ADVANCES IN FOREST FIRE RESEARCH

2022

Edited by
DOMINGOS XAVIER VIEGAS
LUÍS MÁRIO RIBEIRO

ADVANCES IN FOREST FIRE RESEARCH

2022

Edição
Imprensa da Universidade de Coimbra
Coimbra University Press

Email: imprensa@uc.pt
URL: http//www.uc.pt/imprensa
Vendas online: http://livrariadaimprensa.uc.pt

Design da Capa
Carlos Costa

Composição
Luís Mário Ribeiro

ISBN
978-989-26-2297-2

ISBN digital
978-989-26-2298-9

DOI
https://doi.org/10.14195/978-989-26-2298-9

ADVANCES IN FOREST FIRE RESEARCH

2022

Edited by
DOMINGOS XAVIER VIEGAS
LUÍS MÁRIO RIBEIRO
ADAI/CEIF, UNIVERSITY OF COIMBRA, PORTUGAL

ADAI/CEIF

Associação para o Desenvolvimento da Aerodinâmica Industrial (ADAI)

Centro de Estudos sobre Incêndios Florestais (CEIF)

Rua Pedro Hispano nº12

3030 - 289 Coimbra

Telf: +351 239 708580 | Fax: +351 239 708589

www.adai.pt/ceif

https://facebook.com/ceif.adai

https://twitter.com/adai_ceif

Coimbra 2022

Composition

Luís Mário Ribeiro

Contents

Preface

The period between 2018 and 2022 showed us that the problem of wildfires at a global scale is not abating, rather on the contrary. It seems that the consequences of climatic change are already affecting the occurrence of wildfires in various parts of the World in a form that we would expect to happen only several years later. In many countries of Southern Europe, as well in some regions of the USA, Canada and Australia, where we are used to face the presence of very large and devastating fires, we continued to have record breaking events. Some countries, like those of Central and Northern Europe that were not used to having large fires, during these years experienced them.

The previous years were very demanding to the entire World also in other aspects that affected all of us. We refer to the restrictions imposed by the pandemic that limited our meetings and travel, affecting in many cases the health of members of the Wildfire Scientific Community. Fortunately, we were able to find new forms of communication, to overcome those limitations and keep in touch with each other. During weeks and months, for many of us, the personal meetings and group work were replaced by online connections. In spite of the economy of money and time, and the easiness of bringing together a great variety of persons that these meetings provided, we realized that they did not replace the face to face meetings, that bring with them other invaluable dimensions, that are part of personal communication and help to build a scientific community.

Aware of this and of the uncertainties that the various phases of the pandemic brought and of the possibility of having a localized or wide spread worsening of the situation, in the face of a reality that was completely out of our hands, we decided to maintain the organization of our International Conference on Forest Fire Research, now in its 9th Edition, in November 2022, in its traditional form of a face to face meeting.

The good reception of our initiative encouraged us to go ahead with the organization of the Conference, hoping that it will be a hospitable and friendly place where we can all meet and interact. This is our contribution to the common effort to better understand and manage wildfires, to make our Planet a safer and more sustainable place, for many centuries to come.

For the first time in its history, our Conference is partially sponsored by two significant research actions supported by the European Commission. The project FirEUrisk, a Research and Innovation Action of H2020 (Grant 101003890) that aims to propose an innovative framework for managing the risk of wildfires in Europe

by integrating the various phases and scales of the process while focusing on large fires and future climate conditions, will use the Conference to share several of its findings with the scientific and operational communities. The Firelogue Coordination and Support Action, funded by the EU Greendeal program under Grant 101036534, plans to further the dialogue and network among stakeholders within the Wildfire Risk Management community by organizing several networking actions, identifying synergies and conflicts between different interest groups. By bringing together experts from the community, Firelogue will foster mutual discussions and exchange that will lead to just and fair solution to the increasingly threatening wildfires across Europe and the world.

For the second time, the International Association of Wildland Fire honored our Conference by linking it to the 17th International Wildland Fire Safety Summit. The subject of fire safety has always been very dear to our Conference, since its first edition in 1990. This is expressed by the large number of keynotes and papers dedicated to the problem of safety of operational agents and citizens in the face of fire, but also by the Short Courses on Fire Safety that we have organized, since 2002 (the year of the first association to the Safety Summit), in parallel to the Conference, to promote a research culture on fire safety in all countries.

This eBook compiles the valuable contributions to this Conference, made by authors from the scientific community all around the world. Each one of the six major themes of the conference includes different topics in the entire range of fields related to the problem of wildfires management. They compose the six chapters of this eBook, as follows:

Chapter 1) Decision Support Systems and Tools

Topics covered: Fire Detection and Monitoring; Remote Sensing; Fire Behaviour Prediction Systems; Meteorology and other support information; New Technologies

Chapter 2) Fire at the Wildland Urban Interface

Topics covered: Fuel Management; Fire Management; Risk Assessment; Community protection; Fire modelling

Chapter 3) Risk Adaptation

Topics covered: Human and Institutional Factors; Economic Issues; Fire Impacts on Society; Fire Ecology; Fire Climate; Fire Prevention

Chapter 4) Risk Assessment

Topics covered: Fire Risk Assessment; Fire Risk Communication; Fire Effects; Cascading Effects; Evaluation and Management of Burned Areas; Fire History

Chapter 5) Risk Reduction

Topics covered: Fire Behaviour; Fire Prevention; Fuel Management; Fuel Modelling; Fire Preparedness; Climate Change

Chapter 6) Wildfire Management and safety

Topics covered: Fire Behaviour; Firefighting training; Fire Suppression; Large Fires; Fire Safety; Fire protection; Fire Management; Fire Weather

We are sure that this Conference and eBook may serve the purpose of keeping a record of the recent research in these fields and to illustrate the role that is played by the scientific community in the face of the challenges

that these new times bring to fire science. We are sure that it will inspire and trigger more investigation and collaboration.

This e-book, published by the Coimbra University Press, is considered as a publication *per se*, independent from the Conference, and each paper is considered to be part of a chapter.

In the name of the Organizing Committee we wish to thank all the authors for their valuable work and for participating in the Conference.

We wish to thank Dr. Mike Flannigan for having accepted, once more, the role of Head of the Scientific Committee, who with the help of a group of selected experts reviewed and revised the submitted abstracts. Their work was very important to keep the high level of quality that has been the standard of this Conference.

We wish to thank to the distinguished individuals that accepted to be members of the Honorary Committee and to all the entities that sponsored our Conference.

We would like to express our personal thanks to all the members of the Organizing Committee and in particular to our colleagues of the Local Committee and the Secretariat for all their support, work and dedication during the preparation of the Conference. They carried the largest part of the workload that included the performance of large and small tasks that are required to put this Conference together and therefore they deserve thanks from all of us.

Coimbra, 24 August 2022

The Chairman of the Conference

Domingos X. Viegas, ADAI-CEIF, University of Coimbra, Portugal

The Co-Chairman of the Conference

Luis Mario Ribeiro, ADAI-CEIF, University of Coimbra, Portugal

Chapter 1: Decision Support Systems and Tools

A forest fuel dryness forecasting system that integrates an automated fuel sensor network, gridded weather, landscape attributes and machine learning models

Christopher Sean Lyell*[1]; Usha Nattala[2]; Rakesh Chandra Joshi[1]; Zaher Joukhadar[2]; Jonathan Garber[2]; Simon Mutch[2]; Assaf Inbar[3]; Tegan Brown[1]; Tim Gazzard[4]; Alice Gower[4]; Samuel Hillman[4]; Thomas Duff[5]; Gary Sheridan[1]

[1] *School of Ecosystem and Forest Sciences, Faculty of Science, The University of Melbourne. Parkville, VIC 3010, Australia. {clyell, rakesh.joshi, Sheridan}@unimelb.edu.au, {tpbrown@student.unimelb.edu.au}*
[2] *Melbourne Data Analytics Platform, The University of Melbourne. Parkville, VIC 3010, Australia, {usha.nattala, zaher.joukhadar, jonathan.garber, simon.mutch}@unimelb.edu.au*
[3] *Hawkesbury Institute for the Environment, Western Sydney University. Penrith, NSW 2751, Australia, {a.inbar@westernsydney.edu.au}*
[4] *Department of Environment, Land, Water and Planning. Melbourne, Victoria, Australia, {tim.gazzard, alice.gower, samuel.hillman}@delwp.vic.gov.au*
[5] *Country Fire Authority. Burwood East, VIC, Australia, {thomas.duff@cfa.vic.gov.au}*

**Corresponding author*

Keywords

Fuel moisture content; Landscape forecasting; Machine learning; Forest management; Weather forecasting

Abstract

Accurate and timely forecasting of forest fuel moisture is critical for decision making in the context of bushfire risk and prescribed burning. The moisture content in forest fuels is a driver of ignition probability and contributes to the success of fuel hazard reduction burns. Forecasting capacity is extremely limited because traditional modelling approaches have not kept pace with rapid technological developments of field sensors, weather forecasting and data-driven modelling approaches. This research aims to develop and test a 7-day-ahead forecasting system for forest fuel dryness that integrates an automated fuel sensor network, gridded weather, landscape attributes and machine learning models. The integrated system was established across a diverse range of 30 sites in south-eastern Australia. Fuel moisture was measured hourly using 10-hour automated fuel sticks. A subset of long-term sites (5 years of data) was used to evaluate the relative performance of a selection of machine learning (Light Gradient Boosting Machine (LightGBM) and Recurrent Neural Network (RNN) based Long-Short Term Memory (LSTM)), statistical (VARMAX) and process-based models. The best performing models were evaluated at all 30 sites where data availability was more limited, demonstrating the models' performance in a real-world scenario on operational sites prone to data limitations. The models were driven by daily 7-day continent-scale gridded weather forecasts, in-situ fuel moisture observation and site variables. The model performance was evaluated based on the capacity to successfully predict minimum daily fuel dryness within the burnable range for fuel reduction (11 – 16%) and bushfire risk (<11%). The sites with long-term data performed favourably using the LightGBM model. Producing average probability of detection (POD; probability of detecting an event in the specified range) prediction results 1-days out, 5-days out and the average across all seven days of 0.92, 0.81 and 0.80 (<11%), and 0.71, 0.54 and 0.53 (11 – 16%); with R2's of 0.77, 0.59 and 0.55. The machine learning models performed favourably compared to the statistical and process-based models. This demonstrates that accurate, real-time operational fuel moisture forecasting can be achieved by integrating sensor data, weather forecasts, landscape information, and data-driven modelling approaches. The proposed system has the potential to be applied in any wildland fire setting where weather forecasts are available, and the adaptation of this system will greatly enhance the decision-making capabilities of fire managers.

1. Introduction

Bushfires as a natural disaster are the cause of hundreds of fatalities in Australia and across the globe (Blanchi et al., 2014; Haynes et al., 2010, 2019). An important component of bushfire risk is the dead fuel moisture content (DFMC). This is partially due to the ignition probability of fuels having a non-linear relationship, with a significant increase in ignition risk once the fuels reach a threshold moisture content (Ellis, 2015). In

productive forests, fuel moisture is also an important variable which controls the risk of bushfire ignition and spread, with the fuel loads being high enough to maintain a fire once started (Cawson et al., 2018). Fuel moisture also makes planned burning extremely difficult (Slijepcevic et al., 2015). Due to this being able to predict the DFMC into the future would allow for better risk identification and fuel management planning.

Modelling of DFMC has been attempted using processes-based methods which input temperature, relative humidity, solar radiation, and precipitation. With the model proposed by Nelson (2000) being widely used. Recently this model has been surpassed by more mechanistic (Van Der Kamp, 2017) or data driven (Lee et al., 2020; Shmuel et al., 2022) approaches which improve the representation and accuracy of FMC predictions. These methods utilise a larger number of input variables which aim to improve the modelling accuracy by more detailed representation of the physical processes, or through determining the relationships through statistical, data driven techniques (e.g. random forest, neural networks). These methods have not been explored in predictive modelling under varying forest canopies (key driver of FMC (Brown et al., 2021)), forecasting fuel moisture multiple days in advance using forecast data. A forecasting system would be another valuable tool to assist fire managers in early warning risk detection systems or allow fuel reduction burn operations to be moved to a day which will optimise the likelihood of achieving a successful burn.

The overall aim of this study was to develop an automatic fuel moisture monitoring system, capable of forecasting 10-hour fuel moisture. This system is aimed at capturing the change in fuel moisture under varying forest types, located across a large spatial and climatic range. The system integrates advancements in the ability to forecast short-term climate conditions and utilise the ever-expanding, continuous dataset which the automatic fuelsticks provide. For this system to produce the highest accuracy predictions, two specific research questions arose, these being:

1. If you have a high quality and quantity of data how do machine learning models compare with statistical (VARMAX) and process-based models, and which model is likely to be the most reliable in a real-world scenario?
2. How well does the best performing methods in question forecast across a larger network with smaller datasets and varying data quality?

2. Methods

2.1. Overview - Fuel moisture monitoring forecasting system

The Forest Fuel Moisture Forecasting System (FFMFS) comprises four components that come together to allow fuel moisture to be forecast for up to seven days. The conceptual diagram shown in Figure 1 illustrates how these key components are integrated for a continuously retrained spatial/temporal forecast model (gridded weather forecast, gridded landscape attributes, live on ground sensor network, daily re-trained ML model). It integrates spatially forecast climate variables, with the significant advancements in continuous in-situ forest fuel moisture monitoring (Automated fuel moisture sticks), and in remote sensing datasets. These different streams of data and information were brought together in a machine learning algorithm which predicts the minimum, maximum and mean fuel moisture content across the landscape at a daily timescale, seven days in advance. The system was developed in consultation with the Department of Environments, Land, Water and Planning (DELWP, Victorian Government, Australia), this was to ensure that it could be replicated within the government organisation, with the potential to be used in risk and management planning.

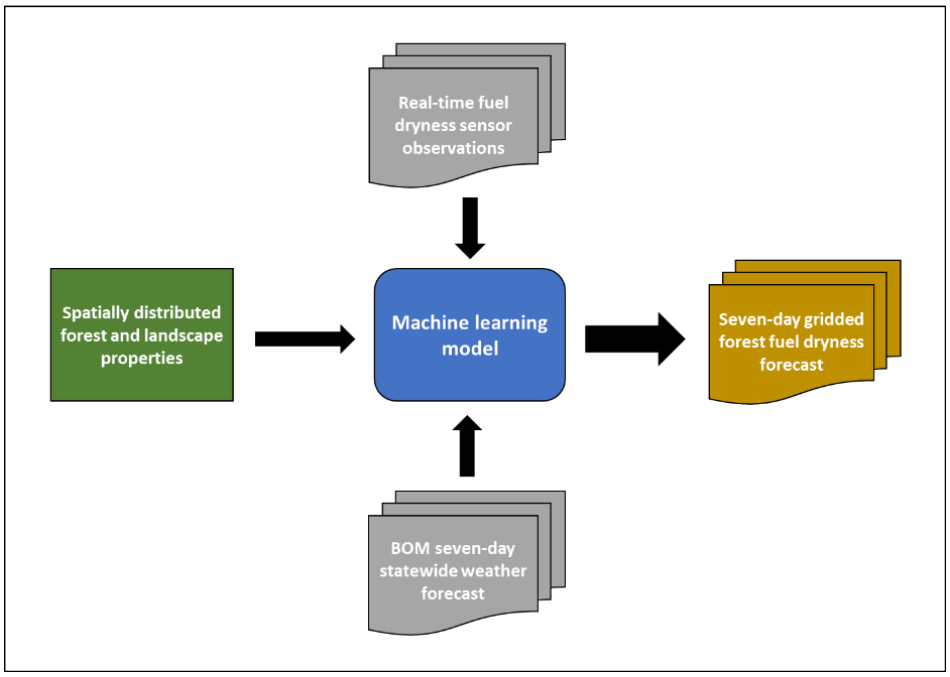

Figure 1- The components of the forest fuel moisture monitoring system

2.2. Study area

The study area was located across Victoria, Australia (Figure 2). On the traditional lands of the First Nations peoples (Victorian Aboriginal Heritage Council Victoria's Current Registered Aboriginal Parties (RAP), 2022). The study comprised of 30 field sites which captured a wide range of physical and environmental variables throughout the region. The long-term climatic conditions vary significantly across the sites, with aridity indexes from 1.13 to 5.90. The study area also covers a range of vegetation types and forest structures, from tall eucalyptus forests to sparse woodlands with shrubs and minimal vertical structural complexity. The sites aimed to capture both open and closed forest conditions.

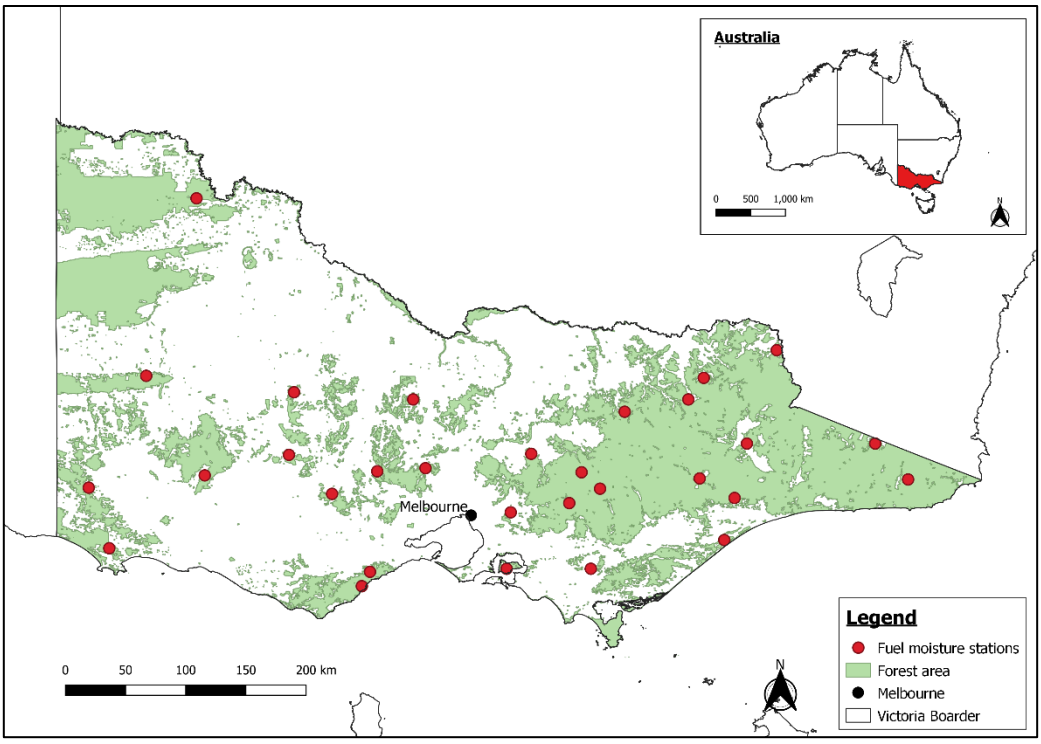

Figure 2- Study area spatial extent across Victoria, Australia.

2.3. Site instrumentation and data collection

The data collection period was from April 2014 to August 2021, with seven sites installed throughout 2014 and 23 in 2019. The sites had fuel moisture content readings collected half hourly using fuel sticks (CS506, Campbell Scientific, Inc., Logan, USA). The fuel moisture sticks were installed 10 - 30cm above the ground to represent elevated ground fuels. Site variables used to represent the vegetation and climate signature includes elevation, slope, aspect, aridity index, long term annual rainfall and vegetation cover fraction. The weather forecast variables were from the Australian Digital Forecast Database (Australian Bureau of Meteorology, 2022). This is a gridded seven day forecast across Victoria, producing daily to sub-daily predictions at ~3km resolution. The daily climate variables used in the model were: Temperature, precipitation, relative humidity, skyview factor, Keetch–Byram Drought Index (Keetch & Byram, 1968), wind direction (predominant) and wind speed (max).

2.4. Modelling

Time Series prediction models fall into three broad categories: Autoregressive, Statistical/machine learning, and process-based/mechanistic. In this study a comparison of these methods for DFMC forecasting is presented.

Autoregressive (AR) models are often the simplest to implement with time series predictions. These models attempt to forecast from the existing dataset using recent values as independent variables. They use linear models with previous values, or residuals from the rolling average of previous values. In addition to recent variables, they may also account for seasonal and long-term trends estimated from time series decomposition, and other independent variables. This study uses an Autoregressive integrated moving average (ARIMA) variation VARMAX as the baseline autoregressive model to determine whether fuel dryness can be predicted using past time series data alone.

The two machine learning methods used were, a boosted regression tree random forest (BRT-RF) model (Breiman, 1998; Elith et al., 2008) and a long short term memory recurrent neural network (LSTM-RNN) model. Boosted regression trees train an ensemble of models (i.e. Random Forest regression models), on subsets of data iteratively to create a decision tree algorithm to predict the response variable. We used the LightGBM python package (Ke et al., 2017) to build and train the random forest model. In addition to BRT's, Neural Networks have also been used effectively for time series forecasting (Fan & He, 2021). We used a Long Short Term Memory Recurrent Neural Networks (LSTM-RNN) to compare ML approaches.

The process–based (PB) model used as a comparison was the model proposed by Van Der Kamp (2017). The model only requires four inputs: temperature, relative humidity, precipitation and radiation. The fuelstick model proposed by Van Der Kamp is an improved version of the Nelson model (2000), representing the radiation loading on the fuelstick in more detail. The original Nelson model has been used operationally in the U.S. National Fire Danger Rating System (NFDRS 2016 version; US National Wildfire Coordinating Group, 2021), as well as in fire behaviour models such as FARSITE and FlamMap.

2.4.1. Long-term climate trends

Time Series Forecasting of environmental systems is a problem in that it typically needs to account for long term trends, seasonal cyclicity, antecedent conditions and lag response to controlling processes (Cheng et al., 2015). Time series data often contain patterns of trend and seasonality that can be extracted to improve predictive capability. To do this, Time Series Decomposition (TSD) is used to split a time series dataset into long term trends, seasonal cycles, and residual error. We use the Facebook prophet python package (Taylor & Letham, 2018), which uses an additive method to decompose the time series. This was used to create a seasonal term for input into the BRT-RF and LSTM-RNN models.

2.5. Model validation and performance metrics

All models were evaluated on the seven original sites installed in 2014. To determine which method performed best with the most high-quality data available. The training dataset was from 2014 to September 2020. The validation dataset was from May 2020 – May 2021. The BRT-RF and PB models were then assessed across the entire range of sites, with the additional sites installed in 2019 having a lesser quality of data. These real-world operational sites, which are centrally managed do not always have the same data quality as research-based sites. Each daily forecast had R^2, RMSE, NSE and MAE calculated, as well as the event-based metrics of the probability of detection (POD) and false alarm ratio (FAR). These event-based metrics predict how the model

performs predicting specific fuel moisture ranges (events), within levels relevant to planned burning (Slijepcevic et al., 2015).

3. Results

The RBT-RF results from the seven long-term sites are presented in Table 1. These results show an overall decrease in the accuracy across the seven days. There was high variability between the sites, with Dimboola, Bendigo and St. Arnaud performing well across all the metrics, while Alexandra and Daylesford performed poorly. The event-based metrics (Figure 3) showed the models performed best at low FMC (<11%), while as the higher two ranges performing worse. The "Patchy Burn" range had the highest FAR, making this range the most unreliable in predictions.

Table 1 – BRT-RF model performance across the seven long term sites from 2014 – 2021.

	R^2				NSE				MAE				RMSE			
Site	**1-D**	**3-D**	**5-D**	**7-D**	**1-D**	**3-D**	**5-D**	**7-D**	**1-D**	**3-D**	**5-D**	**7-D**	**1-D**	**3-D**	**5-D**	**7-D**
Dimboola	0.87	0.73	0.69	0.65	0.86	0.61	0.61	0.23	1.17	1.98	1.97	2.63	1.67	2.79	2.93	3.87
Hattah	0.88	0.74	0.68	0.63	0.84	0.56	0.55	0.35	0.79	1.23	1.39	1.62	1.27	2.11	2.43	2.59
Bendigo	0.87	0.68	0.74	0.65	0.85	0.45	0.69	0.28	1.32	2.39	1.99	2.69	1.87	3.56	2.77	4.04
St. Arnaud	0.79	0.72	0.74	0.63	0.71	0.53	0.49	0.42	1.74	2.39	2.86	2.85	2.71	3.42	3.81	3.80
Casterton	0.73	0.64	0.66	0.56	0.37	-0.82	-0.96	-1.43	3.13	6.20	5.99	7.27	4.70	798	8.00	9.37
Daylesford	0.56	0.17	0.20	0.18	-0.03	-6.10	-7.95	-5.53	2.70	7.35	8.55	7.23	3.95	10.4	11.6	9.95
Alexandra	0.69	0.50	0.47	0.55	0.60	-0.17	-0.17	0.11	1.76	2.69	3.09	2.68	2.45	4.18	4.20	3.64
Overall mean	***0.77***	***0.59***	***0.59***	***0.55***	***0.60***	***-0.70***	***-0.67***	***-0.80***	***1.80***	***3.46***	***3.65***	***3.85***	***2.66***	***4.92***	***4.94***	***5.32***

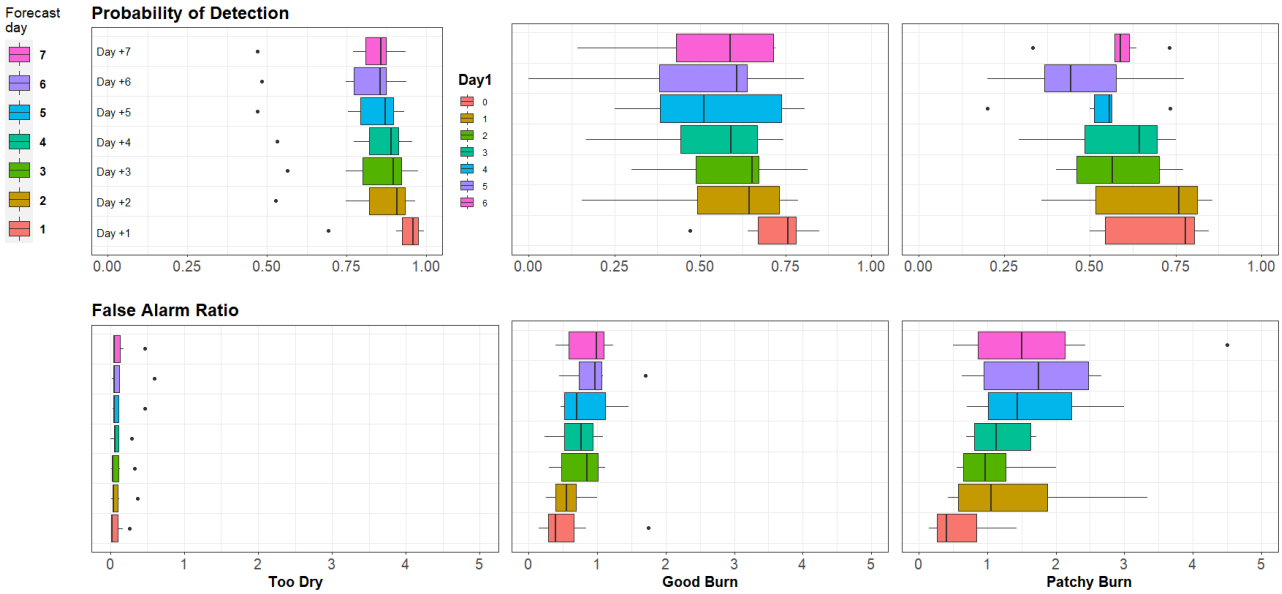

Figure 3 – Event based performance of the BRT-RF model for the daily minimum DFMC forecasts within the range of 11 – 16%, for the seven long term sites. (Top) Probability of detection, (Bottom) false alarm ratios. Left, middle and right columns representing planned burn outcoms proposed in Slijepcevic et al (2015) based on FMC ranges.(left) Too dry and higher risk of burn escaping (0 – 11% FMC); (middle) Good burn representing the FMC range that will sustain a burn but less likely to escape (11 – 16% FMC); and, a Patchy burn due to the FMC being too high and the burn not self sustaining (16 – 21% FMC)

4. Discussion

The BRT-RF managed to incorporate information traditional processed-based modelling cannot, determining how this information relates to the DFMC. The decay in the accuracy, decreasing POD and increasing FAR

across the seven days highlights the increased uncertainty associated with the weather forecast. However, the use of event-based performance metrics showed that although the model decreased in accuracy, it remained within the ranges to predict critical DFMC relevant to planned burning (Slijepcevic et al., 2015). This is critical as while traditional statistics highlight the accuracy in models, they don't reflect the important range for land and fire managers. The results demonstrated that a fuel moisture monitoring forecast system could effectively predict 10-h DFMC up to seven days in advance. Linking ground-based fuel moisture monitoring stations spatially across forested terrain with gridded forecasts allows the complex sub-canopy climate variability to be accounted for in predictions. Grounding the starting DFMC in observations also proved important due to the decay rate across the seven days. If the starting DFMC was incorrect, then adding this uncertainty to the decay rate would decrease the reliability of the forecasts. Lastly, incorporating site variables assisted in the model's ability to account for the transfer of climate relationships from above the canopy to below. The ability to incorporate canopy and landscape variables also has the potential to expand the point-based forecasts into a spatial forecast.

The proposed system differs from previous DFMC forecasting as it incorporates live continuous below canopy measurements with above canopy weather, machine learning techniques and a seasonal rolling term. The assembled dataset represents the largest below canopy comparison of continuous DFMC forecasting using machine learning to our knowledge, across the largest range of forest types. The performance of the model validates the use of ML for predicting DFMC below canopy in closed forests, this being highlighted as an area of limited research by Shmuel et al. (2022). Early results from the other traditional models indicate that the machine learning model performed favourably in comparison, highlighting the value of ML techniques for below canopy moisture forecasting.

5. Conclusion

The proposed Forest Fuel Moisture Forecasting System has demonstrated the ability to incorporate advancements in ML techniques, weather forecasting, ground-based sensors, and remote sensing into a theoretically operational system for land managers. The ability to predict forest fuel moisture multiple days in advance with known levels of uncertainty within relevant DFMC ranges will allow for more informed decisions and planning around fuel reduction burns and bushfire risk. While more work needs to be done on validating the effectiveness of using DFMC forecasting for decision making in bushfire risk and planned burning, the proposed system provides a tool and framework with which this research can be conducted.

6. References

Australian Bureau of Meteorology. (2022). The Australian Digital Forecast Database. Retrieved March 26, 2022, Available online: http://www.bom.gov.au/weather-services/about/forecasts/australian-digital-forecast-database.shtml

Blanchi, R., Leonard, J., Haynes, K., Opie, K., James, M., & Oliveira, F. D. de. (2014). Environmental circumstances surrounding bushfire fatalities in Australia 1901–2011. Environmental Science & Policy, 37, 192–203. https://doi.org/https://doi.org/10.1016/j.envsci.2013.09.013

Breiman, L. (1998). Arcing classifier (with discussion and a rejoinder by the author). The Annals of Statistics, 26(3), 801–849. https://doi.org/10.1214/aos/1024691079

Brown, T. P., Inbar, A., Duff, T. J., Burton, J., Noske, P. J., Lane, P. N. J., & Sheridan, G. J. (2021). Forest Structure Drives Fuel Moisture Response across Alternative Forest States. Fire, Vol. 4. https://doi.org/10.3390/fire4030048

Cawson, J. G., Duff, T. J., Swan, M. H., & Penman, T. D. (2018). Wildfire in wet sclerophyll forests: the interplay between disturbances and fuel dynamics. Ecosphere, 9(5), e02211. https://doi.org/https://doi.org/10.1002/ecs2.2211

Cheng, C., Sa-Ngasoongsong, A., Beyca, O., Le, T., Yang, H., Kong, Z. (James), & Bukkapatnam, S. T. S. (2015). Time series forecasting for nonlinear and non-stationary processes: a review and comparative study. IIE Transactions, 47(10), 1053–1071. https://doi.org/10.1080/0740817X.2014.999180

Elith, J., Leathwick, J. R., & Hastie, T. (2008). A working guide to boosted regression trees. Journal of Animal Ecology, 77(4), 802–813. https://doi.org/https://doi.org/10.1111/j.1365-2656.2008.01390.x

Ellis, P. F. M. (2015). The likelihood of ignition of dry-eucalypt forest litter by firebrands. International Journal of Wildland Fire, 24(2), 225–235. Retrieved from https://doi.org/10.1071/WF14048

Fan, C., & He, B. (2021). A Physics-Guided Deep Learning Model for 10-h Dead Fuel Moisture Content Estimation. Forests, Vol. 12. https://doi.org/10.3390/f12070933

Haynes, K., Handmer, J., McAneney, J., Tibbits, A., & Coates, L. (2010). Australian bushfire fatalities 1900–2008: exploring trends in relation to the 'Prepare, stay and defend or leave early' policy. Environmental Science & Policy, 13(3), 185–194. https://doi.org/https://doi.org/10.1016/j.envsci.2010.03.002

Haynes, K., Short, K., Xanthopoulos, G., Viegas, D., Ribeiro, L. M., & Blanchi, R. (2019). Wildfires and WUI Fire Fatalities BT - Encyclopedia of Wildfires and Wildland-Urban Interface (WUI) Fires (S. L. Manzello, Ed.). https://doi.org/10.1007/978-3-319-51727-8_92-1

Ke, G., Meng, Q., Finley, T., Wang, T., Chen, W., Ma, W., Ye, Q., & Liu, T.-Y. (2017). LightGBM: A Highly Efficient Gradient Boosting Decision Tree. In I. Guyon, U. V Luxburg, S. Bengio, H. Wallach, R. Fergus, S. Vishwanathan, & R. Garnett (Eds.), Advances in Neural Information Processing Systems (Vol. 30). Retrieved from https://proceedings.neurips.cc/paper/2017/file/6449f44a102fde848669bdd9eb6b76fa-Paper.pdf

Keetch, J. J., & Byram, G. M. (1968). A drought index for forest fire control (Vol. 38). US Department of Agriculture, Forest Service, Southeastern Forest Experiment ….

Lee, H., Won, M., Yoon, S., & Jang, K. (2020). Estimation of 10-Hour Fuel Moisture Content Using Meteorological Data: A Model Inter-Comparison Study. Forests, Vol. 11. https://doi.org/10.3390/f11090982

Shmuel, A., Ziv, Y., & Heifetz, E. (2022). Machine-Learning-based evaluation of the time-lagged effect of meteorological factors on 10-hour dead fuel moisture content. Forest Ecology and Management, 505, 119897. https://doi.org/https://doi.org/10.1016/j.foreco.2021.119897

Slijepcevic, A., Anderson, W. R., Matthews, S., & Anderson, D. H. (2015). Evaluating models to predict daily fine fuel moisture content in eucalypt forest. Forest Ecology and Management, 335, 261–269. https://doi.org/https://doi.org/10.1016/j.foreco.2014.09.040

Taylor, S. J., & Letham, B. (2018). Forecasting at Scale. The American Statistician, 72(1), 37–45. https://doi.org/10.1080/00031305.2017.1380080

US National Wildfire Coordinating Group. (2021). Dead Fuel Moisture Content. Retrieved March 25, 2021, Available online: https://www.nwcg.gov/publications/pms437/fuel-moisture/dead-fuel-moisture-content

van der Kamp, D. W., Moore, R. D., & McKendry, I. G. (2017). A model for simulating the moisture content of standardized fuel sticks of various sizes. Agricultural and Forest Meteorology, 236, 123–134. https://doi.org/10.1016/j.agrformet.2017.01.013

Victorian Aboriginal Heritage Council Victoria's Current Registered Aboriginal Parties (RAP). Retrieved March 26, 2022, Available online: https://www.aboriginalheritagecouncil.vic.gov.au/victorias-current-registered-aboriginal-parties

A long-term satellite-based burned area database for the Northern Boreal Region (1982-2020)

José R. García-Lázaro[1]; José A. Moreno-Ruíz[1]; Manuel Arbelo*[2]; Pedro A. Hernández-Leal[2]

[1]Departamento de Informática, Universidad of Almería, 04120 Almería, Spain, {jrgarcia, jaruiz}@ual.es
[2] Departamento de Física, Universidad de La Laguna, 38200 San Cristóbal de La Laguna, Spain, {marbelo, pedro.hernandez}@ull.es

**Corresponding author*

Keywords

Burned Area Mapping; Time Series Analysis; Boreal Forest; LTDR.

Abstract

Burned Area (BA) is an essential variable for studying the Earth's climate evolution. The boreal forest is one of the largest biomes in the world, spanning North America and Eurasia. For North America, two record fire occurrence databases since the 1950s are available: Alaska Fire Service (AFS) database and the Canadian National Fire Database (CNFDB). However, there are currently no reliable burned area data for the boreal region of Eurasia, mainly Siberia, for the 1980s and 1990s. In this work, a Bayesian network algorithm was applied to the Long-Term Data Record (Version 5) to generate a burned area product at a resolution of 0.05 degrees for the entire boreal region above 60°N from 1982 to 2020. An assessment of burnt area estimates was carried out using high-resolution satellite images, official reference data and the MCD64A1 MODIS global burned area product (when were available). The results showed a high correlation with all the reference burned area datasets (95% with AFS-CNFDB, 93% and 95% with MCD64A1 in North America and Eurasia, respectively). The derived database constitutes unique long-term burned area information for studies of fire and carbon dynamics in the Northern Boreal Region, as well as their effects on the climate system.

1. Introduction

Forest fires contribute to greenhouse gas emissions and are responsible for changes in carbon dynamics and their implications for global climate change (Chuvieco *et al.* 2019). One of the regions of the planet where this global change is expected to have the highest impact is the northern boreal region. Boreal forests represent one of the largest sources of carbon storage on our planet (Schuur *et al.* 2015; Young *et al.* 2017).

Images derived from sensors aboard quasi-polar orbiting satellites have in recent years allowed the construction of time series of burned area (BA), providing the scientific community with essential information that could be correlated with other variables involved in global change. Among the main BA products developed are MCD64A1 (Giglio *et al.* 2018) and Fire_CCI (Chuvieco *et al.* 2018), both derived from the MODIS (Moderate Resolution Imaging Spectroradiometer) sensor. However, these products have only been available since 2000, so they do not allow the construction of time series of more than two decades, limiting their application in medium- and long-term fire trend studies.

In this paper, we present and validate a unique database containing annual BA estimates for the northern boreal forest from 1982 to 2020 with a spatial resolution of 0.05°. It is derived from a new BA product, generated by applying a Bayesian network-based classification algorithm to the LTDR (Land Long Term Data Record) v5 dataset (Pedelty *et al.* 2007).

2. Materials and Methods

2.1. Study area

The study area covers all northern boreal regions bounded by 60ºN and 72.5ºN parallels. It was divided into two sub-regions: North America (Alaska and boreal Canada), limited by the 168.5ºW and 43.5ºW meridians and Eurasia (from Scandinavia to the Pacific coast of Siberia), bounded by the 5ºE and 180ºE meridians. The North

American sub-region contains one-third of the boreal ecosystem and the Eurasian sub-region the other two thirds.

2.2. LTDR data set. Pre-processing

The Long-Term Data Record (LTDR) from NASA is a consistent long-term dataset at a spatial resolution of 0.05° (~5 km) based on daily data from the Advanced Very High-Resolution Radiometer (AVHRR) on-board the National Oceanic and Atmospheric Administration (NOAA) satellites and daily data acquired by MODIS on-board NASA's Terra and Aqua satellites (Pedelty *et al.* 2007). Daily global LTDR version 5, download from NASA server (https://ltdr.nascom.nasa.gov/cgi-bin/ltdr/ltdrPage.cgi), was used in this study. The original daily images in HDF (Hierarchical Data Format) format were transformed to BSQ (Band Sequential) format and cropped to the boundaries of the study region. Then, 10-day composites were constructed with the maximum brightness temperature criterion to eliminate atmospheric effects. Simultaneously, vegetation indices derived from the original radiometric bands were calculated for burned area discrimination: NDVI (Normalized Difference Vegetation Index) (Rouse et al. 1973), GEMI (Global Environmental Monitoring Index) (Pinty and Verstraete, 1992) and BBFI (Burned Boreal Forest Index) (Moreno-Ruiz *et al.* 2012).

2.3. Burned area detection

The BA-LTDR classifier initially developed for the NE Siberia region (García-Lázaro *et al.* 2018) was used to generate the corresponding annual BA maps. This classifier is based on the Bayes-Net algorithm of the WEKA (Waikato Environment for Knowledge Analysis) software package (Frank *et al.* 2016).

To assess the accuracy of the BA-LTDR time series for the Northern boreal region, we considered splitting the time series for both sub-regions (Eurasia and North America) into two parts: pre- and post-2000. Since 2000, accuracy assessments for the Eurasian sub-region have been evaluated using only MCD64A1 C6 burned area product with 500 m spatial resolution, according to CEOS validation protocol (Morisette *et al.* 2006). MCD64A1 Collection 6 is currently the product with the highest reliability compared to the other BA products (Padilla *et al.* 2015), and it has the lowest commission and omission errors in the boreal forest region (Boschetti *et al.* 2019). Before 2000, accuracy assessments could not be evaluated in this way because other BA products with a higher spatial resolution for this study sub-region were not available. For the North America boreal sub-region, the BA-LTDR burned area maps obtained (and also BA maps of the MCD64A1 C6 product) were compared with reference data from the Alaska Fire Service (AFS) database (https://afsmaps.blm.gov/imf/imf.jsp?site=firehistory) and Canadian National Fire Database (CNFDB) (http://cwfis.cfs.nrcan.gc.ca/ha/nfdb) (García-Lázaro *et al.* 2018).

The temporal accuracy of the BA-LTDR product in each sub-region was assessed considering the total calculated annual BA. A timing distribution of BA-LTDR product was represented on a chart together with the time series of reference BA and a correlation analysis was carried out. The relative percentages of the annual BA of the BA-LTDR product were calculated concerning the reference data for the common years when available.

3. Results

3.1. Annual burned area maps

The BA-LTDR database contains annually burned area maps for the Northern boreal forest (above 60°N) for the 1982-2020 period in 0.05° (~5 km) resolution Climate Modelling Grid (CMG) cells. Figure 1 presents a decade-by-decade grouping of the annually BA maps for both sub-regions. Burned pixels have been plotted in a dark colour on the green land.

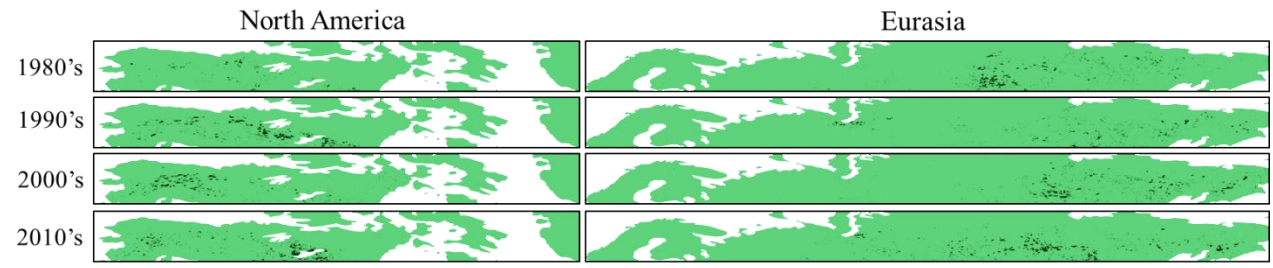

Figure 1- Maps of area burned by decades for the sub-regions of North America and Eurasia. Black: burned area, white: water, green: unburned.

3.1. Temporal Accuracy

Figure 2 shows the annual distribution of the total BA estimated for 1982-2020 in the North America sub-region. BA-LTDR detected 61% of the reference burned area, underestimating the BA in all years of the time series. There was a strong correlation (0.95) between the LTDR-BA data and the reference AFS-CNFDB data. If we divide the time series into two parts (pre-MODIS: 1982-1999, MODIS: 2000-2020), the BA-LTDR algorithm shows a practically homogeneous behaviour both in percentage of burnt area estimation (64% vs 59%) and correlation coefficient (0.98 vs 0.95), concerning the reference data. Making an intercomparison of BA-LTDR with the MCD64A1 C6 product in the common period (2000-2020) in North America, LTDR-BA detected approximately 86% of the area burned, with a correlation coefficient of 0.93.

In the Eurasia sub-region, the assessment of the temporal accuracy of the BA-LTDR burnt area was calculated using the MCD64A1 C6 product as a reference. MCD64A1 C6 estimated an annual BA of around 47.10 millions ha for the period 2000-2020. While BA-LTDR estimated around 66%. BA-LTDR underestimates the BA in all common years except for 2000, but its temporal pattern matches the reference, with a correlation coefficient of 0.95.

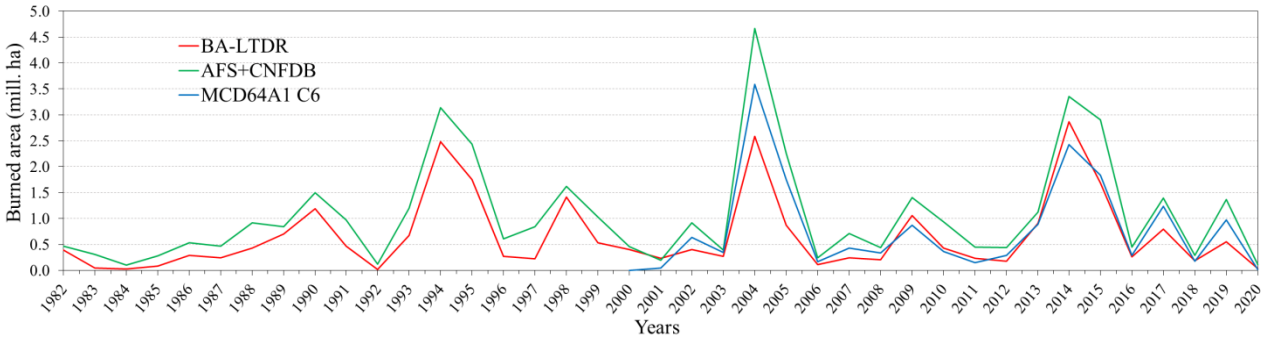

Figure 2- Annual distribution of the burned area estimate (mill. ha) in the North America boreal sub-region from the Alaska Fire Service/Canadian National Fire Database (AFS + CNFDB), BA-LTDR and MCD64A1 C6.

4. Conclusion

A comprehensive burned area database (1982–2020) for the Northern boreal region using a Bayesian network algorithm from the LTDR v5 dataset at 0.05° spatial resolution has been built. This time series is the longest developed for this region at this spatial resolution. It constitutes a unique data source for studies of fire and carbon dynamics in the Northern Boreal Region, as well as their effects on the climate system.

5. Acknowledgments

This research was funded by the Spanish Ministry of Science, Innovation and Universities (MCIU), the State Research Agency (AEI) and the European Regional Development Fund (ERDF) through the project RTI2018-099171-B-I00. The University of Almeria and the Andalusia ERDF Operational Program partially funded this work through projects 2019/006 and UAL18-TIC-A023-B1. The authors would like to thank the LTDR project and its team for the processing and free distribution of the data used in this work.

6. References

Boschetti, L., Roy, D. P., Giglio, L., Huang, H., Zubkova, M., & Humber, M. L. (2019) Global validation of the collection 6 MODIS burned area product. Remote Sensing of Environment, 235(November), 111490. https://doi.org/10.1016/j.rse.2019.111490

Chuvieco, E., Mouillot, F., van der Werf, G. R., San Miguel, J., Tanasse, M., Koutsias, N., García, M., Yebra, M., Padilla, M., Gitas, I., Heil, A., Hawbaker, T.J., Giglio, L. (2019) Historical background and current developments for mapping burned area from satellite Earth observation. Remote Sensing of Environment, 225, 45–64. https://doi.org/10.1016/J.RSE.2019.02.013

Chuvieco, E.; Lizundia-Loiola, J.; Lucrecia Pettinari, M.; Ramo, R.; Padilla, M.; Tansey, K.; Mouillot, F.; Laurent, P.; Storm, T.; Heil, A.; et al. (2018) Generation and analysis of a new global burned area product based on MODIS 250 m reflectance bands and thermal anomalies. Earth Syst. Sci. Data, 10, 2015–2031.

Frank, E., Hall, M. A., Witten, I. H. (2016) The WEKA Workbench. Online Appendix for "Data Mining: Practical Machine Learning Tools and Techniques", Morgan Kaufmann, Fourth Edition, 2016.

García-Lázaro, J. R., Moreno-Ruiz, J. A., Riaño, D., Arbelo, M. (2018) Estimation of burned area in the Northeastern Siberian boreal forest from a Long-Term Data Record (LTDR) 1982-2015 time series. Remote Sensing 10(6), 940. https://doi.org/10.3390/rs10060940

Giglio, L.; Boschetti, L.; Roy, D.P.; Humber, M.L.; Justice, C.O. (2018) The Collection 6 MODIS burned area mapping algorithm and product. Remote Sens. Environ, 217, 72–85.

Moreno Ruiz, J. A., Riaño, D., Arbelo, M., French, N. H. F., Ustin, S. L., Whiting, M. L. (2012) Burned area mapping time series in Canada (1984-1999) from NOAA-AVHRR LTDR: a comparison with other remote sensing products and fire perimeters. Remote Sensing of Environment 117, p. 407-414. https://doi.org/10.1016/j.rse.2011.10.017

Morisette, J. T., Baret, F., Privette, J. L., Myneni, R. B., Nickeson, J. E., Garrigues, S., Shabanov, N. V, Weiss, M., Fernandes, R. A., Leblanc, S. G., Kalacska, M., Sánchez-azofeifa, G. A., Chubey, M., Rivard, B., Stenberg, P., Rautiainen, M., Voipio, P., Manninen, T., Pilant, A. N., … Cook, R. (2006) Validation of Global Moderate-Resolution {LAI} Products : A Framework Proposed Within the {CEOS} {L}and {P}roduct {V}alidation Subgroup. {IEEE} Transactions on Geoscience and Remote Sensing, 44(7), 1804–1817.

Padilla, M., Stehman, S. V., Ramo, R., Corti, D., Hantson, S., Oliva, P., Alonso-Canas, I., Bradley, A. V., Tansey, K., Mota, B., Pereira, J. M., & Chuvieco, E. (2015) Comparing the accuracies of remote sensing global burned area products using stratified random sampling and estimation. Remote Sensing of Environment, 160, 114–121. https://doi.org/10.1016/j.rse.2015.01.005

Pedelty, J.; Devadiga, S.; Masuoka, E.; Brown, M.; Pinzon, J.; Tucker, C.; Vermote, E.; Prince, S.; Nagol, J.; Justice, C.; et al. Generating a long-term land data record from the avhrr and modis instruments. In Proceedings of the 2007 IEEE International Geoscience and Remote Sensing Symposium, Barcelona, July 2007; pp. 1021–1025.

Pinty, B., Verstraete, M. M. (1992) GEMI: a non-linear index to monitor global vegetation from satellites. Vegetatio 101, p. 15-20. https://doi.org/10.1007/BF00031911

Rouse, J. W., Haas, R. H., Schell, J. A., Deering, D. W. (1973) Monitoring vegetation systems in the Great Plains with ERTS. 3rd ERTS Symposium, NASA SP-351 I, pp. 309–317.

Schuur, E.A.G., McGuire, A.D., Schädel, C., Grosse, G., Harden, J.W., Hayes, D.J., Hugelius, G., Koven, C.D., Kuhry, P., Lawrence, D.M., Natali, S.M., Olefeldt, D.k,, Romanovsky, V.E., Schaefer, K., Turetsky, M.R., Treat, C.C., Vonk, J.E. (2015) Climate change and the permafrost carbon feedback. Nature 520 (7546), pp. 171-179. https://doi.org/10.1038/nature14338

Young, A.M., Higuera, P.E., Duffy, P.A., Hu, F.S. (2017) Climatic thresholds shape northern high-latitude fire regimes and imply vulnerability to future climate change. Ecography 40(5), pp. 606-617. https://doi.org/10.1111/ecog.02205

A mechanistic live fuel moisture model

W. Matt Jolly*; Elliott T. Conrad

US Forest Service, Rocky Mountain Research Station, Missoula Fire Sciences Laboratory, 5775 Hwy 10 W, Missoula, MT 59808, USA, {william.jolly, elliot.conrad}@usda.gov

**Corresponding author*

Keywords

Live fuel moisture, density, model

Abstract

Wildland fires are a common global disturbance and many of these fires burn through mixtures of living and dead vegetation. Live fuels are unique because they regulate biomass and water content actively through processes such as photosynthesis or transpiration. The main goal of these processes is to maintain the growth and maintenance demands of the plants while minimising water loss. Historically, live fuel dynamics were assumed to be only driven by evaporative or drying processes and little attention was paid to the interplay between carbon and water dynamics. Here we present a mechanistic model of live fuel moisture (LFM) which is a critical component of live fuel flammability. The model decouples LFM into physical and chemical metrics that are easy to. Each metric serves as a proxy for important components of the seasonal water and carbon cycle or to capture inter-species variations in physical properties. We evaluate this model using field measurements of physical and chemical characteristics for a Douglas Fir (*Pseudotsuga menziesii*), a common intermountain US tree species that commonly burns in crown fires. This simple, mechanistic model was effective at characterising the seasonal variations in LFM across both new and old foliage as a simple function of specific leaf area, surface-area-to-volume ratio, relative water content and a species-specific scalar ($r2=0.995$, $p < 0.05$). Finally, we suggest how this decoupled model can be used to more appropriately parameterize a 3-dimensional computational fluid dynamics-based fire behaviour model to represent an appropriate live fuel moisture as the combined effects of biomass and moisture variations on canopy flammability.

1. Introduction

Wildland fires are a common global disturbance and many of these fires burn through mixtures of living and dead vegetation. While there have been extensive studies exploring the factors that control dead fuel flammability, there have been considerably fewer studies that focus on live fuels. In part, this is due to the difficulty of controlling live fuel characteristics in the lab and considerable variation both seasonally and spatially of those characteristics in the field. These studies are further complicated by historical assumptions that attempt to link live fuel flammability variations to indicators of drought but many studies have found that drought indicators alone are insufficient to capture seasonal live fuel moisture variations (Pellizzaro et al., 2007,, Ruffault et al., 2018). While this is partially accurate, live fuel flammability variations are driven by several interacting factors such as changes in absolute moisture content, variations in needle biomass and structural differences in physical factors such as their surface-area-to-volume ratio. A more complete, mechanistic model of the drivers that influence live fuel moisture variations is needed (Pellizzaro et al., 2007).

2. Methods

We collected new and old live foliar samples bi-weekly from Douglas Fir for the 2021 growing seasons (Apr to October). For each sample we measured live fuel moisture content by weighing samples fresh, drying in a 95 degrees Celsius oven for at least 48 hours and re-weighing samples after drying. After initial fresh weights were taken, a sub-sample of the bulk foliar sample was separated to determine density, surface-area-to-volume ratio and leaf mass area. Foliar volume using an Ohaus density kit on a high precision balance and those samples were retained and dried to compute density. Surface area was measured by scanning the planar surface area and computing the planar surface area using ImageJ. Total surface area was assumed to be 2 time the planar area.

3. The mechanistic live fuel moisture model

We developed and tested a simple, mechanistic model of live fuel moisture. The model decouples factors that are known to influence season variations in live fuel moisture content by varying either their water status / hydration or their dry weight. The model was defined as follows:

$$Live\ Fuel\ Moisture\ (\%\ dry\ wt) = \frac{SLA*RWC*\kappa}{SAV} \qquad \text{Equation 1}$$

SLA is the Specific Leaf Area on a dry weight basis ($m^2\ kg^{-1}$), RWC is the Relative Water Content or a metric of the amount of water in the particle compared to how much water the particle can hold at saturation, *k* is a scalar that represents the amount of water a fuel particle can contain relative to its volume (kg H_20 m-3), SAV is the surface-area-to-volume (SAV) ratio of the particle (m^{-1}). The scalar is a measure of the amount of water a particle can hold relative to its volume and should be species specific but could also be influenced by particle elasticity. When combined, these individual metrics of foliar physical and chemical properties will yield an appropriate metric of live fuel moisture in percent of dry weight.

$$\frac{LFM}{100} = \frac{SLA*RWC*k}{SAV} = \frac{\frac{m^2}{g_{Dry\ Matter}} \times \frac{g_{H_2O}}{g_{H20Sat}} \times \frac{g_{H_2OSat}}{m^3}}{\frac{m^2}{m3}} = \frac{g_{H_2O}}{g_{Dry\ Matter}} \qquad \text{Equation 2}$$

Equation 2 shows that the dimensional analysis of the model will yield a metric with the same units as live fuel moisture content in grams of water per unit gram of dry matter / weight. *k* values were computed from measurements and averaged across needle ages.

4. Results

Seasonal variations in live fuel moisture were most pronounced when comparing new and old growth. During green-up, live fuel moisture contents were over 300% for new foliage, while previous year's foliage had moisture contents near 100% (Figure 1). On average, new foliage moisture content was significantly higher than old foliage moisture content (Figure 2). New foliage had a very low foliar density and very high relative water content while old foliage had a higher density and lower relative water content. Density variations were strongly related to live fuel moisture content variations (Figure 3). Final model predictions showed strong agreement between modelled and predicted live fuel moisture content (rho=0.984, $p < 0.05$) (Figure 4). Mean k values were 736.98 kg H_20 m^{-3} for new growth and 560.17 kg H_20 m^{-3}. Assuming k as fixed for needle ages, we computed the live fuel moisture content using Equation 1 and compared to the final measured live fuel moistures. The model accurately predicted live fuel moisture content $r^2 = 0.995$ across the range of new and old foliage.

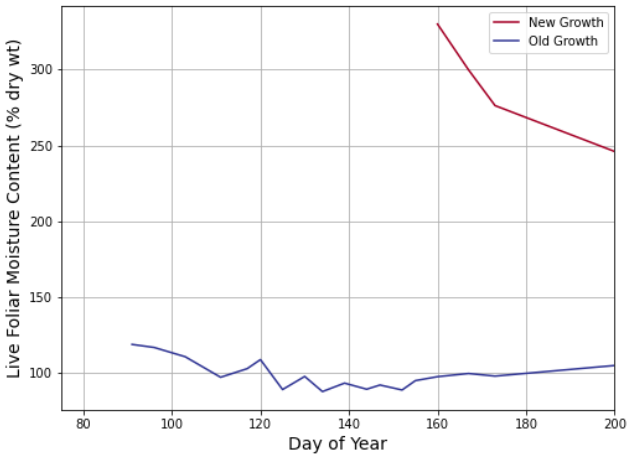

Figure 1 - Seasonal variations in live fuel moisture over the 2021 growing season. New foliage moisture content is shown in Red and previous year's growth in Blue. New growth moisture content was nearly 3 times higher than previous year's growth. Old growth showed a pronounced 'dip' during spring, consistent with other species.

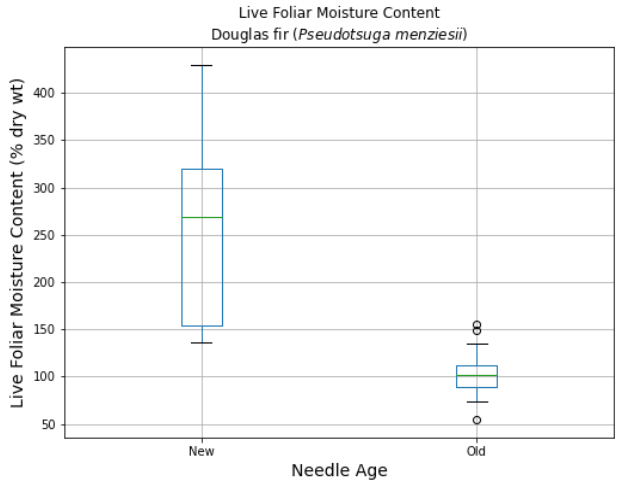

Figure 2 - Difference in live fuel moisture between current year (New) and previous year's growth (Old) for the 2021 growing season of Douglas fir.

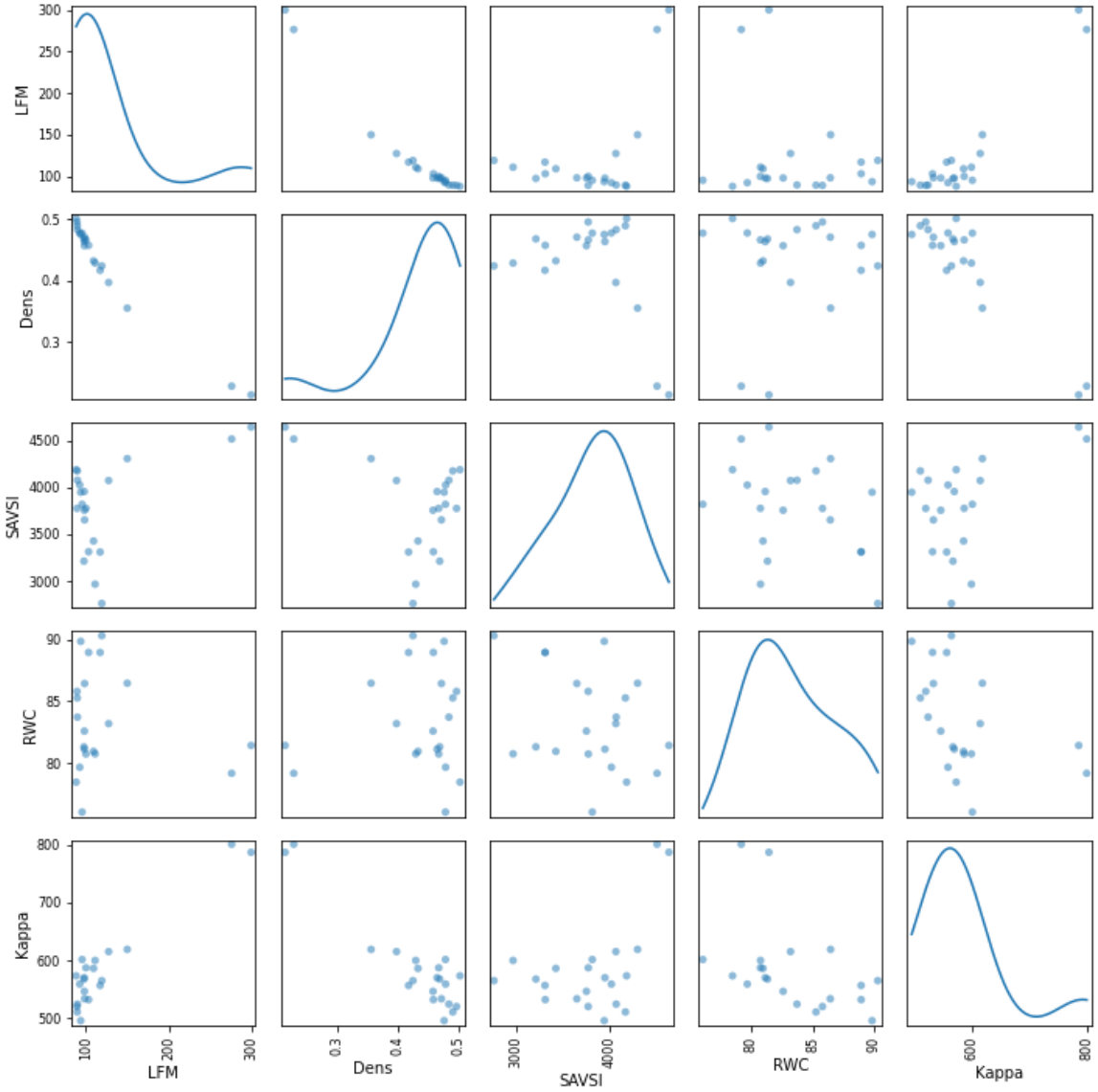

Figure 3 – Cross-scatter plots of input variables to mechanistic live fuel moisture model. LFM is strongly related to density variations and other variables have direct relationships with Live Fuel Moisture (LFM).

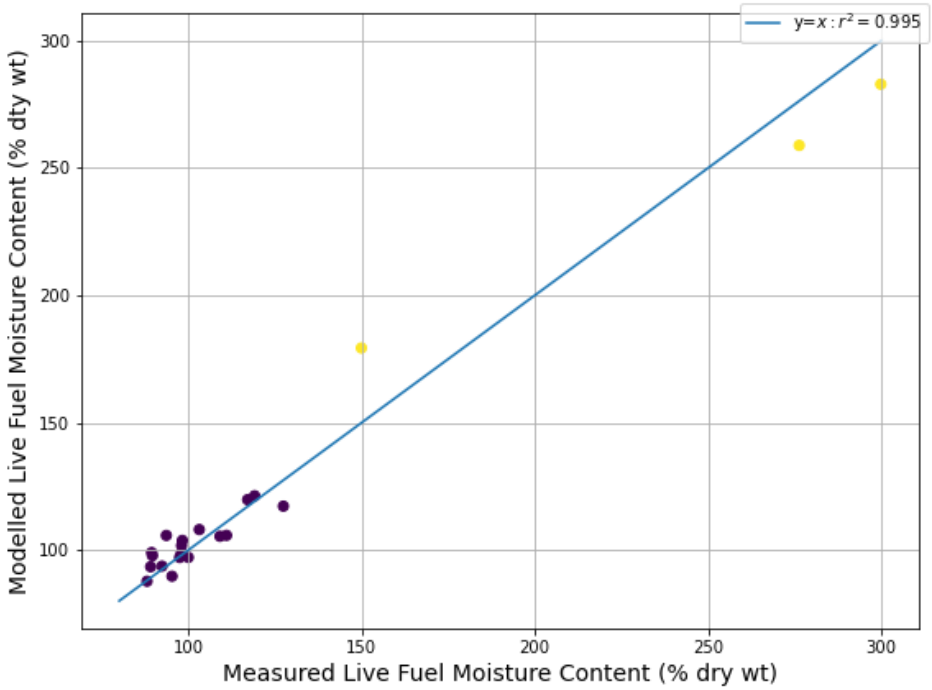

Figure 4 – Preliminary model predictions of live fuel moisture as a function of specific leaf area, relative water content and surface-area-to-volume ratio using a fixed k parameter for new and old foliage.

5. Discussion

This model is the first of its kind to allow the decomposition of live fuel moisture content into components that are easily measured in the field and that allow the decomposition of LFM into components that are important for fire behaviour models. SAV is a critical input to most 2-d and 3-d fire behaviour models because it is primary driver in heat transfer through both radiation and convection. Further, SLA and SAV combine to yield the particle density, which is another very important physical property for heat transfer and subsequent fire behaviour modelling. Finally, RWC is the preferred metric to measure the water status of plants and it dominates plant physiology literature. For example, RWC is strongly linked to soil water potential in Douglas Fir (Barnard et al., 2011) and both metrics correlate well with periods of water stress. Collectively, these variables all yield a framework for better understanding live fuel moisture. As fires grow larger and more intense, understanding the factors that drive live fuel flammability and contribution to overall fire intensity is critical. This mechanistic model of live fuel moisture is one step towards that goal.

6. References

Barnard DM; Meinzer FC; Lachenbruch ; Mcculloh KA*;* Johnson DM*;* Woodruff DR. 2011. Climate-related trends in sapwood biophysical properties in two conifers: avoidance of hydraulic dysfunction through coordinated adjustments in xylem efficiency, safety and capacitance**. Plant, Cell & Environment** 34*:* 643–654.

Pellizzaro, G.; Cesaraccio, C.; Duce, P.; Ventura, A.; Zara, P. 2007. Relationships between seasonal patterns of live fuel moisture and meteorological drought indices for Mediterranean shrubland species. International Journal of Wildland Fire 16, 232–241.

Ruffault, J.; Martin-St Paul, N.; Pimont, F.; Dupuy, J.L. 2018. How well do meteorological drought indices predict live fuel moisture content (LFMC)? An assessment for wildfire research and operations in Mediterranean ecosystems. **Agricultural and Forest Meteorology**, 262, 391–401. doi:https://doi.org/10.1016/j.agrformet.2018.07.031.

A Multilayer Approach to Wildfire Aerial Thermal Image Segmentation Using Unsupervised Methods

Tiago Garcia*[1]; Alexandre Bernardino[2]; Ricardo Ribeiro[2]

[1]*IST. Lisbon, Portugal, {tiagojosegarcia@tecnico.ulisboa.pt}*
[2] *ISR. Lisbon, Portugal, {alex, ribeiro}@isr.tecnico.ulisboa.pt*

**Corresponding author*

Keywords

Thermal Images, Image Segmentation, Airborne Sensors, Wildfire Monitoring, Level Set Segmentation

Abstract

The infrared (IR) thermal images of a propagating wildfire taken by manned or unmanned aerial vehicles can help the firefighting authorities on the ground. The segmentation of such images in regions of fire vs non-fire is a necessary step to measure the fire perimeter and determine the location of the fire front. This work proposes a segmentation method based on level sets, which have the property of handling topology, which makes them suitable to segment wildfire images since the fire areas may be spread out across the image. The results were compared against other common unsupervised segmentation methods, including Otsu, K-means and Mean Shift. The Level Set method was optimized to ensure contour smoothness and reliability, as well as reduce the computation time. Although falling out of use in relation to Deep Learning methods, unsupervised segmentation can still be very useful when annotated datasets are unavailable. The experimental results were compared using hand-drawn labels over a set of images provided by the Portuguese Air Force (FAP) as a ground truth. These labels were carefully drawn by the author to ensure they complied with the requirements indicated by the Portuguese National Authority for Emergency and Civil Protection (ANEPC).

1. Motivation and Objectives

The development of UAVs equipped with cameras and reliable communication and navigation systems enabled a powerful tool in the observation of forest areas, both in the early detection of fires, during the active wildfire combat and the aftermath stage. For early detection, it is important to accurately identify images containing wildfires, while avoiding false positives, for example, with similar color patterns, such as sunsets of dry foliage. During the active stage, it is important to have a tool that allows the authorities to geo-localize the fire front, measure the fire extension, and realize any external effects that can affect the wildfire evolution, such as strong winds. Understanding the evolution of the wildfire and its potential spread areas can help minimize damages and contribute to a more effective combat. When the wildfire is eventually declared as controlled, it is still important to detect if and where reburns occur to quickly extinguish them, preventing a new critical situation.

This work aims at finding the best method for segmenting aerial wildfire thermal images. The thermal cameras can prove extremely useful in situations where smoke and vegetation obscure the field of vision of the aircraft. The algorithms implemented should be able to systematically receive the thermal images and perform multiple segmentations over the same image. Specifically, they should be capable of dividing the image in different areas, sorted according to the fire intensities in each area. The contour lines will then resemble level curves, to eventually construct a thermal map of the image. The contours will also be used to obtain the perimeter of the wildfire and the extension of the fire front in future work.

The layout of this paper is as follows: Section 2 presents the state of the art in thermal image segmentation, Section 3 presents an overview of the theory behind the models used, Section 4 refers some aspects of the implementation, Section 5 presents the datasets used and results obtained. Finally, Section 6 concludes this paper and presents suggestions for future work.

2. Related work

Segmentation of IR images has been done in the past mainly applied to medical images, using watershed (Grau *et al.* 2004), K-means (Ng *et al.* 2006) and level set methods (Banerjee *et al.* 2010). The segmentation of aerial

IR wildfire images for tracking of the active front was attempted using, for example, a combination of Otsu and optical flow (Yuan *et al.* 2017) and Canny edge detectors (Valero *et al.* 2018). However, these methods only present a division of the image in 2 classes.

Multilayer level set methods, like the ones used in Huang and Wu (2010), Huang *et al.* (2013) and Wen *et al.* (2020) were applied to construct thermal mapping of materials. This work applies a similar algorithm but instead to thermal images of wildfires, using only one level set function, which makes the algorithm faster, and adding an edge stopping term.

3. Active Contours

3.1. Level Set Segmentation

The segmentation methods that are based on level sets make use of the idea of implicitly representing a propagating front (or a contour) C through the evolution of a higher dimensional, continuous differentiable function ϕ (dubbed the level set function). In the case of image segmentation, the 2D contour is represented by the level curve of a 3D surface represented by function $\phi: \mathbb{R}^2 \rightarrow \mathbb{R}$. To ensure curve smoothness, the evolution of this function depends on the contour curvature k along its normal direction N which are given by (see Osher and Sethian 1988 for proof)

$$N = \frac{\nabla\phi}{|\nabla\phi|}$$

$$k = \mathrm{div}\left(\frac{\nabla\phi}{|\nabla\phi|}\right)$$

where $\nabla\phi$ represents the gradient of ϕ and $|\nabla\phi|$ the respective norm, while $\mathrm{div}()$ is the divergence operator. The evolution of the level set function is given, according to Osher and Sethian (1988) and Malladi and Sethian (1996), by

$$\frac{\partial\phi}{\partial t} = |\nabla\phi|\mathrm{div}\left(\frac{\nabla\phi}{|\nabla\phi|}\right)$$

For a given open region $\Omega(x, y)$ with smooth boundary, ϕ satisfies

$$\begin{cases} \phi(x,y) > 0, (x,y) \in \Omega \\ \phi(x,y) = 0, (x,y) \in \partial\Omega \\ \phi(x,y) < 0, (x,y) \in \bar{\Omega} \end{cases}$$

where $\partial\Omega$ represents the contour of Ω, which is the contour that is to be obtained. In image processing, all the curve derivatives are taken in a discrete rectangular grid instead of a continuous curve (Malladi and Sethian 1996), which simplifies their calculation.

3.2. Edge-based ACM

Edge-based active contour models use gradient information to stop the contour evolution near strong edges. This can be achieved through the usage of an edge stopping function g that has the property of being positive and decreasing with gradient magnitude, becoming near zero at the edges and neutral when there are no differences in gradient. An example chosen in Caselles *et al.* (1993) is

$$g(\nabla I) = \frac{1}{1 + |\nabla[G_\sigma(x,y) * I(x,y)]|^2} \quad \textbf{(1)}$$

where the image I is convolved with a gaussian kernel G_σ with standard deviation σ.

Edge based methods, such as the Geodesic Active Contour (GAC) model (Caselles *et al.* 1997) are sensible to the placement of the initial contour. If it is initialized away from the object, it may never reach it and instead detect another strong edge, since it has no information about the whole image. This is especially critical if the

image is very noisy, since then the smoothing Gaussian will have to be strong and thus will smooth the edges too.

3.3. Area-based ACM

Area based active contour models use global image information, attempting to divide an image in regions by associating the pixels that share common properties, such as similar intensities. One of the most famous examples is the method introduced by Chan and Vese (Chan and Vese 2001), which is based on the Mumford-Shah functional (Mumford and Shah 1989). The Mumford-Shah formulation for image segmentation comprises the decomposition of an image in *n* regions, such that the intensities vary slowly within each region and briskly across the borders between them.

The Chan-Vese method, initially developed for a two-class segmentation which was achieved by cutting the level set function at level set zero, was generalized to multi-class segmentation (Vese and Chan 2002; Chung and Vese 2005, 2009; He and Osher 2007). For n=m+1 regions, the multi-layer Chan-Vese model determines the evolution of the level set function according to

$$\frac{\partial \phi}{\partial t} = \mu \sum_{i=1}^{m} \left[\delta_\varepsilon(\phi - l_i) div\left(\frac{\nabla \phi}{|\nabla \phi|}\right)\right] + \delta_\varepsilon(l_1 - \phi)|I - c_1|^2 - \delta_\varepsilon(\phi - l_m)|I - c_{m+1}|^2 + \sum_{i=2}^{m} [-\delta_\varepsilon(\phi - l_{i-1}) H_\varepsilon(l_1 - \phi)|I - c_i|^2 + \delta_\varepsilon(l_i - \phi) H_\varepsilon(\phi - l_{i-1})|I - c_i|^2] \quad (2)$$

where δ_ε and H_ε represent the regularized Dirac and Heaviside functions (Chung and Vese 2005), respectively, μ is a weight term, $l_1, \dots, l_m$ are the defined level set positions and $c_1, \dots, c_n$ are the intensity means in each region. The first term in (2) is a regulation term, the rest acts as a 'balloon force' that expands or shrinks the contour to minimize, for each region, the differences between the pixel intensities in the image I and the mean intensity calculated for that region.

4. Implementation

4.1. Multigrid implementation

The calculations required to apply the law in (2) may have an extremely high computational cost if the input image has a high resolution. Even at a resolution of 768x576, which is the most common resolution of the IR images supplied by the FAP, the time needed to achieve convergence on the level set function can be over one minute. To address this issue, we compute several lower resolution images, each one with half the pixels of the previous one in each direction. The level set function is initialized over the coarser grid, evolved until convergence, and extrapolated to the next finer grid. This process is repeated until convergence is reached on the grid with the original image resolution, as explained in Figure 1.

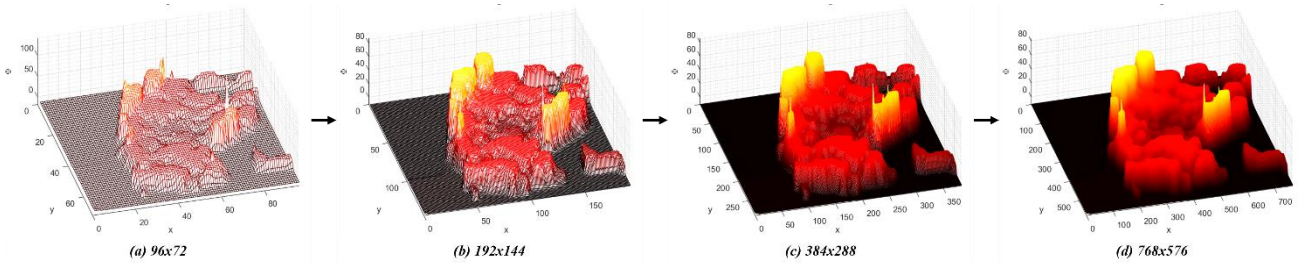

Figure 1 - State of ϕ at the end of the evolution for each resolution. The evolution is processed from the coarser grid (a) to the finer grid (d). Parameters: 6 contours, μ=0.008, α=10000, ε=1, σ=1

4.2. Inclusion of an edge-stopping term

It was verified that with the inclusion of more contours, the outer contours were detecting non-relevant edges or no edges at all, and inner contours were not "sticking" with the borders of the inner-most areas. To correct

this issue, it was decided to add an edge stopping term, like the one in (1), directly to the evolution rule (2), like what was done in Li *et al.* (2010). This term is given by

$$\text{EST} = \alpha g(\nabla I)[\delta_\varepsilon(\phi - l_1) + \delta_\varepsilon(\phi - l_m)] \quad (3)$$

where α is a weight term, $g(\nabla I)$ is given by (1) and $\delta_\varepsilon(\phi - l_i)$ allows for selective application of this term to the i^{th} level set, which is performed since the inclusion of this term has a destabilizing effect on ϕ. The term in (3) approximates the inner contour, given by the level set l_m, to the boundary of the brightest areas and keeps the outermost contour (corresponding to l_1) from propagating outside of the wildfire area.

5. Results

5.1. Datasets

The datasets used for segmentation were provided by the Portuguese Air Force. They consisted of images and videos taken both during real occurrences and during contained tests.

The main video is dubbed FOGO_1. It consists of different points of view of a wildfire, with nearly a minute of IR footage in total between RGB segments. To evaluate the segmentation quantitively, 55 images were selected, 1 second apart from each other, from the total 1342 frames. The ground truth masks were created by hand using MATLAB® Image Labeller App, following the indications given by the ANEPC. These requirements demanded a division of the images in three classes:

- Class 1 (outer): outside of the fire
- Class 2 (middle): region inside the fire that does not belong to the propagating front
- Class 3 (inner): the hottest (brightest) regions, which represent the propagating front

The contours should be smooth to later calculate the perimeter of the burning areas. Additionally, small high intensity 'dots' within the fire are to be classified as class 2, given that they most likely correspond to trees or other objects that are still burning actively but do not represent the fire front that is desired to track.

All the frames of FOGO_1 dataset were subjected to a 6-class segmentation (5 contours) using the level set method in (2) with the addition of the term in (3), with later selection and grouping of the 6 classes in the desired 3 classes (2 contours). The division in 6 classes is also useful to construct thermal maps of the fire. Performing a segmentation with more contours with further reduction, as was done in this case, allows for more reliable results without the need for heavy tuning of parameters. Figure 2 present some of the results obtained.

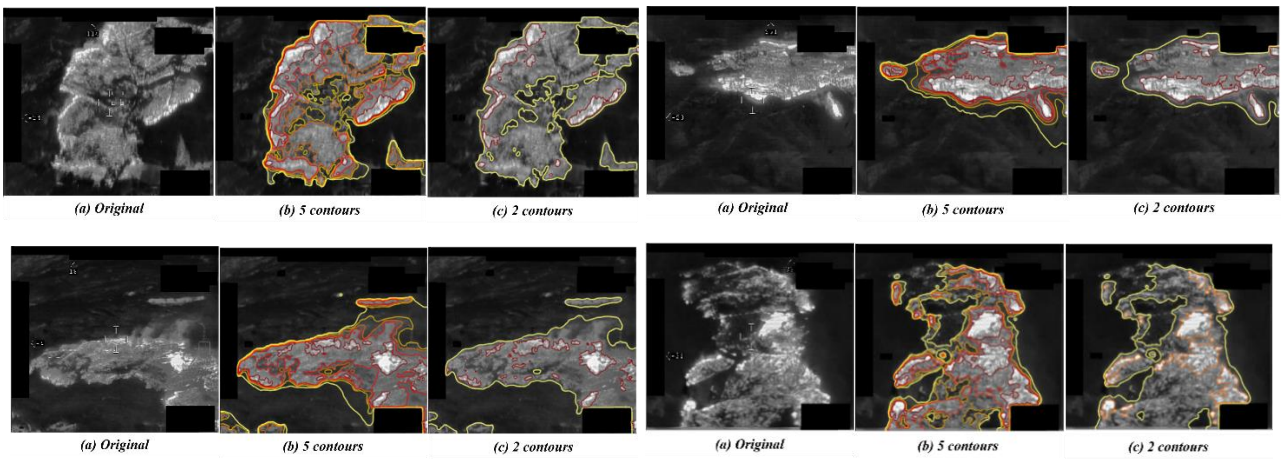

Figure 2 – Segmentation examples of FOGO_1 images using 5 contours with further reduction to 2 contours

To test the algorithm over the whole video sequence, all the frames in FOGO_1 were segmented and compiled in a video that was made available in the following link: https://youtu.be/kD9TEFOaHxw.

5.2. Comparison with other methods

With the objective of finding the best set of parameters for the level set method a grid search of parameters was conducted using the selected 55 frames, and to further compare its performance against other common unsupervised methods, they were also subjected to the application of the multi-layer Otsu (Otsu 1979; Liu and Yu 2009), K-means (Liu and Yu 2009, Sinaga and Yang 2020) and Mean Shift (Fukunaga and Hostetler 1975; Comaniciu and Meer 1999) algorithms. Class grouping was also applied when using these methods.

Experimental results, present in Table 1, were conducted in MATLAB 2020a, using a computer running in Windows 10 64-bit with an Intel® Core™ i7-6700HQ microprocessor and 8 GB of RAM. All metric values displayed correspond to the average of values for the three referred classes. For Mean Shift two types of inputs were tested, a 1-D input corresponding to the pixel intensity (i) and the 3-D input consisting of the pixel intensity (i) and position (x,y), with respective weights 0.8 and 0.2. Since Mean Shift calculates the number of classes automatically, we combine it with Otsu thresholding to aggregate classes. It is important to refer that the ground truths have compromised reliability, since they were not made by the authorities.

Table 1 – Comparison of results using FOGO_1 55 image labelled dataset

Method	Precision	Recall	Accuracy	IoU[1]	WEoS[2]	Time [s]
Proposed	**0.871**	**0.859**	**0.962**	**0.775**	**0.035**	2.86
Otsu	0.812	0.832	0.916	0.688	0.066	**0.15**
K-means	0.803	0.838	0.909	0.682	0.069	1.24
Mean Shift + Otsu (1D input)	0.862	0.741	0.926	0.646	0.056	1.65
Mean Shift + Otsu (3D input)	0.852	0.675	0.902	0.571	0.071	17.3

In terms of computational time, Otsu vastly outperforms by far all the other methods which allows for real-time segmentation. However, to obtain curve regularization, one need to increase the intensity of pre-process blurring, which leads to less reliable contours. Level sets allow for a highly customizable contour regularization therefore they present the best segmentation results.

6. Conclusions and Future Work

This work presented a method based on level sets that can detect the wildfire area and the burning fire front in wildfire thermal images which will enable the calculation and location of the fire perimeter and the most critical areas in future work. It outperforms other common unsupervised methods in terms of segmentation quality, albeit at a cost of computational time.

The lack of a labelled database dictated the non-usage of supervised learning. The hand labels created throughout the development of this work can be used to start such database. It would be interesting to apply state-of-the-art deep-learning methods to these images and compare the results with the ones obtained in this research.

7. Acknowledgements

This work was supported by FCT projects FIREFRONT (PCIF/SSI/0096/2017) and VOAMAIS (PTDC/EEI-AUT/31172/2017, 02/SAICT/2017/31172). The authors would like to thank everyone involved in these projects for the fruitful discussions and collaborations. Furthermore, we would like to express our gratitude to the

[1] Intersection over Union
[2] Weighted Error of Segmentation (same as EoS but a misclassification by just one class counts as a ‘half’ error)

Portuguese Air Force for providing the surveillance images and videos used throughout this work and to the ANEPC for the support and the many suggestions.

8. References

Banerjee, S., & Bhattacharya, M. (2010, October). Segmentation of medical images using Selective Binary and Gaussian Filtering regularized level set (SBGFRLS) method. In *2010 3rd International Conference on Biomedical Engineering and Informatics* (Vol. 2, pp. 541-545). IEEE.

Caselles, V., Catté, F., Coll, T., & Dibos, F. (1993). A geometric model for active contours in image processing. *Numerische mathematik*, *66*(1), 1-31.

Caselles, V., Kimmel, R., & Sapiro, G. (1997). Geodesic active contours. *International journal of computer vision*, *22*(1), 61-79.

Chan, T. F., & Vese, L. A. (2001). Active contours without edges. *IEEE Transactions on Image Processing*, *10*(2), 266–277.

Chung, G., & Vese, L. A. (2005). Energy minimization based segmentation and denoising using a multilayer level set approach. Lecture Notes in Computer Science (Including Subseries Lecture Notes in Artificial Intelligence and Lecture Notes in Bioinformatics), 3757 LNCS, 439–455.

Chung, G., & Vese, L. A. (2009). Image segmentation using a multilayer level-set approach. *Computing and Visualization in Science*, *12*(6), 267–285. https://doi.org/10.1007/s00791-008-0113-1.

Comaniciu, D., & Meer, P. (1999, September). Mean shift analysis and applications. In *Proceedings of the seventh IEEE international conference on computer vision* (Vol. 2, pp. 1197-1203). IEEE.

Fukunaga, K., & Hostetler, L. (1975). The estimation of the gradient of a density function, with applications in pattern recognition. *IEEE Transactions on information theory*, *21*(1), 32-40.

Grau, V., Mewes, A. U. J., Alcañiz, M., Kikinis, R., & Warfield, S. K. (2004). Improved watershed transform for medical image segmentation using prior information. *IEEE Transactions on Medical Imaging*, *23*(4), 447–458.

He, L., & Osher, S. (2007). Solving the Chan-Vese Model by a Multiphase Level Set Algorithm Based on the Topological Derivative. In *Scale Space and Variational Methods in Computer Vision* (pp. 777–788). Springer Berlin Heidelberg.

Huang, Y., & Wu, J. W. (2010). Infrared thermal image segmentations employing the multilayer level set method for non-destructive evaluation of layered structures. *NDT and E International*, *43*(1), 34–44.

Huang, Y., Lee, M. G., Lin, S. Y., & Xiaoyu, Y. I. (2013). Segmenting thermal images of pervious concrete pavement temperature with employing the multilayer level set approach. In *ICSDEC 2012: Developing the Frontier of Sustainable Design, Engineering, and Construction* (pp. 757-764).

Li, C., Xu, C., Gui, C., & Fox, M. D. (2010). Distance regularized level set evolution and its application to image segmentation. *IEEE Transactions on Image Processing*, *19*(12), 3243–3254.

Liu, D., & Yu, J. (2009, August). Otsu method and K-means. In *2009 Ninth International Conference on Hybrid Intelligent Systems* (Vol. 1, pp. 344-349). IEEE.

Malladi, R., & Sethian, J. a. (1996). Level Set and Fast Marching Methods in Image Processing and Computer Vision. 1(4), 0–3.

Mumford, D. B., & Shah, J. (1989). Optimal approximations by piecewise smooth functions and associated variational problems. *Communications on pure and applied mathematics*.

Ng, H. P., Ong, S. H., Foong, K. W. C., Goh, P. S., & Nowinski, W. L. (2006). Medical image segmentation using k-means clustering and improved watershed algorithm. *Proceedings of the IEEE Southwest Symposium on Image Analysis and Interpretation*, *2006*, 61–65.

Otsu, N. (1979). A threshold selection method from gray-level histograms. *IEEE transactions on systems, man, and cybernetics*, *9*(1), 62-66.

Osher, S., & Sethian, J. A. (1988). Fronts propagating with curvature-dependent speed: Algorithms based on Hamilton-Jacobi formulations. *Journal of Computational Physics*, *79*(1), 12–49.

Sinaga, K. P., & Yang, M. S. (2020). Unsupervised K-means clustering algorithm. *IEEE access*, *8*, 80716-80727.

Valero, M. M., Rios, O., Pastor, E., & Planas, E. (2018). Automated location of active fire perimeters in aerial infrared imaging using unsupervised edge detectors. *International Journal of Wildland Fire*, *27*(4), 241–256.

Vese, L. A., & Chan, T. F. (2002). A multiphase level set framework for image segmentation using the Mumford and Shah model. *International Journal of Computer Vision*, *50*(3), 271–293.

Wen, D., Ren, A., Ji, T., Flores-Parra, I. M., Yang, X., & Li, M. (2020). Segmentation of thermal infrared images of cucumber leaves using K-means clustering for estimating leaf wetness duration. *International Journal of Agricultural and Biological Engineering*, *13*(3), 161–167.

Yuan, C., Liu, Z., & Zhang, Y. (2017). Fire detection using infrared images for UAV-based forest fire surveillance. *2017 International Conference on Unmanned Aircraft Systems, ICUAS 2017*, 567–572.

A Platform for Large Scale Application of Remote Sensed Data to Wildland Fire Management

Fredrick Bunt*[1]; Jesse V. Johnson[1]; John Hogland[2]

[1]The University of Montana Department of Computer Science. 32 Campus Drive, Missoula MT 59812, USA, {fredrick.bunt, jesse.johnson}@umontana.edu
[2] Rocky Mountain Research Station, U.S. Forest Service, Missoula, MT 59801, USA, {john.s.hogland@usda.gov}

**Corresponding author*

Keywords

Geospatial processing, remote sensing, fire mitigation, big data, scalable

Abstract

Spatial modelling and machine learning are powerful techniques that can be used to identify patterns within data and build complex relationships between response and predictor variables. While powerful, many of these techniques are computationally intensive and are not designed to fully leverage high performance computing resources, especially when used within a geospatial context. To fully leverage system resources, while facilitating various spatial, machine-learning, and statistical modelling workflows, we developed a Python-based processing library called *raster-tools*. The *raster-tools* library automates delayed reading and parallel processing using Dask and integrates seamlessly into popular spatial, machine learning, and visualisation libraries such as geopandas, rasterio, xarray, scikit-learn, xgboost, pygeos, shapely, matplotlib, plotly, folium, and many more. Combined, these open-source libraries provide users with free and powerful analytical capabilities that can be used at scale and can dynamically display textual, tabular, spatial and graphical data. In this paper, we will provide a brief overview of the *raster-tools* library and demonstrate how the described open-source stack can be used to perform GIS analyses in both a web and desktop environment.

1. Introduction

Our environment is constantly being monitored. Today, satellite and airborne sensors on programs and platforms such as MODIS (MODIS, n.d.), Landsat (USGS, n.d.), Sentinel (EOS, n.d.), and NAIP (NAIP, n.d.) are acquiring data at spatial, spectral, and temporal resolutions that were, until recently, hard to imagine. Similarly, with advancements in drone technology and sensor hardware, the amount of remotely sensed data that is constantly being acquired and used to quantify aspects of natural resources is staggering. The recognition that large volumes of data are not being fully leveraged to inform decision making has led to an increased awareness in the fields of data (Gibert et al, 2018) and decision (Elshawi et al, 2018) science and the potential of what has become known as “Big Data” (Markwo et al, 2017). While there is great potential and promise attributed to “Big Data”, the practical use of data to drive decision making within the natural resource community has not been fully realised (Gibert et al, 2018).

In large part the discrepancy between the potential and use of “Big Data" to aid in natural resource decision making stems from two primary deficiencies: 1) a lack of analysts and technicians trained in the tenets of data science within the natural resources community and 2) software libraries that fully leverage computer resources and integrate tabular, geospatial, and machine learning (ML) domains. Within the first deficiency, common obstacles to implementation include: a lack of education and skills associated with integrating the various mathematical, statistical, ML techniques, computer programming languages, data formats, and the size of the data (Gibert et al, 2018). Less understood issues include leveraging data processing results (e.g. modelled outputs) for efficient decisions, the impact of applying models to new domains, the propagation of errors, and model misspecification. Issues of scale, domain, error, and relevance can have additional meanings within a complex natural resource setting. These issues often prevent studies that convert data into pertinent forest and fire related information from being used to their potential for planning and management decisions.

Within the second identified deficiency (integrated software libraries), geospatial analysis is core to natural resource management and planning. To facilitate geospatial analyses, geographic information systems (GISs) and remote sensing software such as ESRI's software suite (ESRI, n.d.), ERDAS (Hexagon, n.d.), ENVI (L3Harris, n.d.), IDRISI (Clark Labs, n.d.), QGIS (QGIS Dev. Team, n.d.), GRASS (GRASS Dev. Team, n.d.), and Whitebox (Whitebox Geospatial Inc., n.d.) have been developed to support spatial analytics and visualisation. However, commercial software platforms are expensive, typically have only a subset of commonly used routines, have a proprietary code base, do not necessarily integrate well with other processing libraries, and are only partially designed to fully leverage computer hardware, making it challenging to use those systems within a Big Data context. Open-source projects such as QGIS, GRASS, and Whitebox address cost issues but also tend to be plagued by issues similar to their commercial counterparts and typically are less intuitive to use, have stability issues, and often lack documentation.

These obstacles have led some to develop open-source data processing libraries such as gdal (GDAL Contributors., 2022), geopandas (Jordahl et al, 2020), rasterio (Gillies et al, 2013), xarray (Hoyer & Harmon, 2017), scikit-learn (Pedregosa et al, 2011), xgboost (Chen & Guestrin, 2016), shapely (Gillies, 2007), matplotlib (Hunter, 2007), plotly (Plotly Tech. Inc., 2015), and folium (python-visualization, 2020) that build upon common processing frameworks such as numpy (Harris et al, 2020), scipy (Virtman et al, 2020), and pandas (McKinneyl, 2010). However, these libraries alone do not natively address issues of parallel processing, memory management, or excessive use of input and output (Hogland & Anderson, 2017). To address these issues, Dask (Dask Dev. Team, 2016) has built a newer processing framework that builds upon the core processing frameworks of numpy and pandas that can be leveraged to facilitate and integrate tabular, geospatial, and ML analyses through lazy processing and parallelization. Two relatively recent coding projects that have successfully leveraged Dask to facilitate lazy processing, parallelization, and geospatial analyses from a vector and raster perspective include dask-geopandas (Geopandas Dev. Team, n.d.) and xarray-spatial (Makepath, n.d.), respectively. To further address the need for geospatial libraries that fully leverage computer resources and integrate tabular, geospatial, and ML analyses we have developed a new open-source project called *raster-tools*.

Our open-source package leverages the extensive data science, data processing and geospatial ecosystems of Python to provide a platform for developing data-driven decision making tools. Through the use of Python's Dask library (Dask Dev. Team, 2016), *raster-tools* allows users to easily scale their workflow from small laptops up to servers or high-performance computing (HPC) clusters, while fully utilising available resources. It contains a subset of the processing functions offered by ESRI software but can be used to implement many others. *raster-tools* also integrates easily with popular spatial, ML, and visualisation libraries such as geopandas, xarray, scikit-learn, xgboost, shapely, matplotlib, jupyter-lab, folium, and more.

Here, we highlight the use of our *raster_tools* package, in conjunction with an open-source stack, to inform decision making at scale through multiple use cases. Moreover, we demonstrate how this newly developed technology can be easily integrated with other spatial and statistical modelling workflows to realise the potential of Big Data. Finally we discuss the benefits of using *raster-tools* to perform geospatial analyses.

2. Methods

The *raster-tools* project is roughly based on the Rocky Mountain Research Station (RMRS) Raster Utility project (Hogland & Anderson, 2017). While similar in concept, *raster-tools* furthers the intent of the RMRS Raster Utilities project by improving processing efficiencies, increasing the size of datasets that could be processed, expanding possible compute platforms, and providing an open-source set of efficient geospatial, remote sensing, and ML procedures. The *raster-tools* package provides the same lazy processing and execution functionality as RMRS Raster Utility but can easily scale to larger datasets and hardware configurations, run on a wider range of platforms, and directly integrates with Python's wider ecosystem, making it a significant improvement over RMRS Raster Utility project.

The *raster-tools* package is built on the open-source python library Dask (Dask Dev. Team, 2016). Dask is a general-purpose library that embraces lazy operations and data partitioning for parallel data processing. At its core, Dask breaks data into smaller chunks of data, similar to pixel blocks within ESRI's ArcObjects [34], and allows users to apply lazy operations to those data subsets. An operation on the whole dataset is applied as lazy

tasks on the constituent chunks and only takes place when requested by the user. In this way, Dask allows for extensive, lazy data pipelines to be built. For execution, Dask provides robust task scheduling that can distribute per-chunk tasks across available compute resources. This approach to processing automates the parallel aspect of Dask procedures and allows for easy scaling from a single CPU core on a small laptop to distributed HPC clusters. Moreover, processing is performed "out-of-core", making it possible to process large datasets that exceed available memory by only loading chunks into memory at any given time. When chunks are kept small, computation can occur in memory constrained environments, making it feasible to process extremely large datasets quickly and efficiently in a parallel fashion.

To illustrate the benefits of chunking and lazy processing within a geospatial context, we use the *raster-tools* package (Raster-Tools Dev. Team, n.d.) and highlight common and not so common functionality through two use-cases. These are 21st century planning for fire resilient landscapes (Hogland et al, 2021) and burn severity prediction. These use vector and raster based datasets to demonstrate data acquisition, spatial and ML modelling, and visualisation. The rest of the article is separated into Use Case, Discussion, and Conclusion sections that describe the use cases, discuss how *raster-tools* facilitated the analyses within the use cases, and provide concluding remarks, respectively.

3. Use Cases.

3.1. 21st century planning for fire resilient landscapes

The 21st century planning for fire resilient landscapes use case, uses *raster_tools* to perform various spatial analyses to aid in planning forest treatments and quantify the costs and impact of those treatments at scale across a broad landscape. Spatial analyses used in this example include: arithmetic, logical, data format transformations, surface distance, surface allocation, and surface traceback, region grouping, and zonal summaries. Spatial data outputs created in this example include: multiple raster surfaces that quantify desired future conditions (DFCs), actual tonne removal, potential and actual cost, revenue, and profit of treatment implementation for 1.2 million ha in north central Oregon, USA at spatial resolution of 30 m. Primary datasets used within the use case include basal area per ha (BAH: m^2 ha^{-1}), and a most likely classification raster surfaces (Hogland et al, 2021), potential operational delineations (Dunn et al, 2020), United States Census Bureau Tiger/Line files (USCBl, n.d.), the National Hydrography Dataset (NHD) Flowline and Waterbody line and polygon features (NHD, n.d.), and the location of the Malheur Lumber company. All datasets used within the analyses are available for download at Hogland, n.d.a and are explained in further detail in (Hogland et al, 2021).

We provide a Jupyter notebook (Hogland, n.d.b) with an in-depth, dynamic example of the analyses performed within (Hogland et al, 2021) using *raster-tools*. The notebook is meant as a companion piece with (Hogland et al, 2021) and demonstrates everything from installation to final analysis. It is free to download and can be used with Google's Colab for research and educational purposes (Google Research Colab, n.d.).

Key results from the analyses performed in the notebook include spatial surfaces describing estimated treatment cost, revenue, and profit, and the amount of material removed to meet DFCs at 30 m resolution, along with summary reports based on POD boundaries and management priority (Figure 1). Moreover, outputs can be displayed as an interactive map and saved as a HTML file and further embedded within any website. From start to finish the analyses performed within the notebook takes approximately 16 minutes to complete using Colab and represent a substantial improvement in both processing time (minutes vs hours) and storage space (no intermittent datasets were created) over the delivered cost processing technique described in (Hogland et al, 2021).

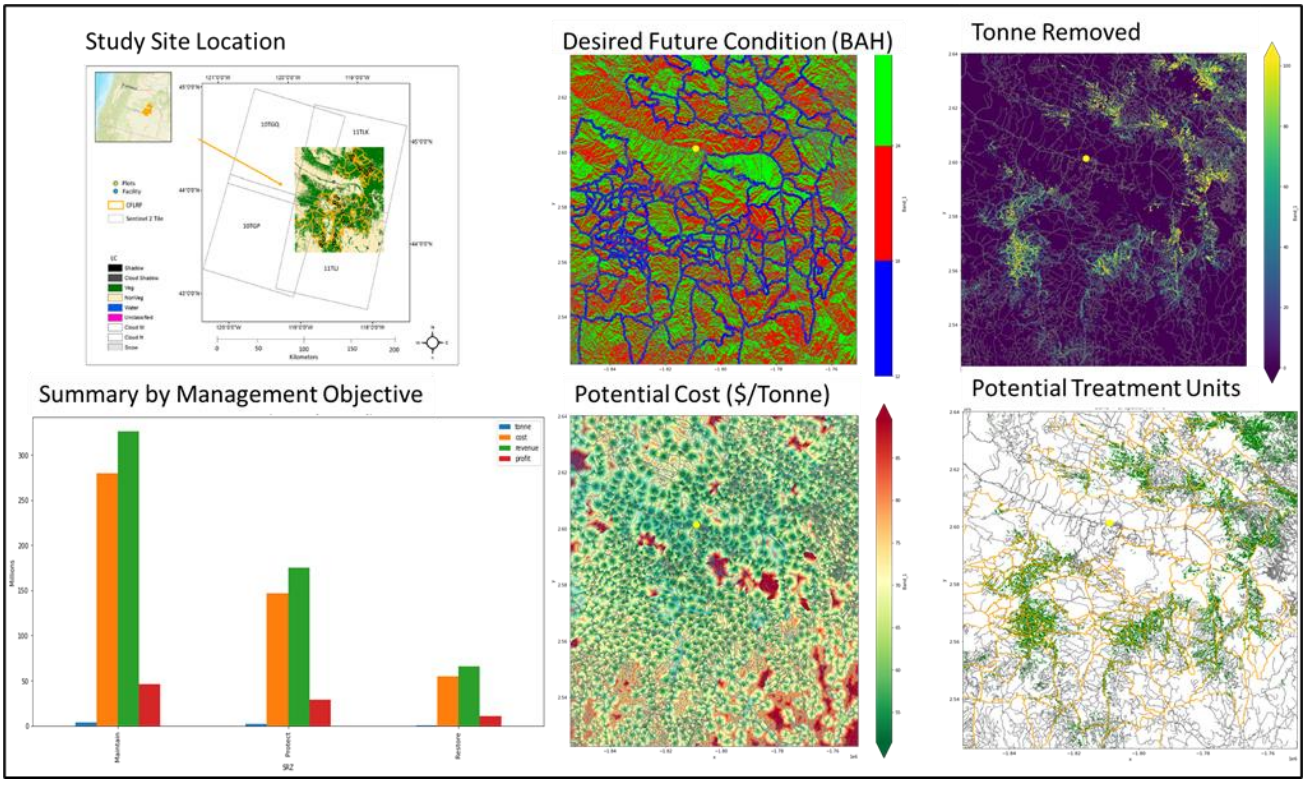

Figure 1- Study site location, Desired Future Condition (DFC), Potential Cost, Removals, Potential Treatment Units, and summarised tonne removed (blue), cost (orange), revenue (green), and profit (red) derived from the 21st century planning notebook.

3.2. Burn Severity Prediction

Our second use case was the development of a burn severity classifier similar to (Parks et al, 2018). For this, we created a training dataset consisting of 29.4 million burn severity labels and predictor values for the state of Montana from 1984–2020. Like (Parks et al, 2018), we used MTBS (Eidenshink et al, 2007) for the severity labels, but increased the number of severity classes used. For the predictors, we used 30 m CONUS EDNA elevation and derivative products (USGS, 2005) and 4 km CONUS gridMET reanalysis products (Abatzoglou, 2013). The training dataset was assembled using *raster-tools* to take MTBS data and pull the corresponding collocated data values from the predictor datasets. Using *raster-tools* allowed us to assemble the training dataset efficiently and in parallel in only a few hours on a desktop computer with limited memory. Figure 2 shows results for a single fire.

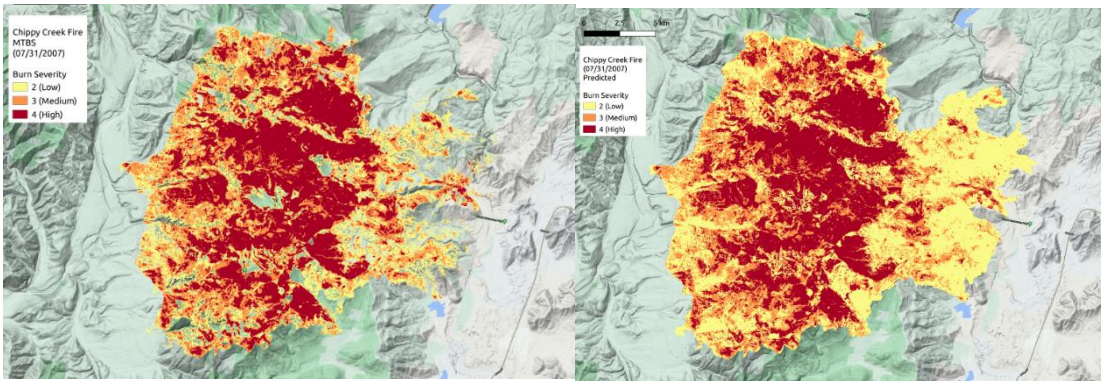

Figure 2- Comparison of MTBS (left) and model predicted (right) burn severity for the 2007 Chippy Creek fire in Montana.

4. Discussion

In both of the above use cases, large, high-resolution rasters and vectors were used as input data. Traditional methods for handling the processing of such data (e.g. ESRI) requires significant investment in computing resources, licensing, and time. With *raster-tools*, we were able to get meaningful, actionable results quickly using relatively small compute platforms. In the first use case, *raster-tools* allowed us to work with large rasters and vectors seamlessly and to carry out a very large number of computations quickly. It eliminated the need to write intermediate results to disk and also allowed us to carry out data analysis on the results with Python's wider data ecosystem.

In the second use case, *raster-tools* allowed us to pull together and work together with nearly 2000 large, high-resolution rasters, simultaneously to produce 29.4 million data points. This would not normally be possible without large investments in computing power, time, and extensive optimization work. Because *raster-tools* uses Python, we were also able to automate this task so that, in the future, we can apply the same processing pipelines to the other parts of the U.S. with only minor changes.

5. Conclusions

Our *raster-tools* package is a free and open-source tool for processing geospatial data. It provides the ability to build automatically scaling processing pipelines that can be run across compute platforms. We think that it can be used as a platform for building data driven applications that produce timely and actionable results at scale.

6. References

MODIS. TERRA The EOS Flagship, Available online: https://terra.nasa.gov/about, (accessed 31 of October, 2019)

United States Geological Survey [USGS]. Landsat 8. Available online: https://www.usgs.gov/land-resources/nli/landsat/landsat-8?qt-science_support_page_related_con=0#qt-science_support_page_related_con (accessed on 23 of October, 2019).

Earth Observing System [EOS]. Sentinel-2. Available online: https://eos.com/sentinel-2/ (accessed on 23 of October 2019).

National Agriculture Imagery Program [NAIP]. National Agriculture Imagery Program (NAIP) Information Sheet. Available online: http://www.fsa.usda.gov/Internet/FSA_File/ naip_info_sheet_2013.pdf (accessed on 14 May 2014).

Gibert, K.; Horsburgh, J.S.; Athanasiadis, I.N.; Holmes, G. Environmental Data Science. Environmental Modelling & Software. 2018, 106, 4-12, doi: 10.1016/j.envsoft.2018.04.005.

Elshawi, R.; Sakr, S.; Talia, D.; Trunfio, P. Big Data Systems Meet Machine Learning Challenges: Towards Big Data Science as a Service, Big Data Research. 2018, 1, 1-11.

Markwo, S.; Braganza, S.; Taska, B. The Quant Crunch - How the Demand for Data Science Skills is Disrupting the Job Market, Burning Glass Technologies Technical Report, 2017, online: https://www.burning-glass.com/wp-content/uploads/The_Quant_Crunch.pdf

Hogland, J.; Dunn, C.J.; Johnston, J.D. 21st Century Planning Techniques for Creating Fire-Resilient Forests in the American West. Forests 2021, 12, 1084. https://doi.org/10.3390/f12081084

Environment Systems Research Institute (ESRI), About ESRI | The Science of Where, Available online: https://www.esri.com/en-us/about/about-esri/overview (accessed on 2 July 2022).

Hexagon, ERDAS Imagine, available online: https://www.hexagongeospatial.com/products/power-portfolio/erdas-imagine, (accessed on 2 July 2022).

L3Harris, Image Processing & Analysis Software | Geospatial Image Analysis Software | ENVI®, available online: https://www.l3harrisgeospatial.com/Software-Technology/ENVI, (accessed on 2 July 2022).

Clark Labs, IDRISI GIS Analysis | Clark Labs, available online: https://clarklabs.org/terrset/idrisi-gis/ (accessed on 2 July 2022).

QGIS Development Team, Welcome to the QGIS project!, https://www.qgis.org/en/site/index.html (accessed 2 July 2022)

GRASS Development Team. GRASS GIS, available online: https://grass.osgeo.org/ (accessed on 2 July 2022).

Whitebox Geospatial Inc. The Whitebox Platform, available online: https://www.whiteboxgeo.com/, (accessed on 2 July 2022).

GDAL/OGR contributors (2022). GDAL/OGR Geospatial Data Abstraction software Library. Open Source Geospatial Foundation. URL https://gdal.org DOI: 10.5281/zenodo.5884351

Jordahl, K. et al. (2020, July 15). geopandas/geopandas: v0.8.1 (Version v0.8.1). Zenodo. http://doi.org/10.5281/zenodo.3946761

Gillies, S. et al.. (2013-). Rasterio: geospatial raster I/O for Python programmers. URL https://github.com/rasterio/rasterio

Hoyer, S. & Hamman, J., (2017). xarray: N-D labeled Arrays and Datasets in Python. Journal of Open Research Software. 5(1), p.10. DOI: https://doi.org/10.5334/jors.148

Pedregosa, F. et al. (2011). Scikit-learn: Machine Learning in Python. Journal of Machine Learning Research, 12, 2825–2830.

Chen, T., & Guestrin, C. (2016). XGBoost: A Scalable Tree Boosting System. In Proceedings of the 22nd ACM SIGKDD International Conference on Knowledge Discovery and Data Mining (pp. 785–794). ACM.

Gillies, S., & others. (2007–). Shapely: manipulation and analysis of geometric objects.

Hunter, J. (2007). Matplotlib: A 2D graphics environment. Computing in Science & Engineering, 9(3), 90–95.

Plotly Technologies Inc. Collaborative data science. Montréal, QC, 2015. https://plot.ly.

python-visualization. (2020). Folium. Retrieved from https://python-visualization.github.io/folium/

Harris, C.R., Millman, K.J., van der Walt, S.J. et al. Array programming with NumPy. Nature 585, 357–362 (2020). DOI: 10.1038/s41586-020-2649-2

Virtanen, P. et al. & SciPy 1.0 Contributors (2020). SciPy 1.0: Fundamental Algorithms for Scientific Computing in Python. Nature Methods, 17, 261–272.

McKinney, W. (2010). Data Structures for Statistical Computing in Python . In Proceedings of the 9th Python in Science Conference (pp. 56 - 61).

Hogland, J.; Anderson, N. Function Modeling Improves the Efficiency of Spatial Modeling Using Big Data from Remote Sensing. Big Data Cogn. Comput. 2017, 1, 3. https://doi.org/10.3390/bdcc1010003

Dask Development Team (2016). Dask: Library for dynamic task scheduling https://dask.org

Geopandas Development Team, dask-geopandas, available online: https://dask-geopandas.readthedocs.io/en/latest/index.html, (accessed on 2 July 2022).

Makepath, xarray-spatial, https://github.com/makepath/xarray-spatial, (accessed on 2 July 2022).

Raster-tools Development Team. raster-tools, Available online: https://github.com/UM-RMRS/ raster_tools (accessed on 2 July 2022)

ESRI. ArcObjects SDK 10 Microsoft .Net Framework—ArcObjects Library Reference (Spatial Analyst), Available online: http://help.arcgis.com/en/sdk/10.0/arcobjects_net/componenthelp/ index.html#/PrincipalComponents_Method/00400000010q000000/ (accessed on 3 March 2017).

Dunn, C.J.; O'Connor, C.D.; Abrams, J.; Thompson, M.P.; Calkin, D.E.; Johnston, J.D.; Stratton, R., Gilbertson-Day, J. Wildfire risk science facilitates adaptation of fire-prone social-ecological systems to the new fire reality. *Environ. Res. Lett.* 2020, *15*, 1–13, doi:10.1088/1748-9326/ab6498.

USCB. TIGER/Line Shapefiles [Machine-Readable Data Files]. Available online: https://www2.census.gov/geo/tiger/TGRGDB20/ (accessed on 12 May 2021).

National Hydrography Dataset [NHD]. Available online: http://prd-tnm.s3-website-us-west-2.amazonaws.com/?prefix=StagedProducts/Hydrography/NHD/State/HighResolution/GDB/ (accessed on 12 May 2021).

Hogland, J. BMFPNotebookdata.zip. Available online: https://drive.google.com/file/d/1zNYZRTgNEX4mNAtU1I3-7RD8VSo8-ATH/view?usp=sharing (accessed on 7/1/2022).

Hogland, J., 21st Century Planning Techniques for Creating Fire-Resilient Forests in the American West: Notebook, available online: https://github.com/jshogland/SpatialModelingTutorials/blob/main/Notebooks/PODs_Integration.ipynb, (accessed on 7/1/2022).

Google Research. Colab, available online: https://colab.research.google.com/, (accessed 7/1/2022)

Parks, S.; Holsinger, L; Panunto, M; Jolly, W Matt; Dobrowski, Solomon; Dillon, Gregory. High-severity fire: evaluating its key drivers and mapping its probability across western US forests, 2018, Environmental Research Letters Vol. 13 No. 4.

Eidenshink, J., Schwind, B., Brewer, K. et al. A Project for Monitoring Trends in Burn Severity. fire ecol 3, 3–21 (2007). https://doi.org/10.4996/fireecology.0301003.

U.S. Geological Survey, 2005, Elevation derivatives for national applications: U.S. Geological Survey Fact Sheet 2005–3049, 2 p., https://doi.org/10.3133/fs20053049

Abatzoglou, J. T. (2013), Development of gridded surface meteorological data for ecological applications and modelling. Int. J. Climatol., 33: 121–131.

A Preliminary Assessment of Tactical Fire Spread Observations during the 2020 California Fire Season

Mario M. Valero*[1]; Christopher Giesige[1]; Eric Goldbeck-Dimon[1,2]; Andrew Klofas[1]

[1]*Department of Meteorology and Climate Science, San Jose State University, San Jose, CA 95192, USA*
{mm.valero, christopher.giesige, andrew.klofas}@sjsu.edu
[2]*Department of Environmental Studies, San Jose State University, San Jose, CA 95192, USA*
{eric.goldbeck-dimon@sjsu.edu}

**Corresponding author*

Keywords

Wildland Fire, Fire Behaviour, Fire Management, Remote Sensing, Infrared Imagery

Abstract

While the undesired effects of wildfire continue to increase in many regions, the fire science community continues to suffer from an important shortage of observational data of fire behaviour, especially at the landscape scale. Observations of landscape-scale fire spread have traditionally been incomplete, infrequent or qualitative. Airborne remote sensing technologies are changing this paradigm with the increasing adoption of infrared and multispectral optical sensors by fire management agencies. However, fire observations acquired during firefighting operations are designed with the goal of supporting tactical fire management decisions and they may not completely meet the needs of a rigorous scientific analysis. In this paper, we discuss tactical fire observations collected by CAL FIRE in 2020 in California (USA), specifically regarding their utility for fire behaviour studies. Generic data properties are summarized and example data is presented for two fire events. Our inspection of the data suggests that the collected imagery will be useful to study fire progression with varying temporal resolution between a few minutes and 24 hours. Imagery was successfully georeferenced and the geographic location of active fire lines could be estimated with a spatial resolution of O(10m). However, the temporal resolution of observations is inconsistent across flights and frequently not enough to study fire behaviour in detail. Furthermore, radiated energy could not be successfully characterized because the sensors utilized were not radiometrically calibrated and saturated at high irradiances. We expect that these observations will be useful to (i) approximate the response of fire behaviour to topographic features as well as changing weather and vegetation conditions, and (ii) validate fire spread simulators at the landscape scale. However, a detailed analysis of local fire rate of spread requires observations made at a higher frequency, while a complete fire behaviour characterization is impossible without accurate measurements of fire radiated energy. Similarly, ecological fire effects and fire emissions can hardly be estimated using such sparse observations.

1. The 2020 California Fire Season

2020 was one of the worst years on record in the Western United States in terms of burned area, social impact and economic losses caused by fire. During the 2020 fire season, 8,648 fires burned over 4.3 million acres in California, more than 4% of the state's total land, making that year the largest wildfire season recorded in California's modern history. 11,116 structures were damaged or destroyed, 33 people died as a consequence of fires, and Emergency Fund expenditures exceeded USD $1B (CAL FIRE, 2020a; CAL FIRE, 2020b). Five fires occurred in 2020 are among the seven largest fires in California's history, and five are listed in the list of 20 most destructive California fires. Among them, the August Complex fire stands out as the first fire that has ever burnt an area larger than 1 million acres. Figure 1 shows the area burned in California during 2020.

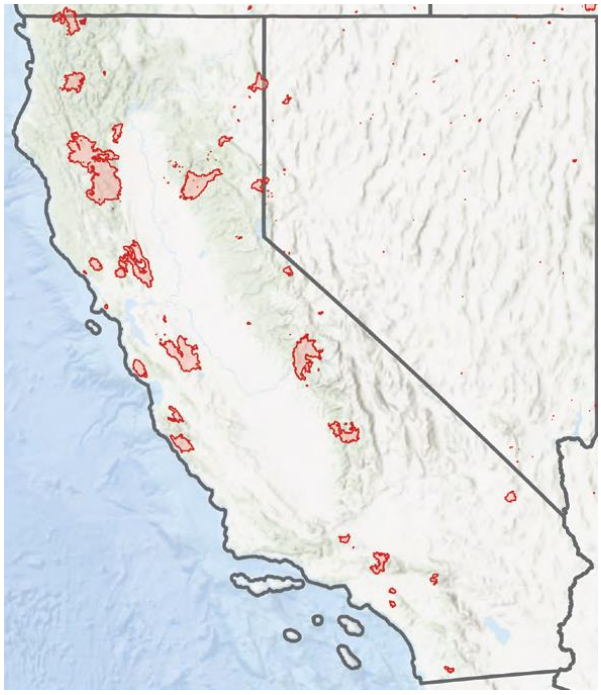

Figure 1- Area burned in California in 2020. Source: CAL FIRE.

2. Tactical Observations of Fire Spread

Fire management agencies deployed airborne imaging sensors during the largest and most impactful fires in 2020. In addition to using the imagery in real time, the data was stored for posterior analysis. This dataset is still being worked on by CAL FIRE. During our preliminary analysis of the dataset, we have identified a subset of the most impactful fires for which there is remote sensing information. The list of selected fires is summarized in Table 1. Two example fires were further selected from this list and are presented in Section 3.

Table 1- High-impact wildfires occurred in 2020 in California which have been selected for analysis based on the existence of fire spread remote sensing information.

Fire name	Location	Start Date	Containment Date	Area burned	Structures damaged	Casualties/Injuries
Creek	San Joaquin River near Mammoth Pool, Shaver Lake, Big Creek, Sierra National Forest	September 4, 2020	December 24, 2020	379,895 acres	71 structures damaged, 856 structures destroyed	26 injuries
North Complex (Clairmont, Bear)	Plumas National Forest	August 17, 2020	November 30, 2020	318,935 acres	2,455 structures destroyed	16 deaths
Glass	Napa county	September 27, 2020	October 20, 2020	67,484 acres	282 damaged, 1555 destroyed	None reported
Slater	Klamath, Six Rivers, and Rogue-Siskiyou National Forests in Siskiyou and Del Norte Counties in California and Josephine County in Oregon	September 8, 2020	November 16, 2020	157,229 acres	440 destroyed, 11 damaged	12 injured 2 dead
LNU	Napa, Sonoma, Lake, Yolo and Solano Counties	August 17, 2020	October 2, 2020	363,220 acres	1491 structures destroyed, 232 damaged	6 killed, 5 injured
Loyalton	Mount Ina Coolbrith, Sierra County, Tahoe National Forest	August 14, 2020	August 26, 2020	47,029 acres	None reported	None reported
Lake	Southwest Lake Hughs, Angeles National Forest	August 12, 2020	September 28, 2020	31,089 acres	33 structures destroyed, 6 damaged	4 injuries

Ranch 2	North San Gabriel Canyon Rd and Ranch Rd, San Gabriel Canyon	August 13, 20	October 2020	4,237 acres	None reported	None reported
CZU	San Mateo and Santa Cruz Counties	August 16, 2020	September 22, 2020	86,509 acres	1,490 Structures Destroyed, 140 Structures Damaged	1 injury, 1 fatality
Bond	Silverado Canyon, near Santa Ana (LA)	December 2, 2020	December 10, 2020	6,686 acres	21 structures damaged, 31 destroyed	None reported
Airport	Near Corona city (Riverside/LA)	December 1, 2020	December 12, 2020	1,087 acres	None reported	None reported
Crews	Crews Rd north of Gilroy	July 5, 2020	July 13, 2020	5,513 acres	1 structure destroyed	None reported
August Complex (Doe Fire - August south, Elkhorn Fire - August north)	Mendocino, Shasta-Trinity and Six Rivers National Forests	August 17, 2020	November 15, 2020	1,032,648 acres	995 structures destroyed	1 fatality
Red Salmon	14 miles northeast of Willow Creek	July 27, 2020	November 17, 2020	144,698 acres	None reported	None reported

3. Description of Remote Sensing Data

The primary source of data is aerial long-wave infrared (LWIR) imagery. Imagery was acquired on multiple flights for each fire. Time intervals between flights vary among fires and go from a few minutes to one day. Each video frame was timestamped and accompanied by camera position and attitude measurements, which allows for image georeferencing and accurate time referencing. The estimated spatial resolution of geocorrected images is in the order of 10m. However, LWIR images are non-radiometric and most of the them are saturated. This prevents retrieving fire radiative properties from this dataset.

4. Examples

This section showcases the available data in two example fire events with high temporal resolution data. In order to create the figures shown in this section, we applied georeferencing transformations to every video frame and stitched together all frames acquired during each flight. The resulting LWIR mosaics were then thresholded to identify active fire pixels. Because images are not radiometric, the optimum thresholding values were determined manually through inspection of image histograms.

4.1. Oak Fire

Fig. 2 shows a subset of the mosaics constructed from aerial LWIR frames captured during the 2020 Oak Fire. The time interval between observations is approximately 20 min. This frequency allows monitoring the fire progression and identifying significant events. For example, Fig. 2.c shows spotting on the south-east section of the fire perimeter. Such spotting significantly contributed to the advance of the fire as depicted in Fig. 2.d-e. Similarly, Fig. 2.f shows how the fire crossed a major highway through spotting.

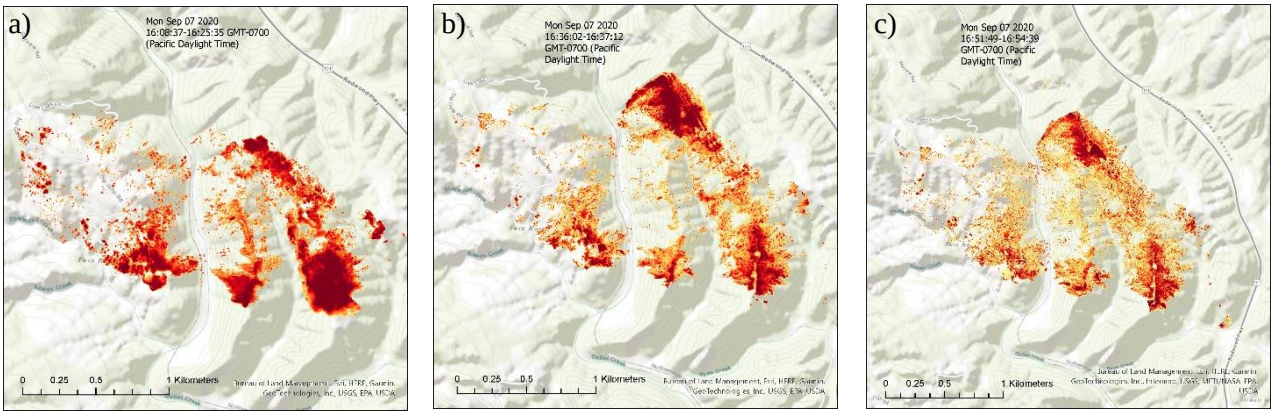

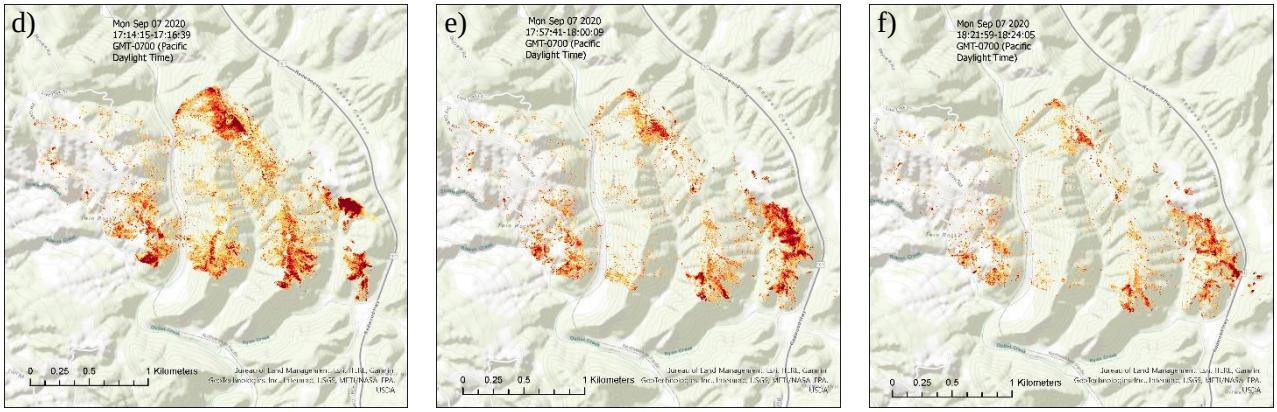

Figure 2. Observations of the 2020 Oak Fire progression. Darker colours represent a higher fire emittance, although images are not radiometric.

4.2. Glass Fire

Fig. 3 depicts the Glass Fire progression. In this case, only one LWIR mosaic is available per day. While the lower temporal resolution hinders the detailed analysis of fire behaviour, fire progression can still be observed in Fig. 3. Fire radiative properties could not be characterized due to the radiometric limitations of the deployed sensor.

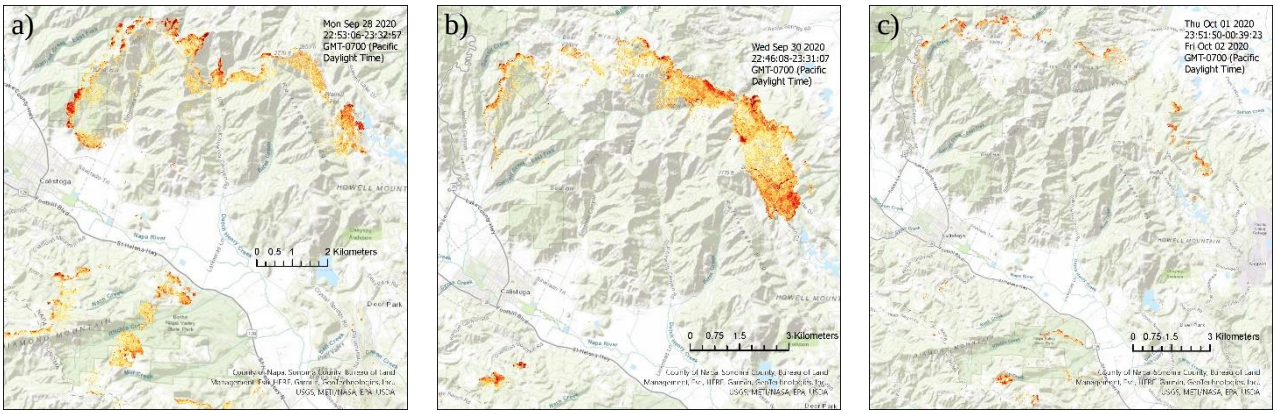

Figure 3. Observations of the 2020 Glass Fire progression. Darker colours represent a higher fire emittance, although images are not radiometric.

5. Discussion, Conclusions and Future Work

Systematic observation of fire behaviour is essential to support ongoing efforts in other areas like fire modelling, fire risk assessment and fire ecological studies. Acquiring fire behaviour observations is challenging, especially at the landscape scale. Remote sensing capabilities provide unprecedented opportunities to overcome the logistical challenges of fire behaviour observation. This paper discusses state-of-the-art data collected during firefighting operations in 2020 in California.

Our preliminary assessment of the data encourages further analysis. The ability to precisely locate active fire lines, track the fire perimeter and detect spot fires allows documenting fire progression and contextualizing it with terrain characteristics, vegetation properties and weather conditions. The primary limitations detected in this dataset relate to the unavailability of accurate radiative measurements and the inconsistent temporal resolution. Suggestions for the improvement of future fire observation systems include the addition of radiometric capabilities and the increase of frequency in observations.

Future work regarding this dataset includes (i) the development of an automated methodology to process the complete dataset, (ii) the development of a database with fire behaviour information collocated with topography, vegetation and weather data, and (iii) the detailed analysis of fire behaviour in individual fire events.

6. References

CAL FIRE, 2020a. "Wildfire Activity Statistics". Available at https://www.fire.ca.gov/media/0fdfj2h1/2020_redbook_final.pdf [last accessed: March 27, 2022].

CAL FIRE, 2020b. "Fire Siege". Available at https://www.fire.ca.gov/media/hsviuuv3/cal-fire-2020-fire-siege.pdf [last accessed: March 27, 2022].

A rule-based semi-automatic method to map burned areas using Landsat and Sentinel-2 images – incorporating vegetation indices into the mapping algorithm

Nikos Koutsias*[1]; Iliana Kalogeropoulou[1]; Anastasia Karamitsou[1]; Nikoletta G. Mili[1]; Magdalini Pleniou[2]

[1] *Department of Environmental Engineering, University of Patras, G. Seferi 2, GR-30100 Agrinio, Greece, {nkoutsia@upatras.gr, up1052692@upnet.gr, up1062187@upnet.gr, akaramitsou@upatras.gr}*
[2] *Forest Research Institute, Hellenic Agricultural Organisation 'DEMETER', GR-57006 Vassilika, Thessaloniki, Greece, {mpleniou@fri.gr}*

**Corresponding author*

Keywords:

Burned land mapping, rule-based, vegetation indices, Landsat, Sentinel-2

Abstract

At local or regional scales, where Landsat has been extensively applied to monitor burned areas, semi- or fully-automated methods are not very common. Koutsias et al. (2013) developed and improved (2021) a semi-automatic method to map burned areas consisted of a set of rules that are valid especially when the post-fire image has been captured shortly after the fire. However, the rule-based approach is not free of errors that eventually create limitations to adopt this method for reconstructing the fire history in a fully automated mode. In this work, we improved the method by incorporating vegetation indices. The vegetation indices evaluated were the: (i) Normalized Difference Vegetation Index (NDVI), (ii) Ratio Vegetation Index (RVI), (iii) Normalized Burn Ratio (NBR), (iv) Normalized Difference Water Index (NDWI) and (v) Shortwave Infrared Water Stress Index (SIWSI).

1. Introduction

There is a long history of mapping burned areas and other forest disturbances using satellite images of multiple resolutions either at research level to develop and improve the mapping methods or to create operational products at global scale (Chuvieco et al. 2019). Maps of fire occurrence can improve our understanding for the protection and restoration of fire-affected natural ecosystems worldwide. Satellite-based remote sensing has been an ideal tool to create maps of fire scars by collecting and processing the required data, as it covers large spatial and temporal extents within a cost- and time-efficient framework (Koutsias et al. 1999).

At global scale, there are unique fire-products, such as those based on MODIS (Justice et al. 2002), however they are mostly devoted to continental scale studies. However, at regional scales, such systematic fire products are not very common mainly due to cost constraints on gathering and processing medium or high-resolution satellite data series that until almost a decade ago were not freely available at no cost although recently such products have started to appear (Hawbaker et al. 2020).

Currently, United States Geological Survey (USGS) archived Landsat images are freely available to the public from the USGS Earth Resources Observation and Science (EROS) Center (http://glovis.usgs.gov/). These historical archives cover large spatial and temporal extents at continental scale and provide a unique opportunity to overcome cost constraints when reconstructing fire history globally at low-to-high spatial resolution. However, one problem that exists is how to process successfully with high accuracy the time series of satellite images consisting of thousands of images without the human interference. The training phase of an algorithm, when needed, is a time-consuming procedure that if omitted would be an advantage of the approach by saving processing time and cost. This is a critical issue in cases where many satellite images need to be analyzed, such as for the spatially explicit reconstruction of fire history, where thousands of images might be used in the processing chain.

2. Mapping burned areas at local scale

2.1. The rule-based approach

There have been efforts to develop automatic or semi-automatic techniques to map burned areas using medium-high resolution satellite images such as those of Landsat satellites (Bastarrika et al. 2014; Hawbaker et al. 2020; Koutsias et al. 2013), Sentinel-2 data (Roteta et al. 2019). Recently, USGS delivered to the users Landsat Level-3 Burned Area (BA) that contains two acquisition-based raster data products that represent burn classification and burn probability using Surface Reflectance data from the U.S. Landsat Analysis Ready Data (ARD) (Hawbaker et al. 2020).

Koutsias et al. (2013) developed a semi-automatic method to map burned areas using multi-temporal acquisitions of Landsat satellite data, considering a pre- and post-fire image as a pair of images that could minimize spectral confusion with unburned surfaces. The proposed method consisted of a set of rules that are valid especially when the pre- and post-fire image has been captured shortly before and after the fire event respectively when the signal has its highest separability from other land cover types.

2.2. Improvement of the method

The rule-based approach is not free of errors (e.g. omission or commission), that eventually create limitations to adopt this method for reconstructing the fire history in a fully automated mode. Therefore, the development of completely automatic techniques to successfully map the burned areas is a challenge. In this work we improved further the method by incorporating vegetation indices.

To revise the old set of rules and create the revised rules we followed the same methodology as in the original paper from Koutsias et al. (2013) where the rules had been developed on the basis of spectral properties of burned areas as compared to the pre-fire unburned vegetation and to the spectral signatures of other land cover types found in post-fire satellite scenes. Therefore, sampling plots that correspond to burned surfaces were located on the post-fire Landsat images to capture the whole variability found within the burned area class. Additionally, other important land cover types were delineated on the satellite images using the pan-European CORINE 2000 Land Cover database.

The digital VI values of the sampling plot pixels were extracted and simple statistics were generated to characterize the spectral properties of the various land cover categories including the burned area class. Histogram and signature data plots were created to graphically represent the spectral profiles for all land cover types including burned areas. It was also used to compare them with patterns of unburned vegetation when using multi-temporal satellite images and with other land cover types when using only single-date post-fire satellite images.

2.3. Vegetation indices

A Vegetation Index (VI) is usually a linear transformation of two or more spectral bands aiming to enhance the spectral signal of the original spectral channels by creating a new spectral space which is sensitive to variations of vegetation attributes as for example leaf area index (LAI), percent green cover, chlorophyll content, green biomass and ab-sorbed photosynthetically active radiation (APAR). In our study we chose few of them that are considered typical and have been extensively applied for vegetation studies or in remote sensing of wildland fires, it is beyond our purpose to make an extensive evaluation of vegetation indices concerning their phenology between low and high fire-prone areas. The vegetation indices chosen were the: (i) Normalized Difference Vegetation Index (NDVI), (ii) Ratio Vegetation Index (RVI), (iii) Normalized Burn Ratio (NBR), (iv) Normalized Difference Water Index (NDWI) and (v) Shortwave Infrared Water Stress Index (SIWSI).

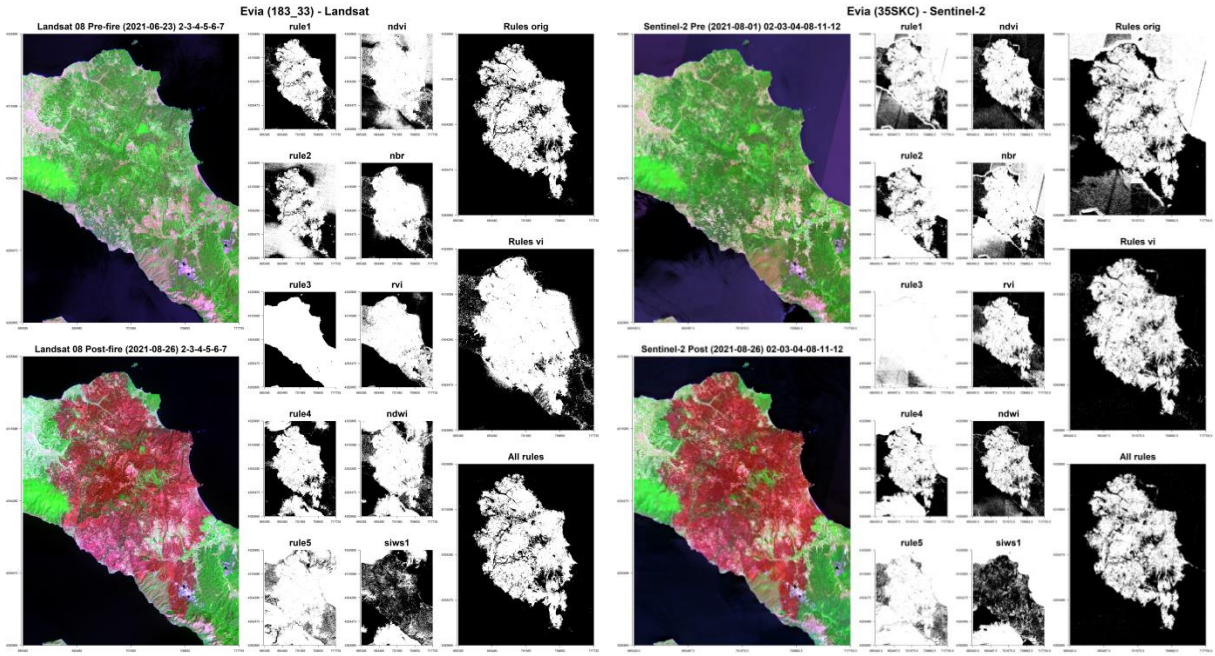

Figure 1- Mapping of burned areas with the rule-based approach as improved by the incorporation of the vegetation indices for Landsat and Sentinel-2 data.

3. References

Bastarrika, A., Alvarado, M., Artano, K., Martinez, M., Mesanza, A., Torre, L., Ramo, R., & Chuvieco, E. (2014). BAMS: A Tool for Supervised Burned Area Mapping Using Landsat Data. Remote Sensing, 6, 12360-12380

Chuvieco, E., Mouillot, F., van der Werf, G.R., San Miguel, J., Tanasse, M., Koutsias, N., García, M., Yebra, M., Padilla, M., Gitas, I., Heil, A., Hawbaker, T.J., & Giglio, L. (2019). Historical background and current developments for mapping burned area from satellite Earth observation. Remote Sensing of Environment, 225, 45-64

Hawbaker, T.J., Vanderhoof, M.K., Schmidt, G.L., Beal, Y.-J., Picotte, J.J., Takacs, J.D., Falgout, J.T., & Dwyer, J.L. (2020). The Landsat Burned Area algorithm and products for the conterminous United States. Remote Sensing of Environment, 244, 111801

Justice, C.O., Giglio, L., Korontzi, S., Owens, J., Morisette, J.T., Roy, D., Descloitres, J., Alleaume, S., Petitcolin, F., & Kaufman, Y. (2002). The MODIS fire products. Remote Sensing of Environment, 83, 244-262

Koutsias, N., Karteris, M., Fernandez-Palacios, A., Navarro, C., Jurado, J., Navarro, R., & Lobo, A. (1999). Burned land mapping at local scale. In E. Chuvieco (Ed.), Remote Sensing of Large Wildfires in the European Mediterranean Basin (pp. 157-187). Berlin Heidelberg: Springer-Verlag

Koutsias, N., Pleniou, M., Mallinis, G., Nioti, F., & Sifakis, N.I. (2013). A rule-based semi-automatic method to map burned areas: exploring the USGS historical Landsat archives to reconstruct recent fire history. International Journal of Remote Sensing, 34, 7049–7068

Koutsias, N. and Pleniou, M., (2021). A rule-based semi-automatic method to map burned areas in mediterranean using Landsat images–revisited and improved. International Journal of Digital Earth, 14 (11), 1602-1623

Roteta, E., Bastarrika, A., Padilla, M., Storm, T., & Chuvieco, E. (2019). Development of a Sentinel-2 burned area algorithm: Generation of a small fire database for sub-Saharan Africa. Remote Sensing of Environment, 222, 1-17

A satellite-based multi-dimensional approach to identify potential post-fire regime shifts in ecosystem functioning

Bruno Marcos*[1,2]; João Gonçalves[1,2,3]; Domingo Alcaraz-Segura[4,5,6]; Mário Cunha[7,8]; João P. Honrado[1,2,9]

[1]CIBIO, Centro de Investigação em Biodiversidade e Recursos Genéticos, InBIO Laboratório Associado, Campus de Vairão, Universidade do Porto, 4485-661 Vairão, Portugal, {bruno.marcos, joao.goncalves}@cibio.up.pt
[2]BIOPOLIS Program in Genomics, Biodiversity and Land Planning, CIBIO, Campus de Vairão, 4485-661 Vairão, Portugal
[3]proMetheus – Research Unit in Materials, Energy and Environment for Sustainability, Instituto Politécnico de Viana do Castelo (IPVC), Avenida do Atlântico, n.º 644, 4900-348 Viana do Castelo, Portugal
[4]iecolab. Interuniversity Institute for Earth System Research (IISTA), University of Granada, Av. del Mediterráneo, 18006 Granada, Spain
[5]Dept. of Botany, Faculty of Sciences, University of Granada, Av. Fuentenueva, 18071 Granada, Spain, {dalcaraz@ugr.es}
[6]Andalusian Center for the Assessment and Monitoring of Global Change (CAESCG), Universidad de Almería, Crta. San Urbano, 04120 Almería, Spain
[7]Departamento de Geociências, Ambiente e Ordenamento do Território, Faculdade de Ciências, Universidade do Porto, 4099-002 Porto, Portugal, {mccunha@fc.up.pt}
[8]Institute for Systems and Computer Engineering, Technology and Science (INESC TEC), Campus da Faculdade de Engenharia da Universidade do Porto, Rua Dr. Roberto Frias, Porto 4200-465, Portugal
[9]Departamento de Biologia, Faculdade de Ciências, Universidade do Porto, 4099-002 Porto, Portugal, {jhonrado.fc.up.pt}

**Corresponding author*

Keywords

Resilience; Spectral post-fire recovery; TCT; MODIS; Iberian Peninsula

Abstract

Wildfires can profoundly impact many aspects of matter flows and energy budgets in ecosystems. Exacerbated by projected shifts in climate, land use, and forest management, changes in fire regimes can lead to decreased ecosystem resilience, regime shifts, and ecosystem collapse. Thorough assessments of ecosystem resilience to wildfires are thus critical to bridge gaps between science, policy, and management. To that end, approaches based on ecosystem functioning offer an integrative view of ecosystem responses to wildfire-induced changes and provide quicker, quantifiable responses to disturbances that are more directly connected to ecosystem services. In that regard, satellite remote sensing can be employed to easily and frequently monitor multiple dimensions of ecosystem functioning over large areas and across time, and to evaluate ecosystem functioning resilience to wildfires. This study describes an approach for identifying potential regime shifts based on satellite-based surrogates of four key dimensions of ecosystem functioning: primary production, water content, albedo, and sensible heat. To that end, we classified the trajectories after wildfires in 2005, in NW Iberian Peninsula, for the 2000–2018 period, into five main types, using two metrics of medium-to-long term spectral post-fire recovery. Then, we derived a synthetic indicator to analyse the overall "strength-of-evidence" of potential regime shifts across dimensions. Potential regime shifts were identified for each dimension of ecosystem functioning considered, with the main effects associated with the sudden removal of vegetation. For primary production, regime shifts may be linked to changes in land cover and use, as well as management. Changes in the concentrations of impervious and radiation-absorbing materials following wildfires may be responsible for regime shifts in water content and albedo, with loss of canopy moisture due to fire-related damage leading to vegetation mortality during post-fire recovery. On the other hand, regime shifts in sensible heat were less frequent, since wildfires tend to have transient effects on this dimension of ecosystem functioning. Overall, our results show that our approach successfully captured different patterns of post-fire recovery and resilience across multiple dimensions of ecosystem functioning. We argue that our approach can provide an enhanced characterization of ecosystem resilience to wildfires, and support the identification of potential regime shifts after such disturbances, ultimately upholding promising implications for post-fire ecosystem management.

1. Introduction

Fire is an integral part of many ecosystems worldwide, playing a key role in their structure, composition, and functioning. However, wildfires can pose a major threat to a wide range of environmental, social, and economic assets (Adámek et al., 2016; San-Miguel-Ayanz et al., 2013). Changes in fire regimes can reduce the ability of ecosystems to recover and persist in the face of disturbances, eroding ecosystem resilience, which can lead to ecosystem collapse, with subsequent impacts on human societies (Folke et al., 2004; Johnstone et al., 2010; Scheffer et al., 2015). Moreover, wildfire disturbances can trigger sudden regime shifts in ecosystems, leading to critical transitions from one dynamic equilibrium to an alternative stable state (Boettiger et al., 2013; Scheffer et al., 2012). Furthermore, fire activity is projected to increase in the next decades, exacerbated by shifts in global climate, land use and forest management (Bowman et al., 2009; Tedim et al., 2013). Therefore, conserving fire-resilient ecosystems is a key priority (Willis et al., 2018).

Thorough assessments of ecosystem state and resilience to wildfires are thus critical to bridge gaps between science, policy, and management, with more comprehensive indicators needed for a better understanding of post-fire processes (Baho et al., 2017; Gouveia et al., 2010; van Leeuwen et al., 2010). To that end, approaches based on ecosystem functioning offer an integrative view of ecosystem responses to wildfire-induced changes, since fire can cause rapid modifications in key aspects of matter and energy flows in ecosystems (B. Marcos et al., 2021; Petropoulos et al., 2009). Furthermore, ecosystem functioning provides quicker, quantifiable responses to disturbances than structure or composition, and are more directly connected to ecosystem services (Alcaraz-Segura et al., 2008). Satellite remote sensing (SRS) has been increasingly employed for a wide range of applications related to both fire and ecosystem functioning, making it a major asset for risk assessment and governance, and post-fire restoration and management (Keeley, 2009; Parks et al., 2019; Smith et al., 2014). Having unlocked our understanding of global fire activity, satellite remote sensing has contributed to advancing wildfire science and management (Szpakowski & Jensen, 2019), allowing us to overcome scale-dependent limitations (Benali et al., 2016). Indeed, multiple aspects of ecosystem functioning — such as carbon and water dynamics, as well as energy budgets — can be easily and frequently monitored over large areas through SRS, due to their strong relation to biophysical properties and ecosystem processes (Villarreal et al., 2018). Nevertheless, multi-dimensional satellite-based assessments of ecosystem functioning resilience to wildfires are still scarce (Frazier et al., 2013). Moreover, the utility of SRS to evaluate ecosystem functioning resilience, and to anticipate potential regime shifts — through the translation of spectral indices into meaningful, informative ecosystem variables — is still largely under-explored (B. Marcos et al., 2021).

In this study, we propose an approach for identifying potential regime shifts based on satellite-based surrogates of four key dimensions of ecosystem functioning, related to the carbon, water and energy exchanges: primary production, water content, albedo, and sensible heat. For each one of those four dimensions of ecosystem functioning, we classified the post-fire trajectories into five main types, using two metrics of medium-to-long term spectral recovery. Finally, we derived a synthetic indicator of "strength-of-evidence" of overall regime shifts across dimensions. We discussed the potential and added value of the proposed approach to improve satellite-based characterization of ecosystem resilience to wildfire disturbances, and to identify potential regime shifts after those disturbances, over multiple dimensions of ecosystem functioning.

2. Materials and Methods

2.1. Study area

To illustrate our approach, we analysed all areas that burned in 2005 in the northwest Iberian Peninsula (NW-IP). This is an area with high wildfire activity, in the last decades — both in terms of ignitions and burned area —, despite the enormous investments in fire suppression (Catry et al., 2009; Moreira et al., 2020). Furthermore, the year 2005 coincided with severe drought, with over 340,000 ha burned in this area (Bastos et al., 2011). The NW-IP features diverse environmental characteristics, with strong environmental gradients, a major climatic and biogeographic transition, diverse land cover classes and land uses, and vegetation types. Moreover, historical land uses and management made this area a highly fire-prone landscape.

2.2. Satellite data preprocessing

Firstly, we identified the areas that burned in 2005, within the study area, with a contiguous area above 100 ha (i.e., "big fires"; following (B. Marcos et al., 2019)), using the MCD64A1 product (Giglio et al., 2018) from the

Moderate Resolution Imaging Spectroradiometer (MODIS). Then, to inform on the four ecosystem functioning dimensions of primary production, water content, and surface albedo, we used time-series of the three Tasselled Cap Transformation (TCT) features of "Greenness" (TCTG), "Wetness" (TCTW), and "Brightness" (TCTB), as well as land surface temperature (LST), respectively. The three TCT features are sensor-specific linear combinations of bands in the visible, near-infrared, and short-wave infrared regions of the electromagnetic spectrum that maximize the association with biophysical parameters such as the amount of photosynthetically active vegetation, water content and soil moisture, and albedo (Lobser & Cohen, 2007; Mildrexler et al., 2009). The LST is a calibrated measure of the thermal emissivity of the land surface. We extracted these satellite image time-series (SITS) from the MODIS MOD09A1 (Vermote, 2015) and MOD11A2 (Wan et al., 2004) products, for the years ranging from 2000 to 2018, with a frequency of 46 images per year (i.e., one image for each 8-day period), at 500m spatial resolution.

Spurious values in each of the four SITS were corrected using a filtering procedure based on the Hampel identifier (Hampel, 1971, 1974). Time-series were seasonally adjusted using Seasonal and Trend decomposition using Loess (STL; (Cleveland et al., 1990; Hyndman & Athanasopoulos, 2018)), to establish pre-fire conditions, by defining reference intervals corresponding to one median absolute deviation around the median, from all values in the three years brfore the date of the fire occurrence. On the other hand, the trend component was used to compute moving-window medians (i.e., incremental steps in the post-fire trajectories).

All data was processed and analysed using software packages within the R statistical programming environment (Busetto & Ranghetti, 2016; Hijmans, 2020; R Core Team, 2019), and the Python programming language (Gillies et al., 2013).

2.3. Extraction of resilience indicators

To support the identification of potential post-fire regime shifts in ecosystem functioning, we first determined — for each pixel and each of the four dimensions of ecosystem functioning — the date of the first directionality inflexion in the trend component curve (t_{INF}) after the date of the wildfire occurrence (t_{FIRE}). This moment represents the first major change of directionality — from divergent to convergent with the pre-fire conditions — in the post-fire trajectory, which can be regarded as an approximation of the date of the start of recovery.

Then, we computed two related but independent "return time"-type metrics related to post-fire (spectral) recovery at medium-to-long term:

- "Return-to-Reference Time" (RRT) — the duration of the period between t_{FIRE} and the first moment in the post-fire recovery when the post-fire trajectory returns to within the pre-fire reference interval — t_{REF}; and
- "Return-to-Equilibrium Time" (RET) — the duration of the period between t_{FIRE} and the moment in the post-fire recovery when the trajectory is stabilized (according to a predefined threshold value for the change rate) — t_{EQ}.

The RRT metric provides an estimate of the amount of time needed to return to the pre-fire conditions (if and when applicable), whereas RET provides an approximate measure of the amount of time needed to achieve a stable state after a fire (if and when applicable) — which can be different from the pre-fire conditions.

2.4. Identification of potential regime shifts

Based on different combinations of the outcomes of the RRT and RET metrics, we classified the post-fire trajectories of each of the four dimensions of ecosystem functioning into four main types of medium-to-long term spectral recovery (Fig. 1):

- "Return to pre-fire" — equilibrium reached within pre-fire reference interval;
- "Under-recovery" — equilibrium reached outside pre-fire reference interval, but pre-fire reference interval not crossed;
- "Over-recovery" — equilibrium reached outside pre-fire reference interval after pre-fire reference interval was crossed;
- "No equilibrium" — pre-fire reference interval crossed, but no equilibrium achieved; and

- "(not detected)" — no recovery detected because either: (i) t_{REF} and t_{EQ} not successfully found; or (ii) inflexion point not found, or not within the pre-fire reference interval.

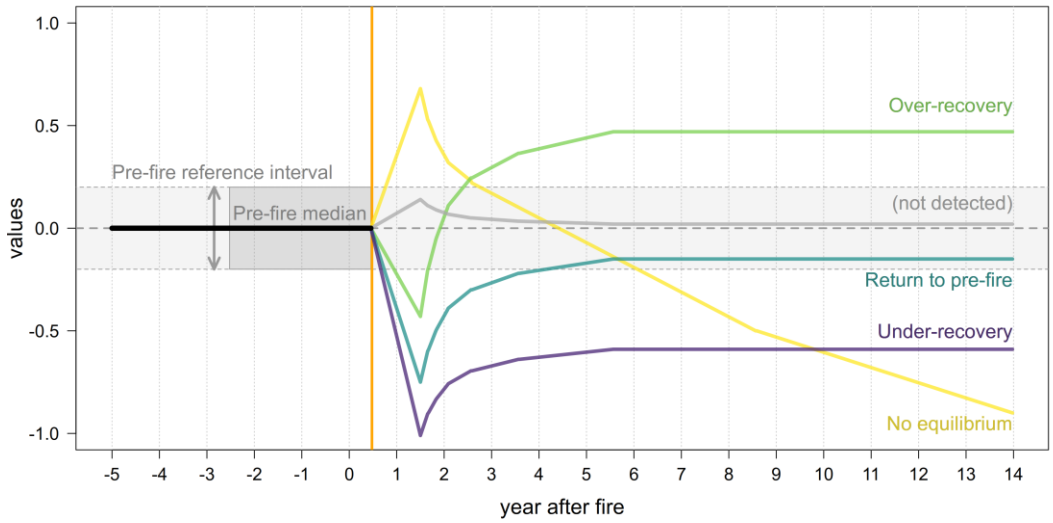

Figure 1 – Illustration of the different classes obtained from the post-fire resilience classification, based on the two independent metrics of "Time to Return-to-Reference" (RRT) and "Time to Return-to-Equilibrium" (RET), respectively measuring the time needed after the wildfire to return to pre-fire conditions, and to achieve a stable state.

Finally, we mapped the percentage of the four dimensions of ecosystem functioning with potential regime shifts (i.e. that were classified as either "Under-recovery" or "Over-recovery"), as a synthetic, multi-dimensional indicator of the overall "Strength-of-Evidence" for potential post-fire regime shifts in ecosystem functioning.

3. Results and Discussion

Overall, most burned pixels in NW-IP were classified as either "Return to pre-fire" or "(not detected)", within each dimension of ecosystem functioning (Fig. 2) — except for albedo ("Albedo"). This suggests an overall high resilience capacity of ecosystems in the study area. Furthermore, the percentage of the "(not detected)" class was highest for sensible heat ("Heat"), corresponding mainly to areas located either near or adjacent to the periphery of the burned patches (Fig. 3). These results, allied to the low percentages of the "Under-recovery" and "Over-recovery" classes, point to the effects of wildfires on Heat being mostly transient (E. Marcos et al., 2018; Quintano et al., 2015). On the other hand, the main effects on primary production ("Productivity"), water content ("Water"), and Albedo can be linked to the sudden removal of vegetation (Veraverbeke et al., 2012).

Regarding potential regime shifts, considerable portions of the analysed burned areas were classified as either "Over-recovery" — with the highest percentage for Productivity and Albedo —, or "Under-recovery" — with the highest percentage for Water and Albedo. Regime shifts in Productivity may translate land cover conversions, particularly when associated with land abandonment (Silva et al., 2011), invasions by exotic plant species (Nunes et al., 2020), or direct human interventions (Silva et al., 2011). Regime shifts in Water can be associated with the loss of moisture in canopy foliage due to fire-related damage — which can sometimes persist for up one year after the fire —, leading to vegetation mortality (Beringer et al., 2003; Senf & Seidl, 2020; Viana-Soto et al., 2020). Also, the increased concentrations of quantities of impervious materials (such as ashes, char, and soot) after a fire can clog soil pores, leading to decreased water retention capacity, and increased post-fire water repellency, surface runoff, and soil erosion rates (Bodí et al., 2014; Hubbert et al., 2012; Ramanathan & Carmichael, 2008). These materials can also be responsible for the observed regime shifts in Albedo, since they absorb visible solar radiation, translating into a darkening effect immediately after the fire that tends to dissipate before the regeneration of vegetation, leading to a temporary brightening effect one to two years after fire (Lentile et al., 2006; Quintano et al., 2019; Ramanathan & Carmichael, 2008; Saha et al., 2019). Whichever the specific driver responsible for regime shifts in each particular case, these qualitative changes can denote a depletion in the resilience capacity of ecosystems, with potentially severe consequences (Gatebe et al., 2014; Saha et al., 2017).

Finally, the "No equilibrium" class may translate either incomplete recovery or unforeseen interferences on the detection of post-fire inflexion points. Nonetheless, the percentages obtained for this class were low across dimensions.

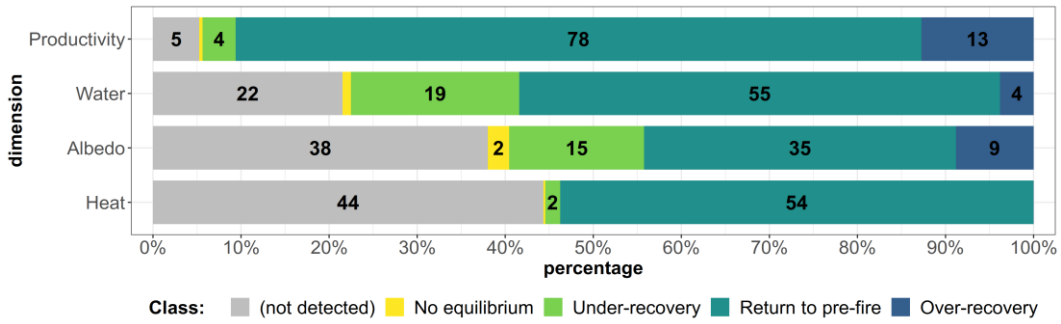

Figure 2 – Relative frequencies obtained for each post-fire resilience class, for each of the four dimensions of ecosystem functioning considered — primary production, water content, albedo, and sensible heat —, across all patches burned in 2005 in NW Iberian Peninsula, up until 2018. Numbers in bold are only shown for percentages above 1%.

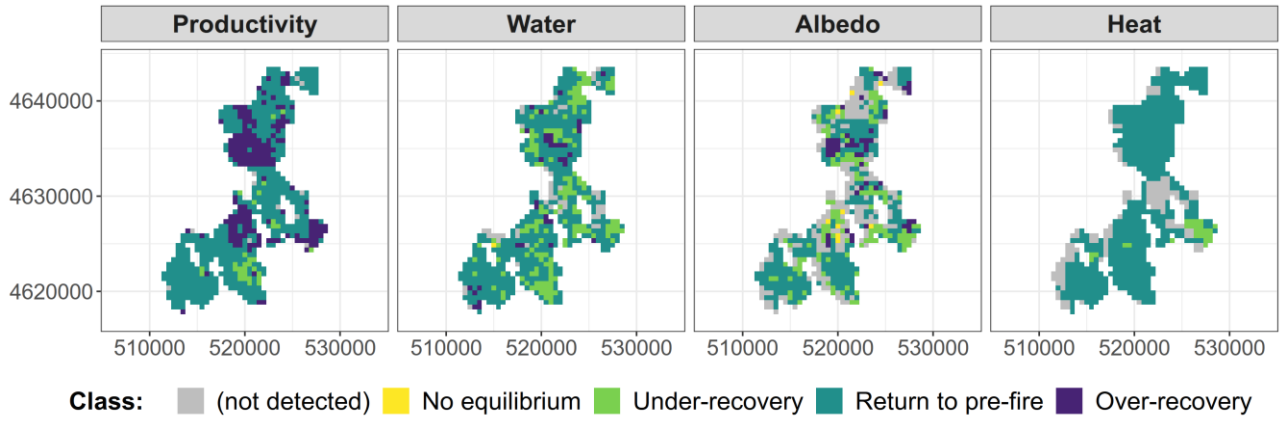

Figure 3 – Post-fire recovery and resilience classification map for a selected burned area, for each of the four dimensions of ecosystem functioning considered — primary production, water content, albedo, and sensible heat.

Maps of the overall "Strength-of-Evidence" of regime shifts, across the four dimensions of ecosystem functioning (Fig. 4), clearly show areas overall more likely to have experienced regime shifts in ecosystem functioning, with particular "hot-spots" being observable in darker colours.

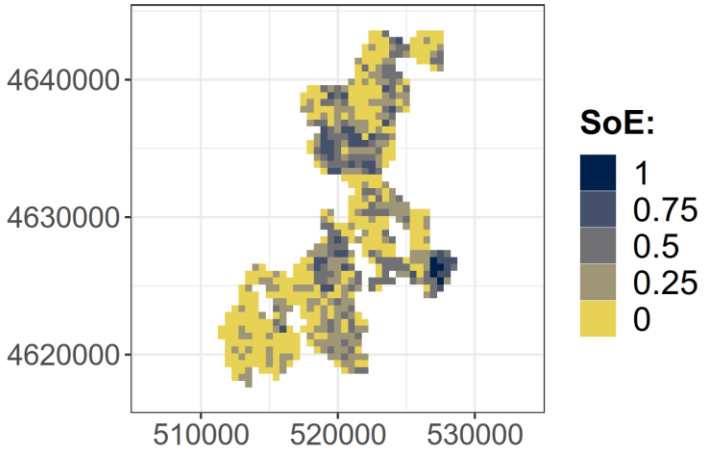

Figure 4 – Maps of "Strength-of-Evidence" for regime shifts across the four dimensions of ecosystem functioning considered — primary productivity, vegetation water content, albedo, and sensible heat —, for a selected burned area.

4. Conclusions and future outlook

In this study, we described an approach for characterizing ecosystem resilience to wildfires, across multiple dimensions of ecosystem functioning, as well as for identifying and mapping potential post-fire regime shifts, using metrics extracted from SITS. Furthermore, the proposed approach can be applied in a wide range of geographic and environmental contexts, using data from different satellite-sensor platforms. Together, the results obtained allowed us to highlight the added value and the potential of the proposed approach. Potential applications include regional-scale, spatially explicit prioritizations for management or conservation purposes, and as a precursor analysis to more detailed, local-scale assessments, investigating specific patterns. Potential future improvements include accounting for the duality in post-fire trajectories of albedo, as well as validating the obtained results through field-collected data such as spectral readings, and aerial ("drone") imagery. Overall, our approach successfully captures different patterns associated with key features of the post-fire processes in ecosystem functioning, pointing to a high degree of complementarity between different dimensions, and highlighting the added value of such multi-dimensional. We argue that such frameworks can provide an enhanced characterization of post-fire ecosystem resilience, ultimately upholding potential implications for post-fire ecosystem management.

5. References

Adámek, M., Hadincová, V., & Wild, J. (2016). Long-term effect of wildfires on temperate Pinus sylvestris forests: Vegetation dynamics and ecosystem resilience. *Forest Ecology and Management*, *380*, 285–295. https://doi.org/10.1016/j.foreco.2016.08.051

Alcaraz-Segura, D., Cabello, J., Paruelo, J. M., & Delibes, M. (2008). Trends in the surface vegetation dynamics of the national parks of Spain as observed by satellite sensors. *Applied Vegetation Science*, *11*(4), 431–440. https://doi.org/10.3170/2008-7-18522

Baho, D. L., Allen, C. R., Garmestani, A., Fried-Petersen, H., Renes, S. E., Gunderson, L., & Angeler, D. G. (2017). A quantitative framework for assessing ecological resilience. *Ecology and Society*, *22*(3), 1. https://doi.org/10.5751/ES-09427-220317

Bastos, A., Gouveia, C. M., DaCamara, C. C., & Trigo, R. M. (2011). Modelling post-fire vegetation recovery in Portugal. *Biogeosciences*, *8*(12), 3593–3607. https://doi.org/10.5194/bg-8-3593-2011

Benali, A., Russo, A., Sá, A., Pinto, R., Price, O., Koutsias, N., & Pereira, J. (2016). Determining Fire Dates and Locating Ignition Points With Satellite Data. *Remote Sensing*, *8*(4), 326. https://doi.org/10.3390/rs8040326

Beringer, J., Hutley, L. B., Tapper, N. J., Coutts, A., Kerley, A., & O'Grady, A. P. (2003). Fire impacts on surface heat, moisture and carbon fluxes from a tropical savanna in northern Australia. *International Journal of Wildland Fire*, *12*(3–4), 333–340. https://doi.org/10.1071/wf03023

Bodí, M. B., Martin, D. A., Balfour, V. N., Santín, C., Doerr, S. H., Pereira, P., Cerdà, A., & Mataix-Solera, J. (2014). Wildland fire ash: Production, composition and eco-hydro-geomorphic effects. *Earth-Science Reviews*, *130*, 103–127. https://doi.org/10.1016/j.earscirev.2013.12.007

Boettiger, C., Ross, N., & Hastings, A. (2013). Early warning signals: The charted and uncharted territories. *Theoretical Ecology*, *6*, 255–264. https://doi.org/10.1007/s12080-013-0192-6

Bowman, D. M. J. S., Balch, J. K., Artaxo, P., Bond, W. J., Carlson, J. M., Cochrane, M. A., D'Antonio, C. M., DeFries, R. S., Doyle, J. C., Harrison, S. P., Johnston, F. H., Keeley, J. E., Krawchuk, M. A., Kull, C. A., Marston, J. B., Moritz, M. A., Prentice, I. C., Roos, C. I., Scott, A. C., … Pyne, S. J. (2009). Fire in the Earth System. *Science*, *324*(5926), 481–484. https://doi.org/10.1126/science.1163886

Busetto, L., & Ranghetti, L. (2016). MODIStsp: An R package for automatic preprocessing of MODIS Land Products time series. *Computers and Geosciences*, *97*, 40–48. https://doi.org/10.1016/j.cageo.2016.08.020

Catry, F. X., Rego, F. C., Bação, F. L., & Moreira, F. (2009). Modeling and mapping wildfire ignition risk in Portugal. *International Journal of Wildland Fire*, *18*(8), 921. https://doi.org/10.1071/WF07123

Cleveland, R. B., Cleveland, W. S., McRae, J. E., & Terpenning, I. (1990). STL: A seasonal-trend decomposition procedure based on loess. *Journal of Official Statistics*, *6*(1), 3–73. https://doi.org/citeulike-article-id:1435502

Folke, C., Carpenter, S., Walker, B., Scheffer, M., Elmqvist, T., Gunderson, L., & Holling, C. S. (2004). Regime Shifts, Resilience, and Biodiversity in Ecosystem Management. *Annual Review of Ecology, Evolution, and Systematics*, *35*(1), 557–581. https://doi.org/10.1146/annurev.ecolsys.35.021103.105711

Frazier, A. E., Renschler, C. S., & Miles, S. B. (2013). Evaluating post-disaster ecosystem resilience using MODIS GPP data. *International Journal of Applied Earth Observation and Geoinformation*, *21*, 43–52. https://doi.org/10.1016/j.jag.2012.07.019

Gatebe, C. K. K., Ichoku, C. M. M., Poudyal, R., Román, M. O. O., & Wilcox, E. (2014). Surface albedo darkening from wildfires in northern sub-Saharan Africa. *Environmental Research Letters*, *9*(6), 065003. https://doi.org/10.1088/1748-9326/9/6/065003

Giglio, L., Boschetti, L., Roy, D. P., Humber, M. L., & Justice, C. O. (2018). The Collection 6 MODIS burned area mapping algorithm and product. *Remote Sensing of Environment*, *217*, 72–85. https://doi.org/10.1016/j.rse.2018.08.005

Gillies, S., Ward, B., & Petersen, A. S. (2013). Rasterio: geospatial raster I/O for Python programmers version 0.36.0 (0.36.0).

Gouveia, C., DaCamara, C. C., & Trigo, R. M. (2010). Post-fire vegetation recovery in Portugal based on spot/vegetation data. *Natural Hazards and Earth System Science*, *10*(4), 673–684. https://doi.org/10.5194/nhess-10-673-2010

Hampel, F. R. (1971). A General Qualitative Definition of Robustness. *The Annals of Mathematical Statistics*, *42*(6), 1887–1896. http://projecteuclid.org/euclid.aoms/1177693054

Hampel, F. R. (1974). The Influence Curve and its Role in Robust Estimation. *Journal of the American Statistical Association*, *69*(346), 383–393. https://doi.org/10.1080/01621459.1974.10482962

Hijmans, R. J. (2020). *raster: Geographic Data Analysis and Modeling. R package version 3.4-5.* (3.4-5). https://cran.r-project.org/package=raster

Hubbert, K. R., Wohlgemuth, P. M., Beyers, J. L., Narog, M. G., & Gerrard, R. (2012). Post-fire soil water repellency, hydrologic response, and sediment yield compared between grass-converted and chaparral watersheds. *Fire Ecology*, *8*(2), 143–162. https://doi.org/10.4996/fireecology.0802143

Hyndman, R. J., & Athanasopoulos, G. (2018). *Forecasting: Principles and Practice* (2nd ed.). OTexts. OTexts.com/fpp2

Johnstone, J. F., Chapin, F. S., Hollingsworth, T. N., Mack, M. C., Romanovsky, V., & Turetsky, M. (2010). Fire, climate change, and forest resilience in interior alaska1. *Canadian Journal of Forest Research*, *40*(7), 1302–1312. https://doi.org/10.1139/X10-061

Keeley, J. E. (2009). Fire intensity, fire severity and burn severity: a brief review and suggested usage. *International Journal of Wildland Fire*, *18*(1), 116. https://doi.org/10.1071/WF07049

Lentile, L. B., Holden, Z. A., Smith, A. M. S. S., Falkowski, M. J., Hudak, A. T., Morgan, P., Lewis, S. A., Gessler, P. E., Benson, N. C., Lentile, L. B., Holden, Z. A., Smith, A. M. S. S., Falkowski, M. J., Hudak, A. T., Morgan, P., Lewis, S. A., Gessler, P. E., & Benson, N. C. (2006). Remote sensing techniques to assess active fire characteristics and post-fire effects. *International Journal of Wildland Fire*, *15*(3), 319. https://doi.org/10.1071/WF05097

Lobser, S. E., & Cohen, W. B. (2007). MODIS tasselled cap: land cover characteristics expressed through transformed MODIS data. *International Journal of Remote Sensing*, *28*(22), 5079–5101. https://doi.org/10.1080/01431160701253303

Marcos, B., Gonçalves, J., Alcaraz-Segura, D., Cunha, M., & Honrado, J. P. (2019). Improving the detection of wildfire disturbances in space and time based on indicators extracted from MODIS data: a case study in northern Portugal. *International Journal of Applied Earth Observation and Geoinformation*, *78*, 77–85. https://doi.org/10.1016/j.jag.2018.12.003

Marcos, B., Gonçalves, J., Alcaraz-Segura, D., Cunha, M., & Honrado, J. P. (2021). A Framework for Multi-Dimensional Assessment of Wildfire Disturbance Severity from Remotely Sensed Ecosystem Functioning Attributes. *Remote Sensing*, *13*(4), 780. https://doi.org/10.3390/rs13040780

Marcos, E., Fernández-García, V., Fernández-Manso, A., Quintano, C., Valbuena, L., Tárrega, R., Luis-Calabuig, E., & Calvo, L. (2018). Evaluation of Composite Burn Index and Land Surface Temperature for Assessing Soil Burn Severity in Mediterranean Fire-Prone Pine Ecosystems. *Forests*, *9*(8), 494. https://doi.org/10.3390/f9080494

Mildrexler, D. J., Zhao, M., & Running, S. W. (2009). Testing a MODIS Global Disturbance Index across North America. *Remote Sensing of Environment*, *113*(10), 2103–2117. https://doi.org/10.1016/j.rse.2009.05.016

Moreira, F., Ascoli, D., Safford, H., Adams, M. A., Moreno, J. M., Pereira, J. M. C. C., Catry, F. X., Armesto, J., Bond, W., González, M. E., Curt, T., Koutsias, N., McCaw, L., Price, O., Pausas, J. G., Rigolot, E., Stephens, S., Tavsanoglu, C., Vallejo, V. R., … Fernandes, P. M. (2020). Wildfire management in

Mediterranean-type regions: paradigm change needed. *Environmental Research Letters*, *15*(1), 011001. https://doi.org/10.1088/1748-9326/ab541e

Nunes, L. J. R., Raposo, M. A. M., Meireles, C. I. R., Pinto Gomes, C. J., & Ribeiro, N. M. C. A. (2020). Fire as a Selection Agent for the Dissemination of Invasive Species: Case Study on the Evolution of Forest Coverage. *Environments*, *7*(8), 57. https://doi.org/10.3390/environments7080057

Parks, S. A., Holsinger, L. M., Koontz, M. J., Collins, L., Whitman, E., Parisien, M.-A., Loehman, R. A., Barnes, J. L., Bourdon, J.-F., Boucher, J., Boucher, Y., Caprio, A. C., Collingwood, A., Hall, R. J., Park, J., Saperstein, L. B., Smetanka, C., Smith, R. J., & Soverel, N. (2019). Giving Ecological Meaning to Satellite-Derived Fire Severity Metrics across North American Forests. *Remote Sensing*, *11*(14), 1735. https://doi.org/10.3390/rs11141735

Petropoulos, G., Carlson, T. N., Wooster, M. J., & Islam, S. (2009). A review of Ts/VI remote sensing based methods for the retrieval of land surface energy fluxes and soil surface moisture. *Progress in Physical Geography*, *33*(2), 224–250. https://doi.org/10.1177/0309133309338997

Quintano, C., Fernández-Manso, A., Calvo, L., Marcos, E., & Valbuena, L. (2015). Land surface temperature as potential indicator of burn severity in forest Mediterranean ecosystems. *International Journal of Applied Earth Observation and Geoinformation*, *36*, 1–12. https://doi.org/10.1016/j.jag.2014.10.015

Quintano, C., Fernandez-Manso, A., Marcos, E., & Calvo, L. (2019). Burn Severity and Post-Fire Land Surface Albedo Relationship in Mediterranean Forest Ecosystems. *Remote Sensing*, *11*(19), 2309. https://doi.org/10.3390/rs11192309

R Core Team. (2019). *R: A Language and Environment for Statistical Computing version 3.5.1* (3.5.1). R Foundation for Statistical Computing. https://www.r-project.org/

Ramanathan, V., & Carmichael, G. (2008). Global and regional climate changes due to black carbon. *Nature Geoscience*, *1*(4), 221–227. https://doi.org/10.1038/ngeo156

Saha, M. V., D'Odorico, P., & Scanlon, T. M. (2017). Albedo changes after fire as an explanation of fire-induced rainfall suppression. *Geophysical Research Letters*, *44*(8), 3916–3923. https://doi.org/10.1002/2017GL073623

Saha, M. V., D'Odorico, P., & Scanlon, T. M. (2019). Kalahari Wildfires Drive Continental Post-Fire Brightening in Sub-Saharan Africa. *Remote Sensing*, *11*(9), 1090. https://doi.org/10.3390/rs11091090

San-Miguel-Ayanz, J., Moreno, J. M., & Camia, A. (2013). Analysis of large fires in European Mediterranean landscapes: Lessons learned and perspectives. *Forest Ecology and Management*, *294*, 11–22. https://doi.org/10.1016/j.foreco.2012.10.050

Scheffer, M., Carpenter, S. R., Dakos, V., & van Nes, E. H. (2015). Generic Indicators of Ecological Resilience: Inferring the Chance of a Critical Transition. *Annual Review of Ecology, Evolution, and Systematics*, *46*(1), 145–167. https://doi.org/10.1146/annurev-ecolsys-112414-054242

Scheffer, M., Carpenter, S. R., Lenton, T. M., Bascompte, J., Brock, W., Dakos, V., van de Koppel, J., van de Leemput, I. A., Levin, S. A., van Nes, E. H., Pascual, M., & Vandermeer, J. (2012). Anticipating Critical Transitions. *Science*, *338*(6105), 344–348. https://doi.org/10.1126/science.1225244

Senf, C., & Seidl, R. (2020). Mapping the forest disturbance regimes of Europe. *Nature Sustainability*, *4*(1). https://doi.org/10.1038/s41893-020-00609-y

Silva, J. S., Vaz, P., Moreira, F., Catry, F., & Rego, F. C. (2011). Wildfires as a major driver of landscape dynamics in three fire-prone areas of Portugal. *Landscape and Urban Planning*, *101*(4), 349–358. https://doi.org/10.1016/j.landurbplan.2011.03.001

Smith, A. M. S. S., Kolden, C. A., Tinkham, W. T., Talhelm, A. F., Marshall, J. D., Hudak, A. T., Boschetti, L., Falkowski, M. J., Greenberg, J. A., Anderson, J. W., Kliskey, A., Alessa, L., Keefe, R. F., & Gosz, J. R. (2014). Remote sensing the vulnerability of vegetation in natural terrestrial ecosystems. *Remote Sensing of Environment*, *154*, 322–337. https://doi.org/10.1016/j.rse.2014.03.038

Szpakowski, D. M., & Jensen, J. L. R. (2019). A Review of the Applications of Remote Sensing in Fire Ecology. *Remote Sensing*, *11*(22), 2638. https://doi.org/10.3390/rs11222638

Tedim, F., Remelgado, R., Borges, C., Carvalho, S., & Martins, J. (2013). Exploring the occurrence of mega-fires in Portugal. *Forest Ecology and Management*, *294*, 86–96. https://doi.org/10.1016/j.foreco.2012.07.031

van Leeuwen, W. J. D., Casady, G. M., Neary, D. G., Bautista, S., Alloza, J. A., Carmel, Y., Wittenberg, L., Malkinson, D., & Orr, B. J. (2010). Monitoring post-wildfire vegetation response with remotely sensed time-series data in Spain, USA and Israel. *International Journal of Wildland Fire*, *19*(1), 75. https://doi.org/10.1071/WF08078

Veraverbeke, S., Gitas, I., Katagis, T., Polychronaki, A., Somers, B., & Goossens, R. (2012). Assessing post-fire vegetation recovery using red–near infrared vegetation indices: Accounting for background and vegetation variability. *ISPRS Journal of Photogrammetry and Remote Sensing*, *68*(1), 28–39. https://doi.org/10.1016/j.isprsjprs.2011.12.007

Vermote, E. (2015). MOD09A1 MODIS/Terra Surface Reflectance 8-Day L3 Global 500m SIN Grid V006. In *NASA EOSDIS Land Processes DAAC.* https://doi.org/10.5067/MODIS/MOD09A1.006

Viana-Soto, A., Aguado, I., Salas, J., & García, M. (2020). Identifying post-fire recovery trajectories and driving factors using landsat time series in fire-prone mediterranean pine forests. *Remote Sensing*, *12*(9), 1499. https://doi.org/10.3390/RS12091499

Villarreal, S., Guevara, M., Alcaraz-Segura, D., Brunsell, N. A., Hayes, D., Loescher, H. W., & Vargas, R. (2018). Ecosystem functional diversity and the representativeness of environmental networks across the conterminous United States. *Agricultural and Forest Meteorology*, *262*, 423–433. https://doi.org/10.1016/j.agrformet.2018.07.016

Wan, Z., Zhang, Y., Zhang, Q., & Li, Z.-L. (2004). Quality assessment and validation of the MODIS global land surface temperature. *International Journal of Remote Sensing*, *25*(1), 261–274. https://doi.org/10.1080/0143116031000116417

Willis, K. J., Jeffers, E. S., & Tovar, C. (2018). What makes a terrestrial ecosystem resilient? *Science*, *359*(6379), 988–989. https://doi.org/10.1126/science.aar5439

A simplified physical propagation model for surface fires designed for an implementation into fire decision making tools

François Joseph Chatelon*[1]; Miguel G. Cruz[2]; Jacques-Henri Balbi[1]; Jean-Louis Rossi[1]; Jacky Fayad[1]; Dominique Morvan[3]; Thierry Marcelli[1]; Nicolas Frangieh[1]; Carmen Awad[1]

[1]UMR SPE 6134. University of Corsica, 20250 Corte, France, {chatelon_j, fayad_j, rossi_j, marcelli_t, Frangieh_n, awad_c}@univ-corse.fr
[2]CSIRO, GPO Box 1700, Canberra, ACT 2601, Australia, {miguel.cruz@csiro.au}
[3]Aix-Marseille Univ, CNRS, Centrale Marseille, M2P2, Marseille, France, {dominique.morvan@univ-amu.fr}

**Corresponding author*

Keywords

Balbi model; physical model; surface fires;

Abstract

Nowadays, the needs for decision making tools useful for people involved in firefighting and/or in landscape management becomes more and more crucial, especially with the dramatic increase of the fire dangerousness and fire severity. These tools have to be accurate enough and faster than real time. Up to now, simulators and other tools are mainly based on empirical or semi-empirical models but the lack of physics in their formulation is a major limitation. The Balbi model is a simplified physical propagation model for surface fires which explicitly depends on the topography, the wind velocity and several fuel characteristics. It is a set of algebraic equations built from usual physical conservation laws (mass, momentum etc.) with some strong assumptions. This work aims at providing a new version of the Balbi model in which the resolution of the rate of spread (ROS) does not need any iterative method any more. This simplification is helpful in implementing the equations set into a fire propagation simulator or a coupled fire-atmosphere simulator. It needs a complete change in the structure of the model and the predicted ROS was tested at the field scale against 179 shrubland fires (burnt in Australia, South Africa, Turkey, Portugal, Spain, New Zealand) and 178 Australian grassland fires with a very good agreement with the observed ROS. Two statistical tools are used to check this agreement (Normalized Mean Square Error, NMSE and Mean Absolute Percentage Error, MAPE) and the Fractional Bias (FB) aims at understanding when the model over-predicts or under-predicts the ROS. The proposed model is accurate and its model parameters are calibrated against a small training dataset which makes it fully predictive whatever the environmental and topographic conditions and the fuel bed characteristics. Its more simple structure allows it to be a good candidate for the heart of a simulation or land management decision making tool.

1. Introduction

Climate change is one of the reason that increases the number of severe wildfires or extreme fire events (European Science & Technology Advisory Group, 2020). The response found by the firefighters to this new type of high intensity fires has to be fast and reliable. Another response consists in shifting from suppression to prevention with efficient fuel mitigation policies or an increase of safety zones and fuel breaks for instance. In both cases, the use of decision making tools is crucial for people involved in firefighting and in landscape management.

The fire behaviour modelling has been considerably improved for the last fifty years. Three main approaches in fire modelling have been emphasized by several authors (Weber, 1991; Perry, 1998; Pastor *et al.* 2003; Sullivan 2009a,b,c): (1) empirical models, (2) semi-empirical models and (3) physical models.

Empirical models are very simple and usually defined thanks to a correlation between ROS and the main parameters influencing the propagation (wind speed, fuel moisture content, fuel height, etc.). They are constructed over a large set of experimental fires (Anderson *et al*. 2015 for instance). Semi-empirical models are based on very simple physics principles but they don't differentiate the heat transfer mechanisms. Because of their simplicity and quickness, both empirical and semi-empirical models were the best candidates to be

incorporated into fire simulators. For instance the semi-empirical Rothermel's model (Rothermel, 1972) is the core of the FARSITE simulator (Finney 1998) or of the coupled fire-atmosphere WRF-SFIRE simulator (Mandel *et al.* 2011). The main limitation of these models is the lack in the physics of the phenomenon and the high cost of the large campaign of experimental burnings.

Detailed physical models — e.g. Firestar 2D (Morvan *et al.* 2009) and 3D (Frangieh *et al.* 2018), Firetec (Linn and Cunningham, 2005), WFDS (Mell *et al.* 2007), are based on multiphase formulations which consists in solving the partial differential equations obtained from the gaseous and solid phases. The main interest of these models lies in improving the comprehension of the fire dynamics but because of their high computational cost, they can't be used to perform numerical simulations in real time situations.

Simplified physical models (Pagni and Peterson, 1973; Albini, 1985; Balbi *et al.* 2010) combines the advantages of the three previous categories. The Balbi model (Balbi *et al.* 2020; Chatelon *et al.* 2022) is a simplified physical propagation model for surface fires at the field scale. It consists in a set of non-linear algebraic equations depending on the triangle of fire (fuel, wind and slope) and built over three heat transfer mechanisms: (1) radiation from the flame base, (2) radiation from the free flame and (3) convection inside the vegetal stratum. The model parameters are calibrated upon a small training dataset of experimental fires found in the literature. The Balbi model is physics-based, fully predictive and faster than real time; it is then designed for an implementation in decision making tools for people involved in firefighting or in fire management.

This work deals with a change in the structure of the Balbi model in order to obtain a brand-new version which aims at simplifying the resolution method for an easier implementation. The predicted ROS is compared to the ROS measured in 179 shrubland fires and 178 grassland fires using some usual statistical tools: (1) Normalized Mean Square Error (NMSE) and Mean Absolute Percentage Error (MAPE) to measure the model's accuracy and (2) Fractional Bias (FB) to check if the observed ROS is overestimated or underestimated.

2. Changes in the structure of the Balbi model

The main equation of the Balbi model presented by Chatelon *et al.* (2022) concerns the calculation of the ROS as the sum of three components derived from: (1) the radiative heat flux from the free flame F1 (see fig.1) on the unburnt fuel (R_r), (2) the radiative heat flux from the flame base (R_b) and (3) the convective heat flux inside the vegetal stratum (R_c) which involves the flame F2. The main equation of the model is then the following:

$$R = R_b + R_c + R_r \tag{1}$$

All details and nomenclature can be found in (Chatelon *et al.* 2022).

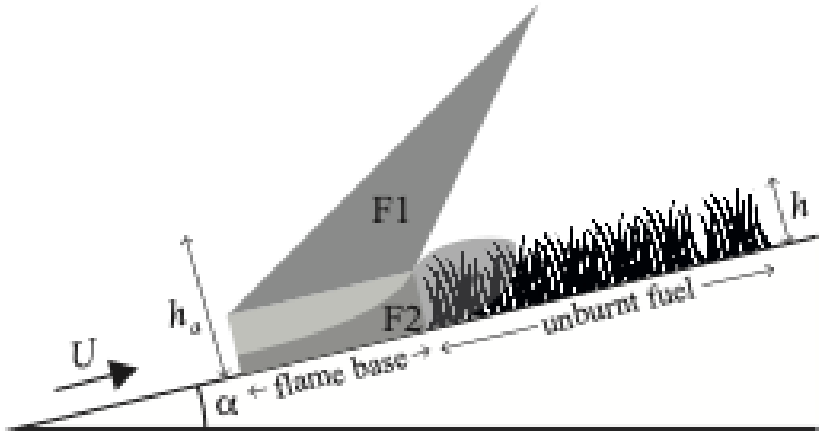

Figure 1- An idealized representation of the flaming zone combustion profile

Both terms R_c and R_r depend on the ROS R and thus, eq. 1 is an implicit algebraic equation that must be solved using an iterative method, which could be difficult to implement in fire simulators. In order to obtain an explicit equation, eq. 1 is changed by the following

$$R = \max(R_b\ ;\ R_c\ ;\ R_r) \tag{2}$$

The term R_b is defined thanks to a usual Stefan-Boltzman modelling that does not depend on the wind speed (Chatelon *et al*. 2022) and:

$$R_c = \frac{b\,U}{1+K\,b\,U} \tag{3}$$

$$R_r = s\,\frac{r_{00}}{u_0}\,(2A-1)(U - u_0\frac{A}{2A-1}) \tag{4}$$

Where *b* is a convective coefficient and *K* represents the drag forces law that are assumed to linearly depend on the total packing ratio. These coefficients (and R_b) mainly depend on fuel characteristics:

$$b = d\ \min\left(\frac{W}{W_0};1\right)\frac{\Delta H}{q\,\tau_0}\,s\sqrt{h} \tag{5}$$

$$K\ = 5\,\beta_t \tag{6}$$

The expressions of the radiative coefficient *A* and the upward gas velocity u_0 are the same as in (Chatelon *et al*. 2022).

The convective coefficient *b* depends on the fuel bed arrangement through the scaling factor *d*. Indeed, at the field scale two different type of fuel arrangement are considered: (1) isotropic (shrub species) and (2) vertical (grass). The expression of this scaling factor is the following:

$$d = d_0 * \begin{cases} 1\ (isotropic\ fuel) \\ 1+\frac{0.3}{h}\ (vertical\ fuel) \end{cases} \tag{7}$$

Finally, all the three components of the ROS (eq. 2) does not depend on the ROS anymore. So eq. 2 has become an algebraic explicit equation.

The value of the radiative coefficient *A* defines the fire regime expressed by eq. 2. Indeed two different regimes can be found:

(1) If $A < ½$, the component Rr (obtained from the free flame radiative heat flux) is a negative term and then:

$$R = \max(R_b\ ;\ R_c) \tag{8}$$

The fire turns into a radiative regime for weak wind values (when $U < U_{bc}$, see fig. 2) and into a convective regime otherwise.

(2) If $A > ½$, the radiation from the flame base is still the dominant heat transfer mechanism for weak wind speeds ($U < U_{bc}$, see fig. 2). Beyond the threshold wind speed U_{bc}, the convective effects are dominating up to a second threshold wind speed U_{cr}. For greater wind speed values, the role of the free flame radiation as heat transfer mechanism on the fire propagation highly increases.

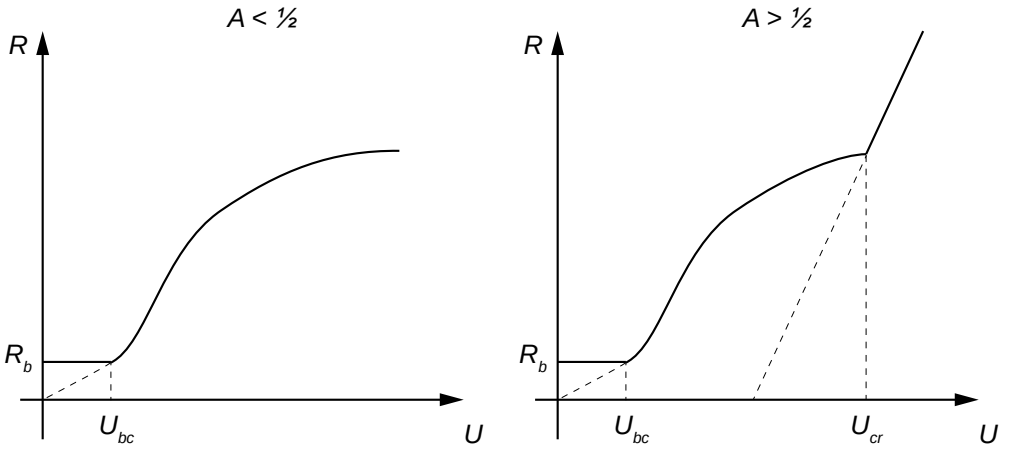

Figure 2- A qualitative representation of the two fire regimes exhibited by the proposed model.

The proposed model is composed of several equations for the calculation of the main physical characteristics of the fire front (flame tilt angle, flame height, flame length, upward gas velocity, flame temperature etc.) and the main equation for the ROS in combining all the previous equations:

$$R = \max\left(R_b\ ;\ \frac{b\ U}{1+K\ b\ U}\ ;\ s\ \frac{r_{00}}{u_0}\ (2A-1)(U-\ u_0\frac{A}{2A-1})\right) \quad (9)$$

As the proposed model is a strong simplification of the Balbi model presented by Chatelon *et al*. (2022), an increase in the overall deviations is expected considering that only the main heat transfer mechanism is taken into account.

The proposed model is fully predictive because its model parameters, especially d_0 (see eq. 7) is fitted once against a small set of experiments. Indeed, this coefficient was derived from the set of 25 fire experiments carried out by Bilgili and Saglam (2003) for shrubland fires and from a subset of 10 grassland fires (location: Ballarat) proposed by Cruz *et al*. (2018).

3. Numerical results and discussion

The proposed model is tested against a large set of fire experiments at the field scale. This set picked up in the literature is composed of 179 shrubland fires (Anderson *et al.* 2015; Bilgili and Saglam, 2003; Marsden-Smedley and Catchpole, 1995; van Wilgen *et al.* 1985) and 178 grassland fires (Cheney *et al.* 1998; Cruz *et al.* 2018) burnt in several regions of the world (Australia, New Zealand, Spain, Portugal, South Africa, Turkey). This set can be distinguished by a wide range of fuel characteristics and wind velocities. Some fires (van Wilgen *et al.* 1985) spread on sloped terrains.

The agreement between observed and predicted rate of spread is assessed using three statistical tools. Both Normalized Mean Square Error (NMSE) and Mean Absolute Percentage Error (MAPE) are useful for estimating the overall deviations and the Fractional Bias (FB) allows to understand if a model shows under-predictions or over-predictions. An ideal model is obtained for a zero NMSE, MAPE and FB.

The comparison between predicted and observed ROS against shrubland fires is presented in Fig. 3. The solid line and the dotted lines are the line of perfect agreement and the ±35% error threshold lines, respectively. As expected, the overall deviations (NMSE = 0.163) are barely higher than the value (NMSE = 0.132) found by Chatelon *et al.* (2022). This increase in the error is kept under control and is mainly due to the fires carried out in Australia where the radiation was found slightly higher than the convective effects. In this case, the NMSE changed from 0.213 (Chatelon *et al.* 2022) to 0.321 (see table 1). Moreover the relative error is equal to 35% which constitutes an acceptable error for ROS models (Cruz and Alexander, 2013). In spite of it, the proposed model provides high NMSE and MAPE for the Portugal fires group (see table 1). Although this fires group was used by Anderson *et al.* (2015) to build their empirical model, both the Anderson's model and the Balbi model (Chatelon *et al.* 2022) generated a poor agreement between predicted and observed ROS. So, it does not seem to be a specific limitation of the proposed model.

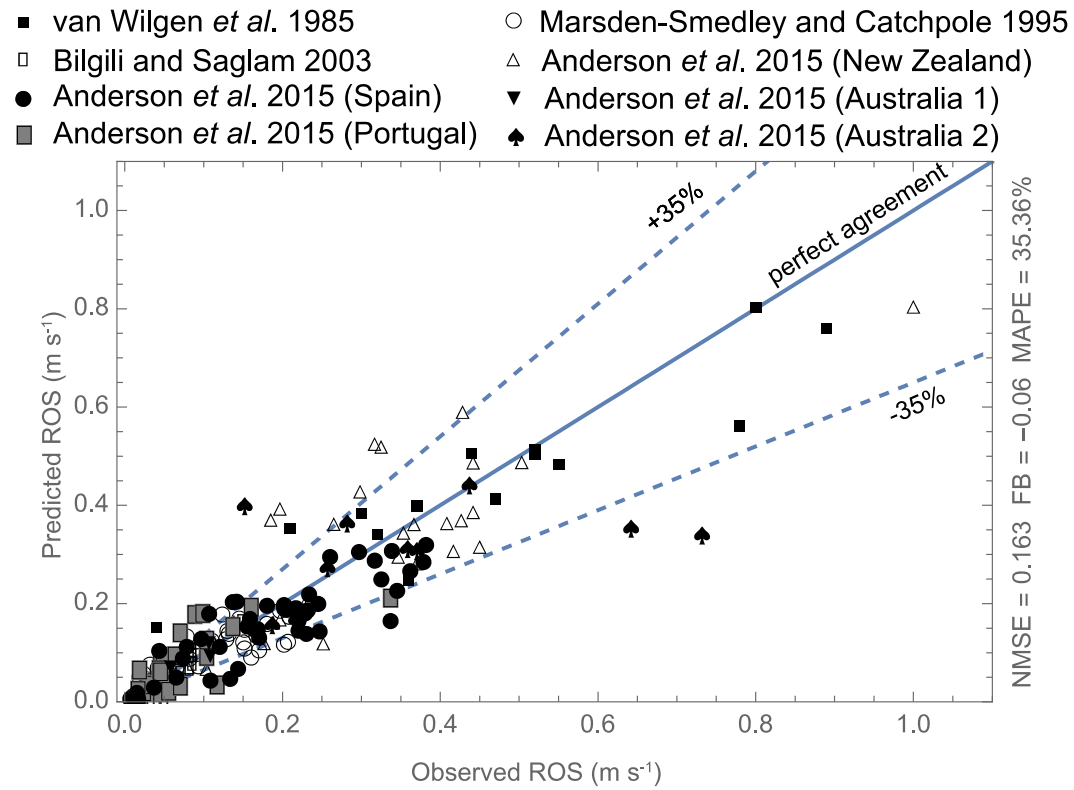

Figure 3- Comparison of predicted ROS vs ROS observed in the shrubland fires dataset.

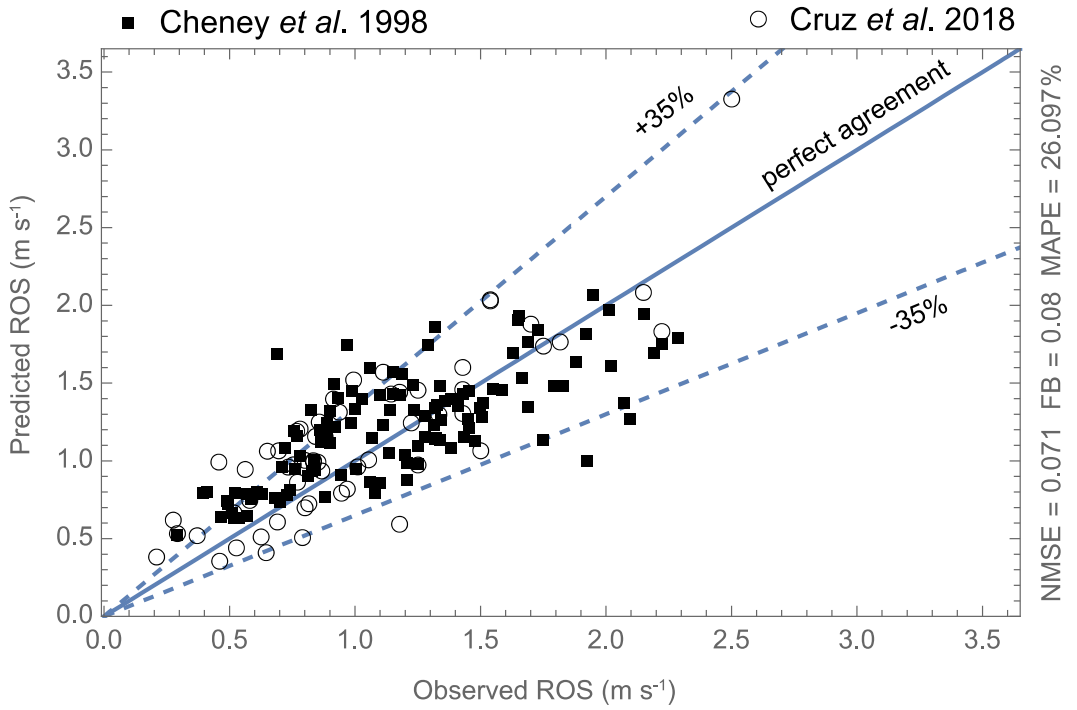

Figure 4- Comparison of predicted ROS vs ROS observed in the grassland fires dataset.

Fig. 4 shows the predicted ROS vs observed ROS in grassland fires. The numerical results provided by the proposed model are very good with small NMSE (0.071) and MAPE (26%). Note that contrary to the shrubland

fires group, the confrontation of the proposed model to grassland fires produces a slight overestimation of the ROS (FB = 0.08).

Table 1- Agreement between observed and predicted rate of spread estimated with three statistical tools (NMSE, Normalized Mean Square Error, MAPE, Mean Absolute Percentage Error and FB, Fractional Bias)

Fuel (location)	Reference	NMSE	MAPE	FB
Shrubs (South Africa)	Van Wilgen *et al.* 1985	0.045	35%	0.06
Shrubs (Turkey)	Bilgili and Saglam 2003	0.046	25%	0.11
Shrubs (Australia)	Marsden-Smedley and Catchpole 1995	0.123	37%	-0.03
Shrubs (New Zealand)	Anderson *et al.* 2015	0.109	29%	-0.02
Shrubs (Portugal)	Anderson *et al.* 2015	0.425	63%	-0.16
Shrubs (Spain)	Anderson *et al.* 2015	0.115	29%	-0.18
Shrubs (Australia)	Anderson *et al.* 2015	0.321	31%	-0.07
Shrubland fires		**0.163**	**35%**	**-0.06**
Grass	Cheney *et al.* 1998	0.068	24%	0.06
Grass	Cruz *et al.* 2018	0.079	30%	0.12
Grassland fires		**0.071**	**26%**	**0.08**

4. Conclusion

This work deals with a simplification of the simplified physical propagation model for surface fires called Balbi model in order to make its incorporation into decision making tools easier. In order to obtain an explicit formula for the ROS, several assumptions are made. The major assumption consists in considering only the main heat transfer mechanism as the mainspring of the propagation. Because of this simplification, the deviations provided by the proposed model are expected to be higher than the ones obtained by Chatelon *et al.* (2022). The numerical results against shrubland fires show a slight increase of the error which remains controlled. The predicted ROS against grassland fires is in a good agreement with the observed ROS. These good results and the characteristics of the proposed model (more simple, accurate, physics-based, fully predictive) confirm that the proposed model can be easily incorporated into decision making tools for operational people (firefighters, landscape managers etc.)

5. References

Albini FA (1985) A model for fire spread in wildland fuels by-radiation. Combustion Science and Technology 42, 229–258. doi:10.1080/ 00102208508960381

Anderson WR, Cruz MG, Fernandes PM, McCaw L, Vega JA, Bradstock RA, Fogarty L, Gould J, McCarthy G, Marsden-Smedley JB, Matthews S, Mattingley G, Pearce HG, Van Wilgen BW (2015) A generic, empirical-based model for predicting rate of fire spread in shrublands. International Journal of Wildland Fire 24, 443–460. doi:10.1071/ WF14130

Balbi J-H, Rossi J-L, Marcelli T, Chatelon F-J (2010) Physical modeling of surface fire under nonparallel wind and slope conditions. Combustion Science and Technology 182, 922–939. doi:10.1080/ 00102200903485178

Balbi JH, Chatelon FJ, Morvan D, Rossi JL, Marcelli T, Morandini F (2020) A convective–radiative propagation model for wildland fires. International Journal of Wildland Fire 29, 723–738. doi:10.1071/ WF19103

Bilgili E, Saglam B (2003) Fire behavior in maquis fuels in Turkey. Forest Ecology and Management 184, 201–207. doi:10.1016/S0378- 1127(03)00208-1

Chatelon, F.-J., Balbi, J.-H., Cruz, M.G., Morvan D., Rossi J.L., Awad C., Frangieh N., Fayad J., Marcelli T. (2022) Extension of the Balbi fire spread model to include the field scale conditions of shrubland fires, International Journal of Wildland Fire, 31(2), 176-192, http://dx.doi.org/10.1071/WF21082.

Cheney N.P., Gould J.S., Catchpole W.R. (1998) Prediction of Fire Spread in Grasslands, International Journal of Wildland Fire, 8(1), 1-13.

Cruz M.G., Alexander M. (2013) Uncertainty associated with model predictions of surface and crown fire rates of spread, Environmental Modelling & Software, 47, 16-28. Doi:10.1016/j.envsoft.2013.04.004.

Cruz M.G., Sullivan A.L., Gould J.S., Hurley R.J., Plucinski M.P. (2018) Got to burn to learn: the effect of fuel load on grassland fire behaviour and its management implications, International Journal of Wildland Fires, 27, 727-741, doi: 10.1071/WF18082.

European Science & Technology Advisory Group (2020) Evolving risk of wildfires in Europe – the changing nature of wildfire risk calls for a shift in policy focus from suppression to prevention. Brussels, Belgium. https:// www.undrr.org/publication/evolving-risk-wildfires-europe-thematic- paper-european-science-technology-advisory.

Finney MA (1998) FARSITE: fire area simulator – model development and evaluation. doi:10.2737/RMRS-RP-4.

Frangieh N, Morvan D, Meradji S, Accary G, Bessonov O (2018) Numerical simulation of grassland fires behavior using an implicit physical multiphase model. Fire Safety Journal 102, 37–47. doi:10.1016/J.FIRESAF.2018.06.004

Linn RR, Cunningham P (2005) Numerical simulations of grass fires using a coupled atmosphere–fire model: basic fire behavior and dependence on wind speed. Journal of Geophysical Research, D, Atmospheres 110, D13107. doi:10.1029/2004JD005597

Mandel J, Beezley JD, Kochanski AK (2011) Coupled atmosphere–wild- land fire modeling with WRF 3.3 and SFIRE 2011. Geoscientific Model Development 4, 591–610. doi:10.5194/GMD-4-591-2011

Marsden-Smedley J.B., Catchpole W.R. (1995) Fire behaviour modelling in Tasmanian buttongrass moorlands II. Fire behaviour, International Journal of Wildland Fire, 5(4), pp 215-228. Doi:10.1071/WF9950215

Mell W, Jenkins MA, Gould J, Cheney P (2007) A physics-based approach to modelling grassland fires. International Journal of Wildland Fire 16, 1–22. doi:10.1071/WF06002

Morvan D, Meradji S, Accary G (2009) Physical modelling of fire spread in grasslands. Fire Safety Journal 44, 50–61. doi:10.1016/J.FIRESAF. 2008.03.004

Pagni PJ, Peterson TG (1973) Flame spread through porous fuels. Sympo- sium (International) on Combustion 14, 1099–1107. doi:10.1016/ S0082-0784(73)80099-2

Pastor E, Zarate L, Planas E, Arnaldos J (2003) Mathematical models and calculation systems for the study of wildland fire behaviour. Progress in Energy and Combustion Science 29, 139–153. doi:10.1016/S0360-1285(03)00017-0

Perry GLW (1998) Current approaches to modelling the spread of wildland fire: a review. Progress in Physical Geography 22, 222–245. doi:10.1177/030913339802200204

Rothermel RC (1972) A mathematical model for predicting fire spread in wildland fuels. USDA Forest Service, Research Paper INT-115, Inter- mountain Forest and Range Experiment Station, Ogden, UT, USA. http://www.snap.uaf.edu/webshared/JenNorthway/AKFireModeling-Workshop/AKFireModelingWkshp/FSPro Analysis Guide Refer- ences/Rothermel 1972 INT-115.pdf.

Sullivan AL (2009a) Wildland surface fire spread modelling, 1990–2007. 1: Physical and quasi-physical models. International Journal of Wildland Fire 18, 349–368. doi:10.1071/WF06143

Sullivan AL (2009b) Wildland surface fire spread modelling, 1990–2007. 2: Empirical and quasi-empirical models. International Journal of Wild- land Fire 18, 369–386. doi:10.1071/WF06142

Sullivan AL (2009c) Wildland surface fire spread modelling, 1990–2007. 3: Simulation and mathematical analogue models. International Journal of Wildland Fire 18, 387–403. doi:10.1071/WF06144

van Wilgen BW, Le Maitre DC, Kruger FJ (1985) Fire behaviour in South African fynbos (macchia) vegetation and predictions from Rothermel's fire model. Journal of Applied Ecology 22, 207–216. doi:10.2307/2403338

Weber RO (1991) Modelling fire spread through fuel beds. Progress in Energy and Combustion Science 17, 67–82. doi:10.1016/0360- 1285(91)90003-6

A study on the 3D Unreal Engine visualization technology of WFDS Plot3Ddata for the development of a virtual forest fire training simulator

Donghyun Kim*[1,2]; Hyunggyen, Choi[3]

[1]*Jeonju University, Jeonju-si Jeonbuk-do, Rep. of Korea, {72donghyunkim@jj.ac.kr}*
[2] *IIASA(International Institute for Applied Systems Analysis). Laxenburg, Austria, {dhkim@iiasa.ac.at}*
[3]*Naviworks, Anyang-si, Rep. of Korea, {hyungkyun.choi@naviworks.com}*

**Corresponding author*

Keywords

VR (Virtual Reality), 3D Visualization, Unreal Engine, WFDS, Virtual Training

Abstract

The expression of flames and smoke in the existing VR engine is an image-based fake flame and smoke that does not have a physics analysis process. In this study, after converting the operation data analyzed in the wildland-urban interface fire dynamics simulator (WFDS) into an FGA file containing vectors and physical quantities at intervals of N seconds, the 3D Unreal engine developed an expression technology for values and vectors movement for smoke and heat. In addition, a visualization program was developed for the movement of flames and smoke according to wind speed and direction in the Unreal engine using a physics analysis model. As a result, the grid data values of the SMV and the UE virtual reality engine showed a 100% coincidence rate, and the visual difference between heat and smoke showed similarity through contrast ratio and lighting effect. The fire visualization expression of the 3D object value of combustibles according to the reduction in mass due to combustion was expressed by automatically updating the 3D object combustible material per unit time through material rendering for each combustion stage.

1. Introduction

The deaths and injuries of firefighters due to forest fires occur continuously around the world every year. In order to effectively suppress forest fires and prevent safety accidents for firefighters, forest fire-related organizations are operating forest fire education programs. Due to the nature of wildfires, firefighters must improve their ability to respond to each forest fire situation for effective suppression at the fire site based on their knowledge of the forest fire environment. However, there are many differences from the actual forest fire suppression environment in theoretical learning and training on the nature of wildfires on a laboratory scale. Recently, building fire education and training simulators using 3D virtual reality technology and game-type forest fire suppression training programs are being developed. Here, the expression of flame and smoke, which are the main components of fire, is used by a training instructor to create each fire situation by adding a simple image as a fire icon. This does not apply chemical species and physical analysis. Therefore, this study proposes to develop a 3D virtual reality education and training authoring tool based on chemical species and physics analysis for more realistic forest fire field experience and effective education by firefighters. This study proposes a technology and method to visualize forest fire flames and smoke through physical analysis in 3D virtual reality UE using the temperature and smoke results analyzed in WFDS.

2. Methods

2.1. WFDS analysis

WFDS was developed to analyze fire spread in open spaces adjacent to forests by applying topography and vegetation fuel by extending FDS developed for structural fire analysis. In this study, the X-axis, Y-axis, and Z-axis were set to 200 m, 160 m, and 50 m, respectively, and the cell spacing was set to 2 m, resulting in a total of 200,000 cells were configured as 100 cells on the X-axis, 80 cells on the Y-axis, and 25 cells on the Z-axis.

For forest fuel, a combustion material, combustion properties were applied to Pinus densiflora with an average height of 17 m and 400 trees/ha, and Cone type was applied for the grid configuration.

2.2. Visualization of VR contents forest fires spread simulation

Result values analyzed with WFDS are stored as Plot3Ddata files, velocity vectors, and physical quantities for fire analysis, and then extracted as vector files FGA files with a cycle of N(3~5) seconds so that they can be imported into 3D Unreal Engine. The FGA file contains data values of vectors and physical quantities in the analysis result. FGA file imported from 3D UE is created as a vector field, and Boundary values such as position, rotation, stile, intensity, and tightness are set. With the generated vector field, the particles are completed by applying the fire and smoke effect used in VR 3D contents. For visualization of forest fire diffusion and forest fuel combustion, first, for visualization of flames and smoke, FGA temperature and smoke (CO, CO_2) concentration data are expressed through particle contrast and lighting effect functions. Second, image change due to forest fuel combustion used the Mesh Decal function as a visualization method with image values created according to the mass reduction rate. Mesh Decal uses the mixed function of semi-transparent Blend Mode and Deffered Decal by updating GBuffer and DBuffer after rendering 3D object surface geometry. In addition, it was configured so that external results such as changes in heat flow of each grid value, wind speed, and wind direction in the UE can be reflected in the impact effect. This is useful for expressing the movement and concentration of smoke in each grid cell differently.

3. Study Results

As a result of expressing the file extracted from the WFDS analysis result as an FGA file with the Unreal Engine, the vector and physical quantity data values such as heat and smoke of each 200,000 grid cells expressed 100% the same value without error even with time series changes. For the visualization of the flame temperature and smoke values for the grid cell, the color and smoke concentration of the flame were adjusted and expressed through the particle contrast and lighting effect on the grid. The results are shown in Figures 1 and 2. The accuracy of the visualization image for the flame intensity and smoke concentration was implemented so that it could be adjusted through the particle lighting function.


Flame #1


Flame #2


Flame #3


Flame #4


Flame #5

Figure 1- Forest fire flame visualization image results in 3D UE

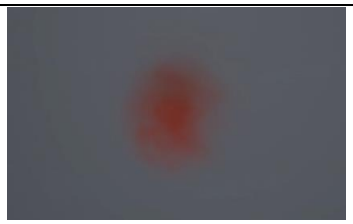
Smoke #1


Smoke #2

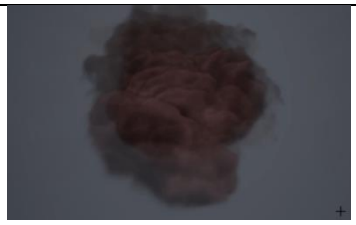
Smoke #3

Figure 2- Forest fire smoke visualization image results in 3D UE

In addition, for the image change according to combustion of the 3D combustion material object data, the Mesh Deca technique was applied to create a material image, and then a method was used to replace the image by mass reduction rate. Figure 3 is a screen visualized in 3D UE according to flame temperature, smoke, and combustion of trees.


Visualization scale 1


Visualization scale 2


Visualization scale 3

Figure 3- Forest fire visualization image results to flame temperature, smoke, trees in 3D UE

Figure 4 shows the simulation results of forest fire spread in Unreal 3D engine using the forest fire diffusion formula of Alexandridis, Alex, et al. There were 2400 grids used for the terrain, and the prediction of wildfire volcanoes was expressed by applying the following conditions to each variable value such as wind, inclination, ambient temperature, and type of fuel material.

- Wind speed: 4.6 m/s

- Wind direction: southwest wind

- Temperature: 32 ℃, FMC (Fuel Moisture Contents): 6.3 %

- Cell size: 5cm²

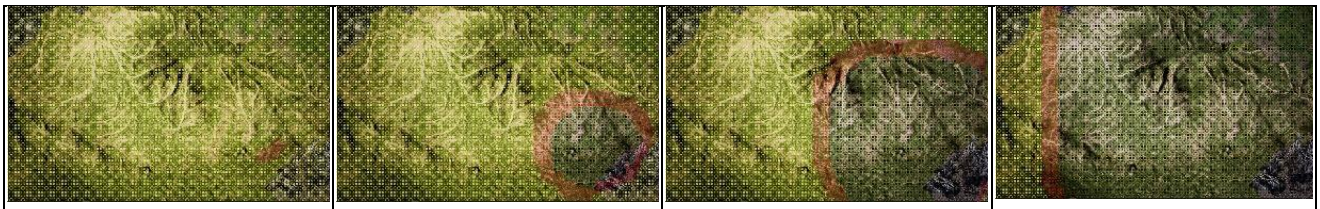
Fire break | after 30 sec. | after 60 sec. | after 120 sec

Figure 4- Result of forest fire spread analysis using Unreal 3D engine

4. Conclusions

As a result of this study on the visualization program of VR UE for virtual reality forest fire training, the following conclusions were obtained.

First, the SMV data and the UE visualization program grid value showed 100% agreement with respect to temperature and smoke, which are the calculation results of WFDS.

Second, in the comparison of the displayed images of flame and smoke concentration, there was a difference in visual brightness and contrast.

Third, the difference in the visual effect was developed to be similar to the SMV visualization data by adjusting the color and smoke concentration of the flame through each particle contrast and lighting effect of the 3D UE.

Fourth, through this study, a methodology for visualizing the accuracy of the properties of forest fires for realistic experience among various element technologies of forest fire education and training contents using virtual reality was presented. However, in this study, visualization studies that reflected real-time changing weather conditions were not yet reflected in the study.

In the future, if the development of fire training contents in virtual space, including the development of educational and training evaluation scenarios, along with the results of this research, is made, it will be a more useful and safe learning tool for forest fire extinguishers.

A study on the standard scenario and training evaluation system for the development of virtual forest firefighters training system

Donghyun Kim

Jeonju University, Jeonju-si Jeonbuk-do, Rep. of Korea, {72donghyunkim@jj.ac.kr}
IIASA(International Institute for Applied Systems Analysis). Laxenburg, Austria, {dhkim@iiasa.ac.at}

Keywords

VR (Virtual Reality), Forest Firefighters, Virtual Training, Training Scenario, Training Evaluation

Abstract

This study relates to the establishment of a virtual reality training system that can reproduce various forest fire situations in a limited indoor space and evaluate the training results quantitatively for fire suppression and evacuation situations of forest fire extinguishers. For individual and team training of firefighters in a virtual space, it is necessary to create SOP-based various forest fire scenario scenarios and training evaluation tools for the development of virtual training contents S/W. In this study, first, a method for creating a standard scenario for virtual reality forest fire extinguishing training was presented and a standard scenario was presented. Scenarios were standardized to be prepared according to 4 types of forest fire environmental data, 4 types of firefighting environmental data, and training difficulty level. Forest fire environmental data was defined as 4 types of forest fire site spatial environment, forest fuel environment, meteorological environment, and fire environment. It was made possible to set the difficulty level of fire drills using 8 types of scenario configuration data. In the survey on the suitability of firefighters for the standard scenario content, it was found to be 95.8±2.5%. In the second scenario-based training competency evaluation tool, forest fire extinguisher CTA (Cognitive Task Analysis) job analysis was conducted to systemize the evaluation items for task performance, mutual cooperation and reporting system for each scenario staged event. Using the CTA model, job structure analysis was conducted on the professional characteristics, procedural skills, best mission performance, and cognitive process for maximizing the training effect of the firefighters. Based on this, a virtual training evaluation item and evaluation score table for each firefighter according to the scenario-based mission performance stage were prepared. In the evaluation of the suitability of the firefighters for each item's evaluation content and points, it was found to be 93.5±2.5% and 97.5±2.5%, respectively.

1. Introduction

In Korea, training of forest firefighters is generally conducted through theory and experiential learning. Theory learning is representative of the principles of forest fire, fire theory, forest fire spread, forestry and meteorology, command system and role, and case study. The experiential learning includes a program to strengthen individual field response capabilities such as how to use hand tools, how to read a map, and evacuation learning, and group training according to the division of roles for each team. Here, experiential learning has a disadvantage in that it is impossible to conduct firefighting training by actually generating a fire in a forest or outdoors. This study intends to establish a virtual reality experience forest fire extinguishing training system that can reproduce various forest fire situations in virtual reality in a limited physical indoor space and quantitatively evaluate the training results. It has been studied that the learning effect using virtual reality is 10 times higher than that of the theoretical lecture in general, and it is known that the training safety and economic feasibility are high. Therefore, this study intends to provide a basis for the production of virtual reality forest fire extinguishing training contents using the virtual reality standard scenario and training evaluation tool proposed through this study. First, an optimal standard scenario was developed by collecting the opinions of firefighters by creating a scenario necessary for virtual reality training by examining and analyzing past forest fire cases. Next, a tool was developed to evaluate the training process of each firefighter based on a scenario through job analysis of each member of the forest fire fighting team.

2. Methods

2.1. Standard scenario development

The virtual reality training system requires an SOPs-based standard training scenario that can be trained by experiencing rescue and evacuation along with the evolution in various forest fire situations in a virtual space.

In this study, in order to create a standard scenario for virtual reality fire training, events for each forest fire situation were defined in a total of four stages through past forest fire cases. Stage 1 (introduction stage: occurrence and growth of wildfires), stage 2 (deployment stage: establishment and implementation of an extinguishing strategy after arrival at the site), stage 3 (growth stage: types of damage caused by spread and accidents, evacuation and rescue request), the fourth stage (end stage: remained fire monitoring and suppression completed), and the worst-case wildfire scenario for the unpredictable dangerous event was written in the third stage.

The details of the standard scenario created by the entire four-step process were prepared by analyzing the time series work of the evolution firefighters. For the standard scenario prepared, more than 90% conformity was verified by surveying 300 forest fire firefighters.

2.2. Training evaluation tool

The evaluation tool for each individual team for virtual reality training based on standard scenario was performed through field work CTA job analysis of forest firefighters. As shown in Figure 1, for the job analysis procedure, procedural technical analysis according to the professional characteristics and firefighting work of the firefighters and the cognitive process structural analysis to maximize the best performance and efficiency are performed. For evaluation items and score distribution table, more than 90% conformity was verified by surveying 300 forest fire firefighters. The training evaluation table was divided into personal equipment, rescue/evacuation equipment, firefighting activity, and rescue/evacuation activity items according to the task of each team member, and detailed evaluation criteria and evaluation methods and weights were applied.

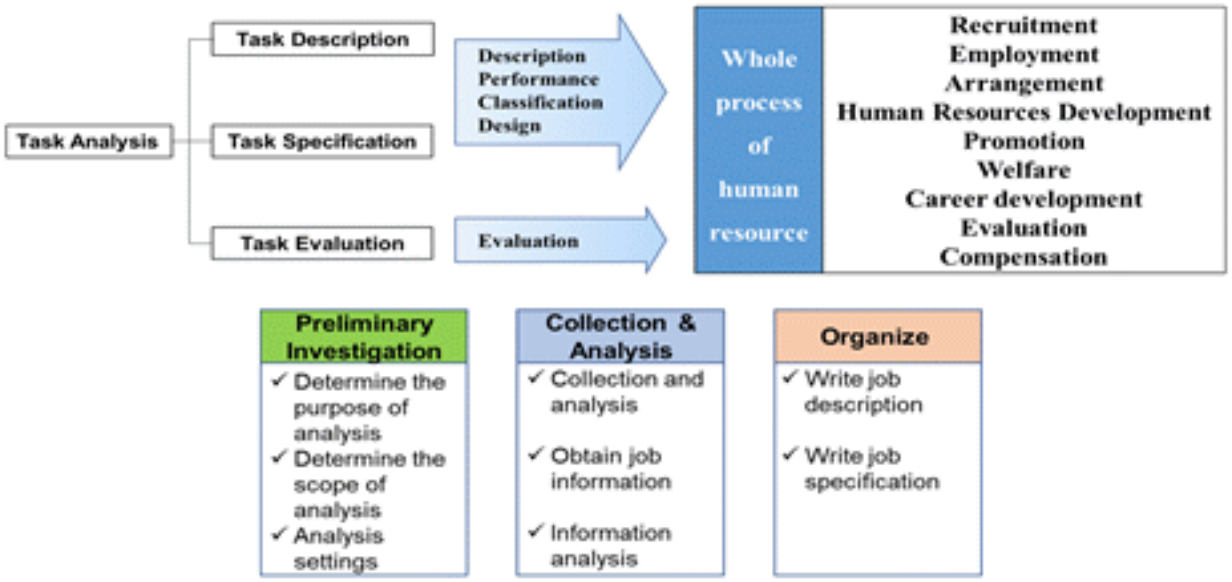

Figure 1- CTA job analysis flow chart and contents

3. Study Results

3.1. Standard scenario

Scenario composition is divided into 4 stages: introduction stage, development stage, growth stage, and termination stage according to the forest fire spread according to the time series. The details are shown in Figure 2.

■ Fire Scenario Composition

S#.	Event	Sub_S#	Contents	Pages
#1	Fire detection and reporting	1	Fire detection and reporting	3~4
#2	Report reception and response	1	Confirmation and Response Preparation	5~6
#3	Arrival at the fire site	1	On-site dispatch	7
#4	Check forest fire situation	5	Fire line, Head fire, Terrain, Weather, Fuels	8
#5	Establish strategy for fire fighting	5	Strategy depends on each fire situaction	8
#6	Start of firefighting work	5	Fire fighting work	9~10
#7	Fire spread growth	3	Crown fire, Spotting Fire, Rapidly fire spread	11~13
#8	Unexpected situation(Spotting, Rolling stone and wood etc.)	5	Observation and congnition, Decision making to work	13~15
#9	Use of fire extinguishing equipments		Proficiency in using the equipment	15~17
#10	Evacuation		Planning, Safety	18~19
#11	Build a fire break line	-	Proficiency in working	20~21
#12	Protected object protection activities		Check for success	22~23
#13	Report to the commander center		Compliance with communication procedures	24
#14	Remaining Embers Management and the end		Check the embers management process	25
Forest Fire Hazard Level 4/5 : Large scale fire spread and damage				

Figure 2- VR training scenario composition for forest firefighters

The scenario details were standardized to be prepared according to 4 types of forest fire environment data, 4 types of firefighting environment data, and training difficulty level. Forest fire environment data is defined as four types of forest fire site spatial environment, forest fuel environment, meteorological environment, and fire environment. It is possible to set the difficulty level of fire drills using a total of 8 types of scenario configuration data. In the survey of firefighters on the training evaluation tool, the suitability evaluation was found to be 95.8±2.5%.

3.2. Training evaluation tool

In this study, evaluation items were classified according to the tasks of each crew member for a team of 10 firefighters in each scenario stage, and the evaluation score was designed to be evaluated as a total score of 100 points through the majority evaluation. The format of the evaluation tool is shown in Figure 3.

Figure 3- Individual virtual reality forest firefighter training evaluation table

A total of 14 evaluation items for each scenario are as follows.

①Whether or not information on forest fire situation is collected and confirmed, ②Establishment and feasibility of firefighting strategy, ③Selection of location for firefighting work, ④Construction of fire line, ⑤Effect of ground firefighting work, ⑥Preparation and use of ground firefighting equipment, ⑦Sudden situation (Spotting fires, Fire Storm, Rolling Stone or wood etc) check and response, ⑧ Use of evacuation equipment, ⑨Secure an evacuation route and a safe place, ⑩Feasibility of evacuation judgment and method, ⑪Arrangement of remaining balance, ⑫Communication by team, ⑬ Report the situation to the command center and make an emergency request, ⑭Protection object protection.

In the survey of firefighters on the training evaluation tool, the suitability evaluation was found to be 97.5±2.5%.

4. Conclusions

The following conclusions were drawn as a result of the study on the scenario writing and training evaluation system, which are the main technologies for the development of the forest fire training system using virtual reality technology.

First, the scenario writing stage through forest fire case analysis was divided into 4 stages, and detailed contents were standardized to be prepared according to 4 types of forest fire environment data, 4 types of firefighting environment data, and training difficulty level.

Second, the evaluation of the suitability of the firefighters for the prepared standard scenario for the virtual forest fire training was found to be effective at 95.8±2.5%.

Third, the evaluation items for each scenario stage through CTA were defined as a total of 14 evaluation items, and a virtual training evaluation system was created with a total of 100 points by assigning different points for each evaluation item.

Fourth, the evaluation of the suitability of the distributed evolution team for the virtual training evaluation tool was found to be effective at 95.8±2.5%.

By using the results of this study on virtual reality scenarios and evaluation tools, virtual reality 3D content work is performed to contribute to the construction of an overall system for individual and team virtual training.

AI-driven Real-time Forecast of Wildfire Development in Hong Kong

Yizhou Li; Xinyan Huang*

Research Centre for Fire Safety Engineering, Department of Building Environment and Energy Engineering, The Hong Kong Polytechnic University, Hong Kong,

**Corresponding author*

Keywords

Fire Perimeters; Wildfire Forecast; TCNN; Smart Firefighting

Abstract

Climate changes have already altered the wildfire regime and increased the wildfire frequency and severity in Hong Kong. Hong Kong is a typical wildland-urban interface, where small high-population urban areas are surrounded by 70% wildland. Statistics show that the burning areas in over 80 % of accidents are less than 1,000 m2, and the burning time cannot last for 24 hours in Hong Kong. To improve the wildfire response and reduce the life and property loss in fires, a real-time fire forecast is required to achieve the most accurate and real-time fire forecast. This study firstly introduced the development of the wildfire spread models and then reviewed the AI-based model emphatically in the wildfire simulation and prediction. The blank parts in the short time series wildfire prediction aroused the attention of authors. Thus, an AI-based method was proposed to predict the wildfire front in real time. This study currently aims to establish the virtual wildfire scenario database in Hong Kong and realizes the AI-driven wildfire prediction model for suppressing fire spreading.

1. Introduction

Wildfire has been a long-existent phenomenon on Earth. It is an important natural process to consume the fuel accumulation in the wildland. The wildfire happens even without human behaviors interfering. However, with the expansion of human living space, urban cities are gradually occupying the wildlands where human behaviors have a great effect on wildfire, increasing the frequency of wildfires. Simultaneously, wildfire can negatively influence the residents who live in the wildland-urban interface (WUI) (Manzello, 2020). The wildfire is a global natural disaster that is concerned by many countries and regions (Fig. 1). Hong Kong is such a typical city full of wildland-urban interfaces (WUIs), as 70% of its land is covered by woodland, Shrubland, and wetland (Civil Engineering and Development Department Hong Kong, 2014; Warren-Rhodes & Koenig, 2001).Thus, Hong Kong cities are constantly threatened by wildfires. There have been more than 1,000 times wildfire accidents reported per year over the last 10 years, according to the data provided by Fire Service Department in Hong Kong (Hong Kong Fire Services Department - Access to Information, 2021). Thus, it is crucial to control the wildfire in time to prevent the hazard from causing huge damage to the city.

(a) California WUI wildfire in 2018 (b) Australia WUI wildfire in 2019 (c) Hong Kong WUI wildfire in 2019

Figure 1- Global wildfire accidents in (a) the USA, (b)Australia, and (c) Hong Kong, China.

After the occurrence of wildfire, grasping the spreading trends is always one of the most effective strategies in controlling the fire. Therefore, Scholars have been devoted to developing the wildfire spreading prediction tools in the last decades (Fig. 2). Overall, the trends are evolving from statistics-based models to physical-based models. The data acquired from the computation tools are no longer the static burning probability. Instead, the

information turns into the intuitive spreading perimeter to guide the fire scientists to locate the flame front based on mathematical physic-based models.

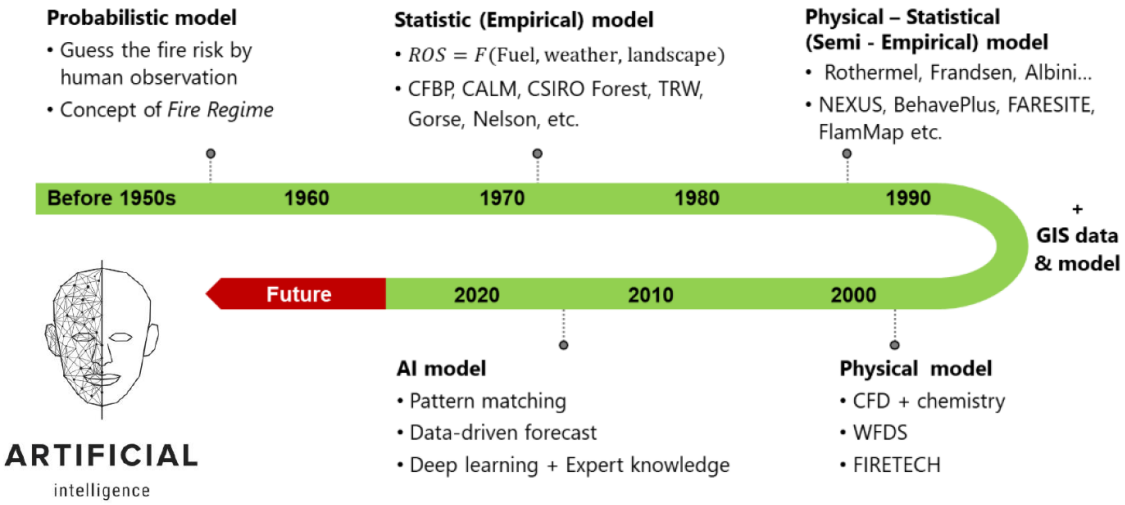

Figure 2- Computational tools for wildfires over the last several decades.

At first, the wildfire spreading models were merely based on static possibility until the empirical models were come up with to transform the likelihood into the statistic question before the 1990s. The turning point was that, according to the empirical models, Finney (1998) developed the FARSITE software to simulate the fire propagation, which was subversive work at that time to make the wildfire visualized in 1998. It combined the GIS data with the statistic data, rendering the prediction convincing. Since the 2000s, a number of numerical methods came out, such as HIGRAD/FIRETEC and Fire Dynamics Simulator (FDS). These numerical methods pay attention to the physical laws of combustion, which make the simulation exquisite but consume a huge amount of time and computation costs.

Gladly, the AI models were proposed to change the way researchers dealt with wildfire spreading. The physical-based computation can be switched into a data-driven matchup in the database. The AI-based models largely decrease the computation time and make real-time prediction possible. In 2019, Hodges (Hodges & Lattimer, 2019) firstly combined FARSITE software with AI algorithms. In his work, he successfully converted the physical-based numerical method into a phenomenological model, which cut the running time when ensuring the prediction accuracy. His job reflected the long-time series wildland fire and the output results were a fire spreading figure in 6 hours. His successful applications in California pave the way for the AI-based wildfire prediction globally.

However, according to the statistics, the burning areas in over 80 % of accidents are less than 1,000 m^2 and the burning time cannot last for 24 hours in Hong Kong. Nevertheless, the short time series real-time wildland fire spreading prediction and local database is blank. There is no current guidance for firefighters, warning them of the wildfire spreading trends. Therefore, it is urgent to make up this field of study in Hong Kong to reduce the danger of wildfire. The real-time wildfire prediction is the basis for the Hong Kong wildland digital twin, which can interact with the firefighters to ensure the city safety.

2. Dataset

FARSITE is widely used by the U.S. Forest Service as an effective tool for simulating the growth of natural fires in wilderness areas (Srivas et al., 2016). It requires an input set that contains different parameters before running the spreading prediction. Due to the lack of real-scenario wildfire data, all the wildfire scenarios are numerical generated by the software FARSITE. It is worth noting that the AI-based algorithm cannot distinguish the difference between numerical simulation results and real-scenario wildfire data, so the model cannot result in huge biases. It is feasible to validate the model in the temporary simulation data. The next action is to replace the original simulation data with real-scenario wildfire data step by step.

FASITE is a mainstream software used by American wildfire researchers. The related input database can be acquired from the Interagency Fuel Treatment Decision Support System (IFTDSS) website. However, it lacks the geography information in Asia. Therefore, it is important to pre-process the local geography parameters to make use of this software in Hong Kong. In this study, the Hong Kong Sunshine Island is chosen as the study area where it is an isolated island in Hong Kong with few species of vegetations. The pixel resolution is 5 m × 5 m, which is much finer than usual 30 m × 30 m.

At the early stage, the software FARSITE is used to add up the dataset. The parameters to be inputted into the software include five compulsory geography information, such as elevation, slope, aspect, fuel model, and canopy cover (Fig. 3). Three optional parameters are stand height, canopy base height, and canopy bulk density respectively to reflect the crown fire. These are the basic information for the wildfire simulation starting. After obtaining all the data, the ignition boundary should be decided. As for the ignition boundary, the ignition locations will start as a point, following the development of a short-time series wildfire. Then the fuel moisture, the temperature, the wind speed, the wind direction, the relative humidity, and cloud cover percentage are required to input, starting the wildfire spreading in the regulated burning periods.

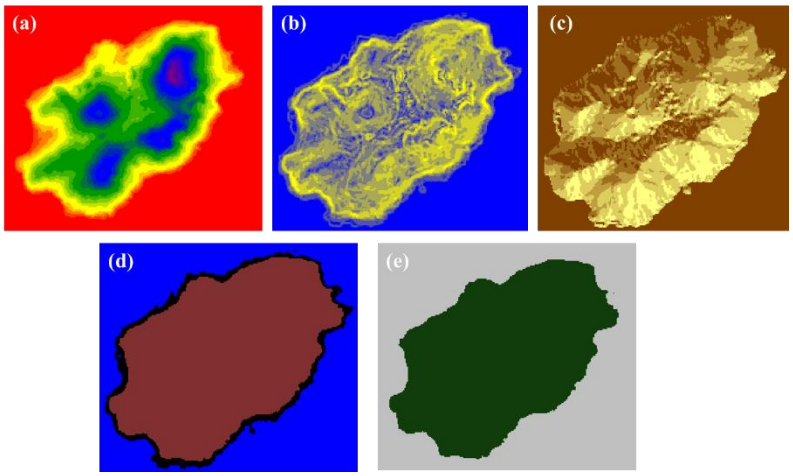

Figure 3- Geography information, (a) elevation, (b) slope, (c) aspect, (d) fuel model, and (e) canopy cover.

To ensure that the dataset has enough data and convincing results, the temperature, the wind speed, the wind direction, the relative humidity, and the cloud cover percentage are seen as five variances to control the simulation results. Because the research area is given and confirmed, while the five parameters in the geography model do not need to change. Likewise, the fuel moisture data is also calculated based on the automatic generation by the software. Once the ignition location is confirmed, the wildfire spreading will get into calculation according to the parameters which is set beforehand.

3. Methodology

3.1. Forward model for spreading simulation

The Rothermel and Albini spread models (Albini, 1985; Rothermel, 1972) were used to calculate the wildfire surface spread rate. In the model, $V_{s,\,peak}$ is calculated according to the following equations:

$$V_{s,peak} = \frac{Q''\zeta}{\rho\epsilon Q_{ig}}(1 + \phi_s + \phi_w) \tag{1}$$

where Q'' is the heat release rate per unit area, ρ is the fuel density, Q_{ig} is the heat of pre-ignition, ζ is the propagating flux ratio (percentage of heat released which pre-ignites fuel), ϵ is the effective heating number (percentage of fuel which is involved in ignition), ϕ_w is the wind coefficient, and ϕ_s is the slope coefficient (Hodges & Lattimer, 2019).

It is widely recognized that the Rothermel and Albini spread models can be applied to predict the wildfire spread perimeter in the peak spreading direction. Therefore, the combined model will be the basis of the spreading model to build the wildfire scenario dataset.

3.2. Forward model for AI-based prediction

The total flow chart of this paper is proposed in Fig. 4. The core of this study is to turn the mathematical spread model into an AI-based algorithm model. The huge difference is that the wildfire front prediction is no longer based on the physical laws proposed by the previous researchers. Instead, the model will find the inner connection among the input parameters to describe the wildfire fronts.

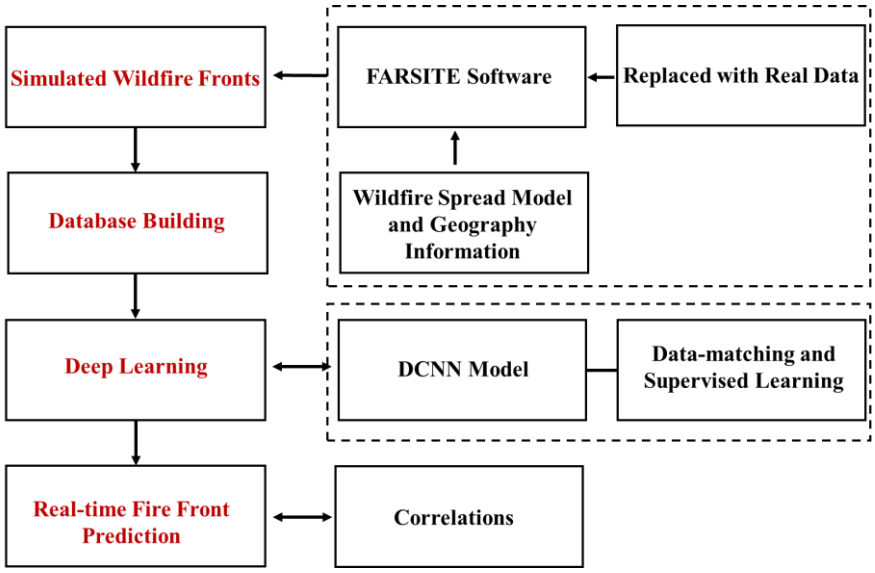

Figure 4- Flow Chart for the AI-based prediction

In order to reasonably find the connection of spreading trends in geo-information, this paper will use Deep Convolutional Neural Network (DCNN) as the basis to build the above-mentioned AI algorithm. The DCNN method (Krizhevsky et al., 2012)consists of many neural network layers. Two different types of layers, convolutional and pooling, are typically alternated. The depth of each filter increases from left to right in the network. The last stage is typically made of one or more fully connected layers (Fig. 5):

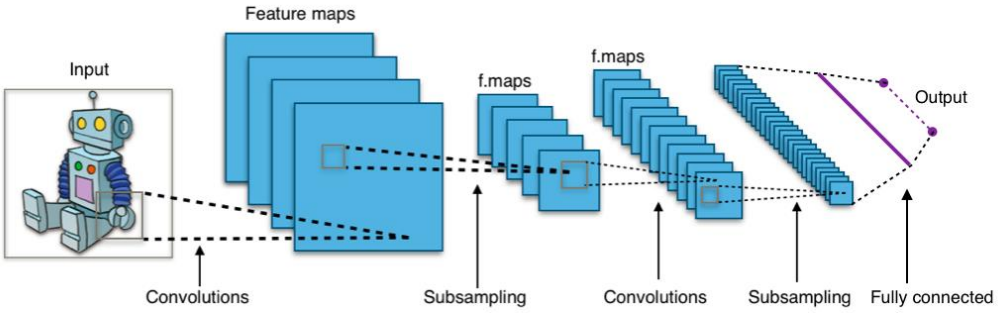

Figure 5- DCNN visualization (Deep Convolutional Neural Network — DCNN | Deep Learning with Keras, n.d.).

The local features of small sub-regions in the images which contain geography information are extracted by neurons, and then the information of these features can be fused into the subsequent processing stage to detect more advanced features such as the probability of fire or spreading trends. Compared with the visual tasks (target detection, classification, segmentation, and motion tracking) in computer vision that involve images with only three color channels as input, the input involved in this paper is more complicated: in addition to basic geographic information, it needs to be added the factors affecting combustion, such as elevation, slope, fuel model, etc. Therefore, the use of mature computer vision DCNN is higher computational cost and poorly robust. For this reason, we have proposed two feasible improvement methods.

First, use a smaller but sparse perception field. In the first layer of DCNN, each convolution kernel is used to connect sub-regions of the picture, and the size of the sub-region is called windows or perceptual field. Traditional visual tasks use overlapping windows to ensure that the convolution kernel can obtain global information. Compared with the computer vision dataset which includes Strenuous sway and changes, the merge of input images has three characteristics: fixed; the field affected by wildfire is limited; the information density of the unified field is large. Therefore, smaller windows can only use the information needed for DCNN learning to associate high-level features. The sparse perception field is to trade off the accuracy and computational cost. As the perception field becomes sparser, the number of convolution kernels that need to be learned will be less, and the weight parameters that need to be updated can usually be reduced exponentially. Although it will bring a loss of accuracy, it is worthwhile for spreading trends tasks that do not require pixel-level accuracy.

Second, partial pooling is performed. The pooling layer in DCNN is used to filter the repetitive and redundant information brought by the convolutional layer. In the images, the information density of the same area under different channels is different. If the same pooling strategy is used for all channels, some of the information in the high-density channel will be lost, while the information of the low-density channel will be retained. Therefore, the DCNN performs small-size pooling on high-density channels (Elevation, Slope, Aspect, Fuel Model, and canopy cover), and large-size pooling on low-density channels (temperature, relative humidity, wind speed, wind direction, and cloud cover).

Besides, the model can be correlated with the updated parameters to realize the data assimilation to some extent. It gets rid of the traditional frameworks that the data cannot be changed during the simulation. In summary, it can be a good reference in the wildfire front prediction in the short-time series wildfire, combined with traditional spread model and geography information using a deep learning method.

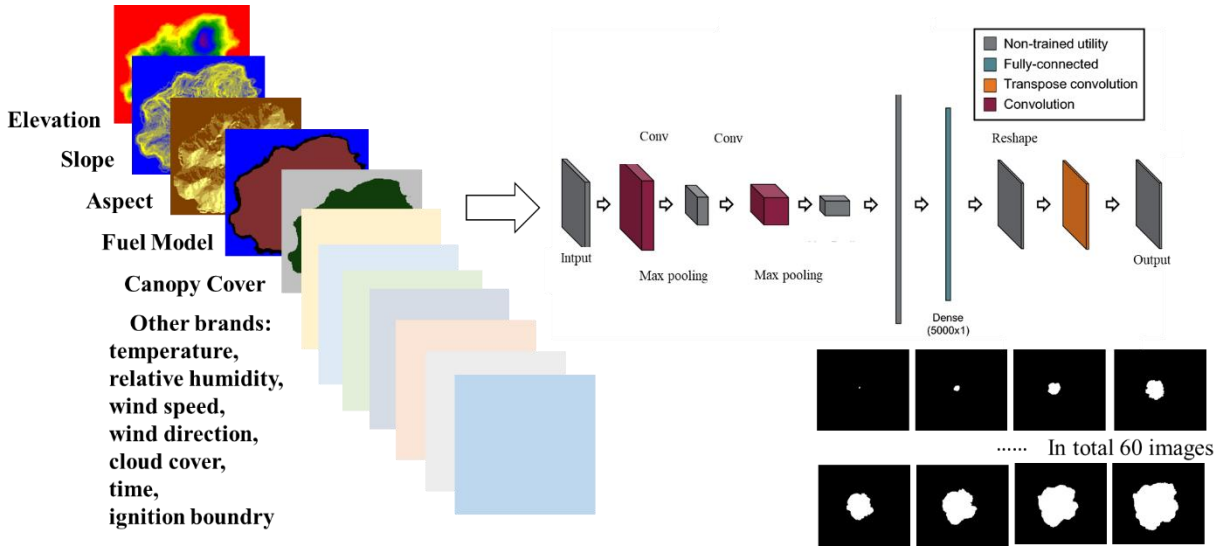

Figure 6- DCNN training model in the paper.

The input images (Tiff format) were 225 × 199 pixels with 12 brands, while 60 output images represent the location of wildfire front with the time step of 5 minutes in five hours (Fig. 6). Six hidden layers are included in the network, including two convolutional, two max pooling, one fully connected classification, and one transpose convolutional layer, which is referred to as Hodges (Hodges & Lattimer, 2019).

The layers in the model made full use of used leaky rectified linear unit (ReLU). The hidden layers in the model are to calculate the pixel possibility whether they need to be colored based on the dataset. In total, the DCNN model works depending on the convolutional layers to form the colored pixel instead of forming the wildfire front according to the traditional spread model.

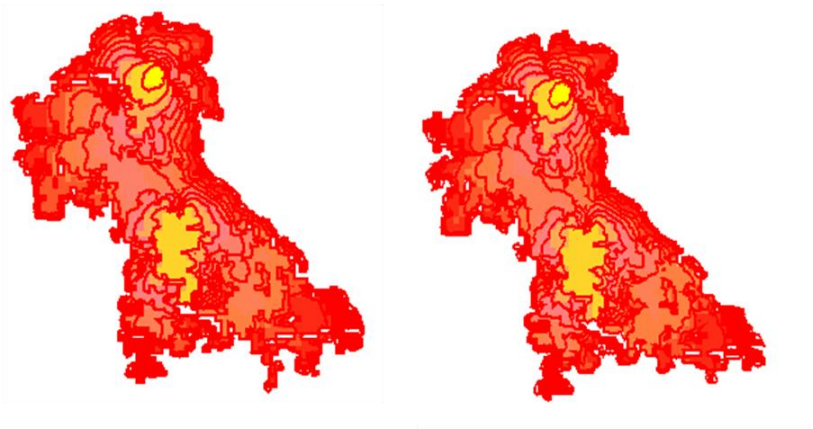

(a) FARSITE simulation (b) DCNN-based Prediction

Figure 7- Wildfire perimeters in (a) FARSITE simulation, and (b) proposed DCNN-based prediction.

4. Conclusion

This paper firstly introduced the development of the wildfire spread models and then reviewed emphatically the AI-based model in the wildfire simulation and prediction. The blank parts in the short-time series wildfire prediction aroused the attention of authors. Thus, a new AI-based method was proposed to predict the wildfire front in a short time response. This study currently aims to establish the virtual wildfire scenario database in Hong Kong, and realizes the AI-driven wildfire prediction model for suppressing fire spreading. The more detailed analysis and applications of this algorithm will be conducted in the future journal paper.

5. Reference

Hernández, L. y cols. (2021). Paisagens corta-fogos. Proposta da ANP|WWF e WWF Espanha para um território ibérico adaptado aos incêndios.

Isenburg, M. (2014). LAStools-efficient LiDAR processing software. Available Online: Lastools. Org (Accessed on 10 October 2017).

Albini, F. A. (1985). A model for fire spread in wildland fuels by-radiation. Combustion Science and Technology, 42(5–6), 229–258.

Civil Engineering and Development Department Hong Kong. (2014). Land Usage Distribution in Hong Kong. 2, 1–7.

Deep convolutional neural network — DCNN | Deep Learning with Keras. (n.d.). https://subscription.packtpub.com/book/big_data_and_business_intelligence/9781787128422/3/ch03lvl1sec24/deep-convolutional-neural-network-dcnn

Finney, M. A. (1998). FARSITE, Fire Area Simulator--model development and evaluation (Issue 4). US Department of Agriculture, Forest Service, Rocky Mountain Research Station.

Hodges, J. L., & Lattimer, B. Y. (2019). Wildland fire spread modeling using convolutional neural networks. Fire Technology, 55(6), 2115–2142.

Ho

ng Kong Fire Services Department - Access to Information. (2021). https://www.hkfsd.gov.hk/eng/access/

Krizhevsky, A., Sutskever, I., & Hinton, G. E. (2012). Imagenet classification with deep convolutional neural networks. Advances in Neural Information Processing Systems, 25, 1097–1105.

Manzello, S. L. (2020). Encyclopedia of wildfires and wildland-urban interface (WUI) fires. Springer.

Rothermel, R. C. (1972). A mathematical model for predicting fire spread in wildland fuels (Vol. 115). Intermountain Forest & Range Experiment Station, Forest Service, US ….

Srivas, T., Artés, T., De Callafon, R. A., & Altintas, I. (2016). Wildfire spread prediction and assimilation for FARSITE using ensemble Kalman filtering. Procedia Computer Science, 80, 897–908.

Warren-Rhodes, K., & Koenig, A. (2001). Ecosystem appropriation by Hong Kong and its implications for sustainable development. Ecological Economics, 39(3), 347–359.

An operational platform for fire danger prevention and monitoring: insights from the OFIDIA2 project

Valentina Bacciu*[1,2] Maria Mirto[1], Sandro Luigi Fiore[3], Costantino Sirca[4], Josè Maria Costa Saura[4], Sonia Scardigno[1], Valentina Scardigno[1], Paola Nassisi[1], Alessandra Nuzzo[1], Alessandro D'Anca[1], Antonio Aloisio[1], Giorgia Verri[1], Giovanni Coppini[1], Ivana Caputo[5], Lucio Pirone[5], Donatella Spano[1,4], Giovanni Aloisio[1,6]

[1]*Euro-Mediterranean Centre on Climate Change (CMCC) Foundation, Italy,{maria.mirto, sonia.scardigno, valentina.scardigno, paola.nassisi, alessandra.nuzzo, alessandro.danca, antonio.aloisio, giorgia.verri, giovanni.coppini, giovanni.aloisio}@cmcc.it*
[2]*Consiglio Nazionale delle Ricerche, Istituto per la BioEconomia, Sassari, Italy, {valentina.bacciu@ibe.cnr.it}*
[3]*Department of Information Engineering and Computer Science, University of Trento, Trento, Italy, {sandro.fiore@unitn.it}*
[4]*University of Sassari, Sassari, Italy, {cosirca, jmcostasaura, spano}@uniss.it*
[5]*Apulia Region - Civil Protection Section, Bari, Italy, {i.caputo, l.pirone}@regione.puglia.it*
[7]*University of Salento, Lecce, Italy, {giovanni.aloisio@unisalento.it}*

**Corresponding author*

Keywords

Decision Support System, Fire Danger indices, Fire behaviour

Abstract

The project OFIDIA2 (Operational FIre Danger preventIon plAtform 2), funded by the Interreg Greece-Italy 2014-2020 Programme, proposed a pragmatic approach to improve the operational capacity of the stakeholders to detect and fight forest wildfires. A data analytics system was designed and implemented within the project to manage, transform, and extract knowledge from heterogenous data sources, through forecasting models such as weather, fire danger, and fire behaviour models, as well as monitoring data from sensors, weather stations, cameras, and drones. Additionally, the project has developed an innovative DSS that provides complete coverage of technical activities to support wildfire hazard management and decision makers in real time.

In this work, we present the OFIDIA2 platform architecture and then we focus on the main findings concerning the component "fire behavior" of the project. Indeed, fires, fuel, topography and weather data were collected from several sources and used to run and calibrate two fire models (FlamMap and Wildfire Analyst) in the project regions. Based on the analyses of recurrent weather conditions leading to large fires, fire metric's maps for prevention and fire-fighting activities were produced. The final information was then included within the DSS to support and improve firefighting and fire management programs.

1. Introduction

Forest fires are a critical problem in Mediterranean regions, especially during summer, threatening ecosystems biodiversity, human life, and high-value assets. High temperatures, strong wind, and low precipitations are the ideal conditions for the occurrence of intense and rapidly spreading fires. In this context, it is of utmost importance to provide fire managers and civil protections with an adequate fire-intelligence system that can provide information to support effective management of wildland fires and decision-making, from the optimization of wildfire prevention and firefighting resources and reducing fire effect impacts on valued resources.

Towards this aim, the project OFIDIA2 (Operational FIre Danger preventIon plAtform 2, https://www.interregofidia.eu/), funded by the Interreg Greece-Italy 2014-2020 Programme, proposed a pragmatic approach to improve the operational capacity of the stakeholders in Apulia (Italy) and Epirus (Greece) regions to detect and fight forest wildfires.

The main goal of OFIDIA2 Project was the development of a software platform for fire danger prevention, able to predict fire risk and danger in case of fire outbreak, based on the constant measurement of several environmental variables detected through appropriate sensors across Apulia and Epirus Regions. The project started in May 2018 and ended in May 2021.

In this short paper, we will present the OFIDIA2 platform architecture and related services (section 2) and then we will focus on the main findings concerning the component "fire behavior" of the project (section 3).

2. OFIDIA2 platform architecture and related services

The project OFIDIA2, based on the results of previous project OFIDIA (Mirto et al., 2015), has implemented a Decision Support System (DSS) for prevention planning and emergency management of forest fire events that incorporates weather data management, fire danger indices, and fire behaviour models, as well as monitoring data from sensors, weather stations, cameras, and drones.

As depicted in Figure 1, the collection, input, storage, management, and analysis of information rely on advanced and automated methodologies using NetCDF (Network Common Data Form) data, digital mapping, and textual data. NetCDF stores multidimensional (variable) scientific data, such as temperature, humidity, pressure, wind speed and direction. The results include i) short-term dynamic fire danger indices developed for improved and realistic prevention and pre-suppression planning; ii) fire behaviour maps to help determine the impact of fire to a considerable extent; iii) an automatic fire detection technology, based on wireless sensors, weather stations, video cameras and drones, successfully tested on several sites.

Additionally, the project has developed an innovative DSS that provides complete coverage of technical activities to support wildfire hazard management and decision makers in real time. The main DSS services are:

- *Forecast Weather maps*: each day an operational chain at the CMCC Supercomputing Center, located in Lecce, produces 72hr forecast data by the WRF meteorological model (Michalakes et al., 2004) with 2x2km resolution. These data are used both for calculating fire danger indices and selecting the fire behaviour maps.
- *Fire Danger indices*: Starting from the WRF data, the maps of three fire danger indices were produced: Canadian, Fosberg and Ichnusa for a time period equal to 72h.
- *Fire Behaviour*: Landscape fire spread and behaviour models have been applied. Two fire simulation models were used for a mean weighted scenario to define the fire weather scenarios and to assess key wildfire characteristics.
- *Dashboard Monitoring*: Regarding sensor monitoring, innovative sensors named Tree Talker Fires send data to a web server every hour. With the same frequency they are downloaded and analyzed at the Supercomputing Center. Data quality and cleaning routines are applied to extract the variables of interest and store them in structured form in the monitoring system. Data are also transferred to the Civil Protection. The variables are displayed in graphs. In the event of an alarm, the system sends an email to the control room manager and commands the cameras to acquire a small piece of video and send it to selected members of the control room.
- *Video cameras*: The system allows monitoring of cameras installed in the forest sites and their geolocation.
- *Historical drone videos*: It is also possible to view the history of the videos acquired with the drones supplied by the Civil Protection.
- *Fleet management*: The fleet management service was born as a support to the group of Civil Protection volunteers. The alarm system implemented in OFIDIA2 allows optimized management of volunteer teams, called teams. Each team is geolocated through our mobile APP. When an alarm occurs, the operator in the control room displays either the single sensor that triggered the alarm or a group of sensors determined by a polygon. Then the operator can see the real position of the teams and select the team that is closest to the site that generated the alarm. Then the system calculates the optimal path that the team must take. The route will be displayed to the team via the mobile App. It is also possible to guarantee the team's interaction with the Control Room operator through a messaging service that remains stored for further analysis.

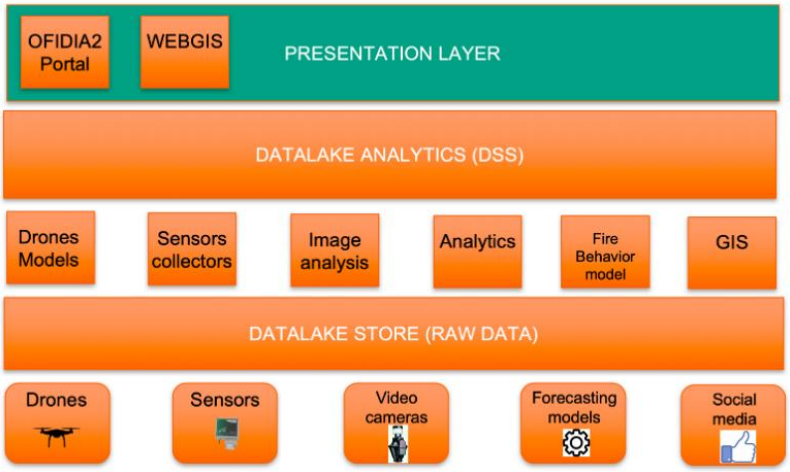

Figure 1- OFIDIA2 architecture

3. Fire behaviour modelling component

In the framework of the "*Fire Behaviour*" DSS service, two fire behaviour modeling tools were run to provide a set of fire behavior characteristics, assessed for a set of fire weather scenarios. This information was then included within the DSS to support and improve firefighting and fire management programs.

3.1. Input data, fire weather scenarios, and fire modelling

We firstly acquired available information on fire ignition for the period 2007-2017 and then the gridded ERA5-Land dataset at 0.1° of resolution through the Copernicus website. A set of multivariate statistical procedures were applied to the database to explore potential associations between fire weather variables and the incidence of large fire events (>100 ha). Clustering technique was applied to weather data looking for groups of observations, evaluating all possible pairs of clusters with the cluster that results in the smallest increase in error sums of squares is used (Everitt and Hothorn, 2011). Thus the parallel coordinate plot (PCP) technique for the visualization of multivariate quantitative data was applied. Finally, to visualize and understand the cluster solution and to highlight an individual observation that represents each cluster, medoids (Kaufman and Rousseeuw, 1990) were calculated to succinctly represent a cluster, also called fire weather scenarios (FWS). Each FWS was made thus of mean wind speed, wind direction, and relative humidity data.To define fuel type and canopy cover layers, the 2012 Corine Land Cover map was reclassified following the methodology in Salis et al. (2013). As a result, 13 fuel types were obtained and associated to the standard or custom fuel models from the original 44 Corine land cover categories present in the study area.

FWS, togheter with information on fire ignition, topography and fuel models, were then used to simulate fire behavior characteristics (e.g., rate of spread, fire intensity, burn probability, fire potential index) through two fire propagation tools, WildFire Analyst (WFA, Monedero et al., 2019; Ramírez et al., 2011) and FlamMap (Finney, 2006). We simulated 36,000 fires (~2 fire per km^2) taking into consideration the historical ignition density of the study area for the period 2007–2017. The simulations were conducted considering constant fuel moisture, wind speed, and wind direction according to the FWS. Fire spread duration was set of 10 h, which is a common average duration of large historical fires in the Mediterranean area. Fire suppression operations as well as barriers to fire spread were not considered.

3.2. Main results

For sake of conciseness, only the results for a mean weighted scenario (i.e. the weighted mean of each single model output according to the relative frequency of each weather scenario) in Apulia region for both simulators WFA and FlamMap are presented here below.

3.2.1. Fire weather scenarios for Apulia region

Analysis of weather data across fire size showed that large fires (>100 ha) mainly occurred under low humidity and high temperatures (Figure 2a). Despite winds from different directions blow in fire days, south west

direction at 15 km hr^{-1} (on average) is one the most common situation in the region (Figure 2b). The cluster analysis revealed four wheatear scenarios in which two have low relative wind speed but contrasting directions whereas the other two have higher wind speed and different directions (north and southwest) (Table 1). Spatial analysis of fire weather scenarios showed that the 1st and 4th clusters (i.e. south west winds) mainly occur in the northern and mid provinces (i.e. Foggia, Barletta-Adria-Trani and Bari). Instead, the other climatic clusters are observed across the Apulia region.

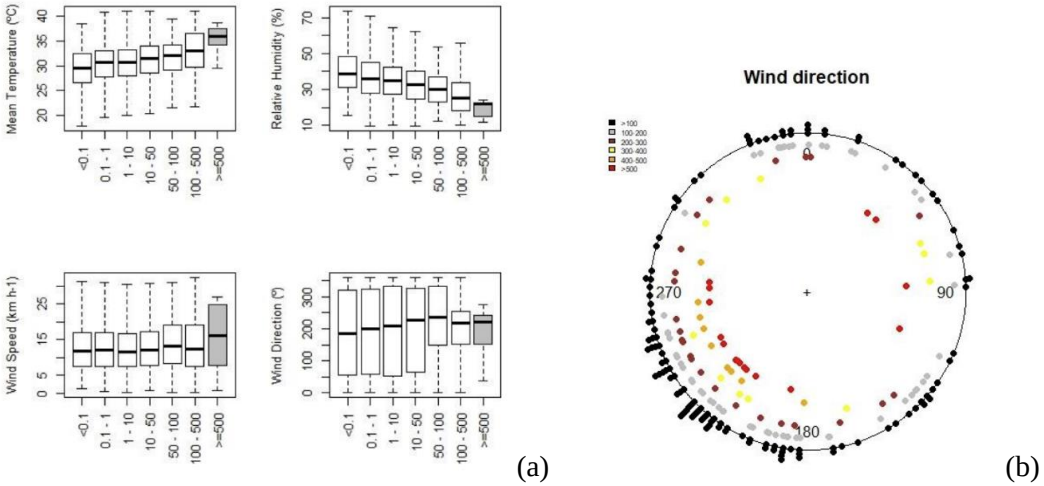

Figure 2 – (a) Distribution of weather variables across fires size categories. (b) Wind direction across fire size categories over 100 ha

Table 1 – FWS according to cluster medoids

Description	*Wind direction (°)*	*Wind speed (km h^{-1})*	*Relative humidity (%)*	*Days (%)*
Sud-ovest calmo	*217*	*6*	*23*	*28*
Est	*72*	*6*	*25*	*19*
Nord	*346*	*18*	*42*	*19*
Sud-ovest forte	*254*	*20*	*19*	*33*

3.2.2. WildFire Analyst simulations

Simulations showed that for all three variables, i.e. flame length, fire intensity and rate of spread, higher values are mainly observed on Foggia, Bari and Taranto provinces. Furthermore, these higher values are mostly observed in the forest protected areas of Gargano, Alta Murgia e Terra delle Gravine (Figure 3). Greatest flame length and fire intensity are projected for shrublands (i.e. maquis) but also in forest of different types whereas fire; rate of spread is projected also higher in maquis and herbaceous vegetation. Fire length and fire intensity are tightly related variables whereas the rate of spread is mostly uncoupled with the previous ones.

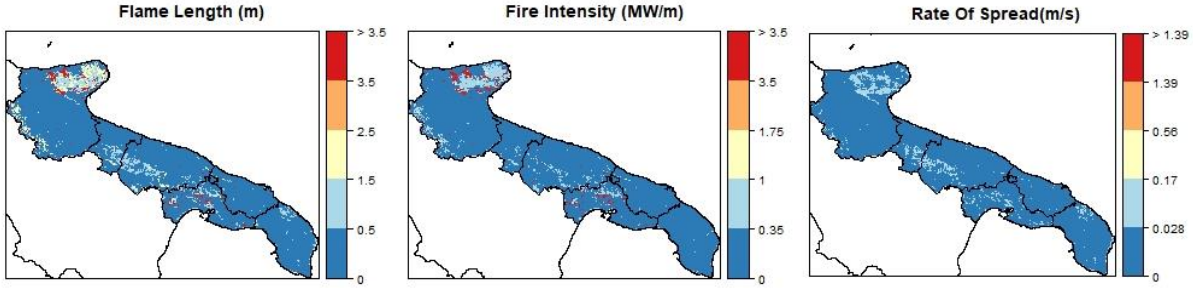

Figure 3 – Flame length (left), fire intensity (center), and rate of spread (right) maps of the Apulia region simulated by WildFire Analyst

3.2.3. FlamMap simulations

FlamMap simulations showed that burning probabilities based on historical fire distribution might be higher in mountain areas of costal Foggia province and along the western axis crossing Barletta-Adria-Trani, Bari and Taranto. Flame length and fire size were also predicted higher over the Gargano in Foggia province. Burn probabilities and fire size showed a quite similar pattern (Figure 4). Based on historical records, burning probabilities, fire size and fire potential index are predicted higher over herbaceous and maquis areas. Instead, conditional flame length might higher in maquis but also in all forest types.

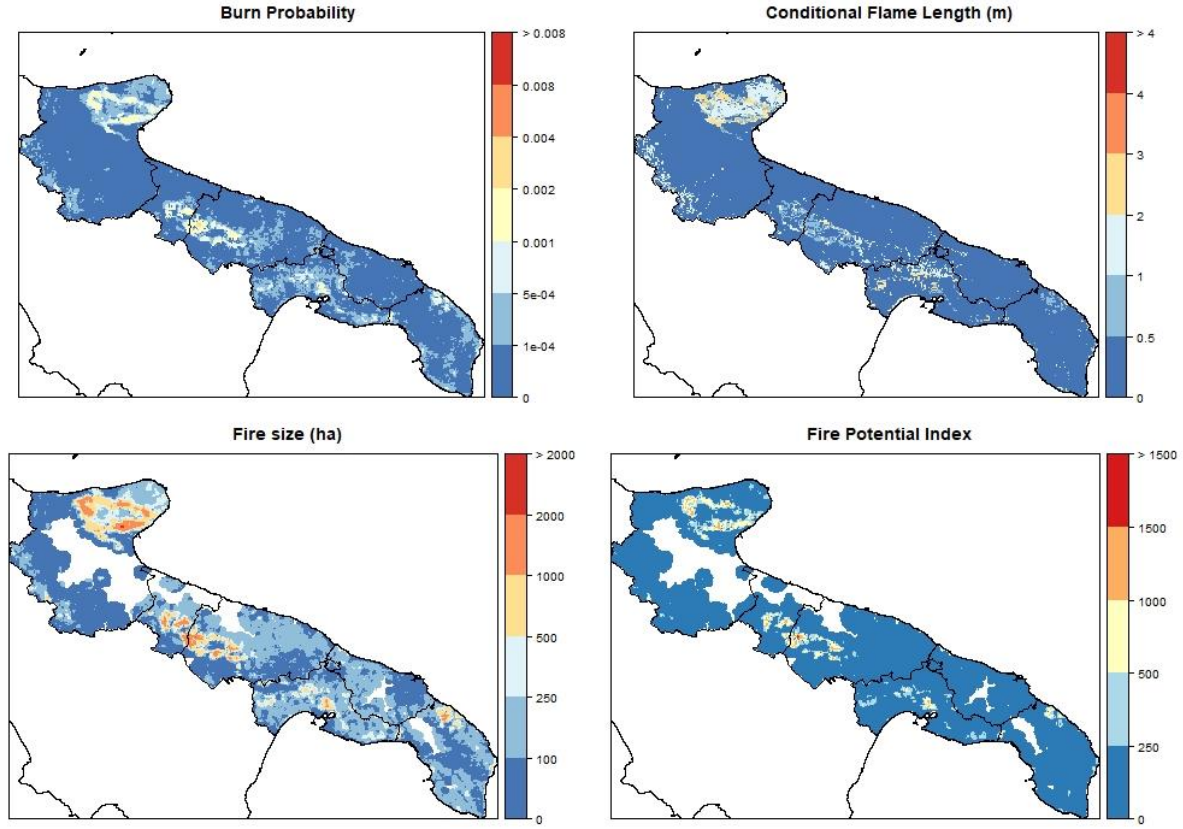

Figure 4 – Burn probability (top left), conditional flame length (top right), fire size (bottom left), and fire potential index (bottom right) maps of the Apulia region simulated by FlamMap

3.3. OFIDIA2 DSS

Finally, fire behaviour characteristic maps for each FWS were imported into OFIDIA2 DSS to allow fast retrieval on user requests. The choice of the FWS depends on the wind speed and direction and relative humidity of that particular day. The variables are request from WRF output. The specific result depends on the definition of the minimum and maximum thresholds (coming from Table 1) that are used to classify a fire day within each FWS. The selected FWS include geotiff images that were imported into a Web GIS (Figure 5). As for the weather forecast of the current day, OFIDIA2 system selects the most appropriate cluster based on the thresholds considered. It is also possible to know the specific value of each variable in the cluster for each latitude and longitude.

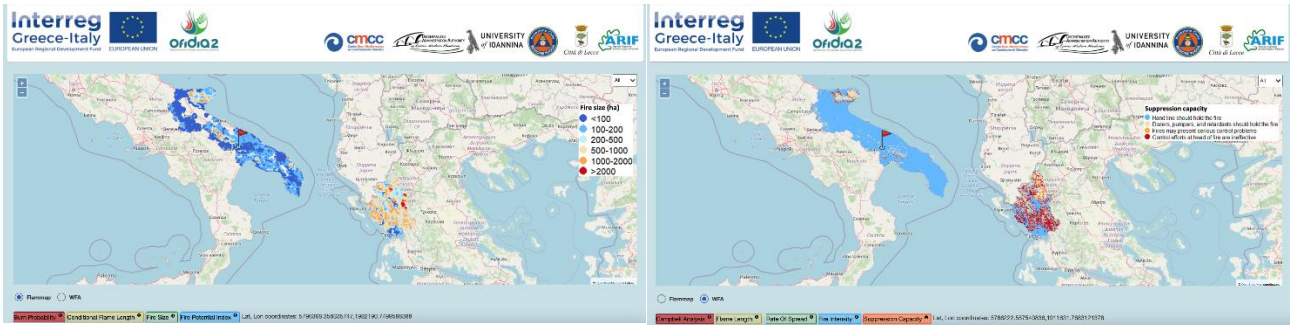

Figure 5 – Examples of the fire behaviour modelling outputs showed by the web GIS of the OFIDIA2 DSS. On the left, fire size calculated by FlamMap; on the right, suppression capacity calculated by WFA.

4. References

Everitt, B., Hothorn, T., 2011. Cluster Analysis, in: An Introduction to Applied Multivariate Analysis with R. Springer New York, New York, NY, pp. 163–200. https://doi.org/10.1007/978-1-4419-9650-3_6

Finney, M.A., 2006. An Overview of FlamMap Fire Modeling Capabilities, in: Andrews, P.L., Butler, B.W. (Eds.), Fuels Management—How to Measure Success. U.S. Department of Agriculture, Forest Service, Rocky Mountain Research Station, Portland, pp. 213–220.

Kaufman, L., Rousseeuw, P.J., 1990. Finding Groups in Data, Wiley Series in Probability and Statistics. John Wiley & Sons, Inc., Hoboken, NJ, USA. https://doi.org/10.1002/9780470316801

Mirto M., Mariello A., Nuzzo A., Mancini M., Raolil A., Marra O., Fiore S., Sirca C., Salis M., Bacciu V., Spano D., Aloisio G., 2015. The OFIDIA Fire Danger Rating System, 2015 10th International Conference on P2P, Parallel, Grid, Cloud and Internet Computing (3PGCIC), 695-700, doi: 10.1109/3PGCIC.2015.115.

Michalakes J., Dudhia D., Gill T., Henderson J., Klemp W., Skamarock W., Wang W., 2004. The Weather Reseach and Forecast Model: Software Architecture and Performance, Proceedings of the 11th ECMWF Workshop on the Use of High Performance Computing In Meteorology, 25-29 October 2004, Reading U.K. Ed. George Mozdzynski.

Monedero, S., Ramirez, J., Cardil, A., 2019. Predicting fire spread and behaviour on the fireline. Wildfire analyst pocket: A mobile app for wildland fire prediction. Ecol. Modell. 392, 103–107. https://doi.org/10.1016/j.ecolmodel.2018.11.016

Ramírez, J., Monedero, S., Buckley, D., 2011. New approaches in fire simulations analysis with Wildfire Analyst. South Africa 9–13. https://doi.org/10.13140/2.1.2045.7766

Salis, M., Ager, A.A., Arca, B., Finney, M.A., Bacciu, V., Duce, P., Spano, D., 2013. Assessing exposure of human and ecological values to wildfire in Sardinia, Italy. Int. J. Wildl. Fire 22, 549–565. https://doi.org/10.1071/WF11060

Autonomous Wildfire Tracking Systems Based on UAV and Perspectives of Wildfire Digital Twin

Yizhou Li; Xinyan Huang*

Research Centre for Fire Safety Engineering, Department of Building Environment and Energy Engineering, The Hong Kong Polytechnic University, Hong Kong,

**Corresponding author: xy.huang@polyu.edu.hk*

Keywords

Digital shadow; Real-time Surveillance; Fire front; Computer vision

Abstract

Digital twin, a new concept, which comes from the manufacturing industries, is introduced to different aspects of life. The ever-burgeoning development of digital twin systems lays the path for a new approach to wildfire monitoring and prevention. A real wildfire digital shadow reflects the fire development, providing a promising platform for firefighting decisions. However, currently, static terrain information cannot be integrated with dynamic wildfire locations, which is a great hindrance to the utilization of digital twin systems. The flame trend fails to be mapped in the digital shadow. The key to solving this issue is to ensure real-time data transfer. Thus, UAVs equipped with vision systems could be leveraged to maintain surveillance, transferring the real-time information to the digital twin systems. Initially, the study reviews the UAVs in wildfires. Specifically, the history of UAV tracking is introduced. Furthermore, the autonomous wildfire tracking system is proposed to assist in locating the fire front. A YOLO-based algorithm is utilized to detect the fire front. The UAVs use an orthographic view to locate the wildfire, controlling and maintaining the gesture with a perspective lock on the flame front. Then, UAVs track and follow the flame front without human intervention. In addition, the combination of UAV location information based on GPS and camera view information depicts the wildfire in the digital twin systems. This study aims to act as a pre-processing step for wildfire digital twin data transfer. It will provide a basis for the precise wildfire portrait in the virtual systems.

1. Introduction

1.1. UAVs in wildfire

The usage of unmanned aerial system (UAS) is not really a new concept, particularly in military uses throughout human civilization. An interesting early use of unmanned aerial technologies was the use of hot air balloons during the US Civil War or the installation of cameras in Kites during the Spanish-American War (Manzello, 2020). Yet, there are also historical accounts that pre-date these events by hundreds of years that have used the concept of unnamed aerial technologies for various purposes.

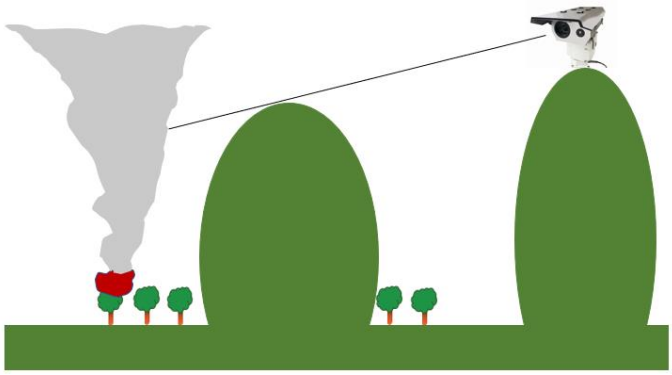

Figure 1- Restrictions of watch towers and fixed cameras installed on mountaintops

In wildland fire detection, monitoring and fighting, a view from higher elevations is desired to gain overall and unique fire information. Compared to a fixed camera network installed on mountain tops and fire watchtowers

(Fig. 1), the airborne monitoring system is more cost-effective and is not limited by the location of the pre-installed infrastructure. Airborne systems usually include high-altitude manned or unmanned aircraft (Allison et al., 2016; Colomina & Molina, 2014) and high-altitude long-duration balloons (Rand, 1994; REGO et al., 2010). As expected, the overall cost of unnamed aircraft and balloons is much lower compared to the manned system. Another important aspect is the risk of having people onboard aircraft during a mission. By using unmanned aircraft, it could avoid putting a crew at risk. Aviation accidents account for 18% of wildland fire fighting fatalities between 2007-2016 (National Wildfire Coordinating Group, 2017). UAVs are undoubtedly one of the most promising technology to ensure the safety of firefighters in wildfires. UAVs can shorten the time of firefighting response and render rescue activities safer, fast er, and more efficient (Khan et al., 2018). It has the ability to access hard-to-reach areas and help gather important data (Reich, 2016). Besides, they can replace the role of helicopters, which may be disturbed by smoke, increasing the risk of pilots in wildfires. The ability to require unmanned control and avoid unnecessary obstacles makes UAVs unique in firefighting. Their safety is not a priority so UAVs could take on more dangerous tasks. The current study about UAV usage in a wildfire is solely about monitoring and putting out fires. Burchan Aydin (Aydin et al., 2019) and his team were entrusted by the fire department of Texas to come up with a fire-distinguishing ball technology and then applied them with UAVs in wildfire fighting. This technology was also utilized to detect and monitor wildfires to reduce false alarms, increasing the efficiency of firefighters (Sudhakar et al., 2020). Since 2021, a platform has been already made use of to manage a number of UAVs in order to spread the liquid on wildland fires (Ausonio et al., 2021). Nowadays, a lot of teams have been focusing on the frameworks of UAV swarms because a single UAV is not enough for a big fire or wildfire so that more UAVs will be applied in the near future (Ausonio et al., 2021; Innocente & Grasso, 2019; Madridano et al., 2021; Roldán-Gómez et al., 2021).

1.2. Digital twin and UAVs

The concept of the digital twin comes from the manufacture industry, and it refers to presenting the real world with virtual methods (Boschert & Rosen, 2016)(Liu et al., 2021), introduced to other industries. Generally, the 3-Dimensional model with real-time data updates is considered as the digital twin/digital shadow, realizing the goal of data assimilation.

The ever-burgeoning development of digital twin systems lays the path for a new approach to wildfire monitoring and prevention. A real wildfire digital shadow reflects the fire development, providing a promising platform for firefighting decisions. However, currently, static terrain information cannot be integrated with dynamic wildfire locations, which is a great hindrance to the utilization of digital twin systems. The digital twin for wildfire is still a terrain model with no updated information. Even when the DJI company launched its newest product in March 2022, Flighthub 2, it simply integrated terrain models with real-time camera information (Fig. 2).

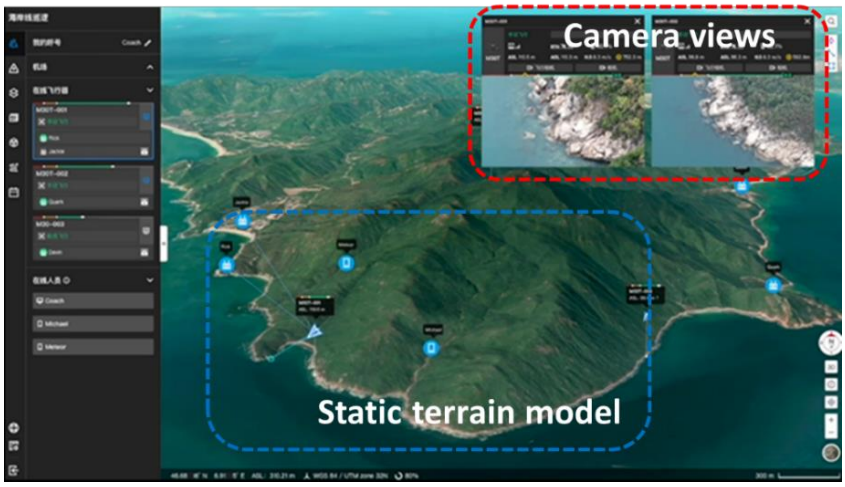

Figure 2- Terrain models integrated with camera views by DJI Company (from DJI FlightHub Website)

The wildfire head fails to be mapped in the digital shadow. The wildfire portrait in the digital twin systems is always a huge difficulty waiting to be solved. The issue lies in the failure of real-time wildfire data transfer. If the fire development trend could be recorded in time. It is possible to depict the wildfire in the digital twin

systems. Gladly, UAVs equipped with vision systems could be leveraged to maintain surveillance, transferring the real-time information to the digital twin systems. However, with the increasing spread of wildfires, it is extremely hard for UAVs to update the geography information of wildfires. Thus, an autonomous wildfire tracking system based on UAVs is proposed to assist in locating the fire front. Since fuels, wind, and other factors resulted in the disordered spreading of wildfire, UAV swarms are utilized to collect information, synchronizing the fire front in the digital twins (Fig. 3).

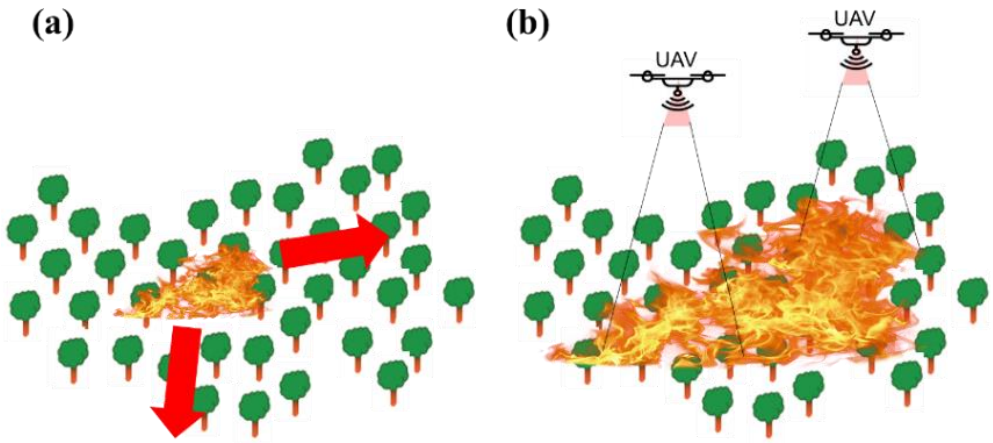

Figure 3- (a) Wildfire spreads following the wind, and (b) UAV follows wildfires in the main directions

The study aims to act as a pre-processing step for wildfire digital twin data transfer. It will provide a basis for the precise wildfire portrait in the virtual systems.

2. Methodology and framework

Object tracking in vision-assisted UAV systems requires three major steps, object detection, object tracking, and relative move of the UAV under control (Lo et al., 2021; Wise & Rysdyk, 2006). The whole structure is shown below (Fig. 4). The UAVs are equipped with both visible and infrared cameras to collect information.

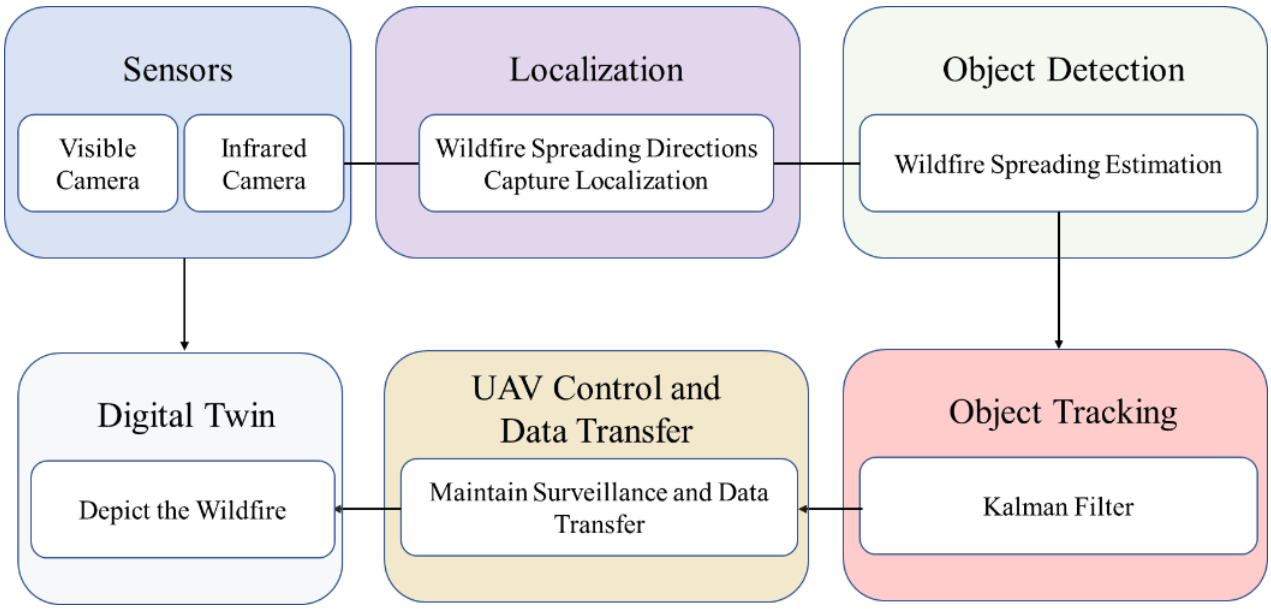

Figure 4- Proposed architecture of autonomous wildfire tracking system

2.1. Fire front detection

Object detection also contains object localization and classification. Compared to traditional algorithms for detecting objects, deep learning-based algorithms have many advantages in robustness, speed, and accuracy. In

this study, a deep learning-based approach has been adopted to detect the wildfire front. It is called You Only Look Once (YOLO), which is a state-of-the-art, real-time object detection system. Many researchers (Lestari et al., 2019; Wu & Zhang, 2018) proved the function of YOLO algorithms in fire detection.

Figure 5- YOLO applied in fire detection (Wu & Zhang, 2018)

2.2. Fire front tracking

Fire front tracking is much more challenging than detection due to faced uncertainties and complexities in aspects. Finally, the Kalman filter method (Welch & Bishop, 1995) was chosen to realize the motion association of object tracking. Compared to normal object detection, the major difference is that fire would spread while UAVs have to follow the wildfire front. To solve this issue, thermal infrared cameras would assist in reducing the uncertainties of flame waves. It conveys the temperature information to the tracking algorithm to ensure a correct path.

Figure 6- Wildfire tracking and UAV moves

2.3. UAV control and data transfer

UAVs are controlled based on the ROS software in the Linux system. Then instructions are programmed into the control commands. In terms of data transfer, the image transmission technology of UAVs themselves can build communication with servers.

2.4. Wildfire portrait

Finally, the combination of UAV location information based on GPS and camera view information could be sent to the virtual systems, promoting to depict of the wildfire fronts in the digital twin systems. The positions on the wildfire front would be updated in time to provide information for wildfire decision makers.

3. Conclusions

In this study, an autonomous wildfire tracking system based on UAV swarms is proposed to assist in locating the fire front. As for this work, we applied the YOLO-v5 object detector and Kalman filter to perform target object tracking. It further proposed an efficient UAV planning to achieve a real-time tracking and autonomous surveillance UAV system. The UAVs use an orthographic view to locate the wildfire, controlling and maintaining the gesture with a perspective lock on the wildfire head. Then, UAVs track and follow the wildfire head without human intervention. In addition, the combination of UAV location information based on GPS and camera view information depicts the wildfire in the digital twin systems. This study aims to act as a pre-processing step for wildfire digital twin data transfer. It will provide a basis for the precise wildfire portrait in the virtual systems.

4. Acknowledgements

This work is funded by the Hong Kong Research Grants Council Theme-based Research Scheme (T22-505/19-N),

5. Reference

Allison, R. S., Johnston, J. M., Craig, G., & Jennings, S. (2016). Airborne optical and thermal remote sensing for wildfire detection and monitoring. Sensors, 16(8), 1–29. https://doi.org/10.3390/s16081310

Ausonio, E., Bagnerini, P., & Ghio, M. (2021). Drone Swarms in Fire Suppression Activities: A Conceptual Framework. Drones, 5(1), 17. https://doi.org/10.3390/drones5010017

Aydin, B., Selvi, E., Tao, J., & Starek, M. J. (2019). Use of fire-extinguishing balls for a conceptual system of drone-assisted wildfire fighting. Drones, 3(1), 1–15. https://doi.org/10.3390/drones3010017

Boschert, S., & Rosen, R. (2016). Digital twin—the simulation aspect. In Mechatronic futures (pp. 59–74). Springer.

Colomina, I., & Molina, P. (2014). Unmanned aerial systems for photogrammetry and remote sensing: A review. ISPRS Journal of Photogrammetry and Remote Sensing, 92, 79–97. https://doi.org/10.1016/j.isprsjprs.2014.02.013

Innocente, M. S., & Grasso, P. (2019). Self-organising swarms of firefighting drones: Harnessing the power of collective intelligence in decentralised multi-robot systems. Journal of Computational Science, 34, 80–101.

Khan, M. A., Safi, E. A., Khan, I. U., & Alvi, B. A. (2018). Drones for Good in Smart Cities : A Review. International Conference on Electrical, Electronics, Computers, Communication, Mechanical and Computing (EECCMC), January, 8.

Lestari, D. P., Kosasih, R., Handhika, T., Sari, I., & Fahrurozi, A. (2019). Fire hotspots detection system on CCTV videos using you only look once (YOLO) method and tiny YOLO model for high buildings evacuation. 2019 2nd International Conference of Computer and Informatics Engineering (IC2IE), 87–92.

Liu, M., Fang, S., Dong, H., & Xu, C. (2021). Review of digital twin about concepts, technologies, and industrial applications. Journal of Manufacturing Systems, 58, 346–361.

Lo, L.-Y., Yiu, C. H., Tang, Y., Yang, A.-S., Li, B., & Wen, C.-Y. (2021). Dynamic Object Tracking on Autonomous UAV System for Surveillance Applications. Sensors, 21(23), 7888.

Madridano, Á., Al-Kaff, A., Flores, P., Martín, D., & de la Escalera, A. (2021). Software Architecture for Autonomous and Coordinated Navigation of UAV Swarms in Forest and Urban Firefighting. Applied Sciences, 11(3), 1258.

Manzello, S. L. (2020). Encyclopedia of wildfires and wildland-urban interface (WUI) fires. Springer.

National Wildfire Coordinating Group. (2017). NWCG report on wildland firefighter fatalities in the United States: 2007-2016. Report, December, 18.

Rand, J. L. (1994). Long duration balloons. Advances in Space Research, 14(2), 183–190. https://doi.org/10.1016/0273-1177(94)90088-4

REGO, F., COLAÇO, C., MARRECAS, P., CATRY, F., MONTIEL, C., & SOMMA, A. (2010). Assessment of the efficiency factors of wildfire detection systems for timely interventions in European countries. Fire Paradox, 036882, 1–46.

Reich, L. (2016). How drones are being used in disaster management. Geo Awesomeness,[Online]. Available: Http://Geoawesomeness. Com/Dronesfly-Rescue/, Accessed Jan, 26.

Roldán-Gómez, J. J., González-Gironda, E., & Barrientos, A. (2021). A survey on robotic technologies for forest firefighting: Applying drone swarms to improve firefighters' efficiency and safety. Applied Sciences (Switzerland), 11(1), 1–18. https://doi.org/10.3390/app11010363

Sudhakar, S., Vijayakumar, V., Kumar, C. S., Priya, V., Ravi, L., & Subramaniyaswamy, V. (2020). Unmanned Aerial Vehicle (UAV) based Forest Fire Detection and monitoring for reducing false alarms in forest-fires. Computer Communications, 149, 1–16.

Welch, G., & Bishop, G. (1995). An introduction to the Kalman filter.

Wise, R., & Rysdyk, R. (2006). UAV coordination for autonomous target tracking. AIAA Guidance, Navigation, and Control Conference and Exhibit, 6453.

Wu, S., & Zhang, L. (2018). Using popular object detection methods for real time forest fire detection. 2018 11th International Symposium on Computational Intelligence and Design (ISCID), 1, 280–284.

BADE, a tool for Burnt Areas Detection & Evolution.

Javier Pérez-Romero*[1]; Antonio del Campo[1]; María González-Sanchis[1]; Antonio J. Molina[1]; Laura Blanco Cano[1]; Manuel Esteban Lucas-Borja[2]

[1] Research Group in Forest Science and Technology (Re-ForeST), Universitat Politècnica de València (UPV), Valencia, Spain {jperrom@upv.es}
[2] Department of Agroforestry Technology, Science and Genetics, School of Advanced Agricultural and Forestry Engineering, Castilla La Mancha University, Campus Universitario s/n, E-02071 Albacete, Spain

**Corresponding author*

Keywords

Wildfire, Remote sensing, dNBR, GEE and Support system.

Abstract

BADE is a support tool for forest researchers and technicians programmed in Google Earth Engine (GEE) platform that serves to detect forest areas that have been burned after a wildland fire, as well as fire severity. It allows the evaluation of vegetation recovery with the visualisation of time series grouped by fire severity and for different spectral indices from which the user can choose. Its use is very simple because of the graphical interface that the user can adjust for a target area of study by selecting the date of the fire, the index to evaluate in the graph and drawing the study area where the dNBR is going to be mapped. Both the map and the graph can be easily downloaded by the user.

1. Introduction

Fire has been a fundamental element in the dynamics of ecosystems in Mediterranean landscapes (Keeley et al. 2012) and for many forest ecosystems, it is the main one (González et al. 2006). These processes were used as a management tool in many rural areas, but the depopulation of these areas in southern Europe during the 20th century has made fires a major environmental problem, as they have become more frequent and more extensive (Pereira et al. 2006). According to data from the European Forest Fire Information System (EFFIS) (http://effis.jrc.ec.europa.eu/), between 2010 and 2019 there were about 19,000 ignitions in Portugal with a burned area of about 140,000 ha. The scenario in Spain during the same period is not much more encouraging, with 12,000 fires burning approximately 123,000 ha in Spain.

After a forest fire, it is necessary to carry out emergency works for the protection of soil and vegetation in the short term and long-term forest management to encourage the recovery of unfavourable areas and the reduction of vegetation in those areas where the fire has been good for recovery (Francos et al., 2016). Planning these types of actions is difficult because covering the entire burned area is costly and time-consuming. Therefore, use is made of remote sensing techniques that assess vegetation recovery by means of spectral indices (White et al. 1996). This is often difficult to apply for untrained technicians in remote sensing applications, who have to carry out a first evaluation followed by forest planning. This is where decision support tools come in to help managers make the right decisions. The objective of this work is to show the creation of the BADE tool, which is an easy-to-use support system for the detection of burned forest areas and that evaluates the recovery of vegetation and is based on remote sensing techniques accessible to everyone.

2. Material and Method

This tool is built on the GEE platform, which allows users to work and download the available large catalog of satellite imagery and other planetary-scale geospatial data. In addition, it allows the use of Google's servers to process and analyse all this information.

GEE allows the use of multiple remote sensing processes with simple steps, which can be replicated and used in other works avoiding repeating long processes. In this way, it makes the work more efficient and avoids human error when repeating the same steps for similar studies.

Such is the power of this platform, that it allows users to create their own applications once they have programmed some processes, and share them with other users who are not so fluent in programming. In this way, advanced users can generate a graphical interface that processes multiple tasks to produce a final result that is the desired result for the creator of the app. For all these reasons, GEE was the solution for the creation of the BADE tool.

2.1. BADE Architecture

BADE is a decision support tool for forest managers who need to detect burnt areas after a wildfire has occurred, along with the severity of the fire and the recovery of the vegetation up to 10 years later. It uses the Landsat mission to work from 1984 to the present day, together with a set of operational processes that can be easily adjusted by the user with its interface to set the survey configuration inputs, such as date of the fire, spectral index to be obtained and region of interest. A map and time series are automatically obtainable and reconfigurable as downloadable results (Fig 1).

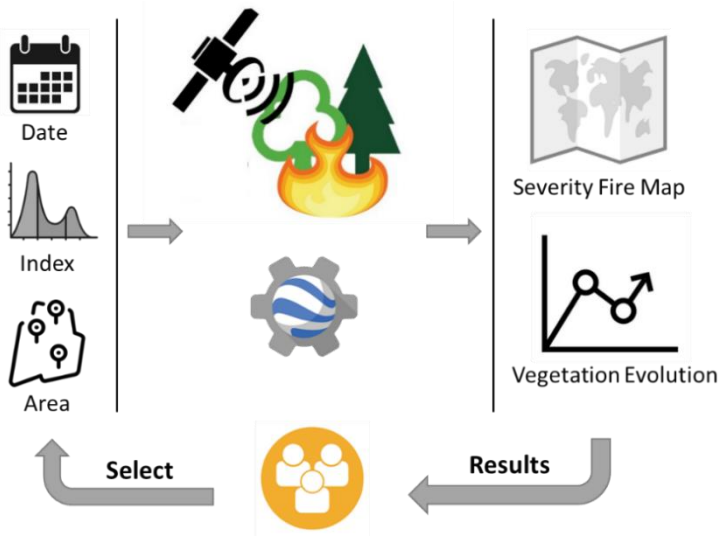

Figure 1: Scheme of the decision support tool, BADE.

BADE performs a large set of geospatial processes in an iterative and replicable way in GEE so that the user obtains its results over and over again each time the process is executed. The steps that this tool continuously performs are as follows:

First, a function is applied to each Landsat mission (5-7-8) that calculates with the spectral bands various indices (Nbr, Ndvi, Msi, Ndii, Rci, Gci, Evi2) for each of the images in each collection, followed by another function that removes to each image the pixels that have clouds or leftovers according to a quality control band that the Landsat images have (pixel_qa). After this, the 3 collections can be combined as a single collection containing the calculated indices and are cloud-free scenes.

Second, is to divide this collection by the date of the fire (that the user enters in the tool) as a pre-fire collection and a post-fire collection; these collections will be used to calculate both the fire severity map and the time series. Therefore, to obtain the severity map to each of these collections, it is filtered by the time span that the user enters to reduce each collection by a similar range. In addition, these collections are filtered one last time by the region of interest that the user draws on the map with the design tools as the region of interest. On these filtered collections, a reduction is generated that converts it into an average pre-fire image and a post-fire image. These images will have the average value of the bands containing the spectral indices. To obtain the burned area, the nbr index is used, which by means of the difference between the scene before and after the fire (dNBR) can calculate the area of vegetation that has changed between the two periods due to the disturbance. The process of generating the dNBR ends with the filtering of the pixels that are considered as loss of vegetation being the value greater than 0.1 and those that are less are masked because they are surfaces that have not been burned.

Third, the image is reclassified into 3 fire severity classes, low, medium and high. Low being those areas where the dNBR value is between 0.1 and 0.25, medium value between 0.25 and 0.5 and high value greater than 0.5, which the user can export as a result in GEOTIFF format. These three classes (low, medium, high severity) are

vectorized to subsequently evaluate their temporal evolution in the recovery of vegetation by the indices. Prior to obtaining these graphs for each severity, these three classes are dissolved to obtain a single vector (fire perimeter) and also those polygons that have small surfaces are filtered to really leave the burned area and eliminate pixels that introduce noise.

Fourth, the three results obtained are mapped in image format, the continuous and masked dNBR, the fire severity classes and the fire perimeter.

Fifth, the time series for each fire severity is calculated for a maximum period of 10 years after the fire, provided that there is information in the Landsat collection. The graph that is generated is the mean value of the pixels within the fire severity polygons and for the dates that there is scene. In addition, the index that the user selects from all the calculated ones is displayed.

Finally, the user can download the results of the image or the graph.

2.2. Workflow

This tool requires very few user steps to display the results. The first step that every user must perform is to delimit the date of the fire that will be analysed. To do this, the user must select the year, month and day of the fire, together with the time span or range before and after the fire that will be used to calculate the dNBR (this step is variable to generate a complete image of the burned area without clouds and therefore with all the pixels) (Fig 2.1). The second thing the user has to do is to select the index to be plotted to see the time series of each severity (Fig 2.2). The third thing to do is to draw the region of interest to filter the Landsat collection to that study area (Fig 2.3). After performing these steps, the results are generated and the 3 layers (continuous dNBR, damage severity classes and fire perimeter) appear in the map viewer (Fig 2.4) which can be downloaded by clicking on the download button (Fig 2.5) and the time series is shown in the blank space (Fig 2.6) which can also be downloaded later.

Figure 2: Parts of the graphical interface of the BADE tool. 1. fire dates; 2. selected index for the time series; 3. draw region of interest where the fire occurred; 4. layers visible on the map; 5. download image of fire severity classes; 6. time series graph of the selected index.

3. Results

The link to use the tool is as follows: https://javierrieju.users.earthengine.app/view/re-forest-fire that to show the results that this tool offers to users, an example of use has been made for a fire that occurred during the summer of 2017 in the municipality of Altura, belonging to the region of Valencia, eastern Spain. Here, we used the date 2017/07/01 and region of interest in rectangle mode on the location of Altura.

It can be seen in Figure 3 how the map has a three-colour image according to the severity of the fire (low, medium, high), along with two other layers which are the perimeter and the continuous dNBR image that can be viewed by selecting them in the layer tab. In addition, the time graph of the selected index is generated, where the average value of each severity class is shown for the years after the fire (Fig. 3).

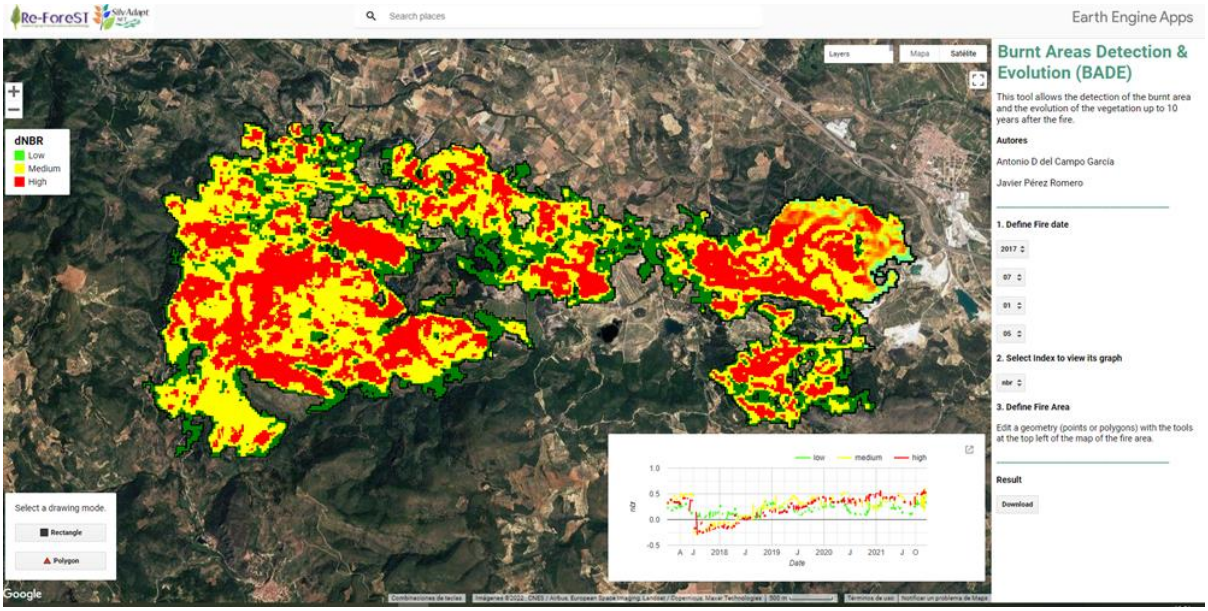

Figure 3: Example execute in BADE tool

These results can be downloaded for use outside the tool. In the first case, the image can be downloaded by clicking on the download button and a new window will open in the explorer for you to choose the directory to save the file in compressed format. The image with the name class_dNBR and the date and time interval set by the user can then be decompressed and is in GEOTIFF format available for use in a GIS (Fig. 4.1).

Finally, you can also download the graph in different formats once you expand it in a new tab. This graph is iterative and the user can consult the values by moving the mouse over the graph. The formats that can be downloaded are CSV, SVG and PNG files (Fig. 4.2).

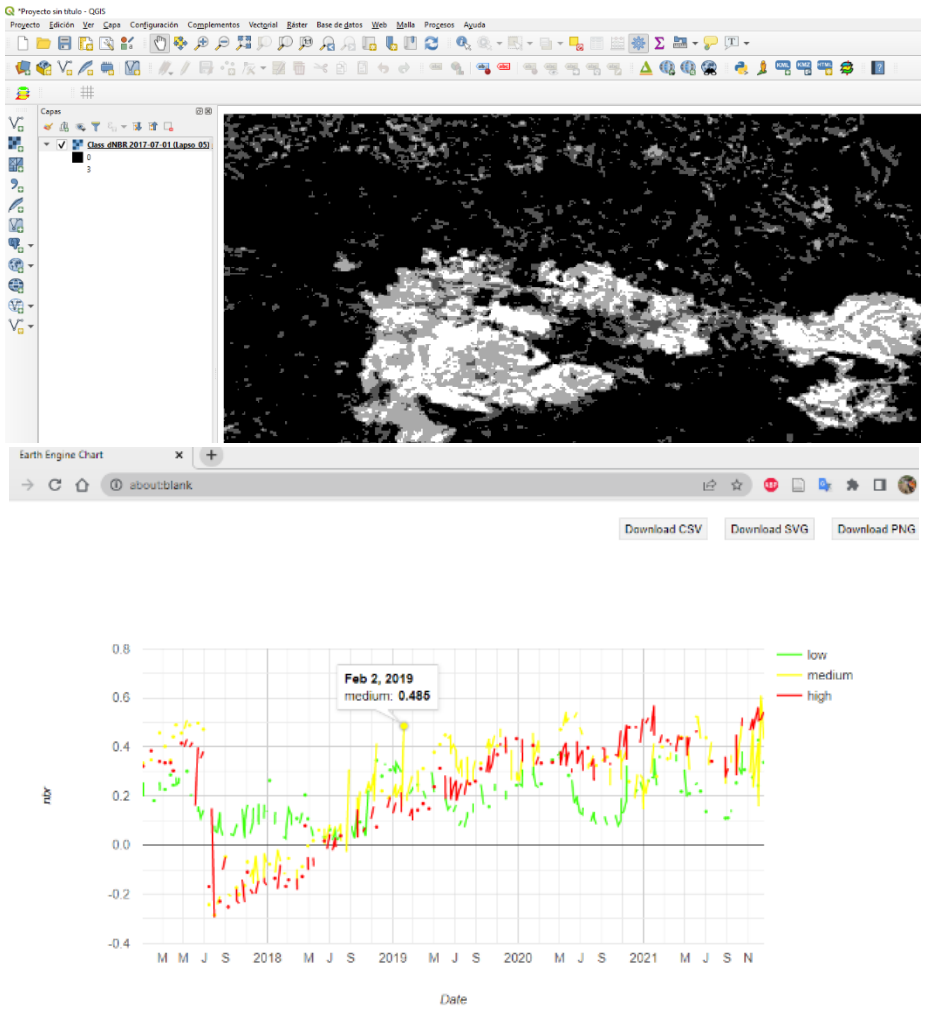

Figure 4: Results provided by BADE tool; 4.1. Map GEOTIFF; 4.2. Iterative Plot.

4. Discussion and Conclusion

The BADE tool allows users to use it easily even if they have no remote sensing experience. Moreover, it is very fast to use and does not require any software or programming knowledge to run it. It simply requires a web browser in which, thanks to its graphical interface, it is easy and intuitive to follow the necessary steps to obtain the results. This makes the tool of great potential for users who are less familiar with computer programs and who work with analysing, assessing or understanding forest fires from three different perspectives. Starting from the technical level, these users can use this support tool to make decisions on forest actions or planning. Then, at the research level, they can use this tool as a method to analyse multiple fires with identical methodologies in order to make meta-analyses or comparisons. At the educational level, this tool allows students to see the potential of remote sensing and new technologies to address the recovery of burned areas.

It is true that BADE needs to continue to incorporate more information for the user to select from all the outputs it generates. These new calculations to be presented and which will be incorporated in future versions will be focused on evaluating with greater precision this evolution, discriminating or differentiating areas with similar characteristics with the help of zonings that consider the physiography of the study area, seeing the trend that the vegetation presents or evaluating how long it takes for burnt areas to reach the pre-fire greenness value. All these improvements will allow managers to evaluate and recognise the study terrain in order to better target the works of action.

Therefore, among the limitations of the current tool are the information on post-fire recovery of vegetation: users know roughly what the average recovery of the entire burned area is like, but there is nothing spatial to help distinguish whether or not, where or when recovery is occurring.

It definitely seems that the tool has the basis to establish itself as a useful tool that should be further developed and complemented so that forest managers who are in contact with fieldwork and that the computer part is a little further away can use it in their daily work. It allows them to know and obtain information on post-fire vegetation quickly and easily without requiring great effort or expertise in remote sensing or programming.

5. Reference

Francos, M., Úbeda, X., Tort, J., Panareda, J.M., Cerdà, A., 2016. The role of forest fire severity on vegetation recovery after 18years. Implications for forest management of Quercus suber L. in Iberian Peninsula. Global and Planetary Change 145, 11–16. https://doi.org/10.1016/j.gloplacha.2016.07.016

González JR, Palahí M, Trasobares A, Pukkala T (2006) A fire probability model for forest stands in Catalonia (north-east Spain). Ann For Sci 63(2):169–176. https://doi.org/10.1051/forest

Keeley JE, Bond WJ, Bradstock RA et al (2012) Fire in Mediterranean ecosystems: ecology, evolution and management. Cambridge University Press.

Pereira JS, Pereira JMC, Rego F et al (2006) Incêndios florestais em Portugal: caracterização, impactes e prevenção. Instituto Superior de Agronomia, Lisboa.

White JD, Ryan KC, Key CC Running SW (1996) Remote Sensing of Forest Fire Severity and Vegetation Recovery. International Journal of Wildland Fire 6, 125-136.

Combining sentinel observations with plume backtrackings to improve wildfire detection

Rocío Baró*[1], Marie D. Mulder[1]; Delia Arnold[1,2]; Stefano Natali[3]; Ramiro Marco Figuera[3]; Marcus Hirtl[1]

[1] Zentralanstalt für Meteorologie und Geodynamik, 1190 Vienna, Austria, {rocio.baro-esteban, marie.mulder, marcus.hirtl}@zamg.ac.at
[2] Arnold Scientific Consulting, 08242 Manresa, Spain {delia.arnold-arias@zamg.ac.at}
[3] SISTEMA GmbH, Tiefer Graben 19 /2 1010 Vienna, Austria {natali, figuera}@sistema.at

**Corresponding author*

Keywords

Sentinel, FLEXPART, detection, smoke plume, backtracking

Abstract

Satellite observations are helpful in detecting wildfires. Especially in areas far from populated regions, satellite observations support the identification of wildfires and issuing warnings in case of a developing event. Occurrences of omission and commission errors have decreased significantly over the years, currently used methods focus mainly on improving and refining the already existing algorithms. Combining state-of-the-art earth observation data, specifically data from Sentinel missions, with modelling approaches may contribute to reduce detection errors. Most of the current methods to detect wildfires by earth observations mainly use a single satellite-based data source to retrieve surface information. Sentinel-3 and Sentinel-5P can be used as complementing data sources, the former is able to detect thermal anomalies in the surface, and the latter is capable of detecting direct fire emissions such as CO and HCHO in the atmosphere. The combined use with the Lagrangian particle dispersion model FLEXPART will allow the backtracking of fire emissions plus the aerosol mid height from Sentinel-5P to better identify wildfires sources. For this purpose, so called 'source-receptor sensitivities' are calculated, that provide information on the times and areas potentially contributing to the observed plume. Finally, identified wildfires can be validated using Sentinel-2 images. The innovation of our approach is to combine sentinel observations with atmospheric smoke plume simulations, by applying a dispersion model in backward mode to backtrack the possible source region of the smoke plume.

1. Introduction

During the last decades, there has been an increase in wildfires around the globe (Liu et al., 2010, Jolly et al., 2015). Climate change, with higher temperatures, lower humidity and significant changes in precipitation patterns, is the main factor raising the fire risk. When detecting wildfires by means of satellite instruments, the occurrence of false alarms is unavoidable. Over the last years, major improvements have been achieved to mitigate false alarms. Regarding wildfire detection errors, there are two types: the commission error (a non-existing fire is identified) and omission error (an existing fire is not detected). The former is the known as false alarm. Currently used methods focus mainly on improving algorithms of existing detection methods.

The main goal of this work is to improve the detection of wildfires by using state-of-the-art earth observation data, specifically data from the Sentinel missions, together with modelling approaches in a combined new methodology. This research-based methodology aims at reducing the number of false alarms while exploiting the new Sentinel data.

2. Methodology

The innovation of this work is to combine sentinel observations with atmospheric smoke plume simulations, by applying a dispersion model (with the Lagrarian particle dispersion model FLEXPART) in backward mode to backtrack the possible source region of the smoke plume. If this region coincides with the ground observation of the satellite instrument, it is expected that the detection has been successful. The method consists of exploiting

currently available data from Sentinel-5P (the first Sentinel instrument that observes atmospheric pollutants) combined with the fire confidence derived from the Fire Radiative Power (FRP) from Sentinel-3.

Figure 1 shows the designed work-flow of the methodology. Firstly, a smoke plume is identified with Sentinel-5P data, then the location of the actual fire can be confirmed or rejected by the fire confidence of Sentinel-3. Subsequently, with the dispersion model FLEXPART in backward mode the origin of the smoke plume can be confirmed. In case a high fire confidence is not given for the suspected fire location, the Sentinel 2 can provide evidence of a fire by showing the burned area.

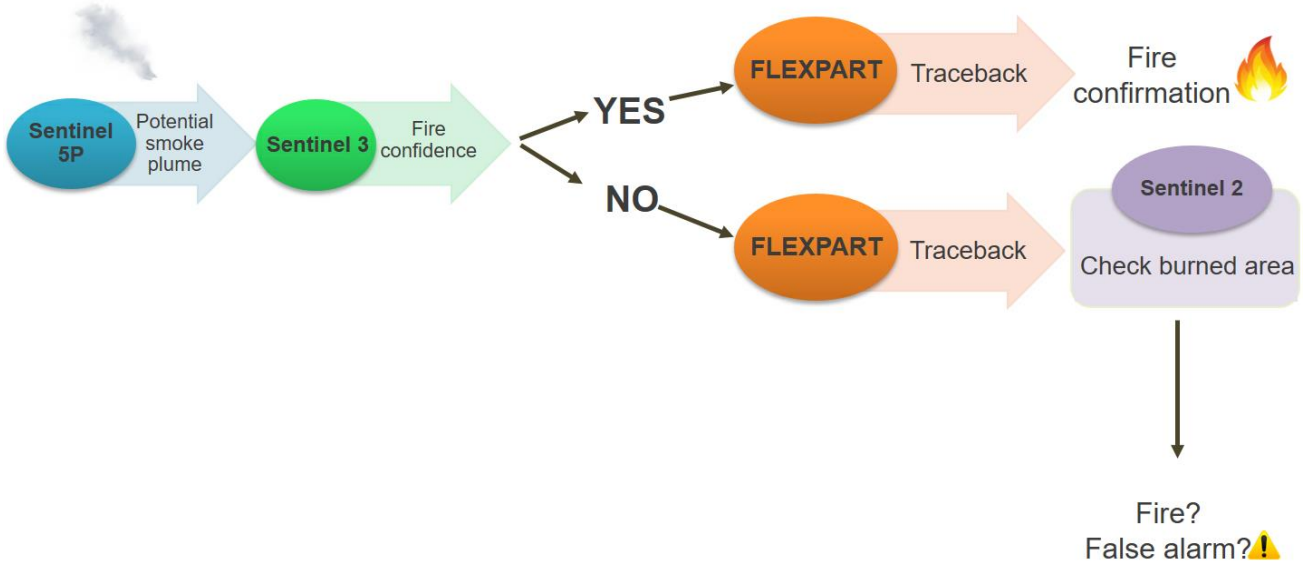

Figure 1. Work-flow including Sentinel-2,-3 and -5P products and dispersion model FLEXPART.

2.1. Sentinel satellites

For the development of this innovative method, the observations from three different Sentinel satellites will be used. Sentinel-5P and -3 provide observations for fire detection, while Sentinel-2 can be used for validation activities.

2.1.1. Sentinel 5P

Sentinel-5 Precursor (Sentinel-5P) is the first Copernicus satellite dedicated to monitor the troposphere, and provides daily global information on concentrations of trace gases (O_3, NO_2, SO_2, HCHO, CHOCHO, CO, CH_4) and aerosols. The mission consists of one satellite carrying the TROPOspheric Monitoring Instrument (TROPOMI) instrument. Its main objective is to perform atmospheric measurements with high spatial resolution (3.5 x 5.5 km), to be used for air quality, ozone and ultraviolet (UV) radiation, and climate monitoring. Because Sentinel-5P observes wildfires emissions (e.g. NO_2, CO, HCHO see figure 9), these observations could potentially be used for the early discovery of wildfires. Once a CO or HCHO plume is selected, in addition, the aerosol layer height product provides the altitude of localized layers of absorbing aerosols in the troposphere for cloud-free conditions.

2.1.2. Sentinel 3

Sentinel-3 has been developed to support ocean, land, atmospheric, emergency, security and cryospheric applications. Its main objective is to measure sea surface topography, sea and land surface temperature, and ocean and land surface colour, with high accuracy and reliability, to support ocean forecasting systems, environmental monitoring and climate monitoring. It carries the SLSTR instrument, a dual-view scanning temperature radiometer, which flies in low Earth orbit (800 - 830 km altitude). There are currently two instruments in orbit, on board the Sentinel-3A and Sentinel-3B satellites. They provide observations across the VIS-to-LWIR spectral range that can be used for active fire detection and FRP retrieval. SLSTR possesses specially designed ‘fire’ channels in the MIR and LWIR, allowing global characterisation of landscape FRP. As stated above, in this work we use the fire confidence derived from FRP, which gives us the information of the probability of a fire pixel.

2.1.3. Sentinel 2

Sentinel-2 consists of two polar-orbiting satellites, and carries an innovative wide swath high-resolution multispectral imager with 13 spectral bands for a new perspective of land and vegetation. The sensor owns one spectral band (band 12, SWIR, 2.190 µm, 20m resolution) that can be used to identify thermal anomalies on the ground. Forest management is included in its main applications. However, using it for validation purposes is not obvious, since it has a long repetition cycle (5 days) and it is difficult to define the fire detection thresholds for SWIR and MIR channels. Therefore, in this work, when available, Sentinel 2 will be used mainly to confirm fires detected by Sentinel 3 and Sentinel 5P and evaluate the accuracy of the method.

2.2. FLEXPART set-up

FLEXPART 10 (Pisso et al., 2019) has been used to simulate the atmospheric transport of wildfire smoke (Pisso et al., 2009, Alvarado et al., 2019 among others), and other types of plumes such as volcanic ash and radionuclides. It can be run in backward mode to provide information on possible source locations. For this purpose, so called 'source-receptor sensitivities' (SRS) are calculated, these provide information on the times and areas potentially contributing to the observed plume. FLEXPART output will also be processed further using a linear regression method. This method is suitable for poorly observed areas, for example, for source apportionment of unusual radionuclides observations, and will here be tested for wildfire plumes. Three selected Sentinel-5P products (CO and HCHO columns and aerosol mid-height) will provide information on plume characteristics needed for the FLEXPART simulations. For this effort, running the backtracking simulations with a tracer is sufficient, while any effort to quantify the sources is out of the scope of this work. FLEXPART will run with meteorological input from the ECMWF fields of the operational stream with a resolution of 0.125°.

3. Results and discussion

Two different test cases will be used from the Californian summer 2020 fire season. To test the developed methodology, the first test case concerns a fire for which observations from all three sentinels will be available. As a second test case, a comission error will be selected: where the Sentinel-3 fire confidence is high, however the combination of Sentinel-5P observations, FLEXPART simulations and, if available, Sentinel 2 data could not provide an estimation of the location of the fire. Here we present the observations of the first test case, where we selected a plume in southern California sensed on the 18th of September 2020. Figure 2 shows the Sentinel-5P CO and HCHO plumes, and in the second row, the Sentinel-5P Aerosol mid-height product and Sentinel 3 Fire confidence are shown.

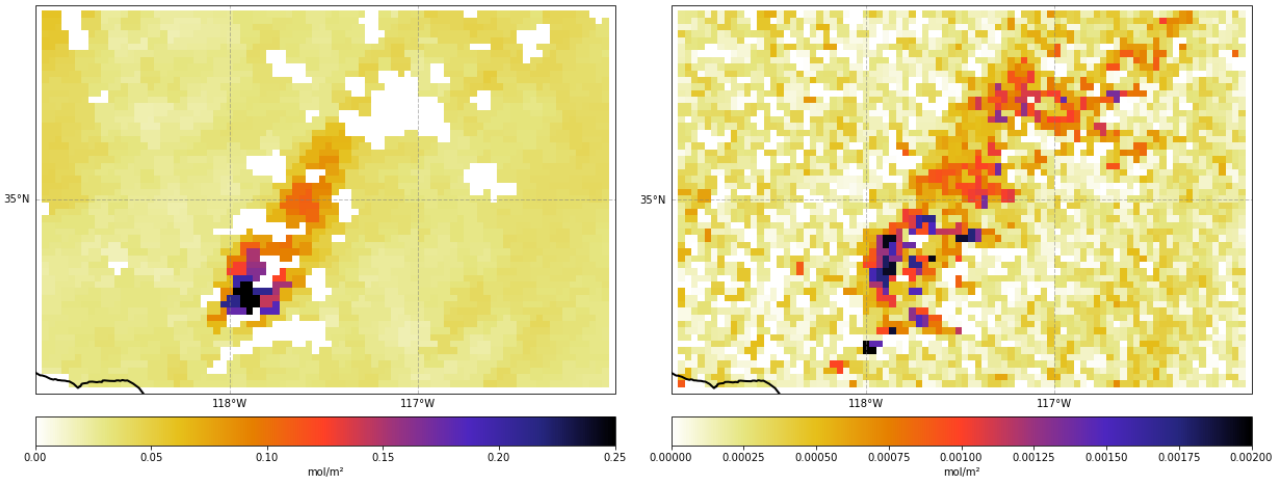

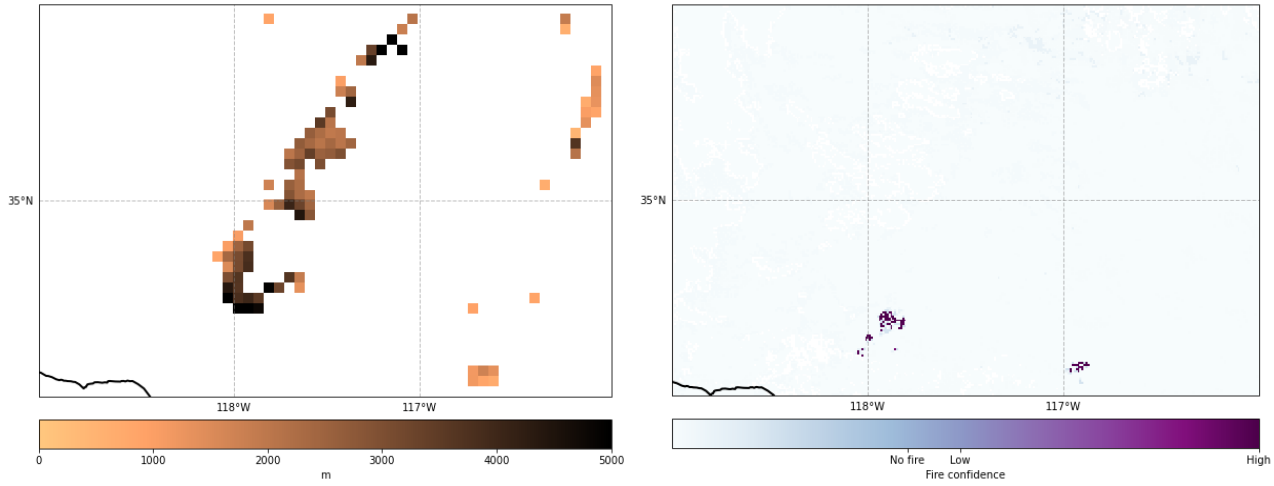

Figure 2. Plots of selected Sentinel satellite products of September 18, 2020. Top left: Sentinel 5P CO column in mol/m^2; Top right: Sentinel 5P HCHO column mol/m^2. Bottom left: Sentinel 5P Aerosol mid-height product in metres; bottom right: Sentinel 3 Fire confidence product derived from FRP.

Subsequently, from the Sentinel-5P products displayed in figure 2, the edges of the CO and HCHO plumes plus the maximum value(s) of the plume will be used as release points in the FLEXPART simulations. Information on the height of the plume will be obtained from the aerosol mid-height product. To evaluate the estimated location of the source of the plume, both the Sentinel-2 images and the Sentinel-3 fire confidence will be used. Finally, the detection is considered successful, if the estimation of the source location coincides with the location identified by the Sentinel-2 images and the Sentinel-3 fire confidence.

The Sentinel-5P CO observations provide relatively clear plume edges, see figure 2, top left, while the HCHO plot (top right) is more noisy yet not interrupted by clouds, hence complementing the CO observations. Circumventing the loss of information due to clouds, can partly abate the disadvantage of long revisiting times, at least of the Sentinel-5P satellite. When successfully tested, our approach paves the way for future applications with Sentinel-4 (launch expected in 2023), which will provide earth observations on a very high temporal resolution (hourly).

The innovation of this work is to combine satellite observations with atmospheric smoke plume observations, and by applying a dispersion model in backward mode to backtrack the possible source region of the smoke plume. To the authors´ knowledge, there are no other studies combining satellite observation and backtracking modelling technique.

4. References

Alvarado, L.M.A., Richter, A., Vrekoussis, M., Hilboll, A., Kalisz Hedegaard, A.B., Schneising, O., and Burrows, J.P.: Unexpected long-range transport of glyoxal and formaldehyde observed from the Copernicus Sentinel-5 Precursor satellite during the 2018 Canadian wildfires, Atmos. Chem. Phys. Discuss., 2020.

Jolly, W.M. et al., Climate-induced variations in global wildfire danger from 1979 to 2013. Nat. Commun. 6, 7537, 2015.

Liu, Y., Stanturf, J. and Goodrick, S., Trends in Global Wildfire Potential in a Changing Climate. Forest Ecology and Management, 259, 685-697, 2010.

Pisso, I., E. Real, K. S. Law, B. Legras, N. Bousserez, J. L. Attie, and Schlager, H., Estimation of mixing in the troposphere from Lagrangian trace gas reconstructions during long-range pollution plume transport, J. Geophys. Res., 114, D19301, 2009.

Pisso, I., Sollum, E., Grythe, H., Kristiansen, N. I., Cassiani, M., Eckhardt, S., Arnold, D., Morton, D., Thompson, R. L., Groot Zwaaftink, C. D., Evangeliou, N., Sodemann, H., Haimberger, L., Henne, S., Brunner, D., Burkhart, J. F., Fouilloux, A., Brioude, J., Philipp, A., Seibert, P., and Stohl, A., The Lagrangian particle dispersion model FLEXPART version 10.4, Geosci. Model Dev., 12, 4955–4997, 2019.

Comparative Analysis of Multisensor Burned Area Products for the Brazilian Amazon – Region of the APA Triunfo do Xingu

Carlos Tamasauskas*[1,2]; Abilio Pereira Pacheco[3,4]; Fantina Tedim[2,5]

[1] Operations and Management Center of the Amazon Protection System (Censipam). 66617-420 Belém-Brazil, {up201902228@g.uporto.pt}
[2] Centre of Studies in Geography and Spatial Planning (CEGOT) – FLUP Pole, Department of Geography, Faculty of Arts, University of Porto. 4150-564 Porto-Portugal
[3] INESC TEC and Faculty of Engineering, University of Porto. 4200-465 Porto-Portugal, {app@fe.up.pt}
[4] ForestWISE, Collaborative Laboratory for Integrated Forest & Fire Management. 5001-801 Vila Real-Portugal, {abilio.p.pacheco@gmail.com}
[5] Department of Geography, Faculty of Arts, University of Porto. 4150-564 Porto-Portugal, {ftedim@gmail.com}

**Corresponding author*

Keywords

Burned Area, Amazon, Fires, APA Triunfo do Xingu, Remote Sensing

Abstract

Fires are not natural phenomena of the Amazon rainforest, therefore, they occur due to human activities, and their occurrences have increased in recent years (Costa et al., 2022). This situation requires continuous monitoring of this vast region, especially in areas where agricultural, livestock, mining, and infrastructure activities are located near protected areas (indigenous lands and nature conservation units). One of the conservation units that has recorded the highest increases in deforestation and fire rates is the Triunfo do Xingu Environmental Protection Area (APA Triunfo do Xingu), which since 2018 has registered the highest rates among other conservation units in the Amazon. The present study aims to develop two databases of burned areas from optical and microwave images for the years 2018, 2019, and 2020 for the APA Triunfo do Xingu using Google Earth Engine; then the results are compared with the DETER, MAPBIOMAS and MCD64A1 burned area bases to estimate existing similarities and divergences. This research uses the images of the Sentinel-2/S-2 and Landsat-8/L-8 optical satellites for the month of August of the years 2018, 2019, and 2020, a period of increased occurrences of active fires in the APA Triunfo do Xingu, to generate the burned area database that will serve as a reference for comparison with other burned area databases. Thus, images with spatial resolution, S-2 with 10 meters and L-8 with 30 meters and spectral (red, near, and medium infrared bands), are suitable for generating information with geometric and thematic quality, as the GEE allows the production of pixel mosaics excluding pixels with cloud and cloud shadows. The Sentinel-1/S-1 images used correspond to the VH cross-polarization, which is the most suitable polarization to map burned area than the VV polarization (Prasasti et al., 2020), having 10 meters of spatial resolution, being with speckle noise filter and with backscatter (DB) values. It is noteworthy that the S-1 images correspond to Band C, the wavelength of 5 cm, which reduces the interference of clouds when imaging the surface. In general, the data sets presented many discrepancies between them, which shows the importance of having a methodology focused on specific areas, such as the Amazon, in order to generate a consolidated information base consistent with the reality of the regime of fire in the studied area. The spatial similarity between the data varied little, with the BA-S1 dataset having the highest overlap rates with the reference base of 19% for 2018, 63% for 2019, and 68% for 2020. Among optical sensor data, the BA-S2L8 datasets for the years 2018 and 2020, and BA-MAPBIOMAS, for the year 2019, presented the highest rates, being, respectively, 13% and 56% for BA -S2L8 and 50% for BA-MAPBIOMAS. We emphasize that the overlaps focused on polygons of burned areas smaller than 6.5 hectares, demonstrating the high spatial similarity between the datasets for small fire areas, despite the BA-MCD64A1 not being the best sensor to detect burns more minor than 100 hectares (Katagis and Gitas, 2022).

1. Introduction

Tropical forests are environments of significant ecological importance, mainly due to their high biodiversity and ecosystem services. However, they have suffered global losses estimated at 420 million hectares since the 1990s (FAO and UNEP, 2020) due to degradation processes and land-use conversion. The Amazon Forest

suffers from this problem, with deforestation and forest fires as the main elements of degradation and transformation of the forest into other uses (Ometto, Aguiar and Martinelli, 2011; dos Reis *et al.*, 2021).

Fires are not natural phenomena of the Amazon rainforest, therefore, they occur due to human activities, and their occurrences have increased in recent years (Costa *et al.*, 2022). This situation requires continuous monitoring of this vast region, especially in areas where agricultural, livestock, mining, and infrastructure activities are located near protected areas (indigenous lands and nature conservation units). One of the conservation units that has recorded the highest increases in deforestation and fire rates is the Triunfo do Xingu Environmental Protection Area (APA Triunfo do Xingu), which since 2018 has registered the highest rates among other conservation units in the Amazon.

The monitoring of fires by remote sensing is performed by recording the brightness temperature to infer high-temperature points that would be active fires (Yao *et al.*, 2020). In addition to registering active fires, mapping the burned area is of great importance for analyzing the fire risk, carbon emissions rates, and the effects of climate change on ecosystems (Liu, Popescu and Malambo, 2019). Although the first study on mapping burned areas was from 1974 and accurately mapped the limits of fire (Hitchcock and Hoffer, 1974) and, in recent decades, produced several data on burned areas on a global scale, such as GLOBCARBON (Plummer *et al.*, 2006), L3JRC (Tansey *et al.*, 2008), Fire_cci (Chuvieco *et al.*, 2018), currently, there is still much uncertainty in the total area affected by fires (Chuvieco *et al.*, 2019) and the products of burned area present many differences between them, which reveals the need for systematic studies on these differences (Humber *et al.*, 2019).

Due to the dense cloud cover that occurs in tropical regions, it is not easy to record phenomena on the surface of these regions. However, a solution is to use optical sensors with high temporal resolution or to use microwave sensors that have a significant ability to cross clouds according to their wavelength. In addition, monitoring large areas, such as Amazon, requires high computing power to process the data, which is currently possible through the Google Earth Engine/GEE platform, enabling access to an extensive collection of remote sensing images.

Thus, the present study aims to develop two databases of burned areas from optical (Sentinel-2 and Landsat-8) and microwave (Sentinel-1) images for the years 2018, 2019, and 2020 at APA Triunfo do Xingu by Google Earth Engine and then compare with the DETER, MAPBIOMAS and MCD64A1 burned area bases to estimate existing similarities and divergences.

2. Materials and Methods

2.1. Study Area

The Triunfo do Xingu Environmental Protection Area was created in 2006 through State Decree 2612 (PARÁ, 2006) with an approximate area of 1,679,280.52 hectares that covers the municipalities of Altamira and São Félix do Xingu. Its objectives are to protect biological diversity, plan the occupation of the territory, and guarantee the sustainable use of its natural resources. However, due to the advancement of farming and livestock activities, there is a growing disorderly occupation and unsustainable use of natural resources through the continuous increase in deforestation and forest degradation by the use of fire. The main economic activity that permeates APATX is cattle ranching, which exerts pressure for the conversion of forest areas into new pasture areas, and this pressure occurs both inside APATX and in the surrounding forests. This situation is reflected in its indication as the conservation unit with the highest rate of deforestation and presence of hotspots over the last few years.

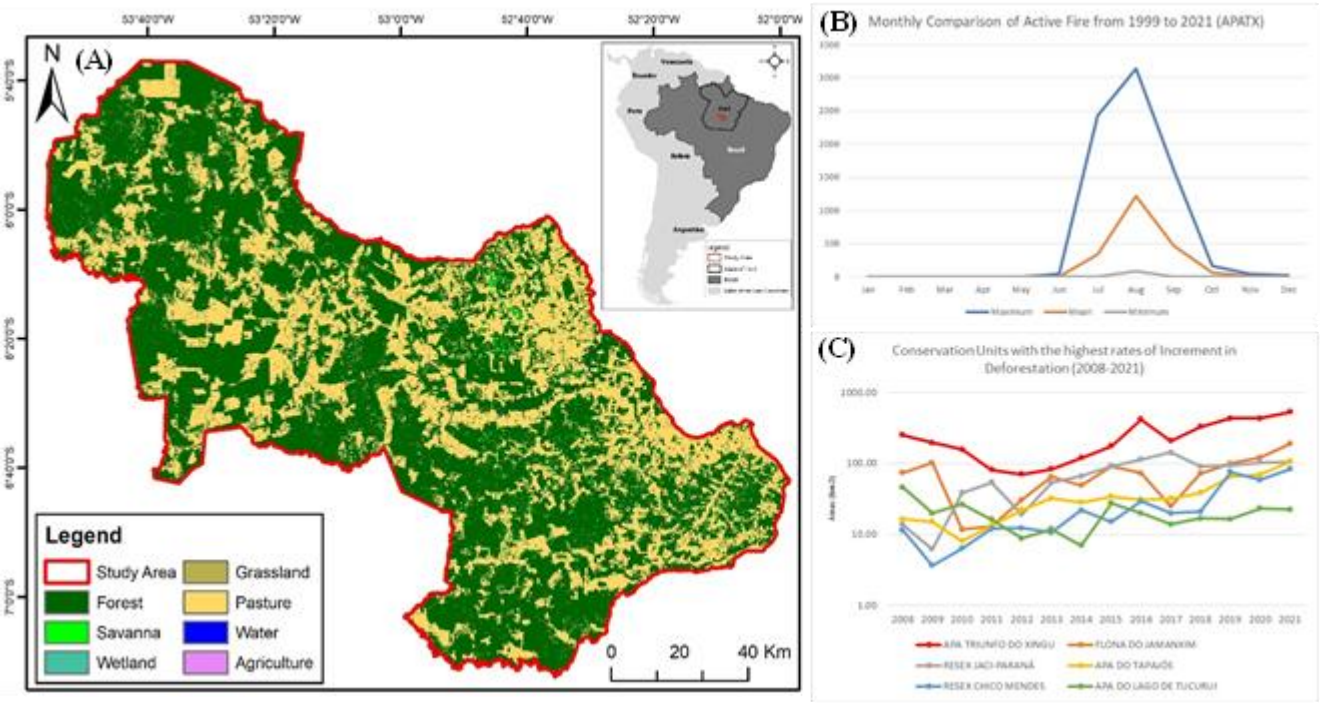

Figure 1- (A) Study Area Location: the APA Triunfo do Xingu located in the southeastern region of the State of Pará/Brazil. Land cover and land use information from the MAPBIOMAS Collection 5 for the year 2020. (B) Monthly comparison of the number of active fires between the years 1999 and 2021 for APATX. Data obtained from the Queimadas Program of INPE/Brazil. (C) Annual comparison of protected areas with the highest deforestation increment rates recorded between 2008 and 2021. Data obtained from the PRODES Program of INPE/Brazil.

2.2. Methodology

The study uses the images of the Sentinel-2/S-2 and Landsat-8/L-8 optical satellites for the month of August of the years 2018, 2019, and 2020, a period of increased occurrences of active fires in the APA Triunfo do Xingu, to generate the burned area database that will serve as a reference for comparison with other burned area databases. Thus, images with spatial resolution, S-2 with 10 meters and L-8 with 30 meters and spectral (red, near, and medium infrared bands) are suitable for generating information with geometric and thematic quality, as the GEE allows the production of pixel mosaics excluding pixels with cloud and cloud shadows.

The Sentinel-1/S-1 images used correspond to the VH cross-polarization, which is the most suitable polarization to map burned area than the VV polarization (Prasasti et al., 2020), having 10 meters of spatial resolution, being with speckle noise filter and with backscatter (DB) values. It is noteworthy that the S-1 images correspond to Band C, the wavelength of 5 cm, which reduces the interference of clouds when imaging the surface.

The processing of the S-2 and L-8 images generated a mosaic of images with minimal presence of clouds and cloud shadows for the month of August of the years 2018, 2019, and 2020. Then, calculate the Burned Area Index (BAI), which highlights pixels with spectral response referring to the absorption of radiation with the biomass burning process. Thus, after identifying the pixels with signs of burning, the image is sliced into determined groups of pixel values and the intersection of the group referring to the burned area with the vectors of active fires obtained from the database of active fires from INPE/Brazil. The intersected pixels are exported as vectors of the burned area class to the GEE database.

The processing of S-1 images starts from the mosaic of images available in each week of the month of August of the year under study. After the mosaic, the change detection processing is performed using the Log-Ratio operator. This logarithmic ratio will highlight the pixels that had a change in values between 2 time periods. Then, I realized the image segmentation process (SNIC), texture index creation (GLCM), and principal component analysis (PCA) to highlight the most significant objects in the images. Subsequently, selected samples for training and classification with the Random Forest classifier. Finally, according to the processing

flow below, intersected the classification results with the active fire data and exported the final result as a burned area database.

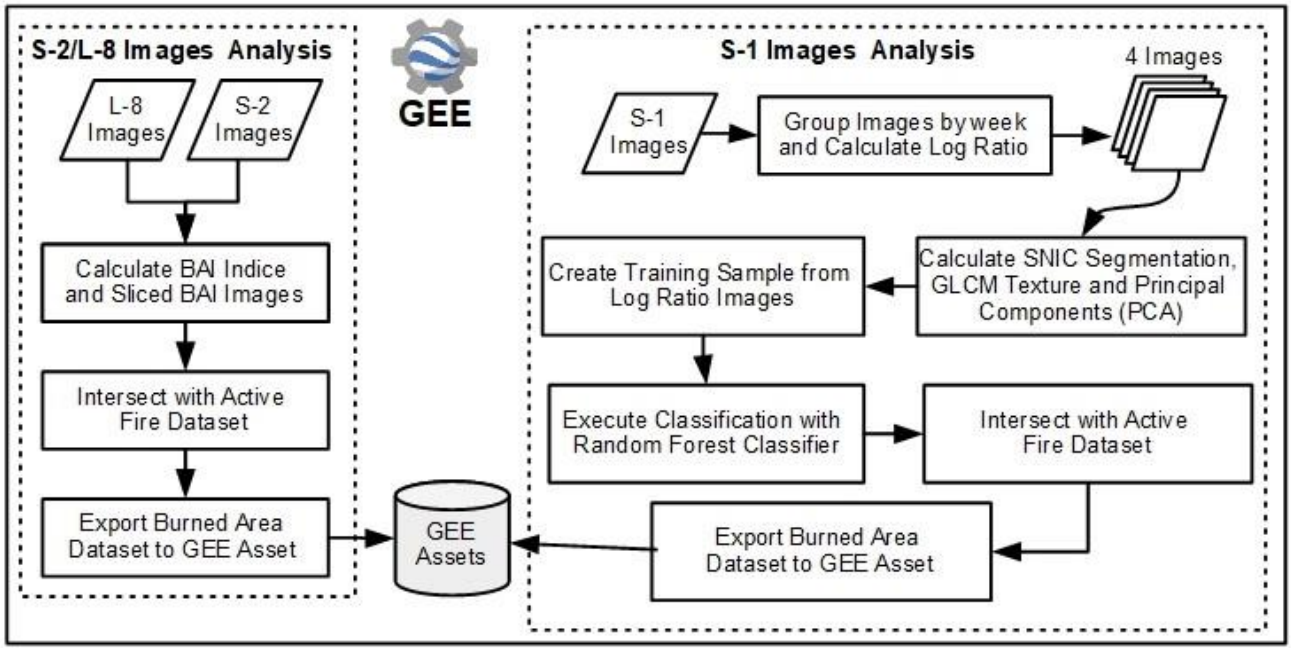

Figure 2 – Images Processing Flow

The burned area data (DETER, MAPBIOMAS, and MCD64A1) are obtained from their electronic addresses and converted into vector shapefile format. It is noteworthy that due to methodological differences between the data, a normalization was carried out with the selection of vectors with a minimum area above 1 hectare. Finally, the comparative analysis evaluated the number of polygons generated in each dataset, their areas, and the overlap rate of the dataset to the reference base, which is the MCD64A1, as the dataset obtained the highest precision for the burned area class at the global level (Padilla *et al.*, 2015).

3. Results and Discussion

The results below demonstrate that for the years 2018, the year with the lowest occurrence of active fires, 2019 and 2020, years that had an increase in active fires, the BA-DETER dataset was the one with the most significant discrepancy in the values of the number of polygons, maximum area and the sum of areas, this is justified because it is a data aimed at alerts and not only to determine the burned area. The reference base (MCD64A1) was different in all the years in the minimum area values, which is due to its spatial resolution being 500 meters. The BA-MAPBIOMAS dataset was the one that had the highest values of the number of polygons in all years, which can be explained by its mapping methodology that operates at the Landsat-8 satellite pixel scale (30 meters). The BA-S1 dataset was the most similar to the reference dataset in terms of maximum area. On the other hand, the BA-S2 dataset was discrepant in all aspects of area in relation to the reference base, which denotes that the difference in spatial resolution has a strong influence on the mapping of the burned area.

Tabela 1- Dataset Area Values

	August 2018 Statistics				
	BA - S2L8	**BA - S1**	**BA - DETER**	**BA - MAPBIOMAS**	**BA - MCD64A1**
Number of Polygons	177	46	4	875	102
Minimum Area	1	1	9	1	24
Maximum Area	2344	189	41	1947	237
Sum of Areas	18537	1048	110	17455	4398
Mean of Areas	105	23	27	20	43

August 2019 Statistics					
	BA - S2L8	**BA - S1**	**BA - DETER**	**BA - MAPBIOMAS**	**BA - MCD64A1**
Number of Polygons	784	1345	153	2048	1861
Minimum Area	1	1	2	1	13
Maximum Area	10066	2375	245	4222	2128
Sum of Areas	152326	36666	4834	69330	93378
Mean of Areas	194	27	32	34	50
August 2020 Statistics					
	BA - S2L8	**BA - S1**	**BA - DETER**	**BA - MAPBIOMAS**	**BA - MCD64A1**
Number of Polygons	772	1471	229	4783	2045
Minimum Area	1	1	1	1	7
Maximum Area	16214	1949	723	3125	1986
Sum of Areas	120419	37585	13877	85217	125222
Mean of Areas	156	26	61	18	61

In general, the data sets presented many discrepancies between them, which shows the importance of having a methodology focused on specific areas, such as the Amazon, in order to generate a consolidated information base consistent with the reality of the regime of fire in the studied area.

The spatial similarity between the data varied little, with the BA-S1 dataset having the highest overlap rates with the reference base of 19% for 2018, 63% for 2019, and 68% for 2020. Among optical sensor data, the BA-S2L8 datasets for the years 2018 and 2020, and BA-MAPBIOMAS, for the year 2019, presented the highest rates, being, respectively, 13% and 56% for BA -S2L8 and 50% for BA-MAPBIOMAS. We emphasize that the overlaps focused on polygons of burned areas smaller than 6.5 hectares, demonstrating the high spatial similarity between the datasets for small fire areas, despite the BA-MCD64A1 not being the best sensor to detect burns more minor than 100 hectares (Katagis and Gitas, 2022).

4. Conclusions

Wildfires are human source phenomena that are present and growing in several areas of the Amazon, being more recurrent in environments naturally prone to fire, such as the cerrado, and areas of expansion of productive activities, mainly livestock and commercial agriculture. The APA Triunfo do Xingu is affected by this dynamic of growth of productive activities and the problems inherent to them, such as deforestation and fires.

The mapping of burned areas in the Amazon still faces many obstacles, especially the limitation of optical sensors in the observing regions with a strong incidence of clouds and the lack of monitoring of the region that uses microwave images, which reduce the problem of limitations of the clouds.

Despite some datasets of burned areas facing the Amazon, there is still a lot of disagreement in the values of burned areas and little spatial similarity between the datasets since we found between 50% and 64% of overlap between some datasets and the reference base. New studies covering longer time intervals and areas with different fire regimes and land use are essential to understanding the limitations that affect the mapping of burned areas. From 2018, the increase in fires inside the APA began, and this problem has worsened since then. Thus, it is of great importance to search for new approaches that allow improving the continuous monitoring of the Amazon, with a focus on deforestation and recording areas burned by fires.

5. References

Chuvieco, E. *et al.* (2018) ‘Generation and analysis of a new global burned area product based on MODIS 250 m reflectance bands and thermal anomalies’, *Earth System Science Data*, 10(4), pp. 2015–2031. Available at: https://doi.org/10.5194/essd-10-2015-2018.

Chuvieco, E. *et al.* (2019) 'Historical background and current developments for mapping burned area from satellite Earth observation', *Remote Sensing of Environment*, 225, pp. 45–64. Available at: https://doi.org/10.1016/j.rse.2019.02.013.

Costa, M.A.M. *et al.* (2022) 'Forest Fires in the Brazilian Amazon and their Effects on Particulate Matter Concentration, Size Distribution, and Chemical Composition', *Combustion Science and Technology*, 0(0), pp. 1–27. Available at: https://doi.org/10.1080/00102202.2021.2019229.

FAO and UNEP (2020) *The State of the World's Forests 2020: Forests, biodiversity and people*. Rome, Italy: FAO and UNEP (The State of the World's Forests (SOFO), 2020). Available at: https://doi.org/10.4060/ca8642enAlso Available in:Chinese Spanish Arabic French Russian.

Hitchcock, H.C. and Hoffer, R.M. (1974) 'MAPPING A RECENT FOREST FIRE WITH ERTS-1 MSS DATA.', *Conf on Earth Resour Obs and Inf Anal Syst, Remote Sensing of Earth Resour*, 3, pp. 449–461.

Humber, M.L. *et al.* (2019) 'Spatial and temporal intercomparison of four global burned area products', *International Journal of Digital Earth*, 12(4), pp. 460–484. Available at: https://doi.org/10.1080/17538947.2018.1433727.

Katagis, T. and Gitas, I.Z. (2022) 'Assessing the Accuracy of MODIS MCD64A1 C6 and FireCCI51 Burned Area Products in Mediterranean Ecosystems', *Remote Sensing*, 14(3), p. 602. Available at: https://doi.org/10.3390/rs14030602.

Liu, M., Popescu, S. and Malambo, L. (2019) 'Feasibility of Burned Area Mapping Based on ICESAT−2 Photon Counting Data', *Remote Sensing*, 12(1), p. 24. Available at: https://doi.org/10.3390/rs12010024.

Ometto, J.P., Aguiar, A.P.D. and Martinelli, L.A. (2011) 'Amazon deforestation in Brazil: effects, drivers and challenges', *Carbon Management*, 2(5), pp. 575–585. Available at: https://doi.org/10.4155/cmt.11.48.

Padilla, M. *et al.* (2015) 'Comparing the accuracies of remote sensing global burned area products using stratified random sampling and estimation', *Remote Sensing of Environment*, 160, pp. 114–121. Available at: https://doi.org/10.1016/j.rse.2015.01.005.

PARÁ (2006) 'Decreto Estadual N. 2612, de 4 de dezembro de 2006. Dispõe sobre a criação da Área de Proteção Ambiental Triunfo do Xingu.' Available at: https://www.semas.pa.gov.br/2006/12/04/9672 (Accessed: 28 June 2022).

Plummer, S. *et al.* (2006) 'Establishing A Earth Observation Product Service For The Terrestrial Carbon Community: The Globcarbon Initiative', *Mitigation and Adaptation Strategies for Global Change*, 11(1), pp. 97–111. Available at: https://doi.org/10.1007/s11027-006-1012-8.

dos Reis, M. *et al.* (2021) 'Forest fires and deforestation in the central Amazon: Effects of landscape and climate on spatial and temporal dynamics', *Journal of Environmental Management*, 288, p. 112310. Available at: https://doi.org/10.1016/j.jenvman.2021.112310.

Tansey, K. *et al.* (2008) 'A new, global, multi-annual (2000–2007) burnt area product at 1 km resolution', *Geophysical Research Letters*, 35(1), p. L01401. Available at: https://doi.org/10.1029/2007GL031567.

Yao, J.Q. *et al.* (2020) 'Amazon Fire Monitoring and Analysis Based on Multi-source Remote Sensing Data', *IOP Conference Series: Earth and Environmental Science*, 474(4), p. 042025. Available at: https://doi.org/10.1088/1755-1315/474/4/042025.

Comparison of the effect of one-way and two-way fire-wind coupling on the modelling of wildland fire propagation dynamics

Mohammad T. Sadrabadi*[1]; Mauro S. Innocente*[1]; Evangelos Gkanas[2]; Ioannis Papagiannis[1,2]

[1]*Autonomous Vehicles & Artificial Intelligence Laboratory (AVAILAB).*
{tavakolsam, Mauro.S.Innocente, papagiai}@uni.coventry.ac.uk
[2]*Centre for Advanced Low Carbon Propulsion Systems (C-ALPS) {evangelos.gkanas@coventry.ac.uk}*
Centre for Future Transport and Cities, Coventry University, Priory Street, Coventry CV1 5FB, UK

**Corresponding authors*

Keywords

Wildland fire, WFDS Level-set, static wind field, two-way coupling.

Abstract

Operational wildland fire propagation models are typically uncoupled from the wind field or they rely either on estimations extracted from an atmospheric model or on meteorological observations. This leads to a frozen wind field (one-way coupling) with a high degree of uncertainty, thus drifting away from the ground truth. In contrast, fully-coupled models (two-way coupling) comprise more accurate representations of the real phenomena, although they are not viable for operational use due to the hefty computational effort they entail. This article investigates and compares the effects of one-way and two-way wind-fire coupling on the predicted propagation of wildfires. The models are validated against experimental data obtained from grassland experiments carried out by the Commonwealth Scientific and Industrial Research Organisation (CSIRO) in Australia. Simulations are carried out on a flat surface and for different wind speeds. Two scenarious are considered, one with and the other without an obstactle affecting both the wind flow and the wildfire propagation. Results from the simulations indicate that the burnt area and the rate of spread (RoS) are both smaller in two-way coupled than in one-way coupled models.

1. Introduction

Wildfire propagation modelling is remarkably challenging due to the complexity that results from its multi-physics and multiscale characteristics (Grasso and Innocente 2020). Chemical energy is converted into thermal energy during combustion as a result of a high-temperature (exothermic) chemical reaction between a fuel and oxygen. This energy is then transferred to the surrounding unburnt fuel, which ignites if a sufficiently high temperature is reached (ignition temperature). Whilst combustion is a chemical phenomenon, energy transfer is a physics phenomenon that occurs on domains ranging from millimetres to kilometres (Sullivan 2009a). Sullivan classified techniques for modelling wildland fire spread into three categories: *physical models* (Sullivan 2009a), *empirical models* (Sullivan 2009b), and *mathematical analogue models* (Sullivan 2009c). In turn, Innocente and Grasso (2019) classified wildfire propagation models into *theoretical models* (mechanistic, possibly physics-based), *data-driven models* (constructed from or fitted to actual or synthetic data), and *mechanistic surrogate models* (mechanisms not directly related to the phenomena being modelled).

A forest fire substantially affects the wind patterns in the immediate area. Rather than regular wind patterns, localised flow structures are generated by the interaction of atmospheric wind and the convection caused by the flaming combustion front. Thus, precisely forecasting fluctuations in wind velocity components produced by the presence of the fire in the boundary layer around its location is critical for effective fire behaviour prediction (Lopes et al., 2017). Several physics-based models such as FIRETEC (Linn et al. 2002), WFDS (Mell et al. 2007), CAWFE (Clark et al. 1996a; Clark et al. 1996b), WRF-FIRE, ForeFire/Mesho-NH (Filippi et al. 2010), and others have been developed and utilised to model wildfire propagation at various scales. However, these models have not been used within operational settings (Marino et al., 2012; Lopes et al., 2017) due to the computational resources required and the resulting slower-than-real-time simulations. Conversely, operational models such as FARSITE (Finney 1996) produce fast simulations at the expense of removing or weakening their links to the laws that govern the underlying physics. These are characteristically data-driven or mechanistic surrogate models, which only provide information on the propagation of fire lines. Furthermore, they are usually

decoupled from or partially coupled with atmospheric models and therefore do not capture the effect of complex wind patterns on the fire dynamics (Bakhshaii and Johnson 2019). They simulate fire propagation using inputs from an atmospheric model and/or meteorological observations resulting in a frozen wind field unaffected by the fire (Bakhshaii and Johnson 2019). These static wind fields are typically calculated by diagnostic models such as WindNinja (Wagenbrenner et al. 2016) and Nuatmos (Ross et al. 1988). The immediate effect of using these models is an increase in the uncertainty of their output (Bakhshaii and Johnson 2019). A more recent study on the effect of two-way fire-wind coupling in (Lopes et al. 2017) suggests that this results in a significantly smaller burnt area than the one obtained with one-way coupled simulations. Later, Lopes et al. (2019) performed simulations with one-way and two-way coupling and reported that, even though both models over predict the fire area, two-way coupling performs better and provides values which are closer to the real data.

To the best of the authors' knowledge, limited research has focused on the effect of one-way and two-way fire-wind coupling on the simulated propagation of wildfires. Since this may differ depending on the combination of fuel, wind and topography, this paper is limited to flat lands covered with short grass. Two scenarios are considered, one with and the other without obstacles to the wind flow and wildfire propagation, aiming to investigate the effect of the formation of complex wind patterns. Simulations are performed using the WFDS level set model for point fire ignition in both two-way and one-way coupled conditions, and results are compared at different times from ignition.

2. WFDS Level-set method

An extension of the structural Fire Dynamics Simulator (FDS) for vegetative fuels developed by the National Institute of Standards and Technology (NIST) in the United States is the so-called Wildland-Urban Interface Fire Dynamics Simulator (WFDS). The governing equations for buoyant flow, heat transfer, combustion, and the thermal degradation of vegetative fuels are solved using computational fluid dynamics techniques. Solving gas-phase equations on computational grids that are too coarse to directly resolve precise physical events requires large-eddy simulations (LES). WFDS offers three models for simulation of wildland fires, including (1) particle mode, (2) boundary fuel model, and (3) level set method. The *Particle Mode* and the *Boundary Fuel Model* rely on physical principles and may employ grid resolutions as fine as 1 m in their basic implementations (Vanella et al. 2021). They require the thermo-physical parameters of the vegetative fuels whilst they calculate the fire rate of spread (RoS). Conversely, the propagation of the fire front in surface wildfires is modelled based on empirical principles only in the *Level Set Method*. A model for vegetation deterioration is not included, and the no-wind no-slope fire rate of spread (RoS_0) for various kinds of vegetation and wind speeds must be set (Vanella et al., 2021). Variations in the way wind and fire interactions are modelled allow for more than one version of this method. In this paper, we adopt the *Level Set Method* due to its capability of carrying out simulations with both one-way and two-way fire-wind coupling.

3. Results and Discussion

3.1. Validation of results

Simulation results are compared to experimental data obtained from grassland experiments carried out by the Commonwealth Scientific and Industrial Research Organisation (CSIRO) in Australia (Cheney et al., 1998). The selected experiment is the C064, which was performed in the midlle of summer with fully dried kerosene grass on a 100×100 m^2 field with wind gusts of 4.6 m/s, grass height of 0.21 m, and a measured RoS of 1.2 m/s.

For the validation of the two-way coupled model, the class 1 Albini fuel models is used with some modifications, including the height changed from 0.3 m to 0.21 m and and Surface Area to Volume Ratio changed form 11500 to 9770. The resulting fire front position for three different mesh sizes of 1, 3 and 5 m is presented in figure 1, which shows that the *Level Set Method* underpredicts the fire propagation when compared to experimental data. Besides, reducing the mesh size appears to decrease the RoS of the simulated fire.

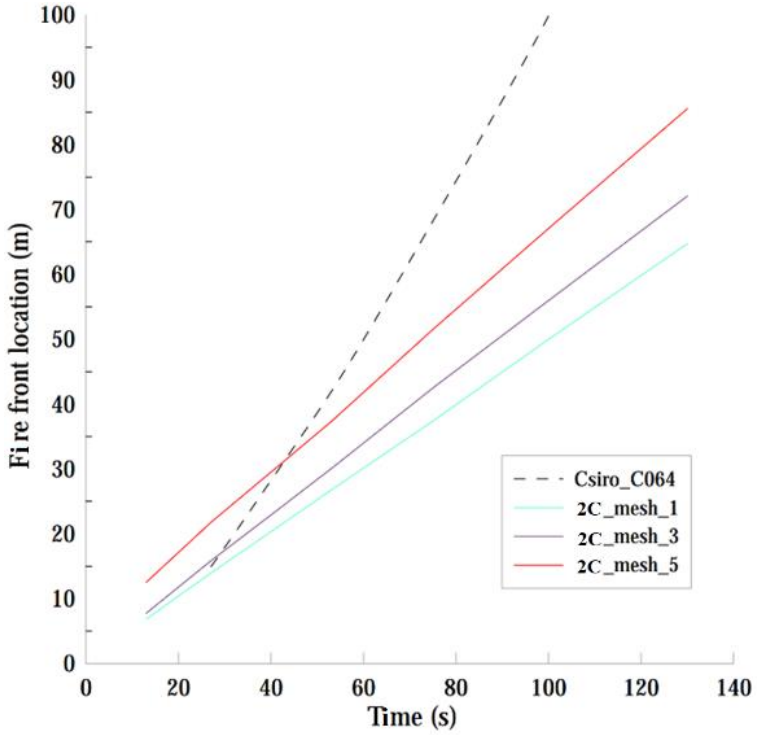

Figure 1- Comparison of fire front position with experimental data of CSIRO-C064 for different mesh sizes.

3.2. Simulations results

The WFDS *Level Set Method* in its two modes, namely one-way (1C) and two-way (2C) fire-wind coupling, is utilised to perform simulations under different conditions to assess the effect of the type of coupling on the prediction of the wildfire propagation. Fire simulations are performed in a 100×100×20 m^3 (x,y,z) domain with a uniform mesh size of 1×1×1 m^3. This results in 100 cells in the x-, 100 cells in the y-, and 20 cells in the z-direction. The fuel is modelled by the type 1 Rothermel-Albini fuel model called "short grass", with a fuel depth of 0.3 m and no-wind no-slope RoS_0 = 0.03 m/s (McGrattan et al. 2019). Fire is ignited at the centre of the fuel area after the wind field has developed. The first mode consists of using a frozen wind field, which is the one developed by the time the fire is ignited. The wind field remains constant for the duration of the simulation. The second mode is a fully coupled simulation, in which the wind is affected by the fire latent heat as it propagates. Figure (2) presents the burnt area 100 s after the fire is ignited, over plain vegetation, for four wind speeds between 1 m/s and 10 m/s, and for both coupling modes: figures (a-d) for one-way coupling or static wind field (1C), and figures (e-h) for two-way coupling or dynamic-wind field (2C). Figure (3) shows the same but in the presence of an obstacle to study the effect of the formation of complex wind structures on the fire propagation.

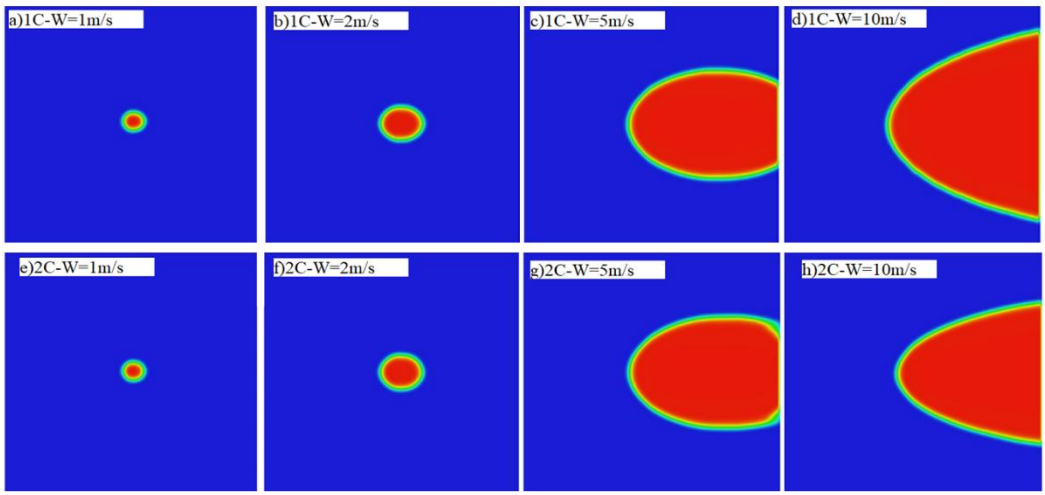

Figure 2- Burnt area at plain surface vegetation in one-way coupling (1C) and two-way coupling (2C) modes.

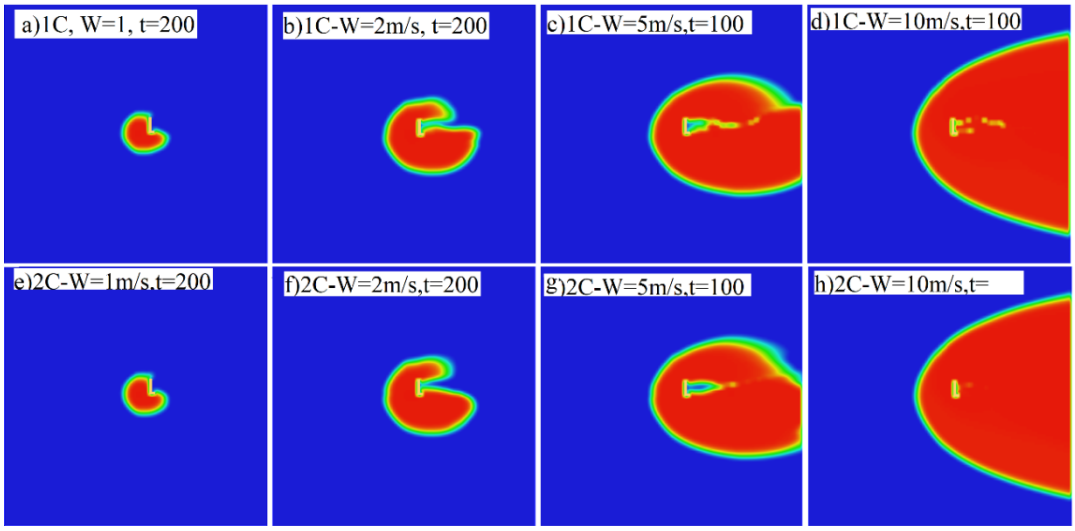

Figure 3- Burnt area at the plain surface with obstacles in one-way coupling (1C) and two-way coupling (2C) modes.

Results indicate that the burnt area is smaller for fully coupled simulations than for frozen wind field, and this difference appears to increase as the fire front propagates. In fact, the RoS is slower in two-way than in one-way coupling, which agrees with (Lopes et al., 2017). For the case with an obstacle, the wind field is highly dynamic, and the fire lines differ significantly depending on the coupling. Furthermore, increasing the wind speed (especially above 5 m/s), the fire intensity increases significantly and the RoS increases exponentially.

Figure (4) presents the fire area for a wind speed of 5m/s at different stages of fire propagation in 1C and 2C modes. As can be seen, the area and shape of the burnt area and fire front at different times of the fire propagation differ substantially. The fire front in two-way coupling is affected significantly by the wind structure. This is directly related to the in-draft flow caused by the convection column, which is not accounted for in the frozen wind field approach and becomes more dominant as the fire propagates over a larger area.

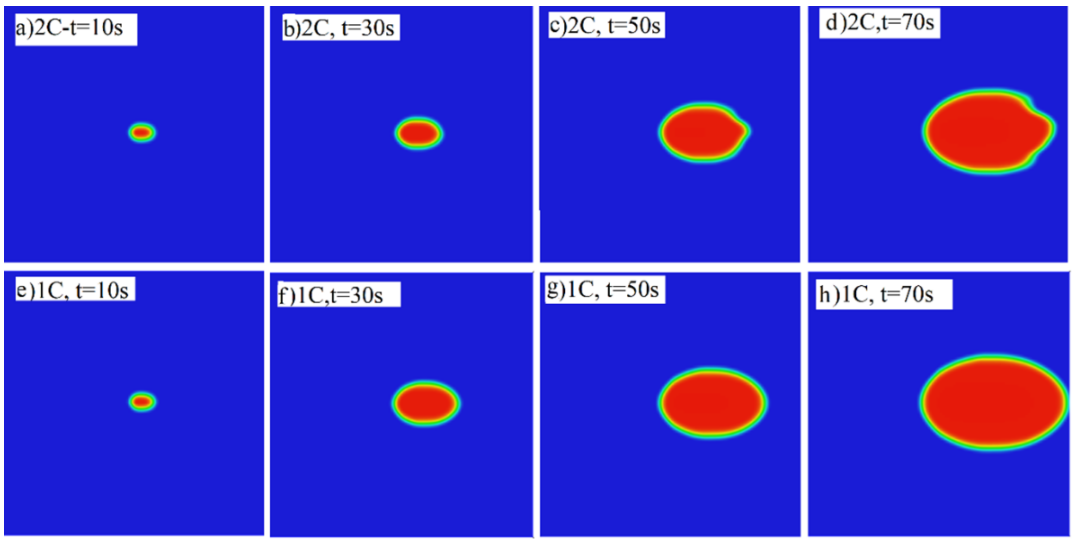

Figure 4- Burnt area at plain surface vegetation in one-way coupled (1C) and two-way coupled (2C) modes at different times.

Figure (5) presents the wind field around and above the fire, which induces the shape of the fire front. The wind which passes above the fire is heated by the latent heat and moves upwards (updraft column). This induces an inward wind field (indraft flow) from the flanks towards the centre line of the fire (green lines), which in turn induces the new shape of the fire front and reduces its RoS compared to the one-way coupling. Figure (6) presents the wind field at different times of the fire propagation for the cases with and without obstacles in wind

speed equal to 5 and 4.6 m/s, respectively, with the fire line depicted in white. The indraft flow at the rear sides of the front fire is clearly visible (figure 6 a-e). Besides, a low-speed zone which turns to recirculation flow forms in front of the fire. This seems to be responsible for reducing the fire RoS in two-way coupled simulations. Variations of the vortex area and structure behind the obstacle is depicted in figure (6 f-j). It is indicated that the area of the vortex behind the obstacle is reduced as the fire front propagates, yet it is the main responsible for the slow propagation of the fire front behind the obstacle, especially in two-way coupled simulations.

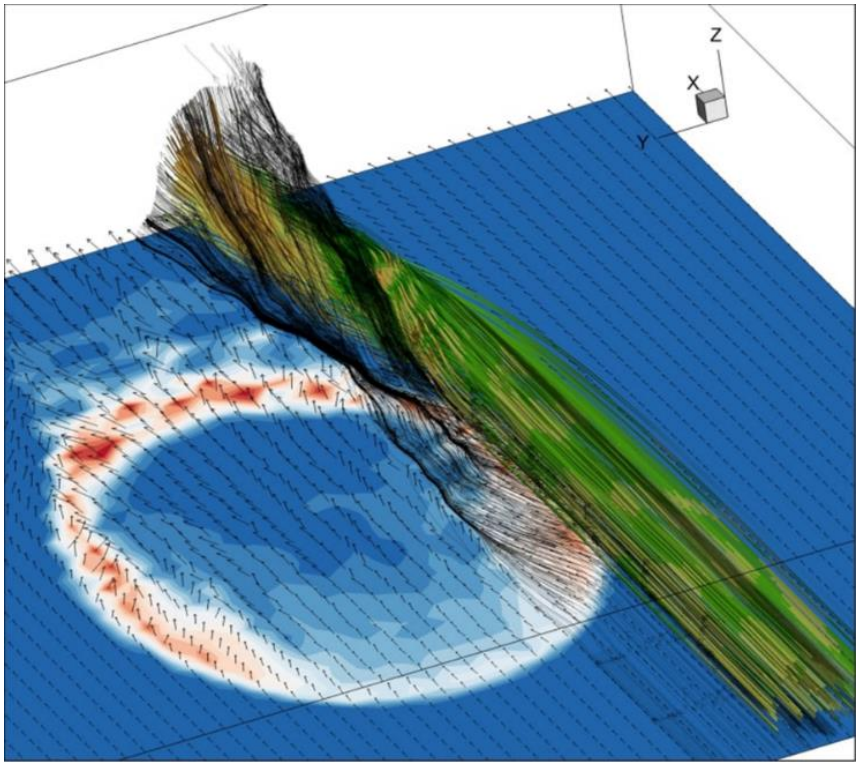

Figure 5- Wind field around and above the fire line.

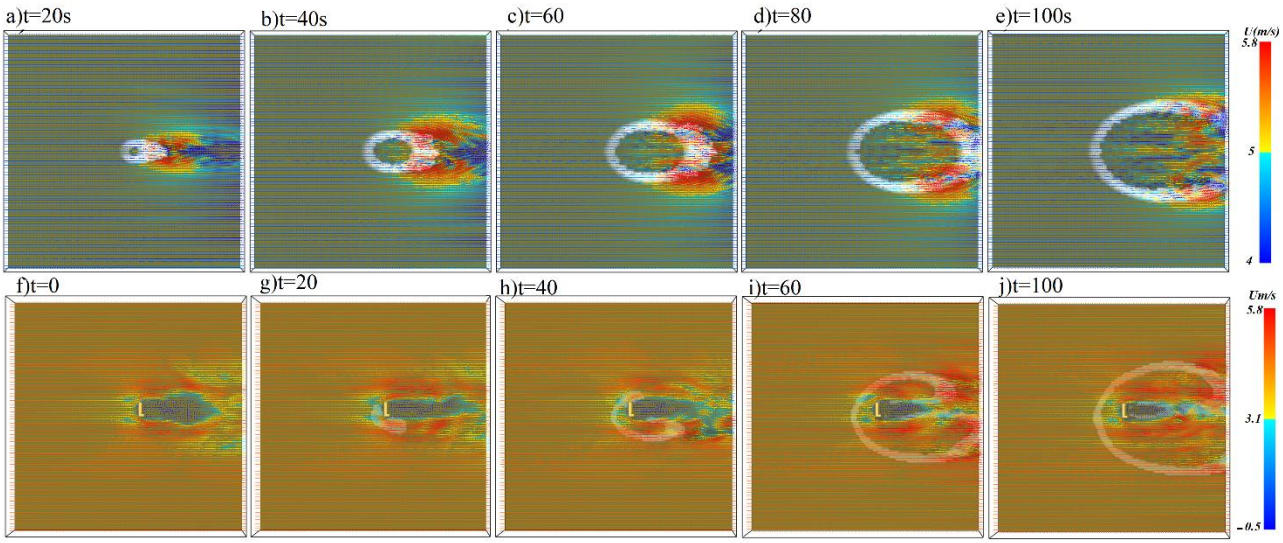

Figure 6- Wind field at z = 1m above the ground in different stages of fire propagation.

4. Conclusion

This paper discusses the effect of utilising one-way and two-way fire-wind coupling strategies on the simulation of wildfire propagation on a flat land covered with short grass, with and without the presence of obstacles. It is observed that the rate of spread (RoS) of the front line in the two-way fire-wind coupling is lower than that for

one-way coupled simulations. It is hypothesised that the main reason for this behaviour is the formation of the indraft flow from the back front and flanks of the fire front caused by the updraft column convection, as well as the formation of wind recirculation (vortex) zones in front of the fire line. It is also observed that the vortex structure behind the obstacle becomes smaller as the fire spreads behind the structure, and yet it reduces the fire propagation speed and its intensity in these areas.

5. Acknowledgements

Part-funded by the Lloyd's Register Foundation International Consortium of Nanotechnologies (ICON-2018-45) and part-funded by Institute for Clean Growth and Future Mobility (CGFM).

6. References

Bakhshaii, A. and E. A. Johnson (2019). "A review of a new generation of wildfire–atmosphere modeling." Canadian Journal of Forest Research, 49(6): 565-574.

Cheney, N., Gould, J., & Catchpole, W. (1998). Prediction of Fire Spread in Grasslands %J International Journal of Wildland Fire. 8(1), 1-13. doi: https://doi.org/10.1071/WF9980001

Clark, T., M. Jenkins, J. Coen and D. Packham (1996). "A Coupled Atmosphere-Fire Model: Role of the Convective Froude Number and Dynamic Fingering at the Fireline". International Journal of Wildland Fire. 6(4): 177-190.

Clark, T. L., M. A. Jenkins, J. Coen and D. Packham (1996). "A Coupled Atmosphere-Fire Model: Convective Feedback on Fire-Line Dynamics", Journal of Applied Meteorology and Climatology. 35(6): 875-901.

Filippi, J. B., F. Bosseur, X. Pialat, P.-A. Santoni, S. Strada and C. J. J. o. C. Mari (2010). "Simulation of Coupled Fire/Atmosphere Interaction with the MesoNH-ForeFire Models". Journal of Combustion, 2011: 1-13.

Finney, M.A., FARSITE: Fire Area Simulator-model development and evaluation 1998, UT: U.S. Department of Agriculture, Forest Service, Rocky Mountain Research Station: Ogden. p. 47.

Grasso, P. and M.S. Innocente (2018). "A two-dimensional reaction-advection-diffusion model of the spread of fire in wildlands". In Advances in Forest Fire Research 2018 (pp. 334-342). Imprensa da Universidade de Coimbra. doi: 10.14195/978-989-26-16-506_36.

Grasso, P. and M. S. Innocente (2020). "Physics-based model of wildfire propagation towards faster-than-real-time simulations." Computers & Mathematics with Applications 80(5): 790-808. doi: 10.1016/j.camwa.2020.05.009.

Innocente, M. S. and P. Grasso (2019). "Self-organising swarms of firefighting drones: Harnessing the power of collective intelligence in decentralised multi-robot systems." Journal of Computational Science 34: 80-101. doi: 10.1016/j.jocs.2019.04.009.

Linn, R., J. Reisner, J. J. Colman and J. Winterkamp (2002). "Studying wildfire behavior using FIRETEC", International Journal of Wildland Fire. 11(4): 233-246.

Lopes, A. M. G., L. M. Ribeiro, D. X. Viegas and J. R. Raposo (2017). "Effect of two-way coupling on the calculation of forest fire spread: model development", International Journal of Wildland Fire. 26(9): 829-843.

Lopes, A. M. G., Ribeiro, L. M., Viegas, D. X., & Raposo, J. R. (2019). Simulation of forest fire spread using a two-way coupling algorithm and its application to a real wildfire. Journal of Wind Engineering and Industrial Aerodynamics, 193, 103967. doi: https://doi.org/10.1016/j.jweia.2019.103967

Marino, E., J.-L. Dupuy, F. Pimont, M. Guijarro, C. Hernando and R. Linn (2012). "Fuel bulk density and fuel moisture content effects on fire rate of spread: a comparison between FIRETEC model predictions and experimental results in shrub fuels.", International Journal of Wildland Fire, 30(4): 277-299.

McGrattan, K., R. McDermott, S. Hostikka and J. Floyd (2019). Fire Dynamics Simulator (Version 5) User's Guide. N. B. a. F. R. Laboratory. National Institute of Standards and Technology (NIST), Maryland, USA., NIST Special Publication 1019-5.

Mell, W. E., M. A. Jenkins, J. S. Gould and P. B. J. I. J. o. W. F. Cheney (2007). "A physics-based approach to modelling grassland fires.", International Journal of Wildland Fire, 16: 1-22.

Ross, D. G., I. N. Smith, P. C. Manins and D. G. Fox (1988). "Diagnostic Wind Field Modeling for Complex Terrain: Model Development and Testing , Journal of Applied Meteorology and Climatology." 27(7): 785-796.

Sullivan, A. L. (2009a). "Wildland surface fire spread modelling, 1: Physical and quasi-physical models", International Journal of Wildland Fire. 18(4): 349-368.

Sullivan, A. L. (2009b). "Wildland surface fire spread modelling, 2: Empirical and quasi-empirical models", International Journal of Wildland Fire. 18(4): 369-386.

Sullivan, A. L. (2009c). "Wildland surface fire spread modelling, 3: Simulation and mathematical analogue models", International Journal of Wildland Fire. 18(4): 387-403.

Vanella, M., K. McGrattan, R. McDermott, G. Forney, W. Mell, E. Gissi and P. Fiorucci (2021). "A Multi-Fidelity Framework for Wildland Fire Behavior Simulations over Complex Terrain.", atmosphere, 12(2): 273.

Wagenbrenner, N. S., J. M. Forthofer, B. K. Lamb, K. S. Shannon and B. W. Butler (2016). "Downscaling surface wind predictions from numerical weather prediction models in complex terrain with WindNinja." Atmos. Chem. Phys. 16(8): 5229-5241.

Creating a forest disturbance dataset for continental Portugal

Eduardo Fernandes*; Carlos Viegas Damásio; João Moura Pires

NOVA LINCS and Departamento de Informática of NOVA School of Science and Technology.
Quinta da Torre, 2829-516 Caparica, Portugal,
{efa.fernandes@campus.fct.unl.pt}, {cd, jmp}@fct.unl.pt

**Corresponding author*

Keywords

Dataset, forest disturbance, changepoint detection, time series, Landsat

Abstract

Quality data is of the utmost importance to effectively evaluate any classification technique. In the realm of remote sensing, more precisely forest disturbance, different studies use different custom datasets. This paper shows the methodology used to create a forest disturbance dataset for continental Portugal. The dataset contains 664 forest points generated from a stratified random sampling based on the tree species and climate zone covering continental Portugal. Every point contains the auxiliary data used and a thorough list of all years where a disturbance occurs and the respective reason for the disturbance; the years span from 1986 until 2019.

The analysis was performed with the Google Earth Engine platform for a fast and flexible solution, tailored to the dataset's needs. To complement the satellite time series, five auxiliary datasets were used to understand the cause of the disturbances and increase confidence.

The resulting dataset shows known differences among various parts of the county. While the north area of the study contains a bigger number of points with multiple disturbances, the south is exactly the opposite with an abundance of undisturbed points. These asymmetries are also reflected in the species present in these different regions.

This dataset may be of interest for studies that need to evaluate forest disturbance techniques, or even changepoint detection techniques, and it may also be useful in studies that focus on differentiating types of forest recovery.

The dataset is available on GitHub at https://github.com/EduardoFAFernandes/portuguese-forest-disturbance-dataset/ 3

1. Introduction

In the remote sensing community, there have been studies that propose or improve disturbance detection techniques, either covering all types of land-covers (Kennedy et al., 2010; Zhu & Woodcock, 2014) or focusing only on forests areas (Brooks et al., 2014; Vogelmann et al., 2012). All face a common challenge: evaluating their approaches. Some make a qualitative evaluation (Vogelmann et al., 2012) while others strive for a quantitative evaluation that inherently needs solid reference data (Brooks et al., 2014; Huang et al., 2010; Vogelmann et al., 2012; Zhu & Woodcock, 2014). Obtaining this type of data is not easy and the aforementioned studies even felt the need to create their datasets. TimeSync (Cohen et al., 2010) was created for this purpose, it is a tool to visualise Landsat time series and collect annotated data; this tool is used in (Kennedy et al., 2010) and (Cohen et al., 2017) to generate disturbance datasets for the USA. We have created our tool to do this type of analysis, the reason will be explained in **Section 2.3**.

This paper will describe the creation of a forest disturbance dataset for continental Portugal and perform a small analysis and interpretation of the collected data.

This work was partially supported by Fundação para a Ciência e a Tecnologia (FCT.IP) through project Floresta Limpa (PCIF/MOG/0161/2019) and NOVA LINCS (UIDB/04516/2020).

2. Materials and Methods

To create the dataset three main steps were taken. The first step was to select points to be analysed. The second step was to gather auxiliary information like fires and land cover data to support evaluation, and to create a sample that would be representative of continental Portugal. The third and final step consisted of individually validating and analysing every point using Landsat time series, auxiliary information, and historical images from Google Earth Engine (GEE) (Gorelick et al., 2017).

2.1. Points to Evaluate

To select only points from forest areas two data sources were used: Inventário Florestal Nacional (IFN) the Portuguese forest inventory and a custom climate region dataset created with feedback from IPMA. To know what species were present at every point we sampled the latest available IFN at the time (2015), using a stratified random sampling based on the species and the climate region. For the species stratification, the classes in IFN 2015 were used, namely: Acacias, Carob Tree, Chestnut, Cork Oak, Eucalyptus, Holm Oak, Maritime Pine, Oak, Other Hardwoods, Other Softwoods, and Stone Pine. Regarding the climate region, five distinct regions were used: North Coastal, North Interior, Centre Coastal, Centre Interior, Alentejo and Algarve.

2.2. Auxiliary Information

Four official data sources were considered relevant for the creation of the dataset describing land cover, species, and burned areas (see **Table 1** and **Figure 1**), the datasets, have been regularly updated throughout the years providing a more complete and detailed history of the forest. Every property in the resulting dataset is represented by a list of values that represent the history of that property across all updates. For instance, if a point has the IFN species list [“Oak”, “Oak”, “Oak”, “Eucalyptus”], this represents that between 2010 and 2015 there was a change in the species present in that point. To gather this information, we intersected the points to evaluate with the auxiliary data sources, and only the precise point locations were taken into account.

Table 1 - Data sources used with their respective updates and the relevant properties that were extracted. (1*https://geocatalogo.icnf.pt/catalogo_tema3.html ; 2*https://geocatalogo.icnf.pt/catalogo_tema5.html ; 3*https://snig.dgterritorio.gov.pt/rndg/srv/por/catalog.search#/search?anysnig=COS&fast=index ; 4*https://land.copernicus.eu/pan-european/corine-land-cover)

Data Source Name	Updates	Relevant properties	Source
Inventário Florestal Nacional (IFN)	1995, 2005, 2010, 2015	id, land cover, species	1*
Burned Area Cartographic Data	Yearly from 1975 until 2018	id, year	2*
Carta de Uso e Ocupação do Solo (COS)	1995, 2007, 2010, 2015	id, land cover	3*
CORINE Land Cover (CLC)	1990, 2000, 2006, 2012	id, land cover	4*

2.3. Point Analysis Methodology

Next, we analysed each point individually supported by our own developed GEE application that, for a particular point, presents the auxiliary information, a Landsat satellite image of the area surrounding the point and the NDVI and NBR time series from 1985 onwards (**Figure 2)**. The index NDVI provides information about vegetation health, while NBR is used to confirm fire occurrences. The time series are interactive; one can click a particular observation and view the respective satellite image for obtaining additional visual context. The time series and RGB images are obtained from the Landsat program remote sensing imagery from missions 4, 5, 7 and 8, collection 1 tier 1 calibrated to top-of-atmosphere reflectance due to the adequate timespan for our objective (as detailed in **Figure 1**). While we could use TimeSync to create this type of dataset, GEE offers a more customizable product at the expense of requiring more user knowledge. The main difference was the temporal resolution of the analysed time series, TimeSync uses annual Landsat composites while our solution uses all the available observations.

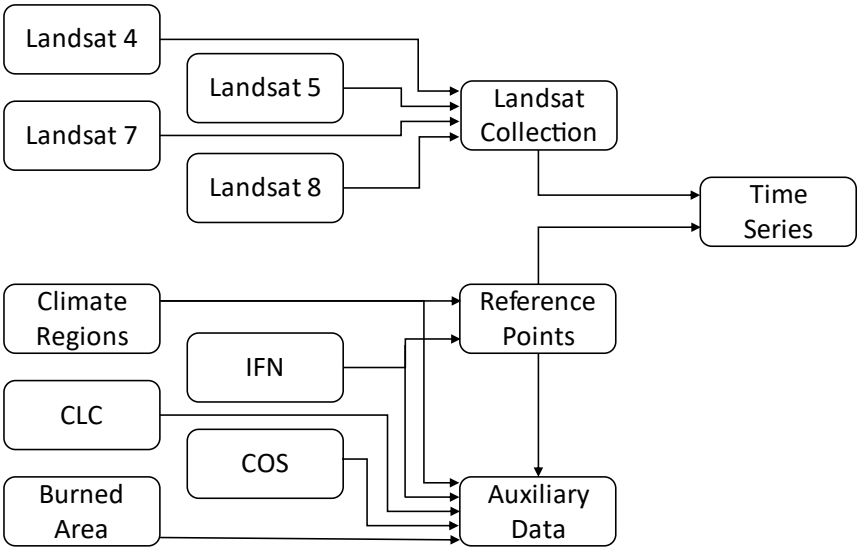

Figure 1 - Diagram of the workflow inputs

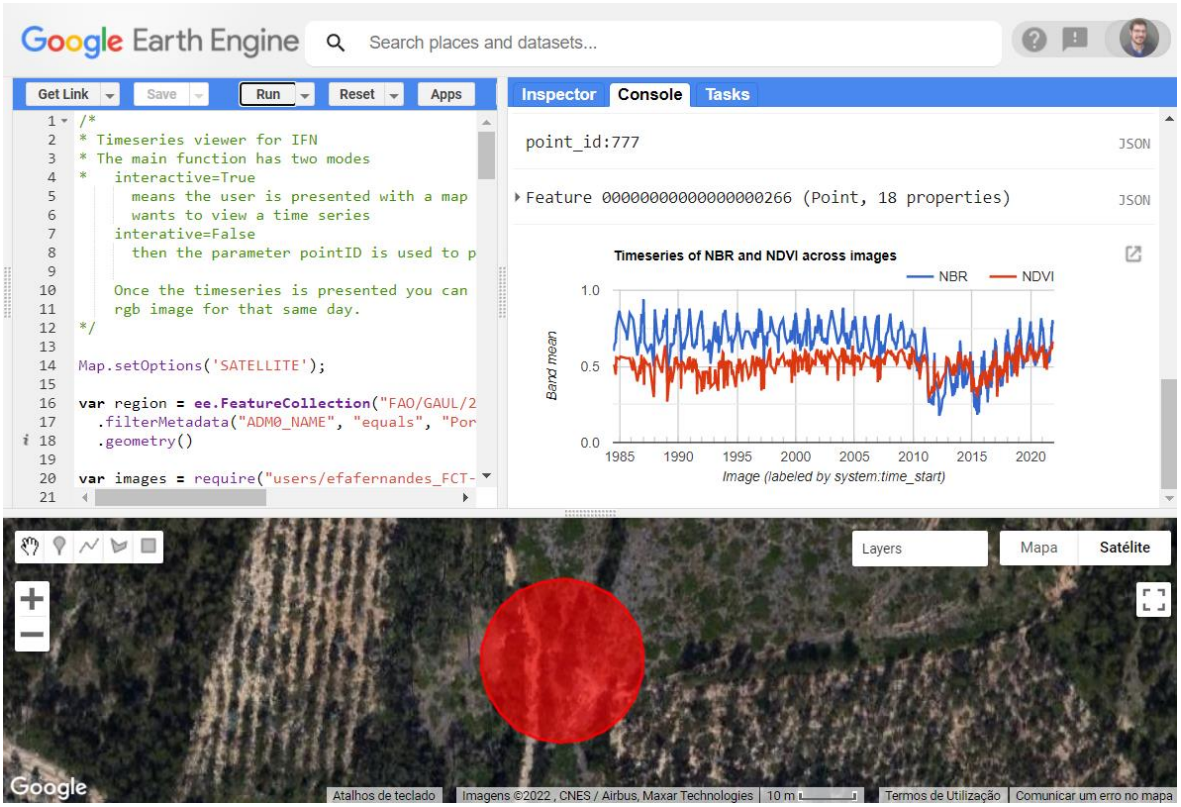

Figure 2 - GEE interface with interactive timeseries, satellite image and auxiliary information. The red circle indicates area to be analysed. In the time series plot we can observe two breakpoints.

The analysis of each point proceeded in three distinct steps described below: validation of the point, selecting changepoints and understanding the cause of the changepoint.

To validate one point, the surrounding circular area with a radius of 15m must meet four conditions. The area must not contain an artificial area, for example, if an area contains buildings or large roads as depicted in **Figure 3a** it is invalidated. The area must not be a low-density tree area, for example, if most of the area is bare soil or ground vegetation as shown in **Figure 3b** the point is considered invalid. The area must be a contiguous plot of land, if the area contains multiple plots of forest area with substantial differences as seen in **Figure 3c** then the

point is invalidated. The final condition is related to the time series, its analysis must be conclusive and decisive, if the time series is somehow erratic, hard to analyse or raises doubt, the point may be invalidated and classified as "other reason".

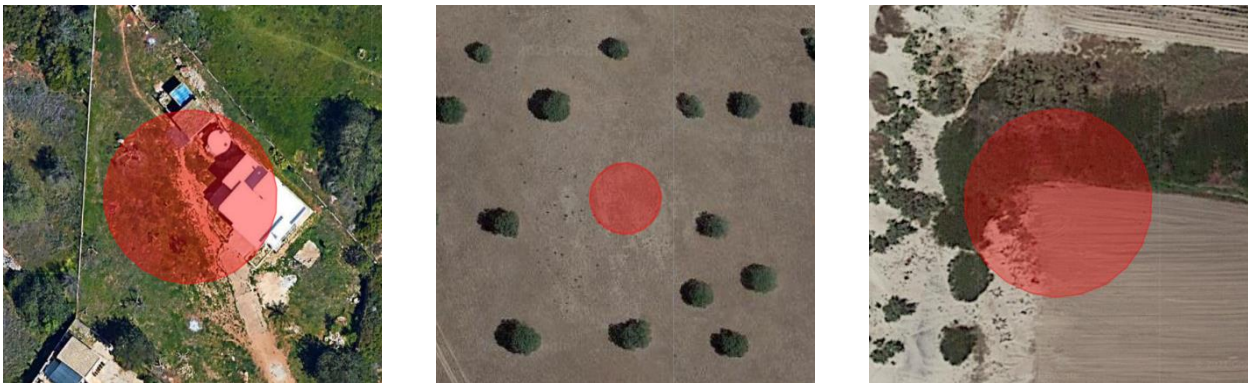

a. Artificial area ***b. Low-density area*** ***c. Different plots of land***

Figure 3 - Examples of three reasons for invalidation

After validating a point, the second step is to look at the time series and determine when the disturbances occur. In Figure 4, we find an NBR index time series with four clear moments where a disturbance occurs, these happen in the years a) 1987, b) 1997, c) 2005 and d) 2015. Not all time series are as clear as this one, some require a more thorough analysis.

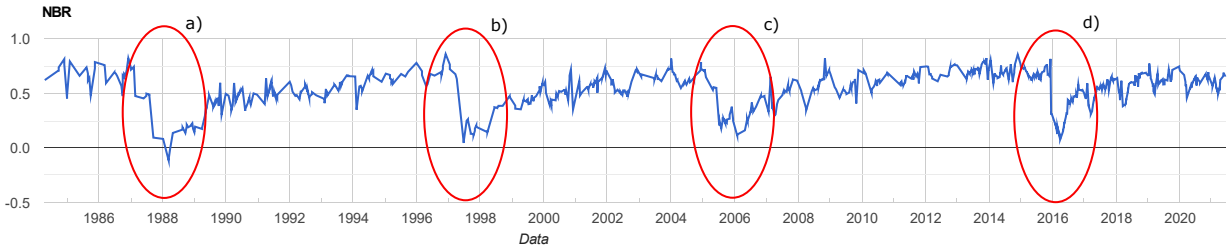

Figure 4 - Example of an NBR time series with four marked changepoints

The third step requires us to understand the cause of the disturbances, this is achieved by cross-referencing information throughout the auxiliary data described in **section 2.2** and using historic high-resolution satellite images from Google Earth Pro (GEP). For this dataset, four changepoint causes were considered: fire, harvest, unknown and other. Continuing with the example in **Figure 4** the auxiliary data says that fires occurred in the years 1987 and 2005, resulting in the annotation of Fire as the cause for changepoint a) and c). The remaining auxiliary data specifies that a eucalyptus forest has always occupied this point. Using GEP, it was possible to deduce that d) is most likely caused by a harvest. With the available data it was not possible to conclude what caused changepoint b) it will be marked as unknown.

3. Results

Having the dataset fully annotated we can turn our attention to its analysis. We will first examine the reason for invalidation, secondly their causes, thirdly we will assess the number of disturbances per valid point and finally evaluate the causes for the disturbances. It should be noted that oak, other softwoods, carob tree and acacias have an extremely small number of samples. Therefore, although represented in the figures, they will not be considered when extracting general conclusions based on species.

3.1. Number of invalidations

From a total of 998 sample points, 664 were considered valid and 334 were deemed invalid. This invalidation is not equally distributed through the species and consequently not uniformly distributed through the study area. When analysing **Figure 5**, we can see that the south and interior of the country have a higher density of invalidated points. The south of Portugal is dominated by cork oak, and we can see that this species is more

affected by invalidation than eucalyptus or maritime pine. The next subsection section will further explain this asymmetry.

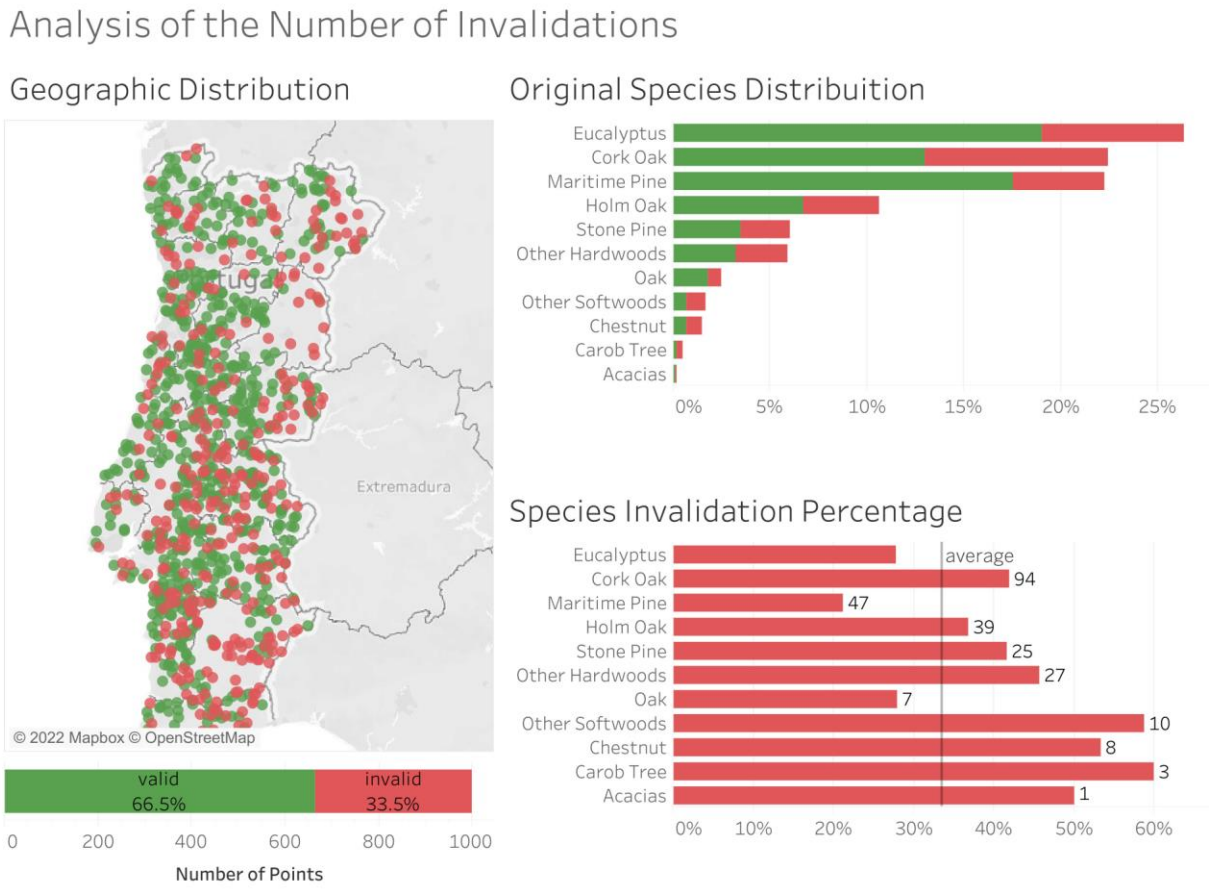

Figure 5 - Dashboard analysing the number of invalidations

3.2. Cause of invalidations

The primary cause for invalidation is low density closely followed by difficult analysis (see **Figure 6**). Once again there is a geographical asymmetry, with low density being predominant in the south and the interior of the country, this is the main reason these areas have a higher density of invalidated points, and consequently why cork oak has a relatively high number of invalidated points. These areas tend to be low density and populated by cork oak just as depicted in **Figure 3b**. We can see that the primary reasons species are invalidated are low density or other. Although this rule is hard to confirm or deny in species with small representation like acacias and carob trees. Additionally, eucalyptus has a high percentage of invalidations caused by complex plot limits.

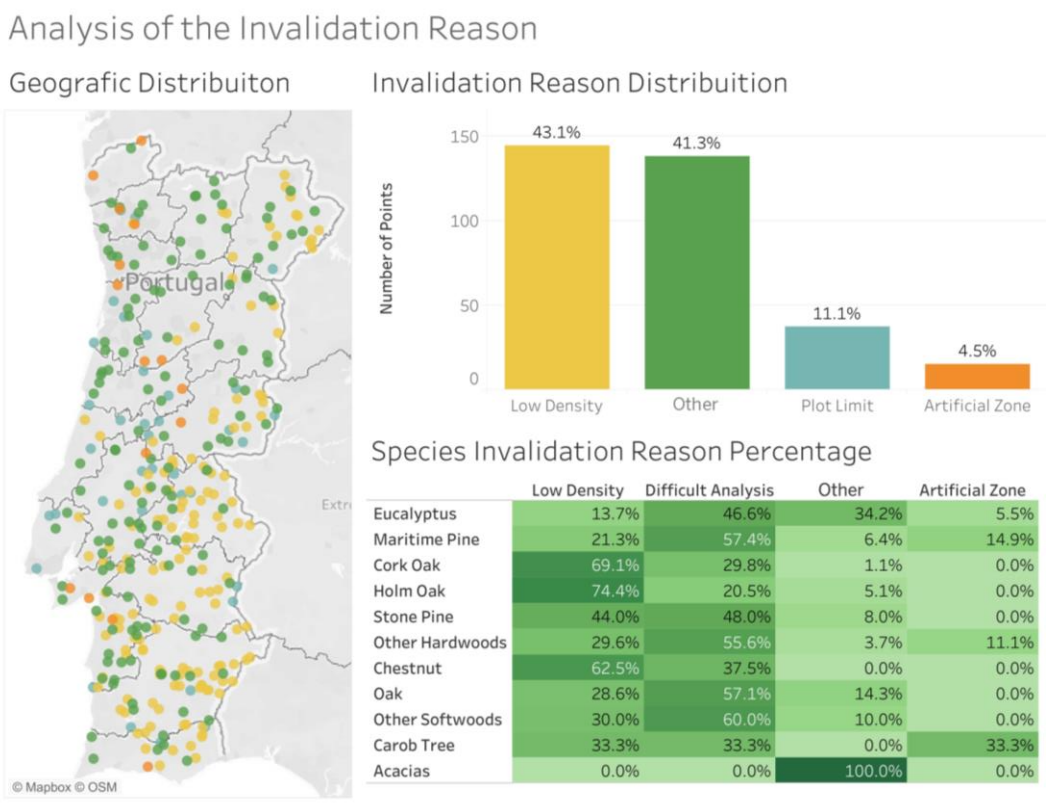

Figure 6 - Dashboard analysing the reason of the invalidation

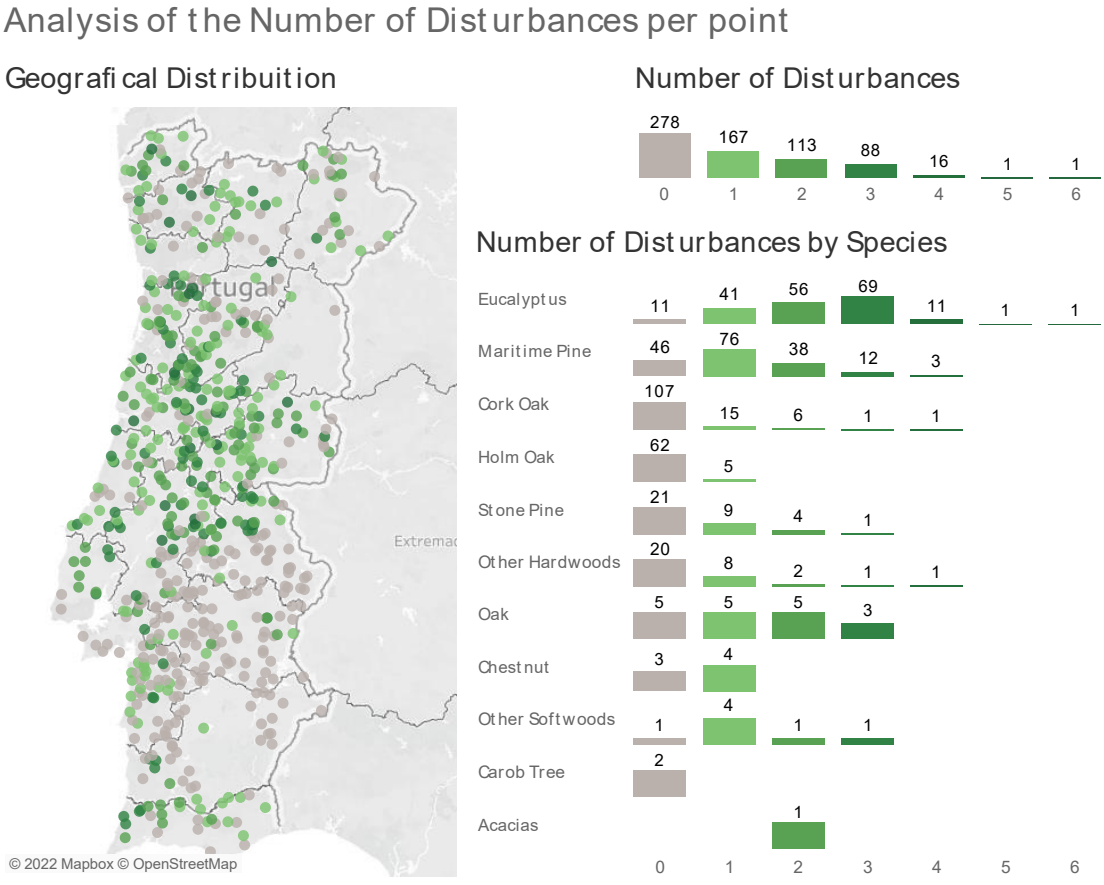

Figure 7 - Dashboard analysing the number of disturbances per point

3.3. Number of changepoints per point

The number of changepoints per point is summarized in **Figure 7,** showing that the mode of changepoints per point for the whole dataset is zero. However, the eucalyptus and the maritime pine classes have respectively a mode of 3 and 1 changepoints. This difference among species is reflected in the geographical distribution of the number of changepoints, the south has almost no changepoints while the center of the country is populated with points that have many disturbances, namely due to fire occurrences.

3.4. Cause of disturbance

Finally, the causes of the disturbances are reported in **Figure 8.** In our dataset, about 20% of the disturbances have an unknown origin, this makes it impossible to conclude if either fire or harvesting is the main cause of forest disturbances. Concerning the temporal distribution of causes, it can be concluded that unknown causes are predominant in the earlier years and tend to later disappear, while harvest cause has the exact opposite behavior. This is due to the lack of information about harvesting since the only way to validate this type of disturbance is either by a landcover change or by high-resolution satellite imagery. GEP only provides significant high-resolution photos after the year 2000. On the other hand, the fire records are in general complete throughout the years. For this reason, it can be assumed that many unknown causes may correspond to harvesting events.

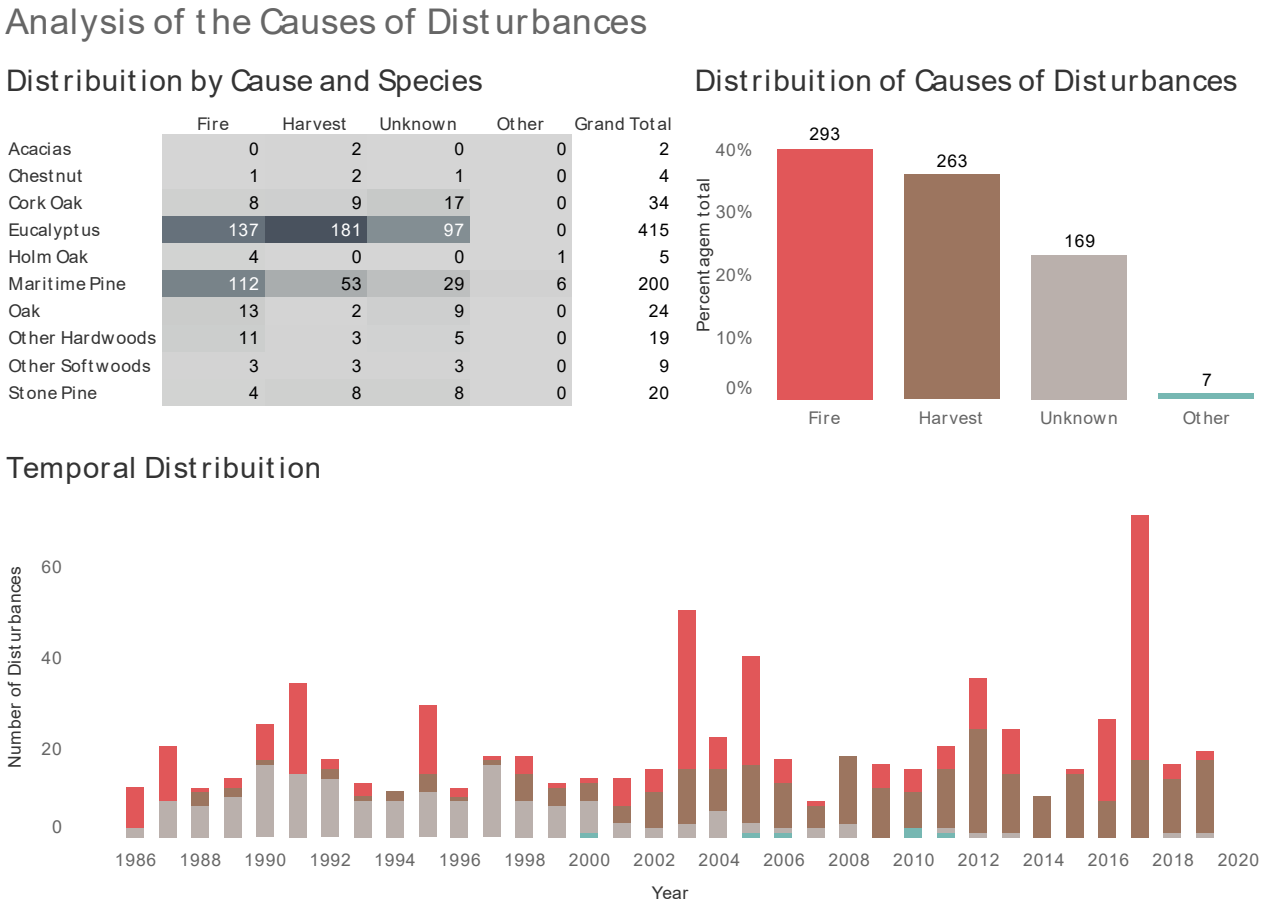

Figure 8 - Dashboard analysing the causes of disturbance

4. Discussion and Conclusions

In this paper, we described the creation of a curated dataset that contains 664 forest points generated from a stratified random sampling based on the tree species and climate zone that cover continental Portugal. Every point contains the auxiliary data used and a thorough list of all years where a disturbance occurs and the respective reason for the disturbance; the years span from 1986 until 2019.

While some of the breakpoints in the dataset can be obtained (with some work) from other sources, this dataset assures that if a breakpoint is not listed then almost certainly a disturbance has not occurred. Furthermore, due to the stratification, it is expected that the number and frequency and type of disturbances present are representative of real-world data for forest areas in Portugal. However, depending on the application, the number of geographic points may not be enough to provide full guarantees. Finally, this dataset only tracked severe disturbances, long term disturbances like droughts were not considered, and thus it may not meet the requirements of some applications.

This dataset can be used in several applications. First, and the main reason motivating the creation of the dataset, it can be used to evaluate algorithms that detect forest disturbances for example or a more generical use as a dataset for evaluating changepoint detection in time series. Finally, it may be employed for differentiating types of forest recovery.

5. References

Brooks, E. B., Wynne, R. H., Thomas, V. A., Blinn, C. E., & Coulston, J. W. (2014). On-the-Fly Massively Multitemporal Change Detection Using Statistical Quality Control Charts and Landsat Data. *IEEE Transactions on Geoscience and Remote Sensing*, *52*(6), 3316–3332. https://doi.org/10.1109/TGRS.2013.2272545

Cohen, W. B., Healey, S. P., Yang, Z., Stehman, S. V., Brewer, C. K., Brooks, E. B., Gorelick, N., Huang, C., Hughes, M. J., Kennedy, R. E., Loveland, T. R., Moisen, G. G., Schroeder, T. A., Vogelmann, J. E., Woodcock, C. E., Yang, L., & Zhu, Z. (2017). How similar are forest disturbance maps derived from different Landsat time series algorithms? *Forests. 8: 98.*, *8*, 98. https://doi.org/10.3390/f8040098

Cohen, W. B., Yang, Z., & Kennedy, R. (2010). Detecting trends in forest disturbance and recovery using yearly Landsat time series: 2. TimeSync — Tools for calibration and validation. *Remote Sensing of Environment*, *114*(12), 2911–2924. https://doi.org/10.1016/j.rse.2010.07.010

Gorelick, N., Hancher, M., Dixon, M., Ilyushchenko, S., Thau, D., & Moore, R. (2017). Google Earth Engine: Planetary-scale geospatial analysis for everyone. *Remote Sensing of Environment*, *202*, 18–27. https://doi.org/10.1016/j.rse.2017.06.031

Huang, C., Goward, S. N., Masek, J. G., Thomas, N., Zhu, Z., & Vogelmann, J. E. (2010). An automated approach for reconstructing recent forest disturbance history using dense Landsat time series stacks. *Remote Sensing of Environment*, *114*(1), 183–198. https://doi.org/10.1016/j.rse.2009.08.017

Kennedy, R. E., Yang, Z., & Cohen, W. B. (2010). Detecting trends in forest disturbance and recovery using yearly Landsat time series: 1. LandTrendr — Temporal segmentation algorithms. *Remote Sensing of Environment*, *114*(12), 2897–2910. https://doi.org/10.1016/j.rse.2010.07.008

Vogelmann, J. E., Xian, G., Homer, C., & Tolk, B. (2012). Monitoring gradual ecosystem change using Landsat time series analyses: Case studies in selected forest and rangeland ecosystems. *Remote Sensing of Environment*, *122*, 92–105. https://doi.org/10.1016/j.rse.2011.06.027

Zhu, Z., & Woodcock, C. E. (2014). Continuous change detection and classification of land cover using all available Landsat data. *Remote Sensing of Environment*, *144*, 152–171. https://doi.org/10.1016/j.rse.2014.01.011

Crowdsourcing Holistic Deep Approach for Fire Identification

Catarina Silva*, Ana Madeira, Alberto Cardoso, Bernardete Ribeiro

University of Coimbra, Faculty of Science and Technology, Informatics Engineering Department, Center for Informatics and Systems, University of Coimbra, Portugal
{catarina, alberto, bribeiro}@dei.uc.pt

**Corresponding author*

Keywords:

Deep Learning, Fire Identification, Crowdsourcing

Abstract

Forest fires have become a global problem that affects large areas of the globe, and has received contributions from citizen science, namely the reporting of fire sighting by citizens with location and images, often using smartphones, which is becoming a frequent source of information to firefighting teams.

Nevertheless, such contributions need validation before resources are deployed and that is the focus of this work. This paper describes a novel approach to identify forest fires in real crowdsourced images using a deep learning (DL) approach.

The approach is based on YOLO networks to train optimized models that identify the real cases that need to be addressed, using a holistic methodology that considers all objects detected in each image before producing a decision. For our experiments, we used benchmark and real datasets of fire and smoke. In the experiments, the performance is compared under different experimental setups. Our approach results show that the proposed crowdsourcing holistic deep approach for fire identification can be successfully used in real scenarios.

1. Introduction

Fire is one of the leading hazards endangering human life, the economy, and the environment (Hall 2014), (Saponara et al. 2020). Identifying a forest fire in its early stages is essential for a faster and more effective response from fire and civil protection authorities. An effective initial response can decrease fire damage and, in certain cases, can prevent the loss of lives and property, e.g., houses and other belongings.

Crowdsourcing approaches (Zanca et al. 2020) involve the use of people to aid in solving problems that technology still struggles. For firefighting, crowdsourcing, or citizen science, can be extremely important in early detection, when communication systems are in place for such reporting. However, such contributions are sometimes malicious with the goal of diverting resources from real fires, often provoked by arsonists, and require validation before resources are deployed.

In this work, citizens are able to report ongoing fires through an app developed in the scope of the Fireloc project (https://fireloc.org), a system that enables the report of forest fires by identifying, locating, and reporting them, using crowdsourced data, i.e. geolocated images with a potential fire. The development of a contribution validation mechanism becomes imperative, allowing for faster and more accurate communication of the occurrence. With the increase of the volume of information received, processing by human visual analysis of each reported situation, even if done by an expert, becomes too time-consuming, and therefore not useful for a rapid response. Therefore, the development of an intelligent system that can automatically identify fire in the submitted images is proposed. This system can then be applied to each report made using the Fireloc application, assessing if there is a current fire or not and discarding false reports, which aims to improve firefighters' intervention. This system can enhance the process of analyzing crowdsourced data, ultimately enhancing firefighters' response.

We explore how the optimization of parameters in YOLO networks (Redmon and Farhadi 2018), (Redmon and Farhadi 2017), (Zhang et al. 2018), (Redmon et al. 2016), a deep architecture for object detection, can be used to allow a better performance in Fireloc project, i.e., to support the determination of validity of an image

obtained through crowdsourcing, a.k.a. citizen science. For this purpose, we construct a dataset with real images obtained in a simulacrum that result in a set of parameters to apply to real situations. We introduce a new concept in post-processing, proposing a holistic approach generalizing the YOLO object detection to an image classification system that fully supports the necessary validation before resources are deployed for firefighting.

In the following, Section 2 describes the related work in deep learning for fire identification. Section 3 describes the proposed holistic deep approach for fire identification, presents and analyses the experimental results. Finally, Section 4 shows the conclusions and future lines of research.

2. Fire Identification with Deep Learning

Fire identification and detection in images using deep learning (DL) (Lecun et al. 2015) have been source of much interest in the research community (Mao et al. 2018), (Qiang et al. 2014), (Lee et al. 2017), (Zhang et al. 2018), (Ayala et al, 2020). In (Mao et al. 2018), a novel fire recognition method based on multi-channel convolutional neural network is proposed, constructing 3 channel color images and using a CNN. The CNN can take as input videos or images and gives as output the probabilities of it belonging to each class considered. All videos are first converted to images frames and all images are then resized to fit the input size of the model. Each image is given to the model as a matrix with each RGB channel, and discriminating features are extracted. Parameter adjustment was achieved using backpropagation. The resulting model could be applied to both video and image inputs, classifying them as belonging the class fire or not.

In (Lee et al. 2017), the images are obtained using an Unmanned Aerial Vehicle (UAV) as a cost-effective means to provide high resolution images for wildfire detection. Results show that such images result in wide range of aerial photographs that can be used for object detection.

In (Zhang et al. 2018), given the difficulty of obtaining real images, a synthetic smoke dataset was constructed by inserting real smoke or simulated smoke into forest background to solve the lack of training data. The published results show that simulated smoke is the better choice, and the model is insensitive to thin smoke.

3. Holistic Deep Approach for Fire Identification

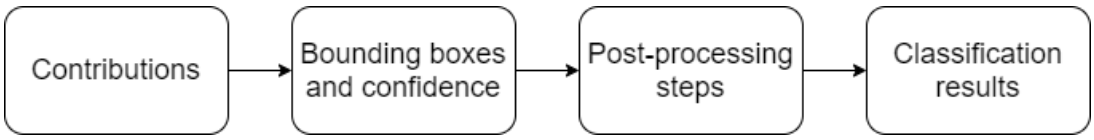

Figure 1- Holistic deep approach for fire identification system

In this work we propose a holistic deep approach for fire identification. Figure 1 shows the operating steps for smoke and fire detection in static images, integrated into the Fireloc project's system. Initially, using the mobile application and the camera of their smartphone or tablet, users can send photos of the forest fire or smoke they observe (contributions).

Then, for each contribution presented to the system, parameter tuning is performed, and the model identifies the parts of the image that contain smoke or fire with bounding boxes and an associated confidence score for each object detected.

Finally, given the specificity of the Fireloc project, a holistic post-processing mechanism is performed before the final classification results are presented to the firefighting team for decision making.

There are several challenges that must be tackled, namely the accurate predictions that avoid misuse of resources and the heterogeneity of submitted contributions in terms of different images formats, sizes, and quality.

The development of the object detection module focuses on the optimization of the parameters: the size of the initial anchors and confidence threshold. The main goal is hence to provide accurate prediction on crowdsourced images on the presence of fire (or smoke) in the given images.

3.1. Datasets

For the fire and smoke detection system implementation, custom datasets were used, manually annotated according to the YOLO format. Two independent sets of images were used to train and test the models, chosen according to the module real conditions of use.

The dataset chosen for the training step was an open source set of images. This dataset is publicly available at https://github.com/DeepQuestAI/Fire-Smoke-Dataset/releases/download and contains an equal number of images with fire and smoke, presenting fires in urban contexts with other objects present in the background and some overlapping objects to be detected (smoke and fire). Although the size of the images is smaller than the typical resolution of photos taken by smartphones and don't contain a high number of images, the variety of examples with smoke and fire makes it use feasible for training YOLO models.

To complement this set of training images, images of smoke and fire were collected in a forest fire context, with characteristics more similar to the actual use of the Fireloc system. These images are, therefore, more suitable for testing the performance of models and were collected in a simulacrum performed by firefighters on May 15, 2019, in tests carried out in Serra da Lousã by Association for Development and Industrial Aerodynamics (ADAI). The manual annotation of the proposed datasets for training and testing the models was carried and the distribution of examples of each class for training and testing datasets is presented in Table I.

Table I- Number of examples present in each dataset

	Total Fire examples	Total Smoke examples
Train dataset	2598	2348
Test dataset	460	421

3.2 Model evaluation

The approach followed to develop the object detection module went through an iterative process, optimizing selected parameters to improve the objects' detection results in the images. The mean Average Precision (mAP) and Average Precision (AP) values per class were analyzed for the evaluation of results. These can be considered standard metrics of YOLO models' performance since they allow an assessment of the relationship between false positives and detected false negatives (Everingham et al. 2010). An adaptation of (Everingham et al. 2010), from the (Cartucho et al. 2018) project, was used.

With the different parameters optimized, the process focused on analyzing the classification results of the images, using the confusion matrices obtained for the classification of the test images to evaluate the models after the application of the post-processing.

3.2. Experiments and results

In the experiments, the trained models were pre-trained with *Imagenet* and the following parameters were considered, defined in the configuration file of each model: (i) Number of classes = 2 (since the classes of objects considered for detection in the images are Smoke and Fire); (ii) Channels = 3 (RGB); (iii) Number of iterations = 6000 (number of iterations recommended by the author of YOLOv4 (Bochkovskiy et al. 2004) for training models with custom datasets).

3.2.1. Experiments and results for anchor adjustment

The definition of the initial anchors of the models can directly influence the detection results obtained. When adjusting the anchors initial size to approximate the bounding boxes sizes in the training dataset, it is possible to suit the boxes size that signals the detected fire and smoke objects in the images. It is to be expected that this approach, by improving the location of objects in the test images, will result in an improvement in the obtained mAP results. In the following experiments, the anchors are adjusted to the bounding boxes marked in the training dataset using the k-means algorithm and aim to improve object detection results.

Table II - Anchor Adjustment Performance Results – Average Precision (AP)

		EPOCHS					
		1000	2000	3000	4000	5000	6000
Fire Smoke	v4	23.08%	41.14%	40.69%	36.20%	46.00%	43.90%
	v4-anch	17.58%	32.53%	37.69%	**40.11%**	38.49%	38.65%
Fire	v4	4.83%	22.30%	15.52%	20.08%	**24.96%**	23.06%
	v4-anch	1.55%	5.92%	7.50%	11.74%	14.56%	13.28%
Smoke	v4	41.34%	59.98%	65.86%	52.32%	67.05%	64.74%
	v4-anch	33.61%	59.13%	67.89%	**68.67%**	64.42%	64.02%

Results show that the YOLOv4 model trained with the default values of anchor size presents better performance in detecting objects of the considered classes. The best result obtained with the model after performing the anchor adjustment is only 40.11% mAP, after 3000 training epochs, inferior to the best result achieved using the original anchors, 46% mAP obtained after 5000 training epochs.

When analyzing the AP results for each class of objects considered, the models present a significant difference in the fire detection performance, reaching a maximum of 24.96% AP/Fire with the model trained with default anchors. In the detection of objects of the Smoke class, both models present good results, reaching 68.47% of AP/Smoke.

3.2.2. Experiments and results for confidence threshold adjustment

This experiment aims to evaluate the effects of the variation of the confidence threshold defined not only on the results of object detection but also on the classification results of the images in the test dataset. In all previous experiments, the specified limit used for this confidence was the default value, used in the studies YOLOv3 (Redmon and Farhadi 2018) and YOLOv4 (Bochkovskiy et al. 2004).

To assess the effects of changing the confidence threshold on the object detections performed, the mAP results obtained after every 1000 iterations of training of the model were evaluated. Values 5%, 10%, 15%, 20%, and 25% were considered for changes in the confidence threshold. The experiment results can be seen in Figure 2, showing the increase of the defined confidence threshold, regardless of the number of training iterations of the model, results in a decrease of mAP results. These results indicate that the higher the defined confidence threshold, the lower the number of correct detections. When considering the results obtained, the confidence thresholds of 5% and 15% stand out positively.

4. Conclusions and future work

We have studied the problem of identifying fire and smoke in crowdsourced images that citizens submit to the Fireloc system to ultimately alert firefighters of ongoing fires. We have explored how the optimization of parameters in YOLO networks can be used to allow a better performance in fire identification. For this purpose, we have constructed a dataset with real images obtained in a simulacrum that result in a set of parameters to apply to real situations. We have additionally introduced a new concept in post-processing, proposing a holistic approach generalizing the YOLO object detection to an image classification system that fully supports the necessary validation before resources are deployed for firefighting.

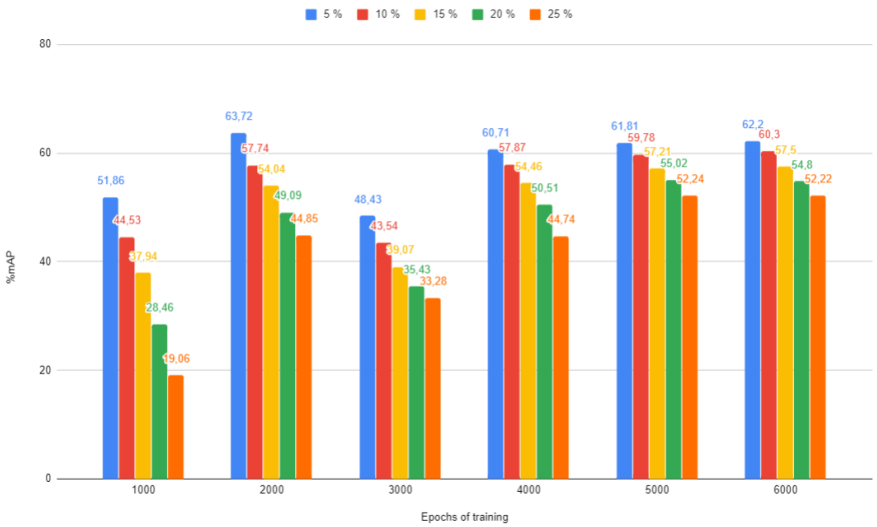

Figure 2 - Results obtained considering varying confidence threshold (5% to 25%)

Figure 3 shows the detection results for comparison of the two operating points. The results obtained with both thresholds are similar, although the image resulting from the detections carried out with 5% threshold shows a more significant number of repeated fire detection. The video is available at https://www.dropbox.com/s/fwtls664s5uukcy/fire_video demo.mp4?dl=0.

Figure 3 - Test results image detection comparison, example 2

Future work is foreseen in two paths. First, the augmentation of the dataset, as it has become clear that it is a potential source of improvement, e.g., through the use of Generative Adversarial Networks (GAN). Second, due to the recent interest in the image and video object recognition the generalization of the post-processing holistic approach to video sequences is also anticipated given that initial tests with video images suggest the viability of the proposed approach.

5. Acknowledgments

This work is funded by the FCT - Foundation for Science and Technology, I.P./MCTES through national funds (PIDDAC), within the scope of CISUC R&D Unit - UIDB/00326/2020 or project code UIDP/00326/2020. This work is also funded by project FireLoc, supported by the Portuguese Foundation for Science andTechnology (Fundação para a Ciência e a Tecnologia - FCT) under project grants PCIF/MPG/0128/2017.

6. References

(Ayala et al, 2020) A. Ayala, B. Fernandes, F. Cruz, D. Macedo, A. L. I. Oliveira and C. Zanchettin, ”KutralNet: A Portable Deep Learning Model for Fire Recognition,” 2020 International Joint Conference on Neural Networks (IJCNN), Glasgow, United Kingdom, 2020, pp. 1-8.

(Bochkovskiy et al. 2004) A. Bochkovskiy, C.-Y. Wang, and H.-Y. M. Liao, “YOLOv4: Optimal Speed and Accuracy of Object Detection,” https://arxiv.org/abs/2004.10934

(Cartucho et al. 2018) J. Cartucho, R. Ventura, and M. Veloso. Robust object recognition through symbiotic deep learning in mobile robots. In 2018 IEEE/RSJ Int Conf Intelligent Robots and Systems, pages 2336–2341, 2018.

(Everingham et al. 2010) M. Everingham, L. Van Gool, C. K. Williams, J. Winn, and A. Zisserman, “The pascal visual object classes (VOC) challenge,” International Journal of

(Hall 2014) Hall, J.R.: The total cost of fire in the United States. National Fire Protection Association, Quincy (2014)

(Lecun et al. 2015) Yann Lecun, Yoshua Bengio, and Geoffrey Hinton. Deep learning. Nature, 521(7553):436–444, 2015.

(Lee et al. 2017) Wonjae Lee, Seonghyun Kim, Yong-Tae Lee, Hyun-Woo Lee, and Min Choi. Deep neural networks for wild fire detection with unmanned aerial vehicle. pages 252–253, Jan 2017.

(Mao et al. 2018) Wentao Mao, Wenpeng Wang, Zhi Dou, and Yuan Li. Fire Recognition Based On Multi-Channel Convolutional Neural Network. Fire Technology, 54(2):531–554, mar 2018.

(Qiang et al. 2014) Y. Qiang, B. Pei, and J. Zhao. Forest Fire Image Intelligent Recognition based on the Neural Network. Journal of Multimedia, 9(3), 2014.

(Redmon et al. 2016) Joseph Redmon, Santosh Divvala, Ross Girshick, and Ali Farhadi, You Only Look Once: Unified, Real-Time Object Detection, CVPR 2016.

(Redmon and Farhadi 2017) J. Redmon and A. Farhadi,” YOLO9000: Better, Faster, Stronger,” 2017 IEEE Conference on Computer Vision and Pattern Recognition (CVPR), Honolulu, HI, 2017, pp. 6517-6525.

(Redmon and Farhadi 2018) Joseph Redmon and Ali Farhadi. YOLOv3: An Incremental Improvement. 2018.

(Saponara et al. 2020) Saponara, S., Elhanashi, A. & Gagliardi, A. Real-time video fire/smoke detection based on CNN in antifire surveillance systems. J Real-Time Image Proc (2020).

(Zanca et al. 2020) D. Zanca, S. Melacci and M. Gori,” Toward Improving the Evaluation of Visual Attention Models: a Crowdsourcing Approach,” 2020 International Joint Conference on Neural Networks (IJCNN), Glasgow, United Kingdom, 2020, pp. 1-8.

(Zhang et al. 2018) Qi Xing Zhang, Gao Hua Lin, Yong Ming Zhang, Gao Xu, and Jin Jun Wang. Wildland Forest Fire Smoke Detection Based on Faster R-CNN using Synthetic Smoke Images. In Procedia Engineering, v.211, 2018.

Deep Learning for High-Resolution Wildfire Modeling

Mark A. Finney[1*], Jason M. Forthofer[1], Xinle Liu[2], John Burge[2], Matthias Ihme[2,3], Fei Sha[2], Yi-Fan Chen[2], Jason Hickey[2], John Anderson[2]

[1]USDA Forest Service, Missoula Fire Sciences Laboratory, 5775 Highway 10 West, Missoula MT 59808, USA, {mark.finney, jason.forthofer}@usda.gov
[2]Google LLC, 1600 Amphitheatre Pkwy, Mountain View, CA 94043, USA, {liuxl, lawnguy, matthiasi, fsha, yifanchen, jyh, janders}@google.com,
[3]Stanford University, 440 Escondido Mall, Stanford, CA 94305, USA

**Corresponding author*

Keywords

Deep learning, wildfire spread modelling, fire behavior

Abstract

We demonstrate the use of a deep learning (DL) approach for representing the behavior of a high-resolution physics-based wildland fire spread model. The ultimate objective is being able to efficiently use the DL model for intensive simulations of large fires while retaining fidelity to the fine-scale physical processes. We begin with a fire model that reduces the spatial domain of the fire spread problem to one dimension (1D). The 1D model explicitly resolves cm-scale fuel variations, heat transfer and heating/drying dynamics of individual fuel particles and burning behavior of the bed. We then ran the fire model for 78,125 factorial combinations of fuel, weather, and topographic conditions as training data for the DL algorithm. The results of the DL analysis show overall agreement of 96% of the variation in fire behavior as represented by steady state rate of spread, flame length and flame zone depth. Exceptions to the DL regression indicate areas where more work is required in refining the resolution in training cases and use of advanced methods of embedding the fire model inside the DL algorithm loop.

1. Introduction

A major challenge for wildfire modelling is the ability to span the range of scales of fire phenomena (Clark et al. 2003). Fuel particle heat transfer and ignition occur over millimetres but wildfires impact landscapes and communities across kilometres. Even if the fine-scale physical processes of fire spread were well known, it is impractical to resolve them computationally for large domains of real fires. Thus, physics-based modelling has been much slower than real time and has not yet become operational for wildfire management. Even for research purposes on relatively small fires (~10^3 m^2) using supercomputing clusters, physical models employing computational fluid dynamics in 3D must compromise spatial resolution to achieve performance and thus fidelity to the fine-scale fuel descriptions, and processes of heat transfer, ignition, and combustion.

An alternative approach, long used in fire spread modelling, is to limit the spatial domain to one-dimension (1D) (Fons 1946). A 1D formulation resolves the heat transfer and sequential ignition of discrete fuel particles at fine-scales and can be unambiguously compared with measured behaviours. In a reprise of this 1D approach, Finney et al. (2021) describe the new research required to understand fuel burning rates, convection heat transfer, and heating and ignition of fuel particles at the fine scales. The fine scale explicitly represents fuel heterogeneity and employs a 1D model for heating, drying, and pyrolysis of fuel particles. It solves a single 1D line spanning domains of about 50-100 m in less than a minute, but this is too slow to be implemented directly in simulations of large fires.

Here we describe the application of deep learning (DL) techniques to the problem of representing modelled fire behaviour. Assuming our high-resolution 1D fire model captures the system behaviour accurately, DL can be used to determine the relations between the resulting fire behaviour outputs and a large list of input variables. Rapid advances in the past decade in DL show it can represent complex and perhaps unknown relations among variables in the system.

A rigorous background on DL is outside the scope of this paper. We refer the interested reader to (Goodfellow et al. 2016). Briefly, DL is a branch of machine learning (ML) that relies on using neural networks with multiple

hidden layers of nodes that do not directly correspond to actual observations. These hidden layers allow DL models to build up rich latent representations of complex systems and are often distinguished from more traditional ML approaches in that they require less feature engineering to be successful, making them ideal candidates for complex domains in the geosciences.

There are many examples of traditional ML applications in wildfire modelling, but more modern DL applications are rare, particularly those modelling fire spread and growth (Piyush et al. 2020). Some examples include Hodges and Lattimer (2019) where a DL model was used to predict the structural evolution of wildfires in two dimensional simulations. Radke et al. (2019) used a DL model to predict how a single real-world fire evolves over the course of a 24-hour period. In a similar vein, we demonstrate that DL can be used to effectively model steady state variables predicted by the 1D fire spread model described below.

2. Methods

2.1. One Dimensional Fire Spread Model

The dynamical nonlinear 1D fire spread model is explained in detail by Finney et al. (2021) and in a companion paper that overviews a more recent version (Forthofer et al., *this conference*). Briefly, the model domain is a 1D transect through a fuel bed with resolution nominally of 1 cm. At these resolutions, variations in fuel structure, such as gaps and clumps can be explicitly resolved in contrast to bulk fuel descriptions (i.e., Scott and Burgan 2005). The simulation proceeds from a specified ignition at one end of the domain, calculating pyrolysis production and flame dimensions from fuel particles heated by radiation (flame and solid fuel) and convection. Convection heat flux to fuel particles from flames is calculated using a mean gas temperature profile and flame tip velocity (Finney et al. 2021). Fuel particle heating and drying response to steep heat flux gradients of an approaching fire (Cohen and Finney 2022a, b) are captured by a 1D conduction model for each size and material in each cell. Fire spread is an outcome of discrete particle ignition, which accelerates from the ignition state and achieves a steady rate of spread (ROS), flame length (FL), and flame zone depth (FZD).

To generate a dataset for training a DL model, the 1D fire spread model was run on a factorial combination of five values for each of the seven input variables, resulting in 78,125 distinct cases, see Table 1 and Table 2 for more details. For this demonstration, we chose only to represent steady state variables of fire spread rate, flame length, and flame zone depth from those data produced by the dynamical model. Others could include acceleration time and energy release from post-frontal combustion.

2.2. Pre-processing

The dataset is filtered to only keep data points where the 1D model reported realistic ROS values of no more than 10 m/s. The dataset is further normalized before model training such that all input variables are normalized into [0, 1] linearly between 0 and the max value of corresponding variable, and output variables are first square-rooted and then normalized in the same fashion as they're skewed and have a long tail. The dataset is randomly split into train (65%), validation (15%) and test datasets (20%) for model development before any filtering. The train dataset is used to learn the parameters of the DL model, while the validation dataset is used to select the best model to avoid overfitting the train dataset. The test dataset is never seen during model development and is reserved to measure the generalization quality of the DL model in the end.

Table 1. Descriptive statistics of input and output variables of the 78,125 full factorial combinations for training the DL model.

Category	Variable	Values (Full factorial design)	Train mean (std)	Validation mean (std)	Test mean (std)
Fuel	Particle Diameter (m)	{0.001, 0.002, 0.004, 0.005, 0.006}	0.0035 (0.0018)	0.0036 (0.0018)	0.0035 (0.0018)
	Moisture (%)	{5, 10, 15, 20, 25}	14.9 (7.0)	15.1 (7.0)	15 (7.0)
	Loading (kg/m3)	{0.1, 0.825, 1.55, 2.275, 3}	1.54 (1.02)	1.54 (1.02)	1.55 (1.02)
	Fuel Depth (m)	{0.01, 0.133, 0.255, 0.378, 0.5}	0.255 (0.173)	0.255 (0.173)	0.255 (0.172)
Weather	Wind Speed (m/s)	{0, 1.25, 2.5, 3.75, 5}	2.49 (1.76)	2.5 (1.77)	2.5 (1.77)
Topography	Terrain Slope (degree)	{0, 7.5, 15, 22.5, 30}	14.9 (10.5)	15.1 (10.6)	15 (10.5)

Fire	Bed Width (m)	{10, 20, 30, 40, 50}	30 (14.1)	29.7 (14.0)	29.9 (14.1)
Dependent variables	ROS (m/s)	N.A.	1.95 (10.11)	1.87 (8.29)	1.93 (10.38)
	Flame Length (m)		3.96 (2.57)	3.95 (2.59)	3.95 (2.56)
	Flame Zone Depth (m)		12.6 (12.0)	12.6 (12.1)	12.5 (12.0)

Table 2: Number of samples for the whole dataset (all) or each split (train, validation, and test). Each row corresponds to a different filtering, no filtering, valid ROSs or zero ROSs only.

Samples	All	Train	Validation	Test
All	78,125	50,681	11,712	15,732
Valid ROS	68,750	44,606	10,302	13,842
ROS == 0	6,666	4,307	1,020	1,339

2.3. Deep Learning Model

We use a two staged approach for predicting the steady-state variables. First, we use a binary classification model that predicts whether there is any fire at all (meaning the fire does not spread under the given conditions). If there is a prediction of *no fire*, then the ROS, FL and FZD are all zero. Otherwise, the regression model is used to perform the final prediction.

Given the relatively few inputs to the model, we chose the quintessential Feed-Forward Neural Network (Goodfellow et al. 2016, Chapter 6) (FFNNs) for both models. More specifically, we use a fully connected FFNN, which allows for a rich latent space that grows exponentially with the number of input features. As such, it is not appropriate for domains with large numbers of input features, but often works surprisingly well for smaller domains (Figure 1).

The DL models are trained on the training dataset such that the Mean Squared Error (MSE) (or binary cross-entropy, i.e., logistic loss) for the regression (or classification) model is minimized. L2 regularization was applied to avoid model overfitting. The learning rate and the learning rate decay rate were empirically determined by training multiple models and then selecting the models with the lowest loss on the *validation* dataset.

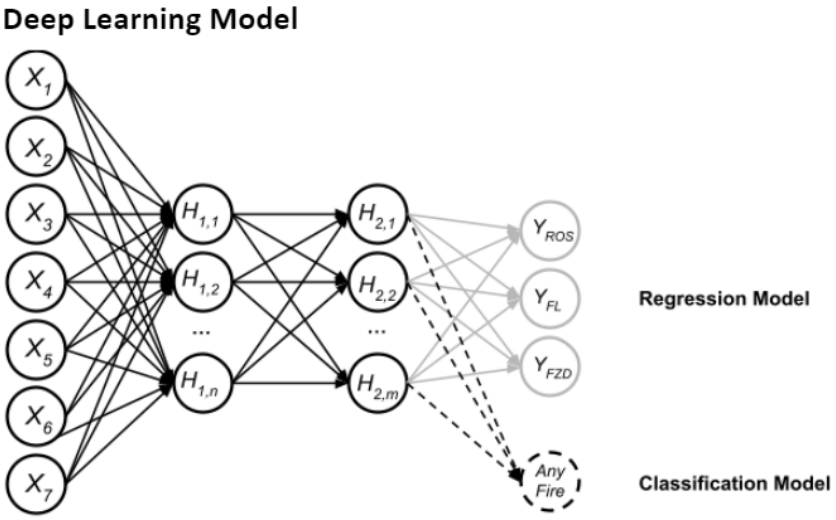

Figure 1. Architecture of feed-forward neural network used for classification and regression, consisting of two hidden layers. Common structures across both models are shown in solid black. The structure unique to the regression model is shown in solid gray. The structure unique to the classification model is shown in dashed-black. Both models take the same seven variables as input that feed into two hidden layers. The classification model requires fewer hidden nodes (n=8, m=8) whereas the regression model benefited from more nodes (n=32, m=8), and they had 145 and 547 parameters respectively. All nodes in the graph are perceptrons (the standard neural network unit) except for the Any Fire node, which also applies a final sigmoid transformation to facilitate binary classification.

3. Results

Use of the detailed 1D fire model as part of a large-scale wildfire simulation (2D or 3D) would provide the correct physics on combustion and steady state statistics but is infeasible due to the computational cost. Therefore, the primary goal for the DL model is to approximate the 1D model as accurately as possible at a dramatically reduced computational cost. For comparison, the average 1D model run time for the training data set was about 70 s for each of the 78,125 cases, whereas the DL model takes about 0.01 s for each case.

We show that the DL model captures the wildfire dynamics well (Figure 2). The scatter plots of the predicted dependent variables versus those from the underlying physical model for the test dataset show that most of the data points are quite close to the perfect reference orange (y = x) line. The mean (standard deviation) of the absolute errors for the dependent variables of ROS, FL, and FZD are 0.078 (0.17) m/s, 0.21 (0.29) m and 0.98 (1.53) m, respectively. Those numbers are close to that for the validation dataset, demonstrating that the DL model is capable of accurately reproducing the fire model's behaviour.

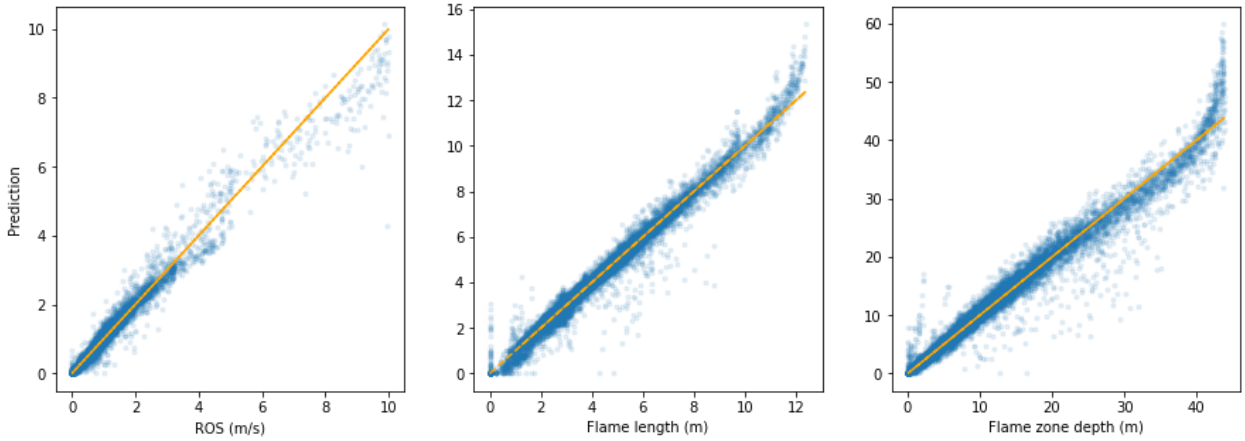

Figure 2: Scatter plot of predictions versus the values from the high-resolution physical model, for all three steady state variables, rate of spread, flame length and flame zone depth.

3.1. Qualitative Analysis

The example fire characteristics represented by ROS, FL and FZD are key descriptors of frontal fire behaviour. We found that errors made by the DL model are at the extremes of the input data. The error around zeros is an indicator that more work is required for the classification model in differentiating the no-fire cases correctly, which is an important problem in practical fire management. The overall underestimate for large ROSs and overestimate for large flames (Figure 2) might be related to dataset filtering, as the wind speed is at most 5 m/s, while we keep ROSs up to 10 m/s for cases with combined wind and high slope angle.

The DL model captured the monotonic dependence of fire behavior on the wind speed and terrain slope (Figure 3). It also and illustrates some extrapolation beyond the training data (recall that the whole dataset training data included only wind speeds up to 5 m/s), not only at the discrete wind speeds reported by the 1D model, but also over the continuous range. However, inevitably, at some point the models' limitations become apparent. Extending the models' accuracy to higher wind speeds can potentially be resolved by including training data at higher wind speeds or considering a probabilistic DL model, e.g. (Dillon et al. 2017), both of which are subjects of ongoing work.

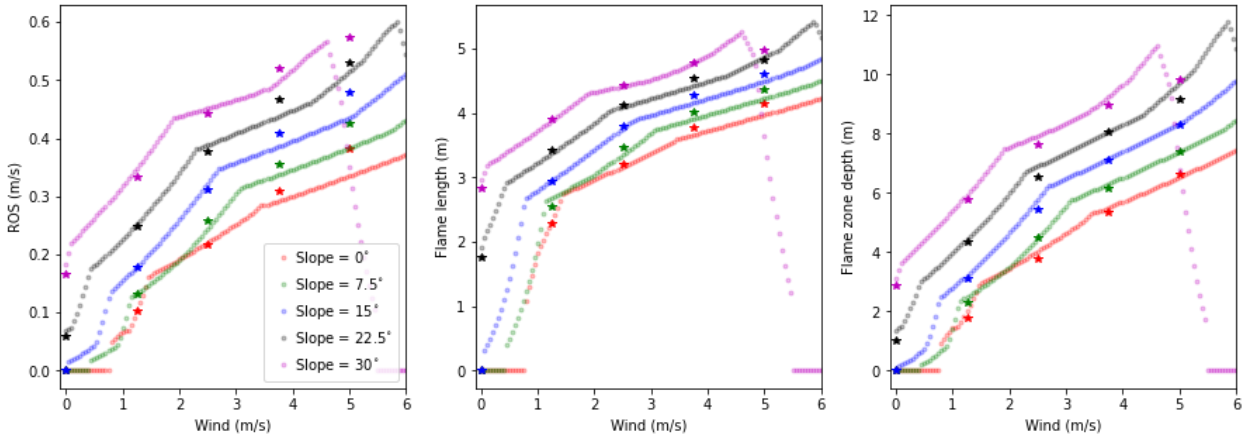

Figure 3: An example of the fit of the DL model (dots) to the 1D model outputs (stars with the same colour) for a range of wind speeds and slopes (0 to 30 degrees), with all other five input variables fixed at their corresponding median values. Extrapolated values are beyond the 5 m/s wind speeds.

4. Discussion

The current demonstration of DL modelling is limited to *homogeneous* fuel, weather, and terrain conditions, which is an oversimplification of the *heterogeneous* conditions where conditions include spatial varying fuels, time varying wind speed, etc. The physical 1D model can deal with this heterogeneity and future work involves investigating the neural network structure that would effectively model such conditions. FFNNs may no longer work as well, but it is likely that more advanced convolutional networks would suffice as demonstrated in Hodges and Lattimer (2019) and Radke et al. (2019).

5. Conclusions

We demonstrated an approach to wildfire modeling that relies on a physical fire spread model in reduced dimension (1D) to resolve the physical processes and DL modeling to produce a computationally efficient representation of the fire behavior. The DL model offers potential implementation in wildfire models at higher dimensions (2D) such as FARSITE (Finney 1998) or 3D where computationally cheap methods are strongly desired. In this capacity, our DL model would perform with low cost compared to the original and be able to address behaviors resulting from fine-scale processes. The DL model accurately associates these steady state variables to the range of input conditions for fuels, weather, and topography, with mean (std) absolute errors of 0.078 (0.17) m/s, 0.21 (0.29) m and 0.98 (1.53) m for ROS, FL and FZD respectively. DL modeling is thus demonstrated as a promising means to represent fine-scale fire behaviors for broad-scale application while maintaining adequate fidelity to the detailed physical processes and inputs. Future work includes modeling heterogeneous input variables and explicitly embedding the DL model in subsequent more sophisticated fire models.

6. Acknowledgements

We thank Zack Ontiveros, Jared Sisk and Carla Bromberg for their helpful discussions, and Lily Hu and Rif A. Saurous for reviewing and approving this manuscript. Isaac Grenfell and Bill Chatham contributed to the 1D model and training data.

7. References

Clark, T.L., Griffiths, M., Reeder, M.J. and Latham, D., 2003. Numerical simulations of grassland fires in the Northern Territory, Australia: A new subgrid-scale fire parameterization. *Journal of Geophysical Research: Atmospheres*, *108*(D18).

Cohen, J.D. and Finney, M.A., 2022a. Fuel particle heat transfer part 1: convective cooling of irradiated fuel particles. *Combustion Science and Technology*, pp.1-27.

Cohen, J.D. and Finney, M.A., 2022b. Fuel Particle Heat Transfer Part 2: Radiation and Convection during Spreading Laboratory Fires. *Combustion Science and Technology*, pp.1-27.

Dillon, Joshua V., Ian Langmore, Dustin Tran, Eugene Brevdo, Srinivas Vasudevan, Dave Moore, Brian Patton, Alex Alemi, Matt Hoffman, Rif A. Saurous. TensorFlow Distributions. arXiv preprint arXiv:1711.10604, 2017.

Finney, M.A., 1998. *FARSITE, Fire Area Simulator--model development and evaluation* (No. 4). US Department of Agriculture, Forest Service, Rocky Mountain Research Station.

Finney, M.A., McAllister, S.S., Forthofer, J.M. and Grumstrup, T.P., 2021. *Wildland Fire Behaviour: Dynamics, Principles and Processes*. CSIRO PUBLISHING.

Fons, W.L., 1946. Analysis of fire spread in light forest fuels. *Journal of Agricultural Research. 72 (3): 92-121*, *72*(3), pp.92-121.

Forthofer, J.M., M.A. Finney, A. Trouve, and M. Ahmad. LIHTFire: a high-resolution physics-based fire spread model in one dimension *This conference*.

Goodfellow I, Bengio Y, Courville A (2016) 'Deep Learning.' (MIT Press)

Hodges JL, Lattimer BY (2019) Wildland Fire Spread Modeling Using Convolutional Neural Networks. Fire Technology55, 2115–2142. doi:10.1007/s10694-019-00846-4.

Piyush Jain, Sean C.P. Coogan, Sriram Ganapathi Subramanian, Mark Crowley, Steve Taylor, and Mike D. Flannigan. (2020) A review of machine learning applications in wildfire science and management. Environmental Reviews. 28(4): 478-505. **https://doi.org/10.1139/er-2020-0019**

Radke D, Hessler A, Ellsworth D (2019) FireCast: Leveraging Deep Learning to Predict Wildfire Spread. **https://glovis.usgs.gov/app?fullscreen=0**

Scott, J.H. and Burgan, R.E., 2005. Standard fire behavior fuel models: a comprehensive set for use with Rothermel's surface fire spread model. *Gen. Tech. Rep. RMRS-GTR-153. Fort Collins, CO: US Department of Agriculture, Forest Service, Rocky Mountain Research Station. 72 p.*, *153*.

Sullivan, A.L., 2009. Wildland surface fire spread modelling, 1990–2007. 1: Physical and quasi-physical models. *International Journal of Wildland Fire*, *18*(4), pp.349-368.

Development of a fire-smoke modelling system to integrate crown fire behaviour

Isilda Cunha Menezes,*[1]; Luiz Rodrigues [2]; Saulo Freitas [2] ; Rodrigo Braz [2]; Mateus Ferreira e Freitas [3]; Karla Longo [2]; Ana Patrícia Fernandes [1]; Diogo Lopes [1]; Joana Ferreira [1]; Myriam Lopes [1]; Ana Isabel Miranda [1]

[1] Center for Environmental and Marine Studies (CESAM), Department of Environment and Planning, University of Aveiro, Campus Universitário de Santiago, 3810-193 Aveiro, Portugal, {isildacm, apsfernandes, diogojlopes, jferreira, myr, miranda}@ua.pt
[2] Center for Weather Forecasting and Climate Studies (CPTEC), Department of Physics, National Institute for Space Research, Cachoeira Paulista, SP, Brazil, {luiz.rodrigues, saulo.freitas, rodrigo.braz, karla.longof}@gmail.com
[3] Multiuser Laboratory of High Performance Computing (LaMCAD), UFG Innovation Agency Building, Federal University of Goiás (UFG), Samambaia Campus, 74690-631, Goiânia , GO, Brazil {mateus.ffreitas@hotmail.com}

**Corresponding author*

Keywords

Atmospheric modelling; wildfire; modelling of fire risk

Abstract

Over the last decades, several real-time air quality forecasting systems have been developed worldwide to support decision-making to control and manage anthropogenic pollution and its impacts. However, the current forecast systems do not, in general, integrate wildfire emissions. In Portugal, from 1996 to 2021, a cumulative area of 3 Mha burnt by rural fires was registered, accounting for roughly half of Portugal's continental area, causing damage to infrastructure and lives, and in particular impacting the quality of the air and human health. The ability of modelling tools to predict the behaviour of fire smoke is fundamental to effectively improve the accuracy of air quality forecasting and preventing public health consequences. There is a wide variety of models available to simulate fire-smoke phenomena. Nonetheless, it is necessary to consider computational aspects, resources, and goals to choose a suitable model to fit the purpose. In the ongoing FIRESMOKE project, the weather forecast model BRAMS-SFIRE version 5.0 is implemented to be part of the new version 5.6.2 of BRAMS. The BRAMS-SFIRE model was coupled to simulate a broad integration between the surface fire fluxes and the atmospheric environment and presented a good accuracy in terms of the physics of the atmosphere and fire interaction. FIRESMOKE also aims to improve the SFIRE model by including the crown fire behaviour. A predictive model for surface fire spread adapted for the timber litter and understory fire behaviour fuel model and conceptual predictions for the behaviour and size of crown fires, including conditions for the crown fire starting and spreading, were incorporated in the SFIRE model by linking these models with the existent surface fire spread and the numerical scheme of propagation. Furthermore, the smoke emitted by the fire, which spread is estimated with the new approach, was entered into the chemistry module of BRAMS. The goal of this paper is to present the BRAMS-SFIRE developments oriented toward the creation design of a FIRESMOKE system for forecasting and monitoring forest fire smoke emissions that also incorporate anthropogenic and biogenic sources of air pollution, to provide a public access service in the scope of air quality over the domain of continental mainland Portugal.

1. Introduction

Smoke integrated framework modelling systems have been implemented worldwide using a combination of independent models, generally providing smoke transport and pollutant concentrations, forecasting air quality, and producing alerts for the risk of high pollution caused by wildland fires. There are three main framework systems in the United States of America, the BlueSky (Wheeler et al., 2010), the United States National Oceanic and Atmospheric Administration smoke prediction system (Stein et al., 2009), and the ClearSky (Jain et al., 2007). Australia has implemented the Australian Bureau of Meteorology Smoke Prediction System for wildfires and prescribed burning (Peace et al, 2020). In Europe, the Copernicus Atmospheric Monitoring Service (CAMS, Akritidis et al., 2020) monitors emissions from fires and atmospheric composition using satellite observations

and numerical modelling. The Center for Weather Forecast and Climate Studies (CPTEC) at the National Institute for Space Research (INPE) in Brazil provides numerical air quality forecasts with the BRAMS modelling system, including emissions both from fires and urban/industrial sources (Freitas et al., 2017; Longo et al., 2013). In Portugal, modelling studies of air pollution from wildfires have been widely developed by the University of Aveiro (Miranda, 2004; Martins et al., 2012; Valente et al., 2007) which maintains the operational Portuguese air quality forecasting system. However, this system does not integrate wildfire emissions into the atmosphere.

Since Portugal is one of the Southern European countries with a higher number of forest ignitions (Rodrigues et al., 2013), the ability to predict the ignition and spread of forest fires, as well as the behaviour of emitted air pollutants, is important to improve resources management's effectiveness and efficiency, for operations of preventing, detecting and fighting forest fires and monitoring air quality, with repercussions on public health.

The application of a fire-smoke modelling system implies the selection of the models to be included that should take into account aspects, such as computational resources, the required accuracy, and physical phenomena representations. In many cases, the available models interact with each other through downscaling. Only a few models include a broad integration of the atmosphere's dynamic and thermodynamic concepts, comprising surface and soil phenomena interaction with the atmosphere's boundary layer. For high-resolution (meters) applications, this ability is limited to case-studies simulations and, still, with inefficient prognosis simulations of the weather state, and therefore, unsuitable for the fire-smoke forecast with high landscape resolution.

The BRAMS-SFIRE system (Menezes et al., 2016, 2021a; Freitas et al., 2017) aims at overcoming this challenge. BRAMS is continuously under development to better simulate atmospheric processes and the coupled SFIRE simultaneously simulates the interactions between the surface fire fluxes and the atmospheric environment, both on the mesoscale and micro-scale. The BRAMS-SFIRE system, which is the representation of fire spread, presented excellent results in terms of the physics of the atmosphere and fire interaction (Menezes, 2016, 2021a) promising a reliable performance for fire-smoke after the development of the crown fire spread model.

The ongoing FIRESMOKE project (Menezes et al., 2021b) aims to improve the meteorological weather forecast model BRAMS-SFIRE, which also integrates an atmospheric chemistry (CCATT - Eulerian Coupled Chemistry, Aerosol and Tracer Transport) model, with the development of a crown behaviour module. This modelling system operates from meso to local scale and in real-time conditions. The present work is part of this project and describes the incorporation in BRAMS, v5.6.2, of the crown fire propagation and fire smoke pollutants in the chemistry model CCATT.

2. Methodology

2.1. Overview of ongoing fire developments on BRAMS

The SFIRE model (Mandel et al., 2009, 2011) coupled to BRAMS (Freitas et al., 2017) by Menezes (2016, 2021a) allows the analysis of surface fire behaviour taking into account the type of fuel bed and its moisture, the topography and the atmospheric wind. Under the FIRESMOKE project, the developments of BRAMS-SFIRE comprise the up-grade for the last version of SFIRE, the introduction of a mathematical model for predicting surface fire spread (Rothermel, 1972) for fire behaviour fuel model 10 (timber litter and understory) (Anderson, 1982) and of the conceptual model for predicting behaviour and size of crown fires from Rothermel (1991), including conditions for the crown fire starting and spreading for coniferous forest fuel types (Van Wagner, 1977), based on the research of Scott and Reinhardt (2001). This new version of BRAMS-SFIRE, part of the current BRAMS model v5.6.2, would be suitable for the operational forecast of fire size and behaviour, weather, and air quality. This development was designed following the scheme in Figure 1. In this scheme, the crown behaviour introduced in the model is represented in the red boxes, in particular in: the "calculation of the fireline advance" and the "calculation of total fireline intensity".

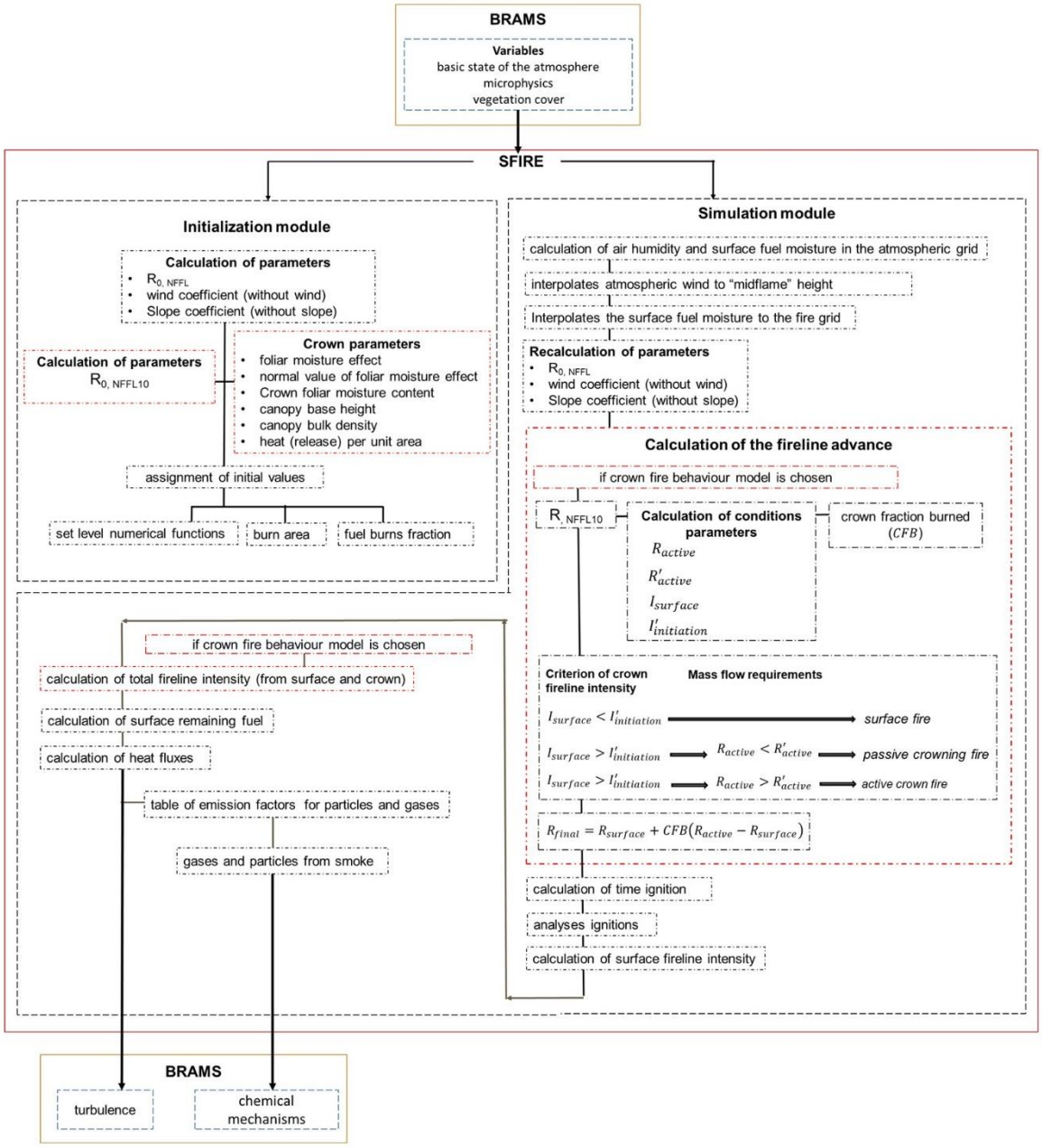

Figure 1- The framework of the BRAMS version 5.6.2 system, with the necessary developments for crown behaviour introduced in the SFIRE model. R is the rate of spread and I is the fireline intensity.

BRAMS-SFIRE, version 5.0, is a one-way coupled fire-atmosphere model. BRAMS injects data from variables of the basic state of the atmosphere, the microphysics, and vegetation cover into the SFIRE, which injects data from variables of sensible and latent heat fluxes from the fire into the boundary layer of the atmospheric model BRAMS, through the turbulence scheme, by carrying out a process of constant exchange during simulation. The SFIRE model uses as surface data high-resolution fuel data on a regular grid, generated using the Northern Forest Fire Laboratory (NFFL) fuel model (Anderson, 1982), and a table with physical and mineral properties, and dendometric measures of the thirteen NFFL fuel models. A new module was built to include the propagation of fire in crown trees by creating new routines and adapting the code of SFIRE's original routines. In this module, the parameters referring to no wind forward rate of spread for a surface fire for NFFL fuel model 10, and the forward rate of spread for NFFL fuel model 10 were programmed. Some considerations were implemented, namely for the crown ignition criteria of Byram's fireline intensity and critical fireline intensity for initiating a crown fire, and the requirements of mass flow, namely, the forward rate of spread for a fully active crown fire

and a critical forward rate of spread for sustaining an active crown fire. Depending on the criteria met, a forward rate of spread for any type of fire - surface, passive crown, or active crown - was associated with the level set numerical method from the SFIRE model, which is the numeric propagation scheme (Osher and Fedkiw, 2003). The assessment of crown fire in SFIRE, requires other estimates of canopy fuel characteristics, namely, canopy bulk density (CBD), canopy base height (CBH), and crown foliar moisture content per cent (FMC) and foliar moisture effect (FME) data. The CBD and FME was programmed from a alometric equation and FMC trough read of data in a "namelist.fire" table, and CBH trough read of a map created from Forest Inventory data from 7964 field plots in Portugal, available from Portuguese Institute for Nature Conservation and Forests (ICNF).With the module "sfclyr_sfire", is made the interaction between BRAMS and SFIRE.

2.2. BRAMS and smoke modelling

Atmospheric emissions during fire events were estimated using the most suitable emission factors ($g.kg^{-1}$), the burning efficiency, the fuel load ($kg.m^{-2}$), and the burned area (m^2). Most of the studies reported in the literature include emission factors for American fuels (e.g. McMeeking et al. 2009; Akagi et al. 2011), savannas/pastures, tropical and extratropical forests (Van Der Werf et al. 2017). For this work, emission factors for Mediterranean conditions were chosen based on a bibliographic review considering values selected by previous studies (Miranda 2004; Alves et al. 2011; Van Der Werf et al. 2017; Vicente et al. 2017, 2012). For Eucalyptus, Acacia and Pinus pinaster species the emission factors were expressed as the average of the emission factors obtained experimentally by Alves et al. (2011) and Vicente et al. (2012, 2017). For the other hardwoods species, the emission factors reported by Van Der Werf et al. (2017) were used. For other resinous, Oak, Chestnut, Cork Oak and Stone pine species the emission factors were obtained by Miranda (2004). Finally, the emission factors obtained for each species were adapted to the NFFL classification considered by the model to update the emission factors parameterization for the Mediterranean conditions.

Within BRAMS concentrations of smoke pollutants are estimated using the species mass released by a fraction of biomass burned (emission factors) dispersed as fluxes, through buoyancy convection and vertical and horizontal advection in dry air along the vertical column in the BRAMS simulated boundary layer, and resolved by chemical mechanisms in the domain of simulation. The selected emission factors of gases and particulate matter from fires, in the domain of simulation, are included in the modelling system through an emission table.

3. Acknowledgements

The authors acknowledge the financial support of FCT – Science and Technology Portuguese Foundation, which funded project FIRESMOKE (PTDC/CTA-MET/3392/2020) through national funds. Thanks are due for the financial support to CESAM by FCT/MCTES (UIDP/50017/2020+UIDB/50017/2020+ LA/P/0094/2020), through national funds.

4. References

Akagi S.K., Yokelson R.J., Wiedinmyer C., Alvarado M.J., Reid JS, Karl T., Crounse J.D., Wennberg P.O. 2011. Emission factors for open and domestic biomass burning for use in atmospheric models. Atmospheric Chemistry and Physics 11, 4039–4072.

Akritidis, D., Katragkou, E., Georgoulias, A. K., Zanis, P., Kartsios, S., Flemming, J., ... & Eskes, H. 2020. A complex aerosol transport event over Europe during the 2017 Storm Ophelia in CAMS forecast systems: analysis and evaluation. Atmospheric Chemistry and Physics, 20(21), 13557-13578.

Alves, C.; Vicente, A.; Nunes, T.; Gonçalves, C.;, Fernandes, A.P.; Mirante, F.; Tarelho, L.; Sánchez de la Campa, A.M.; Querol, X.; Caseiro, A.; Monteiro, C.; Evtyugina, M.; Pio, C. 2011. Summer 2009 wildfires in Portugal: Emission of trace gases and aerosol composition. Atmospheric Environment 45, 641–649.

Anderson, H. E. 1982. Aids to determining fuel models for estimating fire behavior. Gen.Tech. Rep. INT-122. Ogden, UT: U.S. Department of Agriculture, Forest Service, Intermountain Forest and Range Experiment Station. 22 p.

Freitas, S.R., Panetta, J., Longo, K.M., Rodrigues, L.F., Moreira, D.S., Rosario, N.E., ... & Martins, L.D. 2017. The Brazilian developments on the Regional Atmospheric Modeling System (BRAMS 5.2): an integrated environmental model tuned for tropical areas. Geoscientific model development, 10(1), 189-222.

ICNF – Instituto da Concervação da Natureza e das Florestas – Inventário Florestal Nacional [WWW Document]. URL https://www.icnf.pt/florestas/flestudosdocumentosestatisticasindicadores (accessed 27.06.2022).

Jain, R., Vaughan, J., Heitkamp, K., Ramos, C., Claiborn, C., Schreuder, M., ... & Lamb, B. 2007. Development of the ClearSky smoke dispersion forecast system for agricultural field burning in the Pacific Northwest. Atmospheric Environment, 41(32), 6745-6761.

Longo, K. M., Freitas, S. R. D., Pirre, M., Marecal, V., Rodrigues, L. F., Panetta, J., ... & Arteta, J. 2013. The Chemistry CATT-BRAMS model (CCATT-BRAMS 4.5): a regional atmospheric model system for integrated air quality and weather forecasting and research. Geoscientific Model Development.

Mandel, J.; Beezley, J.D.; Coen, J.L.; Kim, M. 2009. Data assimilation for wildland fires: Ensemble Kalman filters in coupled atmosphere-surface models. IEEE Control Systems Magazine, n. June, p. 47-65.

Mandel, J.; Beezley, J.D.; Kochanski, A.K. 2011. Coupled atmosphere-wildland fire modeling with WRF 3.3 and SFIRE 2011. Geoscientific Model Development, v. 4, n. 3, p. 591-610.

Martins, V.; Miranda, A.I.; Carvalho, A.; Schaap, M.; Borrego, C.; Sá, E. 2012. Impact of forest fires on particulate matter and ozone levels during the 2003, 2004 and 2005 fire seasons in portugal. Science of the Total Environment 414, 53–62.

McMeeking, G.R.; Kreidenweis, S.M.; Baker, S.; Carrico, C.M.; Chow, J.C.; Collett, J.L.; Hao, W.M.; Holden, A.S.; Kirchstetter, T.W.; Malm, W.C.; Moosmüller, H.; Sullivan, A.P.; Cyle, E.W. 2009. Emissions of trace gases and aerosols during the open combustion of biomass in the laboratory. Journal of Geophysical Research Atmospheres 114, 1–20.

Menezes, I.; Freitas, S.R.; Ribeiro, N.A.; Corte-Real, J.M.; Surový, P. 2016. Construção de um modelo de interacção atmosfera/fogo aplicado à gestão florestal e avaliação de risco de fogos florestais no Alentejo. Doctoral Thesis from University of Évora, 236 p.

Menezes, I.C., Freitas, S.R., Lima, R.S., Fonseca, R.M., Oliveira, V., Braz, R., ... & Ribeiro, N.A. 2021a. Aplicação dos Modelos de Interação Atmosférica e de Incêndio Florestal BRAMS-SFIRE no sul de Portugal. Revista Brasileira de Meteorologia, 36, 423-440.

Menezes, I.; Miranda, A.I.; Fernandes, A.P.; Lopes, D.; Ferreira, J. Freitas S.R.; Rodrigues L.F.; Braz, R. 2021b. FIRESMOKE - A modelling system for wildfires smoke behaviour [WWW Document]. URL http://firesmoke.web.ua.pt/ (accessed 27.06.2022).

Miranda, A.I. 2004. An integrated numerical system to estimate air quality effects of forest fires. International Journal of Wildland Fire 13, 217–226.

Osher, S. and Fedkiw, R. 2003. Level Set Methods and Dynamic Implicit Surfaces, Springer, New York.

Peace, M.; Charney, J.; Bally, J. 2020. Lessons Learned from Coupled Fire-Atmosphere Research and Implications for Operational Fire Prediction and Meteorological Products Provided by the Bureau of Meteorology to Australian Fire Agencies. Atmosphere, 11(12), 1380.

Rodrigues, M., San Miguel, J., Oliveira, S., Moreira, F., & Camia, A. 2013. An insight into spatial-temporal trends of fire ignitions and burned areas in the European Mediterranean countries. Journal of Earth Science and Engineering, 3(7), 497.

Rothermel, R.C. 1972. A mathematical model for predicting fire spread in wildland fuels. Res. Pap. INT-115. Ogden, UT: U.S. Department of Agriculture, Forest Service, Intermountain Forest and Range Experiment Station. 40 p.

Rothermel, R.C. 1991. Predicting behavior and size of crown fires in the Northern Rocky Mountains. Res. Pap. INT-438. Ogden, UT: U.S. Department of Agriculture, Forest Service, Intermountain Forest and Range Experiment Station. 46 p.

Stein, A. F., Rolph, G. D., Draxler, R. R., Stunder, B., & Ruminski, M. 2009. Verification of the NOAA smoke forecasting system: model sensitivity to the injection height. Weather and Forecasting, 24(2), 379-394.

Scott, J.H. and Reinhardt, E.D. 2001. Assessing crown fire potential by linking models of surface and crown fire behavior. US Department of Agriculture, Forest Service, Rocky Mountain Research Station.

Valente, J., Miranda, A.I., Lopes, A.G., Borrego, C., Viegas, D.X., Lopes, M. 2007. Local-scale modelling system to simulate smoke dispersion. Int J Wildland Fire, 16(2), 196-203.

Van Der Werf, G.R.; Randerson, J.T.; Giglio, L.; Van Leeuwen, T.T.; Chen, Y.; Rogers, B.M.; Mu, M.; Van Marle, M.J.E.; Morton, D.C.; Collatz, G.J.; Yokelson, R.J.; Kasibhatla, P.S. 2017. Global fire emissions estimates during 1997-2016. Earth System Science Data 9, 697–720.

Van Wagner, C.E. 1977. Conditions for the start and spread of crown fire. Canadian Journal of Forest Research. 7: 23–34.

Vicente, A.; Alves, C.; Monteiro, C.; Nunes, T.; Mirante, F.; Cerqueira, M.; Calvo, A.; Pio, C. 2012. Organic speciation of aerosols from wildfires in central Portugal during summer 2009. Atmospheric Environment 57, 186–196.

Vicente, A.; Calvo, A.; Fernandes, A.P.; Nunes, T.; Monteiro, C.; Pio, C.; Alves, C. 2017. Hydrocarbons in particulate samples from wildfire events in central Portugal in summer 2010. Journal of Environmental Sciences (China) 53, 122–131.

Wheeler, N. J. M., Raffuse, S. M., Sullivan, D., Craig, K. J., Reid, S. B., Solomon, R., ... & Larkin, S. 2010. Daily Air Quality Predictions from the Blue Sky Gateway. NATO Science for Peace and Security Series B-Physics and Biophysics, 307-311.

Ecoregion based attribution analysis of the influence of several fire danger indices on the amount of burned area at a global scale by means of pseudo transfer entropy

Antonio Pérez[1], Riccardo Silini[2], Iván Sánchez[1], Joaquín Bedia[3]

[1]Predictia Intelligent Data Solutions SL. Benidorm st. 8 ground floor, 39005, Santander, Spain, {aperez, sanchezi}@predictia.es
[2] Universitat Politècnica de Catalunya. Rambla Sant Nebridi 22, 08222 Terrassa, Barcelona, Spain {riccardo.silini@upc.edu}
[3] Universidad de Cantabria, Dpto. Matemática Aplicada y CC de la Computación. Avda. los Castros s/n. 39005, Santander, Spain {bediaj@unican.es}

**Corresponding author*

Keywords

Fire weather index, fire burned area, attribution, causality, pseudo transfer entropy (pTE)

Abstract

Understanding the current fire-climate relationships is of utmost importance in order to assess the potential impacts that projected climate may exert in the near future. However, the many factors involved in fire activity often prevent a proper attribution of the observed variability. Unlike the many previous correlative studies, here we address this problem using a 'causality' measure known as “pseudo transfer entropy” (pTE), relating three widely used fire danger indices to the global observed burned areas (namely the Canadian Fire Weather Index, the Fire Danger Index from the Australian McArthur Mark 5 Rating System and the Burning Index from the U.S. Forest Service National Fire-Danger Rating System). The study has been performed at an spatial aggregation level defined by the RESOLVE ecoregions, attending to their homogeneous fuel and climatic properties, and considering different spatial and temporal aggregation statistics (mean, 90th percentile, 95th percentile and sum).

We present an open, web-based interactive tool to explore and compare the results derived from the causality of these different fire danger indices with the observed burned area. Our results unveil some consistent patterns and three main conclusions can be drawn: 1) in the overall, all indices exhibit a similar performance in explaining observed burned areas, although regional differences may justify the selection of one index over another in regional studies, 2) the aggregation method used at the ecoregion level affects the causality results, with higher percentiles being better explained by pTE than the mean state and 3) the interactive tool designed may serve as a valuable method of intercomparison and analysis for the vulnerability and impact assessment community involved in fire research.

1. Introduction

Fire is an integral earth system process whose causes are complex (Pausas 2021), often difficult to disentangle, and largely dependent on the scale of analysis. Climate is one of the most important factors affecting fire regimes globally (Bedia 2015; Abatzoglou 2018). Understanding the current fire-climate relationships is of utmost importance in order to assess the potential impacts that projected climate may exert in the near future. However, the many factors involved in fire activity often prevent a proper attribution of the observed variability. Unlike the many previous correlative studies, here we address this problem using a 'causality' measure, in particular “pseudo transfer entropy” (pTE), relating three widely used fire danger indices (the Fire Weather Index from the Canadian Forest Service Fire Weather Index Rating System, the Fire Danger Index from the Australian McArthur Mark 5 Rating System and the Burning Index from the U.S. Forest Service National Fire-Danger Rating System) with global observed burned area records at a monthly scale in the last 20 years. Furthermore, we perform an intercomparison of these fire danger indices taking as spatial reference for the analysis the main terrestrial ecoregions.

2. Data collection

To perform this study, three different datasets have been taken into consideration.

2.1. Fire danger indices

The Copernicus Climate Data Store (CDS) catalogue entry named as "Fire danger indices historical data from the Copernicus Emergency Management Service" [ECMWF 2019] offers historical –1979 to present– information for a set of indices related to fire danger. These indicators are retrieved in a regular latitude-longitude grid which covers the entire globe (180ºW to 180ºE, 90ºS to 90ºN) with a spatial resolution of 0.25º and a daily temporal resolution. From this CDS catalogue entry, data for 3 variables was downloaded: the Fire Weather Index (FWI) from the Canadian Forest Service Fire Weather Index Rating System, the Fire Danger Index (FDI) from the Australian McArthur Mark 5 Rating System and the Burning Index (BI) from the U.S. Forest Service National Fire-Danger Rating System.

2.2. Fire burned area from satellite observations

We have used monthly data of Burned Area (BA) at 0.25◦ resolution from the "Fire burned area from 2001 to present derived from satellite observations" database (C3S 2019a; C3S 2019b) which is publicly available through the Copernicus Climate Data Store (https://cds.climate.copernicus.eu/cdsapp#!/home) as part of Copernicus, the European Union's Earth Observation Programme managed by the European Commission (https://www.copernicus.eu/en). The BA data used are derived through the analysis of reflectance changes from the medium resolution sensors Terra MODIS and Sentinel-3 OLCI, helped by the use of MODIS thermal information. The algorithms used are adapted to the native data from these sensors to produce an homogeneous gridded dataset of global coverage containing monthly data of BA at the grid scale, extending the database to the present.

2.3. RESOLVE Ecoregions dataset (2017)

RESOLVE Biodiversity and Wildlife Solutions provides access to this dataset containing information about 846 in-land ecoregions which depict an overall representation of our living planet (Dinerstein 2017). There is an online visor showing the above mentioned ecoregions: https://ecoregions.appspot.com/

3. Data pre-processing

The process to clean and homogenise the raw data –described in section 2– can be divided in the following tasks (schematized in Figure 1):

Despite having the same spatial resolution (0.25º), the fire danger indices data needed to be regridded to the burned area observations grid due to the fact that their meshes presented some differences. Afterwards, the data is temporally aggregated to the same temporal resolution: 1 Month. Therefore, the fire danger indicators are converted from daily to monthly data and the burned area observations remain in a monthly resolution.

As a last step, the ecoregion's metadata is used to perform a spatial aggregation on both the fire danger indices and the burned area observations.

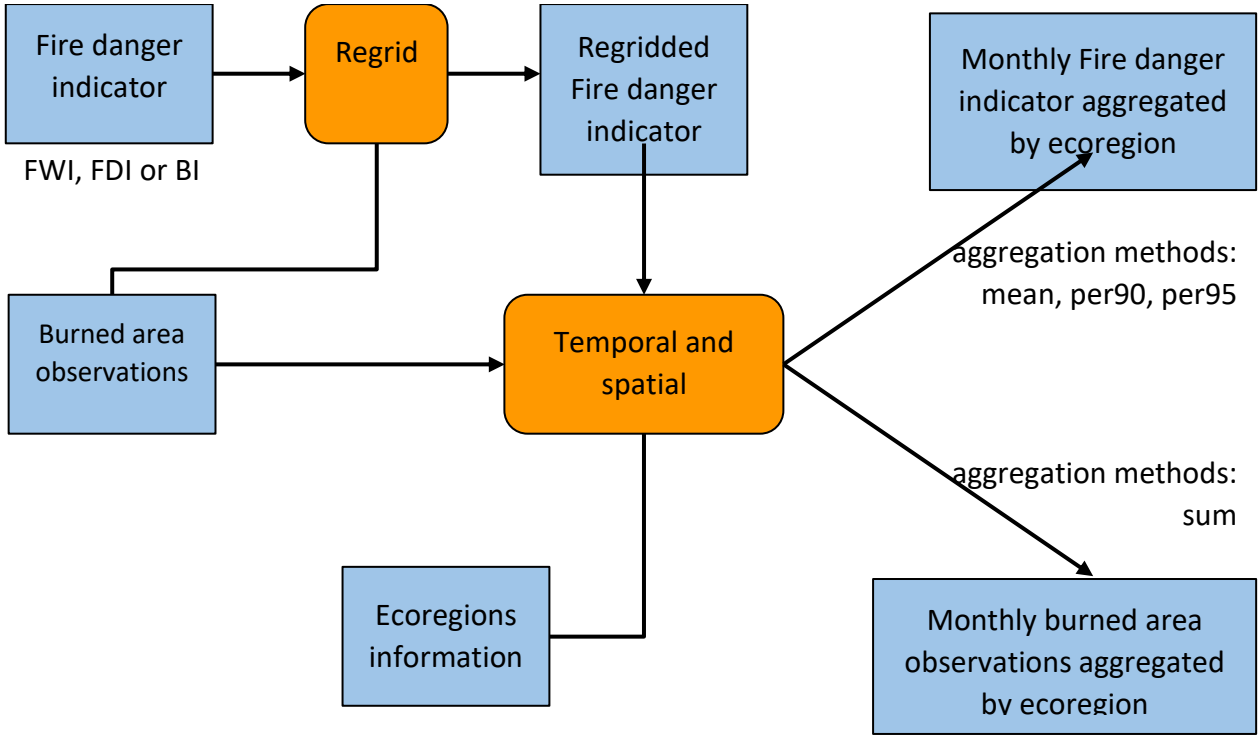

Figure 1- Data pre-processing scheme where the orange boxes represent tasks guided by an algorithm and blue boxes represent data that is used as input/output for the orange boxes.

The aggregation methods used remain constant in both temporal and spatial aggregation algorithms. As established in Table 1, the observed burned area was computed by the sum in order to have the total amount of area burned on time and space. However, the fire danger indices had a different approach and were computed using several statistical options such as the mean, the 90th percentile and the 95th percentile. Other aggregation methods such as the 99th percentile and the maximum were considered, but they presented a lower number of ecoregions with significant results on the causality measure.

Table 1. Combination of variable - aggregation method which were taken into consideration (green).

	MEAN	PERCENTILE 90	PERCENTILE 95	SUM
FWI				
FDI				
BI				
BURNED AREA				

As a consequence, there will be 10 different variables after the preprocessing task (+10 significance test results) for a total number of 693 ecoregions. This number is lower than the total number defined by the RESOLVE dataset due to the following specific facts: 1) some ecoregions do not have enough extent to perform the temporal and spatial aggregation over them –no grid points inside them–, 2) only terrestrial information was provided by both the fire danger indices and the burned area observations, and 3) there are ecoregions with no presence of fire in their surface.

4. Methodology

Once the monthly data is computed, an analysis of the causality from fire danger indices to the fire burned area is performed using a recent fast and effective metric called pseudo transfer entropy (pTE) (Silini 2021). Given

two time series X and Y, we say that X causes Y, if the information contained in the past X, in conjunction with the information contained in the past of Y, can predict the future values of Y, better than the past of Y alone. This means that a fire danger index contains predictive skill on the observed burned area, if a significant pTE from the former to the latter is found. We compute the pTE between the monthly indices, using an embedding size of 2 and a time lag of 1. The embedding size is found by modelling the burned area time series as an autoregressive model.

Once the pTE between fire danger indices and burned area are computed, we have to account for their significance. From the original series we create 100 Iterative Amplitude Adjusted Fourier Transform (IAAFT) surrogates, preserving both the spectra and amplitude distributions, and we compute the pTE between them. The quantiles of the resulting pTE distribution, allow to define significance thresholds. In this study we consider a pTE value above the quantile 90 as significant.

5. Results and discussion

In the context of the research project, a web-app has been designed as a framework to visualise the causality measurement by means of pTE of the different combinations between the set of fire danger indices and the chosen aggregation methods with the total burned area: https://showcase.predictia.es/global-fwi-causality. The aggregation method –as well as the fire danger index– can be chosen on the right side panel. This tool allows the user to browse both the spatial and temporal characteristics of the different types of data. In this way, the user can study the spatial distribution of the causality of the different fire indices (Figure 2), but can also carry out much more in-depth investigations at the ecoregion level (for instance, the Italian Sclerophyllous And Semi-Deciduous Forests), having access to other features such as static data (Figure 3) the analysis of aggregated time series (Figure 4), scatter plot relating the value of the index to the burned area (Figure 5), and a heatmap which compares the index-aggregation method combinations with the burned area on an annual basis (Figure 6).

Some important conclusions can be derived from the web application. Overall, there is not a fire danger index (FWI, FDI or BI) that works globally better since all of them exhibit a similar performance. However, it makes really sense to use some of them over others depending on the ecoregion of interest when performing a local study. Moreover, all three indices follow similar patterns on how the significant ecoregions are distributed because most of them are located in three different main areas: over the boreal strip (Canada, Rusia, Greenland, among others), East-Asia and the Oceanic region, and the centre of Africa –where most of the worldwide area burned is located–.

The use of various aggregation methods allows the analysis of causality depending on whether more intermediate values of fire danger indices or more characteristic values of the extremes of these variables have been taken for the ecoregions of interest. Although there are more ecoregions with significant results when considering the mean value of the fire danger metric (FWI: 298, FDI: 281 and BI: 260) rather than, for instance, the 95th percentile (FWI: 269, FDI: 225 and BI: 240), it seems –as shown in the web-app– that the larger ecoregions are more affected by the extremes than ecoregions with a lower surface area.

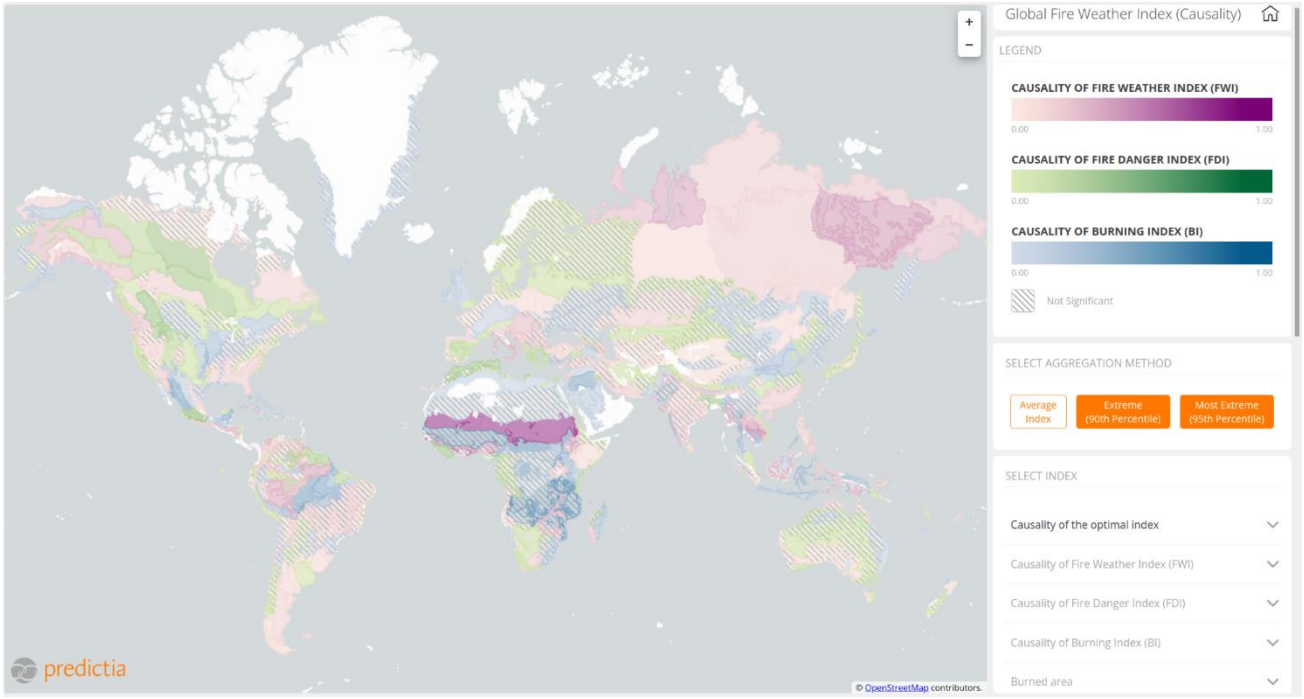

Figure 2- Home page of the web application designed to facilitate access to the processed data. At the left side, the ecoregion map with the 693 ecoregions available during the study. At the right side, there is a panel that acts as a selector to choose the different variables and aggregation methods available.

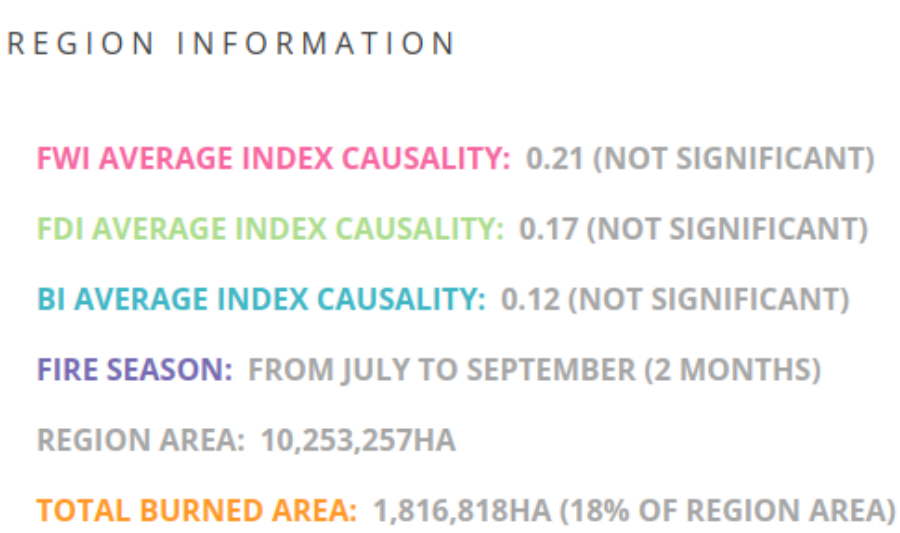

Figure 3- Example of ecoregion static information for the "Italian Sclerophyllous And Semi-Deciduous Forests" ecoregion. This static information contains: the causality of the different indices (FWI, FDI and BI) aggregated by a given aggregation method (95th percentile in this case), the fire season and its length, the ecoregion area and the corresponding total area burned.

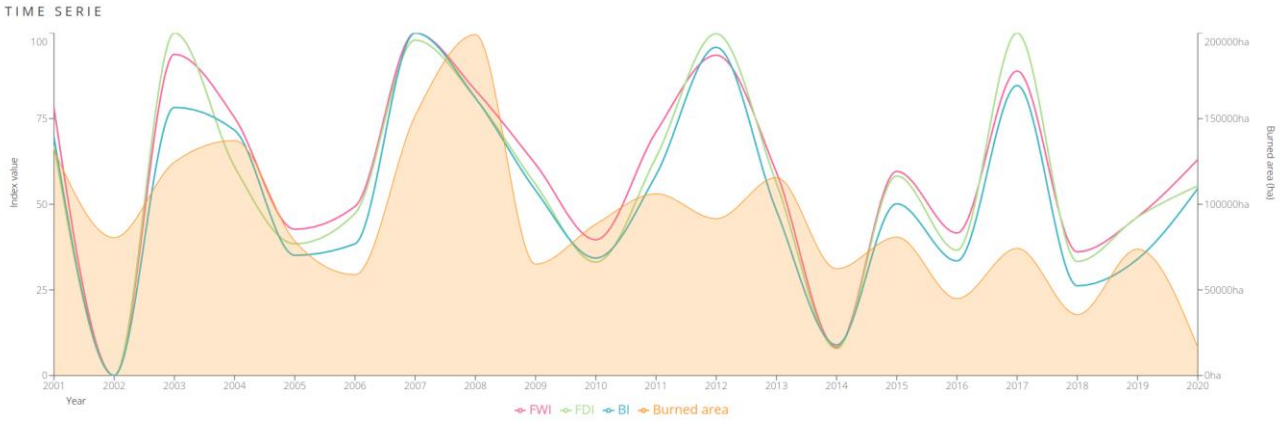

Figure 4- Example of time-serie showing the annual data for different indices (FWI, FDI and BI) aggregated by a given aggregation method (95th percentile in this case) and the total burned area for the "Italian Sclerophyllous And Semi-Deciduous Forests" ecoregion.

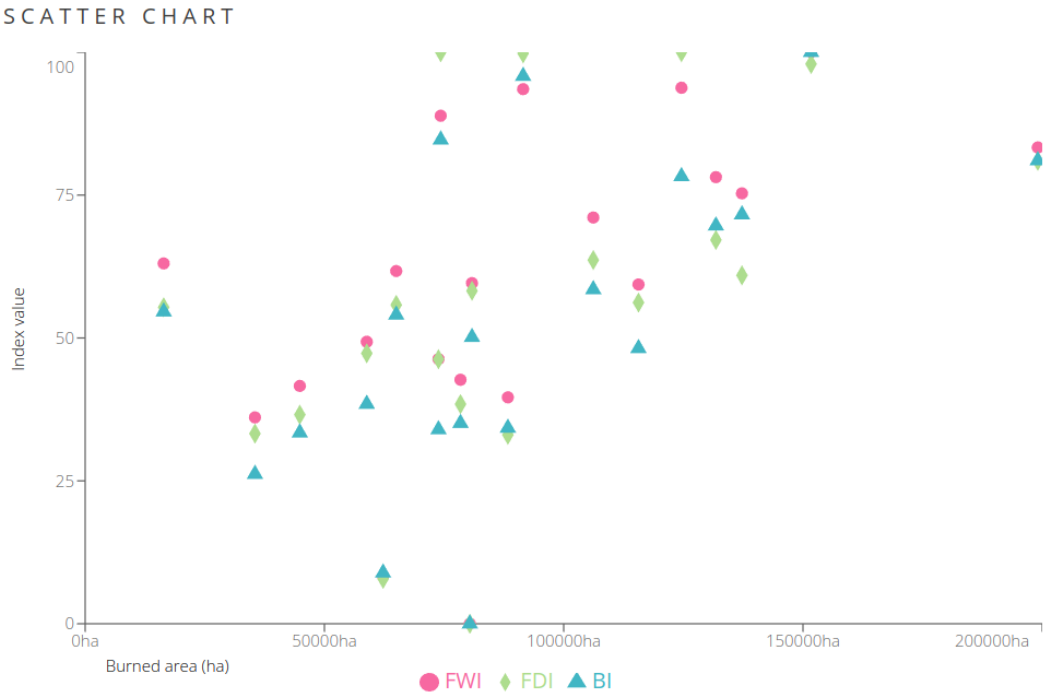

Figure 5- Example of scatter chart showing the relation between the different indices (FWI, FDI and BI) aggregated by a given aggregation method (95th percentile in this case) and the total burned area for the "Italian Sclerophyllous And Semi-Deciduous Forests" ecoregion.

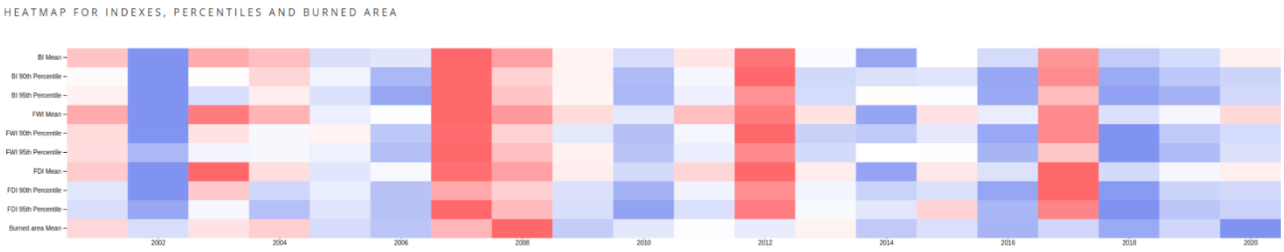

Figure 6- Example of quantile based stripes showing the annual characterisation in comparison with the entire period for all the different combinations of indices (FWI, FDI and BI) and aggregation methods (mean, per90, per95) and the total burned area for the "Italian Sclerophyllous And Semi-Deciduous Forests" ecoregion. From blue to red, it indicates the quantile to which the data belongs: lower, mid-lower, mid-upper, upper.

6. References

Pausas, Juli G. and Jon E. Keeley. Wildfires and global change, Frontiers in Ecology and the Environment, Wiley, nº7, 19, 3 June 2021, p. 387–95. https://doi.org/10.1002/fee.2359.

Bedia, Joaquín et al. Global patterns in the sensitivity of burned area to fire-weather: Implications for climate change, Agricultural and Forest Meteorology, Elsevier BV, 214–215, December 2015, p. 369–79. https://doi.org/10.1016/j.agrformet.2015.09.002

Abatzoglou, John T. et al. Global patterns of interannual climate–fire relationships, Global Change Biology, Wiley, nº11, 24, 24 August 2018, p. 5164–75. https://doi.org/10.1111/gcb.14405

European Centre for Medium-Range Weather Forecasts (ECMWF), (2021): Fire danger indices historical data from the Copernicus Emergency Management Service. v4.0. Copernicus Climate Change Service (C3S) Climate Data Store (CDS). (accessed on 9-Nov-2021), https://doi.org/10.24381/cds.0e89c522.

Copernicus Climate Change Service (C3S) (2019): Fire burned area from 2001 to present derived from satellite observations, OLCI (Ocean and Land Colour Instrument), 5.1.1, Copernicus Climate Change Service (C3S) Climate Data Store (CDS). (Accessed on 9-Nov-2021), https://doi.org/10.24381/cds.f333cf85.

Copernicus Climate Change Service (C3S) (2019): Fire burned area from 2001 to present derived from satellite observations, MODIS (Moderate Resolution Imaging Spectroradiometer), 1.1, Copernicus Climate Change Service (C3S) Climate Data Store (CDS). (Accessed on 9-Nov-2021), https://doi.org/10.24381/cds.f333cf85

Dinerstein, Eric et al. An Ecoregion-Based Approach to Protecting Half the Terrestrial Realm, BioScience, Oxford University Press (OUP), nº6, 67, 5 April 2017, p. 534–45. https://doi.org/10.1093/biosci/bix014

Silini, Riccardo and Cristina Masoller. Fast and effective pseudo transfer entropy for bivariate data-driven causal inference, Scientific Reports, Springer Science and Business Media LLC, nº1, 11, 19 April 2021. https://doi.org/10.1038/s41598-021-87818-3

Effects of wind velocity on predictions of wildland fire rate of spread models: A comparative assessment using surface fuel fire tests

Dionysios I. Kolaitis *; Christos N. Pallikarakis; Maria A. Founti

Fire Engineering Unit, Laboratory of Heterogeneous Mixtures and Combustion Systems,
School of Mechanical Engineering, National Technical University of Athens,
Heroon Polytechneiou 9, Zografou 15780, Greece,
{dkol@central.ntua.gr, pallik@mail.ntua.gr, mfou@central.ntua.gr}

**Corresponding author*

Keywords

Wildland fires, Rate of Spread, Prediction Models, Wind, Laboratory experiments

Abstract

In this work, a collection of ten wildland fire rate of spread prediction models that take into account the effects of wind are reviewed and tested against 166 individual laboratory fire tests, available in the open literature. The investigated models include the well-known semi-empirical models of Rothermel, Wilson and Catchpole et al., the empirical models of Rossa and Fernandes, developed using laboratory fire tests and the empirical models of Burrows et al., Anderson et al., Fernandes et al. and the Canadian Forest Fire Behavior Prediction System, developed using field measurements. The performance of the ten models is evaluated, both qualitatively and quantitatively, by employing a range of statistical error metrics. It is shown that the performance of each model is affected by their specific characteristics, in conjunction with the characteristics of the experiments against which the models were evaluated. It is found that the model of Catchpole et al. yields the lowest statistical error metric values in the specific measurement data set employed here. The empirical models that have been developed using field measurements exhibit significant discrepancies against the experimental data, due to the use of specific parameters regarding fuel type, scale and wind speed. Increasing wind velocities up to 3 m/s result, in the majority of the investigated models, in decreasing discrepancies with the experimental data.

1. Introduction

Prediction of the wildland fire Rate of Spread (ROS) is consistently one significant aim of the fire science community, since knowledge of the spatial-temporal evolution of a wildland fire event provides valuable information for a broad range of activities, ranging from fire defence to civilian evacuation. However, a single, catholic model that can accurately predict any potential wildland fire ROS has yet to be presented. This is, partially, due to the complexity of the involved physical phenomena, comprising a synergy of several interacting physical and chemical processes, e.g. combustion, turbulence, kinetics, heat, mass, and momentum transfer. Moreover, a wildland fire is a multi-scale phenomenon, which can manifest in various types of landscapes with potentially different horizontal (continuous-discontinuous) and/or vertical (surface, understory, over-story) fuel configurations. In this frame, a plethora of models has been developed to predict the ROS in various types of wildland fires, each with its own characteristics and limitations.

Wildland fire ROS prediction models are commonly categorized based on their corresponding level of physical foundation. For instance, a ROS model can be developed based on physical-chemical foundational principles and assumptions (physical model), or using statistical correlations stemmed from experimental data (empirical models), or even a combination of both (semi-empirical models) (Pastor et al., 2003). Experimental measurements, necessary for the development of empirical and semi-empirical models, are provided either from laboratory fire tests, which mainly focus on small-scale surface fires, or from large-scale field experimentation (or field observational studies) that, based on the specific characteristics of the landscape, may potentially account for multiple-scale phenomena.

Among the various parameters that influence the behaviour of a wildland fire, atmospheric wind velocity is of particular interest. Early studies recognized the impact of wind as one of the most influential parameters

affecting the rate of spread and the evolution of a fire front (Rothermel and Anderson, 1966). The majority of the empirical and semi-empirical ROS models is able to incorporate the effects of atmospheric wind, either directly or through a model supplement. More specifically, models developed from field experiments seldom account for the case of a "quiescent" wind environment due to its rarity, as well as the fact that quiescent fires are generally characterised by relatively low ROS values, thus representing a "best case scenario".

In this work, ten different wildland fire ROS prediction models of empirical or semi-empirical nature are being reviewed and validated against 166 individual laboratory fire tests, aiming to quantify their prediction accuracy, by means of various statistical error metrics. Their performance is then discussed in detail, taking into account the specific characteristics and limitations of each model.

2. Investigated ROS models

A collection of ten models has been selected to be evaluated. The investigated models include a first group of the well-known "semi-empirical" models of Rothermel (1972), Wilson (1990) and Catchpole et al. (1998), a second group of the "empirical" models of Rossa and Fernandes (2018a, 2018b) developed using laboratory tests and a third group of the "empirical" models of Burrows et al. (2019), Anderson et al. (2015), Fernandes et al. (2009) and also the Canadian Forest Fire Behavior Prediction System (Forest Canada Fire Danger Group, 1992), which are fuel-specific and have been developed using field measurements.

All three semi-empirical models are based in the theoretical work of Frandsen (1971), where the steady state rate of spread, R (m/s) of an advancing flaming front is expressed as the ratio of thermal power per unit area (called the propagating heat flux) received by a fuel element from the flame, I_p (W/m^2) over the energy density required from the fuel element to reach ignition conditions, L (J/m^3). Rothermel (1972) modified Frandsen's ratio, employing theoretical reasoning as well as laboratory experiments, resulting in a semi-empirical model that is considered to be a "benchmark". In this model, the effects of wind and slope were decoupled from I_p, resulting in a "basic propagating heat flux", $I_{p,0}$ that in turn is assumed to be a fraction, ξ of the energy generated by the flame front, I_R (W/m^3). Through laboratory experiments, Rothermel statistically related the model's theoretical properties with specific measurable properties of the fuel, as well as the wind velocity and the slope angle. Later, Wilson (1990), based on empirical evidence as well as statistical data from a broader range of additional laboratory experiments on quiescent conditions, re-examined the model of Rothermel. One of the main modifications proposed by Wilson is the hypothesis that the energy generated from the flame front contributing to the propagating heat flux, stems only from the heat content of the pyrolyzed gases. Finally, the Catchpole et al. (1998) model was based on laboratory experiments on a wind tunnel as well as on the two previously cited models. One of the main ideas of this model was the re-coupling of the propagating heat flux with the effect of wind.

The empirical work of Rossa and Fernandes (2018a, 2018b) comprises two models that statistically relate the quiescent rate of spread, R_0 (m/s) with fuel related properties, whereas a complementary model that accounts for the effect of wind is used. Their work is based on laboratory experiments and, despite being of empirical nature, selection of some of the related properties is based on theoretical reasoning.

The remaining four empirical models are based on field experiments or observational studies of actual wildland fires on specific flora environments. Burrows et al. (2019) modeled the flame ROS on spinifex grassland (a horizontally discontinuous surface fuel) yielding a "parsimonious" three-parameter model. Anderson et al. (2015) presented a group of empirical models based on a large database of shrubland fires. Fernandes et al. (2009) developed a model for predicting the flame ROS on maritime pine stands. Lastly, the Forestry Canada Fire Danger Group (1992) developed the Fire Behavior Prediction System (FBP) from various types of field experiments and observational studies. This model has been developed to accept fuel specific parameters from various fuel models of Canadian flora environments.

The general form of the ten models investigated in this work are presented in Table 1, where σ (m^{-1}) is the surface-to-volume ratio, β (-) is the packing ratio, m_d'' and m_n'' (kg/m^2) are the dry and net fuel load, respectively, h and h_v (kJ/kg) are the heat content of the fuel and the fuel pyrolysis gas, respectively, M (%) is the fuel moisture content, Q_p (kJ/kg) is the heat of pyrolysis, Q_w (kJ/kg) is the latent heat of evaporation of water, s (m^2/kg) is the particle specific surface, c (%) is the fuel cover (for a discontinuous, horizontal fuel geometry), U (m/s) is the laboratory wind tunnel velocity and U_z (m/s) is the field wind velocity measured at a height z (m

or ft). The rest of the parameters, represented by capital letters, namely A to K, represent specific model constants (different for each model), while the parameters represented by lower case letters, e.g. a, b, and c, represent fuel specific constants for the CFFBPS model.

Table 1 – General form of the main equations corresponding to the investigated ROS models.

Reference	**Model Equations**
Rothermel (1972)	$R = \frac{I_{R,1}(\sigma,\beta,h,M,\eta_S,m_n'')*\xi_1(\sigma,\beta)}{L_1(\sigma,\mathrm{M},\rho_b)}(1+\mathrm{A}(\sigma,\beta)*U^{B(\sigma)})$
Wilson (1990)	$R = \frac{I_{R,2}(\sigma,\beta,\delta,h_v,M,Q_p,Q_w,m_d'')*\xi_2(\sigma,\beta)}{L_2(\sigma,\mathrm{M},\rho_b,Q_p,Q_w)}(1+\mathrm{A}(\sigma,\beta)*U^{B(\sigma)})$
Catchpole et al. (1998)	$R = \frac{I_P(U,\sigma,\beta,\mathrm{M})}{L_2(\sigma,\mathrm{M},\rho_b,Q_p,Q_w)}$
Rossa and Fernandes (2018a, 2018b)	$R = R_0 * K * [1 + E * U^F (R_0 * m'')^G (H + M * I)^J]$, $R_0 = A * M^B * \delta^C$ (1) or $R_0 = A * M^B * \delta^C * \ln(D * s)$ (2)
Burrows et al. (2019)	$R = A * \frac{U_z^B * c^C}{M^D}$
Anderson et al. (2015)	$R = A * U_z^B * \delta^C * e^{D*M}$ or $R = A * U_z^B * \left(\frac{m''}{\delta}\right)^C * e^{D*M}$
Fernandes et al. (2009)	$R = A * U_z^B * e^{C*M} * \delta^D$
CFFBPS (1992)	$R = a * (1 - e^{-b*ISI})^c$, where $ISI = A * e^{B*U_z} * \{C * e^{D*M} * [1 + E * M^F]\}$

3. Methodology

Aiming to evaluate the prediction accuracy of the ten investigated ROS models, a set of 166 individual laboratory fire tests, performed on surface fuels, was collected from the open literature. All the experiments were conducted in wind tunnels, where fuel beds were linearly ignited. The fire tests set includes experiments with various kinds of fuels, namely pine needles, excelsior and wood sticks, which results in a high variety of the fuel parameters. A summary of the experimental studies used in this work is presented in Table 2.

Table 2 – Summary of the experimental studies used for validation.

Reference	**Number of fire tests**	**Fuel**
Lozano et al. (2008)	6	Bamboo sticks
Anderson et al. (2010)	133	Pine Needles (Pinus Ponderosa) / Excelsior
Mendes-Lopez et al. (2003)	7	Pine Needles (Pinus Pinaster)
Korobeinichev et al. (2014)	6	Pine Needles (Pinus Sibirica)
Korobeinichev et al. (2021)	14	Pine Needles (Pinus Sibirica)

In the Atmospheric Boundary Layer, the axial wind velocity decreases with decreasing height, therefore the wind velocity measured at a given height above the flame can be much higher than the wind velocity close to the flame. In order to use the ROS models developed using large-scale field measurements, i.e., Burrows et al., Anderson et al., Fernandes et al., and CFFBPS , the actual "field" wind velocity, U_z, measured at a height *z*, usually in a meteorological station, is required. However, since all fire tests employed in this study were performed in a wind tunnel, there is a need to determine an "equivalent" velocity U_z, using the (usually constant) velocity measured in the wind tunnel, *U*. This wind velocity "adjustment" is performed using the methodology of Albini and Baughman (1979), where the Wind Adjustment Factor (WAF), which corresponds to the ratio of the "mid-flame windspeed" $\overline{\overline{U}}$ to U_z, was introduced. Under the assumption made by Baughman and Albini (1980) that the flame height (above the fuel bed) is considered to be approximately equal to the height of the

fuel bed, the WAF can be estimated using Equation (1), where z and δ are expressed in "ft" (Andrews, 2012). The adjustment of the wind tunnel velocity, U to U_z is based on the additional assumption that the wind tunnel nominal speed (U), due to the small scale of the laboratory fires, is approximately equal to $\overline{\overline{U}}$, an assumption that is commonly made in studies of similar nature (Weise and Biging, 1997).

$$WAF = \frac{\overline{\overline{U}}}{U_z} = \frac{1.83}{\ln\left(\frac{z + 0.36\delta}{0.13\delta}\right)} \tag{1}$$

4. Results and Discussion

The ten ROS models are used to estimate the ROS values in all 166 individual fire tests considered here. Each "predicted" ROS value, R_p (mm/s), is compared against the respective "observed" ROS value, R_o (mm/s); the results are presented both qualitatively, e.g., Figure 1, and quantitatively, by estimating the values of several statistical error metrics. The error metrics selected to evaluate each model's performance are the Mean Absolute Percentage Error (MAPE), the Mean Biased Error (MBE) and the Root Mean Square Error (RMSE), defined in Equations (2), (3) and (4), respectively, where n is the total number of experiments (166 in this case).

$$\text{MAPE} = \frac{\sum_{1}^{n} \frac{\left|R_p - R_o\right|}{R_o}}{n} 100\% \tag{2}$$

$$\text{MBE} = \frac{\sum_{1}^{n} \left(R_p - R_o\right)}{n} \tag{3}$$

$$\text{RMSE} = \left(\frac{\sum_{1}^{n} \left(R_p - R_o\right)^2}{n} \right)^{\frac{1}{2}} \tag{4}$$

The investigated models are evaluated based on their accuracy, i.e., their overall ability to yield predicted values close to the observed ones. The obtained results are graphically presented in Figure 1; the evaluation is assisted by depicting the 10%, 20% and 30% error thresholds, as well.

In Figure 1 (left), results of the semi-empirical and the laboratory-developed empirical models are presented. The models of Catchpole et al. and of Rossa and Fernandes seem to perform well exhibiting, generally, errors lower than ± 30%. The model of Rothermel shows a tendency to under-predict the measured values, thus yielding non-conservative values, a fact that may present an enhanced risk when this model is used in actual operational environments. The model of Wilson, on the other hand, is exhibiting a tendency for over-prediction. Overall, the model of Catchpole et al. seems to yield the most accurate results.

In Figure 1 (right), the performance of the field-developed empirical ROS models is depicted. In general, in this case the results are more sparsely distributed compared to those of the laboratory-developed models. The model of Burrows et al. is found to strongly under-predict the measured values, while the models of Anderson et al. seem to perform slightly better, while still under-predicting the experimental data. The model of Fernandes et al. exhibits the best performance among the five models, while the CFFBPS model predictions are broadly distributed, both over and above the 45 degree slope "line of perfect agreement".

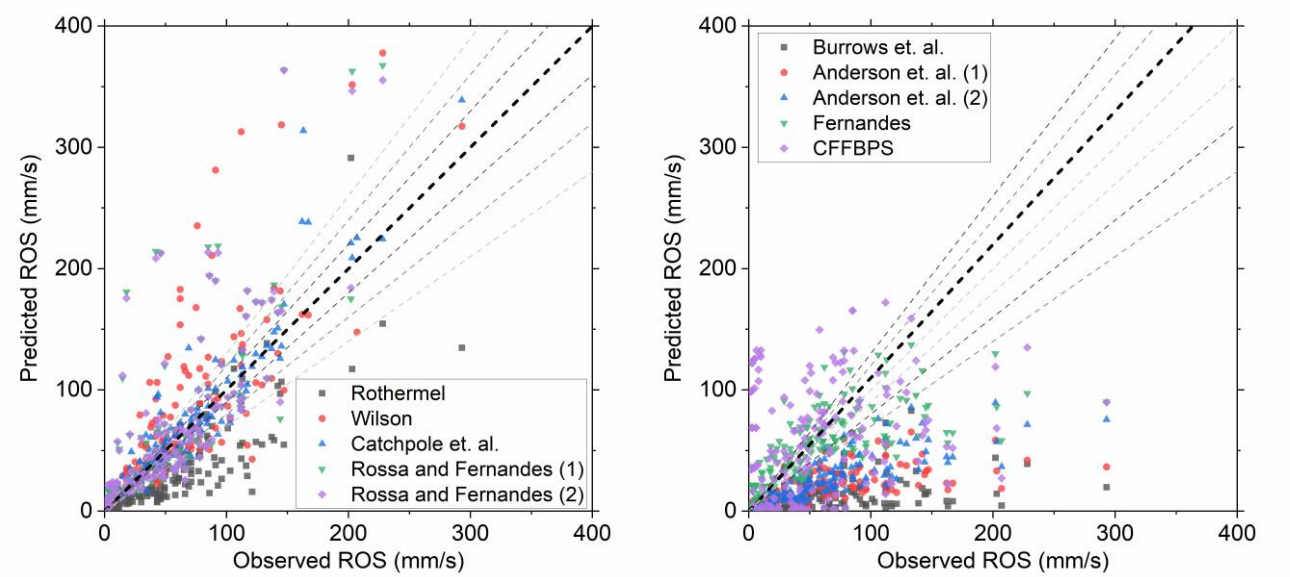

Figure 1 - Comparison of predicted and measured ROS values for the 166 investigated experimental test cases.

The respective values of all calculated statistical error metrics are presented in Table 3. The relative performance of each model may be explained based on their corresponding specific characteristics. For instance, the model of Catchpole et al. exhibits the lowest discrepancies in two out of three error metrics. This may be attributed to the fact that the majority of the experimental data used here (80%, c.f. Table 2) stems from the work of Anderson et al. (2010), who employed the same experimental apparatus used for the development of the Catchpole et al. model. As far as the field-developed models are concerned, their performance mainly depends on four characteristics. Firstly, these models are fuel specific, which means that few fuel-related parameters are required as an input, while the rest of the parameters are integrated in various constants, e.g., statistically fitted coefficient values. For example, the model of Burrows et al. was developed using measurements in fires of spinifex grasslands, a fuel that exhibits horizontal discontinuity. In addition, the only fuel parameter included in the Burrows et al. model is the fuel moisture content. These observations can be related to the fact that the Burrows et al. model exhibited the highest, in absolute terms, MBPE values.

Table 3 - Statistical error metrics for the ten models, validated against the 166 individual fire tests.

Model	**MAPE**	**MBE**	**RMSE**
Rothermel	46 %	-25	40
Wilson	59 %	15	51
Catchpole et al.	**35** %	4	**20**
Rossa and Fernandes (1)	95 %	34	131
Rossa and Fernandes (2)	90 %	33	125
Burrows et al.	79 %	-49	66
Anderson et al. (1)	65 %	-40	58
Anderson et al. (2)	58 %	-35	50
Fernandes et al.	74 %	-6	37
CFFBPS	381 %	**3**	59

Secondly, the fact that field experiments employ live as well as dead fuels may not allow to properly consider the effects of FMC. Thirdly, field experiments usually employ fuel areas exhibiting at least one order of magnitude higher fuel bed width, compared to laboratory tests. Under external wind conditions, the potential ROS depends on the flame front's effective length, which can significantly change during the fire due to the large dimensions of the fuel area as well as the nature of the ever-changing wind (in both magnitude and direction) (Cheney et al., 1993; Cheney and Gould, 1995). Finally, the assumption used to determine the WAF,

i.e. that the height of the flame above the fuel bed is considered to be equal to the height of the fuel bed, is usually not valid in small-scale fires, a fact that might induce further deviations from the observed values.

Figure 2 depicts values of each model's prediction MAPE as a function of wind velocity; the experimentally imposed wind velocities are "clustered" in 4 groups. In the case of ROS models developed using laboratory measurements (Figure 2, left), MAPE is generally decreasing with increasing wind velocity, up to 3 m/s; MAPE values of the Burrows et al. and Anderson et al. models, are not significantly affected by the wind (Figure 2, right).

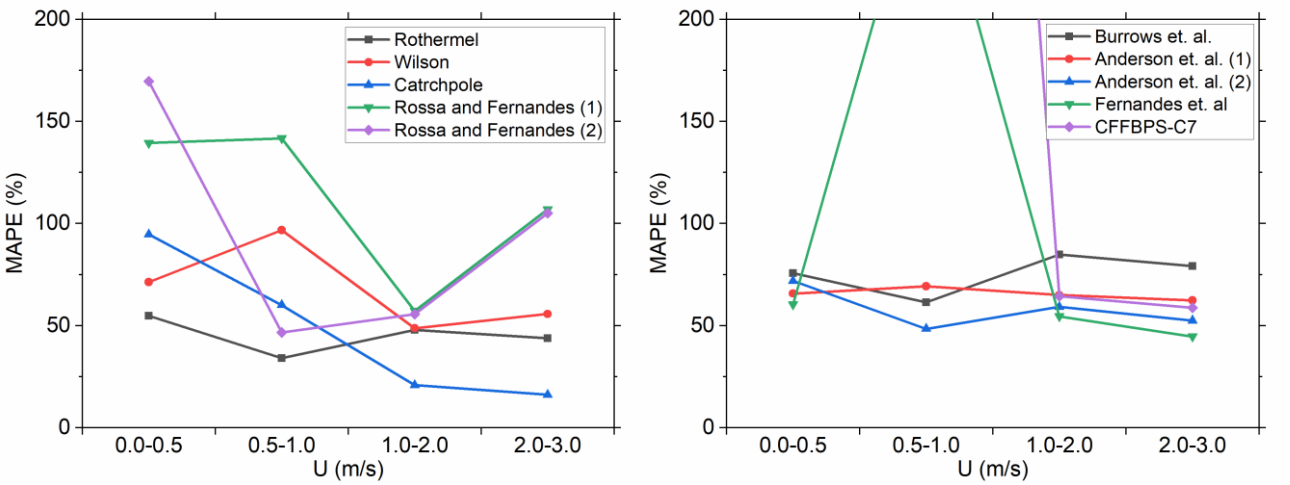

Figure 2 – Effect of wind velocity on the Mean Absolute Percentage Error (MAPE) of each model's predictions.

5. Concluding Remarks

Ten wildland fire rate of spread prediction models were evaluated against laboratory experiments of surface fires. As expected, models that were developed using laboratory data exhibit higher levels of agreement compared to models developed using field data. The field developed models may not be able to accurately predict fires from laboratory experiment due to their fuel specific development (that might differ from the laboratory fuel beds), the fact that field cases are of different scale and are comprised of both live and dead vegetation and, finally, due to the use of severe assumptions in adjusting the laboratory wind speed to the wind velocity. In addition, increasing wind velocities up to 3 m/s result, in the majority of the investigated ROS models, in decreasing discrepancies with the experimental data.

6. References

Albini F.A., Baughman R.G., Estimating Windspeeds for Predicting Wildland Fire Behavior (1979), USDA Forest Service, Research Paper INT-221, Intermountain Forest and Range Experiment Station, Ogden, Utah.

Anderson W.R., Catchpole E.A., Butler B.W., Convective heat transfer in fire spread through fine fuel beds, Int. J. Wildland Fire 19 (2010) 284-298.

Anderson W.R., Cruz M.G., Fernandes P.M., McCaw L., Vega J.A., Bradstock R.A., Fogarty L., Gould J., McCarthy G., Marsden-Smedley J.B., Matthews S., Mattingley G., Pearce H.G., van Wilgen B.W., A generic, empirical-based model for predicting rate of fire spread in shrublands, Int. J. Wildland Fire 24 (2015) 443-460.

Andrews P.L., Modeling wind adjustment factor and midflame wind speed for surface fire spread model. Gen. Tech. Rep. RMRS-GTR-266, U.S. Department of Agriculture, Forest Service, Rocky Mountain Research Station (2012).

Baughman R.G. and Albini F.A. (1980), Estimating Midflame Windspeeds, Northern Forest Fire Laboratory, Missoula, Montana, p. 88-92.

Burrows N., Gill M., Sharples J., Development and validation of a model for predicting fire behaviour in spinifex grasslands of Arid Australia, Int. J. Wildland Fire 27 (2019) 271-279.

Catchpole W.R., Catchpole E.A., Butler B.W., Rothermel R.C., Morris G.A., Latham D.J., Rate of Spread of Free-Burning Fires in Woody Fuels in a Wind Tunnel, Combust. Sci. Technol. 131 (1-6) (1998) 1-37.

Cheney N.P., Gould J.S., Catchpole W.R., The influence of Fuel, Weather and Fire Shape Variables on Fire-Spread in Grasslands, Int. J. Wildland Fire 3(1) (1993) 31-44.

Cheney N.P., Gould J.S., Fire Growth in Grassland Fuels, Int. J. Wildland Fire 5(4) (1995) 237-247.

Fernandes P.M., Botelho H.S., Rego F.C., Loureiro C., Empirical modelling of surface fire behavior in maritime pine stands, Int. J. Wildland Fire 18 (2009) 698-710.

Forestry Canada Fire Danger Group, Development and Structure of the Canadian Forest Fire Behavior Prediction System, Information Report ST-X-3, Forest Canada Science and Sustainable Development Directorate, 1992.

Frandsen W.H., Fire Spread through Porous Fuels from the Conservation of Energy, Combust. Flame 16 (1971) 9-16.

Korobeinichev O., Tereshchenko A., Paletsky A., Shmakov A., Gonchikzhapov M., Chernov A., Kataeva L., Maslennikov D., Liu N., The Velocity and Structure of the Flame Front at Spread of Fire Across the Pine Needle bed Depending on the Wind Velocity, Proceedings of the 10th Asia-Oceania Symposium on Fire Science and Technology (2014), 771-779.

Korobeinichev O., Kumaran S.M., Shanmugasundaram D., Raghavan V., Trubachev S.A., Paletsky A.A., Shmakov A.G., Glaznev R.K., Chernov A.A., Tereshchenko A.G., Experimental and Numerical Study of Flame Spread Over Bed of Pine Needles, Fire Technol. 58 (2022) 1227-1264.

Lozano J., Tachajapong W., Pan H., Swanson A., Kelley C., Princevac M., Mahalingam S., Experimental Investigation of the Velocity Field in a Controlled Wind-aided Propagating Fire Using Particle Image Velocimetry, Fire Safety Science - Proceedings of the 9th International Symposium, 255-266 (2008).

Mendes-Lopez J.M., Ventura J.M., Amaral J.M.P., Flame characteristics, temperature-time curves, and rate of spread in fires propagating in a bed of Pinus Pinaster needles, Int. J. Wildland Fire 12 (2003) 67-84

Pastor E., Zarate L., Planas E., Arnaldos J., Mathematical models and calculation systems for the study of wildland fire behaviour, Prog. Energ. Combust. Sci. 29 (2003) 139-153.

Rossa C.G., Fernandes P.M., Empirical Modeling of Fire Spread Rate in No-Wind and No-Slope Conditions, Forest Sci. 64 (4) (2018a) 358-370.

Rossa C.G., Fernandes P.M, An Empirical Model for the Effect of Wind on Fire Spread Rate, Fire 1 (2) (2018b) 31.

Rothermel R.C., Anderson H.E., Fire Spread Characteristics determined in the Laboratory, (1966), U.S. Forest Service, Research Paper INT-30, Intermountain Forest & Range Experiment Station, U. S. Department of Agriculture, Ogden, Utah.

Rothermel R.C., A Mathematical Model for predicting Fire Spread in Wildland Fuels, USDA Forest Service Research Paper INT-115, 1972.

Weise D.R., Biging G.S., A Qualitative Comparison of Fire Spread Models Incorporating Wind and Slope Effects, Forest Sci. 43 (2) (1997), 170-180.

Wilson R.A., Rothermel's Fire Spread Equations in No-wind and No-slope Conditions, USDA Forest Service Research Paper INT-434, 1990.

Empirical fire propagation potential from a balanced dataset

Ljiljana Šerić*; Antonia Ivanda; Marin Bugarić; Darko Stipaničev

University of Split, Faculty of Electrical Engineering, Mechanical Engineering and Naval Architecture, Rudera Boskovica 32, 21000 Split, Croatia,
{ljiljana.seric, antonia.senta.00, marin.bugaric, darko.stipanicev}@fesb.hr

**Corresponding author*

Keywords

Fire Danger, Fire Propagation Potential, Empirical Model, Machine Learning, Classification

Abstract

In order to assess fire and wildfire risk one must address various features and analyse the danger and vulnerability aspects. Besides fire ignition probability, one of the most important variables for addressing fire danger is fire propagation potential. Fire propagation potential (FPP) can be described as a quantitative description of the circumstances under which, if fire ignites, it leads towards propagation of fire. This means that not all ignitions cause propagation of significant fires. Some ignitions are easily extinguished and pose no danger to vulnerable assets. On the other hand, some ignitions result in large and mega fires, causing large, burned areas and huge casualties. Fire propagation potential (FPP) provides quantitative distinction between these two different circumstances.

Machine learning techniques are more and more applied in fire management tools as they provide us with techniques for learning from the past data and predicting the future outcomes. Majority of previous work is focused on analysis of the large fire events, their causes and development. However, when modelling the FPP, we should consider situations on both ends of the outcome spectrum - situations when fire ignites and propagates and situations when fire ignites and does not propagate. If one uses only data on fires that propagate, without considering the alternative situations data, results that are achieved can be incomplete.

In this paper we propose a novel and more full approach to fire danger assessment by analysing situations of both cases - high and low fire danger. We simplify the value of FPP and consider that in cases the fire propagates the value of FPP is one, and zero otherwise. We used data collected from the events of both cases. We obtained a balanced dataset and trained machine learning model with a data set having representatives of both ends of the FPP spectrum.

The research is demonstrated in the study area of Split and Dalmatia County. We consider past fires that are sensed by satellite and recorded in the EFFIS system as situations when FPP had value 1. To assess the situations when FPP was 0 we analysed the fire intervention database maintained by fire departments. We filtered fire interventions related to forest fires that lasted less than 2 hours and engaged 2 or less firefighters since these records represent time and place of the fire that did not propagate.

For these two cases of events, we collected Sentinel-2 imagery and weather data that consists of temperature and wind speed. Sentinel-2 imagery pixels were extracted for the area associated with both types of events. The dataset was split into train and test datasets, where classifiers were trained by using 80% of data and 20% of remaining data was used for testing the classifier performance. Experiments were conducted by training classifiers using commonly used classifiers - Decision Tree Classifier, K-Nearest Neighbors, Multi-layer perceptron, Random Forest Classifier, Naive Bayes Classifier and Logistic regression. The best performance, according to the R2 score and RMSE is measured on Decision Tree Classifier.

1. Introduction

Assessment of fire danger is done by assessing the probability of occurrence of hazardous fire event. It is obvious that fire poses a hazard or threat in case it ignites, but not all ignitions result in a hazard. In case the fire does not propagate it is not considered dangerous. That is the reason to study the fire propagation potential (FPP) as a limiting factor for fire danger assessment.

Fire danger is studied in literature and various approaches, among which physics-based methods, statistical methods, and machine-learning methods for fire danger predictions are proposed (Pourghasemi 2020). Machine learning methods have shown itself useful for analysis of past events and predicting the future events when

appropriate data is collected (Pham, 2020). Thus, in order to apply Machine learning methods we must obtain a dataset that will be used in the training phase of building the machine learning based model and select the appropriate learning algorithm.

Previous attempts of building a machine learning based model for fire danger prediction mostly relied on data of high fire danger from historical fires (Dimuccio,2011;Tehrany 2019; Pourghasemi 2020) but are neglecting the cases with low fire danger.

In this research we created a balanced dataset covering both cases - fires with burned areas and fire ignitions that did not result in spread. This dataset is used for building a machine learning classifier that distinguishes between situations with high and low FPP.

2. Materials and methods

2.1. Study area

Study area of this research is Split and Dalmatia county, a central-southern county in Croatia with the population of 455,242 (2011) and the land area 4,540 km2.

This region often suffers from large fires especially during the summer season.

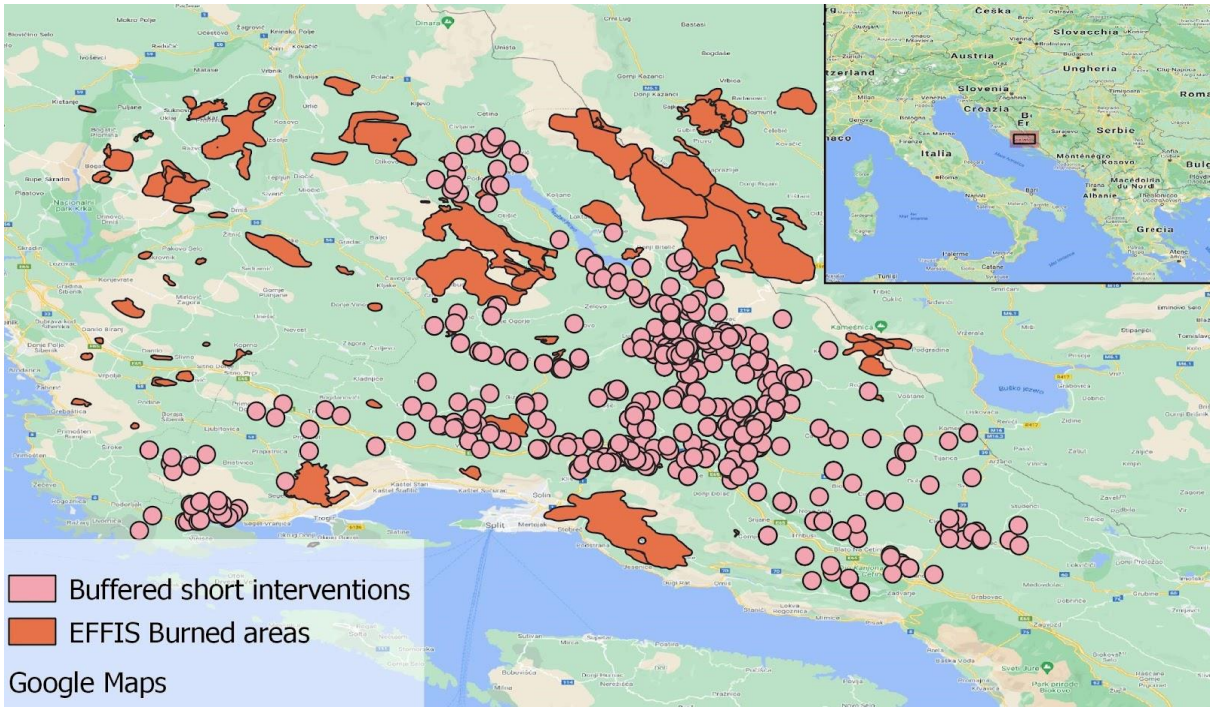

Figure 1- Study area -Split and Dalmatia County with burned areas and locations of interventions without fire spread we used in our research.

2.2. Dataset

In order to observe two cases on both ends of fire propagation potential values we collected data from two different sources.

First, we collected burned area data from the European forest Fire information system (EFFIS) that described burned areas in the study area from 2015 till the end of 2021.

Second dataset was fire departments intervention records from the 2017 till the end of 2021.

These two datasets were used to observe two cases:

Case 1: fire that ignites and propagates to the surrounding area. We observed such situations resulting in burned area noticed by EFFIS system.

Case 2 fire that ignites but is easily extinguished. We observed fire interventions with the description of forest fire, where intervention lasted less than 2 hour and less than 3 firefighters were engaged.

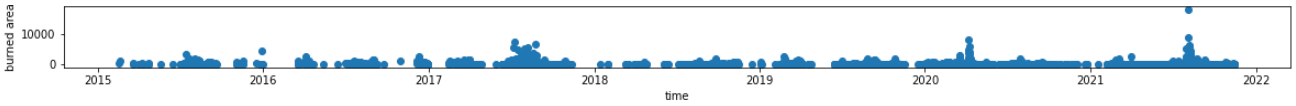

Figure 2- Temporal distribution of burned areas during the period 2015-2022

Reflecting on the fire triangle, the mostly used tool for fire behaviour understanding, propagation of fire is limited by the presence of three variables: fuel, heat, and oxygen. If ignition has happened, heat is present, thus we must determine the presence of fuel and oxygen to enable fire propagation. In our research we used two sources of data that we use as a proxy for quantifying the presence of fuel and oxygen - Sentinel-2 imagery and weather data. Sentinel-2 imagery is collected as Level-2A reflectances in 12 available wavelength bands for the study area. We also collected weather archived data for the period of interest. For each burned area we collected Sentinel-2-L2A pixels value with 60m resolution for each of the 12 bands, representing atmospherically corrected surface reflectances of the 12 wavelength bands, from the imagery taken between 1 and 3 days before the fire.

For the Case 2 events, interventions were described not as an area but as the single point. We collected the same Sentinel-2-L2A pixel values with 60m resolution for the 1 km buffer area surrounding the ignition incident.

This resulted with a dataset each row representing a 60x60m pixel described with 12 values of reflectances for each of the Sentinel-2 band at the time of the event, air temperature for the date of the event, wind speed at the time of the event and value 0 or 1 indicating whether the pixel is burned or not burned.

48604 data items representing burned pixels, and 216376 pixels representing non burned pixels, with a total of 264980 items. However, this dataset is not balanced. We used a common balancing method - down sampling to create a balanced dataset that has a similar number of representatives of both classes. We randomly selected only 25% of majority class samples and created a balanced dataset that consists of total 102698 data items.

B01.tif	B02.tif	B03.tif	B04.tif	B05.tif	B06.tif	B07.tif	B08.tif	B09.tif	B11.tif	B12.tif	B8A.tif	temp	wspd	burn
0.157250	0.231404	0.342539	0.389541	0.585679	1.000000	1.000000	1.000000	1.000000	1.000000	0.662658	1.000000	26.250000	4.000000	1
0.254563	0.214879	0.321657	0.397304	0.686704	0.979826	1.000000	1.000000	1.000000	1.000000	0.851914	1.000000	28.750000	12.750000	1
0.259033	0.302021	0.375166	0.541772	0.635147	0.760511	0.828962	0.901695	0.974500	1.000000	0.977706	0.922368	12.333333	4.666667	0
0.126821	0.193180	0.231912	0.311580	0.462847	0.622117	0.726232	0.784196	0.865924	1.000000	0.760598	0.846687	13.500000	17.500000	0
0.256889	0.237518	0.282364	0.302973	0.405287	0.606758	0.695203	0.741671	0.907718	0.937644	0.646878	0.794378	3.000000	17.333333	0
...	...	...	...	...	...	...	...	...	...	...	...	...	...	...

Figure 3- A sample of the balanced dataset used for classification

2.3. Classification Algorithms

The dataset described in the previous section was randomly splitted into two subsets - train dataset consisting of 80% of the data and test dataset consisting of the remaining 20% of the data. We used the train set to train a classifier that would predict which case the pixel belongs to - case 1 - the pixel will burn if fire ignites, or case 2 the fire will not propagate over the pixel.

The following machine learning algorithm were tested for classifying Case 1 and Case 2 pixels

- Logistic regression
- Naive Bayes Classifier
- K-Nearest Neighbours with 3 neighbours
- Decision Tree Classifier
- Random Forest Classifier with maximum tree depth 5
- Multilayer perceptron with 10 hidden layers

For each classifier we calculated two evaluation measures - R-squared - R^2 score (Chicco, 2021) and Root Mean Square Error (RMSE) (Jierula, 2021). The R^2 and RMSE were calculated both on train and test set in order to check for overfitting.

3. Results

The selected classifiers were trained to predict two classes of propagation potential based on Sentinel 2 imagery and weather features. The classifiers performance measures, as measured on our dataset are shown in Table 1.

Table 1. Performance evaluation measures of classifiers used in the experiment

ML ALGORITHM	TRAIN R^2 SCORE	TEST R^2 SCORE	TRAIN RMSE	TEST RMSE
K-Nearest Neighbors	0.999528	0.999056	0.021728	0.030727
Decision Tree Classifier	1.000000	0.999056	0.000000	0.030727
Multi Layer Perceptron	0.990676	0.990244	0.096559	0.098773
Random Forest Classifier	0.943704	0.938159	0.237269	0.248679
Logistic Regression	0.835045	0.828639	0.406147	0.413958
Gaussian Naive Bayes	0.839293	0.828009	0.400882	0.414717

Ideal value of R^2 measure should be 1. The closer the R^2 value to 1, better the performance of the classifier. We can see that tested algorithms predict the propagation potential that is corelated with our label. The RMSE value should be as small as possible. All tested classifiers have small value of RMSE.

4. Conclusion

From the results shown in Table 1 we can observe that non-linear classifiers result in better performance on our data set. Thus, we can conclude that the relationship between fire propagation potential and land surface reflectances and weather is not linear and straightforward, but rather complex. This was expected since we did not consider different types of land cover, vegetation, and roads, but merely used Sentinel-2 imagery as raw input of low-level land cover features. The resulting empirical propagation potential classifier gives promising results and performs well on test dataset. In future work we will investigate the results on larger study area and cross compare the results on areas with different climate and topographic features. Also, in future work we will investigate the usage of semantic data about the land and weather features to obtain a more general model.

5. References

Chicco D, Warrens MJ, Jurman G. The coefficient of determination R-squared is more informative than SMAPE, MAE, MAPE, MSE and RMSE in regression analysis evaluation. PeerJ Comput Sci. 2021 Jul 5;7:e623. doi: 10.7717/peerj-cs.623.

Copernicus Sentinel data 2015, processed by ESA.

Dimuccio, Luca Antonio, et al. "Regional forest-fire susceptibility analysis in central Portugal using a probabilistic ratings procedure and artificial neural network weights assignment." International Journal of Wildland Fire 20.6 (2011): 776-791.

Jierula A, Wang S, OH T-M, Wang P. Study on Accuracy Metrics for Evaluating the Predictions of Damage Locations in Deep Piles Using Artificial Neural Networks with Acoustic Emission Data. Applied Sciences. 2021; 11(5):2314. https://doi.org/10.3390/app11052314.

Pourghasemi, Hamid Reza, et al. "Application of learning vector quantization and different machine learning techniques to assessing forest fire influence factors and spatial modelling." Environmental research 184 (2020): 109321.

Tehrany, Mahyat Shafapour, et al. "A novel ensemble modeling approach for the spatial prediction of tropical forest fire susceptibility using LogitBoost machine learning classifier and multi-source geospatial data." Theoretical and Applied Climatology 137.1 (2019): 637-653.

Pham, Binh Thai, et al. "Performance evaluation of machine learning methods for forest fire modeling and prediction." Symmetry 12.6 (2020): 1022.

Weather Underground - https://www.wunderground.com/

Evaluating sensitivity to input fuel resolution in popular fire behavior models

Muthu Kumaran Selvaraj[1]; Lydia Carroll[2]; Sonya Sawtelle[2], Jacob Sprague[2], Albert Simeoni[1*]

[1]Department of Fire Protection Engineering, Worcester Polytechnic Institute. Worcester, Massachusetts, USA, {mselvaraj, asimeoni}@wpi.edu
[2] Lockheed Martin. Bethesda, MD 20817 U.S.A., {lydia.m.carroll, sonya.d.sawtelle, jacob.sprague}@lmco.com}

**Corresponding author*

Keywords

Rothermel spread model, fuel sensitivity, remote sensing

Abstract

Fire behavior models ingest a variety of inputs such as weather, topography, and fuel maps to generate predictions of how a fire will behave. Model prediction accuracy is thus to some degree dependent on the fidelity of the input data sources. For many widely used fire models, however, the exact relationship between fuel input quality and model performance is not well understood. This paper seeks to quantify the relationship between input fuel data and output prediction accuracy in popular fire models based on the Rothermel fire spread equation. In particular, it examines how granularity of fuel classes and spatial resolution affect the accuracy of fire behavior predictions. Fuel maps used in the study are generated from remote sensing images using machine learning to map between satellite and ground conditions. Prediction accuracy is evaluated with multiple metrics including rate of spread (ROS) and fire front shape. The outcomes of this study will provide important guidance as to the benefit of producing high fidelity fuel maps when utilizing the Rothermel spread equation to predict fire behavior.

1. Introduction

Fire behavior models use several input data layers such as fuel type (defined as fuel class), moisture content, surface-to-volume ratio, heat content of fuel, bulk density of vegetation, wind velocity and topography of the terrain for predicting rate of fire spread (ROS), flame length (FL) and fire perimeter. All of the aforementioned parameters are subject to spatial and temporal changes by natural occurrences (landslides, change in weather pattern, wildfires, etc.) and human activity (prescribed burns). Therefore, the accuracy of the fire behavior model relies on the accuracy of these input layers data. It is both time-consuming and costly for land managers to keep track of the changes in the fuel type distribution and properties. The use of satellite data can quicky reciprocate the changes (in a matter of days) in fuel type and weather conditions to generate accurate input data (when coupled with machine learning algorithms) for existing fire behavior models.

In this work, an external pre-trained machine learning model will be used to label updated Sentinel-2 MSI data with coarse land cover labels, having a spatial resolution of 10 meters. These labels will be compared pixel-by-pixel, with top-level Scott & Burgan classes (Scott & Burgan, 2005) from the most recent LANDFIRE (LF) fuel product available (resampled to 10-meter resolution, Fig.1). For all pixels, if the land cover model disagrees with the LF Scott & Burgan classification that pixel will be reclassified with the updated derived classification. For example, the most recent LANDFIRE 2020 product may label a pixel as “Timber Litter 1” (TL1) while the updated land cover model – called the Lockheed Martin (LM) land cover model – labels the same pixel with current Sentinel-2 as “Shrub & Scrub” at that same point. Subsequently, this new classification will be stored with this pixel reclassification as, “Shrub 1” (SH1). The output of the LM fuel model will be a raster map of Scott & Burgan classes. This LM fuel model will be validated by predicting the rate of spread and fire perimeter of the Cameron peak fire (for which significant data points are available) which is the largest recorded wildfire in Colorado history.

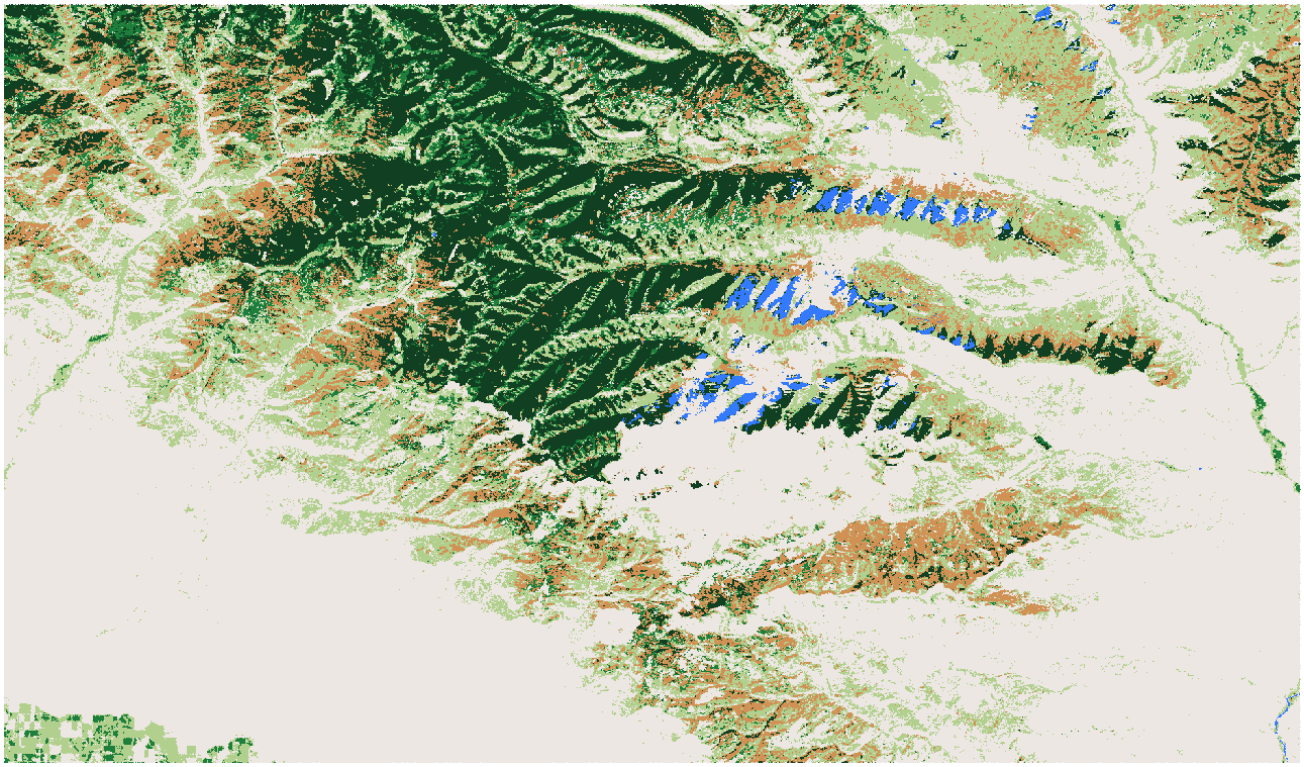

Figure 1 - Sample fuel map generated at 10m pixel resolution using Scott & Burgan fuel classes.

2. Fire Behavior Models in the Field

The most accepted fire prediction models in the United States, the Rothermel-based fire behavior model (Rothermel, 1972) will be used for predicting the rate of spread, flame length and fire perimeter for the LM fuel models.

3. Methods of Evaluation

The fire spread rate and fire perimeter at different times will be used for evaluating the LM fuel model.

4. Sensitivity to Fuel

This section will describe how various fuel map attributes were examined and observations of how each attribute affected prediction accuracy.

4.1. Granularity of Classes

Fuel class granularity will be examined through the comparison of Anderson and Scott & Burgan fuel classes (Scott & Burgan, 2005). Similar maps will be generated with the different fuel models and will be evaluated on how they influence the resulting fire shapes.

4.2. Spatial Resolution

Spatial resolution will be evaluated by generating a high-resolution fuel map and then down sampling it multiple times and comparing with prediction accuracies after each down sampling. Similar procedure will be followed for predicting the influence on fire spread through fire shapes at different times. A sensitivity analysis will also be carried out.

5. Conclusions

Based on the work reported here, recommendations will be made for generating accurate fuel maps to produce optimal prediction results with the Rothermel-based fire behavior models.

6. References

Rothermel, R.C. 1972. A mathematical model for predicting fire spread in wildland fuels. Res. Pap. INT-115. Ogden, UT: U.S. Department of Agriculture, Forest Service, Intermountain Forest and Range Experiment Station. 40 p.

Scott, J.H., Burgan, R.E. 2005. Standard fire behavior fuel models: a comprehensive set for use with Rothermel's surface fire spread model, Gen. Tech. Rep. RMRS-GTR-153. Fort Collins, CO: U.S. Department of Agriculture, Forest Service, Rocky Mountain Research Station. 72 p.

Exploring atmospheric evaporative demand in relation to wildland fire

Timothy Brown[1]*; Daniel McEvoy[1], Andrew Andrade[1], Britt Parker[2]

[1]*Desert Research Institute, Reno, Nevada, {tim.brown, dan.mcevoy, andrew.andrade}@dri.edu*
[2]*NOAA/CIRES University of Colorado, Boulder, Colorado, USA, {britt.parker@noaa.gov}*

**Corresponding author*

Keywords

Evaporative demand, fire danger, wildfire, prescribed fire

Abstract

Evaporative demand, the upper limit of actual evapotranspiration (ET) that could occur given unlimited surface water supply, has a strong connection to drought and wildfire potential in the western United States and globally. A physically based evaporative demand formulation incorporates temperature, wind speed, humidity, and incoming shortwave radiation – components that drive land surface-atmosphere interactions and drying. These are also the primary physically based components in the U.S. National Fire Danger Rating System – some combination of temperature, humidity, and wind speed are also common inputs to other fire danger systems. Thus, association between evaporative demand and fire danger can be expected and this has previously been demonstrated such as via the Evaporative Demand Drought Index (EDDI) indicator. For example, EDDI can be decomposed to examine the weighted physical factors over time leading up to a fire event. Utilizing evaporative demand for monitoring and prediction can serve as an early warning of fire potential depending on climatological persistence patterns for weeks to possibly months in advance though rapid onset anomalies may yield a similar result. Evaporative demand can also inform prescribed burn planning. Based on the exploration of EDDI indicators prior to fire events, this presentation will discuss analyses of evaporative demand in the context of both wildfire and prescribed fire to better understand if and how evaporative demand can be used to inform wildland fire management decisions.

1. Discussion

Evaporative demand (E_0), the upper limit of actual evapotranspiration that could occur given unlimited surface water supply, has a strong connection to drought and wildfire potential globally. Plant water cycle processes including soil water uptake, plant water storage, and water loss through transpiration all influence plant water availability. Extensive transpiration can dominate the plant water cycle leading to increased fuel flammability. A physically based E_0 formulation incorporates temperature, wind speed, humidity, and incoming shortwave radiation (Allen et al. 2005) – components that drive land surface-atmosphere interactions and drying. These are also the primary physically based components in the U.S. National Fire Danger Rating System as well as inputs to other fire danger systems (e.g., temperature, humidity, and wind are primary inputs for the Australia Forest Fire Danger Index).

The Evaporative Demand Drought Index (EDDI; Hobbins et al. 2016; McEvoy et al. 2016) is based only on E_0, which has been shown to signal the onset of rapid drying and flash drought before other indicators such as precipitation, soil moisture, and actual ET. EDDI may better capture short- and long-time scale dry dynamics and provide early warning for fire activity. McEvoy et al. (2019) showed that EDDI generally had higher correlations to fire danger outputs than other commonly used drought indicators.

Figure 1 shows EDDI for three 2018 fire events in California – the Mendocino and Carr fires in July and the Camp fire in November. Colors denote the EDDI percentiles with red colors signifying higher percentiles. In this example these three major fires occurred when EDDI averaged above the 95th percentile for the two months leading up to the fires.

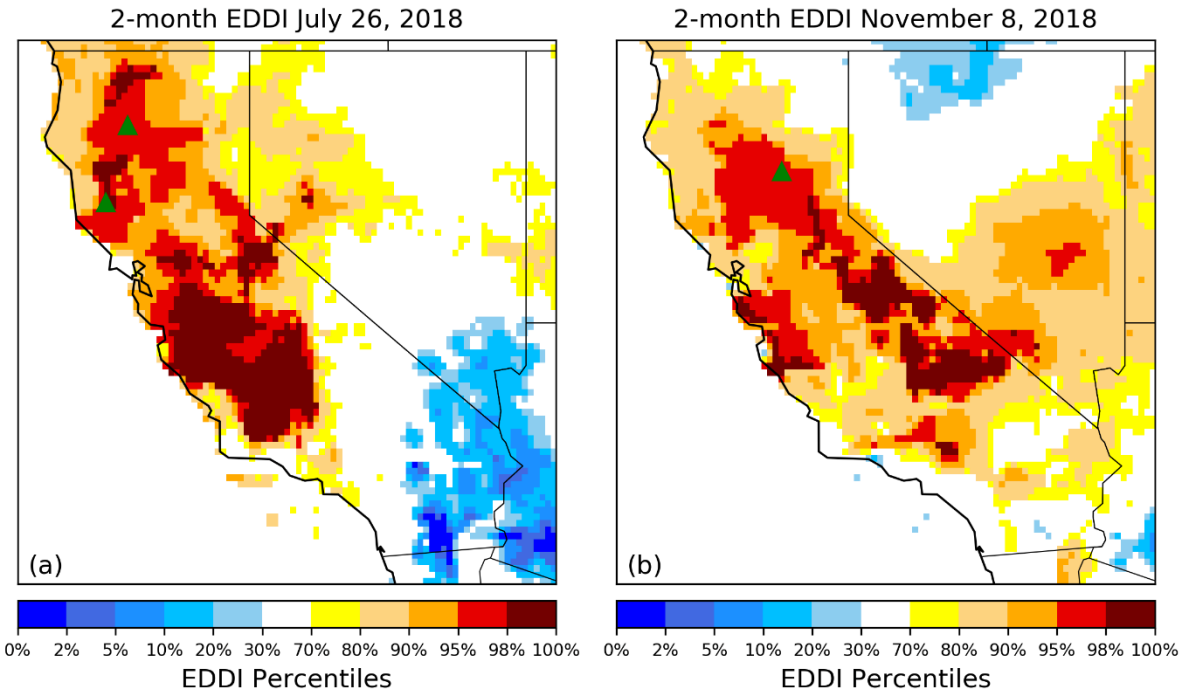

Figure 1 EDDI 2-month percentile categories for (a) 26 Jul 2018, and (b) 8 Nov 2018. Triangles represent the Mendocino (lower) and Carr (upper) fires in(a) and the Camp fire in (b). From Brown et al. (2020).

EDDI can be decomposed to examine the weighted physical factors over time leading up to a fire event. Figure 2 shows the E_0 anomaly and the contributions from each of its drivers aggregated over a two-week window moving forward daily across Sonoma County, California from mid-August through the end of October 2018, a period of eight weeks prior to and three weeks following the ignition of the Tubbs Fire. E_0 is elevated above its climatological median (50^{th} percentile) throughout the period. A notable spike of much above-normal temperatures occurred prior to the fire outbreak from 31 August until 5 September. During the first two weeks of September a positive E_0 anomaly remains but becomes near normal for the second half of September due to the mitigating effects of above-normal humidity and below-normal wind speeds and solar radiation. In early October temperature remains near normal but the combined effects of now-below-normal humidity and above-normal wind speed and solar radiation dominate the E_0 anomaly, which climbs again through the day of the fire ignition (8 October) and afterwards. On the day of ignition, E_0 reaches its second spike when it exceeds its 95th percentile. This indicates that near-surface moisture was decreasing and a drying of the air mass was taking place even during a period of near-normal temperatures. It is also worth noting that wind speed had the largest contributions during the onset of the second spike from 29 September through 2 October. These patterns are suggestive of an important role of rapid (flash) meteorological impacts on fuels. Autumn in California is climatologically dry; an E_0 indicator such as EDDI highlights factors besides soil moisture drought that contributes significantly to drying of fuel moisture. E_0 should work suitably well in other fire prone regions.

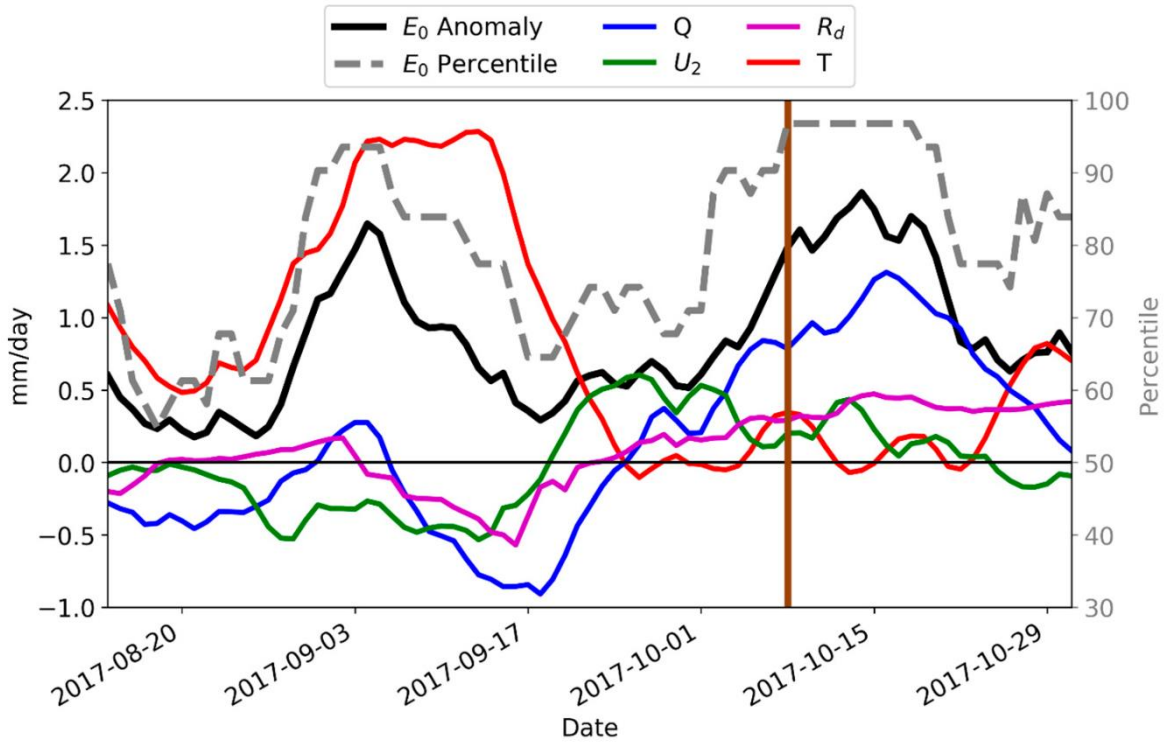

Figure 2 Evaporative demand (E_0) anomaly prior to and during the October 2017 Tubbs fire in Sonoma County, California. The 2-week E_0 anomaly (black line) is spatially averaged across Sonoma County. The contributions from each of its drivers are shown as colored lines (temperature (T) in red, specific humidity (Q) in blue, downwelling shortwave radiation (Rd) in purple, wind speed (U2) in green); percentiles of 2-week E0 are shown in dashed grey (right-hand axis); and the ignition date of the Tubbs fire is shown as a vertical brown line. From McEvoy et al. (2019).

Utilizing E_0 for monitoring and prediction can serve as an early warning of significant fire potential weeks to possibly months in advance especially given persistent climatological patterns though rapid onset anomalies may yield a similar result. The scope of this project is to determine the extent that E_0 can be used as an early warning for significant wildfire potential. Soil moisture drought alone is not always a sufficient indicator of fire potential. Cases of large fires with normal soil moisture conditions but high E_0 have been observed. Short time (e.g., weekly scale) periods of anomalous high E_0 may be sufficient to allow for periods of increased fuel flammability, though this likely will vary depending on vegetation type. Persistence of high E_0 can serve as one indicator of fire potential. That is, while weekly-scale anomalous E_0 can serve as an indicator of increased fire potential, monthly to seasonal scales that are persistent with anomalous E_0 can also serve as an indicator. E_0 could also be used for prescribed burning. For example, if E_0 was calibrated to fuel flammability, then observed E_0 could help inform the potential success of a burn given a specific management goal or serve as indicator of a potential burn escape.

E_0 is already being utilized for some fire activities, especially in California. Examples include successful integration of EDDI into fire management operations with California Predictive Services such as submitting Severity Funding Requests, daily fire weather briefings, seasonal fire potential outlooks, and incorporated into the Fire Behavior Field Reference guide and wildland fire fighter training curriculum (Brent Wachter, *pers. comm.*).

2. References

Allen, R.G.; Walter, I.A.; Elliott, R.; Howell, T.; Itenfisu, D.; Jensen, M., 20-05: The ASCE Standardized Reference Evapotranspiration Equation; American Society of Civil Engineers: Reston, VA, USA, pp. 59.

Brown, T.J., S. Leach, B. Wachter, and B. Gardunio, 2020: The Northern California 2018 Wildfire Season. *Special Supplement to the Bulletin American Meteorological Society*, Vol. 101, No. 1, January 2020, S1-S4. DOI:10.1175/BAMS-D-19-0275.1

Hobbins, M.T.; Wood, A.W.; McEvoy, D.J.; Huntington, J.L.; Morton, C.; Anderson, M.C.; Hain, C.R., 2016: The Evaporative Demand Drought Index: Part I—Linking drought evolution to variations in evaporativedemand. J. Hydrometeorol., 17, 1745–1761.

McEvoy, D.J.; Huntington, J.L.; Hobbins, M.T.; Wood, A.W.; Morton, C.; Anderson, M.C.; Hain, C.R., 2016: The Evaporative Demand Drought Index: Part II—CONUS-wide assessment against common drought indicators. J. Hydrometeorol., 17, 1763–1779.

McEvoy, D. J., Hobbins, M., Brown, T. J., VanderMolen, K.A., Wall, T. U., Huntington, J. L., Svoboda, M., 2019: Establishing Relationships between Drought Indices and Wildfire Danger Outputs: A Test Case for the California-Nevada Drought Early Warning System, *Climate*, 7 (4), https://doi.org/10.3390/cli7040052

Extreme Fire Severity Classification using Clustering and Decision Tree

Henrique Coelho[1]; Susana Nascimento*[1]; Carlos Viegas Damásio[1]; Lourdes Bugalho[2]; Gonçalo Severino[1]

[1]NOVA LINCS and Departamento de Informática da NOVA School of Science and Technology. Quinta da Torre, 2829-516 Caparica, Portugal, {ha.coelho@campus.fct.unl.pt, snt@fct.unl.pt, cd@fct.unl.pt, g.severino@campus.fct.unl.pt}
[2] Instituto Português do Mar e da Atmosfera. IPMA,I.P, Rua C do Aeroporto 1749-077 Lisboa, Portugal, {lourdes.bugalho@ipma.pt}

**Corresponding author*

Keywords

Extreme fires, fire risk scales, Canadian Fire Weather Index, Fuzzy c-means, decision tree

Abstract

With climate change, large, unpredictable, and difficult to suppress forest fires are increasingly frequent. To increase the ability to anticipate and respond to these extreme events it is necessary to characterize the meteorological conditions associated with the risk levels of these events. The main objective of this work is to automatically identify those severity conditions and extract classification rules to characterize extreme forest fires with at least 100ha of burned area (90% percentile) in mainland Portugal for the period 2001-2020.

The conditions characterizing the extreme fires are elicited by applying fuzzy clustering and predictive methods to forest fire data and corresponding fire risk indices, namely the Canadian Forest Fire Risk Index (FWI), and subindices, as well as the Continuous Haines Index (CHI), provided by the Portuguese Institute of Sea and Atmosphere (IPMA). The dates and localization of fires are obtained from the shapefiles provided by the Portuguese Institute for Nature Conservation and Forests (ICNF), and complemented with data from the MODIS Global Burned Area Product MCD64A1 downloaded from the University of Maryland repository.

The popular fuzzy c-means (FCM) algorithm is applied to group fires into five and seven clusters, with no pre-specified ground-truth severity. Then each cluster is labelled with the fire risk scale class assigned to the cluster's prototype considering the EEFIS scale (European-Forest-Fire Information System) for five clusters and IPMA fire risk scale for seven clusters, respectively. Fuzzy Sammon mapping has been used to visualize and validate the fuzzy partitions.

Using the data from 2001-2018, decision trees (DT) were induced in order to obtain the conditions and thresholds that characterize the obtained clusters, and tested with the data from 2019 and 2020. To ensure the quality of the classification results robust validation techniques such as cross-validation and bootstrapping as well as evaluation metrics are applied.

The DT rules described by conjunctions of the fire risk indices and thresholds, were not always in agreement with the reference forest fire risk prediction scales, revealing the importance of adapting the indices values according to the region in question and taking into account several factors (forest fire risk indices) in the analysis of the conditions associated with the level of risk of an extreme forest fire. The proposed approach shown to be a proof of concept to derive an empirical fire severity risk scale for the collection of used indices and to compare the results with the two fire risk scales used by IPMA and EEFIS.

1. Introduction

With climate change, those large, unpredictable, and difficult to suppress forest fires will become increasingly frequent (Petroliagkis et al., 2015). In Portugal, wildfires continue to be one of the most serious natural catastrophes, due to their high frequency and intensity, and with climate change they will become more frequent. To increase our ability to anticipate and respond to these phenomena, it is necessary to study and characterize the meteorological conditions that favor them.

There is no generally accepted definition of what an extreme fire is. This difficulty in defining what an extreme fire is clearly explained by (Viegas, 2012) and (Tedim et al., 2018). However, there is consensus (Tedim et al., 2018; Fernandes, 2005) that three descriptive parameters, burned area (BA), rate of spread (ROS) and fire line intensity (FLI), are necessary indicators to assess what an extreme fire is, as they characterize three essential

aspects of fires: damage caused, unpredictability and suppression capacity, respectively. Table 1 presents the limits used by the authors Tedim et al. (2018) and Fernandes (2005) to define an extreme fire.

Table 1. Adapted from (Tedim et al., 2018; Fernandes, 2005)

Aspects	Parameter	Reference Values
Damage	BA	>= 100 ha
Unpredictability	ROS	>= 50m/min (in forests)
Suppression Capacity	FLI	10000-30000kW/m

Although these descriptive parameters are important to define an extreme fire, in practice, only the burned area (BA) will be used, due to the lack of other data and compatibility problems between them. More specifically, we will use the 90% percentile of the size of fires in Mainland Portugal from 2001 to 2020, which corresponds to about 100 ha, which is in accordance with the criteria in Table 1.

To characterize the meteorological conditions for the occurrence of forest fires, it is used the values of the Continuous Haines Index (CHI) (Mills and McCaw, 2010) and the Fire Weather Index (FWI) (Turner and Lawson, 1978; Van Wagner and Pickett, 1985), and their subindices (FFMC, DMC, DC, BUI and ISI). To characterize the level of risk, the ordinal risk scales based on the Fire Weather Index (FWI) defined by IPMA (IPMA-FWI, 2022) and by the European-Forest-Fire Information System (EEFIS) (Joint Research Centre, 2020) will be adopted in our study.

The objective of this work is to explore fuzzy clustering (Ruspini et al., 2019) to unsupervisedly group fire risk data into distinct fire risk classes, such that a fire may have a positive degree of belongingness to more than one risk class. After the data is clustered, decision tree based methods are used (Quinlan, 1986) to derive if-then classification rules characterizing the meteorological conditions associated with the different classes of risk of fire occurrences.

2. Materials and Methods

The shapefiles of forest fires in Portugal in the period 2001-2020 were obtained from the available geocatalog provided by ICNF (https://geocatalogo.icnf.pt/metadados/area_ardida.html). The data was filtered by burned area in QGIS, and the fires with area >= 100ha were retained (of which 113 are in years 2019 and 2020). When not available, the date of the fire ignition data was obtained from the burned area MODIS Global Burned Area Product MCD64A1 (https://modis.gsfc.nasa.gov/data/dataprod/mod45.php).

The data regarding the FWI, FFMC, DMC, DC, BUI, ISI and CHI indexes were provided by IPMA. The data for the FWI are daily and for the CHI are data every 3 hours, for the period 2001 to 2020, calculated from the operational model analysis data of the European Center for Medium-Term Weather Forecasts (ECMWF), with a regular geographic grid of 0.125º latitude and 0.125º longitude, covering the territory of Mainland Portugal. For each fire, the fire risk indexes corresponding to the ignition date of the network with the largest area of intersection were considered.

There were built two data samples considering fires with burned area greater than to 100ha: one taking the five indices (FWI, CHI, ISI, DC, FFMC), and the other one with seven indices (FWI, CHI, ISI, DC, FFMC, BUI and DMC).

The conducted experimental study comprises three stages: (i) pre-processing and exploratory pre-analysis of fire data and risk indicators; (ii) application of the fuzzy c-means algorithm (FCM) (Bezdek, 1981) to generate fuzzy partitions of fires; and (iii) induction of decision trees (Quinlan, 1986) from the fuzzy clusters.

For each data sample the FCM was run looking for five and seven clusters. The clusters prototypes (centroids) of the obtained fuzzy partitions with five clusters (FCM-5) were labelled according to the EEFIS severity risk scale while the ones of the fuzzy partitioning with seven clusters (FCM-7) use the IPMA scale for the classification. Then, the fire fuzzy partitions, originally in a 5/7-dimensional data space, were projected in 2D with fuzzy Sammon mappings (FUZZYSAM) (Feil et al., 2007) for visual inspection and validation. Finally,

the data fires were assigned to the cluster with highest belongingness and labeled with the classification of the corresponding cluster prototype.

With all observations thus labeled with a certain fire risk class, there were generated decision trees to extract if-then rules that associate meteorological and terrain conditions with a certain level of extreme fire risk.

To avoid overfitting, a decision tree was induced from the data of period 2001-2018 with depth between 1 and 9, with the hyperparameters tuned using stratified shuffle splitting (using a 50%/50% for training and validation). Finally, the data of 2019 and 2020 fires was classified with respect to the FCM prototypes and used to evaluate the performance of the induced trees, namely with the standard precision, recall and F1 metrics.

3. Results

In this Section we discuss the main results of our approach and summarize the assessment of DT classification with the evaluation metrics.

3.1. Phase 1 – Fuzzy Clustering

Figures 2 and 3 show the FUZZYSAM mappings for the four fuzzy partitions resulting from the four combinations of parameters: **some** - five indices (FWI, CHI, ISI, DC, FFMC) or **all** – seven indices (FWI, CHI, ISI, DC, FFMC, BUI and DMC), and **C5** - five clusters or **C7**- seven clusters, hereafter designated as **someC5/C7**, **allC5/C7**, respectively. The projected clustered fires are represented as blue dot points, the colored star points represent the clusters prototypes labelled according to the EEFIS/IPMA severity risk scales, while the iso-lines represent degrees of belongingness (from closest prototypes values of 0.9, 0.8, 0.7 etc) derived from the FCM membership function. This projection guarantees the interpoint fuzzy weighted distances of the projected data approximating the corresponding weighted distance in the original (5D/7D) space. It is useful for interpretation of the clustering results since it is based on the Euclidean distance between the clusters prototypes (representative fires with average indices values) and the data fires.

It is interesting to observe that for the two partitions with five clusters, only the fire risk class labels “Very Low / Low”, “High” and “Very High” are used to classify the clusters. In case of fuzzy partitions with seven clusters, the situation depends on the used data sample with all/some indices. Anyway, the fuzzy partition derived from the configuration someC7 has a continuum of the risk class labels “Very Low”, “Low”, “Moderate”, “High”, and “Extreme”, being the best partition.

3.2. Phase 2 – Induced trees

The decision trees induced from the FCM clustered data (configuration someC7), at depths 3 and 4, are presented in Figures 4 and 5. The obtained trees are human interpretable and show that most fire occurrences are concentrated in three (four) leaves, one for each class, indicating that the result can be quite robust. It is interesting to observe that in both situations are used indices for fuel modelling and fire behaviour, and indices modelling the instability and dryness of the atmosphere. It is clear also that some of the leaves could be pruned, getting the same classification. For the case of seven clusters (someC7) all depth 3 or greater present good quality trees for use (Table 2).

3.3. Evaluation Metrics

The evaluation of the classification results from DT with depths 1 to 9, derived from the fuzzy partition someC7, are presented in Table 2. For DTs with depth above 2 the results appear to be very robust, with score values of recall, precision and F1 above 0.8. However, the metric values for depths above 6 are very close indicating that the deeper trees are overfitted. Furthermore, the shallower depth 3 tree obtains a good performance being very effective at separating the “Very Low’’ and “Extreme’’ fire classes from the others. The confusion occurs essentially in the middle classes and all the risk indices are used except the FWI. So, the decision tree with depth 3 is a good compromise between correct classification and rules simplicity presenting a classification F1 score value above 0.80, which is considered very reliable for real data.

Table 2. Evaluation metrics of the induced trees for configuration some C7

Metric (weighted)	DT depth 1	DT depth 2	DT depth 3	DT depth 4	DT depth 5	DT depth 6	DT depth 7	DT depth 8	DT depth 9
Recall	0.458	0.703	0.838	0.867	0.875	0.919	0.931	0.928	0.928
Precision	0.609	0.736	0.836	0.864	0.873	0.918	0.927	0.927	0.927
F1	0.520	0.712	0.832	0.860	0.873	0.917	0.926	0.926	0.926

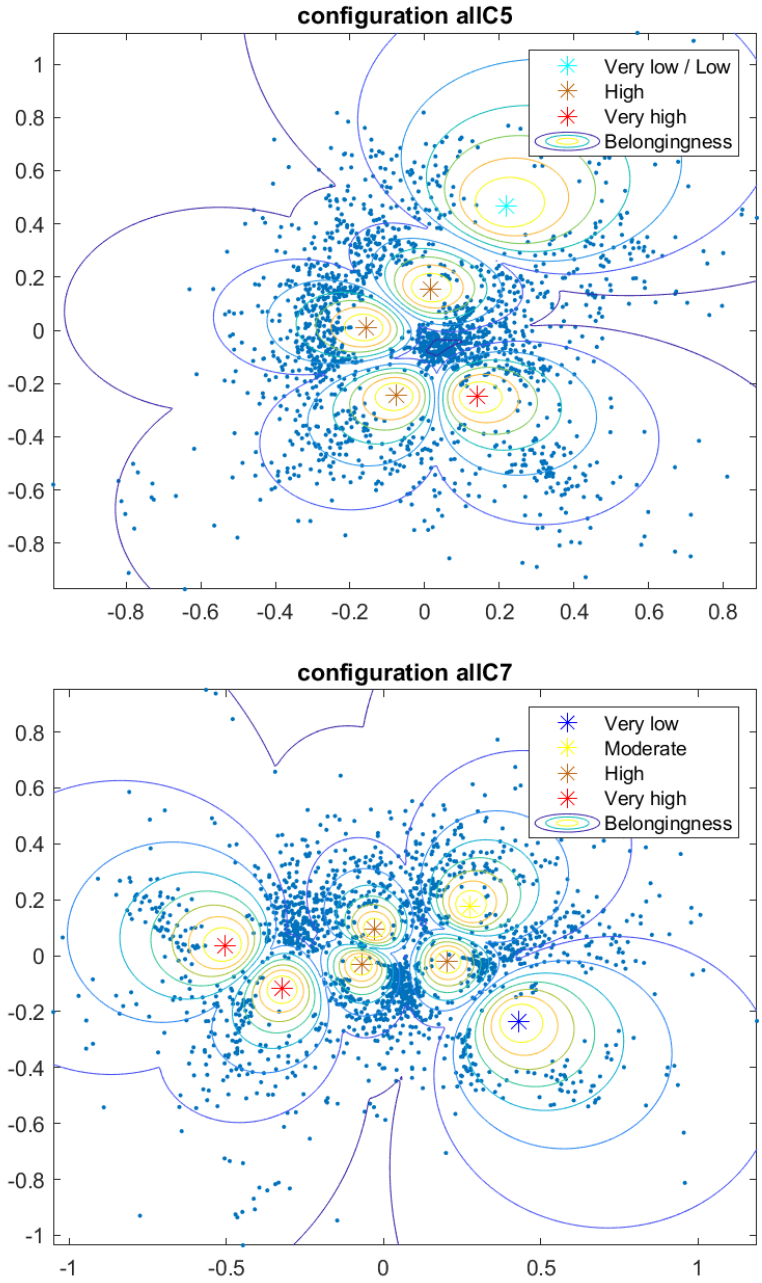

Figure 2. Fuzzy Sammon mapping projection of fuzzy partitions with all the indices: five clusters (top figure) and seven clusters (bottom figure)

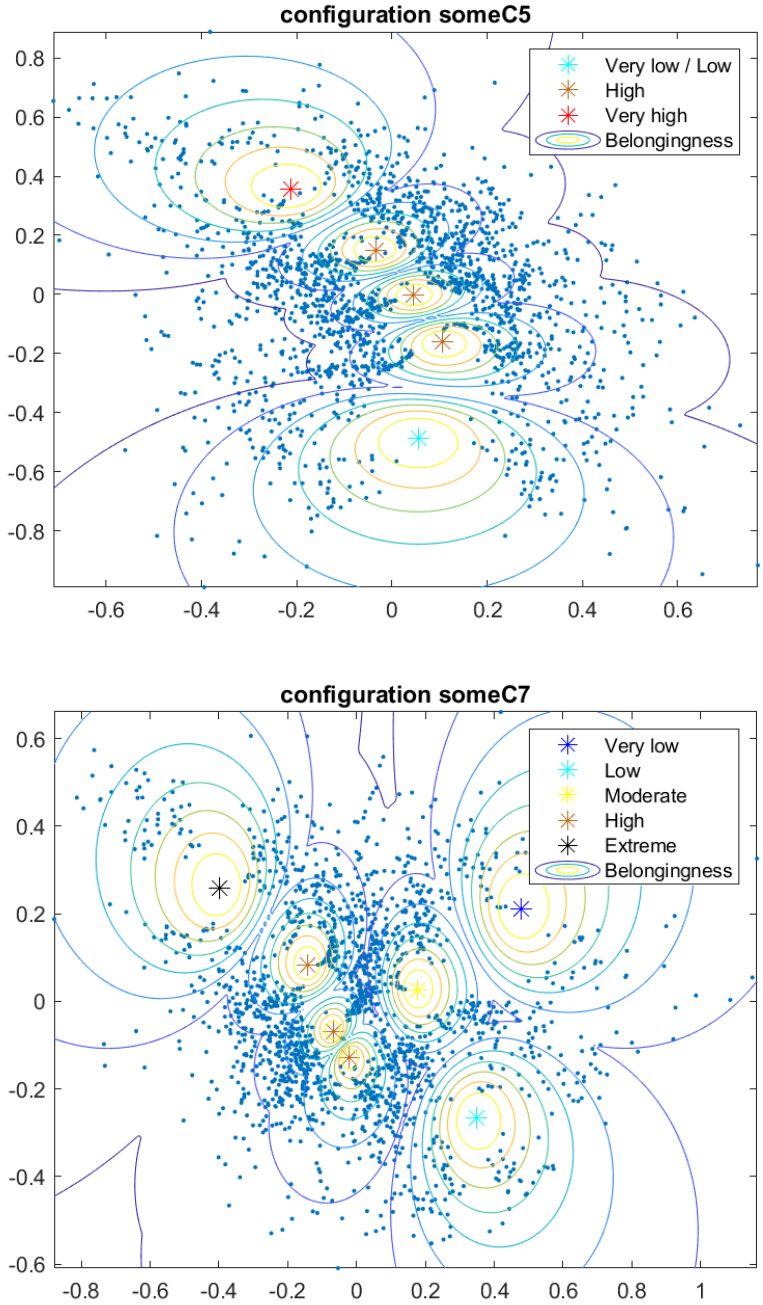

Figure 3. Fuzzy Sammon mapping projection of fuzzy partitions with some of the indices: five clusters (top figure) and seven clusters (bottom figure)

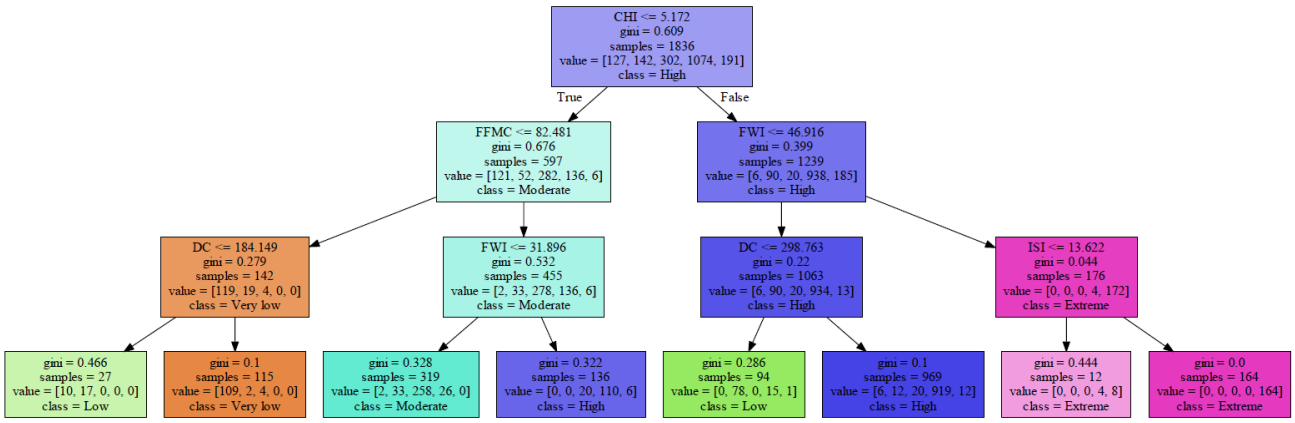

Simplified rules

if (CHI <= 5.172) and (FFMC <= 82.481) and (DC > 184.149) then class: Very low
if (CHI > 5.172) and (FWI <= 46.916) and (DC <= 298.763) then class: Low
if (CHI <= 5.172) and (FFMC <= 82.481) and (DC <= 184.149) then class: Low
if (CHI <= 5.172) and (FFMC > 82.481) and (FWI <= 31.896) then class: Moderate
if (CHI > 5.172) and (FWI <= 46.916) and (DC > 298.763) then class: High
if (CHI <= 5.172) and (FFMC > 82.481) and (FWI > 31.896) then class: High
if (CHI > 5.172) and (FWI > 46.916) then class: Extreme

Figure 4. Induced tree with depth 3 for configuration someC7

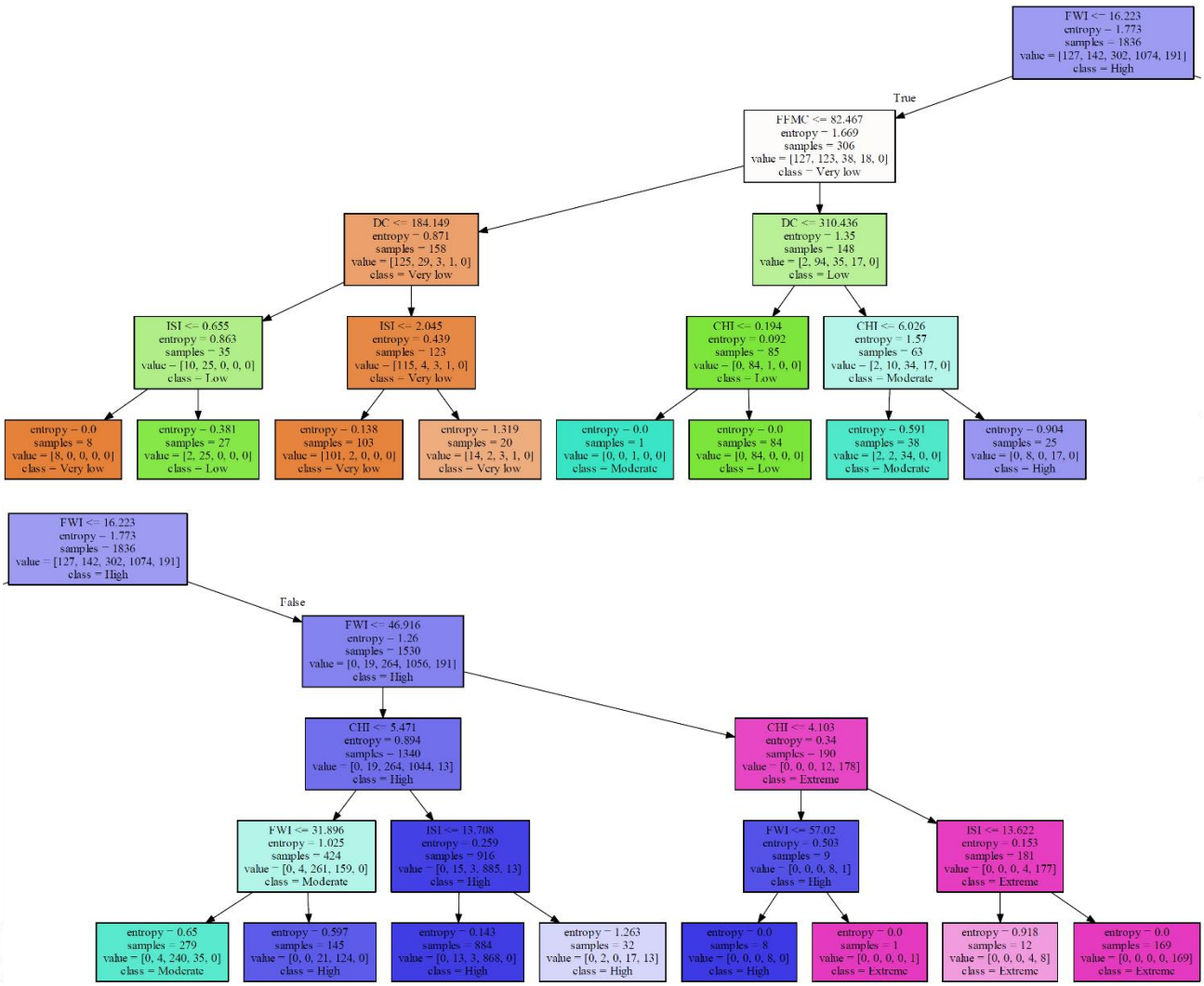

Simplified rules

if (FWI <= 16.223) and (FFMC <= 82.467) and (DC > 184.149) then class: Very low
if (FWI <= 16.223) and (FFMC <= 82.467) and (DC <= 184.149) and (ISI <= 0.655) then class: Very low
if (FWI <= 16.223) and (FFMC > 82.467) and (DC <= 310.436) and (CHI > 0.194) then class: Low
if (FWI <= 16.223) and (FFMC <= 82.467) and (DC <= 184.149) and (ISI > 0.655) then class: Low
if (FWI > 16.223) and (FWI <= 46.916) and (CHI <= 5.471) and (FWI <= 31.896) then class: Moderate
if (FWI <= 16.223) and (FFMC > 82.467) and (DC > 310.436) and (CHI <= 6.026) then class: Moderate
if (FWI <= 16.223) and (FFMC > 82.467) and (DC <= 310.436) and (CHI <= 0.194) then class: Moderate
if (FWI > 16.223) and (FWI <= 46.916) and (CHI > 5.471) then class: High
if (FWI > 16.223) and (FWI <= 46.916) and (CHI <= 5.471) and (FWI > 31.896) then class: High
if (FWI <= 16.223) and (FFMC > 82.467) and (DC > 310.436) and (CHI > 6.026) then class: High
if (FWI > 16.223) and (FWI > 46.916) and (CHI <= 4.103) and (FWI <= 57.02) then class: High
if (FWI > 16.223) and (FWI > 46.916) and (CHI > 4.103) then class: Extreme
if (FWI > 16.223) and (FWI > 46.916) and (CHI <= 4.103) and (FWI > 57.02) then class: Extreme

Figure 5. Induced tree with depth 4 for configuration someC7

4. Discussion and Conclusion

This work consisted of a comparative experimental study between the rules that associate meteorological conditions with extreme forest fire risk levels, generated from data mining and machine learning techniques, with the two ordinal scales of fire risk prediction of reference, the EEFIS scale and the IPMA scale. Specifically, the fuzzy clustering algorithm FCM was explored for the grouping of extreme forest fire data, occurred between 2001 and 2018, into severity fire risk classes, and subsequent visualization in 2D FUZZYSAM maps. Then a classification model was induced by decision tree algorithm for the characterization and extraction of rules, that is, to highlight the meteorological conditions associated with different levels of extreme fire risk. The applicability of these algorithms was tested for this purpose.

The FCM algorithm shown to be effective in the segmentation and classification of extreme fires, for the number of clusters five and seven, providing flexibility to the clustering effort with degrees of membership that may distinguish and rank the fires occurrences with respect to their severity. The partition with seven clusters was chosen with some of the indices (FWI, CHI, ISI, DC, FFMC) because the clusters recognize the "Low''/"Very Low'', "High''/"Very High'' and "Extreme" classes of the classification used in the IPMA. The decision tree classification model, once its hyperparameters have been trained and tuned, through hyper-parameterization and validation techniques, stratified shuffle split, also proved to be effective in extracting the meteorological conditions associated with different levels of extreme fire risk. The decision trees induced from the fire data with 5 indices labelled with the FCM-7 cluster prototypes, presented promising results, with classification validity scores higher than 0.8. The rules generated by these trees were used to determine the meteorological conditions associated with different levels of extreme fire risk, having been analyzed and compared with the EEFIS and IPMA scales, showing that the thresholds do not correspond exactly. This is expected since the EEFIS and IPMA scales were obtained from a single index, while our approach combines conditions of several indices: FWI, subindices and Continuous Haines Index. The generated rules clearly separate "Low'', "High'' and "Extreme''. However, while the rules for "Low'' and "Extreme'' are well defined, for high risk there are several sets of rules that define it. It is also interesting that the danger index CHI, linked to the instability and humidity of the lower atmosphere, is considered as important in the classification of danger (especially extreme) for both rules, with depth 3 (Figure4) and rules with depth 4 (Figure5). In the first case, depth 3, the extreme classification is given for the case of CHI>5.172 and FWI>46.9. Other indices are used to define the low, moderate or high classification rules, always having CHI as the first classification division. In the second case, depth 4, the extreme classification is achieved by two rules: 1) FWI>46.9 and CHI>4.103 or 2) If CHI≤4.103 and FWI>57.02 (extremely high value of FWI), Figure 5. Rules for depth 4 are more complex than those for depth 3, especially for the definition of "Low'', "Moderate'' and "High'' classes.

In the future, the same approach will be applied to particular edaphoclimatic regions of Portugal mainland in order to understand if the results are consistently obtained, as well the expected differences among regions. Furthermore, vegetation and topographic indices will be added in order to be able to induce risk level conditions for wildfires.

5. Acknowledgments

This work was supported by Fundação para a Ciência e a Tecnologia (FCT.IP) through project Floresta Limpa (PCIF/MOG/0161/2019) and NOVA LINCS (UIDB/04516/2020). The authors are indebted to the reviewers for their helpful comments that allowed to improve the paper.

6. References

Bezdek, James C., 1981. Pattern Recognition with Fuzzy Objective Function Algorithms. Plenum press.

Feil, B., Balasko, B. Abonyi, J., 2007. Visualization of fuzzy clusters by fuzzy sammon mapping projection: application to the analysis of phase space trajectories. Soft Computing, 11 (5) 479–488.

Fernandes, P. M., 2005. Estudo de adaptação para Portugal do Sistema Canadiano de Indexação do Perigo de Incêndio. Relatório para a Agência de Prevenção de Incêndios Florestais. Departamento Florestal, Universidade de Trás-os-Montes e Alto Douro.

IPMA-FWI (2022). https://www.ipma.pt/pt/riscoincendio/fwi/ (Accessed 20 June 2022).

Joint Research Centre (2020). EFFIS - fire danger forecast. https://effis.jrc.ec.europa.eu/about-effis/technical-background/fire-danger-forecast (Accessed 20 June 2022).

Mills, G. A. e McCaw, L., 2010. Atmospheric Stability Environments and Fire Weather in Australia - extending the Haines Index. CAWCR Technical Report No. 020, The Centre for Australian Weather and Climate Research.

Petroliagkis, T., Liberta, G, Artes, T., Rodriguez-Aseretto, D., Di Leo, M. e San-Miguel, Ayanz. J., 2015. Stability of atmospheric flow and low-level jets influencing forest fire behavior - An EFFIS report. EUR–Scientific and Technical Research series, EUR 27362, 30, 3-28.

Quinlan, J.R., 1986. Induction of decision trees. Machine Learning 1, 81–106. DOI: https://doi.org/10.1007/BF00116251.

Ruspini, E. H., Bezdek, J. C., Keller, J. M., 2019. Fuzzy clustering: A historical perspective. IEEE Computational Intelligence Magazine 14.1, 45-55.

Tedim, F., Leone, V., Amraoui, M., Bouillon, C., Coughlan, M.R., Delogu, G.M., Fernandes, P.M., Ferreira, C., McCaffrey, S., McGee, T.K. et al., 2018. Defining Extreme Wildfire Events: Difficulties, Challenges, and Impacts. Fire 1, 1, 9.

Turner, J. A. e Lawson, B. D., 1978. Weather in the Canadian Forest Fire Danger Rating System: a user guide to national standards and practices. Environment Canada, Canadian Forest Service, Information Report BC-X-177. Pacific Forest Research Centre: Victoria, BC.

Van Wagner C. E. e Pickett, T.L., 1985. Equations and FORTRAN program for the Canadian Forest FireWeather Index System. Government of Canada, Forestry Technical Report 33, Canadian Forest Service: Ottawa, ON.

Viegas, D.X., Bovio, G., Ferreira, A., Nosenzo, A. e Sol, B., 1999. Comparative study of various methods of fire danger evaluation in southern Europe. International Journal of wildland fire, 9, 4, 235-246.

Viegas, D.X., Reis, R.M., Cruz, M.G. e Viegas, M.T., 2004. Calibração do sistema canadiano de perigo de incêndio para aplicação em Portugal. Silva Lusitana 12, 1, 77-93.

Viegas, D. X., 2012. Extreme fire behaviour. In Forest Management: Technology, Practices and Impact. Bonilla Cruz, AC, Guzman Correa, RE, Eds, 1-56.

Eye in the Sky - Using High-Altitude Balloons for Decision Support in Wildfire Operations

Alexandra Moutinho*[1]; Maria João Sousa[1]; Miguel Almeida[2]; Miguel Bergano[3]; Diogo Henriques[1]; Dário Silva[1], Domingos Barbosa[3], Luis Nero[3,4], António Navarro[3,4]

[1]IDMEC, Instituto Superior Técnico, Universidade de Lisboa. Av. Rovisco Pais, 1049-001 Lisbon, Portugal, {alexandra.moutinho, maria.joao.sousa, carlos.diogo, dario.silva}@tecnico.ulisboa.pt
[2] University of Coimbra, ADAI, Department of Mechanical Engineering, Rua Luís Reis Santos, Pólo II, 3030-788 Coimbra, Portugal, {miguelalmeida@adai.pt}
[3] Instituto de Telecomunicações. Campus Universitario de Santiago, 3810-193 Aveiro, {jbergano,dbarbosa}@av.it.pt
[4]Departamento de Electrónica, Telecomunicações e Informática, Universidade de Aveiro, 3810-193 Aveiro, Portugal {nero, navarro}@ua.pt

**Corresponding author*

Keywords

High-altitude balloon; Aerial imagery; Fire monitoring; Communications; Decision support

Abstract

The large fires that have occurred in recent years around the World have shown that the management of these events becomes much more difficult when the extension of the burnt area or the location of the fire fronts, among other fundamental information for those managing operations in theatre, is not known. In addition, the large involvement of firefighting resources often challenges the operability of the communications system, sometimes making it dysfunctional or with limited operability. This was a reality seen in several large fires, from which we highlight the Fire of Pedrógão Grande that occurred in Portugal in June 2017.

Aware of the need to improve operational technology for fire monitoring, the Eye in the Sky Project has been developed. Our approach within this project is to design and develop an easy to deploy kit that can be launched from anywhere and fulfil these needs, providing quality real-time aerial imagery of the wildfires and guaranteeing emergency communications. The proposed solution consists of a HAB that will carry a flying wing UAV with two different high-value types of payloads that meet these two specific functions of imagery collection in the visible and infrared ranges and communications repeater. The authors like to refer to the Eye in the Sky solution as a satellite dedicated to a specific fire.

Naturally, the development of such solution raises several challenges, particularly in terms of the operational functioning of this solution, the optimised use of the balloon/glider pair with the associated payload, the capture, automatic detection of the fire images and their georeferencing, and the communications system between the payload, the ground station and the users in the command centre. The several challenges that have arisen in the development of this solution, as well as the way found to solve them are hereby exposed.

1. Introduction

The recent increasing number of large wildfires leads to new challenges in the response operations. Involving larger areas and periods of extreme fire behaviour with high fire spread rates, the monitoring of the fire perimeter and the knowledge of the evolution of the fire front is not always possible with the conventional terrestrial means. Thus, drones have been increasingly used to meet this challenge. However, although very useful and versatile in terms of manoeuvrability, drones have some limitations, such as the short autonomy or safety issues due to the sharing of flight height with fire-fighting aircrafts. Another challenge posed by larger fires is associated with the greater number of agents involved in the theatre of operations and consequently the greater number of telecommunications carried out, which sometimes causes the operational communications system to collapse or requires its reinforcement with complementary communications antennas.

The project Eye in the Sky - Using High-Altitude Balloons for Decision Support in Wildfire Operations develops a solution (Figure 1) of a high-altitude balloon (HAB) that transports a flying-wing unmanned aerial vehicle (UAV) carrying a payload with equipment considered of interest for the operation, such as a combination of RGB and IR cameras, which allow monitoring the progress of the fire, or/and a communications link and repeater. Thus, the high-altitude balloon can be seen as an on-demand mini satellite specifically dedicated to the fire event. After being released from the ground, the balloon rises rapidly, leaving the firefighting aircraft operating height in some seconds, so no longer interfering with their activity. The balloon continues to rise until, by decision of the operator or because it has reached the limit of the pressure conditions, it releases the glider which begins its descending phase autonomously or commanded by the operator. This solution allows a continuous operation time that can exceed ten hours.

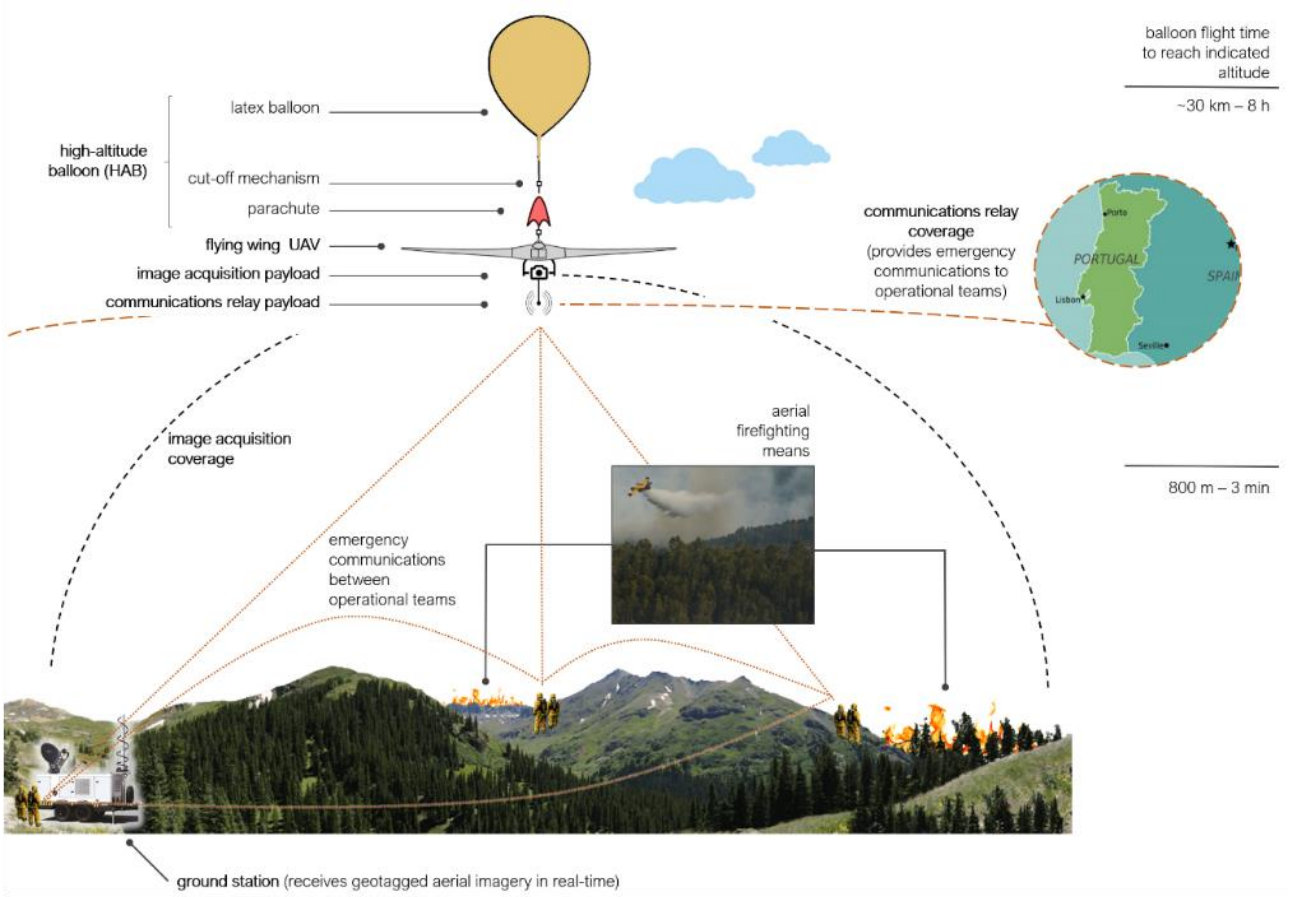

Figure 1 - Representation of the concept of using a high-altitude balloon in fire-fighting operations developed in the Eye in the Sky project (www.adai.pt/eyeinthesky).

In the Eye in the Sky project the described solution is being developed working on three main fronts, namely: a) high-altitude balloon payload stabilization, altitude control and mission prediction, and flying wing mission definition and control, b) automatic detection of fire and hot areas and respective image georeferencing before sending to ground station; and c) ground-to-ground transmission system to establish remote contact with the payload to transmit control orders and to access captured images, as well as to reinforce operational communications in theatre of operations. These topics are described in the following sections.

2. High-altitude balloon in fire-fighting operations

The HAB + UAV hybrid platform proposed incorporates the high cargo capabilities of an aerostat that travels passively through the atmosphere to reach targeted areas, but with low positional accuracy, and the navigation and positioning capabilities of an UAV glider with limited autonomy. These two elements, HAB and UAV together, significantly expand the working envelope of each independent solution, increasing the mission

autonomy when compared with UAV-only-based solutions, making them particularly useful in fire monitoring applications.

A wildfire monitoring test was carried out in the context of the fire event that started in Conqueiros/Proença-a-Nova (Portugal) on the morning of September 13th, 2020. In this test, a balloon equipped with three cameras operating in the visible range was launched from Montalvão, in the municipality of Nisa, at 7 p.m. on 14th September. The balloon reached altitudes greater than 12km, covering the path shown in Figure 2.

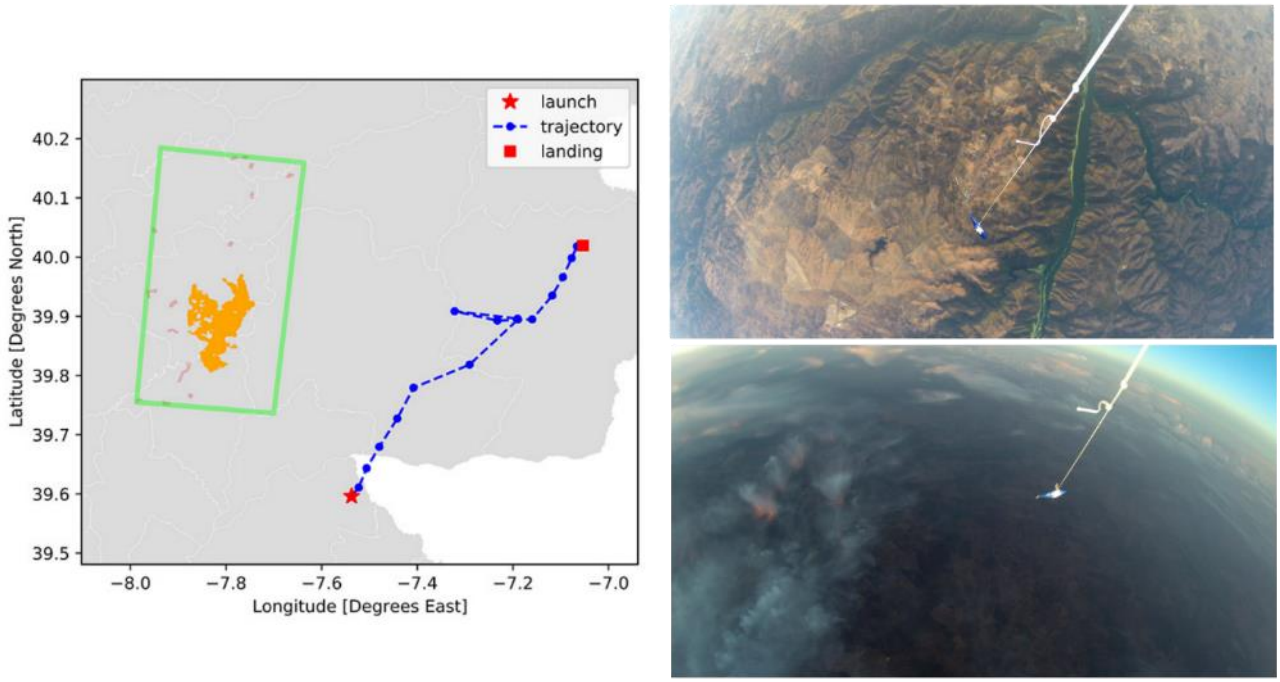

Figure 2 – Left: Balloon trajectory (in blue 'o', launch site '⋆', payload landing site '■') and fire event region (outlined in green) that led to the burned area (in yellow) in Conqueiros/Proença-a-Nova (Portugal). Right: Some images acquired in the same balloon launch at different altitudes by one of the cameras.

This launch had as main objective to test image acquisition at unset, with several cameras operating in the visible range. Although the results were limited by the balloon trajectory that did not pass directly over the fire due to the limitation in the definition of the launch zone and the direction of the existing winds, and the disturbance caused by the smoke column and the excess of artificial lights existing in the captured area, it is still possible to verify the large coverage of the balloon acquired imagery and the potential of the proposed solution.

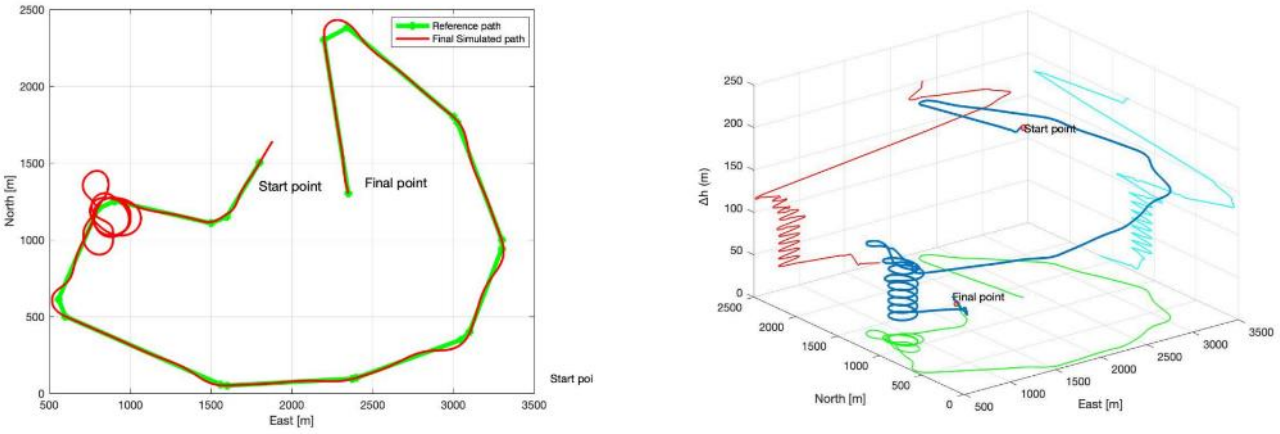

Figure 3 – Example of mission to be executed by the flying wing (reference) and its simulated performance. Vertical range was reduced to limit the loitering turns. (a) North-East visualization; (b) 3D visualization. (Yu (2021))

To guarantee the precision of the aerial imagery coverage, the mission definition of the flying wing UAV after remote cut-off from the HAB, and respective trajectory control, is essential. The implementation of nonlinear control solutions robust to wind disturbances and model uncertainties take gain from its gliding flight capabilities, guaranteeing the mission execution while maximizing flight time (Cordeiro et al. (2021)). An example of a UAV mission after deployment from HAB and stabilization, and simulated execution, is presented in Figure 3, where several points of interest are surveyed (vertical range was greatly reduced to limit the resulting loitering turns on descent).

3. Images

For the image acquisition system, a multimodal payload was developed encompassing thermal and visible range sensors. These two modes have complementary characteristics and enable developing fire detection algorithms that work separately on each of the modalities (Sousa et al. (2019), Sousa et al. (2020a)) or in tandem, allowing for better detection redundancy and robustness to occlusions in the data acquired by each sensor. Extensive field tests have been developed towards the characterization of the sensors, comprising flights with different altitude and horizontal profiles, varying different fire intensity, fire perimeter geometry and different ignition arrangements. These tests enabled identifying the best low-level image processing algorithms for encoding thermal data (Sousa et al. (2020b)). Figure 4 showcases an instance of data acquired including the different approaches taken that are made available in the dataset proposed in (Sousa et al. (2022)). Subsequently, the next steps involve improving the developed off-board automatic data annotation pipelines (Messias et al. (2021)) and applying intelligent system approaches to handle the image processing needs on-board the UAV.

Figure 4 – Examples of aerial images captured in the tests. Left: Tests setup; Middle: Visible range image in RGB color space. Top-Right: Thermal image processed with a linear automatic gain control algorithm, encoded with the GrayRed color palette. Bottom-Right: Thermal image processed with a plateau equalization automatic gain control algorithm, encoded with the Grayscale color palette.

4. Communications

During a fire event, the existence of alternative telecommunication relay systems is of extreme importance. In extreme events, the potential disruption of the communications service can cause severe damage to the firefighting operations. The main goal here is the research and implementation of an autonomous UAV-borne telecommunications service and the respective ground control system. The airborne system is responsible for transmitting all the telemetry data, images, and voice relay, while the ground system will receive these data and send mission controls back to the UAV/HAB. Another goal is the improvement of communications Quality of Service (QoS) between the local forces and the national entities to define adequate firefighting measures.

The image acquisition and respective analysis has an important role. To guarantee the quality of image transmission and reception, a communications relay system is deployed with the aerial platform, equipped with an omnidirectional antenna. This system provides the fire scene information across a high throughput

transmission via radio frequency using the UHF band. The scenes go for an image conversion procedure before transmission like MPEG4, MPEG5, JPEG200, and others. The management of the entire aerial communication system is performed in an SDR device that is responsible to maintain a communication channel with different modulations schemes (AX.25, SARATOGA, DVB-T and others) and properly encrypted. To guarantee the voice relay, a TETRA radio channel is added to comply with the common technology used by the firefighters (SIRESP).

The ground platform includes a fully automated motorized antenna, with high directivity and gain, equipped with a high sensitivity receiver. The system will use the telemetry data of the aerial platform to point the antenna accurately and improve the communication channel characteristics (RSSI, BER, image quality). The images are decompressed and shared with the national entities (CDOS and CNOS) through a satellite internet service.

Figure 5 represents the block diagram of the entire communications system.

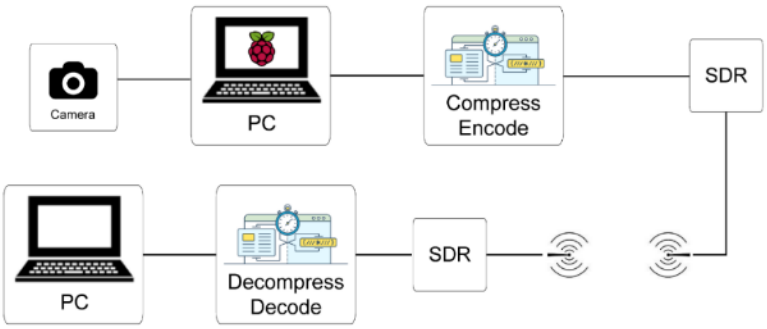

Figure 5 - Block diagram of the communications system.

5. Final Remarks

A solution was presented that is intended to become an important support tool for firefighting operations. This solution involves a high-altitude balloon carrying a glider plane and a payload that can be adapted to each situation. The payload is conceived to have a set of IR and RGB cameras for monitoring the fire and a communications repeater which will reinforce the communications system within the theatre of operations. This is a solution that allows a continuous operation that can exceed ten hours.

Although its main focus is the firefighting phase, as previously described, this solution can also be used in ignition detection operations or even in the aftermath phase in the search for hot spots that deserve greater attention by the forces remaining on the ground to avoid reignitions.

6. Acknowledgments

This work was financed by national funds through FCT – Fundação para a Ciência e Tecnologia, I.P., through IDMEC under project Eye in the Sky (PCIF/SSI/0103/2018), and through IDMEC under LAETA, project UIDB/50022/2020. M.J. Sousa acknowledges the support from FCT through the Ph.D. scholarship SFRH/BD/145559/2019.

7. References

R. A. Cordeiro, A. S. Marton, J. R. Azinheira, J. R. H. Carvalho, A. Moutinho (2021), Increased Robustness to Delay in Incremental Controllers using Input Scaling Gain. *IEEE Transactions on Aerospace and Electronic Systems*. DOI: 10.1109/TAES.2021.3123215

P. Messias, M. J. Sousa, A. Moutinho (2021), in *IEEE International Conference on Fuzzy Systems* (Institute of Electrical and Electronics Engineers Inc. DOI: 10.1109/FUZZ45933.2021.9494421

M. J. Sousa, A. Moutinho, M. Almeida (2019), Classification of potential fire outbreaks: A fuzzy modeling approach based on thermal images. *Expert Systems with Applications*. **129**, 216–232. DOI: 10.1016/j.eswa.2019.03.030

M. J. Sousa, A. Moutinho, M. Almeida (2020a), Wildfire detection using transfer learning on augmented datasets. *Expert Systems with Applications*. **142**. DOI: 10.1016/j.eswa.2019.112975

M. J. Sousa, A. Moutinho, M. Almeida (2020b), Thermal infrared sensing for near real-time data-driven fire detection and monitoring systems. *Sensors (Switzerland)*. **20**, 1–29. DOI: 10.3390/s20236803

M. J. Sousa, A. Moutinho, M. Almeida (2022), MAVFire: Thermal-visual-inertial-GNSS dataset for aerial robotics and fire applications. *(under review)*.

L. Yu (2021), "Pre-flight and real-time path planning of a balloon launched flying wing", MSc thesis, Instituto Superior Técnico, Universidade de Lisboa

Fast and accurate forest fire front reconstruction: A pathway to evaluate fire severity in extreme wildfires

Irene González *; Ana Cortés. Antonio Espinosa, Carles Carrillo, Tomàs Margalef

Universitat Autònoma de Barcelona. Spain,
{irene.gonzalez.fernandez, ana.cortes, antoniomiguel.espinosa, carles.carrillo, tomas.margalef}@uab.cat

**Corresponding author*

Keywords

Fire-front reconstruction; α-shape; FARSITE; Wildfire

Abstract

The increased number of extreme wildfires due to climate change generates new challenges in wildfire modelling and prevention actions. One important aspect is to provide current forest fire spread simulation tools with the capability of being faster and more accurate preserving their forecast abilities. In this paper, we propose an alternative forest fire front reconstruction algorithm that could easily be incorporated in the well-known FARSITE fire spread simulator without affecting its functionality. The fire front reconstruction core part in FARSITE represents up to 60% of its total execution time. The proposal alternative algorithm is based on the α-shape algorithm but including some adaptation considering the particular case of forest fire. Meanwhile, the current FARSITE fire front reconstruction algorithm has a complexity of $O(n^4)$, the adapted α-shape algorithm has a complexity of $O(n\,log(n))$. This new approach has the benefit of being parallelizable using a divide and conquer strategy what will allow to significalty reduce the FARSITE's execution time without modifying its forecat results.

1. Introduction

Climate change is affecting the face of the world. One of the critical aspects of this change is the increase of the average temperature generating long periods of drought in areas that areas not used to. Consequently, in the last decades, one can found extreme wildfires in regions such as Finland, eastern Australia, UK that were typically places with a low rate of huge forest fire (United Nations Environment Programme, 2022-02; Perry et al., 2022). Due to this disrupt new events, there appear new ways of evaluating fire risk indexes according to changing weather conditions such as, for example. the Extreme-Fire Behaviour Index (EFBI) (Artes et al., 2021). These indexes allow to determine whether an ongoing wildfire have the potential to become an extreme forest fire or not. However, once a given wildfire is labelled as potential extreme fire, the next useful step would be to determine the severity of the fire in terms of potential burn area, principal propagation direction and the rate of spread. For that purpose, several forest fire spread simulator have been developed such as FARSITE (Finney, 1998), QUIC-Fire (Linn et al., 2020), Wildfire analyst (Artes et al., 2015) WRF-SFIRE (Mandel et al., 2014) with the aim to be used during an ongoing wildland fire. However, to be useful a forest fire forecast system should provide accurate results faster than real fire propagation, especially when dealing with extreme wildfires. This trade-off has been shown to be difficult to achieve because having higher precision results typically is penalized with higher execution times. This feature is quite relevant in FARSITE when forecasting large forest fires that take place in complex terrain. In particular, the part of the code that consumes most of the computing time is the one devoted to reconstructing the fire perimeter at each time step (Finney, 1998). FARSITE's algorithm has a complexity of $O(n^4)$, that prevents it to be used at real time. In this paper, an alternative algorithm for forest fire perimeter reconstruction is presented, which has a complexity of $O(n\,log(n))$, opening the possibility of turning FARSITE into an operational tool.

The original FARISTE's algorithm for fire front reconstruction is described in section 2. Section 3 introduces the proposal strategy. The experimental study is explained in section 4 and, finally, the main conclusions are reported in section 5.

2. FARSITE: Crossover

FARSITE is a forest fire simulator designed by Finney in 1994 (Finney, 1998). It is an iterative model to construct the evolution of a fire front over a time step. To do that, FARSITE defines a forest fire perimeter as a set of points, whose position in the area is evaluated at each time step applying the so called Rothermel's Model (Rothermel, 1972). In particular, FARSITE has two main steps to evaluate forest fire evolution: the propagation step (step 1) and the fire front reconstruction (step 2).

Step 1 consists of applying Huygens' principal approach for elliptical wave-front modelling. The fire is represented by a set of vertices (points) and for each vertice, the propagation equations of the Rothermel's model (Rothermel, 1972) are applied to evaluate their new positions. Once all vertices have been evaluated, then step 2 is carried out. The fire front reconstruction (called *Crossover* in the FARSITE's code) consists of finding an ordering on the boundary vertices (points) such that there are no intersections between the edges given by any two consecutive points. This is currently done by iteratively comparing all possible combinations of vertices composed by any two edges against each other, in a naïve algorithm. The main objective of such a process is to detect burnt areas and prevent the reconstruction process of generating complex loops and knots without any meaningful. Figure 1 shows this kind of situations. The figures referred as *Before* correspond to fire front obtained once FARSITE' step 1 has finished, and no extra corrections has been performed. Meanwhile the images referred as *After* are the final correct burnt areas (preserving or not preserving an enclave) once FARSITE's step 2 has finished,

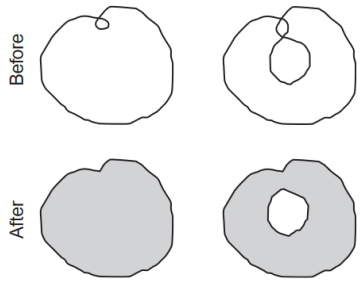

Figure 1- Example of a fire front reconstruction from (Finney, 1998).

As it is stated in the FARSITE's documentation (Finney, 1998), this process could be extremely expensive in terms of execution time. In particular, the *Crossover* routine has a complexity of $\boldsymbol{O(n^4)}$, what clearly penalize the total FARSITE's execution time. In the next section, an alternative algorithm for fire front reconstruction is described, which exhibits a high potential degree of parallelization and, therefore, it arises as a good alternative to accelerate FARSITE's simulations.

3. The boundary α-shape algorithm

The proposal described in this section is based on the α-shape algorithm, which is a generalization of the convex-hull and a subgraph of the Delaunay triangulation (Delaunay, 1934). In a roughly way, given a set of points, the α-shape algorithm could generate different shapes from the Delaunay triangulation of those points, according to the α value selected. This value will control the precision degree of the generated shapes.

A conformal α-shape (Cazals et al., 2005) is very similar to an α-shape but instead of a global parameter α, it uses a local scale parameter. Even so, α-shapes and conformal α-shapes share most of their properties, but the conformal α-shapes are very useful when the data is non-uniformly sampled. In this section, we outline the proposed conformal α-shape algorithm that is designed to substitute the current fire front reconstruction algorithm included in FARSITE.

3.1. Algorithm description

The alternative algorithm that we propose, is based on an α-shape but is adapted to the needs of the problem, making it more akin to a conformal α-shape. In the new algorithm, the inner edges of the Delaunay triangulation will use $\alpha = \infty$, making them irrelevant, while the boundary of the triangulation will use a meaningful α value.

This approach, in addition to saving computation time, allows us to work with a data distribution with which the α-shape might not give us the expected results.

3.2. Inputs & Outputs

The FARSITE fire front reconstruction process starts from a vector of points and returns another vector of ordered points, not necessarily of the same size. Since we want that the new algorithm could be used in an easy plug&play scheme being transparent to the FARSITE's user, we must adapt the inputs and outputs of the alternative algorithm to match those of FARSITE to be able to use it in an interchangeable way.

The desired input for the α shape is a vector of unordered points, but the alternative algorithm previously requires a Delaunay triangulation. As such, the first step to be carried out should be to obtain the Delaunay triangulation by means of an unordered vector of points. Obtaining the Delaunay triangulation is the most time-consuming part of the proposal; however, it exhibits a complexity of $O(n\,log(n))$, what supposes a great improvement considering the original complexity of the current FARSITE algorithm.

The adaptation of the output data of the new proposal algorithm is simple since we already have identified the border of the concave hull.

3.3. Parameter selection

In the *boundary* α-shape algorithm, as in the basic α-shape, it is necessary to choose an α value that will determine the shape obtained. From the context of the problem, the most logical thing to do is to use FARSITE's perimeter resolution parameter, since it is a parameter that the user decides. However, a deeper study of this point should be performed.

4. Experimental results

In this section, we provide the preliminary results obtained in terms of execution time and accuracy of the prediction results when using the original FARSITE fire front reconstruction method and when using the proposal boundary **α**-shape algorithm to generate the new fire perimeter. The performance results reported in this section, are based on running the fire front reconstruction component of FARSITE in an isolated way and compared to the proposed *boundary* α-shape algorithm. Therefore, in order to be fair, the comparison has been done by feeding both programs with the same format of data and generating both the same output data format. Those formats are conformal with the ones used in FARSITE.

4.1. Execution time

The main contribution of the alternative proposal to reconstruct the fire front is the algorithm's complexity reduction. One the one hand, the original naïve FARSITE *Crossover* procedure exhibits a complexity of $\boldsymbol{O(n^4)}$, meanwhile the *boundary* α-shape approach has a complexity of $\boldsymbol{O(n\,log(n))}$ what implies a significant reduction of the execution time of this component of the simulator, which currently represents 60% of the total execution time of FARSITE. In figure 2, one can observe the time spent in executing both reconstruction algorithms when using different numbers of points for the fire perimeter. As we can observe, as the number of points increases, the execution time spent by the new algorithm decreases compared to the time spent by FARSITE approach. This performance improvement is more significative when dealing with a huge number of points being able to achieve a performance improvement of twenty time when using 100000 points. This result could lead to a FARSITE total time execution time of 50%. Describing the fire front with a huge number of points implies to describe the forest fire behavior with better precision but, typically this improvement in the fire front resolution has a direct impact in the execution time. Our proposal has the ability of provide accurate results without penalizing the total execution time.

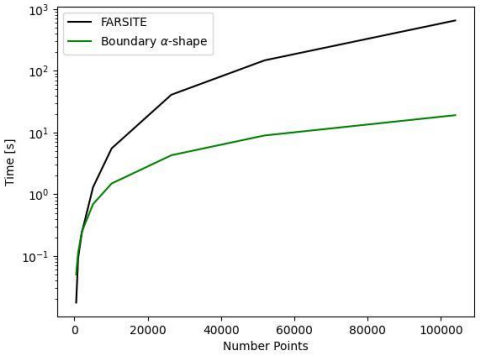

Figure 2 - Execution times of FARSITE Crossover and boundary α-shape with different numbers of points

4.2. Propagation results

The modification of the fire front reconstruction process could lead to different fire behaviour, that is, the output shapes of the simulation tool could be slightly different. However, this substitution should provide similar enough not to modify the overall behavior of the fire. As it is well known, the α-shape algorithm generates quite different results depending on the value of the α parameter. The experimental results shown in this section has been obtained using as α value the resolution of the perimeter, which, in this case, has been set to 30 meters. Figure 3 shows the output provided by the original fire front reconstruction made by FARSITE (black line) and the output provided by the new strategy (green shape). In particular, the two cases depicted in this figure corresponds to two real fires, figure 3(a) is a fire that took place in Pendilhe (Portugal) in 2013 and figure 3(b) was an event that happened in Arkadia (Greece) in 2011. As we can observe, the results are almost the same, however, if we analyze the shape and the line in detail, one can found certain regions where the green shape overpass the black line. Nevertheless, those difference are not significant enough to affect the global behavior of the wildfire,

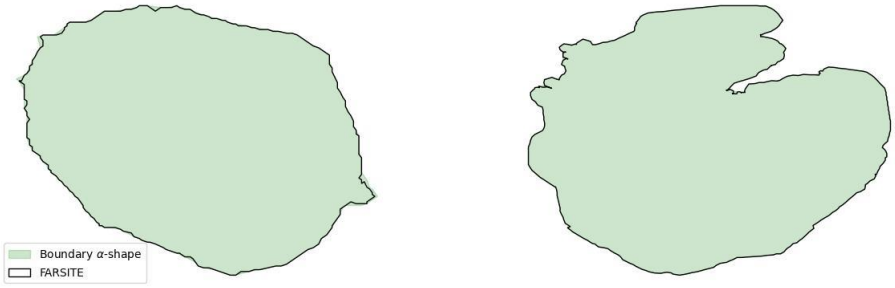

a b

Figure 3- The fire front reconstruction obtained when applying the FARSITE Crossover algorithm and the boundary α-shape proposal to two real wildfires.

5. Conclusions

Climate change generates an increasing number of wildfires, which are growing in intensity and area affected. To tackle such events, current available tools must be enhanced to be faster without loosing their forecast abilities. In this work, an alternative algorithm for FARSITE fire front reconstruction algorithm is presented. The proposal strategy does not affect the simulations results provided by FARSITE but, the preliminary studies show promising results with a reduction of the execution time of 20 times. The initial validation has been done only with the part of the code associated to the fire front reconstruction and the next step is to integrate the new algorithm within FARSITE.

6. Acknowledgments

This research has been supports by Ministerio de Ciencia e Innovación MCIN AEI/10.13039/501100011033 under contract PID2020-113614RB-C21 and by the Generalitat de Catalunya GenCat-DIUiE (GRC) project 2017-SGR-313.

7. References

Artes, T., Cardil, A., Cortés, A., Margalef, T., Molina Terrén, D., Pelegrín, L., & Ramirez, J. (2015). Forest fire propagation prediction based on overlapping dddas forecasts. *Procedia Computer Science*, 51, 1623–1632. https://doi.org/10.1016/j.procs.2015.05.294

Artes, T., Castellnou, M., Durrant, T., & San-Miguel-Ayanz, J. (2021). Wildfire-atmosphere interaction index for extreme fire behaviour. *Natural Hazards and Earth System Sciences*. https://doi.org/10.5194/nhess-2021-122

Cazals, F., Giesen, J., Pauly, M., & Zomorodian, A. (2005). Conformal alpha shapes. *Proceedings Eurographics/IEEE VGTC Symposium Point-Based Graphics*, 2005., 55–61. https://doi.org/10.1109/PBG.2005.194064

Delaunay, B. (1934). Sur la sphère vide. *Bulletin de l'Académie des Sciences de l'URSS. Classe des sciences mathématiques et na*, 1934(6), 793–800.

Finney, M. A. (1998). *FARSITE: Fire area simulator-model development and evaluation* (tech. rep.). Forest Service, U.S. Department of Agriculture. U.S. Department of Agriculture, Forest Service, Rocky Mountain Research Station. https://doi.org/10.2737/rmrs-rp-4

Linn, R., Goodrick, S., Brambilla, S., Brown, M., Middleton, R., O'Brien, J., & Hiers, J. (2020). QUIC-fire: A fast-running simulation tool for prescribed fire planning. *Environmental Modelling & Software*, 125, 104616. https://doi.org/10.1016/j.envsoft.2019.104616

Mandel, J., Amram, S., Beezley, J. D., Kelman, G., Kochanski, A. K., Kondratenko, V. Y., Lynn, B. H., Regev, B., & Vejmelka, M. (2014). Recent advances and applications of wrf-sfire. *Natural Hazards and Earth System Sciences*, 14(10), 2829–2845. https://doi.org/10.5194/nhess-14-2829-2014

Perry, M. C., Vanvyve, E., Betts, R. A., & Palin, E. J. (2022). Past and future trends in fire weather for the uk. *Natural Hazards and Earth System Sciences*, 22(2), 559–575. https://doi.org/10.5194/nhess-22-559-2022

Rothermel, R. C. (1972). A mathematical model for predicting fire spread in wildland fuels. *Research Paper INT-115. USDA Forest Service, Report No. INT-115*.

United Nations Environment Programme, G.-A. (2022-02). Spreading like wildfire: The rising threat of extraordinary landscape fires - a rapid response assessment. https://wedocs.unep.org/20.500.11822/38372

Fire images classification using high order statistical features

Houda Harkat*[1,2]; José Nascimento[1,3]; Alexandre Bernardino[4] ; Hasmath Farhana Thariq Ahmed[5]

[1] Instituto de Telecomunicações, Instituto Superior Tecnico, Av. Rovisco Pais 1, 1049-001 Lisboa, Portugal, {houda.harkat@usmba.ac.ma}
[2] Centre of Technology and Systems (CTS), FCT Campus, NOVA University of Lisbon, 2829-516 Caparica, Portugal.

[3] Instituto Superior de Engenharia de Lisboa, IPL, Lisbon Portugal, {jose.nascimento@isel.pt}
[4] ISR - Instituto de Sistemas e Robotica, Av. Rovisco Pais 1, 1049-001 Lisboa, Portugal, {alex@isr.tecnico.ulisboa.pt}
[5] School of Computer Science and Engineering, Vellore Institute of Technology, Chennai, Tamil Nadu. India. 600127, {hasmath.farhana@vit.ac.in}

**Corresponding author*

Keywords

Forest fire, HOS, Cumulants, Feature Selection, Mutual information, SVM

Abstract

Wildfires and forest fires have devastated millions of hectares of forest across the world over the years. Computer vision-based fire classification, which classifies fire pixels from non-fire pixels in image or video datasets, has gained popularity as a result of recent innovations. A conventional machine learning-based approach or a deep learning-based approach can be used to distinguish fire pixels from an image or video. Deep learning is currently the most prominent method for detecting forest fires. Although deep learning algorithms can handle large volumes of data, typically ignore the differences in complexity among training samples, limiting the performance of training models. Moreover, in real-world fire scenarios, deep learning techniques with little data and features underperform. The present study utilizes a machine learning-based approach for extracting features of higher-order statistical methods from pre-processed images from publicly available datasets: Corsican and FLAME, and a private dataset: Firefront Gestosa. It should be noted that handling multidimensional data to train a classifier in machine learning applications is complex. This issue is addressed through feature selection, which eliminates duplicate or irrelevant data that has an effect on the model's performance. A greedy feature selection criterion is adopted in this study to select the most significant features for classification while reducing computational costs. The Support Vector Machine (SVM) is a conventional machine classifier that works on discriminative features input obtained using the MIFS, feature selection technique. The SVM uses a Radial Basis Function (RBF) kernel to classify fire and non-fire pixels, and the model's performance is assessed using assessment metrics like overall accuracy, sensitivity, specificity, precision, recall, F-measure, and G-mean.

1. Introduction

Millions of hectares of forest have been destroyed by wildfires in recent years (Bhujel, Maskey-Byanju et al. 2017, Mannan, Feng et al. 2017, Nolan, Boer et al. 2020). Nature's balance is protected by forests. Forest fires are usually identified after they have spread across a large area, making management and extinguishment difficult, if not impossible (Alkhatib 2014). Computer vision-based fire detection is gaining active research attention in categorizing surface and crown fires (Guan, Min et al. 2022). Surface fires in the forest can be easily identified with smoke sensors, making classification difficult. Crown fires occur when a surface fire is not controlled immediately. No sensor can withstand the tremendous heat produced by a crown fire, making sensing difficult (Chowdary, Gupta et al. 2018). To detect crown fires early, satellites or unmanned aerial vehicles must continuously monitor the forest landscape. Vision-based techniques also help firefighting teams locate their destination by classifying video or picture information. Apart from preventing flames from spreading, this strategy aims to minimize economic and financial losses to human and forest life. The classification of fire pixels in an image or video can be done using either standard machine learning or deep learning (Bot and Borges 2022, Bouguettaya, Zarzour et al. 2022, Majid, Alenezi et al. 2022).

The conventional machine learning paradigm necessitates feature extraction and selection. Alternatively, deep learning can be used to automatically extract and select features for classification (Farhana Thariq Ahmed, Ahmad et al. 2019). Manual feature extraction is inefficient at capturing discriminative feature information in large data sets. Handcrafted approaches also perform inefficiently and are unreliable as data size increases. While deep learning methods may handle enormous data volumes, they could not account for the variation in complexity across samples. Thus reducing the efficiency of their training models and increasing misclassification (Guan, Min et al. 2022). Moreover, in complex fire scenarios, deep learning with minimal data and features underperforms.

Thus, the current study employed machine learning to extract higher order features (Swami, Mendel et al. 1998) from the image dataset for fire pixel classification. Higher order cumulant features were used since they are resistant to Gaussian noise in the original data. In remote sensing applications like fire monitoring and detection, higher-order statistical features are rarely used (Vijithananda, Jayatilake et al. 2022). The present study evaluates higher order cumulants (order 3) that extract the cumulant coefficients from images using an unbiased approach. Handling multidimensional data to train a model is difficult in machine learning. Through removing redundant or irrelevant data, the model's performance can be improved. To lower the computational cost, information theoretic feature selection approaches have been used in this work with a predefined set of significant feature inputs. Later, the discriminative features are fed into the SVM classifier. To assess the model's performance, the images are classified as either fire or non-fire using an SVM classifier with a Radial Basis Function (RBF) kernel. The current approach uses fire photos from publicly available datasets, notably the Corsican (Toulouse, Rossi et al. 2017) and FLAME (Shamsoshoara, Afghah et al. 2021) datasets. Fire detection was indeed conducted using images from the, Firefront Gestosa , a private dataset.

2. Proposed framework

Figure 1 depicts the current work's process for categorizing fire pixels with handcrafted feature extraction and selection. Three publicly available image datasets have been used in this study: Corsican (Toulouse, Rossi et al. 2017), FLAME (Shamsoshoara, Afghah et al. 2021), and Firefront Gestosa. Furthermore, the present work, combined the three distinct datasets to increase the number of training examples for the presently proposed machine learning model. In this work, the pictures of the adopted datasets are manually labelled and annotated using the data partitioning technique. Prior to the classification task, the images in the image dataset are pre-processed using mask creation and flame localization. Cropping and resizing the photos to 300*300 pixels is then performed using the patch creation approach. Following that, the resized images are divided into training, testing, and validation test sets. The downsized images are then modified using the Radon transform, which reduces the image's dimensionality from two dimensions to one dimension.

The present work applied a projection angle of 0^0 to 360^0 and a step size of 10^0, for performing the Radon transform. As a result, each image is formed contributes to 37 angles. The current study extracts HOS cumulant features from each angle and then concatenates all 37 angles' extracted features into a single feature vector. Since it is impractical to input a larger feature vector to the learning algorithm, the present work incorporates a feature selection approach to reduce computational complexity. The current work examined the extracted features experimentally using a greedy feature selection criterion - Mutual Information Feature Selection (MIFS), with a predefined set of optimal features (30, 50 and 80). Finally, the reduced set of optimal features is sent into the SVM classifier, which performs fire pixel classification. Finally, the machine learning model is used to localize the fire pixels and the classification performance of SVM is evaluated using the following metrics: overall accuracy, sensitivity, specificity, precision, recall, f-measure, and g-mean.

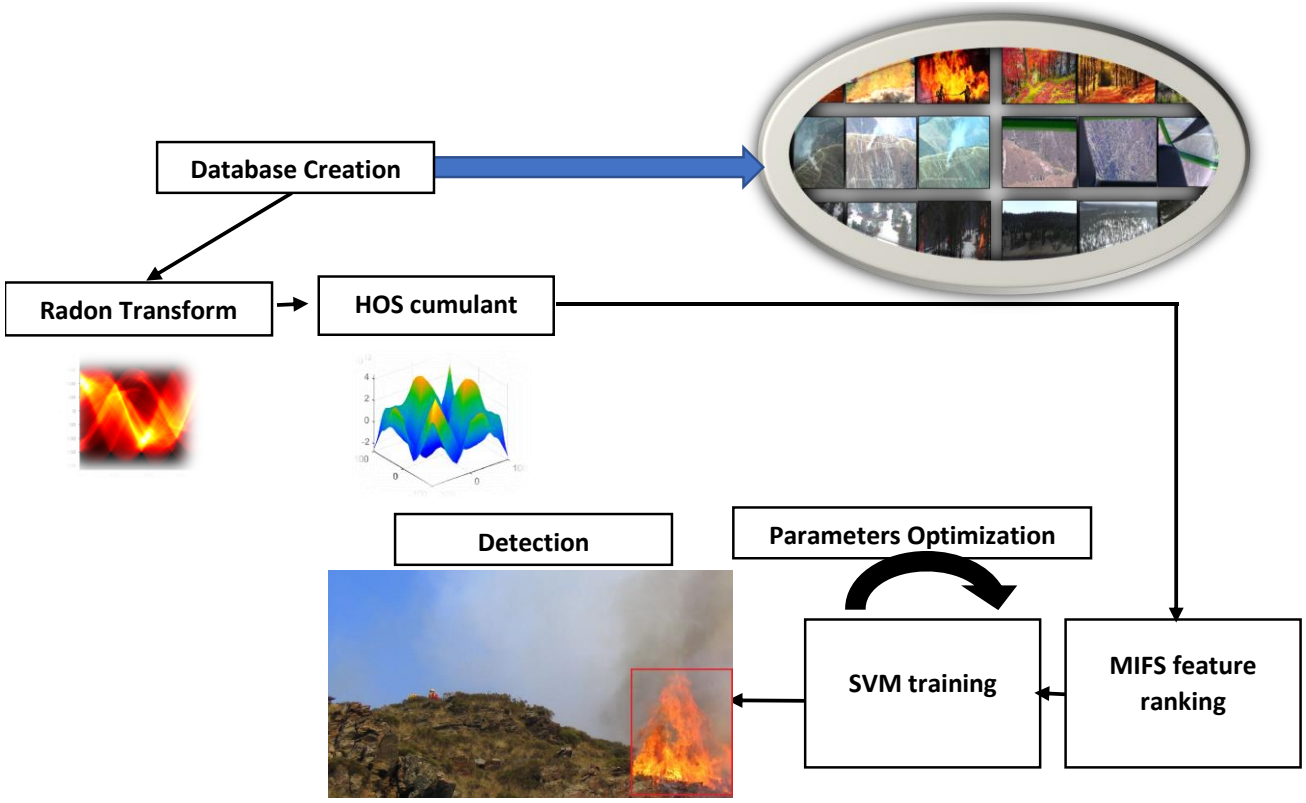

Figure 1- The proposed framework for fire classification adopting a handcrafted approach.

3. Material and methods

3.1. High order cumulants features

The present work, extract higher order statistical features from the pre-processed image. In specific, higher order cumulant features (Mendel 1991, Swami, Mendel et al. 1998) of order three is extracted from the image in an unbiased fashion. By removing the sample mean from the pre-processed image, radon transform (Stanley 1983) was performed to reduce the dimension of the image to a single dimension. Afterwards, cross-cumulant estimates were computed. The third order cumulant represent the normalized skewness and it can recover the cumulant information even in the presence of coloured Gaussian noise present in the image. For a random variable y the cumulant generating function can be expressed as $K(n)$,

$$K(n) = logE[e^{nY}] \qquad (1)$$

The higher order cumulants can further expressed as the central moments with polynomial functions as

$$K_1(\mathrm{Y}) = \mathrm{E}(\mathrm{Y}) \qquad (2)$$

$$K_2(\mathrm{Y}) = \mathrm{var}(\mathrm{Y}) = \mathrm{E}(\big(\mathrm{Y} - \mathrm{E}(\mathrm{Y})\big)^2) \qquad (3)$$

$$K_3(\mathrm{Y}) = \mathrm{var}(\mathrm{Y}) = \mathrm{E}(\big(\mathrm{Y} - \mathrm{E}(\mathrm{Y})\big)^3) \qquad (4)$$

Where, equation 2,3,4 represents the mean (first order), variance (second order), and skewness (third order) respectively.

3.2. Mutual information ranking technique

MIFS (Battiti 1994), a greedy feature selection method, guarantees the selection of highly informative features using mutual information as a metric. This selection paradigm uses a regularisation parameter, β, to identify the

non-linear relationship between selected features and output class. This value β reduces the level of uncertainty among the optimal feature subsets by eliminating duplicate features. Finally, for classification, the ideal feature subset with pre-defined feature information will be fed into machine learning classifier.

MIFS has an advantage over other linear transformation-dependent approaches in that it considers the non-linear relationship between features and the output class labels. As a result, MIFS delivers strong generalisation for training while also reducing computing time.

The MIFS algorithm uses the following approach to ensure that every feature chosen is informative (Battiti 1994):

1. Feature set (empty) $\hat{S}$ initialized with initial features, as $\hat{S} \leftarrow f_0 \ldots, f_n$ features.
2. Mutual information among the feature variables, f to be computed between the feature variables and the class labels (output: O), as I (O: f) in the extracted feature set $\hat{S}_f$
3. Select the features that are highly mutually informative with the output, O and add them to the empty feature set based on the increasing order mutual information as, $\hat{S} \leftarrow \hat{S} \backslash \{f\}$ and $\hat{S} \leftarrow \{f\}$
4. Implement a "greedy" selection of features for a set of pre-determined numbers such as 30, 50 and 80
    a. For every set of feature pair in the set $\hat{S}$, calculate $I(f, \hat{s})$, $\hat{s} \in \hat{S}$, if not calculated already.
    b. The features that are highly related to each other are chosen to satisfy the criteria of mutual information as,

$$I(0 : f) - \beta \sum_{\hat{s} \in \hat{S}} I(f, \hat{s})$$

5. Finally, the set $\hat{S}$ is treated as an ideal feature subset as it contains highly informative features.

4. Results and discussion

The experiments were conducted over a dataset of 8036 pictures, where 4016 represent fire and 4020 are non-fire images. One hundred and twenty-five sun pictures are injected on the database to simulate high intensity pictures that could be misleading to the classifier. The exact contribution of every set of data (Corsican, FLAME and Firefront_Gestosa) into the final dataset is given in table 1. The final dataset was partitioned to training, validation, and test sets with the following ratio: 60%, 20% and 20% respectively. The SVM model, with gaussian kernel, was trained in a loop with varied parameters configurations to find the optimal Gamma and cost parameters.

Table 1- The corresponding parameters of the conducted experiments

Dataset	Corsican Dataset	FLAME Dataset	Firefront_Gestosa Dataset	Sun Pictures
Fire	1775	2003	238	**0**
Non-Fire	0	2782	1113	**125**

Table 3. represent the experimental results by varying the selected features as 30, 50 and 80 from the total set of extracted feature vector. The MIFS paradigm performs the feature selection with regularisation parameter β set to three different values as 0.1, 0.5 and 0.8. The parameters of the conducted experiments are given in table 2., while the corresponding results are given in table 3. The model's performance was measured with overall accuracy, sensitivity, specificity, precision, recall, f-measure and g-mean metrics. The results observed to be better with increasing number of features irrespective of β. Overall performance reported high with set of 80 selected cumulant features with no significant difference in the reported values with β.

Table 2- The corresponding parameters of the conducted experiments

Experiment Nº	*Number of Features*	*Other Parameters*
Experiment 1	30	The regularization parameter β = 0.8
Experiment 2	50	
Experiment 3	80	
Experiment 4	30	The regularization parameter β = 0.5
Experiment 5	50	
Experiment 6	80	
Experiment 7	30	The regularization parameter β = 0.1
Experiment 8	50	
Experiment 9	80	

Table 3- The given results of every experiment

Experiment Nº	*Overall accuracy*	*sensitivity*	*specificity*	*precision*	*recall*	*f-measure*	*g-mean*
Experiment 1	95,78	93,40	98,16	98,07	93,40	95,68	95,75
Experiment 2	96,02	94,05	97,99	97,90	94,05	95,94	96,00
Experiment 3	96,093	**94,15%**	**98,04%**	**97,95%**	**94,15%**	**96,01%**	**96,07%**
Experiment 4	95,981	93,88	98,09	98,00	93,88	95,89	95,96
Experiment 5	96,068	94,12	98,01	97,93	94,12	95,99	96,05
Experiment 6	96,105	**94,17**	**98,04**	**97,95**	**94,17**	**96,03**	**96,09**
Experiment 7	95,856	93,83	97,89	97,79	93,83	95,77	95,83
Experiment 8	96,03	94,12	97,94	97,85	94,12	95,95	96,01
Experiment 9	96,068	**94,07**	**98,06**	**97,98**	**94,07**	**95,99**	**96,05**

5. Conclusions and outlooks

Fire detection is a task that require high precision to localize the exact position of flames. Hence, an accurate and well-trained model need to be developed to make the intervention of the firefighters faster. The current paper divulgates the results of an SVM model trained with 3rd high order cumulant feature set reduced with a mutual information algorithm. The given results are very promising. However, more experiments need to be run using other feature ranking techniques to observes the fluctuation of different parameters and the performance of the classification technique.

6. Acknowledgement

This work was supported by the Institution of Telecommunications and Portuguese Foundation for Science and Technology under the Project UIDB/50008/2020 and Project FIREFRONT with reference PCIF/SSI/0096/2017. Houda Harkat acknowledges the financial support of the Programmatic Financing of the CTS R&D Unit (UIDP/00066/2020).

7. References

"The Amazon in Brazil is on fire - how bad is it?." Retrieved Feb 14, 2022, from https://www.bbc.com/news/world-latin-america-49433767.

"CNN (2020) California wildfires have burned an area almost the size of Connecticut." Retrieved Feb 14, 2022, from https://edition.cnn.com/2020/09/14/us/california-wildfires-monday/index.html

"http://firefront.pt/." Retrieved 07 February 2022.

Alkhatib, A. A. (2014). "A review on forest fire detection techniques." International Journal of Distributed Sensor Networks 10(3): 597368.

Battiti, R. (1994). "Using mutual information for selecting features in supervised neural net learning." IEEE Transactions on neural networks 5(4): 537-550.

Bhujel, K. B., R. Maskey-Byanju and A. P. Gautam (2017). "Wildfire Dynamics in Nepal from 2000-2016." Nepal Journal of Environmental Science 5: 1-8.

Bot, K. and J. G. Borges (2022). "A Systematic Review of Applications of Machine Learning Techniques for Wildfire Management Decision Support." Inventions 7(1): 15.

Bouguettaya, A., H. Zarzour, A. M. Taberkit and A. Kechida (2022). "A review on early wildfire detection from unmanned aerial vehicles using deep learning-based computer vision algorithms." Signal Processing 190: 108309.

Chowdary, V., M. K. Gupta and R. Singh (2018). "A Review on forest fire detection techniques: A decadal perspective." Networks 4: 12.

Farhana Thariq Ahmed, H., H. Ahmad, S. K. Phang, C. A. Vaithilingam, H. Harkat and K. Narasingamurthi (2019). "Higher Order Feature Extraction and Selection for Robust Human Gesture Recognition using CSI of COTS Wi-Fi Devices." Sensors 19(13): 1-23.

Guan, Z., F. Min, W. He, W. Fang and T. Lu (2022). "Forest fire detection via feature entropy guided neural network." Entropy 24(1): 128.

Majid, S., F. Alenezi, S. Masood, M. Ahmad, E. S. Gündüz and K. Polat (2022). "Attention based CNN model for fire detection and localization in real-world images." Expert Systems with Applications 189: 116114.

Mannan, A., Z. Feng, A. Ahmad, M. Beckline, S. Saeed, J. Liu, S. Shah, M. Amir, U. Ammara and T. Ullah (2017). "CO2 emission trends and risk zone mapping of forest fires in subtropical and moist temperate forests of Pakistan." APPLIED ECOLOGY AND ENVIRONMENTAL RESEARCH 17(2): 2983-3002.

Mendel, J. M. (1991). "Tutorial on higher-order statistics (spectra) in signal processing and system theory: Theoretical results and some applications." Proceedings of the IEEE 79(3): 278-305.

Nolan, R. H., M. M. Boer, L. Collins, V. Resco de Dios, H. G. Clarke, M. Jenkins, B. Kenny and R. A. Bradstock (2020). "Causes and consequences of eastern Australia's 2019-20 season of mega-fires." Global change biology.

Shamsoshoara, A., F. Afghah, A. Razi, L. Zheng, P. Z. Fulé and E. Blasch (2021). "Aerial Imagery Pile burn detection using Deep Learning: the FLAME dataset." Computer Networks 193: 108001.

Stanley, R. (1983). "Deans,"The Radon Transform and Some of Its Applications."

Swami, A., J. M. Mendel and C. L. Nikias (1998). "Higher order spectral analysis toolbox, for use with MATLAB, The MathWorks."

Toulouse, T., L. Rossi, A. Campana, T. Celik and M. A. Akhloufi (2017). "Computer vision for wildfire research: An evolving image dataset for processing and analysis." Fire Safety Journal 92: 188-194.

Vijithananda, S. M., M. L. Jayatilake, B. Hewavithana, T. Gonçalves, L. M. Rato, B. S. Weerakoon, T. D. Kalupahana, A. D. Silva and K. D. Dissanayake (2022). "Feature Extraction from MRI ADC Images for Brain Tumor Classification Using Machine Learning Techniques."

Fireline production rate assessment under Mediterranean conditions

Macarena Ortega*[1]; Francisco Rodríguez y Silva[1]; Juan Ramón Molina[1]

[1]University of Córdoba. Forest Fire Laboratory. Edificio Leonardo da Vinci. Campus de Rabanales, Córdoba, Spain, {macarena.ortega, ir1rosif, jrmolina}@uco.es

**Corresponding author*

Keywords

fuel model, firefighter, terrestrial suppression resources, direct and indirect attack, aerial support

Abstract

Global change is raising the occurrence and simultaneity of large wildfires. However, increasing the number of suppression resources is not necessarily the way to manage it and even less if suppression resource assignment is determined based on the experience of the incident commander or incident management team.

This research focuses on the estimation of fireline production rate in wildfires of different size under Mediterranean conditions. Fireline production rate was defined as the expected length of fireline that can be built by a firefighting crew in a period. Their most important explanatory variables were fuel model type, attack type, fire size, working time and support of aerial resources. Fuel models with the highest fireline production rate are those corresponding to grassland. Fireline production rate in indirect attack is lower than in direct attack regardless of fuel model. Fireline production rate decreased with increasing wildfire size. Firefighter production rate was decreased by 41.79% after three hours of work, due to fatigue in stress conditions next to the fire front. Aerial support increased fireline production rate between 8.14% and 20.63%. Finally, according to the findings obtained, the most efficient crew is made up of 7-9 firefighters.

The assessment of the average firefighter production rates based on easily identifiable variables from an incident command post, provides objective information for decision making about the type and number of resources required in wildfires suppression activities. An efficient allocation of suppression resources would reduce crew fatigue and increase the effectiveness of operational plans.

1. Introduction

Although large wildfires constitute less than 2% of the total forest fires (Donovan and Brown, 2005), they are the most severe causing the greatest ecological and socio-economic impacts. Due to their greater virulence and suppression difficulty, large wildfires require the highest suppression costs (Rodríguez y Silva et al., 2020). Moreover, Holmes and Calkin (2013) have indicated that in large wildfires, differences between the standard fireline production rates and estimated rates could be observed.

Fireline production rate was defined as the expected length of fireline that can be built by a firefighting crew in a period (Broyles, 2011). There is a lack of information regarding the productivity and efficiency of wildfires suppression resources (Thompson et al., 2018). Katuwal et al. (2016) used a Stochastic Frontier Analysis to model the production of the suppression resources, including the variability and inefficiency in suppression operations. Rodríguez y Silva (2017) and Rodríguez y Silva and Hand (2018) have generated productivity models based on the combination of suppression resources using econometric techniques.

The main goal of this research is to assess the fireline production rate developed by firefighters in wildfires of different size in Mediterranean ecosystems. Despite difficulties in generating the dataset (Plucinski, 2019a), this research was created through direct observations on active fires. In contrast, other studies estimated rates in firefighter trainings and burn areas and over-estimate fireline production rate (Plucinski, 2019b). Although some studies (Chico, 2001; Jiménez, 2014) have established production rates for fuel models in Mediterranean ecosystems, we try to cover gaps in relation to new psychological and working variables. Firefighter production rate estimated in different wildfire scenarios would constitute a useful and necessary tool for decision-making at two planning level. Before the wildfire, knowing terrestrial firefighting efficiency afford land managers optimize firefighting resources and design crews with an efficient number of firefighters. During a wildfire, it provides a scientific basis on which making technical decisions for the efficient suppression planning and

resources assignment to contain a wildfire. Comparison of production rates based on the use of different suppression resources is a very useful tool for fire managers (Plucinski, 2019b).

2. Material and methods

2.1. Study area

The study area is limited to three spanish regions in southern Iberian Peninsula (Andalucia, Castilla La Mancha and Valencia), which cover a total of 190.000 km^2. Official statistics indicate an annual average of 1,993 fires and an annual burned area of 21,983 ha for them during 2008-2018. The climate of these regions are typically Mediterranean, with dry and hot summers making them fireprone areas.

2.2. Database creation

This study database was generated from direct observation during the firefighting crew work of three Spanish region wildfire agencies during the period 2013-2018. Fire technician or foreman filled in a report for each fire operation. A total of 229 reports were collected, 204 of which were used for this study. Fireline production rate was calculated by the ratio between fireline length and working time per number of firefighters. Fireline effectiveness is defined as the successful containment of the fire in the hand line build during firefighting. In addition to administrative information of each wildfire, the data gathered was (Table 1):

Table 1. Range of the variables gathered.

Variable	Range
Fireline production rate	0.1 - 2.85 m/min*firefighter
Fuel model (Anderson, 1982)	1-10
Fire size	0.5 - 3,400 ha
Working time	10 - 445 min
Temperature	21 - 41.5 ºC
Relative humidity	8 - 52%
Wind speed	2.5 - 60 km/h
Slope	0- 15% (value 1) - > 45% (value 4)
Stoniness	Low (value 1) - Very high (value 4)
Number of firefighters	5-27 firefighters
Type of attack	Direct (value 0) and Indirect (value 1)
Air resources support	No (value 0) and Yes (value 1)
Time interval between releases	3-15 min
Fireline effectiveness	No (value 0) and Yes (value 1)

2.3. Statistical analysis

Statistical analyses were performed by SPSS© software. Kolmogorov-Smirnov test was used to check the normal distribution. Krustal-Wallis and Mann-Whitney tests were used to identify significant differences ($p < 0.05$).

3. Results

In direct attack (Table 2), the highest production rate of firefighting crews was observed working in timber-litter fuel models, however, the lowest rate was found in chaparral fuel models. Fireline production rate in indirect attack (Table 2) was significantly increased in grassland and brushland fuel models in relation to timber fuel models.

Table 2. Fireline production rate for each fuel model group based on type of attack.

Fuel model type	Fireline production rate (m/min*firefighter) Direct attack	Fireline production rate (m/min*firefighter) Indirect attack
Grassland	$0.87(\pm0.45)^a$	$0.40(\pm0.16)^a$
Chaparral	$0.33(\pm0.19)^b$	$0.31(\pm0.12)^a$
Brushland	$0.67(\pm0.34)^c$	
Timber-understory	$0.44(\pm0.17)^b$	$0.16(\pm0.04)^b$
Timber-litter	$1.06(\pm0.1)^d$	

Mean values in a column followed by the same letter are not significantly different ($p < 0.05$).

Aerial resources support increased fireline production rate between the 8.14% (grassland fuel models) and the 20.63% (brushland fuel models) (Table 3).

Table 3. Fireline production rate based on air resources support.

Fuel model type	Fireline production rate (m/min*firefighter) with support of aerial resources	Fireline production rate (m/min*firefighter) without support of aerial resources
Grassland	0.87(±0.30)[a]	0.79(±0.45)[a]
Brushland	0.63(±0.39)[a]	0.51(±0.20)[b]

Mean values in a raw followed by the same letter are not significantly different ($p < 0.05$).

Statistical analysis of production rate did not provide significant differences ($p < 0.05$) according to meteorological conditions and environmental characteristics. However, fireline production rate decreased with increasing wildfire size (Table 4).

Table 4. Fireline production rate based on fire size.

Fire size (ha)	Fireline production rate (m/min*firefighter)
< 1	0.67(±0.55)[a]
1-50	0.55(±0.43)[a]
> 50	0.41(±0.25)[b]

Mean values in a column followed by the same letter are not significantly different ($p < 0.05$).

In addition, in brushland fuel models, fireline production rate was decreased by 41.79% after three hours of work (Table 5).

Table 5. Fireline production rate based on working time.

Working time (min)	Fireline production rate (m/min*firefighter)
< 60	0.67(±0.54)[a]
60-180	0.52(±0.28)[a]
> 180	0.39(±0.27)[b]

Mean values in a column followed by the same letter are not significantly different ($p < 0.05$).

The successful containment increased fireline production rate in both grassland and brushland fuel models (Table 6). The production rate was increased by 84.84% due to a successful containment of the fire perimeter.

Table 6. Fireline production rate based on fire successful containment.

Fuel model type	Unsuccessful fire containment	Successful fire containment
Grassland fuel models	1.09(±0.15)[a]	1.16(±0.42)[a]
Brushland fuel models	0.33(±0.09)[a]	0.61(±0.29)[b]

Mean values in a raw followed by the same letter are not significantly different ($p < 0.05$).

No significant differences in grassland fuel models were observed according to the number of firefighters (Table 7). In the case of brushland fuel models, significant differences were observed from 9 firefighters.

Table 7. Fireline production rate based on crew size.

Fire crew (firefighters)	Fireline production rate in grasslands (m/min*firefighter)	Fireline production rate in brushlands (m/min*firefighter)
< 7	1.02(±0.65)[a]	0.68(±0.47)[a]
7-9	0.77(±0.57)[a]	0.55(±0.35)[a]
> 9	0.90(±0.42)[a]	0.33(±0.26)[b]

Mean values in a column followed by the same letter are not significantly different ($p < 0.05$).

4. Discussion

Fuel models with the highest fireline production rate are those corresponding to grassland. Fireline production rate in indirect attack is lower than in direct attack regardless of fuel model. The fireline production rate estimated in this study is lower than those obtained in other Iberian studies (Chico, 2001; Chico and Poza, 2009; Jiménez, 2014). They overestimated fireline production rate values from simulated conditions or trainings while

we consider direct observations on active fires. In active fires, the working demands, thermal stress conditions and smoke inhalation are different (Rodríguez-Marroyo et al., 2011, 2012). The main differences between our findings and other studies (Chico, 2001; Chico and Poza, 2009; Jiménez, 2014) are found in chaparral and timber-litter fuel models. With regards to chaparral fuel models, the rate is almost half in our study, due to longer periods of work. The timber-litter fuel models have a higher rate due to the absence of tree cutting. Besides, as a finding of this study, it is worth highlighting the production rate increases with the support of aerial resources according to other authors (Holmes and Calkin, 2013; Florec et al., 2019).

Although some studies (Jiménez, 2014) have pointed out that slope and stoniness are important variables in fireline production rates, they have not been identified as representative variables in our research. Similarly, differences in meteorological conditions did not provide significant changes, except for wind speed above 50-60 km/h that reduces production rates. Further studies have highlighted the decline in fireline production rates under extreme fire conditions (Holmes and Calkin, 2013). Moreover, production rate decreased by 45.9% on unsuccessful containment operations. This fact seems to support the idea that productivity models must incorporate psychological variables.

The availability of a reliable dataset for estimating the productivity of fire crews expands wildfire suppression knowledge (Katuwal et al., 2016; Thompson et al., 2018). This study affords to reduce uncertainty about the productivity of suppression resources based on working conditions. As a result, efficiency in the suppression operations will improve (Thompson and Calkin, 2011; Rodríguez y Silva and González-Cabán, 2016).

Further studies should analyse and modelling the effects of aerial resources and the working time in fireline production rate. In this sense, time intervals between releases below 5 minutes greatly increase the productivity of fire crews.

5. Conclusions

Despite the difficulties in generating a fireline production rate dataset, supporting statistical analysis provides us accurate data under Mediterranean Basin conditions. Our findings show that firefighter productivity is lower under active fires than under simulated conditions or trainings. The methodological framework is very flexibility enabling an extrapolation to other territories and fire crew structures. However, more precise information of some variables, such as fuel models, slope and stoniness, is needed.

Several factors were identified as statistically significant to determinate fireline production rates. We emphasize in the idea that productivity models must incorporate working and psychological variables, such as working time, fire size and successful containment. Fire crew productivity increases with the support of aerial resources according to the time interval between releases. Direct attack increases the operational effectiveness of suppression resources. Fireline production rates provide a useful tool for fire managers to assign the right type and number of fire resources, mainly in simultaneous large fires occurrence. Fire managers could quickly predict and evaluate spatial and temporal allocation resources.

6. Acknowledgments

This research was supported by the European Union projects FirEUrisk (H2020-LC-CLA-2020-101003890), CILIFO (POCTEP-0753_CILIFO_5_E) and FIREPOCTEP (POCTEP-0756_FIREPOCTEP_6_E) and the projects VIS4FIRE (RTA2017-00042-C05-01) and ENFIRES (PID2020-116494RR-C44) of the Spanish Ministry of Science, Innovation and Universities. The authors of this study would like to express their gratitude to the engineers and firefighting crews that have contributed to provide the data used.

7. References

Anderson H.E., 1982. Aids to determining fuel models for estimating fire behavior. USDA For Serv Res Pap INT-122.

Broyles G., 2011. Fireline production rates. USDA Forest Service, Pacific. National Technology & Development Program. Fire Management Report. San Dimas, CA, 1151-1805 pp.

Chico F., Poza I., 2009. Rendimiento del personal de extinción. In: Vélez R. La defensa contra incendios forestales. Fundamentos y experiencias. McGrawHill, Madrid, 734-741.

Chico F., 2001. Métodos para la medición de rendimientos y evaluación de los medios aéreos en la extinción de incendios forestales. En: González A.J., Ribas I. (Coord.). La Gestión de los medios aéreos en la defensa contra incendios forestales. I Simposium Internacional. Universidad de Córdoba-Junta de Andalucía. Córdoba, España, 207-222.

Donovan G.H., Brown T.C., 2005. An alternative incentive structure for wildfire management on National Forest land. Forest Science 51, 387-395.

Florec V., Thompson M., Rodríguez y Silva F., 2019. Cost of suppression. In: Mazello S. (Ed.). Encyclopedia of Wildfires and Wildland-urban interface. Springer, Cham.

Holmes T., Calkin D.E., 2013. Econometric analysis of fire suppression production functions for large wildland fires. International Journal of Wildland Fire 22, 246-255.

Jiménez V., 2014. Análisis de la eficacia de la combinación de herramientas de corte en la extinción de incendios forestales. Trabajo Profesional Final de Carrera. ETSIAM. Universidad de Córdoba. Córdoba, Spain.

Katuwal H., Calkin D.E., Hand M., 2016. Production and efficiency of large wildland fire suppression effort: A stochastic frontier analysis. Journal of Environmental Management 166, 227-236.

Plucinski M.P., 2019a. Fighting flames and forging firelines: wildfire suppression effectiveness at the fire edge. Current Forestry Reports 5, 1-19.

Plucinski M.P., 2019b. Contain and control: wildfire suppression effectiveness at incidents and across landscapes. Current Forestry Reports 5, 20-40.

Rodríguez-Marroyo J.A., López-Satue J., Pernía R., Carballo B., García-López J., Foster C., Villa J.G., 2012. Physiological work demands of Spanish wildland firefighters during wildfire suppression. Int Arch Occup Environ Health 85(2), 221-228.

Rodríguez-Marroyo J.A., Villa J.G., López-Satue J., Pernía R., Carballo B., García-López J., Foster C., 2011. Physical and thermal strain of firefighters according to the firefighting tactics used to suppress wildfires. Ergonomics 54(11), 1101-1108.

Rodríguez y Silva F., O'Connor C.D., Thompson M.P., Molina J.R., Calkin D.E., 2020. Modelling suppression difficulty: current and future applications. International Journal of Wildland Fire 29(8), 739-751.

Rodríguez y Silva F., Hand M., 2018. Modeling the productivity of forest fire suppression operations using production functions: a methodological approach. In: Viegas D.X. (Coord.). Advances in Forest Fire Research. University of Coimbra. Portugal. DOI: 10.14195/978-989-26-16-506_128. Part of ISBN: 9789892616506.

Rodríguez y Silva F., 2017. Aproximación metodológica para modelización econométrica de la productividad en la extinción de incendios forestales. Actas Congreso Forestal Español. Sociedad Española de Ciencias Forestales.

Rodríguez y Silva F., González-Cabán A., 2016. Contribution of suppression difficulty and lessons learned in forecasting fire suppression operations productivity: a methodological approach. Journal of Forest Economics 25, 149-159.

Thompson M.P., Lauer C., Calkin D., Rieck J.D., Stonesifer C.S., Hand M.S., 2018. Wildfire response performance measurement: current and future directions. Fire 1, 21: doi:10.3390/fire1020021.

Thompson M.P., Calkin D., 2011. Uncertainty and risk in wildland fire management: A review. Journal of Environmental Management 92, 1895-1909.

Fire Weather Warnings in Croatia

Tomislav Kozarić*; Tomislava Hojsak; Marija Mokorić

Croatian Meteorological and Hydrological Service. Ravnice 48, Zagreb, Croatia, {tomislav.kozaric, tomislava.hojsak, marija.mokoric}@cirus.dhz.hr

**Corresponding author*

Keywords

Fire weather, risk assessment, support tool, vegetation fire, warnings

Abstract

Vegetation fires are among the most dangerous natural hazards. In Croatia, they are most common on the Adriatic coast and in the areas near the Adriatic, especially in summer when the peak of the fire season occurs. Meteorological risk of vegetation fires in Croatia is primarily assessed with the Canadian Forest Fire Weather Index and derived fire danger. However, due to the rare spatial and temporal availability of these data as well as the effects of climate change resulting in frequent enhanced fire danger during the summer, the need for additional risk assessment tool has emerged. In that sense, the fire weather warnings were introduced ten years ago and since then have been constantly improved and adapted to the needs of the firefighting community. The aim is to warn of weather conditions that can lead to the rapid spread and unpredictable behavior of the vegetation fires. As a basic condition, fire weather warnings are issued when the fire danger classes from the Canadian Forest Fire Weather Index are high and very high. Except the meteorological parameters of the Fire Weather Index, the most important of which is wind, the behavior and spread of vegetation fires can be further influenced by atmospheric turbulence and instability in the dry air near the ground and in the lower atmosphere. These parameters also depend on the orography of the terrain and are not included in the Fire Weather Index. Two years ago, three levels of warnings were defined, the thresholds of which depend on the values and duration of wind, turbulence and instability. In addition to the detailed explanation of the method for issuing fire weather warnings, the paper presents textual and graphical warning examples, describes five critical fire weather patterns when conditions for issuing warning are the most common, and in the end gives a brief overview of warnings statistics and the most recent evaluation. According to the feedback from the firefighting community, the warnings proved to be important in the organization of supervisory and preventive activities, as well as fire suppression activities in case of vegetation fire ignition. The evaluation also shows that most of the significant vegetation fires burned in the days and at the locations for which warnings were issued.

1. Introduction

Vegetation fires belong to the most dangerous natural hazards and are closely related to weather and climate. As official institution in Croatia that deals with dangerous weather and weather-related hazards, Croatian Meteorological and Hydrological Service (DHMZ) is responsible for issuing forecasts and warnings on such phenomena. DHMZ cooperates with the Civil Protection Directorate, the Ministry of Defence and the Croatian Firefighting Association - organisations participating in the protection and rescue of people and property.

In Croatia vegetation fires are most common in the warm part of the year on the Adriatic coast and in the areas near the coast with the peak of fire season in the summer months. Therefore, fire protection and related activities are conducted mostly from spring to autumn, usually from May to October. In the fire protection system DHMZ is acting as advisory body, providing specialized meteorological information to the stakeholders of the system, primarily Croatian Firefighting Association (Kozarić et al., 2015).

The assessment of meteorological risk of vegetation fires is primarily based on the Canadian Forest Fire Weather Index (FWI) system, described in Van Wagner C.E. (1987), and on the fire danger classes calculated from the FWI. The analysis and forecasts of these data are unfortunately rarely available, only once a day at 24 meteorological stations. Climatological analysis shows that since 1990s the mean temperature in Croatia has been increasing with prominent positive trend as well as the extreme meteorological events, such as long dry spells and heat waves, particularly in the Adriatic area (Gajić-Čapka et al., 2010). This climate change consequently affects Fire Weather Index which shows positive trend as well, while at the same time, the fire

danger clasess tend to exibit prolonged periods of the highest values during the peak of fire season in summer. On the other hand, FWI does not include information on wind shear or change in direction. For this reasons a need for additional risk assessment tool has emerged and led to the development of the fire weather warnings. They were introduced ten years ago and since then have been constantly improved and adapted to the needs of the firefighting community. Basically, its purpose is to warn of weather conditions that can lead to the rapid spread and unpredictable behavior of the vegetation fires.

2. Method

As a basic condition, the fire weather warnings use the fire danger classes calculated from the Forest Fire Weather Index. A definition of classes is described in Dimitrov (1987) and shown in Table 1. Fire danger classes account for the total amount of fuel available for combustion, represented as the Buildup Index (BUI), and the relevant meteorological parameters included in FWI, the most important of which is wind speed. In terms of fire danger, classes have been assigned the following values: 1-very low, 2-low, 3-moderate, 4-high, and 5-very high. FWI represents the expected intensity of the spreading fire.

Table 1 - Fire danger classes calculated by combining FWI and BUI. Color is assigned to each class.

		Fire Weather Index (FWI)				
		0-4	5-8	9-16	17-32	33+
Buildup Index (BUI)	0-48	1	2	2	3	3
	49-85	2	2	3	3	4
	86-118	2	3	3	4	4
	119-158	2	3	4	4	5
	159+	3	3	4	5	5

The spread rate and the erratic, unpredictable behavior of wildland fires can be strongly increased by the atmospheric turbulence (Heilman and Bian, 2010) and the instability in a dry air (Haines, 1988), both near the ground or in the atmospheric boundary layer. Atmospheric turbulence is most often represented by turbulent kinetic energy (TKE) and instability in dry air by the Haines Index (HI). TKE takes into account an increased influence of orography on the wind, particularly causing gustiness and shear which are not included in the FWI. The highest values of HI are generally coincident with the large burned area and increased number of forest fires which is also the case in the Adriatic region of Croatia (Kozarić and Mokorić, 2014).

Two years ago, three levels of warnings were defined, i.e., yellow, orange, and red, allowing more precise distinction between dangerous weather conditions. The thresholds for levels depend on the values and duration of the three important meteorological parameters – wind speed, TKE and HI. Typically, red warning alerts of the most dangerous fire weather conditions. The latest improvements and adaptation of the fire weather warnings done in 2021 will be explained.

The criteria for fire weather warnings are given in Table 2. Meteorological parameters and fire danger classes are placed in rows of the table. Threshold values for these are in the cells of table columns.

Table 2 - The criteria for fire weather warnings. First condition is monitored in the first row, second condition in the rows 2 to 4.

	Warning level			
	Yellow		Orange	Red
Fire danger class	Moderate	High and/or very high	High and/or very high	High and/or very high
Wind speed (ms^{-1})	>9 (5 hrs or more)	6 to 9 (5 hrs or more)	>9 (2-3 hrs or more)	>9 (18 hrs or more)
TKE (m^2s^{-2})		3 to 5 (5 hrs or more)	>5 (2-3 hrs or more)	>5 (18 hrs or more)
HI		6 (5 hrs or more)		

First condition to be monitored by the DHMZ's forecasters is the fire danger class which should be high and/or very high indicating increased dryness of the fuels. These values tend to be present in most days during peak of the fire season in the Adriatic, particularly in the south. As already mentioned, fire danger classes data are calculated at 24 locations at 12 UTC every day, either as analysis or forecast for next day. It is supposed that classes at 12 UTC represent fire danger for the whole day. Moderate fire danger class is also relevant but only in cases of particularly strong wind lasting for prolonged time.

Second condition to be monitored are the values of parameters of wind speed, TKE and HI, and a duration when exceeding the threshold values in the certain area. These data are available as model fields from numerical weather prediction (NWP) models, e.g., mostly used is in-house mesoscale model ALADIN (Tudor et al., 2016).

If values of at least one meteorological parameter, i.e., wind speed, TKE or HI, or any of their combinations meet the second condition and overlap with the first condition, the warning level is defined. For example, condition for yellow warning will be met if the fire danger class is very high and TKE in the area is from 3 to 5 m^2s^{-2} for 5 or more hours. Special maps in our workstation system have been developed to help forecasters in making these decisions. Note, Haines Index of the highest value 6, can only contribute to yellow warning. According to Croatian firefighters' feedback wind-driven fires cause major problems and the influence of instability (HI) was agreed to be reduced in the alerting process.

In accordance with the criteria, fire weather warnings are produced daily from the beginning of May to the end of October and issued to firefighting community as textual (Figure 1) and graphical product (Figure 2). Warnings are produced separately for the current day, using the analysis of fire danger classes, and for the next day using the forecasted fire danger classes as a first condition. In addition to the warning levels descriptions, a large-scale weather pattern description is included in the textual product.

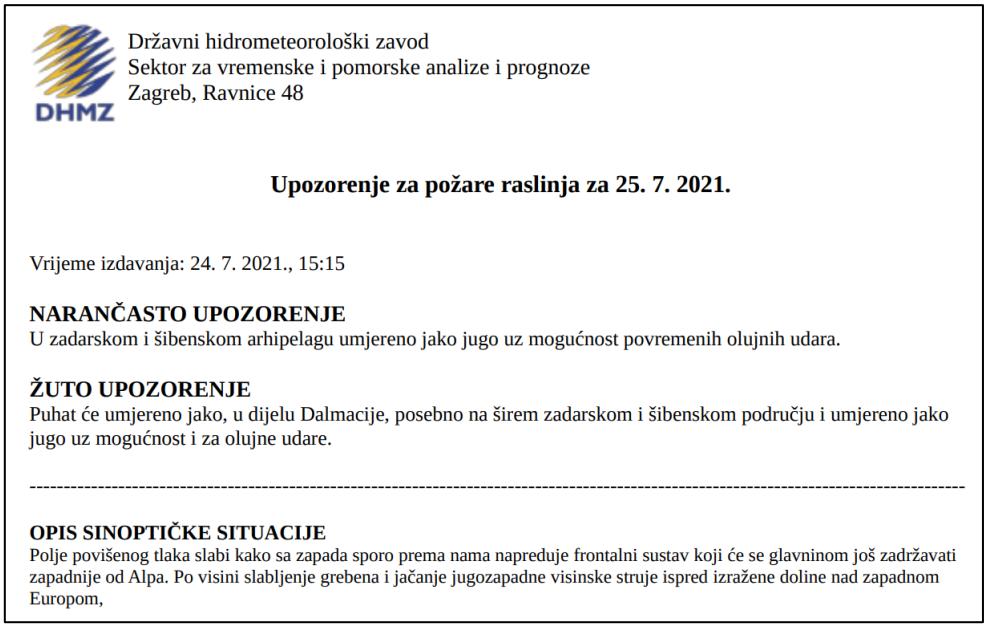

Državni hidrometeorološki zavod
Sektor za vremenske i pomorske analize i prognoze
Zagreb, Ravnice 48

Upozorenje za požare raslinja za 25. 7. 2021.

Vrijeme izdavanja: 24. 7. 2021., 15:15

NARANČASTO UPOZORENJE
U zadarskom i šibenskom arhipelagu umjereno jako jugo uz mogućnost povremenih olujnih udara.

ŽUTO UPOZORENJE
Puhat će umjereno jako, u dijelu Dalmacije, posebno na širem zadarskom i šibenskom području i umjereno jako jugo uz mogućnost i za olujne udare.

OPIS SINOPTIČKE SITUACIJE
Polje povišenog tlaka slabi kako sa zapada sporo prema nama napreduje frontalni sustav koji će se glavninom još zadržavati zapadnije od Alpa. Po visini slabljenje grebena i jačanje jugozapadne visinske struje ispred izražene doline nad zapadnom Europom,

Figure 1 - An example of the textual fire weather warning product (in Croatian). List of warnings sorted by the level is followed by the large-scale weather pattern description.

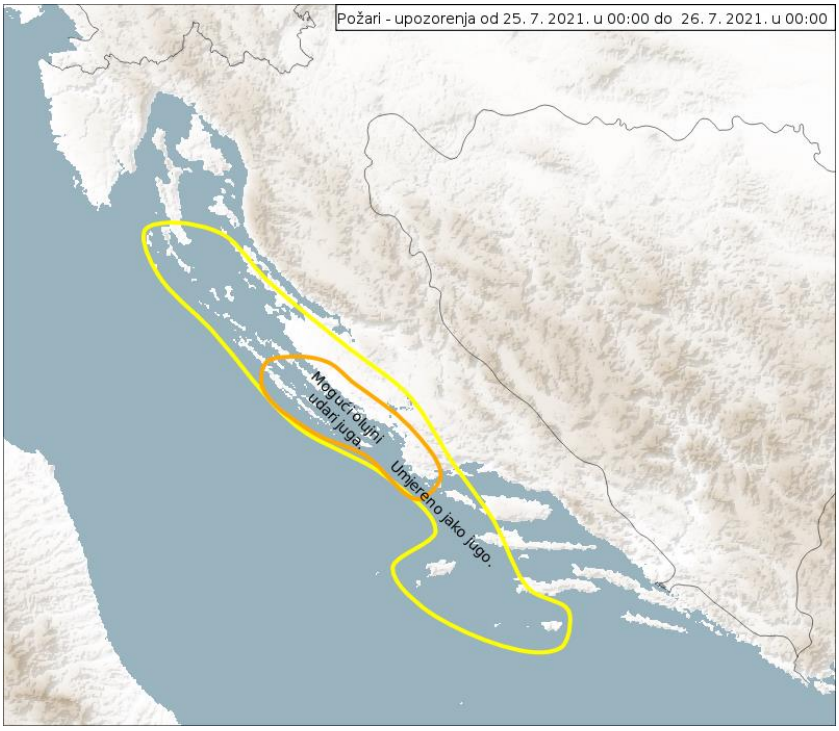

Figure 2 - An example of the graphical fire weather warning corresponding to the textual one (also in Croatian).

3. Critical fire weather patterns

This section describes five critical fire weather patterns when conditions for issuing warnings were most common. These large-scale patterns have been determined by the analysis of synoptic weather situation over Europe, both at surface and aloft, in the days when fire weather warnings were issued due to increased values of meteorological parameters (Mokorić and Hojsak, 2018).

- Pattern 1. Cold front passage followed by high pressure ridge strengthening from the North-west. Usually lasts a few days accompanied by enhanced northeasterly gusty downslope wind, called "Bura", turning to moderate to strong northwesterly wind.
- Pattern 2. Cold front passage with little or no rain ("dry" cold front) and gusty variable winds.
- Pattern 3. Situation of medium or slightly higher air pressure filed, usually non-gradient, accompanied by the instability in dry air (high values of the HI). Usually lasts for several days.
- Pattern 4. Enhanced southeasterly wind (called "Jugo") without rain, prior to approaching cold front.
- Pattern 5. The anticyclonic ridge that extends from northern Europe towards the Adriatic. Often lasts for a few days accompanied by enhanced "Bura".

There are some indications that the annual frequency of these patterns has been increasing in the last ten years, however this has to be explored more thoroughly.

4. Statistics and evaluation of fire weather warnings

Fire weather warnings in Croatia were first introduced in 2012 and since then have undergone changes in terms of improvements and adaptations. In Figure 3 an overview of warnings statistics is presented. It can be seen that in the last ten years the number of days with warnings was gradually increasing. The positive trend in the number of warning days seems to coincide with the positive trend in the fire danger, what can be addressed to the climate change. A notable jump in the last two years in the number of warning days is partly a result of the use of three-level warning method.

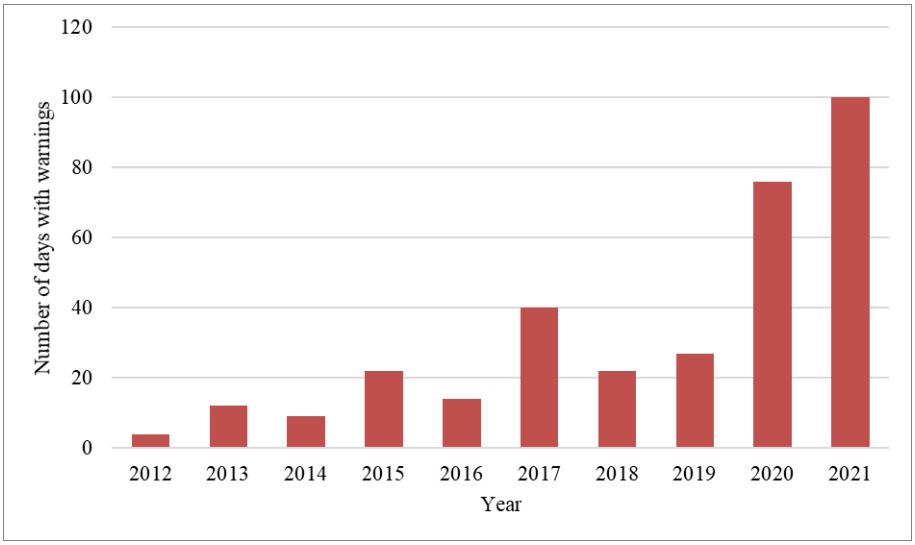

Figure 3 - The number of warning days per fire season in the period from 2012 to 2021.

In order to investigate a possible benefit of fire weather warnings, a simple evaluation was performed with the most recent data from 2021. Forty five days with the significant vegetation fires, i.e., which were hard to suppress or had large burnt area according to reports, were compared with 100 days with issued warnings during fire season. It has to be noted that every warning day is included, no matter how small the warning area was or how short it lasted. With the more strict filtering in terms of coverage and duration of fires, the number of warning days could be reduced significantly, however this was not intention. Furthermore, for the purpose of evaluation only days with the fire occurrence were considered since warnings have not been designed as an indicator of the fire ignition, rather as the indicator of possibility for rapid fire spread and unpredictable behavior. With those restrictions, for 31 out of 45 of the fire days warnings were correctly issued (Figure 4). In case of bigger fires, e.g., 100 ha or more, 7 fire days were covered by the warning and 3 were missed.

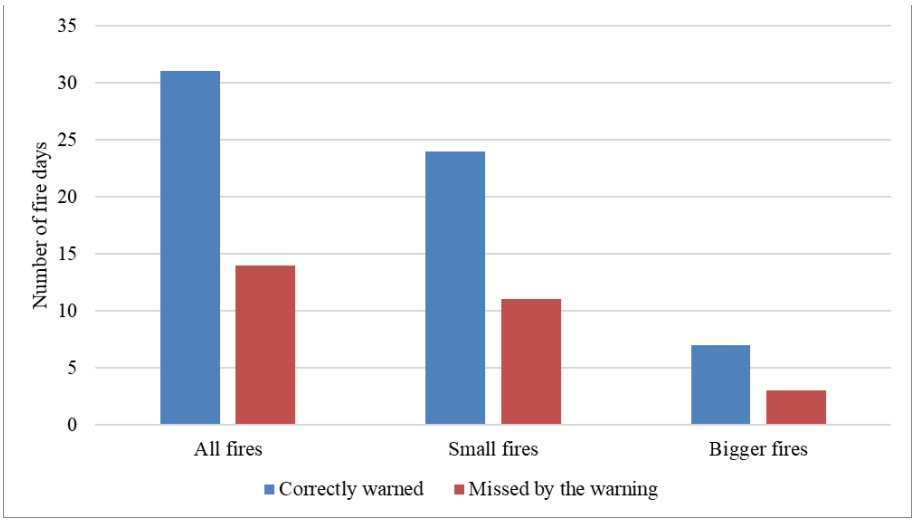

Figure 4 - A simple evaluation of fire weather warnings in the fire season 2021 in case of occurrence of vegetation fires, small and bigger ones. Correctly warned fire days are in blue, missed by the warning are in red.

5. Conclusion

Fire weather warnings in Croatia have been designed to reduce limitations of the assessment of meteorological risk of vegetation fires using only Canadian Fire Weather Index. The limitations are caused by the climate change, poor data availability and the lack of specific meteorological parameters in the FWI, i.e., turbulence and instability.

The main purpose of warnings is to alert to the weather conditions that can lead to rapid spread and unpredictable fire behavior. They are not necessarily an indicator of the fire ignition. The method for issuing is relatively simple, based on predefined criteria, improved over time, and tailored primarily to the needs of firefighting community.

Five critical fire weather patterns have been determined to cause weather conditions favorable for issuing fire weather warnings in Croatia. Most of them are related to strong and gusty wind.

The evaluation showed that most of the significant vegetation fires burned in the days and at the locations for which fire weather warnings were issued. More importantly, according to the feedback from the firefighting community, the warnings have proved to be very useful in the organization of supervisory, preventive and suppression activities.

6. References

Dimitrov T., 1987: Šumski požari i sistemi procjene opasnosti od požara, in: S. Bertović, T. Dimitrov i dr. (Eds.), Osnove zaštite šuma od požara, Centar za informacije i publicitet, Zagreb, 181-251. (in Croatian)

Gajić-Čapka M., K. Zaninović and K. Cindrić, 2010: Climate Change Impacts and Adaptation Measures – Observed Climate Change in Croatia, Fifth National Communication of the Republic of Croatia under the United Nation Framework Convention on the Climate Change, Ministry of Environmental Protection, Physical Planning and Construction, 137-151. https://unfccc.int/resource/docs/natc/hrv_nc5.pdf

Haines D.A., 1988: A lower atmosphere severity index for wildland fire, *Natl. Wea. Dig.*, **13**, 23-27

Heilman W. E. and X. Bian, 2010: Turbulent kinetic energy during wildfires in the north central and north-eastern US, *International Journal of Wildland Fire*, **19**, 346-363.

Kozarić T. and M. Mokorić, 2014: Haines Index and the forest fires in the Adriatic region of Croatia, in: D.X. Viegas (Eds.), Advances in Forest Fire Research, Imprensa da Universidade de Coimbra, Coimbra, 1175-1181. doi:10.14195/978

Kozarić T., M. Mokorić and L. Kalin, 2015: The assessment of meteorological risk for wildfires in the Adriatic region of Croatia, Proceedings of the 2nd IAFSS European Symposium of Fire Safety Science, 86-90. ISBN 978-9963-2177-0-0

Mokorić M. and T. Hojsak, 2018: Specijalne vremenske prognoze u zaštiti od požara raslinja – stručni rad, 11. Međunarodna konferencija i Zbornik radova Dani kriznog upravljanja, 455-463. (in Croatian)

Tudor M., S. Ivatek-Šahdan, A. Stanešić, K. Horvath, M. Hrastinski, I. Odak Plenković, A. Bajić and T. Kovačić, 2016: Changes in the ALADIN operational suite in Croatia in the period 2011-2015, *Hrvatski meteorološki časopis*, **50**, 71–89.

Van Wagner C.E., 1987: Development and Structure of the Canadian Forest Fire Weather Index System, Canadian Forestry Service, Forestry Technical Report 35.

From fire danger to fire risk: an integrative framework for near-term wildfire risk forecasting

W. Matt Jolly*[1], Patrick Freeborn1,

[1]US Forest Service, Rocky Mountain Research Station, Missoula Fire Sciences Laboratory, 5775 Hwy 10 W, Missoula, MT 59808, USA, {william.jolly, Patrick.h.freeborn}@usda.gov

**Corresponding author*

Keywords

Fire danger, wildfire hazard, wildfire risk, forecasting, dynamic

Abstract

Wildfires are a common global disturbance. Many of these fires fill important ecosystem roles but others must be suppressed to prevent loss of life or property. Decision support tools can provide critical information to support effective wildfire management, but the many components of these tools lack a supporting framework to integrate risk components to produce effective and useful wildfire risk forecasts. Here we present a framework to support wildfire preparedness and response decision making that incorporates both static and dynamic components of wildfire hazard to produce risk forecasting. Static model components provide a time-invariant ignition probability for both human and natural caused ignitions and are developed using topographic and fuel quantity metrics. Dynamic model components are evaluated using a combination of fire danger rating indices from the new US National Fire Danger Rating System Version 4.0 released in 2016 and the newly derived Severe Fire Danger Index. Fire danger forecasts can be normalized to percentiles using an appropriate climatology and then used to assess the dynamic, temporally varying wildfire hazard. We show that a simple model using Energy Release Component and Burning Index from the USNFDRS captures the majority of the temporally variability in wildfire occurrence (AUC = 0.823). When combined, we demonstrate the effectiveness of this model forecast system to predict the spatial and temporal locations of new wildfire ignitions across large areas using a blend of high, moderate and low-resolution spatial terrain, fuels and weather forecast data. We demonstrate various components of this framework across the United States and Northern South America specifically across Colombia, Ecuador, and Peru. This work will improve our ability to leverage modern fire danger rating systems with over conventional wildfire risk assessments to provide better decision support products throughout the world and these products have the potential to reduce wildfire impacts to firefighters and communities.

1. Introduction

Wildfires are a common global disturbance. Many of these fires fill important ecosystem roles but others must be suppressed to prevent loss of life or property. Many traditional and / or emerging tools are available to provide effective decision support for wildfire preparedness and response, but these tools are often developed in isolation without an effective framework for integrating the various components of wildfire hazard and risk together to produce meaningful and useful metrics of wildfire potential over the next several days or weeks. Such information is critical to informing resource needs or effectively pre-positioning limited fire response resources in areas of highest potential.

2. A Dynamic Wildfire Risk Forecasting Framework

Wildfire risk has been defined as the product of hazard and vulnerability. However, different types of wildfire risk assessments have never been considered in the context of a larger framework. For example, most spatial wildfire risk assessments only use static factors or scenarios to assess spatial risk and those risks can be assumed static for most purposes. However, when considering the spatial and temporal likelihoods of new wildfire ignition, some of the important factors may be static, such as accessibility from roads or navigable rivers, fuel availability, slope, aspect, elevation and other variables. Dynamic factors generally track seasonal weather severity and are best assessed using fire danger indices from systems such as the Canadian Forest Fire Danger Rating System (Stocks et al., 1989), the US National Fire Danger Rating System (Figure 1) (Jolly et al., 2019)

or other global fire danger metrics. When static and dynamic factors are combined, one can produce spatio-temporal maps of wildfire hazard.

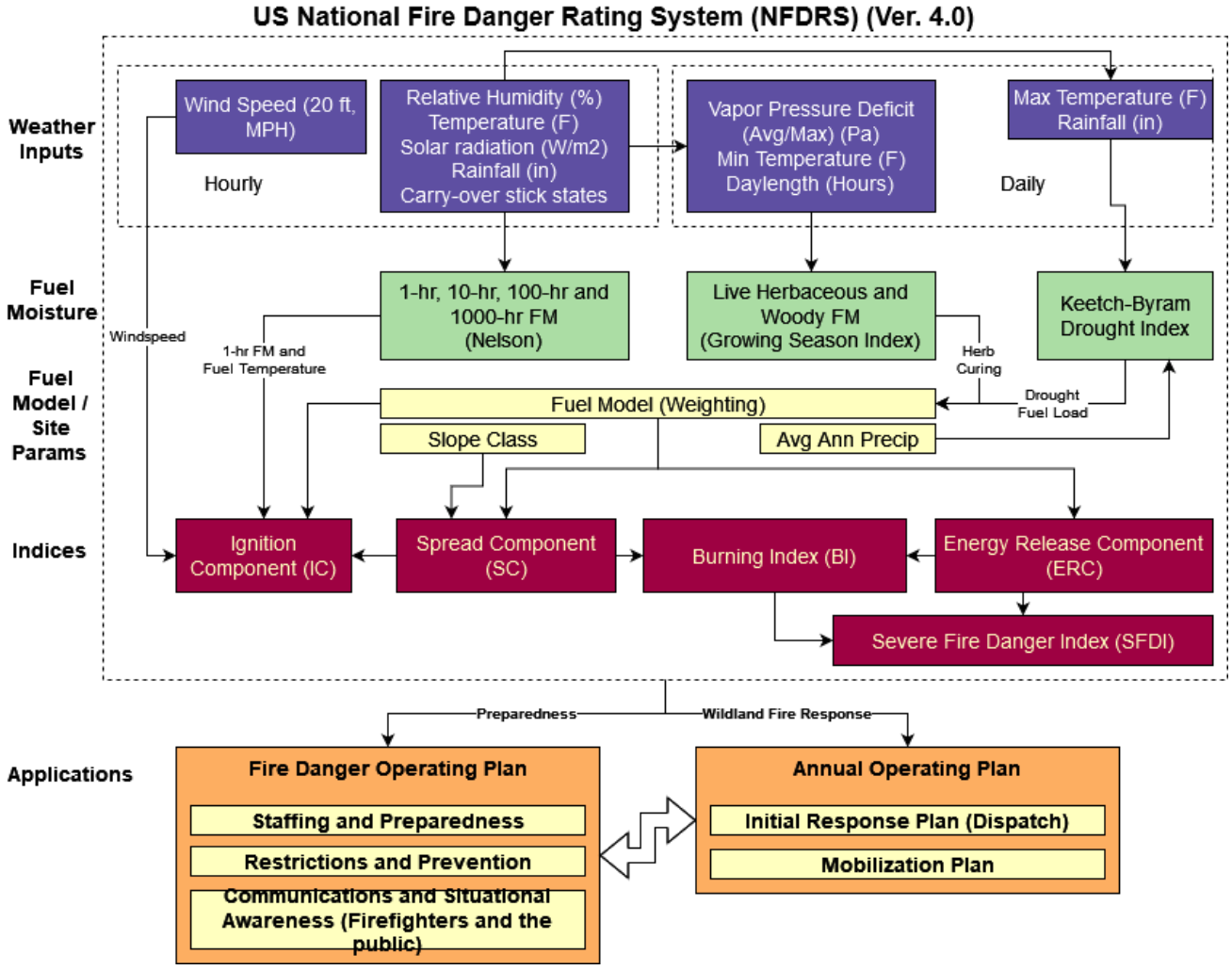

Figure 1 - The new US National Fire Danger Rating System Version 4.0 is one option for modelling and forecasting the dynamic components of wildfire risk. These forecasts can be produced for up to two weeks out.

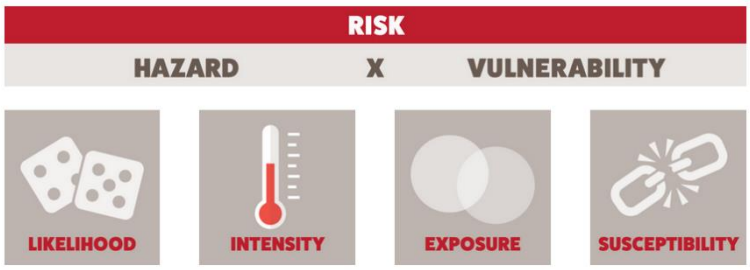

Figure 2 – Definition of Wildfire Risk from the Wildfire Risk to Communities (US Forest Service)

Vulnerability is more difficult to assess but it is generally considered the product of susceptibility and exposure but even these two components have both static and dynamic. Susceptibility is the propensity of a home or community to be damaged if a wildfire occurs and exposure is the spatial coincidence of wildfire likelihood and

intensity with communities (Wildfire Risks to Communities[4]) (Figure 2). Static vulnerability is an instantaneous measure, while dynamic vulnerability recognizes that both exposure and susceptibility can be modified over time to reduce overall risk.

To clarify linkages between static wildfire risk assessment products and dynamic components of risk that vary from day to day or week to week, we need a clearly defined conceptual model of how each piece fits together in the wildfire risk assessment spectrum. Essentially, fire danger rating is a major component of a dynamic wildfire hazard forecast but it can build on some static assessment of ignition risk. For example, terrain variables such as elevation and slope don't vary much over time except when large, geologic events occur and can thus be assumed static. Further, road networks are known to influence the spatial locations of new wildfire ignitions (Monjarás et al., 2020) but road density doesn't vary drastically from year to year except in places with extensive land-use changes.

Two separate models of wildfire hazard were developed. The first was a 'static' ignition hazard model that produces a spatial ignition probability and the second was a 'dynamic' model that include temporally variants factors from NFDRS. The static ignition model was developed separately for human and natural ignitions using slope, distance from roads, maximum NDVI and spatial locations. Fuel availability has been shown to affect fire probabilities in other studies (Briones et al., 2019). The dynamic model used Energy Release Component and Burning Index percentiles. Both models had very high AUC > 0.82. An example ROC for the dynamic model is shown in Figure 5.

The final framework is shown in Figure 6 and an example spatial assessment of dynamic wildfire hazard is shown in Figure 7. This conceptual framework can be used to better characterize the types of wildfire risk products produced for various applications. For example, typical wildfire risk mapping products are static and used for spatial planning. In contrast, fire danger assessment either in real-time or forecast are best used for characterizing dynamic wildfire hazard because they vary over time. When combined, these static and dynamic components of wildfire hazard and vulnerability form a framework that can guide how to leverage the combined components to produce effective wildfire risk forecasts that can support decision making at fine spatial and temporal scales or that can be scaled to larger areas over summarised over time to support longer-term decisions. Finally, we present an example spatial, normalized forecast for three countries in South America (Figure 8).

This framework demonstrates that a unified description of wildfire risk can be obtained when we consider the dynamic and static components of both the hazard and vulnerability. Future work will expand these assessments to the entire Continental United States, will leverage vulnerability assessments from the Wildfire Risk to Communities project across the United States and build on the forecasting system for Latin America to produce similar products and forecasts for Peru, Ecuador and Colombia.

[4] https://wildfirerisk.org/understand-risk/

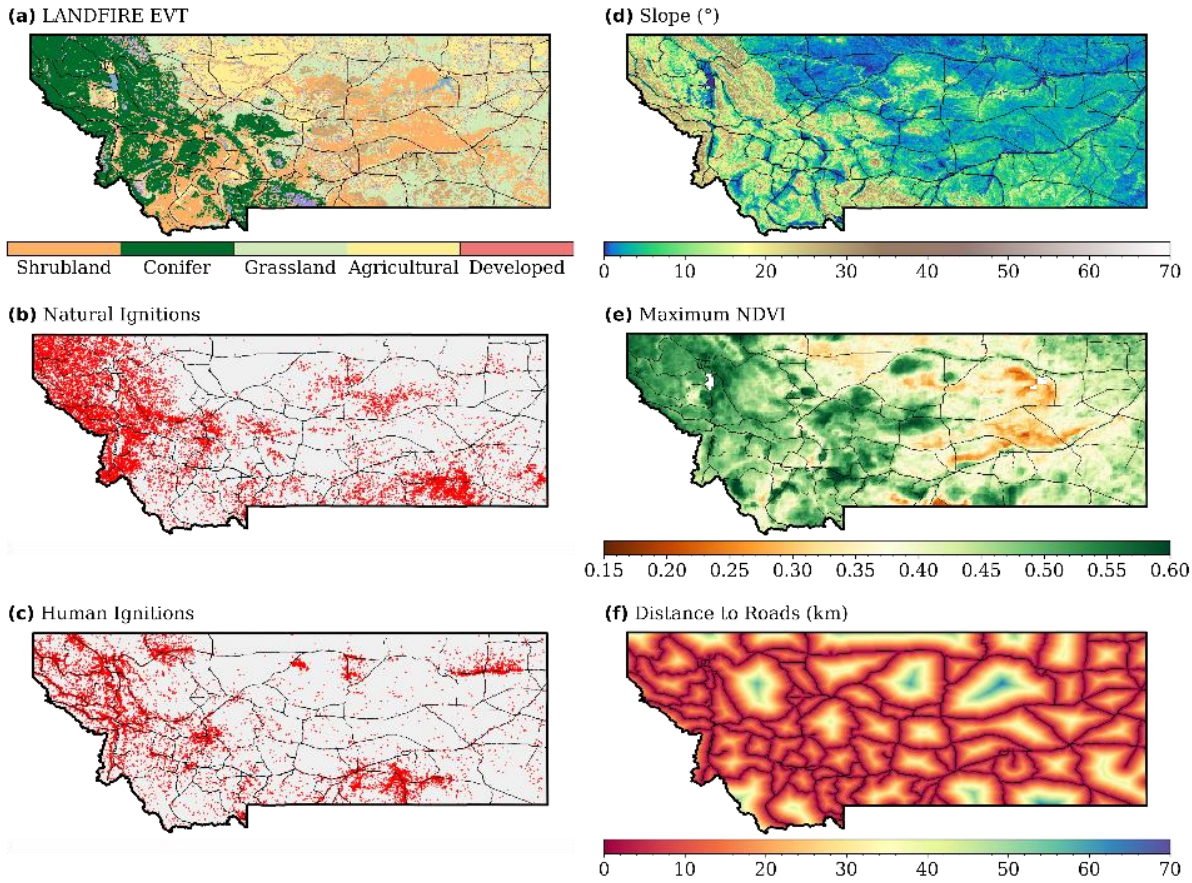

Figure 3 – Spatial inputs to a static ignition probability model. These variables are used to model the temporally invariant aspects of ignition risk.

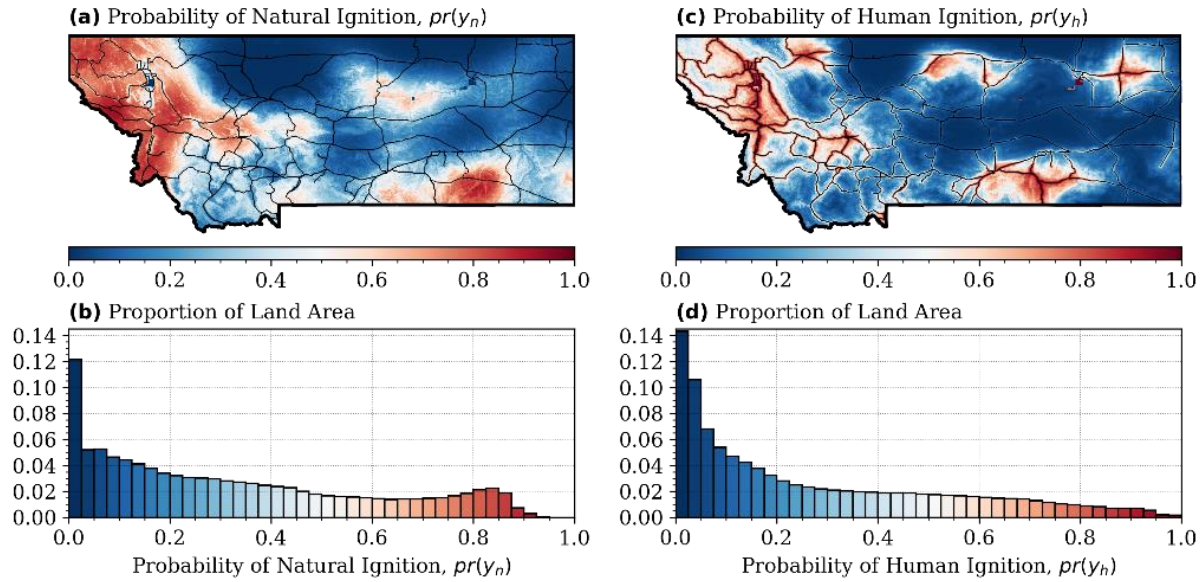

Figure 4 – Final model predicts of ignition risk at 30m resolution across Montana, USA. These maps combine distance to roads, maximum NDVI, slope and spatial location into a static predictive map of ignition risk. These maps can be combined to provide assessments

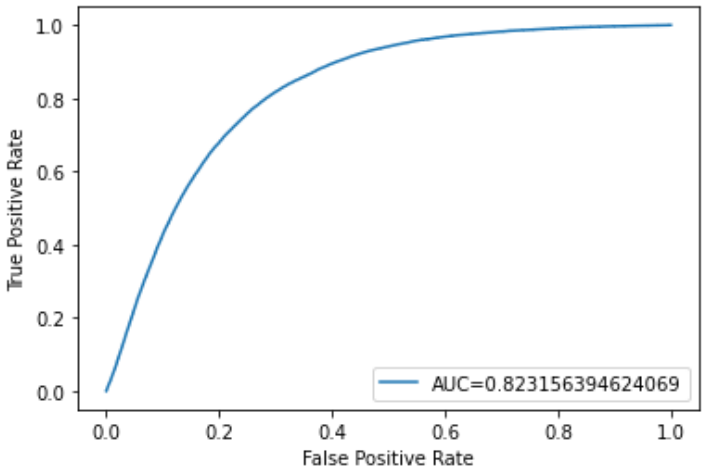

Figure 5 – ROC for dynamic wildfire hazard assessed spatially over Montana, USA. This model uses ERC and BI percentiles from the US National Fire Danger Rating System as inputs. This simple, temporal-only model is very effective at predicted the times when wildfires have historically occurred.

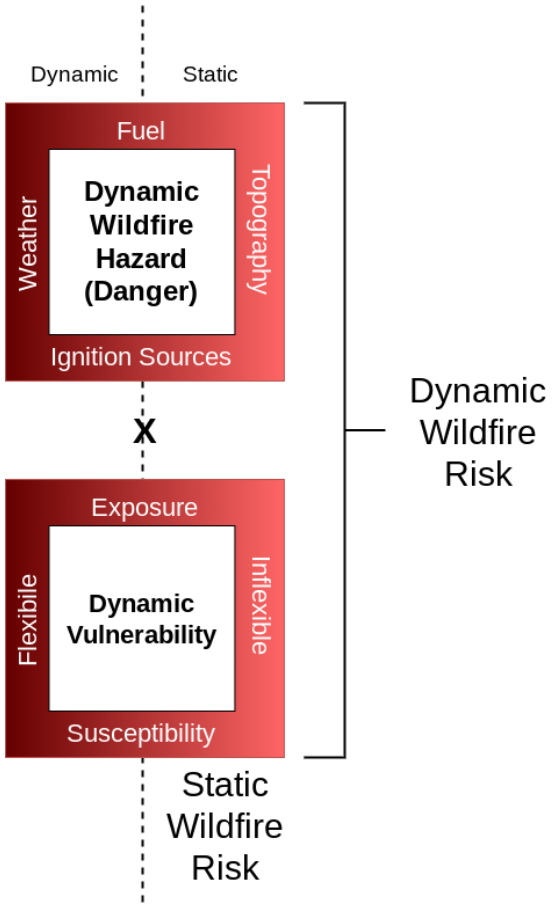

Figure 6 - The conceptual framework linking various static and dynamic wildfire hazard, vulnerability and risk components. Effective forecasts can combine both static and dynamic hazards with snapshots of vulnerability to forecast wildfire risk.

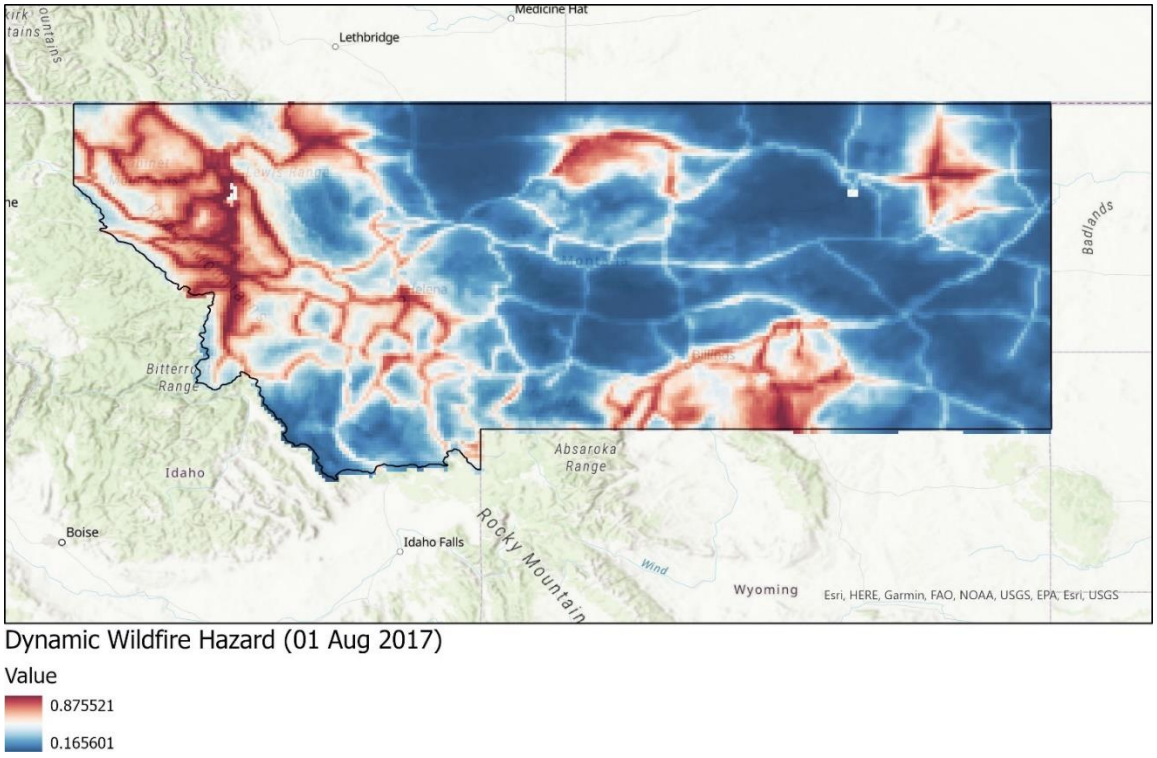

Figure 7 – Final combined dynamic fire hazard assessment for Montana by combining the static human ignition probability with the dynamic wildfire probabilities using the Energy Release Component and Burning Index percentiles from the US NFDRS.

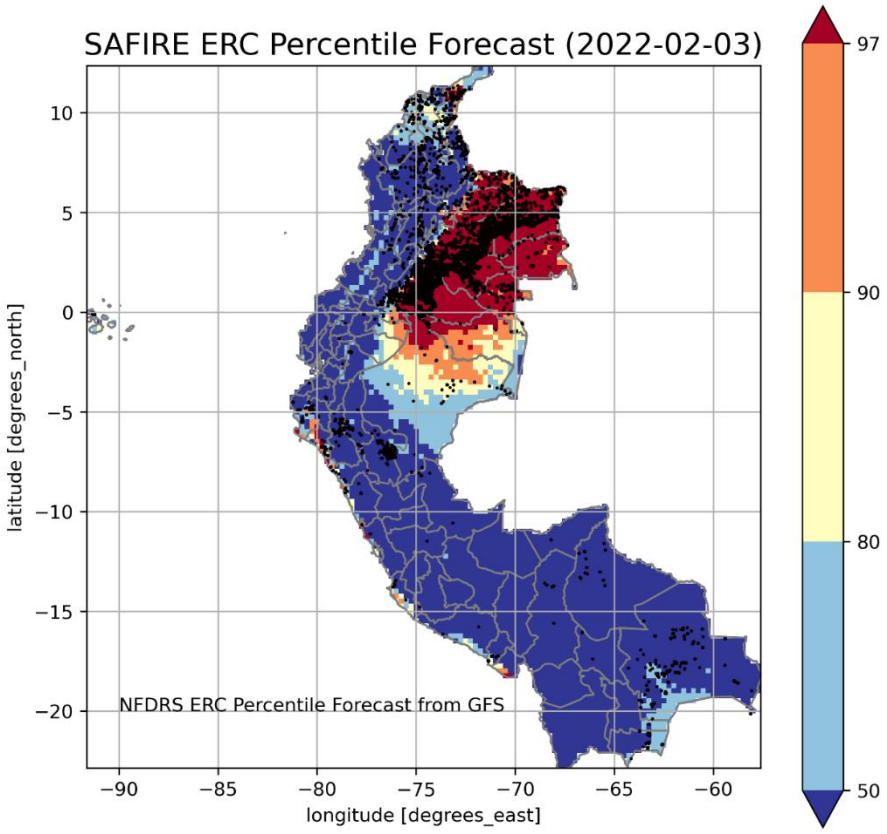

Figure 8 – An example forecast of the Energy Release Component for Peru, Ecuador and Colombia using the Global Forecast System (GFS) with a short climatology of the GFS.

3. References

Briones-Herrera, C.I., Vega-Nieva, D.J., Monjarás-Vega, N.A., Flores-Medina, F., Lopez-Serrano, P.M, Corral-Rivas, J.J., Carrillo Parra, A., Pulgarin-Gámiz, M.Á., Alvarado-Celestino, E., González-Cabán, A. 2019. Modeling and mapping forest fire occurrence from aboveground carbon density in Mexico. **Forests** 10, 402

Jolly, W.M., Freeborn, P.H., Page, W.G., and B.W. Butler. 2019. Severe Fire Danger Index: A Forecastable Metric to Inform Firefighter and Community Wildfire Risk Management. **Fire** 2. doi:10.3390/fire2030047

Monjarás-Vega, N.A., Briones-Herrera, C.I., Vega-Nieva, D.J., Calleros-Flores, E., Corral-Rivas, J.J., López-Serrano,P.M.,Pompa García, M., Rodríguez-Trejo, D.A., Carrillo-Parra, A., González-Cabán, A., Alvarado-Celestino,E., and W.M. Jolly. 2020. Predicting forest fire kernel density at multiple scales with geographically weighted regression in Mexico. **Science of the Total Environment** 87718, 137313. doi:10.1016/j.scitotenv.2020.137313.

Stocks, B. J., Lawson,B.D., Alexander, M.E, Van Wagner,C.E., McAlpine, R.S.,Lynham, T.J. and D. E. Dubé. 1989. The Canadian Forest Fire Danger Rating System: An Overview. **The Forestry Chronicle**. 65(6): 450-457.

Fuel Moisture Content in Croatian wildfire spread simulator AdriaFirePropagator

Darko Stipaničev*[1]; Marin Bugarić[1]; Nera Bakšić[2]; Darko Bakšić[2]

[1]Faculty of Electrical Engineering, Mechanical Engineering. and Naval Architecture, University of Split. R. Boškovića 32, 21000 Split, Croatia, {dstip, mbugaric}@fesb.hr
[2] Faculty of Forestry and Wood Technology, University of Zagreb. Svetošimunska cesta 23, 10000 Zagreb, Croatia {dbaksic@sumfak.hr, neramar@gmail.com}

**Corresponding author*

Keywords

Dead Fine Fuel Moisture Content, Wildfire Spread Simulation, AdriaFirePropagator

Abstract

Fuel moisture content (FMC) is the mass of water contained within vegetation in relation to the dry mass. It is one of the most important variables in all wildfire prediction and spread simulation models. FMC has great influence on wildfire ignition and combustion. For accurate wildfire spread simulations and wildfire risk index estimations, fuel moisture is a very important input variable. Since 2016, Croatian firefighters in everyday practice use Web based System for wildfire behaviour modelling and wildfire spread simulation named AdriaFirePropagator. The simulator is based on semi-empirical Rothermel's surface fire spread model for wildfire behaviour modelling and cellular automata for wildfire spread simulation. Fuel moisture, both live and dead is a very sensitive parameter in wildfire behaviour modelling. Live fuel moisture defines the moisture content of live fuels and dead fuel moisture is defined as moisture of dead fuels with time-lag of 1 hour, 10 hour and 100 hours. In Croatia there is no organised service for daily measurement of fuel moisture content, so values of these variables has to be estimated from meteorological parameters. This paper compares three approaches to fine dead fuel estimation, all implemented in AdriaFirePropagator. The first one, used in most wildfire simulation software, was based on standard mathematical models that relate air temperature, air humidity, 24-hours rainfall and wind speed with fine dead fuel moisture (FFMC). The second one was based on standard Fire Behavior Analysis Tables (FBA Tables) and the third one was based on intensive experimental research of dead fine fuel moisture content of Aleppo pine (*Pinus halepenses* Mill.). After intensive experimental research new Croatian fine dead fuel model PhFFMC was developed, tested in selected pine species stand and applied in AdriaFirePropagator for fuel regions where this pine species dominate. Croatian model is much better correlated with experimental data, therefore for more accurate wildfire simulations, similar models have to be developed also for other typical vegetation fuel types.

1. Fuel Moisture and wildfire spread simulation

Fuel moisture, both live and dead, is a very sensitive parameter in wildfire spread simulation. Live fuel moisture defines the moisture content of live fuels (Moist_live), and dead fuel moisture is usually defined as moisture of dead fuels with time-lag of 1 hour (Mois_dead_1h), 10 hour (Mois_dead_10h) and 100 hour (Mois_dead_100h). To illustrate how important fuel moisture is for wildfire simulations, in Figure 1 we show wildfire spread simulation results where all parameters are the same except live and dead fuel moisture content. The moisture content of **dead fuels** (DFMC) is controlled by fuel properties and external weather conditions: relative humidity, precipitation, temperature, and solar radiation, and the moisture content of **live fuels** (LFMC) is controlled largely by internal physiological mechanisms, so it is difficult to predict them only from meteorological parameters.

2. Determination of Fuel Moisture Content without direct measurement for AdriaFirePropagator simulations

AdriaFirePropagator is a Web base simulation tool for wildfire behaviour modelling and wildfire spread simulation. Since 2016. it is in everyday practice used by Croatian firefighters as one of modules of advanced wildfire surveillance and monitoring system named OiV Fire Detect AI (OiV (2022)).

AdriaFirePropagator is based on semi-empirical Rothermel's surface fire spread model for wildfire behaviour modelling and cellular automata for wildfire spread simulation.

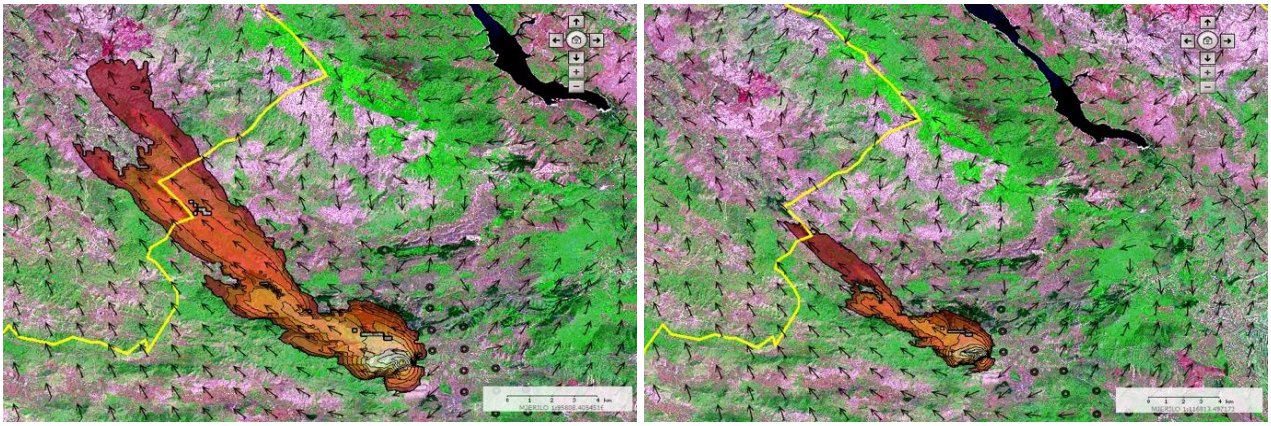

Figure 1 - Wildfire spread simulation using AdriaFirePropagator with the same input parameters except live and deal fuel moisture. In the left simulation the moisture content was 50% of the moisture content used for the right simulation).

In AdriaFirePropagator estimation of the moisture content of dead fuels is estimated by two models. The first one is based on Canadian FWI and its Fine Fuel Moisture Content (FFMC) calculation using air temperature, relative humidity, wind speed and 24-h rainfall. Van Wagner (1987) has proposed the scale equation that connect fine dead fuels moisture content m in % and FFMC:

$$m\ (\%) = 147.2\ (101 - FFMC)/(59.5+FFMC) \quad (1)$$

Formula is valid for the whole FFMC range $FFMC \in [\ 0, 100\ ]$.

Viegas also has shown in Viegas (2005) the correspondence between FFMC and fine dead fuel moisture:

$$m\ (\%) = (9*10^{9})/(FFMC^{4.54}) \quad (2)$$

but this formula is valid only for $FFMC \in [\ 65, 95\ ]$.

In AdriaFirePropagator moisture content m (%) is related to Mois_dead_1h.

Van Wagner (1987) has also proposed scales between Duff Moisture Code (DMC) and real moisture content in %, but AdriaFirePropagator moisture simulation is based on time-lag fuel moisture models corresponding to fuel particle size and not on fuel position used in Canadian FWI moisture codes, therefore here only correlation between FFMC and 1h fuel moisture was used. Other coarser dead fuel particles moisture content (Mois_dead_10h, Mois_dead_100h) is calculated by correlation models based on Scott and Burgan (2005) dead fuel moisture scenarios (very low, low, moderate and high) using simple equations:

$$Mois\_dead\_10h\ (\%) = Mois\_dead\_1 + 1 \quad (3)$$

$$Mois\_dead\_100h\ (\%) = Mois\_dead\_1 + 2 \quad (4)$$

Additionally, according to report published in Scott (2012) we have implemented weighting factors used to combine 1-, 10-, and 100-hr timelag class moisture contents into a single characteristic dead fuel moisture content for standard Scott–Burgan fuel model classes.

The second model for fine dead fuel moisture content estimation was based on standard Fire Behavior Analysis Tables (FBA Tables), published in Rothermel's (1983) guide on fire behavior prediction and implemented in BehavePluse utility named *Fine Dead Fuel Moisture Tool*. In these tables dead fuel moisture content is estimated using as input variables air temperature and relative air humidity. Tables are different for daytime and nighttime with additional corrections for season, time of day, elevation of the projection point relative to the weather observation, slope steepness class, aspect, and whether the fuelbed is shaded as reported in Scott (2012).

Meteorological data for both models are automatically collected from Croatian Meteorological and Hydrological Service server two times a day together with weather predictions calculated by ALADIN forecast model for the next 12 hours in the time resolution of 2 hours.

Moisture content of live fuels unfortunately could not be estimated from meteorological parameters. It is entirely based on field observations using approach published by Scott (2005, 2012) based on estimated by the percentage of cured leaves and introduced in simulator manually.

3. New Croatian model for dead Fine Fuel Moisture Content of two pine species typical for Croatian Adriatic vegetation

In order to improve the models for fine dead fuel moisture estimation, intensive experimental research was initiated at the Faculty of Forestry and Wood Technology, University of Zagreb (Bakšić 2017, Bakšić et al. 2017). As a case study, a typical Adriatic pine species, Aleppo pine (*Pinus halepensis* Mill.) was selected. Equilibrium moisture content (EMC) and response time of dead Aleppo pine needles were determined in the laboratory. These species-specific values were used to modify the Canadian hourly FFMC model. Thus, the basic modifications were changes in the EMC equations and changes in the response time equations of the hourly FFMC model. The input variables were hourly weather data: temperature, relative humidity, and wind speed. At this stage of model development, precipitation phase was not considered, so in case of precipitation the original equation from hourly FFMC should be used. A detailed explanation of the materials and methods as well as the final equations of the new model named PhFFMC (*Pinus halepensis* FFMC) can be found in Bakšić et al. (2017).

For model validation, intensive destructive sampling for moisture content determination was conducted in a mature Aleppo pine forest on Lastovo Island in July 2013. During sampling, a portable weather station was installed in the study site. Figure 2 shows the model validation results: the estimated moisture content for both the hourly FFMC model and the Croatian PhFFMC model compared to the actual observed moisture content.

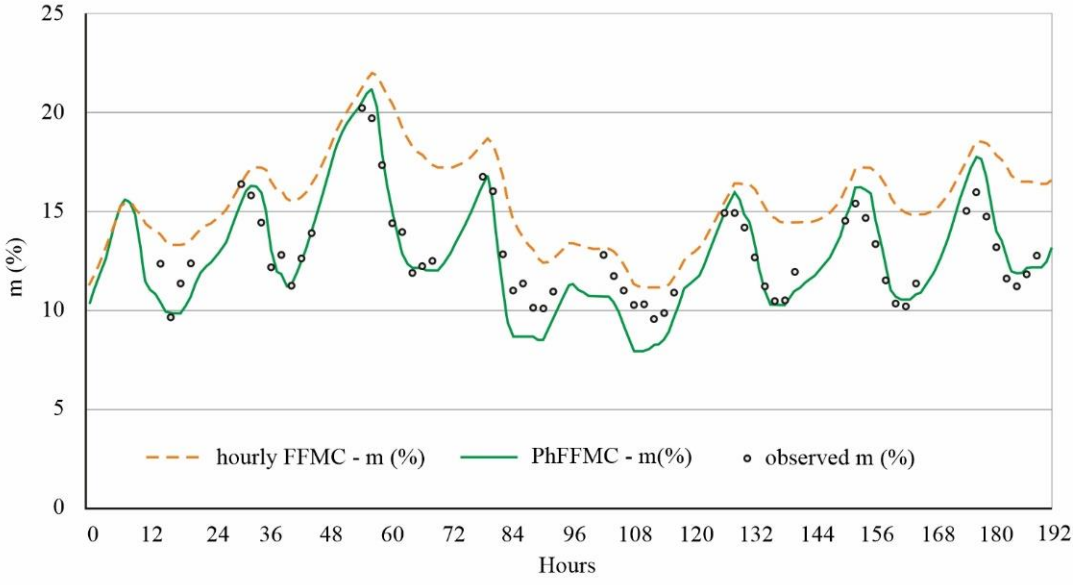

Figure 2 - Estimated moisture content (m) from hourly FFMC and Croatian PhFFMC models compared to actual moisture content (m) (Bakšić 2017).

Model validation results showed that the hourly FFMC model continuously overestimated the moisture content of Aleppo pine needles. Aleppo pine needles lose and gain moisture faster than the hourly FFMC model suggests. This is particularly evident when the actual moisture content reaches a minimum value, as this is when the largest average deviation from the hourly FFMC model occurs. On the other hand, the PhFFMC model follows the moisture content of Aleppo pine needles more closely throughout the period and reduces the mean absolute error in predicting moisture content to only 1%.

4. Comparation of various dead fuel models in AdriaFirePropagator simulator

Croatian model for dead fine fuel moisture content was implemented in AdriaFirePropagator and compared with other standard fuel moisture models based on Van Wagner equation and FBA tables. For testing purposes, we have used the large fire that occurred on the island Lastovo at 0:30 on Sept 4, 2003 and lasted almost 8 days. This fire was very well documented, so we were able to reconstruct its development. Figure 3 shows one of fire images taken by firefighters and ignition point location.

Figure 3 – Lastovo wildfire that has started on Sept 4, 2003 and lasted almost 8 days (left). Ignition point (right).

The weather conditions at the time of fire ignition were: Temperature T = 19.4 ^{0}C (66.92 ^{0}F), Atmospheric pressure at sea level SLP = 1024.7 hPa, Relative Humidity H = 29 %, Total Rainfall PP = 0 mm, Wind Speed W = 27 km/h, Wind Direction WD = 75^0 ('bura' wind). In simulations we have used Albini-Anderson vegetation categories. In its initial stage, fire propagated through vegetation class *"Long Needles and Hardwood Litter"*. Simulation was satisfactory regarding shape, but unfortunately not regarding time as Figure 4 shows. The fire front reaches real fire front in 360 min instead of 150 min. Therefore, we have changed fuel parameters to better fit the real fire spread. The difference was in fuel load and fuel bed depth, that has to be increased.

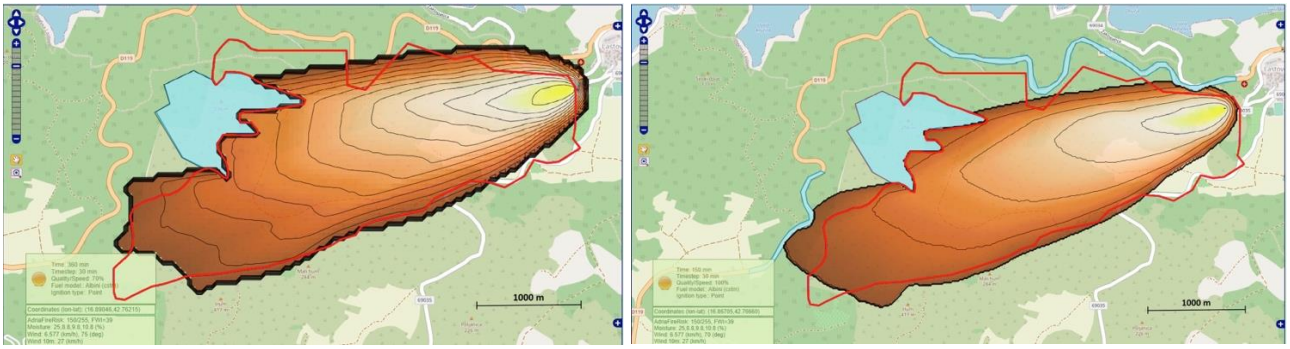

Figure 4 – With original Albini-Anderson fuel model parameters the fire front reaches real fire front (red line) in 360 min (left) instead of real 150 min. After fuel parameters adaptation satisfactory simulation was obtained (right).

Our next step was comparison of various dead fine fuel moisture content models. Live fuel moisture in all simulations was estimated to 80%. Three model for fine dead fuel moisture were compared:

a) Moisture model based on Canadian Fine Fuel Moisture Content (FFMC) calculation: Moisture 1h: 9.6; Moisture 10h: 10.6; Moisture 100h: 11.6 (same for the whole simulation)
b) Croatian model based on PhFFMC (Dominant vegetation on Lastovo island is Aleppo pine): Moisture 1h: 8.8; Moisture 10h: 9.8, Moisture 100h: 10.8 (same for the whole simulation)
c) Moisture model based on standard Fire Behavior Analysis Tables (FBA Tables): Moisture 1h: 6; Moisture 10h: 7; Moisture 100h: 8 (same for the whole simulation)

Figure 6 shows AdriaFirePropagator simulations for various moisture content models in comparison with real fire front recorded by firefighter commander Miloslavić (2003).The red line represents the real fire front.

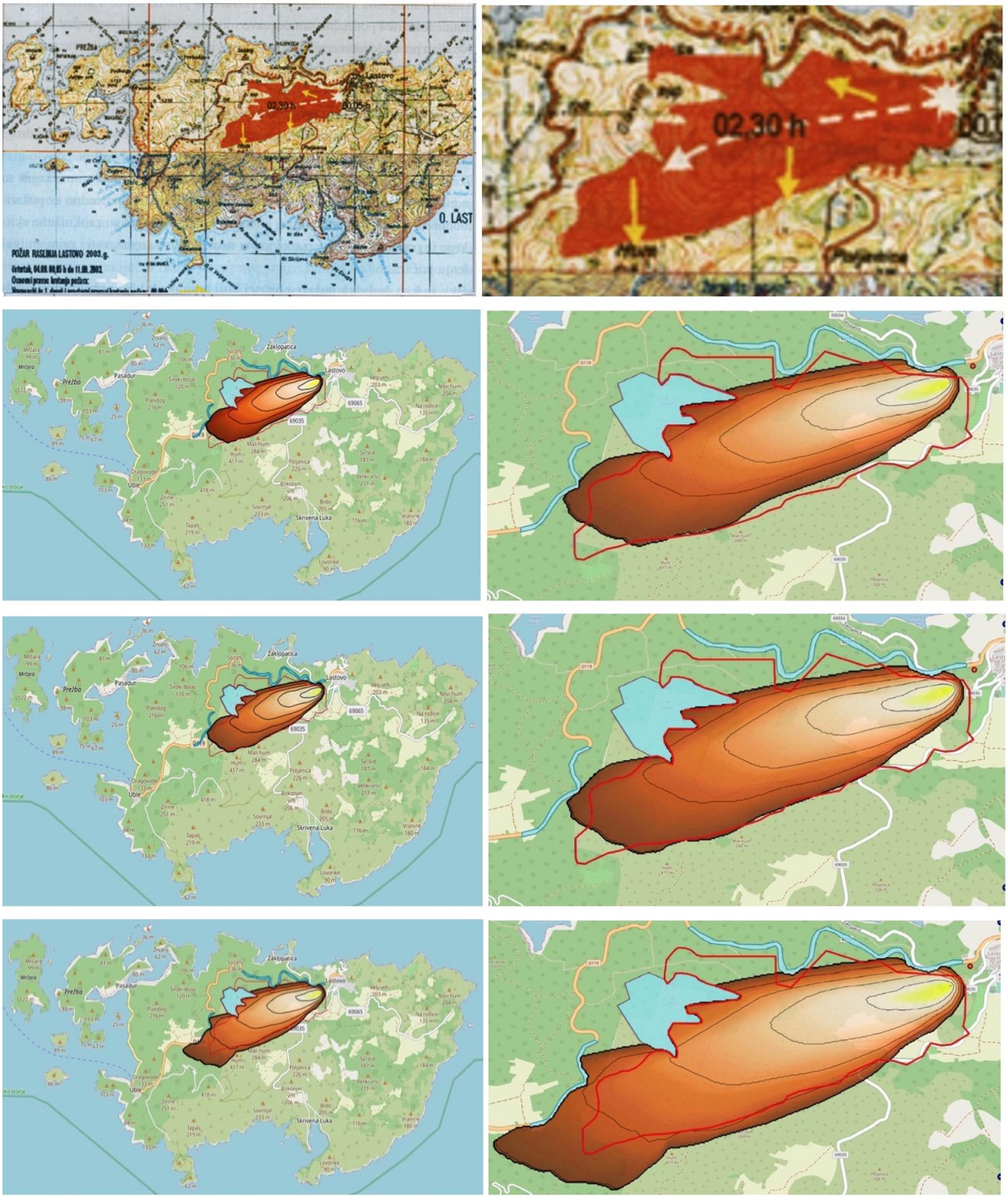

Figure 6 – Comparison of real fire front (1st row and red line on simulations) and AdriaFirePropagator simulations for various moisture models: 2nd raw – Canadian FFMC, 3rd raw– Croatian PhFFMC model, 4th raw – FBA Tables.

Table 1 summarise obtained results and shows precision, recall, F1 score and Intersection over Union (IoU).

Table 1 – Statistical comparison of simulation results from Figure 6 for various moisture models

	Precision	Recall	F1 score	IoU
Canadian FFMC	**0,93811805**	0,79243403	0,854375306	0,753069534
Croatian	0,929727814	0,827800566	**0,880604881**	**0,779056441**
FBA tables	0,742912923	**0,878384288**	0,804988789	0,673624466

Simulation based on Croatian PhFFMC model gave the best result in cumulative measures, because simulated fire front for this model was the closest to the actual fire front. FFMC based model gives the biggest moisture content, therefore the simulated fire front is smaller than the actual fire front. The situation is opposite for FBA tables model: the moisture content is the smallest and the simulated fire front is bigger than the actual one.

5. Conclusion

AdriaFirePropagator is a wildfire simulation software used in everyday practice by Croatian firefighters as a part of the advanced wildfire surveillance and monitoring system named OiV Fire Detect AI. Fuel moisture, both live and dead is a very sensitive parameter in wildfire spread simulations. Paper compares three different models for dead fuel moisture estimation: model based on Canadian FFMC, model based on Fire Behavior Analysis Tables (FBA Tables) and a new Croatian model based on intensive experimental and field research for fine dead fuel model for Aleppo pine PhFFMC. A well-documented 2003 Lastovo fire was used as a case study. From aforementioned models, the Croatian PhFFMC model has shown the best fit with real fire front, therefore our suggestion is that similar models should be made for all other vegetation categories characteristic for Adriatic region. The authors of PhFFMC model also have developed the similar model for Dalmatian black pine (*Pinus nigra* (Arnold) subsp. *dalmatica* (Vis.) Franco)) named PnFFMC (Bakšić 2017, Bakšić & Bakšić 2022). We hope that similar models will be develop for all other typical Adriatic vegetations. Also, we have shown that the original parameters of Albini-Anderson vegetation models do not give good results, especially in relation to the time component of fire spread, therefore we had to adjust them to match the actual fire spread. We hope that new vegetation models proposed through FirEUrisk project will resolve this problem.

6. Acknowledgements

This project has received funding from the European Union's Horizon 2020 research and innovation programme under grant agreement No 101003890.

7. References

Bakšić, N. (2017) Moisture of dead forest fuel as a factor of influencing forest fire occurrence, PhD Thesis, Faculty of Forestry, University of Zagreb

Bakšić, N.; Bakšić, D.; Jazbec, A. (2017) Hourly fine fuel moisture model for Pinus halepensis (Mill.) litter, *Agricultural and forest meteorology*, 243, 93-99

Bakšić, N; Bakšić, D. (2022) Predicting the fine fuel moisture content in Dalmatian black pine needle litter. International Journal of Wildland Fire, https://doi.org/10.1071/WF21092

Miloslavić, M. (2003) Wildfire on Lastovo island 2003, Vatrogasni vjesnik, 10/2003, 9–14 (in Croatian)

OiV (2022). *OiV Fire Detect AI* - https://oiv.hr/hr/usluge-i-platforme/brosure/usluge/oiv-fire-detect-ai/

Rothermel, R. C. (1983) How to predict the spread and intensity of forest and range fires. *Gen. Tech. Rep. INT-143. Ogden, UT: U.S. Department of Agriculture, Forest Service*, Intermountain Forest and Range Exp. Station

Scott, J. H.; Burgan, R. E. (2005) Standard fire behavior fuel models: a comprehensive set for use with Rothermel's surface fire spread model, *Gen. Tech. Rep. RMRS-GTR-153.* U.S. Department of Agriculture, 72p

Scott, J. H. (2012) Introduction to Wildfire Behavior Modeling, *National Interagency Fuels, Fire & Vegetation Technology Transfer* - http://pyrologix.com/wp-content/uploads/2014/04/Scott_20121.pdf

Van Wagner, C.E., (1977). A Method of Computing Fine Fuel Moisture Content Throughout the Diurnal Cycle. Information Report PS-X-69. Canadian Forestry Service, Chalk River, Ontario, Canada.

Van Wagner, C.E. (1987). Development and Structure of the Canadian Forest Fire Weather Index System. *Technical Report No. 35. Canadian Forestry Service*, Chalk River, Ontario, Canada.

Viegas D.X. (2005) Forest Fire Meteorology Reaearch and Application, *Presentation at WWRP Wildfire Workshop*, Melburn, Australia, 6-10 June 2005 - http://www.powershow.com/view1/1c2a52-ZDc1Z/Forest_Fire_Meteorology_Research_and_Application_powerpoint_ppt_presentation

Fuelbreaks design: from CFD modelling to operational tools

Nicolas Frangieh[1] , Gilbert Accary[2] , Jean-Louis Rossi[1] , Dominique Morvan*[3] , François-Joseph Chatelon[1], Thierry Marcelli[1], Sofiane Meradji[4] , Lucile Rossi[1], Carmen Awad[1], Jacky Fayad[1], Patrice Briot[5]

[1] UMR CNRS SPE 6134 Université de Corse, Corte, France, {frangieh_n, rossi_j, chatelon_j, marcelli_t, rossi_l, awad_c, fayad_j}@univ-corse.fr
[2]Scientific Research Center in engineering Lebanese University, Beirut, Lebanon, {gaccary@ul.edu.lb}
[3]Aix-Marseille Univ., CNRS, Centrale Marseille, M2P2, Marseille, France {dominique.morvan@univ-amu.fr}
[4] IMATH Laboratory, EA 2134, Université de Toulon, Toulon, France, {sofiane.meradji@univ-tln.fr}
[5] Service Régional DFCI, Hôtel de Région, Ajaccio, France, {patrice.briot@isula.corsica}

**Corresponding author*

Keywords

Wildfire modelling, Fuelbreak, Fire Safety Engineering

Abstract

Dimensioning a fuelbreak remains always a challenging problem. For a long time, this problem was tackled using an empirical approach from the experience of operational users such as the fire fighters and the foresters. During the last decades, new approaches coming from fire safety engineering have completed the set of tools adapted to study this problem. These tools are all based on physical considerations, more or- less sophisticated. The simplest ones, consist in assimilating the flame as a radiant panel, calculating the distribution of radiant heat flux as a function of the distance separating the flame to a potential target and defining at what distance this heat flux reached a critical threshold level susceptible to produce damages on this target (pain for people or ignition for materials). The most complex ones, consist in solving the conservation equations (mass, momentum, energy ...) governing the behaviour of complex coupled problem formed by the vegetation, the flame front and the surrounding atmosphere. This new generation of engineering tool, based on CFD approach allows to directly predict the behaviour of a fire front propagating toward a fuelbreak, in order to evaluate its efficiency as a function of the amount of surface fuel (grass, shrubs) removed to reduce locally the fuel load and therefore the intensity of an incoming fire. These two approaches are fully complementary, only the first one has the potentiality to be spread operationally on the field, whereas the second one can contribute to improve the first one and to study with more detail some very sensitive situations such as those encountered in the wildland urban interface (WUI). The main part of this study concerns numerical simulations of the propagation of a fire front through a homogeneous vegetation layer (a grassland) in the vicinity of a fuelbreak represented by a band more or less wide inside which all the fuel was removed. The simulations were performed using a fully physical wildfire model (FIRESTAR3D), three variable parameters were considered in this study: the 1m open wind speed (U1 ranged between 3 and 10 m/s), the fuel height (HFuel ranged between 0.25 and 1m) and the fuelbreak width (LFB). With these conditions, the simulations covered a large range of values of the Byram's convective number NC ($0.3 < NC < 60$) in order to explore wind as well driven fires ($NC < 2$) and plume dominated fires ($NC > 10$). The 72 simulations carried out in this study have been classified in three categories: 1/ Propagation (if the fire has crossed the fuelbreak with a propagation after); 2/ Overshooting or Marginal (if the fire has crossed the fuelbreak without a propagation after); 3/ No-propagation (if the fuelbreak has stopped the fire). The main objective of this study was to determine the optimal fuelbreak width LFBx separating between the Propagation and the No-propagation regimes, in order to generalize the conclusion, the results have been presented in dimensionless form (similitude theory) in representing as an example the ratio LFBx/HFuel versus the Byram's convective number NC.

1. Introduction and numerical configuration

Most of criteria used to design the optimal width of a fuelbreak are based on the assumption that the ignition of the fuel located beyond the fuel break will be due to radiation heat transfer. One of the first formula proposed by Emmons (1964) assumed that the ignition of the solid fuel located ahead of the fire front was initiated from the foot of the fire (1D vision), conducting to an expression including the extinction length scale characterizing the solid fuel layer and the depth of the fire front. Whereas other ones included the role played by the flame inside and above the vegetation layer (2D vision), proposed criteria based on the geometry (length or height) of

the flame (Rossi & al, 2011; Butler & Cohen, 1998). We propose with this work to explore this problem with more details and without a priori ideas, using numerical simulations based on a fully physical approach, with the objective to study both the influence of heat transfers coming from radiation and convection upon the effectiveness of a fuelbreak built in an homogeneous grassland. The spotting phenomena, which can play also a great role for this problem, was not taken into account in this study.

A set of 72 numerical simulations of the propagation of a quasi-infinite fire front has been carried out in a grassland inside which a x-meter width (L_{FB}) fuelbreak has been positioned. Outside the fuelbreak the vegetation layer was constituted as follows: a dry grass (FMC = 5%) with a fuel load ranged between 0.25 and 1 kg/m^2. In order to reproduce a quasi-infinite fire front (to avoid some effects, such as the curvature of the fire front resulting from finite ignition line), periodic boundary conditions have been imposed on the lateral sides of the domain (see Figure 1) (Frangieh & al, 2021). As indicating in the abstract, a quite large set of conditions (wind, fuel height) has been tested to cover the two regimes of propagation identified in the literature, namely the wind-driven fires and the plume-dominated fires. As suggested in many previous studies, the transition between these two regimes of propagation can be defined from the Byram's convective number N_C representing the power ratio between the buoyancy (plume) and the inertia (wind) forces (see Eq.1): $N_C < 2$ for wind-driven fires and $N_C > 10$ for plume-dominated fires (Morvan, 2014).

$$N_C = \frac{2\ g\ I}{\rho\ C_P T_0 (U_{10} - ROS)^3} \quad (Eq.1)$$

Where g and I represent respectively the acceleration of gravitation and the fireline intensity, ρ, C_P and T_0 the density, the specific heat and the temperature of the ambient air, U_{10} and ROS the 10m open wind velocity and the fire rate of spread.

The numerical simulations have been performed using a multiphase formulation, consisting in solving the balance equations (mass, momentum, energy …) governing the evolution of the coupled system formed by the vegetation and the surrounding atmospheric layer. The main advantage of this approach is its ability in reproducing main physical phenomena, such as the thermal decomposition of the vegetation, the mass and heat transfer between the vegetation and the atmosphere, the combustion process both in the gas phase (the flame) and in the solid phase (embers), the radiation heat transfer, the atmospheric turbulence, and the interactions (drag effect) with the vegetation and so on … To achieve these objectives a relative fine grid must be used for the representation of the computational domain. As shown in previous studies, the size of the grid must respect some criteria in order to represent correctly the radiative heat transfer between the flame and the vegetation (at least the grid size must be smaller than the extinction length scale characterizing the vegetation layer). But this level of details needs also to pay a high price in terms of computational resources and to collect numerous data on the field to describe the structure and the state of the fuel. For these reasons, this kind of formulation is presently limited to describe a fire front at a relatively small scale (< 1 km), however sufficient in many fire safety engineering problems, such as the present one, the evaluation of the effectiveness of fire breaks (Frangieh & al, 2021; Morvan, 2015), or others more fundamental problems associated to wildfires physics (Morvan, 2014, 2013; Frangieh & al, 2020).

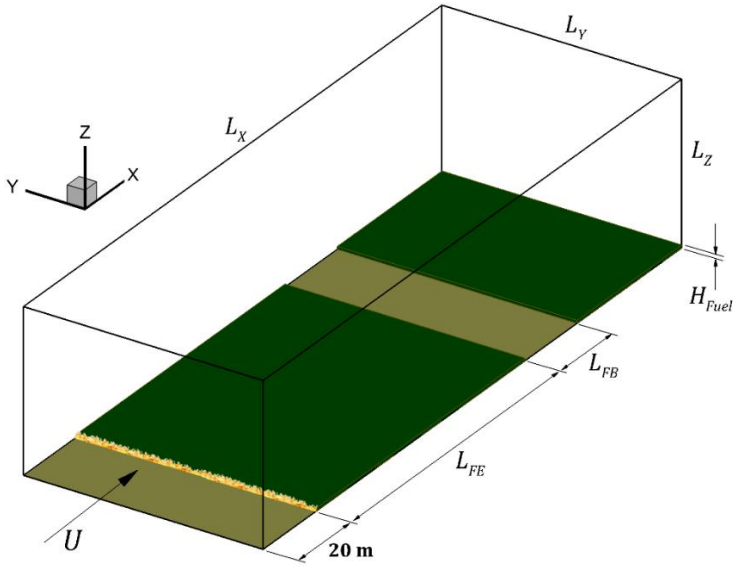

Figure 1- Numerical configuration: L_{FB} fuelbreak width .

2. Some numerical results

After analysis, the set of numerical results was classified in three categories: 1/ Propagation; 2/ Overshooting or Marginal; 3/ No-propagation. The first and the last ones are easily understanding, they correspond respectively to the cases for which the fire front was able to propagate (1) or was stopped (3) beyond the fuelbreak. The middle case (2) includes two sub-cases: Overshooting (2.a) for which some pocket ignition was observed beyond the fuelbreak followed by a propagation along a short distance and an extinction; Marginal (2.b) very similar to Overshooting, the fire behaviour switch to No-propagation if the fuelbreak width increased by 1 m. A 3D view of a fire front crossing a 6.5 m wide fuelbreak is shown in Fig.2. This representation illustrates how a fire front was able to cross such fire prevention device. As the fire front reached the border of the fuelbreak, the fuel located on the opposite side is ignited punctually (see Fig.2), forming a set of burning pockets. Then these punctual fires merged in forming a continuous fire front which can then propagate again through the solid fuel layer. In comparison the Overshooting situation was observed when the ignition points were too distant to be able to merge and to sustain a continuous propagation of the fire (Frangieh & al, 2021).

The yellow surface represents the isovalue surface (T = 1000 K in the gas phase), therefore this zone includes both the flaming zone and the smoldering zone. It is for this reason that it seems so wide.

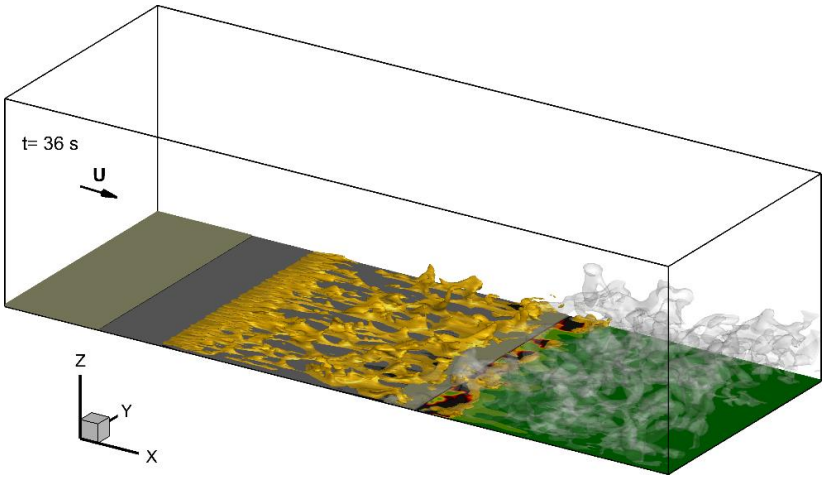

Figure 2- 3D visualization of grassland fire obtained for U_1 =8 m s^{-1} and W = 0.35 kg m^{-2} (Nc = 1.95) as it crosses a 6.5-m wide fuelbreak. The yellow surface is the isovalue surface T = 1000 K of the gas temperature and the semi-transparent grey surface is the isovalue surface $Y_{H2O} = 10^{-3}$ of the mass fraction of water vapor.

The ratio between the critical fuel break width with the fuel height (L_{FBx}/H_{Fuel}) versus the Byram's convective number N_C is reported in Fig.3. This curve shows clearly the role played by the regime of propagation. The range of variation of the ratio L_{FBx}/H_{Fuel} seemed to be particularly important for wind-driven fires ($N_C < 2$), between 30 and 80 (for the present cases), whereas the same parameter varied between 25 and 10 for plume-dominated fires ($N_C > 10$). This effect can be attributed to the mechanisms of heat transfer between the flame and the fuel located beyond the fuel break: for plume-dominated fires the fuel is exclusively heated by radiation whereas for wind-driven fires heat transfer by convection and sometimes by flame contact (the flame can be significantly tilted by the wind flow) plays an increasing role (Emmons, 1964; Butler & Cohen, 1998). These results highlight that the optimal design of a fuel break cannot be only reduced to a constant ratio between the fuel break width and the upwind fuel depth (and therefore the fuel load), this ratio must necessarily depend on the wind flow conditions and also of the slope (not study in this work). However, in looking the worst case (wind driven fire with $N_C << 1$), a ratio LFBx / HFuel nearly equal to 100 (see Fig.3) seems to be quite secure to avoid a crossing of an incident fire front.

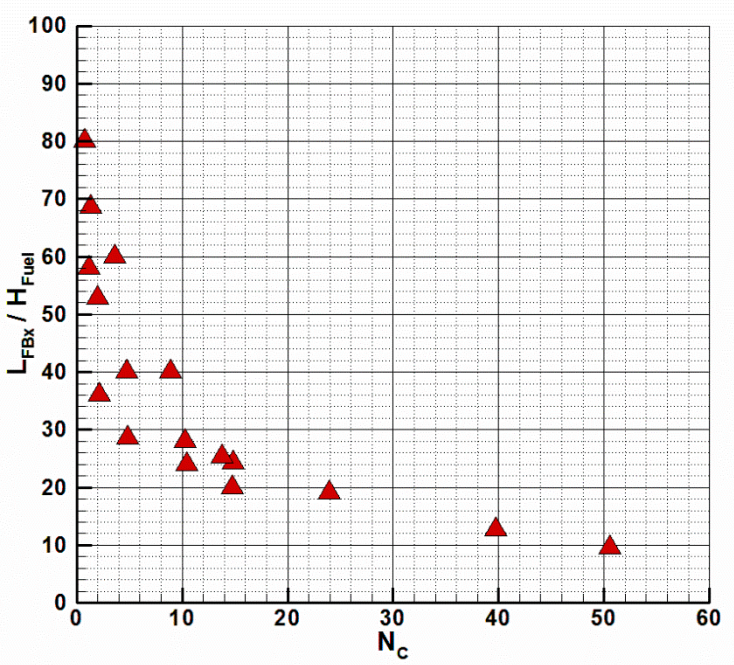

Figure 3- Optimal fuelbreak width L_{FBx} (lower limit of extinction) scaled by the fuel height H_{Fuel} versus Byram's convective number N_C (Frangieh & al, 2021).

The results obtained at various fireline intensity in the present study, have been also confronted to those predicted with a more operational tool (DIMZAL), based on a simplified physical analysis (mainly the radiant panel theory) (Rossi & al, 2011; Bisganbiglia & al, 2017). This comparison has allowed to highlight some agreements but also some differences between the two set of data, allowing to foresee some progress in a new version of this operational tool. Better agreement between these two approaches can be noticed in Fig.4 for relatively less critical configurations, obtained here for weak wind conditions, i.e. plume dominated fires mainly piloted by radiation heat transfer. This result is not surprising in considering the scientific base retained in DIMZAL tool. As suggest in (Frangieh & al, 2021), a adaptative evolution of the critical heat flux implemented in DIMZAL to evaluate the optimal fuel break width could be an interesting way to cover a larger spectra of fire behaviour, from plume dominated fire to wind driven fire. This work is already in progress and could be presented in a future publication.

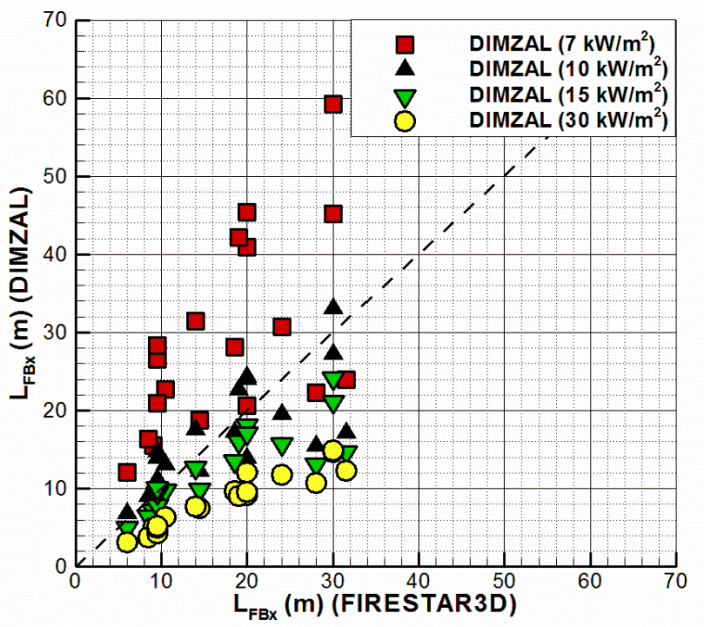

Figure 4- Optimal fuelbreak width obtained by numerical simulations (FIRESTAR3D) and from DIMZAL operational tool for critical heat flux values (Rossi & al, 2011; Frangieh & al, 2021).

3. Acknowledgments

This work was funded by the Corsican Collectivity and the French state in the framework of the collaborative project GOLIAT (CPER: 40031). "Centre de Calcul Intensif d'Aix-Marseille" is acknowledged for granting access to its high-performance computing resources. The authors acknowledge the three reviewers that have allowed to improve the original manuscript.

4. References

Emmons H. (1964) Fire in the forest, Fire research abstracts and reviews 5 163-178.

Rossi J.L., Simeoni A., Moretti B., Leroy-Cancellieri V. (2011) An analytical model based on radiative heating for the determination of safety distances for wildland fires, Fire Safety Journal 46 520-527.

Butler B.W., Cohen J.D. (1998) Firefighter safety zones: a theoretical model based on radiative heating, Int. J. Wildland Fire 8(2) 73-77.

Frangieh N., Accary G., Rossi J.L., Morvan D., Meradji S., Marcelli Th., Chatelon F.J. (2021) "Fuelbreak effectiveness against wind-driven and plume-dominated fires: a 3D numerical study", *Fire Safety Journal*, 121 103383.

Morvan D. (2014) "Wind effects, unsteady behaviours and regimes of propagation of surface fires in open field", *Combustion Science and Technology*, 186(7) 869-888.

Morvan D. (2015) "Numerical study of the behaviour of a surface fire propagating through a fuel break built in a Mediterranean shrub layer", *Fire Safety Journal*, 71 34-48.

Morvan D. (2013) "Numerical study of the effect of fuel moisture content (FMC) upon the propagation of a surface fire on a flat terrain", *Fire Safety Journal*, 58 121-131.

Frangieh N., Accary G., Morvan D., Meradji S., Bessonov O.(2020) "Wildfires front dynamics: 3D structures and intensity at small and large scales", *Combustion and Flame*, 211 54-67

Bisgambiglia P.A., Rossi J.L., Franceschini R., Chatelon F.J., Rossi L., Marcelli Th. (2017) DIMZAL : A software tool to compute acceptable safety distance, Open Journal of Forestry 7 11-33.

Generic burning rate curve for porous fuel beds

Sara McAllister*; Isaac Grenfell; Mark Finney

RMRS Missoula Fire Sciences Lab, USDA Forest Service. 5775 W US Highway 10, Missoula, MT 59808, USA, {sara.mcallister; isaac.c.grenfell; mark.finney}@usda.gov

**Corresponding author*

Keywords

Burning rate, wood cribs, design fire

Abstract

A new wildfire spread model is being developed to alleviate many of the limitations of current operational models. This new model consists of sub-models for ignition, burning and heat release rate, and heat transfer. Unfortunately, the factors that control the burning rate of wildland fuels are not well understood. In this work, we use an extensive database of experimental data with wood cribs to examine curve forms that can be used to describe the time-dependent nature of the burning rate of porous fuel beds. Fifty crib designs and 148 individual mass data curves of cribs burned with unrestricted airflow were available for analysis. Both a power law and a Weibull-distribution-like curve are shown to capture the main shape of the experimental data. Further work will incorporate data with restricted airflow, wind, and moisture content.

1. Introduction

Operational fire behaviour models are either empirically (such as the Canadian and Australian systems (Fire Danger Group 1992, Cruz et al. 2015)) or semi-empirically derived (Rothermel model in the US system (Rothermel 1972). Because of their origin, there are inherent limitations to their use. For example, these three systems consist of fire spread models, designed to output a spread rate for a given set of conditions. There is no built-in ability to determine if a fire will even spread, a question that is relevant to planning prescribed fires and determining the burning period for long duration modelling. In order to alleviate such limitations, a new fire behaviour model is being developed by the Missoula Fire Sciences Lab that treats fire spread as a series of ignitions (Finney et al. 2021). Once an initial ignition is realized, the fuel begins to burn releasing heat at a given rate, and some of that heat is transferred to the unburnt fuel ahead. The new fire behaviour model thus consists of several sub-models: ignition, burning and heat release rate, and heat transfer. This paper focuses on work towards the burning and heat release rate sub-model.

Unfortunately, the burning rates of wildland fuels beds are not well understood. Though it is not actually used in spread prediction, the related residence time of a wildland fire is predicted in BehavePlus as simply 8 times the fuel diameter in inches, which does not take into consideration the variety of other parameters that are likely at play, such as packing, moisture content, and wind (Albini 1976, Anderson 1969). Studying the burning rate in natural fuels beds during a spreading fire is very challenging and it is difficult to accurately manipulate the relevant variables to understand the underlying governing physical processes. For this reason, a simplified fuel bed is often used called a wood crib. Wood cribs have been used to study wildland fire for decades (Fons 1963, Byram 1964, Rothermel 1971, Thomas 1973, Anderson 1990). Wood cribs are frequently used in fire protection engineering as ignition sources and there are several correlations to predict their burning rates (Gross 1962, Block 1971, Heskestad 1973, Thomas 1973). Previous work (McAllister and Finney 2016a) has shown that a slightly modified version (from McAllister and Finney 2016a) of the correlation from Thomas (1973) works best to predict the burning rate for a wide variety of crib designs and stick thicknesses:

$$\frac{100\dot{m}}{A_s\rho_o(gh)^{0.5}} = \frac{0.85}{(0.26h/s)} \qquad \text{(Eq. 1)}$$

where $\dot{m}$ is the burning rate (g/s), A_s is the exposed surface area (cm^2), ρ_o is the air density (g/cm^3), h is the crib height (cm), and s is the spacing between sticks (cm). The new fire behaviour model under development currently uses a simple empirical relation based on a somewhat limited set of laboratory experiments as a place

holder for a more complete sub-model. This place holder consists of a burning rate that is constant in time, which is a gross simplification for the time-dependent burning rate so often seen in actual scenarios where the fire builds in intensity, reaches a peak, and then decays to extinction. The goal of this paper is to develop a more physically-based time-dependent relation for the burning rate based on experiments using wood cribs. Such a "design fire" is common in the fire protection literature (for example see Bwalya 2008, Quintiere 2017).

2. Methods

McAllister et al. have conducted a wide range of experiments using wood cribs and have generated an extensive database of experimental data that will be exploited for this work (see McAllister and Finney 2016a, McAllister and Finney 2016b, McAllister 2019, McAllister 2021, McAllister 2022). For a detailed description of the experimental procedures, please see the original papers. The same general procedure was followed. The cribs were conditioned in a conditioning chamber at 35°C and 3% RH for at least three days so that the moisture content was about 1%. The cribs were place on 7.62 cm tall rectangular steel tubes to create a sufficient space between the crib and the weighing platform (see McAllister and Finney 2016a). The cribs were ignited by briefly dunking them in 99% isopropyl alcohol and allowing them to drain. The mass was measured with three 6-kg load cells recording at 10 Hz for the majority of tests. The reported burning rates were found by determining the maximum slope of a linear fit to the data. In all, the database consists of 50 crib designs with a wide variety of stick thickness (0.16-1.27 cm), stick lengths (6.4-60.96 cm), crib heights (1.27-31.75 cm), and porosities (0.00196-0.211 as evaluated by the Heskestad (1973) formulation). See Appendix A for a full list of crib designs. Most cribs were tested three times so a total of 148 mass loss curves were available for analysis.

To prepare the data for analysis, the data was trimmed to only include the time when the crib was actively burning. The ignition point was manually determined, but the burnout time was chosen to be the time when the burning rate, found from a spline fit with ten degrees of freedom, dropped to 5% of the peak value. The consumed mass (initial mass – mass(t)) was then scaled by the initial mass minus the residual mass, and the time scaled by the burnout time so that both mass and time ranged between 0 and 1. The scaled burning rate was found by a spline fit of the scaled mass and scaled time. The scaling can be done for both the consumed mass and burning rate with the measured values ("observed scaling") as well as predicted values ("predicted scaling") based on the number of sticks, wood density, and peak burning rate estimated from the Thomas correlation (Equation 1). Because the peak burning rate only occurs in most cases for a short period of time, an average burning rate would be more appropriate to estimate the burnout time. To estimate this average burning rate as a proportion of the peak, a subset of the data was examined, and it was found that the average burning rate was approximately 60% of the peak value. Thus, an average scaled burning rate of 0.60*(peak burning rate) was used to estimate the predicted burnout time for scaling the data (predicted burnout time = predicted initial mass / average predicted burning rate). Two curve forms were then fit to this collection of scaled data, first with the scaled consumed mass then the scaled burning rate. The first curve form, a power-law relation, was used based on experience:

$$m^*_{consumed} = \left(\frac{2t^*}{1+t^{*\alpha}}\right)^{\beta} \qquad \text{(Eq. 2)}$$

The second was found from a literature survey to be quite useful for fitting heat release rate curves from cone calorimeter tests to passenger vehicles (Numajiri and Furukawa 1998, Ingason 2005, Tohir et al. 2021):

$$m^*_{consumed} = \left[1 - e^{-\gamma t^*}\right]^{\delta} \qquad \text{(Eq. 3)}$$

where $m^*_{consumed}$ is the scaled consumed mass (dimensionless), t* is the scaled time (dimensionless), and α, β, γ, and δ are fitting constants. Note that Equation 3 is similar to the Weibull distribution but will be referred to here as the "N&F" fit in reference to the work by Numajiri and Furukawa (1998). The derivatives of Eqs. 2 and 3 were used to fit the scaled burning rate:

$$\dot{m}^* = 2\beta\left(\frac{2t^*}{1+t^{*\alpha}}\right)^{\beta-1}\frac{1+(1-\alpha)t^{*\alpha}}{(1+t^{*\alpha})^2} \qquad \text{(Eq. 4)}$$

$$\dot{m}^* = \gamma\delta e^{-\gamma t^*}\left[1 - e^{-\gamma t^*}\right]^{\delta-1} \qquad \text{(Eq. 5)}$$

where $\dot{m}^*$ is the scaled burning rate (dimensionless).

3. Results and Discussion

Table 1 shows the fitting constants in Equations 2 and 3 that best fit the experimental scaled consumed mass ("mass curve fits") and the fitting constants in Equations 4 and 5 for the scaled burning rate ("rate curve fits"). Also included in Table 1 are measures of fit including the coefficient of determination (r^2), root-mean-square error/deviation (RMSE), and the median absolute error/deviation (MDAE).

Table 1 – Curve fit constants and measures of fit for "observed scaling."

	Power law mass curve fit (Eq. 2)	N&F mass curve fit (Eq. 3)	Power law rate curve fit (Eq. 4)	N&F rate curve fit (Eq. 5)
Fitting constant 1 [ ]	$\alpha = 1.450$	$\gamma = 3.784$	$\alpha = 1.687$	$\gamma = 3.212$
Fitting constant 2 [ ]	$\beta = 1.845$	$\delta = 3.265$	$\beta = 2.160$	$\delta = 3.250$
r^2 to mass [ ]	0.9593	0.9535	0.9620	0.9614
RMSE to mass [ ]	0.0659	0.0713	0.0688	0.1044
MDAE to mass [ ]	0.0407	0.0519	0.0448	0.0846
r^2 to rate [ ]	0.5206	0.4879	0.6006	0.5470
RMSE to rate [ ]	0.3281	0.3735	0.3093	0.3203
MDAE to rate [ ]	0.2652	0.2690	0.2329	0.2418

Figure 1 compares the "mass curve fits" to the experimental mass consumed data using both the "observed scaling" on the left and the "predicted scaling" on the right. Immediately, it is observed that there is considerably more spread in the data when the "predicted scaling" is used. This is due to the accumulation of errors in estimating the initial mass (7.7% average difference from observed), the residual mass (29-31% for 1.27 and 0.64 cm sticks; 110-117% for 0.32 and 0.16 cm sticks), and the burning time (30% average difference from observed). A noticeable portion of the spread is from a handful of crib designs whose burning rate (and thus burning time) was not well predicted by the Thomas correlation (Eq. 1). In general, however, both curve fits are centred in the data cloud, with the power law (red) curve appearing to increase at a slightly earlier time than the N&F (blue) curve and pass through the point (1, 1).

Figure 2 compares the "mass curve fits" to the scaled burning rates using both the "observed scaling" on the left and the "predicted scaling" on the right. Here again, as expected, when the "predicted scaling" is used there is more spread in the data for the same reasons as above. What is more problematic is that the time when the peak burning rate occurs does not seem to be well predicted when the consumed mass is used for fitting. Key metrics for the burning rate are compared in Table 2. The "experimental" values are averages from each individual data file. By considering the first three columns in Table 2, it appears that power law fit to the consumed mass data might be slightly better at matching the time to the peak scaled burning rate, but the N&F curve fit to the consumed mass data is better for capturing the mean and peak scaled burning rates.

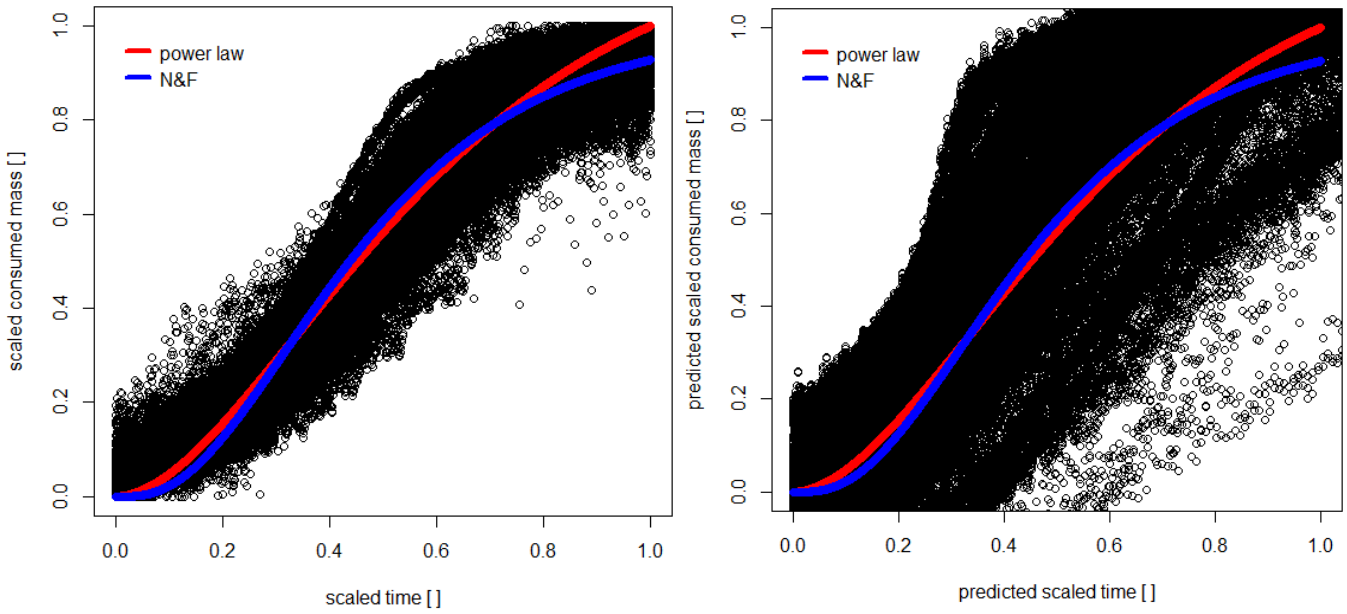

Figure 1 – "Mass curve fits" for consumed mass versus time using observed scaling (left) and predicted scaling (right).

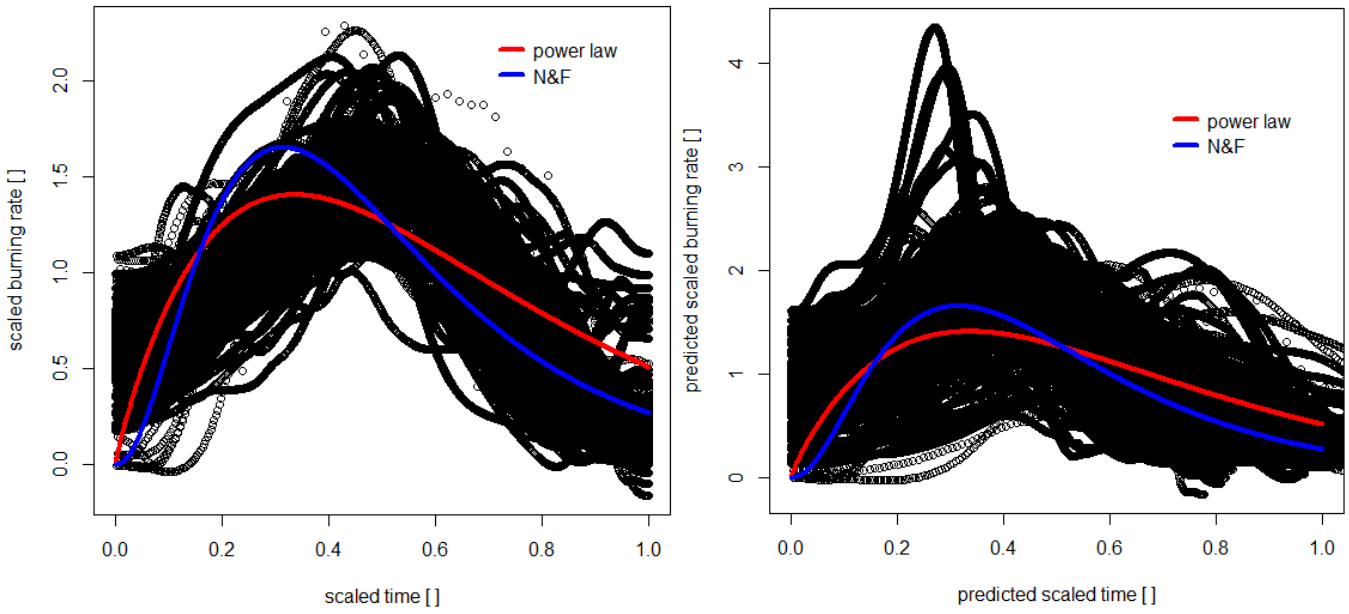

Figure 2 – "Mass curve fits" applied to scaled burning rate using observed scaling (left) and predicted scaling (right).

Table 2 – Key burning rate parameters as measured in the database and calculated from curve fits.

Burning rate parameter	Experimental average	Power law to mass data (Eq. 2)	N&F to mass data (Eq. 3)	Power law to rate data (Eq. 4)	N&F to rate data (Eq. 5)
Mean scaled burning rate [ ]	0.9286	1.000	0.9276	0.9992	0.8742
Peak scaled burning rate [ ]	1.5940	1.4057	1.6527	1.5477	1.4041
Time to peak scaled rate [ ]	0.4949	0.333	0.312	0.386	0.367

Figure 3 shows the results if the curves in Eqs. 4 and 5 are fit to the scaled burning rate (using the "observed scaling"). As shown in Table 1, the curve fitting constants and goodness of fits are slightly different. As expected, the measures of fit to the rate data have improved, while the fitness has decreased slightly for the consumed mass. Though the differences between the two curve fits are still slight, Table 2 shows that when the burning rate is fit, the time to peak is shifted somewhat to match the experimental average more closely but is

still skewed slightly early. The power law fit now slightly better predicts the peak burning rate, while the N&F still better matches the average.

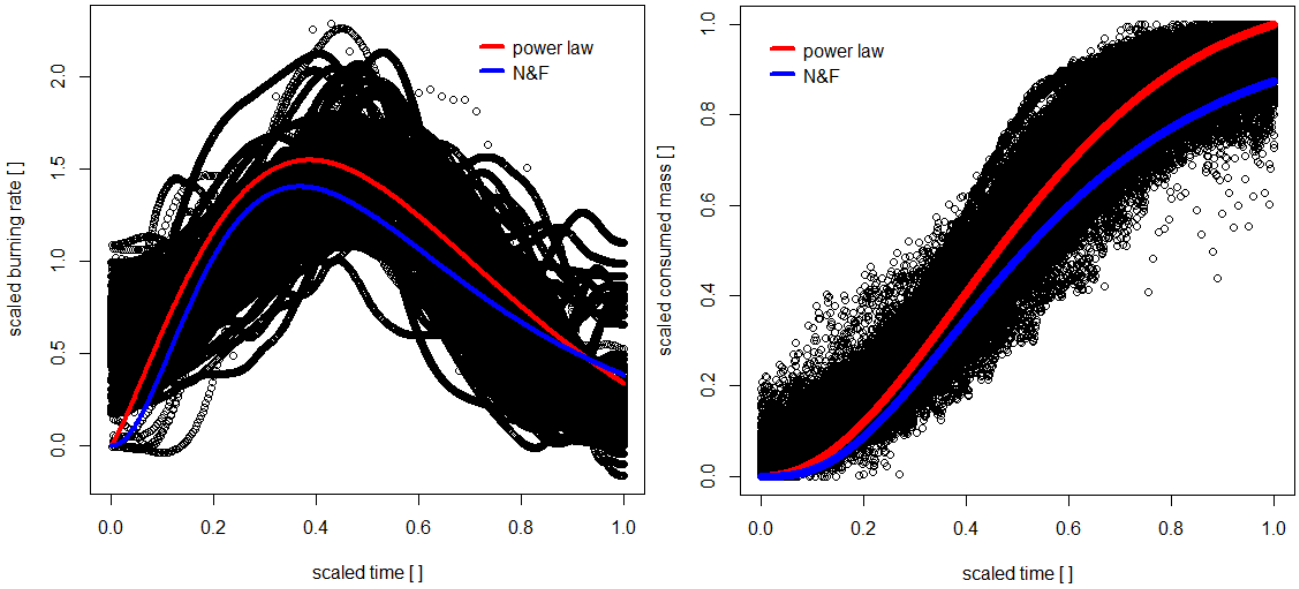

Figure 3 – "Rate curve fits" plotted with scaled burning rate data (left) and scaled consumed mass (right).

4. Summary and Future Work

Two curve forms were fit to an experimental database of crib burns. Both curve forms show promise and captures features of the data slightly differently. Determination of which curve form is most appropriate will likely depend on which feature is more important to the application. Further data also needs to be incorporated that includes the effect of restricted air flow, wind, and moisture content.

5. Acknowledgements

This work was funded by the National Fire Decision Support Centre. The authors want to thank James McGuire, Jennifer Kennedy, Sophia Vernholm, and Chelsea Phillips for building the many cribs and help performing the experiments; Randy Pryhorocki and Josh Deering for building the apparatuses used for the experiments; and Cyle Wold for setting up the data acquisition system.

6. References

F.A. Albini. 1976. Estimating wildfire behavior and effects. General Technical Report INT-30, Intermountain Research Station, USDA Forest Service. (Ogden, UT)

H.E. Anderson. 1969. Heat transfer and fire spread. Research Paper INT-69, Intermountain Research Station, USDA Forest Service. (Ogden, UT)

H.E. Anderson. 1990. Relationship of fuel size and spacing to combustion characteristics of laboratory fuel cribs,'' Research Paper INT-424, Intermountain Research Station, USDA Forest Service.

G.M. Byram, H.B. Clements, E.R. Elliott, P.M. George. 1964. An experimental study of model fires, Technical Report No. 3, Forest Service, USDA Southeastern Forest Experiment Station.

A. Bwalya. 2008. An Overview of Design Fires for Building Compartments. *Fire Technol* **44,** 167–184.

M.G. Cruz, J.S. Gould, M.E. Alexander, A.L. Sullivan, W.L. McCaw, S. Matthews. 2015. A guide to the rate of fire spread models for Australian vegetation. Australasian Fire and Emergency Service Authorities Council Ltd. And Commonwealth Scientific and Industrial Research Organisation, Melbourne, Vic, 123 pp.

M.A. Finney, S.S. McAllister, T.P. Grumstrup, J.M. Forthofer. 2021. Wildland fire behavior: dynamics, principles and processes, CSIRO Publishing, Clayton South, Victoria, Australia, 360 pp.

Fire Danger Group. 1992. Development and Structure of the Canadian Forest Fire Behavior Prediction System. Vol. 3. Forestry Canada, Science and Sustainable Development Directorate.
G. Heskestad. 1973. Modeling of enclosure fires, *Symp. (Int.) Combust.* 14, 1021-1030.
H. Ingason. 2005. Fire development in large tunnel fires, Fire Saf. Sci. 8, 1497–1508,
S. McAllister, M. Finney. 2016a. Burning rates of wood cribs with implications for wildland fires. *Fire Technol* 52, 1755-1777.
S. McAllister, M. Finney. 2016b. The effect of wind of burning rate of wood cribs, Fire Technol 52, 1035-1050.
S. McAllister. 2019. The Role of Fuel Bed Geometry and Wind on the Burning Rate of Porous Fuels, *Front. Mech. Eng.* 5, 11. doi: 10.3389/fmech.2019.00011
S. McAllister. 2021. Effect of reduced plume entrainment on the burning rate of porous fuel beds. Progress in Scale Modeling, an International Journal 2(2), 6. doi: 10.13023/psmij.2021.02-02-06
S. McAllister. 2022. Burning rate and flow resistance through porous fuel beds: axisymmetric versus line fires, *Combust Sci Technol* DOI: 10.1080/00102202.2021.2019233
J.G. Quintiere. 2017. Principles of Fire Behavior, 2nd edition, CRC Press, New York, 413 pp.
R.C. Rothermel. 1972. A mathematical model for predicting fire spread in wildland fuels. Research Paper INT-115, Intermountain Research Station, USDA Forest Service, 40 pp.
P.H. Thomas. 1973. Behavior of fires in enclosures – some recent progress, *Symp. (Int.) Combust*. 14, 1007-1020.
M.Z.M. Tohir, M. Spearpoint, C. Fleischmann. 2021. Probabalistic design fires for passenger vehicle scenarios, Fire Safety Journal 120, 103039. Doi: https://doi.org/10.1016/j.firesaf.2020.103039

Table A.1 – Crib designs in database. The crib porosity is calculated using the method from Heskestad (1973). Cribs with a porosity less than 0.05 cm are considered densely packed.

crib design no	stick thickness (b, [cm])	height (h, [cm])	No sticks per layer (n, [])	No. layers (N, [])	stick length (l, cm)	packing ratio	Heskestad porosity (cm)
1	1.27	31.75	2	25	12.7	0.20	0.1205
2	1.27	12.7	3	10	12.7	0.30	0.1060
3	1.27	17.78	3	14	15.24	0.25	0.1169
4	1.27	12.7	5	10	12.7	0.50	0.0215
5	1.27	12.7	7	10	12.7	0.70	0.0039
6	1.27	17.78	6	14	20.3	0.38	0.0390
7	1.27	26.67	4	21	25.4	0.20	0.1202
8	1.27	2.54	11	2	25.4	0.55	0.0625
9	1.27	6.35	10	5	30.48	0.42	0.0757
10	1.27	3.81	13	3	40.64	0.41	0.1313
11	1.27	3.81	14	3	43.18	0.41	0.1257
12	1.27	5.08	13	4	45.72	0.36	0.1414
13	0.64	6.35	3	10	6.4	0.30	0.0530
14	0.64	6.35	5	10	6.4	0.50	0.0108
15	0.64	6.35	7	10	6.4	0.71	0.0020
16	0.64	15.24	6	24	12.7	0.30	0.0205
17	0.64	8.89	4	14	15.24	0.17	0.1293
18	0.64	5.715	5	9	15.24	0.21	0.1246
19	0.64	22.23	10	35	15.24	0.42	0.0057
20	0.64	8.89	8	14	19.05	0.27	0.0454
21	0.64	9.53	5	15	19.05	0.17	0.1174

22	0.64	10.16	8	16	19.69	0.26	0.0429
23	0.64	28.58	3	45	20.32	0.10	0.1213
24	0.64	10.16	8	16	20.32	0.25	0.0460
25	0.64	10.16	10	16	20.32	0.32	0.0270
26	0.64	8.89	9	14	20.96	0.28	0.0429
27	0.64	9.53	9	15	21.59	0.27	0.0429
28	0.64	5.08	8	8	22.86	0.23	0.1179
29	0.64	6.35	6	10	25.4	0.15	0.211
30	0.64	3.81	10	6	25.4	0.25	0.1197
31	0.64	6.35	10	10	25.4	0.25	0.0725
32	0.64	9.53	14	15	25.4	0.36	0.0213
33	0.64	1.91	27	3	25.4	0.69	0.0074
34	0.64	8.89	8	14	30.48	0.17	0.1210
35	0.64	3.81	12	6	30.48	0.25	0.1188
36	0.64	4.45	20	7	30.48	0.42	0.0270
37	0.64	5.72	20	9	60.96	0.21	0.1163
38	0.32	3.81	6	12	15.24	0.13	0.1232
39	0.32	3.81	8	12	20.32	0.13	0.1206
40	0.32	1.27	14	4	20.32	0.22	0.1173
41	0.32	1.91	14	6	25.4	0.18	0.1242
42	0.32	9.54	14	30	25.4	0.18	0.0252
43	0.32	6.36	27	20	25.4	0.34	0.0087
44	0.32	12.72	6	40	30.48	0.06	0.1215
45	0.32	2.86	14	9	30.48	0.15	0.1178
46	0.16	1.59	9	10	15.24	0.10	0.1191
47	0.16	11.11	3	70	15.24	0.03	0.1173
48	0.16	1.27	13	8	20.32	0.10	0.1272
49	0.16	5.72	15	36	20.32	0.12	0.0220
50	0.16	1.27	16	8	25.4	0.10	0.1298

GOLIAT, a project to develop tools for firefighting and land use planning

Thierry Marcelli*[1]; Lucile Rossi[1]; Gilbert Accary[2], Carmen Awad[1], Antoine Burglin[1], Dominique Cancellieri[1], Valérie Cancellieri[1], François-Joseph Chatelon[1], Jacky Fayad[1], Lila Ferrat[1], Nicolas Frangieh[1], Hugo Grossi[1], Sofiane Méradji[3], Frédéric Morandini[1], Dominique Morvan[4], Antoine Pieri[1], Clément Wandon[1], Agence Arobase.fr[5], Jean-Louis Rossi[1]

[1] *UMR CNRS SPE 6134, Université de Corse - CNRS, 20250 Corte, France, {marcelli_t, rossi_l,awad_c, burgling_a, cancellieri_d, leroy_v, chatelon_j, fayad_j, ferrat_l, frangieh_n, grossi_h, morandini_f, pieri_a, rossi_j, wandon_c}@univ-corse.fr*
[2] *Scientific Research Center in Engineering, Lebanese University, Museum Square, 1106 Beirut, Lebanon, {gaccary@ul.edu.lb}*
[3] *IMATH laboratory, EA 2134, Toulon University, 83160 Toulon, France, {sofiane.meradji@univ-tln.fr}*
[4] *Aix-Marseille Université, CNRS, Centrale Marseille, M2P2, Marseille, France, {dominique.morvan@univ-amu.fr}*
[5] *Agence Arobase.fr, 1 Avenue de la République, 20250 Corte, France, info@arobase.fr*

**Corresponding author*

Keywords

Decision support tools, past fires database, behavior and impact Simulator, hot spot geolocation, guide to prescribed fires

Abstract

The GOLIAT project is a consortium of academics and firefighting operators and land-use planning professionals of Corsica. One goal of GOLIAT project is to provide four operational decision support tools. To reach this goal, a survey of past fires occurred in Corsica since the twentieth century beginning is made. This inventory contributes to build up a database with a web display interface easy to use as fire patterns history. A fire behavior and impact simulator prototype for vegetation fires, a geolocation tool for hot spots using UAV images, and a guide of good practices of prescribed fires in the undergrowth are building. At the same time, experimental fires are carried out to improve knowledge about high intensity fire and the experimental results were compared to the predictions provided by a complete physical 3D model, namely FireStar3D.

1. Introduction

The GOLIAT project brings together academics from the University of Corsica, Aix-Marseille University, University of Toulon and Lebanese University with Corsican fire-fighting operators and land-use planning professionals and a company carrying out computer developments. The partners are : the National Forestry Office, Fire and rescue Service of Southern Corsica, Fire and Rescue Service of Northern Corsica, Regional Nature Park of Corsica and Arobase company. The aim of the program is to develop tools, studies, guides, and awareness-raising activities to provide a response to wildfire issues. This program is co-financed by the Corsican Collectivity and the French State. It started in January 2020 and will last for three and a half years.

The GOLIAT project is divided into three main objectives. The first objective is to deepen the phenomenological and historical knowledge of vegetation fires in Corsica. Research is carried out to increase knowledge of the behavior of vegetation fires, the fires that have occurred in Corsica, and the methods used to control fire in traditional Corsican society. The second objective is to build decision-making tools prototypes that meet the needs of firefighting and land-use planning operators. Four prototype tools are under development: 1) A database associated with an information display tool dedicated to fires that have taken place in Corsica 2) A behavior and impact simulator for vegetation fires 3) A geolocation tool for hot spots using UAV images 4) A guide to prescribed burning in the undergrowth. The third objective is to carry out many awareness-raising and prevention actions on the vegetation fire problem in Corsica, aimed at schools, public and local authorities.

In the context of global warming that we are experiencing, intense fires affect several countries growing and over larger periods. Prescribed burnings are used by operators for land-management thanks to its low cost and high efficiency in hard-to-reach areas. In the context of this program, high intensity fires across Corsican *Genista salzmannii* vegetation and prescribed burnings on a Mediterranean pine forest are instrumented and studied mixing numerical and experimental approaches and disciplines such as physics, chemistry, ecology, and UAV vision.

2. Decision support tools

From the needs expressed by the firefighting and land-use managers, the GOLIAT project has been elaborated to provide decision support tools usable by them when fire occurs.

Three tools are created to give to firefighters in a web display information about the past and the future of Corsican fires.

When a fire will occur, using the GPS position of the ignition point, operators will have web server services to see (1) the past fires information correlated with meteorological data, (2) the prediction of the future fire front positions and heat fluxes and (3) the geolocation tool for hot spots obtained from UAV IR images.

One tool is created specifically for land managers, it concerns a guide to prescribed burning in the undergrowth in *Pinus laricio* forest.

2.1. Fire database associated with an information display tool

A survey of past fires occurred in Corsica since the twentieth century beginning is made. This inventory contributes to build up a database. This last contains information about fires, which size is greater than 10 ha, occurring in Corsica since 1904. It also contains meteorological data (Fig. 1) and noteworthy events in relation with the firefighting. 2 048 fire contours and 1 593 ignition points are included, a work is in progress to show this information in a web server in a format display adapted for firefighters easy to use as a fire patterns history.

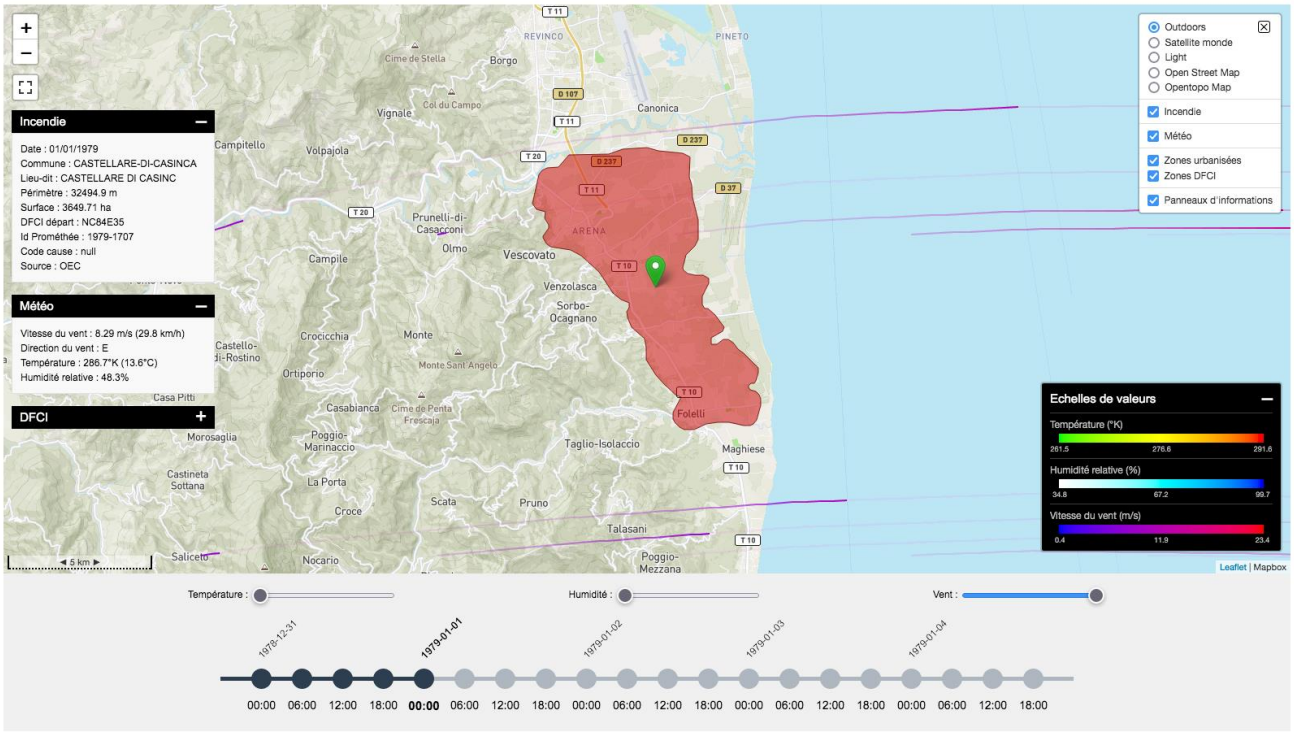

Figure 1- Screenshot of the web interface presenting data associated to a past fire

The meteorological data which allowed this representation come from the Copernicus project (https://cds.climate.copernicus.eu/cdsapp#!/dataset/reanalysis-uerra-europe-complete?tab=overview) (Fig. 2). A script has been created that collects the dates of all fires and collects weather data from T-24h to T+96h with a 6h time step.

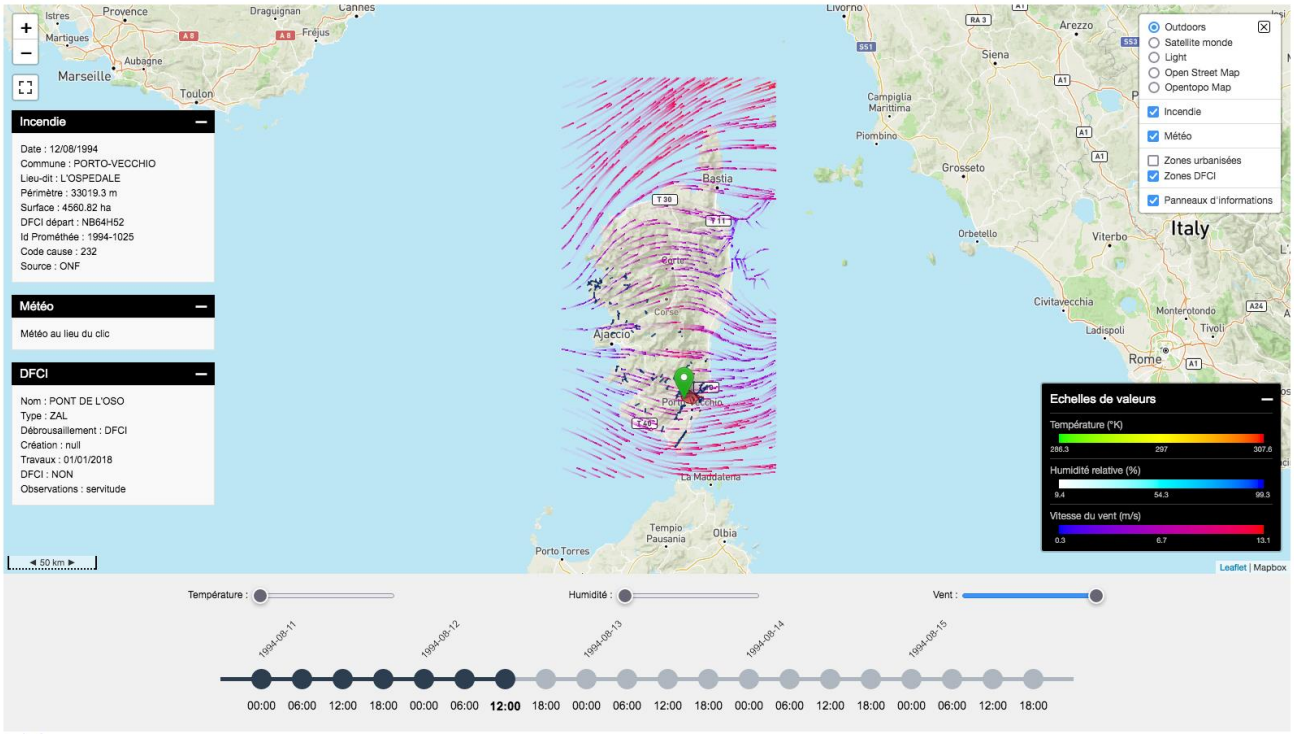

Figure 2- Wind flow all over Corsica screenshot

2.2. A behavior and impact simulator for vegetation fires

The behavior and impact fire simulator is developed on the requirements drawn up between researchers and operators. Physics used to predict fire behavior is the last version of the Balbi model (Balbi *et al*. 2020) developed at the University of Corsica. This simulator will predict from an ignition point or a contour (Fig. 3) the fire front evolution (Fig. 4) and an acceptable safety distance (Rossi *et al*. 2011). Indeed, the knowledge of the impact zone in front of flames is a relevant information for firefighters to stay in safety conditions when they fight fire.

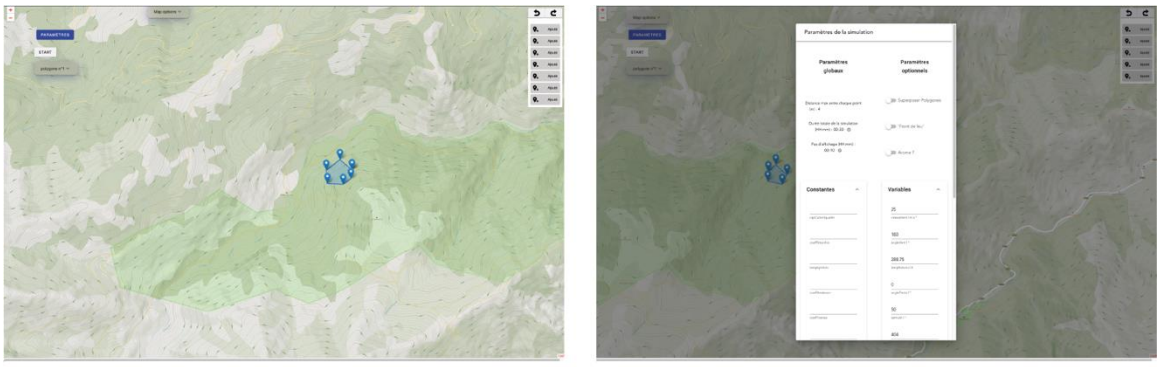

Figure 3- (a) Start contour screenshot (b) Simulation parameters configuration panel

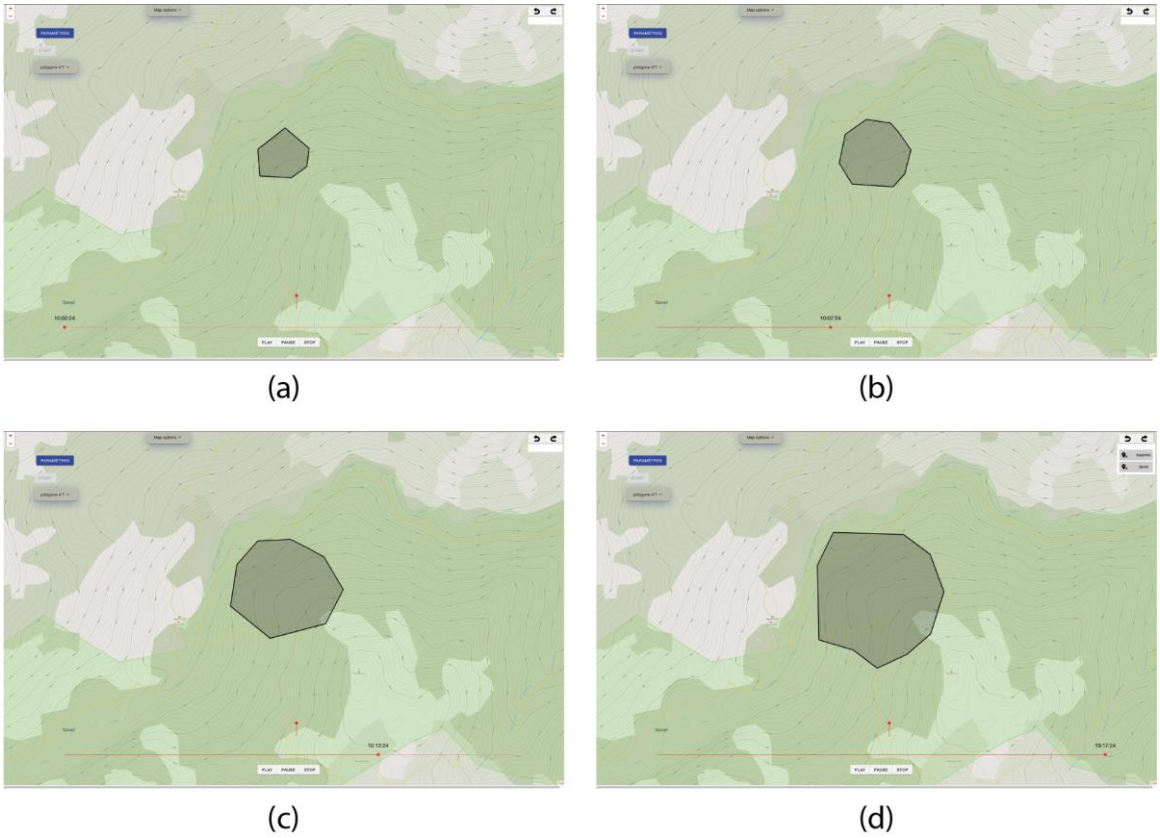

Figure 4- Fire front evolution simulation (a) t = …

Experimental fires were conducted with the main objective of providing data to test the predictions of the theoretical physical fire models, in the case of a high-intensity fire spreading upslope at field scale (Fig. 5). To understand and investigate the different phenomena encountered in this type of fires, the experimental results were compared to the predictions provided by the multiphase code FireStar3D (Fig. 6) (Frangieh *et al*. 2020). These predictions were used to examine the fire front dynamics, to evaluate the fire intensity that was difficult to accurately assess during the experiment (Fayad *et al*. 2022).

Figure 5- Experimental fire at Speluncatu (Corsica)

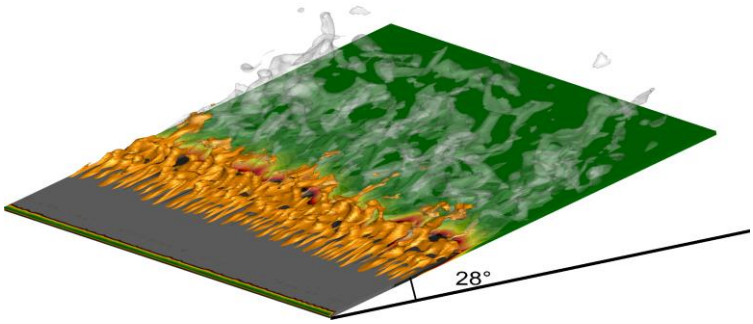

Figure 6- FireStar3D simulation on the Speluncatu experiment

2.3. A geolocation tool for hot spots using UAV images

The geolocation tool answers the needs expressed by the Fire and Safety Services of Corsica. When the fire is stopped, it is necessary to keep an eye on for several days and they need to cover burnt aeras for extinguishing hot spots whom are potential resumption of fire.

Thank to DJI SDK, programs have been developed to automate the pattern of the drone with cameras on board working simultaneously on the UAV and far IR, to detect and to geolocate the hot spots (Fig. 7).

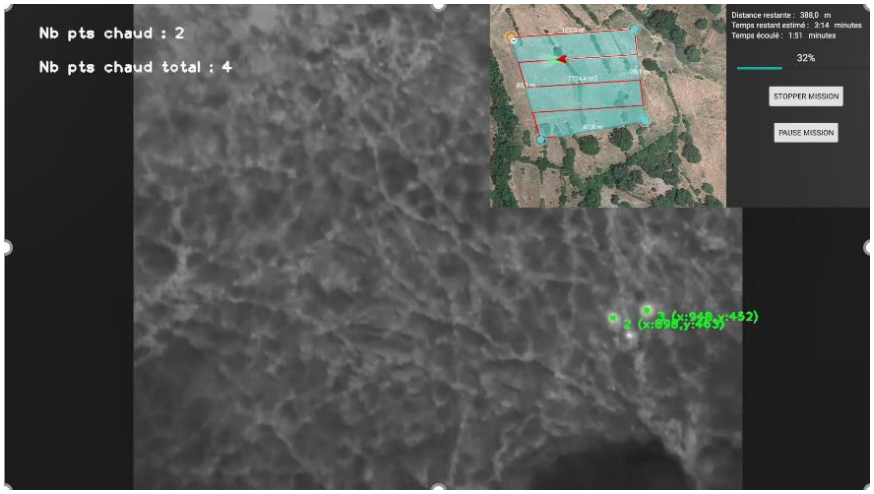

Figure 7- Hot spot software screenshot

2.4. A guide to prescribed burning in the undergrowth

Research works are conducted to improve the knowledge on fire resistance of *Pinus laricio* forests. Undergrowth prescribed fires are carried out (Fig. 8). Samples of vegetation, soil, insects, and pine needles are taking on witness parcels. Sensors for tree growth, sap fluxes, temperatures are located on these parcels.

The analysis of the collected data will allow to give recommendations on undergrowth prescribed fires to minimize impact on *Pinus laricio* forests.

Figure 8- Prescribed fire on a* Pinus laricio *forest in Corsica

3. Conclusion

The GOLIAT project is based on the research developed at the University of Corsica and develops new work to meet the needs for tools, studies and knowledge expressed by firefighting and land-use operators. It allows synergy between academics and fire professionals, technology transfer to build decision support tools: a database of fires occurred in Corsica with a display tool, a behavior and impact simulator for vegetation fires, a geolocation tool for hot spots using UAV images and a guide of good practices to prescribed fires in the undergrowth of *Pinus laricio* forest.

The improvement of knowledge on the phenomenology of vegetation fires will make it possible to increase the effectiveness of the prediction of fire behavior and, thanks to the strong interaction with the operational staff, to develop tools that meet their needs.

4. References

Balbi JH, Chatelon FJ, Morvan D, Rossi JL, Marcelli T, Morandini F. A convective–radiative propagation model for wildland fires. International Journal of Wildland Fire 2020; 29:723–738. https://doi.org/10.1071/WF19103.

Fayad J, Rossi L, Frangieh N, Awad C, Accary G, Chatelon F-J, Morandini F, Marcelli T, Cancellieri V, Cancellieri D, Morvan D, Pieri A, Planelles G, Costantini R, Meradji S, Rossi J-L (2022) Numerical study of an experimental high-intensity prescribed fire across Corsican Genista salzmannii vegetation. *Fire Safety Journal* 103600. doi:10.1016/J.FIRESAF.2022.103600.

Frangieh N, Accary G, Morvan D, Méradji S, Bessonov O. Wildfires front dynamics: 3D structures and intensity at small and large scales. Combustion and Flame 2020; 211:54-67. https://doi.org/10.1016/j.combustflame.2019.09.017.

Rossi JL, Simeoni A, Moretti B, Leroy-Cancellieri V. An analytical model based on radiative heating for the determination of safety distances for wildland fires. Fire Safety Journal 2011; 46:520–527. https://doi.org/10.1016/j.firesaf.2011.07.007.g

Identifying the most influential parameters in experimental grass fire spread modeling using global sensitivity analysis

Flore C. Roubelat[1,2]; Aurélien Costes[1]; William P. Antolin[1], and Mélanie C. Rochoux[1]*

[1] CECI, CNRS, Cerfacs, Université de Toulouse. 42 Avenue Gaspard Coriolis, 31057 Toulouse cedex 1, France, {aurelien.costes, william.antolin, melanie.rochoux}@cerfacs.fr
[2] École Nationale de la Météorologie, Météo-France, Institut National Polytechnique, Université de Toulouse. 42 Avenue Gaspard Coriolis, 31057 Toulouse cedex 1, France, {flore.roubelat@meteo.fr}

**Corresponding author*

Keywords

Wildland fire-spread, Rate-of-spread parameterization, Perturbed physics ensemble, Parameter uncertainty, Sensitivity analysis

Abstract

Coupled atmosphere/fire models are recognized as an efficient and representative way to simulate wildland fire behavior at geographical-to-meteorological scales by representing the two-way interactions between the fire front propagation and the surrounding atmosphere. These coupled models rely on a rate-of-spread (ROS) parameterization to represent the fire front propagation speed as a parametric function of environmental factors characterizing biomass fuel properties and moisture content, near-surface wind conditions and terrain slope. In actual wildland fires, these input parameters are only partially known and induce significant uncertainties in the coupled model predictions. To estimate the envelope of plausible wildland fire behavior, we aim at designing a perturbed-physics ensemble prediction capability based on a coupled atmosphere/fire model. To make the approach feasible, it is essential to identify the relevant subset of parameters to perturb to generate an ensemble of fire front positions and shapes. In the present study, we carry out a global sensitivity analysis based on Sobol' indices to rank the environmental factors by order of influence on the Balbi's ROS parameterization applied to typical conditions for grass fire experiments. Results show, for the given experimental conditions, the predominance of the near-surface wind speed on the ROS variability, followed by the leaf area index LAI, the ignition temperature T_i, the dead fuel moisture content M_d, the dead fuel particle mass density ρ_d, and the fuel layer height e. Results also show that the sensitivity of each fuel parameter to the ROS is not constant with respect to the near-surface wind speed, and that the most influential input parameters differ between the head and the back of a fire. This indicates the importance of exploring the spatial and temporal dependencies of coupled model sensitivities in future work. The subset of input parameters already identified as influential allows to reduce the dimension of the uncertain space over which to analyze the coupled model response, and thereby the perturbed-physics ensemble size. This is a key aspect to extend the global sensitivity analysis to the coupled model framework. While the present sensitivity analysis is limited to experimental grass fire conditions, this approach could be easily extended to more wildland fire configurations - to analyze to what extend the sensitivity analysis results obtained here are applicable to different biomass fuels.

1. Introduction

Coupled atmosphere/fire models (Kochanski *et al.* 2013; Filippi *et al.* 2018; Costes *et al.* 2021) provide an efficient but representative way to simulate wildland fire behavior at landscape-to-meteorological scales. They predict the propagation of the fire front at the land surface, the dynamics of the fire plume, and their mutual interactions. These two-way interactions can modify the near-surface wind and enhance the fire front propagation during a wildland fire. The fire model requires from the atmospheric model the near-surface wind at a given height to evaluate the rate of spread (ROS) and propagate the fire front. It also provides the surface heat fluxes as surface boundary conditions to the atmospheric model. Both ROS (Rothermel 1972; Balbi *et al.* 2009) and surface heat fluxes are evaluated through parameterizations, which require as inputs a large number of environmental factors related to biomass fuel, near-surface wind and terrain slope. These input parameters are partially known (Jimenez *et al.* 2008) and thereby introduce uncertainties in the coupled simulations. They also have their own intrinsic variability. For these reasons, it is necessary to adopt a stochastic viewpoint, i.e., to

run ensembles of the coupled atmosphere/fire model to represent the range of possible wildland fire behavior over a given time window (Costes *et al.* 2021).

To limit the computational cost of ensemble simulations while obtaining a physically and spatially-consistent ensemble, an appropriate experimental design is essential. The main issue addressed in this work is to identify a subset of input parameters that contributes most to the ROS variability along the fire front, and thus on the fire front propagation through variance-based global sensitivity analysis (Wilks 2011). The influential input parameters will be good candidates to perturb to build a perturbed-physics ensemble that is representative of fire front uncertainties in coupled atmosphere/fire modeling.

2. Global Sensitivity Analysis Method

2.1. Principles

The objective of sensitivity analysis is to quantify how uncertainties in each input parameter influence the output variability in a given model. This is useful to spot the most influential parameters on a given model response (factor prioritization), and to constrain irrelevant parameters to an arbitrary value (factor fixing) (Wilks 2011). There are two main types of sensitivity analysis methods. On the one hand, local methods are centered around one point in the parameter space, and, for each parameter, the impact of small parameter perturbations on the model output is calculated. They have some limitations if the model response is subject to nonlinearity since the local output variability may not be representative of the model response for all possible values of the input parameters. On the other hand, in the global methods, the entire parameter space is considered and the model response is analyzed in a multi-query framework, meaning that multiple model evaluations of simultaneously-modified input parameters are performed and that the induced model variability provides a measure of the parameter influence on the model output. Global methods are known to be very efficient, even for a nonlinear and non-monotonic model, where interactions between input parameters can occur. Still, their results largely depend on the parameter space boundaries and sampling.

2.2. Sobol' Sensitivity Indices

In the present study, we consider a global sensitivity analysis method based on variance decomposition (the model output variance is used as the measure of the input parameter influence on the overall model output variability) to estimate Sobol' sensitivity indices (Sobol 1990; Saltelli *et al.* 2008).

The model output Y is a function of d independent and uncertain input parameters, i.e., $Y = \mathcal{M}(X_1, \dots, X_d)$, where X_i is the ith parameter that is considered as a random variable, $\boldsymbol{X} = (X_1, \dots, X_d)$ is a random vector of dimension d, and $\mathcal{M}$ is the model operator. By using Hoeffding's decomposition theorem, the output variance $V = V(Y)$ can be written as

$$\mathrm{V} = \sum_{i=1}^{d} V_i + \sum_{1 \le i < j \le d} V_{ij} + \cdots + \mathrm{V}_{1\dots\mathrm{d}},$$

where V_i is the output variance only due to parameter i, V_{ij} is the output variance due to the pair of parameters i and j, and $V_{1\dots d}$ is the output variance due to the d parameters. Using these notations, Sobol' first-order index for the ith parameter X_i (Sobol 1990) is defined as

$$S_i = \frac{V_i}{V}.$$

S_i varies between 0 and 1, and represents the proportion of the model output variance due to the ith parameter (if S_i = 1, this means that 100% of the model output variance is explained by the ith parameter alone). By analogy, higher-order indices represent the proportion of the model output variance due to a set of parameters. The full contribution of the ith parameter (including interaction effects with other parameters) can be estimated using total-order indices S_i^T (Saltelli *et al.* 2008):

$$S_i^T = S_i + \sum_{j>i}^{d} S_{ij} + \cdots + S_{1,\dots,d}.$$

The first-order index S_i represents the main effect of the *i*th parameter X_i that is used in factor privatization, and the total-order index S_i^T represents the total effect of the parameter that is used in factor fixing. The difference between the two indices represents to which extent the parameter effects on the model response comes from an interaction with the other parameters (if the total-order index for a given parameter is equal to its first-order index, this implies that there are no interaction effects for this parameter).

3. Sensitivity Analysis Application to Rate-Of-Spread (ROS) Parameterization

The model due to Rothermel (1972) is the most well-known ROS parameterization. Its formulation relies on the energy conservation principle and provides a ROS value only at the head of the fire front (i.e., in the upwind direction). In practice, Rothermel's formulation is combined with geometrical relationships to evaluate the ROS all along the fire front. This is the main difference with Balbi's parameterization (Balbi *et al.* 2009) that directly provides a ROS value that varies all along the fire front, even if the fuel is homogeneous. Balbi's formulation is based on mass, momentum and energy conservation, but still provides an analytical formulation for the ROS through flame geometry simplifications.

In this study, we consider Balbi's ROS parameterization adapted for landscape-scale wildland fires (Santoni *et al.* 2011) and already implemented in the Meso-NH/BLAZE coupled model. It was, for instance, used for the coupled model evaluation against the FireFlux I grass experimental data (Costes *et al.* 2021). The change made by Santoni *et al.* (2011) compared to Balbi *et al.* (2009) is the consideration of the different properties of live and dead fuels, and their impacts on the ROS. Following previous work by Costes *et al.* (2021), we consider here the conditions of a grass fire experiment, without slope, to carry out the sensitivity analysis. The slope parameter is therefore not among the perturbed input parameters.

3.1. Sobol'-Saltelli Estimation Approach and Experimental Design

We adopt the well-known Saltelli's approach (Saltelli *et al.* 2008) to estimate first- and total-order Sobol' indices (altogether $2 \times d$ indices, where d is the number of uncertain input parameters). This approach corresponds to a Monte Carlo estimation of the Sobol' indices at a total cost of $N \times (d + 2)$ ROS evaluations (where N is the ensemble size), and thereby provides a confidence interval for the resulting Sobol' indices estimates.

In this study, the uncertain space is made by all the input parameters of Balbi's ROS parameterization (fifteen parameters including the near-surface wind speed U_0, Table 1). This space is sampled by N points using Sobol' low-discrepancy sequence. This is a quasi-random Monte Carlo method, where the generated sequence has many interesting properties: *i)* the sequence has a low discrepancy (i.e., there is a more homogeneous coverage of the parameter space than in a classical Monte Carlo method for a limited number of samples N), and *ii)* the sequence is coherent (the N first points of a sequence with $(N + 1)$ points are the same as for a sequence with N points, implying that, if more samples must be generated, it is not necessary to recompute the previous points and that a large model dataset can be generated in an incremental way). It is worth noting that we consider here a large number of samples N to guarantee convergence of the Sobol' indices (N = 20,000). This is feasible here since the ROS parameterization can be evaluated at a low cost (the sampling strategy will have to be adapted when switching to a coupled atmosphere/fire model, which is very demanding in terms of computing resources). Table 1 provides a detailed description of the fifteen input parameters. Without further information, they are perturbed according to a uniform statistical distribution, which is characterized by a variation interval. The center of this interval corresponds to a so-called standard value, which corresponds to a tall grass fuel typical of the FireFlux I experiment that was simulated in Costes *et al.* (2021) using the Meso-NH/BLAZE coupled model configured with the Balbi's ROS parameterization. We consider here a large variation interval to study how the ROS changes for a wide set of environmental conditions, and to identify which are the most influential input parameters that could then be used to generate ensemble coupled model simulations and study the coupled model response in a variety of situations.

3.2. Results

3.2.1. Predominant wind factor

Figure 1 shows the first- and total-order sensitivity indices for all parameters presented in Table 1 (d = 15). For example, the first-order index for the dead fuel particle density ρ_d is equal to 0.05 (circle symbol), and the

associated total-order index is equal to 0.06 (square gray symbol). This means that ρ_d is responsible for 6% of the ROS variability within the ensemble (5% without accounting for the interaction with the other parameters).

Table 1- Input parameters (Balbi's ROS parameterization) perturbed in the sensitivity analysis

Name	Symbol	Unit	Standard value	Lower bound	Upper bound	Coefficient of variation
Fuel calorific capacity	c_p	J kg^{-1} K^{-1}	1,912	1,720.8	2,103.2	6%
Fuel layer height	e	m	1.5	1.0	2.0	19%
Leaf area index	LAI	—	4	2	6	29%
Dead fuel moisture content	M_d	%	10	5	15	29%
Living fuel moisture content	M_l	%	80	60	100	14%
Dead fuel particle surface-to-volume ratio	s_d	m^{-1}	5,000	4,250	5,750	9%
Living fuel particle surface-to-volume ratio	s_l	m^{-1}	5,000	4,250	5,750	9%
Ignition temperature	T_i	K	590	490	690	10%
Near-surface wind speed	U_0	m s^{-1}	4	0	8	58%
Combustion enthalpy	ΔH	MJ kg^{-1}	15.43	14.66	16.20	3%
Air density	ρ_a	kg m^{-3}	1.2	1.0	1.4	10%
Dead fuel particle mass density	ρ_d	kg m^{-3}	400	300	500	14%
Living fuel particle mass density	ρ_l	kg m^{-3}	400	300	500	14%
Dead fuel surface loading	σ_d	kg m^{-2}	1	0.8	1.2	12%
Living fuel surface loading	σ_l	kg m^{-2}	0.1	0.05	0.15	29%

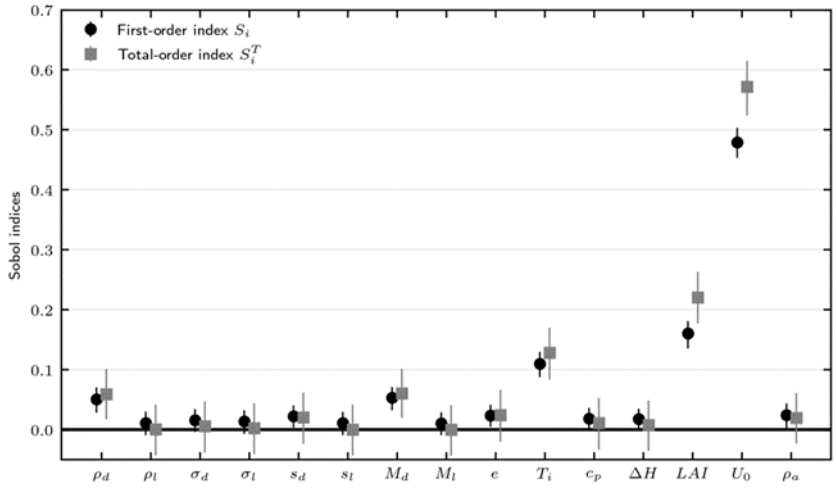

Figure 1- Sobol' indices quantifying the sensitivity between the 15 perturbed parameters and the ROS as evaluated by Balbi's parameterization at the fire front head. Circles represent first-order indices. Squares represent total-order indices. Vertical bars represent estimation uncertainties.

From Figure 1, the most influential parameters on the Balbi's ROS parameterization can be identified. The near-surface wind speed U_0 is the predominant factor by explaining by itself 48% of the ROS variability (57% in total). The difference between the first- and total-order indices is important for U_0, implying that there are important interaction effects between the wind factor and the other parameters. Other influential parameters are by order of importance the leaf area index LAI, the ignition temperature T_i, the dead fuel moisture content M_d, and the dead fuel particle mass density ρ_d for which the first-order Sobol' index is equal to 16%, 11%, 5% and 5%, respectively.

3.2.2. Sensitivity analysis by near-surface wind speed level

Previous results correspond to the ROS at the head of the fire front. We now apply the same sensitivity analysis method when the near-surface wind speed U_0 is equal to 0 m s^{-1}, in order to represent the situation of a back fire (fourteen parameters are perturbed). The most influential parameters are by order of importance the fuel

layer height e, the ignition temperature T_i, the combustion enthalpy ΔH, the dead fuel moisture content M_d and the dead fuel surface loading σ_d for which the first-order Sobol' index is equal to 38%, 21%, 9%, 8% and 8%, respectively. This shows that T_i and M_d are influential parameters at the head and at the back of a fire.

This results also indicates that the sensitivity of the ROS to the different fuel parameters is variable according to the value of the near-surface wind speed U_0. This is consistent with the difference previously-observed between the first- and total-order Sobol' indices for the near-surface wind speed U_0 indicating significant interaction effects. Since the wind velocity seen by the fire front changes all along the fire front (the wind speed used in the ROS parameterization corresponds to the normal component of the wind velocity to the fire front), the order of importance of the input parameters may change along the fire front. To further analyze this dependency, the near-surface wind speed U_0 is removed from the perturbed parameters and Sobol' indices are estimated for different wind levels varying between 0 and 20 m s^{-1} (the mean ROS within the ensemble changes from 0.39 to 3.82 m s^{-1}). We focus the sensitivity analysis on the eight most influential parameters identified in the previous steps (the near-surface wind speed U_0 is no longer included in the perturbed parameters to generate the N samples). Figure 2 presents Sobol' first-order indices obtained for the different wind levels. Results confirm that the order of importance of the input parameters largely depends on the wind level. Without wind, more than 60% of the ROS variability is explained by two parameters, the fuel layer height e and the ignition temperature T_i. When the wind speed increases, for instance for U_0 = 5 m s^{-1}, the fuel layer height e is far less important (4%), and the leaf area index LAI becomes very influential (41%). This is consistent with Balbi's ROS parameterization. First, the parameter e is only involved in the radiation submodel to estimate the radiant panel size, and radiation is assumed to be independent of the wind speed. Second, as part of the definition of the upward velocity of the combustion gases, the parameter LAI is involved in the tilt angle estimation that depends on the wind speed. This study indicates that the most influential parameters that are relevant to perturb to generate an ensemble depend on the portion of the fire front that is considered (head, flanks or back).

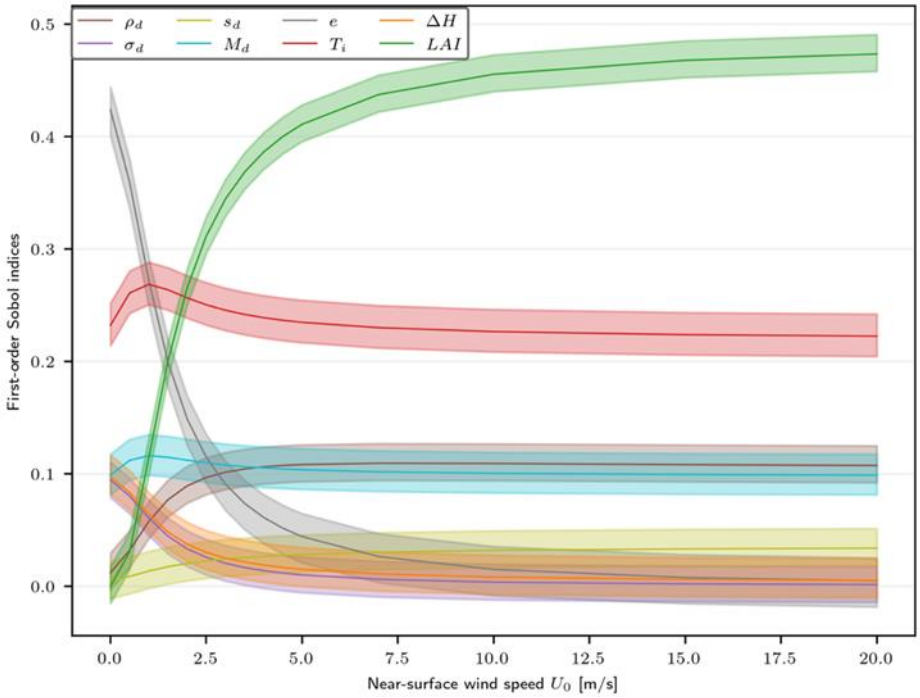

Figure 2- First-order Sobol' indices relating the ROS and 8 perturbed inputs, which are obtained for different levels of the near-surface wind speed U_0. One input parameter corresponds to one color. Shaded intervals represent estimation uncertainties.

4. Conclusions

This study identifies the most influential parameters involved in Balbi's ROS parameterization through Sobol'-Saltelli sensitivity analysis approach to estimate the first- and total-order Sobol' indices. The most influential

parameter is the near-surface wind speed U_0. The influence of the other parameters depends on the value of the near-surface wind speed U_0, but overall, the five most influential fuel parameters are the leaf area index LAI, the ignition temperature T_i, the fuel layer height e, the dead fuel particle mass density ρ_d, and the dead fuel moisture content M_d. The next step is to extend this sensitivity analysis approach to a coupled atmosphere/fire model to represent the spatio-temporal impact of input parameters on the wildland fire behavior. This will provide access to the fire-induced wind and to the temporal and spatial variability of the near-surface wind speed, which in turn has an influence on the spatial and temporal variability of the fire front. This will also be helpful to define a protocol for generating a perturbed-physics ensemble and estimating the range of plausible wildland fire behavior for a given event. For this purpose, the sensitivity analysis approach will include different ROS parameterizations and different environmental conditions to go beyond the conditions of a flat grass fire experiment, and thus have sensitivity analysis results that cover a wider range of wildland fire conditions.

5. References

A.K. Kochanski et al. “Real time simulation of 2007 Santa Ana fires”. In*: Forest Ecology and Management* 294 (2013), pp. 136–149. DOI: 10.1016/j.foreco.2012.12.014.

J.-B. Filippi et al. “Simulation of a large wildfire in a coupled fire-atmosphere model”. In: *Atmosphere* 9.6 (2018). DOI: 10.3390/atmos9060218.

A. Costes et al. “Subgrid-scale fire front reconstruction for ensemble coupled atmosphere-fire simulations of the FireFlux I experiment”. In: *Fire Safety Journal* 126 (2021), p. 103475. ISSN: 0379-7112. DOI: 10.1016/j.firesaf.2021.103475.

Rothermel; Richard C. *A mathematical model for predicting fire spread in wildland fuels*. Technical report, Research Paper INT-115. (1972) U.S. Department of Agriculture, Forest Service, Ogden, Utah, USA.

J.-H. Balbi et al. “A physical model for wildland fires”. In: *Combustion and Flame* 156.12 (Dec. 2009), pp. 2217–2230. DOI: 10.1016/j.combustflame.2009.07.010. URL: https://hal.archives-ouvertes.fr/hal-00593608.

E. Jimenez; M.Y. Hussaini and S. Goodrick. “Quantifying parametric uncertainty in the Rothermel model”. In: *International Journal of Wildland Fire* 17.5 (2008), pp. 638–649.

D. Wilks. “Statistical Methods in the Atmospheric Sciences”. In: vol. 100. International Geophysics. Academic Press (2011). Chap. 3 - Empirical distributions and exploratory data analysis, pp. 23–70.

I.M. Sobol. “On sensitivity estimation for nonlinear mathematical models”. In: *Matematicheskoe Modelirovanie* (*Russian*) 2 (1990), pp. 112–118.

A. Saltelli; M. Ratto; T. Andres; F. Campolongo; J. Cariboni; D. Gatelli; M. Salsana and S. Tarantola. *Global Sensitivity Analysis: The Primer*. Wiley (2008).

P.-A. Santoni et al. “Wildland fire behaviour case studies and fuel models for landscape-scale fire modeling”. In: *Journal of Combustion* 2011 (2011), p. ID613424. DOI: 10.1155/2011/613424.

Improved prediction of drought for wildland fire danger rating in Canada

Chelene C. Hanes*[1,2]; Mike Wotton[2]; Douglas G. Woolford[3]; Laura Bourgeau-Chavez[4]; Stéphane Bélair[5]; David Martell[2]; Mike Flannigan[6]

[1]Great Lakes Forestry Centre, Canadian Forest Service, Natural Resources Canada, 1219 Queen St. E, Sault Ste. Marie, ON, P6A 2E5, Canada {chelene.hanes@nrcan-rncan.gc.ca}
[2] Institute of Forestry and Conservation, John H. Daniels Faculty of Architecture, Landscape and Design, University of Toronto, 33 Willcocks Street, Toronto, ON M5S 3B3, Canada {mike.wotton, david.martell}@utoronto.ca
[3] Statistical and Actuarial Sciences, University of Western Ontario, 1151 Richmond St., London, ON, N6A 3K7, Canada {dwoolfor@uwo.ca}
4. Michigan Technological University, Michigan Tech Research Institute, 3600 Green Ct. Suite 100, Ann Arbor, MI 48105, United States {lchavez@mtu.edu}
5. Canadian Meteorological Centre, Environment and Climate Change Canada, 2121, route Transcanadienne, Dorval, Quebec H9P 1J3, Canada {stephane.belair@ec.gc.ca}
6. Natural Resource Science, Thompson Rivers University, 805 TRU Way, Kamloops, BC V2C 0C8, Canada {mflannigan@tru.ca)

**Corresponding author*

Keywords

Boreal forest; fuel moisture; in situ; modeling; remote sensing

Abstract

Canadian fire management agencies track drought conditions using the Drought Code (DC). The DC is one of three fuel moisture codes in the Fire Weather Index System, which is part of the Canadian Forest Fire Danger Rating System. The DC represents the moisture of deep organic layers (15-18 cm nominal depth) and is used operationally to assess potential lightning ignition holdover, persistent deep smoldering, and mop-up problems. As the climate changes and drought conditions arise more frequently, our understanding of drought and how to measure it become more important. Determining what the DC means in areas without deep organic soils is a question commonly proposed by fire operations personnel. Recent studies have indicated that some more complex models (e.g. the Canadian Land Data Assimilation System – CaLDAS) may provide added intelligence about the fire environment and drought conditions, something that has not been explored in Canada. To shed light on these questions we carried out field studies in the provinces of Alberta and Ontario. Four field sites were included in our study, two in Alberta near Edson and Red Earth Creek, and two in Ontario near Dryden and Chapleau. At each of the seven plots within these four sites, we installed 8-12 water content reflectometry (WCR) probes at two different depths. The probes were installed from the surface through the organic layers, and in some cases, into the mineral soil. Overall, our results indicated that the simple DC model predicted the moisture content of the deeper organic layers (10-18 cm depths) well, even compared to the more complex CaLDAS model. The WCR probes at these depths, exhibited good agreement with how the DC model estimated moisture changes. The DC may therefore be representative of changes in moisture content in a wide range of depths and soil horizons. Issues with model inputs, particularly missed precipitation events and incorrect DC spring starting values, had a greater influence on DC model fit than other factors. Calibration and validation of the CaLDAS model to mineral soils may be the cause of its consistent under prediction of organic layer moisture.

1. Introduction

Throughout most typical fire seasons the principal day-to-day short-term indicators of fire danger, ignition potential and rate of spread, are of primary concern to fire managers. The moisture content of the litter layer and underlying fine to medium organic fuels heavily influence fire behaviour through their interaction with local weather and topography. Hot, dry and windy conditions can quickly dry out these layers, which can lead to more fire activity and more intense fires. Longer-term drought and continuous drying into deeper, denser organic fuels can make a challenging fire season quickly turn to something much worse.

Drought in the Canadian Forest Fire Danger Rating System (CFFDRS) is measured by the Drought Code (DC), one of three moisture codes in the Fire Weather Index (FWI) System. Similar drought indices used for fire danger rating exist in other jurisdictions, such as the Keetch-Byram Drought Index (Keetch and Byram, 1968) and the Palmer Drought Index (Palmer, 1965). One significant, but subtle difference is that the DC is designed to directly estimate the lack of moisture in denser organic layers rather than using hydrologic drought in the mineral soil as a proxy for fuel moisture deficiencies. The layer of the forest floor tracked nominally by the DC has depth of 15-18 cm and nominal fuel load of 25 kg/m^2, in keeping with the standard pine fuel on which the FWI System is based (Van Wagner, 1987).

Since the development of the DC, most efforts to account for carrying-over drought from fall into spring and its impact on fire activity in Canada has focused on how to establish the starting spring values and field validation of the DC using destructive sampling methods (Otway et al., 2007, Stocks, 1979, Alexander, 1982, Lawson and Dalrymple, 1996). Most of Canada is snow covered, or receives significant precipitation during the winter months. More recent studies have developed correlations with organic soil moisture using electronic moisture probes (Terrier et al., 2014, Elmes et al., 2018, Keith et al., 2010). Such methods are less time consuming and allow greater temporal and spatial variability in measurements. Those instruments rely on soil dielectric properties, which can vary with soil composition, clay content and organic content (Bourgeau-Chavez et al., 2010, Kellner and Lundin, 2001). Despite good correlations with the measurements produced with these probes, questions remain operationally around probe installation and use and what layers best correlate with the DC.

The DC has also been shown to have strong correlation to C-band (~6 cm wavelength) Synthetic Aperture Radar (SAR) backscatter in low-biomass areas (Bourgeau-Chavez et al., 1999, Bourgeau-Chavez et al., 2007). An algorithm developed by Bourgeau-Chavez was shown to be useful to initialize DC start-up values in Alaska. Further work by Bourgeau-Chavez using polarimetric C-band SAR (Radarsat2) was successful at improving the soil moisture estimation in higher biomass areas (Bourgeau-Chavez et al., 2013). Although such research demonstrates the potential use of earth observation to map organic soil moisture, there remain limitations to remote sensing of soil moisture in forested regions (Jin et al., 2017, Magagi et al., 2013, Pan et al., 2016).

More sophisticated land surface models may alleviate some of the remote sensing issues; studies in other regions have shown improved drought estimation by incorporating land surface modelling outputs (Vinodkumar and Dharssi, 2019, Cooke et al., 2012, Yang et al., 2015) into fire danger methods to represent soil moisture changes. This approach has not been explored for the dense boreal forests in Canada. Inclusion of earth observations from an existing product, like the ECCC's (Environment and Climate Change Canada) Canadian Land Data Assimilation System (CaLDAS) (Carrera et al., 2019, Carrera et al., 2015) is an emerging area for fire science in Canada. CaLDAS integrates information from L-band satellite SMOS (Soil Moisture Ocean Salinity) as well as the geostationary satellite GOES (Geostationary Operational Environmental Satellite) with high-resolution land surface modelling and ground level observations to produce estimates of soil moisture across Canada every three hours. To further explore what organic depths the DC is tracking and determine the potential added intelligence electronic soil moisture content probes and land surface modelling data could provide, a field-based study was conducted in the provinces of Alberta and Ontario. This study had the following three objectives:

1. Determine how well the DC correlates to organic soil moisture and at which depths, using WRC (water content reflectometry) probes.
2. Explore the use of land surface models (CaLDAS) to represent moisture changes in these deep organic layers.
3. Determine if CALDAS estimates of soil moisture can be used to estimate/correct the DC.

2. Methods

We installed 8-12 WCR probes at depths of 10 and 18 cm in seven forest plots (Figure 1), from the surface through the organic layers, and in some cases, into the mineral soil. We compared these observed moisture contents with the DC model estimates of moisture and CaLDAS estimated Volumetric Moisture Content (VMC). DC values were estimated from nearby fire weather stations. The version of CaLDAS used included short-range forecasts calculated from ECCC's High Resolution Deterministic Prediction System every three hours. Precipitation within the model was assimilated from the Canadian Precipitation Analysis (CaPA)

(Mahfouf et al., 2007), in addition to other atmospheric variables, using an Ensemble Kalman Filter methodology. The land surface model was built around the SVS (Soil, Vegetation and Snow) scheme also developed by ECCC (Alavi et al., 2016, Husain et al., 2016). Daily soil moisture outputs from CaLDAS were obtained from ECCC for our analysis.

The field measurements of moisture content observed at depths of 10 cm and 18 cm were compared to the following: 1) daily DC values, converted to VMC, 2) CaLDAS VMC estimates at all three depths (0-5 cm, 5-10 cm and 10–20 cm) and 3) daily DC values (expressed as VMC) to CaLDAS VMC at three depths. All analysis were first conducted on daily time series of VMC during the fire season from late spring (May) until early fall (September) for 2019-2021 where available. The hydroGOF R package was used to calculate goodness of fit statistics for these time series comparisons including: R^2 (Coefficient of Determination), RMSE (Root Mean Square Error), Pbias (Percent Bias), and NSE (Nash Sutcliffe Efficiency; Nash and Sutcliffe, 1970). Goodness of fit statistics were first calculated for the entire 2019-2021 time series (May through September), then again for each individual year separately to show annual variations.

3. Results

Overall results indicated that the simple DC model did a good job of predicting the moisture content of the deeper organic layers (i.e. 10-18 cm) depths (Table 1), even compared to the more complex land surface model CaLDAS (Table 2). The WCR probes installed through the litter, fermentation and humus layers, and in some cases into the mineral soil, had good agreement with the DC model estimated VMC (Figure 2). Therefore, the DC may be representative of moisture changes in a wider range of depths, soil horizons and forest types. There was greater variability between different forest plots than between years and probe depths (Table 1). Model inputs, particularly precipitation and DC starting values had a large influence on DC model fit.

Differences in statistics and time series plots showed a clear trend that the DC had the best fit with the observed VMC in the wetter and deeper mixedwood Chapleau plot (Figure 2). In contrast, much poorer goodness of fit statistics were observed at the shallower and drier aspen plot also at the Chapleau site (Figure 2). Beyond those bookends there was no obvious indication of what is influencing overall organic moisture changes and the ability of the DC to represent them (i.e. duff depth, moisture regime, forest type); more advanced analyses may be required to investigate this further.

Results showed that better representation of precipitation is a simple way to improve DC tracking of forest floor moisture. This is not surprising as other studies have shown that FWI System codes and indices overall were improved compared to basic interpolation of stations with better precipitation inputs (i.e., gridded precipitation especially with radar) estimates (Hanes et al., 2017, Cai et al., 2019). Although the CaLDAS model includes high-resolution gridded precipitation products (Carrera et al., 2015) its outputs still consistently underestimated observed moisture contents (Table 2, Figure 3). It also had little skill in predicting DC values directly and consistently underestimated DC moisture content (Table 3, Figure 4). This strong bias is most likely due to the validation and calibration of CaLDAS to focus primarily on agricultural areas and mineral soil moisture (Carrera et al., 2019). This is similar to other remote sensing soil moisture calibrations/validations (Magagi et al., 2013, Pan et al., 2016). Although land surface models have been proposed as an alternative to drought modelling for fire danger in some areas (Vinodkumar and Dharssi, 2019, Cooke et al., 2012, Vinodkumar et al., 2017) the majority of studies assume mineral soil moisture as proxy measure of fuel moisture content. It is clear that overall, drier conditions are more conducive to fire, but it is the day-to-day changes in fine fuel moisture that are of primary importance, influencing daily variability in fire behaviour (Van Wagner, 1985). Many remote sensing and fire danger studies to date largely ignore the organic layer and focus only on “surface soils”, which can include litter but are essentially mineral soil. Organic material contains more pore space and are therefore generally wetter than mineral soils (Otway et al., 2007). Therefore, to better model organic moisture directly, remote sensing retrieval algorithms and land surface models need to refine the soil dielectric models based on soil organic carbon properties (e.g., higher porosity and typically lower bulk density) (Jin et al., 2017). Organic soils typically have a lower dielectric content than mineral soil with same VMC (Jin et al., 2017, Bourgeau-Chavez et al., 2010). Integration of national maps of organic layer thickness (e.g., Hanes et al. 2022) into CaLDAS in combination with organic layer specific algorithms are needed to improve model skill for estimating drought indices for fire. Doing so would allow greater use of land surface models directly as additional sources

of fire intelligence, especially for regions without good weather station coverage; this would also allow fire managers to take advantage of the forecast capabilities of these complex models.

4. Conclusions

Our results indicate that the relatively simple DC model does a reasonable job of representing observed moisture changes in deeper organic layers over a wide range of forest types for depths of 10 to 18 cm. Electronic probes that use the dielectric content of soil moisture, installed at these depths, can be used to supplement or correct DC estimates. Physically based hydrologic models have been proposed because we have the capacity to use them (i.e., Johnson et al., 2013, Keith et al., 2010). Yet the simplicity of the DC model and ease of application without the necessity to parameterize to a specific region still outweigh any validation improvements in moving to a more complex model. Although land surface models like CaLDAS hold much promise to integrate earth observation and high-resolution numerical weather prediction outputs into wildfire danger prediction, their bias to mineral soils limit their use at this time. We anticipate better performance in the future once organic soils are integrated into CaLDAS and the SVS land surface scheme. This is not to say the DC model is perfect. Much clarity could come from expanding the definition of what the DC model represents (i.e. beyond the elusive standard 15-18 cm depth in a standard pine forest). This may require a shift in the definition from an exact moisture value for a specific soil horizon towards a definition that includes a wider range of slower drying organic layers/fuels as data permits.

5. References

ALEXANDER, M. E. 1982. Calculating spring Drought Code starting values in the Prairie provinces and northwest Territories. Forest Management Note #12. Edmonton, AB: Northern Forestry Centre, Canadian Forestry Service.

BOURGEAU-CHAVEZ, L. L., GARWOOD, G., RIORDAN, K., CELLA, B., ALDEN, S., KWART, M. & MURPHY, K. 2007. Improving the prediction of wildfire potential in boreal Alaska with satellite imaging radar. Polar Record, 43, 321-330.

BOURGEAU-CHAVEZ, L. L., GARWOOD, G. C., RIORDAN, K., KOZIOL, B. W. & SLAWSKI, J. 2010. Development of calibration algorithms for selected water content reflectometry probes for burned and non-burned organic soils of Alaska. International Journal of Wildland Fire, 19, 961-975.

BOURGEAU-CHAVEZ, L. L., KASISCHKE, E. S. & RUTHERFORD, M. D. 1999. Evaluation of ERS SAR Data for Prediction of Fire Danger in a Boreal Region. International Journal of Wildland Fire, 9, 183-194.

BOURGEAU-CHAVEZ, L. L., LEBLON, B., CHARBONNEAU, F. & BUCKLEY, J. R. 2013. Evaluation of polarimetric Radarsat-2 SAR data for development of soil moisture retrieval algorithms over a chronosequence of black spruce boreal forests. Remote Sensing of Environment, 132, 71-85.

CAI, X. L., WANG, X. L., JAIN, P. & FLANNIGAN, M. D. 2019. Evaluation of Gridded Precipitation Data and Interpolation Methods for Forest Fire Danger Rating in Alberta, Canada. Journal of Geophysical Research-Atmospheres, 124, 3-17.

CARRERA, M. L., BÉLAIR, S. & BILODEAU, B. 2015. The Canadian Land Data Assimilation System (CaLDAS): Description and Synthetic Evaluation Study. Journal of Hydrometeorology, 16, 1293-1314.

CARRERA, M. L., BILODEAU, B., BELAIR, S., ABRAHAMOWICZ, M., RUSSELL, A. & WANG, X. H. 2019. Assimilation of Passive L-band Microwave Brightness Temperatures in the Canadian Land Data Assimilation System: Impacts on Short-Range Warm Season Numerical Weather Prediction. Journal of Hydrometeorology, 20, 1053-1079.

COOKE, W. H., MOSTOVOY, G. V., ANANTHARAJ, V. G. & JOLLY, W. M. 2012. Wildfire Potential Mapping over the State of Mississippi: A Land Surface Modeling Approach. Giscience & Remote Sensing, 49, 492-509.

ELMES, M. C., THOMPSON, D. K., SHERWOOD, J. H. & PRICE, J. S. 2018. Hydrometeorological conditions preceding wildfire, and the subsequent burning of a fen watershed in Fort McMurray, Alberta, Canada. Natural Hazards and Earth Systems Science, 18, 157-170.

HANES, C. C., JAIN, P., FLANNIGAN, M. D., FORTIN, V. & ROY, G. 2017. Evaluation of the Canadian Precipitation Analysis (CaPA) to improve forest fire danger rating. International Journal of Wildland Fire, 26, 509–522.

HANES, C. C., WOTTON, M., WOOLFORD, D. G., MARTELL, D.L., & FLANNIGAN, M.D. 2022. Mapping organic layer thickness and fuel load of the boreal forest in Alberta, Canada. Geoderma, 417, 115827.

JIN, M. J., ZHENG, X. M., JIANG, T., LI, X. F., LI, X. J. & ZHAO, K. 2017. Evaluation and Improvement of SMOS and SMAP Soil Moisture Products for Soils with High Organic Matter over a Forested Area in Northeast China. Remote Sensing, 9, 17.

JOHNSON, E. A., KEITH, D. M. & MARTIN, Y. E. 2013. Comparing measured duff moisture with a water budget model and the duff and drought codes of the Canadian Fire Weather Index. . Forest Science 59, 78-92.

KEETCH, J. J. & BYRAM, G. M. 1968. A Drought Index for Forest Fire Control. Asheville, NC: Southeastern Forest Experiment Station.

KEITH, D. M., JOHNSON, E. A. & VALEO, C. 2010. Moisture cycles of the forest floor organic layer (F and H layers) during drying. Water Resources Research, 46, W07529.

KELLNER, E. & LUNDIN, L.-C. 2001. Calibration of Time Domain Reflectometry for Water Content in Peat Soil. Nordic Hydrology, 32, 315-332.

LAWSON, B. D. & DALRYMPLE, G. N. 1996. Ground-truthing the Drought Code: Field Verification of Overwinter Recharge of Forest Floor Moisture. In: FRDA (ed.). Canadian Forest Service and the British Columbia Ministry of Forests.

MAGAGI, R., BERG, A. A., GOÏTA, K., BÉLAIR, S., JACKSON, T. J., TOTH, B., WALKER, A., MCNAIRN, H., O'NEILL, P. E., MOGHADDAM, M., GHERBOUDJ, I., COLLIANDER, A., COSH, M. H., BURGIN, M., FISHER, J. B., KIM, S.-B., MLADENOVA, I., DJAMAÏ, N., ROUSSEAU, L.-P. B., BELANGER, J., SHANG, J. & MERZOUKI, A. 2013. Canadian Experiment for Soil Moisture in 2010 (CanEx-SM10): Overview and Preliminary Results. IEEE Transactions on Geoscience and Remote Sensing, 51, 347-363.

NASH, J. & SUTCLIFFE, J. 1970. River flow forecasting through conceptual models part I-A discussion of principles. Journal of Hydrology, 10, 282-290.

OTWAY, S. G., BORK, E. W., ANDERSON, K. R. & ALEXANDER, M. E. 2007. Relating changes in duff moisture to the canadian forest fire weather index system in Populus tremuloides stands in elk island national park. Canadian Journal of Forest Research-Revue Canadienne De Recherche Forestiere, 37, 1987-1998.

PALMER, W. C. 1965. Meteorological Drought. U.S. Weather Bureau, Research Paper No. 45. Washington, DC. 39pp.

PAN, M., CAI, X. T., CHANEY, N. W., ENTEKHABI, D. & WOOD, E. F. 2016. An initial assessment of SMAP soil moisture retrievals using high-resolution model simulations and in situ observations. Geophysical Research Letters, 43, 9662-9668.

STOCKS, B. J. The 1976-1977 drought situation in Ontario. WMO Symp. For. Meteorol., Aug. 21-25, 1978 1979 Ottawa, ON. World Meteorol. Organization Publ. 527, 97-98.

TERRIER, A., DE GROOT, W. J., GIRARDIN, M. P. & BERGERON, Y. 2014. Dynamics of moisture content in spruce-feather moss and spruce-Sphagnum organic layers during an extreme fire season and implications for future depths of burn in Clay Belt black spruce forests. International Journal of Wildland Fire, 23, 490-502.

VAN WAGNER, C. E. 1985. Drought, timelag, and fire danger rating. Eighth Conference on Fire and Forest Meteorology. Society of American Foresters.

VAN WAGNER, C. E. 1987. Development and Structure of the Canadian Forest Fire Weather Index System. Ottawa: Petawawa National Forestry Institute.

VINODKUMAR & DHARSSI, I. 2019. Evaluation and calibration of a high-resolution soil moisture product for wildfire prediction and management. Agricultural and Forest Meteorology, 264, 27-39.

VINODKUMAR, DHARSSI, I., BALLY, J., STEINLE, P., MCJANNET, D. & WALKER, J. 2017. Comparison of soil wetness from multiple models over Australia with observations. Water Resources Research, 53, 633-646.

YANG, Y., UDDSTROM, M., PEARCE, G. & REVELL, M. 2015. Reformulation of the Drought Code in the Canadian Fire Weather Index System Implemented in New Zealand. Journal of Applied Meteorology and Climatology, 54, 1523-1537.

6. Figures and Tables

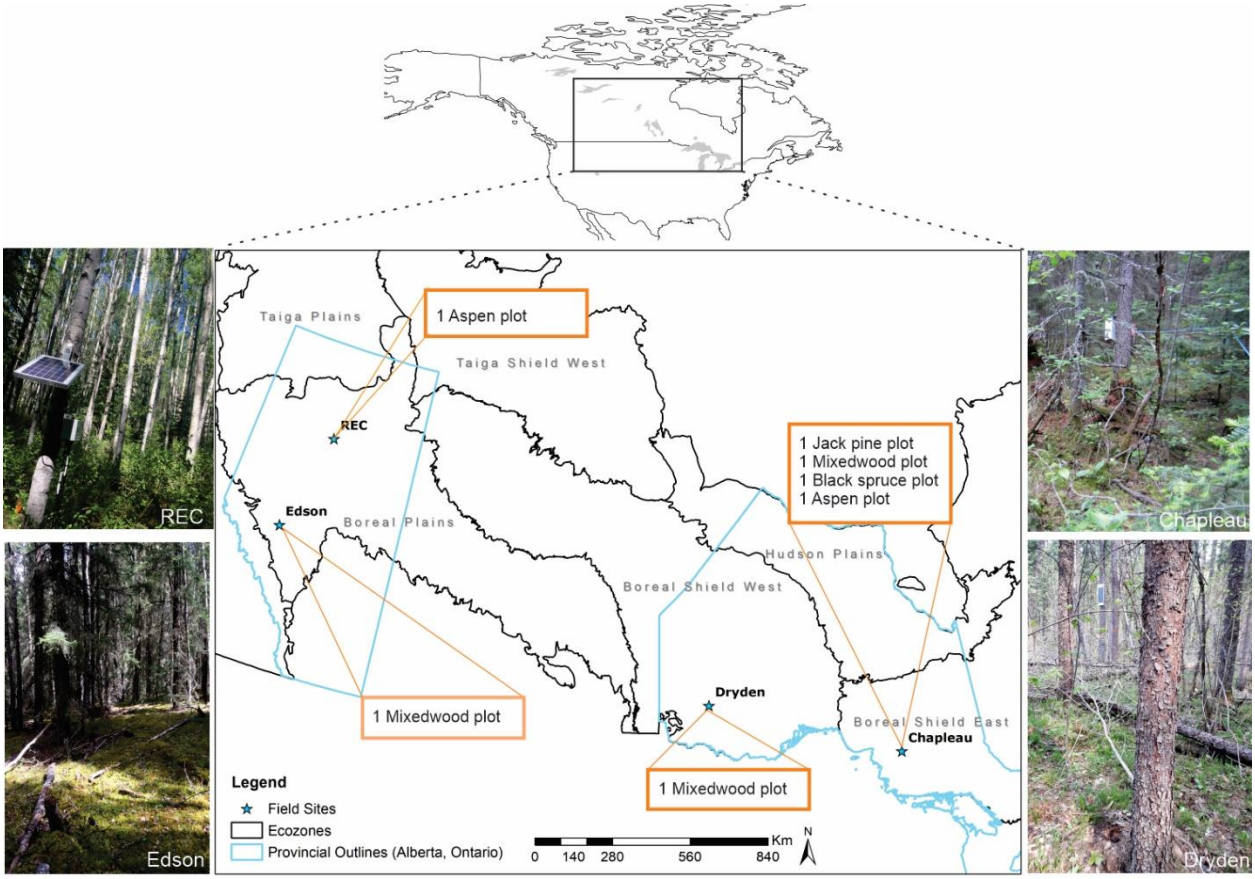

Figure 1. *Top: A map of North America with Canadian and United States borders highlighting the general area of our study region (box). Bottom: The four moisture probe field sites (shown as stars) in Alberta and Ontario; REC on this map designates the Red Earth Creek site. The number and vegetation type of each plot, within the different sites, are indicated in the orange boxes.*

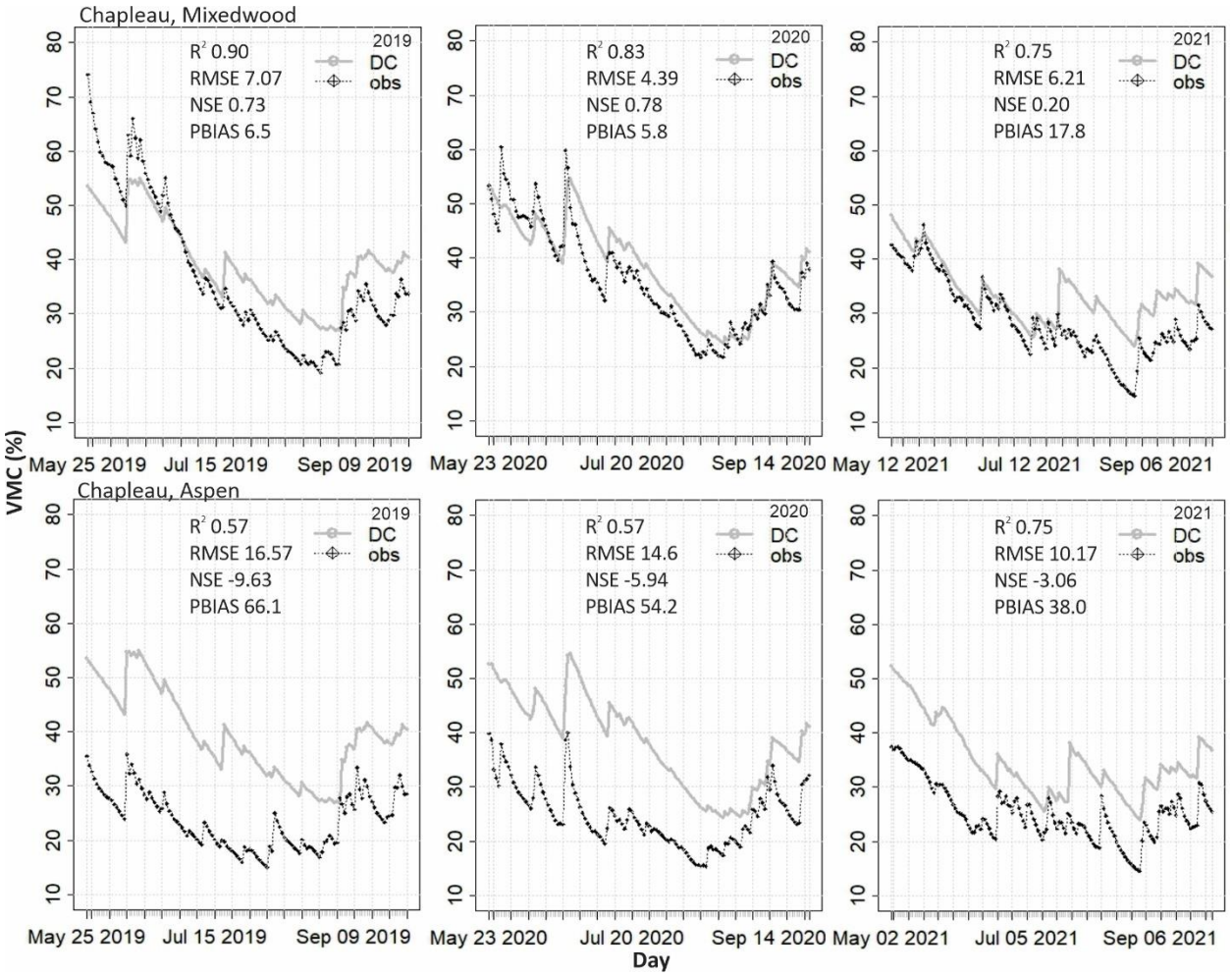

Figure 2. Goodness of fit statistics and time series comparisons for each fire season (2019-2021) for the Chapleau site. Mixedwood (top row) is contrasted with aspen (bottom row). The black line is the observed (obs) Volumetric Moisture Content (VMC) (field measured at 18 cm). The grey line is the DC estimated VMC.

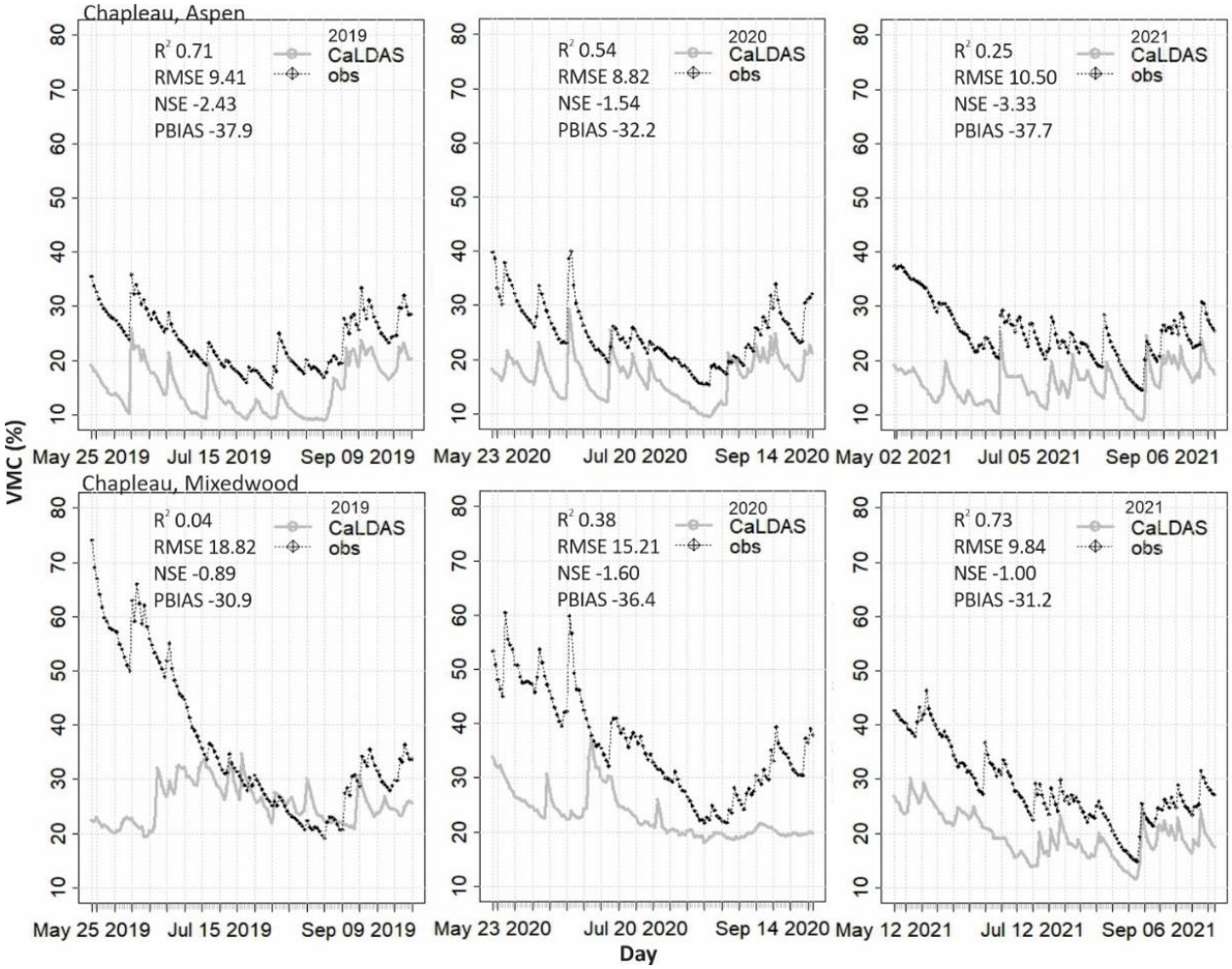

Figure 3. Example of a better match between observed (18 cm) and CaLDAS (Canadian Land Data Assimilation System) volumetric moisture content (VMC) for 10-20 cm moisture for Chapleau, aspen plot (top row) and a worse match for the Chapleau, mixedwood plot (bottom row). Goodness of fit statistics and time series are shown for 2019-2021.

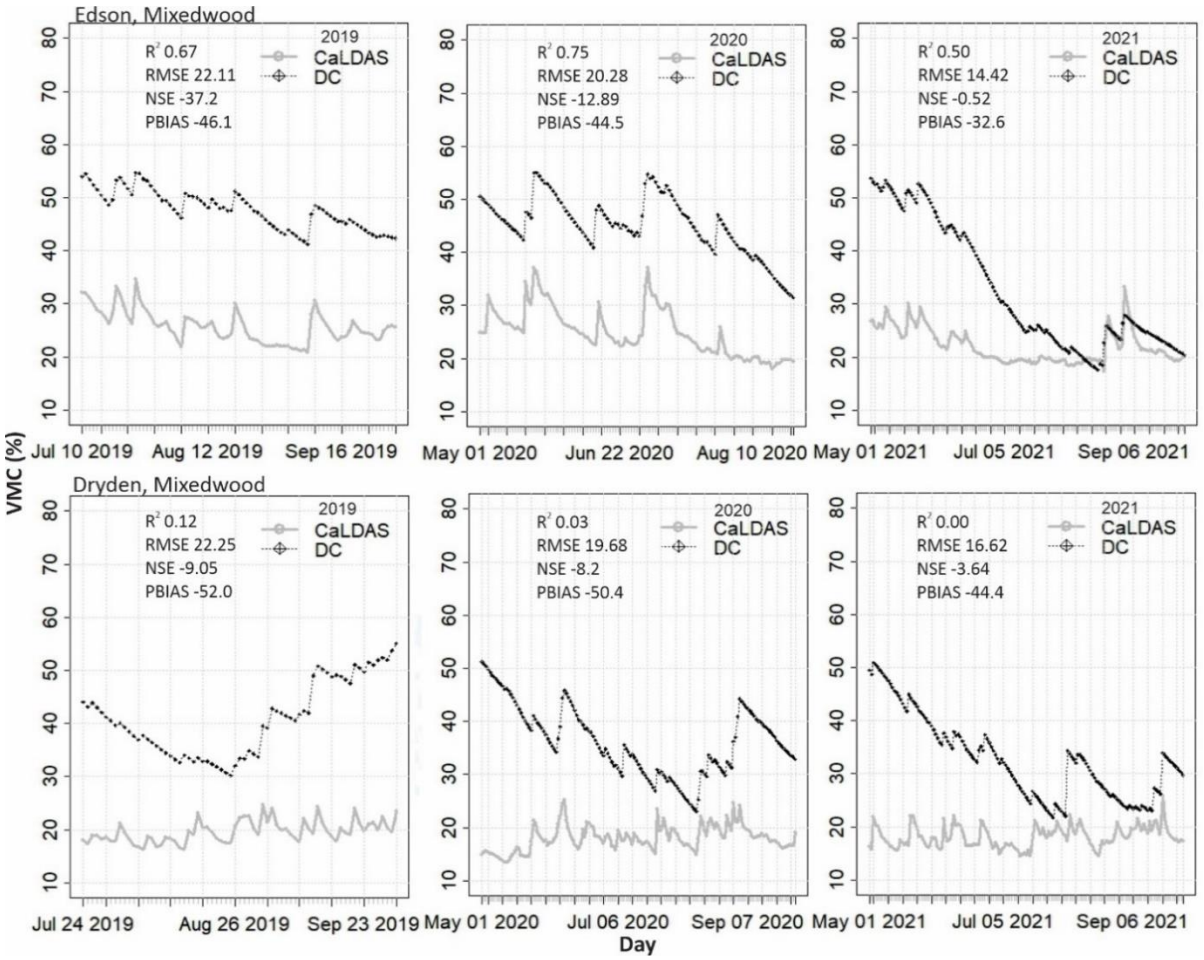

Figure 4. Example of a better match between DC (Drought Code) VMC (volumetric moisture content) and CaLDAS (Canadian Land Data Assimilation System) moisture for the Edson, mixedwood plot (top row) and a worse match for Dryden, mixedwood plot (bottom row). Goodness of fit statistics and time series are shown for 2019-2021. The black dotted line is the DC VMC. The grey line is the simulated CaLDAS estimated VMC for 10-20 cm.

Table 1. Goodness of fit statistics comparing field measured volumetric moisture content (VMC %) of the duff layer up to various depths compared to Drought Code (DC) estimated VMC calculated from the nearest fire weather station. Statistics listed (R^2, RMSE (Root Mean Square Error), NSE (Nash Sutcliffe Efficiency), Pbias (Percent Bias)) are for time series from 2019 – 2021, May until September, where field data permitted.

Site	Plot	Field Depth (cm)	R^2	RMSE	NSE	Pbias
Chapleau	Aspen	10	0.55	11.93	-2.44	39.8
		18	0.53	13.85	-5.95	51.7
	Jack pine	10	0.53	14.69	-5.28	58.2
		18	0.59	11.37	-1.57	37.5
	Black spruce	10	0.49	11.62	-2.37	37.1
		18	0.46	13.54	-5.81	48.6
	Mixedwood	10	0.74	9.64	-1.01	31.1
		18	0.83	5.99	0.70	9.6
Dryden	Mixedwood	10	0.73	7.39	0.6	11.3
		18	0.76	6.89	0.64	-8.3
Edson	Mixedwood	6	0.68	10.86	-0.70	-18.4
		10*	0.64	10.74	-0.56	-19.5
		30	0.69	16.05	-2.44	-28.3
REC	Aspen	10	0.55	0.47	0.32	-11.3
		18	0.58	0.51	0.43	-9.1

*no data for 2019

Table 2. Goodness of fit statistics comparing field measured volumetric moisture content (VMC %) of the duff layer up to various depths compared to Drought Code (DC) estimated VMC calculated from the nearest fire weather station. Statistics listed (R^2, RMSE (Root Mean Square Error), NSE (Nash Sutcliffe Efficiency), Pbias (Percent Bias)) are for time series from 2019 – 2021, May until September, where field data permitted.

Site	Plot	CaLDAS Depth (cm)	Field Depth (cm)	R^2	RMSE	NSE	Pbias
Chapleau	Aspen	0-5	10	0.27	11.89	-2.19	-37.5
			18	0.28	9.25	-2.10	-32.3
		5-10	10	0.34	11.2	-2.03	-37.1
			18	0.35	8.92	-1.88	-31.7
		10-20	10	0.46	11.94	-2.45	-41.0
			18	0.48	9.65	-2.37	-36.0
	Jack pine	0-5	10	0.11	7.72	-0.74	-22.2
			18	0.05	11.30	-1.53	-32.4
		5-10	10	0.14	7.65	-0.71	-22.7
			18	0.07	11.24	-1.51	-32.8
		10-20	10	0.18	7.92	-0.83	-25.0
			18	0.11	11.55	-1.65	-34.8
	Black spruce	0-5	10	0.18	11.00	-4.61	-35.7
			18	0.17	14.46	-4.24	-42.2
		5-10	10	0.20	10.95	-4.56	-35.7
			18	0.19	14.43	-4.22	-42.2
		10-20	10	0.24	11.32	-4.94	-37.4
			18	0.24	14.81	-4.50	-43.7
	Mixedwood	0-5	10	0.05	10.02	-1.17	-22.2
			18	0.10	15.94	-1.10	-35.0
		5-10	10	0.04	8.55	-0.58	-15.0
			18	0.08	14.49	-0.74	-28.9
		10-20	10	0.10	8.89	-0.71	-19.7
			18	0.18	14.94	-0.85	-32.9
Dryden	Mixedwood	0-5	10	0.10	17.40	-1.22	-41.8
			18	0.04	23.16	-3.06	-52.0
		5-10	10	0.11	17.38	-1.22	-41.7
			18	0.05	23.12	-3.05	-52.0
		10-20	10	0.11	17.63	-1.28	-42.7
			18	0.05	23.40	-3.15	-52.8
Edson	Mixedwood	0-5	10*	0.61	20.69	-4.80	-48.2
			30	0.44	29.52	-10.65	-56.2
		5-10	10*	0.58	19.23	-4.01	-44.2
			30	0.40	28.30	-9.71	-53.6
		10-20	10*	0.61	19.04	-3.91	-43.6
			30	0.41	28.16	-9.60	-53.3
REC	Aspen	0-5	10	0.04	30.20	-5.51	-61.5
			18	0.04	28.81	-5.53	-60.4
		5-10	10	0.19	29.01	-5.01	-59.6
			18	0.22	26.82	-4.87	-57.7
		10-20	10	0.33	29.49	-5.21	-61.1
			18	0.36	28.06	-5.20	-59.9

**does not include 2019*

Table 3. Goodness of fit statistics comparing Volumetric Moisture Content (VMC %) of the Drought Code (DC) to CaLDAS (Canadian Land Data Assimilation System) estimated VMC at three depths. Statistics listed summarize time series from 2019 – 2021, May until September where field data permitted, without considering any autocorrelation from day-to-day. Statistics listed include R^2, RMSE (Root Mean Square Error), NSE (Nash Sutcliffe Efficiency) and Pbias (Percent Bias).

Site	Plot	CaLDAS Depth (cm)	R^2	RMSE	NSE	Pbias
Chapleau	Aspen	0-5	0.04	22.27	-6.87	-55.3
		5-10	0.07	21.98	-6.66	-55.0
		10-20	0.15	22.82	-7.26	-57.8
	Jack pine	0-5	0.01	20.61	-5.95	-50.8
		5-10	0.01	20.62	-5.95	-51.1
		10-20	0.03	21.06	-6.25	-52.6
	Black spruce	0-5	0.01	20.48	-5.99	-50.8
		5-10	0.01	20.43	-5.95	-50.9
		10-20	0.02	20.82	-6.23	-52.1
	Mixedwood	0-5	0.19	16.78	-3.67	-40.7
		5-10	0.08	15.21	-2.83	-35.2
		10-20	0.29	15.82	-3.14	-38.8
Dryden	Mixedwood	0-5	0.02	21.44	-4.97	-51.1
		5-10	0.02	21.38	-4.94	-51.1
		10-20	0.02	21.65	-5.09	-51.9
Edson	Mixedwood	0-5	0.43	19.75	-2.31	-44.4
		5-10	0.46	18.65	-1.95	-41.1
		10-20	0.53	18.48	-1.9	-40.8
REC	Aspen	0-5	0.09	20.19	-1.5	-49.4
		5-10	0.35	18.774	-1.16	-46.3
		10-20	0.34	19.21	-1.27	-47.8

Increasing the resilience of transmission power lines to extreme events

Luis Mario Ribeiro*[1]; Miguel Almeida[1]; Domingos Viegas[1]; Pedro Marques[2]; João Gaspar[2]; Tiago Rodrigues[1]

[1]Forest Fire Research Centre. University of Coimbra, ADAI, Department of Mechanical Engineering, Rua Luís Reis Santos, Pólo II, 3030-788 Coimbra, Portugal.
{luis.mario, miguelalmeida, tiago.rodrigues}@adai.pt; xavier.viegas@dem.uc.pt
[2] REN, Portugal,{pedro.marques, joao.gaspar}@ren.pt

**Corresponding author*

Keywords

Infrastructure resilience; power lines; fire impact; fuel management; WUI

Abstract

Electricity transmission power lines are critical infrastructures in a country's electrical system, and wildfires represent extreme events that jeopardize their function. In addition, in the absence of proper vegetation management, these infrastructures can be the cause of ignition. The management of vegetation, or fuel, near these structures has specific rules, at least in Portugal, with the objective of protecting the infrastructure itself and minimizing the risk of ignition due to an electrical discharge or the physical contact of the vegetation with the conductors. The extent of the transmission power line network may hinder the application of extensive fuel management actions, and in many cases the trees that falls outside the fuel management that goes with it may also pose a danger.

This work explores the possibility of combining LiDAR with ancillary data and specific algorithms to identify those trees that may put the power line in danger in case they fall due to any external or internal circumstances. As a result of the application of the proposed methodology, it was possible to classify individual trees according to a risk class, as well as critical areas of intervention. With this information the Portuguese company REN, responsible for the transmission power line network, was able to plan and calendarize critical fuel management interventions in trees that fell outside the fuel breaks that they manage, but that posed imminent risk to the infrastructure.

1. Introduction

Urban infrastructures, such as power lines, are sometimes the cause of ignition (Miller et al., 2017; Viegas et al., 2017, 2019), and in case of a wildfire, their extension and diffusion in the landscape exposes them to a high probability of damage (Viegas et al., 2011). Some infrastructures have characteristics that, when hit by a fire, can lead to episodes of great danger. Besides being critical, many of these infrastructures are also strategic, since their affectation can compromise the response to the fire. The power (electric) network, water supply and natural gas infrastructures are good examples of this reality (Ribeiro et al., 2021).

In Portugal, as in many other countries, fuel breaks are maintained in the areas where the power lines are installed. This fuel (vegetation) management strategy aims fundamentally at 1) minimizing the probability of electrical cables producing ignitions, either by contact with vegetation or by discharges to the ground and 2) minimizing the probability of the fire affecting the structure itself, causing interruptions in the power supply. Although the importance of these strips may be higher in medium and low tension lines, because they are usually placed closer to the ground, the high and very high tension (VHT) lines have the same problems (Viegas et al., 2020). The width of these linear strips of fuel management depends on the voltage of the lines, and for the VHT that value is of 10 m for each side, counting from the most external line (Figure 1).

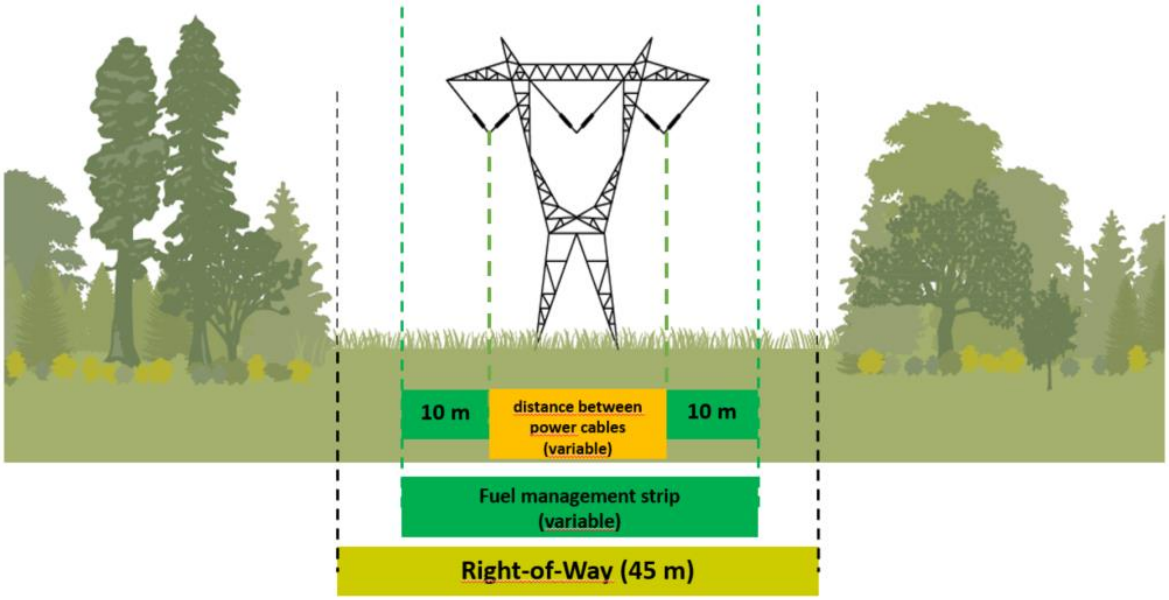

Figure 1. Power lines Fuel management strip vs. power lines right-of-way (RoW).

REN (*Rede Elétrica Nacional, SA*) is the Portuguese Transport System Operator (TSO) and is responsible for the operation and maintenance of the electric transport infrastructures. In their planning they have extended the fuel break width to at least 45 m, more than the legally mandatory distances, in what is called a "right-of-way" (RoW) strip, in a demonstration that their concern with all externalities that may pose danger to the infrastructure is very real. Nevertheless, often they identified several cases with the presence of trees that fall outside these linear fuel breaks that in case of falling, could potentially impact the cables. Trying to identify where and when this could happen was the genesis of this work, proposed to us by REN.

2. Objectives and methodology

The main goal of the work was to identify both individual trees that could impact on the electric power cables and critical areas of intervention where one or more trees could also pose danger to the infrastructure. The reason for having both outputs was to have a redundant mechanism, as the identification of individual trees may be subject to errors. Having in mind that the current fuel management is implemented in the RoW strip of at least 22.5m for each side of the line axis, it was a requisite that the analysis should be performed in an extension of that strip until 40 meters were reached (also counting from the axis of the line). The methodology consists in a series of algorithms implemented a sequence of models in ArcGIS Pro, allowing for a semi-automatization of the process of identification. It is based on the analysis of LiDAR and other ancillary data, mostly the possibility of identification of each pixel's height to the ground. Generically, for each point on the terrain of the analysis area, a critical tree height was calculated, from which, in case of a fall, trees may eventually contact the power line. The critical tree height is nothing more than the height relative to the ground of each pixel of the vegetation height layer created during the processing phase ($H_{critical\_pixel}$ in Figure 2). For this purpose, the height of the vegetation in the analysis area, the height of the lower power line and its maximum deflection (corresponding to the maximum arrow), i.e. the maximum deviation that the line can assume in relation to an imaginary line horizontally joining the two supports where it is inserted (Figure 3), were taken into account.

Figure 2 schematically presents the reasoning behind the process described and Figure 3 illustrates the concept of "maximum arrow".

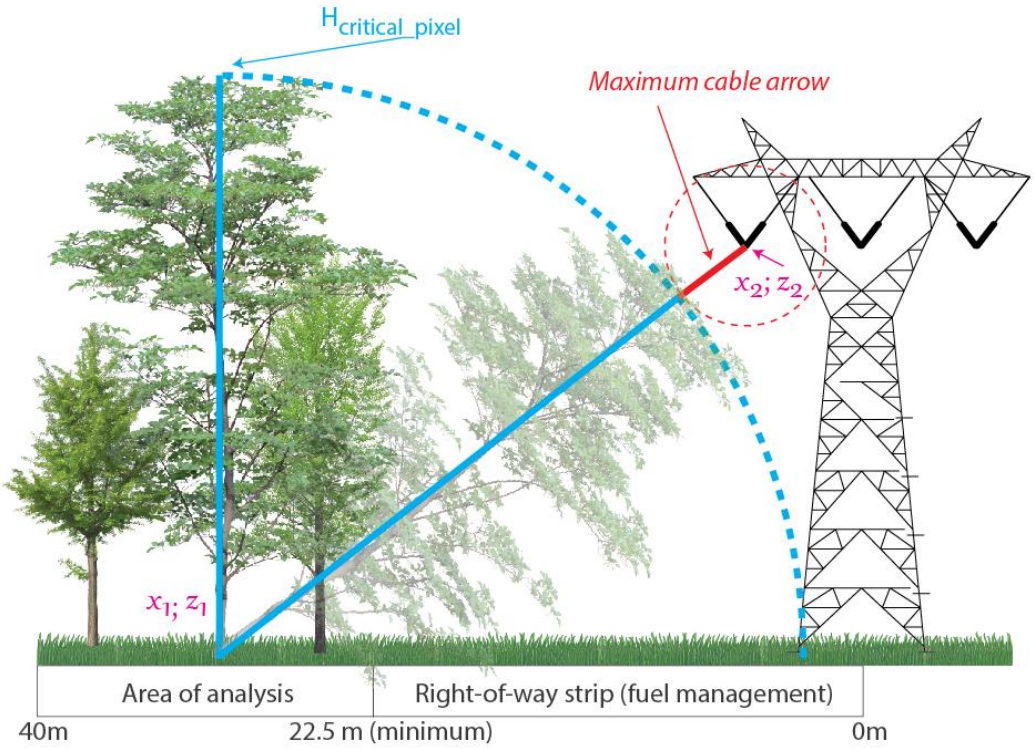

Figure 2. Simplified scheme of the relationship between critical vegetation height and maximum arrow (deflection).

The critical height was considered to be the height at which, if the tree falls, the curve it describes will cause it to touch the line, considering its arrow in the position closest to that curve. We also assumed the worst case scenario, i.e., that the tree falls with its axis of rotation at the point of contact with the ground, towards the line, while the cable wobbles with maximum deflection in its relative position on the line, towards the tree. Note that no whiplash effect was considered, although it can happen. Also, to simplify the algorithms, all power lines were considered to be of the same type (*Zambeze*) and the power line deflection to be in straight lines, forming 2 triangles between the imaginary straight line connecting the poles (black line connecting them in Figure 3) and the point of maximum deflection where the cable arrow is maximum (dashed blue line in Figure 3). The possible errors incurred by these assumptions are not significant in the overall analysis and having straight lines allows for the establishment of trigonometric relationships in the process.

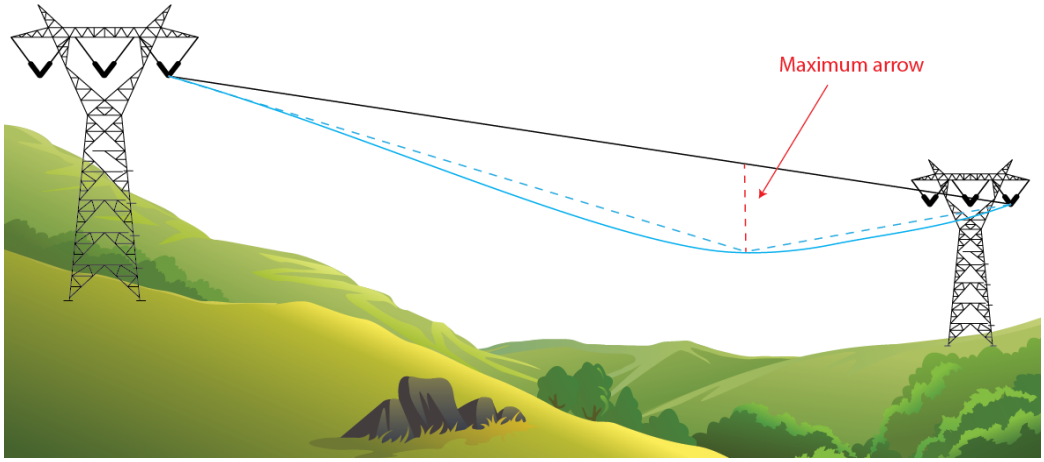

Figure 3. Concept of maximum arrow of deflection.

The calculation of this critical tree height, or pixel height, was performed using Equation 1.

$$\boldsymbol{H_{critic\_pixel}} = \sqrt{(x_1 - x_2)^2 + (z_1 - z_2)^2} - maximum\ arrow \qquad \textbf{Equation 1}$$

Where

$\boldsymbol{x_1}$ – Horizontal coordinate of each pixel to be analyzed, perpendicular to the line at point $\boldsymbol{x_2}$.
$\boldsymbol{x_2}$ – Horizontal coordinate of the line at each point, at the intersection location of a perpendicular of the line with the pixel being analyzed ($\boldsymbol{x_1}$).
$\boldsymbol{z_1}$ – Altitude of each pixel (= real height above ground).
$\boldsymbol{z_2}$ – The actual altitude that the line assumes at the intersection location of a perpendicular of the line with the pixel under analysis.
$\boldsymbol{maximum\ arrow}$ – Maximum distance of the horizontal line joining the two fixation points at the tangent to the maximum arc it actually makes.

Data preparation involved several consecutive operations, modelled in ArcGIS, and a brief resume is shown here.

2.1. Preparing and homogenizing data

The collected data from all lines was analysed for inconsistencies and stored with a common reference system in specific Geodatabases. The main datasets used were vectorial data from electric towers and power lines, alphanumeric data for tower characteristics (total height, height of cable insertion, dimension of cable connectors and width of cables insertion in relation to the axis) and LiDAR data.

2.2. LiDAR analysis and processing

The LiDAR data processing was divided in three steps. First the production of the raster layers for elevation (DEM), surface (DSM) and object height (or canopy height in the literature, CHM), based on the methodology described in ESRI (2020). This step included the metadata analysis, the quality assessment and the masking of the analysis area. The second step related to the individual trees identification, and was based on processes described in the existing literature, e.g. Popescu & Wynne 2004, Khosravipour et al., 2014 and Millikan et al., 2019. Finally, a visual inspection on LiDAR analysis, eliminating false positives, such as roofs, communication or electric towers, or other artificial or natural structures that were not trees. Figure 4 shows, from left to right, a) the insertion of one tower (yellow and black dot), the power line (orange line), the analysis area (red lines), b) the object height layer (CHM) and c) the individual trees identification prior to the visual inspection, showing the misidentification on roofs.

Figure 4. Example of the CHM and individual tree identification.

2.3. Powerlines and towers data processing

The maximum arrow for each line segment between poles was calculated following Sequeira (2009) and REN (2016). To achieve the best resolution possible in the final analysis, the power lines were then split into 1 m segments (to match the resolution of the DEM) and each segment was parametrized with all the needed variables for the models' calculation. Also, the towers were characterized with the needed parameters. Using trigonometric relations, the following variables were calculated: altitude of each 1-meter segment ($\boldsymbol{z_2}$), distance of each 1 meter segment to the axis of the line ($\boldsymbol{x_2}$) and the maximum arrow in each 1 meter segment (taking into account the real altitude of insertion of each tower).

2.4. Buffering variables to the analysis area

For the analysis of the possible intersection of the cables with the trees a raster processing methodology was adopted. The analysis area was populated with the variables needed at 1 meter resolution, with a process of buffering all the 1-meter segments of the power lines. The process was repeated for all the needed variables, creating as many raster files.

3. Results

The critical height of each pixel was calculated according to Equation 1 for each 1-meter cell of the analysis area. This height refers to the height a pixel should have (in this case the tree that stands on it) to impact on the power line in case it falls and in the worst possible conditions. The resulting raster layer with the critical height was then compared to the actual height of each pixel to assess if the trees were in fact posing a threat to the line, i.e., if the pixel was critical or not. The value of this critical pixel is the difference, in meters, between the height a tree should have to impact the line (if falling) and its real height. A risk scale was created assigning to each class a priority of intervention, as depicted in Table 1, allowing for the classification into critical areas of intervention.

The results of the analysis were obtained in the form of a raster layer for the critical areas of intervention and a vector layer for the individual critical trees. The critical height for each vector point was obtained from the respective raster layer.

Table 1. Risk levels, critical pixel value and priority of intervention.

Risk class	Risk	Critical pixel value (Pc)	Interpretation (in case a tree falls, for the worst scenario)	Priority of intervention
N/A	None	Pc < -7	No risk/no trees at risk of collision with the line	Ignored
I	Low	-7 ≤ Pc <-5	Tree has to grow at least 5-7 meters to reach the line	4
II	Medium	-5 ≤ Pc < -3	Tree has to grow at least 3-5 meters to reach the line	3
III	High	-3 ≤ Pc < 0	The tree is at the limit of being able to reach the line or not	2
IV	Very high	Pc ≥ 0	The tree has a height equal to or greater than the critical value from which it can hit the line	1

Figure 5 shows the result of the identification process, in the same area as the earlier example. From left to right we can see *a)* the raw critical pixel evaluation (the colours are merely indicative), *b)* the critical areas of intervention, as reclassified based on Table 1 (with the colours of the classes), and *c)* the respective critical trees.

Figure 5. Example of the processing results.

In total, 11 power lines were analysed, in a cumulative extension of more than 600 km and with an area subject to analysis of more than 2000 ha. Table 2 resumes the results for the priority of intervention 1 and 2.

Table 2. Resume of the results for priority levels 1 and 2.

Line	Entension (Km)	Analysis area (ha)	Area of intervention in priority 1 (ha)	Area of intervention in priority 2 (ha)	Number of trees in priority 1	Number of trees in priority 2
1	98.9	296.75	3.61 (1.22%)	3.81 (1.28%)	2137	2075
2	83.56	290.7	2.82 (0.97%)	2.48 (0.85%)	1729	1405
3	85.26	256.7	4.92 (1.92%)	3.81 (1.48%)	2994	2314
4	99.39	300.4	1.59 (0.53%)	1.39 (0.46%)	794	813
5	59.57	194.9	2.42 (1.24%)	1.44 (0.74%)	1155	580
6	21.18	63.9	1.18 (1.85%)	0.62 (0.97%)	553	568
7	75.54	226.6	1.51 (0.67%)	1.29 (0.57%)	709	753
8	23.25	70.2	0.41 (0.58%)	0.34 (0.48%)	216	176
9	34.49	130.4	3.40 (2.61%)	1.12 (0.86%)	1302	433
10	29.4	88.2	0.23 (0.26%)	0.31 (0.35%)	143	155
11	32.87	98.6	0.79 (0.80%)	0.67 (0.68%)	325	289

About 1.13 % of the total area was deemed as posing level 1 danger to the power line infrastructure, i.e., immediate risk of contact in case of falling. A total of 39205 trees were identified, being 12057 in class 1 and 9561 in class 2.

4. Validation and application

The validation of the methodology was performed by a series of field visits to the identified critical areas. In those areas, the critical trees were visually identified, and its height measured with a digital laser hypsometer. A total of 103 trees were visited and the relation between the observed and predicted height resulted in a R^2 of 0.98, which is representative of the good accuracy of the methodology. In terms of identification of trees, in some cases we identified points that were very close and referred to the same tree. This highlights the value of also producing the results as a raster of critical areas.

Since this work was developed, REN used the results to implement extraordinary fuel management actions in the areas identified, consisting of individual trees extraction (Figure 6), hence increasing the resilience of its infrastructure. Until now around 35500 trees were removed, but the work is still ongoing.

Figure 6. Example of an individual tree extraction, after being identified as critical.

5. References

ESRI. (2020). Data area delineation from lidar points—Help | Documentation. https://desktop.arcgis.com/en/arcmap/latest/MANAGE-DATA/LAS-DATASET/LIDAR-SOLUTIONS-DATA-AREA-DELINEATION-FROM-LIDAR-POINTS.htm

Khosravipour, A., Skidmore, A. K., Isenburg, M., Wang, T., & Hussin, Y. A. (2014). Generating pit-free canopy height models from airborne lidar. Photogrammetric Engineering and Remote Sensing, 80(9), 863–872. https://doi.org/10.14358/PERS.80.9.863

Miller, C., Plucinski, M., Sullivan, A., Stephenson, A., Huston, C., Charman, K., Prakash, M., & Dunstall, S. (2017). Electrically caused wildfires in Victoria, Australia are over-represented when fire danger is elevated. Landscape and Urban Planning, 167(July 2016), 267–274. https://doi.org/10.1016/j.landurbplan.2017.06.016

Millikan, P. H. K., Silva, C. A., Rodriguez, L. C. E., Oliveira, T. M. de, Carvalho, M. P. de L. C. e, & Carvalho, S. de P. C. e. (2019). Automated individual tree detection in amazon tropical forest from airborne laser scanning data. CERNE, 25(3), 273–282. https://doi.org/10.1590/01047760201925032630

Popescu, S. C., & Wynne, R. H. (2004). Seeing the trees in the forest: Using lidar and multispectral data fusion with local filtering and variable window size for estimating tree height. Photogrammetric Engineering and Remote Sensing, 70(5), 589–604. https://doi.org/10.14358/PERS.70.5.589

REN. (2016). Planeamento e Engenharia Projeto. Abertura da Linha Palmela – Fanhões, a 400 Kv para a Subestação de Alcochete. Memória Descritiva (Rev. 1).

Ribeiro, L. M., Viegas, D. X., Almeida, M., Alves, D., Barbosa, T., & Modarres, M. (2021). Planeamento da gestão de combustíveis : Efeito da distância e da frequência das limpezas na proteção das estruturas e rede viária. Relatório do Projeto financiado pela AGIF ao ForestWISE e subcontratado ao Centro de Estudos sobre incêndios Florestais da ADAI (Universidade de Coimbra).

Sequeira, N. (2009). Projecto de Linha Aérea de Alta Tensão conforme a norma EN50341-1. Relatório de Projecto Realizado No Âmbito Do Mestrado Integrado Em Engenharia Electrotécnica e de Computadores Major Energia. FEUP.

Viegas, D.X., Ribeiro, L. M., & Rossa, C. (2011). Incêndios Florestais (D.X. Viegas (ed.)). Verlag Dashöfer.

Viegas, Domingos Xavier, Almeida, M. A., & Ribeiro, L. M. (2020). Faixas de gestão de combustíveis. In M. J. Antunes, D. Lopes, & C. Oliveira (Eds.), Florestas e legislação: Planos Municipais Da Defesa Da Floresta Contra Incêndios. Instituto Jurídico Faculdade de Direito da Universidade de Coimbra. https://www.uc.pt/fduc/ij/publicacoes/pdfs/EbookFlorestas2019pdf

Viegas, Domingos Xavier, Almeida, M. A., Ribeiro, L. M., Raposo, J., Viegas, M. T., Oliveira, R., Alves, D., Pinto, C., Rodrigues, A., Ribeiro, C., Lopes, S., Jorge, H., & Viegas, C. X. (2019). Análise dos Incêndios Florestais Ocorridos a 15 de outubro de 2017. https://www.portugal.gov.pt/pt/gc21/comunicacao/documento?i=analise-dos-incendios-florestais-ocorridos-a-15-de-outubro-de-2017

Viegas, Domingos Xavier, Almeida, M. F., Ribeiro, L. M., Raposo, J., Viegas, M. T., Oliveira, R., Alves, D., Pinto, C., Jorge, H., Rodrigues, A., Lucas, D., Lopes, S., & Silva, L. F. (2017). O complexo de incêndios de Pedrógão Grande e concelhos limítrofes, iniciado a 17 de junho de 2017. Centro de Estudos sobre Incêndios Florestais (CEIF/ADAI/LAETA). https://www.portugal.gov.pt/pt/gc21/comunicacao/documento?i=o-complexo-de-incendios-de-pedrogao-grande-e-concelhos-limitrofes-iniciado-a-17-de-junho-de-2017

Influence of a sea-breeze front over a fire plume, Pedrogão Grande wildfires (20 June 2017)

Paulo Pinto*[1]; Álvaro Silva[1]; Domingos Viegas[2], Miguel Almeida[2], Luís Mário Ribeiro[2]

[1] Portuguese Institute for Sea and Atmosphere (IPMA), Rua C do Aeroporto, 1749-077 Lisbon, Portugal, {paulo.pinto, alvaro.silva@ipma.pt}
[2]Forest Fire Research Centre. University of Coimbra, ADAI, Department of Mechanical Engineering, Rua Luís Reis Santos, Pólo II, 3030-788 Coimbra, Portugal., {miguelalmeida, luis.mario}@adai.pt, xavier.viegas@dem.uc.pt

**Corresponding author*

Keywords

Sea-breeze front, pyroCumulus, weather radar, Dual-polarization

Abstract

During the afternoon of 20 June 2017, two massive wildfires were ongoing more than 30 km to the east-southeast of the city of Coimbra, central Portugal. There were no clouds over the location and surrounding areas. As these fires were progressing, smoke plumes were observed with their tops at around 6-7 km a.m.s.l. However, as a sea-breeze front arrived at the buoyancy sources it was observed an outstanding vertical growth of the plumes. One of these developments was particularly analyzed and it was found that the plume topped at nearly double that altitude in less than 60 min. As a result of this interaction, an impressive pyroCumulus cloud formed. This process was analyzed using weather radar with Dual polarization capabilities.

1. Introduction

The fire complex of Pedrogão Grande, during 17-22 June 2017, was considered as the worst on record in Portugal due to the large burnt area and related fatalities, as described in Viegas et al. (2017). The influence of a mesoscale convective system over the fires was analyzed in Pinto et al. (2022) for an event of 17 June.

Further from convective flows induced by meteorological systems, the progression of sea-breeze fronts (SBF's) over fire areas has also been described as an important mechanism of interaction with smoke plumes, generating transient, though significant, increase in fire intensity, as discussed by Hanley et al (2013). A SBF is the outcome of a thermally-driven mesoscale circulation that results from the differential heating over land and oceanic bodies. During the day, warmer and less dense air over land generates lower air pressure than over the ocean where cooler, denser air, resides. As a result, the mesoscale front propagates inland as the cooler air flows towards land to replace warmer air. These phenomena are known to trigger convection inland, as increased low-level convergence lifts the air and facilitates moisture convergence, Pielke et al. (1991). As a SBF propagates over a location, air moisture usually increases, temperature drops, wind direction may suddenly shift, gusts may be produced and air quality may also change, as shown by Miller et al. (2003). Coupled atmosphere-fire models are required to understand, in detail, the interaction between SBF's and the fires, as pointed out by Hanley et al (2013). However, the monitoring of the interaction between the SBF and the pyroconvective plume may suggest important impacts on the fire. During the afternoon of 20 June, a SBF was observed to propagate across the area where two fires were progressing.

2. Sea-breeze front

2.1. Numerical Weather analysis and forecast

At 12:00 (all times are UTC) of 20 June 2017, the UK Met Office mean sea-level pressure analysis showed a low to the west of Portugal and an anticyclone over central Mediterranean that was promoting the advection of a hot and dry airmass over western Iberia (Figure 1a). Over central Portugal the low-level flow was weak from the east-southeast, inland, and also light, but from the west-northwest along the coast as shown by the 12:00

ECMWF forecast (Figure 1b). Above 500 hPa (5900 m a.m.s.l.), at 12:00, the flow was from the west according to the rawinsonde from Lisbon (Figure 2). The sounding also showed an inverted-V type profile with relatively moist air in the 700-600 hPa layer but a dry airmass below 700 hPa (Figure 2). This typical profile has been referred in pyrocloud case studies such as Fromm et al. (2012) and Peterson et al. (2017).

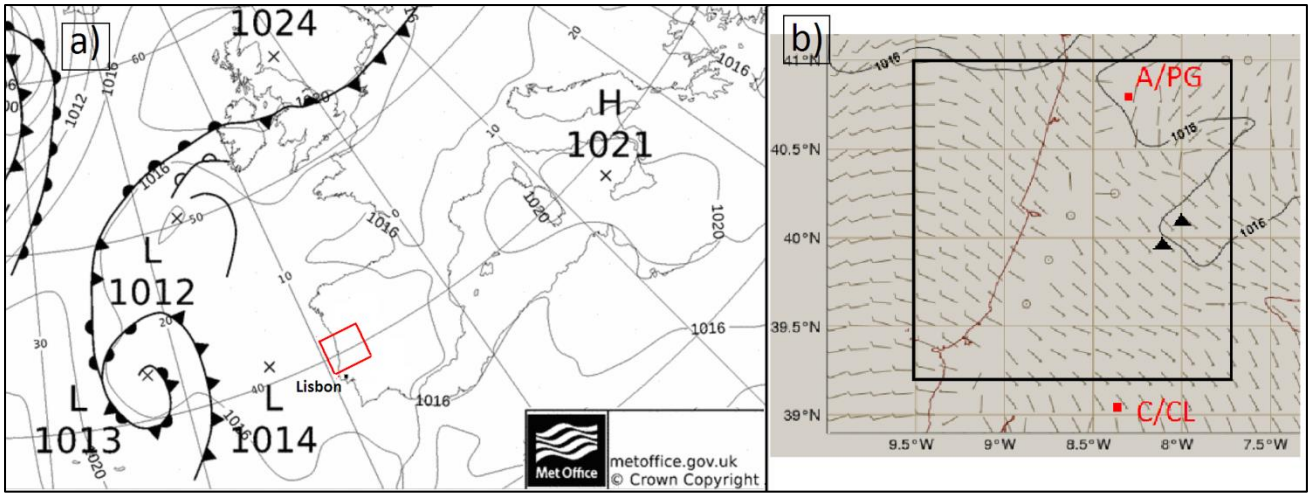

Figure 1- (a) Mean sea-level pressure analysis (solid contours, 4-hPa intervals) over the Northeast Atlantic (adapted from Uk Met Office), red square defines area in (b), Lisbon sounding station represented by a dot and (b) Zoomed-in area from (a) 10 m wind speed and direction (wind barbs notation) over mainland Portugal, ECMWF forecast H+12, black square defines central Portugal, A/PG and C/CL radars are represented by a red square symbol and fire locations are represented by black triangles, 12:00 UTC, 20 June 2017.

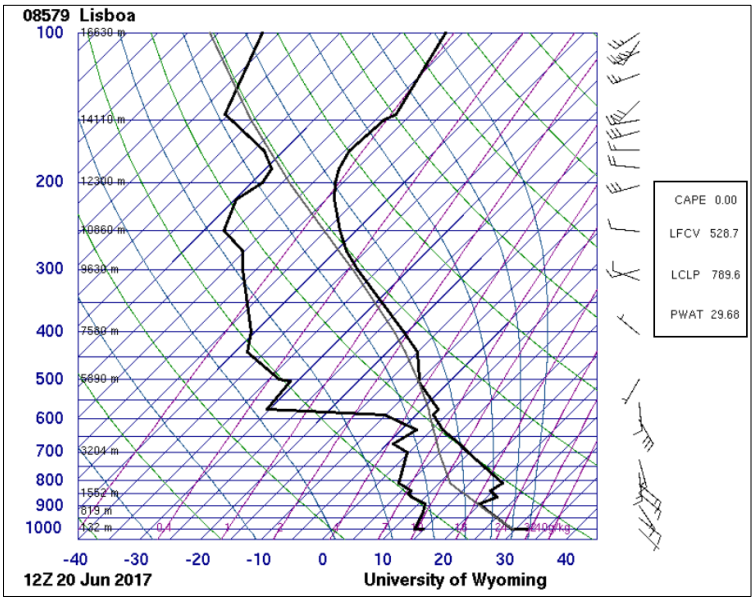

Figure2- Skew-T chart for rawinsonde profile for Lisboa station (08579) at 12:00 UTC, 20 June 2017 (location is indicated in Figure 1a). Dry bulb air temperature (black line, right), dew point temperature (black line, left), parcel trajectory (grey line, middle) and wind barbs at different levels are represented. Sounding indices: CAPE (J/Kg), LFCV (Level of free convection using virtual temperature, hPa), LCLP (Lifting condensation level, hPa) and Precipitable water for the entire sounding(8mm), adapted from University of Wyoming (http://weather.uwyo.edu/upperair/europe.html)

An area of low-level convergence (LLC) was identified to the west of the fires along a coastal strip in the 10 m wind forecast, at 12:00 (Figure 1b), coinciding with a large horizontal gradient in relative air humidity (Figure 3a). Dry air (<35%) was located to the east of the LLC whereas moister air was forecasted to the west of it (Figure 3a). Forecasts also showed that the LLC was separating warmer air to the east, from cooler air to the west, at 12:00 (not shown). Forecasts from 12:00, 15:00 and 18:00 anticipated that the LLC would propagate

eastwards, over the fires area (not shown) always separating cooler, moister air (Figure 3b,c) to its west, from warmer, drier air (Figure 3b,c) to its east. This was materializing the propagation of a SBF.

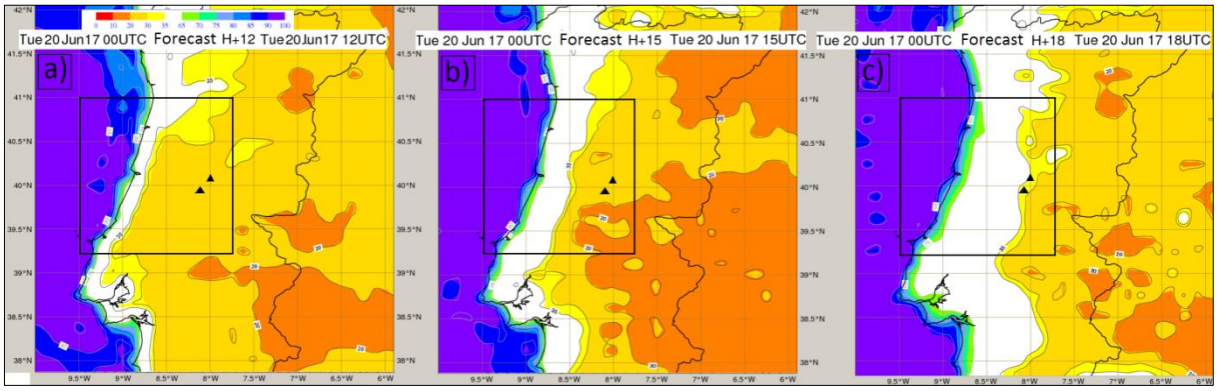

Figure 3- (a) 10 m Relative humidity (shaded, %) ECMWF forecast H+12, 12:00 UTC, (b) H+15, 15:00 UTC, and (c) H+18, 18:00 UTC, 20 June 2017. Fire locations are represented by black triangles.

2.2. Radar and surface observations

Two Doppler radars from the Instituto Português do Mar e da Atmosfera (IPMA) network were used. The Porto radar (A/PG), a dual polarization system (DP), it is located 100 km to the north of the fires (Figure 1b) and at 1100 m a.m.s.l.. The Lisbon radar (C/CL), a single polarization system (SP), it is located 100 km to the south of the fires (Figure 1b) and at 200 m a.m.s.l.. From each of the radar, reflectivity scan observations were extracted every 10 min. C/CL observations offered the best view of the low-level reflectivity due to the lower altitude of the beam, thus low elevation plane position indicators of reflectivity (PPZ) were extracted from this radar. The A/PG radar processed the correlation coefficient (ρhv) due to its DP technology.

Low-level reflectivity from C/CL radar was detected 400 m above two main active fires that were progressing in central Portugal (Figure 1b). The follow-up of reflectivity allowed the identification of the buoyancy sources (Figure 4). Visible channel satellite imagery (not shown) has confirmed that the sky was clear in the area, thus the fire plume was the only object detected on radar. Orientation of the plume and its evolution were derived from a reflectivity pattern extending downwind of the buoyancy sources (Figure 4b).

As a result of fires intensification, there is an increase in the combustion processes and in buoyancy that transport more and larger pyrometeors (McCarthy et al., 2019) upwards, according to McCarthy et al. (2019) and Jones et al. (2010). These effects will increase reflectivity (considering its dependency on the sixth power of the backscatterers diameter) and generate taller plumes. Thus, magnitude of low-level reflectivity close to the fire site and the vertical extent of the plume are good indicators of the general intensity of the strong convective processes caused by the fire (pyroconvection).

The parameter ρhv is a correlation, in a time series, between horizontally and vertically polarized echoes and is a fine particle type discriminator according to Balakrishnan et al. (1990). Lang et al. (2014), LaRoche et al. (2017) showed that fire particles exhibit ρhv values lower than those associated to hydrometeors. In accordance with Pinto et al. (2022), this study assumes that atmospheric volumes with $\rho hv \leq 0.7$ are mainly filled in by pyrometeors without significant condensation, whereas larger values correspond to atmospheric volumes with significant condensation/glaciation of pyrometeors.

Thin reflectivity lines that are traceable on radar may result from the local increase in reflectivity that is associated with the stacking of scatterers generated by low-level convergence. This can be associated with convective outflows, Srivastava et al. (1987), but also, as shown by Hanley et al (2013), with SBF's. A thin reflectivity line was identified on the lowest tilt from the C/CL scan during the afternoon of the 20 June (Figure 4).

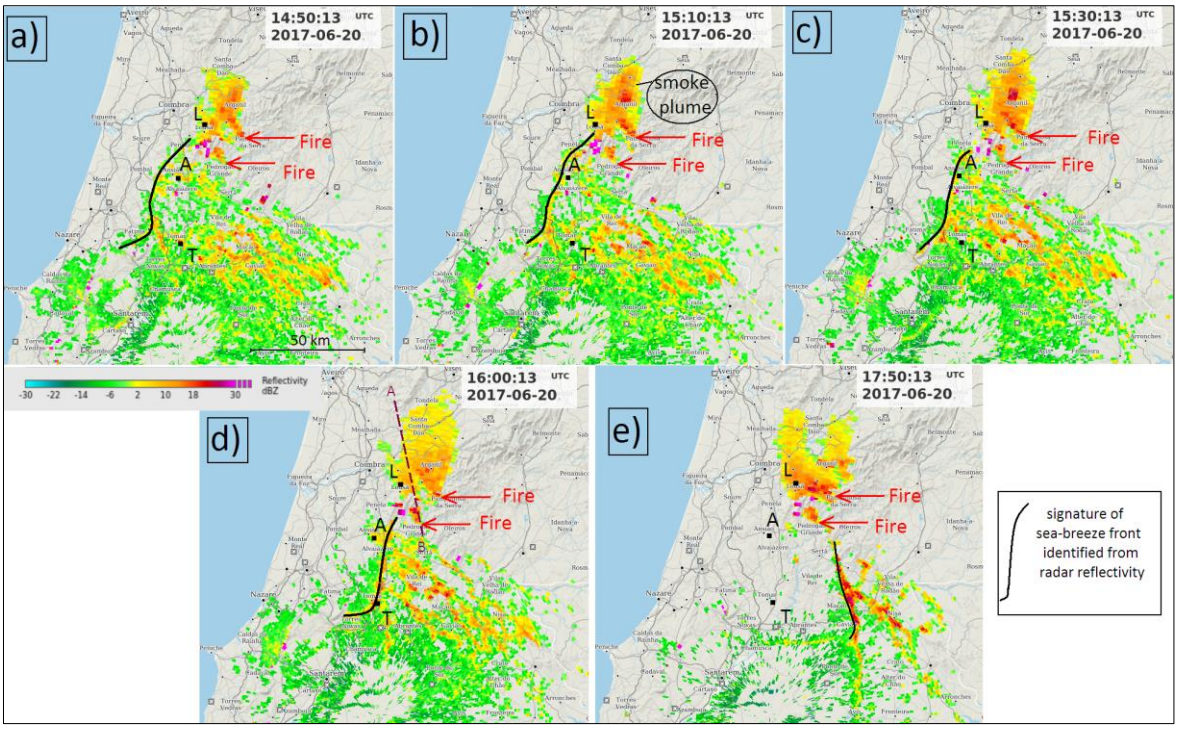

Figure 4- PPI of reflectivity, 0.1° tilt, 20 June 2017, C/CL radar. (a) 14:50 UTC, (b) 15:10 UTC, (c) 15:30 UTC, (d) 16:00 UTC, (e) 17:50 UTC. "L" Lousã, "A" Ansião, "T" Tomar AWS's. Buoyancy sources are represented by red arrows and "FIRE". "AB" dashed segment in (d) represents transect of the vertical section represented in Figure 7(a). "Smoke Plume" in a black circle in (b) highlights the pattern of a smoke plume.

The line started to be identified at 14:50, still to the west of three automatic weather stations (AWS) of IPMA (Figure 4a). Two-meter air temperature and relative humidity, 10m wind gusts and average wind speed and direction, were recorded every 10min. At this time AWS's ("L", Lousã; "A", Ansião; "T", Tomar) were influenced by a hot and dry airmass (40 °C, < 25%) and light winds from the south or southeast (Figure 5). The line was propagating eastwards and as it arrived at "L" by 15:10 the AWS started to record a decrease in air-temperature and an increase in relative humidity. However, the sudden shift to a westerly flow was the most noticeable change (Figure 5c). The other AWS's remained under the influence of a hot and dry airmass (Figure 5a,b). By 15:30, as the line arrived at "A" (Figure 4c) the AWS started to record a substantial decrease in air-temperature and increase in relative humidity (Figure 5b). It was also observed a shift to a westerly flow and average wind and gusts increment (Figure 5b). "T" AWS, still located to the east of the line (Figure 4c), remained under the influence of a dry and hot airmass in southeasterly winds (Figure 5a). At 16:00, as the thin line finally arrived at "T" (Figure 4d), the AWS recorded the same qualitative changes observed in the other AWS, concurrently with the thin line arrival (Figure 5a). By this time, the three AWS were being influenced by a cooler and moister airmass than before. These observations showed that the thin reflectivity line that was identified on low-level reflectivity was, indeed, coherently associated with the propagation of a SBF. The findings were similar to those documented by Hanley et al. (2013). This behavior confirmed the forecasts of the ECMWF and highlighted the fine performance of the model for this event (Figure 3).

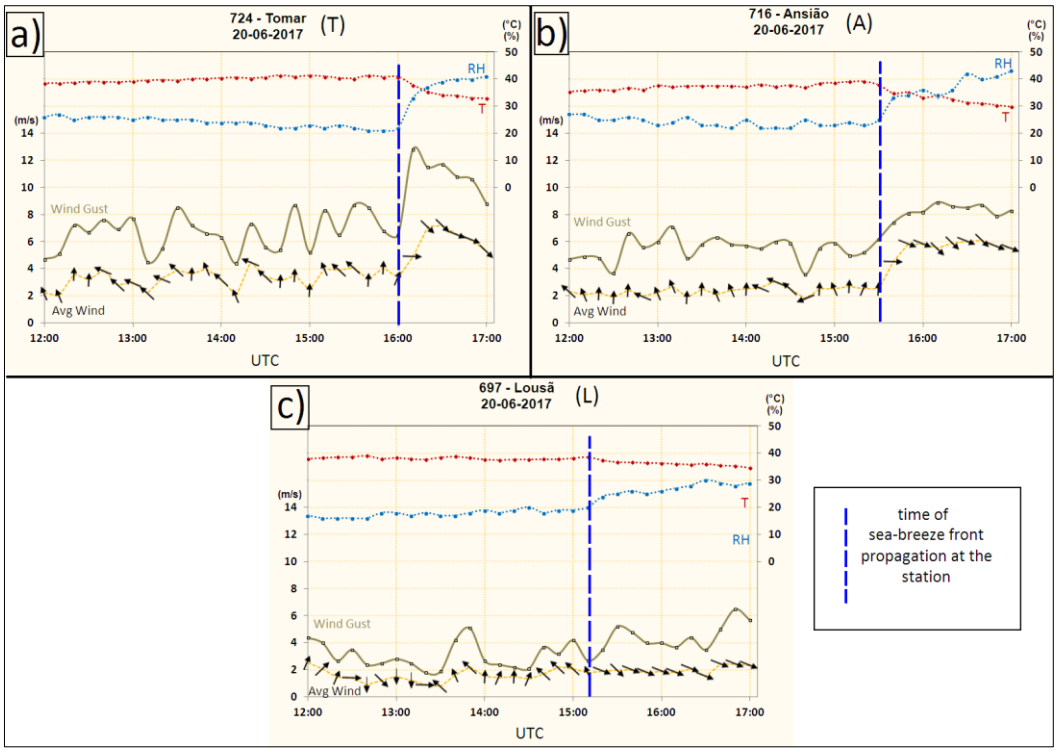

Figure 5- Weather observations at the AWS (a) Tomar ("T"), (b) Ansião ("A"), (c) Lousã ("L"). 2m air temperature (T, red), relative humidity (RH, blue), magnitude of 10 m wind gusts (green cyan), magnitude of 10 m average wind (dotted black line) and direction (arrows) observed during 12:00-17:00 UTC, 20 June 2017.

3. Influence of the sea-breeze front over the fire plume: pyroCumulus formation

The magnitude of low-level reflectivity close to buoyancy sources was monitored according to a method described in Pinto et al. (2022). The monitoring for the southwest fire (Figure 4) yielded magnitudes of 9-16 dBZ for the period 14:50-15:50 (Figure 4a,b,c). Then, from 15:50 to 16:00, an increase from 16 to 21 dBZ was noticed for this fire. At 16:10 a similar value was observed and slightly lower values were found afterwards (not shown).

Miller et al. (2003) show a diagram (their figure 9) of the simplified two-dimensional flow of a gravity current such as a SBF. Their study refers to a SBF head that may extend for more than 2000 m above the surface and explains that the flow of the pre-frontal area may promote convective activity due to the favored vertical motions. On this concern Hanley et al. (2013) have noticed that the reflectivity of a smoke plume increased substantially when a SBF was approaching the fire, but still 5-7 km upwind of it (their Figure 7.3) and considered that this was the result of enhanced low-level convergence and vertical motion ahead of the front.

The increase observed in reflectivity at 16:00, however seeming small in dBZ units, it equates to a large difference in base linear reflectivity units, since the factor is logarithmic due to its dependency on the sixth power of the scatterers diameter. Thirty minutes before this increase has occurred, the SBF was 15 km to the west of the buoyancy source (Figure 4c) but at 16:00 it was only 5 km to the west of it (Figure 4d). This sudden and transient increase on low-level reflectivity by 16:00-16:10 is considered as a result of the direct influence of the approaching SBF over the plume, similar to the case studied by Hanley et al. (2013). The SBF continued to propagate eastwards and at 17:50 was still detectable on radar but displaced to the east of the fires (Figure 4e).

The pyroconvective plume was observed in low-level reflectivity at 500 m above the fires, as a V-shape pattern extending northwest of the buoyancy sources, driven by the flow at that level (Figure 4, Figure 6). Two independent plumes were identified as departing from each buoyancy source, but merged downwind of them due to fires proximity (Figure 4, Figure 6). The plume of the southwest fire looked discontinuous due to strong clutter cancelation effects over the mountainous area located to the northwest of the buoyancy source. This can be seen with the C/CL radar (Figure 6) but also with the A/PG radar (Figure 7). Still, it can be observed a larger

magnitude of the reflectivity in the area of the plume slightly downwind of the fire, close to "L" at 16:30 (Figure 6a), when compared to the value observed at 16:00 (Figure 4d). At 16:40 an even larger reflectivity (41, 5 dBZ) was observed in the same area of the plume (Figure 6b).

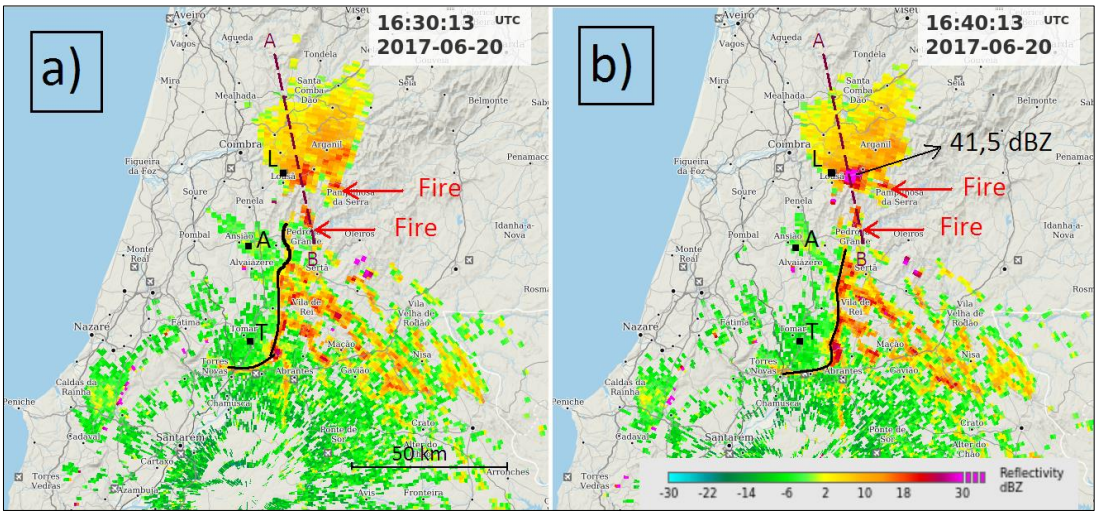

Figure 6- PPI of reflectivity, 0.1° tilt, 20 June 2017, C/CL radar. (a) 16:30 UTC, (b) 16:40 UTC. "L" Lousã, "A" Ansião, "T" Tomar AWS's. Buoyancy sources are represented by red arrows and "FIRE". "AB" dashed segment in (a) represents transect of the vertical section represented in Figure 7(c). "41,5 dBZ" highlights large magnitude reflectivity.

A sequence of static vertical sections of reflectivity and ρhv illustrates the vertical growth of the smoke plume and its transition to a pyrocumulus cloud (Figure 7). At 16:00 the smoke plume top was at 6000-7000 m a.m.s.l., as in previous observations (not shown). Its reflectivity (Figure 7a, upper) was produced by pyrometeors (ρhv ≤ 0.7, greenish colors in Figure 7a, lower), without significant condensation. This was consistent with the observed LFCV (Level of Free Convection from virtual temperature) at 5600 m a.m.s.l. at 12:00 (Figure 2). However, as the SBF started to influence the plume, it was noticed a vertical expansion of it, so that by 16:30 the top was at 9000 m (Figure 7b, upper). By then there were signs of condensation/glaciation in upper levels (ρhv > 0.7; yellowish colors in Figure 7b, lower). At 16:50 its top was at 12500 m, reflectivity attained 50.5 dBZ in the convective core (3500 m a.m.s.l.), 40 dBZ at 1200 m altitude (Figure 7c, upper) and condensation arrived at low levels (Figure 7c, lower). The hydrometeor algorithm (not shown) classified as *rain*, *graupel* and *hail* large fractions of the pyrocumulus transect, suggesting that some precipitation may have reached ground levels but there was no ground truth to verify it. This pyrocumulus peaked at 13000 m by 17:00 (not shown) and started to lose buoyancy afterwards, lowering as observed at 17:20 (Figure 7d). A photograph taken from Coimbra, 25 km to the west, shows the outstanding pyroCu at 16:48 (Figure 8).

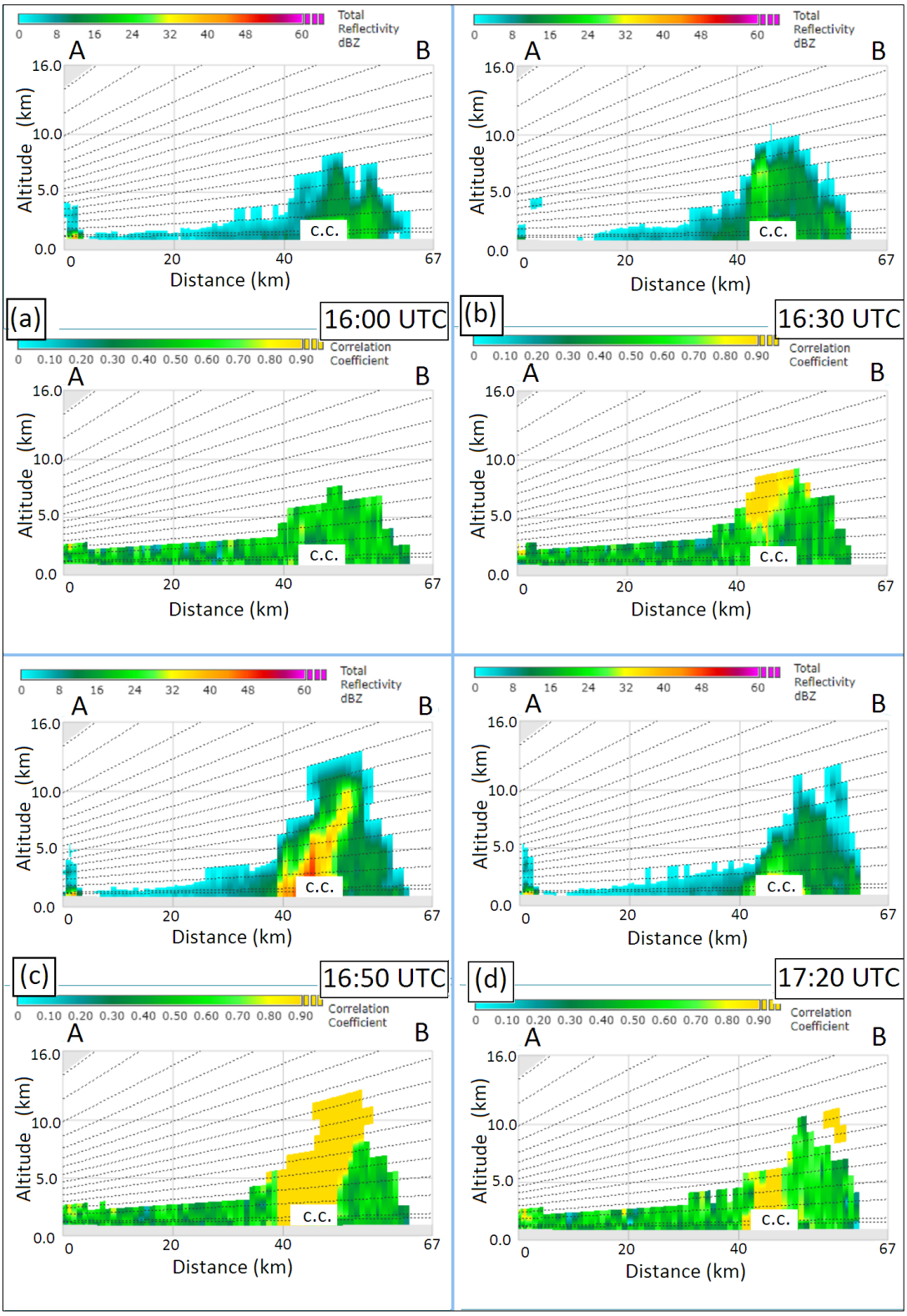

Figure 7- Vertical sections of reflectivity ((a), (b, (c), (d), upper) and of ρhv ((a), (b), (c), (d), lower), 20 June 2017, A/PG radar. (a) 16:00 UTC, (b) 16:30, (c) 16:50 UTC, (d) 17:20 UTC. Horizontal axis with distance marks every 20 km up to 67 km. Vertical axis with distance marks every 5 km up to 16 km."C.C." white rectangle depicts the area contaminated by strong clutter cancelation. Greenish colors represent smoke, yellowish colors represent condensation/glaciations of pyrometeors. (see figures 4 and 6 for reference of the transect location).

Figure 8- Photograph of the pyrocumulus cloud taken from Coimbra, at 16:48 UTC, 20 June 2017 (note: confront with Figure 7c). Extracted fromViegas et al. (2017).

4. References:

Balakrishnan, N.; Zrnic, D.S. Use of Polarization to Characterize Precipitation and Discriminate Large Hail. J. Atmos. Sci. 1990, 47, 1525–1540. https://doi.org/10.1175/1520-0469(1990)047<1525:UOPTCP>2.0.CO;2

Fromm, M. D., R. H. D. McRae, J. J. Sharples, and G. P. Kablick III, 2012: Pyrocumulonimbus pair in Wollemi and Blue Mountains national parks, 22 November 2006. Aust. Meteor. Oceanogr. J., 62, 117–126, *https://doi.org/10.22499/2.6203.001*.

Hanley, D., Cunningham, P., Goodrick, S. 2013. Interaction between a wildfire and the sea-breeze front. In Qu, John J., Sommers, William T., Yang, Ruixin; Riebau, Allen R. (eds.). Remote sensing and modelling applications to wildland fire. Beijing, China: Tsinghua University Press and New York Spirnger. Pgs. 81 - 98

Jones, T.A.; Christopher, S.A. Satellite and radar observations of the 9 April 2009 Texas and Oklahoma grassfires. Bull. Am. Met. Soc. 2010, 91, 455–460. https://doi.org/10.1175/2009BAMS2919.1

LaRoche, K.T.; Lang, T.J. Observations of Ash, Ice, and Lightning within Pyrocumulus Clouds Using Polarimetric NEXRAD Radars and the National Lightning Detection Network. Mon. Weather Rev. 2017, 145, 4899–4910. *https://doi.org/10.1175/MWR-D-17-0253.1*.

Lang, T.J.; Rutledge, S.A.; Dolan, B.; Krehbiel, P.; Rison, W.; Lindsey, D.T. Lightning in Wildfire Smoke Plumes Observed in Colorado during Summer 2012. Mon. Weather Rev. 2014, 142, 489–507. https://doi.org/10.1175/MWR-D-13-00184.1.

McCarthy, N.; Guyot, A.; Dowdy, A.; McGowan, H. Wildfire and Weather Radar: A Review. J. Geophys. Res. 2019, 124, 266–286. https://doi.org/10.1029/2018JD029285

Miller, S.T.K., Keim, B.D., Talbot, R.W., Mao, H. Sea breeze: Structure, forecasting, and impacts.. Reviews of Geophysics, Volume 41, Issue 3

Peterson, D. A., E. J. Hyer, J. R. Campbell, J. E. Solbrig, and M. D. Fromm, 2017: A conceptual model for development of intense pyrocumulus in western North America. Mon. Wea. Rev., 145, 2235–2255, *https://doi.org/10.1175/MWR-D-16-0232.1*.

Pielke, R.A., Song, A., Michaels, P.J., Lyons, W.A., Arritt, R.W.. The predictability of sea-breeze generated thunderstorms. Atmósfera, vol. 4,. núm. 2, abril, 1991, pp. 65-78. Universidad Nacional Autónoma de México. Distrito Federal, México

Pinto, P.; Silva, A.P.; Viegas, D.X.; Almeida, M.; Raposo, J. Influence of Convectively Driven Flows in the Course of a Large Fire in Portugal: The Case of Pedrógão Grande. Atmosphere 2022, 13, 414. https://doi.org/10.3390/atmos13030414

Srivastava, R. A model of intense downdrafts driven by the melting and evaporation of precipitation. J. Atmos. Sci. 1987, 44, 12, 1752–1774. https://doi.org/10.1175/1520-0469044<1752:AMOIDD>2.0.CO;2

Viegas, D.X.; Almeida, M.; Ribeiro, L.; Raposo, J.; Viegas, M.T.; Oliveira, R.; Alves, D.; Pinto, C.; Humberto, J.; Rodrigues, A.; et al. O Complexo de Incêndios de Pedrógão Grande e Concelhos Limítrofes, Iniciado a 17 de Junho de 2017. ADAI-CEIF, Coimbra. 2017 (In Portuguese). Available online http://www.portugal.gov.pt/donwload-ficheiros/ficheiro.aspx?v=3bb97773b-59fb-4099-9de5-a22fdcad1e3b (accessed on 12 November 2021).

k-PERIL: probabilistic creation of trigger boundaries for rural communities evacuating from a wildfire

Nikolaos Kalogeropoulos; Harry Mitchell; Guillermo Rein*

Imperial College London. South Kensington Campus, SW7 2AZ, London, UK
{nikolaos.kalogeropoulos17, harry.mitchell15, g.rein}@imperial.ac.uk

**Corresponding author*

Keywords

Evacuation Modeling, Evacuation planning, Management Support System, WUI Fires, Decision Support

Abstract

Evacuation is a critical part of wildfire emergencies. Emergency managers must be prepared to issue evacuation notices to areas that could be in the path of a wildfire to protect lives. There are methods of establishing when an evacuation should be called for any given urban area. One option is the creation of trigger boundaries around populated areas. This boundary is formed so that, should the wildfire cross it, a triggered evacuation will be complete before the wildfire becomes a threat to the area by threatening the community.

Models already exist for calculating the trigger boundary around an area, and each have their strengths and limitations. WUIVAC by Li et. al. (2015) is a robust tool that can calculate the trigger boundary of an urban area, for any one simulated fire. However, it can only model trigger boundaries for one wildfire at a time and thus cannot capture the susceptibility of the area to any possible wildfire. Ramirez et. al. (2019) created a tool to calculate the probabilistic trigger boundary of an area by simulating all possible fires that may threaten the urban area. This tool is effective for management and planning, but is incredibly resource-intensive and limited in terms of letting the user specify which area is most likely to suffer from a wildfire.

To address this, the k-PERIL algorithm was developed to calculate the trigger boundary of an urban area, as an upgraded version of the PERIL algorithm (Mitchell et. al, 2019). The user can load a single simulated wildfire, through software like FARSITE, and an evacuation time and get an exact trigger boundary for a specified urban area. The user can also load multiple wildfire simulation results for a given area, and K-PERIL will then generate a probabilistic trigger area. The user can then choose to retrieve a singular boundary of the area based on a probability value; It was made as part of the WUINITY project, by Ronchi et. al (2020), a self-contained wildfire simulation and evacuation planning tool.

To introduce k-PERIL as a tool of calculating trigger boundaries, this paper presents the a study on creating trigger boundaries for Roxborough Park, an urban area near Denver, CO, USA. A fire ignition area was specified and a number of wildfires with varying weather inputs were created, and a probabilistic boundary was created. The testing program allowed the user to specify the average weather values and standard deviations of their area of interest, specify an area where ignition is most likely, and specify the number of simulated wildfires. Testing for single-wildfire boundaries will be conducted in the full paper.

The results show that the results follow the current understanding of wildfire propagation. The resulting shapes are more accurate when more test cases are loaded, and are wider when the input variables are more varied. K-PERIL can thusly be used to create both specific and probabilistic boundaries around an inhabited area, either for immediate response or long-term planning.

1. Introduction

Wildfire emergency managers currently rely on their experience and intuition to call an evacuation when a Wildlife-Urban Interface (WUI) area is at risk [Pyne, Andrews, Laven 1996]. If the evacuation is called too soon, critical resources may be diverted from an area that needs them more; if it is called too late, lives may be at risk [Thomas, McAlpine 2010]. Trigger boundaries are a method of calculating the ideal time to trigger an evacuation, by coupling the decision-making process with the physical position of the fire.

1.1. Trigger Boundaries

Trigger boundaries set an area around an urban area at risk. For a given Wildfire Required Safe Egress Time (WRSET), the boundary is formed so that, when the fire reaches any point in the boundary, the urban area has

an ASET amount of time before the fire reaches the urban area. This can be explained schematically using Figure 1.

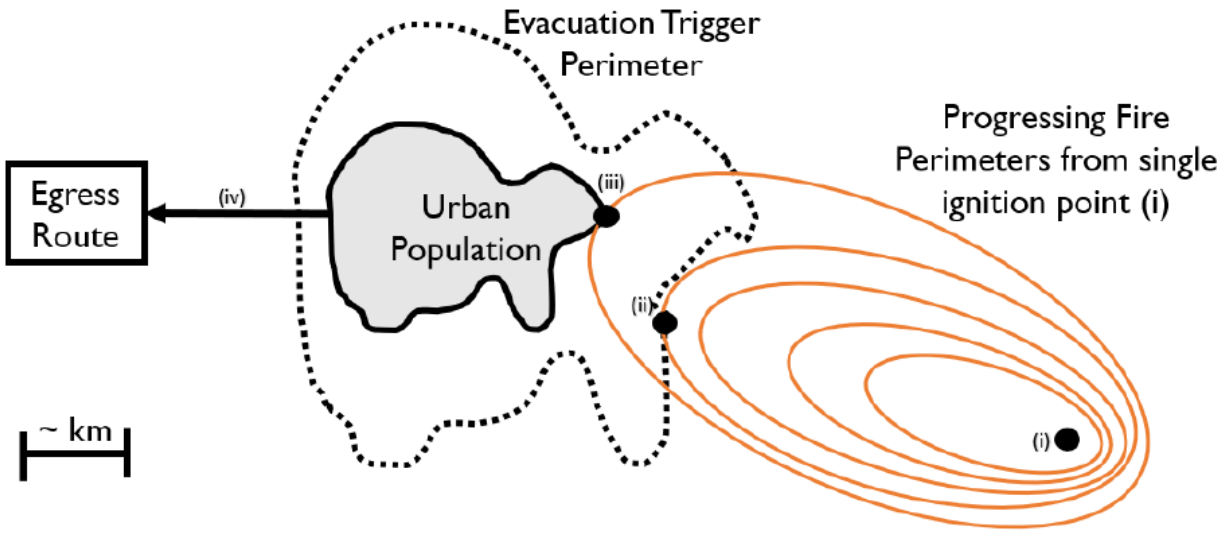

Figure 1- Schematic of the function of trigger boundaries (here referred to as trigger perimeters) [6]. A fire starts at timestep (i). At timestep (iii) the fire has reached a designated urban population. An ASET amount of time before timestep (iii), the fire was at timestep (ii). The locus of all the points where the fire is an ASET amount of time away from the urban node is the trigger boundary.

Currently there is no universally used method of analytically deducing trigger buffers by practitioners, but there is a number of models that attempt to calculate the safety boundary. The most popular such model is HURREVAC [A Hurricane Decision Support Tool For Government Emergency Managers] although it is made to calculate trigger boundaries for hurricane-prone coastal areas. Below is a presentation of trigger boundary calculation programs created specifically for wildfire risk.

1.2. Previous models

1.2.1. WUIVAC

WUIVAC [Dennison, Cova, Mortiz 2007] [Li, Cova, Dennison 2015] is an open-source model that uses Rate of Spread data from wildfire simulations to calculate the trigger boundary for any given urban area. WUIVAC has been used in applied test cases such as one involving the 2003 Cedar Creek fire [Larsen et. al. 2011], though none of them have been experimentally validated. One setback of the program is it can only be used to create one boundary at a time, so if a sensitivity or long-term planning study was needed, the program would be cumbersome to use.

1.2.2. Ramirez et. Al.

Ramirez et. Al [Ramirez et. al. 2019] calculate safety buffers using a different approach. They simulate wildfires as well, but set the simulated time duration equal to WRSET, and then run one hundred simulations, with normally distributed starting conditions. While this method is very thorough, it is also computationally expensive and inefficient. It also does not account for the acceleration phase of wildfires or other effects that fully developed wildfires may induce [Thomas, McAlpine 2010]. It also cannot run a study for a singular fire, should that need arise.

1.2.3. PERIL and K-PERIL

PERIL [Mitchel, Rein 2019a] [Mitchell et al. 2019b] is a program created based on the working principles of WUIVAC. It too uses wildfire simulations to calculate arrival times, and then creates a weighted point network to find the trigger boundary. The long-term goal of PERIL is to be integrated in the greater WUINITY project [Mallick, 2021] [Ronchi et al. 2020] [Wahlqvist et al. 2021]. WUINITY is a project aiming to provide a coupled wildfire-evacuation model that accounts for wildfire propagation, pedestrian and vehicular evacuation.

k-PERIL is the next iteration of the PERIL program, which enables the running of both single-fire studies and probabilistic studies. It uses the same core algorithm as PERIL but outputs a matrix of all the points that are inside the trigger boundary. It can then compound each output matrix for multiple cases and thus create a probabilistic boundary based on how many boundaries include each point. PERIL has been used in a real case before, but k-PERIL has only been verified in simple cases, when compared to PERIL. This is the first study where k-PERIL is used in a real-life situation.

2. Objectives

In this study, we set out to test k-PERIL in a real-life case. The urban area selected for the test is an area around Roxborough Park, an urban area south of Denver, CO, USA (figure 2) that has undergone extensive evacuation testing and documenting thereof as part of the WUI-NITY studies [Mallick 2021]. The primary risk of fire considered is ignition in the shrubland south of the area, with southern winds guiding the fire towards the urban area.

3. Methods

For this analysis, a custom testing suite was created, that generated several custom FARSITE [Finney 1998] simulations and run them through a command-line version of FARSITE [Fire Behavior Applications and libraries 2021]. The results were then given to k-PERIL and the boundary of each simulation was calculated. The boundaries were then summed to a probabilistic overall boundary around the urban area. FARSITE was used here because of its position as a universally accepted accurate wildfire simulation model, and because of the availability of the command line version. However, any wildfire simulation software (or, in fact, any Rate of Spread data) can be used to create the inputs, such as WFDS or Prometheus.

The inputs to FARSITE were specified assuming a normal distribution of all the available weather input values. A sample of the normal distribution of the input data for a test case is given in Figure 3. The fuel moisture was specified as constant and identical for all fuels, as fuel moisture data is difficult to obtain. The wind direction was made to always point towards the urban area to ensure the simulated wildfire would always reach the urban area (this was in accordance with the average wind direction given by the closest Remote Automatic Weather Station (RAWS)). The temperature and moisture data were extrapolated to a diurnal profile. The ignition location was chosen randomly from a specified area in the raster (figure 2). The WRSET time was set at 110 minutes, from [Mallick, 2021].

The parameters used for the fuel moisture are:

- Fuel models: 0 -245
- 1-Hour Fuels: 4 tons m^{-2}
- 10-Hour Fuels: 6 tons m^{-2}
- 100-Hour Fuels: 13 tons m^{-2}
- Live Herbaceous moisture content: 30%
- Live Woody moisture content: 60%

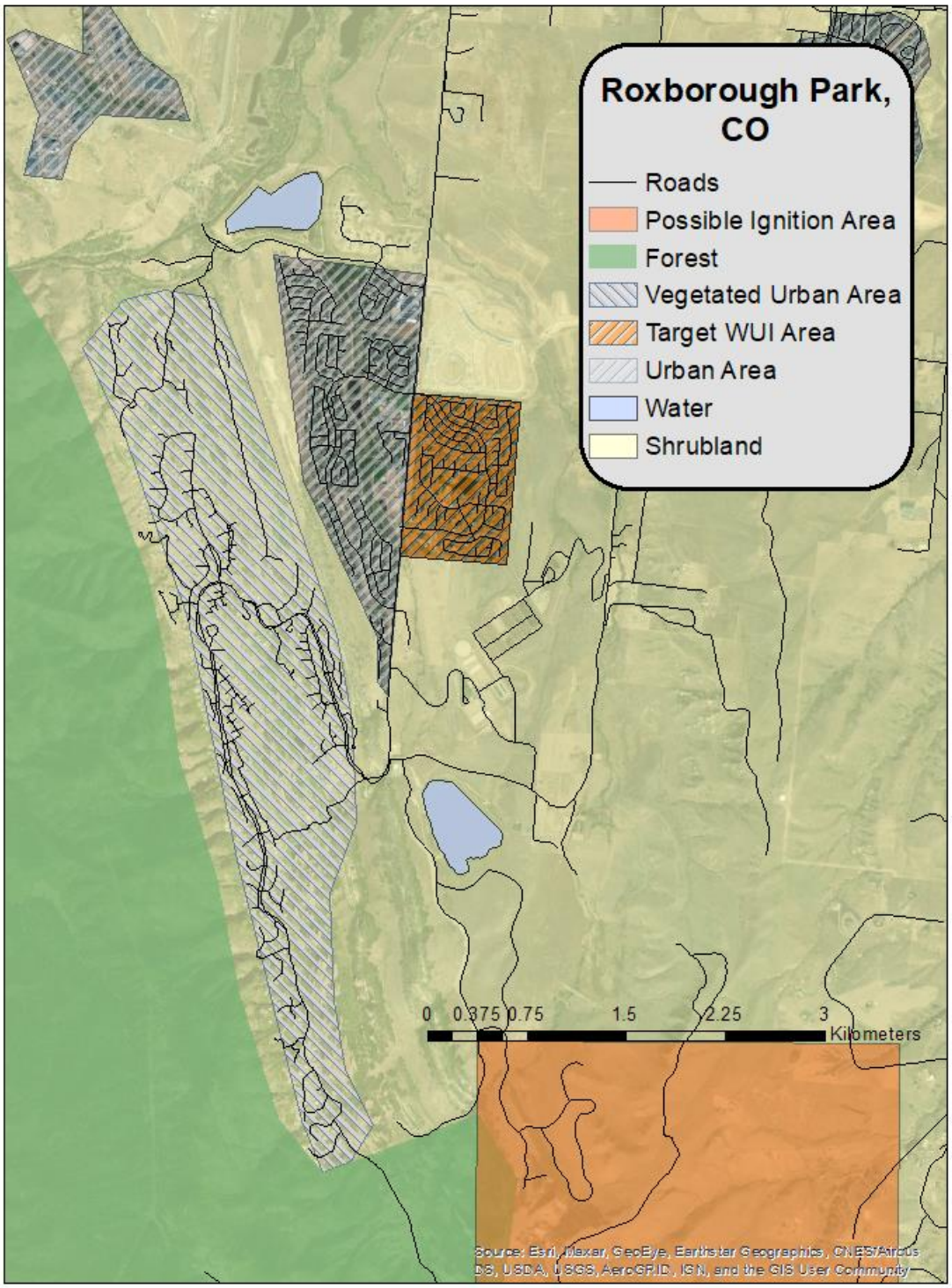

Figure 2- ArcGIS map of area selected for this study - a neighbourhood in Roxborough Park, CO, USA. Target urban area is highlighted in Pink. A populated region of Roxborough Park was chosen as the at-risk community. The fire risk has been identified as any fire starting on the south, with northwards winds.

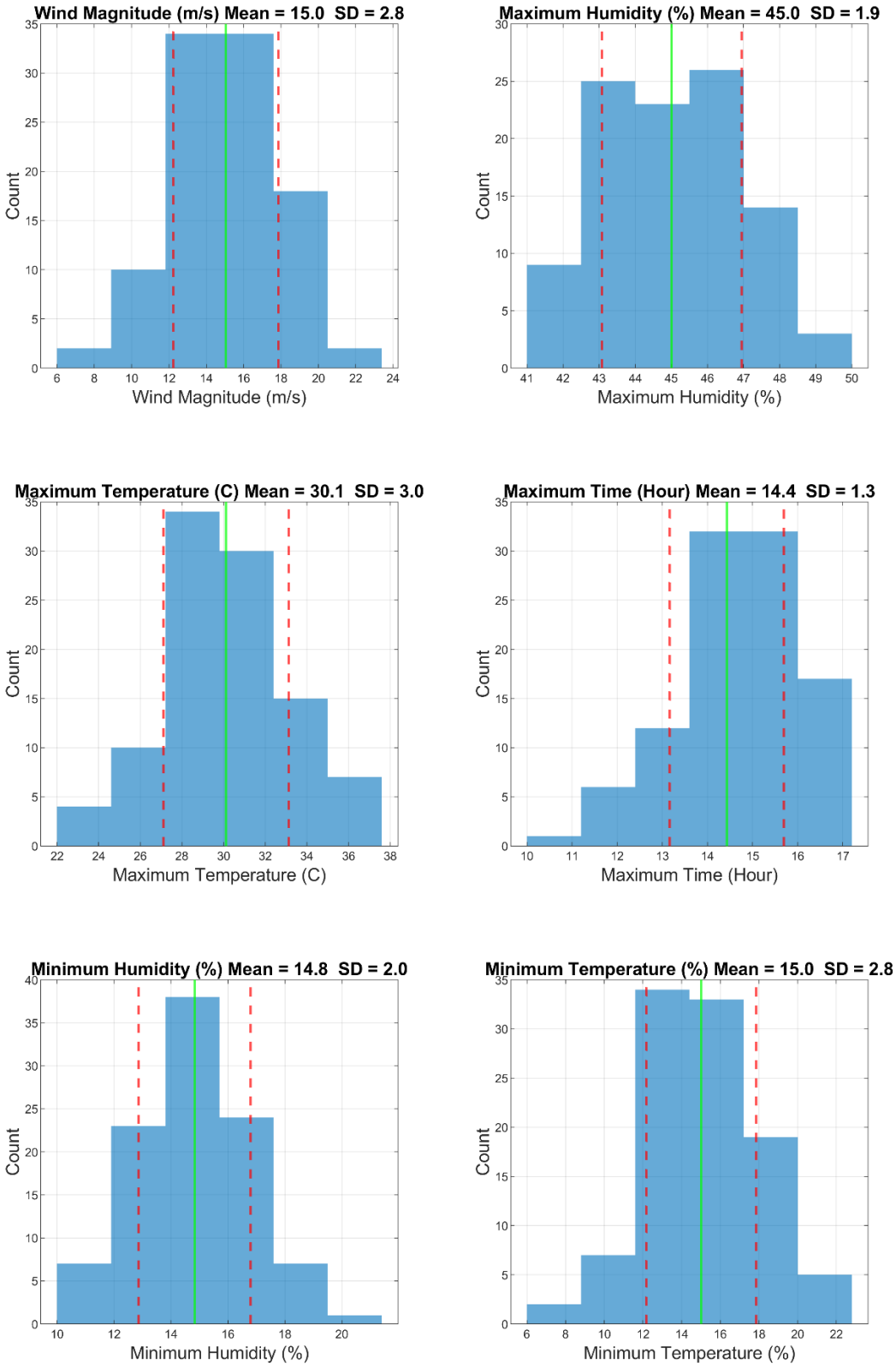

Figure 3- All the weather related values are given as normally distributed values. This data is plotted above for a simulation with 100 cases.

4. Results

A number of studies were conducted with varying input data, as shown in table 1. The first three sets of tests examine the effect of number of simulated cases to the probabilistic boundaries. The latter three cases test the effect of wind magnitude (both average value and standard deviation) for a larger ASET, to exaggerate the effect of the change.

Table 1- Input variables for the simulated cases.

Case No.	ASET (min)	Wind Magnitude (ms^{-1})	Wind Standard Deviation (ms^{-1})	Simulated cases
1	110	15	3	10
2	110	15	3	25
2	110	15	3	100
3	300	15	3	100
4	300	35	3	100
5	300	35	15	100

The results of the studies are shown in Figures 4, 5, and 6. Specific discussion on the results and what they suggest is given in the Discussions section.

The probabilistic boundaries are given as probability values on a raster. One can choose whether to keep all the nonzero cells as their trigger boundary, and get a conservative boundary that would cover all simulated cases. One could equivalently choose the boundary where 90% of all the boundaries meet, to exclude any outliers or one-off glitches. The user could ultimately even choose the 0% boundary value, which only shows the area common to all the boundaries. To illustrate the shape and gradient of the trigger boundaries, values ranging from 100% inclusion to 0% inclusion are shown in figures 4 and 5.

5. Discussion

The studies ran in this paper have a level of uncertainty due to uncertainties in the input data. While the wind data is consistent with the average readings of the nearest RAWS station, said RAWS station is more than 20 miles away from the target area. The generated wind magnitude and direction data are also considered temporally uniform which is inaccurate for any area.

For all the reasons above, it is challenging to tell whether the probabilistic or direct results of k-PERIL are accurate to the target area. What can be done is a qualitative analysis of the boundaries based on their characteristics and their change based on changing input variables. In this analysis, the formed boundaries seem to agree with the expected results. In figures 4, 5, and 6 the boundaries are uniform which stems from the fact that the fire spread is steady and uniform in a uniform shrubland. The boundary's southern border is thicker as it is meeting the faster-spreading head of the fire. On the northern border there is a large area on the north-western corner, which also makes sense since the fire turns when it is past the urban area as it is spreading upwards and to the unburned area. Figure 4 shows that more simulations form a better boundary as they filter out outlier simulations; 25 to 100 simulations are enough for a consistent 75% Boundary. Figure 5 shows that a larger ASET does result to larger boundaries as expected, but larger wind or deviation thereof does not seem to affect the probabilistic boundaries. This might be because the wind magnitude is not as strong an influence for

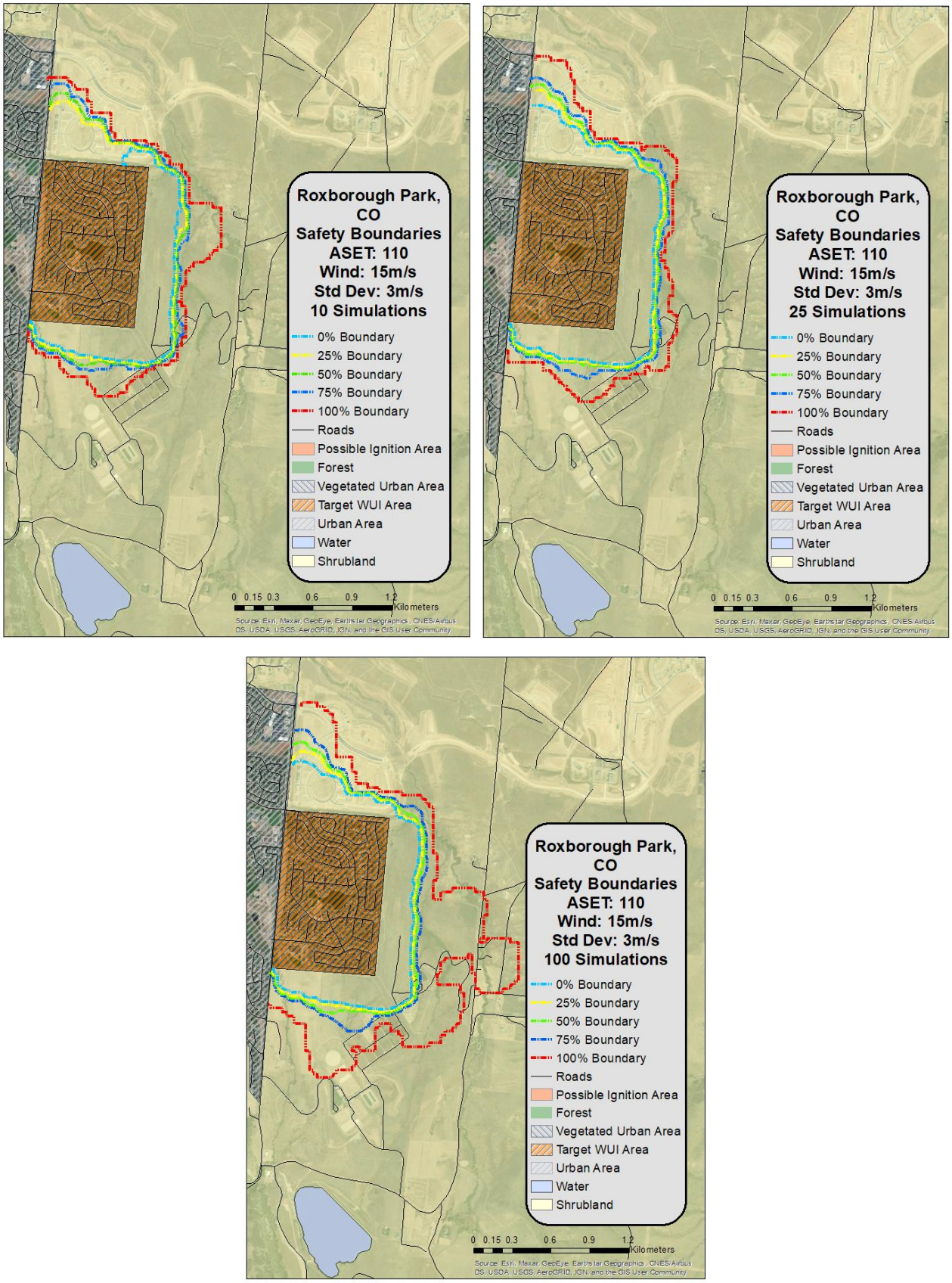

Figure 4- Top Left: Probabilistic safety Boundary for an ASET of 110 minutes, wind magnitude of 15 ms^{-1} with a standard deviation of 3 ms^{-1} and 10 simulated cases. Top Right: Safety boundary for the same case as the Left, with 25 simulated cases. Bottom: Safety boundary for the same case as previous, with 100 simulated cases.

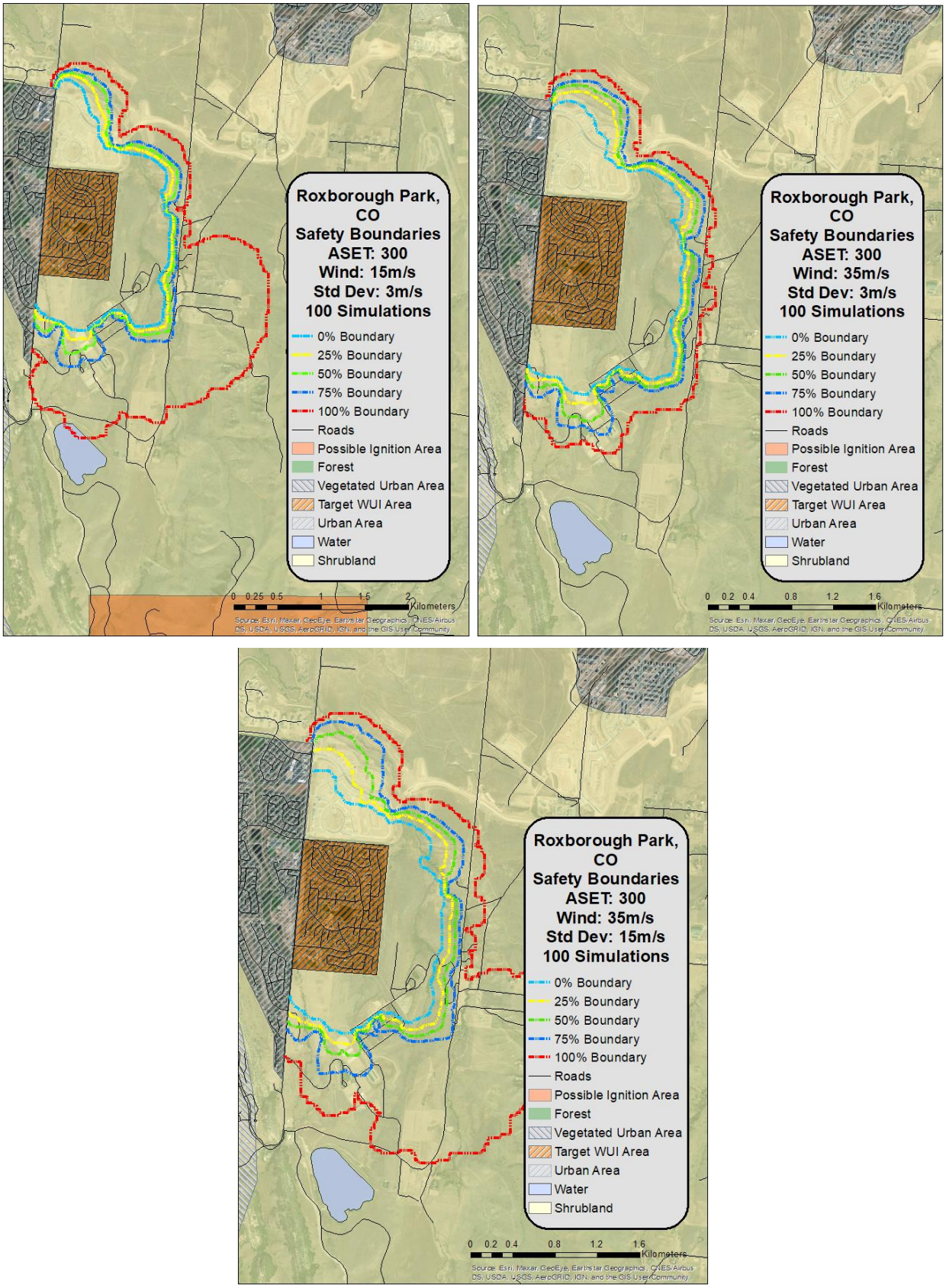

Figure 5- Top Right: Safety Boundary for an ASET of 300 minutes, wind magnitude of 15 ms^{-1} with a standard deviation of 3 ms^{-1} and 100 simulated cases. Top Left: Similar case to A with a wind magnitude of 35 ms^{-1}. Bottom: Similar to B with a wind magnitude standard deviation of 15 ms-1.

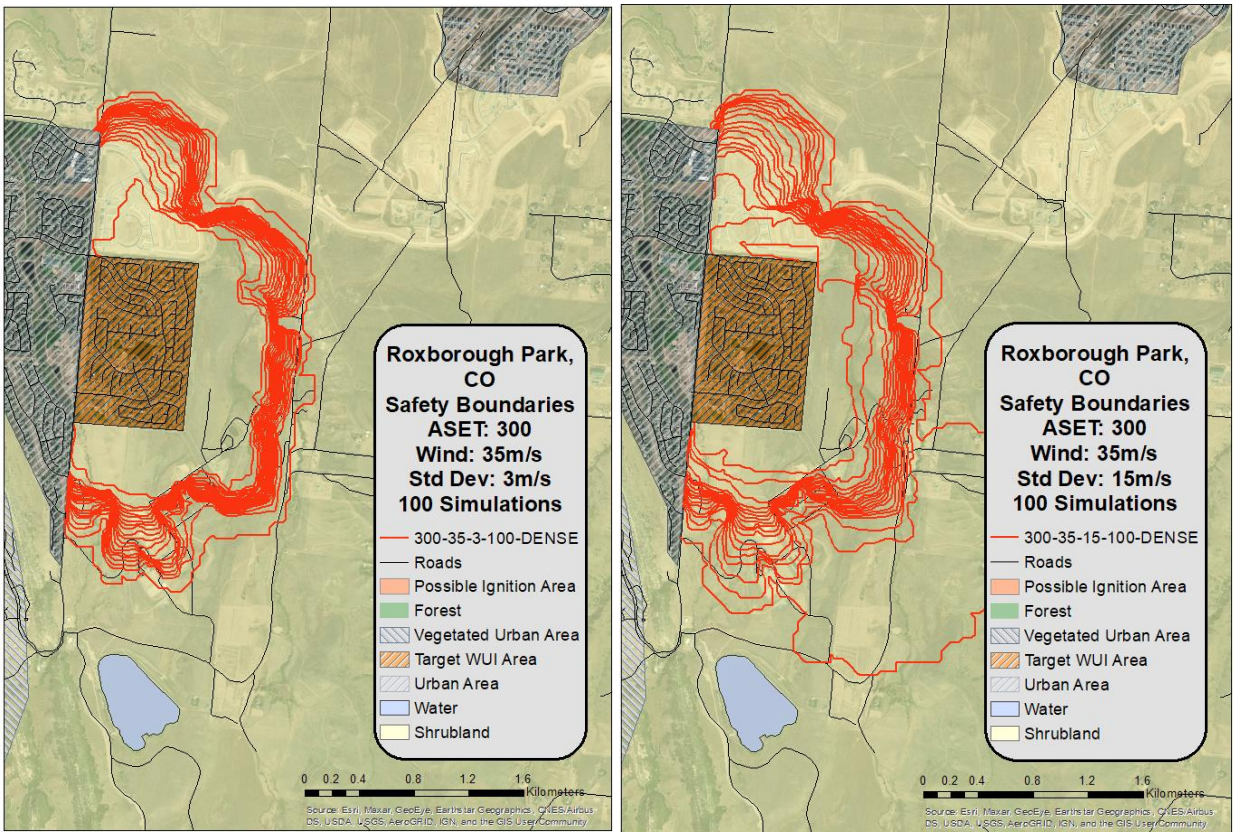

Figure 6- Right: Safety Boundary for an ASET of 300 minutes, wind magnitude of 35 ms^{-1} with a standard deviation of 3 ms^{-1} and 100 simulated cases. Left: Similar case to A with a standard deviation of 15 ms^{-1}. Both plots have equal isoprobabilistic boundaries.

this type of vegetative fuel. From Figure 6 it is evident that a greater standard deviation in wind input results in wider probability boundaries, although the magnitude of the change is small compared to the change in standard deviation. The difference in output between the last two cases can be better appreciated when more probability lines are drawn, as in Figure 6.

6. Limitations

Although k-PERIL is an upgrade compared to previous versions, it is still limited in many aspects. One critical limitation is that verification and validation can only be done with real wildfire data. Using simulated wildfire data to validate k-PERIL would only verify that the program is self-consistent, since these data are an input layer to the algorithm. To truly verify k-PERIL, the trigger boundaries would need to be generated for a real area, then a wildfire should be initiated, and the propagation of the fire and time of arrival should be recorded and compared with the predicted trigger boundary. The accuracy of k-PERIL will then be limited by the accuracy of the modelling engine used to obtain the simulated spread data. A point of future work is to find recorded rate of spread data of a real wildfire, and use it to test the validity of k-PERIL.

Another critical limitation of k-PERIL is that its results are limited by the accuracy and abilities of the wildfire model used to create the ROS input data. Most such programs can model surface fires, crown fires and spotting effectively. However, most models cannot model complex physical effects, such as long-range spotting, plume collapse, sudden wind shift, or other eruptive fire events. These are avenue of future work but may require radical changes.

7. Future work

Two future work possibilities have been discussed on the Limitations section above. Another critical area of improvement is expanding the coupling between the wildfire propagation and the evacuation simulations.

Currently the model reduces the entire evacuation procedure into one number (WRSET) and cannot account for event such as egress route blockage, probability of traffic accidents, or lane reversals initiated while the fire has crossed the trigger boundary. There is little real-time interaction between evacuation modelling and wildfire modelling; k-PERIL is supposed to be a link between the two, but at its current form it does not provide a robust coupling of the two models.

8. Conclusion

The above analysis shows that the boundaries are reasonable according to current wildfire behaviour understanding, and as such k-PERIL creates boundaries appropriate for future application. K-PERIL's results are as close to verified or tested as they can feasibly be, and as such k-PERIL has been proven to produce actionable results.

9. References

Dennison, P. E., Cova, T. J. & Mortiz, M. A. (2007) WUIVAC: a wildland-urban interface evacuation trigger model applied in strategic wildfire scenarios. Natural Hazards (Dordrecht). 41 (1), 181-199. 10.1007/s11069-006-9032-y.

Fire Behavior Applications and l ibraries. (2021) https://www.alturassolutions.com/FB/FB_API.htm .

Finney, Mark A. 1998. FARSITE: Fire Area Simulator-model development and evaluation . Res. Pap. RMRS-RP-4, Revised 2004, Ogden, UT: U.S. Department of Agriculture, Forest Service, Rocky Mountain Research Station. 47 p.

A Hurricane Decision Support Tool For Government Emergency Managers. https://www.hurrevac.com/ .

Larsen, J. C., Dennison, P. E., Cova, T. J. & Jones, C. (2011) Evaluating dynamic wildfire evacuation trigger buffers using the 2003 Cedar Fire. Applied Geography (Sevenoaks). 31 (1), 12-19. 10.1016/j.apgeog.2010.05.003.

Li, D., Cova, T. J. & Dennison, P. E. (2017) Using reverse geocoding to identify prominent wildfire evacuation trigger points. Applied Geography (Sevenoaks). 87 14-27. 10.1016/j.apgeog.2017.05.008.

Li, D., Cova, T. & Dennison, P. (Nov 3, 2015) An open-source software system for setting wildfire evacuation triggers. Proceedings of the 1st ACM SIGSPATIAL International Workshop on the use of gis in emergency management. , ACM. pp.1-6http://dl.acm.org/citation.cfm?id=2835600.

Mallick, Afroza. (2021) Testing the wildland-urban interface fire evacuation tool WUI-NITY: A case study of a rural community. Lund, Sweden, Lund University.

Mitchell, H. & Rein, G. (2019a) PERIL: Toolkit for the design of wildfire trigger buffers in WUI evacuations. EWWF.

Mitchell, H., Rein, G., Gwynne, S. & Ronchi, E. (2019b) PERIL: Calculating the safe evacuation trigger time of a WUI population because of a wildfire.

Pyne, S. J., Andrews, P. L. & Laven, R. D. (1996) Introduction to wildland fire. [unknown] 2. ed. edition. New York [u.a.], Wiley.

Ramirez, J., Monedero, S., Silva, C. A. & Cardil, A. (2019) Stochastic decision trigger modelling to assess the probability of wildland fire impact. The Science of the Total Environment. 694 10.1016/j.scitotenv.2019.07.311.

Ronchi, E., Wahlqvist, J., Gwynne, S., Kinateder, M., Benichou, N., Ma, C., Rein, G., Mitchell, H. & Kimball, A. (2020) WUI-NITY: a platform for the simulation of wildland-urban interface fire evacuation. Quincey, MA, NFPA.

Thomas, P. A. & McAlpine, R. S. (2010) Fire in the Forest. Cambridge, Cambridge University Press.

Wahlqvist, J., Ronchi, E., Gwynne, S. M. V., Kinateder, M., Rein, G., Mitchell, H., Bénichou, N., Ma, C., Kimball, A. & Kuligowski, E. (2021) The simulation of wildland-urban interface fire evacuation: The WUI-NITY platform. Safety Science. 136 105145. 10.1016/j.ssci.2020.105145.

Large eddy simulations of the structure of spreading line fires at flame scale

Mohamed M. Ahmed*[1]; Arnaud Trouvé[1]; Jason M. Forthofer[2]; Mark A. Finney[2]

[1]University of Maryland, Department of Fire Protection Engineering, College Park, MD 20742 (USA) {mmahmed, atrouve}@umd.edu
[2]USDA Forest Service, Missoula Fire Sciences Laboratory, 5775 Highway 10 West, Missoula MT 59808 (USA) {jason.forthofer, mark.finney}@usda.gov

**Corresponding author*

Keywords

Fire behavior; Flame spread; Particle burning rate model; Pyrolysis; Computational Fluid Dynamics

Abstract

Our general objective in the present study is to develop tools to better describe the coupling between solid phase and gas phase processes that control the dynamics of flame spread in wildland fire problems. We focus on a modelling approach that resolves processes occurring at flame scales, i.e., the formation of flammable vapors from the biomass vegetation due to pyrolysis, the subsequent combustion of these fuel vapors with ambient air, the establishment of a turbulent flow because of heat release and buoyant acceleration, and the thermal feedback to the solid biomass through radiative and convective heat transfer. The modelling capability is based on a general-purpose Computational Fluid Dynamics (CFD) library called OpenFOAM and an in-house Lagrangian particle model that treats drying, thermal pyrolysis, oxidative pyrolysis and char oxidation using a one-dimensional porous medium formulation that allows descriptions of thermal degradation processes occurring during both flaming and smoldering combustion.

The modelling capability is calibrated for pine wood and is first applied to simulations of fire spread across a surrogate vegetation bed corresponding to thin, monodisperse, cylindrical-shaped sticks of pine wood with prescribed particle and environmental properties (i.e., bed height, surface-to-volume ratio, packing ratio, moisture content, and wind velocity). While the model can be used in sloped terrain, the present simulations are limited to a flat ground surface. The current emphasis is on determining threshold conditions for successful spread, differences between the plume-dominated and wind-driven flame regimes, possible transitions to a steady or time-dependent flame structure, and differences in the relative weights of the flaming and smoldering regions.

1. Introduction

The dynamics of wildland fires involve multi-physics phenomena occurring at multiple scales. Computational Fluid Dynamics (CFD) models have the potential to provide detailed information on the interactions between physical phenomena occurring at all these different scales. However, because of computational cost, the domain of application of CFD models is typically limited to a particular range of scales. Thus, current CFD-based wildland fire models are scale-specific and belong to one of the following three classes: combustion solvers aimed at describing the coupling between pyrolysis, combustion, radiation and flow occurring at the vegetation and flame scales (Porterie *et al*. (2000), Morvan and Dupuy (2001), Morvan and Dupuy (2004), Fire Dynamics Simulator (FDS), Verma *et al.* (2022)); wildfire solvers aimed at describing the coupling between combustion and flow occurring at fireline scales and/or geographical scales (Linn and Cunningham (2005), Canfield *et al.* (2014), Mell *et al.* (2007)); and atmospheric boundary layer solvers aimed at describing the coupling between combustion and flow occurring at meteorological scales (Clark *et al.* (2004), Mandel *et al.* (2011), Kochanski *et al.* (2013), Coen *et al.* (2013), Filippi *et al.* (2009), Filippi *et al.* (2013)).

We focus in this study on the development of a combustion solver aimed at describing the physics of wildland fire spread at flame scale. The solver couples a one-dimensional, Lagrangian-based, solid particle model that describes the biomass vegetation phenomena (drying, pyrolysis, char oxidation) with a three-dimensional, Eulerian-based, CFD model that describes the gas phase phenomena (flow, combustion, radiative and convective heat transfer processes). The gas phase model uses a Large Eddy Simulation (LES) approach and is based on a general-purpose CFD library called OpenFOAM. The Lagrangian particle model uses an in-house solver developed both for fast one-dimensional simulations of flame spread (Forthofer *et al.* (2022)) and for

detailed LES simulations of the flame structure in wildland fire configurations. The model considers the particle as thermally-thick and composition-thick and includes descriptions of thermal degradation processes occurring during both flaming and smoldering combustion.

2. Numerical Model

The vegetation bed is treated as a population of porous particles, which can have different geometries and different sizes. Each porous particle is described as a system with a solid phase and a gas phase, which allows for a detailed treatment of the particle-to-external-gas outflow of volatile mass and the external-gas-to-particle diffusion of oxygen mass; this detailed treatment is required to account for in-depth oxidative pyrolysis and char oxidation. We consider here thermally-thick and composition-thick particles featuring in-depth variations of temperature and composition. The particles geometry can be modelled as rectangular (leaves or sticks), cylindrical (needles or stems) or spherical (embers or firebrands).

2.1. Lagrangian particle model

In the Lagrangian viewpoint, the thermo-chemical degradation of each porous particle is tracked individually in space and time. We consider each porous particle to experience four heterogenous (gas/solid) reactions: a drying reaction; a thermal pyrolysis reaction; an oxidative pyrolysis reaction; and a char oxidation reaction. We follow the work of Lautenberger and Fernandez-Pello (2009) by describing the particle as a matrix of pores featuring a solid phase and a gas phase. We discretize the porous particle into a set of one-dimensional control volumes that contain information about the porosity, thermophysical properties, chemical composition, temperature and pressure. In the following case studies, we consider thermo-chemical degradation and flame spread of pine sticks. We combine the thermophysical properties of pine wood provided in Lautenberger and Fernandez-Pello (2009) with the reaction kinetic parameters provided in Anca-Couce *et al.* (2012); this combination was found to achieve a good fit of experimental data at both micro-scale and bench-scale, as shown in the next section.

The governing equations of mass, momentum, and energy conservation inside each control volume of the porous particle are solved numerically using an implicit approach that treats convection and diffusion through a second-order, Crank-Nicolson method and chemical reaction through a first-order, backward Euler method. An in-house object -oriented C++ solver of this Larangian particle model was developed. This code can serve as a stand-alone solver of thermo-chemical degradation of solids, or it can be implemented into larger frameworks to model fire spread over vegetation as discussed in the following section. This code also features an adaptive time-stepping technique (for speed, stability, and robustness) and a re-meshing capability (for deforming particles due to swelling or shrinking).

2.2. Vegetation bed model

In order to describe gas-solid mass, momentum and energy exchanges in simulations of fire spread across a given set of porous vegetation layers, ambient air conditions and a given terrain, we developed a LES solver that couples the open-source C++ library OpenFOAM and the Lagrangian particle solver presented in the previous section.

The LES solver adopts a multiphase formulation similar to previous work proposed by Porterie *et al*. (2000), Morvan and Dupuy (2001) and Morvan and Dupuy (2004). In the current work, the Favre-filtered reactive-radiative Navier-Stokes equations are solved using a low Mach number approach. Source terms are added to the governing equations to represent the contributions of solid particles to the mass production or consumption of gaseous species, the flow momentum through a drag force, and the energy exchange through radiative and convective heat transfer. These source terms are treated as subgrid-scale (SGS) terms using the Lagrangian particle model and are accumulated to account for multiple particles existing inside each elementary control volume of the vegetation bed. The number of particles is determined from the fuel loading and the geometric parameters of the vegetation bed. A three-dimensional representation of a typical computational configuration is shown in Fig. 1.

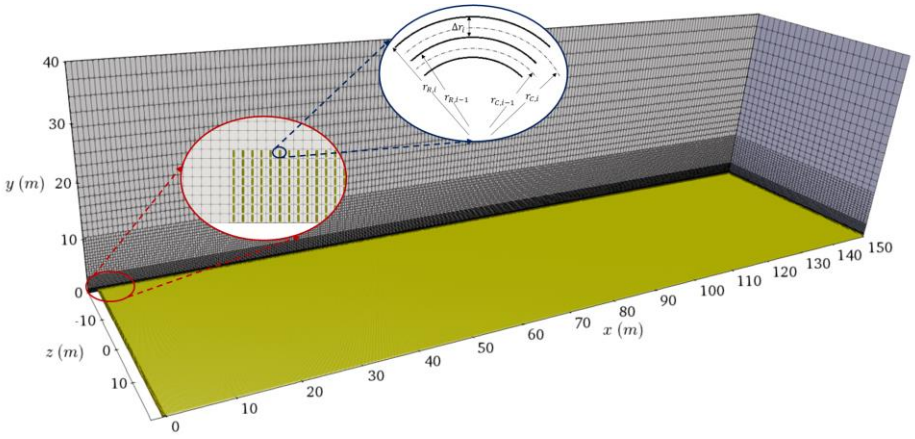

Figure 1- A view of the computational domain used in spreading line fire simulations. The solid particles are colored in yellow. A zoom into the 1D cylindrical mesh used for individual solid particles is shown.

The solver can leverage various SGS turbulence models implemented in the native OpenFOAM library. We use the WALE model proposed by Nicoud and Ducros (1999). The homogenous combustion of the gaseous fuel produced by pyrolysis reactions is treated by assuming a global reaction equation and using a modified version of the Eddy Dissipation Model (Magnussen and Hjertager (1976)) that we recently developed to account for the variations of the laminar diffusion characteristic time with LES filter size. The solver also features a radiation model based on a multi-phase radiative transfer equation (MRTE) that includes absorption/emission by the solid particles and by the gases (Consalvi *et al.* (2002)); the MRTE is solved using the finite volume Discrete Ordinate Method (DOM) implemented in the OpenFOAM library. The radiation absorption/emission by the gases is modeled by either a Prescribed Global Radiant Fraction (PGRF) approach or a Weighted-Sum-of-Gray-Gases (WSGG) model (Ahmed and Trouvé (2021)). The PGRF approach is adopted in the present study in the flame region, while the absorption and emission in the plume region are calculated using Plank-mean absorption coefficients of CO_2 and H_2O. Convective heat transfer is modeled using empirical Nusselt number correlations developed for a wide range of Reynolds numbers under no blowing conditions (Churchill and Bernstein (1977)). The blowing effect due to outflowing volatiles is accounted for through a Couette flow approximation (Lautenberger and Fernandez-Pello (2009)). The vegetation bed drag force is modeled using a drag coefficient that has been determined experimentally for isolated particles in crossflow (Mueller (2012)). It should be noted that there might be some uncertainties in the choices of the drag coefficient and the heat transfer coefficient, and more elaborate models that represent actual vegetation patches may be required.

3. Results and Discussion

3.1. Bench-scale validation of the Lagrangian particle model

We present here validation results of the Lagrangian particle model introduced in section 2.1. Numerical simulations were performed for a single particle exposed to prescribed heating conditions. The spatial resolution inside the particle is 0.1 mm. The first set of simulations corresponds to the experiment of Anca-Couce et al. (2012) in which a micro-scale pine wood sample is exposed to a heating rate of 5 K/min, while the second set of simulations corresponds to the experiment of Kashiwagi *et al.* (1987) in which a 3.8 cm-thick white pine sample is exposed to an irradiation intensity of 40 kW/m^2. Both sets of experiments consider different nitrogen-air atmospheres and thereby evaluate the ability of the model to correctly describe the contributions of oxidative pyrolysis and char oxidation. Figure 2 shows that the model predictions in terms of particle mass evolution and spatial distributions of temperature inside the particle are in very good agreement with the experimental data at both micro- and bench-scales.

3.2. Flame scale simulations of quasi-infinite line fires

We now turn to LES of a quasi-infinite line fire over a surrogate vegetation bed corresponding to vertical cylinders made of the same pine wood material tested in the previous section. A computational domain with periodic boundary conditions on the lateral sides is used to mimic quasi-infinite line fires. As shown in Fig. 1, the computational domain has a cross-section of $40 \times 40\ m^2$. The vegetation bed of pine wood cylinders starts

at 2 m from the domain entrance and extends to a length of up to 150 m to achieve steadily-propagating line fires. Preliminary tests show that a shorter domain that extends to only 50 m is sufficient to achieve steadily-propagating plume dominated fires. The pine wood cylinders have a diameter of 2 mm and a total height of 0.4 m. The packing ratio and the surface-to-volume ratio of the vegetation bed are 0.005 and 2000 m^{-1}, respectively, which give a radiation absorption length-scale of about 0.4 m (Consalvi *et al.* (2002)). The initial moisture content of the fuel bed is 5%. The composition of the gaseous fuel produced from thermal and oxidative pyrolysis reactions is assumed to be $C_{3.4}H_{6.2}O_{2.5}$ with a heat of combustion of 15.6 MJ/kg and a global radiant fraction of 0.35. External wind velocity is imposed at the domain's west boundary using a power-law profile with a nominal velocity evaluated at an elevation of 2.0 m. Turbulence fluctuations are introduced corresponding to 10% intensity. Ignition is achieved using a hot plate placed underneath the fuel bed. The plate has a length of 0.5 m and a temperature of 1600 K and is activated for 5 seconds.

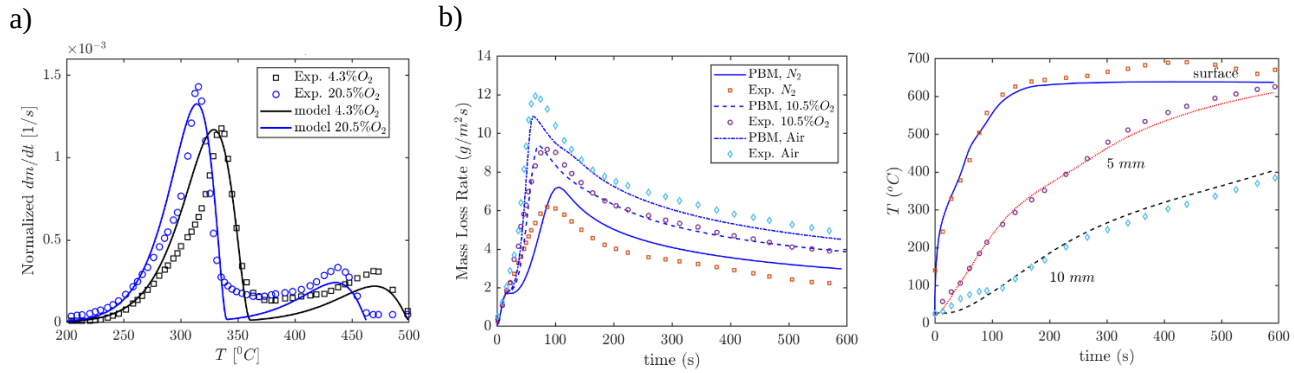

Figure 2- Series of validation tests of the Lagrangian particle model calibrated for pine wood: a) Mass loss rate in different atmospheres in micro-scale experiments taken from Anca-Couce et al. (2012) (5 K/min heating rate); b) Mass loss rate and surface/in-depth temperatures in different atmospheres in bench-scale experiments taken from Kashiwagi et al. (1987) (40 kW/m² irradiation).

The computational domain is divided into 4 regions with cells of equal size in the *x*- and *y*-directions: the grid resolution in the vegetation bed region from the ground to 0.8 m elevation is 0.1 m; the grid resolution in the flame region between 0.8 and 3 m elevation is 0.2 m; and the grid resolution in the plume region between 3 and 10 m elevation is 0.4 m; the grid resolution in the far-field region above 10 m elevation starts from 0.2 meters and is slowly decreased with elevation through stretching. The grid resolution in the span-wise direction (z-direction) is twice that in the *x*- and *y*-directions. The total number of grid cells is about 3.6 million with approximately 1.2 million particles. The time-step is controlled using a Courant–Friedrichs–Lewy condition and is of the order of ~0.001 s. The radiation field is updated every 5 time-steps using 144 solid angles. The simulations are carried out on a distributed-memory parallel cluster using Message Passing Interface (MPI) technique. A simulation of 60 seconds fire spread requires 96 hours using 160 processors (~15 kCPU hours).

We present here results from two cases corresponding to nominal wind speeds of 1.0 and 5.0 m/s. The corresponding Byram's convection number is 79 and 1.5, respectively. These two conditions are representative of the plume-dominated and wind-driven flame regimes. The corresponding values of the rate of spread (ROS) as predicted by the classical Rothermel model are 0.09 m/s and 0.34 m/s, respectively. A three-dimensional rendering of the simulated cases is presented in Fig. 3. The comparison between the left and right plots in Fig. 3 shows the expected differences between a low-wind-velocity flame that is vertical and develops above the vegetation bed and a high-wind-velocity flame that is horizontal, is attached to the ground and develops mostly within the vegetation bed. It also shows that the simulated fires feature a peak-and-trough structure (and a finger-like structure) similar to those observed in wildland fires.

Figure 4 shows the time evolution of the locations of the flame front (defined as the maximum *x*-location where the mixture fraction is greater than the stoichiometric mixture fraction), the back and front edges of the pyrolysis region (defined as the minimum and maximum *x*-locations where the pyrolysis reactions take non-zero values), and the smoldering front (defined as the maximum *x*-location where the char oxidation reaction takes non-zero values). The flame front location predicted by the Rothermel model is included for comparison. The simulation results show that the fireline intensity is 0.56 MW/m for the plume-dominated flame and 4.3 MW/m for the wind-driven flame; the corresponding values of the ROS are 0.082 and 0.52 m/s, respectively.

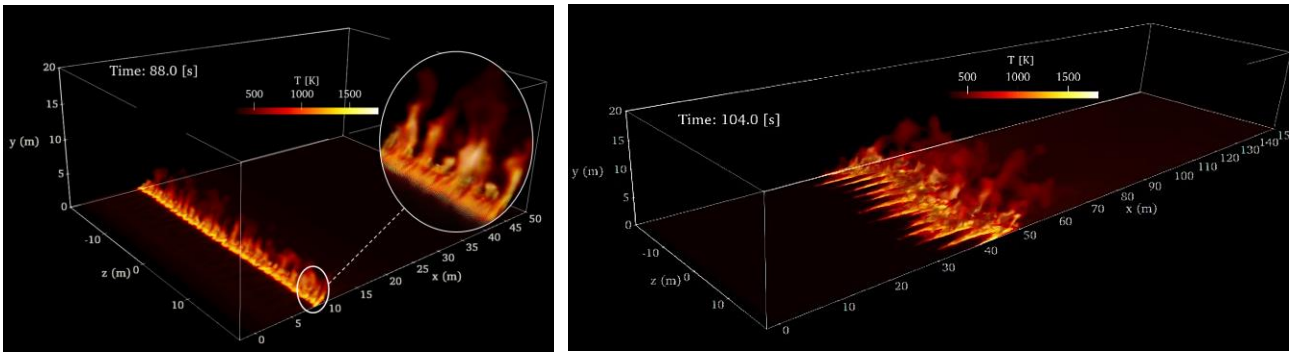

Figure 3- A 3D rendering of the structure of the line fire at a wind velocity of 1 m/s (left) and 5 m/s (right). The fire is visualized using an iso-volume of the region where the gas temperature is above 450 K.

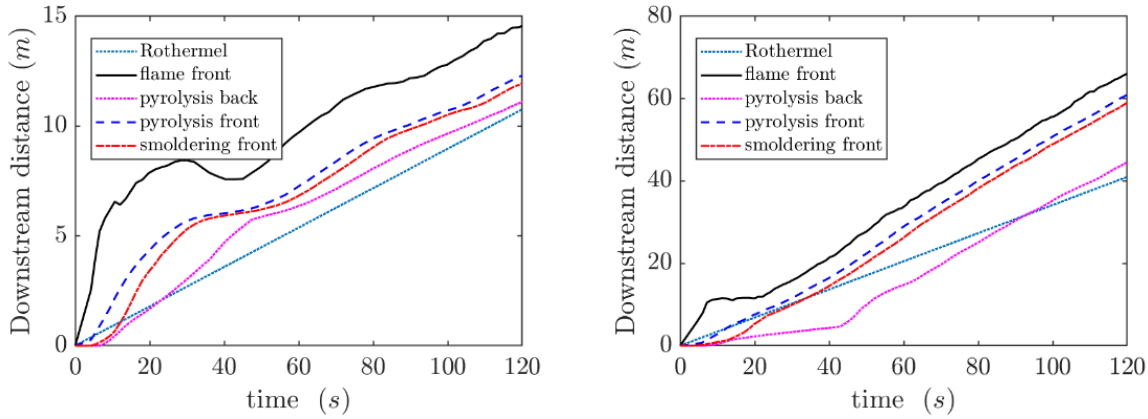

Figure 4- Time evolution of the position of the line fire at a wind velocity of 1 m/s (left) and 5 m/s (right).

4. Conclusion

This paper presents preliminary results obtained with a new modelling capability aimed at bringing fundamental information on the coupling between solid phase and gas phase processes that control the dynamics of flame spread in wildland fire problems. This modeling capability uses sub-millimetre-scale spatial resolution in the solid biomass solver and centimetre-scale spatial resolution in the gas phase solver and thereby resolves the exchanges of mass, momentum and heat associated with pyrolysis, combustion, radiation and flow at flame scales. The modeling capability is based on the OpenFOAM CFD library and an in-house Lagrangian model that treats particles as a one-dimensional porous medium and includes descriptions of thermal degradation processes occurring during both flaming and smoldering combustion.

5. Acknowledgements

This project is financially supported by the USDA Forest Service, Missoula Fire Sciences Laboratory. The project is also supported by supercomputing resources made available by the University of Maryland (https://www.glue.umd.edu/hpcc/) and by the US National Science Foundation (XSEDE Program, Grant #TG-CTS140046, https://www.xsede.org).

6. References

Porterie B, Morvan D, Loraud JC, Larini M (2000) Firespread through fuel beds: Modeling of wind-aided fires and induced hydrodynamics. Physics of Fluids 12, 1762-1782.

Morvan D, Dupuy JL (2001) Modeling of fire spread through a forest fuel bed using a multiphase formulation. Combustion and Flame 127, 1981-1994.

Morvan D, Dupuy JL (2004) Modeling the propagation of a wildfire through a Mediterranean shrub using a multiphase formulation. Combustion and Flame 138, 199-210.

Fire Dynamics Simulator (FDS), developed by the National Institute of Standards and Technology. https://pages.nist.gov/fds-smv/

Verma S, Ahmed M, Trouvé, A (2022) The Structure of Line Fires at Flame Scale. In K. Speer and S. Goodrick (Eds.), Wildland Fire Dynamics (pp. 35-62). Cambridge: Cambridge University Press.

Linn RR, Cunningham P (2005) Numerical simulations of grass fires using a coupled atmosphere-fire model: Basic fire behavior and dependence on wind speed. Journal of Geophysical Research 110, D13107.

Canfield JM, Linn RR, Sauer JA, Finney N., Forthofer J (2014) A numerical investigation of the interplay between fireline length, geometry, and rate of spread. Agricultural and Forest Meteorology, 189-190, 48-49.

Mell W, Jenkins MA, Gould J, Cheney P (2007) A physics-based approach to modeling grassland fires. International Journal of Wildland Fire 16, 1-22.

Clark TL, Coen J, Latham D (2004) Description of a coupled atmosphere-fire model. International Journal of Wildland Fire 13, 49-64.

Mandel J, Beezley JD, Kochanski AK (2011) Coupled atmosphere-wildland fire modeling with WRF 3.3 and SFIRE 2011. Geoscientific Model Development 4, 591-610.

Kochanski AK, Jenkins MA, Mandel J, Beezley JD, Clements CB, Krueger S (2013) Evaluation of WRF-SFIRE performance with field observations from the FireFlux experiment. Geoscientific Model Development 6, 1109-1126.

Coen JL, Cameron M, Michalakes J, Patton EG, Riggan PJ, Yedinak KM (2013) WRF-Fire: Coupled weather-wildland fire modeling with the Weather Research and Forecasting model. Journal of Applied Meteorology and Climatology 52, 16-38.

Filippi JB, Bosseur F, Mari C, Lac C, Le Moigne P, Cuenot B, Veynante D, Cariolle D, Balbi JH (2009) Coupled atmosphere-wildland fire modelling. Journal of Advances in Modeling Earth Systems 1, 11.

Filippi JB, Pialat X, Clements CB (2013) Assesment of ForeFire/Meso-NH for wildland fire/atmosphere coupled simulation of the FireFlux experiment. Proceedings of the Combustion Institute 34, 2633-2640.

OpenFOAM, developed by the OpenFOAM Foundation. http://www.openfoam.org

Forthofer JM, Finney MA, Grumstrup TP, Ahmed MM, Trouvé A (2022) LIHTFire: A high resolution 1D physics-based wildfire spread model. In IX International Conference on Forest Fire Research, Coimbra, Portugal, accepted for presentation.

Lautenberger C, Fernandez-Pello C (2009) A model for the oxidative pyrolysis of wood. Combustion and Flame 156, 1503-1513.

Anca-Couce A, Zobel N, Berger A, Behrendt F (2012) Smouldering of pine wood: Kinetics and reaction heats. Combustion and Flame 159 1708-1719.

Nicoud F, Ducros F (1999) Subgrid-scale stress modelling based on the square of the velocity gradient tensor Flow. Turbulence and Combustion 62, 183-200.

Magnussen BF, Hjertager BH (1976) On mathematical modeling of turbulent combustion with special emphasis on soot formation and combustion. Proceedings of the Combustion Institute 16, 719-729.

Consalvi JL, Porterie B, Loraud JC (2002) A formal averaging procedure for radiation heat transfer in particulate media. International Journal of Heat and Mass Transfer 45(13), 2755-2768.

Ahmed MM, Trouvé A (2021) Large eddy simulation of the unstable flame structure and gas-to-liquid thermal feedback in a medium-scale methanol pool fire. Combustion and Flame 225, 237-254.

Churchill SW, Bernstein M (1977) A correlating equation for forced convection from gases and liquids to a circular cylinder in crossflow. Journal of Heat Transfer 99, 300-306.

Mueller EV (2012) LES modeling of flow through vegetation with applications to wildland fires. Doctoral dissertation, Worcester Polytechnic Institute.

Kashiwagi T, Ohlemiller TJ, Werner K (1987) Effects of external radiant flux and ambient oxygen concentration on nonflaming gasification rates and evolved products of while pine. Combustion and Flame 69, 331-345.

Leveraging a wildfire risk prediction metric with spatial clustering

Ujjwal KC[1]; Jagannath Aryal*[2]

[1]*CSIRO|Agriculture and Food, St Lucia, Australia, {Ujjwal.KC@csiro.au}*
[2] *Faculty of Engineering and IT, The University of Melbourne, Melbourne, Australia; {Jagannath.Aryal@unimelb.edu.au}*

**Corresponding author*

Keywords

Wildfire, risk metric, risk characterization, clustering, data-driven approach

Abstract

Fire authorities have started widely using operational fire simulations for effective wildfire management. These fire simulation outputs, when aggregated on a massive scale, create an opportunity to apply the evolving data-driven approach to closely estimate wildfire risks even without running computationally expensive simulations. We explored this opportunity in one of our previous works where we proposed a probability-based risk metric that gives a series of probability values for fire starting at a location under a given weather condition, to fall into different risk categories. The metric considered each fire start location as a unique entity, which could face scalability issues when the metric is used for a larger geographic area and make the metric hugely compute-intensive. As spatial clusters are significantly fewer than fire start locations, such spatial clusters may leverage the metric by reducing the computational requirements. In this work, we investigate if the spatial clustering of fire start locations based on historical fire areas can address the scalability issue without significantly compromising the accuracy of the metric.

1. Introduction

With an increased understanding of phenomena and advancements in computing technologies and observational sciences, natural disasters can be modeled and studied with greater detail (Razavi et al., 2012, Kaizer et al., 2015). Several wildfire models and tools have been developed that can estimate the wildfire behaviors and propagation accurately. Consequently, fire authorities have started widely using operational fire simulations for making better-informed decisions for wildfire management. These fire simulations when aggregated on a massive scale have created a unique opportunity to apply the evolving data-driven approach to closely estimate wildfire risks even without running a single computationally expensive simulation amidst the process being highly compute-intensive otherwise.

In one of our previous works (KC et al., 2022), we validated the application of the data-driven approach to facilitate rapid wildfire risk using a Bayesian probabilistic model. The wildfire risk metric detailed in the study gave a series of probability values for fire starting at a location under a given weather condition to fall into different risk categories. Despite the application of the model being computationally inexpensive, building the inference model was tedious and comparatively compute-intensive as each possible fire start location was considered a unique entity and the probability values conditioned on fire start location had to be calculated for each location. Such a consideration can face serious scalability issues when the geographical area undertaken for wildfire risk estimation is large and has a significantly large number of possible fire start locations. As such, in this work, we investigate if the spatial clustering based on historical data (the data used to build the inference model) could address this scalability issue of the risk metric without significantly compromising the accuracy of the metric. The concept of spatial clusters was envisioned to leverage the risk metric as the number of spatial clusters is significantly lower than the number of possible fire start locations in a geographical area, which could further reduce the overall computational requirements of the metric.

2. Methods and Procedures

2.1. Study Area

We chose Tasmania as the study area to validate the proposed idea of characterizing geographical regions into different risk zones using spatial clustering. The choice was made for several reasons - frequent occurrences of wildfires in the region, the prevalence of readily available high-quality land data sets for the region usable in operational wildfire simulation tools, and a well-studied and systematic grid configuration of fire start locations in the region (Service, 2019; KC et al., 2020a). Tasmania Fire Service (TFS) has maintained a grid configuration of 68,048 possible fire start locations at an interval of 1 km irrespective of land. Any start locations falling on the water bodies are shifted to the nearest land location.

2.2. Wildfire Simulation Tool – Spark

We used the Spark framework (Miller et al., 2015) to run wildfire simulations. Spark offers a flexible platform to simulate the progression of wildfires and their behaviors in different vegetation types. Each wildfire simulation in Spark requires input data sets for fire behavior models, maps of land classification, fuel load, topographical data sets, and weather data to produce output metrics such as total area burnt by fire, the intensity of the fire, and the number of urban cells burnt. All the calculations in Spark are parallelized using the OpenCL framework. All the simulations and their outputs used in this study are available in (KC et al., 2021).

2.3. Fire simulations inputs

We chose four weather inputs - temperature, relative humidity, wind speed, and wind direction for this study following the experimental setup of one of our previous works (KC et al., 2020a, KC et al., 2020b). The ranges for these inputs considered for spatial clustering for risk zones are listed in Table 1. Five equally spaced discrete values of each weather input (except wind direction) were considered along with four distinct directions (east, west, north, and south) for wind directions. Wildfires grow aggressively under weather conditions characterized by high values of wind speed, temperature, and low values of relative humidity when the wind is pushing the fire away from the water bodies. All other static inputs to fire simulations were used as per the configurations and records maintained by TFS and the Tasmanian Government (Tasmania, 2021). All fire simulations were run for five hours, and the cumulative areas burnt by fire in the period were reported as a simulation output.

Table 1 - Range and discretization of the factors for fire weather

Parameters	Range	Labels with Interval
Air Temperature	[10, 40]	Low (L) [10,18] Medium (M)(18, 33) High (H) [33, 40]
Relative Humidity	[10, 90]	Low (L) [70,90] Medium (M) (30, 70) High (H) [10, 30]
Wind Speed	[10,60]	Low (L) [10,23] Medium (M) (23,48) High (H) [48, 60]

2.4. Wildfire risk zones assignment using spatial clustering

We employed spatial clustering enabled by k-means clustering (Likas et al., 2003) based on the values of area burnt by fires starting at the location to assign a risk zone to the fire start location. It should be noted that for any fire start location closer to any water bodies, the information on the fire burnt areas should be interpreted carefully. For example, under a given weather condition, a fire starting at a location with a water body to its east with the wind driving the fire towards the east ceases immediately giving an unburnt landscape, while any fire starting at the same location with the wind driving the fire in other directions not east, may burn a significant area of land. To overcome such circumstances, we adapted the clustering mechanisms based on the mean and median values of fire burnt areas for all locations. The characteristics of the clusters obtained from clustering mechanisms were interpreted to label all fire start locations in Tasmania under three risk zones - low, medium, and high.

3. Experimental setting

3.1. Computing environment for wildfire simulations

All the wildfire simulations used for this study were run using the cloud-based frameworks as designed in (KC et al., 2020) over the cloud infrastructure of Nectar Cloud (Nectar, 2018) and Google Cloud (Google, 2020). Several types of Cloud instances were used as this study does not include any time-related evaluation metrics.

3.2. Evaluation metrics

We compared the accuracy of the proposed clusters-based risk zone characterization against that of the baseline McArthur Forest Fire Danger Index (FFDI) (McArthur, 1967) and our previously proposed risk metric. We also compared the proportions of underfits (predicted area less than the true values) and overfits (predicted area more than the true values). The comparison was done for three and two risk zones as initially explained in our previous work (KC et al., 2022).

4. Results and Discussion

4.1. Risk zones characterization using spatial clustering

Figure 1 shows all possible fire start locations in Tasmania characterized as low, medium, and high-risk areas as given by the spatial clustering. Out of 68,048 fire start locations, about 66 % of the locations were characterized as low-risk zones while the compositions for the medium and the high-risk zone stood at about 24 % and 10 % respectively. Most of the fire start locations closer to water bodies were labeled as low wildfire risk zones while the fire-starting inwards were labeled as high-risk zones. The high-risk zone had a range of average fire area between 3,900 and 10,400 hectares while the low-risk zone had the same range between 2 and 1,700 hectares.

4.2. Comparison against the FFDI and the risk metric

Table 2 shows the comparison of the cluster-based risk metric against the baseline FFDI and the previous wildfire risk metric for three and two risk categories. The accuracy of the cluster-based metric for three distinct risk categories stood at about 70 % while the same for the FFDI and the previous metric stood at about 55 % and 75 % respectively. Similarly, for two distinct risk categories, the numbers stood at about 85 %, 88 %, and 77 % for the cluster based, FFDI, and previous metric respectively. As expected, the accuracy of the cluster-based risk metric is less than that of the previous risk metric. However, the accuracy is still better than that of the McArthur FFDI and is not considerably far from the accuracy of the previous metric. The cluster-based risk metric had more proportion of underfits than the previous metric which could be due to a wider range of fire areas for the low-risk zone compared to the original range of low-risk zone in our previous metric. Conversely, the overfit proportion with the cluster-based metric is marginally less than in the previous metric, which could minimize the overestimation of resources during wildfire management.

In this investigative study, we were able to cut down the location-specific probability calculations from 68,048 to a clustering mechanism and a significantly fewer number of 3 (clusters). Such a provision in the risk metric could theoretically reduce the computational requirements of the calculations of location-specific probability values by a factor in thousands. The most important fact in the findings is that the change in the accuracy of the metric is a mere 8 % and 3 % for three and two distinct risk categories respectively. A comprise of less than 5 % in accuracy at such a scale for a significant reduction in the computational requirements outlines the spatial clustering as discussed in this paper to be a good alternative for fire start location risk characterization in the data-driven probability-based wildfire risk metric.

Table 2 - Performance comparison against the McArthur FFDI

Evaluation metrics	**Three Categories**			**Two Categories**		
	Cluster-based	Previous metric	McArthur FFDI	Cluster-based	Previous metric	McArthur FFDI
Accuracy	66.81	74.55	51.99	84.87	87.43	76.03
Underfits	24.9	15.88	38.87	13.31	10.27	13.49
Overfits	8.2	9.66	9.14	1.81	2.3	13.49

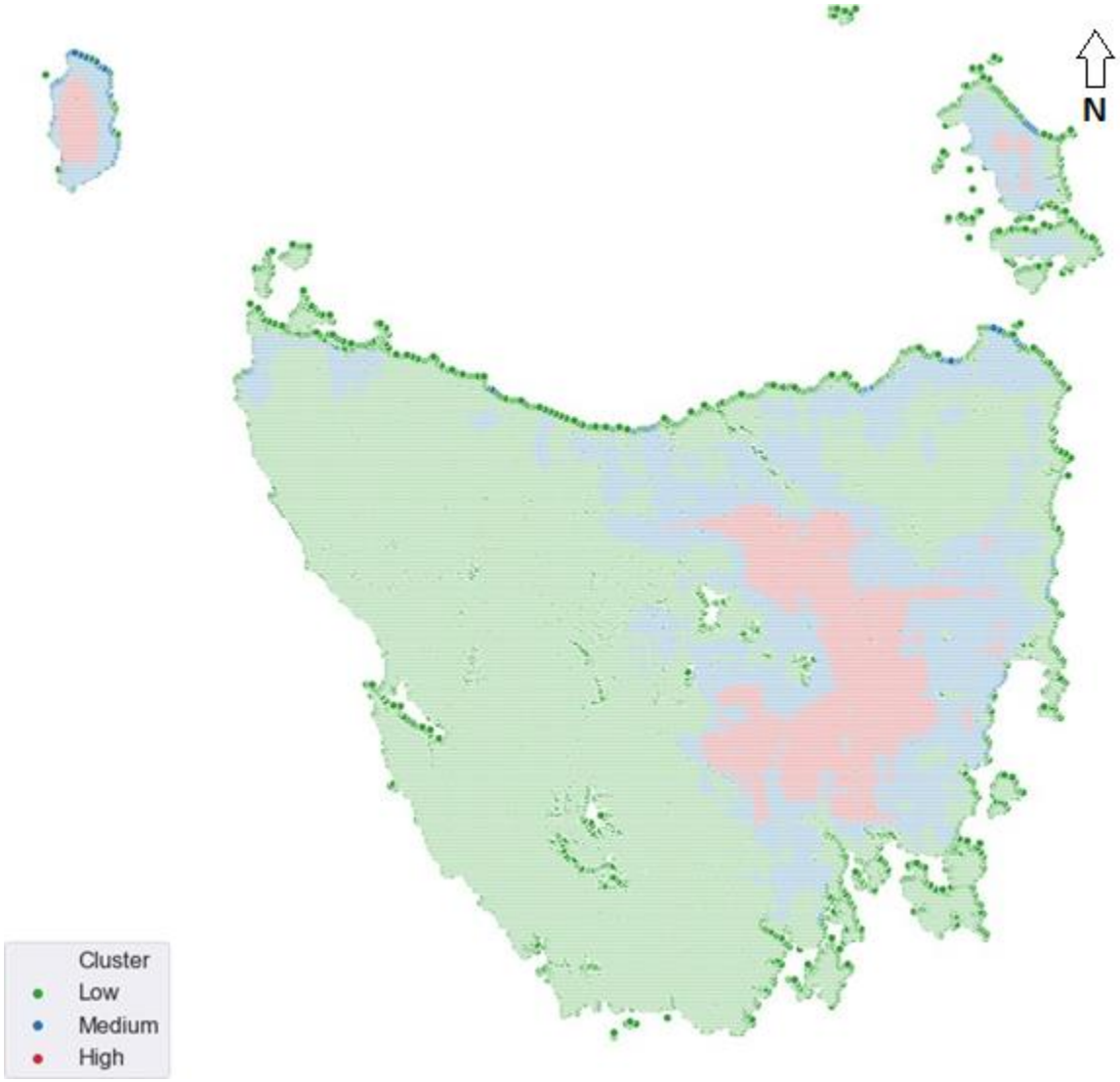

Figure 1 - Risk zone characterization of all possible fire start locations in Tasmania.

5. Conclusions and future research

The ever-evolving data-driven approach can be a computationally efficient alternative to rapidly estimate wildfire risks using several inference models. One such model was detailed in one of our previous works to build a probability-based risk metric, which was quite accurate in risk estimation. But the metric was subjected to scalability issues as each fire start location was considered a unique entity for location-related probability calculations. In this brief study, we investigated if spatial clustering could address the scalability issue of the metric without significantly compromising the accuracy of the metric. We found that the spatial clusters to characterize the risk of each start location could help solve the scalability issues by drastically reducing the number of calculations required by a theoretical factor in thousands with a mere compromise of about 5 % in accuracy. Such an inexpensive estimation of wildfire risk with a data-driven metric can help fire authorities to prioritize resource allocation and make better-informed decisions at various stages of fire emergencies to

minimize the possible losses. We expect future works to verify the numbers around the factor by which the computational requirements of the probability-based risk metric are poised to get reduced with spatial clustering. Similarly, the studies around the influence of the number of spatial clusters on the accuracy of the metric could also be studied further.

6. References

(Google, 2020) Google (2020). Google cloud. https://cloud.google.com/. Accessed: 2020-05-12.

(Kaizer et al., 2015) Kaizer, J. S., Heller, A. K., and Oberkampf, W. L. (2015). Scientific computer simulation review. *Reliability Engineering & System Safety*, 138:210–218.

(KC et al., 2020a) KC, U., Garg, S., and Hilton, J. (2020). An efficient framework for ensemble of natural disaster simulations as a service. *Geoscience Frontiers*, 11(5):1859–1873.

(KC et al., 2020b) Ujjwal, K., Garg, S., Hilton, J., and Aryal, J. (2020b). A cloud-based framework for sensitivity analysis of natural hazard models. *Environmental Modelling & Software*, 134:104800.

(KC et al., 2021) KC, U., Garg, S., Hilton, J., and Aryal, J. (2021). Fire simulation data set for Tasmania

(KC et al., 2022) Ujjwal, K., Hilton, J., Garg, S., and Aryal, J. (2022). A probability-based risk metric for operational wildfire risk management. *Environmental Modelling & Software*, 148:105

(Likas et al., 2003) Likas, A., Vlassis, N., and Verbeek, J. J. (2003). The global k-means clustering algorithm. *Pattern recognition*, 36(2):451–461.

(McArthur, 1967) McArthur, A. (1967). Fire behavior in eucalypt forest. canberra, department of development. *Forestry and Timber Bureau*.

(Miller et al., 2015) Miller, C., Hilton, J., Sullivan, A., and Prakash, M. (2015). Spark–a bushfire spread prediction tool. In *International Symposium on Environmental Software Systems*, pages 262–271. Springer.

(Nectar, 2018)Nectar (2018). Nectar cloud. https://nectar.org.au/research-cloud/. Accessed: 2018-05-12.

(Razavi et al., 2012) Razavi, S., Tolson, B. A., and Burn, D. H. (2012). Review of surrogate modeling in water resources. *Water Resources Research*, 48(7).

(Service, 2019) Service, T. F. (2019). *STATE FIRE COMMISSION ANNUAL REPORT*.

(Tasmania, 2021) Tasmania (2021). List data. https://listdata.thelist.tas.gov.au/opendata/. Accessed: 2021-03-12.

Lidar Instrumentation for the California Fire Dynamics Study

Amanda Makowiecki*[1,2], Edward Strobach[1,2], Sunil Baidar[1,2],
Neil Lareau[3], Craig Clementsu[4], W. Alan Brewer[2]

[1]*Cooperative Institute for Research in Environmental Sciences, University of Colorado-Boulder. Boulder, CO, USA, {amanda.makowiecki@noaa.gov}*
[2] *Chemical Sciences Laboratory, National Oceanic and Atmospheric Administration. Boulder, CO, USA*
[3] *University of Nevada-Reno. Reno, NV, USA*
[4] *Wildfire Interdisciplinary Research Center, San Jose State University. San Jose, CA, USA*

**Corresponding author*

Keywords

Doppler lidar, fire dynamics, mobile Doppler lidar

Abstract

The California Fire Dynamics Study (CalFiDE) is a collaborative effort between the Chemical Sciences Laboratory (CSL) at National Oceanic and Atmospheric Administration (NOAA), Wildfire Interdisciplinary Research Center (WIRC) at San Jose State University (SJSU) and the University of Nevada Reno (UNR), to investigate wildfire dynamics in Northern California in late Summer and Fall 2022. Further information on the instrumentation and scope of this study can be found in the Valero et al. short paper. During CalFiDE, the contributing organizations plan to deploy four Doppler lidar systems in addition to infrared imaging and chemical measurements to quantify the fire dynamics and atmospheric coupling of large scale wildfires. These systems will be installed on a range of mobile platforms including; a Twin Otter aircraft, pickup trucks, and trailers. The mobile ground based installations allow researchers to rapidly deploy the systems to areas of interest during the study, while the aircraft installation will cover a larger range of spatial scales. Systems will operate in scanning modes to quantify 3D winds, vertical stares to resolve fine scale vertical velocities, and coordinated scans where the measurement volumes of nearby systems are overlapped to provide high resolution measurements of 3D winds. The coordinated scanning technique will be used to target fine scale features within fire plumes such as helical updrafts, counter-rotating vortices, and inflow/outflow dynamics. Collectively these lidar observations will provide validation data sets for simulated fire-generated winds.

1. Introduction

Doppler lidar is a proven technology to study atmospheric dynamics and recently has expanded its scope to measurements of wildfire dynamics (Charland et al. 2013, Lareau et al. 2017). These systems can provide measurements of 3D wind fields, boundary layer dynamics, and aerosol backscatter intensity allowing for characterization and ultimately a better understanding of the dynamics which govern wildfire behavior. Coupling Doppler lidars with mobile platforms enables measurements of both the spatial and temporal evolution of wildfires. Additionally, these mobile installations enable fast deployment of the lidar systems for time sensitive and dynamic deployments such as wildfires. Here we present the Doppler lidar instrumentation which will be deployed for the California Fire Dynamics Study (CalFiDE) in Northern California in August-September 2022. A total of four Doppler lidar systems will be deployed for this experiment consisting of; one aircraft based Doppler lidar, one ground based mobile Doppler lidar, and two ground based stationary Doppler lidars. The aircraft based measurement will primarily focus on profiling incoming winds and measuring plume structure. The ground based mobile system will perform continuous measurements while driving the periphery of the fire. The two ground based stationary systems will be located at the fire front to monitor fire generated winds.

Deploying multiple Doppler lidars within the same geographic region allows for more complete measurement coverage. Additionally, by overlapping measurement volumes from multiple Doppler systems, measurement resolution of 3D winds can be drastically improved (Newman et al. 2016, Choukulkar et al. 2017). This technique will allow for targeted measurements of smaller scale features such as entrainment/lateral mixing of core updrafts over wildfire fire plumes, and will help address the horizontal and vertical structure of the dynamics governing transport.

2. Aircraft Based System

2.1. Installation on the Twin Otter

Dynamics of the plume and wind fields surrounding the fires will be measured using a Doppler lidar installed on board the NOAA Twin Otter aircraft. The Doppler lidar is a microjoule-class pulsed Doppler lidar designed by the NOAA Chemical Sciences Laboratory (Schroeder et al. 2020). The lidar will provide measurements of turbulence intensity and 3-D winds around the fire as well as aerosol intensity backscatter distributions as seen in Figure 1b. The system has a maximum range of 7.2 km with a resolution of 60m. The lidar is paired with a partial hemispheric scanner which will extend out the port-aft window of the aircraft (Figure 1a) allowing for measurements below the aircraft as well as above the aircraft, which will be used when flying at low altitudes for in-situ sampling. The scanner can be operated in a scanning mode for measurements of 3-D wind fields around the fire. An inertial navigation system feeds back to the scanner for real-time stabilization of aircraft motion during the flight. This stabilization enables vertical stares and target tracking.

Ultimately these scanning data will provide the upstream wind profile impacting the plume development and thus important context for other plume rise observations. The motion compensated stares and target tracking will provide data on fine scale structures occurring within the plume and the surrounding flows.

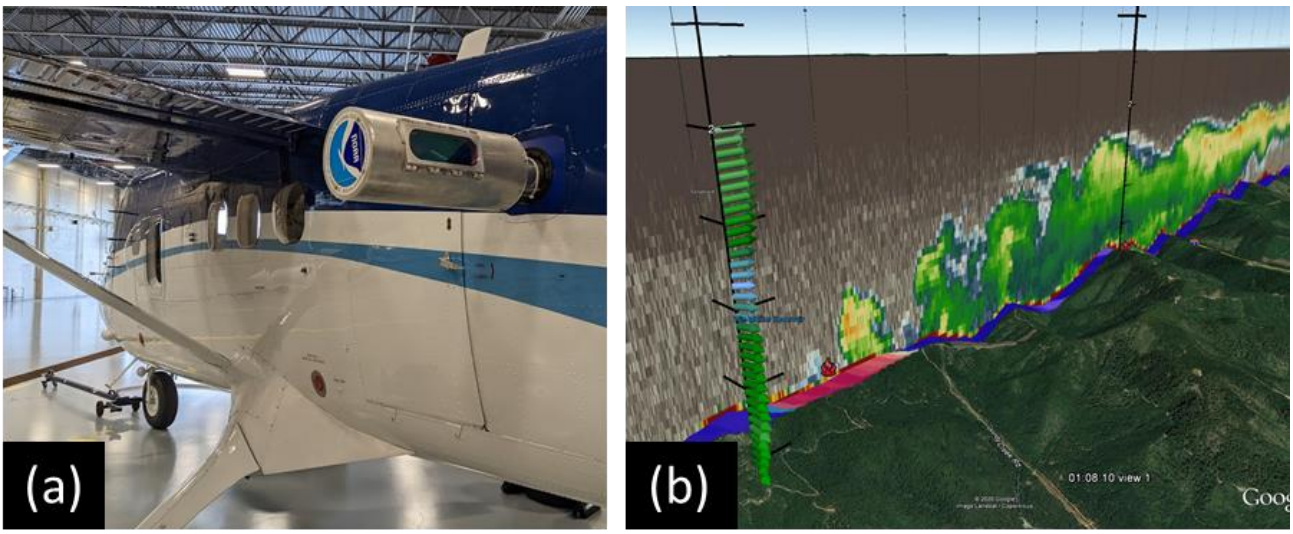

Figure 1- a) Doppler lidar scanner installed on the NOAA Twin Otter. b) Data from a wildland fire during a 2019 measurement campaign. The red area at the surface indicates the fire area. Arrows on the left axis indicate wind speed and direction. Coloration indicates aerosol backscatter intensity.

3. Ground Based Systems

In addition to the aircraft based Doppler lidar, there will be three ground based Doppler lidars deployed for the CalFiDE experiments. Fire-generated winds close to the fire front, including convergent and rotating inflow winds will be sampled by two Doppler lidar systems from UNR and SJSU. These data are critical for understanding the coupling of fire and atmospheric processes that can drive rapid fire spread and intensification.

A NOAA motion-stabilized truck-based lidar will measure convective boundary layer (CBL) depth, vertical velocity, and horizontal wind profiles proximal to the fire, but away from the fire front. The Doppler lidar installed in the NOAA F-250 pickup truck, known as the PickUp based Mobile Atmospheric Sounder (PUMAS), is shown in Figure 2. The Doppler lidar system itself has also been designed by the ARS group within NOAA CSL. The system has similar operating characteristics as the system installed on the Twin Otter, with an effective range of 7.2 km and 60m along path resolution. The unique characteristic of this system is it has two output beams. One beam is coupled with an optical wedge scanner for continuous scans for 3D wind fields. The second channel is directed vertically for continuous measurements of vertical velocities. The optical head of the lidar is housed in a motion stabilizing cradle which stabilizes the platform in both pitch and roll, enabling continuous measurements while the truck is underway.

Figure 2- Doppler lidar and scanner installed in the bed of an F-350 pickup truck.

4. 3-D Measurements of Wildfire Winds: Improved Scan Patterns and Multi-Lidar Systems

The NOAA airborne Doppler lidar system has previously flown on the Twin Otter for the 2019 FIREX-AQ campaign to study the impact of fires on air quality and climate. During this campaign, the system was outfitted with an optical wedge scanner which allowed for scans and motion compensated vertical stares below the aircraft, but did not allow for more complex scan geometries or upward looking measurements. The partial hemispheric scanner which will be deployed for CalFiDE was developed in response to this need for improved scanning strategies and coordinated scans between multiple lidar systems which was noted in the FIREX-AQ data.

The wildfires sampled from the Twin Otter during FIREX-AQ were done with a single Doppler lidar. While the vertical stare captured the spatial distribution of updrafts/downdrafts within a wildfire, the conical scan attempted to characterize the inflow/outflow structure near the fire front. Analysis of the data collected during FIREX-AQ revealed that features central to transport, such as rigorous updrafts centered over wildfire hotspots, offered an opportunity to study the structural variability of these updrafts and dynamics associated with lateral mixing during parcel ascent.

A key shortcoming of this dataset, however, was the lack of temporal information related to the evolution of the updraft as well as the rather narrow observation window associated with beam slice intersecting the updrafts/downdrafts along track. Measurements which were not completely centered on core updrafts/downdrafts made quantifying their role in transport challenging, and thus has led to the development of new and improved strategies that are planned for CalFiDE.

To address the temporal evolution of hotspots and the updrafts therein, an inverted triangle, either vertically pointing or off-angle, will be used to target specific core features over areas of high FRP as the Twin Otter flies within range of the fire front. The inverted triangle will have a denser cluster of points near the base of the updraft which will widen with height. Additionally, two ground-based mobile systems – one upwind and one downwind – will be used in conjunction with the inverted triangle scan to map out the 3-D structure in order to quantify the spatiotemporal characteristics and associated dynamics. Figure 3 shows a proposed configuration of the three Doppler lidar systems that would be coordinating in real-time, such that the beams from the respective Doppler lidar systems will intersect to construct the 3-D wind vector in a gridded format. The idea is not only to quantify the spatiotemporal characteristics over wildfires, but to determine the vortical structure associated with counter-rotating vortices at the flanks of updrafts, whether there is a helical component associated with certain core updraft features, and how the inflow/outflow dynamics assists in the spatial structure and temporal evolution of the most rigorous updrafts.

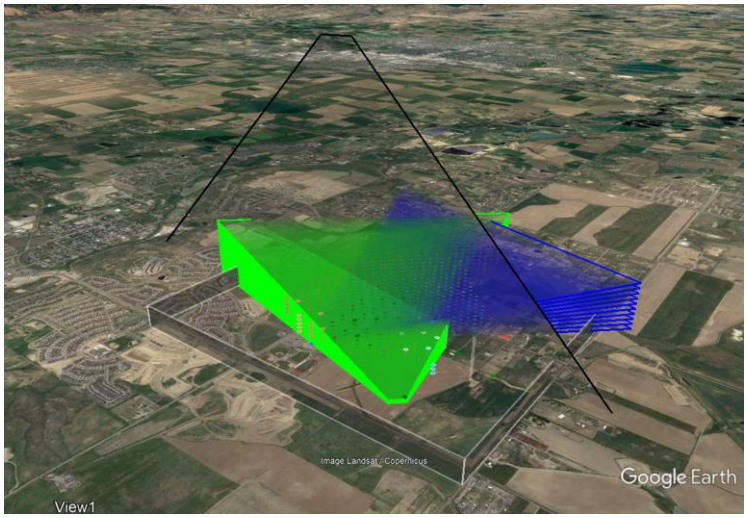

Figure 3- Demonstration of scan geometry for CalFiDE multi-Doppler coordinated scans.

5. References

Lareau, N. P., & Clements, C. B. (2017). "The Mean and Turbulent Properties of a Wildfire Convective Plume", Journal of Applied Meteorology and Climatology

Charland, A. M., and Clements, C. B. (2013), "Kinematic structure of a wildland fire plume observed by Doppler lidar", J. Geophys. Res. Atmos.

Newman, J. F., Bonin, T. A., Klein, P. M., Wharton, S., and Newsom, R. K. (2016) "Testing and validation of multi-lidar scanning strategies for wind energy applications," Wind Energy.

Choukulkar, Aditya, W Alan Brewer, Scott P Sandberg, Ann Weickmann, Timothy A Bonin, R Michael Hardesty, Julie K Lundquist, et al. (2017) "Evaluation of Single and Multiple Doppler Lidar Techniques to Measure Complex Flow during the XPIA Field Campaign," Atmos. Meas. Tech.

Schroeder, P., Brewer, W. A., Choukulkar, A., Weickmann, A., Zucker, M., Holloway, M. W., & Sandberg, S. (2020). "A Compact, Flexible, and Robust Micropulsed Doppler Lidar", Journal of Atmospheric and Oceanic Technology

Monitoring wildfire smoke dispersion using concentrations of PM10 and PM2.5

Lourdes Bugalho*[1]; Luisa Mendes[2]; Maria José Monteiro[1]; Paulo Pinto[1]; João Rio[1]; Manuel João Lopes[1]

[1]IPMA,I.P., Lisboa, Portugal, {lourdes.bugalho, maria.monteiro, paulo.pinto, joao.rio, manuel.lopes}@ipma.pt,
[2] FCT NOVA, Portugal, {lc.mendes@fct.unl.pt}

**Corresponding author*

Keywords

Smoke wildfire, PM_{10}, $PM_{2.5}$, Aerosol Optical Depth

Abstract

Portugal as a member of the European Union (EU) follows the air quality legislation regulated by Directive 2008/50/EC that states that "Member States shall ensure that timely information about actual or predicted exceedances of alert thresholds, and any information threshold is provided to the public". The southern European countries, have biogenic contributions, mainly resulting from the long-distance transport of particulate matter, originating in arid regions, and from large forest fires, whose pollutants loads cannot be imposed limits. These sources lead to an additional contribution of atmospheric pollutants mainly during the spring and summer season. Climate change is increasing the vulnerability of the environment to extreme events, such as those that enhance the likelihood of forest fires. Due to the predicted increase in temperatures, the decrease in precipitation and humidity, an increase in the frequency and intensity of forest fires is expected, namely in regions of the Mediterranean basin, as is the case of Portugal. Monitoring the concentration of particles (PM10 and PM2.5) in the network of air quality stations can be a way of detecting the dispersion of smoke and giving possible alerts to affected populations. The analysis of PM10 and PM2.5 of the air quality network stations, from 2010 to 2020 only for June to October, shows very high concentration values that are associated with to the periods of forest fires. These data were analysed for all seasons by districts, considering a daily average. The daily concentration average was performed by including the observations on the period spanning from two days before and after the registration of a fire with daily burned area larger than 500 ha by district. Trajectory analysis was performed to confirm the origin of the particles observed at the stations. It was verified that, for the period 2010-2020, the daily average value of PM10 concentration is variable and generally increases from the day before to the day of the event by an average percentage of 26%. This variation depends on the proximity of the forest fire, the burned area as an indication of its strength, the stability of the atmosphere and the height of the boundary layer. During the summer season, dust episodes also occur, originating in the Sahara, especially in the southern regions of Portugal, increasing the observed concentration of PM10 and PM2.5 particles. In this way, for the summer period, the days with high values of PM10 and PM2.5 that could have been originated by dust particles, with larger dimensions, were identified and separated from those which referred to smoke particles from forest fires, usually smaller. For this purpose, the relationship between the concentrations of PM2.5 in relation to PM10, in the studied period, was taken in to account. For the large fires of 2017, a more detailed characterization of these features was made, analysing the optical thickness of the aerosols and the Angstrom exponent of the VIIRS radiometer on board the Suomi NPP satellite.

1. Introduction

Climate change is increasing the vulnerability of the environment to extreme events, which happen more frequently, namely those likely to promote forest fires (EEA, 2021). Due to the expected increase in temperatures (Andrade et al., 2014, 2015) and decrease in precipitation and humidity, it is expected an increase in the frequency and intensity of forest fires in certain regions of the Mediterranean basin, considered climatic hotspots, such as Portugal. It is also expected an increase in the duration of the current forest fire season, revealed by the analysis of the last 30 years. Furthermore, the fire regime is expected to change almost everywhere in Europe, southern countries being the ones that concentrate most of the annual burned area (San-Miguel-Ayanz et al, 2018). In 2017 the burnt area in Portugal was 539921 ha, which represented 498% of the average of the

previous decennium. Indeed, the wildfires that occurred in 2017 in Portugal, and more recently in 2019 in Australia, have raised awareness towards the need for further studies on the many relevant impacts of wildfires.

Biomass burning is an important source of gases and particulate matters (PM) that can significantly change local, regional and global atmospheric chemistry, with impact on air quality, which can affect human health (Crutzen & Andreae, 1990). Smoke emissions from forest fires present a highly variable composition between wildfires and with time for the same wildfire, leading to different particle sizes distribution, particle light absorption, and spectral dependence on absorption based on the type of fuel, its amount, burning characteristics, and weather conditions (Dubovik, O et al, 2002; Shi, S. et al, 2019). The released particles and gases can affect the tropospheric chemistry and cause several respiratory and cardiovascular diseases (Cardoso de Mendonça et al., 2006; Reid et al., 2019). Exposure to wildfires pollutants has been associated with an increase in respiratory and cardiovascular hospitalizations (Cardoso de Mendonça et al. 2006; Finlay et al. 2012). Therefore, it is important to monitor the concentration of particles in the ambient air. Monitoring can be done by warnings based on observations of air quality network stations and complemented by observations of the aerosols optical thickness (AOD) for wavelength between 400 to 800 nm, together with the Angstrom exponent, which indicates the particles size distribution in the air column, or with the aerosol index (AI), which gives information on absorbent aerosols. Both aerosols may present high values of AOD (for 500nm), but with large differences in the Angstrom exponent (dust aerosol is characterized by low values, around 0.5, while forest burning aerosols are characterized by high values often higher than 1.5). It is known that the main absorbing aerosols in the atmosphere are dust and aerosols resulting from forest burning. In the great fires of June 17th and October 15th 2017 in Portugal, the coexistence of these two types of aerosols was observed.

2. Material and Methods

2.1. Study Data

In this study, PM_{10} and $PM_{2.5}$($\mu g/m^3$) observational data from surface air quality monitoring stations, was used, from June 2010 to October 2020. These stations are the responsibility of the Portuguese Environment Agency (APA) in coordination with the corresponding Commission for Coordination and Regional Development (CCDR). The data measured continuously at the various stations are reported, in near real time, and made available to the public by QUALAR online database (https://qualar.apambiente.pt/indices).

Back and forward trajectory performed by HYSPLIT Model, (https://www.ready.noaa.gov/hypub-bin/trajtype.pl)

Daily values of burned area in Portugal, by district, were accessed from June to October, 2010 to 2020. The days in which the daily burned area, for each of the districts, exceeded 500 ha were identified.

Optical thickness data from OLCI-SENTINEL3A, with the XBAER algorithm (product C3S from Copernicus) and satellite Angstrom exponent from VIIRS (NOAA) data were used for June 16th to 20th, 2017 and October 14th to 17th, 2017.

Two Doppler weather radars from the IPMA network were accessed to analyze several fire plumes as they were being tracked near ground air quality stations.

2.2. Methods

All PM_{10} and $PM_{2.5}$ concentration values were analyzed for forest fires with a burned area larger than 500ha. For each case, the period spanning from two days before the fire occurrence to two days after the fire suppression was considered. The variation of the daily average of PM_{10} between the days before and after was calculated. For stations where a positive variation was observed, the back trajectory was computed for 24h and 48h in order to verify the origin of the particles in order to confirm the areas they came. In the large fires of 2017, data from AOD 550nm and Angstrom exponent of aerosols were also used, the latter mainly for splitting dust and smoke from forest fires. Data from the IPMA radar network was also used to monitor smoke plumes from the large forest fires that occurred in Portugal in 2017.

One of the radars, Arouca/Pico do Gralheiro (A/PG), is a dual polarization (DP) system located northeast of the observed plumes, with a beam around 1100 m a.m.s.l.(above mean sea level), while the other, Coruche/Cruz do

Leão (C/CL), is a single polarization system located to the southeast of the plumes, with a beam around 200 m a.m.s.l.. Low-level plane position indicators of reflectivity (PPZ) were extracted every 10 min from the A/PG radar and used to identify fire plume patterns in the case of high PM10 values observed at the air quality station Ilhavo (number 2018) from 20UTC of 15th October to 01UTC of 16th October 2017, the radar beam being at approximately 800 m a.g.l. (above ground level). PPZs were also used to identify fire plume patterns in the case of observation of PM_{10} at station Ervedeira (number 2019) and station Montemor-o-Velho (number 2022), but in this case the C/CL radar was used, the beam being at approximately 400 m a.g.l., due to the lower altitude of the radar.

As fires intensify, heat flux increases combustion and buoyancy, and more pyrometeors are transported upward, according to Jones et al, (2010). Thus, the magnitude of low-level reflectivity observed near the fire site is a good indicator of the overall intensity of strong convective processes caused by fire. A/PG radar was additionally used to verify if the suspected plume patterns were, in fact, originating from fire activity, based in the magnitude of the correlation coefficient that is processed in DP mode (Balakrishnan et al. (1990), Pinto et al. (2022)). Within the range of 100 km, the spatial resolution of the radar observations was 1 km or better. The evolution of plume patterns observed in the low-level PPZ was followed in the vicinity of ground stations as shown on a georeferenced map. A comparison was made between ground station air quality observations and low-level radar observations. Every 10 min, the magnitude of the reflectivity value of the plume that was being observed was estimated, at each moment, in an area of 3 x 3 km^2 (in polar coordinates). The center of this area was selected to be 5 km upstream from the ground station in relation to the identified buoyancy source and for each instant an average reflectivity was derived.

3. Results and Discussion

The variation in PM_{10} concentration between the day before and the day of the forest fire, for the stations whose back trajectory indicated this origin, was on average, 26%, ranging between 22% and 31% for the 2010-2020 period.

The 2017 forest fire season in Portugal was considered as a complex of extreme forest fire events, with two noticeable events, one in June and the other in October, not only because of the amount of total area burned, but because of the high number of casualties (more then 100 in two days). We studied, in detail, the behavior of the air quality stations for these two events. These events were also characterized by having dust events associated.

During the forest fires episodes, the proportion between $PM_{2.5}$ and PM_{10} varies in the sense of increasing the percentage of $PM_{2.5}$, indicating an increase of smaller particles, with greater damage to health. In the case of the large fires in Pedrogão Grande, 17th to 22th of June 2017, Figure 1 shows this ratio for stations 3096-Chamusca, 3089-Mem Martins, 2020-Fundão. By analyzing the back trajectory for the Fundão station (2020) it appears that on the 16th, 20th and 21th, the concentration of PM were due to dust, coinciding with the periods in which the $PM_{2.5}/PM_{10}$ values were lower, while on the 18th and 19th they were due to large fires in the central region of Portugal, with higher values of the $PM_{2.5}/PM_{10}$ ratio, Figure1. In the intermediate periods, a mixing of particles may have occurred, with intermediate values of the ratio. With the same methodology applied to Chamusca (3096, in blue in Figure 1) it was confirmed that the concentration of particles was essentially due to the forest fires in Pedrogão Grande and Góis on the 17th to 19th of June and the variation in the type of particles from the afternoon of the 19th of June.

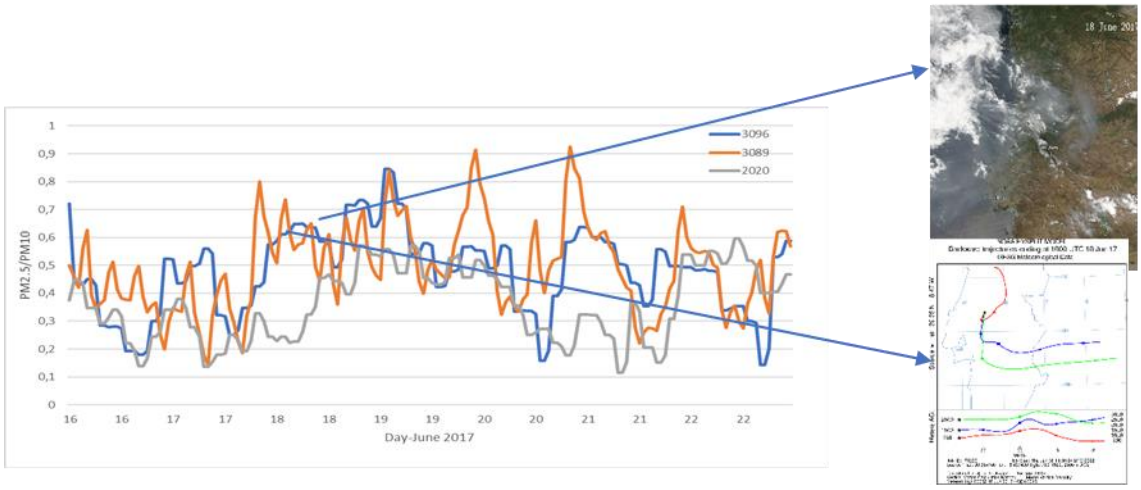

Figure 1- Hourly variation of the ratio between $PM_{2.5}$ and PM_{10} on three air quality monitoring stations (3096-Chamusca, 3089-Mem Martins, 2020-Fundão) the 16th to 22th of June 2017. Satellite image (MODIS/VIIRS) and backtrajectory for Chamusca Station for 18th June 2017.

Optical thicknesses of aerosols at 550nm allow a good identification of regions affected by smoke particles from fires (Figure **2**), when available.

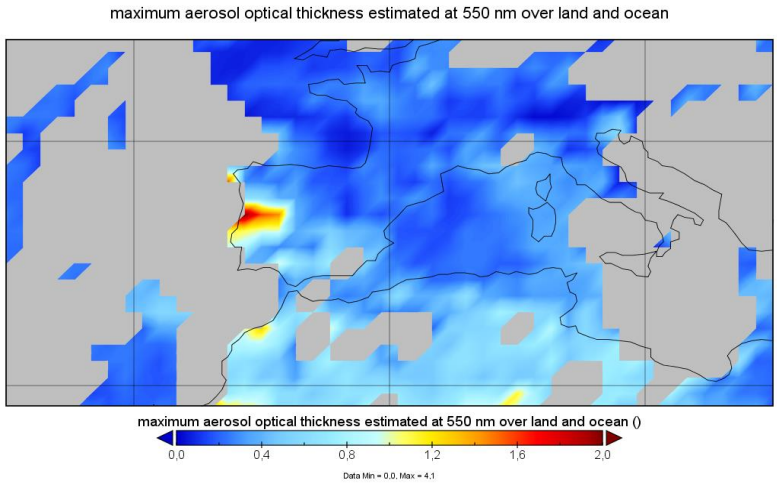

Figure 2- Maximum aerosol optical thickness estimated at 550nm on 18th June 2017(C3S from Copernicus)

Combining the optical thickness of the aerosols and the variation of the PM_{10} concentration (negative, in the direction of decrease, above 50% of variation, and positive with a variation above 50%), monitoring maps are obtained. These maps can allow the monitoring of the most serious episodes.

During the great fires of October, several stations had $PM_{2.5}$ observation´s gaps, especially the stations in the North and Central region of Portugal, where due to the location of forest fires and the predominant south-north flow will have been the most affected

In the wildfire events of October, the stations with PM_{10} observation located in the north and central region of Portugal were analyzed, jointly with the analysis of trajectories, dispersion of the point of fire and mainly with the analysis of smoke by radar observation. In the case of Ilhavo station (number 2018), two rapid increases in PM_{10} concentration were observed, one from 21UTC on the 15th to 2 UTC on the 16th and the other on the 17th of October, Figure 3. For the first PM_{10} observation period, low-level radar observations were analyzed every

10 minutes, monitoring the advection of the smoke plume from the forest fire, Figure 4. In the second period, no smoke was identified by the radar, being observed, by satellite, a mass of dust driven by a strong southerly flow.

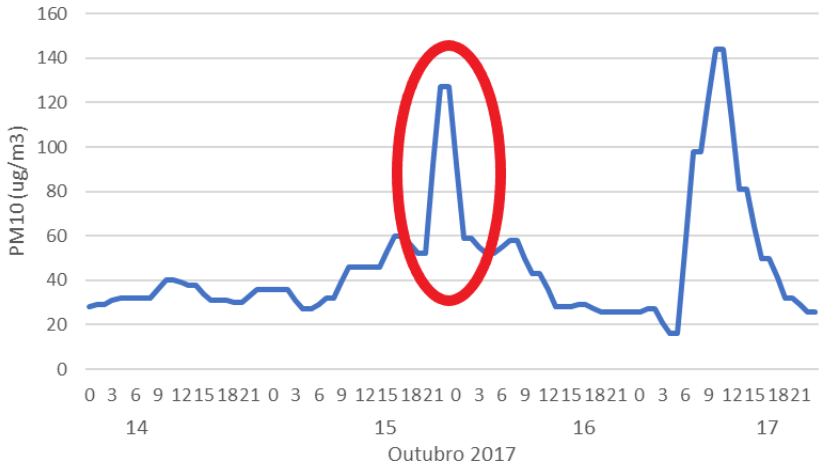

e

Figure 3- Hourly variation of PM_{10}, on air quality monitoring station 2018 (Ilhavo), on October 14th to 17th October 2017r

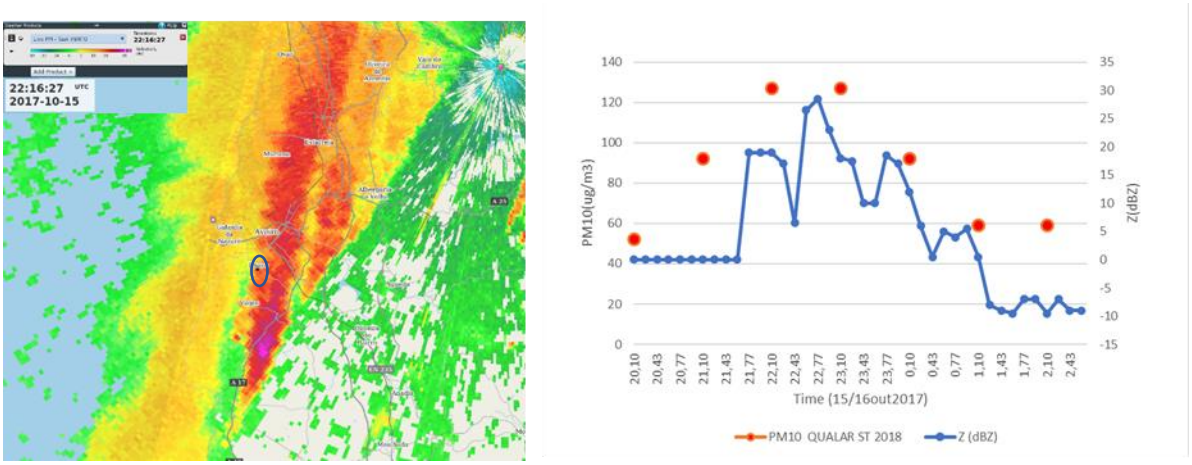

Figure 4- Low-level PPZ radar observation in an area matrix 3X3km² at 22:16 UTC of 15thOctober. The Ilhavo station is marked with a circle, (right). Hourly variation of PM_{10}, (red), on air quality monitoring station 2018 (Ilhavo), on October 15th at 20:00UTC to 16th at 2:00UTC, 2017, and low-level PPZ radar observation every 10 minutes in an area matrix 3X3km² between 15that 20:06 UTC and 16th at 2:36 UTC October (blue), (left)

4. Future Work

Combining multiple sources of information (RADAR reflectivity observations; surface air quality observations; AOD from remote sensors observations on board of satellite) we can early warn local authorities for atmospheric pollution events, caused by forest fires, in order to prevent population health issues.

As future work, this study should be extended to other severe forest fire events in Portugal, and it will also be necessary to study how to combine, operationally, all the existing information from observation.

5. Acknowledgment

The authors are grateful for the financial support of the Foundation for Science and Technology, I.P., through national funds (PIDDAC), under the SmokeStorm project (PCIF/MPG/0147/2019).

6. References

EEA (2021). European Environment Agency available online at: https://www.eea.europa.eu/ims/forest-fires-in-europe (accessed March 25, 2022)

Andrade and Contente 2020 Andrade C, Contente J (2020) Climate change projections for the Worldwide Bioclimatic Classification System in the Iberian Peninsula until 2070. Int J Climatol joc.6553. doi:10.1002/joc.6553

Balakrishnan, Narayanaswamy & Zrnic, D.. (1990). Use of Polarization to Characterize Precipitation and Discriminate Large Hail. Journal of The Atmospheric Sciences - J ATMOS SCI. 47. 1525-1540. 10.1175/1520-0469(1990)047<1525:UOPTCP>2.0.CO;2.

Cardoso de Mendonça MJ, Sachsida A, Loureiro PRA (2006) Estimation of damage to human health due to forest burning in the Amazon. J Popul Econ 19:593–610. doi:10.1007/s00148-006-0066-y

Crutzen, P. J., & Andreae, M. O. (1990). Biomass burning in the tropics: Impact on atmospheric chemistry and biogeochemical cycles. Science, 250, 1669– 1678. https://doi.org/10.1126/science.250.4988.1669

Dubovik, O.; Holben, B.; Eck, T.F.; Smirnov, A.; Kaufman, Y.J.; King, M.D.; Tanre, D.; Slutsker, I. Variability of Absorption and Optical Properties of Key Aerosol Types Observed in Worldwide Locations. J. Atmos. Sci.2002, 59, 19.

Finlay et al., 2012 Finlay SE, Moffat A, Gazzard R, et al (2012) Health Impacts of Wildfires. PLoS Curr. doi: 10.1371/4f959951cce2c

Jones,T. A., and S. A.Christopher,2010:Satellite and radar observations of the 9 April 2009 Texas and Oklahoma grassfires. Bull. Amer. Meteor. Soc., 91 , 455–460.

Pinto, P.; Silva, Á.P.; Viegas, D.X.; Almeida, M.; Raposo, J.; Ribeiro, L.M. Influence of Convectively Driven Flows in the Course of a Large Fire in Portugal: The Case of Pedrógão Grande. Atmosphere 2022,13, 414. https://doi.org/10.3390/atmos13030414.

Reid CE, Considine EM, Watson GL, et al (2019) Associations between respiratory health and ozone and fine particulate matter during a wildfire event. Environ Int 129:291–298. doi: 10.1016/j.envint.2019.04.033

Shi, S.; Cheng, T.; Gu, X.; Guo, H.; Wu, Y.; Wang, Y. Biomass Burning Aerosol Characteristics for Different Vegetation Types in Different Aging Periods. Environ. Int. 2019, 126, 504–51

More than just the FWI: Exploring all components of the Canadian Fire Weather Index System for International Fire Danger Rating Systems

Natasha Jurko*[1]; Mike Wotton [1,2]; Chelene Hanes[1]

[1] Great Lakes Forestry Centre, Canadian Forest Service, Natural Resources Canada.
1219 Queen St. E, Sault Ste. Marie, ON, P6A 2E5, Canada
{Natasha.Jurko, Chelene.Hanes}@nrcan-rncan.gc.ca

[2] Institute of Forestry and Conservation, John H. Daniels Faculty of Architecture, Landscape and Design, University of Toronto. 33 Willcocks Street, Toronto, ON M5S 3B3, Canada
{Mike.Wotton@utoronto.ca}

**Corresponding author*

Keywords

Fire Weather, Adaptation, Fire Danger Rating Systems, Preparedness

Abstract

The Canadian Fire Weather Index (FWI) System has its origins in early Canadian fire research and resultant hazard rating systems dating back to the 1930s. Today the FWI System is one cornerstone of the larger Canadian Forest Fire Danger Rating System (CFFDRS), which is comprised of several sub-systems, each evaluating fire potential at different scales and resolutions. The other major sub-system in the CFFDRS is the Fire Behaviour Prediction (FBP) System, designed to give quantitative predictions of fire behaviour in specific situations under constant conditions. Whereas the FBP System requires information on fuels, weather and landscape features to calculate potential fire behaviour on variable timescales, the FWI System provides a set of six daily outputs derived from weather observations, each indicative of different aspects of potential fire activity useful in fire management planning.

The basic design of the FWI System and simple inputs has made it a popular choice for adaptation in other regions. The System outputs can be readily adapted to act as the foundation for a new fire danger rating system or as an enhancement to an existing system. Research exploring the utility of the FWI System for characterizing fire activity in a region often focus on the final indicator, the FWI (not to be confused with the System namesake). While the FWI (the indicator) is a highly useful indicator of potential fire intensity, it is not necessarily the most appropriate indicator from the System to capture specific fire management needs. In adapting the FWI System to a new jurisdiction to support fire management, each indicator from the System should be evaluated on how it informs specific fire management needs in a region; that is, which of the System's six outputs relate most closely to important aspects of fire activity. Furthermore, it is important to understand how the standard Canadian pine fuel type might differ from those in the region in question.

This paper will review examples of how each of the indicators of the FWI System are used in operational fire management planning in Canada, and present Canadian Forest Service (CFS) experience in adapting the FWI System to other jurisdictions. We will evaluate each of the six components of the FWI System and their use to describe different aspects of fire potential in the wildland fire environment. While grounding this discussion in the way the System outputs are used to inform operational fire management decision-makers in Canada, we will also discuss their potential adaptation to support fire management planning in other locations. We will touch on the question of adaptation of the System to different fuels, and how these might affect the interpretation of each component and, how these considerations can lay the foundation to building local fire behaviour predictors.

While there is no set recipe for adaptation of the FWI System to a new region, understanding what each element of the wildland fire environment the FWI System outputs are designed to track is a critical first step.

The Canadian Forest Fire Danger Rating System (CFFDRS) is the national system for fire danger rating used throughout Canada. The two main sub-systems of the CFFDRS are the Fire Weather Index (FWI) System and Fire Behaviour Prediction (FBP) System. The FWI System uses daily weather observations to create six indicators, each capturing different aspects of potential fire activity important in daily fire management planning. The simple design and use in Canadian fire management planning has made the FWI System a popular choice for adaptation to other regions. When adapting the FWI System to a new jurisdiction, each of its six

indicators should be calibrated to the regional landscape and evaluated with respect to how each can inform local fire management planning. In this paper, we discuss the fire management structure in Canada, the development of the FWI System and its outputs, describe fire management decision-aid tools and provide examples of the use and adaptation of each components of the FWI System to other regions.

1. Fire management and danger rating in Canada

Wildland fire management in Canada is largely the responsibility of its ten provinces and three territories, each organizing and operating a fire management agency independent of each other, conforming to policies and regulations specific to their jurisdictions. However, they engage collectively in risk-sharing by agreeing to share suppression resources during periods of heightened activity that overload the resource capacity in a specific geographic area. To support preparedness and response planning each agency relies upon its own internal fire intelligence capacity, running their own fire weather monitoring networks and fire danger calculation activities. The CFFDRS provides a 'common language' for characterizing potential fire activity in the wildland environment across the country; however, local interpretation and decision-making tools are as unique as each region.

2. International evaluations and adaptations

When considering the FWI System for adaptation to other regions outside Canada, a variety of methods have been used to evaluate its effectiveness and to adapt the System. Such studies tend to focus on evaluating the final component of the FWI System, also known as the Fire Weather Index (FWI). While the FWI component is a good indicator of general fire danger, evaluating the association between FWI and information about different aspects of the fire environment (e.g., number of fires, ignition date, weather or total area burned) may not identify the most useful relationships between different aspects of fire activity and the FWI System as a whole. Other components of the FWI System may be better suited to inform specific fire management decision-making needs (Table 1). When adapting the FWI System to new regions, the evaluation of how each indicator best reflect the different aspects of fire potential is an important first step in generating effective FWI System based decision-aids.

Table 1, Examples of each Fire Weather Index System indicator and their fire management decision-aid associations.

FWI indicator	Physical association	Primary association in fire management	Examples of fire management associations
FFMC	Forest litter moisture	Flaming ignition sustainability	- Human-caused fire occurrence - Spot fire ignition - Vigor of surface spread
DMC	- Duff moisture (F-layer) - Medium woody debris	Lightning fire ignition	- Depth of burn
DC	- Deep duff moisture (H-layer) - Logs, large woody debris	Sustained smouldering	- Depth of burn - Lightning fire holdover - Fuel consumption - Live moisture deficit - Suppression difficulty
ISI	Fire Spread	Fire spread rate	- Crown fire potential
BUI	Surface fuel moisture levels	Surface fuel consumption	- Depth of burn - Sustained smouldering - Fire intensity
FWI	Fire intensity	Suppression resource effectiveness	- Public facing assessment of fire danger - Flame size

Understandably, methods of evaluation and adaptation are dependent on a number of factors; analysis is constrained by data availability, such as historical weather data and accurate area burned datasets. While field campaigns can add invaluable information in the adaptation of the System, these are often limited due to resource or timeliness constraints. Evaluation may start as a data driven exercise and be re-evaluated as more

historical data and statistical methods for classification become available (e.g., de Jong et al., 2016, Dentoni, 2015). Strategies of calibrating the FWI System components over very different landscapes while maintaining a consistent calibration have been developed by the European Forest Fire Information (EFFIS) System by introducing additional layers to provide context (Camia and Amatulli, 2010). Others may have additional information from field data to examine the relationship between the different FWI System indicators and regional fuel composition (e.g., de Groot et al., 2007, Dimitrakopoulos et al., 2011, Fogarty et al., 1998) allowing local adaptations to be tailored to the specific effects of weather on forest floor fuel types. Re-evaluating each FWI System component after initial adaptation as data is collected can lead to better understanding and evaluation of each indicators use as a decision-aid. Fire management agencies in Canada have been developing the expert knowledge to use the FWI System over several decades and research continues to provide FWI System indicators and classification methods to reflect the changing demands in wildland fire management (Hanes et al., 2021).

3. The outputs of the FWI System and their use

The FWI System contains six indicators, calculated daily based on solar noon observations of temperature, relative humidity, wind speed and 24hr accumulated precipitation (Figure 1). The first three indicators of the FWI System are the moisture codes; they act as a bookkeeping system to track moisture in dead fuels in different layers of the forest floor. The three moisture codes are then used to calculate three fire behaviour indexes, which are general indicators of potential fire spread, fuel availability and fire intensity. The outputs of all indicators are on an increasing numerical scale, where higher numbers signify higher danger during the peak burning period of the day, generally late afternoon.

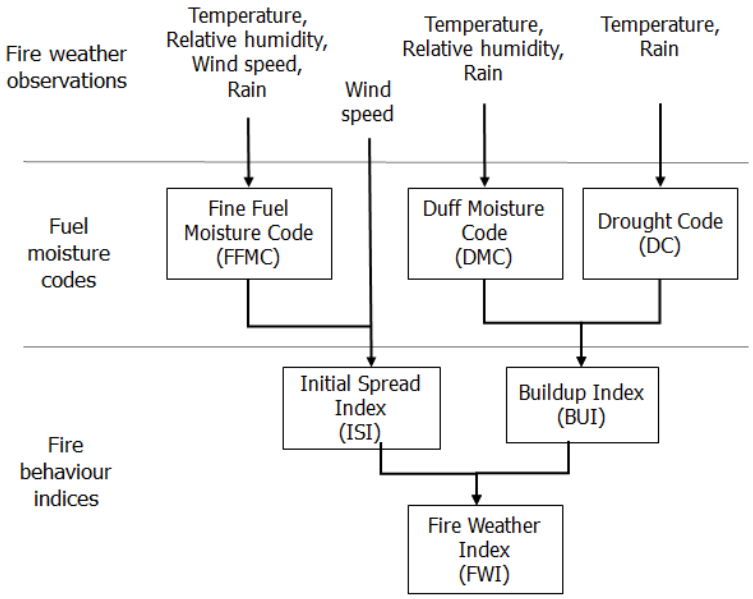

Figure 1: Structure of the Canadian Fire Weather Index (FWI) System.

The first of the three moisture codes in the FWI System is the Fine Fuel Moisture Code (FFMC), which tracks the moisture content of the fine dead fuels on the forest floor. Moisture content in fine fuels is a primary factor controlling the sustainability of a flaming ignition in fuel beds. The FFMC therefore plays a role as an indicator of the readiness of forest floor fine fuels to sustain flaming ignition; its utility in this regard has been demonstrated in many fuel types (e.g. Beverly and Wotton 2007). From the perspective of fire management agencies, this makes the FFMC well suited as an indicator of the day-to-day changes in the number of human-caused fires expected in regions with human activity in the wildland (this has been demonstrated throughout different fuel types in Canada). When the FWI System has been adapted to other regions, the relationship between FFMC and sustainable flaming ignition has been calibrated to other fuel types. For example, de Groot et al. (2005) calibrated dead grass fuel with FFMC using fuel moisture measurements and small-scale ignition

field experiments in three grassland sites of Indonesia. In this case, dead grass was chosen as the fuel type as it was a common fuel source and a fuel of concern for fire managers in Indonesia.

The Duff Moisture Code (DMC) tracks the moisture content in the loosely packed layer of decaying dead organic fuel directly beneath the fine litter (FFMC) layer. Moisture content in organic layers has been shown in both lab and field-based studies to indicate the sustainability of smouldering combustion; tracking moisture in this layer is of value for users looking to estimate the potential for consumption in this layer (i.e., depth of burning) or to estimate the ability of ignitions to 'holdover'. In day-to-day fire management planning in Canada, the DMC is used to indicate the potential for ignitions from lightning, (a significant cause of wildfires throughout most of the country).

The Drought Code (DC), tracks the compact decaying organic material deep (typically >10cm deep) in the forest floor, often associated with the humus layer of the organic horizon. While such deep layers are not always present throughout mature upland pine forests in Canada, tracking the impacts of drought is considered an important part of understanding conditions in the wildland fire environment. Operationally the DC is considered in lightning fire ignition and when examining the potential for deep burning and requirements for extended periods of suppression resource utilization for mop-up and the mitigation of the risk of restarts. In Canada, the DC has been studied in fen and bog peatlands to explore a relationship with the water table and volumetric moisture content (Waddington 2012). In South East Asia fire danger rating system applications, the DC has been calibrated to track drought in peatlands where fire activity has caused major haze disasters affecting health and industry (Field et al. 2004). In other more arid regions without deep organic layers the DC might have most utility as an indicator of drought effects on live fuel moisture.

The three moisture codes: FFMC, DMC, and DC are inputs used to calculate the three remaining FWI System indicators, which reflect different aspects of fire behaviour. The Initial Spread Index (ISI) provides an indication of the potential rate of spread of a fire by capturing the interaction between the dryness of fine dead surface fuels (which carry flaming) and the wind. The FBP System provides explicit characterization of the relationships between spread rate and ISI over a wide range of fuel types found in Canada; ISI is a good indicator of spread in all these types. In other regions, where grass fuel type is the main concern for wildland fire activity, the ISI has been adapted as an indicator for general fire intensity. For example, fire management guidelines in Indonesia indicate difficulty of wildfire control (and suppression resource effectiveness) as associated with the ISI (de Groot et al., 2007).

The Build-Up Index (BUI) is a weighted average of the DMC and DC and is a general indicator of the potential heavier fuel available for consumption by a passing fire. The FBP System uses the BUI as the primary variable influencing surface fuel consumption across a broad range of forest types. Because of this association with surface fuel consumption, as a daily planning aid the BUI is used to inform fire managers about the potential for increased fire intensity due to the long-term dryness of surface fuels. Because it provides a weighted indication of moisture content throughout the forest floor, it can also be used as a general indicator of potential below surface smoldering.

The final primary fire behaviour output of the FWI System is the Fire Weather Index (FWI). In the scaled, unitless world of the FWI System the FWI is an expression of Byram's fireline intensity concept, capturing the interaction between spread rate (ISI) and fuel consumption (BUI) in a relative way (Van Wagner 1987). In Canada, many agencies use the FWI when communicating 'fire danger levels' to the public, because it combines information from other parts of the system on ignition potential, spread potential, and the difficulty of suppression of a fire, into a single number. However, in operational fire management planning, the different elements of the FWI System that more directly influence each of those separate aspects of fire activity are used directly.

The FWI System remains an important tool for daily planning at the regional scale, providing fire management personnel an overview of potential fire activity over large landscapes. Increased fire activity, which increases demands for resources along with changing priorities in managing fire in Canadian forests has made decision-making in wildland fire planning increasingly challenging across the country. To support these complex demands and new technologies, updates to the CFFDRS are underway to incorporate new data sources and new modular, process-based approaches. Updates to the FWI System include a modification to the fire danger calculations to better reflect peaks in daily fire weather, and new fire danger indicators specific to grasslands and peatlands (Canadian Forest Service Fire Danger Group, 2021). The addition of the grassland and peatland

moisture codes and intensity indexes will widen the adaptability of the FWI System in other regions outside Canada. As the threat from wildland fire increases in many parts of the world, the FWI System indicators can be a foundation for local decision-support tools. Evaluation of the adaptability of the System to any new region must start with an evaluation of the information needs specific to fire management decision-making and then an evaluation of how the different indicators within the FWI System structure can inform those fire management decision-making needs.

4. References

Beverly, J. L., & Wotton, B. M. (2007). Modelling the probability of sustained flaming: predictive value of fire weather index components compared with observations of site weather and fuel moisture conditions. International Journal of Wildland Fire, 16(2), 161-173.

Camia, A., & Amatulli, G. (2010). Climatology of FWI over Europe: fire danger anomalies and index percentile rankings. VI International Conference on Forest Fire Research, 15–18 November 2010, ADAI/CEIF, Coimbra, Portugal, edited by: Viegas, D. X, p.12.

Canadian Forest Service Fire Danger Group. 2021. The Vision for the Next Generation of the Canadian Forest Fire Danger Rating System (Information Report GLC-X-26). Natural Resources Canada, Canadian Forest Service, Great Lakes Forestry Centre. Information Report GLC-X-26. 70 p.

de Groot, WJ, Wardati, Y Wang (2005). Calibrating the Fine Fuel Moisture Code for grass ignition potential in Sumatra, Indonesia. International Journal of Wildland Fire 14(2), 161-168.

de Groot, W. J. D., Field, R. D., Brady, M. A., Roswintiarti, O., & Mohamad, M. (2007). Development of the Indonesian and Malaysian fire danger rating systems. Mitigation and Adaptation Strategies for Global Change, 12(1), 165-180.

de Jong, M. C., Wooster, M. J., Kitchen, K., Manley, C., Gazzard, R., & McCall, F. F. (2016). Calibration and evaluation of the Canadian Forest Fire Weather Index (FWI) System for improved wildland fire danger rating in the United Kingdom. Natural Hazards and Earth System Sciences, 16(5), 1217-1237.

Dimitrakopoulos, A. P., Bemmerzouk, A. M., & Mitsopoulos, I. D. (2011). Evaluation of the Canadian fire weather index system in an eastern Mediterranean environment. Meteorological Applications, 18(1), 83-93.

Field, R. D., Wang, Y., & Roswintiarti, O. (2004). A drought-based predictor of recent haze events in western Indonesia. Atmospheric Environment, 38(13), 1869-1878.

Fogarty, L. G., Pearce, H. G., Catchpole, W. R., & Alexander, M. E. (1998). Adoption vs. adaptation: lessons from applying the Canadian forest fire danger rating system in New Zealand. In Proceedings, 3rd International Conference on Forest Fire Research and 14th Fire and Forest Meteorology Conference, Luso, Coimbra, Portugal. pp. 1011-1028.

Hanes, C. C.; Wotton, B.M; McFayden, C; Jurko, N. (2021). An Approach for Defining Physically Based Fire Weather Index System Classes for Ontario (Information Report, GLC-X-29). 42p.

Van Wagner, C. E. (1987) Development and Structure of the Canadian Forest Fire Weather Index System. Ottawa: Petawawa National Forestry Institute. 36p.

Waddington, J. M., Thompson, D. K., Wotton, M., Quinton, W. L., Flannigan, M. D., Benscoter, B. W., & Turetsky, M. R. (2012). Examining the utility of the Canadian Forest Fire Weather Index System in boreal peatlands. Canadian Journal of Forest Research, 42(1), 47-58.

Optimization with fire spread simulation for forest management

Filipe Alvelos*[1,2]; Isabel Martins[3,4]; Susete Marques[3,5]; Mariana Dias[3]; Eduardo Cunha[2]; David Neto[2]

[1] *Departamento de Produção e Sistemas, Escola de Engenharia, Universidade do Minho, Portugal, {falvelos@dps.uminho.pt}*
[2] *Centro Algoritmi, Escola de Engenharia, Universidade do Minho, Portugal*
[3] *Instituto Superior de Agronomia, Universidade de Lisboa, Portugal {isabelinha@isa.ulisboa.pt, smarques@isa.ulisboa.pt, marii.plant@gmail.com}*
[4] *Centro de Matemática, Aplicações Fundamentais e Investigação Operacional*
[5] *Centro de Estudos Florestais e Laboratório Terra*

**Corresponding author*

Keywords

Forest management, fire spread simulation, mixed integer programming, decision making, software.

Abstract

We propose a method for forest management in which wildfire is modelled explicitly through the integration of optimisation and simulation. Given a forest, the decision problem is to select a plan (i.e. a prescription and a periodicity for shrub cleaning) for each of its stands. Each plan is associated with values for a set of criteria for each period of the temporal horizon. Considered criteria are net present value, biodiversity, carbon stock, and erosion. The problem is modelled by a mixed integer programming (MIP) with the objective of maximizing the net present value and imposing limits for the remaining criteria.

A fire spread simulator, based on shortest path algorithms following the minimum travel time principle, is responsible to identify sets of plans that are not acceptable together as they result in a high rate of fire spread. That information is included in the MIP as constraints. This cycle optimization-simulation is repeated until the plans provided by the MIP are acceptable in all scenarios.

Data from a real landscape case-study has been collected and processed to obtain management and fire parameters required to validate the proposed method, which is being implemented in Python (with Gurobi as a MIP solver, GeoPandas for managing and processing geospatial data, and NetworkX implementation of graph algorithms).

1. Introduction

Forest management problems have been addressed with optimisation techniques for decades as surveyed in Kaya et al. (2016).

We consider the forest management problem of deciding which prescription and shrub cleaning periodicity to apply in each stand. Different variants of this problem have been approached before with mixed integer programming, being harvest scheduling with spatial constraints one of the most studied (for a broader view, see Yoshimoto (2018) for the problem with constraints on clearcut area and Neto (2020) for the problem with habitat fragmentation concerns). Recent works (e.g. Marques et al. 2017) consider, among the net present value, carbon stock and others, fire resistance indicators.

Our main contribution is to explicitly incorporate fire spread simulation in forest management. Optimization is used to select promising plans with respect to forest management indicators (net present value, biodiversity, carbon stock, erosion). Fire spread simulation is used to exclude plans that, taken together, may lead to wildfires with high damage potential.

We consider two modules: an optimization module and a fire spread simulation module. The optimization module, which consists in a mixed integer programming (MIP) model, is responsible for the selection of a global plan, i.e. the calendar of silvicultural operation including shrub cleaning periodicity for each stand, further called prescription, that maximizes the net present value taking into account limits on the biodiversity, carbon stock,

soil erosion, standing timber volume, and harvested timber fluctuations between planning periods. The first three limits are imposed to ensure a certain quality of the respective ecosystem services and soil functions. The last constraints aim at maintaining the availability of timber in the forest and simultaneously a stable timber supply.

The fire spread simulation module represents the landscape as a grid network and, using the minimum travel time principle (MTT) (Finney 2002) and an all-pair shortest paths algorithm (Ahuja et al. 1993) allows to obtain the fire paths and fire arrival times at each node of the network for any ignition node. The assessment of the fire potential damage is made by the distance travelled by fire in the quickest path (in a given time interval, i.e. the rate of spread (ROS) of fire is measured in all nodes that have the same fire arrival time) in a set of scenarios.

The interaction between the two models occurs in both directions. The optimization module provides to the simulation module the current plan of each stand. The simulation module generates a set of scenarios that share the fuel model and canopy characteristics derived from the current plan of each stand and have different wind and ignition locations. For each scenario, the fire transmission time between each pair of adjacent nodes is obtained and the ROS is calculated. If the ROS of a fire path is higher than a given threshold, the path is termed unacceptable. The set of stands belonging to an unacceptable path cannot have the current plan because lead to a ROS higher than the acceptance threshold. In that case, a corresponding constraint is inserted in the MIP model. If the simulation module does not identify an unacceptable fire path, the global plan is optimal with respect to all fire scenarios considered.

This paper is organized as follows. In section 2 we detail the optimization module. In section 3, we detail the fire spread simulation module. In section 4, we provide an overview of a landscape being used as a case-study, describe the data gathered, and how the proposed approach is being implemented. In section 5, conclusions are drawn, and extensions are discussed.

2. Optimizing plans

We consider a forest divided into stands. The set of stands is denoted by S. For each stand $s, s \in S$, we represent its area (in ha) with a_s and its set of available plans by P_s.

A plan p, $p \in P_s$, is defined by a prescription and by a brush cleaning periodicity. For example, for an eucalyptus stand, available plans may be characterized by an harvest periodicity (e.g., 10, 11 or 12 years), and a shrub periodicity (e.g, 5, 10 years or never, resulting in nine plans).

We denote by T the set of periods of the planning horizon, being the number of periods of the planning horizon its cardinality $|T|$.

The consequences of applying a plan p to a stand s are measured for each time period, which is indexed by $t, t \in T$, and are the following:

npv_{sp}^{t} − net present value (€);
bd_{sp}^{t} − biodiversity (*index*);
es_{sp}^{t} − soil erosion (ton);
cb_{sp}^{t} − stock of carbon (ton) ;
vol_{sp}^{t} − volume (m^3) of timber removed by thinning and harvest.

For the end of the planning horizon, we define:

$stv_{sp}^{|T|}$ − standing timber volume (m^3).

We consider the following limits that cannot be violated in each period:

b_{min} − biodiversity index;
c_{min} − carbon stock (ton/ha);
e_{max} − soil erosion (ton/ha).

Two further parameters are considered:

$stv_s^0 -$ standing timber volume (m^3) in stand s at the beginning of the first period;
$\Delta -$ deviation allowed from the reference volume of timber removed.

The decision variables are:

$$x_{sp} = \begin{cases} 1, \text{if stand } s \text{ is managed with plan } p \\ 0, \text{otherwise} \end{cases}, s \in S, p \in P_s;$$

$w -$ reference level for the volume of removed timber over the planning horizon.

The model is:

$$Max \sum_{s \in S} \sum_{p \in P_s} \sum_{t \in T} npv_{sp}^t x_{sp} \quad (1)$$

$subject\ to$:

$$\sum_{p \in P_s} x_{sp} = 1, s \in S \quad (2)$$

$$\frac{\sum_{s \in S} a_s (\sum_{p \in P_s} bd_{sp}^t x_{sp})}{\sum_{s \in S} a_s} \geq b_{min}, t \in T \quad (3)$$

$$\frac{\sum_{s \in S} \sum_{p \in P_s} es_{sp}^t x_{sp}}{\sum_{s \in S} a_s} \leq e_{max}, t \in T \quad (4)$$

$$\frac{\sum_{s \in S} \sum_{p \in P_s} cb_{sp}^t x_{sp}}{\sum_{s \in S} a_s} \geq c_{min}, t \in T \quad (5)$$

$$\sum_{s \in S} \sum_{p \in P_s} vol_{sp}^t x_{sp} \geq (1 - \Delta) w, t \in T \quad (6)$$

$$\sum_{s \in S} \sum_{p \in P_s} vol_{sp}^t x_{sp} \leq (1 + \Delta) w, t \in T \quad (7)$$

$$\sum_{s \in S} \sum_{p \in P_s} stv_{sp}^{|T|} x_{sp} \geq \sum_{s} stv_s^0 \quad (8)$$

$$x_{sp} \in \{0,1\}, s \in S, p \in P_s \quad (9)$$

$$w \geq 0 \quad (10)$$

The objective function (1) states the management objective of maximizing the net present value. Constraints (2) state that each stand is managed with one and only one prescription and shrub cleaning periodicity, i.e. one plan. Constraints (3) ensures a minimumfor the average biodiversity index value of the forest for each period. Constraints (4) guarantees a maximum for the average erosion of the forest for each period. Constraints (5) imposes a minimum for the average carbon stockage of the forest for each period. Constraints (6) and (7) impose a limit on the fluctuation of the volume of timber removed in each period in relation to a reference value. Constraint (8) states that the volume of standing timber of the forest at period T is greater than or equal to that at the beginning of the first period. Constraints (9) and (10) define the domain of the decision variables.

After the optimization of the model just introduced, a global plan is obtained. This plan is provided to the fire spread simulation which is responsible to identify stands belonging to unacceptable paths. Let U represent the stands belonging to an unacceptable fire path, and, with a slight abuse of notation for clarity, $s\bar{p}$ represent stand s and its current plan, $\bar{p}$. Constraint (11) excludes the use of the current plans of the stands in U together:

$$\sum_{s \in U} x_{s\bar{p}} \leq |U| - 1 \quad (11)$$

At a given iteration, the MIP model to optimize is (1-10) plus the set of all constraints (11) identified in the previous iterations.

Feasibility issues may arise in the first MIP if the limits are too narrow or the plans are not suited. After the insertion of constraints on unacceptable paths, the MIP may become infeasible – meaning that no global plan respecting the unacceptable path criterion can be found. In that case, the identification of the path may be used to drive other fire related measures (e.g. implement fire barriers).

3. Simulating fire spread

Fire spread simulation is based on the minimum travel time principle (MTT) (Finney 2002) which states that fire arrival time at any location is given by the duration of quickest path from the ignition to the location.

We define a grid network representing the landscape. Nodes are associated with locations and arcs are associated with potential fire transmission between adjacent locations. Each arc has a fire transmission time, which depends on the slope, wind and fuel model. The set of transmission times, together with one ignition location, defines a scenario for which the quickest path in a given period is identified.

After the optimization module obtains a global plan, i.e. as a set of plans, a set of fire scenarios is considered. The slope and fuel moisture are the same for all scenarios. For each period, the fuel model and canopy measures are constant (given by the plan selected for each stand). Different transmission times are obtained by varying the wind. For a given set of transmission times, all-pairs quickest paths are determined efficiently. Based on those transmission times, for each potential ignition location, the quickest fire path (in a given period, with a minimum length) is identified and checked against a pre-defined threshold. If the ROS of the fire path is greater then the fire path is unacceptable, and its plans and the corresponding stands are returned to the optimization module which will derive the constraints as (11).

4. Implementation and case-study

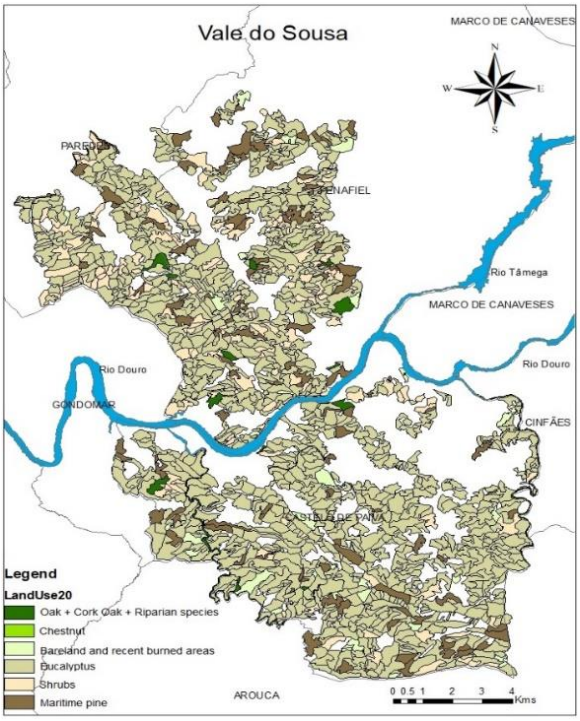

Figure 1 – Case study area location and land occupation in 2020.

The proposed approach is being implemented and validated with data from the Zona de Intervenção Florestal (ZIF) Paiva and Entre-Douro e Sousa in Portugal.

ZIF is a forested landscape located in Northwest Portugal, 100 Km from Oporto. The Associação Florestal do Vale do Sousa, a forest owners association, is the entity responsible for developing the management plan for the whole area. ZIF is divided in 1406 stands with a total area of 14313 *ha*. Data required for the approach was collected and estimated as follows.

The wSADfLOR decision support toolbox was used to automate data processing (Marto et al., 2019). The prescription writer and simulation modules were used to generate the prescriptions and their outputs according to the management planning criteria (Table 1). We also computed several ecosystem services provided by the forested landscape (Barreiro et al 2016, Botequim et al 2021, Marques et al 2021, Rodrigues et al 2021). We considered a planning horizon extending over ten years, with a period corresponding to one year.

A fuel model for each stand from the set of national fuels models proposed in (Cruz and Fernandes 2008, Fernandes and Loureiro 2021) was identified and assigned to each prescription each year of the planning horizon

Table 1- Silvicultural models characteristics and growth models used in simulation.

Species	Stand	Density (trees/ha)	Beat up (%)	Pruning and thinning (year)	Wilson factor	Harvest (year)
***Pinus pinaster* Ait.**	Mixed Pure	1100 1100	15 15	10[1], 25 to 45 (every 10)	0.27	35 to 50
***Eucalyptus* sp. Labill**	Mixed Pure	1400 1400	15 15	3[2] 3[2]	-	10 to 12
***Castanea sativa* Mill.**	Pure	1250	20	According to site index	-	40 to 55
***Quercus robur* L.**	Pure	1600	20	20, 23[3], 27, 37, 45	0.20	40 to 60
***Quercus suber* L.**	Pure	833	20	15, 30, 40, 58, 76	-	30, 40, then every 9[4]
Riparian sp.	Pure	4000	-	-	-	-

[1]Pre-commercial thinning; [2]Stool thinning in 2nd and 3rd coppice cycles, with 1.6 intensity; [3]Prunning; [4]Debarking (cork extraction).

Examples of three attributes of the landscape are given in Figure 2 (altitude, fuel models, and canopy cover).

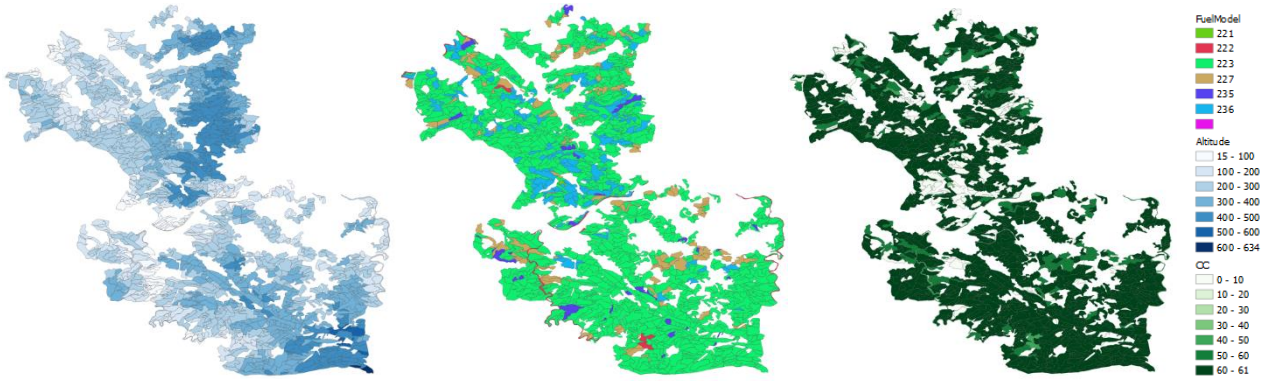

Figure 2- Altitude (600 meters amplitude), fuel models and canopy cover for ZIF.

Geographical information is processed and managed with GeoPandas, Transmission times are calculated with the Rothermel model (with R_0 obtained with BehavePlus6 for each portuguese fuel model and following Andrews (2018) to derive the slope and wind factors in any direction), NetworkX is used for shortest path calculations and visualization, and Gurobi / Gurobipy is used for optimization.

5. Conclusions

We proposed a method for fire-aware forest management based on the interaction of optimization and simulation. Optimization suggests plans respecting limits for different criteria (e.g. biodiversity) and maximizing the net present value, while simulation asserts the plans are acceptable for a different set of scenarios or identify which plans cannot be selected together. In the latter case, the optimization model is updated taking into account that information and the process is repeated. Short-term future work includes the validation with a case-study.

At the time of writing, most of the parameters required for validating the approach in a real landscape are gathered and an implementation in Python is being conducted.

Extensions of the proposed approach may explore four relevant issues:
i) include fire suppression resources and their optimized positioning (Alvelos 2018, Mendes and Alvelos 2022) in the fire spread model;ii) characterize unacceptable scenarios with other measures (or combinations), e.g, fire perimeter, fire area, and average ROS;

iii) address strategic plans where the planning horizon covers several decades;
iv) consider multiple objectives (in fact, the described model can be seen as the one of an iteration of the

epsilon-constraint method for multi-objective optimization) and additional spatial constraints (e.g. clearcut related).

6. Acknowledgments

This research was supported by project PCIF/GRF/0141/2019 ”An Optimization Framework to reduce Forest Fire” and in the scope of Norma Transitória—DL57/2016/CP1382/CT15 both funded by FCT – Fundação para a Ciência e Tecnologia. We thank Paulo Fernandes for providing us the files with the Portuguese fuel models.

7. References

Ahuja, R., Magnanti, T. & Orlin, J. (1993) Network Flows, Prentice-Hall.

Andrews, P. L. (2018). The Rothermel surface fire spread model and associated developments: A comprehensive explanation. Gen. Tech. Rep. RMRS-GTR-371. Fort Collins, CO: US Department of Agriculture, Forest Service, Rocky Mountain Research Station. 121 p., 371.

Alvelos, F. (2018). Mixed Integer Programming Models for Fire Fighting. In International Conference on Computational Science and Its Applications (pp. 637-652). Springer, Cham.

Borges, J.G., Garcia-Gonzalo, J., Bushenkov, V.A., McDill, M. E., Marques, S. & Oliveira, M.M. (2014). Addressing multi-criteria forest management with Pareto Frontier methods: an application in Portugal. Forest Science, 60, 63-72.

Barreiro, S.; Rua, J.; Tomé, M. (2016) StandsSIM-MD: A Management Driven forest SIMulator. Forest Systems, 25, eRC07, 5 pages.

Botequim, B.; Bugalho, M.N.; Rodrigues, A.R.; Marques, S.; Marto, M.; Borges, J.G. (2021) Combining Tree Species Composition and Understory Coverage Indicators with Optimization Techniques to Address Concerns with Landscape-Level Biodiversity. Land, 10, 126, 26 pages.

Fernandes, P., Gonçalves, H., Loureiro, C., Fernandes, M., Costa, T., Cruz, M. G., & Botelho, H. (2009, July). Modelos de combustível florestal para Portugal. In Actas do 6o Congresso Florestal Nacional. SPCF, Lisboa, Portugal (pp. 348-354).

Fernandes, P., Loureiro, C., (versão 2021). Modelos de combustível florestal para Portugal. Departamento de Ciências Florestais e Arquitetura Paisagista, UTAD, CITAB, 16 pages.

Finney, M. A. (2002). Fire growth using minimum travel time methods. Canadian Journal of Forest Research, 32(8), 1420-1424.

Kaya, A., Bettinger, P., Boston, K., Akbulut, R., Ucar, Z., Siry, J., Merry, K. & Cieszewski, C. (2016). Optimisation in forest management. Current Forestry Reports, 2(1), 1-17.

Marques, S., Bushenkov, V., Lotov, A., G. Borges, J. (2021) Building Pareto Frontiers for Ecosystem Services Tradeoff Analysis in Forest Management Planning Integer Programs. Forests, 12, 1244, 20 pages. https://doi.org/10.3390/f12091244

Marto, M., K. M. Reynolds, J. G. Borges, V. A. Bushenkov, S. Marques, M. Marques, S. Barreiro, B. Botequim and M. Tomé. 2019 A Web-based Architecture for a Forest Resources Management Decision Support System. Forests, 10, 1079, 21 pages

Mendes, A. B., & e Alvelos, F. P. (2022). Iterated local search for the placement of wildland fire suppression resources, European Journal of Operational Research, 2022, ISSN 0377-2217, https://doi.org/10.1016/j.ejor.2022.04.037.

Neto, T., Constantino, M., Martins, I. & Pedroso J.P. (2020). A multi-objective Monte Carlo tree search for forest harvest scheduling. European Journal of Operational Research, 282 (3), 1115-1126,

Rodrigues, A.R.; Marques, S.; Botequim, B.; Marto, M.; Borges, J.G. (2021) Forest management for optimizing soil protection: A land-scape-level approach. Forest Ecosystems, 8, 50, 13 pages.

Yoshimoto, A. & Asante, P. (2018), A new optimization model for spatially constrained harvest scheduling under area restrictions through maximum ow problem. Forest Science, 64(4), 392-406.

Physics-based modelling of junction fires: Sensitivity and Validation studies

Ahmad Hassan*[1]; Gilbert Accary[2]; Duncan Sutherland[3]; Sofiane Meradji[4]; Khalid Moinuddin[1]

[1] Institute for Sustainable Industries and Liveable Cities, Victoria University, Melbourne, Vic. 8001, Australia, {ahmad.hassan6@live.vu.edu.lb, Khalid.Moinuddin@vu.edu.au}
[2] Scientific Research Centre in Engineering, Lebanese University, Lebanon, {gaccary@ul.edu.lb}
[3] School of Science, University of New South Wales, Canberra, PO Box 7916, Canberra BC, ACT 2610, Australia, {duncan.sutherland@adfa.edu.au}
[4] IMATH Laboratory, Toulon University, EA 2134, France, {sofiane.meradji@univ-tln.fr}

**Corresponding author*

Keywords

Fire modelling, fully-physical model, fire behaviour, slopping terrain, detailed physical fire model.

Abstract

The process of modelling and replicating extreme fire behaviour like junction fire, which is the intersection occurred between two contiguous fire lines, is essential for understanding the phenomena associated with extreme fires. Numerical simulations of junction fires, replicating laboratory-scale experiments, with no imposed wind, were performed for a shrub fuel bed with slopes ranging from 0° to 30°. The simulations of junction fires were conducted for two junction angles 30° and 45°. For each scenario, the sensitivity to a range of numerical parameters was investigated.

The rate of spread (ROS) is a key parameter for assessing risks from vegetation fires. Experimental spreading junction fires, conducted at laboratory scale at Coimbra University (Portugal), were simulated using FIRESTAR3D −a three-dimensional physics-based fire model. To ensure the robustness of simulations, sensitivity analyses were carried out by varying the grid resolution, domain size and fuel characteristics −using two descriptions levels of the shrub: the vegetation was represented using only one cylindrical-shaped solid-fuel type (excelsior fuel using the characteristic parameters for Erica shrub), or two fuel by adding the contribution of twigs of various diameters up to 6 mm while keeping the same packing ratio. Finally, the validation of FIRESTAR3D simulations was achieved through the comparison of predicted and experimentaly-measured ROSs.

The experimental trends of the compared quantities were well reproduced by the simulations. Accelerating and decelerating propagation phases were observed in all simulations, with a dependence on the slope angle, while the maximum ROS depends critically on the junction angle. As it was the case of other wildfires simulated by FIRESTAR3D, it was found that this physics-based model is capable of simulating junction fire propagation.

There are several processes associated with the development of a junction fire behaviour, in which dramatic changes in fire behaviour can occur with little change in various fuel, weather and topographical parameters. In a subsequent study, we aim to develop an understanding of junction fire behaviour taking into account essential parameters that affect the behaviour, namely: slope, junction angle, and driving wind velocity.

1. Introduction

Fire behaviour in extreme form is one of the major natural disasters in many parts of the world given their devastating effects. The intersection of multiple fire lines is among the strongest form of extreme fire behaviour. A junction fire, also called jump fire or eruptive fire, is the case of merging of two fire fronts, enhancing their propagation speed through strong interaction that occurs between the two fire lines. A particularly serious example took place during the 2003 Canberra (Australia) fire, where fire merging led to a devastating intense fire which spawned the first known pyrogenic tornado (McRae, et al., 2013). To mitigate the impact of this natural hazard, there is a need to better understand the wildfire behaviour. Simulation tools are designed to forecast fire behaviour and the course of a fire front over landscapes on a broad scale, while describing the intricacies of the interaction between flames and possible targets on a smaller scale (houses, vegetation, etc.).

The present study is focused on the specific eruptive fire mechanism of the merging of contiguous fire fronts, called junction fires. The analysis and the estimation of the evolution of the junction fire fronts were conducted using a physics-based model FIRSTAR3D (Morvan, et al., 2018). This three-dimensional model, developed in close collaboration between Aix-Marseille University, the Lebanese University, and Toulon University, is based on a multi-phase formulation and solves the conservation equations of the coupled system formed by the vegetation and the surrounding gaseous medium. The model takes into account the vegetation degradation processes (drying, pyrolysis, and combustion), the interaction between the atmospheric boundary layer and vegetation (aerodynamic drag, heat transfer by convection and radiation, and mass transfer), and the transport in the gaseous phase (convection, turbulence, and combustion).

There has been limited research into the interactions of junction fires especially using a physics-based model, and it is desirable to count this study as an endeavour to replicate the behaviour and examine the influence of the critical parameters: slope and junction angle.

Physics-based modelling is a very complex approach and the complexity comes also from the numerous thermo-physical and numerical parameters used in the simulations. The sensitivity of the simulations to the grid resolution, domain size and fuel description level were investigated in this study. Sensitivity analysis to numerical parameters has been carried out with a twofold objectives: to assess the suitability of the numerical implementation of the junction fire configuration and show the advantage of considering several fuel types to represent the vegetation, and to determine the most appropriate grid resolution to be used within the vegetation, as well as the acceptable size of the computation domain.

2. Methodology and Numerical modelling

Raposo, et al. (2018) conducted a large series of experimental junction fire tests at laboratory and field scales. The laboratory experiments were carried out at the Forest Fire Research Laboratory (LEIF) of the University of Coimbra, Portugal. The experiments reported in Raposo, et al. (2018) provide many experimental measurements that could be used to validate the present simulation results. The rate of spread (ROS) is the quintessential parameter to quantify the dynamic behaviour, although other simulation outputs such as fire intensity, dominant heat transfer quantities, and flame geometry are also important.We examined the capability of FIRESTAR3D to reproduce the results of such experiments for slope angles ranging from 0 to 30°, and for two values of the junction angle (30° and 45°), and for multiple values of fuel moisture content (see Table 1). Additional simulations were carried out (simulation 6 in Table 1) as a part of the parametric study. Simulations of this kind, are computationally expensive due to the high spatial resolution (grid size of 5 cm in the propagation direction) and temporal resolution (10^{-3} to 10^{-2} s) required to accurately solve the governing equations of the problem.

Table 1- Physical parameters of the junction fires cases considered in the validation study.

Simulation Number	ID in (Raposo, et al., 2018)	Fuel moisture content, m_f (%)	Junction angle, Θ (º)	Slope angle, α (º)
1	10-L48	23.91	45	30
2	11-L49	23.91	30	0
3	12-L50	21.65	30	30
4	13-L51	18.76	30	20
5	17-L56	13.63	30	30
6	-	20	60	30

Numerical simulations were conducted using a V-shaped vegetation region immersed inside a larger computational domain (29 m long, 29 m wide, and 12 m high) as shown in Figure 1. The homogeneous fuel bed, of height 0.15 m, is 5 m long and is located 12 m away from the inlet boundary and at least 12 m (depending on the junction angle) away from the lateral boundaries. Solid-fuel particles are assumed to have a cylindrical shape and to behave as a black body. Both the solid-phase and the fluid-phase grids are characterised by cells sizes below the extinction length scale (0.073 m) within the vegetation, given by $\frac{4}{\alpha\sigma}$, where α is the packing ratio and σ is the surface-to-volume ratio (see Table 2).

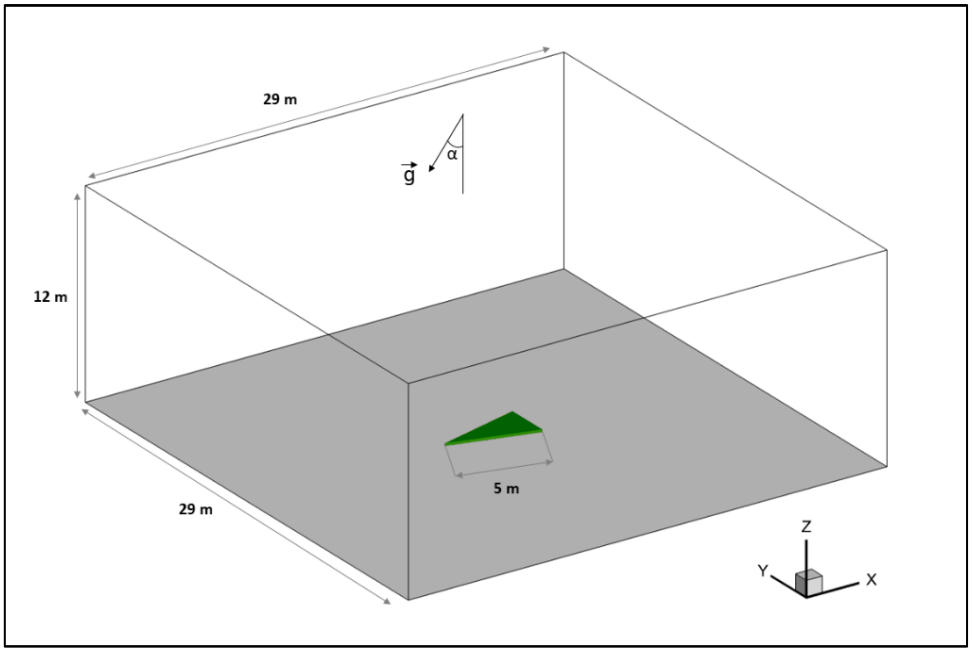

Figure 1 - Perspective view of the computational domain and the vegetation cover used to simulate the junction fire.

The fire lines are ignited in the model by activating a burner. A 10-cm wide burner is activated instantaneously along the entire ignition lines by injecting CO gas at 1600 K from the bottom of the computational domain for the duration of 5 s. Open boundaries are applied on the computational domain sides (except the bottom one), which allows the fire to create its own induced air flow. The main physical parameters that were used in all the configurations are tabulated in Table 2.

Table 2- Geometric and physical properties of the shrubland vegetation (Raposo, et al., 2018; Gilliers, et al., 2002).

Vegetation height δ	Solid-fuel volume fraction, α	Surface/Volume ratio, σ	Dry material density, ρ	Drag Coefficient, C_D	Thermal emissivity	Vegetation particles shape
(m)		(m^{-1})	($Kg.m^{-3}$)			
0.15	0.00784	6900	500	0.42	1	Cylindrical

The fuels used in this study were shrubs composed of a mixture of genus Erica, often called Heather, the fuel load was kept constant at the value of 0.6 $kg.m^{-2}$, used experimentally.

The physical properties of the shrub mentioned in Table 2 are characteristic properties (Pereira, et al., 1995). Realistic simulations should take into account the heterogeneity of fuel in terms of distribution of twigs and leaves, their percentages, as well as their specific surface-to-volume ratio. Most of the physical properties of shrubs used by (Raposo, et al., 2018) can be found in the literature (Fernandes, 1997) and a complex method of describing shurb (combination of leaves and twigs) is presented as Table 3. A simulation was carried out using this fuel description to observe any difference of fire behaviour compared to fuel of Table 2. For both descriptions, the same fuel moisture content was considered (same to experimental value).

Table 3- Geometric and physical properties of leaves and twigs of shrub vegetation (Fernandes, 1997).

	Surface/Volume ratio, σ (m^{-1})	Dry material density, ρ ($Kg.m^{-3}$)	Solid-fuel volume fraction, α
Leaves (d < 2.5mm)	7200	253	0.0108 (70%)
Twigs (2.5 < d < 6 mm)	920	970	0.001212 (30%)

Although the grid resolution is chosen below the extinction length, (Perez-Ramirez, et al., 2017) recommended to use a grid cell size three times less than the extinction length. Mesh and domain size sensitivity tests have been carried out by increasing and decreasing of the cell size by 30%. To that end, several simulations were carried out using cells of different sizes: 3.5, 5 and 6.5 cm. Moreover, three sizes of the computational domain with a distance from the vegetation region to the open boundaries of 10, 12 and 15 m have been considered, as detailed in Tables 4 and 5.

Table 4- Mesh parameters (for a computational domain size of 29×29×12 m^3).

Minimum cells size in the xy plane	3.5 cm	5 cm	6.5 cm
Mesh size of the solid phase	284×284×18	200×200×12	152×152×8
Mesh size of the fluid phase	202×202×163	160×160×160	136×136×158

Table 5- Domain size (with a cell size of 5 cm).

Size	***1***	***2***	***3***
Domain size	25×25×10 m^3	29×29×12 m^3	35×35×15 m^3
Mesh size of the fluid phase	150×150×134	160×160×160	176×176×199

3. Results and Discussion

In order to capture the effects of parameters and to consistently compare flame properties, quasi-steady regions of acceleration and deceleration were identified. These regions were duly identified for all selected simulations, similarly to the experimental work that proves a pattern of behaviour directly related to the selected parameters.

Six duly-chosen configurations (see Table 1 for details) were simulated using FIRESTAR3D. the comparison between the simulations and the experiments is based on the measurement of the ROS of the junction point assumed to lie in the mid plane of the computational domain.

3D views of the fire flame obtained for a simulation 5 is represented in Figure 2. These results show clearly the potential of FireStar3D in reproducing numerically the junction fire in shrubland.

Assuming a symmetrical propagation, we computed the ROS by tracking the local consumption of dry material in the central vertical plane along the streamwise direction inside the vegetation (at 5cm from the bottom). The ROS estimation was obtained from the time derivative of the position of the junction point.

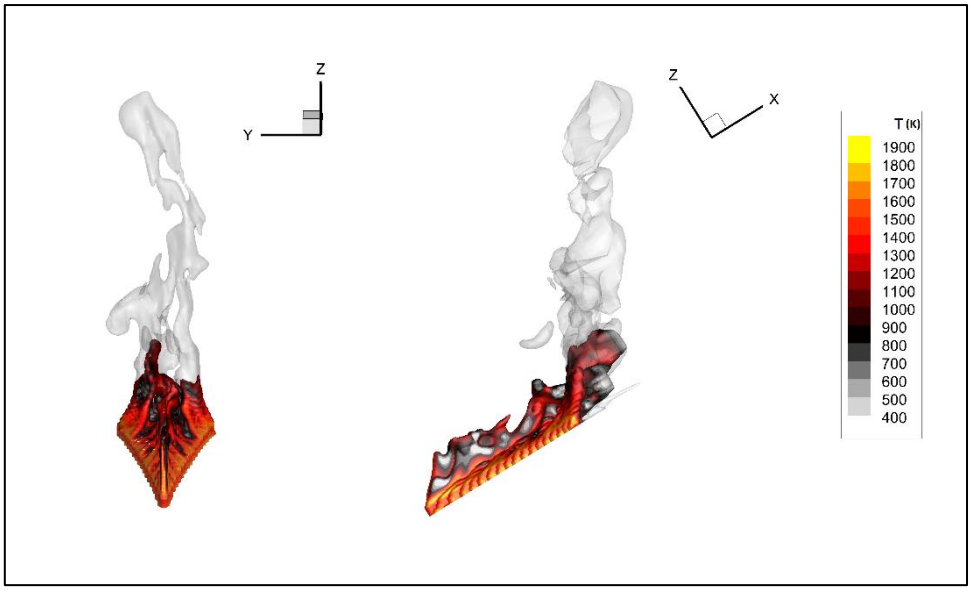

Figure 2- 3D front (left) and side (right) views of an isovalue surface of the soot volume fraction (1.6×10^{-7}) coloured by the gas temperature and an isovalue surface of the water mass fraction (9×10^{-3}) (in grey with 50% of transparency) obtained in the case of simulation 5, 10s after ignition.

3.1. Sensitivity analysis results

Figure 3 shows simulation results of junction point position as function of time from the cases listed in Tables 4-5. Minimal effects of the grid resolution and the domain size on the junction point propagation are observed. Consequently, the considered domain size and mesh (Size 2 – Mesh 5 cm) allow to obtain a solution that is quasi-independent of these parameters as far as global fire behaviour is concerned (ROS, fire intensity, etc).

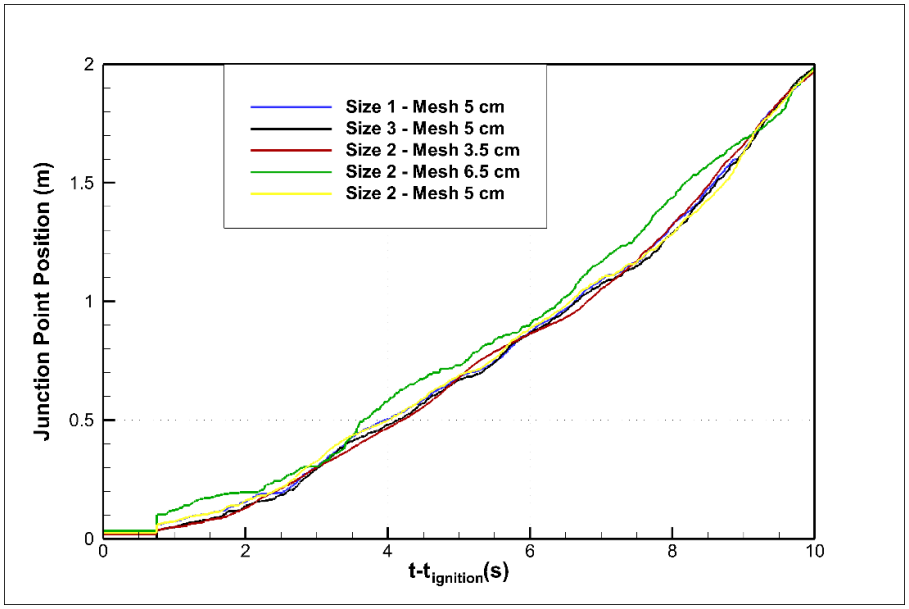

Figure 3- Junction point position for simulation 2 in five sensitivity tests.

Regarding fuel description level, the shrub was described using two methods. In both cases the total initial volume fraction and mass were kept the same (see Table 3) and they are identical to those reported in (Raposo, et al., 2018). A more realistic description of the vegetation (by accounting for different sizes of solid fuel particles) better reproduced the fire dynamics, especially the mass loss process.

Regarding the ROS, a good similarity of the junction point propagation for single and two types of fuel is observed (see Figure 4). The propagation is slightly quicker in the two-fuel case and we attributed that to the low percentage of large diameter particles and very small surface to volume ratio (diameter) of small particles comparing it to the characteristic value adopted first (6900 m^{-1}). Besides that, the limited information about moisture content of leaves and twigs, accounts for the slight overestimation. Overall, the use of multiple description level manages to estimate the ROS in a similar order of magnitude.

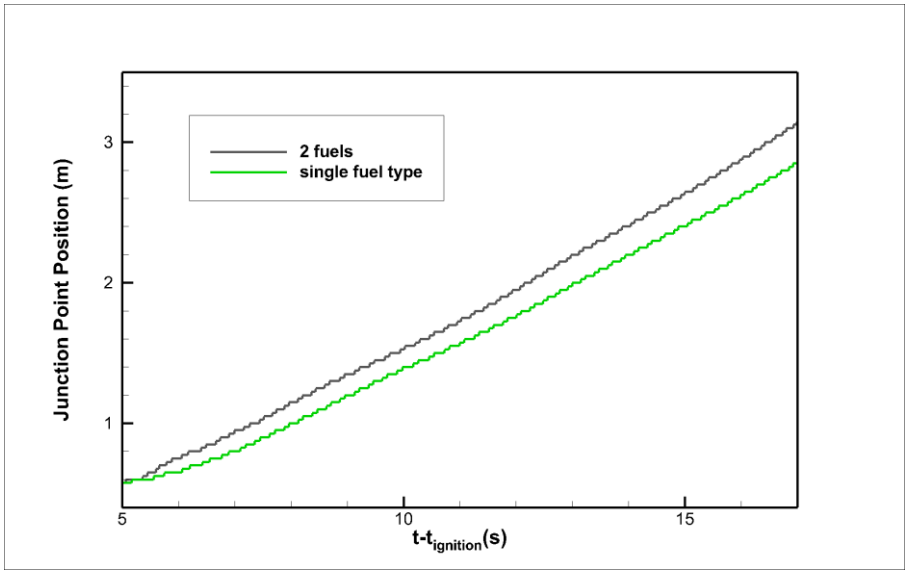

Figure 4- Junction point position for the different fuel combinations

3.2. Validation results

Figure 5 shows the evolution of fire perimeters. It can be observed that the junction fire angle is not fixed during the propagation, instead, it (on average) increases continuously.

The process of merging of these fires is not the closure of the space between the fire lines by a reduction of their respective angle, similar to the closure of scissors. On the contrary, it is the junction point that advances, tending to form a single straight fire line resulting from the two original fire fronts.

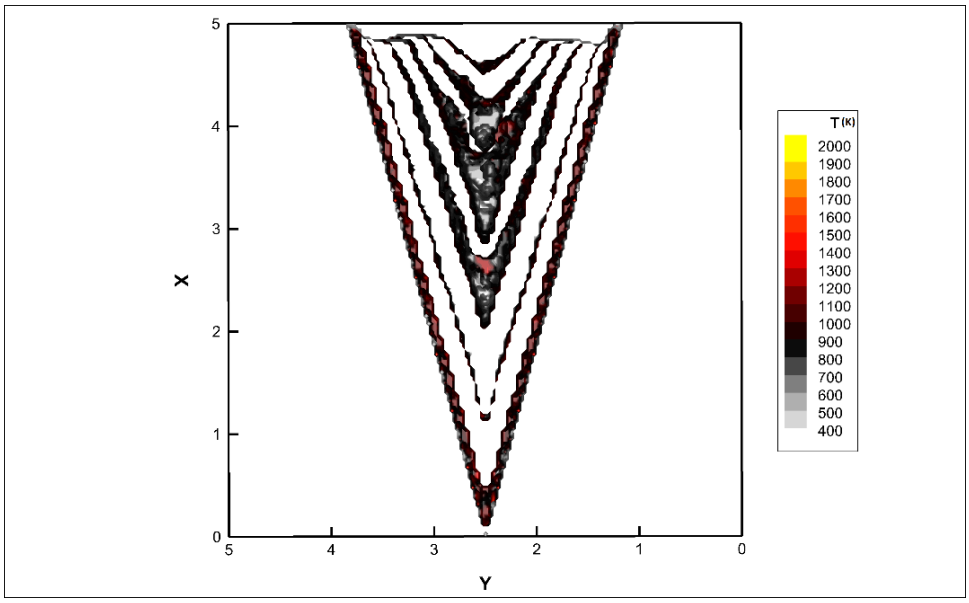

Figure 5- Evolution of fire perimeter according to pyrolysis edge (dry material 0.001 kg.m^{-3}) for simulation 2. The first perimeter is at t – $t_{ignition}$ = 5s and the time difference between each perimeter is 5s.

Simulations 2, 3 and 4 have the same junction angle (30°) and close fuel moisture content values (21.35±2.55%), whilst the slope angle varies (0°, 20° and 30°). Figure 6 shows the simulation and experimental results of ROS for these three simulations.

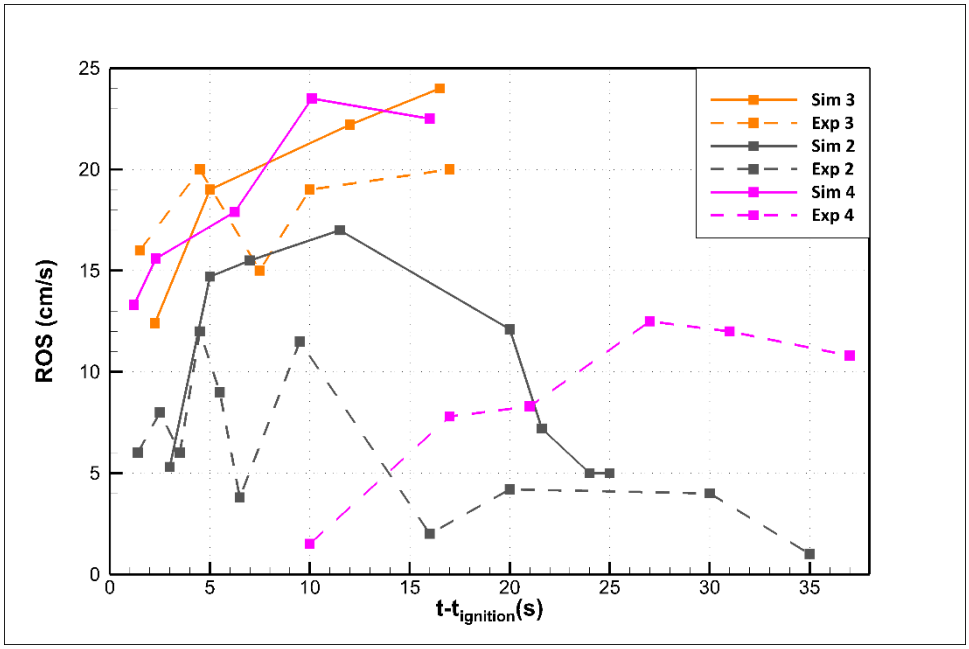

Figure 6- Evolution of the value of ROS for three different slope values (α) as a function of time.

First and foremost, the behaviour under the change of slope angle is prominent in the simulated ROS' results. Taking the maximum ROS into consideration, the value increases with the increase of slope angle (cm.s^{-1} for

slope 0°, 23.5 cm.s^{-1} for slope 20° and 25 cm.s^{-1} for slope 30°). Experimentally, case number 4 seems to be not reflecting this effect as the maximum value (12.5 cm.s^{-1}) is close to the maximum value for experiment 2 (12 cm.s^{-1}) and way far from 20 cm.s^{-1}, maximum value for case 3. This could be attributed to fluctuations that occurred in experiments or ROS measurement error.

The existence of acceleration and deceleration propagation phases has been observed in simulations as observed in experiments. The deceleration phase was significant in simulation 2 (α=0°), slight in simulation 4 (α=20°) and absent in simulation 3 (α=30°).

Experiments 3 and 5 were conducted with the same angles but the fuel in experiment 5 was drier (8% fuel moisture content difference). The simulations capture this difference only by a slight increase in the maximum ROS, however, the accelerative behaviour did not change.

3.3. Parametric study

In Simulations 1, 3 and 6, the slope is 30° and the junction angles are 45°,30° and 60°, respectively. The fuel moisture content values are close; therefore, the effect of junction angle could be deduced. The results are depicted in Figure 7.

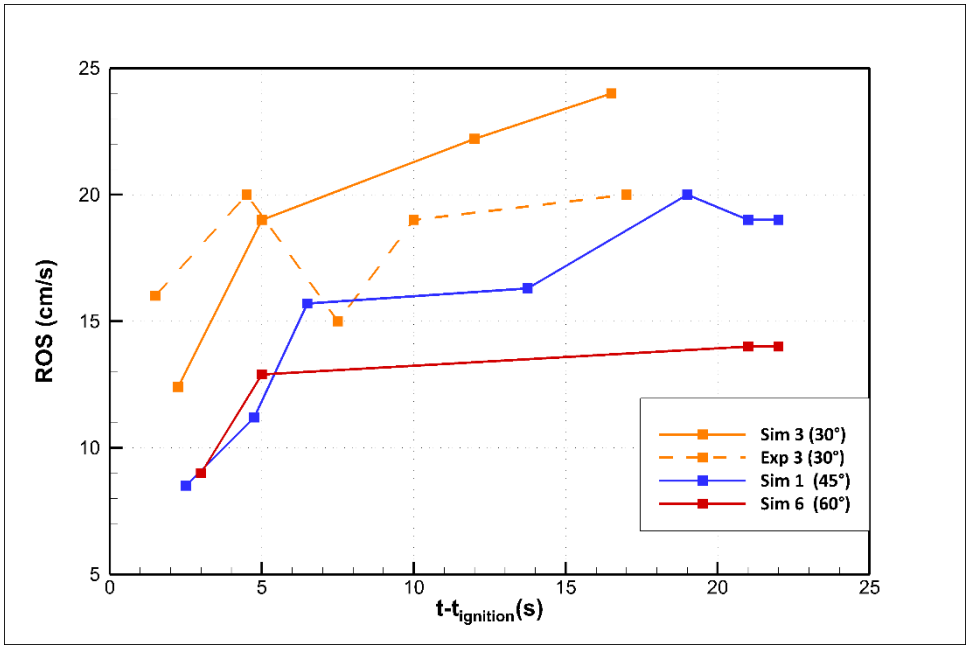

Figure 7- Evolution of the value of ROS for three different junction angles (θ) as a function of time.

Comparing Figures 6 and 7, it appears that the junction angle is more important parameter on the fire spread, consistent with the findings of (Viegas, et al., 2012) for non-slope conditions. A thorough investigation for the influence of critical parameters for a wider range were done in a full parametric study published in a forthcoming paper (Hassan, et al., 2022). Considering simulation 3 and 1, an increase of 15° of junction angle decreased the maximum ROS by 5 cm.s^{-1}, which correctly reflected the experimental results.

4. Conclusion

A set of junction fire simulations was conducted numerically using a physics-based model. The use of physics-based models to simulate extreme fires offers the possibility to study, in detail and at a low cost, the burning of vegetation according to a wide set of parameters that are difficult to control experimentally. FIRESTAR3D has been validated for junction fire simulations by comparison ROS estimation to an experimental data set, proving an excellent quantitative and qualitative accordance. The ultimate objective of the study is to investigate the effects of the slope, the junction angle and the wind speed on fire behaviour during the different propagation phases and on the ROS, endeavouring to build a better understanding of the junction fire phenomenon and its underlying physics.

5. References

Fernandes, P., 1997. Caracterização Do Combustível E Do Comportamento Do Fogo Em Comunidades Arbustivas Do Norte De Portugal, Vila Real: Universidade De Trás-Os-Montes E Alto Douro - Curso De Mestrado Em Engenharia De Recursos Florestais.

Gilliers, J., Nickling, W. & King, J., 2002. Drag coefficient and plant form response to wind speed in three plant species: Burning Bush (Euonymus alatus), Colorado Blue Spruce (Picea pungens glauca.), and Fountain Grass (Pennisetum setaceum). JOURNAL OF GEOPHYSICAL RESEARCH, Volume 107 NO. D24, 4760.

Hassan, A., Accary, G., Sutherland, D. & Moinuddin, K., 2022. Physics-based modelling of junction fire: Parametric study. International journal of wildland fire.

McRae, R., Sharples, J., Wilkes, S. & Walker, A., 2013. An Australian pyro-tornadogenesis event. Natural Hazards, Volume 65(3), pp. 1801-1811.

Morvan, D. et al., 2018. A 3D physical model to study the behavior of vegetation fires at laboratory scale. Advances in Forest Fire Research, October, Volume 101, pp. 39-52.

Pereira, J., Sequeira, N. & Carreiras, J., 1995. Structural Properties and Dimensional Relations of Some Mediterranean Shrub Fuels. International Journal of Wildfire, Volume 5(1), pp. 35-42.

Perez-Ramirez, Y., Santoni, P., Tramoni, J. & Bosseur, F., 2017. Examination of WFDS in Modeling Spreading Fires in a Furniture Calorimeter. Fire Technology, Volume 53, pp. 1795-1832.

Raposo, J. et al., 2018. Analysis of the physical processes associated with junction fires at laboratory and field scales.. International Journal of Wildland Fire, Volume 27, p. 52–68.

Viegas, D., Raposo, J., Davim, D. & Rossa, C., 2012. Study of the jump fire produced by the interaction of two oblique fire fronts. Part 1. Analytical model and validation with no-slope laboratory experiments.. International Journal of Wildland Fire, Volume 21, p. 843–856.

Predicting fire severity in Montana using a random forest classification scheme

Jesse V. Johnson*[1]; Anthony Marcozzi[1]; Frederick Bunt[1]; Jacob Bova[1]; John Hogland[2]

[1]University of Montana Department of Computer Science, USA, {jesse.johnson@umontana.edu, anthony.marcozzi@umconnect.umt.edu, fredrick.bunt@umontana.edu, jacob.bova@umconnect.umt.edu}
[2]US Forest Service Rocky Mountain Research Station, USA, {john.s.hogland@usda.gov}

**Corresponding author*

Keywords

Fire prediction, new technologies, machine learning, fire severity, risk assessment

Abstract

Fire managers often make decisions about wildfire incidents on a landscape scale. While several well developed models can predict fire behaviour at these scales, the limited data they draw upon restricts their range of validity. Other models explicitly represent the physical complexities of the fire environment, but with increased computational costs and increased sensitivity to boundary conditions. In this paper, we explore a middle ground between landscape level, data-driven fire behaviour predictions and physics-based, computationally expensive models. Machine learning is used to predict fire severity from a set of well recognized covariate features related to weather, fuel, and topography. A random forest is used for the classification task, and the model covariates are tested to determine their importance in the classification. The model demonstrates considerable skill in prediction of burn severity, with overall classification accuracy of 71%, and lower accuracy in moderate severity predictions. Our results are similar in accuracy to previous work, but distinctive in that we have made no attempts to train the model on specific ecoregions. We determine that topographic variables like elevation, slope, and aspect are the most important in this classification problem.

1. Introduction

Between 1985 and 2017, the Western United States experienced increases in both the severity and the area burned by wildfires (Center, 2017). During the same period of time, the wildland urban interface, WUI, became the fastest growing land use type in the United States (Radeloff et al., 2018), leading to increased economic consequences of wildfires (Center, 2017). Yet, wildfires have historically been an integral part of North American ecosystems, and by pursuing a policy of wildfire suppression since the early 20th century, land managers have altered fire regimes in much of North America, potentially driving some of the increases in fire frequency and intensity (Arno & Brown, 1991). In addition to a more complicated landscape from expanded WUI settlement and increased fuel loading, fire managers now have to account for a warming climate. Thus, the areas threatened by wildfires have increased, and are projected to increase still more under nearly all climate change scenarios (Flannigan et al., 2009).

Management practices aimed at mitigating the threat of wildfire have traditionally involved treatments of a landscape with a combination of thinning projects and prescribed burns (Arno & Brown, 1991). Assessment of the impact of these practices is a critical phase of planning, and involves predictive modelling of fire on the landscape being considered for treatment. Several predictive fire models exist, and have distinctive features that may be suited to requirements arising from operational use, predictive capabilities, computational cost, or model complexity (Sullivan, 2009a, 2009b, 2009c).

Sullivan (Sullivan, 2009a, 2009b, 2009c) divides existing fire models into six groups, organised by two broad classes. One class of fire models, data-driven models, are based on empirically derived formulas for fire spread, operate on large landscape level domains, are computationally efficient, and see broad operational use. The other class of fire models, called physics-based models, use physical principles to determine fire spread, operate on stand or individual fuel element levels, are computationally expensive, and are limited to research applications in fire science. Both classes of model offer various benefits and costs, and there is a lively debate to each class' relative merits (Cruz et al., 2017, 2018).

Nowadays, machine learning (ML) may offer a novel approach to fire modelling as it has the fast computation associated with data-driven models, yet may capture the complexities of fire physics. Several authors have applied ML techniques to predict fire behaviour from burn characteristics and covariates such as climate, topographic elevation and slope, and fuel descriptions (Jain et al., 2020).

In this paper we focus on predicting burn severity measured by the differenced normalised burn ratio (dNBR) (Eidenshink et al., 2007). We are not the first to apply machine learning methods to the problem of predicting burn severity. (S. A. Parks et al., 2018) predicted high severity fires using boosted regression trees using a suite of features (covariates) grouped into live fuel, topographic, climate, and fire weather. Moreover, they successfully predict high severity fires in 19 distinctive ecoregions of the American west and report that fuels descriptors have the greatest importance for prediction. S. Parks et al., 2018 predicted the probability of *low-severity* fires using a similar approach. More recently, Huang et al., 2020 carried out a similar analysis for Northern California's coastal mountains and achieved a 79% overall classification accuracy and found topographic features to have the greatest explanatory power.

Here, as in Parks et al., 2018, we set out to characterise landscapes by the severity of fire (Eidenshink et al., 2007) that would result if the landscape were to burn. Unlike Parks et al., 2018, but following Huang et al., 2020 we formulate our problem as a multi-label classification problem, using features to determine unburned, low, moderate, and high severity fires. We also include new features in our classification scheme by adding higher order products of features. Our region of interest is the state of Montana, which is broader and includes a greater variety of ecoregions than (Huang et al., 2020). In terms of data volumes, we evaluate 29 million pixels, which is 70 times the volume in (S. A. Parks et al., 2018) and more than 14 times more data than (Huang et al., 2020).

2. Methods

2.1. Collection of the Features and Training Data

Covariates considered in this work fit into three broad categories; topography, weather, and fuels. In Table 1 we detail the features, resolutions, and sources used in this analysis. To improve the classification, these 9 fields were multiplied by themselves and each other in order to create a total of 54 features (9 features plus 45 squares or products of features). The Monitoring Trends in Burn Severity (MTBS)(Eidenshink et al., 2007), provides fire perimeters and burn severity during the 35 year period from 1985-2020, totaling to 825 unique wildfires.

Table 1: The data used in the analysis, the resolution, and the source.

	Feature	**Resolution**	**Source**
Topography	Elevation	30 m, Constant	EDNA (Layers, 2005)
	Slope	30 m, Constant	EDNA (Layers, 2005)
	Aspect	30 m, Constant	EDNA (Layers, 2005)
Weather	Solar Radiation	4 km, weekly average	gridMET (Abatzoglou, 2013)
	Min Relative Humidity	4 km, weekly average	gridMET (Abatzoglou, 2013)
	Max Temperature	4 km, weekly average	gridMET (Abatzoglou, 2013)
	Precipitation	4 km, annual average	gridMET (Abatzoglou, 2013)
Fuels	Landfire Vegetation Type	30 m, 2014 Update	LANDFIRE (Rollins, 2009)
	Landfire Fuels Model 40	30 m, 2014 Update	LANDFIRE (Rollins, 2009)

2.2. Model Selection

The statistical modelling is done with Scikit-learn's RandomForestClassifier [17]. This method employs randomly created ensembles of classification trees. Through averaging of trees the variance of model output is reduced without a commensurate increase in model bias. This approach is well-suited to the large number of samples in the training dataset and the underlying physics of the classification problem, which is not overly dependent on spatial or temporal gradients in the feature set. The lack of gradient dependence justifies the decision to avoid convolutional neural networks (CNNs). It is also true that compared to deep CNNs, the RandomForestClassifier is easier to train and interpret, especially with regard to feature importance.

2.3. Model Training

For model training we split 75% of the pixel level feature vectors into training data with the remaining 25% reserved for testing. The test and training data were randomly sampled from the complete data set of 29,379,900 feature vectors. To avoid a class imbalance the training data are sampled in proportion to the number of records in each of the severity classes. Gini impurity was used for the loss function, and 100 trees were grown.

3. Results

To measure performance, we report the confusion matrix (Table 2), precision, recall and F1 scores for each category (Table 3), and a pair of summary statistics. Our classes are relatively well balanced and the summary statistics are a reasonable means of expressing our overall success. Tables 1 and 2 reveal the detailed structure of classifications.

The first summary statistic is the accuracy score for the classification, which was 0.711. The second summary statistic is the area under the receiver operating characteristics (AUROC) and was found to be 0.872.

An impurity method was used to evaluate the importance of the features. The results for the ten most important features appear in Table 4. We also map predicted and observed fire severities in Figures 1-3. These provide a means of visually inspecting fires to determine where predictions are failing. In considering these figures, it is important to note that the extent of the fire is determined by the outline provided in the MTBS data, our prediction method does not determine fire perimeters.

Table 2: A confusion matrix documents the performance of our classification algorithm. Diagonal elements represent instances of successful classification. Off-diagonal values indicate the number of times misclassification took place in each class.

	Low Severity	Moderate Severity	High Severity
Low Severity	**2,853,697**	**544,457**	**134,909**
Moderate Severity	**725,985**	**1,165,844**	**210,226**
High Severity	**120,313**	**285,448**	**1,204,096**

Table 3: A classification report summarises the values of various metrics for each class. Precision is true positives divided by the sum of true and false positives. Recall is true positives divided by the sum of true positives and false negatives. F1 is twice the ratio of precision times recall divided by the sum of precision and recall. Support refers to the number of labels in each class.

Category	Precision	Recall	F1	Support
Low Severity	**0.77**	**0.81**	**0.79**	**3,533,063**
Moderate Severity	**0.58**	**0.53**	**0.56**	**2,202,055**
High Severity	**0.73**	**0.75**	**0.74**	**1,609,857**
Accuracy			**0.71**	**7,344,975**
Weighted Average	**0.71**	**0.71**	**0.71**	**7,344,975**

Table 4: The fractional importance of the 10 most relevant features in the model.

Feature	Importance
Elevation × Annual Precipitation	**3.96%**
Elevation × Solar Radiation	**3.67%**
Elevation × Vegetation Type	**3.16%**
Elevation^2	**3.14%**
Elevation × Fuel Type	**3.05%**
Elevation	**3.00%**
Elevation × Minimum Daily Humidity	**2.83%**
Slope × Annual Precipitation	**2.59%**
Elevation × Aspect	**2.58%**
Elevation × Slope	**2.51%**

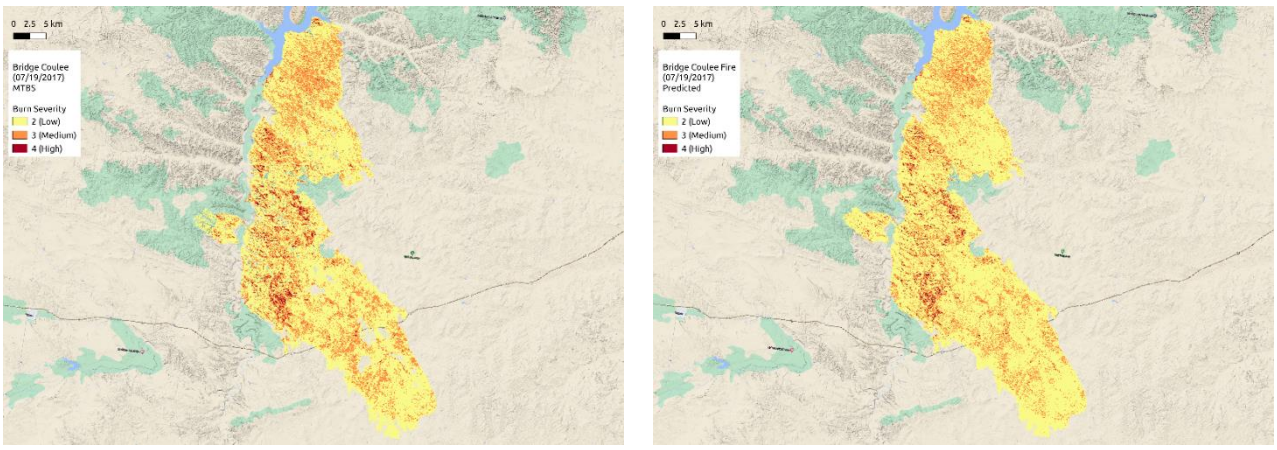

Figure 1: The Bridge Coulee fire, 7/19/2017. Left panel shows the fire severity determined by MTBS (Eidenshink et al., 2007). Right panel shows the fire severity predicted by our random forest classifier.

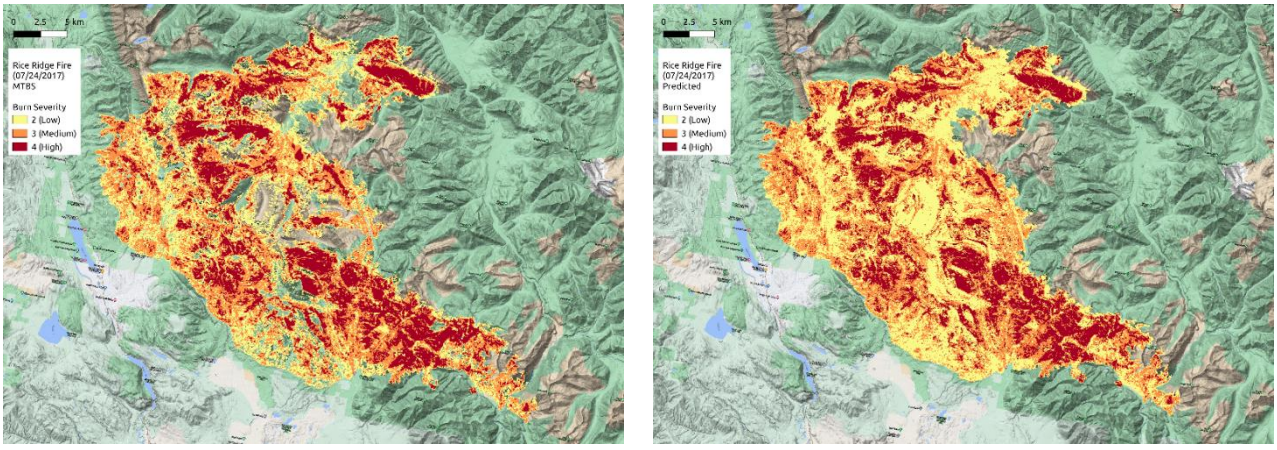

Figure 2: The Rice Ridge fire, 07/24/2017. Left panel shows the fire severity determined by MTBS (Eidenshink et al., 2007). Right panel shows the fire severity predicted by our random forest classifier.

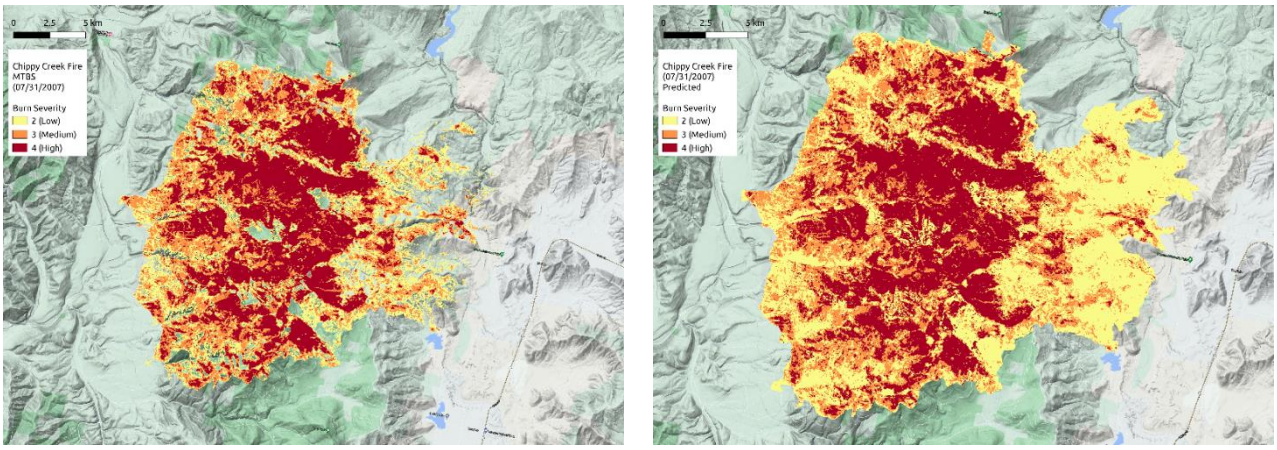

Figure 3: The Chippy Creek fire, 07/31/2007. Left panel shows the fire severity determined by MTBS (Eidenshink et al., 2007). Right panel shows the fire severity predicted by our random forest classifier.

4. Discussion and Conclusions

A number of favourable outcomes were achieved in this work. First, we achieve nearly the accuracy reported in (Huang et al., 2020), which reported 79%. Our reported accuracies do not take into consideration the ecoregions used in both (Huang et al., 2020; S. A. Parks et al., 2018). We attribute our relative success within

the inhomogeneous state of Montana to the large volumes of data we used in training; nearly 29 million feature vectors for our work, compared to 462 thousand in (Huang et al., 2020) and 100 thousand per ecoregion in (S. A. Parks et al., 2018). (S. A. Parks et al., 2018) do not report accuracy, and have a boolean classification variable. This makes direct comparison difficult, however our AUC of 0.87 compares favourably to their value of 0.72.

We tested a large number of features and dropped ones determined to be less significant. So far as we know, we are the first investigators to use products of features in our analysis. The results show that some of these products have considerable explanatory power. The ability to account for some curvature in subdividing feature vectors appears to improve classification.

The lower scores for classification of moderate burn severity are noteworthy. We know burn severity suffers from classification errors due to the thresholding of its classification(Kolden et al., 2015), and expect those inherent difficulties to become prominent when classifying across inhomogeneous terrain, where the differences in severity might reflect changes in fuel composition and climate more than genuine thresholds in the classification.

We only classified low, moderate, and high because it is difficult to interpret land that burned but undisturbed. Nevertheless, we carried out analyses that included the unburned category and found overall classification accuracy fell to 65%. This is important to consider when comparing our results to (Huang et al., 2020).

Our software framework for carrying out these analyses is robust and highly scalable. We expect that the addition of more features such as primary productivity derived variables and climate data will improve our accuracy rates. It would also be a straightforward matter to begin identifying ecoregions and training a unique random forest within each of those. Our most significant advance may be to demonstrate that classification of burn severity can achieve near to cutting-edge results by simply increasing the volumes of data used in the analysis.

5. References

Abatzoglou, J. T. (2013). Development of gridded surface meteorological data for ecological applications and modelling. *International Journal of Climatology*, *33*(1), 121–131.

Arno, S. F., & Brown, J. K. (1991). *Overcoming the paradox in managing wildland fire*. National Emergency Training Center Emmitsburg, Maryland, USA.

Center, N. I. C. (2017). *National Interagency Coordination Center Wildland Fire Summary and Statistics Annual Report 2020*. National Interagency Coordination Center Boise, ID, USA.

Cruz, M. G., Alexander, M. E., & Sullivan, A. L. (2017). Mantras of wildland fire behaviour modelling: facts or fallacies? *International Journal of Wildland Fire*, *26*(11), 973–981.

Cruz, M. G., Alexander, M. E., & Sullivan, A. L. (2018). A response to "Clarifying the meaning of mantras in wildland fire behaviour modelling: reply to Cruz et al. (2017)." In *International Journal of Wildland Fire* (Vol. 27, Issue 11, p. 776). https://doi.org/10.1071/wf18161

Eidenshink, J., Schwind, B., Brewer, K., Zhu, Z.-L., Quayle, B., & Howard, S. (2007). A Project for Monitoring Trends in Burn Severity. *Fire Ecology*, *3*(1), 3–21.

Flannigan, M. D., Krawchuk, M. A., de Groot, W. J., Mike Wotton, B., & Gowman, L. M. (2009). Implications of changing climate for global wildland fire. *International Journal of Wildland Fire*, *18*(5), 483–507.

Huang, Y., Jin, Y., Schwartz, M. W., & Thorne, J. H. (2020). Intensified burn severity in California's northern coastal mountains by drier climatic condition. *Environmental Research Letters: ERL [Web Site]*, *15*(10), 104033.

Jain, P., Coogan, S. C. P., Subramanian, S. G., Crowley, M., Taylor, S., & Flannigan, M. D. (2020). A review of machine learning applications in wildfire science and management. *Environmental Review*, *28*(4), 478–505.

Kolden, C. A., Smith, A. M. S., & Abatzoglou, J. T. (2015). Limitations and utilisation of Monitoring Trends in Burn Severity products for assessing wildfire severity in the USA. *International Journal of Wildland Fire*, *24*(7), 1023–1028.

Layers, E. (2005). *Elevation Derivatives for National Applications*. pubs.usgs.gov. https://pubs.usgs.gov/fs/2005/3049/fs20053049.pdf

Parks, S. A., Holsinger, L. M., Panunto, M. H., Matt Jolly, W., Dobrowski, S. Z., & Dillon, G. K. (2018). High-severity fire: evaluating its key drivers and mapping its probability across western US forests. *Environmental Research Letters: ERL [Web Site]*, *13*(4), 044037.

Parks, S., Dobrowski, S., & Panunto, M. (2018). What Drives Low-Severity Fire in the Southwestern USA? In *Forests* (Vol. 9, Issue 4, p. 165). https://doi.org/10.3390/f9040165

Radeloff, V. C., Helmers, D. P., Anu Kramer, H., Mockrin, M. H., Alexandre, P. M., Bar-Massada, A., Butsic, V., Hawbaker, T. J., Martinuzzi, S., Syphard, A. D., & Stewart, S. I. (2018). Rapid growth of the US wildland-urban interface raises wildfire risk. In *Proceedings of the National Academy of Sciences* (Vol. 115, Issue 13, pp. 3314–3319). https://doi.org/10.1073/pnas.1718850115

Rollins, M. G. (2009). LANDFIRE: a nationally consistent vegetation, wildland fire, and fuel assessment. *International Journal of Wildland Fire*, *18*(3), 235–249.

Sullivan, A. L. (2009a). Wildland surface fire spread modelling, 1990 - 2007. 3: Simulation and mathematical analogue models. In *International Journal of Wildland Fire* (Vol. 18, Issue 4, p. 387). https://doi.org/10.1071/wf06144

Sullivan, A. L. (2009b). Wildland surface fire spread modelling, 1990–2007. 1: Physical and quasi-physical models. *International Journal of Wildland Fire*, *18*(4), 349–368.

Sullivan, A. L. (2009c). Wildland surface fire spread modelling, 1990–2007. 2: Empirical and quasi-empirical models. *International Journal of Wildland Fire*, *18*(4), 369–386.

Prediction of soil properties immediately after fire using SAR backscatter data

José Manuel Fernández-Guisuraga*[1]; Elena Marcos[1]; Susana Suárez-Seoane[2]; David Beltrán-Marcos[1]; Alfonso Fernández-Manso[3]; Carmen Quintano[4,5]; Leonor Calvo[1]

[1] Area of Ecology, Department of Biodiversity and Environmental Management, Faculty of Biological and Environmental Sciences, University of León, 24071 León, Spain {jofeg, elena.marcos, dbelm, leonor.calvo}@unileon.es
[2] Department of Organisms and Systems Biology (Ecology Unit) and Research Unit of Biodiversity (IMIB; UO-CSIC-PA), University of Oviedo, Oviedo, Mieres, Spain {s.seoane@uniovi.es}
[3] Agrarian Science and Engineering Department, School of Agricultural and Forestry Engineering, University of León, 24400 Ponferrada, Spain {alfonso.manso@unileon.es}
[4] Electronic Technology Department, School of Industrial Engineering, University of Valladolid, 47011 Valladolid, Spain {carmen.quintano@uva.es}
[5] Sustainable Forest Management Research Institute, University of Valladolid-Spanish National Institute for Agriculture and Food Research and Technology (INIA), 34004 Palencia, Spain

**Corresponding author*

Keywords

ALOS-2; nutrients; organic carbon; radar; wildfire

Abstract

The physical sense of synthetic aperture radar (SAR) backscatter data is of particular interest for characterizing soil spatial variability in burned areas. The objective of this study was to evaluate the potential of SAR backscatter data in L-band (Advanced Land Observing Satellite-2; ALOS-2) for assessing fire effects on soil organic carbon, total nitrogen and available phosphorous immediately after wildfire in a burned landscape of the western Mediterranean Basin. ALOS-2 backscatter coefficients were used to estimate soil properties measured in the field in immediate post-fire situation through generalized linear models. The retrieval of soil properties from ALOS-2 L-band SAR backscatter data featured a high overall fit (R2 = 0.37-0.59) and low error (nRMSE = 12.7%-22.5%). ALOS-2 co-polarized channel showed the highest sensitivity to spatial variation in soil properties, and there were no noticeable under and overestimation effects. These results support the applicability of SAR sensors operating at long wavelengths for monitoring fire effects on soil properties, reducing data gathering costs within large burned landscapes.

1. Introduction

Wildfires are a frequent disturbance in the Mediterranean Basin, entailing shifts in the multifunctionality of terrestrial ecosystems as a consequence of fire impacts on the (i) composition and structure of vegetation communities (Fernández-Guisuraga et al., 2019) and (ii) soil properties, among others processes. Fire effects on physical and biochemical soil properties have been widely documented from in-situ field research (e.g. Fernández-García et al., 2019; Huerta et al., 2020). However, the identification of fire effects on soil properties through conventional methods based on field trials is not functional for assessing large burned landscapes due to the fine scale of variation of soil effects, even more when dealing with high environmental variability in plant communities.

Remote sensing techniques (RST) based on multispectral and hyperspectral passive optical data, acquired from space-borne and aerial platforms, have been extensively used for retrieving soil properties in agroforestry systems (e.g. Mirzaee et al., 2016; Gholizadeh et al., 2018). However, the remote estimation of soil properties using multispectral and hyperspectral passive optical sensors might be limited to secondary correlations in vegetated areas, since the reflectance signal is mostly determined by top-of-canopy traits (Healey et al., 2020), and this behaviour may lead to soil properties overestimation (Angelopoulou et al., 2019). To deal with this constraint, active remote sensing data acquired by synthetic aperture radar (SAR) sensors are among the most

reliable RST for digital mapping of soil properties because SAR signal can penetrate the soil through vegetation canopy, especially with increasing wavelength (Jagdhuber, 2012).

In the field of fire disturbance, SAR backscatter data have been used to map burnt area (Belenguer-Plomer et al., 2019) and fire severity (Tanase et al., 2014) with high confidence. Nonetheless, the characterization of soil spatial variability in burned landscapes leveraging SAR strengths for this purpose, remains completely unexplored. For that reason, we aimed to evaluate the potential of L-band SAR backscatter data acquired from Advanced Land Observing Satellite-2 (ALOS-2) satellite for assessing fire effects on soil properties in a burned landscape of the western Mediterranean Basin.

2. Material and methods

The study site is located within the perimeter of a wildfire that burned 9,940ha of shrubland and forest communities in the Sierra de Cabrera mountain range (N-NW Iberian Peninsula; Figure 1) between 21th and 27th August 2017. The following plant communities were affected by the wildfire: (i) gorse shrublands dominated by *Genista hystrix* Lange; (ii) heathlands dominated by *Erica australis* L.; (iii) broom shrublands dominated by *Genista florida* L.; (iv) Pyrenean oak forests dominated by *Quercus pyrenaica* Willd.; and (v) Scots pine forests dominated by *Pinus sylvestris* L.

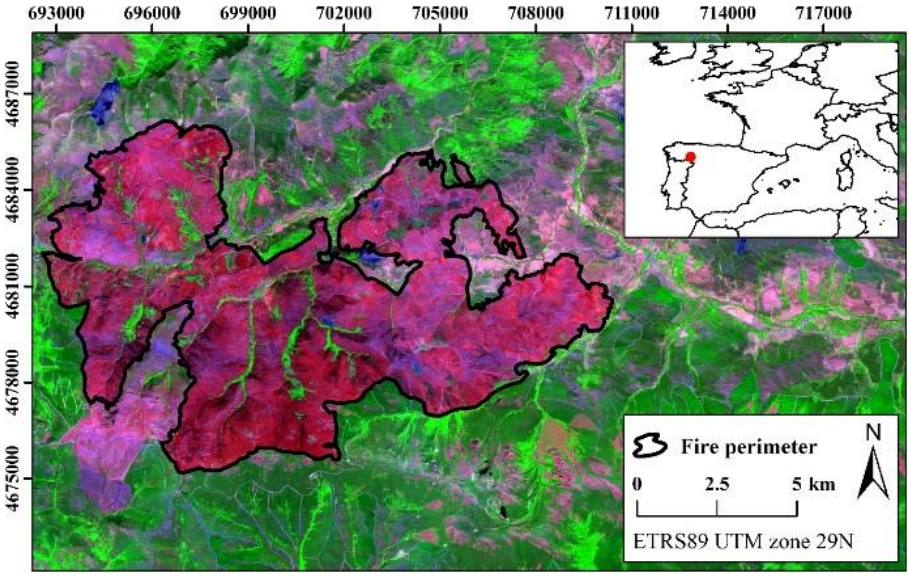

Figure 1- Sierra de Cabrera wildfire (NW Spain). Background image corresponds to a Sentinel-2 false-colour composite (SWIR-NIR-red) in immediate post-fire situation.

In September 2017, the month following the wildfire, a set of 35 plots of 30m x 30m were established in the field following a stratified random design using the dominant plant communities as strata. The area occupied by each plot was homogeneous regarding vegetation legacies and soil characteristics. Two composite soil samples were systematically collected at a depth of 3cm within the plots for obtaining a representative sample. Soil samples were homogenized, air dried and sieved in the laboratory (2mm mesh). Soil organic carbon (SOC; %) was determined following the combustion method (Dumas, 1831). We analysed soil total nitrogen (STN; %) by the Kjeldahl procedure (Bremner and Mulvaney, 1982) and available P (mg/kg) was determined through Olsen et al. (1954) method.

Remote sensing data used to predict soil properties in immediate post-fire situation consisted on ALOS-2 L-band SAR backscatter at dual polarization. ALOS-2 mission carries the Phased Array L-band SAR-2 (PALSAR-2) instrument, with a long operating wavelength of 23.6cm. Starting from 2015, the Japan Aerospace Exploration Agency (JAXA) has delivered 25m ALOS-2 global mosaics of Fine Beam Dual-polarization (FBD) SAR data strips (stripmap mode) acquired in ascending orbits with HH and HV polarizations. Mosaic data for the study site were acquired on 3rd October 2017 from JAXA Earth Observation Research Centre (https://www.eorc.jaxa.jp/). The product was pre-processed by JAXA using the mosaicking algorithm developed by Shimada and Ohtaki (2010), which includes (i) radiometric calibration, (ii) slope correction and

(iii) orthorectification. Product data stored in digital numbers were converted to γ^0 backscatter intensity in dB units. The values of ALOS-2 predictors (HH and HV γ^0 backscatter coefficients, as well as and HV/HH ratio) were extracted for each 30m x 30m field plot.

Soil properties in immediate post-fire situation were modelled by means of ALOS-2 predictors using generalized linear models (GLMs). The response variables were: (i) soil organic carbon, (ii) total nitrogen and (iii) available phosphorous, which were modelled following a Gamma error distribution with a log link function. Prediction performance of soil properties in immediate post-fire situation was evaluated through the coefficient of determination (R^2), the root-mean-squared error (RMSE) and the normalized RMSE (nRMSE). All statistical analyses were implemented in R (R Core Team, 2021).

3. Results and Discussion

ALOS-2 L-band SAR backscatter data featured a high overall fit (R^2 = 0.37-0.59) and predictive capacity (nRMSE = 12.7%-22.5%) for predicting each of the soil properties in immediate post-fire condition (Table 1). This could be attributed to the increased interaction of L-band SAR backscatter signal with soil surface properties because of the long operating wavelength of the instrument (Tanase et al., 2014), namely with soil moisture and surface roughness (Zribi and Dechambre, 2003), these properties being highly correlated with soil carbon and nutrients content (Moser et al., 2009). The soil property best predicted by ALOS-2 data was organic carbon (nRMSE = 12.7%), followed by total nitrogen (nRMSE = 14.1%) and available phosphorous (nRMSE = 22.5%). The slightly better predictive capacity of soil organic carbon content may be related to the lower carbon spatial variability in the plant communities of the study site immediately after fire relative to total nitrogen and available phosphorous content (Huerta et al., 2020).

Table 1- Soil organic carbon, total nitrogen and available phosphorous model performance evaluated through the coefficient of determination (R^2), root-mean-squared error (RMSE) and normalized RMSE (nRMSE).

	Organic C	Total N	Available P
R^2	0.59	0.48	0.37
RMSE	4.107	0.213	26.772
nRMSE	12.7%	14.1%	22.5%

All ALOS-2 predictors (HH and HV γ^0 backscatter coefficients and HV/HH ratio) featured a high signification in the models (*p-values* ≤ 0.01), being noticeable the strength of the correlation of the ALOS-2 HH polarization with all soil properties ($R^2 > 0.3$) (Table 2). This behaviour could be explained by the higher sensitivity of co-polarized SAR backscatter to soil dielectric properties as compared to cross-polarized data (Burgin et al., 2011).

Table 2- Relationship between ALOS-2 backscatter predictors and soil organic carbon, total nitrogen and available phosphorous evaluated through the coefficient of determination (R^2).

	Organic C	Total N	Available P
HH γ^0	0.30	0.33	0.31
HV γ^0	0.22	0.26	0.30
HV/HH	0.32	0.24	0.11

Soil organic carbon, total nitrogen and available phosphorous model predictions in immediate post-fire situation based on ALOS-2 fitted data were closely tailored to the 1:1 line, with the absence of under or overestimation effects for the entire range of field values of soil properties (Figure 2), which could be attributable to the lower attenuation of SAR backscatter signal in the L-band by vegetation canopies than in shorter wavelengths (Tanase et al., 2014).

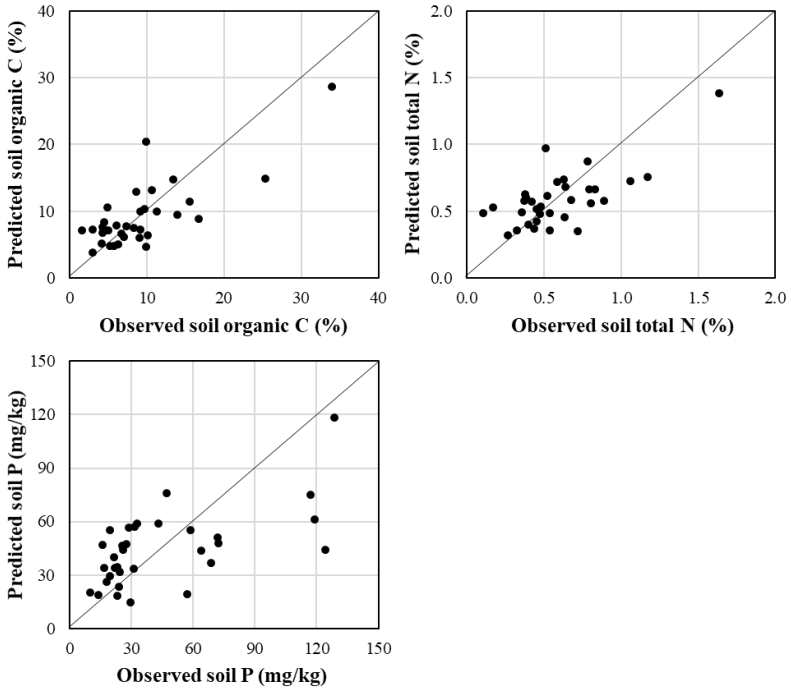

Figure 2- . Relationship between observed and predicted soil organic carbon, total nitrogen and available phosphorous in immediate post-fire situation from ALOS-2 backscatter data. The dotted black line represents the 1:1 line. Overall fit and predictive statistics are displayed in the Table 1.

The mean soil organic carbon, total nitrogen and available phosphorous content within the burned scar immediately after fire, extracted from spatially explicit prediction maps of GLM objects (Figure 3), were 4.78%, 0.65% and 34.13 mg/kg, respectively.

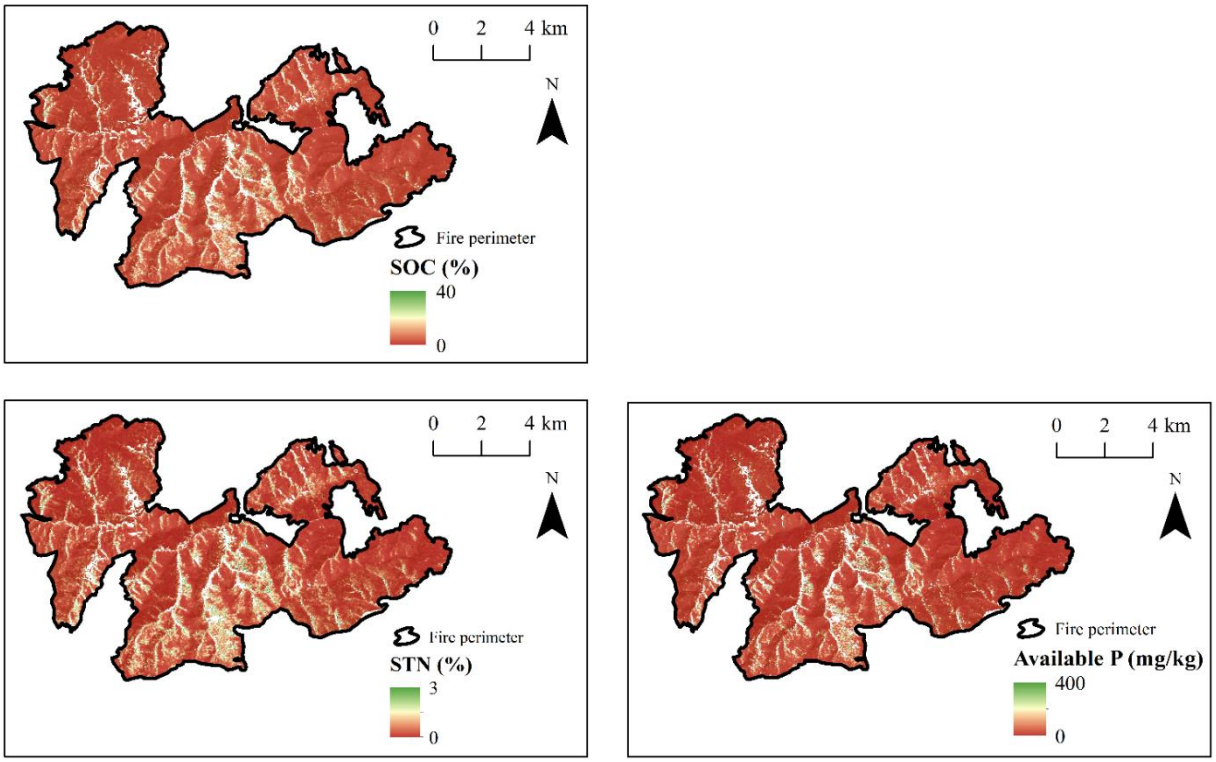

Figure 3- . Spatially explicit maps of predicted soil organic carbon, total nitrogen and available phosphorous. Blank regions within the fire perimeter correspond to unburned valley-bottom areas.

4. Conclusions

The use of remote sensing techniques for monitoring fire impact on soils is essential to determine the implementation of post-fire emergency actions aimed at mitigating soil degradation in extensive burned landscapes. This is a pioneer study evaluating the potential of L-band SAR data for this purpose. The estimation of soil organic carbon and nutrients content immediately after fire from L-band SAR backscatter featured a high performance because of the low attenuation of backscatter signal in the L-band by vegetation canopies and increased interaction with soil surface properties. The results of this study support the applicability of SAR sensors operating at long wavelength for monitoring fire effects on soil properties, reducing field data gathering costs.

5. Acknowledgements

This study was financially supported by the Spanish Ministry of Economy and Competitiveness, and the European Regional Development Fund (ERDF), in the framework of the FIRESEVES (AGL2017-86075-C2-1-R) project; and by the Regional Government of Castilla and León in the framework of the WUIFIRECYL (LE005P20) project.

6. References

Angelopoulou, T., Tziolas, N., Balafoutis, A., Zalidis, G., Bochtis, D., 2019. Remote Sensing Techniques for Soil Organic Carbon Estimation: A Review. Remote Sensing, 11: 676.

Belenguer-Plomer, M.A., Tanase, M.A., Fernandez-Carrillo, A., Chuvieco, E., 2019. Burned area detection and mapping using Sentinel-1 backscatter coefficient and thermal anomalies. Remote Sensing of Environment, 233: 111345.

Bremner, J.M., Mulvaney, C.S., 1982. Nitrogen total. Page, A.L., Miller, R.H., Keeney, D.R. (Eds.), Methods of Soil Analysis. Part 2: Chemical and Microbiological Properties (second ed.). ASA, Madison, United States, pp. 595-624.

Burgin, M., Clewley, D., Lucas, R.M., Moghaddam, M., 2011. A Generalized Radar Backscattering Model Based on Wave Theory for Multilayer Multispecies Vegetation. IEEE Transactions on Geoscience and Remote Sensing, 49: 4832-4845.

Dumas, J.B.A., 1831. Procedes de l'analyse organic. Annales de chimie et de physique, 247: 198-213.

Fernández-García, V., Marcos, E., Fernández-Guisuraga, J.M., Taboada, A., Suárez-Seoane, S., Calvo, L., 2019. Impact of burn severity on soil properties in a Pinus pinaster ecosystem immediately after fire. International Journal of Wildland Fire, 28: 354-364.

Fernández-Guisuraga, J.M., Suárez-Seoane, S., Calvo, L., 2019. Modeling Pinus pinaster forest structure after a large wildfire using remote sensing data at high spatial resolution. Forest Ecology and Management, 446: 257-271.

Gholizadeh, A., Žižala, D., Saberioon, M., Borůvka, L., 2018. Soil organic carbon and texture retrieving and mapping using proximal, airborne and Sentinel-2 spectral imaging. Remote Sensing of Environment, 218: 89-103.

Healey, S.P., Yang, Z., Gorelick, N., Ilyushchenko, S., 2020. Highly Local Model Calibration with a New GEDI LiDAR Asset on Google Earth Engine Reduces Landsat Forest Height Signal Saturation. Remote Sensing, 12: 2840.

Huerta, S., Fernández-García, V., Calvo, L., Marcos, E., 2020. Soil Resistance to Burn Severity in Different Forest Ecosystems in the Framework of a Wildfire. Forests, 11: 773.

Jagdhuber, T., 2012. Soil Parameter Retrieval under Vegetation Cover Using SAR Polarimetry. Thesis Dissertation, University of Potsdam, Germany.

Mirzaee, S., Ghorbani-Dashtaki, S., Mohammadi, J., Asadi, H., Asadzadeh, F., 2016. Spatial variability of soil organic matter using remote sensing data. Catena, 145: 118-127.

Moser, K.F., Ahn, C., Noe, G.B., 2009. The Influence of Microtopography on Soil Nutrients in Created Mitigation Wetlands. Restoration Ecology, 17: 641-651.

Olsen, S.R., Cole, C.V., Frank, S.W., Dean, L.A., 1954. Estimation of Available Phosphorus in Soils by Extraction with Sodium Bicarbonate. USDA Circular No. 939, US Government Printing Office. Washington DC, USA, p. 19.

R Core Team (2021). R: A language and environment for statistical computing. R Foundation for Statistical Computing, Vienna, Austria. URL https://www.R-project.org/.

Shimada, M., Ohtaki, T., 2010. Generating large-scale high-quality SAR mosaic datasets: Application to palsar data for global monitoring. IEEE Transactions on Geoscience and Remote Sensing, 3: 637-656.

Tanase, M.A., Santoro, M., Aponte, C., de la Riva, J., 2014. Polarimetric properties of burned forest areas at C- and L-band. IEEE Journal of Selected Topics in Applied Earth Observation and Remote Sensing, 7: 267-276.

Zribi, M., Dechambre, M., 2003. A new empirical model to retrieve soil moisture and roughness from C-band radar data. Remote Sensing of Environment, 84: 42-52.

QUIC-Fire: Initial capabilities of a fast-running simulation tool for prescribed fire applications

Rodman Linn *[1]; Scott Goodrick [2]; Sara Brambilla [1]; David Robinson [1]; Michael Brown [1]; Carolyn Sieg [3]; Joseph O'Brien [2]; Russell Parsons [4]; John Kevin Hiers [5]

[1]Los Alamos National Laboratory. Los Alamos, NM, {rrl, sbrambilla, drobinson, mbrown}@lanl.gov
[2] USDA Forest Service Southern Research Station. Athens, GA, USA, *{scott.l.goodrick, joseph.j.obrien}@usda.gov*
[3] USDA Forest Service Rocky Mountain Research Station. Flagstaff, AZ, USA, {carolyn.sieg@usda.gov}
[4] USDA Forest Service Rocky Mountain Research Station. Missoula, MT, USA, {russell.a.parsons@usda.gov}
[5] Tall Timbers Research Station, Tallahassee, FL, {jkhiers@talltimbers.org}

**Corresponding author*

Keywords

Prescribed Fire, fire modeling, coupled fire/atmosphere

Abstract

Prescribed fire is increasingly being looked to as a tool that can support land and fire managers in their efforts towards ecological sustainability and wildfire risk management. As prescribed fire use is considered for treatment of more acres and in more complex settings, practitioners are having to work harder to meet their expanding treatment goals in a safe and environmentally responsible manner. In the context of a prescribed fire, the role of multiple ignitions and complex fire geometries depends heavily on feedbacks between the fire and atmosphere and accentuates the need for explicit representation of these processes in any modeling tools that are to be used to support prescribed fire managers. Computational fluid dynamics models like FIRETEC and WFDS are inherently capable of representing this interaction, but they are too computationally expensive for widespread uses by practitioners for exploration and analysis. We have developed a new simulation tool called QUIC-Fire to capture these fire/atmosphere feedbacks while being orders of magnitude less computationally expensive by coupling the fast-running 3-D rapid wind solver QUIC-URB to a physics-based cellular automata fire spread model Fire-CA. Here we describe some of the model basics and provide initial demonstration capabilities of a new fast-running modeling tool, QUIC-Fire, that can be applied to prescribed fire planning. QUIC-Fire provides a self-determining fire prediction capability that represents the critical coupled fire/atmosphere feedbacks at scales relevant for prescribed fire. Although, the development of this model is in the nascent stages, initial results show an encouraging capability to capture basic trends in fire behavior, response of fire spread to size of fire, consumption of canopy fuels in prescribed fire scenarios, interaction between multiple firelines and response to heterogeneity in vegetation. Its ability to model response to both ignition patterns and a temporally and spatially variable fire environment without computational expense of CFD solutions is encouraging.

1. Introduction

Prescribed fire is one option that land and fire managers can use in their efforts towards wildfire risk management and ecological sustainability and thus a variety of programs are working to escalate its use. Intentional ignitions are used to manage 5 million hectares annually in the US (Melvin, 2015) with several millions more burned globally (Bond and Keeley, 2005; Guyette et al., 2017; Ichoku et al., 2008). As prescribed fire use is considered for treatment of more acres and in more complex settings, practitioners are faced with the challenge of meeting their expanding treatment goals in a safe and environmentally responsible manner. Planning prescribed fire practices and defining their prescription windows to meet objectives depends on anticipating the fire's response to variation in fuels and weather conditions (Chiodi et al., 2018; O'Brien et al., 2018; Wade et al., 1989). Thus, it is desirable to have simulation tools that can be used to assist with planning and exploration of potential prescribed fire scenarios.

2. Models Applied to Prescribed Fires

Predicting prescribed fire behavior can depend on factors that are not as significant in rapidly spreading or intense wildfire, which have been the focus of much wildfire modeling to date. One factor that complicates the prediction of prescribed fire behavior compared to wildfire scenarios is the significant influence of the rates and patterns of ignition on ensuing fire behavior. The role of multiple ignitions and complex fire geometries, which are present in many prescribed fire scenarios, depends heavily on feedbacks between the fire and atmosphere, accentuates the need for explicit representation of this coupling in any such simulation tools that are to be used to support prescribed fire managers. Also, the interaction between the fire environment and practitioner-designed ignition practices depends on landscape-scale fuel, weather, and topographic conditions as well as their localized spatial and temporal variability (Canfield et al., 2014; Furman, 2018).

The absence of strong driving conditions such as strong winds, steep slopes, or extremely low fuel moistures increases the challenge of predicting prescribed fire behavior (Linn et al., 2021) In the absence of such strong drivers the three-dimensional heterogeneities of the forest structure increase in importance. Additionally, since the metrics for success of a prescribed fire often depend on meeting ecological or fuel reduction objectives without breaching safety constraints the interaction between the fire and the heterogeneities vegetation structure is important. Thus, an important characteristic for simulation tools focused on supporting prescribed fire planning is the ability to capture the interaction between three-dimensional heterogenous forest structure, and fire behavior.

Many fire behavior models have been developed to predict fire spread and energy release using a variety of approaches ranging from empirical one-dimensional spread models to three-dimensional CFD models (Sullivan, 2009a; Sullivan, 2009b), but ultimately all wildland fire models must balance representing the complexity of fire-fuel-atmospheric feedbacks and the speed of predictions (Hilton et al., 2018). Firefighter safety and rapid assessments of fire spread have dominated the objectives for much of the wildland fire modeling to date, leading to development of tools producing rapid outputs for common or dangerous wildland fire scenarios. Unfortunately, the speed of these tools is often achieved by eliminating complexity and computational cost, which can frequently means reduction of generality. Simplifications are often made to the representation of the coupling between the fire and atmosphere to fit the conceptual model of a free-burning head fire. This conceptual paradigm does not always capture phenomena associated with the complex fire geometries and multiple fires that exist in prescribed fire scenarios. These tools often do not explicitly represent the heterogeneity of the fuel or three-dimensional structure of the vegetation and thus make assumptions about the structure. Although, these simplifications are often acceptable for many intense wildfire scenarios they ignore the sensitivity of prescribed fires to subtle changes in fire environment. Computational fluid dynamics (CFD) models like FIRETEC (Linn et al., 2002 and WFDS (Mell et al., 2007) are inherently capable of representing the sensitivity of fires to their environment and important interactions at scales relevant to prescribed fires, but they are primarily research tools and are currently are too computationally expensive for widespread use by practitioners for exploration and analysis.

Tools are now being developed with more specific intent of supporting prescribed fire planning. QUIC-Fire (Linn et al., 2019) is an example of a new simulation tool designed to capture fire/atmosphere feedbacks that are pertinent to prescribed fires while being orders of magnitude less computationally expensive than CFD tools. QUIC-Fire provides a self-determining fire prediction capability that represents the critical coupled fire/atmosphere feedbacks at scales relevant for prescribed fire. This was accomplished by exploiting the capabilities of the QUIC-URB wind field solver (Pardyjak and Brown, 2003; Singh et al., 2008) coupled with a new CA-based fire spread model, referred to here as FIRE-CA. QUIC-URB is a fast-running wind field solver that was originally designed for computing flow fields around buildings in urban settings (Pardyjak and Brown, 2003). Although, the development of QUIC-Fire is in the nascent stages, initial results show an encouraging capability to capture basic trends in fire behavior, response of fire spread to size of fire, consumption of canopy fuels in prescribed fire scenarios, interaction between multiple firelines and response to heterogeneity in vegetation. Its ability to model response to both ignition patterns and a temporally and spatially variable fire environment without computational expense of CFD solutions is encouraging.

3. Looking forward

Significant efforts to refine this simulation tool are expected to improve its ability to meet the needs of prescribed fire practitioners including additional smoke and fire effects capability. It is also extremely important to continuously assess strengths and weaknesses of this tool, as with all models, through comparison against observations and the expectations of experienced prescribed fire managers. These assessments can be challenging because of the complexity of many prescribed fire scenarios and the dependence of prescribed fire behavior on heterogeneity of the fire environment, but they are crucial for identifying fire regimes warranting increased confidence or refinement in the model. When examining the behavior of models like QUIC-Fire is important to look beyond spread rate to broader context of fire and smoke behavior.

4. References

Bond, W.J., Keeley, J.E., 2005. Fire as a global 'herbivore': the ecology and evolution of flammable ecosystems. Trends in Ecology & Evolution 20(7) 387-394.

Canfield, J., Linn, R., Sauer, J., Finney, M., Forthofer, J., 2014. A numerical investigation of the interplay between fireline length, geometry, and rate of spread. Agricultural and Forest Meteorology 189 48-59.

Chiodi, A., Larkin, N., Varner, J.M., 2018. An analysis of Southeastern US prescribed burn weather windows: seasonal variability and El Niño associations. International Journal of Wildland Fire 27(3) 176-189.

Furman, J., 2018. Next Generation Fire Modeling for Advanced Wildland Fire Training. Fire Management Today 78(4) 48-53.

Guyette, R., Stambaugh, M.C., Dey, D., Muzika, R.M., 2017. The theory, direction, and magnitude of ecosystem fire probability as constrained by precipitation and temperature. PloS one 12(7) e0180956.

Hilton, J., Sullivan, A.L., Swedosh, W., Sharples, J., Thomas, C., 2018. Incorporating convective feedback in wildfire simulations using pyrogenic potential. Environmental Modelling & Software 107 12-24.

Ichoku, C., Giglio, L., Wooster, M.J., Remer, L.A., 2008. Global characterization of biomass-burning patterns using satellite measurements of fire radiative energy. Remote Sensing of Environment 112(6) 2950-2962.

Linn R, Winterkamp J, Williams B, Furman J, Hiers JK, Jonko A, O'Brien Joseph, Yedinak K, Goodrick S,, 2021. Modeling Low Intensity Fires: Lessons Learned from 2012 RxCADRE. Fire

Linn, R., Reisner, J., Colman, J.J., Winterkamp, J., 2002. Studying wildfire behavior using FIRETEC. International Journal of Wildland Fire 11(4) 233-246.

Linn RR, Goodrick S, Brambilla S, Brown M, Middleton R, O'Brien JJ, Hiers JK, 2019, QUIC-Fire: A fast running simulation tool for prescribed fire planning. Environmental Modeling and Software.

Mell, W., Jenkins, M.A., Gould, J., Cheney, P., 2007. A physics-based approach to modelling grassland fires. International Journal of Wildland Fire 16(1) 1-22.

Melvin, M., 2015. 2015 National prescribed fire use survey report, Technical Report 02-15 Coalition of Prescribed Fire Councils, Inc.

O'Brien, J., Hiers, J., Varner, J., Hoffman, C., Dickinson, M., Michaletz, S., Loudermilk, E., Butler, B., 2018. Advances in mechanistic approaches to quantifying biophysical fire effects. Current Forestry Reports 4(4) 161-177.

Pardyjak, E.R., Brown, M., 2003. QUIC-URB v. 1.1: Theory and User's Guide. Los Alamos National Laboratory, Los Alamos, NM.

Singh, B., Hansen, B.S., Brown, M.J., Pardyjak, E.R., 2008. Evaluation of the QUIC-URB fast response urban wind model for a cubical building array and wide building street canyon. Environmental fluid mechanics 8(4) 281-312.

Sullivan, A.L., 2009a. Wildland surface fire spread modelling, 1990–2007. 1: Physical and quasi-physical models. International Journal of Wildland Fire 18(4) 349-368.

Sullivan, A.L., 2009b. Wildland surface fire spread modelling, 1990–2007. 2: Empirical and quasi-empirical models. International Journal of Wildland Fire 18(4) 369-386.

Wade, D.D., Lunsford, J.D., Dixon, M.J., Mobley, H.E., 1989. A Guide for Prescribed Fire in Southern Forests. USDA Forest Service: Atlanta, GA, p. 56.

Remote characterization of fire behavior during the FireFlux II experiment

Mario M. Valero*; Adam K. Kochanski; Craig B. Clements

Wildfire Interdisciplinary Research Center, Department of Meteorology and Climate Science, San Jose State University, San Jose, CA 95192, USA, {mm.valero, craig.clements, adam.kochanski}@sjsu.edu

**Corresponding author*

Keywords

Fire Behavior, Remote Sensing, Thermal Infrared, FireFlux II, Wildfire Experiment

Abstract

The FireFlux II field experiment was conducted on January 30th, 2013 in south-east Texas, USA, under high fire danger conditions. The experiment was designed to study the behavior of a head fire progressing through a flat, tall grass prairie, and it was informed by the use of a coupled fire-atmosphere model. Vegetation properties and fuel moisture were measured shortly before the experiment. Near-surface atmospheric conditions were monitored during the experiment using an elaborate meteorological instrumentation array. Fire behavior was observed through a combination of remote and in-situ sensors. Clements et al. (2019) presented the analysis of the experiment micrometeorology and in-situ fire behavior observations acquired using a thermocouple array. In this paper, we extend the study of fire behavior during the FireFlux II experiment with the analysis of remote sensing observations. Two thermal infrared and two visible cameras were deployed during the experiment. One thermal and one visible camera were mounted on a helicopter, whereas the other two cameras were installed on a 40-m-height tower next to the burn unit. The tower infrared camera covered a reduced area of interest coincident with the thermocouple array and it allowed monitoring the fire spread as well as measuring the spatially-resolved evolution of brightness temperature. Imagery collected from the helicopter allowed extending fire behavior measurements to the complete burn unit. While airborne IR footage was saturated and did not allow estimation of emitted radiant heat, its analysis allowed tracking fire progression through the plot and therefore estimating rate of spread and fire time of arrival. The existence of in-situ temperature observations provides an outstanding opportunity to validate remote sensing methodologies. In addition, the combination of remote observations with in-situ fire and fuel measurements allows a comprehensive characterization of fire behavior, including spatially-resolved fire rate of spread and fire time of arrival, fire radiative power, Byram's fire line intensity, and air temperature during fire front passage. This paper presents preliminary results from this analysis. Such results demonstrate the usefulness of the selected datasets and the potential of the proposed methodology, encouraging further work. Possible applications of the resulting dataset include (i) the validation of existing fire behavior models that are able to predict any of the measured variables, (ii) the development of data-driven fire behavior models, and (iii) the investigation of the relative contribution of radiative and convective heat transfer mechanisms to fire spread.

1. The FireFlux II field experiment

This section summarizes the aspects of the FireFlux II experiment that are the most relevant for the present study. A complete description of the experiment design, instrumentation and measurements can be consulted in Clements et al. (2019). **Experimental site**

The FireFlux II experiment was conducted at the University of Huston Coastal Center (HCC) in Galveston County near La Marque, Texas, approximately 45 km south-east of Huston and 22 km north-west of Galveston Bay. The burn unit used in this experiment was a Texas Gulf Coast tall grass prairie, 40 ha in extension and situated 5 m above mean sea level (MSL). The last time it had been burned before FireFlux II was in 2006 during the first FireFlux experiment.

1.1. Experiment design

This fire experiment took place on 30 January 2013 under a regional burn ban and high fire danger conditions. The main goal of FireFlux II was to measure the behavior of a high-intensity head fire and monitor the corresponding near-surface atmospheric conditions. This was achieved by deploying a multifaceted set of instruments. Various platforms were used to deploy the sensors, including meteorological towers, surface fireproof sensors, and one helicopter. Figure 1 shows the experiment layout.

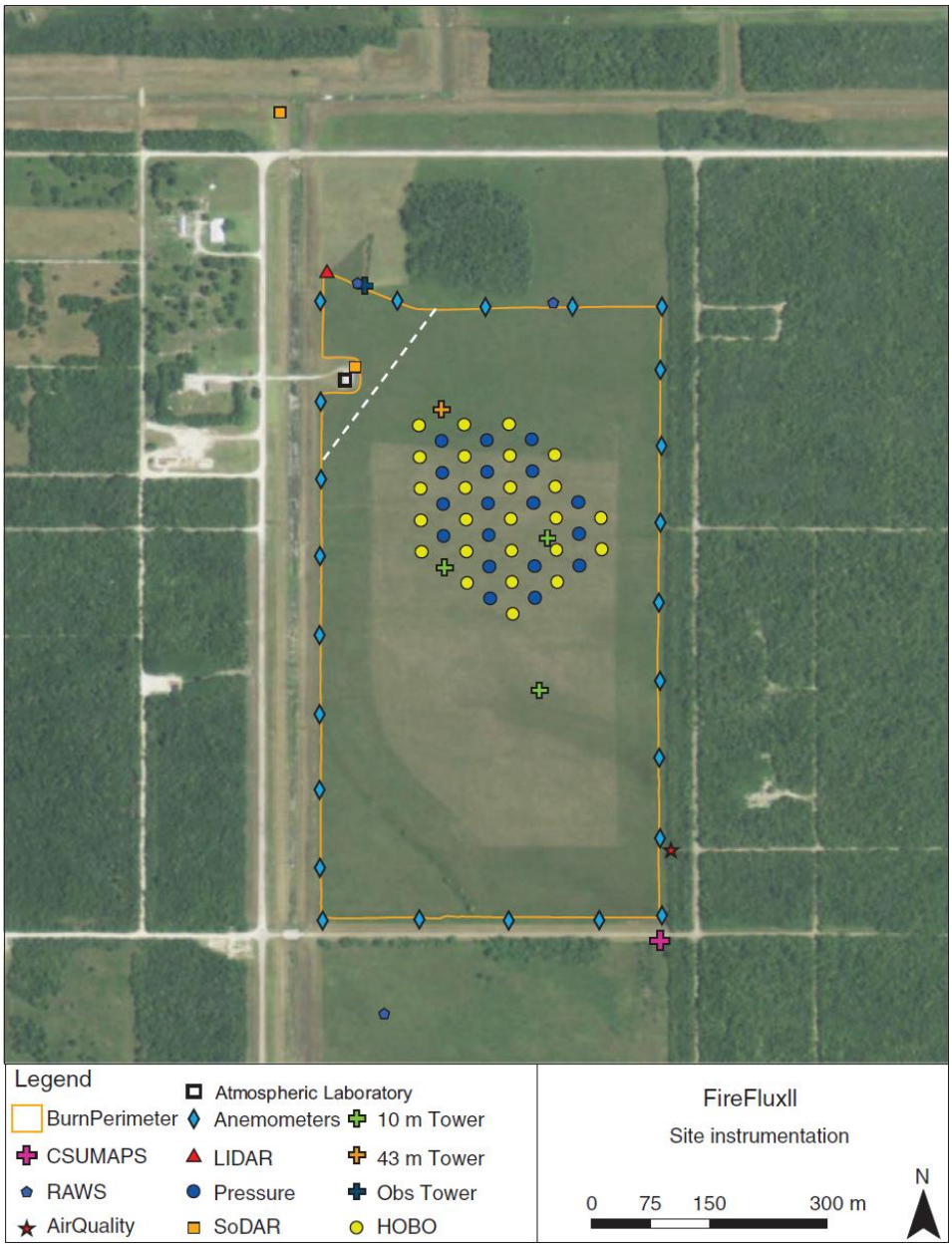

Figure 1- FireFlux II experiment layout (figure reproduced from (Clements et al. 2019)).

1.2. Atmospheric measurements

An array of towers distributed inside the burn unit constituted the primary source of meteorological data. A permanent 43-m meteorological tower is situated in the middle of the northern half of the burn unit. Additionally, three 10-m meteorological towers were installed south of the 43-m tower following a diamond pattern. Each tower was instrumented with arrays of 3D sonic anemometers, thermocouples, barometric pressure sensors, and radiometers. An additional meteorological tower was located outside the burn unit on the south-east corner and collected thermodynamic and wind profiles using 3D and 2D sonic anemometers, temperature and relative humidity probes.

Other instrumentation outside the burn unit included two Doppler sodars that provided 10-m average vertical wind profiles between 10 and 600 m above ground level (AGL), a Doppler lidar that captured radial velocities and backscatter intensities within the plume, three automated weather stations which measured wind speed and direction, air temperature and relative humidity, and an array of anemometers deployed along the burn unit perimeter to measure surface winds. Twenty-four cup-vane anemometers were installed at a height of 3.3 m AGL and spaced approximately 20 m apart from each other.

Finally, a radiosonde was launched before the ignition and recorded vertical atmospheric profiles of temperature, dew point temperature, and wind speed and direction.

1.3. Fuel sampling

Vegetation was sampled four weeks before the experiment to characterize the structure and loading of combustible material within the burn unit. Twenty destructive clip plots were established on a systematic grid within the burn unit at 25-m spacing. Fuel loading was determined from net dry vegetation weights measured after oven-drying vegetation samples at 70°C and surface-area-to-volume ratio was estimated by a detailed analysis of fuel particle geometry. Fuel loading was measured again after the experiment following a similar procedure in order to determine biomass consumption. Fuel moisture was sampled within 30 min of ignition.

2. Experimental Setup to Measure Fire Behavior

Fire behavior was monitored using a combination of in-situ and remote sensors. In-situ air temperature was measured by an array of thermocouples located at ground level and spaced 30 m apart (identified as *HOBOs* in Fig. 1). Remote instrumentation consisted of optical sensors working in the visible (VIS) and long-wave infrared (LWIR) spectral ranges. One VIS and one LWIR cameras were installed on a 40-m observation tower located at the north-west corner of the burn unit. Another VIS and another LWIR camera were installed on a helicopter that flew above the experimental site at about 450 m AGL. Figure 2 shows example frames from the different video sequences.

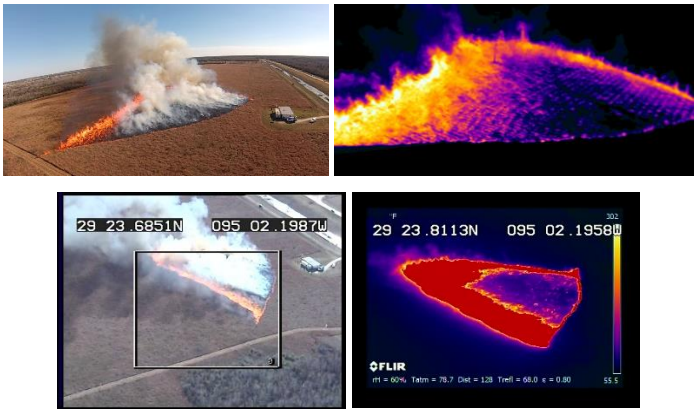

Figure 2- Example frames acquired by the four deployed cameras. Left: VIS, right: LWIR; top: tower-mounted; bottom: airborne.

3. Fire Behavior Characterization

Fire spread was monitored independently using three distinct data sources: the in-situ thermocouple array, the tower cameras, and the helicopter cameras. The observations from these three data sources overlap partially, which is leveraged in this study to accomplish a twofold objective. First, the overlapping regions are used to conduct a comparative analysis of different methodologies that are designed to yield the same result. Second, outcomes obtained from each methodology complement each other, and they are therefore combined to produce a unified dataset that contains comprehensive fire behavior metrics for the complete duration of the experiment.

3.1. In-Situ Thermocouples

Temperature profiles measured by in-situ thermocouples were used to identify the time of arrival of the fire to each sensor. Due to the lack of a unified criterion to identify fire arrival based on temperature time series, we explored three common approaches: identifying fire time of arrival as (a) the time at which the maximum temperature is reached, (b) the time at which the temperature gradient is the greatest, and (c) the time at which the temperature first exceeds a specified threshold. The three strategies produced similar results, although not identical (Fig. 3). Point estimations of fire time of arrival were interpolated to create a 2D map, as shown in Figure 4.

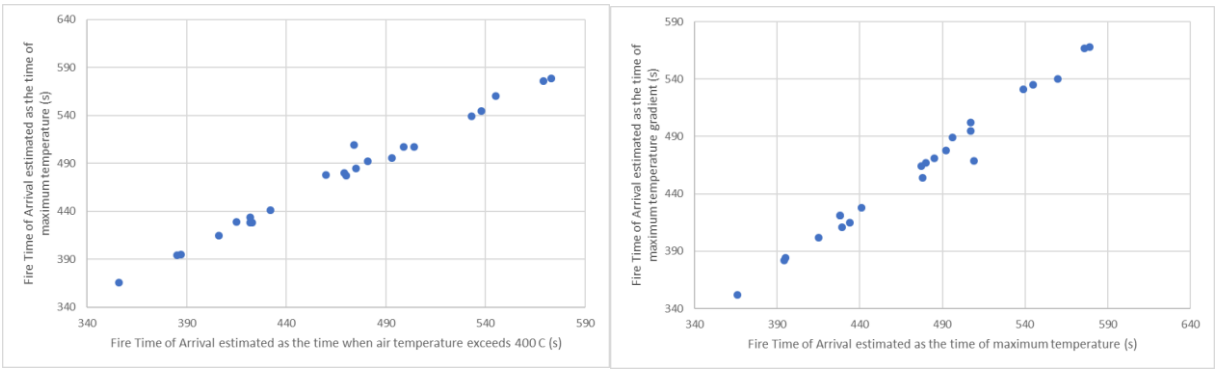

Figure 3- Comparison of different strategies to estimate fire time of arrival from in-situ air temperature measurements.

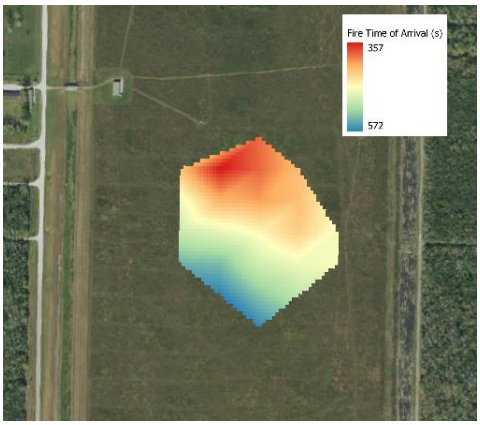

Figure 4- Fire time of arrival, relative to time of ignition, derived from in-situ air temperature measurements. Base image provided by the USDA National Agriculture Imagery Program.

3.2. Tower Remote Sensing

LWIR imagery acquired from the 40-m tower was still and provided a clear view of fire spread in a reduced area of interest, which allowed tracking the fire progression with high resolution and high positioning accuracy. The oblique imagery was geocorrected using ground control points. Resulting georeferenced brightness temperature fields were used to quantify fire progression and estimate fire time of arrival (Fig. 5). Fire progression was tracked using the methodology described in (Valero et al. 2018), whereas fire time of arrival was estimated as the time of maximum brightness temperature.

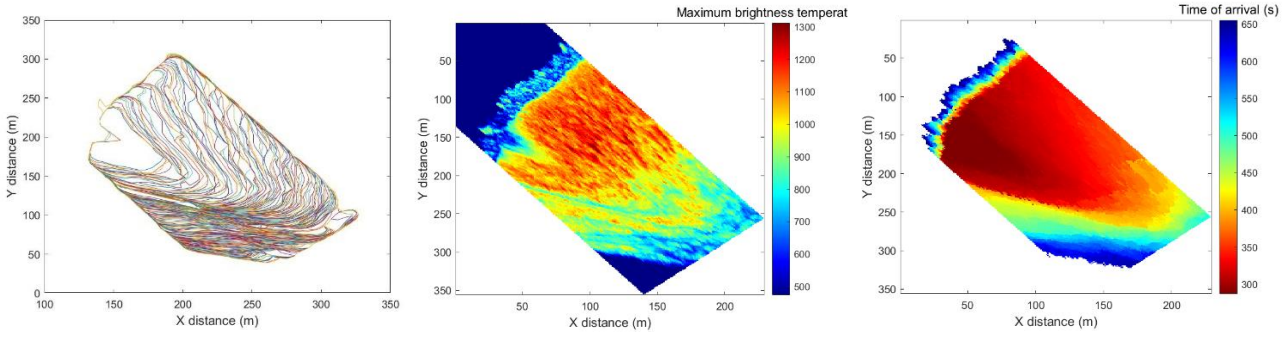

Figure 5- Fire progression (left), maximum brightness temperature registered at each location (center) and fire time of arrival relative to time of ignition (right) derived from the tower LWIR camera footage.

3.3. Airborne Remote Sensing

Airborne imagery complemented the information collected by in-situ and fixed remote sensors by covering a significantly larger area and tracking fire progression during the complete duration of the experiment. The LWIR airborne camera saturated and it therefore did not allow measuring the radiant heat emitted by the fire.

However, it was useful to track fire progression and estimate fire times of arrival for the complete burn unit (Fig. 6).

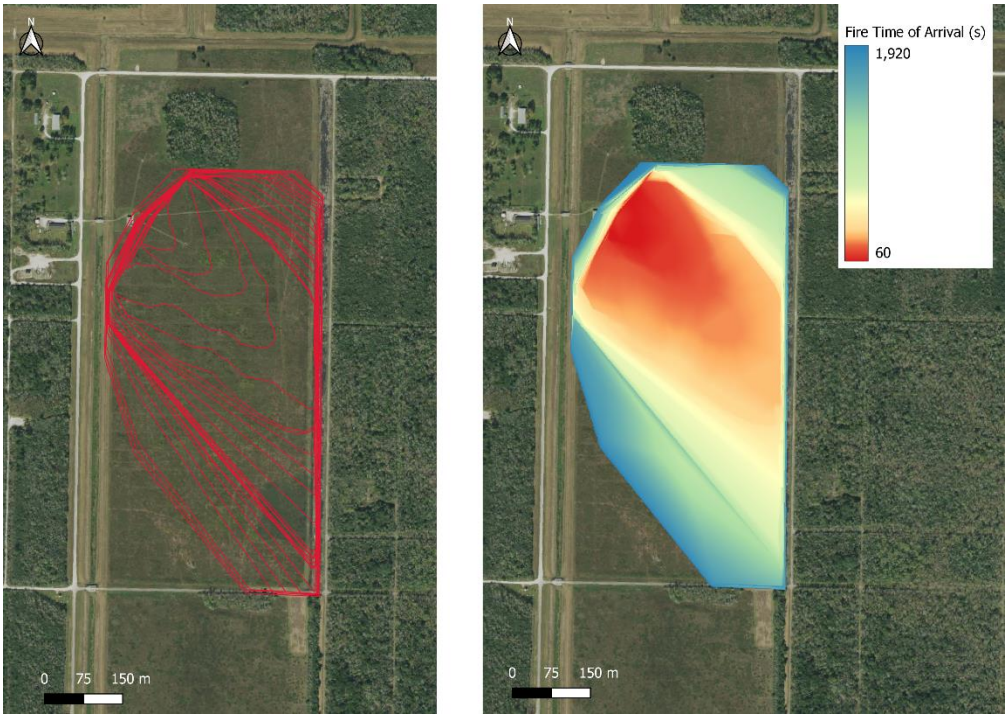

Figure 6- Fire progression derived from the airborne IR imagery. Left: fire perimeter at 60-s intervals. Right: fire time of arrival at every location in the burn unit, relative to the time of ignition. Base image provided by the USDA National Agriculture Imagery Program.

4. Conclusions and Future Work

In this paper, we present preliminary results of a detailed fire behavior analysis during the FireFlux II experiment. The results achieved so far demonstrate the utility of the three analyzed datasets and encourage further processing. Planned future work includes (i) conducting a detailed comparison of the measurements derived from each sensing technique, (ii) expanding the calculated results with additional fire behavior metrics, such as fire radiative power, rate of spread, and fire line intensity, and (iii) homogenizing the results and producing a comprehensive dataset that can be used in model validation exercises.

5. References

Clements, Craig B., Adam K. Kochanski, Daisuke Seto, Braniff Davis, Christopher Camacho, Neil P. Lareau, Jonathan Contezac, et al. 2019. “The FireFlux II Experiment : A Model-Guided Field Experiment to Improve Understanding of Fire – Atmosphere Interactions and Fire Spread.” International Journal of Wildland Fire 28: 308–26. https://doi.org/10.1071/WF18089.

Valero, M. M., O. Rios, E. Pastor, and E. Planas. 2018. “Automated Location of Active Fire Perimeters in Aerial Infrared Imaging Using Unsupervised Edge Detectors.” International Journal of Wildland Fire 27 (4): 241–56. https://doi.org/10.1071/WF17093.

Remotely sensed time series reveal varying levels of association between burned area and severity across regions in mainland Portugal

João Gonçalves*[1,2,3]; Bruno Marcos[1,2]; João P. Honrado[1,2,4]

[1]CIBIO, Centro de Investigação em Biodiversidade e Recursos Genéticos, InBIO Laboratório Associado, Campus de Vairão, Universidade do Porto, 4485-661 Vairão, Portugal, {joao.goncalves, bruno.marcos}@cibio.up.pt
[2]BIOPOLIS Program in Genomics, Biodiversity and Land Planning, CIBIO, Campus de Vairão, 4485-661 Vairão, Portugal
[3]proMetheus – Research Unit in Materials, Energy and Environment for Sustainability, Instituto Politécnico de Viana do Castelo (IPVC), Avenida do Atlântico, n.º 644, 4900-348 Viana do Castelo, Portugal
[4]Departamento de Biologia, Faculdade de Ciências, Universidade do Porto, 4099-002 Porto, Portugal, {jhonrado.fc.up.pt}

**Corresponding author*

Keywords

Fire severity, Burnt area, Spatiotemporal trends, Remote Sensing, Earth Observation

Abstract

Wildfires can pose severe threats to human lives and assets as well as to biodiversity on a global scale. Due to climate, land-use changes, and often inadequate forest management, wildfire regimes are also in transition, causing modifications in these disturbance events' spatial distribution, timing, size, frequency, and severity. In particular, increasing fire severity causes slower post-fire recovery times and a depletion in the resistance and resilience capacities which potentially trigger regime shifts in the state of ecosystems.

Satellite remote sensing (SRS) Earth Observations (EO) allow us to characterize the ecological impacts of wildfires and assess spatiotemporal trends in fire severity. The SeverusPT project is currently pursuing the objective of harnessing SRS/EO time series to characterize wildfire severity and assess its impacts on ecosystems. Our primary objectives of this exploratory research paper are two-fold: (i) assess national and regional spatiotemporal trends in fire severity and burnt area, and (ii) evaluate if fire severity regionally scales up with the total burnt area. Satellite image time series (SITS) from Terra/MODIS were obtained to calculate fire severity through the Normalized Burn Ratio (NBR) and the difference between pre- and post-fire (ΔNBR). Trend analyses were employed to quantify fire severity and burned area spatiotemporal patterns. Linear regression assessed the association between total burnt area by year/region (predictor) and fire severity (response).

Preliminary results show that at a national level, from 2001 until ca. 2008 - 2009 there was a general decrease in fire severity, followed by a reversal of this trend. This turning point has led to a general increase, with new severity highs formed in 2017 and 2020. We also found wide variation in fire severity at the regional level (NUTS-III), and trend analysis displayed that most regions increased both in burned area and severity. Linear regression showed that burned area and fire severity are correlated despite this association being highly structured at the regional level, forming a continuous spectrum from highly area-severity coupled regions (e.g., AM Porto, Médio Tejo, Viseu, Coimbra, Alto-Minho) to less coupled ones (e.g., Cávado, Trás-os-Montes, Alentejo). These results may support that the increasing amount and size of burnt area will scale up into higher fire severity for specific regions. These preliminary results from the SeverusPT project show that MODIS image time series allow assessing the spatial variation and the temporal trends of fire severity in a standardized and synoptic fashion. Future research using Landsat time series will aim to further assess these trends and profit from the data archive and the increased spatial resolution of this satellite mission. Mapping fire severity, its spatiotemporal variation and addressing its environmental drivers are now more crucial than ever to understand its dynamics and support fire management and prevention.

1. Introduction

Fire can relevantly introduce (socio-)ecological disturbances worldwide, impacting ecosystem composition, structure, functioning, and the provision of ecosystem services to humanity (Bowman et al., 2009). Modification

of fire regimes due to global environmental changes is thus at the forefront of social concerns motivating the improvement of policy and planning instruments regarding fire risk management and land tenure/use, natural resource management, and territorial governance.

Despite the vast investments in fire suppression, extreme fire events have increased across Mediterranean Europe. These extreme events, exacerbated by global climate change and fuel accumulation, often override the capacity of fire-suppression systems, putting human lives and livelihoods at risk. Assessing and predicting the effects of those events on ecosystems (i.e., fire severity), especially under a changing climate, is paramount for adequate fire prevention and fighting.

Surprisingly, there is a significant gap of publicly available, standardized and validated datasets on fire severity. Overcoming this gap is the central goal of SeverusPT, which is currently developing a framework for assessing, mapping and predicting fire severity based on satellite indicators of ecosystem functioning. A combination of metrics derived from satellite multi-spectral images (e.g. the difference Normalized Burn Ratio; ΔNBR), with data collected in-field (e.g. through the Composite Burn Index; CBI) is being exploited to assess fire severity (e.g. Cardil et al., 2019), conveying post-fire measures of environmental and ecological impacts due to fire (e.g., Koutsias et al., 2013; Tedim et al., 2017).

Our primary objectives with this exploratory research are two-fold: (i) assess national and regional spatiotemporal trends in fire severity and burned area, and (ii) evaluate if fire severity regionally scales up with total burnt area (i.e., a putative and here tentatively called "fire area – severity coupling" hypothesis).

2. Methods

2.1. Study area

This study area comprises mainland Portugal covering an area of approximately 89,100 Km^2, considered one of the countries of southern Europe with a greater incidence of forest fires in the last decades. Elevation ranges from 0 to 1993 meters, with the mountain areas occurring mainly in the north. The climate ranges from temperate Atlantic in the northwest to dry Mediterranean in southern regions. The average annual temperature varies from 4 °C in the northern mountainous interior to 18 °C in the south.

2.2. Time series data and statistical analyses

Satellite image time series (SITS) from Terra/MODIS product MOD13Q1 (version-006) containing vegetation indices at 16-day/250m were obtained to calculate fire severity through the Normalized Burn Ratio (NBR) index. NBR consists of the normalized difference between the near-infrared band #2 (NIR, 858 nm) and the shortwave-infrared band #7 (SWIR, 2130 nm), as:

$NBR = (NIR_{b2} - SWIR_{b7})/(NIR_{b2} + SWIR_{b7})$ (Eqn. 1).

A high NBR value typically characterizes normal or "healthy" vegetation, whereas low values indicate bare ground and/or recently burnt areas. Delta NBR, calculated as the difference between the pre-fire and the post-fire NBR, was used as an estimate of fire severity as:

$\Delta\text{NBR} = \text{NBR}_{pre\_fire} - NBR_{post\_fire}$ (Eqn.2).

A higher value of ΔNBR generally indicates more severe damage, whereas negative values may indicate less severely affected areas or even short-term recovery following a fire. To calculate a standardized annual time-series of ΔNBR between 2001 and 2020 for mainland Portugal, we considered the characteristic phenology of fire mostly concentrated around summer/early-fall months (Marcos et al., 2019) and defined the post-fire period from September-November and the pre-fire between March-May. Within the pre- and post-fire periods, all available NBR images were averaged through the median hence applying the following formula:

$\Delta\text{NBR} = \text{median}(\text{NBR}_{\{Mar-May\}}) - \text{median}(NBR_{\{Sep-Nov\}})$ (Eqn.3).

As a non-parametric/rank-based measure, the median is less affected by cloud cover and noise in the data. All Eqn.1-3 calculations were performed using Google's Earth Engine planetary-scale geospatial analysis platform (Gorelick et al., 2017). Based on the annual ΔNBR time series, we extracted the values only for fire perimeters (at annual time steps) identified in the National Burnt Area Database (NBAD) for mainland Portugal from

2001to 2020 (ICNF, 2022). NBAD was also employed to calculate the total burnt area and the distribution of fire perimeters at the regional NUTS-III inter-municipal level using R statistical software and the *terra* package (Hijmans, 2022). National and regional-level statistics of fire severity based on quantiles were calculated. Annual time-series plots (employing loess/moving-average smoother) were employed to assess spatiotemporal patterns of severity. Linear regression was employed to assess the relation (i.e., the degree of coupling) between total burnt area by year/region (predictor) and fire severity (response). The coefficient-of-determination (R^2) and the F-statistic p-value were estimated to convey the strength of this association and its statistical significance.

3. Results and Discussion

3.1. General trends of fire severity in the last two decades (2001 – 2020) in mainland Portugal

These preliminary results from the SeverusPT project show that MODIS image time series allow assessing the spatial variation and the temporal trends of fire severity in a standardized and synoptic fashion. Satellite data is particularly useful to assess micro- to mesoscale variation in severity (Fig.1–a) and identify slightly scorched or unburnt "islands" which hold particular relevance for post-fire biological/ecological recovery (e.g., Santos et al., 2022) across different time-frames (Torres et al., 2018) and ecosystem dimensions (Marcos et al., 2021). Such variations in fire severity can be caused by a multitude of factors such as the spatial distribution, type, state, shape, and vertical structure of fuels, as well as microclimate and weather conditions, topography, geomorphology and fire suppression efforts. These factors combine to shape the fine-scale and anisotropic variations, with fire edges typically exhibiting lower severity (Fig.1–a). SITS also excel in characterizing temporal trajectories in severity with widely different profiles from triangular patterns (potentially showing cyclical decreases and increases in biomass triggered by highly frequent fires with, respectively, less and more severity, Fig.1–b). In contrast, we also found areas with increasing fire severity where, potentially, biomass decreases caused by fire are unmatched by fast recovery times and progressive post-fire biomass accumulation coupled with fire-prone weather conditions in subsequent events.

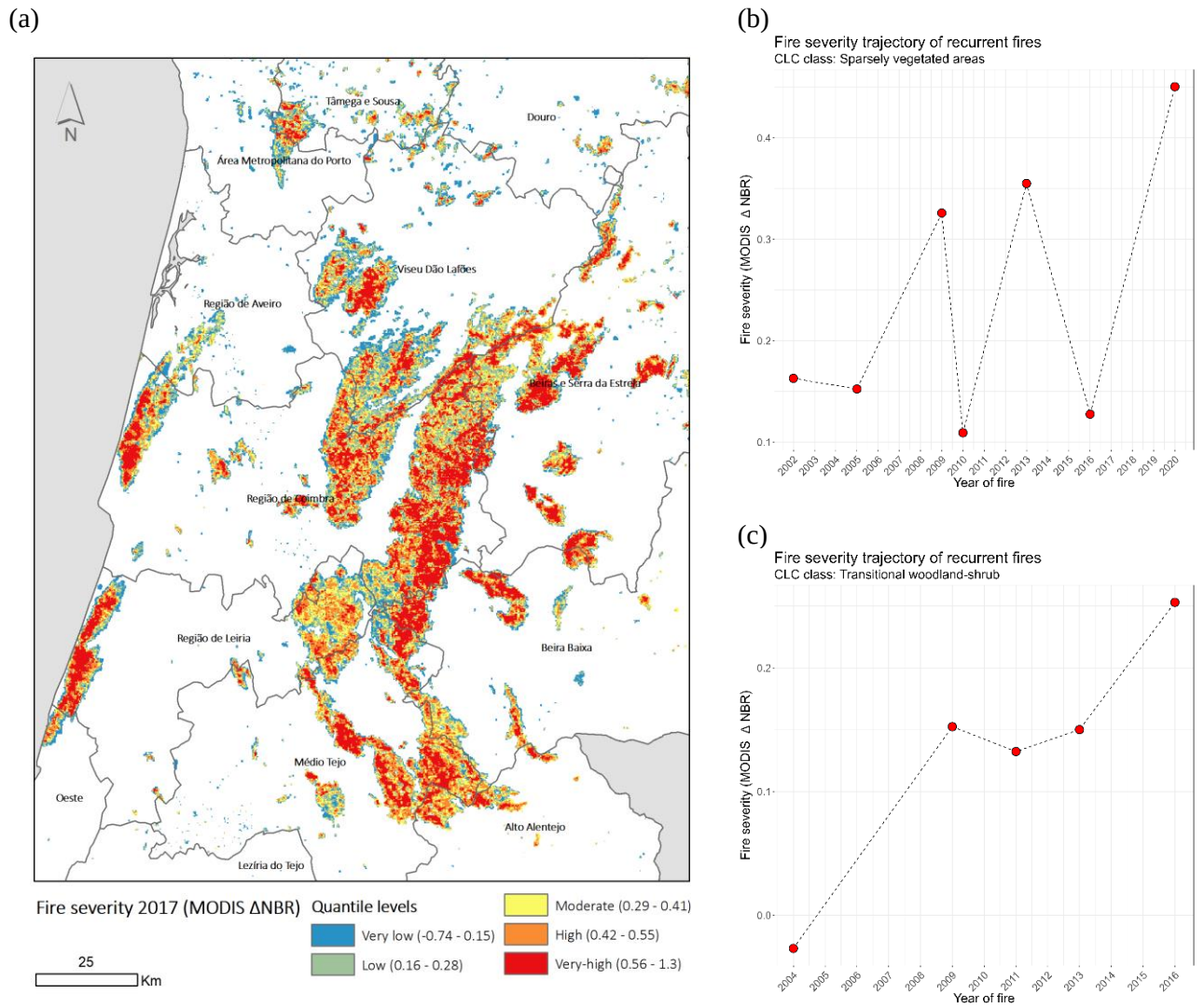

Figure 1 – (a) MODIS ΔNBR image shows the spatial variation of fire severity within and between fire perimeters of 2017. Each severity level is based on the 20% quantiles of the annual distribution. (b) and (c) comprise two illustrative severity trajectories for recurrent fires in a sparsely vegetated area following a triangular pattern (b) and transitional woodland-shrubland (c) with a monotonic linear increase trend in severity. Each point in these plots shows the severity of each fire event for a given area.

Preliminary results also show that, at a national level from 2001 until ca. 2008 - 2009 there was a general decrease in fire severity, followed by a reversal of this trend. This turning point has led to a general increase with new severity highs formed in 2017 and 2020 (Fig.2). This trend reversal also led us to separately consider this nested period of 2008 – 2020 for subsequent analyses.

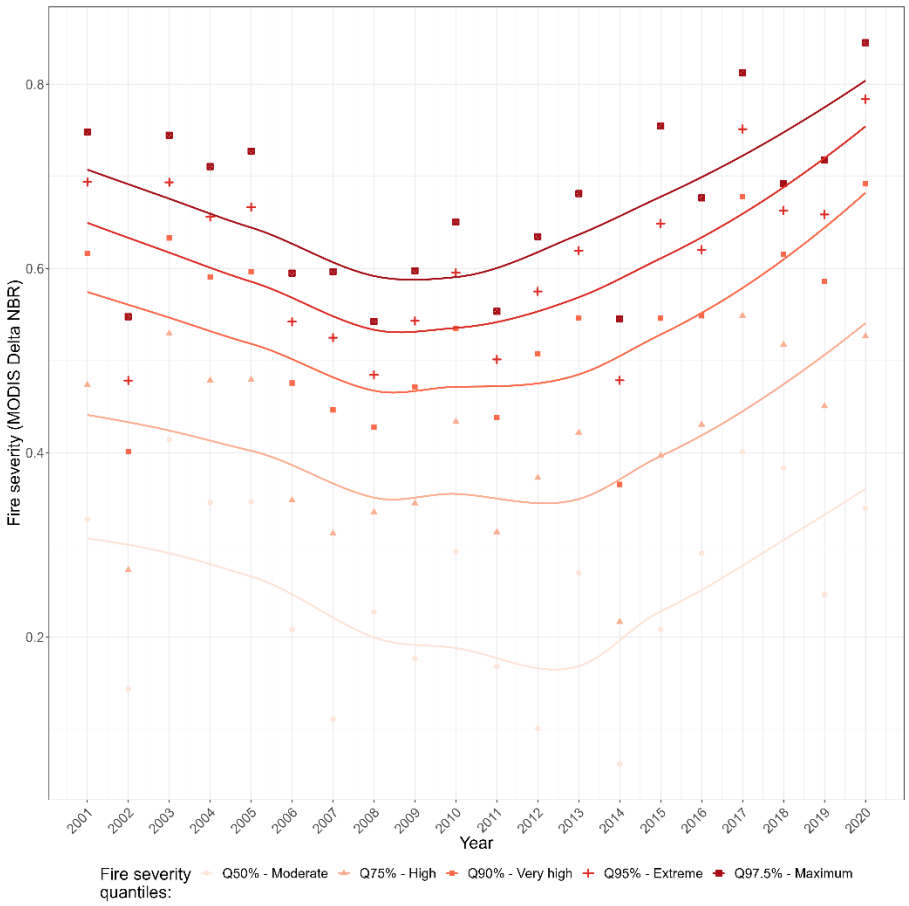

Figure 2 – Fire severity trends for mainland Portugal between 2001 and 2020 across different severity levels based on distribution quantiles (Q50% - moderate, Q75% - High, Q90% - very-high, Q95% - extreme and Q97.5% - maximum).

Moreover, preliminary results also show that there is wide variation in fire severity at the regional level (considering NUTS-III inter-municipal units; Fig.3) with the Region of Aveiro, Ave, Área Metropolitana do Porto, Médio Tejo, Terras de Trás-os-Montes and Alto-Minho recording the most significant increases since 2008 from average (50% quantile) to very high severity fires (97.5% quantile).

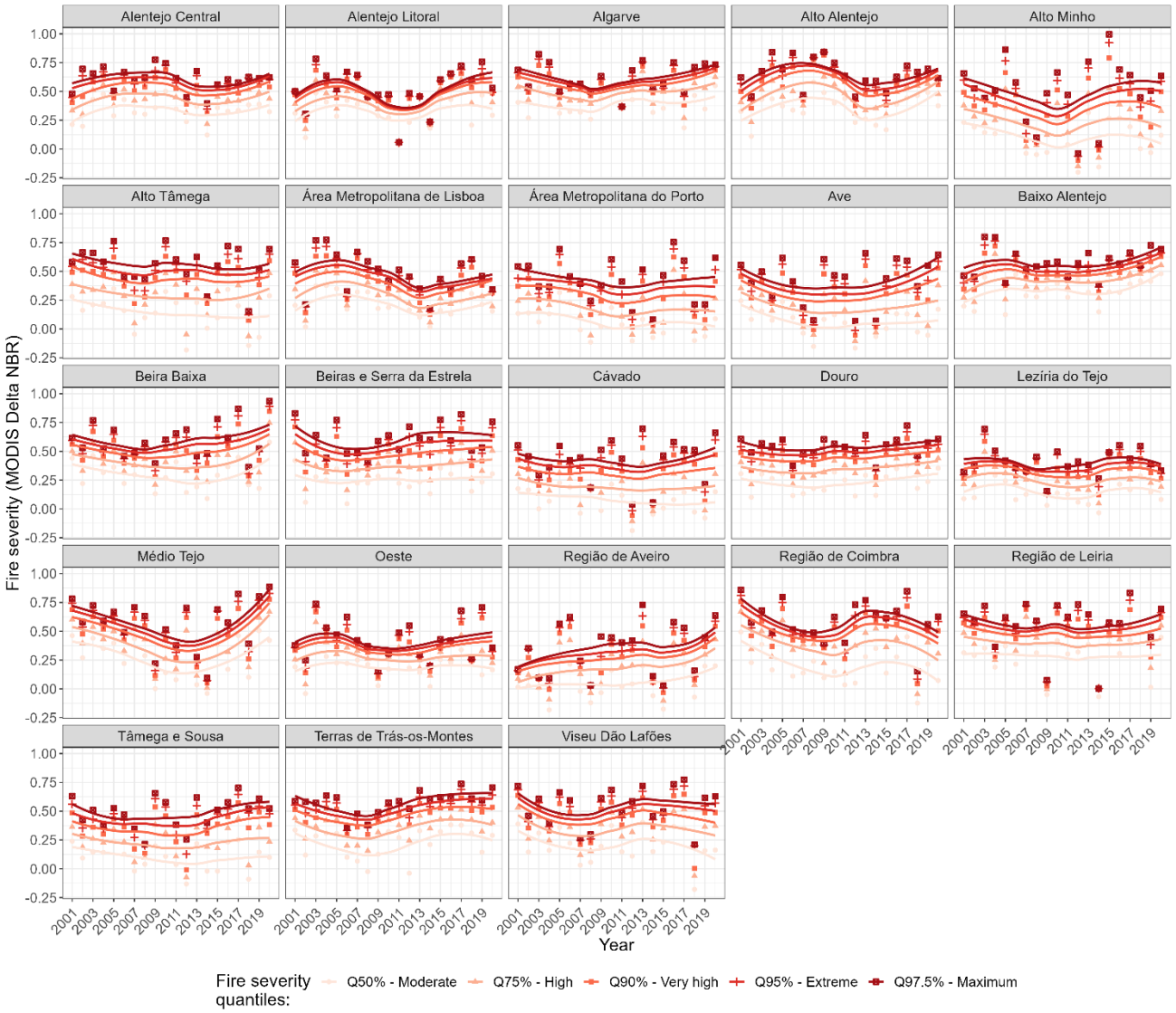

Figure 3 – Fire severity trends for mainland Portugal intermunicipal regions (NUTS-III) between 2001 and 2020 across different severity levels based on distribution quantiles (Q50% - moderate, Q75% - High, Q90% - very-high, Q95% - extreme and Q97.5% - maximum).

When comparing the temporal trends of burnt area *vs* median fire severity across NUTS-III regions (for 2008-2021; following the trend reversal period), preliminary results show that the most frequent class is the one combining the increase of both burnt area and severity (Fig. 4). These regions are primarily located in the country's centre portion (from AM Porto to Lezíria do Tejo) and south (Alentejo Litoral/Sul) portions. Slightly more complex combinations occur in the north with decreased trends in burnt area and severity for Cávado and Alto Tâmega regions. In contrast, a combination of burnt area decrease and severity increase is found for Alto Minho, Ave, Tâmega-Sousa, Douro and Trás-os-Montes regions. We found few regions with burnt area increase and severity increase trends, including Viseu-Dão-Lafões, and Alto/Central Alentejo.

(a)

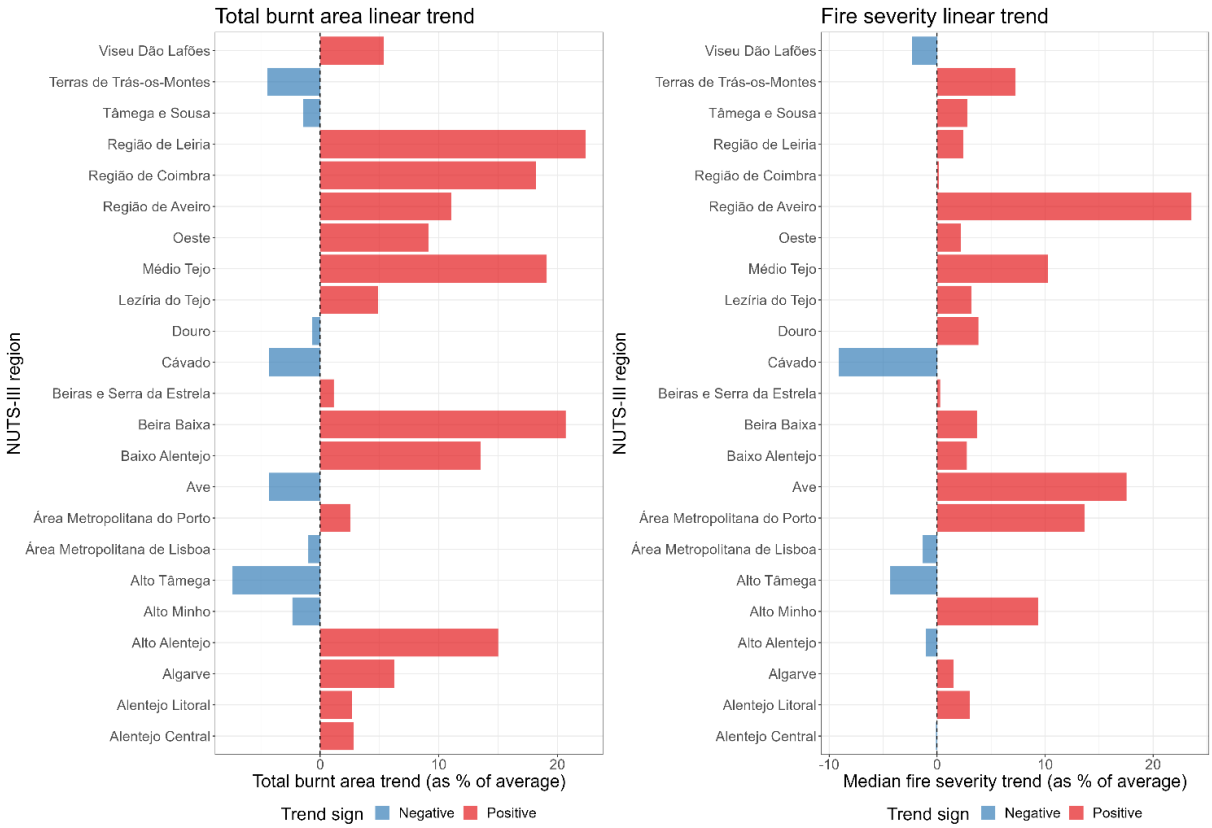

(b)

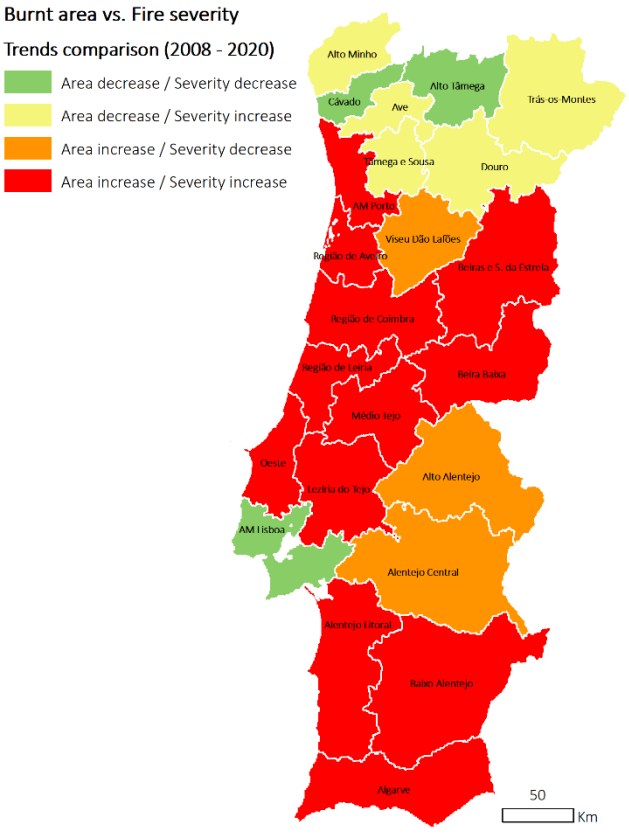

Figure 4 – Comparison of temporal trends of total burnt area vs fire severity across inter-municipal regions of mainland Portugal (NUTS-III), considering the period 2008-2021

(a) Linear trend analysis was employed and expressed as the percentage of average change. The trend sign is positive, i.e., increasing impact across time in the burnt area and/or fire severity, and negative if otherwise.

(b) Map depicting the combination of trends for the burnt area and fire severity for different NUTS-III regions.

Linear regression analyses allowed us to evaluate that burnt area and fire severity are indeed correlated. However, the nature of this relationship is highly structured at the regional level, forming a continuous spectrum of variation from highly area-severity coupled regions – with a higher coefficient of determination (R^2) values (e.g., AM Porto, Médio Tejo, Viseu, Coimbra, Alto-Minho; Fig.5) – to uncoupled regions (e.g., Cávado, Alentejo) with lower regression R^2's.

These results may support the (tentatively called) "fire area – severity coupling" hypothesis, in which, for specific regions (Fig.6), the increasing amount and size of burnt area will scale up into higher fire severity.

Overall, "coupled" regions are located in the northern and central portions of the country (exceptions to Cávado, and Trás-os-Montes; Fig.6) and the southern-most region of Algarve. For these regions, the observed fire area-severity scale-up will potentially cause a higher depletion of ecosystems functioning capacities and resilience and trigger longer recovery times (Marcos et al., 2021; Torres et al., 2018).

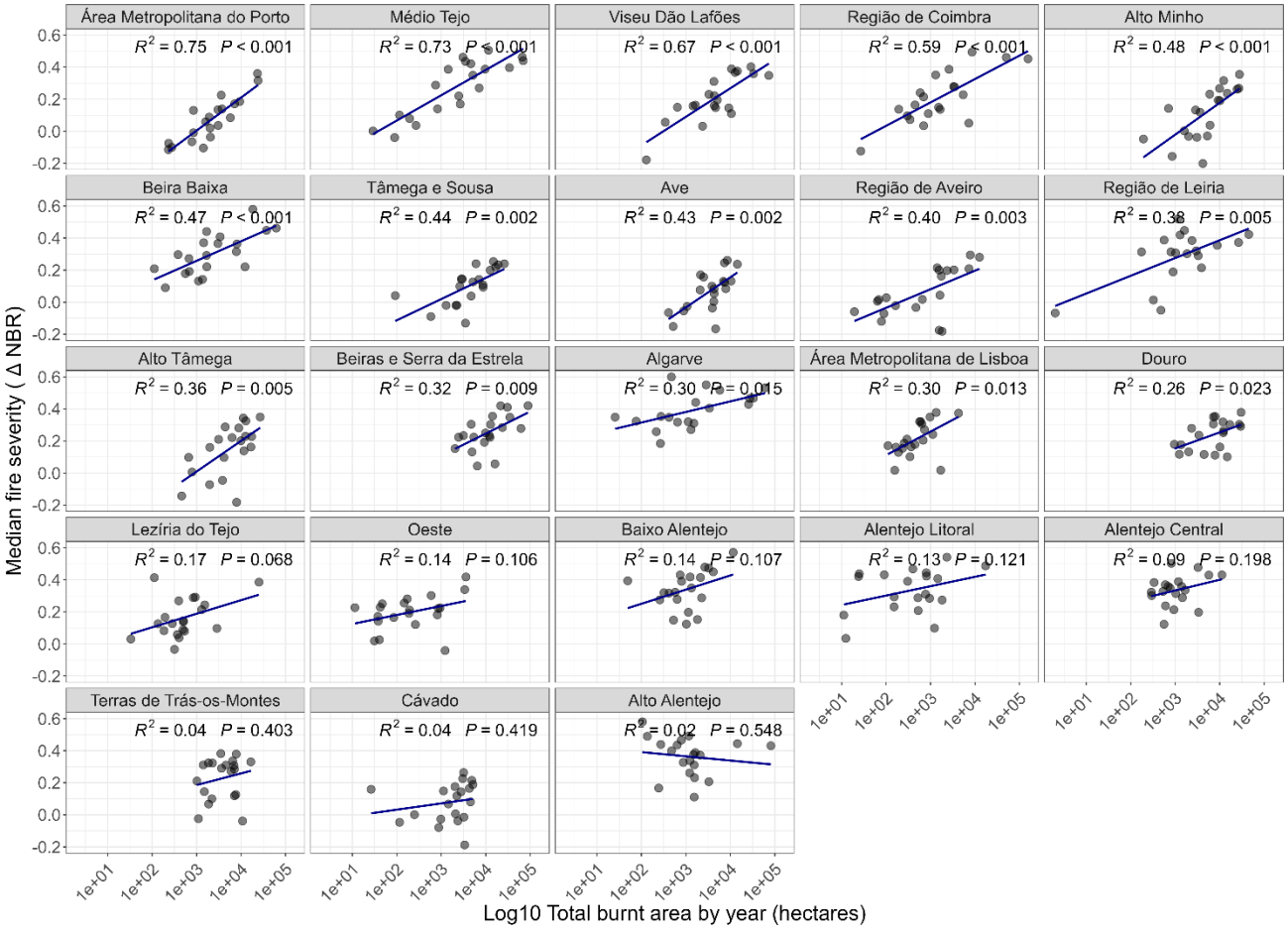

Figure 5 – Linear regression plots between total burnt area per year (2001-2020) and median fire severity (MODIS ΔNBR). Plots are shown for are all mainland NUTS-III regions and displayed by decreasing R^2 value.

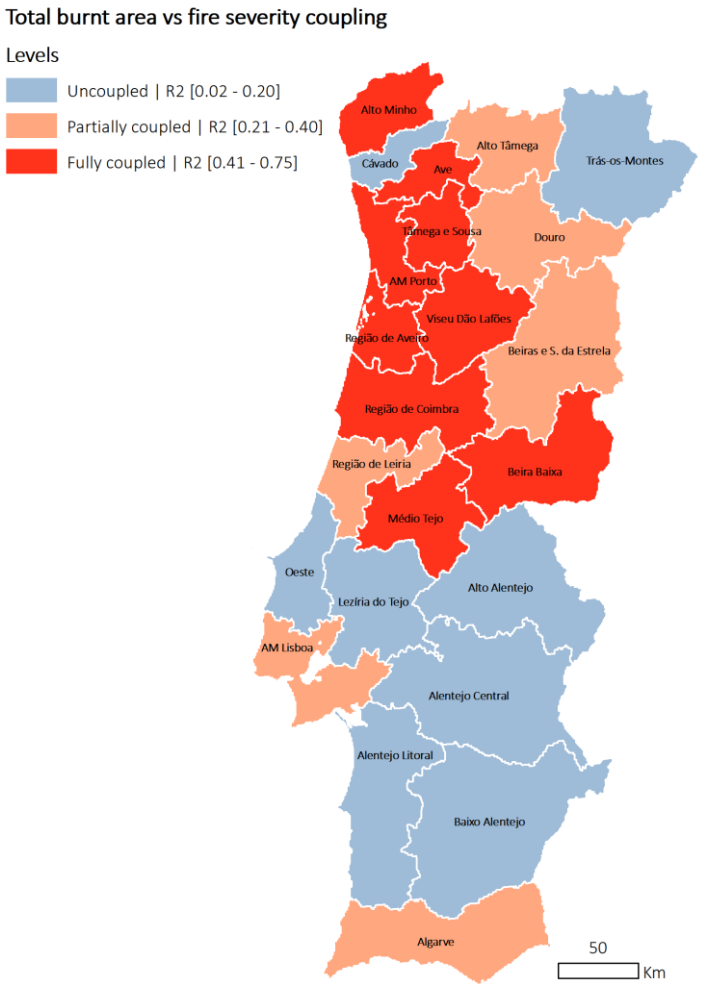

Figure 6 – Coupling between total burnt area (2001-2020) and fire severity assessed through MODIS ΔNBR.

4. Final remarks and future work

Mapping fire severity, its spatiotemporal variation and addressing its environmental drivers are now more crucial than ever to understand its dynamics and support fire management and prevention. This exploratory research shows preliminary results from the SeverusPT project addressing these goals and exploring trends and the regionally varied scaling between burned area and fire severity.

Such phenomena must be adequately addressed with different strategies across distinct regions to contain and prevent further damage from wildfires to ecosystems. Future work will examine and attempt to model the drivers of the "*fire area – severity coupling" hypothesis* and exploit finer-scale satellite image time series and improved algorithms to expand current results. In particular, Landsat time series will aim to further assess these trends and profit from the long historical data archive and the increased spatial resolution of this satellite mission.

5. References

Bowman D et al., Fire in the Earth system., Science, vol. 324, no. 5926, pp. 481–4, Apr. 2009, doi: 10.1126/science.1163886.

Cardil, A., B. Mola-Yudego, Á. Blázquez-Casado, and J. R. González-Olabarria, Fire and burn severity assessment: Calibration of Relative Differenced Normalized Burn Ratio (RdNBR) with field data, J. Environ. Manage., vol. 235, pp. 342–349, Apr. 2019, doi: 10.1016/j.jenvman.2019.01.077.

Gorelick, N., M. Hancher, M. Dixon, S. Ilyushchenko, D. Thau, and R. Moore. 2017. Google Earth Engine: Planetary-scale geospatial analysis for everyone. Remote Sensing of Environment 202:18-27.

Hijmans, R.J. 2022. terra: Spatial Data Analysis. R package version 1.5-21. https://CRAN.R-project.org/package=terra

ICNF, 2022. Territórios ardidos (National Burnt Area Database for mainland Portugal 1975-2020). Creation date: 28/04/2020, Updated in: 26/01/2022, Visit date: Feb-2022. URL: https://sig.icnf.pt/portal/home/item.html?id=983c4e6c4d5b4666b258a3ad5f3ea5af

Koutsias, N, B. Allgöwer, K. Kalabokidis, G. Mallinis, P. Balatsos, and J. G. Goldammer, Fire occurrence zoning from local to global scale in the European Mediterranean basin: Implications for multi-scale fire management and policy, IForest, vol. 9, no. APR2016, pp. 195–204, Apr. 2016, doi: 10.3832/ifor1513-008.

Marcos, B., J. Gonçalves, D. Alcaraz-Segura, M. Cunha, and J. P. Honrado. 2019. Improving the detection of wildfire disturbances in space and time based on indicators extracted from MODIS data: a case study in northern Portugal. International Journal of Applied Earth Observation and Geoinformation 78:77-85.

Marcos, B., J. Gonçalves, D. Alcaraz-Segura, M. Cunha, and J. P. Honrado. 2021. A Framework for Multi-Dimensional Assessment of Wildfire Disturbance Severity from Remotely Sensed Ecosystem Functioning Attributes. Remote Sensing 13.

Santos, X., J. Belliure, J. Gonçalves, and J. G. Pausas. 2022. Resilience of reptiles to megafires. Ecological Applications 32:e2518.

Tedim, F, R. Remelgado, C. Borges, S. Carvalho, and J. Martins, Exploring the occurrence of mega-fires in Portugal, For. Ecol. Manage., vol. 294, pp. 86–96, Apr. 2013, doi: 10.1016/j.foreco.2012.07.031

Torres, J., Gonçalves, J., Marcos, B., and Honrado, J. 2018. Indicator-based assessment of post-fire recovery dynamics using satellite NDVI time-series. Ecological Indicators 89:199-212.

Sensitivity of LIDAR Derived Fuel Cells to Fire Modeling at Laboratory Scale

Anthony Marcozzi*[1]; Jesse Johnson[1]; Russell Parsons[2]; Jacob Downs[1]

[1]University of Montana. 32 Campus Dr, Missoula, MT 59812, USA, {anthony.marcozzi@umconnect.umt.edu, jesse.johnson@mso.umt.edu, jacob.downs@umconnect.umt.edu}
[2] USDA Forest Service, Rocky Mountain Research Station, Fire Sciences Laboratory. 5775 Hwy 10 West, Missoula, MT 59808, USA, {russell.a.parsons@usda.gov}

**Corresponding author*

Keywords

CFD, Fire behavior, LIDAR, DAKOTA, Fuel modeling

Abstract

Computational models of wildfires are an important tool for fire managers and scientists. However, fuel inputs to wildfire models can be difficult to represent with sufficient detail to be both computationally efficient and representative of observations. Recent advances in fuel mapping with airborne and terrestrial laser scanning (LIDAR) techniques present new opportunities to capture variation in fuels within a tree canopy and on a landscape. In this paper, we develop a technique for building 3D representations of vegetation from point clouds created by Terrestrial Laser Scans (TLS). Our voxel based approach can be extended to represent heterogeneous crown fuels as collections of fuel cells in modern 3D Computational Fluid Dynamics wild fire models such as FDS, QUIC-Fire, or FIRETEC. We evaluated the effectiveness of our technique at different fuel cell resolutions by using the DAKOTA optimization toolkit to compare simulated fire behavior in FDS with observed burn data collected during a series of experiments at the Missoula Fire Sciences Laboratory. The primary finding was that within the search space of point cloud derived fuel cells, we find accurate descriptions of observed fire behavior with the FDS model. We also find that within our search space, regions of global minima are consistent across fuel cells at different resolutions. This finding suggests that while new techniques are capable of characterizing fuel models with a high degree of fidelity, high resolution 3D fuel models do not improve parity with observed fire behavior in the FDS fire model. The results of this paper offer fire modelers guidelines for translating LIDAR data to 3D fire models, and what fuel cell resolution can best capture accurate fire behavior.

1. Introduction

Wildfires are an increasingly visible natural phenomenon across the globe. In the United States, 43,371 structures were lost due to wildfires from 2016-2019 (National Interagency Fire Center 2019), and the Wildland Urban Interface (WUI), the area where houses and vegetation intersect, was the fastest growing land use type in the United States from 1990-2015 (Radeloff et al. 2018). Despite the threat to homes in the WUI, wildfires have historically been an integral part of North American forest, brush, and grassland ecosystems, and by pursuing a policy of wildfire suppression since the early 20th century, land managers have altered fire regimes in much of North America (Arno and Brown 1991). In addition to a more complicated landscape from an expanded WUI and altered fire regimes from fuel loading, fire managers also have to account for the effects of a warming climate on fire conditions. The number of areas with the potential to be adversely affected by wildfires has increased in the 21st century. Tools for mitigating the threat of wildfire to fire sensitive areas, such as the WUI, have traditionally included a combination of thinning projects and prescribed burns (Arno and Brown 1991). Unfortunately, the tools developed to evaluate the efficacy of such projects on a local scale rely on limiting assumptions, cannot be generalized across landscapes, and do not account for rapidly changing fire regimes due to climate change (Parsons et al. 2018).

Physics based Computational Fluid Dynamic (CFD) models present a possible solution to these problems by providing a mechanism to study fire behavior in heterogeneous vegetation and dynamic fire environment conditions (Linn et al. 2020). However, CFD models must be coupled with accurate models of fuel to realistically represent fire behavior (Parsons et al. 2011, Atchley et al. 2021).

Fortunately, rapid advancements in remote sensing techniques have introduced new methods capable of meeting the data requirements of physics based fire models. LIDAR is a promising remote sensing technology for the 3D characterization of vegetation and fuels (Hudak et al. 2017). Point clouds are capable of measuring vegetation height, cover, and relative density – all of which play important roles in determining fire behavior. Critically, these fuel measurements play an important role in determining the transition relationship between quasi steady-state surface fires and more extreme fire behavior such as torching and crowning, which can be crucial to understanding the fire risk of a given landscape (Parsons et al. 2017).

Despite these promising advancements in fire and fuels modeling, there are still significant gaps in the research linking fuel models to the fire modeling environment. Fire modelers must balance careful tradeoffs between computational expense, data collection, and grid resolution when deciding how to represent vegetation as 3D gridded input data. To date, no comparisons have been published between observed fire behavior and simulated fire behavior of LIDAR-derived fuel cells. This paper explores the concept of altering three-dimensional fuel cells in terms of moisture content, bulk density, and resolution to provide an algorithmic approach to translating LIDAR point clouds into a CFD based simulation environment.

Leveraging TLS and mass over time data collected in 2021 on burning saplings at the Missoula Fire Sciences Laboratory, we developed a methodology for representing complex vegetation in three-dimensional fuel cells. Then, we tested the effect of fuel cell descriptors such as fuel moisture content, bulk density, and resolution on modeled fire behavior in the FDS model. We present our methodology, which can be used to translate point cloud data to any CFD fire model with gridded fuel inputs such as FDS, FIRETEC, or QUIC-Fire. Lastly, we provide fire modelers with heuristics for making decisions on fuel cell fidelity in order to balance simulation accuracy with computational requirements using the FDS model.

2. Methods

The sapling burn experiments reported here were conducted in the Missoula Fire Sciences Laboratory burn chamber. The experiment was designed to examine the effect of drought stress on tree mortality when exposed to two controlled levels of fire intensity. We acquired 123 saplings of two species, Engelmann spruce (*Picea engelmannii*) and Ponderosa pine (*Pinus ponderosa*), from a local nursery. Saplings were acquired in May and stored in planter containers filled with soil and with the roots intact. During this storage period, half of the saplings from each species were given a low water treatment of water every one to two weeks so as to mimic conditions of a drought environment. The other half were adequately watered every three days so as to encourage normal development.

Each day of the experiment, saplings were transported to the burn chamber and ignited over a pair of concentric ring gas burners. During the ignition period, each sapling was exposed to one of three fire intensity categories: no fire treatment, low burner treatment, or high burner treatment. At the time of the fire treatment, a tree was placed through the hole such that the tree stand rested on a scale. Additionally, the weight of the sapling was recorded during the burning period with a load balance transmitting at 0.5 Hz.

For each sapling, three-dimensional scans were collected from a Leica Geosystems BLK360 Terrestrial Laser Scanner. Two scans were taken from the same location before and after the burn treatment. The TLS was run at a high density setting with a reported resolution of 5mm at 10 meters. Because the scans were taken in the same location, static references in the burn chamber were present to facilitate spatial referencing. The two scans were co-registered using Cyclone Register 360 software from Leica Geosystems in order to create a single 3D point cloud. Figure 1 shows the experimental setup with LIDAR scanner.

Figure 1- Experimental setup with LIDAR scanner at the Missoula Fire Sciences Laboratory

There are several challenges associated with correlating 3D point clouds to fine fuel mass and location without the use of destructive sampling. A higher point cloud density does not necessarily correlate to a higher density of foliage or stem biomass. A voxel based representation of the experimental saplings offers numerous advantages. Duplicated points from stitching multiple scans are represented as a single voxel, voxels represent points returned to the scanner in addition to points occluded by overlapping woody material, and voxels are one step closer to the concept of a 3D fuel cell necessary for input to a CFD fire model (Hosoi and Omasa 2006).

Our voxelization technique begins by identifying reference voxels. A reference voxel is the smallest possible voxel representation of a point cloud given the physical constraints of the TLS device and the scanning environment. Reference voxels have a Boolean value indicating the presence or absence of points within the voxel. We chose 1cm x 1cm x 1cm voxels for our reference voxel size due to the reported 5mm point density at 10 meters of the TLS device. We construct voxels at coarser resolutions by creating a voxel grid in the point cloud domain and counting the number of reference voxels that occur within the voxel at the desired resolution. When the voxel is converted to a fuel cell, biomass is distributed in proportion to the number of contained reference voxels.

We conducted a multidimensional parameter study using the DAKOTA optimization toolkit. Each n-dimensional sample generated by DAKOTA contains parameters for fuel cell resolution, fuel moisture content, and total dry foliage mass. We used the FDS lagrangian particle model to simulate the experimental burn for each sapling at five different fuel cell resolutions. FDS outputs foliage mass at 100 Hz which we used to compute a loss function between simulated and modeled fire behavior. Figure 2 shows a complement of five FDS simulations of the same sapling across five different fuel cell resolutions.

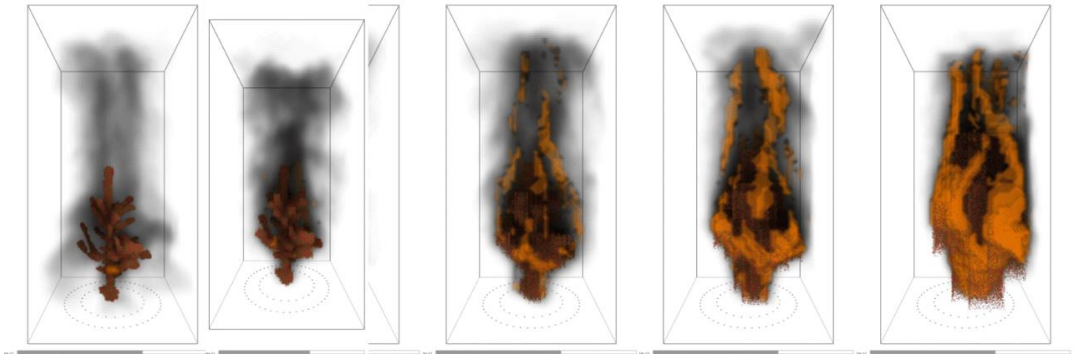

Figure 2 - FDS simulations of a burning sapling at different fuel cell resolutions

3. Results

We computed the RMSE of each simulation in the parameter sweep across sixteen saplings. For each sapling, we found the minimum RMSE determined from comparing the mass loss curves for observed and simulated burns. Figure 3 shows the minimum RMSE found in the set of simulations for Engelmann spruce sapling S63. We observe close parity between the simulated and observed mass loss in both the shape of the curves and the resulting change in mass.

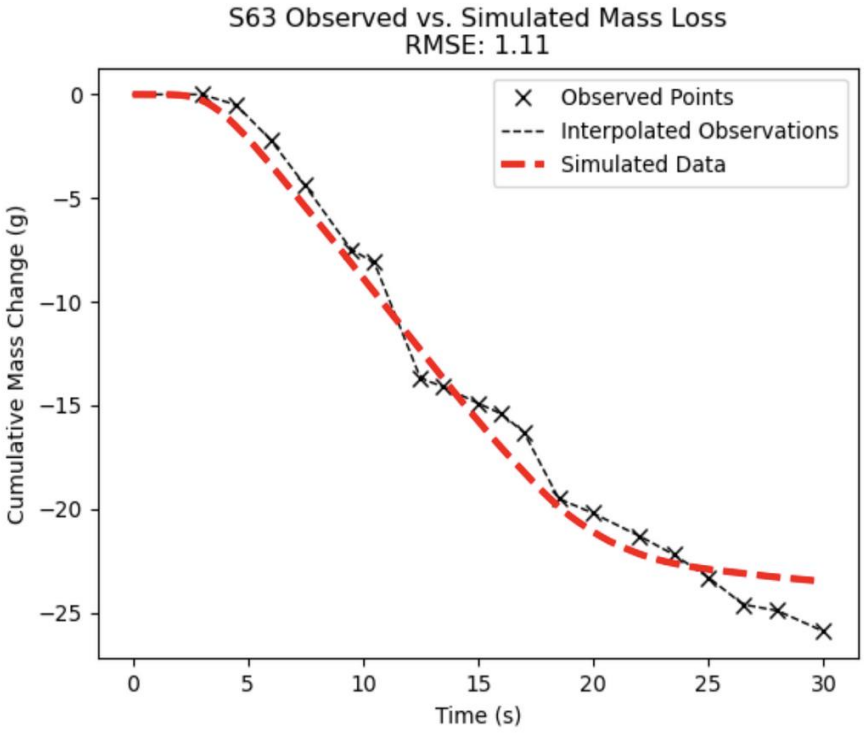

Figure 3 - Comparison between simulated and observed curves of cumulative mass change. This is the lowest RMSE value found out of the 16,384 model runs.

The correspondence between RMSE and the independent variables allows us to examine the space sampled by DAKOTA in our multidimensional parameter study. Figure 4 shows the results of the numerical experiment as described above for one Engelmann spruce sapling. Each pane in the image represents a parameter sweep across 2D points for a given fuel cell resolution. Each pixel has a value for fuel moisture content and dry foliage mass. Fuel moisture content was sampled uniformly in the range [20, 350]%, and dry foliage mass was sampled in the range [10, 80]g for a total of 256 points for each sampled fuel cell resolution.

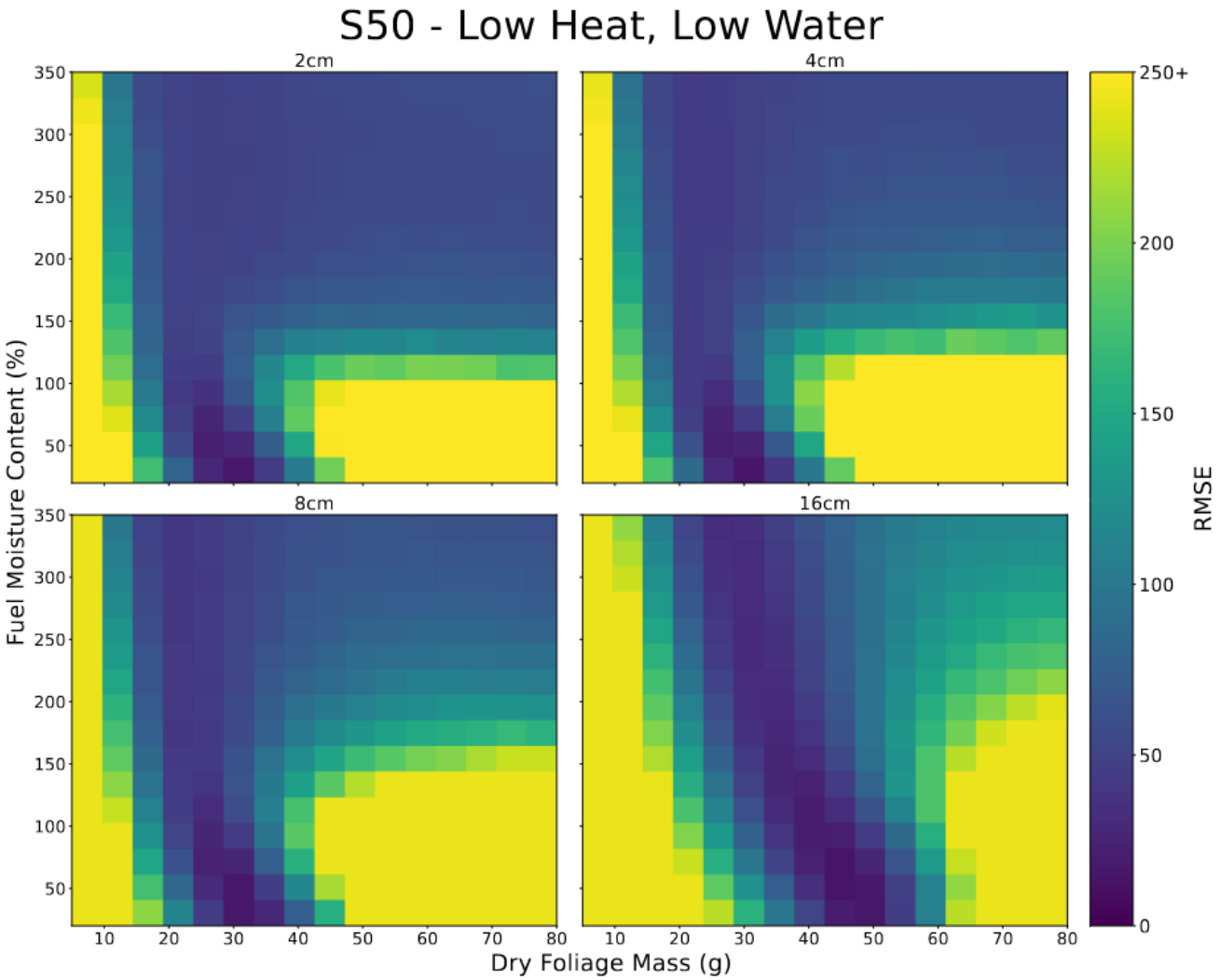

Figure 4 - Distribution of RMSE values for the full 1,024 samples in the parameter sweep for sapling S50. The upper left pane is for simulations with a fuel cell resolution of 2cm, upper right for 4cm, bottom left for 8cm, and bottom right for 16cm. The x and y axis of each pane correspond to the sampled range of dry foliage mass and fuel moisture content. Each pixel is colored according to the RMSE resulting from the comparison between the simulated model output and the observed data for sapling S50.

The multidimensional parameter study identifies a region of consistent minima across all fuel cell resolutions. The model is sensitive to dry foliage mass values as evidenced by the areas of high RMSE below 25g and above 50g along the x-axis in figure 4. Minimum RMSE values occur at higher dry foliage mass values for the coarsest fuel cell resolution of 16cm x 16cm x 16cm. Additionally, the model shows sensitivity to fuel moisture content. This effect is more pronounced when dry foliage mass is high, and the model appears less sensitive to fuel moisture content when the dry foliage mass is low. The parameter sweep identifies a consistent region of minima across all fuel cell resolutions. We find that the coarsest fuel cell resolution expands the area of RMSE minima across a larger range of dry foliage mass values.

In addition to the parameter space plots for individual saplings, we also analyze the effects of independent variables on RMSE. We compute the Pearson correlation coefficients between dry foliage mass, fuel moisture content, and fuel cell resolution on the logarithm of RMSE for each of the sixteen multidimensional parameter studies. The distribution of correlation coefficients are displayed in Figure 6. This result suggests that fuel cell resolution has a significantly lower ability to predict RMSE than dry foliage mass or fuel moisture content.

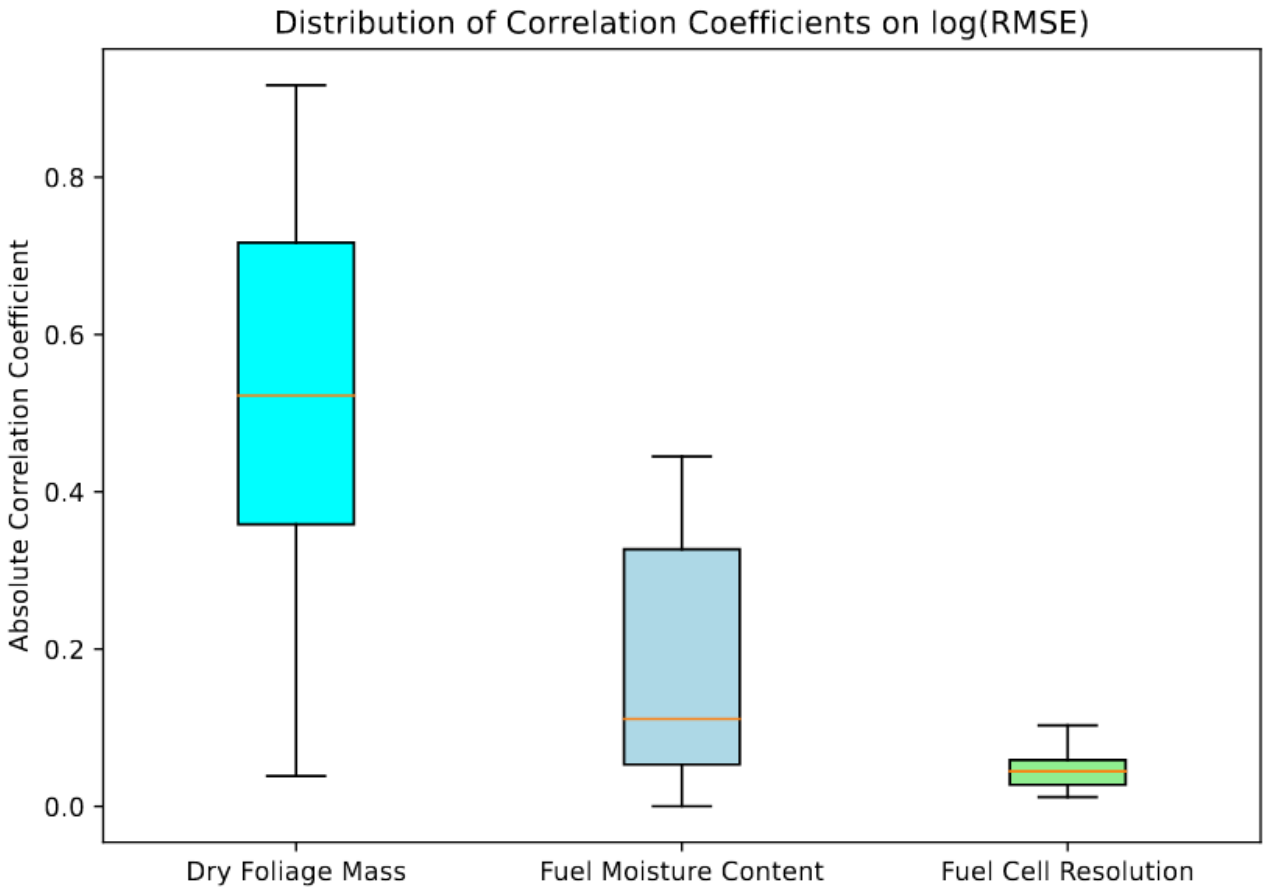

Figure 6 - Box and whisker plot of the distribution of correlation coefficients between log(RMSE) and three independent variables: Dry Foliage Mass, Fuel Moisture Content, and Fuel Cell Resolution for n=16 saplings. The box extends from the first quartile (Q1) to the third quartile (Q3) of the data, with a line at the median. Whiskers extend from the lowest correlation coefficient to the highest correlation coefficient in the data. We take the absolute value of the correlation coefficient in order to capture the magnitude, but not the direction, of the correlation.

4. Discussion

In this study we developed a methodology for describing heterogeneous canopy fuel loads using LIDAR point clouds. Next, we conducted a series of numerical experiments examining the effectiveness of this technique by comparing FDS model output with observed load balance data taken from a series of experimental tree burns. We used DAKOTA to conduct a parameter sweep on fuel moisture content and dry foliage mass and identified physically plausible local minima. Additionally, we found that our sampling technique identified an area of RMSE minima for all fuel cell resolutions, and that the area was consistent for 2-8cm resolution fuel cells.

Our fuel cell methodology represents a first step at achieving this goal of linking data from LIDAR points clouds and coupled fire-atmospheric models. While we found close parity between our fire simulations in FDS and observational data using our 3D fuel models, many opportunities for further research and refinement exist. For example, our technique tends to over-sample reference voxels associated with the stem of the saplings. The result of this phenomenon is the over-weighting of combustible thermally thin foliage concentrated in the middle of the 3D fuel model. This phenomenon likely results in an overestimation of mass loss when the vegetation is exposed to a heat source in a fire effects model. Future research can expand on previous work segmenting foliage from woody material in LIDAR point clouds (Seielstad *et al.* 2011) in order to improve our methodology by characterizing reference voxels by vegetative return type.

Both fine and coarse fuel cell grids were capable of accurately characterizing observed mass loss in a simulation environment. Based on these results, we conclude that if the primary goal of a simulation is to reproduce the burning behavior of a 3D fuel model, then a coarse fuel cell grid can successfully balance tradeoffs between

computational complexity and representative heterogeneity. While high resolution LIDAR data can improve the representative heterogeneity of 3D fuel models, we find that high resolution fuel descriptions do not improve model results.

Additionally, the importance of dry foliage mass and fuel moisture content suggest that fire modelers should have a high level of confidence in their fuel attributes in order to have confidence in model results. Non-destructive biomass estimates of vegetation are an active area of research. Our study suggests that obtaining accurate biomass estimates is crucial for achieving model accuracy. More work is needed to examine the relationship between biomass measurements from traditional field techniques or derived from LIDAR data, and fuel inputs to couple fire-atmospheric models.

One major shortcoming of our study is that we were unable to evaluate the relationship between numerically identified fuel attributes from RMSE minima and actual fuel attributes measured from vegetation samples. While the majority of parameter spaces resulted in physically plausible fuel attributes, regions of RMSE minima also contained physically implausible minima. For example, our numerical experiments consistently identified regions of high dry foliage mass and low fuel moisture content as minima. This often contradicted known high water treatments applied to the sapling.

Future research can examine the role of branchwood in thermal degradation, velocity fields, and moisture content. The role of DAKOTA can expand to include additional parameters, simulation designs, and more advanced analysis techniques. Additional investigations into the effects of more detailed 3D fuel models on fire behavior models will help us better understand how to apply coupled fire-atmospheric fire models to real world problems like prescribed burn planning.

5. References

Atchley, A. L., Linn, R., Jonko, A., Hoffman, C., Hyman, J. D., Pimont, F., Sieg, C., & Middleton, R. S. (2021). Effects of fuel spatial distribution on wildland fire behavior. International Journal of Wildland Fire, 30(3), 179–189. https://doi.org/10.1071/WF20096

Arno, S. F., and J. K. Brown. (1991). Overcoming the paradox in managing wildland fire. Western Wildlands 17:40-46.

Hiers, J. Kevin, Joseph J. O'Brien, J. Morgan Varner, Bret W. Butler, Matthew Dickinson, James Furman, Michael Gallagher, et al. 2020. "Prescribed Fire Science: The Case for a Refined Research Agenda." Fire Ecology 16 (1). https://doi.org/10.1186/s42408-020-0070-8.

Hosoi, F., & Omasa, K. (2006). Voxel-based 3-D modeling of individual trees for estimating leaf area density using high-resolution portable scanning lidar. *IEEE Transactions on Geoscience and Remote Sensing*, *44*(12), 3610–3618. https://doi.org/10.1109/TGRS.2006.881743

Hudak, A., Prichard, S., Keane, R., Loudermilk, L., Parsons, R., Seielstad, C., Rowell, E., & Skowronski, N. (2017). *Hierarchical 3D fuel and consumption maps to support physics-based fire modeling* (Issue June). www.firescience.gov

Linn, R. R., Goodrick, S. L., Brambilla, S., Brown, M. J., Middleton, R. S., O'Brien, J. J., & Hiers, J. K. (2020). QUIC-fire: A fast-running simulation tool for prescribed fire planning. *Environmental Modelling and Software*, *125*, 104616. https://doi.org/10.1016/j.envsoft.2019.104616

Loudermilk, E. Louise, J. Kevin Hiers, Joseph J. O'Brien, Robert J. Mitchell, Abhinav Singhania, Juan C. Fernandez, Wendell P. Cropper, and K. Clint Slatton. 2009. "Ground-Based LIDAR: A Novel Approach to Quantify Fine-Scale Fuelbed Characteristics." International Journal of Wildland Fire 18 (6): 676–85. https://doi.org/10.1071/WF07138.

Mell, W., Jenkins, M. A., Gould, J., & Cheney, P. (2007). A physics-based approach to modelling grassland fires. *International Journal of Wildland Fire*, *16*(1), 1–22. https://doi.org/10.1071/WF06002

Mell, W., Maranghides, A., McDermott, R., & Manzello, S. L. (2009). Numerical simulation and experiments of burning douglas fir trees. *Combustion and Flame*, *156*(10), 2023–2041. https://doi.org/10.1016/j.combustflame.2009.06.015

National Interagency Fire Center (U.S.). (2019). *Wildland fire statistics*. Boise, Idaho : National Interagency Fire Center

Parsons, R. A., Mell, W. E., & McCauley, P. (2011). Linking 3D spatial models of fuels and fire: Effects of spatial heterogeneity on fire behavior. *Ecological Modelling*, *222*(3), 679–691. https://doi.org/10.1016/j.ecolmodel.2010.10.023

Parsons, R., Linn, R., Pimont, F., Hoffman, C., Sauer, J., Winterkamp, J., Sieg, C., & Jolly, W. (2017). Numerical Investigation of Aggregated Fuel Spatial Pattern Impacts on Fire Behavior. *Land*, *6*(2), 43. https://doi.org/10.3390/land6020043

Parsons, R.A. *et al.* (2018) 'Modeling thinning effects on fire behavior with STANDFIRE', *Annals of Forest Science*, 75(1). doi:10.1007/s13595-017-0686-2.

Pimont, Fraņois, Jean Luc Dupuy, Rodman R. Linn, and Sylvain Dupont. 2009. "Validation of FIRETEC Wind-Flows over a Canopy and a Fuel-Break." International Journal of Wildland Fire 18 (7): 775–90. https://doi.org/10.1071/WF07130.

Radeloff, V.C. *et al.* (2018) 'Rapid growth of the US wildland-urban interface raises wildfire risk', *Proceedings of the National Academy of Sciences of the United States of America*, 115(13), pp. 3314–3319. doi:10.1073/pnas.1718850115.

Rowell, Eric, E. Louise Loudermilk, Carl Seielstad, and Joseph J. O'Brien. 2016. "Using Simulated 3D Surface Fuelbeds and Terrestrial Laser Scan Data to Develop Inputs to Fire Behavior Models." Canadian Journal of Remote Sensing 42 (5): 443–59. https://doi.org/10.1080/07038992.2016.1220827.

Seielstad, Carl, Crystal Stonesifer, Eric Rowell, and Lloyd Queen. 2011. "Deriving Fuel Mass by Size Class in Douglas-Fir (Pseudotsuga Menziesii) Using Terrestrial Laser Scanning." Remote Sensing 3 (8): 1691–1709. https://doi.org/10.3390/rs3081691.

Simple firefighting demand modelling and its use for estimation of the potential influence of fuel treatment scenarios on the number of required firetrucks on the island of Kythira, Greece

Gavriil Xanthopoulos[1]*; Miltiadis Athanasiou[1]; Vassiliki Varela[2], Konstantinos Kaoukis[1], Panagiotis Xanthopoulos[1]

*[1]*Hellenic Agricultural Organization "Demeter", Institute of Mediterranean Forest Ecosystems. Terma Alkmanos, 11528, Athens, Greece, {gxnrtc@fria.gr, info@m-athanasiou.gr, kako@fria.gr, panosxant@hotmail.com}*
[2] Center for Security Studies (KEMEA). 4, P. Kanellopoulou str., 101 77, Athens, Greece, {v.varela@kemea-research.gr}

**Corresponding author*

Keywords

forest fire, fire suppression, firefighting demand, fuel management

Abstract

The island of Kythira, in Greece, suffered a devastating forest fire that started on August 4, 2017. After that, it became evident that the location of the island, away from aerial fire suppression resources bases and with limited capacity for quick arrival of significant ground firefighting reinforcements, necessitates careful fire prevention and presuppression planning to avoid repetition of the disaster. The study presented here aimed to examine the adequacy of the available 13 firetrucks on the island to successfully carry out initial attack under similar conditions to those of 2017, and to evaluate what could be the effect of four alternative fuel treatment scenarios on reducing the potential of a future disaster. A map of the forest fuels on the island, a weather scenario similar to the conditions at the start of the 2017 fire, and the Digital Elevation Model (DEM) of the island were used with a fire spread simulator (G-FMIS) first to simulate the actual fire and to examine if it matches the observed fire spread in 2017. Once good agreement was verified, four fuel treatment scenarios were applied on the fuels. The accordingly adjusted fuel map was used for further simulations. The resulting fire perimeter growth, taking flame length into consideration, was examined against the capacity of ground forces (firetrucks) to control lengths of the perimeter using a simple but effective fire suppression model, that is based on an equation developed earlier for assessment of the effectiveness of such forces in Greece. The results showed that under broadcast grazing on the island the risk of escaped fires can be minimized, reducing the need for heavy aerial support in case of a fire.

1. Introduction

In Greece, the island of Kythira, which lies south of Peloponnese, suffered a devastating forest fire that started on August 4, 2017, and spread actively for three days. It finally burned 2,471 ha (8.91% of the island) creating significant problems to the environment and the economy of Kythira including its important tourism sector. In the frame of a post-fire effort to reduce the chance of repetition of such a disaster (Xanthopoulos et al. 2022) it was needed to estimate the requirement of firefighting resources for suppression of potential fires and compare it with those currently available on the island. The island's location, away from the bases of aerial resources, and with a long time requirement (4-6 hours) before significant ground reinforcements can arrive by boat, means that the initial attack must be handled by the locally stationed 13 firetrucks with their crews. An analysis of the firefighting requirement was identified as important for highlighting the need for effective fire prevention to the local authorities and population, both in regard to mitigation of fire starts and to fuel treatment for biomass reduction. Furthermore, it can demonstrate the importance of quick and strong mobilization of resources in case of a fire start under weather conditions that could lead to a failure of initial attack and repetition of the 2017 disaster. The effort for estimation of the firefighting requirement, using fire spread simulation both with the actual fuels and those under different fuel management scenarios, is described here. The study uses the area of the August 4, 2017 burn as an example, because it spans the most typical fuel types on the island.

2. Methodology

In the frame of the post-fire fire prevention effort on Kythira, a forest fuels map was developed for the island (Xanthopoulos et al. 2022). The fire behavior and the growth of the August 2017 fire was documented in detail and it was possible to reconstruct fire evolution with good accuracy. Next, the G-FMIS fire spread simulator, was used for simulating fire spread (Xanthopoulos et al. 2022). Inputs included a weather scenario similar to the conditions at the start of the 2017 fire, the forest fuels map and the DEM of Kythira. The outcome was a realistic simulation, matching well the true evolution of the fire (Xanthopoulos et al. 2022). Once good agreement was verified, G-FMIS was used to examine the effect on fire spread, that four potential fuel treatments could have if they had been applied, prior to the fire event, to the area that burned. The four scenarios were:

- Scenario 1: Mechanical treatment (tractor) only in agricultural areas
- Scenario 2: Mechanical treatment (hand tools) only in agricultural areas
- Scenario 3: Grazing everywhere (in all types of vegetation)
- Scenario 4: Intense grazing everywhere (in all types of vegetation)

Modified post-treatment fuel models were estimated for the four scenarios, based on scientific literature review, the forest fuel map was adapted accordingly, and new fire spread simulations, using the same weather conditions as those at the time of the 2017 fire, tested the effect of the fuel treatment on fire perimeter growth and flame length under the four scenarios. Fire spread was simulated for six hours in time steps of 1 hour. The fire perimeter of the simulated fires under the four scenarios, for each time step, were traced manually and the perimeter length for each of five classes of flame length (m) was calculated. The classes were a) 0-1.5 m, b) 1.5-2.5 m, c) 2.5-3.5 m d) 3.5-10 m e) >10 m.

The effect of the fuel treatments on the firefighting demand (firetrucks) was assessed using a published formula for calculating the length of the flank of a fire that can be extinguished by a firetruck having a water carrying capacity of 2500 l, as a function of flame length (Simos and Xanthopoulos 2014). The formula is as follows:

$$EXT2500L\_Flank = 20.756 + 57.493 / FLflank$$

Where the extinction length EXT2500L_Flank and the flank flame length FLflank are expressed in meters. Table 1 is based on the equation above.

Table 1- Length of the fire perimeter of a fire (EXT2500L_Flank) that can be extinguished by a 2500 l firetruck, as a function of flame length

Flame length class	**FL value used in simulation**	**Extinction of perimeter (m) per 2500l firetruck load**
1: up to 1.5 m	1.2	68.7
2: up to 2.5 m	2.2	46.9
3. up to 3.5 m	3.5	37.2
4. up to 10 m	10.0	26.5
5. more than 10m	20.0	23.6

In order to develop a more realistic firefighting requirement estimation, the reduction in the effectiveness of the firetrucks due to the need for refilling with water needs to be taken into consideration, as well as the average time for emptying the load of a firetruck to the fire (Joerscke 1999). Assuming a typical average distance of 4 km to water sources at Kythera, a fire truck travel speed of 50 km h^{-1} on the winding and narrow road network of the island, and a time of 15 minutes for using-up one water load on the fireline, the truckloads that can be achieved by a firetruck per hour were calculated as shown in Table 2.

Table 2- Estimated fight and reload rounds per hour (LOADS_PER_HOUR) that can be achieved by a firetruck with a 2500 l water carrying capacity on Kythira island.

Average distance (km)	ADIST	4.00
Firetruck speed (km/h)	SPEED	50.00
Water loading time with delays	WLT	5.00
Travel time (min)	TRAVEL=WLT+((2*ADIST/SPEED)*60)	14.60
Time for using-up one water load (min)	WUT	15.00
Total time needed per truckload for each round (min)	TT=TRAVEL+WUT	29.60
Fight & reload rounds per hour	LOADS_PER_HOUR=60/TT	2.03

The required firetruck loads for extinguishing a length of the perimeter of each flame length class at each time step, was estimated by dividing the length of the perimeter by the corresponding EXT2500L_Flank for that flame length. The number of hours for each time step (1 to 6 hours), divided by the LOADS_PER_HOUR, provided an estimate of the truckloads that can be delivered by a firetruck in this step's hours. Thus, the required number of firetrucks to deliver the needed truckloads at each time step was calculated by dividing the required firetruck loads for extinguishing the perimeter until then, with the truckloads that can be delivered by a firetruck.

3. Results

Figure 1 shows the simulated growth of the August 4, 2017 fire, in hourly steps, indicating through different colours the flame length along the perimeter. The flame length classes correspond to the broadly accepted limits for firefighting (Tedim et al. 2018). It is noted that at no point across the perimeter, a flame length over 10 m is predicted. Figure 2 illustrates the effect that the four fuel treatment scenarios would have on the burned area and flame length along the perimeter

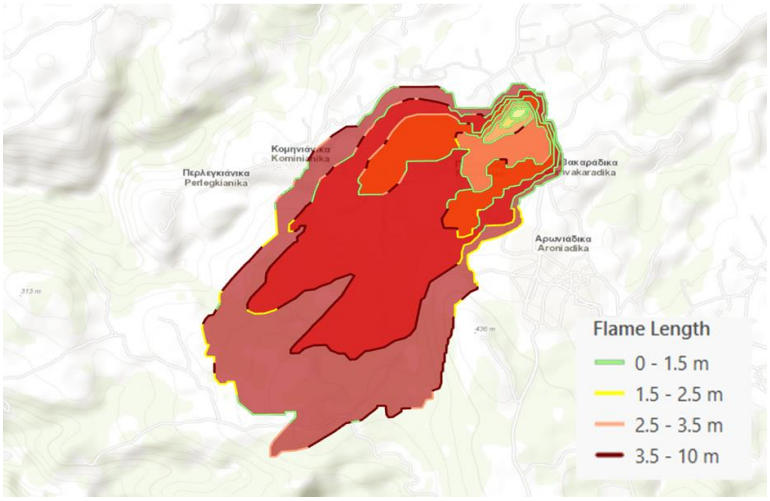

Figure 1- Simulation of the August 4, 2017 fire on Kythira based on the existing fuels at the time, showing the flame length classes along the perimeter at each (hourly) simulation step.

Figure 3 presents the growth of the perimeter with time along the 6-hour simulation, including the simulation with the "real" fuel situation (i.e. the fuels that actually burned in the 2017 fire) and the simulations with the four fuel treatment scenarios. The significant effect of grazing (treatments 3 and 4) is obvious. On the other hand, treatments 1 and 2 seemingly have little effect. This is explained by the relatively small percentage (7.19%) that agricultural areas that receive these treatments, occupy within the specific burned area.

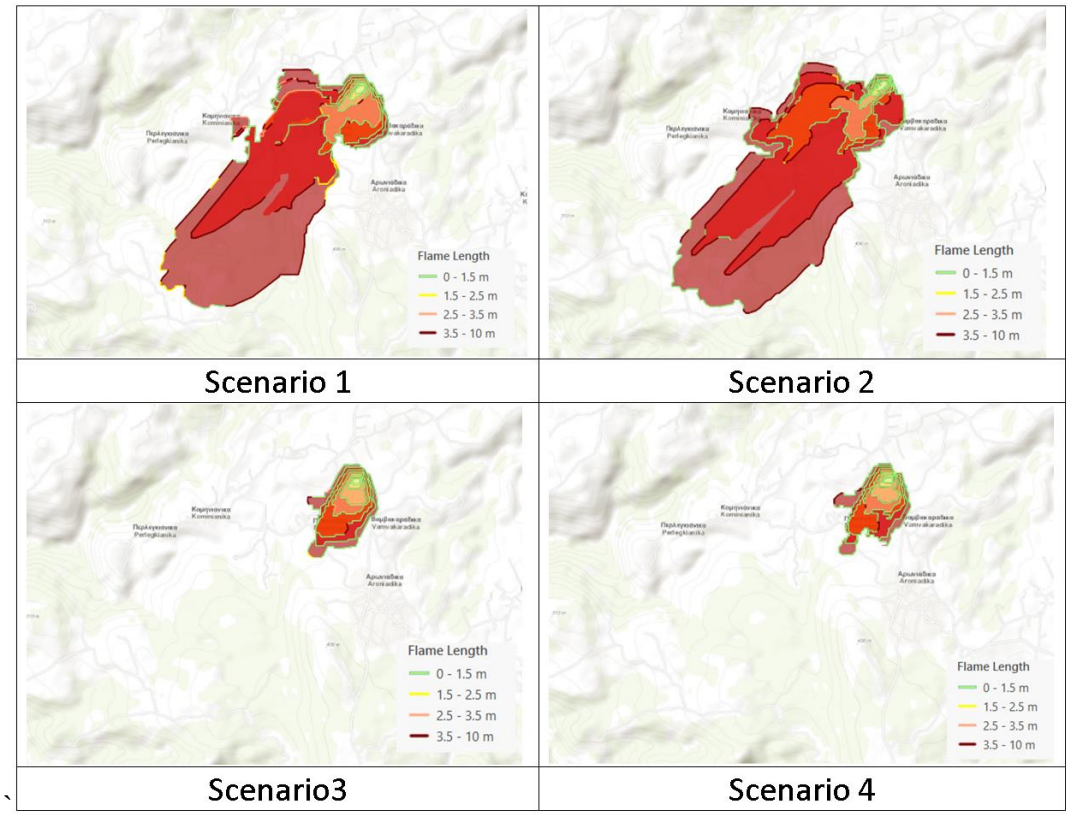

Figure 2- Influence of the four fuel treatment scenarios on burned area and flame length along the perimeter (simulation of 6 hours)

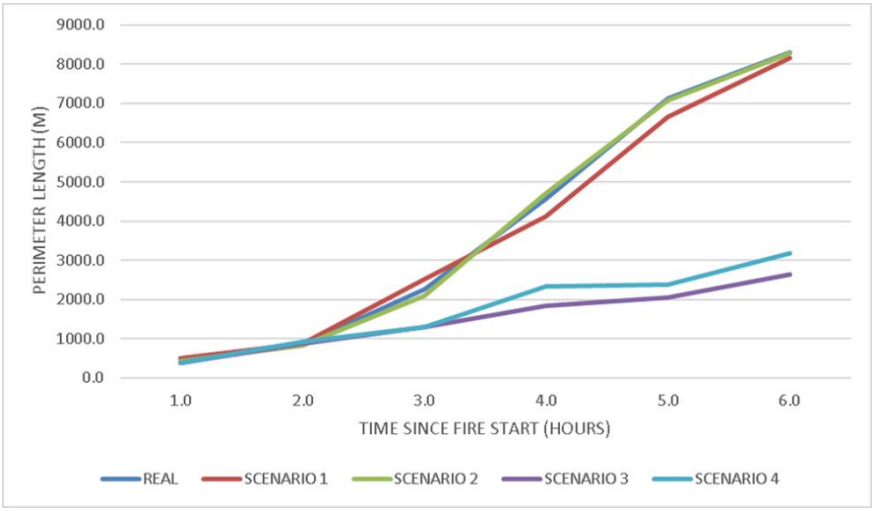

Figure 3- Fire perimeter length growth with time for the simulations with the real fuels and under four fuel treatment scenarios

The treatments also have an effect on flame length along the perimeter, which influences the firefighting requirements, as shown in table 4 which presents the required of firetruck loads (T) with time. As an example, the perimeter length after 3 hours of simulation with the real fuels, indicated as PL_3 in table 4, is 2271.4 m. It consists of 1924.5 m of FL class 1 (i.e. 1.2 m), 85.5 of FL class 2 (2.2 m), 121.2 m of FL class 3 (3.5 m) and 140.2 of FL class 4 (10.0 m). Taking table 1 into consideration, the 1924.5 m of FL class 1 require 1924.5/68.7= 28.0 truckloads. The other parts of the perimeter require 1.8, 3.3, and 5.3 truckloads respectively for a total requirement of 38.4 truckloads in 3 hours.

Table 4- Estimated requirement of 2500 l firetruck loads (T) for extinguishing the fire Perimeter at each time step (i=1-6), taking the Flame Length of all the parts of the perimeter (in classes) into consideration (PL_i)(m)

Fuels	PL_1	T	PL_2	T	PL_3	T	PL_4	T	PL_5	T	PL_6	T
Kythira fire fuels	505.8	7.4	864.3	14.2	2271.4	38.4	4572.6	88.2	7117.3	204.0	8302.3	202.4
Scenario 1	504.3	7.3	867.4	14.1	2516.8	40.8	4118.6	76.7	6654.9	162.3	8153.4	175.9
Scenario 2	438.1	6.4	841.2	12.3	2093.8	36.2	4703.6	102.8	7084.1	183.5	8275.3	189.6
Scenario 3	394.0	5.7	875.9	12.8	1292.2	19.3	1839.0	29.0	2060.6	30.0	2629.0	41.4
Scenario 4	388.6	5.7	917.7	13.4	1292.7	19.7	2328.8	36.2	2379.6	34.7	3190.1	51.2

Continuing on the previous example, using LOADS_PER_HOUR = 2.03 from table 2, it is calculated that a firetruck can transport and use 3 x 2.03= 6.1 truckloads in 3 hours. The number of firetrucks that can achieve the required 38.4 truckloads, are 38.4/6.1 = 6.3 firetrucks. Figures 4 and 5, present the estimated evolution of required truckloads as the fire spreads, and ultimately the number of the required firetrucks for the 6 hours of the simulation.

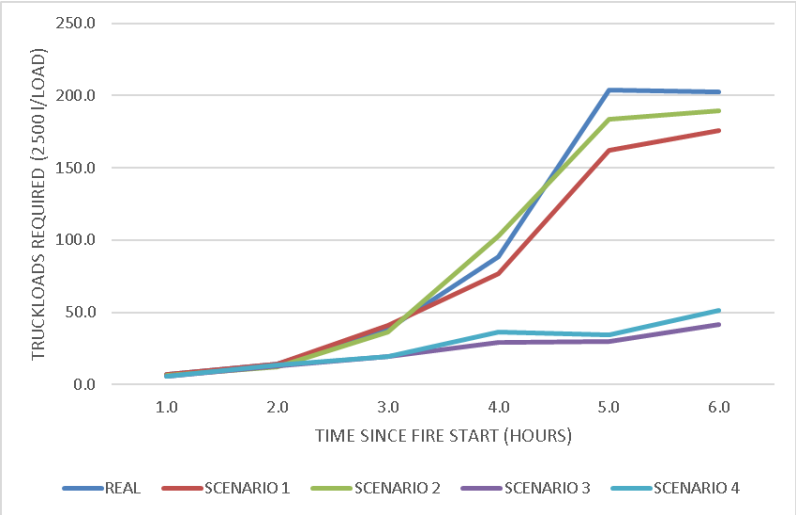

Figure 4- Number of required truckloads of 2500 l for extinguishing the fire perimeter with time, for the five simulations

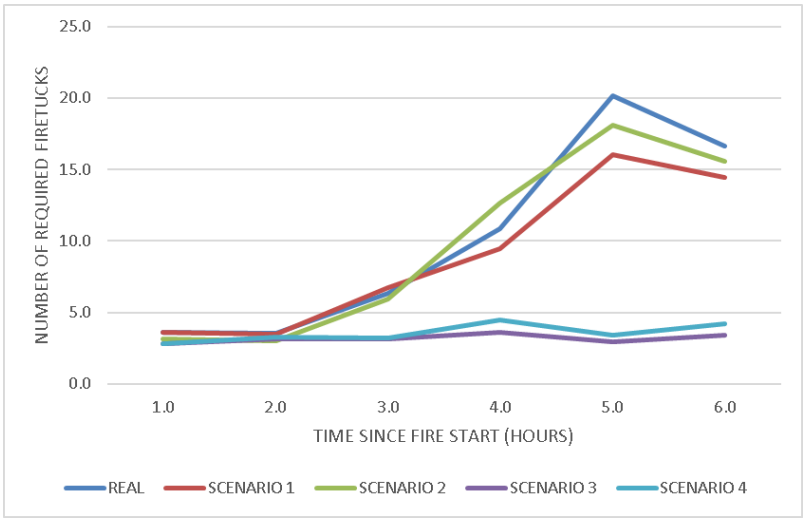

Figure 5- Evolution of the required number of firetrucks for controlling the perimeter of the fire as a function of time, for the five simulations

4. Conclusions

In conclusion, the simple method developed here for estimating ground firefighting demand has produced some very interesting results. It demonstrated the need for increased prevention and better presuppression planning and the value of systematic broadcast grazing as a fuel treatment across the island. Under such fuel treatment the 13 available firetrucks could be able to control starting fires even under difficult conditions. Aerial resources, if dispatched, could have an auxiliary role. The concept presented here can be used for similar analyses elsewhere.

5. Acknowledgements

The study was supported by the project "PREVAIL PREVention Action Increases Large fire response preparedness" (826400 — PREVAIL — UCPM-2018-PP-AG), funded by the European Union Humanitarian Aid and Civil Protection (DG-ECHO).

6. References

Joerscke, J. D. (1999). Pumping Apparatus: Driver Operator's Handbook. International Fire Service Training Assn.

Simos, M., & Xanthopoulos, G. (2014). Assessment of the effectiveness of the forest fire fighting ground forces in Greece. In proceedings of the 7th International Conference on Forest Fire Research on "Advances in Forest Fire Research", November 17-20, 2014. Coimbra, Portugal. Viegas D. X., (editor). ADAI/CEIF, University of Coimbra, Portugal. pp. 665-672.

Tedim, F., Leone, V., Amraoui, M., Bouillon, C., Coughlan, M. R., Delogu, G. M., Fernandes, P., Ferreira, C., McCaffrey, S., McGee, T., Parente, J., Paton, D., Pereira, M., Ribeiro, L.M., Viegas, D. X., & Xanthopoulos, G. (2018). Defining extreme wildfire events: difficulties, challenges, and impacts. Fire, 1(1), 9.

Xanthopoulos, G., Athanasiou, M., Nikiforaki, A., Kaoukis, K., Mantakas, G., Xanthopoulos, P., Papoutsakis, C., Christopoulou, A., Sofronas, S., Gletsos, M., & Varela, V. (2022). Innovative Action for Forest Fire Prevention in Kythira Island, Greece, through Mobilization and Cooperation of the Population: Methodology and Challenges. Sustainability, 14(2), 594.

Simulating wildland surface fire behaviour to support emergency management

Debora Voltolina*[1, 2]; Giacomo Cappellini[2]; Tiziana Apuani[1]; Simone Sterlacchini[2]

[1]Institution. Department of Earth Sciences "Ardito Desio", University of Milan, Via Luigi Mangiagalli 34, 20133 Milan, Italy {debora.voltolina, tiziana.apuani}@unimi.it
[2] Institute of Environmental Geology and Geoengineering, National Research Council, Via Mario Bianco 9, 20131 Milan, Italy {debora.voltolina, giacomo.cappellini, simone.sterlacchini}@igag.cnr.it

**Corresponding author*

Keywords

Fire Behaviour; Remote Sensing; Rothermel's Model; Agent-Based Modelling; Decision Support Systems

Abstract

The recent upsurge in the incidence of extreme wildfire events, the expected impact of climate change on the frequency and severity of fires, and the progressive expansion of wildland-urban interface areas highlight the tangible need for improvement in our ability to predict, mitigate and manage the growing risk to which communities are exposed. The aim of this research is to contribute to deepen the knowledge on the spatial simulation of the complex dynamics of wildland surface fire behaviour through the development and application of a spatially distributed predictive model for the simulation of wildland surface fire spread intended for operational purposes. Given the position of one or more ignition points, the developed model allows to (i) obtain near real time dynamic estimates of the geo-environmental parameters that control the fire spread, (ii) compute the direction and intensity of the maximum rate of fire spread in heterogeneous environments, and (iii) simulate the surface fire spread using agent-based models. The final aim is to provide competent authorities with timely information on the expected evolution of the flame front to optimise decision-making processes. The model, developed under synthetic conditions, is then applied to case studies recorded in the territory of the Autonomous Region of Sardinia, that offers institutional information on the ignition location, the evolution of the flame front, and the completed fire suppression activities, which are implemented in the model as well. Overall, the model showed a promising predictive capacity evaluated in quantitative terms of morphological matching between the observed and predicted fire spread patterns, returning more accurate results in areas with less complex morphologies and dominated by herbaceous rather than shrubby fuels. The model also made it possible to obtain simulations with processing times compatible with its operational application as a tool for optimising and planning fire risk prevention and mitigation strategies and policies as well as fire management activities. Future research will be aimed at estimating the propagation of the parametric uncertainty through the model and applying the model to fire events occurred across different Mediterranean-type climate regions to consistently evaluate its predictive capacity.

1. Introduction

Wildland fires are a global and pervasive phenomenon whose incidence and intensity are expected to further increase in the next decades in response to the complex interactions between climatic and anthropogenic factors (Jolly et al. 2015; Flannigan et al. 2016; Williams and Abatzoglou 2016; Turco et al. 2018; Forkel et al. 2019; Dupuy et al. 2020; Jones et al. 2020). Mediterranean-type climate regions appear to be particularly prone to suffer for such an exacerbated fire activity (Turco et al. 2016; Bowman et al. 2017; Kelley et al. 2019; Salis et al. 2019; Mantero et al. 2020). Contextually, recent studies have highlighted that wildfire management policies in Mediterranean-type climate regions are predominantly focused on reactive fire suppression strategies, while struggling with proactive preparation and mitigation actions (Moreira et al. 2020; Ganteaume et al. 2021). Hence, the latest report by the European Commission's Directorate-General for Research and Innovation, which was aimed at providing evidence-based scientific support to the European policymaking process, warned about the emerging risk of a disproportionate increase in uncontrolled extreme wildfire events and the consequent urgent need for a reassessment of wildland fire management policies and strategies at the European level (Rego et al. 2018). An integrated wildfire risk management requires contribution from multiple disciplines, ranging

from susceptibility mapping to early active fire detection and fire spread simulation modelling. Accurate predictions of the spatiotemporal evolution of both predicted and ongoing events are of crucial importance for planning and optimising emergency response strategies, which are essential to control the fire spread before it could overwhelm suppression capabilities (Tedim et al. 2018).

The development of a comprehensive model for simulating the spread of surface fires includes (i) a method for converting a multi-dimensional set of geo-environmental data into a set of parameters describing the spread of wildland surface fires and (ii) a method for extending these one-dimensional measurements in space and time and simulate the evolution of the flame front. Sullivan (2009a, 2009b, 2009c) and then Papadopoulos and Pavlidou (2011) conducted exhaustive comparative reviews of the strategies adopted and developed to model the fire spread, (i.e., physical and quasi-physical or empirical and quasi-empirical models), and to simulate the fire growth, (i.e., raster and vector implementations). Modelling fire spread and growth is a complex task due to multiple factors including the spatiotemporal heterogeneity and variability of geo-environmental conditions as well as the uncertain effect of fire suppression interventions (Alexander and Cruz 2013). Especially in the last decades, the increasing computational resources and the growing availability of remotely sensed datasets have fuelled the development of a considerable number of wildland surface fire behaviour models (Szpakowski and Jensen 2019; Jain et al. 2020). However, the optimisation of near real-time simulation of fire spread and growth in operational environments remains an open issue.

The objective of this study is to support the optimisation of the decision-making processes of wildland surface fire risk management in the island of Sardinia, Italy, which is preliminary assumed as representative of Mediterranean-type climate regions. This project intends to pursue the main objective of developing and validating a spatially distributed predictive model for the simulation of wildland surface fire spread intended to be implemented as a geospatial decision support system aimed at providing strategies and tools for an integrated wildfire risk management.

2. Methods

2.1. Model development

When considering models that can be used as decision support tools for operational fire management, some constraints become evident: (i) short decision time frame; (ii) fine-scale spatiotemporal resolution; (iii) input data retrievability in operational environment; (iv) low complexity of laboratory and field experiments; (v) minimum computational requirements at the desired spatiotemporal resolution. The simulation model design and implementation are aimed at providing competent authorities with near real-time multi-temporal maps of the expected evolution of the surface fire spread and growth capable of accurately and dynamically capturing the spatiotemporal variability of the geo-environmental drivers of fire spread.

The quasi-empirical mathematical model defined by Rothermel (1972), one of the most extensively employed method for simulating fire behaviour in operational environments, has been adopted for the prediction of the maximum rate of fire spread. In fact, despite their site-specificity and their tight dependence on local geo-environmental conditions, the empirical and quasi-empirical models boast calculation promptness and usability compared to physical and quasi-physical models. To obtain more flexibility in handling the model equations (Rothermel 1972; Albini 1976; Andrews 2012, 2018), an independent algorithm capable of estimating the same parameters defined by the model has been implemented. The algorithm takes as input combinations of the drivers of fire spread, including geo-morphometrical parameters, horizontal wind speed and direction, fuel types, and their characterisation in terms of live and dead fuel moisture contents, and performs pixel-based evaluations of the magnitude and direction of the maximum rate of spread relative to upslope, the flame length, the intensity of the flame front, and the eccentricity of the ellipse which represents the analytical approximation of the spatial pattern produced by a wildland fire spreading under ideal homogeneous conditions. The algorithm has been then integrated into a spatial simulation model which adopts a hybrid raster-vector approach to simulate the spatiotemporal growth of the flame front. Indeed, while vector implementations for simulating fire growth generally offer greater accuracy, the advantages of raster implementations include simplicity, better portability to parallel computing environments, and higher computational efficiency. Therefore, an agent-based model has been implemented to simulate fire growth with discrete time intervals of 1-minute length and discrete spatial

units with a modular area. Spatial units are represented by hexagonal cells, each of which can host at most one and only one agent. An agent instantiated in a cell might represent both the actual ignition point of an active fire or a simulated ignition originating from the elliptical vector simulation propagated from one of the adjacent cells (Figure 1).

2.2. Model application to case studies

The model has been developed under synthetic conditions to verify its conceptual validity and then, applied to case studies referring to historical wildland fire events recorded in the fire database of the Autonomous Region of Sardinia to evaluate its accuracy and predictive capacity.

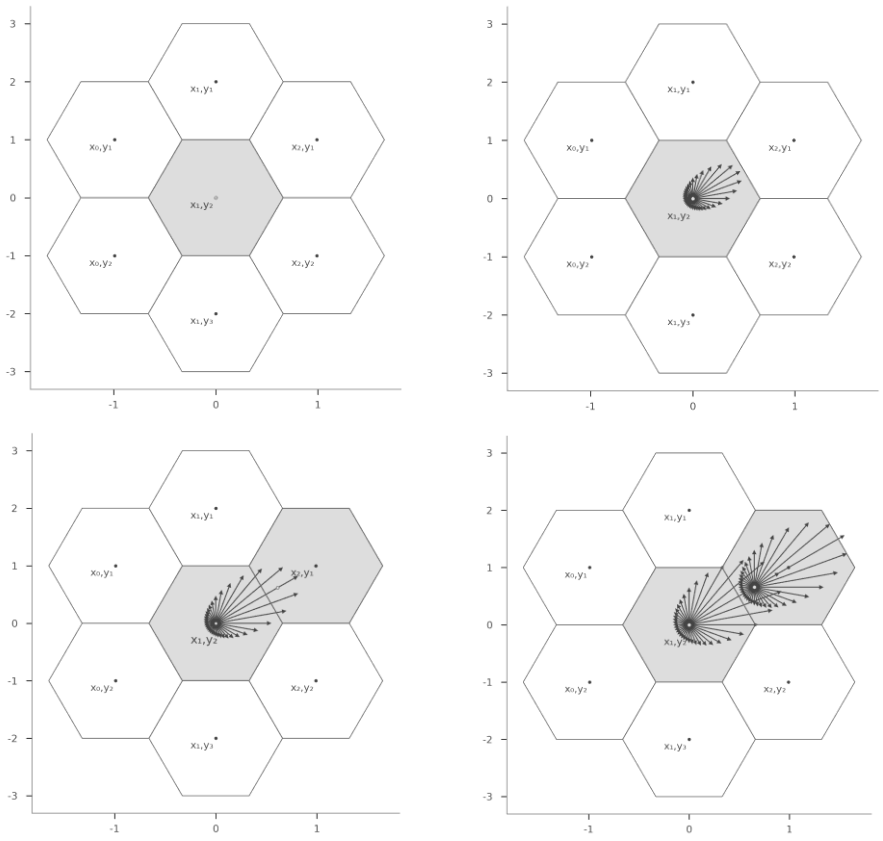

Figure 1- Agent-based model behaviour. A single ignition agent is instantiated in the centroid of the grey hexagonal cell at time t0 (a). After a time t1, an elliptic vector simulation has started from that agent spreading according to the rate and direction of fire spread calculated for that cell by the Rothermel's model (b). After a time t2, the elliptical vector simulation has generated a new agent in one of the white adjacent hexagonal cells (c). After a time t3 a new elliptical vector simulation has started from the new agent (d).

Obtaining dynamic estimates of the geo-environmental parameters that control the fire spread and growth, is essential for the model to compute the direction and intensity of the maximum rate of spread and to simulate the spatiotemporal patterns of fire growth. The near real-time simulation of the evolution of expected and ongoing fire events requires a continuous monitoring of the spatiotemporal variability of the geo-environmental drivers, including wind speed and direction and fuel moisture content. Remote sensing methodologies, making use of either airborne or spaceborne active and passive sensors, provide exceptional advantages over traditional methods for the estimation of geo-environmental parameters, especially in an operational context. Dynamic estimates of the drivers of fire spread have been derived from remotely sensed datasets and global reanalysis with suitable spatial and temporal resolutions. Information on the spatiotemporal variability of live and dead fuel moisture fractions have been derived by adopting empirical relationships already defined in literature for plant communities in Mediterranean-type climate regions (Chuvieco et al. 2004; García et al. 2008; Frey et al. 2012; Nolan et al. 2016), which relate vegetation indices (MODIS Terra NDVI; Vermote and Wolfe 2015) with

land surface temperature estimates (MODIS Terra LST; Wan et al. 2015). Horizontal wind speed and direction have been obtained from the ERA5-Land climatic reanalysis, produced by ECMWF, which provides measurements at 10 m above the ground with a spatial resolution of 9 km and a temporal resolution of 3 hours (Muñoz Sabater 2019). Both standard and custom fuel models for Sardinia (Duce et al. 2012) have been assigned to land cover units (Autonomous Region of Sardinia, 2008) according to the literature (Salis et al. 2013).

The availability of accurate institutional information regarding the evolution of the fire spread and growth as well as of successful fire suppression activities, such as control lines, have been also simulated. Finally, standard quantitative indices such as the Sørensen similarity coefficient or sensitivity and specificity measures, have been computed to estimate the model performance in terms of spatiotemporal agreement between the observed and simulated fire spread and growth patterns.

The procedure for estimating the drivers of fire spread has been automated by means of the Google Earth Engine platform (Gorelick et al. 2017) and the spatial model simulating fire spread and growth is entirely developed in Python (Kluyver et al. 2016).

3. Results and Discussion

The predictive patterns resulting from fire growth simulations exhibited a satisfying level of agreement with theoretical knowledge on fire behaviour modelling. It has been observed that wind speed and direction play a decisive role in determining the speed and direction of maximum spread of the flame front. Similarly, fuel continuity and its vertical structure have shown a significative impact on the predicted patterns of fire growth.

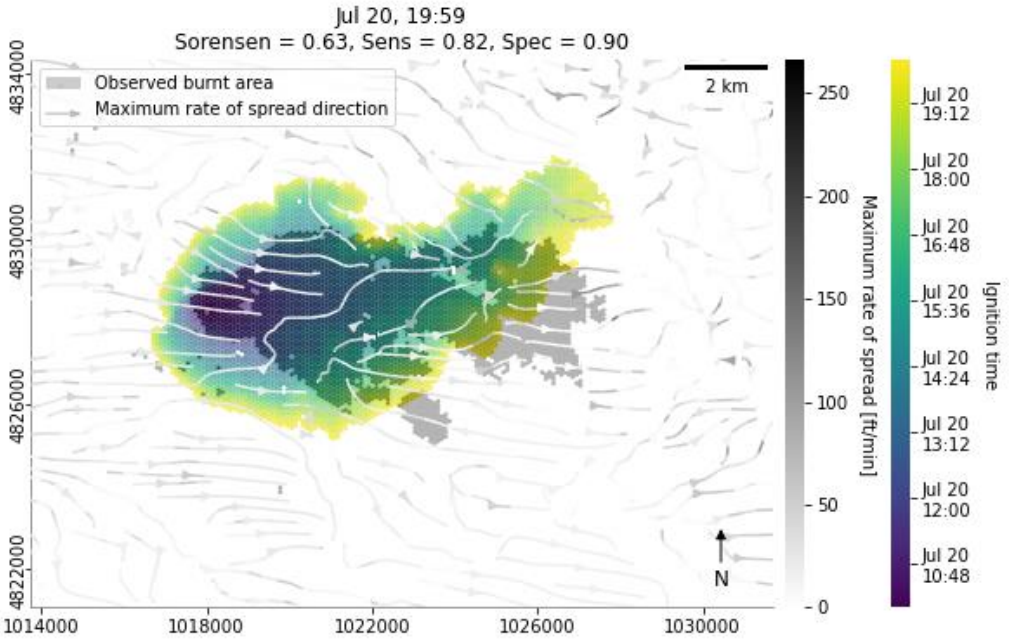

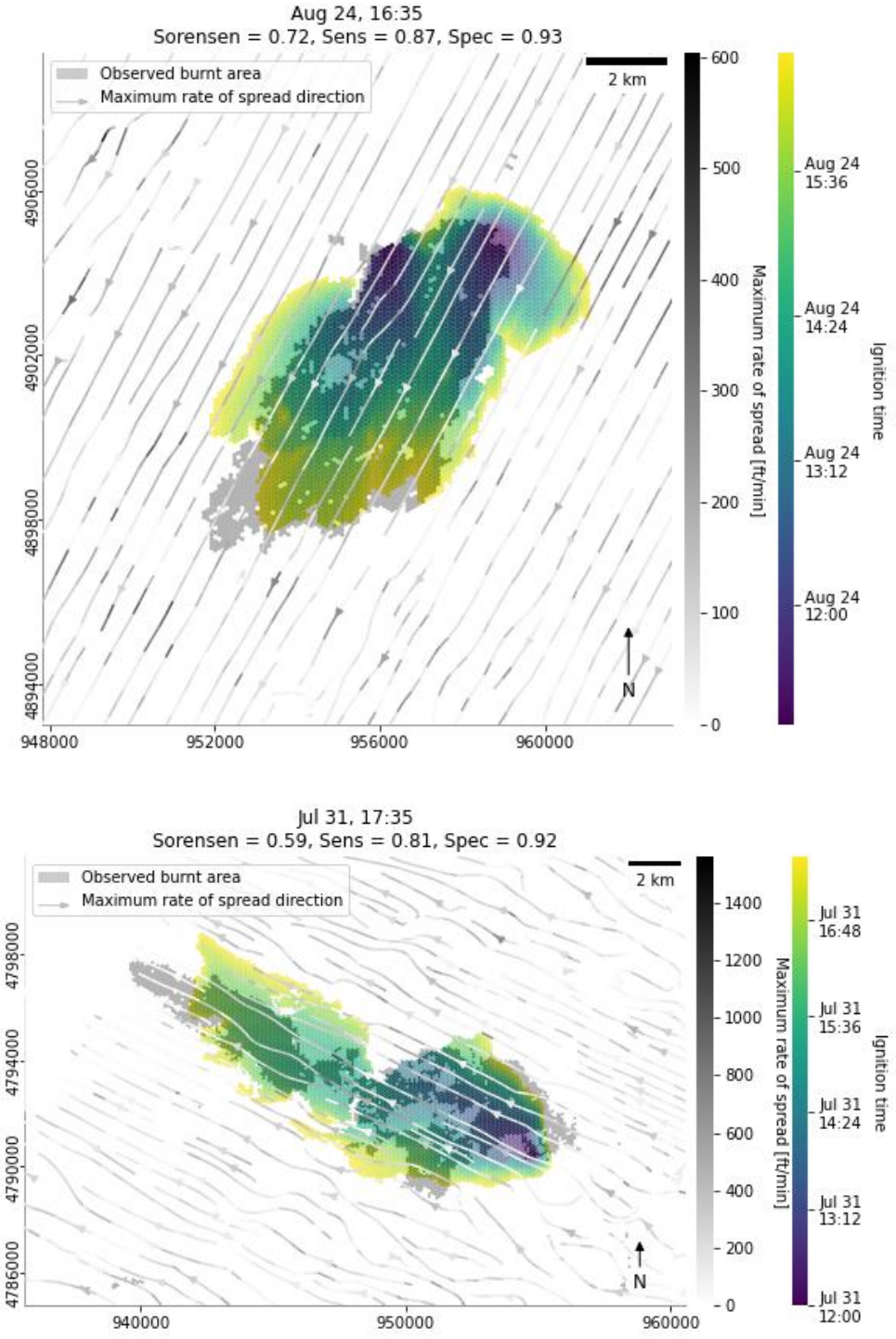

Figure 2- Predicted patterns of fire growth for the case studies of Isili (CA), July 20th, 2016 (a), Sagama (OR), August 24th, 2016 (b), and Gonnosfanadiga (VS), July 31st, 2017 (c). Grey shadows indicate the observed burnt area while the predicted patterns of fire growth are represented with a colormap referring to the hexagonal cell ignition time. Sensitivity and specificity measures and the Sørensen similarity coefficient are reported. Grey arrows indicate the magnitude and direction of the maximum rate of spread according to the Rothermel's model.

Although not fully representative of the complexity and diversity of the geo-environmental conditions in the study area, the selection of case studies for the model application strived to capture heterogeneous geo-environmental conditions. Predicted patterns of fire growth exhibited probability of omission or commission errors lower than 20% (Figure 2), even without the simulation of active fire suppression interventions, which

played a significant role in reducing commission errors. A greater model predictive capacity has been observed in the absence of complex morphologies (Figure 2b), reflecting intrinsic limitations of the Rothermel's model and the complexity of properly simulating wind fields, found to be critical for the estimation of both the magnitude and direction of maximum surface fire spread. A higher predictive capacity also emerged in the presence of herbaceous fuels (Figure 2a-b) compared to fuels characterized by sclerophyllous shrubs typical of the Mediterranean maquis and garrigue (Figure 2c), hence, highlighting the need to obtain more accurate estimates of the horizontal and vertical fuel continuity. Omission errors might be attributable to (i) uncertainties connected with the estimation of geo-environmental parameters and their propagation within the model, but also to (ii) ground fire spread phenomena or secondary outbreaks triggered by embers carried by the wind.

Comprehensively, the model developed for the simulation of the propagation of surface forest fires showed a satisfactory predictive capacity in terms of morphological correspondence between the observed and simulated perimeter. Results of the model application to case studies recorded by the Autonomous Region of Sardinia suggest the model suitability for operational use as a tool for the near real-time forecast of the magnitude and direction of the maximum rate of surface fire spread.

Future studies will aim to: (i) calibrate and validate the methodology for the estimation of the geo-environmental parameters; (ii) propagate the parametric uncertainty through the model; (iii) simulate the occurrence of secondary outbreaks due to reignitions or spotting events; (iv) implement a wider range of fire suppression activities and techniques; (v) apply the model to fire event occurred across different locations in Mediterranean-type climate regions to consistently evaluate its predictive capacity.

4. References

Albini FA (1976) Estimating Wildfire Behaviour and Effects.

Alexander ME, Cruz MG. (2013) Limitations on the accuracy of model predictions of wildland fire behaviour: A state-of-the-knowledge overview. The Forestry Chronicle, 89(3), 370–381.

Andrews PL (2012) Modeling Wind Adjustment Factor and Midflame Wind Speed for Rothermel's Surface Fire Spread Model.

Andrews PL (2018) The Rothermel Surface Fire Spread Model and Associated Developments: A Comprehensive Explanation.

Autonomous Region of Sardinia. (2008). Carta dell'Uso del Suolo in scala 1:25.000. http://webgis2.regione.sardegna.it/catalogodati/

Autonomous Region of Sardinia. (2010) Modello Digitale del Terreno (DTM) SAR, passo 10 m. https://www.sardegnageoportale.it/areetematiche/modellidigitalidielevazione/

Bowman DMJS, Williamson GJ, Abatzoglou JT, Kolden CA, Cochrane MA, Smith AMS (2017) Human exposure and sensitivity to globally extreme wildfire events. Nature ecology & evolution 1, 1–6. doi:10.1038/s41559-016-0058

Chuvieco E, Cocero D, Riaño D, Martin P, Martínez-Vega J, de la Riva J, Pérez F (2004) Combining NDVI and surface temperature for the estimation of live fuel moisture content in forest fire danger rating. Remote Sensing of Environment 92, 322–331. doi:10.1016/j.rse.2004.01.019

Duce, P., Pellizzaro, G., Arca, B., Ventura, A., Bacciu, V. M., Salis, M., … Perez, Y. (2012). Fuel types and potential fire behaviour in Sardinia and Corsica islands: a pilot study. In Modelling fire behaviour and risk (pp. 2–8). Retrieved from http://www.cmcc.it/wp-content/uploads/2013/04/P_Book_Modelling-Fire-Behaviour-and-Risk.pdf

Dupuy J-L, Fargeon H, Martin-StPaul N, Pimont F, Ruffault J, Guijarro M, Hernando C, Madrigal J, Fernandes P (2020) Climate change impact on future wildfire danger and activity in southern Europe: a review. Annals of Forest Science 77. doi:10.1007/s13595-020-00933-5

Flannigan MD, Wotton BM, Marshall GA, de Groot WJ, Johnston J, Jurko N, Cantin AS (2016) Fuel moisture sensitivity to temperature and precipitation : climate change implications. Climatic Change 134, 59–71. doi:10.1007/s10584-015-1521-0

Forkel M, Dorigo W, Lasslop G, Chuvieco E, Hantson S, Heil A, Teubner I, Thonicke K, Harrison SP (2019) Recent global and regional trends in burned area and their compensating environmental controls. Environmental Research Communications 051005

Frey CM, Kuenzer C, Dech S (2012) Quantitative comparison of the operational NOAA-AVHRR LST product of DLR and the MODIS LST product V005. International Journal of Remote Sensing 33, 7165–7183. doi:10.1080/01431161.2012.699693

Ganteaume A, Barbero R, Jappiot M, Maillé E (2021) Understanding future changes to fires in southern Europe and their impacts on the wildland-urban interface. Journal of Safety Science and Resilience, 2(1), 20–29. doi.org/10.1016/j.jnlssr.2021.01.001

García M, Chuvieco E, Nieto H, Aguado I (2008) Combining AVHRR and meteorological data for estimating live fuel moisture content. Remote Sensing of Environment 112, 3618–3627. doi:10.1016/j.rse.2008.05.002

Gorelick N, Hancher M, Dixon M, Ilyushchenko S, Thau D, Moore R (2017) Google Earth Engine: Planetary-scale geospatial analysis for everyone. Remote Sensing of Environment, 202, 18–27. doi.org/10.1016/j.rse.2017.06.031

Jain P, Coogan SCP, Subramanian SG, Crowley M, Taylor S, Flannigan MD (2020) A review of machine learning applications in wildfire science and management. Environmental Reviews, 28(4), 478–505. doi.org/10.1139/er-2020-0019

Jolly WM, Cochrane MA, Freeborn PH, Holden ZA, Brown TJ, Williamson GJ, Bowman DMJS (2015) Climate-induced variations in global wildfire danger from 1979 to 2013. Nature Communications 6, 1–11. doi:10.1038/ncomms8537

Jones MW, Smith AJP, Betts RA, Canadell JG, Prentice IC, Le Quéré C (2020) Climate Change Increases the Risk of Wildfires. ScienceBrief Review.

Kelley DI, Bistinas I, Whitley R, Burton C, Marthews TR, Dong N (2019) How contemporary bioclimatic and human controls change global fire regimes. Nature Climate Change 9, 690–696. doi:10.1038/s41558-019-0540-7

Kluyver T, Ragan-Kelley B, Pérez F, Granger BE, Bussonnier M, Frederic J, Kelley K, Hamrick J, Grout J, Corlay S, Ivanov P, Avila D, Abdalla S, Willing C (2016) Jupyter Notebooks – a publishing format for reproducible computational workflows. Positioning and Power in Academic Publishing: Players, Agents and Agendas – Proceedings of the 20th International Conference on Electronic Publishing, ELPUB 2016, 87–90. doi.org/10.3233/978-1-61499-649-1-87

Mantero G, Morresi D, Marzano R, Motta R, Mladenoff DJ, Garbarino M (2020) The influence of land abandonment on forest disturbance regimes: a global review. Landscape Ecology 35, 2723–2744. doi:10.1007/s10980-020-01147-w

Moreira F, Ascoli D, Safford H, Adams MA, Moreno Rodriguez JM, Pereira JMC, Catry FX, Armesto J, Bond W, González ME, Curt T, Koutsias N, McCaw L, Price O, Pausas JG, Rigolot E, Stephens S, Tavsanoglu C, Vallejo Calzada VR, Van Wilgen BW, Xanthopoulos G, Fernandes PM (2020) Wildfire management in Mediterranean-type regions: Paradigm change needed. Environmental Research Letters 15. doi:10.1088/1748-9326/ab541e

Muñoz Sabater J (2019) ERA5-Land hourly data from 1981 to present [data set]. Copernicus Clim. Chang. Serv. Clim. Data Store. doi:10.24381/cds.e2161bac

Nolan RH, Resco de Dios V, Boer MM, Caccamo G, Goulden ML, Bradstock RA (2016) Predicting dead fine fuel moisture at regional scales using vapour pressure deficit from MODIS and gridded weather data. Remote Sensing of Environment 174, 100–108. doi:10.1016/j.rse.2015.12.010

Papadopoulos GD, Pavlidou F (2011) A Comparative Review on Wildfire Simulators. IEEE Systems Journal, 5(2), 233–243.

Rego FMCC, Moreno Rodriguez JM, Vallejo Calzada VR, Xanthopoulos G (2018) Forest Fires - Sparking firesmart policies in the EU. Directorate - General for Research and Innovation - Climate Action and Resource Efficiency, doi:10.2777/248004

Rothermel RC (1972) A Mathematical Model for Predicting Fire Spread in Wildland Fuels. US Department of Agriculture, Forest Service, Intermountain Forest and Range Experiment Station Research paper INT-115.

Salis, M., Ager, A. A., Arca, B., Finney, M. A., Bacciu, V. M., Duce, P., Spano, D. (2013). Assessing exposure to human and ecological values in Sardinia, Italy. International Journal of Wildland Fire, 22, 549–565. https://doi.org/10.1071/WF11060

Salis M, Arca B, Alcasena FJ, Massaiu A, Bacciu VM, Bosseur F, Caramelle P, Dettori S, Fernandes de Oliveira AS, Molina-Terren D, Pellizzaro G, Santoni P-A, Spano D, Vega-Garcia C, Duce P (2019) Analyzing the recent dynamics of wildland fires in Quercus suber L. woodlands in Sardinia (Italy), Corsica (France) and Catalonia (Spain). European Journal of Forest Research 138, 415–431. doi:10.1007/s10342-019-01179-1

Sullivan AL (2009a) Wildland surface fire spread modelling, 1990-2007. 1: Physical and quasiphysical models. International Journal of Wildland Fire, 18(4), 349–368. doi.org/10.1071/WF06143

Sullivan AL (2009b) Wildland surface fire spread modelling, 1990-2007. 2: Empirical and quasi-empirical models. International Journal of Wildland Fire, 18(4), 369–386.

Sullivan AL (2009c) Wildland surface fire spread modelling, 1990-2007. 3: Simulation and mathematical analogue models. International Journal of Wildland Fire, 18(4), 387–403.

Szpakowski DM, Jensen JLR (2019) A review of the applications of remote sensing in fire ecology. Remote Sensing, 11, 2638–2669. doi.org/10.3390/rs11222638

Tedim F, Leone V, Amraoui M, Bouillon C, Coughlan MR, Delogu GM, Fernandes PM, Ferreira C, McCaffrey S, McGee TK, Parente J, Paton D, Pereira MG, Ribeiro LM, Viegas DX, Xanthopoulos G (2018) Defining Extreme Wildfire Events: Difficulties, Challenges, and Impacts. Fire 1, 1–28. doi:10.3390/fire1010009

Turco M, Bedia J, Di Liberto F, Fiorucci P, Von Hardenberg J, Koutsias N, Llasat MC, Xystrakis F, Provenzale A (2016) Decreasing fires in mediterranean Europe. PLoS ONE 11. doi:10.1371/journal.pone.0150663

Turco M, Rosa-Cánovas JJ, Bedia J, Jerez S, Montávez JP, Llasat MC, Provenzale A (2018) Exacerbated fires in Mediterranean Europe due to anthropogenic warming projected with non-stationary climate-fire models. Nature Communications 9, 1–9. doi:10.1038/s41467-018-06358-z

Vermote E, Wolfe RE (2015) MOD09GA MODIS/Terra Surface Reflectance Daily L2G Global 1kmand 500m SIN Grid V006 [data set]. NASA EOSDIS Land Processes Distributed Active Archive Center (LP DAAC). doi.org/10.5067/MODIS/MOD09GA.006

Wan Z, Hook S, Hulley G (2015) MOD11A1 MODIS/Terra Land Surface Temperature/Emissivity Daily L3 Global 1km SIN Grid 006 [data set]. NASA EOSDIS Land Processes Distributed Active Archive Center (LP DAAC). doi.org/10.5067/MODIS/MOD11A1.006

Williams AP, Abatzoglou JT (2016) Recent Advances and Remaining Uncertainties in Resolving Past and Future Climate Effects on Global Fire Activity. Current Climate Change Reports 2, 1–14. doi:10.1007/s40641-016-0031-0

Simulation of induced-wind-dominated fire on sloping terrain

Gilbert Accary*[1]; Jacky Fayad[2]; François-Joseph Chatelon[2]; Nicolas Frangieh[2]; Carmen Awad[2]; Sofiane Meradji[3]; Thierry Marcelli[2]; Jean-Louis Rossi[2]; Dominique Morvan[4] ; Lucile Rossi[2]

[1] Scientific Research Centre in Engineering, Lebanese University. Museum Square, 1106 Beirut, Lebanon {gaccary@ul.edu.lb}
[2] UMR CNRS SPE 6134, Université de Corse – CNRS. 20250 Corte, France {fayad_j, chatelon_j.fr, frangieh_n, awad_c, marcelli_t, rossi_j, rossi_l}@univ-corse.fr
[3] IMATH laboratory, EA 2134, Toulon University. 83160 Toulon, France {sofiane.meradji@univ-tln.fr}
[4] Aix-Marseille University, CNRS, Centrale Marseille, M2P2. Marseille, France {dominique.morvan@univ-amu.fr}

**Corresponding author*

Keywords

Extreme fire; fire behavior, physical fire model; FireStar3D, numerical simulation

Abstract

Using the fully physical model FireStar3D, numerical simulations of grassland fires were carried out on a sloping terrain (10°, 25°, and 40° inclinations) for a 10 m-open wind speed of 1, 2, and 3 m/s. To reproduce the behaviour of a quasi-infinite fire front, periodic conditions were considered in the fireline direction. The simulations highlight the role played by the additional wind induced by the fire (that reaches about 10 m/s at 10 m above ground) and its feedback action on fire behaviour. This interaction results in the transition of the fire behaviour to induced-wind-dominated fire, and this goes along with a substantial increase of the fireline heat release rate that reaches 20 MW/m. In addition, the simulations highlight the acceleration of the fire spread resulting from flame attachment observed for the inclinations of 25° and 40°. The fire regime was characterized by Byram's convection number, based on the effective crosswind speed, that drops by two orders of magnitude once fire-induced wind takes effect on fire behaviour.

1. Introduction

Fire blow-up or flare-up (Viegas, 2005) is considered a very dangerous aspect of wildfire events, and is characterized by a sudden change in its behavior within a very short lapse of time. Therefore, this phenomenon presents a significant threat and one of the main causes of human losses, because of its unpredictable behavior that surprises firefighters and engulfs them with flames. There have been too many accidents imputed to blow-up fires, for instance: Mann Gulch fire in the USA, 1949 (13 victims), Storm King fire in the USA, 1994 (14 victims), Palasca in France, 2000 (2 victims), Guadalajara in Spain, 2005 (11 victims), Kornati in Craotia, 2007 (11 victims) … Many explanations have been proposed for this phenomenon (Viegas & Simeoni, 2011; Werth, 2016) and the first kind of interpretations is based on the external conditions related to stability in the atmosphere and change in the wind velocity or direction. However, real fires showed that fire blow-up could occur in the presence of contrary wind (Countryman, 1968), and laboratory experiments showed flare-up behaviors under no wind conditions (Viegas & Pita, 2004; Dold & Zinoviev, 2009). The second kind of interpretations proposed the interaction between the spreading fire and other factors like wind and topography. Indeed, the majority of blow-up fires have been observed to occur in connection with canyons or steep slopes. Thus, many models have taken into account the topographic effects in order to study flare-up behavior (Viegas, 2005; Viegas & Pita, 2004; Dold & Zinoviev, 2009; Viegas, 2006; Wu et al., 2000; Drysdale & Macmillan, 1992) and many have highlighted the role played by flame attachment to explain this fire behavior. For instance, Wu et al., 2000, carried out laboratory scale experiments on inclined surfaces and obtained a critical inclination angle of 24° for flame attachment, that separates fire spread dominated by radiative heat transfer and convective one (Dold & Zinoviev, 2009), while Drysdale & Macmillan, 1992, had noticed a change in fire behavior around 15° inclination angle. The role played by induced wind and its feed-back action on fire propagation is still an open question, but it is sure that this indraft provides oxygen to the combustion zone and contributes to fire propagation. At field scale, the accident of Freixo de Espada-a-Cinta reported by Viegas, 2005 is a good example of the presence of induced wind in a canyon. Moreover, Viegas & Pita, 2004, showed clearly the presence of

the induced wind and its effect on the fire behavior during laboratory experiments of fires spreading in canyons. In order to better understand the role played by induced wind on the behavior of fire on sloping terrain, a 3D Large Eddy Simulation (LES) was conducted using a complete physical model, namely FireStar3D (Morvan et al., 2020; Frangieh el al., 2018). The configuration was set up to allow for fire-induced wind to take place and interact consequently with the fire that induced it.

2. Modelling and Numerical Method

The mathematical model used in FireStar3D is based on a multiphase formulation (Grishin, 1997). The model consists of two parts that are solved on two distinct grids. The first part consists of the equations governing the reacting and turbulent flow of the gas mixture of fresh air and the gaseous products resulting from the degradation of the solid fuel (by drying, pyrolysis, and heterogeneous combustion) and the homogeneous combustion in the flaming zone. The second part consists of the equations governing the thermal degradation, the state and the composition, of the solid phase subjected to an intense heat flux coming from the flaming zone. The interaction between the gaseous and the solid phases, is obtained through coupling terms that appear in both parts of the model. The reader is invited to consult references (Morvan et al., 2020; Frangieh el al., 2018; Morvan & Dupuy, 2004) for more information about FireStar3D model. To avoid border effects induced by a finite-length ignition line on the fire behaviour, the simulation was carried out using periodic boundary conditions along the two lateral sides of the computational domain, as shown by Fig. 1. The homogeneous vegetation layer, of height δ = 0.6 m and whose physical properties are given in Tab. 1, is located at 30 m from the domain inlet. Domain inclination (α = 10°, 25°, or 30°) was specified through two non-zero gravity components: $g_x = -g\sin(\alpha)$ and $g_z = -g\cos(\alpha)$, where $g = 9.81$ m/s^2 is Earth gravity.

Table* 1. *Main physical properties of the vegetation

Particle density, ρ_v (kg/m^3)	1000
Volume fraction, β	0.003
Fuel moisture content, FMC (%)	60
Fuel bed depth, e (m)	0.6
Fuel load, σ (kg/m^2)	1.8
Surface-area to volume ratio, s (m^{-1})	3000
Thermal emissivity, ε	1
Fuel particles shape	Cylindrical

Initially (i.e., at t = 0), a one-seventh power horizontal velocity profile was imposed in the entire computational domain with a 10-m open wind speed U_{10} = 1, 2, or 3 m/s, and the hydrodynamic module of the code was run long enough until reaching a statistically-steady state. During this purely dynamic phase, the one-seventh power velocity profile was imposed at the domain inlet and a homogeneous Neumann outlet conditions were imposed for all primary variables of the problem. At the top boundary, a constant wind speed $U_{Top} = 1.43 \times U_{10}$ (obtained from the one-seventh power wind velocity profile) was imposed during the entire simulation time. Once the flow had reached a statistically-steady state, a 2 m wide burner was activated along the entire fuelbed width by injecting CO gas at 1600 K from the bottom boundary of the domain. The burner was activated during 10 s (at most) or until the consumption of a solid-fuel mass equal to that available above the burning area.

For the solid phase, a uniform grid with (Δx,Δy, Δz) = (0.2m, 0.2 m, 0.03 m) was used, while for the fluid phase, a uniform grid with (Δx, Δy, Δz) = (0.4 m, 0.4 m, 0.015 m) was used within the vegetation before being gradually coarsened both in the x and in the z directions. Both these grids are characterized by cells sizes below the radiation extinction length scale (Morvan, 2011) within the vegetation, given by $4/s\beta$, where s is the surface to volume ratio of the vegetation (m^{-1}) and β is the volume fraction of the solid phase (see Tab. 1); this characteristic length is equal to 0.445 m in present case. A variable time stepping strategy was used, based on a truncation-error control, with time step values varying between 0.001 s and 0.01 s. At each time step, the solution is assumed to be obtained when the residuals of all conservation equations had reached 10^{-4} in normalized form.

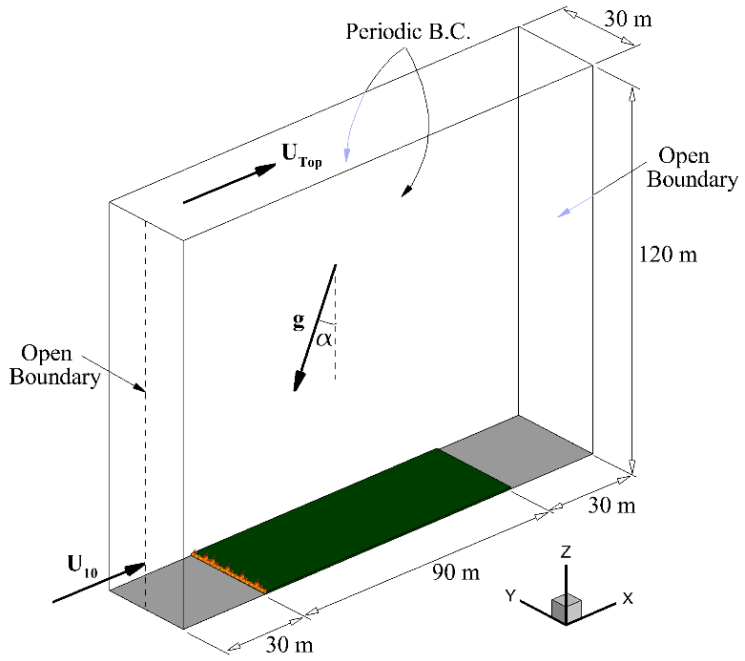

Figure 1- Computational domain and boundary conditions used to simulate an induced-wind-dominated fire on a sloping terrain.

3. Results and discussion

Figure 2 shows the time evolution of the pyrolysis front position (average at the vegetation surface), as well as the fireline heat release rate (HRR) obtained for two cases. For $\alpha = 10°$ and $U_{10} = 1$ m/s, we notice that a quasi-constant rate of spread (ROS) (the curve slope) of about 0.45 m/s is obtained, while the fireline HRR increases from about 6 to 12 MW/m after steady state of fire propagation was reached. For $\alpha = 40°$ and $U_{10} = 3$ m/s, in addition to the substantial increase of the HRR that reaches 20 MW/m, we notice a transitional phase in fire propagation where the ROS increases between 60 and 80 s after ignition from 0.5 m/s to 0.7 m/s.

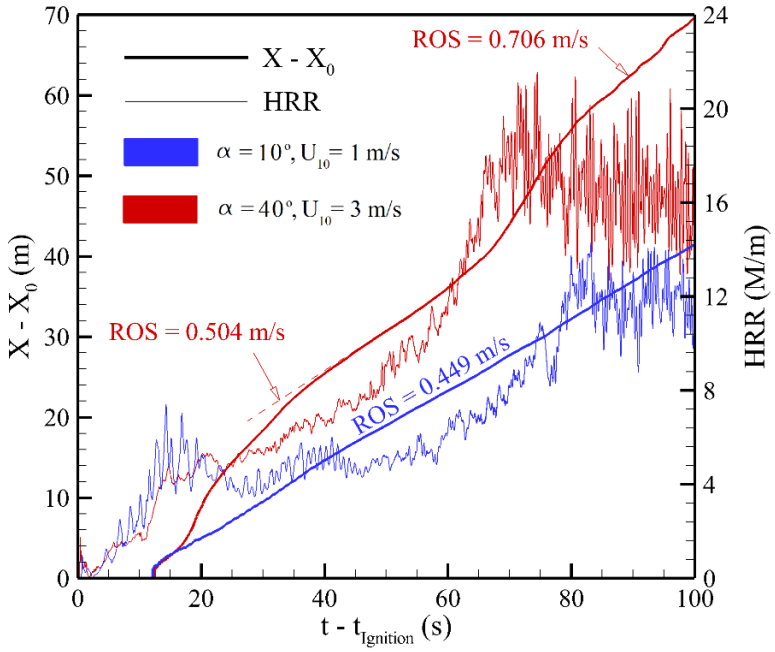

Figure 2- Time evolution of the pyrolysis front distance from burner position ($X-X_0$) and of the fireline HRR obtained for the two extreme considered cases.

To better understand the substantial increase in the HRR, figure 3(a) shows the time evolution of the 10-m open wind speed, shown in Fig. 1 at the domain inlet, for three different cases. We notice that U_{10} starts at the value imposed by the initial conditions, then it increases continuously during the simulation. This additional wind speed is induced the fire itself, it provides fresh air to the combustion zone, pushes the flames onto the unburned vegetation, and increases substantially the extend of the flaming zone, as shown in Fig. 4, and consequently the fireline HRR. Figure 3(b) shows the time evolution of the wind velocity profile along the vertical dashed-line shown in Fig. 1 at the domain inlet for $\alpha = 25°$ and $U_{10} = 2$ m/s; similar results were obtained for the other two cases. We notice how the shape of the velocity profile changes over time, with a maximum wind speed located at about 10 m above ground.

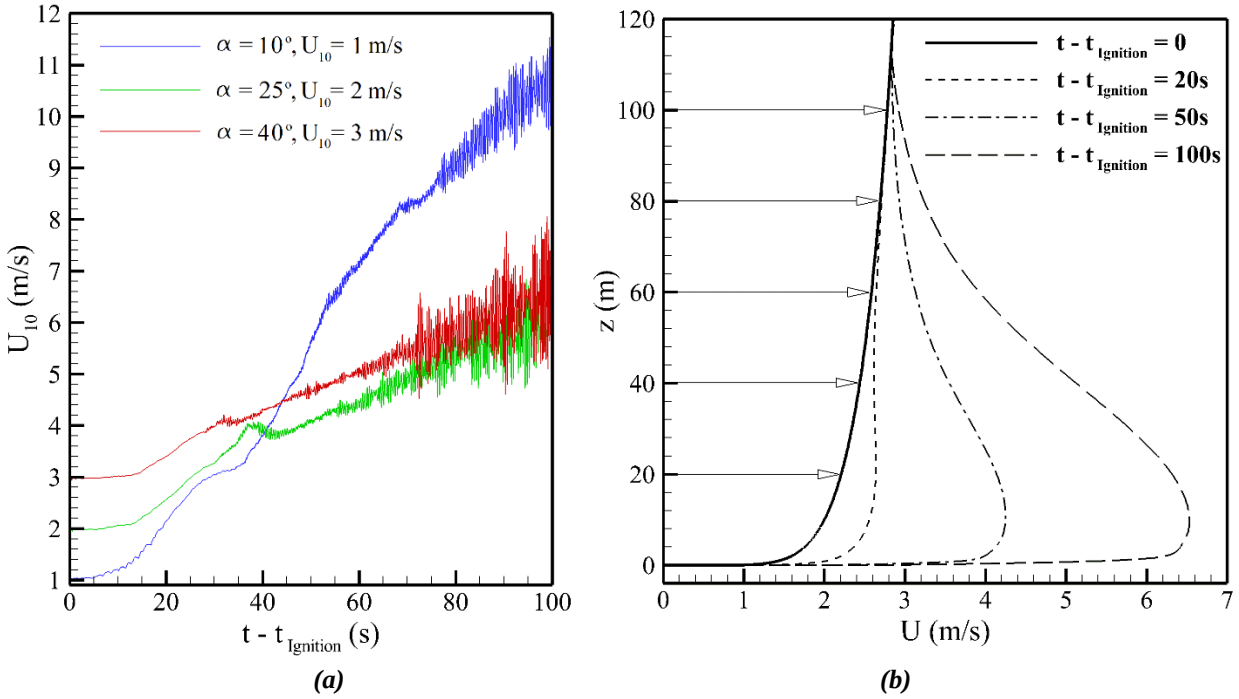

Figure 3- (a) Time evolution of the 10-m open wind speed, U_{10}, at the inlet (x = 0, y = 15 m, z = 10 m) for different simulated cases. (b) Inlet wind profile along the vertical dashed line shown in Fig. 1 at different simulation times for $\alpha = 25°$ and $U_{10} = 2$ m/s.

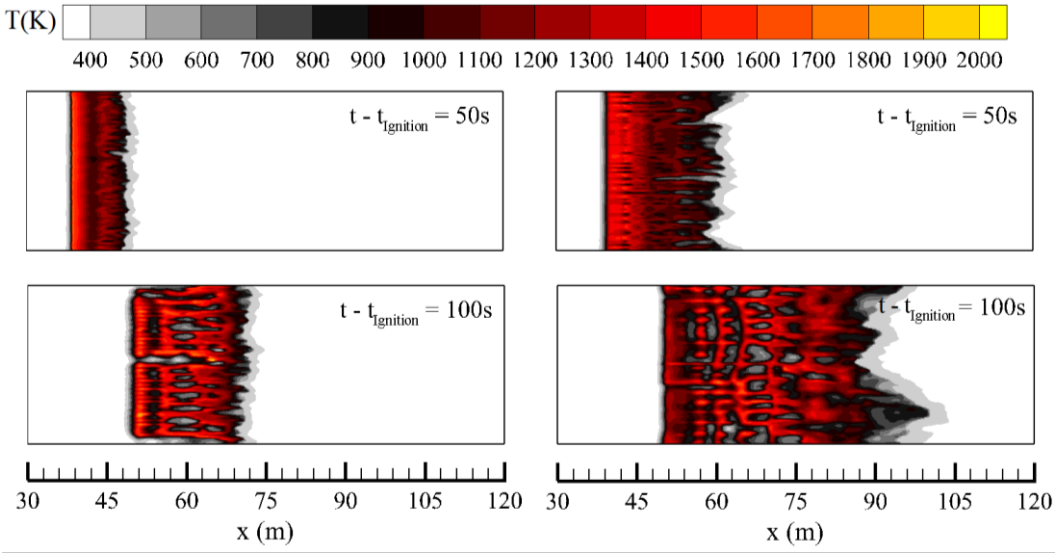

Figure 4- Distribution of the fuel particles temperature at the fuel-bed surface and for two simulation times. Left: $\alpha = 10°$ and $U_{10} = 1$ m/s, right: $\alpha = 40°$ and $U_{10} = 3$ m/s.

The transitional phase in fire propagation observed in Fig. 2 for α = 40° and U_{10} = 3 m/s (also obtained with less intensity for α = 25° and U_{10} = 2 m/s) seems to result mainly from flame attachment, as shown in Fig. 5, while it was not observed for α = 10° and U_{10} = 1 m/s, which is consistent with literature (Wu et al., 2000).

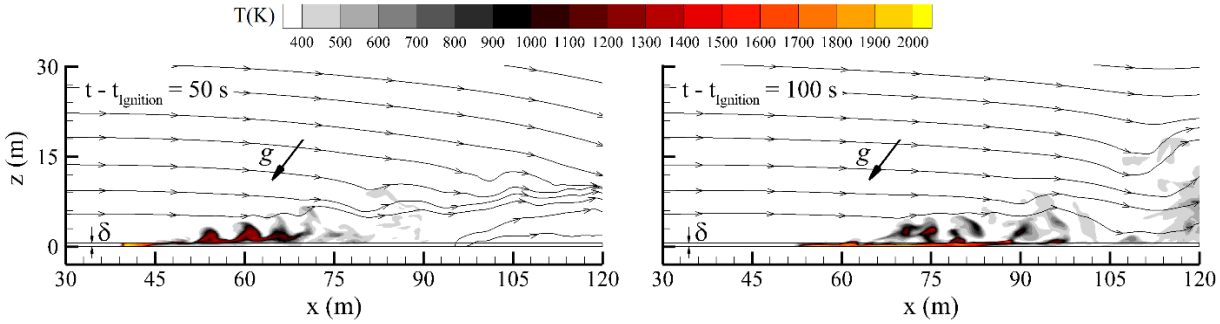

Figure 5- Temperature field and streamlines in the vertical median plane (y = 15 m) obtained for α = 40° and U_{10} = 3 m/s before ($t - t_{Ignition}$ = 50 s) and after ($t - t_{Ignition}$ = 100 s) flame attachment.

The transition between plume-dominated and wind-dominated regimes is piloted by the ratio between the two forces governing flames trajectory: buoyancy contributing to maintain the flames more or less vertical and the wind inertial force pushing the flames towards the unburned vegetation. The ratio between the power of these two forces defines a dimensionless parameter, Byram's convective number (Nelson, 2015), defined by Eq. (1).

$$N_C = \frac{2\, g\, I\, cos^3\alpha}{\rho_0\, C_{P0}\, T_0\, (U_{10}^e - ROS)^3} \tag{1}$$

where, ρ_0 and C_{P0} represent the density and the specific heat of air in standard conditions at temperature T_0, g is the acceleration of gravity, I is the fireline intensity (aberage value of the HRR), and U_{10}^e is the effective 10 m-open wind speed (accounting for the fire-induced wind). The thresholds for the transition between the two regimes of propagation are: $N_C < 2$ (wind-driven fire) and $N_C > 10$ (plume-dominated fire) (Morvan & Frangieh, 2018; Byram, 1959). Figure 6 shows the evolution time of Byram's number, obtained from Eq. (1), for the three considered cases. We notice that Byram's number decreases by the action of the additional wind induced by the fire itself and eventually corresponds to wind-driven fires for all considered cases. Also, the signature of flame attachement is visible between 60 and 80 s after ignition on the evoluation of Byram's number.

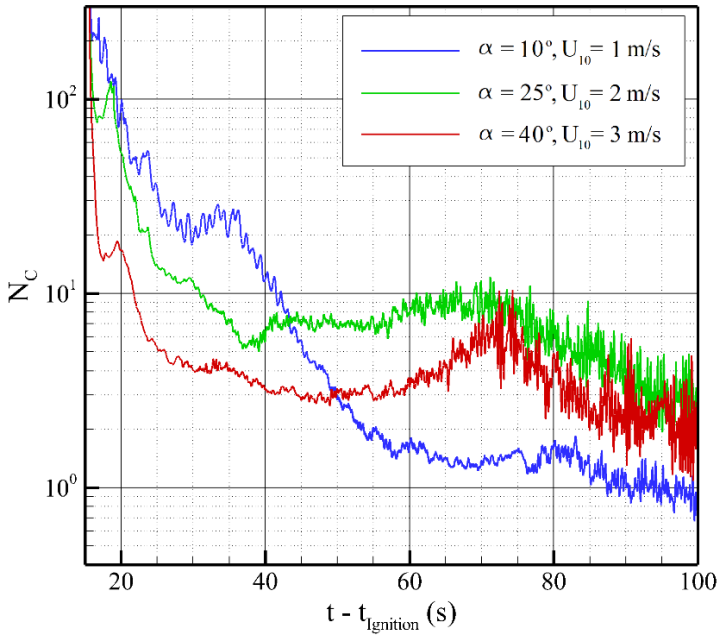

Figure 6- Time evolution of Byram's number obtained from Eq. (1) for the different simulated cases.

4. Conclusion

Induced-wind-dominated fire has been simulation numerically on a sloping terrain using FireStar3D. The action of the induced wind results within few seconds in a substantial increase of the HRR. This is coupled to the flare-up effect of flame attachment that was observed for an inclination angle higher than 25°. This study is, to our knowledge, the first to numerically demonstrate the feed-back action of fire-induced wind. This pioneering work paves the way to other numerical studies that could address open questions related to the role played by induced wind, such as: What are the conditions that favour the development of this mechanism? Does it develop in the case of a finite fireline? Answering these questions will certainly improve our understanding this type of fires and its triggering mechanisms.

5. References

Byram, G. M. (1959). Combustion of forest fuels, in: Davis, K. P. (Eds.), Forest Fire Control and Use, McGraw-Hill, New York.

Countryman, C. M., Fosberg, M. A., Rothermel, R. C., and Schroeder, M. J. (1968). Fire Weather and Fire Behaviour in the 1966 Loop Fire. Fire Technology 4, 126-41.

Dold, J. W., and Zinoviev, A. (2009). Fire Eruption through Intensity and Spread Rate Interaction Mediated by Flow Attachment. Combustion Theory and Modelling 13, 763-93.

Drysdale, D. D., Macmillan, A. J. R. (1992). Flame spread on inclined surfaces. Fire Safety Journal 18, 245-254.

Frangieh, N., Morvan, D., Accary, G., Méradji, S., Bessonov, O. (2018). Numerical simulation of grassland fires behavior using an implicit physical multiphase model. Fire Safety Journal 102, 37-47.

Grishin, A. M., Albini, F.A. (1997). Mathematical modelling of forest fires and new methods of fighting them. Publishing House of the Tomsk University: Russia.

Werth, P.A., Potter, B.E., Alexander, M.E., Clements, C.B., Cruz, M.G., Finney, M.A., Forthofer, J.M., Goodrick, S.L., Hoffman, C., Jolly, W.M., McAllister, S.S., Ottmar, R.D., Parsons, R.A. (2016). Synthesis of knowledge of extreme fire behavior: Volume 2 for Fire Behavior Specialists, Researchers, and Meteorologists, Gen. Tech. Rep. PNW-GTR-891. 258.

Morvan, D., Dupuy, J. L. (2004). Modeling the propagation of a wildfire through a Mediterranean shrub using a multiphase formulation. Combustion and Flame 138, 199-210.

Morvan, D. (2011). Physical Phenomena and Length Scales Governing the Behaviour of Wildfires: A Case for Physical Modelling, Fire Technol. 47, 437-460.

Morvan, D., Frangieh, N. Wildland fires behaviour: Wind effect versus Byram's convective number and consequences upon the regime of propagation, Int. J. Wildl. Fire. 27 (2018) 636-641.

Morvan, D., Accary, G., Méradji, S., Frangieh, N., Bessonov, O. (2020). A 3D physical model to study the behavior of vegetation fires at laboratory scale. Fire Safety Journal 101, 39-52.

Nelson, R. M. (2015). Re-analysis of wind and slope effects on flame characteristics of Mediterranean shrub fires, Int. J. Wildl. Fire. 24, 1001-1007.

Viegas, D. X., and Pita, L. P. (2004). Fire Spread in Canyons. International Journal of Wildland Fire 13, 253-274.

Viegas, D.X. (2006). Parametric study of an eruptive fire behaviour model. International Journal of Wildland Fire 15, 169-177.

Viegas, D.X. (2011). A mathematical model for forest fires blowup. Combust. Sci. Technol. 177, 27-51.

Viegas, D.X. Simeoni, A. (2011). Eruptive Behaviour of Forest Fires, Fire Technol. 47, 303-320.

Wu, Y., Xing, H. J., Atkinson, G. (2000). Interaction of fire plume with inclined surface. Fire Safety Journal 35, 391-403.

Spectral monitoring of a system for the rehabilitation of burned soils based on inoculation with cyanobacteria and microalgae

João Gonçalves*[1,2,3], Bruno Marcos[1,2], Márcia Bessa da Silva[4,5], Inês Conceição[6], João Pissarra[7], Jéssica Roque[7], Paula Tamagnini[6,7], Paula Melo[4,6], Ruth Pereira[4,6], João Honrado[1,2,6]

[1]CIBIO, Centro de Investigação em Biodiversidade e Recursos Genéticos, InBIO Laboratório Associado, Campus de Vairão, Universidade do Porto, 4485-661 Vairão, Portugal, {joao.goncalves, bruno.marcos}@cibio.up.pt
[2]BIOPOLIS Program in Genomics, Biodiversity and Land Planning, CIBIO, Campus de Vairão, 4485-661 Vairão, Portugal
[3]proMetheus – Research Unit in Materials, Energy and Environment for Sustainability, Instituto Politécnico de Viana do Castelo (IPVC), Avenida do Atlântico, n.º 644, 4900-348 Viana do Castelo, Portugal
[4]GreenUPorto – Centro de Investigação em Produção Agroalimentar Sustentável & Departamento de Biologia, Faculdade de Ciências, Universidade do Porto, Portugal.
[5]CITAB – Centro de Investigação e Tecnologias Agroambientais e Biológicas, Universidade de Trás-os-Montes e Alto Douro, Vila Real, Portugal.
[6]Departamento de Biologia, Faculdade de Ciências, Universidade do Porto, 4099-002 Porto, Portugal,
[7]i3s – Instituto de Investigação e Inovação em Saúde & Departamento de Biologia, Faculdade de Ciências, Universidade do Porto, Portugal.

**Corresponding author*

Keywords

Burned soil rehabilitation, Spectral monitoring, handheld spectrometer, multispectral, unoccupied aerial system (UAV), remote sensing

Abstract

Inocula containing photosynthetic microorganisms such as cyanobacteria and microalgae can promote the formation of biocrusts, improving the soil properties and allowing ecosystem recovery. The GreenRehab project aims to develop a low-cost, eco-friendly, and easy-to-implement system to rehabilitate burned soils and protocols to evaluate the success of an ecosystem after-fire recovery. For this purpose, native cyanobacteria and microalgae were isolated from soil/biocrusts and tested, with selected strains being cultivated on a large scale. To evaluate the performance of the proposed rehabilitation system (based on the inoculation of native cyanobacteria and microalgae), we analyzed spectral data scanned from a portable visible/near-infrared spectrometer that indirectly estimates top-soil photosynthetic activity. Several spectral indices based on the normalized difference combination of spectral bands were calculated and compared for their ability to assess photosynthetic activity over time. Results showed that treatments with microalgae and cyanobacteria effectively enhanced photosynthetic activity, with Trichocoleus stimulating soil rehabilitation the most. Moreover, the best performing normalized difference index was the one combining the 660 nm and 860 nm wavelengths. Parallelly, very-high resolution imagery obtained from a UAV equipped with a multispectral camera is currently being tested to assess the performance of different inocula previously selected from microcosm experiments in environmental conditions closer to real ones in post-fire scenarios. Preliminary results led us to develop an integrated protocol for image acquisition, radiometric calibration and photogrammetric post-processing. This allowed us to characterize baseline conditions in the test area, including geomorphology, vegetation and portray fine-scale patterns in greenness and photosynthetic activity. Overall, spectral measurements from portable spectrometers and UAVs open the possibility of assessing which treatments exploited in the GreenRehab project effectively enhance soil rehabilitation and recovery from frequent fires. Such innovation may translate into other "real-world" applications in ecology, forestry, and agronomy.

1. Introduction and context

The GreenRehab project aims to develop a system for rehabilitating burned soils by applying inocula composed of native and locally-harvested cyanobacteria and microalgae. These photosynthetic microorganisms promote

the formation of biocrusts improving the soil properties and allowing the re-establishment of the ecosystem (Rossi et al. (2012), Colina et al. (2014), Büdel et al. (2016), Lababpour et al. (2016)). For this purpose, native cyanobacteria and microalgae were isolated from soil/biocrusts and tested in microcosm experiments to select soil conditioners and plant growth enhancers. Selected strains will be cultivated on a large scale, and different microbial consortia and distinct dispersion methods will be tested in restricted burned areas. Finally, the soil properties, microbial community, edaphic fauna and vegetation recovery will be assessed before and after re-inoculation. By the end of the project, we intend to have a low-cost, eco-friendly, and easy-to-implement system to rehabilitate burned soils and a protocol to evaluate the success of an ecosystem after-fire recovery.

2. Approach

(I) A microcosm experiment was developed to select which native cyanobacteria and algae performed best for enhancing soil activity. This experiment was divided into controls (soil not inoculated) and four different inoculation treatments with soil, perlite and photosynthetic organisms isolated from biological soil crusts – one microalga: *Klebsormidium*; and three cyanobacteria: *Oscillatoria*, *Trichocoleus* and, *Nodosilinea*.

We evaluated the implementation and performance of rehabilitation of these treatments by analyzing the spectral data scanned from a portable visible/near-infrared (VNIR) spectrometer (LinkSquare-1, URL: https://linksquare.io, hereafter LS1, covering the VNIR region from 350 nm to 1100 nm) that indirectly estimates the top-soil photosynthetic activity.

Several spectral indices based on the normalized difference combination of spectral bands were calculated and compared in R statistical software (R Core-Team, 2019) for their ability to assess photosynthetic activity over time. Measures were collected weekly and systematically based on a predefined mesh placed over each soil tray. Ten spectral measurements per tray were collected weekly using LS1 handheld spectrometer.

(II) Mesocosm experiments are also being performed in GreenRehab to assess the effectiveness of each cyanobacteria and microalgae inocula in environmental conditions closer to real ones found in post-fire scenarios. This effort involves developing a detailed framework to support post-fire severity and recovery monitoring (e.g., Torres et al. 2017), characterizing baseline conditions in the field site selected for the in-situ, and designing a tailored experimental setup (e.g., Gonçalves et al., 2016). In particular, very-high resolution imagery obtained from an unoccupied aerial vehicle (UAV, DJI Phantom-4) equipped with a multispectral camera (Parrot Sequoia+) is being tested to assess the performance of different inocula previously selected from microcosm experiments. Predefined semi-automated flights were used to collect images from the study area and later used for 3D photogrammetric assembly. Ground control points were collected with a centimetre-precision GNSS station to improve the accuracy of 3D reconstructions using Agisoft Metashape Pro software (Agisoft, 2021). Radiometric corrections were applied for multispectral VNIR images. A dense point cloud, orthomosaic, digital surface model (DSM) and spectral indices were obtained to characterize reference conditions.

3. Preliminary results

3.1. Microcosm experiments – hyperspectral monitoring

The results showed that the portable spectrometer LinkSquare-1 could provide reliable and relevant information for detecting VNIR spectral data. Treatments with microalgae and cyanobacteria effectively enhanced photosynthetic activity. When comparing the different treatments and their performances with spectral indices, *Trichocoleus* (T3) seemed to stimulate soil rehabilitation the most. Although *Nodosilinea* (T4) and *Klebsormidium* (T1) treatments showed an inferior performance to *Trichocoleus*, they still increased over time. *Oscillatoria* (T2) obtained the lowest results in stimulating top-soil photosynthetic activity based on spectral data. The best performing normalized difference index was the one combining the 660 nm (red) and 860 nm (NIR) using the infrared light source of the LS1 device.

(a)

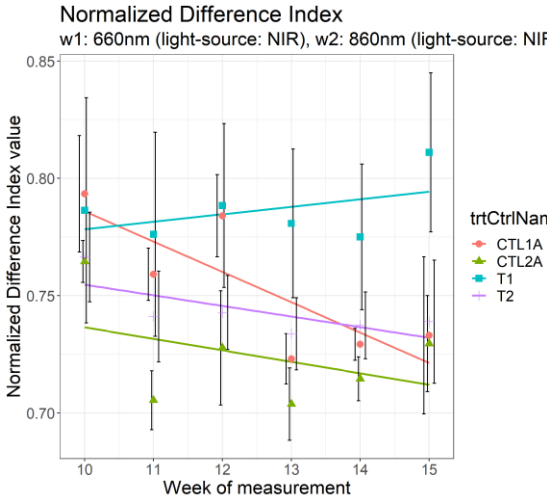

(b)

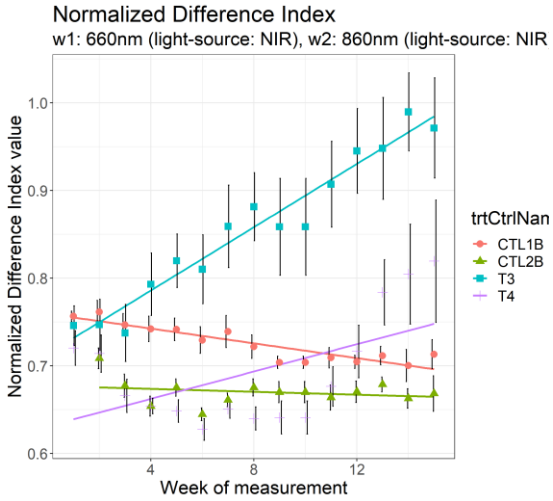

(c)

Figure 1 – Growth of the different microorganisms on the microcosm experiment monitored using a handheld LinkSquare-1 spectrometer for the collection of hyperspectral measurements for treatments (T): (a) T1 – Klebsormidium (microalga) and T2 – Oscillatoria (cyanobacterium); (b) T3 – Trichocoleus and T4 – Nodosilinea (cyanobacteria). CTL1A/CTL1B – burned soil moistened with BG11 medium; CTL2A/CTL2B – burned soil covered with perlite soaked in BG11 medium. (c) Spectral data collected with LS1 handheld spectrometer using a mesh over the soil surface.

3.2. Mesocosm experiments – UAV multispectral monitoring

Results from GreenRehab project have allowed us to devise a conceptual and analytical framework for fire severity assessment and post-fire recovery monitoring based on remote Earth observations (Marcos et al. 2021). Furthermore, field tests with the UAV/multispectral imagery have allowed us to detail the protocol for image acquisition, radiometric calibration and photogrammetric post-processing. Initial results point out that UAV imagery and DSM can be used to characterize baseline conditions in the test area, contributing to understanding geomorphology and vegetation patterns as well as dominant plant species (Fig.2 a–c). In addition, Normalized Difference Indices based on radiometrically calibrated images (Fig.2 d) can portray fine-scale patterns in greenness and photosynthetic activity.

(a)

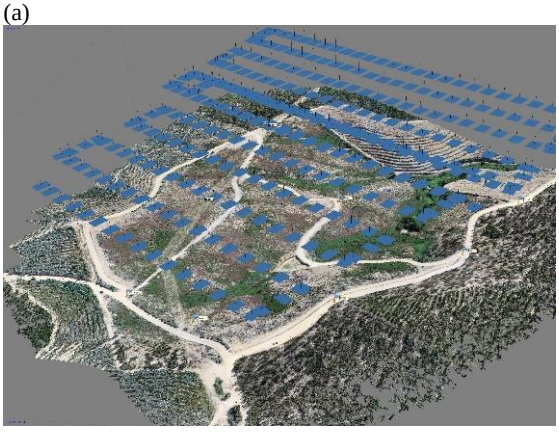

(b)

(c) (d)

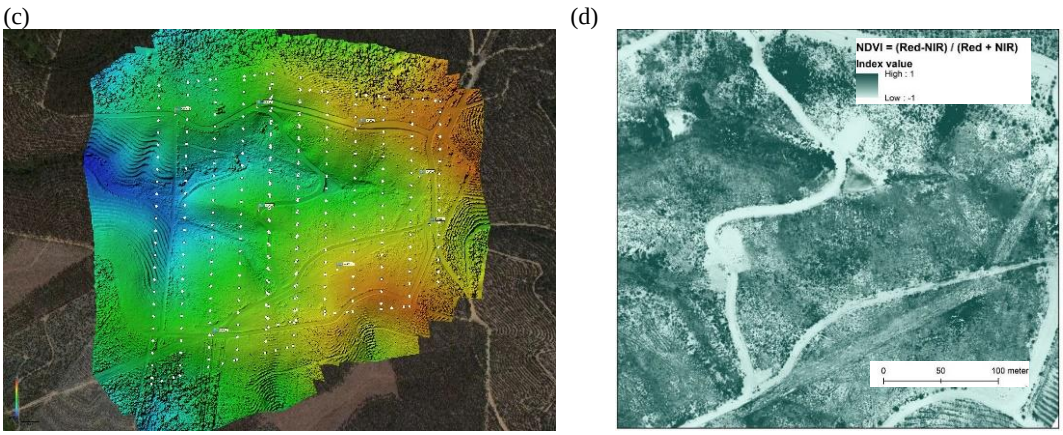

Figure 2 – Outputs from UAV surveys obtained for monitoring the macrocosm experiments in the field: (a) densified point-cloud, (b) orthomosaics with ultra-high resolution (2.5 cm), (c) digital surface model (blue and 'colder' colors indicate lower altitudes whereas reds and warmer ones indicate higher elevations), and (d) image depicting the normalized difference vegetation index (calculate from red and near-infrared spectral bands). Darker greens show higher amounts of vegetation in the test/experimental site.

4. Final remarks and future research

Spectral measurements and indices from portable spectrometers and UAVs open the possibility of assessing which treatments exploited in GreenRehab project enhance soil rehabilitation and recovery from frequent fires. Such innovation may translate into other "real-world" applications in ecology, forestry, and agronomy.

Future research will continue to expand these results and explore how image time series, collected at regular time steps, can aid in monitoring the effectiveness and velocity of different treatments to provide a low-cost and easy-to-implement system to rehabilitate burned soils.

6. References

Agisoft (2021) Agisoft Metashape Pro v-1.7.0 software. URL: https://www.agisoft.com

Büdel, B. Dulić, T., Darienko, T., Rybalka, N., Friedl, T. (2016). Cyanobacteria and algae of biological soil crusts. In Biological Soil Crusts: An Organizing Principle in Drylands. Ecological Studies 226 (pp. 55-80). Springer Berlin Heidelberg.

Colina et al (2014). Microbial secreted exopolysaccharides affect the hydrological behavior of induced biological soil crusts in desert sandy soils. Soil Biol. Bioch 68: 62-70

Gonçalves, J., Henriques, R., Alves, P., Sousa-Silva, R., Monteiro, A. T., Lomba, Â., Marcos, B. and Honrado, J. (2016). Evaluating an unmanned aerial vehicle-based approach for assessing habitat extent and condition in fine-scale early successional mountain mosaics. Appl Veg Sci, 19: 132–146.

Lababpour (2016). Potentials of the microalgae inoculant in restoration of biological soil crusts to combat desertification. International Journal of Environmental Science and Technology, 13(10), 2521-2532

Marcos, B., J. Gonçalves, D. Alcaraz-Segura, M. Cunha, and J. P. Honrado (2021). A Framework for Multi-Dimensional Assessment of Wildfire Disturbance Severity from Remotely Sensed Ecosystem Functioning Attributes. Remote Sensing 13

R Core-Team (2019). A Language and Environment for Statistical Computing version 3.5.1 (2019), URL: https://www.r-project.org

Rossi et al (2012). The role of the exopolysaccharides in enhancing hydraulic conductivity of biological soil crusts. Soil Biol. Bioch. 46:33-40

Torres, J., Marques, J., Alves, P. et al. (2017). Local lithological drivers of post-fire vegetation recovery and implications for fire-prone regions. Ecological Research, 32: 37. https://doi.org/10.1007/s11284-016-1415-2

Structure characterization on Mediterranean forest stand using terrestrial laser scanning

Roberto Ferrara; Stefano Arrizza; Andrea Ventura; Bachisio Arca; Michele Salis; Angelo Arca; Pierpaolo Masia; Pierpaolo Duce; Grazia Pellizzaro*

Consiglio Nazionale delle Ricerche; Istituto per la BioEconomia; Sassari; Italy;
{roberto.ferrara, stefano.arrizza, andrea.ventura, bachisio.arca, michele.salis, angelo.arca, pierpaolo.masia, pierpaolo.duce, grazia.pellizzaro}@ibe.cnr.it

**Corresponding author*

Keywords

Terrestrial Lidar, Forest inventory, DBSCAN, point cloud, segmentation, trees.

Abstract

The definition of the structural parameters of forest stands and its vertical and horizontal continuity is relevant for a number of environmental applications, such as carbon dynamics studies, sustainable forest management, ecological studies, and fire risk mitigation and management.

Obtaining detailed information on tree structures and canopy variables requires extensive and time- consuming field campaigns. Recently, proximal sensing techniques as Terrestrial Laser Scanning (TLS) have been used for forest monitoring studies and have demonstrated their potential to overcome the limitations of conventional ground-based forest inventory techniques. However, accuracy and applicability of TLS techniques for canopy characterization of broadleaf evergreen forests still require further investigation. In particular, a proper separation between points representing woody material, leaves and small branches is fundamental for the estimation of tree attributes and crown characterization.

In this work, we developed and tested an automatic procedure based on the DBSCAN point density algorithm to accurately separate points derived from terrestrial Lidar measurements at plot level. The objective was to identify volume of woody material, tree density, and canopy cover of a forest stand.

The study was conducted in an area located in southeastern Sardinia (Italy) covered by evergreen forests dominated by holm oaks, with different types of understorey (sparse and dense). Destructive and non-destructive measurements were carried out within three circular plots of 20 m, 25 m and 30 m diameter, respectively. TLS data were collected in field by multiple scans of the three plots. 3D point clouds were processed to isolate trees, soil and understorey. The point clouds were then transformed into voxel clouds (cubic volumes) that were used as input to classify woody and non-woody components by applying both DBSCAN point density clustering algorithms and principal component analysis.

The results show that the proposed method enables the correct identification of crown, trunk, and main branches through an automatic procedure that requires the setting of only a few parameters. Moreover, the procedure does not need excessive computing power and takes only a few minutes to complete the process. Our approach represents a step forward in improving the procedure for measuring forest structure from three-dimensional point clouds. However, further studies are needed to test the capabilities of this method in forest stands characterized by higher and denser understorey and with different tree species (e.g. mixed forests).

1. Introduction

Information on forest canopy structure and reconstruction of tree geometry is required at a wide range of spatial scales for several environmental applications such as carbon dynamic and ecological studies, ecological and forest management, ecosystem productivity model, forest fuel studies and fire risk management.

In particular, an accurate description of fuel is crucial for fire hazard mitigation planning by predicting potential fire behaviour and effects of fuel treatment. Obtaining landscape-level fuel maps, allows the description of the parameters needed to interpret the fire behaviour models, increasingly used to support fire management processes. A correct characterization and classification of fuel needs accurate estimates of vegetation structure

and crown attributes. However, many fuel characteristics are often operationally hard to be measured requiring manual field measurements and cutting.

Because to obtain detailed information on forest stand and canopy variables estimation, extensive, difficult and laborious field campaigns are required, remote and proximal sensing techniques for forest monitoring have become popular in recent decades. Specifically, Terrestrial Laser Scanner (TLS) has demonstrated its potentials to overcome the limitations of the conventional ground-based forest inventory techniques. TLS is a LiDAR system from which detailed 3D information called point clouds can be collected. Using a laser beam, TLS provide a high-resolution 3D view on vegetation structure right down to branch and leaf scales, making it superior to data obtained through traditional field work. Using the intensity of the returned laser pulses, TLS can be used to estimate the water content and photosynthetic capacity of the vegetation. TLS allows accurate estimation of traditional structural metrics used in forest monitoring and management, such as basal area per hectare, tree height, and diameter at breast height-DBH, and also offers a non-destructive approach to estimate quantify canopy and stem volume with high accuracy, thus allowing estimation of AGB parameters with reduced uncertainties, as well as development and improvement of reliable allometric equations.

Although several studies highlight the effectiveness of TLS in describing forest parameters, the accuracy and applicability of TLS techniques for canopy characterization of broadleaf evergreen forests needs further investigations. In particular, estimation of tree attributes such as canopy density, crown bulk density, branch size distribution, etc., in evergreen plants presupposes a correct separation between points representing shrubs, woody material, leaves and small branches. Separation of photosynthetically active material (leaves) from non-photosynthetically active material (wood) is particularly challenging in the case of non-deciduous broadleaf trees, which are characterized by complex crown architecture and where measurements must be performed under foliage conditions.

In a previous work (Ferrara et al., 2018) we proposed an approach based on the point density algorithm DBSCAN for wood-leaf separation from terrestrial LIDAR point clouds of single trees. The TLS data set collected in field by multiple scanning on single trees were partitioned in cubic volumes (voxels) that were used as input to generate clusters through DBSCAN. The most highly populated cluster, due to continuous bark shape versus chaotic leaf distribution, represented wood voxels. So that process led to the identification of wood and non-wood voxels.

In this work we applied the previous DBSCAN based approach at plot level in order to evaluate performance of the proposed procedure in estimating woody material volumes, tree density and canopy cover in holm oak forest stand.

2. Materials and methods

The study was carried out in an area located in South-East Sardinia, Italy. The area was covered by evergreen forests dominated by holm oaks with associated species consisting of Arbutus unedo, Erica arborea, etc. Destructive and non-destructive measurements were done inside three circular plots of 20 m, 25 m and 30 m diameter, respectively. Data sets were collected in field by multiple scanning of the three plots using a Leica HDS6100 laser scanner in super high-resolution mode, it means 3.1 x 3.1mm point spacing at 10 m range. The TLS data set collected in field were processed as reported in figure 1 with the purpose of isolating trees from understorey and separating wood from foliage. The whole process was carried out by algorithms in the opensource R platform.

The first step of the process is the discretization of the point cloud, going from scattered points to voxels ordered in a grid. A voxel is a cubic element, that we choose of 2 cm edge, that contains n points. This step allows to reduce the amount of data in the further computation and also to reduce the noise characteristic of laser scanner acquisition.

The second step is to classify voxels as ground or above ground biomass. Ground voxels will be useful to determinate the height in each point of the plot, needed for example in DBH determination, but are not useful in the following process to determinate wood, leaf and understorey biomass.

Third step; with respect to the single tree approach which used DBSCAN cluster algorithm, in this case the identification of wood voxel clusters was made by applying the principal component analysis and setting a minimum threshold of number of voxels per cluster.

3. Results and Discussion

Due to significant advances in technology and refinement of analysis methods over the past decade, several approaches have been proposed to separate leaf and wood points in a TLS point cloud. These separation methods can be divided into: 1) methods based on the geometric characteristics of point clouds; 2) methods based on the radiometric characteristics of point clouds; 3) methods with machine learning algorithms. Most of the methods developed focus on the geometric attributes of the point clouds.

The results obtained show that the separation method which uses density-based spatial clustering of application with noise (DBSCAN) algorithm proposed, allows the discrimination of the woody groups from the foliar ones and consequently to correctly identify foliage, trunk and main branches at plot level. It is a fully automated procedure that requires the choice and setting of few parameters in order to work properly. Unlike other developed methods, it does not require excessive computational power and takes only a few minutes to complete a good classification. Not being bound to the use of a specific instrument and requiring open source software, it can easily be replicated and applied to any point cloud.

The approach used represents a further step in the improvement of the measurement procedure of the forest structure from clouds of 3D points, in particular as regards the estimation of the woody material, the density of the trees and the projection area of the foliage, especially when the underlying layer is dominated by a not high herbaceous vegetation.

However, further studies are needed to assess the ability of this method in forest stands characterized by high and dense understorey and with different species of trees.

4. References:

Ferrara R, Virdis SGP, Ventura A, Ghisu T, Duce P, Pellizzaro G (2018) An automated approach for wood-leaf separation from terrestrial LIDAR point clouds using the density based clustering algorithm DBSCAN. AGR FOREST METEOROL 262:434-444. https://doi.org/10.1016/j.agrformet.2018.04.008

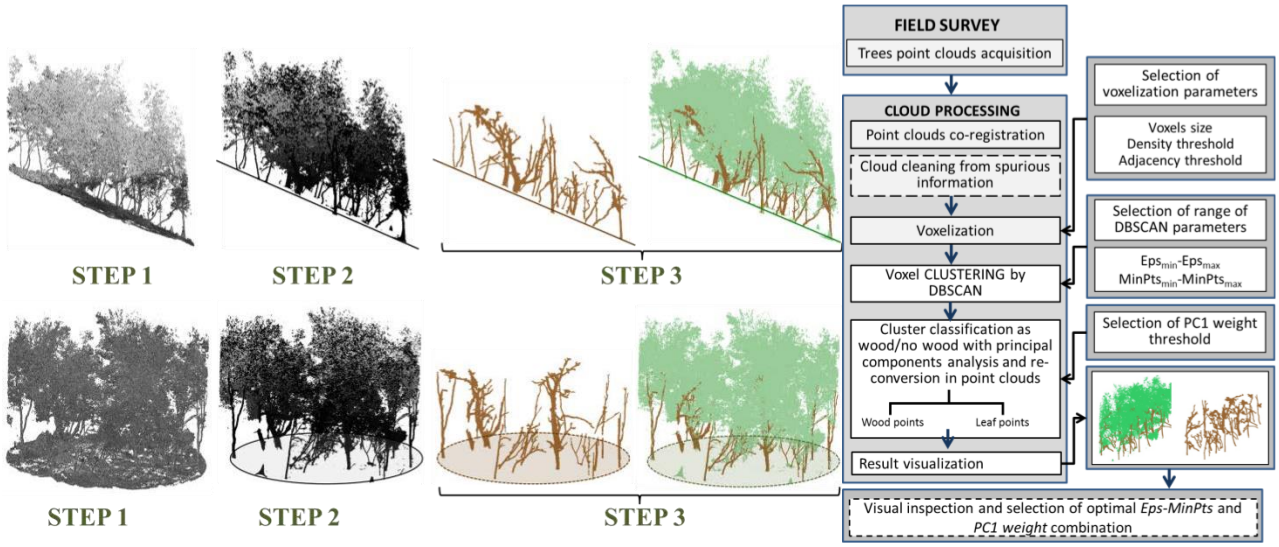

Figure 1. Scheme of proposed approach at plot level for wood separation (a) and an example of qualitative final segmentation results from the elaboration of the plot scans (b)

The California Fire Dynamics Experiment (CalFiDE): Developing Validation Data Sets for Coupled Fire-Atmosphere Simulations

Mario M. Valero*[1]; Amanda Makowiecki[2,3]; Alan Brewer[3], Craig B. Clements[1], Neil P. Lareau[4], Adam K. Kochanski[1], Edward Strobach[2,3]

[1]*Wildfire Interdisciplinary Research Center, Department of Meteorology and Climate Science, San Jose State University, San Jose, CA 95192, USA {mm.valero, craig.clements, adam.kochanski}@sjsu.edu*
[2]*Cooperative Institute for Research in Environmental Sciences, University of Colorado Boulder. Boulder, CO 80309, USA*
[3]*Chemical Sciences Laboratory, National Oceanic and Atmospheric Administration. Boulder, CO 80305, USA {amanda.makowiecki, alan.brewer, edward.strobach}@noaa.gov*
[4]*Department of Physics, University of Nevada-Reno, Reno, NV 89557, {nlareau@unr.edu}*

**Corresponding author*

Keywords

Wildland Fire, Fire Behavior, Remote Sensing, Doppler Lidar, Radar

Abstract

The California Fire Dynamics Experiment (CalFiDE) is a 6-week study of wildfire behavior and its response to spatially and temporally evolving wind fields in California, USA. It is the result of a partnership between the Chemical Sciences Laboratory (CSL) at the National Oceanic and Atmospheric Administration (NOAA), the Wildfire Interdisciplinary Research Center (WIRC) at San Jose State University (SJSU) and University of Nevada, Reno. A Twin Otter aircraft will be instrumented and flown over landscape-scale wildfires in California between August 14 and September 30, 2022. Onboard instrumentation includes (i) a scanning Doppler lidar system capable of measuring vertical profiles of 3D wind speed and turbulence, (ii) a multispectral infrared imaging system designed to remotely sense fire behavior, (iii) NightFox fire radiative power sensors (iv) AIMMS probe to measure flight-level winds, temperature, and water vapor content, and (v) Chemistry instruments to sample flight level NOX , NOY, O3, CO and GHG. Airborne measurements will be complemented with ground-based mobile scanning radars and lidars, which will be positioned around the fire to characterize the spatial structure and internal dynamics of the smoke plume. This combination of sensors will provide a unique opportunity to characterize landscape-scale wildfire behavior, fire weather and fire atmospheric chemistry in a synchronized manner. We expect that the datasets resulting from this experiment will have a broad applicability in fundamental fire dynamics studies, fire model validation exercises and the calibration of spaceborne remote sensing fire observations.

1. Introduction

Rigorous observation of fire behavior and fire meteorology during landscape-scale wildfires is essential to develop and validate wildfire models. Validation of coupled fire-atmosphere models, for example, poses unique data challenges that have so far limited rigorous model assessment. In order to validate coupled fire models, observational data must be comprehensive enough to validate all of the model components. For fire spread focused implementations, coupled fire models involve an atmospheric component, a fuel moisture component, and a fire spread component, while air quality applications require additional emission, aerosol and chemical transport modules. As these model components are interlinked, an error in one module can impact the final fire simulation results beyond the specific physical processes modeled by that module. For example, model inaccuracies in the rate of spread may be a result of the deficiencies of the fire spread component itself, but also due to the model's inability to resolve ambient weather conditions, or limitations in representing the local fire-induced circulation. An example of the fire-induced circulation simulated by a coupled fire-atmosphere model (WRF-SFIRE) is presented in Figure 1.

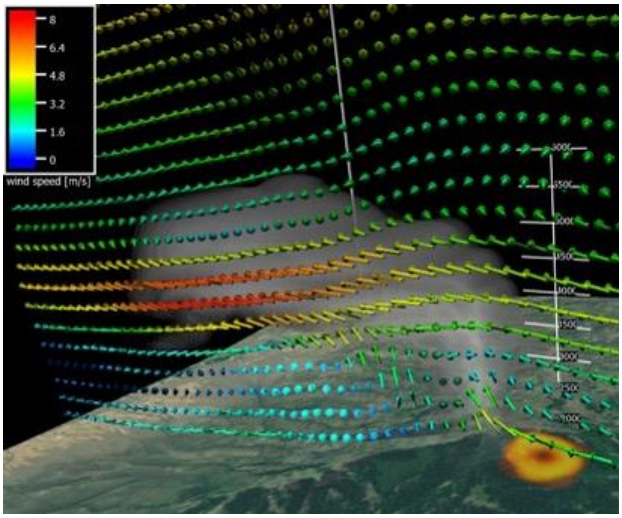

Figure 1. Example of a fire-induced circulation simulated by WRF-SFIRE, a coupled fire-atmosphere model, for Langdon Burn in Utah National Forest, November 7th 2019.

At present, no suitable datasets exist for validating and improving current and future coupled fire-atmosphere models that predict the spread and impact of landscape-scale wildfires (i.e., 1000s of acres). While validation datasets exist for small-scale fires (e.g., Craig B Clements et al. 2007; C B Clements et al. 2014; Craig B. Clements et al. 2019; Ottmar et al. 2016), the physics of landscape-scale fires are different, with processes such as long-range spotting, strong fire-induced winds, large vortex formation, and pyrocumulonimbus (pyroCB) development impacting fire processes.

CalFiDE has been designed to address this problem by integrating airborne and terrestrial remote sensing systems to simultaneously characterize fire behavior, plume dynamics and local circulations near the fireline. Data will be acquired using a rapid deployment strategy during active fires with a combination of airborne infrared (IR) camera systems, airborne Doppler lidar, truck-mounted scanning Doppler radar, and a suite of truck/trailer mounted scanning Doppler lidars. These observations will resolve process-level details of the fire (rate of spread, fire radiative power, etc.), fire-induced winds, plume rise dynamics, and pyroCb development. This sampling approach will provide the necessary data to validate model forecasts and diagnose deficiencies in model physics.

2. Sensor description

The primary objective of CalFiDE is the spatially and temporally resolved observation of fire dynamics and micrometeorology in the fire environment. Consequently, the main sensing packages designed to be deployed during this experiment include (a) an airborne Doppler lidar to characterize the wind field around the fire and plume, (b) an infrared multispectral imaging system to track fire progression and measure fire behavior, and (c) a set of ground-based mobile radar and lidar sensors to characterize vertical winds, smoke plume dynamics and boundary layer evolution. In addition, a number of physical and chemistry sensors will be installed on the aircraft to make in-situ measurements of flight-level thermodynamic conditions as well as air chemical composition. Table 1 summarizes CalFiDE's sensing capabilities, whereas the rest of this section provides additional detail on the main instrumentation.

Table 1: Summary of CalFiDE's sensing capabilities.

Sensor	Deployment strategy	Measuring capabilities	Resulting data products
Airborne Doppler Lidar	Airborne	Partial hemispheric scans of wind speed and direction	Horizontal wind profiles and vertical motion in the fire area
Visible camera	Airborne	3-band color images	Contextual visual information about the fire scene
Mid-wave IR camera	Airborne	Broad-band irradiance in the midwave infrared range	Fire Radiative Power, Brightness Temperature, identification of flaming vs. smoldering areas
Long-wave IR camera	Airborne	Broad-band irradiance in the longwave infrared range	Fire geometry, fire line location, fire rate of spread, identification of flaming vs. smoldering areas
NightFox	Airborne	Scanning radiometers @ 1.6μm & 4μm (± 30°)	Spatially resolved Fire Radiative Power
NOxCaRD & PICARRO	Airborne	NO_x , NO_Y, O_3, CO and GHG	Ozone Photochemistry and Fire Impacted Urban O_3
Ka-Band Polarimetric Doppler Radar	Ground-based, mobile	Radar reflectivity, radial velocity, and polarization	Fine-scale kinematics and microphysical properties of active wildfire smoke plumes
Scanning Doppler Lidars	Ground-based, mobile	Lidar backscatter intensity and radial velocity	Smoke plume dynamics, kinematics, horizontal wind fields and turbulent properties

2.1. Airborne Doppler Lidar

Dynamics of the plume and wind fields surrounding the fires will be measured using a Doppler lidar installed on board the NOAA Twin Otter aircraft. Combined with a partial hemispheric scanner that allows for measurements both below and above the aircraft, the lidar will provide profiles of the horizontal wind field, vertical motions, and aerosol backscatter intensity throughout the boundary layer. Figure 2 shows the morphology (a) and vertical motions (b) of a fire plume emanating from a fire shown as a red hot spot in the ground track. The horizontal wind profile, shown as colored arrows pointing in the direction of flow in the foreground, indicates 5 m/s flow with a strong directional shear layer at 1000m. In Figure 2b upward motions in the plume are shown in warm colors.

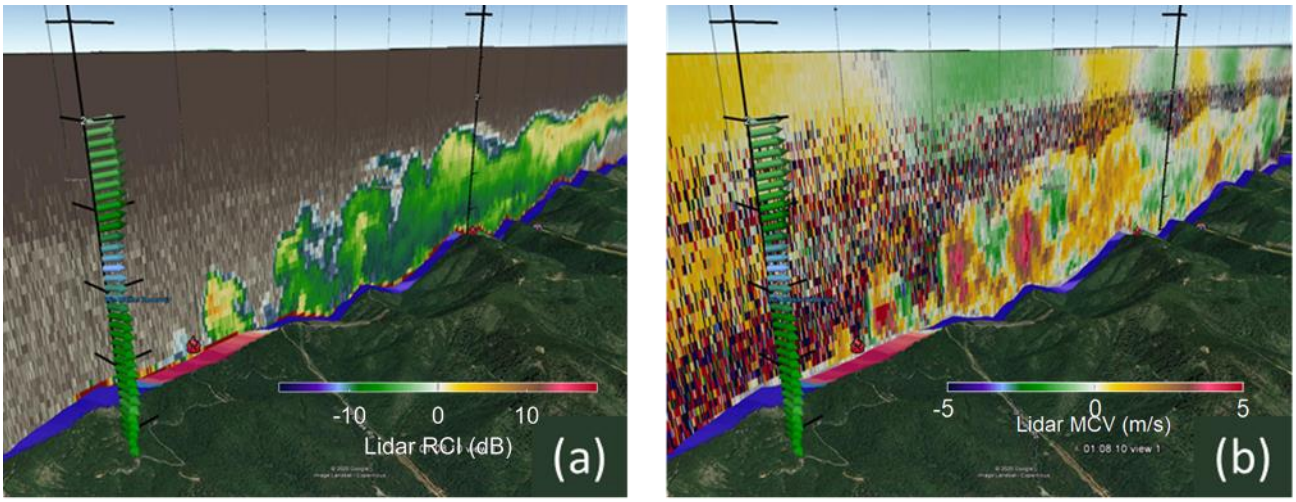

Figure 2: Doppler lidar data from a wildland fire during a previous NOAA field campaign on the Twin Otter. The red area at the surface indicates the fire area. Arrows on the left axis of each figure indicate horizontal wind speed and direction. The colored fields indicate; (a) aerosol backscatter intensity, and (b) vertical velocity.

2.2. Airborne Infrared Imaging System

Fire behavior will be monitored using a combination of optical sensors operating in the visible, medium-infrared (3.9 μm), and thermal-infrared (8-14 μm) spectral ranges. This selection of bands will allow measuring fire

location, fireline geometry, rate of spread, and fire radiative power with a spatial resolution of about 3m for a nominal flight altitude of 11,000 ft. The across-track swath sampled by the camera system will be ~2 km. All optical sensors will be mechanically coupled to an inertial navigation system (INS) which will provide geolocation and attitude information for image direct georeferencing. Raw inertial navigation measurements taken in real time will be corrected after the mission using Post-Processing Kinematics (PPK). Furthermore, direct georeferencing outcomes will be refined using image processing algorithms like those described in (Valero, Jimenez, et al. 2018; Valero et al. 2021). The resulting georeferenced imagery will be analyzed using the methodology developed by (Valero, Rios, et al. 2018) and it will also be used for the identification of spot fires. Figure 3 shows an example of observations collected using this methodology in a previous small-scale experiment.

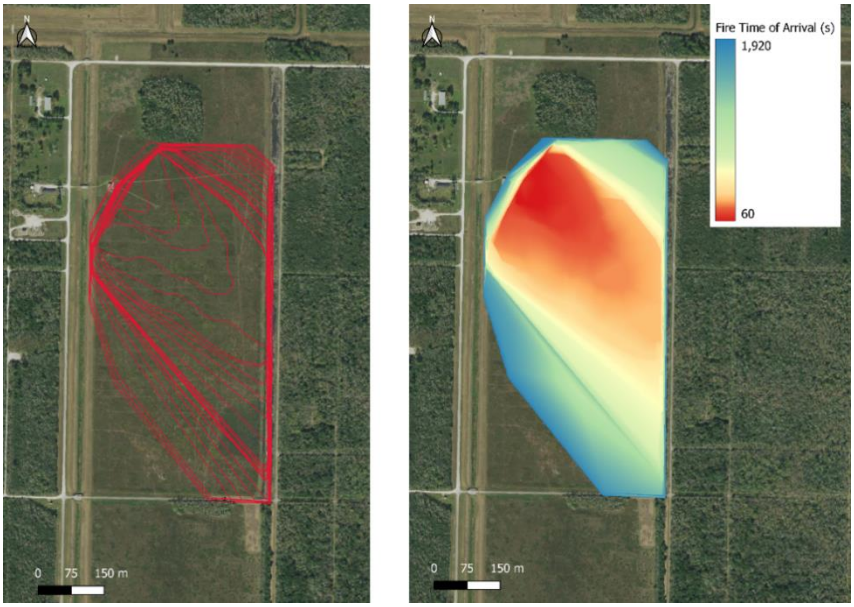

Figure 3. Fire progression during the FireFlux II experiment (Clements et al., 2019) derived from airborne IR imagery. Left: fire perimeter at 60-s intervals. Right: fire time of arrival at every location in the burn unit, relative to the time of ignition. Base image provided by the USDA National Agriculture Imagery Program.

2.3. Ground-Based Mobile Radar

Time-and-space resolved observations of wildfire plume structure will be generated with SJSU's truck-mounted scanning Ka-band (35 GHz, 8-mm) fully polarimetric Doppler radar (SKAR). These data will quantify plume volume, plume injection height, and pyroCu/Cb initiation. SKAR has a narrow beam width (0.33°), 15 km range, and range gate resolution of up to 5 m, and scans the full upper hemisphere in ~ 2 minutes. The SKAR's capabilities in probing wildfire plumes is well-established (Aydell and Clements 2021). Figure 4 shows SJSU's truck mounted Doppler radar (a) and Doppler lidar (b).

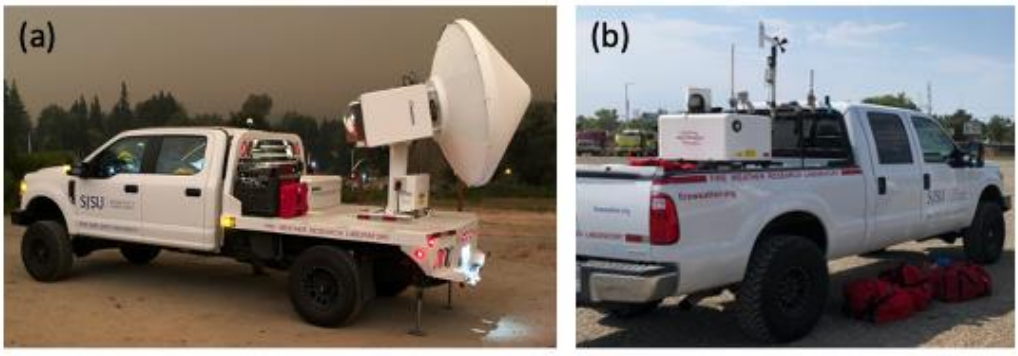

Figure 4. SJSU's Doppler Ka-band radar (a) and Doppler lidar (b).

2.4. Ground-Based Mobile Lidars

Two scanning Doppler lidars (SJSU, UNR) will be deployed within 1-2 km of the fire front to characterize plume structures and dynamics and atmospheric vertical wind profiles and boundary layer evolution. These data are critical for understanding the coupling of fire and atmospheric processes that can drive rapid fire spread and intensification.

Additionally, a NOAA motion-stabilized truck-based lidar will measure convective boundary layer (CBL) depth, vertical velocity variance, and horizontal wind profiles proximal to the fire, but away from the fire front.

3. Experiment design

The project will be headquartered in San Jose, CA between August 14 and September 30, 2022. Ground-based instruments will be staged on the SJSU campus. The research aircraft will be staged at the San Jose International Airport (KSJC), or other ad-hoc flight bases as necessary. Instruments and crews will deploy to wildfires on a day-to-day basis within intensive observing periods (IOPs).

IOPs will be declared one to three days in advance. Five IOPs are planned, each up to 3 days, yielding a total of 15 research days for the ground assets. Observations will typically occur from 12 AM to 8 PM (local time) in order to capture peak fire behavior. The aircraft will make two afternoon flights, separated by refueling. Operations meetings will be held each morning and evening to examine weather and fire conditions, research objectives, and instrument sitting.

Potential “blow-up” fires will be identified through a combined examination of weather, fire and plume development, fuels, topography, and simulated fire growth. UNR and SJSU forecasters will provide daily weather briefings to monitor conditions conducive for “blow up” fires. Satellite IR and NIROPS fire perimeters will be used to track day-to-day fire growth. NEXRAD radar, visible satellite, and webcam networks will be used to track plume development. Maps of topography, fuel type, fuel load, and fire history will be used to estimate growth potential for active fires. Finally, once a fire of interest is identified, an existing “point-and-click” web interface for the WRF-SFIRE simulator (WRFXPY) will be used to predict the expected mesoscale weather evolution and fire growth for a 54-hour window.

Aircraft flight paths will typically follow a “lawn mower” crosswind pattern just upwind of the plume core. An emphasis will be placed on keeping the head fire within the 2 km scan swath of the IR instrumentation. Flight altitudes will be confined between the Temporary Flight Restriction (TFR, ~10,000 ft) and 16,000 ft, which is the flight ceiling. Truck-mounted radars and lidars will deploy to safe locations within 5 km of the head fire. Where possible the locations will be distributed to provide view angles with >30° of separation to measure different components of the wind. Previous deployments have used scenic overlooks, rest stops, reservoirs, ski areas, helipads and airports, and open meadows as safe locations with good field of view.

4. References

Aydell TB, Clements CB (2021) Mobile Ka-band Polarimetric Doppler Radar Observations of Wildfire Smoke Plumes. Monthly Weather Review 1247–1264. doi:10.1175/mwr-d-20-0198.1.

Clements CB, Davis B, Seto D, Contezac J, Kochanski A, Fillipi J-B, Lareau N, Barboni B, Butler B, Krueger S, Ottmar R, Vihnanek R, Heilman E, Flynn J, Jenkins M, Mandel J, Teske C, Jimenez D, O’Brien J, Lefer B (2014) Overview of the 2013 FireFlux II grass fire field experiment. ‘Adv. For. fire Res. - Proc. 7th Int. Conf. For. Fire Res.’ pp. 392–400 doi:10.14195/978-989-26-0884-6_43.

Clements CB, Kochanski AK, Seto D, Davis B, Camacho C, Lareau NP, Contezac J, Restaino J, Heilman WE, Krueger SK, Butler B, Ottmar RD, Vihnanek R, Flynn J, Filippi J-B, Barboni T, Hall DE, Mandel J, Jenkins MA, O’Brien J, Hornsby B, Teske C (2019) The FireFlux II experiment : a model-guided field experiment to improve understanding of fire – atmosphere interactions and fire spread. International Journal of Wildland Fire 28, 308–326. doi:10.1071/WF18089.

Clements CB, Zhong S, Goodrick S, Li J, Potter BE, Bian X, Heilman WE, Charney JJ, Perna R, Jang M, Lee D, Patel M, Street S, Aumann G (2007) Observing the Dynamics of Wildland Grass Fires: FireFlux - A Field

Validation Experiment. Bulletin of the American Meteorological Society 88, 1369–1382. doi:10.1175/BAMS-88-9-1369.

Ottmar RD, Hiers JK, Butler BW, Clements CB, Dickinson MB, Hudak AT, O'Brien JJ, Potter BE, Rowell EM, Strand TM (2016) Measurements, datasets and preliminary results from the RxCADRE project–2008, 2011 and 2012. International Journal of Wildland Fire 25, 1–9.

Valero MM, Jimenez D, Butler BW, Mata C, Rios O, Pastor E, Planas E (2018) On the use of compact thermal cameras for quantitative wildfire monitoring. 'Adv. For. Fire Res. 2018'. (Ed DX Viegas) pp. 1077–1086. (University of Coimbra Press) doi:10.14195/978-989-26-16-506_119.

Valero MM, Rios O, Pastor E, Planas E (2018) Automated location of active fire perimeters in aerial infrared imaging using unsupervised edge detectors. International Journal of Wildland Fire 27, 241–256. doi:10.1071/WF17093.

Valero MM, Verstockt S, Butler BW, Jimenez D, Rios O, Mata C, Queen L, Pastor E, Planas E (2021) Thermal Infrared Video Stabilization for Aerial Monitoring of Active Wildfires. IEEE Journal of Selected Topics in Applied Earth Observations and Remote Sensing 14, 2817–2832. doi:10.1109/JSTARS.2021.3059054.

The FireLoc System - Geolocating Forest Fires with Crowdsourced Data

Cidália C. Fonte*[1,2]; Alberto Cardoso[3]; Jacinto Estima[3,4]; José-Paulo de Almeida[1,2]; Joaquim Patriarca[2,3]

[1] University of Coimbra, Department of Mathematics, Apartado 3008, EC Santa Cruz, 3001-501 Coimbra, Portugal, {cfonte@uc.pt}, {zepaulo@mat.uc.pt}
[2] INESC Coimbra, DEEC, Rua Sílvio Lima, Pólo II, 3030-290 Coimbra, Portugal, {jpatriarca@mat.uc.pt}
[3] University of Coimbra, Department of Informatics Engineering, Center for Informatics and Systems of the University of Coimbra (CISUC), Rua Sílvio Lima, Pólo II, 3030-290 Coimbra, Portugal, {alberto, estima}@dei.uc.pt
[4] IADE, Universidade Europeia, Av. Dom Carlos I 4, 1200-649 Lisboa, Portugal

**Corresponding author*

Keywords

Wildfire detection; crowdsourced data; smartphones; geolocation

Abstract

The FireLoc system aims to allow the reporting of forest fires observed by citizens using a dedicated app developed for mobile devices. The collected data includes the observer's geolocation, a photograph of the observed event, and the orientation of the observer towards the fire. These data are integrated into the FireLoc system, which also includes other types of georeferenced data about the terrain, including, e.g., land cover and slope information. The system processes the collected data and identifies the geolocation of the observed events in near real-time. This may enable a fast geolocation of fire events and also assist in monitoring the progress of the fire. This short paper briefly describes the FireLoc System that comprises three components: 1) a data collection component developed for mobile platforms; 2) a data integration and processing component, in charge of processing the collected data and assessing the most probable location of the fire event considering the reliability of the contributed data; and 3) a component for providing information to relevant institutions and the general public, which is developed for both mobile and desktop platforms and allows to monitor the progress of the reported events.

1. Introduction

Due to climatic changes and human intervention in the environment, the frequency and severity of forest fires are increasing in several regions, a phenomena that is likely to increase even further in the next few years (e.g., Cleetus & Mulik, 2014). As these events may become uncontrollable over the right atmospheric, land cover and topographic conditions (e.g., Liu et al., 2015; Viegas, 2012; Rossa, 2015), as occurred in Portugal in 2017, it is very important to be able to geolocate ignitions as soon as possible. Several types of systems are used for this purpose, including human observers at observation towers or complex systems using digital cameras and Unmanned Aerial Vehicles (UAV). However, these systems have limitations and do not cover all locations. In some cases, they are not able to collect data near the event or, such as the UAV systems, are only able to monitor a relatively limited region and therefore may only be used when a given event has already been detected. On the other hand, many regions include villages and roads crossing forested areas, which means there may be citizens in the proximity that may help to geolocate fires at an early stage by sending data in real time, should a system be available to facilitate those contributions. This is the aim of the FireLoc system (https://fireloc.org), currently under development in the context of a project funded by the Portuguese Foundation for Science and Technology (Fundação para a Ciência e Tecnologia - FCT). This paper briefly describes the components of the FireLoc system, with emphasis on the ones that enable the interaction with users.

Other approaches based on crowdsourced data have been proposed, using, e.g., data extracted from social media (e.g., Al-Salehi et al., 2021; Tavra et al., 2021; Arapostathis & Karantzia, 2019) or dedicated apps, such as the CITISENS project in Greece (Bogdos & Manolakos, 2019). However, the geolocation with data collection from social media has many limitations, including the data and metadata obtained using the available social media

APIs (Fontes et al., 2017). Regarding projects using dedicated apps, to the best of the authors knowledge, none is available for general use. Also, none uses the FireLoc methodology to geolocate the observed events, which is based on the intersection of estimated lines of sight. For example, the CITISENS project uses a methodology that geolocates the events using additional data collected from the smartphone, such as gyroscope and accelerometer data, to identify the observer's line of sight and geolocates the observed fire events by intersecting the estimated line of sight with a Digital Elevation Model. The authors stated that the geolocation estimated following such methodology provided accurate results (Bogdos & Manolakos, 2019), even though it assumes that the observer has a direct line of sight to the fire (i.e., it would not work in case the observer is just seeing a column of smoke). Therefore, it would be interesting, in a subsequent stage, to compare the geolocation accuracy obtained with both approaches and determine if the fusion of both methodologies is able to increase the accuracy of the geolocation of observed events.

2. The FireLoc System

The FireLoc system is composed by three main components that include several modules (Fonte et al., 2021), namely: 1) a data collection component, which includes a mobile app enabling citizens to upload data, and modules to collect other types of geospatial data, such as satellite imagery, meteorological data, or data from the OpenStreetMap project (https://www.openstreetmap.org/); 2) the data processing and validation component, containing a central core module complemented by modules to: a) geolocate the observed events using data uploaded by citizens, b) assess the reliability of citizen contributions and classify the uploaded photographs as showing fire or smoke, and c) estimate the risk associated to the computed location of the observed events and its neighbourhood; 3) the interfaces component, which includes a graphical user interface to be used by end-users, and a back-office interface for system administrators. Further details on the components that enable the interaction with the citizens are given in section 3, for the FireLoc app, and section 4, for the FireLoc portal.

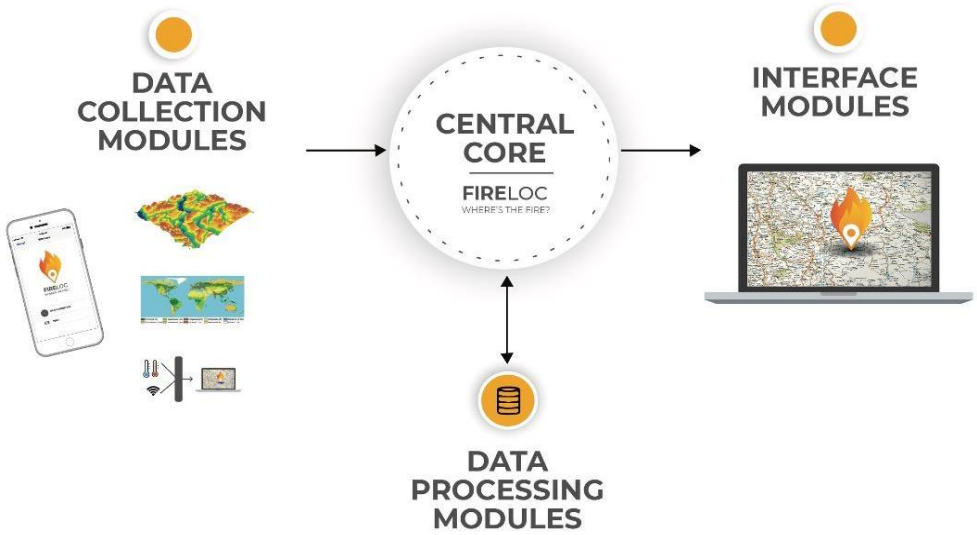

Figure 1- The FireLoc system.

3. The FireLoc app

The FireLoc app was developed to collect the data contributed by citizens. So far it is only available in Portuguese. Figure 2 shows the interfaces of some of the steps related to the data collection process, namely the geolocation, the orientation towards the fire, and the photograph collection steps.

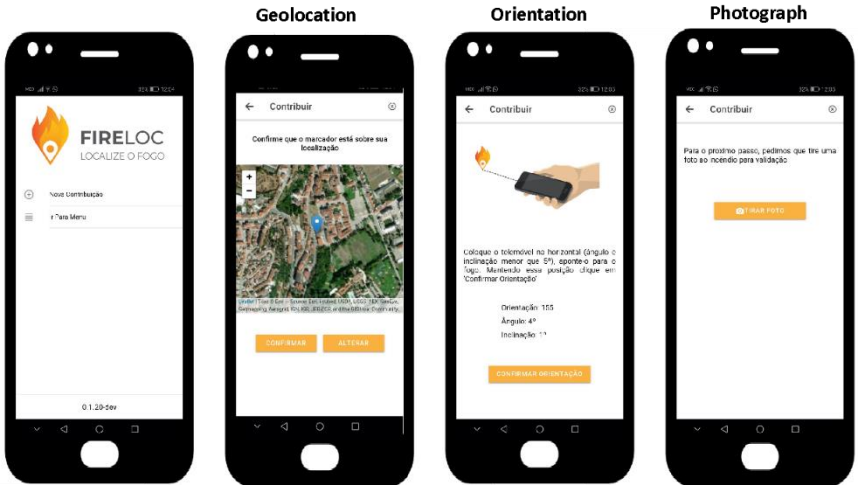

Figure 2- The FireLoc app

Part of the data required by the system are collected automatically by the app using the mobile device sensors when the volunteer starts a contribution, such as the observer geolocation (even though the volunteer may correct it over a map), the date and the time of observation. To collect other necessary data, the volunteer needs to follow a set of steps, indicated by the app, which include:

1. Orientation towards the observed fire and recording of the magnetic azimuth;
2. Orientation towards the fire and taking a photograph of the observed event.

The collection of the above-mentioned data is mandatory, and the contribution can only be uploaded if these steps are followed. However, the volunteer may also upload additional data, which will be useful to assess the quality and validity of the contribution. As in any projects involving citizen participation, a crucial aspect is related to their willingness to contribute. Therefore, there has to be a balance between the data that system administrators would like to collect and the data the volunteers are willing to provide. Due to this constraint, even though potentially useful, the contribution of additional data was considered to be optional at the current version, to avoid overloading the volunteer with too many mandatory steps. These additional data include:

1. Orientation towards the volunteer's shadow and measurement of the magnetic azimuth;
2. Additional geolocation after the volunteer moves backward or forward in the direction of the fire;
3. The indication of the approximate distance to the fire;
4. A short text message with any information the volunteer may consider useful.

The measurement of the magnetic azimuth in the direction of the volunteer's shadow is useful to compare the bearing measured by the mobile device with the known bearing of the shadow at the observation location, date and time. This will provide information about the order of magnitude that can be expected in the orientation measured by the mobile device, which can help avoiding large errors usually associated with the bearings measured by mobile devices (Fonte et al. 2022). The repeated geolocation after the volunteer's movement in the direction of the fire provides additional data to estimate the orientation towards the event. The estimate distance to the fire, even though difficult to provide by a volunteer, may be a useful insight to determine if the fire is in the close proximity of the observer's position (i.e., a few hundreds of metres) or farther away (i.e., several kilometres away). Finally, text messages may provide additional information about, for example, the stage, severity or level of dangerousness of the event.

4. The FireLoc portal

The FireLoc portal (see Figure 3) includes a webpage where information about the project is available, and a Geoportal where several types of data may be visualized (Figure 4). The data available for visualization depends upon the type of user. Four types of users were considered:

1. Common users, not registered in the system;
2. Registered users with the "volunteer profile";
3. Registered users with privileged permissions (e.g., civil protection agents or firefighters)
4. System administrators.

Among the data available for visualization are:

- The events geolocation and evolution identified with the data provided by the citizens, within a specific interval of time or a selected region. When the user has the required permissions, these may be visualized in real time, or only in the aftermath of the event;
- Citizen contributions (different data are available depending on the type of user);
- Statistical analyses and graphs about the reported events and contributions;
- Several types of ancillary geospatial data, including land-use/land-cover maps, digital elevation models, slope maps, cartography of built-up areas, or maps of the burnt areas obtained, e.g., from satellite imagery classification.

Data available in the portal may be used in real-time to geolocate events reported by citizens. The analysis of these data may help to geolocate the event and provide a better insight about the fire, e.g., through the observation of collected photographs, which may offer useful details about the event to decision makers (e.g., the dimension or spread at the time of the contribution, or the characteristics of the landscape). Other geospatial datasets available in the system may provide additional useful information, such as the proximity to inhabited areas or the regions vulnerability to fire propagation.

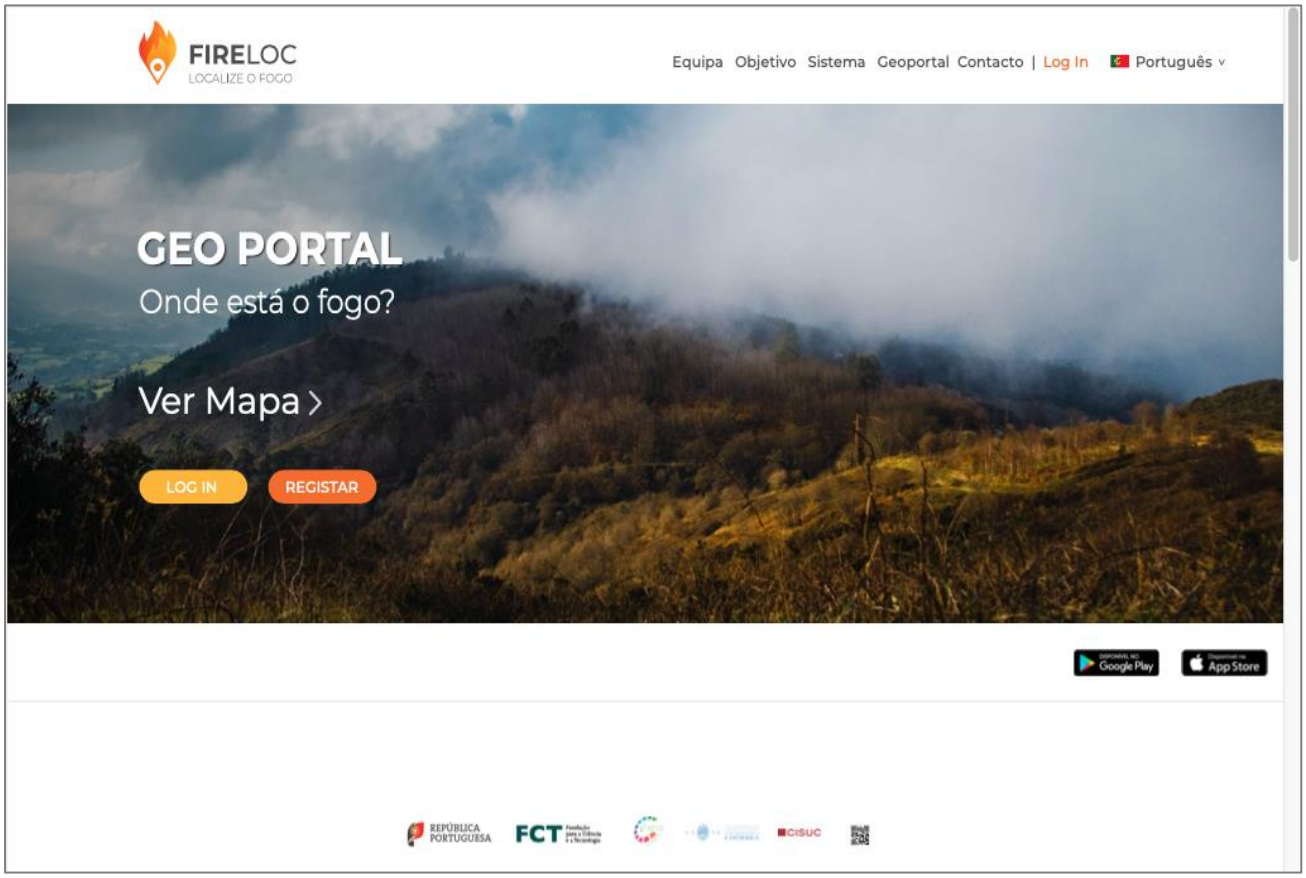

Figure 3- The FireLoc portal initial page.

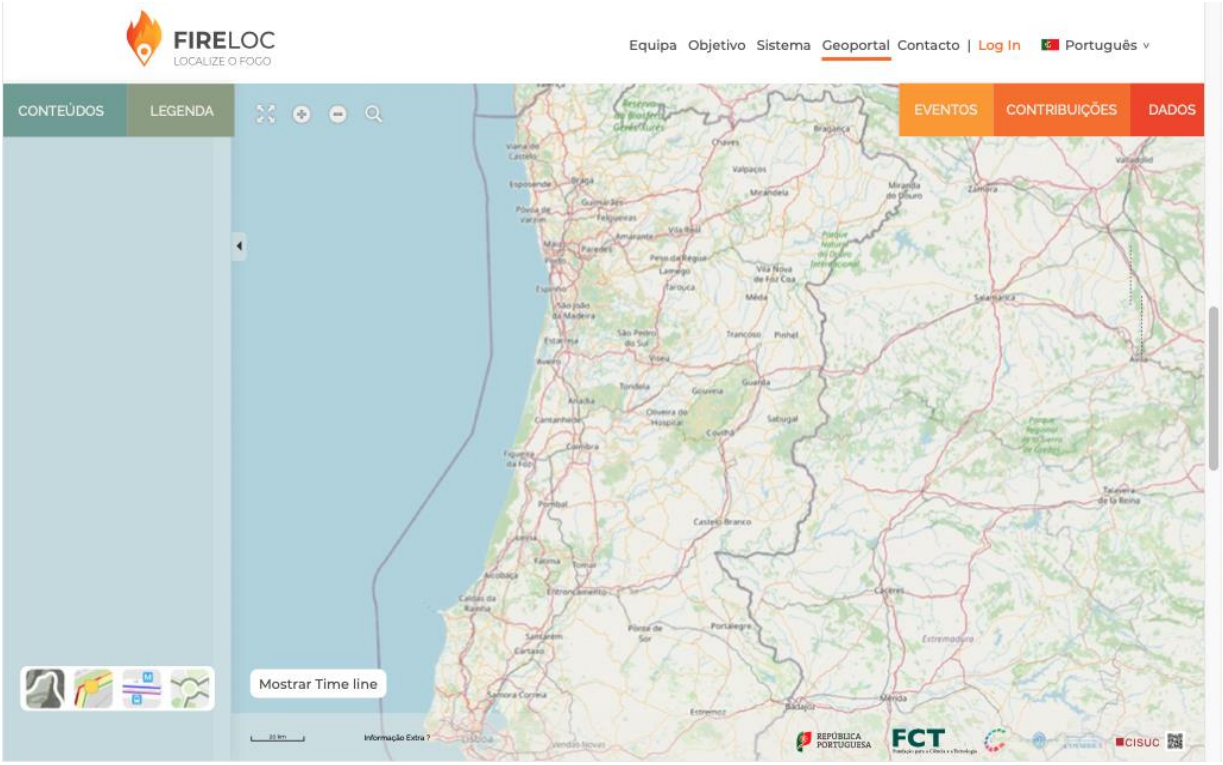

Figure 4- The FireLoc geoportal.

5. Conclusions

The FireLoc system will enable the collection of geospatial data provided by citizens that may assist in fire detection and monitoring. The uploaded photographs will enable the early visualization of the event by authorities, which proved to be crucial in previous experiments (Albuquerque et al. 2016). The geolocation of both the observer and the event may provide key information, especially in cases where reported events are not spotted by official personnel in observation towers or more complex systems, but only through a phone call to the emergency number 112 (where the geolocation of the event is made only based on the observer's oral description). Moreover, the processing of the collected data will provide additional information about the fires, that may be very useful both in real time analysis but also when analysing past events.

6. References

Albuquerque, J. P. D, Fonte, C.C., de Almeida, J.-P., Cardoso, A. (2016). How volunteered geographic information can be integrated into emergency management practice? First lessons learned from an urban fire simulation in the city of Coimbra. Proceedings ISCRAM 2016 Conference - 13th Annual Conference for Information Systems for Crisis Response and Management, 22-25 May 2016, Rio de Janeiro, Brazil. http://idl.iscram.org/files/joaoportodealbuquerque/2016/1353_JoaoPortodeAlbuquerque_etal2016.pdf

Al-Salehi, M., Nerantzis, E., Masa, G., & Rossi, C. (2021). SAFERS - Structured Approaches for Forest fire Emergencies in Resilient Societies—Deliverable D6.8 (D6.8; p. 46). SAFERS Consortium. file:///C:/Users/cfonte/AppData/Local/Temp/SAFERS_D6.3_Dissemination%20and%20communication%20plan%20-%20Issue%201.pdf

Arapostathis, S., & Karantzia, M. (2019). Mapping Information of Fire Events, from VGI Source (Twitter), for Effective Disaster Management (in Greece); The Fire of North-East Attica, August 2017, (Greece) Case Study: IEREK Interdisciplinary Series for Sustainable Development (pp. 257–260). https://doi.org/10.1007/978-3-030-01440-7_6

Bogdos, N., & Manolakos, E. S. (2019). Crowd-Sourced Wildfire Spread Prediction With Remote Georeferencing Using Smartphones. IEEE Access, 7, 102102–102112. https://doi.org/10.1109/ACCESS.2019.2931456

Cleetus, R., Mulik, K. (2014). Playing with Fire - How Climate Change and Development Patterns Are Contributing to the Soaring Costs of Western Wildfires. Union of Concerned Scientists. Accessed March 25th 2021, at: https://www.ucsusa.org/sites/default/files/legacy/assets/documents/global_warming/playing-with-fire-report.pdf

Fonte, C.C., Cardoso, A., Estima, J., de Almeida, J.-P., Patriarca, J. (2021). The FireLoc Project: Identification, Positioning and Monitoring Forest Fires with Crowdsourced Data. FIG e-Working Week 2021. 21-25 June 2021, Amsterdam, The Nederlands.

Fonte, C.C., Patriarca, J., de Almeida, J.-P., Cardoso, A., Estima, J., Silvestre, D. (2022). Quality assessment of positioning and orientation data collected by mobile devices. Research Report INESC Coimbra. ISSN 1645-2631.

Fontes, D., Fonte, C. C., Cardoso, A., Almeida, J. P., & Estima, J. (2017). A platform to integrate crowdsourced, physical sensor and official geographic information to assist authorities in emergency response. Proceedings of the 20th AGILE International Conference on Geographic Information Science. 20th AGILE International Conference on Geographic Information Science, Wageningen, Netherlands.

Liu N., Wu J., Chen H., Zhang L., Deng Z., Satoh K., Viegas D. X., Raposo J.R. (2015). Upslope spread of a linear flame front over a pine needle fuel bed: The role of convection cooling. Proceedings of the Combustion Institute, Volume 35, Issue 3, 2015, pp. 2691- 2698.

Viegas, D.X., (2012). Extreme Fire Behaviour. In: Armando C. Bonilla Cruz and Ramona E. Guzman Correa (Ed.), Forest Management: Technology, Practices and Impact. Nova Science Publishers, pp. 1-56.

Rossa C.G., Davim D., Viegas D.X., (2015). Behaviour of slope and wind backing fires. International Journal of Wildland Fire. Volume 24, Issue 8, pp. 1085-1097.

The FireLoc system - methodologies for geolocating the observed fires

Cidália C. Fonte*[1,2]; Ismael Jesus[2,3], Cédric Pereira[4]; Alberto Cardoso[3]; Jacinto Estima[5,6]; Joaquim Patriarca[2,3]; José-Paulo de Almeida[1,2]

[1] University of Coimbra, Department of Mathematics, Apartado 3008, EC Santa Cruz, 3001-501 Coimbra, Portugal, {cfonte@uc.pt}, {zepaulo@mat.uc.pt}
[2] INESC Coimbra, DEEC, Rua Sílvio Lima, Pólo II, 3030-290 Coimbra, Portugal, {ijesus@uc.pt}, {jpatriarca@mat.uc.pt}
[3] University of Coimbra, Department of Informatics Engineering, Center for Informatics and Systems of the University of Coimbra (CISUC), Rua Sílvio Lima, Pólo II, 3030-290 Coimbra, Portugal, {alberto@dei.uc.pt}
[4] Instituto de Astrofísica e Ciências do Espaço, Department of Physics, Faculty of Sciences, University of Lisbon, Campo Grande, 1749-016 Lisboa, Portugal, {cppereira@fc.ul.pt}
[5] IADE, Universidade Europeia, Av. Dom Carlos I 4, 1200-649 Lisboa, Portugal {jacinto.estima@universidadeeuropeia.pt}
[6] INESC-ID, Rua Alves Redol 9, 1000-029 Lisboa, Portugal

**Corresponding author*

Keywords

Crowdsourced data; event geolocation; GNSS positioning; bearing measurement; error

Abstract

The FireLoc system aims at geolocating forest fires observed by the citizens using data uploaded by them through a dedicated app developed for mobile devices. The collected data includes the location of the observer (determined with the Global Navigation Satellite System receiver embedded in the device), the magnetic bearing registered by the mobile device when facing the fire and the approximate distance to the fire. However, due to the errors that may be associated with the measurement of the magnetic bearing an additional measurement is collected with the app, which is the magnetic bearing measured when the volunteer is facing his/her shadow. Even though the collection of this data is not mandatory to upload a contribution at the current version of the app, it may be very useful to estimate the error associated with the measurement of the magnetic bearing. This short paper describes the process to determine the location of the observed fire with the collected data, without considering the error associated with the measurement of the orientation and when this error is considered by using a fuzzy approach to identify the region where the fire is more likely to be located.

1. Introduction

The FireLoc project aims to provide to the citizens a tool that can be used to upload data about forest fires. This data is collected using a dedicated app, and includes the geolocation of the observer, computed with the Global Navigation Satellite System (GNSS) receiver embedded in the mobile device, the magnetic bearing measured when facing the fire, the approximate distance to the fire and the magnetic bearing measured when facing the observer's shadow. This last two values are not mandatory in the present version of the app, so that the process to contribute does not include too many steps, which may demotivate the volunteer. However, this last data may turn out to be very useful to estimate the orientation errors, which may be very large (e.g., Kuhlmann et al., 2021; Fonte et al., 2022, Novakova, 2017). In this short paper we present the procedure used to geolocate the fires using these data.

2. Base strategies for fire positioning

The fire positioning is based upon the following approaches:

1. Positioning with the observer's geolocation and the distance between the observer and the fire.
2. Positioning considering the intersection of at least two contributions.
3. Positioning considering the intersection of at least two contributions and the estimated error in the orientation extracted from the orientation to the observer's shadow.

The first two approaches are further explained in the next subsections, while the third is explained in section 3.

2.1. Positioning with the observer's location and the distance

If only one observation is uploaded, it is possible to know in which direction the event was observed but not to position it exactly unless the observer indicates the distance to the fire. In this case the coordinates of the fire location are obtained with equations (1) and (2), where (X_{Fire}, Y_{Fire}) are the coordinates of the fire in a projected reference systems, $(X_{Observer}, Y_{Observer})$ are the coordinates of the observer in the same reference system, *D* is the distance between both and CB_{Fire} is the cartographic bearing, computed using the measured magnetic bearing and the cartographic declination.

$$X_{Fire} = X_{Observer} + D\ sin\ (CB_{Fire}) \quad (1)$$

$$Y_{Fire} = Y_{Observer} + D\ cos\ (CB_{Fire}) \quad (2)$$

2.2. Positioning with the intersection of at least two contributions

This positioning approach requires the contribution of at least two volunteers. Figure 1 illustrates the process when four volunteers send data corresponding to the same event. Angles MB_i $(i = 1, \ldots 4)$ represent the magnetic bearings measured with the mobile device when the observers are oriented towards the fire. They are measured in the clockwise direction and vary between 0° and 360°. The intersection of each set of two observations identifies a point. If the time interval between the contributions is below a specified value (selected by the system administrator) the event location is the convex bounding box containing the points obtained with all intersections (orange polygon in Figure 1).

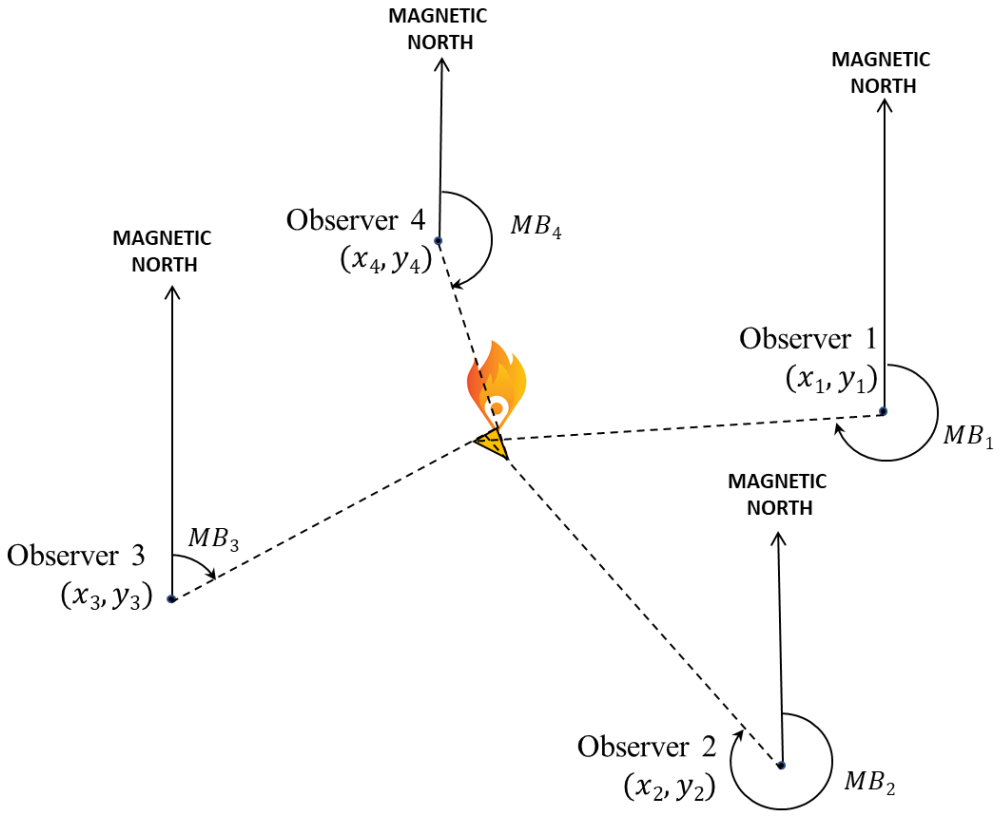

Figure 1- Event geolocation principle with the volunteers' contributions

3. Strategies for minimizing errors in the fire positioning

The positioning strategy presented in section 2.1 has always low accuracy due to the difficulty in estimating the distance to the event. Therefore, it is only used in solo if no other contributions are available. Strategy 2.2

enables the geolocation of the observed events if the observations correspond to the same event and if no significant errors are associated with both the observer's geolocation and the measure magnetic bearing. However, there are errors associated with these measurements. There may be also a time interval between the contributions, which means that the event may have moved between them. In this short paper only the first two sources of error will be addressed.

3.1. Errors associated with the measurements

The observer's positioning errors may be due to several factors, such as multipath, number and position over the horizon of the satellites used to compute the location, and the GNSS receiver characteristics. These errors are usually lower than a few hundreds of meters, even though outliers may occur (e.g., Fonte et al., 2022; Zhang et al., 2018). The errors associated with the orientation measurement may be due to, e.g., the lack of calibration of the mobile device compass, the influence of external objects with magnetic fields, the quality of the mobile device and its handling by the user. Tests have shown that these errors may have large magnitudes, which may reach a few tens of degrees. Even though these two sources of error influence the quality of the fire's geolocation, the influence of the observer's location error only generates a translation of the fire position with the same magnitude. Therefore, the effect of these errors over the fire geolocation is not important due to the level of accuracy required for this type of application, where a geolocation with an accuracy of a few hundred of meters is enough. On the other hand, the influence of the orientation errors increases with the distance between the observer and the observed fire (Fonte et al., 2021). For example, an error of 10° corresponds to a displacement perpendicular to the observation direction of 174 m if the fire is 500 m away from the observer, but it is already 3,5 km if it is 10 km away. Therefore, a strategy was developed to estimate the order of magnitude that may be associated with the measured magnetic bearing in each contribution, based on its measurement towards a known direction: the observer's shadow.

3.2. Observation strategies used to minimize the effect of observation errors

Even though the errors associated with the observer's geolocation are not critical due to the reasons explained above, the app keeps registering the geolocation during the whole time the volunteer is contributing. This enables the FireLoc system to perform a statistical analysis of its variation, including the mean location and the associated standard deviation, which is an indicator of the expected quality of the coordinates. Moreover, the volunteer can see the computed geolocation over a map and correct it if it is incorrect.

Regarding the orientation, the FireLoc app asks the user to orient himself/herself towards his/her shadow, so that the magnetic bearing can be registered. As the magnetic bearing of the shadow is known at any location over the Earth at any time, this enables the comparison of the measured value with the known value. Figure 2 illustrates this procedure, where δ represents the magnetic declination (its value is computed by the magnetic observatories and is regularly updated), AZ_{Sun} is the Sun's azimuth, MB_{SHADOW} is the shadow magnetic bearing $MB_{SHADOW}^{MEASURED}$ is the measured shadow magnetic bearing, $MB_{FIRE}^{MEASURED}$ is the magnetic bearing measured towards the fire, and ε is the estimated error in the magnetic bearing. Equation (3) shows how the magnetic bearing of the shadow is computed. Depending on the location on Earth the magnetic declination may have to be added or subtracted to the Sun's Azimuth, and, as the magnetic bearing varies between 0° and 360°, 180° needs to be added or subtracted if the Sun's azimuth is, respectively, lower or larger than 180°. Equation (4) shows how the magnetic bearing measurement error ε is computed and equation (5) how the corrected magnetic bearing towards the fire (MB_{Fire}) is obtained.

$$MB_{SHADOW} = AZ_{Sun} \mp \delta \mp 180° \quad (3)$$

$$\varepsilon = MB_{SHADOW} - MB_{SHADOW}^{MEASURED} \quad (4)$$

$$MB_{Fire} = MB_{FIRE}^{MEASURED} + \varepsilon \quad (5)$$

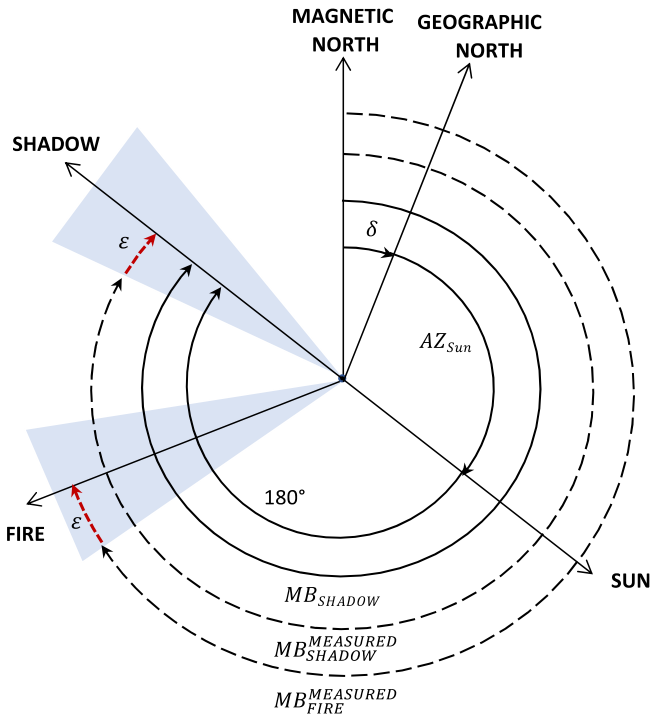

Figure 2 – Relation between the measured and computed orientations

A procedure was implemented to compute the Sun's Azimuth (AZ_{Sun}) given the observer's coordinates (latitude and longitude), the date and the time of observation. Other necessary parameters are considered constant, namely the distance between the centre of the Earth and the Sun, and the ecliptic obliquity. The algorithm requires the computation of the sideral time corresponding to the Gregorian date in the Julian calendar. Then, the Geocentric Sun's right ascension and declination is computed using the NREL's Solar Position Algorithm (SPA) (https://midcdmz.nrel.gov/solpos/spa.html) and the hour angle is computed. These data enable the computation of the altitude and azimuth of the Sun and the given location and time. The Sun's apparent position is then computed using the atmospheric refraction and geocentric parallax, and the Sun's azimuth is corrected with the diurnal aberration, computed with the observer's location (e.g., Green, 1985).

3.3. Strategies to geolocate the fire with the available data

Given the impact of the orientation errors over the fire geolocation, an approach was developed that considers the orientation towards the fire not as a line but as a region, centered at the MB_{Fire} direction and with a maximum amplitude of ε to both sides, as shown in Figure 3. A fuzzy approach was applied to express the variability of the likelihood of the fire location, considering trapezoidal fuzzy sets perpendicular to the line of sight, having a support with an amplitude of 2ε and the core an amplitude of ε as shown in Figure 3. The intersection of these fuzzy regions enables the identification of the expected fire location, where the most likely region corresponds to the core of the fuzzy region obtained with the intersection of all contributions, and the support of the fuzzy region shows all possible locations given the considered contributions (see Figure 4).

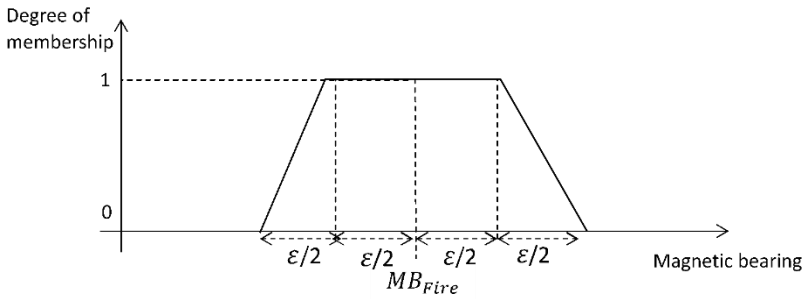

Figure 3 – Trapezoidal fuzzy intervals perpendicular to the line of sight expressing the orientation uncertainty.

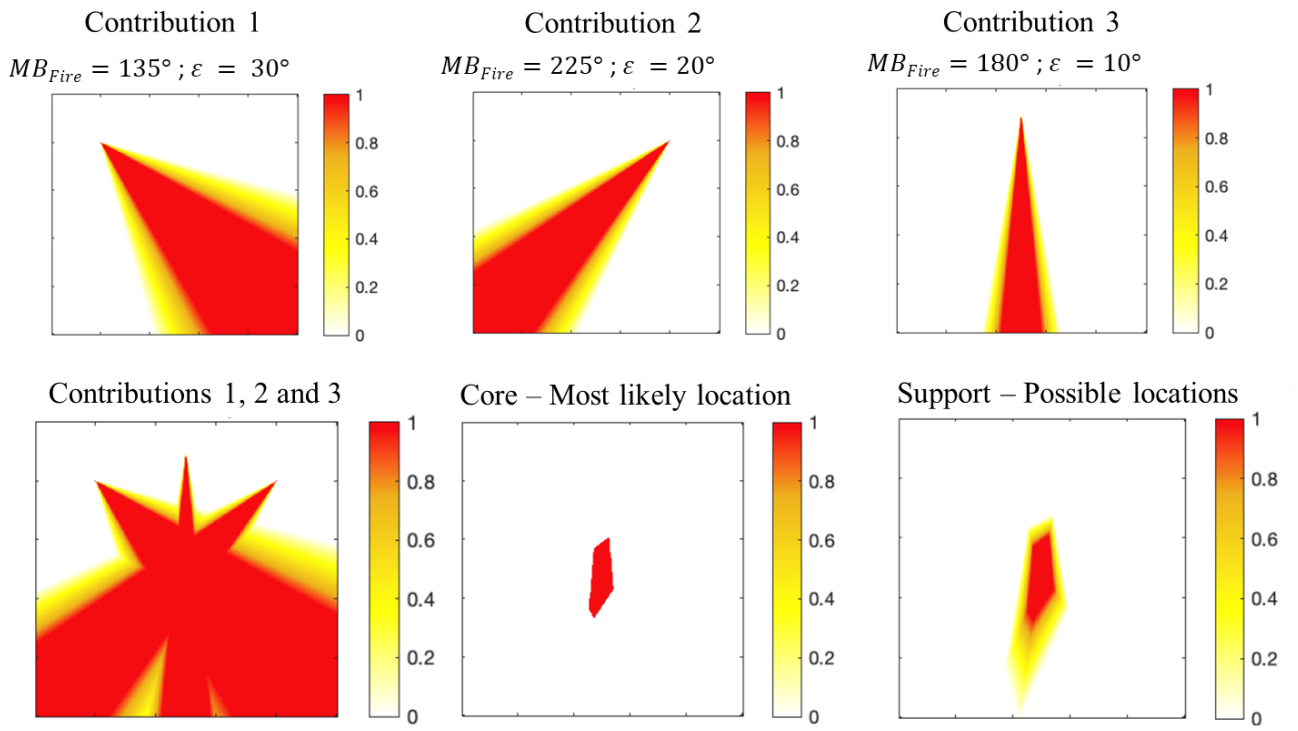

Figure 4 - Event geolocation considering the orientation errors.

4. Conclusions

This short paper describes some of the strategies developed to geolocate the fires observed by citizens with the data collected with the FireLoc app. Additional strategies will be developed based on statistical approaches and outliers' detection, so that the best strategy can be identified based on the data collected by the app.

5. References

Fonte, C.C., Cardoso, A., Estima, J., de Almeida, J.-P., Patriarca, J. (2021). The FireLoc Project: Identification, Positioning and Monitoring Forest Fires with Crowdsourced Data. FIG e-Working Week 2021. 21-25 June 2021, Amsterdam, The Nederlands.

Fonte, C.C., Patriarca, J., de Almeida, J.-P., Cardoso, A., Estima, J., Silvestre, D. (2022). Quality assessment of positioning and orientation data collected by mobile devices. Research Report INESC Coimbra. ISSN 1645-2631 (https://www.uc.pt/en/org/inescc/res_reports_docs/RR_01_2022).

Green, Robin M. (ed.) (1985) Spherical Astronomy. ISBN: 9780521317795

Novakova, L.; Pavlis, T.L. (2017) Assessment of the Precision of Smart Phones and Tablets for Measurement of Planar Orientations: A Case Study. *Journal of Structural Geology*, *97*, 93–103, doi:10.1016/j.jsg.2017.02.015.

Kuhlmann, T.; Garaizar, P.; Reips, U.-D. (2021) Smartphone Sensor Accuracy Varies from Device to Device in Mobile Research: The Case of Spatial Orientation. *Behav Res*, *53*, 22–33, doi:10.3758/s13428-020-01404-5.

Zhang, X.; Tao, X.; Zhu, F.; Shi, X.; Wang, F. (2018) Quality Assessment of GNSS Observations from an Android N Smartphone and Positioning Performance Analysis Using Time-Differenced Filtering Approach. *GPS Solut*, *22*, 70, doi:10.1007/s10291-018-0736-8.

The Impact of Terrain and Fire Duration on Boreal Fires in the LPJmL-SPITFIRE Fire-Enabled Dynamic Global Vegetation Model

Luke Oberhagemann*[1]; Markus Drüke[2]; Werner von Bloh[2]; Maik Billing[2]; Boris Sakschewski[2]; Henning Rust[3]; Kirsten Thonicke[2]

[1] *Institute of Environmental Science and Geography, University of Potsdam. Karl-Liebknecht Str. 24-25, Potsdam, Germany, {oberhagemann@uni-potsdam.de}*
[2] *Potsdam Institute for Climate Impact Research. Telegrafenberg, Potsdam, Germany, {Drueke, Bloh, Maik.Billing, Boris.Sakschewski, Kirsten.Thonicke}@pik-potsdam.de*
[3] *Institute of Meteorology, FU Berlin. Address, Kaiserswerther Str. 16-18, Berlin, Germany {henning.rust@fu-berlin.de}*

**Corresponding author*

Keywords

Dynamic Global Vegetation Model, Landscape Fragmentation, Multiple-Day Fires

Abstract

Fire-enabled Dynamic Global Vegetation Models (DGVMs) are used to model fire-vegetation interactions and their impacts on global vegetation dynamics. Previously, these DGVMs have performed poorly in the boreal zone. The challenge of modelling fires in the boreal zone has been addressed by several DGVMs by increasing fire durations, from previous limits of less than a day, to multiple days. We investigate improvements to modelling boreal fires in the LPJmL-SPITFIRE DGVM by implementing a multiple-day fire spread algorithm. In addition, we include an empirically derived terrain fragmentation function to account for the impact of terrain ruggedness on limiting fire spread for larger, longer-duration fires. Our work is conducted in two parts: first, we use satellite data to investigate the impact of terrain ruggedness on burnt area at the 0.5° by 0.5° resolution typical of DGVMs, for latitudes greater than 50°. We demonstrate that terrain fragmentation acts as a significant limit on fire size, and derive an empirical function based on our data analysis that describes this effect. The second part of our work consists of the implementation of a multiple-day fire spread algorithm in combination with the terrain ruggedness limitation function in the LPJmL-SPITFIRE model. We find that this results in a significant improvement of fire spread calculations in the boreal zone. The results of this work represent a useful addition to LPJmL-SPITFIRE, in addition to DGVMs in general that do not incorporate the effects of terrain-based landscape fragmentation.

1. Introduction

Dynamic Global Vegetation Models (DGVMs) model processes including vegetation establishment, growth, and mortality as they respond to solar radiation and global water and carbon cycles. An important component of many such models is the incorporation of a coupled fire model to calculate fire-related plant mortality as well as fire impacts on the global carbon cycle. The Lund-Potsdam-Jena managed Land (LPJmL) Dynamic Global Vegetation Model calculates vegetation dynamics on a grid with cells of size 0.5° × 0.5° and is coupled to the Spread and InTensity of FIRE (SPITFIRE) global fire model (Schaphoff et al., 2018; Thonicke et al., 2010). SPITFIRE models ignition events and fire danger, and takes a process-based approach to modelling the spread of the resulting fires, based on the Rothermel equation (Thonicke et al., 2010; Rothermel, 1972; Albini 1976). The work described herein focuses on the fire spread component of SPITFIRE, coupled with the latest version of LPJmL, LPJmL5.3.

A common issue in DGVMs has been inaccuracy in predicting fire in boreal regions (Ward et al., 2018). Fires in boreal forests often have longer durations (Andela et al., 2019). Therefore, several models have sought to improve fire modelling in boreal regions by introducing longer fire durations (Ward et al., 2018). LPJmL-SPITFIRE currently limits fire duration to a maximum of 241 minutes, relying on a modelling approach that replaces large fires with a larger number of small fires (Thonicke et al., 2010). While this approach is successful at lower latitudes, the model currently under-predicts burnt area in the boreal zone to a significant extent.

To improve upon this, we examine the impact of introducing longer fire durations in LPJmL-SPITFIRE. As a consequence of introducing these longer in duration, and therefore larger, fires, the impacts of various fuel bed fragmentation barriers on fire size become more significant. We therefore examine the impact of terrain ruggedness on limiting fire spread, and implement a function to represent this in the model.

While some fire-enabled DGVMs account for the effect of landscape fragmentation on limiting burnt area, the functions used for this are based on heuristic arguments, and are not derived from theoretical calculations or observed data, and many models omit this effect entirely (e.g. Pfeiffer et al., 2013, Rabin et al., 2017). We seek to improve upon this by deriving an empirical function, based on a satellite data analysis, that can be implemented in DGVMs. A combination of this function and multiple-day fire spread results in significant improvements to the fire spread component of LPJmL-SPITFIRE in the boreal zone.

2. Terrain Limits on Fire Spread

We examine the impact of terrain ruggedness on fire spread using the 250 m GMTED2010 Digital Elevation Model (DEM), courtesy of the U.S. Geological Survey. We compute the Vector Ruggedness Measure (VRM) at the original resolution of the DEM and take the median of this value over 0.5° × 0.5° grid cells, matching the resolution of LPJmL-SPITFIRE, using Google Earth Engine (Gorelick et al., 2017). We then compare these values for each grid cell to the size of individual fires in the grid cells from 2003 to 2016 using data from the Global Fire Atlas (Andela et al., 2019). We divide fires by the main landcover type burned and report results for landcover types with over 10 000 observed fires that have ignition points at latitudes greater than 50°.

We bin fires by VRM, with bin widths calculated using the Freedman-Diaconis rule found to produce the most consistent results. We find that the most significant impact of VRM on fire size is its role as a limit on the size of the largest fires, with significantly less impact on the median fire size calculated in each bin. The left panel in Figure 1 shows functions of the form: $\text{maximum fire size} = \frac{a}{\text{VRM}+b}$, where a and b are constants, fit to the maximum fire size in each bin using least squares regression, with R^2 values shown in the legend.

These functions collapse into two bands, with Evergreen Needleleaf Forests, Mixed Forests, and Grasslands generally having higher maximum fire sizes and Open Shrublands, Deciduous Needleleaf Forests, and Woody Savannas having smaller maximum fire sizes. A potential explanation may be that additional causes of fuel bed fragmentation beyond those due to terrain ruggedness may result in reduced fuel bed connectivity for the lower band of functions, amplifying the effect of terrain fragmentation. However, further study is required to examine the differences between the two bands.

We use the function derived for Mixed Forests for the initial implementation of a maximum fire size function in LPJmL SPITFIRE. This is due to several factors, including that 70% of fires in the landcover types we examine at latitudes over 50° fall into the upper band of maximum fire size functions, of which the mixed forest function imposes the largest limit, and that the landcover types in the lower band are not well represented in the LPJmL DGVM. The function is:

$$\text{maximum fire size} = \frac{60}{\text{VRM} + 1.6 * 10^{-4}},$$

and is plotted in the right panel of Figure 1. Maximum fire sizes in each bin, to which the function is fit, are shown in black, and raw individual fire sizes are shown in grey. This limit is significantly closer to the bulk of the fire size distribution for VRM values above 0.003, potentially due to fires before this value being extinguished before they can reach their significantly higher and, at low VRM values, potentially non-existent, maximum terrain limits. While our current implementation treats this as a fixed maximum fire size, further work should be undertaken to examine the conditions under which this limit can be surpassed due to extreme fire behaviour, in particular to avoid artificially strong fire size limitation under extreme fire conditions.

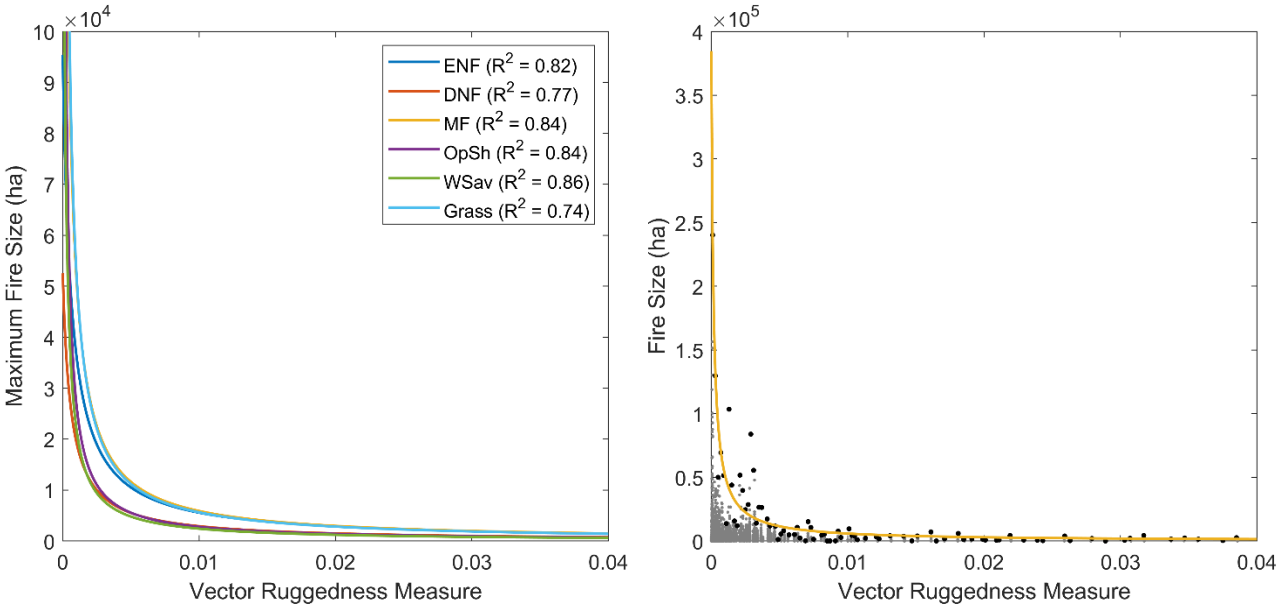

Figure 1 – Derived functions for the maximum fire size as a function of median vector ruggedness measure over a 0.5° × 0.5° grid cell for various landcover types (left panel). Abbreviations are as follows: ENF – Evergreen Needleleaf Forests, DNF – Deciduous Needleleaf Forests, MF – Mixed Forests (combinations of broadleaf and needleleaf trees), OpSh – Open Shrublands, WSav – Woody Savannas, Grass – Grasslands. The function for Mixed Forests is shown in the right panel with the bin maxima to which this function is fit as black points and individual fires from the Global Fire Atlas shown in grey.

3. Implementation into LPJmL-SPITFIRE

To improve the modelling of boreal fires in LPJmL-SPITFIRE we implement a function that calculates fire spread over multiple days. This function calculates burnt area based on fire spread in an elliptical shape, as in the original SPITIFRE formulation by Thonicke et al. (2010), with ellipses continuing their growth on subsequent days in the absence of extinction events, or the reaching of terrain limits. All active fires in a grid cell are extinguished if there is no calculated increase in fire size for any fires on a given day, or if the Fire Danger Index (FDI), which we calculate based on the Vapour Pressure Deficit (VPD) as in Drueke et al. (2019), falls below a threshold value of 0.005. While this produces reasonable results, further investigation is required to implement a more sophisticated approach to fire extinction caused by, e.g., precipitation in future versions of this model. At present we rely on the impact such events have on reducing the Fire Danger Index.

To avoid excessive computational costs, we limit the number of days that fires burn to 14. This is longer than 95% of fires in the Global Fire Atlas and should therefore not be excessively limiting. In addition, we modify the fire duration function from Thonicke et al. (2010) to allow for longer burning on individual days. The current function results in very short median fires, lasting about 1 hour even when allowing for a maximum fire duration of 12 hours. We set a fixed fire duration of 12 hours per day, relying on a reduced rate of spread to limit fire sizes under wetter conditions. We choose 12 hours per day as fire spread often reduces significantly at night (e.g. Balch et al., 2022). This may be further refined in future, e.g. by limiting fire spread to times when the VPD thresholds derived by Balch et al. (2022) are exceeded.

We examine the impact of this change in fire duration by starting a fire in the model on the day, and in the same grid cell of each fire in the Global Fire Atlas. We then compare the burnt area in the model to the Global Fire Atlas, effectively comparing the fires in the model to their observed counterparts. This approach allows for an examination of the model's fire spread calculations without the additional ambiguity introduced by the parametrization of ignition events and their conversion into spreading fires based on an FDI. Because the FDI, which requires some tuning, is only implemented in the extinction threshold, this significantly reduces the impact of tuning on the model results examined here.

Figure 2 shows a timeseries of burnt area for model simulations with multiple-day fires compared to the Global Fire Atlas, and to a previous version of SPITFIRE (described in Schaphoff et al., 2018). The implementation of multiple-day fires results in a significant improvement in the model at latitudes greater than 50°, and the implementation of terrain fragmentation fire size limits improves the model further. The previous version of SPITFIRE simulates a negligible amount of burnt area for these fires due to the low fire duration.

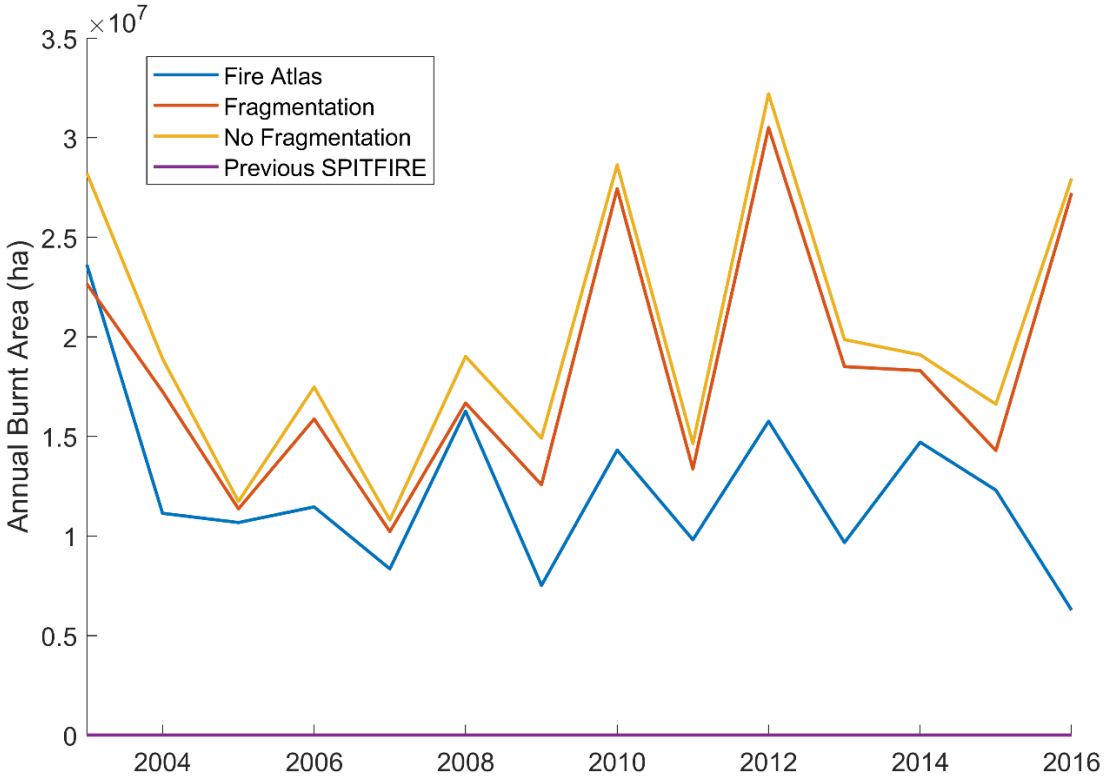

Figure 2 – Annual burnt area as a function of time for latitudes over 50° in LPJmL-SPITFIRE and for the same fires in the Global Fire Atlas. The two implementations of LPJmL-SPITFIRE with multiple-day fires (Fragmentation and No Fragmentation) show a significant improvement in reproducing these fires over a previous version of SPITFIRE.

Therefore, the parametrization introduced here represents a significant improvement at the examined latitudes. However, modelled values appear to diverge slightly from the Global Fire Atlas burnt areas in later years. One potential cause for this may be that the Global Fire Atlas divides large burn patches into too many individual fires, e.g. as described by Artés et al. (2019), which grow into individual large fires in LPJmL-SPITFIRE. An additional cause for the difference may be that LPJmL simulates significant encroachment of vegetation into higher latitudes over the examined time period.

This increase in vegetation in the model may also explain excessively high values of burnt area at higher latitudes shown in Figure 3. Of additional interest, a difference map between model runs with terrain fragmentation limits imposed and those without, shown in the bottom right panel, shows the locations where the terrain fragmentation function has the greatest impact. Modelled fires in eastern Russia and Alaska are particularly prone to reaching the terrain fragmentation limits. Therefore, accounting for these limits may be particularly important for studying fires in these areas.

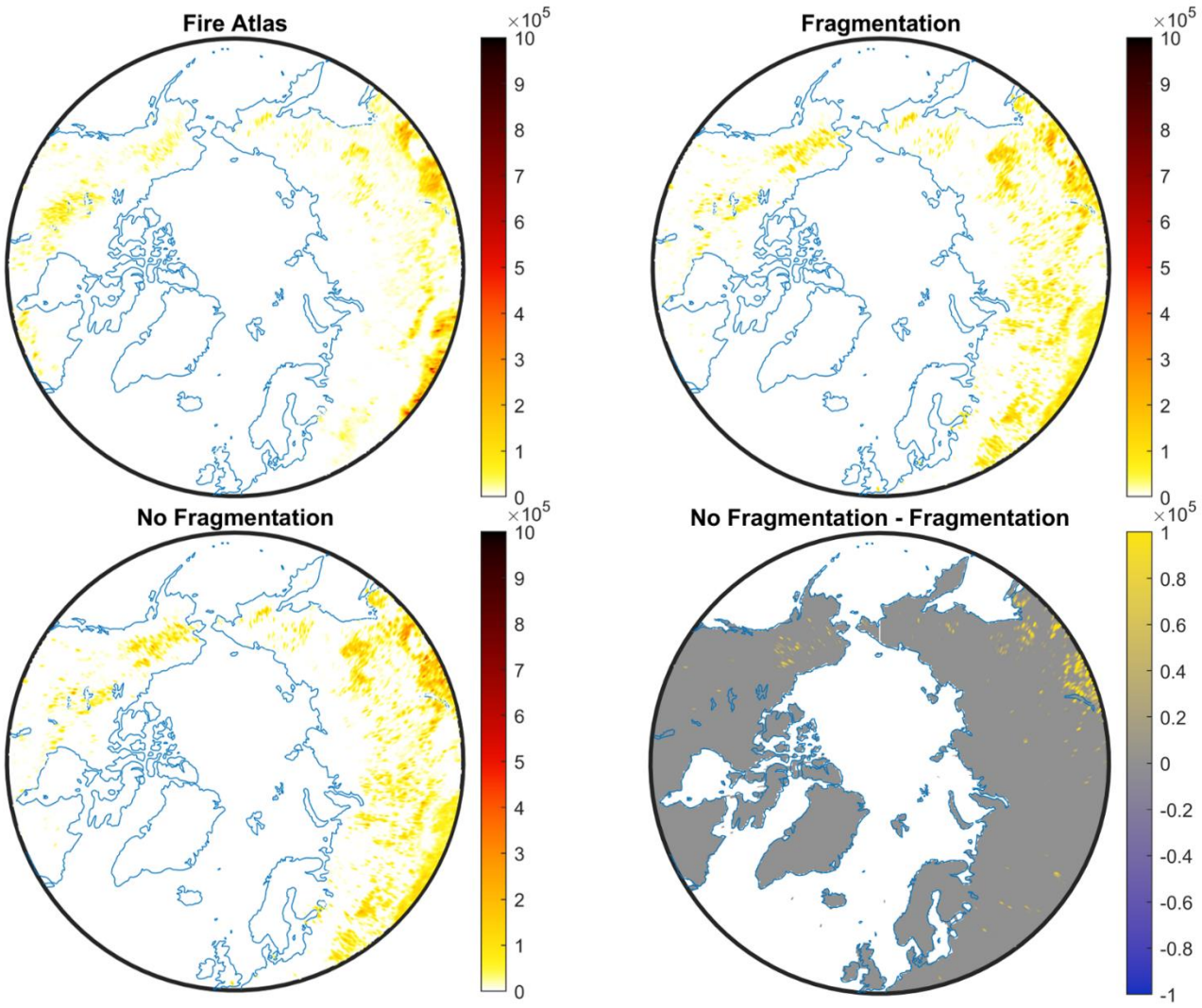

Figure 3 – Burnt area per 0.5° × 0.5° grid cell (in ha) at latitudes over 50°, summed from 2003 to 2016, due to fires in the Global Fire Atlas and the same fires implemented in LPJmL-SPITFIRE with and without fuel bed fragmentation due to terrain ruggedness in the model. The bottom right panel shows the difference between these two sets of results. Colour maps were obtained from www.colorcet.com, based on Kovesi (2015).

4. Conclusions

We implement a multiple-day fire spread algorithm, and a function to account for the effect of terrain fragmentation in LPJmL-SPITFIRE at latitudes greater than 50°. Terrain fragmentation is accounted for by fitting a function of the Vector Ruggedness Measure to the maximum fire sizes observed in the Global Fire Atlas. This function is then implemented as a limit to fire sizes in the model. The multiple-day fire spread algorithm allows fires to burn for 12 h per day up to a maximum of 14 days. In general, our model results compare favourably with the Global Fire Atlas burnt area when simulating the same fires, with differences likely caused in large part by inaccuracies in vegetation modelling at high northern latitudes. Therefore, our results show a significant improvement on LPJmL-SPITFIRE in the boreal zone.

5. References

Albini, Frank A. 1976. Computer-based models of wildland fire behavior: a user's manual. Ogden, UT: USDA Forest Service, Intermountain Forest and Range Experiment Station. 71 p.

Andela, N., Morton, D. C., Giglio, L., Paugam, R., Chen, Y., Hantson, S., van der Werf, G. R., & Randerson, J. T. (2019). The Global Fire Atlas of individual fire size, duration, speed and direction. *Earth System Science Data*, *11*(2), 529–552. https://doi.org/10.5194/essd-11-529-2019

Artés, T., Oom, D., de Rigo, D., Durrant, T. H., Maianti, P., Libertà, G., & San-Miguel-Ayanz, J. (2019). A global wildfire dataset for the analysis of fire regimes and fire behaviour. *Scientific Data*, *6*(1), 296. https://doi.org/10.1038/s41597-019-0312-2

Balch, J. K., Abatzoglou, J. T., Joseph, M. B., Koontz, M. J., Mahood, A. L., McGlinchy, J., Cattau, M. E., & Williams, A. P. (2022). Warming weakens the night-time barrier to global fire. *Nature*, *602*(7897), 442–448. https://doi.org/10.1038/s41586-021-04325-1

Drüke, M., Forkel, M., von Bloh, W., Sakschewski, B., Cardoso, M., Bustamante, M., Kurths, J., & Thonicke, K. (2019). Improving the LPJmL4-SPITFIRE vegetation–fire model for South America using satellite data. *Geoscientific Model Development*, *12*(12), 5029–5054. https://doi.org/10.5194/gmd-12-5029-2019

Gorelick, N., Hancher, M., Dixon, M., Ilyushchenko, S., Thau, D., & Moore, R. (2017). Google Earth Engine: Planetary-scale geospatial analysis for everyone. *Remote Sensing of Environment*, *202*, 18–27. https://doi.org/10.1016/j.rse.2017.06.031

Haas, O., Prentice, I. C., & Harrison, S. P. (2022). Global environmental controls on wildfire burnt area, size, and intensity. *Environmental Research Letters*, *17*(6), 065004. https://doi.org/10.1088/1748-9326/ac6a69

Kovesi, P. (2015). *Good Colour Maps: How to Design Them* (arXiv:1509.03700). arXiv. https://doi.org/10.48550/arXiv.1509.03700

Pfeiffer, M., Spessa, A., & Kaplan, J. O. (2013). A model for global biomass burning in preindustrial time: LPJ-LMfire (v1.0). *Geoscientific Model Development*, *6*(3), 643–685. https://doi.org/10.5194/gmd-6-643-2013

Rabin, S. S., Melton, J. R., Lasslop, G., Bachelet, D., Forrest, M., Hantson, S., Kaplan, J. O., Li, F., Mangeon, S., Ward, D. S., Yue, C., Arora, V. K., Hickler, T., Kloster, S., Knorr, W., Nieradzik, L., Spessa, A., Folberth, G. A., Sheehan, T., … Arneth, A. (2017). The Fire Modeling Intercomparison Project (FireMIP), phase 1: Experimental and analytical protocols with detailed model descriptions. *Geoscientific Model Development*, *10*(3), 1175–1197. https://doi.org/10.5194/gmd-10-1175-2017

Rothermel, R. C. (1972). *A Mathematical Model for Predicting Fire Spread in Wildland Fuels*. Intermountain Forest & Range Experiment Station, Forest Service, U.S. Department of Agriculture.

Schaphoff, S., von Bloh, W., Rammig, A., Thonicke, K., Biemans, H., Forkel, M., Gerten, D., Heinke, J., Jägermeyr, J., Knauer, J., Langerwisch, F., Lucht, W., Müller, C., Rolinski, S., & Waha, K. (2018). LPJmL4 – a dynamic global vegetation model with managed land – Part 1: Model description. *Geoscientific Model Development*, *11*(4), 1343–1375. https://doi.org/10.5194/gmd-11-1343-2018

Thonicke, K., Spessa, A., Prentice, I. C., Harrison, S. P., Dong, L., & Carmona-Moreno, C. (2010). The influence of vegetation, fire spread and fire behaviour on biomass burning and trace gas emissions: Results from a process-based model. *Biogeosciences*, *7*(6), 1991–2011. https://doi.org/10.5194/bg-7-1991-2010

Ward, D. S., Shevliakova, E., Malyshev, S., & Rabin, S. (2018). Trends and Variability of Global Fire Emissions Due To Historical Anthropogenic Activities. *Global Biogeochemical Cycles*, *32*(1), 122–142. https://doi.org/10.1002/2017GB005787

Tools supporting planning and organizing rescue actions in state forests in Poland as an example of the practical implementation of scientific research

Ryszard Szczygieł*[1]; Mirosław Kwiatkowski[2]; Jan Kaczmarowski[3]

[1,2]Forest Research Institute, SękocinStary, 3 BraciLeśnej Street, 05-090 Raszyn, Poland, {R.Szczygiel, M.Kwiatkowski}@ibles.waw.pl
[3]General Directorate of the State Forests, 127 Grójecka Street, 02-124 Warsaw, Poland, {Jan.Kaczmarowski@lasy.gov.pl}

**Corresponding author*

Keywords

Fire management, fire risk assessment, fuel models, forest fire modeling

Abstract

In terms of the average number of forest fires (7,188) in 2010-2019, Poland was third in Europe after Portugal (19,362) and Spain (11,860). The average burnt area, which is a kind of efficiency indicator for the forest fire protection system, in the analyzed period was 0.42 ha in Poland. The functioning fire protection system in the State Forests, which covers 76.9% of the forest area in the country, is constantly improved thanks to close cooperation with the Forest Research Institute. The results of the research conducted by the Institute are thus implemented in forestry practice, examples of which are presented in this article.

The basis for planning and organizing rescue operations is the assessment of potential forest fire risk, which is carried out using the method of classifying forest areas to the forest fire risk category. It is determined for the forest district (average area 17500 ha) for 10 years on the basis of the frequency of fires, forest stand, climatic and anthropogenic conditions according to the formulas developed for each of the factors. The category determines the distribution of funds for fire protection and the method of forest preparation in the event of a fire, concerning fire detection, communication and alarm systems, the density of fire access roads and water supply points, and fire extinguishing equipment. The macroscopic method of forest fire risk categorization is complemented by the method of forest stand flammability classes, which determines their susceptibility to fire due to the presence of flammable material. It is based on the forest habitat type and soil cover type and is determined at the level of separation (average area 3 ha), with the possibility of generalization to the division (20 ha) and forestry (1300 ha). Both methods are used to map the potential fire risk of forests in Poland. The method of determining the degree of forest fire risk on the basis of air temperature and relative humidity, precipitation and direct measurements of moisture content of pine litter (*Pinus sylvestris*) is used to assess the dynamic forest fire risk, shaped by weather conditions. Determining the degree of risk is performed from the 1st of March to the 30th of September, daily at 9.00 and 13.00 in 60 forecast zones with the use of an automated network of 145 meteorological measuring points. Information on the degree of risk determines the operational readiness of ground and air forces. In the event of a fire and determination of its forest address, we can download from the Information System of the State Forests, data on the flammability class of the forest stand and the characteristics of the flammable material (type, fuel load), using the developed fuel models for 7 types of soil cover, the fires of which constitute nearly 90 % of all events.

The possibility of a soil cover fire turning into a crown fire is determined based on the developed algorithms, taking into account the age of the forest stand, habitat and stand conditions, meteorological conditions and the duration of the fire. Organizing a firefighting action, including in particular having the right amount of forces and resources to extinguish a fire with the smallest possible area, can be supported by the application "Model of a forest fire", which the forest service has at its disposal. It was developed on the basis of laboratory and field research on the conditions of the emergence and spread of forest fires. The result of these works was the development of algorithms in the form of mathematical equations, enabling the calculation of the basic parameters of a forest fire (speed of the front, surface and perimeter of the fire) depending on the wind speed, moisture content of the flammable material, fuel load and the time of free fire development. Model calculations can be performed for forest bed, grass, heather and total fires. Early fire detection, reliable alarming and extinguishing action at the earliest possible stage of fire development, supported by the above-mentioned actions contribute to the effective protection of state forests in Poland. The examples cited and discussed above indicate a high level of usefulness, practical application and full implementation at the national level of the results of the research work of the Forest Research Institute in the structures of the functioning and constantly improved system of fire protection of the State Forests in Poland.

1. Introduction

According to EFFIS data {Forest fires in Europe, Middle East and North Africa 2020. JRC Technical Report. 2021], in Poland in the years 2010-2019, on average, 7188 forest fires occurred in Poland. More fires were recorded only in Portugal (19,362) and Spain (11,860). Taking into account the average burnt area, which can be treated as a kind of efficiency indicator for the organization of the forest fire protection system, in the analyzed period it amounted to 0.42 ha in Poland. For comparison, the average in Portugal and Spain was at a similar level, amounting to 7.13 and 7.97 ha per fire, respectively. The maximum average burnt area was in Croatia (56.48 ha), followed by Serbia (28.10 ha), Greece (25.60 ha) and North Macedonia (21.40 ha). The functioning fire protection system in the State Forests, which cover 76.9% of the forest area in the country, is constantly improved thanks to close cooperation with the Forest Research Institute. Thanks to this, the results of the conducted research are implemented in practice, and selected examples of them in the field of supporting the planning and organization of firefighting actions are presented in this article. Its beginning is the assessment of the potential and dynamic fire risk, then the acquisition of forest stand data from the place where the fire started from the IT system and finally forecasting the spread of the fire.

2. Assessment of the potential risk to the forest

The basis for the operational planning and organization of rescue activities is the assessment of the potential fire risk of forests. The analysis determining the forest susceptibility to fire is performed by determining the potential fire risk at the following levels: national - classification of the Regional State Forests Directorates, of regions (NUTS 2) and subregions (NUTS 3), regional - classification of forest districts and counties, and local - classification of stands. The method of classifying forest areas into the forest fire riskcategory {Szczygiel et al, 2020] and the method of forest fire risk classification according to flammability classes [Kaczmarowski et al, 2021], developed by the Forest Research Institute, are used to evaluate the fire risk. The forest fire risk category is determined on the basis of the frequency of fires, forest stand, climatic and anthropogenic conditions according to the formulas developed for each of the factors. It decides on the distribution of funds for fire protection and the method of forest preparation in case of fire, concerning fire detection, communication [Szczygiel et al, 2020] and alarm systems, the density of fire access roads and water supply points, and fire extinguishing equipment. The categorization of forest fire risk is made on a macroscopic scale, because the minimum area for which it is determined is the area of a forest district, amounting to an average of 17.5 thousand hectares. The macroscopic method of forest fire risk categorization is complemented by the method of forest stand flammability classes, which determine their susceptibility to fire due to the presence of combustible material. It is based on the forest habitat type and the type of soil cover and is determined at the level of separation (average area 3 ha), with the possibility of generalization to the compartment (20 ha) and forest range (1300 ha). The classification of forest stand flammability can be used: when carrying out rescue and extinguishing actions of small and medium forest fires (risk assessment at the level of sub-compartment), when planning the target network of fire access roads and water supply points, and conducting rescue and firefighting actions when extinguishing large fires (risk assessment at the level of sub-compartment, compartment) and in determining the location of observation points and equipment bases for extinguishing forest fires (risk assessment at the forest range level).

3. Assessment of dynamic forest fire risk

To assess the dynamic forest fire risk, shaped by weather conditions, the method of determining the degree of forest fire risk is used on the basis of air temperature and relative humidity, precipitation and pine litter moisture content (*Pinus sylvestris*) [Szczygiel et al, 2017]. The determination of the degree is performed from March 1 to September 30, daily at 9.00 am and 1.00 pm in 60 forecast zones with the use of an automated network of 145 meteorological measurement points, making measurements with a 10-minute frequency. Their distribution density depends on the forest fire risk category. The method makes it possible to determine the current degree of risk on the basis of the measurements made, and to calculate the projected degree 24 hours in advance. The projected degree of risk is calculated on the basis of the forecasted values of meteorological parameters obtained from the numerical weather model (COSMO) and the projected moisture content of pine litter, calculated on the basis of equations developed for this purpose. Information on the degree of risk provided to the forest service and fire brigade determines the operational readiness of the ground and air forces.

4. Determining the data on the place where a forest fire occurred

In the event of a fire and determination of its forest address, we have the option of downloading from the Information System of the State Forests, data about the stand (habitat type, species, age, type of soil cover), which allow to determine the flammability class of the forest stand and the characteristics of the combustible material. For the fire characteristics (eg type, fuel load), developed fuel models are used for 7 types of soil cover, where fires account for nearly 90% of all events [Kwiatkowski et al, 2016]. The main features that characterize the type of fuel (fuel model) were: fuel load (kg / m^2), moisture of combustible material (%), heat of combustion and calorific value (KJ / kg) and fuel volume density (kg / m^3). In order to facilitate the mapping of the existing types of combustible materials, a matrix of the occurrence of fuel models was developed depending on the habitat type of forest and the type of cover, which allows to generate a map for any forest area after collecting forest stand assessment data.
The typology of fuels enables the identification of the occurring fire risk and is used in the fire spread forecasts.

5. Modeling of fire spread

From the point of view of the person managing the rescue operation, the key information is the type of fire, the expected size and speed of fire spread, which affects the amount of forces and resources necessary to extinguish the fire. The "Forest Fire Model" application is used to forecast fire development, which was developed on the basis of laboratory and field research on the conditions of the formation and spread of forest fires. The result of these works was the development of algorithms in the form of mathematical equations, enabling the calculation of the basic parameters of a forest fire (speed of the front, surface and perimeter of the fire) depending on the wind speed, moisture content of the flammable material, fuel load and the time of free fire development (time from the start of the fire to the start of the extinguishing). The amount of extinguishing agents needed (water and foam) is also calculated for the three fire extinguishing variants (extinguishing the entire surface, extinguishing the edges or location with barrier zones). Model calculations can be performed for litter cover, grass, heather and total fires [Szczygiel 1991, Szczygiel et al, 2013]. The possibility of a soil cover fire turning into a crown fire is determined based on the developed algorithms, taking into account the age of the forest stand, habitat and stand conditions, meteorological conditions and the duration of the fire [Szczygiel 1991]. The use of the application for forecasting the development of a fire can be used by the commander of the firefighting operation, because all alarm and disposition points of forest districts are equipped with it. This application can also be used for post-fire analysis and training purposes.
The process of supporting planning and organizing firefighting actions discussed in this article is presented in figure 1.

6. Summary

The forest fire protection system operating in Poland is based on three principles: early fire detection, immediate alerting of the rescue forces and starting fire extinguishing at the earliest stage of its development. Rapid fire detection is ensured by a comprehensive forest fire detection system, consisting of 693 lookout towers, 7 patrol planes and 320 patrol and firefighting vehicles. Moreover, nearly 50% of forest fires are reported by outsiders. Quick alarming about a fire is possible thanks to the created network of communication and alerting the forest service and fire brigade, which means that the average time of starting fire extinguishing is from 30 to 45 minutes. IT tools supporting operational planning, from the assessment of potential forest fire risk, through the assessment of fire risk depending on meteorological conditions, have an impact on the readiness of rescue forces to act. Data on the place of the fire allow assessing the risk of fire spreading there and at the same time are used to forecast the basic parameters of the fire, which allows you to have the required amount of forces adequate to the local risk and fire situation. This procedure of actions undoubtedly has a decisive influence on the effectiveness of extinguishing actions, expressed in the average area burned, and consequently also on the amount of losses caused by fires in the forest.

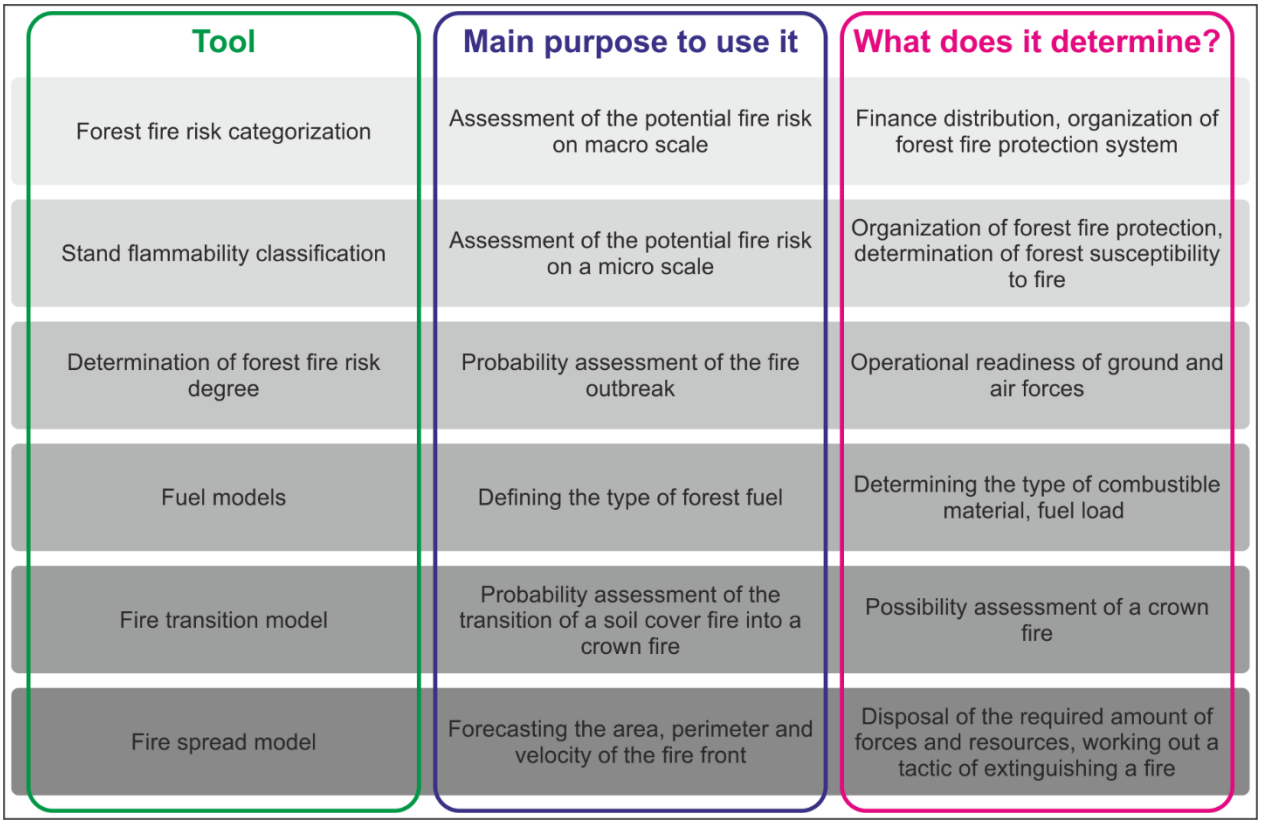

Figure 1. The process planning and organizing firefighting actions

7. Literature

Forest fires in Europe, Middle East and North Africa 2020. JRC Technical Report. European Commission, 2021.

Szczygieł R., Kwiatkowski M., Kołakowski B., Piwnicki J. 2020. Potential forest fire hazard evaluation in Poland. Folia Forestalia Polonica, Vol. 62(1) (doi:10.2478/ffp-2020-0005).

Kaczmarowski J., Parapura H., Kwiecień J. Tłumienie fali radiowej w środowisku leśnym/Damping of radio waves in the forest environment. Sylwan, Vol. 165 (4) 2021. (doi:10.26202/sylwan.2021026).

Szczygieł R., Kwiatkowski M., Kołakowski B., Piwnicki J. 2020. Dynamic forest fire risk evaluation in Poland. Folia Forestalia Polonica, Vol. 62(2) (doi:10.2478/ffp-2020-0014).

Szczygieł R., Kwiatkowski M., Kołakowski B. 2017. Opracowanie modeli paliw leśnych materiałów roślinnych pokrywy gleby / Development of forest fuel models for soil cover vegetation.FRI report..

Kwiatkowski M., Szczygieł R., Kołakowski B. 2016. Określenie warunków przejścia pożaru pokrywy gleby w pożar całkowity w zależności od typów siedliskowych lasu, składu gatunkowego i wieku drzewostanów / Determination of the conditions for the transition of a soilcoverfire to a crown fire depending on forest habitat types, species composition and age of stands. FRI report..

Szczygieł R. 1991. A model of forest fire. Actes proceedings (Actas 2) 10th World Forestry Congress, Paris.

Szczygieł R., Kwiatkowski M., Kołakowski B. 2013. Opracowanie aplikacji modelu pożaru lasu. FRI report..

Towards real-time predictions of large-scale wildfire scenarios using a fully coupled atmosphere-fire physical modelling framework

Qing Wang*[1]; Matthias Ihme[1,2]; Yi-fan Chen[1]; Vivian Yang[1]; Fei Sha[1]; John Anderson[1]

[1]Google Inc. 1600 Amphitheatre Pkwy, Mountain View, CA 94043, USA, {wqing, matthiasi, yifanchen, vivianyang, fsha, janders}@google.com
[2] Stanford University. 440 Escondido Mall Building 530, Stanford, CA 94305, USA

**Corresponding author*

Keywords

Wildfires, Coupled fire-atmospheric modelling, High-performance computing, Large-scale fire simulations

Abstract

With the changing climate, fire-exclusion, and expansion of wildland-urban interfaces, the frequency and severity of wildfires are expected to increase, putting substantial stress on fire management and authorities to mitigate the risk of wildfires. Improved physical models in conjunction with advanced high-performance computing resources offer new opportunities for operational use in examining potential fire-spread scenarios and planning. This work presents an open-source, high-fidelity modelling framework for simulating large-scale wildfire scenarios, taking into consideration atmospheric/fire coupling, complex terrain, and heterogeneous fuel loading. The framework is implemented using the TensorFlow programming environment on tensor processing units (TPUs). TPUs are a dedicated high-performance computing architecture to accelerate machine-learning applications and high-performance scientific computing. This framework solves the Favre-filtered reacting Navier-Stokes equations and the unclosed terms describing turbulence/chemistry interaction and turbulence transport are modelled using large-eddy simulation (LES) closures. Wildfire dynamics is described by a one-step solid-fuel pyrolysis/combustion model that is coupled to atmospheric flow dynamics using a Boussinesq-type approximation. A second-order finite-difference discretization is employed in a variable-density, low-Mach number formulation to discretize the governing equations, and an immersed-boundary method is adapted to represent complex terrain. In conjunction with the coupled atmosphere/fire model and physical models for turbulence/atmosphere/fire interaction, the resulting simulation framework enables high-resolution simulations (with spatial resolution below 2m) of large-scale fires that cover up to ~100,000 acres. Following the summary of validation results against a prescribed fire experiment to assess the overall accuracy at well-controlled conditions, we employ this coupled atmosphere/fire modelling framework to simulate a large-scale wildfire scenario that is representative of the 2017 California Tubb's fire. To this end, we extract the terrain of the North Bay region of Calistoga and Santa Rosa, spanning an area of 20×20 km2, and consider a North-Eastern wind. The simulation results illustrate the rapid fire-spread dynamics and the coupling of the fire with the terrain and atmosphere. With relevance to operational and research applications that include parametric studies to examine effects of wind, fuel-density, other environmental factors, and fire-management strategies, we discuss the scalability and further extensions of the physical fidelity towards enabling real-time applications on TPU-compute architectures.

1. Introduction and Motivations

Wildfires can threaten livelihood and properties and impact the environment and health [Kollanus et al., 2016; van der Werf et al., 2017]. Over the last few decades, wildfire management has changed profoundly, facing longer fire seasons and more severe fires with more acres burned on average each year [Westerling et al., 2006]. Now, extreme fire events are becoming the norm rather than the exception [Zhongming et al., 2020], with some of the most destructive wildfires in California's history occurring over the last ten years [Khorshidi et al., 2020]. While the number of total fires in the United States has stayed the same, the scale of these extreme fires and subsequently the cost to suppress them and the devastation they cause on forests and communities has grown [Hazard HQ Team, 2021]. In addition, wildfires significantly impact the climate and are estimated to contribute to 10% of the CO2 emissions per year worldwide. Main issues in reliably predicting wildfires are variability in atmospheric conditions, fuel loading, moisture content, and uncertainties in physical models. Therefore, ensemble simulations are required, which provide a statistical representation of the effects of wildfire behaviour

and the prediction of extreme-fire dynamics, ultimately to improve early-detection, prevent, and mitigate impacts [Brillinger et al., 2003].

By leveraging emerging computing architectures, the objective of this work is to develop a scalable high-performance simulation tool that enables the reliable prediction of realistic wildfire scenarios under consideration of representative terrain topographies, fuel distribution, and atmospheric conditions. Here, we will present recent progress toward the development of such a simulation framework using the TensorFlow programming environment. The underlying combustion-physical models and the key features of this solver to efficiently run on Tensor Processing Units (TPU) are presented. The application of this solver is demonstrated by performing simulations of a wildfire scenario that is representative of 2017 Tubbs fire.

2. Numerical Methods

2.1. Governing Equations and Discretization

In this work, we present a simulation framework that solves the three-dimensional Navier-Stokes equations in a low-Mach formulation. The physical model describes the interaction between wildfire spread behaviour and atmospheric flow dynamics. The combustion of the fine-grained fuel is described using a single-step reaction that accounts for solid-fuel pyrolysis and combustion. The states of the solid fuel, including the fuel density, moisture content, and solid temperature, are modelled with a set of ordinary differential equations. The fire behaviour is represented by two prognostic variables, namely the potential temperature and the oxygen mass fraction. The evolution of these variables is modelled by two transport partial differential equations in conjunction with the Navier-Stokes equations, which couples the fire dynamics with the hydrodynamics of air flows using a Boussinesq formulation [Linn & Cunningham, 2005]. Effects of turbulence are considered using eddy-diffusivity-based subgrid models through LES filtering. Specifically, the Smagorinsky-Lilly model [Lilly, 1962] is used as the sub-grid scale closure to represent small-scale turbulence in atmospheric flows.

The governing equations are discretized using a finite-difference formulation with a time-explicit iterative scheme. This simulation framework was examined through benchmark simulations for non-reacting and turbulent conditions [Wang et al., 2022], confirming second-order temporal and spatial accuracy, and excellent weak and strong scalability thanks to the graph-based computing architecture and the optimization through the accelerated linear algebra compiler for TPUs.

To consider complex terrains, we employ the immersed boundary method with feedback-force [Zhang & Zheng, 2007]. In this method, an additional forcing term is added to the momentum and scalar transport equations for the potential temperature and oxygen mass fraction. With this method, the ground is represented as a non-slip isothermal interface. The boundary conditions were tested in canonical flow configuration to confirm expected solution accuracy.

2.2. Tensor Processing Unit

A main contribution of this work is the implementation of the wildfire simulation framework on TPU platforms using the TensorFlow programming interface. The TPU architecture is an application-specific integrated circuit that specifically targets accelerated dense matrix multiplications for machine-learning applications and high-performance scientific computing. The simulation framework is based on a recently developed CFD-solver [Wang et al., 2022] that was developed for high-fidelity reacting and non-reactions fluid-flow applications.

To provide context, we briefly summarise salient features of the TensorFlow TPU implementation. The TPU architecture consists of a TPU board with four independent chips. Each chip contains two tensor compute cores that are optimised for vectorized operations and dense-matrix operations. Up to 1024 chips are connected through a dedicated high-speed inter core interconnect network, forming a TPU pod [Jouppi et al., 2017, 2021]. Main benefits of this computer architecture, making it particularly interesting for large-scale wildfire simulations, are high-peak performance, the flexible programming environment, and the compilation of the executable taking into consideration data management, memory allocation, hardware execution, and inter-chip communication.

3. Results

3.1. Validations for prescribed fire experiments

We validate our wildland fire simulation framework against the FireFlux II experiment [Clements et al., 2019], which is a prescribed grassland fire over a flat ground with homogeneous fuel distribution. Extensive parametric studies have been performed and will be published in a forthcoming study [Wang et al. 2022], and this presentation focuses on illustrating key results from this study. Simulations were performed in a Cartesian domain of size $1\,km \times 0.5\,km \times 0.6\,km$ along the wind-direction, lateral, and height. The domain is discretized using a structured regular mesh with resolution $2\,m \times 2\,m \times 0.5\,m$ along the three respective directions. The atmospheric boundary layer is prescribed by a logarithmic velocity profile with a bulk-velocity of 5 m/s and neutrally stratified atmosphere [Clements et al., 2019], and is modelled by the Monin-Obukhov similarity theory [Porté-Agel et al., 2000]. We consider a homogeneous grassland that is 1.5 m tall, having a fuel density of 0.4 kg/m^3. The simulation is advanced over a total of 200 s at a time-step size of 0.01 s, which corresponds to a CFL number of 0.4. The simulation is performed using 128 TPU cores, taking 0.15 s wall-clock time to complete one temporal iteration. Considering the scaling to a full TPU-pod with 1024 cores and linear scalability, suggest that these simulations can be performed at near real-time conditions, opening unique opportunities for operational services.

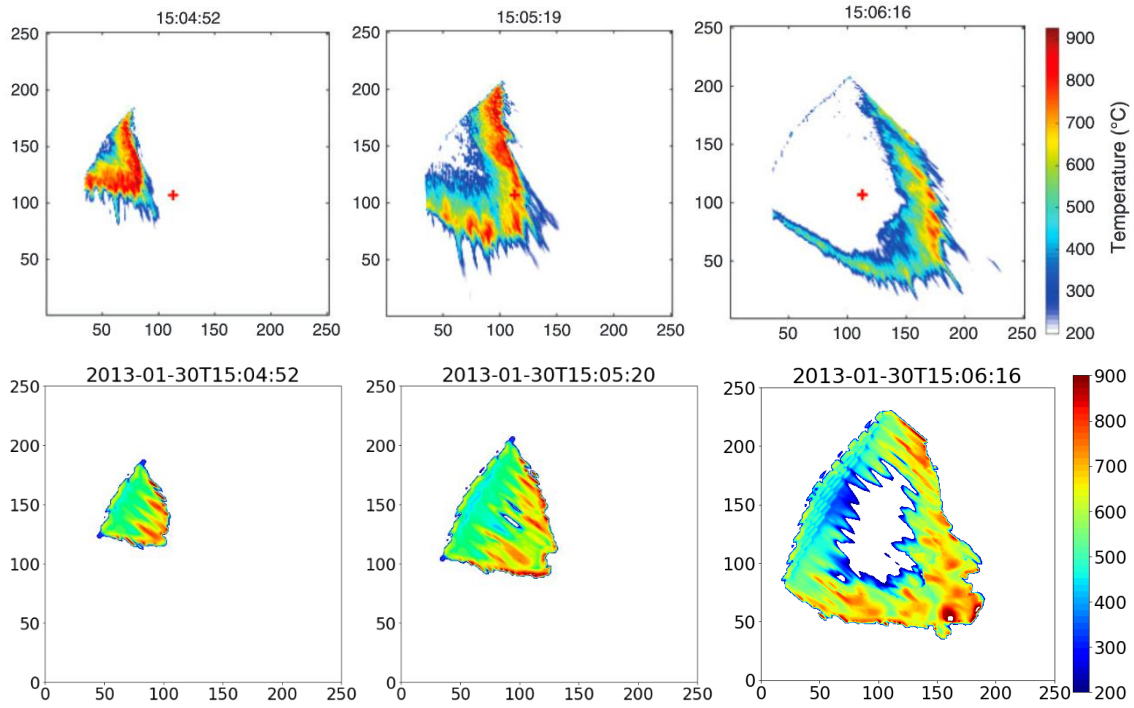

Figure 1- Time sequences of the temperature profile. The first row shows results from the experiment [13] , and the second row is results from the simulation at the corresponding time.

Quantitative comparison of simulation results against published measurements for temperature fields are presented in Figure 1, with the top row showing experimental data (taken from LIDAR) and the bottom row showing temperature fields at a fuel-bed height of 0.5 m above the ground. Results for three different time instances are shown, indicating overall good agreement in predicting the head-fire spreading rate and lateral extent of the fire. The perimeter and key topology of the fire are captured by the simulation. Additionally, the overall good agreement in peak temperature suggests that the heat release and corresponding fire intensity is well captured by the simulation. Differences are evident for the backfire, with the simulation overpredicting the fire residence time. We attribute these differences to the ignition and variability in the fuel load [Wang et al. 2022].

3.2. Large-scale wildfire simulation

Following the validation of the wildfire simulation framework against a prescribed fire experiment, we proceed by considering a large-scale fire scenario. For this, we consider a fire scenario that is representative of the Tubbs fire [Martinez et al. 2017]. The domain for this simulation takes a size of $20\,km \times 20\,km \times 2\,km$, as shown

in Fig. 2, with the *x*-axis aligned with the north-eastern wind direction [Martinez et al. 2017]. The mesh resolution is 20 m horizontally and 4 m in vertical direction. The elevation map is obtained from the USGS database [The National Map-Data Delivery, n.d.] with the latitudes and longitude coordinates sampled in the selected area, which are then interpolated onto the computational mesh. We assume that the ground is covered by homogeneously distributed tall grass of height 1.35 m with a bulk density of 1 kg/m^3, which corresponds to a fuel load of 1.35 kg/m^2. The velocity field is initialised with a Blasius boundary layer that conforms with the terrain. The inflow velocity profile is set to a bulk flow of 10 m/s on which we superimpose turbulence fluctuations that are generated with a digital filter [Klein et al., 2003] with a turbulence intensity of 20%. A convective outflow boundary condition is applied at the downstream exit of the domain. The two boundaries at the lateral sides are set as free-slip walls. A Reighley damping layer is applied at the top boundary, covering 10% of the domain. Within this layer, we prescribed values for all velocity components and prognostic variables. Before ignition, the flow is advanced for one flow-through time (corresponding to 2000 s) to establish a fully developed atmospheric boundary layer. Following this initialization period, we ignite a square region of size 500 m^2 at the location where the fire was first spotted. The solution is advanced for another 4000 s until the fire reaches the end of the domain (near the region of Santa Rosa).

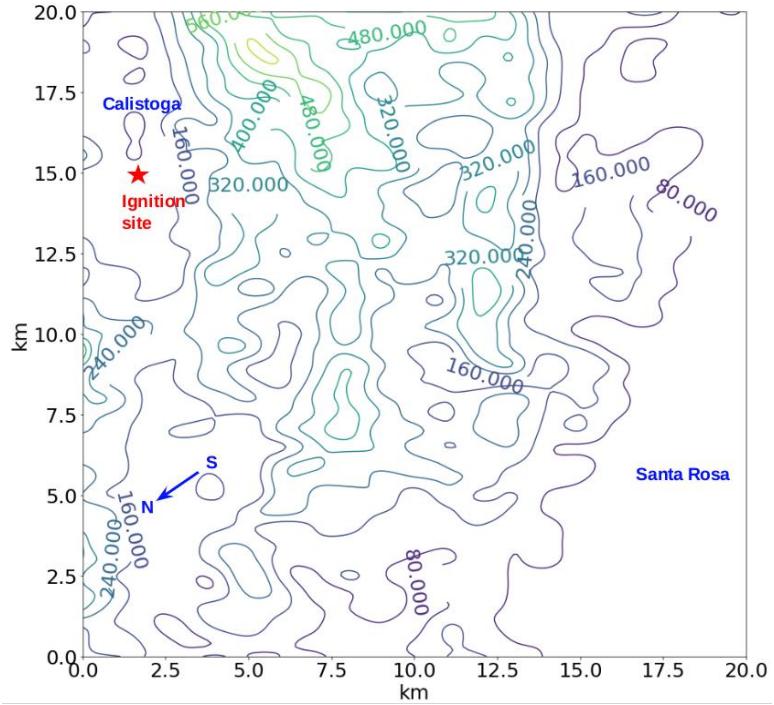

Figure 2- Simulation domain over (20 km)^2 area covering the spread of the Tubbs fire in the first 2 hours.

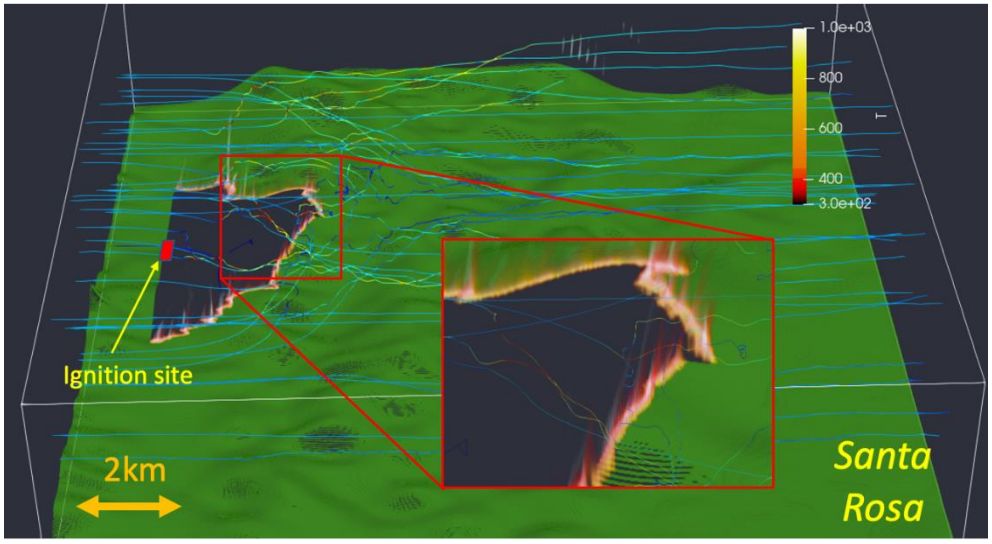

(a) time: 1000 s

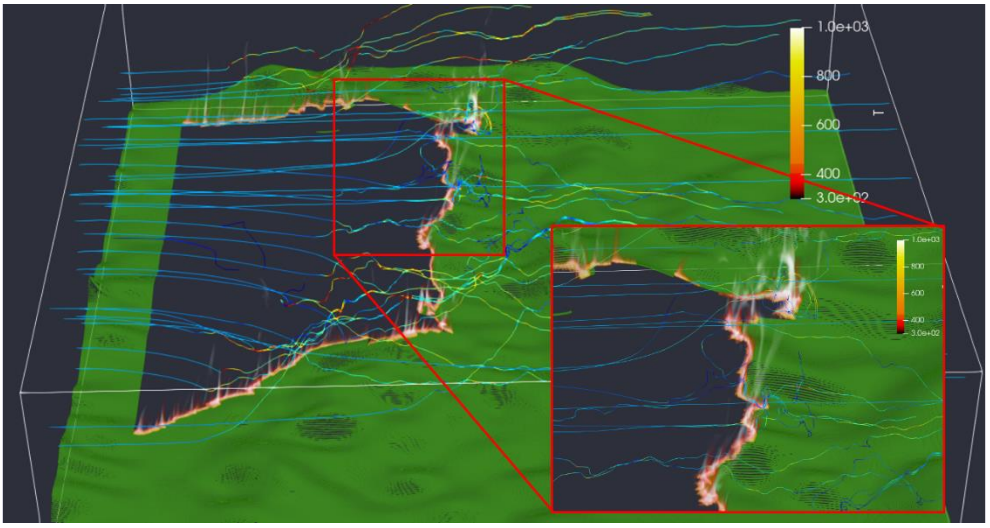

(b) time: 2000 s

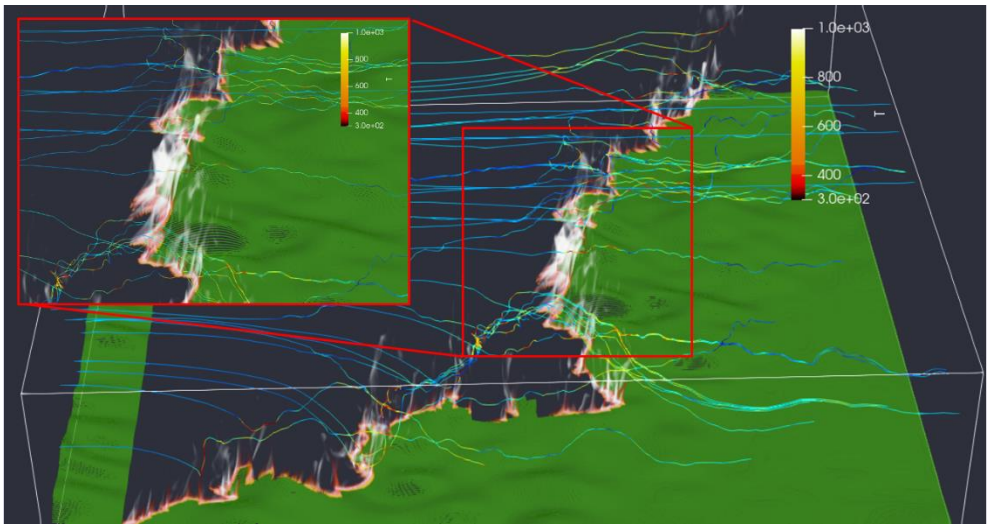

© time: 3000 s

Figure 3- Simulation of large-scale wildfire behaviour over (20 km)^2 area in Northern California near Santa Rosa, representative of the Tubbs fire, showing time-sequence of fire front (colored by temperature at a height of 6 metres above the ground) over the topography (with elevation map shown in green, scaled by a factor of 2.5). The red square in (a) indicates the ignition location.

A time-sequence at three instances after the ignition is shown in Fig. 3, together with an enlarged view of the fire front. This transient fire sequence illustrates the coupling of the fire plumes with approaching wind. The fire front exhibits severe corrugation due to the conforming terrain and increasing spreading rate on uphill slopes. It can be seen that after 1000 s (~15mins) the fire completely traversed the valley and approached the mountain ridge to Santa Rosa. We note that our current simulations consider homogeneous fine grassland, which is not representative of the vegetation in this area. Because of these important differences in the vegetation and time-dependent wind, we note that these results are not fully representative of the Tubbs fire scenario, but illustrate the capability in predicting large-scale fire events at affordable computational cost.

4. Conclusions

High-fidelity numerical simulations for realistic wildfires are helpful for physical analyses of atmosphere/fire coupling yet too expensive to generate. In this study, we demonstrate that these simulations are within reach using advanced HPC architectures by showing simulations of two realistic fire scenarios. The first scenario considers a prescribed grassland fire over a flat ground. Validations with the experimental results show good predictability of the simulation framework regarding fire statistics including rate of spread, perimeter, and fire intensity. The second scenario considers a historical fire in California 2017. This simulation covers an area of $400\ km^2$ with 0.5 billion mesh points. With the current simulation setup and partition, we simulate the 1 hour duration of the fire that propagates from Calistoga to Santa Rosa in a 12-hour wall-clock period. The performance of this simulation can be further improved by optimising the time step size and refining the partitioning strategy, which makes the simulation close to real time.

5. Acknowledgment

We thank Rod Linn from Los Alamos National Laboratory for helpful discussions on the model development. Craig Clements is acknowledged for sharing the Fire-Flux II validation data. We also thank Mark Finney from the United States Forest Services for helpful discussion on the wildfire dynamics.

6. References

Brillinger, D. R., Preisler, H. K., & Benoit, J. W. (2003). Risk assessment: a forest fire example. Institute of Mathematical Statistics Lecture Notes - Monograph Series (pp. 177–196). Institute of Mathematical Statistics.

Clements, C. B., Kochanski, A. K., Seto, D., Davis, B., Camacho, C., et al. (2019). The FireFlux II experiment: a model-guided field experiment to improve understanding of fire–atmosphere interactions and fire spread. International Journal of Wildland Fire, 28(4), 308–326.

Hazard HQ Team. (2021). The 2021 Wildfire Risk Report. CoreLogic.

Jouppi, N. P., Hyun Yoon, D., Ashcraft, M., Gottscho, M., Jablin, T. B. et al. (2021). Ten Lessons From Three Generations Shaped Google's TPUv4i : Industrial Product. 2021 ACM/IEEE 48th Annual International Symposium on Computer Architecture (ISCA), 1–14.

Jouppi, N. P., Young, C., Patil, N., Patterson, D., Agrawal, G., et al. (2017). In-Datacenter Performance Analysis of a Tensor Processing Unit. Proceedings of the 44th Annual International Symposium on Computer Architecture, 1–12.

Khorshidi, M. S. Dennison, P. E. Nikoo, M. R. AghaKouchak, A. Luce, C. H. Sadegh, M. (2020). Increasing concurrence of wildfire drivers tripled megafire critical danger days in Southern California between 1982 and 2018. Environmental Research Letters: ERL [Web Site], 15(10), 104002.

Klein, M., Sadiki, A., & Janicka, J. (2003). A digital filter based generation of inflow data for spatially developing direct numerical or large eddy simulations. Journal of Computational Physics, 186(2), 652–665.

Kollanus, V., Prank, M., Gens, A., Soares, J., Vira, J., Kukkonen, J., Sofiev, M., Salonen, R. O., & Lanki, T. (2016). Mortality due to vegetation fire–originated PM2.5 exposure in Europe—assessment for the years 2005 and 2008. Environmental Health Perspectives, 125(1). https://doi.org/10.1289/ehp194

Lilly, D. K. (1962). On the numerical simulation of buoyant convection. Tell'Us, 14(2), 148–172.

Linn, R. R. (1997). A Transport Model for Prediction of Wildfire Behavior (No. LA-13334-T) (F. H. Harlow (ed.)) [Ph.D]. Los Alamos National Lab., NM (United States).

Linn, R. R., & Cunningham, P. (2005). Numerical simulations of grass fires using a coupled atmosphere–fire model: Basic fire behavior and dependence on wind speed. Journal of Geophysical Research, 110(D13), 287.

Martinez, J. Bergland, V. Franklin, M. Frits, M. Lohse, S. Roath, G. Thompson, M. (2017). Incident Report (No. 17CALNUO10045). California Department of Forestry and Fire Protection.

Pierce, C. D. (2001). Progress-Variable Approach for Large-Eddy Simulations of Turbulent Combustion (P. Moin (ed.)) [Ph.D]. Stanford University.

Porté-Agel, F., Meneveau, C., & Parlange, M. B. (2000). A scale-dependent dynamic model for large-eddy simulation: application to a neutral atmospheric boundary layer. In Journal of Fluid Mechanics (Vol. 415, pp. 261–284).

The National Map-Data Delivery. (n.d.). topoBuilder Application. USGS Topographic Maps. Retrieved November 8, 2021, from https://topobuilder.nationalmap.gov/

van der Werf, G. R., Randerson, J. T., Giglio, L., van Leeuwen, T. T., Chen, Y., Rogers, B. M., Mu, M., van Marle, M. J. E., Morton, D. C., Collatz, G. J., Yokelson, R. J., & Kasibhatla, P. S. (2017). Global fire emissions estimates during 1997–2016. Earth System Science Data, 9(2), 697–720.

Wang, Q., Ihme, M., Chen, Y.-F., & Anderson, J. (2022). A TensorFlow simulation framework for scientific computing of fluid flows on tensor processing units. Computer Physics Communications, 274, 108292.

Wang, Q. Ihme, M. Chen, Y.-F. Yang, V. Anderson, J. Linn, R. R. Clements, C. (2022). Ensemble simulations for predicting wildfire spread dynamics. In Preparation.

Westerling, A. L., Hidalgo, H. G., Cayan, D. R., & Swetnam, T. W. (2006). Warming and earlier spring increase western U.S. forest wildfire activity. Science, 313(5789), 940–943.

Zhang, N., & Zheng, Z. C. (2007). An improved direct-forcing immersed-boundary method for finite difference applications. Journal of Computational Physics, 221(1), 250–268.

Zhongming, Z Linong, L Xiaona, Y Wangqiang, Z Wei, L. (2020, October 20). California's Mega Fires Have Arrived 30 Years Early. Scientific American. http://119.78.100.173/C666//handle/2XK7JSWQ/300076

Transforming Rural Landscape towards Fire Resilience and Landscape Sustainability

Manuela R. Magalhães*; Selma B. Pena*; Natália S. Cunha, Luísa M. Franco, Ana Müller

Linking Landscape, Environment, Agriculture and Food (LEAF), Instituto Superior de Agronomia, Universidade de Lisboa, Tapada da Ajuda, 1349-017 Lisboa, Portugal {mmrm@tecnico.ulisboa.pt} {selmapena, natcunha, luisafranco, anamuller}@isa.ulisboa.pt

**Corresponding authors*

Keywords

Fire resilience, ecological network, native forest, landscape planning, Geographic Information System

Abstract

After the fires that occurred in 2017 and 2018 in Portugal, the imperative need to plan for sustainable and fire resilient landscapes led to the implementation of the Landscape Transformation Program. However, it is still lacking a landscape planning methodology to achieve those resilient landscapes. This paper presents a landscape plan for a fire-prone landscape located in the Centre region of continental Portugal - Serras da Lousã e Açor. This landscape is characterised by steep slopes (70% of the total area) and is dominated by highly combustible coverings, such as eucalyptus (27.89 %), maritime pine (28.06 %), other coniferous (10.08 %) and shrubs (18.91 %). Fires have occurred frequently and 96 % of the case study's total area was burned between 1975 and 2020.

The landscape plan here presented was based on the FIRELAN model and goes a step further by proposing a progressive landscape transformation. FIRELAN integrates fire resilience, ecological sustainability, and economic viability. In this model, the landscape components, which can be physical, biological or cultural, are organised in two main infrastructures - the Ecological Network and the Fire Resilient Landscape Network - and in Complementary Areas.

The Ecological Network ensures the ecological functioning of the landscape by emphasising the quality or potentiality of biophysical components, in articulation with the nature conservation and at-risk areas, underlying the provision of multiple functions valuable to society.

The Fire Resilient Landscape Network integrates fire behaviour knowledge related to land morphology, promotes the landscape discontinuities according to it, is made of less combustible land uses, and includes the cultural management in the urban-rural interface, roads, and power grid. This network is divided in two, the Primary and the Secondary Fire Resilient Landscape Networks. The last one includes the areas with slopes greater than 25%, located outside the Fire Resilient Primary Network.

As to the Complementary Areas, these correspond to the interstices (compartments with slopes less than 25%) of both of networks. Since these areas have low ecological value, they can allocate more artificial land uses.

The implementation of the landscape plan is defined in two temporal phases: the landscape plan for the Scenario 2030, which consists on the implementation of the Primary Fire Resilient Landscape Network (51%), and the landscape plan for the Scenario 2050, that adds the implementation of the Secondary Fire Resilient Landscape Network (37%) and Complementary Areas (9 %). This landscape plan represents a paradigm shift from a landscape dominated by eucalyptus and maritime pine to a dominant forest of native species (such as oaks), archetypical species (such as chestnut, walnut - both for wood or fruit - the wild cherry and others) and also riparian species (alder, willows, poplar, ash, elm, etc.).

Differentiating the final proposal into two phases makes it possible to distinguish implementation priorities, since the application of the model implies a substantial transformation of the current landscape, with high implementation costs. The payment for ecosystem services to the landowners during the paradigm transition period, which is expected to be 20 to 30 years, is recommended to allow the plan implementation.

1. The landscape planning model

Despite long Portuguese forest legislation, only in 2020 the transformation of vulnerable into sustainable and fire resilient landscapes via landscape planning has been formally introduced in legislation with the Landscape Transformation Program (RCM No. 49/2020). However, the methodology to achieve those resilient landscapes

is not regulated. The planning of rural landscapes to prevent rural fires must include sustainable land uses and well-defined management measures. This approach goes beyond obtaining marketable goods of materials and energy since it delivers other ecosystem services provided by a multifunctional and biodiverse forest, including water quality, soil and biodiversity conservation, climate regulation, tourism and scientific data. In addition, it offers intangible benefits such as human contact with nature, recreation and leisure. The availability of forest ecosystem services depends on forest planning and management to avoid and prevent uncontrollable fires.

The three major factors influencing rural fires are climatic conditions, land morphology and land cover. Assuming that it is impossible to radically change the first two factors, the proposed landscape planning methodology assumes that the transformation of the landscape by changing the land cover and land use reorganisation should guarantee the three significant vectors of sustainability: fire resilience, ecological sustainability, and economic viability. Landscape fire resilience is determined by several interrelated factors, namely: fire behaviour as a function of the land morphology (Viegas, 2006), combustibility of plant species (Calviño-Cancela et al., 2017; Silva et al., 2009), landscape discontinuities (Agee et al., 2000, Cui et al., 2019, Povak et al., 2018), and rural-urban interface (Gibbons et al., 2018, Badia et al., 2019). Ecological sustainability of the landscape is achieved by the delimitation of the Ecological Network (EN) (Forman, 1995; Magalhães, 2001; Cunha e Magalhães, 2019) and its correct implementation, supported by land suitability analysis for land uses (McHarg, 1967).

Regarding fire behaviour, biophysical factors can contribute to some extent to reducing fire risk and therefore should be taken into account when planning, namely: i) slopes facing north, with a slope greater than 25%, as they receive less radiation throughout the year, burn less than other slopes (Oliveira et al., 2014); ii) The rate of fire progression doubles for every 10º (about 17%) increase in slope and can increase continuously on steep slopes, from bottom to top, at approximately 5-6 km/h fire speed (Viegas, 1989); iii) Above slopes greater than 30º (57%), the relationship between slope and fire velocity is almost exponential (Viegas, 2006); iv) When the fire reaches the top of the watershed (the ridge), if it does not advance to the opposite slope, due to the slope's breeze, it starts to plough along the contour lines, losing speed. Thus, steep slopes, ridgelines, headwaters and valley bottoms should be strategically covered with less combustible vegetation, to break fire progression.

The proposed landscape planning methodology is based on the landscape transformation model named FIRELAN (Magalhães et al., 2021; Pena et al., 2021) developed in the SCAPEFIRE research project (PCIF/MOS/0046/2017) that includes the present study area as case study), integrates fire resilience, ecological sustainability, economic viability and the simulation of fire behaviour. This paper focuses on fire resilience and ecological sustainability. Other sub-teams dealt with the last two issues which are not covered in this presentation.

The planning design unit of the FIRELAN model is the watershed and is defined by the configuration of landscape infrastructures in its biophysical and cultural systems. Those landscape infrastructures consist of a **Primary and a Secondary Fire Resilient Landscape Networks,** including many components of the Ecological Network. The EN ensures the ecological functioning of the landscape by improving the quality and quantity of biophysical components (water, soil, and biodiversity) in articulation with the nature conservation and at-risk areas, underlying the provision of multiple functions valuable to society (Magalhães, 2013; Cunha & Magalhães, 2019).

Furthermore, the Fire Resilient Network assures the landscape discontinuities recommended by current knowledge of fire behaviour (Viegas, 2006) related to land morphology namely on streams and valley bottoms, ridges lines (Cunha et al., 2018), and the headwaters system areas (Pena et al., 2018). These discontinuities are obtained from less combustible land uses and vegetation types, as well as cultural system management/measures namely in the urban-rural interface, roads, and power grid. The protection buffers around rural settlements and roads contemplated in law and integrated in this methodology, are high priority intervention areas, as they contribute to the direct safety of local population and land properties in case of fire. The different FIRELAN components are presented in Table 1.

The FIRELAN model includes also the Complementary Areas that correspond to the interstices (compartments) of the infrastructures with low ecological value. Those areas have relevant socio-economic functions although less critical from an ecological point of view, therefore can allocate more artificial land uses (Magalhães, 2001; Magalhães et al., 2007).

Table 1 - FIRELAN components and its organisation in ecological network, fire resilient landscape network and complementary areas

System	***Sub-systems***	***Landscape Components***	***Ecological Network***	***Fire Resilient Landscape Network***		***Complementary Areas***
				Primary Network	***Secondary Network***	
Physical	*Water*	*Streams*				
		Valley bottoms				
		Water bodies				
		Headwater system areas				
	Soil	*Rocky outcrops*				
		Steep slope areas (slope> 25%)				
Biological	*Biodiversity*	*Vegetation with conservation interest*				
		Natura 2000				
		Low ecological value				
Cultural	*Agriculture*	*Existent agriculture*				
	Rural settlements	*Rural protection buffer area*				
		Rural protection buffer area in steep slopes (> 25%)				
		Rural settlements				
	Cultural Network	*Power infrastructure protection buffer area*				
		Road infrastructure protection buffer area				
		Road Network				

The proposed methodology promotes a paradigm shift from a landscape dominated by eucalyptus and maritime pine to a dominant forest of native species (such as oaks), archetypical species (such as chestnut, walnut - both for wood or fruit - the wild cherry and others) and also riparian species (alder, willows, poplar, ash, elm, etc.). The economy of this new forest is increasingly valued since it is composed of woody and non-woody products.

However, it can be noted that its profitability comes from producing much more valuable hardwoods that are scarce in the market and valuable non-wood products such as cork, mushrooms, honey, aromatic and medicinal plants, berries, etc. In addition, in a region where today there are few and mostly aged people, the installation of new activities as a result of the multifunctional and biodiverse landscape as management shepherding, hunting, tourism and management will involve new jobs and the settling of people.

2. Case study

The case study is located in the central region with an area of 54839 ha (Figure 1A). This area covers part of the Mondego river basin to the North, and the Tagus river basin to the South. Its dominant characteristics are hilly and rugged terrain with predominating altitudes above 500 m, such as Serra do Açor (1418 m) and Serra

da Lousã (1205 m). The geological formations are mainly schist with some quartzite outcrops, giving rise to an enclosed valley bottoms with abrupt and extensive hillslope morphology.

About 70% of the total area is characterised by steep slopes (greater than 25%). The southern area is represented by a less rugged morphology, although hillslopes between 12 and 25 % of slope predominate. It is noteworthy that only 7% of the intervention area has slopes below 12%, which are mainly in the surroundings of the two largest urban agglomerations of Castanheira de Pera and Pedrógão Grande.

The land use map (DGT, 2019) (Figure 1B) shows an occupation dominated by eucalyptus (27.89 %), maritime pine (28.06 %), other coniferous (10.08 %), shrubs (18.91 %), which together make up about 85 % of the area with highly combustible coverings. This situation significantly contributed to the fires between 1975 and 2020 (Figure 1C), corresponding to 52.656 ha of burned area, representing 96 % of the case study's total area.

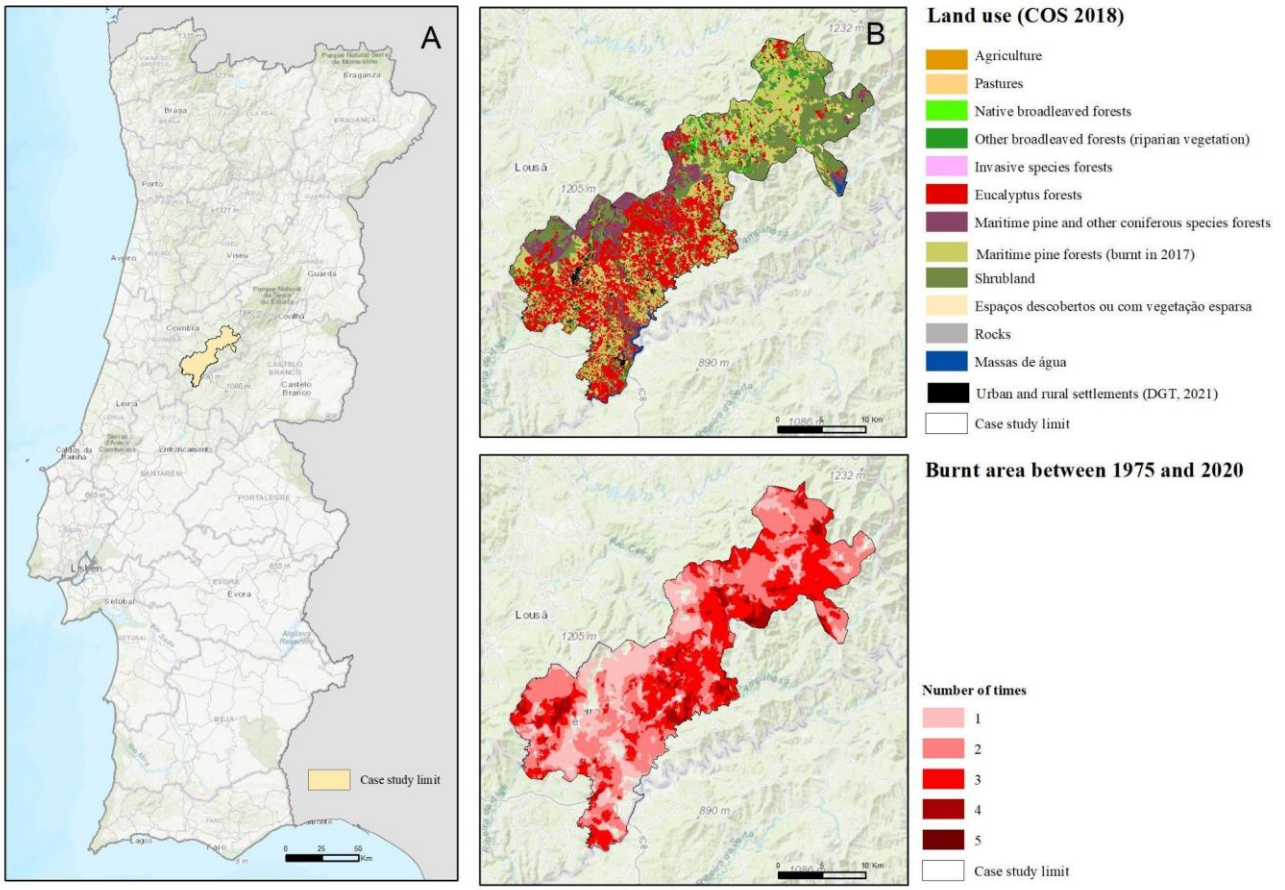

Figure 1 - Case study location (A), current land use (B) and fire frequency between 1975 and 2020 (C)

3. Landscape Plan of Serras da Lousã and Açor

The landscape plan of Serras da Lousã and Açor is the result of FIRELAN model application to the case study area. It corresponds to the biophysical and cultural systems according to the mapped landscape components (Table 1) and a set of potential land uses for each situation.

The implementation of the landscape plan is defined in two temporal phases, presented in the Scenario 2030 and Scenario 2050. The first temporal phase runs until 2030, an important goal in fulfilling European commitments, such as the Biodiversity Strategy 2030 (EC, 2020) and the New Forest Strategy for 2030 (EC, 2021), included in the European Green Deal (EC, 2019). The 2050 Scenario is coincident with the implementation of other long-term European targets up to 2050, such as the Climate Neutral Strategies by 2050 (EC, 2018). This phasing is intended to allow for a progressive transformation of the Landscape. The desired situation is one that should be considered as the "benchmark of a new economy of rural territories, which promotes a multifunctional, biodiverse and resilient forest that is more profitable, with greater capacity for

carbon sequestration and capable of producing better services from ecosystems" (RCM No. 49/2020). This will be achieved after the implementation of the two scenarios by 2050.

The 2030 Scenario (Figure 2) represents the first phase of implementation of the proposal and consists of Primary Fire Resilient Landscape Network (51% of the case study area), implemented with less combustible land uses, integrating the essential components for compartmentalised landscape:

- the two fundamental landforms/features that simultaneously play a role at the ecological level and in fire resilience:
  - i) streams and associated valley bottoms (riparian gallery; riparian forest or agriculture) - 2737 ha;
  - ii) headwater systems (native and archaeophytes mixed forest) - 15362 ha.
- the existing land uses:
  - iii) natural vegetation with conservation interest - 4239 ha;
  - iv) agriculture - 1694 ha.
- buffer protection areas:
  - v) to rural settlements (agriculture/pastures/native forest) - 1472 ha;
  - vi) to road network (pasture/native forest) - 1112 ha;
  - vii) to power grid (agriculture/pasture/lowland scrubland) - 582 ha.
- the Natura 2000 Network (to be intervened by structures and to guarantee the conservation of existing Habitats)

In this Scenario (2030), to be carried out in a first phase, also included is the intervention in all areas with invasive forests (114 ha), the "compartments" generated by the FRLPI, maintain their use until financing and other conditions for their implementation are in place. These areas are fundamentally characterised by:

- hillslopes with slopes greater than 25 % located outside the FRLPI (20085 ha);
- Low ecological value areas with slopes of less than 25% (4899 ha).

Although there is no intervention at this stage, these areas should be subject to silvo-environmental measures.

The 2050 Scenario (Figure 3) represents the second phase of the proposed landscape plan. It assumes the implementation of the Fire Resilient Landscape Primary Network 2030 and the implementation of interventions located in the Secondary Fire Resilient Landscape Network and Complementary Areas.

The Secondary Fire Resilient Landscape Network includes areas with slopes greater than 25%, located outside the Primary Network, occupying about 37% of the case study area (20085 ha). These areas present high risks of soil erosion, high velocity of water runoff, which decreases infiltration (this condition is aided by the nature of the geological substrate consisting of shale). These conditions together lead to soil loss and thus infertility in these areas and contribute to a faster rate of fire progression. The proposed uses are native hardwoods or native bushland.

The Complementary Areas are the "compartments" with slopes less than 25% generated by the Fire Resilient Landscape Network (4899 ha), represented in pink in Figure 3. In the case study area these areas are of low ecological value. Their use is more flexible, and alternatives depend on the suitability of the soil to the various trees and shrubs species or crops and the choice of their promoters.

Regarding soil and water conservation management techniques, minimum mobilization and the use of manual or mechanical-manual practices are recommended above slopes of 35%. Also, reforestation should be based on the promotion of natural regeneration and intensive forest management should be replaced by close-to-nature forestry (Carvalho, 2018), semi-intensive, extensive or very extensive.

Other recommended techniques are the green firebreaks, which are strips of vegetation with low combustibility, cultivated in strategic locations on the landscape with the aim of slowing down or stopping the progress of a fire. The headwaters, riparian galleries and other suitable hedges can be considered green firebreaks. When compared to the fuel management buffers contemplated in law, characterised by the absence of vegetation, green firebreaks represent a more sustainable option, with benefits such as increasing biodiversity, restoring ecosystems (soil, water and air) and the economic value associated with its products (Wang et al., 2021). In addition, although their installation is more demanding than that of the fuel management buffers, the maintenance costs are reduced in the medium to long term.

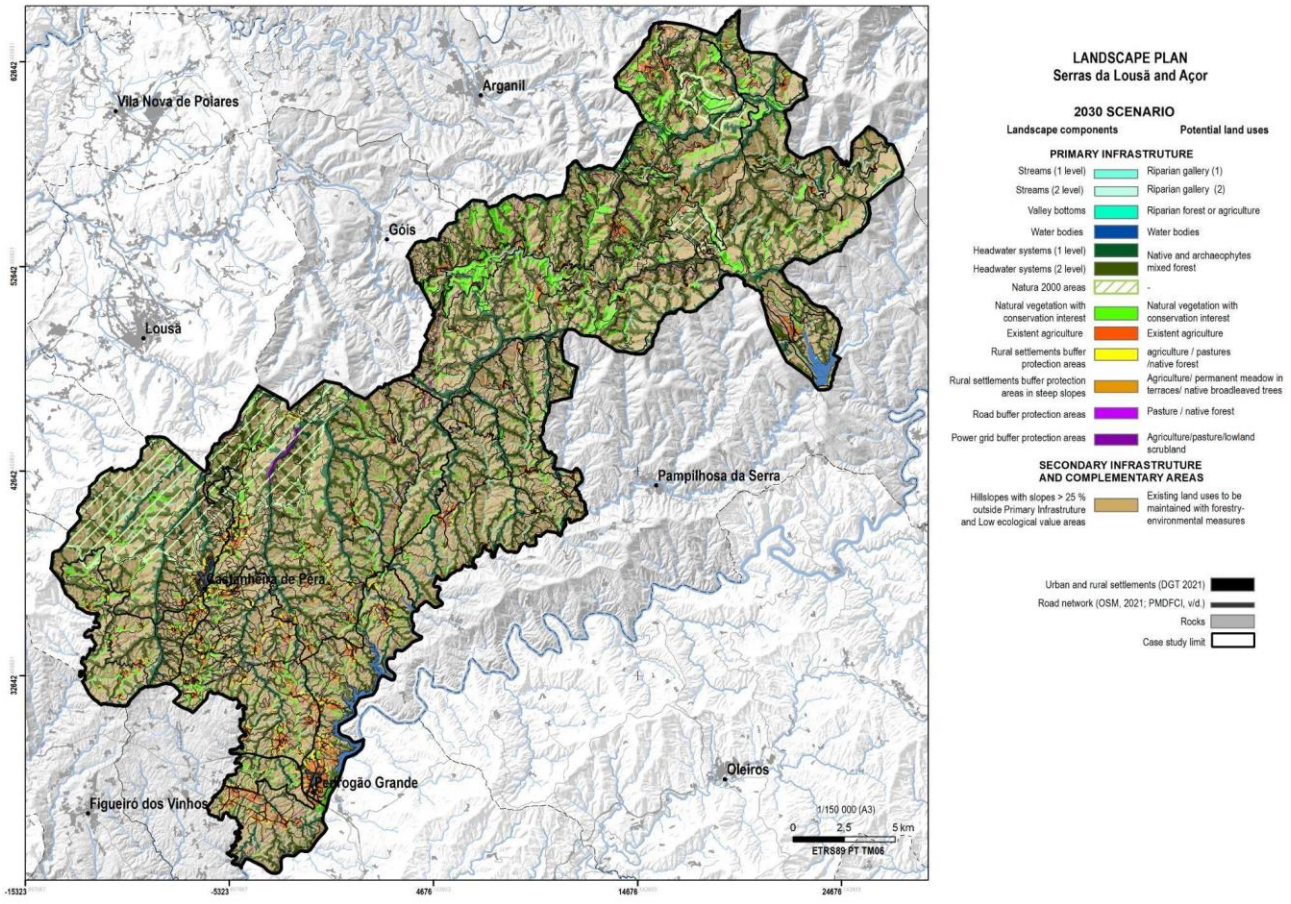

Figure 2 - Landscape Plan - 2030 Scenario

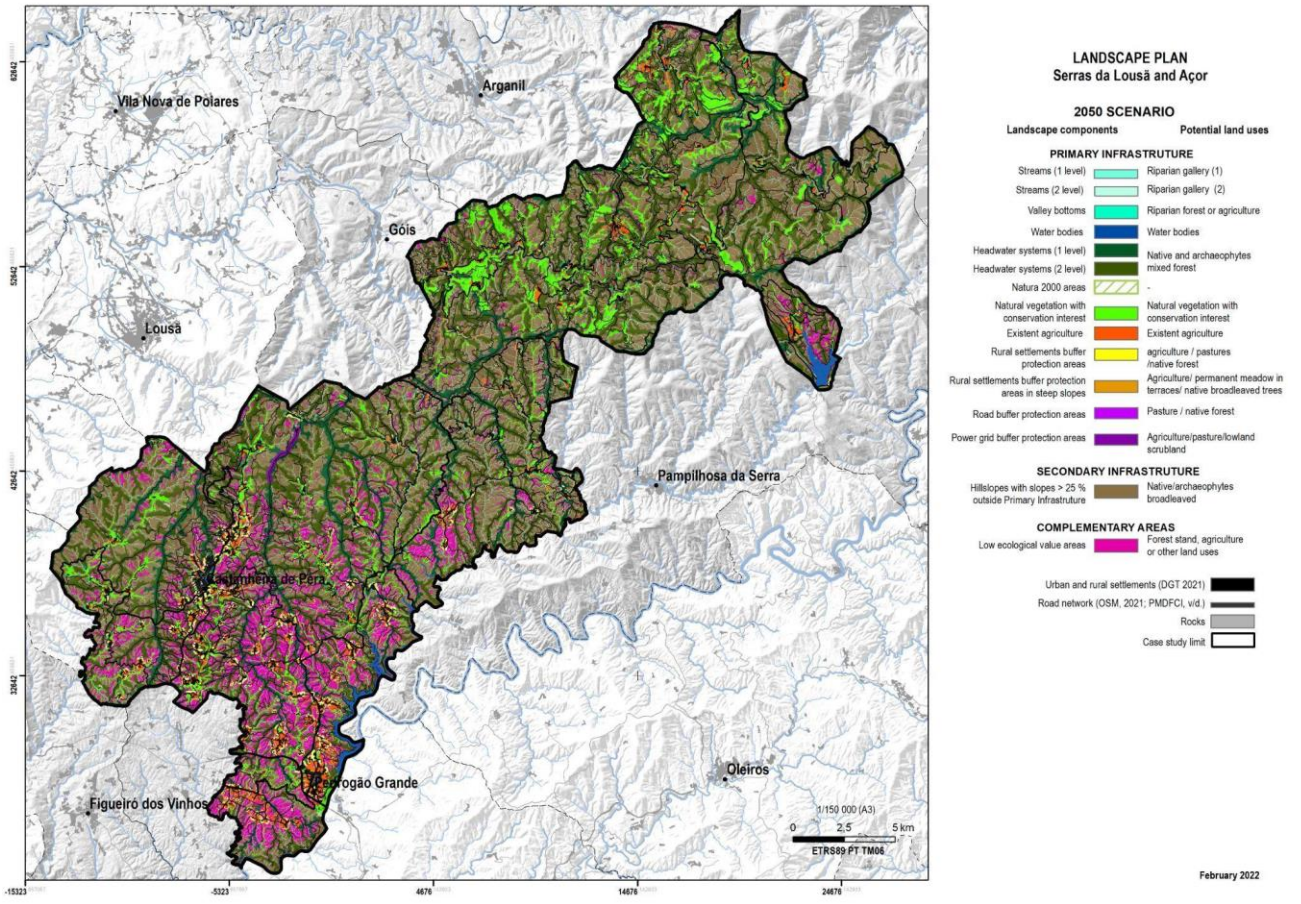

Figure 3 - Landscape Plan - 2050 Scenario

This landscape plan was accompanied by several public participation workshops, involving representatives of the landscape transformation stakeholders who were open to the transformation, except for pulp/paper companies and large landowners whose properties are covered with eucalyptus.

Specialised teams in the simulation of fire behaviour, the evaluation of implementation costs and also the evaluation of ecosystem services evaluated these two phases (Scenario 2030 and Scenario 2050). These components of the Landscape Plan are not developed in this paper. However, we refer to some of the conclusions obtained by specific teams.

The simulation of fire behaviour shows that the transformations proposed for the landscape leads to a reduction in fire intensity levels (and all associated characteristics), especially from the 2018 scenario to the long-term scenario (2050).

Regarding the evaluation of ecosystem services (ES), this was conducted in two phases. In a first phase, the evaluation of the ES (Biomass supply, Food supply, Regulation of water cycles, Soil protection, Carbon Sequestration, Biodiversity, Cultural Functions) in the current landscape and proposed transformations was based on a qualitative exercise of the supply potential. In a second phase, a quantitative assessment of the flow of ES in the different landscape scenarios and respective economic valuation was carried out. The analysis allowed to conclude that the proposed transformation improve the landscape's ability to provide regulatory and cultural services.

4. Conclusion

The final proposal of the FIRELAN model application to the case study was differentiated in two phases (scenarios) to allow for the distinction of implementation priorities, since the proposed transformation implies a substantial change of the current landscape, with high implementation costs.

It was therefore considered that, in a first phase, the linear components of the Fire Resilient Landscape Network should be implemented, fundamentally made up of the primary and secondary streams and valley bottom systems and the watershed headwaters, as these are the ones that, conceptually, will have a determining role in fire containment. Although the transformation of the Secondary Fire Resilient Landscape Network has been relegated to the 2nd phase, it is admitted that, given its characteristics, areas with slopes greater than 25%, also these, when covered by highly combustible uses such as eucalyptus and maritime pine, contribute greatly to fire risk, so it is also considered very important to implement these areas according to the plan.

The rationale for the option of low combustible land uses was based on existing literature and observation of post-fire landscape cases. This option implies a very significant change in the existing areas of eucalyptus and maritime pine (from 56% to a maximum of 9% in the 2050 scenario), so it is proposed to pay for ecosystem services to the landowners during the paradigm transition period, which is expected to be 20 to 30 years, depending on the species to be used.

5. References

Agee, J.K.; Bahro, B.; Finney, M.A.; Omi, P.N.; Sapsis, D.B.; Skinner, C.N.; Wagtendonk, J.W.; Weatherspoon, P.C. (2000) The use of shaded fuelbreaks in landscape fire management. For. Ecol. Manag., 127, 55–66.

Badia, A.; Pallares-Barbera, M.; Valldeperas, N.; Gisbert, M. (2019) Wildfires in the wildland-urban interface in Catalonia: Vulnerability analysis based on land use and land cover change. Sci. Total. Environ., 673, 184–196.

Calviño-Cancela, M.; Chas-Amil, M.L.; García-Martínez, E.D.; Touza, J. (2017) Interacting effects of topography, vegetation, human activities and wildland-urban interfaces on wildfire ignition risk. For. Ecol. Manag., 397, 10–17.

Carvalho, J. (2018). Silvicultura Próxima da Natureza. Conciliar Economia e Ecologia para uma Silvicultura Multifuncional, Rentável e Sustentável. Agrobook. 279 pp.

Cui, X., Azharul, M. A., Perry, G. L.W., Paterson, A. M., Wyse, S. V., Curran, T. J. (2019) Green firebreaks as a management tool for wildfires: Lessons from China. Journal of Environmental Management, Volume 233, Pages 329-336, ISSN 0301-4797, https://doi.org/10.1016/j.jenvman.2018.12.043.

Cunha, N.S., Magalhães, M.R., Domingos, T., Abreu, M.M., Withing, K. (2018). The land morphology concept and mapping method and its application to mainland Portugal. Geoderma, 2018. 325: 72-89. DOI: 10.1016/j.geoderma.2018.03.018.

Cunha, N.S. & Magalhães, M. R. (2019). Methodology for mapping the national ecological network to mainland Portugal: A planning tool towards a green infrastructure. Ecological Indicators 104C: 802-818. https://doi.org/ 10.1016/j.ecolind.2019.04.050.

EC, (2018). A clean planet for all – a European strategic long-term vision for a prosperous, modern, competitive and climate neutral economy. European Commision.

EC, (2019). The European Green Deal. COM/2019/640 final

EC (2020). EU Biodiversity Strategy for 2030. Bringing Nature Back into Our Lives. COM (2020) 380 Final. 2020.

EC, (2021). New EU Forest Strategy for 2030. COM/2021/572 final

DGT, 2019. Carta de Uso e Ocupação do Solo de Portugal Continental para 2018 - COS 2018. Direcção Geral do Território, Lisboa

Forman, R.T.T. (1995) Land Mosaics: The Ecology of Landscapes and Regions; Cambridge University Press: Cambridge, UK.

Gibbons, P.; Gill, A.M.; Shore, N.; Moritz, M.A.; Dovers, S.; Cary, G.J. (2018). Options for reducing house-losses during wildfires without clearing trees and shrubs. Landsc. Urban. Plan., 174, 10–17.

Magalhães, M.R. (2001). A Arquitectura Paisagista - morfologia e complexidade, Editorial Estampa, Lisboa, 525 pp.

Magalhães, M. R., Abreu, M.M., Lousã, M. & Cortez, N. (2007). Estrutura Ecológica da Paisagem. Conceitos e Delimitação - Escalas Regional e Municipal, ISApress, Lisboa

Magalhães, M. R. (2013). Estrutura Ecológica Nacional – uma proposta de delimitação e regulamentação, ISApress, Instituto Superior de Agronomia, Universidade de Lisboa, Isbn: 978-972-8669-53-9

Magalhães, M.R., Cunha, N.S., Pena, S.B. & Müller, A. (2021). FIRELAN—An Ecologically Based Planning Model towards a Fire Resilient and Sustainable Landscape. A Case Study in the Center Region of Portugal. Sustainability 2021, 13, 7055. https://doi.org/10.3390/su13137055

McHarg, I. (1967). Design with Nature; John Wiley and Sons: New York, NY, USA.

Oliveira, S.; Moreira, F.; Boca, R.; San-Miguel-Ayanz, J.; Pereira, J.M.C. (2014). Assessment of fire selectivity in relation to land cover and topography: A comparison between Southern European countries. Int. J. Wildland Fire, 23, 620–630.

PCIF/MOS/0046/2017. SCAPEFIRE A Sustainable Landscape Planning Model For Rural Fires Prevention. FCT funded project. https://www.isa.ulisboa.pt/proj/scapefire/en/

Pena, S.B., Franco, M.L., Magalhães, M.R. (2021). Contributing to Healthy Landscapes by Sustainable Land Use Planning [Online First], IntechOpen, DOI: 10.5772/intechopen.99666. Disponível em: https://www.intechopen.com/online-first/78391

Pena, S.B., Magalhães, M.R., Abreu, M.M. (2018) Mapping headwater systems using a HS-GIS model. An application to landscape structure and land use planning in Portugal. Land Use Policy 2018. 71, 543-553. DOI: 10.1016/j.landusepol.2017.11.009

Povak, N.A.; Hessburg, P.F.; Salter, R.B. (2018) Evidence for scale-dependent topographic controls on wildfire spread. Ecosphere, 9, e02443.

RCM No. 49/2020. Criação do Programa de Transformação da Paisagem. Diário da República n.º 121/2020, Série I de 2020-06-24, páginas 6 - 18.

Silva, J.S.; Moreira, F.; Vaz, P.; Catry, F.; Godinho-Ferreira, P. (2009). Assessing the relative fire proneness of different forest types in Portugal. Plant Biosyst., 143, 597–608.

Viegas, D. X. (2006). Parametric study of an eruptive fire behaviour model. International Journal of Wildland Fire, 15(2), 169–177. https://doi.org/10.1071/WF05050

Viegas, D. X.; Lourenço, L. (1989). Os Incêndios Florestais na Região Centro; Revista Sociedade e Território: Porto, Portugal.

Wang, H., Finney, M., Song, Z., Wang, Z., Li,X. (2021). Ecological techniques for wildfire mitigation: Two distinct fuelbreak approaches and their fusion, Forest Ecology and Management, Volume 495, 2021, 119376, ISSN 0378-1127, https://doi.org/10.1016/j.foreco.2021.119376.

Using cellular automata to assess the role played by wind direction in two large fire episodes in Portugal

Bárbara Mota[1]; Joana G. Freire[2]; Mariana Oliveira*[2]; Sílvia A. Nunes[2]; Rui Dilão[3]; Carlos C. DaCamara[2]

[1] Department of Computational Biology, Faculty of Biology and Medicine, University of Lausanne, CH-1015 Lausanne, Switzerland, {Barbara.Mota@unil.ch}
[2] Instituto Dom Luiz (IDL), Faculty of Sciences, University of Lisbon, 1749-016 Lisbon, Portugal, {jcfreire, mdpoliveira, sanunes, cdcamara}@fc.ul.pt
[3] Non-Linear Dynamics Group, Department of Physics, IST, University of Lisbon,1049-001 Lisbon, Portugal, {ruidilao@tecnico.ulisboa.pt}

**Corresponding author*

Keywords

Cellular automata; wildfire simulation; wind direction; Pataias and Quiaios wildfire;

Abstract

Portugal is recurrently affected by severe wildfires, the fire season of 2017 representing the most tragic year with half a million of hectares burned and 115 deaths. The events that took place on October 15 deserve special attention, not only because the area burned on that day represents more than 50% of that burned during the entire year, but also because it resulted from the combination of very strong winds steered by the passage of hurricane Ophelia, very dry vegetation because of a prolonged drought affecting the country, very low atmospheric relative humidity and a record number of ignitions. Meteorological fire danger is usually rated using the Fire Weather Index (FWI) that is part of the Canadian Forest Fire Weather Index System. However, wind direction is not taken into account when defining FWI, and therefore it is worth investigating how this factor may affect the evolution of a given fire keeping all the remaining factor unaltered. The role played by wind direction is assessed using a cellular automata (CA) model to simulate two wind-driven wildfires that took place at Pataias-Burinhosa and Quiaios on October 15, 2017. The CA model is first calibrated using winds derived from a regional weather forecasting model and sensitivity studies are then performed by systematically rotating the forecasted winds keeping all the other parameters constant. Results indicate a progressive decrease in probability of burning from a 45º to a 90º counterclockwise rotation. These results suggest improving FWI by defining an FWI vector, whose direction is that of the wind and magnitude is that of FWI. This vector should then be compared against the prevailing vegetation patch orientation, and the closer the alignment between the two directions, the greater the meteorological fire danger.

1. Introduction

Portugal is recurrently affected by severe wildfires with strong adverse impacts at social, economic, ecologic and environmental levels (Costa et al., 2011; Pereira et al., 2011). A recent tragic case is the year of 2017 with the highest record of total burned area since 1980 (above half a million hectares), 115 deaths and an involvement of about 1.5 thousand firefighters (ICNF, 2017).

Information about the likelihood of a large fire event on a given day and in a given location is of vital importance for fire management and fire prevention. The likelihood of a fire event is usually rated by means of meteorological fire danger indices (Finney, 2005), and in this respect the Canadian Forest Fire Weather Index System (Stocks et al., 1989) has shown to be particularly useful for the ecosystems of Mediterranean Europe (San-Miguel-Ayanz et al., 2012). The Canadian System consists of six components that account for the effects of fuel moisture and wind on fire behaviour and all components are derived from surface weather observations at local 12 noon, namely air temperature, air relative humidity, wind speed and cumulated precipitation. Wind direction is not considered in the Canadian System but, especially in cases of wind-driven fires, it is expected that the total area burned will also depend on the relationship between wind direction and the orientation of major flammable vegetation patches, with fire propagating longer distances when wind direction is closer to patch orientation.

The large fire events that started on October 15, 2017 in Central Portugal are especially worth being studied from the point of view of the relationship between wind direction and vegetation patch orientation. That day was marked by strong and persistent southerly winds associated to the passage of hurricane Ophelia; around 500 ignitions started on October 15 that combined with the extremely dry state of the vegetation due to a persistent drought that had affected Portugal and with the very low values of atmospheric humidity resulted in a daily amount of burned area representing more than 50% of the total burned area of that year (Pinto et al. 2022). Two of the events, at Pataias-Burinhosa and at Quiaios, took place along two coastal elongated bands of forested terrain, with 94% of pine and 2% of eucalyptus forests in Pataias and 64% of pyne and 18% of eucalyptus forests in Quiaios (Guerreiro et al. 2018). The orientation of the two coastal bands was very close to the prevailing south-north wind direction of the winds, a situation that is not common in Portugal at that time of the year.

The aim of this work is to assess the role played by wind direction on total area burned in the events of Pataias and Quiaios. After calibrating a cellular automata model to fire propagation observed in the two events using winds as derived from a regional weather forecast model, the models are run with winds rotated by constant amounts and keeping the remaining parameters constant and, finally, a sensitivity study is performed on total burned area to wind rotation.

2. Methods and Data

2.1. The Alexandridis CA model of fire spread

Cellular automata (CA) models are built up on a set of rules defined at a local level that yield global complexity that can resemble fire propagation. Space is defined by a regular grid where each cell is found to be in one of a number of possible states. Cells can only interact with cells in a neighbourhood by means of evolution rules. For every time step, each cell's state is updated according to these rules and depending on the previous states of the cell as well as of its neighbours (Wolfram 2002). We will use a simplified version of the Alexandridis CA fire spread model (Alexandridis et al. 2008) to simulate fire spread. Fire modelling is probabilistic in the sense that a set of simulations is performed and the probability that a given cell will burn is derived from the fraction of simulations where the cell did burn.

In order to run the model first we need to identify the cell that is burning, then consider a squared-cell grid around it, the eight surrounding cells, called neighbours, translating the eight directions along which the fire can propagate. Each cell can be in one of four states: 1) void of fuel content (being assumed that it cannot be ignited at any future instant); 2) contains fuel (it can be ignited); 3) has been ignited (fire can propagate in the next time step to its neighbours); 4) the fire is extinguished (the cell remains in that burnt state until the end of the run).

The model considers three factors when evaluating the likelihood of fire propagating from a cell to another cell in its neighbourhood: wind, slope of the terrain, and type of vegetation. The three factors considered are included in the weight of the probability of a fire to spread to a cell (p_{burn}) in the neighbourhood of a cell classified as in fire, according to the expression:

$$p_{burn} = p_h(1 + p_{veg})p_w p_s \qquad (1)$$

where p_s, p_{veg} and p_w are the slope, the vegetation type and the wind contributions, respectively, and where p_h corresponds to the value of p_{burn} for a certain cell with no slope or wind ($p_h = 0.58$ by optimisation).

Four transition rules are then applied:

1) If $state(i,j) = 1$ at t, $state(i,j) = 1$ at $t + \Delta t$.
2) If $state(i,j) = 3$ at t, $state(i,j) = 4$ at $t + \Delta t$.
3) If $state(i,j) = 4$ at t, $state(i,j) = 4$ at $t + \Delta t$.
4) If $state(i,j) = 2$ at t, $state(i \pm 1, j \pm 1) = 3$ at $t + \Delta t$ if the factor p_{burn} is higher than a value obtained by a random generator.

Following Freire and DaCamara (2019), a wind rule was added in order to simulate spotting. This rule allows fire to spread to a number of cells placed along the wind direction instead of only spreading to the direct neighbour as described in the baseline model. The number of cells to be burned when applying the wind rule was obtained from a step function of the wind speed. According to the rule, i) only cells whose p_{veg} value is greater than a certain threshold can be set on fire when applying this rule, and ii) fire can jump over cells with no fuel or with low values of p_{veg} so that spotting effect is captured.

2.2. Case studies

The model was used to simulate the two coastal wildfires of Pataias-Burinhosa and Quiaios, that started on October 15, 2017. As shown in Figure 1, the two fire events present an elongated shape which reflects the strong influence of the prevailing wind (from south to north). The Pataias-Burinhosa wildfire started with an ignition in Pataias at 2:01 pm, followed by a second ignition at 2:33 pm, in Burinhosa (northeast from the first ignition). Most of the 16,949.6 ha of burned area did occur on the first day. The Quiaios wildfire originated from a single ignition located at the most southern point of its fire perimeter. It was first reported at 2:36 pm. This wildfire was dominated at 11:16 pm on the following day. During that period, an area of 19,025.5 ha was consumed by fire.

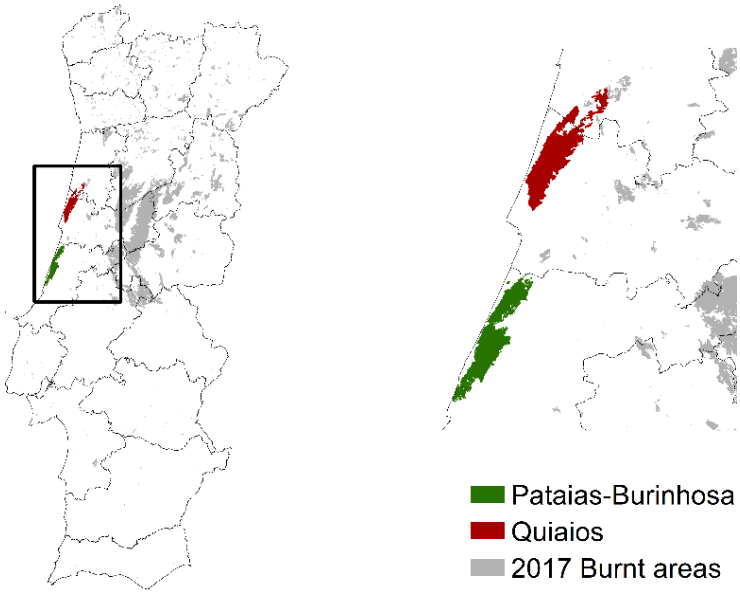

Figure 1- The burned areas of the Pataias-Burinhosa (in green) and the Quiaios (in red) fire events within the context of the burnt areas in 2017 (in grey).

2.3. Input data

Elevation profiles were provided by SRTM (Shuttle Radar Topography Mission) digital model (Farr et al., 2007). Land cover data were extracted from 100-m resolution CORINE land cover maps (CLC2012) to build the initial state and vegetation type matrices. The regional model WRF (Weather Research Forecast, version 4.0) (Skamarock et al., 2019) was run to obtain wind data which was subsequently corrected for wind interaction with topography with software WindNinja (version 3.4.1) (Forthofer et al., 2014). Wind information was updated every hour in the simulation. Information on starting ignitions and duration of fire events was provided by ICNF (Instituto da Conservação da Natureza e das Florestas) burned area maps (ICNF, 2022; ICNF, 2017). We also resorted to the official report (Guerreiro et al., 2018) to check the data.

Calibration of the model was performed by comparing the simulated burned area against shapefile maps provided by EFFIS (European Forest Fire Information System) (San-Miguel-Ayanz et al., 2012) in the case of the Pataias-Burinhosa event and, in the case of Quiaios, against a Sentinel-2 product of burned areas and implementing the methodology described in the RUS-Copernicus tutorial (RUS-Copernicus, 2017).

3. Results and discussion

Results presented in Figure 2 are the outcomes of ensembles of 100 simulations with time steps of $\Delta t = 4$ min covering a period of 21 hours for Pataias-Burinhosa and 35 hours for Quiaios, these values corresponding to the period where virtually all the area was burnt.

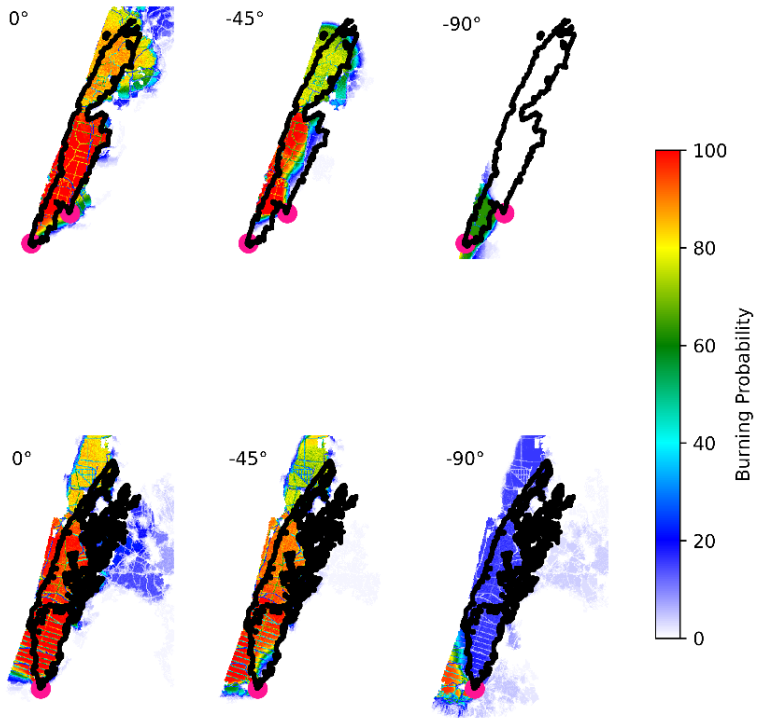

Figure 2- Maps of burning probability (%) as obtained for the simulations of the Pataias-Burinhosa (top panel) and the Quiaios (bottom panel) events. Left column shows the results from model calibration using winds derived from the regional weather forecast model, and the middle and right columns show the results from simulations when the winds are rotated counterclockwise of 45º and 90º, respectively. Black lines represent the real fire perimeters and the pink circles indicate locations of the ignition points.

Maps of probability of burning that resulted from the 100 simulations for model calibration, i.e. using winds derived from the regional weather forecast model (Fig. 2, left column) show an overall agreement with the observed fire perimeter (lines in black), and it is worth stressing that no barriers were defined representing actions of firefighting. Simulations using winds rotated counterclockwise show a progressive decrease in probability of burning from a 45º (Fig. 2, central column) to a 90º (Fig. 2, right column) rotation. In this latter case, simulations for the Pataias-Burinhosa event indicate that most of the area does not even burn, whereas for Quiaios most of the area presents values of probability lower than 20%.

Results obtained suggest that incorporation of wind direction in the Canadian System represents an added value when rating meteorological fire danger. For instance, this information could be incorporated in the Fire Weather Index (FWI), that rates fire intensity, leading, e.g. to the definition of an FWI vector, whose direction is that of the wind and magnitude is that of FWI. This vector should then be compared against the prevailing vegetation patch orientation, and the closer the alignment between the two directions, the greater the meteorological fire danger.

4. Ackowledgements

This work was supported by national funds through FCT (Fundação para a Ciência e a Tecnologia, Portugal) under project FIRECAST (PCIF/GRF/0204/2017) and IDL (UIDB/50019/2020).

5. References

Alexandridis A, Vakalis D, Siettos CI, Bafas GV. 2008. A cellular automata model for forest fire spread prediction: The case of the wildfire that swept through Spetses Island in 1990. *Appl. Math. Comput*. **204**, 191 - 201. https://doi.org/10.1016/j.amc.2008.06.046.

CLC2012: The CORINE Land Cover CLC dataset produced in 2012. Accessed 01 March, 2022. https://land.copernicus.eu/pan-european/corine-land-cover/clc-2012?tab=download.

Costa L, Thonicke K, Poulter B, Badeck FW. 2011. Sensitivity of Portuguese forest fires to climatic, human, and landscape variables: subnational differences between fire drivers in extreme fire years and decadal averages. *Reg. Environ. Change*. **11**, 543–551. https://doi.org/10.1007/s10113-010-0169-6.

Farr TG, Rosen PA, Caro E, Crippen R, Duren R, Hensley S, Kobrick M, Paller M, Rodriguez E, Roth L, Seal D, Shaffer S, Shimada J, Umland J, Werner M, Oskin M, Burbank D, Alsdorf D. 2007. The shuttle radar topography mission. *Rev. Geophys*. **45**. https://doi.org/10.1029/2005RG000183.

Finney MA. 2005. The challenge of quantitative risk analysis for wildland fire. *Forest Ecology and Management*. **211**, 97–108. https://doi.org/10.1016/j.foreco.2005.02.010.

Forthofer JM, Butler BW, Wagenbrenner NS. 2014. A comparison of three approaches for simulating fine-scale surface winds in support of wildland fire management. Part I. Model formulation and comparison against measurements. *Int. J. Wildland Fire*. **23**, 969-981. https://doi.org/10.1071/WF12089.

Freire JG, DaCamara CC. 2019. Using cellular automata to simulate wildfire propagation and to assist in fire management. *Earth Syst. Sci*. **19**, 169–179. https://doi.org/10.5194/nhess-19-169-2019.

Guerreiro J, Fonseca C, Salgueiro A, Fernandes P, Lopez Iglésias E, de Neufville R, Mateus F, Castellnou M, Silva J, Moura J, Rego F, Caldeira D. 2018. Avaliação dos incêndios ocorridos entre 14 e 16 de outubro de 2017 em Portugal Continental. Relatório Final. *Comissão Técnica Independente*. Relatório, Lisboa: Assembleia da República.

ICNF. 2017. "Relatório provisório de incêndios florestais 2017: 01 de Janeiro a 31 de Outubro." Accessed June 30, 2022. https://www.icnf.pt/api/file/doc/2c45facee8d3e4f8.

ICNF. 2022. Territórios Ardidos. Accessed June 28, 2022. https://sig.icnf.pt/portal/home/item.html?id=983c4e6c4d5b4666b258a3ad5f3ea5af.

Pereira, MG, Malamud BD, Trigo RM, Alves PI. 2011. The history and characteristics of the 1980–2005 Portuguese rural fire database. *Nat. Hazards Earth Syst. Sci.* **11**, 3343–3358. https://doi.org/10.5194/nhess-11-3343-2011.

Pinto P, Silva ÁP, Viegas DX, Almeida M, Raposo J, Ribeiro LM. Influence of Convectively Driven Flows in the Course of a Large Fire in Portugal: The Case of Pedrógão Grande. 2022. *Atmosphere* **13**, 414. https://doi.org/10.3390/atmos13030414.

RUS-Copernicus. 2017. Training kit - HAZAO2: Burned area mapping with Sentinel-2 using SNAP June, Portugal. Accessed March 09, 2019. https://rus-copernicus.eu/portal/wp-content/uploads/library/education/training/HAZA02_BurnedArea_Portugal_Tutorial.pdf.

San-Miguel-Ayanz J, Schulte E, Schmuck G, Camia A, Strobl P, Liberta G, Giovando C, Boca R, Sedano F, Kempeneers P, McInerney D, Withmore C, Oliveira SS, Rodrigues M, Durrant T, Corti P, Oehler F, Vilar L, Amatulli G. 2012. Comprehensive Monitoring of Wildfires in Europe: The European Forest Fire Information System (EFFIS), Approaches to Managing Disaster – Assessing Hazards, Emergencies and Disaster Impacts, edited by: Tiefenbacher J. *InTech*, Rijeka, Croatia, 87–108. https://doi/10.5772/28441

Skamarock WC, Klemp JB, Dudhia J, Gill DO, Liu Z, Berner J, Wang W Powers JG, Duda MG, Barker DM, Huang X-Y. 2019. A Description of the Advanced Research WRF Version 4.1 NCAR Tech. Note NCAR/TN-556+STR. https://doi.org/10.5065/1dfh-6p97.

Stocks BJ, Lawson B D, Alexander ME, Van Wagner CE, McAlpine RS, Lynham TJ, Dube DE. 1989. The Canadian Forest Fire Danger Rating System: An Overview. *For. Chron.* **65**, 450–457, https://doi.org/10.5558/tfc65450-6.

Wolfram S. 2002. 'A New Kind of Science'. 1st Edition. Wolfram Media Inc.

Validation of operational fire spread models in California

Adrián Cardil*[1,2,3]; Santiago Monedero[1]; Miguel Ángel Navarrete[1]; Sergio de-Miguel[2,3]; Carlos A. Silva[4]; Raúl Quilez[1]; Scott Purdy[1]; Joaquin Ramirez*[1]

[1] Technosylva Inc, La Jolla, CA, USA
{acardil, smonedero, manavarrete, rquilez, spurdy, jramirez}@tecnosylva.com
[2] Department of Crop and Forest Sciences, University of Lleida, Lleida, Spain, {sergio.demiguel@udl.cat}
[3] Joint Research Unit CTFC - AGROTECNIO - CERCA, Solsona, Spain
[4] Forest Biometrics and Remote Sensing Laboratory (Silva Lab), School of Forest, Fisheries, and Geomatics Sciences, University of Florida, PO Box 110410, Gainesville, FL 32611, USA , {carlos_engflorestal@outlook.com}

**Corresponding author*

Keywords

Fire modelling, Wildfire Analyst,

Abstract

The use of wildfire simulators allows estimating fire spread and behaviour in diverse and complex fire environments, supporting fire planning and analysis of incidents in operational environments. However, uncertainty derived from the spatio-temporal estimation of input variables and model's inherent inaccuracies related to its limitations and assumptions may undermine the utility of such predictions. Here, we assessed the performance of well-known operational surface and crown fire spread models used in California through the analysis of the rate of spread (ROS) of 1,853 wildfires occurring in the State from 2019 to 2021. For each detected wildfire, we retrieved the observed fire progression using the FireGuard (FG) database which provides the fire progression through geo-spatial polygons every 15 minutes approximately. Based on this data, we developed an algorithm that characterises the ROS for each FG polygon and the average ROS in the first 8 hours of the fire. Also, we ran a fire simulation for each wildfire with Wildfire Analyst Enterprise using high-resolution fuel and weather data to estimate the rate of spread. Then, we assessed 1) the accuracy of the fire simulations by comparing the real and simulated ROS based on the Mean Absolute Error (MAE), Mean Bias Error (MBE) and Mean Absolute Percentage Error (MAPE); 2) the most important factors influencing the accuracy of fire simulations, including the wind speed, and fuel types. Although the models clearly underestimated ROS in timber fuels, especially when no crown fire behaviour was predicted, most of the fire simulations had an acceptable error to be used in operational environments given the new techniques to adjust and calibrate the fires with field data. Finally, we used this analysis to present new approaches to optimise the fire predictions, including the optimisation of new custom fuels through genetic algorithms and enhancement of crown fire spread models.

1. Introduction

Wildfires are a natural disturbance of many ecosystems (Pausas and Keeley 2009) although they suppose a growing threat to the environment, economical assets and population (Molina-Terrén *et al.* 2019). Important amounts of financial resources have been invested in fire management aiming to reduce the substantial damage of wildfires and ensure safety for the population (Liang *et al.* 2008; Cardil and Molina 2015; Stocks and Martell 2016). In this sense, the estimation of the wildfire rate of spread (ROS) across complex landscapes is essential for effective planning and fire suppression, including the release of timely and operative public warnings for disaster management and evacuation orders (Cruz *et al.* 2018; Monedero *et al.* 2019; Ramirez *et al.* 2019).

Several mathematical approaches have been developed in the last decades aimed at predicting fire behaviour. The capability of accurately predicting the fire spread is directly linked to the model's inherent inaccuracy derived from its limitations and assumptions (Albini 1976; Ascoli *et al.* 2015; Vacchiano and Ascoli 2015) and input data, factors that may undermine the utility of such predictions for decision-making (Cruz and Alexander 2013; Benali *et al.* 2017; Ramirez *et al.* 2019). Cruz and Alexander (2013) quantified errors and biases of several wildfire ROS models after conducting a comprehensive survey of studies gathering a database comprising 1,278 paired predicted vs observed ROS values. Other studies assessed model's performance in several fire-prone

areas and analysed how new improvements in fire spread models may enhance the performance to their previous ones (Cruz *et al.* 2018).

This work assesses the predictive accuracy of fire spread models currently used in California in operational settings under different environmental conditions using 1,853 fires from 2019 to 2021. The analysis identifies in what conditions the models may over or under-estimate the ROS and, subsequently, the burned area and associated fire impacts on buildings or other assets. The analysis is based on well-known error metrics and statistical approaches (Cruz *et al.* 2018) aiming to compare the predicted with observed ROS values. Finally, we propose several improvements in the current fire spread models to enhance their performance.

2. Methodology

2.1. Study area

This study was developed in California, a region dominated by Mediterranean climatic conditions, known to foster recurrent large wildfires (Pyne *et al.* 1998). Fire-prone weather situations such as long and dry summers with thunderstorms episodes, low relative humidity and strong dry winds are typical of this region (Sugihara and Barbour 2006).

2.2. Fire progression data (FireGuard)

The National Fireguard Detections product (FG) provides wildfire detection and monitoring across the USA at all times. It allows the detection of new wildfires as well as areas of significant fire growth which is especially useful in remote regions and during the first 24 - 48 hours when this information is usually scarce. Updates on the fire progression are often provided every 15 minutes.

We retrieved all FG polygons in California from October 2019 to November 2021 and removed prescribed fires. Then, we clustered FG polygons based on distance and fire arrival time to aggregate them to real incidents and create progression maps of individual fires (Figure 1). For each cluster, we selected the first FG polygon later used as ignition source. As a result, the progression of 1,853 wildfires was obtained for further analysis. We used the first burning period (8 hours from the fire start) to compare the simulated ROS with the real ROS obtained through FG. We developed an algorithm to analyse the ROS for each FG polygon (see ROS vectors for some fires in Figure 1) to finally estimate the average ROS during the first burning period. Also, for each fire we retrieved a set of environmental variables for identifying in what conditions the models may over or under-estimate the ROS and, subsequently, the burned area and associated fire impacts on buildings or other assets. This set of variables includes surface fuel types, canopy characteristics, weather conditions (forecast and stations), dead and live fuel moisture content.

2.3. Fire modelling with Wildfire Analyst Enterprise (WFA-e)

Fire modelling was carried out using Wildfire Analyst Enterprise (WFA-e) that provides real-time analysis of wildfire behaviour and simulates the spread of wildfires to directly support multi-agency wildfire incident management. Currently, many public and private entities, such as natural resource agencies, electrical investor-owned utilities, insurance and forestry companies strongly rely on WFA-e which facilitates optimal decision-making. We simulated 1,853 fires using the first FG polygon as an ignition source based on well-known semi-empirical fire spread models currently used in California including the Rothermel's (1972) surface fire spread model, van Wagner's (1977) crown fire initiation model, Rothermel's (1991) crown fire spread model, Albini's (1979) spotting model, and Andrews' (2012) conversion factor and wind profile and Minimum Travel Time time evolution algorithm (Finney 2002). We calculated the average hourly ROS and average simulated ROS during the real fire duration based on the FG fire progression up to 8 hours after the fire start (first burning period).

Improved high-resolution surface fuel types (Scott and Burgan 2005) and canopy characteristics maps (canopy cover, canopy height, canopy base height and canopy bulk density) were collected to perform the fire simulations. These maps were modelled by Technosylva Inc based on an Object-based Image Analysis by grouping homogeneous vegetation areas into vector objects later classified with machine learning algorithms and ground truth data with an accuracy of 90%. We used high-resolution weather data at 2 km using the Weather Research and Forecasting model, a mesoscale numerical weather prediction system designed for operational

forecasting applications. Nelson's 2000 model was used to estimate dead fuel moisture content and live fuel moisture content was retrieved from the US National Fuel Moisture Database (WFAS; https://www.wfas.net/index.php/national-fuel-moisture-database-moisture-drought-103).

2.4. Statistical analysis

We compared the ROS predicted by WFA-e and observed through FG based on four different metrics (Cruz *et al.* 2018): 1) *ROS residual* representing the difference between the predicted and observed ROS. Therefore, a positive residual indicates an over-prediction; 2) *Mean Absolute Error (MAE)*, representing an average of the absolute error (eq. 1); 3) *Mean Bias Error (MBE)*, representing an average bias between the predicted and observed values (eq. 2); 4) *Mean Absolute Percentage Error (MAPE)*, a measure of prediction accuracy of a forecasting method in statistics. It expresses the accuracy as a ratio (eq. 3).

$$\mathrm{MAE} = \frac{\sum_{i=1}^{n} |WFA_i - FG_i|}{n} \quad \text{(equation 1)}$$

$$\mathrm{MBE} = \frac{\sum_{i=1}^{n} (WFA_i - FG_i)}{n} \quad \text{(equation 2)}$$

$$\mathrm{MAPE} = \frac{100}{n} \sum_{i=1}^{n} \left| \frac{FG_i - WFA_i}{FG_i} \right| \quad \text{(equation 3)}$$

where *FGi* represents the ROS measures through FG, *WFAi* is the estimated ROS by WFA-e and *n* the number of wildfires.

We analysed the simulation accuracy based on these metrics considering input data for fire simulations and enhancements in our models through the use of simulated local wind fields (Windninja (Wagenbrenner *et al.* 2016)) and improved crown fire spread models.

3. Results and discussion

Rothermel (1972) model is the most widely evaluated fire spread model on Earth based on prescribed fires and some wildfires (Cruz and Alexander 2013). However, the amount, nature and quality of data provided in this work allows a better understanding of the model's performance under different environmental conditions in California. The observed (FG) and predicted (WFA-e) fire progression were compared analytically based on the methods described in section 2.4. However, as an example, we showed four fires in figure 1 to illustrate the ROS vectors calculated automatically from the FG data and the fire simulation for each fire. Although this visual assessment is useful to clarify how we compared the predicted and observed ROS, a statistical analysis was carried out to assess the performance of models for all the fires retrieved from FG in the study period considering the different combinations of environmental conditions influencing fire behaviour (fuels, weather, topography, etc).

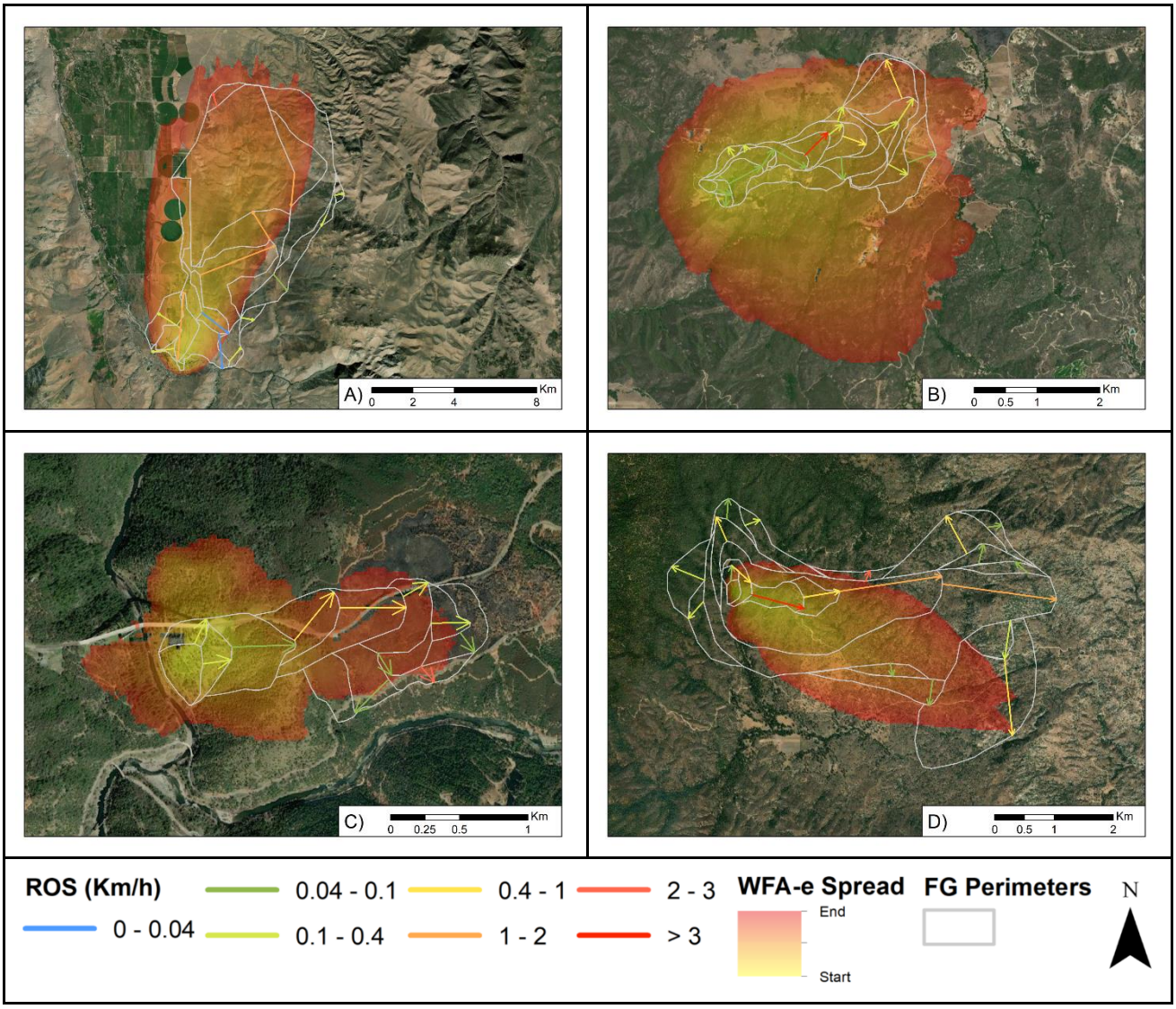

Figure 1. Fire progression and simulation of four wildfires in California. A) Mountain View fire (lat = 38.515; lon = -119.465; 2020/11/17); B) Chaparral fire (lat = 33.485; lon = -117.399; 2021/08/28); C) Bridge fire (lat = 38.921; lon = -121.037; 2021/09/05); D) French fire (lat = 35.687; lon = -118.55; 2021/08/18); Note that the FG polygons and WFA-e simulated fire progression have the same time duration.

Overall, the model produced the best predictions for Grass (GR), Grass-Shrub (GS) and Shrub (SH) Scott and Burgan (2005) fuel types with MAPE values of approximately 60% (Fig. 2) similarly to other studies (Cruz *et al.* 2018). The lowest MAE (0.31 km/h), MBE (0.016 km/h) and MAPE (59 %) values were found for the SH fuel types, followed by GS and GR fuel types. Thus, we found the highest error and bias in timber fuel types (Fig 2) with a MAPE value of 80%, also in line with other studies assessing the performance of Rothermel's model (Cruz *et al.* 2018). The histogram of ROS residuals showed a normal distribution for GR, GS and SH Scott and Burgan (2005) fuel types (Fig. 2A) with low bias in the predictions (MBE; Fig 2C). However, the models had a preponderant ROS under-prediction bias in most timber fires as shown by the histogram of ROS residuals, MAE and MBE metrics (Fig 2), an error type leading to potentially negative consequences in operational decision-making (Cheney and Gould 1995). This analysis suggests that new enhancements are needed to decrease the error and bias of fire spread models in line with other studies developed in other regions such as Australia (Cruz *et al.* 2018). Previous studies found the lowest MAE values in timber and logging slash fuel types but also the largest MAPE (76 %) values. This was derived from the range of observed ROS values in these fuel types that were substantially lower than in grasslands and shrublands fuel types (Cruz *et al.* 2018). However, in our study, we also found the highest MAE and MBE values in timber fuel types since the database contained fires with high ROS. The simulated ROS tended to be under-predicted in extremely fast fires (average observed ROS > 1.5 km/h) in all fuel types and specially in timber fuel types. This may be related to convective fire behaviour leading to local winds in the fire front not considered by the weather models.

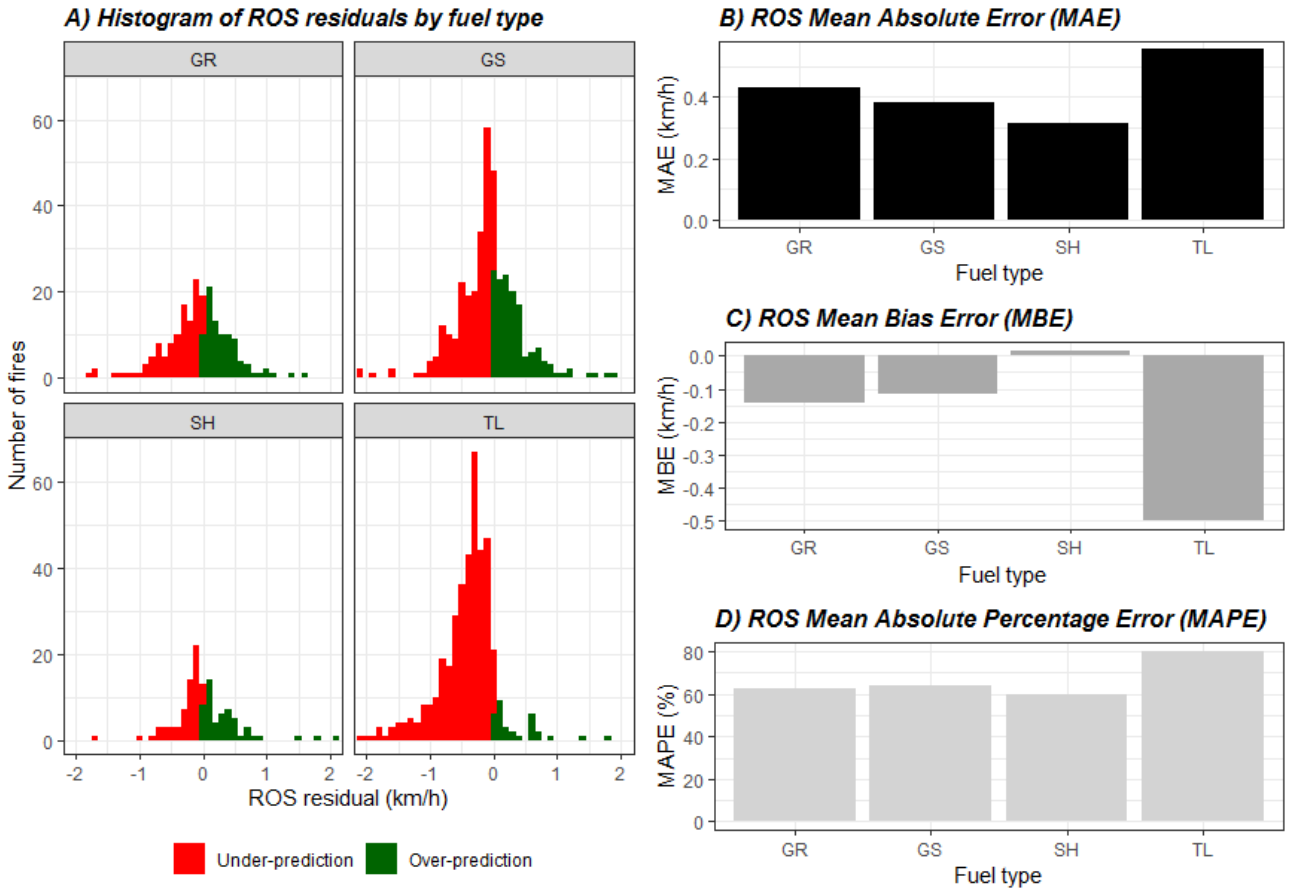

Figure 2. Fire spread model's performance analysis for 1,853 wildfires occurred in California in the 2019-2021 period. A) Histogram of ROS residuals by fuel type based on Scott and Burgan (2005); B) ROS mean absolute error (MAE); C) ROS mean bias error (MBE); D) ROS mean absolute percent error (MAPE). GR: Grass Fuel Types 101 to 109; GS: Grass-Shrub Fuel Types 121 to 124; SH: Shrub Fuel Types 141 to 149; TL: Timber-Litter-Understory Fuel Types 161 to 189.

Fire spread model's accuracy was also influenced by other environmental variables beyond fuel types (fuel moisture content, wind speed, etc), a fact not deeply studied in previous research studies. In general, high wind speeds led to ROS overprediction and low wind speed to underprediction, especially in GS and TL fires. This effect may be amplified in TL fuel types given that the crown fire spread models often require high wind speeds to forecast crown fire activity. Also, these models often behave binarily given a specific set of environmental conditions dramatically influencing the predicted ROS. We tried to address this issue in this work decreasing the MAPE up to 60% by smoothing the active crown ratio as follows:

$$ROS = surfaceROS * (1-\alpha) + \alpha * crownROS \quad \text{(Equation 4)}$$

where surfaceROS is the surface ROS fire spread by Rothermel 1972, crownROS represents the crown ROS by crown fire behaviour models and $\alpha = activeRatio^{1/factor}$ is the active crown ratio that is modulated by a factor defined by the fire analyst.

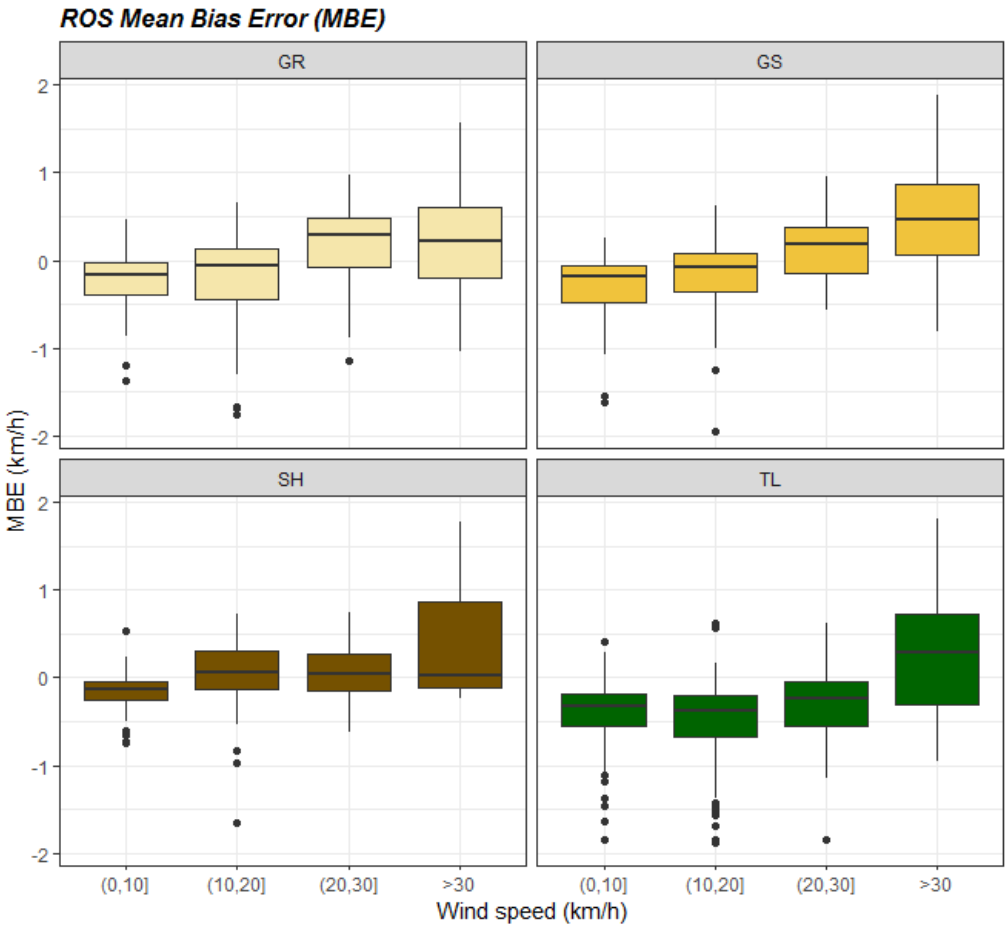

Figure 3. Boxplot of the ROS bias error (MBE) by fire and fuel type based on Scott and Burgan (2005) for 1,853 wildfires occurred in California in the 2019-2021 period. GR: Grass Fuel Types 101 to 109; GS: Grass-Shrub Fuel Types 121 to 124; SH: Shrub Fuel Types 141 to 149; TL: Timber-Litter-Understory Fuel Types 161 to 189.

4. Conclusions and further research

This work concludes that the fire spread model's performance for California is in line with previous studies developed in other regions and the accuracy of fire behaviour outputs are modulated by environmental conditions, especially wind speed. Therefore, the models are accurate enough to be used in real-time operations, especially with the use of adjustment modes that allow the calibration of predictions using field data (Artès *et al.* 2015; Cardil *et al.* 2019). However, we also recognize that there are challenges regarding the effect of pyroconvection on local wind fields and the estimation of ROS in timber areas. The results of this evaluation suggest that the accuracy of fire simulations may be improved with newer models aiming to address the modelling of crown fire behaviour.

The FG data and the algorithms developed in this research work to calculate ROS vectors represent a crucial enhancement to better analyse the fire spread model's performance and calibrate and provide new models and fuel families. Our approach addresses issues arising from the use of long fire runs, encompassing at times variations in fuel types, the estimation of fuel characteristics across the landscape, and the averaging of wind speed over broad spatial and temporal scales.

5. References

Albini F (1976) "Estimating wildfire behavior and effects. Intermountain forest and range experiment station." (Utah)

Albini F (1979) Spot fire distance from burning trees: a predictive model. (USDA Forest Service, Intermountain Forest and Range Experiment Station, Technical Report INT-56. Ogden, UT)

Andrews P (2012) "Modeling wind adjustment factor and midflame wind speed for Rothermel's surface fire spread model." (USDA Forest Service, Rocky Mountain Research Station, General Technical Report RMRSGTR- 266.: Fort Collins, CO)

Artès T, Cardil A, Cortés A, Margalef T, Molina D, Pelegrín L, Ramírez J (2015) Forest Fire Propagation Prediction Based on Overlapping DDDAS Forecasts. Procedia Computer Science 51, 1623–1632. doi:10.1016/j.procs.2015.05.294.

Ascoli D, Vacchiano G, Motta R, Bovio G (2015) Building Rothermel fire behaviour fuel models by genetic algorithm optimisation. International Journal of Wildland Fire 24, 317–328. https://doi.org/10.1071/WF14097.

Benali A, Sá ACL, Ervilha AR, Trigo RM, Fernandes PM, Pereira JMC (2017) Fire spread predictions: Sweeping uncertainty under the rug. Science of The Total Environment 592, 187–196. doi:10.1016/j.scitotenv.2017.03.106.

Cardil A, Molina DM (2015) Factors Causing Victims of Wildland Fires in Spain (1980–2010). Human and Ecological Risk Assessment: An International Journal 21, 67–80. doi:10.1080/10807039.2013.871995.

Cardil A, Monedero S, Silva CA, Ramirez J (2019) Adjusting the rate of spread of fire simulations in real-time. Ecological Modelling 395, 39–44. doi:10.1016/j.ecolmodel.2019.01.017.

Cheney NP, Gould JS (1995) Fire Growth in Grassland Fuels. International Journal of Wildland Fire 5, 237–247. https://doi.org/10.1071/WF9950237.

Cruz M, Alexander M (2013) Uncertainty associated with model predictions of surface and crown fire rates of spread. Environmental Modelling and Software Software 47, 16–28.

Cruz MG, Alexander ME, Sullivan AL, Gould JS, Kilinc M (2018) Assessing improvements in models used to operationally predict wildland fire rate of spread. Environmental Modelling and Software 105, 54–63. doi:10.1016/j.envsoft.2018.03.027.

Finney M (2002) Fire growth using minimum travel time methods. Canadian Journal of Forest Research 32, 1420–1424. doi:10.1139/X02-068.

Liang J, Calkin DE, Gebert KM, Venn TJ, Silverstein RP (2008) Factors influencing large wildland fire suppression expenditures. International Journal of Wildland Fire 17, 650–659. doi:10.1071/WF07010.

Molina-Terrén DM, Xanthopoulos G, Diakakis M, Ribeiro L, Caballero D, Delogu GM, Viegas DX, Silva CA, Cardil A (2019) Analysis of forest fire fatalities in Southern Europe: Spain, Portugal, Greece and Sardinia (Italy). International Journal of Wildland Fire 85–98. doi:10.1071/wf18004.

Monedero S, Ramirez J, Cardil A (2019) Predicting fire spread and behaviour on the fireline. Wildfire analyst pocket: A mobile app for wildland fire prediction. Ecological Modelling 392, 103–107. doi:10.1016/j.ecolmodel.2018.11.016.

Nelson RJ (2000) Prediction of diurnal change in 10-h fuel stick moisture content. Canadian Journal of Forest Research 30, 1071–1087.

Pausas JG, Keeley JE (2009) A burning story: the role of fire in the history of life. BioScience 59, 593–601. doi:10.1525/bio.2009.59.7.10.

Pyne S, Andrews P, Laven R (1998) "Introduction to wildland fire." (Wiley: New York)

Ramirez J, Monedero S, Silva C, Cardil A (2019) Stochastic decision trigger modelling to assess the probability of wildland fire impact. Science of The Total Environment 694, 133505. doi:10.1016/j.scitotenv.2019.07.311.

Rothermel R (1972) A mathematical model for predicting fire spread in wildland fuels. USDA Forest Service, Intermountain Forest and Range Experiment Station Research Paper INT-115 Ogden, UT.

Rothermel R (1991) Predicting behavior and size of crown fires in the Northern Rocky Mountains. Predicting Behavior and Size of Crown Fires in the Northern Rocky Mountains US Department of Agriculture, Forest Service, Intermountain Research Station INT-438 Ogden, UT.

Scott J, Burgan R (2005) Standard fire behavior fuel models: a comprehensive set for use with Rothermel's surface fire spread model.

Stocks B, Martell D (2016) Forest fire management expenditures in Canada 1970–2013. The Forestry Chronicle 92, 298–306.

Sugihara N, Barbour M (2006) Fire and California vegetation. "Fire in California's Ecosystems." (Eds N Sugihara, J van Wagtendonk, J Fites-Kaufman, K Shaffer, A Thode)(University of California Press: Berkeley, California)

Vacchiano G, Ascoli D (2015) An Implementation of the Rothermel Fire Spread Model in the R Programming Language. Fire Technology 51, 523–535. doi:10.1007/s10694-014-0405-6.

Wagenbrenner NS, Forthofer JM, Lamb BK, Shannon KS, Butler BW (2016) Downscaling surface wind predictions from numerical weather prediction models in complex terrain with WindNinja. Atmospheric Chemistry and Physics 16, 5229–5241. doi:10.5194/acp-16-5229-2016.

van Wagner C (1977) Conditions for the start and spread of crown fire. Canadian Journal of Forest Research 7, 23–34.

Vegetation Mapping with Random Forest using Sentinel 2- A case study for Lousã region, Portugal

Pegah Mohammadpour*[1,2]; Crismeire Isbaex [1]; Emilio Chuvieco[2]; Xavier Viegas[1]; Carlos Viegas[1]

[1] *Univ of Coimbra, ADAI, Department of Mechanical Engineering, Rua Luís Reis Santos, Pólo II, 3030-788 Coimbra, Portugal. {Pegish2014@gmail.com or pegah@adai.pt}*
[2] *University of Alcala, Department of Geology, Geography and the Environment, Alcalá de Henares, Spain*

**Corresponding author*

Keywords

Vegetation classification, Sentinel 2, Random Forest, Accuracy Assessment, Independent Variables, GLCM texture feature

Abstract

Vegetation mapping requires accurate information to allow its use in applications such as sustainable forest management against the effects of climate change and the threat of wildfires. Remote sensing provides a powerful resource of fundamental data at different spatial resolutions and spectral regions, making it an essential tool for vegetation mapping and biomass management. Due to the ever-increasing availability of free data and software, satellites have been predominantly used to map, analyze, and monitor natural resources for conservation purposes. This study aimed to map vegetation from Sentinel-2 (S2) data in a complex and mixed vegetation cover of the Lousã district in Portugal. We used ten multispectral bands with a spatial resolution of 10 m, and four vegetation indices, including Normalized Difference Vegetation Index (NDVI), Green Normalized Difference Vegetation Index (GNDVI), Enhanced Vegetation Index (EVI), and Soil Adjusted Vegetation Index (SAVI). After applying Principal Component Analysis (PCA) on the 10 S2A bands, four texture features, including Mean (ME), Homogeneity (HO), Correlation (CO), and Entropy (EN), were derived for the first three Principal Components. Textures were obtained using the Gray-Level Co-Occurrence Matrix (GLCM). As a result, 26 independent variables were extracted from S2. After defining the land use classes by object-based, the Random Forest (RF) classifier was applied. The map accuracy was evaluated by the confusion matrix, using the metrics of Overall Accuracy (OA), Producer Accuracy (PA), User Accuracy (UA), and Kappa Coefficient (Kappa). The described classification methodology showed a high OA of 90.5% and Kappa of 89% for vegetation mapping. Using GLCM texture features increased the accuracy up to 2%. The ME and CO had the highest contribution to the accuracy of the classification among the GLCM textures. GNDVI had outperformed other vegetation indices in variable importance. Also, using only S2A spectral bands, especially bands 11, 12, and 2, showed a high potential to classify the map with an OA of 88%. This study showed that adding at least one GLCM texture feature and at least one vegetation index into the S2A spectral bands may effectively increase the accuracy metrics and tree species discrimination.

Notation

B_2 S2A band2
B_3 S2A band3
B_4 S2A band4
B_8 S2A band8
N Number of grey levels
P Normalized symmetric GLCM of dimension $N \times N$
$P(i, j)$ Normalized grey level value in the cell i, j of the co-occurrence matrix
d Distance
θ Direction
$\bar{x}$ Mean of P_x
$\bar{y}$ Mean of P_y
σ_x Standard deviation of P_x
σ_y Standard deviation of P_y

1. Introduction

Wildfires have wide-ranging effects on people's lives, wildlife, the natural environment, and the economy worldwide. Wildfire is a key component of the Mediterranean landscapes and ecosystems due to climate change, changes in the Land Cover and Land Use (LCLU), agriculture abandonment and expansion of forests and shrublands, expansion of Wildland-Urban Interfaces (WUI), and reduction in forest management (Xavier et al. 2006). Southern European nations such as Spain and Portugal with Mediterranean Basin (MB) forests would face the greatest fire dangers, given they are already prone to severe and frequent wildfires (Investment in Disaster Risk Management in Europe 2021, Costa H et al. 2020). Portugal experienced an unprecedented fire season in 2017, with a record of 540,000 ha burnt, 119 deaths, and millions of euros in losses and damage (Benali and Fernandes 2021, Monterio-Henriques and Fernandes 2018). Severe drought and the emergence of meteorological conditions conducive to large wildfires amplified the Portuguese 2017 fire season (Benali and Fernandes 2021). According to the Portuguese Institute of the Sea and the Atmosphere (IPMA), May 2022 was the warmest May in the past 92 years because of severe drought conditions, unusually high temperatures, and low average precipitation (IPMA 2022). Consequently, MB forests' protection from wildfire and climate change will be critical, necessitating large-scale fuel mapping and management (Kolström et al. 2011).

Conventionally, vegetation mapping has been performed using field surveys, image interpretation, and ancillary data analysis. Nowadays, remote sensing data with active and passive sensors are the main source of information for earth observation and producing up-to-date LCLU classification (Aragoneses and Chuvieco 2021, Xie et al. 2008, Chaves et al. 2020). Forest mapping and monitoring can be significantly improved by using freely available middle-resolution remote sensing data such as the Sentinel constellation. Sentinels' data provide high temporal frequency, different spatial coverage, and characterize various fuel types and their conditions with several spectral bands ((Aragoneses and Chuvieco 2021, Xie et al. 2008, Zeng et al. 2020, Kaplan 2021). Sentinel-2 mission with two satellites, Sentinel 2 level A (S2A) and Sentinel 2 level B (S2B), was launched by the European Union's Copernicus Earth Observation program of the Europe Space Agency (ESA) in 2015 and 2017, respectively. Sentinel-2 mission offers spatial resolution varying between 10 m and 60 m and a revisit frequency of 5 days (Sentinel-2 User Handbook. Vol. 2). Sentinel-2 includes three red-edged vegetation and the SWIR bands that are highly susceptible to chlorophyll content and amend distinguishing different vegetation types and LCLU classification accuracy (Chaves et al. 2020). Several studies found Sentinel-2 data with high potential in different applications such as crop classification (Hernandez et al. 2020), tree species classification (Costa et al. 2022, Wessel et al. 2018, Persson et al. 2018), mapping burned area (Pacheco et al. 2021), and forest type classification (Kaplan 2021). Most of the recent studies have shown that non-parametric machine learning approaches such as Artificial Neural Network (ANN), Support Vector Machine (SVM), and Random Forest (RF) have a great potential to classify heterogeneous land covers (Wessel et al. 2018, Pacheco et al. 2021, Sheykhmousa et al. 2020). Ma et al. (2017) found RF as the mostly used supervised classifier and more stable object-based image analysis (OBIA) with the highest mean accuracy of 85.81%, followed by SVM through reviewing 173 publications on supervised object-based classification. For example, Wessel et al. (2018) classified tree species based on multitemporal Sentinel-2 data with the highest overall classification accuracy of 91% for the SVM object-based algorithm. Persson et al. (2018) also studied the classification of common tree species in Sweden by applying RF classifier on multitemporal Sentinel-2 data. They achieved the highest overall accuracy of 88.2% for the combination of all spectral bands for four image dates.

Several operational programs are undergoing to produce global land cover maps, such as CORINE Land Cover (CLC), Land Change Monitoring, Assessment, and Projection (LCMAP), North American Land Change Monitoring System (NALCMS), and recently WorldCover produced by ESA at 10m resolution (Costa et al. 2018). These harmonized LCLU mappings have great potential for providing valuable information on Earth's surface; however, they face several challenges. The thematic accuracy of these global or continental land cover maps is spatially dependent on a low-frequency basis (e.g., every five years or more). Usually, they cannot comply with the user-specific requirements in space and time (Costa et al. 2018). Several researchers found the Mediterranean countries, such as Portugal and Spain, with the lowest overall accuracy, below 70% out of all European countries mapped (Costa et al. 2022, Liu et al. 2021). National land cover mapping with higher accuracy and up-to-date and detailed data can use as a complementary product for larger mapping scales (Costa et al. 2022).

SMOS (Sistema de Monitorização de Ocupação do Solo) is the land cover monitoring system for mainland Portugal which is in preparation by Directorate General for Territory (DGT) based on COS (Cartografia de Uso

e Ocupação do Solo), the traditional LCLU map of Portugal. An annual land cover cartography product of mainland Portugal (COSsim) based on sentinel-2 was started to overcome the limitation of COS. Costa et al. (Costa et al. 2022) presented an approach to map COSsim for 2018 with an overall accuracy of 81.3% using Random Forest (RF) classification and Sentinel-2 multi-temporal data. Although they achieved an accuracy of over 90% for southern Portugal, the classification overall accuracy for the center and North Portugal was below 80%, especially for the Coimbra district with approximately 75%. Their methodology was developed based on the following stages such as image classification, spatial stratification, knowledge-based rules (combination of expert knowledge and auxiliary data), intra-annual change, and manual editing. They classified this map into 13 thematic classes including the predominant species such as evergreen oaks, Eucalyptus, Maritime pine, and Stone pine (Costa et al. 2022). Costa et al. (2018) also studied a methodology with the combination of supervised and rule-based classification under the scope of the Land Use and Coverage Area frame Survey (LUCAS) to produce annual land cover statistics over Portugal from 2010 to 2015. They collected temporal Landsat data and auxiliary data such as Land Use and Land Cover map (COS2010) and Land Parcel Identification System (LPIS). ANN, SVM, and RF have been used for classification in their study and final classification with 15 classes obtained through the voting process. They reached the highest overall accuracy of 87.5% for the year 2010 and the lowest accuracy of 86.4% for the years 2014 and 2015.

The main objective of this study is to apply RF classification algorithms on S2A data to map the vegetation in the Lousa region, Portugal. The specific purpose of this study is to increase the interclass separability of forest and vegetation classes. According to the literature, no up-to-date vegetation mapping with Sentinel-2 and high overall accuracy was seen for the mentioned study area. Principal component analysis (PCA) was applied to the S2A spectral bands resampled to 10m resolution. Four common Vegetation Indices (VIs) and 12 GLCM-based textural variables, extracted from three first principal components (PCs), were integrated into the S2A spectral bands to better classify various vegetation in complex land cover. A comparison has been performed between the classification with all 26 independent variables and three different combinations of S2A spectral bands, vegetation indices, and GLCM textures. The importance of input variables has been analyzed based on Mean Decrease Accuracy (MDA) and Mean Decrease Gini (Gini). The obtained high-accuracy vegetation map can be used for biomass management and wildfire risk assessment.

2. Materials and Methodology

2.1. Study area

The study area is in the central region of Portugal. The study area is 138.4 km^2 (13840 ha) in size, latitudes 40º and 40º 3' N and longitudes 8º 09' and 8º 19' W, and is located in the municipality of Lousa in the Coimbra district of Portugal, as shown in **Figure 1**. The Lousa district has an elevation ranging from 57 m near the River Ceira in the north to 1205 m at Trevim in the south, which is the highest point of Serra da Lousa. Over 68% of the territory is below 400 meters of altitude. Slope values vary from the flat region in the northwest, with slopes typically less than 10°, to mountainous areas in the southeast, with slopes larger than 20° (Plano Municipal de Defesa da Floresta Contra Incêndios 2020).

The forest area (about 10,385 ha) is the municipality's dominant land use, accounting for approximately 75% of the municipality's total area. Agriculture land occupies 1399.27 ha. As a result, forestry and agricultural areas comprise most of the land, covering approximately 85% of the total area (Incêndios 2020). The predominant vegetation cover includes *Pinus pinaster* and *Eucalyptus globulus* species represent about 50% and 25% of the total forest species in the municipality, respectively (Incêndios 2020).

The climate of Lousa is the Mediterranean, with moderate, rainy winters and hot, dry summers. The months of autumn, winter, and early spring see the most precipitation. Their values are highly dependent on altitude and range, on average, between 1000 and 1800 mm annually. In 2017, 28 distinct wildfires burned about 4560 ha of forest in the municipality. The largest fires detected in Lousa municipality happened during the summer when temperatures average above 30 C°, and relative humidity falls below 30%, except for October 2017, which was affected by Storm Ophelia (Incêndios 2020). The severity of the Portuguese 2017 wildfires was exacerbated by a severe drought and the occurrence of meteorological conditions conducive to large wildfires (Viegas et al. 2017).

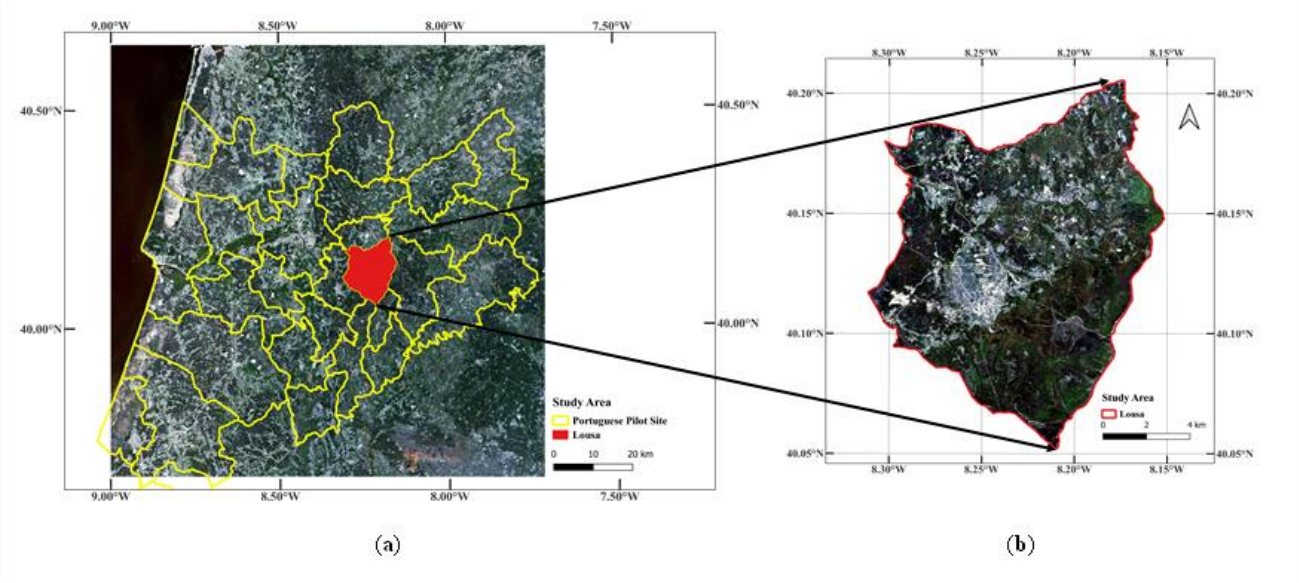

Figure 1- Geographical framework of the location and limits of the study area within a firEUrisk project and mainland Portugal: a) Sentinel-2 false-color composite image and b) study area- Lousa.

2.2. Materials, Data, and Model Algorithm

The S2A image processing procedures are synthetically represented in the workflow (**Figure 2**). Several processing stages were needed to achieve the vegetation mapping.

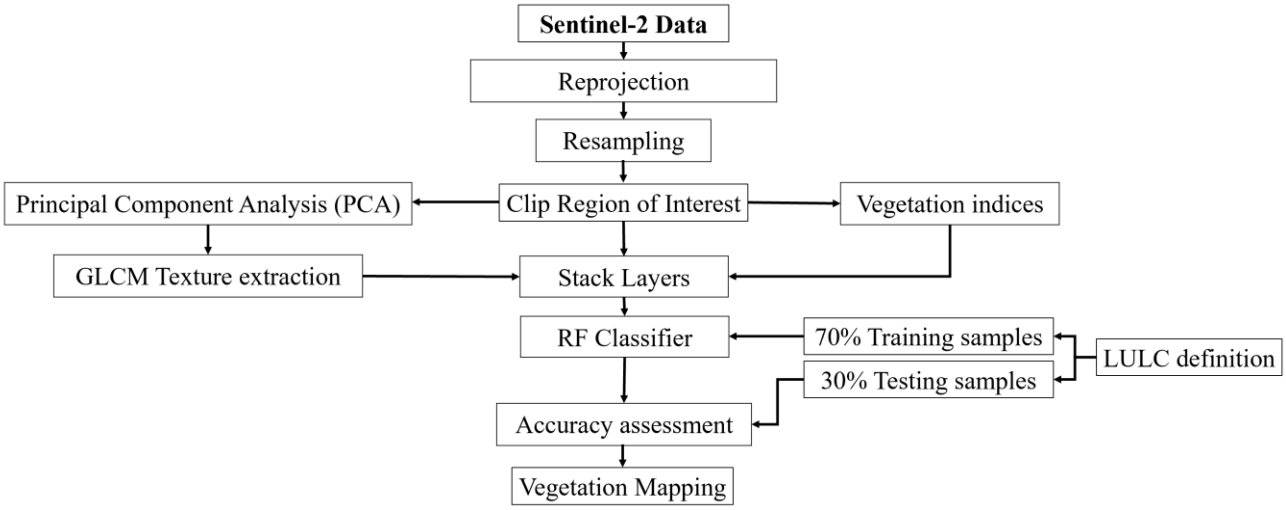

Figure 2- Scheme of vegetation mapping with Sentinel-2 data.

2.3. Dataset and preprocessing

Sentinel-2A MSI Level-2A images taken on July 18th, 2020, were derived from the Sentinels Scientific Data Hub for the study area (https://scihub.copernicus.eu/). The image was taken during the dry season to have less cloud coverage percentage (0.25%). The image was projected from WGS84 Geographic latitude/longitude coordinates to EPSG:3763 - ETRS89 / Portugal TM06, which preserves the area measure.

Sentinel-2 is equipped with MultiSpectral Instrument (MSI), which has four 10 m bands (visible and infrared – NIR), six 20 m bands (red-edge vegetation and short-wave infrared – SWRI), and three 60 m bands (Kaplan 2021). It is possible to increase the spatial resolution of all bands to 10 m using the resampling method and downscale the coarse resolution to fine resolution (Kaplan 2021, Sentinel-2 User Handbook. Vol. 2 2015, Zheng et al. 2017). Pixels of 20 m bands were resampled to the pixel size of 10 m with the Nearest Neighbor technique using ArcGIS Pro (version 2.8).

The high spectral resolution of Sentinel-2 imagery enables the extraction of different features. Based on the literature review and the sensitivity of optical features to biomass, four common spectral vegetation indices (VIs) were derived, including Normalized Difference Vegetation Index (NDVI), Green Normalized Difference Vegetation Index (GNDVI), Enhanced Vegetation Index (EVI), Soil Adjusted Vegetation Index (SAVI) using ArcGIS Pro(Noi Phan et al. 2020, Xia et al. 2017). The complete list of formulas can be found in Table 1 (B2, B3, B4, and B8 are the correspondence S2A bands). NDVI is strongly related to vegetation content, and NDVI high values indicate denser and healthier vegetation. GNDVI is a modified form of NDVI that can detect varying chlorophyll concentration rates by using green reflectance instead of red reflectance (Gitelson et al. 1996). EVI was developed to increase the sensitivity of vegetation signals in high biomass locations (Bhatnagar et al. 2021). SAVI also is a vegetation index that aims to reduce the impact of soil luminance, particularly in areas with low vegetation cover (Somvanshi and Kumari 2020).

Table 1- Vegetation indices (VIs) and applications from S2A.

Vegetation Indices	Formulation	Application
NDVI	$\frac{B_8 - B_4}{B_8 + B_4}$	Detection of vegetation communities in various seasons (29) Estimating changes in vegetation state (28) Determining the density of greenness (31)
GNDVI	$\frac{B_8 - B_3}{B_8 + B_3}$	Determining water and nitrogen uptake in the crop canopy (32)(28)
EVI	$\frac{B_8 - B_4}{B_8 + (6 \times B_4) - (7.5 \times B_2) + 1} \times 2.5$	Detection of vegetation communities in various seasons (29) Land cover classification (26)
SAVI	$\frac{B_8 - B_4}{B_8 + B_4 + 0.5} \times 1.5$	Minimizing soil brightness influences (33) (30) Land cover classification (26)

In addition to VIs, the previous research proves that using textural features significantly improves classification accuracy, especially for the species with similar spectral characteristics but different spatial patterns (Gini et al. 2018). PCA is commonly used in data mining to explore data and reduce data dimensionality (Guo et al. 2002, Xiao 2010). It reduces dimensionality by identifying a new set of variables that is smaller than the original set and captures big principal variability in data while disregarding minor variability (Xiao 2010). The three first PCs with cumulative eigenvalues of more than 99% were extracted from the spectral bands in ArcGIS Pro, as shown in **Appendix A (Table A1)**.

A total of four textural variables, including Mean (ME), Entropy (EN), Homogeneity (HO or also called Inverse Difference Moment- IDM), and Correlation (CO), were derived using the first three PCs (Kattenborn et al. 2019). These textures were obtained through the Gray-Level Co-Occurrence Matrix (GLCM) statistical approach with Probabilistic Quantizer (Quantization levels of 32), the inter-pixel distance of 1, and window size of 5×5 using SNAP (version 8.0.0). The window size was optimized based on this particular study area since the texture measures are dependent on the window size (Chatziantoniou et al. 2017). The formulas of textures and their application are listed in **Table 2**. The GLCM method examines the distribution of gray levels across adjacent pixels by considering the pixels' spatial position in an image (Humeau-Heurtier 2019, Xu and Gowen 2020, Zhang et al. 2017). Humeau-Heurtier (2019) defined the GLCM $P(i,j \mid d,\theta)$ as a relative frequency of the occurrence of the same intensity value i (reference pixel) adjacent to the different intensity value j (neighbor pixel) in a specific spatial relation at the distance d and direction of θ. Based on these parameters, ME used the frequency of occurrence of a certain neighboring pixel to weight the pixel value (Held 1998). EN assesses the degree of disorder and complexity of the texture distribution in GLCM (Humeau-Heurtier 2019, Zhang et al. 2017). HO shows the level of homogeneity (Humeau-Heurtier 2019), and CO measures the linear relationship between pixel values for the grayscale in the horizontal or vertical direction (Humeau-Heurtier 2019,Xhang et al. 2017).

Table 2- Texture metrics Formula

Texture Metrics	Formulation	Application
ME	$\sum_{i}^{N}\sum_{j}^{N} i \times P(i,j\|d,\theta)$	Weighting pixel value based on the frequency of its occurrence in conjunction with a specific neighbor pixel value (42,43) Calculating the mean processing window value (44)
EN	$-\sum_{i}^{N}\sum_{j}^{N} P(i,j\|d,\theta)\log_2 P(i,j\|d,\theta)$	Assessing the disorder of the GLCM (39) Reflecting the complexity of the texture distribution (41)
HO	$-\sum_{i}^{N}\sum_{j}^{N} \frac{P(i,j\|d,\theta)}{1+(i-j)^2}$	Measuring the level of homogeneity in pairs of pixels (39)
CO	$\frac{\sum_{i}^{N}\sum_{j}^{N}(i-\bar{x})(j-\bar{y})P(i,j\|d,\theta)}{\sigma_x\sigma_y}$	Measuring grey level linear relation between pixels (39,41,45)

2.4. Reference Data

Training samples for each ground object must be selected separately since RF is a supervised classifier. The basis for the selection of training and validation samples was acquired visually from Portugal Directorate-General for the Territory (DGT; Direção-Geral do Território 2018), Portugal Institute for Nature Conservation and Forests (ICNF; Instituto da Conservação da Natureza e das Florestas 2015), and Google Earth (orthophoto maps). Vegetation category was selected and verified based on dominant species, as presented in **Table 3**, such as *Pinus pinaster*, *Eucalyptus*, *Castanea*, *Pinus pinea*, *Quercus (*including *Quercus robur*, *Quercus suber*, and *Quercus ilex)*, *Acacia*, and other land use including cropland and agriculture land, shrubland and grassland, Water and barren (area without vegetation including roads and urban area) (Incêndios C 2020). Therefore, samples' polygons were manually created based on visual interpretation and reference sources.

Table 3- Dominant species represented in ha and percentage adapted from (Incêndios C 2020).

Species	Area (ha)	Percentage of the Study Area (%)
Pinus pinaster	5190.17	37.5
Eucalyptus	2611.95	18.9
Quercus	1273.36	9.2
Castanea	510.93	3.7
Acacia	506.26	3.6
Pinus Pinea	11.18	0.1

2.5. Image Classification

A total of 26 independent variables (including 10 spectral bands, four vegetation indices, and 12 texture measures) were used as an input to supervised classification to improve the classification performance (Aragoneses and Chuvieco 2021). RF algorithm was applied as a machine learning algorithm for vegetation classification in RStudio (version 2022.02.3+492). RF algorithm, an ensemble classifier that produces multiple decision trees, is commonly used in LULC due to its' high accuracy results achieved, solving highly non-linear problems on relatively small-size databases, and handling a large number of input features (Kluczek and Zagajewski 2022, Wójtowicz et al. 2021, Adeli et al. 2022). Furthermore, RF enables input feature ranking through random permutation, which has been studied in this paper using the RandomForest package in R (Zheng et al. 2017). The number of trees (ntree) and the number of random samples per node (mtry) were 500 and five, respectively. As shown in **Appendix A (Figure A1**), by increasing the ntree, out-of-bag (OOB) Error decreases and becomes stable at around 200 (Feng et al. 2015, Hanes et al. 2022). Researchers showed satisfactory results with the default parameter for the RF classifier which is ntree of 500 trees (Immitzer et al. 2016,Wang et al.

2015). In addition, a mtry that is excessively small or large reduces the individual tree's prediction ability. The optimum value for mtry calculates through 1/3 or the square root of the number of input variables (43,53). In this paper, the optimum mtry was calculated as five through the tuneRF function in R, as it is shown in **Appendix A (Figure A2)**. Samples were randomly subdivided into 70% for the training of the classification algorithm and 30% to validate the model. Finally, an accuracy assessment of vegetation classification has been performed by calculating the confusion matrix.

2.6. Accuracy Assessment

Accuracy assessments have traditionally relied on a confusion matrix (Stehman and Foody 2019). The confusion matrix measures OA, PA, UA, and Kappa to describe the fitness between the generated classes and the reference data (Xie et al. 2008, Sheykhmousa et al. 2020). OA is directly correlated to the percentage of the study area that is correctly classified, and the Kappa is also measuring the performance of RF (Stehman and Foody 2019, Landis and Koch 1977). OA is a relatively coarse measurement since it does not provide information on class-specific accuracy, while PA and UA respectively provide class-specific accuracy on the reference and classified area per class (Stehman and Foody 2019). The AO, PA, and UA may consider high precision with accuracy above 79% (56), and the Kappa greater than 80% represents a high degree of agreement (Landis and Koch 1977).

3. Results and Discussion

A total of 26,100 pixels were selected for the training and validation samples by visual interpretation using reference sources, including DGT, ICNF, and Google Earth. The effective sample size is suggested to be between 0.2% to 3% of the total dataset pixels (Blatchford et al. 2021). The sampling size of this study is approximately 1.3% of the total pixels. Increasing the training sample size generally boosts classification accuracy. Many researchers have found a positive correlation between classification accuracy and sample size (Ma et al. 2017). According to Moraes et al.(2021), there is no recommended minimum sample size, and the sufficient sample size depends on several parameters such as the classifier, predictor variables, class definition, and size and spatial features of the study area. They analyzed the influence of sample size on the LCLU in the North of Portugal using S2 data and the RF classifier. They compared OA for the sample size of 50 to 6000 per class. They found a similar OA value with a variation of 2%, and the highest value of 73.7% indicated the low sensitivity of the RF classifier to the sample size (Moraes et al. 2021). According to the actual occupied area in (Incêndios C 2020), Pinus pinaster and Eucalyptus have the greatest number of pixels, and other classes have a similar proportion of actual occupied. Samples were divided into 70% (17394 pixels) as training samples and 30% (8706 pixels) as validation samples using Stratified random sampling in R. **Appendix B (Table B1)** shows the total of 10 classes for this study.

Accuracy assessment of the classification was evaluated based on the confusion matrix and OA, PA, UA, and Kappa metrics. The rows and columns of the confusion matrix shown in **Table 4** indicate the map classification and the reference classification, respectively. Diagonal cells of the matrix show the correct classifications, and off-diagonal cells indicate misclassifications. The repetition of 10 times was conducted for an unbiased evaluation, and the mean accuracy metrics are presented in **Table 5**. OA 90.9% (±1) and Kappa of 89% (±1) have achieved for this classification, indicating a high classification accuracy. The lowest and highest PA was obtained for *Acacia* and Water, respectively. The other classes have a high accuracy of over 90%, except for *Quercus,* with a PA of 79.5%. In the case of UA, barren has the highest accuracy of 97.1%, while *Acacia* has the lowest with a value of 70.1%. Predominant species of *Pinus pinaster* and *Eucalyptus* has a high UA and PA of over 90%.

Table 4- Confusion Matrix and statistical measures for RF vegetation classification.

		Reference										**Total**	**PA**
Classification	**Classes**	**1**	**2**	**3**	**4**	**5**	**6**	**7**	**8**	**9**	**10**	N° Pixels	%
	1	**2136**	40	36	18	63	0	0	5	4	0	2302	92.8
	2	101	**2052**	13	11	4	11	26	51	1	7	2277	90.1
	3	32	10	**580**	64	7	0	17	20	0	0	730	79.5
	4	24	2	41	**333**	1	0	0	1	0	0	402	82.5
	5	30	2	6	9	**176**	0	0	0	0	0	223	78.8
	6	0	0	0	0	0	**43**	0	3	0	1	47	91.5
	7	10	5	5	6	0	2	**638**	1	0	17	684	93.3
	8	19	21	13	1	0	3	11	**1083**	0	0	1151	94.1
	9	0	0	0	0	0	0	0	0	**39**	0	39	100
	10	0	2	1	0	0	0	9	0	0	**831**	843	98.6
Total	N° Pixels	2352	2134	695	442	251	59	701	1164	44	856	**8706**	
UA	%	90.8	96.2	83.5	75.3	70.1	72.9	91	93	88.6	97.1		
OA	**90.9%**												
K	**89%**												

Figure 3 shows the classified vegetation map based on the proposed methodology. **Figure 4** represents the area and percentage of each class in the classified map and reference data. According to the result, the largest area is occupied by *Pinus pinaster* followed by *Eucalyptus* mostly in the south and north of the study area, respectively. However, the Pinus pinaster has the majority in the reference data and occupied approximately 37% of the study area (Incêndios C 2020,DGT 2018,ICNF 2016). Since the reference data were based on COS2018 (DGT 2018), they were not up-to-date and accurate. It is necessary to perform a field measurement to detect the changes and assess the final classification of this paper. Land cover changes may happen due to wildfire or cutting trees either for commercial purposes by private land owners or forest management. In addition, the study area is very heterogeneous and has several areas with mixed species that it is also hard to distinguish visually using Google Earth. Also, Cropland/Agriculture land class has a greater area than the reference data mentioned in **Section2.1**. Some of these misclassifications were due to the new plantation field of tree species and confusion with the Shrubland/Grassland class. Both of these fields have a similar pattern and spectral features of Cropland/Agriculture land class. The other six classes' areas predicted similar results compared to the reference data with an error of less than 3%, referring to **Appendix B (Table B1)** for more information. According to Costa et al. (2022), there is always expected to have spectral confusion between shrubland and tree species or grassland and agricultural land because of similar spectral features of some classes. They also mentioned the broad conceptual definition of the classes as another factor of misclassification (Costa et al. 2022). Shrubland/Grassland class may have a broad conceptual definition since it includes natural, semi-natural, and agricultural grassland and also shrubs. Costa et al. (2022) also found several classification contradictions between their LCLU classified map and COS2018 (DGT 2018) for the land cover of mainland Portugal. They presented a significant increase in the occupied area of shrubland and grassland as one of the major land covers of Portugal in comparison with COS (DGT 2018). Problematic classes may also result from the fragmented species distribution, either rare or mixed with other classes, especially for tree stands (Immitzer et al. 2016). The major reasons for different classification statistics may relate to the higher resolution imagery of S2A with 10 m compared with traditional maps, including COS, class definition, and impact of the 2017 wildfire and burnt area on land cover changes (DGT 2018). Immitzer et al. (2016) mentioned the effect of a parameter such as a stand age and density, crown coverage, and understory on the spectral behavior of the tree species and their intra-class separability. Several Pine and Eucalyptus stands have been seen in this study area with different ages due to the plantation or cutting. All these effective factors have been considered in this study while comparing the result with the reference data.

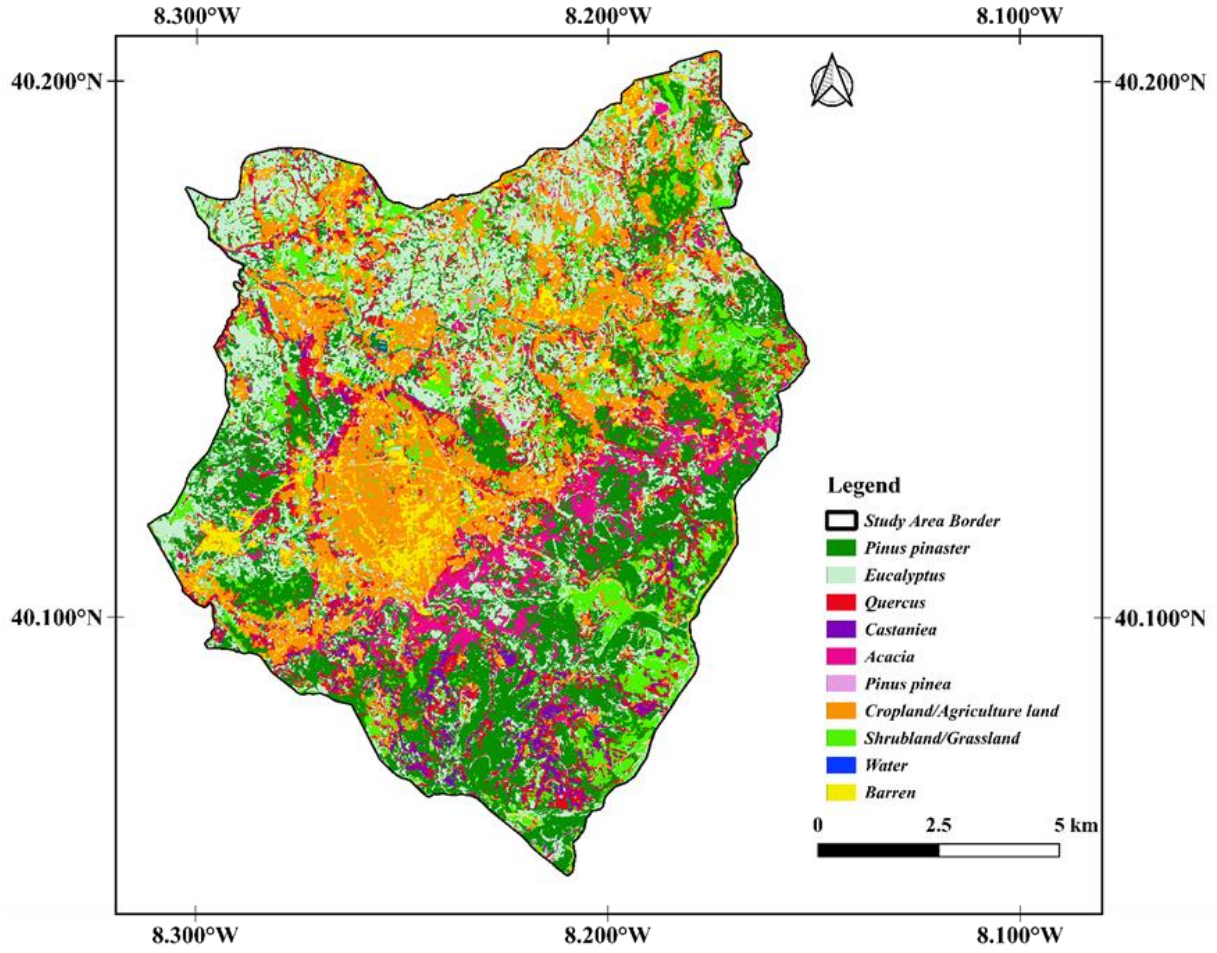

Figure 3- Vegetation map generated based on 26 independent variables of S2A imagery using RF classification for Lousa, Portugal.

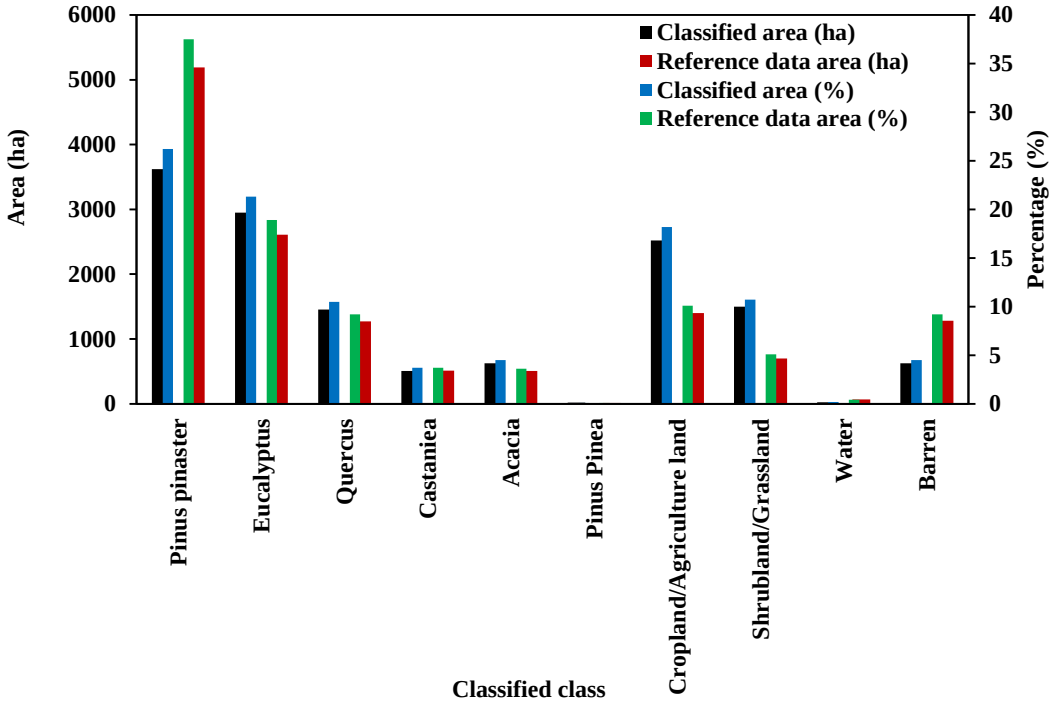

Figure 4- Comparison of classification result and reference data represented in the area (ha) and percentage.

3.1. Importance of Independent Variables

In order to assess the importance of each variable in RF classification accuracy, MeanDecreseAccuracy (MDA) and MeanDeacreseGini (Gini) have been used through random permutation. **Figure 5 (a) and (b)** show the ranking of the variables based on their contribution to distinguishing the classes. This ranking was almost the same for all the repetitions. Band 11 and 12 (SWIR) and band 2 (Blue) have the highest MDA and Gini among the S2A spectral bands, although the NIR band of 8 achieved low scores. In the case of the GLCM textures, the ME and CO of the PC3 have the highest rank among all 26 variables in MDA. Generally, the ME and CO for the PC1 and PC3 were ranked among the top five variables in both MDA and Gini. Additionally, GNDVI and NDVI have the highest contribution among VIs.

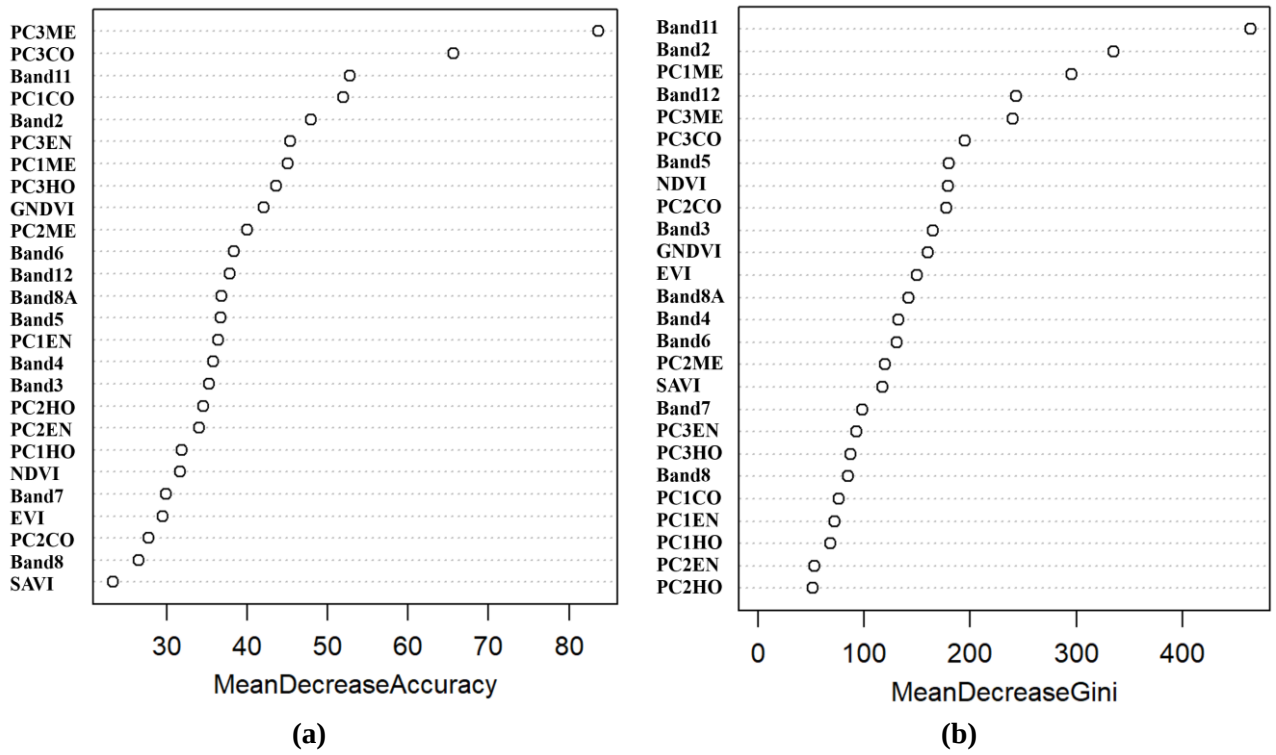

Figure 6 - Band Importance ranking based on mean decrease accuracy and mean decrease Gini.

The methodology has been applied to different independent variables input to analyze the importance of the GLCM textures. The classification was repeated for three additional scenarios of input bands: (I) Only S2A spectral bands, (II) S2A spectral bands and VIs, and (III) S2A spectral bands and GLCM textures. The Rf classifier based on S2A spectral band and GLCM texture achieved the maximum OA and Kappa, as presented in **Table 7**. Using all 26 variables has ranked second with a difference of 1.2%, lower than the combination of spectral bands and GLCM textures. Wang *et al. (2015)* also achieved high accuracy of 97.1% by using only GLCM feature on IKONOS multispectral bands, which is higher than the accuracy of the combination of all spectral bands and GLCM and GI features (96.9%). They believed that lower accuracy of all bands is associated with increasing omission and commission errors of some Gi features. In this paper, the lower accuracy of classification with all bands may cause by vegetation indices. However, the combination of spectral bands and four vegetation indices yielded higher accuracy than only spectral bands and improved the accuracy. The minimum OA and Kappa also were obtained for employing only S2A spectral bands. Adding GLCM texture to S2A spectral bands has increased the accuracy metrics by 4%.

Table 6- OA and Kappa for RF classification with different combinations of independent variables.

	All bands	**Spectral bands**	**Spectralbands+ VIs**	**Spectralbands+ GLCM texture**
OA (%)	90.8	88	88.6	92
Kappa (%)	89	86	86.1	90.2

Appendix B (Figures B1) shows the band importance for these three additional classifications. In all of the four scenarios of input variables, band11 and band 2, ME and CO of PC1 and PC3 outperformed other variables with the high value of MDA and Gini. It can be concluded that adding at least one GLCM texture may improve the classification accuracy. In this paper, the ME and CO have enhanced the RF classification with higher accuracy. Several studies have indicated the importance of texture feature extraction in increasing the accuracy of the classified map (Zheng et al. 2017, Zhang et al. 2017,Adeli et al. 2022). Wang et al. (2015) found the ME as the most important variable in mapping forest health conditions using IKONOS imagery. Zhang et al. (2017) emphasized the importance of GLCM texture feature extraction on classification accuracy improvement. These textures provide information about different objects with the same spectral, while spectral bands provide the data for the same objects in the different spectrums (Zheng et al. 2017). Zheng et al. (2017) have suggested using Extended Attribute Profiles (EAPs) in addition to GLCM textures, which can improve shrubland, agricultural land, and barren discrimination. Furthermore, S2A spectral bands have shown a high potential in the LCLU classification of the regional study area of this paper without using additional variables, which were also mentioned previously in several research studies (Chaves et al. 2020,Zheng et al. 2017, Immitzer et al. 2016). In this paper, bands 11 (SWIR) and band 2 (blue) were almost among the five first important variables in all combinations. Immitzer et al. (2016) found bands 2 and 11 as the highest score while NIR band 8A was the lowest score for forest species classification. Feng et al.(2015) declared that spectral features contribute the most in their study with the UAV for flood mapping. In their study, the red and blue bands followed by ME were the most important variables.

3.2. Effect of Bootstrap Sample Size

Rf classifier uses bootstrap aggregation, randomly creating different training subsets of the original training dataset to grow the individual regression trees (Immitzer et al. 2016, Wang et al. 2015). Wang et al.(2015) suggested using two-thirds of the validation dataset per subset for bootstrap sample size. The minimum value of the bootstrap sample size in this paper was equal to the minimum class pixels (Water), and the largest sample size was approximately equal to the extraction of highest and lowest class pixels (*Pinus pinaster* and Water). As shown in **Figure 7**, the lowest and highest OA and Kappa were calculated for the sampling size of 137 and 7000, respectively. The highest OA was increased by around 15.7%, and Kappa was increased by 19.3%. According to UA and PA, the lowest UA and PA has appeared in the sample size of 137 with zero percentage of water and *Pinus pinea* detection; more information was presented in **Appendix B (Table b2)**. The minimum PA remained below 70% until the sample size of 5000. Thomlinson et al.(1999) proposed the minimum OA and per-class accuracy of 85% and 70% for high precision classification, respectively. Although the bootstrap sample size of 6000 and 7000 has increased OA and Kappa by approximately 1%, the sample size of 5000 was used for this research to avoid overfitting and high computational process based on previous studies (Zheng et al. 2017, Thomlinson et al. 1999). 5000 bootstrap sample size is also equal to two-thirds of the validation dataset in this paper. Furthermore, the lowest and highest OOB error were obtained for the samples of 5000 and 137, respectively.

This paper has achieved high value for the accuracy metrics based on a single image of medium resolution S2A multispectral bands compared with previous studies that used multi-temporal or high-resolution imagery (Costa et al. 2022, Immitzer et al. 2016). The main purpose of this study was to increase the interclass separability of forest and vegetation classes and to provide up-to-date data based on S2A for the Lousa region, Portugal. However, the major limitation is the lack of recent reference data or fieldwork in Portugal. To better analyze the accuracy of the classified map, field measurement data and reliable and up-to-date ground truth data as reference data are needed. For future study, adding Light Detection and Ranging equipment (LiDAR) data, UAV imagery with finer resolution, Sentinel-1 SAR data, and knowledge of local experts are expected to increase the discrimination of the LCLU classes and provide more information on vertical features of the species. Recently, Portugal has started capturing LiDAR data for the whole country. Nevertheless, it is not yet covered in the study area of this paper.

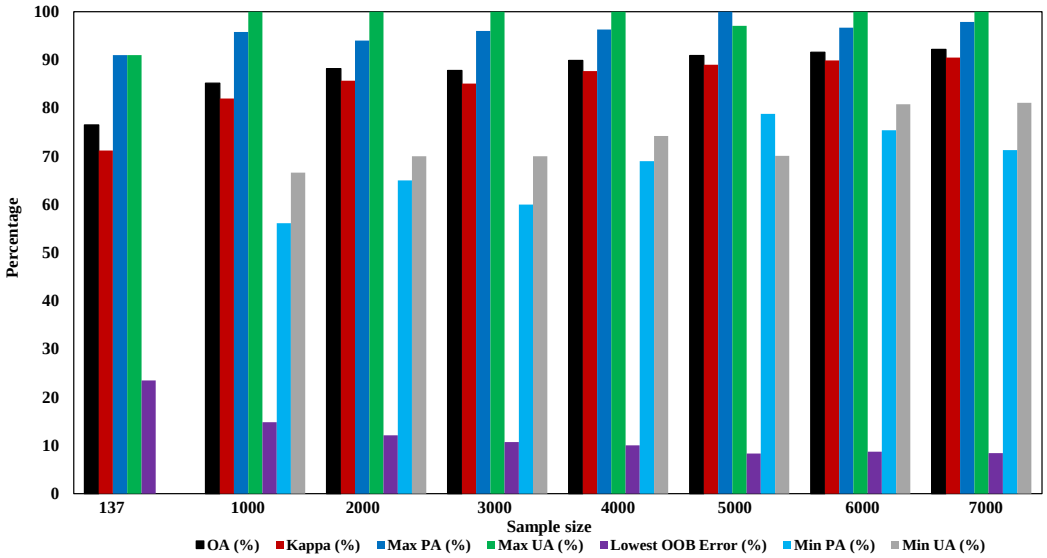

Figure 7- Effect of sample size on OA, UA, PA, Kappa, and OOB Error in RF classification.

4. Conclusion and Future Works

This paper proposed a methodology for vegetation mapping by applying a Random Forest classifier on the Sentinel2-A image. Twenty-six independent variables were used by combining ten S2A multispectral bands resampled to 10 m pixel size with four vegetation indices and 12 GLCM texture feature variables. These GLCM texture features were calculated from the three first principal components of downscaled S2A spectral bands using PCA. Training and validation data was acquired through forestry data of ICNF and DGT and visual interpretation using Google Earth. RF classifier with 500 *ntree* and 5 *mtry* was used to classify the study area into ten classes, including the predominant tree species. A high precision classification was performed with an overall accuracy of 90.5% and a Kappa coefficient of 89%. Nevertheless, employing all 26 variables did not achieve the highest accuracy compared to the combination spectral bands and GLCM textures with an OA of 92%. The comparison of classification accuracy for four different combinations of input variables shows the importance of GLCM textures especially ME and CO in improving the performance of the RF classifier. Spectral bands 11 and 2 also have high scores in MDA and GINI for all the scenarios. Generally, S2A 10m spectral bands have a strong potential for precise and rapid vegetation classification. GNDVI contributes the most to the accuracy of classification amongst vegetation indices. The results of this study indicate that incorporating at least one GLCM texture feature and at least one vegetation index into the S2A spectral bands can effectively improve the accuracy of assessment and tree species classification.

Few studies explored vegetation mapping with high accuracy in Portugal, mainly in the Lousa region, using Sentinel 2 images. Exploring the multispectral band and texture feature analysis can contribute to the spectral separability of vegetation, facilitating studies of aboveground biomass estimation and wildfire simulation. Accuracy assessment of the implemented methodology has shown a high potential for generating high-accuracy vegetation mapping over forestry areas. It is foreseen to expand the methodology for the data fusion of Sentinel 2 and Sentinel 1 to include data regarding the vertical structure of the vegetation and canopy. This data will enable the creation of a fuel type tridimensional semantic map to be used by fire behavior models and allow the definition of biomass management strategies towards wildfire risk reduction or accurate fire spread simulations for the decision support during wildfire occurrences. These results are relevant for the ESA 2025 Agenda, whose challenge is integrating information from Copernicus mapping carbon to promote sustainable land management and improved resilience against natural risks and impacts of climate change. Therefore, more studies are necessary to be conducted in order to cover more datasets in Portugal.

5. Acknowledgments

This work is financed by national funds through FCT - Foundation for Science and Technology, under grant agreement 2021.05971.BD attributed to the 1st author. The authors gratefully acknowledge the Portuguese

Foundation for Science and Technology (FCT) for its support under the framework of the research projects PCIF/SSI/0096/2017 – FIREFRONT and IMFire - Intelligent Management of Wildfires, ref. PCIF/SSI/0151/2018, fully funded by national funds through the Ministry of Science, Technology, and Higher Education and project FirEURisk – Developing a Holistic, Risk-Wise Strategy for European Wildfire Management, funded by the European Union's Horizon 2020 research and innovation programme under grant agreement No 101003890.

6. Author Contributions

Pegah Mohammadpour: Writing – review & editing, Writing – original draft, Data processing, Map generation, Visualization, Validation, Software, Methodology and study design, Formal analysis, Data curation**.** Crismeire Isbaex: Writing – review & editing**.** Emilio Chuvieco: Writing – review & editing, Supervision**.** Xavier Viegas: Writing – review & editing, Supervision**.** Carlos Viegas: Writing – review & editing, Supervision.

7. Conflicts of Interest

The authors declare no conflict of interest.

Appendix A

Table A1- Percent and accumulative eigenvalues of three first PCs.

PC Layer	Percent of Eigenvalues (%)	Accumulative of Eigenvalues (%)
PC1	92.5	92.5
PC2	6.3	98.8
PC3	0.6	99.4

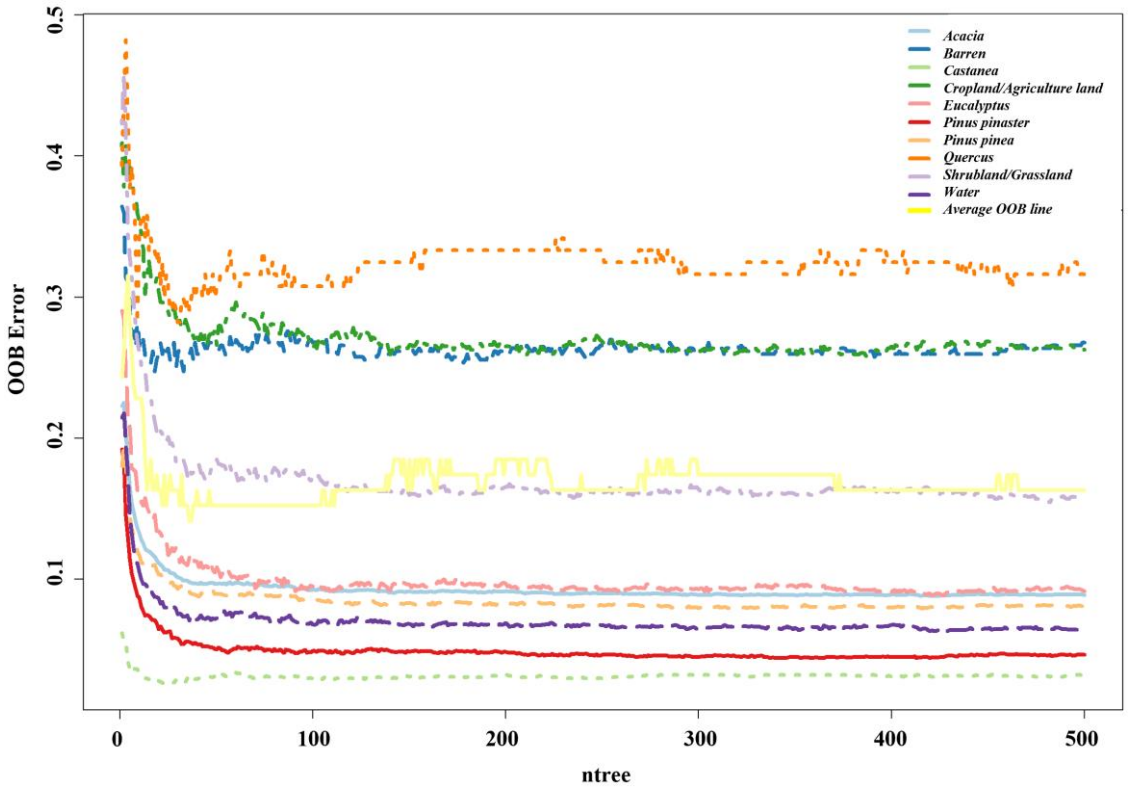

Figure A1- OOB Error of the number of RF trees, ntree.

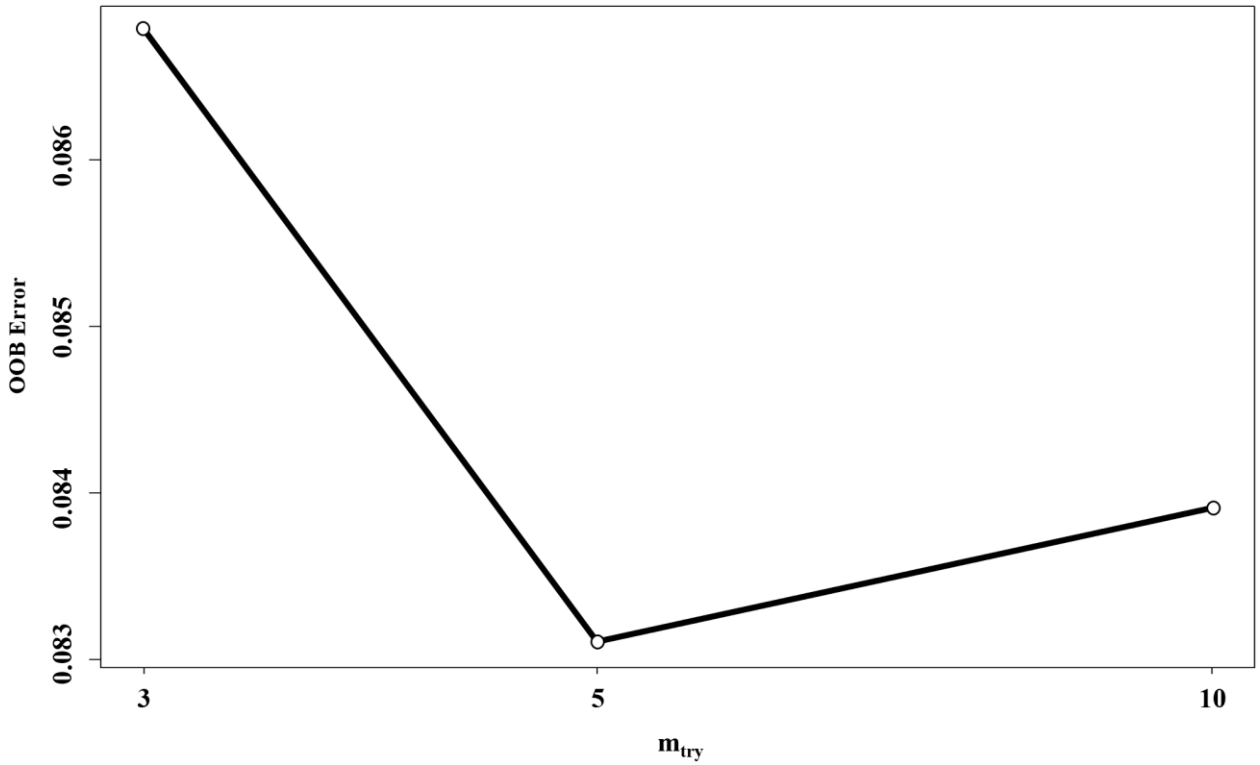

Figure A2- OOB Error of the number of RF mtry.

Appendix B

Table B1- Classification result represented in the area (ha) and percentage.

Class ID	Classified Class	Classified area (ha)	Percentage (%)	The difference with reference data area (ha)	The difference with reference data area (%)
1	*Pinus pinaster*	3619.1867	26.2	-1570.9833	-11.3
2	*Eucalyptus*	2951.4365	21.3	+339.4865	+2.4
3	*Quercus*	1453.5870	10.5	-180.227	-1.3
4	*Castanea*	506.3817	3.7	-4.5483	-0.0
5	*Acacia*	626.2897	4.5	+120.0297	+0.9
6	*Pinus Pinea*	17.1625	0.1	+5.9825	+0.0
7	Cropland/Agriculture land	2518.3886	18.2	+1119.0689	+8.1
8	Shrubland/Grassland	1499.6008	10.7	+798.0708	+5.6
9	Water	21.9260	0.2	-42.914	-0.2
10	Barren	625.9895	4.5	-655.2805	-4.7

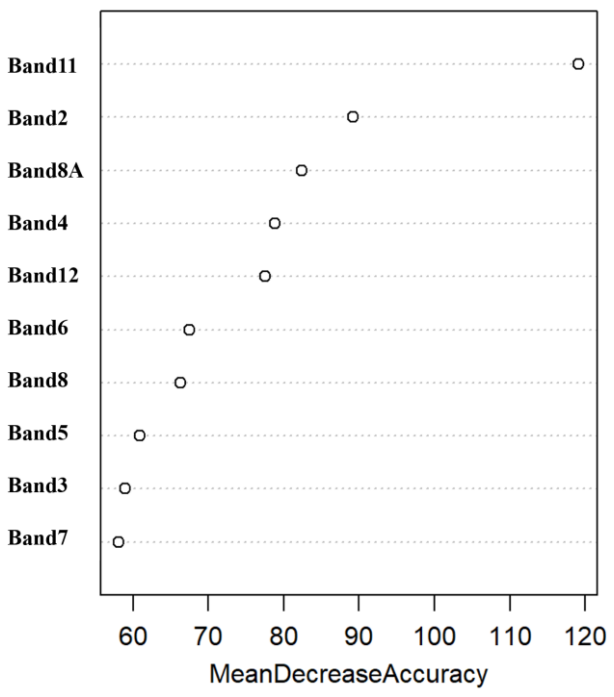
Band11
Band2
Band8A
Band4
Band12
Band6
Band8
Band5
Band3
Band7
60
70
80
90
100
110
120
MeanDecreaseAccuracy

(a)

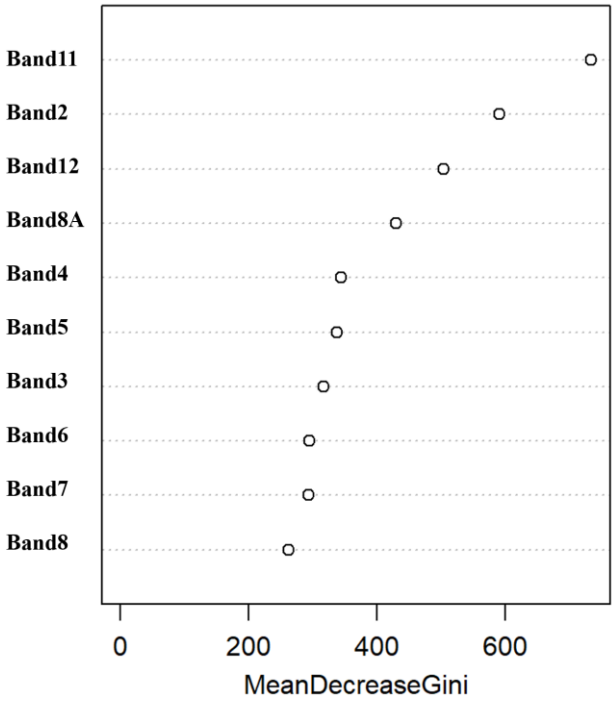
Band11
Band2
Band12
Band8A
Band4
Band5
Band3
Band6
Band7
Band8
0
200
400
600
MeanDecreaseGini

(b)

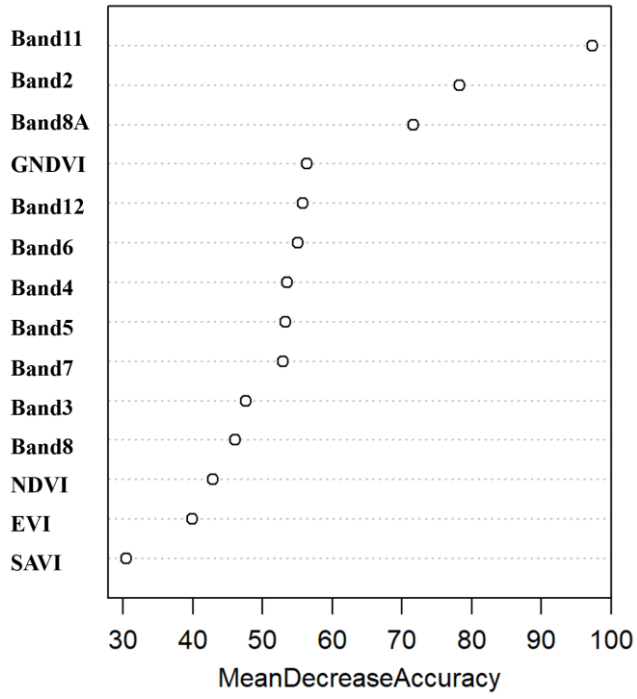
Band11
Band2
Band8A
GNDVI
Band12
Band6
Band4
Band5
Band7
Band3
Band8
NDVI
EVI
SAVI
30
40
50
60
70
80
90
100
MeanDecreaseAccuracy

(c)

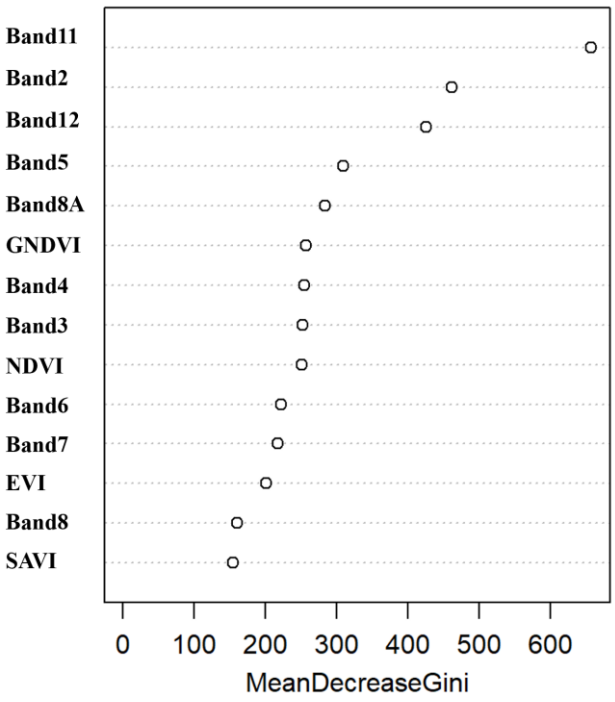
Band11
Band2
Band12
Band5
Band8A
GNDVI
Band4
Band3
NDVI
Band6
Band7
EVI
Band8
SAVI
0
100
200
300
400
500
600
MeanDecreaseGini

(d)

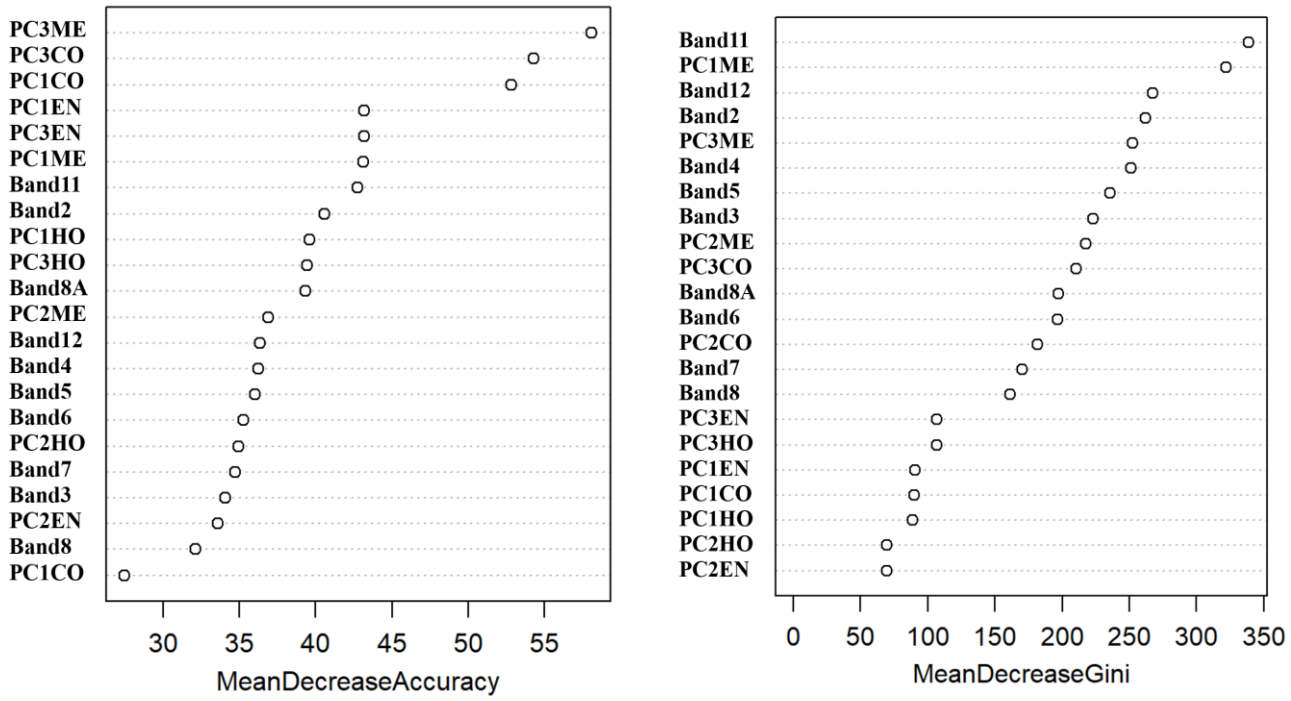

Figure B1- Mean decrease accuracy and mean decrease Gini for three different combinations of variables: (I) Spectral bands (a)-(b), (II) Spectral bands + VIs (c)-(d), and (III) Spectral bands+ GLCM texture (e)-(f).

Table B2- Effect of sample size on OA, UA, PA, and Kappa in RF classification.

Sample Size	**137**	**1000**	**2000**	**3000**	**4000**	**5000**	**6000**	**7000**
OA (%)	76.5	85.2	88.2	87.8	89.9	90.9	91.6	92.2
Kappa (%)	71.2	82	85.7	85.1	87.7	89	89.9	90.5
Max PA (%)	91 Barren	95.8 Barren	94 *Eucalyptus*	96 Barren	96.3 Barren	100 water	96.7 Barren	97.9 Barren
Min PA (%)	0 Water & *Pinus pinea*	56.1 *Pinus pinea*	65 *Acacia*	60 *Acacia*	69 *Castanea*	78.8 *Acacia*	75.4 *Castanea*	71.3 *Pinus pinea*
Max UA (%)	91 Barren	100 Water	100 Water	100 Water	100 *Pinus pinea*	97.1 Barren	100 Water	100 Water/P*inus pinea*
Min UA (%)	0 Water & *Pinus pinea*	66.6 *Quercus*	70 *Quercus*	70 *Quercus*	74.2 *Quercus*	70.1 *Acacia*	80.8 *Quercus*	81.1 *Quercus*
Lowest OOB Error (%)	23.5	14.83	12.1	10.7	10	8.3	8.7	8.4
Optimum mtry	10	10	5	10	10	5	5	5
ntree	Not stable	Stable	Stable	Stable	Stable	Stable	Stable	Stable

8. References

(ICNF) PI for NC and F. No Title [Internet]. 2015. Available from: https://geocatalogo.icnf.pt/catalogo_tema3.html

Adeli S, Quackenbush LJ, Salehi B, Mahdianpari M. THE IMPORTANCE OF SEASONAL TEXTURAL FEATURES FOR OBJECT-BASED CLASSIFICATION OF WETLANDS : NEW YORK STATE CASE STUDY. 2022;XLIII(June):6–11.

Agarwal A, Kumar S, Singh D. Development of neural network based adaptive change detection technique for land terrain monitoring with satellite and drone images. Def Sci J. 2019;69(5):474–80.

Alam MJ, Rahman KM, Asna SM, Muazzam N, Ahmed I, Chowdhury MZ. Comparative studies on IFAT, ELISA & DAT for serodiagnosis of visceral leishmaniasis in Bangladesh. Bangladesh Med Res Counc Bull. 1996;22(1):27–32.

Aragoneses E, Chuvieco E. Generation and mapping of fuel types for fire risk assessment. Fire. 2021;4(3).

Benali A, Fernandes P. Understanding the impact of different landscape-level fuel management strategies on wildfire hazard Understanding the impact of different landscape-level fuel management strategies on wildfire hazard. 2021;(March).

Bhatnagar S, Gill L, Regan S, Waldren S, Ghosh B. A nested drone-satellite approach to monitoring the ecological conditions of wetlands. ISPRS J Photogramm Remote Sens [Internet]. 2021 Apr;174:151–65. Available from: https://linkinghub.elsevier.com/retrieve/pii/S0924271621000125

Blatchford ML, Mannaerts CM, Zeng Y. Determining representative sample size for validation of continuous, large continental remote sensing data. Int J Appl Earth Obs Geoinf [Internet]. 2021;94(September 2020):102235. Available from: https://doi.org/10.1016/j.jag.2020.102235

Chatziantoniou A, Petropoulos GP, Psomiadis E. Co-Orbital Sentinel 1 and 2 for LULC mapping with emphasis on wetlands in a mediterranean setting based on machine learning. Remote Sens. 2017;9(12):1–19.

Chaves MED, Picoli MCA, Sanches ID. Recent applications of Landsat 8/OLI and Sentinel-2/MSI for land use and land cover mapping: A systematic review. Remote Sens. 2020;12(18).

Costa H, Almeida D, Vala F, Marcelino F, Caetano M. Land cover mapping from remotely sensed and auxiliary data for harmonized official statistics. ISPRS Int J Geo-Information. 2018;7(4).

Costa H, Benevides P, Moreira FD, Moraes D, Caetano M. Spatially Stratified and Multi-Stage Approach for National Land Cover Mapping Based on Sentinel-2 Data and Expert Knowledge. Remote Sens. 2022;14(8).

Costa H, de Rigo D, Libertà G, Houston Durrant T, San-Miguel-Ayanz J. European wildfire danger and vulnerability in a changing climate: towards integrating risk dimensions. 2020. 59 p.

ESA. Sentinel-2 User Handbook. Vol. 2, European Space Agency ESA Standard Document. 2015. 64 p.

Feng Q, Liu J, Gong J. Urban flood mapping based on unmanned aerial vehicle remote sensing and random forest classifier-A case of yuyao, China. Water (Switzerland). 2015;7(4):1437–55.

Gini R, Sona G, Ronchetti G, Passoni D, Pinto L. Improving tree species classification using UAS multispectral images and texture measures. ISPRS Int J Geo-Information. 2018;7(8):1–18.

Gitelson A, Merzlyak MN. Quantitative estimation of chlorophyll-a using reflectance spectra: Experiments with autumn chestnut and maple leaves. J Photochem Photobiol B Biol. 1994;

Gitelson AA, Kaufman YJ, Merzlyak MN. Use of a green channel in remote sensing of global vegetation from EOS- MODIS. Remote Sens Environ. 1996;58(3):289–98.

Guo Q, Wu W, Massart DL, Boucon C, De Jong S. Feature selection in principal component analysis of analytical data. Chemom Intell Lab Syst. 2002;61(1–2):123–32.

Hanes CC, Wotton M, Woolford DG, Martell DL, Flannigan M. Mapping organic layer thickness and fuel load of the boreal forest in Alberta, Canada. Geoderma [Internet]. 2022;417:115827. Available from: https://doi.org/10.1016/j.geoderma.2022.115827

Haralick RM, Shanmugam K, Dinstein I. Textural Features for Image Classification. SEG Tech Progr Expand Abstr. 1973;3:610–21.

Held M, Committee TIB. GLCM TEXTURE: A TUTORIAL. 17th Int Symp Ballist. 1998;2(March):267–74.

Hernandez I, Benevides P, Costa H, Caetano M. Exploring sentinel-2 for land cover and crop mapping in portugal. Int Arch Photogramm Remote Sens Spat Inf Sci - ISPRS Arch. 2020;43(B3):83–9.

Humeau-Heurtier A. Texture feature extraction methods: A survey. IEEE Access. 2019;7:8975–9000.

ICNF IC da N e das F. 6.o Inventário Florestal Nacional. Relatório Final 2015. 2016.

Immitzer M, Vuolo F, Atzberger C. First experience with Sentinel-2 data for crop and tree species classifications in central Europe. Remote Sens. 2016;8(3):1–27.

Incêndios C, Base I, Florestal GT. Plano Municipal de Defesa da Floresta Contra Incêndios. 2020;

Instituto Português do Mar e da Atmosfera (IPMA). May Climatological Bulletin [Internet]. 2022. Available from: https://www.ipma.pt/pt/media/noticias/news.detail.jsp?f=/pt/media/noticias/textos/Boletim_climatologico_maio.html

Investment in Disaster Risk Management in Europe Makes Economic Sense. Invest Disaster Risk Manag Eur Makes Econ Sense. 2021;

Kaplan G. Broad-Leaved and Coniferous Forest Classification in Google Earth Engine Using Sentinel Imagery. 2021;(November 2020):64.

Kattenborn T, Lopatin J, Förster M, Christian A, Ewald F. Remote Sensing of Environment UAV data as alternative to fi eld sampling to map woody invasive species based on combined Sentinel-1 and Sentinel-2 data. Remote Sens Environ [Internet]. 2019;227(January):61–73. Available from: https://doi.org/10.1016/j.rse.2019.03.025

Kluczek M, Zagajewski B. Airborne HySpex Hyperspectral Versus Multitemporal Sentinel-2 Images for Mountain Plant Communities Mapping. 2022;

Kolström M, Vile T, Lindner M. Climate Change Impacts and Adaptation in European Forests. EFI Policy Br 6. 2011;(February):14.

Landis JR, Koch GG. The Measurement of Observer Agreement for Categorical Data. Biometrics. 1977;33(1):159–74.

Liu H, Gong P, Wang J, Wang X, Ning G, Xu B. Production of global daily seamless data cubes and quantification of global land cover change from 1985 to 2020 - iMap World 1.0. Remote Sens Environ [Internet]. 2021;258:112364. Available from: https://doi.org/10.1016/j.rse.2021.112364

Ma L, Li M, Ma X, Cheng L, Du P, Liu Y. A review of supervised object-based land-cover image classification. ISPRS J Photogramm Remote Sens [Internet]. 2017;130:277–93. Available from: https://doi.org/10.1016/j.isprsjprs.2017.06.001

Ma L, Li M, Ma X, Cheng L, Du P, Liu Y. A review of supervised object-based land-cover image classification. ISPRS J Photogramm Remote Sens. 2017;130:277–93.

Monteiro-Henriques T, Fernandes PM. Regeneration of native forest species in Mainland Portugal: Identifying main drivers. Forests. 2018;9(11).

Moraes, Daniel, Benevides P, Costa H, FranciscoD. MF, Caetano M. INFLUENCE OF SAMPLE SIZE IN LAND COVER CLASSIFICATION ACCURACY USING RANDOM FOREST AND SENTINEL-2 DATA IN PORTUGAL. IGARSS 2021 - 2021 IEEE Int Geosci Remote Sens Symp. 2021;

Nizalapur V, Vyas A. Texture analysis for land use land cover (LULC) classification in parts of Ahmedabad, Gujarat. Int Arch Photogramm Remote Sens Spat Inf Sci - ISPRS Arch. 2020;43(B3):275–9.

Noi Phan T, Kuch V, Lehnert LW. Land cover classification using google earth engine and random forest classifier-the role of image composition. Remote Sens. 2020;12(15):1–22.

Pacheco ADP, Junior JADS, Ruiz-Armenteros AM, Henriques RFF. Assessment of k-nearest neighbor and random forest classifiers for mapping forest fire areas in central portugal using landsat-8, sentinel-2, and terra imagery. Remote Sens. 2021;13(7):1–25.

Persson M, Lindberg E, Reese H. Tree species classification with multi-temporal Sentinel-2 data. Remote Sens. 2018;10(11):1–17.

Portugal Directorate-General for the Territory (DGT). No Title [Internet]. 2018. Available from: https://www.dgterritorio.gov.pt/Carta-de-Uso-e-Ocupacao-do-Solo-para-2018

Sheykhmousa M, Mahdianpari M, Ghanbari H, Mohammadimanesh F, Ghamisi P, Homayouni S. Support Vector Machine Versus Random Forest for Remote Sensing Image Classification: A Meta-Analysis and Systematic Review. IEEE Journal of Selected Topics in Applied Earth Observations and Remote Sensing. 2020.

Somvanshi SS, Kumari M. Comparative analysis of different vegetation indices with respect to atmospheric particulate pollution using sentinel data. Appl Comput Geosci [Internet]. 2020;7(June):100032. Available from: https://doi.org/10.1016/j.acags.2020.100032

Stehman S V., Foody GM. Key issues in rigorous accuracy assessment of land cover products. Remote Sens Environ [Internet]. 2019;231(May):111199. Available from: https://doi.org/10.1016/j.rse.2019.05.018

Story M, Congalton RG. Remote Sensing Brief Accuracy Assessment: A User's Perspective. Photogramm Eng Remote Sensing. 1986;52(3):397–9.

Thomlinson JR, Bolstad P V., Cohen WB. Coordinating methodologies for scaling landcover classifications from site-specific to global: Steps toward validating global map products. Remote Sens Environ. 1999;70(1):16–28.

Viegas DX, Figueiredo Almeida M, Ribeiro LM, Raposo J, Viegas MT, Oliveira R, et al. O Complexo de Incêndios de Pedrogão Grande E Concelhos Limítrofes, Iniciado a 17 de Junho de 2017. 2017. Iniciado a [Internet]. 2017;2017:238. Available from: https://www.portugal.gov.pt/pt/gc21/comunicacao/documento?i=o-complexo-de-incendios-de-pedrogao-grandee-%0Aconcelhos-limitrofes-iniciado-a-17-de-junho-de-2017

Wang H, Zhao Y, Pu R, Zhang Z. Mapping Robinia pseudoacacia forest health conditions by using combined spectral, spatial, and textural information extracted from IKONOS imagery and random forest classifier. Remote Sens. 2015;7(7):9020–44.

Wessel M, Brandmeier M, Tiede D. Evaluation of different machine learning algorithms for scalable classification of tree types and tree species based on Sentinel-2 data. Remote Sens. 2018;10(9).

Wójtowicz A, Piekarczyk J, Czernecki B, Ratajkiewicz H. A random forest model for the classification of wheat and rye leaf rust symptoms based on pure spectra at leaf scale. J Photochem Photobiol B Biol. 2021;223(February).

Xavier AC, Rudorff BFT, Shimabukuro YE, Berka LMS, Moreira MA. Multi-temporal analysis of MODIS data to classify sugarcane crop. Int J Remote Sens. 2006;

Xia H, Zhao W, Li A, Bian J, Zhang Z. Subpixel inundation mapping using landsat-8 OLI and UAV data for a wetland region on the zoige plateau, China. Remote Sens. 2017;9(1):1–22.

Xiao B. Principal component analysis for feature extraction of image sequence. 2010;

Xie Y, Sha Z, Yu M. Remote sensing imagery in vegetation mapping: a review. J Plant Ecol. 2008;

Xu JL, Gowen AA. Spatial-spectral analysis method using texture features combined with PCA for information extraction in hyperspectral images. Vol. 34, Journal of Chemometrics. 2020.

Zeng L, Wardlow BD, Xiang D, Hu S, Li D. A review of vegetation phenological metrics extraction using time-series, multispectral satellite data. Remote Sens Environ. 2020;

Zhang X, Cui J, Wang W, Lin C. A study for texture feature extraction of high-resolution satellite images based on a direction measure and gray level co-occurrence matrix fusion algorithm. Sensors (Switzerland). 2017;17(7).

Zheng H, Du P, Chen J, Xia J, Li E, Xu Z, et al. Performance evaluation of downscaling sentinel-2 imagery for Land Use and Land Cover classification by spectral-spatial features. Remote Sens. 2017;9(12).

VESPRA-Vulnerable Elements in Spain and Portugal and Risk Assessment

Emilio de Diego Lázaro*[1]; Jaime Ribalaygua Batalla[1]; Ana Miranda[2]; Johnny Reis[2] ;Miguel Almeida[3]; Luis Mario Ribeiro[3] ; Alba Àgueda[4] ; Eulalia Planas Cuchi[4]

[1]Meteogrid S.L. Gran Vía, 22 duplicado 28013 Madrid, España, {ediego, jrb}@meteogrid.com
[2] CESAM, Department of Environment and Planning, University of Aveiro, Campus Universitario de Santiago, Aveiro, 3810-193, Portugal, {Miranda, johnnydreis}@ua.pt
[3] Associação para o Desenvolvimento da Aerodinâmica Industrial(ADAI). Rua Pedro Hispano nº12 3030 - 289 Coimbra, {miguelalmeida, luis.mario}@adai.pt
[4] Universitat Politècnica de Catalunya · Barcelona Tech (UPC). EEBE. Avinguda Eduard Maristany, 16. 08009-Barcelona {alba.agueda, eulalia.planas}@upc.edu

**Corresponding author*

Keywords

Vulnerable elements, Cross-border risk assessments, GIS-based platform, Extreme events, Emergencies

Abstract

The VESPRA project (Vulnerable Elements in Spain and Portugal and Risk Assessment), financed by the Union Civil Protection Mechanism UCPM-2020-PP-AG, is designed in a context of increased frequency and intensity of extreme events and emergencies, and in a current context where those responsible for the emergency often do not have sufficiently updated information on vulnerable elements. Indeed, there is cartography of these elements, but it is very quickly becoming outdated. It is therefore necessary to design a strategy that allows continuous updating of this information, and this is one of the main functionalities of the proposed solution in VESPRA.

VESPRA arises for the improvement of the risk management mechanisms for local risks such as forest fires, and also for other generic ones like those related to adverse meteorological phenomena or the dispersion of pollutants in wide areas. It is focused on the border area between Spain and Portugal and within the project, an international protocol will be defined for the collection of vulnerable elements and their characterisation regarding different hazards, and for their integration into a GIS-based platform specially designed to optimize their management and continuous updating. VESPRA will result in a system to assist decision-making in the event of an emergency in order to improve the harmonised identification and mapping of vulnerable elements and the integration of vulnerability in a joint information system for the evaluation and assessment of the transnational emergency response. The project targets three end-user groups: (I) the local authorities, (II) the general population, and (III) relevant institutions in civil protection.

Although the implementation for demonstration and validation purposes will be actually implemented as a baseline in three study cases, along the transboundary area between Spain and Portugal, VESPRA is developed with an European vocation aimed at the future adoption of the technological and procedural models in other transboundary European regions. These will be international, trans-boundary operational exercises based on the VESPRA system and on simulated scenarios in the selected study case regions. The first one will be a forest fire starting in Spain and moving towards Portugal. The exercise will evaluate the capability of the VESPRA system to help in the joint evaluation of potential risks and the coordination of responding forces, as well as the primary actions for the protection of the population and infrastructures. The second exercise will develop a combination of simultaneous nuclear and industrial emergency, one in each country, and will focus on the ability of VESPRA to provide accurate information and a channel of seamless interchange of key aspects for the ranking, evaluation and final decision making on such combined scenarios. The third one will be the simulation of an extreme weather episode, similar to the pass of Ophelia in 2017, affecting population and critical transportation and other infrastructures in both countries.

1. Introduction and objectives

We are in a new paradigm of change regarding emergencies, on the one hand due to the need for new scopes in the treatment of information across borders, and on the other hand in the context of global climate change. Most natural and man-made disasters imply risks that cross borders, due to their spatial dimension (earthquakes, forest fires, extreme weather events, floods) or their spread (pandemics, livestock epidemics, nuclear/industrial accidents).

Climate change has already led to an increase in the frequency and intensity of new extreme weather events such as the storm Ophelia, that occurred in 2017 and affected Portugal and Spain through a wave of fires never seen before. The increasing human, economic or environmental impacts of these new hazards, as well as their also increasing probability of occurrence, affect boths sides of the borders between countries. This increasing complexity and the emergence of new threats require greater intersectoral, transdisciplinary and cross-national cooperation at all stages of risk management (Benelux; 2016).

Risk analysis services and early warning systems have become basic tools in civil protection. Recent technological changes related to big-data, artificial intelligence, communication networks, and remote-sensing have created a shift in awareness of the emergency. In addition, the advances on the global and local weather forecast have led to an increasing improvement of their accuracy. Authorities and end-users of these services demand high quality, tailor-made information and solutions to their very specific problems in emergency management. To address this demand it is necessary to provide more innovative and holistic services with higher added-value, in an increasingly competitive market.

One of the main needs of emergency response services is to have updated information. They used to have vulnerable elements in cartography, but it became outdated very quickly, as changes in their location, characteristics, operating status, etc., as well as the appearance of new elements (for example, a new point of interest where visitors congregate), are very frequent. Thus, if for example an access road has been damaged last winter and is no longer suitable for emergency vehicles, or if there is a new point to protect in the event of a disaster, this information is essential for the emergency managers, and the outdated mapping is no longer useful, or may even be harmful. In this context, they need a solution allowing the constant updating of these vulnerable elements' information, and therefore allowing the assessment of the territory's vulnerability in a robust way..

VESPRA arises as an answer adapted to the new demands and offers flexible and demand-driven services that fit the end-users specific needs. Specialized end-users demand innovative solutions and bespoke system features. The main objectives of the VEPRA project are:

(I) The design, development and operationally implementation of a system for the evaluation and analysis of the transboundary vulnerability to the identified risks (forest fires, industrial/nuclear pollution cloud dispersion and extreme weather). It will be an open-source computer platform for vulnerable elements data and information exchange with a common methodology for: the harmonised collection and updating of data, vulnerability and impact assessment and assistance in operational and preventive decision-making in the emergency; and

(II) The other major objective is to improve emergency management through cross-border collaboration, taking into account civil protection and emergency management structures in each country. This requires the implementation of a network of competent authorities at national and sub-national level for the use of the platform applied to the identified risks, including: Technical specifications and protocols for the development and generation of operational vulnerability mapping to enhance cross-border interoperability and Design and implementation of joint cross-border small-scale exercises for previously identified risks.

2. Methodology

The VESPRA project seeks to establish an environment where vulnerability can be assessed prior to an emergency. To do so, it is necessary to know the vulnerable elements that could be affected, as well as current state of the art regarding vulnerability. For this purpose, available databases of vulnerable elements are reviewed along with an analysis of vulnerability in real events. These results form the basis for the establishment of a harmonised cross-border catalogue of typologies of vulnerable elements. This step is crucial for the subsequent development and implementation of a GIS system that will be fed by these typologies, and subsequently by the vulnerability models.

The system (VESPRA platform) is developed and adapted in two phases, a first phase that allows the collection of vulnerable elements (WP2) and a second phase that allows the design, development and implementation of vulnerability assessment models (WP4).

VESPRA platform is used to collect the vulnerable elements of the Spanish-Portuguese border in a database which is harmonized for both countries. In addition, the system allows the cartographic representation of all the results, so that possible cartographic alternatives can be analysed using the most modern representation techniques (WP3).

During the project, work is also carried out on the characterisation of vulnerable elements using different methodologies derived from the risks studied in the project (forest fires, industrial / nuclear accidents and extreme weather events, WP4). To this end, different models are applied according to the nature of the risk and the vulnerable element. All this is integrated in the GIS platform already developed to have a final system that allows the vulnerability assessment (WP5). This system has the following characteristics:

- Simplicity. The handling of the platform is practical and simple, as it should be used by non-technical people, without requiring any training, beyond reading the help and, occasionally, consulting the support centre;
- Flexibility. The platform allows the creation of new typologies of vulnerable elements, and new information related to each typology through its administration module without the need for software modifications. It also allows, through the administration module, the modification of the symbology and styles of the elements represented;
- Immediacy. Any change produced in the territory must be able to be immediately validated and incorporated into the system and into the systems connected to it. This is an essential characteristic, in order to allow the continuous updating of the vulnerable elements information;
- No licenses. As it will be 100% developed on free software libraries, operating system, database and languages, future maintenance costs will be limited to the maintenance of the hardware where it is installed;
- Transferability. The system is able to be subject to technology transfer, so it is easy to administer and easy to modify, with a clean and clear data model and a structured and commented code.

Once the system has been completed, it is validated by means of an operational implementation in which the results it provides, both cartographic and numerical, are evaluated. In addition, the platform is used in the three cross-border trainings in order to see its applicability and operability in quasi-real situations. Subsequently, all evaluation results are used to make adjustments in the final version of the platform(WP6).

Finally, the last work package (WP7) has as its main objective to promote the use and exploitation of the main VESPRA results ensuring their contribution to risk reduction in transboundary regions. This is done through dissemination and diffusion of technical and scientific documentation, organisation of workshops and the creation of public awareness and media working groups, among others, aimed at two relevant target groups: technicians and researchers; and different stakeholders (e.g. potentially affected populations or the media).

3. Preliminary results

The VESPRA project has achieved the objectives expected for the basic line of work of study and harmonisation of data, focusing on a rigorous analysis of the specific state of the art in the field, on which the fundamental bases of the VESPRA project have been built, searching for unmet needs in this area and technological innovation to make the most of them. Specifically, these first lines of work have been based on the following:

(I) the survey and harmonisation of the conceptual framework of vulnerability, hazard and risk and of the databases of vulnerable elements available in the regions, Member States and the Union. A total of 45 databases covering different geographical scales - global, European, cross-border, national, regional and local - have been evaluated, taking into account the data format, as well as their time frame and spatial resolution.

(II) the creation of an agreed catalogue of vulnerable elements (Annex 1), including a hierarchical classification by type and nature groups (i.e. static, dynamic), a universal definition and a preliminary description of the undesired consequences in case of exposure to hazard levels observed in real events. This catalogue includes more than 100 vulnerable elements divided into six main types related to each hazard: people, utilities, commercial and service facilities, industrial facilities, environmental elements and cultural heritage facilities and services. Each vulnerable element typology is divided into several sub-typologies with a simple attribute scheme that is used to analyse its vulnerability to emergencies.

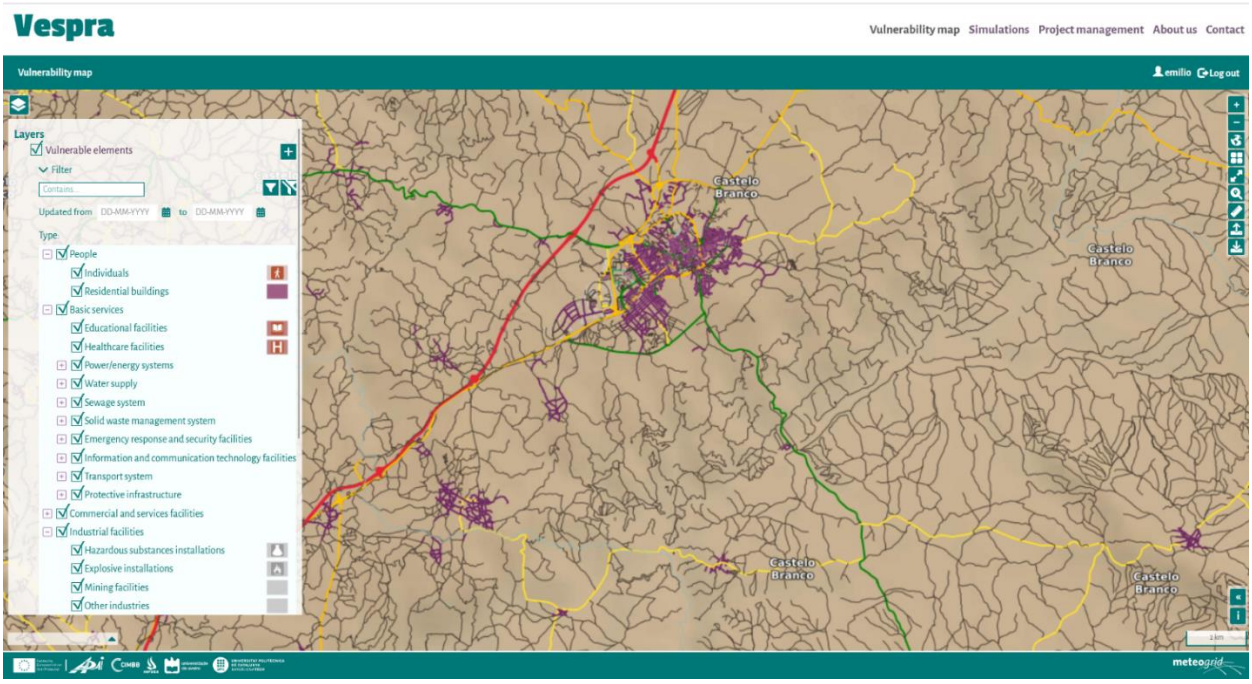

Figure 1. Overview of the system

As a result of the above it has been possible to complete a survey of the main databases of vulnerable elements and of the main hazards in the Member States, as described in the relevant Civil Protection Organisations, and to review and draw lessons learned from recent relevant events involving vulnerable elements, especially in population, infrastructures and the environment.

In parallel, the VESPRA project has devoted effort to the design, development and implementation of a data collection system and procedure linking several territorial levels. Given the trans-scalar and cross-border nature of the data collection, a special effort has been made for the interoperability of the process between Spain and Portugal, for which a multilingual graphical user interface has been developed. Portability and modularity have been at the core of the system design, including the use of mobile phones and tablets to facilitate its use down to a local level. The tools are based on a GIS-WEB with different solutions to manage the cartographic information generated with different user profiles (Figure 1). A mapping strategy has also been developed based on existing standards for the mapping coding of vulnerable elements and consistent with the rapid mapping of the Copernicus service. This makes VESPRA perfectly compatible with the products used by and for the Union Civil Protection Mechanism (UCPM).

The next step in the VESPRA project has been the study, definition, analysis and description of the vulnerability and risk models to be incorporated into the VESPRA tool. For each of the four hazards considered, the vulnerability models available in the state of the art have been studied and the most interesting ones have been selected for the purposes of the project taking into account the previous results. Once the models have been analysed and selected, the next step has been to describe an algorithm for their use and implementation in the VESPRA tool.

The risk assessment model followed in the VESPRA Project comprises several sequential steps. Each of these steps provides the user with a set of information of great operational and preventive interest, making the VESPRA tool usable in the prevention, preparedness and response phases, i.e. in the hypothesis of a future hazard event and in the course of a hazard event.

Figure 2 shows the general data flow and processing of the VESPRA approach to obtain mapping information on vulnerability and potential damage. This general approach has been specified for each of the hazards.

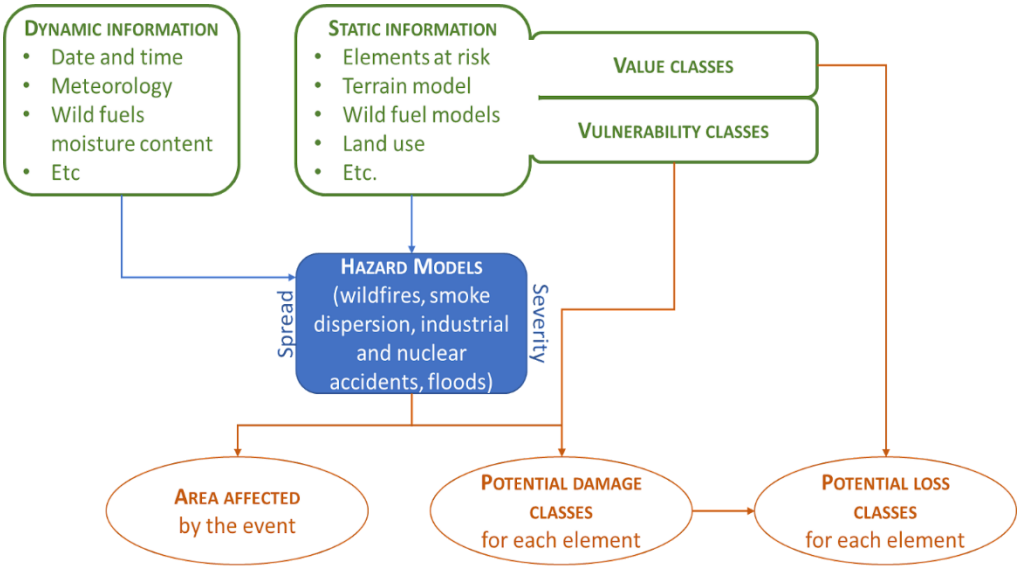

Figure 2. Data flow of the VESPRA Tool.

The VESPRA team is currently implementing these models in the decision support system (Figure 3), contributing to the specific end goal (cross-border disaster risk management through prevention and preparedness in Europe).

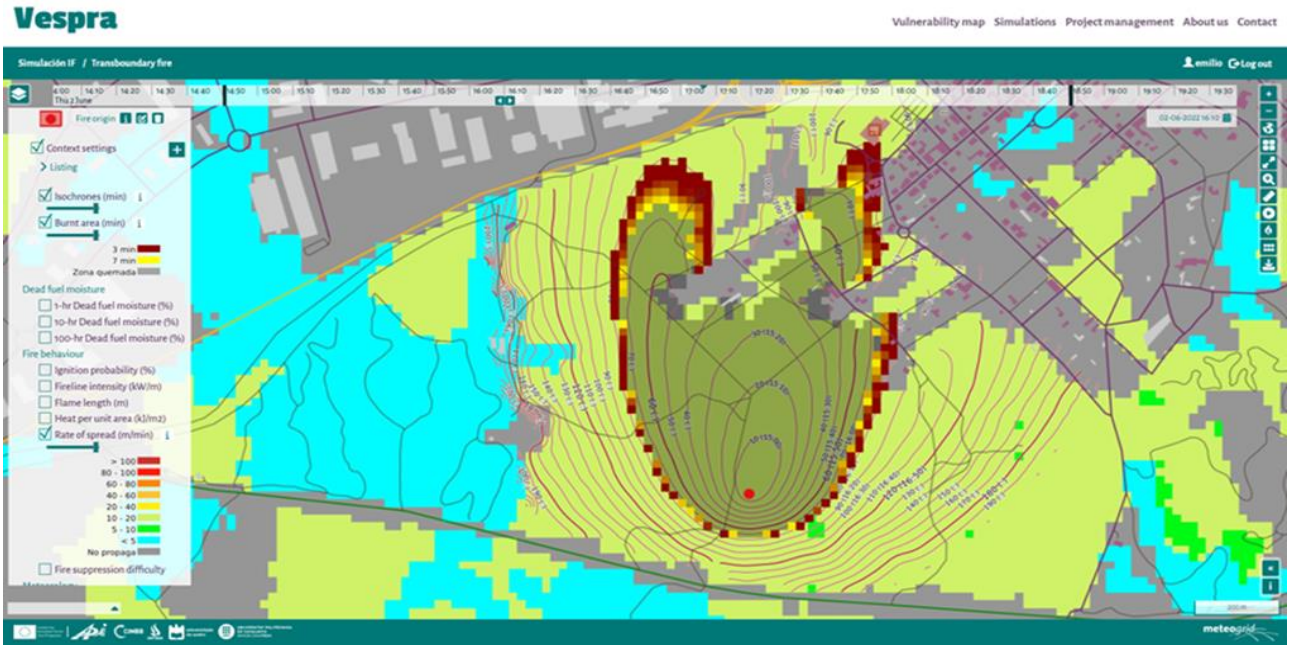

Figure 3. Potential Loss of the exposed elements for the demonstration area in the scenario.

4. Conclusions

VESPRA is a system based on web services that will incorporate the vulnerability geo-database, the catalogue, the weather forecasting services and the different vulnerability analysis models in diverse risk domains. This includes the capacity to project meteorological processes, the identification of possible scenarios, the estimation of possible consequences and the identification of possible vulnerable elements affected. In this sense, this last line of innovation is especially dedicated to the integration of all the components of the system under a single user interface, which will comply with the degree of interoperability required by the cross-border nature of the services. The system will be fully compatible with the existing legacy systems in the two selected countries (Portugal and Spain), but will also be fully interactive and allow information sharing in both countries.

5. Acknowledgements

This research is funded by theEuropean Union Civil Protection Mechanism (Project UCPM-2020-PP-AG–VESPRA – 101004896)

6. References

Benelux; 2016. Inventaire Benelux des Risques Transfrontaliers. Secrétariat général de l'Union Benelux. Bruxelles. Available at: https://www.benelux.int/files/4714/6960/8568/SennRisk-DEF_WEB.pdf

7. Annex 1

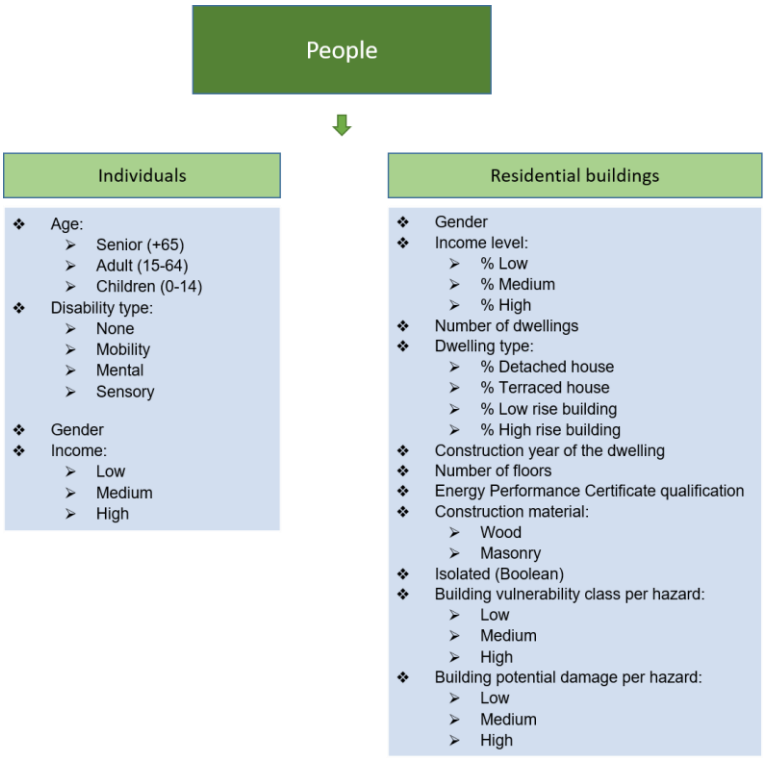

Figure 1. Specific attributes for people sub-typologies.

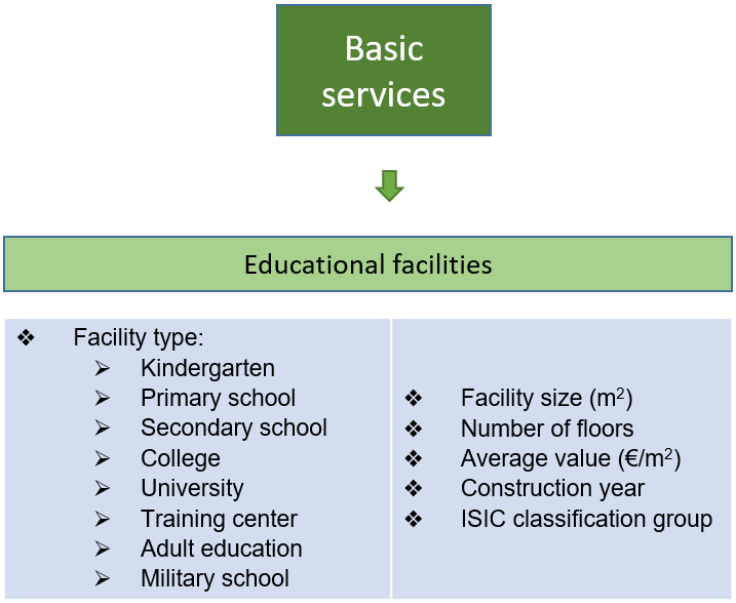

Figure 2. Specific attributes for educational facilities sub-typologies.

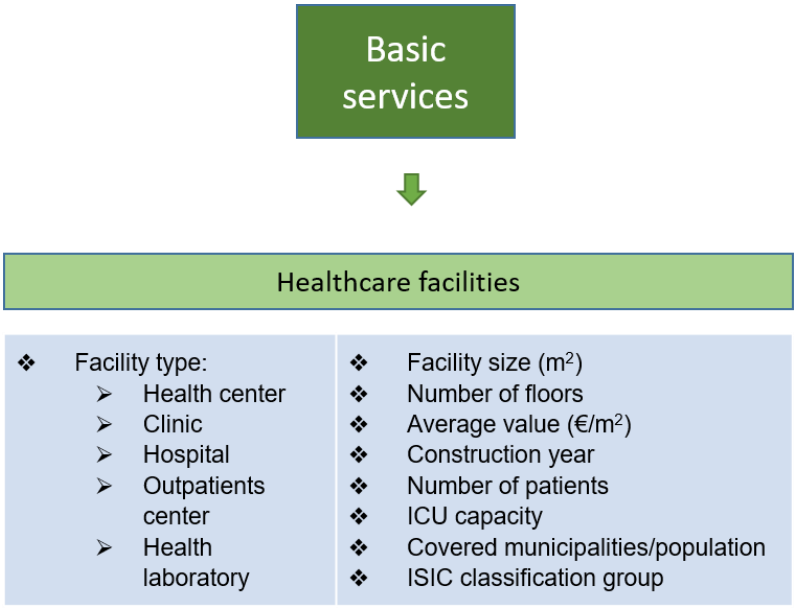

Figure 3. Specific attributes for health care sub-typologies.

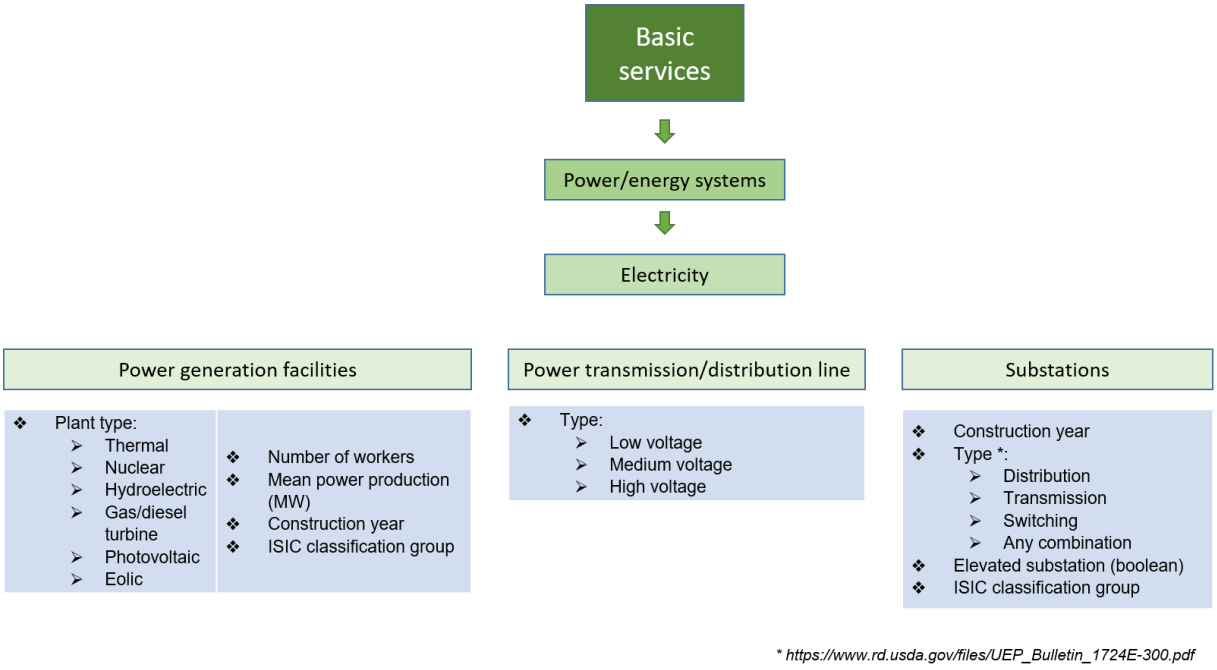

Figure 4. Specific attributes for electricity sub-typologies.

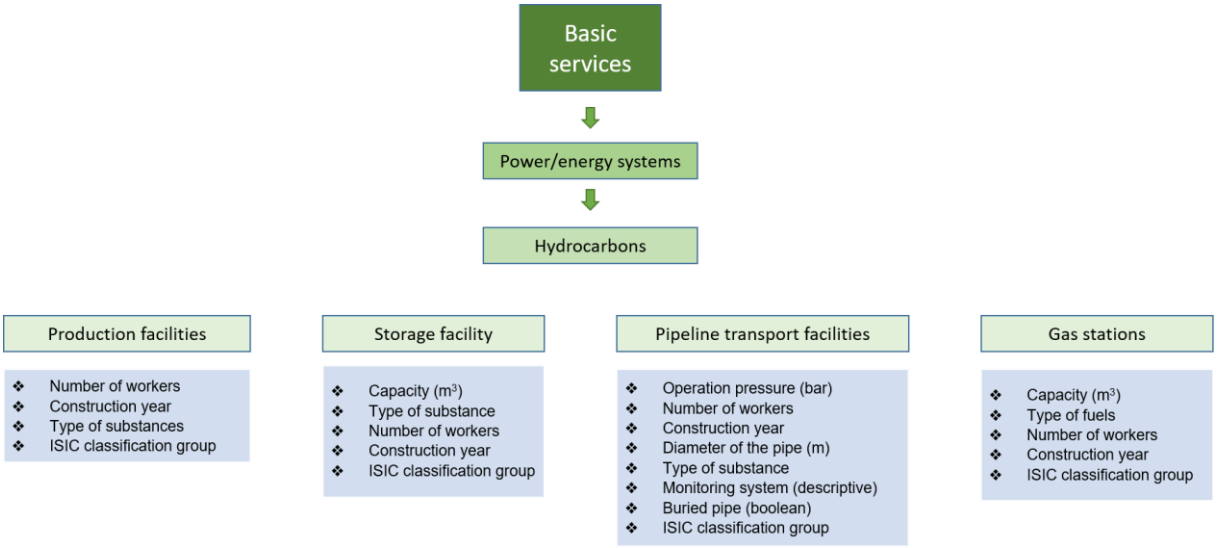

Figure 5. Specific attributes for hydrocarbons sub-typologies.

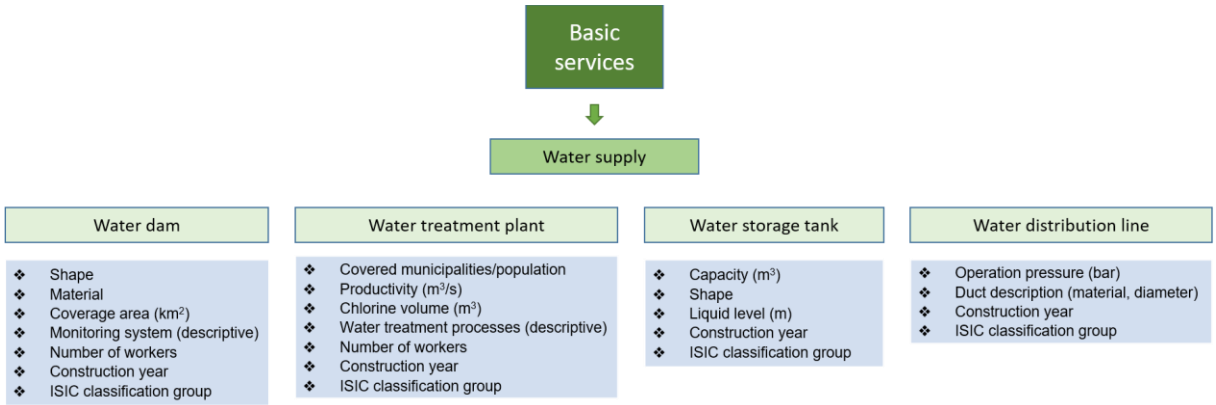

Figure 6. Specific attributes for water supply sub-typologies.

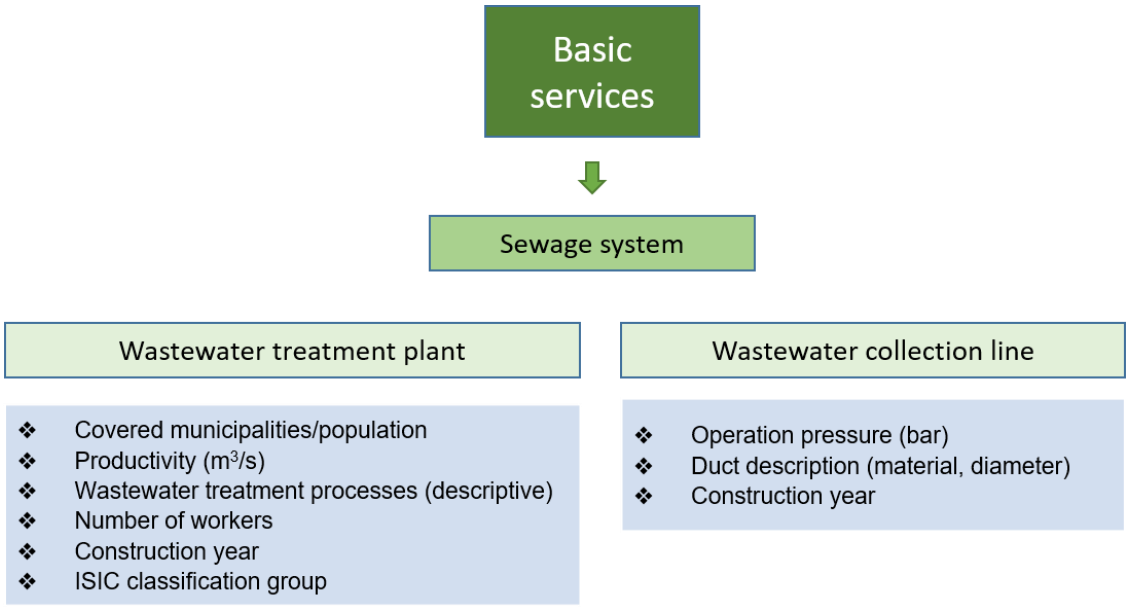

Figure 7. Specific attributes for sewage system sub-typologies.

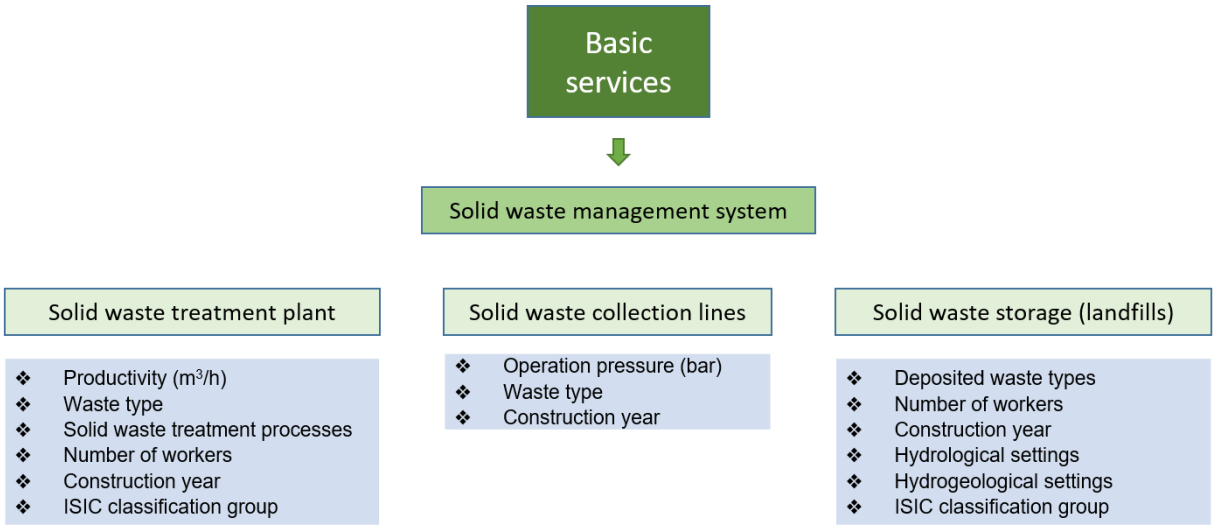

Figure 8. Specific attributes for solid waste management system sub-typologies.

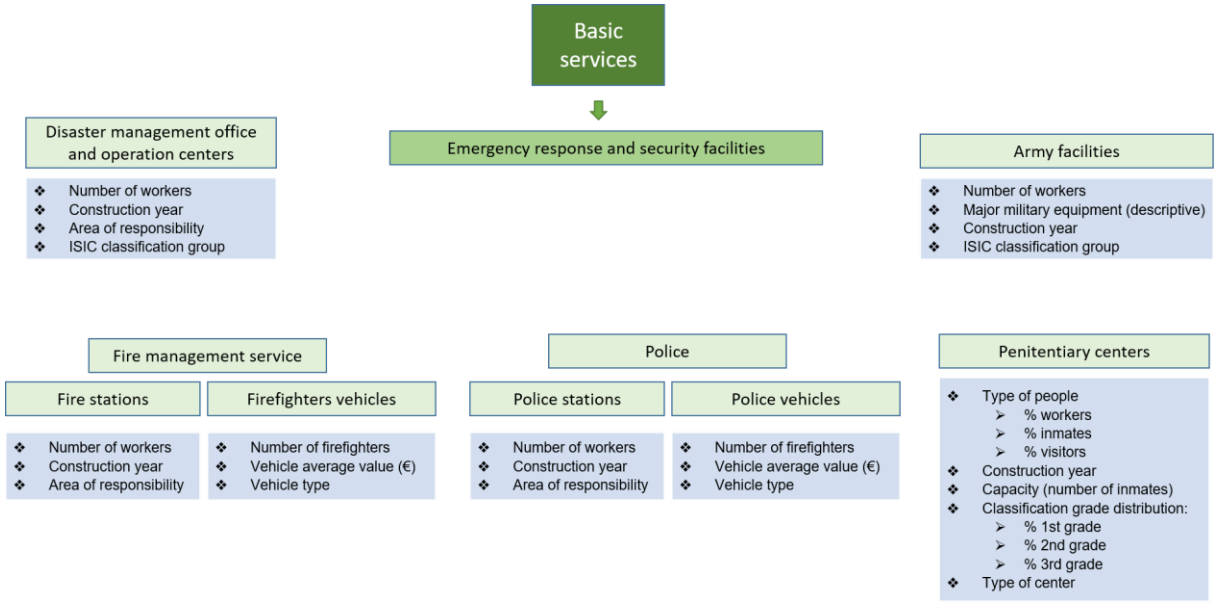

Figure 9. Specific attributes for emergency response and security facilities sub-typologies.

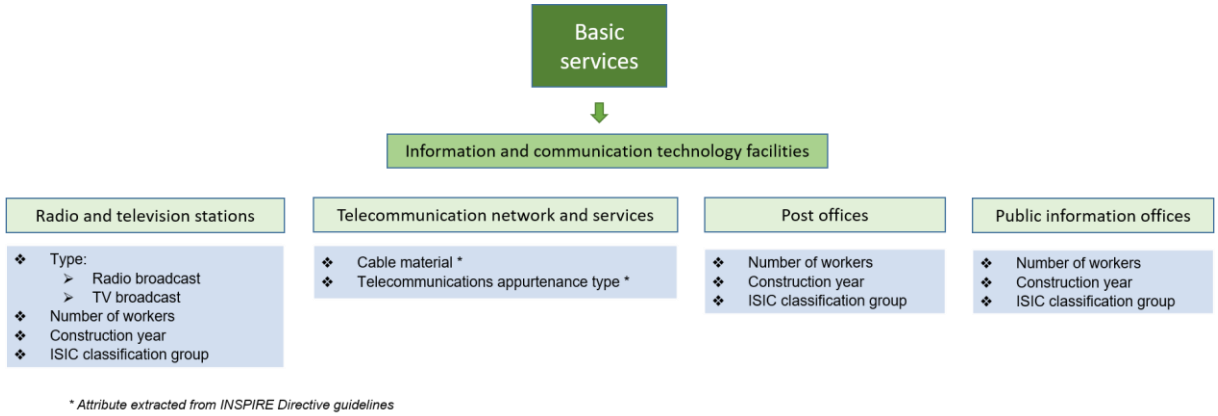

Figure 10. Specific attributes for information and communication technology facilities sub-typologies.

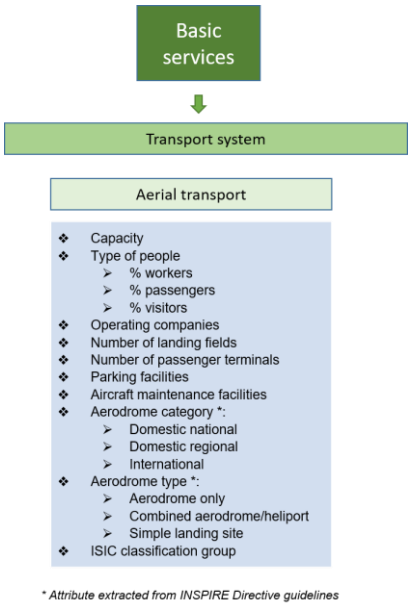

Figure 11. Specific attributes for aerial transport.

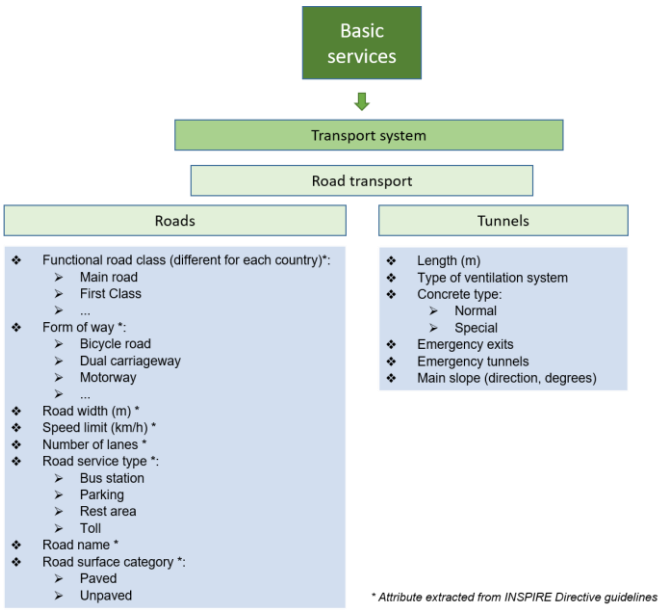

Figure 12. Specific attributes for road transport sub-typologies.

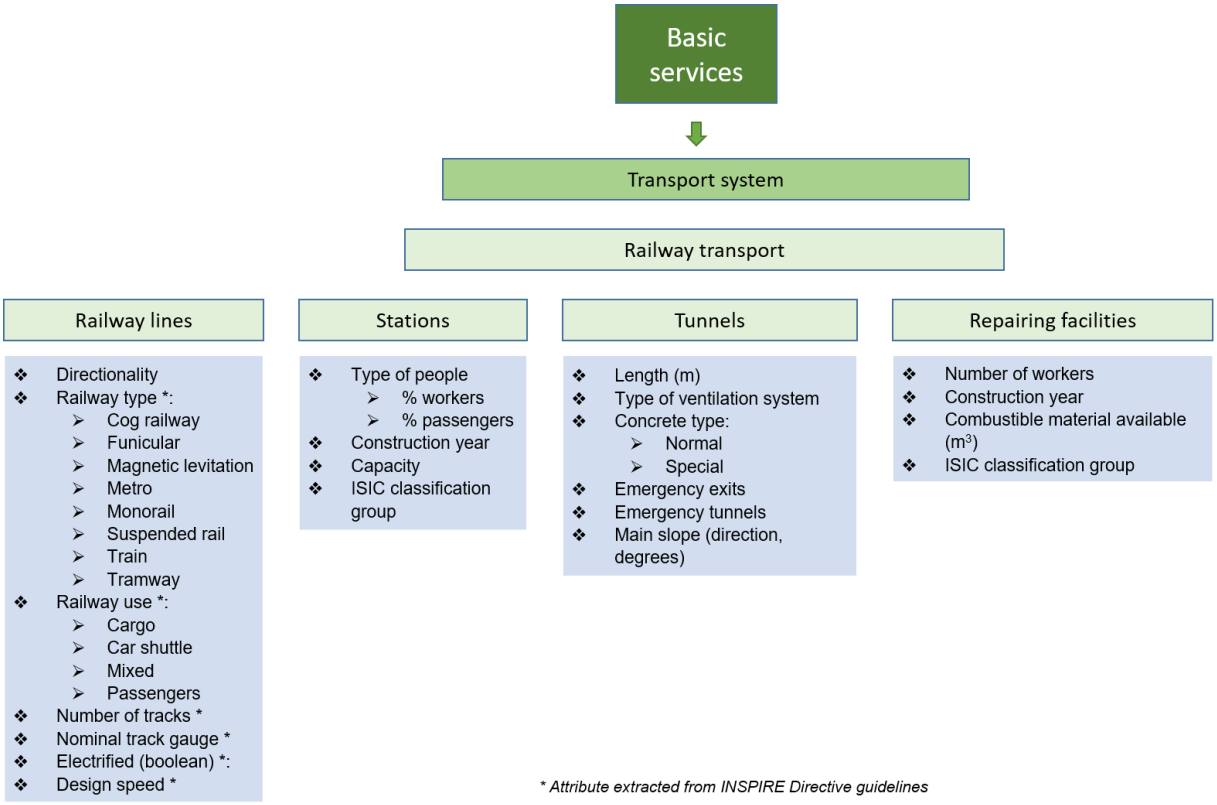

Figure 13. Specific attributes for railway transport sub-typologies.

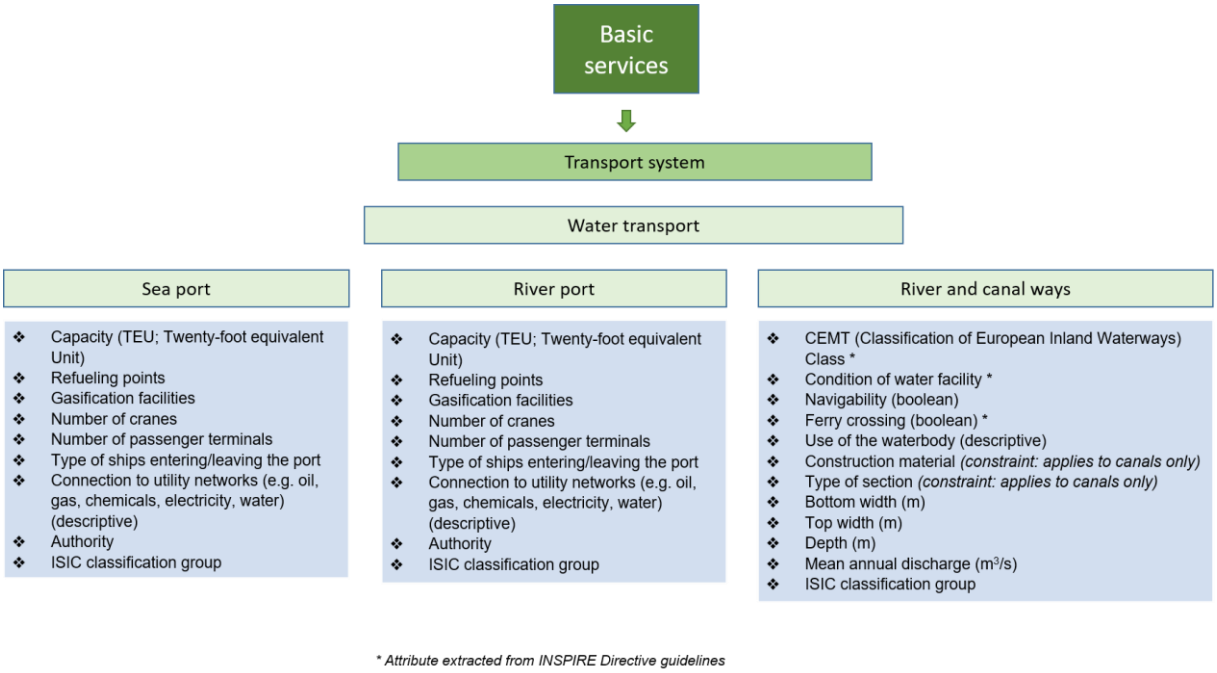

Figure 14. Specific attributes for water transport sub-typologies.

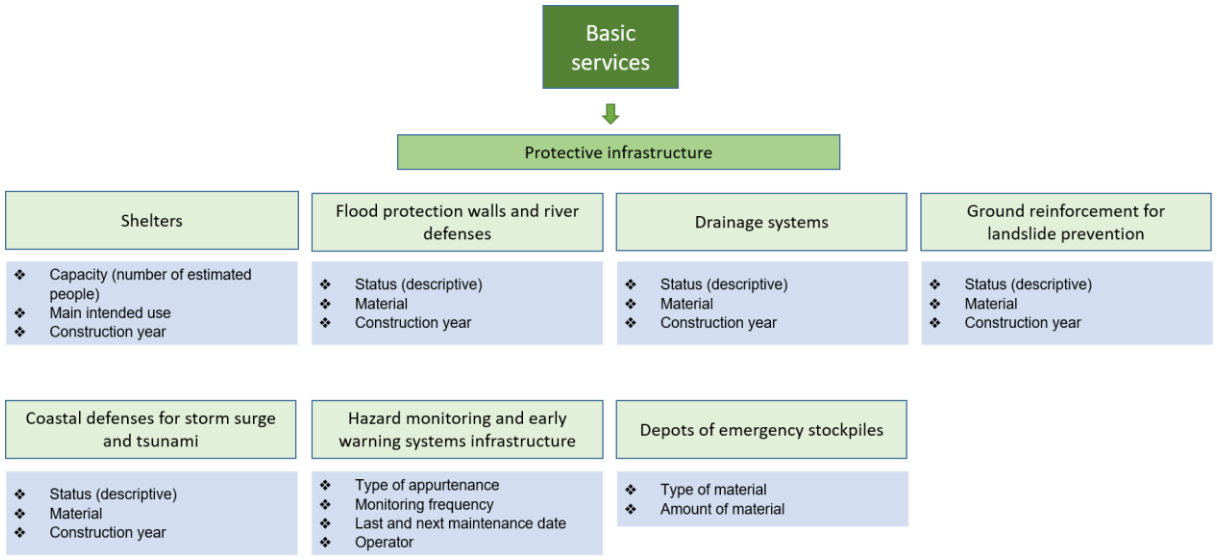

Figure 15. Specific attributes for protective infrastructure sub-typologies.

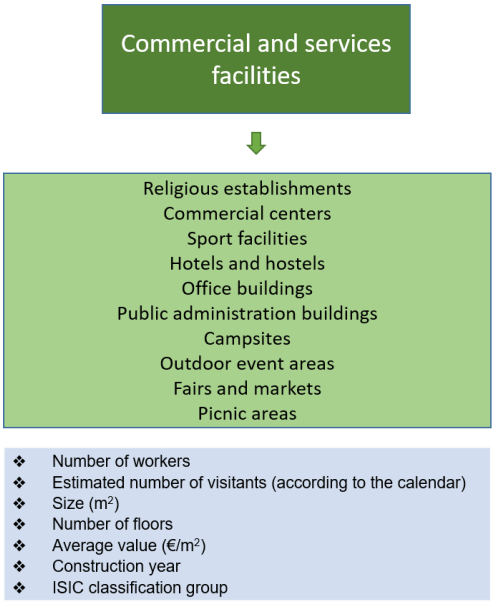

Figure 16. Specific attributes for commercial and services sub-typologies.

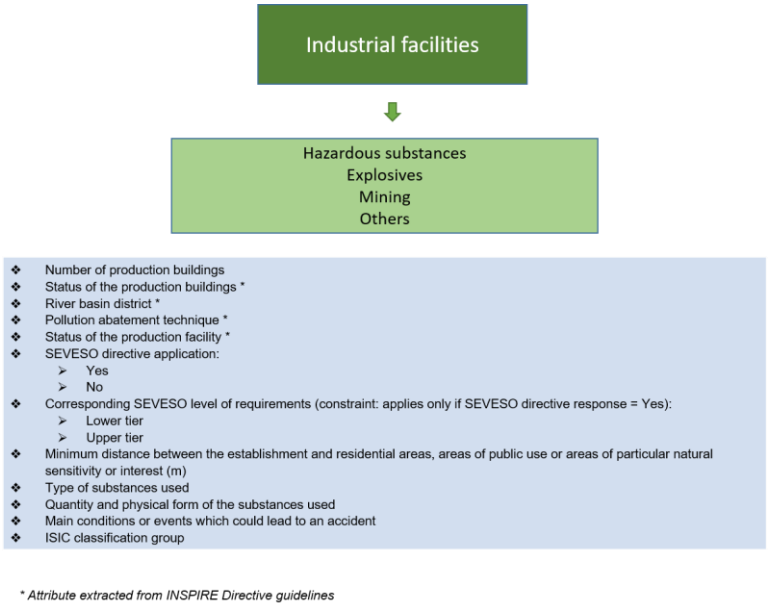

Figure 17. Specific attributes for industrial facilities sub-typologies.

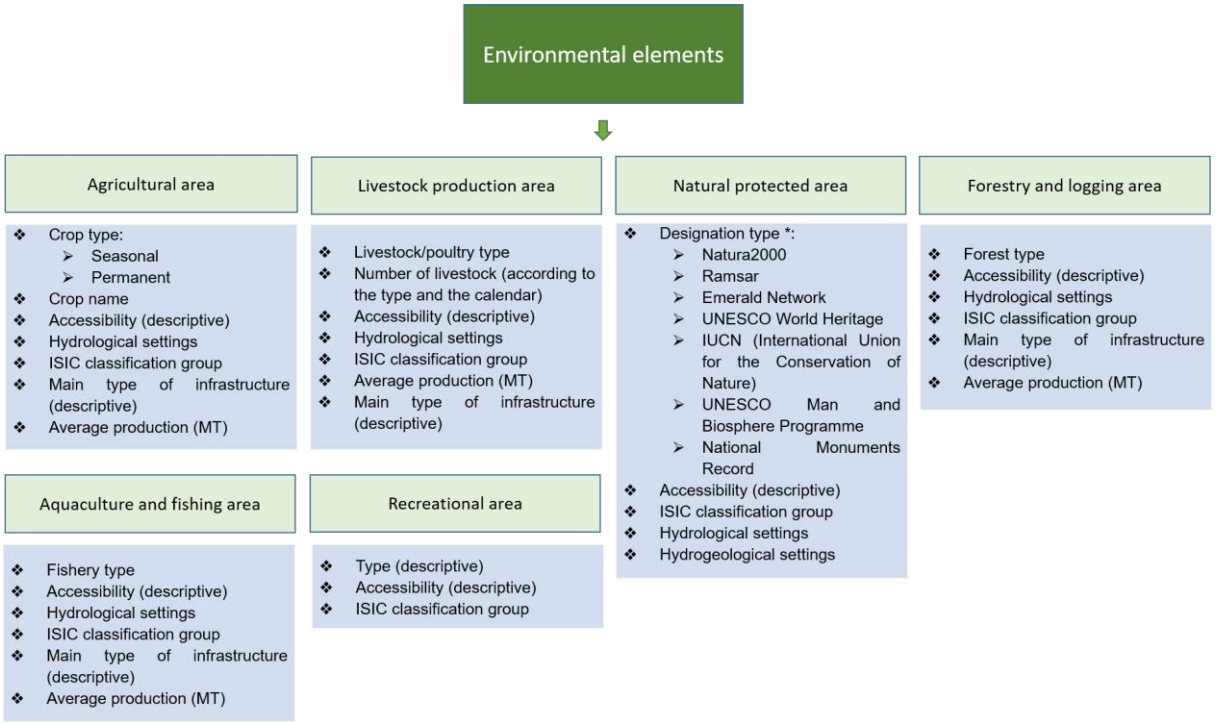

Figure 18. Specific attributes for environmental elements sub-typologies.

Figure 19. Specific attributes for cultural heritage facilities and services sub-typologies.

Chapter 2:
Fire at the Wildland Urban Interface

A Comparison of Particulate Morphology of Wildland Fuels and Human-Made Fuels at the Wildland-Urban Interface

Samuel L. Manzello*[1]; Sayaka Suzuki[2]

[1]Reax Engineering, Berkeley, CA, USA, {manzello@reaxengineering.com}
[2]National Research Institute of Fire and Disaster (NRIFD), Chofu, Tokyo, Japan, {sayakas@fri.go.jp}

**Corresponding author*

Keywords

Particulates; Wildland-Urban Interface (WUI) Fires; Scanning Electron Microscopy (SEM)

Abstract

A major outcome of large outdoor fires is the production of combustion products. The most well-known type of large outdoor fires are wildland fires that spread into developed, urban areas, known as wildland-urban interface (WUI) fires. Particulate emissions from WUI fires in California in 2018 resulted in almost a complete closure of San Francisco. Improved knowledge of large outdoor fire particulate emissions is needed at the laboratory-scale. Here, samples of oriented strand board (OSB), a common human-made fuel abundant in cities, were ignited using a radiant heater coupled to a spark igniter. Particulate samples were taken to begin to look at the morphology of the generated particulates. Using a simple experimental setup affords the capability to investigate particulates produced from smoldering combustion as well as those collected from flaming combustion. In this short paper, some initial results are presented fro OSB combustion. Further comparison to vegetative fuels will be presented at the conference.

1. Introduction

A consequence of large outdoor fires is the production of combustion products. These combustion products are known to cause extreme visibility issues and worries about health. Globally, the combustion of vegetative fuels is thought to be the prime supplier of particulate emissions and the second most supplier of gaseous emissions [Akagi *et al.*, 2011]. Particulate emissions from WUI fires in California in 2018 resulted in almost a complete closure of San Francisco.

Methodologies to determine emissions from wildland fires or biomass have centered on the concept of developing specific emissions factors (EF) [Akagi *et al.*, 2011]. EFs are usually reported for carbon monoxide, carbon dioxide, and particulate matter less than 2.5 microns. In many cases, EF do not account for the combustion of human-made fuels. It is obvious the vegetation species are not solely suppling the gaseous and particulate emissions but also the combustion processes from buildings, cars, buses, and other human-made combustibles only add to the assortment of emissions. Yet, it is not obvious how to addresses these additional complications.

Another overlooked, key shortcoming is that many of the EFs for vegetative fuels are predicated on controlled/prescribed fires. Specifically, these are well-controlled fires conducted for a variety of fire/fuel management intentions. Such controlled burning has benefits since it is performed over real terrain, but the fire exposure conditions cannot possibly recreate what is observed in the most dangerous fires. Typically, controlled fires are undertaken, under low ambient wind conditions to ensure safety yet massive, destructive fires rarely occur in low winds.

Complimenting EF research, there have been studies that have looked at the particulates formed in the context of wildland fires and as well as from biomass [Akagi *et al.*, 2011, Posfai *et al.*, 2003, Reid *et al.*, 2005]. None of this important research has been extended to WUI fires, where many non-vegetative fuels exist. What has been observed is that the nature of particles formed depend highly on the nature of the smoldering or flaming combustion properties of the wildland fires or biomass.

The reasons for this lie in the details of the combustion processes. In the case of smoldering combustion, and therefore smoldering fires, this is a surface process. Oxygen moves to the surface and reacts with fuels at

relatively low temperatures. Since polycyclic aromatic hydrocarbons (PAH) are known to form at higher temperatures, smoke particles contain less soot for smoldering combustion as compared to flaming combustion. Particle formation are also known to occur around other nuclei other than PAHs [Lighty *et al.*, 2000]. For any type of large outdoor fire, there have been few studies of particulate formation in the smoldering phase and to the authors knowledge, almost no studies for engineered wood products found in WUI fires.

Results reported that for wildland fires or biomass that are in a state of smoldering combustion, the combustion processes are generally dominated by lower temperature regimes and therefore the collected particles have a liquid-like structure [Akagi *et al.*, 2011, Posfai *et al.*, 2003, Reid *et al.*, 2005]. For wildland fires or biomass that have higher temperatures, and are in a state of flaming combustion, these fires produce particles with more well-known fractal agglomerates and structure often seen in most soot formation studies in a state of flaming combustion (**see Figure 1).**

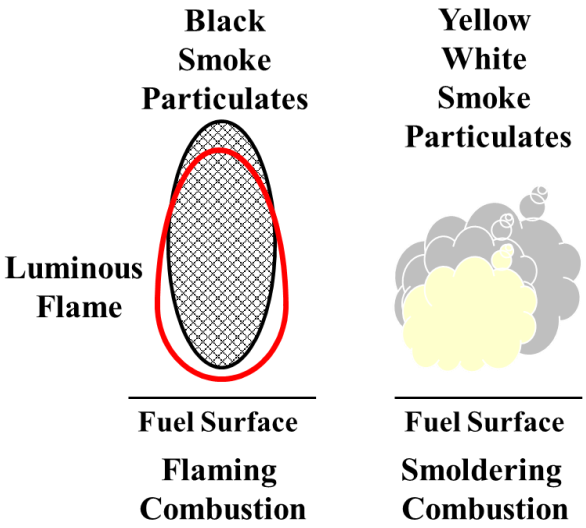

Figure 1- Differences in particulates observed during flaming combustion and smoldering combustion states.

Improved knowledge of large outdoor fire particulate emissions is needed at the laboratory-scale. Here, samples of oriented strand board (OSB), a common human-made fuel abundant in cities, were ignited using a radiant heater coupled to a spark igniter. Particulate samples were taken to begin to look at the morphology of the generated particulates. Using a simple experimental setup affords the capability to investigate particulates produced from smoldering combustion as well as those collected from flaming combustion.

As the nature of particulate samples were expected to be sensitive to the voltage of the electron beam for smoldering combustion in particular, scanning electron microscopy (SEM) was used as first step to investigate the morphology. Transmission electron microscopy (TEM) operates at higher acceleration voltages and this is expected to influence the samples. In this short paper, some initial results are presented fro OSB combustion. Further comparison to vegetative fuels will be presented at the conference.

2. Experimental Description

The experimental setup consisted of a radiant heater coupled to spark igniter (see **Figure 2**). Samples of OSB were cut into sizes of 100 mm by 100 mm. As commercial samples of OSB was used, the thickness was fixed at 11 mm.

The use of engineered wood products has been common worldwide. In the United States of America, there has been a move to replace plywood with OSB. In the past, plywood was more common. OSB is manufactured from smaller trees and is manufactured primarily of wood fragments, so it is cheaper to produce. Plywood requires thin, long sheets of wood veneers. Similar trends have been seen in other countries, including Japan.

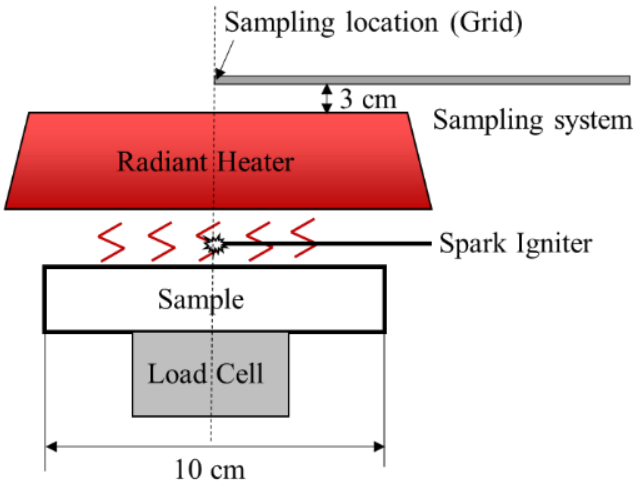

Figure 2- Schematic of Experimental Setup.

A radiant heat flux of 25-30 kW/m^2 was applied and the spark was operated continuously to produce flaming combustion. Under these conditions, the OSB samples ignited with sustained flaming ignition within 90 sec. Experiments were also conducted using a radiant heat flux of 25 kW/m^2, without the application of the spark, to produce smoldering combustion.

To sample particulates that are generated, the well-known principle of thermophoretic sampling was used. In the presence of a temperature gradient, the hot particles will be collected using cold grids that may be used for Scanning Electron Microscope (SEM) and Transmission Electron Microscopy (TEM) analysis. Presently, SEM was used a first step to image the overall structure of the particulate samples.

3. Results and Discussion

Experiments were conducted for one applied heat flux level and all samples were taken at the same time after the onset of sustained flaming combustion of the OSB sample. The total sampling time was varied from 1 sec to 3 sec. Figure 3 displays agglomerates imaged with the SEM for one of these sampling times.

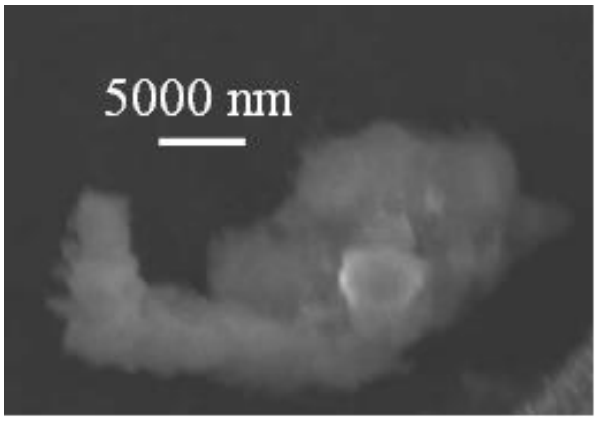

Figure 3 SEM image of particles collected from OSB in a state of flaming combustion (25 kW/m^2).

A series of experiments were conducted to sample the particulates generated from OSB samples in a state of smoldering combustion. The radiant heat flux was applied to the specimens and no spark was applied. Typical SEM images for the collected particulates from OSB undergoing smoldering combustion will be presented at the conference.

It is clear that the morphology of the particulates is indeed different depending on whether the OSB samples are in a state of flaming as opposed to smoldering combustion. Owing the higher temperatures during flaming combustion, the more well-known fractal agglomerate structures are observed for the OSB samples in a state of flaming combustion

4. Summary

Improved knowledge of large outdoor fire particulate emissions is needed at the laboratory-scale. Particulate samples were taken during both flaming combustion states and smoldering combustion states using thermophoretic sampling. As the nature of particulate samples were expected to be sensitive to the voltage of the electron beam for smoldering combustion in particular, scanning electron microscopy (SEM) was used as first step to investigate the morphology The nature of the combustion state resulted in vast differences in the morphology of the collected samples. Further comparison to vegetative fuels will be presented at the conference.

5. References

S.K. Akagi, R.J. Yokelson, *et al*., (2011) Emissions Factors for Open and Domestic Biomass Burning for Use in Atmospheric Models, *Atmos. Chem. Phys*. 11 4039-4072

J.S. Lighty, J. Vernath, and A Sarofim (2000) Combustion Aerosols: Factors Governing Their Size and Composition and Implications to Human Health, *J. of the Air & Waste Management Association*, 50 1565-1618.

M. Posfai, R. Simonics, J. Li, P. V. Hobbs, and P. R. Buseck, (2003) Individual Aerosol Particles from Biomass Burning in Southern Africa: 1. Compositions and Size Distributions of Carbonaceous Particles, *J. Geophysical Research* 108 8483-8496.

J. S. Reid, R. Koppmann, T. F. Eck, and D. P. Eleuterio, (2005) A Review of Biomass Burning Emissions Part II: Intensive Physical Properties of Biomass Burning Particles, *Atmos. Chem. Phys.* 5 799–825.

A comparison of two methods to measure pyrolysis gases in a wind tunnel and in prescribed burns

David R. Weise *[1], Timothy J. Johnson[2], Tanya L. Myers[2], Wei Min Hao[3], Stephen Baker[3], Javier Palarea-Albaladejo[4,5]

[1] USDA Forest Service, Pacific Southwest Research Station, 4955 Canyon Crest Dr., Riverside, CA, 92507, USA, {david.weise@usda.gov}
[2] Pacific Northwest National Laboratory, Richland, WA, USA, {Timothy.Johnson, Tanya.Myers}@pnnl.gov
[3] USDA Forest Service, Rocky Mountain Research Station, Missoula, MT, USA {wei.hao, stephen.baker1}@usda.gov
[4] Department of Computer Science, Applied Mathematics and Statistics, University of Girona, Girona, Catalonia, Spain {javier.palarea@udg.edu}
[5] Biomathematics and Statistics Scotland, Edinburgh, Scotland, UK

**Corresponding author*

Keywords

FTIR, GC/FID, Pinus palustris, compositional data, prescribed burning

Abstract

Pyrolysis products from wildland fuels are typically measured under tightly controlled conditions using fuels which have been processed to remove water content and physical shape. Different instruments can be used to identify and quantify the composition of these gases. Measurement of pyrolysis gases under conditions typical of wildland fires has seldom occurred. We used FTIR spectroscopy and GC/FID analysis to measure pyrolysis gases produced in wind tunnel experiments and small prescribed burns in longleaf pine needle fuel beds with live shrubs. Use of compositional data techniques on the 8 common gases measured by both methods showed that the compositions were affected by the measurement method and interaction between method and location was significant.

1. Introduction

A wide variety of methods and instruments are available to identify and quantify the hundreds of gaseous and particulate compounds produced by the heating and combustion of wildland fuels. The methods and instrumentation have been compared (e.g., Fehsenfeld *et al.* 1987; Christian *et al.* 2004; Li *et al.* 2019) as well as used in a complementary fashion to increase the detection and quantification of as large a suite of compounds as possible (e.g., Yokelson *et al.* 2013). Linking laboratory results to field scale phenomena has long been a topic of interest and the field of wildland fire and smoke emissions is no exception (Ward and Radke 1993).

Ward and Radke (1993) compared different methods of describing smoke emissions from bench-scale measurement to aircraft and satellite measurement. Combustion efficiency, defined as the ratio of CO_2 to the sum of CO_2, CO, hydrocarbons, and particulate matter emitted by a fire, was proposed as a measure to link results across scales. Further development of this concept led to the use of CO/CO_2 and modified combustion efficiency (MCE) as descriptors of a fire and as an "independent" predictor of other smoke components (Ward and Hao 1991; Yokelson *et al.* 1996) because MCE was often "well-correlated" with other emission components. However, the problematic use of correlation measures on proportional and relative data has long been known (Pearson 1896; Aitchison 1986) and the measured gas mixtures formally correspond with multivariate relative data known as compositional data. Thus, the widely assumed convention that CO/CO_2, and thus MCE, was an independent predictor for other smoke components has been shown to be in error (Weise *et al.* in press). Given the above, the objective of this manuscript is to properly compare the composition of pyrolysis gases measured in a series of wind tunnel and field fires by FTIR spectroscopy and GC/FID using a compositional data analysis (CoDA) approach to determine if the two sampling methods produced similar results.

2. Methods

Gas sampling was performed in a series of wind tunnel experiments and field prescribed burns in longleaf pine (*Pinus palustris* Mill.) needle fuel beds containing a live shrub component. See Scharko *et al.* 2019 and Weise *et al*. 2022 for details of the sampling methodology and analytical methods used to determine quantity and composition of the gases. Eight gases (CO_2, CO, CH_4, C_2H_2, C_2H_4, C_3H_6, C_4H_6 and C_4H_8) were measured by both FTIR and GC/FID. The relative amounts of these gases will be analyzed in this paper using version 4.1.2 of the public domain software R (R Core Team 2021). The data were preprocessed using the *multLN* function to impute random values below the minimum observed concentrations (Palarea-Albaladejo and Martín-Fernández 2013, 2015).

The common approach to analysis of compositional data is to express them through adequate log-ratios coordinates (balances) and then applying ordinary statistical techniques (Egozcue *et al.* 2003). The purpose of the various log-ratio transformations used in CoDA is to put the data in ordinary real space as opposed to their original simplex space. Seven log-ratio balances representing meaningful contrasts between subsets of gases were obtained by sequential binary partitioning (Egozcue and Pawlowsky-Glahn 2005). Multivariate analysis of variance (MANOVA) tested the effects of method (FTIR, GC/FID) and location (wind tunnel, field) on the entire composition and ANOVA tested the effects on these 7 balances individually. The data were unbalanced (Table 1); there are a variety of approaches to use ANOVA to test the significance of effects for unbalanced data. Based on Langsrud (2003), we used the *Anova* function which calculated Type II sums of squares to test the effects. Because there are only two levels of each factor, the significance of the difference between the two levels is tested by default; the probability was adjusted to account for the multiple t-tests using Benjamini and Hochberg's (1995) false discovery rate. A total of 21 t-tests (7 balances x 3 effects (method, location, interaction)) were performed because the intercept term was not included.

3. Results

The gases common to the GC/FID and FTIR samples were CO, CO_2, CH_4, C_2H_2, C_2H_4, C_3H_6, C_4H_6 and C_4H_8. These gas concentrations, constituting a subcomposition of the original composition, were "normalized" ("closed" in the CoDA parlance) to put them on a proportion (0,1) scale. Note that within a CoDA framework, these values can be expressed in the original ppm units, proportions or be converted to percentages without affecting the statistical results (scale invariance property). The relative amounts of the gases were similar in terms of highest to lowest proportions (Table 2); however, the relative amount of CO measured by FTIR at Ft. Jackson was an order of magnitude larger than the wind tunnel or GC/FID measurements. The MANOVA showed that the GC/FID and FTIR methods had a significant effect on the relative composition of the common gases (Table 2) and there was a significant interaction between location and method.

Because of the significant interaction, the mean values of the 4 combinations of location and method were calculated for each balance (Table 4). The overall mean for each balance is a weighted mean so the values were strongly influenced by the large number of GC/FID observations in the wind tunnel. The presence of significant interaction prevents clearly attributing differences in the balances to method alone. Since location was not significant as a main effect, the probability values are not presented.

Method significantly affected 4 of the 7 balances and the interaction term for method and location significantly affected a single balance. The 1st two balances containing CO_2 were smaller for the FTIR measurements at Ft. Jackson; relatively less CO_2 and more CO and CH_4 were measured (Table 2) resulting in smaller balances. The FTIR measured more CO relative to CH_4 than GC/FID; however, relatively more CH_4 was measured by GC/FID in the field burns. The interaction term affected the CO_2 vs CO & CH_4 balance. The FTIR balance values were smaller than GC/FID for Alkenes vs Alkynes. Note that the GC/FID values for this balance were close to zero which implies that the actual ratio between these subsets of gases was close to 1 in the original units, suggesting that the relative amounts of these two groups are approximately equal. The propene vs isobutene balance suggested that more propene relative to isobutene was present in the FTIR samples compared to the GC/FID.

Table 1. Number of pyrolysis gas samples analyzed by FTIR and GC/FID in the wind tunnel (RFL) and prescribed fires in Ft. Jackson, SC (FJ).

Method	Location	
	RFL	FJ
FTIR	22	5
GC/FID	88	7

Table 2. Mean relative amount of pyrolysis gases common to two sampling methods in wind tunnel (RFL) and prescribed fires in Ft. Jackson, SC (FJ). Expressed in proportions.

	RFL FTIR	RFL GC/FID	FJ FTIR	FJ GC/FID
Carbon dioxide (CO_2)	9.22E-01	9.43E-01	8.07E-01	9.81E-01
Carbon monoxide (CO)	6.85E-02	4.82E-02	1.58E-01	1.47E-02
Methane (CH_4)	5.25E-03	6.13E-03	1.64E-02	3.32E-03
Ethene (C_2H_4)	2.38E-03	1.87E-03	9.86E-03	3.33E-04
Acetylene (C_2H_2)	1.23E-03	4.89E-04	6.29E-03	1.48E-04
Propene (C_3H_6)	4.15E-04	8.56E-05	1.45E-03	3.65E-05
1,3-butadiene (C_4H_6)	9.92E-05	3.87E-05	4.29E-04	2.47E-05
Isobutene (C_4H_8)	3.86E-06	2.15E-05	7.43E-05	1.44E-05

Table 3. Summary of multivariate analysis of variance testing effects of sampling method (FTIR, GC/FID) and fire location (wind tunnel, Ft. Jackson) on mean relative composition of pyrolysis gases measured by both methods.

Source	df[a]	Pillai's[b] trace	F[c]	Num df	Den df	Pr(>F)
Method	1	0.39	10.66	7	112	<0.0001
Location	1	0.07	1.15	7	112	0.34
Interaction	1	0.16	2.97	7	112	0.007

a. Degrees of freedom of effect.
b. Pillai's trace used to test equality of means.
c. F-statistic associated with Pillai's trace.

4. Discussion and Conclusions

Direct comparison of gas measurements in a fire environment produced with different instruments is challenging and influenced by many factors. Different instruments and analytical techniques may measure the same gases with differing resolution or are unable to detect the same compounds (Ward and Radke 1993). Because of this, a wide variety of instrumentation is deployed to measure a large suite of compounds (e.g., Yokelson *et al*. 2013). The present study used two methods readily adapted to field use. The inherent spatial, temporal and compositional variability in fuels as well as the conditions under which the fuels were heated can affect the composition of the pyrolysis and combustion products. Some of this variability can be controlled by using a common sample line or assuming sample collection points in close proximity are true replicates. In small-scale experiments, fuel variability is reduced by homogenizing samples to eliminate shape and moisture effects and heating methods are closely controlled. In the present study, the assumption was made that samples taken in proximity in wind tunnel fuel beds or in small, prescribed burns in natural fuels each represented true replicates. In 3 of the 4 location × method combinations, samples were collected in canisters for subsequent analysis (either later in the day (FTIR) or several weeks after collection (GC/FID). The wind tunnel FTIR spectroscopic measurements were collected in real time.

While all these factors may affect the values of the absolute values for the pyrolysis gases collected, it is the relative values which are important since these are compositional data. Based on the subcomposition of gases measured by both FTIR and GC/FID, it is not possible to state that fire location (wind tunnel versus field) did not significantly affect relative composition of pyrolysis gases based on the presence of significant interaction. While the analytical method effect was significant, it cannot be separated from location. In the present study, the FTIR sampling was confounded with real-time measurement in the wind tunnel versus analysis of canister samples from the field. Canisters were used as a necessary safety precaution since the field fires were much less

controlled than the wind tunnel burns and the FTIR setup precluded field use. Use of real-time measurement by FTIR provided other benefits (Banach *et al.* 2021).

Pyrolysis gases have been successfully measured in a wind tunnel and in small field prescribed burns using two different methods: FTIR-spectroscopy and GC/FID analysis. Using CoDA techniques on the subcomposition of gases measured by both methods showed that the compositions were affected by the measurement method.

Table 4. Estimated mean values for selected log-ratio balances of pyrolysis gases by method, location and overall mean. P-values adjusted to control false discovery rate (Benjamini and Hochberg 1995) < 0.05 are in bold.

Balance	Gases involved	RFL		FJ		Mean	p-values	
		FTIR	GC/FID	FTIR	GC/FID		Method	Interaction
Dominant gases vs Hydrocarbons	$\frac{[CO_2, CO, CH_4]}{[C_2H_2, C_2H_4, C_3H_6, C_4H_6, C_4H_8]}$	7.90	8.36	6.35	8.82	8.22	**0.043**	0.262
CO_2 vs CO & CH_4	$\frac{[CO_2]}{[CO, CH_4]}$	3.17	3.27	2.26	4.04	3.25	**0.001**	**0.004**
CO vs CH_4	$\frac{[CO]}{[CH_4]}$	1.82	1.46	1.60	1.05	1.51	0.375	0.763
Alkenes vs Alkynes	$\frac{[C_2H_4, C_3H_6, C_4H_8]}{[C_2H_2, C_4H_6]}$	-0.88	0.10	-0.52	-0.09	-0.11	**0.043**	0.474
Ethene vs Alkenes	$\frac{[C_2H_4]}{[C_3H_6, C_4H_8]}$	3.34	3.08	2.78	2.18	3.06	0.478	0.763
Acetylene vs 1,3-butadiene	$\frac{[C_2H_2]}{[C_4H_6]}$	1.78	1.79	1.90	1.27	1.77	0.474	0.474
Propene vs isobutene	$\frac{[C_3H_6]}{[C_4H_8]}$	3.31	0.98	2.10	0.66	1.43	**0.001**	0.474

5. Literature Cited

Aitchison J (1986) 'The statistical analysis of compositional data.' (Chapman and Hall: London ; New York)

Banach, Catherine A., Ashley M. Bradley, Russell G. Tonkyn, Olivia N. Williams, Joey Chong, David R. Weise, Tanya L. Myers, and Timothy J. Johnson. 2021. "Dynamic infrared gas analysis from longleaf pine fuel beds burned in a wind tunnel: observation of phenol in pyrolysis and combustion phases." *Atmospheric Measurement Techniques* 14 (3): 2359–76. doi:10.5194/amt-14-2359-2021.

Benjamini Y, Hochberg Y (1995) Controlling the false discovery rate: a practical and powerful approach to multiple testing. *Journal of the Royal Statistical Society Series B (Methodological)* 57, 289–300.

Christian TJ, Kleiss B, Yokelson RJ, Holzinger R, Crutzen PJ, Hao WM, Shirai T, Blake DR (2004) Comprehensive laboratory measurements of biomass-burning emissions: 2. First intercomparison of open-path FTIR, PTR-MS, and GC-MS/FID/ECD. *Journal of Geophysical Research* 109. doi:10.1029/2003JD003874.

Egozcue JJ, Pawlowsky-Glahn V (2005) Groups of parts and their balances in compositional data analysis. *Mathematical Geology* 37, 795–828. doi:10.1007/s11004-005-7381-9.

Egozcue JJ, Pawlowsky-Glahn V, Mateu-Figueras G, Barceló-Vidal C (2003) Isometric logratio transformations for compositional data analysis. *Mathematical Geology* 35, 279–300. doi:10.1023/A:1023818214614.

Fehsenfeld FC, Dickerson RR, Hübler G, Luke WT, Nunnermacker LJ, Williams EJ, Roberts JM, Calvert JG, Curran CM, Delany AC, Eubank CS, Fahey DW, Fried A, Gandrud BW, Langford AO, Murphy PC, Norton

RB, Pickering KE, Ridley BA (1987) A ground-based intercomparison of NO, NO_x, and NO_y measurement techniques. *Journal of Geophysical Research* **92**, 14710. doi:10.1029/JD092iD12p14710.

Langsrud, Ø. 2003. ANOVA for unbalanced data: use Type II instead of Type III sums of squares. *Statistics and Computing* 13 (2): 163–67. doi:/10.1023/A:1023260610025.

Li H, Lamb KD, Schwarz JP, Selimovic V, Yokelson RJ, McMeeking GR, May AA (2019) Inter-comparison of black carbon measurement methods for simulated open biomass burning emissions. *Atmospheric Environment* 206, 156–169. doi:10.1016/j.atmosenv.2019.03.010.

Palarea-Albaladejo J, Martín-Fernández JA (2013) Values below detection limit in compositional chemical data. *Analytica Chimica Acta* 764, 32–43. doi:10.1016/j.aca.2012.12.029.

Palarea-Albaladejo J, Martín-Fernández JA (2015) zCompositions — R package for multivariate imputation of left-censored data under a compositional approach. *Chemometrics and Intelligent Laboratory Systems* 143, 85–96. doi:10.1016/j.chemolab.2015.02.019.

Pearson K (1896) Mathematical contributions to the theory of evolution.--on a form of spurious correlation which may arise when indices are used in the measurement of organs. *Proceedings of the Royal Society of London* (1854-1905) 60, 489–498. doi:10.1098/rspl.1896.0076.

Quick, J. 2011. "R Tutorial Series: Two-Way ANOVA with Unequal Sample Sizes." R-Bloggers (blog). February 28, 2011. https://www.r-bloggers.com/2011/02/r-tutorial-series-two-way-anova-with-unequal-sample-sizes/.

R Core Team (2021) 'R: A Language and Environment for Statistical Computing.' (R Foundation for Statistical Computing: Vienna, Austria) https://www.R-project.org/.

Scharko NK, Oeck AM, Myers TL, Tonkyn RG, Banach CA, Baker SP, Lincoln EN, Chong J, Corcoran BM, Burke GM, Ottmar RD, Restaino JC, Weise DR, Johnson TJ (2019) Gas-phase pyrolysis products emitted by prescribed fires in pine forests with a shrub understory in the southeastern United States. *Atmospheric Chemistry and Physics* 19, 9681–9698. doi:10.5194/acp-19-9681-2019.

Ward DE, Hao WM (1991) Projections of emissions from burning of biomass for use in studies of global climate and atmospheric chemistry. Air and Waste Management Association: Vancouver, British Columbia, Canada http://www.treesearch.fs.fed.us/pubs/43258.

Ward DE, Radke LF (1993) Emissions measurement from vegetation fires: a comparative evaluation of methods and results. 'Fire in the environment: the ecological, atmospheric, and climatic importance of vegetation fires: report of the Dahlem Workshop, held in Berlin, 15-20 March 1992'. (Eds PJ Crutzen, JG Goldammer) pp. 53–76. (John Wiley & Sons Ltd.) http://www.fs.fed.us/rm/pubs_other/rmrs_1993_ward_d001.pdf.

Yokelson RJ, Burling IR, Gilman JB, Warneke C, Stockwell CE, de Gouw J, Akagi SK, Urbanski SP, Veres P, Roberts JM, Kuster WC, Reardon J, Griffith DWT, Johnson TJ, Hosseini S, Miller JW, Cocker III DR, Jung H, Weise DR (2013) Coupling field and laboratory measurements to estimate the emission factors of identified and unidentified trace gases for prescribed fires. *Atmospheric Chemistry and Physics* 13, 89–116. doi:10.5194/acp-13-89-2013.

Yokelson RJ, Griffith DWT, Ward DE (1996) Open-path Fourier transform infrared studies of large-scale laboratory biomass fires. *Journal of Geophysical Research* 101, 21067. doi:10.1029/96JD01800.

Weise DR, Palarea-Albaladejo J, Johnson TJ, Jung H (2020) Analyzing wildland fire smoke emissions data using compositional data techniques. *Journal of Geophysical Research: Atmospheres* 125, e2019JD032128. doi:10.1029/2019JD032128.

Weise DR, Hao WM, Baker S, Princevac M, Aminfar A-H, Palarea-Albaladejo J, Ottmar RD, Hudak AT, Restaino JC, O'Brien JJ (in press) Comparison of fire-produced gases from wind tunnel and small field experimental burns. *International Journal of Wildland Fire* WF21141, 63 p.

A Landscape Mediation on WUI fires to develop collective knowledge and prevention actions at the local community level

Ondine Le Fur*[12]; Marielle Jappiot[1]; Pierre Dérioz[2]

[1]RECOVER, INRAE, Aix-Marseille Université. Aix-en-Provence, France, {ondine.le-fur, marielle.jappiot}@inrae.fr
[2]Espace-Dev 228 IRD, Avignon Université. Avignon, France, {pierre.derioz@univ-avignon.fr}

**Corresponding author*

Keywords

Wildland-Urban Interface; landscape; collaborative approach; mediation.

Abstract

The WUI expansion and climates changes are causing an increasing number of dramatic consequences on the socio-ecosystem in Southern Europe. In France, to reduce the fire threat to infrastructure and human lives, a specific prevention policy provides for many regulatory measures to address forest fire risk in urban planning and forest management. This approach to assessing risk is highly technical and hazard-centred. The shortcomings are the difficulty in appropriating the issue for those who do not have this standardised approach and legitimise less attention paid to individual and collective practices having an effect on vulnerability.

Our research focuses on landscape as a means of analysing the representation of forest fire risk by local stakeholder groups. According to the European Landscape Convention, landscape is defined as 'an area, as perceived by people, whose character is the result of the action and interaction of natural and/or human factors'. Landscape therefore has both a factual and a subjective value. As an intermediary tool, the landscape allows an inclusive dialogue between various stakeholders since it belongs to the common register and does not have an immediate scientific connotation (Dérioz, 2008).

On this basis, we develop a landscape mediation on forest fire risk to analyse how can landscape help to build a shared knowledge of risk in local communities. Landscape mediation is an engineering of public involvement applied to the landscape which eases mobilising stakeholder experience and feelings in territorial diagnostic and spatial planning (Paradis, 2010). We experiment the benefits of landscape mediation to develop a local risk culture by using a case study in Martigues city in the southeast of France. The study site is subject to strong development pressure due to its proximity to the Aix-Marseille Provence metropolitan area, is located nearby two forested areas - Côte Bleue and Castillon forests -, which are regularly affected by fires, and has a scattered residential area and therefore a relatively large WUI zone.

The landscape mediation project consists of two stages. In spring 2022, residents of the study site are invited to participate in a walking tour through their living area. Using a booklet, the participants assess the characteristics of the landscape and describe the uses of the WUI and its associated fire risk attributes. A collective risk knowledge emerges from sharing contrasting feelings and opinions on WUI and ways to limit vulnerability individually and collectively. In a second stage, the participants present their landscape diagnostic and their views and concerns on forest fire risk prevention management to a group of local stakeholder representatives of spatial planning and forest fire risk experts. The diversity of thought reveals new ideas that benefit spatial planning initiatives. This landscape mediation is a collaborative approach to increase public acceptance of forest fire management placing the inhabitant in a collective consideration of vulnerability reduction in his living area. The research helps sharing residents' perceptions of forest fire with decision-makers and fire risk experts to better understand how the community influences action or inaction on forest fire risk prevention management.

1. French fire risk prevention is complex in its implementation and understanding

Public policies for wildfire risk management operate mainly in 32 departments in the south of France, with coordination of the local strategy at the regional level (articles L.133-1 and L.133-2, Forestry Code). Local government agencies are principally in charge of wildfire prevention policies. However, certain competences are shared with local territorial authorities in particular the maintenance of firefighter infrastructures in the forest, equipping neighbourhoods with fire hydrants, clearing regulation around houses and roads, public

information on the wildfire risk and ensuring that urban development considers natural hazards. Those local jurisdictions adopt regulatory wildfire prevention tools in different ways according to local political will, which creates variations in prevention strategy between territories.

As a result, residents have to deal with regulations that affect the design of their garden, their house and their development project. Resident common practice is to make comparisons with the neighbour's situation, but it hardly helps to understand the individual case. Requests for information to clarify the fire risk management measures are therefore inevitable. People then face with the complexity of the stakeholder network, each jurisdiction acting in line with its own competencies in reducing the vulnerability of wildland-urban interfaces (WUI) - the area where combustible vegetation intermingles with buildings -. Given the regulatory measures that affect residents, their involvement in wildfire prevention strategy is necessary. They are resident experts on local knowledge of the territory and are therefore a source of realistic solutions to reduce vulnerability.

How can we develop a local risk culture that could facilitate dialogue between residents and spatial planning stakeholders and encourage collective initiatives to reduce vulnerability in neighbourhoods prone to wildfire? In this respect, we propose to develop a local fire risk culture using a landscape mediation event.

2. Landscape mediation for wildfire risk prevention

2.1. What is a landscape mediation?

EU members signed the Landscape Convention in 2000. According to this act, "Landscape" means an area, as perceived by people, whose character is the result of the action and interaction of natural and/or human factors. This definition gives recognition to all types of landscapes - including common everyday landscape -, a continuous temporal dynamic, but also a feeling dimension. The feeling dimension of the landscape corresponds to the description that the person makes of a place based on the experienced moments and feelings. When description of a place is shared, then certain aspects of the landscape are collectively valued (Bouisset & Degrémont, 2015). Thus, the landscape is subjective, and the transition from an individual representation to a collective culture depends on the degree of information sharing in the community (Devine-Wright, 2011; Raymond et al., 2015).

A landscape mediation is a public participation engineering applied to the landscape which eases mobilising stakeholder experiences and feelings in territorial diagnostic (Paradis, 2010). Spatial planning studies regularly employ this type of process (Labat & Donadieu, 2013). It was initially developed as an analysis tool for landscape enhancement, for example in the diagnostic of landscape charters. Also thereafter, landscape mediation has been used as a medium for analysing land-use management mainly in rural territories with environmental concerns (Dérioz, 2008; Ferrario, 2018), for example in regional natural park plans or in urban planning schemes. With regard to natural risk management, landscape mediation approaches serve to facilitate the development of a risk culture. They are not yet well developed and are mainly found in flood risk management (Wake, et al., 2020). We have not found any example of landscape mediation for wildfire risk prevention in the literature.

Thematic landscape mediation on wildfire risk has specific aspects. Generally, landscape analysis leads to imagining landscapes at their best value. For wildfire risk, we try to imagine the situation of a landscape on fire. The task could be therefore difficult, because the landscape valorisation only comes into play when visualizing the least critical crisis scenario for the territory. Moreover, in participatory approaches using landscape, participants are usually asked to imagine the territory at a fixed moment in the future (e.g in 2050). The temporal dimension is more complex for wildfire risk prospective; because the projected moment is not a date, but the next fire event, thus a phenomenon that occurs randomly in the forest and is not predictable. Furthermore, landscape is a common term and has no immediate scientific connotation. Conversely, wildfire risk is a complex concept that requires knowledge and a technical vocabulary for its management. Applying landscape mediation to the context of WUI materializes the wildfire risk to a known and shared place and makes the subject accessible to all for discussion.

2.2. Case study: the “walk-workshop” event on the WUI in Martigues

The study case is the city of Martigues (Bouches-du-Rhône), in southeastern France. This municipality is facing strong urban development pressure due to its inclusion in an attractive metropolitan area, the Aix-Marseille

Provence metropolis. The urban fringes are fragmented, which increases the length of the linear contact between the inhabited and the natural areas. Wildfires in Martigues often threaten dwellings, campsites and industrial areas. The issue of managing the WUI is a major concern and involves considering the consequences of wildfires from a landscape and ecological perspective as well as for community safety.

For the landscape mediation we develop, the landscape analysis focuses on the WUI (Calkin et al., 2014). Our research focuses on the use of landscape as a means of analysing and sharing the representation of fire risk by the inhabitants. Our objectives are i) to mobilise and interact between inhabitants and land management actors around the issue of fire risk ii) to carry out a shared diagnosis of the landscape focused on vulnerability to wildfire in WUI iii) to identify good planning practices at different spatial scales.

The main stakeholder in the project is the local authority of the Aix-Marseille Provence Metropolitan Area. To ensure the event's success, the local authority should support the landscape mediation. The Martigues City Council and the Metropolitan Council were interested in the project because they had ongoing spatial planning documents dealing with the wildfire risk and landscape management (the Metropolian Landscape Plan and the Intercommunal Urban Planning Scheme). The local authorities and the researchers are jointly building the event to ensure that it corresponds to everyone's expectations. In our case, the event takes place in two stages, first a walk with the residents to examine the surrounding landscape and wildfire risk context in their neighbourhood, and then a workshop where the residents report on their landscape analysis and discuss it with a group of professionals responsible for the spatial planning and the wildfire risk (Figure 1).

To conduct the walk and the workshop, we have developed tools for analysing landscape atmospheres and for sharing opinions on landscape objects characterising wildfire risk management in the WUI. The tour walk first passes behind the houses to study the direct line of contact with the forest, then returns by the main road to study the landscape in the neighbourhood. It goes through different depths of view to investigate the context of the risk and its management at several spatial scales (e.g. the plot, the street, the neighbourhood). For the workshop, we set up inclusive communication medium (e.g. A0 map of the study site, video with a local goatherd, photos of the walk).

Figure 1- Concept of Landscape Mediation on wildfire risk in Martigues. A two-step process, a walk and a workshop.

3. Analysis of the results: many ideas are waiting to be realised

3.1. Using sociology to describe landscapes

The walk itinerary was close to a fire that had covered almost 1000 ha in 2020 and had caused the evacuation of 2,700 people and the destruction of two campsites. The recent memory of a fire with significant damage seemed to be a reason enough to mobilise the population to attend the event. Still we went door-to-door to distribute flyers and explain the approach to the inhabitants and to some shop owners, relatively few people

came to the landscape mediation event. One reason for the limited involvement is the location of the study area, which was in an attractive urban municipality (48,500 inhabitants) but in its rural part. It is middle-class neighbourhoods and the locals are mainly families who have lived there for a long time. There is not much traffic except from the local residents and they appreciate this privacy.

Consequently, the residents who took part were in their sixties and older, and had been living in the area for decades, or even had family members in the community of more than two generations. For example, one resident had experienced two wildfires on her lot, in 1989 and 2020. This resident profile provided an ideal opportunity to discuss landscape dynamics over time. Participants had already been involved in wildfire crisis with their neighbours, thus they were in a way the voice of the other locals. They proposed several actions, including having goats graze near the residential fringes and supporting original agricultural initiatives that could be established in abandoned agricultural lands. The residents' opinion was a fine expertise on local vulnerability issues (Figure 2).

The inhabitants appreciated to express to the local authorities their thoughts on wildfire treat and their ideas for actions to improve the situation in their neighbourhoods. All parties involved in the workshop shared the difficulty of identifying the different regulations on risk prevention and the complexity of the stakeholder network involved. We found the inhabitant's knowledge had equal legitimacy with the expertise of professionals in spatial planning and wildfire risk management.

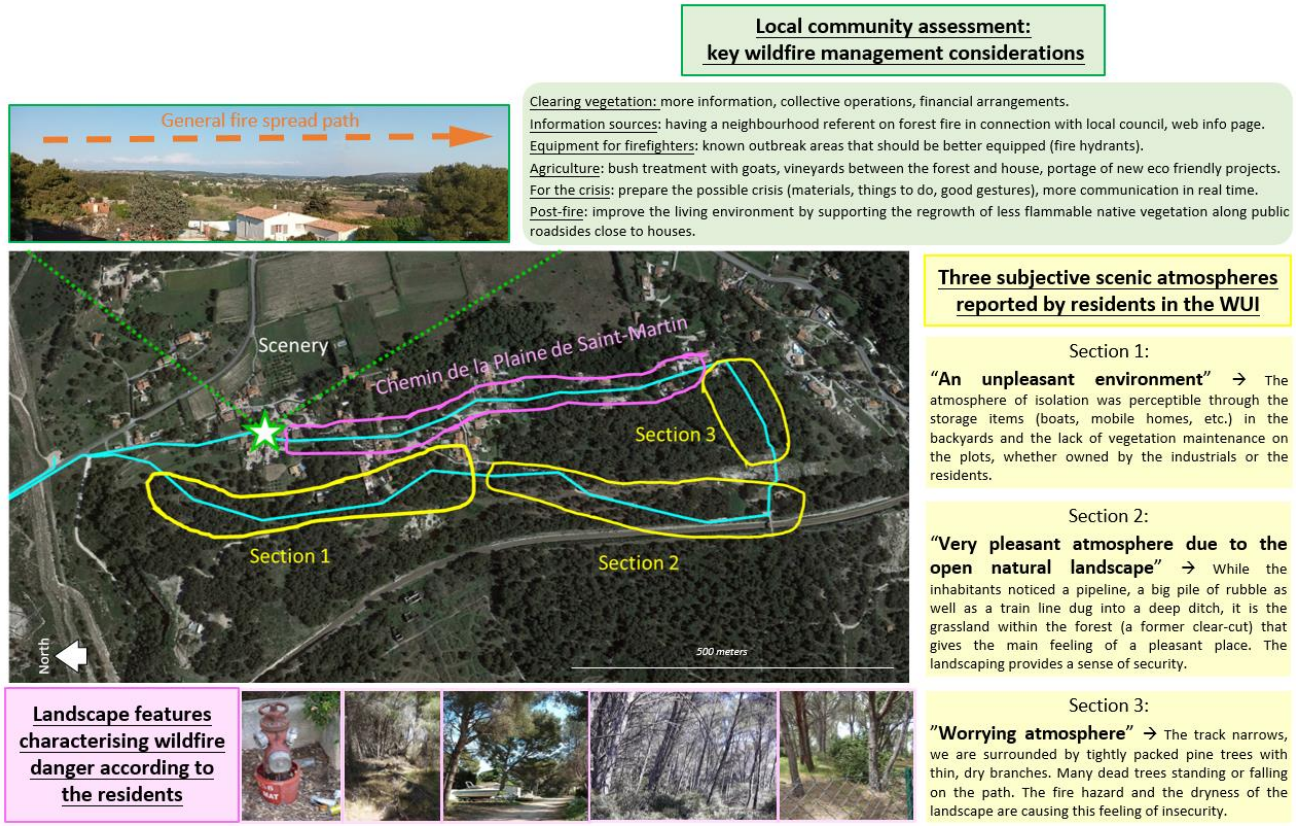

Figure 2- Analysis of WUI vulnerability produced during the walk with the residents. The walk itinerary is blue (3km).

3.2. The event is part of the ongoing process of wildfire risk culture

This exploratory research study shows the means for mobilizing stakeholders in a context where public services have limited capacities to take part in original wildfire risk management approach. Some of the essential spatial planners and wildfire risk managers were not represented in the workshop (e.g. the firefighters). They are brought back into the process afterwards by distributing the report and conducting an interview with them. Also, the strong involvement of the partners present and the quality of the experience sharing, opinions and initiative proposals are guarantees of the success of the mediation tools mobilized. A path has already been found in the Metropolitan Landscape Plan to conduct an action in Martigues with inhabitants. The landscape mediation could

be multiplied over several vulnerable districts and repeated each year, as an annual appointment for a walk and a workshop to discuss wildfire risk and its prevention management. The study case has proved its worth, and the perpetuation of landscape mediation is possible if the communities decide to take up the concept (Figure 3).

The suggested landscape mediation is punctual, whereas the risk culture is a permanent information to share over time. Therefore, organizing such an event around wildfire risk is an opportunity that only makes sense if the participants value together the ideas shared during this time. This communication (article in a local media, reports to stakeholders) contributes to the risk culture by marking the meeting between the local agencies and the population and disseminating the ideas exchanged to other potential interested parties.

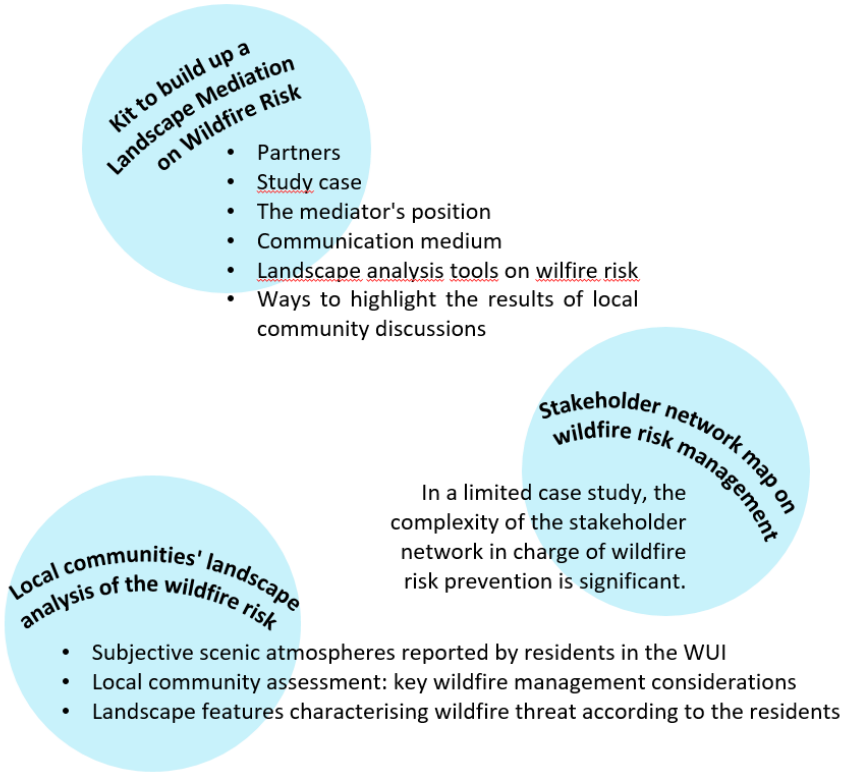

Figure 3- Outcomes from the exploratory research project on Landscape Mediation

4. Conclusion

We have described the benefits of landscape mediation on developing local wildfire risk culture. The landscape mediation event we assessed in the city of Martigues is a study case in line with participatory research actions. For local jurisdictions, it helps to share the risk perception in a collaborative approach, through constructive dialogues with the locals. Furthermore, while the stakeholder system for wildfire risk management is complex, the legislation and responsibilities are evolving, and parties directly in charge are sometimes struggling to define their own role. The landscape mediation clarify the comprehension of this set of functions and then favour the emergence of local and original initiatives. It encourages local authorities to consider residents' perspectives in their spatial planning strategies.

5. References

Bouisset, C., & Degrémont, I. (2015) The Role of Local Inhabitants in Shaping City-Forest Interfaces Representations and Practises on the Urban Fringes of the Landes de Gascogne, *Projets de paysage. Revue scientifique sur la conception et l'aménagement de l'espace,* (13).

Calkin, D. E., Cohen, J. D., Finney, M. A., & Thompson, M. P. (2014) How risk management can prevent future wildfire disasters in the wildland-urban interface, *Proceedings of the National Academy of Sciences of the United States of America, 111*(2), 746–751.

Dérioz, P. (2008) L'approche paysagère : un outil polyvalent au service de l'approche opérationnelle et interdisciplinaire des problématiques environnementales, p. 23 Presented at 1ères Journées Scientifiques ARPEnv, (Nîmes, France: https://halshs.archives-ouvertes.fr/halshs-00363625).

Devine-Wright, P. (2011) Place attachment and public acceptance of renewable energy: A tidal energy case study, *Journal of Environmental Psychology, 31*(4), 336–343.

Ferrario, V. (2018) The landscape as a tool. The case of renewable energy, *Ri-Vista. Research for Landscape Architecture, 16*(2), 34–51.

Labat, D., & Donadieu, P. (2013) *Le paysage, levier d'action dans la planification territoriale, L'Espace géographique, Tome 42*(1), 44–60.

Paradis, S. (2010) La médiation paysagère, levier d'un développement territorial durable ?, *Développement durable et territoires, 1*(2).

Raymond, R., Béringuier, P., Bonin, S., Darly, S., Dérioz, P., Fourault-Cauët, V., Germaine, M.-A., Loireau, M., Milian, J., Noël, B., Temple-Boyer, E., & Toublanc, M. (2015) Les paysages des franges périurbaines, transitions ou parois de verre ?, 7–25.

Wake, C., Kaye, D., Lewis, C. J., Levesque, V., & Peterson, J. (2020) Undercurrents: Exploring the human dynamics of adaptation to sea-level rise, *Elementa: Science of the Anthropocene, 8*(1), 060.

A Study of FDS Computational Performance in Heterogeneous Hardware Architectures -Applied for grassland fires

Donghyun Kim[1,2]; Jae-Ryul Shin[*3]; Hwang-Hui Jeong[3]

[1]Jeonju University, Jeonju-si Jeonbuk-do, Rep. of Korea, {72donghyunkim@jj.ac.kr}
[2] IIASA(International Institute for Applied Systems Analysis). Laxenburg, Austria, {dhkim@iiasa.ac.at}
[3]NEXTfoam, Geumcheon, Seoul, Rep. of Korea, {jrshin, hhjeong}@nextfoam.co.kr

**Corresponding author*

Keywords

FDS, Computational Fluid Dynamic, Message Passing Interface, Open Accelerator, Kokkos

Abstract

Fire Dynamic Simulator (FDS), a fire simulation program, applies Message Passing Interface (MPI) and Open Multi Processing (OpenMP) libraries for large-scale simulation. FDS can be executed by dividing simulation problems in a computing cluster using MPI. The main point is to divide the entire domain to be interpreted into several sub-domains and allow each sub-domain to be calculated by an individual computer with an individual processor. When performing parallel computation, FDS first decomposes each sub-domain, then supports two-step parallelization in which multi-threading is applied within each sub-domain, and uses the OpenMP library to implement multi-threading. In this study, OpenACC, a parallelization technique capable of using heterogeneous hardware architectures, was partially applied to FDS. As an application problem, the calculation performance is evaluated through CSIRO Grassland Fires, a verification case of FDS. The hardware for evaluation was a personal computer consisting of dual Xeon 2678-V3 and GeForce GTX 1070. The FDS source code applies OpenACC using PGI Fortran as a compiler in Linux environments. In calculation performance, calculations using CPU and GPU together show 1.89 times faster performance than calculations using a single CPU. In case of using 1 GPU and 16 CPUs (MPP + OpenACC), the analysis result is 21 times faster. In this regard, analysis of grassland fire of WFDS was performed.

1. Introduction

Central Process Unit (CPU), the brain that performs calculations, has been increasing exponentially in unit performance in accordance with Moore's law over the past half century, but the improvement trend has been saturated by the 21st century. Since then, performance has been increased by increasing the number of cores, and now it is trying to overcome the scaling limitations of systems composed only of CPU by accelerators. Therefore, heterogeneous hardware architectures are widely used, and the well-known AlphaGo has 280 Graphic Process Units (GPU) of Tesla accelerators for deep learning. The adaptive parallel technique in heterogeneous hardware architecture proposed in this study is a new technique using the Kokkos library, in which the practical version was released by 2014, and is a very experimental and innovative technology. Therefore, few literatures have been published so far, and its application has recently been introduced by conferences in the field of high-performance supercomputing and international combustion conferences. There is currently the only alternative called Open Computing Language (OpenCL) in a way that does not use Kokkos while pursuing the same goal of adapting to heterogeneous hardware architectures, but this is a new programming language. Compilers that support this must develop together, but there have been no cases applied to the engineering or computational fluid fields yet. On the other hand, because Kokkos uses templates, which are existing features of general-purpose C++ languages, it has the advantage of being able to use dedicated high-performance compilers that are optimized according to architectures such as GNU, PGI, Intel, Cray, and CUDA.

Fire Dynamics Simulator (FDS) is a dedicated fire simulation program written in the Fortran programming language by introducing computational fluid dynamics techniques to analyze the fluid flow phenomenon driven by fire. FDS numerically solves the Navier-Stokes equation for low-velocity heat-driven flows focusing on smoke and heat transfer from fire.Therefore, FDS provides a model that can analyze basic fire dynamics and combustion. FDS has been developed by the National Institute of Standards and Technology in the United States with the goal of interpreting real fire problems. However, the computational cost increases to analyze very

detailed physical phenomena. To overcome this, FDS is written so that the central processing unit (hereinafter referred to as CPU) is executed on various hardware platforms and operating systems sequentially or in parallel. FDS uses a Message Passing Interface (MPI) to divide and execute analysis problems in a computing cluster. This is a method in which the entire area to be analyzed is divided into multiple meshes and each mesh is computed by a separate processor on a separate computer. FDS supports two-step parallelization by first decomposing each computational domain into a mesh of distributed memory and then applying multi-threading within each mesh in performing parallel analysis, and uses the OpenMP (Open Multi Processing) library to implement multi-threading.In this study, Open ACCelerator (OpenACC), a parallelization technique that can use heterogeneous hardware architectures, was partially applied to FDS to speed up FDS operation. The speed verification application case was conducted on Grassland fire tested in Australia in 2010. The computational performance is evaluated through the verification case of FDS, CSIRO Grassland Fires. The hardware for evaluation was configured in parallel with a personal computer consisting of dual Xeon 2678-V3 and GeForce GTX 1070. FDS source code applies OpenACC using PGI Fortran as a compiler in Linux environment.

2. Parallel Computing Method

MPI and OpenMP are standard methods for performing parallel computation in distributed memory system and shared memory system environment. Parallel computation has been supported since FDS version 5.4, and two parallel processing methods are provided, OpenMP and MPI. These two methods can be simultaneously applied to FDS according to the hardware configuration. In section 3.1.2 of the FDS User's Guide, it was reported that the maximum speed improvement of OpenMP is approximately doubled, and that when MPI and OpenMP are used together, most of the reduction in analysis time is achieved by MPI.

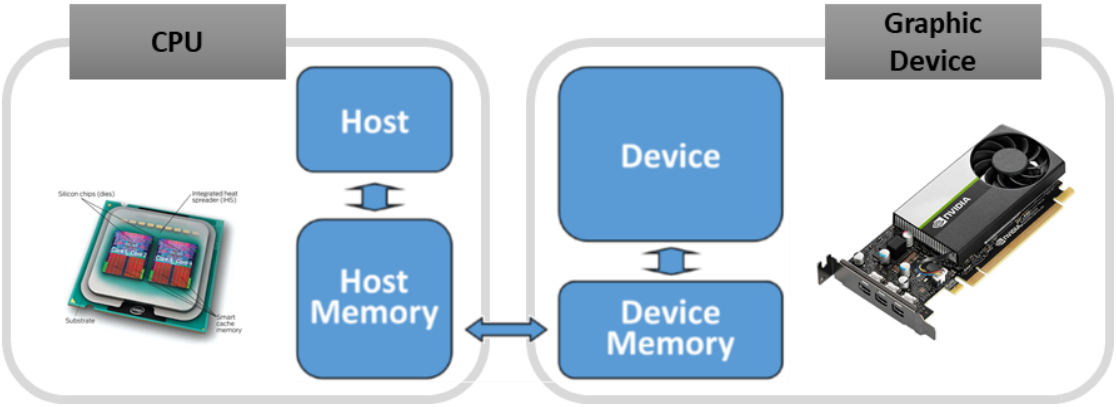

Figure 1- OpenACC's Abstract Accelerator Model

2.1. MPI

MPI is a standard that describes information exchange in distributed and parallel processing. The Message Passing method is an operation model in which data to be exchanged between processors is exchanged using a message passing function. MPI defines the standard of the Message Passing Library, which is a collection of these functions, and several MPI libraries have been developed accordingly. Subroutines that require parallelization in sequence code are constructed in parallel through appropriate parallelization techniques.

2.2. OpenMP

OpenMP is an application programming interface that supports shared memory multi processing of programs in programming languages such as C, C++, and Fortran on various computer platforms. OpenMP provides users with a simple and flexible interface for developing a variety of parallel applications from desktops to supercomputers, and is easily extensible. And by using OpenMP and MPI, the application program can also be built as a Hybrid OpenMP/MPI model.

2.3. OpenACC

OpenACC is a data parallel programming model designed to provide portability between CPU/GPU hardware architectures. Like OpenMP, OpenACC is directive-based, so there are fewer changes to the original code

compared to CUDA or OpenCL. Also, compilers such as PGI and GCC support OpenACC. OpenACC is a method in which the compiler detects directives in a program and determines how to parallelize loops.

3. Computing Performance

The computational performance is evaluated through the verification case of FDS, CSIRO Grassland Fires. As hardware for evaluation, a personal computer composed of dual Xeon 2678-V3 and GeForce GTX 1070 was used. FDS source code applies OpenACC using PGI Fortran as a compiler in Linux environment. In the FDS source code, '!$ACC PARALLEL LOOP' of OpenACC was partially applied to 'PRESSURE_ITERATION_LOOP', the part that determines convergence during calculation.

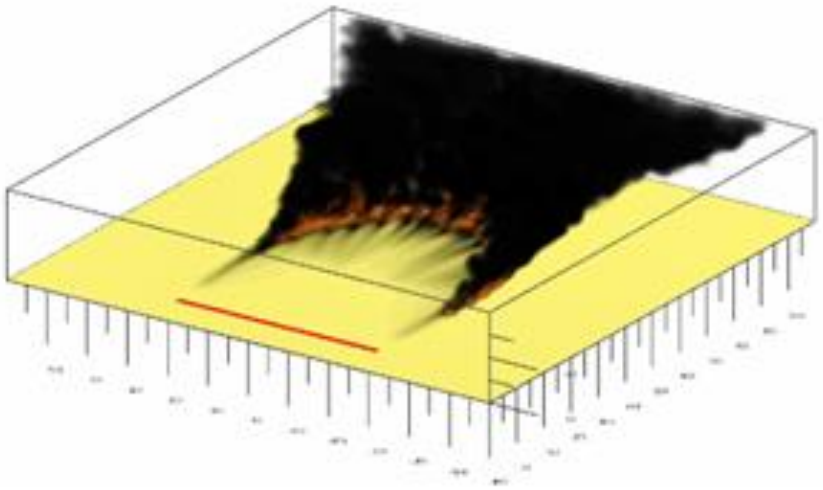

Figure 2- WFDS result of Grassland Fires in CSIRO Austrailia

Table 1- Computing Performance

MPI	Analysis time [hr]	OpenACC with MPI	Analysis time [hr]
1 CPU	109	1 CPU + 1 GPU	57
2 CPU	59	2 CPU + 1 GPU	32
4 CPU	31	4 CPU + 1 GPU	16
8 CPU	17	8 CPU + 1 GPU	9
16 CPU	9	16 CPU + 1 GPU	5

In the case of MPI, when 16 CPUs are used compared to one CPU, the analysis time is 12 times faster from 109 hours to 9 hours. On the other hand, when one CPU and one GPU are used together by applying OpenACC, the calculation time is 1.89 times faster than the result using one CPU. In the case of using 1 GPU and 16 CPUs (MPP + OpenACC), the analysis time is 5 hours, which is about 21 times faster.

Table 2 shows the results of measuring the parallel performance of MPI+OpenACC according to the increase in the size of the computation area. When parallelization was performed with MPI, the performance improvement was evident as the number of CPUs and the size of the problem increased. On the other hand, in the case of MPI+OpenACC, the performance of MPI+OpenACC with 2 CPUs or more is lower than that of MPI. It can be seen that the amount of CPU allocated during MPI parallelization is also allocated to the GPU as much as the number of CPUs, which increases the load and decreases performance. In addition, if the size of the calculation area is about 100 million and 8 CPUs are used, the memory performance of the GPU, GTX 1070, is exceeded, and calculation cannot be performed. However, when one or two CPUs are used, it can be seen that the performance of MPI+OpenACC is significantly superior to that of MPI depending on the size of the calculation area.

Table 2- 2D Heat Conduction SpeedUp with Problem Size and Parallel Method

Problem Size	1024x1024 (@1 million)		2048x2048 (@4 million)		10240x10240 (@100 million)	
Parallel Method	MPI	MPI + OpenACC	MPI	MPI + OpenACC	MPI	MPI + OpenACC
1 CPU	1	1.48	1	2.93	1	4.96
2 CPU	1.96	1.41	1.99	2.82	2.63	4.69
4 CPU	3.70	0.85	4.15	1.70	4.06	2.88
8 CPU	7.21	0.59	6.46	1.08	8.02	Out of GPU memory
16 CPU	15.12	0.31	16.84	0.74	16.71	

4. Conclusion

In this study, OpenACC, a parallelization technique that can use heterogeneous hardware architectures, was partially applied to FDS. As an application problem, computational performance was evaluated through CSIRO Grassland Fires, a verification case of FDS. As hardware for evaluation, a personal computer composed of dual Xeon 2678-V3 and GeForce GTX 1070 was used. In computational performance, the computation using the CPU and GPU is 1.89 times faster than the computation using one CPU. In the case of using 1 GPU and 16 CPUs (MPP + OpenACC), the analysis time is 5 hours, which is about 21 times faster. In the future, it is expected that the hardware parallelization technology can be used to shorten the calculation time for forest fire spread fire analysis using a personal computer.

A Study of the Ignition Mechanism for Dead Pinus Palustris Needles

Weixuan Gong*; Juan Cuevas; Albert Simeoni

Department of Fire Protection Engineering, Worcester Polytechnic Institute, MA 01605, USA, {wgong@wpi.edu}

**Corresponding author*

Keywords

Wildfire, Ignition criterion, Pyrolysis gas evolution, Modified Cone Calorimeter, FTIR spectrometry

Abstract

Combinations of cumulative impacts of drought, invasive species, climate variability, and ever-expanding wildland-urban interface make landscapes more susceptible to devastating wildland fires. To treat the increasing risks of wildland fires, one of the ways is to mitigate the risk of ignition, which requires a solid understanding of the ignition mechanism of vegetation fuels. This can be achieved mainly through discerning the degradation stage and the ignition criteria. Scaling up the experiments for the degradation stage and evaluating the suitability of existing ignition criteria are two of the primary challenges for ignition studies on vegetation fuels.

Motivated by the challenges, two series of experiments were conducted using a modified Cone Calorimeter to understand the mechanisms driving the ignition of dead Pinus palustris needles. In the first set of experiments, the ignition of pine needles was studied for varied incident heat fluxes (20-35 kW/m2) and air flow rates (buoyancy-induced - 100 l/min forced flow). In the second set of experiments, Fourier transform infrared spectroscopy (FTIR) was used to characterize the composition of the pyrolysis gases generated from the thermal degradation of pine needles when exposed to various incident heat fluxes (20 and 30 kW/m2) under an inert atmosphere obtained using a flow of pure nitrogen.

The results for the first series of experiments show that the critical mass loss rate at ignition increase with both flow rates and heat flux. From the second set of experiments, it was found that methane (CH4), carbon monoxide (CO), carbon dioxide (CO2), and water vapor (H2O) are the main constituents of the pyrolysis gases. The predominance of these compounds was found to be independent of the external heat flux while their concentrations are sensitive to it. The flammability of pyrolysis gas was found to increase with external heat flux.

1. Introduction

There is an urgent need to advance wildland fire management due to the increasing risk of wildfires (Richer et al., 2006). One of the ways to reduce the risk of wildfires is to avoid ignition, which requires a solid understanding of the occurrence of the flaming combustion of the vegetation fuels.

Characterizing the pyrolyzing process and the ignition moment are the two primary challenges of understanding the ignition of wildland fuels. Mass-loss kinetics and pyrolysis gas characterization are the focuses of pyrolyzing process research. Although the mass loss kinetics has been well studied on a micro-scale experimental basis (Leroy et al., 2010; Liu et al., 2002), it is necessary to scale up the experiments while maintaining fuel properties. For the pyrolysis gas aspect, the technology for identifying the components is advanced (Nunes et al., 2018), while there is a gap in quantifying the dynamics of each component over time.To characterize the occurrence of ignition, the condensed-phase criteria, including ignition temperature, critical mass loss rate, and heat release rate at ignition are widely accepted. However, the suitability of these criteria needs to be checked and verified because of the broad ranges of these values reported by the literature.(Delichatsios, 2020; Lyon & Quintiere, 2007)

Motivated by the challenges, the objectives of this work are dual. The first is to explore the influence of external heat flux on the pyrolysis process of dead Pinus palustris needles. The evolution of pyrolysis gas is expected to be characterized and quantified by FTIR spectroscopy. The second one is to investigate the relationships between a solid-phase ignition criterion and different experimental conditions.

2. Materials and Experimental Design

2.1. Experimental Design

A modified cone calorimeter, shown in Figure 1, was used to study the pyrolysis and ignition mechanisms of pine needles.

Two series of experiments were conducted to understand the mechanisms driving the ignition of dead Pinus palustris needles. In the first set of experiments, FTIR spectroscopy was used to characterize the composition of the pyrolysis gases generated from the thermal degradation of pine needles when the fuel bed was exposed to incident heat fluxes of 20 and 30 kW/m^2, and a nitrogen inflow of 50 l/min being fed from the bottom of the combustion chamber. The main constituents of the pyrolysis gas were identified by the characteristic bands shown in FTIR scans and were quantified by applying Beer-Lambert's law (Plummer, Reagen & Logan, 2003).

In the second set of experiments, the ignition of pine needles was studied for incident heat fluxes ranging from 20 to 35 kW/m^2 and air inflows of 0 l/min to 100 l/min. In these tests, the time-to-ignition (t_{ig}), and the critical mass-loss rate at ignition ($\dot{m}''_{cr}$) were evaluated.

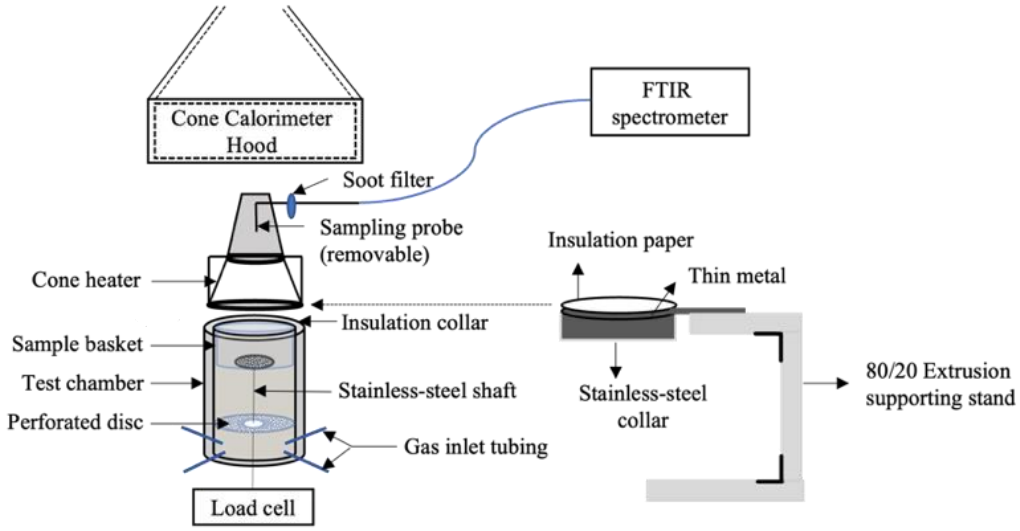

Figure 1 – Experimental apparatus: modified cone calorimeter allowing the inflow with desired flow rates

2.2. Materials

The fuel samples were oven-dried at 60°C for 24 h for conditioning and measuring their residual moisture content. After this, the conditioned pine needles were stored in sealed containers until testing. All the samples had an average fuel moisture content of 4.6 % on a dry weight basis.

For the experiments, 20 g of conditioned pine needles were placed in a cylindrical sample holder 12.6 cm in diameter and 3 cm in depth. Two different types of sample holders, shown in Figure 2, were used; for the experiments with no inflow of oxidizer being fed through the bottom of the combustion chamber (buoyancy-induced flow), a sample holder with 0% porosity was used. For experiments with a forced inflow being supplied, a sample holder with 63% porosity was used.

(a) (b)

Figure 2 - Fuel samples for the tests with (a) buoyancy-induced flow using the basket of 0% opening and (b) forced flow using the basket of 63% opening.

3. Results and Discussion

3.1. FTIR analysis of pyrolysis gas

3.1.1. Pyrolysis gas component identification

Figure 3 presents the FTIR spectra of the pyrolysis gas samples collected during the experiments conducted at 20 kW/m^2 and 30 kW/m^2, respectively. The main constituents of the pyrolysis gas determined by the characteristic bands shown in FTIR scans include CH_4, CO, CO_2, and H_2O. The characteristic bands at 2880-3180 cm^{-1}, 2010-2250 cm^{-1}, and 2290-2390 cm^{-1} indicate the formation of CH_4, CO, and CO_2. The characteristic bands at 1390-2020 cm^{-1} and 3500-3998 cm^{-1} represent the occurrence of H_2O. Similar pyrolysis gas components of plant species are also found in other literature (Granada et al., 2012).

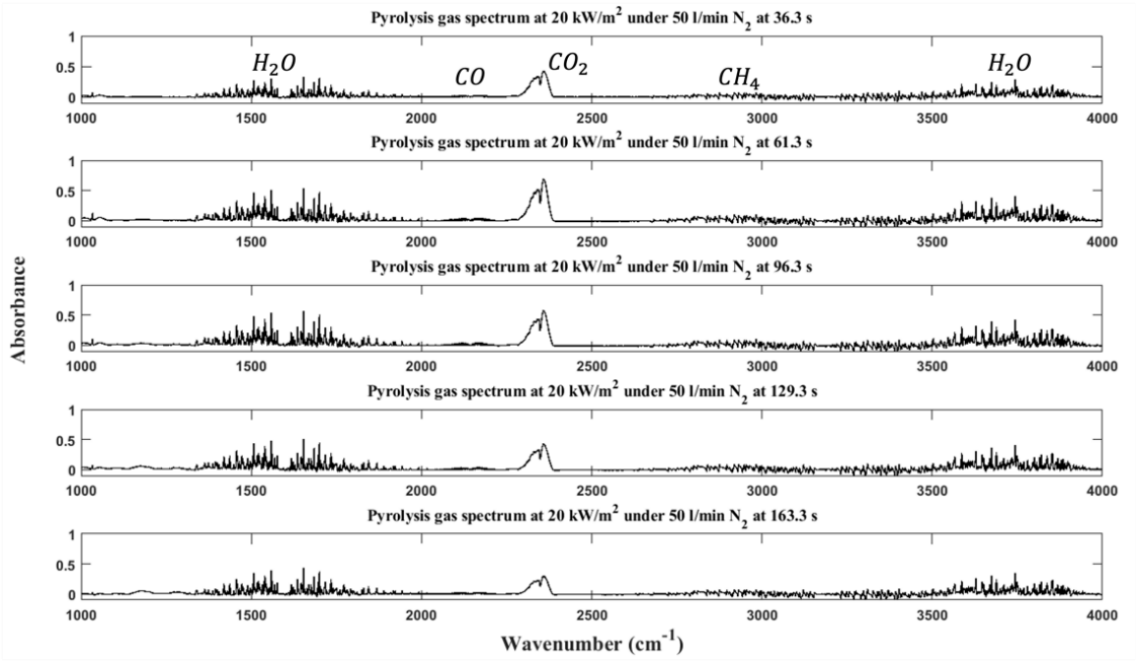

(a)

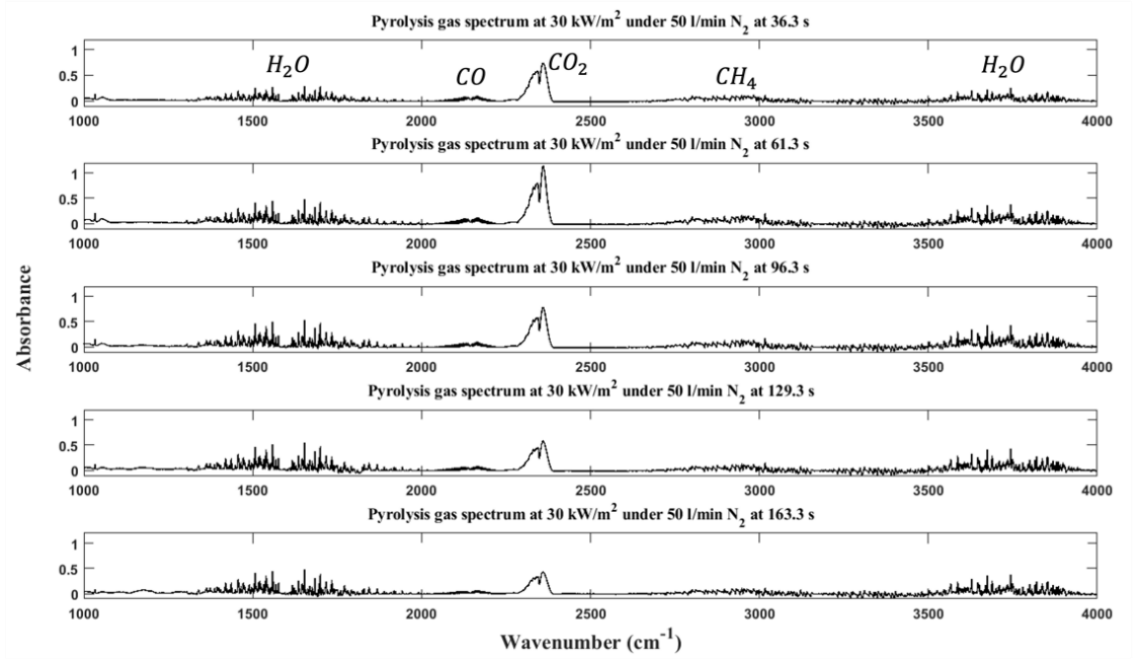

(b)

Figure 3 - Pyrolysis gas FTIR spectra at 50 l/min N_2 and (a) 20 kW/m^2, 50 l/min N_2 and (b) 30 kW/m^2.

3.1.2. Quantification of the pyrolysis gas constituents

Figure 4 shows the evolution of the concentration of the different gas species identified in the pyrolysis gas samples collected at both heat flux levels. All the results are averaged from three repetitions. It is essential to highlight that the calculated concentration of each component at each moment is not the instantaneous concentration at that moment, but the average concentration over time of the data collection (26.3 s).

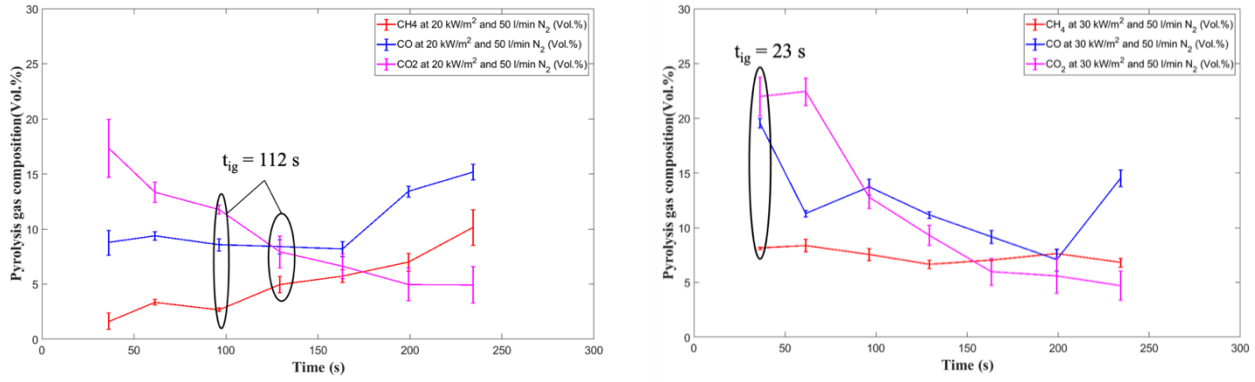

(a) ***(b)***

Figure 4 - Pyrolysis gas concentration evolution at 50 l/min N2 and (a) 20 kW/m2, 50 l/min N2 and (b) 30 kW/m2.

Combining these results with the time-to-ignition under the same conditions (see Section 3.2), it is possible to evaluate the composition of the pyrolysis gases at ignition. For an incident heat flux of 20 kW/m^2, the concentration of CH_4, CO, CO_2, and H_2O at ignition are found to be 3.8, 8.5, 9.9, and 77.8 vol.%. For an incident heat flux of 30 kW/m^2, the concentrations of CH_4, CO, CO_2, and H_2O at ignition are 8.1, 19.6, 22.0, and 44.1 vol.%.

Thus, the effective heat of combustion of the pyrolysis gases (H_{c_py}) can be evaluated as the weighted sum of the heat of combustion of each species, defined by Eqs. (1) and (2).

$$H_{c\_py} = Y_{CO} \cdot H_{c\_CO} + Y_{CH_4} \cdot H_{c\_CH_4} \quad \text{Eq (1)}$$

$$Y_i = \frac{X_i M_i}{\sum X_i M_i} \quad \text{Eq (2)}$$

where X_i, M_i, Y_i, and H_{c_i} are the mole fraction, molecular weight, mass fraction, and heat of combustion of a given gas species. The reference values of the heat of combustion of CH_4 and CO are 50.1 and 10.1 kJ/g, respectively (Quintiere, 2006).

The resulting effective heat of combustion of the pyrolysis gases was evaluated to be 2.6 kJ/g and 6.4 kJ/g for 20 and 30 kW/m^2, respectively. This result is in general agreement with the range of values (from 4.62 to 5.38 kJ/g) reported by (Cancellieri et al., 2005). The variation of the heat of combustion on different heat fluxes indicates that the pyrolysis gas obtained at a higher heat flux is of greater flammability.

3.2. Ignition tests(tig)

3.2.1. Time-to-ignition (tig)

Table 1 presents the mean ignition time (t_{ig}), mean thermal penetration depth (δ), and dimensionless thermal depth (x) measured at external heat fluxes ranging from 20 to 35 kW/m^2, and airflow rates of 0, 50, and 100 l/min air.

Table 1: Mean time-to-ignition, thermal penetration depth, and dimensionless thermal depth for a 30 mm fuel bed under different external heat fluxes and flow rates.

Flow rate (l/min)	Heat flux (kW/m^2)	t_{ig} (s)	δ (mm)	x (-)
0	20	66.67 (3.54)	9.16 (0.25)	3.28 (0.09)
	25	19.33 (3.76)	4.88 (0.43)	6.28 (0.50)
	30	13.00 (0.82)	4.04 (0.12)	7.44 (0.22)
	35	5.67 (0.27)	2.67 (0.07)	11.26 (0.28)
50	20	124.33 (18.47)	12.39 (1.04)	2.48 (0.23)
	25	35.67 (9.06)	6.51 (0.92)	4.95 (0.81)
	30	22.67 (2.37)	5.32 (0.28)	5.68 (0.29)
	35	12.33 (2.76)	3.87 (0.43)	8.01 (0.80)
100	20	No ignition	-	-
	25	88.67 (5.18)	10.56 (0.27)	2.85 (0.07)
	30	38.33 (3.17)	6.92 (0.34)	4.36 (0.21)
	35	20.00 (2.41)	4.98 (0.35)	6.10 (0.39)

The thermal penetration depth, defined in Eq. (3), represents the depth pyrolysis layer (Delichatsios, 2020). The dimensionless thermal depth is defined as the ratio of the fuel sample thickness to the thermal penetration depth (Delichatsios, 2020), and it is used to discriminate whether the fuel bed shows thermally-thick or thermally-thin behavior at ignition based on the criterion presented in Eq. (4) (M. Delichatsios, 2020).

$$\delta = \sqrt{\alpha t_{ig}} \qquad \text{Eq (3)}$$

$$x = \frac{\tau}{\delta} = \begin{cases} < 0.8 & thermally\ thin \\ 0.8 < x < 2 & thermally\ intermediate \\ 2 < & thermally\ thick \end{cases} \qquad \text{Eq (4)}$$

For a thermal diffusivity of pine needles (α) of 1.26 × 10-6 m^2/s (Korobeinichev et al., 2018), it appears that the 30 mm-thick pine needle bed behaves thermally thick for all testing conditions.

From the table, it can be seen that t_{ig} and δ increase when increasing the airflow rate and decrease when increasing the magnitude of the external incident heat flux over the fuel bed. When increasing airflow rates, the net heat delivered to the fuel bed decreases due to an enhanced convective cooling through the fuel bed, which reduces the pyrolysis reaction rate of the fuel bed and the quantity of the released fuel vapor. Meanwhile, the generated fuel vapor through the pyrolysis is diluted by the incoming airflow.

On the other hand, the decrease of t_{ig} and δ when increasing the external incident heat flux over the fuel bed is due to the steepness of the temperature profile developed inside the fuel bed; higher incident heat fluxes will increase the amount of energy available to promote the pyrolysis reaction, increasing its rate. Thus, less time is required until a sufficient fuel rate for ignition is achieved. Furthermore, higher incident heat fluxes will produce steeper temperature profiles, causing a decrease in the relative distance between the thermal propagation depth and the pyrolysis front depth. Thus, as the time-to-ignition decreases with the magnitude of the external heat flux, the thermal wave can only propagate into depths closer to the surface of the fuel bed.

3.3. Critical mass loss rate ($\dot{m}''_{cr}$)

The results of the critical mass-loss rate **($\dot{m}''_{cr}$)** are shown in Figure 5. The uncertainties of the results are determined by one standard deviation of three repetitions for each test.

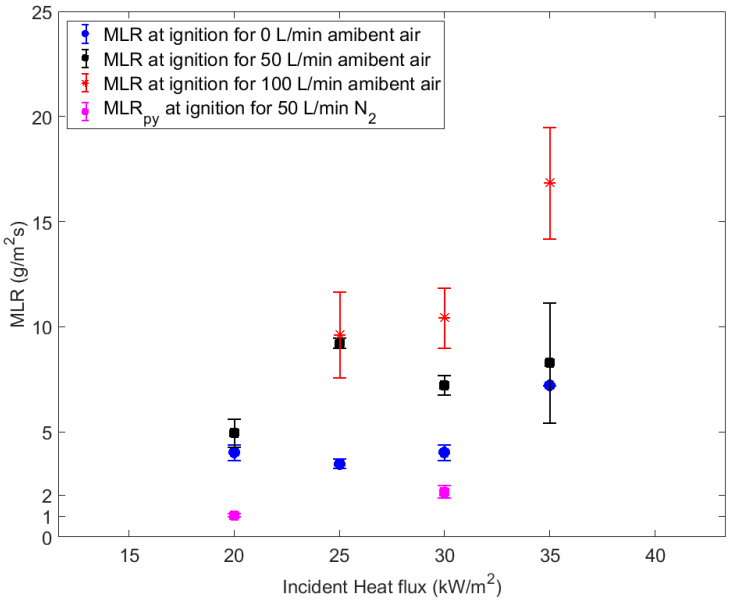

Figure 5 – Critical mass loss rate (MLR) for sustained flaming ignition

The critical mass-loss rate at ignition was found to increase when increasing the external incident heat flux and the airflow rate. Two mechanisms mainly drive the mass loss of the fuel bed. One part of the mass loss is due to pyrolysis, while the other one is due to the smoldering combustion of the fuel bed. Both reactions have been found to increase their rate when provided more energy (Bartlett & Bisby, 2015). Thus, increasing the magnitude of the external incident heat flux over the fuel bed increases the pyrolysis rate, smoldering combustion, and consequently, the mass-loss rate of the fuel bed. The reason for the increase of $\dot{m}''_{cr}$ when increasing the airflow rate is due to the dilution of the flammable mixture. As the chemical reaction at flaming ignition is near stoichiometric (Lyon & Quintiere, 2007), the fuel vapor concentration needs to increase with the airflow rates so that the equivalence ratio meets the requirements for ignition. Therefore, to obtain sufficient fuel, as shown in Eq (5), the thermal depth or the pyrolysis reaction rate needs to be increased. The increase in thermal depth with airflow rates has been shown in the analysis in 3.2.1. The pyrolysis reaction rate can also be locally increased by the appearance of smoldering spots, which is consistent with the observation that smoldering was detected before ignition for all tests conducted under forced flow conditions.

4. Conclusion

The work presented herein attempted to enhance our understanding of the conditions that lead to the ignition of Pinus palustris pine needles through a series of experiments aimed at characterizing the pyrolysis gases and the conditions under which piloted ignition occurs.

In pyrolysis tests, the influence of different heat fluxes on pyrolysis gas yields was investigated. The yield, generation rate, and flammability of pyrolysis gas were all found to increase with increasing heat fluxes.

In ignition tests, the influences of external heat fluxes and airflow rates on the time to ignition and mass loss rate at ignition were analyzed. The analysis of time-to-ignition results indicated that the thermal behavior of the fuel bed at ignition was influenced by both heat fluxes and airflow rates. The analysis of mass loss rate suggested significant contributions of smoldering combustion to the flaming ignition under low heat fluxes and high airflow rate conditions.

5. References

Bartlett, A., & Bisby, L. A. (2015). Analysis of cross-laminated timber upon exposure to non-standard heating conditions Structural behaviour of cross-laminated timber elements in fires View project FireComp View project. https://www.researchgate.net/publication/270875737

Cancellieri, D., Leoni, E., & Rossi, J. L. (2005). Kinetics of the thermal degradation of Erica arborea by DSC: Hybrid kinetic method. Thermochimica Acta, 438(1–2), 41–50. https://doi.org/10.1016/j.tca.2005.07.013

Delichatsios, M. (2020). Effects of material thickness on ignition times and creeping flame spread in the thermal regime: Theory, analytical solution and experimental justification. Fire Safety Journal, 116. https://doi.org/10.1016/j.firesaf.2020.103204

Granada, E., Eguía, P., Vilan, J. A., Comesaña, J. A., & Comesaña, R. (2012). FTIR quantitative analysis technique for gases. Application in a biomass thermochemical process. Renewable Energy, 41, 416–421. https://doi.org/10.1016/j.renene.2011.11.020

Korobeinichev, O. P., Shmakov, A. G., Osipova, K. N., Kumar, A., & Kambam Meetei, N. (2018). Experimental Study and Numerical Modeling of Downward Flame Spread Along a Single Pine Needle: Part 1 (Experiments). Combustion Science and Technology, 190(1), 164–185. https://doi.org/10.1080/00102202.2017.1380001

Leroy, V., Leoni, E., & Cancellieri, D. (2010). Thermal Degradation of Lignocellulosic Fuels: Biopolymers Contribution. In Biopolymers. Sciyo. https://doi.org/10.5772/10267

Liu, N. A., Fan, W., Dobashi, R., & Huang, L. (2002). Kinetic modeling of thermal decomposition of natural cellulosic materials in air atmosphere. In Journal of Analytical and Applied Pyrolysis (Vol. 63). www.elsevier.com/locate/jaap

Lyon, R. E., & Quintiere, J. G. (2007). Criteria for piloted ignition of combustible solids. Combustion and Flame, 151(4), 551–559. https://doi.org/10.1016/j.combustflame.2007.07.020

Ningbo, G., Baoling, L., Aimin, L., & Juanjuan, L. (2015). Continuous pyrolysis of pine sawdust at different pyrolysis temperatures and solid residence times. Journal of Analytical and Applied Pyrolysis, 114, 155–162. https://doi.org/10.1016/j.jaap.2015.05.011

Nunes, L. J. R., de Oliveira Matias, J. C., & da Silva Catalão, J. P. (2018). Applications for Torrefied Biomass. In Torrefaction of Biomass for Energy Applications (pp. 203–214). Elsevier. https://doi.org/10.1016/b978-0-12-809462-4.00011-0

Plummer, G., M., Reagen, W., K., & Logan, P., W. (2003). Organic and inorganic gases by extractive FTIR spectrometry. NIOSH Manual of Analytical Methods, Fourth Edition. https://www.cdc.gov/niosh/docs/2003-154/pdfs/3800.pdf

Richer, H. B., Anderson, J., Brewer, J., Davis, S., Fahlman, G. G., Hansen, B. M. S., Hurley, J., Kalirai, J. S., King, I. R., Reitzel, D., Rich, R. M., Shara, M. M., & Stetson, P. B. (2006). Probing the faintest stars in a globular star cluster. Science, 313(5789), 936–940. https://doi.org/10.1126/science.1130691

Setchkin, N. P. (n.d.). A Method and Apparatus for Determining the Ignition Characteristics of Plastics.

A study on urban forest fire risk analysis and forest fire management plan suitable for each region -Focus on Nowongu Seoul

Donghyun Kim

Jeonju University, Jeonju-si Jeonbuk-do, Rep. of Korea, {72donghyunkim@jj.ac.kr}
IIASA(International Institute for Applied Systems Analysis). Laxenburg, Austria, {dhkim@iiasa.ac.at}

Keywords

WUI (Wildland Urban Interface), Urban Forest Fire Management, Fire Risk Analysis, Fire Policy, Fire Management

Abstract

The risk of fire in urban forests is high due to housing and living infrastructure adjacent to the forest, resulting in large human and property damage and high frequency of occurrence. It is very important to identify the forest fire environment and potential risk factors for each city in order to manage the forest fire risk in the cities adjacent to the forest. In this study, urban forest fire management measures were suggested by conducting a survey on the causes of forest fires and the entire adjacent forests in Nowon-gu, which has the most urban-forest adjacent areas in terms of administrative districts among Seoul, which has the highest population density in Korea. The forest fire investigation has been conducted for the last 5 years, and in addition to analyzing the forest, topography, and meteorological environment, an analysis of fire-vulnerable areas in the event of a forest fire in downtown Seoul was conducted. Eight action plans were presented by dividing the actionable forest fire management into prevention, preparation, and response stages for areas adjacent to forests and areas vulnerable to forest fire risk. First, in prevention, fuel management that can reduce the risk of forest fires, map production and risk reduction management for temples in the forest, and selection of appropriate locations to install forest fire long-distance around monitoring cameras and drone autonomous monitoring stations were suggested. Second, in the preparation stage, a fuel blocking method was presented to establish a safe zone for hiking trails, prepare a mountaineering safety map for forest fire evacuation, and prevent the spread of residential fires in forest interface area. Third, in the response stage, the installation of a multi-purpose outdoor fire hydrant for suppression of forest fires and house fires adjacent to the forest, the activities of forest fire extinguishing vehicles and marking of the entry area, and the establishment of an urban forest disaster integrated control system were suggested.

1. Introduction

As forests and adjacent forests are developed as residential or commercial areas due to urban expansion, the number of cases in which forest fires become urban fires and building fires spread into forest fires is increasing. In the case of WUI forest fires, due to spatial characteristics, not only forest fires, but also complex fire-fighting activities such as the evacuation of people, extinguishing fires in buildings, and protection of dangerous facilities are required, and organic cooperation between the forestry department and the urban fire-fighting department is more necessary. In the case of the United States and Canada, community-based forest fire management is implemented according to the FireWise and FireSmart programs, respectively. In Korea, the risk of forest fires is high due to the continuous increase in urban expansion and use of urban forests, but there are no forest fire management activities and programs in the local community. Therefore, this study intends to propose a forest fire management plan for the forest adjacent to the Nowon-gu of Seoul, which has the highest population density in Korea. In Nowon-gu, the forest area occupies 1,546ha, which is 44% of the total administrative district, and a total of 18 forest fires have occurred since 2015 in forest. In Nowon-gu, 7 cultural assets including the royal tombs of the Joseon Dynasty, designated as UNESCO cultural assets, and 26 temples are distributed in the adjacent forest area.

2. Methods

2.1. Forest fire risk analysis to Nowon-gu WUI

Forest fire risk analysis was conducted on the forests of Bulam Mt. and Surak Mt. of 1,456 ha in Nowon-gu, WUI houses and buildings, temples and facilities in the forest, and shelters on hiking trails. The following four items were investigated.

① Forest fuel density and forest fuel type

② Risk of fire spread due to forest fires in WUI houses and structures

③ Possibility of casualties during forest fire spread

④ Ease of firefighting environment

WUI forest fire risk analysis was conducted by analyzing correlations with topography, weather, and forests along with past forest fire cases to select areas vulnerable to forest fires. was classified, and predictive factors such as topography, forest, and weather were quantified using a spatial analysis program.

2.2. Forest Fire Management Plans to Nowon-gu WUI

Nowon-gu WUI forest fire management measures were divided into three stages: prevention, preparation, and response, and the existing countermeasures and activities of local administrative agencies were analyzed and methods to reduce and prevent risks were suggested based on the results of analysis of areas vulnerable to forest fire risk. The risk felt by residents was investigated through the on-site residents briefing session, and WUI risk environment improvements were heard to manage the risk of forest fires.

3. Study Results

3.1. Standard scenario

As shown in Figure 1, the risk of release of forest fires in the forest adjacent to Nowon-gu was classified on a scale of 0 to 1, and the maximum risk of forest fire occurred within a radius of 300m of the WUI. As for the risk of spreading of crown fire, the area with the highest risk was found to be around 20 m in the lower radius of the ridge. The risk of damage from forest fires was analyzed as high risk 9, high risk 6, moderate 5, and low 6.

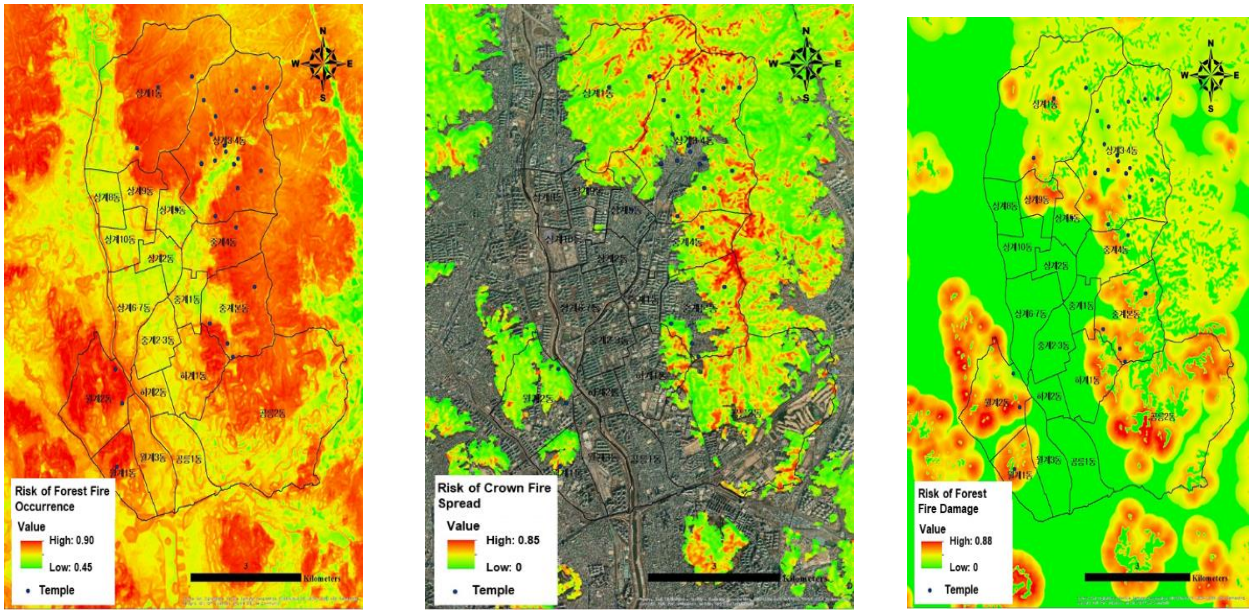

(a) Risk Map Forest Fire Occurrence ***(b) Risk Map of Crown Fire*** ***(c) Temple fire damage risk map***

Figure 1- Results of forest fire risk analysis in Nowon-gu, Seoul

3.2. WUI Forest fire management measures

For the project to strengthen the capacity for forest fire management in Nowon-gu, 8 projects were presented in the areas of prevention, preparation, and response. In the field of prevention, ① fuel reduction project to lower the risk of forest fire, ② the risk rating mapping and risk reduction project for temples, ③ selection of appropriate locations to install forest fire long-distance around monitoring cameras and drone autonomous monitoring stations were presented. In the field of preparation, ① project to establish a safe zone on hiking trail and prepare a mountaineering safety

map for forest fire evacuation, ② a fuel continuity blocking project to prevent house fires in WUI were presented. In response fields, ① a multi-purpose outdoor fire hydrant installation project for suppressing forest fires and house fires to WUI, ② forest fire extinguishing vehicle entry and activity area indication project, ③ urban forest disaster integrated control system construction project were presented. Including the preparation of detailed implementation plans and required budgets for a total of 8 projects in 3 areas, it suggested a method to strengthen forest fire management capabilities in stages by year with the utilization of public workers and public relations for residents from 2021. Figure 2 is a schematic diagram for a total of 8 projects, and is a conceptual diagram of fuel reduction in the prevention field and the construction of a safety zone for hiking trails in the preparedness field.

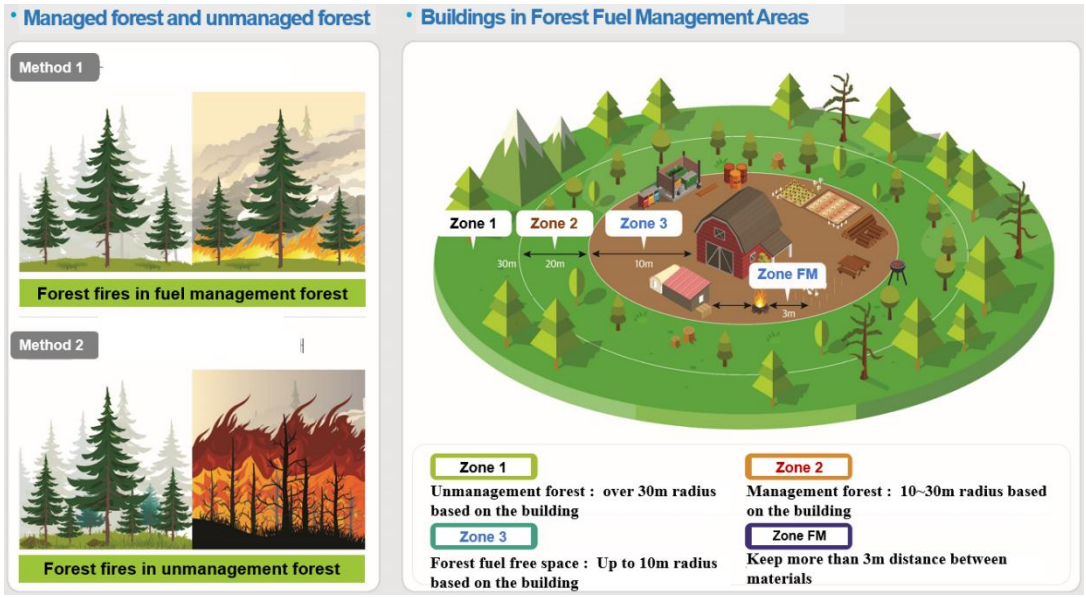

(a)

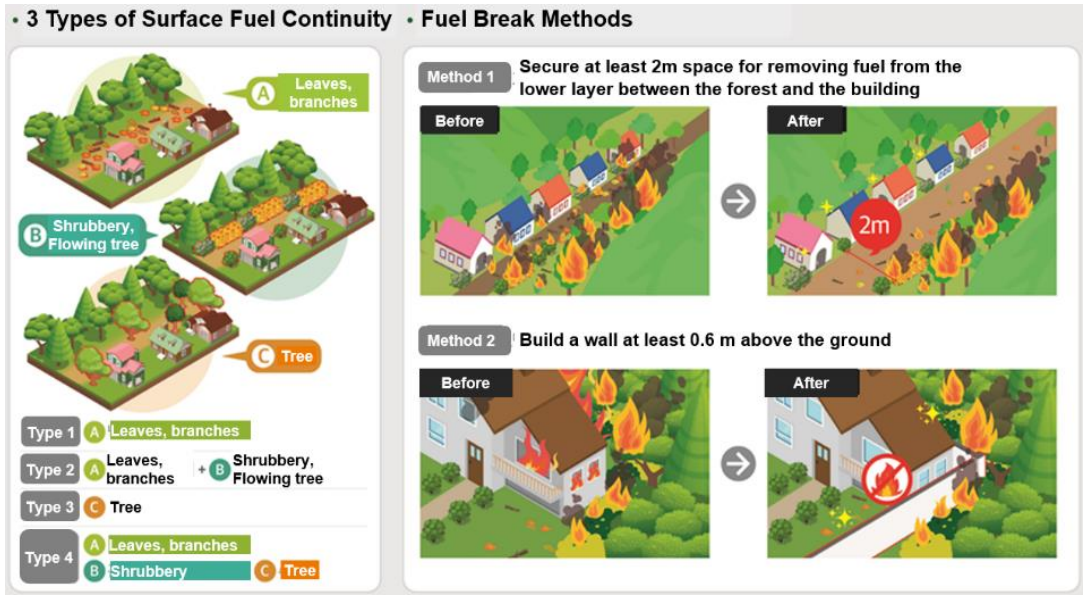

(b)

(c)

Figure 2- Nowon-gu WUI Forest Fire Management Measures Conceptual Map; (a) Prevention field: Measures to reduce fuel, (b) staging area: WUI fuel continuity cut off, (c) Response field: Fire engine access road marking

A total of 14 evaluation items for each scenario are as follows.

①Whether or not information on forest fire situation is collected and confirmed, ②Establishment and feasibility of firefighting strategy, ③Selection of location for firefighting work, ④Construction of fire line, ⑤Effect of ground firefighting work, ⑥Preparation and use of ground firefighting equipment, ⑦Sudden situation (Spotting fires, Fire Storm, Rolling Stone or wood etc) check and response, ⑧Use of evacuation equipment, ⑨Secure an evacuation route and a safe place, ⑩Feasibility of evacuation judgment and method, ⑪Arrangement of remaining balance, ⑫Communication by team, ⑬Report the situation to the command center and make an emergency request, ⑭Protection object protection.

In the survey of firefighters on the training evaluation tool, the suitability evaluation was found to be 97.5±2.5%.

4. Conclusions

The results of the WUI forest fire risk analysis and risk management measures suitable for the region in Nowon-gu, which has the largest forest area in Seoul, which has the highest population density in Korea, are as follows.

First, a forest fire risk map for the Nowon-gu, a temple fire risk map in the forest, and a tree crown fire occurrence risk map were produced.

Second, for temples with a high risk of forest fires, a risk mitigation method was suggested so that they could be maintained below normal.

Third, a total of 8 countermeasures were presented in the field of prevention (3 items), preparedness (2 items), and response (3 items) as Nowon-gu forest fire management plan.

Based on the method of promoting this research and preparing countermeasures, it is intended to be used in preparing various forest fire prevention measures through application to other regions, thereby contributing to forest fire management in WUI.

An Equivalent Fuel Model for Wildland Urban Interface – Application to Risk Management

Mehdi Karzar-Jeddi

Impact Forecasting, Aon, 200 E Randolph St, Chicago, IL 60601, USA, {mehdi.karzar.jeddi@aon.com}

Keywords

Wildland urban interface, equivalent fuel, thermal equivalency

Abstract

Wildfires are imposing increasingly greater risk to people and insured properties. The frequency and intensity of destructive wildfires has increased significantly in past decades. Most wildfire damage to properties occurs in the wildland-urban interface (WUI), where properties are either exposed to wildfire directly and burn or are ignited by firebrands. Many wildfire models are focused on modelling the spread of fires in wildland; however, the studies of the spread of wildfires into urban areas is limited. This paper presents a new model for fuel load in urban area using an equivalent fuel load as wildland fuel to simulate wildfire spread when they approach wildland and urban interface/intermix. The model is to estimate the heat release rate from a typical single house and determine the combination of different fuel sizes. Then, according to the density of structures based on satellite imagery the fuel from LANDFIRE fuel is updated with the model urban fuel. A similar method of equivalent fuel load for agriculture area is developed and the LANDFIRE fuel is updated with the agriculture fuel. Using the updated landscape fuel and terrain, Rothermel-based simulation of wildfire is performed in FARSITE. This simulation is helpful in determining the risk of wildfires for properties and communities.

1. Introduction

In recent decades the frequency and significance of wildfires have increased significantly in many parts of the world including the United States (Manzello *et al.* (2018)). Recent fire seasons in the western United States are some of the most damaging and costly on record. Data from California's fire department shows that in 2021 alone, there have been 8,835 wildfires in California which have burned 2,568,948 acres and damaged 3,629 structures. A United Nations report warns that the risk of highly devastating fires may increase by more than 50 percent by the end of the current century, Sullivan (2022). A better understanding of the spatial distribution of wildfire risk will help to mitigate the catastrophic loss of life and properties. This can help by ignition prevention, fuel and vegetation management, enhancing preparedness, and suppression response in high-risk areas as well as reducing human development and increasing home resistance to ignition in fire-prone areas, Calkin *et al.* (2014). This will also help property- and casualty-related industries, such as (re-)insurance industries, to mitigate their financial losses, by designing policies such that the risk of wildfire is considered more accurately (Hazra and Gallagher (2022)).

To estimate the threat of wildfires a stochastic simulation of probabilistic fire scenario is needed (Finney *et al* (2011)[a,b]). This simulation process requires the prediction of occurrence of probabilistic wildfires and simulation of fire growth based on the physical properties of the fuel and terrain and the associated simulated weather. Many models have been developed by researchers including FARSITE and Prometheus, which are simulating the growth of wildland fires (Finney (2004) and Tymstra (2010)). These models simulate the spread of wildfires based on Rothermel (1972)'s Fire Spread in wildland area. A model for the probabilistic simulation of fires in wildland has been developed and a probabilistic risk component of wildland fires has been calculated for the continental United States (Finney *et al* 2011[a,b]). The required wildland fuel models in United States can be acquired from the LANDFIRE website. Landfire data provides a model environment in the form of eight bands raster that includes fuel properties as well as terrain specifications for wildland. But the model environment is limited to wildland and many other applications including urban areas and agriculture lands are considered non-burnable. This work presents a model based on the energy release properties of burning houses and assigns an equivalent fuel model for urban and WUI area as well as agricultural lands. The LANDFIRE fuel is updated with urban and agriculture fuel models for the urban area. The new model can be uploaded to FARSITE or other

wildfire simulator that uses LANDFIRE data which enables wildfire simulator to simulate the spread of the wildfires in WUI.

2. Model description

2.1. The heat release of a single house

A model fuel load for houses is designed such that it can produce the same amount of thermal energy as reported in earlier works of Trelles and Pagni (1997) and Rehm *et al.* (2001). The estimated energy release process can be divided in three stages, first the fire grows exponentially and burns at maximum heat release rate for about an hour, and then burning dies down slowly within two steps. At the peak of burning of the involved house, the vegetation around the structure burns and releases thermal energy simultaneously (Trelles and Pagni (1997)). Summation of the heat release rate yields a total energy release for combustion of an involved house, which includes heat release from the structure and its contents. The energy release from burning of the contents is obtained from experimental studies by Blais *et al.* (2020) of burning the contents of a typical U.S. living room. Assuming fuel load of the typical house is distributed uniformly throughout the entire house and considering the footprint of the house, the total fuel load of the content of a typical house is calculated. The model fuel is designed based on the equivalent amount of thermal energy release from structure and content.

2.2. Estimating the fuel load for WUI

The potential fuel loading of urban areas also depends on the number of the houses in each raster cell of LANDFIRE data. The ratio of vegetation fuel load to structure fuel load decreases once we move from the wildland to urban area as the areal density of structures increases (Rehm *et al.* (2001)). To account for the change in fuel type due to the structure density, the structure density in the simulation area is calculated from the US Building Footprint datasets developed by Microsoft (2022). Considering the density of the buildings, the LANDFIRE fuel in urban areas is updated from non-burnable to the new urban fuel.

2.3. Equivalent fuel for agricultural land

Similar to WUI and urban areas, LANDFIRE considers agricultural lands as non-burnable areas. An estimate of the fuel load for agriculture fields is provided by South Carolina's Forestry Commission, which we used for updating LANDFIRE fuel model

3. References

https://www.fire.ca.gov/

Manzello, S.L., Almand, K., Guillaume, E., Vallerent, S., Hameury, S., Hakkarainen, T., The growing global wildland urban interface (WUI) fire Dilemma: priority needs for research. Fire Saf. J. 100, 64-66 (2018)

Sullivan, A., Spreading like Wildfire: The Rising Threat of Extraordinary Landscape Fires - A Rapid Response Assessment, 2022

Calkin, D. E., Cohen, J. D., Finney, M. A. & Thompson, M. P. How risk management can prevent future wildfire disasters in the wildland-urban interface. Proc. Natl Acad. Sci. USA 111, 746–751 (2014)

Hazra, D. and Gallagher, P., Role of insurance in wildfire risk mitigation, Economic Modelling, 108, 105768, (2022)

Finney, M.A., Grenfell, I.C., McHugh, C.W., Seli, R.C., Trethewey, D., Stratton, R.D., Brittain, S., A Method for Ensemble Wildland Fire Simulation, Environmental Modeling and Assessment 16, 153–167, 2011

Finney, M.A., McHugh, C.W., Grenfell, I.C., Riley, K.L., and Short, K.C., A simulation of probabilistic wildfire risk components for the continental United States. Stochastic Environmental Research and Risk Assessment 25: 973–100 (2011)

Finney, M.A., FARSITE: Fire Area Simulator-model development and evaluation, USDA report, 2004

Tymstra, C., Bryce, R.W., Wotton, B.M., Taylor, S.W., and Armitage, O.B., Development and structure of Prometheus: the Canadian wildland fire growth simulation model. Edmonton, Alberta: Canadian Forest Service, Northern Forestry Centre, Information Report NOR-X-417, 2010.

Rothermel, R.C., A mathematical model for predicting fire spread in wildland fuels, Res. Pap. INT=115 Ogden, UT: U.S. Department of Agriculture, Forest Service, Intermountain Forest \& Range Experiment Station, 1972

http://www.landfire.com

Trelles, J. and Pagni, P., Fire-induced Winds In The 20 October 1991 Oakland Hills Fire, Fire Safety Science, 5, 911-922 (1997)

Rehm, R.G., Hamins, A., Baum, H.R., Mcgrattan, K.B. and Evans, D.D., Community-Scale Fire Spread, California's 2001 wildfire conference, 126-139, (2001)

Blais, M. S., Carpenter, K., and Fernandez, K., Comparative Room Burn Study of Furnished Rooms from the United Kingdom, France and the United States, Fire Technology, 50, 489-514 (2020).

https://github.com/Microsoft/USBuildingFootprints

Fuel Load Estimation Guide for South Carolina, South Carlina Forestry Commission.

Analysis of fires at Wildland-urban interface in an observation plot in Hungary

László Bodnár*[1]; Péter Debreceni[2]; Ágoston Restás[3]

[1]University of Public Service, Faculty of Law Enforcement, Institute of Disaster Management. 1101 Budapest, Hungary krt. 9-11, {bodnar.laszlo@uni-nke.hu}
[2] National Food Chain Safety Office. 1024 Budapest, Petrezselyem u. 7. {debrecenip@nebih.gov.hu}
[3] University of Public Service, Faculty of Law Enforcement, Institute of Disaster Management. 1101 Budapest, Hungary krt. 9-11, {restas.agoston@uni-nke.hu}

**Corresponding author*

Keywords

Wildland- urban interface (WUI), observation plot, combustible fuel, wildfire statistic, integrating housing density.

Abstract

The Wildland- urban interface (WUI) is an area, where houses meet or intermingle with undeveloped wildland vegetation. The identification of these areas is not yet present in all countries. Although scientific research on this topic is still incomplete in Hungary, there are already initiatives and some results to identify WUI areas and analyse their risks. Authors approach the WUI fire risk from two directions. On the one hand, wildland is a combustible biomass, so wildfires pose a direct threat to the built environment. The reason for this threat is that residential buildings are located along the forest, which, as a flammable material, provides an opportunity for the spread of fire. This allows fire to spread from wildland vegetation to the populated area, endangering human life and property. Authors examine the characteristics of WUI fires in Hungary through analysis of observation plots. In the short paper Authors present the direct and indirect interface WUI and analyse the risk of WUI fires by using GIS spatial analyses. Authors also analyse the combustible fuel, the number of fires, and the integrating housing density in the observation plot.

1. Introduction

The Wildland- urban interface (WUI) is an area, where houses meet or intermingle with undeveloped wildland vegetation (Cohen, 2003), (Radeloff, 2005). The concept of WUI is still less known in some part of Europe (also in Hungary), but in the Mediterranean region it is the biggest challenge of fires caused by human negligence. Fires at the WUI are a huge challenge in many countries. One example is the United States, where millions of people and homes on both west and east coasts are at risk from these fires (Radeloff, 2018). In Canada, such areas cover more than 30 million hectares (Johnston 2018). Australia has also WUI fire danger, therefore, a study on fire prevention has been carried out, focusing on priorities and perceptions of wildfire risk (Koksal, 2019). In Europe, countries of the Mediterranean region are especially high vulnerable. In Spain, there are emergency plans against the wildfires (Caballero 2007). In Portugal, the emphasis is also on the prevention, as the risk of wildfires is one of the highest in Europe almost every year (Viegas, 2012). France is also a good example, where a topological matrix has been established to identify WUI areas (Lampin-Maillet, 2009). In Hungary, the national literatures on wildfires focuses less on the prevention of WUI fires and more on the effectiveness of firefighting (Restás, 2018) and the detection (Bodnár, 2018).

2. Methods

During our research we have examined and analysed the relevant literatures in the topic as well as findings of other authors. We present each findings, and in some cases, we discuss or agree with them. In addition, we conducted discussions with international experts on the subject. In order to present the WUI areas developed in Hungary, we made image analyses in an observation plot. Our main observation plot is in South Hungary, in Bacs- Kiskun County nearby the town Kiskőrös. On this observation plot we have made fuel analyses, examined the wildfire statistics from the last 10 years, and examined the integrating housing density along the wildland area. For each risk, we determined the risk of fire hazard. In addition, spatial analyses allowed us to quantify

patterns and relationships in data and display the results as maps, tables, and charts. So we performed GIS Spatial analyses with topoXmap, developed by Hungarian GIS experts. TopoXmap is an efficient, powerful GIS (Geographic Information System) data collection, visualization and processing software which includes GIS tools. It can use and process raster and vector datasets. It possesses powerful GIS visualization tools and supports to build database and to analyse GIS datasets.

3. Results

On the first observation plot (not the above mentioned territory nearby Kiskőrös) we show that in Hungary direct and also indirect interfaces developed. So Figure 1 is a WUI area and the location is part of the village of Nagykovácsi in Hungary (Pest County), but the area belongs to the **urban agglomeration** of Budapest. During the image analysis, we performed a graphical delimitation, where the direct interface of WUI was marked with a red and the indirect interface with yellow. We considered as a **direct interface**, where the areas of wildland and urban environment are adjacent to each other and the distance between them is minimal. **Indirect interface** is where the distance between wildland and residential area is significantly longer, but there are agricultural lands or other combustible materials between the two areas.

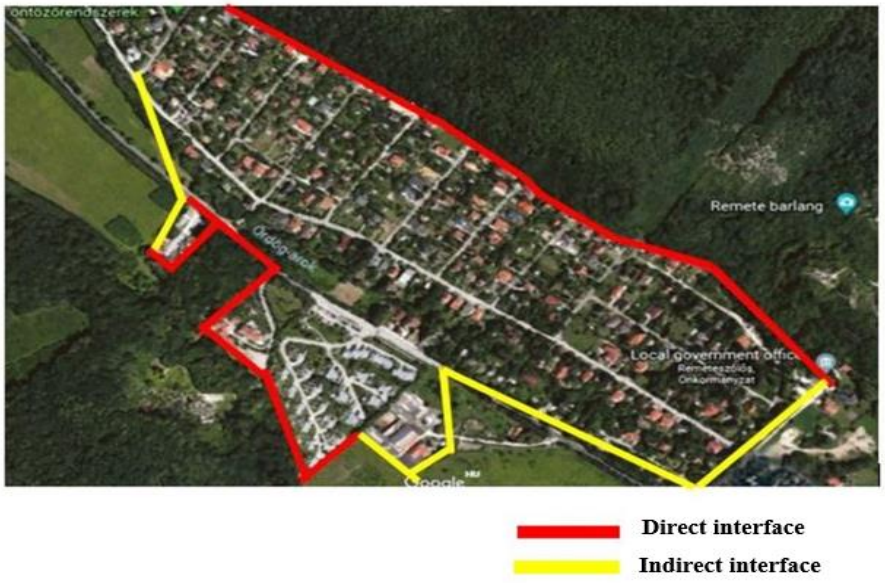

Figure 1- Direct and indirect interface at the WUI.

After that we examined another observation plot for fires at the WUI in 3 steps. We analyse the combustible fuel (first step), the number of fires (second step) and the integrating housing density (third step) in our second observation plot.

In the first step, we **analyzed the combustible fuel** in the observation plot (Bacs-Kiskun County-Kiskőrös) and we distinguished three main groups such as *low dangered forest lands*, *medium dangered forest lands* and *high dangered forest lands* (Figure 2). Pine and juniper vegetation are classified as high endangered forestland (red). Mixed forest and oak forest stands higher than 5 meters are classified as moderately endangered vegetation (yellow). Other native and planted tree species (for example poplar, ash, beech, maple, acacia,) are classified as low endangered forest land (green).

In the second step we **examined the wildfire statistics** in the observation plot from the last 10 years. We distinguished the fires according to their distance from the settlement. We put fires in WUI-1 zone that occurred 500 metres from the residential area. The additional zones were as follows: WUI-2 zone – 1 000 m; WUI-3 zone 1 500 m – WUI-4 zone 2 000 m and WUI-5 zone 2 500 m. In Figure 2, fires in WUI-1 and WUI-2 zones (red and orange hoops) are important for the analysis.

Table 1- Number of wildfires in the WUI zones in the observation plot.

Year	Number of wildfires	WUI-1	WUI-2	WUI-3	WUI-4	WUI-5
2011	103	42	17	9	9	26
2012	278	114	42	25	21	76
2013	66	23	11	8	6	18
2014	78	35	5	5	9	24
2015	50	18	6	2	5	19
2016	69	24	10	12	4	19
2017	145	32	30	21	22	40
2018	45	8	9	10	5	13
2019	180	41	25	22	34	58
2020	85	26	11	8	15	25
2021	123	29	23	20	16	35

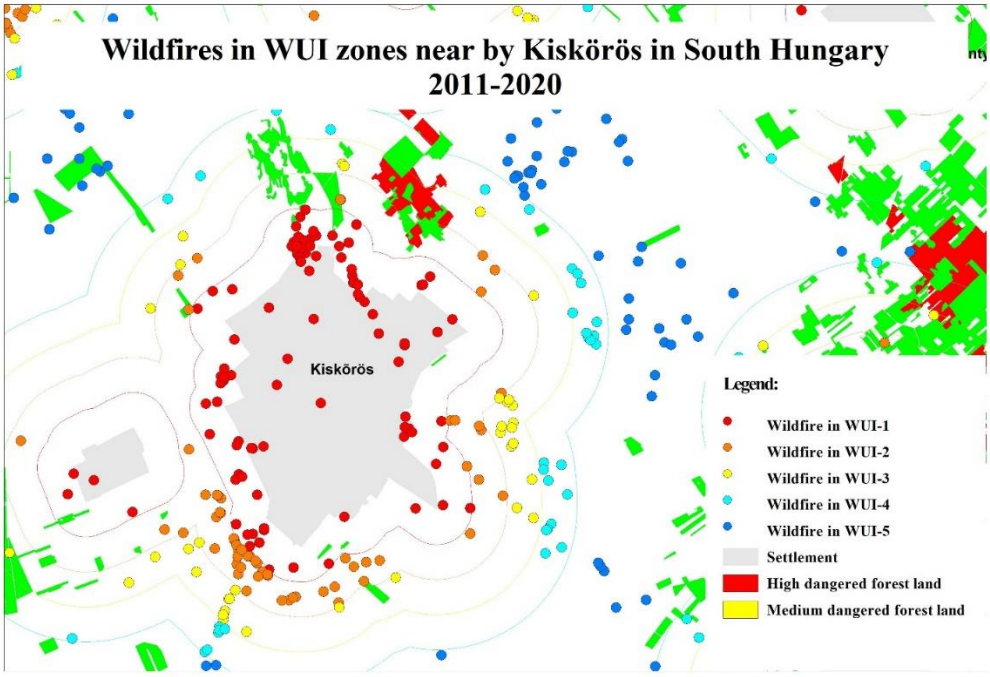

Figure 2 - The distance of fires from the residential area in the observation plot.

We performed GIS Spatial analyses with topoXmap on Figure 2, which presents the fires that occurred in the wildland areas of the settlements in the observation plot. The red colour indicates fires that occur within 500 metres from the residential area (WUI 1 zone) and the yellow those that occur within 1 km (WUI 2 zone). It is clear that a significant part of wildfires occurred close to the residential areas (marked in red and orange). Because of this, buildings were endangered from wildfires. The cause of fires is primarily the human factors.

In the third step of our three-step analysis, we examined the **housing density** along the wildland area at the WUI. Our observation plot is small, so in this case we have examined the integrating housing density of the entire county (Bacs-Kiskun Coutnty). We used Google Earth (open access) for this purpose, where we made an image analysis. We classified the integrating housing densities in three categories. In the first category (green) there are only farms nearby the forest. The second category is where the residential buildings are scattered relative to each other along the forest edge (10 m < >30 m, yellow). We classified the areas into the third category, where residential building very close to each other (<10 m, red).

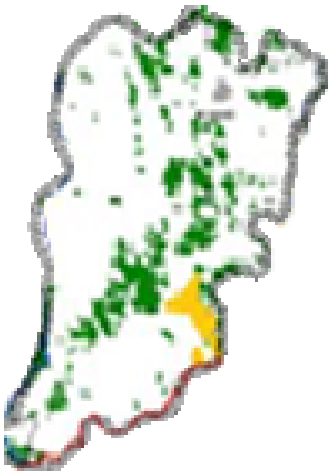

Figure 3- Integrating housing densities at the WUI in Hungary.

After the analysis we determine that there are many farms in the county. So the integrating housing density is low, mainly due to farmlands, and therefore it results in a low fire risk.

4. Conclusion

As a result of our analysis, we prove that WUI areas have developed also in Hungary. As WUI areas endangers human life and and property, these areas must also be identified in Hungary. To summarize our research above, we state that the preventive fire protection of Wildland-urban interface areas is a complex nature, which is still a research gap in Hungary, regardless of the research and guidelines already available in the international references. Taking into account international trends, we examined the risk of WUI fires of a national observation plot. The risk was determined as a result of a three-step analysis. As a result of the analysis, we consider the observation plot, as a high vulnerable WUI area. WUI risk is primarily due to the risk of fuel and fire occurrence. To sum up our results we determined that WUI fires can develop primary due to combustible fuel and number of fires in the observation plot we have analysed. However, they mainly endanger residential buildings and farms at the forest edge, and there is less chance of further residential buildings being damaged from fires.

5. References

Bodnár, L., Restás, Á. 2018: Examination of the forest fires detection: the relationship between the fire and the detection. In: Viegas, Domingos Xavier (ed.) - Advances in forest fire research 2018. Imprensa da Universidade de Coimbra. 995-1001.

Caballero D., Beltrán J., Velasco A. 2007: Forest fires and wildland-urban interface in Spain: types and risk distribution. In: IV Conferencia Internacional sobre Incendios Forestales. Sevilla, Espana, 13 -17 mayo 2007, Organismo Autónomo de Parques Nacionales, Ministerio de Medio Ambiente, 13-17.

Cohen, J. D. 2003: Preventing residential fire disasters during wildfires. In: Proceedings of the international workshop, Forest fires in the wildland-urban interface and rural areas in Europe: an integral planning and management challenge, Athens. Greece. 5-12.

Johnston L., Flannigan M. 2018: Mapping Canadian wildland fire interface areas. *International Journal of Wildland Fire*, XXVII. 1. 1-14.

Koksal K., Mc Lennan J. 2019: - Every Danielle: Australian wildland-urban interface householders' wildfire safety preparations: 'Everyday life' project priorities and perceptions of wildfire risk. *International Journal of Disaster Risk Reduction,* 33. 1. 142-154.o

Lampin-Maillet C., Marielle J., Long M 2009: Mapping wildland-urban interfaces at large scales integrating housing density and vegetation aggregation for fire prevention in the South of France. *Journal of Environmental Management*, XCI. 3. 732-741.

Radeloff C.V., Hammer R. B., Stewart S. I., Fried J. S, Holcomb S. S. and McKeefry J. F 2005: The Wildland-Urban Interface in the United States. *Ecological Application*, XV. 799-805.

Radeloff C.V., Helmers D., Kramer A. 2018: Rapid growth of the US wildland-urban interface raises wildfire risk. *Proceedings of the National Academy of Sciences*, CXV. 3314-3319.

Restás Á 2018: Results of I4F technology making aerial firefighting more effective. In: X. D. VIEGAS: Forest Fire Research Abstracts Book 2018. Coimbra, Portugal: ADAI/CEIF, University of Coimbra, (2018) pp. 115-115. ISBN: 978- 989-99- 0809-3.

Viegas X. D., Figueiredo R., Almeida E. 2012: *Wildland fire report of Tavira/São Brás de Alportel Centro de Estudos sobre Incêndios Florestais*, ADAI/LAETA. Coimbra University. Coimbra.

Anatomy of the *Las Máquinas* wildfire using remote sensing tools

Jorge Valdivia[1]; Israel Avila[1]; Fernando Auat-Cheein[2]; Andrés Fuentes[2]; Pedro Reszka*[1]

[1]Universidad Adolfo Ibáñez, Av. Diagonal Las Torres 2640, Peñalolén, Santiago, Chile
{jorvaldivia@alumnos.uai.cl, jiavilaosses@gmail.com, pedro.reszka@uai.cl}
[2] Universidad Técnica Federico Santa María, Avda. España 1680, Valparaíso, Chile
{fernando.auat, andres.fuentes}@usm.cl

**Corresponding author*

Keywords

WUI fires, Chile, FWI, Earth Observation satellites, spectral indices

Abstract

The Las Máquinas wildfire took place in central Chile in the austral summer season of 2017 and became the most severe event in Chilean history, causing loss of life, property and the destruction of native forest, crops, large areas of commercial plantations and biodiverse habitats. Since this event has no precedent in Chilean wildfire history, it was used as an example to carry out a detailed analysis of the conditions before (pre-), during (per-) and after (post-) the fire from a remote sensing perspective. The goal of this work is to develop a framework to carry out detailed analyses of catastrophic fires for forensic and public policy purposes, making use of the advantages posed by Earth Observation satellites, including the simultaneous imaging of large areas with a good spatial resolution, and an ever-increasing temporal resolution, coupled with a sophisticated suite of instruments which allow measuring many parameters simultaneously. This study examines the biophysical, meteorological and physical variables like the evolution of the Normalized Difference Vegetation Index (NDVI), weather conditions, maximum temperature evolution, the Canadian Fire Weather Index (FWI), the burned area, the maximum fire radiative power, among others, for the five municipalities that were affected by the fire: Cauquenes, Chanco, Empedrado, Constitución and San Javier, all of which are located in the Maule Region. The results indicate that Las Máquinas wildfire took place under exceptional meteorological conditions. In particular, the conditions before the night when Santa Olga was destroyed were characterized by extreme values of the FWI, which caused a significant increase in the burned area and overwhelmed any response by the fire brigades.

1. Introduction

Central Chile experienced tragic wildfire events in the 2016-2017 season, which killed 11 people, destroyed over 1000 structures, including the complete destruction of the village of Santa Olga, burned down approximately one half of the protected forests of *Nothofagus alessandrii*, an endangered southern beech species endemic to Chile. The total burned area for the fires was of about 575,000 ha, with the damage occurring especially in the Maule Region (CONAF 2017, ONEMI 2017), which saw the destruction of ~10% of its total area. The *Las Máquinas* fire consumed 190,000 ha in a few days, becoming the most devastating event in Chilean history. This wildfire is analyzed in this paper solely relying on Earth Observation (EO) tools. The goal of this work is to develop a framework to carry out detailed analyses of catastrophic fires for forensic and public policy purposes, making use of the advantages given by EO satellites, including the observation of large tracts of landscapes with a good spatial resolution, and an ever-increasing temporal resolution, coupled with a sophisticated suite of instruments which allow measuring many parameters simultaneously. For this purpose, we analyzed the landscape conditions before the fire (*pre*-fire), the propagation of the fire front (*per*-fire) and the evolution of the vegetation in the years after the event (*post*-fire), using open-access satellite imagery obtained from multiple remote sensing instruments, giving a new perspective to the description of this event. Additionally, the *pre*- and *per*-fire Canadian Fire Weather Index (FWI) was calculated for the entire Region of Interest on a daily basis, based on remotely sensed data and physical simulations.

2. Methods & materials

2.1. Study area

The Maule region is located in Central Chile (35° 25' 36'' S, 71° 39' 79'' W), with an area of 30,296 km^2 (see Figure 1). The climate is prototypical Mediterranean. Forestry is one of the main economic activities, with large continuous *Pinus radiata* and *Eucalyptus globulus* plantations. The Region of Interest (ROI) corresponds to five municipalities within the Maule region, where the wildfire took place. These municipalities are: Cauquenes, Empedrado, San Javier, Chanco and Constitución, which correspond to the five zones shown in Figure 1 that are delimited by a thick black line filled with a gray hatched fill.

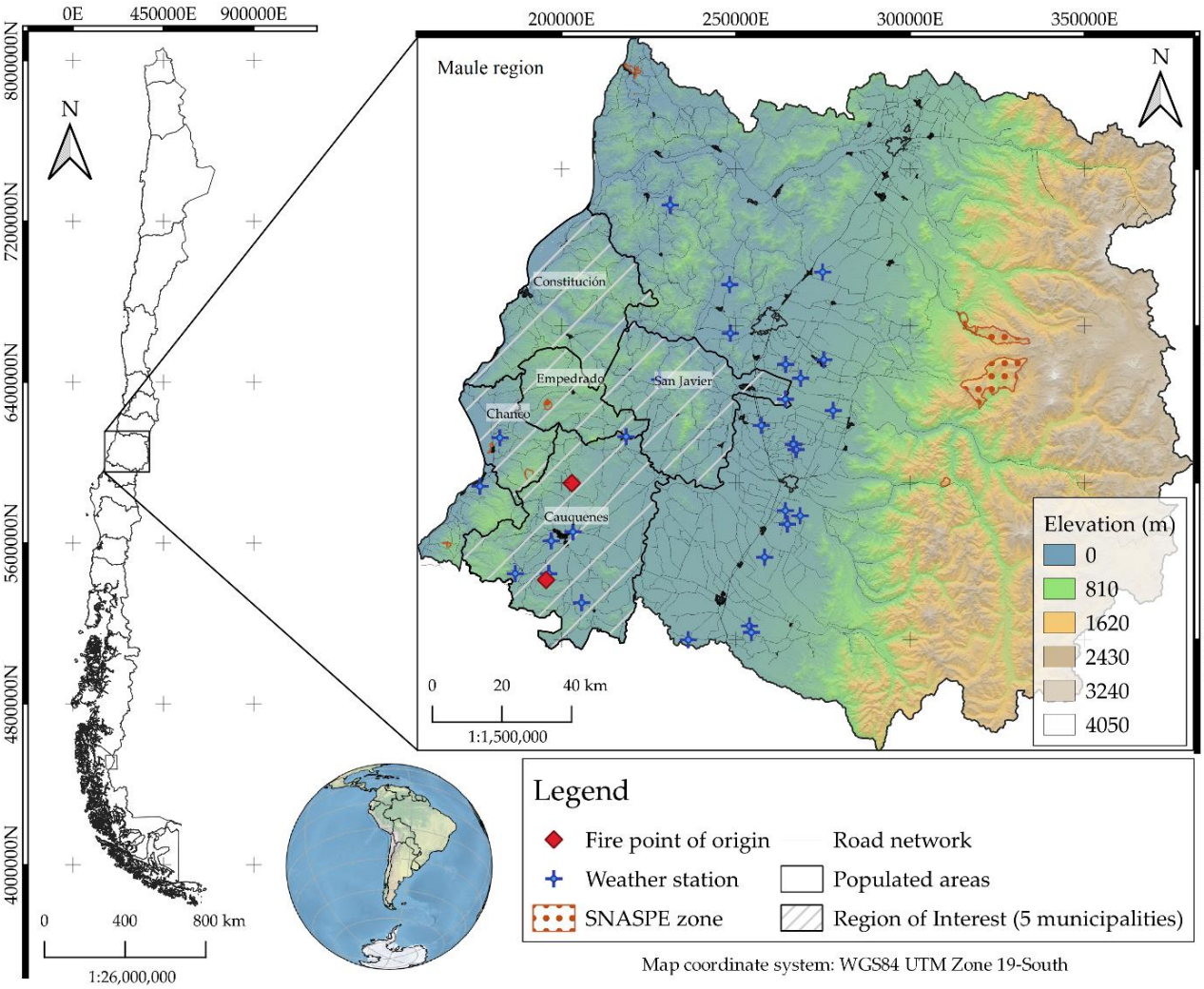

Figure 1. ROI with topography, weather stations, points of fire origins, and populated areas. SNASPE zones correspond to protected wilderness areas.

2.2. Burned area

Three different satellite products were used to calculate the burned area of the event: MODIS (product MCD64A1 v006 Burned Area (Giglio et al., 2015a), Landsat-8 pre- and post-fire images at Level-2 (surface reflectance with atmospheric correction), and Sentinel-2 pre- and post-fire images at Level-1C. The "sen2r" package (Ranghetti et al., 2020) was used in R to perform atmospheric, terrain and cirrus correction at the Top-Of-Atmosphere (TOA) for Sentinel-2 data, delivering Bottom-Of-Atmosphere (BOA) reflectance images. Landsat-8 and Sentinel-2 images were obtained from NASA's EarthExplorer. All images had < 0.5% cloud pixels within the ROI. Three images of Landsat-8 and Sentinel-2 were assembled to build the ROI, while only one MODIS Tile was required. The images were cropped and masked to the extent of the ROI. For Landsat-8 and Sentinel-2 BOA data, the following spectral indices were computed: Normalized Difference Vegetation Index (NDVI) (Rouse 1973), Normalized Difference Water Index (NDWI) (McFeeters 1996), Normalized Burn

Ratio (NBR) (Key & Benson 2006) and its temporal difference between pre, and post fire, i.e. the delta Normalized Burn Ratio (dNBR), which can represent the optimal separation of burned pixels from unburned ones and provide an scaled index representing the burn severity (Van Wagtendonk 2004). The two following filters were applied to the data: (i) NDVI pre-fire must be greater than 0.25, and (ii) NDWI must be lower than zero, meaning that only vegetation (El-Gammal et al., 2014) and non-water pixels can burn. Several threshold values for the dNBR were studied.

2.3. Vegetation evolution

Using MODIS product MOD13A1 (Vegetation indices 16-Day) (Didan 2015), the NDVI (Rouse 1973) was calculated. The average NDVI value for each municipality was computed from January 2010 to January 2022.

2.4. Fire weather

2.4.1. Standardized precipitation index

The Standardized Precipitation Index (SPI) (McKee et al., 1993) is based on the deviation of rainfall from normal data, and is computed by summing precipitations over k months, and fitting these accumulated precipitation values to a parametric statistical distribution from which probabilities are transformed to the standard normal distribution ($\mu = 0$, $\sigma = 1$). The precipitation data corresponded to the Integrated Multi-satellitE Retrievals for Global Precipitation Measurements (IMERG-GPM) monthly accumulated precipitation data product (GPM 3IMERGM.06) at a 0.1 degree × 0.1 degree spatial resolution (Huffman et al., 2019a), acquiring monthly accumulated precipitations from January 2001 to January 2016. SPI was computed using the "SPEI" package (Beguería & Vicente-Serrano 2017) in R, based on the Pearson Type III distribution, i.e. 3-parameter Gamma distribution function (Guttman 1999). In addition, the area under the curve (AUC) of the SPI was also studied.

2.4.2. Temperature evolution

Temperature evolution was carried out using the maximum monthly temperature from 1979 to 2019 grid product of Chile's CR^2. The product was built using statistical regionalization of the ERA-Interim atmospheric reanalysis data, while adding local information (such as topography and temperature observations) and surface temperature estimates by MODIS Land Surface Temperature product (M*D11A1) (Wan et al., 2015). The raster pixel-data was extracted for the whole ROI and then the average value was computed and stored.

2.4.3. FWI

The FWI was calculated using remote sensing products and physical simulations. $FWI = f(T_a, U_r, PP, RH)$, where T_a is the ambient temperature or NSAT (near-surface air temperature, in °C), U_r is the wind speed at 10 m height (km/h), PP is the precipitation (mm), and RH is the relative humidity (%). Wind speed was simulated using WindNinja V3.6.0 (Forthofer et al., 2014), with a landscape file for the ROI built by using primarily the information of the National Land Use Inventory (LUI) (CONAF 2016). NSAT was calculated using multiple linear regression models and machine learning random forests regression algorithms. The variables used are those proposed by Zhang et al., 2014. The regression training dataset was built by using daily images of NDVI, PW (precipitable water vapor, cm) and T_s (land surface temperature) from 2010 to 2016 for the month of January only. The pixels at the location of the weather stations within the ROI were extracted, as well as the air temperature measured by the weather station at the closest acquisition time of the satellite-product.

Precipitation was obtained from the IMERG-GPM (Huffman et al., 2019b), where the product GPM IMERG Final Precipitation L3 Daily at a 0.1 degree × 0.1 degree spatial resolution was used. Relative humidity was obtained by calculating the quotient of the actual vapor pressure, e_a, and the saturation vapor pressure, $e°(T_a)$. The only variables required are the near-surface air temperature (NSAT) and the dew-point temperature (T_{dew}) (Allen et al., 1998; Lawrence 2005). The latter was obtained from MODIS M*D07 product (atmospheric profiles) (Borbas et al., 2016). Finally, the FWI was computed in R using the "cffdrs" package (Wang et al., 2017) with adjusted latitude and initial conditions of the Fine Fuel Moisture Code (FFMC), Duff Moisture Code (DMC) and Drought Code (DC) derived from the fire danger indices historical data from the Copernicus Emergency Management Service (Vitolo et al., 2019).

3. Results

3.1. Burned area

Landsat-8 and Sentinel-2 burned area for several dNBR threshold values is shown in Figure 2. The upper bound of the red rectangle corresponds to the burned area reported by the authorities (218,076 ha), while the lower bound corresponds to the burned area calculated by means of the MODIS MCD64A1 product. Figure 3 shows the burned area obtained from MODIS, and both Landsat-8 and Sentinel-2 for certain dNBR threshold values. Figure 4 exhibit the evolution of the daily burned area.

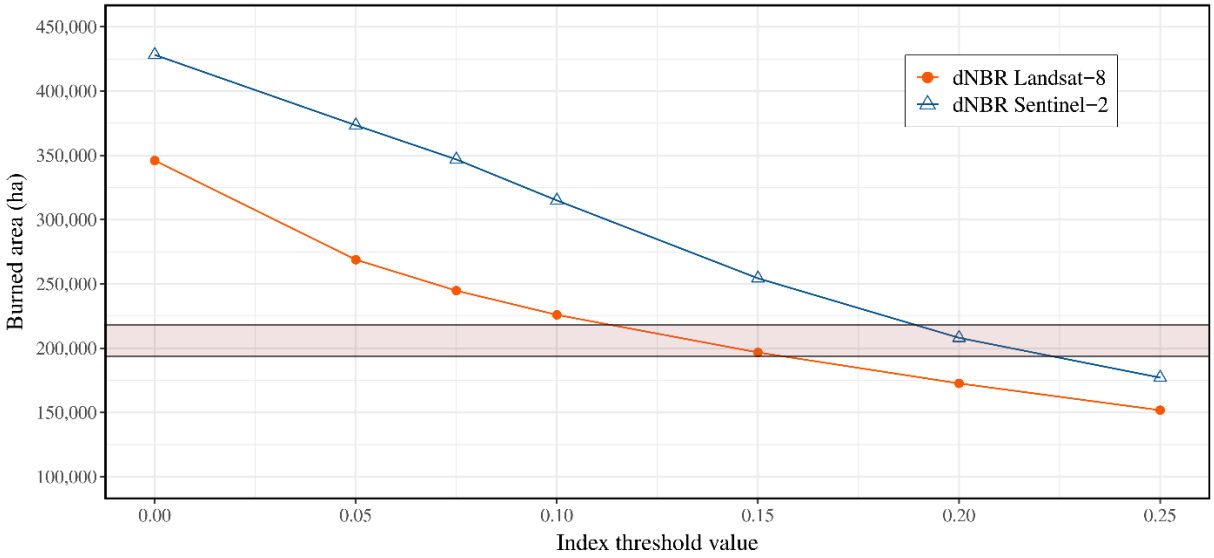

Figure 2. Burned area versus dNBR threshold values for Landsat-8 and Sentinel-2 images.

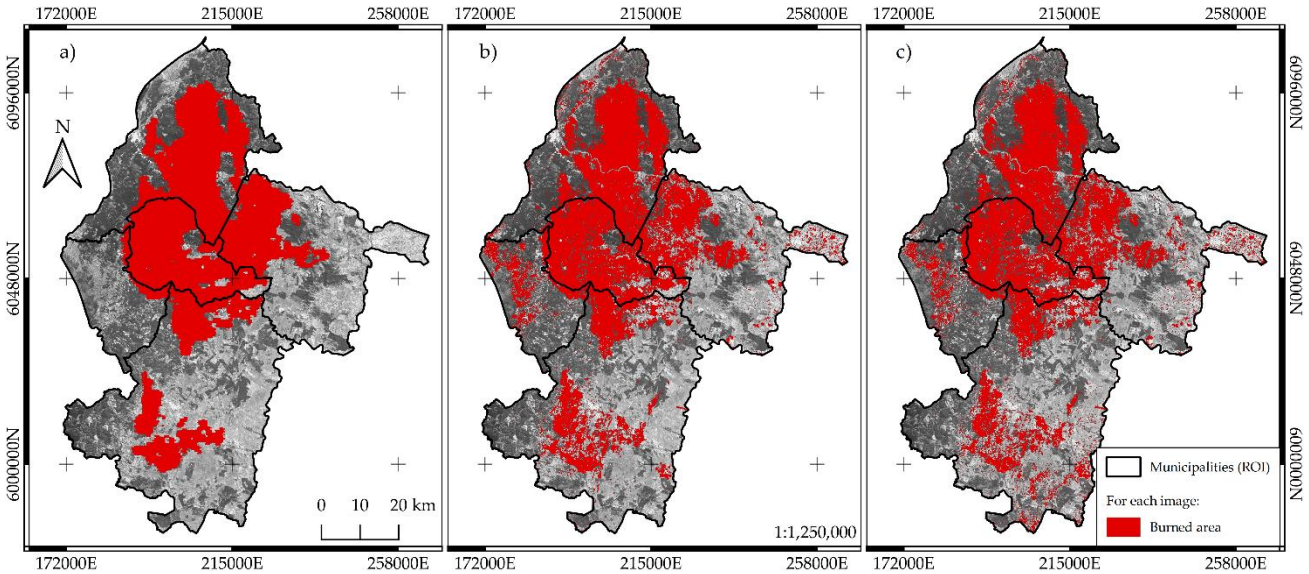

Figure 3. Burned area for a) MODIS MCD64A1 product, b) Landsat-8 with dNBR=0.135, and c) Sentinel-2 with dNBR=0.205. Considering the dNBR threshold values mentioned before, the Landsat-8 and Sentinel-2 burned area results were 204,440 ha and 204,450 ha, respectively. While the affected surface with MODIS MCD64A1 was 193,804 ha. Map coordinate system is WGS84 UTM Zone 19-South.

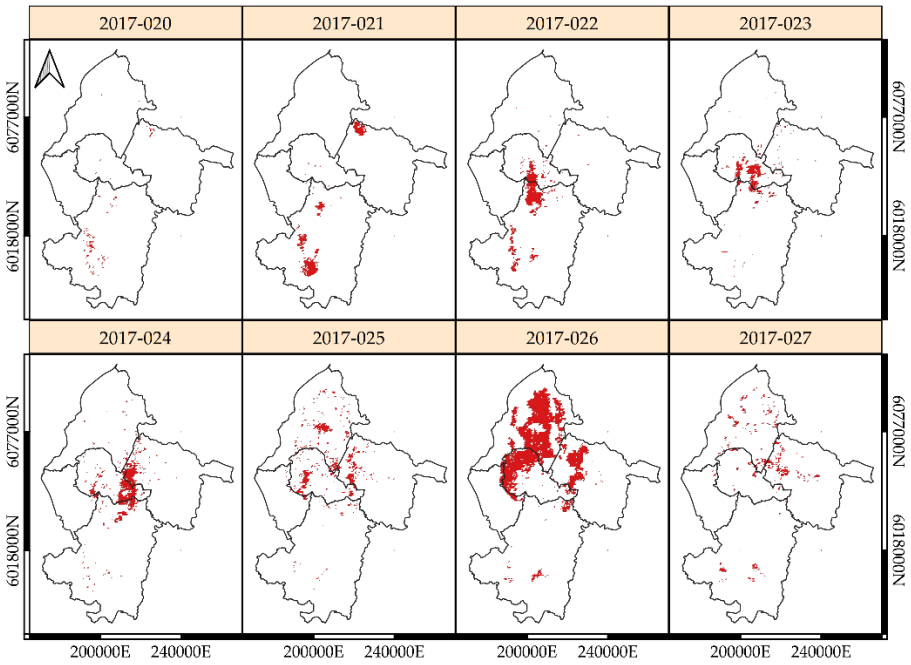

Figure 4. Burned area evolution (MODIS MCD64A1 product) between Julian days 020 – 027 (January 20th to January 27th, 2017) within the ROI. Each image corresponds to daily data.

3.2. Vegetation evolution

The results in Figure 5 shows that the most affected municipality within the ROI in terms of its flora was Empedrado. Note that around 89% of Empedrado surface-area was burned.

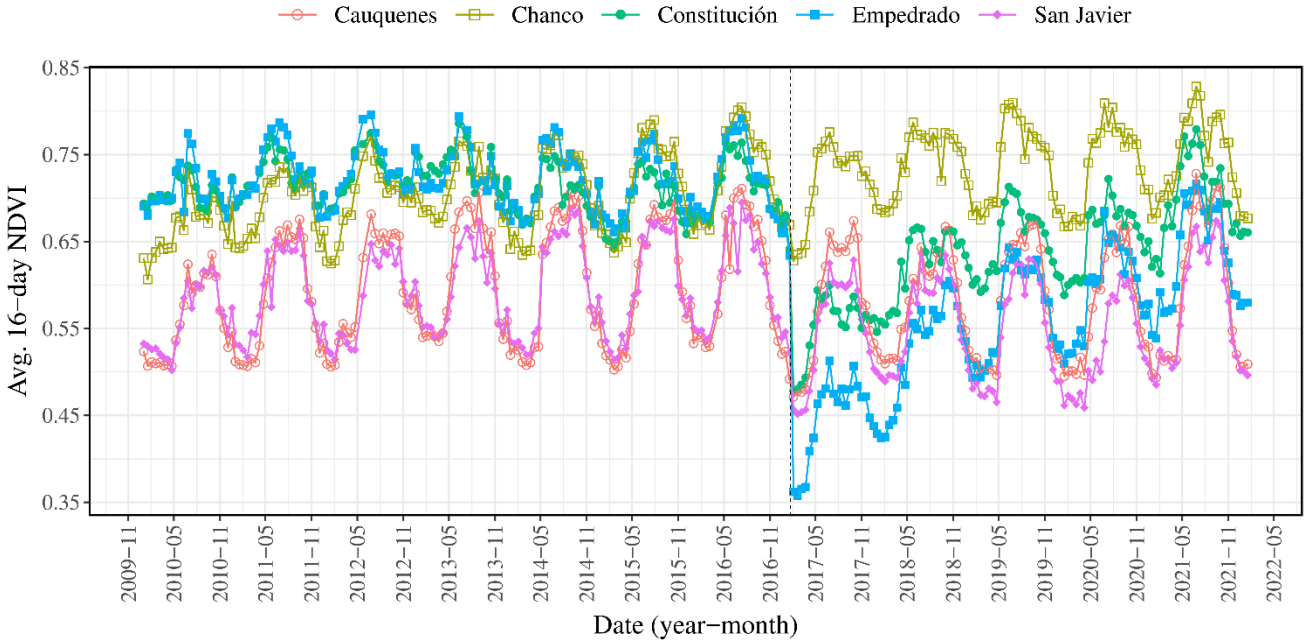

Figure 5. Average NDVI evolution from January 2010 to January 2022 for each municipality within the ROI. The vertical dashed line corresponds to the fire start date (January 20, 2017).

3.3. Standardized precipitation index

Severe drought values were found the year prior to the event (see Figure 6a). Furthermore, the downward trend displayed by the cumulative SPI AUC in Figure 6b corresponds to a persistent drought from 2009 onwards.

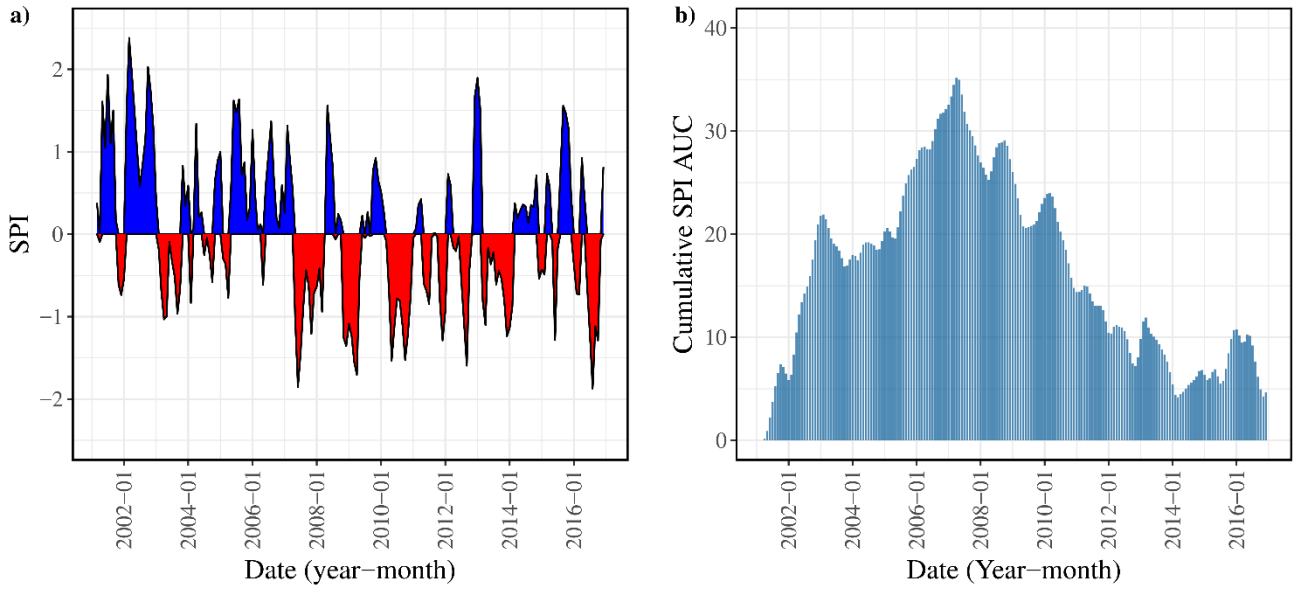

Figure 6. Standardized precipitation index (SPI) a) evolution and b) AUC analysis within the ROI from 2001 to 2016.

3.4. Temperature evolution

Record temperature of around 29°C were found on December 2016, the month prior to the event and the highest since 1979 within the ROI.

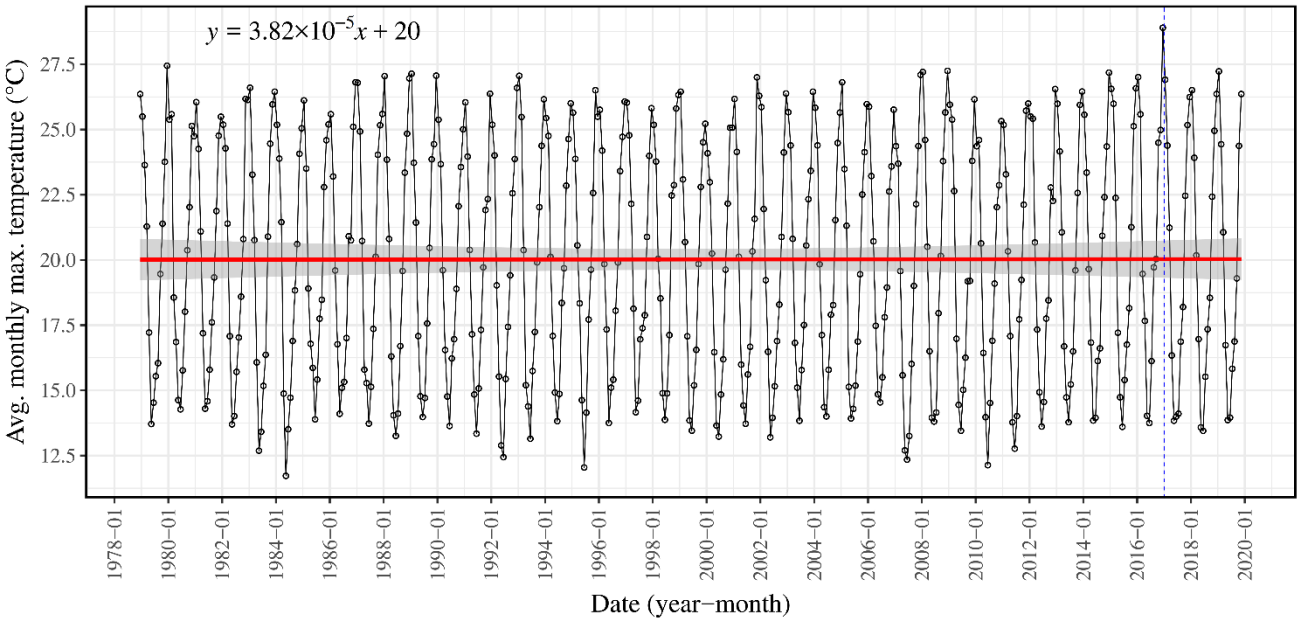

Figure 7. Average maximum temperature within the ROI from January 1979 to December 2019. Red line corresponds to the data trendline, the gray zone is the confidence interval, and the vertical dashed line is the fire start date.

3.5. Canadian FWI

FWI evolution and validation are shown in Figure 8. All datasets exhibit an increase in the FWI during the event (Figure 8a, 8c and 8e). On the other hand, a FWI map is shown in Figure 9. As it is possible to observe, on January 24th, Aqua FWI values at the north of the ROI exhibit extreme FWI values of 52.4±5.5, which is a day prior to the catastrophic events that destroyed the village of Santa Olga.

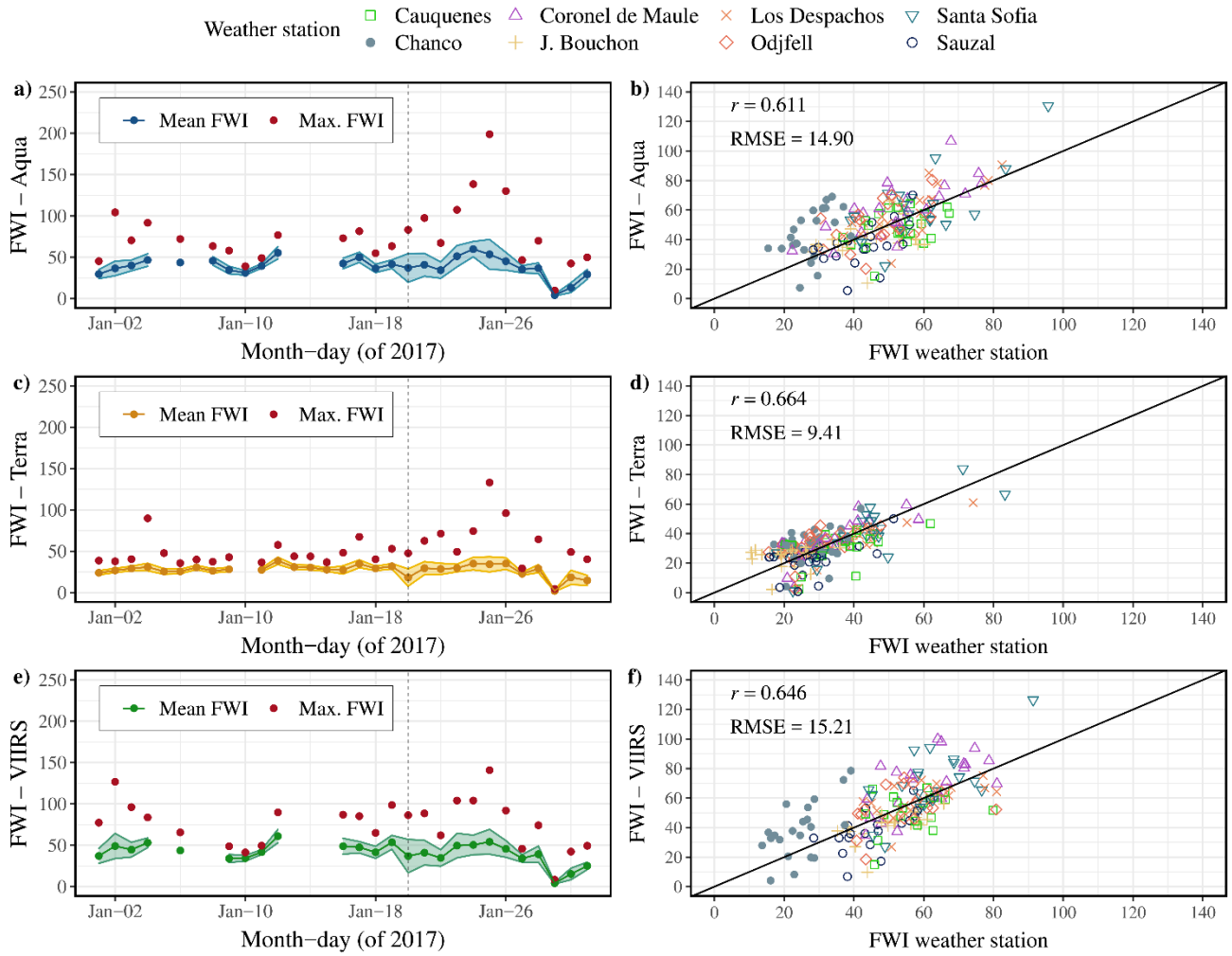

Figure 8. Canadian FWI evolution for a) Aqua, c) Terra and e) VIIRS-SNPP, and validation for b) Aqua, d) Terra, and f) VIIRS-SNPP. The colored areas in a), c) and e) represent the standard deviation of the FWI. The vertical dashed line corresponds to the fire start date.

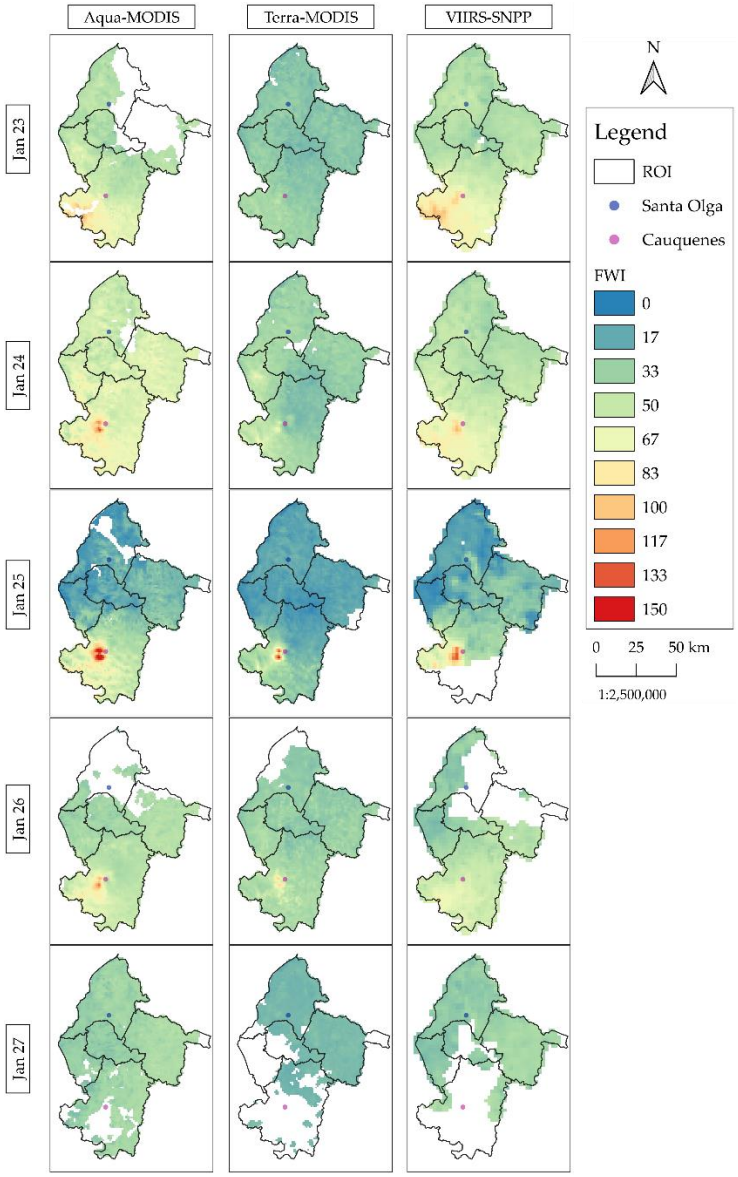

Figure 9. Canadian FWI estimated with Aqua-MODIS, Terra-MODIS, and VIIRS-SNPP, from January 23 to 27, 2017.

4. Conclusion

The *Las Máquinas* wildfire took place under exceptional meteorological conditions. The lowest NDVI values were registered for Empedrado during the event. On the night of January 25, the wildfire propagated at a peak rate, particularly among Empedrado (center), Constitución (north) and San Javier (east) (Fig. 4). The SPI data shows a consistent moderate-to-severe drought in the ROI, in agreement with the mega-drought observed in central Chile (Garreaud et al., 2020). The fire also occurred in a period with a record averaged maximum temperature (Fig. 7).

FWI results show that the index can be calculated on a daily basis from remotely sensed data (and wind-speed simulations), and that a day prior to the catastrophic events in Santa Olga, extreme FWI values were observed within the Constitución municipality. Moreover, the pre-fire FWI trend analysis (from January 1 to 19) showed positive slope values, which might be an indicator of wildfire risk.

From the FWI validation results, it is possible to conclude that the use and application of a remote sensing methodology to calculate the FWI is feasible, since the results were neither strongly overestimated nor underestimated.

Through remote sensing, we were able to compile a large amount of open-access satellite-based information with a good spatial and temporal resolution. This detailed information, and the reported framework for retrieving and processing the data, can contribute to the forensic study of large wildfires, particularly those occurring in remote areas or countries without a sophisticated wildfire safety and response infrastructure.

5. Acknowledgements

This work was funded by ANID SCIE/ANILLO ACT210052.

6. Bibliography

Allen, R. G., Pereira, L. S., Raes, D., & Smith, M. (1998). Crop evapotranspiration-Guidelines for computing crop water requirements – FAO Irrigation and drainage paper 56. FAO, Rome, 300(9), D05109.

Beguería, S. & Vicente-Serrano, S. M. (2017). SPEI: Calculation of the Standardized Precipitation-Evapotranspiration Index. R package version 1.7.

Borbas, E. E., Seemann, S., Li, Z., Li, J., Kern, A., & Menzel, W. P. (2016). MODIS Atmosphere Profiles Product (07_L2). NASA MODIS Adaptive Processing System. Goddard Space Flight Center.

CONAF (2016). Catastro de uso de suelo y vegetación. Comisión Nacional Forestal. Obtained in March 2022 from Infraestructura de Datos Espaciales (IDE).

CONAF (2017). Análisis de la afectación y severidad de los incendios forestales ocurridos en enero y febrero de 2017 sobre los usos de suelo y los ecosistemas naturales presentes entre las regiones de coquimbo y los ríos de chile. Corporación Nacional Forestal, Informe Técnico. 56 p. Santiago, Chile.

Didan, K., Huete, A. (2015). MOD13A1 MODIS/Terra Vegetation Indices 16-Day L3 Global 500m SIN Grid. NASA LP DAAC.

El-Gammal, M.; Ali, R.; Samra, R., *J Am Sci.* 2014, 10, 108–113.

Forthofer, J. M., Butler, B. W., & Wagenbrenner, N. S., *Int. J. Wildland Fire* 2014, 23(7), 969-981.

Garreaud, R. D., Boisier, J. P., Rondanelli, R., Montecinos, A., Sepúlveda, H. H., Veloso-Aguila, D., *Int J Climatol* 2020, 40(1), 421-439.

Giglio, L., Justice, C., Boschetti, L., Roy, D. (2015a). MCD64A1 MODIS/Terra+ Aqua Burned Area Monthly L3 Global 500 m SIN Grid V006 Burned Monthly 500m. NASA EOSDIS Land Processes DAAC: Sioux Falls, SD, USA.

Guttman, N. B., *J Am Water Resour As* 1999, 35(2), 311-322.

Huffman, G.J., E.F. Stocker, D.T. Bolvin, E.J. Nelkin, Jackson Tan (2019a), GPM IMERG Final Precipitation L3 1 month 0.1 degree x 0.1 degree V06, Greenbelt, MD, Goddard Earth Sciences Data and Information Services Center (GES DISC).

Huffman, G.J., E.F. Stocker, D.T. Bolvin, E.J. Nelkin, Jackson Tan (2019b), GPM IMERG Final Precipitation L3 1 month 0.1 degree x 0.1 degree V06, Greenbelt, MD, Goddard Earth Sciences Data and Information Services Center (GES DISC)

Key, C.H.; Benson, N.C. Landscape assessment (LA) – Sampling and analysis methods. Technical Report RMRS-GTR-164-CD, USDA Forest Service, 2006.

Lawrence, M.G., *B. Am. Meteorol. Soc*. 2005, 86, 225–234.

McFeeters, S.K., *Int J Remote Sens* 1996. 17, 1425–1432.

McKee, T. B., Doesken, N. J., & Kleist, J., In *Proceedings of the 8th Conference on Applied Climatology* 1993 17(22), 179-183.

ONEMI (2017). Monitoreo para la Región del Maule por incendios forestales. Oficina Nacional de Emergencia del Ministerio del Interior, Gobierno de Chile. https://www.onemi.gov.cl/alerta/monitoreo-para-la-region-del-maule-por-incendios-forestales/.

Rouse, J.W.; Haas, R.H.; Schell, J.A.; Deering, D.W.; Harlan, J.C. Monitoring the vernal advancement and retrogradation (greenwave effect) of natural vegetation. Technical Report E74-10676, Texas A&M University, Remote Sensing Center, College Station, Texas, United States. Prepared for Goddard Space Flight Center, 1973.

Ranghetti, L., Boschetti, M., Nutini, F., Busetto, L *Comp Geosci* 2020. 139, 104473.

Van Wagtendonk, J.W., Root, R.R. and Key, C.H., *Remote Sens Environ* 2004, 92(3), 397-408.

Wan, Z., Hook, S., Hulley, G. (2015). MOD11A1 MODIS/Terra Land Surface Temperature/Emissivity Daily L3 Global 1km SIN Grid V006. NASA EOSDIS Land Processes DAAC.

Wang, X., Wotton, B. M., Cantin, A., Parisien, M-A., Anderson, K., Moore, B., Flannigan, M. D., *Ecol Proc*ess 2017, 6(1), 5.

Zhang, H., Wu, B., Yan, N., Zhu, W., & Feng, X., *J Geophys Res-Atmos* 2014, 119(21), 12-256.

Anticipation of future risk due to land cover change and WUI extend. Application to the Baronnies Provençales Regional Natural Parc (France)

Eric Maillé*, Christophe Bouillon

[1]French National Research Institute for Agriculture, Alimentation and Environment (INRAE), RECOVER joined research unit, Aix-en-Provence, France {eric.maille, christophe.bouillon}@inrae.fr

**Corresponding author*

Keywords

Land Use Land Cover Change, Wildland-Urban Interface, Dynamic Modelling, Simulation, Risk Mapping

Abstract

We propose a modelling framework aimed at representing change in fire risk level due to land cover change, and more specifically to change in the map of Wildland Urban Interface (WUI). The framework is composed of one module that simulates transitions between classes of the land cover matrix using a "state-transition" model, while a gravity-like model is used to represent discontinuous urban spread in relation to the land cover matrix dynamic. The WUI map is calculated using the WUIMap model at each step of time: this later method crosses some fuel types and classes of scattered buildings spatial distribution. A risk level is associated to each interface type based on a rules based assessment of hazard and vulnerability components.

The methodology was applied to the French sub-mediterranean Baronnies Provençales Regional Natural Parc. This area was up to now few prone to forest fire, mainly due to its elevation, but climate change scenarios let anticipate the average climate fire risk level will drastically increase in this area during the next decades. The objective was to assess the increase part of risk level originated by land cover change, and provide a spatial representation of this change. Results show that although spread of scattered buildings will remain low in terms of number of buildings, its impact on risk components, and specifically on territorial vulnerability, is considerable, as a low number of buildings may impact very large portion of the territory in terms of risk. In a further step of this research, new multicriteria models will be used to refine risk assessment.

1. Introduction

Drivers of wildfire risk change are numerous, including climate change and land cover change (FUME 2013). Because of climate change, wildfire risk will raise in both latitude (toward the North) and altitude. However, in many situations, climate change may be considered uniform at the scale of local territories. On the other hand, land cover change affects the spatial distribution of the risk within local territories, especially if the global risk, associating hazard, vulnerability and exposure components (IPCC 2014), is considered. Together with change in vegetation fuel, dynamic of wildland urban interfaces is a key factor of change in such global risk.

Anticipating future fire risk at local scale is a key element for land management and planning activities in wild fire prone areas. We propose a method of evaluation of risk change in relation to WUI dynamic. It is applied to one backside French South-Eastern supra-Mediterranean protected area: the Baronnies Provençales Regional Natural Parc area (Parc Naturel Régional des Baronnies Provençales). It gathers some 116 Eurostats Local Administrative Units (LAU, formerly NUTS 5), ie. "communes". Due to its elevation (from 300m up to 1500m), and the attenuation of the Mediterranean influences, this area was up to now relatively little prone to forest fires. Different works (Chatry et al., 2010, Galizia et al. 2021, Romero and Ganteaume, 2020) show that this situation will change in the next few decades due to climate change and land cover change.

2. Objectives

The objective is to provide an assessment of future change in risk spatial distribution related to change in WUI extend in a low mountain protected area. The risk to be assessed is the global risk, integrating hazard, vulnerability and exposure (Birkmann et al, 2014). The temporal perspective, ie. the simulation time period of the modelling exercise, is the next two to three decades (2050-2060).

3. Method

3.1. Risk assessment at WUI

WUI typologies, which characterizes the relationship between fuel areas and areas of vulnerabilities, are used as estimators of global risk level. Change in risk spatial distribution is assessed based on change in WUI map. The WUI typology used is the WUIMap (Lampin-Maillet and Bouillon, 2011) model one. A scale of risk associated to WUI types is proposed, combining a hazard component and a vulnerability component to calculate a global risk index for each WUI type (figure 3).

3.2. Future WUI change

Future WUI change are simulated based on a couple of Land Use/Land Cover Change (LULCC) change models (Maillé and Espinasse, 2012). This approach separates two main types of Land Cover Change (LULCC): i) scattered buildings diffusion-densification simulated by a gravity-like model and ii) the change in land cover "matrix" simulated by a "state-transitions" model. It also separates and articulates land cover change processes (physical) and some land uses change processes (symbolic).

On a conceptual level, the model considers land cover classes, representing land cover types. However, land cover classes are endowed with attributes (similarly to computer sciences "classes") and have their own behavior (dynamic). We call legend (or nomenclature) the list of the land cover classes. Patches are spatial instances of a class (polygon, pixel, continuous set of pixels…). The model then represents two types of dynamic: semantic transitions (change of classes) and state change (change in attribute values).

The model is based on a very simple legend (nomenclature) of 4 (plus 1) land uses/land cover dynamic classes: i) F: Forest lands, ii) W: non-forest wildlands (opened and half-opened, including some pastoral lands), iii) A: agriculture (cultivated, excluding pastoral lands), and iv) U: urban and other artificialized lands (including roads and infrastructures). One last land cover class gathers land covers supposed static (water areas and some mountain mineral areas). WUI land cover classes are not part of the legend (nomenclature), but are derived from the model outputs.

The state of land cover classes is represented by attributes, depending on the LC class. 3 main state attributes are represented: fuel load (concerns the only W land cover class), potential of building density (all non-urban dynamic land cover classes) and anthropogenic pressure (only W land cover class). Attributes values are normalized between 0 and 1:

- for fuel load, 0 is the minimum load (herbaceous stratum only), 1 is the forest state ;
- for potential of building density, 0 is a non-buildable area, 1 is an area that can evolve up to continuous urban, according to the land planning document ;
- for anthropogenic pressure, 1 represents "fully" used area (no free ecological dynamic possible: urban and periurban lands, cultivated areas, high pressure pastoral area), 0 represents area with free (or quasi-free) ecological dynamics (totally abandoned areas).

Among the land use change processes represented by the model, the buildable state of land patches is a key factor of WUI dynamics, linked to land planning activity. However, our approach is purely geographic, as the only variables that drive the dynamic are than land cover and topography. The underlying anthropogenic and/or natural processes determining land cover changes are not explicitly represented. For example, change of one given land patch from not buildable (0) to fully buildable (1) (symbolic state) only depends on initial land cover class of the patch, continuity with other buildable areas, local initial building density and some other topographical variables defining an "urban potential" (average altitude, slope and aspect of the patch). A stochastic residual comes to modulate the results of the deterministic calculation, in order to propose a normal representation of the spatial distribution of the unknown information (typically, personal human decisions).

Finally, an interface map is calculated at each step of time using the WUIMap model. This one cross some specific classes of building density and classes of vegetation aggregation. This model was demonstrated to provide good indicators of the global (hazard/vulnerability) risk (Lampin-Maillet & Bouillon, 2011). The different classes of WUI stemming from the WUIMap model are provided in the legend of fig 3.

The following table proposes a synoptic view of the model and its relationship with the WUIMap risk model.

Table 1: Synoptic view of the WUI change model and its relationship with the WUIMap risk model. *Note that W->F semantic transition results from two possible dynamics: forest spread or afforestation, for which the W->F transition automatically occurs when the fuel load of a W patch reaches 1. **Also the Non-U -> U transition automatically occurs when building density overcomes the WUI very high-density threshold.

	Buildings overlay	**Land use/land cover "matrix"**							
		Physical land cover				**Symbolic land use**			
Class of spatial dynamic	Diffusion	Semantic transitions (change in LULC class)			Attribute change	Semantic transitions		Attribute change	
Dynamic	Scattered buildings diffusion/densification	Forest advance (W -> F)*	Afforestation (W->F)*	Urbanization** (NonU→U)	Natural fuel load increase of W FL ∈ [0-1]	Not buildable -> buildable	Land abandonment (A->W)	Potential of building density pBD ∈ [0, 1]	Antropogenic pressure AP ∈ [0, 1]
Concerned classes	A,F,W	W	W	A,F,W	W	A,F,W	A	A,F,W	W
Spatial representation	Point	Pixel	Polygon	Polygon	Polygon	Polygon	Polygon	Polygon	Polygon
Main dynamic factors of the change	- Local building density - Potential building density	Anthropogenic pressure (AP) -Forest neighborhood	-Fuel load (FL=1)	-local building density (lBD)	-Anthro-pogenic pressure (AP)	-Urban neighborhood -Local building density lBD -Urban potential	-Urban neighborhood -Local building density lBD -Agriculture potential	-Urban neighborhood (UNB) -Local building density lBD	-Building density (lBD) -urban neighborhood
Main static factors of the dynamic	- Urban potential	-Forest potential			-Forest potential			-Urban potential	-Pastoral potential
Derived outputs	Local building density lBD ∈ [0,1]	Forest land and neighborhood		Urban neighborhood (UNB)	Fuel load and structural index			Wildlands state and neighborhood	
⇩	⇩	⇩		⇩	⇩		⇩		
WUIMap inputs	Buildings density (low-high)	High fuel aggregation WUI types		Very high building density WUI type	Intermediate fuel aggregation WUI types		Low fuel aggregation WUI types		

3.3. Data for calibration (diachronic mapping), validation and scenarios

Parameters of the model are calibrated based on diachronic mapping. Three main data sources are used:

- French cadastral database ("DGI Majic 3") allowed assessing the "scattered building dynamic", for each of the commune. This database contains the buildings, georeferenced, with their date of construction, unless for ancient one (before 1930). It is so possible to assess an historical rate of spread of scattered buildings for each commune.
- Land cover database, including Corine Land Cover 1988/1990, 2000, 2006, 2012, 2018, and *Crige* regional land cover database 2006, 2014, 2018. These database are jointly used:
- Satellite images for date older than 1988 as well as downscaling the oldest land cover database, CLC1988 notably, in order to improve inter-date consistency.

These data allowed calculating different parameters for different contexts (for each of the communes (LAU) – for instance) of the model including notably:

- rate of spread of scattered building, in relation to topography and urban environment (urban potential)
- rate of spread of forest land on opened and semi-opened wildlands, in relation to topography (forest potential)
- speed of closure of wildlands in relation to the forest potential
- etc.

More complex "atomic models", ie elementary models that are not modules of other higher lever models, are also calculated. Typically, an atomic model is specified, based on GLM analysis of past data, for assessing the

rate of land use transitions such as land abandonment probability, in relation to agriculture potential (topography, shape of the patch, urban neighborhood…). A GLM model of change from not buildable to buildable classes (potential of building density different from 0) in relation to the contextual building density and urban neighborhood is also specified. To do so, sample of patches are drawn at random and transition model are calculated by logistic modelling. Sub-samples of the patches are kept for validation.

Based on these parameters assessments, different scenarios are defined, which are specified by tuning the values of some of the parameters: protection of the environment, conservation of agriculture and forest, economic development, and one projective scenario (simple projection of the current dynamics):

- ***Scenario "protection of the environment":*** Preservation of natural spaces is favored without strong demographic impetus, which retains its trends (lower rate of discontinuous urban spread than measured in the past). On the other hand, the scenario promotes livestock farming to maintain open natural spaces (low rate of wildland closure).
- **Scenario "*conservation of agriculture and forest*"**: it promotes the maintenance of agricultural activity and production (low rate of agriculture land abandonment), as well as livestock farming to maintain open relict natural spaces (low rate of wildland closure). It also promotes logging.
- ***Scenario "*economic development*"***: it promotes "urban" economic activities as well as tourism that may have an impact on space: this is reflected in particular by a possible extension, even local, of high-stakes areas within or in contact with little artificialized areas (high rate of spread of discontinuous urban areas).

3.4. Periods and step of time

The past period for model calibration is 1974-2018. The step of time of simulations is annual.

4. Results

Examples of results showing the map of scattered urban spread and land cover matrix change simulations using the projected scenario are proposed in the following figures.

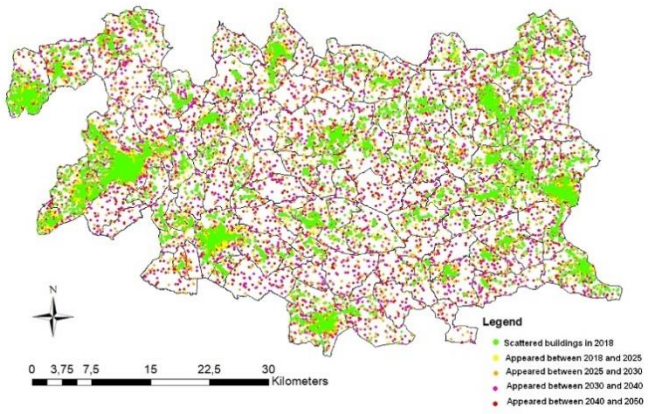

Fig 1. simulation of future scattered urban spread between 2018 and 2050 (projective scenario)

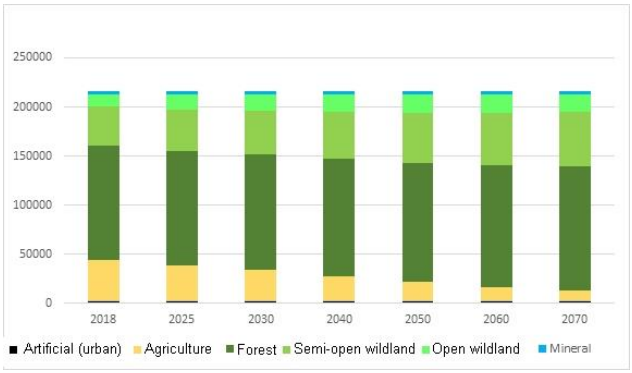

Fig 2. Quantitative change of the land cover matrix 2018 and 2050 (projective scenario)

A WUI maps are calculated based on these land cover map simulations. These maps are indicators of the global risk at local scale.

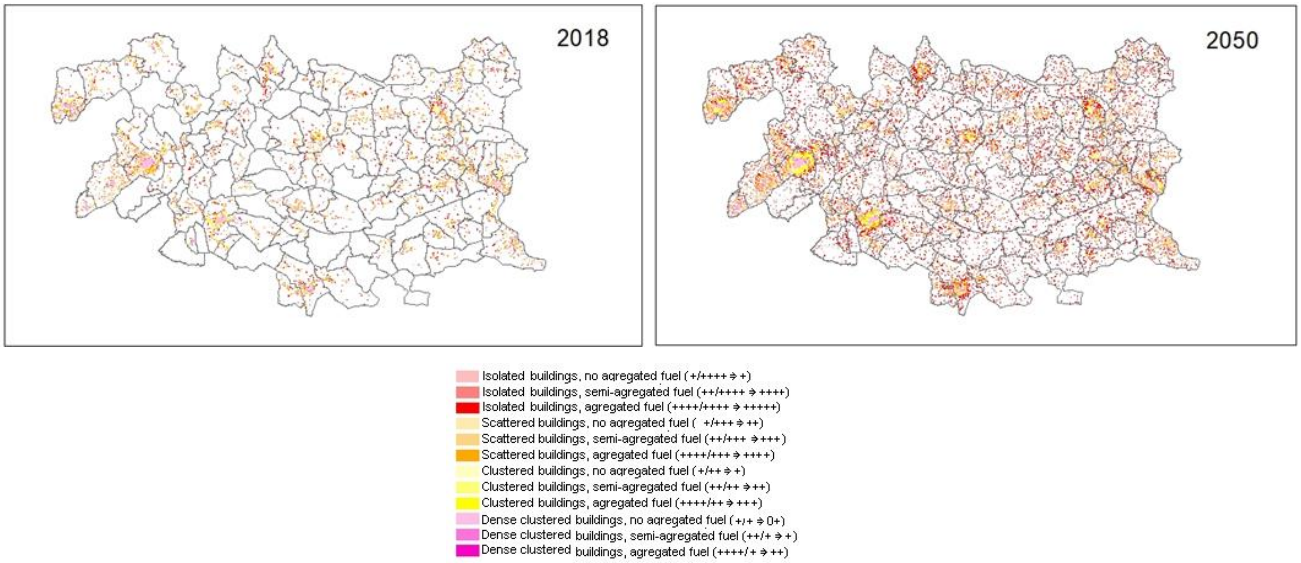

Fig 3. Simulated change in WUIMap interface types spatial distribution between 2018 and 2050, as indicator of risk. The legend mention the risk indicator associated to each WUI type in the form of:

hazard indicator / vulnerability indicator => global risk indicator

The vulnerability here considered is an "intensive" vulnerability, assessing the vulnerability of each building related to the type of interface it belongs to. The extensive vulnerability has also to be calculated, taking into account the number of buildings within the interface patches.

5. Conclusion

Anticipation of future wildfire risk in areas up to now little prone to that risk, is a key decision support for land management and planning. We propose a model for WUI spread simulation as the result of several land cover change, including scattered buildings and urban spread, as well as fuel spread on abandoned agriculture and pastoral areas. The objective of the model is not to preview the future risk absolute value, but rather to assess the possible effect of different land management scenarios on the future spatial distribution of wildfire risk. It is a support for today decisions. The risk model is simply based on WUI types. Results shows spectacular future increase of risk levels on most of the territories, while land cover change remain relatively modest: the spread of low density scattered built area results in some large areas risk increase, as low density built areas have the highest risk as soon as a significant fuel biomass is present. As a perspective, one other more complex analytical risk model (Chai-Allah & Maillé, 2020) is also used allowing better assessing the different components of the risk, including hazard, vulnerability and exposure. This later model is an expert-opinion based multicriteria one, where the interface type is one of the criteria for some of the components calculation. A panel of experts assessed the weight of this criterion for each of the relevant components. Up to now purely static, such a multicriteria risk model will be used in the future to assess change in risk level because of land cover change at territorial scale.

6. References

Birkmann, J., Kienberger, S., Alexander, D. (Eds.), 2014. Assessment of vulnerability to natural hazards. A European Perspective. Elsevier, UK.

Chai-Allah, A. & Maillé, E., 2020. « Mapping Forest Fire Risk in the Mediterranean forests—A Case Study of Provence-Alpes-Côte d'Azur region (France) ». In , 3:8107. https://doi.org/10.3390/IECF2020-08107.

Chatry, C., Le Gallou, J. , Le Quentrec, M. , Lafitte, J. , Laurens, D. , Creuchet, D. & Grelu. J., 2010. « Rapport de la mission interministérielle 'Changements climatiques et extension des zones sensibles aux feux de forêts' ». Rapport Min. Alimentation Agriculture Pêche, no 1796.

Galizia, L. F., Curt, T., Barbero, R., Rodrigues, M., 2021. Understanding Fire Regimes in Europe. International Journal of Wildland Fire 31 (1): 56-66. https://doi.org/10.1071/WF21081.

IPCC, 2014. Climate change 2014. Impact, Adaptation and Vulnerability, Summary for Policymakers, Working Group II (WGII) Contribution to the Fifth Assessment Report of the Intergovernmental Panel on Climate Change, WMO, UNEP,
https://www.ipcc.ch/site/assets/uploads/2018/02/ar5_wgII_spm_en.pdf.

Lampin-Maillet, C., Bouillon, C., 2011. WUImap: A Software Tool for Mapping Wildland-Urban Interfaces in Mediterranean European Context. Indian journal of environmental health, 2011, 5 (5), pp.631-642. ⟨hal-02595104⟩

Maillé, E. & Espinasse, B. 2012. Pyroxene: A Territorial Decision Support System Based on Spatial Simulators Intergration for Forest Fire Risk Management, in. Petraq, Papajorgji. 2012. New Technologies for Constructing Complex Agricultural and Environmental Systems. IGI Global

Maillé, E. & Espinasse, B., 2009. Spatial Agents for scale integration of spatial dynamics models. European Journal of Geomatics and Spatial Analysis, 19(4), 523-549.

Romero, B. & Ganteaume, A., 2020. « Does Recent Fire Activity Impact Fire-Related Traits of Pinus Halepensis Mill. and Pinus Sylvestris L. in the French Mediterranean Area? » Annals of Forest Science 77 (4): 1-19. https://doi.org/10.1007/s13595-020-01016-1.

Application of the Computational Fluid Dynamics in Forest Fires Investigations for Mitigation of the Wildland-Urban Interface Fires' Risks

MohammadReza Modarres; Miguel Almeida*

[1] Department of Mechanical Engineering, University of Coimbra, ADAI, Rua Luís Reis Santos, Pólo II, 3030-788 Coimbra, Portugal, {mohammad, miguelalmeida}@adai.pt

**Corresponding author*

Keywords

CFD, FDS, Forest fires, Vegetation fuels, HRR, WUI

Abstract

Realistic modeling of the vegetation fires based on reliable data from laboratory experiments is a key factor in the prediction of the fire dynamics behavior and its spread rate in wildlands. A robust understating of the fire behavior in different species can provide a pragmatic insight to take precautionary steps to mitigate the fire risks in Wildland-urban interfaces. Computational Fluid Dynamics (CFD) modeling of wildland fires offers a considerably high load of information needed for engineers and policymakers. This paper addresses the numerical modeling of the Ivy (Hedera helix) and grapevine (Vitis) plants using the fire dynamics simulation for the fire behavior analysis. Other species which authors have conducted experiments are Acacia, Apple tree, Arizona cypress, Bay laurel (Laurus nobilis), Blueberry tree (Prunus Spinosa), Cherry Tree, Fig tree, Gum rockrose (Cistus ladanifer), Hydrangea, Kiwi tree, Leyland cypress, Lindens (Tilia), Loquat (Eriobotrya japonica), Nerium oleander, Olive tree, Pacific madrone (Arbutus menziesii), Rhus typhina (Anacardiaceae), The Holly (Ilex Aquifolium), Thuja occidentalis (white cedar), and Wild Blackberry (Rubus Ulmifolius) shrub, in alphabetical order. The corresponding mathematical modelings of these experiments are being carried out by the authors.

The current numerical study was performed using the NIST open-source FDS code, developed by the National Institute of Standards and Technology with specific emphasis on the heat release rate from fires in different types of indigenous plants common in the Mediterranean climate, especially in Portugal. The validations of the numerical results are realized based on the observations from the experiments conducted at the Laboratório de Estudos Sobre Incêndios Florestais (LEIF) by the authors. The large-eddy simulation (LES) is used in these sets of simulations to close the turbulence equations in the low-Mach regime. The 2nd order accurate finite difference approximation scheme is used to discretize the governing equations on uniformly spaced three-dimensional staggered grids. The flow obstructions are treated using the simple immersed boundary method. Comparing the results of the FDS with those from the practical experiments, it is concluded that mathematical modeling of the vegetation fires can provide reasonably accurate results based on the fuel's physical and chemical characteristics along with operating boundary conditions.

1. Introduction

Forest fires as uncontrolled and non-prescribed combustion or burning of plants are considered a serious threat not only to the forests by jeopardizing the fauna and flora, mistuning the biodiversity in forest ecosystems but also in severe cases of extended fires, the residential areas. During drought seasons, especially in summers, with escalating effects imposed by global warming, the forests become more vulnerable caused by scattered litters of dry senescent leaves, twinges, and twigs as potent fuel types to make forests susceptible to lethal fires with colossal loss of the vegetation cover. Wildfires can become more intensified based on the environmental conditions (e.g., meteorological conditions, and terrain topography) which in turn can lead to irreparable casualties for the residential sites nearby or even farther. A forest fire may exist as surface, underground, ground, crown fires, and in severe cases as firestorms with natural or man-made causes. According to the European Commission report on forest fires, in 2020, southern European countries, e.g., Spain, France, Portugal, Italy, and Greece were the most affected regions losing thousands of acres of forest lands, including Romania, which is an expanding threat to the central and northern Europe. Based on the recent forest fires in Portugal, especially in 2017, the concept of WUI fires becomes more important than ever, which necessitates more laboratory experiments as the basic requirement for theoretical investigations. Since performing tests on different

vegetation fuels is limited due to the dimensions of the species with complex arrangements and diversities in nature, FDS can be an efficient tool to simulate the fire behavior based on the data gathered from laboratory-sized burnings. The FDS results can be subsequently applied to the diverse species in size and arrangements to have a realistic vision to define precautionary measures and policies. This paper intends to address the computational fluid dynamics modeling (CFD) of the fire behavior in Ivy and grapevine plants, using the FDS based on the experimental data conducted by the authors at LEIF located in Lousã, Coimbra (Portugal). This methodology is an efficient way to broaden the vision of engineers and down the road the policymakers in urban planning sectors.

2. Solution Methodology in FDS

The current FDS formulation applies the low Mach number assumption which yields in filtering out the acoustics from the equations and allowing the variations both in temperature and density, Rehm and Baum (1978). This approximation converts the governing equations into the elliptic format in the LES turbulence model. The FDS code utilizes Deardorff's turbulent eddy viscosity sub-grid closure model by default, Deardorff (1980). Turbulent Schmidt and Prandtl numbers are set to the constant values. The fast chemistry eddy dissipation concept by Magnussen and Hjertager (1977) is used for the formulations of the turbulence-chemistry interaction with the single-step reaction for the fuel and oxidizer combustion using the lumped species method, Fox (2003), discussed in McGrattan et al. (2013).

The Runge-Kutta discretization with high stability-preserving (SSP) is used over time for flow variables. This scheme is second order in both space and time. The Poisson equation is solved using the direct fast Fourier transform (FFT) solver. The mesh is uniform and staggered. The immersed boundary method is applied to treat the flow obstructions in the computational domain.

3. Experimental Tests

Five samples of each type of vegetation fuel were used for the experiments. Tables 1 and 2 contain the characteristics of the samples of the Ivy and the Grapevine in detail:

Table 1 – Details of case studies for the Ivy.

Case Nº	Initial Mass (kg)	Final Mass (kg)	FMC_w (%)	Length (cm)	Height (cm)	Depth (cm)
1	13.73	11.35	49.00	70	80	25
2	5.40	4.30	47.00	65	70	20
3	8.40	7.20	46.30	75	80	25
4	13.26	12.00	36.70	80	80	25
5	17.96	16.70	52.40	75	80	28

Table 2 – Details of the samples of the Grapevine.

Case Nº	Initial Mass (kg)	Final Mass (kg)	FMC_w (%)	Length (cm)	Width (cm)	Depth (cm)
1	1.12	0.14	60.40	124	68	14
2	1.12	0.05	61.20	130	67	16
3	1.10	0.08	51.50	130	68	14
4	1.16	0.12	56.67	133	69	15
5	1.18	0.12	59.21	127	67	13

In Tables 1 and2, the initial and final masses refer to the mass of the plants before and after the burning process in kilograms measured by the instantaneous mass acquisition system. The wet basis moisture content of the species is measured using the digital moisture analyzer.

The first experimental case, the Ivy plant, fixed to a massive vertical plate to mimic the common ivy-green-wall, in which the length in Table 1 refers to the horizontal distance from the point A to B, and the height refers to the distance from B to C, as pointed out in Figure 1. In the case of the Grapevine, the sample has a horizontal configuration on a metal grid, in order to create the scenario of a pergola of vines that is so often seen next to houses. The length in Table 2 is the distance from the point D to E, and width refers to the EF length as illustrated

in Figure 2. Depth (cm) in both cases defines the distance between the opposite sides of each sample. The experiments have been carried out in the environmental conditions with a mean temperature of 26.7 ºC, 23.6 ºC, and relative humidity of 42.4%, and 58.2% for the Ivy and the Grapevine, respectively.

Figure 1. Laboratory tests, Ivy.

Figure 2. Laboratory tests, Grapevine.

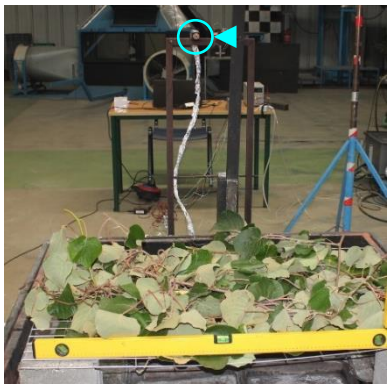

Figure 3. The location of the heat flux sensor.

Figure 4. S-type pitot tube in the experiments.

Fire evolution was recorded by three RGB and two IR cameras. Having the calibration rod at the RHS of Figure 3 (distance between red/white tapes is 20 cm), one can determine the flame dimensions. The thermal behavior of the fire was captured by installing the sets of thermocouples to measure temperatures at different points and the heat release rate was measured using the heat flux sensor installed at a 1.0 m height. The S-type pitot tube is used to detect the uprising convective gas flow velocity from fire installed at a 3.5 m height, as illustrated in Figure 4. The mass-loss rate is measured continuously using the load cells installed at 3 points beneath the test stand with a precision of 10 gr, connected to the summing junction, before connection to the digital indicator.Two trays of denatured alcohol (96% v/v) each containing 200 ml and four trays each containing 250 ml, were used to ignite the Ivy and the Grapevine plants, respectively. The reason for utilizing the trays of alcohol is to imitate the fire in the understory in wildfires and use a sustainable energy source to keep the fire lit in the primitive stages of the experiments.

The dry basis moisture content of each species was measured based on the mass difference between the wet and oven-dry conditions for both pre and post-burn cases as reported in Tables 3 and4**,** as follows

Table 3 – Details of the samples of the Ivy.

	Pre-burn			**Post-burn**		
Plant segment	m_0 (g)	m_f (g)	FMC_d (%)	m_0 (g)	m_f (g)	FMC (%)
Foliage	177.10	63.23	1.80	98.79	54.86	80
0 < Ø < 3 mm	517.60	299.57	0.73	197.84	129.13	53
3 < Ø < 6 mm	300.33	122.44	1.45	281.86	150.64	87
6 < Ø < 10 mm	365.00	166.60	1.19	208.22	93.60	122
Ø > 10 mm	2350.00	973.70	1.41	3202.75	1461.60	119

Table 4 – Details of the samples of the Grapevine.

	Pre-burn			Post-burn		
Plant segment	m_0 (g)	m_f (g)	FMC_d (%)	m_0 (g)	m_f (g)	FMC (%)
Foliage	368.99	137.29	1.69	52.14	31.38	66
0 < Ø < 3 mm	62.32	22.89	1.72	13.22	8.08	64
3 < Ø < 6 mm	147.33	60.82	1.42	93.46	51.90	80
6 < Ø < 10 mm	33.68	17.52	0.92	18.18	13.86	31

In Tables 3 and 4, m_0 is the initial mass, m_f is the final oven-dry mass in grams, and FMC_d is the dry basis moisture content. Different classes of species' segments are divided into 5 categories: i) foliages; ii) parts with a diameter/thickness (Ø) less than 3 mm; iii) from 3 to 6 mm; iv) 6 to 10 mm; and v) larger than 10 mm for both pre and post-burn cases.

4. FDS Modeling

4.1. The Computational Domain

To study the fire behavior and specifically the heat release rate, as an important factor from each species, the structured, staggered grid is generated for two computational domains. For the Ivy case study, the 3D sketch corresponds to Figure 1, and the domain has a dimension of 0.9 m × 1.0 m × 3.7 m in the x, y, and z directions, and contains 3,971,968 grid cells as illustrated in Figure 5, with two trays of alcohol (colored in red). The computational domain for the Grapevine corresponds to Figure 2 and has a dimension of 6.0 m × 6.0 m × 6.0 m in the x, y, and z directions, containing 2,979,200 mesh cells, as depicted in Figure 6. In this case, four trays of alcohol were used to ignite the plant. The details of the samples correspond to the Case Nº 2 of the laboratory tests reported in Tables 1 and 2.

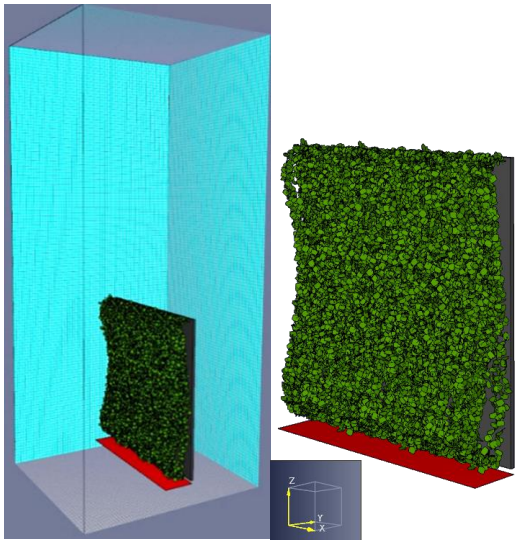

Figure 5. 3D Computational Model, Ivy.

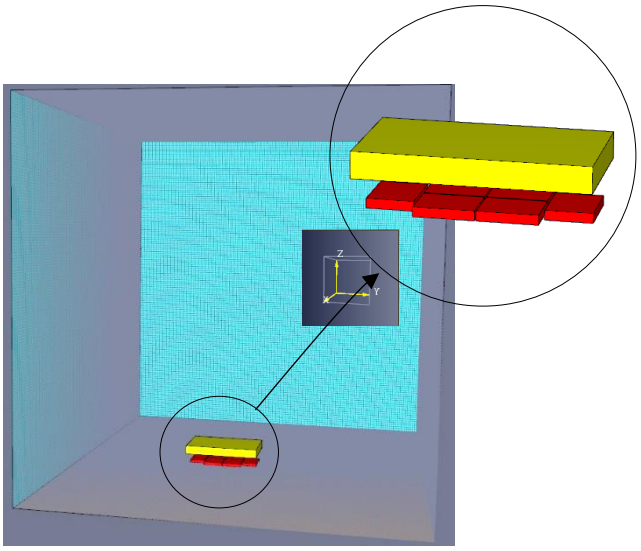

Figure 6. 3D Computational Model, Grapevine.

The boundaries of the CFD of fire in both plants correspond to the details mentioned in Tables 1 to 4. The 3D model for the Ivy is sketched in 3D-CAD SOLIDWORKS software. In the second stage, the geometry is translated into the parallelepiped volume using MATLAB code. In the Grapevine test case, the Lagrangian particle cloud approach is used to model the presence of leaves and twigs along with a possibility for the flow penetration through the cuboid. In both cases, the XY planes beneath the sample are set to be solid and adiabatic, while other boundaries are set as air vents to allow the passage of flows from either side corresponding to the test conditions.

5. Results and Discussion

The FDS simulations of both plants were performed using the equivalent hydrocarbons with CHON contents of 1.0, 1.7, 0.72, 1.0E-3, and 2.0, 3.7, 0.72, 1.0E-3, for the Ivy and the Grapevine, respectively. The Ivy plant is

simulated as a porous obstruction with a 3D configuration inspired by the factual test sample. The Grapevine is modeled using the Lagrangian particle cloud method. The plant is simulated as an ensemble of 4 different classes mentioned inTable 4. The results of the transient LES simulations for both cases are demonstrated in Figures 7 and 8 for the corresponding time-lapse of 0, 5, 15, 20, and 40 seconds in both real-time laboratory experiments and CFD simulations. The heat release rate from FDS for each case study is compared with the corresponding HRR from the laboratory tests conducted at LEIF, in Figures Figure and Figure .

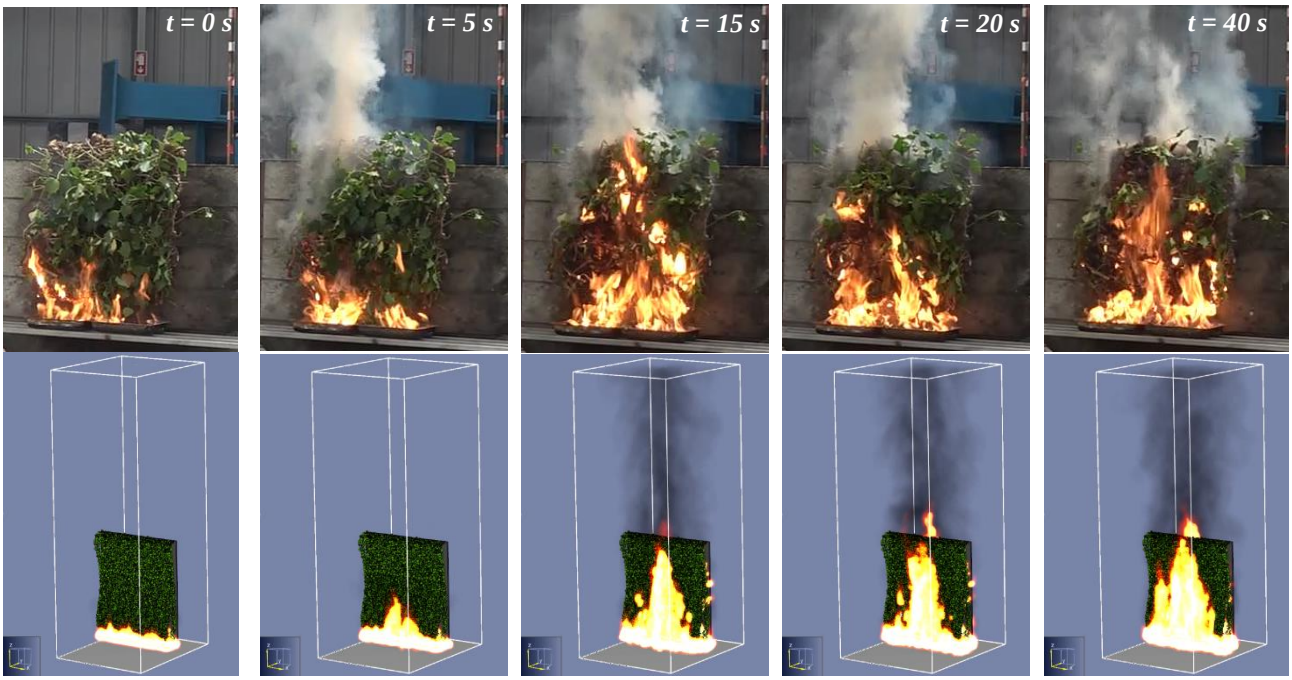

Figure 7. Comparison of the real-time lab experiments with numerical modeling from FDS for the Ivy plant at 0; 5; 15; 20; and 40 s.

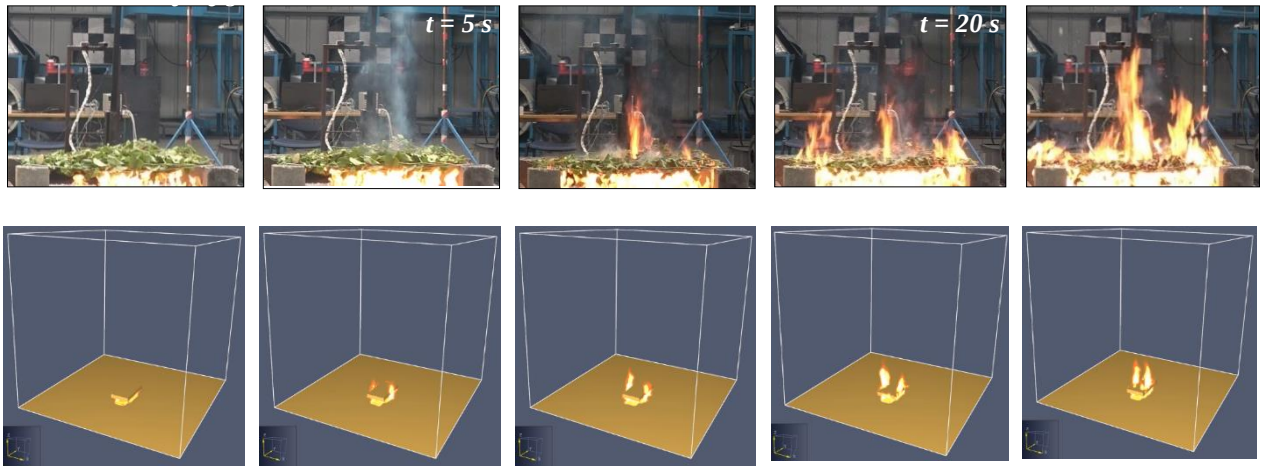

Figure 8. Comparison of the real-time lab experiments with numerical modeling from FDS for the Grapevine plant at 0; 5; 15; 20; and 40 s.

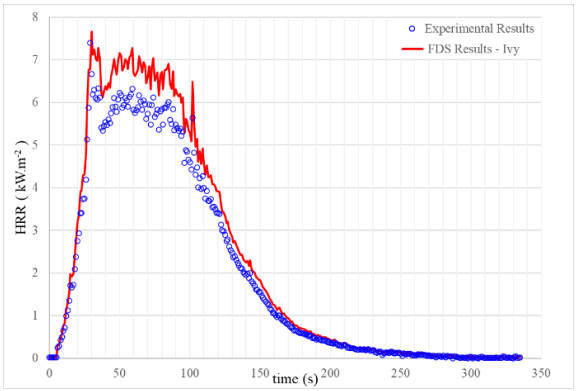

Figure 9. Comparison of HRR for experimental and numerical cases, Ivy.

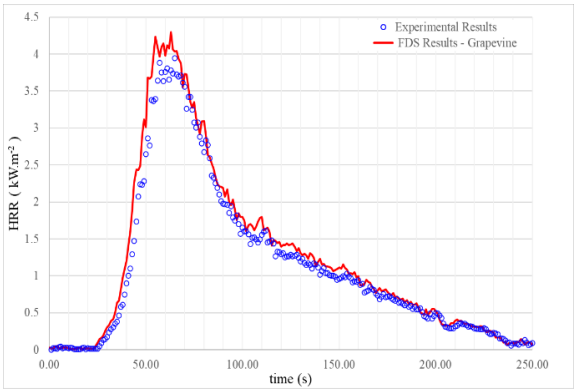

Figure 10. Comparison of HRR for experimental and numerical cases, Grapevine.

6. Conclusion

In this paper, both experimental and numerical modeling of the fire behavior for the Ivy and the Grapevine plants are addressed. Utilizing the capability of FDS in the simulation of fires can be very helpful for fire researchers and experts. The heat release rate from each vegetation species is an important factor that needs to be analyzed for further fire risk analysis and management. Since FDS solely cannot materialize this goal, experimental observations for reliable fire calculations are mandatory. Modeling the fire behavior using the FDS, developed by NIST, the authors could simulate the fire behavior in two forest species with a promising agreement with the experimental data. Moreover, the authors have carried out multiple experiments using different types of plants indigenous to the Mediterranean climate, especially in Portugal. For future work, it is intended to perform FDS modelings based on the available laboratory data to have a complete database for thermal characteristics of the vegetation fuels, their interactions with the surrounding environment, and their contribution to the wildfires. Last but not the least, the final purpose of the ongoing reach is to categorize the forest species as less vulnerable to the hazardous types which can jeopardize lives and residential sites, especially in WUI regions.

7. References

Deardorff, J. W. (1980). Stratocumulus-capped mixed layers derived from a three-dimensional model. Boundary-layer meteorology, 18(4), 495-527.

Fox, R. O. (2003). *Computational models for turbulent reacting flows*. Cambridge university press.

Magnussen, B. F., & Hjertager, B. H. (1977, January). On mathematical modeling of turbulent combustion with special emphasis on soot formation and combustion. In Symposium (international) on Combustion (Vol. 16, No. 1, pp. 719-729). Elsevier.

McGrattan, K., Hostikka, S., McDermott, R., Floyd, J., Weinschenk, C., & Overholt, K. (2013). Fire dynamics simulator user's guide. NIST special publication, 1019(6), 1-339.

Rehm, R. G., & Baum, H. R. (1978). The equations of motion for thermally driven, buoyant flows. Journal of research of the National Bureau of Standards, 83(3), 297.

Basic rules for developing fire sprinkler system in the forest

Ágoston Restás*[1]; Miguel Almeida[2]; Saeid Lotfi[2]; László Bodnár[1]; Domingos Xavier Viegas[2]

[1] University of Public Service, Institute of Disaster Management. 1101 Budapest, Hungary krt. 9-11., {restas.agoston, bodnar.laszlo}@uni-nke.hu
[2] ADAI Association for the Development of Industrial Aerodynamics 3030 289 Coimbra, Portugal {miguelalmeida, saeid.lotfi}@adai.pt; {xavier.viegas@dem.uc.pt}

**Corresponding author*

Keywords

Active protection, sprinkler system, circle footprint, effectiveness, water flow

Abstract

It is a well-observed phenomenon in developed societies that, in order to return to nature, a part of the society seeks to settle near forests or in the forest creating wildland – urban interface (WUI) areas. It has special features and generates significant risk of fire on the experts try to find responds. In the present study, the authors intend to explore the theoretical foundations of the application of the sprinkler system in forest protecting built environment from fires. Understanding and finding basic rules for the effective sprinkler system application can contribute to reduce the impacts caused by fire. As research methods, the authors based their study mostly on geometric calculation and the physics of evaporation, moreover the basic mathematical formulas as well as logical conclusions were also used. Authors found geometry of circle overlapping generates always problems regarding the effectiveness of sprinkler systems. 50% overlapping in longitudinal axis seems to be acceptable solution. In this case overlapping rate is 78% per circle with 1.6 kg.m-2 water coverage levels and 22% of the circles have 0.8 kg.m-2 water coverage level. As another solution, sequentially used system seems good solution for replacing the evaporated water, where 75% of the coverage level is accepted as lowest threshold of the effective rate.

1. Introduction

It is a well-observed phenomenon in developed societies that, in order to return to nature, the middle class of the society seeks to settle near forests or in the forest (Petrov and Marinov 2020). The extent of the danger and the significance of the risk are shown by the emergence of the concept of WUI (Wildland Urban Interface) in recent decades (Caballero et al. 2007; Johnston 2018), which refers to the mixing of the natural and the built environment. The characteristics of fires in the WUI environment have been examined in a number of studies that suggest that both fire prevention and firefighting face new types of challenges (Radeloff et al. 2018; Koksal et al. 2019). There are a number of answers to the questions generated by the challenges, one of which the authors seek to address in this article. The essence of the question in this article, i.e., the aim of the research, is to examine the possibility that sprinkler systems used in closed areas to extinguish fires could be suitable or not for use in open areas, especially for the forest-related built environment to protect them from the destructive effects of fire. There are many researches focusing on the application of sprinkler system, mostly in closed areas, both residential (Bénichou at al. 1999; Butry at al. 2007; Moinuddin 2019) and industrial environments (Garis et al. 2018; Vishnoi 2017), however the option examination of their effectiveness in open space is missing. Therefore, in the present study, the authors intend to explore the theoretical foundations of the application of the sprinkler system in forest fires, and what principal criteria such a system should meet. Authors believe that this contributes to find basic rules for the effective application.

2. Methods

Authors have examined and analysed the relevant literatures focusing on the sprinkler systems to adapt closed areas experiences to open areas. In addition, they conducted discussions with fire engineers to be expert on this subject. As research methods, the authors based their study mostly on geometric calculation and the physics of evaporation, moreover the basic mathematical formulas as well as logical conclusions were also used. Finding

the basic criteria for the effective application of the sprinkler systems this study uses some simplifications and ideal assumptions.

3. Results

Based on Byram's formula (Byram 1959), 2 m flame length takes about 1.2 MWm^{-1} fire intensity, 1 MWm^{-1} assumed in this study. Based on firefighter practice 2 m flame length requires about 5 m wide watered shrub or vegetation strip to stop fire (Bell 1987). Sprinkler heads create circles footprint; in this study, watered circles are 5 m in diameters. 5 m width is effective at cross axis, but left or right side of this axis watered width is less than 5 m, meaning that it is not effective (it is zero at radius distance at the longitudinal axis in case of a simple circle). Therefore, more than 5 m in diameters circles are required or some parts of the circle footprints accepted as limited effectiveness. In this study, authors count with latter option, that is, some parts of the circle footprints have limited effectiveness.

To raise the effective parts of the footprints, authors use overlapping of the circles to ensure the adequate width of the watered strip. In case of 50% overlapping in longitudinal axis the water amount is double in overlapping areas that is 78% (2 x 39%) of the total circle footprint. In case of 5 m in diameter the maximum overlapping is about 4.33 m in cross lane that is 0.67 m less than 5 m.

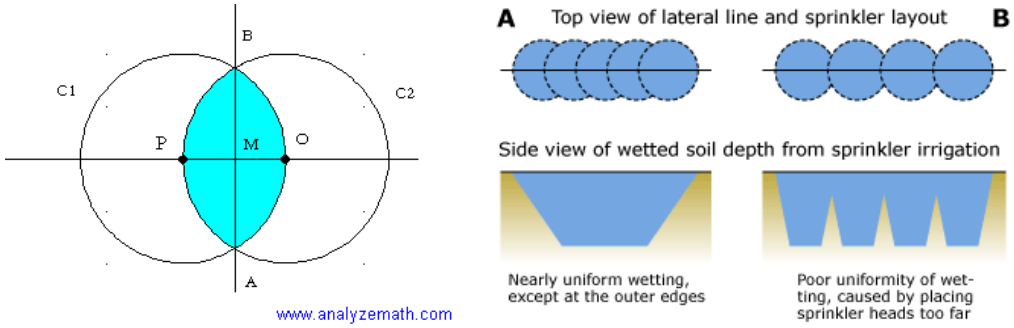

Figure 1. Circle overlapping (left) (Wolfram MathWorld) and footprints of sprinkler systems (right) (Salinity Management Guide 2007)

The 50% overlapping requires more sprinkler head that is 1 head per 2.5 m. Higher position of sprinkler would mean bigger diameter of watered surface however more than 5 m means waste in water use. About 50% overlapping means the optimal water use. It is economical question how many water wasted can balance the higher price of using more sprinkler head. In short time water use is not very important but as a stable, long time existing system can be.

The 1 MWm^{-1} fire intensity, like a shrub or bush fires, requires about 1.2 – 1.8 kgm^{-2} water for stopping fire spread (Murgatroyd 2002; Solarz and Jordan 2010, Delforge 2011). As a thumb rule authors take 1.6 $kg.m^{-2}$ water as effective amount in this study. Each vegetation surface has limited capability of keeping water on its surface. More water than the maximum means that it will flow down the ground and it has no cooling effect. Because of the geometry there is no ideal solution for the effectiveness however it should be optimized or use thumb rules. In this example, 78% (2 x 39%) of overlapping of each circle footprint with 1.6 kgm^{-2} amount of water should be accepted as effective cover rate.

Because of the overlapping of sprinklers' footprint each sprinkler head should produce 0.8 kgm^{-2} water. Top view area of the 5 m in diameter circle is about 20 m^2; it means 1 sprinkler head should produce 16 kg of water (0.8 kgm^{-2} x 20 m^2 = 16 kg). After producing the required amount of water in theoretic and economic view sprinkler heads should stop the water not to waste it.

High temperature as well as low humidity assumed in case of intensive shrub fire; authors count with above 30 ^{0}C degrees. At this temperature thin water layer (or small droplets) on leaves can evaporate quickly. It depends mainly on the temperature, humidity, wind and the surface area of leaves (or the rate of water and surface). Because of the surface tension of the water some additives (e.g., foam agent) is required (ca. 0.1 – 0.5%) to cover the vegetation surface (leaves) with water steadily (or "drops on leaves" is accepted). In case of shrub the leaf area index (LAI) is about 2 that mean a 5 m in diameter circle has 20 m^2 top view area but 40 m^2 of 3D leaf

surfaces. This means that the evaporation surfaces of a 5 m in diameter circle shrub land is about 40 m^2. In ideal case on 31 m^2 leaf surface (78% of 40 m^2) has 0.8 kgm^{-2} water amount, on 9 m^2 (22% of 40 m^2) has 0.4 kgm^{-2} water amount, however it means 1.6 kgm^{-2} and 0.8 kgm^{-2} water amount in top view case.

Rate of water evaporation depends on many factors (Ward and Fang 1999; Marek and Straub 2001), however in this case – sunshine, above 30 ^{0}C degrees, less than 15% humidity, slight wind – as a thumb rule, we can calculate with about 1.5 mmh^{-1}, meaning that overlapping area became totally dry again in 32 minutes, not overlapped area in 16 minutes. After producing the required water – 16 kg per 20 m^2 top view footprint of sprinkler head – because of the evaporation theoretically there are two options:

A) Continuously used sprinklers to compensate the evaporation.

B) Sequentially used sprinklers to replace the evaporated amount of water.

Case A): Because the evaporation is 16 kg per 20 m^2 (40 m^2 leaf surface) per 16 min, the rate is 1 $kg.min^{-1}$ per sprinkler head footprint area (20 m^2); it means requirement for compensate evaporation loss is 1 $kgmin^{-1}$ per sprinkler head. It can be very difficult to find applicable sprinkler head. Moreover, in case of continuously used sprinklers water mist will change the circumstances drastically – cool down the sprayed area and humidity up to 100% – meaning that the evaporation will be reduced even more, as an end point of the function at 100% air humidity actually there is no evaporation.

In case B) the question is that, what is the effective frequency of switching on and off the sprinkler heads. This frequency should depend on the acceptable coverage level of water comparing to the required 16 kg per sprinkler head footprint (20 m^2). Authors think 75% of the coverage level – that is 12 kg per sprinkler head footprint (20 m^2) – is acceptable. It means 22% will be covered by 0.6 kgm^2 (in 3D with LAI: 0.3 kgm^{-2}) while 78% of the head footprint will be covered by 1.4kgm^{-2} (in 3D with LAI: 0.7 kgm^{-2}). Taking into account the evaporation rate that is 1.5 $mm.h^{-1}$ the required switch on frequency is 4 min (0.1 kgm^{-2} evaporated water per 1.5 mmh^{-1} = 1.5 $kgm^{-2}h^{-1}$ evaporation rate). Counting with 4 min sequentially used sprinkler heads the coverage level of non-overlapping area swings between 75-100%, that is 0.6-0.8 $kg.m^{-2}$ on top view footprint, however in case of overlapping area it swings between 87.5-100% that is 1.4-1.6 kgm^{-2}.

Theoretically, on the overlapping area the coverage level should jump up to 1.8 kgm^{-2} that is 112.5% however leaves have limited capability to keep water on its surface[5]. In case of shrubs, it is about 1.2 – 1.8 kgm^{-2}, in this example 1.6 kgm^{-2}. More water than enough means lost as well as the amount above the upper limit of effectiveness. This means that 12.5% as an extra is not effective because it goes down to the ground. Logically each sprinkler head footprint has one overlapping part that is 39% of the total area. In case of 5 m in diameter circle it takes 7.8 m^2 of 20 m^2. The lost water is 0.2 kgm^{-2} x 7.8 m^2 = 1.56 kg. This amount takes 23.4 kg wasted water of the total of 60 kg used water per hour.

The 300 m long wetting zone requires 120 sprinkler heads (2.5 m per head). Total water amount – to reach the protection capability (120 heads x 20 m^2 x 0.8 kgm^{-2}) – takes 1,920 kg water. Water consumption of the system – in case of 4 min sequential use of heads replacing the evaporated water (60 kgh^{-1} per head x 120 heads) – takes about 7,200 kg water per hour. Wasted part of the used water during service is 39% that means 2,808 kg water per hour.

4. Conclusions

There are many studies dealing with the application of sprinkler systems to suppress fires or to stop fire spread in residential settlements or in industrial environments but there is no study focusing on the usage of sprinkler system stopping fire propagation in open spaces or rural area. Du to serious fires happened in the near past all around the world this study try to find some fundamentals to help future studies focusing on similar topics.

Results say that the geometry of circle overlapping generates always problems regarding the effectiveness of sprinkler systems. 50% overlapping in longitudinal axis seems to be acceptable solution (2.5 m per head). In this case overlapping rate is 78% per circle with 1.6 $kg.m^{-2}$ water coverage levels and 22% of the circles have

[5] In case of aged forest crown it is about 5 kgm^{-2}.

0.8 kgm^{-2} water coverage level. Sequentially used system seems good solution for replacing the evaporated water, where 75% of the coverage level is accepted as lowest threshold of the effective rate. As an example, 300 m long protection zone requires 120 sprinkler heads. Building up this zone it requires 1,920 kg water for wetting up, then keeping it in service it requires 7,200 kgh^{-1} water. In this case 39% of the service water is lost because it is above the upper limit of effectiveness.

As a final conclusion, sprinkler system can be an effective solution against fire creating a barrier or for stopping it in a professional point of view however both the issue of economic and the technical optimization require further study.

5. Acknowledgements

Three of the co-authors of this paper participate in the House Refuge Project (PCIF/AGT/0109/2018) which is funded by the Portuguese Foundation for Science and Technology (www.fct.pt), to whom they would like to express their acknowledgement.

6. References

Bell A, (1986/87) Water bombing of fires: no magic solution. Ecos 50 Summer http://www.ecosmagazine.com/?act=view_file&file_id=EC50p18.pdf (available: 04.03.2022)

Bénichou N, Yung D, Hadjisophocleous G, (1999) Impact of fire department response and mandatory sprinkler protection on life risks in residential communities. National Research Council: Ottawa, Canada

Butry D.T, (2012) Comparing the performance of residential fire sprinklers with other life-safety technologies. *Accident Analysis and Prevention*, **48** 480-494.

Butry D.T, Brown M.H, Fuller S.K, (2007) Benefit-cost analysis of residential fire sprinkler systems. Technical Report, NISTIR 7451, National Institute of Standards and Technology: Gaithersberg, MD. United States

Byram G.M., (1959) Combustion of Forest Fuels. In Forest Fire: Control and Use; McGraw-Hill: New York, NY, USA, 61–89.

Delforge P, (2001) Guide d'emploi des moyens aeriens en feux de forets, Minister de L'Interieur, (Aerial Firefighting Handbook) Paris, France

Garis L, Singh A, Clare J, Hughan S, Tyakoff A, (2018) Sprinkler Systems and Residential Structure Fires-Revisited: Exploring the Impact of Sprinklers for Life Safety and Fire Spread Background to Sprinkler Systems and Life Safety. Technical Report, University of the Fraser Valley https://www.researchgate.net/publication/324680385 (available 10.01.2022)

Koksal K, Mc Lennan J, Every D, (2019). Australian wildland-urban interface householders' wildfire safety preparations: 'Everyday life' project priorities and perceptions of wildfire risk. *International Journal of Disaster Risk Reduction*, **33** (1) 142-154.

Marek R, and Straub J, (2001) Analysis of the evaporation coefficient and the condensation coefficient of water. *International Journal of Heat Mass Transfer*, **44**,39–53.

Moinuddin K, (2019) Reliability of Fire Sprinkler System. Conference presentation, 16th International Fire & Safety Expo Korea, doi: 10.13140/RG.2.2.31752.06408

Murgatroyd I.R, (2002) Forest and Moorland Fire Suppression. Technical Note, Forestry Commission, Edinburg, United Kingdom

Petrov K, Marinov P, (2020). Development of suburbanization in Europe. *Journal of Bio-based Marketing* **3** (1) 71-81.

Radeloff C.V, Helmers D, Kramer A, (2018). Rapid growth of the US wildland-urban interface raises wildfire risk. Proceedings of the National Academy of Sciences, 95 3314-3319.

Salinity Management Guide: Effect of irrigation application method on salinity of soil water. https://watereuse.org/salinity-management/lz/lz_5.html (available: 15.03.2022)

Solarz P, Jordan C, (2000) Airtanker drop guides; USDA Forest Service, Technology and Development Program, 0057-2848-MTDC, September 2000, 5100/5700

U.S. Fire Administration (2008) USFA position on residential fire sprinklers. http://www.usfa.fema.gov/about/position_ statements/sprinklers_position.shtm (available 26.02.2022)

Vishnoi K, (2017). Piping layout for fire sprinkler system: An overview. *International Journal of Engineering and Applied Sciences* **4** (3) 17-21

Ward C, and Fang G, (1999) Expression for predicting liquid evaporation flux: Statistical rate theory approach. *Physical Review* E, **59**, 429–440.

Wolfram MathWorld, (2022) Circle – Circle Intersection. https://mathworld.wolfram.com/Circle-CircleIntersection.html (available: 18.01.2022)

Burnover events identified during the 2018 Camp Fire

Eric D. Link*; Alexander Maranghides

National Institute of Standards and Technology, 100 Bureau Dr, Gaithersburg, MD 20899, USA, {eric.link, alexander.maranghides}@nist.gov

**Corresponding author*

Keywords

Burnover; Camp Fire; entrapment; evacuation; wildland-urban interface

Abstract

The most destructive and deadly wildland-urban interface (WUI) fire in California history burned through communities in Butte County, California on November 8, 2018. Characterized by strong winds, dry fuel conditions, and steep terrain, the fire spread more than 12 km in the first 2 hours after ignition, triggering mass evacuations. The fire destroyed over 18 000 structures and caused 85 fatalities, mostly within the first 12 hours of the incident. Extensive data collection was conducted after the fire, gathering detailed first-hand account information from technical discussions with 157 first responders, photos and videos, emergency call recordings, and first responder radio logs, among other data to support an in-depth case study of the incident. Subsequent analysis and data integration yielded a complete timeline reconstruction of the first 24 hours of the event, as well as additional observations of the fire behavior. This report presents novel findings related to 23 identified life-threatening entrapment/burnover events, in which fire trapped or overtook people and compromised escape routes. These events affected the safety of hundreds of civilians and dozens of first responders, and occurred throughout the fire area. Many entrapments/burnovers impacted civilians evacuating in heavy traffic on major artery roadways or otherwise blocked evacuation routes and first responder access. Some resulted in injuries and fatalities. As the frequency of fast-moving fires requiring last-minute large-scale evacuations increases, the risk of similar events is high, particularly in intermix communities where the presence of primarily wildland vegetation along evacuation routes and some secondary roadways, likely amplified by local topography and wind, can result in significant entrapments/burnovers.

1. Introduction

1.1. The 2018 Camp Fire

The Camp Fire, which occurred in Butte County in northern California in 2018, was the most destructive and deadly fire in California history (CAL FIRE 2022). The fire first ignited shortly before dawn on November 8, 2018 near Camp Creek Road (for which the fire is named), in the community of Pulga, located in the Feather River Canyon (CAL FIRE 2019a). Dry fuel conditions, a strong wind event, and steep wind-aligned topography presented conditions conducive to rapid fire spread. By 07:30, just over one hour after ignition, high winds up to 22 m/s had driven the fire from the origin, over a ridge, and into the community of Concow 6.4 km to the southwest. By 08:00, numerous spot fires were igniting throughout the eastern portion of the town of Paradise an additional 6 km southwest of Concow. Structures in Paradise were burning by 08:30 as thousands of civilians began evacuating. The rapid fire spread led to 85 fatalities (Butte County Sheriff 2019; CAL FIRE 2019b; Butte County District Attorney 2020), and within 12 hours a majority of the structures in Paradise had burned. Ultimately, over 18 000 structures were destroyed and over 700 structures were damaged by the fire (Wallingford 2018; CAL FIRE 2022). Figure 1 depicts the location of Butte County within the state of California with the final fire perimeter shown in red.

After a preliminary reconnaissance (Maranghides *et al.* 2020a; Maranghides *et al.* 2020b), it was determined that an in-depth case study of the incident was feasible due to the data available and would provide scientific merit. Subsequent data collection and data integration were conducted to reconstruct a detailed timeline of the fire to provide a foundation for additional data analysis (Maranghides *et al.* 2021). The results presented here constitute findings related to the numerous life-threatening burnover events that were identified during the case study (Maranghides *et al.* 2021; Maranghides *et al.* 2022). The interested reader is encouraged to study (Maranghides *et al.* 2021) for the most detailed fire progression data available. While over 2200 data points

were included, the spatial resolution and detail required to provide accurate temporal contours is incredibly high and is not possible at this scale without consistent widespread aerial measurement. An animation of the analyzed fire observation data showing the fire progression is available from (National Institute of Standards and Technology 2021) which provides a non-interpolated view of fire progression.

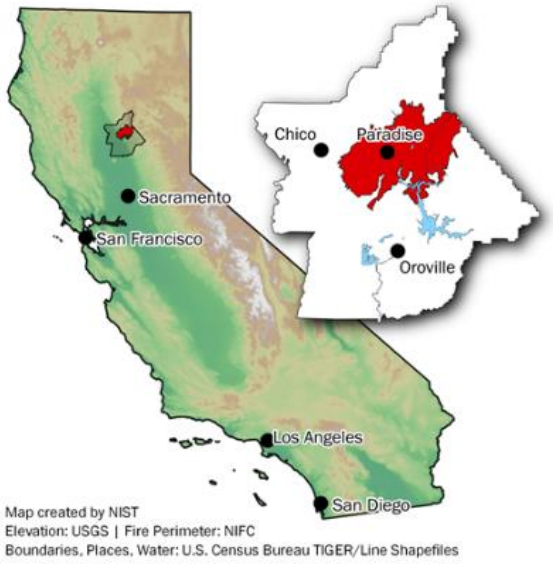

Figure 1 – Location of Butte County in California and the Camp Fire (red).

1.2. Entrapments and Burnovers

Entrapments in wildland fires are defined by the National Wildfire Coordinating Group (NWCG) as "a situation where personnel are unexpectedly caught in a fire behavior-related, life-threatening position where planned escape routes or safety zones are absent, inadequate, or compromised. An entrapment may or may not include deployment of a fire shelter for its intended purpose. These situations may or may not result in injury. They include 'near misses.'" (Page and Freeborn 2019; National Wildfire Coordinating Group n.d.-a). A burnover is further defined as an entrapment in which "fire moves through a location or overtakes personnel or equipment…often resulting in personal injury or equipment" (Page and Freeborn 2019; National Wildfire Coordinating Group n.d.-b). A recent report by Page et al. (Page *et al.* 2019), considering a comprehensive database of firefighter entrapments in the US, indicates entrapment rates have been steady at about 9 incidents per year.

In the US, most entrapment documentation is related to firefighters during operations, rather than civilians. Internationally, there are few studies about burnover events involving civilians unless they are focused on fatalities (Blanchi *et al.* 2014; Diakakis *et al.* 2016; Haynes *et al.* 2019; Molina-Terrén *et al.* 2019). In general, the number of entrapments or burnover events involving civilians is likely undercounted because they are not widely publicized, reported, or studied. As more fires burn rapidly into WUI areas with little time to evacuate, the potential for burnovers is increasing. Recent events with civilian fatalities while attempting evacuation have been documented in Portugal (Viegas *et al.* 2017; Viegas *et al.* 2019) and Greece (Horowitz 2018; Xanthopoulos and Athanasiou 2019).

During the Camp Fire, numerous events occurred where fire temporarily restricted through-access on a major traffic artery or a secondary road, or trapped civilians or first responders amid dangerous conditions. The events varied in intensity and duration. Some impacted civilian evacuation while others impacted first responders only. Some burnovers resulted in civilian fatalities, civilian and first responder injuries, and destruction and damage of civilian and first responder vehicles. In many cases, burnovers did not result in fatalities, injuries, or damage. These were instances in which fire blocked the road and civilians caught in traffic and/or first responders attempting to access the scene either waited for conditions to improve or opted to take another route, if available. These events could be interpreted as entrapments or "near misses" with respect to the NWCG definitions but are included in this report as they have significant impact on civilian and first responder life safety. All identified

events were grouped and labeled as burnovers in this report for simplicity, acknowledging the uncertainty in the data regarding exact extent and accounting for all potential people in the event.

Specifically understanding the fire development and progression associated with individual burnover events will require in-depth spatial and temporal (pre-, during, and post-fire) data collection of local fuels, weather, and topography. This detailed data was beyond the scope of the current work, which identified the prevalence of these types of events during the Camp Fire.

2. Identified Burnovers

The fire progression timeline report (Maranghides *et al.* 2021) includes 23 technical findings related to fire progression and fire behavior. Four of the findings relate to the burnover events that were identified during the case study data analysis. The findings were:

F15. Multiple burnovers occurred during the Camp Fire.

F16. Burnovers adversely affected pre-planned evacuation routes and led to use of Temporary Refuge Areas (TRAs).

F17. Intense vegetation and structure fires occurred along roadways and resulted in multiple road closures which adversely impacted response and evacuation activities.

F18. Fire resulted in downed utility poles along roadways and throughout the communities. The downed poles, along with the associated electrical and utility lines, blocked multiple streets and impaired access for response and evacuation.

Nearly two dozen entrapment/burnover events were identified in the analysis and compilation of data collected from 157 individual first responder accounts as well as numerous photos and videos. Additional detail about the data collection and data integration processes can be found in (Maranghides *et al.* 2021). The detailed narrative of each event is beyond the scope of this paper, but is documented in (Maranghides *et al.* 2021; Maranghides *et al.* 2022), and conveys the range of different scenarios under which burnovers occurred. The presented list does not include an analysis of the local conditions associated with the 85 documented fatalities. Additional burnovers may have occurred that were not captured during the data collection process; however, there is high confidence that nearly all of the large burnover events are accounted for based on the total combined dataset of fire observations (Maranghides *et al.* 2021), traffic conditions, burned vehicles, and TRAs (Maranghides *et al.* 2022).

The 23 documented burnover events occurred throughout the fire area within the first 26 hours of the incident, beginning almost immediately as fire impacted the community of Concow. The location of each event is marked in Fig. 2 with their corresponding ID number, with additional details listed in Table 1. These events affected civilian and/or first responder evacuation and movement, with 12 occurring on major egress arteries (identified by bold type in Table 1).

Many of the entrapments/burnovers significantly impacted evacuation (n=17) and required the formation/utilization of TRAs (n=9) to maintain life safety for residents and firefighters. In at least two cases, fire shelters were deployed by firefighters to reduce radiative exposures to civilians and first responders. Several entrapments/burnovers resulted in civilian or first responder injuries and civilian fatalities.

The burnovers were divided into two categories with respect to risk of injury or death. Fourteen burnovers were identified as “Category 1,” representing the highest potential of death/injury (highlighted red in Table 1), and nine as less-hazardous “Category 2” events. Of the 11 burnovers that occurred before 10:00 on November 8, nine were listed as Category 1, and two as Category 2. All but one of the Category 1 burnovers on the morning of November 8 significantly impacted civilian evacuations. Seven of the 14 Category 1 burnovers resulted in the formation of Temporary Refuge Areas (TRAs). Significant civilian evacuation traffic played a major role in the population exposed to these burnover events.

Local conditions dictated the spatial and temporal extent of each burnover. Burnover durations averaged nearly two hours and were influenced by the type and quantity of vegetative and other fuels in the area, as well as the spatial extent of the event. Overall, vegetation setbacks from the roadway (estimated using photos, video, and imagery) ranged from 0 m to 10 m; however, in most instances the setbacks were 3 m or less. Many events

affected significant lengths of roadway, on average estimated over 800 m per burnover, and ranged from 150 m up to 3 km. Road widths ranged from 3 m on narrow tertiary local roads to 23 m wide multi-lane primary arteries.

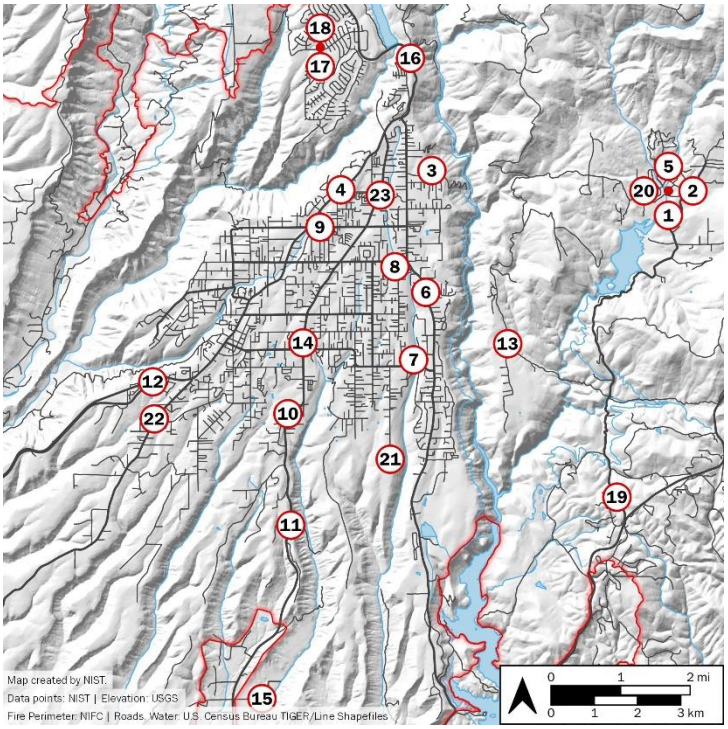

Figure 2 – Locations of the 23 NIST-identified burnover events.

Table 1 – List of burnover details.

ID[a]	Location[b]	Burnover Initiation	Burnover Duration (min)	Road Width (m)	Vegetation Setback (m)	Roadway Length Affected[c] (m)	Impacted Civilian Evacuation (Y if yes)	Fire Shelter(s) Deployed (Y if yes)	TRA Formed (Y if yes)
1	Hoffman Rd	07:50	40	3	0–2, more at creek	250	Y	Y	Y
2	**Concow Rd**	07:50	70	7	0–1	1000	Y		
20	Camelot Ln	07:55[d]	50	6	0	n/a	Y		Y
3	Chapman Ln	08:30	n/d[e]	3	0–3	250			
4	**Skyway** (upper)	08:30	360	8	0–10	2600	Y (street was gridlocked)		Y
5	Windermere Ln	08:35[d]	n/d	4	0–2	1100	Y (fatality)		
6	**Pentz Rd**	08:45	150	8	0–1	1300	Y (street was gridlocked)		Y
7	**Pearson Rd**	09:15	60	11	1–3	800	Y (street was gridlocked)	Y	Y
8	**Bille Rd**	09:25	140	8	0–2	500	Y (street was blocked)		Y
21	Edgewood Ln	09:30	n/d	3	0–3	250	Y (fatalities)		
9	**Wagstaff Rd**	09:30	60	8	0–3	500	Y		
10	**Clark Rd** / American Way	10:00	120	11	1–3	700	Y		
11	**Clark Rd** / Airport Rd	10:00	90	9	1	1500	Y		
12	**Skyway** (lower)	10:15	90	7–20	1–3	1000	Y		
13	Jordan Hill Rd / Granite Hill Rd	11:30	n/d	5	0–4	800	Y		
22	**Neal Rd**	11:30	90	6	1–3	800	Y (street was gridlocked)		
23	**Clark Rd**/Cypress Ln	11:45	n/d	8	0–6	1300	Y		
14	**Clark Rd** / Black Bear Diner	13:10[d]	n/d	23	3 (structure)	150			
15	Rattlesnake Flats Rd	15:15	15	3	0	300			
16	Coutolenc Rd	00:00 (Nov 9)	120	7	0–2	3000			Y
17	Chestnut Cir	06:00 (Nov 9)	n/a	9	0–1	150			
18	Ponderosa Way	07:15 (Nov 9)	n/d	12	0–3	400	Y		Y
19	Concow Fire Station 37	07:15 (Nov 9)	n/d	9	0–3	600			Y

[a] Events are listed chronologically. ID #20–23 are out of sequence because they were added in a second round of analysis.
[b] Roadways in **bold** denote major artery roads significant for evacuation.
[c] The roadway segment affected by each burnover was estimated from the technical discussions.
[d] First time of observation. Burnover conditions existed prior to the first recorded observation.
[e] No data.

3. Discussion / Implications of Findings

One may first notice the large number of identified events. The mission focus of the fire service, the relatively specific definition of burnovers versus entrapments, as well as the potential negative stigma of burnovers (Strohmeyer *et al.* 2018), may all combine to a general under-reporting of such events (Jolly *et al.* 2019). Additionally, the majority of reported entrapments are likely reported in wildland fire settings opposed to WUI fire settings in more developed infrastructure with additional urban fire service mutual aid. The fact that 23 individual instances were identified within one incident suggests that this may be a more frequent issue, specifically in the context of WUI fires. Fourteen incidents were labeled “Category 1,” indicative of higher severity and significant threat to life.

It is important to note that these events also had a significant impact on civilians. Overall, these events have a different narrative compared to many firefighter-only burnovers experienced during suppression efforts. Of the 23 events, only 2 include officially documented firefighter injuries sustained during fire suppression efforts.

Those events, #15 and #18, injured 5 firefighters and were reported in an after action "Green Sheet" report (CAL FIRE 2018). The rest of the identified events were dominated by civilian presence, often with the assistance or guidance of first responders to locate a safer TRA. In very few cases was active suppression used or available to protect civilians from fire exposures.

Half of the events occurred in Paradise during overlapping time windows (IDs 4, 6, 7, 8, 21, 9, 10, 11, 12, 22, 23) early in the incident, stressing emergency resources. Simultaneous events, particularly across large spatial areas, significantly stretch the resources available to respond to each event to protect evacuating civilians. Early evacuation is key; however, this may not always be feasible. In rapidly developing events, a well-planned and efficient evacuation plan will need to be tailored to local conditions. The need to protect civilian evacuations may significantly change the operations of the fire service, resulting in additional fire spread and structure/infrastructure loss.

While 14 of the 23 incidents occurred before 11:00 on Day 1 (when more civilians were involved), several did occur the following day on November 9, impacting first responder operations. The potential for such events must be considered throughout the entire incident, not only for first responders but also for situations where fire continues to progress and impact additional populated areas. There are also significant long-lasting effects of burnovers in WUI areas, particularly as abandoned/burned vehicles and burned and downed power poles and lines can block passage for hours, impacting evacuation and first responder operations.

4. Conclusions

This portion of a greater case study into the 2018 Camp Fire in Butte County, California presents a unique dataset of burnover events that impacted mass evacuations during a WUI fire. Twenty-three burnover events threatening the safety and trapping or restricting movement of first responders and hundreds of evacuating civilians, were identified through in-depth analysis of data collected from technical discussions with first responders. Seventeen burnovers directly impacted the evacuation of civilians, 12 of which occurred on major evacuation roadways. Most burnover events lasted between 1 and 2 hours in duration and impacted an average roadway length of 800 m. Two events injured firefighters and were documented by the incident in official "Green Sheet" reports.

This is an important area of study as the frequency of fast-moving fires requiring last-minute large-scale evacuations increases. In intermix communities, the presence of primarily wildland vegetation along evacuation routes and some secondary roadways, likely amplified by local topography and wind, can result in significant entrapments/burnovers. There is limited technical information to provide reliable guidance on the relationship among vegetative fuel type, density, and setback from the roadway, along with topography and exposures, that can be used to develop reliable guidance for the protection of egress arteries against burnovers. Additional research is needed to characterize fire behavior that leads to burnovers and to quantify burnover severity. Such a study would need to capture the necessary fuels, weather, and fire behavior information. This work must be undertaken immediately following the event, as much of the data will originate from first-hand observations and perishable field data, such as post-fire fuel consumption measurements. This information would inform fuel setback guidance for primary egress arteries and provide technical input to evacuation plans.

5. Acknowledgements

The authors would like to acknowledge Ruddy Mell, Steven Hawks, Mike Wilson, Will Brewer, Chris Brown, Bob Vihnaneck, and Doug Walton for their contributions to the overall case study effort. The authors would also like to acknowledge the many first responders and community officials who contributed their time and information to the case study, as well as the data collection teams who participated in the technical discussions to collect much of the data used to compile the information in this report.

6. References

Blanchi, R, Leonard, J, Haynes, K, Opie, K, James, M, Dimer de Oliveira, F (2014) Environmental circumstances surrounding bushfire fatalities in Australia 1901–2011. *Environmental Science & Policy* **37**, 192–203. https://doi.org/10.1016/j.envsci.2013.09.013

Butte County District Attorney (2020) The Camp Fire Public Report: A Summary of the Camp Fire Investigation. Butte County District Attorney, (Oroville, CA) Available at https://www.buttecounty.net/Portals/30/CFReport/PGE-THE-CAMP-FIRE-PUBLIC-REPORT.pdf?ver=2020-06-15-190515-977 [Verified June 2022].

Butte County Sheriff (2019) Camp Fire Update. Press Release, September 25, 2019. Oroville, CA. Available at http://www.buttecounty.net/sheriffcoroner/News-Center/ArtMID/4964/ArticleID/1370/Camp-Fire-Update [Verified June 2022]

CAL FIRE (2018) Informational Summary Report of Serious or Near Serious CAL FIRE Injuries, Illnesses and Accidents (Green Sheet). Available at https://www.firefighterclosecalls.com/wp-content/uploads/2018/12/18-CA-BTU-016737-Camp-Green-Sheet.pdf [Verified June 2022].

CAL FIRE (2019a) CAL FIRE Investigators Determine Cause of the Camp Fire. Press Release, May 15, 2019. Available at https://www.fire.ca.gov/media/5121/campfire_cause.pdf [Verified June 2022]

CAL FIRE (2019b) Top 20 Deadliest California Wildfires. (Updated August 8, 2019). Available at https://www.fire.ca.gov/media/5512/top20_deadliest.pdf [Verified August 2019]

CAL FIRE (2022) Top 20 Most Destructive California Wildfires. (Updated January 13, 2022). Available at https://www.fire.ca.gov/media/t1rdhizr/top20_destruction.pdf [Verified June 2022]

Diakakis, M, Xanthopoulos, G, Gregos, L (2016) Analysis of forest fire fatalities in Greece: 1977–2013. *International Journal of Wildland Fire* **25**, 797–809. https://doi.org/10.1071/WF15198

Haynes, K, Short, K, Xanthopoulos, G, Viegas, D, Ribeiro, LM, Blanchi, R (2019) Wildfires and WUI Fire Fatalities. In 'Encyclopedia of Wildfires and Wildland-Urban Interface (WUI) Fires'. (Ed S Manzello) (Springer, Cham). https://doi.org/10.1007/978-3-319-51727-8_183-1

Horowitz, J (2018) As Greek Wildfire Closed In, a Desperate Dash Ended in Death. The New York Times, July 24, 2018. Available at https://www.nytimes.com/2018/07/24/world/europe/greece-wildfire.html [Verified June 2022]

Jolly, M, Butler, B, Page, W, Freeborn, P (2019) An Assessment of Research Needs Related to Wildland Firefighter Safety. Final Report JFSP Project ID: 18-S-01-1. Available at https://www.firescience.gov/Publications/Final_Report_JFSP_18-S-01-1.pdf [Verified June 2022].

Maranghides, A, Mell, W, Hawks, S, Wilson, M, Brewer, W, Link, E, Brown, C, Murrill, C, Ashley, E (2020a) Preliminary Data Collected from the Camp Fire Reconnaissance. National Institute of Standards and Technology, NIST Technical Note 2128. (Gaithersburg, MD). https://doi.org/10.6028/NIST.TN.2128

Maranghides, A, Mell, WR, Hawks, S, Wilson, M, Brewer, W, Link, E, Brown, C, Murrill, C, Ashley, E (2020b) Camp Fire Preliminary Reconnaissance. National Institute of Standards and Technology, NIST Technical Note 2105. (Gaithersburg, MD). https://doi.org/10.6028/NIST.TN.2105

Maranghides, A, Link, E, Mell, W, Hawks, S, Wilson, M, Brewer, W, Brown, C, Vihnaneck, B, Walton, WD (2021) A Case Study of the Camp Fire — Fire Progression Timeline. National Institute of Standards and Technology, NIST Technical Note 2135. (Gaithersburg, MD). https://doi.org/10.6028/NIST.TN.2135

Maranghides, A, Link, E, Mell, W, Hawks, S, Brown, C, Walton, WD (2022) A Case Study of the Camp Fire — Notification, Evacuation, Traffic, and Temporary Refuge Areas. National Institute of Standards and Technology, NIST Technical Note In Progress. (Gaithersburg, MD).

Molina-Terrén, DM, Xanthopoulos, G, Diakakis, M, Ribeiro, L, Caballero, D, Delogu, GM, Viegas, DX, Silva, CA, Cardil, A (2019) Analysis of forest fire fatalities in Southern Europe: Spain, Portugal, Greece and Sardinia (Italy). *International Journal of Wildland Fire* **28**, 85–98. https://doi.org/10.1071/WF18004

National Institute of Standards and Technology (2021) Camp Fire—Fire Progression (animated .gif). (Updated February 8, 2021). Available at https://www.nist.gov/el/fire-research-division-73300/wildland-urban-interface-fire-73305/nist-investigation-california-3 [Verified June 2022]

National Wildfire Coordinating Group (n.d.-a) Entrapment. Available at https://www.nwcg.gov/term/glossary/entrapment [Verified June 2022]

National Wildfire Coordinating Group (n.d.-b) Burnover. Available at https://www.nwcg.gov/term/glossary/burnover [Verified June 2022]

Page, WG, Freeborn, PH (2019) Entrapment. In 'Encyclopedia of Wildfires and Wildland-Urban Interface (WUI) Fires'. (Ed S Manzello) (Springer, Cham). https://doi.org/10.1007/978-3-319-51727-8_183-1

Page, WG, Freeborn, PH, Butler, BW, Jolly, WM (2019) A review of US wildland firefighter entrapments: trends, important environmental factors and research needs. *International Journal of Wildland Fire* **28**, 551–569. https://doi.org/10.1071/WF19022

Strohmeyer, J, Burbridge, B, Carey, S, Zimmerlee, R, Weaver, T, Apuzzo, G, Dotson, T (2018) Horse Park Fire Entrapment Facilitated Learning Analysis. Available at https://www.wildfirelessons.net/HigherLogic/System/DownloadDocumentFile.ashx?DocumentFileKey=6b7b737c-1ab1-a04d-bf39-27b9d97e5883&forceDialog=0 [Verified June 2022]

Viegas, DX, Almeida, MF, Ribeiro, LM, Raposo, J, Viegas, MT, Oliveira, R, Alves, D, Pinto, C, Jorge, H, Rodrigues, A, Lucas, D, Lopes, S, Silva, LF (2017) O Complexo de Incêndios de Pedrógão Grande e concelhos limítrofes, iniciado a 17 de junho de 2017. Centro de Estudos sobre Incêndios Florestais (CEIF/ADAI/LAETA), (Coimbra, Portugal).

Viegas, DX, Almeida, MA, Ribeiro, LM, Raposo, J, Viegas, MT, Oliveira, R, Alves, D, Pinto, C, Rodrigues, A, Ribeiro, C, Lopes, S, Jorge, H, Viegas, CX (2019) Análise dos Incêndios Florestais Ocorridos a 15 de outubro de 2017. Centro de Estudos sobre Incêndios Florestais (CEIF/ADAI/LAETA), (Coimbra, Portugal).

Wallingford, N (2018) Camp Incident Damage Inspection Report. CAL FIRE, (Sacramento, CA).

Xanthopoulos, G, Athanasiou, M (2019) The Fire Globe: Attica Region, Greece (July 2018). *Wildfire* (Century Publishing: Post Falls, Idaho) **28**(2), 18–21.

Community-level risk assessment of structure vulnerability to WUI fire conditions in the 2017 Tubbs Fire

Raquel S.P. Hakes[1,2,‡]; Maria Theodori[3,4,‡]; Chris Lautenberger[4]; Linda Qian[5]; Michael J. Gollner*[3]

[1]*University of Maryland, College Park. College Park, Maryland, USA*
[2] *Current Affiliation: Sandia National Laboratories[†]. Livermore, California, USA, {rshakes@sandia.gov}*
[3] *University of California Berkeley. Berkeley, California, USA, {theodori, mgollner}@berkeley.edu*
[4]*Reax Engineering. Berkeley, California, USA, {lautenberger@reaxengineering.com}*
[5] *University of Chicago. Chicago, Illinois, USA, {q.linda1998@gmail.com}*

**Corresponding author*

Keywords

Wildland-urban interface; WUI fires; risk assessment; wildfires

Abstract

This study presents a risk analysis for structures in the wildland-urban interface (WUI) using fragility curves. Reconstruction modelling using the model ELMFIRE is conducted to reproduce exposure conditions for the 2017 Northern California Tubbs Fire as a case study. The reconstruction simulates the distribution of embers, expanding the ability of fire reconstruction to represent conditions during the fire event which are not represented by the flaming fire front. Results from the Tubbs Fire simulation are used to provide exposure conditions to investigate the relationship between exposure conditions, structure and community characteristics, and the damage sustained by a structure in the fire event. A methodology using fragility curves to estimate the probability of destruction, used for risk analysis in other disaster fields, is modified and developed here for application to wildland-urban interface fires. Results of the fragility analysis find that increased ember exposure increases the likelihood of damage or destruction. Relatively low levels of ember exposure still result in relatively high likelihoods of destruction, highlighting the importance of ember spread. Current models cannot simulate structure-to-structure fire spread; additional limitations are highlighted for future work.

1. Introduction

In the last decade, large wildland fires threatening communities, called wildland-urban interface (WUI) fires, have become increasingly frequent and severe, causing increasing damage and destruction to structures. For example, fifteen of California's twenty most destructive wildland fires (measured in terms of homes destroyed) have occurred from September 2015 onward (CAL FIRE, 2022), with the most destructive, the 2018 Camp Fire, destroying over 18,000 structures. Globally, in the last five years alone, major destructive fires have occurred in Australia (2020), Chile (2019), Greece (2021), and Portugal (2017), to name a few. The increase in destructive WUI fires is anticipated to continue, due to the combined effects of climate change and increasing development in the WUI, the area where structures and wildland fuels interface or intermix.

Current mitigation strategies to protect homes from wildfire vary extensively and, for the most part, have little quantitative data supporting their effectiveness. One approach to addressing effectiveness of mitigation efforts is to investigate the risk to structures from wildfire. Risk can be defined, generally, as the product of hazard and vulnerability (Scott et al., 2013). Hazard consists of the probability of a given exposure level being achieved, and vulnerability consists of the susceptibility of a structure to a given exposure level. Current hazard and risk assessment of wildland fires focuses primarily on fire risk at a landscape scale, used for land and resource management (Scott et al., 2013). Despite the importance of fire exposure from the wildland, risk assessment at

[‡] These authors have contributed equally to this work.
[†] Sandia National Laboratories is a multimission laboratory managed and operated by National Technology & Engineering Solutions of Sandia, LLC, a wholly owned subsidiary of Honeywell International Inc., for the U.S. Department of Energy's National Nuclear Security Administration under contract DE-NA0003525.

the community scale has neglected to include the conditions to which a structure was or may have been exposed (Alexandre et al., 2016; Syphard & Keely, 2019), primarily because such information has been out of reach.

An objective of the present work is to develop a quantitative wildfire risk assessment framework, applicable to structures and communities in the WUI that can inform pre-disaster community design and emergency planning and support strategic operations that ensure fire and life safety during a wildfire. The methods detailed herein include leveraging reconstruction wildland fire modelling and statistical analysis to connect hazard exposure conditions and urban vulnerability characteristics to the amount of damage a structure or community experiences. As a preliminary case study, we investigate the 2017 Tubbs Fire in California, the second most destructive fire in California history. This fire directly exposed over 8,000 structures in a period of under six hours, thus providing a large database of structure information. This work addresses a major gap in current WUI risk assessment which has, to-date, not included ember exposure, a key cause of fire ignition in WUI fires.

2. Methods

2.1. Fire Hazard Modelling

The Tubbs Fire ignited at 9:45 PM local time on 8 October 2017 (CAL FIRE, 2017). The area of the fire is characterized by a combination of grass, shrubs, understory, and timber litter fuels, such as herbaceous grasses and shrubs, and live oaks (Coen et al., 2018). Due to severe south-westerly foehn winds, the fire spread over 19 km in the 5 hrs following ignition, reaching the city of Santa Rosa in the early morning of 9 October 2017. Before containment, the fire burned 36,807 acres, destroyed 5,636 structures, and caused 22 fatalities (CAL FIRE, 2022).

An operational fire model that could be used in real time during a fire event, ELMFIRE (Eulerian Level Set Method of Fire Spread) (Lautenberger, 2013, 2019a, 2019b), was chosen to model the Tubbs fire. While it has many of the same limitations as other semi-empirical models, it is used here for its relatively fast computational run time, its ability to simulate ember deposition of multiple embers (a feature not available in other models), and its implementation of Monte Carlo analysis techniques (Lautenberger, 2017) to address the stochasticity and uncertainty of physical phenomena inherent in simulating wildland fires.

2.1.1. Model Inputs

ELMFIRE requires geospatial inputs which describe the vegetation in the simulation domain (represented as a fuel model (Scott & Burgan, 2005)), environmental conditions (i.e., fuel moisture content, weather, winds), and topographical information. Fuel and topographical data were downloaded from LANDFIRE at a resolution of 30 m (Rollins, 2009). One of the difficulties of applying wildland fire modelling methods to WUI areas is that there are differing physical scales and processes involved in fire ignition and spread across wildland fuels versus structural or urban fuels. Fuel models used in wildland fire modelling assume that urban areas are non-burnable. Despite the problems inherent in this assumption, there are no current operational models available to describe the spread of fire in WUI areas.

Weather and winds were modelled using the Weather Research and Forecasting (WRF) model, a mesoscale numerical weather prediction model. The WRF model for the Tubbs fire was initialized based on meteorological conditions at the start of the fire. The computational resolution of the WRF model was down-sampled in the fire model domain to match the limiting resolution of the fuels (30 m). In total, the model simulated 7 hours of the fire with a temporal resolution ranging from 1-15 s.

2.1.2. Model Outputs

Fire spreads into the WUI via radiation, direct flame contact, and ember exposure. Thus, key quantitative outputs from fire modelling that are subsequently used as hazard intensity metrics for risk analysis include flame length and ember count. Flame length is linearly related to fireline intensity (kW/m) by Byram's Equation (Byram, 1959), and, while the fire model does not directly output radiation, flame length is used to represent the impact of the main fire front on ignition and fire spread. Ember count is the number of embers ignited per grid cell over the course of the fire simulation.

2.2. Structure Dataset

2.2.1. Vulnerability Characteristics

Data on pre- and post-fire structure characteristics and post-fire structure damage is available for the Tubbs Fire (and many other fires) through damage inspection (DINS) reports produced by California's Department of Forestry and Fire Protection. The DINS data is obtained as a geospatial vector file with point geometry representing the location of structures. Since the defensible space around a structure is known to heavily influence its vulnerability to fire (Valachovic et al., 2021), the dataset geometry is converted so that structures are represented by polygons using a building footprints database published by Microsoft (2018). This allows for calculation of additional attributes such as minimum structure-to-structure distance and vegetation-to-structure distance (or defensible space), the latter using LiDAR data for vegetation. These two characteristics of structural vulnerability were included in the risk analysis to understand the impact of community layout on structure ignition, as structure-to-structure spread is known to be a driver of fire spread in the WUI. Year built of the structure was also included, as it influences the materials and methods of construction due to changes in building code requirements.

2.2.2. Damage States

Each structure in the DINS dataset is assigned one of six damage states ranging from "No Damage", to some percentage indicating the level of partial damage, to "Destroyed". These damage states are a key component to the risk analysis described below. Although a small selection of undamaged structures is recorded, the DINS reports preferentially include damaged and destroyed structures. Yet to draw conclusions about the relationship between structure damage level and fire exposure, it is necessary to include structures that survived the fire, as well as those that were destroyed. Therefore, this dataset has been supplemented to include structures that were likely to have been exposed to fire or embers, as assumed by their location compared against fire modelling outputs. These structures are assumed to have incurred no damage, given their omission from the DINS report. Finally, since a low number of partially damaged structures were recorded, the analysis considers only three overall damage levels (as shown in Figure 1): no damage (DS0), some damage (DS1); and destroyed (DS2). This combination is consistent with previous work that has looked at home destruction (Penman et al., 2015).

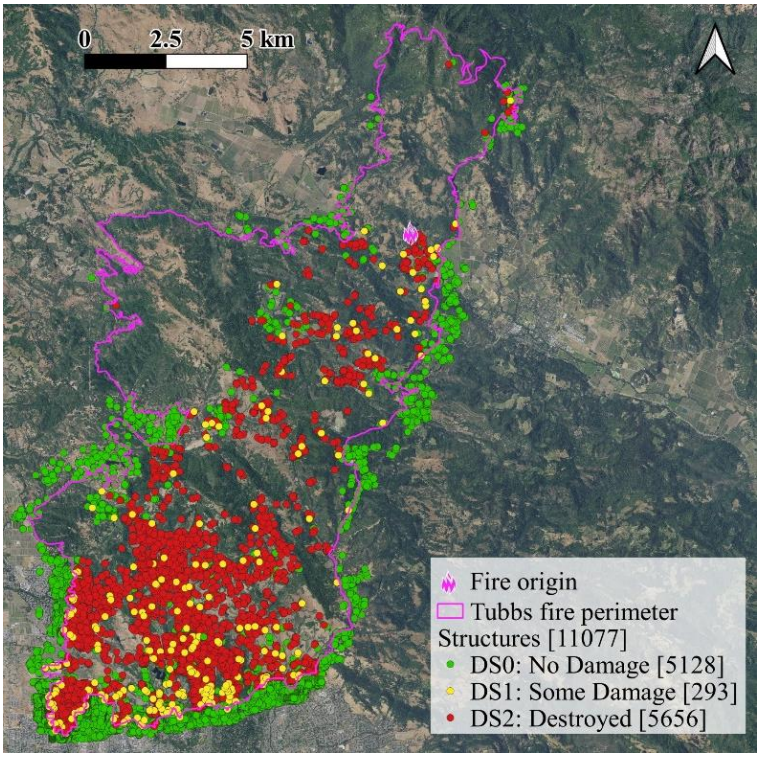

Figure 1- Tubbs fire perimeter outlined in pink with the ignition location indicated by a yellow star. The red dots indicate the location of structures that were destroyed in the Tubbs fire, the yellow dots indicated those that incurred partial damage, and the green dots are structures that were undamaged.

2.3. Risk Analysis Framework

We explore a risk analysis framework, following Rossetto et al. (2014), that incorporates fire hazard intensity metrics, structure vulnerability data, and structure loss inventory. Fragility curves, which are used in damage and loss models for flood and hurricane events, such as HAZUS (FEMA, 2001), represent a probability of exceeding a certain damage state given a level of intensity. The fragility curves are fitted using a generalized linear model with the explanatory variable considered to be the intensity measure (ember density) as well as the year built, defensible space, and the distance to the nearest structure. Other measures of intensity such as the flame length and additional structure and community characteristics can be incorporated and will be presented in future work. The response variable is modelled using a binomial probability density function.

The analysis of probability can be applied on a general level to all structures or by splitting the structures into different building classes. These building classes may be characterized by certain structure features (such as the presence/absence of combustible roofing) that could cause a structure to react differently from another structure under identical exposure conditions. The goodness-of-fit of the model is assessed using the *p*-value and the confidence interval. These metrics are used to determine the appropriate explanatory variables to include, the best link function, and to develop the building classes for significance. Initial results using all structures are presented here. The effect of building classes will be explored in further work.

3. Results and Discussion

To understand the relationship between exposure and damage, fragility curves with all structures for each intensity measure were produced. Figure 2 shows the fragility curve for all structures as a function of the number of embers ignited in a given cell. The probability shown in Figure 2 also incorporates the correlated influence of structure year built, defensible space as measured by vegetation distance via LiDAR, and the distance to the nearest structure. Here DS1 includes both partially damaged and destroyed structures, as the fragility curve represents an exceedance rather than an equivalence. In other words, the line representing DS1 indicates the probability that a structure surpasses the no-damage threshold at a given intensity level. The probability of both damage and destruction increases as the intensity measure increases. Structures require only low ember exposure to reach damaged and destroyed states (i.e., a single ember per cell is often sufficient). For high ember loads, probability of destruction of nearly all structures increases steeply.

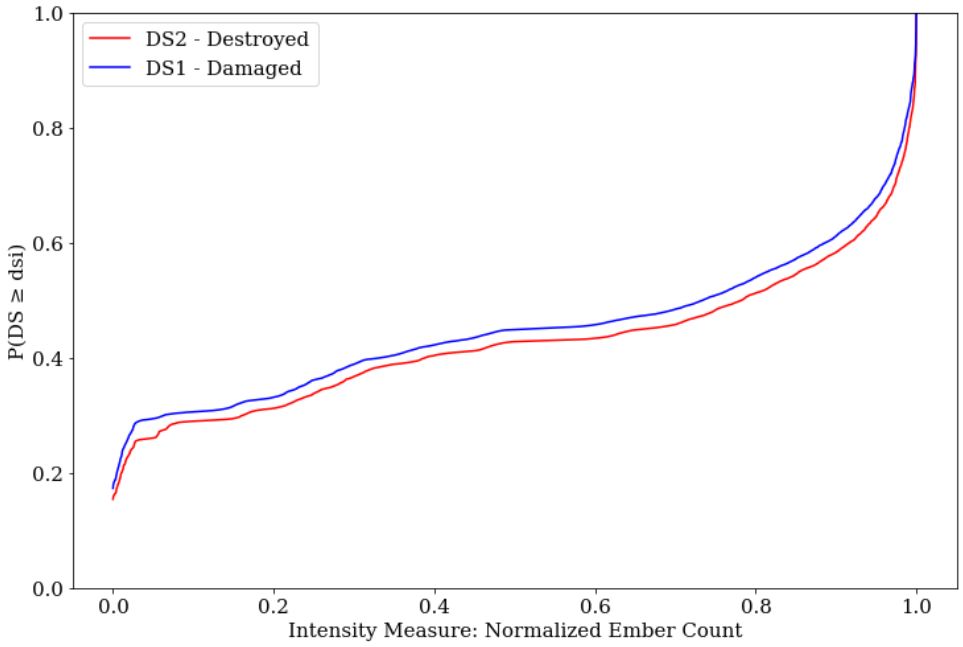

Figure 2- Fragility curve representing probability that the damage state of a structure exceeds either DS1 or DS2 as a function of a normalized ember count, which represents higher or lower numbers of embers ignited in a given cell. Ember count, year built of the structure, defensible space, and structure-to-structure distance are considered as explanatory variables.

The initial results of the fragility curve analysis show a clear relationship between exposure and destruction. Similar trends, not shown here, are found when considering flame length in the explanatory variables, though flame length is found to have a weaker correlation than embers with probability of damage or destruction. Overall, far fewer structures are exposed to flames than to embers, highlighting how critical it is to include embers in our models and in our risk analyses. While previous work (Duff & Penman, 2021) highlights that ember and fire exposure are both important in determining structure damage, the present work elucidates the relationship between ember exposure and destruction across a range of intensity conditions.

4. Conclusions and Future Work

This work shows a strong correlation between ember exposure and destruction, consistent with reports that embers are responsible for the majority of home ignitions (Mell et al., 2010). Future work will assess how local features, such as topography and fuels, compare to using embers for risk assessment. Further work should consider additional mechanisms of exposure, such as structure-to-structure spread (and the best way to capture that information). Similarly, this study focused on specific fire and structure characteristics expected to have an impact on risk, based on the literature; however, additional features may be relevant. Structure and community characteristics (defensible space, distance to nearest structure, year built of a structure) were considered individually here; however, another study has found that some characteristics are only significant when combined with others (Duff & Penman, 2021). Future work should consider interactions between features.

5. Acknowledgments

The authors would like to thank Evan Ellicott, Steve Hawks, Sophie Marxer, Charles Scawthorn, Katrina Sharonin, David Shew, and Xiaoxu Tian for their assistance and advice. This work was funded by the National Science Foundation award 1854952 and in part by the Gordon and Betty Moore Foundation. RH acknowledges financial support from NSF GRFP, the Clark Doctoral Fellows Program, and the PEO Scholar Award. LQ acknowledges financial support from the Jeff Metcalf Grant. This paper describes objective technical results and analysis. Any subjective views or opinions that might be expressed in the paper do not necessarily represent the views of the U.S. Department of Energy or the United States Government.

6. References

Alexandre, P. M., Stewart, S. I., Keuler, N. S., Clayton, M. K., Mockrin, M. H., Bar-Massada, A., Syphard, A. D., & Radeloff, V. C. (2016). Factors related to building loss due to wildfires in the conterminous United States. *Ecological Applications; Ecol Appl*, *26*(7), 2323-2338. https://doi.org/10.1002/eap.1376

Byram, George M. (1959). Combustion of forest fuels. Pages 61-89 In: Davis, K. P., editor. Forest fire: control and use. New York, NY: McGraw-Hill.

CAL FIRE. (2022, January 13). Top 20 most destructive California wildfires. California Department of Forestry and Fire Protection. Retrieved March 22, 2022, from https://www.fire.ca.gov/media/t1rdhizr/top20_destruction.pdf

CAL FIRE. (2017, October). Tubbs fire (Central LNU Complex). California Department of Forestry and Fire Protection. Retrieved March 23, 2022, from https://www.fire.ca.gov/incidents/2017/10/8/tubbs-fire-central-lnu-complex

Coen, J., Schroeder, W., & Quayle, B. (2018). The Generation and Forecast of Extreme Winds during the Origin and Progression of the 2017 Tubbs Fire. *Atmosphere, 9*(12), 462. https://doi.org/10.3390/atmos9120462

Duff, T. J., & Penman, T. D. (2021). Determining the likelihood of asset destruction during wildfires: Modelling house destruction with fire simulator outputs and local-scale landscape properties. *Safety Science, 139*, 105196. https://doi.org/10.1016/j.ssci.2021.105196

Federal Emergency Management Agency (FEMA), 2001. Hazus99 Technical Manual. Service Release 2. (Washington, D.C., FEMA).

Lautenberger, C. (2019a). ELMFIRE – Eulerian level set model of fire spread technical reference. Technical report, Reax Engineering.

Lautenberger, C. (2019b). ELMFIRE – Eulerian level set model of fire spread users' guide. Technical report, Reax Engineering.

Lautenberger, C. (2017). Mapping areas at elevated risk of large-scale structure loss using Monte Carlo simulation and wildland fire modeling. *Fire Safety Journal, 91*, 768-775. https://doi.org/10.1016/j.firesaf.2017.04.014

Lautenberger, C. (2013). Wildland fire modeling with an Eulerian level set method and automated calibration. *Fire Safety Journal, 62*, 289-298. https://doi.org/10.1016/j.firesaf.2013.08.014

Mell, W. E., Manzello, S. L., Maranghides, A., Butry, D., & Rehm, R. G. (2010). The wildland–urban interface fire problem – current approaches and research needs. *International Journal of Wildland Fire, 19*(2), 238-251. https://doi.org/10.1071/WF07131

Microsoft. (2018). US building footprints. Retrieved March 23, 2022, from https://github.com/Microsoft/USBuildingFootprints

Penman, T. D., Nicholson, A. E., Bradstock, R. A., Collins, L., Penman, S. H., & Price, O. F. (2015). Reducing the risk of house loss due to wildfires. *Environmental Modelling & Software: With Environment Data News, 67*, 12-25. https://doi.org/10.1016/j.envsoft.2014.12.020

Rollins, M. G. (2009). LANDFIRE: a nationally consistent vegetation, wildland fire, and fuel assessment. *International Journal of Wildland Fire, 18*(3), 235-249. https://doi.org/10.1071/WF08088

Rossetto, T., Ioannou, I., Grant, D. N., & Maqsood, T. (2014). *Guidelines for the empirical vulnerability assessment.* GEM Technical Report 2014-08 V1.0.0, 140 pp., GEM Foundation, Pavia, Italy, doi: 10.13117/GEM.VULN-MOD.TR2014.11.

Scott, J. H., & Burgan, R. E. (2005). *Standard fire behavior fuel models: a comprehensive set for use with Rothermel's surface fire spread model.* Gen. Tech. Rep. RMRS-GTR-153. U.S. Department of Agriculture, Forest Service, Rocky Mountain Research Station. 72 p. https://doi.org/10.2737/RMRS-GTR-153

Scott, J. H., Thompson, M. P., & Calkin, D. E. (2013). *A wildfire risk assessment framework for land and resource management.* Gen. Tech. Rep. RMRS-GTR-315. U.S. Department of Agriculture, Forest Service, Rocky Mountain Research Station. 83 p. https://doi.org/10.2737/RMRS-GTR-315

Syphard, A., & Keeley, J. (2019). Factors associated with structure loss in the 2013–2018 California wildfires. *Fire, 2*(3), 49-64. https://doi.org/10.3390/fire2030049

Valachovic, Y., Quarles, S., Swain, S. (2021). *Reducing the Vulnerability of Building to Wildfire: Vegetation and Landscaping Guidance*. University of California Agriculture and Natural Resources, Publication Number 8695. 12 p. DOI: 10.3733/ucanr.8695

Distinguishing between mitigation and adaptation as wildfire prevention actions

Maria João Canadas*[1]; Miguel Leal[1,2]; Filipa Soares[3]; Ana Novais[1]; Paulo Flores Ribeiro[1]; Ana Delicado[3]; Rafaello Bergonse[2]; Sandra Oliveira[2]; Francisco Moreira[4,5,6]; Luísa Schmidt[3]; José Lima Santos[1]

[1]Forest Research Centre and Associated Laboratory TERRA, School of Agriculture, Universidade de Lisboa. Tapada da Ajuda, 1349-017 Lisbon, Portugal, {mjcanadas, ananovais, pfribeiro, jlsantos}@isa.ulisboa.pt, {mleal@campus.ul.pt}
[2] Centre of Geographical Studies and Associated Laboratory TERRA, Institute of Geography and Spatial Planning, Universidade de Lisboa. Edifício IGOT, Rua Branca Edmée Marques, 1600-276 Lisbon, Portugal, {rafaellobergonse, sandra.oliveira1}@campus.ul.pt
[3] Institute of Social Sciences, Universidade de Lisboa. Avenida Professor Aníbal de Bettencourt 9, 1600-189 Lisbon, Portugal, {filipa.soares, ana.delicado, mlschmidt}@ics.ulisboa.pt
[4] CIBIO, Centro de Investigação em Biodiversidade e Recursos Genéticos, InBIO Laboratório Associado, Instituto Superior de Agronomia, Universidade de Lisboa. Tapada da Ajuda, 1349-017 Lisbon, Portugal, {fmoreira@isa.utl.pt}
[5] CIBIO, Centro de Investigação em Biodiversidade e Recursos Genéticos, InBIO Laboratório Associado. Campus de Vairão, Universidade do Porto, 4485-661 Vairão, Portugal
[6] BIOPOLIS Program in Genomics, Biodiversity and Land Planning, CIBIO. Campus de Vairão, 4485-661 Vairão, Portugal

**Corresponding author*

Keywords

Wildfire policies; wildfire responses; collective action; owner collaboratives; local governments

Abstract

There is actually a broad consensus over the need to shift from fire suppression to fire prevention strategies. To inform policies that effectively promote this shift, we distinguish between actions aimed at more fire-resilient landscapes and those focused on the protection of people, i.e., wildfire mitigation and adaptation (WM&A), respectively.

With the goal of discussing the usefulness of this distinction and identifying local factors and external resources that promote preventive actions, we developed an analysis of collective WM&A actions across 116 parishes in a wildfire-prone region in Portugal, Pinhal Interior. Two principal component analyses were used to explore relationships between variables expressing collective WM&A actions. Random forest was used to model how those actions are related to local factors (land use/land cover, population, institutions) and external resources for wildfire prevention.

Our results showed that collective mitigation and adaptation responses to wildfire are independent, in coherence with their distinct goals, actors involved, and policy domains. Mitigation through owners' collaboration proved to be strongly related to policy funding, local economic dynamism, and demographic vitality, unlike community adaptation. In fact, adaptation responses from the local governments and the very few existing residents' collaboratives are very incipient. We conclude, on one hand, that mitigation and adaptation actions are currently supported by two unequally consolidated policy domains and, on the other hand, that both domains are equally underfunded, namely because of the difficulties in expanding owner collaboratives beyond favorable local conditions, i.e., in socioeconomically depressed regions.

1. Introduction

The shift from fire suppression to fire management through prevention has been increasingly discussed in the scientific and policy communities (Ager et al., 2018; EC, 2018; Leone and Tedim, 2020; Moreira et al., 2020; Fernandes et al., 2020). Within preventive actions we distinguish between mitigation and adaptation, taking into consideration the action itself, its objectives, and the actors involved, in line with the need to identify the policy recipients. Mitigation actions are primarily designed to reduce the susceptibility of the landscape to wildfire,

while protecting forest assets. Adaptation actions mainly seek to safeguard people and goods through reducing their exposure and vulnerability. Mitigation includes actions taken by landowners to reduce the amount or modify the kind and arrangement of fuel loads in forest and agricultural areas, thereby contributing to reduce wildfire hazard (Fernandes et al., 2014; Martins et al., 2021; Oliveira et al., 2013). Adaptation actions are taken by residents, homeowners, or communities to create defensible space on their properties and territories (Alcasena et al., 2019; Bihari and Ryan, 2012; Stidham et al., 2014) or to get insurance policies that allow a quicker recovery after a damaging event (Gan et al., 2015). Adaptation includes actions such as fuel treatments and protection strips in the surroundings of rural settlements and infrastructure, escape strategies, and shelters (Everett and Fuller, 2011).

These wildfire mitigation and adaptation (hereafter WM&A) actions can be carried out at different levels (Busenberg, 2004; Gill, 2005). This study is focused on the WM&A actions at a collective level (private owner groups, local communities, and local governments), unlike most empirical studies, which mainly address the individual responses (e.g., Fischer, 2011; Rodríguez-Carreras et al., 2020, Brenkert-Smith et al., 2012; Martin et al., 2009; McCaffrey et al., 2011; McGee et al., 2009; Olsen et al., 2017). The collective level is relevant because, to be effective, WM&A actions need to be coherently executed at a scale larger than the individual.

This study also aims to inform an effective paradigm shift from suppression to prevention by analysing collective WM&A actions within a wildfire-prone Portuguese region: Pinhal Interior. The WM&A actions are included in the same analysis, resorting to the same explanatory factors, but clearly distinguishing between mitigation and adaptation based on their different nature and goals and the actors involved in their implementation. We seek to define relationships between WM&A actions and both local factors (natural resources, population, and institutions) and external resources (access to policy funding) that favour or hinder mitigation and adaptation. The main goal of this study is to explore the usefulness of distinguishing mitigation and adaptation, and to identify local factors and external resources that promote each of them.

2. Data and methods

Data collection and analysis were executed at a parish level from primary and secondary data. A survey was applied to the presidents of Parish Councils to identify WM&A actions during the 2015-2020 period. These correspond to a set of 14 actions related to investments in firefighting, awareness and protection, land clearing, grazing and plantations. Five of the 121 parishes were excluded for non-answer reasons. Secondary data includes Forest Intervention Zones (FIZ), land use/land cover (LULC), population, institutions, public funding, or burnt areas.

A principal component analysis (PCA) was applied to the 116 parishes to understand the relationship between mitigation and adaptation. Four variables were used in the PCA: 1) number of adaptation actions (Numb_actions); 2) existence of an approved Forest Management Plan (FMP_approved); 3) proportion of the parish covered by FIZ (FIZ_extent); and 4) age of FIZ (FIZ_age). The last three variables express the FIZ's success in the implementation of collective mitigation actions. The principal components (PC) with eigenvalues greater than 1 were extracted.

Random forest modelling was used to determine relationships between PC scores (dependent variables) and a set of 51 independent variables, which were grouped in five dimensions: 1) LULC or resource system characteristics; 2) people and their relationships; 3) institutions; 4) external resources; and 5) wildfires. Mean squared error (MSE) was used to measure the effect of each independent variable in the models.

3. Results and discussion

3.1. Collective mitigation progression and adaptation effort display two locally independent dynamics

Two PC were extracted from the PCA, retaining together 88% of the total variance (table 1). PC1 (mitigation under FIZ) collects 64% of the variance and is associated with FMP_approved, FIZ_extent and FIZ_age. PC2 (community adaptation) represents 24% of the variance and is only associated with Numb_actions. These PC can be considered as orthogonal because all variables related to mitigation only contribute to PC1 and the

variable related to adaptation only contributes to PC2. Therefore, these PC are independent and not spatially related, which means that there is no association between progression of mitigation and adaptation effort.

It was possible to achieve this innovative result by comparing both responses to wildfire (actions for landscape protection and people's protection) across different territorial units for the first time. In fact, research on collective responses to wildfires are mostly confined to single territorial contexts and case studies (Danley et al., 2021). On the other hand, landowners' mitigation and residents' adaptation are either analysed separately or just assimilated (Everett and Fuller, 2011; Górriz-Mifsud et al., 2019; McLennan and Birch, 2005).

Table 1- Unrotated component matrix extracted from the PCA.

Acronym	Variable	Component	
		Mitigation under FIZ (PC1)	**Community adaptation (PC2)**
Numb_actions	Number of WM&A actions	-0.264	0.964
FMP_approved	Forest Management Plan approved	0.915	0.151
FIZ_extent	Proportion of the parish covered by FIZ	0.910	0.085
FIZ_age	Age of FIZ	0.909	0.042

3.2. Socioeconomic vitality, ownership structure, and leadership are key factors for WM&A action, unlike wildfire experience

Random forest models (figure 1) showed a much better fit for PC1 than for PC2 (58.5% *vs*. 6.8% of variance explained). This can be partly explained by the different territorial levels between actions and local and external resources. Data for some of the variables were only available at the municipal level, not allowing to fully capture the reality in each parish of the same municipality.

The highest scores of PC1 were obtained for parishes with higher values of built-up areas (*Built_up*), population densities (*PopDens*), agriculture areas (*Agricult* and *AgricBuff*), landscape heterogeneity (*Shannon*), younger people (*Young*), livestock (*LivStock*), tourism (*AccomCap* and *NightSty*), properties' dimension (*AvgUAA*), and capacity to raise public funding (*ForFund*). The propensity for landowners' collective mitigation under FIZ occur in parishes with more heterogeneous landscapes, larger built-up and agricultural areas, higher social dynamism, larger properties, higher amounts of money from public funding, and recent wildfires. On the contrary, there are no FIZ in parishes where people are older (and more vulnerable), landscape is more homogeneous, eucalyptus prevails, properties are smaller, and there have been fewer recent fires.

The PC2 model shows that only land registry (*LandReg*) stands out in variable importance (figure 1). The active role played by local governments in the promotion of land registry suggests that community adaptation depends on stronger leadership by local governments (Harris et al. 2011; Labossière & McGee, 2017). The PC2 scores are not clearly related to the other considered variables.

Historic and recent fires, namely the catastrophic years of 2003, 2005 and 2017, did not have significant effects on local collective mitigation or adaptation actions. This means that wildfire experience and awareness at the local level may not represent an effective trigger of collective mitigation and adaptation action, unlike what has been suggested in other studies (Jakes and Sturtevant, 2013; Mockrin et al. 2018; Muller and Schulte, 2011; Steelman and Kunkel, 2004).

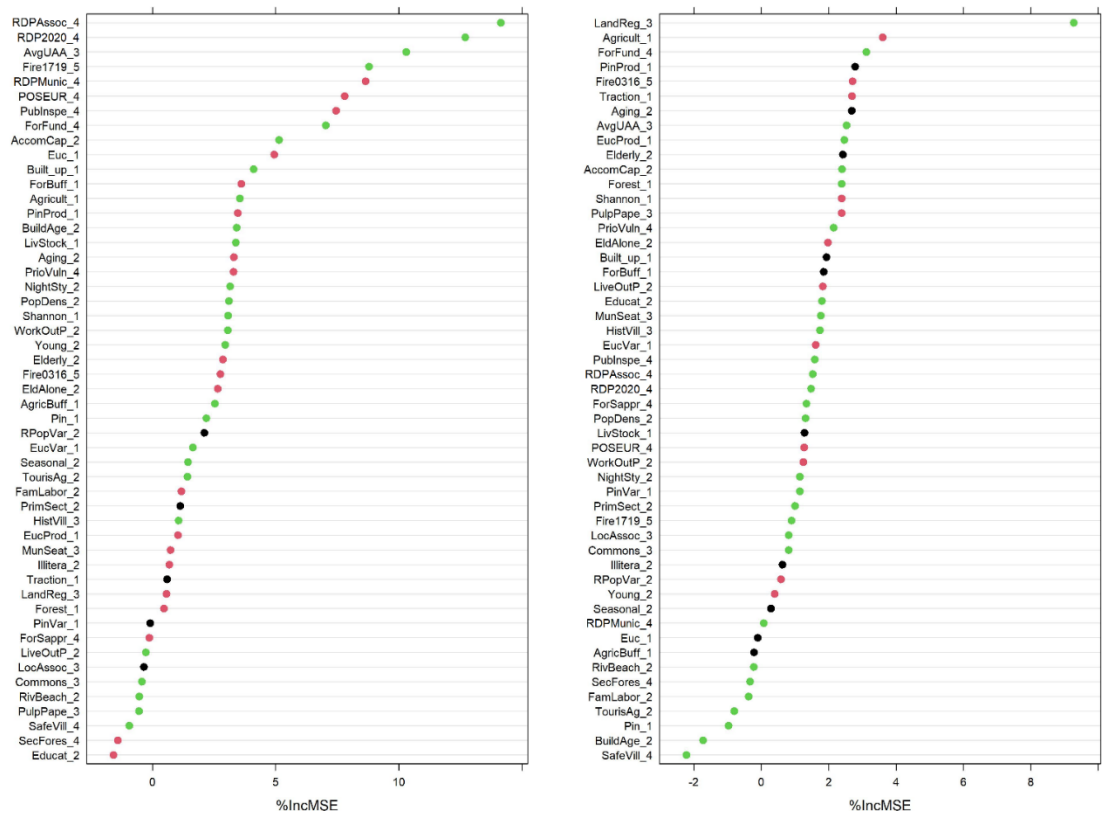

Figure 1- Variable importance for the random forest models for PC1 (left) and PC2 (right). Green, red, and black dots identify positive, negative, or unclear marginal effects of the variable on the scores of the PCs, respectively. Numbers following variable names refer to the corresponding dimension (see data and methods section).

3.3. Mitigation and adaption: a distinction supported by different policy domains

Most of the top variables in the PC1 model are included in the external resources dimension, demonstrating the vital role of public funding for collective mitigation progression (Canadas et al., 2016; OECD, 2013). This association is positive for public funding aimed at mitigation and negative for programmes aimed at adaptation. These associations reinforce the usefulness of distinguishing the two action spheres that are also supported by two distinct policy domains (OECD, 2016). Mitigation under FIZ is positively associated with landscape protection, agricultural and rural development policies.

Mitigation and adaptation actions on the ground are related to distinct policy domains, which are promoted by different policy actors and tend to protect different interests (table 2). However, these two policy domains seem to be unequally consolidated. The mitigation domain is supported by a set of well-established public and private agencies, policy measures and funding allocation already in place. The adaptation domain is more recent and less established, unlike what happens in the Anglo-Saxon countries (Everett and Fuller, 2011; McLennan and Birch, 2005).

Table 2- Programmes, entities, and policy domains supporting collective WM&A actions.

Programme	**Executing/funding entities**	**Policy domain**
"Secure Forests" Operation	National Republican Guard (Ministry of Internal Administration and Ministry of National Defence)	Adaptation
"Safe Village, Safe People" Programme	National Emergency and Civil Protection Authority (Ministry of Internal Administration), National Associations of Municipalities and Parishes	Adaptation
Rural Development Programme 2014-2020 (RDP 2020)	Ministry of Agriculture Co-financed by the European Agricultural Fund for Rural Development (EAFRD) and the Portuguese State Budget	Predominantly Mitigation
Permanent Forest Fund	National Forest Authority	Mitigation
Programme for Sustainability and Efficient Use of Resources [*POSEUR*]	Ministry of Environment Financed by the European Commission's Cohesion Fund	Predominantly Adaptation

Nevertheless, several drawbacks affect both action spheres and policy domains. Underfunding is among the main drawbacks pointed to mitigation policies (Santos et al., 2021). In fact, as in other countries, fire suppression has repeatedly attracted most public funds related to wildfires, thus limiting the resources for prevention (Calkin et al., 2011; Fernandes et al., 2020; North et al., 2015). The average investment in suppression in Portugal during the 2007-2016 period was three times higher when compared to prevention (Beighley and Hyde, 2018; Viegas et al., 2017). On the other hand, the results have demonstrated that the adaptation effort on the ground does not have a strong association with any funding or policy priority.

4. Conclusions

The proposed distinction between mitigation and adaptation has enabled us to reveal that, on the one hand, collective mitigation and adaptation are independent, i.e., mitigation action does not go along with adaptation action, and, on the other hand, WM&A are associated to different territorial variables and policy domains. The visibility given to the unequal consolidation levels between the two policy domains is an important outcome of that distinction.

The results suggest the local context, namely the economic and social vitality, ownership structure, and leadership by local governments, as the key factors to explain the different involvement of the territories in collective WM&A action. Unlike what is dominantly assumed in the literature the wildfire experience seems to play a minor role. Therefore, awareness campaigns targeted at landowners and local communities may prove insufficient to promote the desired WM&A action.

Although territorial differences are recognized in the wildfire literature, the consequences of those differences have not yet been fully explored, namely concerning the role of local government versus self-organization for collective WM&A actions. In the study area, owners' collaboration for mitigation has developed in parishes with higher demographic vitality and economic dynamism and resident collaboration for collective adaptation is almost absent. High levels of aging, low profitability of land-using activities and land management abandonment hinder both WM&A on strictly self-organization grounds. In fact, self-organization unlikely arises and thrives in similar regions, where local socioeconomic conditions markedly differ from those reported in the WUI literature.

5. Acknowledgements

The authors were financed by national funds through FCT – Portuguese Foundation for Science and Technology, I.P., under the framework of the project People&Fire: Reducing Risk, Living with Risk (PCIF/AGT/0136/2017). This research was also supported by the Forest Research Centre (UID/AGR/00239/2019), Centre of Geographical Studies (UIDB/00295/2020 and UIDP/00295/2020) and Associated Laboratory TERRA. Sandra Oliveira was funded through FCT, within the contract 2020.03873.CEECIND. Francisco Moreira was supported by contract IF/01053/2015.

6. References

Ager, A.A., Barros, A.M.G., Day, M.A., Preisler, H.K., Spies, T.A., Bolte, J., 2018. Analyzing fine-scale spatiotemporal drivers of wildfire in a forest landscape model. Ecol. Modell. 384, 87–102. https://doi.org/10.1016/j.ecolmodel.2018.06.018

Alcasena, F.J., Ager, A.A., Bailey, J.D., Pineda, N., Vega-García, C., 2019. Towards a comprehensive wildfire management strategy for Mediterranean areas: Framework development and implementation in Catalonia, Spain. J. Environ. Manage. 231, 303–320. https://doi.org/10.1016/j.jenvman.2018.10.027

Beighley, M., Hyde, A.C., 2018. Portugal Wildfire Management in a New Era: Assessing Fire Risks, Resources and Reforms.

Bihari, M., Ryan, R., 2012. Influence of social capital on community preparedness for wildfires. Landsc. Urban Plan. 106, 253–261. https://doi.org/10.1016/j.landurbplan.2012.03.011

Brenkert-Smith, H., Champ, P.A., Flores, N., 2012. Trying not to get burned: Understanding homeowners' wildfire risk-mitigation behaviors. Environ. Manage. 50, 1139–1151. https://doi.org/10.1007/s00267-012-9949-8

Busenberg, G., 2004. Wildfire Management in the United States: The Evolution of a Policy Failure. Rev. Policy Res. 21, 145–156. https://doi.org/10.1111/j.1541-1338.2004.00066.x

Calkin, D.C., Finney, M.A., Ager, A.A., Thompson, M.P., Gebert, K.M., 2011. Progress towards and barriers to implementation of a risk framework for US federal wildland fire policy and decision making. For. Policy Econ. 13, 378–389. https://doi.org/10.1016/j.forpol.2011.02.007

Canadas, M.J., Novais, A., Marques, M., 2016. Wildfires, forest management and landowners' collective action: A comparative approach at the local level. Land use policy 56, 179–188. https://doi.org/10.1016/j.landusepol.2016.04.035

Danley, B., Caputo, J., Butler, B.J., 2021. A Burning Concern: Family Forest Owner Wildfire Concerns Across Regions, Scales, and Owner Characteristics. Risk Anal. https://doi.org/10.1111/risa.13816

EC, 2018. Forest fires: sparking firesmart policies in the EU. European Comission, Directorate-General for Research and Innovation, Brussels. https://doi.org/10.2777/248004

Everett, Y., Fuller, M., 2011. Fire safe councils in the interface. Soc. Nat. Resour. 24, 319–333. https://doi.org/10.1080/08941920903313835

Fernandes, P.M., Loureiro, C., Guiomar, N., Pezzatti, G.B., Manso, F.T., Lopes, L., 2014. The dynamics and drivers of fuel and fire in the Portuguese public forest. J. Environ. Manage. 146, 373–382. https://doi.org/10.1016/j.jenvman.2014.07.049

Fernandes, P.M., Delogu, G.M., Leone, V., Ascoli, D., 2020. Wildfire policies contribution to foster extreme wildfires, in: Tedim, F., Leone, V., McGee, T.K. (Eds.), Extreme Wildfire Events and Disasters: Root Causes and New Management Strategies. Elsevier, pp. 187–200. https://doi.org/10.1016/B978-0-12-815721-3.00010-2

Fischer, A.P., 2011. Reducing Hazardous Fuels on Nonindustrial Private Forests: Factors Influencing Landowner Decisions. J. For. 109, 260–266. https://doi.org/10.1093/jof/109.5.260

Galiana, L., Aguilar, S., Lázaro, A., 2013. An assessment of the effects of forest-related policies upon wildland fires in the European Union. Applying the subsidiarity principle. For. Policy Econ. 29, 36–44. https://doi.org/10.1016/j.forpol.2012.10.010

Gan, J., Jarrett, A., Gaither, C.J., 2015. Landowner response to wildfire risk: Adaptation, mitigation or doing nothing. J. Environ. Manage. 159, 186–191. https://doi.org/10.1016/j.jenvman.2015.06.014

Gill, A.M., 2005. Landscape fires as social disasters: An overview of 'the bushfire problem.' Environ. Hazards 6, 65–80. https://doi.org/10.1016/j.hazards.2005.10.005

Górriz-Mifsud, E., Burns, M., Marini Govigli, V., 2019. Civil society engaged in wildfires: Mediterranean forest fire volunteer groupings. For. Policy Econ. 102, 119–129. https://doi.org/10.1016/j.forpol.2019.03.007

Harris, L.M., McGee, T.K., McFarlane, B.L., 2011. Implementation of wildfire risk management by local governments in Alberta, Canada. J. Environ. Plan. Manag. 54, 457–475. https://doi.org/10.1080/09640568.2010.515881

Jakes, P.J., Sturtevant, V., 2013. Trial by fire: Community Wildfire Protection Plans put to the test. Int. J. Wildl. Fire 22, 1134–1143. https://doi.org/10.1071/WF12156

Labossière, L.M.M., McGee, T.K., 2017. Innovative wildfire mitigation by municipal governments: Two case studies in Western Canada. Int. J. Disaster Risk Reduct. 22, 204–210. https://doi.org/10.1016/j.ijdrr.2017.03.009

Leone, V., Tedim, F., 2020. How to create a change in wildfire policies, in: Tedim, F., Leone, V., McGee, T.K. (Eds.), Extreme Wildfire Events and Disasters: Root Causes and New Management Strategies. Elsevier, pp. 217–232. https://doi.org/10.1016/B978-0-12-815721-3.00012-6

Martin, W.E., Martin, I.M., Kent, B., 2009. The role of risk perceptions in the risk mitigation process: The case of wildfire in high risk communities. J. Environ. Manage. 91, 489–498. https://doi.org/10.1016/j.jenvman.2009.09.007

Martins, A., Novais, A., Santos, J.L., Canadas, M.J., 2021. Experts' multiple criteria evaluations of fuel management options to reduce wildfire susceptibility. The role of closer knowledge of the local socioeconomic context. Land use policy 108, 105580. https://doi.org/10.1016/j.landusepol.2021.105580

McCaffrey, S.M., Stidham, M., Toman, E., Shindler, B., 2011. Outreach programs, peer pressure, and common sense: What motivates homeowners to mitigate wildfire risk? Environ. Manage. 48, 475–488. https://doi.org/10.1007/s00267-011-9704-6

McGee, T.K., McFarlane, B.L., Varghese, J., 2009. An examination of the influence of hazard experience on wildfire risk perceptions and adoption of mitigation measures. Soc. Nat. Resour. 22, 308–323. https://doi.org/10.1080/08941920801910765

McLennan, J., Birch, A., 2005. A potential crisis in wildfire emergency response capability? Australia's volunteer firefighters. Environ. Hazards 6, 101–107. https://doi.org/10.1016/j.hazards.2005.10.003

Mockrin, M.H., Fishler, H.K., Stewart, S.I., 2018. Does Wildfire Open a Policy Window? Local Government and Community Adaptation After Fire in the United States. Environ. Manage. 62, 210–228. https://doi.org/10.1007/s00267-018-1030-9

Moreira, F., Ascoli, D., Safford, H., Adams, M.A., Moreno, J.M., Pereira, J.M.C., Catry, F.X., Armesto, J., Bond, W., González, M.E., Curt, T., Koutsias, N., McCaw, L., Price, O., Pausas, J.G., Rigolot, E., Stephens, S., Tavsanoglu, C., Vallejo, V.R., Van Wilgen, B.W., Xanthopoulos, G., Fernandes, P.M., 2020. Wildfire management in Mediterranean-type regions: Paradigm change needed. Environ. Res. Lett. 15, 011001. https://doi.org/10.1088/1748-9326/ab541e

Muller, B., Schulte, S., 2011. Governing wildfire risks: What shapes county hazard mitigation programs? J. Plan. Educ. Res. 31, 60–73. https://doi.org/10.1177/0739456X10395895

North, M.P., Stephens, S.L., Collins, B.M., Agee, J.K., Aplet, G., Franklin, J.F., Fule, P.Z., 2015. Reform forest fire management. Science 349, 1280–1281. https://doi.org/10.1126/science.aab2356

OECD, 2013. Providing Agri-environmental Public Goods through Collective Action. Organisation for Economic Cooperation and Development, Paris. https://doi.org/10.1787/9789264197213-en

OECD, 2016. Better Policies for Sustainable Development 2016: A New Framework for Policy Coherence, Better Policies for Sustainable Development 2016. Organisation for Economic Cooperation and Development, Paris. https://doi.org/10.1787/9789264256996-en

Oliveira, S., Moreira, F., Boca, R., San-Miguel-Ayanz, J., Pereira, J.M.C., 2013. Assessment of fire selectivity in relation to land cover and topography: a comparison between Southern European countries. Int. J. Wildl. Fire 23, 620. https://doi.org/10.1071/WF12053

Olsen, C.S., Kline, J.D., Ager, A.A., Olsen, K.A., Short, K.C., 2017. Examining the influence of biophysical conditions on wildland–urban interface homeowners' wildfire risk mitigation activities in fire-prone landscapes. Ecol. Soc. 22. https://doi.org/10.5751/ES-09054-220121

Paveglio, T.B., Moseley, C., Carroll, M.S., Williams, D.R., Davis, E.J., Fischer, A.P., 2015. Categorizing the Social Context of the Wildland Urban Interface: Adaptive Capacity for Wildfire and Community "Archetypes." For. Sci. 61, 298–310. https://doi.org/10.5849/forsci.14-036

Rodríguez-Carreras, R., Úbeda, X., Francos, M., Marco, C., 2020. After the Wildfires: The Processes of Social Learning of Forest Owners' Associations in Central Catalonia, Spain. Sustain. 12, 6042. https://doi.org/10.3390/su12156042

Santos, J.L., Martins, A., Novais, A., Canadas, M.J., 2021. A Choice-Modeling Approach to Inform Policies Aimed at Reducing Wildfire Hazard through the Promotion of Fuel Management by Forest Owners. Forests 12. https://doi.org/10.3390/f12040403

Steelman, T.A., Kunkel, G.F., 2004. Effective community responses to wildfire threats: Lessons from New Mexico. Soc. Nat. Resour. 17, 679–699. https://doi.org/10.1080/08941920490480697

Stidham, M., McCaffrey, S., Toman, E., Shindler, B., 2014. Policy tools to encourage community-level defensible space in the United States: A tale of six communities. J. Rural Stud. 35, 59–69. https://doi.org/10.1016/j.jrurstud.2014.04.006

Viegas, D.X., Almeida, M.F., Ribeiro, L.M., 2017. O complexo de incêndios de Pedrógão Grande e concelhos limítrofes, iniciado a 17 de Junho de 2017.

Evaluation of the flammability of forest species for fire management in wildland urban interface areas of Brazil.

Antonio Carlos Batista*, Daniela Biondi

[1]*Universidade Federal do Paraná, Rua Lothario Meissner 632, Campus III, Curitiba, Brazil, {batistaufpr, dbiondi}@ufpr.br*

**Corresponding author*

Keywords

Forest fuels, fire prevention, brazilian forest species, WUI.

Abstract

Classification of forest fuels according to their flammability is an essential component of fire risk assessment in the context of forest fire management planning. Surveys on the flammability of forest fuels are useful for fire management because they provide information on the reaction of individual fuels in heating a fire, make it possible to classify different plant species within an ecosystem in terms of fire hazard, and help with selection of suitable species to reduce the danger of fires in reforestation. The flammability characteristics of vegetation have been fundamental in recent methodologies for risk assessment of forest fires in several regions of the world. In addition, knowledge of how species differ in their flammability characteristics is necessary to draw up lists of recommended plants for urban and residential afforestation in wildland urban interface areas. In Brazil, there are no methodologies for classifying tree and shrub species according to the flammability characteristics of the vegetation. The choice of these species is made empirically, considering only the local experiences of vegetation specialists. This research aimed to consolidate in the country a methodology that has been adopted in several countries to characterize plant species according to the degree of flammability, facilitating the use of these species in protection activities against forest fires. The general objective of this research was to evaluate the flammability of native and exotic forest species from forest fragments and wildland urban interfaces (WUI) areas of Curitiba-PR and Gurupi-TO in Brazil, to support fire management planning in these environments. To achieve this objective, fifty-eight species were chosen from the fragment forests and wildland urban interfaces of Curitiba-PR and Gurupi-TO, Brazil, belonging to the southern and northern regions of Brazil, respectively, where forest activities are very important for the regional economy and to which fires cause significant damage. One of the analysis criteria for the selection of species were the morphological characteristics of the species. The selected species were submitted to flammability tests in the Forest Fire laboratories of the Federal University of Paraná and of the Environmental Monitoring and Fire Management Center (CEMAF) of the Federal University of Tocantins (Gurupi-TO)., The results indicated that of the analysed species, 44% had low flammability (IF = 0), and therefore, have potential for use in fire prevention activities at the wildland urban interfaces areas of the cities of Curitiba and Gurupi.

1. Introduction

The behavior of forest fires and the mechanisms involved in this process are highly complex. Studies on the behavior of fire in forest fuels have intensified a lot since the 20th century due to the growing need to develop fire prediction and simulation models to improve systems for preventing and fighting forest fires or, using a broader current concept, to provide more effective instruments for fire management.

Classification of forest fuels according to their flammability is an essential component of fire risk assessment in the context of forest fire management planning. Researchers and administrators have long identified the need to classify the flammability of forest species for use in fire prevention and combat plans and for the improvement of fire behavior prediction models. Surveys on the flammability of forest fuels are useful for fire management because they provide information on the reaction of individual fuels in the combustion process, make it possible to classify different plant species within an ecosystem in terms of fire hazard, and help with selection of suitable species to reduce the danger of fires in reforestation (DIMITRAKOPOULOS AND PAPAIOANNOU, 2001).

From the point of view of natural resource management, the interaction between natural and urban areas is called “wildland urban interface” (WUI). Forest fire prevention and mitigation programs educate and help communities in WUI areas to understand and be prepared for forest fires, including access, buildings and the

urban landscape. The techniques and measures to prevent forest fires in the urban landscape around the residences allow access of personnel and firefighting equipment and reduce the risks and damages due to fires. Usually the most effective measures are obtained through the vertical and horizontal separation of vegetation and in these cases the use of less flammable plant species is essential. (BEHM et al, 2004). Therefore, knowledge of how species differ in their flammability characteristics is necessary to draw up lists of recommended plants for urban and residential afforestation in WUI areas (WHITE and ZIPPERER, 2010).

Modeling has become an essential tool in research on forest fires and is currently a crucial tool in studies on risk mapping, fire propagation, as well as forest management (MADRIGAL et al, 2009). Experimental studies are needed both to calibrate and to validate the prediction models. Ignition, fire behavior, risk assessment and fire control require a thorough understanding of the chemical and physical processes involved in wildfires. How forest fuels burn and which parameters have the greatest influence on the combustion process are issues that need to be addressed (BARTOLI et al, 2011).

Forest fires affect vegetation which, in turn, affects fire behavior, as the plant species that provide the fuel for fires have specific flammability (CURT et al, 2011).

Climate change over the last few decades has been cited in numerous reports and surveys as one of the main causes of the increase in the frequency and magnitude of wildfires. Several climatological and ecophysiological models project drier and warmer conditions and, therefore, with greater risk of forest fires (MORENO, 2009, WESTERLING & BRYANT, 2008). But the frequency and magnitude of fires do not depend only on meteorological conditions, they also depend on the characteristics of the vegetation, especially its flammability (ALESSIO et al, 2008).

Flammability can be considered as the ease with which the material ignites and can also be understood as the resistance of the plant species to start and propagate fires (NUÑEZ-REGUEIRA et al, 2004). It can also be defined as the ease with which the material catches fire, both spontaneously and when exposed to certain conditions (ZHANG et al, 2011).

Flammability was initially defined based on three components (ANDERSON, 1970):

a- Ignition potential – time required for the fuel to reach ignition, after being exposed to a source of heat;

b- Sustainability – is the ability to maintain combustion after ignition;

c- Combustibility – is the burning rate after ignition.

Martin et al. (1994) added a fourth component: the amount of fuel burned (consumability).

The concept of flammability can be reduced to different aspects of combustion, according to the type of metric used in its evaluation, as can be seen in Table 1 (WHITE and ZIPPERER, 2010).

Flammability is experimentally evaluated by burning fuels in the laboratory, either in the form of the discrete elements (e.g. a leaf, a branch) for which the concept was coined, or as a bed of fuel or a heterogeneous set of individual units (FERNANDES and CRUZ, 2012).

Scale is an important issue when defining the methodology to be used to measure flammability. Vegetation flammability can be assessed at three levels: plant parts, whole plant and plant groups. In general, small-scale combustion tests are used to assess the flammability of plant parts. Large combustion tests are used to evaluate whole plants and groups of plants (GILL & ZYLSTRA, 2005).

Flammability characteristics are affected by several factors that can be classified into two groups: physical structures and components (twig size, leaf size and shape, dead material retention); and physiological and cellular elements (volatile oils and resins, moisture content, mineral content, lignin and greases), which are described in table 1 (WHITE and ZIPPERER, 2010).

Table 1. Criteria associated with favourable and unfavourable characteristics for determining plant fire resistance.

Favourable characteristics	Unfavourable characteristics
Architecture and Structure	
- Easy maintenance and pruning	- No maintenance and no periodic pruning
- Drought tolerant	- Fuel accumulator, including dry twigs, branches and leaves
- Free from dead leaves or needles and twigs	- Producer of large amounts of litter
- Thick, fleshy leaves and branches	- Dry or dead underground material
- Slow growing, with characteristics of - Prostrate or vine growth	- Dry and leathery leaves
- Little volume of leaves and small branches	- Needle-like or very thin leaves
- Difficult to ignite	- Compact and dense shape
- Does not keep flames for a long time	- Dense, abundant foliage
- Broad leaves	- Rough (shaggy) bark
- Produces limited dead and fine material	
- Low foliage density	
Physiological and Cellular	
- Low levels of volatile oils and resins	- High content of oils or resins, including gums and terpenes
- High moisture content, juicy	
- High ash and mineral content	

Source: WHITE e ZIPPERER, 2010.

2. Objectives

The general objective of this research was to evaluate the flammability of forest species used in forest fragments and (WUI) areas to support fire management planning in these environments. To achieve this objective, the following specific objectives were established: selection of species of frequent occurrence in urban and interface forest fragments of the cities of Curitiba-PR and Gurupi-TO, according to the favourable morphological characteristics of fire resistance and to determine, in laboratory, the flammability characteristics of the selected species.

3. Material and Methods

The flammability tests were carried out in the Forest Fire Laboratories of the Federal University of Paraná and CEMAF (Environmental Monitoring and Fire Management Center) of Federal University of Tocantins, Brazil.

Fifty-seven species were chosen from the fragment forests and wildland urban interfaces of Curitiba-PR and Gurupi-TO, Brazil, belonging to the southern and northern regions of Brazil, respectively, where forest activities are very importante for the regional economy and to which fires cause important damage. The criteria used for the selection of the species followed the recommendations of Biondi and Batista (2010). The selected species were: *Allophylus edulis, Anacardium occidentale, Antonia ovata, Araucaria angustifolia, Aristida sp., Aspilia montevidensis, Bauhinia rufa, Bougainvillea glabra, Byrsonima verbascifolia, Camellia japonica, Casearia sylvestris, Chytraculia concinna, Clethra scabra, Copaifera langsdorffi, Cupania vernalis, Curatella americana, Dalbergia miscolobium, Davilla elliptica, Dimorphandra mollis, Diospyros lasiocalix, Eriotheca gracilipes, Eryngium elegans, Eugenia uniflora, Euonymus japonicus, Guettarda viburnoides, Himatanthus obovatu, Hirtella ciliate, Hyptis meridionalis, Jasminum mesnyi, Lafoensia pacari, Lantana camara, Leandra australis, Leucena leucocephala, Ligustrum lucidum, Luehea divaricate, Macrolobium limbatum, Magnolia grandiflora, Michelia champaca, Mollinedia clavigera, Myrcia splendens, Ocotea puberula, Ouratea hexasperma, Persea americana, Pinus taeda, Pseudobombax grandiflorum, Psidium cattleianum, Qualea multiflora, Rhododendron simsii, Schinus terebentifolius, Tabebuia aurea, Tachigali aurea, Tapirira obtuse, Trachypogon spicatus, Vatairea macrocarpa, Verbena rigida, Viburnum odoratissimum, Ziziphus Cinnamomum.*

Flammability was determined according to the methodology recommended by Valette (1990) and Petriccione (2006). For each evaluated species, 50 firing repetitions were performed in the epirradiator, each one consisting of 1 ± 0.1 g of fresh fine forest fuel (< 0.7 cm in diameter). In the tests, the following combustion characteristics

were analysed: ignition time (IT), in seconds, time of complete combustion (TC), in seconds, maximum flame height (FH), in centimetres and ignition frequency (iF), in percentage. iF is the percentage of repetitions in which ignition occurred, considering a maximum IT of 60 seconds. The burnings that exceeded this time were classified as "negative burning" and received standardized values: IT equal to 61 seconds; TC equal zero seconds and FH equal zero centimetres. The flammability index (FI) of the selected species was obtained according to the iF and IT, varying as follow: 0 = very low flammable; 1 = low flammable; 2 = moderately flammable; 3 = flammable; 4 = very flammable; and 5 = extremely flammable (Table 2).

The data obtained were submitted to the flammability rating value (FI) and Cluster analysis, with the objective of validate the classification and identify the variables that present higher influence in the species flammability

Table 2. Classification of flammability according to the ignition time (IT), in seconds, and ignition frequency (iF), in percentage.

IT (s)	**iF (%)**					
	≤ 50	**50 - 79**	**80 - 84**	**85 - 89**	**90 – 94**	**> 94**
> 32.5	0	0	0	1	1	2
27.6 – 32.5	0	0	1	1	2	2
22.6 – 27.5	0	0	1	2	2	3
17.6 – 22.5	0	1	2	2	3	3
12.6 – 17.5	1	1	2	3	3	4
< 12,6	1	2	3	3	4	5

Source: Valette (1990).

4 Results and discussion

The results of the cluster analysis indicated that of the 57 species analysed, 44% were classified as very low flammable (22 native and 3 exotic species), 14 % as low flammable (8 native species), 15,8 % as moderately flammable (7 native and 2 exotic species), 8.8 % as flammable (2 native and 3 exotic species), 5,2 % as very flammable (2 native and 1 exotic species) and 12,2 % as extremely flammable (5 native and 2 exotic species).

The criterion used in this research for the selection of species through morphological characteristics proved to be adequate as a preliminary analysis to the flammability tests, considering that 74% of the analysed species presented low or null flammability. These preliminary results provide a good basis for continuing flammability studies for the potential use of low flammability species in wildland urban interface (WUI) areas and in forming safety green barriers highways and for forest fire prevention. The promising species to continue the flammability studies in the studied WUI areas are presented in table 3.

Regarding the origin of the species, 31% of the species classified as low or null flammability (FI = 0 or 1) belong to the Cerrado biome, a region heavily impacted by forest fires, although many of these species are naturally occurring in fire-adapted environments. This information reinforces the importance of knowing the flammability of the species for fire management in Brazil.

Table 3. Species with low flammability (FI = 0) with potential for use in the cities of Curitiba and Gurupi to prevent forest fires.

Species	**Origin**
Araucaria angustifolia	Native
Aristida sp.	Native
Aspilia montevidensis	Native
Bougainvillea glabra	Native
Cupania vernalis	Native
Dalbergia miscolobium	Native
Davilla elliptica	Native
Dimorphandra mollis	Native
Eriotheca gracilipes	Native
Eryngium elegans	Native
Eugenia uniflora	Native

Euonymus japonicus	Exotic
Hyptis meridionalis	Native
Lantana camara	Native
Leandra australis	Native
Ligustrum lucidum	Exotic
Luehea divaricata	Native
Macrolobium limbatum	Native
Myrcia splendens	Native
Ocotea puberula	Native
Persea americana	Exotic
Pseudobombax grandiflorum	Native
Psidium cattleianum	Native
Schinus terebentifolius	Native
Verbena rigida	Native

4. References

ALESSIO, G. A.; PEÑUELAS, J.; LLUSIÀ, J.; OGAYA, R.; ESTIARTE, M.; DE LILLIS, M. 2008. Influence of water and terpenes on flammability in some dominant Mediterranean species. International Journal of Wildland Fire, 17, 274–286

ANDERSON, H. E. 1970. Forest fuel ignitibility. Fire Technology, New York, v. 6, p.312–319.

BARTOLI, P.; SIMEONI, A.; BITEAU, H.; TORERO, J.L.; SANTONI, P. A. 2011.Determination of the main parameters influencing forest fuel combustion dynamics. Fire Safety Journal, 46, 27–33.

BEHM, A. L.; DURYEA, M. L.; LONG, A. J.; ZIPPERER, W. C. 2004. Flammability of native understory species in pine flatwood and hardwood hammock ecosystems and implications for the wildland–urban interface. International Journal of Wildland Fire, 13, 355–365.

BIONDI, D.; BATISTA, A. C. 2010. Ornamental plant species of Brazil and their potential use as fire breaks. In: VI International Conference on Forest Fire Research, Coimbra. Abstractcs - VI International Conference on Forest Fire Research - CD-ROM. Coimbra - Portugal: ADAI/CEIF - Ed. Domingos X. Viegas, 2010. v. 1. p. 1-8.

CURT, T.; SCHAFFHAUSER, A.; BORGNIET, L.; DUMAS, C.; ESTÈVE, R.; GANTEAUME, A.; JAPPIOT, M.; MARTIN, W.; N'DIAYE, A.; POILVET, B. 2011. Litter flammability in oak woodlands and shrublands of southeastern France. Forest Ecology and Management, 261, 2214–2222.

DIMITRAKOPOULOS, A. P.; PAPAIOANNOU, K. K. 2001. Flammability Assessment of Mediterranean forest fuels. Fire Technology, 37, 143-152.

FERNANDES, P.M.; CRUZ, M.G. 2012. Plant flammability experiments offer limited insight into vegetation–fire dynamics interactions. New Phytologist, 194, 606-609.

GILL, A. M.; ZYLSTRA, P. Flammability of Australian Forests. 2005. Australian Forestry, 68 (2):87-93.

MADRIGAL, J.; HERNANDO, C.; GUIJARRO, M.; DIEZ, C.; MARINO, E.; CASTRO, A.J. 2009. Evaluation of forest fuel flammability and combustion properties with an adapted mass loss calorimeter device. Journal of Fire Sciences, V. 27, 321-342.

MARTIN, R. E.; GORDON, D. A.; GUTIERREZ, M.E; LEE, D. S.; MOLINA, D. M.; SCHROEDER, R.A.; SAPSIS, D. B.; STEPHENS, S. L.; CHAMBERS, M. 1994. Assessing the flammability of domestic and wildland vegetation. Proceedings of the International Conference on Fire and Forest Meteorology, v. 12, p. 130-137.

MORENO, J. M. Impactos en el riesgo potencial de incendios debidos al cambio climático. 2009. In: BIROT, Y. (Ed). Convivir con los incendios forestales: lo que nos revela la ciencia. EFI Discussion Paper 15, European Forest Institute, p. 77-80.

NUNEZ-REGUEIRA, L.; RODRIGUEZ-ANON, J. A.; PROUPIN CASTINEIRAS, J. 2004. "Using calorimetry for determining the risk indices to prevent and fight forest fires," Thermochimica Acta, vol. 422, no. 1-2, p. 81–87.

PETRICCIONE, M.; MORO, C.; RUTIGLIANO, F. A. 2006. Preliminary studies on litter flammability in Mediterranean region. Forest Ecology and Management, v. 234, p. 128-128.

VALETTE, J. C. Inflammabilités des espèces forestières méditerranéennes. 1990. Rev. Forest. Fr., v. 42, p.76-92.

VÉLEZ, R. 2000. La defensa contra Incendios Forestales: Fundamentos y experiencias. Madrid: McGraw Hill.

WESTERLINT, A. L.; BRYANT, B. P. 2008. Climate Change and Wildfires in California. Climate Change 87 (Suppl 1): S231-S239.

WHITE, R. H.; ZIPPERER, W. C. 2010. Testing and classification of individual plants for fire behaviour: plant selection for the wildland–urban interface. International Journal of Wildland Fire, 19, 213–227.

ZHAN, Z.; ZHANG, Z.; ZHOU, D. 2011. Flammability characterization of grassland species of Songhua Jiang-Nen Jian Plain (China) using thermal analysis. Fire safety Journal, v. 46, n.5, p. 283-288.

Factors Influencing Ember Accumulation Near a Building

Stephen L. Quarles[1]; Christine Standohar-Alfano[2]; Faraz Hedayati[1], Daniel J. Gorham*[1]

[1] Insurance Institute for Business & Home Safety. 5335 Richburg Rd, Richburg, SC 29729, USA, {steveq0629@gmail.com}, {fhedayati, dgorham}@ibhg.org
[2] Haag Engineering. 2224 E. 117th St, Burnsville, MN 55337, USA, {Christine.Standohar@gmail.com}

**Corresponding author*

Keywords

Ember; firebrand; accumulation; building; structure

Abstract

Embers, also known as firebrands, are the leading cause of building ignition during wildland-urban fires. This is attributed to direct ignitions of materials on, in, or attached to the building, and indirect ignition when they ignite vegetation or other combustible material near the building which can result in radiant heat and / or direct flame contact that ignites the building. Where and when embers accumulate near a building and ignitable fuel presents the potential for indirect ember ignition of the building. Factors that influence ember accumulation near a building include building geometry, such as flat wall and re-entrant corners, building wind angle, wind speed and the surface roughness characteristics of the horizontal landscape close to the building. Experiments conducted at the Insurance Institute for Business & Home Safety (IBHS) Research Center, using full-scale buildings with the above-mentioned factors provided a means to quantify ember accumulation on a mass per unit area basis.

1. Introduction

One of the main challenges to combating wildfires is that they spread through three main mechanisms, including flame impingement, radiant heat, and wind-blown embers, also referred to as firebrands. Ignition of a structure can be caused by direct flame contact from the primary fire front or from fires caused by localized fuel sources (i.e. vegetation, fences, etc.) near the structure (Potter and Leonard 2010, Quarles et al. 2010). Regardless of the source of the flame, ignition of the exterior of the building can result in ignition of internal contents. Buildings near flames are subjected to radiant heat and their vulnerability depends on both the intensity of the radiation as well as the duration (Potter and Leonard 2010).

The third mechanism of wildfire spread is by exposure to embers. This mode is the most important cause and accounts for up to 90% of structural ignitions (Potter and Leonard 2010). For example, two of every three homes destroyed in the 2007 Witch Creek fire in San Diego County, CA were ignited by ember accumulation (Quarles et al. 2010). The risk of ignition from embers depends on several features, including the number of embers, the ember characteristics, the amount of and type of combustible debris or materials near the building, duration of the ember attack, and environmental conditions. In some cases, ember attacks can result in the ignition of a building 12 hours after the initial fire front passes (Potter and Leonard 2010). The delayed ignition can be explained by either the continued production of embers from burning fuels after the fire front passed, or the smoldering combustion of a component or assembly that eventually transitioned to flaming combustion.

The lifecycle of embers that cause destruction of homes and building can be described in three stages: 1) production and release of embers from burning fuel; 2) transport of embers from the source to where they are deposited, including accumulation; and given sufficient accumulation and receptive fuel 3) ignition. Given the dominant role that embers play in wildfire spread and home ignition (Manzello et al. 2020) a considerable amount of research has been conducted and is underway on this topic. Experiments conducted by Suzuki and Manzello (2017) also studied accumulation zones created by stagnation planes in front obstacles. These investigations found that wind speed (6, 8, and 10 m/s) influenced the accumulation of firebrands in the stagnation plane on the windward side of obstacles and suggest experiments at wind speeds greater than 10 m/s would be desirable. In the stagnation zone roughness of horizontal surface affects the accumulation of embers (Suzuki & Manzello 2017). Later work investigated the effect of structure separation distance on firebrand

accumulation (Suzuki and Manzello 2021) which highlighted the role of firebrand behaviour between two structures. The heat flux, and ignition potential, from a pile of accumulated embers is distinctly different than from an individual ember (Hakes et al. 2019).

Nguyen and Kaye (2022) conducted a series of small-scale wind tunnel experiments investigating non-combustible ember accumulation on building rooftops and found that building geometry and wind angle were important factors for accumulation rates. Separate from and prior to these previous studied a set of experiments were conducted at IBHS to study the accumulation of embers near a building as a function of wind speed, building geometry, and wind angle. This work is the focus of the present paper.

2. Methodology

These ember accumulation experiments were conducted as part of the 2015 wildfire experimental campaign at the IBHS Research Center in Richburg, South Carolina. This research facility includes a wind tunnel large enough to hold full-scale one- and two- story residential and small commercial buildings, allowing for investigations to evaluate the performance of buildings subjected to high winds (Standohar-Alfano et al. 2017). The facility is able to generate wind speeds greater than 71.5 m/s (100 mph) using a 105-fan array. The wind tunnel can generate a constant wind speed or replicate observed, fluctuating wind records from hurricanes, thunderstorms, or open country conditions. For the 2015 wildfire experimental campaign, an open country wind record was used and was scaled to generate wind time histories defined as medium and high. The medium and high wind speed traces were fluctuating records with an average wind speed of 10.3 and 17.4 m/s (23 and 39 mph), respectively. Figure 1 shows the medium and high wind speed traces used in the experiments. In addition, an idle fan speed was used which ranged between 4.5-5.4 m/s (10-12 mph).

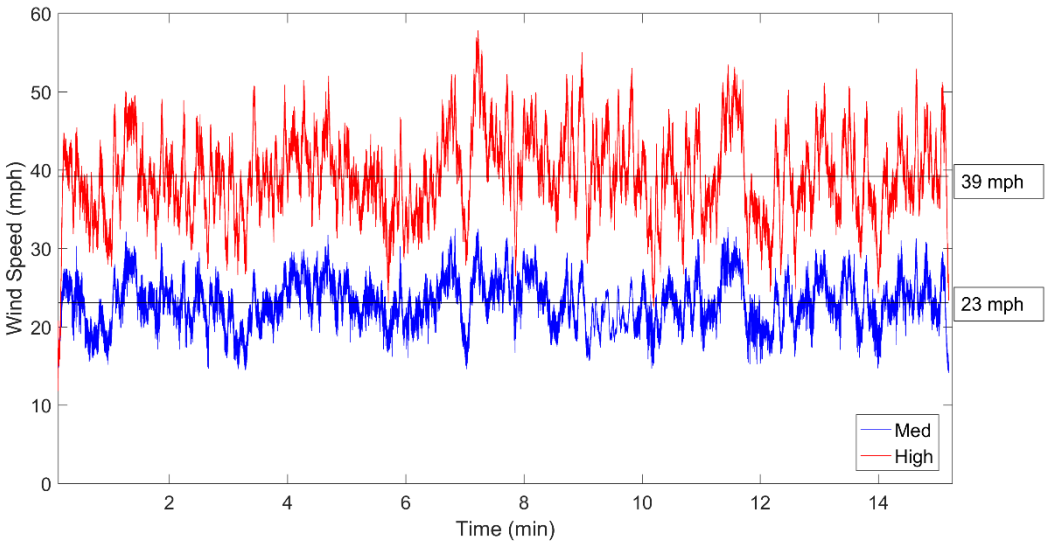

Figure 1. Medium and high wind speed records used in the 2015 wildfire experimental campaign (1 mph = 0.45 m/s). The average wind speeds for the "medium" and "high" wind speeds are boxed to the right of the respective record.

The wind tunnel utilizes a large turn table with a radius of 16.8 m (55 ft) which can rotate 360°, allowing for the full rotation of the test building and therefore the evaluation of the effect of wind speed and direction on the deposition of embers around the test building.

The 2015 wildfire experimental campaign used a custom-made system to deliver fuel and generate embers. The fuel was a mixture of southern yellow pine wood chips and wooden dowels processed from midwestern hardwood species, with a ratio of 80% and 20%, by weight, respectively. All raw material was dried to a moisture content less than 10%. The generators were used to burn fuel and create embers, as shown in Figure 2. The fuel was delivered into the generator by the auger feed line shown by Figure 2A. The fuel dropped on top of a metal grate immediately above a gas burner (not shown). A fan located under the burner (Figure 2B) pushed embers up and out of the exhaust chute indicated by Figure 2C. Eight generators were placed at equally spaced increments in front of the fan array.

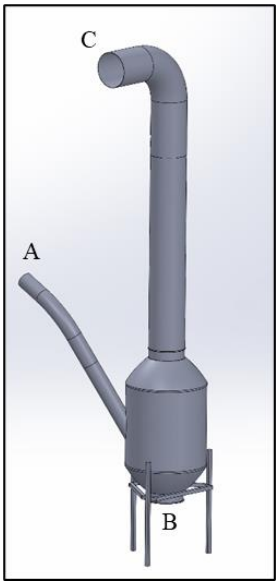

Figure 2. Schematic of the ember generators used. A is the auger feed line which introduced the fuel into the generator; B is the location of the vertically oriented fan; and C is the exhaust chute.

An overview of the auger system, generators, and test building is shown in Figure 3. Prior to testing, fuel was placed in the hoppers shown in Figure 3A. Five augers (not shown) dropped fuel into the pneumatic feed lines. The feed rate was controlled by powering the augers on and off. The desired feed rate was obtained when individual augers were turned on for a predetermined length of time between 3-5 seconds and then off for 10-20 seconds. Establishing the on/off times for each individual auger was determined based on visual inspection of ember output and observed overheating of the generators. The goal of using the intermittent fuel delivery was to ensure a consistent output of embers by all generators without damaging the generators from excessive heat.

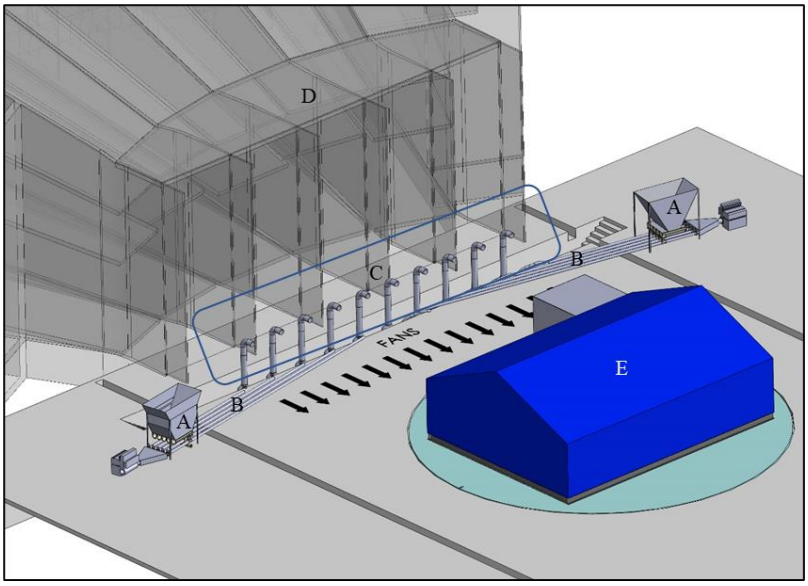

Figure 3. Experimental setup, including auger feed and ember generator system. The left and right hoppers are shown in A; B indicates the auger feed lines which deliver fuel to the 10 generators indicated in C; D is the fan array behind the generators; and E is the test building.

The auger delivered fuel to feed lines shown as B in Figure 3. These feed lines delivered the fuel to the generators (Figure 2A and Figure 3C). As described earlier, the generators burned the fuel and a fan pushed embers up the exhaust chute. Using the wind traces shown in Figure 1, the fan array (Figure 3D) created the wind flow in the test chamber. The test building shown by E in Figure 3 was then subjected to an ember exposure. The duration of the exposure was 15-minutes. The system used in this study is shown in Figure 4. By placing a building in the wind field and exposing it to embers, embers were collected at various near-building locations.

Figure 4. Test building and ember generator system used in the accumulation study. As shown, the collection trays were initially covered with a solid panel until steady flow from the generators was observed.

To evaluate ember accumulation in the vicinity of a building, a full-scale structure was positioned in the wind tunnel (Figure 3E and Figure 5). The structure was one-story with a building footprint of 9.1 m x 12.2 m (30 ft x 40 ft). To evaluate the vulnerability of a re-entrant corner, a 3 m x 3 m (10 ft x 10 ft) cube was placed on one corner of the long axis, as shown in Figures 4 and 5. This cube detached and re-attached at different locations on the test building. The building and cube were clad with fiber-cement panels. The orientation of the building was varied to assess the impact of wind direction on ember accumulation.

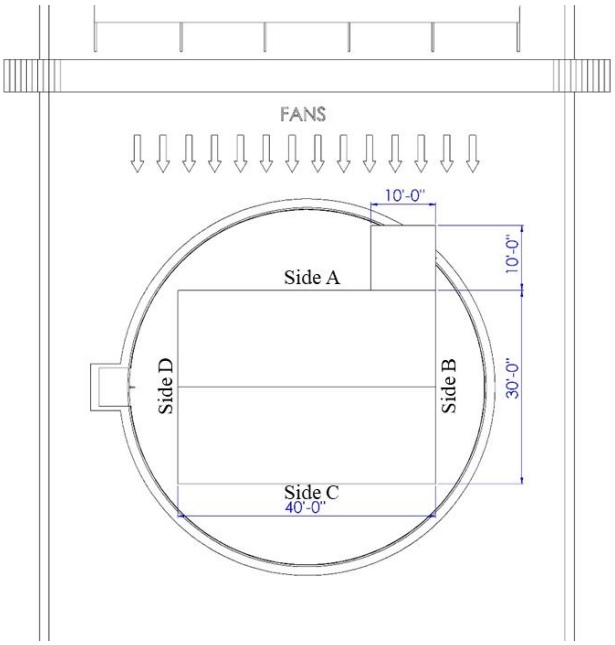

Figure 5. Plan view of the test building used in the accumulation experiments.

2.1. Ember Accumulation and Characterization

For the ember accumulation portion of the experiments, water-filled pans were placed at various locations on the test building. The building was then subjected to an ember exposure for 15 minutes. Thirteen scenarios were

examined at both medium and high wind speeds, as shown in Table 1. With the exception of the 270 orientation, a water-filled pan was placed in the re-entrant corner. Two additional water-filled pans (defined as WP 1 and WP 2) were positioned at selected locations along the building, as indicated in Table 1. Location information is also provided in Figure 6.

Table 1. Ember Accumulation Test Matrix.

	Pan		
Orientation	Corner	WP 1	WP 2
0°A	Yes	1.5 m (5 ft)	1.5 m (5 ft)
15°A	Yes	1.5 m (5 ft)	1.5 m (5 ft)
330°B	Yes	0 m (0 ft)	0 m (0 ft)
345°B	Yes	0 m (0 ft)	0 m (0 ft)
0°B	Yes	0 m (0 ft)	0 m (0 ft)
15°B	Yes	0 m (0 ft)	0 m (0 ft)
30°B	Yes	0 m (0 ft)	0 m (0 ft)
60°	Yes	0 m (0 ft)	3.8 m (12.5 ft)
75°	Yes	0 m (0 ft)	3.8 m (12.5 ft)
90°	Yes	0 m (0 ft)	3.8 m (12.5 ft)
105°	Yes	0 m (0 ft)	3.8 m (12.5 ft)
120°	Yes	0 m (0 ft)	3.8 m (12.5 ft)
270°	No	1.5 m (5 ft)	3.1 m (12 ft)

As indicated in Table 1, there were four main parent orientations investigated, shown in bold (0°A, 0°B, 90°, and 270°). With these four scenarios, the face closest to the fans was perpendicular to the wind field. For three of the main orientations (0°A, 0°B, and 90°) the re-entrant corner was directly impacted by the wind field (i.e., not on the leeward side of the building). In order to assess the impact of wind direction on ember accumulation the building was rotated in 15° increments. The location of the re-entrant corner on the test building was assessed with two of the main orientations (0°A and 0°B). For scenarios with an A orientation, the cube was in its original location at the end of the building as indicated in Figure 5. For the cases with a B orientation, the cube was moved to the mid-length of the building (centered at 6.1 m (20 ft)).

The pan location is also included in Table 1. The corner pan was located in the re-entrant corner and there was only one orientation where it was not utilized. There were two wall pans (WP 1 and WP 2) used in the ember accumulation experiments. The location is given as the distance from the closest corner. For the A scenarios, both pans were placed 1.5 m (5 ft) from the corners of the windward side. For the B scenarios, both of the wall pans were placed at the corner (0 m). For the cases where the main (parent) orientation was 90°, one pan was placed at the corner and the second pan was placed 3.8 m (12.5 ft) from the same corner. This resulted in a spacing of 2.3 m (7.5 ft) between the pans. For the 270° orientation, one pan was placed 1.5 m (5 ft) from one corner and the second pan was placed 3.1 m (12 ft) from the other corner.

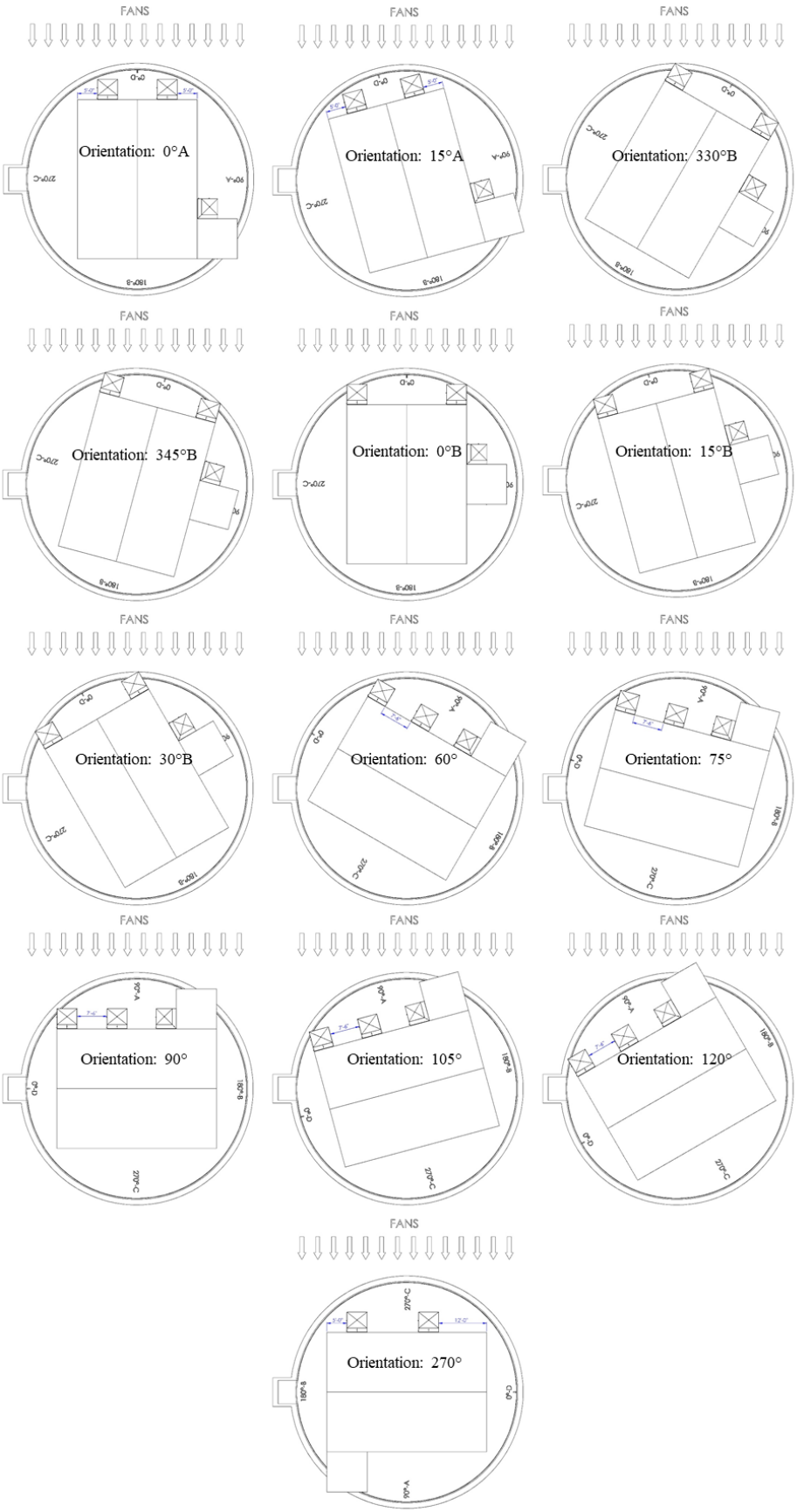

Figure 6. Pan location for all orientations.

At the beginning of each test, during the time the generators were starting up and output was non-uniform, the pans were covered. Once the generators reached a steady state the cover was removed and the wind speed record began, marking the start of the 15-minute exposure. The orientations summarized in Table 1 were subjected to both the medium and high wind speed traces.

The water-filled pans used in the ember accumulation study measured 1.5 m x 1.5 m (5 ft x 5 ft) and were divided into two sections defined as field and wall. The wall section was the area closest to the exterior wall. For all pans, this was 0.3 m (1 ft) from the wall edge. The field section was larger than the wall section and was the remaining portion of the water-filled pan that was not immediately adjacent to the building. Figure 7 shows an image of the two types of pans used in the accumulation study. Figure 7a illustrates the pan that was placed in the re-entrant corner. Since this pan had two edges against a wall, the wall section was larger than the pans placed elsewhere on the building.

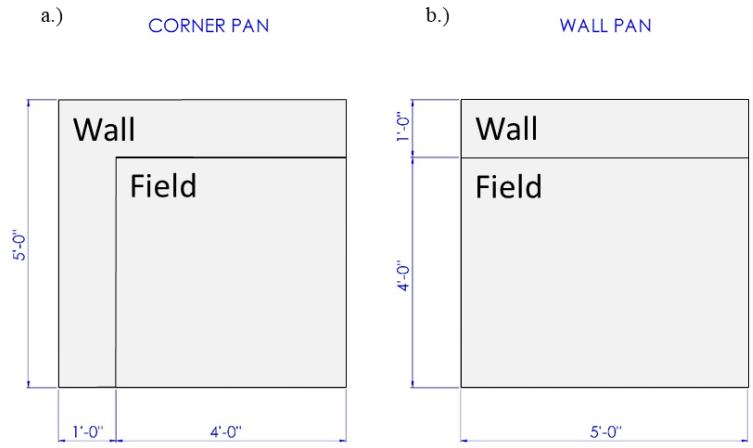

Figure 7. Water-filled pan dimensions and sections where a.) is the pan at the re-entrant corner and b.) is the pan placed along the flat wall (WP 1 and WP 2).

In addition to estimating the ember accumulation in the water-filled pans, the mass and surface area of individual embers was also measured. This was done to study the variability in ember characteristics. The surface area was calculated using image processing software and the mass was found using a high-precision electronic scale.

3. Results and Discussion

Results from the accumulation study are shown in Figures 8 through 11. There was variability in the accumulation depending on orientation, wind speed, pan section (wall or field), and pan placement along the wall of the test building. Thirteen orientations were investigated. The orientation of the test building with Side A facing the fans, as shown in Figure 5, was designated as the 90°orientation. Side B was designated 180°, Side C was designated 270° and Side D was designated 0°.

The results for the 270°orientation are shown in Figure 8. This was the only orientation that was tested at the idle (non-fluctuating) wind speed. This orientation positioned the cube on the leeward side of the building, so no embers were collected in the corner pan. The results for this orientation indicated that maximum ember accumulation occurred in the wall sections. At this orientation, the difference in accumulation between the wall and field sections increased with increasing wind speed.

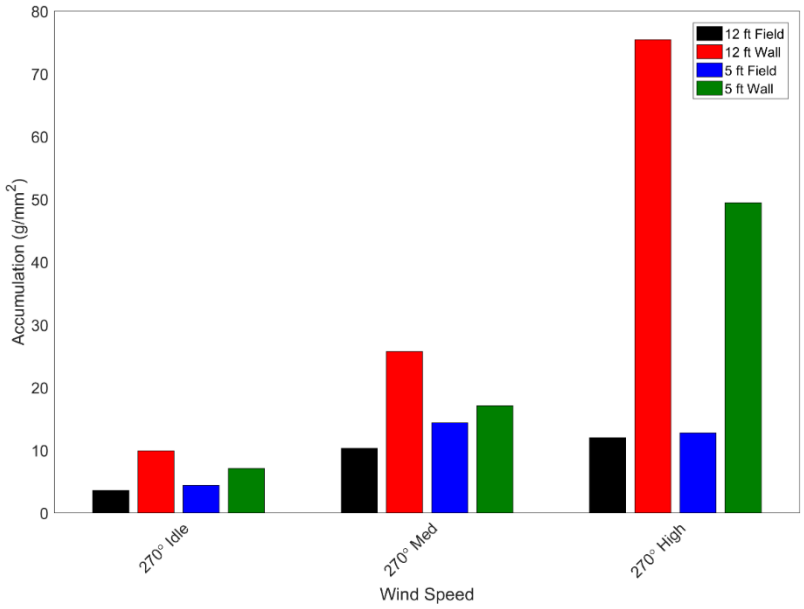

Figure 8. Ember accumulation in water-filled pans. The length direction of the test building faced the fans.

For the orientations in the 90° parent orientation (Figure 9), the 60° had the highest accumulation for both the medium and high wind speeds. At this orientation, WP 1 and WP 2 were closer to the ember generators and the re-entrant corner was positioned so that embers were naturally caught in the corner pan. For this reason, accumulation values were relatively high. At 105° and 120°, ember accumulation decreased. For these orientations, the cube used to simulate the re-entrant corner did provide some shelter for locations on the leeward side of the cube where the water-filled pans were placed.

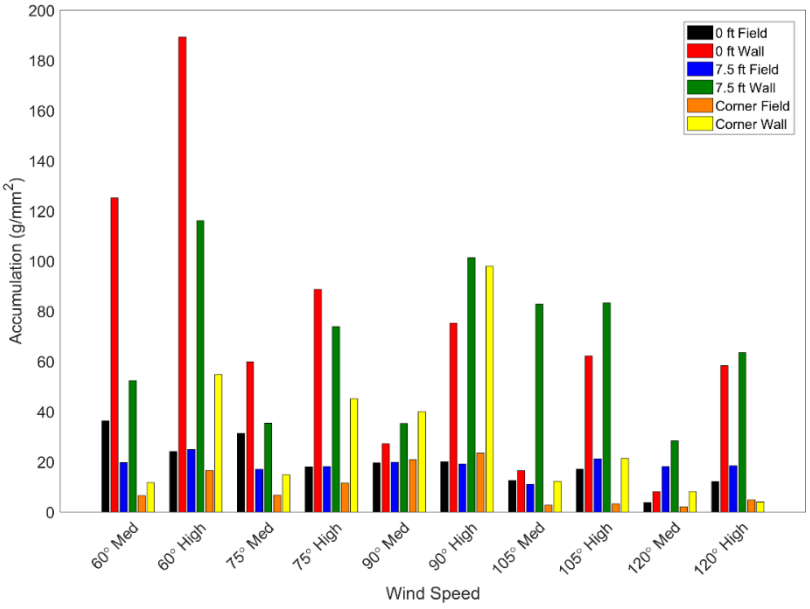

Figure 9. Ember accumulation in water-filled pans. Results are presented for the 90° parent orientation.

The results of accumulation for the 0°A and 15°A orientation is shown in Figure 10. As with previous orientations, the wall section of the pans had higher accumulations than the field sections for a given wind speed. Likewise, the high wind speed record did result in higher values of accumulation. Since the re-entrant corner was located 9.1 m (30 ft) from the windward edge of the building, ember accumulation in the corner pan was minimal due to the distance from the ember generators.

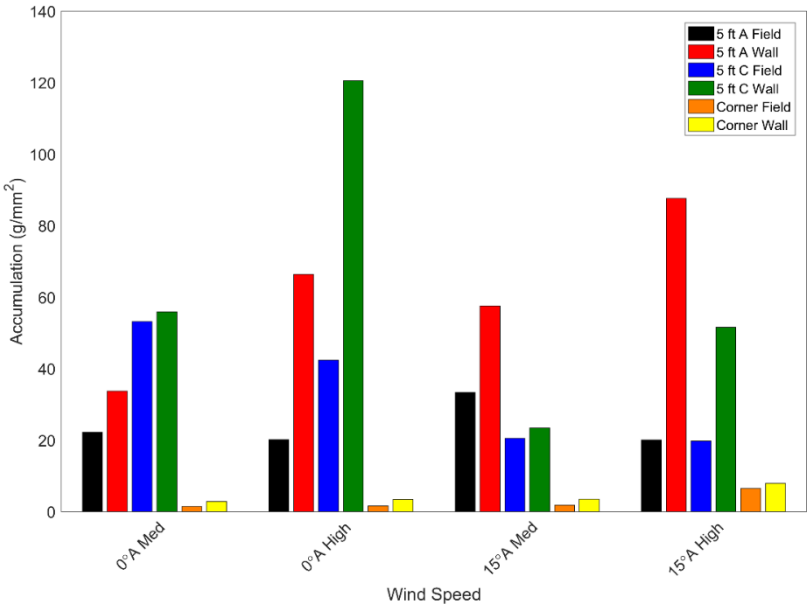

Figure 10. Ember accumulation in water-filled pans. Results are presented for the 0°A parent orientation.

Finally, the results of the 0°B parent orientation are shown in Figure 11. For these orientations, the re-entrant corner was located at the mid-span of the test building and was closer to the ember generators. As with other orientations, the wall section of the water-filled pans saw larger values of ember accumulation as compared to the field section. Likewise, high wind speeds typically resulted in higher values of accumulation. The 330°B and 345°B orientations had higher accumulations in the water-filled pan located on the C side of test building. With these orientations, the test building was rotated such that the C side was closer to the generators, so this result was not surprising. Similarly, for the 15°B and 30°B orientation, the A side of the building was closest to the generators, so accumulation was greatest in the water-filled pan located on the A side of the windward wall. Likewise, as the test building was rotated counter-clockwise from 0°B, the re-entrant corner moved closer to the generators and there was an observed increase in ember accumulation at the corner pan.

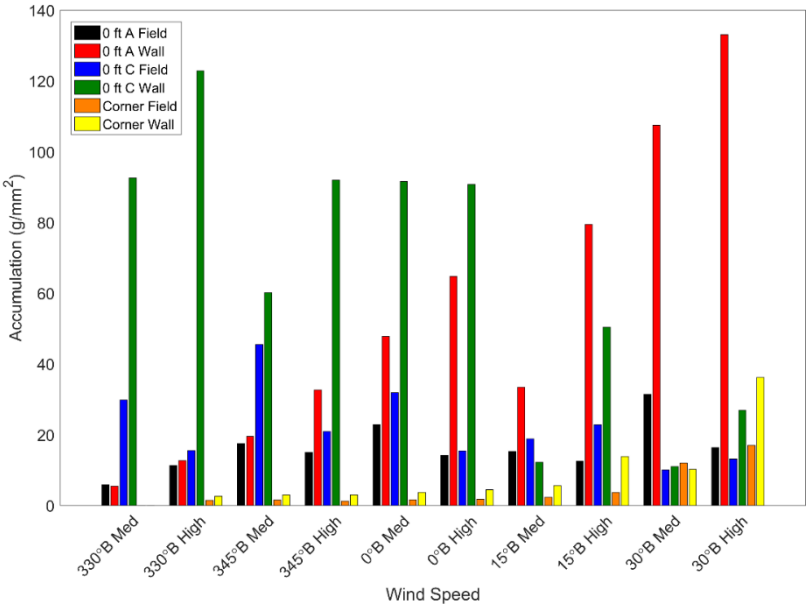

Figure 11. Ember accumulation in water-filled pans. Results are presented for the 0°B parent orientation.

In addition to quantifying ember accumulation, characterization of individual embers was also performed by measuring mass and surface area. The goal of this portion of the work was to add to the knowledge base regarding the quantification of ember exposure since this is an area of needed research. Due to the large number

of orientations investigated, only embers from the four parent orientations (270°, 90°, 0°A, and 0°b) were included.

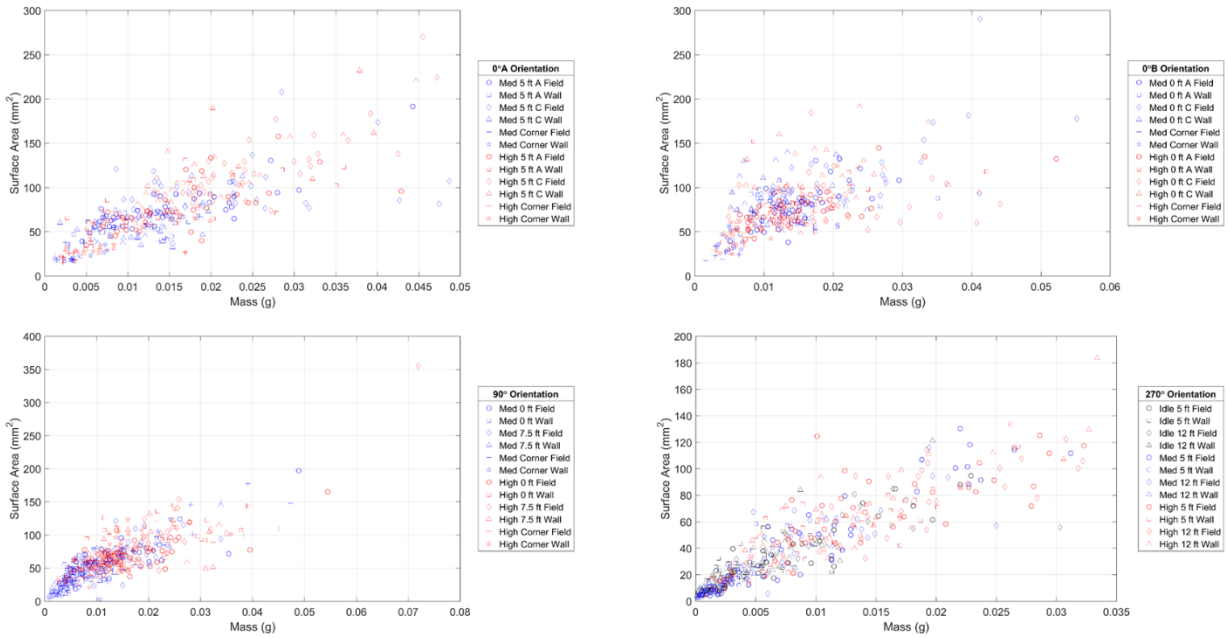

Figure 12. Ember characteristics, mass and surface area, from ember generators and collected in water-filled pans.

The relationship between mass and surface area is relatively linear and as the surface area increases, so does the mass. There did not appear to be any strong dependency between wind speed and ember surface area or mass. Likewise, the orientation did not appear to have an important impact on ember surface area or mass. This was not surprising since fuel type plays a larger role in ember characteristics than building orientation. As data regarding ember characteristics from active wildfires becomes available, a comparison can be made to the embers created with the IBHS generators. Using that information, the generators and/or fuel can be modified to better replicate embers collected in the field.

4. Conclusion

Overall, the data suggested that the accumulation for the wall section was higher than the accumulation for the field section, thus indicating greater vulnerability at locations immediately adjacent to the building. For the wall sections, higher wind speeds resulted in greater accumulation. Higher wind speeds allowed more embers to reach the building and become caught in the recirculation where they were forced into the water-filled pans. For the field sections, accumulation values were typically largest for the medium wind speed record, however, the dependency of accumulation on wind speed was lower. This likely resulted in the relatively large size of the field section, so at medium wind speed, lower momentum embers could land directly in the field section since they were unable to reach the building.

These results have important implications, especially for rough ground surfaces immediately adjacent to buildings. If embers strike a building and become contained in the recirculation, they can be forced down to the ground. If the ground surface is rough (i.e., mulch), it will capture the embers and allow them to accumulate closer to the building. Any combustible material near accumulated embers can potentially ignite which would result in direct flame contact or elevated levels of radiant heat near a building.

5. References

Manzello SL, Suzuki S, Gollner MJ, Fernandez-Pello, AC (2020) Role of firebrand combustion in large outdoor fire spread. Progress in Energy and Combustion Science. doi: 10.1016/j.pecs.2019.100801

D. Nguyen, N.B. Kaye, Quantification of ember accumulation on the rooftops of isolated buildings in an ember storm, Fire Saf. J. 128 (2022), https://doi.org/10.1016/j. firesaf.2022.103525.

Potter M and Leonard J (2010). Spray System Design for Firebrand Attack – Research Findings and Discussion Paper. CSIRO – Sustainable Ecosystems, Report No. EP103159, 1-27.

Standohar-Alfano CD, Estes H, Johnston T, Morrison MJ, Brown Giammanco TM (2017) Reducing losses from wind-related natural perils: research at the IBHS Research Center. Frontiers in Built Environment 3, 9. doi:10.3389/FBUIL.2017.00009

Suzuki S and Manzello SL (2017) Experimental investigation of firebrand accumulation zones in front of obstacles. Fire Safety Journal. doi: 10.1016/j.firesafe.2017.08.007

Manzello, S.L.; Suzuki, S.; Gollner, M.J.; Fernandez-Pello, A.C. The role of firebrand combustion in large outdoor fire spread. Prog. Energy Combust. Sci. 2020, 76, 100801.

Suzuki S and Manzello SL (2021) Investigating the Effect of Structure to Structure Separation Distance on Firebrand Accumulation. Front. Mech. Eng 6:628510. doi: 10.3389/fmech.2020.628510

Quarles, Stephen L., Valachovic, Yana, Nakamura, Gary M., Nader, Glenn A., and De Lasaux, Michael J, (2010). Home Survival in Wildfire-Prone Areas: Building Materials and Design Considerations. University of California Agriculture and Natural Resources. ANR Publication 8393.

Fire propagation from surface to canopy on ornamental species under wind in laboratory conditions

Anthony Streit [1]; Bruno Guillaume *[1]; Bertrand Girardin [1]; Lucas Terrei [2]; Anthony Collin [2]; Alexis Marchand [3]

[1] Efectis France, Saint Aubin, France, {bruno.guillaume@efectis.com}
[2] LEMTA, Université de Lorraine, CNRS, Vandoeuvre-lès-Nancy, France
[3] SCALIAN, Rennes, France

**Corresponding author*

Keywords

Wildfires at Urban Interface, Fire propagation in parcels and structures, Wind-driven laboratory tests, WUI numerical modelling

Abstract

Fires in wildland-urban interfaces (WUIs) are resulting from intertwined physical processes at different scales: landscape, settlement, parcel, building and material (Vacca et al., 2020) and are causing growing damage worldwide in context of climate change and large urban sprawl.

The significant damage caused by these fires requires effective reinforcement of the resistance of structures and parcels against exposure to fire. Recent methodologies (Vacca et al., 2020 ; Benichou et al., 2021; Maranghides et al., 2022) have emphasised the need to look at these objectives by considering the spatial relationships between fuels, exposures and building resistance, in the perspective of a fire propagating in WUI according to so-called "fire pathways". At parcel scale, the fire pathways often involve ornamental vegetation, that highly raises the damaging potential of the wildfire, this vegetation being at short distance to the structures and having a comparable size with buildings. Horizontal and vertical discontinuities in this vegetation do largely impact the exposure (Cohen, 2008) and installing such discontinuities is becoming part of the protection regulation against wildfires in different countries (Maranghides et al., 2022).

While the impact of embers has been extensively studied in the Insurance Institute for Business and Home Safety (IBHS) facilities (Manzello and Suzuki, 2014; Suzuki and Manzello, 2020), the effect of the fuel discontinuities on the reduction of thermal attack when approaching the building has been poorly addressed. This study aims at simulating in laboratory conditions a moving fire front pushed by wind and propagating from the surface to a canopy of ornamental vegetation, with fuel discontinuities. The experimental setup is composed of a fire lit in a surface excelsior fuelbed, propagating to a nearby vertical ornamental structure (excelsior and cypress) exposed to controlled high wind exposure (up to 3 m/s). The work is completed by a comparison of numerical modelling between the WFDS and FDS models.

The first steps of this study are shown here, showing a coherent sensitivity of the rate of spread to fuelbed width and fuelbed load, and showing the ability of WFDS and FDS to reasonably reproduce this rate of spread. The ability of FDS to propagate to an isolated vertical tree with the same modelling processes is also well established.

1. Introduction

Significant efforts have been made to understand the development and expansion of fires at the wildland-urban interface (WUI) (Cohen, 2008; Vacca et al., 2020), showing how the nearest combustible elements to the building are crucial for the propagation of the fire to the building. On the other hand, tree canopy fire contamination in native forests have independently been subject to various studies (Rothermel, 1991; Fernandes et al., 2009).

At homeowner scale, ornamental vegetation (isolated garden trees, hedges, climbing plants, ...) strongly enhances the danger coming initially from the native forest. In most tests and numerical simulations of WUI fires, these elements, located between the native forest and the building, are generally not represented. However, if represented they burn under very low wind conditions (Suzuki and Manzello, 2020; Li et al., 2021; Di Cristina et al., 2021), though in real fires (particularly true in South-East of France), fires in these ornamental elements occur under very gusty and chaotic wind conditions.

This study aims at experimentally reproducing a surface fire (excelsior fuelbed) propagating to a nearby vertical ornamental structure (excelsior and cypress), under high wind exposure (3 m/s) in the laboratory (*i.e.* at reduced scale). Additionally, a numerical setup composed of the models WFDS/FDS is used to compare and validate the codes against the experimental data.

This contribution describes the first steps of this study: the first section describes how zero-wind surface fire experimental data are generated to evaluate the sensitivity of Rate Of Spread (ROS) to fuel load and fuel width. The second section describes the setup of FDS and WFDS models that will be used in the entire study. Then results of some nominal and intermediate model configurations are presented. The last section is dedicated to the intermediate conclusions and to introduce the next steps of the study.

2. Calibration of the zero-wind surface fire in the experimental setup

The first step consisted in evaluating the ROS of a surface fire under zero-wind condition, in order to gain in reproducibility of surface fires for the full experimental setup. This is a first validation before developing the full experimental setup composed of a surface fire propagating to an ornamental vegetation under high wind exposure (Figure 1b). 85 experiments were performed with zero-wind surface fires (Marchand et al., 2014, 2019). They were carried out on excelsior as fuelbed (Figure 1a) and the sensitivity to fuelbed width and fuelbed load was investigated. The combustible material was fully characterised in a previous work by Marchand et al. (2019). The first 45 experiments were conducted with a constant vegetation load (0.5 kg/m²) and with fuelbed width ranging from 25 cm to 3.5 m. The excelsior was spread onto the table in order not to exceed a maximum average height of 8.5 cm. The fire was ignited on a line along the whole bed width. The last 40 fire tests were conducted with a constant fuelbed width of 2 m and with a fuel load ranging from 0.1 kg/m² to 1 kg/m². Visible cameras combined with image processing (Otsu algorithm) were used and a direct linear transformation (DLT) algorithm was developed in order to quantify fire behaviour properties (ROS, fire length, etc.).

(a)  (b) 

Figure 1 - Zero-wind fire spread test on the surface fuelbed, (b) View of the high wind exposure facility

A summary of main results is shown in Figure 2. For the sensitivity of ROS to fuelbed width, ROS is shown to increase at low values of fuel bed width and seems to reach a constant value of about 1.5 cm/s for a 2 m fuel bed width and beyond. In such configurations, the fire fronts are near-parabolic, but the front curvature varies with the line width and the rate of spread is also affected. For the sensitivity to fuelbed load, ROS is shown to globally increase with fuel loads from 0.3 cm/s for the lowest load to 2.6 cm/s in average for the highest load. The repeatability of tests showed discrepancy up to 0.5 cm/s as compared to the average value that can be significant but explained by ambient conditions (different seasons and ambient conditions).

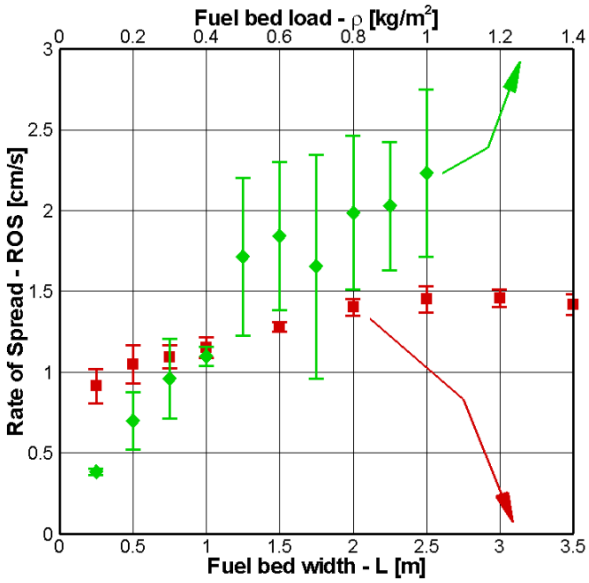

Figure 2 - Distribution in the 85 experiments of the rate of spread as a function of fuelbed width (red colour) for a constant vegetation load of 0.5 kg/m² and as a function of fuelbed load (green colour) for a constant fuelbed width set at 2 m.

3. Wind-driven surface fire experiments

A second step consisted in evaluating the ROS of the wind-driven surface fire. Five different wind fans of the "wind wall" were activated with the same constant frequency in each individual experiment. The wind measurements collocated to the fans and at different horizontal distances from the fans, at 0 m and 1m ground heights are shown in Figure 3. The wind at z= 0 m ground height is more affected by the distance to the fans than the wind at z= 1 m. All fan frequencies cannot be used when burning the vegetation since above 30 Hz the excelsior is heavily washed from the table by the wind.

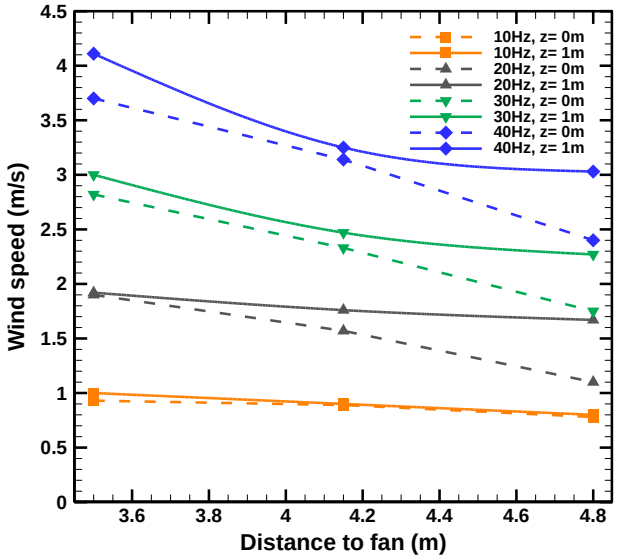

Figure 3 – Wind speed wih horiztonal distance to the fans, and at two different ground heights (z=0m and z=1m)

Different tests of excelsior burning under different wind speeds have been conducted at two different vegetation loads, set at 0.23 kg/m² and 0.4 kg/m². The excelsior fuelbed was positioned at a distance of 1.3 m from the fans.

As shown on Figure 4, the ROS exhibits a strong increase when going from zero-wind to 0.88 m/s wind speed, with a multiplication of ROS by 4 for the 0.23 kg/m^2 case and by 6 for the 0.4 kg/m^2 case. Then a plateau of ROS is observed between 0.88 m/s wind speed and 1.9m/s wind speed and finally another strong ROS increase occurs when reaching 2.4 m/s wind speed.

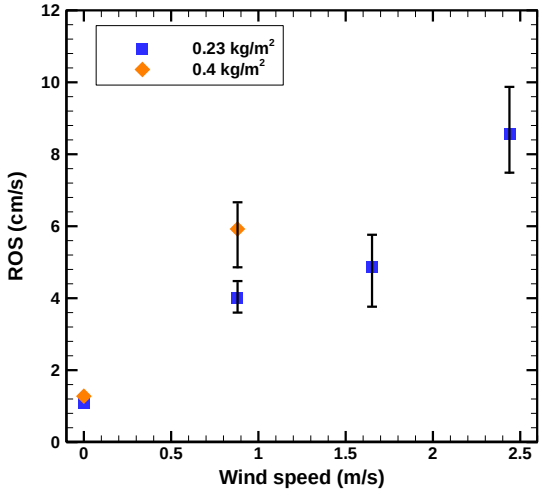

Figure 4 – Rates of spread in function of the wind speed for two different loads (0.2 kg/m^2 and 0.4 kg/ m^2)

4. Calibration of the surface and canopy fires, with wind, in the experimental setup

Finally, the full experimental setup composed of a surface fire propagating from excelsior to an ornamental vegetation in form of a very thin hedge, with and without wind exposure, has been tested, with the same objective of monitoring ROS.

Two types of vegegation were sampled to constitute the hedge: cypress and oleander. This vegetation was arranged with equal fuel load on a vertical mesh of 1 m large and 1.5 m height, by intertwinning the branches with the fine diameter coarse galvanized steel mesh, which has the advantage of preventing the vegetation from collpasing when burning. A simple evaluation showed that the very fine diameter of the mesh would not modifiy significantly the fire power or the ROS over the hedge. Same fuel load was imposed on the entire mesh with respectively about 1.2 kg/m^2 and 4 cm depth for cypruss and about 1.2 kg/m^2 and 6 cm depth for oleander, collected in gardens and let drying for a minmum of 15 days. Size distribution of <2mm, 2-4 mm, and 4-6 mm diameters were found for cypress of 34.7 %, 55.1%, and 10.2 %. Size distribution of 2-4 mm, 4-6 mm, and 6-8 mm diameters were found for oleander of 48 %, 44 %, and 8 %. The Figure 5 shows cypress and oleander branches and the bulk density evaluation by tube test.

Figure 5 – Property measurements: (left) oleander weighting, (middle) cypress branches clustering for size distribution evaluation, (right) cypress bulk density evaluation

The Fuel Moisture Content (FMC) was sampled 1 day before the experiment. FMC of cypress was about 23.8 % on dry matter basis. FMC of oleander was about 10.7 %. The FMC for cypress has been measured 15 times with a SD (standard deviation) of 9.6%, 6 times with a SD of 1.3% for oleander, and 5 times with a SD of 0.7% for excelsior. For ROS measurements, a total of 8 thermocouples (TCs) were vertically-positioned, 4 being vertically aligned along the middle of the hedge and 4 others vertically aligned along the exterior side of the

hedge. Each TC is 50 cm distant from another, covering a distance of 0.1 m to 1.6 m over the table. Two visible cameras were also placed, one at the back of the hedge and another one on the side.

A series of 2 experiments were conducted with cypress under zero-wind conditions, while 1 experiment was conducted with cypress under 10 Hz wind conditions (around 0.88 m/s) (outputs not shown here), and 2 experiments were conducted with oleander under zero-wind conditions. Under zero-wind conditions, the fire contaminates the hedge only after the excelsior fire has arrived very close to the foot of the hedge (Figure 6).

Figure 6 – Fire contamining from excelsior fire to the hedge under zero-wind conditions, (upper) for cypress and (lower) for oleander. Propagation visualized in 5 phases (from left to right): excelsior fire approaches, excelsior fire at the foot of the hege (reference time t=0s), fire at maximum development in the hedge, fire largely decreasing, fire in extinction phase

ROS of the fire in the hedge was quantatively extracted from the vertically-positioned TCs under zero-wind conditions, but the oscillatory flames did contaminate the vertical sensors in an erratic sequence (with higher TCs contaminated prior to lower TCs), preventing from getting the ROS this way. The measurements from visibles cameras revealed a robust way to measure ROS, the imagery being preliminatorily distance-referenced (Figure 7). Cypress fire exhibited ROS values respectively between 35 cm/s and 43 cm/s under zero-wind condition, and 55 cm/s under 10 Hz wind condition. The oleander exhibited ROS values between 22 and 24 cm/s under zero-wind condition. More experiments have been scheduled to gain statistical robusntess of these results. Additionally the calibration of the WFDS and FDS models is in ongoing process on these data.

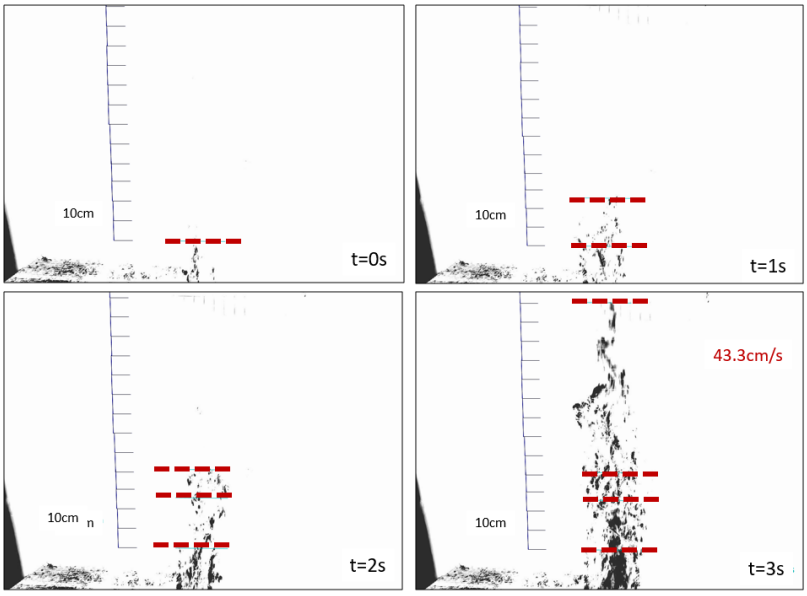

Figure 7 – Zero-wind condition cypress ROS measured by manual interpretation on distance-referenced thermal camera imagery

5. Numerical setup

The two versions of "FDS" (Fire Dynamic Simulator), the classical FDS and its WFDS derivation (Widland Fire Dynamic Simulator) are used in this study. Each numerical model has its own parameters to represent the vegetation fuel and should be calibrated. In the literature, grid resolution to reproduce laboratory "forest fire" experiments may vary from 2 cm (Morandini et al. (2019) for rockrose shrubs) or 5 cm (Wickramasinghe et al. (2020) for Douglas fir) and up to 10 cm (Mell et al. (2009) for the same Douglas fir).
The WFDS model in 7.6 version is used here with a uniform spatial resolution along the three directions of Δ= 2 cm. The linear pyrolysis model is employed in WFDS.
The Fire Dynamic Simulator (FDS) in version 6.7.5 is used here with either (1) a uniform spatial resolution along the three directions of Δ= 2 cm, or (2) with $\Delta x=\Delta z$ =1 cm and Δy= 2 cm. The pyrolysis and char oxidation processes are driven by an Arrhenius model.

6. Nominal WFDS and FDS calibration on the intermediate setup of a zero-wind surface fire

The tests modelled with WFDS for the zero-wind surface fire require to attribute values to eight key parameters of the pyrolysis model: the maximum value allowed for the MLR [MLRmax in kg/m^3/s], the bulk density of vegetation [ρbulk in kg/m^3], the density of vegetative fuel [ρ in kg/m^3], the surface-to-volume ratio of vegetation [σ in 1/m], the moisture fraction Hu in %wt calculated on a dry mass basis), the fraction of dry virgin vegetation that becomes char τchar (in %wt), the heat of combustion [ΔHr in kJ/kg] and an adimensional multiplicative drag coefficient Cf.

Raw values of these parameters have been previously obtained by Marchand et al. (2019) and are presented in Table 1. Simulations were made to determine the ROS evolution as a function of the fuelbed width for a 0.5 kg/m² vegetation load using these raw values as input data. Despite that, the global trend is well captured as the ROS increases with the fuel bed width, these simulations exhibited a strong underestimation (60 % differences with the experimental data). Therefore, these values have been fitted: a local sensitivity analysis revealed that MLRmax and ΔH_r were the most significantly sensitive parameters for the ROS predicted by the WFDS model. An identification algorithm (Particle Swarm Optimisation method according to Kennedy and Eberhart (1995)) was then used to identify the best values for these two input parameters, keeping all others at their initial experimental values. As presented in Figure 8, with these new parameters, the numerical trend of ROS with fuelbed width is in a good agreement with the experimental data.

The tests modelled with FDS for the same test configuration require to attribute values to several parameters driving the thermal decomposition and char oxidation. More details about model formulation can be found in Mell et al. (2009), Perez-Ramirez et al. (2017) and Morandini et al. (2019) or Porterie et al. (2009). Most of the parameters are extracted from these previous studies. Namely, the parameters describing the dehydration of the vegetation are taken as $E_{H_2O} = 5800K$, $A_{H_2O} = 6 \times 10^5 s^{-1}K^{-1/2}$ and $\Delta H_{H_2O} = 2.2596 \times 10^3 J.kg^{-1}$ (endothermic). The parameters describing the decomposition of the vegetation into combustible duel are $E_{pyr} = 7250K$, $A_{pyr} = 3.63 \times 10^4 s^{-1}$ and $\Delta H_{pyr} = 1.297 \times 10^3 J.kg^{-1}$ (endothermic). The latter parameter is the only parameter that is not extracted from Perez-Ramirez et al. (2017) or Porterie et al. (2009), its value was fitted so the predicted ROS under zero-wind condition was similar to the experimental one with a fuelbed of 0.5 kg/m² and a fuel width of 0.25 m. The char oxidation model and its inputs was extracted from Perez-Ramirez et al. (2017). Namely, the following parameters were used in our study : $E_{char} = 9000K$, $A_{char} = 430\ m.s^{-1}$ and $\Delta H_{pyr} = 32 \times 10^3 J.kg^{-1}$ (exothermic).

Table 1 -Input parameters used for WFDS: comparison between raw experimental values and fitted optimised values

Features	Initial experimental values	Fitted Optimal values
MLRmax [kg/m³/s]	0.22	0.43
ρbulk [kg/m³]	5.55	
ρ [kg/m3]	519	
σ [1/m]	14 600	
Hu [-]	0.12	
τchar [-]	0.31	
ΔHr [kJ/kg]	16 480	14 497
Cf [-]	0.375	

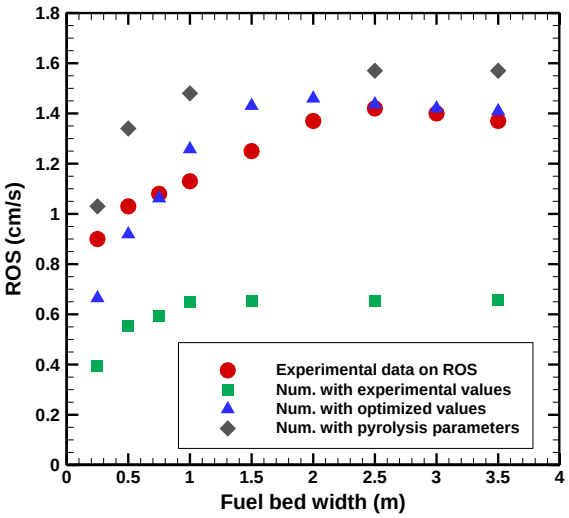

Figure 8 - Results of the two sets of WFDS simulations of ROS, with raw experimental values of the pyrolysis model parameters, and fitted optimal values

Simulations of FDS conducted with too low fuel loads (0.23 kg/m²) did exhibit no propagation, and calibrating different char oxidation parameters did not change this limiting model behavior. As seen in next section, when using a value of 0.3 kg/m² as in Meerpoel-Pietri et al. (2022) did not exhibit this problem.

7. Nominal FDS simulation on the intermediate setup of a wind-driven surface fire

The configuration of Figure 4 is simulated using the FDS model, using a fuel load of 0.5 kg/m². The model shows a coherent tendency in respect to the observations, with a lower increase of ROS with wind. More experiments at 0.4 kg/m² with wind have been scheduled to gain statistical robusntess of these results, to be compared with simulation at 0.4 kg/m².

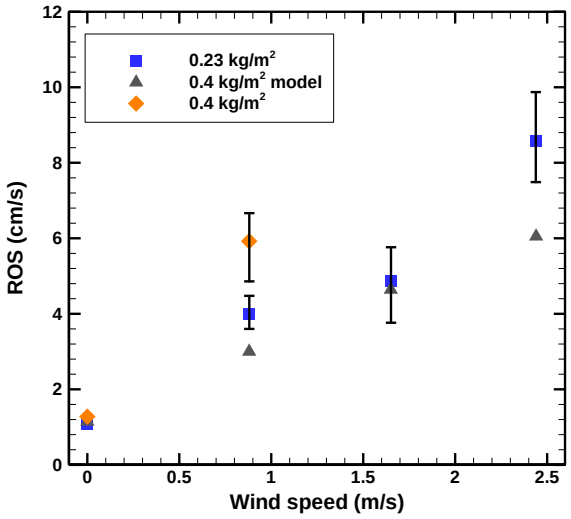

Figure 9 – Comparison of rates of spread varied with wind intensity, for two different loads (0.2 kg/m² and 0.4 kg/m²) for the experiments, and for one load (0.5 kg/m²) for the model

8. Nominal FDS simulations in similar setups

A simulation setup is used to illustrate the ability of FDS model to reproduce a zero-wind surface fire, extracted from Meerpoel-Pietri et al. (2022) referred hereafter as MP2022, with additional 20 % slope of the fuelbed. The fuelbed is also there composed of excelsior. The configuration from MP2022 as well as the input values given by the authors for the Arrhenius pyrolysis model are used within the FDS model, while the authors used the WFDS model.

As shown in Figure 10, the FDS outputs have a very similar intensity curve as the WFDS at 2 cm resolution from MP2022 , while being globally 22 % higher in intensity in the period between 5 s and 77 s. The difference in terms of intensity may be explained by the difference of the two codes. However, the ROS is coherent with the WFDS results and with the experimental data.

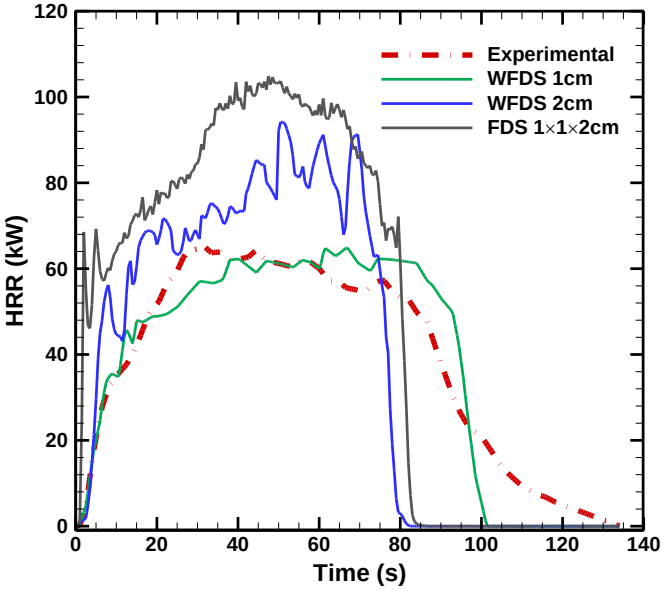

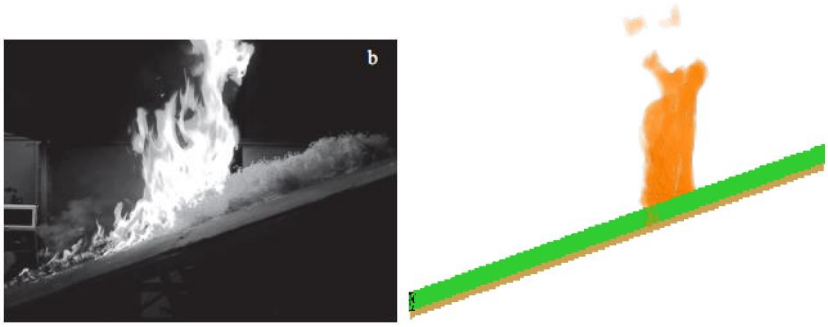

Figure 10. (upper row): Comparison of the intensity-time curves: the WFDS 1 cm and 2 cm and the experimental data are taken from MP2022 while the FDS is from current study, (lower row): Comparison in side view along the full slope of the observed (left) and modelled (right) flame height at timestep 51 s (source: observed flame photo is from Meerpoel Pietri et al. (2022))

A second similar setup as the full ornamental vegetation setup of this study is the single-tree canopy fire under zero wind provided by Mell et al. (2009), referred hereafter as M2009. The Mass Loss Rates (MLR) are calculated with FDS in this study for two different grid resolution, 10 cm and 25 cm, together with two different pyrolysis schemes: Arrhenius (same scheme as in the previous nominal zero-wind surface fire test) and simplified Arrhenius (scheme from older FDS versions). As shown in Figure 11 for a 5 m tree, the M2009 WFDS simulation is the closest to the experimental data, but all simulations from our study vary here only with a delay of less than 5 seconds in the peak MLR value, and with less than 20 % difference in peak value.

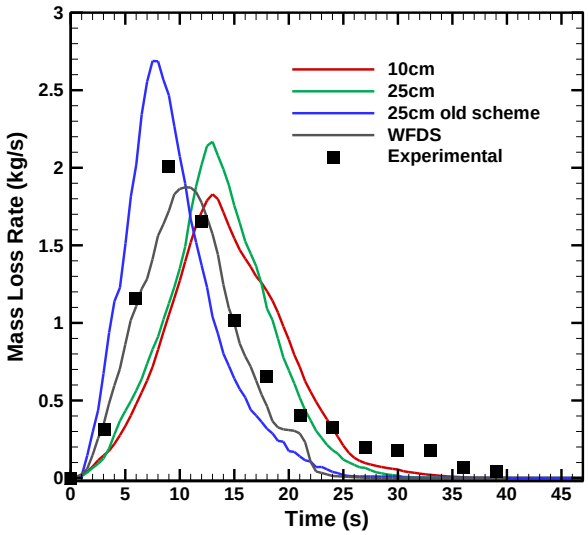

Figure 11 - Time evolution of MLR in current FDS version with both pyrolysis schemes and both resolutions (10 cm and 25 cm), compared with the Mell et al. (2009) experiment data and numerical WFDS outputs

These nominal simulations of FDS based on current state model should be confronted with observations of next coming surface and canopy fire tests in the study.

9. Conclusions

Based on experimental data on zero-wind surface fire propagation, this contribution showed promising results on the ability of WFDS and FDS to reproduce well the fire front behaviour. Moreover, the ability of FDS to propagate to an isolated vertical tree with the same modelling processes is also presented and validated.

A new experimental setup allowing simulating a scenario of fire contamination from the surface to an ornamental vegetation, under high wind conditions, is in ongoing development. It involves a surface fire

scenario, represented by a fire in Excelsior, which contaminates an ornamental vegetation. Some targeted nominal intercomparisons with the WFDS and FDS models will be presented in the final contribution. This new experimental setup will allow in a coming future to evaluate the impact of vertical discontinuities (low branches position of the ornamental vegetation), as well as effect of wind intermittency.

10. References

Benichou N., Adelzadeh M., Singh J., Gomaa I., Elsagan N., Kinateder M., Ma C., Gaur A., Bwalya A., and Sultan M. (2021). National Guide for Wildland-Urban Interface Fires. National Research Council Canada: Ottawa, ON. 192 pp

Cohen J (2008) The wildland-urban interface fire problem: A consequence of the fire exclusion paradigm. Forest History Today. Fall: 20-26.

Di Cristina G., Kozhumal S., Simeoni A., Skowronski N., Rangwala A.; Im, S.-K. (2021). Forced convection fire spread along wooden dowel array. Fire Safety Journal. 120: 103090. https://doi.org/10.1016/j.firesaf.2020.103090.

Fernandes P.-M. (2009). Combining forest structure data and fuel modelling to classify fire hazard in Portugal. Annals of Forest Science, Springer Nature (since 2011)/EDP Science (until 2010), 66 (4).

Kennedy J. and Eberhart R. (1995) « *Particle swarm optimization* », *IEEE International Conference on Neural Networks, 1995. Proceedings*, vol. 4, p. 1942–1948.

Li B. , Ding L. ,Simeoni A. , Ji J. ,Wan H.,Yu L. (2021) Numerical investigation of the flow characteristics around two tandem propane fires in a windy environment, Fuel, 286, 119344.

Manzello L. and Suzuki S. (2014), Exposing Wood Decking Assemblies to Continuous Wind-Driven Firebrand Showers, Fire Safety Science 11: 1339-1352.

Maranghides A., Link E., Nazare S., Hawks S., McDouglad J, Quarles S., Gorham D. (2022) WUI Structure/ Parcel/ Community fire hazard mitigation methodology, NIST Technical Note 1600. National Institute of Standards and Technology, Gaithersburg, MD.

Marchand A., Trevisan N., Collin A. and Boulet P. Fire propagation, *Cellular automaton model, Fire front width effect, Radiative transfer*, in Advances in forest fire research, Imprensa da Universidade de Coimbra, 2014.

Marchand A., Ferrière S., Collin A., Boulet P. Acem Z., Demeurie F. and Morel J.-Y. Vegetation fire spread database : 85 wood wool shaving experiments at laboratory scale. Fire Safety Journal, Vol. 109, 102870, 2019.

Suzuki S. and S.L. Manzello (2020) Investigating coupled effect of radiative heat flux and firebrand shower on ignition of fuel beds, Fire Technology.

Maranghides, A. , Link, E. , Nazare, S. , Hawks, S. , McDougald, J. , Quarles, S. and Gorham, D. (2022), WUI Structure/Parcel/Community Fire Hazard Mitigation Methodology, Technical Note (NIST TN), National Institute of Standards and Technology, Gaithersburg, MD, [online], https://doi.org/10.6028/NIST.TN.2205,

McGrattan, K.B., Klein, B., Hostikka, S., and Floyd, J (2008). Fire Dynamics Simulator Users Guide. NIST Special Publication 1019-5, National Institute of Standards and Technology, U.S. Department of Commerce, Gaithersburg, MD.

Meerpoel-Pietri K., Tihay-Felicelli V., Graziani A.,Santoni P.-A., Morandini F., Perez-Ramirez Y., Bosseur F.,Barboni T., Sánchez-Monroy X., Mell W. (2022): Modeling with WFDS Combustion Dynamics of Ornamental Vegetation Structures at WUI: Focus on the Burning of a Hedge at Laboratory Scale, Combustion Science and Technology, DOI: 10.1080/00102202.2021.2019235

Mell W, Jenkins MA, Gould J, Cheney P (2007) A physics based approach to modeling grassland fires. 2007. International Journal of Wildland fire. 16(1): 1-22.

Mell W., Maranghides A., McDermott R., and Manzello S.L. (2009) Numerical simulation and experiments of burning douglas fire trees, Combustion and Flame, vol. 156, no. 10, pp. 2023–2041.

Morandini, F.; Santoni, P.A.; Tramoni, J.B.; Mell, W.E. (2019) Experimental investigation of flammability and numerical study of combustion of shrub of rockrose under severe drought conditions. Fire Safety Journal. 108: 102836

Perez-Ramirez Y., Mell W.E., Santoni P.-A., Tramoni J.-B., Bosseur F., 2017, Examination of WFDS in Modeling Spreading Fires in a Furniture Calorimeter. Fire Technology, Springer Verlag, 2017, 53 (5), pp.1795-1832.

Porterie B., J. L. Consalvi , A. Kaiss & J. C. Loraud (2005) Predicting Wildland fire behavior and emissions using a fine scale physical model, Numerical Heat Transfer, Part A: Applications, 47:6, 571-591

Rothermel, Richard C. 1991. Predicting behaviour and size of crown fires in the northern Rocky Mountains. Res. Pap. INT-RP-438. Ogden, UT: U.S. Department of Agriculture, Forest Service, Intermountain Research Station. 46 p.

Vacca, P.; Pastor, E.; Planas, E.; Caballero, D. 2020 WUI I fire risk mitigation in Europe: A performance-based design approach at home-owner level, Journal of safety science and resilience, 1 (2), p. 97-105

Vanella M, McGrattan K, McDermott R, Forney G, Mell W, Gissi E, Fiorucci P. A (2021) Multi-Fidelity Framework for Wildland Fire Behavior Simulations over Complex Terrain. Atmosphere. 12(2):273.

Wickramasinghe A, Khan N and Moinuddin K (2020) Physics-based simulation of firebrand and heat flux on structures in the context of AS3959. Project Report. Bushfire and Natural Hazard CRC, Melbourne, Victoria

Fire-spotting modelling: A comparative study of an Italian test case

Marcos López-De-Castro*[1]; Andrea Trucchia[2]; Umberto Morra di Cella[2]; Paolo Fiorucci[2], Antonio Cardillo [3], Gianni Pagnini [1, 4]

[1] BCAM-Basque Center for Applied Mathematics. Calle Alameda de Mazarredo 14, Bilbao, 48009, Basque Country, Spain, {malopez, gpagnini}@bcamath.org
[2] CIMA Research Foundation. Via Armando Magliotto 2, Savona, 17100, Italy, {andrea.trucchia, paolo.fiorucci, umberto.morradicella}@cimafoundation.org
[3] Regione Molise, Centro Funzionale Decentrato del Molise, Contrada Selva del Campo, Campochiaro,86020, Italy, {cardillo@protezionecivile.molise.it}
[4] Ikerbasque-Basque Foundation for Science. Plaza Euskadi 5, Bilbao, 48009, Basque Country, Spain.

**Corresponding author*

Keywords

Wildfire simulation, fire-spotting, RandomFront, PROPAGATOR, cellular automata.

Abstract

Wildfire propagation is a non-linear and multiscale system in which there are involved multiple physical and chemical processes. One critical mechanism for the spreading of wildfires is the so-called fire-spotting: a random phenomenon which occurs when embers are transported over large distances by the wind, and causing the start of new spotting ignitions which jeopardize the fire-fighting actions. Due to its nature, fire-spotting is usually modeled as a probabilistic process. Three principal processes are involved during the fire-spotting: firebrands generation, transport joined with landing, and spot ignition. In this work, the physical parametrization of fire-spotting RandomFront (Trucchia et al. 2019) has been implemented into the operational wildfire spread simulator PROPAGATOR (Trucchia et al. 2020), which is based on a cellular automata approach. In the routine RandomFront, the downwind landing distribution of firebrands is modeled by means of a lognormal distribution, which is parameterized by taking into account the physics involved in the phenomenon. The considered physical parameters are: wind field, fire-line intensity, fuel density, firebrand radius, maximum loftable height, as well as factors related to atmospheric stability and flame geometry (Trucchia et al. 2019; Egorova et al. 2020,2022). As a matter of fact, similarity analysis cannot be applied to wildifres (Egorova et al. 2022, Section 2) thus the outputs of the simulations are checked against a real test case. In particular, we have considered the evolution of a real wildfire occured in Italy in August 2021 during which the fire-spotting played a critical role. In addition, we have implemented into PROPAGATOR also other two schemes for fire-spotting already available in literature and suitable for cellular automata-based wildfire simulators (Alexandridis et al. 2011; Perryman et al. 2013). We compared the performance of these three fire-spotting models. The results show that, on the one hand, the RandomFront parametrization reproduces the main spotting effects similarly to the available literature models (Alexandridis et al. 2011; Perryman et al. 2013), and, on the other hand, RandomFront generates also a variety of fire-spotting situations together with long-range fluctuations of the burning probability by allowing for complex patterns.

1. Brief introduction

Fire-spotting occurs when firebrands are transported away from fire and start new fires known as spot-fires (Brown and Davis 1973; Werth et al. 2011). These new fires can occur near the fire propagation front, accelerating the spread of fire, or kilometers away from the source fire, causing new secondary ignitions that increase the extinction difficulty and in which civilians and firefighters can result trapped (Koo et al. 2010). The conducted research to understand this phenomenon has been done in two ways. On one hand, there are extensive experimental studies focused on the characterization of the firebrands generation and transport process (Manzello et al. 2007, 2008; Suzuki et al. 2012; Thomas et al. 2017; Himoto and Iwami 2021; Wickramasinghe et al. 2022). Unfortunately, the short scales of the experiments limit its application into the calculation of the landing distribution (Pérez et al. 2011; Sullivan and Cruz 2015). On the other hand, firebrand transport models

have been developed to estimate the landing distribution and flight paths of the firebrands (Tarifa et al. 1965, 1967; Albini 1979, 1983; Himoto and Tanaka 2005; Sardoy et al. 2007, 2008; Wang 2011; Kaur et al. 2016). We highlight that the validation of these models in reduce-scale experiments are unreliable, in particular, in cases with important wind-fire or multiple fire interactions (Egorova et al. 2022, Section 2).

Wildfire modeling has been studied from several approaches (Sullivan 2009a; b; c), but Cellular Automata (CA) based methods have demonstrated to be a quick, efficient, and versatile approach to simulate the wildfire spreading (Clarke et al. 1994, Duarte 1997, Hargrove et al. 2000, Encinas et al. 2007, Gharakhanlou and Hooshangi 2021). Some of the developed CA-based models include the effect of the fire-spotting. We highlight the model developed by Alexandridis et al. (2008, 2011), which was revisited by Freire and Dacamara (2019) to reproduce a forest fire in Portugal, and the model developed by Perryman et al. (2013).

In this work, we have implemented into the operational wildfire spread simulator PROPAGATOR (Trucchia et al. 2020) the recently developed parametrization RandomFront (Trucchia et al. 2019; Egorova et al. 2020, 2022) as well as both previously cited CA-based fire-spotting models to be compared. In addition, we have reproduced a wildfire that occurred in Italy in August 2021, in which the fire-spotting effects were critical, for validating the results.

2. Fire propagation model and firebrand landing parametrizations description

2.1. Propagator fire-spread simulator

In this work, PROPAGATOR (Trucchia *et al.* 2020) was used to simulate the spread of fire. PROPAGATOR is an operational software based on a CA approach and assisted with high resolution data from the topography and land fuel cover. The fire spread is computed through vegetation type, slope, wind direction and speed, and fuel moisture content, therefore, the burned surface evolves in a stochastic sense. The input parameters are the wind intensity and direction, the start point of fire and the adopted ROS model. PROPAGATOR is designed to compute an ensemble of simulations in a fast way, being its basic and natural output a georeferenced map which represents the probability of each cell to be affected by fire.

2.2. Alexandridis *et al.* (2011) firebrand landing parametrization

The model developed by Alexandridis et al. (2008, 2011) , consist of a CA approach focused on the efficient simulation of wildfire spreading. The first part of their fire-spotting parametrization models the firebrand landing distance as follows:

$$d_p = r_n \cdot P_w = r_n \, exp\left(U_{C_2}(Cos\,\varphi - 1)\right), \qquad (1)$$

where r_n is a random number drawn from a normal distribution, φ is the angle between the direction of the wind and the direction of the blasting, and $U_{C_2} = U \cdot C_2$ is the mean-wind velocity times a fitted constant. In addition, the probability of spot ignition, *i.e.*, when a blasting firebrand will ignite or not a new spot-fire, is computed as:

$$P_C = P_{C0}\,(1 + P_{cd}), \qquad (2)$$

where P_{c0} is a constant probability corrected by P_{cd}, which is a factor that depends on type and fuel density.

2.3. Perryman *et al.* (2013) firebrand landing parametrization

The model developed by Perryman et al. (2013) consists of an ensemble of four sub-models adapted to a CA environment. Their firebrand landing distribution was implemented following the statistical model developed by Sardoy et al. (2008) for the firebrands which are blasted parallel to the wind, and the Himoto and Tanaka (2005) results for firebrands blasted perpendicular to the wind field. The landing distance of the parallel firebrands are computed following a lognormal distribution function:

$$p(d) = \frac{1}{\left(\sqrt{2\pi}\,\sigma_{FB}\,d\right)}\, exp\left(\frac{-\left(ln(d) - \mu_{FB}\right)^2}{\left(2\sigma_{FB}^2\right)}\right), \qquad (3)$$

where d is the distance away from the line front. The mean μ_{FB} and standard deviation σ_{FB} depend on the current wind intensity U, the fireline intensity I_f, fitted constants and if the firebrands are buoyancy driven or wind driven. To discern between both cases, the Froude number Fr is computed:

$$Fr = \frac{U}{\sqrt{g\left(\frac{I_f}{(\rho\, c_p\, T_A\, g^{1/2})}\right)^{2/3}}}, \qquad (4)$$

where g is the acceleration of gravity, I_f is the fire intensity, ρ is the ambient gas density, c_p is the specific heat of gas and T_A is the ambient temperature. If Froude number is less or equal to one, buoyancy driven regime is considered and for Froude number greater than one, wind driven plume regime. The firebrand distance of the embers generated parallel to the wind are modeled by means of a normal distribution, assuming zero mean and standard deviation $\sigma_v = L/2$, where L is the cell size.

2.4. RandomFront firebrand landing parametrization

The landing distance is parameterized by means of a log-normal distribution (*i.e.*, Eq. (3)) combined with the physics involved in the firebrand transport (Trucchia *et al.* 2019). The mean of the distribution μ^* depends strongly on the atmospheric conditions, specifically on the Atmospheric boundary layer (Egorova et al. 2020):

$$\mu^* = H\left(\frac{3\rho C_d}{2\,\rho_f}\right)^{1/2}, \qquad (5)$$

where C_d is de Drag coefficient and ρ_f is the density of the wildland fuels. The maximum liftable height of the firebrands H is computed as a fraction of the injection height $H = 0.4 \cdot H_{smoke}$. The injection height of the smoke H_{smoke} is described by the formula (Sofiev et al. 2012, formula (10)):

$$H_{smoke} = \alpha\, H_{ABL} + \beta\left(\frac{I_f}{d\, P_{f_0}}\right)^{\zeta} exp\left(-\frac{\delta_{FT}\, N_{FT}^2}{N_0^2}\right), \qquad (6)$$

where H_{ABL} is the height of the atmospheric boundary layer, $N^2{}_0$ and $N^2{}_{FT}$ are the Brunt-Väisälä frequency at the current height and in the free troposphere respectively, and P_{f0} is the ratio of reference fire power. The standard deviation σ involves the effects of the horizontal wind, flame geometry and the slope over the fire-spotting landing distance Egorova et al. (2020, 2022):

$$\sigma = \sigma(\varphi,\omega) = \frac{1}{z_p} ln\left\{\frac{U\,Cos\,\varphi}{\sqrt{gr\left(1+Tan^2\,\omega\right)}} + \beta_2\sqrt{\frac{2\rho_f}{3\rho C_d}}\,\frac{1.4U\,Cos\,\varphi + \sqrt{gh_0\left(1+\phi_{wind}+\phi_{slope}\right)^{2/3}\,Tan\,\omega}}{\sqrt{gh_0\left(1+\phi_{wind}+\phi_{slope}\right)^{2/3}} - 1.4U\,Cos\,\varphi\,Tan\,\omega}\right\}, \qquad (7)$$

where φ is the angle between the wind and the direction in which a firebrand is ejected, ω is the slope of the cell in which the ember is generated and:

$$L_f = h_0\left(1+\phi_{wind}+\phi_{slope}\right)^{2/3} = \beta_0\, I_f^{2/3}, \qquad (8)$$

where:

$$\beta_0 = \left(\frac{1}{2g\left(\rho c_p T_A\right)^2}\right)^{1/3}. \qquad (9)$$

Fire-spotting in the RandomFront parametrization is considered as a downwind phenomenon. A critical angle φ_0 is defined as the angle for which the ember is not considered ($\sigma <= 0$). By means of the probabilistic distribution, this is the angle for which σ becomes negative.

3. Area of study and simulations

3.1. Area of study

The reproduced wildfire took place 1st August 2021 in the municipality of Campomarino, in the Adriatic coast of Italy (Fig. 1).

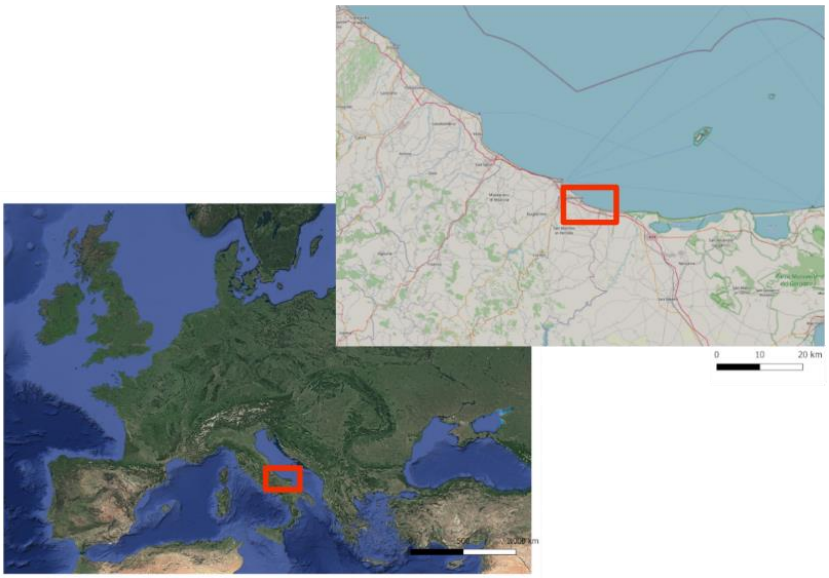

Figure 1- Study area.

The burnt perimeter is exposed in Fig. 2 – (a). The wildfire started burning around 12:00 am and finished around 5:00 pm. The fire-spotting effects were reported around 3:00 pm from the East to the West part of the port. We defined a rectangular area of study with 2.98 km^2 around the wildfire extension to run the simulations. Each cell of the cellular automaton has a resolution of 20 m^2. The fuel types have been adapted from the Corine Land Cover (CLC) classification (Feranec et al. 2016) t o the propagator classes (Fig. 2 – (b)). Specifically, we took *Pinus pinaster Aiton* as the reference tree specimen associated with the fire-prone conifers fuel type (Tihay *et al.* 2009). The data labeled as "non-burnable" have a low but non-zero probability of being burnt. The orography data were obtained from a Digital Elevation Model (DEM) but due to the proximity to the sea, a null or very tiny variation of the slope is reported over the fire-prone conifers.

3.2. Methodology and simulations

For each parametrization an ensemble of 100 independent realizations was generated under the same conditions (Trucchia *et al.* 2020). The computational time for each ensemble is less than two minutes. Each simulation was stopped after 5 hours of simulated time. The weather was reported to be unstable and turbulent when the wildfire occurred, with peaks up to 70 km/h. To reproduce these conditions, we consider a constant wind speed of 40 km/h and, each 15 minutes of simulated time, a stochastic constant derived from a normal distribution with mean 0 and standard deviation 20 is added to the mean wind speed. In addition, the main wind direction, which came mainly from south, is also perturbed each 15 min with a stochastic variable derived from a normal distribution with mean 0 and standard deviation $\pi/8$. Two processes still needed to be characterized for a complete fire-spotting description: firebrand generation and spot ignition. Despite the considerable number of studies focused on both previous phenomena at the laboratory scale, there is a lack of research focused on the development of a physics-guided probabilistic model to characterize them. Due to this reason, we have modeled the firebrand generation for each burning cell by means of a Poisson distribution and the spot probability through Eq. (2). Next, we show the probability maps computed from the ensemble of simulations after 3 and 5 hours, which are the times at which fire-spotting was reported and the fire stopped, respectively.

3.2.1. Alexandridis et. al. (2011) sub-model results

The port separates both coniferous areas with 190 m, so the mean of the normal distribution which will generate r_n in the Alexandridis parametrization Eq. (1) was implemented as 190. We also consider to implement the

standard deviation equal to 25 as reasonable value. The computed burn probability map for this firebrand landing distribution after 3 and 5 hours is exposed in Figure 3 respectively.

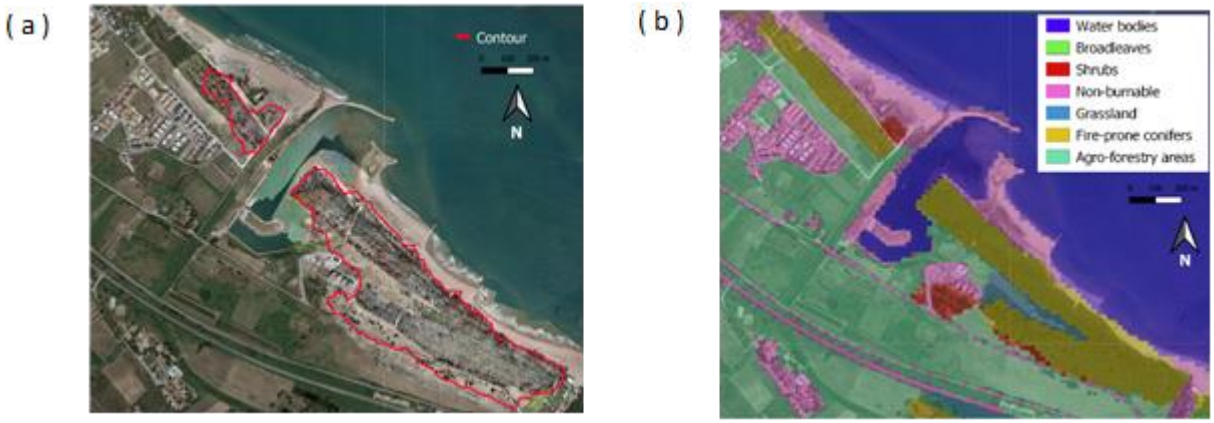

Figure 2- Studied area. Figure 2-(a) shows the true color orthomosaic derived by UAV survey done after the wildfire occurs. The red line defined the burnt area, based on high resolution photointerpretation. Figure 2-(b) displays the land cover classification used.

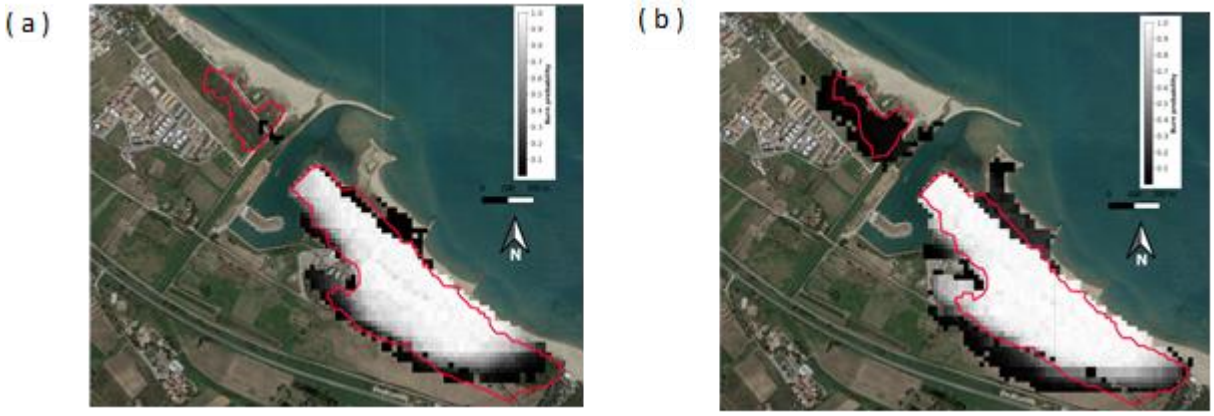

Figure 3- Computed burn probability map with the Alexandridis parametrization implemented. Figure 3-(a) shows the burn probability after 3 hours and Figure 3-(b) after 5 hours.

3.2.2. Perryman et. al. (2013) sub-model results

The burn probability map after 3 and 5 hours with the Perryman firebrand landing distribution is shown in Figure 4.

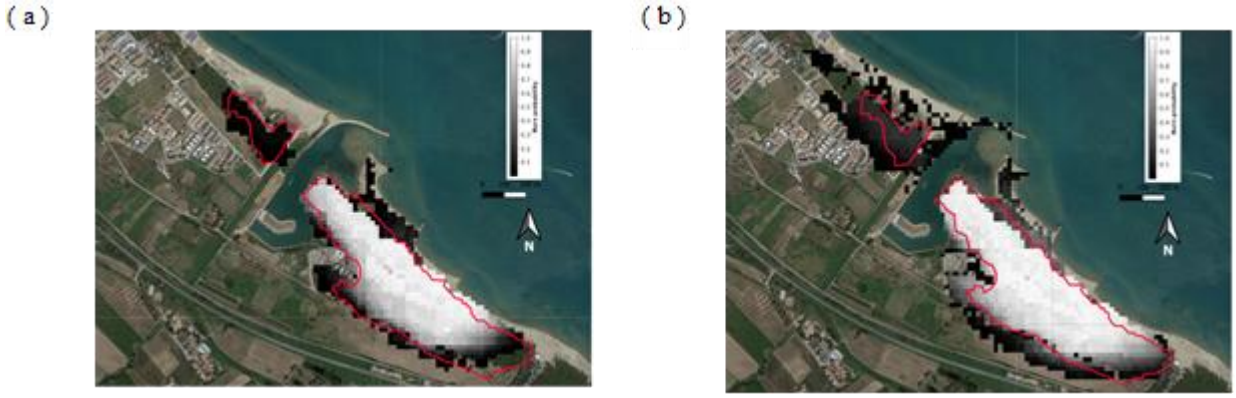

Figure 4- Computed burn probability map with the Perryman parametrization implemented. Figure 4-(a) shows the burn probability after 3 hours and Figure 4-(b) after 5 hours.

3.2.3. RandomFront sub-model results

The burn probability map after 3 and 5 hours with the RandomFront firebrand landing distribution is shown in Figure 5. Due to the instability of the weather and the summer conditions we consider the height of the Atmospheric Boundary Layer equal to H_{abl} = 2600 m.

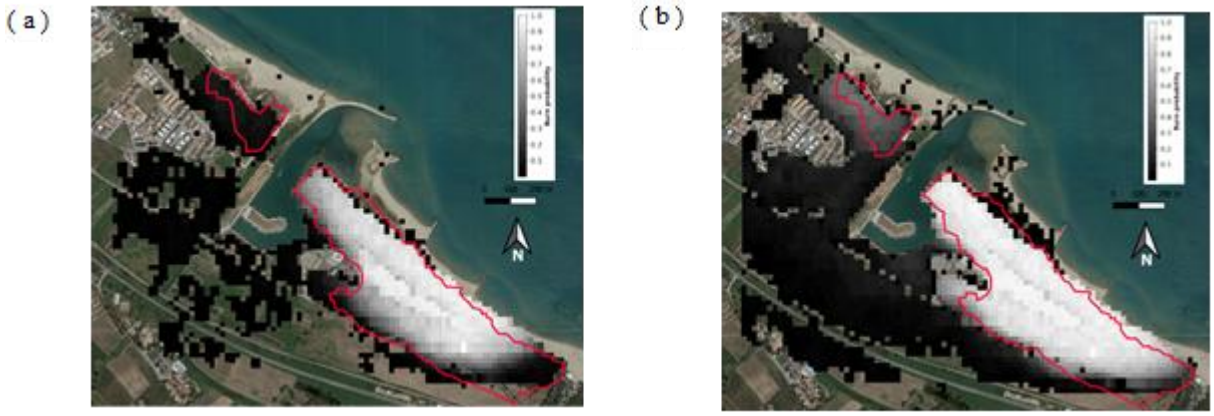

Figure 5- Computed burn probability map with the RandomFront parametrization implemented. Figure 5-(a) shows the burn probability after 3 hours and Figure 5-(b) after 5 hours

4. Brief discussion

To validate the model against the shape of the reference wildfire and quantify the obtained results, the averaged probability was computed for the two reference areas at both sides of the port, see Table 1. This measure is defined as the sum of the probabilities associated to each cell in the reference domains divided by the number of cells inside the reference domains.

Table 1- Averaged probabilities computed inside the reference perimeters.

Area	Alexandridis *et al. (2011)*	Perryman *et al. (2013)*	RandomFront
East	0.7937	0.7370	0.7303
West	0.0358	0.1330	0.2868

Table 1 shows that the averaged probability in the reference area at the West part of the port is, in the ensemble generated with RandomFront parametrization, one order of magnitude higher than the one obtained by using Alexandridis *et al.*, and more than twice when compared with the Perryman *et al.* parametrization. This agrees with Figures 3, 4 and 5 displayed results. Figure 3 shows how Alexandridis *et al.* parametrization is unable to assign any burning probability to the West part of the port when the fire-spotting was indeed reported. In addition, at the end of the simulation, a poor spread pattern is observed. The Perryman *et al.* parametrization of the firebrand's landing distribution displayed in Figure 4 generates a bit more complex spread pattern than by using Alexandridis *et al.*, but a low burn probability remains assigning to the West part of the port. By contrast, RandomFront firebrand's landing parametrization can generate a clear but low burn probability when the fire-spotting was reported. In addition, at the end of the simulation, an averaged burnt probability of 28.6% is assigned to the reference area at the West part of the port, as well as quite complex spread pattern is observed.

The implementation of fire-spotting routines causes deviation between simulations output when performed with different fire-spotting models (but fixed input data), see Figures 3, 4 and 5. In particular, from both the spread pattern and the probability to burn, we have that that the fire-spotting parametrization RandomFront performs better than the other two models.

5. Main conclusions

In this work, we have implemented the recently developed RandomFront fire-spotting landing distribution into the operational software PROPAGATOR. In addition, we have compared against other two fire-spotting models developed for a cellular automaton setting. To compare the performance of these three parametrizations, a real wildfire affected by fire-spotting effects was reproduced and used as validation test: actually, because results at laboratory scale are unreliable due to the multi-scale nature of wildfires. The ensemble computed with the

RandomFront parametrization displays a more complex spread pattern than the other parametrizations and a non-zero burnt probability in the West area of the port where the fire-spotting was indeed reported. In addition, at the end of the simulation in the area affected by the fire-spotting, RandomFront provides higher burnt probabilities than the other implemented parametrizations. Firebrand rate generation and spot ignition probability, which are still poorly for probabilistic modelling approaches, embody future development of the present research.

6. Acknowledgements:

This research has been supported by the Basque Government through the BERC 2022–2025 programme; by the Spanish Ministry of Economy and Competitiveness (MINECO) through the BCAM Severo Ochoa excellence accreditation SEV-2017-0718 and also through the project PID2019-107685RB-I00; by the European Regional Development Fund (ERDF) and the Department of Education of the regional government, the Junta of Castilla y León (Grant 574 contract SA089P20); and by the Interreg IPA CBC Italy- Albania - Montenegro programme through the project The flOod and Big firE foREst, prediction, forecAst anD emergencY management (TO BE READY).

7. References:

Albini F (1979) Spot fire distance from burning trees -a predictive model. USDA Forest Service, Intermountain Forest and Range Experiment Station, General Technical Report INT-56. (Odgen, UT).

Albini F (1983) Potential spotting distance from wind-driven surface fires. USDA Forest and Range Experiment Station, Research paper INT-309. (Odgen, UT).

Alexandridis A, Russo L, Vakalis D, Bafas GV, Siettos CI (2011) Wildland fire spread modelling using cellular automata: evolution in large-scale spatially heterogeneous environments under fire suppression tactics. International Journal of Wildland Fire 20, 633. doi:10.1071/WF09119.

Alexandridis A, Vakalis D, Siettos CI, Bafas GV (2008) A cellular automata model for forest fire spread prediction: The case of the wildfire that swept through Spetses Island in 1990. Applied Mathematics and Computation 204, 191–201. doi:10.1016/j.amc.2008.06.046.

Brown AA, Davis KP (1973) 'Forest fire: control and use.' (McGraw-Hill: New York)

Clarke K, Brass J, Riggan P (1994) A Cellular Automaton Model of Wildfire Propagation and Extinction. Photogrammetric Engineering and Remote Sensing 60(11), 1355–1367.

Duarte JAMS (1997) Bushfire Automata and Their Phase Transitions. International Journal of Modern Physics C 08, 171–189. doi:10.1142/S0129183197000175.

Egorova VN, Trucchia A, Pagnini G (2020) Fire-spotting generated fires. Part I: The role of atmospheric stability. Applied Mathematical Modelling 84, 590–609. doi:10.1016/j.apm.2019.02.010.

Egorova VN, Trucchia A, Pagnini G (2022) Fire-spotting generated fires. Part II: The role of flame geometry and slope. Applied Mathematical Modelling 104, 1–20. doi:10.1016/j.apm.2021.11.010.

Encinas LH, White SH, Rey AM del, Sánchez GR (2007) Modelling forest fire spread using hexagonal cellular automata. Applied Mathematical Modelling 31, 1213–1227. doi:https://doi.org/10.1016/j.apm.2006.04.001.

Feranec J, Soukup T, Hazeu G, Jaffrain G (Eds) (2016) 'European Landscape Dynamics.' (CRC Press) doi:10.1201/9781315372860.

Freire JG, DaCamara CC (2019) Using cellular automata to simulate wildfire propagation and to assist in fire management. Natural Hazards and Earth System Sciences 19, 169–179. doi:10.5194/nhess-19-169-2019.

Gharakhanlou NM, Hooshangi N (2021) Dynamic simulation of fire propagation in forests and rangelands using a GIS-based cellular automata model. International Journal of Wildland Fire 30, 652-663. doi: 10.1071/WF20098.

Hargrove WW, Gardner RH, Turner MG, Romme WH, Despain DG (2000) Simulating fire patterns in heterogeneous landscapes. Ecological Modelling 135, 243–263. doi:10.1016/S0304-3800(00)00368-9.

Himoto K, Iwami T (2021) Generalization framework for varying characteristics of the firebrand generation and transport from structural fire source. Fire Safety Journal 125, 103418. doi:10.1016/j.firesaf.2021.103418.

Himoto K, Tanaka T (2005) Transport Of Disk-shaped Firebrands In A Turbulent Boundary Layer. Fire Safety Science 8, 433–444. doi:10.3801/IAFSS.FSS.8-433.

Kaur I, Mentrelli A, Bosseur F, Filippi J-B, Pagnini G (2016) Turbulence and fire-spotting effects into wild-land fire simulators. Communications in Nonlinear Science and Numerical Simulation 39, 300–320. doi:10.1016/j.cnsns.2016.03.003.

Koo E, Pagni PJ, Weise DR, Woycheese JP (2010) Firebrands and spotting ignition in large-scale fires. International Journal of Wildland Fire 19, 818. doi:10.1071/WF07119.

Manzello SL, Maranghides A, Mell WE (2007) Firebrand generation from burning vegetation. International Journal of Wildland Fire 16, 458. doi:10.1071/WF06079.

Manzello SL, Shields JR, Cleary TG, Maranghides A, Mell WE, Yang JC, Hayashi Y, Nii D, Kurita T (2008) On the development and characterization of a firebrand generator. Fire Safety Journal 43, 258–268. doi:10.1016/j.firesaf.2007.10.001.

Pérez Y, Pastor E, Àgueda A, Planas E (2011) Effect of Wind and Slope When Scaling the Forest Fires Rate of Spread of Laboratory Experiments. Fire Technology 47, 475–489. doi:10.1007/s10694-010-0168-7.

Perryman HA, Dugaw CJ, Varner JM, Johnson DL (2013) A cellular automata model to link surface fires to firebrand lift-off and dispersal. International Journal of Wildland Fire 22, 428. doi:10.1071/WF11045.

Sardoy N, Consalvi JL, Kaiss A, Fernandez-Pello AC, Porterie B (2008) Numerical study of ground-level distribution of firebrands generated by line fires. Combustion and Flame 154, 478–488. doi:10.1016/j.combustflame.2008.05.006.

Sardoy N, Consalvi J, Porterie B, Fernandezpello A (2007) Modeling transport and combustion of firebrands from burning trees. Combustion and Flame 150, 151–169. doi:10.1016/j.combustflame.2007.04.008.

Sofiev M, Ermakova T, Vankevich R (2012) Evaluation of the smoke-injection height from wild-land fires using remote-sensing data. Atmospheric Chemistry and Physics 12, 1995–2006. doi:10.5194/acp-12-1995-2012.

Sullivan AL (2009a) Wildland surface fire spread modelling, 1990 - 2007. 1: Physical and quasi-physical models. International Journal of Wildland Fire 18, 349. doi:10.1071/WF06143.

Sullivan AL (2009b) Wildland surface fire spread modelling, 1990 - 2007. 2: Empirical and quasi-empirical models. International Journal of Wildland Fire 18, 369. doi:10.1071/WF06142.

Sullivan AL (2009c) Wildland surface fire spread modelling, 1990 - 2007. 3: Simulation and mathematical analogue models. International Journal of Wildland Fire 18, 387. doi:10.1071/WF06144.

Sullivan AL, Cruz MG (2015) Small-scale flame dynamics provide limited insight into wildfire behavior. Proceedings of the National Academy of Sciences 112, E4164–E4164. doi:10.1073/pnas.1506877112.

Suzuki S, Manzello SL, Lage M, Laing G (2012) Firebrand generation data obtained from a full-scale structure burn. International Journal of Wildland Fire 21, 961. doi:10.1071/WF11133.

Tarifa CS, Marañón PP del NM de, Moreno FG, Villa AR (1967) Transport and Combustion of Firebrands. Final Report of Grants FG-SP-114 and FG-SP-146 Vol. II. INTA, Informe Técnico (Madrid) http://oa.upm.es/6521/.

Tarifa CS, Notario PP del, Moreno FG (1965) On the flight paths and lifetimes of burning particles of wood. Symposium (International) on Combustion 10, 1021–1037. doi:10.1016/S0082-0784(65)80244-2.

Thomas JC, Mueller EV, Santamaria S, Gallagher M, El Houssami M, Filkov A, Clark K, Skowronski N, Hadden RM, Mell W, Simeoni A (2017) Investigation of firebrand generation from an experimental fire: Development of a reliable data collection methodology. Fire Safety Journal 91, 864–871. doi:10.1016/j.firesaf.2017.04.002.

Tihay V, Simeoni A, Santoni P-A, Rossi L, Garo J-P, Vantelon J-P (2009) Experimental study of laminar flames obtained by the homogenization of three forest fuels. International Journal of Thermal Sciences 48, 488–501. doi:10.1016/j.ijthermalsci.2008.03.018.

Trucchia A, D'Andrea M, Baghino F, Fiorucci P, Ferraris L, Negro D, Gollini A, Severino M (2020) PROPAGATOR: An Operational Cellular-Automata Based Wildfire Simulator. Fire 3, 26. doi:10.3390/fire3030026.

Trucchia A, Egorova V, Butenko A, Kaur I, Pagnini G (2019) RandomFront 2.3: a physical parameterisation of fire spotting for operational fire spread models – implementation in WRF-SFIRE and response analysis with LSFire+. Geoscientific Model Development 12, 69–87. doi:10.5194/gmd-12-69-2019.

Wang H-H (2011) Analysis on Downwind Distribution of Firebrands Sourced from a Wildland Fire. Fire Technology 47, 321–340. doi:10.1007/s10694-009-0134-4.

Wickramasinghe, A.; Khan, N.; Moinuddin, K. (2022) Determining Firebrand Generation Rate Using Physics-Based Modelling from Experimental Studies through Inverse Analysis. Fire 5, 6. doi: 10.3390/fire5010006

Werth PA, Potter BE, Clements CB, Finney MA, Goodrick SL, Alexander ME, Cruz MG, Forthofer JA, McAllister SS (2011) Synthesis of knowledge of extreme fire behavior: volume I for fire managers. U.S. Department of Agriculture, Forest Service, Pacific Northwest Research Station, PNW-GTR-854. (Portland, OR) doi:10.2737/PNW-GTR-854.

Flammability characteristics of typical garden species

Miguel Almeida*[1]; MohammadReza Modarres[1]; Juan Antonio Muñoz[2]; Luís M. Ribeiro[1]

[1] University of Coimbra, ADAI, Department of Mechanical Engineering, Rua Luís Reis Santos, Pólo II, 3030-788 Coimbra, Portugal, {miguelalmeida, Mohammad, luis.mario}@adai.pt
[2] Polytechnic University of Catalonia. Center for Technological Risk Studies, Eduard Maristany St., 16 Building I - 5th floor 08019 Barcelona, Catalonia, Spain, {juan.antonio.munoz@upc.edu}

**Corresponding author*

Keywords

Wildland urban interface; WUI; fuel characteristics; plants, trees, fire behavior, fire modelling

Abstract

The large fires in recent years have caused tragic episodes that have led to the death of many hundreds of people and the loss of buildings of great social and economic value. Several of these impacts could have been avoided if the fuel management around buildings had been appropriate. Many studies on flammability are dedicated to wild fuels present in the forests, shrublands or grasslands. However, the existing data on the vegetation typical of the surroundings closest to the constructions (e.g., gardens) is scarce. Besides being the fuels closest to the buildings, these are fuels that normally can be effectively managed by the building owners, i.e., their management is within the reach of the common citizens.

This work aimed to characterize the flammability parameters for several typical garden species in the Mediterranean Basin. An extensive experimental program was carried out to characterize individual plants of the following species: holly (Ilex aquifolium), linden (Tilia nobilis), anacardia (Rhus typhina), laurel (Laurus nobilis), olive tree (Olea europaea), pacific madrone (Arbutus menziesii), apple tree (Malus sylvestris), cherry tree (Prunus avium), sloe (Prunus Spinosa), fig tree (Ficus carica), loquat (Eriobotrya japonica), kiwi plant (Actinidia deliciosa), grapevine (Vitis vinifera), hydrangea (Hydrangea macrophylla), oleander (Nerium oleander), ivy (Hedera helix). In this work, the results for only three of those plants will be presented, namely: oleander, fig tree and laurel. The following parameters will be presented: mass-loss rate, vertical profile of temperature, heat flux and flame dimensions.

This study has two main objectives: 1) to provide data that allows fire behavior modelling in the proximity of dwelling houses; and 2) the determination of the acceptable safety distance that species must be from buildings to prevent their ignition. Some of the tests performed showed that the presence of some species in the proximity of buildings (not attached) can be beneficial due to their low inflammability and because they can constitute an obstacle to the passage of firebrands, which can ignite the construction.

1. Introduction

The greatest impacts that have been registered in the last decade as a result of wildfires highlighted the relevance of the wildland-urban interface (WUI), with a special focus on the potential loss of people and animals' lives, as well as the destruction of buildings. The various studies concerning large wildfires (Viegas et al., 2017; Viegas et al., 2019) concluded that improper fuels management in the vicinity of constructions is among the main causes of its destruction. In addition, the lower confidence of citizens regarding the fire resistance of buildings leads to people often feeling impelled to leave their homes putting their lives at risk due to untimely evacuation processes.The fuel management in the WUI scenario requires knowledge of the flammability characteristics of the fuels. For example, it is important to know the minimum distance at which a certain tree shall be planted from a construction, to avoid ignitions by direct heat transfer from vegetation to houses. Moreover, this knowledge is important for selecting the species that should be placed closer to buildings or those that should not exist in their immediate vicinity. Naturally, the probability of ignition of a structure depends not only on the characteristics of the surroundings, but also on the construction characteristics and the self-protection capacity (e.g., sprinkler systems) that may exist.

The fuels around buildings can be divided into natural fuels (e.g., trees, ornamental plants) and man-made fuels (e.g., vehicles, plastic covertures, GPL tanks). The present work is exclusively dedicated to natural fuels, namely typical garden plants. Thus, any mention of fuels in this text shall be understood in that context.

In the analysis of fire behavior modelling in WUI, the knowledge of the flammability characteristics of the species that feed the combustion processes is essential. Although there is some information on the flammability of wild species (e.g., forests, shrublands or grasslands), the characterization of the typical species of the areas in the immediate surroundings of the buildings is poorly developed – Weise et al. (2005), Ganteaume et al. (2013) and Zhang et al. (2011) are examples of exceptions. Thus, the accuracy of the fire behavior simulators applied to the WUI is compromised. Physical properties of the fuel, e.g., fuel moisture content (FMC), bulk density, porosity, thermochemical characteristics such as the equivalent hydrocarbon (CHON) content for gas-phase reactions, and applying realistic boundary conditions are major factors to be considered in the fire dynamics simulations (FDS) (Weise et al., 2005). The boundary conditions entail several parameters, e.g., domain characteristics, heat release rate per unit area (HRRPUA) of the burner, environmental conditions with a trade-off between the grid size, and the computational capacity of the solver.

A laboratory work program was carried out to determine the flammability characteristics of typical garden plants, specifically: holly (*Ilex aquifolium*), linden (*Tilia nobilis*), anacardia (*Rhus typhina*), laurel (*Laurus nobilis*), olive tree (*Olea europaea*), pacific madrone (*Arbutus menziesii*), apple tree (*Malus sylvestris*), cherry tree (*Prunus avium*), sloe (*Prunus Spinosa*), fig tree (*Ficus carica*), loquat (*Eriobotrya japonica*), kiwi plant (*Actinidia deliciosa*), grapevine (*Vitis vinifera*), hydrangea (*Hydrangea macrophylla*), oleander (*Nerium oleander*), ivy (*Hedera helix*). The results of this study apply to other scenarios where these species are present – for example, the road sides, the surroundings of industrial facilities or the periphery of settlements. The main objective of this work is to provide relevant data for modelling fire behavior in the WUI and to increase the knowledge that allows defining with scientific support the best practices of fuel management in the immediate surroundings of buildings. In this manuscript, as an example, the results for one shrub – oleander – and for two trees – laurel and fig tree – will be presented (Figure 1). Besides the flammability data a valuation of the acceptable safety distance between those plants and a building will be provided.

(a) (b) (c)

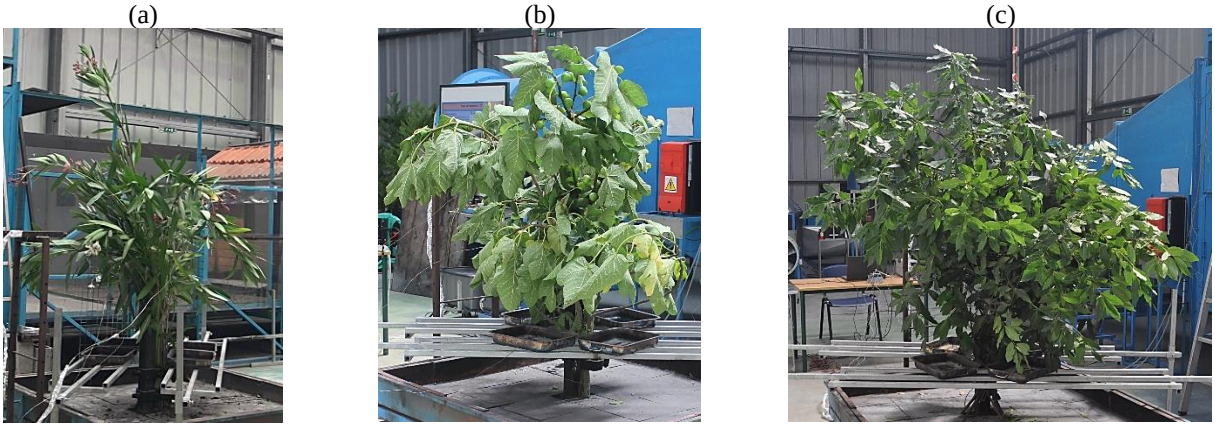

Figure 1: Image of the species used in the tests that will be described: a) oleander; b) fig tree; c) laurel.

2. Methodology

The laboratory tests were performed at the ADAI's Laboratory for Forest Fire Studies, in Lousã - Coimbra (Portugal). All tests were performed between July and August 2021.

2.1. Experiments description

Fuel sampling

Each plant to be tested was collected from its natural environment no more than 24 hours before being burnt. After their transport to the laboratory, the plants were kept in a shady environment, with indoor conditions never exceeding 25ºC.

Experimental setup

The plants were burnt in the "Tree Burning Platform" (Ganteaume et al., 2013) that has attached a weighing system allowing the determination of the mass decay throughout the burning. A *Pitot* tube and a thermocouple

were placed above the plant at a fixed height of 3.5m to determine the convective flow velocity. Besides the thermocouple at a height of 3.5m, in the same vertical axis connecting the center of the plant to the *Pitot* tube, two thermocouples were also placed in the middle and at the top of the plant's crown. A radiative heat flux meter was installed at 1.0m height and 50cm from the edge of the plant canopy. Furthermore, the tests were recorded with a pair of IR cameras and another pair of RGB cameras, settled parallel and transversally to the flame front. The analysis of the images captured by these cameras allowed the determination of the flame dimensions - height, length and depth - along with the test. Figure 2 presents the experimental setup described.

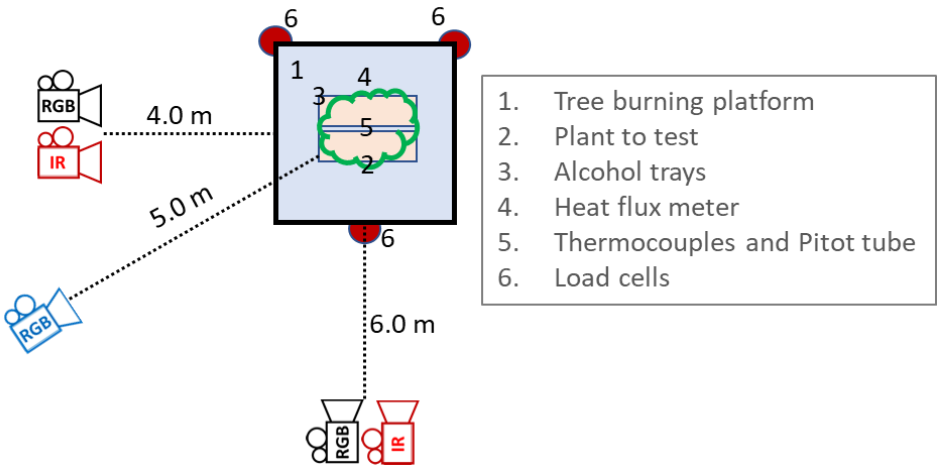

Figure 2 – Experimental setup.

Experimental procedure

Ignition: Since the plants tested alone could not sustain the fire, it was necessary to add a heat source. Thus, 20cm below the base of the plant crowns, trays were placed with denatured alcohol (96% v/v) allowing the ignition and sustaining the fire, just like what happens with the understory in real fire events. The trays were used to distribute the heat evenly to the entire base of the canopy. It was used an area of trays per horizontal projected area of the crown of 0.75 m^2/m^2, which corresponds to 1.6 L of alcohol per cm^2 of the horizontal projected area of the plant.

To facilitate data synchronization, the measuring equipment was started simultaneously with the ignition that occurred at the same time in all trays.

The trays were installed on a shelf that did not interfere with the mass acquisition system so it was not necessary to make the correction of this parameter. A reference burning test was performed only with alcohol in order to understand the influence of this fuel on the heat flux acquisition values during the regular tests. The methodology used throughout these experiments was the same as described in Almeida et al. (2021). Five repetitions per plant were carried out.

2.2. Calculations

Mass loss coefficient

The mass loss was analyzed based on the mass loss coefficient *k* of Equation 1 for determining the absolute value of mass *m* and for Equation 2 which allows the determination of the relative mass m_r. In these equations m_0 corresponds to the initial mass and *t* is the time elapsed since ignition.

$$m = m_0 \times e^{-k \times t} \quad \text{[Equation 1]}$$

$$m_r = \frac{m}{m_0} = e^{-k \times t} \quad \text{[Equation 2]}$$

Figure 3 shows an example of mass loss determination with the respective curve for each test carried out for the same species. The final *k* value for each species is determined based on of the mean value of the *k* values obtained in the five test repetitions.

(a) (b)

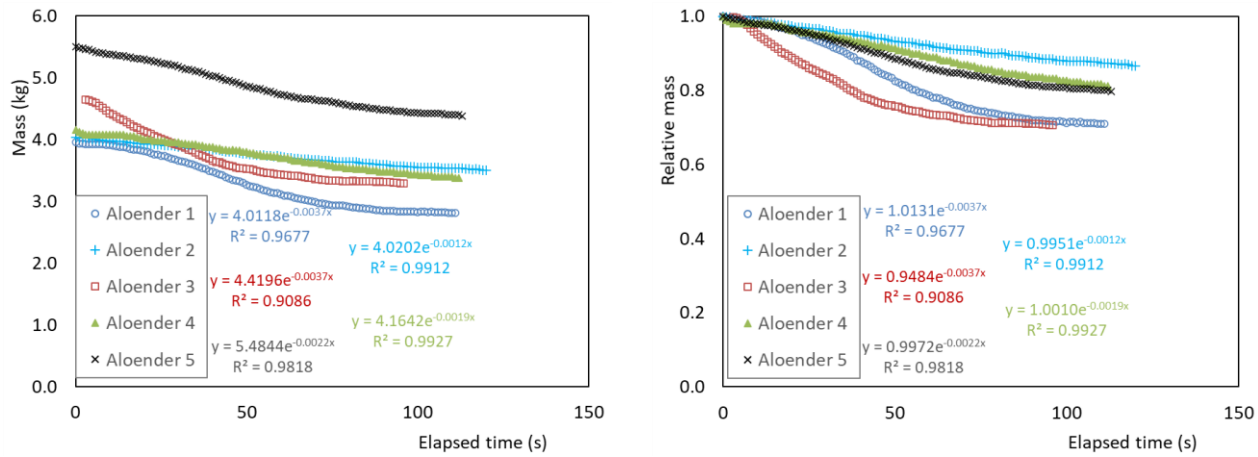

Figure 3: Example of the mass loss curves for the five tests performed with oleander: a) absolute mass values (Equation 1); b) relative mass values (Equation 2).

Heat flux reference tests

Reference tests were performed with the same configuration and quantity of trays containing the same amount of denatured alcohol used during the experiments with plants. It was found that the heat flux recorded is higher than in some tests with plants (Figure 4). This is because the plants are themselves a barrier to heat flux from the alcohol. Thus, the error associated with the burning of alcohol is assumed not to be very high and so is not considered.

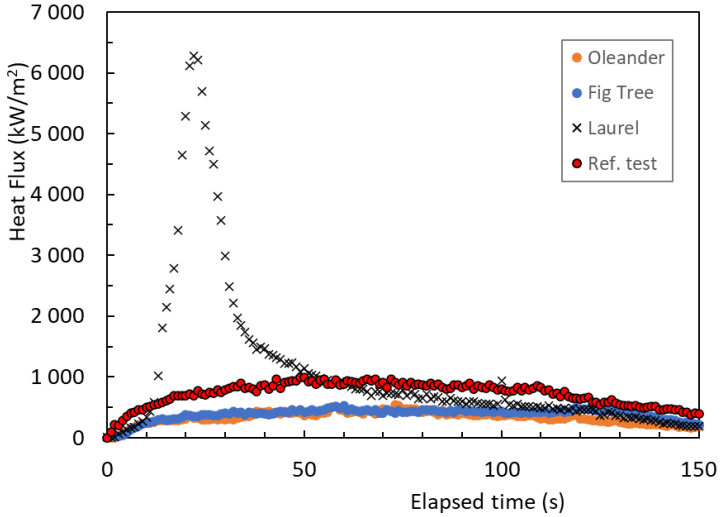

Figure 4: Heat flux values emitted by denatured alcohol and plants.

Acceptable safety distance

The acceptable safety distance *ASD* was determined using the model developed by Rossi et al. (2011), presented by Equation 3. Table 1 expresses the details of the Rossi's *ASD* definition.

$$ASD = \left[\frac{L_f \cos(\gamma)\sqrt{-4\Phi^2+\left(BT_f^4\varepsilon\tau\right)^2}}{2\Phi_{thres}} + L_F \sin(\gamma)\right] \times \left[1 - exp\left(-\frac{2L}{L_f}k\right)\right] \quad \textit{[Equation 3]}$$

Table 1: Description of the variables in Equation 3 and presentation of the values used in the simulations.

Symbol	Parameter	Values used
ASD	Acceptable safety distance	Variable
L_F	Flame length (m)	Variable

Φ	Heat flux limit (W.m-2)	Variable
h	Height difference between the base of the flame and the target (m)	1.7
k	Empirical parameter	1
L	Half of the length of the flame front (m)	20
γ	Angle of inclination of the flame (°)	0
B	Stephan-Boltzmann constant ($W.m^{-2}.K^{-4}$)	5.670374419×10^{-8}
Tf	Average flame temperature (K)	1350
τ	Atmospheric transmittivity	0.9
ε	Equivalent flame emissivity	0.8

2.3. Resume

Table 2 – Summary of the experiments: m_0- initial mass; m_f- final mass; FMC- fuel moisture content; CH- crown height; CD- average crown diameter; CBH- crown base height.

Species type	*Case*	m_0 (kg)	m_f (kg)	FMC%	CH (m)	CD (m)	CBH (cm)
Oleander	1	3.98	2.89	50.4	0.90	0.90	15
	2	3.97	3.10	36.2	1.75	1.15	15
	3	4.57	3.63	36.2	1.80	1.05	30
	4	4.00	3.28	36.9	1.85	1.55	17
	5	5.50	4.30	37	1.70	1.00	15
Fig tree	1	5.25	4.82	43.6	1.5	1.15	25
	2	5.94	5.49	58.8	1.4	1.30	25
	3	5.41	4.85	59.2	1.3	1.15	25
	4	6.10	4.88	58.8	1.4	1.25	25
	5	5.46	4.58	58.9	1.35	1.15	25
Laurel	1	3.89	2.24	53.7	1.50	1.30	15
	2	4.44	3.12	53.7	2.00	1.35	15
	3	3.45	2.12	53.7	1.30	1.10	20
	4	3.17	2.04	57.7	1.85	1.00	15
	5	3.97	2.89	63.4	2.00	1.05	10

3. Results and discussion

Mass loss

As previously mentioned, the mass loss is presented through the average value of the mass loss coefficient *k* for each species, as presented below. Fig tree is clearly the species that presents the lowest value of *k*, i.e., a slower mass decay. On the other side, the laurel presents a very high value of *k*, which is a reflection of its great inflammability, which was verified in the tests.

Table 3: Average mass loss coefficient determined for each species. In parentheses the standard deviation values are shown.

Parameter	Oleander	Fig tree	Laurel
Mass loss coefficient *k* (s^{-1})	0.00254 (0.0012)	0.00106 (0.00058)	0.00776 (0.00425)

Temperature

The temperature values were measured in the central longitudinal axis of the plant at various heights, as previously mentioned. Figure 5 (a, b, c) presents the temperature variation along the tests, for several heights. Figure 5d presents the temperature variation measured in several tests in the thermocouple located at half the height of the plant. The values obtained for the oleander and fig are very close, while the temperature values for the laurel are much higher. In the first two species, the thermocouple located at 20 cm is the one that reaches higher temperatures because it is close to the trays with alcohol. However, in the tests with the laurel, due to the higher intensity of the flame, the highest temperature value was obtained for the thermocouple located at mid-height of the plant.

(a) (b)

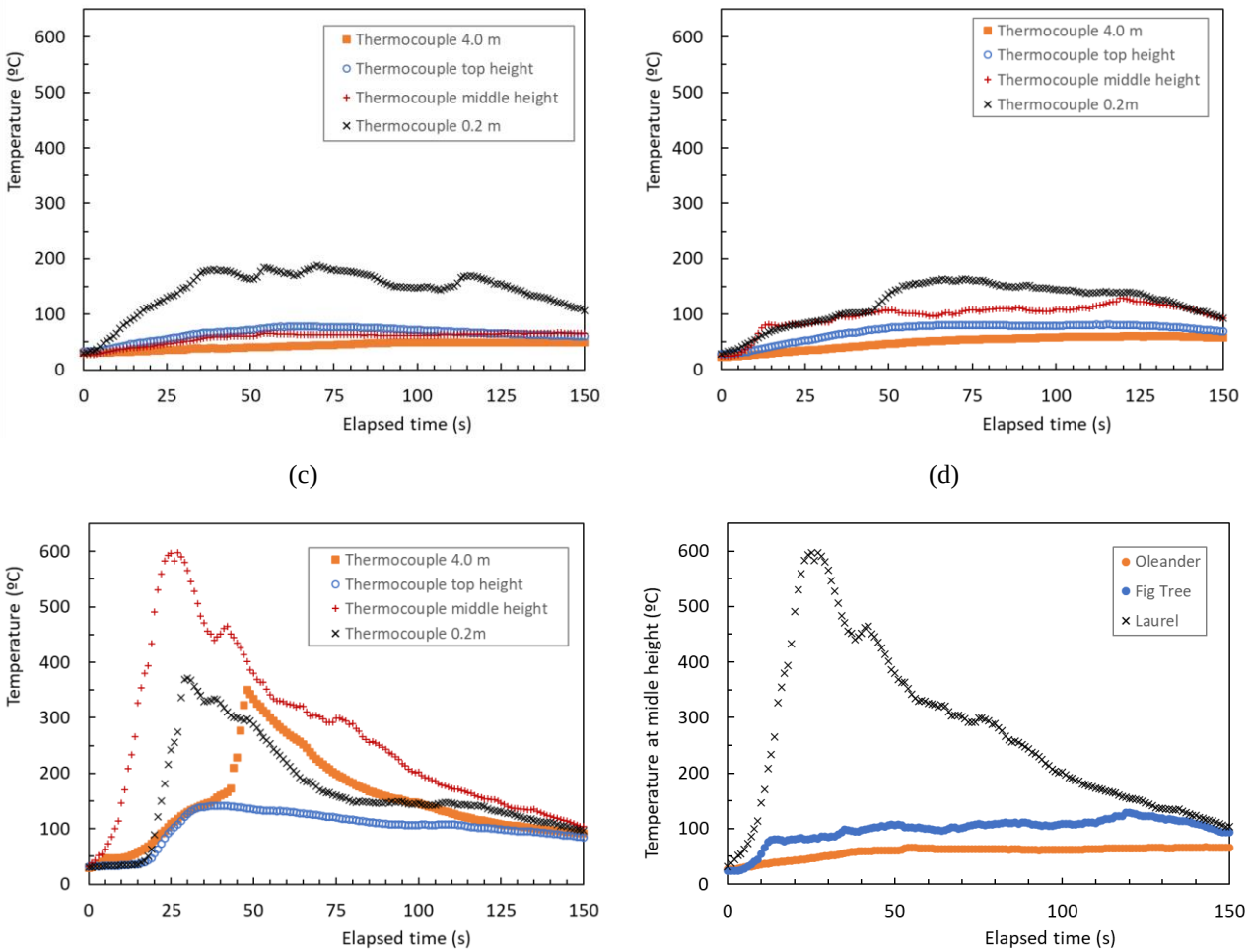

(c) (d)

Figure 5- Temperature variation along the tests since ignition (t=0s). a), b) and c) refer to the measurements obtained at the different thermocouples for the oleander, fig tree and laurel, respectively; d) comparison between the temperature variation recorded at the thermocouple located at mid-height of the plant.

Heat flux and flame dimensions

Figure 6a presents the heat flux variation values for the three species. Once again, the heat flux measured in the tests with oleander and fig tree are merely residual, while the values reached for laurel present a maximum of 6281 kW/m^2.

(a) (b)

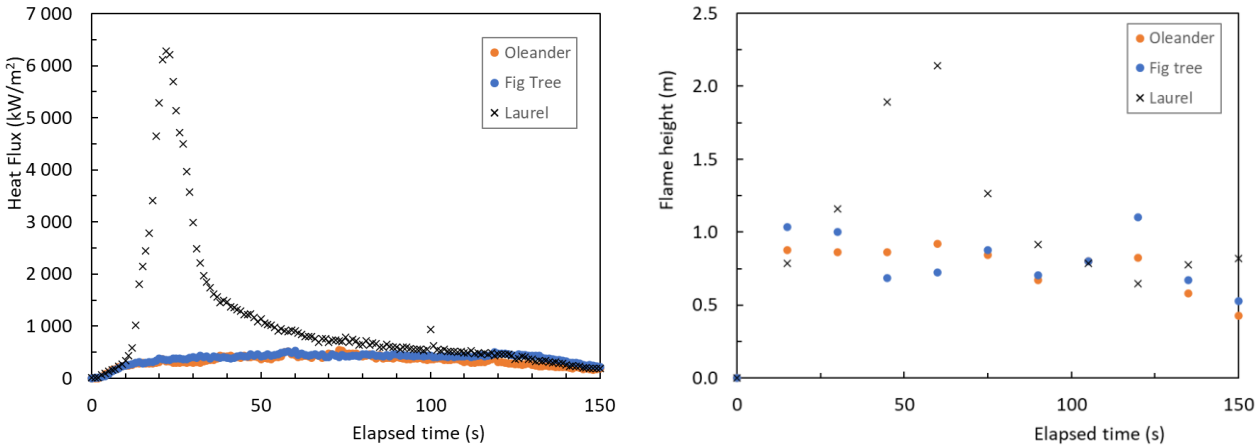

Figure 6 – Variation of heat flux (a) and flame height (b) during the tests performed for each species

Figure 6b presents the values of the flame height for the various species. Once again, the flame size of the laurel burning stands out from the other species due to its high burning intensity.

Acceptable safety distance

The table below presents the ASD values determined for the three species. In the sequence of the results presented above, it is easy to understand that laurel is the species that should be more distant from a building.

Table 4: Resume of the Acceptable safety distance determined for each species.

Species	Oleander	Fig tree	Laurel
Acceptable safety distance (m)	1.4	1.4	12.8

4. Conclusions

Values of flammability parameters for three species typically used in gardens, namely oleander, fig and laurel, were presented. These results may be of great interest for simulations of fire behavior in areas where these species exist. The laurel was the species that exhibited the highest flammability.

In addition, these test results allow the determination of what should be the acceptable safety distance that these species should be from a building. Normally, the regulations and standards in the scope of these matters do not distinguish between the species of shrubs and trees. However, as could be seen, trees such as laurel should be much more distant from buildings than, for example, fig trees. Given its low flammability, the existence of trees such as fig tree in the WUI can be beneficial to reduce the wildfires risk since they hardly spread fire to buildings, constituting a barrier to the projection of firebrands and reducing the turbulence in these areas.

5. Acknowledgements

The authors developed this work through the House Refuge Project (PCIF/AGT/0109/2018) which is funded by the Portuguese Foundation for Science and Technology (www.fct.pt), to whom they would like to express their acknowledgement.

6. References

Ganteaume, A., Jappiot, M., Lampin, C., Guijarro, M., & Hernando, C. (2013). Flammability of Some Ornamental Species in Wildland–Urban Interfaces in Southeastern France: Laboratory Assessment at Particle Level. Environmental Management, 52(2), 467–480. https://doi.org/10.1007/s00267-013-0067-z

Viegas, D. X., Almeida, M. A., Ribeiro, L. M., Raposo, J., Viegas, M. T., Oliveira, R., Alves, D., Pinto, C., Rodrigues, A., Ribeiro, C., Lopes, S., Jorge, H., & Viegas, C. X. (2019). Análise dos Incêndios Florestais Ocorridos a 15 de outubro de 2017. Centro de Estudos sobre Incêndios Florestais (CEIF/ADAI/LAETA).

Coimbra, Portugal. https://www.portugal.gov.pt/pt/gc21/comunicacao/documento?i=analise-dos-incendios-florestais-ocorridos-a-15-de-outubro-de-2017

Viegas, D. X., Almeida, M. F., Ribeiro, L. M., Raposo, J., Viegas, M. T., Oliveira, R., Alves, D., Pinto, C., Jorge, H., Rodrigues, A., Lucas, D., Lopes, S., & Silva, L. F. (2017). O complexo de incêndios de Pedrógão Grande e concelhos limítrofes, iniciado a 17 de junho de 2017. Centro de Estudos sobre Incêndios Florestais (CEIF/ADAI/LAETA). Coimbra, Portugal. https://www.portugal.gov.pt/pt/gc21/comunicacao/documento?i=o-complexo-de-incendios-de-pedrogao-grande-e-concelhos-limitrofes-iniciado-a-17-de-junho-de-2017

Weise, D. R., White, R. H., Beall, F. C., & Etlinger, M. (2005). Use of the cone calorimeter to detect seasonal differences in selected combustion characteristics of ornamental vegetation. International Journal of Wildland Fire, 14(3), 321–338. https://doi.org/10.1071/WF04035

Zhang, Z., Zhang, H., & Zhou, D. (2011). Flammability characterisation of grassland species of Songhua Jiang-Nen Jiang Plain (China) using thermal analysis. Fire Safety Journal, 46(5), 283–288. https://doi.org/10.1016/j.firesaf.2011.03.004

Gas cylinder accidents and incidents during Wildland Urban-Interface fires: an overview of the events

Thiago F. Barbosa*[1, 2]; Luís Reis[2]; Jorge Raposo[2]; Luís M. Ribeiro[2], Domingos Viegas[2]

[1] Univ Coimbra, ADAI, Department of Civil Engineering. Rua Luís Reis Santos, Pólo II, 3030-788 Coimbra, Portugal. {thiago.barbosa@adai.pt}
[2] Univ Coimbra, ADAI, Department of Mechanical Engineering. Rua Luís Reis Santos, Pólo II, 3030-788 Coimbra, Portugal, {luis.reis, jorge.raposo, xavier.viegas}@dem.uc.pt, {luis.mario@adai.pt}

**Corresponding author*

Keywords

LPG cylinders, Wildland Urban-Interface, Forest Fire, Accidents

Abstract

Incidents or accidents involving domestic liquefied petroleum gas (LPG) tanks have occurred at Wildland-Urban Interface (WUI) areas in Portugal, the USA, Spain and Greece, among others. The presence of LPG tanks in the WUI may cause severe events, especially when they are stored close to wildlands or artificial fuels. This work is a review aimed at presenting an overview of the cases related to accidents/incidents with LPG tanks stored during WUI fires. Fourteen recent accidents/incidents are described and lessons are taken in order to make recommendations to homeowners.

1. Introduction

Accidents and incidents related to Liquefied Petroleum Gas (LPG) stored at Wildland Urban-Interface (WUI) areas have been mentioned by authors (Barbosa et al., 2022; Caballero et al., 2019; Scarponi et al., 2020; Viegas et al., 2017, 2019). Due to the amount of energy stored, the vessel may become a hazard when a wildfire occurs.

Heating an LPG cylinder can cause severe events. For instance, it may trigger a boiling liquid expanding vapor explosion (BLEVE). The BLEVE occurs in pressurized vessels, which can cause severe damage to people and surrounding infrastructure. The main BLEVE effects are thermal radiation from a fireball (when the fluid is combustible), fragments projected and overpressure, all of which jeopardize the surroundings (Casal and Salla, 2006; B. Hemmatian et al., 2017; Behrouz Hemmatian et al., 2017; Planas-Cuchi et al., 2004). The BLEVE may be avoided if the cylinders have a PRD coupled, given the fact that the valve may prevent exacerbated pressure increment. However, in the few cases that heat dose is high, the BLEVE can still happen. If the PRD works, instead of explosion, a less dangerous event, a jet fire may occur. However, either event can trigger a domino effect.

This work is a review aimed at presenting an overview of the cases related to LPG stored at WUI fires. Fourteen accidents and incidents are described in this work as well as their effects.

2. Some recent events with gas storing occurred during WUI fires

2.1. Cases 1 and 2: Wildfire in Funchal, Portugal, August 2016

In August 2016, adverse weather conditions caused by an anticyclone in the northeast of the Iberian Peninsula and a depression in Morocco led Madeira Islands to have extreme values of temperature and relative humidity between 5 – 10th August. In the south of Madeira, the air humidity reached 10-20% and temperatures around 38ºC. On August 9th, the most extreme weather conditions were registered: the wind reached 35 km·h-1 with wind gusts of 80 km·h^{-1}; the minimum temperature registered was 29.6 ºC, which is 3.7 ºC higher than the last highest value registered in 1976 (Caballero et al., 2019; IPMA, 2016).

On August 8th, around 15:30h, an ignition occurred in forest area close to the WUI area. The local conditions of high temperatures, low humidity and strong wind, increased fire spread, namely to WUI areas, and ultimately, to urban areas. The fire spread initially up the hill through the forest zone, coming down the hill afterwards due to the prevailing wind direction. These extreme conditions exposed houses, the water treatment plant and a five-star hotel. Even on the 9th, 36 houses burned, 600 habitants were moved, the João de Almada Hospital was evacuated and three fatalities occurred.

In two houses, LPG cylinders were directly affected by the fire. Non-natural fuels and forest fuels in the surroundings of the house contributed to the cylinder´s fire impingement.

In the first house (case 1), the cylinder burst. Damages made by the BLEVE were found in the door and windows.

In the second house (case 2), four LPG cylinders were impinged by flames. The house was destroyed by the fire, but a BLEVE did not happen.

No fatalities related to LPG cylinders were registered for cases 1 and 2.

2.2. Cases 3 and 4: Pedrógão Grande Fire Complex, Portugal, June 2017

Pedrógão Grande Wildfire was a large fire in Portugal, possibly the second worst in Portuguese history. It caused 65 fatalities and around 200 injuries and 45328 hectares were burned. This large wildfire was caused by at least two different ignitions, on the same day, June 17th, at around 14:30h and 15:30h (local time), respectively in Escalos and Regadas. On June 17th, the Portuguese Institute for Sea and Atmosphere (IPMA) registered 80% of the Portuguese territory having dry conditions. The accumulated precipitation was close to the lowest in the period registered (1970-2017). The Fire Weather Index (FWI) was 26, which means a very high risk (Ribeiro et al., 2020; Tedim et al., 2020; Viegas et al., 217).

2.2.1. Case 3

In the early morning of the 18th a blind person who lived alone in a house in Balsa, did not realize that the fire had ignited an annex of the house where a gas cylinder was kept. The subsequent explosion destroyed that part of the house where the lady lived and killed her (Viegas et al., 2017).

2.2.2. Case 4

In the fire zone, near Louriceira, there was a motorhome that was used for summer vacation by an immigrant. On June 20th, the fire reached the motorhome at around 17:00h. An explosion was heard by firefighters that were nearby and they saw a dense smoke spreading upwards. A save and rescue team was sent, but they soon realized that a cylinder burst had happened. Inside the motorhome there were two mobile LPG cylinders. The first cylinder burst and became fragmented. The second one was hit by the burst that created a hole in cylinder´s surface causing LPG release and burning until the cylinder became empty (Viegas et al., 2017).

2.3. Cases 5 - 7: October Wildfire, Portugal, October 2017

Due to the long dry season, the same cited in case 3, combined with the Ophelia Hurricane (level 2-3 in the Saffir-Simphson scale), which caused powerful winds (50 $km \cdot h^{-1}$), many ignitions occurred on October 15th, leading to fast fire spread in multiple locations. October 2017 was the warmest since 1931 and the driest since 1997. In 24 hours, 220 thousand hectares were burned. On this day, 10% of moisture content of fine forest fuels was registered and in some places values close to 5% were found. The dry season, powerful winds and the low moisture content triggered a large wildfire, resulting in the largest burned area registered in Portugal. The FWI was 82 (maximum risk) and 532 ignitions were registered on October 15th. This wildfire caused 51 fatalities (Viegas et al., 2017, 2019)

Cases 5, 6 and 7 happened during the October Wildfire.

2.3.1. Case 5

In Oliveira do Hospital, a house on a hill was reached by a fire spreading very fast up the hill. The house had walls built with stone. The kitchen and its roof were totally destroyed and only the stone walls were left standing. After visiting the house ruins, a cylinder burst was suggested by the research team as the cause for the greater destruction. A fatality that happened in this house may have been related to the burst (Viegas et al., 2019).

2.3.2. Case 6

Around 16:00h, the wildfire had reached a small village called Vale do Laço. Citizens and firefighters were trying to save themselves, their houses and their belongings. A house nearby, situated on a slope and close to forest fuels, was affected by the wildfire. There were two brothers living there. It wasn't until around 20h, in the aftermath of the fire, that firefighters and habitants mentioned a previous suggestion made to the two brothers, asking them to leave and go into the town. However, the brothers had declined this advice and remained at home. They later observed smoke coming from the attic, probably caused by an ember that entered through an open window. They tried to extinguish it, but unsuccessfully which led to one fatality. On the day after, during the fire aftermath, an LPG cylinder burst destroying a large part of the house, but fortunately without causing casualties (Viegas et al., 2019).

2.3.3. Case 7

In Oliveira do Hospital, a warehouse was severely damaged by fire. 21 LPG cylinders with a volume of approximately 0.026 m^3 each were found. The cylinder´s size is usually the domestic size. It can be filled with up to 13 kg of LPG if it is butane or up to 11 kg of propane. Thus, up to 271 kg of LPG was stored, and this very large amount of energy caused great concern and damage to the surrounding structures when the various cylinders exploded. In this case, only the destruction of infrastructure was observed (Viegas et al., 2019).

2.4. Cases 8 e 9: Benitatxell Fire, Spain, September 2016

This fire is a consequence of an arsonist, on a day with a temperature of 35 ºC, relative humidity below 25% and wind gusts of 52 $km \cdot h^{-1}$. During this fire, around 1400 persons were evacuated, 470 received medical care, and 200 structures were affected by fires, but only three structures were severely damaged. The burned area was 898 hectares (Caballero et al., 2019; Rodríguez-García et al., 2022; Vacca et al., 2020).

Two LPG tanks placed nearby forest fuels were affected by the fire. In both cases jet fires were registered, being both LPG tanks equipped with PRD that were able to prevent the BLEVE (Caballero et al., 2019; Scarponi et al., 2020).

2.5. Cases 10 and 11: Mati Fire, Greece, July 2018

This wildfire is cited as the most lethal natural disaster in the history of the Modern Greek state. The wildfire broke out in the forest surroundings of the Ntaou region on Peneli Mountain, approximately 20 km northeast of Athens. On July 23rd, the temperature was nearly 40 ºC, relative air humidity was 19% and wind gusts were up to 100 $km \cdot h^{-1}$. The fire caused 100 fatalities, 200 people injured and 998 structures were destroyed (Caballero et al., 2019; Efthimiou et al., 2020; Molina-Terrén et al., 2019; Palmos et al., 2021; Tedim et al., 2020; Vacca et al., 2020).

During this fire, several explosions were reported and at least two LPG related cases were registered. The first one (case 10) is related to an LPG tank with at least 1 m3 exposed to fire. Case 11 was related to a mobile cylinder. Both vessels were found seriously damaged (Caballero et al., 2019).

2.6. Case 12: Llutxent, Spain, August 2018

This fire began on August 6th on a slope in the municipality of Llutxent. The ignition was caused by a thunderstorm and five fires were registered at the same time. The burned area was 3270 hectares, 163 persons were evacuated, 50 structures were affected and 10 houses were destroyed. The fire was completely extinguished by August 13th and no fatalities were reported (Caballero et al., 2019).

Five LPG mobile cylinders were burned during the fire and were found on a porch. BLEVE and jet fire were not reported, which may be explained by residual amount of LPG in the cylinders.

2.7. Case 13: Quinta do Colaço Fire, Portugal, August 2015

This fire occurred during the summer of 2015, in the District of Coimbra, reaching the municipalities of Almalaguês, Ceira, Semide and Rio de Vide. The burned area was 5500 hectares. 722 civil protection agents and firefighters worked to suppress the fire while they kept receiving new alert calls. The fire broke out in Quinta do Colaço around 12:42h. Unfortunately at 16:13h, the air support reported another 7 spot fires, which were suppressed by 7 fire trucks (Almeida, 2015).

A small building in a hill, probably used as a workshop and close to trees was affected by fire. Gas cylinders were placed inside the building and one of them burst. In principle, those cylinders were used to do metallurgic works using acetylene and oxygen. The cylinders were seriously damaged, and it was not possible to identify the fluid previously stored in them. The small building collapsed after the exposure to the fire and BLEVE (Almeida, 2015).

2.8. Case 14: Calabasas Fire, The USA, June 2016

During the summer of 2016 a brush fire occurred threatening thousands of homes in Calabasas. The burned area was around 208 hectares. Due to the fire, mandatory evacuations at Calabasas Highlands, Eddingham and Adamsville and voluntary evacuations in adjacent areas forced around 5000 people to leave their homes. The fast-moving wildfire swept through hills in Calabasas, it reached a preschool complex, burning outbuildings and heating a propane storage tank that caused a jet fire (Bartholomew 2016; Weber 2016; Scarponi et al. 2020).

3. Recommendation

Through the information gathered in the cases of accidents related to gas stored at WUI, we found some unsafe practices that occurred in more than one case, which should not be done. The accidents could be avoided through good practices carried out by the users, for instance: place the cylinder at a safe distance from the forest and artificial fuels; only one cylinder should be stored; and forest fuels (and other types of fuels) in the house´s surroundings should be eliminated.

Steel cylinders that are still being traded without PRD are not recommended to be used in houses that might be exposed to wildfires. For domestic applications we encourage the use of steel cylinders filled with butane and always with PRD coupled to the valve.

A protection made with a non-combustible fabric, low cost and easy to build was suggested by Barbosa et al. 2022

The users should consider the eventual jet fire direction through the PRD opening and its length before placing the cylinder. These safe practices may avoid future LPG accidents at the WUI.

4. References

Almeida, M.A. de F.B. de, 2015. Relatório resumo do Incêndio da Quinta do Colaço (Almalaguês).

Barbosa, T.F., Reis, L., Raposo, J., Viegas, D.X., 2022. A Protection for LPG Domestic Cylinders at Wildland-Urban Interface Fire. Fire 5, 63. https://doi.org/10.3390/ fire5030063

Bartholomew, D., 2016. Old Fire in Calabasas burns more than 500 acres, threatens thousands of homes [WWW Document]. Los Angeles Dly. News. URL https://www.dailynews.com/2016/06/04/old-fire-in-calabasas-burns-more-than-500-acres-threatens-thousands-of-homes/ (accessed 5.13.22).

Caballero, D., Sjöström, J., Pastor, E., 2019. Inventory of pattern scenarios. Wuiview 1–70.

Casal, J., Salla, J.M., 2006. Using liquid superheating energy for a quick estimation of overpressure in BLEVEs and similar explosions. J. Hazard. Mater. 137, 1321–1327. https://doi.org/10.1016/j.jhazmat.2006.05.001

Efthimiou, N., Psomiadis, E., Panagos, P., 2020. Fire severity and soil erosion susceptibility mapping using multi-temporal Earth Observation data: The case of Mati fatal wildfire in Eastern Attica, Greece. Catena 187, 104320. https://doi.org/10.1016/j.catena.2019.104320

Hemmatian, Behrouz, Casal, J., Planas, E., 2017. A new procedure to estimate BLEVE overpressure. Process Saf. Environ. Prot. 111, 320–325. https://doi.org/10.1016/j.psep.2017.07.016

Hemmatian, B., Planas, E., Casal, J., 2017. Comparative analysis of BLEVE mechanical energy and overpressure modeling, Process Safety and Environmental Protection.

IPMA, 2016. Análise Preliminar do Período 5 a 10 Agosto 2016 na Madeira [WWW Document]. URL https://www.ipma.pt/pt/media/noticias/news.detail.jsp?f=/pt/media/noticias/arquivo/2016/madeira-5-10-ago-2016.html (accessed 3.2.22).

Molina-Terrén, D.M., Xanthopoulos, G., Diakakis, M., Ribeiro, L., Caballero, D., Delogu, G.M., Viegas, D.X., Silva, C.A., Cardil, A., 2019. Analysis of forest fire fatalities in Southern Europe: Spain, Portugal, Greece and Sardinia (Italy). Int. J. Wildl. Fire 28, 85–98. https://doi.org/10.1071/WF18004

Palmos, D., Papavasileiou, C., Papakitsos, E.C., Vamvakeros, X., Mavrakis, A., 2021. Enhancing the environmental programmes of secondary education by using web-tools concerning precaution measures in civil protection: The case of Western Attica (Greece). Saf. Sci. 135, 105117. https://doi.org/10.1016/j.ssci.2020.105117

Planas-Cuchi, E., Salla, J.M., Casal, J., 2004. Calculating overpressure from BLEVE explosions. J. Loss Prev. Process Ind. 17, 431–436. https://doi.org/10.1016/j.jlp.2004.08.002

Ribeiro, L.M., Rodrigues, A., Lucas, D., Viegas, D.X., 2020. The impact on structures of the pedrógão grande fire complex in June 2017 (Portugal). Fire 3, 1–22. https://doi.org/10.3390/fire3040057

Rodríguez-García, E., Santana, V.M., Alloza, J.A., Ramón Vallejo, V., 2022. Predicting natural hyperdense regeneration after wildfires in Pinus halepensis (Mill.) forests using prefire site factors, forest structure and fire severity. For. Ecol. Manage. 512. https://doi.org/10.1016/j.foreco.2022.120164

Scarponi, G.E., Pastor, E., Planas, E., Cozzani, V., 2020. Analysis of the impact of wildland-urban-interface fires on LPG domestic tanks. Saf. Sci. 124. https://doi.org/10.1016/j.ssci.2019.104588

Tedim, F., Leone, V., Mcgee, T.K., 2020. Extreme Wildfire Events and Disasters. https://doi.org/10.1016/B978-0-12-815721-3.00002-3

Vacca, P., Caballero, D., Pastor, E., Planas, E., 2020. WUI fire risk mitigation in Europe: A performance-based design approach at home-owner level. J. Saf. Sci. Resil. 1, 97–105. https://doi.org/10.1016/j.jnlssr.2020.08.001

Viegas, D.X., Figueiredo Almeida, M., Ribeiro, L.M., Raposo, J., Viegas, M.T., Oliveira, R., Alves, D., Pinto, C., Jorge, H., Rodrigues, A., Lucas, D., Lopes, S., Silva, L.F., 2017. O complexo de incêndios de Pedrógão o Grande e concelhos limítrofes, Iniciado a 17 de junho de 2017.

Viegas, X., Almeida, M.F., Ribeiro, M., Almeida, M.A., Raposo, J., Viegas, M.T., Oliveira, R., Alves, D., Pinto, C., Rodrigues, A., Ribeiro, C., Lopes, S., Jorge, H., Viegas, C.X., 2019. Análise Dos Incêndios Florestais Ocorridos a 15 De Outubro De 2017 - Principais incêndios e resposta operacional.

Weber, C., 2016. Evacuations canceled near Calabasas wildfire [WWW Document]. Press Democr. URL https://www.pressdemocrat.com/article/news/evacuations-canceled-near-calabasas-wildfire/?artslide=1 (accessed 5.22.22).

Impact of forest gaps on wind turbulence and potential wildfire behavior at the rural-urban interface

Jiawei Zhang*[1,2], Marwan Katurji[2], James Brasington[2], James Hilton[3], Peyman Zawar-Reza[2], Tara Strand[1]

[1] *New Zealand Forest Research Institute, Scion, New Zealand, {jiawei.zhang@scionresearch.com}*
[2] *School of Earth and Environment, University of Canterbury, New Zealand,*
[3] *Commonwealth Scientific and Industrial Research Organization (CSIRO), Australia,*

**Corresponding author*

Keywords

Forest gaps, firebreaks, rural-urban interface, wind gust, Large Eddy Simulation

Abstract

Forest canopy can impact fire behavior through modulating both subcanopy atmospheric turbulence and wake turbulence at the forest edge. The 2020 Lake Ōhau fire happened at a rural-urban interface where the heavily fire-damaged village was surrounded by a heterogeneous forest canopy. Evidence shows that high wind speeds with strong gusts were present throughout the fire outbreak, indicating a strong wind-driven wildfire. Since the village was surrounded by complex terrain including a forest canopy, the forest canopy might play an important role in modifying the wind conditions within the village which could impact the fire spread behavior.

This research uses Large Eddy Simulation (LES) to study wind gusts and other near-surface wind characteristics in the Lake Ōhau area under the weather conditions of the 2020 Lake Ōhau fire. The work especially focuses on how the forest canopy around the village could change the wind gust within and around the village area. To do so, a LiDAR field campaign was also undertaken to obtain ultra-high resolution (grid resolution < 10m) forest canopy and other geoinformation.

Results also show that the village was impacted by two mesoscale wind systems - an offshore westerly downslope wind from west of the village and a northerly wind coming down over Lake Ōhau. The LES results were also used to further explore how simulated forest gap orientation might impact the downstream wind. Previous studies have shown that creating forest gaps or firebreaks can significantly change the wind characteristics within and at the edge of the forest. Three additional scenarios were studied by modifying the forest canopy around the village, including one without any forest canopy, one with horizontal (West-East orientation) forest gaps and one with vertical (North-South orientation) forest gaps. Total removal of the forest canopy increased the average wind gust in almost all areas within the village while the changes were spatially more heterogeneous in the horizontal and vertical gap scenarios. Differences of the spatial wind gust distribution might be related to how different forest gap alignments change the dominant inflow wind component. Next steps of this work will utilize passive tracers and temporal analysis to identify the processes driving these differences.

1. Introduction

The 2020 Lake Ōhau fire was one of the largest fires in recent New Zealand history with 54 residential buildings damaged and all residents forced to evacuate (Fire and Emergency New Zealand, 2021). The fire started at about 2.00am, October 4th local time (1.00pm October 3rd UTC) and burnt 5043 hectares of land in total. The extent of the fire can be seen in the short-wave infrared (SWIR) imagery from the Sentinel 2 satellite (Figure 1, the brown patches). The FENZ 2021 report highlighted the extremely high wind gusts (up to 167.2 km/h) measured at the closest automatic weather station (AWS) during the incident. The presence of such strong wind gusts suggests that atmospheric flow, especially surface atmospheric turbulence, will play an important role in the fire spread behavior.

The Lake Ōhau village settlement (Lat: -44.271, Lon:169.847) lies at the confluence zone of complex valley outlet systems to the west, the lake coastline to the north and east, and a relatively large pine forest to the northwest (Figure 2). With the complex terrain features (including topography and forest canopy) in this rural-

urban interface, it is paramount to understand how these features modulated localized wind turbulence during the fire. Due to the limited on-site measurements (the closest long-term weather station is more than 50km away and situated in a different valley), high resolution turbulence-resolving numerical simulations are the best tools available to study the wind behavior.

Figure 1: The Lake Ōhau fire from Sentinel 2 satellite short wave infrared (SWIR) imagery, October 3rd 2020 (UTC).

This research focused on the forest canopy around the village. Studies have shown that both the vertical structure of the forest canopy and forest gap location can impact the fire-atmospheric interaction through modifying fire-induced atmospheric turbulence (Kiefer et al., 2016, 2018). Forest gaps or firebreaks can be naturally formed or intentionally created. They have been used in recent decades as a silvicultural tool to reduce wildfire risks (Scarascia-Mugnozza et al., 2000). Most studies on forest gaps or firebreaks focus on the efficiency of the gaps in delaying or stopping fire from spreading further. However, a few studies have investigated the role of forest gaps on wake turbulence and how the turbulence mixing and flow reattachment at the wake of the forest canopy can impact fire behaviors like ember transport (Chung & Koseff, 2021). These studies are mostly based on idealized simulations using homogenous (evenly distributed) vegetation canopy. Questions remain about how different alignment of forest gaps can impact the near-surface atmospheric turbulence within a highly heterogenic environment such as the rural-urban interface (RUI).

Previous studies have compared the Large Eddy Simulation (LES) to field measurements and shown that LES models with a vegetation canopy module is capable of simulating atmospheric turbulence within and at the wake of the forest canopy (Kiefer et al., 2022; Mueller et al., 2014). Thus, an LES model was used in this study to investigate the role of the forest canopy in modulating the atmospheric flow during the Lake Ōhau fire.

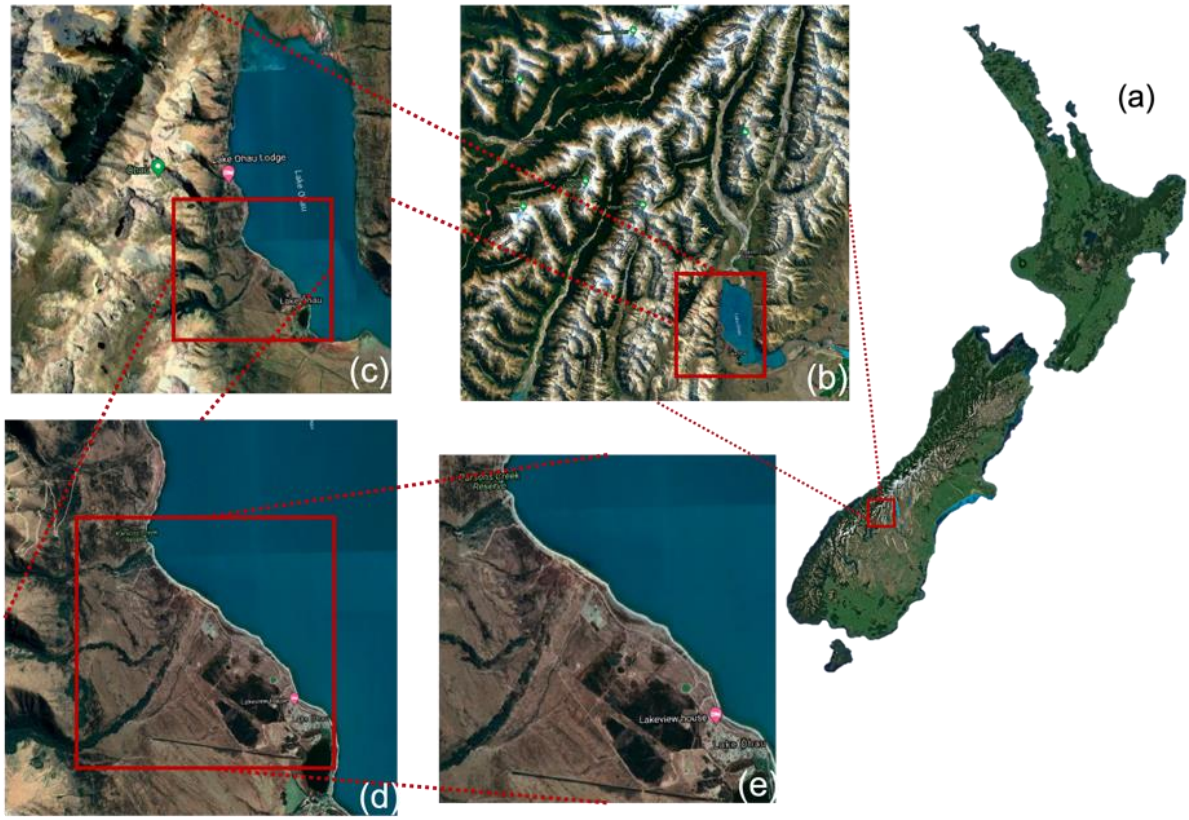

Figure 2 - Image of Lake Ōhau and surrounding topography from Google Earth. Areas from (b) to (e) are covered in our nested large eddy simulations as domain D2 to D5.

2. Methods

2.1. Mesoscale weather condition during the fire

Mesoscale weather information was obtained through the Weather Research and Forecast (WRF) simulation (Figure 3a). The simulation results aligned well the nearest AWS observation (Figure 3, the location is about 50km northeast of the Ōhau village). The AWS data was consistent with synoptic charts and showed a high intensity northwest downslope wind with hourly average wind speed around 10m/s during the event. The simulated mesoscale wind speeds on the majority of the downwind slopes of the region, as shown in Figure 3, were around 20m/s or greater

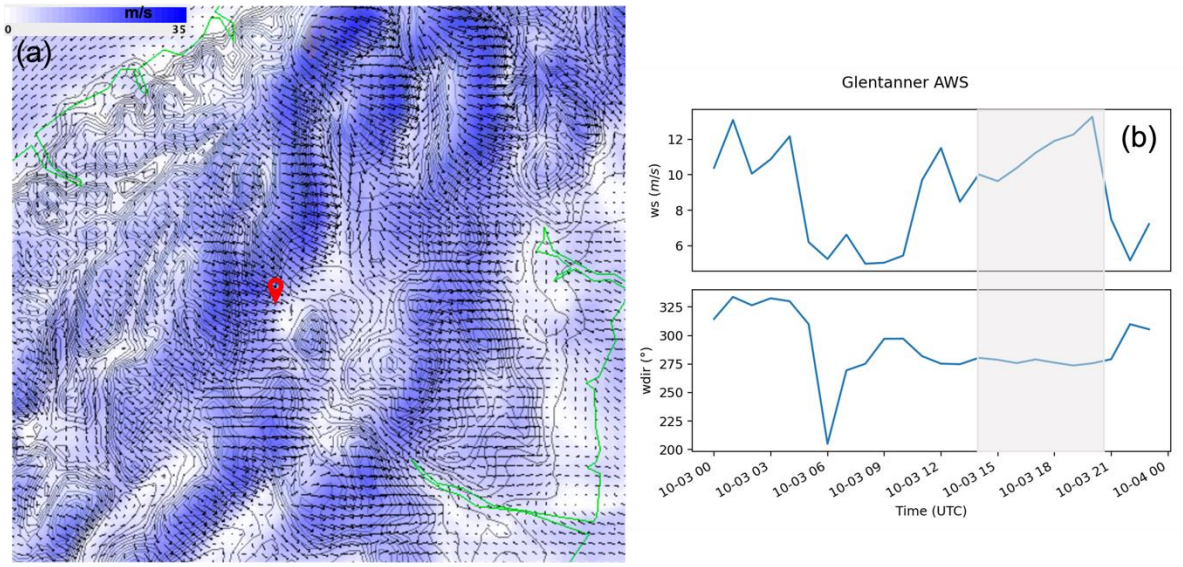

Figure 3- a) Hourly surface wind speed (10m AGL) at 2020-10-03 21:00 (UTC) from a 3km WRF simulation. The marker indicates the Lake Ōhau village area. b) Hourly wind speed and wind direction from the Glentanner AWS (-43.91498S, 170.12862E). The grey area indicates the fire ignition and early spread period.

2.2. Model description and initialization

The LES model used in this study is called the PALM model (B. Maronga et al., 2015; Björn Maronga et al., 2020; Raasch & Schröter, 2001). The model was set up using nested simulation domains with the second largest domain covering 62km in both horizontal dimensions around the Lake Ōhau area to allow a well-developed terrain-induced atmospheric inflow to the village area. The inner-most domain was focused on the Lake Ōhau village area with very fine horizontal (9m) and vertical (3m) grid resolutions to resolve the small scale near-surface atmospheric turbulence. The detailed domain configuration can be found in Table 1 and Figure 2.

Table 1. LES simulation domain setup. D1 domain was used to avoid numerical instability caused by steep terrain. For D2 and D3, the terrain information (DEM and land cover information) is taken from Land Information New Zealand (LINZ). For D4 and D5, merged terrain information was used based on both the LINZ datasets and our LiDAR field campaign. The vegetation and urban canopy were used only in the finer domains (D4 and D5). Detailed information can be found in section 2.2.2.

Domain name	Domain size ($L_x \times L_y \times L_z$) (km)	Domain resolution ($\Delta x \times \Delta y \times \Delta z$) (m)	Terrain information	Vegetation and urban canopy
D1	93×78×12	243×243×81	Flat and homogeneous	No
D2	62×62×10	243×243×81	Yes	No
D3	16×16×4	81×81×27	Yes	No
D4	5.8×5.8×1.3	27×27×9	Yes	Yes
D5	3.5×3.5×1.2	9×9×3	Yes	Yes

2.2.1. Field campaign and geoinformation reconstruction

To carry out an ultra-high resolution LES simulation, same-resolution geoinformation is needed including land cover information (vegetation type, urban land type etc.), leaf area density (LAD) profiles at all spatial locations, and urban building location and height information. The land cover information and urban building locations are taken from the Land Cover Database version 5.0 and NZ Building Outlines created by Land Information New Zealand (LINZ). The LAD and building height information is derived from the data obtained during our terrestrial LiDAR helicopter campaign. To simulate the pre-fire vegetation/urban canopy impact on the near-surface atmospheric turbulence, the work also reconstructed the pre-fire vegetation/urban canopy information (Figure 4 shows the detailed process). The reconstructed vegetation shows more consistency with the pre-fire satellite image from Google Earth (Figure 5).

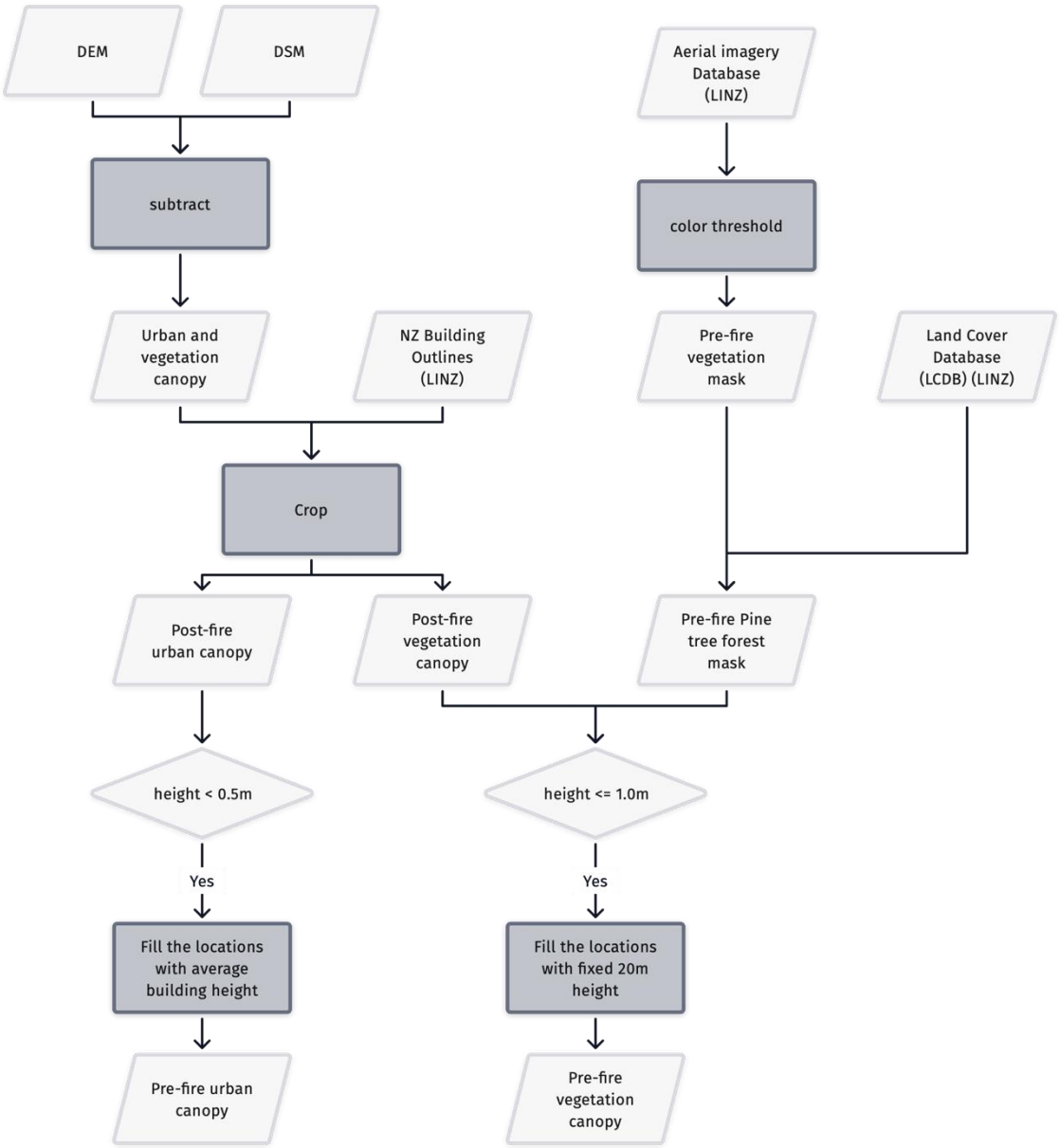

Figure 4- Process diagram - reconstructing the pre-fire vegetation and urban canopy.

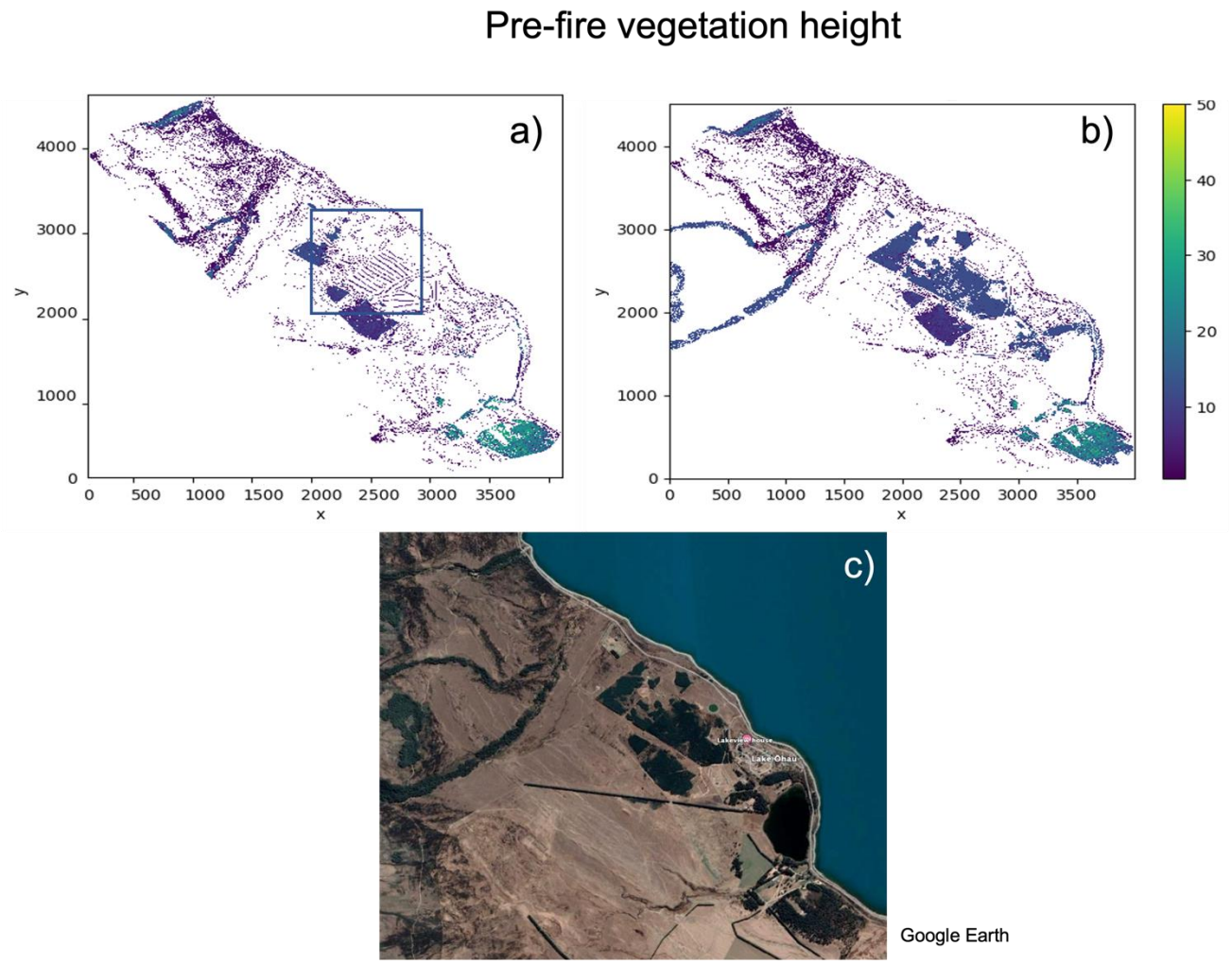

Figure 5- Vegetation height derived from LiDAR (a) reconstructed vegetation height (b) and pre-fire satellite image (c) from Google Earth image taken on 19/9/2019.

2.2.2. Simulation cases

Four scenarios were studied to address the impact of vegetation on the near-surface atmospheric turbulence during the fire: (i) the base case (Original) with the original reconstructed pre-fire geoinformation, (ii) all the vegetation around the village was completely removed (Noveg), (iii) 27m-wide horizontal (East-West orientation) gaps were created for all the trees around the village (Hgap) and (iv) 27m-wide vertical (North-South orientation) gaps were created for all the trees around the village (Vgap) (Figure 6). To incorporate the mesoscale forcing in the LES simulations, all the simulations carried out were initialized using average vertical profiles of velocity and temperature from the WRF simulation. In all scenarios, the LES model used the same initialization conditions from the WRF simulation data; the only differences being the modified vegetation canopy information. All simulations were run for 2 hours with the first 1.5 hours as model spin-up time. The last 30 minutes of data is analyzed below.

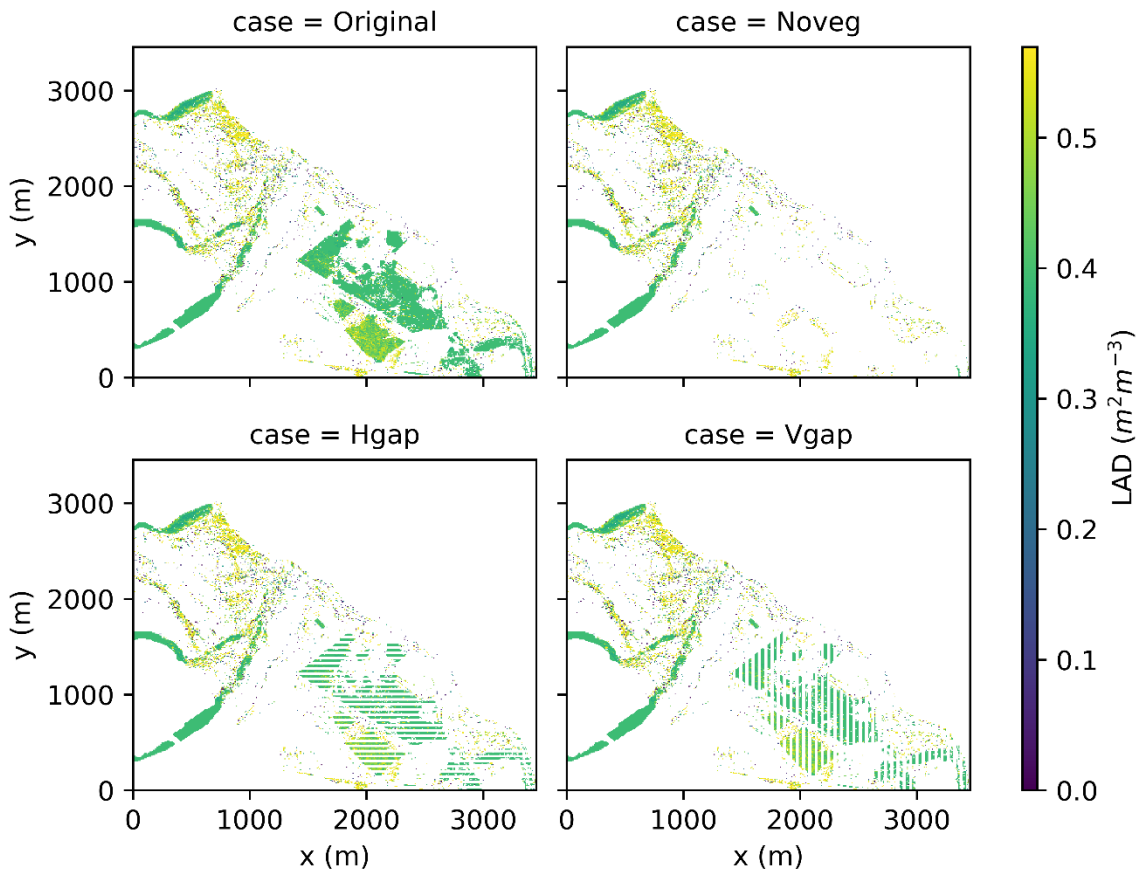

Figure 6- Leaf Area Density (LAD) at the first grid level above the ground (1.5m AGL) from four simulation cases. Original represents the original reconstructed pre-fire vegetation, Noveg represents removing all the trees around the village, Hgap represents the horizontal tree gap scenario, Vgap represents the vertical tree gap scenario.

3. Results and discussion

The base (Original) simulation shows that the village and the surrounding area were impacted by two main wind components. One is westerly downslope wind descending from the steep slope to the west of the village and the other one is the northerly down valley wind that traveled down across the lake (Figure 7). The result is consistent with the larger scale forcing from the WRF simulation.

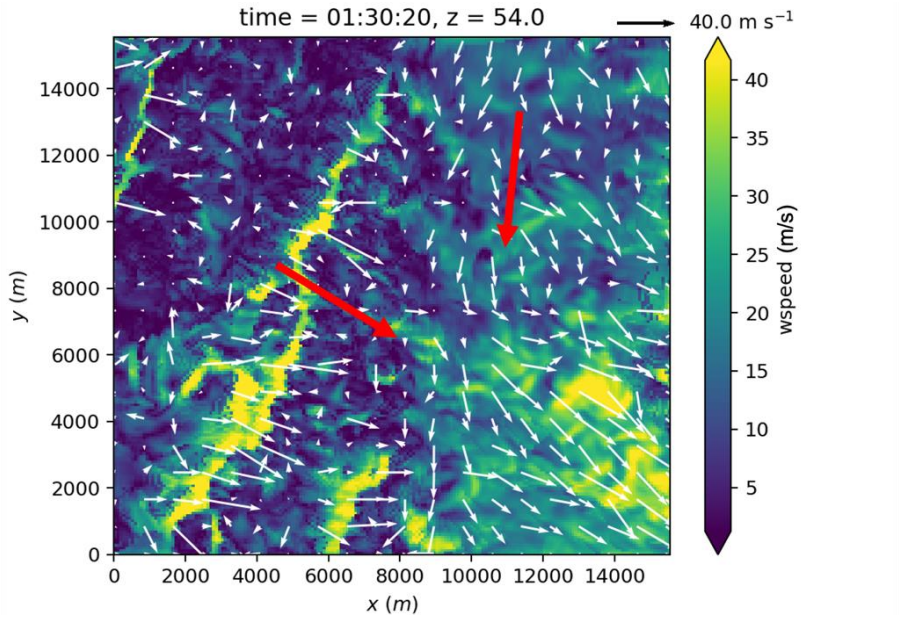

Figure 7- Instantaneous wind speed at 54m AGL from D3 domain. The red annotation shows two upstream incoming wind components that impacted the Lake Ōhau area during the fire event. Evidence of these two upstream wind components can be found from the instantaneous wind vector (white arrows) in the figure. Although not shown here, the two upstream components exist throughout the simulation.

Wind gusts are one of the important factors representing fire danger, especially in complex terrain where we still lack understanding of the spatial-temporal characteristics of wind gusts (Cheney & Sullivan, 2008; Letson et al., 2019). By simulating four different scenarios, the work found that modifying the vegetation canopy around the village can change the wind gust characteristics not only within the village but also in surrounding areas. Wind gust is calculated based on the World Meteorological Organization (WMO) standard (maximum value of the 3 second running average wind speed within one minute).

Figure 8 shows zoomed-in view of the differences in average wind gusts between the modified vegetation canopy simulations and the base case (Original) simulation from the D5 domain. Without surrounding vegetation (Noveg), almost all areas in the village experience an increase in wind gusts. A decrease in average wind gusts is only found in the wake of the buildings. This might indicate a more constant predominant wind direction resulting from the removal of vegetation which could act as a barrier to hinder the merging of the two wind components. Wind gust differences have more spatial variability in the horizontal forest gap (Hgap) and vertical forest gap (Vgap) simulations. The average wind gust is stronger in the central left area (solid boxes in Figure 8) in the Vgap scenario compared to the Hgap scenario. Both forest gap scenarios have weaker wind gusts in the bottom right of the village (dashed box in Figure 8). However, the wind gust decrease is more significant in the Vgap simulation than the Hgap one.

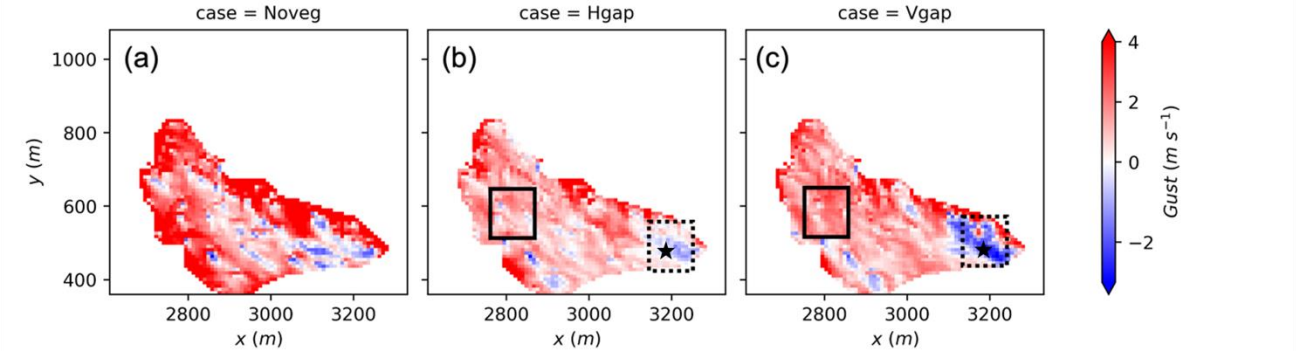

Figure 8- The difference of the average wind gust between each simulation with modified canopy and the base simulation during the last half hour simulation. Solid boxes in (b) and (c) show the area where the vertical gap simulation has stronger average wind gust compared to the horizontal gap simulation. The dashed boxes show the area where the horizontal forest gap simulation has stronger average wind gust than the vertical forest gap simulation. The star marker shows the location of which the wavelet analysis was carried out.

Areas with the average wind gust surpassing 30 m/s or 108 km/h can be found mainly over the lake area close to the village (Figure 9). Both the Noveg scenario and Hgap scenario have higher average wind gusts in the lake area while the Vgap scenario has similar wind gusts to the Original scenario.

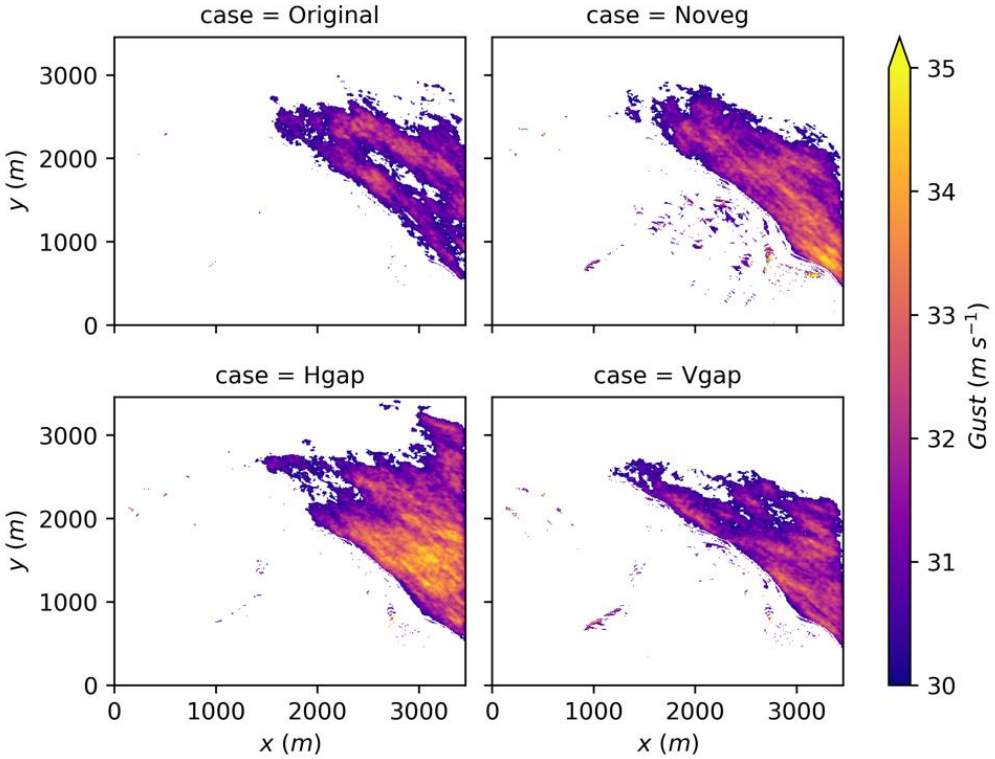

Figure 9- The average wind gust higher than 30 m/s at 6m AGL from the D5 domain.

4. Discussion and future work

The above results suggest that, with the two inflow wind streams (offshore westerly downslope wind and onshore northerly wind), different forest gap alignment might change the predominant inflow wind component by channeling one inflow stream and/or blocking the other. Time series analysis (Figure 10) shows slightly different integral scales between different forest gap alignments. At the selected location (star maker in Figure 8), the Horizontal gap (Hgap) scenario have more high frequency signals with period shorter than 32s (dashed blue line in Figure 10). This suggests more small-scale turbulence which might be caused either by shifting the predominant inflow components or locally generated turbulence coherent structures within the canopy. Further spatial/temporal signal analyses are needed to confirm the mechanism behind the spatial heterogeneity of the wind gust changes among different forest configurations. Future work will also use a passive tracer released at different sides of the forest patch edge (Figure 11) to further evaluate the fire risk (potential ember transport etc.) associated with atmospheric flow around the RUI.

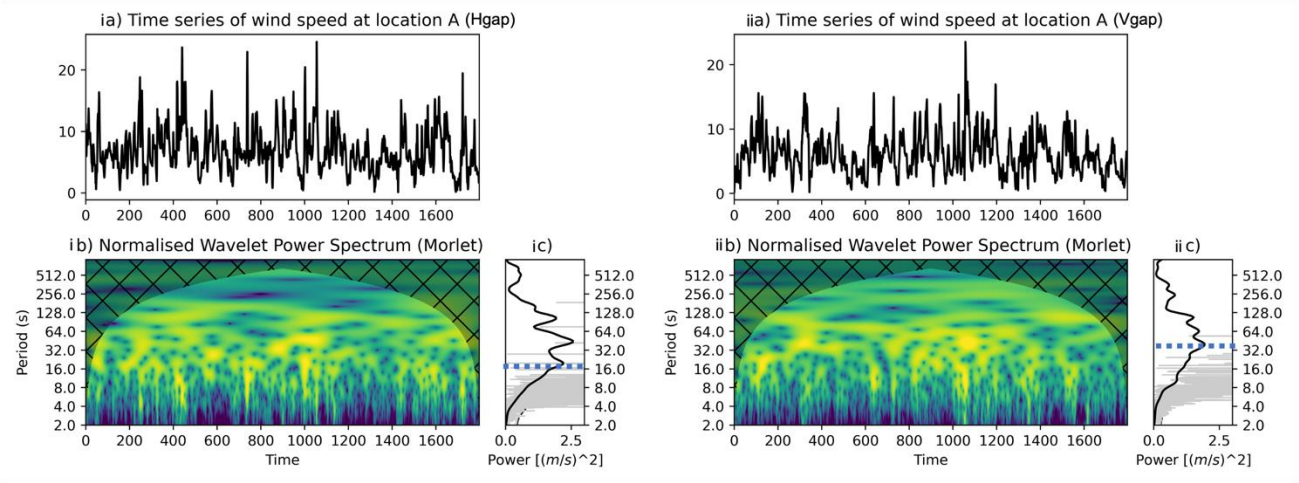

Figure 10- Wavelet analysis of the wind speed (1Hz) taken at the same location (star marker in Figure 8) for Hgap (left) and Vgap (right) simulations. ia) and iia) are the time series, ib) and iib) show the wavelet power spectrum using Morlet mother wavelet function, ic) and iic) show the global wavelet spectrum (black line, dashed blue line shows the first power peak) and Fourier power spectrum (grey line).

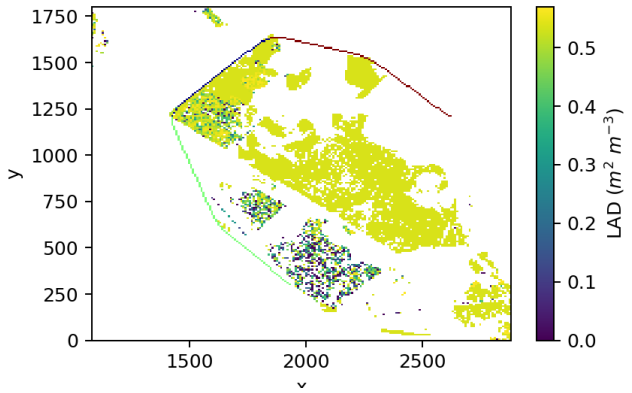

Figure 11- The passive tracer release location map. Green, blue and red curved lines indicate three different tracer groups that will be released at different sides of the vegetation canopy around the village. The rest of the image shows the leaf area density (LAD) at 7.5m AGL to indicate the relative location of the tracers to the vegetation canopy.

5. Conclusion

Preliminary results show that the vegetation canopy surrounding Lake Ōhau village can modulate wind gusts within and around the village. Removal of surrounding trees can alter the spatial wind gust distribution in different ways. In our case study simulations, the total removal of forest vegetation around the village resulted in increasing the average wind gusts of about 4m/s and higher in almost all areas within the village. On the other hand, forest gaps created through partial removal of the trees resulted in varying changes to the wind gusts in the village, depending on the direction of the gaps. Comparisons of the spatial distribution of wind gusts over the lake adjacent to the village also show that the influence of the vegetation canopy changes can extend far beyond the village area. Our current results suggest that the alignment of the forest gap might impact the dominant inflow component which might then impact the fire spread through changing wind speed and wind gust intensities, Further spatial and temporal analysis of the wind field and passive tracer distribution will help further verify these hypothesis.

6. Acknowledgement

We would like to give thanks to FNEZ for supporting the LiDAR field campaign. We also want to thank New Zealand eScience Infrastructure (NeSI) and University of Canterbury's high performance computational center

for proving computational resources and support. We would like to give special thanks to Paul Bealing and other UC technical team members for their support. The WRF data in this work was from the WRF database provided by the Center of Atmospheric Research, University of Canterbury, We would like to thank Tony Dale who runs and maintains the WRF simulation database. This research was co-funded by Ministry of Business, Innovation and Employment (MBIE), New Zealand (Grant No. C04X1603 - "Preparing New Zealand for Extreme Fire" and C04X2103 – "Extreme wildfire: Our new reality – are we ready?") and by the Royal Society of New Zealand (Grant No. RDF-UOC1701).

7. Bibliography

Cheney, P., & Sullivan, A. (2008). Grassfires: Fuel, Weather and Fire Behaviour. Csiro Publishing.

Chung, H., & Koseff, J. (2021). Turbulence structure and scales in canopy-wake reattachment. Physical Review Fluids, 6(11), 114605. https://doi.org/10.1103/PhysRevFluids.6.114605

Fire Emergency New Zealand. (2021, November 18). The Lake Ōhau Fire - A Summary of Events. Retrieved from https://fireandemergency.nz/assets/Documents/Research-and-reports/lakeOhau/Lake-Ohau-Fire-a-Summary-of-Events.pdf

Kiefer, M. T., Heilman, W. E., Zhong, S., Charney, J. J., & Bian, X. (2016). A study of the influence of forest gaps on fire–atmosphere interactions. Atmospheric Chemistry and Physics, 16(13), 8499–8509. https://doi.org/10.5194/acp-16-8499-2016

Kiefer, M. T., Zhong, S., Heilman, W. E., Charney, J. J., & Bian, X. (2018). A Numerical Study of Atmospheric Perturbations Induced by Heat From a Wildland Fire: Sensitivity to Vertical Canopy Structure and Heat Source Strength. Journal of Geophysical Research: Atmospheres, 123(5), 2555–2572. https://doi.org/10.1002/2017JD027904

Kiefer, M. T., Heilman, W. E., Zhong, S., Charney, J. J., Bian, X., Skowronski, N. S., et al. (2022). Representing low-intensity fire sensible heat output in a mesoscale atmospheric model with a canopy submodel: a case study with ARPS-CANOPY (version 5.2.12). Geoscientific Model Development, 15(4), 1713–1734. https://doi.org/10.5194/gmd-15-1713-2022

Letson, F., Barthelmie, R. J., Hu, W., & Pryor, S. C. (2019). Characterizing wind gusts in complex terrain. Atmospheric Chemistry and Physics, 19(6), 3797–3819. https://doi.org/10.5194/acp-19-3797-2019

Maronga, B., Gryschka, M., Heinze, R., Hoffmann, F., Kanani-Sühring, F., Keck, M., et al. (2015). The Parallelized Large-Eddy Simulation Model (PALM) version 4.0 for atmospheric and oceanic flows: model formulation, recent developments, and future perspectives. Geoscientific Model Development Discussions, 8(2), 1539–1637. https://doi.org/10.5194/gmdd-8-1539-2015

Maronga, Björn, Banzhaf, S., Burmeister, C., Esch, T., Forkel, R., Fröhlich, D., et al. (2020). Overview of the PALM model system 6.0. Geoscientific Model Development, 13(3), 1335–1372. https://doi.org/10.5194/gmd-13-1335-2020

Mueller, E., Mell, W., & Simeoni, A. (2014). Large eddy simulation of forest canopy flow for wildland fire modeling. Canadian Journal of Forest Research, 44(12), 1534–1544. https://doi.org/10.1139/cjfr-2014-0184

Raasch, S., & Schröter, M. (2001). PALM–a large-eddy simulation model performing on massively parallel computers. Meteorologische Zeitschrift, 10(5), 363–372.

Scarascia-Mugnozza, G., Oswald, H., Piussi, P., & Radoglou, K. (2000). Forests of the Mediterranean region: gaps in knowledge and research needs. Forest Ecology and Management, 132(1), 97–109. https://doi.org/10.1016/S0378-1127(00)00383-2

Impact of the WUI vegetation management on damage to building: comparing post-fire damage assessment and CFD modelling results.

Anne Ganteaume[*1], Bruno Guillaume[2], Bertrand Girardin[2]

[1]*INRAE, RECOVER, Aix-en-Provence, France, {anne.ganteaume@inrae.fr}*
[2]*EFECTIS, Bordeaux, France, {bruno.guillaume, bertrand.girardin}@efectis.com*

**Corresponding author*

Keywords:

Vegetation management; post-fire damage; CFD modelling; Wildland-Urban Interface

Abstract

In most Wildland-Urban Interface (WUI) fires, damage to building can result from poor vegetation management, comprising a lack of mandatory brush-clearing around building or an unwise location of trees (e.g. too close to building or overhanging the roof). It was interesting to check if post fire damage can be predicted by CFD fire modelling in different scenarios of vegetation management (treated vs untreated) according to different past-fire events. Ultimately, this work will help to assess if the fuel treatment regulation in the framework of fire prevention is efficient and to pinpoint possible limitations.

Different scenarios of vegetation treatments were tested on four study cases of dwellings surrounded by gardens juxtaposed to wildland vegetation (therefore submitted to the regulation on fuel management in WUI) that were affected by the Rognac fire in 2016 (SE France). In each case, comparisons of modelled and observed fire behaviour and impacts on buildings were performed using the Fire Dynamic Simulator model (FDS) and very accurate georeferenced ornamental vegetation mapping, especially around buildings.

Despite problems to adapt FDS modelling to the high fuel moisture content (FMC) of some species, results showed that overall brush-clearing mitigated fire intensity and propagation and therefore damage to building and ornamental vegetation, sometimes highlighting that this fuel management measure could be softened (decreasing the radius treated) or, on the contrary, strengthened according to the topography and wind. The fuel biomass treatment involving vegetation residues left on site was also found as deleterious as the lack of treatment.

Overall, the modelling using FDS, at the WUI scale and taking into account a very refined vegetation distribution, was mostly successfully validated by post-fire damage recorded during the past-fire events, which was rarely attempted in the complex environment of forest fires in the French Mediterranean area. The current scientific limitations of the model did not allowed obtaining realistic results in terms of heat flux received by the building, even if they were coherent in global intensity comparing treated and untreated vegetation, and have to be addressed in future improvements of the model.

1. Introduction

In some Mediterranean countries, the culture of fire risk has declined slowly with the decreasing trend of fire occurrence and burned area over the past decades (Fox et al. 2015). However, peaks of large fire occurrence still occur during extreme weather events (e.g. 2003, 2016 in SE France), often resulting in catastrophic fires difficult to suppress (Maditinos & Vassiliadis 2011; Jones et al. 2016). As a prevention measure in SE France, implementing the regulations on fuel reduction around housing (i.e. mandatory brush-clearing) at the wildland-Urban Interfaces (WUI) is of the upmost importance to mitigate the fire effects on buildings and to keep safer people and firefighters during a fire. However, these regulations are difficult to control and little respected, even if experience feedbacks also showed that the environment surrounding the housing (e.g. location of hedges, no fuel areas, etc.) can play an important role during WUI fires, especially on the resulting damage (Syphard et al. 2019).

In order to improve the fire prevention at WUI along identifying the different environmental factors surrounding the housing that can contribute to increase or decrease its vulnerability (usually, vegetation types, slope, and

wind), it is also necessary to verify if the regulations in terms of fuel reduction are still efficient in critical scenarios of wind and slope or if they can be softened or strengthened in some cases.

Previous studies revealed that WUI fire issue is mostly due to the building susceptibility to fire rather than a difficulty to control the fire (Cohen 2000, Cohen 2008). Fire behaviour modelling is a useful alternative tool, when properly calibrated and validated, to forecast the fire intensity and propagation as well as the fire impact on building in different scenarios of vegetation, terrain, and weather conditions. Despite several fire behaviour models (Sullivan, 2009) applied to forest fires, few are used for simulation at WUI, for instance, because WUI vegetation differs from that of wildland (more heterogeneous in terms of species composition and spatial distribution; Ganteaume 2018). Only complex CFD physics-based models (e.g. the wildland-urban fire dynamics simulator WFDS, Mell et al., 2007) or raster-based models (e.g. SWIFFT, De Gennaro et al. 2017; Fernandez et al. 2018), for instance, have achieved this goal. HRR and heat fluxes received have been validated on isolated dry tree experiment (Mell et al, 2009) at the laboratory scale but there is a gap on the validation at meso scale (i.e. the scale of the garden). The current study is therefore an attempt to validate simulation results using post-fire damage.

This work aimed at comparing post-fire damage recorded during past-fires to results of CFD modelling run on different scenarios of vegetation management (brush-clearing *vs* no brush-clearing) to validate the modelling results and assess the role of the regulation on fuel reduction on the fire mitigation at WUI.

2. Material & Methods

2.1. Study cases

Three study cases of housing, located at WUI and differently affected (from partial damage to total destruction) by a large past fire event in SE France (Rognac fire that occurred in 2016 ; Fig. 1) was considered in this work. Regarding this fire, three areas have been selected: « Griffons » (community of Vitrolles) as well as « Barnouins » and « Château » (community of Les Pennes-Mirabeau). Damage recorded during post-fire surveys were used as a validation of the modelled fire behaviour and impact on buildings. According to the French regulation, buildings located at WUI were theoretically subjected to fuel reduction within a 50 m-radius. Depending on the case, this regulation was implemented, sometimes partially, or not at all. Some cases presented, around the building, an area corresponding to a garden, with ornamental lawn, trees and shrubs, others presented a home ignition zone (HIZ) composed of natural vegetation, brush-cleared or not, similar to the neighbouring natural vegetation (Table 1).

2.2. Modelling

So far, the models FDS (version 6.7.5) (Vanella et al., 2021) and WFDS developed by NIST (McGrattan et al. 2013) regarding wildfires have been validated by laboratory experiments (e.g. Mell et al. 2009, Perez-Ramirez et al. 2017 ; Morandini et al. 2019) or grass fires (Mell et al. 2007).

In this work, the inputs used for the simulations (see table 1) were :

(i) topographical data (EU-DEM-v1.1 COPERNICUS program, available with a resolution of 25m) ;

(ii) vegetation data : Vegetation was recorded with as much as precision as possible (in the field during the post-fire survey and using aerial or satellite images available before the fire), given its strong heterogeneity, according to three strata (litter and grass, understorey, and overstorey). The WUI vegetation can be composed, according to the study case, of exotic species and/or native species similar to the wildland vegetation and was managed or not according to the regulation;

(iii) wind data : the wind direction was taken from the fire-fighter reports of the events. The wind speed considered is 11 m s^{-1} on average over 5 min. The intermittent wind is modelled by a simple alternation every 15s of 2 m s^{-1} and 20 m s^{-1} (typical of the dominant wind, Mistral, in the study area).

The outputs of the modelling are the flame front position and vegetation mass loss variation at different times of simulation, and the temporal variation of the total power and of heat fluxes (located at different heights on buildings) during the simulation.

The modelling was run for each study case on the two vegetation management scenarios (with or without brush-clearing), except in the study case « Château » which was divided into three different scenarios (one of them comparing the ignition by firebrands and by flame propagation from a hedge) given the extended area damaged by the fire (Fig. 2).

3. Results and discussion

Post-fire surveys carried out in the four study cases showed a large range of damage from scorched vegetation to building destruction (Fig. 3).

Overall, the results of the modelling run on brush-cleared vegetation showed a fire behaviour less intense than when the fuel treatment was not implemented (Fig. 4), however, with a fire heat release similar during the first 10 to 20s (up to 40s in the case Château C2) according to the study case.

3.1. Griffon

Post-fire damage assessment : Only the windward house was severely burned and it sheltered the neighbouring house, which was undamaged (Fig. 3). The facade exposed to the fire was the most damaged (window with broken glass allowing the fire to impact the inside) mostly because the close by ornamental hedge acted as a vector for fire propagation. The southern hedge was burned by a surface fire fueled by the brush-clearing residues and spread the flame to the neighbouring ornamental shrubs located in the garden.

Modelling : During the first part, flames propagated further in the modality brush-cleared because the lower tree density (Fig. 5) and possibly because of the tilt angle between the flame and the slope located between the forest and the garden. Beyond 20s of simulation, the HIZ (and thus the ornamental vegetation) seems to be unaffected by the fire in this modality in contrast to the other scenario.

This study case allowed highlighting the importance of cleaning the residues after treatment. Indeed, the modality with brush-clearing, without vegetation residues, showed that the fire intensity would have been decreased avoiding the damage to the building.

3.2. Barnouins

Post-fire damage assessment : The fire propagated uphill in the brush-cleared garrigue towards the house (slope of ~50%), the damage was mostly due to a windward window that had been left open, allowing the firebands generated by the pine stand downhill to enter the building and set it on fire. A large part of the windward ornamental vegetation (located on the left of the house) was also impacted in contrast of the leeward side of the house (Fig. 3).

Modelling : Regarding the fire spread (Fig. 6), after the first 15s of simulation, the flames were more scattered in the modality with brush-clearing, especially at T0+50s and T0+65s and the tree canopy burned (higher tree mass loss), probably because of the low simulated FMC. Flux sensors located at different heights on the house windward facage, in both modalities, were quickly reached by the flames and intensities higher than 80kW m^{-2} were recorded, showing that the contribution of the vegetation, even brush cleared in this case, was significant (Fig. 7).

The heat sensor positioned the highest (13m) was strongly affected by the wind gusts. It is then possible that, even if the window had been closed, the combination between the steep slope and the strong wind could have provoked intensity to break the window pane allowing the fire propagation into the house and its destruction. With this combination of two important factors (terrain and wind), the limitation of the mandatory brush-clearing is reached, showing that the area treated should have been extended beyond the mandatory 50m.

3.3. Château

Post-fire damage assessment C1 : In this case, the fire propagated from the NNW to the SSE, first in an untreated wildland vegetation (pine stand) and reached the tall northern cypress hedge located to the South of the south-werstern building that completely burned.

Modelling : In the modality with brush-clearing, the fire propagated less intensely, limiting the spread on the flanks, therefore avoiding the cypress hedge and the other trees around the building (Fig. 8). This was due to

two main factors : i) a lower intensity in all of the vegetation strata in the modelling and ii) a stronger wind in the HIZ in the modality with brush-clearing because of the lower tree density. In contrast, in the modality without brush-clearing the hedge partially burned.

In this case, the scenario without brush-clearing underestimated the fire effects on the hedge which did not totally burned, despite the simulated low FMC, unless the ignition be provoked or enhanced by the firebrand shower generated by the burning pine stand (highly likely synergy). In contrast, in the modality with brush-clearing, the fire impact on the ornamental vegetation located East of the building was low, highlighting the importance of the mandatory fuel treatment.

Post-fire damage assessment C2 : In this case, the fire behaviour was assessed when the flame front reached the northern building. The tall pine (11m) located close to the building (overhanging the roof) completely burned participating to the building destruction.

Modelling : Beyond the first 40s of simulation in the modality with brush-clearing, the fire spread in the pine stand and in the brush-cleared area but with decreasing intensity when approaching the buildings. After 45s, the tall pine was reached by the fire in both modalities but more intensively (totally burned) in the modality without brush-clearing (Fig. 9) according to the post-fire damage assessment.

In this case, the impact of the fire on the pine was moderate highlighting once more the effect of the vegetation treatment, especially in the area submitted to the dominant wind, therefore to the fire.

Post-fire damage assessment C3 : In this case, three tall trees, a cedar, a palm tree, and a linden tree, located close to the southernmost building (and partially overhanging the roof) have been impacted by the fire (the two formers having mostly or totally burned while the latter was heavily scorched), participating to the building destruction.

Modelling : The simulation presenting the fire propagation due to firebrands showed that the fire could ignite the tree canopy and spread progressively towards the ground (Fig. 10), igniting then the lower branches and the vegetation close by. This was possible thanks to local wind currents of different directions generated by neighbouring obstacles (buildings, trees, etc.) during wind gusts (i.e. 11.7 m s^{-1}). This result was not observed in the post-fire survey, especially for the linden, possibly because the higher FMC than in the modelling.

The simulation presenting the fire propagation involving the cypress hedge located to the North (Fig. 11) showed that the tall cedar burned. The fire then reach the side of the building where the linden tree was located, but without succeeding in its ignition while, at 100s, the fire ignited the southern cypress hedge. According to the post fire damage recorded, the linden tree was less impacted than the cedar, even with a lower simulated FMC. However, the synergy with the firebrand shower is also probable.

4. Conclusions

This work consisted in implementing the CFD model FDS on three different study cases impacted by a past fire event and comparing the results to the post-fire damage recorded in the field for validation. For each case, two scenarios of vegetation management were tested (brush-clearing *vs* no brush-clearing). Simulations results could mostly be validated by the post-fire survey and underlined once more the relevance of the fuel reduction measures in terms of fire mitigation. In some cases, they highlighted the necessity to strengthen this regulation. This work also proved the functional capacities of the model used to assess the fire behaviour at the WUI scale despite the bias inherent to the model, mainly regarding the simulated FMC, which was lower than in the field. This hypothesis is common to all of the calculation codes (e.g. Swifft, WFDS, etc.) and cannot be by-passed in the current state of knowledge

5. Acknowledgements

This work was funded by the French Ministry of Environment (Ministère de la Transition Ecologique) and by the Interreg program Marittimo InterMed IT-FR Maritime.

6. References

Cohen J (2000) Preventing disaster: Home ignitability in the wildland-urban interface. Journal of Forestry 98(3): 15-21.

Cohen J (2008) The wildland-urban interface fire problem: A consequence of the fire exclusion paradigm. Forest History Today. Fall: 20-26.

De Gennaro M, Billaud Y, Pizzo Y, Garivait S, Loraud J-C, El Hajj M, Porterie B (2017) Real-time wildland fire spread modeling using tabulated flame properties. Fire Safety Journal 91, 872-881. doi: 10.1016/j.firesaf.2017.03.006.

Fernandez F., Guillaume B., Porterie B., Ganteaume A., Guerra F., 2018. Modelling fire spread and damage in wildland-urban interfaces. VIII International Conference on Forest Fire Research, Coimbra, Portugal, 12 - 16 Novembre 2018.

Fox D. M., Martin N., Carrega P., Andrieu J., Adnes C., Emsellem K. & Fox E. A. (2015), "Increases in fire risk due to warmer summer temperatures and wildland urban interface changes do not necessarily lead to more fires", Applied Geogra- phy 56, pp. 1-12.

Ganteaume A ,2018 Ornamental Vegetation, in: S. Manzello (Ed.), Encyclopedia of Wild- fires and Wildland-Urban Interface (WUI) Fires, Springer, Cham, 2018 .

Jones GM, Gutiérrez RJ, Tempel DJ, Whitmore SA, Berigan WJ, Peery MZ, 2016.Megafires: an emerging threat to old-forest species, Front. Ecol. Environ. 14 300–306, doi: 10.1002/FEE.1298 .

Maditinos Z, Vassiliadis C, Mega fires: can they be managed effectively? Disaster Prevent. Manage. 20 (2011) 41–52, doi: 10.1108/09653561111111072 .

McGrattan K, Hostikka S, McDermott R, Floyd J, Weinschenk C, Overholt K (2013) Fire Dynamics Simulator user's guide. National Institute of Standards and Technology, Technical Report NIST Special Publication 1019–6. (Gaithersburg, MD, USA)

Mell W, Jenkins MA, Gould J, Cheney P (2007) A physics based approach to modeling grassland fires. 2007. International Journal of Wildland fire. 16(1): 1-22.

Mell W., Maranghides A., McDermott R., and Manzello S.L. (2009) Numerical simulation and experiments of burning douglas fire trees, Combustion and Flame, vol. 156, no. 10, pp. 2023–2041.

Mell, W.; Jenkins, M.A.; Gould, J.; Cheney, P. 2007 A physics based approach to modeling grassland fires. 2007. International Journal of Wildland fire. 16(1): 1-22

Morandini, F.; Santoni, P.A.; Tramoni, J.B.; Mell, W.E. 2019. Experimental investigation of flammability and numerical study of combustion of shrub of rockrose under severe drought conditions. Fire Safety Journal. 108: 102836

Perez-Ramirez Y, Mell WE, Santoni PA, Tramoni J-B, Bosseur F (2017) Examination of WFDS in modeling spreading fires in a furniture calorimeter. Fire Technology 53(5), 1795–1832. doi:10.1007/s10694-017-0657-z

Sullivan A (2009) Wildland surface fire spread modelling, 1990–2007. 1: Physical and quasi-physical models. International Journal of Wildland Fire. 18. 349-368. 10.1071/WF06143.

Syphard A. D., Rustigian-Romsos H., Mann M., Conlisk E., Moritz M. A. & Ackerly D. (2019), "The relative influence of climate and housing development on current and projected future fire patterns and structure loss across three California land- scapes", Global Environmental Change 56, pp. 41-55.

Vanella M, McGrattan K, McDermott R, Forney G, Mell W, Gissi E, Fiorucci P. A (2021) Multi-Fidelity Framework for Wildland Fire Behavior Simulations over Complex Terrain. Atmosphere. 12(2):273.

Table 1 - Characteristics of the three study cases. Wind direction is given according to the World Meteorological Organisation.

Study case	**Wind/Fire direction (°)**	**Topography between building and natural vegetation**	**Type of vegetation outside HIZ**	**Mandatory brush-clearing (legal fuel management : 50m-buffer around the building)**	**Damage**
Griffon (Rognac fire 2016)	300	Slope	*Quercus pubescent* stand, understorey, grass	Yes but vegetation treated left on site resulting in a modality equivalent to a lack of brush-clearing (high amount of dead fuel)	Partial damage to the building and to ornamental vegetation
Barnouins (Rognac fire 2016)	345	Slope	*Quercus coccifera* shrubland and *pinus halepensis* stand, grass	Yes	Building destroyed and ornamental vegetation mostly burned
Château (Rognac fire 2016)	350	Flat	*Pinus halepensis* stand, shrubland, grass	Not implemented windward	Building destroyed and ornamental vegetation burned or scorched

FIGURES

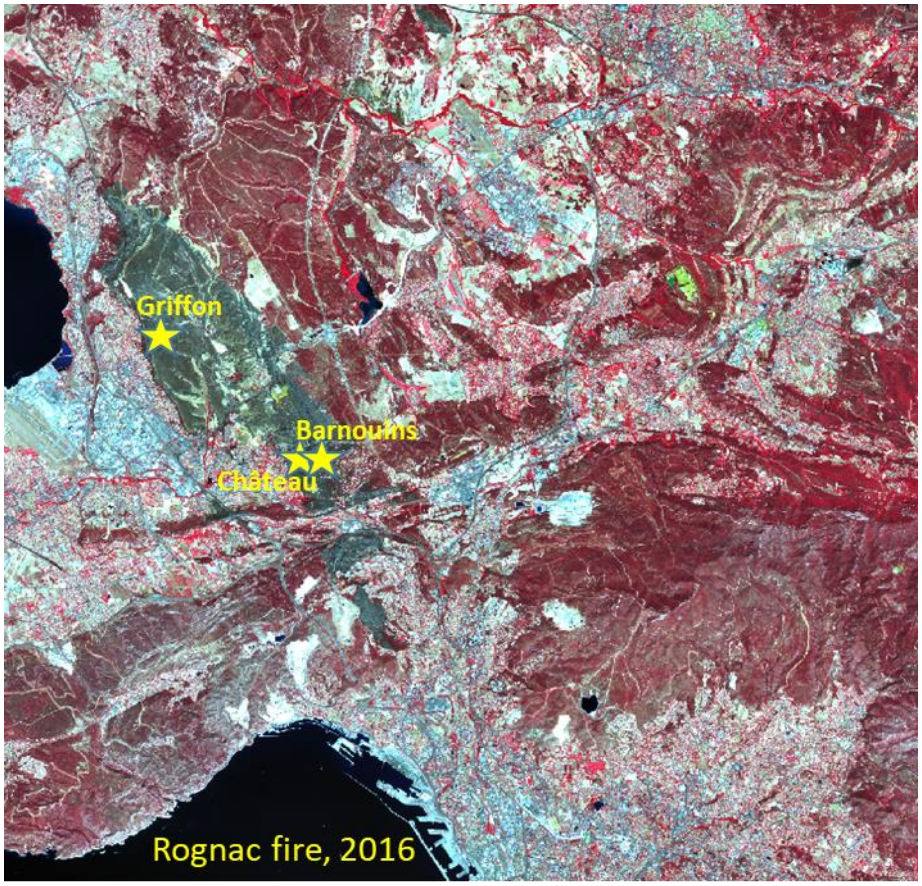

Figure 1 - Near Infra Red aerial imageries of the Rognac fire and locations of the three study cases.

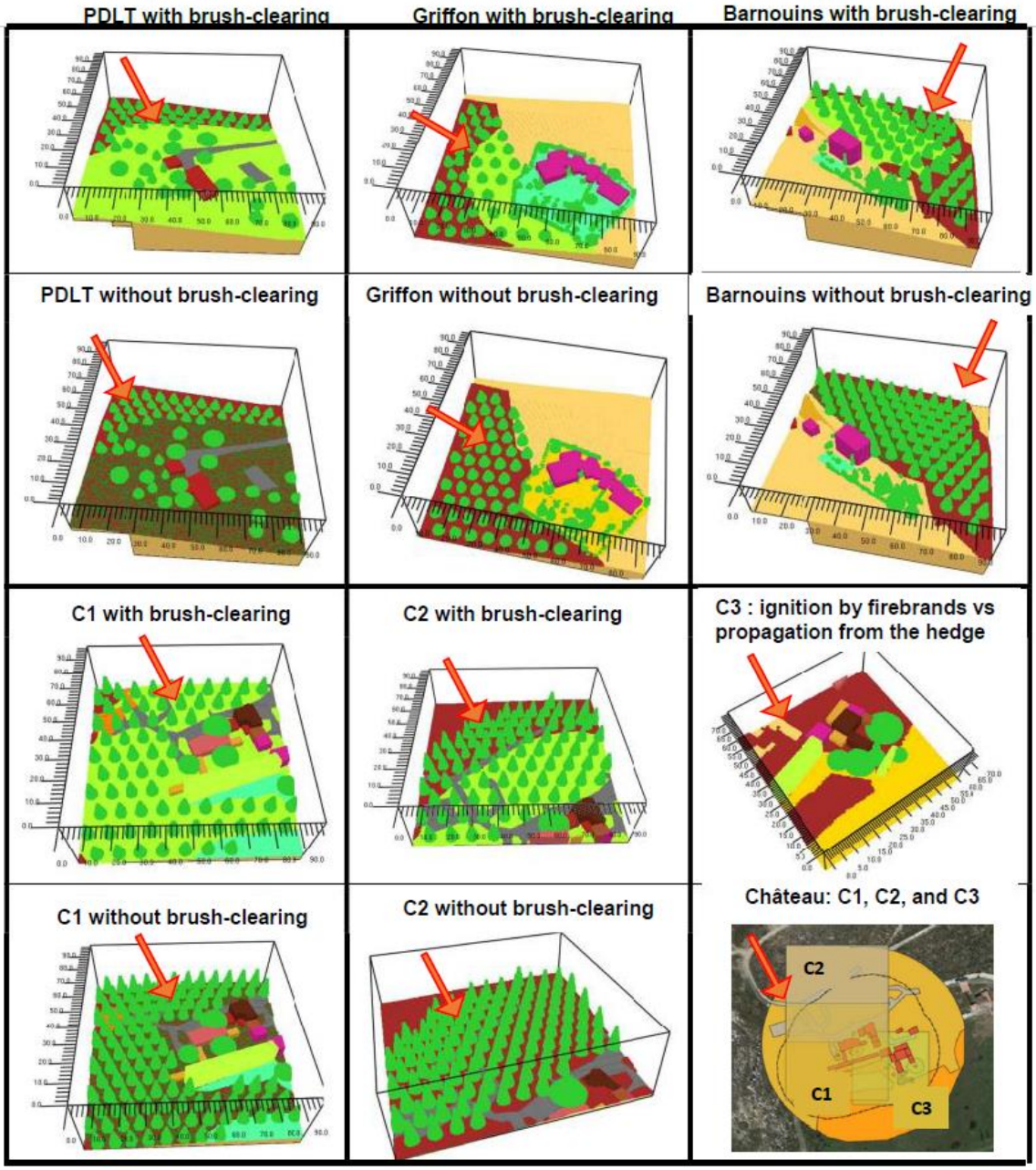

Figure 2 - The different configurations (with or without brush-clearing) of the 4 study cases (PDLT : Plan de la Tour) used in the modelling. The arrow shows the fire direction.

Figure 3 – Pictures of the post-fire damage recorded in the three study cases.

Figure 4 - Temporal evolution of the power released by the fire in the entire simulation domain (« Château C1 ») according to the fuel treatment.

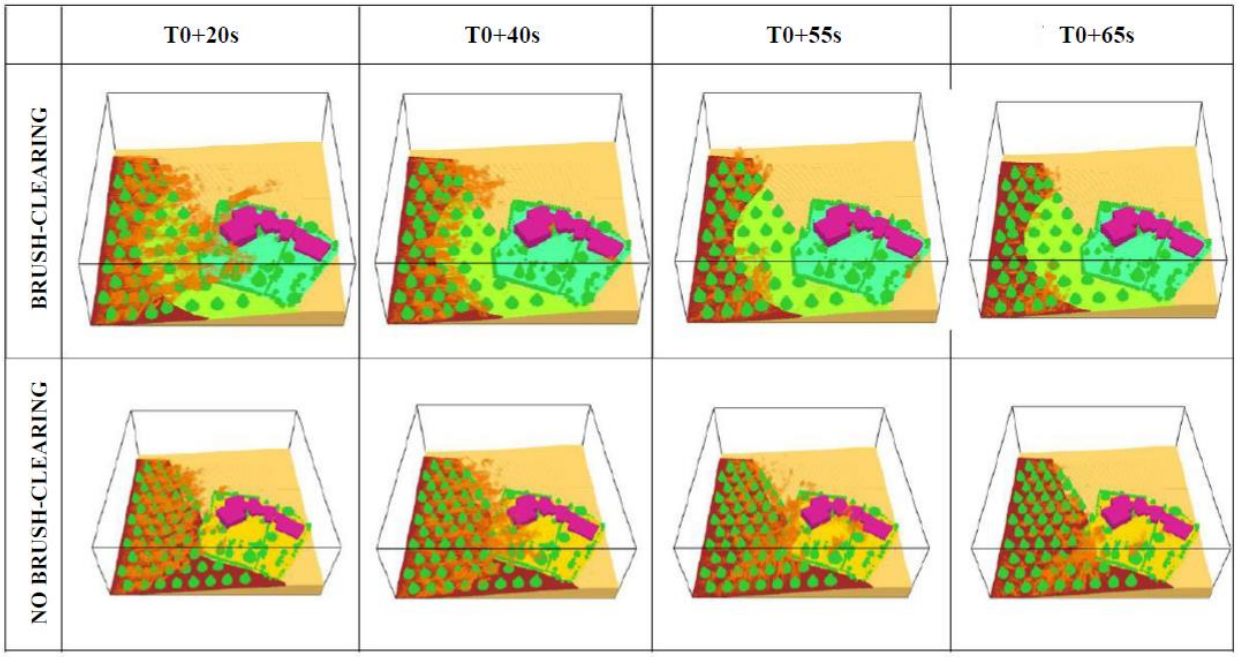

Figure 5 - Temporal evolution of the simulated flame front (« Griffon ») according to the fuel treatment.

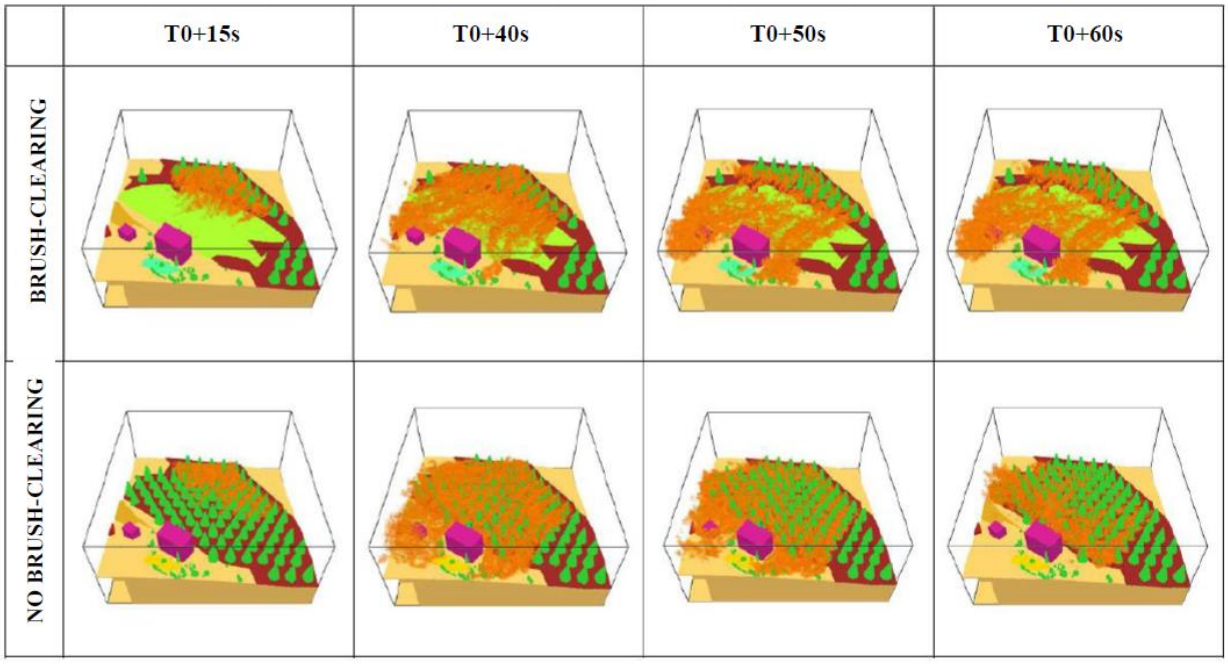

Figure 6 - Temporal evolution of the simulated flame front (« Barnouins ») according to the fuel treatment.

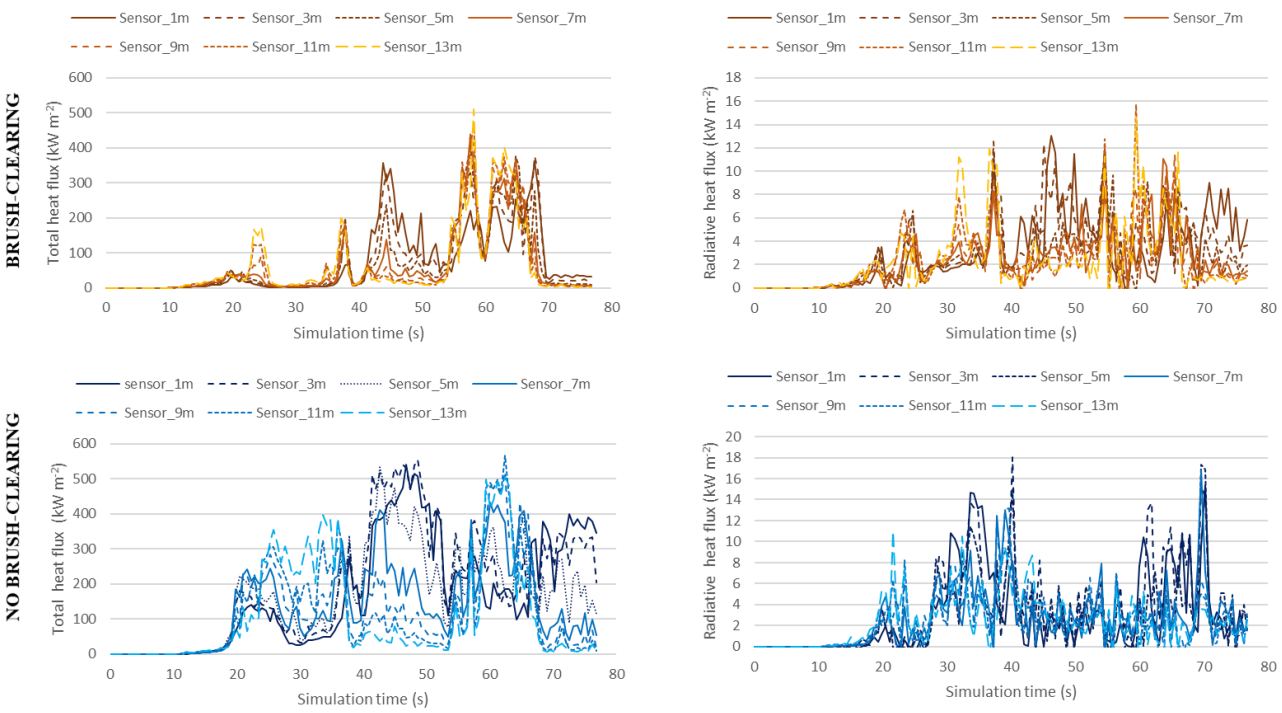

Figure 7 - Temporal evolution of the simulated heat flux (total and radiative) recorded by flux sensors located at different heights on the side of the house (« Barnouins ») exposed to the flame front according to the fuel treatment.

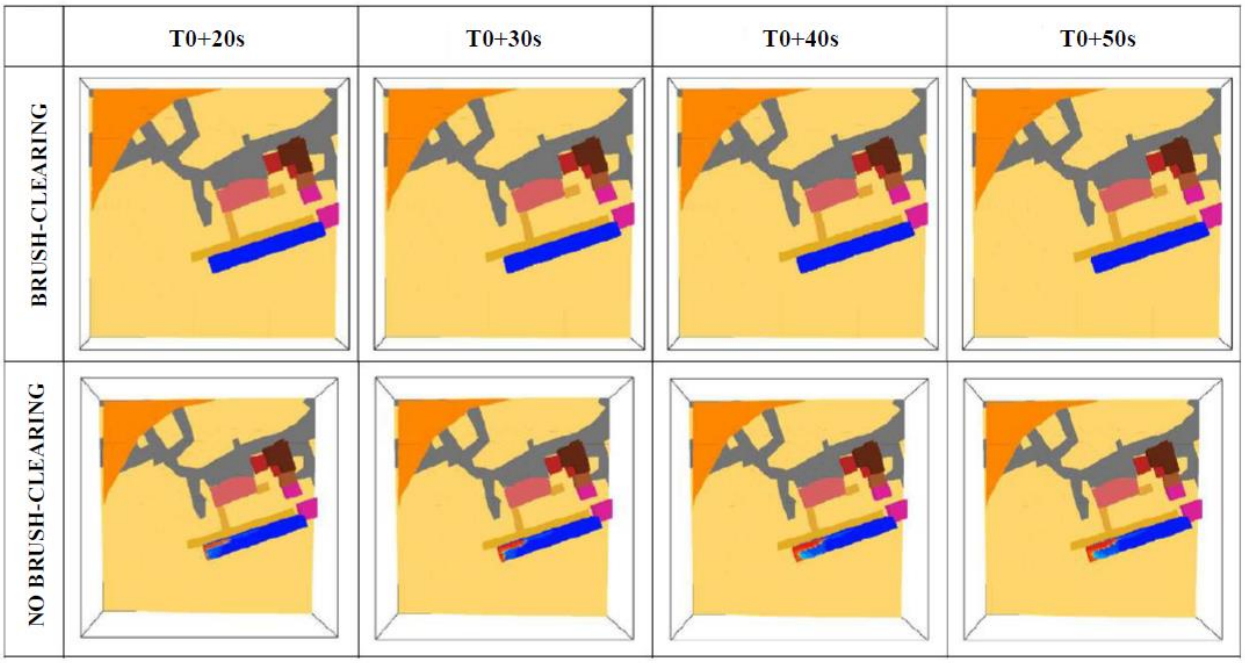

Figure 8 - Temporal evolution of the simulated mass loss of the northern cypress hedge (« Château C1 ») according to the fuel treatment (Colors ranging from blue to red: initial to totally burned fuel mass).

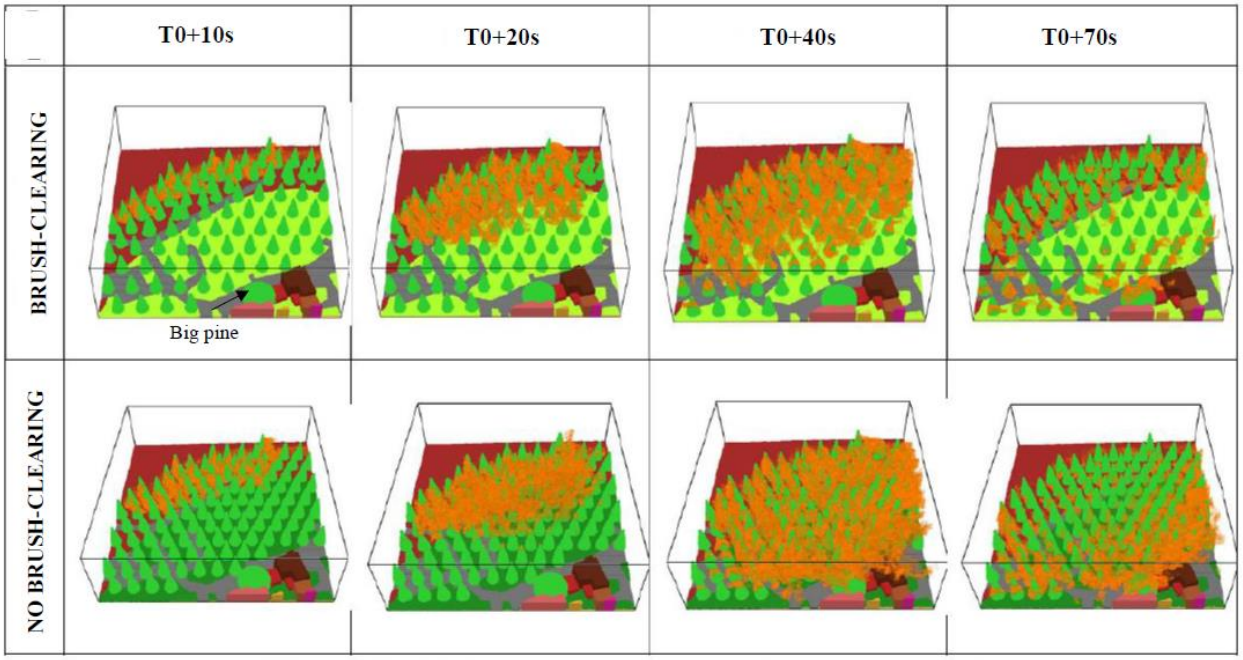

Figure 9 - Temporal evolution of the simulated flame front (« Château C2 ») according to the fuel treatment.

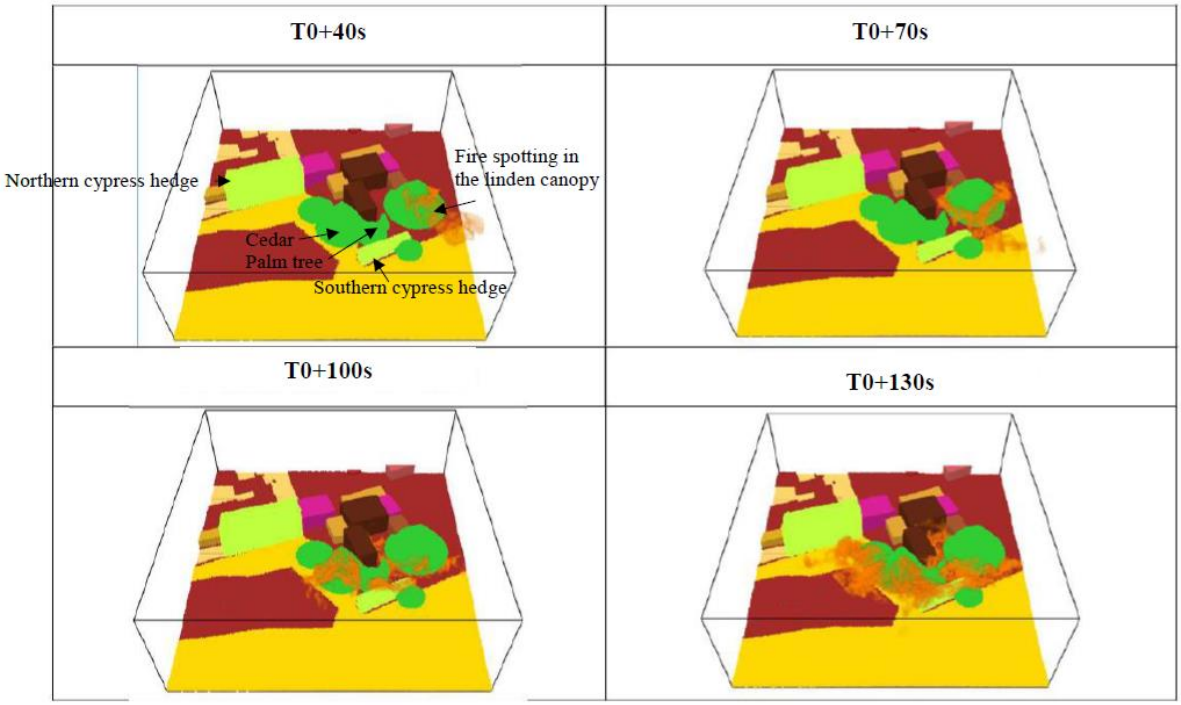

Figure 10 - Temporal evolution of the simulated flame propagation after ignition by fire spotting of the linden canopy (« Château C3 »).

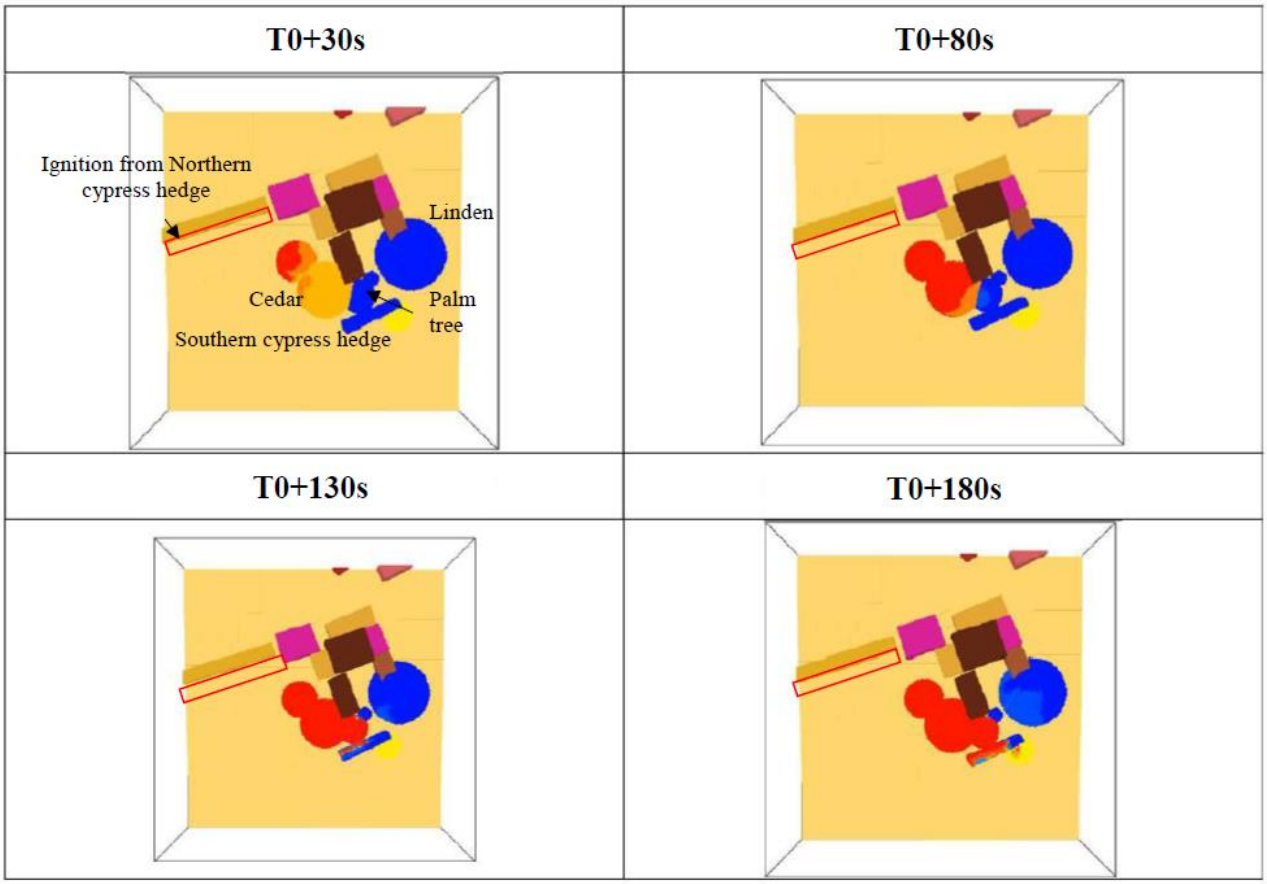

Figure 11 - Temporal evolution of the simulated mass loss of the ornamental vegetation ignited by the burning northern cypress hedge (« Château C3 ». Colors ranging from blue to red: initial to totally burned fuel mass)

.

Implementation of "Safe Villages" settlements with surrounding areas of high hazard to wildfire: Outlook from the Algarve Region

Ana Gonçalves*[1]; Sandra Oliveira1; José Luís Zêzere[1]

[1]Centro de Estudos Geográficos, Instituto de Geografia e Ordenamento do Território, Universidade de Lisboa, Lisboa, Portugal; Laboratório Associado TERRA, {acng, sandra.oliveira1, zezere}@campus.ul.pt

**Corresponding author*

Keywords

Safe village; Safe people; Hazard; Algarve; Wildfires

Abstract

Wildfires in Portugal are increasingly putting the population and existing assets at risk. In the aftermath of the fires of 2017, there was a renovated concern to increase the protection of settlements and the self-protection abilities of the population; as such, several initiatives were developed with the aim of increasing the resilience and safety of communities. This study analyzes the implementation of the "Safe Village and Safe People" program, created by the National Emergency and Civil Protection Authority, in the municipalities of the Algarve region, taking into account its spatial distribution and the relationship with hazard levels in the immediate surroundings of settlements (100 m). It also aims to analyze whether this program can be combined with other ongoing initiatives associated with fuel management and landscape transformation in the area surrounding the settlements. For this, a database was created with the location of the Safe Villages already implemented in the Algarve region, with the geographic coordinates defined by a point that intersects the village. This point was then spatially joined with the polygon of the matching built-up area, retrieved from the cartography of Built-up Areas of Portugal, to obtain the boundaries of the villages and delimit the 100 m buffer around. Then, the total hazardous area (of high and very high wildfire hazard) in the 100 m buffer around each Safe Village was retrieved. Finally, the hazardous area around the Safe Villages was analysed in relation to the total hazardous area around all the settlements of the region, to assess the adequacy of "Safe Villages" location with regard to hazard levels for the whole region. Results show that 135 Safe Villages are implemented in 9 municipalities of Algarve. Around 6.6% of the 100 m area surrounding all the settlements in the region presents high and very high hazard. The municipalities of Monchique and Aljezur have the largest hazardous area in the surrounding 100m of all their settlements (61.96% and 20.86%, respectively). When analyzing the implementation of Safe Villages program, the ones implemented in the municipality of Alcoutim cover a greater percentage of surrounding hazardous area (58.08%) in relation to the total. The efficiency of this program and, therefore, the protection of local communities, can be improved by selecting the villages with higher hazardous area around and by combining its implementation with different programs that focus on fuel management that promotes hazard reduction, such as the "Condominium of Villages", created by the Directorate General of the Territory.

1. Introduction

In the last decades, wildfires in Portugal have been increasing significantly, either by the high extent of burned area or by the high material damage and human losses they have caused (Bergonse et al., 2021; Gonçalves et al., 2021; Nunes et al., 2016; Oliveira et al., 2020; Vilar et al., 2016). These events put at risk local rural communities as well as urban areas, which increasingly expand into the wildland-urban interface (Tonini et al., 2018). Since the 1980s, these problems have been rising, essentially due to the rural exodus and farmland abandonment, with the subsequent accumulation of fuels in the areas surrounding settlements (areas that were once occupied by agriculture will now be covered by shrubland and/or forest) and the aging population that remains in rural communities (Ferreira-Leite et al., 2013; Nunes et al., 2016). All these factors increase the susceptibility to wildfires in these areas and increase the exposure of people, assets and natural areas (Ager et al., 2013; Gallardo et al., 2016; Vieira et al., 2009). The year 2017 was the most devastating to date in Portugal, with the largest recorded burned area (~ 500 000 ha) and more than hundred fatalities in the June and October fires (Comissão Técnica Independente, 2018; Instituto da Conservação da Natureza e das Florestas, 2017). These events renovated the need to improve the protection of human communities and to increase the coping capacity of the population (Alcasena et al., 2019; Costafreda-Aumedes et al., 2017; Gonçalves et al., 2021;

O'Connor et al., 2016; Oliveira et al., 2020; Palaiologou et al., 2019). Since then, several initiatives have been developed in Portugal to deal with these challenges; one such measure is the Safe Village Safe People program, initiated in 2018 and coordinated by the National Emergency and Civil Protection Authority (ANEPC). This program aims at creating structural measures for the protection of people and assets located in rural villages or in the wildland-urban interface, through the implementation of strategic infrastructures, the identification of critical points and places of shelter and refuge or the creation of evacuation routes. For a settlement to be classified as a "safe village", it must have implemented several measures, among which:

a) prevention of risky behaviour, by developing awareness actions to reduce the number of ignitions caused by anthropogenic actions;

b) awareness of the population about wildfire risk levels and self-protection practices they should adopt, by organizing fire drills in coordination with local authorities;

c) creating evacuation plans for when a fire is approaching the village;

d) creation of shelter and places of refuge able to protect the population during the passage of the fire, in cases where it is the most viable option (Autoridade Nacional de Proteção Civil, 2018).

By implementing these strategies at the local level, it is intended to increase the self-protection capacity of the population and mitigate the consequences of large wildfires. This is especially important in a context of climate change, where fires will be more frequent and severe (Ager et al., 2014; Birkmann et al., 2013; Dupuy et al., 2020; Marques et al., 2011; Moreira et al., 2010). The objective of this study was to analyze the implementation of the "Safe Village Safe People" program, considering the spatial distribution and the relationship with the level of wildfire hazard in the surrounding area, specifically in the 100m protection area around settlements (defined by Decree Law No. 82/2021, October 13). With this analysis, it is also possible to analyse whether the "Safe Village Safe People" program can be aligned with other initiatives, associated with fuel management and landscape transformation in the surrounding area of villages, such as the " Condominium of Villages" program, coordinated by the Directorate General of Territory (DGT). The implementation of several programs in an integrated manner, which concur to the same objective of wildfire mitigation and communities' protection, can promote a more efficient management of resources and increase the effectiveness of the implemented strategies.

2. Methods

2.1. Study area

The analysis of Safe Villages was carried out for the municipalities of the Algarve region (NUTS III) (figure 1). The Algarve region has an area of 4 996 km^2 and is composed of 16 municipalities. Regarding land use and occupation, 63.02% of the Algarve region corresponds to forest and shrubland and 23.31% to agriculture and pasture. In terms of hazard, 30.65% of the region is at high and very high hazard of fire. According to the provisional results of the 2021 Census, the Algarve has 467,475 inhabitants, showing a positive variation of 3.7% compared to 2011. Monchique is the municipality with the most significant hazard level as 90.74% of its area falls into high or very high hazard while Lagoa records the lowest percentage (1.27%). The municipality of Monchique with the highest percentage of forest and shrubland (91.96%) and the one with the lowest percentage is Faro (17.79%). Over the last decade, Vila do Bispo recorded the highest population growth (+8.7%) while Alcoutim recorded a significant population loss in the same period (-13.5%).

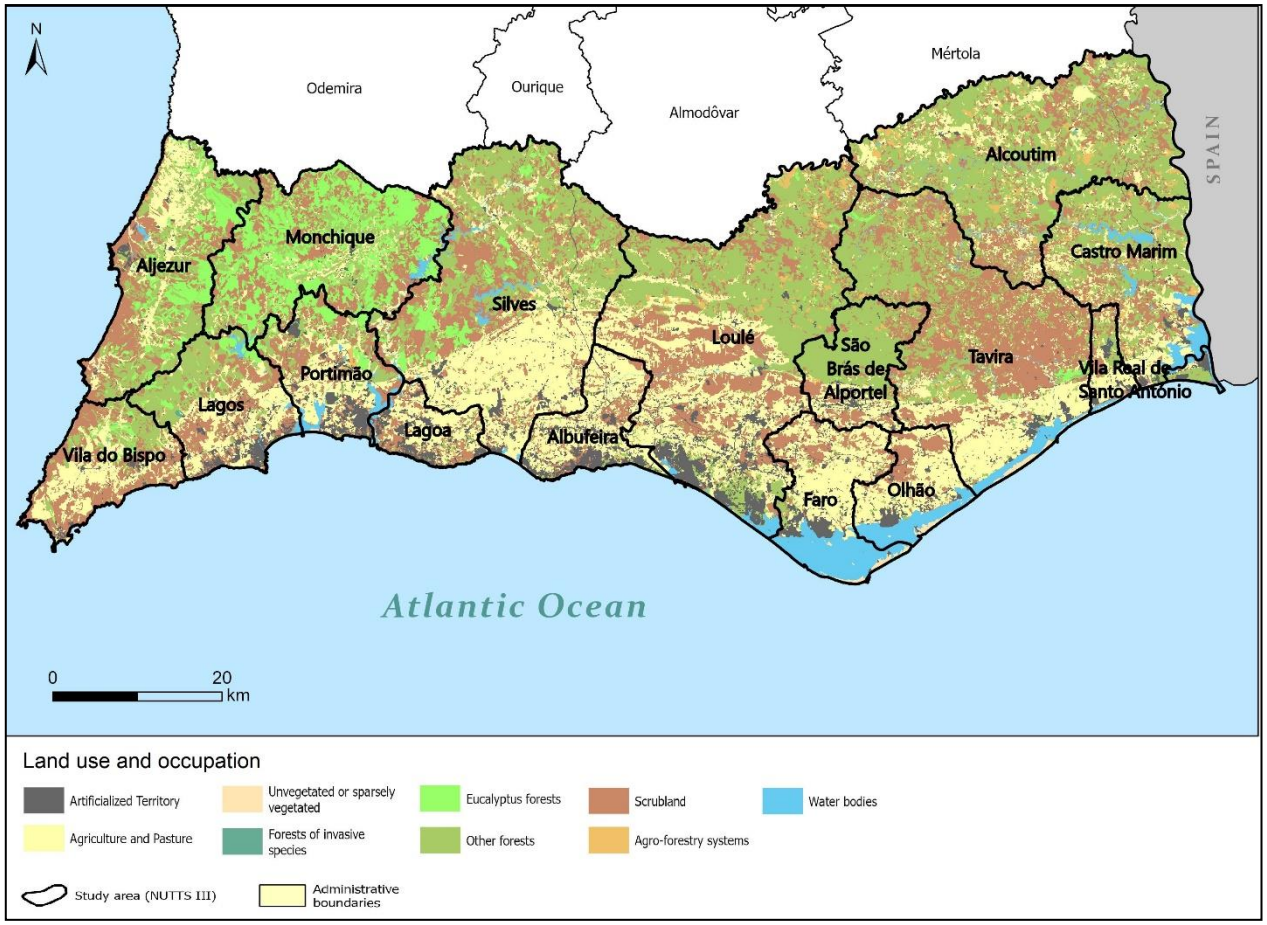

Figura 1 - Geographical setting and hazard level of the study area (Source: ICNF, 2020)

2.2. Data collection and processing

For this analysis, a database was first built with the location of the safe villages already implemented in the Algarve region. For this task, the geographic coordinates of a point that intersects the settlements designated as safe villages were retrieved from the website of the program "Safe Villages"[6] . To obtain the boundaries of the settlements, the built areas made available by the DGT were taken, mapped from the artificialized classes of the 2018 Land Use and Occupation (COS2018) combined with the geographic base of classic residential buildings of the National Statistics Institute (INE) (2011). Although a settlement is generally defined as a group of 10 or more residential buildings (Instituto Nacional de Estatística, 2001), this database of built-up areas includes several typologies: type 1 concentrated settlement (settlements with 10 or more residential buildings); type 2 dispersed settlement (isolated houses or places with less than 10 residential buildings); type 3 non-residential areas. For this analysis, all non-residential areas (type 3) and all isolated houses defined as type 2 were excluded, keeping the dispersed settlement that corresponds to at least 2 residential buildings. This option is connected to the application of fuel management areas (FGC) of 100 m around a settlement, since in the cases of isolated houses the FGC defined by law are of 50m. The definition of the FGC for the protection of settlements around built areas was accomplished by creating a 100 m buffer in the surroundings, using *ArcGIS tools*. Then, the area of high and very high hazard existing in these surrounding buffers was calculated, being considered the most critical or priority area. The hazard layer corresponds to the structural assessment of wildfire hazard levels for 2020-2030, based on probability from historical burned area and susceptibility resulting from landcover and topography (Oliveira et al., 2020) and it was obtained from the Institute for Nature Conservation and Forests (ICNF). The following step was to calculate the proportion of critical area (high and very high hazard) in the

[6] https://aldeiasseguras.pt/aldeias-seguras/)

buffer zones around the safe villages, in relation to the critical area within all buffer zones in the settlements of the municipality.

3. Results and Discussion

In Algarve the high and very high hazard levels cover 6.6% of the 100 m buffers around the built-up areas of the region, which are composed of 8060 individual polygons. In these polygons, 25% have high or very high hazard area in the surrounding 100 m buffer. In these settlements with hazardous surrounding area, 22% have more than 50% of critical area in their buffer.

Up to 2021, 135 safe villages were implemented (figure 2), in 9 municipalities (table 1). These villages (SV), cover 6.7% of the critical area around the settlements where hazardous levels are found.

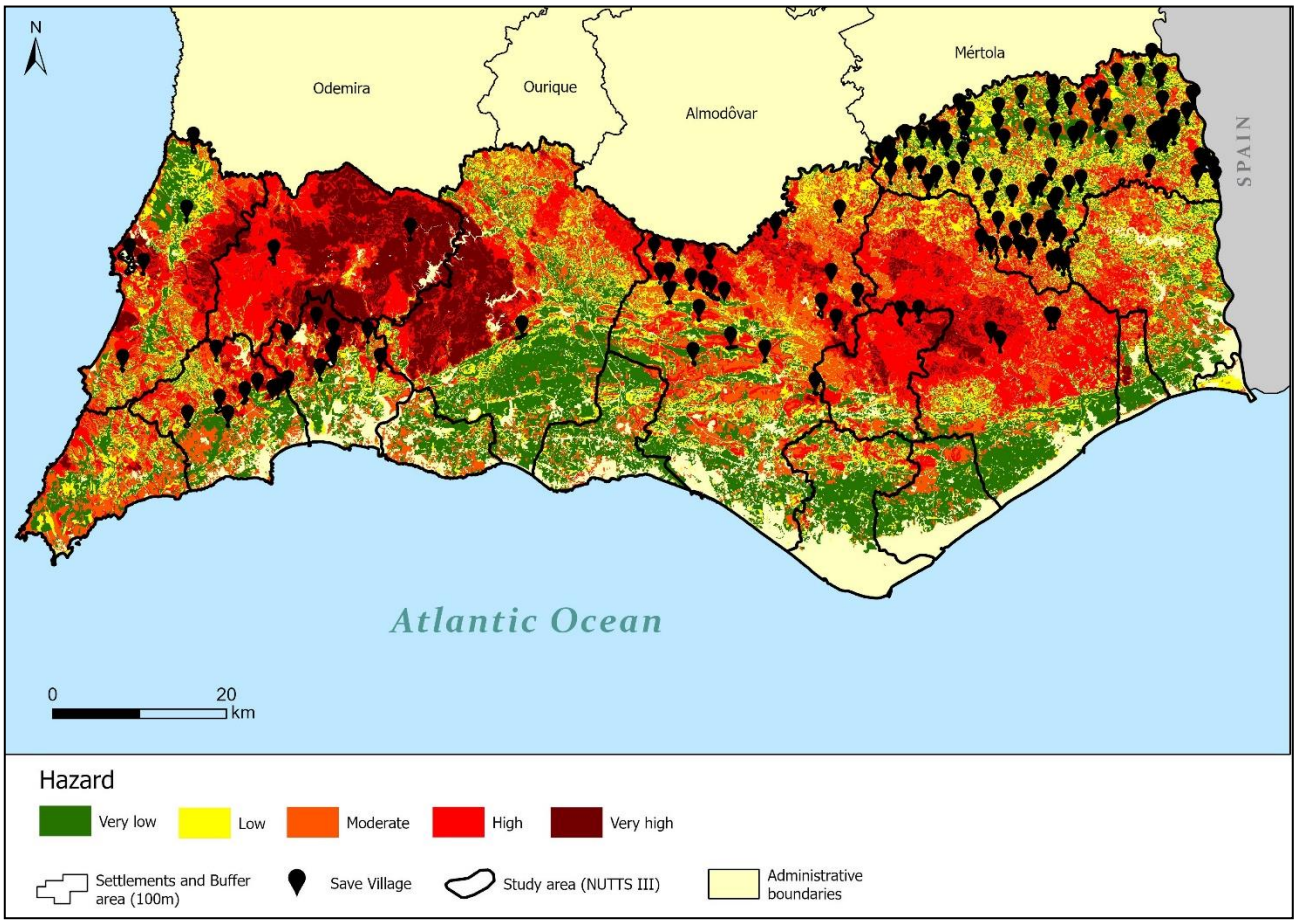

Figure 2 - Location of Safe Villages and wildfire hazard levels in the Algarve region

Overall, Monchique has the highest percentage of critical area in the surrounding 100m of its settlements (61.9%), followed by far by Aljezur (20.9%) (figure 3). However, the municipality of Alcoutim and Aljezur (figure 3a) are the ones where the SV implemented cover a higher percentage of critical area around (58.1% and 32.7%, respectively). The SV in Monchique cover 2.2% of the hazardous area around its settlements. These results suggest that the implementation of SV is done in view of conditions other than the hazard levels around the settlements. Alcoutim, for example, shows a low amount of critical area surrounding the settlements (<1%), but it is the municipality with more SV, whose implementation has covered nearly 60% of the critical area. It should also be noted that the 100m buffer here considered may not suffice to protect a settlement in case of large fires, nor match the size of the wildland-urban interface that should be considered in wildfire management strategies (Sirca et al., 2017).

Table 1 - Percentage of critical areas in implemented Safe Villages

Municipalities	% high and very high hazard in the FGC of SV (with total FGC of settlements)	% high and very high hazard in total FGC of settlements	Number of Safe Villages	% of Safe Villages
Albufeira	0	1.98	0	0
Alcoutim	58.08	0.86	84	62.22
Aljezur	32.69	20.86	5	3.70
Castro Marim	0	2.21	0	0
Faro	0	4.18	0	0
Lagoa	0	1.50	0	0
Lagos	4.16	3.59	7	5.19
Loulé	12	4.12	20	14.81
Monchique	2.28	61.96	2	1.48
Olhão	0	0.52	0	0
Portimão	3.29	5.47	8	5.93
São Brás de Alportel	11.32	13.57	2	1.48
Silves	5	3.28	1	0.74
Tavira	2.09	13.27	6	4.44
Vila do Bispo	0	6.92	0	0
Vila Real de Santo António	0	1.17	0	0

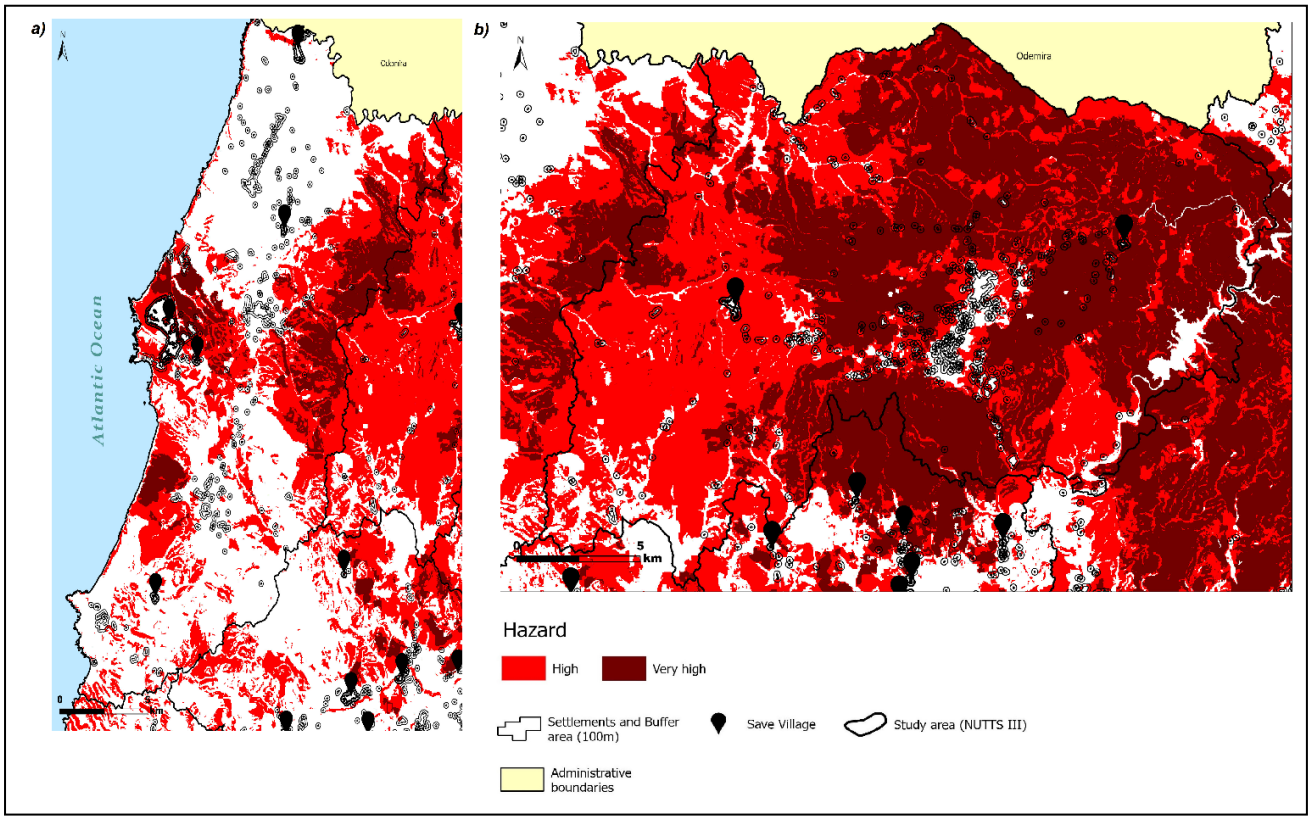

Figura 3 - Safe Villages and critical areas in the municipality of Aljezur (a) and Monchique (b)

To accelerate the implementation of protection measures around human settlements, the connection and integrated application of different but complementary initiatives can be helpful. One example is the

"Condominium of Villages", a program created by the DGT in 2020 that is directed towards fuel management around settlements. Its main purpose is to support actions aimed at changing landcover-landuse and promoting fuel management around built areas, to improve the resilience of vulnerable villages, particularly those located in parishes with at least 40% of critical area in their territory.

The articulation of measures will enable a better definition of priorities, namely in the the location of safe villages, but also a better implementation of fuel management around the village. Although this interconnection is important, at this moment the implementation of the "safe village" program does not depend only on the physical factors of the territory, but also on the involvement of the resident population, namely the existence of a volunteer to be a Safety Officer in the settlement. This officer must also have knowledge of the geographic and social context and of existing structures at the local level. If we consider demographic aging and rural exodus, especially in the inner part of the country, it is challenging to designate a Security Officer, since many villages only have elderly residents, who do not have the required profile to assume this role.

4. Conclusions

In the ideal scenario, all settlements should be Safe Villages. The creation of different initiatives in Portugal should increasingly allow an interconnection in the implementation of measures that contribute to the protection of people and assets. That said, a main objective must be a better articulation between entities and local communities, for the application of this type of programs. This becomes even more pertinent in a context of climate change, which can increase the frequency and magnitude of wildfire events, but also in a context of sociodemographic changes that increase the vulnerability of territories, thus making it necessary to have a better definition of mitigation and prevention strategies for wildfires.

5. Acknowledgments

Ana Gonçalves was supported by FCT in the scope of her PhD dissertation *"The influence of land use transition and socio-demographic dynamics in the evolution of fire risk in Portugal"*. [2020.07651.BD]. Sandra Oliveira was funded through FCT, I.P., under the programme of 'Stimulus of Scientific Employment—Individual Support' within the contract '2020.03873.CEECIND'.

6. References

Ager, A. ., Buonopane, M., Reger, A., & Finney, M. A. (2013). Wildfire exposure analysis on the national forests in the pacific northwest, USA. Risk Analysis, 33(6), 1000–1020. https://doi.org/10.1111/j.1539-6924.2012.01911.x

Ager, A. ., Preisler, H. K., Arca, B., Spano, D., & Salis, M. (2014). Wildfire risk estimation in the Mediterranean area. Environmetrics, 25(6), 384–396. https://doi.org/10.1002/env.2269

Alcasena, F., Ager, A. ., Bailey, J., Pineda, N., & Vega-García, C. (2019). Towards a comprehensive wildfire management strategy for Mediterranean areas: Framework development and implementation in Catalonia, Spain. Journal of Environmental Management, 231, 303–320. https://doi.org/10.1016/j.jenvman.2018.10.027

Autoridade Nacional de Proteção Civil. (2018). Aldeia Segura, Pessoas Seguras - Guia de Apoio à Implementação. https://aldeiasseguras.pt/wp-content/uploads/2020/05/Guia-de-Apoio-a-Implementacao.pdf

Bergonse, R., Oliveira, S., Gonçalves, A., Nunes, S., Camara, C., & Zêzere, J. L. (2021). Predicting burnt areas during the summer season in Portugal by combining wildfire susceptibility and spring meteorological conditions. Geomatics, Natural Hazards and Risk, 12(1), 1039–1057. https://doi.org/10.1080/19475705.2021.1909664

Birkmann, J., Cardona, O., Carreño, M., Barbat, A., Pelling, M., Schneiderbauer, S., Kienberger, S., Keiler, M., Alexander, D., Zeil, P., & Welle, T. (2013). Framing vulnerability, risk and societal responses: The MOVE framework. Natural Hazards, 67(2), 193–211. https://doi.org/10.1007/s11069-013-0558-5

Costafreda-Aumedes, S., Comas, C., & Vega-Garcia, C. (2017). Human-caused fire occurrence modelling in perspective: A review. International Journal of Wildland Fire, 26, 983–998. https://doi.org/10.1071/WF17026

Dupuy, J. luc, Fargeon, H., Martin-StPaul, N., Pimont, F., Ruffault, J., Guijarro, M., Hernando, C., Madrigal, J., & Fernandes, P. (2020). Climate change impact on future wildfire danger and activity in southern Europe: a review. Annals of Forest Science, 77(2). https://doi.org/10.1007/s13595-020-00933-5

Ferreira-Leite, F., Bento-Gonçalves, A., Lourenço, L., Úbeda, X., & Vieira, A. (2013). Grandes Incêndios Florestais em Portugal Continental como resultado das perturbações nos regimes de fogo no mundo Mediterrâneo. Silva Lusitana, 9(Especial), 129–144. http://www.scielo.gpeari.mctes.pt/pdf/slu/v21nEspecial/v21a09.pdf%5Cnhttp://hdl.handle.net/1822/25046

Gallardo, M., Gómez, I., Vilar, L., Martínez-Vega, J., & Martín, M. P. (2016). Impacts of future land use/land cover on wildfire occurrence in the Madrid region (Spain). Regional Environmental Change, 16(4), 1047–1061. https://doi.org/10.1007/s10113-015-0819-9

Gonçalves, A., Oliveira, S., Sá, A., Benali, A., Zêzere, J. L., & Pereira, J. M. (2021). Avaliação da Exposição das Comunidades Locais a Incêndios Florestais. O caso de Alvares, Góis. Finisterra, 56(117), 29–53. https://doi.org/10.18055/Finis19277

Independente, C. T. (2018). Avaliação dos incêndios ocorridos entre 14 e 16 de outubro de 2017 em Portugal Continental.

Instituto da Conservação da Natureza e das Florestas. (2017). 10o Relatório Provisório de Incêndios Florestais. 3–19. http://www2.icnf.pt/portal/florestas/dfci/Resource/doc/rel/2017/10-rel-prov-1jan-31out-2017.pdf

Instituto Nacional de Estatística. (2001). BGRI - Base Geográfica de Referenciação de Informação informação. Revista de Estudos Regionais - Região de Lisboa e Vale Do Tejo, 67–73.

Marques, S., Borges, J. G., Garcia-Gonzalo, J., Moreira, F., Carreiras, J. M. B., Oliveira, M. M., Cantarinha, A., Botequim, B., & Pereira, J. M. (2011). Characterization of wildfires in Portugal. European Journal of Forest Research, 130(5), 775–784. https://doi.org/10.1007/s10342-010-0470-4

Moreira, F., Catry, F., Rego, F., & Bacao, F. (2010). Size-dependent pattern of wildfire ignitions in Portugal: when do ignitions turn into big fires? Landscape Ecol, 25, 1405–1417. https://doi.org/10.1007/s10980-010-9491-0

Nunes, A. N., Lourenço, L., & Meira, A. C. C. (2016). Exploring spatial patterns and drivers of forest fires in Portugal (1980–2014). Science of the Total Environment, 573, 1190–1202. https://doi.org/10.1016/j.scitotenv.2016.03.121

O'Connor, C., Thompson, M., & Rodríguez y Silva, F. (2016). Getting Ahead of the Wildfire Problem: Quantifying and Mapping Management Challenges and Opportunities. Geosciences, 6(3), 35. https://doi.org/10.3390/geosciences6030035

Oliveira, S., Gonçalves, A., & Zêzere, J. L. (2020). Reassessing wildfire susceptibility and hazard for mainland Portugal. Science of the Total Environment, 1–16. https://doi.org/10.1016/j.scitotenv.2020.143121

Oliveira, S., Gonçalves, A., Benali, A., Sá, A., Zêzere, J. L., & Pereira, J. M. (2020). Assessing risk and prioritizing safety interventions in human settlements affected by large wildfires. Forests, 11(8). https://doi.org/10.3390/F11080859

Palaiologou, P., Ager, A. ., Nielsen-Pincus, M., Evers, C. R., & Day, M. A. (2019). Social vulnerability to large wildfires in the western USA. Landscape and Urban Planning, 189, 99–116. https://doi.org/10.1016/j.landurbplan.2019.04.006

Sirca, C., Casula, F., Bouillon, C., García, B. F., Ramiro, M. M. F., Molina, B. V., & Spano, D. (2017). A wildfire risk oriented GIS tool for mapping Rural-Urban Interfaces. Environmental modelling & software, 94, 36-47.

Tonini, M., Parente, J., & Pereira, M. (2018). Global assessment of rural-urban interface in Portugal related to land cover changes. Natural Hazards and Earth System Sciences, 18(6), 1647–1664. https://doi.org/10.5194/nhess-18-1647-2018

Vieira, A., António Bento, G., Lourenço, L., Martins, C., & Leite, F. (2009). Risco de incêndio florestal em áreas de interface urbano-rural : o exemplo do Ave. Territorium, 16, 139–146. https://doi.org/:http://dx.doi.org/10.14195/1647-7723_16_13

Vilar, L., Camia, A., San-Miguel-Ayanz, J., & Martín, M. P. (2016). Modeling temporal changes in human-caused wildfires in Mediterranean Europe based on Land Use-Land Cover interfaces. Forest Ecology and Management, 378, 68–78. https://doi.org/10.1016/j.foreco.2016.07.020

Intermittent fireline behavior over porous vegetative media in different crossflow conditions

Abhinandan Singh*; Reza M. Ziazi; Albert Simeoni

Department of Fire Protection Engineering, Worcester Polytechnic Institute, Worcester, MA, USA, {asingh4, rziazi, asimeoni}@wpi.edu

**Corresponding author*

Keywords

Fire spread, Flame pulsations, Flame residence, Ignition, Flame leaping

Abstract

Detailed physical understanding of fire spread is important in the face of the increasing frequency of wildland fires around the globe. Historically, fire spread across porous vegetative media has been considered a continuous phenomenon. Most studies neglect the influence of flame pulsations on the ignition of fuel particles ahead of the fire front, hence approximating the fire spread to a steady and continuous process. This research explores the dynamic nature of fire propagation by experimentally examining the instantaneous flame pulsations and their impact on the ignition of virgin fuel particles. Fire spread experiments were conducted over a longleaf pine needle (Pinus Palustris) testbed under varying crossflow conditions. In addition to introducing a flame tilt, the presence of crossflow strongly enhances the pulsating nature of a free-burning fire. The flame region of influence ahead of the fireline was augmented by the flame tilt and flame pulsations thereby leading to point ignitions at a distance. If sustained, these point or flash ignitions merge with the fireline, leading to flame spread in the form of leaps. Fire behavior was evaluated by conducting detailed image analysis of videos acquired by placing various cameras around the testbed. Additionally, local temperature and flow velocity were measured by placing a series of thermocouple trees and bi-directional probes within the fuel bed. A curved flame profile was observed under wind-aided conditions, and the curvature was seen to increase with the increasing velocity. Alternatively, a flat temperature profile was observed for no wind conditions. Under forced flow conditions, the bi-directional probes within the testbed measured the flow blocking effect (drag forces) and the presence of flame greatly enhanced the local flow velocity.

1. Introduction

Rapid changes in the global climate (Ellis et al. 2021) and years of inefficient land management techniques (Hann and Bunnell 2001) are the major reasons behind the increased frequency of high-intensity wildland fires. The future global average temperature is expected to follow an increasing trend (Arnell et al. 2009), which will further reduce the fuel moisture content (Keeley and Syphard 2016) and thereby increase the frequency and intensity of large wildland fires. Proximity of the human population to the forested regions and increase in the wildland urban interface (WUI) (Radeloff et al. 2018) adds urgency to this problem. Reliable fire spread models require a thorough physical understanding of the fire spread phenomenon under varying atmospheric conditions. A significant portion of wildland fire literature focuses on understanding flame spread across vegetative fuel, which has further been utilized to build and validate various fire spread models.

The pulsating nature of free-burning fires under the influence of crossflow has been studied using burners (Tang et al. 2019), pool fires (Lin et al. 2021), cribs (McAllister and Finney 2016), engineered cardboard (Finney et al. 2015), and most importantly vegetative fuel (Simpson et al. 2014). Non-spreading flames are helpful in evaluating the fire behavior under changing external conditions but with limited conclusions that may or may not be applicable to the flame spread problem. This work draws an understanding from the pulsating nature of non-spreading flames and furthers it to evaluate the influence of flame pulsations on particle ignition and flame spread behavior. Flame spread is mostly considered as a continuous movement of fire through spontaneous ignitions ahead of the fire front. However, the non-continuous nature of flame spread has been recently studied (Viegas et al. 2021) through various experimental studies. This research focuses on the non-continuous and dynamic motion of the fire front through a pine needle testbed. The multi-scale interaction between wind, fire,

and topography makes the fire spread a dynamic phenomenon, that can influence the development of a fire. Hence, the quantification of this dynamic fire behavior is important for accurate fire prediction.

Flame pulsations during flame spread was first explored in the context of the *trench effect* (Atkinson et al. 1995, Smith 1992, Drysdale et al. 1992) where pressure pulsations were measured by placing probes along the flame spread direction. The controlling physical mechanism generating these pressure variations was observed to change with the trench orientation. Frequency and magnitude of these pulsations were inversely related (Atkinson et al. 1995). Recent work by Finney et al. (2015) examined the flame intermittencies and described the importance of convective heating for fire propagation. Delayed ignition due to intermittent particle heating was also analyzed and continuous flame presence was shown to be necessary for particle ignition and hence fire spread. In the current research, flame pulsations and their impact on particle ignition and fire spread are explored using image analysis and video observations. Delayed fire movement is also examined using temperature measurements while local flow measurements show flow blocking and air entrainment.

2. Experimental details

Fire spread experiments were conducted under various crossflow conditions using a well-characterized wind tunnel, shown as a schematic in Fig. 1(a). These experiments used a *Pinus Palustris* testbed (1650mm by 600mm) placed inside the tunnel with an ignitor embedded in the sand at the leading edge. Sand was used as the pine needles' base to emulate a natural setting. Baked insulation board was used to make the ignitor wick of width 600mm and length 15mm which was soaked with ~20ml of liquid methanol. The ignitor flame was initiated using a heated Nichrome wire placed across the width of the wick top surface. Since methanol generates a clean fast-burning flame, fire spread independent of the ignitor was observed within the first 400mm of the testbed. Fire spread behavior was qualitatively and quantitatively analyzed for five different flow conditions, namely 0, 0.23, 0.28, 0.42, and 0.75m/s. The fuel loading was kept constant at 0.5kg/m^2 and the fuel moisture content (FMC) varied between 5 and 7% on a dry basis.

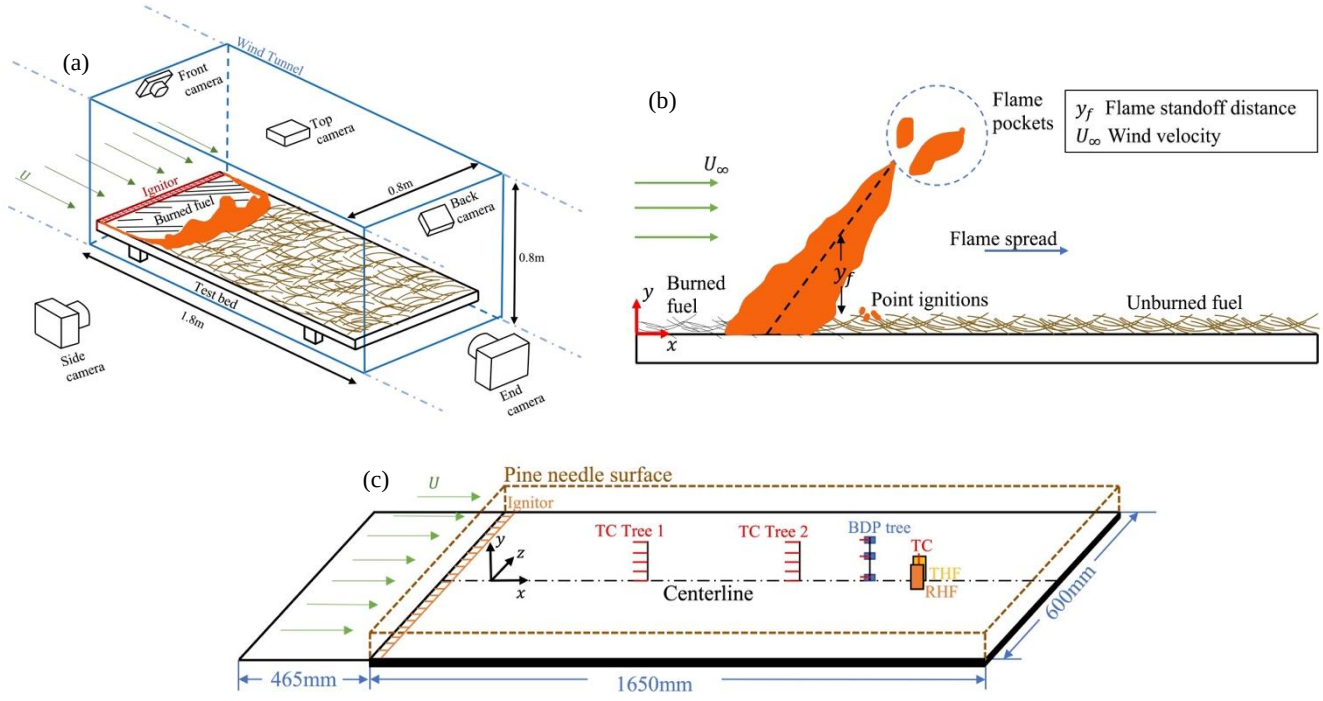

Figure 1 - (a) Schematic of the testbed placed inside the wind tunnel along with the cameras. (b) Fire spread behavior through a pine needle testbed (c) Testbed with the sensor setup.

A schematic of the sensor layout within the testbed is shown in Fig. 1(c). The testbed consisted of two thermocouple trees composed of five K-type thermocouples of 150µm wire-diameter each placed at x = 540mm and x = 1040mm from the leading edge. Five thermocouples were placed in each tree at five different heights with equal increments of 23mm starting from the bottom of the bed (z = 0, 23.3, 46.6, 70, and 93.2mm). Three 10mm diameter bi-directional probes (BDPs) were also placed in a tree-like arrangement (z = 0, 70 and

93.2mm) at x = 1250mm from the leading edge. A K-type thermocouple was attached to each BDP for density correction and flame location. Heat flux measurements were conducted by placing a radiometer and total heat flux gauge at x = 1400mm along with a K-type thermocouple to assess the flame location. Temperature and heat flux measurements were carried out at a sampling rate of 75Hz while pressure was measured at a frequency of 220Hz. Five cameras were placed above and around the testbed to observe the fire behavior as the flame front moved along the testbed.

A detailed image analysis algorithm was developed using the previously established technique (Singh and Singh 2021) of generating flame probability contour profile for non-spreading flames by assuming negligible fire front movement within 0.5s. Side-view cameras acquired the videos at 120 frames per second and every 60 frames (0.5s) were binarized and averaged to build an instantaneous contour profile, which was used to extract the mean and intermittent flames. Additionally, the videos were qualitatively analyzed to observe the flame pulsations and their influence on particle ignition and fire spread.

3. Results and discussions

A detailed qualitative analysis is presented in this section by conducting visual observations using various videos acquired from cameras placed around the testbed. This qualitative analysis is verified by comparison with the temperature and velocity measurements. To understand fuel particle ignition and fire front movements, flame pulsations in the form of mean and intermittent flame are evaluated. The increased region of influence of the fire front is seen to cause point ignitions leading to flame leaping, which is observed from the side, top and back cameras.

3.1. Flame pulsations – Mean and intermittent flame

Buoyancy-induced instabilities and air entrainment lead to flame pulsations generating a mean and intermittent flame. This intermittent flame appears in the form of flame pockets separating from the mean fire front along the direction of flame orientation. A robust image analysis technique was used to evaluate the mean and intermittent flame regions (Singh and Singh 2021, Sun et al. 2021) using the videos acquired from the side-view camera. It is observed from Fig. 2 that for the same wind velocity, the flame region of influence increased due to the presence of the intermittent flame and the area of intermittent flame increased with increasing crossflow momentum. Furthermore, the flame tilt generated under the influence of crossflow decreased the *flame standoff distance* (see Fig. 1(b)), leading to an increased preheating of the unburnt fuel particles ahead of the fire front.

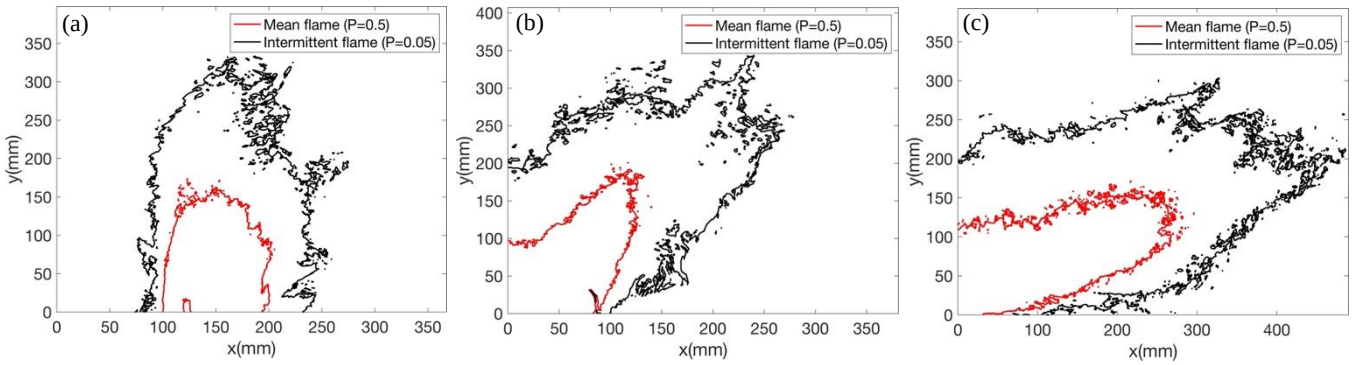

Figure 2 – Mean and intermittent flame contour profiles evaluated using 60 frames (0.5s) for (a) 0m/s, (b) 0.23m/s, and (c) 0.75m/s flow.

3.2. Ignition and fire line movement

Fire front acts as an obstacle for the flow, which intermittently breaks through this barrier, pushing the hot gases towards the unburnt fuel (Finney et al. 2015). This increases the flame region of influence and causes intermittent point ignitions ahead of the flame. This phenomenon is presented in Fig. 3 using the back view for 0.42m/s case with time t = 0s taken as the first frame. Point ignitions, represented by the dotted blue line, have dynamic nature, and depend upon the instantaneous heating conditions. Under low heating conditions, these point ignitions are seen to extinguish and then re-ignite, as observed between t = 0.099s and t = 0.132s. The fire front stagnates at a given *x*-location until the point ignitions merge with the fire front, leading to *flame leaping*

over the top surface (at t = 0.198s). This behavior is seen to continue throughout the testbed and under varying wind velocities.

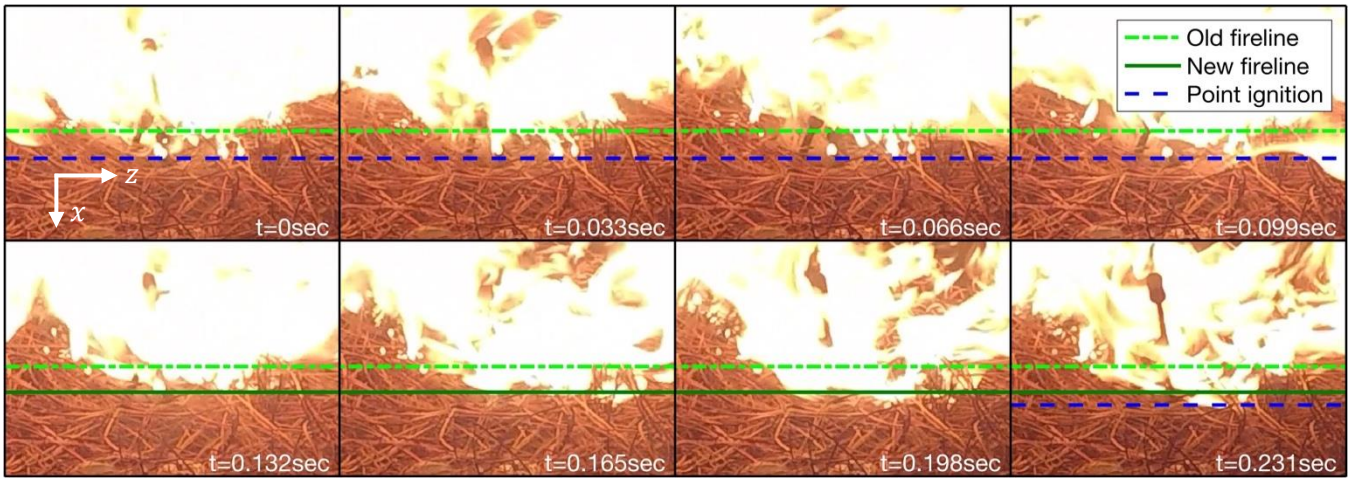

Figure 3 – Intermittent point ignitions and flame spread in the form of leaps for a wind velocity of 0.42m/s. The frames are extracted from the video captured using the back camera.

3.3. Local temperature and flow variations

Two thermocouple trees were placed along the testbed centerline to evaluate the flame behavior during fire front stagnation. Flame presence at a location was acquired using a threshold temperature of 300°C (Mueller et al. 2018). Figure 4 contains the flame profile measured by both the thermocouple trees for wind velocity of 0m/s, 0.28m/s and 0.75m/s. Fire spread under no-flow condition shows a flat flame profile, while this flatness was lost with the introduction of cross wind. For wind-aided fire spread, the flame skimmed over the top surface of the fuel bed, while a delayed movement was observed through the bed, leading to a curved flame profile throughout the bed.

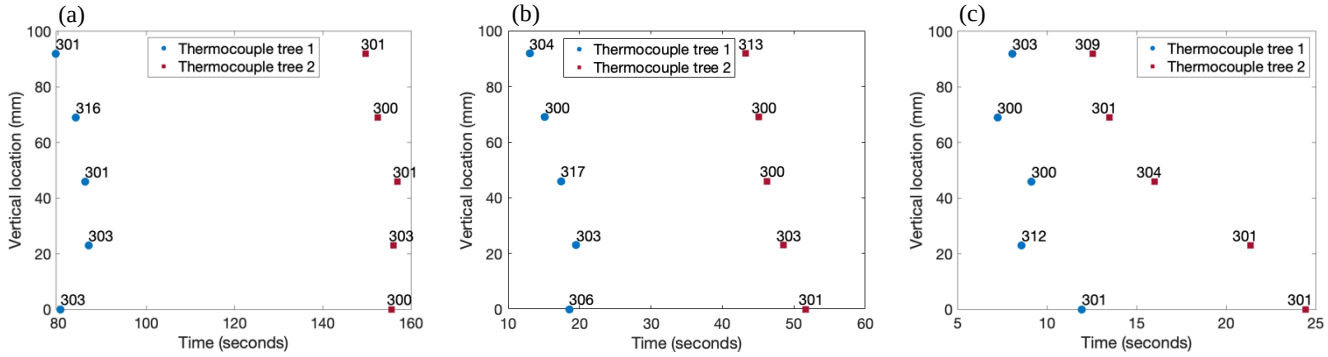

Figure 4 – Flame profile measured using two thermocouple trees consisting of five thermocouples at various vertical locations for wind velocities of (a) 0m/s, (b) 0.28m/s, and (c) 0.75m/s.

The flow velocity measured at the fuel bed surface (=70mm) using a bi-directional probe is presented in Fig. 5 for crossflows of 0m/s, 0.28m/s and 0.75m/s. Temperature measurements at the same location are also presented in the same graph. Near-zero velocity fluctuations were initially observed for all the crossflow wind speeds, representing the flow blockage effect by the porous vegetation. This flow blockage delays the fire movement through the fuel bed, thereby causing the flame to skim over the top surface. For no-flow and low-wind conditions, a significant reduction in the velocity, leading to negative or reverse flow can be seen. This reverse flow represents cold-air entrainment that leads to convective cooling and possible extinction of the point-ignitions ahead of the fire front. No reverse flow is observed for a wind velocity of 0.75m/s because the forced momentum dominates over the induced air entrainment near the fire front.

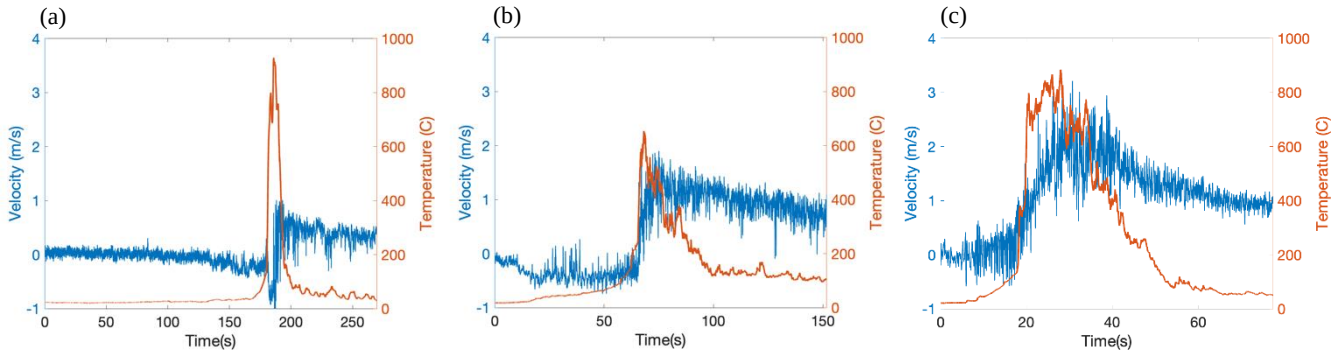

Figure 5 – Local flow velocity and corresponding temperature measured along the top surface of the testbed for wind velocities of (a) 0m/s, (b) 0.28m/s, and (c) 0.75m/s.

4. Conclusions

This work experimentally investigated the dynamic nature of flame spread over a pine needle testbed under varying crossflow conditions. Buoyancy-induced flame pulsations and their interaction with wind was seen to increase the flame region of influence. The flame standoff distance was also seen to decrease with the crossflow momentum, thereby enhancing fuel preheating. The increased flame influence leads to point ignitions in the unburnt fuel ahead of the fire front. These point ignitions can grow under suitable conditions and eventually merge with the fire front leading to flame spread in the form of leaps. Fire front is observed to halt before leaping to a new downstream location. During this flame front pause, it was seen that the fuel bed top surface experiences the flame while flow blockage within the fuel bed delays the fire spread through the bed. Furthermore, the cold air entrainment ahead of the fire front causes convective cooling of point ignitions, leading to extinction and re-ignition. On re-ignition, these point sources grow and merge with the fire front, leading to flame spread. Quantification of the observed point ignitions and leaping phenomenon will be conducted in the future work alongside building a theoretical understanding for intermittent fireline movement.

5. Acknowledgements

This work was funded by the U.S. Department of Defense Strategic Environmental Research and Development Program, project RC20-1304, and the U.S. Environmental Protection Agency, grant number 84006801.

6. References

Arnell, N.W., Lowe, J.A., Challinor, A.J. and Osborn, T.J., 2019. Global and regional impacts of climate change at different levels of global temperature increase. *Climatic Change*, *155*(3), pp.377-391. https://doi.org/10.1007/s10584-019-02464-z

Atkinson, G.T., Drysdale, D.D. and Wu, Y., 1995. Fire driven flow in an inclined trench. *Fire safety journal*, *25*(2), pp.141-158. https://doi.org/10.1016/0379-7112(95)00039-9

Drysdale, D.D., Macmillan, A.J.R. and Shilitto, D., 1992. The King's Cross fire: Experimental verification of the 'Trench effect'. *Fire Safety Journal*, *18*(1), pp.75-82. https://doi.org/10.1016/0379-7112(92)90048-H

Ellis, T.M., Bowman, D.M., Jain, P., Flannigan, M.D. and Williamson, G.J., 2021. Global increase in wildfire risk due to climate-driven declines in fuel moisture. *Global change biology*. https://doi.org/10.1111/gcb.16006

Finney, M.A., Cohen, J.D., Forthofer, J.M., McAllister, S.S., Gollner, M.J., Gorham, D.J., Saito, K., Akafuah, N.K., Adam, B.A. and English, J.D., 2015. Role of buoyant flame dynamics in wildfire spread. *Proceedings of the National Academy of Sciences*, 112(32), pp.9833-9838. https://doi.org/10.1073/pnas.1504498112

Hann, W.J. and Bunnell, D.L., 2001. Fire and land management planning and implementation across multiple scales. *International Journal of Wildland Fire*, 10(4), pp.389-403. https://doi.org/10.1071/WF01037

Keeley, J.E. and Syphard, A.D., 2016. Climate change and future fire regimes: examples from California. *Geosciences*, 6(3), p.37. https://doi.org/10.3390/geosciences6030037

Lin, Y., Hu, L., Zhang, X. and Chen, Y., 2021. Experimental study of pool fire behaviors with nearby inclined surface under cross flow. *Process Safety and Environmental Protection*, *148*, pp.93-103. https://doi.org/10.1016/j.psep.2020.10.011

McAllister, S. and Finney, M., 2016. Burning rates of wood cribs with implications for wildland fires. *Fire technology*, *52*(6), pp.1755-1777. https://doi.org/10.1007/s10694-015-0543-5

Mueller, E.V., Skowronski, N., Thomas, J.C., Clark, K., Gallagher, M.R., Hadden, R., Mell, W. and Simeoni, A., 2018. Local measurements of wildland fire dynamics in a field-scale experiment. *Combustion and Flame*, *194*, pp.452-463. https://doi.org/10.1016/j.combustflame.2018.05.028

Radeloff VC, Helmers DP, Kramer HA, Mockrin MH, Alexandre PM, Bar-Massada A, Butsic V, Hawbaker TJ, Martinuzzi S, Syphard AD, Stewart SI. Rapid growth of the US wildland-urban interface raises wildfire risk. Proceedings of the National Academy of Sciences. 2018 Mar 27;115(13):3314-9. https://doi.org/10.1073/pnas.1718850115

Simpson, C.C., Sharples, J.J. and Evans, J.P., 2014. Resolving vorticity-driven lateral fire spread using the WRF-Fire coupled atmosphere–fire numerical model. *Natural Hazards and Earth System Sciences*, *14*(9), pp.2359-2371. https://doi.org/10.5194/nhess-14-2359-2014

Singh, A., and Singh, A.V., 2021. Burning behavior of mixed-convection wind-driven flames under varying freestream conditions. *Fire Safety Journal*, *122*, p.103320. https://doi.org/10.1016/j.firesaf.2021.103320

Smith, D.A., 1992. Measurements of flame length and flame angle in an inclined trench. *Fire safety journal*, *18*(3), pp.231-244. https://doi.org/10.1016/0379-7112(92)90017-7

Sun, X., Hu, L., Zhang, X., Ren, F., Yang, Y. and Fang, X., 2021. Experimental study on flame pulsation behavior of external venting facade fire ejected from opening of a compartment. *Proceedings of the Combustion Institute*, *38*(3), pp.4485-4493. https://doi.org/10.1016/j.proci.2020.06.181

Tang, W., Finney, M., McAllister, S. and Gollner, M., 2019. An experimental study of intermittent heating frequencies from wind-driven flames. *Frontiers in Mechanical Engineering*, *5*, p.34. https://doi.org/10.3389/fmech.2019.00034

Viegas, D.X.F.C., Raposo, J.R.N., Ribeiro, C.F.M., Reis, L.C.D., Abouali, A. and Viegas, C.X.P., 2021. On the non-monotonic behaviour of fire spread. *International journal of wildland fire*, *30*(9), pp.702-719. https://doi.org/10.1071/WF21016

Investigating Conifer Tree Flame Spread Under an Applied Wind Field

Sayaka Suzuki*[1]; Samuel L. Manzello[2]

[1]*National Research Institute of Fire and Disaster (NRIFD), Chofu, Tokyo, Japan, {sayakas@fri.go.jp}*
[2]*Reax Engineering, Berkeley, CA, USA, {manzello@reaxengineering.com}*

**Corresponding author*

Keywords

Flame Spread; Vegetation; Ignition; Firebrands

Abstract

The most well-known type of large outdoor fires are wildland fires that spread into developed, urban areas, known as wildland-urban interface (WUI) fires. More than a decade ago, the state of California in the USA identified the need to develop an approach to harden communities to WUI fires exposure. The term harden simply indicates to make infrastructure in communities more ignition resistant. The premise has its roots in the development of standards and codes developed to mitigate urban fire disasters that were observed in the USA, such as the 1871 Great Chicago Fire or 1904 Baltimore Fire. The urban fire codes and standards provide the basis for fire resistant construction in many countries throughout the world. In the USA, the concept of WUI fire building codes and standards is far newer, due to the more recent WUI fire problem in this country. It is important to note that the exposure conditions used in these test methods are best guess estimates of what exposure conditions would be in a WUI fire and were developed with the best available information at that time. For these reasons, it is not surprising WUI communities will continue to be lost in the future. The lack of physical understanding is a major barrier to developing computational methods to be able to predict and understand how WUI fires spread well as develop sorely needed scientifically-based building codes and standards need to ensure resilience to these threats. There has been little in the way of quantification of firebrand production from vegetative fuel sources. Three ignition sources were utilized. The first considered a custom propane burner, the second made use of firebrand showers using a custom firebrand generator, and the third utilized one tree to ignite another tree. In this short paper, some results are presented using the firebrand generator igntion method for one conifer tree species, Douglas-fir.

1. Introduction

The large outdoor fire problem is a global issue that shows no signs of stopping in the future. The most well-known type of large outdoor fires are wildland fires that spread into developed, urban areas, known as wildland-urban interface (WUI) fires. In the USA, the size of areas burned in 2020 is simply staggering. In California, the August Complex fire itself consumed more than 1 million acres. WUI fires continue to occur throughout the Americas, Australia, Europe, and in Asia. Studies have linked climate change to increased wildland fire hazards [Abatzoglou, and Williams, 2016]. Significant WUI fires were observed in South Korea in 2019 [Lee and Lee, 2020**]** and in Australia in 2019 and 2020 [Deb et al., 2020]. It is important to distinguish WUI fires from wildland fires [Mell et al., 2010]; WUI fires include the combustion of both vegetative fuels and entire communities whereas wildland fires include the combustion of vegetative fuels and occur in uninhabited areas. Estimates place at least 70,000 communities, nearly 46 million structures at risk from WUI fires, which amounts to nearly 120 million people in the USA [Manzello *et al*., 2018].

More than a decade ago, the state of California in the USA identified the need to develop an approach to harden communities to WUI fires exposure. The term harden simply indicates to make infrastructure in communities more ignition resistant. The premise has its roots in the development of standards and codes developed to mitigate urban fire disasters that were observed in the USA, such as the 1871 Great Chicago Fire or 1904 Baltimore Fire. The urban fire codes and standards provide the basis for fire resistant construction in many countries throughout the world. In the USA, the concept of WUI fire building codes and standards is far newer, due to the more recent WUI fire problem in this country. Developing test standards for outdoor fire exposures presents significant challenges. Based on post-fire studies of ignition vulnerabilities in WUI fires, standard test methods were devised by the office of the State Fire Marshal (SFM) in California to address ignition vulnerabilities to exterior walls, exterior windows, horizontal projections such as eaves, decking assemblies,

and the use of ignition resistant materials. It is important to note that the exposure conditions used in these test methods are best guess estimates of what exposure conditions would be in a WUI fire and were developed with the best available information at that time. For these reasons, it is not surprising WUI communities will continue to be lost in the future. To put in it lightly, the science is not there and is dangerous to even reside in many places in California or other areas prone to WUI fires. The international standards organization (ISO) has just begun to address the large outdoor fire problem, as WUI fires are occurring all over the globe [Manzello, 2020].

An important missing piece to better grasp WUI fire spread processes are firebrands. Firebrands are new far smaller combustible fragments from the original fire source. Firebrands signifies any hot object in flight that are capable to ignite other fuel types. Firebrands are produced or generated from the combustion of vegetative and structural fuels. Firebrand processes include generation, transport, deposition, and ignition of various fuel types, leading to fire spread processes at distances far removed from the original fire source. There has been little in the way of quantification of firebrand production from vegetative fuel sources [Manzello *et al*., 2020]. The lack of physical understanding is a major barrier to developing computational methods to be able to predict and understand how WUI fires spread well as develop sorely needed scientifically-based building codes and standards need to ensure resilience to these threats. In this study, discrete fuel packages, manifested as conifer trees, were spaced apart, and the flame spread processes through these fuel packages were observed under an applied wind field. The experiments were conducted using wind facilities at the National Research Institute of Fire and Disaster (NRIFD) in Japan. Three ignition sources were utilized. The first considered a custom propane burner, the second made use of firebrand showers using a custom firebrand generator, and the third utilized one tree to ignite another tree. In this short conference paper, some results are presented using the firebrand generator igntion method for one conifer tree species.

2. Experimental Description

There was interest to see if firebrand showers alone could result in tree ignition and combustion. For these experiments, the reduced-scale firebrand generator was used to generate firebrand showers (see **Figure 1**). The firebrand generator has the ability to produce continuous firebrand showers. In this experimental series, Japanese cypress chips were used to produce firebrands. For a detailed description of the firebrand generator technology and procedures, please see Suzuki and Manzello (2017). A brief description is provided here.

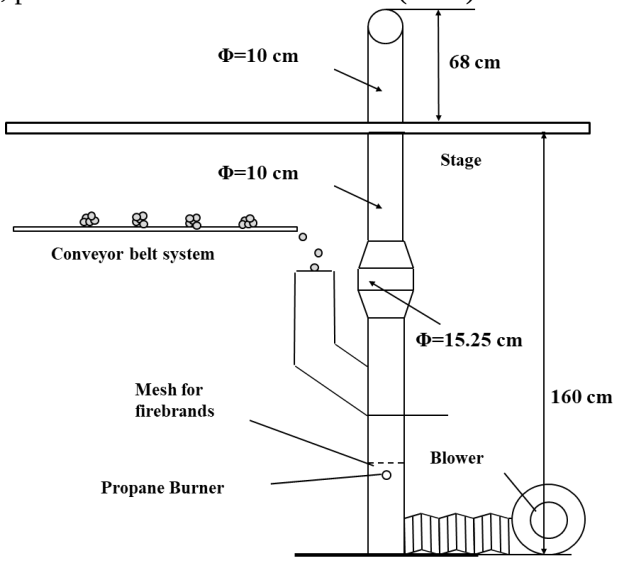

Figure 1- Reduced Scale Firebrand Generator

The reduced-scale continuous-feed firebrand generator consisted of two parts; the main body and continuous feeding component. The capability of a smaller-sized firebrand generator to develop continuous firebrand showers has been described [Suzuki and Manzello 2011]. Japanese Cypress wood chips, which represent firebrands generated from *structures*, and Douglas-fir wood pieces, which represent firebrands generated from *vegetation*, were used to produce firebrands. The Japanese Cypress wood chips had dimensions of 28 mm ±7.5 mm (L) by 18 mm ± 6.3 mm (W) by 3 mm ± 0.8 mm (H) (average ± standard deviation), respectively, before combustion. These were provided from a supplier and filtered to remove really small wood chips by using a 1

cm mesh. Douglas-fir wood pieces were machined to dimensions of 7.9 mm (H) by 7.9 mm (W) by 12.7 mm (L). Similar to the authors' prior full-scale studies, firebrands made from Japanese Cypress wood chips have approximately double the projected areas at a certain mass, compared to firebrands generated from Douglas-fir wood pieces as also seen in [Suzuki and Manzello, 2017]. The difference of wind speeds on characteristics was not observed. In this case, a tree was placed at Δx = 500 mm, from the exit of firebrand generator, similar to prior work that exposed structural fuels to firebrand showers **[**Suzuki and Manzello 2017].
In this short paper, the confier tree species used was Douglas-fir. These trees were collected a tree farm in Japan. The trees were not being grown for inside use. Nearly all the previous confier tree research in laboratory settings used conifers that were collected from Christmas Tree farms in order to have a full, uniform tree for easy comparison. Rather, in these experiments, it was of interest to determine if a tree growing in a more natural state may be ignited by wind-driven firebrand showers.

3. Results and Discussion

Figure 2 displays the results for the interaction of firebrand showers and a Douglas-fire tree of 1.5 m in height. In this experiment, the applied wind speed was 4 m/s. The firebrand generator was fed with Japanese Cypress wood chips to simulate an attack from a near-by adjacent structure. It is interesting to observe that even conifer trees with an open shape may be ignited from firebrand showers. As will be presented at the conference, the authors have recently investigated conifer tree ignition processes under and applied wind field for Nobel-fir conifers [Manzello and Suzuki 2021]. For both species, ignition was possible from firebrand showers. Perhaps the most striking feature is that combustion dynamics are vastly different under an applied wind.

Figure 2- Douglas-fir tree ignited by the firebrand generator under a 4 m/s wind

4. Summary

An important missing piece to better grasp WUI fire spread processes are firebrands. Firebrands are new far smaller combustible fragments from the original fire source. There has been little in the way of quantification of firebrand production from vegetative fuel sources. In this study, discrete fuel packages, manifested as conifer trees, were spaced apart, and the flame spread processes through these fuel packages were observed under an applied wind field. The experiments were conducted using wind facilities at the National Research Institute of Fire and Disaster (NRIFD) in Japan. Three ignition sources were utilized. The first considered a custom propane burner, the second made use of firebrand showers using a custom firebrand generator, and the third utilized one tree to ignite another tree. In this short paper, some results were presented using the firebrand generator igntion method for one conifer tree species, Douglas-fir. Results indicated that it was possible to ignite Douglas-fir trees using wind-driven firebrand showers. Once ignited, the combustion dynamics of a real-scale tree combusting under wind were markedly different than all the studies performed under no-wind conditions.

5. References

Abatzoglou, J.T., and Williams, A.P., (2016) Impact of Anthropogenic Climate change on Wildfire Across Western US Forests, Proceedings of the National Academy of Sciences, 113: 11770-11775.

Deb, P., Moradkhani, H., et al., (2020). Causes of the widespread 2019–2020 Australian bushfire season. Earth's Future, 8, e2020EF001671.

Lee, S.-J., & Lee, Y.-W. (2020). Detection of Wildfire-Damaged Areas Using Kompsat-3 Image: A Case of the 2019 Unbong Mountain Fire in Busan, South Korea. Korean Journal of Remote Sensing, 36(1), 29–39.

Manzello, S.L., (2020), Introduction to the Special Section on Global Overview of Large Outdoor Fire Standards, Fire Technology, 56:1827-1829.

Manzello, S.L., Almand, K., et al., FORUM Position Paper - The Growing Global Wildland-Urban Interface (WUI) Fire Problem: Priority Needs for Research, Fire Safety Journal: 100: 64-66, 2018.

Manzello, S.L., Suzuki, S., et al., (2020), Role of Firebrand Combustion in Large Outdoor Fire Spread, Prog. Energy Combust. Sci., 76, 100801.

Manzello, S.L., and Suzuki, S., (2021), The Combustion of Noble-Fir Trees in the Presence of an Applied Wind Field, Proceedings of the 12th U. S. National Combustion Meeting Organized by the Central States Section of the Combustion Institute May 24–26, 2021 (Virtual).

Mell, W.E, Manzello, S.L. et al., (2010) Wildland-Urban Interface Fires: Overview and Research Needs, Int'l J. Wildland Fire, 19: 238-251.

Suzuki, S., and Manzello, S.L., (2011) On the Development and Characterization of a Reduced-Scale Continuous Feed Firebrand Generator, Fire Safety Science 10:1437-1448.

Suzuki, S., and Manzello, S.L., (2017) Experiments to Provide the Scientific-Basis for Laboratory Standard Test Methods for Firebrand Exposure, Fire Safety Journal, 91:784-790.

Investigation of firebrand production from Douglas-Fir

Gabriel Setti; Juan Cuevas; Albert Simeoni*; Rory Hadden

Department of Fire Protection Engineering, Worcester Polytechnic Institute, Worcester, MA, USA, {gsetti, jcuevas, asimeoni}@wpi.edu, {r.hadden@ed.ac.uk}

**Corresponding author*

Keywords

Wildfire, Firebrands, Fire spread

Abstract

Firebrands are one of the leading mechanisms of spread during wildfire and WUI fires, where hot firebrands can be transported several kilometers ahead of the fire front, potentially creating new fires. Thus, a better understanding of the parameters affecting firebrand generation and characteristics is mandatory to develop better simulation models and predict the "firebrand potential" of different species. The goal of this study is to create a test procedure to characterize the firebrand generation efficiently and to analyze the reproducibility and relevance of the results. The experiments were conducted inside an 11m-long wind tunnel with two variable speed fans. Trunks and branches from Douglas-Fir (*Pseudotsuga menziesii*) samples were dried and tested separately using a 30cm-by-30cm propane burner under wind velocities that ranged from 0.4 m/s to 2.0 m/s. For each experiment, the firebrands generated were collected using water-filled pans with fine meshes inside. The mass distribution of the firebrands over the test section was measured using a load cell. It was observed that the heaviest firebrands only reach the pans next to the tree. Moreover, these pans contained most firebrands produced during the experiments. Thus, at low wind velocity (0.4 m/s), the wind is not strong enough to propagate the firebrands on a large area.

1. Introduction

Firebrands are primarily generated from burning wildland fuels (trees, shrubs, branches) and wooden structures (roofs, structural members). They are produced when the burning fuel thermally decomposes, loses structural integrity, and breaks down into smaller burning portions (Cohen & Deeming, 1985). These smaller portions will eventually separate from the main structure due to the drag forces generated by the airflow surrounding the burning element. Then, they will be lofted in the air by the fire-induced buoyant plume in a flaming or smoldering state (Sánchez Tarifa et al., 1965).

Several parameters have an impact on the geometric characteristics of the firebrands such as the fire behavior, the characteristics of the fuel and the environmental conditions (Bahrani, 2020). Furthermore, the ignition-by-firebrand potential depends on the number of firebrands landing in the same area, the thermal properties of the recipient fuel (moisture content, thermal inertia, density) and the properties of the firebrands (temperature, area, mass) (Cohen & Deeming, 1985).

This work presents the preliminary results of a series of experiments focused on studying the generation of firebrands from 1 m tall Douglas-fir (Pseudotsuga menziesii) samples as a function of wind velocity and for a set fire exposure in the controlled setting of a large-scale wind tunnel. First, a description of the experimental design will be given. Then, the different test parameters and the test matrix will be presented. Finally, the results of the preliminary experiments, including the mass distribution and the characterization of the firebrands, will be presented.

2. Experimental design

2.1. Experimental setup

The wind tunnel used in these experiments comprises a conditioning section, a test section, and a discharge section. The structure of the wind tunnel is shown in Fig. 1.

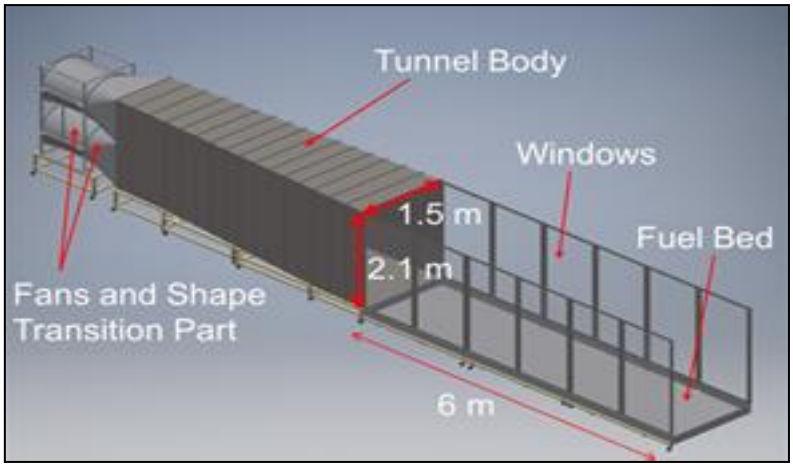

Fig.1: Schematic of the wind tunnel

In the conditioning section, two variable speed fans, along with the diffuser and straighteners, provide a stable and well-characterized inflow at the inlet of the test section.

The 6 m long test section is attached to the exit of the conditioning section and has a cross-sectional area of 1.5 m (width) by 2 m (height). It is equipped with tempered windows for flow and flame diagnostics. Within the test section, a 1.5 m width by 6 m long test bed is placed.

At the beginning of the test bed, a 30cm-by-30cm propane burner was installed. The heat release rate (HRR) of the burner is set by a mass flow controller regulating the volumetric flow of propane being delivered. The size of the burner was selected based on the maximum diameter of the samples used to ensure complete flame engulfment and avoid edge effects over the sample, as shown in Fig. 2a.

Downstream from the burner, the vegetation sample is mounted over a 60cm-by-45cm platform and held in place with a steel bracket, as shown in Fig. 2b. A 0.2 g sensitivity scale sampling at 1 Hz is placed below the platform to record the mass loss of the sample during testing.

To collect the firebrands, a layout of aluminum pans of 53cm-by-33cm was placed on the test section downstream from the sample (Fig. 2b). These pans were filled with water to extinguish the firebrands when they landed. A fine mesh (0.6mm-by-0.6mm grid size) was placed below the water level to collect the firebrands inside the pan after each experiment.

At the discharge section, a deflector is placed to prevent the firebrands from escaping the confined test environment.

Two cameras were used to record the experiments and to track the firebrands:

- A high-speed camera on the side of the tunnel facing the glass panels was used to track the firebrands throughout the test section. The data collected from this camera allowed for estimating firebrand velocities during flight.
- A GoPro camera placed close to the fuel sample, behind the glass panels, was used to record its ignition at the beginning of the experiments

After each experiment, the firebrands were collected, dried, and weighted using a 0.01g-accurate load cell to determine the mass distribution.

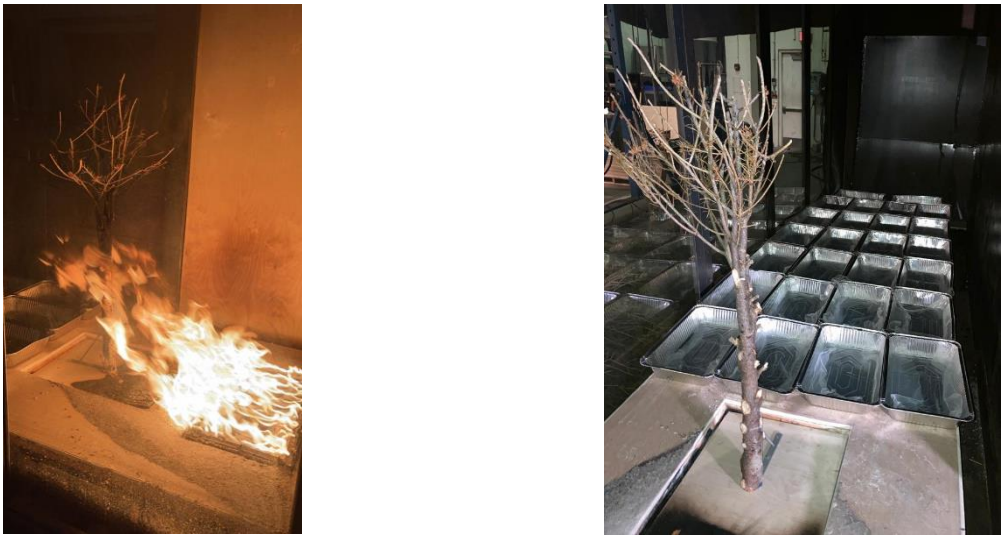

(a) (b)

Fig. 2: Testbed. (a) Propane burner. (b) Mounting platform and aluminum pan array used to collect the firebrands generated

2.2. Fuel selection

For the current study, Douglas-Fir (*Pseudotsuga menziesii*) samples were used. The species was selected due to its geographical accessibility and the availability of data and results from the literature (Manzello et al., 2006; Baker, 2011; Manzello et al., 2008).

The moisture content inside vegetative fuels significantly impacts the fire behavior and the firebrand generation. A quantitative analysis of the effect of the different moisture content of vegetative fuels is given in (Manzello et al., 2008). Three different levels can be found (mass basis); With a moisture content of 70% or above, no sustained burning after the ignition will be observed, and thus no firebrand generation. When the moisture content is between 30% and 70%, a transition regime occurs where the tree will be partially burned after the ignition. For moisture content below 30%, the tree will be entirely consumed after the ignition and firebrand generation will occur. Moreover, Douglas-Fir will not produce firebrands if its moisture content exceeds 30% (mass basis) (Baker, 2011).

Thus, a fuel conditioning chamber was built to reduce the moisture content of the vegetative fuels used for the experiments. This chamber will also allow us to dry the wet firebrands after the experiments to then characterize and analyze them. An operational temperature of 61°C was achieved inside the chamber.

The samples were prepared from locally sourced two-meter-tall live trees as follows:

First, the branches were separated from the trunks and stacked in different packages. Then, the trunks were cut in half to fit inside the test section, labeled, and placed in the drying chamber. The moisture content and the weight of each trunk were checked every day to follow the evolution of the drying procedure.

Before testing, the moisture content was determined using a wood moisture meter able to measure the moisture content (volume basis) between 1.5% and 50 % with a +/- 2% accuracy. Through the drying procedure described above, the samples achieved a moisture content of 15% before testing.

2.3. Experimental matrix

Preliminary experiments were conducted to determine the most suitable HRR and wind velocities inside the tunnel. The different wind velocities selected are shown in Table 1. A HRR of 300 kW/m^2 was selected as it was the minimum HRR to achieve sufficient flame engulfment given the characteristics of the burner and the rest of the experimental setup.

The branches and the trunks were tested separately to see the difference in terms of firebrand production with the same parameters.

Table 1: Experimental matrix.

Fuel Type	Wind velocity (m/s)	HRR (kW/m^2)	Repetitions
Trunk	0.4	300	3
	1.0		3
	2.0		3
Branches	0.4	300	3
	1.0		3
	2.0		3

3. Results

In the following section, the preliminary results of some experiments conducted using tree trunk samples are presented to illustrate the approach in practice. These experiments were conducted at a 0.4 m/s wind velocity and 300 kW/m^2 HRR.

3.1. Weight distribution

The primary trend observed in the mass distribution is that the heaviest firebrands only reach the first row of pans. Figure 3 shows the weight distribution of the firebrands under a 0.4 m/s wind velocity. Because of the low velocity, none of the firebrands generated reached the pans furthest from the fuel sample. Further experiments using higher wind velocities are required to determine the impact of the wind on the distance traveled and the mass distribution of the firebrands.

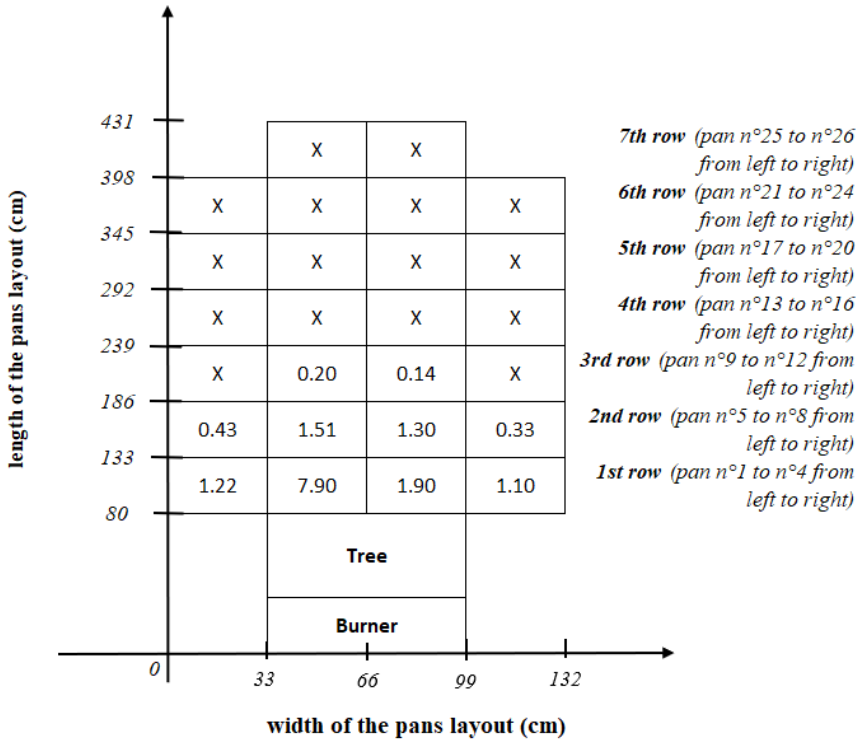

Fig. 3: Weight distribution of the firebrands for a preliminary test

3.2. Characterization of the firebrands generated

After each experiment, the meshes containing the firebrands were removed from the pans and dried for two hours. Pictures from two different pans are shown in Fig. 4a and Fig. 4b.

The primary trend observed during the preliminary experiments is that the number of firebrands per pan and their size decreases when the distance from the tree increases. Moreover, for the same row, the pans placed on the sides of the test section will receive fewer and smaller firebrands than the pans placed in the middle.

(a) (b)

Fig. 4: Firebrands collected at different locations during preliminary experiments with a 0.4 m/s wind velocity. (a) Firebrands collected in the first row (pan n°2). (b) Firebrands collected in the second row (pan n°5).

3.3. Firebrand velocity

From Figure 5, it can be seen that the absolute velocity of the firebrands correlates well with the imposed wind velocity. The variation in the range of velocities measured is attributed to the variation in mass and geometry of the firebrands collected. Both parameters will alter the contribution of buoyancy and aerodynamic drag over the firebrands. As mentioned earlier, further experiments are required to analyze the influence of wind velocity over the absolute velocity of the firebrands generated.

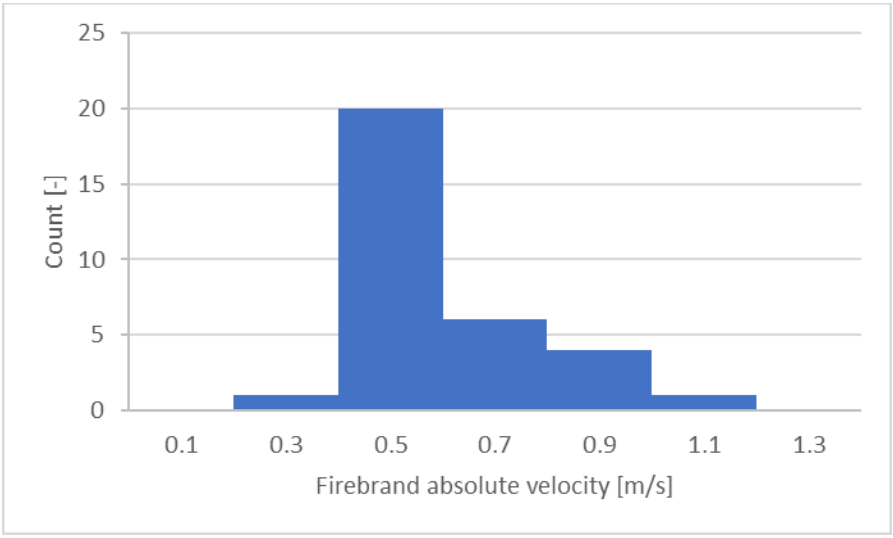

Figure 5: Aggregated firebrand velocity distribution for an experiment conducted using a flow velocity of 0.4 m/s.

4. Conclusion

A series of experiments were conducted using Douglas-fir under different wind conditions to analyze the firebrands' characteristics and mass distribution as a function of fuel type and crossflow velocity.

The preliminary results presented here demonstrate the methodology under which the study is conducted. The complete version of the study will showcase a detailed analysis of the results obtained for the complete experimental matrix proposed.

5. References

Bahrani, B. (2020). Characterization of Firebrands Generated From Selected Vegetative Fuels in Wildland Fires. The University of North Carolina at Charlotte.

Baker, E. S. (2011). Burning Characteristics of Individual Douglas-Fir Trees in the Wildland/Urban Interface. Worcester Polytechnic Institute.

Cohen, J. D., & Deeming, J. E. (1985). The national fire-danger rating system: basic equations. In Gen. Tech. Report. https://doi.org/10.2737/PSW-GTR-82

Manzello, S. L., Cleary, T. G., Shields, J. R., Maranghides, A., Mell, W., & Yang, J. C. (2008). Experimental investigation of firebrands: Generation and ignition of fuel beds. Fire Safety Journal, 43(3), 226–233. https://doi.org/10.1016/j.firesaf.2006.06.010

Manzello, S. L., Maranghides, A., Mell, W. E., Cleary, T. G., & Yang, J. C. (2006). Firebrand production from burning vegetation. Forest Ecology and Management, 234, S119. https://doi.org/10.1016/j.foreco.2006.08.160

Manzello, S. L., Suzuki, S., Gollner, M. J., & Fernandez-Pello, A. C. (2020). Role of firebrand combustion in large outdoor fire spread. Progress in Energy and Combustion Science, 76, 100801. https://doi.org/10.1016/j.pecs.2019.100801

Sánchez Tarifa, C., Pérez Del Notario, P., & García Moreno, F. (1965). On the flight paths and lifetimes of burning particles of wood. Symposium (International) on Combustion, 10(1), 1021–1037. https://doi.org/10.1016/S0082-0784(65)80244-2

Legal Regulation of Fuel Management Areas

Dulce Lopes*[1]; Karoline Tavares Vitali[2]

[1] *UCILeR, Univ Coimbra, Portugal, {dulcel@fd.uc.pt}*
[2] *UCILeR, Univ Coimbra, Portugal, {karoline.vitali@gmail.com}*

**Corresponding author*

Keywords

Fuel Management, Fuel Management Areas, Firebreaks, Fuelbreaks, Legal Regulation; Integrated Rural Fire Management System (Portugal)

Abstract

Fuel management areas (FMA) can be classified depending on their different objectives, as primary, secondary and tertiary, and can be made up of firebreaks when fuels are totally removed, fuelbreaks and shaded fuelbreaks when land remains covered by vegetation, but fuels are reduced in volume and flammability. Given the recognized importance of these areas (as defensible spaces), but also their variety, they may be found in several legislations but regulated in quite different modes. In general terms, however, it is possible to observe that there are common features which are considered in the legal regulation of fuel management, mostly at the wildland-urban interface: the location of the land; its wildfire hazardousness and the type of activity and vegetation present on the property and its surroundings. Portuguese legislation distinguishes between primary, secondary and tertiary fuel management areas, but adopts a very simplified approach to secondary FMA, considering only the type of activity at hand and the type of land (forest or agricultural) in the surroundings, and no other relevant factors as topography, climate and concrete vegetation. This contribution focuses on secondary areas and defines their main traits, from the point of view of legal regulation, and also the difficulties in their operationalisation. This article is an output of the project House Refuge (PCIF/AGT/0109/2018), funded by the Portuguese Foundation for Science and Technology.

1. Introductory remarks

Fuel management plays a crucial role in preventing forest fires and especially mega-fires and their consequential damages to lives, environment and property (ANDERSON/ANDERSON, 2012).

However, because they involve actions with long term results, highly complex and technical, and because the technical precepts that fuel management involves are very hard to translate into law, they ended up receiving little attention for many years within the legal field, when the focus on forest fire policies was placed on actions of suppression of forest fires, which have more immediate result, especially in countries affected by large fires, such as Portugal (BENTO-GONÇALVES, 2021) and USA (BUSENBERG, 2004; ANDERSON/ANDERSON, 2012; STEPHENS, 2016). Yet the increase in the incidence and size of fires has highlighted the importance of adequate regulation of fuel management and investment in this sector.

Fuel management areas (FMA) can be classified depending on their different objectives, as primary, secondary and tertiary. Also, they can be made up of firebreaks when fuels are totally removed or extremely reduced in usually linear areas, in order to diminish the intensity of a fire and allow for an easier access to fire related departments and forces; fuelbreaks, when fuels are greatly reduced in volume and flammability and shaded fuelbreaks that include vegetation but at a low density, in order to break up the continuity of fuel and limit the fire progression (ASCOLI et.al., 2020).

Given the recognized importance of these areas as *defensible spaces*, but also the various factors that influence fire behaviour and therefore the technical requirements for fuel management, they may be found in several legislations but regulated in quite different modes, as the particularities of the place where management is carried out must be taken into consideration (VIEGAS, 2005).

The purpose of this contribution is to give a broad framework of the international regulation models of fuel management in particular at the wildland-urban interface (WUI) and also to analyse in more detail the legal solutions in Portugal.

2. Regulation types of fuel management areas

Although the legal regulation of FMA in WUI in different countries is not uniform, common features can be found regarding fuel management conditions, the size of fuel management strips and those responsible for rule-making, implementation and, eventually, enforcement.

In the table below we highlight some examples of foreign regulation of fuel management in what regards fuelbreaks, such as the state of Victoria in Australia, the state of California in the USA and France. Note that in the first two countries, the regulation of the fuel management rule is left to the states, while France establishes a general rule that can be altered by regulations drawn up by fire-prone regions (Code Forestier, Article L131-14).

Country	**Rules of fuel management**	**Responsible entity**
Australia (State of Victoria)	10/50 and 10/30 rules of fire management: building a firebreak area within 10 meters of the house, with the removal of all the vegetation in this area, and one fuelbreak area within 30 or 50 meters – depending on the hazardousness of the area	Owners or those with administration powers
USA (State of California)	Three different zones of fuelbreaks: 1st: area up to five feet around the house in which the responsible person has to build a fuelbreak area removing the flammable vegetation. 2nd: 5 to 30 feet zone, requires management actions such as the creation of fuel breaks with driveways and decks, spacing trees and the removal of the fuel under them. The 3rd zone (30 to 100 feet) only takes place if the administration considers that the other areas are not sufficient due to accentuated risks (NFPA, 2022).	Id.
France	Around buildings: General rule to reduce the vegetable fuel within a 50 m area surrounding the buildings on lands located up to 200 meters from forests.	Id. The owners can request the municipalities to carry out fuel management and its maintenance, but they remain responsible for the costs of these operations (Code Forestier, article L131-14).

In general terms, it is possible to observe that there are common features which are considered in the legal regulation of fuel management in those countries and that influence the different dimensions and practices of fuel management: the location of the land; its wildfire hazardousness; the presence of homes in the surroundings; the type of the activity undertaken and the kind of the vegetation present on the property and vicinities.

There has been some consensus on the main factors that lead to a wildfire, on the need to take action to reduce hazardous fuel levels and safeguard wildland-urban interface communities, and on the range of conditions that should be considered when delimiting FMA's. Naturally, since many firebreaks are located in private areas, legislations place legal duties on owners or administrators of the property to prepare and maintain them. Therefore, it is necessary to translate technical requirements into law so that those demands are complied with, and, in case of failure to comply, so that legal consequences are applied (for instance administrative or criminal sanctions or civil responsibility claims).

For law to be effective it is necessary that rules are consistent and understandable and also that their scope (which rules apply to whom, when and where) is clearly defined, so that their addressees know what is expected from them at any point in time and space. This means that in the wildland-urban interface, unless specific

planning instruments are adopted that detail rules based on susceptibility of wildfires in concrete defined areas, it is difficult to include a wide range of variables when defining which legal rules to apply.

This is particularly apparent when considering the situation of homes or other human activities near slopes. Despite the fact that this is the most dangerous location for such uses (https://www.portugalwildfires.com/wildfires-on-slopes/), it is quite challenging to define a general rule on firebreaks (for a whole country, a state, a department or even a municipality) that complies with the legal demands of certainty and predictability. The wildfire hazardousness of an area could and should indeed take into consideration this factor (if the area of reference is mainly slopy or not); however, this is an approximate exercise that might not lead to the best definition of the concrete conditions under which firebreaks should be established.

Nonetheless, this need not be an unsurmountable task. Law is not a straitjacket (KEITER, 2006) and allows for moments of flexibility, as long as applicable legal solutions are duly framed into specific instruments (for instance territorial or land management plans) made known to the public. In addition, law is a tool for engagement and change and can, therefore, play an important role in addressing relevant societal challenges, such as wildfires. This implies the involvement of all actors, public and private, and the adoption of balanced solutions that are technically adequate, but also legally sound.

3. Portuguese regulation of fuel management areas

After this bird veil on existing types of regulation across several countries and the importance of an adequate legal regulation, a more precise look should be directed to the Portuguese Legal System. Let's start without delay, observing firstly that Portugal is undergoing a period of normative change. Decree Law no. 124/2006, 28 June, established the National Defense of Forest against Fires System (SNDFCI), and regulated, among many other instruments, FMA of primary, secondary and tertiary nature (Articles 13 to 15). Despite the fact that Article 15 of Decree Law no. 124/2006, that regulates secondary FMA is still in force in many Municipalities, according to article 79(4) of Decree-Law no. 82/2021, 13 October, this new piece of legislation is, from the 1st of January 2002 onwards, the basic framework of the Integrated Rural Fire Management System (SIGFR).

According to SGIFR, fuel management is defined as the creation and maintenance of horizontal or vertical discontinuity of the fuel load, through modification or partial or total removal of the plant biomass and the composition of plants, using the most recommended techniques with the intensity and frequency appropriate to meet the objectives of the intervened spaces [Article 3(1)(g)]. FMA functions are referred to in Article 47(2).

Three FMA are established. Primary FMAs correspond to linear strips in rural areas that have a standard width of 126 m and compartmentalize areas that should preferably have between 500 and 10,000 ha. These areas are managed and executed by the Portuguese State and defined in Regional Action Programs (Article 49). On the other side of the spectrum tertiary FMAs are of local interest and are to be defined in more concrete forest management instruments (Article 51).

As for secondary FMAs, they are established in Article 49 and can be summarized in the following table:

Type of activity	**General rule of fuel management**	**Responsible entity**
Road network	10 m outside the limits of the carriageway	Entities (public/private) responsible for the infrastructures
Railway network in operation	10 m from the outer rails	Id.
Very high voltage and high voltage electric power transport and distribution lines	Strip corresponding to the vertical projection of the outer conductor cables + a strip 10 m wide on each side	Id.
Medium voltage electric power distribution lines	Strip corresponding to the vertical projection of the outer conductor cables + a strip 7 m wide on each side	Id.

Low voltage electrical power distribution lines, with conductor cables without electrical insulation	Strip not less than 3 m wide on either side of the vertical projection of the conductor cable	Id.
Gas and oil products transportation network	7 m from the duct axis to each side	Id.
SIRESP (communication system for emergency and security) support infrastructures	Surrounding strip with a width of 7 m	Id.
Camping and caravan parks, hotels, hazardous activities that may lead to grave accidents, industrial establishments and entrepreneurial areas, fuel stations, logistics platforms, electricity or gas production and storage facilities and sanitary landfills	Surrounding strip with a standard width of 100 m	Owners, lessees, usufructuaries or entities that, in any title, administer the land within the strip
Surroundings of built-up areas, when bordering forest land	Surrounding strip with a standard width of 100 m from the interface of built-up areas	Id.
Buildings that are being used for housing or economic activities, if the 50 m band covers forest land	Standard width of 50 m, measured from the outer masonry of the building	Id.
Buildings that are being used for housing or economic activities, if the band covers agricultural land	Standard width of 10 m, measured from the outer masonry of the building	Id.

These rules are applicable to all areas except for built-up areas where fuel management is carried out in accordance with municipal regulations [Article 49(9) and Article 3(1)(b)], regardless of their wildfire hazardousness or location in fire prone areas. Also, the size of the FAM is "watertight" and does not take into account the specific conditions of the terrain, being too large in some cases and insufficient in others (i.e. properties located in slopes, for instance).

The legal regulation in Portugal is therefore oversimplified, taking only in consideration the type of activity at hand and the type of land (forest or agricultural) in the surroundings, and no other relevant factors as topography, climate and concrete vegetation, and, therefore, not being sufficiently multidisciplinary and multifunctional in its scope (VIEGAS et al., 2020).

The SGIFR tends nonetheless to introduce some plasticity to this general legal framework in two different ways:

a) the admissibility of *compatible uses* in the FMA, seen as the occupation of land in a manner different from that foreseen in the fuel management standards, as long as it is compatible with the objective of fuel management, reducing its availability for the ignition and progression of fire, and generates value for the owners or communities [Article 3(1)(k)];

b) and the *flexibility* of the FMA width, in duly justified cases, and depending on the hazard and wildfire fire risk, up to 50 /prct. greater or less than that established in these paragraphs 4 to 7 may be adopted [Article 49(2)].

These possibilities need to the included into the newly introduced (and not yet in adopted) subregional programs (Article 34). Hence, so far, the terms of such compatibility and flexibility possibilities are indeterminate.

4. Conclusive remarks

Translating technique into law is not an easy task. The demands of a dynamic and flexible framework that prevents wildfires and reduces the devastation of their effects, needs to be compatibilized with the logic of law, that aims at fair, but also, stable rules and results (LOPES, . The legal regulation of secondary fire management

areas tends to such a balance, at the price of, in some cases, excessively reducing the technical complexity of fire management techniques, as can be seen in the Portuguese case.

5. References

ANDERSON, Sara E.; ANDERSON, Terry L. 2012. "The Political Economy of Wildfire Management: Saving Forests, Saving Houses, or Burning Money", *in Wildfire Policy: Law and Economics Perspectives*, BRADSHAW, Karen M.; LUEK, Dean (Eds.), Abingdon, RFF Press, pp. 110-126. ISBN13: 978-1-933115-95-5

ASCOLI, Davide, et. al. 2020. "Firebreaks and Fuelbreaks". *In: Encyclopedia of Wildfires and Wildland-Urban Interface (WUI) Fires*, MANZELLO, Samuel (ed.), Vol. I, Springer, Cham, DOI: https://doi.org/10.1007/978-3-319-51727-8_151-1

BENTO-GONÇALVES, António. 2021. *Os Incêndios Florestais em Portugal*, Fundação Francisco Manuel dos Santos, Lisboa

BUSENBERG, George. 2004, "Wildfire Management in the United States: The Evolution of a Policy Failure›", *in Review of Policy Research*, vol. 21, n. 2, pp. 145-156

KEITER, Robert B., 2006. "The Law of Fire: Reshaping Public Land Policy in an Era of Ecology and Litigation", *in: Environmental Law*, 36, pp. 301-384

LOPES, Dulce. 2020. "As Políticas Florestais em Portugal, Bases e Principais Instrumentos*", In: e-Pública – Revista Eletrónica de Direito Público*, Vol. 7, No. 2. Available at: https://**e**-publica.pt/volumes/v7n2/pdf/v7n2a2.pdf

NFPA. 2022. *Preparing Homes for Wildfires.* Available at: https://www.nfpa.org/Public-Education/Fire-causes-and-risks/Wildfire/Preparing-homes-for-wildfire/

Prescrizioni Regionali Antincendi. 2021. Aggiornamento 2021(Regione Autónoma de Sardigna), available at: https://delibere.regione.sardegna.it/protected/54987/0/def/ref/DBR54958/

Prescrizioni Regionali Antincendi - Regione Autònoma De Sardigna, 2020 – 2022. Available at: https://delibere.regione.sardegna.it/protected/54987/0/def/ref/DBR54958/

Règlement Interdépartemental de Protection de la Forêt contre Incendies, 2016. Available at https://www.gironde.gouv.fr/content/download/49981/337387/file/R%c3%a8glement%20interd%c3%a9partemental%20de%20protection%20de%20la%20for%c3%aat%20contre%20l'incendie%20-%202016.pdf

STEPHENS, Scott L. 2016. "U.S. federal policy and forest policy: emphasizing resilience in dry forests", *in: Ecosphere*, volume 7 (11): e01584. 10.1002/ecs2.1584.

VIEGAS, Domingos Xavier. 2005. "Os incêndios florestais e as leis", *In: Polícia e Justiça*, n. 6, pp. 337-346. ISSN 0870-4791

VIEGAS, Domingos Xavier et al. 2020. "Faixas de Gestão de Combustíveis", *In: Florestas e Legislação – Planos Municipais de Defesa das Florestas contra Incêndios*, ANTUNES et al. (coord), Instituto Jurídico da Universidade de Coimbra. Available at: https://www.uc.pt/site/assets/files/433549/lc_florestas_e_legislac_a_o-planos_municipais.pdf

Victoria Planning Provisions, 2020. Available at https://planning-schemes.delwp.vic.gov.au/schemes/vpps/52_12.pdf?_ga=2.106824387.170620406.1621282691-2119954253.1620513567

Local response to extreme wildfire events in populated areas: practices and lessons learned from the Mati/Attica (2018) and North Evia (2021) fires, Greece

Vassiliki Varela [1*]; George Eftychidis[1]; Sofia Papageorgiou[2]; Georgia Legaki[2]

[1] *Center for Security Studies(KEMEA), 4, P. Kanellopoulou str. Athens GR-101 77 Greece, {v.varela,, g.eftychidis}@kemea-research.g*
[2] *Municipality of Rafina-Pikermi, 12,Arafinidon Alon GR-190 09, Rafina, Greece, {spapageorgiou@4059.syzefxis.gov.gr, glegaki@0164.syzefxis.gov.gr}*

**Corresponding author*

Keywords

Extreme events, wildfires, lessons learned, resilience

Abstract

Managing extreme wildfires requires a more holistic approach where proactive governance, citizens, and local communities play a central role.

Two recent devastating wildfires in Greece, the one in July 2018 in Mati/Attica and the other in August 2021 in North Euboea, demonstrated to a large extent the weaknesses and gaps in the Civil Protection mechanism as well as the inadequate preparedness of the local population to deal with such fires. In addition, both fires had a high societal and political impact and raised a lot of criticism and opposition.

Both fires burned under extreme weather conditions (i.e., extreme winds in Mati and prolonged heatwave in Euboea) and in parallel with other major fires in the country. However, they were characterized by quite different fire regimes, ecosystem and landscape features, and the local community type they affected.

This paper studies and analyses the combined response of the civil protection authorities and the local communities during these significant fire events.

Focused surveys, questionnaires, interviews, onsite discussions, and round tables with local authorities, citizens, first responders, and representatives of the touched communities were organized to collect information on problems, challenges, and risks, as well as response practices that proved to be effective during the response phase.

This work aims to identify lessons learned for suggesting a revision of current practices and policies to bridge the gap among the actors involved in wildfire management and to facilitate the development of local adaptation plans to increase the resilience of the local communities to wildfire risk.

1. Introduction

The new context of extreme wildfires requires implementing a more holistic fire management approach. Environmental management, climate adaptation, safety concerns, and cultural and socio-economic opportunities need to be coupled with proactive governance to mitigate disastrous situations in the near future. Furthermore, revision of forest management practices and large-scale and community-based actions are necessary for reducing the risk, increasing awareness, and improving preparedness. In this puzzle, citizens, local communities, the forestry, and bio-economy sectors have to play a significant role. (Cordis-European Commission, 2021)

Furthermore, the intermix of settlements with natural ecosystems and the fires occurring between wildlands and rural and peri-urban settlements cause severe wildfire challenges that often become the subject of intense political debate and confrontation.

Wildfires that break out the recent years under severe weather conditions, exacerbated by the ongoing climate change, can rapidly grow across the intermingled structures and vegetation, and firefighters can hardly control their propagation. Such fires can potentially burn large wooded and rural areas and destroy houses, properties, infrastructures, and livestock, while they may also result in severe injuries or even fatalities.

Recent major wildfire disasters in Greece and other EU countries have proved that the government organizations, the public authorities, and the citizens are not sufficiently prepared to handle the worsening of fire regimes. Therefore, the communities need to adapt landscape management to prevent and reduce the risk of wildfires, defend the rural communities and the natural resources, and protect human lives against the adverse direct and indirect impacts and consequences of wildfires. (Goldammer et al., 2013, Dimitrakopoulos, 2019)

Becoming a fire-resilient community that can cope with the wildfire challenges is linked to a continuous, iterative process of adaptation to the landscape and the socioeconomic factors in these areas. Unfortunately, the way the threatened communities may pursue adaptation remains entirely unclear. There is also inconsistency in how citizens perceive risk and how the civil protection authorities do so. This fact contributes to a risk perception-action gap (Wachinger et al., 2012; Margolis, 1996) that often sub-optimizes both efforts.

Fire disasters offer lessons on organizational weaknesses and allow to identify good and bad practices. Moreover, there is a specific "window of opportunity" following the disastrous event to integrate the outcome of such lessons into local government policy changes. (Mockrin, 2018)

This paper studies and analyzes the combined response of the civil protection authorities and the local communities during two recent major wildfires in Greece. The purpose is to identify lessons learned to suggest a revision of current practices and policies and bridge the gap among the efforts of the actors involved in wildfire events. In addition, organizational and societal adaptation to the risk of large wildfires must be considered to increase the local communities' resilience and protect the natural ecosystems in fire-prone areas.

Focused surveys, questionnaires, interviews, and round tables with local people, first responders, and representatives of the touched communities were organized to collect information on identified problems and practices that proved effective during the response phase. The aim is to use this material to develop a proper local adaptation plan to increase the resilience of the local communities to wildfire risk.

1.1. Fire events

The fires under consideration are characterized as "extreme events" and had a very high impact on society and at a political level. However, they had pretty different features regarding the fire regime, the ecosystem environment, landscape patterns, and the local communities' attributes that they affected.

Both occurred in parallel with other important fires in the country, which had started earlier and occupied most suppression forces; the authorities initially underestimated or overlooked their severity. Thus, the initial attack effort was inadequate.

1.1.1.Mati fire – July 2018

On the 23rd of July 2018, at 16.30', a fire ignited north of Athens in the settlement of Daou-Penteli, which belongs to the municipality of Penteli. Due to very strong and gusting winds in the area, blowing from an unusual direction, the fire spread quickly as a crown fire and headed east towards the sea. It propagated across the wildland-urban interface causing significant damages and losses in the settlements Neos Voutzas, Mati, and Kokkino Limanaki, which are sited north of Rafina port.

Due to the extremely fast fire spread in a built forested area with thousands of houses mixed with forest vegetation and narrow streets, several people were blocked in their homes or trapped in their cars trying to flee from the area. In addition, several people were caught by the fire as they attempted to reach the sea to be safe. In a fire that lasted less than six hours, hundred two (102) people lost their lives, several were injured or inhaled toxic smoke, while many houses suffered partial damage or total collapse. The fire propagation stopped when it reached the sea after a few hours and burned only 1400 ha.

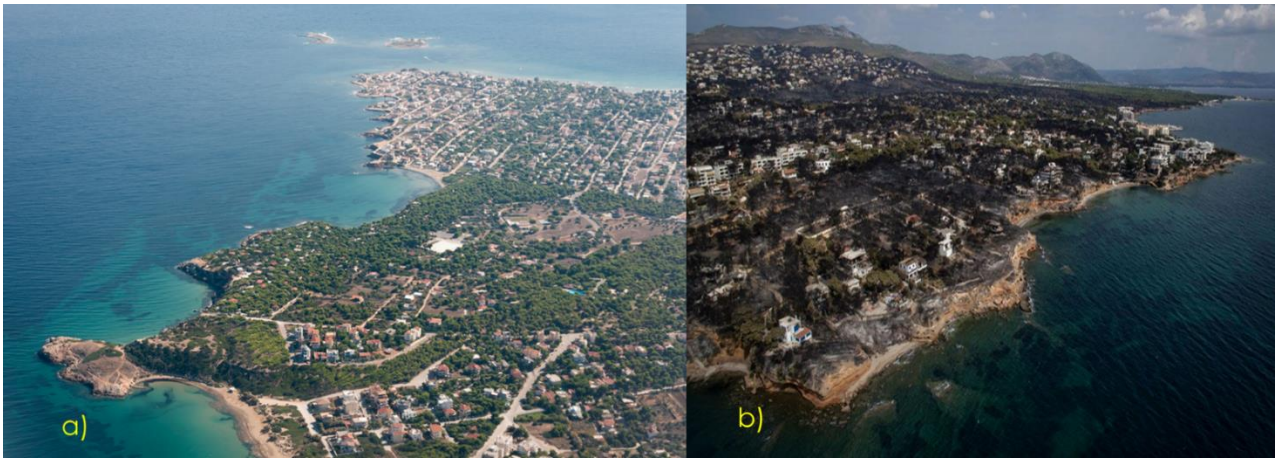

Figure 1.View of Mati area a) before[7] the fire and b) after[8] the fire

1.1.2.*N. Euboea fire – August 2021*

The fire ignited on 03/08/2021 at 15:30 and was finally contained and secured on the 17th of August. The total burned area was 51245 ha and affected two municipalities of the Northern part of the Euboea island, namely Istiaia-Aidipsos & Mantoudi-Limni-Agia Anna.

Figure 2. Burned area of N.Euboea mega-fire (2021)

Figure 3. Burned area of Mati-Neos Voutzas fire (2018)

The fire weather conditions were characterized by the extreme heatwave affecting Greece, Turkey, and the southern Balkan peninsula, lasting from the last days of July until the first ten days of August. The heatwave was the most intense of the past 30 years. It was a high-intensity surface & crown fire, especially in places of dense pine stands, with a low rate of spread due to low wind speed during combustion, in combination with a considerable accumulation of fuel, due to inadequate forest management for fire prevention through fuel treatment actions.

[7] https://upload.wikimedia.org/wikipedia/commons/4/40/2014-10-22_11-32-46_Greece_Attika_-_Raf%C3%ADna.jpgand
8 https://www.bbc.com/news/world-europe-44968581

Figure 4. The fire threatened the town of Limni in N.Euboea[9]

Figure 5. Several losses in Mati were due to the trap of cars in the narrow streets of the settlement

2. Methodology

To identify diverse approaches and understand the role, the practices, and the interaction among local actors during the fires, targeted surveys/interviews and dialogue meetings were applied with Local Civil Protection Authorities, first responders, and representatives of local communities.

Two workshops were also organized in the areas of interest, with thirty-two (32) and forty-six (46) participants, in Mati/Attika and North Euboea, respectively, in which round-table discussions took place and provided a lot of information input for the local response, community and volunteers involvement, the impact of the fire and the activities after the fire events. The topics discussed during the interviews and dialogue meetings and the round table discussions during the workshops concerned:

a) general aspects of the operation of local civil protection authorities and community groups, such as existing resources and operational framework and knowledge and training background, perception of resilience

b) Relationship and interaction with other authorities, community groups, and also citizens during a forest fire emergency

c) Response actions during the specific fire events

d) Evaluation of actions and suggestions for improvement after the fire

The information extracted was analyzed, and shared elements were grouped to identify common aspects of local fire management and response during fire events, and to understand problems, discrepancies, strengths, and potential for development through lessons learned.

3. Results & Discussion

According to the results of this study, regional and predominantly local authorities are in direct communication with various community groups, organized volunteers, and active citizens who are active in their area. Typically, there is good collaboration with these groups, and they perform jointly several actions related to the fire management phases, including the response.

As many interviewees stated, the authorities tend to be more rational and objective in their perception of risk and try to be guided by circumstances and statistics. In contrast, the population tends to react more emotionally. (Varela et al.,2022)

The authorities highlighted the opinion that citizens do not understand the risks they face and that they need to become more self-reliant.

[9] https://www.ekathimerini.com/news/1165654/six-villages-evacuated-in-evia-as-fire-burns-through-forest/

However, it is expected that local voluntary groups often specialize in forest fires in their area, especially in the rural and forested areas, and have a good perception of the fire risk. Therefore, voluntary groups, which were self-organized, played an essential role during the mega-fire in Euboea.

Technological systems (the 112-emergency line) and social media communicate the fire emergency with the community. However, the challenge is to disseminate information to vulnerable groups, the elderly and children, who do not have access to the Internet. The civil protection plans provide specific provisions and practices for vulnerable groups of citizens.

Despite the overall cooperation, a problem commonly mentioned is the lack of an interoperable Operational Centre. All the local, regional and national authorities can use such an organizational structure to have a complete operational picture of the event, facilitate the coordination suppression effort, and provide specific instructions to the volunteer firefighters and the citizens.

It is worth mentioning that according to most local authorities, a fire disaster provides opportunities for improvement. Nevertheless, many interviewees commented on the weaknesses of their organization due to limited resources or coordination problems and the insufficient actions for risk management and communication. However, after evaluating and criticizing the management's actions during the fire events, they provided ideas and suggestions for the future. For example, in the region of Mati, after the fire in July 2018, gathering places were created, signs marking routes to the sea were erected, and special spatial plans (SPPs) began to be drafted.

Some of the actions at a national and local level after the catastrophic fire in Mati/Attica are the following:

- 112 Emergency Service was activated

- the responsibility of evacuation was transferred from the first and second levels of local government to the central authority in the Ministry of Climate Crisis and Civil Protection.

- local government officials are trained in Civil Protection by institutions such as the Centre for Training and Lifelong Learning and the National University of Athens.

- Independent Civil Protection Offices have been established both at the first & second level of local government and at the Central Authority

- Updated natural disaster plans were created.

- The Municipality is funded by the relevant Ministry of Climate Change and Planning in addition to the low funding it received until recently from the Central Government

- G-Polis web application was organized as a means tool to inform the residents of the Municipality directly on their mobile phones about any dangerous - alarming event that takes place and "guide" the residents for its evolution.

Nevertheless, the excessive use of evacuation orders and the misleading instructions during the fire in North Evia led to non-compliance with state recommendations and relative loss of trust. This fact was confirmed by the majority of local authorities and residents interviewed, demonstrating the need to reorganize and update the plans and procedures and the doctrine for evacuating areas during wildfires, considering the fire situation, landscape conditions, and the capabilities of the local population. The possibility of partial evacuation should be given case-by-case (evacuation of children, elderly and vulnerable groups to a safe place). This approach will allow the competent/healthy people from the area to support the response mechanism since the local population knows the site better than the firefighters, who are often sent as reinforcements from services that arrive from distant municipalities or regions. The above presupposes that the volunteers know how to protect themselves, i.e., that they have received training, are adequately equipped, and are collaborating with the firefighters in an organized manner.

The study of local response to extreme fire events that occurred in two geographic areas that significantly differ in landscape and socioeconomic aspects allows the broader analysis of the applied practices at the local level. It can also be used to understand the deficiencies and weaknesses of the response actions comprehensively. There are a need to integrate, monitor, and coordinate fire management activities from the local to the central level in the context of the civil protection organization. However, to improve the effectiveness and efficiency

of protection, it seems necessary to strengthen the involvement and preparedness of the local actors during significant wildfire events.

Properly designed adaptation plans aiming to increase the resilience of the local communities to wildfire risk can benefit from the results and the analysis envisaged in this paper.

4. Acknowledgment

This research has been performed in the context of the European Research projects FIREURISK (https://fireurisk.eu) and RISKPACC (https://www.riskpacc.eu). These projects have received funding from the European Commission's Horizon 2020 research and innovation program under the Grant agreements No. 101003890 and No. 101019707, respectively.

5. References

Cordis, European Commission (2021). Preventing and fighting extreme wildfires with the integration and demonstration of innovative means. https://cordis.europa.eu/programme/id/H2020_LC-GD-1-1-2020

Dimitrakopoulos, A., Eftichidis, G., Xanthopoulos, G., & Mitsopoulos, I. (2019). Report of the Independent Committee tasked to Analyze the Underlying Causes and Explore the Perspectives for Future Management of Landscape Fires in Greece (pp. 1-81, Tech.). Athens, GR: Global Fire Monitoring Center.

Goldammer J.G., Mitsopoulos I, Byambasuren O., Sheldon P. (2013). Defense of Villages, Farms, and Other Rural Assets against Wildfires Guidelines for Rural Populations, Local Communities, and Municipality Leaders in the Balkan Region. Published by the Global Fire Monitoring Center (GFMC) on behalf of the European and Mediterranean Major Hazards Agreement (EUR-OPA) Council of Europe.

Margolis H. (1996) Dealing with Risk: Why the Public and the Experts Disagree on Environmental Issues. Chicago: University of Chicago Press.

Mockrin, Miranda H.; Fishler, Hillary K.; Stewart, Susan I. (2018). Does Wildfire Open a Policy Window? Local Government and Community Adaptation After Fire in the United States. Environmental Management. 62(2): 210-228. https://doi.org/10.1007/s00267-018-1030-9.

Varela V., Knudsen S., Pitidis V, (2022). CPA Consultation Report and Repository of Best Practices. RiskPACC project deliverable D1.2. European Union's Horizon 2020 research and innovation programme under grant agreement No. 101021271

Wachinger, G., Renn, O., Begg, C., & Kuhlicke, C. (2013). The Risk Perception Paradox—Implications for Governance and Communication of Natural Hazards. Risk Analysis, 33(6), 1049-1065.

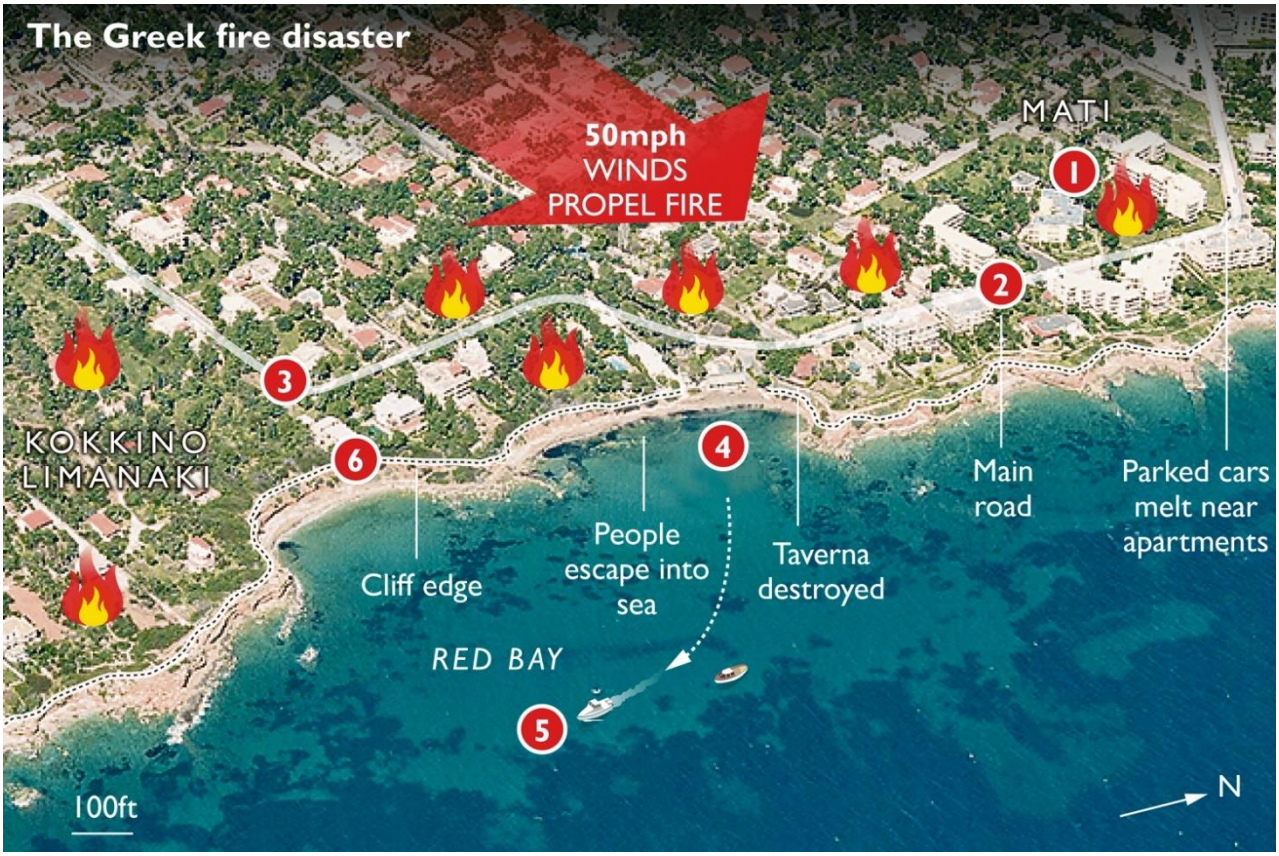

Photo by The Times – Infographic shows the situation

Managed grazing as wildfire risk reduction. A case study in Castilla - La Mancha, province of Cuenca (Spain)

Clara Quesada-Fernández*; José Félix Mateo-Fernández

Junta de Comunidades de Castilla-La Mancha. Cuenca, Spain, {claraquesada@gmail.com}

**Corresponding author*

Keywords

Rural development, forest management, fire prevention, environmental service, SDG (Sustainable Development Goals)

Abstract

Controlled grazing is a useful tool to manage and control fuel in the bush and reduce the risk of forest fires. In Castilla-La Mancha, an eminently agrarian region with a vast forest area, forest management of fuels has traditionally been carried out by crushing or burning waste in piles. Recently, this work is beginning to be carried out through prescribed burning. In recent years, experimental efforts have also been made to reintroduce controlled grazing to eliminate forest fuels through continuous browsing of forest vegetation in fire defense areas, previously carried out through preventive forestry work, avoiding or delaying the maintenance of these areas, assuming significant economic savings. Effectively reducing fuel, using local cattle ranches as a resource for fixing the population in the territory and recovering some autochthonous breeds of cattle contributes to the rural development of these regions of emptied Spain and helps to mitigate climate change. The present work analyzes the results of using cattle for the maintenance of the defense areas of Castilla-La Mancha with the results in the province of Cuenca, in approximately 1,100 annual hectares of management through managed grazing.

1. Introduction & antecedents

Extensive livestock farming can be considered a strategic sector, since as it is less dependent on external factors (fuel prices, fluctuation in feed prices, etc.) it can become essential as a method of exploitation dependent on its own resources.

The objective is to increase the periods in which a defense infrastructure against forest fires requires maintenance by means of mechanical tools. With this, the cost of maintaining the infrastructure is achieved in order to continue fulfilling the purpose for which it was designed. In this way, the creation and maintenance of a silvopastoral system was achieved, combining fire defense actions and the sustainable use of livestock, thus achieving the elimination and control of forest fuels and the maintenance of the defense areas of Castilla - La Mancha.

2. Objectives, methods

The feasibility of applying managed grazing in an area must be evaluated taking into account the area, the type of vegetation cover, accessibility, the presence of nearby cattle herds, as well as available infrastructure (sheepfolds, corrals, etc.) and possibility of having water. The economic justification is obtained by comparing the costs of treatment or maintenance through mechanical or manual clearing (which is the most common treatment) of a typical defense area in which, due to the plant formation and the quality of the site, it would have to be repeat the treatment in cycles of 5 years, with the maintenance costs of that same area through intensive controlled grazing.

The province of Cuenca has a long tradition of transhumance livestock related to ranches in the west of the community, Valle de Alcudia (Ciudad Real) and the north of Sierra Morena in the province of Córdoba and Sierra de Cazorla in Jaén. Extensive grazing has been carried out in a traditional way since ancient times (Figure 1) and participation in this program tries to give value and recognition to this activity.

Figure 1- Example of the effects of previous continuous grazing and observed in 2016 before the start of the program on mount 1097 in the municipality of Vega del Codorno (Cuenca).

The GENERAL OBJECTIVE is to maintain the defense infrastructures against forest fires or defense areas (AACC or AAEE) that make up the RAD in optimal conditions for the use for which they were made, reducing maintenance costs. To achieve this objective, it has been essential to have the coordinated work between shepherds and shepherds with their respective farms, the environmental agents Corps and forest engineers of the Ministry of Sustainable Development of the *Junta de Comunidades de Castilla - La Mancha* and *GEACAM*.

3. Results, conclusion

The line of work with controlled grazing was received differently depending on the provinces of Castilla-La Mancha, but in all of them actions were carried out on more or less surface. The provinces that best received this incentive were Cuenca and Guadalajara, executing 80% of the total area of the community in them. In this section we will focus on the results obtained in the province of Cuenca.

The year 2018 was the beginning of the journey with 7 contracts and 115 hectares grazed in the municipalities of Cuenca and Vega del Codorno. In 2019, the number of assigned hectares was increased and 873.57 hectares could be worked on, including the initial area of 2018 to add others in various municipal terms. In 2020, the last year of the program, the expansion was even greater and the 2018 and 2019 areas were joined by some more of them until reaching 1011.95 hectares.

The herds were homogeneous, for the most part, finding sheep, goats and cattle as the main species. Some farms were mixed, especially in the case of sheep with some goats. The breeds of each herd were varied.

The result of browsing was similar between flocks of sheep or mixed flocks of sheep and goats in equal plant formations. Better yields were obtained with herds of pure goats, mainly due to the increase in browsing on the shrubby species and the regrowth of Quercus. Cattle farms also showed good results in terms of vegetation control, since these animals uproot grasses and legumes, which means longer regeneration times, in addition to the effect of trampling in those areas where the presence of weeds is intensified cattle, also delaying the growth of vegetation.

One of the strengths of the program has been the involvement and perseverance of the work team, especially the shepherds, which has made it possible to obtain an optimal result on maintaining the infrastructures that have been worked on.

At the same time, the links between shepherds and the regional government were strengthened and it was shown that by carrying out this work it was possible to be more efficient in preventing forest fires.

The economic interest has made it possible to involve and motivate existing shepherds in the area who have actively participated by contributing with their experience and knowledge.

Figure 2. Example of the final result of cattle grazing in 2020 in Cañizares (Cuenca) (left) and in Monteagudo de las Salinas (Cuenca) (right). Photos: Clara Quesada, 2020. José Félix Mateo, 2020.

4. References

HERNANDO, C; MADRIGAL. J; ORTEGA, M; GUIJARRO, M. 2011. El pastoreo controlado como medida de prevención de incendios forestales: la opinión de expertos españoles. En: Cuadernos de la Sociedad Española de Ciencias Forestales, nº 33. ISSN 1575-2410, ISSN-e 2386-8368, (Ejemplar dedicado a: Actas de la IV Reunión sobre Sistemas Agroforestales. El papel de la ganadería extensiva en la silvicultura preventiva y la gestión del medio natural), pp. 33-39.

JUNTA DE COMUNIDADES DE CASTILLA – LA MANCHA. 2016. Plan Director de Defensa contra Incendios Forestales de Castilla-La Mancha.

JUNTA DE COMUNIDADES DE CASTILLA – LA MANCHA. 2017. Plan estratégico para la ganadería extensiva en Castilla-La Mancha. Consejería de Agricultura, Medio Ambiente y Desarrollo Rural.

JUNTA DE COMUNIDADES DE CASTILLA – LA MANCHA. CONSEJERÍA DE DESARROLLO SOSTENIBLE. 2017. Plan silvopastoral para el mantenimiento de la red de áreas de defensa contra incendios forestales en Castilla – La Mancha. Provincia de Cuenca.

JUNTA DE COMUNIDADES DE CASTILLA – LA MANCHA. 2017. Plan Especial de Emergencias por Incendios Forestales (Plan INFOCAM).

VÉLEZ, R. 2004. Europa: desarrollo y fuego. En: II Simposio sobre políticas, planificación y economía en la defensa contra incendios forestales. Córdoba (España).

Mapping methodological analysis of wildland-urban interface for wildfires in south of Brazil

Heitor Renan Ferreira*[1]; Antonio Carlos Batista[1]; Kendra Zamproni[1]; Josamar Gomes da Silva Júnior[1]; João Francisco Labres dos Santos[1]

[1] Federal University of Paraná, Curitiba, Brazil,
{bmheitorf, batistaufpr, kendra.zam, josamargomes}@gmail.com, {joaolabres@ufpr.br}

**Corresponding author*

Keywords

Urban-rural interface; Forest fire; Vegetation fire; Wildfire prevention and combat; Risks map

Abstract

Wildfires cause several damages to flora, fauna, soil, atmospheric air and human health. The places where there is a concentration of forest fuels in contact or very close to the homes represent a great risk, because the human presence can contribute to the start of fires and can also be drastically affected in the event of a fire. These environments are called wildland-urban interface, represented by places where human beings and anthropic structures meet or mix with vegetation. There are different methodologies for the classification of the wildland-urban interface, aiming to serve as a subsidy for preventive and vegetation fire-fighting policies. In Brazil, discussions about the theme are incipient. Campina Grande do Sul and Quatro Barras are two Brazilian municipalities with an extensive vegetative area with social interaction (areas of wildland-urban interface) and, in addition, suffer from the presence of wildfires. From 2011 to 2020, a total of 797 occurrences were registered in this area. The objective of the present study was to delimit the wildland-urban interface for Campina Grande do Sul and Quatro Barras municipalities, located in the state of Paraná, Brazil, relating to the occurrence of wildfires. To achieve the proposed objective, it was necessary to use a methodology for classifying wildland-urban interface areas, already established globally, based on the density of households and forest cover, dividing into intermix and interface zones. Two methodologies from the Brazilian Institute of Geography and Statistics were used to obtain the density of households (statistical grid and census sectors). The statistical grid presents fixed cells of 0.04 km² for urban areas and 1 km² for rural areas, while the census sectors have variable areas. The results showed that when using the statistical grid, Campina Grande do Sul and Quatro Barras had coverage of 12.5 and 15.2% of the municipal areas classified as wildland-urban interface, respectively. In the use of census sectors, Campina Grande do Sul presented 25.7% and Quatro Barras 13.6% of the areas as a wildland-urban interface. This discrepancy observed when using the census sector may be related to an overestimation of household densities due to the variable size of the census sectors. When distributing the 314 geolocation of fires that occurred in the municipalities from 2011 to 2016, it was observed that when using the statistical grid, 15.3% of these were present in areas of wildland-urban interface and using the census sectors, 17.2 % of occurrences located in these areas. Based on the results obtained, it can be concluded that the delimitation of the wildland-urban interface using the method of household information contained in the statistical grid presented greater detail than use of the census sectors. However, it is necessary to evaluate the methodology used to quantify coverage forestry. The presence of fires in areas with a wildland-urban interface demonstrates the need for preventive policies to be applied to the habitants of these places. Finally, it is recommended to continue studies, as well as to create or adapt methodologies for classifying the wildland-urban interface based on local characteristics.

1. Introduction

Forest fires are directly and indirectly responsible for numerous environmental, economic and social damages. Its occurrences are increasingly affecting the daily lives of communities present in areas adjacent to vegetation cover, especially in areas classified as wildland-urban interface.

Wildland-urban interface (WUI) zones can be generically conceptualized as areas where urban and vegetational aspects merge. This promotes human influence both in the generation of combustible residue and in the burning of different materials. Also, when preventive measures are not adopted, the presence of buildings close to vegetated areas may present susceptibility to damage in the event of a fire in vegetation.

Until part of the 20th century, the distinction between forest, farm and city was generally well defined (CHANDLER, 1983), but the advance of urban areas and the population increase from urban centers towards peripheral areas has mixed these different zonings, creating zones of wildland-urban interface (VÉLEZ, 2009). The different classification methodologies of wildland-urban interface, differ in classification methods, but converge in presenting buildings, population and vegetation as the main variables used.

In Brazil, there is no explicit definition of the wildland-urban interface areas for purposes related to the fuels involved in the wildfire occurrences. According to Prudente (2014) and Sakakibara (2019) the distinctions between urban and rural areas are not clear. According to Caballero (2019), this situation can bring about possible harm in the elaboration of preventive policies and actions to minimize the occurrence of fires

The cities of Campina Grande do Sul and Quatro Barras are located in the metropolitan region of Curitiba, capital of Paraná, Brazil, and have an extensive vegetative area with social interaction (presence of buildings). In addition, these municipalities suffer from the occurrence of wildfires, with a total of 797 records from 2011 to 2020.

The application of methodologies consolidated in other countries for wildland-urban interface characterization can be a first step towards future adaptations and elaboration of specific classification methodologies for the reality of Paraná, contributing to science and society. Thus, the present study aims to delimit the wildland-urban interface of the municipalities of Campina Grande do Sul and Quatro Barras, relating it to the occurrence of wildfires.

2. Material and methods

2.1. Study area

The study area is the municipalities of Campina Grande do Sul and Quatro Barras, located in the state of Paraná, belonging to the south region of Brazil (Figure 1). The Campina Grande do Sul city hall presents the coordinates UTM fuse 22S N 7.199.737 and E 695.805 e and the Quatro Barras city hall presents the coordinates UTM fuse 22S N 7.193.123 e E 693.494 (*INSTITUTO BRASILEIRO DE GEOGRAFIA E ESTATÍSTICA* - IBGE, 2011).

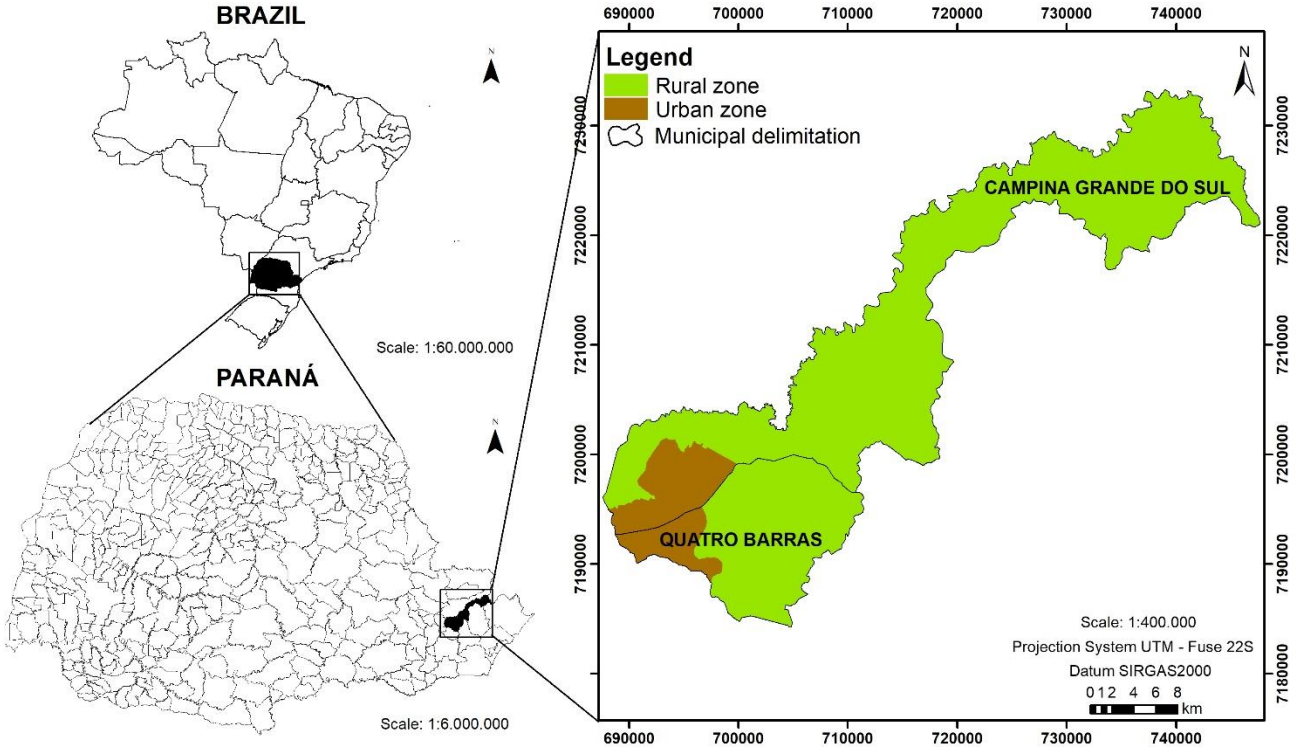

Figure 1- Localization map

The municipality of Campina Grande do Sul has an area of 539.25 km² and Quatro Barras 180.47 km² (IBGE, 2019). According to the 2010 demographic census (IBGE, 2011), they have a population of 38,769 and 19,851,

respectively. Campina Grande do Sul has 9.6% of its area considered as urban and Quatro Barras 15.6% (IBGE, 2011).

According to data obtained by Alvares *et al.* (2013), the study area is located in a climate type Cfb and Cfa region according to the Köppen classification. The study area is inserted in the Atlantic Forest biome, presenting the phytogeographic domains: araucaria moist forests, dense rainforest and natural grasslands (*INSTITUTO DE TERRAS, CARTOGRAFIA E GEOGRAFIA DO PARANÁ* - ITCG, 2009).

2.2. Data collection and analysis

An adaptation of the methodology proposed by Radeloff *et al.* (2005) was carried out. These authors are supported on USDA and USDI (2001) definitions, which show the division into intermix WUI and interface WUI. Figure 2 presents the decision flowchart for classifying the wildland-urban interface.

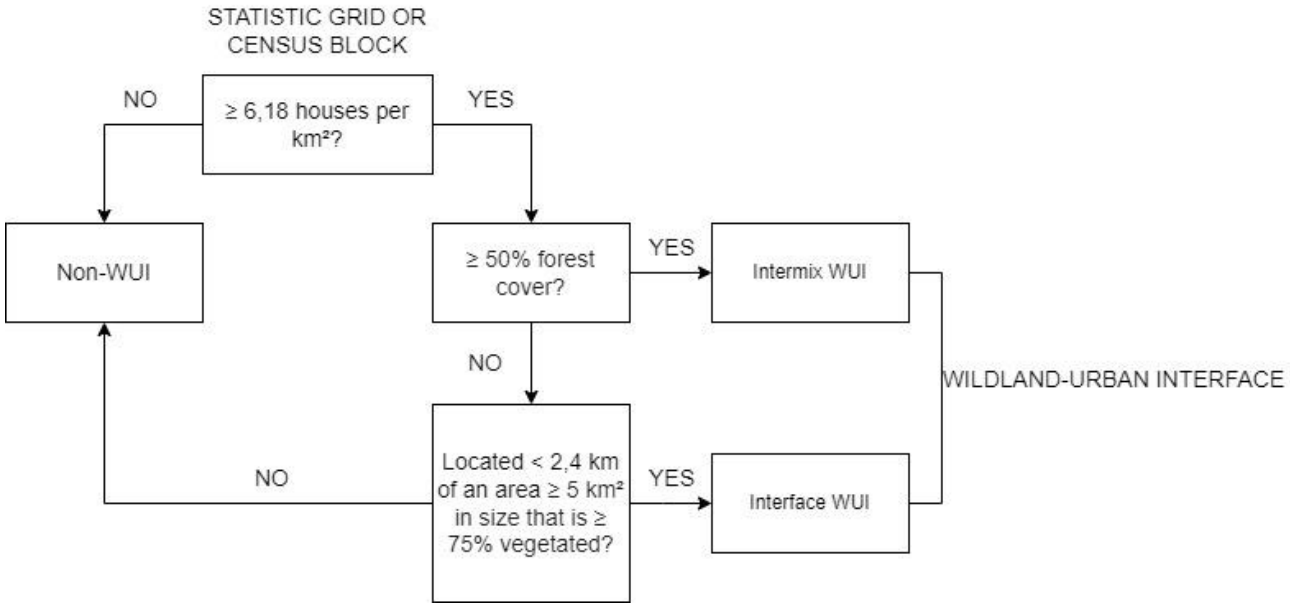

SOURCE: MARTINUZZI *et al.* (2015), adapted by the authors.

Figure 2 – Decision flowchart for wildland-urban interface classification

The results of the 2010 IBGE demographic census (IBGE, 2011) were used to obtain data on the number of households per square kilometer. The data are arranged by statistical grid and by census sectors, with limits defined by the institute. The IBGE divides the statistical grid into cells of 1 km² (1 x 1 km) for areas considered rural and 0.04 km² (200 x 200 m) for areas considered urban. Census sectors are defined using IBGE's own methodology and have variable areas. Thus, it was necessary to calculate their area and then proceed with the division of the total number of households per square kilometer.

Land cover and use was obtained through the 2019 year 5.0 collection of the *Projeto de Mapeamento Anual de Cobertura e Uso de Solo do Brasil* (MAPBIOMAS, 2020). In order to obtain exclusive forest cover, the polygons classified as "forest formation" and "planted forest" were extracted.

"Planted forests" were considered in the present study, because in addition to the lack of information on their silvicultural management (providing greater or lesser probability of fires), planted forests are relevant in the quantification of forest fuels, which may affect households close to cultivation.

By superimposing the statistical grid and the census sectors with the forest formations and planted forests, it was possible to obtain the percentage of forest cover for each polygon, classifying them with coverage equal to or greater than 50% or with coverage less than 50%.

Also, based on forest cover, polygons with areas greater than 5 km² and with at least 75% of forest cover were grouped. A 2.4 km buffer was subsequently applied to verify the centroids of the statistical grid and census sectors present in the area of operation of these polygons, enabling interface zone classification when applicable.

The geolocation of wildfire data was obtained through the database obtained by Ferreira (2021) when analysing the occurrences of wildfires in the metropolitan region of Curitiba, from 2011 to 2016.

Subsequently, was verified the number of fires that occurred in the wildland-urban interface classification zones obtained by the two census methods.

Data were manipulated using ArcGis (version 10.5), QGIS (version 3.10) and Excel (version 2016).

3. Results and discussion

3.1. Wildland-urban interface delimitation

Figures 3a and 3b present the results obtained through the application of the methodology for classifying wildland-urban interface areas, based on the IBGE's statistical grid and census sectors.

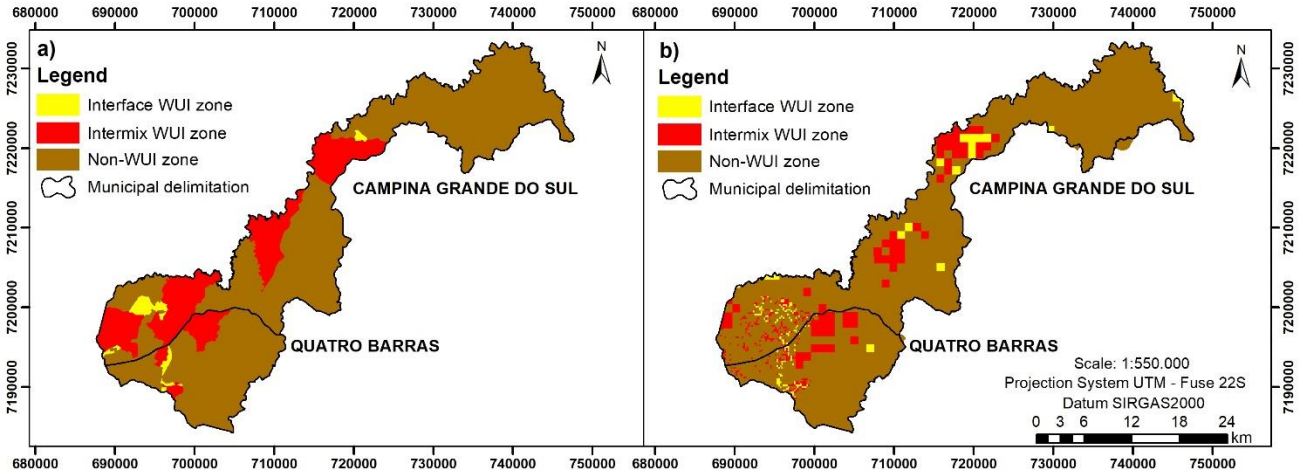

Figure 3 – Classification of wildland-urban interface areas according to: a) census sectors e b) statistical grid

It is observed that the fragmentation performed by the statistical grid (Figure 3b) presents greater detail than the use of census sectors (Figure 3a), mainly in areas classified as urban areas by the IBGE, located to the west of both municipalities.

The statistical grid presented in urban areas classified separately as intermix zones without the presence of interface zones, which may have as a possible reason the influence of "urban forest" in the study area. According to Biondi (2015), urban forest represents all vegetation cover located in the urban perimeter. Thus, vegetation cover equal to or greater than 50% of the cell area, regardless of the size of the forest fragment, combined with household density, allows the classification of the cell as intermix, even if it is present in zoning classified by the IBGE as urban.

When using the census sectors, a less refined classification was generally found, extrapolating mainly the intermix zones to areas not considered as such by the statistical grid.

In the city of Campina Grande do Sul, the intermix zone presented a total area of 129.17 km² through the census sector methodology, and when comparing with the statistical grid methodology (49.41 km²), an overestimation of 160.9% is observed. n the city of Quatro Barras, the census sector showed 21.51 km² and the statistical grid 23.27 km² for that zone.

Regarding the interface zones, the statistical grid presented higher values for both municipalities, especially Campina Grande do Sul, which obtained a total area of 17.87 km², representing 83.3% more coverage when compared to the method of census sector (9.55 km²). This value may be related to the greater distribution of cells in the statistical grid, providing greater territorial coverage and, consequently, greater possibility of fitting the parameters necessary for its classification as an interface zone.

Analysing all the wildland-urban interface, it is observed that in the city of Quatro Barras the total area occupied was very similar between both methods used, with values of 27.5 km² for the statistical grid and 24.62 km² for the census sector. In Campina Grande do Sul, the census sector, with an area of 138.73 km², was 106.2% higher than the area obtained by the statistical grid, which presented an area of 67.28 km².

The reason that may be associated with this discrepancy in value observed in Campina Grande do Sul is the high density of households in small areas of the census sectors. The census sectors may present a high concentration of households in part of the polygon and be considered as a wildland-urban interface, even if only a small portion of the polygon has households.

The observed refinement of the statistical grid allows for a better classification and segmentation than the census sectors, which, in turn, can classify the zones in a rough way, presenting the possibility of the occurrence of overestimates in certain areas and failures in non-classification of others. However, as the presence of intermix zones in urbanized areas is observed, it is necessary to evaluate the methodology used when considering the percentage of forest cover present in cells of 0.04 km², located in areas considered urban by the IBGE.

3.2. Wildfire distribution in the wildland-urban interface

Based on the results obtained by Ferreira (2021), in the period from 2011 to 2016 there were 460 wildfires in both municipalities (282 in Campina Grande do Sul and 178 in Quatro Barras), but only 314 occurrences were geolocated (68.3%).

It is observed that using the statistical grid, 15.3% (48 occurrences) were present in wildland-urban interface areas and using the census sectors, 17.2% (54 occurrences) were located in these areas.

When using the statistical grid, 19 occurrences (6.1%) were present in the intermix zone and 29 occurrences (9.2%) in the interface zone. When using the census sector methodology, 25 occurrences (8.0%) were present in the intermix zone and 29 occurrences (9.2%) in the interface zone.

As the geolocation of occurrences is dependent on addresses with registered streets, 146 occurrences (31.7%) that were unable to obtain geolocation may be related to these areas.

With the increase in population, the tendency is to have an expansion of households from urban areas towards rural areas. This can increase the tension between human occupations and vegetation, consequently increasing fire records.

The results obtained demonstrate that in the study area there is part of the wildfires at the wildland-urban interface, regardless of the methodology used to obtain the density of households. This demonstrates the need to develop prevention and combat policies focused on these areas. The peculiar characteristics of these places and the increase in anthropic pressure can cause future damage to life.

4. Conclusion

Based on the results obtained, we concluded that:

• The delimitation of the wildland-urban interface using the method of household information contained in the statistical grid presented greater detail than the use of census sectors. However, it is necessary to assess whether the cells present in the zoning outlined as urban by the IBGE should be considered, since there was an influence of the urban forest on the forest coverage percentage of the cells.

• The geolocation of the wildfire occurrences recorded in the years 2011 to 2016 showed a low presence in areas classified as wildland-urban interface. As 31.7% of the occurrences were not geolocated, there is a possibility that the presence in these areas has been larger. Regardless of the quantification, occurrences were observed in these places, thus demonstrating the need for prevention and combat policies focused on the inherent characteristics of the wildland-urban interface.

• It is recommended the continuity of studies related to the wildland-urban interface, as well as the creation or adaptation of methodologies for classification based on local characteristics.

5. References

ALVARES, C. A.; STAPE, J. L.; SENTELHAS, P. C.; GONÇALVES, J. L. M.; SPAROVEK, G. Köppen's climate classification map for Brazil. **Meteorologische Zeitschrift**, Stuttgart, v. 22, n. 6, p. 711-728, 2013.

BIONDI, D. Floresta urbana. In: BIONDI, D. **Floresta urbana**. Curitiba, 2015. 202 p.

CABALLERO, D. **Utilización, interpretación y limitaciones del índice de interfaz WUIX**. Madrid, 2019. 65 p. Série: Cadernos Técnicos.

CHANDLER, C.; CHENEY, P.; TRABAUD, L.; WILLIAMS, D. **Fire in forestry**. Volume II – Forest fire management and organization. Canada: John Wiley & Sons, 1983.

FERREIRA, H. R. **Análise das ocorrências de incêndios em vegetação na região metropolitana de Curitiba-PR, no período de 2011 a 2016**. 137 f. Dissertation (Master in Forestry Engineering) - Universidade Federal do Paraná, Curitiba, 2021.

INSTITUTO BRASILEIRO DE GEOGRAFIA E ESTATÍSTICA (IBGE). Censo demográfico de 2010: características da população e dos domicílios – resultados do universo. Rio de Janeiro, 2011. In: <https://www.ibge.gov.br/estatisticas/sociais/saude/9662-censo-demografico-2010.html?edicao=9673&t=downloads>. Acess: 05 set. 2020.

_____. Malha municipal. 2019. In: <https://www.ibge.gov.br/geociencias/organizacao-do-territorio/15774-malhas.html?=&t=downloads>. Access: 05 nov. 2020.

INSTITUTO DE TERRAS, CARTOGRAFIA E GEOCIÊNCIAS (ITCG). Mapa de fitogeografia do Estado do Paraná. 2009. In: <http://www.itcg.pr.gov.br/arquivos/File/Produtos_DGEO/Mapas_ITCG/PDF/Mapa_Fitogeografico_A3.pdf>. Access: 20 mar. 2020.

MARTINUZZI, S.; STEWART, S. I.; HELMERS, D. P.; MOCKRIN, M. H.; HAMMER, R. B.; RADELOFF, V. C. **The 2010 Wildland-Urban Interface of the Conterminous United States.** 2015. 123 p.

PROJETO DE MAPEAMENTO ANUAL DE COBERTURA E USO DE SOLO DO BRASIL (MAPBIOMAS). Coleção 5.0 da Série Anual de Mapas de Cobertura e Uso de Solo do Brasil. 2020. In: <https://mapbiomas.org/>. Access: 20 nov. 2020.

PRUDENTE, L. T. O lugar da interface rural-urbana no planejamento territorial: estudo de caso da região metropolitana de Porto Alegre/RS**. 1° Congresso brasileiro de geografia política, geopolítica e gestão territorial**, p. 1258-1269, 2014

RADELOFF, V. C.; HAMMER, R. B.; STEWART, S. I.; FIRED, J. S.; HOLCOMB, S. S.; MCKEEFRY, J. F. The wildland-urban interface in the United States. **The ecological society of America**, Washington, v. 15, n. 3, p. 799-804, 2005.

SAKAKIBARA, G. M. **Classificação de áreas urbanas e rurais no Brasil: uma discussão a partir do território municipal.** 165 f. . Dissertation (Master in Geography) – Universidade Federal do Rio Grande do Sul, Porto Alegre, 2019.

UNITED STATES DEPARTMENT FOR AGRICULTURE (USDA); UNITED STATES DEPARTMENT OF THE INTERIOR (USDI). Urban wildland interface communities within vicinity of Federal lands that are at high risk from wildfire. **Federal Register**, v. 66, n. 3. p. 751–777, 2001.

VÉLEZ, R. La proteción contra incêndios en la interfaz urbano-forestal. In: VÉLEZ, R. (Coord.) **La defensa contra incendios forestales**: fundamentos y experiencias. 2.ed. Madrid: McGraw-Hill, 2009. p. 282-287

Measuring fire risk perception of residents before and after a fire

Sven Christ*; Nina Schwarz; Richard Sliuzas

PGM Department, ITC Faculty, University of Twente. 99 Hengelose Straat, Enschede, Overijssel, The Netherlands, {s.i.christ, n.schwarz, r.sliuzas}@utwente.nl

**Corresponding author*

Keywords

Wildfire, Wildland urban interface, Settlement fire, Risk perception

Abstract

Few studies have the opportunity to empirically investigate changing risk perception before and after a fire event. Here, we study the impact a fire within a settlement fire has on the risk perception of residents in a high wildfire risk informal settlement in South Africa. We measured risk perception concerning wildfires and settlement fires. Findings from our questionnaire indicate a fire event raises the perception of wildfire and settlement fire risk. Residents respond differently whether they are directly impacted by the fire or not, with unaffected residents more concerned about personal risk than community risk. While other studies found that a fire event raises the likelihood of residents enacting risk reduction efforts, our results dispute this, with residents indicating they are less likely to commit to personal risk reduction efforts. Finally, a fire event appears to lower the likelihood of residents leaving a settlement due to the perception of wildfire or settlement fire risk.

1. Introduction

Wildfire risk management at the wildland-urban interface (WUI) relies on institutions, politicians and residents who are often at opposing ends with policies and other risk reduction efforts cooperating (Christ et al. 2022). Risk perception is key for understanding how humans respond to interventions to reduce risk and, therefore, successful implementation (Arvai et al., 2006; McGee et al., 2009). Furthermore, experiencing disaster events changes perceptions of the specific disaster and other disasters (ibid). Thus, understanding how fire events change risk perception can improve making tailor-made interventions.

Recently, Dupey & Smith (2019) found that a wildfire can trigger residents to participate in risk mitigation behaviours. Flores Quiroz et al. (2021) disputed this claim after they investigated fire risk perception in Imizamo Yethu (IY) but focused on what the elements residents believe cause fire in IY, not how they perceive the hazard of fire itself. Few studies have empirical data collected on residents' fire perception before and directly after a fire event. Here, we define wildfires as fires that start in the wildland and potentially move into the settlement, whereas settlement fires are those that start in the settlement and may move into wildland.

We investigated IY, an informal settlement, to evaluate what impact a recent settlement fire had on residents' perceptions of wildfires and settlement fires in relation to:

- Perceived fire risk
- Vulnerability to fire and the consequences of fire
- Perceived coping capacity
- Implementation of risk reduction efforts
- Residents' intentions to remain in the area

2. Study Area

IY (0.57 km^2) is an informal settlement in the City of Cape Town, bordering the Table Mountain National Park (TMNP), South Africa (Figure 1) (Kahanji et al., 2019). TMNP forms part of the fire-prone and fire-dependent fynbos biome. Over the years, IY has experienced multiple fires, including threats from wildfires in 2009, 2015 and 2022 (African News Agency, 2015; Engel, 2022; Eyewitness News, 2009). Access to IY is difficult due to

the steep incline and the narrow and informal structure of the roads (Gibson et al., 2019). Settlement fires in IY are likely to run up the mountain if wind conditions are favourable (Gibson et al., 2019; Kahanji et al., 2019).

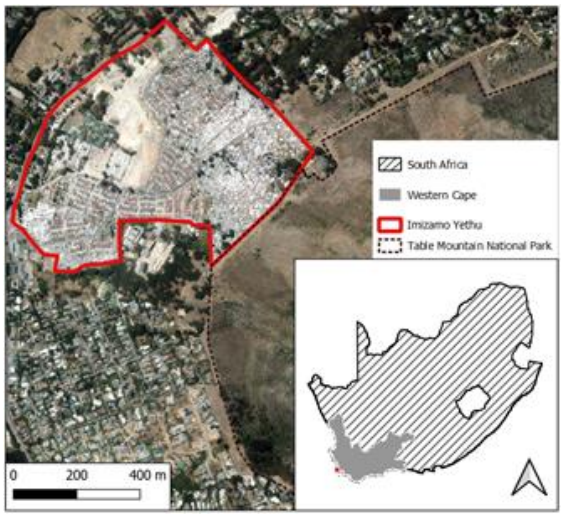

Figure 1- Imizamo Yethu in South Africa

The two most recent fires were on 6 September 2020, 9 months before our first survey and 15 August 2021, 1 month before our second survey (Ntseku, 2021; Stent, 2020).

3. Methods

We developed a questionnaire based on the works of authors who focussed on fire risk perception, housing decision making and fire management (Brenkert-Smith et al., 2012; CapeNature, n.d.; Dupey & Smith, 2019; Ghasemi et al., 2020; Martin et al., 2007; Pharoah, 2012; Statistics South Africa, 2020; Turner, 1968). A fieldwork team surveyed residents using Epicollect (https://five.epicollect.net/). First with a battery of 106 questions, using non-probability sampling to capture specific areas for another study. Data collection occurred between 21 June and 08 August 2021 (244 respondents.

To measure changes in perception, we modified the second questionnaire (127 questions) to include factors such as whether a respondent was directly affected by the fire on August 15 or not. Data was collected between 21 September and 3 October 2021. With limited funding, we captured 109 responses (56 directly impacted, 53 not directly impacted).

For this report, we focussed on a selection of 18 questions that address the research objectives. We measured perceptions on a Likert scale 1-7, with 1 representing completely disagree and 7 completely agree. To evaluate if the differences between the groups of residents were statistically significant we used the non-parametric Mann-Whitney U test in SPSS (28.0.1.0) (McKnight & Najab, 2010).

4. Results and discussion

4.1. Basic description

Respondents had a mean age of over 34, and over 11 years in IY (Table 1). Most were employed and about half were owners, indicating potential means for implementing risk reduction efforts if deemed important and effective enough.

Table 1- Basic statistics of groups

	Before fire %	After fire – direct impact %	After fire – no direct impact %
Mean Age	34	44	38
Mean Time in IY	11	15	14
Housing status			
Living rent-free	18	2	25
Owner	55	50	66
Tenant	27	48	9
Employment status			
Full time employed	19	80	68
Part-time employed	37	11	17
Self-employed	17	2	6
Unemployed	26	7	9

*Percentages may not total 100 due to rounding

4.2. Fire risk perception

All residents felt their property was more at risk after the fire, with those that experienced direct impact more aware of the risk of settlement fire (Figure 2). Those experiencing a direct impact considered the community at a higher level of risk of wildfire and settlement fire than before. Those without a direct impact, however, perceived both risks lower than before the fire. These findings agree with what McGee et al. (2009) found comparing residents who lost their homes in a wildfire and those that were at home during the fire but had no losses.

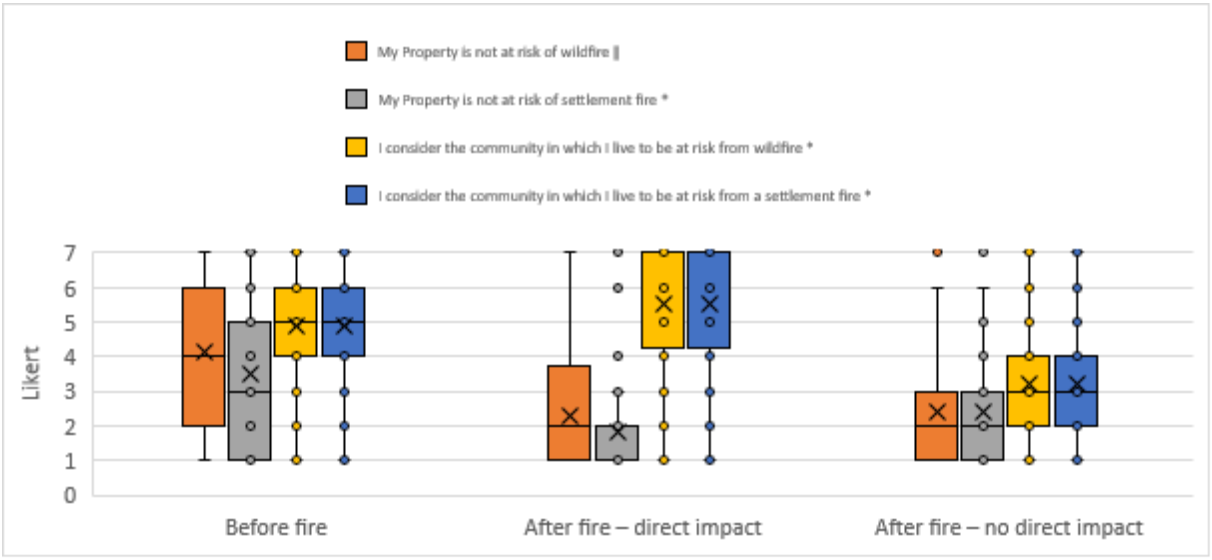

Figure 2- Property and community risk (X represents the mean, * $p \leq 0.05$ between all groups, ‖ $p \leq 0.05$ between before fire and direct impact as well as between before fire and no direct impact only)

Although all residents perceived a raised property risk perception of both wildfire and settlement fire, those that experienced the fire have a more acute sense of settlement fire than of wildfire. Those that did not experience the fire considered both risks equal.

4.3. Vulnerability and consequences

Respondents have always felt vulnerable to fires, with a slightly higher vulnerability to settlement fires (Figure 3). After the fire, those who were directly affected had an increased sense of vulnerability to both fires. They, however, felt the severity will be lower for where they live, indicating they feel it had a direct impact on them, but not so great an impact on their neighbours who may not have been affected. Interestingly, those who were not directly affected by the fire felt less vulnerable than before the fire as well as the impact less severe. It could be that residents now have a tangible idea of what a fire event looks like and believe that they are not as

vulnerable and could recover post-fire as Wachinger et al. (2013) indicated can be the case with people who only witness a disaster but do not experience losses.

Figure 3- Vulnerability (X represents the mean, * p ≤ 0.05 between all groups)

4.4. Perceived coping capacity

Before the fire, most residents believed that they could defend their properties. This, however, reduced post-fire, with respondents believing they are not able to defend their homes against either type of fire (Figure 4).

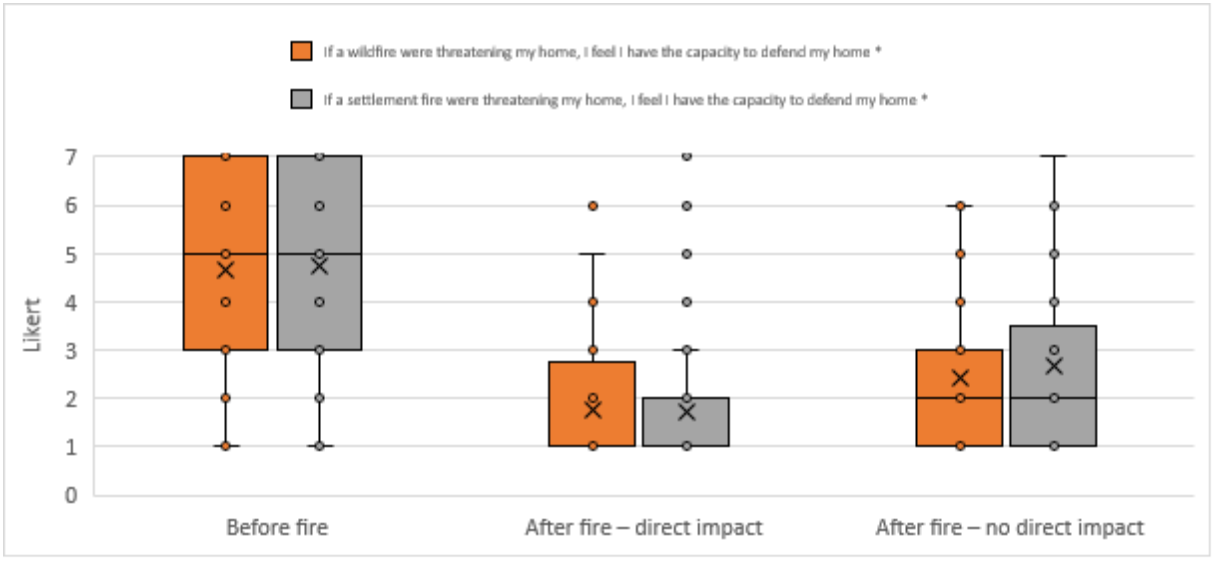

Figure 4- Coping capacity (X represents the mean, * p ≤ 0.05 between all groups)

4.5. Implementation of risk reduction

Respondents that experienced the fire were less likely to implement risk mitigation efforts (Figure 5). This contrasts with Dupey & Smith, (2019), who found residents more likely to participate in mitigation efforts after a near-miss fire event. However, our finding is in agreement with McGee et al. (2009) who found that those who lost their homes felt it was not possible to mitigate against wildfires. Those with no direct fire impact were still more likely to implement mitigation efforts than those who experienced the fire. This may be as they still believe it to be effective and thus more likely to partake in it (Bubeck et al., 2012). Most respondents were still

willing to implement the low-cost action of keeping their plots free from garbage and vegetation, but the likelihood was reduced and more spread between individuals.

Figure 5- (X represents the mean, * p ≤ 0.05 between all groups, ‖ p ≤ 0.05 between before fire and direct impact as well as between before fire and no direct impact only)

The reduction of the intention to keep roads clear of cars can be interpreted as keeping a vehicle close by as a means of escape in case of a fire, but also as a way to protect the asset in high-crime areas such as South Africa (Cheteni et al., 2018). This is illustrated in South Africa through residents fortifying homes for safety from crime but making it difficult to escape in emergencies (Zweig et al., 2018).

South African informal settlers perceive open fire cooking and settlement density as the greatest hazard for fire ignitions and irresponsible drinking in IY (Flores Quiroz et al., 2021; Zweig et al., 2018). However, implementing electrical cooking and settlement density reduction requires a multi-stakeholder approach.

These findings confirm “windows of opportunity” for different mitigation actions that have been theorised by Wachinger et al. (2013) to close even faster for those who did not directly experience the disaster.

4.6. Intention to stay in IY

Residents who experienced the fire directly were more likely to stay in IY even with the fire hazards (Figure 6). The self-selection bias that they are the ones who returned and, thus, are less likely to leave has to be acknowledged. Unaffected residents were more likely to leave due to the fire hazards than residents before the fire. Those that experienced the fire, however, were as likely as before to move to a safer location within IY due to wildfire, but less likely for settlement fires. Indicating that residents are aware of the spatial element of wildfire, and the random nature of settlement fires. Leaving IY due to settlement fire and wildfire, however, agreed with those that experienced fire and those that did not with their intention to leave.

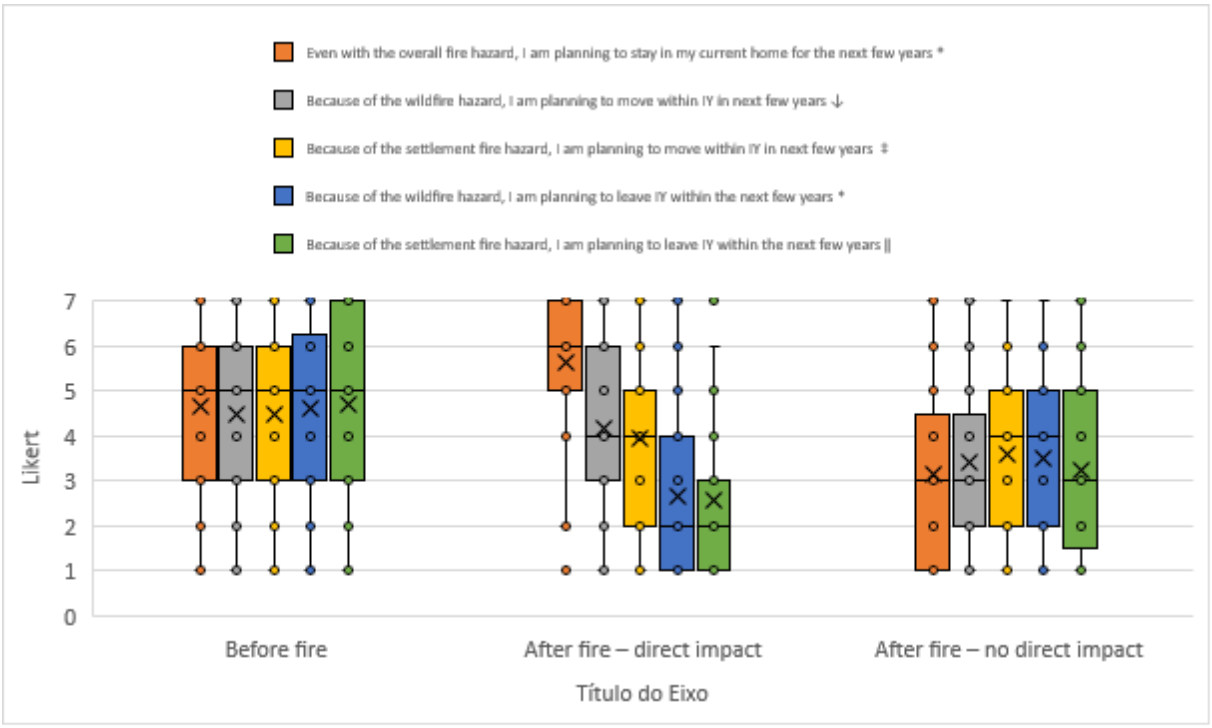

Figure 6- Intention to remain in IY (X represents the mean, * $p \leq 0.05$ between all groups, ‡ $p \leq 0.05$ only between direct impact and no direct impact, ‖ $p \leq 0.05$ between before fire and direct impact as well as between before fire and no direct impact only, ↓ $p \leq 0.05$ between before fire and no direct impact as well as between direct impact and no direct impact only)

5. Conclusions

We highlighted that any fire event affects the perceptions of residents. The level of impact on community risk perception depends on whether a resident was directly impacted. All residents, however, perceived increased fire risk after a fire occurred in the settlement. Those directly affected feel more vulnerable to fires whereas factors such as seeing the recovery may reduce the feelings of vulnerability of other residents. In IY, fires appear to make residents less likely to implement mitigation measures.

Those that experienced the fire and returned are not likely to leave, yet are also less likely to implement risk mitigation efforts and feel the most vulnerable to fire events. Importantly, these perceptions peak briefly after a fire event but are likely to regress towards the pre-fire level as early as nine months after the fire. Interventions relying on residents' perception of self-efficacy are best addressed when residents' perception of their coping capacity improves. Whereas interventions relying on external education and group action could best be implemented while residents feel they are powerless to help themselves individually.

6. References

African News Agency. (2015). Fire rages on slopes above Hout Bay. *IOL News*. https://www.iol.co.za/news/south-africa/western-cape/fire-rages-on-slopes-above-hout-bay-1840937

Arvai, J., Gregory, R., Ohlson, D., Blackwell, B., & Gray, R. (2006). Letdowns, Wake-Up Calls, and Constructed Preferences: People's Responses to Fuel and Wildfire Risks. *Journal of Forestry*, 104(4), 173–181.

Brenkert-Smith, H., Champ, P. A., & Flores, N. (2012). Trying Not to Get Burned: Understanding Homeowners' Wildfire Risk–Mitigation Behaviors. *Environmental Management*, 50(6), 1139–1151. https://doi.org/10.1007/s00267-012-9949-8

Bubeck, P., Botzen, W. J. W., & Aerts, J. C. J. H. (2012). A Review of Risk Perceptions and Other Factors that Influence Flood Mitigation Behavior. *Risk Analysis*, 32(9), 1481–1495. https://doi.org/10.1111/j.1539-6924.2011.01783.x

CapeNature. (n.d.). Fire Management. CapeNature. https://www.capenature.co.za/care-for-nature/conservation-in-action/integrated-catchment-management/fire-management/

Cheteni, P., Mah, G., & Yohane, Y. K. (2018). Drug-related crime and poverty in South Africa. *Cogent Economics & Finance*, 6(1), 1534528. https://doi.org/10.1080/23322039.2018.1534528

Christ, S., Schwarz, N., & Sliuzas, R. (2022). Wildland urban interface of the City of Cape Town 1990–2019. *Geographical Research*, 1-18 1534528. https://doi.org/10.1111/1745-5871.12535

Dupey, L., & Smith, J. (2019). Close but No Cigar: How a Near-miss Wildfire Event Influences the Risk Perceptions and Mitigation Behaviors of Residents Who Experienced a Recent, Nearby Wildfire. https://digitalcommons.usu.edu/extension_curall/1959/

Engel, K. (2022). Seven-day wildfire at Gysmanshoek Pass almost entirely contained. *IOL News*. https://www.iol.co.za/capeargus/news/seven-day-wildfire-at-gysmanshoek-pass-almost-entirely-contained-19ab309c-cbc1-4cb9-9b93-5d3322962c84

Eyewitness News. (2009). Veld fire threatens informal settlement. https://ewn.co.za/2009/03/29/Veld-fire-threatens-informal-settlement

Flores Quiroz, N., Walls, R., & Cicione, A. (2021). Towards Understanding Fire Causes in Informal Settlements Based on Inhabitant Risk Perception. *Fire*, 4(3), 39. https://doi.org/10.3390/fire4030039

Ghasemi, B., Kyle, G. T., & Absher, J. D. (2020). An examination of the social-psychological drivers of homeowner wildfire mitigation. *Journal of Environmental Psychology*, 70, 101442. https://doi.org/10.1016/j.jenvp.2020.101442

Gibson, L., Engelbrecht, J., & Rush, D. (2019). Detecting historic informal settlement fires with Sentinel 1 and 2 satellite data - Two case studies in Cape Town. *Fire Safety Journal*, 108, 102828. https://doi.org/10.1016/j.firesaf.2019.102828

Kahanji, C., Walls, R. S., & Cicione, A. (2019). Fire spread analysis for the 2017 Imizamo Yethu informal settlement conflagration in South Africa. *International Journal of Disaster Risk Reduction*, 101146. https://doi.org/10.1016/j.ijdrr.2019.101146

Martin, I. M., Bender, H., & Raish, C. (2007). What Motivates Individuals to Protect Themselves from Risks: The Case of Wildland Fires. *Risk Analysis*, 27(4), 887–900. https://doi.org/10.1111/j.1539-6924.2007.00930.x

McCain, N. (2021). Hout Bay residents scramble for shelter after fire displaces 300. *News24*. Hout Bay residents scramble for shelter after fire displaces 300

McGee, T. K., McFarlane, B. L., & Varghese, J. (2009). An Examination of the Influence of Hazard Experience on Wildfire Risk Perceptions and Adoption of Mitigation Measures. *Society & Natural Resources*, 22(4), 308–323. https://doi.org/10.1080/08941920801910765

McKnight, P. E., & Najab, J. (2010). Mann-Whitney U Test. *In The Corsini Encyclopedia of Psychology*. John Wiley & Sons, Inc. https://doi.org/10.1002/9780470479216.corpsy0524

Ntseku, M. (2021). Imizamo Yethu fire leaves almost 1 000 people homeless. *IOL News*. https://www.iol.co.za/capeargus/news/imizamo-yethu-fire-leaves-almost-1-000-people-homeless-ae506663-3484-4f50-85c8-e0eb2c5e0c34

Pharoah, R. (2012). Disaster Risk Reduction. In M. Pelling & B. Wisner (Eds.), *Disaster risk reduction: Cases from urban Africa*. Routledge. https://doi.org/10.4324/9781849771016

Statistics South Africa. (2020). General household Survey 2018. http://www.statssa.gov.za/publications/P0318/P03182018.pdf

Stent, J. (2020). The smell of fire hangs in the air in Imizamo Yethu. *Daily Maverick*. https://www.dailymaverick.co.za/article/2020-09-10-the-smell-of-fire-hangs-in-the-air-in-imizamo-yethu/

Turner, J. C. (1968). Housing Priorities, Settlement Patterns, and Urban Development in Modernizing Countries. *Journal of the American Planning Association*, 34(6), 354–363. https://doi.org/10.1080/01944366808977562

Wachinger, G., Renn, O., Begg, C., & Kuhlicke, C. (2013). The Risk Perception Paradox-Implications for Governance and Communication of Natural Hazards. *Risk Analysis*, 33(6), 1049–1065. https://doi.org/10.1111/j.1539-6924.2012.01942.x

Zweig, P., Pharoah, R., Eksteen, R., & Walls, R. (2018). *Installation of Smoke Alarms in an Informal Settlement Community in Cape Town*, South Africa.

Microscale fire modelling at the Wildland-Urban Interface

Cesare Fiorini; Hélder D. Craveiro*; Aldina Santiago; Luís Laim; Luís Simões da Silva

ISISE, Department of Civil Engineering, University of Coimbra,
Rua Luís Reis Santos – Pólo II 3030-218, Coimbra, Portugal,
{gerson.fiorini, heldercraveiro.eng, aldina, luislaim, luisss}@dec.uc.pt

Keywords

Wildland-urban interface; Physics-based modelling; Performance-based approach; CFD; Heat transfer

Abstract

The direct and indirect impacts of Wildland-Urban Interface fires on infrastructures and communities have become more severe in the last few decades, mainly due to the disproportionate growth of urban areas lacking planning and management, the abandonment of rural areas and activities, and climate changes. Many regions of the southern Mediterranean, the United States, Australia, and South America have been severely affected with catastrophic losses.

Building codes addressing the problem of WUI fires in the vicinity of the built environment are still scarce, but already with a few good examples, namely the Australian Standard AS 3959-2009, Construction of Buildings in Bushfire Prone Areas. But with the increasing risks, nowadays mainly driven by climate change, it is necessary to develop new approaches and codes for existing and new buildings effectively contributing to enhancing the resilience of the built environment and communities in the WUI. Moreover, taking advantage of new and ever-evolving computational tools, the use of a performance-based approach, replacing or complementing prescriptive codes, shows great potential to enable a deeper understanding of the complex fire spread mechanisms from forest fires to urban fires, namely radiant heat, direct flame contact and firebrands.

Physics-based modelling enables a better understanding of such phenomena, bearing in mind that up to date no accurate and reliable models for firebrands can be found. In this investigation, a performance-based approach is considered, exploring the capabilities of computational fluid dynamics and the software Fire Dynamics Simulation (FDS) to investigate and quantify WUI fire exposures. This was achieved by considering available experimental data on vegetation burning and developing and calibrating the numerical models using FDS. A Particle Method, based on Lagrangian particles was selected for this investigation since this model is particularly suitable to simulate surface and raised vegetation fire spread. With this strategy all thermo-physical properties of the fuels must be used as input, ensuring that the fire spread can be computed by the model.

Based on the calibrated models for a single tree, a new case study scenario was created (structure exposed to wildfire) and investigated aiming to assess in detail WUI fire exposures under different conditions by varying several parameters, such as wind speed and direction, distance to the structure and elevation of the terrain. Since a performance-based approach was selected and considering the basic principles associated with Fire Safety Engineering (FSE), 3 basic components must be assessed, namely the fire modelling, the thermal analysis of the structure and finally the structural analysis considering temperature increase and degradation of mechanical properties of materials. From the fire modelling investigated in this paper, some attention was devoted to assessing Adiabatic Surface Temperatures in the structure and consequently defining in a simple way to couple CFD field models to Finite Element Models (FEM) that will enable the understanding and development of ignition resistant structures in the WUI.

1. Introduction

The direct and indirect impacts of Wildland-Urban Interface (WUI) fires on infrastructures and communities have become more severe in the last few decades, mainly due to the disproportionate growth of urban areas lacking planning and management, the abandonment of rural areas and activities, and climate changes. Catastrophic loss of lives, property damage and environmental destruction have been observed on several occasions, such as the 2005 and 2017 wildfires in Portugal (Independent Technical Commission 2022; Chas-Amil et al. 2020; Independent Technical Commission 2018), the 2009 Victorian bushfires (Teague B. et al., 2009), the 2018 Camp Fire in Northern California (P. Eavis et al. 2020; Spearing et al. 2020; Ager et al. 2021), the Australian bushfires (I. Kwai 2020); Mclennan et al. 2015) or the wildfires in Eastern Attica, Greece (Efthimiou et al. 2020). The severity of the problem is relevant and may be intensified in the next few years by climate changes. In the Sixth Assessment Report of the Intergovernmental Panel on Climate Change (IPCC

2021), it is stated that in southern Europe, northern Asia, the USA, and Australia, the weather conditions promoting the occurrence of wildfires, are becoming more likely. The increasing frequency of such events shows the urgent need to understand these phenomena and the existing risks, aiming to predict their consequences and implement adequate mitigation measures, strengthening the resilience of communities and the built environment (Ager et al. 2021; Álvares-Miranda et al. 2018; Syphard et al. 2017). Understanding the fire spread mechanisms from wildfires to the built environment in the vicinity of forest areas is a complex task requiring extensive investigation considering not only the WUI fire exposure (radiant heat, direct flame contact and firebrands) but also the vulnerability of infrastructures (Quarles and Standohar-Alfano 2018) for the development of science-based resilient solutions/methods for retrofitting existing structures and to design new structures in the WUI, that can be incorporated in future codes.

Exploring the versatility of advanced computational tools, it is possible to adopt a Performance-Based Design (PBD) approach to investigate in detail fire spread mechanisms from forest fires to the built environment using similar strategies as the ones presented by Vacca et al. (2020) in the scope of the research project WUIVIEW - Wildland-Urban Interface VIrtual Essays Workbench ((ECHO/2018/826522), considering that serious limitations still exist mainly related to the behaviour of firebrands and their interaction with structures and how external fires impact buildings. In this investigation, physics-based models, using the software Fire Dynamics Simulator (FDS) (McGrattan et al. 2020), were developed to calibrate experimental tests on single burning trees (Douglas-fir experiments conducted at NIST) reported by Mell *et al*. (2009). Then some case study scenarios were designed, incorporating surface vegetation and trees in the vicinity of a building. Additionally, the influence of elevation and wind speed on the fire behaviour was considered to evaluate the possible fire spread mechanisms from wildfires to buildings.

2. Methodology

2.1. Modelling of single-burning trees

To conduct parametric numerical studies, it is necessary to accurately calibrate the developed models using available experimental results. In this study, the experimental tests performed by Mell *et al*. (2009) on single-burning Douglas-fir trees were reproduced using FDS 6.7.7 (McGrattan et al. 2020). The calibration was performed for 2 m and 5 m Douglas-fir trees, with a moisture content of 14% and 26%, respectively. The Particle Method was used to model the vegetation in fire. In this case, the trees are represented by a collection of Lagrangian particles that are heated up by convection and radiation, as explained by Vanella *et al*. (2021). Using the Particle Method, it is necessary to use as input all relevant thermo-physical properties of fuels, allowing the model to compute the fire spread. Physical and thermal properties/parameters used in the simulations are presented in Table 1. It is worth mentioning that different fuel chemical compositions were assumed, namely $C_{3.4}H_{6.2}O_{2.5}$ (Hostikka and McGrattan 2001), $C_6H_{10}O_5$ (Browne 1958) and $CH_{1.7}O_{0.74}N_{0.002}$ (McGrattan et al. 2021). The heat of combustion was 17500 kJ/kg.

Table 1 – Physical and Thermal Parameters used in FDS

Quantity	Value	Quantity	Value
Drag Coefficient [--]	2.8	Heat of Combustion [kJ/kg]	14516|17500
Moisture Vegetation [%]	14|26	Soot Yield [kg/kg]	0.02
Vegetation Density	514	Initial Temperature [º C]	28
Fuel Geometry Tree	Cone	Heat of Reaction [kJ/kg]	418
Crown Width (radius) [m]	0.85|1.45	Specific Heat Capacity [kJ/kg K]	2.0|1.5|4.184
Crown Base Height [m]	0	Thermal Conductivity [1][W/ m K]	0.11
Tree Height [m]	1.9|4.3	Density [2] [kg/m^3]	300|67
N_PARTICLES_PER_CELL	1	Reference Temperature [º C]	300 [3], 100 [4]
PACKING_RATIO (s, m, l) [5]	68, 48, 44| E-5	Shape	Cylindrical

[1] Vegetation; Char and Ash.; [2] Moisture, Char Veg and Dirt.; [3] Vegetation Grass. [4] Moisture. (small, medium, large) [5]

Mesh sensitivity tests were also performed, considering two mesh sizes, namely 10 and 25 cm. It was observed that mesh size played a very relevant role in the accuracy of the developed model. Overall, it was observed that the FDS can accurately reproduce the observed experimental behaviour in terms of Mass Loss Rate for both

single Douglas-fir burning trees using a mesh size of 10 cm and a fuel chemical composition of $C_{3.4}H_{6.2}O_{2.5}$ (S. Hostikka and K. MacGrattan, 2001). As in the experimental test, a circular shape burner was prescribed with a heat release rate of 30 kW.

2.2. WUI case study

The selected case study comprised a small industrial warehouse (15 × 10 m^2) facing a set of trees. The maximum height of the building is 12 m. Two doors (3.5 x 8 m^2) are located on the eastern and western sides. Two square gates (8 × 8 m^2) are placed on the northern and southern wall perimeters. The trees are on a slope, as depicted in Figure 1. The dimensions of the computational domain are the following: X = 57 m, Y = 36 m and Z = 40 m. Four meshes were created to optimize the computation time. Three meshes, with a cubic cell of 25 cm were created (Z direction ranging from 0 to 24 m). The fourth mesh with cubic cells of 50 cm was created in the Z direction from 24 to 40 m. A total of 3.414.528 cells are generated. The cladding of the walls is made of a concrete panel with a thickness of 25 cm. The glass surfaces are 15 mm thick. The terrain has two flat planes with an 8 m difference in altitude. The warehouse is located on the higher ground (west side), where there is no vegetation. The flat ground has an extension of 37 x 36 m^2 and an elevation of 8 m above the bottom level (east side). The ground area covered with grass is 20 x 36 m^2. A slope of 46 º (*i.e.*, 80 %) is considered. Grass and nine trees, having a height of 15 m and a girth of 1.5 m, are positioned on the slope. The wind is a critical parameter and was considered in the model, using different wind speeds aiming to assess its influence on the fire behaviour. The wind was modelled using the Monin-Obukhov (Vanella et al. 2021) similarity theory, considering neutral stability with an Obukhov length of 1000000 m and a Davenport-Wieringa roughness length classification of 0.03 (classification: open; grass prairie, farm fields, tundra, airports, heather) (McGrattan et al. 2021). For the detailed case study, the following wind speeds were assessed: 4.15 m/s, 5.80 m/s and 6.7 m/s.

To assess the impact of the forest fire in the structure, aiming to easily transfer data from the fire model to the heat transfer model and mechanical model and understand heat transfer to solids, several Adiabatic Surface Temperature (AST) devices were used. The AST concept is useful to calculate temperatures in fire-exposed structures (expressing the thermal exposure of a surface).

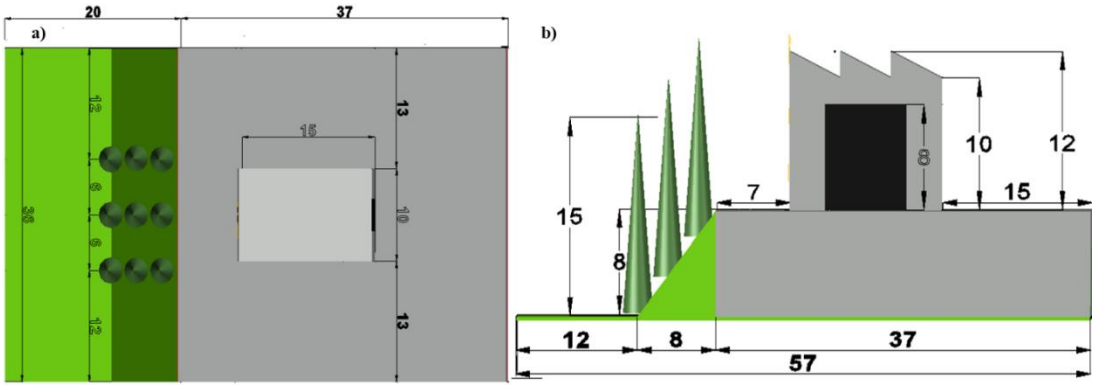

Figure 1 – Schematic representation of the selected case study. a) Top view. b) Lateral view.

3. Results

3.1. Calibration of single-burning trees

The previously described modelling strategies and assumptions provided accurate estimations using a more refined mesh size of 10 cm, but with significantly higher needs in terms of computational resources. The comparison between experimental and numerical results is depicted in Figure 2. The peak mass loss monitored in the experimental test of the Douglas-fir tree with 2 m (moisture of 14%) was 0.417 kg/s, whereas the numerical model provided an estimation of 0.409 kg/s. The results show an excellent agreement, hence enabling additional parametric studies. Regarding the case of a tree with 5 m (moisture of 26%), as depicted in Figure 2b), the peak mass loss rate was 1.90 kg/s in the experimental test and 2.03 kg/s in the numerical simulation considering a mesh size of 10 cm (showing a difference of less than 7%).

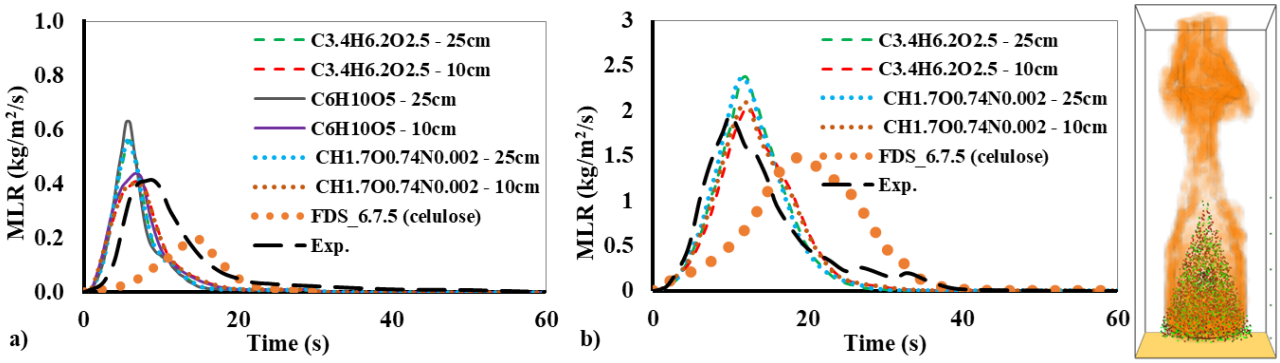

Figure 2 - Calibration of the numerical models against single burning Douglas-fir trees. Mass loss rate comparison. a) Tree with 2 m with a moisture content of 14%. b) Tree with 5 m with a moisture content of 26%.

3.2. Case study

Figure 3 shows values referring to Radiative Heat Flux obtained in the investigated scenario. Two quantities are displayed, F and R, respectively from the façade and the roof, considering three different wind speeds expressed in m/s (4.15, 5.85 and 6.70). Figure 4 depicts the obtained Adiabatic Surface Temperatures (AST) at different locations.

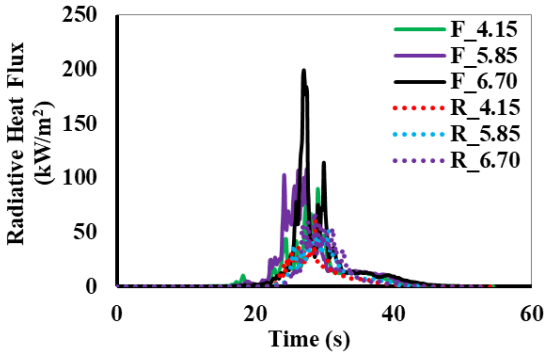

Figure 3 – Radiative Heat Flux as a function of the adopted wind speed.

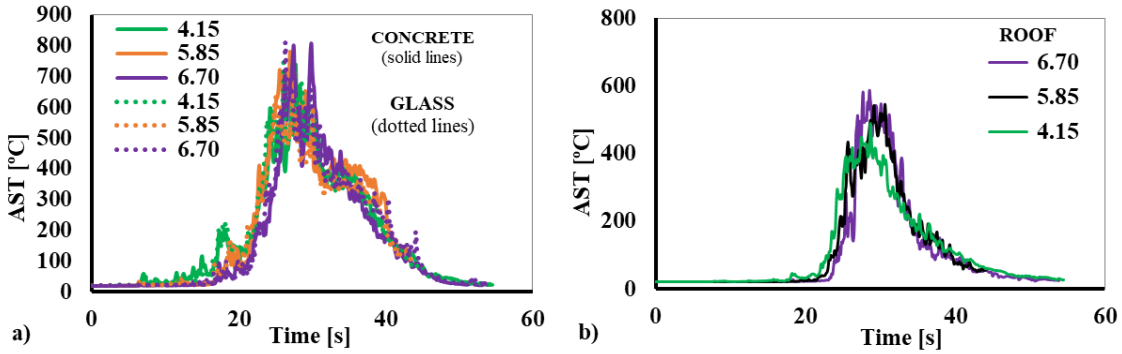

Figure 4 – Adiabatic Surface Temperatures at different locations of the building as a function of wind speed. a) AST in concrete and glass. b) AST in the roof.

The highest values are obtained on the façade (around 200, 108, and 90 kW/m^2 respectively, for 6.70, 5.85 and 4.15 m/s). The higher values were obtained when the higher wind speeds were considered, which caused a greater deflection of the flames. The average maximum value of the radiative flux measured on the roof was about 60 kW/m^2.

AST temperatures on concrete and glass (placed on the façade) and on the roof are depicted in Figure 4 a) and b), respectively. All the curves in Figure 4 a) are very close. For concrete, the peak value was 806ºC, and for glass, it was 813ºC. Both values were reached for a wind velocity equal to 6.70 m/s. Figure 4 b) shows that the difference between the maximum peak values is 100ºC, with the highest value of 587ºC with the wind blowing

at 6.70m/s. The obtained information allows coupling CFD results with finite element software, enabling the mechanical analysis of buildings in the WUI and consequently the analysis and design of fire-resistant and resilient buildings.

4. Conclusions

Fire spread mechanisms from wildfires to the built environment are complex phenomena that still require extensive research, especially when related to the behaviour of firebrands and their interaction with structures (different levels of vulnerability of structures may lead to new secondary fires). However, existing tools already show the potential for further developments for a better understanding and more accurate quantification of fire exposures in the WUI. This will lead to relevant developments in terms of new design methodologies for buildings in the vicinity of forest areas incorporating Performance-based principles.

In this study, numerical models were developed and calibrated against experimental results, enabling new parametric studies focusing on the relevant heat transfer phenomena from wildfires to the built environment. Wind speed was one of the key parameters investigated. Its impact on the radiative heat flux and AST was assessed and reported. For the selected case study, the higher the wind speed the higher the incident radiative heat flux and AST in the structure.

Further studies on firebrands and new mathematical models must be developed to better simulate their behaviour and interaction with surrounding infrastructures.

5. Acknowledgements

The authors gratefully acknowledge FCT for its support under the framework of the research project PCIF/AGT/0062/2018 – INTERFACESEGURA, financed by FCT through National funds.

6. References

Ager, A. Alan, Michelle A. Day, Fermin J. Alcasena, Evers, Cody R., Karen C Short, Isaac Grenfell, (2021), Science of the Total Environment, 784, 147057. https://doi.org/10.1016/j.scitotenv.2021.147057

Álvarez-Miranda, Eduardo, et al., (2018) A multicriteria optimization model for sustainable forest management under climate change uncertainty: An application in Portugal, European Journal of Operational Research, 269, pp. 79-98. https://doi.org/10.1016/j.ejor.2017.04.052

Chas-Amil, María-Luisa, García-Martínez, Eduardo, Touza, Julia, (2020). Iberian Peninsula October 2017 wildfires: Burned area and population exposure in Galicia (NW of Spain), International Journal of Disaster Risk Reduction, vol. 48, 101623. https://doi.org/10.1016/j.ijdrr.2020.101623

Efthimiou, N., Psomiadis, E., Panagos, Panos, (2020). Fire severity and soil erosion susceptibility mapping using multi-temporal Earth Observation data: The case of Mati fatal wildfire in Eastern Attica, Greece, Catena, vol. 187, 104320. https://doi.org/10.1016/j.catena.2019.104320

F.L. Browne (1958), Theories of the combustion of wood and its control: A survey of the literature, Report 2136, Forest Products Laboratory, US, Department of Agriculture, 1958.

I. Kwai, (2020) What to read on Australia's bushfire crisis. New York Times. Retrieved February. https://www.nytimes.com/2020/01/10/world/australia/bushfire.html (2020), 17-2020.

Independent Technical Comission, Guerreiro J. et al. (2018) Avaliação dos incêndios ocorridos entre 14 e 16 de outubro de 2017 em Portugal Continental, Relatório final. Comissão Técnica Independente. Assemnly of the Portuguese Republic, Lisboa, 2018, p. 274.

Independent Technical Commission, Coord. Guerreiro, J., et al (2022), Análise e apuramento dos factos relativos aos incêndios que ocorreram em Pedrogão Grande, Castanheira de Pera, Ansião, Alvaiázere, Figueiró dos Vinhos, Arganil, Góis, Penela, Pampilhosa da Serra, Oleiros e Sertã, entre 17 e 24 de Junho de 2017, Final Report, Assembly of the Portuguese Republic, Portugal.

IPCC, 2021: Summary for Policymakers. In: Climate Change 2021: The Physical Science Basis. Contribution of Working Group I to the Sixth Assessment Report of the Intergovernmental Panel on Climate Change [Masson-Delmotte, et al.]. Cambridge University Press. In Press.

M. Vanella, K. McGrattan, R. McDermott, G. Forney, W. Mell, E. Gissi and P. Fiorucci (2021), A Multi-Fidelity - Framework for Wildland Fire Behavior Simulations over Complex Terrain, Atmosphere, vol. 12, no. 273, pp. 1-16. https://doi.org/10.3390/atmos12020273

McGrattan K., Hostikka S., Floyd J., McDermott R., Vanella M. (2020), Fire Dynamics Simulator Technical Reference Guide, Volume 3: Validation- NIST Special Publication 1018-3 6th ed., pp. 27–29, 896, 897. http://dx.doi.org/10.6028/NIST.SP.1018

McGrattan K., Hostikka S., Floyd J., McDermott R., Vanella M. (2021), Fire Dynamics Simulator, User's Guide, NIST Special Publication 1019 6th ed., http://dx.doi.org/10.6028/NIST.SP.1019

Mclennan, Jim, Paton, Douglas, Wright, Lyndsey, (2015). At-risk householders' responses to potential and actual bushfire threat: An analysis of findings from seven Australian post-bushfire interview studies 2009-2014, International Journal of Disaster Risk Reduction, vol. 12, 319-327.

Mell W., Maranghides A., McDermott R, Manzello S.L. (2009), Numerical simulation and experiments of burning douglas fir trees, 641 Combustion and Flame, Volume 156, Issue 10, pp. 2023-2041. https://doi.org/10.1016/j.combustflame.2009.06.015

P. Eavis, I. Penn. (2020) California says PG&E power lines caused camp fire that killed 85, New York Times (2019, May 15). https://www.nytimes.com/2019/05/15/business/pge-fire.html, Accessed 20th sept. 2020.

Quarles, S. L.; Standohar-Alfano C. D. (2018), Ignition Potential of Decks Subjected to an Ember Exposure - Wildfire Research, Technical Report, pp. 2,3,5,7,17. https://ibhs.org/wp-content/uploads/Ignition-Potential-of-Decks-Subjected-to-an-Ember-Expo- 603sure.pdf

Simo Hostikka, K.B. McGrattan (2001), Large-eddy simulation of wood combustion, Interfalm'2001, International Interflam Conference, 9th Proceedings. Volume 1. September 17-19, Edinburgh, Scotland, Interscience Communications LTD, London, England, 755-762, 2001.

Spearing, Lauryin A., Faust, Kasey M. (2020). Cascading system impacts of the 2018 Camp Fire in California: The interdependent provision of infrastructure services to displaced populations, International Journal of Disaster Risk Reduction, Vol. 50, November 2020, 101822. https://doi.org/10.1016/j.ijdrr.2020.101822

Syphard, A. D., Brennan T.J., Keeley J. E. (2017), The importance of building construction materials relative to other factors affecting structure survival during wildfire, International Journal of Disaster Risk Reduction, Volume 21, Pages 140-147. https://doi.org/10.1016/j.ijdrr.2016.11.011

Teague B., McLeod R., Pascoe S., (2009), Victorian Bushfires Royal Commission, Final Report, Parliament of Victoria, Melbourne, Australia.

Vacca P., Caballero D, Pastor E., Planas E. (2020) WUI fire risk mitigation in Europe: A performance-based design approach 2020, Journal of Safety Science and Resilience 1 97–105.

Mobile LPG cylinders at WUI fires: an alternative to avoid accidents

Thiago Barbosa*[1,2]; Luís Reis[2]; Jorge Raposo[2]; Domingos Viegas[2]

[1]Univ Coimbra, ADAI, Department of Civil Engineering. Rua Luís Reis Santos, Pólo II, 3030-788 Coimbra, Portugal.
[2]Univ Coimbra, ADAI, Department of Mechanical Engineering. Rua Luís Reis Santos, Pólo II, 3030-788 Coimbra, Portugal, {luis.reis, jorge.raposo, xavier.viegas}@dem.uc.pt

**Corresponding author*

Keywords

LPG cylinders, Wildland-Urban Interface fires, BLEVE, Protection, Safety.

Abstract

Wildland fires are frequent events worldwide, particularly in the European-Mediterranean region, USA, and Australia. These fires have been more frequent and intense in recent years due to climate changes and may cause significant damage, especially when reaching theWildland-Urban Interface (WUI) areas. The presence of liquefied petroleum gas (LPG) cylinders may cause severe events in WUI areas, as occurred in Portugal during the large wildfires of 2017, which could have been avoided if the cylinders were protected. Devices for protecting the parts of houses under WUI fire were previously presented, but a protective device for cylinders was not. In this work, a protective device for LPG cylinders made with a thin fabric with an aluminum coating on the external face was tested in laboratory and field conditions. The cylinder and the fabric were equipped with thermocouples and heat flux sensors attached to their surfaces. The tests showed that the device gave effective protection to the cylinder, decreasing the radiative heat flux that reaches it and keeping it in a safe condition when exposed to a fire; consequently preventing extreme behavior such as an explosion.

1. Introduction

Wildfires cause huge socio-economic damages, particularly when they occur in Wildland-Urban Interface (WUI) areas. These fires are becoming more frequent and severe in recent years due to climate change (Barbosa et al., 2022; Oliveira et al., 2020; Pastor et al., 2020; D. X. Viegas et al., 2021). Liquefied petroleum gas (LPG) cylinders are widely used in many countries for different domestic purposes, such as cooking, heating water, and keeping homes warm (Heymes et al., 2013; Scarponi et al., 2020) . Given the fact that the majority of rural WUI areas do not have a gas distribution network, the presence of mobile gas cylinders near each house is common. When a wildfire occurs nearby, the cylinders become a relevant hazard for the people and structures because of the enormous amount of energy stored.

Accidents related to LPG cylinders have been registered in Portugal during at least five large fires and in other countries (Table 1). Regarding the effects caused by an LPG cylinder's explosion, experimental tests with an LPG cylinder were carried out by other authors (Stawczyk, 2003; Tschirschwitz et al., 2017): the flying projectiles could reach up to 300 meters from the initial position; the overpressure presented high values at distances shorter than 10 meters from the explosion. These effects may jeopardize the safety of persons and structures in the surroundings.

Table 1: Summary of events related to LPG stored at WUI

id	Place	Type	Year	Event	Reference
1	Quinta do Colaço, Portugal	Cylinder	2015	BLEVE	(Almeida, 2015)
2	Funchal, Madeira, Portugal (2 cases)	Cylinder	2016	BLEVE	(Barbosa et al., 2022; Caballero et al., 2019; Scarponi et al., 2020)
3	Calabassas, California, USA	Domestic tank	2016	Jet fire	(Scarponi et al., 2020;Bartholomew, 2016)
4	Benitatxell, Spain (2 cases)	Domestic tank	2016	Jet fire	(Scarponi et al., 2020; Caballero et al., 2019)
5	Louriceira, Portugal	Cylinder	2017	BLEVE	(Viegas et al., 2017)

6	Oliveira do Hospital, Portugal (2 cases)	Cylinder	2017	BLEVE	(Barbosa et al., 2022; Viegas et al., 2019)
7	Vale do Laço, Portugal	Cylinder	2017	BLEVE	(Viegas et al., 2019)
8	Balsa, Portugal	Cylinder	2017	BLEVE	(Viegas et al., 2017)
9	Mati, Greece (2 cases)	Domestic tank	2018	Jet fire	(Scarponi et al., 2020)
10	Llutxent, Spain	Cylinder	2018	Jet Fire	(Caballero et al., 2019)

Protective devices were presented to protect house walls and roofs in a WUI fire case (Barbosa et al., 2022; Takahashi, 2019; C. Viegas et al., 2021) . However, the LPG cylinders are commonly placed outside of the houses as a safety recommendation. Thus, cylinders should also be protected to avoid accidents.

To fill the gap related to the LPG cylinder's protection, this study presents a light and cheap protection for LPG cylinders capable of keeping them in a safe condition when exposed to WUI fires (Barbosa et al., 2022; Takahashi, 2019; C. Viegas et al., 2021).

2. Materials and Methods

2.1. The protective device

The protective device (PD1) was manufactured with two main parts. The first and most external one is made with a fabric manufactured with fiberglass with an aluminum coating on the external face to decrease the radiative heat flux. The fabric is classified "A" (non-combustible) according to the European fire classification for construction products (EN 13501). The second one is a structure made with a square metal tube, with geometry the same as a cube, with opened faces and a handle on top used for moving. On one face, near the bottom, there is a small vent square of 15 x 15 cm to pass the gas tube. This tube was wrapped in the fabric. The goal of the protection device is to reduce the heat flux that reaches the cylinder and prevent the LPG stored in the cylinder from getting warm. It is an alternative system for people living in rural areas without access to an industrialized or commercial protection system; it is easy to be built, cheap, light, mobile, and ergonomic. The protective device was built for cylinders of 11 kg of propane or 13 kg of butane and manufactured in accordance with European codes (EN 12245:2009+A1; EN 1442). It has the following dimensions: 65 cm in height and 45 cm in length and width. The cost of the protection was 56 Euros, and the total system weight was 6.4 kg.

2.2. Laboratory tests

Seventeen tests were carried out (Table 2), sixteen at the laboratory and one in the field. The laboratory tests were performed in the Forest Fire Research Laboratory (LEIF) in Lousã, Portugal, at four different flame distances, to evaluate the protection efficiency related to the heat flux at flame distances similar to those found in fires near rural houses. The field test was aimed at evaluating the cylinder protection in a real fire scenario and validating the laboratory tests.

Table 2: Summary of the tests

Test	Reference	Distance (m)	Content Moisture (%)	Room Temperature (ºC)
1	F25-1	0.25	16	24.3
2	F25-2	0.25	11.5	19.7
3	F25-3	0.25	11.5	19.5
4	F50-1	0.5	14.3	15.1
5	F50-2	0.5	11.5	19.7
6	F50-3	0.5	11.5	19.7
7	F75-1	0.75	16	25.6
8	F75-2	0.75	11.5	19.7
9	F75-3	0.75	11.5	19.7
10	F100-1	1	16	22.5
11	F100-2	1	10	20
12	F100-3	1	10	19.8
13	Ref25	0.25	16	11.9
14	Ref50	0.5	16	12

15	Ref75	0.75	16	11.6
16	Ref100	1	16	11.8
17	PSS	surrounded	40	21

The cylinders were placed at four different distances ”D”. These distances from the flames used were 0.25, 0.5, 0.75, and 1 meter. For each test were used 10 kg of shrubs. Shrubs were used according to previous studies placed (Pinto et al., 2017; Rodrigues et al., 2019; D. X. Vegas et al., 2021; Viegas et al., 2006), and it is the same fuel present in the field test. This fuel was in a basket with a volume of 1 m^3. Reference tests with the cylinder and without protection were performed to obtain the heat flux and temperature on the cylinder’s surface.

The cylinders were equipped with the temperature and heat flux sensor IHF01 Hukseflux attached to the external surface (FI 1, TI 1) halfway up the cylinder’s height; the same was attached to the external surface of the fabric (FI 2, TI 2) (Figure 1). Two thermocouple type K were used; the first thermocouple was attached to the floor at 10 cm from the fuel basket (TI 3); and the second was attached to a wall surface, far from the influence of the flame (TI 4). The flux sensors were connected to the model 9211 (±80 mV) from National Instruments (NI), and it was plugged into the chassis 9174, also from NI. These instruments allow for the continuous measurement of the signal from the sensor with a frequency of 1 Hz, being able to load and process the data directly to a computer. The thermocouples were connected to a model 9213 from NI.

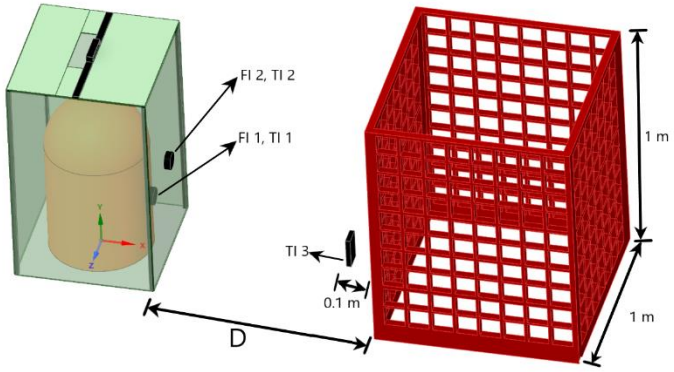

Figure 1- Schematic drawing of laboratory test: protective device at the four distances “D” from the fuel basket, and the instrument’s position on the cylinder’s surface (FI 1, TI 1), fabric’s surface (FI 2,TI 2), and thermocouple 3 – credit Barbosa et al. (2022).

2.3. Field Test

In the field test, the instrumental apparatus used was the same as in the laboratory tests. The field test was performed on a slope of 30% covered by shrubs with less than 50 cm in height and an average moisture content of 40%. The LPG cylinder was covered by the protective device and surrounded by shrubs. The ignition was made on the bottom of the hill (Figure 2 b).

(a) (b)

Figure 2- (a) Laboratory teste, and (b) field test

3. Results and discussion

3.1. Laboratory tests

A significant difference was found (Figure 3) related to the heat flux that reached the cylinder´s surface and the fabric´s surface, showing that the high level of heat flux decreased, and this factor is decisive in keeping the conditions safe in a fire scenario. If there is no high heat flux reaching the vessel, the fluid pressure and temperature will not be high enough to produce an explosion.

The flux sensor attached to the surface cylinder showed values with no significant changes. For the test at 0.25 m from the flames, the difference related to the heat flux that reaches the cylinder´s surface and the fabric´s surface was up to 10 kW· m^{-2} (87%), which shows that the protection device works even at a short distance from the flames. The heat flux registered in the reference tests (Ref) without protection, and the flux on the cylinder´s surface under protection (Cylinder), show a significant difference in the flux that reaches the cylinder.

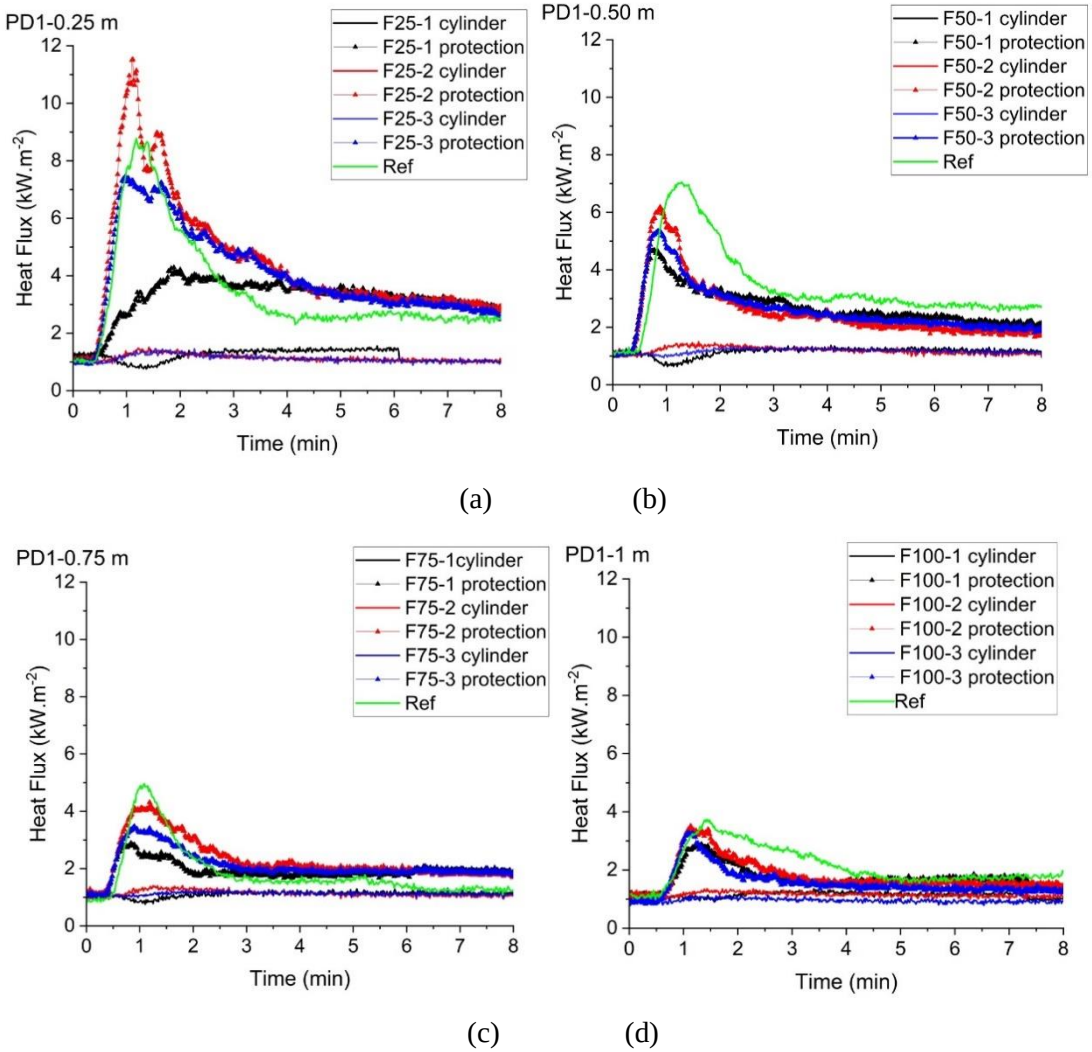

Figure 3- Heat flux on the protection, cylinder, and reference tests at (a) 0.25, (b) 0.50), (c) 0.75, and (d) 1 m from the basket fuel

In all tests with the protective device and during the time of fire exposure, the cylinder surface temperature remained close to the laboratory environmental temperature (Figure 4). Thus, the LPG cylinder was not heated and stayed under safe conditions, even when the fabric was reached by the intense heat flux of up to 12 kW· m^{-2} .

Figure 4 shows the temperature on the cylinder´s surface (Cylinder) and the temperature on the fabric´s surface (Protection). There is a great difference between the cylinder and fabric surfaces, reaching 80 °C. The cylinder´s surface temperature was kept at safe values, close to the laboratory temperature, and below the temperature

needed to cause high pressure and open a pressure relief valve (26 bar). The temperature registered in the reference tests (Ref) without protection and the temperature on the cylinder´s surface under protection (Cylinder) shows a significant difference in the cylinder´s temperature, up to 80 °C (Figure 4).

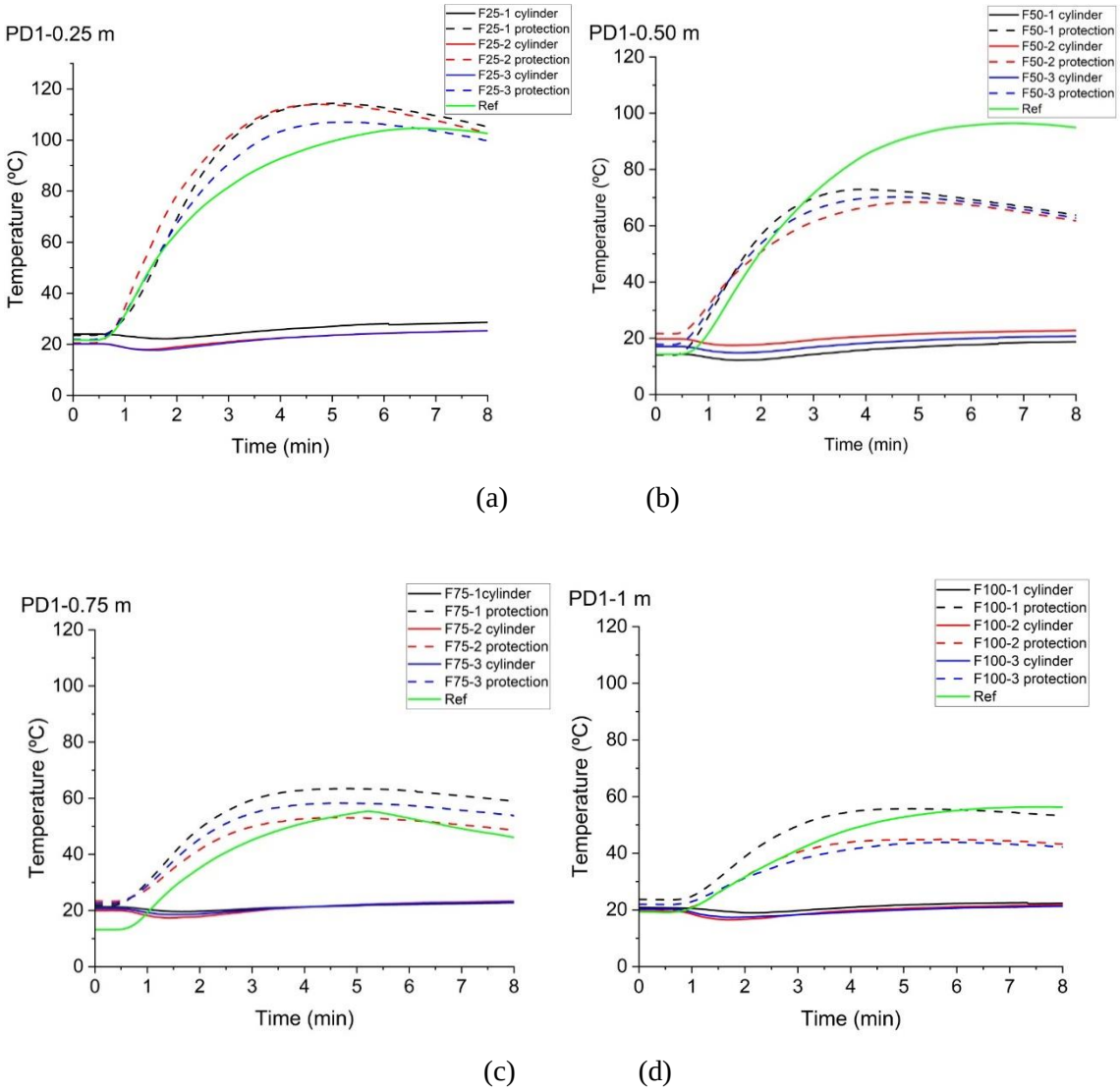

Figure 4- Temperature profile in the laboratory, on protection, cylinder, and reference tests at (a) 0.25, (b) 0.50), (c) 0.75, and (d) 1 m from the basket fuel

3.2. Field Test

In the field test, the behavior of the cylinder and protection was similar to the laboratory tests. There was a large difference between the temperatures of the cylinder´s surface and the fabric's surface, and the same occurred for the heat flux (Figure 5). On the outer face of the protection, the thermal radiation peak was 7 $kW \cdot m^{-2}$ and the peak temperature was 174 °C; on the face of the cylinder, the radiation peaked at 2.5 $kW \cdot m^{-2}$, and the surface temperature had a maximum of 51 °C.

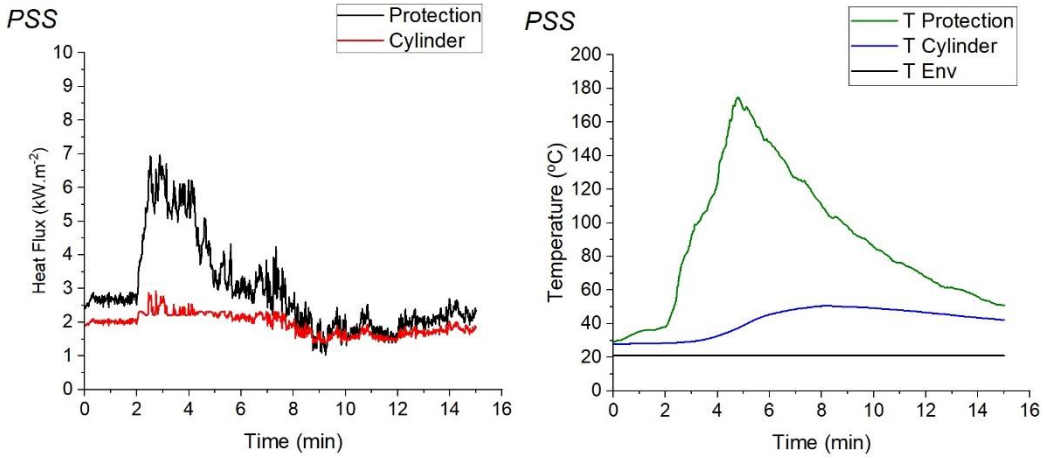

Figure 5- Field test (PSS): (a) Heat Flux and (b) temperatures on the surfaces of the protection and cylinder

4. Conclusion

WUI fires are frequent events, and they may cause accidents related to LPG stored. In this work, the efficiency of a protective device manufactured in an insulating fabric with a reflective external surface to cover an LPG cylinder and block the heat flux when a WUI fire occurs was assessed.

Laboratory and field tests were carried out with the protective device at different distances from the fire to find the block rate of the heat flux and determine if the protective device works in a real fire event.

The protective device could block up to 87% of the heat flux and keep the cylinder's temperature close to room temperature even under high heat flux and at a short distance from the flame.

Regarding the accidents mentioned, the protective device tested in this work could have avoided these burst vessel cases. It shows the importance of a protection system and how positive its use can be in avoiding the heating of the fluid, and hence the material rupture, decreasing the probability of extreme events, such as a BLEVE. The proposed protective device is an alternative to prevent accidents related to LPG cylinders in WUI fires.

5. References

Almeida, M.A. de F.B. de, 2015. Relatório resumo do Incêndio da Quinta do Colaço (Almalaguês).

Barbosa, T.F., Reis, L., Raposo, J., Viegas, D.X., 2022. A Protection for LPG Domestic Cylinders at Wildland-Urban Interface Fire. Fire 5, 63. https://doi.org/10.3390/ fire5030063

Bartholomew, D., 2016. Old Fire in Calabasas burns more than 500 acres, threatens thousands of homes [WWW Document]. Los Angeles Dly. News. URL https://www.dailynews.com/2016/06/04/old-fire-in-calabasas-burns-more-than-500-acres-threatens-thousands-of-homes/ (accessed 5.13.22).

Caballero, D., Sjöström, J., Pastor, E., 2019. Inventory of pattern scenarios. Wuiview 1–70.

European Committee for Standardization, 2017. EN 1442.

European Committee for Standardization, 2018. EN 13501.

European Committee for Standardization, 2012. EN 12245:2009+A1.

Heymes, F., Aprin, L., Forestier, S., Slangen, P., Baptiste Jarry, J., François, H., Dusserre, G., 2013. Impact of a distant wildland fire on an LPG tank. Fire Saf. J. 61, 100–107. https://doi.org/10.1016/j.firesaf.2013.08.003

Oliveira, R., Oliveira, S., Zêzere, J.L., Viegas, D.X., 2020. Uncovering the perception regarding wildfires of residents with different characteristics. Int. J. Disaster Risk Reduct. 43. https://doi.org/10.1016/j.ijdrr.2019.101370

Pastor, E., Muñoz, J.A., Caballero, D., Àgueda, A., Dalmau, F., Planas, E., 2020. Wildland–Urban Interface Fires in Spain: Summary of the Policy Framework and Recommendations for Improvement. Fire Technol. 56, 1831–1851. https://doi.org/10.1007/s10694-019-00883-z

Pinto, C., Viegas, D., Almeida, M., Raposo, J., 2017. Fire whirls in forest fires: An experimental analysis. Fire Saf. J. 87, 37–48. https://doi.org/10.1016/j.firesaf.2016.11.004

Rodrigues, A., Ribeiro, C., Raposo, J., Viegas, D.X., André, J., 2019. Effect of Canyons on a Fire Propagating Laterally Over Slopes. Front. Mech. Eng. 5, 1–9. https://doi.org/10.3389/fmech.2019.00041

Scarponi, G.E., Pastor, E., Planas, E., Cozzani, V., 2020. Analysis of the impact of wildland-urban-interface fires on LPG domestic tanks. Saf. Sci. 124. https://doi.org/10.1016/j.ssci.2019.104588

Stawczyk, J., 2003. Experimental evaluation of LPG tank explosion hazards, Journal of Hazardous Materials.

Takahashi, F., 2019. Whole-House Fire Blanket Protection From Wildland-Urban Interface Fires. Front. Mech. Eng. 5. https://doi.org/10.3389/fmech.2019.00060

Tschirschwitz, R., Krentel, D., Kluge, M., Askar, E., Habib, K., Kohlhoff, H., Neumann, P.P., Storm, S.U., Rudolph, M., Schoppa, A., Szczepaniak, M., 2017. Mobile gas cylinders in fire: Consequences in case of failure. Fire Saf. J. 91, 989–996. https://doi.org/10.1016/j.firesaf.2017.05.006

Viegas, C., Batista, R., Albino, A., Coelho, M., Andrade, J., Alves, D., Viegas, D.X., 2021. Active Barrier Combining Fire-Resistant Fiberglass Fabric and Water Sprinkler System for Protection Against Forest Fires. Fire Technol. 57, 189–206. https://doi.org/10.1007/s10694-020-00991-1

Viegas, D.X., Figueiredo Almeida, M., Ribeiro, L.M., Raposo, J., Viegas, M.T., Oliveira, R., Alves, D., Pinto, C., Jorge, H., Rodrigues, A., Lucas, D., Lopes, S., Silva, L.F., 2017. O complexo de incêndios de Pedrógão o Grande e concelhos limítrofes, iniciado a 17 de Junho de 2017.

Viegas, D.X., Palheiro, P.M., Pita, L.P., Ribeiro, L.M., Cruz, M.G., Ollero, A., Arrue, B., Ramiro, M.D., 2006. Analysis of fire behaviour in Mediterranean shrubs: The Gestosa fire experiments (Portugal). For. Ecol. Manage. 234, S101. https://doi.org/10.1016/j.foreco.2006.08.137

Viegas, D.X., Rodrigues, A., Abouali, A., Almeida, M., Raposo, J., 2021. Fire downwind a flat surface entering a canyon by lateral spread. Fire Saf. J. 122, 103349. https://doi.org/10.1016/j.firesaf.2021.103349

Viegas, X., Almeida, M.F., Ribeiro, M., Almeida, M.A., Raposo, J., Viegas, M.T., Oliveira, R., Alves, D., Pinto, C., Rodrigues, A., Ribeiro, C., Lopes, S., Jorge, H., Viegas, C.X., 2019. Análise Dos Incêndios Florestais Ocorridos a 15 De Outubro De 2017 - Principais incêndios e resposta operacional.

Modelling pyro-convective activity in Pedrógão Grande mega fire

Flavio T. Couto *[1,2]; Jean-Baptiste Filippi[3]; Roberta Baggio[3]; Rui Salgado [1,2,4]

[1]Instituto de Ciências da Terra—ICT (Polo de Évora), Universidade de Évora, Rua Romão Ramalho, 59, 7000-671 Évora, Portugal, {fcouto, rsa}l@uevora.pt
[2] Earth Remote Sensing Laboratory (EaRS Lab), Universidade de Évora, Évora, Portugal.
[3] Centre National de la Recherche Scientifique (CNRS), Sciences Pour l'Environnement – Unite ì Mixte de Recherche 6134, Università di Corsica, Campus Grossetti, Corte, France, {filippi_j@univ-corse.fr, roberta.baggio.colpi@gmail.com}
[4] Departamento de Física, Escola de Ciências e Tecnologia, Universidade de Évora, Évora, Portugal

**Corresponding author*

Keywords

Mega fires; PyroCb; Meso-NH model; ForeFire model.

Abstract

The development of PyroCumulonimbus (PyroCb) clouds during mega fire events has high impact in the evolution of the fire fronts and have been observed more frequently in the last years. In 2017, Portugal was affected by several episodes of extreme wildfires with associated cloud systems. The present study aims to investigate the development of pyro-convective activity during the Pedrógão Grande episode. The study used the reference fire propagation deduced from the official investigation (forced fire) as well as reference boundary condition from atmospheric analysis to simulate the coupled simulation with a mesoscale atmospheric model at high temporal and spatial resolution. The Meso-NH model has been configured into three nested domains with horizontal resolutions of 2000 m, 400 m and 80 m. The emission of heat and vapour into the atmosphere was made using the ForeFire model. The results highlight the importance of the use of cloud resolving models configured with very-high spatial and temporal resolutions for representing the development of phenomena associated to pyro-convective activity, namely those occurring in the micro-scale from the cloud microphysics processes, like very-localised microbursts.

1. Introduction

Extreme wildfires are frequently associated with strong convective processes due the heat and moisture released from the fires. Such a fire-atmosphere coupling environment lead the formation of convective clouds, also referred as PyroCumulus (PyroCu) or PryroCumulonimbus (PyroCb) clouds. The first are more common and can form as relatively small clouds above fire plumes. The second can be observed in plume dominated wildfires characterized by an intense convection column, above which a cloud resembling towering cumulonimbus (Cb) may form. The microphysics processes, as condensation of moisture in the fire plume can enhance convection by releasing latent heat, for example. Their updraughts manage, sometimes, to penetrate into the stratosphere. PyroCb activity can have a significant impact on fire behaviour through feedback processes between the atmosphere and the fire, including the increase of burn and spread rates by strong variations in surface wind direction and speed associated with convective inflows and downdraughts, and ignition of new fires by PyroCb lightning (e.g., Tory et al., 2018; Dowdy et al., 2019).

In 2017, an extreme fire season affected Portugal. The first deadly event occurred in June in the region of Pedrógão Grande and caused more than 60 fatalities (e.g., Couto et al., 2020; CTI Report, 2017). In mid-October, extreme wildfires spread across the Central region of Portugal mainland resulting in 48 fatalities (Guerreiro et al., 2018). The present study aims to investigate how a wildfire can influence the occurrence of violent pyro-convective activity.

2. Methodology

In general, the atmospheric models do not account for fire-atmosphere interactions. To investigate the pyroconvective activity, a numerical simulation was run with the Meso-NH model coupled to the ForeFire model. The Meso-NH is a non-hydrostatic model able to represent the atmospheric motions in different scales, and implemented with a rather complete parametrization package of physical processes in the atmosphere (Lac et al., 2018), whereas ForeFire is a fire propagation model (Filippi et al., 2009, 2018). The present study considers the wildfires occurred in Pedrógão Grande and Góis on June 17, 2017. The fire propagation map was constructed based in the fire propagation map presented in the CTI Report (2017).

In order to resolve the development of the fire/weather system, the two-way nesting capability of the Meso-NH model was used with three nested domains (Figure 1). Several simulations were made aiming to obtain the more realistic scenario of the event. The horizontal grid size is 2000 m for the outer domain covering 600 km × 600 km. The inner computational grids have grid increments of respectively 400, 80 m, covering a total area of respectively 120 km × 120 km, 24 km × 24 km for the innermost model. The time step is 10 s for the outermost model and decreases to 2 s, 0.5 s for the finer models. Initial and lateral boundary conditions for the outer domain are provided by ECMWF analysis, with updates every 6 h. The simulation with the coarsest resolution began on 17th June 2017 at 0600 UTC, with a progressive downscaling up to the finest resolution beginning at 1300 UTC. The vertical resolution is identical for all the nested domains, with 50 levels up to 20 km and a first level above the ground at 30 m height. All the nested models used the one and a half order closure turbulence scheme with a prognostic TKE: the two finest resolution domains use the 3D version of the scheme, while the first one only considers the 1D version, neglecting the horizontal turbulent fluxes.

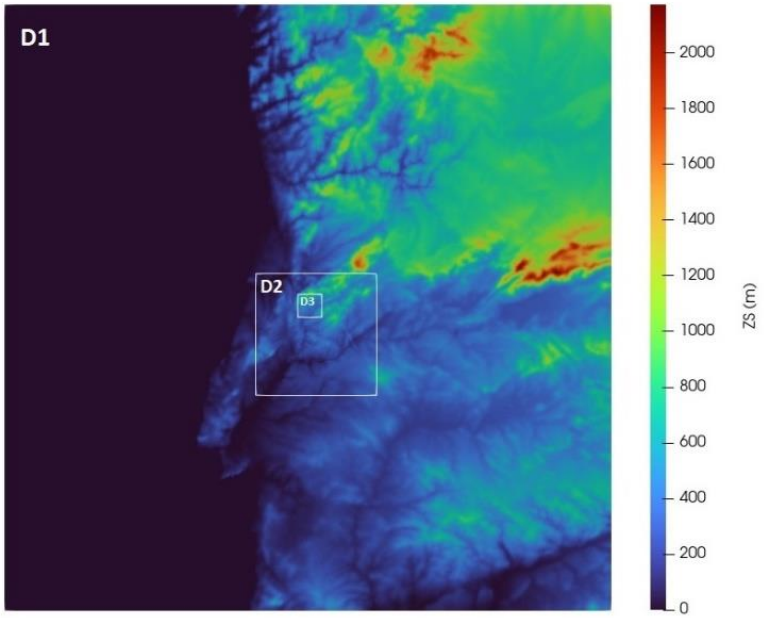

Figure 1- Meso-NH configuration with orography obtained from the SRTM database.

3. Results

Figure 2 shows the fire line representing the fire front propagation as well as the strong fire-atmosphere interaction, with the fire leading to intense convective updraughts. The role of the fire in this episode is presented by the development of a deep convective cloud. In the figure, the plume is associated with a PyroCb cloud, which result from condensation inside the plume. Such a cloud is represented by five hydrometeos species (e.g., cloud droplet, raindrops, graupel, snow or aggregates, pristine ice crystals). The convection was likely enhanced by the strong wildfire activity and penetrated into the higher troposphere above 10 km altitude. The extreme pyro-convective activity was also verified in the simulation by the development of microbursts originated from the PyroCb cloud (not shown).

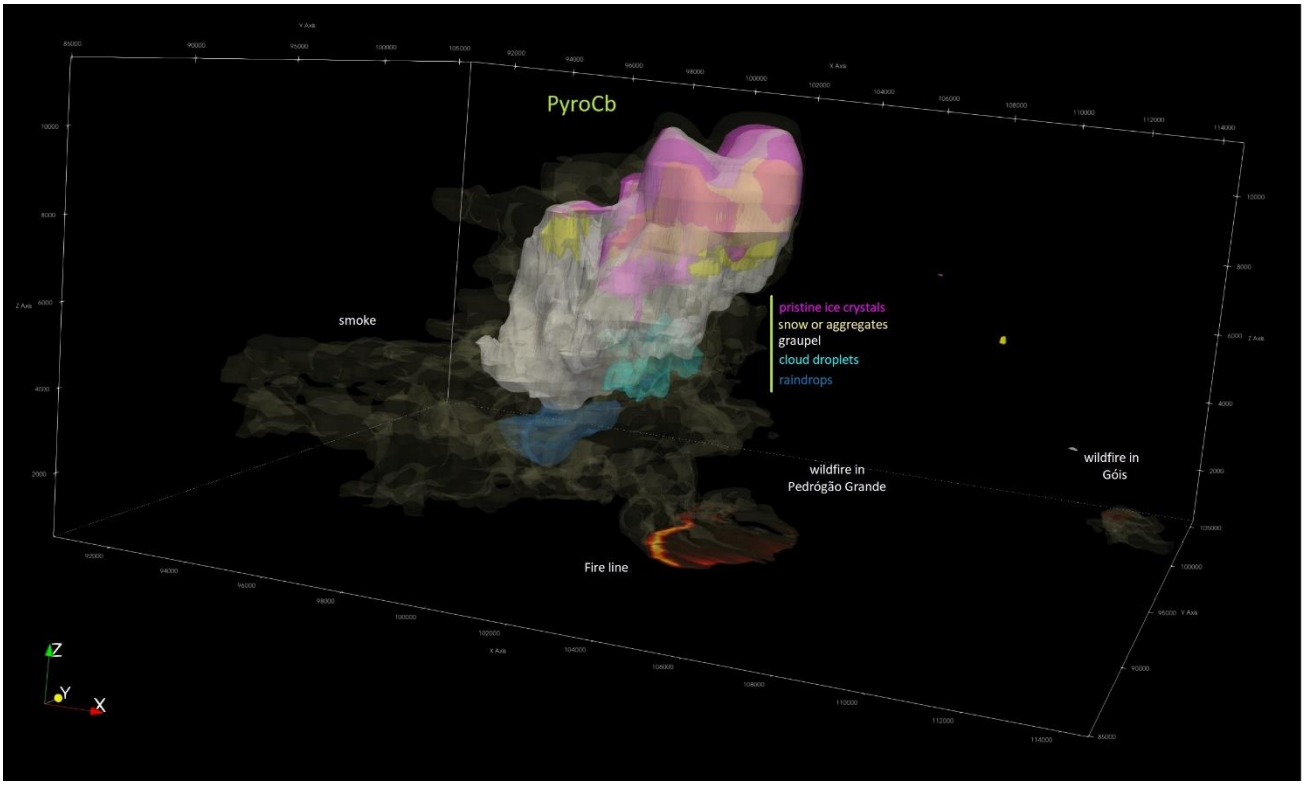

Figure 2- Anatomy of the PyroCb cloud simulated in the Pedrógão Grande mega fire episode. Animation available online at https://youtu.be/vn7PaFh88ss.

4. Conclusions

Fire spread associated with extreme pyro-convective activity is currently highly unpredictable and difficult to suppress. In this study, the findings show the benefits of the use of cloud-resolving models in order to assess the potential for dangerous fire conditions associated with pyroconvection. Moreover, the preliminary results indicate that the model, when configured in high temporal and spatial resolution, is able to represent the pyro-convective plume height from a wildfire and the main processes associated to the interaction of the fire with the atmosphere. In the Pedrógão Grande mega fire event, the violent fire-driven convection manifested as a PyroCumulonimbus cloud. It is important to note that one of the goals was to obtain a reference high resolution (10s, 80m) weather analysis for the reference fire line behaviour from the official report, so fire is forced in the simulation (the impact of the atmosphere in the fire front evolution is not represented).

The study is on-going and will help us to better understand pyro-convective events, namely the atmospheric processes in a micro-scale context, and also in terms of fire behaviour to associate local wind and temperature and humidity to the fire line evolution and local rate of spread. Overall, an improved understanding of these events is important for a range of fields related to the pyroconvection and extreme fire events.

6. Acknowledgments

This research is funded by the European Union through the European Regional Development Fund in the framework of the Interreg V A Spain – Portugal program (POCTEP) through the CILIFO project (Ref.: 0753_CILIFO_5_E), FIREPOCTEP project (0756_FIREPOCTEP_6_E), RH.VITA project (ALT20-05-3559-FSE-000074), H2020 FIRE-RES (GA: 101037419), and also by Portuguese national funds through FCT - Foundation for Science and Technology, I.P. under the PyroC.pt project (Refs. PCIF/MPG/0175/2019) and ICT project (Refs. UIDB/04683/2020 and UIDP/04683/2020).

7. References

Couto, F.T.; Iakunin, M.; Salgado, R.; Pinto, P.; Viegas, T.; Pinty, J.-P. Lightning modelling for the research of forest fire ignition in Portugal. Atmos. Res. 2020, 242, 104993.

CTI Report 2017. In Análise e Apuramento dos Factos Relativos aos Incêndios que Ocorreram em Pedrógão Grande, Castanheira de Pera, Ansião, Alvaiázere, Figueiró dos Vinhos, Arganil, Góis, Penela, Pampilhosa da Serra, Oleiros e Sertã, entre 17 e 24 de junho de 2017; Comissão Técnica Independente (CTI), Assembleia da República: Lisboa, Portugal, 2017; p. 296.

Dowdy, A.J.; Ye, H.; Pepler, A.; et al. (2019) Future changes in extreme weather and pyroconvection risk factors for Australian wildfires. Sci Rep 9, 10073.

Filippi, J.-B.; Bosseur, F.; Mari, C.; Lac, C.; Le Moigne, P.; Cuenot, B.; Veynante, D.; Cariolle, D.; Balbi, J.H. (2009) Coupled atmosphere-wildland fire modelling. Journal of Advances in Modeling Earth Systems, 1, 11.

Filippi, J.B.; Bosseur, F.; Mari, C.; Lac, C. Simulation of a large wildfire in a coupled fire-atmosphere model. Atmosphere 2018, 9, 218.

Guerreiro, J.; Fonseca, C.; Salgueiro, A.; Fernandes, P.; Lopez Iglésias, E.; de Neufville, R.; Mateus, F.; Castellnou Ribau, M.; Sande Silva, J.; Moura, J.M.; et al. Avaliação dos Incêndios Ocorridos Entre 14 e 16 de Outubro de 2017 em Portugal Continental. Relatório Final; CTI Report 2018; Comissão Técnica Independente (CTI), Assembleia da República: Lisboa, Portugal, 2018; p. 274.

Lac, C.; Chaboureau, J.P.; Masson, V.; Pinty, J.P.; Tulet, P.; Escobar, J.; Leriche, M.; Barthe, C.; Aouizerats, B.; Augros, C.; et al. Overview of the Meso-NH model version 5.4 and its applications. Geosci. Model Dev. 2018, 11, 1929–1969.

Tory, K.J.; Thurston, W.; Kepert, J.D. (2018) Thermodynamics of Pyrocumulus: A Conceptual Study. Mon. Wea. Rev., 146, 2579–2598.

Modelling wildfire firebrand accumulation in front of walls perpendicular to the wind

Simona Dossi; Guillermo Rein*

Department of Mechanical Engineering, and Leverhulme Centre for Wildfires, Environment, and Society, Imperial College London, London, UK, {g.rein@imperial.ac.uk}

**Corresponding author*

Keywords

Embers, Firebrands, WUI, ignition, building damage, safety, accumulation

Abstract

Windblown embers, also known as firebrands, can be generated in large numbers during wildfires and ignite fuels as far as kilometers away from their origin. Firebrands are often cited as the leading cause of building wildfire ignition in the wildland-urban interface. Building ignition via firebrands can occur directly, by landing on or inside the building, or indirectly, by igniting adjacent fuel and creating adjacent flame exposure. Studies have investigated firebrands generation from various fuels, wind-driven transport, and ignition mechanisms on different materials and building features. Less research has been conducted on how firebrands deposit and accumulate around buildings; this knowledge is critical in designing buildings safer to firebrand ignition. Here, we address this need and computationally investigate firebrand landing and accumulation in front of obstacles. We present work on a computational fluid dynamic Fire Dynamics Simulator (FDS) model simulating the published experimental data by Suzuki and Manzello measuring the firebrand accumulation region in front of a vertical wall under firebrand exposure generated by the NIST Dragon and varying wind speeds (4, 6, 8, and 10 m/s) (Suzuki and Manzello, 2017). T he simulated firebrand accumulation areas in front of the wall are compared to the experimental observations. The wall obstacle dimensions and wind speeds are varied; and the accumulation patterns and sizes are studied to define the critical design parameters affecting firebrand accumulation. Here we present the current progress, simulation results, and future vision for this research project.

1. Introduction

Wildfires pose a significant risk to life and property, and can cause extensive damage to residential communities. Understanding how wildfire spreads is crucial to mitigate this risk. There are three main wildfire spread pathways: flame radiation, direct flame contact, and firebrand ignition. Embers more generally describe small and hot carbon-based fuel particles; firebrands specifically describe airborne burning particles, which travel through wind-driven transport (Babrauskas, 2018). The type of fuel, flames, and surrounding conditions impact these particles' size, shape, and burning conditions. When firebrands land, they may ignite the target fuel they have contact with, this process is called spotting and the new ignited fires are called spot fires. Firebrand ignition of spot fires includes numerous sub-processes occurring on various spatial scales. Firebrands are first generated by flaming fuel, then transported in the wind, and lastly land of target fuel, possibly igniting it; these processes are illustrated in figure 1 and figure 2. Here we present Fire Dynamics Simulator (FDS) simulations of firebrand exposure of a simple geometric obstacle, a rectangular wall perpendicular to wind flow, under varying wind speeds and varying wall thicknesses. Results are compared and validated with published experimental results.

Figure 1: Schematic diagram of the five subprocesses of wildfire firebrand building ignition and damage: 1) firebrand generation, 2) wind-driven transport, 3) landing and accumulation, 4) building ignition and 5) fire spread.

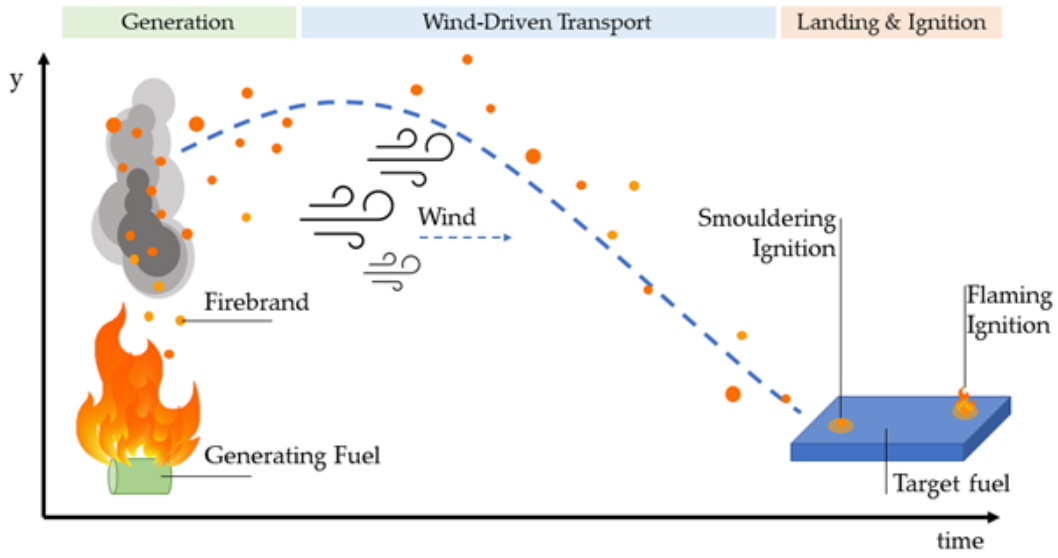

Figure 2: Schematic diagram of firebrand generation, wind-driven transport, and landing and ignition on target fuel, adapted from (Fernandez-Pello, 2017).

1.1. Firebrand Generation and Transport

Firebrands can be generated from a variety of fuels including both vegetative and urban fuel. Extensive research has been produced characterising the firebrand characteristics generated from specific fuels; including Douglas-fir trees (Manzello, Maranghides and Mell, 2007), full scale burning buildings (Suzuki et al., 2012), different roof materials and designs (Waterman, 1969), prescribed fires (El Houssami et al., 2016; Filkov et al., 2017) and actual wildland-urban interface fires (Manzello and Foote, 2014). Figure 3 is a photograph from the 2018 Delta fire in California, and shows the high number of firebrands which can be produced under certain wildfire conditions. Characterisation parameters include, mass and size distribution of firebrands, number of firebrands, projected area of landed firebrands; researchers stress the need for more data of firebrand characterisations from real wildfires and wildland-urban interface fires. The physical firebrand characteristics impact the forces acting on them during wind-driven transport, and therefore their trajectory; their physical and chemical characteristics, and initial conditions determine the type of combustion.

Figure 3: Firebrand shower during the 2018 Delta Fire in the Shasta-Trinity National Forest, California, USA. Photo courtesy of Noah Berger/Associated Press (noahbergerphoto.com). Photo shows numerous airborne firebrands and flames on the grass appears to be ignited by the landing firebrands

Models describing the breakage of firebrands during generation have been developed; Barr and Ezekoye used simple mechanical breakage models coupled with thermal decomposition model which predicts the size distribution of firebrands lofted from a fractal tree which can be combine with plume models to describe the breakage, transport, and mass loss of firebrands in wildfire conditions (Barr and Ezekoye, 2013). Tohidi et.al. studied the mechanical response of wooden elements under external loading after having been heated in wildfire conditions to mimic the firebrand breakage fuel during firebrand generation (Tohidi et al., 2017).

The breakage conditions determine the initial position and conditions of the firebrand's wind-driven transport. Extensive research has been conducted in the field of firebrand transport. Transport models calculated the maximum horizontal transport (spotting) distance for different firebrand conditions: firebrand particles lofted by transitory flaming group of trees (Albini, 1979), by the persistent flaming fuel piles (Albini, 1981) by the thermal fields transporting firebrands by the wind field (Albini, 1983).

Sardoy et al. calculated the wind flow trajectories and burning rates of disk-shaped firebrands initially lofted by crown fire plumes for carrying wind speeds and fire intensities (Sardoy et al., 2007). Anthenien et.al created a numerical model describing the burning and wind transport processes for spherical cylindrical, and disk firebrands lofted by fire plumes (Anthenien, Tse and Carlos Fernandez-Pello, 2006). Detailed review papers cover and compare the many firebrand transport and combustion models developed (Koo et al., 2010).

1.2. Firebrand Landing and Ignition

Firebrands can be transported to, and land on vegetative fuel or urban fuel; spot fires can spread wildfire in the wildland and to the wildland-urban interface (WUI) igniting homes and communities. Here we consider the landing and accumulation of firebrand in front of solid obstacles mimicking building components to investigate WUI fire ignition by firebrands. There are three main general pathways for firebrand ignition of buildings:

1. Indirect ignition: firebrands ignite vegetation or combustibles near the building, the flaming fire spreads and ignite the building.
2. Direct ignition - building interior: firebrand enter the building structure through openings and ignite combustibles inside the building.
3. Direct ignition - building exterior: firebrands accumulate on the building exterior and ignite the building exterior material

Experimental research has characterized firebrand ignition conditions of various objects and materials. the NIST dragon is an experimental apparatus which creates a continuous feed of adaptable speed airflow with burning firebrands (Manzello and Suzuki, 2013). The dragon generates firebrands which match the size and mass flux distribution of real wildfire scenarios, thus allowing the experimental investigation of realistic firebrand exposure. The NIST dragon has been used to study the response of many building targets including: roofing assemblies (Manzello et al., 2010), wall sidings and eaves set ups (Manzello, Suzuki and Hayashi, 2012), decking assemblies (Manzello and Suzuki, 2014), fences (Suzuki et al., 2016). IBHS has used an adaption of the dragon to test full scale buildings in a wind tunnel under various conditions.

For a firebrand to be able to ignite spot fires, the firebrands must heat the target fuel to ignition temperature. Studies have investigated the necessary firebrand mass and temperature to ignite various materials including: structural wood (Santamaria et al., 2015), and fuel beds with varying properties, including: water content, vegetation, geographical origin (Hadden et al., 2011)(Viegas et al., 2014)(Urban et al., 2019).

1.3. Modelling Landing and Accumulation

Models calculating firebrand landing locations and distributions considering varying surrounding conditions and firebrand material and combustion properties have been developed. Such models allowed calculation of ground level mass distribution of disk-shaped firebrands for varying fire intensities and wind speeds (Sardoy et al., 2008). To investigate more specficially at firebrand landing patterns near or on buildings, and the various material fire responses possible, requires more detail. Research has started focusing on firebrand landing position and distributions, around solid obstacles resembling building constructions or building components.

Ngyugen investigated the accumulation patterns of particles resembling firebrands on different rooftop deisgns in wind tunnel experiments and found numerous complex factors, including roof design details, wind speed and wind direction, which determined where and how firebrands land and accumulate on rooftops (Nguyen and Kaye, 2021). Experiments looking at the response and accumulation patterns in front of obstacles and in between

cuboid obstacles representing inter-building distance in the WUI (Butler et al., 2017; Suzuki and Manzello, 2017; Mankame and Shotorban, 2021).Results advance understanding indirect ignition, and direct ignition of building exterior, by increasing insight on where and for how long firebrands are most likely to land under varying conditions and ignite buildings. Firebrand deposition around cubic obstacles has been modeled using Large Eddy Simulations for turbulence and Lagrangian particle tracking for firebrand trajectory (Mankame and Shotorban, 2021).

With the objective of investigating how building design parameters affect the firebrand landing and accumulation around buildings, here we use the Fire Dynamics Simulator (FDS) to model firebrand exposure and ground level distribution with varying windspeeds perpecndicular to a vertical wall of varying heights. We model the experimental set up conducted by Suzuki and Manzello in 2017, to compare results and validate this model (Suzuki and Manzello, 2017). By comparing the landing distribution of firebrands with published experimental results, and varying obstacles shapes, we comment on using models to determine the most hazardous designs and conditions for firebrand ignition in wildfire conditions.

2. Methodology

2.1. Simulation parameters

We present FDS simulations mimicking the experimental set up of a published study investigating firebrand accumulation zones in front of walls (Suzuki and Manzello, 2017). In the experiment, Douglas-fir wood firebrands are fed continuously toward a wall 7.5 m away, perpendicular to feed. The wind tunnel speed and the wall dimensions are varied to test the effect on firebrand accumulation pattern in front of the wall. The experimental set up is shown in figure 4 by a schematic diagram and photos from (Suzuki and Manzello, 2017). The area of the firebrand accumulation piles, and the distance between the pile and the wall were measured and presented. Different FDS computational domain dimensions were tested in order to minimize computational resources, without compromising result accuracy. Figure 5 presents a schematic and screenshot of the final FDS computational domain dimensions. Table 1 compares the properties of the firebrands, wind flow, and wall obstacle in the experimental investigation, and in the FDS simulation.

The wind profile, and firebrand positions are calculated by FDS, and MATLAB image analysis is used to calculate the accumulated area of firebrands. The wall size and shape is varied as in the experimental investigation: sizes 2.4 m x 2.4 m and 1.3 m x 2.4 m were first simulated. The wind speed was also varied as in the experimental investigation; wind speeds 4, 6, 8, and 10 m/s are considered. Simulations with varying wall length and width, and additional solid obstacles will be conducted when the model is validated.

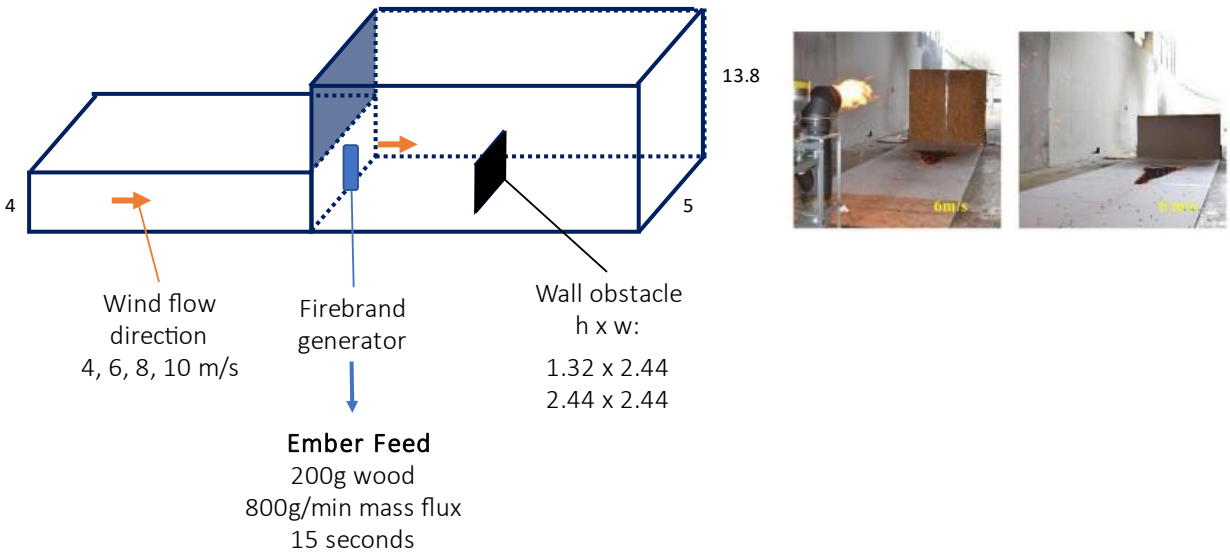

Figure 4: (left): Schematic of wind tunnel, with dimensions in meters, and experimental set up (right:) Photos of experimental set up from (Suzuki and Manzello, 2017)

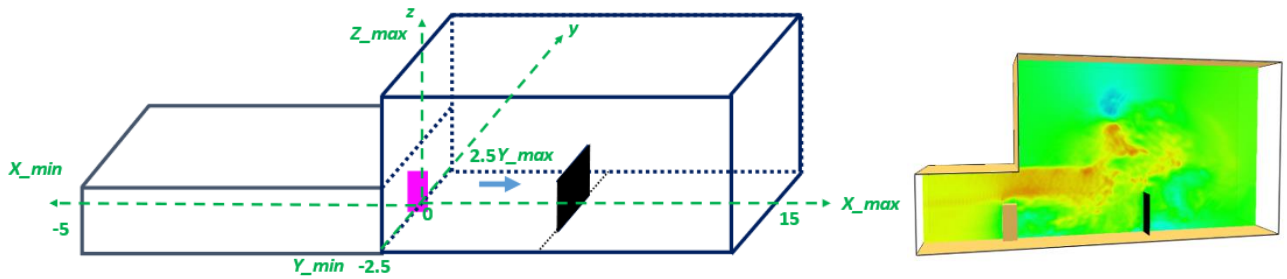

Figure 5: (left): Schematic of FDS computational domain (right:) FDS computational domain with wind speed of 4 m/s at y=0 and t=5 seconds

Table 1: Properties and parameters of the firebrand particles, wind speed, and walls, tested in the experimental investigation, and simulated in this FDS simulation

	Experiment: (Suzuki and Manzello, 2017)	**FDS simulation**
Firebrand *[Size, shape, mass flux, material]*	7.9 mm x 7.9 mm x 12.7 mm Cuboid 17.1 g/m^{2}s Douglas-fir wood	D = 8 mm, L = 13.5 mm Cylindrical 17 g/m^{2}s Includes particles with both wood and char densities to simulate range of possible particle weights (further physical and chemical properties are defined in model)
Wind speed	4 m/s, 6m/s, 8m/s, 10m/s	4 m/s, 6m/s, 8m/s, 10m/s
Wall *[Size]*	2.44 m x 2.44 m 1.32 m x 2.44 m	2.4 m x 2.4 m 1.3 m x 2.4 m

2.2. Particle Tracking and Turbulence Model

FDS uses Lagrangian particle tracking to calculate particle position and trajectory in the computational domain, and Large Eddy Simulation (LES) to calculate turbulent flow. By default firebrand particles are modelled as cylindrical particles. Simulated particles do not experience thermal degradation, to mitigate this limitation particles with both unburned wood densities, and wooden char densities are introduced to simulate a spectrum of possible particle densities. Lagrangian Particle Tracking method computes a force balance on each singular particle based on Newton's second Law, given in Equation 1. The momentum transferred from particles to surrounding gas is calculated in FDS by Equation 2; and the acceleration of the particles is solved via Equation 3. Where m_p is the particle mass, u_p is the particle velocity, f_b is the momentum transferred from particles to gas, ρ_f is the fluid density, C_D is the drag coefficient, u_f is the fluid velocity, ρ_p is the particle density, A_p is the particle surface area, g is the gravitational constant and V_p is the particle volume.

$$m_p \frac{du_p}{dt} = F_{drag} + F_{bouyancy} + F_{other} \quad (1)$$

$$f_b = \frac{1}{V}\sum[\frac{\rho}{2} C_d A_{pc}(u_p - u_f)|u_p - u_f| - \frac{dm_p}{dt}(u_p - u_f)] \quad (2)$$

$$\frac{du_p}{dt} = g - \frac{\frac{1}{2}(\rho C_d A_{pc})}{m_p}(u_p - u_f)|u_p - u_f| \quad (3)$$

In FDS, turbulence is calculated with LES, with the default Deardoff model. The default near-wall model in FDS uses Wall-Adapting Local Eddy-viscosity model. All solid boundaries are set to have no slip conditions, and wind is introduced and exited in the domain via open boundary conditions.

3. Results

The modeling and data analysis of this project is ongoing. This section current results and explains the result objectives for future work.

3.1. Firebrand Accumulation Distribution

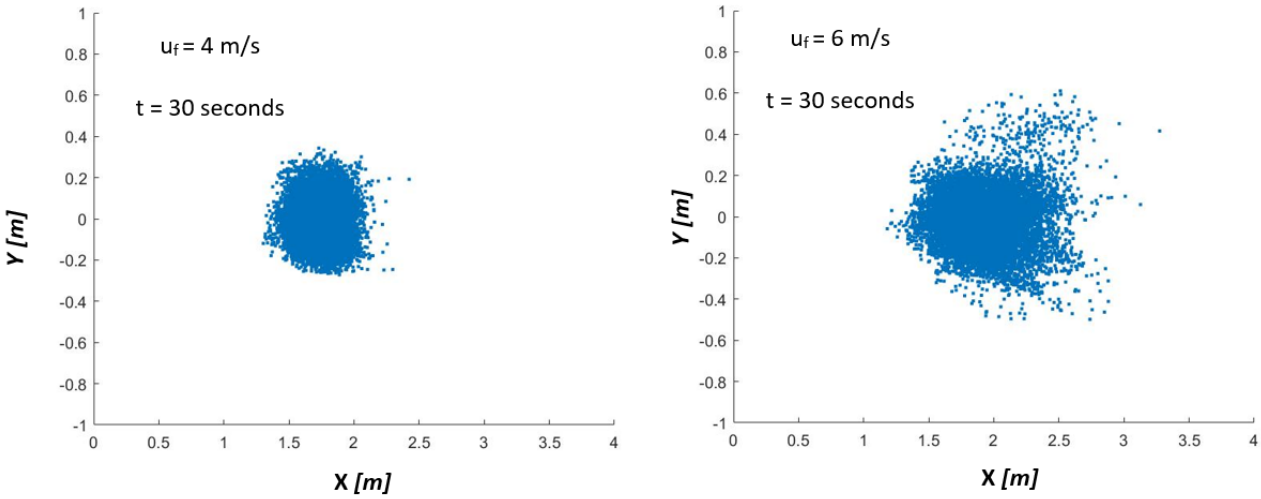

Figure 6: Particle distribution on the floor (z = 0) after 15 seconds of firebrand exposure under 4 m/s wind (left) and 6 m/s wind (right).

Figure 6 presents the particle distribution on the floor (z = 0) after 15 seconds of firebrand exposure under 4 m/s wind, and 6 m/s wind produced in the FDS simulations. These results show that the accumulated area increases as the wind speed increases, this is the opposite trend presented in (Suzuki and Manzello, 2017). Authors are investigating which parameters are determining this disagreement in simulation results, and experimental observations; especially focusing on the solid boundary conditions of the computational domain, and the particle geometry and related drag coefficient – which have been simplified in the simulation to conserve computational resources.

3.2. Separation Distance

The distance between the firebrand accumulation zone, where firebrands land and stop moving, and the side of the wall facing the firebrand feed is measured in both the experimental investigation, and in the FDS simulations computed. For the FDS simulations, the separation distance is calculated from the final firebrand particle positions at the end of the simulations; these are graphed for each particle in for wind speed of 4 m/s and 6 m/s in figure 7. For a wind speed of 4 m/s the separation distance ranges from 5.1m to 6.2m, for 6 m/s wind the separation distance ranges from 4.2 m to 6.2m. These distances greatly overestimate the separation distances reported in (Suzuki and Manzello, 2017). Furt hermore, FDS inaccurately the trend direction of changing separation distance for changing wind speed: experimental measurement confirm that separation distances increase as the wind speed increases, while FDS calculates the opposite trend.

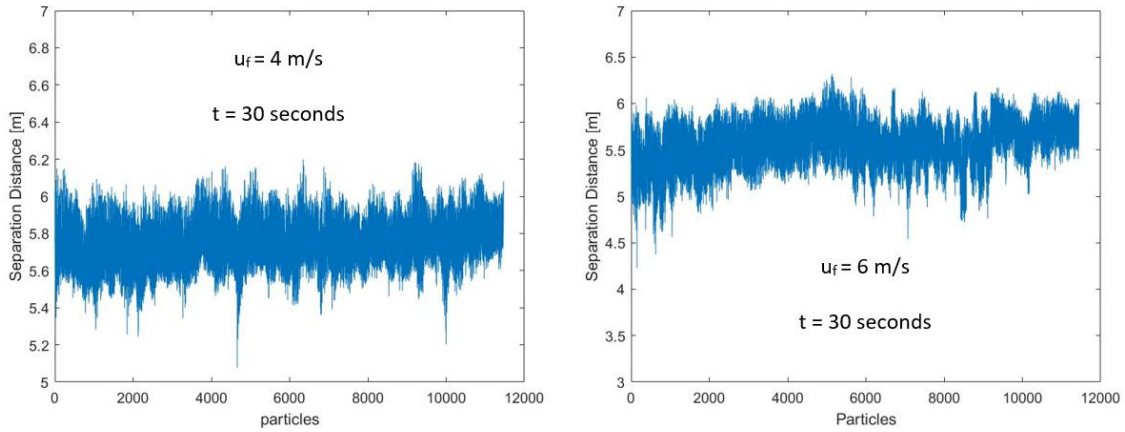

Figure 7: Separation distances between all particles at the end of the simulation (t = 30 seconds, after 15 seconds of firebrand exposure) and wall obstacle (located at x = 7.5m), for 4 m/s wind (left) and 6 m/s wind (right).

3.3. Upcoming Work

MATLAB image analysis is being conducted to calculate the projected area of firebrands that have landed and accumulated at z = 0 in front of varying obstacles. Numerous simulations varying significant parameters are being carefully analysed to conclude the most significant parameters to simulate firebrand accumulation. Especially, changes to the wind profile simulated in the wind tunnel, and more accurate firebrand particle geometries and drag coefficients are being studied to improve model accuracy.

If the model can be successfully validated with experimental measurements, it will be used to study the building design significance in affecting firebrand accumulation patterns. By varying the wall dimensions, and adding additional solid obstacles to the simulation, the impact of varying building design on firebrand exposure (separation distances, projected area, mass accumulation profile) will be presented. Studying the impact of design considerations on the landing distribution of firebrands in front of walls and sidings is important in designing wildfire resistant WUI buildings and communities.

4. References

Albini, F. A. (1979) Spot Fire Distance from Burning Trees: A Predictive Model. Edited by U. Intermountain Forest and Range Experiment Station (Ogden. USDA, Forest Service (General technical report INT).

Albini, F. A. (1981) 'Spot fire distance from isolated sources - extensions of a predictive model', USDA Forest Service Research Note, INT-309, p. 9p.

Albini, F. A. (1983) 'Transport of firebrands by line thermalst', Combustion Science and Technology, 32(5–6), pp. 277–288. doi: 10.1080/00102208308923662.

Anthenien, R. A., Tse, S. D. and Carlos Fernandez-Pello, A. (2006) 'On the trajectories of embers initially elevated or lofted by small scale ground fire plumes in high winds', Fire Safety Journal, 41(5), pp. 349–363. doi: 10.1016/j.firesaf.2006.01.005.

Babrauskas, V. (2018) 'Firebrands and Embers', in Manzello, S. L. (ed.) Encyclopedia of Wildfires and Wildland-Urban Interface (WUI) Fires. Cham: Springer International Publishing, pp. 1–14. doi: 10.1007/978-3-319-51727-8_3-1.

Barr, B. W. and Ezekoye, O. A. (2013) 'Thermo-mechanical modeling of firebrand breakage on a fractal tree', Proceedings of the Combustion Institute, 34(2), pp. 2649–2656. doi: 10.1016/j.proci.2012.07.066.

Butler, K. M. et al. (2017) 'Wind effects on flame spread and ember spotting near a structure', 15th International Conference and Exhibition on Fire and Materials 2017, 2, pp. 681–693.

Fernandez-Pello, A. C. (2017) 'Wildland fire spot ignition by sparks and firebrands', Fire Safety Journal, 91(May), pp. 2–10. doi: 10.1016/j.firesaf.2017.04.040.

Filkov, A. et al. (2017) 'Investigation of firebrand production during prescribed fires conducted in a pine forest', Proceedings of the Combustion Institute, 36(2), pp. 3263–3270. doi: 10.1016/j.proci.2016.06.125.

Hadden, R. M. et al. (2011) 'Ignition of Combustible Fuel Beds by Hot Particles: An Experimental and Theoretical Study', Fire Technology, 47(2), pp. 341–355. doi: 10.1007/s10694-010-0181-x.

El Houssami, M. et al. (2016) 'Experimental Procedures Characterising Firebrand Generation in Wildland Fires', Fire Technology, 52(3), pp. 731–751. doi: 10.1007/s10694-015-0492-z.

Koo, E. et al. (2010) 'Firebrands and spotting ignition in large-scale fires', International Journal of Wildland Fire, 19(7), pp. 818–843. doi: 10.1071/WF07119.

Mankame, A. and Shotorban, B. (2021) 'Deposition Characteristics of Firebrands on and Around Rectangular Cubic Structures', Frontiers in Mechanical Engineering, 7(June), pp. 1–14. doi: 10.3389/fmech.2021.640979.

Manzello, S. L. et al. (2010) 'Quantifying the vulnerabilities of ceramic tile roofing assemblies to ignition during a firebrand attack', Fire Safety Journal, 45(1), pp. 35–43. doi: 10.1016/j.firesaf.2009.09.002.

Manzello, S. L. and Foote, E. I. D. (2014) 'Characterizing Firebrand Exposure from Wildland-Urban Interface (WUI) Fires: Results from the 2007 Angora Fire', Fire Technology, 50(1), pp. 105–124. doi: 10.1007/s10694-012-0295-4.

Manzello, S. L., Maranghides, A. and Mell, W. E. (2007) 'Firebrand generation from burning vegetation', International Journal of Wildland Fire, 16(4), pp. 458–462. doi: 10.1071/WF06079.

Manzello, S. L. and Suzuki, S. (2013) 'Experimentally simulating wind driven firebrand showers in wildland-urban interface (WUI) fires: Overview of the NIST firebrand generator (NIST dragon) technology', Procedia Engineering, 62, pp. 91–102. doi: 10.1016/j.proeng.2013.08.047.

Manzello, S. L. and Suzuki, S. (2014) 'Exposing decking assemblies to continuous wind-driven firebrand showers', Fire Safety Science, 11, pp. 1339–1352. doi: 10.3801/IAFSS.FSS.11-1339.

Manzello, S. L., Suzuki, S. and Hayashi, Y. (2012) 'Exposing siding treatments, walls fitted with eaves, and glazing assemblies to firebrand showers', Fire Safety Journal, 50, pp. 25–34. doi: 10.1016/j.firesaf.2012.01.006.

Nguyen, D. and Kaye, N. B. (2021) 'Experimental investigation of rooftop hotspots during wildfire ember storms', Fire Safety Journal, 125(August), p. 103445. doi: 10.1016/j.firesaf.2021.103445.

Santamaria, S. et al. (2015) 'Investigation of Structural Wood Ignition By Firebrand Accumulation', The First International Conference on Structural Safety under Fire and Blast, (July 2016), pp. 1–13.

Sardoy, N. et al. (2007) 'Modeling transport and combustion of firebrands from burning trees', Combustion and Flame, 150(3), pp. 151–169. doi: 10.1016/j.combustflame.2007.04.008.

Sardoy, N. et al. (2008) 'Numerical study of ground-level distribution of firebrands generated by line fires', Combustion and Flame, 154(3), pp. 478–488. doi: 10.1016/j.combustflame.2008.05.006.

Song, J. et al. (2017) 'The Wind Effect on the Transport and Burning of Firebrands', Fire Technology, 53(4), pp. 1555–1568. doi: 10.1007/s10694-017-0647-1.

Suzuki, S. et al. (2012) 'Firebrand generation data obtained from a full-scale structure burn', International Journal of Wildland Fire, 21(8), pp. 961–968. doi: 10.1071/WF11133.

Suzuki, S. et al. (2016) 'Ignition of Wood Fencing Assemblies Exposed to Continuous Wind-Driven Firebrand Showers', Fire Technology, 52(4), pp. 1051–1067. doi: 10.1007/s10694-015-0520-z.

Suzuki, S. and Manzello, S. L. (2017) 'Experimental investigation of firebrand accumulation zones in front of obstacles', Fire Safety Journal, 94(April), pp. 1–7. doi: 10.1016/j.firesaf.2017.08.007.

Tohidi, A. et al. (2017) 'Thermo-mechanical breakage mechanism of firebrands', 10th U.S. National Combustion Meeting, 2017-April(April).

Urban, J. L. et al. (2019) 'Ignition of a spot smolder in a moist fuel bed by a firebrand', Fire Safety Journal, 108(May), p. 102833. doi: 10.1016/j.firesaf.2019.102833.

Viegas, D. X. et al. (2014) 'Ignition of Mediterranean Fuel Beds by Several Types of Firebrands', Fire Technology, 50(1), pp. 61–77. doi: 10.1007/s10694-012-0267-8.

Waterman, T. E. (1969) Experimental Study of Firebrand Generation. Chicago. Available at: https://apps.dtic.mil/sti/pdfs/AD0695640.pdf.

Numerical and experimental study on the moisture content of a pine tree

Eusébio Conceição*[1]; João Gomes[2]; Mª Manuela Lúcio[1]; Domingos Viegas[3]; Mª Teresa Viegas[3]

[1] FCT – Universidade do Algarve, Campus de Gambelas,
8005-139 Faro, Portugal, {econcei@ualg.pt, maria.manuela.lucio@gmail.com}
[2] CINTAL, Campus de Gambelas,
8005-139 Faro, Portugal, {jgomes@ualg.pt}
[3] FCT – Universidade de Coimbra - Pinhal de Marrocos - Pólo II,
3030 Coimbra, Portugal, {xavier.viegas, maria.viegas}@dem.uc.pt

**Corresponding author*

Keywords

Experimental Tests, Mass and Energy Transmission, Moisture Content, Numerical Simulation, Pine Tree

Abstract

This article presents a validation study of the numerical model for assessing the moisture content of a pine tree based on experimentally obtained results, considering the surrounding external environmental conditions. In this work, the moisture content of the leaves of a pine tree is evaluated, taking into account the air temperature and the relative humidity conditions around the tree. The experimental work consisted of collecting maritime pine leaves, measuring their moisture content with a moisture analyzer and recording the environmental conditions, obtained by a meteorological station, at the time of this collection. In this work, data obtained during the year 2021 are considered. The experimental results obtained in the meantime were compared with the results obtained numerically. The numerical simulation was done by a research software developed by the authors called Hygrothermal Tree Modelling. In the conceiving of the numerical model, the processes of water circulation and energy transmission were included. The values of leaf moisture content predicted by the numerical model differ slightly from the values obtained experimentally, whose relative error calculated was 1.45%.

1. Introduction

Mass and heat transmission processes must be known when evaluating the thermal response and existing water circulation in trees. Phenomena such as water distribution, diffusion, transpiration and temperature are taken into account in this type of process.

Studies carried out by Janott et al. (2011), Wang et al. (2012), Simon et al. (2018), and Green et al. (2003) present very relevant models for understanding and simulating phenomena concerning the way in which mass transmission takes place in trees. Janott et al. (2011) proposed a concept of water flow in soil-plant systems. Wang et al. (2012) defined a model of tree structure and functioning to include biomass production, organ sharing and water availability solutions to simulate plant and environment interaction. Simon et al. (2018) developed a model to evaluate leaf temperatures and transpiration rates of trees. Green et al. (2003) presented a soil water balance numerical model.

Vegetation moisture and dry matter content can be used as important indicators in fire spread models and also to predict how fire evolves (Adab et al., 2016). For example, Adab et al. (2016) concluded that the scaling up of moisture content indices could be useful to apply as a previous forest fire alert system. Evaluating forest fire risk is a challenge task due to several uncertainties such as fuel flammability and ignition potential (Rao et al., 2020). In research works of Lifang et al. (2019) and Nolan et al. (2020) and Rao et al. (2020) the application of moisture content indices, their implications, challenges and details of use in this type of forecast were evaluated.

The model of water transfer, used in the study presented in this paper, includes the distribution, diffusion and transpiration processes. This model was developed from models of blood and water flow processes in the human body (Conceição and Awbi, 2021).

The grid generation is important to evaluate the temperature distribution and to feature the thermal phenomena (by conduction, evaporation, radiation and convection) that occur in the tree. The grid generation theory applied

in this is founded on that used to obtain the geometries of buildings, vehicles or human bodies, utilized to assess the radiative exchanges (Conceição and Lúcio, 2010; Conceição et al., 2010).

The thermal response model of the pine tree used here is founded on thermal and radiative numerical models applied to other type of geometries, such as buildings (Conceição et al., 2018) and vehicles (Conceição et al., 2000).

The objective of this study is to validate the sub-model of the Hygrothermal Tree Modelling numerical model used to calculate the moisture content, mainly in the leaves, of a pine tree. Therefore, a periodic collection of pine leaves and subsequent measurement in the laboratory of their moisture content were carried out over the last two years. The experimental results obtained during the year 2021 were chosen to be compared with the results obtained numerically, maintaining the same external environmental conditions as those recorded experimentally.

2. Numerical Model

The numerical model is based on a system of equations of mass and energy transmission. The conduction, convection, radiation and transpiration phenomena are considered when establishing the system of energy transmission equations. The water mass evaluation, the water distribution, and the processes of diffusion and transpiration are considered when establishing the system of mass transmission equations.

The pine tree three-dimensional (3D) geometry model consists of cylindrical elements used to define the trunks, branches and leaves. The dimensions of each cylindrical element, consisting of several layers, are given by its length and diameter. This 3D geometry model will be an input of the pine tree thermal response numerical model.

The pine tree thermal response numerical model is founded on the human thermal response numerical model (Conceição and Lúcio, 2001), removing the thermoregulatory system and arising new pathways for water circulation. This numerical model considers a set of balance integral equations of energy for the pine tree body tissues and of mass for the water in the pine tree. The solution of the system of equations thus constituted is obtained by applying the Runge-Kutta-Fehlberg algorithm with error control.

The following phenomena are considered by the tree thermal response numerical model:

- Heat conduction existing between the various layers of each element of the tree;
- Heat convection existing between the outer surface of the elements and the surrounding air environment;
- Heat evaporation, assuming simultaneously the mass and heat transfer and the water phase change, existing between the outer surface of the elements and the surrounding air environment.

The following phenomena are considered in the mass transmission:

- Water distribution: the water is conveyed from the trunk to the branches and leaves;
- Water diffusion: water is conveyed within the trunk from the internal tissues to the external tissues; in this calculation, the cylindrical elements that constitute the trunk are divided into several layers (one inner, one outer, and a set of central layers located between them);
- Water transpiration: water is evaporated by convection from the outer layer to the environment, considering evaporative phenomena.

3. Methodology

Numerical simulation was carried out considering only one pine branch and its 90 leaves. Figure 1 presents the grid generation of this branch with its leaves. As input data for the numerical simulation, the average values of wind speed, ambient air temperature and ambient air relative humidity were considered, corresponding to the average of values recorded experimentally throughout the year 2021. These values are as follows:

- Average ambient air temperature: 20.60ºC;
- Average air relative humidity: 58.39%;

- Average wind speed: 4.29 m/s.

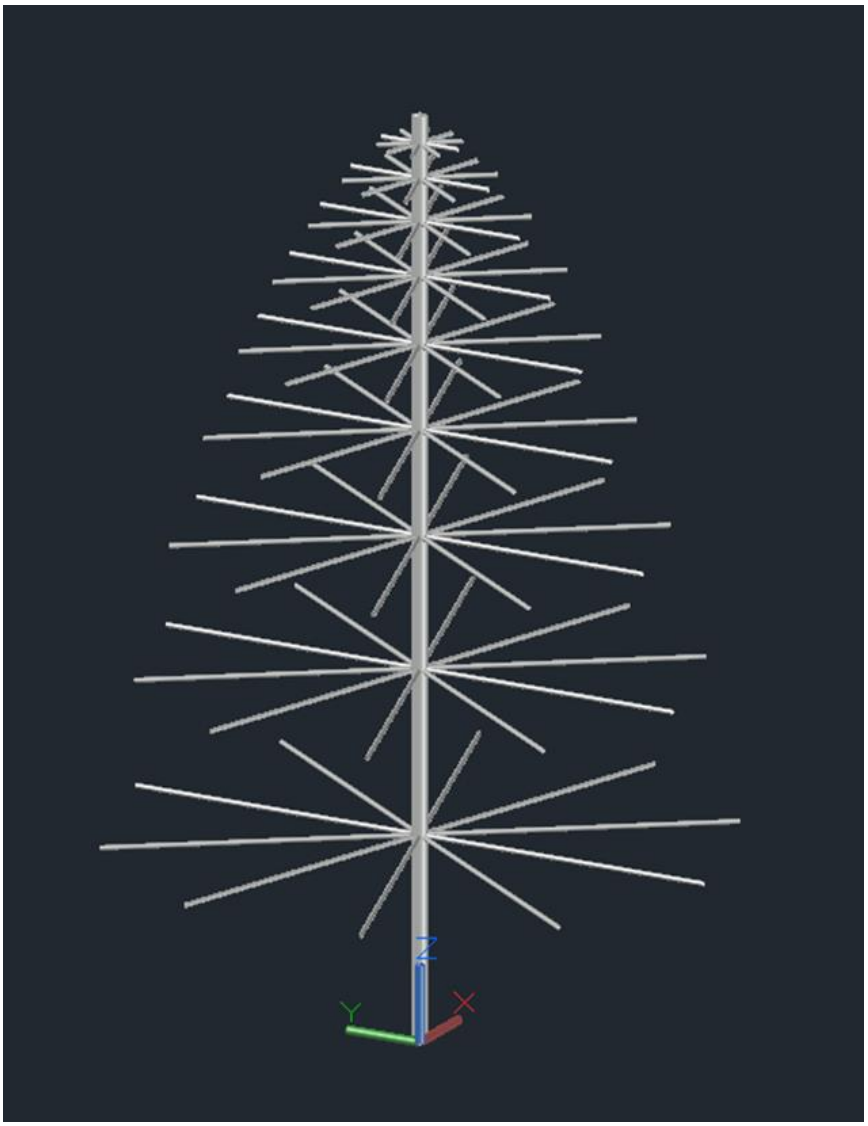

Figure 1 – Grid generation of the pine branch with its leaves.

The experimental work involves a periodic collection of a sample of maritime pine leaves, among other tree species, in a previously delimited area. This collection work has been going on since June 2019. This sample is taken to the laboratory in a closed environment for experimental tests. Upon arrival at the laboratory, its moisture content is measured. The tests carried out later are not presented in this work. Moisture content measurement is done using a Kern moisture analyzer. During this process, records of air temperature, relative humidity and wind speed measured on the day of collection are obtained by a weather station located in the vicinity of the collection area.

4. Results and Discussion

The experimental data obtained are shown in Table 1. The experimental results chosen to be analyzed and compared with the numerical results refer to the year 2021. From the measurements carried out, 61 were selected to be analyzed. Table 1 shows the monthly average values obtained from the measured moisture content of maritime pine leaves, as well as the monthly average of air temperatures and relative humidity recorded on the days of leaf sampling.

The average numerical moisture content obtained in the leaves of the pine branch was 56.41%. Note that this value corresponds to the numerical simulation carried out considering the mean values of air temperature and relative humidity obtained experimentally (see Table 1).

The numerical average results of the moisture content in the leaves are very similar to the monthly average results obtained experimentally in the measurement of the moisture content in the leaves. Comparing the numerically calculated value of the moisture content of the leaves with the annual mean value of the experimental measurements, it appears that the relative error is 1.45%. It can be concluded that the numerical model implemented in the calculation of the moisture content of the leaves of a pine tree allows to obtain results very close to the real ones, so the use of this numerical model is considered valid.

Table 1 – Experimental data obtained during 2021 (average monthly results).

Month	Moisture content (%)	Air temperature (ºC)	Relative Humidity (%)
1	55.20	15.10	83.00
2	55.29	16.03	78.29
3	54.76	17.54	62.20
4	55.32	17.95	65.50
5	54.24	21.10	55.00
6	54.06	25.82	44.00
7	57.87	26.71	38.11
8	56.60	26.42	53.67
9	54.53	26.50	48.00
10	61.85	22.74	50.60
11	54.14	17.70	53.00
12	53.38	13.63	69.33
Average	**55.60**	**20.60**	**58.39**

5. Conclusions

This article introduced a numerical model developed to calculate the moisture content available in the leaves of a tree, considering the surrounding external environmental conditions given by air temperature, relative humidity and wind speed. In this study, in particular, maritime pine leaves were used. The results obtained numerically were compared with experimental measurements done under similar environmental conditions. Experimental data used throughout the year 2021 were used.

The main conclusion reached is that the numerical model proposed here allows obtaining results on the moisture content of maritime pine leaves very close to those obtained experimentally. Comparing the numerical result with the annual average value of the experimental results, it is verified that there is a relative error of 1.45%.

Therefore, the authors consider that the numerical model proposed in this work can be effectively used to calculate the moisture content of tree leaves and, particularly, of maritime pine.

6. Acknowledgments

The authors would like to acknowledge the support of the project reference PCIF/MPG/0108/2017, funded by the Portuguese Foundation of Science and Technology (FCT). The authors grateful the collaboration of the Camilo Portela.

7. References

Adab, H., Kanniah, K., Beringer, J.: Estimating and up-scaling fuel moisture and leaf dry matter content of a temperate humid forest using multi resolution remote sensing data. Remote Sensing 9, 961 (2016).

Conceição, E., Silva, M., André, J., Viegas, D.: Thermal behaviour simulation of the passenger compartment of vehicles. International Journal of Vehicle Design 24(4), 372-387 (2000).

Conceição, E., Lúcio, M.: Numerical and subjective responses of human thermal sensation. In: 6th Portuguese Conference on Biomedical Engineering, BIOENG'2001, Faro, Portugal, 11-12 June (2001).

Conceição, E., Nunes, A., Gomes, J., Lúcio, M.: Application of a school building thermal response numerical model in the evolution of the adaptive thermal comfort level in the Mediterranean environment. International Journal of Ventilation 9(3), 287-304 (2010).

Conceição, E., Lúcio, M.: Numerical study of the influence of opaque external trees with pyramidal shape in the thermal behaviour of a school building in summer conditions. Indoor and Built Environment 19, 657-667 (2010).

Conceição, E., Santiago, C., Lúcio, M., Awbi, H.: Predicting the air quality, thermal comfort and draught risk for a virtual classroom with desk-type personalized ventilation systems. Buildings 8(2), 35 (2018).

Conceição, E., Awbi, H.: Evaluation of integral effect of thermal comfort, air quality and draught risk for desks equipped with personalized ventilation systems. Energies 14(11), 3235 (2021).

Green, S., Vogeler, I., Clothier, B., Mills, T., Dijssel, C.: Modelling water uptake by a mature apple tree. Australian Journal of Soil Research 41, 365-380 (2003).

Janott, F., Gayler, S., Gessler, A., Javaux, M., Klier, C., Priesack, E.: A one-dimensional model of water flow in soil-plant systems based on plant architecture. Plant Soil 341, 233-256 (2011).

Lifang, C., Qun, D., Zhiming, Z., Zehao, S.: Moisture content variations in soil and plant of post-fire regenerating forests in central Yunnan Plateau, Southwest China. Journal of Geographical Sciences 29(7), 1179-1192 (2019).

Nolan, R., Blackman, C., Dios, V., Choat, B., Medlyn, B., Li, X., Bradstock, R., Boer, M.: Linking forest flammability and plant vulnerability to drought. Forests 11, 779 (2020).

Rao, K., Williams, A., Flefil, J., Konings, A.: SAR-enhanced mapping of live fuel moisture content. Remote Sensing of Environment 245, 111797 (2020).

Simon, H., Lindén, J., Hoffmann, D., Braun, P., Bruse, M., Esper, J.: Modeling transpiration and leaf temperature of urban trees – A case study evaluating the microclimate model ENVI-met against measurement data. Landscape and Urban Planning 174, 33-40 (2018).

Wang, F., Letort, V., Lu, Q., Bai, X., Guo, Y., Reffye, P., Li, B.: A functional and structural Mongolian Scots pine (Pinus sylvestris var. mongolica) model integrating architecture, biomass and effects of precipitation. PLoS ONE 7(8): 43531 (2012).

Numerical characterization of structures heat exposure at WUI

Yolanda Pérez-Ramirez*[1]; Anthony Graziani[1]; Paul-Antoine Santoni[1]; Virginie Tihay-Felicelli[1]; William (Ruddy) Mell[2]

[1]Université de Corse - CNRS UMR 6134 SPE, Campus Grimaldi, 20250, Corte, France, {perez_y@univ-corse.fr}, {graziani_a, santoni_p, tihay_v}@univ-corse.fr
[2] U.S. Forest Service, Pacific Wildland Fire Sciences Lab, 400 N. 34th St., Suite 201, Seattle, WA, 98103, USA, {ruddymell@gmail.com}

**Corresponding author*

Keywords

Wildfire, Heat transfer, Fuel treatments, Numerical simulations, WFDS

Abstract

In the forthcoming years, self-protection of communities will be a first priority over fire suppression in order to tend to more fire-resistant and resilient WUI communities. All around the world, countries facing WUI fires apply different recommendations or regulations often issued from post-fire surveys. Still, more efforts are necessary to understand how and why dwellings are damaged or completely destroyed under WUI fires attack. In particular, there is a need to quantitatively assess the effectiveness of the current legal prescriptions for homeowners concerning the defensible space around dwellings. Three-dimensional, time dependent, computational fluid dynamics fire behavior models can take into account the factors interacting and contributing to WUI fires (i.e., weather conditions, terrain configuration, fire, vegetation and structures). Moreover, they allow the spatially-explicit modelling of vegetation elements (i.e., trees, shrubs, etc.). Thus, they can be supporting tools to quantitatively assess the heat (radiative and convective) exposure of structures during the approach of a WUI fire, in order to investigate how the characteristics of the defensible space can protect a dwelling or not against such a fire. This study addresses the characterization of heat exposure conditions of a dwelling in common Mediterranean WUI scenarios by using the three-dimensional, time dependent, computational fluid dynamics forest fire behavior model WFDS. To this purpose, WUI fire simulations have been carried out at the landscape scale, taking into account the different zones that a fire burns before it might approach and reach a home structure. This is, a forested area and the defensible space or cleared area around a dwelling. Two different scenarios have been studied, where different spatial patterns for the raised vegetation at the defensible space have been considered. One vegetation pattern has a low level of aggregation corresponding to a sparse spatial distribution of plants, whereas the other vegetation pattern has a higher level of aggregation representative of a clumpy distribution of plants. Both scenarios, in agreement with the current regulations in Corsica, have the same amount of available fuel load, as well as, the same number and characteristics of raised vegetation elements. Fire simulations for these two scenarios have been carried out at different wind and ambient conditions representatives on one side of normal dry summer conditions and on the other side of severe dry summer conditions. Heat exposure conditions have been characterized in terms of radiative and convective heat fluxes received by the structure. Special attention has been given on the role of fire – vegetation – wind interactions for the results and discussion.

1. Introduction

Fire events occurring at the Wildland Urban Interface (henceforth WUI), are responsible not only for important structure losses but also for human fatalities. In order to plan successful mitigation actions, it is necessary to understand the complex interactions between weather conditions, terrain configuration, fire, vegetation and structures during a WUI fire.

The existing wildfires risk mitigation strategies and the associated regulations concern different scales, from community scale (i.e., land use and fire regulations) to individual dwelling scale (i.e., building codes) (Duerksen et al., 2011). However, the susceptibility of a dwelling to undergo wildfire damages is strongly determined by its characteristics in relation to the immediate surroundings (Calkin et al., 2014), as already demonstrated by several studies (Cohen 2000; Cohen & Stratton, 2003; 2008).

The most common strategies to reduce dwelling's loss at individual property scale involve building construction materials (i.e., combustible, non-combustible, fire resistant), building design features (i.e., details of its different

parts and the weak points in the building envelope like openings), and a defensible space around the dwelling by clearing ornamental vegetation and other material or secondary structures (i.e., sheds, fences, etc.) which can burn and impact the dwelling. However, self-protection plans of WUI settlements mainly concern the defensible space around dwellings since generally, building policies at WUI are only mandatory for new structures.

In the forthcoming years, self-protection of communities will be a first priority over fire suppression in order to tend to more fire-resistant and resilient WUI communities (Pastor et al., 2020). All around the world, countries facing WUI fires apply different recommendations or regulations often issued from post-fire surveys (Laranjeira & Cruz, 2014; Intini et al., 2019). Still, more efforts are necessary to understand how and why dwellings are damaged or completely destroyed under WUI fires attack. In particular, there is a need to quantitatively assess the effectiveness of the current legal prescriptions for homeowners concerning the defensible space (Mell et al., 2010).

Three-dimensional, time dependent, computational fluid dynamics fire behavior models can take into account the factors interacting and contributing to WUI fires (i.e., weather conditions, terrain configuration, fire, vegetation and structures). Moreover, they allow the spatially-explicit modelling of vegetation elements (i.e., trees, shrubs, etc.). Thus, they can be supporting tools to quantitatively assess the heat (radiative and convective) exposure conditions of structures during the approach of a WUI fire, in order to investigate how the characteristics of the defensible space around a dwelling can protect it or not against such fire.

This study addresses the characterization of heat exposure conditions of a dwelling in common Mediterranean WUI scenarios by using the three-dimensional, time dependent, computational fluid dynamics fire behavior model WFDS (Mell et al., 2007; 2009; Pérez-Ramirez et al., 2017). Heat exposure conditions have been characterized in terms of radiative and convective heat fluxes received by the structure, paying special attention to the openings in the building envelope (e.g., windows, shutters, etc.). It is worth noting that even though different exposure conditions are responsible for dwellings damage at WUI, this is, flame radiation, direct flame contact and firebrands (Caton et al, 2017), only the two first mechanisms have been considered in this study.

2. Numerical Modelling

WUI fire simulations with WFDS have been carried out at the landscape scale to take into account the different zones that a fire has to burn before the fire front might approach and reach the home structure. This is, a forested area and the defensible space around the dwelling. The defensible space includes ornamental vegetation in the immediate surroundings of the dwelling and a cleared area.

2.1. Vegetation modelling

The forested area implemented corresponds to a high-density cork oak forest, composed by a canopy stratum of cork oaks (*Quercus suber*), a shrub layer of plants of rockrose (*Cistus monspelliensis*), tree heath (*Erica arborea*) and strawberry tree (*Arbutus unedo*) and a litter layer. To model the cork oak forest, data from field sampling, as well as, from the literature were used. Several hypotheses were considered to model trees and shrubs; this is, plants per species have the same dimensions and they have a uniform distribution of fine particles in the crown. Spatial patterns of raised vegetation plants were modelled by using spatial statistics and in particular a point process based on a hard core pairwise interaction model.

The defensible space was modelled by taking into account the current regulation in Corsica which concerns its dimensions (i.e., distance between the house and the forest), the specifications on tree thinning and the required tree spacing (i.e., trees/shrubs and/or hedges spacing in this area). The immediate surroundings to the dwelling are composed by grass and a hedge, which is a common ornamental vegetation structure used in Mediterranean WUI communities to delimit properties. The area in between the forested area and the immediate surroundings of the dwelling is the result of the clearing of the cork oak forest stand, and is thus constituted by a canopy layer of cork oaks and the resprouting of the shrub layer (i.e., 20 cm height).

The same hypothesis and methods were used for the modelling of the canopy layer in the cleared area. Two different vegetation patterns in terms of the spatial distribution of cork oaks were tested in this area, resulting in two different scenarios. These two vegetation patterns are in agreement with the regulation in Corsica but present a different level of aggregation for the canopy layer. One vegetation pattern has a low level of aggregation (cleared area type 1) corresponding to a sparse spatial distribution of trees, whereas the other

vegetation pattern has a higher level of aggregation (cleared area type 2) representative of a clumpy distribution of trees (Figure 1). Both scenarios have the same amount of available fuel load, as well as, the same number and characteristics of trees. Consequently, only the spatial distribution of trees changes between these two configurations.

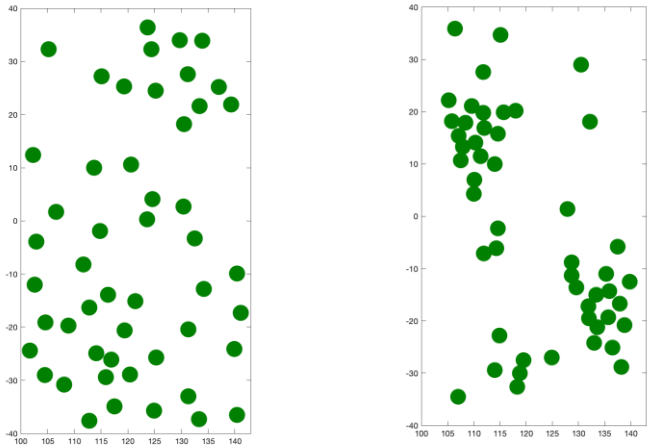

a) *b)*

Figure 1 – Vegetation spatial patterns in the cleared area. a) Sparse distribution. b) Clumpy distribution.

2.2. Numerical cases setup

Fire simulations for the two scenarios (i.e., forest – cleared area type 1 – ornamental vegetation – dwelling and forest – cleared area type 2 – ornamental vegetation – dwelling) were carried out for different wind and ambient conditions. Two wind velocities were tested corresponding to a mild to moderate wind and a strong wind, representative for more extreme conditions. In the same way, two sets of ambient conditions and fuel moisture content were studied, one set being characteristic of normal dry summer conditions and the other set being representative of severe dry summer conditions. Fuel moisture content values for the different species considered were obtained from historical records of the French operational network called "Reseau Hydrique" (Martin-StPaul et al, 2018). Table 1 summarizes the different scenarios and conditions tested in this study.

Table 1- Specifications of the different scenarios and conditions tested (RH: Relative Humidity, FMC: fuel moisture content on dry basis)

Forested area	**Cleared area**	**Wind conditions**	**Ambient conditions – Fuel moisture content**
High-density cork oak forest stand	**Vegetation distribution type 1**	**Low-moderate wind**	**Dry conditions**
	Low aggregation pattern	25 km/h	32°C, 20 % RH 52 % - 81 % FMC
	Vegetation distribution type 2	**Strong wind**	**Severe dry conditions**
	High aggregation pattern	45 km/h	40°C, 10 % RH 23 % - 60 % FMC

The computational domain size was 275 m x 80 m x 70 m (Figure 2). The domain was subdivided into two area, the first one covering all the surface of the domain up to 32 m height, and the second one covering the upper part of the domain. In the first area, where combustion takes place, the grid cell size was $\Delta x=\Delta y=\Delta z=25$ cm, whereas in the second area the grid cell size was $\Delta x=\Delta y=\Delta z=50$ cm. A 1/7th power law profile was used at the inlet of the domain to implement the wind condition. Ignition was delayed to allow the wind field to fully develop in the whole domain. Periodic conditions were applied at both left and right sides of the domain. A free slip conditions was used for the top boundary, while an open boundary condition was prescribed at the outlet of the domain.

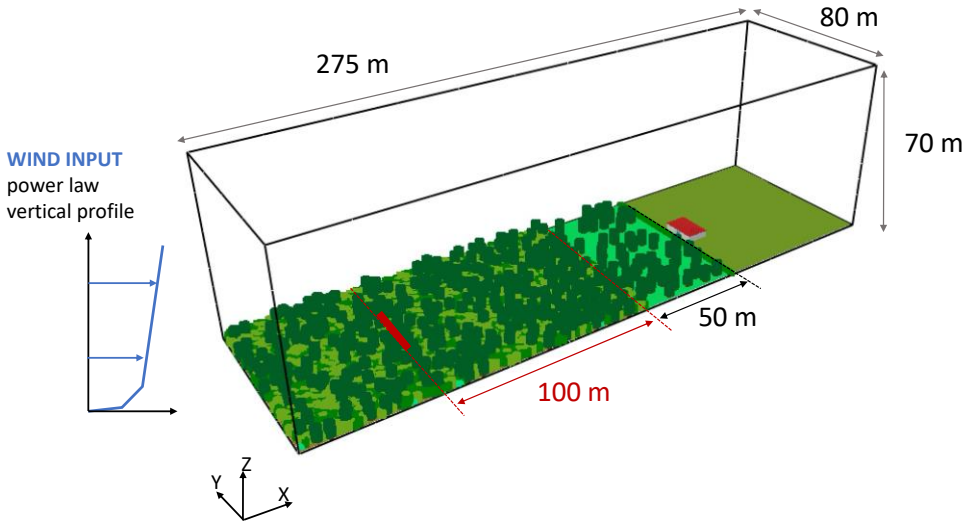

Figure 2 – Numerical domain implemented

Surface fuels (i.e., litter, grass and the shrubs regrowth in the cleared area) were implemented by using the fuel boundary model coupled with a linear pyrolysis sub-model for the thermal degradation of the solid-phase. The other vegetation elements were implemented by using the fuel element model combined to an Arrhenius type model for solid-phase degradation including char oxidation.

Different openings were implemented in the dwelling façade the most exposed to the fire, this is, a central French window and two windows on both sides of the French window.

3. Results and Conclusions

The distribution pattern of trees in the cleared area affects the wind patterns nearby the dwelling, which in turn affect the burning dynamics. As it can be seen in Figure 3 for the worst-conditions cases, this is cases spreading under a strong wind and very dry conditions, the position of the fire front and its shape at the same instant of time differ from one case to another. For the vegetation pattern corresponding to a low level of aggregation (Figure 3a)) the fire front shape is not symmetric to the centerline and thus the heat exposure conditions vary from one window to another (Figure 4a)). For the other vegetation scenario (Figure 3b)), the fire front profile is almost symmetric to the centerline so that the heat exposure conditions in terms of the duration and maximum heat exposure of windows are similar even though some differences are observed that can be explained by the presence of a group of trees in front of one of the windows (Figure 4b)).

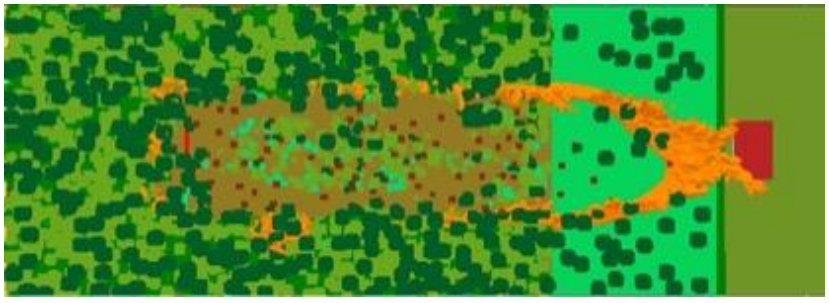

a)

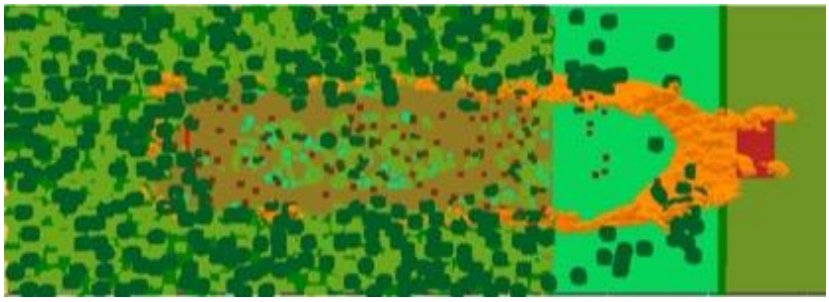

b)

Figure 3 – Snapshots as rendered by Smokeview for the worst-conditions cases at the same instant of time. a) Vegetation distribution type 1. b) Vegetation distribution type 2.

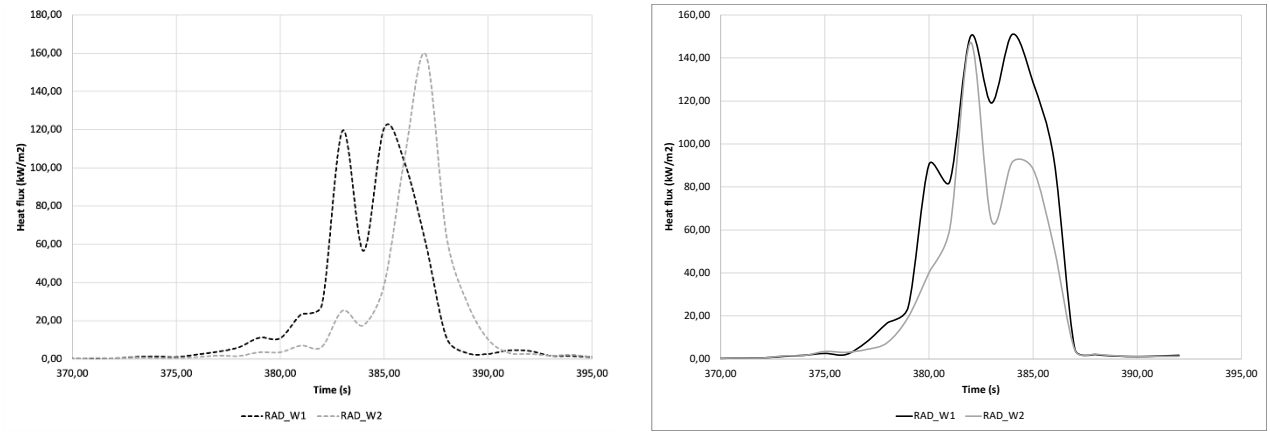

a) *b)*

Figure 4 – Total heat fluxes received by side windows for the worst-conditions cases. a) Vegetation distribution type 1. b) Vegetation distribution type 2.

As illustrated in Figure 5, heat release rate tendencies for both cases are similar during the combustion phase in the forested area and differences are observed once the fire front reaches the cleared area (at about 340 seconds) due to the differences in combustion dynamics in this area. Results for the cases run in the other conditions (Table 1) are in agreement with these results.

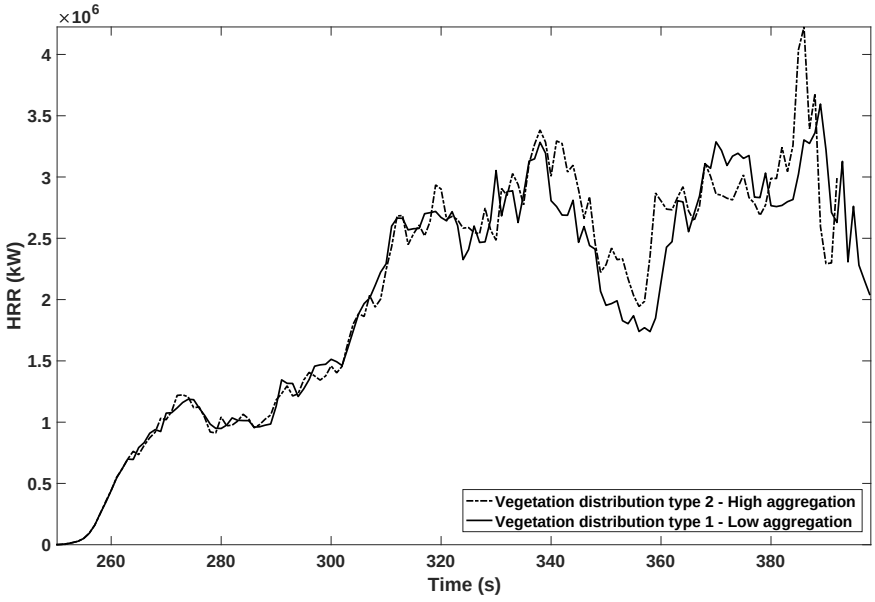

Figure 5 – Heat Release Rate for the worst-conditions cases

This study highlights the role of heterogenous patterns of vegetation on the burning dynamics for a WUI fire scenario and thus on the thermal exposure conditions of a dwelling, due to the interactions between vegetation, wind and fire itself. However, a deeper analysis including simulations of other vegetation patterns, is need to obtain statistically significant conclusions.

4. Acknowledgements

This research was supported by the projects "MED-STAR" (Strategie e misure per la mitigazione del rischio di incendio nell'area Mediterranea) and "INTERMED" (Interventions pour gérer et réduire le risque d'incendie à l'interface habitat-espace naturel) financed by the fund PC IFM 2014-2020 (http://interreg-maritime.eu/fr/web/med-star).

5. References

Calkin DE, Cohen JD, Finney MA, Thompson MP (2014) How risk management can prevent future wildfire disasters in the wildland-urban interface. Proceedings of the National Academy of Science of the United States of America, 111 (2): 746 – 751.

Caton SE, Hakes RSP, Gorham DJ, *et al.* (2017) Review of Pathways for Building Fire Spread in the Wildland Urban Interface Part I: Exposure Conditions. Fire Technology, 53: 429-473.

Cohen JD (2000) Preventing disaster, home ignitability in the wildland-urban interface. Journal of Forestry 98(3):15–21.

Cohen J, Stratton RD (2003) Home destruction within the Hayman fire perimeter. Hayman Fire Case Study. Gen. Tech. Rep. MRS-GTR-114, ed Graham RT (US Forest Service Rocky Mountain Research Station, Fort Collins, CO).

Cohen JD, Stratton RD (2008) Home Destruction Examination: Grass Valley Fire, Lake Arrowhead, CA. R5-TP-026b (US Forest Service, Portland, OR).

Duerksen C, Elliott D, Anthony P (2011) Addressing Community Wildfire Risk: A Review and Assessment of Regulatory and Planning Tools. The Fire Protection Research Foundation, Quincy, MA, USA.

Intini P, Ronchi E, Gwynne S, Bénichou N (2019) Guidance on Design and Construction of the Built Environment Against Wildland Urban Interface Fire Hazard: A Review. Fire Technology, 56: 1853-1883.

Laranjeira J & Cruz H (2014) Building vulnerabilities to fires at the wildland urban interface. In Viegas DX (Ed): Advances in Forest Fire Research. Chapter 3 – Fire Management, 673 – 684.

Martin-StPaul N, Pimont F, Dupuy JL, Rigolot E, Ruffault J, Frageon H, Cabane E, Duché Y, Savazzi R, Toutchkov M (2018) Live fuel moisture content (LFMC) time series for multiple sites and species in the French Mediterranean area since 1996. Annals of Forest Science, 75: 57.

Mell WE, Jenkins MA, Gould J, Cheney P (2007) A physics-based approach to modelling grassland fires. International Journal of Wildland Fire, 16: 1-22.

Mell WE, Manzello SL, Maranghides A, Butry D, Rehm R (2010) The wildland-urban interface fire problem – current approaches and research needs. International Journal of Wildland Fire, 19: 238-251.

Mell WE, Maranghides A, McDermott R, Manzello S (2009) Numerical simulation and experiments of burning Douglas fir trees. Combustion and Flame, 156: 2023-2041.

Pastor E, Muñoz JA, Caballero D, Agueda A, Dalmau F, Planas E (2020) Wildland-Urban Interface Fires in Spain: Summary of the Policy Framework and Recommendation for Improvement. Fire Technology, 56: 1831-1851.

Pérez-Ramirez Y, Mell WE, Santoni PA, Tramoni JB, Bosseur F (2017) Examination of WFDS in Modeling Spreading Fires in a Furniture Calorimeter. Fire Technology, 53: 1795-1832.

Numerical investigation of the effect of wind speed on wildfire interaction with an idealized building

Maryam Ghodrat *[1]; Ali Edalati-nejad [2]; Phillip L. Davies[1]

[1]School of Engineering and Information Technology, University of New South Wales, UNSW Canberra. Campbell, ACT, Australia, {m.ghodrat@unsw.edu.au}
[2]School of Science, UNSW Canberra, Canberra, ACT 2612, Australia, {a.edalatinejad@adfa.edu.au}

**Corresponding author*

Keywords

Wildfire; wind-driven surface fire; wildland-urban interface; LES; FireFOAM

Abstract

This paper presents an investigation into the impact of wind speed on the interaction of wind driven surface fire with an idealized building structure. The open-source large eddy simulation (LES) fire dynamic solver, FireFOAM, was used to simulate fires burning with an intensity of 10 MW/m under different wind speeds. The numerical data was validated using a wind only simulation which compared aerodynamic data to the previous full size experimental and numerical studies. The results show the aerodynamic flow characteristics and their interaction with the idealized structure located downstream of the fire source. Increase in wind speed showed a linear relationship to increase in the coefficient of lift on the building. The local coefficient of pressure on the building was calculated which indicated significant risk of damage due to aerodynamic lift caused by buoyant fire updraft. The results also show that at a constant fire intensity, increasing wind speed leads to an increase in the average temperature of the domain downstream of the fire to a certain value and then decreases.

1. Introduction

Wildfires are a natural disaster which can cause significant damage to the local environment, both natural and man-made. Whilst many plants and animals have adapted to wildfire and require regular fires to maintain biodiversity (Walker et al., 2019), urban structures face high risk of damage and destruction. With large wildfires becoming a more likely occurrence (Theobald & Romme, 2007) and urban sprawl into wildland areas, there is a need for continued study into reducing the risk wildfires pose to urban structures in the wildland-urban interface. Research in this area is useful for improving the design of wildfire resistant buildings, thereby reducing the socioeconomic impact of wildfires in the future.

Wildfire studies using CFD solvers have been used since the 1980s when Grishin and his team developed the first fully physical multiphase wildfire model (Grishin, Zverev, & Shevelev, 1986). From this model more advanced wildfire simulation software has been developed including Wildland Fire Dynamics Simulator (WFDS) (Mell, Charney, Jenkins, Cheney, & Gould, 2013) and FIRETEC code (Frangieh, Accary, Morvan, Méradji, & Bessonov, 2020; Morvan, Accary, Meradji, Frangieh, & Bessonov, 2018; Pimont, Dupuy, Linn, & Dupont, 2011). Several wildfire prediction software programs have been developed to provide fast predictions in an operational environment through simplification of wildfire spread. These are tools based on the Rothermel model (Rothermel, 1972), BehavePlus (Andrews, 2007) and FARSITE (Finney, 1998). These programs perform well during a wildfire but cannot provide accurate data to help improve the understanding of fire spread and damage to buildings on a small scale. This is where accurate fire modelling CFD tools are required, as they provide data that are rather difficult to obtain experimentally. He and his team were the first to carry out a numerical analysis of wind-driven wildfire interaction with an idealized building in 2011 (He, Kwok, Douglas, & Razali, 2011). Since then, studies by Fryanova and Perminov (Fryanova & Perminov, 2017), and Pimont, Dupuy, and Linn (Pimont, Dupuy, & Linn, 2014) investigated the likelihood of structure ignition and the minimum clearing distance to avoid ignition caused by radiation and convective effects. In 2020 Ghaderi and his team used fireFOAM to investigate wind-driven wildfire interaction with an idealized building focusing on the radiative heat flux experienced by the building (Ghaderi, Ghodrat, & Sharples, 2020). Further research is

required into the interactions between wind-driven wildfires and urban environments to prevent loss of life and property. In the present study, the effect of wind speed, at a constant fire intensity, on the fire-line dynamics, downstream temperature, and local pressure coefficient along the centrelines over the front, top and rear surfaces of an idealised building investigated. The results of this research will help inform decisions in building design in the Wildland Urban Interface.

1.1. Model description

1.1.1.Case design

The modeling case was designed to be a simplified representation of a wildfire interaction with an idealised building. The line fire is a fixed mass flow rate inlet of methane. The mass flow rate is fixed to produce a 10 MW/m line fire intensity, representing a typical grassland fuel fire propagating at a rate of spread of 0.75m/s and a fuel load of 0.4kg/m^2 (Byram, 1959). The idealized building was chosen to be a six-meter cube, as was used in several previous studies on wind-building interactions (Castro & Robins, 1977; Ghodrat, Shakeriaski, Nelson, & Simeoni, 2021; Richards & Hoxey, 2012). This provides reference data for qualitative and quantitative validation of the modeling case. The size of the computational domain was chosen to be 50 ×30 × 25 m to minimize adverse boundary condition effects as per the recommendations by Richards and Norris (Richards & Hoxey, 2012) in their work on LES modelling of unsteady flow around the Silsoe Cube (Figure 1a). The five-meter distance from the inlet to the line fire was chosen to provide proper boundary layer development and reduce the sensitivity to the inlet velocity profile at the price of greater simulation cost.

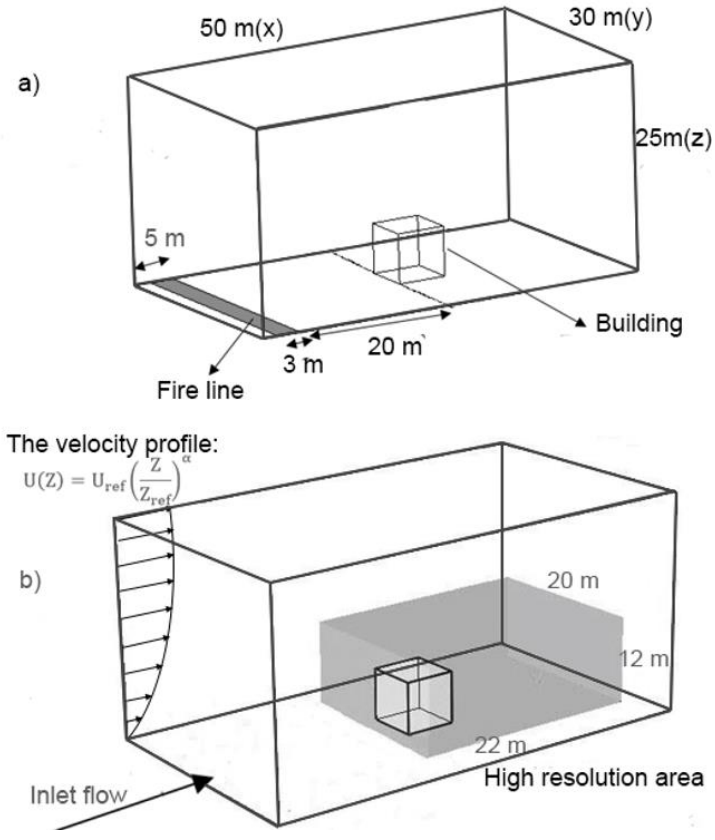

Figure 1- Schematic of the computational domain and the location of fire source and the building. (a) the calculated domain (b) Subdomain configuration

The inlet velocity profile is a power-law inflow velocity profile superimposed with random noise to simulate a realistic turbulent wind (Equation 1). This equation simulates the expected boundary layer formation, allowing for a reduction in the length of the flow development section prior to the fire, thereby reducing simulation cost (Bonnet, Delville, & Lamballais, 2003; Lund, Wu, & Squires, 1998).

$$u^* = \frac{U(Z)}{U_{ref}} = (\frac{Z}{Z_{ref}})^{\alpha} \quad (1)$$

Where u* is the velocity at each height, U_{ref} is the reference velocity, Z_{ref} is the reference height (6 m). γ is an exponent which corrects for terrain characteristics and assumed to be 0.16 based on the terrain at the experiment site (Lund et al., 1998). The roof and outlet of the simulation were set at atmospheric pressure to allow inflow and outflow as required. The walls are set to be free slip boundaries as suggested by Launder and Spalding (Launder & Spalding, 1983).

The mesh was created using consecutive reginal refinement. First a subdomain of size 22×20×12m was determined all over the building to make sure the complex vortical flow structures generated behind the building were recorded precisely (see Figure 1b). The next level of mesh refinement was arranged to sort out the near-wall regions around the building. In addition a high-resolution mesh near the floor was defined and provided all over the domain.

1.2. Numerical modeling

In the present paper, FireFOAM, as a well-known computational tool in fire research, was employed. FireFOAM is an open-source CFD code based on OpenFOAM, capable of being used for diffusion flames modeling. It has been successfully used for many practical applications such as solid fuel pyrolysis (Liu, Wang, & Zhang, 2020), fire suppression (Myers, Trouvé, & Marshall, 2018), and fire-wall interaction (Ren, Wang, Vilfayeau, & Trouvé, 2016).
The Favre-filtered formulation of the fully compressible Navier-Stokes equations representing the fire dynamics in the most common form is written as a set of conservation equations of mass, momentum, energy, and chemical species mass fraction (Poinsot & Veynante, 2005):

$$\frac{\partial \bar{\rho}}{\partial t} + \nabla.(\bar{\rho}\tilde{u}) = 0 \quad (2)$$

$$\frac{\partial \bar{\rho}\tilde{u}}{\partial t} + \nabla.(\bar{\rho}\tilde{u}\tilde{u}) = -\nabla\bar{p} + \nabla.\left[\left(\mu + \mu_{sgs}\right)\left(\nabla\tilde{u} + (\nabla\tilde{u})^T - \frac{2}{3}(\nabla.\tilde{u})I\right)\right] + \bar{\rho}g \quad (3)$$

$$\frac{\partial \bar{\rho}\widetilde{Y_k}}{\partial t} + \nabla.(\bar{\rho}(\tilde{u} + \tilde{u}_c)\tilde{Y}_k) = \nabla.\left[\left(\frac{\mu_{sgs}}{Sct} + \bar{j}_k\right)\nabla\widetilde{Y_k}\right] + \overline{\dot{\omega}_k'''} \quad k = 1, \dots, N_s - 1 \quad (4)$$

$$\frac{\partial \bar{\rho}\widetilde{h_s}}{\partial t} + \nabla.(\bar{\rho}\tilde{u}\tilde{h}_s) = \frac{D\bar{p}}{Dt} + \nabla.\left[\left(\alpha + \alpha_{sgs}\right)\nabla\tilde{h}_s\right] - \nabla.\overline{\dot{q}_r''} + \overline{\dot{q}_c'''} + \nabla.(\alpha\sum_{k=1}^{N_s}(h_{s,k}\nabla\tilde{Y}_k)) + \nabla.(\sum_{k=1}^{N_s}(\bar{j}_k h_{s,k})) \quad (5)$$

In these equations, ρ, P, u, h_s, Y, Sct are the density, pressure, velocity, sensible enthalpy, mass fraction, and turbulent Schmidt number. The symbols "–" and "~" show spatial and Favre filtering. $\overline{\dot{q}_c'''}$ is the heat generated by combustion (assuming complete combustion, i.e., $\chi = 1$) and $\overline{\dot{q}_r''}$ is the total radiation heat transfer emission intensity (W/ m^2) of the gas mixture. The eddy dissipation concept (EDC) (Magnussen & Hjertager, 1977) was used for combustion modeling. The infinitely-fast reaction assumption was applied to determine the reaction mechanism as the EDC in coupled with the infinitely-fast combustion model reveals higher superiority in modeling well-ventilated diffusion flames (Wang, Chatterjee, & de Ris, 2011).

1.3. Validation

Two methods of validating the numerical model were used to ensure both simulation accuracy and grid independency. Validation of simulation accuracy of the aerodynamic component of FireFOAM was achieved through a wind-off test. The coefficients of pressure measured on the building were compared to previous experimental results and numerical results by Castro and Robins (Castro & Robins, 1977) and He et al. (He et al., 2011), respectively. Both tests were run in a similar condition with an identical building (6 m cube) and wind speed (U_{ref}= 6m/s), and the measured and calculated coefficients of pressure can therefore be directly compared. Experimental data to validate grid independence was created by running three cases with differing mesh refinement. The grid numbers were set to 6, 8, and 10 million. The result of the validation cases showed

good similarity in the area from 0-1 and 2-3 but not between 1-2. The three mesh refinements produced very similar results and therefore the 8 million cell grid was selected for all simulations.

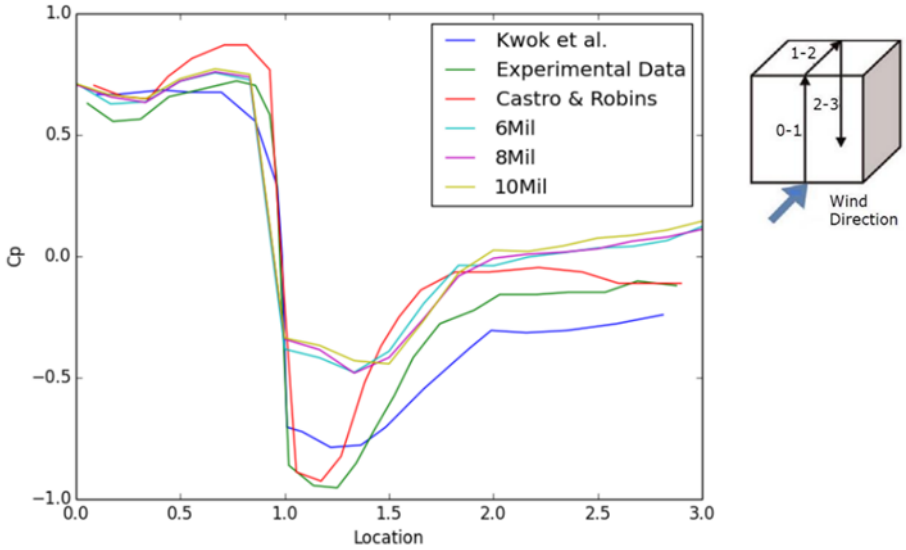

Figure 2- Comparison of the measured mean pressure coefficients on the building centreline, U_{ref}=6 m/s (no-fire case).

2. Results and discussion

The present study examined the simulated impact of a dynamically varying wind-field on a motionless heat source, correspond to a line fire configuration. The modeling results allowed analysis of the transient fire behaviour under different wind velocities (4.5 m/s, 6m/s and 7.5 m/s) and constant fire intensity of 10 MW/m. Figure 3 shows the time dependent flow pattern of wind speed variation in the fire field. As shown, increasing wind speed leads the fire front to be leaned towards the ground downstream of the line-fire bed. This is largely associated with the inertia forces becoming more dominant in this region with rising wind speed. Furthermore, as can be seen from the wind speed contours, air entrainment hooked on the turbulent surface line fire generates a low-pressure zone in the flame-ground area in front of the fire and due to this the fire plume is accelerated and create an area attached to the ground.

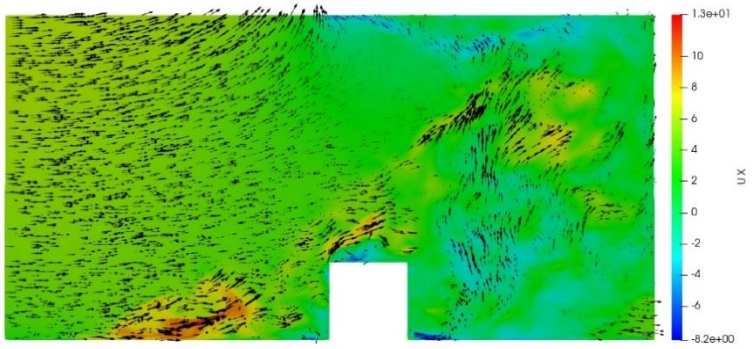

(a)

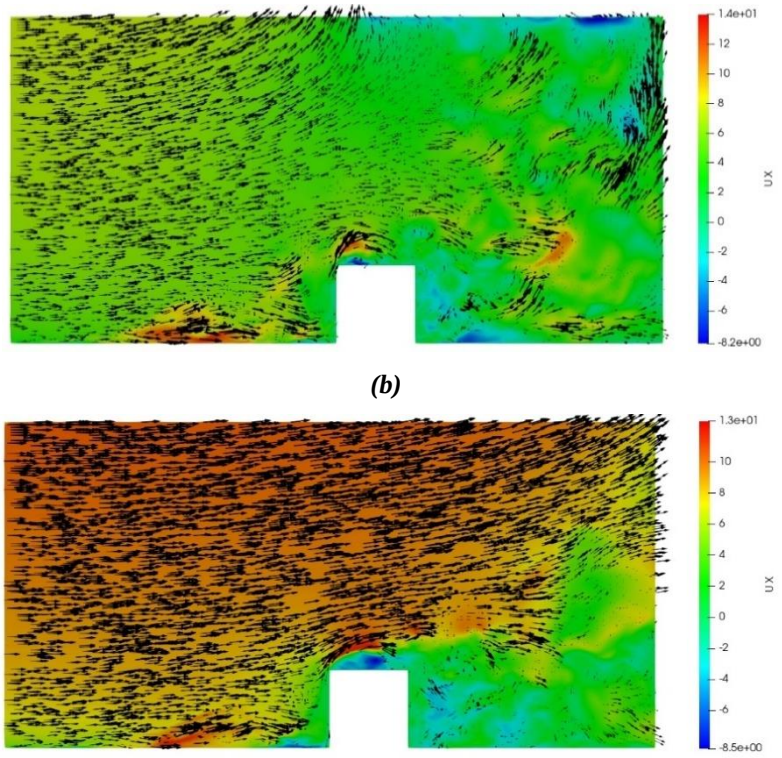

(b)

(c)

Figure 3- Vertical transects of instantaneous streamwise wind speed component and corresponding velocity vectors at different lateral locations. (a) U_{ref}=4.5 m/s (b)U_{ref}=6 m/s (c) U_{ref}=7.5m/s

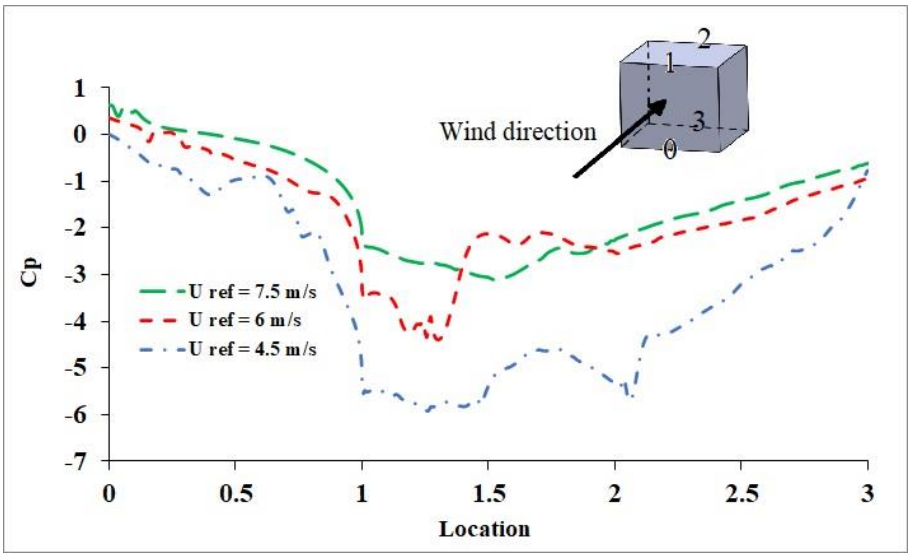

Figure 4- Coefficients of pressure on different location on the building under different wind speed

Figure 4 compares the coefficients of pressure on different location of the building with the focus on the front and back surface and the roof of the building during the three test cases for three wind velocities. The result shows strong negative coefficient of pressure primarily on the roof of the building, between locations one and two. The strong updraft created by the buoyant fire combined with the vortex's development on the roof of the building, seen in the visual analysis above, are responsible for creating this. The lowest negative coefficient of pressure decreases with increasing wind velocity, meaning higher wind velocities generate more lift on the roof and may have the potential to cause both window and roof failure (Castro & Robins, 1977).

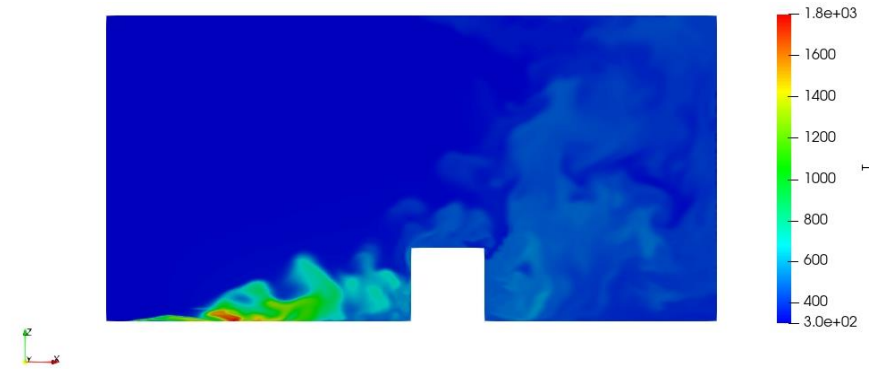

(a) 4.5 m/s

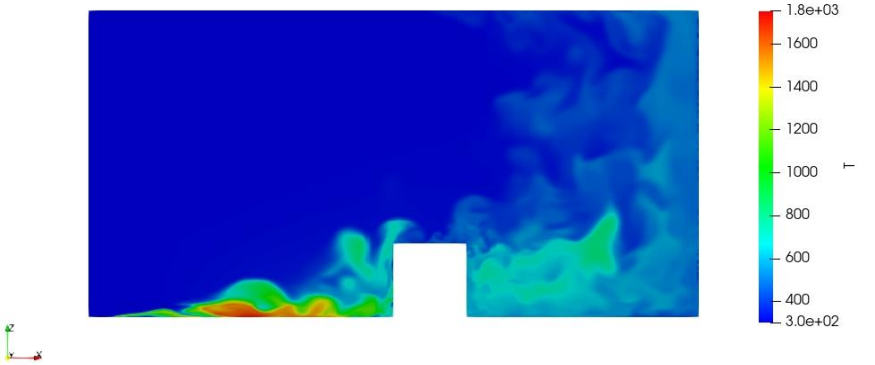

(b) 6m/s

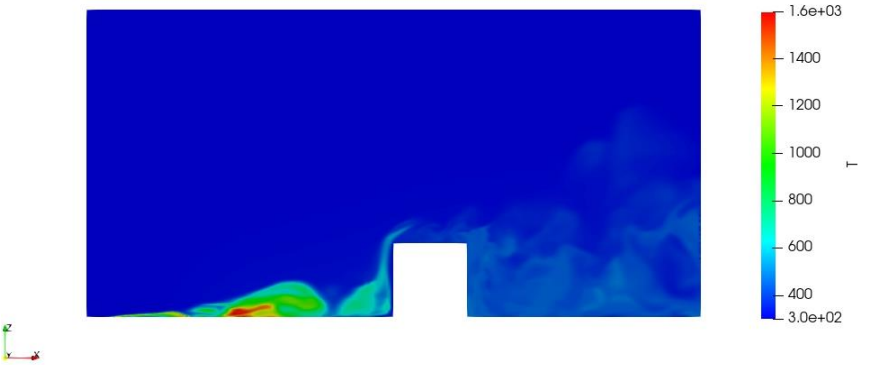

(c) 7.5 m/s

Figure 5- Temperature profile downstream of the line-fire source under different wind speed

Figure 5 shows the effect of wind speed variation on the temperature distribution downstream of the fire source at constant burning intensity of 10 MW/m. As can be seen in this figure increasing wind speed causes the flame to tilt further towards the building. Comparing the temperature contours under wind speed of 4.5 m/s and 6 m/s highlights that both average and local temperature intensified with raising wind speed and reached to a maximum value at wind speed of 6m/s (Fig. 5 a). Further increase in wind speed up to 7.5 m/s decreases the temperature of domain downstream of the fire source as the convective cooling become (Fig 5 c).

3. Conclusion

This paper detailed a numerical investigation into the effect of varying wind velocity in a simulated idealised structure using FireFOAM. The results show the flow characteristics expected in the wildfire structure interactions as well as the associated effects. The coefficient of pressure on the roof decreases dramatically with increased wind speed creating a large lifting force which has the potential to cause failure. The results also show

that at a constant fire intensity, increasing wind speed leads to an increase in the average temperature of the domain downstream of the fire to a certain value and then decrease.

4. Reference

Andrews, P. L. (2007). *BehavePlus fire modeling system: past, present, and future.* Paper presented at the In: Proceedings of 7th Symposium on Fire and Forest Meteorology; 23-25 October 2007, Bar Harbor, Maine. Boston, MA: American Meteorological Society. 13 p.

Bonnet, J.-P., Delville, J., & Lamballais, E. (2003). *The Generation of Realistic 3D, Unsteady Inlet Conditions for LES.* Paper presented at the 41st Aerospace Sciences Meeting and Exhibit.

Byram, G. M. (1959). Combustion of forest fuels. *Forest fire: control and use*, 61-89.

Castro, I., & Robins, A. (1977). The flow around a surface-mounted cube in uniform and turbulent streams. *Journal of fluid Mechanics, 79*(2), 307-335.

Finney, M. A. (1998). *FARSITE, Fire Area Simulator--model development and evaluation*: US Department of Agriculture, Forest Service, Rocky Mountain Research Station.

Frangieh, N., Accary, G., Morvan, D., Méradji, S., & Bessonov, O. (2020). Wildfires front dynamics: 3D structures and intensity at small and large scales. *Combustion and flame, 211*, 54-67.

Fryanova, K., & Perminov, V. (2017). Impact of forest fires on buildings and structures. *Magazine of Civil Engineering*(7 (75)), 15-22.

Ghaderi, M., Ghodrat, M., & Sharples, J. J. (2020). LES Simulation of Wind-Driven Wildfire Interaction with Idealized Structures in the Wildland-Urban Interface. *Atmosphere, 12*(1), 21.

Ghodrat, M., Shakeriaski, F., Nelson, D. J., & Simeoni, A. (2021). Existing improvements in simulation of fire–wind interaction and its effects on structures. *Fire, 4*(2), 27.

Grishin, A., Zverev, V., & Shevelev, S. V. (1986). Steady-state propagation of top crown forest fires. *Combustion, Explosion and Shock Waves, 22*(6), 733-739.

He, Y., Kwok, K. C., Douglas, G., & Razali, I. (2011). Numerical investigation of bushfire-wind interaction and its impact on building structure. *Fire Saf. Sci, 10*, 1449-1462.

Launder, B. E., & Spalding, D. B. (1983). The numerical computation of turbulent flows. In *Numerical prediction of flow, heat transfer, turbulence and combustion* (pp. 96-116): Elsevier.

Liu, H., Wang, C., & Zhang, A. (2020). Numerical simulation of the wood pyrolysis with homogenous/heterogeneous moisture using FireFOAM. *Energy*, 117624.

Lund, T. S., Wu, X., & Squires, K. D. (1998). Generation of turbulent inflow data for spatially-developing boundary layer simulations. *Journal of computational physics, 140*(2), 233-258.

Magnussen, B. F., & Hjertager, B. H. (1977). *On mathematical modeling of turbulent combustion with special emphasis on soot formation and combustion.* Paper presented at the Symposium (international) on Combustion.

Mell, W., Charney, J., Jenkins, M. A., Cheney, P., & Gould, J. (2013). Numerical simulations of grassland fire behavior from the LANL-FIRETEC and NIST-WFDS models. In *Remote Sensing and Modeling Applications to Wildland Fires* (pp. 209-225): Springer.

Morvan, D., Accary, G., Meradji, S., Frangieh, N., & Bessonov, O. (2018). A 3D physical model to study the behavior of vegetation fires at laboratory scale. *Fire Safety Journal, 101*, 39-52.

Myers, T., Trouvé, A., & Marshall, A. (2018). Predicting sprinkler spray dispersion in FireFOAM. *Fire safety journal, 100*, 93-102.

Pimont, F., Dupuy, J.-L., & Linn, R. (2014). Fire effects on the physical environment in the WUI using FIRETEC. *Chapter*.

Pimont, F., Dupuy, J.-L., Linn, R. R., & Dupont, S. (2011). Impacts of tree canopy structure on wind flows and fire propagation simulated with FIRETEC. *Annals of Forest Science, 68*(3), 523-530.

Poinsot, T., & Veynante, D. (2005). *Theoretical and numerical combustion*: RT Edwards, Inc.

Ren, N., Wang, Y., Vilfayeau, S., & Trouvé, A. (2016). Large eddy simulation of turbulent vertical wall fires supplied with gaseous fuel through porous burners. *Combustion and Flame, 169*, 194-208.

Richards, P., & Hoxey, R. (2012). Pressures on a cubic building—Part 1: Full-scale results. *Journal of wind engineering and industrial aerodynamics, 102*, 72-86.

Rothermel, R. C. (1972). *A mathematical model for predicting fire spread in wildland fuels* (Vol. 115): Intermountain Forest & Range Experiment Station, Forest Service, US ….

Theobald, D. M., & Romme, W. H. (2007). Expansion of the US wildland–urban interface. *Landscape and Urban Planning, 83*(4), 340-354.

Walker, X. J., Baltzer, J. L., Cumming, S. G., Day, N. J., Ebert, C., Goetz, S., . . . Schuur, E. A. (2019). Increasing wildfires threaten historic carbon sink of boreal forest soils. *Nature, 572*(7770), 520-523.

Wang, Y., Chatterjee, P., & de Ris, J. L. (2011). Large eddy simulation of fire plumes. *Proceedings of the Combustion Institute, 33*(2), 2473-2480.

Numerical prediction of the thermal stress induced by the burning of an ornamental vegetation at WUI

Anthony Graziani*[1]; Karina Meerpoel-Petri[1]; Virginie Tihay-Felicelli[1]; Paul-Antoine Santoni[1]; Frédéric Morandini.[1]; Yolanda Perez-Ramirez[1]; Antoine Pieri[1]; William Mell[2]

[1] Université de Corse – CNRS UMR 6134 SPE, Campus Grimaldi, 20250, Corte, France, {graziani_a@univ-corse.fr}
[2] U.S. Forest Service, Pacific Wildland Fire Sciences Lab, 400 N. 34th St., Suite 201, Seattle, WA, 98103, USA

**Corresponding author*

Keywords

Physics-based simulation, Thermal stress, WFDS, WUI

Abstract

Over the last decades, urban expansion and global warming have increased the occurrence of wildland fires propagating at the vicinity of buildings at WUI. In this scenario, ornamental vegetation is one of the vectors of fire propagation close to habitations, which can significantly increase the risk of damage (Maranghides et al (2009), Maranghides et al (2015), Etlinger et al (2004), Ganteaume et al (2013)). In such context, it is necessary to quantify the thermal stress generated by an ornamental plant over a building to predict the vulnerability of construction materials. To this end, numerical simulation is a good candidate to easily multiply burning cases at field scale and explore the effects. The present study focuses on the predictions of the thermal stress induced by the burning of an ornamental vegetation over targets facing the fire.

The study involves a numerical modelling of the burning of rockrose hedges at field scale using the physics based code WFDS. The solver uses a large eddy simulation approach for fluid dynamics and energy transfer through the fluid phase. The thermal degradation of the solid fuel is modelled (dehydration, pyrolysis, char oxidation) by a three steps mechanism with Arrhenius laws (Mell et al (2009)). The raised vegetation is represented with a Fuel Element approach, which models the solid fuel as a set of static Lagrangian particles of different sizes and distributed within the volume to reproduce the arrangement of the shrub. The ability of WFDS to reproduce the combustion of plants has already been studied at laboratory scales (Mell et al (2009), Perez-Ramirez et al (2017), Morandini et al (2019), Sanchez-Monroy et al (2019), Moinuddin et al (2020)) but investigations at field scale involving raised vegetation are few.

A set of experiments was carried out at field scale. Fire tests consist of the burning of reconstructed rockrose hedges of 6m length, 1m width and two heights (1m and 2m). The geometry mimics the typical shape of ornamental hedges that can be found to separate buildings in south of France. Visible cameras are distributed around the setup to capture the geometry of the flame front. Four couples of heat flux meters are positioned at 3m in front of the centreline and side of the hedge, which represents the theoretical position of the wall of a building according to the current fire safety regulation in France.

Comparison between predictions and experimental data shows good agreement for the local measurement of the heat stress at the location of the targets. Total and radiant heat fluxes fit with experimental data during the fire growth and the fully developed phases, which represent the period where the thermal stress is the highest. Peaks of total and radiant heat flux are the same order value but can be overestimated depending of the location of the sensors due to the wind dynamics that is not fully implementable in WFDS. Results show that the accuracy of the numerical model is satisfying to predict the thermal stress received by targets during the fully developed fire at field scale. It could be used to numerically determine the vulnerability of material buildings in different scenarios.

1. Introduction

The combination of climate change and cities expansion have risen the risk of fire at wildland urban interfaces (WUI) which can lead to house damages and human fatalities. Indeed, one of the identified vectors of fire spreading nearby a dwelling is ornamental vegetation, which can significantly increase the risk of material failure depending of their distance to the walls (Maranghides et al (2009), Maranghides et al (2015), Etlinger et

al (2004), Ganteaume et al (2013)). Predicting material thermal stress under wildland fire conditions is a key challenge to help authorities make more efficient fire safety regulations and facilitate the work of firefighters. To achieve this, numerical simulation is a suitable tool that allows to easily multiply fire scenarios at field scale in addition to experiments. While field experiments can be time consuming and expensive, numerical simulations are easier to deploy and lead to a larger number of physical quantities to analyze. However, numerical modeling can involve strong hypothesis compared to actual ambient conditions, especially at field scale since reproducing variable wind conditions is always challenging. Thus, it is required a first step to validate the predictions of the model at field scale by direct comparison with dedicated experiments, which is the topic of the present study. Consequently, this paper is focused on the numerical prediction of the thermal stress induced by the burning of an ornamental vegetation over targets facing the fire and the comparison to experiments. The paper is organized as follow. First, a full description of the experimental scenario at field scale is given. The numerical model employed is then presented, followed by a comparison with the experimental results. Finally, the paper ends with concluding remarks.

2. Experimental setup.

The main goal of this set of experiments is to quantify fire risk incurred by a facade that faces a burning ornamental hedge during summer for two configurations: one that is in accordance with the fire safety regulation in France, and another which is not. The quantification of such risk is directly estimated by measuring the heat flux received at the location of the wall.

Field scale experiments involved a rectangular reconstructed rockrose hedges of 6 m long and 1 m width with 2 different heights (1 m and 2 m) which reproduces the geometry of a common ornamental hedge used to separate buildings in south of France. The hedges were made with steel cages filled with dried rockrose branches rearranged to mimic the natural shape of a shrub. Rockrose (*i.e: Cistus Montpeliensis*) is a common species that can be found in the south of France and which contributes in propagating wildland fires during summer. A $6 \times 2 \times 0.2$ m^3 litter made of commercial wooden wool was positioned upstream of the reconstructed hedge to generate a surface spreading fire that ignited the rockrose by direct contact of the flame. The two setups involved 48 kg and 96 kg of vegetation fuel for respectively 1m and 2m height of the hedge, which represents a bulk density of 8 kg/m^3. Rockrose branches were weighted using a weight cell and meticulously introduced into the cage to have the required mass of fuel. Beforehand, rockrose was dried at ambient air to achieve a moisture content on dry basis of 10% in order to consider fuels in extremely dried conditions.

Experiments were carried out during summer under dry atmospheric conditions ($T_{air} = 37.93° \pm 0.37$, $RH_{air} = 16.6\% \pm 1.2$) and low wind conditions ($U_w = 2.29\ m/s \pm 0.17$). Tests were conducted during the same day to avoid variations of weather conditions between 2 consecutive days. Table 1 summarizes the three cases studied. The significant change in wind direction during the tests explain the difference between case n°1 and the others.

Three visible cameras were located around the hedge (2 on the sides, 1 at the back) in order to record the flame geometry. Four couples of radiant and thermal heat fluxes were positioned at 3 m in front of the hedge to assess the heat stress. This distance between the hedge and the heat fluxmeters corresponds to the minimal distance required between an ornamental vegetation and the wall of a building according to the current fire safety regulation in France. The first two couples of fluxmeters were aligned with the hedge centerline at heights of respectively 1 m (R1+T1) and 1.5 m (R3+T3) from the ground. The last two couples were aligned with the side of the hedge at the same z-coordinate i.e. 1 m for (R2+T2) and 1.5 m for (R4+T4). Each couple of fluxmeters was wall-mounted over an $1 \times 0.6 \times 0.05$ m^3 insulator plate to protect the wiring and the electronic from the fire. During each experiment, time history of upcoming wind velocity and direction was also recorded using an anemometer placed 15 m upstream from the setup and 2 m height from the ground. The cameras, the fluxmeters and the anemometer were recorded synchronously at 1 Hz using a data logger. Figure 1 presents a photo (a) and a layout (b) of the experiment setup.

Table 1 – Cases setup for the experimental burning of rockrose hedges at field scale

Case n°	Hedge dimension (m^3)	Accordance with Regulation?	Wind speed (m/s)	Wind direction (°)	Relative air humidity (%)	Temperature of air (°C)
1	6 × 1 × 1	Yes	2.34 (±0.73)	-12 (±33)	16.6	37.9
2	6 × 1 × 1	Yes	2.47 (±1.3)	47 (±51)	18.1	37.5
3	6 × 1 × 2	No	2.06 (±0.73)	44 (±43)	15.2	38.4

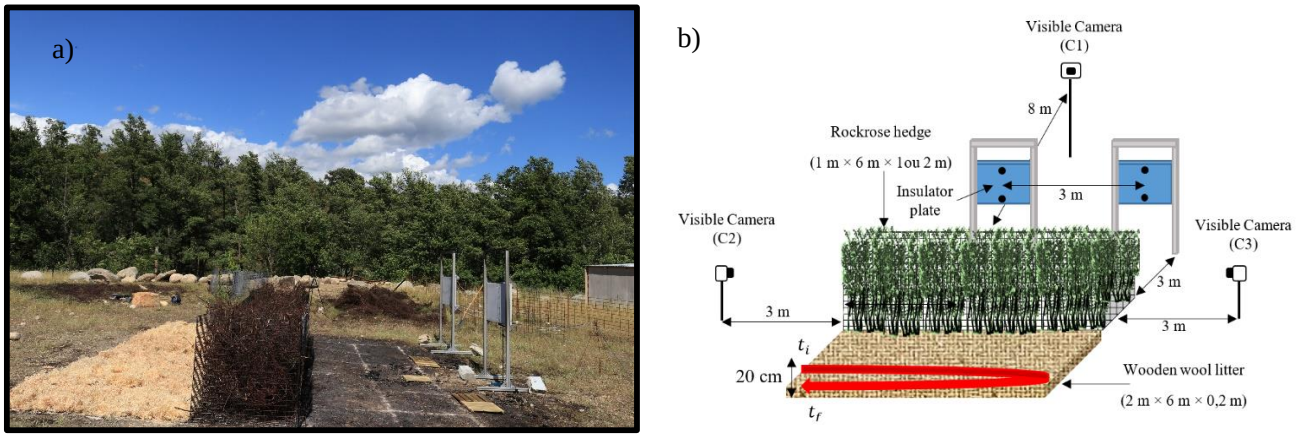

Figure 1 – Experimental setup at field scale: (a) photo of the setup, (b) layout of the setup.

3. Numerical modelling

Wildland-Urban interface Fire Dynamic Simulator (WFDS) is a physics-based CFD solver derived from NIST's code Fire Dynamics Simulator (McGrattan et al (2013a)) that includes the modelling of burning vegetation through a solid fuel approach [2]. Over the last decade, the code was widely use to simulate different types of vegetation fires, ranging from the burning of pine needles at laboratory scale to wildland fires at field scale walls (Mell et al (2009), Perez-Ramirez et al (2017), Morandini et al (2019), Sanchez-Monroy et al (2019), Moinuddin et al (2020)).

WFDS solves a solid-gas phase problem over a numerical domain discretized into a Cartesian grid mesh using the conservation equations of mass, momentum and energy transport. The turbulent gas phase is modelled with a Large-Eddy Simulation (LES) approach and a low-Mach formulation of the Navier-Stokes equations. The solid phase is represented by a "Fuel Element" (FE) approach, which consists in modelling the raised vegetation as static Lagrangian particles of different sizes and properties distributed within a volume that represents the plant. The heat transfer, drag force and thermal degradation for each particle of vegetation are approximated with a one-dimensional approach (thermally thin elements). The degradation of the solid fuel is represented by a three steps mechanism including dehydration, pyrolysis and char oxidation. Each stage is modelled with an Arrhenius law. The combustion of the pyrolysis gas is simplified by a single step combustion equation of a $C_xH_yO_z$ fuel. More details about the solver are in Mell *et al* (2009).

In order to simulate the experiments of the burning hedges, the volume of the numerical domain was set to $50 \times 50 \times 50$ m^3 with the hedge positioned at the center. This domain size allows avoiding any interaction between the boundary conditions and the numerical solution close to the hedges. The domain was meshed using two different sizes of hexahedral cells to save computational time. For a zone of $20 \times 20 \times 10$ m^{3}around the hedge, the cell size was $\Delta x = \Delta y = \Delta z = 12.5$ cm which was the best compromise between accuracy and computational cost. In the rest of the numerical domain, the mesh size was $\Delta x = \Delta y = \Delta z = 25$ cm. To reproduce the wind conditions of the experiments, a 1/7th power law profile was used at the inlet for which the averaged wind velocity and direction recorded during the test was considered. At the outlet, an outflow condition was set. On the top and bottom, a free-slip and a wall condition were respectively used. On the sides of the domain, periodic boundary conditions were considered to take into account the wind direction. The rockrose hedge was modeled using a Fuel Element approach and was decomposed into 6 classes of particles: flowers,

leaves, twigs of 0-2 mm, 2-4 mm, 4-6 mm and 6-25 mm in diameter. Characteristics and spatial distribution of each particle class were obtained from laboratory measurements. The Arrhenius coefficients associated to the thermal degradation process came from Morandini *et al* (2019). The wooden wool litter was also modeled with a fuel element approach using a three-step thermal degradation model with Arrhenius coefficient taken from Sanchez-Monroy et al (2019). Numerical heat flux sensors (radiant and total) were positioned at the same location as the experimental ones. Figure 2 presents snapshots of the simulations using the rendering of software SmokeView for both cases of hedge height.

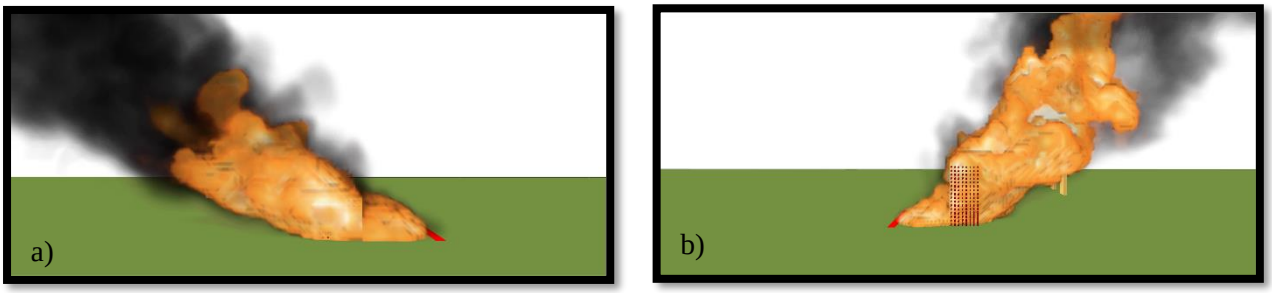

Figure 2 – Snapshots (200 kW/m^3 isosurface) of numerical simulation of burning hedges for two heights: (a) 1m, (b) 2m, rendered in Smokeview

4. Results and discussion

Experimental results show that three combustion stages mainly occur during the burning of the hedge: growth, fully developed fire and extinguishment. The present study focused on the heat fluxes during the developed fire stage. Figure 3 presents an example of the comparison between experiments and simulations for sensors T3 and T4 for case n°1. Red and black dashed lines represent the extinguishment time for the simulations and the experiments respectively. The first observations show that predicted heat fluxes fit better the experiments for the sensors facing the hedge centerline than those located at the side in terms of magnitude and curve shape tendencies.

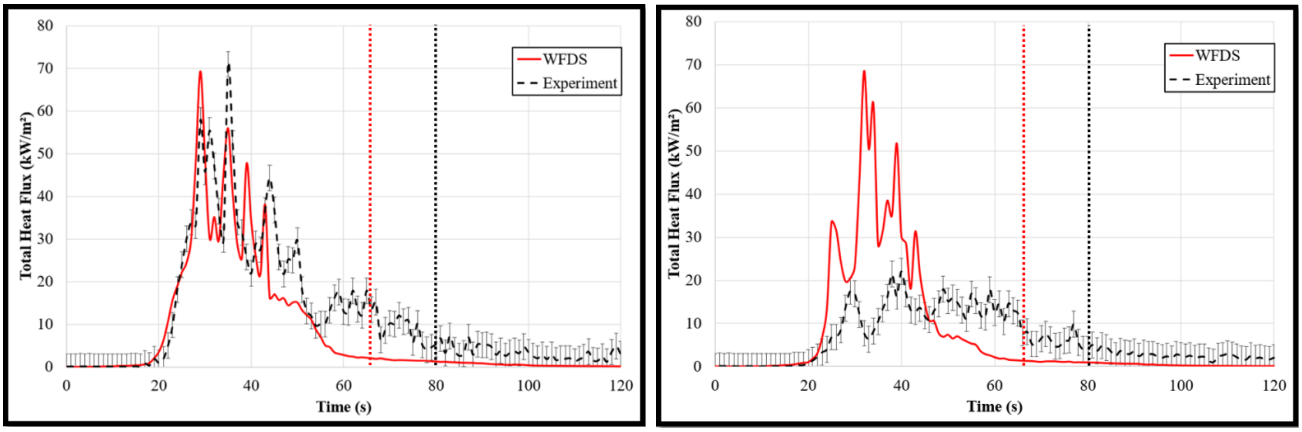

Figure 3 – Comparison between simulation and experiment for the total heat flux line for case n°1: left sensor T3; right sensor T4.

For the sensor T3, the numerical model predicted well the heat flux impinging on the sensor during the first half of the fully developed stage, which shows the highest magnitude of the heat flux. During the second half of the stage, the simulation failed to reproduce the particle collapse observed in the experiments, which deviates the prediction from the measurement. This also causes fire extinguishment occurring 19% to 33% faster in the simulation depending on the case simulated. The edge effects mainly explain the overestimation of the heat flux magnitude received by the numerical sensor at the side. Indeed, experiments have shown that the heat fluxes received by the sensors located at the edge of the hedges are more sensitives to the flame dynamics, and even more when large changes in wind direction occur and lean the flame away from the sensors. The current version of WFDS do not allow reproducing changes in wind speed and direction over time. This leads to a constant orientation of the simulated flames that point toward sensor T2 and T4 during the numerical simulation. The

predicted heat fluxes are therefore overestimated the heat fluxes for theses sensors. Overall, comparisons between simulations and experiments are in agreements with observations made by Perez-Ramirez & al (2017) and Meerpeol-Pietri & al (2022) at laboratory scale for pine needles and reconstructed hedges respectively.

Table 2 – Comparison between experimental and numerical exposure times for sensor T3 for each cases at different heat flux threshold.

Heat flux threshold (kW/m²)	Exposure time for sensor T3 (s)								
	Case n°1			Case n°2			Case n°3		
	Experiment	WFDS	E (%)	Experiment	WFDS	E (%)	Experiment	WFDS	E (%)
5	62	36	-42	49	37	-24	89	34	-62
8	52	33	-37	39	33	-15	62	31	-50
12	41	30	-27	32	30	-6	51	27	-47
15	33	27	-18	28	28	0	49	26	-47
30	14	11	-21	20	19	5	31	16	-48
35	10	9	-10	18	18	0	26	15	-42
40	7	7	0	14	16	14	20	12	-40
	Average relative difference (%)		-22%	**Average relative difference (%)**		-5%	**Average relative difference (%)**		-48

To evaluate the thermal stress due to the hedge burning, we choose to quantify the exposure times for different heat fluxes thresholds at the sensor location (Meerpoel-Pietri (2021)). Table 2 presents the average predicted and measured exposure time at sensor T3 for each case estimated from the total heat flux curves. According to literature, exposure time measured and predicted are high enough to damage PVC. For instance, for 5 kW/m², the loss of mechanical properties for PVC windows or gutters occurs for an exposure time higher than 32 s. This value was exceeded for the experiments and the simulations for all the cases studied.
With regard to the accuracy of the predictions, for all the cases, the accuracy increases when heat flux increases. The hedge collapsing which leads to a longer period of low heat flux measurement during the experiments that cannot be reproduced by WFDS induces this result. In addition, it can be observed that simulation results for case n°3 involving a 2 m high hedge, underestimate the exposure time from 40% to 62% depending on the threshold considered. The hedge collapse observed experimentally and not predicted by the simulation has more impact on the overall hedge combustion for this case. Predictions of the exposure time for cases n°1 and 2 show good agreement. While average relative difference is around 5% for case n°2, case n°1 underestimates the exposure time by 22% in average and up to 42% for the lower heat flux because of changes in wind dynamics as explained previously. According to these results, this study validates the capability of WFDS to be used for the prediction of material failure at field scale for cases that includes vegetation up to 1 m height.

5. Conclusion

Comparison between dedicated experiments and numerical simulations were carried out to demonstrate the capability of WFDS to predict thermal stress induced by the burning of reconstructed hedges at field scale. Three sets of experiments involving 2 sizes of hedges were carried out in summer to reproduce two configurations: the first one that corresponds to the current fire safety regulations in France and the second one that does not agree. Results are in accordance with literature and show that WFDS gives good predictions of the total heat flux received and the exposure time at the hedge centerline during the period where the fire is the most intense. However, predictions deviate from the experimental data when changes in wind direction occur during the experiment and for the 2 m high hedge which strongly collapsed during the burning phase.

6. Acknowledgments

The experiments were supported by the projects "MED-STAR" (Strategie e misure per la mitigazione del rischio di incendio nell'area Mediterranea) and "INTERMED"(Interventions pour gérer et réduire le risque d'incendie à l'interface habitat-espace naturel) financed by the fund PC IFM 2014-2020 (http://interreg-maritime.eu/fr/web/med-star).

The field scale simulation of this research was supported by the project "Structure Heat Exposure – Simulations and Experiments", contract number 21-IJ-11261987-002, funded by the USDA (US Forest Service).

7. References

Maranghides, W. E. Mell, A Case Study of a Community Affected by the Witch and
Guejito Fires, NIST TN 1635, 2009.

Maranghides, A. , D. , Vihnanek, R. , Restaino, J. and Leland, C. (2015), A Case Study of a Community Affected by the Waldo Fire Event Timeline and Defensive Actions, Technical Note (NIST TN), National Institute of Standards and Technology, Gaithersburg, MD, (https://doi.org/10.6028/NIST.TN.1910)

Etlinger MG, Beall FC, Development of a laboratory protocol for fire performance of landscape plants. Int J Wildl Fire 13:479–488, 2004. doi:10.1071/WF04039

A. Ganteaume, M. Jappiot, C. Lampin, M. Guijarro, C. Hernando, Flammability of Some Ornamental Species in Wildland-Urban Interfaces in Southeastern France: Laboratory Assessment at Particle Level, Environmental Management 52:467-480, 2013. DOI :10.1007/s00267-013-0067-z

W. Mell, A. Maranghides, R. McDermott, S.L. Manzello, Numerical simulation and experiments of burning douglas fir trees, Combustion and Flame 156:2023-2041, 2009.

Y. Perez-Ramirez, W.E. Mell, P.A. Santoni, J.B. Tramoni, F. Bosseur, Examination of WFDS in Modeling Spreading Fires in a Furniture Calorimeter, Fire Technology. 53 (2017) 1795–1832. https://doi.org/10.1007/s10694-017-0657-z

F. Morandini, P.A. Santoni, J.B. Tramoni, W.E. Mell, Experimental investigation of flammability and numerical study of combustion of shrub of rockrose under severe drought conditions, Fire Safety Journal. 108 (2019) 102836. https://doi.org/10.1016/j.firesaf.2019.102836

K.A.M. Moinuddin, D. Sutherland, Modelling of tree fires and fires transitioning from the forest floor to the canopy with a physics-based model, Mathematics and Computers in Simulation. 175:81-95 (2020)

K. Meerpoel-Pietri, V. Tihay-Felicelli, A. Graziani, P.A. Santoni, F. Morandini, Y. Perez-Ramirez, F. Bosseur, T. Barboni, X. Sánchez-Monroy, W. Mell, Modeling with WFDS Combustion Dynamics of Ornamental Vegetation Structures at WUI: Focus on the Burning of a Hedge at Laboratory Scale, Combustion Science and Technology, (2022) DOI:10.1080/00102202.2021.2019235

Sanchez-Monroy X., Mell, W.F, Torres-arenas, J., Butler, B.W. Fire spread upslope : Numerical simulation of laboratory experiments. Fire Safety Journal. – 2019

McGrattan, K., Hostikka, S., McDermott, R., Floyd, J., Weinschenk, C., Overholt, K., 2013a. Fire dynamics simulator technical reference guide volume 1: mathematical model. NIST special publication 1018, 175.

Le bâti face à un aléa technologique thermique | LNE, Laboratoire national de métrologie et d'essais, (2008). https://www.lne.fr/fr/guides-techniques/bati-face-alea-technologique-thermique.

K. Meepoel-Pietri, Prédiction de la vulnérabilité des constructions lors des incendies à l'interface milieu naturel/constructions, Thèses, Université de CORSE - Pascal PAOLI ; Ecole doctorale Environnement et Société ; UMR CNRS 6134 SPE, 2021.

Performance of Attached Decks Subjected to Ember Top-of-deck and Flame Impingement Under-deck Exposures

Faraz Hedayati*; Stephen L. Quarles

Insurance Institute for Business & Home Safety, Richburg, SC, USA, {fhedayati, squarles}@ibhs.org

**Corresponding author*

Keywords

Embers, flame-impingement, deck, wildfire

Abstract

Attached decks are a vulnerable component of a building in wildfire-prone areas. Once ignited, decks can expose a building's cladding (siding), exterior wall components such as windows and doors, and the under-eave area to flames and radiant heat. This exposure can result in severe damage or destruction of the building.

In a wildfire, decks are typically exposed to embers (firebrands) on their top surface and flame impingement to their bottom side. In this research, the vulnerability of decks to ember attack on the top surface and flame impingement at the bottom was investigated. Moreover, the ability of the current deck standards (State Fire Marshal (SFM) Standard 12-7A-4A and ASTM E2632) to predict the performance of different decking assemblies during a wildfire was assessed from experimental and computational perspectives.

Deck research at IBHS began with the evaluation of the vulnerability of decks to wind-blown embers. This research provided evidence that the top surface of redwood (Sequoia sempervirens) decks was particularly vulnerable to ignition by embers. Ignition typically occurred from ember accumulation in gaps between deck boards at joist crossings, which is an area where wind-blown vegetative debris can accumulate. This finer fuel can facilitate ignition by embers. After ignition, fire propagated both parallel and perpendicular to the test building. Although the mechanism was different, propagation did not depend on the orientation of the deck boards (or support joists).

The research on decks was followed up by testing deck assemblies exposed to under deck flame impingement. Several combinations of substructure (i.e., the structural support system) and walking surfaces were evaluated. These results highlighted the vulnerability of joists in the deck assembly. In North America, a wood or plastic composite walking surfaces installed over a wood substructure is the most common decks are built. Our tests showed that once the joist ignites due to the initial flame impingement exposure, it can burn for an extended period and expose the bottom side of the deck boards to flames. It was observed that if a joist was not engulfed in flames, the boards above them do did burn. Hence, one major finding from this study was regarding the impact of the substructure overall deck performance and the importance of explicitly considering the structural support system in any standard test method used to evaluate performance. It also supported the benefit of advocating the use of a noncombustible structural support system in new construction.

While using metal substructures significantly reduced the vulnerability of decks to wildfires (considering both ember and flame exposures), it might not be an affordable option to retrofit existing decks. To address this issue, different types of walking surfaces were tested. It was concluded that continuous noncombustible walking surfaces such as no-gap metal boards or a concrete slab surface limited the availability of oxygen and stalled flame spread in the under-deck area.

1. The IBHS Research Center Test Chamber

The Insurance Institute for Business & Home Safety (IBHS) is a non-profit corporation that operates a natural hazards research facility located in Richburg, South Carolina. The experiments take place at the center square of the test chamber, measuring 145 ft x 145 ft (44.2 m x 44.2 m). The west wall of the chamber is equipped with 105 fans. Each fan is 5.5 ft (1.68 m) in diameter and collectively can create a time history of fluctuating wind speeds from 12 mph (5.3 m/s) to 120 mph (53m/s). The test chamber is also equipped with eight ember generators, each one with the capacity to produce about 120 embers per second with mass between 0.01 to 1 gram. Figure 1a and 1b show IBHS test chamber. Figure 1c shows a snapshot of a deck exposed to embers [Alfano et al. 2017].

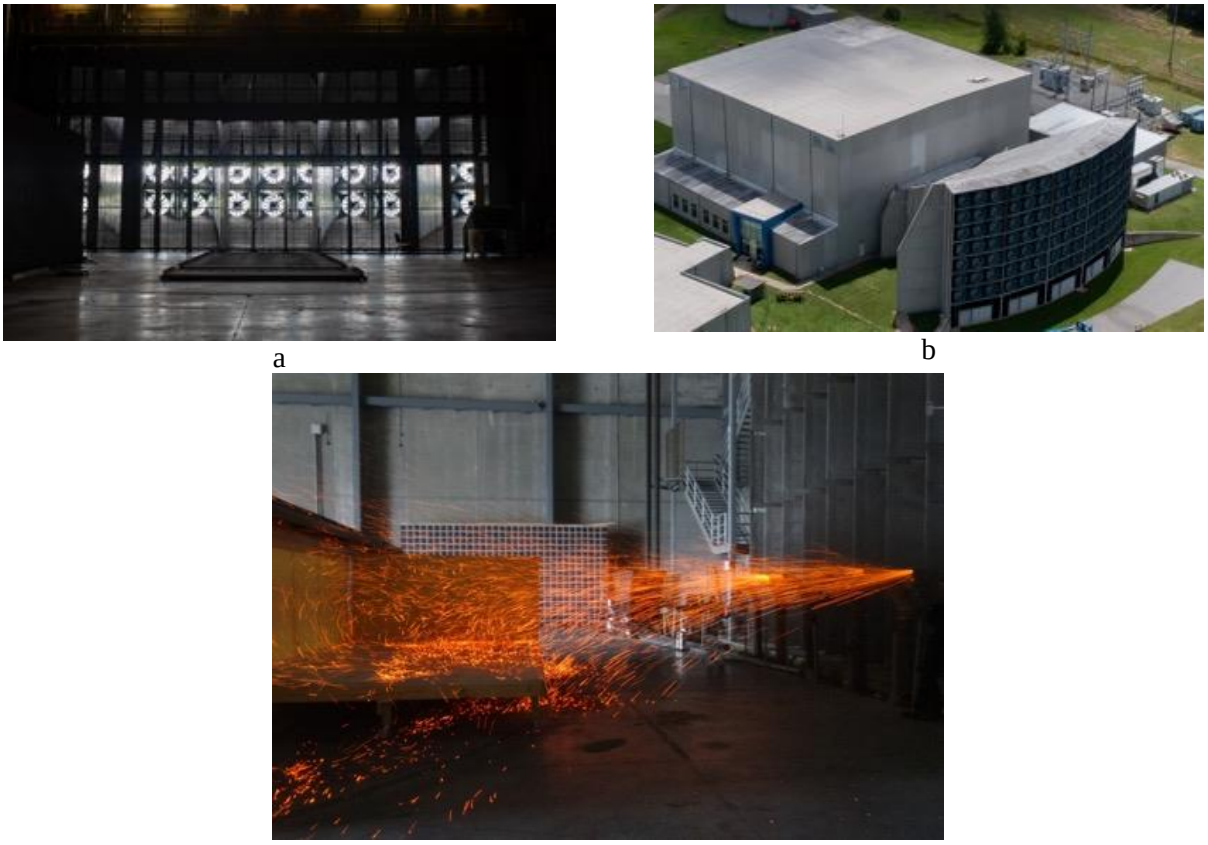

a b c

Figure 1. IBHS test chamber (a) inside (b) outside (c) ember generators schematic

2. Ember Exposure to Decks

This series of experiments investigated the ignition potential of eight different types of deck boards exposed to wind-blown embers. The materials evaluated included solid wood and plastic composite deck board products. Six of the products evaluated complied with the provisions specified in Chapter 7A of the California Building Code [CBC 2019], but two did not. Each deck was subjected to an ember exposure of up to one hour and both quantitative and qualitative observations were made. Overall, most of the decks performed well in that they did not ignite and transition to flaming combustion. At locations where embers accumulated, however, smoldering was often observed.

The medium-density softwood product (CBC Chapter 7A compliant) and one of the plastic composite products (CBC Chapter 7A non-compliant), exhibited sustained flaming when subjected to an ember exposure. Transitory flaming was observed in the high-density hardwood decking product (CBC Chapter 7A compliant). The time-to-ignition (flaming) for the decking products varied from 12 minutes for the non-FRT softwood deck to 47 minutes for one of the plastic composite products. Photographs of ignited non-FRT softwood deck is shown in Figure 2. Although neither the number nor mass flux of the ember exposure was quantified, this variation in time-to-ignition provides relative information on the susceptibility of decking products to ignition from wind-blown embers. It was observed that for decks where joists were installed perpendicular to the building, once ignition occurred the fire spread in a smoldering phase along the joist toward and away from the building under an average wind speed of 18 mph. At the deck board gaps, the smoldering combustion transitioned to flaming as a result of airflow between the deck boards. This allowed fire to continue to propagate all the way to the building.

Figure 2. Top of deck (left) and under-deck (right) views of ignited decks during the ignition potential series of experiments. Table 1 tablulates a summary of all the ember exposure tests.

Table 1. Summary of the ember exposure tests

Deck Name	Chapter 7A Compliant	Density[1] (g/cm^3)	Performance	
			Replication 1	Replication 2
PVC Composite	Yes	0.68	Smoldering	Smoldering
PE Composite 1	No	0.97	Smoldering	Sustained Flaming[2]
PE Composite 2	Yes	1.19	Smoldering	Smoldering
PE Composite 3	Yes	1.03	Smoldering	Smoldering
PE Composite 4	No	1.21	Smoldering	Smoldering
High-Density Tropical Hardwood	Yes	1.15	Smoldering	Transitory Flaming[3]
Medium-Density Softwood	Yes	0.51	Sustained Flaming	Sustained Flaming
FRT Wood	Yes	0.50	Smoldering	Smoldering

1. Nominal moisture content, 8% (oven dry basis). Density on current mass, current volume basis.
2. Continuous flaming for more than five seconds.
3. Continuous flaming for less than five seconds

It was also observed that embers dropped into and through the gap, onto the surface below and had the potential to ignite fine fuels underneath (Figure 3). This highlights the risk of underdeck flame impingiment and importance of removing combustible materials from the under-deck área, even if vertically enclosed around the deck perimeter.


(a) (b)

Figure 3. Ember penetration through gaps between deck boards; (a) embers falling to ground and (b) resulting in the ignition of pine needles that accumulated under the deck.

3. Underdeck Flame Exposure to Decks

Although maintaining the under-deck area is necessary to reduce the vulnerablity of decks in a wildfire, post-event investigations have shown that these recomendation are often overlooked. Depending on the frequency of maintenance around a building, a noticeable amount of fuel can accumulate under a deck. If this fuel is ignited

by wind-blown embers, the flame might be tall enough (depending on fuel load, wind speed, and deck height) to reach the deck structure. People also store combustibles, such as firewood, under decks [Maranghides et al. 2015]. Ignition of these materials intensifies the under-deck flame exposure. In this case, the under-deck flame exposure would be more intense and may last longer than exposure from burning wind-blown debris.

Provisions in Chapter 7A of the California Building Code allow the use of many combustible deck board products. These materials include non-fire-retardant treated wood (e.g., redwood and western red cedar) and plastic composites. These decking products can be installed over combustible or noncombustible joists. Whereas the current standard test method includes the substructure in the tested assembler, the arrangement is fixed, and therefore does not consider the substructure system as a variable. To sumarize, the current standard test method evaluates a (1) 2ft x 2.4 ft deck, (2) a "no wind" condition and (3) does not consider the structural support system as a variable[CBC 2019].

To assess the efficacy of the current test methods, all three of the above-mentioned assumptions were challanged by more realistic wildfire conditions. Six-foot by six foot (1.8 x 1.8 m) deck assemblies were exposed to under deck flame in the presence of a 19 mile per hour (8.5 m/s) constant wind speed. The deck assemblies had different combinations of substructure and walking surfaces. Metal and Southern yellow pine substructures were tested with redwood, plastic composite and metal deck boards. It was observed that all the currently compliant deck boards burn extensively and expose the cladding adjacent to the under-deck portion of the attached building to a high thermal insult. Figures 4 and 5 show the progression of fire for redwood deck boards installed over southern yellow pine and the respective wall temperature for different products respectively.

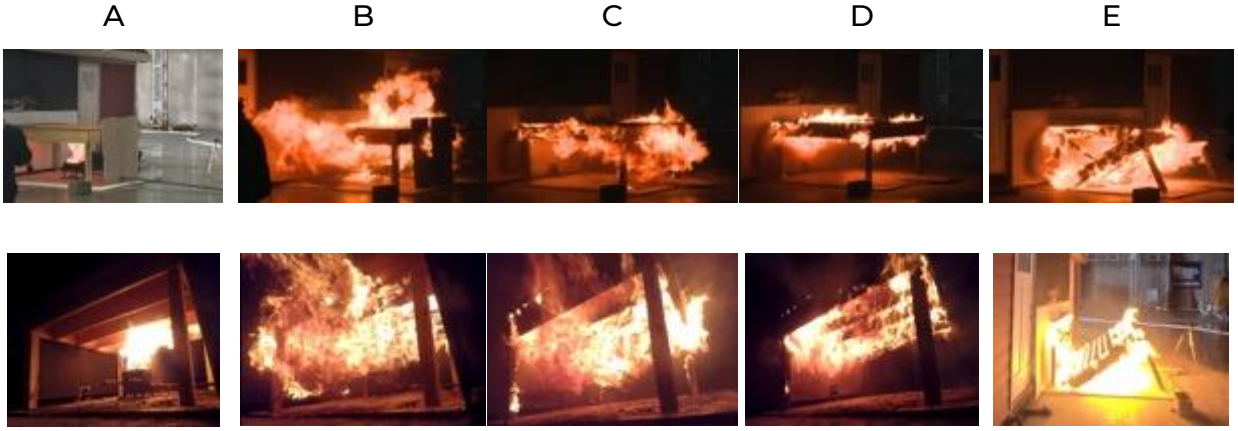

Figure 4. Time-lapse of a redwood deck with Southern Yellow Pine joists test from two angles. (A) After 5 seconds. (B) After 2 minutes. (C) After 5 minutes. (D) After 7 minutes. (E) After 10 minutes

These tests highlighted the contribution of the deck's substructure in the fire. It was observed that if a joist was not engulfed in flames, the boards above them do did burn. To evaluate this observation in detail, the wood and plastic composite combustible decks boards were installed over a metal substructure and exposed to the same under-deck fire source. Figures 6 and 7 show the progression of fire for redwood deck boards installed over southern yellow pine and the wall temperature for different products respectively.

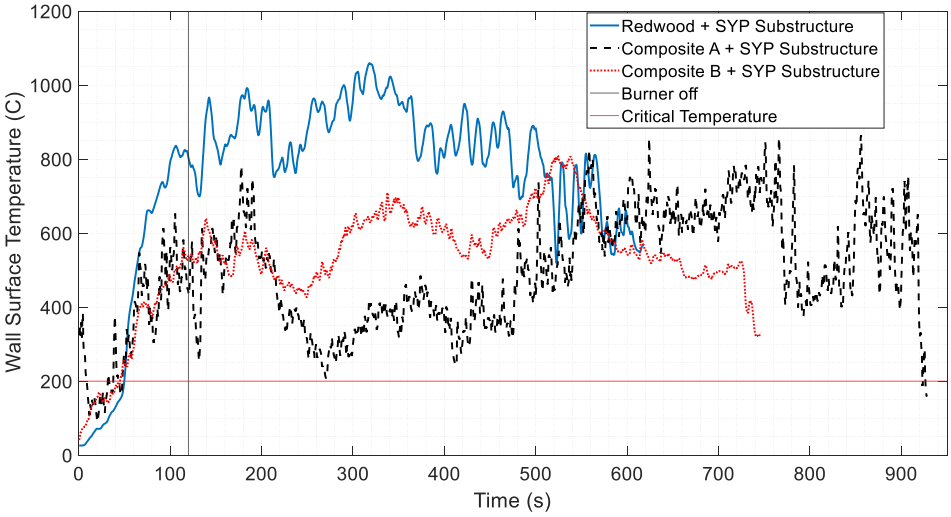

Figure 5. Siding temperature at the under-deck area for different deck boards over Southern Yellow Pine structure.

A (start of the test) B (after 5 minutes) C (after 15 minutes)

Figure 6. Time-lapse of redwood (first row), composite A (second row), and composite B (third row) decks with metal joist test.

The ignition temperature of wood depends on samples' thermophysical properties (moisture content, geometry, ,density, and some external parameters such as the test apparatus, and piloted/autoignition conditions. The resuts of ignition temperature of wood show a wide span of ignition temperatures of 210–497_C for piloted ignition and 200–510_C for autoignition. [Babrauskas 2002]. From these observations, it can be concluded that that "if a wood specimen is ignited under external heating barely sufficient to ignite it, it will ignite at approximately 250_C regardless of the type of heating arrangement [Babrauskas 2002]."

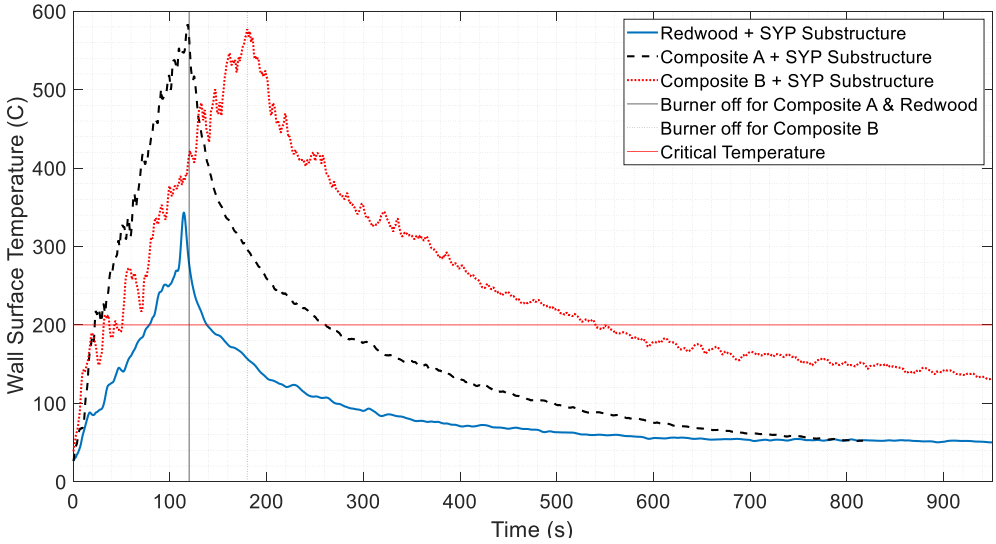

Figure 7. Siding temperature at the under-deck area for different deck boards over metal structure (exposure duration for Composite B is 1 minute longer).

Comparing the wall temperature variations in Figures 5 and 7 shows the contribution of a combustible substructure in the fire. After shutting off the burner after 2 or 3 minutes, in all cases (as shown in Figure 7), the temperature rapidly dropped. The results of these experiments demonstrate the benefits of using metal substructures for new decks. However, for existing decks changing the entire substructure could be cost prohibitive. To address this issue, the performance of two types of metal deck boards were evaluated. The Type 1 walking surface was aluminum and marketed as a waterproof product. The installation instructions for this product specified that there be no spacing between boards. These deck boards are engineered to properly address water drainage and thermal expansion. The Type 2 walking surface was also an aluminum product, however, installation instructions called for spacing between deck boards. Figure 8 shows the status of decks during the experiment from two views. As can be seen, the intensity of the fire between walking surfaces Type1 and 2 were notably different. For the Type1 walking surface the fire was in a smoldering phase while for Type2 walking surface the flames length extnding form under the deck was observed to be as high as two feet (0.6 m).

(a)
SYP structure and walking surface Type1

(b)
SYP structure and walking surface Type2

Figure 8. Comparing Type1 (a) and Type2 (b) walking surfaces installed over a SYP substructure

Table 2 summarizes the results of the underdeck tests. The time between twice of the exposure time and the end of the experiment was analysed for critical temperatures [Babrauskas 2002]. The last column of Table 2 shows if the temperature of the wall exceeded 250 degrees Celsius during this time.

Table 2. Summary of the results of the underdeck tests.

Board	Sub-structure	Currently Chapter7A compliant	Wall temperature exceeds 250 C?
Redwood	SYP	Yes	Yes
Redwood	Metal	Yes	No
Composite A	SYP	Yes	Yes
Composite A	Metal	Yes	No
Composite B	SYP	No	Yes
Composite B	Metal	No	No
Metal No Gap	SYP	Yes	No
Metal Gapped	SYP	Yes	Yes
Metal No gap	Metal	Yes	No
Metal gapped	Metal	Yes	No

4. References

Christine D. Standohar-Alfano et. Al. Reducing Losses from Wind-Related Natural Perils: Research at the IBHS Research Center, Front. Built Environ., 24 February 2017 | https://doi.org/10.3389/fbuil.2017.00009

Materials and construction methods for exterior wildfire exposure, California Building Codes, Chapter 7A, 2019

Maranghides A, McNamara D, Vihnanek R, Restaino J, Leland C. A Case Study of a Community Affected by the Waldo Fire. 2015.

Babrauskas, V., Ignition of wood: a review of the state of the art. Journal of Fire Protection Engineering, 2002. 12(3): p. 163-189.

Physics-Based Modelling for Mapping Firebrand Flux and Heat Load on Structures in the Wildland-Urban Interface

Amila Wickramasinghe[1]; Nazmul Khan[1]; Alexander Filkov[2], Khalid Moinuddin[1]

[1]Institute for Sustainable Industries and Liveable Cities, Victoria University, Melbourne, VIC 3030, Australia {p.wickramasinghe@live.vu.edu.au; {Nazmul.khan, Khalid.Moinuddin}@vu.edu.au
[2] School of Ecosystem and Forest Sciences, Faculty of Science, University of Melbourne, VIC 3363, Australia, {alexander.filkov@unimelb.edu.au}

**Corresponding author*

Keywords

Physics-based modelling, firebrands, wildland fire, bushfire attack level, AS3959

Abstract

The mechanisms of wildfire attack on structures are classified into direct flame contact, radiant heat, firebrand attack and a combination of two or all of them. Arguably, airborne firebrands play a vital role as one of the main causes of structure ignition and fire propagation by forming spot fires far from the fire front. Firebrand flux (the number of firebrands landed on a unit area per unit time) and the heat load are important parameters to calculate the wildfire risk on structures. Australian Building Standard AS3959 is developed based on radiation heat flux and it does not quantify the effects of firebrand flux on structures to assess the wildfire risk completely. To improve the assessment of the Bushfire Attack Level (BAL) in AS3959, there is a need for the quantification of firebrand flux at different scales of wildfires. Lacking information about firebrand generation from various vegetation species under different environmental conditions creates a gap to estimate the firebrand flux accurately. In this study, we aim to use a physics-based model to quantify the firebrand generation rate of Eucalyptus dominant forest vegetation at different severities of wildfires expressed by the Fire danger indices (FDI) of 100, 80, and 50. The wind speed was chosen while keeping the temperature, relative humidity, and drought factor as constants to obtain the focused FDIs. A 40 m height Eucalyptus forest was modelled with 25 t/ha understorey and 10 t/ha canopy fuel loads as per AS3959 forest vegetation classification. The forest fires were prescribed with the intensities of 53.4, 43.1, and 27 MW/m with 100 m length to replicate the fire events explained by FDIs. The depth of the fireline was approximated according to the fire residence time and the spread rate. The firebrand size, shape, and quantity were taken from our previous firebrand generation study (Wickramasinghe et al. 2022) and the particles were injected randomly through the forest volume which is engulfed by the fire. The distances between the modelled structure that follows an Australian standard house design and the vegetation were maintained according to the BALs. We obtained the radiative heat flux on the houses close to the algorithm provided in AS3959 for each BAL. In this study, both firebrand and heat flux were quantified at strategic locations of the house. We find a logarithmic relationship exists between firebrand flux and radiative heat flux in the range of R2 0.96 to 0.99. Hence, for a certain BAL, the firebrand flux increases with the FDI similar to radiative heat flux. Results from this study can be used to quantify the firebrand flux on various house patterns from different vegetation fires, which may improve the design standards and construction requirements of buildings to mitigate the vulnerability of houses at the wildland-urban interface (WUI).

1. Introduction

Firebrand generation from burning vegetation is a potential threat to people and infrastructure in the wildland-urban interface due to the unpredictable nature of spotting[1]. This phenomenon can be severe with the scale of the wildfire and structural ignition becomes harder to control. Postfire investigations reveal more than 50% of houses destroyed by the wildfires are from firebrands and 2/3 of homes ignited directly or indirectly by the wind

[1] The phenomenon of ignition and starting a new fire front by burning material like wood chips, bark, twigs, leaves, or nuts ahead of the central fire front.

dispersed firebrands (Maranghides & Mell, 2011). Leonard et al.(2004) claim firebrands caused the ignition of over 90% of houses in Australia during a number of wildfire events.

The firebrand generation has received the least attention compared to the latter three aspects of the key processes of firebrand studies: transport, spotting, and secondary ignition. It is difficult to build an integrated system to replicate a realistic wildfire scenario and quantify the risk without adequate knowledge of firebrand generation. Safety issues, the need for advanced instruments, and large financial and human resources to measure firebrand generation at the fire front make the quantification of firebrand generation more difficult. However, physics-based modelling is identified as a viable alternative to finding the firebrand generation associated with the influence of vegetation species and different environmental conditions. Some physics-based models show the capability of predicting firebrand transport and short-range spotting through validation processes (Wadhwani et al., 2017). The validation of physical models requires thermophysical properties of vegetation, characteristics of firebrands including shapes, size, number, the intensity of the fire, the environmental conditions such as wind, fuel moisture content (FMC), and relative humidity, temperature etc. Various bench-scale and field-scale experiments have been conducted to understand the importance of these parameters to use in physics-based models.

Collecting firebrands from tree torching and management scale fires is a widely used technique to investigate the morphologies, characteristics and landing distribution of firebrands. The effects of vegetation species, fuel load, FMC, and wind speed are examined to understand the firebrand generation and their ignition propensity. Manzello et al.(2007) , Hudson et al.(2020) and Adusumilli et al.(2021) found firebrand collection significantly increases with the decrement of FMC. Most of the vegetation species investigated by Bahrani et al.(2020) show the number of firebrands collection increase with the wind speed. The parametric studies conducted through physics-based models by Thurston et al.(2017), Bhutia et al.(2010), and Tse et al.(1998) conclude the significance of firebrand characteristics, wind speed, and intensity of the fire for spotting. The relationship between fire intensity and the firebrand flux was firstly investigated by Thomas et al.(2017) through a prescribed forest fire experiment. With these experimental data of Thomas et al.(2017) the firebrand generation of a Pitch Pine forest was estimated through physics-based modelling by Wickramasinghe et al.(2022) using an inverse analysis technique. This modelling maintains fire intensities, wind climate, fuel properties, and firebrand characteristics (shape, size, composition) to replicate the field experiment and found the firebrand generation rate as 4.18 pcs/MW/s (pcs: pieces).

To the best of the authors' knowledge, there is no standard document that provides quantitative information about firebrand flux on structures in the WUI. Having a substantial understanding of firebrands flux is important to establish building standards to mitigate the wildfire risk with fidelity. Australian standard AS3959 – the prescription for constructing buildings in wildfire-prone areas – qualitatively presents the increment of firebrand attack with the radiative heat flux. The radiative heat flux is expressed in terms of Bush fire Attack Level (BAL) which describes the safe distance to the structure from the edge of the vegetation.

In the present work, we conduct a series of physics-based simulations to quantify the firebrand flux on structures incorporated with the radiative heat flux given in AS3959 for forest vegetation classification. As firebrand attack is the main cause of house ignition during wildfires in Australia, including quantified firebrand flux correlated to the current radiative heat flux is important to implement the BAL of AS3959 standard to better counter the wildfire risk on houses in WUI.

2. Methodology

The simulations are conducted using a physics-based model Fire Dynamic Simulator (FDS) (McGrattan et al., 2005) which is a product of National Standards Technology, USA. FDS uses the multiphase modelling technique, and the gas phase is simulated by Large Eddy Simulation (LES), while the solid firebrands are introduced in the domain by Lagrangian particle-based transport scheme.

2.1. Firebrand generation rate calibration for vegetation species, wind, and FMC

The firebrand generation rate (4.18 pcs/MW/s) found for Pitch Pine at 31% FMC and 2 m/s wind speed (Wickramasinghe et al., 2022) is used as the base information for calibration of the firebrand generation rate for Eucalyptus. The Eucalyptus and Pitch pine vegetations are relatively similar species in terms of the average tree

height, crown shape, orientation of leaves etc. Due to the scarcity of data, we assume the firebrand generation rate of Eucalyptus is the same as the Pitch pine at the same wind speed and FMC. Therefore the numerical effect of vegetation species in between these two fuels for firebrand generation could be approximated as 1:1. To calibrate the effect of wind speed for firebrand generation of Eucalyptus, we use the experimental data of Barani et al.(2020) obtained for the Loblolly Pine at different wind speeds. The physical appearance of Loblolly Pine and Eucalyptus are similar to use in the analysis. It shows increasing wind speed results in a higher number of firebrand production. Based on these experimental data, we obtain the mathematical relationship as presented in equations 1(a) and 1(b), for the number of generated firebrands against the wind speed to estimate the firebrand generation number at the wind speeds for FDI 100, 80, and 50:

$$fb_{generation} = 33.39 \times U_{wind} + 202.03 \;\; when \; 0 < U_{wind} < 8.19 \; ms^{-1} \quad 1(a)$$

$$fb_{generation} = 575 \;\; when \; 8.19 \; ms^{-1} \; < U_{wind} \quad 1(b)$$

where $fb_{generation}$ is the number of firebrand generation and U_{wind} is the wind speed at the burning vegetation. The firebrand generation ratio is calculated in reference to the number of firebrands generated at 2 m/s as shown in Table 1.

Table 1: Firebrand generation ratio according to the wind conditions for FDIs 50, 80, and 100.

Similar vegetations	Firebrand generation rate (pcs/MW/s)	Wind speed (m/s)	Number of firebrands	Generation ratio to 2 m/s
Loblolly Pine	4.18	2.00 (reference)	298	(298/298)=1.00
		5.48 (FDI 50)	454	(454/298)=1.52
Eucalyptus	(Pitch Pine at 2 m/s)	8.88 (FDI 80)	575	(575/298)=1.93
		10.38 (FDI 100)	575	(575/298)=1.93

The effect of FMC is evaluated as per Hudson et al.(2020) where higher FMC is associated with a lower number of firebrand production. Ponderosa Pine is the matching vegetation species to Eucalyptus in this tree burning experiments and the relationship between firebrand production and FMC is mathematically derived as presented in equation (2):

$$fb_{generation} = -4.7 \times FMC + 538.32 \quad (2)$$

where FMC is the dry basis fuel moisture content. By that, the firebrand generation ratio of Eucalyptus is estimated reference to the 31% of FMC as shown in Table 2.

Table 2: Firebrand generation ratio according to the FMC for FDIs 50, 80, and 100.

Similar vegetations	Firebrand generation rate (pcs/MW/s)	FMC (%)	Number of firebrands	Generation ratio to 3.84% FMC
Ponderosa Pine	4.18	31 (reference)	393	(393/393)=1.00
Eucalyptus	(Pitch Pine at 31%)	3.84 (all FDIs)	520	(520/393)=1.33

The final firebrand generation rates are approximated by the multiplication of the quantified individual generation ratios of species, wind, and FMC with the reference firebrand generation rate of Pitch Pine. Hence, the firebrand generation rates of forest vegetation for FDI 50, 80, and 100 are found as 8.43, 10.68, and 10.68 pcs/MW/s to use as inputs in the FDS model.

2.2. Model set up

The simulation domain size is chosen as 336 m× 102 m × 90 m with a 1.5 m grid size at the wind developing region and 0.75 m grid size at the area where fireline, firebrand generation and landing occur. These grid sizes are determined according to the grid convergence analysis of Wickramasinghe et al.(2022). Fig. 1 illustrates the developed wind flow introduced with eddies as per Jarrin et al.(2006), prescribed fire, fire-induced buoyancy, and the firebrand landing on the modelled house.

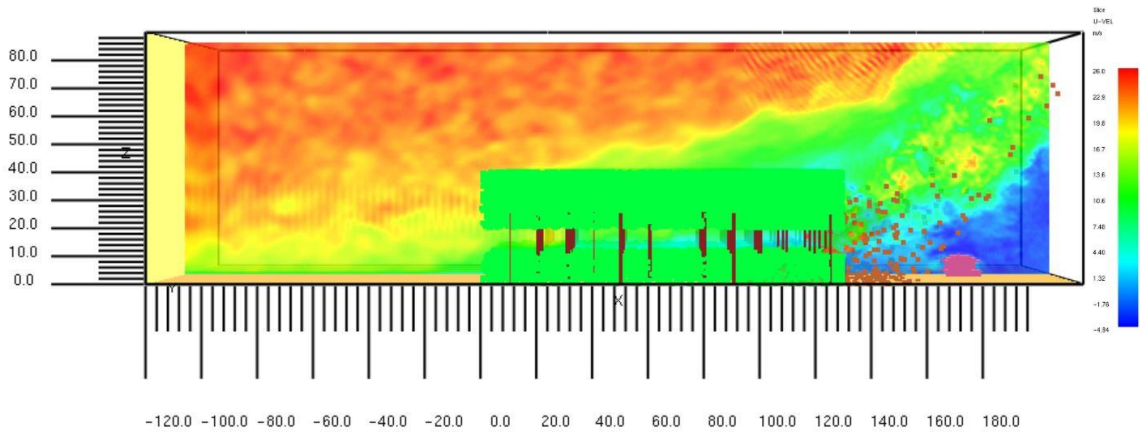

Figure 1- A Smokeview (the visual companion software of FDS) representation of the simulation of Forest fire at FDI 100 and BAL 12.5. The distance between the house and the forest edge is maintained as 50 m according to the BAL.

15 simulations were conducted varying the three different FDIs and five different BALs to calculate the firebrand flux and heat load on the house. The firebrand flux was measured at the strategic locations (gutter, deck, roof, window corners, sub-floor) of the house where firebrands can accumulate and start a secondary ignition. The radiative heat flux was also recorded at the same locations. The total firebrand flux is calculated based on the total number of firebrands received on a unit area of the house at a unit time. The maximum radiative heat flux is taken as the highest value obtained by a heat flux device at any strategic location. We plot the total firebrand flux against the radiative heat flux for FDIs as shown in Fig. 2. Each data point is related to a BAL (or the location of the house downwind).

3. Results and discussion

We use the maximum radiative heat flux and the total firebrand flux on the house to develop a mathematical correlation. According to Fig. 2, the firebrand flux on the house shows a logarithmic relationship with the radiative heat flux with an R^2 of 0.96, 0.98 and 0.99 for FDI 100, 80, and 50 respectively. Both FDI 100 and 80 curves are located over FDI 50 implying the higher firebrand risk for the same radiative heat flux. Although the curves are quite close for the lower three BALs, the FDI 100 has positioned above the FDIs 80 and 50 after BAL 29. This indicates that the firebrand attack is higher for FDI 100 than the FDIs 80 and for some BALs when the house is located close to the fireline.

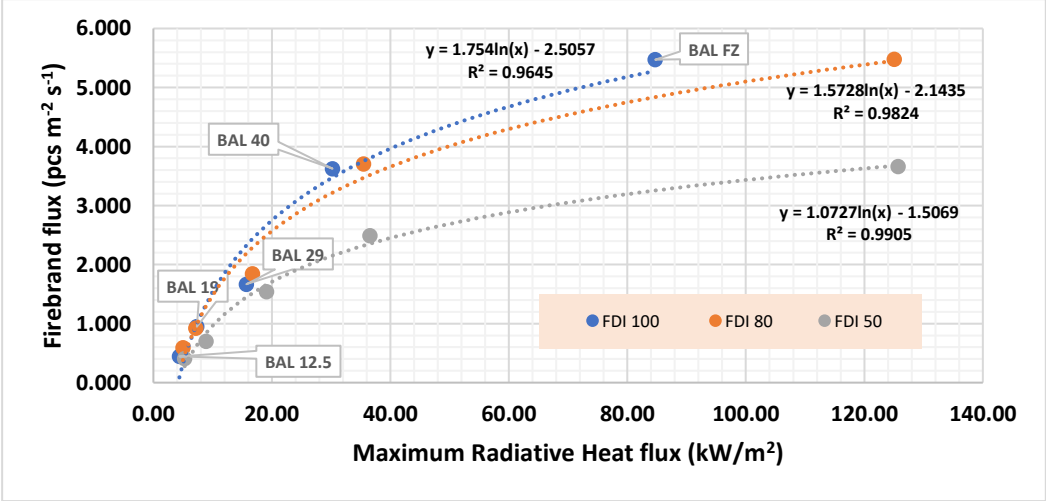

Figure 2- The correlation of the firebrand flux and the radiative heat flux for forest vegetation at FDI 100, 80, and 50.

4. Conclusion

A series of physics-based simulations have been conducted to quantify the firebrand flux on a structure located in the downwind direction of a burning forest. The influences of vegetation species, wind speed, and FMC were calibrated to find the resultant firebrand generation rate to use as inputs in the Eucalyptus tree burning model. The thermophysical data were taken from the literature and the model was set up according to the fuel loads, FDIs, and BALs as given in the AS3959 standard. The firebrand flux and the radiative heat flux on the house were calculated and found a logarithmic relationship between the two parameters. The quantification of firebrand attack was correlated with the existing radiative heat flux to improve the building construction requirements of AS3959 to mitigate the wildfire risk on buildings in the WUI.

5. References

Adusumilli, S., Hudson, T., Gardner, N., & Blunck, D. L. (2021). Quantifying production of hot firebrands using a fire-resistant fabric. International Journal of Wildland Fire, 30(2), 154-159.

Bahrani, B. (2020). Characterization of Firebrands Generated from Selected Vegetative Fuels in Wildland Fires The University of North Carolina at Charlotte].

Bhutia, S., Ann Jenkins, M., & Sun, R. (2010). Comparison of firebrand propagation prediction by a plume model and a coupled–fire/atmosphere large–eddy simulator. Journal of Advances in Modeling Earth Systems, 2(1).

Hudson, T. R., Bray, R. B., Blunck, D. L., Page, W., & Butler, B. (2020). Effects of fuel morphology on ember generation characteristics at the tree scale. International Journal of Wildland Fire, 29(11), 1042-1051.

Jarrin, N., Benhamadouche, S., Laurence, D., & Prosser, R. (2006). A synthetic-eddy-method for generating inflow conditions for large-eddy simulations. International Journal of Heat and Fluid Flow, 27(4), 585-593.

Leonard, J., Blanchi, R., & Bowditch, P. (2004). Bushfire impact from a house's perspective. Earth Wind and Fire–Bushfire 2004 Conference, Adelaide,

Manzello, S. L., Maranghides, A., & Mell, W. E. (2007). Firebrand generation from burning vegetation. International Journal of Wildland Fire, 16(4), 458-462.

Maranghides, A., & Mell, W. (2011). A case study of a community affected by the Witch and Guejito wildland fires. Fire technology, 47(2), 379-420.

McGrattan, K. B., Forney, G. P., Floyd, J., Hostikka, S., & Prasad, K. (2005). Fire dynamics simulator (Version 5): User's guide. US Department of Commerce, Technology Administration, National Institute of Standards and Technology.

Thomas, J. C., Mueller, E. V., Santamaria, S., Gallagher, M., El Houssami, M., Filkov, A., Clark, K., Skowronski, N., Hadden, R. M., & Mell, W. (2017). Investigation of firebrand generation from an experimental fire: Development of a reliable data collection methodology. Fire Safety Journal, 91, 864-871.

Thurston, W., Tory, K. J., Fawcett, R. J., & Kepert, J. D. (2017). Long-range spotting by bushfire plumes: The effects of plume dynamics and turbulence on firebrand trajectory.

Tse, S. D., & Fernandez-Pello, A. C. (1998). On the flight paths of metal particles and embers generated by power lines in high winds-a potential source of wildland fires. Fire Safety Journal, 30(4), 333-356.

Wadhwani, R., Sutherland, D., Ooi, A., Moinuddin, K., & Thorpe, G. (2017). Verification of a Lagrangian particle model for short-range firebrand transport. Fire Safety Journal, 91, 776-783.

Wickramasinghe, A., Khan, N., & Moinuddin, K. (2022). Determining firebrand generation rate using physics-based modelling from experimental studies through inverse analysis. Fire, 5(1), 6.

Preventive irrigation for fire defence in Mediterranean wildland-urban interface areas based on the ecosystem water status

Laura Blanco-Cano*; A. J. Molina-Herrera; M.C. González-Sanchis; J. Pérez-Romero, A.D. Del Campo-García

[1] *ETSI Agronómica y del Medio Natural. Dep. Ing. Hidráulica y Medio Ambiente. Re-ForeST. Universitat Politécnica de Valencia, Spain, {blancocanolaura@gmail.com}*

**Corresponding author*

Keywords

Eco-Hydro-Voxel, system water status, fire behaviour, preventive irrigation, pyro-eco-hydrology

Abstract

In highly anthropized Mediterranean environments, more intense and persistent droughts alter the characteristics of the soil substrate and consequently the water status of the vegetation. Causing an increase water stress of the forest stands implies an increase in dead fuel availability and fire risk. This situation together with the current trend of urbanisation in areas adjacent to forest areas, generating the wildland-urban interface (WUI) areas, represents a new field in the firefighting, which presents both regulatory and technical deficits. This paper presents a management model based on the water quantification of the soil-plant-atmosphere system that defines the optimal amount of irrigation needed to decrease fire intensity to a suppression stage in the WUI of La Vallesa forest in the Natural Park of Túria (Valencia, Spain). Mainly highlighted is the ability to manipulate the fire behaviour by intervening the water status of the system through prescribed irrigation. We report that by means of irrigation, the moisture content of the forest system can be increased by 5.49 ± 3.97 %, which translated to energy, implies an increase in the capacity of the system to absorb 14.24 ± 10.32 kJ/kg and this translates into a decrease in a potential flame length of 0.10 ± 0.26 m above its height.

1. Introduction

The tendency in the Mediterranean areas to urbanize in areas adjoining natural systems (mainly forests), has generated a territorial concept called the wildland-urban interface (WUI), which is susceptible to risk since it connects the territorial dynamics with the problem of forest fires (Martín, 2012). Therefore, a fire in a WUI has direct consequences on the adjacent population, which can translate into economic losses due to the burning of agricultural land, buildings, vehicles, etc., and even endangers the safety of the inhabitants.

Historically, social awareness of this problem has been lower to that of wildland fires, which may have influenced the lack of current legislation, technical methods, and experimental evidence to deal with this new situation (Vacca et al., 2020). One key aspect in this WUI context is the possibility to deploy irrigation-based protection systems (e.g. www.sideinfo.es).

This work aims to provide a vision based on eco-hydrology that addresses the problem of fires in WUI areas. The capacity to manipulate forest-water relationships and hence the hydration of the ecosystem can consequently reduce the risk and danger of fires. The main objectives considered are: i) relate irrigation dosage with the water status of the system and fire behaviour parameters and ii) quantify the effect of system hydration on fire behaviour.

Abbreviations

EHV	Eco-Hydro-Voxel	σ	surface-area-to-volume ratio (ft^2/ft^3)
RH	relative humidity (%)	σ_x	surface-area-to-volume ratio specific to each fuel size and fuel type (ft^2/ft^3)
1-h	dead fuel with a diameter of less than 0.6 cm	*wo*	oven-dry fuel load (lb/ft^2)
10-h	dead fuel with a diameter of between 0.6 and 2.5 cm	wo_x	oven-dry fuel load specific to each fuel size and fuel type (lb/ft^2)
100-h	dead fuel with a diameter of between 2.5 and 7.5 cm	δ	fuel bed depth (ft)

h	low heat content (btu/lb)	M_x	dead fuel moisture of extinction (%)
S_T	total mineral content (fraction)	M_f	moisture content (%)
S_e	effective mineral content (fraction)	Q_{ig}	heat of preignition (kJ/kg)
p_p	oven-dry particle density (lb/ft^3)	F_B	flame length (m)

2. Material

2.1. Study area

The study area is located in a private forest called La Vallesa, which is part of the Turia Natural Park in the province of Valencia (Spain). The climate is typically Mediterranean with a marked summer drought. The main land use is forestry with some abandoned agroforestry areas. However, there is also a strong anthropic influence, as the forest is surrounded by residential developments, with an estimated potential impact of 15,000 inhabitants in the event of a fire. Research plots were established in the forest in a representative area dominated by a *Pinus halepensis* stand and constituting a TU2 fuel model (Scott & Burgan, 2005).

2.2. Water status monitoring

The plots have a network of sensors that continuously measure the variables necessary to know the water status of the system. The quantification and therefore monitoring of the actual water status of the forest is done through the "Eco-Hydro-Voxel" (EHV) concept. The EHV is a typified volume of space based on the SPAC, which allows quantifying the amount of water stored in the different compartments or tanks of the volume along the SPAC. Tanks are defined according to the most representative compartments of the SPAC: saprolite/deep soil, surface soil, duff/litter, scrub, trunks, branches, canopy/living leaves and atmosphere.

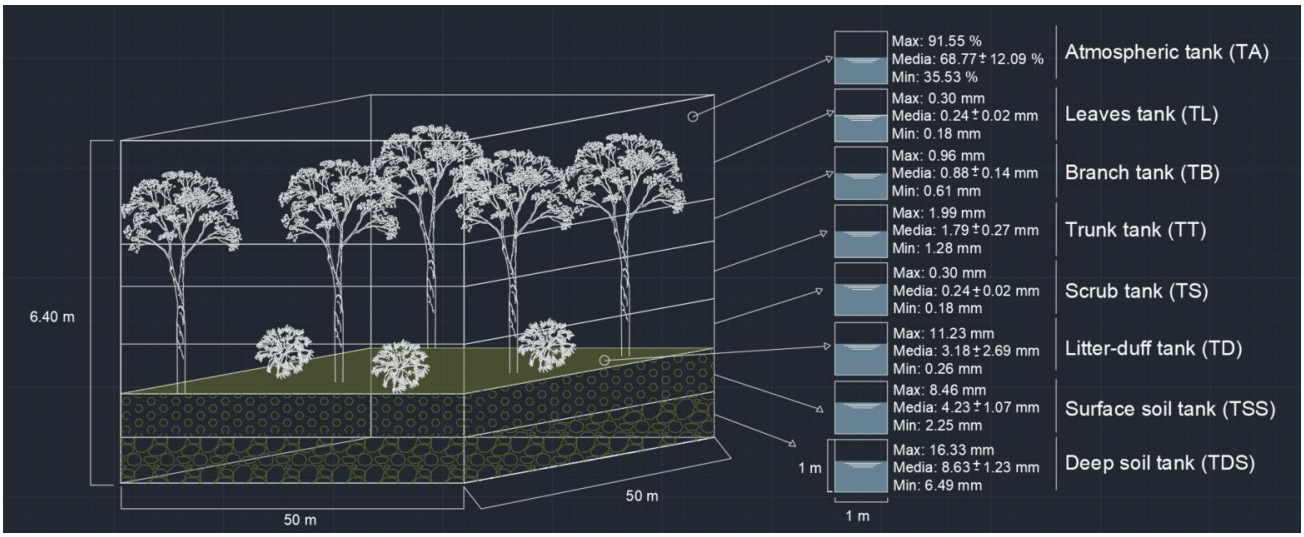

Figure 1- Schematization of the Eco-Hydro-Voxel (EHV) with its subdivisions or tanks. In addition, the basic statistics (maximum, mean ± standard deviation and minimum) of each water content of the tanks are presented.

For the present study, focusing on surface fire, duff/litter, scrub and atmospheric tanks have been used. Litter/duff tank moisture (%) is measured by soil moisture sensors installed between the litter layer and the decomposing organic horizon. Scrub tank moisture (%) is estimated by using an empirical model based on vapour pressure deficit, which was calibrated and trained with real measurements made in different sampling campaigns. Atmosphere tank moisture has the relative humidity (%) and vapour pressure deficit (kPa) as its main proxies for moisture content. These variables are measured by a weather station installed 2 m above the canopy, which also measures the wind speed (m/s) and the temperature (ºC).

Based on the EHV, the calculation of the moisture content (M_f, %) parameter is made, which is a measure of the amount of water in an environment available to a fire. Therefore, this parameter will be the link between the water status of the system and the energy of the fire. Classically this measure of M_f was composed of dead fuels (1-h, 10-h and 100h) and live fuels (herbaceous and woody). Specifically, 1h-moisture was estimated through the moisture content of litter/duff and the atmospheric tank (Rakhmatulina et al., 2021), and in this study it has

been considered that each tank represents 50 % of the total moisture content. The moisture of litter/duff tank that represents this 50 % was included without transformation, however, for the value of the atmosphere tanks, relative humidity and temperature were selected and these two variables were combined using the Baksic et al. (2017) procedure, thus obtaining the value that will represent the other 50% of the humidity of 1h. On the other hand, 10-h and 100-h moisture content dynamics were obtained following Balaguer-Romano et al. (2020). These authors consider constant proportions between the different dead moisture contents; thus, we follow this approach to calculate 10-h and 100-h moisture contents as a function of the 1-h moisture content. Finally, the moisture content of the live woody material is taken directly from the moisture content of the scrub tank.

2.3. Effect of irrigation on fire behaviour

The design of preventive (prescribed) irrigations is based on two fundamental objectives: i) to increase the operational capacity of the system and ii) to reduce the danger and potential risk of a fire. Operational capacity refers to the energy absorption capacity of the system through its moisture content. This concept has been studied through the heat of preignition (Q_{ig}, Rothermel, 1972), which is the energy required for one unit of fuel to reach ignition and it is directly related to its moisture content. Fire danger is represented by the flame length (F_B, Byram, 1959) i.e., the distance measured from the tip of the average flame to the center of the flame zone at the base of the fire, and has been considered as potentially dangerous when it exceeds 1.2 m. It is calculated as a function of fire intensity (I_B). For the inputs related to the fuel particle properties, we used standard values: h = 8,000 Btu/lb, S_T = 0.0555 lb minerals/lb wood, S_e = 0.010 (lb minerals – lb silica)/lb wood and p_p = 32 lb/ft3. Some fuel array properties were calculate based on weight method, where σ = 1813.42 ft2/ft3 [σ_{1h} = 2000; σ_{10h} = 109; σ_{100h} = 30] and *wo* = 0.22 lb/ft2 [wo_{1h} = 0.06; σ_{10h} = 0.10; σ_{100h} = 0.05; σ_{1h} = 0.01], the parameter δ was measured (0.33 ft or 10 cm), and the M_x = 30 % (TU2 model as in Scott & Burgan, 2005). Finally, the environmental parameters correspond to real measurements carried out in the experimental plots (weighted moisture content and wind velocity at midflame height). As the plot is very flat, a value of slope = 2.5 % is considered.

3. Results

Detailed quantification of the EHV water reservoirs has shown a clear response of fire behaviour to water input as related to seasonality. With the onset of dry season, the tanks had low moisture content values and Q_{ig} is low and therefore the F_B is high (Figure 2). The accumulated water input (precipitation) in this dry period (dehydrated system) was 60 mm; and the average M_f was 11.63 ± 3.17 %, (average litter/duff humidity of 4.63 ± 3.90 %, scrub humidity of 75.50 ± 7.35 % and atmospheric humidity of 68.33 ± 12.12 %), resulting in an average Q_{ig} of 611.69 ± 8.23 kJ/kg and F_B of 0.84 ± 0.16 m. However, in the humid period (hydrated system), there was a total precipitation of 320 mm, the mean M_f increased to 19.34 ± 3.86 % (litter/duff with 13.75 ± 3.84 %, scrub with 89.02 ± 4.57 % and atmospheric with 74.43 ± 15.26 %), Q_{ig} increased to 631.71 ± 10.02 kJ/kg and F_B decreased to 0.75 ± 0.29 m.

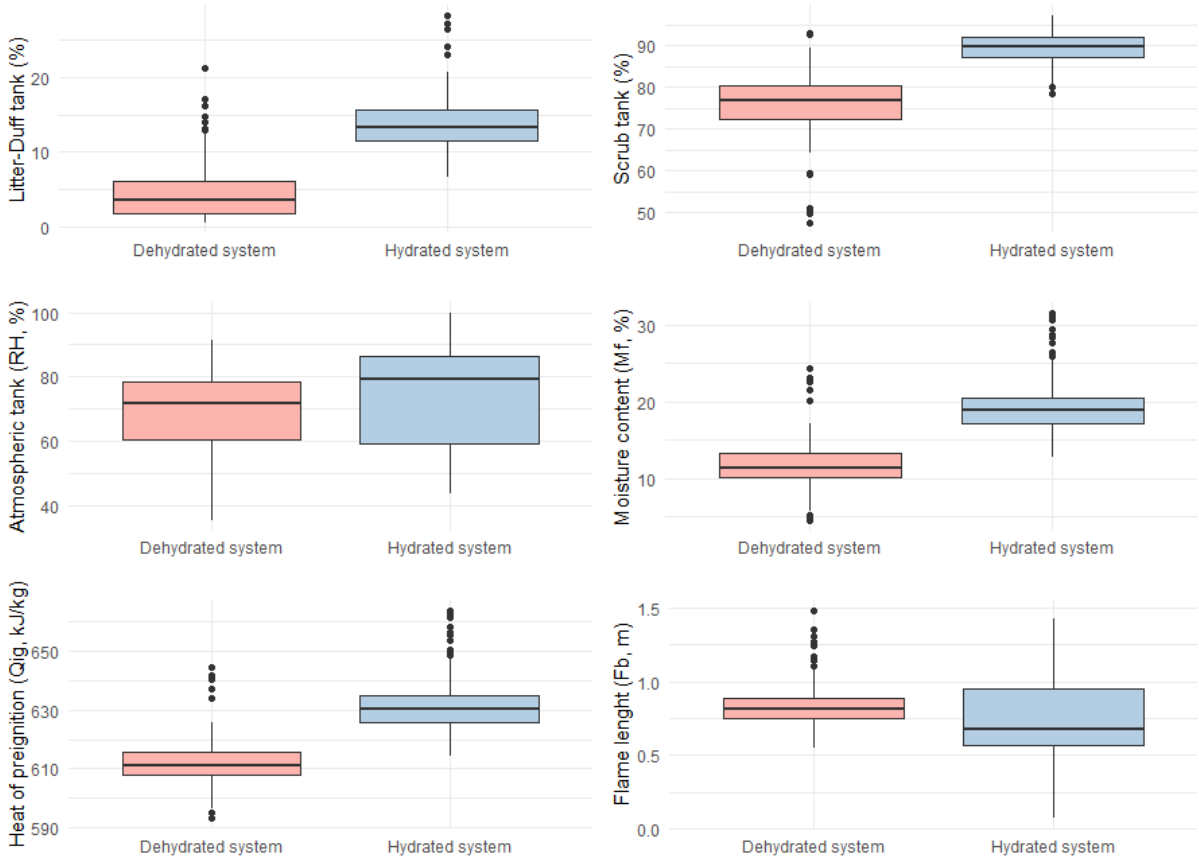

Figure 2- Comparison of the parameters studied in relation to a period of hydration and dehydration.

Regardless of the amount of precipitation and the previous hydration status of the system, the variation observed in M_f between the day before (dry condition) and the day of the water input suffered an increase of 5.49 ± 3.97 %, specifically the moisture content of the litter/duff increased 2.00 ± 3.87 %, the scrub 7.76 ± 7.21 % and the atmosphere 7.47 ± 8.57 %, this translates into a change in fire behaviour of an increase in Q_{ig} of 14.24 ± 10.32 kJ/kg and a decrease in F_B of 0.10 ± 0.26 m. In a particular case where a rainfall of 3 mm occurred (wind speed remained comparable, 1.24 m/s the day before and 1.06 m/s the day of the rain), the system in the day before had a litter/duff tank moisture content of 4.62 %, the scrub tank of 75.10 % and the atmospheric of 49.94 %, being a total M_f of 10.62 %, which makes its potential fire behaviour a Q_{ig} of 609.08 kJ/kg and an F_B of 0.90 m. However, after the occurrence of this precipitation, the system elevated its hydric status to a litter/duff moisture content of 5.82 %, 79.90 % in the scrub tank and 72.72 % in the atmospheric tank, with a total M_f of 12.81 %, implying an increase in Q_{ig} to 614.76 kJ/kg and a reduction in F_B , which became 0.80 m (Figura 3).

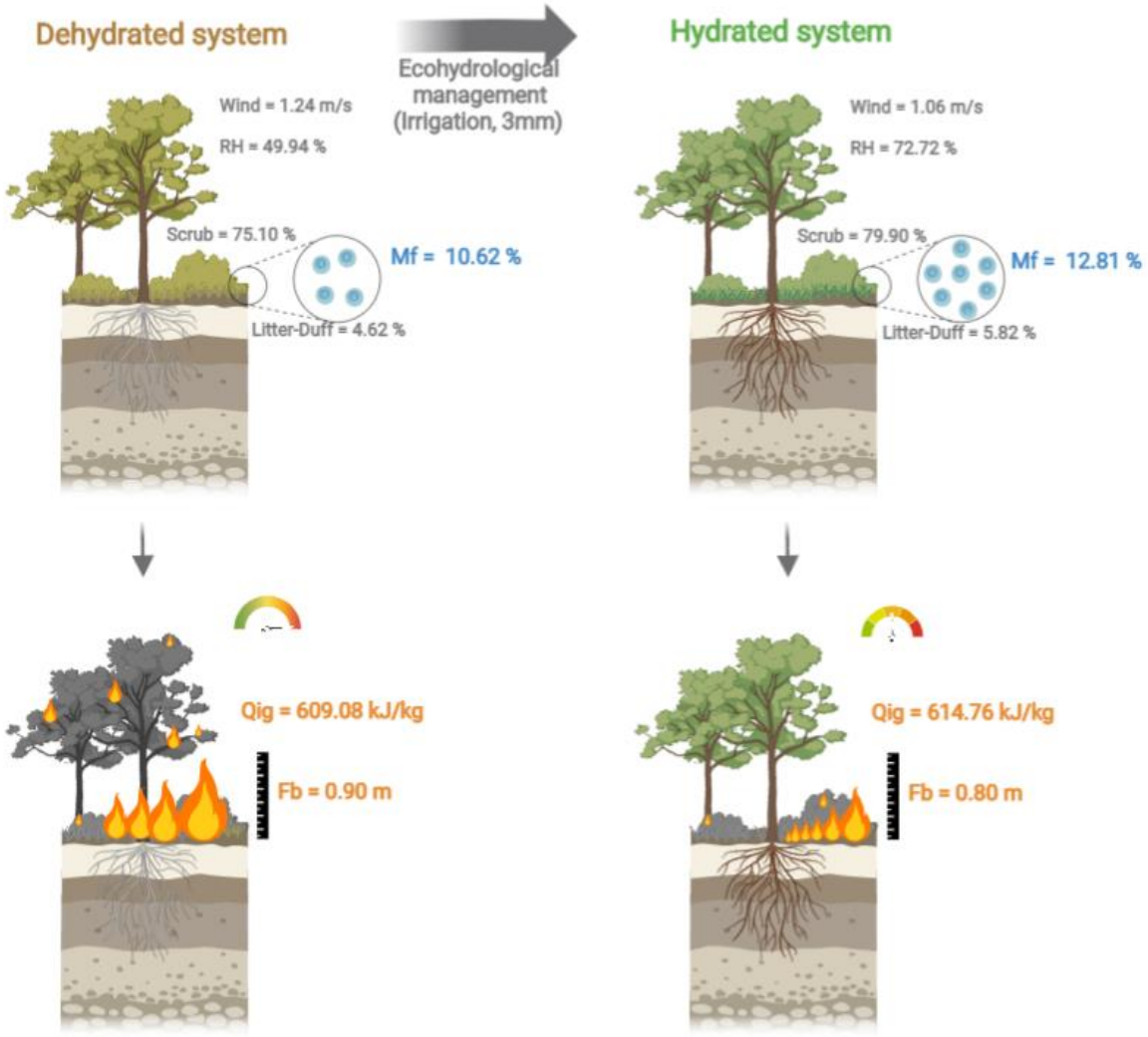

Figure 3- Case study of the change in moisture content (Mf), the EHV tanks used for its estimation (atmospheric or RH, scrub and litter-duff) and associated fire behaviour (flame length (Fb) and heat of preignition (Qig)) of the same system after a 3 mm rainfall.

4. Discussion

The EHV concept, through which the hydric state of the system has been quantified, has been a key point to study the irrigation-system-fire relationship. The main nexus of this relationship has been the transformation of system hydration into fire terms, i.e. the estimation of M_f (input for fire behaviour calculation) through the quantification of the EHV tanks (litter/duff, scrub and atmosphere). Furthermore, eco-hydrological monitoring of the system has allowed us to know the capacity and the real manipulation range of the hydration of the system through irrigation and thus the potential for the variation of fire behaviour.

The quantification of water and fire behaviour relationships is useful in fire-prone areas as it provides key information related to fire risk, availability of fuels, capacity for fire suppression, threats and danger to inhabitants as in the case of WUI areas. In this study it has been seen that through irrigation it is possible to increase the operational capacity of the system by 14.24 ± 10.32 kJ/kg on average, making a fire have to consume this additional heat amount before spreading, even decreasing the potential flame length by 0.10 ± 0.26 m on average, thus reducing the potential danger of the fire and increasing the probability to put the fire out. In addition, this approach that relates irrigation-fire makes it possible to develop irrigation algorithms, which will have the objective of minimizing the water supplied to obtain the greatest benefit of the characteristics of the fire behaviour (Blanco-Cano et al., 2022).

The practicality of the approach of increasing water status through irrigation could be a problem in areas affected by droughts, as water availability is low. This situation can be solved through: i) Use of reclaimed water, ii) eco-hydrological management: thinning and planting of green firebreaks. In reference to the use of reclaimed water the GUARDIAN project (https://proyectoguardian.com/) is a real-life solution and is currently installed in a semi-arid Mediterranean area. On the other hand, thinning, beyond reducing fuel load (which is the classic view in forest fire prevention), is known to increase the water status in the remaining trees (Del Campo et al., 2019; Manrique-Alba et al., 2020) and it should be included in the design of such treatments. Finally, the planting of green firebreaks consists of planting vegetation with low flammability and water retention mechanisms that allow them to have a relatively higher water content. In addition, these firebreaks can generate more humid and shaded areas, which allows for better water retention (Cui et al., 2019). This vision of hydric manipulation through eco-hydrological management for areas where water limitation is a critical factor in water supply through irrigation.

It can be concluded that fire management in WUI zones must bet on taking a pyro-eco-hydrological approach, understanding that the moisture content of the system can be modified and manipulated within certain ranges and that these modifications will have direct changes in the fire behaviour.

5. Acknowledgements

This work has been funded by Urban Innovation Actions – European Union (UIA03-338 GUARDIAN Project).

6. References

Bakšić, N., Bakšić, D., & Jazbec, A. (2017). Hourly fine fuel moisture model for Pinus halepensis (Mill.) litter. *Agricultural and Forest Meteorology*, 243, 93-99.

Balaguer-Romano, R., Díaz-Sierra, R., Madrigal, J., Voltas, J., & Resco de Dios, V. (2020). Needle senescence affects fire behavior in Aleppo pine (Pinus halepensis Mill.) stands: a simulation study. *Forests*, 11(10), 1054.

Blanco-Cano, L., Molina-Herrera, A.J., González-Sanchis, M.C., Pérez-Romero, J., Dalmau-Rovira, F2., Quinto-Peris, F., Gorgonio-Bonet, E., Pastor, E., Del Campo García, A.D. (2022). GUARDIAN: Sistema de gestión contra incendios forestales para la prevención y defensa de la interfaz urbano-forestal mediterránea. *8º Congreso Forestal Español*.

Byram, G. M. (1959). Combustion of forest fuels. *Forest fire: control and use*, 61-89.

Cui, X., Alam, M. A., Perry, G. L., Paterson, A. M., Wyse, S. V., & Curran, T. J. (2019). Green firebreaks as a management tool for wildfires: Lessons from China. *Journal of environmental management*, 233, 329-336.

Del Campo, A. D., González-Sanchis, M., Molina, A. J., García-Prats, A., Ceacero, C. J., & Bautista, I. (2019). Effectiveness of water-oriented thinning in two semiarid forests: The redistribution of increased net rainfall into soil water, drainage and runoff. *Forest Ecology and Management*, 438, 163-175.

Manrique-Alba, À., Beguería, S., Molina, A. J., González-Sanchis, M., Tomàs-Burguera, M., Del Campo, A. D., ... & Camarero, J. J. (2020). Long-term thinning effects on tree growth, drought response and water use efficiency at two Aleppo pine plantations in Spain. *Science of the total environment*, 728, 138536.

Martín, L. G. (2012). Las interfaces urbano-forestales: un nuevo territorio de riesgo en España. *Boletín de la Asociación de Geógrafos Españoles.*

Rakhmatulina, E., Stephens, S., & Thompson, S. (2021). Soil moisture influences on Sierra Nevada dead fuel moisture content and fire risks. *Forest Ecology and Management*, 496, 119379.

Rothermel, R. C. (1972). A mathematical model for predicting fire spread in wildland fuels. *Intermountain Forest & Range Experiment Station, Forest Service, US Department of Agriculture*. (Vol. 115).

Scott, J., & Burgan, R. E. (2005). A new set of standard fire behavior fuel models for use with Rothermel's surface fire spread model. *USDA Forest Service Rocky Mountain Research Station*. General Technical Report RMRS-GTR-153.

Vacca, P.; Caballero, D.; Pastor, E.; & Planas, E. (2020). WUI fire risk mitigation in Europe: 546 A performance-based design approach at home-owner level. *Journal of Safety Science and Resilience*, 1(2), 97-105.

Rural fires – Causes of human losses in Portugal

Andreia Rodrigues[1*], Domingos Viegas[2], José Zêzere[3], Aldina Santiago[1], Luis Laím[1]

[1] ISISE, University of Coimbra, Department of Civil Engineering, Coimbra, Portugal, {andreia.rodrigues, aldina}@dec.uc.pt, {luislaim@uc.pt}
[2] University of Coimbra, Department of Mechanical Engineering, Portugal {xavier.viegas@dem.uc.pt}
[3] University of Lisbon, Institute of Geography and Spatial Planning, Portugal, {zezere@campus.ul.pt}

**Corresponding author*

Keywords

Rural Fires, victims, paradigm change, self-evacuation, risk factors

Abstract

Wildfires are the cause of many fatalities in Portugal and around the world. Extreme fire phenomena are increasingly rising to intense and uncontrolled fires, with dimension and destructive potential greater than what was used to be seen and dealt with.

In the past, "rural communities" had a history of peaceful coexistence with fire, and the population consider themselves to be prepared to fight it. However, the widespread abandonment of rural landscape, the decrease of the agricultural activities around the villages and the aging population, lead to villages no longer naturally protected and the wildfires get closer to the houses with increasing intensity. Generally, population still has a poor awareness of fire risk, making, sometimes, wrong last-minute decisions. Therefore, it is crucial to protect rural communities that are now more vulnerable to wildfire threat.

2017 comes with a milestone in the history of wildfires in Portugal due to the high number of fatalities, in two different occurrences spaced in time, but geographically close. In both events 92% of deaths occurred in urban forest interface areas. Analysing the location of mortal victims, it is possible to identify risk factors that lead to the death civilians in rural fires. This paper presents an analysis of the characteristics and causes of death of the victims of the June and October 2017 fires in Portugal, recognizing risk factors that led to their death.

1. Introduction

Rural fires with extreme and unpredictable behaviour are a growing and critical problem around villages, often requiring mass evacuations to protect people and ensure safety (Manzello, 2018). However, the application of these actions in Portugal needs a more detailed analysis because the type of construction is mostly safe. Severe fires cause high devastation in communities, which could include the loss of human lives. The safety of populations at risk depends on accurate risk assessment, emergency planning and the emergency management.

Portugal, like other Southern European countries, faces unparallel circumstances nowadays, where large and uncontrollable fires are becoming more frequent, exceeding the capabilities of existing suppression resources and increasing community exposure (Fernandes, 2017). Sociodemographic changes in rural areas, climate change issues and vegetation changes lead to unprecedented circumstances that require the adjustment of fire use strategies and planning tools (Oliveira, 2021).

Zones where humans and their development, as infrastructures, meet or intermix with wildland fuel, has the designation of urban-forest interface (UFI); called also by urban-rural interface (URI) by some authors due to the translation from the Anglo-Saxon bibliography, as wildland-urban interface (WUI) (Fidalgo, 2012). The UFI areas present the typical problems of urban management, simultaneously with those of forest land management, due to the interaction between the two types of land that in the absence of fires, would be advantageous. However, these areas also have high risk of rural fires. UFI Communities hardly recognise the potential for destruction of forest fires, before experience the fire approaching (Fidalgo, 2012). In Portugal, the interface problem is also an emerging problem, with increasing importance due to the increase of the various

factors associated with it: the aggravation of forest fires, the growth in population on the outskirts of large cities and the frequency of extreme risk situations of a meteorological nature (Ribeiro, 2016).

A recent study reviewed the susceptibility and danger of forest fires in Portugal, introducing new data and extending the study period (Oliveira et al., 2021). This study indicates that in Portugal about 2% of the municipalities have more than 90% of their territory classified as dangerous, while 32% of the municipalities have, on the contrary, less than 10% of classified dangerous area.

Until 2003, rural fires in Portugal were known for the destruction of large areas of forests that affected the population only indirectly through high income losses due to loss of eucalyptus or pine trees, but which only occasionally affected buildings leading to loss of dwellings and consequently of human lives. 2003 and 2005 were as remarkable years due to the civilian's losses. Until then, human losses in rural fires were mainly combatants. Loss of civilian lives as a result of forest fires is a recent reality in Portugal.

The study and discussion of the type of victim, and the conditions that led to their death, is essential for a better understanding of this phenomenon and, from there, to infer the processes of change to be adopted so that these types of situations do not happen again. This paper aims to identify the factors that lead to the loss of human lives during rural fires, studying the characteristics of the fatal victims of the 2017 fires in Portugal, trying to identify their last actions and their last choices, based on analysis of data from the Independent Technical Commission and from the Centre for Studies on Forest Fires of the University of Coimbra from both June and October fires of 2017.

2. Change in the paradigm of rural fires in Portugal

Climatic conditions related to the environment and meteorological surroundings have proved to be of great importance in the development of fire and its propagation conditions. Under certain optimal weather conditions, the probability of massive wildfires increases significantly, as in the case of Pedrógão Grande in 2017 in Portugal (Viegas et al, 2017). Extreme meteorological phenomena appear with increasing frequency giving rise to this type of fire. They are known to be severe and complex, capable of reaching a very large size and high intensity, causing major environmental and socio-economic impacts.

Portugal, like other Mediterranean countries, is experiencing a confluence of two long-term trends: the widespread abandonment of the rural landscape that has become economically irrelevant, together with a strong reluctance by governments to create effective policies to deal adequately with the fire.

According to the legislation of the Portuguese government, in Ordinance n. 301/2020 of 24 December, it is recognized that the divestment in forestry, which contributed to the emergence of a monocultural landscape with a high fuel load and fire risk potential, wich "*when in the presence of severe meteorological episodes, this situation has resulted in large fires, devastating extensive forest and agricultural areas, infrastructure and heritage and putting human life at risk. These episodes, in turn, feed the vicious circle of abandonment, with consequences in terms of ecosystem degradation and the social and economic vulnerability of these territories*." (Portaria nº 249/2020, 2020). It is assumed that the policies implemented so far have not been enough and that populations are increasingly vulnerable to both the social and economic aspects.

Additionally, Portugal is also characterised by dispersed urban agglomerations, mainly in the countryside. Thus, it is essential that rural fire risk assessments consider not only hazard and exposure, but also social vulnerability (Oliveira et al., 2021). Dispersed urban agglomeration was synonymous of small villages of compact construction, but isolated in the landscape. Especially in the north and centre of Portugal, there are other types of villages called "*Avulso*" and "*Espraiado*" settlements that also contributed to this dispersed urban agglomeration. "*Espraiado*" settlement is briefly characterised by being consolidated in a network of rural paths spread out in all directions and is also characterised by having a vegetable garden or farm at the back; while *Avulso* settlement is characteristically off-center, presenting a loose building on a rural matrix., many of them are used as second homes, without permanent occupation.

In the scope of rural fire risk, the affected people are generally in rural areas, but recent cases have shown that this is not always the case, and the fire has been increasingly taking on such a dimension that it crosses borders, incoming urban areas as well. In 2005, a fire devastated the outlying of Coimbra, even going into the urban area due to spotting. The fire started on August 19 in Vila Nova de Poiares, but it was a re-ignition that gave rise to

a new fire, which, covering several kilometres, entered the city of Coimbra on August 21. Ten years earlier, in August 1995, a similar event also affected the same city, causing the damage of an apartment and of some vehicles.

These events highlight a change in the exposure of populations to danger, as it is no longer just a problem in rural areas but also in some urban areas, where this risk is not yet considered. People who live in urban or residential areas, among patches of forests, hardly recognise the potential for destruction of forest fires, before experiencing a situation of an approaching fire (Fidalgo, 2012).

In rural areas, despite the high risk of exposure, residents are used to live with forest fires and over the years have developed ways to protect themselves against this problem. The villages were protected by surrounding natural containment strips (agricultural fields) and in case of fire the active population came together to protect the distressed housing. However, with the abandonment of agricultural practices and the exodus of younger people to urban areas, this natural protection is decreasing. Quite often the abandoned agricultural areas are replaced by forest plantations, bringing trees closer to the houses.

Additionally, elderly residents keep the same feeling that they are safe, but the context in which they live has changed. In this way, we can consider that the inhabitants of these villages may have a false sense of security, which will make them stay close to the houses and refuse to evacuate their village, thus increasing their vulnerability.

If, on the one hand, there is urban expansion in rural areas towards forested areas in some areas of the country, especially in the north and centre of Portugal, due to tourism and demand for country houses for second homes, on the other hand, the abandonment of activities such as agriculture and grazing, the depopulation of rural areas and the continuous exodus to large urban environments by young people, lead to the abandonment of these areas, leaving elderly populations vulnerable, even on the outskirts of cities, making the forest and areas of bush to get closer and closer to the buildings.

3. Human losses in wildfires in Portugal

The loss of a human life due to forest fires will always be the greatest loss regardless of the area burned by the fire or the cumulative number of fires each year. In Portugal, records of the loss of human lives due forest fires are available since 1966.

3.1. Historical wildfire deaths around the world

Year after year, wildfires are killing people around the world and some of the fires led to the loss of a large number of people in a single occurrence. In Greece in 2018, around 100 people died in just one event in the town of Matti; in Australia in 2009 at least 173 people died in several fires that occurred in what became known as Black Saturday and in Russia in 2010 where, during one of the hottest summers ever registered, wildfires killed 60 people in July. There would be many other examples, even in the more distant past, but the fire known as “Peshtigo Firemost” that killed at least 1200 people in the United States of America in 1871 has being recognized as the deadliest event in history.

In Portugal, this is a recent reality. Over the years, there are negative milestones in history, remembering the years of 2003 and 2005 where respectively 21 and 23 people died (Viegas, 2004) and the fateful year of 2017, with the loss of a total of 66 casualties in June and 57 in October. The year of 2017 was a milestone in history due to the high number of fatalities, in two different occurrences spaced in time, but geographically close, where most deaths occurred in urban forest interface areas.

Australia's Country Fire Authority (CFA) conducted a retrospective study of civilian deaths that occurred in the fires in Victoria. The investigation used the coroners' reports to determine the circumstances of each death. Many of the case studies illustrate the risk resulting from late evacuation and poor understanding of fire behaviour. Three categories of victims were identified:

-victims who recognized the real threat to their safety with enough time to save their lives, but chose an ineffective survival strategy;

- victims who did not recognize the real threat to their security in time to implement an effective survival strategy; and

- victims physically unable to implement effective survival strategies. (Handmer, 2005)

These victim typologies, according to the analysis of deaths related to the 2017 fire in Portugal, are remarkably similar.

3.2. Analysis of fatalities in the June 2017 occurrence in Portugal

The June 2017 fire complex will go in the history of rural fires in Portugal, as it caused 66 fatalities, making it one of the most serious fire disasters in our country, and one of the worst in Europe. It consisted of several events, the most critical being those that started in Pedrógão Grande, and in Góis, which were associated with three other fires that consumed a total area of 45,328 ha (Viegas et al, 2017).

Following these fires, the Portuguese government created, through Law nº 49-A/2017, of 10 July, the Independent Technical Commission (ICT) with a mandate to carry out an independent assessment of those fires. At the same time the Government requested to The Centre for Studies on Forest Fires (CSFF- ADAI) of the University of Coimbra to also carry out a study on the conditions of occurrence, initiation, and propagation of fire, with particular emphasis on the study of its propagation and the analysis of fatal accidents (Viegas et al, 2017). Both studies led in the same direction, and they are complementary.

The ICT report identified 64 fatalities due to the fire and carried out an exploratory analysis of the conditions and particularities of the human victims who died because of this fire. Note that the ADAI report counts one more victim accounting 65 victims because this report counted one victim who died two days later, following serious injuries. This victim was the only firefighter among the other victims, all civilians. Neither of the two studies count the number of injuries. Later one other injured person died in the hospital bringing the total number of fatalities to 66.

Analysing the age of the victims, most were between 30 and 70 years old, active people, without limitations in the process of escape or risk perception (figure 1). As for gender, the number of victims is very close, so it was not considered a risk factor or characteristics related to the cause of death.

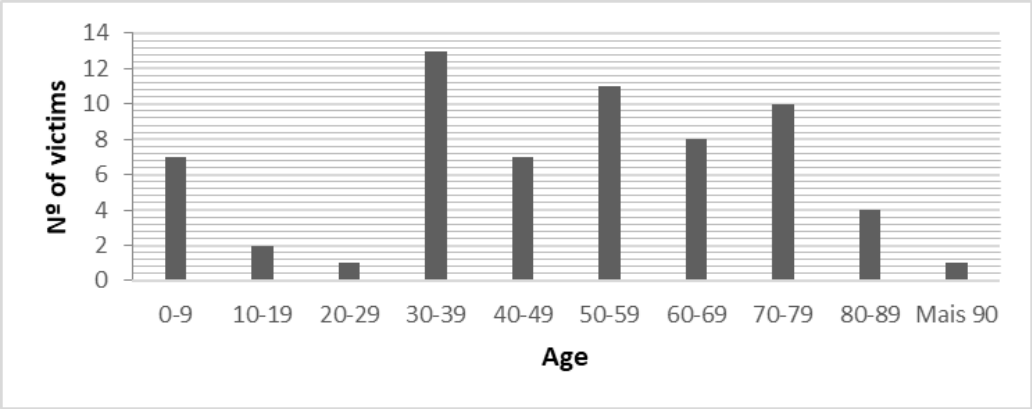

Figure 1- Distribution of the age of the victims– June 2017 (CSFF- ADAI 2017)

An important factor in this analysis is the relationship of the victims with the place where they died. According to the data of CTI report, half of the victims were residents of the villages affected by the fire. However, it is the high number of occasional visitors that needs special attention (figure 2).

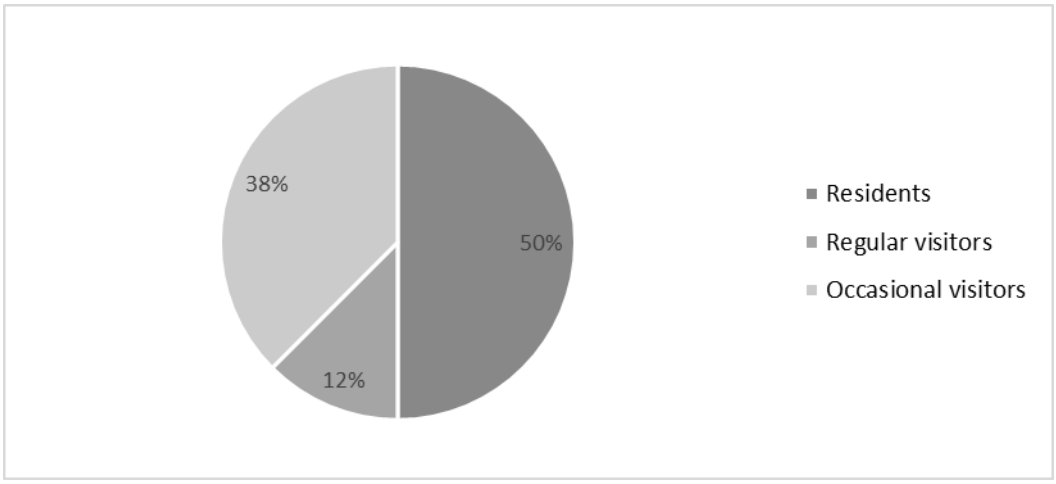

Figure 2- Relationship between the residence for the victims and the place of death – June 2017(ICT 2017)

It should be noted that this is a very popular zone in the summer, mainly for its river beaches and for leisure activities. The violence of the fire, the lack of knowledge of escape routes, self-protection measures for rural fire situations, combined with the lack of the presence of competent authorities to give indications, significantly increase the panic of these people, looking for escape routes became their way to death. Only 4 of the 66 victims died inside their homes.

Regarding the distance from the place of death to the victims' homes, 47% die more than 5 km from home. These victims are tourists and visitors, who, whether or not they have a relation with this zone, they were on a occasional visit (figure 3).

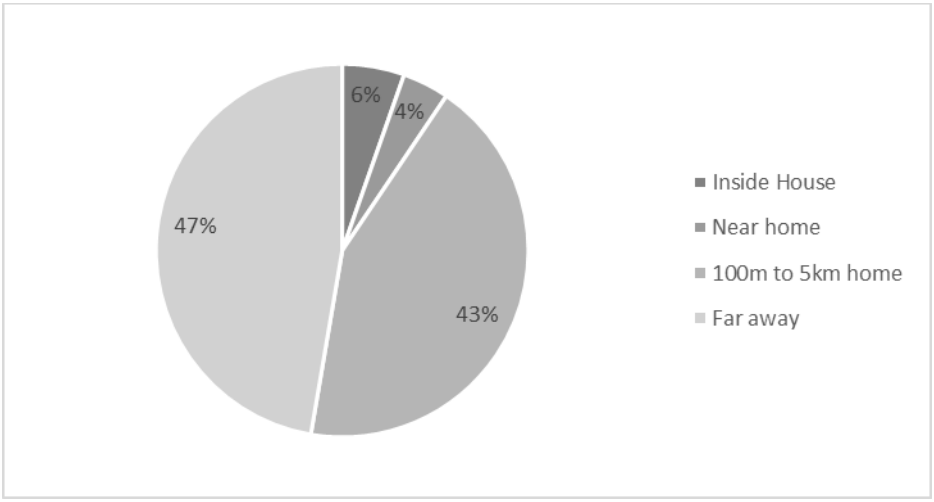

Figure 3- Relationship between the victims and the place of death – June 2017 (ICT 2017)

However, 43% of the victims died between 100 meters and 5 km away from their homes, which indicate that the victims tried to run away in the face of the approaching fire, considering that they were going to get safety. Additionally, regarding the circumstances of death, from the analysis of data, it is considered that 70% of the victims were running away from the fire (figure 4).

Figure 4- Relationship between leave and stay on the number of deaths - June 2017 (ICT 2017)

In the group of victims who did not run away the fire, the report identified evidence that, in addition to the 4 victims who remained in their homes and who were caught by the fire there, the remaining victims who were not running away were passing through that area, returning home or to their accommodation after a day of sightseeing in the mountains. Regarding how the victims fled the fire, the CSFF- ADAI report identifies that 89% of victims chose the car as a means of escape.

3.3. Analysis of fatalities in the October 2017 occurrence in Portugal

In the sequence of the June fires, also in the 15 October fires, the Portuguese Parliament also requested the constitution of the Independent Technical Commission and the Portuguese Government requested to CSFF-ADAI a study of the most relevant facts of these fires, with the Country still in the aftermath of the June fires and still in shock from this new disaster.

Although both reports work in the same direction, the number of victims identified in both is not coincident, and the CSFF- ADAI report identifies and analyses 51 fatalities and the ICT only recognize 48 victims. This discrepancy is mainly due to the fact that the ICT report considers the direct victims of the fire (and that were investigated by the Judiciary Police) only, while CSFF- ADAI report analysed victims directly and indirectly related to the fire, based on 40 accidents that resulted in these deaths.

While in the fires of June 2017, all victims perished in a short time and limited zone, in October 2017 the victims were dispersed for a complex of different fires. In the October fire, more than 50% of the victims were 50 years of age or older (Figure 5). This fact, important in the following analyses, shows that the victims of these fires were mostly elderly, in many cases with health problems and mobility difficulties. As for gender, in this complex of fires, 65% of the victims were men and 35% women.

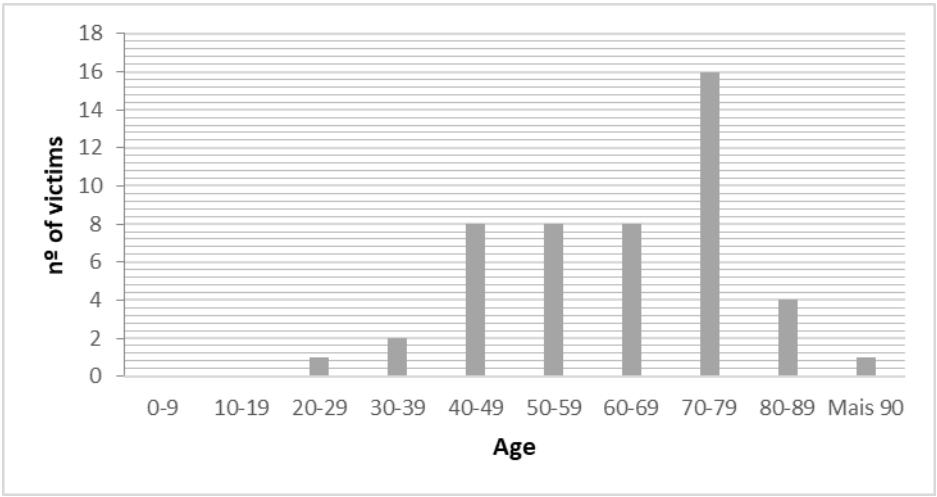

Figure 5- Distribution of the age of the victims– October 2017 (ICT 2018)

The analysis of the relationship of the victims with the place of death shows that 86% of the victims were residents in the area. In addition, since most victims were old people, they end up dying either inside their homes or nearby. (Figure 6).

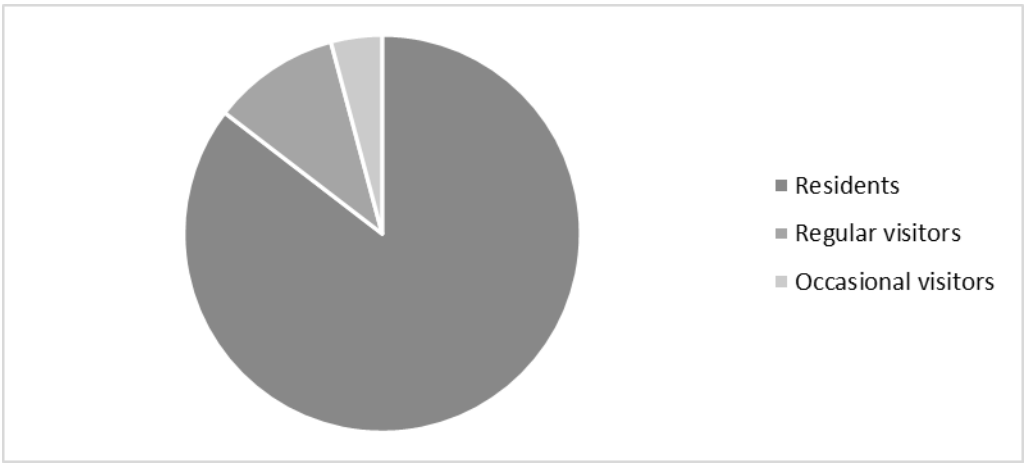

Figure 6- Relationship between the residence for the victims and the place of death - October 2017 (ICT report 2018)

The distribution of distances from the place of death to the home is more heterogeneous in October fire (Figure 7), allowing to conclude that there were different circumstances and decision-making by the victims.

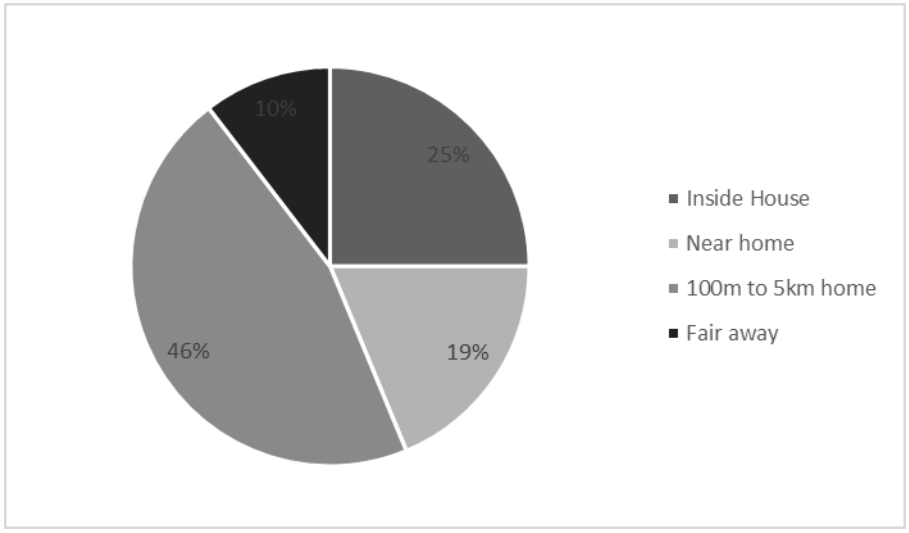

Figure 7- Distance between the residence for the victims and the place of death - October 2017 (ICT report 2018)

There are about 44% of victims who died inside or near houses, but a large percentage of people, about 46% tried to run away. It should be noted that, according to the ICT report, 60% of the houses of the victims of this fire did not burn. In this case, 63% of the people tried to run away (figure 8).

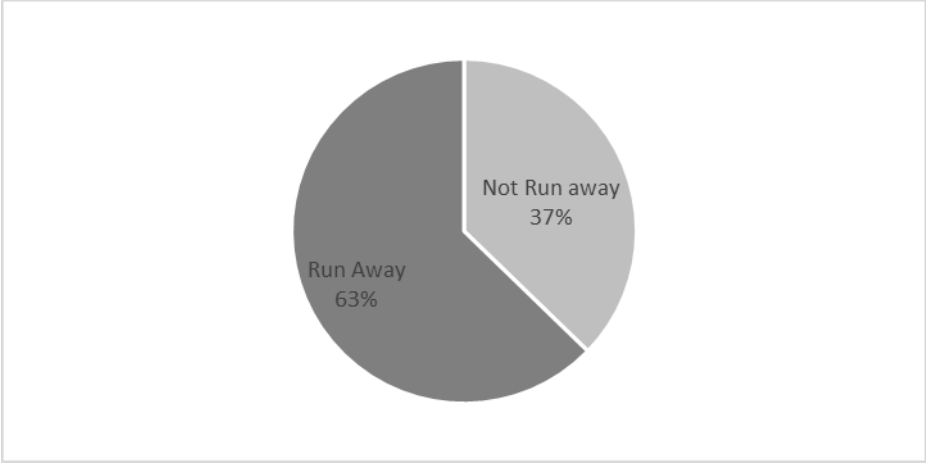

Figure 8- Relationship of leak with the death process – October 2017 (Viegas et al 2018)

After the June fires it was expected that people would have learned and chosen to stay in their homes and not choose to run away. But even so, a large percentage of people died while trying to run away.

4. Discussion of results

The analysis and discussion of the type of victims, and the conditions that led to their death, is an essential tool for a better understanding of this phenomenon and, from there, to infer the processes of change to be adopted in order to avoid such disastrous events. In this study and from both analysed fires, it was observed that the victims have very different characteristics.

The fire of June 2017 is a fire with great severity on the surface (CTI, 2017), and the fatalities were mostly young people and adults, who took advantage of a weekend for leisure activities. Many of them, faced with the imminence of a major fire, decided to use their vehicles and move away from the scene of the fire. With limited information about the area, they followed the only path they knew and were caught by the front of the fire along the way. Regarding the victims who lived in the area of the fire, it is observed that none of the houses of the victims who decided to flee were affected, and staying at home would have been the best option. These people would be safe, and the option of escape became their exposure factor, leading to their death.

From the analysis of both reports, the conclusions stated that after June 2017, the population would have been left with the idea that fleeing would be the most dangerous option. However, and not contradicting the validity of this thesis, it is important to understand here that the typology of victims is different in the occurrence of October 2017.

The victims of October 2017 were elderly people, some of them with limitations in perception and reaction to danger as well as in mobility. Thus, according to the reading and analysis of the survivors' reports, contained in the CEIF-ADAI report, a large number of victims were surprised by the flames already in the vicinity of their home or during the night.

It is also important to point out that, with the change in the fire paradigm, as mentioned above, the elderly populations maintain their belief that they are safe in the villages, not recognizing the risk situation they are in. Adding to this idea, the disbelief in the authorities of fire fighting forces, make the populations stay to the limit near their homes with the idea of protecting them.

In this way, and as a way of summarising the conclusions stated above, the following risk factors were identified:

- Growing demand for nature-based tourism: With the change in the dynamics of fires in Portugal, they take on more and more proportions and dynamics that are difficult to identify in advance. The high demand for rural and forested areas for tourism and leisure, essentially by residents of urban areas, significantly increases the number of people dispersed in these spaces. In addition, visitors are mostly people who are poorly prepared and unaware of the risk of forest fire, thus increasing their vulnerability.

- False feeling of inhabitants in rural areas: inhabitants in rural areas have become used to living with fires. With the abandonment of rural areas, the forest tends to invade the villages, significantly increasing the urban-forest interface. The feeling of safety that the inhabitants had before is no longer real and currently the rural settlements are very vulnerable to fires, being a relevant risk for their inhabitants.
- Demand for rurality and nature-based experience: although the exodus of permanent inhabitants from the villages in the countryside in recent decades, there is an increasing demand for accommodation and/or housing in rural areas, essentially by foreigners. There is also an increase in the return of retired people to their origins, in search of an end of life in the tranquillity of the countryside. This factor has further contributed to the fact that, in addition to the forest entering the alleys, new construction often "enters" the forest in search of tranquillity through contact with nature;
- Strong exposure of vulnerable communities to risk: With the exodus of young people to cities, villages become increasingly aged. The sense of neighbourhood ceased to exist, and it is increasingly common for the elderly to be debilitated in their homes, cared for and often visited by employees of social solidarity institutions. In the face of a fire situation, and in addition to the difficulties associated with age and illness, indirect fire products such as smoke and gases substantially affected these people;
- Understanding the escape process: The lack of preparation and awareness make the population wait for the fire to arrive at the houses. In the face of very intense fire phenomena, combined with poor information and the lack of competent authorities on the ground to guide their exit process, last-minute self-evacuation will increase people's exposure to the fire from which they are fleeing.

5. Conclusions

Forest fires continue to be the source of many fatalities both in Portugal and around the world.

The analysis of fatalities resulting from the 2017 fires in Portugal shows that people still have a poor perception of fire risk, making wrong last-minute decisions that lead to death. The lack of awareness combined with the lack of credible information means that, in the face of a fire, people make decisions based on what they know from their experience on past events. The disrepute in public policies and in action also increase it.

With the analysis of the location and of some characteristics of the mortal victims it is possible to identify risk factors that lead to the death of civilians due to wildfires, such as the increase in demand for rurality, both for permanent and tourist housing, of inhabitants coming from urban areas, which are not familiar with wildfires.

Another problem, very evident in the October fires, is the false sensation of security of elderly population. The habitants in rural areas have a history of peaceful coexistence with fire and consider that they are prepared to face it. However, the abandonment of rural areas, abandonment of the agricultural activities that were developed around the villages, mean that villages are no longer naturally protected and that a fire gets closer to the houses with greater intensity. The strong relationship of belonging to their place of residence means that specially the elderly people want to stay close to their homes, believing that they are naturally protected, something that used to happen in the past. This fact makes these populations even more exposed and vulnerable.

Finally, the lack of preparation and awareness make the population wait for the fire to arrive at their homes. In the face of very intense fire phenomena, combined with poor information and the lack of competent authorities on the ground to guide their exit process, last-minute self-evacuation will increase people's exposure to the fire from which they are fleeing.

The conclusions obtained with this study are intended to be the stepping stone for future work on the creation of methodologies for the protection of civilians in the face of forest fires.

6. References

Carvalho, A. F. (2010). Bases para o Ordenamento do Povoamento. Dissertação para atribuição de grau mestre em Ordenamento da cidade, Universidade de Aveiro.

CTI, C. T. (2017). Relatório Comunidade Independente – Análise e apuramento dos factos relativos aos incêndios que ocorreram em Pedrogão Grande, Castanheira de Pera, Ansião, Alvaiázere, Figueiró dos Vinhos, Arganil, Góis, Penela, Pampilhosa da Serra. Relatório Técnico.

CTI, C. T. (2018). Avaliação dos Incêndios ocorridos entre 14 e 16 de Outubro de 2017 em Portugal.

Decreto-Lei nº249/2020. (2020). Aprova a delimitação dos territórios vulneráveis com base nos critérios fixados no artigo 2.º do Decreto-Lei n.º 28-A/2020, de 26 de junho. Diário da República n.º 249/2020, Série I de 2020-12-24, páginas 25 - 48.

Duarte, J. (2005). "Os Fogos Florestais em Portugal: O Planeamento do espaço na Interface UrbanoFlorestal e a segurança das populações". Actas do X Colóquio Ibérico de Geografia, Universidade de Évora, Évora.

ELBEIN, S. (2019). https://nationalgeographic.pt/. Obtido de National Geografic: https://www.natgeo.pt/ciencia/2019/12/como-viver-com-grandes-incendios-florestas-portuguesas-podem-ajudar-responder

Fernandes, P. (2017). Entender porque arde tanto a floresta em Portugal. Pp. 69-91 In Árvores e Florestas de Portugal, Vol. 8 Proteger a Floresta - Incêndios, Pragas e Doenças.

Fidalgo, E. (2012). Territórios em mudança e os incêndios na interface urbano-florestal. Estudo de caso em Baião. Cadernos de Geografia Coimbra, FLUC - pp. 87-98.

Handmer, J. A. (2005). Is Staying at Home the Safest Option During Bushfires? Historical Evidence for an Australian Approach. Environmental Hazards 6: 81–91.

Leite, F. F. (2013). Grandes incêndios florestais em Portugal Continental como resultado das perturbações nos regimes de fogo no mundo mediterrâneo. Silva Lusitana.

Lourenço, L. (2007). Incêndios florestais de 2003 e 2005. Tão perto no tempo e já tão longe na memória! Colectâneas Cindínicas VII.

Manzello, S. L., Blanchi, R., Gollner, M. J., Gorham, D., McAllister, S., Pastor, E., ... & Suzuki, S. (2018). Summary of workshop large outdoor fires and the built environment. Fire safety journal, 100, 76-92.

Oliveira, S., Bergonse, R., Santos, P. P., Gonçalves, A., Melo, R., & Zêzere, J. (2021). Avaliação de Risco de Incêndio Rural à escala local na região Centro de Portugal. Geografia, Riscos e Proteção Civil: Homenagem ao Professor Doutor Luciano Lourenço, 79-89.

Oliveira, S., Gonçalves, A., & Zezere, J. L. (2021). Reassessing wildfire susceptibility and hazard for mainland Portugal. Science of the total environment, 762, 143121.

Portaria n. 301/2020 de 24 de Dezembro. (2020). Aprova a delimitação dos territórios vulneráveis com base nos critérios fixados no artigo 2.º do Decreto-Lei n.º 28-A/2020, de 26 de junho. Diário da república.

Viegas, D. A. (2017). O complexo de incêndios de Pedrogão Grande e concelhos limítrofes, iniciado a 17 de junho de 2017. Centro de Estudos sobre Incêndios Florestais da Universidade de Coimbra.

Viegas, D. A. (2019). Análise dos incêndios florestais ocorridos a 15 de outubro de 2017. Centro de Estudos sobre Incêndios Florestais da Universidade de Coimbra.

Viegas, D. A. (2004). Cercados pelo fogo - 1ª ed. - Coimbra : MinervaCoimbra,- ISBN 972-798-105-4

Ribeiro, L.M (2016) Os incêndios na interface urbano-florestal em Portugal: uma análise de diagnóstico. Dissertação para atribuição de grau mestre em Dinâmicas Sociais, Riscos Naturais e Tecnológicos. Universidade de Coimbra

Simulated flame shape and heat transfer of quasi-equilibrium grass fires at transitional Byram numbers

Duncan Sutherland*[1]; Jason Sharples[1], Khalid Moinuddin[2]

[1]School of Science, UNSW Canberra, Australia, {duncan.sutherland, j.sharples}@adfa.edu.au
[3] Institute for Sustainable Industries and Liveable Cities, Victoria University, Australia, {khalid.moinuddin@vu.edu.au}

**Corresponding author*

Keywords

Physics-based simulation, grass fires, quasi-equilibrium spread

Abstract

There are two basic modes of fire spread: buoyancy driven where the fire plume is approximately vertical, and wind driven where the fire plume is attached to the surface. The buoyancy driven mode is usually identified by Byram number Nc>10, and the wind driven mode identified by Nc<2. Grass fires at field scale over a range of Byram numbers are simulated using a physics-based model and the mechanisms of heat transfer to the unburnt fuel are analysed. The wind speed is varied to give different Byram number and different fire behaviour. The current thresholds on Byram number are found to correctly classify the behaviour of the fire plume. Previously it was thought that radiative heating dominates convective heating for buoyancy dominated fires, and convective heating dominates radiative heating for wind dominated fires. However, the radiative boundary heat flux is found to dominate the convective boundary heat flux in all cases. The convective heat flux along the centreline ahead of the main fire front increases with wind speed. The results imply that the heat transfer mechanisms, at least for this fire configuration, is more complicated than previously thought. Further research is required to understand if the convective heat transfer mechanisms are adequately reproduced in the simulations.

1. Introduction

The Byram convective number Nc (Morvan and Frangieh, 2018) is used in various parts of the literature in an attempt to classify fires as wind-driven (wind-dominated, shear force dominated, or sometimes called the boundary layer mode) or buoyancy-driven (buoyancy dominated, plume driven, or plume mode). In wind-driven fires the flame is elongated and at an acute angle to the ground. Radiative and convective heat transfer to unburnt fuel is thought to be enhanced by the flame geometry. In buoyancy-driven fires the flame is roughly vertical and therefore it is hypothesised that the heat transfer to the unburnt fuel is almost exclusively by radiation (Morvan and Frangieh, 2018). The importance of convective structures and convective heating on fuel ignition and fire spread has been studied experimentally (Finney et al., 2015). The equation for Nc is

$$Nc = \frac{2gQ/(\rho\, c_p\, T_a)}{(U_{10} - R)^3}$$

where U_{10} is the wind speed at 10 m, Q is the fire intensity, g is the acceleration due to gravity, R is the rate of spread, ρ (1.2 kg m^{-3}) is the gas density, c_p is the gas specific heat capacity (1.0 kJ kg^{-1} K^{-1}), and T_a is the ambient temperature. Therefore, the Byram number can be thought of as measuring the relative importance of the buoyant or convective force and the shearing force upon a fire. The thresholds proposed for the Byram number are $Nc < 2$ is a wind-driven fire, $Nc > 10$ is a buoyancy-driven fire, and $2 \leq Nc \leq 10$ is some intermediate fire behaviour.

Physics-based simulations are becoming a popular tool for wildfire investigation. Here we use the Wildland-Urban Fire Dynamics Simulator (WFDS, subversion 9977, based upon FDS version 6.0), which has been validated against field scale fires (Mell et al., 2007, Moinuddin et al., 2018).

Four simulations are conducted, with the driving wind speed the only parameter varied across the simulation set. Specifically, we consider the following wind speed: $U = 3$, 4, 6, and 10 ms^{-1}, which are referred to as the

U3, U4, U6, and U10 cases, respectively. The U6 simulation replicates the CO64 experiment conducted during the Annaburoo campaign (Cheney et al., 1993). The rate of spread data for the U3, U6, and U10 cases were presented in (Moinuddin et al., 2018) (averaged quasi-equilibrium value only) and (Sutherland et al., 2020) (values for all time). The Byram number for U3, U6, and U10 at all times was also presented in (Sutherland et al., 2020). All other results, namely the heat transfer and flame shape results, presented here are novel.

2. Methodology

WFDS is a fully physics-based fire spread simulator, that is, the solid fuel degradation, gas-phase combustion, heat transfer and fluid flow are explicitly simulated with as few parameterisations as possible. The simulation methodology for grass fire is also well established and the method used here is identical to (Moinuddin et al., 2018, Sutherland et al., 2020).

Several simplifying assumptions are used to model the fuel bed. The fuel is considered as a thin layer on the ground and heat transfer by conduction between the fuel elements is neglected. The fuel dehydrates at 393 K and pyrolyses between 400 and 500 K following a linear mass loss rate [7].

The heat transfer is modelled with several simplifying assumptions. Heat transfer by convection is approximated using an empirical correlation based on approximating the fuels as cylindrical particles. The fuel height and structure are modelled as an aerodynamic drag force term in the fluid momentum equation. The parameters of the convective heat transfer and aerodynamic drag model are deduced from experimental measurements. The flame emits radiation, and the radiation transport equation is solved by the discrete ordinates method. The combustion zone is difficult to resolve using LES, and therefore the gas temperature inside the flame can be underpredicted. Because the emitted radiation depends on the fourth power of gas temperature an underprediction can result in large errors in the radiation term. Therefore, within the flaming zone the source of radiation is a function of local heat release rate per unit volume. Outside the flaming zone, gas temperature is well resolved and the usual fourth power of temperature relation is used. Full details of the WFDS model can be found in (Mell et al., 2007).

3. Results and discussion

3.1. Quasi-equilibrium fire spread

The contours of burning area over time, are extracted from the boundary temperature, T, data. The $T = 400$ K contour at time t represents the extent of the burning region.

The burnable region of the simulation domain and example fire isochrones for the U4 case, are shown in Figure 1.

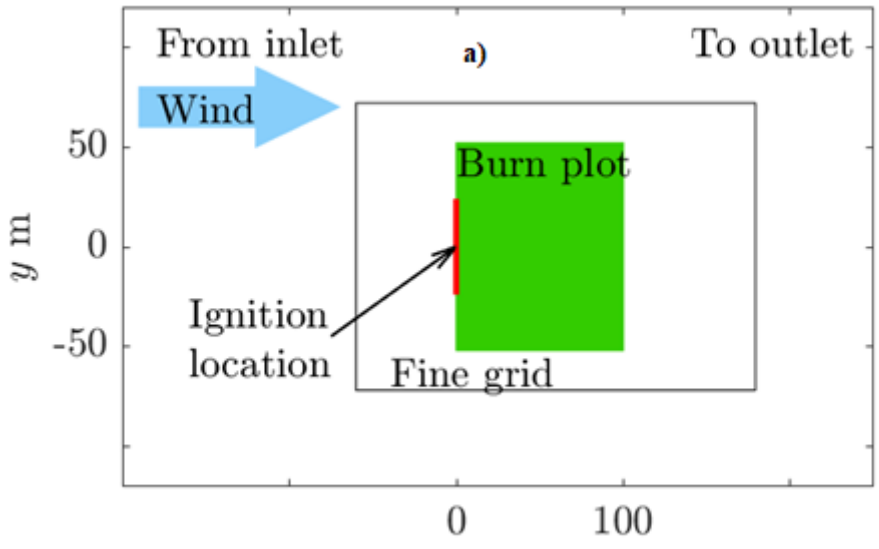

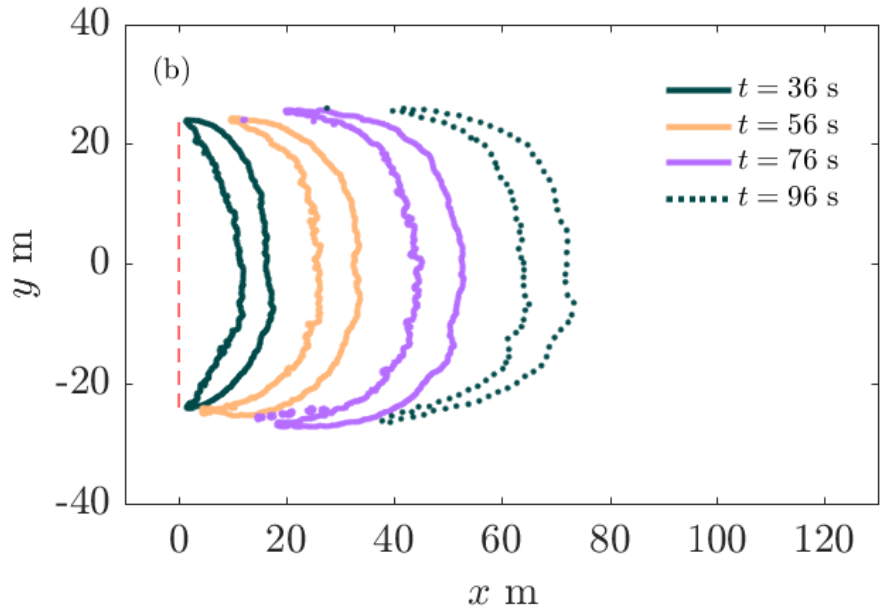

Figure 1- (a) a schematic of the simulation (b) example fire isochrones for the U4 case.

The rate of spread of the fire is estimated from the boundary temperature along the domain centreline. The location of the burning region, x_* is identified from the centre of the interval along $y = 0$ where $T_s > 400$ K. The time dependent rate of spread is then the time derivative of x_*; the derivative is approximated from the simulation data using the standard first-order forward difference scheme:

$$\mathrm{R(t)} = \frac{dx_*}{dt} \approx \frac{\mathrm{x_*(t_{n+1})} - \mathrm{x_*(t_n)}}{t_{n+1} - t_n}$$

The time interval between the data points is 1 s.

Because the data is noisy, the results are smoothed by a 5-point moving average. The quasi-equilibrium rate of spread R_{qe} is then judged manually from the region where $R(x_*)$ is approximately constant. $R(x_*)$ is shown for the quasi-equilibrium regions for all cases in Figure 2(a). Plotting against location stretches $R(t)$ for the higher speed cases to provide a consistent abscissa and allow easier comparison between the different wind speed cases. R_{qe} is achieved at different times for different driving wind speeds. However, the distance from ignition at which a fire can be deemed quasi-equilibrium is approximately the same: 50 m, which is the threshold used here. $R(x_*)$ decreases rapidly from approximately $x_* = 95$ m as the fire reaches the end of the plot, and these data are omitted from the plots and subsequent analysis. Figure 2(b) shows the corresponding Byram numbers.

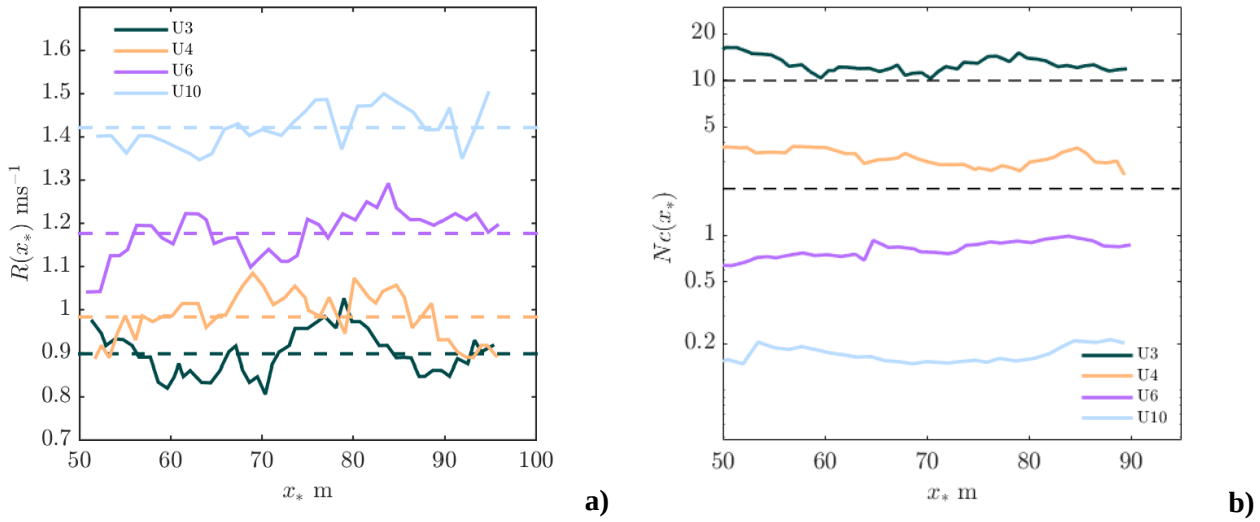

Figure 2- (a) Rate of spread as a function of distance from the ignition line, in the quasi-equilibrium range. (b) the Byram number. The black dashed lines indicate the threshold limits of Nc=2 and Nc=10.

3.2. Quasi-equilibrium flame shape

Because the fires spread at a quasi-equilibrium rate, and the head fire geometry is approximately constant during this phase of spread, ensemble averages of pyrolysis front, boundary radiative heat flux, boundary convective heat flux, centreline heat release rate, and centreline wind velocities can be constructed in a reference frame that moves with the fire. Similar ideas were used by Mueller (2107) to analyse flame geometry.

To construct the ensembles, all data outside of the quasi-equilibrium region were discarded. The trailing edge of the fire was selected as the reference point. At each output step the data was circularly shifted such that the reference point was located at $x = 0$. That dataset was then averaged in time. Errors are introduced by the circular shift; however, these occur far upstream ($x < -100$ m) and far downstream ($x > 100$ m) and can be discarded.

The ensemble averaged u-velocity contours (shaded colours) and the contour of 10% of maximum heat release rate (red) are shown in Figure 3. The red contours were selected as a representation of the flame shape: most of the heat released by the flame is on the inside of this contour. The white arrows in the plot are vector representation of the ensemble averaged u- and v-velocities. In the U3 case, the u-velocity is negative on the downstream side of the flame. To highlight this, the $u = 0$ contour is shown in black. This, and the velocity vector field (white arrows), indicates that the flame and plume entrain fresh air from both sides and is therefore truly a buoyancy dominated fire, consistent with the Byram number prediction. No other cases exhibit two-sided entrainment into the plume. The U4 and U6 cases exhibit roughly vertical flames like the U3 case. The U4 and U6 case exhibit downstream enhancement of the u-velocity, however, this is more prominent in the U6 case. In the U4 case the velocity enhancement decays after approximately 25 m but the enhancement persists for at least 50 m in the U6 case. This suggests that the plume of the U6 case has attached to the ground and this attachment persists for some distance. The plume attachment is consistent with the Byram number prediction of a wind dominated fire. The U4 case has an intermediate Byram number, although with $Nc \approx 3.26$ this fire is notionally closer to wind dominated than buoyancy dominated. The single sided entertainment is consistent with a wind dominated fire, but the u-velocity enhancement does not persist for significant distances, suggesting that the plume has detached close to the flaming region. The U10 case shows an elongated heat release rate contour and significant downstream enhancement of the u-velocity; consistent with a wind dominated fire.

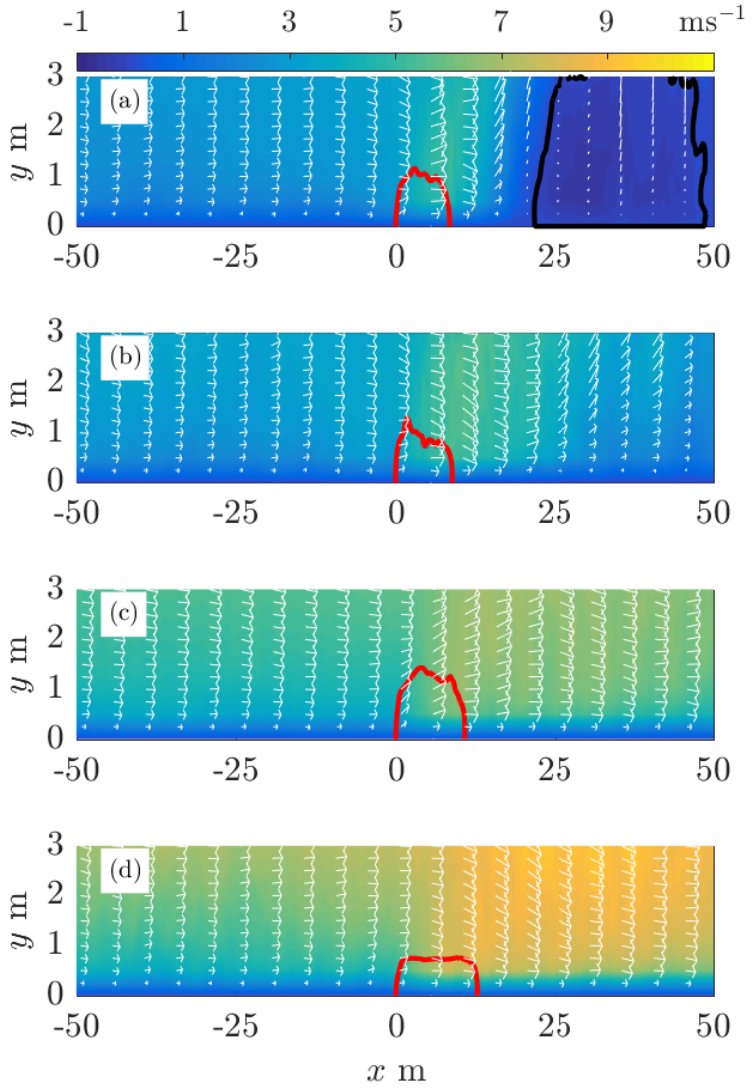

Figure 3- Contours of 10% of maximum heat release rate (red) per unit volume along the line y = 0 averaged in time over the quasi-steady regime superposed on colour contour plot of averaged u−velocity (a) U3 case (b) U4 case (c) U6 case (d) U10 case. To to highlight the region of negative u−velocity in the U3 case, the u = 0 contour is plotted in black. The white arrows show the direction of the ensemble averaged wind field along the centreline

3.3 Analysis of heat transfer

To investigate how the mechanisms of heat transfer change with the mode of fire propagation, the total radiative and convective heat fluxed received by the unburnt fuel is computed. However, the data may still include cooling of the unburnt fuel by radiation and convection, and such cooling is expected at the flanks and trailing edge regions of the fire. To examine the regions of heat transfer, the contours of ensemble-averaged boundary (z=0 m) heat flux are shown in Figure 4 (radiative) and Figure 5 (convective).

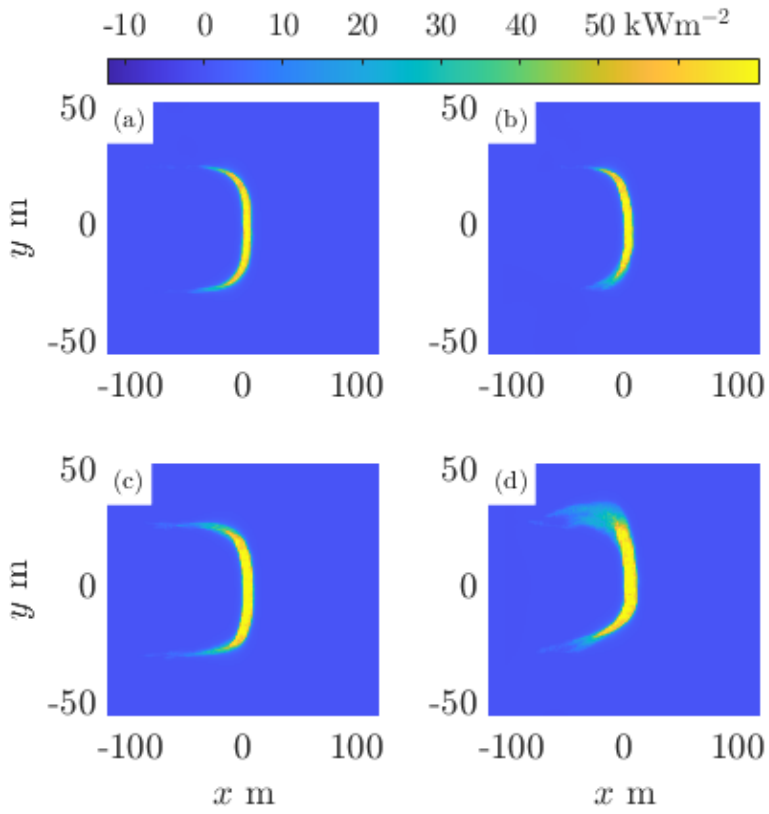

Figure 4- Ensemble averaged radiative heat transfer (a) U3 (b) U4 (c) U6 (d) U10

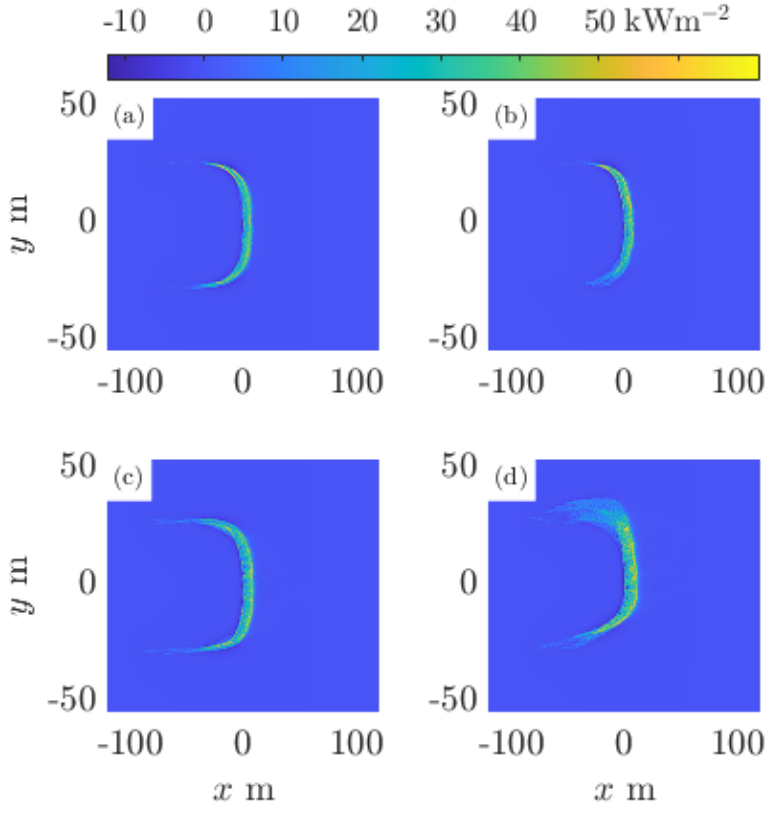

Figure 5 Ensemble averaged convective heat transfer (a) U3 (b) U4 (c) U6 (d) U10

The shape of the contour is like the shape of the pyrolysis zone. The heat fluxes are most intense in the straighter near-centreline head region of the fire. However, at the edges and trailing regions of the fire, the averages appear

indistinct. This phenomenon is strongest around $y = 40$ m in the U10 case. The flanks of the fires, unlike the near centreline behaviour of the fires, are somewhat intermittent and cannot be in a quasi-equilibrium state.

There is little to no radiative cooling, however, there is strong evidence of convective cooling, located at the trailing edge of the fire. The variation in the convective heat flux across the head fire may be associated with the vortex structures identified by Finney et al. (2015). Because these structures appear in the ensemble average, these structures must persist in approximately the same y-location over the quasi-equilibrium propagation.

To identify if there is a dominant mechanism of heat transfer along the centreline, the ensemble averaged boundary heat fluxes are shown upon the centreline in Figure 6. The vertical dotted lines are the locations of the leading edge of the heat release rate contour shown in Figure 3. The centreline radiative heat flux exhibits a single broad peak, which stretches in the positive x-direction as U increases. The centreline convective heat flux has a more complicated shape. There is a region of cooling before the trailing edge, followed by a peak in heating at the trailing edge ($x = 0$ m). The magnitude of the cooling and heating peaks are similar for all wind speeds. There is a region of decreased heat transfer at approximately $x = 2$ m, even extending to a region of cooling in the U10 case. The magnitude of this trough does not appear to follow a systematic trend. It is possible that this region is associated with the previously identified vortex structures that occurs near the centreline in all cases.

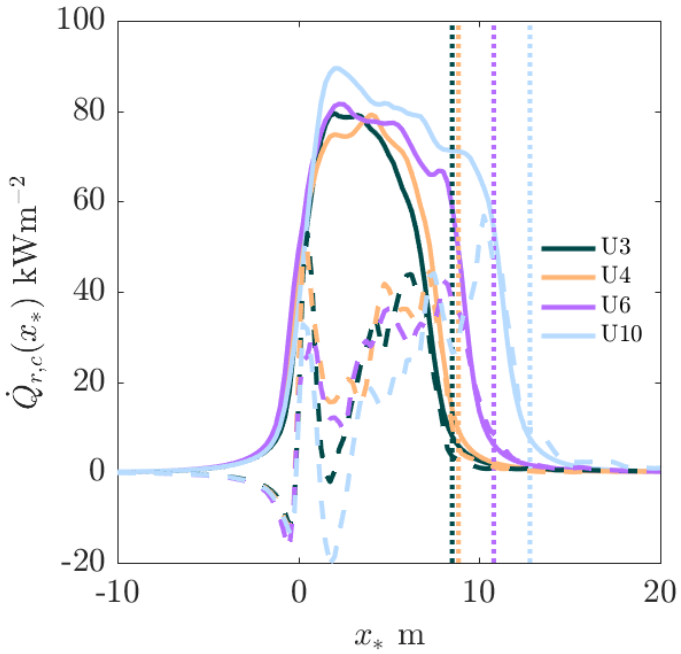

Figure 6- Centreline radiative (solid) and convective (dotted) heat transfer to the unburnt fuel. The vertical dotted lines are the leading edge of the heat release contour shown in Figure 3.

The main peak convective heat flux does increase and stretch in the positive x-direction like the radiative heat flux. The U10 case has a peak of convective heat flux of similar magnitude to the value of radiative heat flux at $x = 10$ m. Similar trends are observable at lower velocities. Therefore, it appears that at the leading edge of the fire, for these cases, both centreline radiative and convective heat fluxes are of approximately equal magnitude. The convective heat flux in the U10 case exceeds the radiative heat flux at $x \approx 15$ m, consistent with the observations of Finney et al. (2015). However, Finney et al. do not look directly at convective heat flux in the flaming region, as we have done. Instead, they observe particle temperature ahead of the main fire front and infer the behaviour of the convective heat flux. The simulated convective heat flux is $\dot{q}'' = h\,(T_w - T_g)$ where h is the convective heat transfer coefficient based upon natural and forced convection empirical correlations. The T with subscripts w and g represent the wall (fuel) and gas temperature respectively. WFDS has been validated by comparing the simulated rate-of-spread to observations (Mell et al. 2007, Moinuddin et al. 2018) however, there is little direct (i.e. measuring and simulating fuel temperature ahead of the front) validation for the convective heat transfer model in surface grass fires and further research is required to investigate the heat transfer further.

4. Conclusions

The Byram number correctly predicts the plume dynamics as expected. Low Nc cases have elongated and attached flames with one-sided entrainment into the plume; whereas higher Nc cases have a more vertical flame with two-sided entrainment.

For these simulations, the dominant heat transfer mechanism was found to be radiation in all cases. The radiative heat transfer was always approximately twice as much as the convective heat transfer, even if the flame was attached in a wind dominated fire. On the centreline, considered representative of the head fire behaviour, convective heating emerges to be of approximately equal magnitude as radiative heating at the leading edge of the fire. This is contrary to the hypothesis that convective heating takes over as the dominant mechanism of heat transfer in wind driven cases. While the results presented here are specific to this fire geometry and represent only a relatively small window of near transitional Nc, the hypothesised behaviour of heat transfer mechanisms are likely more complicated than currently thought and understood.

5. References

Morvan, D., & Frangieh N., Wildland fires behaviour: wind effect versus Byram's convective number and consequences upon the regime of propagation, International Journal of Wildland Fire 27 (9) (2018) 636–641

Finney, M. A., Cohen, J. D., Forthofer, J. M., McAllister, S. S., Gollner, M. J., Gorham D. J., Saito, K., Akafuah, N. K., Adam, B. A., & English, J. D., Role of buoyant flame dynamics in wildfire spread, Proceedings of the National Academy of Sciences 112 (32) (2015) 9833–9838.

Mell, W., Jenkins, M., Gould, J., & Cheney, P., A physics-based approach to modelling grassland fires, International Journal of Wildland Fire 16 (1) (2007) 1–22

Moinuddin, K. A. M., Sutherland, D., & Mell, W., Simulation study of grass fire using a physics-based model: striving towards numerical rigour and the effect of grass height on the rate-of-spread, International Journal of Wildland Fire 27 (12) (2018) 800–814

Cheney P., Gould, J., & Catchpole, W., The influence of fuel, weather and fire shape variables on fire-spread in grasslands, International Journal of Wildland Fire 3 (1) (1993) 31–44

Sutherland, D., Sharples, J. J., Moinuddin, & K. A. M. The effect of ignition protocol on grassfire development, International journal of wildland fire 29 (1) (2020) 70–80

Morvan, D., & Dupuy, J., Modeling the propagation of a wildfire through a Mediterranean shrub using a multiphase formulation, Combustion and flame 138 (3) (2004) 199–210.

Mueller, E. V., Examination of the underlying physics in a detailed wildland fire behavior model through field-scale experimentation (2017) PhD Thesis, University of Edinburgh.

The effect of downslope terrain on wildfire dynamics in the presence of a cubic structure

Ali Edalati-nejad[1]; Maryam Ghodrat*[2]; Jason J. Sharples*[1]

[1]School of Science, UNSW Canberra, Canberra, ACT 2612, Australia, {a.edalatinejad, j.sharples}@adfa.edu.au
[2] School of Engineering and Information Technology, UNSW Canberra, Canberra, ACT 2612, Australia, {m.ghodrat@unsw.edu.au}

**Corresponding authors*

Keywords

Wildfire; Downslope; wildland–urban interface; wind–fire interaction; terrain slope; wind structure

Abstract

In the current work, a numerical study is performed to investigate the effect of the downslope field by a wind driven surface fire in the presence of an idealised building structure. Fires burning with different intensity values of 4, and 15 MW/m on inclined terrain with various downslope angles of 0, -10, -20, and -30°, and under two different wind speed of 6, and 12 m/s are simulated using a large eddy simulation (LES) solver, implemented in open-source platform FireFOAM. The results are validated with experimental measurements of a full-scale cubic building model. The presented outcomes highlight the physical effect of sloped terrain on a building in the vicinity of a line-fire. The results show that at high wind velocity values, the buildings at the higher downslope terrains are at higher risk of wildfire damages

1. Introduction

Wildfire is a highly complex phenomenon and while it is an important ecological process, it can also have detrimental effects when it spreads from wildland areas and impacts the wildland-urban interface (Verma, 2019). They are important elements of ecosystem management and functional ecosystems (Menage, Chetehouna, & Mell, 2012).

To mitigate the disastrous impact of wildfire and manage its environmental and economic impacts, people interact with wildfires in different ways. This includes the use of prescribed fires to reduce fire hazard and thereby lessen the associated likelihood of damage to assets, particularly in the Wildland-Urban Interface (WUI) (Canfield, Linn, Sauer, Finney, & Forthofer, 2014). The growing pace of urbanization resulting in increasing encroachment of urban development into forested areas, is considered one of the most significant reasons for landscape transformation in many countries including Australia (Manzello et al., 2018).

Protection of assets (dwellings, associates structures and other infrastructure) in areas likely to be impacted by wildfire requires precise assessment of factors, such as wind and topography, that might affect the many facets of a wildfire and its impact on assets in the WUI (Cruz, Sullivan, & Alexander, 2014; Ghodrat, Shakeriaski, Nelson, & Simeoni, 2021a; Hilton et al., 2017; Mell, Manzello, Maranghides, Butry, & Rehm, 2010).

Terrain slope is generally considered to be a key element impacting the way in which wildfires spread (Abouali, Viegas, & Raposo, 2021; Butler, Anderson, & Catchpole, 2007). It is commonly accepted that fires increase speed up a hill and many deadly incidents have been reported linked with the hilly terrain (Butler et al., 2007; Dupuy, Maréchal, Portier, & Valette, 2011).

Wildfire behaviour reflects a wide range of complex physical and chemical processes (Ghaderi, Ghodrat, & Sharples, 2020; Verma, 2019) that encompasses aerodynamic behaviours, topographic impacts (such as terrain slope) (Edalati-nejad, Ghodrat, & Simeoni, 2021; Verma, 2019), atmospheric conditions (Ghodrat et al., 2021a; Ghodrat, Shakeriaski, Nelson, & Simeoni, 2021b)(wind speed and direction, temperature, and humidity), the rate of fire spread (ROS) (Canfield et al., 2014), and the effects of fuel type and state (Edalati-nejad, Ghodrat, Fanaee, & Simeoni, 2022), including fuel moisture content (FMC) (Morvan, 2013). As such, it is infeasible to

comprehensively account for the myriad effects driving fire behaviour. Instead, researchers have conducted targeted studies that focus on understanding the effects of a small subset of the most significant driving factors, such as Viegas (Viegas, 2004) who carried out an experimental investigation of the combined effect of terrain slope and wind. In this study a plane fuel bed under uniform wind and slope conditions was studied.

These studies provide valuable information about the effect of terrain slope on fire dynamics when fires are spreading upslope. However, there has been considerably less attention paid to scenarios where fires are burning downslope. Sullivan and his co-authors, (Sullivan, Sharples, Matthews, & Plucinski, 2014) developed a rate of spread correction for fires burning downslope, but there is still much to be understood about the dynamics of line fires burning downslope. For example, questions about how negative slopes interact with pyroconvective flows and how they affect the temperature profile downstream of the line-fire source are still relatively unexplored and require further study. Such studies are critical in informing further development of wildfire risk mitigation measures. The outcome of the present study contributes to alleviate the wildfire damages and helps the risk managements, for example, Australian Standard AS 3959 (Debnam, Chow, & England, 2005), the Australian Standard for Building in Bushfire Prone Areas.

In the present investigation, the effect of downslope terrain, at a constant wind speed and fire intensity, on the fire-line dynamics and downstream temperature has been investigated. Moreover, the pattern of heating on an idealised building structure is investigated to better understand the impacts of downslope fires on built assets.

2. Physical model

In the present work, an idealized (cubic) building structure with a size of 6 × 6 × 6 m is located downstream of a fire line. As can be seen in Fig. 1, the size of the computational domain is 50 ×30 × 25 m. The building structure is located 20 m downstream of the fire line.

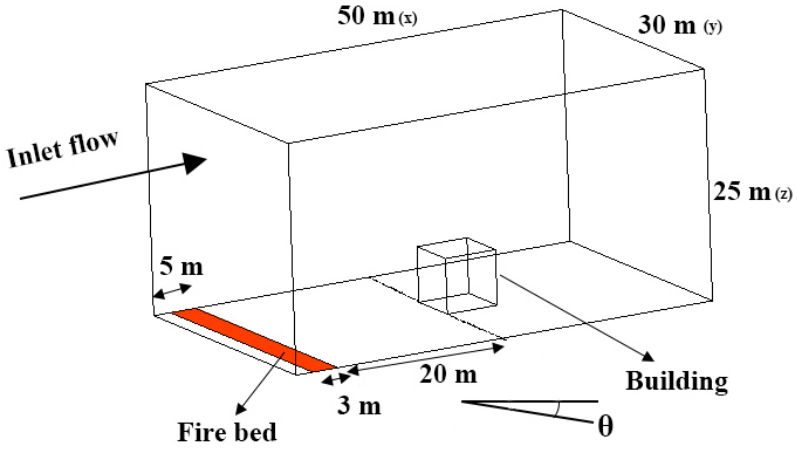

Figure 1- Computational domain and physical model

The fire-line is placed at the edge (near the inlet) of the domain, which is inclined at various downslope angles, with a constant fire intensity and wind velocity to investigate the impact of slope-fire interactions on downstream temperature and air density in the presence of the building structure. In this investigation, a constant fire intensity (Byram, 1959) equal to 15 MW/m is considered, which is equivalent to a forest wildfire (Smith, 2014), and is provided by invoking model parameters in FireFOAM, corresponding to the burning of methane with a heat of combustion equal to 45,435 kJ/kg (Kremer & Schäfer, 1973).

In this model, the boundary layer in the vicinity of the ground has been considered by applying a power-law velocity profile:

$$U(Z) = U_{ref}\left(\frac{Z}{Z_{ref}}\right)^{\alpha} \quad (1)$$

Where U_{ref} is the reference velocity which in this paper is considered 12 m/s, Z_{ref} is the reference height, which is equal to the building's height (6 m), and α is a constant taken equal to 0.16 based on the terrain category of the experimental study (Tominaga et al., 2008).

The angle of inclination of the terrain, θ, is the angle of gravitational acceleration to the z direction, which is defined via:

$$g_x = -g \sin(\theta) \text{ and } g_z = -g \cos(\theta) \tag{2}$$

3. Numerical modelling

To numerically solve the governing equation of the problem, the FireFOAM solver of OpenFOAM, which is an open-source CFD software, is used. FireFOAM is an efficient tool to simulate wildfire behaviour (El Houssami, Lamorlette, Morvan, Hadden, & Simeoni, 2018; Le et al., 2018). To account for the effects of turbulence, the Large Eddy Simulation (LES) (Wang, Chatterjee, & de Ris, 2011) method is utilized. The governing equations for the problem are as follows:

$$\frac{\partial \bar{\rho}}{\partial t} + \frac{\partial(\bar{\rho}\tilde{u}_i)}{\partial x_i} = 0 \tag{3}$$

$$\frac{\partial(\bar{\rho}\tilde{u}_i)}{\partial t} + \frac{\partial(\bar{\rho}\tilde{u}_i\tilde{u}_j)}{\partial x_i} = \frac{\partial}{\partial x_j}\left[\bar{\rho}(\upsilon + \upsilon_t)\left(\frac{\partial(\tilde{u}_i)}{\partial x_j} + \frac{\partial(\tilde{u}_j)}{\partial x_i} - \frac{2}{3}\frac{\partial(\tilde{u}_k)}{\partial x_k}\delta_{ij}\right)\right] - \frac{\partial(\bar{P})}{\partial x_i} + \bar{\rho}\, g_i \tag{4}$$

$$\frac{\partial(\bar{\rho}\tilde{h})}{\partial t} + \frac{\partial(\bar{\rho}\tilde{u}_j\tilde{h})}{\partial x_j} = \frac{D\bar{P}}{Dt} + \frac{\partial}{\partial x_j}\left[\bar{\rho}\left(\alpha_t + \frac{\upsilon_t}{Pr_t}\right)\left(\frac{\partial\tilde{h}}{\partial x_j}\right)\right] + \dot{q}''' - \nabla.\dot{q}_r'' \tag{5}$$

$$\frac{\partial(\bar{\rho}\widetilde{Y_m})}{\partial t} + \frac{\partial(\bar{\rho}\tilde{u}_j\widetilde{Y_m})}{\partial x_j} = \frac{\partial}{\partial x_j}\left[\bar{\rho}\left(D_c + \frac{\upsilon_t}{Sc_t}\right)\frac{\partial(\widetilde{Y_m})}{\partial x_j}\right] + \omega_m \tag{6}$$

$$\bar{P} = \bar{\rho}R\tilde{T} \tag{7}$$

where "¯" and "~" show spatial and Favre filtering, respectively, h is the total enthalpy, Y_m represents the mass fraction of species m, P is the static pressure, and g is the gravitational acceleration. $Sc_t, Pr_t, \upsilon, D_c, \upsilon_t, \rho, \alpha_t, R, \delta$ and ω_m are the turbulent Schmidt number, the turbulent Prandtl number, the laminar viscosity, the laminar diffusion coefficient, the turbulent viscosity, density, thermal diffusion coefficient, gas constant, Kronecker delta, and production/sink rate of species m due to gas reaction, respectively. The PIMPLE algorithm (Jasak, 1996)for pressure-velocity coupling, is applied. The differencing scheme of first order upwind is also used.

In order to validate the simulations, the mean pressure coefficients around the idealized building structure for the current work and an experimental measurement of Richards and Hoxey (Richards & Hoxey, 2012) in the absence of fire were compared as shown in Fig. 2. The pressure along the vertical and horizontal centrelines of the Silsoe cube, at the Silsoe Research Institute, UK, has been measured. In this figure, X-axe corresponds the yellow dashed line shown on the cube, starts from point 0, goes to the point 1, passes point 2, and continues to the point 3.

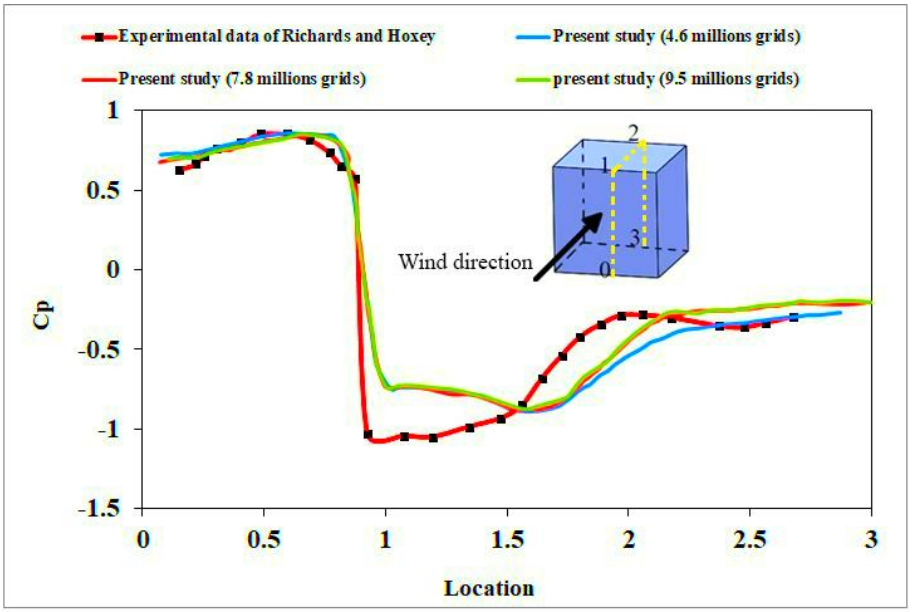

Figure 2- Comparison between the mean pressure coefficient for three different grids number of the current investigation and the experimental measurement (Richards & Hoxey, 2012)

In addition, to study the grid dependency, three different grid numbers of 4,600,000, 7,800,000, and 9,500,000 into the domain have been applied and tested. At the first, increasing the mesh number, changes the mean pressure coefficient, then a further increase will not affect the results. Therefore, the second mesh numbers have been selected for the present study. As can be observed in Fig. 2, there is an acceptable agreement between the present work's results and the experimental measurements.

4. Results

Figure 3 shows the effect of downslope terrain angles on the temperature distribution for the cases at U_{ref} = 6 m/s and fire intensities 4, and 15 MW/m. As can be seen in this figure, at all cases, the wind causes the flames to tilt towards the building. The flame tilt angle is defined as the angle between the centreline of flame and the vertical direction (Li et al., 2021; Li, Wan, Gao, & Ji, 2019). Also, the flame tilt angle decreases as the terrain slope becomes more negative increasing the terrain downslope. This is due to the fact that buoyancy forces cause the flame to rise in the direction opposing gravity, thus reducing the tilt angle. Looking at the figures in more detail, they reflect that in the mentioned cases (U_{ref} = 6 m/s and fire intensities 4, and 15 MW/m), the increasing in the negative downslope, leads to decreasing the risk of being the building in the exposure of high temperature air, caused by the fire.

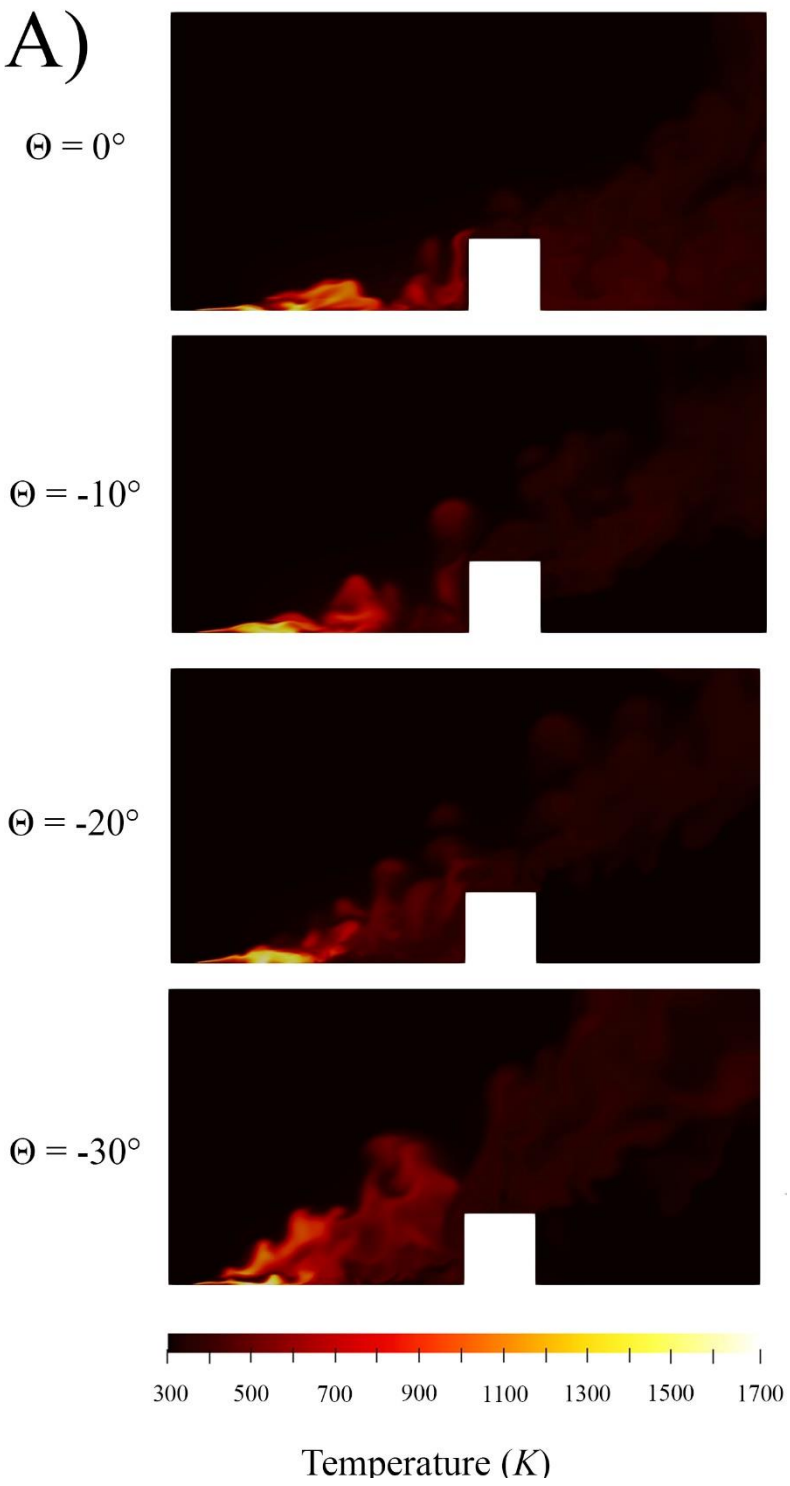
A)
Θ = 0°
Θ = -10°
Θ = -20°
Θ = -30°
300
500
700
900
1100
1300
1500
1700
Temperature (K)

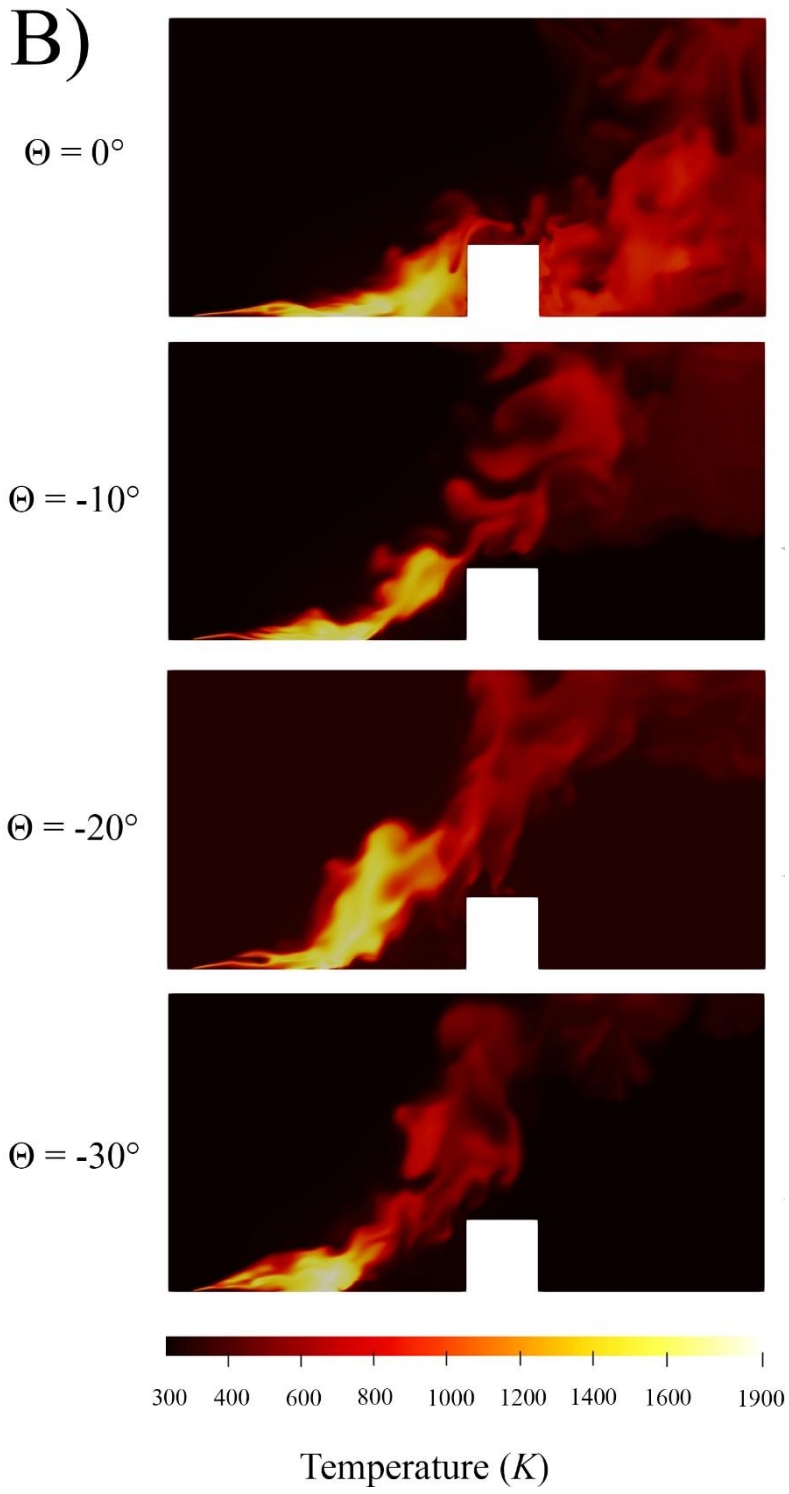

Figure 3- Temperature distribution for the cases at fire intensity (A): 4 MW/m and (B): 15Mw/m and wind velocity 6 m/s for different downslope degrees

Figure 4 shows how the average temperature downstream of the fire-line and the building surface varies with the downslope terrain angle. Considering the effect of wind, the fire plume is directed in the downstream direction so that in the case with no slope, the fire plume is close to the ground. This is due to the effect of wind on enhancing the tilt angle toward to the building. Increasing the downslope angle, decreases the flame tilt angle and the takes the plume closer to the higher altitude surfaces of the building structure. So, for the cases with U_{ref} = 12m/s, an increase in the downslope inclination leads to an increase in the higher temperature region downstream of the fire, which can be seen in Fig. 6. It can also be observed that by increasing the downslope terrain angle, the building temperature increases, for the mentioned cases. This is also due to the combination

of the wind speed and the downslope terrain, which have contrary effects on the flame tilt angle in the current cases. For the cases with U_{ref} = 12 m/s (I = 4, and 15 MW/m), increasing the downslope angles from 0˚ to -30˚, increases the average temperature of the building surface by 14%, and 30%, and increases the temperature of the zone downstream of the fire by 3%, and 9%, respectively.

On the other hand, the effect of increasing in the downslope angles, on the temperature of the building surface and downstream, for the cases with U_{ref} = 6m/s, is in the contrast with the cases with U_{ref} = 12 m/s. Because the wind velocity is lower and the fire plume is not that close to the ground, compared to the cases with U_{ref} = 12 m/s. Accordingly, for the cases with U_{ref} = 6 m/s (I = 4, and 15 MW/m), increasing the downslope angles from 0˚ to -30˚, decreases the average temperature of the building surface by 15%, and 30%, and decreases the temperature of the zone downstream of the fire by 3%, and 17%, respectively.

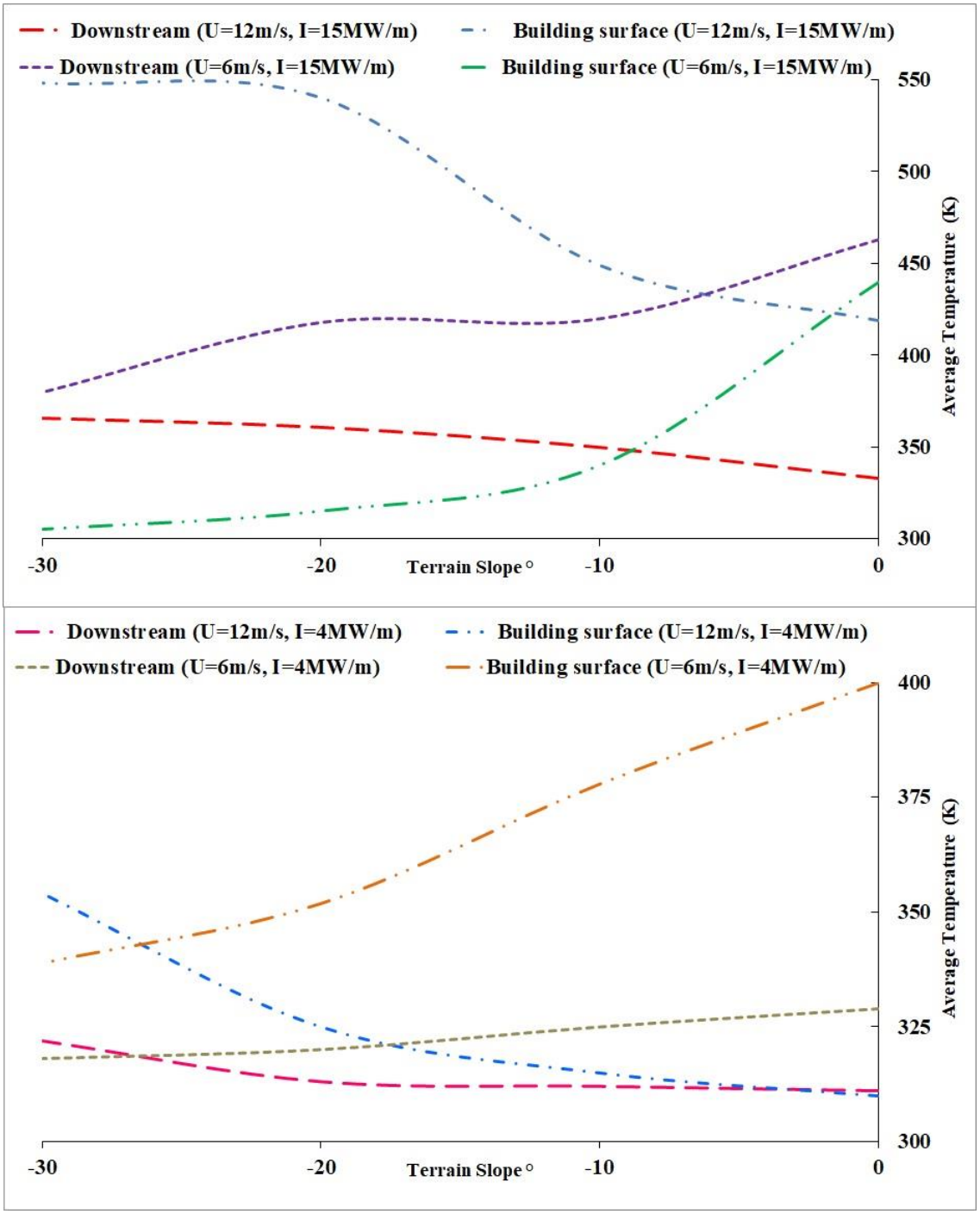

Figure 4- Average temperature of the downstream of the domain and the building surface versus the terrain slope for the cases with U_{ref} = 6, and 12 m/s and fire intensities 4, and 15 MW/m.

5. Conclusion

In the present work, the effect of downslope terrain on fire-line dynamics and downstream temperature, at a constant wind and fire intensity, in the presence of an idealized building structure has been numerically studied. The downslope angles varied from 0˚ to -30° and a wind-field with reference velocity of 6, and 12 m/s and fire intensity 4, and 15 MW/m are considered. The main results of the present investigation are summarized as follows:

- The calculated results show an acceptable agreement with the empirical measurements in the absence of fire.
- At constant wind velocity of 12 m/s, the buildings at the higher downslope terrains are at higher risk of wildfire damages, in contrast, at constant wind velocity of 6 m/s, the buildings at the higher downslope terrains are at lower risk of wildfire damages.
- For the cases with U_{ref} = 12 m/s, increasing the downslope angles from 0˚ to -30˚, increases the average temperature of the building surface by 14%, and 30%, and for the cases with U_{ref} = 6 m/s, increasing the downslope angles, decreases the average building temperature by 15%, and 30%, respectively.

6. References

Abouali, A., Viegas, D. X., & Raposo, J. R. (2021). Analysis of the wind flow and fire spread dynamics over a sloped–ridgeline hill. *Combustion and flame, 234*, 111724.

Butler, B., Anderson, W., & Catchpole, E. (2007). *Influence of slope on fire spread rate.* Paper presented at the In: Butler, Bret W.; Cook, Wayne, comps. The fire environment--innovations, management, and policy; conference proceedings. 26-30 March 2007; Destin, FL. Proceedings RMRS-P-46CD. Fort Collins, CO: US Department of Agriculture, Forest Service, Rocky Mountain Research Station. CD-ROM. p. 75-82.

Byram, G. M. (1959). Combustion of forest fuels. In 'Forest fire: control and use'.(Ed. KP Davis) pp. 61–89. In: McGraw-Hill: New York.

Canfield, J., Linn, R., Sauer, J., Finney, M., & Forthofer, J. (2014). A numerical investigation of the interplay between fireline length, geometry, and rate of spread. *Agricultural and Forest Meteorology, 189*, 48-59.

Cruz, M., Sullivan, A., & Alexander, M. (2014). Fire behaviour knowledge in Australia: knowledge gaps and Fire Behaviour Analyst (FBAN) training revision plan. In: CSIRO Ecosystems Sciences and CSIRO Digital Productivity and Services ….

Debnam, G., Chow, V., & England, P. (2005). AS 3959 CONSTRUCTION OF BUILDINGS IN BUSHFIRE-PRONE AREAS–DRAFT FOR PUBLIC COMMENT (DR 05060) REVIEW OF CALCULATION METHODS AND ASSUMPTIONS.

Dupuy, J.-L., Maréchal, J., Portier, D., & Valette, J.-C. (2011). The effects of slope and fuel bed width on laboratory fire behaviour. *International journal of wildland fire, 20*(2), 272-288.

Edalati-nejad, A., Ghodrat, M., Fanaee, S. A., & Simeoni, A. (2022). Numerical Simulation of the Effect of Fire Intensity on Wind Driven Surface Fire and Its Impact on an Idealized Building. *Fire, 5*(1), 17.

Edalati-nejad, A., Ghodrat, M., & Simeoni, A. (2021). Numerical investigation of the effect of sloped terrain on wind-driven surface fire and its impact on idealized structures. *Fire, 4*(4), 94.

El Houssami, M., Lamorlette, A., Morvan, D., Hadden, R. M., & Simeoni, A. (2018). Framework for submodel improvement in wildfire modeling. *Combustion and flame, 190*, 12-24.

Ghaderi, M., Ghodrat, M., & Sharples, J. J. (2020). LES Simulation of Wind-Driven Wildfire Interaction with Idealized Structures in the Wildland-Urban Interface. *Atmosphere, 12*(1), 21.

Ghodrat, M., Shakeriaski, F., Nelson, D. J., & Simeoni, A. (2021a). Existing improvements in simulation of fire–wind interaction and its effects on structures. *Fire, 4*(2), 27.

Ghodrat, M., Shakeriaski, F., Nelson, D. J., & Simeoni, A. (2021b). Experimental and numerical analysis of formation and flame precession of fire whirls: a review. *Fire, 4*(3), 43.

Hilton, J., Leonard, J., Blanchi, R., Newnham, G., Opie, K., Rucinski, C., & Swedosh, W. (2017). *Dynamic modelling of radiant heat from wildfires.* Paper presented at the Proceedings of the 22nd International Congress on Modelling and Simulation (MODSIM2017), Tasmania, Australia.

Jasak, H. (1996). Error analysis and estimation for the finite volume method with applications to fluid flows.

Kremer, H., & Schäfer, G. (1973). *Rates of fuel conversion and heat release in turbulent combustion of methane-air mixtures in tunnel burners.* Paper presented at the Symposium (International) on Combustion.

Le, D., Labahn, J., Beji, T., Devaud, C. B., Weckman, E. J., & Bounagui, A. (2018). Assessment of the capabilities of FireFOAM to model large-scale fires in a well-confined and mechanically ventilated multi-compartment structure. *Journal of fire sciences, 36*(1), 3-29.

Li, B., Ding, L., Simeoni, A., Ji, J., Wan, H., & Yu, L. (2021). Numerical investigation of the flow characteristics around two tandem propane fires in a windy environment. *Fuel, 286*, 119344.

Li, B., Wan, H., Gao, Z., & Ji, J. (2019). Experimental study on the characteristics of flame merging and tilt angle from twin propane burners under cross wind. *Energy, 174*, 1200-1209.

Manzello, S. L., Almand, K., Guillaume, E., Vallerent, S., Hameury, S., & Hakkarainen, T. (2018). Forum position paper the growing global wildland urban interface (wui) fire dilemma: Priority needs for research. *Fire Safety Journal, 100*.

Mell, W. E., Manzello, S. L., Maranghides, A., Butry, D., & Rehm, R. G. (2010). The wildland–urban interface fire problem–current approaches and research needs. *International journal of wildland fire, 19*(2), 238-251.

Menage, D., Chetehouna, K., & Mell, W. (2012). *Numerical simulations of fire spread in a Pinus pinaster needles fuel bed.* Paper presented at the Journal of Physics: Conference Series.

Morvan, D. (2013). Numerical study of the effect of fuel moisture content (FMC) upon the propagation of a surface fire on a flat terrain. *Fire Safety Journal, 58*, 121-131.

Richards, P., & Hoxey, R. (2012). Pressures on a cubic building—Part 1: Full-scale results. *Journal of wind engineering and industrial aerodynamics, 102*, 72-86.

Smith, S. (2014). The Performance of Distribution Utility Poles in Wildland Fire Hazard Areas. *Technical Bulletin: Newport Beach, CA, USA*.

Sullivan, A. L., Sharples, J. J., Matthews, S., & Plucinski, M. P. (2014). A downslope fire spread correction factor based on landscape-scale fire behaviour. *Environmental modelling & software, 62*, 153-163.

Tominaga, Y., Mochida, A., Yoshie, R., Kataoka, H., Nozu, T., Yoshikawa, M., & Shirasawa, T. (2008). AIJ guidelines for practical applications of CFD to pedestrian wind environment around buildings. *Journal of wind engineering and industrial aerodynamics, 96*(10-11), 1749-1761.

Verma, S. (2019). *A large eddy simulation study of the effects of wind and slope on the structure of a turbulent line fire.* University of Maryland, College Park,

Viegas, D. X. (2004). Slope and wind effects on fire propagation. *International journal of wildland fire, 13*(2), 143-156.

Wang, Y., Chatterjee, P., & de Ris, J. L. (2011). Large eddy simulation of fire plumes. *Proceedings of the Combustion Institute, 33*(2), 2473-2480.

The enemy lives next door: ecological consequences of woody encroachment in a grassland ecosystem in southern Brazil

Tiago de Souza Ferreira*; Alexandre França Tetto; Ronaldo Viana Soares; Antonio Carlos Batista; Amanda Köche Marcon

Federal University of Paraná. Av. Pref. Lothario Meissner, 632, Jardim Botânico, Curitiba-PR . 80210-170. Brazil, {tiagoferreira@florestal.eng.br}, {tetto, rvsoares, batistaufpr}@ufpr.br, {amandakoche@gmail.com}

**Corresponding author*

Keywords

Woody encroachment, forest-grassland mosaic, fire ecology, landscape dynamic, biome shift.

Abstract

The replacement of grasslands by woody plants represents one of the main threats to the biodiversity conservation in open landscapes around the world. This transformation occurs when ecological processes that are essential to avoid the canopy closure are prevented, such as fire. We sampled trees and shrubs and evaluated the effects of fire in an old-growth grassland remnant released from fire for 18 years in Southern Brazil. Our main objective was to analyze whether woody encroachment promotes a biome shift of the grassland ecosystem. We hypothesized if woody encroachment is deterministically structured towards a dominance of forest species and a significant decrease in fire intensity and severity along the encroachment gradient occurs. Then, the woody encroachment does not represent a simple process of woody densification, but a biome shift towards an alternative forest state, that change the ecology of the system in a positive feedback loop and get stability as the woody community expands. We found clear evidences that woody encroachment promotes a biome shift from an open grassland state to an alternative forest state. In this process, our results indicated that woody encroachment was structured deterministically in the multivariate space with the occurrence of indicator species in the early and late stages. Throughout the entire encroachment gradient analyzed, a significant dominance of forest species was found, indicating that Southern Brazilian grasslands have the potential to be converted into forests more rapidly than savannas in the absence of fire. A significant decrease in fire intensity was found as the process of woody encroachment increased, indicating a change in the system behaviour that favoured the occurrence of a positive feedback loop between the canopy cover and the recruitment of shade-tolerant forest species. Simultaneously to fire intensity decrease, we observed that the reversion of the woody encroachment process was significantly reduced as the woody dominance increased. Thus, the woody encroachment mediated by fire suppression can be considered a degradation factor in our study area, since it can shift the system balance to another alternative stable state. By elucidating the ecological consequences behind woody encroachment, we recommend the use of prescribed fires to the conservation of the grasslands landscapes in Southern Brazil.

1. Introduction

Temporal analyses based on satellite images indicated that Araucaria Forest areas are expanding in Soutern Brazil, specially in forest-grasslands ecotones where fire has been avoided (OLIVEIRA; PILLAR, 2004). However, its is still unclear whether woody encroachment represent only a process of woody densification or a general biome shift towards a generation of a new alternative forest state. Furthermore, if woody encroachment actually results in a change in the fundamental state of the ecosystem, we still don't know the level of stability of this new state.

To address these issues, we studied an old-growth grassland remnant that was encroached by woody species due to fire suppression for a period of 18 years (from 1999 to 2017). In 2017, this same area was hit by a wildfire, then we analyzed the fire effects over the woody plants community with the objective of to evaluate the fire intensity and severity along the woody encroachment gradient. We hypothesized if woody encroachment is deterministically structured towards a dominance of forest species and a significant decrease in fire intensity and severity along the encroachment gradient occur. Then, the woody encroachment does not represent only a simple process of woody densification, but a biome shift towards an alternative forest state, that change the ecology of the system in a positive feedback loop and get stability as the woody community expands.

2. Material and Methods

2.1. Study area

This study was conducted in Vila Velha State Park (VVSP) located in the municipality of Ponta Grossa, Paraná State, Brazil (latitude: 25º 13' 30" S, longitude: 50º 0' 0" W) (Table 1). The VVSP was created in 1953 (PARANÁ, 1953), in an area of 3,122 ha considered as a remnant of the original vegetation of Campos Gerais region (INSTITUTO AMBIENTAL DO PARANÁ, 2004). The Campos Gerais region comprises areas of old-growth grassland vegetation associated with Araucaria Forest fragments forming mosaics (MAACK, 2012).

2.2. Data collection

2.2.1. Vegetation sampling

We sampled trees and shrubs in five permanent transects measuring 50 m wide per 100 m long (subdivided in 20 plots of 250 m² - 10 x 25 m). The plots were randomly distributed over an area mapped in the VVSP management plan as steppe-savanna transition vegetation (INSTITUTO AMBIENTAL DO PARANÁ, 2004). In this place, we previously assumed that there is a natural tendency of forest expansion over grasslands and that the current vegetation pattern is associated with fire suppression policies, which guided the park management during the past decades. In each plot, tree and shrub data were collected according to the inclusion criterion of DBH equal to or greater than 3 cm.

2.2.2. Assessment of fire intensity and severity

We inferred the intensity of fire by measuring the height of bark-char left on the tree boles after the fire passage. We adopted as standard measure the highest stem-bark char height.

We determined fire severity by calculating the proportion of basal area lost as a result of fire in each plot. For this, one year after fire, trees and shrubs were reassessed according to survival and complete mortality or topkill. Then, the basal area obtained in each plot were compared with the basal area obtained in the first survey. The fire severity ranged from 0 to 1, with 1 being noted for complete mortality or topkill of all woody individuals present in the plot and 0 for complete absence of mortality or topkill of all woody individuals present in the plot.

2.3. Data analyses

2.3.1. Community structure and dominance of forest specialist species along the encroachment gradient

To verify if the woody encroachment was deterministically structured towards a dominance of forest species, we firstly evaluated the floristic-structural relationship among the plots by the construction of a hierarchical cluster dendrogram. Then, the occurrence of multivariate structure among the plots was analyzed by similarity profile test (SIMPROF) (CLARK; SOMERFIELD; GORLEY, 2008). Later, the multivariate structure captured by SIMPROF test was analyzed by a Principal Coordinate Analysis (PCoA) with the adjustment of generalized additive model (GAM) *a posteori*.

In each cluster identified in the SIMPROF test, we verified the occurrence of indicators woody species through the IndVal analysis (DUFRÊNE; LEGENDRE, 1997). In addition, the species were classified into three distinct functional groups according to the habitat preference: savanna specialists, generalists and forest specialists. To verify the existence of significant associations between the number of individuals in each functional group and the stages of woody encroachment, a chi-square test was applied to a contingency table.

To verify the patterns of change in species richness of each functional group along the woody encroachment gradient, we used a generalized linear model (GLM), in which the absolute and relative species richness was adjusted as a function of the density of woody plants per plot.

2.3.2. Effect of woody encroachment in fire intensity and severity

We analyzed the effect of woody encroachment in fire intensity by a Kruskal-Wallis variance analysis and beta regression models with logit link was applied to model the fire severity as a function of the sum of the basal in each plot.

3. Results

The SIMPROF analysis rejected the null hypothesis ($p < 0.01$) of absence of community structuring associated with the woody encroachment process, indicating the formation of six significantly different floristic-structural groups (Figure 1).

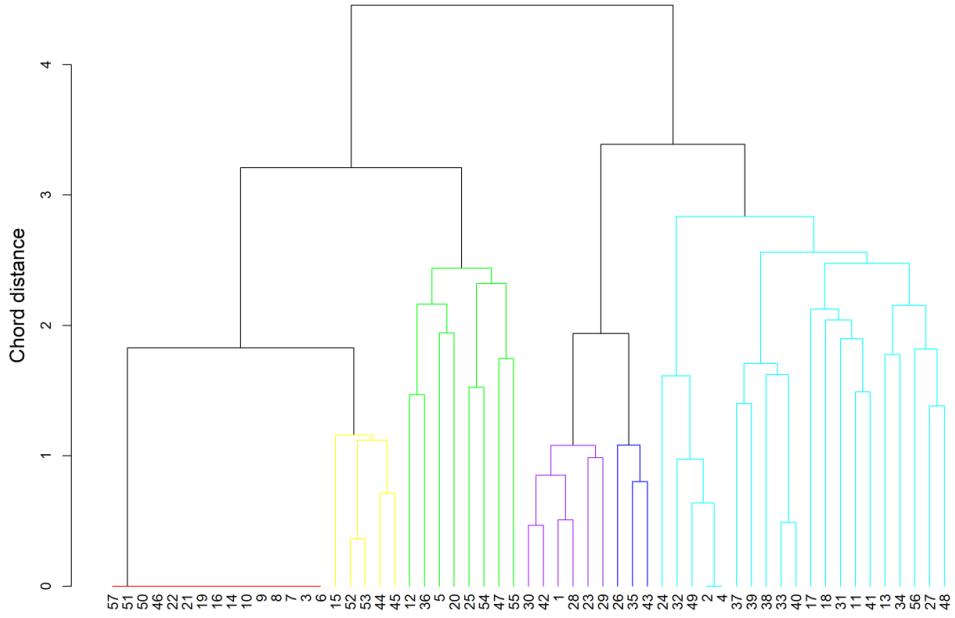

Figure 1 - Similarity profile analysis (SIMPROF)

The ordination produced with the smoothed surface adjusted *a posteriori* by GAM indicated that 55.4% of the floristic-structural variation was explained by the density of woody individuals ($R^2 = 0.502$; $p \leq 0.05$) (Figure 2). Thus, the floristic-structural groups established by the SIMPROF analysis were significantly associated in the multivariate space in response to woody encroachment gradient.

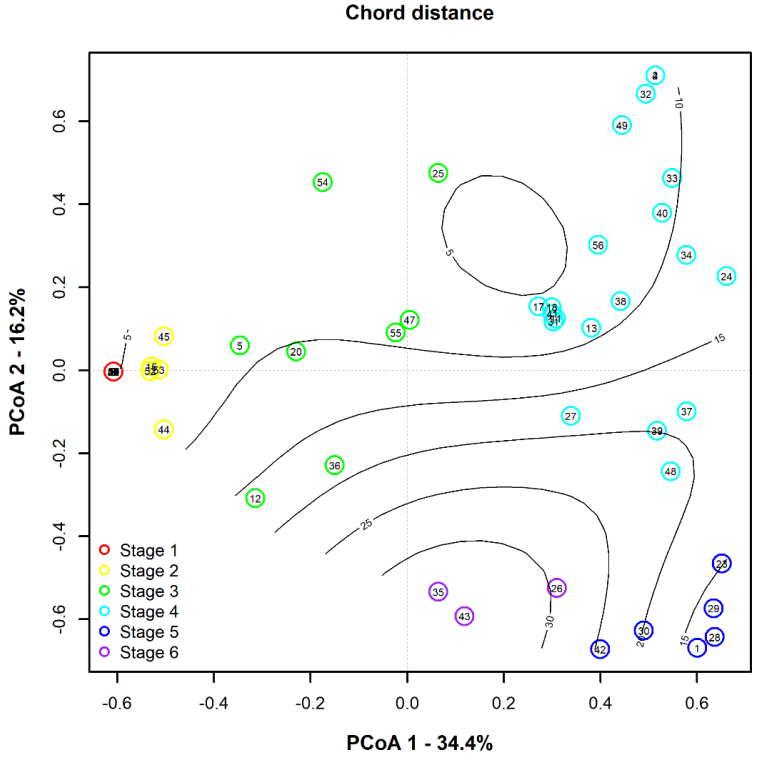

Figure 2 - Principal coordinate analysis with smoothed surface lines of woody abundance per plot adjusted a posteriori by GAM

The IndVal analysis recognized the occurrence of typical species in the initial (1 and 2) and advanced (5 and 6) stages of woody encroachment. In early stages 1 and 2, *Clethra scabra* Pers. (IndVal = 38.85%; p = 0.015) and *Myrcia splendens* (Sw.) DC. (IndVal = 46.74%; p = 0.014) were recognized as indicator species, respectively. In late stages 5 and 6, the indicator species were: *Myrsine umbellata* Mart. (IndVal = 51.84%; p = 0.010) and *Miconia sellowiana* Naudin (IndVal = 29.95%; p = 0.034), respectively.

We observed significant associations among functional groups and the stages of woody encroachment according to the chi-square test (χ^2 = 51.098; p = 0.01; Cramer's V = 0.2072). The analysis of the standardized residuals of chi-square test showed that forest specialist individuals were positively associated with initial and advanced stages of woody encroachment (Figure 3).

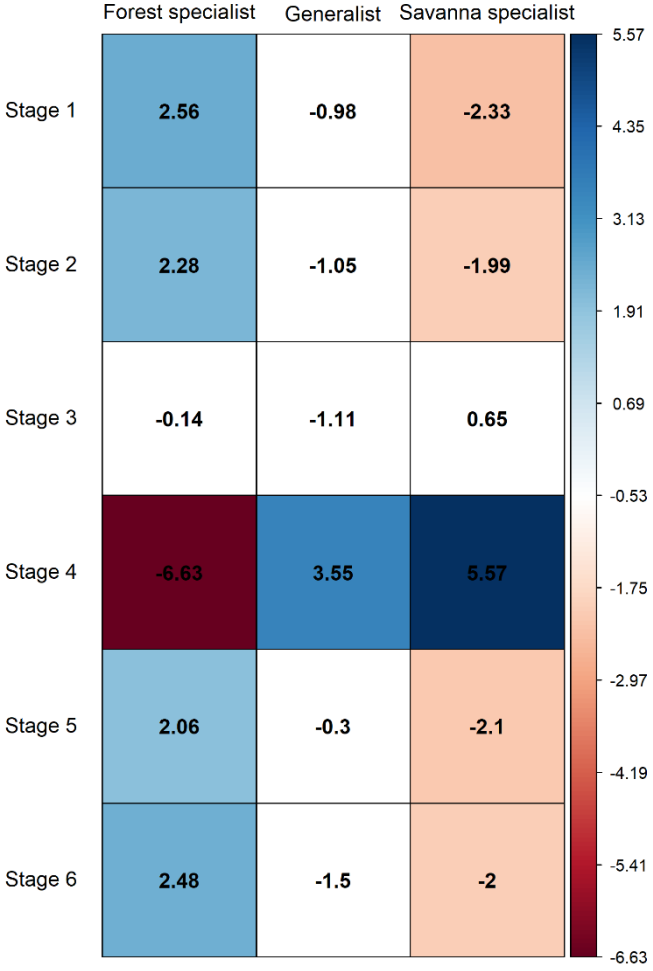

Figure 3 – Pearson's chi-square test (χ^2) between functional groups and stages of woody encroachment

The increase of woody encroachment process resulted in a significant increase in the absolute richness of savanna specialist (F = 5.45; R^2 = 0.23; p < 0.01; Deviance explained = 12.74%) and forest specialist species (F = 33.72; R^2 = 0.34; p < 0.01; Deviance explained = 40.84%). The same pattern was not observed for generalist species (F = 0.21; R^2 = 0.002; p = 0.65; Deviance explained = 0.86%), which showed constant species richness along the woody encroachment gradient (Figure 4A). Proportionally, the species richness of all functional groups maintained constant along the woody encroachment gradient, with forest specialist species being responsible for leading the encroachment process from early to advanced stages (Figure 4B).

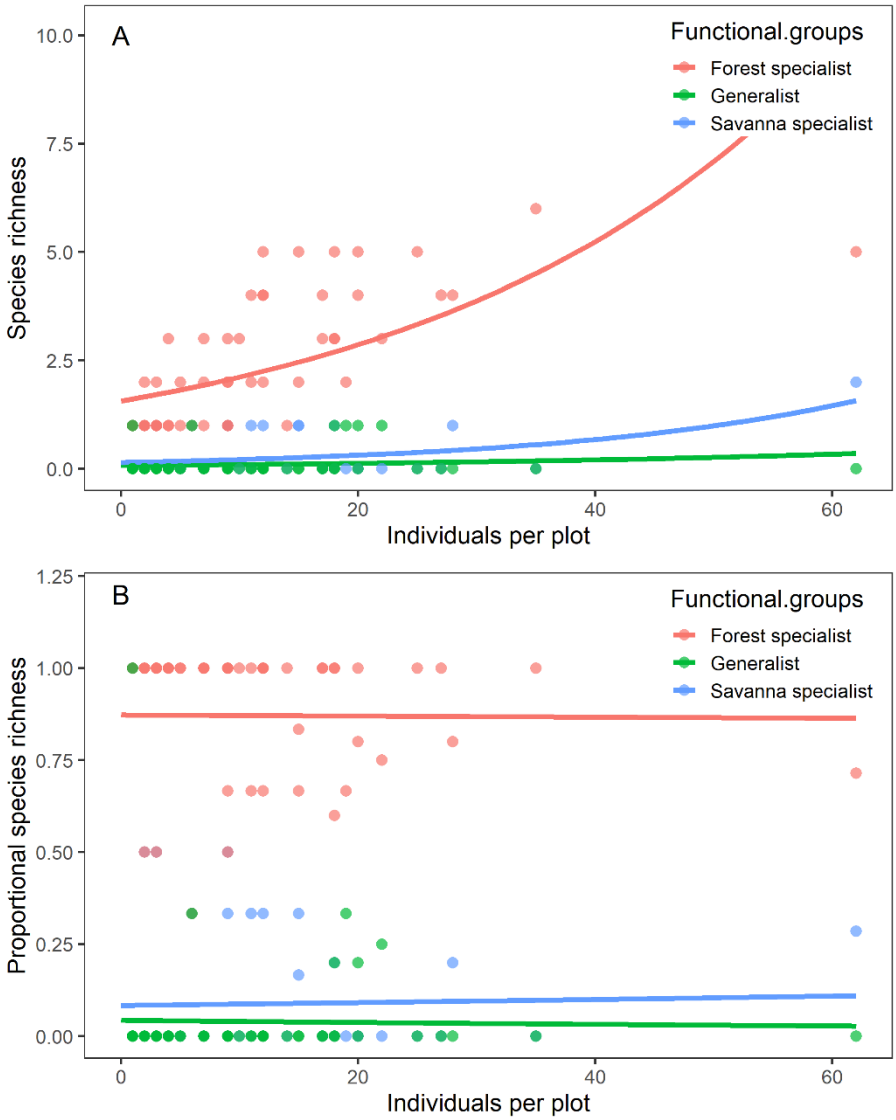

Figure 4 - Changes in absolute (a) and relative (b) species richness of the functional groups along the gradient of woody encroachment

The fireline intensity showed a significant reduction along the woody encroachment gradient (Kruskal-Wallis χ^2= 18.37; df = 5; p = 0.0002). The Dunn *post-hoc* test of multiple comparison showed that stage 6 (0.81 ± 0.79 m) had a significantly lower carbonization height than the other stages of encroachment, with the exception of stage 5 (0.93 ± 0.73 m). Stage 5, in turn, showed a significantly lower carbonization height than stages 1 (1.12 ± 0.74 m) and 2 (1.20 ± 0.85 m). The other stages of invasion did not show significant differences among them in relation to the stem-bark char height (Figure 5).

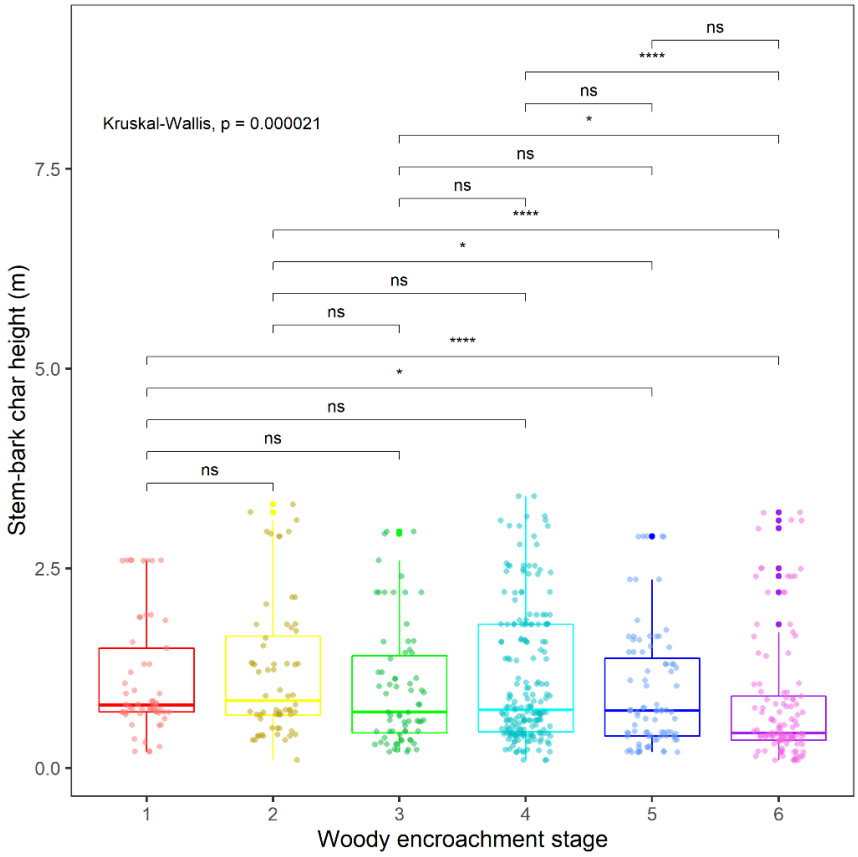

Figure 5 – Kruskal-Wallis's test and Dunn post-hoc test of multiple comparison of the height of stem-bark char and woody encroachment stages

Fire severity significantly decreased as the woody encroachment process advanced (p = 0.0001). The fitted GLM model showed that 39% of the variability in fire severity was explained by the increase in basal area per hectare (Figure 6). The value of basal area per hectare needed to reach the fire severity threshold corresponding to 0, i.e., complete absence of mortality and/or topkill, was estimated at 32.3 $m^2.ha^{-1}$.

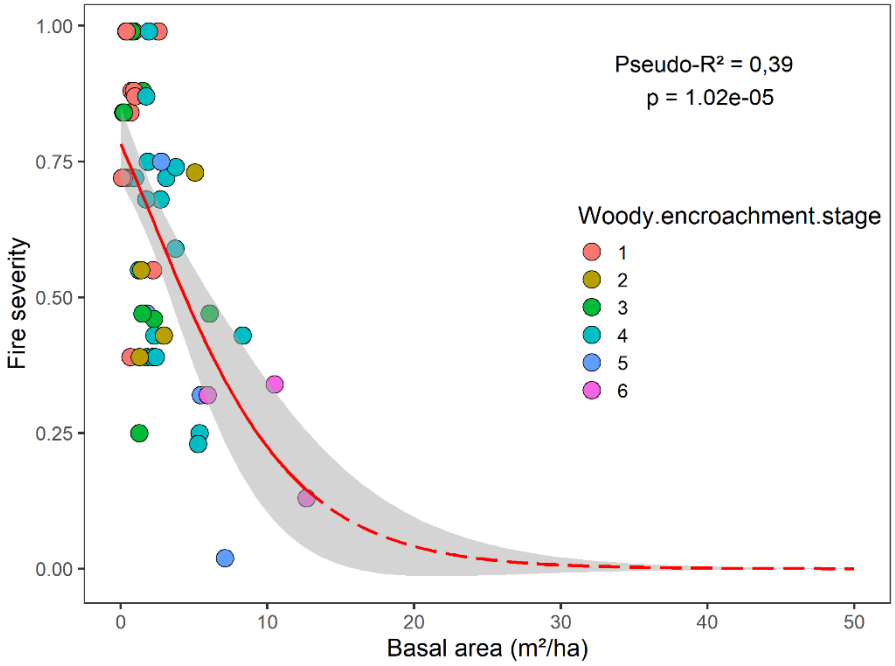

Figure 6 – Beta regression between fire severity and basal area of plots

4. Discussion and concluding remarks

Our results support the assumption that subtropical highland grasslands of the Atlantic Forest Biome are ecosystems that depend of fire for their maintenance (OVERBECK et al., 2018). Studies carried out in the region have shown that in the absence of fire, the remnants of grassland vegetation are likely to be invaded and replaced by woody species (*e.g.* OLIVEIRA; PILLAR, 2004; SÜHS; GIEHL; PERONI, 2020).

Although the woody encroachment has been extensively documented worldwide, few studies explored if this phenomenon exclusively represents a process of woody densification that does not interfere in the flammability of the system, or if it is associated with a change in the fundamental state of the ecosystem towards an alternative forest state. Specifically, the flammability of Southern Brazilian grassland ecosystems is of particular interest for their conservation, because it allows the occurrence of periodic fires, which are capable of sustaining vegetation in an open state, since the climate could otherwise way, promote the forest (BEHLING; PILLAR, 2007). On the other hand, the shading provided by canopy closing of woody species is a critical factor for the survival of light-demanding grassland vegetation (PARR; GRAY; BOND, 2012). Here, we observed that the flammability was negatively affected by the progress of woody encroachment, indicating a change in the behavior of the system.

In the process of state transition between grassland and forest ecosystems, the increase in canopy cover, provided by the woody encroachment, results not only in the reduction of herbaceous biomass, but also in lower air temperature, higher relative humidity, lower wind speed and higher moisture content of the combustible material (HOFFMANN et al., 2012b). Furthermore, as the density of trees and shrubs increases, the fuel bed becomes increasingly dominated by leaf litter, which is less flammable than grasses (PRIOR et al., 2017). Thus, grass loss in response to canopy closure indicates the transition from a fire-maintained state to a fire-independent state (HOFFMANN et al., 2012a). Identifying the transition from one state to another provides a basis for understanding how fire governs the distribution of different types of vegetation under the same climatic conditions. Hoffmann et al. (2012a) indicated that when an ecosystem reaches sufficient canopy cover to suppress fire and exclude grasses, a fire suppression threshold is reached. In order to find an analogous threshold for our study system, we analyzed fire severity along a gradient of basal area per hectare and found that the ability of fire to reverse the invasion process is significantly reduced as the woody encroachment progresses until reaching the threshold of 32.3 $m^2.ha^{-1}$, which is when the forest state reaches stability and becomes independent from fire.

Understanding the consequences of woody encroachment is important because grassland ecosystems are undergoing widespread degradation worldwide (HOEKSTRA et al., 2005). In Southern Brazil, the practice of cattle grazing and the preservation of the endemic biodiversity of the highland grasslands fundamentally depend on the maintenance of the ecosystem in an open state, which makes woody encroachment a prominent concern for both the local economy and biodiversity conservation (OVERBECK et al. al., 2007; SÜHS; GIEHL; PERONI, 2018, 2020). In this way, the integration of the woody invasion process into a coherent strategy for the management of natural resources can help the management and restoration of grassland ecosystems. Therefore, we recommend the use of prescribed fires to the conservation of the grasslands landscapes in Southern Brazil.

5. References

BEHLING, H.; PILLAR V.D. Late Quaternary vegetation, biodiversity and fire dynamics on the Southern Brazilian highland and their implication for conservation and management of modern Araucaria forest and grassland ecosystems. Philosophical Transactions Royal Society B, v. 362, p.243-251, 2007.

CLARKE, K.R.; SOMERFIELD, P.J.; GORLEY, R.N.Testing of null hypotheses in exploratory community analyses: similarity profiles and biota-environment linkage. Journal of Experimental Marine Biology and Ecology, v. 366, p. 56-69, 2008.

DUFRÊNE, M.; LEGENDRE, P.Species assemblages and indicator species:the need for a flexible asymmetrical approach. Ecological Monographs, v. 67, p. 345-366, 1997.

HOEKSTRA, J.M. et al. Confronting a biome crisis: global disparities of habitat loss and protection. Ecology Letters, v. 8, p. 23-29, 2005.

HOFFMANN, W.A. et al. Ecological thresholds at the savanna-forest boundary: how plant traits, resources and fire govern the distribution of tropical biomes. Ecological Letters, v. 15, p. 759-768, 2012a.

HOFFMANN, W.A. et al. Fuels or microclimate? Understanding the drivers of fire feedbacks at savanna–forest boundaries. Austral Ecology, v. 37, p. 634-643, 2012b.

INSTITUTO AMBIENTAL DO PARANÁ - IAP. Plano de manejo do Parque Estadual de Vila Velha. Curitiba, 2004.

MAACK, R. Geografia física do estado do Paraná. 4° edição, Editora UEPG, Ponta Grossa, 2012. 526 p.

OLIVEIRA, J.M.; PILLAR, V.D. Vegetation dynamics on mosaics of Campos and Araucaria forest between 1974 and 1999 in Southern Brazil. Community Ecology, v. 5, n. 2, p.197–202, 2004.

OVERBECK, G.E. et al. Brazil's neglected Biome: the South Brazilian Campos. Perspectives in Plant Ecology Evolution and Systematics, v. 9, n. 2, p. 101-116, 2007.

OVERBECK, G.E. et al. The South Brazilian grasslands – A South American tallgrass prairie? Parallels and implications of fire dependency. Perspectives in Ecology and Conservation, v. 16, n. 1, p. 24-30, 2018.

PARANÁ. Lei n° 1293 de 12 de outubro de 1953. Cria, no município de Ponta Grossa, nas terras denominadas "VILA VELHA" e "LAGOA DOURADA", um parque estadual. Diário Oficial do Estado, Curitiba, PR, 16 out. 1953.

PARR, C.L.; GRAY, E.F.; BOND, W.J. Cascading biodiversity and functional consequences of a global change–induced biome switch. Diversity and Distributions, v. 18, p. 493-503, 2012.

PRIOR, L.D. et al. Does inherent flammability of grass and litter fuels contribute to continental patterns of landscape fire activity? Journal Biogeography, v. 44, p. 1225-1238, 2017.

SÜHS, R.B.; GIEHL, E.L.H.; PERONI, N. Interaction of land management and araucaria trees in the maintenance of landscape diversity in the highlands of southern Brazil. PLOS ONE, v. 13, n. 11, e0206805, 2018.

SÜHS, R.B.; GIEHL, E.L.H.; PERONI, N. Preventing traditional management can cause grassland loss within 30 years in southern Brazil. Scientific Reports, v. 10, n. 783, 2020.

The last landscape gardeners: Incident analysis of traditional burns in Portugal

Emanuel Oliveira[1]; Raquel Lobo-do-Vale [2]; Maria Conceição Colaço *[3]

[1]Universidad Santiago de Compostela, Departamento de Ingeniería Agroforestal, Rúa Benigno Ledo, 27002. Lugo, Spain, {emanuelrenato.sousadeoliveira@rai.usc.es}
[2] Centro de Estudos Florestais, Instituto Superior de Agronomia, Universidade de Lisboa, Tapada da Ajuda, 1349-017 Lisboa, Portugal, {raquelvale@isa.ulisboa.pt}
[3] Centro de Ecologia Aplicada Baeta Neves (CEABN-InBIO), Instituto Superior de Agronomia, Universidade de Lisboa, Tapada da Ajuda, 1349-017 Lisboa, Portugal, {ccolaco@isa.ulisboa.pt}

**Corresponding author*

Keywords

Fire use, Tradtional fire, Wildfire, Fatalities, Rural population

Abstract

In Portugal, there are countless historic and legislative references about fire use in rural areas. This popular use of fire to manage the huddled of agricultural and forestry leftovers and small burns to clean the farmed lands continues nowadays, to be used in rural environments. However, these environments are becoming depopulated, with aged populations which are often isolated.

Every year, in the social media, there are news about fatalities or injuries from elder people when using fire in the landscape. In 2018 the number of incidents were much higher than usual. For that, the objective of this work was to identify which were the factors that could explain this anomaly.

To obtain a systematic data of the incidents, a thorough analysis of the regional and national newspapers, both in paper and online, was performed from 2008 to 2020. Variables like date, place, sex, age and other were gathered. All the incidents variables were complemented with meteorological data associated with wildfire risk, sociodemographic variables and the legislative context.

From 2008 to 2020 there were 50 incidents, with 78% of fatalities. The anomaly of incidents in 2018 corresponded to 42% of cases. Most of the incidents occurred with elder (75%) and male (82%) people. The predominant months of occurrence were April and October particularly in the year 2018. The majority of fatalities (69%) occurred when the victim was burning alone. Legislative, social and meteorological analysis showed that the most probable factor that lead to the incidents anomaly of 2018 was the extreme pressure to manage the vegetation, held by police forces, legislation and fines value if you didn't comply.

1. Introduction

In Portugal, there are countless historic and legislative references about fire use in rural areas (OTI, 2021). This popular use of fire to manage the huddled of agricultural and forestry leftovers and small burns to clean the farmed lands continues nowadays, to be used in rural territories. However, these areas are becoming depopulated, with aged populations remaining, and often isolated.

If in the 50´s of the XX century, the territory had a network of patches with agriculture and woodlands, maintained by the local farmers, at the present, this no longer occurs. Consequently, there is an increase of the biomass accumulated in unused areas creating fuel-loads prone to wildfires. The remaining population continues to use fire for the management of the land, however not always with the strength to control it (Colaço, 2019). As mentioned in the report of WWF (2019), "under these circumstances, the traditional use of fire in the maintenance of pasture and agricultural land can have disastrous effects when the flames spread onto abandoned plots and turn into uncontrollable wildfires".

Not only wildfires can start by these traditional burns, but this practice can lead to injuries or even fatalities. Every year, all over Europe, in the social media, there are news about fatalities or injuries from elder people when using fire in the landscape. In 2018 the number of incidents in Portugal was much higher than the usual

yearly three or four records. Thus, the objective of this work was to identify all the injuries and fatalities that occurred by the use of fire, analysing which were the factors that could explain 2018 increase of numbers.

2. Methodology

To obtain a systematic data of the incidents, a thorough analysis of the regional and national newspapers, both in paper and online, was performed from the years 2008 to 2020. For the search online the terms used were "incidents, death, fatalities, injury" cross over with "agricultural burns, traditional burn, stubble burn, farmer, elder population". Variables like date, place, sex, age and other information considered relevant were gathered from the newspapers. All the incidents variables were complemented with meteorological data associated with wildfire risk provided by the Information Management System of Wildfire (ICNF, 2021), sociodemographic variables obtained from the National Statistical Institute (INE, 2020) and the legislative context. A statistical analysis was performed crossing over the incidents with meteorological data (FWI indices), sociodemographic data and to the legislation context.

3. Results and discussion

From 2008 to 2020 there were 50 incidents, with 78% of fatalities. The anomaly of incidents in 2018 corresponded to 42% of cases (figure 1).

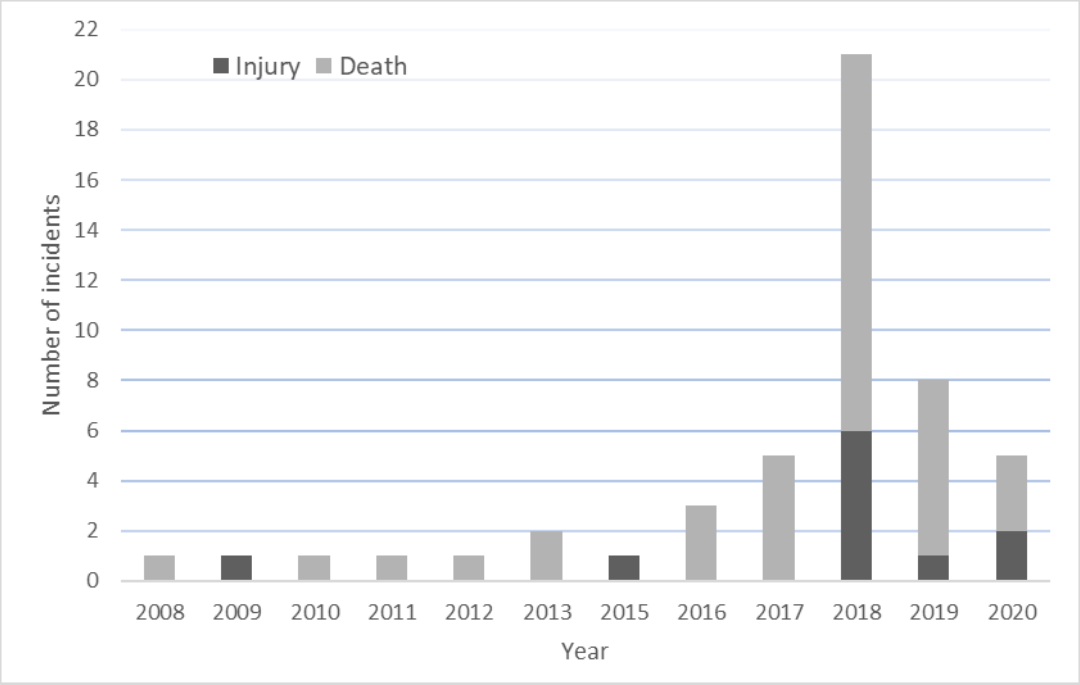

Figure 1- Number of incidents (injury and death) during the 2008-2020 period in Portugal.

The predominant months of incident occurrence were March/April and October particularly in the year 2018. While the first period of the year coincides with the deadline for the fuel management mandatory by law before the fire season, the second period in October coincides with the preparation of the fields to plant new agricultural cultures.

Between the months of December until April, the incidents only occurred after the year 2015 with a greater predominance on the years of 2018 and 2019. Instead, the incidents occurring in October and November ranged most of the study period (2008-2020).

3.1. Sociodemographic characteristics

Age can be considered a critical factor. Most of the incidents (from 2008 to 2020) happened with people above 66 years old (72%) and male (84%). All the incidents occurred with women above 70 years old. Traditionally in southern Europe, field work that uses fire is a gender issue, with predominance for men to perform it (Proxecto

Batefogo, 2019). Most of the incident with women are related with burnings that the couple were performing together. However, the majority of fatalities (69%) occurred when the victim was burning alone and only 10% burned with company, usually with their wives. The information for all the incidents is incomplete since the newspapers in 21% of the news didn't mentioned how was this context (alone vs. with company).

In what relates to the sociodemographic context, most of the incidents (64%) occur in regions with high ageing index (people above 65 years / people bellow 15 years x 100) and 41% in areas with very low population density (values bellow 50 inhab/km^2).

These factors could roughly explain the risk associated with the use of fire by an elder population, isolated and conditioned by the lack of renewal of the population that allows maintaining traditional practices safely, where the use of fire as a rural tool is included. However, these factors don't explain the increase in 2018.

3.2. Meteorology analysis

Meteorology is a factor that influence greatly fire behaviour and its control. Among other meteorological data, and analysis of the Daily Severity Rating (DSR) of the day and area where the incident occurred was performed. This index indicates the difficulty in fire extinguishing operations reflecting the effort required to its deletion (Rego & Colaço, 2013). So, the higher the value of DSR, the most complex and difficult will be fire control and extinction. The analysis showed that 75% of the incidents occurred on days with very low values, so it did not indicate a relationship with the difficulty of burning and consequent incidents.

Once more the meteorology does not explain the increase of 2018.

3.3. Legislation context

Immediately after the extreme wildfires that affected Portugal in 2017, prevention and the responsibility to do fuel management was considered a priority. In particular, around houses and roads, with a bigger demand from the government and from the authorities that control it. Although the legislation already existed (DL 124/2006), in 2018 the authorities increased public announces, doubled the fines if the citizen don't comply, and the police forces were more present doing inspection. These impositions, led to a real race to comply with the law, leading to the speculation of the prices, which were very high for the majority of the population, particularly the elderly without resources (in many cases with very low retirement pensions).

The pressure about fuel management around the houses felt by the citizens it is well expressed in figure 2, where google trends shows the interest on this subject on google searches.

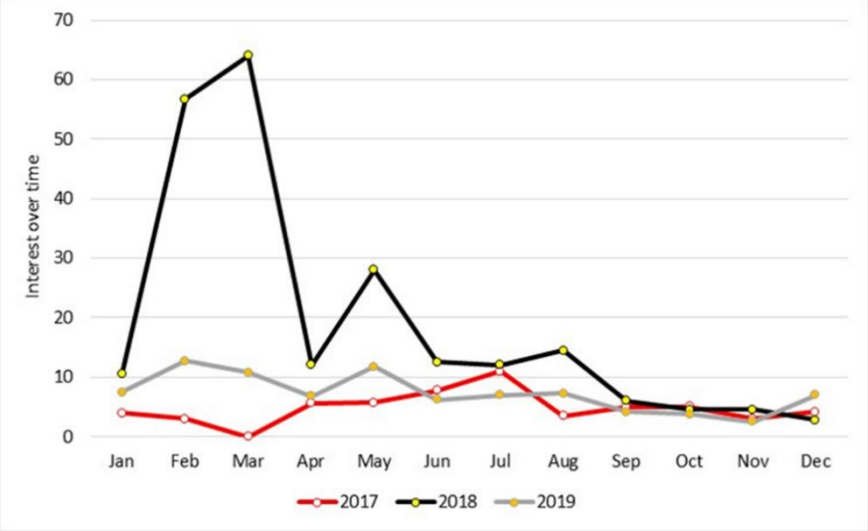

Figure 2- Internet search interest on the topic "Fuel clearing around the houses" on google trends

4. Final remarks

Since 2019, in Portugal, to burn agricultural debris it is necessary to ask permission on an Mobile app. The numbers for 2020 and 2021 reach more than one million permits (personal communication Oliveira, E.).

Although 50 incidents on a universe of millions can be considered very low, we should consider that our goal is to have zero fatalities performing these actions in the field.

Legislative, social and meteorological analysis showed that the most probable factor that lead to the incidents anomaly was the extreme pressure to manage the vegetation, held by police forces, legislation and fines value if you didn't comply.

Several actions from the forest authorities to support and to monitor the traditional burns and to know who is going to perform it have been taken. Considering the results above, it is important that the burns done with elder people who are alone and on a high or very high structural fire risk zone, should be supported by fire teams in the field.

Also, in here there are evidences that a mandatory law with high pressure from the authorities, should always be complemented with pedagogical and support actions. When that doesn't happen, it can lead to unsecure actions leading to injuries or fatalities.

5. Bibliography

Colaço, M.C. (2019). Reaprender a vivir cos incendios forestais nun contexto de cambio climático. *In* Proxecto Batefogo - Coord. *Árbores que non arden. As mulleres na Prevención de Incendios Forestais*. Editora Catro Ventos, Vigo, Espanha. pp.127-146

ICNF (2021). Sistema de Gestão Informação de Incêndios Florestais. https://fogos.icnf.pt/sgif2010/login.asp

INE (2021). Instituto Nacional de Estatística. https://censos.ine.pt/

Observatório Técnico Independente, Castro Rego F., Fernandes P., Sande Silva J., Azevedo J., Moura J.M., Oliveira E., Cortes R., Viegas D.X., Caldeira D., e Duarte Santos F. - Coords. (2020). *O Uso do Fogo em Portugal – tradição e técnica.* Assembleia da República. Lisboa. 133 pp.

Proxecto Batefogo (2019). *Árbores que non arden. As mulleres na Prevención de Incendios Forestais*. Editora Catro Ventos, Vigo, Espanha.

Rego, F.C. & Colaço, M.C. (2013). Wildfire Risk Analysis. In Abdel H. El-Shaarawi & Walter P. Piegorsch (eds.), *Encyclopedia of Environmetrics* (2nd ed.). United Kingdom: John Wiley & Sons, Ltd.

WWF (2017). *Forests ablaze Causes and effects of global forest fires.* Study D. WWF Deutschland.

Turbulent Wildland Fire Spread by Ember Wash

Kevin Speer*[1,2]; Bryan Quaife[1,2]; Xin Tong[1,2]

[1] *Geophysical Fluid Dynamics Institute. Florida State University, Tallahassee, FL, 32306 USA, {kspeer@fsu.edu}*
[2] *Department of Scientific Computing. Florida State University, Tallahassee, FL, 32306 USA, {bquaife, xtong}@fsu.edu*

**Corresponding author*

Keywords

Fire-atmosphere interaction, rate-of-spread, ember wash, spotting, dynamics

Abstract

We implement an ember spotting and ember wash model within an idealized 2D coupled fire-atmosphere model. To do this, we add a stochastic transport to the background or total coupled wind field. An exponentially distributed or a normally distributed velocity anomaly added to the total wind vector represents a turbulent transport of the probability of ignition near ground by intermittent processes. These bed load transport processes may include including gusts, tumbling, and near-front small-scale coherent wind eddies that trap embers and transport them forward, hence carrying the fire along the near-surface total wind field.

1. Introduction

Short range spotting can be difficult to distinguish from fire front movement in higher winds, typical of strong spotting conditions. Some of this short range spotting is due to firebrands that did not rise in the fire's plume but rather spread nearly horizontally in the surface boundary layer. These and the heavier embers and burning debris that emerge from the main fire frontal region carried by strong winds are responsible for rapid movement and widening of the front. We use the phrase "*ember wash*" to denote this part of the fire.

Models have demonstrated the important role of plume intensity and turbulence in the degree and range of spotting, and suggested an exponential-like distribution of spotting downwind of the fire (Martin and Hillen, 2016; Bhutia et al., 2016). Data analyses confirm some aspects of this short-range behavior (Page et al., 2019; Storey et al., 2021). A possible example of this behavior appears in the "Northwest Oklahoma Fire Complex" of three large wildfires that burned about 800,000 acres in Oklahoma and Kansas (Figs. 1 and 2).

Our objective is to represent in an idealized fashion some of the most important processes for surface wind-driven fire in a turbulent flow. We show below how complex fire fronts and effects emerge from the interaction of background wind, fire-induced flow, and a new ember wash effect near intense fires.

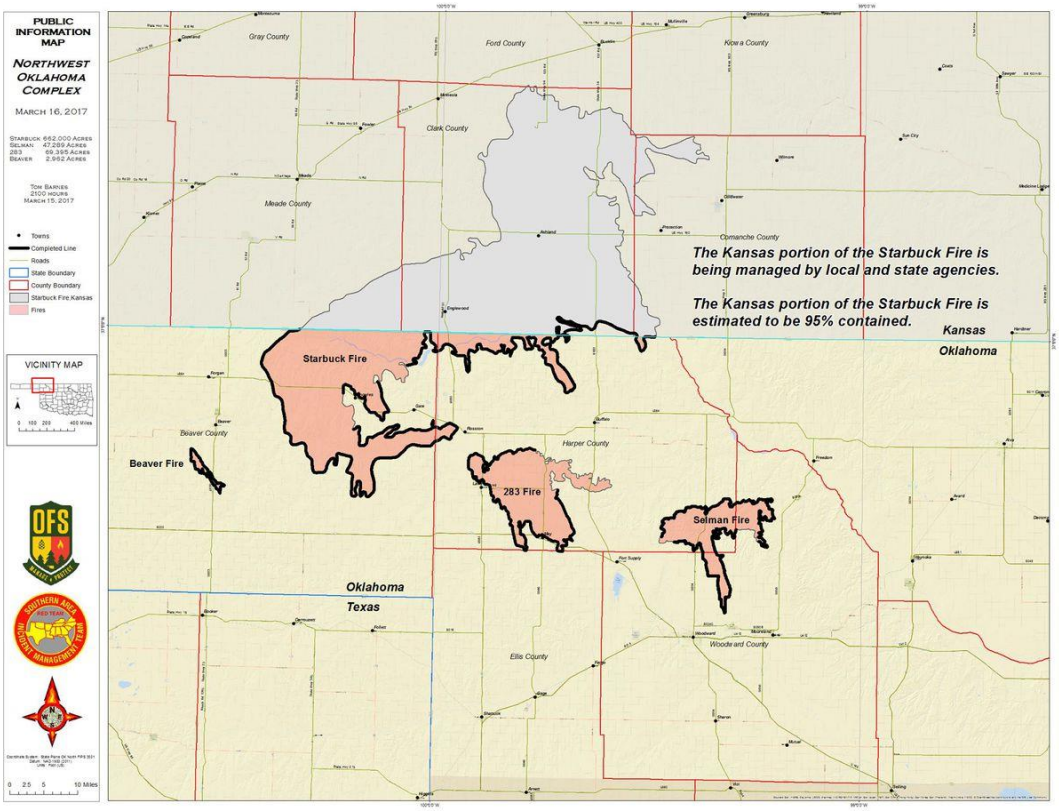

Figure 1- The 2017 NW Oklahoma Complex Fire consisted of several major fires and burned over 834,000 acres. Wind speeds were over 30 mph (15 m/s) with gusts up to 50 mph (25 m/s) in places. Source: Public Information Map of the OK Forest Service.

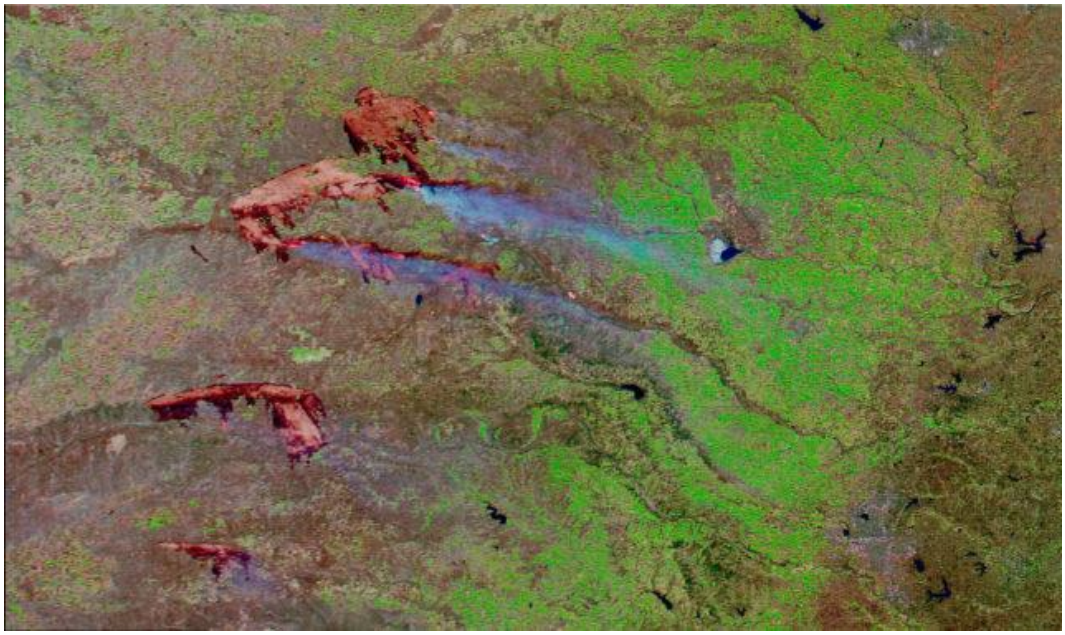

Figure 2- Infrared imagery of the 2017 NW OK Complex Fire near Woodward showing the intense fingering and complex spread behavior, some associated with wind and fuel variations and river drainage slopes. Flame heights were reported in places at over 40 ft.

2. Idealized Surface Wind Model

We use an idealized 2D model for near-surface wind in the presence of fire to investigate ember-enhanced spread in the presence of fire-atmosphere interaction (Quaife and Speer, 2021). The divergent flow is induced

by the rising buoyant fire plume that entrains surrounding air, and the rotational flow at the surface is induced by the lifting of horizontal background vorticity by the buoyant plume. Turbulent diffusion is incorporated into fire spread to represent the fluctuations in hot gases and flames at the near-surface boundary due to small-scale horizontal turbulent motion of the wind within and above the fuel. QS2021 provided a suite of runs that demonstrate various effects of fire-atmosphere interactions on spread rate and geometry of the fire. Standard phenomena such as a parabolic fire front shape, accelerated merging of flank fires, fingering, and other effects are well represented in the idealized model. In QS2021 the *first arrival time* or *time-of-arrival* heat map was emphasized as well as the rigorous relationship between this map and the rate-of-spread in any direction.

We solve for the flow generated by each burning elemental cell in a cellular automata (CA) model of combustion. A simple combustion term with fixed burn time is used. In the CA framework, we specify small-scale divergence and vorticity sources to the flow around individual fire elements which sum to produce the total wind on the fire front.

2.1. Solution Method

The model CA domain is defined by a two-dimensional rasterized grid and solved by decomposing the velocity into the sum of an irrotational and a solenoidal velocity field (Quaife and Speer, 2021). The first component is a background velocity that we take to be the uniform velocity U_{BG}. The other two velocity components are fire-induced, arising from flow convergence into the fire plume and from specified vorticity sources. Hilton et al 2018 call the divergent component the *pyrogenic potential*. At the flanks of the fire, we impose a vorticity source that, depending on the intensity of the fire, may be clockwise or counterclockwise on the fire flank. The model and velocity fields with and without the vorticity model are illustrated in Fig. 2.

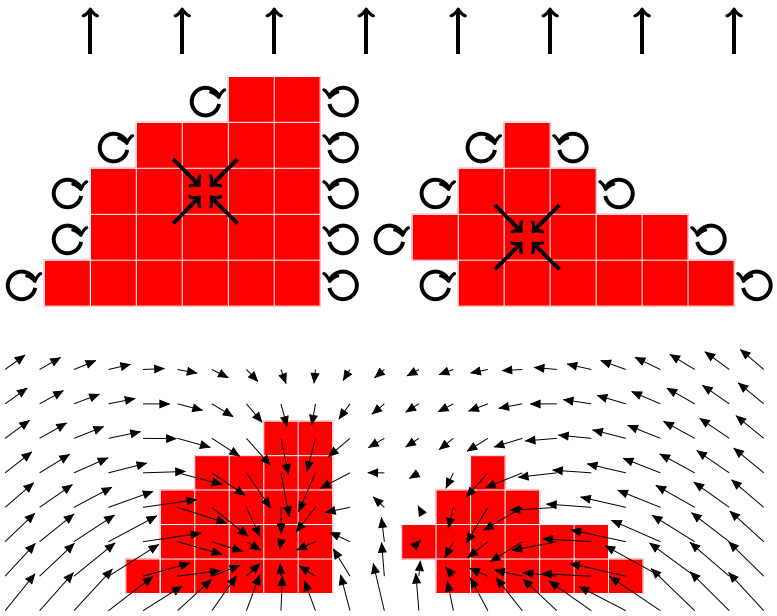

Figure 3- Wind around combusting elements (indicated by red cells). The atmospheric velocity is the sum of three components: a background flow, a pyrogenic potential or divergent term, and vorticity along the flanks.

Computing the flow field requires solving the two-dimensional Poisson equation with a known (and evolving) forcing function. We use the standard second-order central difference formula to discretize the Laplacian, and we impose a constant Neumann boundary condition. The resulting sparse linear system is solved with Matlab's backslash operator. With the total velocity field in hand, new cells must be ignited downwind. We use Bresenham's line algorithm to carry the fire downwind. This algorithm is a line drawing algorithm that determines cells of a rasterized geometry that are between a start and end point. We modify the algorithm since we only have a starting point at a burning cell and wind speed and direction. In addition, we stop igniting cells along the line if it reaches a cell that is either combusting or has no remaining fuel.

2.2. Model Configuration

Here, the cell size is 1m on a side, and the time evolution occurs over minutes to hours. The full model domain is rectangular, flat, and 200 m on a side. The only fuel parameter in the model is a constant burn time. This

parameter depends on the fuel and combustion process and is regarded here as an observed parameter, estimated from observations (Currie et al., 2018). While the range of this quantity can be large, mean values of a few seconds to minutes are typical in light to moderate fuels. The strength of the pyrogenic source is related to fire intensity by standard plume scaling.

We introduce a stochastic term that allows cells to ignite neighboring cells the time step before the original cells extinguish, with a probability of 0.4. This diffusion-based ignition occurs independently of the convection-based ignition due to wind. The rate of spread under diffusion is simply related to the burn time and probability of ignition since the model waits for the cell to burnout before igniting a neighboring cell.

The wind in our CA model is kinematic, and satisfies mass conservation but not a full set of momentum equations. Its role is to act as a "convective agent" for the probability of fire in a cell, and the added stochastic terms are designed to reflect the statistics of a multitude of processes and interactions in the surface boundary layer ahead of the fire front. In this implementation we relax this assumption and carry the fire stochastically down the local wind direction to simulate short-range spotting and ember wash.

3. Extension to Ember Spotting Effects

We extend this model with simple spotting and ember wash representations. We first consider an idealized spotting model to illustrate how embers may be distributed down the ambient wind when they are lofted, and the resulting flow complexity induced by the fire. Next we introduce *ember wash* that is induced by ember transport down the local near-surface wind. Representation of the latter is substantially different from spotting since the embers may roll or bounce along the ground as well as be carried by the wind hence their transport is more complicated, but also more localized to the fire front.

Spot fires are introduced based on a Gaussian-distributed lifetime (Tohidi and Kaye, 2017) with mean 20s and standard deviation 5s downwind *using the background flow* (not the total wind which include fire-induced flow). The reason for this is that aloft the main influence on trajectories is the background wind, with the plume effects secondary once the embers have been released by the plume into the surrounding environment. The ignition probability of the spot is given by a Poisson process with Bernoulli distribution and probability p=0.01. Higher probabilities produce too much fire with new fronts emerging rapidly mirroring the initial front; lower probabilities produce infrequent spotting. This is a useful idealization of the overall spotting process that reflects actual physical processes in an idealized manner. The subsequent spread of the fire is strongly influenced by the presence of spotting, which draws air in toward the new fire and dramatically changes the local flow (Fig. 4).

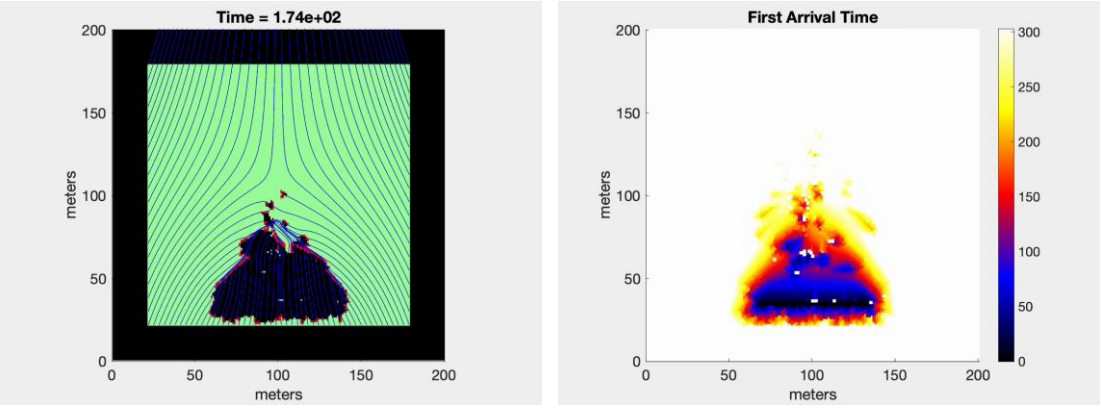

Figure 4- Idealized example of fire spread due to spotting. Fire progression map at 174s after ignition (left) and first arrival time heat map (right; seconds in color, with darker colors showing earlier arrival times). The addition of spot fires produces a complex fire-induced surface wind that affects subsequent spread. Streamlines of the wind (solid curves) indicate the interaction of a constant background wind of 1 m/s from the south (bottom) with the fire-induced wind; combusting elements are shown as red cells. The atmospheric velocity is the sum of three components: a background flow, a pyrogenic potential or divergent term, and vorticity along the flanks.

4. Extension to Ember Wash Effects

In contrast to spotting, *ember wash* or *ember blizzards* show a tendency for embers to spread near the surface rather than aloft. Much of this may occur in a tumbling or *bed load* mode of transport with embers bouncing, rolling, and being re-suspended and carried rapidly forward again in wind gusts. Thus we represent this process by a highly localized probability of ignition with an exponential decay away from the fire front. Such a shape may be justified as a subset of the observed close-range, exponential, spotting distributions in observations of spotting distance (Storey et al, 2021; Page et al, 2019) and sediment transport (Furbish and Schmeeckle, 2020).

A dot-fire ignition pattern is used to generate a fire and illustrate the ember wash effect on spread (Fig. 5). To model the ember wash, the magnitude of the velocity of each burning cell is increased with a probability of p=0.2. The increase in magnitude is sampled from an exponential random variable with a mean of 1 m/s. Streamlines show the very different effect of fire-atmosphere interactions in the case of ember wash that produces a much stronger perturbation to the ambient wind due to the larger area on fire at any given time compared to a simpler continuous, front with a relatively narrow width. The combination of ember wash and fire-induced wind generates a spread geometry not well described by exponential alone from a single well-defined front. Intense fingering due to dynamics with ember wash can also enhance total spread rates. Interactions with structures will be described in our presentation.

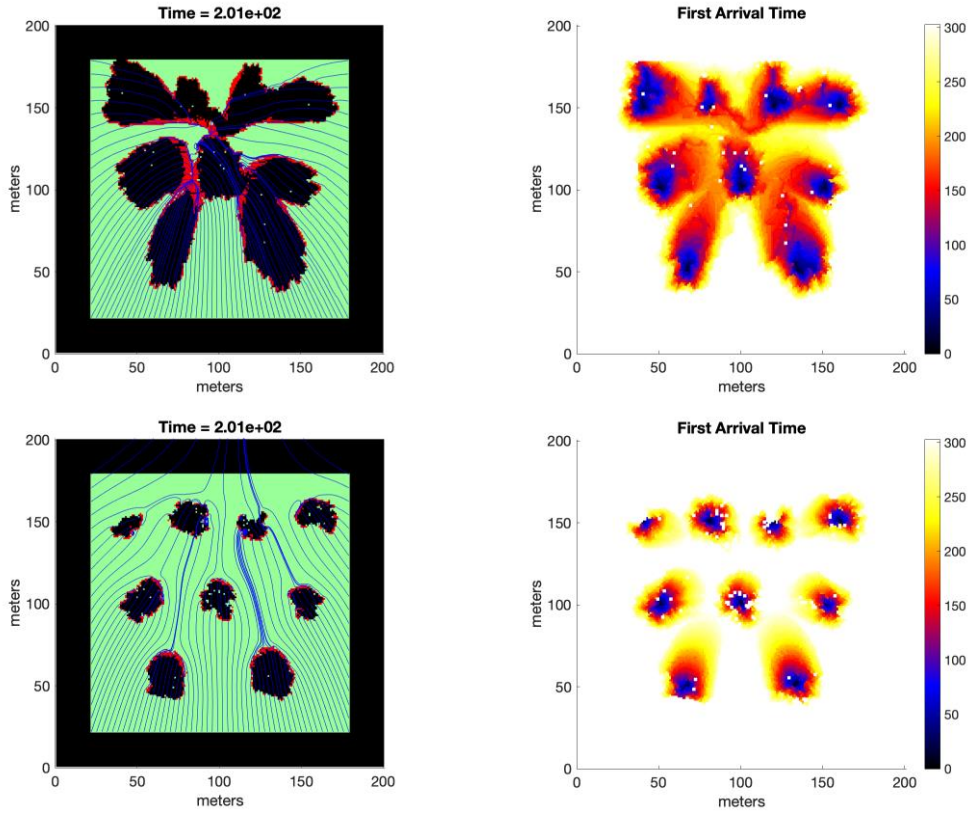

Figure 5- Fire spread with ember wash (top) and without ember wash (bottom). Fire progression map at 201s after ignition (*left****) and first arrival time heat map (****right****); seconds in color, with darker colors showing earlier arrival times. The ignition pattern is nine isolated spots. With ember wash a large region of ignition appears following the direction of the coupled fire-induced wind field. Streamlines of the wind (solid curves) indicate the interaction of a constant background wind from the south (bottom) with the fire-induced wind; combusting elements are shown as red cells. The atmospheric velocity is the sum of three components: a background flow, a pyrogenic potential or divergent term, and vorticity along the flanks.***

5. References

Bhutia, Sangay, Mary Ann Jenkins and Ruiyu Sun, Comparison of Firebrand Propagation Prediction by a Plume Model and a Coupled–Fire/Atmosphere Large–Eddy Simulator J. Adv. Model. Earth Syst., 2(1), 2010.

Currie, Miles, Kevin Speer, J. Kevin Hiers, Joe J. O'Brien, Scott Goodrick, and Bryan Quaife, Pixel-level statistical analyses of prescribed fire spread, Can. J. For. Res., 49.1:18026, 2019.

Albini Frank, A., Martin E. Alexander B, C, E and Miguel G. Cruz, A mathematical model for predicting the maximum potential spotting distance from a crown fire International Journal of Wildland Fire, 21:609–627, 2012.

Furbish, D. J., and M. W. Schmeeckle (2013), A probabilistic derivation of the exponential-like distribution of bed load particle velocities, Water Resour. Res.,49, 1537–1551, doi:10.1002/wrcr.20074.

Martin, Jonanthan and Thomas Hillen, The Spotting Distribution of Wildfires, Appl. Sci., 6(6):177, 2016.

Page, Wesley G.,, Natalie S. Wagenbrenner, Bret W. Butler, and David L. Blunck, An analysis of spotting distances during the 2017 fire season in the Northern Rockies, USA, Can. J. For. Res., 49:317–325, 2019.

Quaife, Bryan, and Kevin Speer, A Simple Model for Wildland Fire Vortex-Sink Interactions, Atmosphere, 12(8):1014, 2021.

Storey, Michael, A., Owen F. Price, Ross A. Bradstock, and Jason J. Sharples, Analysis of Variation in Distance, Number, and Distribution of Spotting in Southeast Australian Wildfires, Fire, 3(10), 2020.

Tohidi, Ali and Nigel B. Kaye, Stochastic modeling of firebrand shower scenarios, Fire Safety Journal, 91:91-102, 2017.

Using fuzzy logic to evaluate fire vulnerability of dwellings located at the wildland-urban interface

Alba Àgueda; Pascale Vacca; Eulàlia Planas; Elsa Pastor*

Department of Chemical Engineering, Centre for Technological Risk Studies, Universitat Politècnica de Catalunya·BarcelonaTech, Barcelona, Spain,
{alba.agueda, pascale.vacca, eulalia.planas, elsa.pastor}@upc.edu

**Corresponding author*

Keywords

Fire risk awareness, homeowners, probability of failure, fuel management, experts' poll

Abstract

WUI fires are posing great challenges to firefighting services, which are overwhelmed by the need to not only suppress the fire, but also protect the community. The need for self-protection is therefore growing, as is the need for the creation of fire-adapted communities. A tool that can aid homeowners and residents of the WUI is therefore created, so that they can identify the vulnerabilities present on their properties and consequently reduce them in order to diminish the risk of damage due to a wildfire. This Vulnerability Assessment Tool is based on a fault tree analysis that includes possible structural vulnerabilities as well as the different ways a fire could spread on a property to finally enter and damage the building. The identification of the probabilities of the different events in the fault tree is obtained through the use of fuzzy logic, for which inputs, outputs and rules are identified. A questionnaire targeted to homeowners and based on the fault tree and linked to the probability identified with fuzzy logic is then developed. By filling in this questionnaire, homeowners at the WUI will be able to know what the probability of a fire entering their house is. The result of the questionnaire also indicates which are the issues on the property that need to be addressed in order to lower this probability. Finally, the tool is validated with a case study of several houses affected by a fire in Spain.

1. Introduction

Fires at the Wildland-Urban Interface (WUI) are annually expanding in frequency and severity, resulting in catastrophic events that take a heavy toll in human life and structure losses (Ganteaume et al. 2021). These events often overwhelm firefighters' capacities due to the need of a simultaneous response to wildfire suppression, community evacuation and structure protection, therefore highlighting the need of the creation of fire-adapted communities, which can safely co-exist with fire (Vacca et al. 2020). Risk reduction strategies which include preventive actions not only at the community scale, but also at the residents' scale (i.e., the WUI microscale) are needed to reach this goal, as case studies indicate that a home's structural characteristics and its immediate surroundings determine a home's ignition potential in a WUI fire, thus influencing its chances of survival (Cohen 2000), (Hakes et al. 2017).

The analysis of past fire events all over the world has resulted in the identification of the different pathways leading to building ignition, which have been summarized by Hakes et al. (2017). Consequently, some countries that have historically been affected by wildfires at the WUI have created standards and guidelines for new and/or existing buildings that include WUI microscale risk reduction strategies related to both building and property characteristics. These are mainly general rules based on experience, but frequently poorly supported by scientific evidence and studies, thus without taking into account the appropriate parameters and processes that explain fire behaviour and effects on assets at the relevant scale (Pastor et al. 2019). In the Mediterranean region, standards and guidelines do not always include building construction or maintenance, or it is not analysed with the appropriate detail.The focus of this work lies in creating a Vulnerability Assessment Tool (VAT) specific for Mediterranean WUI microscale settings, directed to WUI homeowners and residents that is supported by scientific evidence and studies and can give quantitative information on the vulnerability of a property to an incoming wildfire, and can thus identify the main issues that need to be addressed. The tool is presented in form of a checklist that can be easily filled in by the homeowners or residents themselves.

2. Methodology

In order to reduce the risk of home loss at the WUI, a coupled approach that reduces the vulnerability of a home to fire along with the probability of its exposure conditions is necessary (Calkin et al. 2014), (Caton et al. 2017). The causes of fire entrance inside a building located at the WUI can be summarized therefore in two intermediate events of a fault tree, as shown in Figure 1: one involving the exposure conditions and the other involving structural vulnerabilities typical of Mediterranean constructions. For the fire to enter a building, both of these events should occur. The different paths that lead to these two intermediate events in a Mediterranean environment, identified through a literature review of past events (Vacca et al. 2020), are further explored to develop the sketch model in Figure 2.

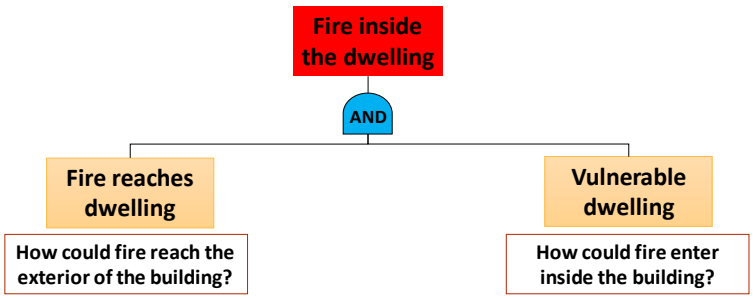

Figure 1: Events that lead to fire enetring a buidling at the WUI

When it comes to the ways the fire can reach the building, two areas around the dwelling have been identified: zone 1 includes the area within a radius of 10 m from the dwelling, while zone 2 consists of a 10 m to 30 m ring around the dwelling. In both zones, three types of fuels are considered: ornamental vegetation, artificial fuels (e.g., LPG tanks, garden furniture, sheds, etc.) and wildland vegetation. A set of fuel management guidelines (based on a review of existing guidelines as well as from observations from past fires and fire tests) has been established for each type of fuel. Failure occurs when compliance to these guidelines is not met.

The same method is applied to elicit the structural vulnerability of the dwelling according to the different paths through which fire could enter. According to Vacca et al. (2020), there are four main paths: glazing systems, roof, vents and structural damage to the dwelling's envelope due to heat accumulation in semi-confined spaces. The failure sequence for each one of these elements is identified as shown in Figure 2. For example, the failure of a glazing system depends on the thickness of the glass pane and the type of shutters, with different degrees of protection depending on the material.

Quantification of the probability of failure of each of these events has proven to be difficult, as information on paths that lead to ignition during past fires is not always available or reliable, as it is mostly collected without the possibility of thorough investigation due to lack of information or resources. To deal with this difficulty, a model that combines fuzzy logic with classical logic has been developed, that uses fuzzy sets that provide means to model the uncertainties associated with lack of information (Sivanandam et al. 2007).

2.1. Model Description

The structure of the developed model is given in Figure 2. Note that, according to Figures 1 and 2, two system variables lead to the final output of the model (i.e., fire inside the dwelling) through a classical logical AND gate, these are: (i) Probability of fire reaching the dwelling (POF_1) and (ii) Probability of failure of the dwelling due to its vulnerabilities to fire (POF of the dwelling). In the same way, this last variable (ii) is obtained through a classical logical OR gate according to the values obtained for the probabilities of failure of the four elements that constitute pathways for the fire into the house, i.e. glazing systems, roof, vents and semi-confined spaces that can suffer structural damage due to heat accumulation. The probability (i) (POF_1) depends on the compliance to different rules set for fuels located in the two considered zones previously described. All the probabilities of failure are obtained through the use of fuzzy logic. Seven fuzzy inference systems (FIS) are defined, as shown in Figure 2.

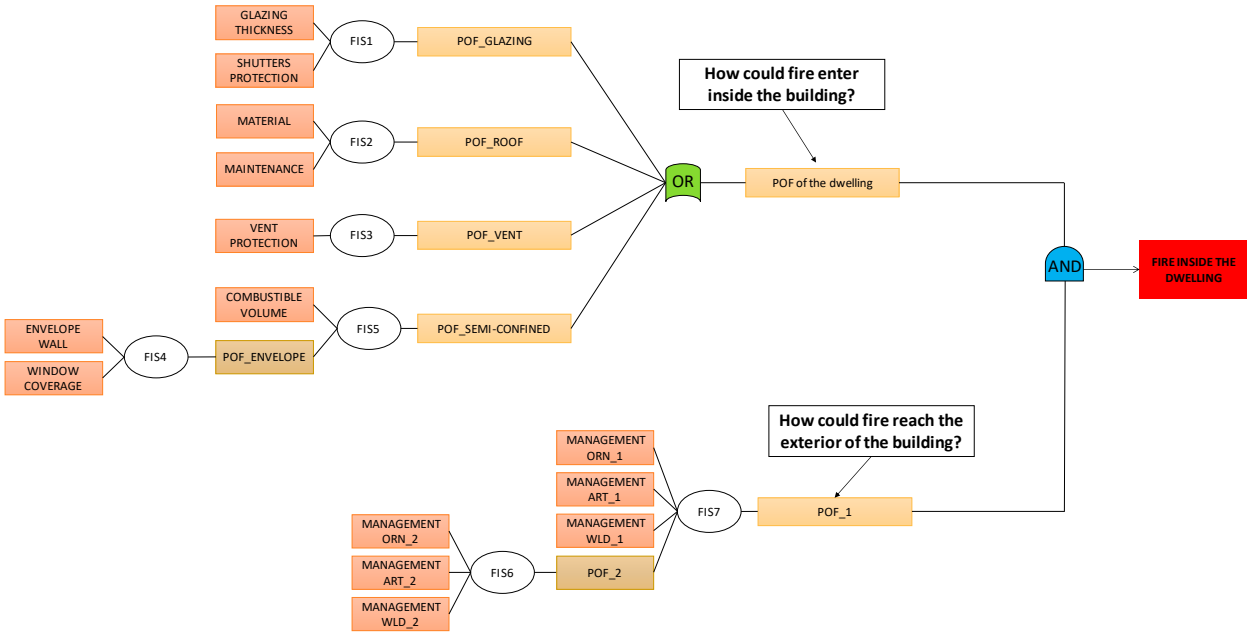

Figure 2: Scheme for vulnerability assessment to wildland fires for dwellings at the WUI. FIS: Fuzzy Inference System; POF: Probability Of Failure; ORN: Ornamental; ART: Artificial; WLD: Wildland; _1: Refers to zone 1; _2: Refers to zone 2.

When a FIS is defined, the generic process shown in Figure 3 must be followed. Initially, the variables that are relevant in the system must be identified (inputs and outputs). These variables must then be fuzzified, meaning that they need to be defined as fuzzy sets by identifying their universe of discourse and selecting a set of linguistic terms (i.e., fuzzy subsets) that accurately describes them. Subsequently, a membership function for each fuzzy subset must be defined to quantify the degree of belonging of any value in the universe of discourse to each fuzzy subset (Sivanandam et al. 2007). Then the inferring process is performed by using a set of rules that connect antecedents (input variables) with the consequent (output variable). These rules usually have a structure such as: "IF …, THEN …". An aggregation process is required to take into account the different rules that activate according to the inputs. Then, since the output is also defined as a fuzzy set, a defuzzification process is necessary in order to transform the fuzzy results into a precise output.

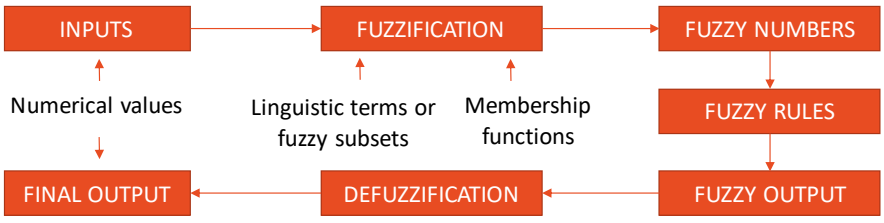

Figure 3: Generic Fuzzy Inference Process - bas ed on (Darbra et al. 2008)

2.2. Poll for experts

A poll for experts on WUI fires and vulnerabilities was prepared to calibrate this fuzzy model. It was filled in by 13 experts. Their expertise helped to determine membership functions, as the poll consisted in giving the most characteristic value (or range of values) for the fuzzy subsets that defined each set present in the model. Additionally, the poll included the fuzzy rules, for which the experts could choose the linguistic value of the output variable. When more than one input variable was combined, the logical operator AND was used. An example of the selection for the rules' consequent is shown in Figure 4.

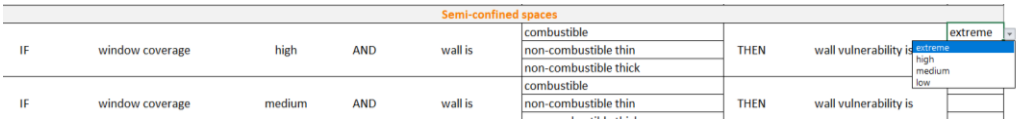

Figure 4: Example of rules present in the questionnaire prepared to synthetize experts' knowledge

2.3. Homeowners questionnaire

The previously presented model has to be used together with a questionnaire that homeowners can fill in autonomously. Questions can be answered mainly with YES or NO and they include all information needed to run the vulnerability model for a specific property. An example of the type of questions is shown in Figure 5.

	Building characteristics	
	Shutters	
1	Do you have protection for all your windows/glazing systems (i.e. shutters)? made of non-combustible materials (solid core wood fire-resistant, metal like aluminium)?	◻ Yes ◻ No
2	What material are the shutters made of?	◻ Wood ◻ Aluminium ◻ PVC ◻ Fire resistant materials
	Glazing panes	
3	What is the thickness of the glazing systems (in mm)?	
	Roof material	
4	Is your roof covering or your roof assembly made of fire-rated material (e.g. clay tiles, concrete tiles, asphalt glass fibre composition singles, slate, etc.)?	◻ Yes ◻ No
	Roof maintenance	
5	Are there missing, displaced or broken tiles?	◻ Yes ◻ No
6	Is the underlying roof sheeting exposed?	◻ Yes ◻ No
7	Are there unsealed spaces between the roof and the external walls or between the roof covering and the roof decking?	◻ Yes ◻ No
8	Do you perform regular cleaning of debris piling up on roof or gutters?	◻ Yes ◻ No

Figure 5: Example of questions included in the homeowners questionnaire.

Once the questionnaire is completed, the replies are introduced into the fuzzy model to calculate the probabilities of failure of the different considered elements, which are then used to calculate the probability of a fire entering a building.

3. Case study

This vulnerability model was tested using information gathered from five homeowners affected by a WUI fire that took place in July 2021 in Lloret de Mar, Spain. These homeowners replied to the questionnaire and we used their answers to quantify the probability of fire entrance in their dwelling (Table 1). They got our feedback and could identify the different issues (fuel management, structural constraints, etc.) that needed to be addressed in order to reduce this probability.

The WUI fire under study prompted evacuation orders and several homes were threatened, various elements present outdoors were burned (e.g. vehicles, fences and garden furniture), and one house was severely damaged (H02) due to the fire entering the building as a result of the breakage of a window pane.

Table 1. Probability of fire entrance in the dwellings according to the elements identified in the scheme for vulnerability assessment to wildland fires presented in Figure 2. FIS: Fuzzy Inference System; POF: Probability Of Failure; _1: Zone 1 (10-m around the dwelling); _2: Zone 2 (10-m to 30-m ring around the dwelling).

FIS / Classical logic results (%)	**Dwellings**				
	H01	**H02**	**H03**	**H04**	**H05**
POF_GLAZING	39	48 (70*)	65	16	16
POF_ROOF	14	14	65	14	14
POF_VENT	0	0	88	0	0
POF_ENVELOPE	0	14	39	39	39
POF_CONFINED	0	41	32	21	21
POF_2	71	71	88	65	88
POF_1	55	87	83	63	66
POF of the dwelling	47	74 (85*)	99	42	42
Probability of fire entrance	26	64 (74*)	82	27	28

* Values obtained considering no-shutters, since PVC shutters were not pulled down during the fire.

According to Table 1 the dwellings with the highest probability of fire entrance were H03 (82%) and H02 (74% considering no-shutters). H03 presented the highest probability of failure of the dwelling itself (99%). Vulnerable elements in H03 structure were the shutters' material, glazing thickness and vents design. Moreover, regarding the probability of fire reaching the dwelling (POF_1), H03 had a value of 83%. This value was not the highest one from the set of dwellings monitored, since H02 reached a slightly higher value (87%), but it was quite high nonetheless. The dwelling H02 had the highest probability of fire reaching the building (POF_1 = 87%), because compliance with fuel management rules was low in both zones.

4. Conclusions

The tool we have developed (i.e. VAT) considers the complex nature of the WUI microscale fire risk problem through the use of fuzzy logic. The end users of this tool are intended to be not only fire safety practitioners, but also the homeowners and residents of the WUI. The use of this VAT will lead to the improvement of fire safety practices at the microscale; i.e. it will increase WUI fire risk awareness of homeowners by identifying systematically major problematic conditions present on their property and in its surroundings. While the building of the tool is complex, the final product that is presented to the user is straightforward and easy to use. Moreover, a planned use of this tool at a local level would be key to improving fire protection at the community level.

5. Acknowledgements

This research was funded by the project PID2020-114766RB-100 of MCIN/ AEI /10.13039/501100011033.

6. References

Australian Standards (2018) AS 3959: Construction of buildings in bushfire-prone areas.

Autoridade Florestal National (2011) Gestão de Combustíveis Para Protecção de Edificações - Manual. https://fogos.icnf.pt/sgif2010/InformacaoPublicaDados/gestao_comb_final.pdf.

Calkin DE, Cohen JD, Finney MA, Thompson MP (2014) How risk management can prevent future wildfire disasters in the wildland-urban interface. Proceedings of the National Academy of Sciences of the United States of America 111, 746–751. doi:10.1073/pnas.1315088111.

Caton SE, Hakes RSP, Gorham DJ, Zhou A, Gollner MJ (2017) Review of Pathways for Building Fire Spread in the Wildland Urban Interface Part I: Exposure Conditions. Fire Technology 53, 429–473. doi:10.1007/s10694-016-0589-z.

Cohen JD (2000) Preventing Disaster: Home Ignitability in the Wildland-Urban Interface. Journal of Forestry 98, 15–21. http://www.fs.fed.us/rm/pubs_other/rmrs_2000_cohen_j002.pdf.

Darbra RM, Demichela M, Murè S (2008) Preliminary risk assessment of ecotoxic substances accidental releases in major risk installations through fuzzy logic. Process Safety and Environmental Protection 86, 103–111. doi:https://doi.org/10.1016/j.psep.2007.10.015.

Ganteaume A, Barbero R, Jappiot M, Maillé E (2021) Understanding future changes to fires in southern Europe and their impacts on the wildland-urban interface. Journal of Safety Science and Resilience 2, 20–29. doi:10.1016/j.jnlssr.2021.01.001.

Generalitat de Catalunya (2019) Protegeos de los incendios forestales. Pla INFOCAT.

Government of Alberta (2013) 'FireSmart Guidebook for Community Protection: A Guidebook for Wildland/Urban Interface Communities.' http://wildfire.alberta.ca/firesmart/documents/FireSmart-GuideCommunityProtection-Nov2013.pdf.

Hakes RSP, Caton SE, Gorham DJ, Gollner MJ (2017) A Review of Pathways for Building Fire Spread in the Wildland Urban Interface Part II: Response of Components and Systems and Mitigation Strategies in the United States. Fire Technology 53, 475–515. doi:10.1007/s10694-016-0601-7.

International Code Council (2021) 'International Wildland-Urban Interface Code (IWUIC).'

Intini P, Ronchi E, Gwynne S, Bénichou N (2019) Guidance on Design and Construction of the Built Environment Against Wildland Urban Interface Fire Hazard: A Review. Fire Technology 56, 1853–1883. doi:10.1007/s10694-019-00902-z.

Manca T, López M (2014) Guía Metodológica de Actuaciones de Prevención, Defensa y Autoprotección en la Interfaz Urbano-Forestal. 1–60.

Ministère de l'Écologie et du Développement durable (2002) Plans de prévention des risques naturels (PPR): Risques d'incendies de forêt.

National Fire Protection Association (2018) NFPA 1144: Standard for reducing structure ignition hazards from wildland fire.

NFPA (2022) Prepare Your Home Wildfire Risk Reduction Steps That Can Make Your Home Safer During a Wildfire. https://www.nfpa.org//-/media/Files/Firewise/Fact-sheets/FirewiseHowToPrepareYourHomeForWildfires.pdf.

Papathoma-Köhle M, Schlögl M, Garlichs C, Diakakis M, Mavroulis S, Fuchs S (2022) A wildfire vulnerability index for buildings. Scientific Reports 12, 1–15. doi:10.1038/s41598-022-10479-3.

Pastor E, Muñoz JA, Caballero D, Àgueda A, Dalmau F, Planas E (2019) Wildland-Urban Interface Fires in Spain: Summary of the Policy Framework and Recommendations for Improvement. Fire Technology. doi:https://doi.org/10.1007/s10694-019-00883-z.

Regione Autonoma della Sardegna (2021) 'Prescrizioni regionali antincendi.'

Regione Piemonte (2021) Piano regionale per la programmazione delle attività di previsione, prevenzione, e lotta attiva contro gli incendi boschivi.

Sivanandam SN, Deepa SN, Sumathi S (2007) 'Introduction to fuzzy logic using MATLAB.' (Springer)

Vacca P, Caballero D, Pastor E, Planas E (2020) WUI fire risk mitigation in Europe: A performance-based design approach at home-owner level. Journal of Safety Science and Resilience 1, 97–105. doi:10.1016/j.jnlssr.2020.08.001.

Vulnerability analysis to wildland-urban interface fires in metropolitan areas: an integrated approach

Elsa Pastor*[1]; David Caballero[1], Israel Rodríguez[2], Miriam Arenas[2], Pepa Morán[3], Guillem Canaleta[4], Pascale Vacca[1], Alba Àgueda[1], Eulàlia Planas[1]

[1] Department of Chemical Engineering, Centre for Technological Risk Studies, Universitat Politècnica de Catalunya·BarcelonaTech, Barcelona, Spain, {elsa.pastor, pascale.vacca, alba.agueda, eulalia.planas}@upc.edu, {davidcaballero@europe.com}
[2] CareNet Research Group, Internet Interdisciplinary Institute, Universitat Oberta de Catalunya. {irodriguezgir, marenasc}@uoc.edu
[3] Department of Urbanism and Regional Planning , DUOT, Universitat Politècnica de Catalunya·BarcelonaTech, Barcelona, Spain {pepa.moran@upc.edu}
[4] Pau Costa Foundation, c.Mossèn Cinto Verdaguer, 42 esc. A bxs 2A, Taradell, Spain. {gcanaleta@paucostafoundation.org}

**Corresponding author*

Keywords

Structural vulnerability, social vulnerability, ecosystem vulnerability, Barcelona wildfire risk.

Abstract

Wildfires pose a growing threat to populated areas around the world and especially in the Mediterranean Basin. Numerous Mediterranean cities have typically developed neighbourhoods that expand into forest land in which basic aspects for an efficient WUI fire management have not been considered. In this paper, we present a holistic approach to analyse threats to metropolitan areas due to WUI fires, accounting for infrastructural, societal and ecosystems vulnerability at settlement scale. Based on design fires and the key parameters responsible of fire impact and percolation through communities of most probable WUI fire events, we define key indicators to describe how vulnerable structures are in WUI metropolitan areas. Following, urban and societal indicators are selected to account for population's vulnerability and, finally, ecosystems potential losses are accounted by ecosystem vulnerability indicators such as ecosystem sensitivity and adaptability. We have implemented this methodology to analyse vulnerability in Barcelona WUI areas and identified those that can be more threatened in case of wildfire. Results of this study will be key to inform risk-reduction public policies, as they provide particular insights on those WUI areas within Barcelona municipality that should be prioritized along with the specific issues that should be tackled.

1. Introduction

Wildfires pose a growing threat to populated areas around the world and especially in the Mediterranean Basin. In 2018, the residential area of Mati, Greece, suffered a fire that killed 102 people and reduced more than 600 buildings to ashes. In the summer of 2021, numerous fires ravaged southern Turkey, killing 9 people and destroying hundreds of homes. Algeria also suffered several fires, with 65 deaths, and Greece, southern France, southern Italy, Cyprus and Sardinia had also severe outbreaks with multiple affected towns and resorts (Figure 1).

Climate change is affecting the synoptic weather patterns in the Mediterranean, with episodes of more intense and lasting Saharan air advections involving high temperatures and very low relative humidity, as well as extreme weather events with episodes of strong winds and hurricanes (medicanes). Although the number of ignitions has not risen significantly, the consequences are observed to be more and more severe.

Figure 1- Left: fires in Athens – Greece, 2021 (source: Aggelos Barai); Right: fires in Marmaris – Turkey, 2021 (source: Yetkin Report)

Built-up areas located in the wildland-urban interface (WUI) are increasingly threatened. Buildings, facilities and infrastructure are in direct touch with or very close to vegetation, which, in the event of a fire, suffer the direct consequences of flame contact, radiation and smoke exposure. Numerous Mediterranean cities have typically developed neighbourhoods that expand into forest land. Those wild areas, which provide basic ecosystem services (e.g. biodiversity conservation, water availability, air quality improvement, recreation, etc.), are usually on high slopes and are frequently visited by non-residents and tourists. In the development of such districts, the basic aspects for an efficient WUI fire management have not been considered, such as access roads, fire-resilient urban planning, fuel-reduced fringes, water points, etc.

In addition, evacuation processes in WUI fires are often very complex and, in some cases, end in disaster. Education, awareness, and training are critical issues for building resilient communities, as well as trust, engagement and interaction between experts, managers, and communities (McCaffrey et al., 2013). Giving all parties the opportunity to express their opinions, exchange knowledge and clear up misunderstandings, are central to meet social needs and improve community preparedness, response, and recovery (Mort et al. 2020).

In this paper, we present a holistic approach to analyse threats to metropolitan areas due to WUI fires, accounting for infrastructural, social and ecosystems vulnerability indicators at settlement scale. Our method is applied to Barcelona WUI area as a case study showing great potential to be replicated to other vulnerable metropolitan WUI areas.

2. Methodology

WUI fire vulnerability can be defined by the characteristics and circumstances of a WUI area that make it susceptible to the damaging effects of a wildfire (Gaunteaume et al., 2021). The magnitude of wildfire effects (i.e. heat from flames and toxic dose of smoke components) depend on the spread and intensity of the fire, driven by environmental parameters such as weather, topography and fuel. In turn, wildfire effects can lead to tremendous consequences in urbanized areas, ruining assets and infrastructures, killing and injuring people, and destroying basic ecosystem services.

In line with this definition, our methodology to analyse vulnerability to fires in WUI metropolitan areas is based on two main grounds (Figure 2). On the one hand, WUI fire vulnerability is intimately linked to the type of wildfire that can potentially threat a WUI zone, which may be different depending on the synoptic weather conditions. Fires generally follow particular behaviour patterns according to weather and topography, which have led to the definition of the so-called design fires in many Mediterranean regions (e.g. Costa et al., 2011). Design fires are thus the basis to infer fire impact and effects in WUI zones, and have to be well understood and parametrized for a comprehensive vulnerability analysis. On the other hand, vulnerability of WUI areas has to be explored covering three main axes to account for all possible damages: vulnerability of structures and infrastructures, social vulnerability and ecosystem vulnerability.

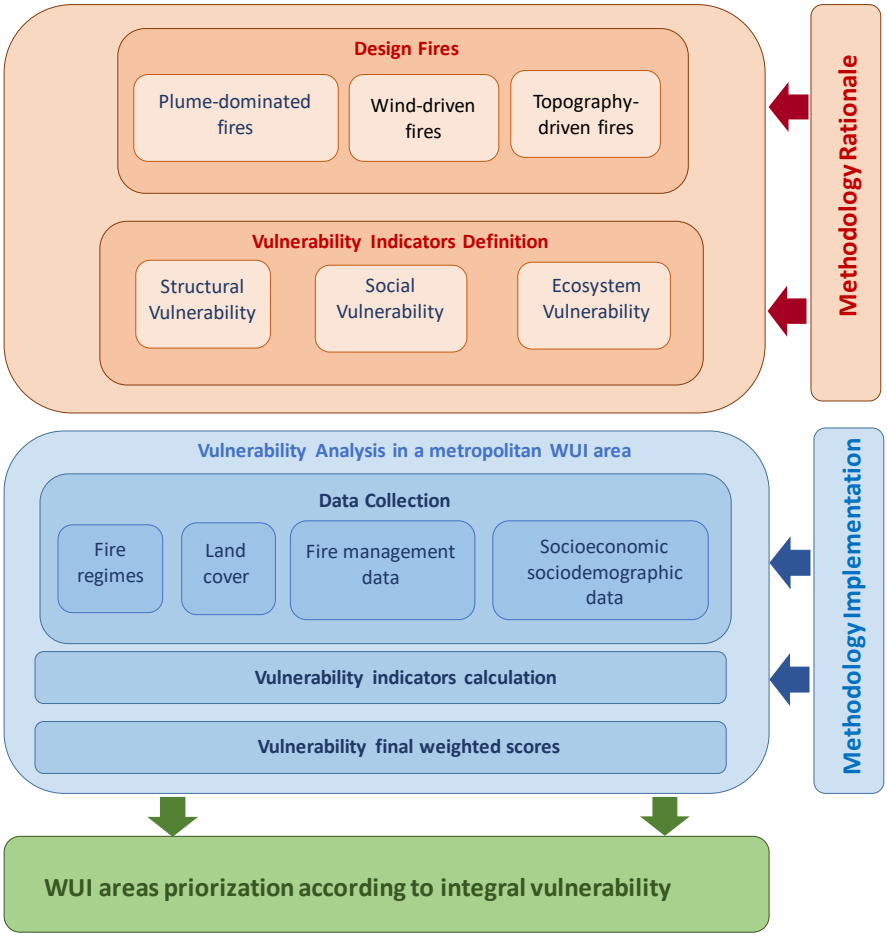

Figure 2- WUI fire vulnerability analysis. Methodology rationale

We have defined key indicators for structural vulnerability (Table 1) in line with the different fire exposure phases – pre-impact, impact and fire transfer (Vacca et al., 2020) that a WUI settlement faces in a fire incident. During the pre-impact phase, it is likely that firebrands will reach the settlement and initiate a spot fire within. This probability can be associated to the area of flash fuels (i.e. grasses and other fine fuels that ignite readily) present in the settlement, which will favour spot fire development. During the impact phase, the magnitude of the consequences in a WUI settlement due to direct flames/smoke exposure of the main fire perimeter will depend on the type of design fire and on the fire propagation mode (head, flank or back fire propagation). Fire permeability within the settlement (i.e. the easiness at which the fire propagates through the community) will largely depend on the type of WUI (e.g. interface, intermix or occluded, as defined by Mell et al, 2010) and is mainly driven by the vegetation continuity and channelling effects due to complex topography. Following, we have identified several severity-escalating factors that may increase fire risk, to account for *i)* the spatial arrangement of the structures with the surrounding vegetation (e.g. length of friction between structures-vegetation or roads-vegetation), *ii)* the presence of critical infrastructure that in case of fire impact may result in the escalation of the fire consequences; *iii)* the operation response (both regarding firefighting response and population response) and *iv)* the degree implementation of preventive measures. Finally, the last component of infrastructural vulnerability deals with the likelihood of a settlement to become itself a fire source term to consolidated adjacent wildlands.

Regarding social vulnerability, it is well known that socio-economic and socio-demographic variables closely correlate with levels of risk, vulnerability, and disaster within and between communities. Wildfires may be especially harmful to people who suffer from exclusion or discrimination on economic grounds, age (particularly the elderly, children, and young people), gender, origin, functional diversity, among others (Eriksen, 2014). According to this, we use these indicators to identify and further understand, in a more nuanced and qualitative examination, the social dimensions and intersections mediating and influencing WUI fire vulnerability

Table 1 – Infrastructural vulnerability components and indicators. (Qn) stands for quantitative indicator. (Ql) stands for qualitative indicator

Vulnerability component	**Indicators**
Pre-impact (firebrands exposure)	Area with flash fuels within the settlement (Qn)
Impact of the main fire perimeter (flames and smoke exposure)	Type of design fire (Ql)
	Propagation mode (Ql)
Fire transfer	Type of WUI (Ql)
	Degree of vegetation continuity (Qn)
	Presence of canyons within the settlement (Ql)
Severity escalating factors	Structure-vegetation and road-vegetation friction (Qn)
	Presence of critical infrastructure potentially exposed (Ql)
	Firefighting arrival time (Qn)
	Population response time (notification, decision and action) (Ql)
	Compliance with water network provisions (Ql)
	Compliance with fuel-reduced fringes provisions (Ql)
Fire source term potential	Perimeter length with flash fuels around the settlement adjacent to consolidated wildlands (Qn)

As for ecosystem vulnerability analysis within the wildfire context, it has to be highlighted that it has been receiving increasing attention during these last years. Several methods can be found in the literature (e.g. Chuvieco et al., 2010; Duguy et al., 2012; Tedim et al., 2013; Aretano et al., 2015) which basically differ on the components that make up ecosystem vulnerabilty and on the type of key issues under study, wether they mainly focus on habitats of greatest ecological value, on socioeconomic aspects or on a wider range of paramaters. In an holostic approach, ecosystem vulnerability analysis in WUI areas must integrate biodiversity indicators as well as other significant landscape and ecosystem values relevant for metropolitan areas, like residential areas, areas with historical-artistic heritage elements, and leisure equipment or infrastructure. In order to consider all these different aspects with a good trade-off between scope and computational cost, in our methodology we consider ecosystem vulnerability to be fairly represented by two basic indicators: sensitivity and adaptability. Ecosystem sensitivity represents the degree to which exposed elements may be affected by fire disturbances, while ecosystem adaptability considers the socioecological adaptive capacities of both ecosystems and communitties that allow to generate recovery and regeneration strategies when facing fire disturbance. Sensitivity and adaptabiltiy are usually infered by considering parameters such as types of habitat, forest cover and community facilities (Aleksandrova et al., 2021; Birkmann et al. 2013).

3. Case study: analysing vulnerability of WUI fires in Barcelona

Barcelona is a large metropolis with a WUI area of remarkable extension, coinciding with the urbanized perimeter within the Collserola Natural Park (NP). Inserted within or in contact with a continuous forest mass, buildings, streets and highways, facilities and infrastructure could be potentially threatened by large forest fires. WUI areas of Barcelona are densely inhabited with population with diverse socio-demographic and socio-economic characteristics. They are also frequently visited for recreational and sports purposes. It has to be highlighted that Collserola NP ecosystem has a direct impact on the health of the millions of people living around it, supplying key ecosystem services to the metropolitan area of Barcelona. The many functions that Collserola generates are air quality (through the absorption of CO_2 and the release of O_2), the regulation of water resources through uptake and evapotranspiration, and the regulation of the urban climate. In addition, Collserola provides habitat for valuable biodiversity.

3.1. Design wildfires

According to Ballart and Pagès (2021), the WUI area of Barcelona can be affected by two different types of wildfires: *A)* a plume-dominated fire, under a synoptic weather pattern of southern heat wave, involving synoptic westerly hot winds from the Iberian Peninsula; and *B)* wind-driven fires (sea winds) with upslope propagation which may occur under southern heat waves or anticyclones. The scenario involving higher risk corresponds to type A fires, as those would involve larger burnt areas with high intensity (Figure 3).

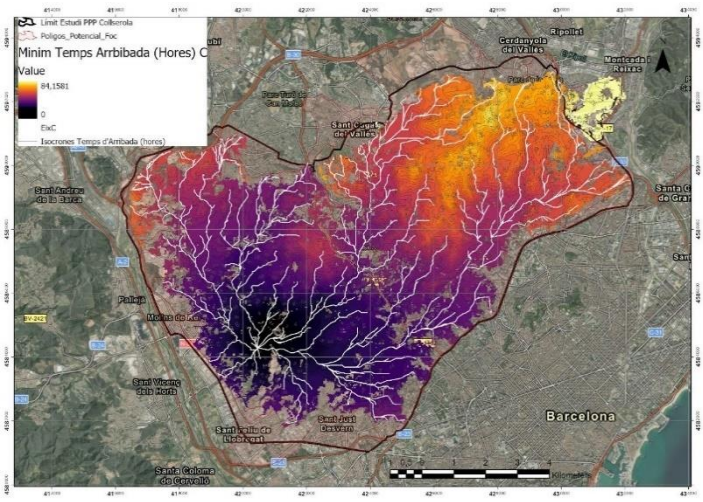

Figure 3- FlamMap simulation of a fire initiated in the metropolitan area of Barcelona (Molins de Rei) including all potential fire runs. The enormous destructive potential of the fire can be observed, as almost the overall Collserola NP area would be affected (Collserola NP perimeter is drawn with a brown solid line).

3.2. Vulnerability analysis

Vulnerability has been analysed in nine 1x1 km-areas of interest (AoI) within the WUI area of Barcelona (Figure 4) in which a preliminary screening of structural, social and ecosystems indicators has been done.

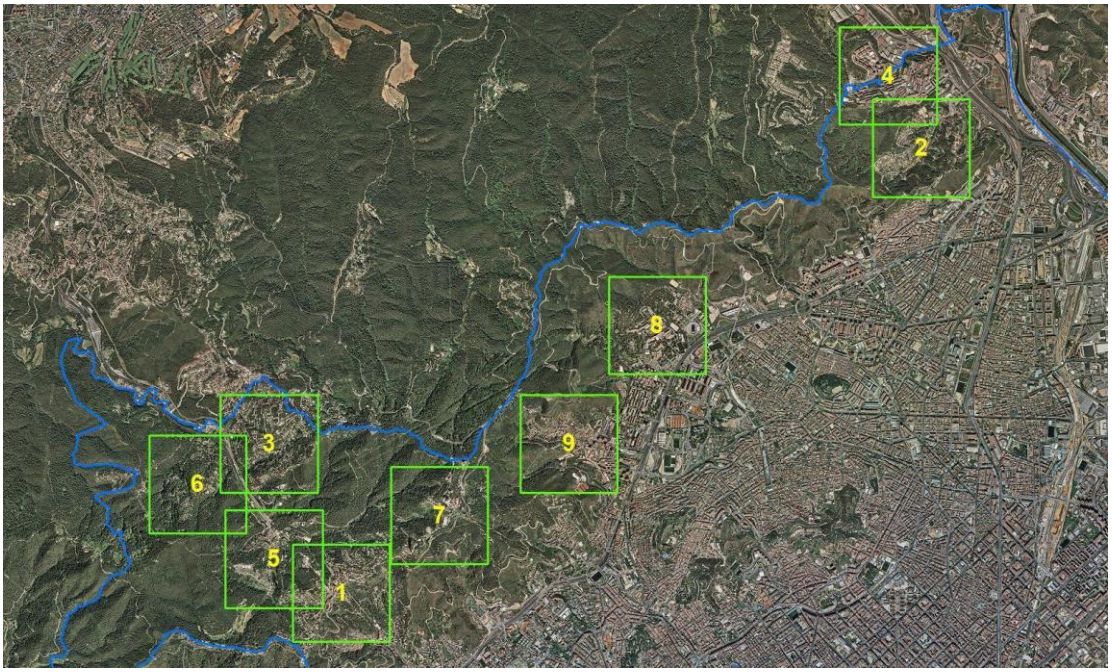

Figure 4- Location of the areas of interest within the WUI area of Barcelona. 1) Vallvidrera, 2) Torre Baró, 3) Can Rectoret, 4) Ciutat Meridiana, 5) Mas Sauró, 6) Mas Guimbau, 7) el Tibidabo, 8) Universitat de Barcelona Campus Mundet, 9) Sant Genís dels Agudells.

Regarding structural vulnerability, the indicators of the different components (i.e. firebrands exposure, fire and smoke impact, permeability, severity escalating factors and fire source potential) have been analysed and weighted across the nine AoIs. As for fire and smoke impact, the two design fires have been considered (i.e. plume-dominated fire with W-E direction and sea wind-driven fire with SE-NW direction) examining both potential head and flank impact. Permeability has been qualitatively analysed by classifying all AoIs in the study area in the two different types of WUI present in Barcelona (i.e. intermix and interface). Moreover, a quantitative analysis of vegetation continuity has been undertaken by using the WUIX algorithm (Caballero, 2019). The same software has also been used to compute the section of the WUI perimeter adjacent to consolidated grasslands or other wildlands with flash fuels, to obtain the potentiality of the AoI to become a wildfire source

term egressing from the main fire perimeter. Firebrands' exposure has been inferred by computing the area of flash fuels in all AoIs. The main severity escalating factors have been investigated with data provided by the Barcelona fire agency (Bombers de Barcelona), and Barcelona city and provincial councils. As for structure-vegetation and road-vegetation friction length, again the WUIX algorithm has been used. The three AoIs with higher structural vulnerability have appeared to be Vallvidrera, Torre Baró and Can Rectoret.

In terms of social vulnerability, the main indicators of social and urban vulnerability most used to inform public policies at municipal and metropolitan level in Barcelona have been identified. These are indicators that are essentially based on socio-demographic and economic variables at neighbourhood level. In particular, we should mention the Social Vulnerability Index (SVI), based on three basic variables such as aging, migrant status and income (Ruiz et al, 2020) and the Urban Vulnerability Index (UVI, Antón-Alonso et al., 2021) that integrates information on social and residential exclusion. Mean normalized values of SVI and UVI have been calculated for the nine AoIs. Torre Baró, Ciutat Meridiana, UB Mundet and Sant Genís dels Agudells, have appeared to be the WUI areas with higher social vulnerability.

As for ecosystem vulnerability, Barcelona WUI area has been analysed both in terms of ecosystem sensitivity and adaptability according to the methodology developed in Moran (2020). Both parameters have been combined to obtain a final value of ecosystem vulnerability. The maximum ecosystem vulnerability corresponds to those elements of maximum sensitivity and minimum adaptability. In our case study, maximum values have been found in areas of scattered intermix or settlements surrounded by dense forest coverage. According to these criteria, Vallvidrera, Can Rectoret, and Torre Baró have appeared to be the WUI areas with higher ecosystem vulnerability.

4. Conclusions

A holistic methodology to analyse vulnerability to wildfires in metropolitan areas has been designed and implemented for the case study of the WUI areas of Barcelona. It considers three main vulnerability components: infrastructural, social and ecosystem vulnerability. Relying on different types of indicators, this integrated vulnerability analysis is key to inform risk-reduction public policies, as it provides particular insights on those WUI areas within a municipality that should be prioritized along with the specific issues that should be tackled.

5. Acknowledgements

This research is funded by the Barcelona City Council and "La Caixa" Foundation (project WUICOM-BCN, 21S09274-001) and by the project PID2020-114766RB-100 of MCIN/ AEI /10.13039/501100011033.

6. References

Aleksandrova, M., Balasko, S., Kaltenborn, M., Malerba, D., Mucke, P., Neuschäfer, O., Radtke, K., Pütz, R., Strupat, C., Weller, D., Wiebe, N. (2021). World Risk Report 2021. Bündnis Entwicklung Hilft. 74 pp.

Antón-Alonso, F., Porcel, S., Cruz, I., Pujol, F. C. (2021). La vulnerabilitat urbana a Barcelona. Papers: Regió Metropolitana de Barcelona: Territori, estratègies, planejament, (63), 50-67.

Aretano, R., Semeraro, T., Petrosillo, I., De Marco, A., Pasimeni, M.R., Zurlini, G. (2015). Mapping ecological vulnerability to fire for effective conservation management of natural protected areas. Ecological Modelling, 295, 163e175.

Ballart, H., Pagès, J. (2021). Projecte d'infraestructures de prevenció de grans incendis forestals del perímetre de protecció prioritària de Collserola. Fundació Pau Costa. Generalitat de Catalunya. Departament d'Acció Climàtica, Alimentació i Agenda Rural.

Birkmann, J., Cardona, O.D., Carreno, M.L., Barbat, A.H., Pelling, M., Schneiderbauer, S., Kienberger, S., Keiler, M., Alexander, D., Zeil, P., Welle, T. (2013). Framing vulnerability, risk, and societal responses: the MOVE framework. Natural Hazards 67, 193e211.

Caballero, D. (2019). Utilización, interpretación y limitaciones del índice de interfaz WUIX. Cuadernos Técnicos.

Chuvieco, E., Aguado, I., Yebra, M., Nieto, H., Salas, P.J., Martín, M.P., Vilar, L., Martínez, J., Martín, S., Ibarra, P., Salas, J., Martín, M.P., Vilar, L., Martínez, J., Martín, S., Ibarra, P., De la Riva, J., Baeza, J., Rodríguez, F., Molina, J.R., Herrera, M.A., Zamora, R., (2010). Development of a framework for fire risk assessment using remote sensing and geographic information system technologies. Ecological Modelling, 221, 46e58.

Costa, P., Castellnou, P., Larrañaga, A., Miralles, M., Kraus, D. (2011). La prevenció dels grans incendis forestals adaptada a l'incendi tipus. FireParadox Project, Unitat Tècnica GRAF, 89 pp.

Duguy, B., Alloza, J.A., Baeza, M.J., De la Riva, J., Echeverría, M., Ibarra, P., Llovet, J., Cabello, F.P., Rovira, P., Vallejo, R.V., (2012). Modelling the ecological vulnerability to forest fires in mediterranean ecosystems using geographic information technologies. Environmental Management, 50, 1012e1026.

Eriksen, C. (2014). Gendered Risk Engagement: Challenging the Embedded Vulnerability, Social Norms and Power Relations in Conventional Australian Bushfire Education. Geographical Res., 52(1), 23–33.

Ganteuame, A., Barbero, R., Jappiot, MN., Maillé, E. (2021). Journal of Safety Science and Resilience, 2, 20-29.

McCaffrey et al. (2013). Social science research related to wildfire management: an overview of recent findings and future research needs. Int. J. Wildland Fire, 22(1), 15.

Mort, M., Rodríguez-Giralt, I., & Delicado, A. (2020). Children and young people's participation in disaster risk reduction: Agency and resilience (p. 204). Policy Press.

Mell, W.E., Manzello, S.L., Maranghides, A., Butry, D., Rehm, R.G. (2010). The wildland-urban interface fire problem – current approaches and research needs. International Journal of Wildland Fire, 19, 238-251.

Moran, P. (2020) Paisatges Disruptius: La representació dels incendis forestals en el paisatge mediterrani (Tesis doctoral) Barcelona: Escola Tècnica Superior d'Arquitectura (ETSAB) UPC.

Ruiz, E., Marco, C., Velasco, A. (2020). Desigualtat i vulnerabilitat social a Barcelona i el seu entorn metropolità. Secció d'Estudis Territorials. Àrea Metropolitana de Barcelona. 87 pp.

Tedim, F., Remelgado, R., Borges, C., Carvalho, S., Martins, J., 2013. Exploring the occurrence of mega-fires in Portugal. For. Ecol. Manage. 294, 86e96.

Vacca, P., Caballero, D., Pastor, E., Planas, E. (2020). WUI fire risk mitigation in Europe: a performance-based design approach at home-owner level. Journal fo Safey Science and Resilience, 1, 97-105.

Wildfire and evacuation simulation: An overview of research, development, and practice

Shahab Mohammad Beyki; Aldina Santiago; Luís Laím; Helder D. Craveiro

University of Coimbra, ISISE, Department of Civil Engineering, Coimbra, Portugal, {Shahab.m.beyki@gmail.com, aldina@dec.uc.pt, luislaim@uc.pt, heldercraveiro.eng@uc.pt}

Keywords

Wildfire, Fire spread simulation, Evacuation modeling, Wildland-urban interface

Abstract

Wildfires have been growing dramatically over the past decades due to climate changes, global warming, droughts and forest-landscape, and vegetation changes. Increasing losses due to wildfires have been a significant concern; therefore, wildfires have become an important field of study and research. This paper assesses and reviews the wildfire simulation approaches to predict the fire spread characteristics. These simulations are essential to analyze the potential risks and impacts of wildfire, predict the fire rate of spread (RoS), fireline intensity, and flame length, which are the most crucial parameters for fire management and first responders, and determine the evacuation necessity or requirement. The assessment of evacuation triggers is investigated according to the available literature, and studies on wildfire and fire spread simulation based on different approaches such as physical, numerical, or computational fluid dynamic (CFD) modeling and empirical are reviewed. All mentioned simulations are modeled on different scales, i. e. microscale, mesoscale, and macroscale, based on the desired criteria assessment of each case study. These approaches are distinguished basically by their ability to model an area of a certain extent or scale, and their accuracy in attaining the desired analysis, data, and prediction, and selecting one approach over the others is always a trade-off between these two criteria.

1. Introduction

Wildland fires have been recognized as a crucial field for research by the International Association for Fire Safety Science (IAFSS) agenda 2030 for a fire-safe world (McNamee *et al., 2019*). Wildland-urban interface (WUI) communities are defined as places "where humans and their development meet or intermix with wildland fuel" (Us Department of Agriculture, 2001), which are the most vulnerable to wildfires given their proximity. Moreover, other risks usually exist in WUI communities, such as insufficient transportation systems that fall behind in comparison to urban development and an increase in population; for instance, many WUI communities have only one road in and out of them, which can cause difficulties during evacuation (Cova, 2005). Multiple fatalities have been reported as the consequence of a wildfire or occurred during evacuations due to the inadequacy of the rural road. The inadequacy of the rural roads can cause congestion and trap the evacuees (e.g., Pedrogão Grande). Moreover, delayed evacuation triggers alarm or delays in evacuation advice implementation are other problems, which can cause locals to stay until the last minute and face hazardous situations (Haynes *et al. 2010*).

Wildfire modelings play a crucial role in fire management, determining the fire risk exposure, mitigating fire risk, evacuation management, and evacuation planning. The ability to forecast the wildfire behavior accurately will ensure the safety and effectiveness of wildfire control and fire management (Countryman, 1972). Different aspects of fire in the wildland context, such as intensity of the fire, direction of spread, and the rate of fire spread in the wildland, are the main desired quantities, which are modeled in accordance to conditions that affect the wildfire, e.g., weather, topography, vegetation, etc. (Dhall, 2020). A flow diagram is presented in Fig. 1 to grasp an idea of different factors of uncertainty that would affect the characteristics of fire.

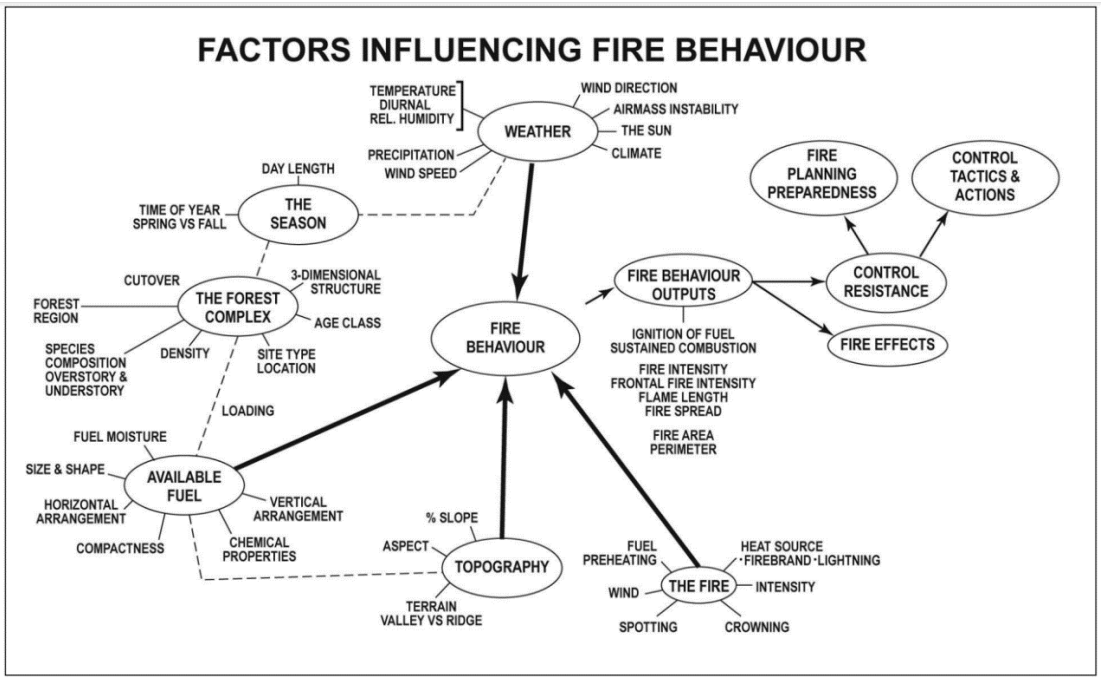

Fig. 1. Factors influencing wildland fire behavior and in turn, the complexities involved in its prediction (Santoni et al. 2011).

Wildfires, especially at the wildland-urban interface, raise various challenges for the residential population and the governing authorities in terms of producing a safe and effective plan to preserve the society, protect the infrastructure and residents' assets, and, if necessary, evacuation. To ensure life safety and evacuation effectiveness, various social and environmental characteristics of WUI communities, which pose different challenges, need to be addressed (Cohn *et al.* 2006). Heterogeneity of the household density over the WUI, layout and the positioning of the roads, insufficiency of the roads due to the WUI community growth, and the topography and geography of the surrounding environment are the physical factors that need to be considered to produce an effective and safe evacuation (Cova, 2005), in addition to social factors, e.g., age, sex, income, race, and culture of the residents (Folk *et al. 2019,* McCaffrey *et al.* 2018, McLennan *et al.* 2019, Vaiciulyte *et al.* 2018). Even though it is not yet the standard protocol, evacuation simulation models are increasingly used to develop better evacuation strategies for WUI communities (Pel *et al.* 2012, Alsnih *et al.* 2004). These simulation models enable the authorities to manage and plan an effective evacuation by deciding the evacuation trigger or start time, evacuation roads and routes, and traffic management for different wildfire scenarios. This is achieved by forecasting evacuation-affecting factors, i.e., departure time and pattern, travel duration, the mean speed of the evacuees, the traffic length, and flow rate (Pel *et al.* 2012).

2. Wildfire modeling

Wildfire simulation models are distinguished into two basic categories regarding their fundamental approach: physical models and empirical or semi-empirical models. The actual development of the combustion process is not the aim of empirical or semi-empirical simulations but rather be used in the management and decision-making process (Papadopoulos and Fotini-Niovi 2011). Many identified a coupling of both approaches as the best solution to better simulate the characteristics of wildfire and fire behavior (Cruz and Gould 2009).

Richard Rothermel (1972) published a detailed mathematical model of wildfire to predict the fire rate of spread in wildland fuels, which is the basis of many other models and simulations. This model could not be used to incorporate the crown fires, while it could only predict the fire's intensity and its spread rate in a continuous fuel bed on the ground. Finally, with the development of such models and programs, computer calculations started their use for operational and research purposes in the field of wildfires in the 1970s (Frandsen 1973, Burgan 1979).

The cellular automata (CA) model was used by Karafyllidis and Thanailakis (1997) for the very first time to predict the fire spread in homogenous and heterogeneous forests (also referred to as the KT model). The most outstanding advantage of this model was the ability to incorporate weather conditions and land topography. Later on, in an attempt to create software to simulate small-scale fires in the Mediterranean regions, with the scope of fire management and deployment of firefighters, Giorgio and Baracani (2002) combined the mathematical model introduced by Rothemermel for the simulation of fire spread with the CA theory.

In the following years, various research was carried out to improve the KT model to get more accurate results. Hernandez Encinas *et al.* (2007) improved the former developed KT models with two different approaches. First, the wildfire spread in homogenous and heterogeneous environments was modeled by changing the square cellular into a hexagonal cellular automaton. Second, a more realistic simulation was achieved by improving the KT model, which was modeling the circular fire front spread coming from the diagonal cell over linear spreading.

Tiziano *et al*. (2015) presented a CA approach that can mitigate the problem of distorted fire shapes thanks to a redefinition of the spread velocity. With the same method, the Spatio-temporal evolution of fire bands simulation with more simulated fire properties was carried out by Yuxuan *et al*. (2018). Fire shape distortion simulation was improved without any mathematical correction.

Onur Satir *et al*. (2016) manipulated the artificial neural network method to map forest fire probability in Mediterranean forestland using multiple data assessments. A new method called Evolutionary Statistical System (ESS) was developed by Bianchini *et al.* (2015) to simulate forest fire spread. This method addressed the challenges raised by the input parameters' uncertainty.

The cellular automata theory was then combined with a data-driven parallel fuzzy theory approach to simulate the wildfire spread by Ntinas *et al.* (2017). The introduced fuzzy cellular automata (FCA) model enables data incorporation from real wildfires to improve its accuracy due to a data-driven approach based on evolutionary optimization. Nevertheless, the application of this method for real-time wildfire scenarios would be restricted due to its computational complexity. Zhong Zheng *et al.* (2017) applied extreme machine learning (EML) to the traditional wildfire prediction CA method and validated the newly introduced model with five fires in the western United States. Significant improvement in the simulation accuracy was observed as a result of the method implementation.

In recent years, extensive studies have been conducted concerning wildland-urban interface fire spread modeling. Jiang *et al*. (2021) proposed a fire spread model based on the heterogeneous Cellular Automata model for large-scale complex wildland-urban interface (WUI) areas using thermal principles and empirical statistics. Valero *et al.* (2021) enabled uncertainty quantification in wildfire CFD models using multi-fidelity strategies. Attempting to overcome the wildfire modeling uncertainties, which are mainly due to the computing constraints, these authors improved the classic Monte Carlo method and achieved simulation speedups of up to 100 times; this improvement was used to quantify uncertainties and assess the sensitivity of the fire rate spread (RoS) to weather and fuel parameters. Agranat and Perminov (2020) developed a physics-based multiphase Computational Fluid Dynamics (CFD) model of wildfire initiation and spread to create a user-friendly computational tool for analyzing wildland fire behavior and its effect on urban and other structures.

3. Evacuation modeling

On the other side of this field of research stands the evacuation simulations. Wildfires necessitate the evacuation of large groups of people from large locations, often across long distances. The increasing frequency of these catastrophes shows that suitable evacuation strategies for wildfire-prone areas are required.

There is a scarcity of household data on wildfire evacuation behavior to support and design evacuation models. Most wildfire research has focused on forecasting who would flee, and how to anticipate traffic needs, however, they are still restricted in scope. Evacuation models also require information on decisions and behaviors made during the evacuation process, such as which and how many cars will be utilized, which routes evacuees will take to reach safety, which destinations will be chosen as safe spots, and many other aspects (Alsnih and Stopher 2004). In the absence of such data, most models default to ideal household behaviors, such as Leon and March (2017), and/or only consider one method of transportation (e.g. on foot (Veeraswamy *et al.* 2018) or vehicles

(Shahparvari *et al.* 2019)). Because evacuation data from WUI fires is scarce, models that integrate behavioral features frequently rely on users' judgment or defaults, which are not always anchored in fire evacuation data (Carole and Gaudo 2017, Cova and Johnson 2002).

Traditional evacuation simulation models have been demonstrated to be too optimistic regarding clearance timeframes and other results (Murray-Tuite and Mahmassani 2003). According to a study by Wu *et al.* (2012), evacuees are unlikely to organize themselves optimally along major corridors during hurricanes. When compared to models using ideal assumptions, simulating actual behavior (e.g., individuals delaying evacuation and/or choosing regular routes) (Bulumulla *et al.* 2017) can considerably reduce evacuation "effectiveness" (Chiu and Mirchandani 2008). Incorrect assumptions regarding evacuation behavior in WUI fires might jeopardize the safety of a WUI community. Models that incorrectly account for evacuee decision-making and behavior might understate evacuation results (e.g., clearance time), leading to emergency officials using ineffective traffic management measures or delaying warnings until it is too late.

Multiple time periods are involved in the household evacuation procedure. Ronchi et al. (2019) describe a generic WUI fire evacuation timetable, which lists emergency officials' and households'/evacuees' activities chronologically. After being alerted and deciding to leave, a household's evacuation timetable may include time to finish preparations, time to go on foot, time to travel by car, and time to board at a safe location. Trip generation (which predicts the number of people who will evacuate and when they will leave), trip distribution (which predicts where [the destination] people travel to reach safety), modal split (which predicts the types of transportation chosen for evacuation), and traffic assignment (which predicts the routes chosen to reach the destination) are the four steps traditionally followed by traffic models to simulate households' evacuation timelines. Driving parameters (such as speeds and flows) are included in the traffic assignment (Koligowski 2021).

The type and structure of data required for each phase vary depending on the modeling approach. Macroscale, microscale, and mesoscale modeling methodologies are employed to simulate household behavior and mobility in evacuation models. To detect larger patterns in evacuation behavior, macro models describe households/traffic behavior at the aggregate level, needing data on traffic speed and flows, capacity, and densities. Individuals (agents or vehicles) can be simulated using microscale models, which require data about household decisions, behaviors, and/or movements within the broader evacuation community. Mesoscale models offer a middle ground between the two approaches, representing traffic entities in greater depth and their interactions at a lower resolution (Murray-Tuite and Wolsohn 2013). All modeling methods require data on WUI fire evacuation decision-making and behavior. Data on evacuation decisions and timing are required to give models and users information on the number of individuals, homes, and cars entering the traffic system at various points throughout the evacuation. To offer the models/users an evacuation endpoint, data on the destinations or zones to which evacuees would be moving is also required. Following that, data on mode choice reveals how evacuees are distributed across various modes of transportation of various sizes and capabilities. Finally, data on traffic assignment is required to inform models and consumers about how various modes are dispersed and move along the road network (Murray-Tuite and Wolsohn 2013).

Cova *et al*. (2005) developed a new method for delimiting wildfire evacuation trigger points using fire spread modeling and geographic information system (GIS). It was suggested that using data on wind, topography, and fuel in conjunction with estimated evacuation time, a trigger buffer can be computed for a community whereby an evacuation is recommended if a fire crosses the edge of the buffer. Additionally, in an attempt to couple the fire simulation, pedestrian evacuation, and traffic, Wahlqvist *et al*. (2021) developed the WUI-NITY platform, which simultaneously models fire and evacuation to enhance situational awareness in evacuation scenarios.

Ronchi *et al*. (2019) focused their study on the modeling of wildland-urban interface fire evacuations. Since the most important "layers" of a WUI wildfire, including wildfire, pedestrians, and traffic, were mainly modeled in isolation, this research presented a framework for evacuation simulation, including all the layers.

An agent-based simulation model (ABM) was developed by Grajdura *et al*. (2022), to study the behavior of evacuees in case of a fast-moving wildfire toward a community. A "Post-disaster Survey" and decision tree methods were used to model agent movements and decisions. Another study modeled awareness of the residents, departure, and preparation time in case of a no-notice wildfire evacuation (Grajdura *et al*. 2021). The effects of age, race, income and other characteristics of a resident at the time of being alerted to a wildfire were

assessed. It was shown that smartphones and community evacuation plans have a large and positive effect on no-notice fire awareness time (Grajdura *et al*. 2021).

4. Gaps, challenges, and conclusions

As discussed above, in the field of wildfires and evacuation caused by wildfires simulation and modeling, there is always a challenge: the trade-off between computation power or availability and the accuracy of the results obtained by models. As a result, studies made step-by-step improvements, including considering more factors that influence the actual case to attain a more accurate result and changing the whole simulation model or the approach toward the problem. With advances in computer hardware and sophisticated processing resources, the "fully physical" models had exponential growth over the past two decades. Many factors which were considered for modeling by empirical correction coefficients are now modeled physically, and almost the exact phenomenon is implemented into the model. The distinction between radiation heat transfer and convection heat transfer, the existence of two different fire propagation regimens (wind-driven and plume-dominated), identification of surface fire and crown fire, and the transition of surface to crown fire, ignition by firebrands, fire whirlwinds, along with many other physical phenomena. Yet still, many other issues remain a challenge. Empirical factors that are used in the models need to be corrected and updated constantly; the weather data available for the fire propagation simulation are not completely exact and are based on forecasting, in which the intervals of forecasts are from hour to hour, the fuel models i. e., fuel types and fuel moisture content, vary from time to time in each location, and many other issues that need to be addressed to be able to make a more exact prediction on wildfire behavior.

As for the evacuation simulation models, none of the models that were overviewed are specially designed for WUI wildfire evacuation scenarios. But as discussed, they can be modified to provide useful data for evacuation planning and management regardless of their original mission. These models either focus on vehicle transport through the road systems as a mass concept or on individual cars through an urban area or even pedestrians. Usually, the integration between vehicles and pedestrian are not considered, which can cause serious challenges during a wildfire evacuation. The models usually lack detailed features which take the interaction between wildfire behavior and WUI residents' evacuation behavior. Different factors like age, sex, culture, race, and income affect each evacuee's decision-making process. Even the proximity to wildfire hazards has a great deal of influence on the behavior of evacuees.

Nevertheless, these models can be of great use in identifying critical points in a transportation system and roads that might cause problems during evacuations. The evacuee decisions can be estimated by a professional analyst and implemented into the model. In order to have a complete and effective evacuation simulation software, a model should be provided that integrates the wildfire characteristics, and smoke spread with the evacuee behaviors and the transportation and network system.

5. References

Margaret McNamee, Brian Meacham, Patrick van Hees, Luke Bisby, W.K. Chow, Alexis Coppalle, Ritsu Dobashi, Bogdan Dlugogorski, Rita Fahy, Charles Fleischmann, Jason Floyd, Edwin R Galea, Michael Gollner, Tuula Hakkarainen, Anthony Hamins, Longhua Hu, Peter Johnson, Björn Karlsson, Bart Merci, Yoshifuni Ohmiya, Guillermo Rein, Arnaud Trouvé, Yi Wang, Beth Weckman, IAFSS agenda 2030 for a fire safe world, Fire Safety Journal, Volume 110, 2019, 102889, https://doi.org/10.1016/j.firesaf.2019.102889.

Us Department of Agriculture, Fed. Regist., 66 (2001), pp. 751-777

Cova, Thomas J. "Public safety in the urban–wildland interface: should fire-prone communities have a maximum occupancy?" Natural Hazards Review 6.3 (2005): 99-108.

Haynes, Katharine, et al. "Australian bushfire fatalities 1900–2008: exploring trends in relation to the 'Prepare, stay and defend or leave early-policy." environmental science & policy 13.3 (2010): 185-194.

Countryman, C.M. 1972. The fire environment concept. USDA For. Serv., Pac. Southwest For. Range Exp. Stn., Berkeley, CA. 12 p.

Dhall, Aditya, et al. "A survey on systematic approaches in managing forest fires." Applied Geography 121 (2020): 102266.

Santoni, P.-A., J.-B. Filippi, J.-H. Balbi and F. Bosseur. 2011. Wildland fire behavior case studies and fuel models for landscape-scale fire modeling. J. Combust. 2011: Article ID 613424. 12 p.

Cohn, Patricia J., Matthew S. Carroll, and Yoshitaka Kumagai. "Evacuation behavior during wildfires: results of three case studies." Western Journal of Applied Forestry 21.1 (2006): 39-48.

Folk, Lauren H., et al. "A provisional conceptual model of human behavior in response to wildland-urban interface fires." Fire technology 55.5 (2019): 1619-1647.

McCaffrey, Sarah, Robyn Wilson, and Avishek Konar. "Should I stay or should I go now? Or should I wait and see? Influences on wildfire evacuation decisions." Risk analysis 38.7 (2018): 1390-1404.

McLennan, Jim, et al. "Should we leave now? Behavioral factors in evacuation under wildfire threat." Fire technology 55.2 (2019): 487-516.

Vaiciulyte, S., et al. "Insight into behavioral itinerary impact on evacuation time delay in wildfires." ESFSS18. Nancy, France (2018).

Pel, Adam J., Michiel CJ Bliemer, and Serge P. Hoogendoorn. "A review on travel behavior modeling in dynamic traffic simulation models for evacuations." Transportation 39.1 (2012): 97-123.

Alsnih, Rahaf, and Peter R. Stopher. "Review of procedures associated with devising emergency evacuation plans." Transportation Research Record 1865.1 (2004): 89-97.

Papadopoulos, George D., and Fotini-Niovi Pavlidou. "A comparative review on wildfire simulators." IEEE Systems Journal 5.2 (2011): 233-243.

Cruz, Miguel G., and Jim Gould. "National fire behavior prediction system." Proceedings of the Biennial Conference of the Institute of Foresters of Australia. Institute of Foresters of Australia, Yarralumla, ACT, 2009.

Rothermel, Richard C. A mathematical model for predicting fire spread in wildland fuels. Vol. 115. Intermountain Forest & Range Experiment Station, Forest Service, US Department of Agriculture, 1972.

Frandsen, William H. "Rothermel's fire spread model programed for the Hewlett-Packard 9820." (1973).

Burgan, Robert E. Estimating live fuel moisture for the 1978 national fire danger rating system. Vol. 226. Intermountain Forest and Range Experiment Station, Forest Service, US Department of Agriculture, 1979.

Karafyllidis, Ioannis, and Adonios Thanailakis. "A model for predicting forest fire spreading using cellular automata." Ecological Modelling 99.1 (1997): 87-97.

Guariso, Giorgio, and Matteo Baracani. "A simulation software of forest fires based on two-level cellular automata." Proceedings of the IV International Conference on Forest Fire Research. 2002.

Encinas, L. Hernández, et al. "Modelling forest fire spread using hexagonal cellular automata." Applied mathematical modeling 31.6 (2007): 1213-1227.

Tiziano Ghisu, Bachisio Arca, Grazia Pellizzaro, Pierpaolo Duce, An optimal Cellular Automata algorithm for simulating wildfire spread, Environmental Modeling & Software, Volume 71, 2015, 1-14.

Satir, Onur, Suha Berberoglu, and Cenk Donmez. "Mapping regional forest fire probability using artificial neural network model in a Mediterranean forest ecosystem." Geomatics, Natural Hazards and Risk 7.5 (2016): 1645-1658.

Bianchini, Germán, Paola Caymes-Scutari, and Miguel Méndez-Garabetti. "Evolutionary-Statistical System: A parallel method for improving forest fire spread prediction." Journal of Computational Science 6 (2015): 58-66.

Ntinas, Vasileios G., et al. "Parallel fuzzy cellular automata for data-driven simulation of wildfire spreading." Journal of computational science 21 (2017): 469-485.

Zheng, Zhong, et al. "Forest fire spread simulating model using cellular automaton with extreme learning machine." Ecological Modelling 348 (2017): 33-43.

Wenyu Jiang, Fei Wang, Linghang Fang, Xiaocui Zheng, Xiaohui Qiao, Zhanghua Li, Qingxiang Meng, Modeling of wildland-urban interface fire spread with the heterogeneous cellular automata model, Environmental Modeling & Software, Volume 135, 2021

Mario Miguel Valero, Lluís Jofre, Ricardo Torres, Multifidelity prediction in wildfire spread simulation: Modeling, uncertainty quantification, and sensitivity analysis, Environmental Modeling & Software, Volume 141, 2021.

Vladimir Agranat, Valeriy Perminov, Mathematical modeling of wildland fire initiation and spread, Environmental Modeling & Software, Volume 125, 2020

León, Jorge, and Alan March. "Taking responsibility for 'shared responsibility': urban planning for disaster risk reduction across different phases. Examining bushfire evacuation in Victoria, Australia." International Planning Studies 22.3 (2017): 289-304.

Veeraswamy, Anand, et al. "The simulation of urban-scale evacuation scenarios with application to the Swinley forest fire." Safety science 102 (2018): 178-193.

Shahparvari, Shahrooz, et al. "Fleet routing and scheduling in bushfire emergency evacuation: A regional case study of the Black Saturday bushfires in Australia." Transportation Research Part D: Transport and Environment 67 (2019): 703-722.

Adam, Carole, and Benoit Gaudou. "Modelling human behaviours in disasters from interviews: application to Melbourne bushfires." Journal of Artificial Societies and Social Simulation 20.3 (2017).

Cova, Thomas J., and Justin P. Johnson. "Microsimulation of neighborhood evacuations in the urban–wildland interface." Environment and Planning A 34.12 (2002): 2211-2229.

Murray-Tuite, Pamela M., and Hani S. Mahmassani. "Model of household trip-chain sequencing in emergency evacuation." Transportation Research Record 1831.1 (2003): 21-29.

Wu, Hao-Che, Michael K. Lindell, and Carla S. Prater. "Logistics of hurricane evacuation in Hurricanes Katrina and Rita." Transportation research part F: traffic psychology and behaviour 15.4 (2012): 445-461.

Bulumulla, Chaminda, et al. "The importance of modelling realistic human behaviour when planning evacuation schedules." Proceedings of the 16th Conference on Autonomous Agents and MultiAgent Systems. 2017.

Chiu, Yi-Chang, and Pitu B. Mirchandani. "Online behavior-robust feedback information routing strategy for mass evacuation." IEEE Transactions on Intelligent Transportation Systems 9.2 (2008): 264-274.

Enrico Ronchi, Steven M.V. Gwynne, Guillermo Rein, Paolo Intini, Rahul Wadhwani, An open multi-physics framework for modeling wildland-urban interface fire evacuations, Safety Science, Volume 118, 2019, 868-880.

Kuligowski, Erica. "Evacuation decision-making and behavior in wildfires: Past research, current challenges and a future research agenda." Fire Safety Journal 120 (2021): 103129.

Murray-Tuite, Pamela, and Brian Wolshon. "Evacuation transportation modeling: An overview of research, development, and practice." Transportation Research Part C: Emerging Technologies 27 (2013): 25-45.

Jonathan Wahlqvist, Enrico Ronchi, Steven M.V. Gwynne, Max Kinateder, Guillermo Rein, Harry Mitchell, Noureddine Bénichou, Chunyun Ma, Amanda Kimball, Erica Kuligowski, The simulation of wildland-urban interface fire evacuation: The WUI-NITY platform, Safety Science, Volume 136, 2021.

Grajdura, Sarah, Sachraa Borjigin, and Deb Niemeier. "Fast-moving dire wildfire evacuation simulation." Transportation research part D: transport and environment 104 (2022): 103190.

Grajdura, Sarah, Xiaodong Qian, and Deb Niemeier. "Awareness, departure, and preparation time in no-notice wildfire evacuations." Safety science 139 (2021): 105258.

Will Concentrated Sunlight Ignite a Wildfire?

Shaorun Lin[1], Siyan Wang[2], Yanhui Liu[1], Xinyan Huang[1,*], Michael J. Gollner[2]

[1]Research Centre for Fire Safety Engineering, Department of Building Environment and Energy Engineering, The Hong Kong Polytechnic University, Hong Kong, {flynn.lin@connect.polyu.hk, myname.yanhui@connect.polyu.hk, xy.huang@polyu.edu.hk}
[2]Deparment of Mechanical Engineering, University of California, Berkeley, CA, USA, {siyan_wang, mgollner}@berkeley.edu

**Corresponding author*

Keywords

Smouldering; Point Heating Source; Irradiation Spot; Ignition Energy; Modelling.

Abstract

Concentrated sunlight is a potential ignition source of wildfires, but its ignition mechanism is still poorly understood. Herein, we study the smoldering ignition of tissue paper (a common fuel that was abandoned by human in wildland) by a concentrated sunlight spot with heat fluxes up to 780 kW/m2, which is focused by a transparent glass sphere. The diameter of the sunlight spot on the paper sample ranges from 1.5 to 20.0 mm by varying the paper position within the focal length, where a smaller spot has a larger intensity of sunlight irradiation. We found that the concentrated sunlight can easily ignite the tissue paper. The measured minimum spot irradiation for smoldering ignition is not a constant but is much higher than 11 kW/m2 measured in a traditional cone-calorimeter test. As the diameter of the irradiation spot decreases from 20 to 1.5 mm, the minimum irradiation for smoldering ignition increases from 17.5 to 205 kW/m2. A 2-D computational model was successfully applied to reproduce the experimental observations and validate the results. This work ultimately quantifies the potential fire risk from concentrated sunlight spots and helps elucidate the underlying mechanisms leading to smoldering ignition.

1. Introduction

The ignition of wildland fuels defines the initiation of devastating fire events. Many ignition events leading to wildland fires occur remotely by a point heating source (Caton et al. 2017), such as the deposition of lofted firebrands, lightning strikes, and concentrated sunlights (Fernandez-Pello 2017a; Wang et al. 2022). Significant studies have focused on spotting ignition by lofted firebrands (Fernandez-Pello 2017b). Comparatively, a lesser-studied source of ignition is a concentrated sunlight spot, which can be focused by a dew droplet, curved glass window and decorations, transparent fish bowls, or cylindrical bottles filled with water (Fig. 1a). In 2018, sunlight concentrated by shards of broken glass had burned roughly 80 acres near Reardan, Washington (Fig. 1b). However, our understanding on this potential ignition source is still limited.

Once an intense irradiation spot is applied, a recipient fuel may first be heated, dried, decompose, and then begin to smolder (Drysdale 2011). Smoldering can be easily initiated by a weaker ignition source or even self-ignited, providing a shortcut to severe fire events through the smoldering-to-flaming transition (Rein 2014; Santoso et al. 2019). Therefore, it is of vital significance to fully understand smoldering ignition. So far, little research has studied the smoldering ignition by concentrated irradation spots, and the ignition criteria are still poorly understood.

This work investigates the smoldering ignition of multiple-layered tissue paper samples by sunlight spots concentrated by a spherical glass ball. Within the focus length, the diameter of the heating spot was varied from 1.5 mm to 20 mm, and the intensity of irradiation was varied up to 780 kW/m2. The ignition delay time, critical heat flux of smoldering by the irradiation spot were quantified. Eventually, a 2-D model will be established to vlidate the experimental results.

(a) (b)

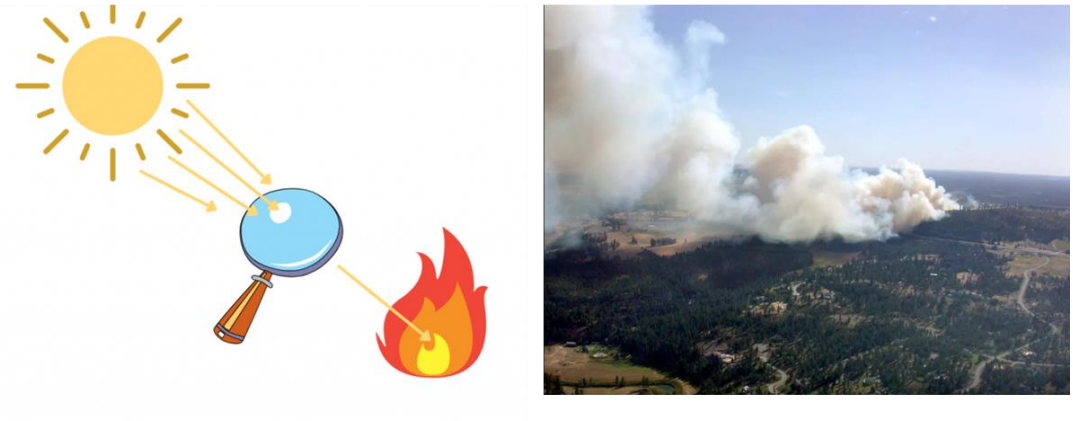

Figure 1- (a) schematic diagram of ignition by concentrated sunlight (copyright: Survival Guide), (b) a wildfire triggered by sunlight concentrated in US (copyright: The Spokesman-Review).

2. Experimental Method

2.1. Materials and setups

Thin tissue paper was used in the experiment, as it was a typical thin fuel abondoned by humans in wildlands. Before the test, the tissue paper was first oven-dried at 75 ℃ for 48 h, and its dried bulk density was measured to be 98 ± 5 kg/m^3. For the test, the tissue was first cut into a size of 60 mm × 60 mm, and six layers of tissue were packed into a sample with an overall thickness (δ) of about 2 mm (see Fig. 2a).

In the experiment, natural sunlight was concentrated by a 150-mm K9 crown glass sphere with a refractive index (n_c) around 1.53. The focal length and back focal length of the crown glass sphere were theoretically calculated to be 108 mm and 33 mm, as illustrated in Fig. 2b.

A solar power meter was fixed at the front towards the sunlight direction to record real-time solar irradiation ($\dot{q}_s''$). The sample frame was a hollow box that was inserted into the sample holder. The sample holder was installed on a slide that can adjust its distance between the tissue sample and the glass sphere with a precision of 0.5 mm.

2.2. Quantification of solar irradiaiton heat flux

To quantify the high irradiation of concentrated sunlight spot, an optical simulation performed in *TracePro* (TracePro) was first used to c orrelate the size of the light spot and theoretical irradiation ($\dot{q}_c''$) concentrated by a 150-mm crown glass sphere.

In the optical simulation, the overall concentration factor (C) is a ratio of irradiation level after and before concentrating which could be used to quantify the concentrated irradiation flux in this study. Fig. 2b shows the overall concentration factor (C) vs. light spot diameter (D) of a 150-mm glass sphere based on an optical simulation performed in *TracePro* (TracePro).

With the instant solar irradiation ($\dot{q}_s''$) and the overall concentration factor (C) for different light spots determined, the actual concentrated solar irradiant heat flux to the fuel sample can be calculated as

$$\dot{q}_c'' = C\dot{q}_s'' \qquad (1)$$

Four different positions (x) of 3 mm, 13 mm, 19 mm, and 33 mm within the glass sphere's back focal length were tested, with respect to four heating diameters (D) of 20.0 mm, 9.0 mm, 5.5 mm, and 1.5 mm.

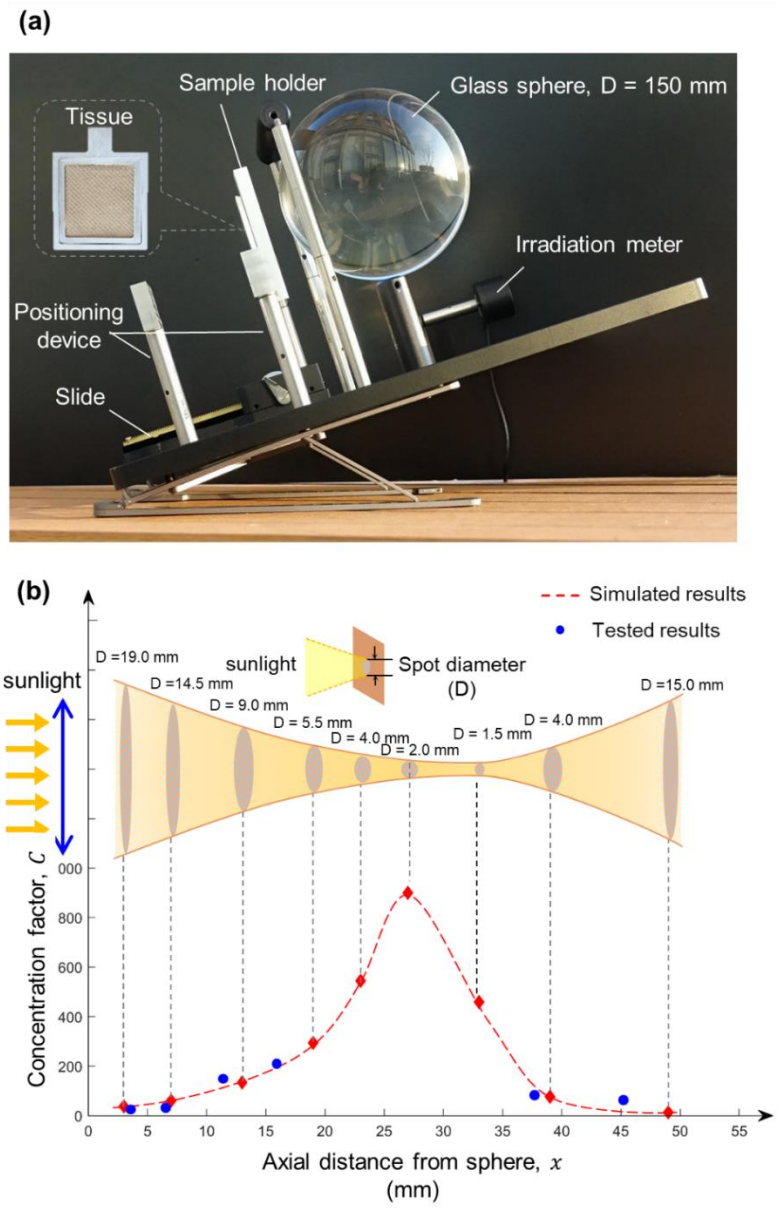

Figure 2- (a) Photos the experiment apparatus, and (b) overall concentration factor at different axial distance from sphere.

3. Experimental results

3.1. Smoldering ignition phenomena

Fig. 3a shows an example of a successful smoldering ignition process by a concentrated irradiation spot with a diameter of 1.5 mm and a resultant irradiation heat flux of 560 kW/m^2. Once the irradiation spot was applied on the sample surface, some smoke was released (Lin et al. 2019). Continuing the heating, the surface layer within the light spot turned black (or charred) and cracked, allowing the light beam to heat the lower layers directly. After heating for about 8 s, the sample detached from the apparatus but remained in the controlled environment (without wind) for another 5 min. As a result, the black spot expanded outwards evenly, expanding at a stable rate, and eventually burned out the sample. Fig. 3b shows an example of a failed smoldering ignition process by the concentrated irradiation spot with a diameter of 1.5 mm and a resultant radiant heat flux of 300 kW/m^2. Initially, smoke and a charring tendency were also observed. However, after heating for 8 s, no smoldering propagation phenomenon was observed, indicating a failed ignition.

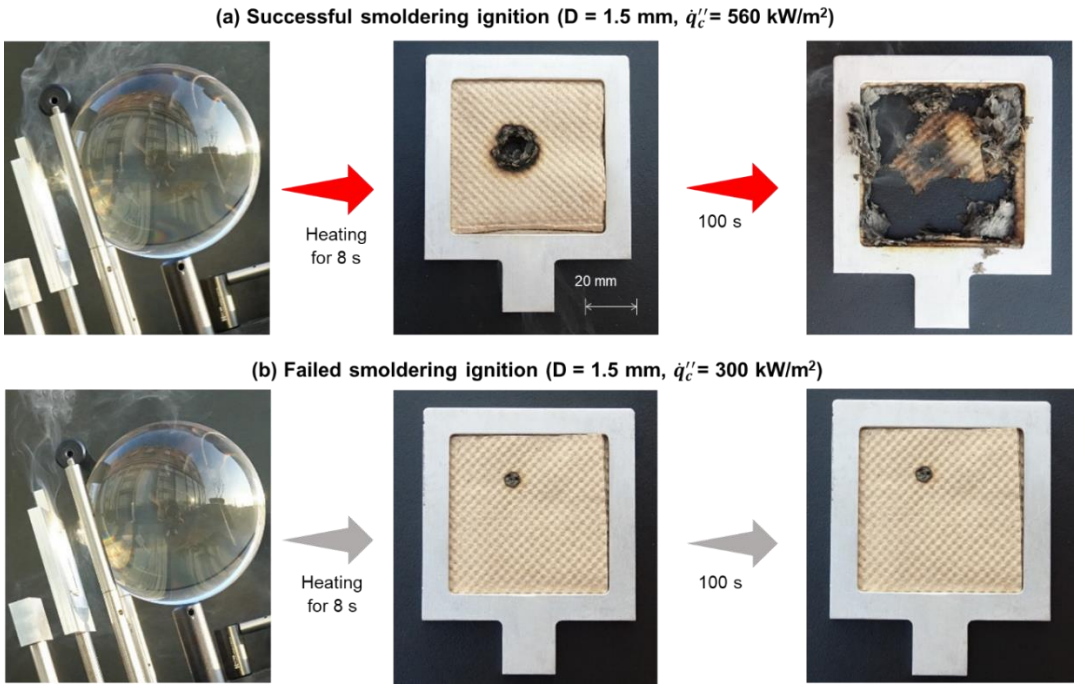

Figure 3- Smoldering ignition of dried tissue samples by concentrated irradiation spot with a diameter of 1.5 mm for 8 s, (a) successful ignition under irradiation of 560 kW/m², and (b) failed ignition under irradiation of 300 kW/m².

3.2. Critical heat flux

Fig. 4a plots the critical irradiation heat fluxes for smoldering ignition vs. the spot diameters. Interestingly, as the diameter of concentrated irradiation spot decreases from 20 mm to 1.5 mm, the critical heat flux increases dramatically from 18 kW/m^2 to 205 kW/m^2. Moreover, as the diameter of the irradiation spot increases, eventually, the critical heat flux for smoldering ignition approaches a near-minimum value obtained from the cone calorimeter (about 11 kW/m^2).

To scientifically understand the effect of the small irradiation spot on the critical heat flux of smoldering ignition, a simplified 2-D heat transfer analysis was applied. To achieve ignition, the critical irradiation heat flux ($\dot{q}''_{crt}$) should balance the environmental heat losses from the top and back sides ($\dot{q}''_{\infty}$) and the radial conductive heat loss to the virgin fuel ($\dot{q}''_{cond}$) (Lin et al. 2019; Huang and Gao 2020) a t the smoldering temperature (T_{sm}) as

$$\dot{q}''_{crt}\left(\frac{\pi D^2}{4}\right) = \dot{q}''_{\infty}\left(\frac{\pi D^2}{4}\right) \times 2 + \dot{q}''_{cond}(\pi D\delta) \qquad (2)$$

which can be further expressed and simplified as

$$\dot{q}''_{crt} = 2\dot{q}''_{\infty} + \frac{4\delta\dot{q}''_{cond}}{D} \quad \text{(small spot)} \qquad (3)$$

Therefore, as the diameter of the irradiation spot increases, the critical heat flux for smoldering ignition decreases, agreeing with the trend in Fig. 4a.

As the diameter of the irradiation spot (D) increases, the effect of conduction in Eq. (3) gradually approaches zero. Thus, for a larger irradiation spot, heat transfer can be approximated as a conventional 1-D process. The critical heat flux for smoldering ignition then approaches 11 kW/m^2, which approximately equals the environmental heat losses from the top and back surfaces as

$$\dot{q}''_{crt} = 2\dot{q}''_{\infty} = 2[\varepsilon\sigma(T_{sm}^4 - T_{\infty}^4) + h(T_{sm} - T_{\infty})] \quad \text{(large spot)} \qquad (4)$$

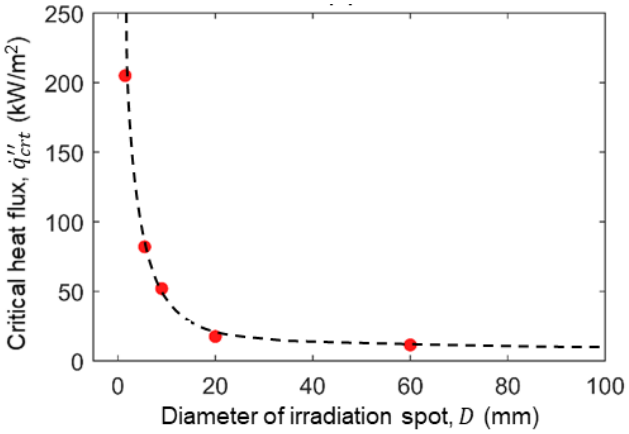

Figure 4-The relationship between diameters of irradiation spots (D) and critical ignition heat fluxes ($\dot{q}''_{crt}$).

4. Numerical modelling

To simulate the experimental observation, a 2-D numerical model is developed using Gpyro v0.8 (Lautenberger 2016). The governing conservation equations include the conservation of mass (Eq. 5), species (Eq. 6) and energy (Eq. 7) in the condensed phase as well as the mass (Eq. 8), species (Eq. 9), and momentum (Darcy's law) (Eq. 10) in the gas phase (see details in (Lautenberger 2016)). The schematic diagram of the computational domain has the same sample thickness (2 mm) and length (60 mm) as experiments. To save computational cost, the domain can be half of the actual sample owing to geometrical symmetry (Lin et al. 2022), as illustrated in Fig. 5.

$$\frac{\partial \bar{\rho}}{\partial t} = -\dot{\omega}'''_{fg} \quad (5)$$

$$\boldsymbol{\frac{\partial(\bar{\rho} Y_i)}{\partial t} = \dot{\omega}'''_{fi} - \dot{\omega}'''_{di}} \quad (6)$$

$$\boldsymbol{\frac{\partial(\bar{\rho}\bar{h})}{\partial t} = k\frac{\partial}{\partial x}\left(\frac{\partial T}{\partial x}\right) + k\frac{\partial}{\partial z}\left(\frac{\partial T}{\partial z}\right) + \dot{\omega}'''_{di}(-\Delta H_i)} \quad (7)$$

$$\frac{\partial}{\partial t}\left(\rho_g \overline{\psi}\right) + \frac{\partial \dot{m}''_x}{\partial x} + \frac{\partial \dot{m}''_z}{\partial z} = \dot{\omega}'''_{fg} \quad (8)$$

$$\frac{\partial}{\partial t}\left(\rho_g \overline{\psi} Y_j\right) + \frac{\partial}{\partial x}\left(\dot{m}''_x Y_j\right) + \frac{\partial}{\partial z}\left(\dot{m}''_z Y_j\right) = -\frac{\partial}{\partial x}\left(\overline{\psi}\rho_g D_{eff}\frac{\partial Y_j}{\partial x}\right) - \frac{\partial}{\partial z}\left(\overline{\psi}\rho_g D_{eff}\frac{\partial Y_j}{\partial z}\right) + \dot{\omega}'''_{fj} - \dot{\omega}'''_{aj} \quad (9)$$

$$\dot{m}''_z = -\frac{\kappa}{\nu}\frac{\partial p}{\partial z}\ \dot{m}''_x = -\frac{\kappa}{\nu}\frac{\partial p}{\partial x}\ \left(\rho_g = \frac{P\overline{M}}{RT}\right) \quad (10)$$

For the symmetrical plane ($x = 0$), adiabatic and impermeable boundary conditions are applied. At the top free surface ($z = 0$), initially ($t \le t_h$), irradiation ($\dot{q}''_{ir}$) with a heating diameter of $D/2$ is applied for a prescribed duration (t_h), and both convective ($h_{c,z=0} = 10\ \mathrm{W/m^2 \cdot K}$) and radiative heat losses are considered. Afterwards ($t > t_h$), the irradiation spot is removed. The mass transfer of gas species on the top free surface is considered. Based on the heat-mass transfer analogy, the mass transfer coefficient can be approximated as $h_{m,z=0} = h_{c,z=0}/C_g = 9.09\ \mathrm{g/m^2 \cdot s}$ (Lautenberger 2016). At the right and bottom boundary ($z = \delta$ and $x = L/2$), similar to the top free surface, both convective ($h_{c,z=0} = 10\ \mathrm{W/m^2 \cdot K}$) and radiative heat loss are considered, and the same mass transfer of gas species as the top surface is applied on the bottom surface. TThe whole computational domain has the same initial gas composition as the ambient air ($Y_{O_2} = 0.232$ and $Y_{N_2} = 0.768$). The solution starts to converge at $\Delta z = \Delta x = 0.1$ mm and $\Delta t = 0.01$ s.

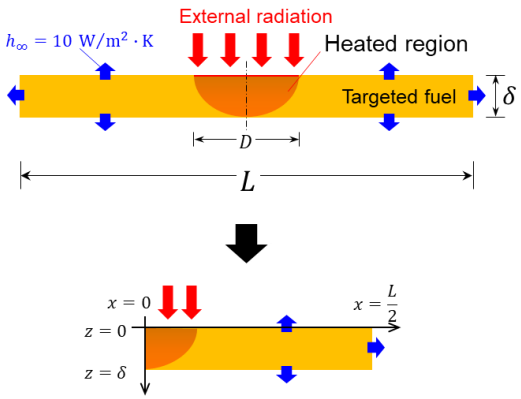

Figure 5- Schematic diagram of the 2-D computational domain for smoldering ignition using solar irradiation spots.

A previously developed 5-step kinetic scheme of typical biomass was applied here (Eq. 11-15) (Li et al. 2014; Yang et al. 2016; Huang et al. 2017). The kinetic parameters for the smoldering of biomass are obtained by optimizing the TG data in both inert and oxidative atmospheres using the Kissinger-Genetic Algorithm method ((Li et al. 2014)) and are listed in Table 1. The detailed species thermophysical properties can be found in (Huang et al. 2017).

$$\text{Water} \rightarrow \text{Water vapor} \quad [\text{dr}] \quad (11)$$

$$\text{Hemicellulose} \rightarrow \text{Char} + \text{Pyrolyzates} \quad [\text{hp}] \quad (12)$$

$$\text{Cellulose} \rightarrow \text{Char} + \text{Pyrolyzates} \quad [\text{cp}] \quad (13)$$

$$\text{Lignin} \rightarrow \text{Char} + \text{Pyrolyzates} \quad [\text{lp}] \quad (14)$$

$$\text{Char} + O_2 \rightarrow \text{Ash} + \text{gas} \quad [\text{co}] \quad (15)$$

Table 1- Chemical kinetic parameters and yields of 5-step reaction for biomass, where the reaction expression is $A_k + \nu_{O_2,k} O_2 \rightarrow \nu_{B,k} B_k + \nu_{g,k}$gas, and $\Delta H > 0$ is endothermic.

Parameter	*dr*	*hp*	*cp*	*lp*	*co*
$\lg Z_k$ (lg (s^{-1}))	8.12	8.2	11.4	21.4	12.9
E_k (kJ/mol)	67.8	106	154	229	184
n_k (-)	3	1.49	0.95	8.7	1.27
n_{k,O_2} (-)	0	0	0	0	1
$\nu_{B,k}$ (kg/kg)	0	0.24	0.27	0.40	0.06
ΔH_k (MJ/kg)	2.26	0.2	0.2	0.2	-20
$\nu_{O_2,k}$ (kg/kg)	0	0.5	0.5	0.5	1.5

5. Modelling results

Fig. 6(a) summarizes the modeled ignition time and compares it with the experimental data (uncertainty shown by shadowed area). Considering the complex nature of the smoldering process, a good agreement can be observed between predictions and experiments. Also, the effect of irradiation level ($\dot{q}''_{ir}$) on the ignition time is well predicted by the model; that is, the ignition time decreases as the irradiation level increases. For example, given an irradiation spot of 5 mm, as the radiant heat flux increases from 60 kW/m^2 to 150 kW/m^2, the predicted ignition time decreases from 85 s to 8 s.

Fig. 6(b) further summarizes the predicted minimum heat fluxes of smoldering ignition for different irradiation spots and compares them with the experimental data. For example, as the diameter of the irradiation spot increases from 2 mm to 10 mm, the predicted minimum heat flux for smoldering ignition decreases from

85 kW/m^2 to 43 kW/m^2. In general, simulations show an excellent agreement with experimental measurements with a relative error of less than 10%.

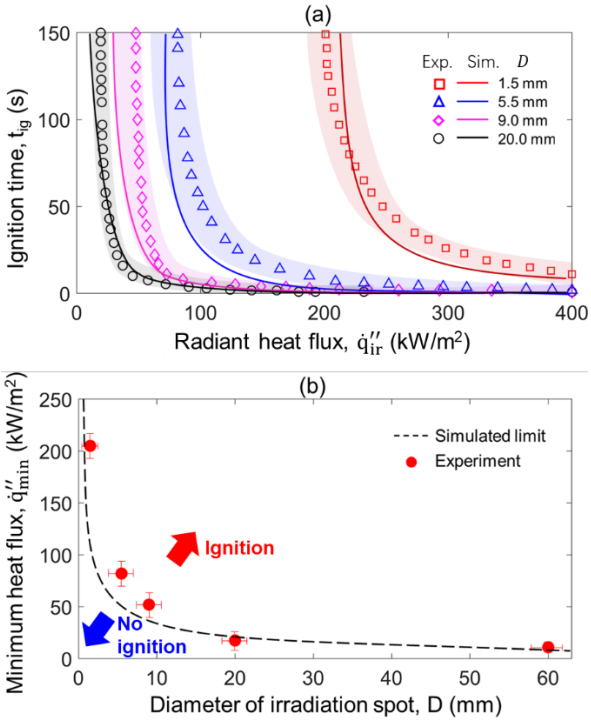

Figure 6- (a) Comparison between the experimental and modelled ignition time under different irradiation spots, (b) predicted minimum heat flux of smoldering ignition vs. test data.

6. Conclusion

In this work, we investigated the smoldering ignition of multi-layered thin tissue paper (common fuels in wildland abandoned by humans) by small irradiation spots. We found that the measured minimum spot irradiation for smoldering ignition is not constant but remains much higher than the 11 kW/m^2 measured from cone-calorimeter tests. As the diameter of irradiation spots decreases from 20.0 mm to 1.5 mm, the minimum irradiation necessary for smoldering ignition increases from 17.5 kW/m^2 to 205 kW/m^2. A simplified heat transfer analysis was proposed, which explains the critical smoldering ignition heat flux for solar irradiation spots by including two-dimensional cooling effects.

Afterwards, a 2-D computational model was successfully established to reproduce the experimental observations and validate the results. Future numerical simulations are needed to further reveal the underlying physical and chemical process of smoldering spot ignition for other fuels.

7. Acknowledgement

This research is funded by the National Natural Science Foundation of China (NSFC) No. 51876183.

8. Reference

Caton SE, Hakes RSP, Gorham DJ, Zhou A, Gollner MJ (2017) Review of Pathways for Building Fire Spread in the Wildland Urban Interface Part I: Exposure Conditions. Fire Technology 53, 429–473. doi:10.1007/s10694-016-0589-z.

Drysdale D (2011) 'An Introduction to Fire Dynamics.' (John Wiley & Sons, Ltd: Chichester, UK) doi:10.1002/9781119975465.

Fernandez-Pello AC (2017a) Wildland fire spot ignition by sparks and firebrands. Fire Safety Journal 91, 2–10. doi:10.1016/j.firesaf.2017.04.040.

Fernandez-Pello AC (2017b) Wildland fire spot ignition by sparks and firebrands. Fire Safety Journal 91, 2–10. doi:10.1016/j.firesaf.2017.04.040.

Huang X, Gao J (2020) A review of near-limit opposed fire spread. Fire Safety Journal 103141. doi:10.1016/j.firesaf.2020.103141.

Huang X, Li K, Zhang H (2017) Modelling bench-scale fire on engineered wood : Effects of transient flame and physicochemical properties. Proceedings of the Combustion Institute 36, 3167–3175. doi:10.1016/j.proci.2016.06.109.

Lautenberger C (2016) Gpyro-A Generalized Pyrolysis Model for Combustible Solids: Users'Guide. (Berkeley)

Li K, Huang X, Fleischmann C, Rein G, Ji J (2014) Pyrolysis of Medium-Density Fiberboard : Optimized Search for Kinetics Scheme and Parameters via a Genetic Algorithm Driven by Kissinger's Method. Energy & Fuels 28, 6130−6139. doi:10.1021/ef501380c.

Lin S, Sun P, Huang X (2019) Can peat soil support a flaming wildfire? International Journal of Wildland Fire 28, 601–613. doi:10.1071/wf19018.

Lin S, Yuan H, Huang X (2022) A Computational Study on the Quenching and Near-Limit Propagation of Smoldering Combustion. Combustion and Flame 238,. doi:10.1016/j.combustflame.2021.111937.

Rein G (2014) Smoldering Combustion. SFPE Handbook of Fire Protection Engineering 2014, 581–603. doi:10.1007/978-1-4939-2565-0_19.

Santoso MA, Christensen EG, Yang J, Rein G (2019) Review of the Transition From Smouldering to Flaming Combustion in Wildfires. Frontier in Mechanical Engineering 5,. doi:10.3389/fmech.2019.00049.

TracePro Software for design and analysis of illumination and optical systems.

Wang S, Lin S, Liu Y, Huang X, Gollner MJ (2022) Smoldering Ignition using a Concentrated Solar Irradiation Spot. Fire Safety Journal 129,. doi:10.1016/j.firesaf.2022.103549.

Yang J, Chen H, Zhao W, Zhou J (2016) TG-FTIR-MS study of pyrolysis products evolving from peat. Journal of Analytical and Applied Pyrolysis 117, 296–309. doi:10.1016/j.jaap.2015.11.002.

Chapter 3:
Risk Adaptation

After an off-season fire: the behavior of exotic *Eucalyptus globulus* and invasive *Acacia longifolia* in Portugal

Andreia Anjos[1,2]; Joana Jesus[1,2]; Cristina Marques[3]; Nuno Borralho[3]; Helena Trindade[2]; Sérgio Chozas[2]; Cristina Máguas[2,*]

[1] Universidade de Lisboa, Faculdade de Ciências, Departamento de Biologia Vegetal, 1749-016 Lisboa, Portugal
[2] cE3c – Centre for Ecology, Evolution and Environmental Changes, Faculdade de Ciências, Universidade de Lisboa, 1749-016 Lisboa, Portugal; {cmhanson@fc.ul.pt}
[3] RAIZ – Forest and Paper Research Institute, 3800-783 Eixo, Portugal

**Corresponding author*

Keywords

Sapling establishment; Pre-fire management; Nodulation; *Bradyrhizobium* spp.

Abstract

The introduction of species into exotic areas results in serious transformations on introduced areas. In Portugal, Eucalyptus globulus (exotic species) and Acacia longifolia (exotic invasive species) occupy a vast forested area. Eucalyptus globulus was extensively planted due to its role in pulpwood industries and, while the majority of plantations are managed, some are poorly managed along with isolated trees dispersed in the landscape (seed-trees) that are very huge and old, potentially increasing the risk of dispersal. Acacia longifolia was introduced for dune stabilization, but quickly expanded, becoming invasive without human intervention. As a leguminous species, the ability to establish symbiosis with nitrogen-fixing bacteria seems to be crucial to potentiate this invasiveness; however, these mutualistic interactions will interfere with soil microbiota, altering plant communities and affecting local biodiversity. Being two species adapted to post-fire regeneration, their behavior changes after fire occurrence, however after off-season fires, there is a gap in knowledge about their establishment dynamics. Eucalyptus globulus plantations and surrounding areas of seed-trees affected by June and October 2017 fire events were sampled, as well as unburnt areas. Acacia longifolia root-nodules were collected from unburnt and burnt areas affected by 2017 October fire and bacterial community was isolated and identified. Our results showed that the fire date and pre-fire management restrained E. globulus natural regeneration, with greater establishment in unmanaged plantations affected by the October fire. The presence of seed-trees seems to be less influenced by these factors (fire date and management), and can be considered an important seed source. Also, A. longifolia bacteriome has lower diversity after fire, but the main symbionts seem to be nitrogen-fixing bacteria, indicating a more specialized symbiosis that could enhance post-fire invasion. Bradyrhizobium spp. were the main partners in both studied zones, revealing its role as a facilitating microorganism. Off-season fires specific conditions seem to create more favourable conditions for E. globulus establishment, while A. longifolia seems to be able to establish promiscuous symbioses, but simultaneously adapt to a disturbed environment, managing to outcompete effectively with other plant species.

1. Introduction

Globally, the introduction of plant exotic species has increased due to economic interests and with ecosystems' rehabilitation purposes. However, these introduced species have negative impacts on novel ecosystems, such as disrupting ecosystems' functioning by altering water and soil cycles (Thompson *et al*., 2014; Liao *et al*., 2012), increasing fire hazard (Calviño-Cancela *et al*., 2018), reducing local biodiversity and modifying natural landscape (Vilà *et al*., 2011). In Portugal, the main exotic species are *Eucalyptus globulus* Labill. (Myrtaceae) and *Acacia longifolia* Andrews. (Leguminosae), two species native from Australia and introduced in the 19th century for different reasons (Alves *et al*., 2007; Peperkorn *et al.*, 2005). In the case of *E. globulus*, due to its fast growth, high productivity, and wood product quality (Turnbull, 1999), it was extensively planted for pulpwood production industries and occupies nowadays ca. one quarter of the forested area (ICNF, 2019). Most plantations have been planted intentionally and are managed with short rotation systems with 10-12 years tree cutting cycles and periodic clearing of the understory vegetation (Soares et al., 2007). Nonetheless, isolated *E. globulus* trees are often left uncut, hereafter referred as seed-trees, and many plantations are poorly managed, resulting in the presence of older trees with great reproductive capacity, potentially increasing the risk of

dispersal. However, *E. globulus* potential invasive capacity is a controversial topic, since qualitative studies classified it as invader in some parts of the world (Sanz-Elorza *et al*., 2001; Rejmánek and Richardson, 2013; Marchante *et al*., 2014), while other authors classified this species with a moderate risk of invasion, including in well managed plantations, which reduces its expansion beyond plantation edges (Larcombe *et al*., 2013; Fernandes *et al*., 2016; Ziller *et al*., 2018).

Another important exotic species is *A. longifolia*, considered nowadays as one of the most aggressive invaders, accounting with 18 % of the Portuguese mainland area occupied by alien species (Morais *et al*., 2017). This species was introduced for dune stabilization and recently, it has been described as an "ecosystem-engineer" (Stock *et al.*, 1995; Marchante *et al*., 2004; Yelenik *et al*., 2006) mostly determined by its inherent ability to fix atmospheric nitrogen through Legume–Rhizobia symbioses. Biological nitrogen fixation occurs inside root nodules, which includes a complex and reciprocal signalization process between the host plant and compatible bacteria (Andrews and Andrews, 2017). *Acacia* spp. do not have a specific bacterial partner, being a promiscuous woody species, that possibly exploits soil bacterial diversity to find partners for symbiotic success, particularly relevant in the context of invasion (Rodríguez-Echeverría *et al*., 2007; 2011). The identification of who is taking part in nodule's bacteriome remains a major challenge. Until now, several studies showed *Bradyrhizobium* as the most common partner in native and introduced environments, followed by *Rhizobium* (Rodríguez-Echeverría *et al*., 2010), while *Mesorhizobium* and *Sinorhizobium* appear mostly in the native range (Lafay *et al*., 2001; Marsudi *et al*., 1999; Nick *et al.*, 1999a, b). In fact, nitrogen-fixers are among the functional and taxonomically diverse rhizosphere communities (Kamutando *et al*., 2018).

Once *E. globulus* and *A. longifolia* are native from Australia, they are highly adapted to post-fire regeneration, both by bud resprouting and massive seed germination (Silva and Marchante, 2012; Águas *et al*., 2014, Calviño-Cancela *et al.*, 2018; Carvalho *et al*., 2010). In fact, fires are common perturbations in regions with Mediterranean type-climates (such as Portugal and Australia), characterized by long dry summers (Salis *et al.*, 2014). Under the current climate change scenario, it is known that the Mediterranean region will be undoubtably challenged, since it is expected an all year round warming more determinant in summer, and a widespread dryness ascribed to modifications in precipitation patterns (IPCC, 2021), resulting in a shift in fire regime extending the normal summer fire season (from July to September) with increasing off-season fires (Turco *et al*., 2019). For example, in Portugal, 2017 was a particularly dry and warm year, which resulted in several large wildfire events from June (early in the season) to mid-October (late in the season). As a consequence of the June fires ca. 52.000 hectares (ha) burned, while the October fires devastated an even larger area (ca. 190.000 ha) (ICNF, 2017). Fire events are a critical factor in these species' behavior, on one hand, regarding *E. globulus* dispersal dynamics that under off-season fires is still unknown and on the other hand, what happens on *A. longifolia* nodulation and bacterial diversity inside root nodules.

In this study, we aim to assess (1) the effects of off-season fires and pre-fire management alongside with the presence of seed-trees in *E. globulus* sapling dispersal and (2) if fire alters bacterial community inside *A. longifolia* root nodules.

2. Material and Methods

Eucalyptus globulus managed and unmanaged plantations and seed-trees surrounding areas were selected on areas affected by the off-season fires that occurred in June (early in the season) and in October (late in the season) of 2017 and in unburnt areas nearby; plots were sampled through distance transects composed by 3x3 m plots where sapling cover was assessed. Regarding *A. longifolia*, 5x5 m plots were selected in unburnt and burnt areas affected by October fire, where root nodules were collected by digging up saplings. Nodules were disinfected and bacterial diversity was isolated in YMA plates to identify symbiotic partners, through fingerprinting with M13 and rRNA 16S amplification.

Data analysis

Generalized Linear Mixed Model (GLMM) was performed in order to assess the factors that influenced *E. globulus* natural regeneration using Fire occurrence (No fire, June or October fire event), Management (managed and unmanaged) and Type (plantation or isolated seed-trees). To compare *A. longifolia* diversity between unburnt and burnt zones, Shannon-Wiener diversity index and Pielou evenness index were used.

3. Results and Discussion

3.1. *Eucalyptus globulus* behavior after off-season fire

Firstly, GLMM showed that Fire occurrence and pre-fire Management were the main factors influencing *E. globulus* saplings cover ($p < 0.001$). This species natural regeneration is very limited in absence of fire, since vegetation presence will compete with seedlings (Garau *et al.*, 2009) and litter accumulation constrain seedling emergence (Águas *et al*., 2017) (tab.1). After fire, seeds will find favorable conditions to germinate, however it is dependent on post-fire climatic conditions. In fact, after the June fire followed by summer months, regeneration was lower comparing with October fire followed by rainy season, given that seeds require wet and bare soil to germinate (Rejmánek and Richardson, 2011). However, pre-fire management highly restrain this species dispersal, since seed accumulation in the canopies is limited by frequent tree cutting cycles, preventing trees from reaching their full potential of seed production that occurs from 7 years old (Kirkpatrick, 1975). Furthermore, unmanaged conditions showed higher sapling cover especially after an October fire, representing the worst-case scenario, since trees are older leading to a greater accumulation of capsules up in the canopy. Additionally, seed-trees are an important propagules' source due to their age and seed production potential, being less sensitive to post-fire conditions and pre-fire management actions, influencing this species dispersal dynamics.

Table 1 – Eucalyptus globulus sapling cover (mean ± SE, %) for managed and unmanaged plantations and managed and unmanaged surrounding areas of seed-trees in absence of fire (no fire) and after June and October 2017 fires. Different letters indicate significant differences between no fire and the two fire dates (post hoc pairwise Tukey tests).

	Plantation		**Seed-tree**	
	Managed	**Unmanaged**	**Managed**	**Unmanaged**
No fire	0.58 ± 0.13^{a}	0.02 ± 0.02^{a}	0.07 ± 0.03^{a}	0.07 ± 0.04^{a}
June fire	0.10 ± 0.10^{ab}	1.38 ± 0.82^{ab}	2.56 ± 0.74^{ab}	9.35 ± 2.45^{cd}
October fire	1.70 ± 0.53^{a}	19.70 ± 4.35^{d}	6.72 ± 1.84^{bc}	14.00 ± 2.78^{e}

3.2. *Acacia longifolia* behavior after off-season fire

Considering *A. longifolia* nodulation, it seems that this process is potentiated after fire with a higher number of nodules present in young acacia saplings in post-fire environment (mean value of 14.0 comparing to 10.1 in unburnt zones), despite no statistically significant differences. However, there were differences in diversity and composition of bacteriome inside root nodules, with higher diversity present in unburnt zone (H' = 1.0) comparing to burnt zone (H' = 0.74) (tab. 2), underlining its promiscuity (Thrall *et al*., 2005). This higher diversity was expected once, under unburnt conditions, soils are inhabited by a greater abundance and diversity of bacteria in rhizospheric environment (Kamutando *et al*., 2018). After fire, symbiosis seems to be more specialized towards nitrogen-fixing bacteria, considering the disruption of plant-soil-biota feedbacks (Kulmatiski and Kardol, 2008) and a higher dominance of nitrogen-fixing bacteria observed. This more specialized bacteriome could be determinant for *A. longifolia* post-fire regeneration, increasing fitness, along with the absence of interspecific competition.

In this study, cultivable bacteria belonged to 5 different classes, including Alphaproteobacteria with *Bradyrhizobium* sp. as the most represented genera in both zones, Betaproteobacteria with *Paraburkholderia* sp. as the second most represented genera, and Gammaproteobacteria, mostly represented by *Pseudomonas* sp., from phylum proteobacteria; Actinobacteria from phylum actinobacteria and Bacilli from phylum firmicutes. Furthermore, there was also present an intraspecific diversity with *Bradyrhizobium cytisi* as the most abundant species in both zones.

Pielou evenness index showed a dominance of a genera in both unburnt and burnt zones (J' = 0.75 and J' = 0.67, respectively), which corresponds to the presence of *Bradyrhizobium* genus; in fact, this genus is the most common partner included among nitrogen-fixers and rhizobia group (Madigan and Martinko, 2006). Indeed, this genus has been already described as an important partner in native and introduced environments (Rodríguez-Echeverría *et al*., 2010), and its presence in both studied conditions reveals a close relationship with *A. longifolia* that may have a facilitating role. Furthermore, Paraburkholderia spp. and Pseudomonas spp. were also highly represented among isolates and are already included in Plant Growth Promoting Bacteria (PGPB), that could perform different functions apart from possible nitrogen fixation, once *Paraburkholderia* was already described

as nitrogen-fixing inducer and *Pseudomonas* was identified as non-rhizobial nodule inducing bacterial endophytes (NRE) (Martínez-Hidalgo and Hirsch, 2017). This apparently multifunctional bacteriome could be the reason why *A. longifolia* is such an effective invader.

Table 2 – Diversity of cultivated bacteria (%) isolated from A. longifolia root nodules from young saplings sampled in unburnt and burnt zones.

	Genera	Unburnt zone	Burnt zone
Alphaproteobacteria	*Althererythrobacter* sp.	1.0	0
	Bradyrhizobium sp.	36.2	45.8
	Paracoccus sp.	1.0	0
	Rhizobium sp.	1.0	0
Betaproteobacteria	*Caballeronia* sp.	2.0	0
	Duganella sp.	9.0	0
	Paraburkholderia sp.	16.0	13.6
Gammaproteobacteria	*Moraxella* sp.	2.0	0
	Pseudomonas sp.	13.8	10.2
Actinobacteria	*Micrococcus* sp.	2.0	6.8
	Nocardioides sp.	1.0	1.6
Bacilli	*Paenibacillus* sp.	2.0	0
-	Not identified	13.0	22.0

4. Conclusions

Fire seems to have a determinant role in these exotic species behavior in studied areas, influencing dispersal dynamics of *E. globulus* and altering *A. longifolia* bacteriome inside nodules. *Eucalyptus globulus* establishment is highly dependent on fire occurrence and also on post-fire climatic conditions, but also the management practices implemented prior to fire. It is important to highlight the potentiated dispersal after October fire, as well as, the presence of seed-trees as a key propagule source. Furthermore, *A. longifolia* symbiosis seems to be influenced by fire, with a more specialized interaction with nitrogen-fixing bacteria that can be referred as the "first settlers" within symbiosis reestablishment after fire. However, unburnt conditions highlighted for the fact that this invasive species is a generalist mutualist, capable of establishing symbiosis with a greater diversity of rhizospheric bacteria.

5. References

Águas, A.; Incerti, G.; Saracino, A.; Lanzotti, V.; Silva, J.S.; Rego, F.C.; Mazzoleni, S.; Bonanomi, G. 2017. Fire effects on litter chemistry and early development of Eucalyptus globulus. Plant Soil 422: 495–514;

Alves, A.M., Pereira, J.S., Silva, J.N. 2007. O Eucaliptal em Portugal – Impactes Ambientais e Investigação Científica. ISAPress, Lisbon;

Andrews, M.; Andrews, M. 2017. Specificity in Legume-Rhizobia Symbioses. International Journal of Molecular Sciences, 18:705;

Calviño-Cancela, M., Lorenzo, P., González, L. 2018. Fire increases Eucalyptus globulus seedling recruitment in forested habitats: Effects of litter, shade and burnt soil on seedling emergence and survival. Forest Ecology and Management, 409:826–834;

Carvalho, L.; Antunes, P.M.; Martins-Loução, M.A.; Klironomos, J.N. 2010. Disturbance influences the outcome of plant-soil biota interactions in the invasive Acacia longifolia and in native species. Oikos, 119:1172–1180;

Fernandes, P.; Antunes, C.; Pinho, P.; Máguas, C.; Correia, O. 2016a. Natural regeneration of Pinus pinaster and Eucalyptus globulus from plantation into adjacent natural habitats. Forest Ecology and Management 378;91–102;

Garau, A.M.; Ghersa, C.M.; Lemcoff, J.H.; Barañao, J.J. 2009. Weeds in Eucalyptus globulus subsp. maidenii (F. Muell) establishment: effects of competition on sapling growth and survivorship. New Forests, 37:251–264;

ICNF. 2017. 10º Relatório Provisório de Incêndios Florestais. Departamento de Gestão de Áreas Públicas e de Proteção Florestal do Instituto da Conservação da Natureza e das Florestas. RIF102017;

ICNF. 2019. IFN6 – Anexo Técnico. [pdf], 31 pp, versão 1.0 Instituto da Conservação da Natureza e das Florestas, Lisboa;

IPCC. 2021. Climate Change 2021: The Physical Science Basis. Contribution of Working Group I to the Sixth Assessment Report of the Intergovernmental Panel on Climate Change [Masson-Delmotte, V.P.; Zhai, A.; Pirani, S.L.; Connors, C.; Péan, S.; Berger, N.; Caud, Y.; Chen, L.; Goldfarb, M.I.; Gomis, M.; Huang, K.; Leitzell, E.; Lonnoy, J.B.R.; Matthews, T.K.; Maycock, T.; Waterfield, O.; Yelekçi, R. Yu; B. Zhou (eds.)]. Cambridge University Press. In Press.

Kamutando, C.N.; Vikram, S.; Kamgan-Nkuekam, G.; Makhalanyane, T.P.; Greve, M.; Le Roux, J.J.; Richardson, D.M.; Cowan, D.A.; Valverde, A. 2018. The Functional Potential of the Rhizospheric Microbiome of an Invasive Tree Species, Acacia dealbata. Microbial Ecology, 77:191–200;

Kirkpatrick, J.B. 1975. Natural distribution of Eucalyptus globulus Labill. Austalian Geographer, 13:22-35.

Kulmatiski, A.; Kardol, P. 2008 Getting plant-soil feedbacks out of the greenhouse: experimental and conceptual approaches. Progress in Botany, 69:449–472;

Lafay, B.; Burdon, J.J. 2001. Small-Subunit rRNA Genotyping of Rhizobia Nodulating Australian Acacia spp. Applied and Environmental Microbiology, 67:396–402;

Larcombe, M.J.; Silva, J.S.; Vaillancourt, R.E.; Potts, B.M. 2013. Assessing the invasive potential of Eucalyptus globulus in Australia: quantification of wildling establishment from plantations. Biological Invasions 15:2763–2781;

Liao, C.; Luo, Y.; Fang, C.; Chen, J.; Li, B. 2012. The effects of plantation practice on soil properties based on the comparison between natural and planted forests: a meta-analysis. Global Ecology and Biogeography, 21:318–327;

Madigan, M.; Martinko, J. 2006. Brock, Biology of Microorganisms, 11th edition, Chapter 17 Metabolic Diversity, pp. 504-506; 586-587; Chapter 19, p. 641;

Marchante, H.; Marchante, E.; Buscardo, E.; Maia, J.; Freitas, H. 2004. Recovery Potential of Dune Ecosystems Invaded by an Exotic Acacia Species (Acacia longifolia) Weed Technology, 18:1427–1433;

Marchante, H.; Morais, M.; Freitas, H.; Marchante, E. 2014. Guia prático para a identificação de Plantas Invasoras em Portugal. Imprensa da Universidade de Coimbra, Coimbra;

Martinez-Hidalgo, P.; Hirsch, A. 2017. The nodule microbiome: N2-fixing rhizobia do not live alone. Phytobiomes, 1:70-82;

Marsudi, N. 1999. Identification and characterization of fast- and slow-growing root nodule bacteria from South-Western Australian soils able to nodulate Acacia saligna. Soil Biology and Biochemistry, 31:1229–1238;

Morais, M.C.; Marchante, H.; Marchante, H. 2017. Big troubles are already here: Risk assessment protocol shows high risk of many alien plants present in Portugal. Journal for Nature Conservation, 35:1–12;

Nick, G.; De Lajudie, P.; Eardly, B.D.; Suomalainen, S.; Paulin, L.; Zhang, X.; Gillis, M.; Lindström, K. 1999. Sinorhizobium arboris sp. nov. and Sinorhizobium kostiense sp. nov., isolated from leguminous trees in Sudan and Kenya. International Journal of Systematic and Evolutionary Microbiology, 49:1359–1368;

Nick, G.; Jussila, M.; Hoste, B.; Niemi, M.; Kaijalainen, S.; Lajudie, P.; de Gillis, M.; Bruijn, F.J.; de Lindström, K. 1999. Rhizobia isolated from root nodules of tropical leguminous trees characterized using DNA-DNA dot-blot hybridization and rep-PCR genomic fingerprinting. Systematic and Applied Microbiology, 22:287–299;

Peperkorn, R.; Werner, C; Beyschlag, W. 2005. Phenotypic plasticity of an invasive acacia versus two native Mediterranean species. Functional Plant Biology, 32:933– 944;

Rejmánek, M.; Richardson, D.M. 2011. Eucalypts. In: Simberloff, D., Rejmánek, M. (Eds.), Encyclopedia of biological invasions. University of California Press, Berkeley, pp. 203–209;

Rejmánek, M.; Richardson, D.M. 2013. Trees and shrubs as invasive alien species-2013 update of the global database. Diversity and Distributions. 19:1093–1094;

Rodríguez-Echeverría, S.; Crisostomo, J.; Freitas, H. 2007. Genetic Diversity of Rhizobia Associated with Acacia longifolia in Two Stages of Invasion of Coastal Sand Dunes. Applied and Environmental Microbiology, 73:5066–5070;

Rodríguez-Echeverría, S. 2010. Rhizobial hitchhikers from Down Under: Invasional meltdown in a plant-bacteria mutualism? Journal of Biogeography, 37:1611–1622;

Rodríguez-Echeverría, S.; Le Roux, J.J.; Crisostomo, J.; Ndlovu, J. 2011. Jack-of-all-trades and master of many? How does associated rhizobial diversity influence the colonization success of Australian Acacia species? Diversity and Distributions, 17:946–957;

Salis, M.; Ager, A.A.; Finney, M.A.; Arca, B.; Spano, D. 2014. Analyzing spatiotemporal changes in wildfire regime and exposure across a Mediterranean fire-prone area. Natural Hazards, 71:1389–1418;

Sanz-Elorza, M.; Dana, E.D.; Sobrino, E. 2001. Checklist of invasive alien plants in Spain (Iberian Peninsula and Balearic Islands). Lazaroa, 22:121–131;

Silva, J.S.; Marchante, H. 2012. Post-fire management of exotic forests. In: Moreira, F.; Heras, J.; Corona, P.; Arianoutsou, M. (Eds.), Post-Fire Management and Restoration of Southern European Forests. Springer, Dordrecht, pp. 223–255;

Soares, P.; Tomé, M.; Pereira, J.S. 2007. A produtividade do eucaliptal, in: Alves, A.M.; Pereira, J.S.; Silva, J.M.N. (Eds.), O Eucaliptal Em Portugal – Impactes Ambientais E Investigação Científica. Lisbon, pp. 27–60;

Stock, W.D.; Wienand, K.T.; Baker, A.C. 1995. Impacts of invading N2-fixing Acacia species on patterns of nutrient cycling in two Cape ecosystems: Evidence from soil incubation studies and 15N natural abundance values. Oecologia 101:375–382;

Thrall, P.H.; Millsom, D.A.; Jeavons, A.C.; Waayers, M.; Harvey, G.R.; Bagnall, D.J.; Brockwell, J. 2005. Seed inoculation with effective root-nodule bacteria enhances revegetation success. Journal of Applied Ecology, 42:740-751;

Thompson, I.D; Okabe, K.; Parrotta, J.A; Brockerhoff, E.: Jactel, H.; Forrester, D.I.; Taki, H. 2014. Biodiversity and ecosystem services: lessons from nature to improve management of planted forests for REDD-plus. Biodiversity and Conservation, 23:2613–2635;

Turco, M.; Jerez, S.; Augusto, S.; Tarín-carrasco, P.; Ratola, N.; Jiménez-Guerrero, P.; Trigo, R.M. 2019. Climate drivers of the 2017 devastating fires in Portugal. Scientific Reports, 9:13886;

Turnbull, J.W. 1999. Eucalypt plantations. New. Forest 17:37-52;

Vilà, M.; Espinar, J.L.; Hejda, M.; Hulme, P.; Jarošík, V.; Maron, J.; Pergl, J.; Schaffner, U.; Sun, Y.; Pyšek, P. 2011. Ecological impacts of invasive alien plants: A meta-analysis of their effects on species, communities and ecosystems. Ecology letters. 14:702-8;

Yelenik, S.G.; Stock, W.D.; Richardson, D.M. 2006. Functional Group Identity Does not Predict Invader Impacts: Differential Effects of Nitrogen-fixing Exotic Plants on Ecosystem Function. Biological Invasions, 9:117–125;

Ziller, S.R.; Dechoum, M.S.; Zenni, R.D. 2018. Predicting invasion risk of 16 species of eucalypts using a risk assessment protocol developed for Brazil. Austral Ecology.

Analyzing the EU forestry sector to seek new market opportunities using Minimum Spanning Tree based clustering analysis

Jongmin Han[1*]; Abílio Pereira Pacheco[2]; José Coelho Rodrigues[3]

[1,2,3] INESC TEC and Faculdade de Engenharia, Universidade do Porto, Rua Dr. Roberto Frias, 378, 4200-465, Porto, Portugal
[2]ForestWISE - Collaborative Laboratory for Integrated Forest and Fire Management, Quinta de Prados, 5000-801 Vila Real, Portugal
{jongmin.han, app, jpcr}@fe.up.pt

**Corresponding author*

Keywords

Clustering analysis; MST based clustering; selection of variables; EU 27 classification; European forest

Abstract

To enhance the economic viability and address the labour shortage in the forestry industry, alternative solutions using robotization and automation are emerging. However, due to technological barriers and lack of solid business models, successful commercialization in the forestry sector is yet to be challenging. As an initial market analysis for developing a business model for new forestry machineries, this study was conducted to reveal clusters of EU countries to seek the potential market opportunities outside of Portugal. To identify similar market conditions and restrictions, EU countries were clustered using Minimum Spanning Tree (MST) based clustering analysis clustering algorithm and selection of variables while considering the geographic, economic, and social conditions of each country.

1. Introduction

Robotization and automation of forestry machinery are emerging as an alternative to address significant challenges in the forestry industry in terms of economic viability, safety, labour shortages, and environmental performance (Lideskog, Karlberg, and Bergsten 2015; Couceiro et al. 2019)). However, such a technological shift has not yet had significant commercialization in the forestry sector except for logging due to technological challenges and a lack of solid business models (Teece 2010; Lideskog, Karlberg, and Bergsten 2015). A well-developed business model is essential for increasing the value of technology and opportunities into economic outputs through customers and markets leading to the success of a business (Chesbrough 2002; 2010). Thoroughly analyzing the main components of a business model is an essential process to create a solid framework for developing the business model (Couceiro et al. 2019). Especially, determining the value proposition and market segments are crucial in measuring and predicting the potential of new products and services.

In most developed countries, the forestry sector is highly internationalized, concerned with its sustainability, diversity and increasing complexity, responding to the growing competition (Melo, Cunha, and Ferreira 2017). Although the forestry industry in Portugal is rich in opportunities, mainly due to the abandonment of rural and deprived areas and the lack of investment in maintenance and conservation, the potential has not yet been fully exploited (Melo, Cunha, and Ferreira 2017). Different countries around the world have distinct levels of economic, social, and environmental issues in forestry due to several factors that each country faces, e.g. geographic characteristics, economic capabilities. The possibility of such issues which may directly lead to potential risks is influenced by the situations that a given country has. For example, damages from natural disasters may vary depending on a country's risk management capabilities. According to literature (Toya and Skidmore 2007), countries with higher income and educational attainment, greater openness, more complete financial systems, and smaller government are more likely to experience fewer losses. Thus, there is a need to investigate the geographic, economic, and social features to draw implications in a variety of scenarios, including potential market opportunities. In this sense, the use of different indicators can be a solution for analyzing the current situation of the forest sector at a national level.

As an initial phase for building a business model for new forestry machines, this study was conducted to reveal clusters of EU countries to seek the potential market opportunities outside of Portugal. To identify similar market conditions and opportunities, EU countries were clustered using a hierarchical clustering algorithm, an unsupervised learning branch from the Artificial Intelligence.

2. Methodology

2.1. Data collection

The main statistical data source used for the analysis was from major international organizations such as the Food and Agricultural Organization of the United Nations (FAO). The FAO statistical databases (FAOSTAT) platform is freely accessible and contains the largest statistical database on agriculture, fishery, and forestry in the world, with approximately 20,000 indicators covering 245 countries and territories, with around 2,000,000 users each year (FAOSTAT, 2022). The FAOSTAT database is used widely in peer-reviewed literature, serving as the basis for many Agriculture, Forestry, and Other Land Use (AFOLU)-related analyses (Tubiello et al. 2013). FAOSTAT is useful to make the cross-country comparisons because it has the user-friendly interface and the possibility to track the different items that we need in one place. To reflect the economic, social, and environmental issues in the forestry sector, twenty-seven indicators for 2015 (year) were selected related to forest production, land use, and social capital in FAOSTAT. The selected indicators had to respect the following criteria: (i) be fact based; (ii) be based on available data for twenty-seven EU countries; (iii) be easily interpreted. In creating the final list of indicators, new ad hoc indicators were created. One of the ad hoc indicators was, for example, "The production quantity of Pulpwood (m^3) per Forest Land (1000 ha)"

2.2. Data pre-processing

As the variables were reported in different units, to determine distances between the EU countries, it was necessary to standardize them and eliminate dependence. According to (Arabie et al. 1996), when the number of variables is large, there is a possibility that variables that do not contribute to cluster classification exist, and these variables may interfere with finding a cluster structure. Finding structure in a high-dimensional variable space with a small dataset is a general problem in both classification and cluster analysis. This may be due to the presence of several "noisy" noninformative variables and/or redundant features from strongly correlated or more generally strongly dependent variables that may produce, for instance, multicollinearity (Fraiman, Justel, and Svarc 2008). The basic methodology for the detection of redundant variables is correlation analysis under unsupervised dataset that there are no output variables to predict. The most used measures are Pearson correlation coefficient for a linear correlation, and Spearman and Kendall correlation coefficient for a nonlinear correlation (Marshall 1996; Chok 2010). According to previous research, the use of Pearson correlation coefficient is not robust in forms of associations other than linear or normal associations (Kowalski 1972; Speed 2011).

2.3. Clustering analysis based on Minimum Spanning Tree (MST)

Hierarchical cluster analysis as a multivariate statistical tool has also been widely used to group the data by simultaneously clustering objects and variables (Newman 2004). Hierarchical clustering has the advantage that it does not require a knowledge on the number or size of groups to look for beforehand. However, it does not tell us how many groups should be used to get the best division (Jain, Murty, and Flynn 1999; Xu and II 2005; Fortunato 2010). Another problem is the lack of the ability to detect clusters which are not defined by regular geometric curves (Grygorash, Zhou, and Jorgensen 2006; Zhong, Miao, and Fränti 2011; Wu et al. 2013; Tewarie et al. 2015) Detecting clusters with irregular boundaries has become a research interest in recent years. In particular, the clustering algorithm using the Minimum Spanning Tree (MST) has recently attracted a lot of attention (Gower and Ross 1969). MST is a tree that minimizes the total weight or lengths of the edges of the tree under a weighted, undirected graph.

3. Results and Discussion

As a result of the Shapiro-Wilk test for normality, twenty-nine indicators in 2010 and twenty-six indicators in 2015 did not follow a normal distribution. With large enough sample sizes (> 30 or 40), the violation of the

normality assumption should not cause major problems (Ghasemi and Zahediasl 2012). However, the dataset which this research dealt with is small sample size and its normality is violated. Thus, for variable reduction, the Kendall correlation measure was employed. It is known to be more robust and slightly more efficient than the Spearman correlation coefficient (Croux and Dehon 2010).

Following the above-mentioned methodology, the first step was the elimination of some higher correlated dependent and statistically significant variables (significance level = 5%) for the selection of appropriate features. The three indicators, such as "Share of Net value added of forestry in total net value added", "Proportion of naturally regenerating forest in forest area", "Proportion of land under meadows and pastures in agricultural area", consequently had been eliminated by correlation analysis. Finally, the analysis enabled the grouping of twenty-seven EU countries into clusters using thirty-seven different variables. When analyzing the similarity without SDG indicators between EU countries, twenty-nine indicators were used except eight SDG indicators.

Before correlation analysis, normalization (Min-Max scaling) was used to make variables comparable to each other on equal grounds. The variables were shift and rescaled so that they end up ranging between 0 and 1. The method did not change the shape of the distribution of data while adjusting the values. If the shape of the distribution is changed, it introduces bias into analysis because the distribution of a lot of collected data is not Gaussian. Applying Prim's algorithm for shaping a complete graph based on Manhattan distance among monitored features into MST. Finally, a network community detection technique was applied to identify the clusters of EU countries.

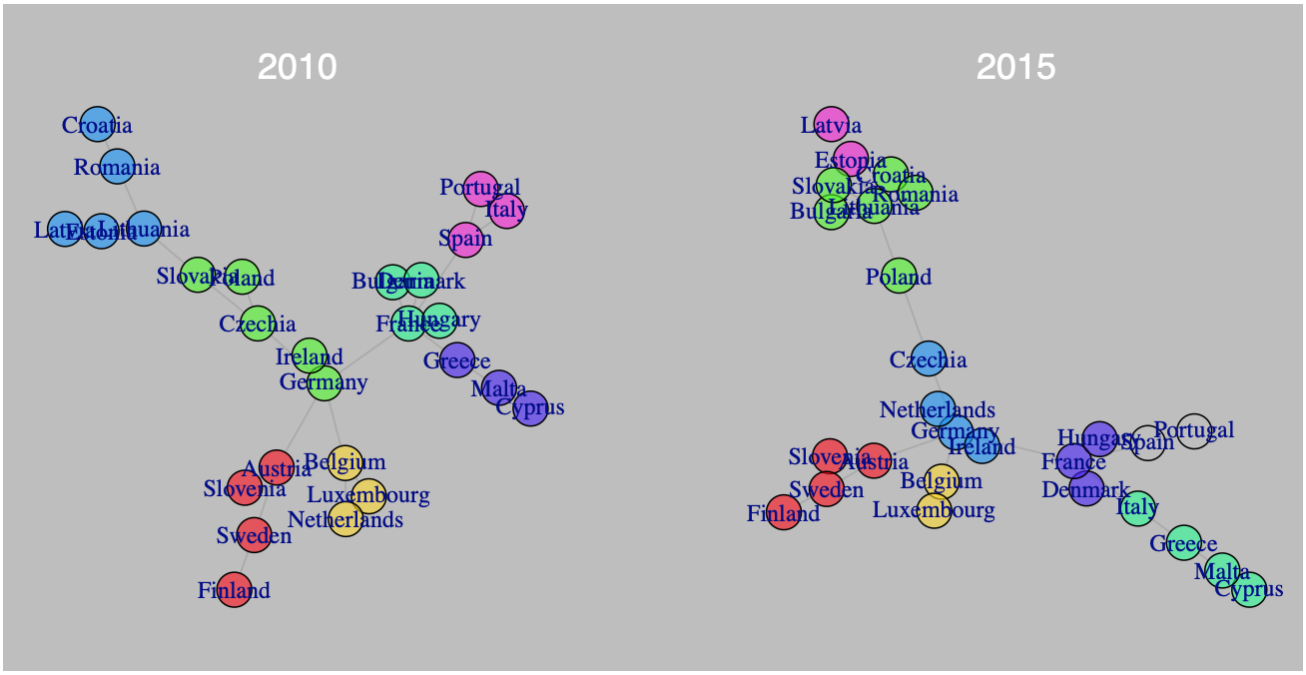

Figure 1- ***Network communities of EU countries with MST based on the Manhattan distance, and each cluster is identified by a special color***

Our analysis of the different indicators related to forestry through clustering analysis based on MST was performed on the EU27 countries for two time periods 2010 and 2015. Fig. 1 shows that there is a difference in the network community composition depending on different periods. There were six clusters created, representing the seven groups of EU-27 countries in 2010, while eight clusters were created in 2015.

Table1. Sorting countries into clusters using dataset 2010

1	2	3	4	5	6	7
Austria	Belgium	Czechia	Bulgaria	Croatia	Cyprus	Italy
Finland	Luxembourg	Germany	Denmark	Estonia	Greece	Portugal
Slovenia	Netherlands	Ireland	France	Latvia	Malta	Spain
Sweden		Poland	Hungary	Lithuania		
		Slovakia		Romania		

The results of year 2010 are presented by two clusters of five members, two of four members and three of three members (Table 2). On the other hand, the results of year 2015 are presented by one cluster of three members, one of five members, two of three members and three of three members (Table 2). The group consisting of Austria, Finland, Slovenia, and Sweden did not change during the two periods in 2010 and 2015, and Portugal and Spain, which were in the same group in 2010, were analyzed as belonging to the same group in 2015 as well. On the other hand, in Italy and Luxembourg, the group to which they belonged also changed over time.

Table 2. Sorting countries into clusters using dataset 2015

1	2	3	4	5	6	7	8
Austria	Belgium	Bulgaria	Cyprus	Czechia	Denmark	Latvia	Portugal
Finland	Luxembourg	Croatia	Greece	Germany	France	Estonia	Spain
Slovenia		Lithuania	Malta	Ireland	Hungary		
Sweden		Poland	Italy	Netherlands			
		Romania					
		Slovakia					

4. References

Arabie, P, L J Hubert, G De Soete, and Glenn W Milligan. 1996. "Clustering and Classification," 341–75. https://doi.org/10.1142/9789812832153_0010.

Chesbrough, Henry. 2002. "The Role of the Business Model in Capturing Value from Innovation: Evidence from Xerox Corporation's Technology Spin-off Companies." *Industrial and Corporate Change* 11 (3): 529–55. https://doi.org/10.1093/icc/11.3.529.

———. 2010. "Business Model Innovation: Opportunities and Barriers." *Long Range Planning* 43 (2–3): 354–63. https://doi.org/10.1016/j.lrp.2009.07.010.

Chok, Nian Shong. 2010. "Pearson's Versus Spearman's and Kendall's Correlation Coefficients for Continuous Data."

Couceiro, Micael S., David Portugal, João F. Ferreira, and Rui P. Rocha. 2019. "SEMFIRE: Towards a New Generation of Forestry Maintenance Multi-Robot Systems." *2019 IEEE/SICE International Symposium on System Integration (SII)* 00: 270–76. https://doi.org/10.1109/sii.2019.8700403.

Croux, Christophe, and Catherine Dehon. 2010. "Influence Functions of the Spearman and Kendall Correlation Measures." *Statistical Methods & Applications* 19 (4): 497–515. https://doi.org/10.1007/s10260-010-0142-z.

FAOSTAT. 2022. Database on Agriculture. Food and Agriculture Organization of the United Nations. Rome, Italy. Food and Agriculture Organization of the United Nations. 2022. https://www.fao.org/faostat/en/#home.

Fortunato, Santo. 2010. "Community Detection in Graphs." *Physics Reports* 486 (3–5): 75–174. https://doi.org/10.1016/j.physrep.2009.11.002.

Fraiman, Ricardo, Ana Justel, and Marcela Svarc. 2008. "Selection of Variables for Cluster Analysis and Classification Rules." *Journal of the American Statistical Association* 103 (483): 1294–1303. https://doi.org/10.1198/016214508000000544.

Ghasemi, Asghar, and Saleh Zahediasl. 2012. "Normality Tests for Statistical Analysis: A Guide for Non-Statisticians." *International Journal of Endocrinology and Metabolism* 10 (2): 486–89. https://doi.org/10.5812/ijem.3505.

Gower, J. C., and G. J. S. Ross. 1969. "Minimum Spanning Trees and Single Linkage Cluster Analysis." *Journal of the Royal Statistical Society: Series C (Applied Statistics)* 18 (1): 54–64. https://doi.org/10.2307/2346439.

Grygorash, Oleksandr, Yan Zhou, and Zach Jorgensen. 2006. "Minimum Spanning Tree Based Clustering Algorithms." *2006 18th IEEE International Conference on Tools with Artificial Intelligence (ICTAI'06)*, 73–81. https://doi.org/10.1109/ictai.2006.83.

Jain, A. K., M. N. Murty, and P. J. Flynn. 1999. "Data Clustering: A Review." *ACM Computing Surveys (CSUR)* 31 (3): 264–323. https://doi.org/10.1145/331499.331504.

Kowalski, Charles J. 1972. "On the Effects of Non-Normality on the Distribution of the Sample Product-Moment Correlation Coefficient." *Journal of the Royal Statistical Society: Series C (Applied Statistics)* 21 (1): 1–12. https://doi.org/10.2307/2346598.

Lideskog, Håkan, Magnus Karlberg, and Urban Bergsten. 2015. "Development of a Research Vehicle Platform to Improve Productivity and Value-Extraction in Forestry." *Procedia CIRP* 38: 68–73. https://doi.org/10.1016/j.procir.2015.07.014.

Marshall, Albert W. 1996. "Copulas, Marginals, and Joint Distributions." *Lecture Notes-Monograph Series* 28.

Melo, A., J. Cunha, and P. Ferreira. 2017. "Business Model for Forest Management." *Procedia Manufacturing* 13: 940–47. https://doi.org/10.1016/j.promfg.2017.09.164.

Newman, M. E. J. 2004. "Detecting Community Structure in Networks." *The European Physical Journal B* 38 (2): 321–30. https://doi.org/10.1140/epjb/e2004-00124-y.

Speed, Terry. 2011. "A Correlation for the 21st Century." *Science* 334 (6062): 1502–3. https://doi.org/10.1126/science.1215894.

Teece, David J. 2010. "Business Models, Business Strategy and Innovation." *Long Range Planning* 43 (2–3): 172–94. https://doi.org/10.1016/j.lrp.2009.07.003.

Tewarie, P., E. van Dellen, A. Hillebrand, and C.J. Stam. 2015. "The Minimum Spanning Tree: An Unbiased Method for Brain Network Analysis." *NeuroImage* 104: 177–88. https://doi.org/10.1016/j.neuroimage.2014.10.015.

Toya, Hideki, and Mark Skidmore. 2007. "Economic Development and the Impacts of Natural Disasters." *Economics Letters* 94 (1): 20–25. https://doi.org/10.1016/j.econlet.2006.06.020.

Tubiello, Francesco N, Mirella Salvatore, Simone Rossi, Alessandro Ferrara, Nuala Fitton, and Pete Smith. 2013. "The FAOSTAT Database of Greenhouse Gas Emissions from Agriculture." *Environmental Research Letters* 8 (1): 015009. https://doi.org/10.1088/1748-9326/8/1/015009.

Wu, Jianshe, Xiaoxiao Li, Licheng Jiao, Xiaohua Wang, and Bo Sun. 2013. "Minimum Spanning Trees for Community Detection." *Physica A: Statistical Mechanics and Its Applications* 392 (9): 2265–77. https://doi.org/10.1016/j.physa.2013.01.015.

Xu, Rui, and Donald Wunsch II. 2005. "Survey of Clustering Algorithms." *IEEE Transactions on Neural Networks* 16 (3): 645–78. https://doi.org/10.1109/tnn.2005.845141.

Zhong, Caiming, Duoqian Miao, and Pasi Fränti. 2011. "Minimum Spanning Tree Based Split-and-Merge: A Hierarchical Clustering Method." *Information Sciences* 181 (16): 3397–3410. https://doi.org/10.1016/j.ins.2011.04.013.

Arctic fires and smouldering combustion: influence of soil and air temperature on fire spread

Eirik G Christensen[1], Yuqi Hu[1], Muhammad A. Santoso[1], Wuquan Cui[1], Guillermo Rein*[1]

[1]Department of Mechanical Engineering, and Leverhulme Centre for Wildfires, Environment and Society, Imperial College London, London, SW7 2AZ, United Kingdom, {e.christensen16, y.hu15, m.santoso16, w.cui17, g.rein}@imperial.ac.uk

**Corresponding author*

Keywords

Smouldering, Frozen, Peat, Arctic, Permafrost

Abstract

Recent wildfires in Arctic regions have burned unprecedented swaths of land, demonstrating a detrimental change in the arctic fire regime and release large amounts of ancient carbon that have been stored for millennia in the organic soils into the atmosphere. These events highlight the vulnerability of these biomes to climate change and the importance of protecting them. Arctic fires are poorly understood and difficult to be detected due to their remote location. Here, we present a novel rig capable of studying smouldering arctic fires at the lab scale by reducing environmental and soil temperatures. The rig consists of a chamber with low air temperatures, a reactor with a temperature-controlled base to imitate the influence of permafrost, and the fuel sample of organic soil with preconditioned temperatures. The smouldering of organic soil was investigated across a range of realistic temperatures in the Arctic: -7 °C, 2 °C, and 21 °C. The experimental results show that smouldering can be sustained in soil temperatures below the freezing point of water. While insignificantly affect spread rate, the range of temperature in this study was found to have profound effect on the depth of burn, increasing by up to 66% as base temperature decreased from 21 to -7 °C. The critical moisture content above which smouldering is not self-sustain was found to be between 110% and 120% which is lower than the value in the literature because the lower temperature of the reactor base in this study resulted in higher heat losses than the reactor in the literature. As the average soil temperature increases with climate change, the critical moisture content will increase and may lead to more frequent fires in the Arctic. This study is the first experimental work on smouldering Arctic wildfires with findings that can improve our understanding on the effect of cold temperatures, and presents a novel methodology to investigate Arctic fires at laboratory scale.

1. Introduction

In pristine condition, the organic soil in peatland is protected from fire, due to the cold and high moisture conditions (Turetsky *et al*. 2015). With global warming and land-use changes, the condition of peatland is disturbed and can lead to the drying of the organic soil. Once dry, the soil can be ignited and burn for weeks to months (Page *et al*. 2002) because the fire of the organic soil is governed by smouldering combustion, which is the slow, low temperature, flameless burning of charring porous fuel, and the most persistent type of combustion phenomena (Rein 2016). The difficulty in peat fire mitigation has been reported to requires abundant resources of million to billion L of waters that was often difficult to fulfil, leading to the persistent emission of carbon (Ramadhan *et al*. 2017).

In the Arctic, there are reports of fires that were ignited during the summer, survived the winter season by burning underground, and returned to the surface once the snow has melted (Rein and Huang 2021). Such fires that resurface after winter season have been referred to as overwintering fires. In the summer, both flaming and smouldering are part of the wildfire. The flames of the wildfires will be extinguished by rainfall, cold weather or firefighting. However, smouldering hotspots can survive below ground and not be quenched by water or winter because of the insulation effect of the topsoil and snow cover. In the Spring, the overwintering fires grow helped by the dry conditions and warmer temperatures (Scholten *et al*. 2021).

Smouldering dynamics have, primarily, been studied to understand wildfires in tropical and temperate peatlands. Lin *et al*. (2021) investigated the critical MC to ignition in regard to temperatures in the Arctic. However, no laboratory experiments have explored the dynamics of smouldering wildfires in the Arctic, such as spread rate and burning depth. Here we introduce a novel experimental set-up to address this gap by conducting experiments varying both temperature and MC to understand their effects on the dynamics of smouldering wildfires in the Arctic.

2. Method

The effect of temperature on smouldering dynamics was explored by using a novel rig developed by Christensen (2020). The rig was designed to control three parameters: the ambient air (or chamber) temperature (T_c), the soil temperature (T_0), and the temperature of the bottom boundary of the reactor (T_b) in which the peat was burned. To control the air temperature, a large chamber with an internal dimension of 120 × 80 × 80 cm was constructed using vermiculite and lined with a fibreboard insulating material (Figure 1). A 40 × 40 cm extraction hood was mounted through the top of the chamber with a variable speed mechanical fan installed to control the extraction rate of the smoke from the smouldering samples. A fine metal mesh (0.5 mm) skirt extends down from the hood, as illustrated in Figure 1, to reduce any significant air currents from developing which would affect the smouldering dynamics. The experiments were conducted inside the mesh skirt. A compressed airline was passed through a vortex tube which directed cold air with adjustable temperature (T_i) through an inlet at the bottom of the chamber. A thermocouple was placed within the mesh cage at the same height as the top edge of the reactor to measure T_c. T_c was varied from ~20°C down to ~10°C by adjusting T_i down -7 ± 2°C.

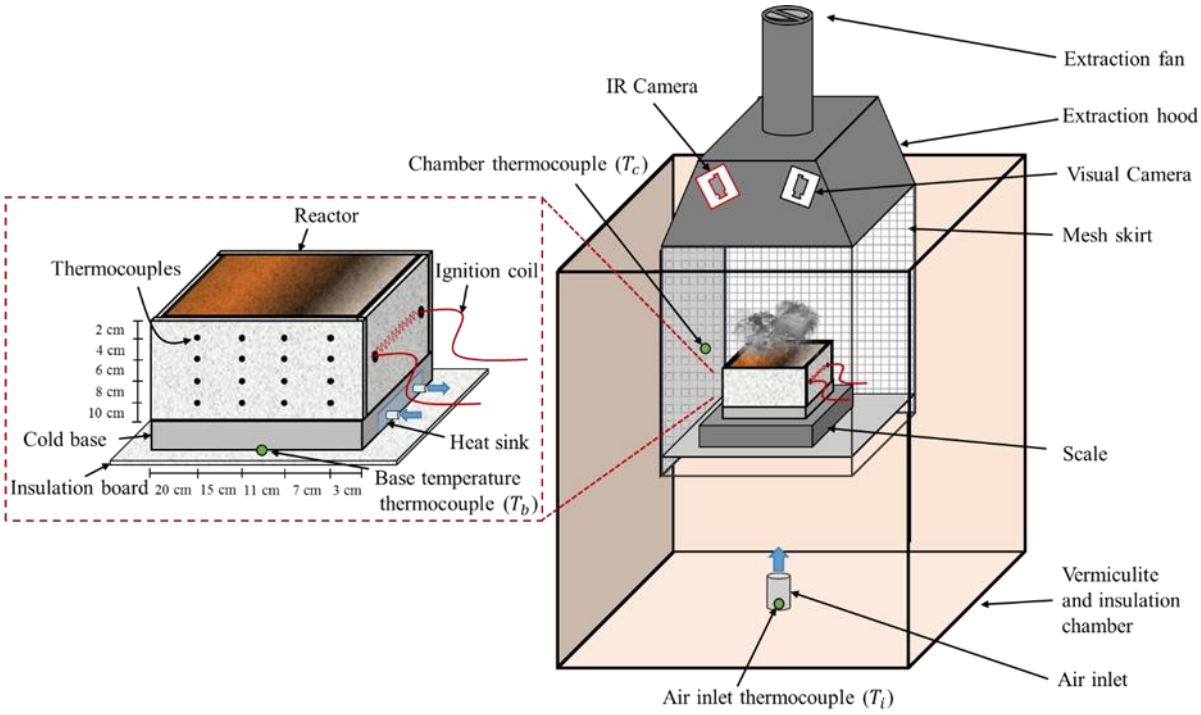

Figure 1- Illustration of the Experimental Low-temperature Smouldering Apparatus (ELSA). Left figure shows key features of the reactor which is filled peat soil. The internal dimension of the reactor measures 20 × 20 × 10 cm. On the right, key features of the rig are highlighted. The dimensions of the chamber are 120 × 80 × 80 cm.

The reactor has internal dimensions of 20 × 20 × 10 cm (Figure 1). The walls were constructed from an insulating fibreboard (k= 0.7 W·m^{-1}·K^{-1}, ρ= 310 kg·m^{-3}, c_p= 1090 J·kg^{-1}·K^{-1}). The bottom of the reactor was a thin aluminium plate so to allow for the effective conduction of heat. To control the temperature of the bottom boundary of the reactor, an aluminium base (22 × 22 × 2.5 cm) was placed. The base was designed with an inset heat sink through which a temperature-controlled water – glycol mixture was pumped. The temperature of the mixture was varied by a benchtop recirculating chiller (Polyscience LS-series compact chiller). A thermocouple was mounted to the base to measure the temperature at the interface between the base and the aluminium plate (T_b) as indicated in Figure 1.

A commercial peat (Shamrock Irish Moss Peat, Bord na Móna Horticulture) was used due to its accessibility, material consistency and frequent use in literature (Huang *et al*. 2016), allowing for improved isolation of peat soil variability and comparison to literature results. This soil has a C/H/N/S proportion of 54.1/5.1/1.3/0.5% by mass respectively, and an inherent inorganic content of 2.5 ± 0.6% (Hu *et al*. 2019). Sample preparation was conducted according to Christensen *et al*. (2019). The peat was dried at 80 °C until no mass loss was observed in measurements of 6 h apart. Water was added to the dried peat to achieve a desired MC, and the peat was put in a sealed container to homogenise for 24 h. MC is considered as the mass of the water divided by the mass of

the dry matter. The MC was verified by taking a 100 g subsample of the peat and drying it in an oven at 90°C for 6 hours (this was found to sufficiently dry sub samples of any moisture content). Where the initial temperature of sample (T_0) was required to be altered, the reactor and sample was placed in a fridge or freezer for at least 12 hours before starting the experiment.

The samples were ignited using an 18 cm, helically wound nichrome coil, 1 cm in diameter through which 100 W of power is supplied, which has been shown to be a strong ignition source (Huang *et al*. 2016). A scale is used to measure the mass of the sample every minute. 16 thermocouples were inserted along the centreline of the reactor at 3, 7, 11 and 15 cm from the ignition side and at 2, 4, 6 and 8 cm depths, as illustrated in Figure 1. This is a similar thermocouple array to that used in (Huang *et al*. 2016). Both infrared (FLIR Duo R) and visual cameras (GoPro) were mounted above the reactor to capture the behaviour and spread of the smouldering.

To explore the effect of soil temperature on smouldering dynamics, three temperature conditions were targeted: below zero, near zero, and room temperature. This covered a range of temperatures from frozen conditions to summer conditions in Arctic regions, where the active layer is warm. Temperature condition (T_{cond}) was defined as a set of three temperatures set up: base temperature (T_b), chamber temperature (T_c), peat soil initial temperature (T_0). Table 1 shows T_{cond} setup in this work. Experiments with MC of 50% and 100% were conducted at all three condition temperatures, with one to three experiments conducted per soil condition.

Table 1- Summary of average temperatures for the three temperature conditions (T_{cond}) in this study: below freezing point (-7°C), at freezing point (2°C), and at room temperature (21°C). The uncertainties reported here are the standard deviation of measured temperature across all experiments at the given condition temperature.

Condition temperature (T_{cond})	Below freezing point -7°C	Freezing point 2°C	Room temperature 21°C
Base temperature (T_b)	-6.8 ± 0.6°C	2.1 ± 1.3°C	20.7 ± 0.3°C
Chamber temperature (T_c)	10.1 ± 1.4°C	9.5 ± 2.2°C	21.8 ± 1.5°C
Initial soil temperature (T_0)	-11.3 ± 1.5°C	3.8 ± 0.4°C	18.0 ± 0.1 °C

3. Results

Figure 2a presents the spread rates measured using the IR images and shows a slightly decreasing relationship with decreasing condition temperature. This is likely due to the increased sensible energy required to heat the fuel at low temperatures and to melt the frozen MC. Figure 2b shows that MC has a more substantial effect on spread rate than condition temperature, with horizontal spread rates decrease with MC. For samples with 50% MC, the spread rate decreased 14% between 21°C and -7°C conditions. This difference increased to 18% in samples of 100% MC. As such, condition temperature was found to have a minor but insignificant influence on horizontal spread rates as confirmed by a nonsignificant linear regression ($p>0.05$), but was significantly influenced by MC as confirmed by a significant 2-sample t-test ($p<0.05$).

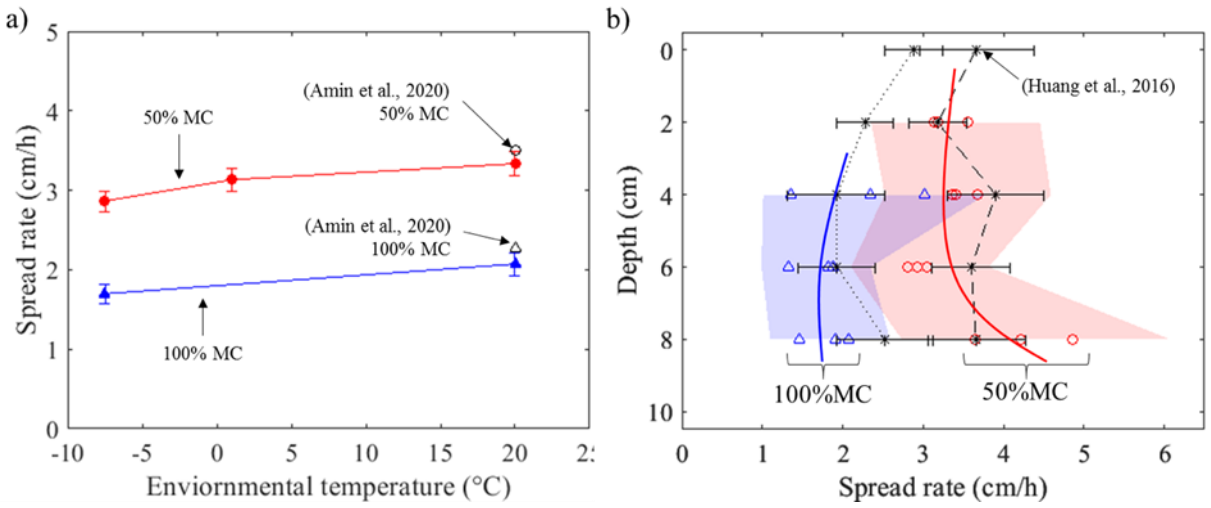

Figure 2- a) illustrating the effect of condition temperature on spread rate, measured using infrared (IR) imaging, in sample of 50% and 100% moisture content (MC). Results are also compared against IR spread measurements of a

similar reactor with an insulated base at room temperature presented by Amin et al. (2020). IR data was not available for samples with 100% moisture at 2°C. b) showing the effect of depth on spread rate on both samples with 50% and 100% MC at various temperature conditions and compared to spread rates presented by Huang et al. (2016). Error bars are based on uncertainties in measurement. Triangle and circle symbols represent spread rate from samples of 100% MC and 50% MC. Blue and red lines are approximate trends of horizontal spread rate with depth from samples of 100% MC and 50% MC. Temperature at 2 cm depth in samples of 100% moisture never exceeded 100°C and so could not be measured. Data from Huang et al. (2016) are represented by black lines: dotted line for sample of 100% MC and dashed line for sample of 50% MC.

The depth of burn is found by linearly interpolating between the peak temperatures of adjacent thermocouples and finding the location of the 200°C threshold. The burning depths in this study are presented in Table 2 along with the burning depth found in (Huang *et al*. 2016). Two effects are noticeable in the depth of burning in regard to both condition temperature and MC. Firstly, decreasing condition temperatures increases the burning depth, with a linear model confirming the significance of this trend ($p<0.05$). At 50% MC the burning depth increased by 66% between 21°C and -7°C, while in samples of 100% MC the increase was 13%. This change in depth of burning is likely due to the additional energy required to melt and heat the soil causing the optimal balance between oxygen supply and heat losses to exist deeper within the soil. Secondly, comparing the depth of burning estimated here to that presented by Huang *et al*. (2016) who conducted experiments at room temperature, using the same source of peat and a similar reactor but with an insulated bottom face, it is evident that the effect of the energy loss through the base results in shallower burning depths. This difference is enhanced with MC.

Table 2- Estimated burning depth by using 200°C as an indicator of char formation and linearly interpolating between peak temperatures measured by thermocouples. Depth of burning measured by Huang et al. (2016), is also presented for comparison.

	Depth of burning (cm)			
	-7 °C	2°C	21°C	Huang *et al*. (2016)
50% MC	2.5 ± 0.2	1.8 ± 0.3	1.5 ± 0.3	3 ± 1
100% MC	5.4 ± 0.6	4.6 ± 0.2	4.8 ± 0.5	9 ± 1

Additional experiments were performed to explore how the condition temperature influenced the critical MC of ignition in this work. It was found that smouldering could be successfully sustained in MC of 110% however would fail at 120%. This was true across all condition temperatures, and is lower than the value of 160% MC found by Hu *et al*. (2019) who used the horizontal reactor with an insulated base.

4. Conclusions

In this work, we have studied the smouldering dynamics of peat fire in the Arctic using a novel experimental rig able to separately control the temperature of the ambient air (10 to 21°C) and bottom boundary of the smouldering sample (-7 to 21°C). The initial temperature of the peat sample was varied from -11 to 18°C. We found that the range of ambient air, bottom boundary, and initial soil temperatures in this study have insignificant effect on spread but reduce burning depth up to 66% as the bottom boundary temperature decreased from 21 to -7°C. The critical moisture content to ignition in this study was found to be between 110 and 120% which is lower than the value in the literature (160%). This study is the first experimental work on smouldering Arctic wildfires with findings that can improve our understanding on the effect of cold temperatures on the smouldering dynamics of peat fires, and presents a novel methodology to investigate Arctic fires at laboratory scale.

5. Reference

Amin HMF, Hu Y, Rein G (2020) Spatially resolved horizontal spread in smouldering peat combining infrared and visual diagnostics. Combustion and Flame 220, 328–336. https://doi.org/10.1016/j.combustflame.2020.06.039

Christensen EG (2020) Experimental investigation of the effects of soil and environmental conditions on smouldering wildfires, PhD Thesis, Imperial College London. https://doi.org/https://doi.org/10.25560/87186

Christensen E, Hu Y, Restuccia F, Santoso MA, Huang X, Rein G (2019) Experimental methods and scales in smouldering wildfires. In 'Fire Effects on Soil Properties'. (Eds P Pereira, J Mataix-Solera, X Ubeda, G Rein, A Cerdà) pp. 267–280. (CSIRO Publishing). https://doi.org/10.1071/9781486308149

Hu Y, Christensen EG, Amin HMF, Smith TEL, Rein G (2019) Experimental study of moisture content effects on the transient gas and particle emissions from peat fires. Combustion and Flame 209, 408–417. https://doi.org/https://doi.org/10.1016/j.combustflame.2019.07.046

Hu Y, Christensen E, Restuccia F, Rein G (2019) Transient gas and particle emissions from smouldering combustion of peat. Proceedings of the Combustion Institute 37(3), 4035–4042. https://doi.org/10.1016/J.PROCI.2018.06.008

Huang X, Restuccia F, Gramola M, Rein G (2016) Experimental study of the formation and collapse of an overhang in the lateral spread of smouldering peat fires. Combustion and Flame 168, 393–402. https://doi.org/10.1016/J.COMBUSTFLAME.2016.01.017

Lin S, Liu Y, Huang X (2021) Climate-induced Arctic-boreal peatland fire and carbon loss in the 21st century. Science of The Total Environment 796. https://doi.org/https://doi.org/10.1016/j.scitotenv.2021.148924

Page SE, Siegert F, Rieley JO, Boehm HDV, Jaya A, Limin S (2002) The amount of carbon released from peat and forest fires in Indonesia during 1997. Nature 420(6911), 61–65. https://doi.org/10.1038/nature01131

Ramadhan ML, Palamba P, Imran FA, Kosasih EA, Nugroho YS (2017) Experimental study of the effect of water spray on the spread of smoldering in Indonesian peat fires. Fire Safety Journal 91, 671–679. https://doi.org/10.1016/J.FIRESAF.2017.04.012

Rein G (2016) Smoldering Combustion. In 'SFPE Handbook of Fire Protection Engineering'. (Eds MJ Hurley, D Gottuk, JR Hall, K Harada, E Kuligowski, M Puchovsky, J Torero, JM Watts, C Wieczorek) pp. 581–603. (Springer: New York). https://doi.org/10.1007/978-1-4939-2565-0_19

Rein G, Huang X (2021) Smouldering wildfires in peatlands, forests and the arctic: Challenges and perspectives. Current Opinion in Environmental Science & Health 24. https://doi.org/https://doi.org/10.1016/j.coesh.2021.100296

Scholten RC, Jandt R, Miller EA, Rogers BM, Veraverbeke S (2021) Overwintering fires in boreal forests. Nature 593(7859), 399–404. https://doi.org/10.1038/s41586-021-03437-y

Turetsky MR, Benscoter B, Page S, Rein G, van der Werf GR, Watts A (2015) Global vulnerability of peatlands to fire and carbon loss. Nature Geoscience 8(1), 11–14. https://doi.org/10.1038/ngeo2325

Bridging the gap in the knowledge on the role of spatial planning in the reduction of wildfire risk: insights from Portugal

Fantina Tedim[1*]; André Samora-Arvela[1*]; Catarina Coimbra[2], Fernando Correia[1]; Diogo Pinto[1]; José Aranha[3]

[1] Centre for Studies in Geography and Spatial Planning, CEGOT, Geography Department, Faculty of Arts and Humanities, University of Porto, 4150-564 Porto, Portugal, {ftedim@letras.up.pt, anesamora@gmail.com, up201107231@edu.letras.up.pt, up201304874@letras.up.pt}
[2] Guarda's Town Hall, Serviço Florestal e Desenvolvimento Rural, Praça do Município 5A, 6300-854 Guarda, Portugal, {catarina.coimbra@mun-guarda.pt}
[3] Centre for the Research and Technology of Agroenvironmental and Biological Sciences (CITAB), University of Trás-os-Montes and Alto Douro, 5001-801 Vila Real, Portugal, {j_aranha@utad.pt}

**Corresponding author*

Keywords

Wildfire; Risk Reduction; Spatial Planning; Hazard Index; Threats

Abstract

The 2017 wildfires marked a dramatic milestone in Portuguese society, which corresponded to extreme intensity and the inherent loss of life, property, and thousands of burned forest hectares. This high impact led to a paradigm shift regarding prevention and firefighting, highlighting the need for an integrated fire management approach and assuming as imperative the integration of wildfire risk reduction on spatial planning at the municipal level. This turning point was expressed in the prolific legislative production, namely in the guidelines for preventing and fighting wildfires, given by the Resolution of the Council of Ministers (RCM) n.º 157-A/2017; on the principles set out in the Directive for Preventing and Fighting Wildfires, defined by the RCM n.º 20/2018; in the approval of the National Plan for the Integrated Management of Wildfires (PNGIFR), emanated from the RCM n.º 45-A/2020, which established the need to implement an Integrated Management System for Wildfires (SGIFR), whose vision and objectives were defined in the RCM n.º 12/2019, and its operating rules were enacted in the Decree-Law n.º 82/2021.

As such, the SGIFR establishes, at a national level, strategic guidelines with a view to risk reduction, changing the behaviour of owners, users, and other beneficiaries of the rural territory. In addition, SGIFR proposes integrating wildfire risk reduction in spatial planning through the insertion of a fire hazard map, namely in the master plan's constraints map (i.e., the map where are identified the administrative easements and public utility restrictions that may constitute limitations or impediments to any specific form of land use). The constraint map is one of the documents of the Municipal Master Plan, i.e., the fundamental legal instrument in the management of the municipal territory that defines the strategic framework for territorial development and the spatial organization model of the municipal territory.

This paper identifies the weaknesses of the approach proposed by the SGIFR to promote wildfire risk reduction through spatial planning. Firstly, we used an online questionnaire answered by 175 municipalities of Portugal, in order to examine the local technicians' experience in applying the legislation of spatial planning and wildfire management policies. In a second step, we collected data from a Delphi survey with 27 experts and from a focus group with 9 experts with the aim to confirm or disconfirm the importance of each need for integration between land use planning and rural fire management, indicated by the questionnaire of 175 municipalities. One of the main weaknesses is related with the integration of the fire hazard map in the constraints map of the Municipal Master Plan, considering the high inter-annual variability of fire hazard and the long-term definition of the municipal development model. This procedure will create building permit constraints which can limit the development and continue to favour the depopulation of the rural areas.

This paper contributes to bridging a critical gap in knowledge on the role of spatial planning in the reduction of wildfire hazard and exposure, given that the characteristics of fire hazard are distinctive from other natural hazards (e.g., floods, costal erosion, earthquakes).

1. Introduction

Wildfire losses are increasing in many parts of the world related with the expansion of wildland urban interfaces and the occurrence of extreme wildfires, whose intensity and frequency are expected to increase due to climate

change (Keeley & Syphard, 2016). As these events overwhelm the control capacity (Tedim et al, 2018; Tedim et al., 2020), a stronger focus on prevention and mitigation, within a adaptative planning framework, is required. Spatial planning and development regulations are recognized as an instrument for reducing wildfire hazard and exposure across wildland-urban-interface (Mowery et al., 2019, Mockrin et al., 2020; Gatti & McGee,2021; Gonzalez-Mathiesen et al., 2021). While among other natural hazards (e.g., floods, coastal erosion, earthquakes) there is a long experience using spatial planning to reduce risk, in wildfire domain remain some critical gaps in knowledge and operationalization strategies (Mockrin et al., 2020), as wildfires are complex socio-ecological processes that mostly has anthropic origin.

In Portugal, the National Plan for the Integrated Management of Wildfires (PNGIFR), emanated from the Resolution of the Council of Ministers (RCM) n.º 45-A/2020, which established the need to implement an Integrated Management System for Wildfires (SGIFR), and its operating rules enacted in the Decree-Law n.º 82/2021, intent to integrate wildfire management into spatial planning instruments. The main instrument for this integration is the hazard map that is going to be one more layer of the Constraints Map of the Municipal Master Plans. The national hazard map was published in March of 2022 by the Portuguese Institute for the Conservation of Nature and Forests and was produced using a methodology that considers deterministic factors (Verde & Zêzere, 2010; Oliveira, Gonçalves, & Zêzere, 2021). The Municipal Master Plans (PDM's) inform spatial planning development and the buildings permits. The Master Plans regulate, at spatial level, the land use in order to promote the sustainable development in a given municipal territory, while its Constraints Map express restrictive areas that limit the desirable development at a site, safeguarding the biophysical and cultural character of the territory, as well as avoiding the occupation of areas with the highest hazard index. In this context, SGIFR determines that the interdiction of building permits in high and very high wildfire hazard areas (APPS) and major restrictions in very low, low and medium hazard areas, which have, by a SGIFR legal obligation, to be integrated in the Constraints Map of Master Plans.

This paper contributes to research on the difficulties, needs, and impact of the integration of wildfire hazard map into spatial planning namely into the Municipal Master Plans, first stablished by the Forest Fire Defence System (SDFCI - Decree-Law n.º 124/2006, of 28 June) and now determined by the Integrated Management System for Wildfires in the Continental Territory (SGIFR - Decree-Law n.º 82/2021. First, it identifies the difficulties that local governments face in the implementation of the new legislation, namely in the integration of wildfire hazard map into spatial planning. Second, it measures the consensus among experts. Third, pertinent recommendations are presented.

The overall research question is: What are the benefits and disadvantages of the hazard map integration in the Constraints Map of the Master Plans? The paper is organized as follows: Section 2 summarizes the mixed – methods used to collect and analyse data; Section 3 is dedicated to the analysis of legal environment of spatial planning and wildfire management integration; Section 4 presents the results about the identification of major difficulties and suggestions of local technicians, collected by an online survey and a Delphi survey, concerning the risk reduction in spatial planning at municipal level; Section 5 formulates the discussion about the challenges and opportunities regarding the integration of fire hazard map in the constraints map of the municipal Master Plans; and Conclusions are stated in Section 6.

2. Data and methods

2.1. Review of government documents

To prepare the two steps method used in this research, we started by reviewing government documents.

2.2. Data collection

As a first step, an online survey was sent between April and June of 2022, to 275 municipalities (the municipalities of Lisbon, Porto and São João da Madeira, were excluded because are urban areas). The questionnaire was formed by two questions: i) "*What are the main difficulties you face with the implementation of the SGIFR (DL n.º 822021, of October 13, in its latest version)?"*; ii) "*Do you agree with the decision to integrate the wildfire hazard map in the Constraint Map of the spatial plans? Please justify your reply.*". The response rate was 64%. It exceeds the necessary minimum sample size (161 replies for a confidence level of 95% and a margin of error of 5%), using Kish (1995) and Laureano (2013) equation**,** for extrapolating conclusions from the results.

The 175 municipality responses were organized by five territorial regions within the SGIFR governance structure: North (with 53 replies; 62% of the region's municipalities), Centre (with 50 replies; 73% of the region's municipalities), Lisbon and Tejo River Valley (with 24 replies; 44% of the region's municipalities), Alentejo (with 25 replies: 53% of the region's municipalities) and Algarve (with 10 replies; 63% of region's municipalities) (Figure 1). Thirteen (13) municipalities chose to remain anonymous.

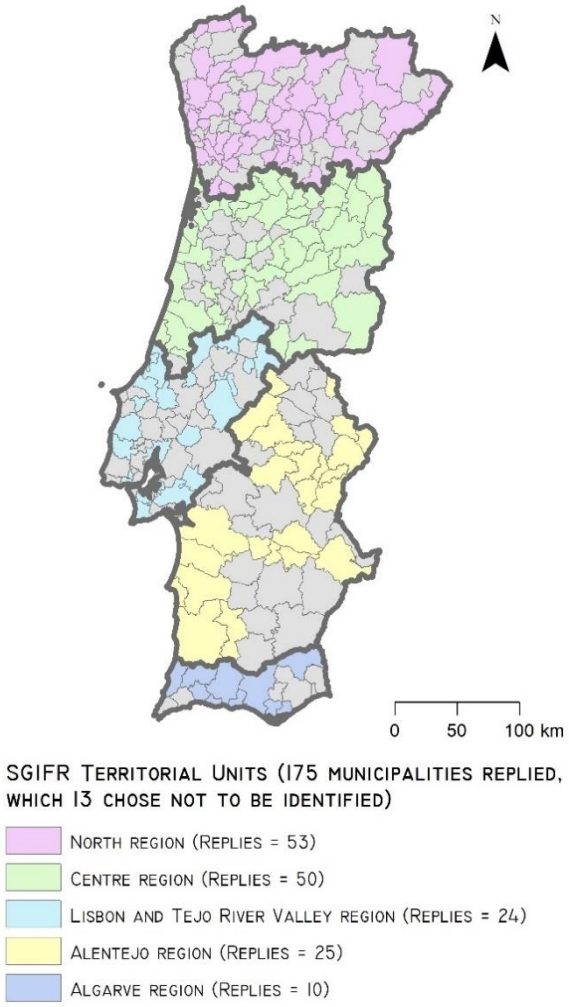

Figure 1 – Municipalities that responded the online survey per region.

The data collected was analysed in NVivo software, version 1.6.1 (1137). Coding in NVivo enabled to categorization of the survey open responses and consequently made it possible to count the frequency of each response.

In a second step, a workshop was held at Guarda Municipal Council on June 3, 2022, where a Delphi questionnaire was operated with 27 experts in spatial planning and wildfire management in order to differentiate the importance of the main categories emanated from the previous step. Thus, an one round real-time Delphi survey was supported by a 5-point *Likert* scale (*1 - Completely disagree; 2 - Disagree; 3 - Fairly agree; 4 - Agree; 5 - Completely agree*).

Procedures for measuring consensus vary widely, so there are several methods available to determine the convergence of opinion among Delphi participants (Rayens & Hahn, 2000; Gracht, 2012; Beiderbeck et al., 2021). These authors support the use of the interquartile range (IQR), where the low values are an indicator of consensus *([0 - 1] Most agreement]1 - 2[Average agreement [2 - 3] Low agreement*) (Gracht, 2012). According to Rayens & Hahn, (2000), a null interquartile range indicates complete consensus. Despite this, it was still decided to use the arithmetic mean (Mean). In this sense, an arithmetic mean value above 3.5 (integrating the answers *4 - Agree*; *5 - Completely agree*) expresses a tendency of concordant answer, while an average value lower than 2.5 (*1 - Completely disagree*; *2 - Disagree*) reflects a discordant trend. On the other hand, another indicator was used, namely the percentage of concordant answers (*Level of Agreement Responses*), which helps

the analysis of the response trend. The IQR of Delphi responses was calculated in Statistical Package for the Social Sciences 26 (IBM, 2022).

Finally, a focus group, in the workshop held in Guarda municipality with nine experts in spatial planning and wildfire management, was conducted to elicit, spontaneously, knowledge that had not been collected by the online questionnaire and the Delphi survey due to its more formatted nature.

3. Spatial planning and wildfire management integration: legal environment

The National Program for Spatial Planning Policy (PNPOT), the main Portuguese instrument for spatial planning on a national scale, in its revised version of 2019, approved by the Law n.º 99/2019, of September 5, stated that the "*articulation of the master plans with the instruments of forest management, forest defence and wildfire fighting, is paramount in order to build a more integrated planning approach that better responds to the challenges of the territories and to safeguard people and goods*".

RCM n.º 12/2019, of January 21, approved the mission of the Integrated Management System for Wildfires (SGIFR), namely the protection of people and property from wildfires, based on the clear definition of responsibilities concerning the management of the rural territory and the protection of people and buildings against wildfires, integrating all actors in a joint action within prevention and suppression processes. The same initiative enshrined the urgent establishment of the National Plan for the Integrated Management of Wildfires (PNGIFR) as a replacement for the previous National Plan for the Defence of Forests against Wildfires (PNDFCI), which saw its goals exceeded as a result of the accumulation of fuel and systemic frailties aggravated by heat waves or extreme weather events with increasing personal and property damage.

This context of vegetation accumulation and of perception bias of risk by populations that did not change risk behaviours required to the adoption of multiple and integrative solutions. Thus, the RCM n.º 45-A/2020, June 16th, gave the motto for the PNGIFR: guiding the integrated management of wildfires in a territory that seeks to be lived by a population with context-sensitive behaviours under efficient risk management options. The PNGIFR introduced an innovative risk governance model, identified strategic objectives and measures to be implemented, clarifying the roles and responsibilities of the various entities that cooperate to achieve the defined goals.

Subsequently, the Integrated Management System for Wildfires in the Continental Territory (SGIFR) promulgated by Decree-Law (DL) n.º 82/2021, defined the norms and institutional articulation processes in the integrated management of wildfires with two axes of intervention: protection against wildfires, oriented towards the safeguarding of people and buildings, and rural fire management, oriented towards the defence and valorisation of rural territories, considering its protection role by reducing conditions for the occurrence and progression of wildfires.

The SGIFR revoked the previous Forest Fire Defence System (SDFCI). which had been instituted by Decree-Law n.º 124/2006, of 28th June. As such, the previous requirement to draw up Municipal Plans for the Defence of Forests against Wildfires (PMDFCI) of the SDFCI was replaced by the requirement of Municipal Programs for the Execution of Integrated Management of Wildfires of the SGIFR.

Unlike the Master Plans (PDM's), the PMDFCI's and its hazard maps, as they were not, legally, spatial plans, were not directly binding on individuals as they did not meet the requirements of public advertising and public discussion, essential for the production of effects by any normative act, as enshrined in the respective paragraph 2 of article 119 and paragraph 5 of article 64 of the Portuguese Republic Constitution (Oliveira, 2018), situation only solved by the Law n.º 76/2017, 17th August.

In light of this goal of spatial planning and wildfire risk reduction alignment, the SGIFR, as the previous SDFCI, stipulates the integration of fire hazard index classes (very low, low, medium, high, very high) in the constraints map of the PDM's, and defines constraints on building permits within and outside the areas of high and very high fire hazard index classes, which are designated Priority Areas for Prevention and Safety (APPS).

4. Results

4.1. Main difficulties faced by the municipalities with the implementation of the SGIFR

4.1.1. The results from the online survey

The forestry technicians that responded to the online survey identified several difficulties regarding the integration of hazard map into the constraint map of Master Plans (table 1).

The main difficulties (table 1) are:

i) "new hazard map does not correspond to the existing reality in the territory" due to the spatial resolution; the fact that is not based on the Master Plan's urban spaces; the redundancy of the previous hazard maps, among others aspects. The greatest worries regions are from Centre region (22% of replies) and from North region (19% of replies) (supplementary table S1) that have around 50% of their territory in high and very high hazard index (table S2), but also from Alentejo (16% replies), where 56% of the surface presents low or no wildfire risk

ii) "land use map (COS) 2018 does not reflect the existing reality at the local level", which is a main worry from Algarve region (10% of replies);

iii) "obstacles to cultural and sporting activities)" as the articles 67 and 68 of SGIFR establish the prohibition of many activities in high and very high hazard areas and in days with high weather risk. This is a worry of the Centre region (4% of replies) (1% of national replies);

iv) "difficulties in surveying and mapping burned areas", being a worry of Alentejo municipalities ($% of replies) (1% of national replies);

v) "confusion between the concept of Hazard (structural) and Fire weather index (daily)", stated by 4% of Centre region replies (1% of national replies);

vi) "difficulty in understanding the criteria for defining hazardous areas", evidenced by 2% of Centre replies (1% of national replies);

vii) "the execution of the fuel management strips has contributed to colossal forest destruction", conduced by North region (2% of replies) (1% of national replies);

viii) "the current dimensions of the fuel management strips [around the houses] are not justified, as there is no gain in defence beyond 30 meters in size", concluded by North region (2% of North replies) (1% of national replies).

Table 1 – Main difficulties faced by the municipalities with the implementation of the SGIFR: responses to online survey (N=175).

	Responses (N=175)	**%**
RISK MANAGEMENT TOOLS		
New hazard map does not correspond to the existing reality in the territory (spatial resolution; not based on the Master Plan's urban spaces; redundancy of the previous hazard maps, among others)	30	17 %
Land use and land cover map (COS 2018) does not reflect the existing reality at the local level	2	1%
Obstacles to cultural and sporting activities (articles 67 and 68 of the SGIFR)	2	1%
There are difficulties in surveying and mapping burned areas	2	1%
Confusion between the concept of Hazard (structural) and Fire Weather Index (daily)	1	1%
Difficulty in understanding the criteria for defining hazardous areas	1	1%
The execution of the fuel management strips has contributed to colossal forest destruction	1	1%
The current dimensions of the fuel management strips are not justified, as there is no gain in defence beyond 30 meters in size	1	1%

4.1.2. Consensus of the Delphi panel

Subsequently, the robustness of the consensus in the Delphi survey responses (N = 27 experts) regarding the difficulties and needs regarding the integration of the hazard map in the constraint map of Master Plans was analysed. Those who generate a strong consensus were "hazard map does not correspond to the existing reality in the territory (spatial resolution; not based on the Master Plan's urban spaces; redundancy of the previous hazard maps, among others)" (mean=4.41; IQR=1; level of agreement responses=85%), "Land use map (COS) 2018 does not reflect the existing reality at the local level" (mean=4.11; IQR=1; level of agreement responses=85%); "confusion between the concept of Hazard (structural) and Fire Weather Risk (daily)" (mean=3.93; IQR=1; level of agreement responses=78%); and "difficulty in understanding the criteria for defining hazardous areas" (mean=4.37; IQR=1; level of agreement responses=89%) (table 2).

Table 2 – Main difficulties faced by the municipalities with the implementation of the SGIFR: consensus analysis of Delphi panel responses (N=27).

	Mean of Delphi Group (N = 27)	**Interquartile Range (IQR) [0 - 1] Most agreement]1 - 2[Average agreement [2 - 3] Low agreement**	**Level of Agreement Responses = Agreements / S opinions expressed**
RISK MANAGEMENT TOOLS			
Hazard map does not correspond to the existing reality in the territory (spatial resolution; not based on the Master Plan's urban spaces; redundancy of the previous hazard maps, among others)	4.40	1	85%
Land use map (COS) 2018 does not reflect the existing reality at the local level	4.11	1	85%
Confusion between the concept of Hazard (structural) and Fire Risk (daily)	3.92	1	78%
Difficulty in understanding the criteria for defining hazardous areas	3.85	1	70%
Obstacles to cultural and sporting activities (articles 67 and 68 of the SGIFR)	3.75	2	54%
The execution of the fuel management strips has contributed to colossal forest destruction	3.41	3	48%
The current dimensions of the fuel management strips are not justified, as there is no gain in defence beyond 30 meters in size	3.41	2	48%
There are difficulties in surveying and mapping burned areas	3,00	2	33%

4.2. Agreement with the decision to integrate the wildfire hazard map in the Constraints Map of the Master Plans

4.2.1. Results from the online survey

Regarding the integration of the wildfire hazard in the constraints map of Master Plans, most municipalities agree with their integration (74%) (table 3). Within the regions, the results are:

i) Lisbon and Tejo River Valley respondent municipalities agree with the integration (96% of replies, where high and very high hazard represent 24% of the territory);
ii) Alentejo respondent municipalities agree with the integration (92% of replies, where high and very high hazard represent 5% of the territory);
iii) North region respondent municipalities agree with the integration (79% of replies, where high and very high hazard represent 49% of the territory);
iv) Centre region respondent municipalities agree with the integration (74% of replies, where high and very high hazard represent 51% of the territory);

v) Algarve region respondent municipalities agree with the integration (60% of replies, where high and very high hazard represent 34% of the territory).

Table 3 - Agreement with the decision to integrate the wildfire hazard map in the Constraints Map of Master Plans: responses to online survey (N=175).

	Responses (N=175)	**%**
YES	130	74%
DECISION MARKING		
The integration of the hazard map facilitates decision making regarding the licensing of construction and expansion of buildings in rural areas depending on the hazard	37	21%
The integration of the hazard map in Constraint Map of Master Plan is necessary in order to bind individuals	5	3%
The hazard map must be integrated into the Master Plan constraint map only if it is prepared by the municipality	1	1%
HAZARD MAP METHODOLOGY		
The methodology of the hazard map standardizes the criteria, at a national level, for the elaboration of this cartography, leaving no room for discrepancies	5	3%
The methodology for executing the hazard map should be reviewed and should be dynamic	4	2%
The artificialized territories in the Land Use Map (COS 2018) do not correspond to the urban spaces of the Master Plan, which makes procedural analysis difficult in the context of the constraints to the construction of the SGIFR	2	1%
EXPECTED IMPACTS		
But the structural hazard map leads to major restrictions	3	2%
The hazard map must not lead to the prohibition of occupation of rural areas, increasing their vulnerability, abandonment, and inherent increase in hazardousness	1	1%
Hazard index encourages the management of rural areas insofar as the less dangerous nature of the plots will increase their financial value	1	1%
NO	45	26%
EXPECTED IMPACTS		
The structural hazard map leads to major restrictions	9	5%
MISMATCHES IN THE PLANNING FRAMEWORK		
Hazard index, due to its dynamic nature, becomes impracticable to be transposed to Master Plan's Constraints Map	5	3%
There is an incompatibility between the rigidity of the Spatial Plans and the dynamics of transformation of the Territory	1	1%
The hazard map must maintain its independent character from the Spatial Plans, supporting forestry planning and rural fire management	1	1%
LEGAL ENVIRONMENT		
The hazard map binds individuals without having been published for public consultation	3	2%
HAZARD MAP METHODOLOGY		
The hazard map should be carried out by the municipalities	1	1%
The hazard map was created by identifying spaces with high fire recurrence and from a standpoint of definition of defence areas, so it cannot be used as a building constraint	1	1%

However, both those who agree and those who disagree present suggestions for improvement in this subject.

The concordant responses were categorized in Decision Making, Hazard Map Methodology, and Expected Impacts.

Regarding decision making, the concordant respondents stated that "the integration of the hazard map facilitates decision making regarding the licensing of construction and expansion of buildings in rural areas depending on the hazard" (21% of national replies; 33% of Lisbon and Tejo River Valley; 24% of Alentejo region replies; 21% of North region replies; 20% of Algarve region replies; 14% of Centre region replies)

In addition, "the integration of the hazard map in Constraints Map of Master Plans is necessary in order to bind individuals" (3% of national replies; 4% of North region replies; 4% of Centre region replies; 4% of Alentejo region replies).

However, there are municipalities that consider that "hazard map must be integrated into the Master Plan constraint map only if it is prepared by the municipality" (1% of national replies; 2% of North region replies) explaining.

Concerning hazard map methodology one of the positive aspects is that "the methodology of the hazard map standardizes the criteria, at a national level, for the elaboration of this cartography, leaving no room for discrepancies" (3% of national replies; 8% of Lisbon and Tejo River Valley replies; 2% of North region replies).

Nevertheless, the are municipalities that establish some conditions like "the methodology for executing the hazard map should be reviewed and should be dynamic" (2% of national replies; 6% of North region replies), and that "the artificialized territories in the Land Use Map (COS 2018) do not correspond to the urban spaces of the Master Plan, which makes procedural analysis difficult in the context of the constraints to the construction of the SGIFR" (1% of national replies; 10% of Algarve region replies; 2% of Centre region replies).

About the expected impacts, the concordant respondents acknowledge that "the structural hazard map leads to major restrictions" (2% of national replies; 4% of Centre region replies), "the hazard map must not lead to the prohibition of occupation of rural areas, increasing their vulnerability, abandonment, and inherent increase in hazardousness" (1% of national replies; 10% of Algarve region replies), and "hazard index encourages the management of rural areas insofar as the less dangerous nature of the plots will increase their financial value" (1% of national replies; 4% of Lisbon and Tejo River Valley replies).

Discordant respondents, on the other hand, presented answers that were grouped into four themes: Expected Impacts, Mismatches in the Planning Framework, Legal Framework and Hazard Map Methodology.

For these respondents, the main expected impacts are related to major restrictions determined through the hazard map (5% of national replies; 10% of Algarve region replies; 6% of North region replies; 6% of Centre region replies).

Within mismatches in the planning framework, they say that "hazard index, due to its dynamic nature, becomes impracticable to be transposed to Master Plan's Constraint Map" (3% of national replies), "there is an incompatibility between the rigidity of the Spatial Plans and the dynamics of transformation of the Territory" (1% of national replies; 2% of Centre region replies) and that "the hazard map must maintain its independent character from the Spatial Plans, supporting forestry planning and rural fire management" (1% of national replies; 10% of Algarve region replies).

Among legal environment, they state that the hazard map binds individuals without having been published for public consultation" (2% of national replies; 10% of Algarve region replies; 4% of Centre region replies).

In regard to hazard map methodology, "the hazard map should be carried out by the municipalities" (1% of national replies; 2% of North region replies) and "the hazard map was created by identifying spaces with high fire recurrence and from a standpoint of definition of defence areas, so it cannot be used as a building constraint" (1% of national replies; 2% of North region replies).

4.2.2. Consensus of the Delphi panel

Regarding the justification of the concordant and discordant answers, and the suggestions for improvement, there is a consensus in: "the methodology for executing the hazard map should be reviewed and should be dynamic" (mean=3.56; IQR=1; level of agreement responses=89%); "the artificialized territories in the Land Use Map (COS 2018) do not correspond to the urban spaces of the Master Plan, which makes procedural analysis difficult in the context of the constraints to the construction of the SGIFR" (mean=3.56; IQR=1; level of agreement responses=63%); "the methodology of the hazard map standardizes the criteria, at a national level, for the elaboration of this cartography, leaving no room for discrepancies" (mean=3.15; IQR=1; level of agreement responses=37%); "the structural hazard map leads to major restrictions" (mean=3.96; IQR=0; level of agreement responses=81%); "the hazard map binds individuals without having been published for public consultation" (mean=4.15; IQR=1; level of agreement responses=77%); and "hazard index, due to its dynamic nature, becomes impracticable to be transposed to Master Plan's Constraint Map" (mean=3,52; IQR=1; level of agreement responses=52%).

Table 4 – Agreement with the decision to integrate the wildfire hazard map in the Constraints Map of Master Plans: responses to online survey (N=175): consensus analysis of Delphi survey responses (N=27).

	Mean of Delphi Group (N = 27)	**Interquartile Range (IQR) [0 - 1] Most agreement]1 - 2[Average agreement [2 - 3] Low agreement**	**Level of Agreement Responses = Agreements / S opinions expressed**
YES			
HAZARD MAP METHODOLOGY			
The methodology for executing the hazard map should be reviewed and should be dynamic	4.37	1	89%
The artificialized territories in the Land Use Map (COS 2018) do not correspond to the urban spaces of the Master Plan, which makes procedural analysis difficult in the context of the constraints to the construction of the SGIFR	3.56	1	63%
The methodology of the hazard map standardizes the criteria, at a national level, for the elaboration of this cartography, leaving no room for discrepancies	3.15	1	37%
EXPECTED IMPACTS			
But the structural hazard map leads to major restrictions	3.96	0	81%
The hazard map must not lead to the prohibition of occupation of rural areas, increasing their vulnerability, abandonment and inherent increase in hazardousness	3.85	2	63%
Hazard index encourages the management of rural areas insofar as the less dangerous nature of the plots will increase their financial value	3.15	2	44%
DECISION MARKING			
The integration of the hazard map in Constraint Map of Master Plan is necessary in order to bind individuals	3.89	2	63%
The hazard map must be integrated into the Master Plan constraint map only if it is prepared by the municipality	3.7	2	1%
The integration of the hazard map facilitates decision making regarding the licensing of construction and expansion of buildings in rural areas depending on the hazard	3.59	2	63%
NO			
LEGAL ENVIRONMENT			
The hazard map binds individuals without having been published for public consultation	4.15	1	77%
MISMATCHES IN THE PLANNING FRAMEWORK			
There is an incompatibility between the rigidity of the Spatial Plans and the dynamics of transformation of the Territory	3.81	2	62%
Hazard index, due to its dynamic nature, becomes impracticable to be transposed to Master Plan's Constraint Map	3.52	1	52%
The hazard map must maintain its independent character from the Spatial Plans, supporting forestry planning and rural fire management	3.15	2	42%
EXPECTED IMPACTS			
The structural hazard map leads to major restrictions	3.96	0	81%
HAZARD MAP METHODOLOGY			
The hazard map should be carried out by the municipalities	4,00	2	69%
The hazard map was created by identifying spaces with high fire recurrence and from a standpoint of definition of defense areas, so it cannot be used as a building constraint	3.69	2	54%

It is not surprising that the highest participation rate and greatest concern with hazard related restrictions was from municipalities in the North region and the Center region, as these are the regions that have around of 50% of their territory in high and very high hazard index (table S2).

As discussed in the focus group, the constraints on building in areas with high and very high hazards are stranglers for the territorial development and could increase the depopulation of the interior, which will generate even less human capacity for fuel management and, thus, could increase the hazard. As for the integration of the hazard map in the Master Plan constraint map, it was discussed that the hazard map is a cartography that can undergo annual changes and it makes no sense to integrate it into a constraint map of the Master Plan that is only reviewed every 10 years.

5. The integration of the fire hazard map in the constraints map of the municipal master plan: challenges and opportunities

The Portuguese authorities estimate fire hazard, based on a deterministic approach (Verde & Zêzere, 2010; Oliveira, S., Gonçalves, A., & Zêzere, J. L., 2021). This approach uses fire probability, slope and land cover factors, aggregating it in quintiles, which correspond to five hazard classes, in order to create the fire hazard map as specified by SDFCI (Decree-Law n.º 124/2006). Therefore, the fire hazard map has usually been the product of multiplying probability and susceptibility to wildfires, while potential damage has been the product of multiplying the economic value and vulnerability (AFN, 2012). As such, the fire risk assessment is based on multiplying the Fire Hazard with the Potential Damage. In the case of the Fire Hazard inputs, it should be noted that the probability results from dividing the number of recorded wildfire occurrences and the number of years in its series, expressed as a percentage. As such, the time series of wildfire occurrences must be as long as possible (Parente et al., 2016).

Using the number of occurrences as a methodological input for the hazard map calculation works for the majority of fires and it is a prolific exercise, but do not apply to extreme fires conditions (Tedim et al., 2020), whose intensity and recurrence are expected to increase with a changing climate (Keeley & Syphard, 2016).

Susceptibility, on the other hand, derives from the multiplication of susceptibility classes depending on two factors, namely slope and land use/cover. In this context, the susceptibility is increasing as the slope increases. Regarding land use, forest land use classes are associated with greater susceptibility, while agricultural classes have a low to medium susceptibility. At this point, several methodological challenges arise. Regarding the slope calculation, it is imperative to use a Digital Terrain Model with the maximum possible spatial resolution, so that the areas with the greatest susceptibility are identified with high accuracy.

The accuracy between reality and what is mapped is also a challenge in terms of land use mapping. In this subject, the Corine Land Cover (CLC) cartography with a minimum mappable unit of 25 hectares (ha) and a time series with five reference years (1990, 2000, 2006, 2012 and 2018), or the Land Use and Occupation Map (COS) with a minimum mappable size of 1 ha and time series with five reference years (1995, 2007, 2010, 2015 and 2018), are commonly used. Even concerning cartography with a smaller and, therefore, more exact mappable size unit, it is important to consider the disadvantages of the COS use at local scale, depending on its level of accuracy and generalization rules adopted at the time of its preparation.

The COS vectorial map derives from the orthophotomaps interpretation, related to the previous years (up to 2 years before), with a spatial resolution of 20 linear meters and the mentioned 1 ha in terms of minimum mappable area. By this combination of factors, the COS map, when used, is already out of date. Another issue is that its spatial resolution is not compatible with the identification of isolated housing, scattered housing, or road network. In the case of the master plans, the maps should be done at a scale of at least 1/1000, so that human infrastructures are effectively represented (buildings and local road network). In this context, an opportunity in the calculation of the fire hazard is the use of land use maps with higher resolution and smaller mappable units that allow greater accuracy to the real land use, carried out with a constant periodicity that allows the expression of the dynamic influence of land use and land cover changes on fire hazard index of a given territory.

However, the integration of the fire hazard map in the constraint map of the master plans can be an opportunity or a threat, depending on the spatial resolution and degree of generalization of the COS that serves as an input of fire hazard index.

This integration can, therefore, generate a spatialization of the areas with the greatest fire hazard that is crystallized in the municipal master plans, thus, failing to assume the impact on the hazard index reduction of the fuel management initiatives and the dynamics of land use and land cover change. Another threat can arise from the trend that master plans are only revised in 10, 20 or more years.

In this way, it emerges the challenge to improve the calculation of fire hazard due to the constant search for inputs permanently updated and with greater accuracy, considering that integrating fire hazard into the constraint map of the municipal master plans could fail the risk reduction strategy due to the lack of recognition of its dynamic character.

Regarding the factors currently considered for the calculation of the hazard index, it is important to mention that extreme wildfires do not comply with them, given their intensity and degree of uncertainty (Tedim et al. 2018; 2020). As such, integrating risk reduction in spatial planning is paramount, but the strategy to be carried out must be dynamic and adaptive, without falling into the temptation of completely eliminating uncertainty and risk, which is impossible.

6. Conclusions

The integration of the fire hazard map in the constraints map of the Municipal Master Plans, proposed by the SGIFR, represents a challenge, considering the high inter-annual variability of fire hazard, the long-term definition of the municipal development model and the methodology (including the data accuracy) used to assess hazard. The procedure imposed by the current wildfire policy will create building permit constraints that can limit the development of rural areas and the growth of rural agglomeration. These restrictions could continue to favour the depopulation of the rural areas and the creation of more hazardous landscapes by abandonment.

The current existing static regulation system poses growing mismatches, economic, environmental, and social losses. The integration of spatial planning and wildfire risk reduction policies should more comprehensive. Multisector approaches able to mobilize synergies in an adaptive regulation system are paramount and, in this sense, the present paper identified the most pressing opportunities to improve the hazard map and spatial plans alignment.

7. Author Contributions

Conceptualization, F.T. and A.S.A.; methodology, F.T. and A.S.A.; formal analysis, F.T. and A.S.A.; investigation, F.T. and A.S.A.; resources, F.T. and A.S.A.; data curation, A.S.A., F.C., and D.P.; writing—original draft preparation, F.T., A.S.A. and J.A.; writing—review and editing, F.T. and A.S.A.; supervision, F.T; project coordination, F.T. All authors have read and agreed to the published version of the manuscript.

8. Acknowledgments

This research was done in the frame of project ‘AVODIS – Understanding and building on the social context of rural Portugal to prevent wildfire disasters’ (FCT Ref: PCIF/AGT/0054/2017), financed by national funds through FCT-Foundation for Science and Technology, Portugal.

9. Conflicts of Interest

The authors declare no conflict of interest.

10. References:

AFN (2012). Plano Municipal de Defesa da Floresta contra Incêndios – Guia Técnico. Lisboa: Autoridade Florestal Nacional.

Beiderbeck, D., Frevel, N., Gracht, H., Schmidt, S. L., & Schweitzer, V. M. (2021). Preparing, conducting, and analyzing Delphi surveys: Cross-disciplinary practices, new directions, and advancements. MethodsX, 8, 101401.

Blanchi, R., Jappiot, M., Alexandrian, D. (2002). Forest fire risk assessment and cartography. A methodological approach. In Viegas, D. (ed.) Proceedings of IV International Conference on Forest Fire Research. Luso, Portugal.

Gatti, E., McGee, T. (2021). Survey of Municipal Land Use Planning for Wildfire Risk Mitigation in Alberta. Canada, Edmonton: University of Alberta, Department of Earth and Atmospheric Sciences.

Gonzalez-Mathiesen, C., Ruane, S., March, A. (2021). Integrating wildfire risk management and spatial planning – A historical review of two Australian planning systems. International Journal of Disaster Risk Reduction, 53, 101984. DOI https://doi.org/10.1016/j.ijdrr.2020.101984

Gracht, H. (2012). Consensus measurement in Delphi studies: review and implications for future quality assurance. Technological forecasting and social change, 79(8), 1525-1536.

IBM. 2022. "Statistical Package for the Social Sciences 26." United States, New York: International Business Machines Corporation. 2022. https://www.ibm.com/support/pages/downloading-ibm-spss-statistics-26.

Lampin-Maillet, C., Mantzavelas, A., Galiana, L., Jappiot, M., Long, M., Herrero, G., Karlsson, O., Iossifina, A.,Thalia, L., Thanassis, P. (2010). Wildland Urban Interfaces, Fire Behaviour and Vulnerability: Characterization, Mapping and Assessment. In Joaquim Sande Silva, Francisco Rego, Paulo Fernandes and Eric Rigolot (eds.) European Forest Institute Research Report 23 - European Towards Integrated Fire Management – Outcomes of the European Project Fire Paradox. European Forest Institute.

Laureano, R. (2013). Teste de Hipóteses com o SPSS – 2ª Edição. Lisbon: Edições Sílabo.

Jakes, P.J., Sturtevant, V. (2013). Trial by fire: community wildfire protection plans put to the test. International Journal of Wildland Fire, 22, 1134–1143. DOI: https://doi.org/10.1071/WF12156

Jappiot, M., Gonzalez-Olabarria, J., Lampin-Maillet, C., Borgniet, L. (2009). Assessing wildfire risk in time and space. Living with wildfires: what science can tell us. A Contribution to the Science-Policy Dialogue. Yves Birot (ed.) EFI Discussion Paper 15. European Forest Institute, Joensuu, pp. 41–47.

Kish, L. (1995). Survey Sampling. USA, Nova Iorque: Wiley Classics Library.

Mockrin, M.H., Fishler, H.K., Stewart, S.I. (2020). After the fire: Perceptions of land use planning to reduce wildfire risk in eight communities across the United States. International Journal of Disaster Risk Reduction 45, 101444. DOI: https://doi.org/10.1016/j.ijdrr.2019.101444

Mowery, M., Read, A., Johnston, K., Wafaie, T. (2019). Planning the Wildland-Urban Interface PAS Report 594, p. 194. https://www.planning.org/publicati ons/report/9174069/.

Muller, B. H., L. Yin, L. (2010). Regional governance and hazard information: the role of co-ordinated risk assessment and regional spatial accounting in wildfire hazard mitigation. J. Environ. Plan. Manag., 53, 1–21.

Oliveira, F. P. (2018). Algumas notas sobre as alterações ao Decreto-Lei n.º 124/2006, de 28 de junho operadas pela Lei n.º 76/2017, de 17 de agosto que define o Sistema de Defesa da Floresta Contra Incêndios. E-PUBLICA – Revista Eletrónica de Direito Público, Vol. 4, nº 3. 26-40.

Oliveira, S., Gonçalves, A., & Zezere, J. L. (2021). Reassessing wildfire susceptibility and hazard for mainland Portugal. Science of the Total Environment, 762, 143121. DOI: https://doi.org/10.1016/j.scitotenv.2020.143121

Parente, J., Pereira, M. G. (2016). Structural fire risk: The case of Portugal. Science of the Total Environment, 573, 883-893. DOI: http://dx.doi.org/10.1016/j.scitotenv.2016.08.164.

QSR (2022). NVivo Release 1.6.1 software. QSR International Pty Ltd NVivo Release 1.6.1 software.

Rayens, K., Hahn, J. (2000). Building consensus using the policy Delphi method. Policy, politics, & nursing practice, 1(4), 308-315.

Keeley J., Syphard A. (2016). Climate Change and Future Fire Regimes: Examples from California. Geosciences, 6(3):37. DOI: https://doi.org/10.3390/geosciences6030037

Verde, J., Zêzere, J. (2010). Assessment and validation of wildfire susceptibility and hazardin Portugal. Natural Hazards and Earth System Sciences, 10, 485–497. DOI: https://doi.org/10.5194/nhess-10-485-2010.

Tedim F, Leone V, Amraoui M, Bouillon C, Coughlan MR, Delogu GM, Fernandes PM, Ferreira C, McCaffrey S, McGee TK, Parente J, Paton D, Pereira MG, Ribeiro LM, Viegas DX, Xanthopoulos G. (2018). Defining Extreme Wildfire Events: Difficulties, Challenges, and Impacts. Fire, 1(1):9. https://doi.org/10.3390/fire1010009

Tedim, F., McCaffrey, S., Leone, V., Delogu, G. M., Castelnou, M., McGee, T. K., & ArAnhA, J. (2020). What can we do differently about the extreme wildfire problem: An overview. Extreme Wildfire Events and Disasters, 233-263.

Design and Radiative heat transfer in a fireman in wildfire environment

Eusébio Conceição*[1]; João Gomes[2]; Mª Manuela Lúcio[1]; Domingos Viegas[3]; Mª Teresa Viegas[3]

[1] FCT – Universidade do Algarve, Campus de Gambelas,
8005-139 Faro, Portugal, {econcei@ualg.pt, maria.manuela.lucio@gmail.com}
[2] CINTAL, Campus de Gambelas,
8005-139 Faro, Portugal, {jgomes@ualg.pt}
[3] FCT – Universidade de Coimbra - Pinhal de Marrocos - Pólo II,
3030 Coimbra, Portugal, {xavier.viegas, maria.viegas}@dem.uc.pt

**Corresponding author*

Keywords

Numerical simulation, fireman thermal response, energy balance integral equations, mass balance integral equation

Abstract

This work presents the design and radiative heat transfer in a fireman in wildfire environment. The fireman body model, used in this work, is divided into 35 elements. Each element is subdivided into several layers, constituted by fat, muscle, core and skin, and can be protected from the outside environment by several clothing layers. The geometry of the fireman and the fire front are developed using numerical models. Fireman thermal systems consider energy and mass balance integral equations. The energy balance integral equations consider the conduction, convection, evaporation and radiation, amount other phenomena, while the mass balance integral equations consider the convection and diffusion, amount other phenomena. The fireman has subjected two vertical fire fronts. The fireman and the fire front geometry was developed and are used to evaluate the view factors that each fireman section is subjected. The view factors are used to evaluate separately the influence of the two fire front and the Mean Radiant Temperature are used to evaluate integrated the influence of both fire front.

1. Introduction

In this study the influence of two fire fronts in the fireman are analysed. The view factors are used to evaluate separately the influence of each one in the fireman, while the Mean Radiant Temperature (see (ISO, 2005), (Fanger, 1970), (ASHRAE, 2017)) is used to evaluate integratelly the influence of the two fire front in the fireman. However, in order to evaluate the view factors and the Mean Radiant Temperature the fireman and fire front geometry are important to generate in detail.

The numerical model used in this study considers the fireman geometry and the fireman thermal response. In the fireman thermal response special attention is made in the radiative phenomenon.

The human body geometry considers 34 cylindrical elements and 1 sphere element (see (Conceição and Lúcio, 2001), (Conceição et al., 2018) and (Conceição and Awbi, 2021)). In the cylindrical elements are considered the neck, chest, upper abdomen, lower abdomen, right upper shoulder, right lower shoulder, right upper arm, right lower arm, right hand, left upper shoulder, left lower shoulder, left upper arm, left lower arm, left hand, right upper thigh, right lower thigh, right upper leg, right lower leg, right foot, left upper thigh, left lower thigh, left upper leg, left lower leg, left foot and 10 fingers. In the sphere element the head is considered.

In the fireman thermal response, it is important to consider the radiative heat exchanges to evaluate the thermal interaction between the surrounding surfaces and the fireman body surfaces. In this study the shading devices is also considered. See this methodology applied in plan surfaces in (Conceição et al., 2010), (Conceição, Gomes and Awbi, 2019) and (Conceição and Lúcio, 2010). The numerical model considers also the convective heat exchanges between the body surface and the surrounding airflow, the heat conduction through the bodies' tissues, water heat loss by evaporation from the skin surface and clothing of the fireman. In the numerical model the energy and mass balance integral equations is used.

In the radiative heat exchange the view factors between the fire front and the fireman should be evaluated. The view factors, among others works, can be analysed in (Jiang et al., 2017), (Vorre, Jensen and Le Dréau, 2015) and (Lai, Maing and Ng, 2017).

2. Numerical model

The fireman thermal response is based on the energy balance integral equations for the body tissues and clothing and the mass balance integral equation for the water in the body tissues and clothing.

The energy balance integral equations consider the following phenomena:

- The conduction phenomenon appears between the various layers of each body element and between the various layers of clothing.
- The convection phenomenon appear between the bodies external surface (skin and clothing) and the surrounding air environment.
- The evaporation phenomena appear between the bodies external surface (skin and clothing), subjected to water vapour, and the surrounding air environment.
- The radiation phenomenon appears between the bodies external surface and the fire front, whose modelling uses the Mean Radiant Temperature values. Between the clothing levels and between the skin and the clothing the radiation phenomenon are also verified.

The mass balance integral equations consider the following phenomena:

- The water vapour convection appear between the bodies external surface (skin and clothing) and the surrounding air environment.
- The diffusion phenomenon appears between the clothing bodies and between the skin and the clothing surfaces.

The systems of equations defined above are solved by the Runge-Kutta-Fehlberg algorithm with error control.

3. Numerical methodology

The fireman model has a height of 1.8 m and consists of 35 elements. It is equipped with three layers of clothing, the outer layer corresponding to the typical equipment (including the helmet) of a fireman fighting a forest fire.

In this study two fire front, being static in the numerical simulation, are considered:

- The fire front number 1 has 10 m wide and 1 m high and is located in front to the fireman;
- The fire front number 2 has 8 m wide and 1 m high and is located in the side to the fireman.

The fireman distance between each fire front is:

- 5 m from the fireman to the fire front number 1;
- 6.5 m from the fireman to the fire front number 2.

The fireman is placed at a distance of 5 m perpendicular to the central zone of the fire front, as shown, respectively, in Figure 1 and Figure 2.

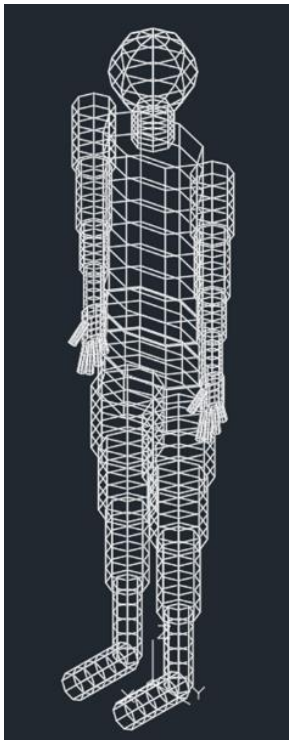

Figure 1- Fireman three-dimensional model

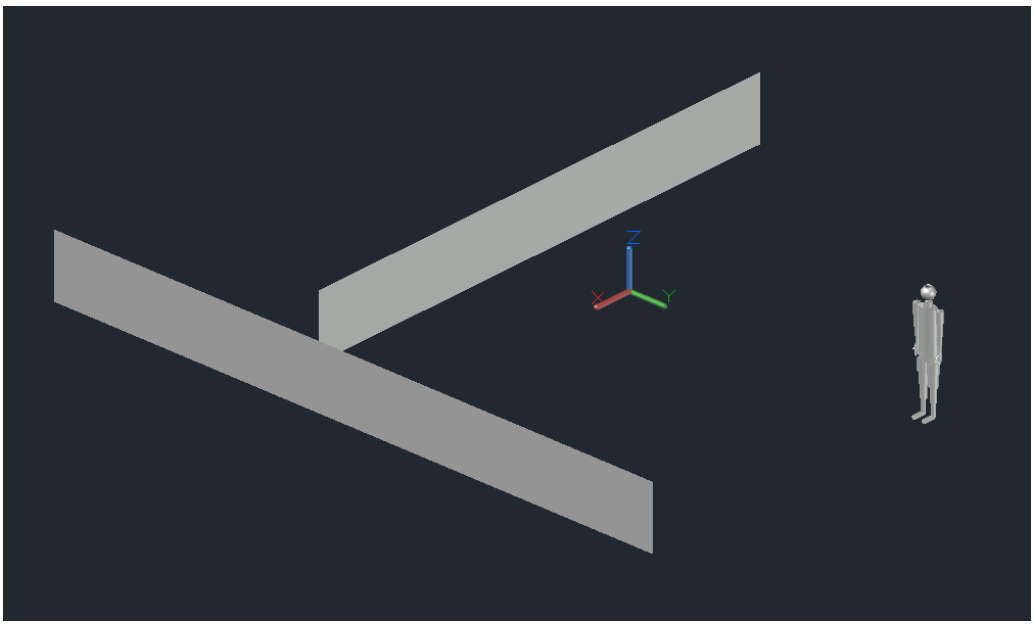

Figure 2- Location of the fireman in relation to the fire front number 1 and number 2

4. Results

This section presents the results obtained in the view factors for the fire front number 1 (see figure 3) and the view factors for the fire front number 2 (see figure 4). The Mean Radiant Temperature distribution, that is influence of the two fire front is presented in Figure 5.

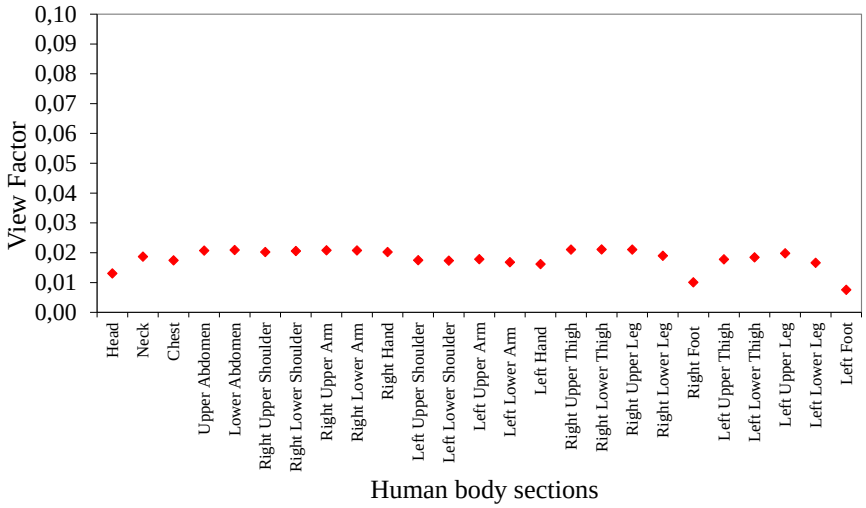

Figure 3. View factor that the fireman are subjected in the fire front number 1.

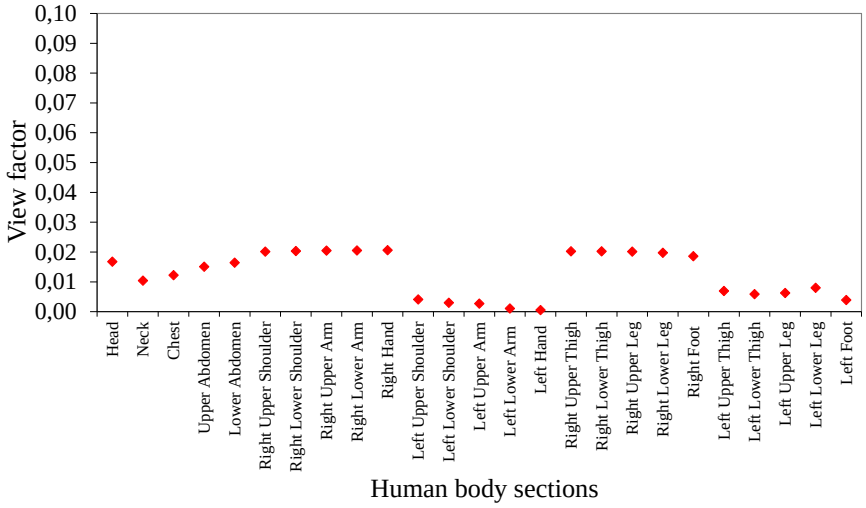

Figure 4. View factor that the fireman are subjected in the fire front number 2.

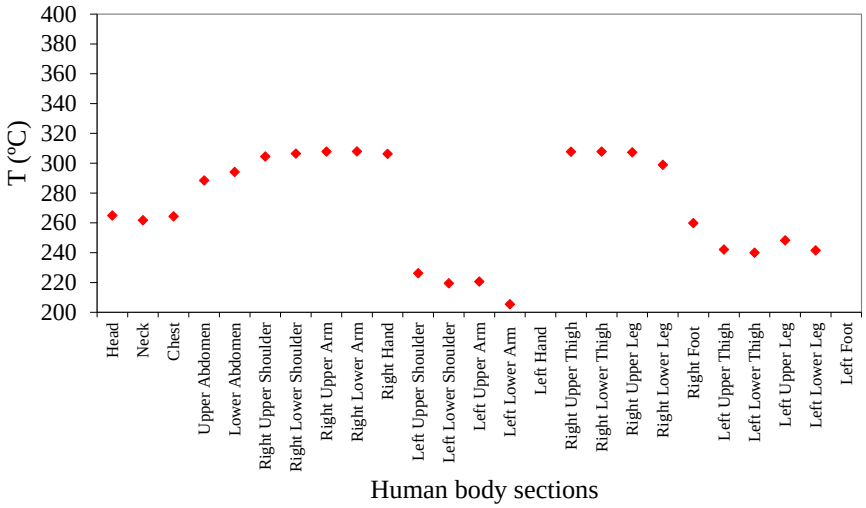

Figure 5. Mean Radiant Temperature distribution in the fireman.

In accordance with the obtained results the fire front located in front to the fireman present similar distribution of the view factor in the human body. In general, the view factor value is similar, however the head and the feet's presents slight low values.

When the fire front is localized in the lateral area to the fireman, the left upper and the left lower member, mainly the upper arm, present lower view factor values. Thus, these human body sections are protected from the radiation flux of the fire front number 2.

Finally, the Mean Radiant Temperature present the contribution of the radiant heat flux come from the two fire fronts, calculated trough the view factors. In the present study, namely in the fire front number 2, the protection promoted by the trunk is verified in the left arm. The low view facts verified also in the foot and hear are also verified in the Mean Radiant Temperature.

Thus, this kind of situation, namely when the occupant are subjected simultaneous to several fire front, this methodology consider simultaneously the real radiative effect that the fireman are subjected.

5. Conclusions

In this paper a design and radiative heat transfer in a fireman in wildfire environment is evaluated. In accordance with the obtained results, the fireman and the fire front geometry is very important in the calculation of the view factors and the Mean Radiant Temperature used to evaluate the heat exchanges that the fireman is subjected.

The human body geometry considers 35 human body elements. The grid generation refinement considered in cylinders and sphere is important in the view factors calculus. In the fire front geometry, considered as a plan vertical surface, the grid generation refinement is also an important factor in the view factors calculus.

The Mean Radiant Temperature is calculated based in the view factors obtained individually in each fire front.

This methodology is important to evaluate individual the effect that each fire front promoted in the fireman, using the view factor concept, and is important to evaluate simultaneously the integral effect that all fire front promoted in the fireman, using the Mean Radiant Temperature.

6. Acknowledgments

The authors would like to acknowledge the support of the project reference PCIF/MPG/0108/2017, funded by the Portuguese Foundation of Science and Technology (FCT).

7. References

ASHRAE (2017) 'ANSI/ASHRAE Standard 55-2017 : Thermal Environmental Conditions for Human Occupancy', ASHRAE Inc.

Conceição, E. and Awbi, H. (2021) 'Evaluation of integral effect of thermal comfort, air quality and draught risk for desks equipped with personalized ventilation systems', Energies. doi: 10.3390/en14113235.

Conceição, E., Gomes, J. and Awbi, H. (2019) 'Influence of the airflow in a solar passive building on the indoor air quality and thermal comfort levels', Atmosphere, 10(12). doi: 10.3390/ATMOS10120766.

Conceição, E. Z. E. et al. (2010) 'Application of a school building thermal response numerical model in the evolution of the adaptive thermal comfort level in the Mediterranean environment', International Journal of Ventilation, 9(3). doi: 10.1080/14733315.2010.11683887.

Conceição, E. Z. E. et al. (2018) 'Predicting the air quality, thermal comfort and draught risk for a virtual classroom with desk-type personalized ventilation systems', Buildings, 8(2). doi: 10.3390/buildings8020035.

Conceição, E. Z. E. and Lúcio, M. (2001) 'Numerical and subjective responses of human thermal sensation', Proceedings of the BioEng.

Conceição, E. Z. E. and Lúcio, M. M. J. R. (2010) 'Numerical study of the influence of opaque external trees with pyramidal shape on the thermal behaviour of a school building in summer conditions', Indoor and Built Environment, 19(6). doi: 10.1177/1420326X10377546.

Fanger, P. O. (1970) Thermal comfort. Analysis and applications in environmental engineering., Copenhagen: Danish Technical Press. Danish Technical Press.

ISO (2005) 'ISO 7730: Ergonomics of the thermal environment Analytical determination and interpretation of thermal comfort using calculation of the PMV and PPD indices and local thermal comfort criteria', Management. doi: 10.1016/j.soildyn.2004.11.005.

Jiang, F. et al. (2017) 'Accuracy analysis and improvement of the Blind Enclosure Model to calculate the longwave radiative heat transfer for a façade with louver blinds', Energy and Buildings. doi: 10.1016/j.enbuild.2017.01.065.

Lai, A., Maing, M. and Ng, E. (2017) 'Observational studies of mean radiant temperature across different outdoor spaces under shaded conditions in densely built environment', Building and Environment. doi: 10.1016/j.buildenv.2016.12.034.

Vorre, M. H., Jensen, R. L. and Le Dréau, J. (2015) 'Radiation exchange between persons and surfaces for building energy simulations', Energy and Buildings. doi: 10.1016/j.enbuild.2015.05.005.

Do wildfires burn tourism intentions? The case of Portugal

João Cerejeira*[1,2]; Rita Sousa[1]; Carolina Bernardo[1]

[1]School of Economics and Management, University of Minho, and NIPE – Economic Policies Research Unit - Campus de Gualtar, 4710 - 057 Braga, Portugal, {joao.cerejeira, ritasousa}@eeg.uminho.pt, {caroltsbernardo@gmail.com}
[2] CIPES – Centro de Investigação de Políticas do Ensino Superior, R. 1º Dezembro 399, 4450-227 Matosinhos, Portugal, {joao.cerejeira@eeg.uminho.pt}

**Corresponding author*

Keywords

Tourism demand, wildfires, spatial econometrics, climate change

Abstract

Fire intensity and size incite visitation decrease and recreational losses, relevant tourism variables for European economies. As a result of climate change, the wildfires recurrence is becoming more evident. Due to significant gaps in analyzing the relationship between wildfires and tourism demand, this paper aims to explain how tourism demand reacts to wildfires in Portugal. We use a spatial econometric model to analyze the relationship between total burned areas and overnight stays in a touristic establishment in a given municipality and its neighboring municipalities. Our results show that wildfires negatively affect the overnight stays in the same location but also cause spillover effects in neighboring municipalities. Also, the wildfire occurrences are positively related to the number of overnight stays after three months, suggesting a delay in tourism activities.

1. Introduction

Climate change relates to shifts in the mean climate and variations in the frequency and intensity of extreme weather events. The increased frequency and intensity of extreme precipitation, droughts, tropical cyclones, and compound extremes, including fire weather, are evident, as shown in the IPCC 6th Assessment Report (IPCC 2021). In particular, the recurrence and duration of wildfires, as a result of climate change, has increased in many countries all over the world, including Greece, Spain, and Portugal (Giannakopoulos, Kostopoulou et al. 2011, Hall, Scott et al. 2011, Marques, Borges et al. 2011, Doerr and Santín 2016). Consequently, economic activities, specialization, and other economic geography variables are also predicted to shift in the coming years (Yohe and Schlesinger 2002, Conte, Desmet et al. 2021). A region that is expected to be severely affected by climate change and fires is the Mediterranean.

In the Mediterranean, tourism constitutes a significant economic activity, totalizing 217 billion euros in international tourism receipts, 23% of the world total, in 2014. The Mediterranean climate is the principal element tourists consider regarding travel planning, especially relevant for summer tourism (Giannakopoulos, Kostopoulou et al. 2011, Roson and Sartori 2014). Hence, the dependence of tourism activities on climate resources makes the industry one of the most vulnerable to climate change (Dogru, Bulut et al. 2016, Dogru, Marchio et al. 2019).

Portugal, as a Mediterranean country, has historical wildfires. Natural ignitions in the European Mediterranean basin, such as lightning, are standard where the atmospheric conditions feature low humidity and little or no precipitation. However, the modified socio-economic, environment and land patterns, in Portugal, as well as in other European Mediterranean countries, led to changes in the traditional causes of fire ignition in recent decades, whose origins have predominantly become anthropogenic instead of natural (Pereira, Trigo et al. 2005, de Zea Bermudez, Mendes et al. 2009). Currently, Portugal has the highest incidence of wildfire events in the Mediterranean basin and the whole of Europe, which have also become larger and more intense (Meira Castro, Nunes et al. 2020).

As in other similar regions, wildfires in Portugal are more prone to occur in the summer, when high temperatures and relative air humidity are low. In the same period, tourism activities are at their highest, and studies already

look to patterns of seasonality and global warming implications in summer tourism (Vergori 2017, Koutroulis, Grillakis et al. 2018). The tourist accommodation sector registered 2.5 million guests and 7.5 million overnight stays in August 2021 in Portugal, versus 1.5 million guests and 3.6 million overnight stays in November 2021. This summer tourism peak is responsible for a seasonal increase in the income of associated economic sectors, such as food and hospitality. The average daily rate (ADR) amounted to EUR 115.8 in August, and EUR 98.7 in July, versus EUR 47.1 in February (INE 2021).

Although the broad impacts of climate change in tourism have been analyzed (Scott, Gössling et al. 2012, Kaján and Saarinen 2013, Dogru, Marchio et al. 2019, Scott, Hall et al. 2019), more specific studies only focus on tourism activities that will suffer most immediately from climate change, expectedly, the decrease in snow and skiing activities (Dawson and Scott 2013, Gilaberte-Búrdalo, López-Martín et al. 2014, Steiger, Scott et al. 2019). Some of these studies use simplified regression models to evaluate the effect on ski tourism variables resulting from increased temperatures (Demiroglu, Kučerová et al. 2015, Damm, Greuell et al. 2017).

Studies on wildfire impacts in tourism are even in more remarkable absence, as noted by Arabadzhyan, Figini et al. (2021) in a review on coastal tourism. Such may be explained both by the difficulty in collecting and treating data and coordinating analysis between two vastly different scientific areas and by the fact that the tourism boom is still very recent in some wildfire-prone regions, such as Portugal. Additionally, the years of the pandemic and substantial restrictions on travel further hinder the collection of information, although new analyses are emerging (Marques, Guedes et al. 2021). Existing analyses include Sánchez, Baerenklau et al. (2016) that develop a Kuhn–Tucker model of recreation demand, with survey data, to look to relationships between wildfires and wilderness access, looking to the effects on visits, showing significant potential welfare loss. In Portugal, Otrachshenko and Nunes (2022) use yearly data in a two-level analysis in a panel regression model with fixed effects to reveal that burned areas negatively impact the number of tourist arrivals.

As evidenced, the literature presents significant gaps in analyzing the relationship between wildfires and tourism demand. In the context of climate change, with perspectives of future worsening of extreme events in the Mediterranean region, and with the growing importance of the tourism sector for regional socio-economic development, it becomes critical to understand how tourists change their journeys in the evidence of those events.

This paper aims to understand how tourism demand reacts to wildfires and how tourists adjust their destination / monthly travel intentions within monthly time lags. Do tourists postpone their trips for a few months when faced with the evidence of the fires? Will they change their intentions to visit at similar times in the following years? This study builds on previous analysis and develops a model to address these questions. Looking at all mentioned works, we conclude that regression analyses, adequately tuned to the variables in question, can produce valuable results. We apply spatial econometric techniques not yet used in this field to develop a novel spatial regression model that considers the possibility of spillovers in time and space, contributing to the economic geography literature on climate change impacts. The model analyses wildfires over monthly time units and municipalities, capturing their effects on the variation in the distribution of tourism along with the municipalities mentioned above.

2. Data and Methodology

2.1. Data

This study uses wildfires data provided by the Portuguese Institute for Conservation of Nature and Forests (ICNF) (ICNF 2021). The database includes monthly distributed data on the burned area in hectares by municipalities from 2017 to 2020. The total burned area includes forests and shrubs lands and rural areas. The percentage of wildfires events during summers increased severely from 49% to 70% from 2019 to 2020.

As a proxy for tourism demand, the municipality's number of tourist guests and monthly overnight stays were obtained from the Statistics Portugal website (INE) from 2020 to August 2021 (INE 2021b, INE 2021c).Figure 1 and 2 shows the occurrence of wildfires of more than 1000ha in continental Portugal during summers 2019 and 2020, respectively. Comparing figure 2 with tourism demand, in 2020 and 2021 summers (Figure 3), it is possible to see the lowest tourism records in the same municipalities with the most significant fires. In Proença-a-Nova (Pr-a-Nova in Figure 2), for example, had the most significant wildfire in 2020 summer (Figure 2), and

this municipality registered the lowest tourism demand rate in 2020 and 2021 (Figure 3). This data shows possible wildfires interfering in summer tourism demand in the same year and one year later after the wildfire event.

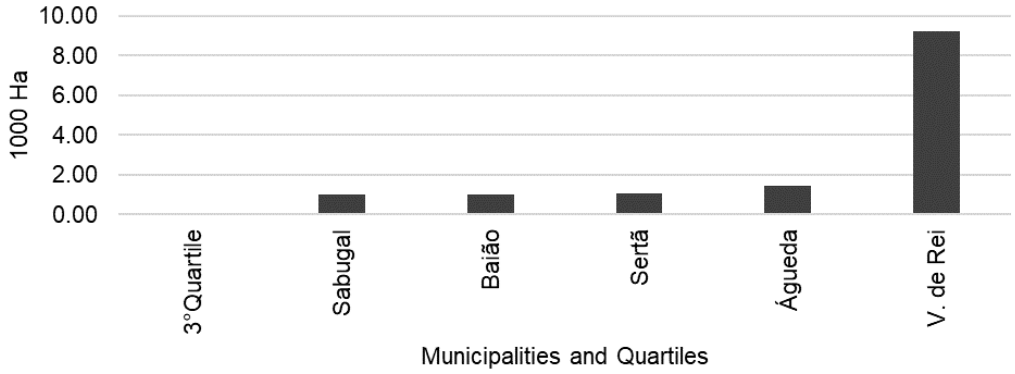

Figure 1- Burned areas per Municipalities of the 4th Quartile, summer 2019. Source: (ICNF 2021).

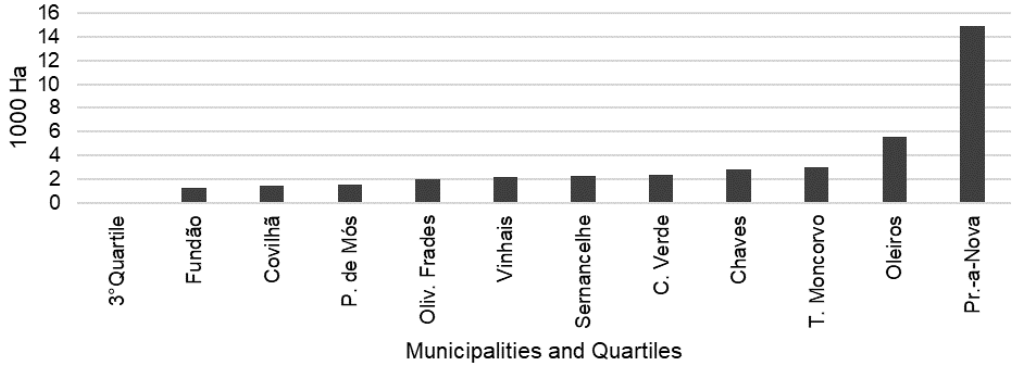

Figure 2- Burned areas per Municipalities of the 4th Quartile, summer 2020. Source: (ICNF 2021).

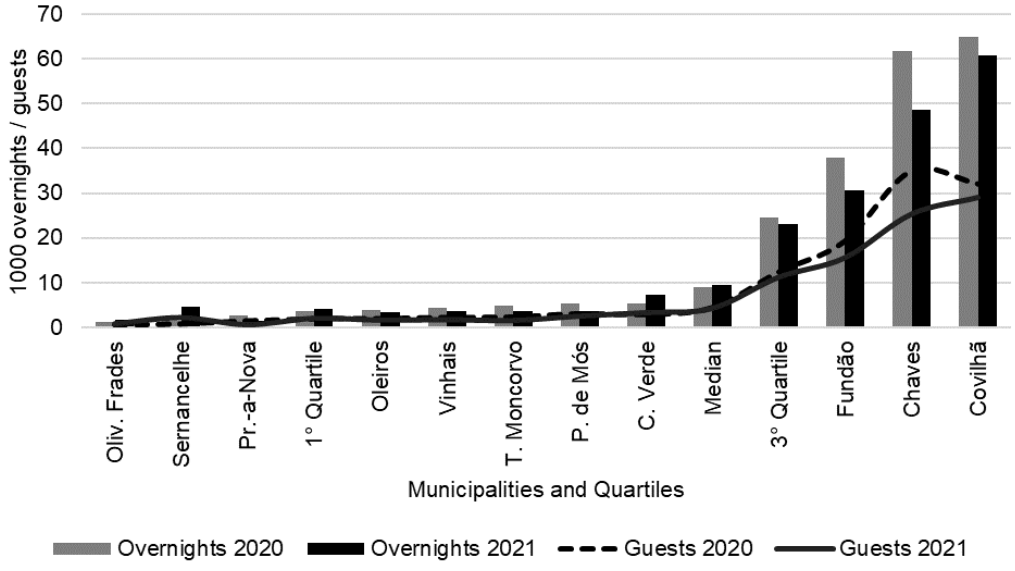

Figure 3- Tourism demand, per representative Municipalities with wildfires in 2020 - summers 2020 and 2021. Source: INE (2021b); INE (2021c).

In the same way, a similar effect appeared when comparing figure 4 with the tourism demand in 2020 summer for the same municipalities illustrated in figure 1. For example, Vila de Rei municipality, wherein 2019 had the

most significant wildfire registered during summer (Figure 1), and in the next year (2020) had the lowest summer tourism demand recorded (Figure 4), showing a one-year later effect.

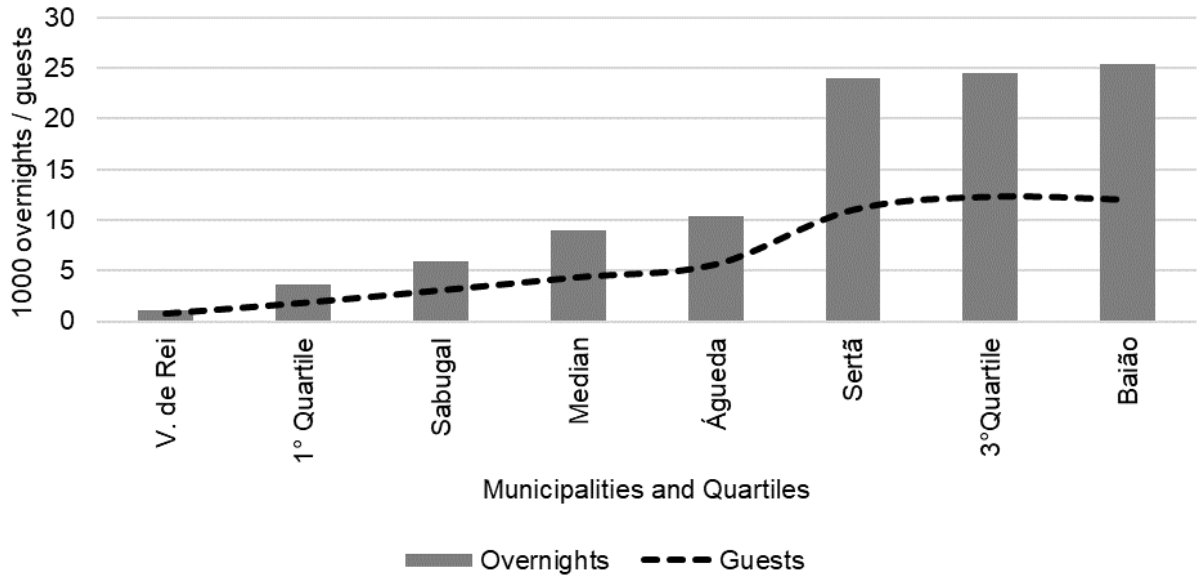

Figure 4- Tourism demand, summer 2020, per Municipalities with wildfires in 2019. Sourc e: INE (2021b); INE (2021c).

2.2. Methodology

In this paper, we use a spatial econometric regression to look at the effects on neighbor regions. We estimate the relationship between total burned areas and overnight stays in a touristic establishment in a given municipality by month. The main equation has the following specification:

$$Stays_{i,m,y} = \beta_0 + \beta_1 Burned_{Area\,i,m,y} + \theta_i + month_m + year_y + \varepsilon_{ii,y}$$

where $Staysi,m,y$ is the number of overnight stays, considered in relation to each person, by municipality, $Burnedi,m,y$ stands for the total area of burned forest, agriculture land, and shrub. The terms θi, $monthm$, and $yeary$, are the municipality, month and year fixed effects, respectively.

The municipality fixed effects control for time-invariant unobserved local characteristics that may affect the number of overnight stays, such as the area of the municipality, the landscape, the location or the supply of cultural and environmental amenities that do not vary in 2020 and 2021. Monthly and yearly fixed effects control for any common changes across municipalities and for the seasonal nature of the touristic demand as well as COVID19 restrictions implemented nationally wide.

The coefficient of interest is $\beta 1$ which measures the change in the number of overnight stays due to an increase in one hectare in burned area.

The model is estimated with contemporaneous information for overnight stays and burned area, but the $\beta 1$ estimator potentially suffers from omitted variable bias, if there are other factors that affect tourist demand and the burned area simultaneously.

Wildfires in one given municipality can also affect tourism demand in neighboring municipalities. In order to control for that, we estimate a set of models including a spatial lag of the burned area in other municipalities, weighted by a spatial weight matrix. This matrix is row-standardized and is based on the power functional form as follows:

$$w_{ij} \begin{cases} \dfrac{d_{ij}^{-2}}{\sum_{j=1}^{n} d_{ij}^{-2}}, i \neq j \\ 0, \end{cases}$$

The model with spatially lagged burned area has the following specification:

$$Stays_{i,m,y} = \beta_0 + \beta_1 Burned\_Area_{i,m,y} + \beta_2 WBurned\_Area_{i,m,y} + \theta_i + month_m + year_y + \varepsilon_{ii,y}$$

where $WBurnedi,m,y$ denotes the spatial lag of $Burnedi,m,y$.

3. Results

The analysis of effects on the number of overnights spent by tourists resulting from wildfires is presented below in Table 1. The model comprises 1, 3, 6, 9 and 12 monthly temporal lags, identified with *"L#"*, to capture the changes in intentions. For each temporal lag, a spatial lag, noted with *"W"*, is also considered, showing the effects of wildfires on neighboring municipalities in local tourism demandable. These results are presented in Table 2.

According to Table 1, burned area is positively related to the number of overnight stays after three months. This can be the result of postponed reservations or the decrease in prices that might occur if wildfires reduce the attractiveness of the municipality in the following days. The negative effect appears to be statistically significant after twelve months of the wildfires. On average, one hectare of burning area reduces overnight stays in almost 3 units.

Table 1 - Results of the spatial regression model with time lags.

	(1) Overnights	(2) Overnights	(3) Overnights	(4) Overnights	(5) Overnights	(6) Overnights
Burned Area	-0.535					
	(0.382)					
L. Burned Area		-0.251				
		(0.434)				
L3. Burned Area			0.887**			
			(0.404)			
L6. Burned Area				0.0662		
				(0.439)		
L9. Burned Area					0.598	
					(0.524)	
L12. Burned Area						-2.953*
						(1.637)
Mun. fixed effects	Yes	Yes	Yes	Yes	Yes	Yes
Month fixed effects	Yes	Yes	Yes	Yes	Yes	Yes
Year fixed effects	Yes	Yes	Yes	Yes	Yes	Yes
N	2636	2815	3137	3783	4259	4259
R^2	0.055	0.054	0.056	0.034	0.048	0.048
adj. R^2	0.051	0.049	0.052	0.031	0.045	0.045

Table 2 presents the results of the model with the temporal and spatially lags of the burned area. The negative effects of the burned area on overnight stays are now statistically significant on the contemporaneous month of the wildfire, as well as on the twelve months lag. A novel result is the impact of wildfires in neighboring municipalities. The magnitudes are much higher than the magnitude of the coefficient for the same location. The positive effect after three months is also significant, as in Table 3, as well as the effect of the neighboring wildfires.

We construct the model considering fixed effects from external variables, such as climate temperature and the occurrence of COVID 19. However, a further analysis that may be carried out is to consider the effect of COVID 19 on the tourism demand in Portugal. In addition, we hope to analyze further the effects of wildfires on tourism revenues and their impact on regional and national GDP.

Table 2 - Results of the spatial regression model with time and space lags.

	(1) Overnights	(2) Overnights	(3) Overnights	(4) Overnights	(5) Overnights	(6) Overnights
Burned Area	-0.706*					
	(0.407)					
W_Burned Area	-28.96**					
	(13.06)					
L. Burned Area		-0.252				
		(0.424)				
L.WBurned Area		-0.227				
		(4.428)				
L3. Burned Area			0.728**			
			(0.324)			
L3.W_Burned Area			27.98**			
			(12.80)			
L6. Burned Area				0.0958		
				(0.427)		
L6.W_Burned Area				-7.286		
				(5.082)		
L9. Burned Area					0.612	
					(0.507)	
L9.W_Burned Area					7.707	
					(7.254)	
L12. Burned Area						-2.623*
						(1.477)
L12.W_Burned Area						-26.11***
						(8.929)
Mun. fixed effects	Yes	Yes	Yes	Yes	Yes	Yes
Month fixed effects	Yes	Yes	Yes	Yes	Yes	Yes
Year fixed effects	Yes	Yes	Yes	Yes	Yes	Yes
N	2636	2815	3137	3783	4259	4259
R^2	0.055	0.054	0.056	0.034	0.048	0.048
adj. R^2	0.051	0.049	0.052	0.031	0.045	0.045

4. References

Arabadzhyan, A., P. Figini, C. García, M. M. González, Y. E. Lam-González and C. J. León (2021). "Climate change, coastal tourism, and impact chains – a literature review." Current Issues in Tourism 24(16): 2233-2268.

Conte, B., K. Desmet, D. K. Nagy and E. Rossi-Hansberg (2021). "Local sectoral specialization in a warming world." Journal of Economic Geography 21(4): 493-530.

Damm, A., W. Greuell, O. Landgren and F. Prettenthaler (2017). "Impacts of +2°C global warming on winter tourism demand in Europe." Climate Services 7: 31-46.

Dawson, J. and D. Scott (2013). "Managing for climate change in the alpine ski sector." Tourism Management 35: 244-254.

de Zea Bermudez, P., J. Mendes, J. Pereira, K. Turkman and M. Vasconcelos (2009). "Spatial and temporal extremes of wildfire sizes in Portugal (1984–2004)." International Journal of Wildland Fire 18(8): 983-991.

Demiroglu, O. C., J. Kučerová and O. Ozcelebi (2015). "Snow reliability and climate elasticity: case of a Slovak ski resort." Tourism Review 70(1): 1-12.

Doerr, S. H. and C. Santín (2016). "Global trends in wildfire and its impacts: perceptions versus realities in a changing world." Philosophical Transactions of the Royal Society B: Biological Sciences 371(1696): 20150345.

Dogru, T., U. Bulut and E. Sirakaya-Turk (2016). "Theory of vulnerability and remarkable resilience of tourism demand to climate change: Evidence from the Mediterranean Basin." Tourism Analysis 21(6): 645-660.

Dogru, T., E. A. Marchio, U. Bulut and C. Suess (2019). "Climate change: Vulnerability and resilience of tourism and the entire economy." Tourism Management 72: 292-305.

Giannakopoulos, C., E. Kostopoulou, K. V. Varotsos, K. Tziotziou and A. Plitharas (2011). "An integrated assessment of climate change impacts for Greece in the near future." Regional Environmental Change 11(4): 829-843.

Gilaberte-Búrdalo, M., F. López-Martín, M. R. Pino-Otín and J. I. López-Moreno (2014). "Impacts of climate change on ski industry." Environmental Science & Policy 44: 51-61.

Gomes, J. F. P. (2006). "Forest fires in Portugal: how they happen and why they happen." International Journal of Environmental Studies 63(2): 109-119.

Gomes, J. F. P. and M. Radovanovic (2008). "Solar activity as a possible cause of large forest fires — A case study: Analysis of the Portuguese forest fires." Science of The Total Environment 394(1): 197-205.

Gómez-González, S., F. Ojeda and P. M. Fernandes (2018). "Portugal and Chile: Longing for sustainable forestry while rising from the ashes." Environmental Science & Policy 81: 104-107.

Hall, C. M., D. Scott and S. Gössling (2011). "Forests, climate change and tourism." Journal of Heritage Tourism 6(4): 353-363.

ICNF. (2021). "Informação sobre áreas ardidas e ocorrências de 2001 a 2021 - Relatórios de Incêndios rurais." accessed 2022-01-31, from http://www2.icnf.pt/portal/florestas/dfci/relat/rel-if.

INE. (2021). "Survey on Guests Stays on Hotel Establishments and Other Accommodations: Global results.", accessed 2022-01-31, from https://www.ine.pt/xportal/xmain?xpid=INE&xpgid=ine_destaques&DESTAQUESdest_boui=472730931&DESTAQUESmodo=2.

INE. (2021b). "Nights (No.) in tourist accommodation establishments by Geographic localization and Place of residence; Annual.", accessed 2022-01-31, from https://www.ine.pt/xportal/xmain?xpid=INE&xpgid=ine_indicadores&contecto=pi&indOcorrCod=0009183&selTab=tab0.

INE. (2021c). "Guests (No.) in tourist accommodation establishments by Geographic localization (NUTS - 2013) and Type (tourist accommodation establishment); Monthly." accessed 2022-01-31, from https://www.ine.pt/xportal/xmain?xpid=INE&xpgid=ine_indicadores&contecto=pi&indOcorrCod=0009812&selTab=tab0.

IPCC (2021). Climate Change 2021: The Physical Science Basis. Contribution of Working Group I to the Sixth Assessment Report of the Intergovernmental Panel on Climate Change. V. Masson-Delmotte, P. Zhai, A. Pirani, S.L., Connors, C. Péan, S. Berger, N. Caud, Y. Chen, L. Goldfarb, M.I. Gomis, M. Huang, K. Leitzell, E. Lonnoy, J.B.R. Matthews, T.K. Maycock, T. Waterfield, O. Yelekçi, R. Yu, and B. Zhou.

Kaján, E. and J. Saarinen (2013). "Tourism, climate change and adaptation: a review." Current Issues in Tourism 16(2): 167-195.

Koutroulis, A. G., M. G. Grillakis, I. K. Tsanis and D. Jacob (2018). "Mapping the vulnerability of European summer tourism under 2 °C global warming." Climatic Change 151(2): 157-171.

Lynch, D. L. (2004). "What Do Forest Fires Really Cost?" Journal of Forestry 102(6): 42-49.

Marques, C. P., A. Guedes and R. Bento (2021). "Rural tourism recovery between two COVID-19 waves: the case of Portugal." Current Issues in Tourism: 1-7.

Marques, S., J. G. Borges, J. Garcia-Gonzalo, F. Moreira, J. M. B. Carreiras, M. M. Oliveira, A. Cantarinha, B. Botequim and J. M. C. Pereira (2011). "Characterization of wildfires in Portugal." European Journal of Forest Research 130(5): 775-784.

Meira Castro, A. C., A. Nunes, A. Sousa and L. Lourenço (2020). "Mapping the Causes of Forest Fires in Portugal by Clustering Analysis." Geosciences 10(2): 53.

Molina, J. R., A. González-Cabán and F. Rodríguez y Silva (2019). "Wildfires impact on the economic susceptibility of recreation activities: Application in a Mediterranean protected area." Journal of Environmental Management 245: 454-463.

Otrachshenko, V. and L. C. Nunes (2022). "Fire takes no vacation: impact of fires on tourism." Environment and Development Economics 27(1): 86-101.

Parente, J., M. G. Pereira, M. Amraoui and E. M. Fischer (2018). "Heat waves in Portugal: Current regime, changes in future climate and impacts on extreme wildfires." Science of The Total Environment 631-632: 534-549.

Pereira, M. G., L. Caramelo, C. V. Orozco, R. Costa and M. Tonini (2015). "Space-time clustering analysis performance of an aggregated dataset: The case of wildfires in Portugal." Environmental Modelling & Software 72: 239-249.

Pereira, M. G., R. M. Trigo, C. C. da Camara, J. M. C. Pereira and S. M. Leite (2005). "Synoptic patterns associated with large summer forest fires in Portugal." Agricultural and Forest Meteorology 129(1): 11-25.

Rego, F., G. Louro and L. Constantino (2013). "The impact of changing wildfire regimes on wood availability from Portuguese forests." Forest Policy and Economics 29: 56-61.

Roson, R. and M. Sartori (2014). "Climate change, tourism and water resources in the Mediterranean." International Journal of Climate Change Strategies and Management 6(2): 212-228.

Sánchez, J. J., K. Baerenklau and A. González-Cabán (2016). "Valuing hypothetical wildfire impacts with a Kuhn–Tucker model of recreation demand." Forest Policy and Economics 71: 63-70.

Scott, D., S. Gössling and C. M. Hall (2012). "International tourism and climate change." WIREs Climate Change 3(3): 213-232.

Scott, D., C. M. Hall and S. Gössling (2019). "Global tourism vulnerability to climate change." Annals of Tourism Research 77: 49-61.

Steiger, R., D. Scott, B. Abegg, M. Pons and C. Aall (2019). "A critical review of climate change risk for ski tourism." Current Issues in Tourism 22(11): 1343-1379.

UNWTO (2015). UNWTO Mediterranean Tourism Trends, 2015 edition. UNWTO Tourism Trends Snapshot. W. T. Organization.

Vergori, A. S. (2017). "Patterns of seasonality and tourism demand forecasting." Tourism Economics 23(5): 1011-1027.

Viegas, D. X. (2018). "Wildfires in Portugal." Fire Research 2(1).

Yohe, G. and M. Schlesinger (2002). "The economic geography of the impacts of climate change." Journal of Economic Geography 2(3): 311-341.

Firefighters' lifestyle and well-being

Laura Carmona*[1]; Raquel Pinheiro[2]; Joana Faria-Anjos[3]; Sónia Namorado[4]; Maria José Chambel[5]

[1]Faculdade de Psicologia da Universidade de Lisboa, Portugal {lauracarmona@campus.ul.pt}
[2] Escola Nacional de Bombeiros, Portugal {raquel.pinheiro@enb.pt}
[3]CicPsi, Faculdade de Psicologia da Universidade de Lisboa, Instituto de Emergência Médica, Portugal (joana.f.anjos@gmail.com)
[4] Instituto Nacional de Saúde Dr. Ricardo Jorge, Portugal (sonia.namorado@insa.min-saude.pt)
[5] CicPsi, Faculdade de Psicologia da Universidade de Lisboa, Portugal {mjchambel@psicologia.ulisboa.pt}

**Corresponding author*

Keywords

Lifestyle; Flourishing; FANTASTIC checklist; physical activity, sleep

Abstract

The firefighters' lifestyle has important consequences in their well-being. A sample of 861 Portuguese firefighters answer an adapted version of the FANTISTIC checklist that included questions related to family and friends' relationships, physical activity, nutrition, sleep and stress, alcohol and tobacco consumption's, and heath behaviors. We observed that the majority did not have physical activity in the professional context, only sometimes had a healthy nutrition, was overweight, had a tobacco consumption higher than that observed in the Portuguese population and a consumption of alcohol identical to that observed in Portuguese population, about 10% never sleep well and about 50% sometimes sleep well, about 40% only sometimes had capacity to manage stress and about 49% only sometimes relax in free time. Furthermore, we observed that the firefighter's lifestyle was an important predictor of his(er) general well-being, namely his(er) flourishing (e.g., meaning and purpose in life, positive relationships, self-esteem, feelings of competence, optimism, and involvement in daily activities), after control the gender, age, marital status, tenure as firefighter, and hours of work per week. We concluded that is important to develop an intervention to promote the lifestyle of Portuguese firefighters: encouraging the practice of physical exercise, healthy eating, non-consumption of tobacco or dangerous consumption of alcohol and promoting of a healthy sleep and management of stress. These programs must adjust to the idiosyncrasies of corporations and transform those same idiosyncrasies in valid and essential resources. In fact, some of the cultural or operational characteristics (e.g, combination of professionals and volunteers) must be considered so that these programs can be successfully implemented.

1. Lifestyle and Well-being on Firefighters

Previous research has supported the influence that lifestyle factors and behaviors, namely food, sleep, physical activity, body mass index, social, alcohol consumption and tobacco consumption, have on well-being. (e.g. Dale, Brassington & King, 2014; Kilani et al., 2020; Prendergast, Schofield & Mackay, 2016), particularly in firefighters in the UK (Siddall et al., 2014) and Finland (Airila, 2015).

2. FANTASTIC as a valid measure to evaluate lifestyle

The FANTASTIC Lifestyle Assessment Inventory is a lifestyle assessment tool that incorporates physical, emotional, and social factors. There are several advantages of this tool: having only one page, it can be completed quickly; components are easily remembered; it is holistic; can be used for self-assessment; scores are benchmarks for ongoing assessments; results are available immediately; can be immediately combined with a personalized prescription and follow-up plan; saves time by incorporating lifestyle data into a single fill; issues are relevant and based on daily life; it includes only behaviors that can be controlled, minimizing "victim blaming".

Several studies have been using the FANTASTIC Inventory to study lifestyle of the general population (Ramírez-Vélez & Agredo, 2012; Ramírez-Vélez et al., 2015; Rodriguez-Añez, Reis & Petroski, 2008), healthy

individuals (Kim, Kim, & Kim, 2007) and different population groups (e.g., paramedics and Armed Forces (Wilhelm et al., 2016), students (Decina, Mcgregor & Hagino, 1990; Kamien & Power, 1996; Kim, Park, Joe & Cho, 2006; Lo, Francis-Cracknell, & Hassed, 2017), individuals with suicidal behaviors (Wilhelm et al., 2016), deliberate self-harm (Wilhelm et al., 2007), hypertension (López-Carmona et al., 2000), diabetes (Rodríguez Moctezuma et al., 2003), metabolic syndrome (Triviño et al., 2009), cancer (Dennis, Waring, Payeur, Cosby & Daudt, 2013), elderly (Deluga et al., 2018), and patients from family practice (Kason & Ylanko, 1984)).

In this study was used an adaptation of the FANTASTIC Lifestyle Assessment Inventory to the Portuguese firefighter population. The first aim was to know the lifestyle of the Portuguese firefighters, namely related to physical activity, nutrition habits, alcohol and tobacco consumption's, sleep quality and management of stress. The second aim was relating the lifestyle with the firefighters' well-being, namely their flourishing, which refers to the existence of meaning and purpose in life, positive relationships, self-esteem, feelings of competence, optimism, and involvement in daily activities Diener et al., 2010).

3. Hypothesis

In order to test whether there is an influence of lifestyle on the well-being of Portuguese firefighters, the following hypothesis was put forward:

Hypothesis: Firefighters with a better lifestyle have better well-being (i.e. flourishing).

4. Procedure and Sample

The National School of Firefighters sent an email to all the commanders of the different corporations in the Portuguese mainland, asking that it be disseminated by its operational staff. This email had a link to access the questionnaire placed on the Qualtrics platform for two weeks. The anonymity of the participants was ensured.

The sample consisted of 861 firefighters: 578 (67%) men and 283 (33%) women; 540 (62.7%) aged up to 40 years and 321 (37.3%) over 40 years old; 53,4% was married, 45,8% was single and 0,3% was Widower; 472 (54.8%) firefighters for more than 10 years; 492 (57.1%) working less than 40 hours a week as a firefighter and 369 (42.9%) working more than 40 hours a week as a firefighter, with a mean of 34.72 hours (SD = 22.92).

Flourishing was measured through 8 items (Silva e Caetano, 2012) (e.g. I lead a purposeful and meaningful life), answered on a 7-point scale, 1 (strongly disagree) to 7 (strongly agree), where a higher score is indicative of better well-being (Cronbach's alpha = 0.83).

5. Results and conclusions

5.1. Firefighters' Lifestyle

Table 1. Synthesis of FANTISTIC results

Physical Activity	**Individual**	**Collective in professional Context**
Never	18%	58,4%
1 time a week	44,8%	28,8%
3 or more time a week	36,7%	12,8%
Nutrition	**Healthy eating**	**Consumption of high-calorie foods**
Never/almost never	14,3%	12%
Sometimes	59%	81,2%
Always/almost always	26,7%	6,9%
Tobacco consumption	**Yes**	**No**
	36,2%	63,88%
Alcohol consumption	**More than 7 drinks per week**	**Sometimes more than 4-5 drinks per time**
	6,8%	42,3%

Sleep	**Good quality**	**Difficulties**
Almost never	9,6%	31,9%
Sometimes	50,2%	50,9%
Almost always	40,2%	17,2%
Stress	**Management of stress**	**Relax during free time**
Almost never	1,9%	8%
Sometimes	41,5%	48,9%
Almost always	56,7%	43,1%

5.2. Firefighters' lifestyle and flourishing

After controlling for the effect of demographics (gender, age, marital status, time as a firefighter, working hours per week), lifestyle is a significantly predictor of flourishing (cf. Table 2). Thus, the Hypothesis that firefighters with a better lifestyle have better well-being (i.e. flourishing) was supported.

Table 2. Hierarchical Regression of Firefighters' Lifestyle in Flourishing

	Flourishing	
Step 1	*Beta*	*Beta*
Gender	.24	.20
Age	.04	.05
Marital status	.05	.03
Tenure as firefighter	.02	.04
Work hours per week	.05	.01
Step 2		
Lifestyle		.35**
F	1.20	19.67**
Adj. R-Sq.	0	.12
R-Sq. Change	.01	.12**

** $p < .01$

This study found that the lifestyle habits of Portuguese firefighters are mainly very good and excellent, which is in line with the studies by Deluga et al. (2018) (with seniors), Triviño et al. (2009) (with middle-aged adults), Ramírez-Vélez e Agredo (2012) (with colombian adults) and Ramírez-Vélez et al. (2015) (with colombian university students). We can observe critical factors regarding each one of the considered categories.

Although the FANTASTIC Lifestyle Assessment Inventory is a measure from 1984, it has had a lot of use in recent years. Its small size and ease of response proved to be especially suited for firefighters.

We can conclude that to improve the firefighters' well-being we must increase their lifestyle, namely the practice of healthy habits related to physical activity, nutrition, alcohol and tobacco consumption, sleep, and stress management.

6. References

Airila, A. (2015). Work characteristics, personal resources, and employee well-being: A longitudinal study among Finnish firefighters. Finnish Institute of Occupational Health, People and Work Research Reports, 109.

Dale, H., Brassington, L., King, K. (2014). The impact of healthy lifestyle interventions on mental health and wellbeing: A systematic review. *Mental Health Review Journal, 19* (1), 1-26.

Decina, P., Mcgregor, M., & Hagino, C. (1990). Lifestyle analysis: A comparative study between freshman, second and fourth year chiropractic students. *Journal of the Canadian Chiropractic Association*, 34: 69–81.

Deluga, A., Kosicka, B., Dobrowolska, B., Chrzan-Rodak, A., Jurek, K., Wrońska, I., Ksykiewicz-Dorota, A., Jędrych, M., & Drop, B. (2018). Lifestyle of the elderly living in rural and urban areas measured by the FANTASTIC Life Inventory. *Annals of Agricultural and Environmental Medicine*, 25(3): 562–567. doi: 10.26444/aaem/86459.

Dennis, D., Waring, J., Payeur, N., Cosby, C., & Daudt, H. (2013). Making lifestyle changes after colorectal cancer: Insights for program development. *Current Oncology*, 20: e493–e511.

Diener, E., Wirtz, D., Tov, W., Kim-Prieto, C., Choi, D. W., Oishi, S., & Biswas-Diener, R. (2010). New well-being measures: Short scales to assess flourishing and positive and negative feelings. *Social Indicators Research, 97*(2), 143-156.

Kamien, M. & Power, R. (1996). Lifestyle and health habits of fourth year medical students at the University of Western Australia. *Australian Family Physician*, 25(Suppl. 1): S26–S29.

Kason, Y., & Ylanko, V. (1984). FANTASTIC lifestyle assessment: Part 5 measuring lifestyle in family practice. *Canadian Family Physician*, 30, 2379.

Kilani, H., Bataineh M., Al-Nawayseh A., Atiyat K., Obeid O., Abu-Hilal M., et al. (2020). Healthy lifestyle behaviors are major predictors of mental wellbeing during COVID-19 pandemic confinement: A study on adult Arabs in higher educational institutions. *PLoS ONE 15*(12): e0243524.

Kim, K. A., Kim, J. S., & Kim, M. S. (2007). Predictors of coronary heart disease risk in healthy men and women. *Journal of Korean Academy of Nursing*, 37(7), 1039-1048.

Kim, N., Park, D., Joe, H., & Cho, B. (2006). Health behaviors and health perceptions among medical and law students. *Journal of the Korean Academy of Family Medicine*, 27: 376–383.

Lo, K., Francis-Cracknell, A., & Hassed, C. (2017). A Health Enhancement Programme for physiotherapy students: a mixed methods pilot study. *New Zealand Journal of Physiotherapy*, 45(3), 143-153.

López-Carmona, J., Rodríguez-Moctezuma, R., Munguía-Miranda, C., Hernández-Santiago, J., & Csas de la Torre, E. (2000). Validity and reliability of the Fantastic instrument for measuring life-style in Mexican patients with hypertension. *Atención Primaria*, 26: 542–549.

Prendergast, K., Schofield, G. & Mackay, L. (2015). Associations between lifestyle behaviours and optimal wellbeing in a diverse sample of New Zealand adults. *BMC Public Health 16*, 62.

Ramírez-Vélez, R., & Agredo, R. (2012). The Fantastic instrument's validity and reliability for measuring Colombian adults' life-style. *Revista de salud pública*, 14: 226–237.

Ramírez-Vélez, R., Triana-Reina, H., Carrillo, H., Ramos-Sepúlveda, J., Rubio, F., Poches-Franco, L., Rincón-Párraga, D., Meneses-Echávez, J., & Correa-Bautista, J. (2015). A crosssectional study of Colombian University students' self-perceived lifestyle. *Springer Plus*, 4: 289. DOI 10.1186/s40064-015-1043-2.

Rodriguez-Añez, C., Reis, R., & Petroski, E. (2008). Brazilian version of a lifestyle questionnaire: Translation and validation for young adults. *Arquivos Brasileiros de Cardiologia*, 91: 92–98.

Rodríguez-Moctezuma, J., López-Carmona, J., Munguía-Miranda, C., Hernández-Santiago, J., & Martinez-Bermúdez, M. (2003) Validez y consistencia del instrumento FANTASTIC para medir estilo de vida en diabéticos. *Revista Médica del Instituto Mexicano del Seguro Social*, 41: 211–220.

Siddall, A., Turner, P., Stevenson, R., Standage, M., Bilzon, J. (2014). Lifestyle behaviours, well-being and chronic disease biomarkers in UK Operational firefighters. Conference *Medicine and Science in Sports and Exercise*, Orlando, Florida.

Silva, A. J., & Caetano, A. (2013). Validation of the flourishing scale and scale of positive and negative experience in Portugal. *Social Indicators Research, 110*(2), 469-478.

Triviño-Quintero, L., Dosman-González, V., Uribe-Vélez, Y., & Agredo-Zuñiga, R. (2009). A study of lifestyle and its relationship with risk factors for metabolic syndrome in middle-aged adults. *Acta Medica Colombiana,* 34: 158–163.

Wilhelm, K., Finch, A., Kotze, B., Arnold, K., McDonald, G., Sternhell, P., & Hudson, B. (2007). The Green Card Clinic: Overview of a brief patient-centred intervention following deliberate self-harm. *Australasian Psychiatry*, 15: 35–41.

Wilhelm, K., Handley, T., & Reddy, P. (2016). Exploring the validity of the Fantastic Lifestyle Checklist in an inner city population of people presenting with suicidal behaviours. *Australian & New Zealand Journal of Psychiatry*, 50(2) 128–134. DOI: 10.1177/0004867415621393.

Wilson, D., & Ciliska, D. (1984). Lifestyle assessment: Development and use of the FANTASTIC Checklist. *Canadian Family Physician, 30*, 1527-1532.

GAMBUT field experiment of peatland wildfires in Sumatra: infrared measurements of smouldering spread rate

Muhammad A. Santoso[1]; Eirik Christensen[1]; Hafiz M. F. Amin[1;5]; Pither Palamba[3]; Yuqi Hu[1;6]; Dwi M. J. Purnomo[1]; Wuquan Cui[1]; Agus Pamitran[2]; Franz Richter[1]; Thomas E. L. Smith[4]; Yulianto S. Nugroho[2]; Guillermo Rein*[1]

[1]Department of Mechanical Engineering, and Leverhulme Centre for Wildfires, Environment and Society, Imperial College London, London, SW7 2AZ, United Kingdom, {m.santoso16, e.christensen16, hafiz.amin, y.hu15, dwi.purnomo16, w.cui17, franz.richter11, g.rein}@imperial.ac.uk
[2]Department of Mechanical Engineering, Universitas Indonesia, 16424, West Java, Indonesia, {pamitran@eng.ui.ac.id, yulianto.nugroho@ui.ac.id}
[3]Department of Mechanical Engineering, Universitas Cenderawasih, Jayapura, Indonesia, {pither.palamba@yahoo.com}
[4]Department of Geography & Environment, London School of Economics & Political Science, United Kingdom, {t.e.l.smith@lse.ac.uk}
[5]School of Computing, Engineering & Digital Technologies, Teesside University, Middlesbrough, United Kingdom {H.Amin@tees.ac.uk}
[6]Sichuan Fire Research Institute of the Ministry of Emergency Management, Chengdu, China, {huyuqi@scfri.cn}

**Corresponding author*

Keywords

Peat, smouldering, fire, field, infrared

Abstract

Peatland wildfires present challenge to the mitigation of climate change due to the large amount of ancient carbon emission. Once ignited, the organic soils in peatland can burn for a long periods (weeks to months) and are difficult to extinguish. Peat fire is governed by smouldering combustion which is the slow, low temperature, flameless burning of charring porous fuel, and the most persistent type of combustion phenomena. The detection and monitoring of peatland wildfires are often conducted by remote sensing like satellite. However, there is currently a missing gap between spread of peat fires in the small laboratory scale and the large field scale. This work covers this gap by conducting field-scale controlled experiment of peatland wildfires. The experimental campaign, GAMBUT, was conducted in the peatland of Sumatra, Indonesia, covering an area of 408 m2. Smouldering spread rate was measured by infrared cameras and subsurface thermocouples. The smouldering sustained up to 10 days and nights, and survived against three rainfalls. Observation from infrared images show that horizontal smouldering spread rate fluctuates during propagation. However, no significant difference was found between average horizontal spread rates from the measurements of infrared camera and thermocouples, i.e. 0.3±0.13 cm/h to 0.8±0.2 cm/h. The spread rates here agree with the trend in the literature of laboratory experiments, fit within in the ranges of high moisture (MC) and inorganic (IC) contents of the soil (MC between 23 to 141% and IC between 49 to 72%). Even though slower, the fires thrived up to 10 days and against three rainfalls, demonstrating the persistency of smouldering peat fires and calling for a consideration of degraded peatland with high inorganic content to be consistently included in the mapping and monitoring of peatland area. GAMBUT presents a unique understanding of peatland wildfires at field conditions and aims to contribute to the better monitoring and mitigation acts.

1. Introduction

Peatlands contribute to the massive amount of carbon storage in the world, estimated to be up to 700 Gt (Yu 2012). In pristine conditions, the organic soil in peatland is protected from fires either due to the high moisture content, and the cold condition such as the case of permafrost in the Arctic region. However, recent increase of frequency of severe wildfires around the world, especially those of peatlands in the Arctic region, identifies that the ancient carbon that has been stored in peatlands for millennia is under threat to be released to the atmosphere

(Young *et al.* 2016). Once ignited, the organic soil (peat) can burn for weeks to months and difficult to be extinguished, surviving against rainfalls and firefighting responses (Rein 2016).

Peat fire is dominantly governed by smouldering combustion, which is the slow, low temperature, flameless burning of charring porous fuel, and the most persistent type of combustion phenomena. Smouldering peat fire spreads in both horizontal and vertical direction (in-depth into the subsurface layer). Recent laboratory studies have been conducted to understand both directions of smouldering spreads (Huang *et al.* 2016; Huang and Rein 2017; Christensen *et al.* 2020), and reveal the heat transfer effect on the faster spread in the subsurface layer than the surface layer. This phenomena can cause an overhang formation in which the surface layer stays unburned while the subsurface continues to propagate (Huang *et al.* 2016).

Currently, there is limited controlled experiment in the field to explain the different smouldering behaviour between surface and subsurface layers to improve the monitoring and mitigation of peatland wildfires in the field scale. Most studies in the field were conducted forensically such as the measurements were conducted on actual peatland wildfires with minimum control on the ignition methods, measurements location, and fire spread area (Page *et al.* 2002; Usup *et al.* 2004; See *et al.* 2007; Simpson *et al.* 2016; Smith *et al.* 2018). Pastor et al. (Pastor *et al.* 2017) conducted systematic peat fire experiment in the peatland of Peruvian Andes with each experimental area of 50×50 cm, and 1 out of 18 tests show temperatures up to 400°C and 3 show temperature above 100°C. This work aims to add to the previous field studies, contribute to the systematic methodology of peatland wildfires experiment in the field, and better understanding of surface peat fires spread in the field scale.

2. Methodology

The experimental campaign, GAMBUT, was conducted in Rokan Hilir regency, Sumatra, Indonesia, from 19 to 29 August 2019 (Santoso 2021). More detailed discussion of the study area can be found in Santoso (2021). The site in this study is in a tropical wet climate with a mean annual rainfall of 2,080 mm (Badan Pusat Statistik Kabupaten Rokan Hilir 2015); mostly covered by palm trees, ferns, and sedges; and closely located with an artificial reservoir (water pond) (Figure 1). The experiments were conducted in 12 days across changing precipitations. Three rainfall events equated to 4.8 mm of water column height occurred in the afternoon of day 6, 1.4 mm in the night of day 6, and 2.5 mm in the night of day 9 (Santoso 2021).

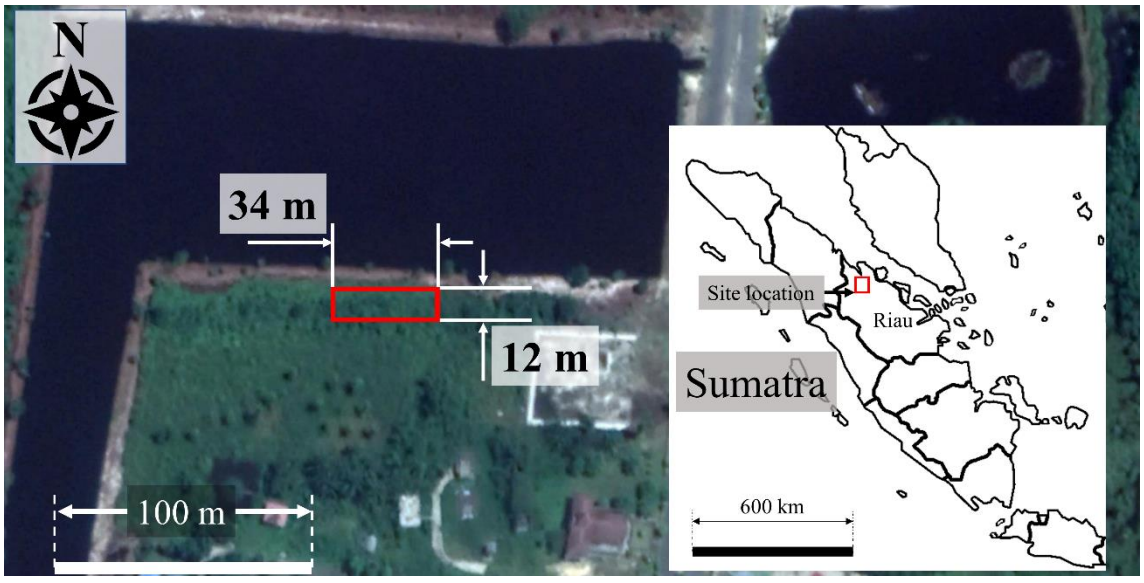

Figure 1- Top view of the site for GAMBUT experiment near a reservoir (Google Earth, 2021). The experiment area is indicated by the red rectangle. The site is a secondary peat swamp forest in Rokan Hilir, Sumatra, Indonesia (1°36'17.1"N 100°58'30.5"E). Inset picture shows Sumatra Island in which the site is indicated by a red rectangle (Golbez, 2021, CC BY) (Santoso 2021).

The experiments in this study were conducted in three plots of land, each with dimensions of 10 by 10 m (Figure 2a). Firebreaks were made around the perimeter of each plot by digging trenches of 50 cm wide and 50 cm deep which were filled with sand to prevent fires from spreading beyond these plots. From the left to right of Figure

2, the plots are indicated as Plot 1, Plot 2, and Plot 3. In each plot, two peat fire experiments were conducted (Figure 2b). In Plot 1, these two peat fire experiments are indicated as fire area of Plot 1 North (P1N) and Plot 1 South (P1S). In Plot 2, the fire area are Plot 2 North (P2N) and Plot 2 South (P2S), while the fire area in Plot 3 are Plot 3 North (P3N) and Plot 3 South (P3S). In total, six peat fire experiments were conducted during this field experiment campaign. In this study, fires in the north and south sides of the plots were well separated and did not spread into each other. Ignition was conducted by slash-and-burn and ember ignition. Slash-burn ignition was conducted by burning piles of dried surface vegetation of a dimension of 8 m length, 1 m wide, and 50 cm high, while ember ignition was conducted by filling an ignition pit shown in Figure 2b with smouldering charcoals. Details of ignition methods can be seen in (Santoso 2021).

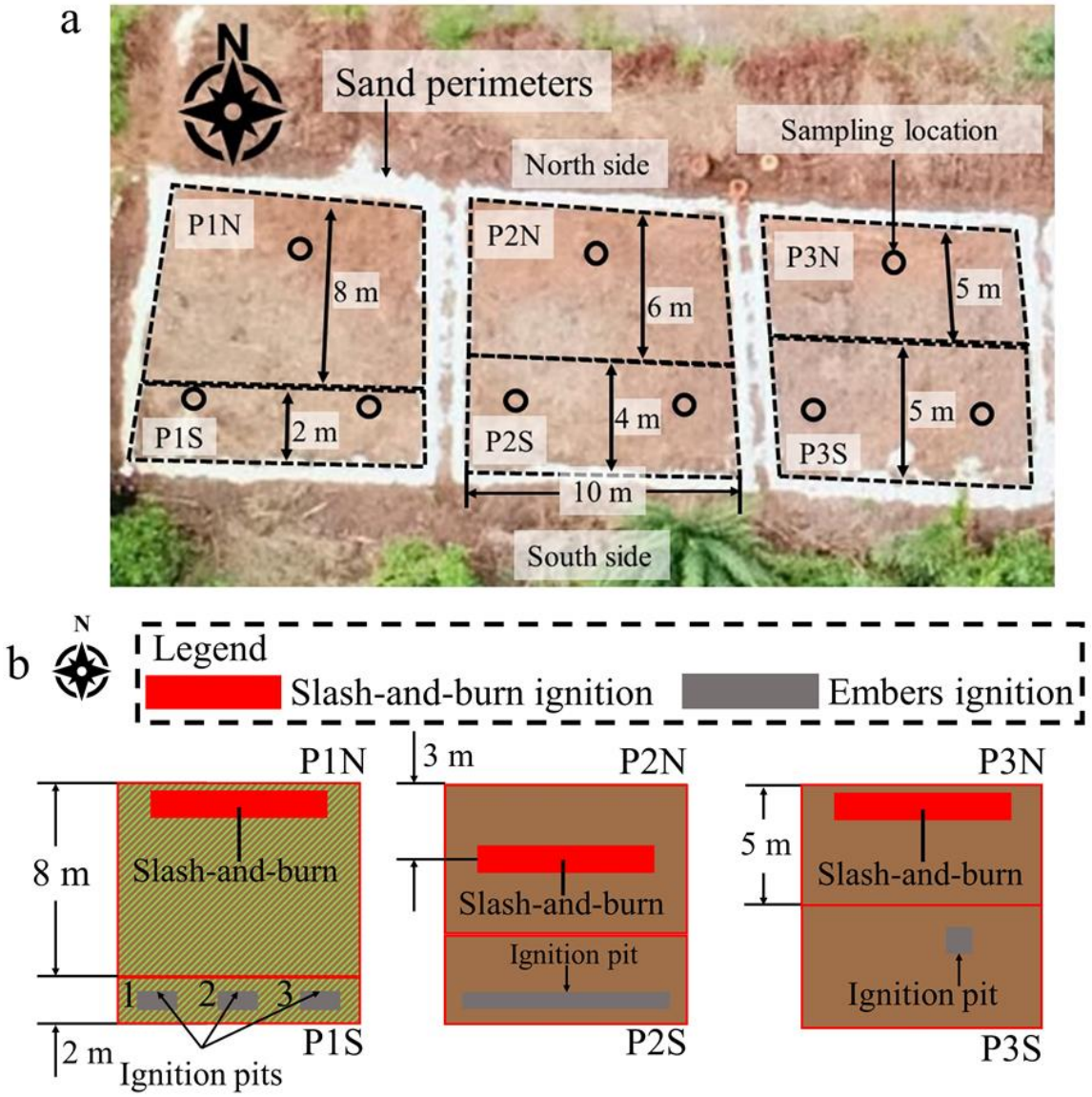

Figure 2- a) Top view of the 12 × 39 m of experimental area after surface vegetation treatment (Nugroho, 2018, CC BY). Black circles represent peat sampling locations for measurements of bulk density, moisture content (MC), inorganic content (IC), and elemental content. b) Schematic of the fire areas and different ignition methods. Red and grey rectangles refer to slash-and-burn and ember ignitions, respectively. Green diagonal lines refer to the surface litter that is kept intact on plot 1. Fire areas indicated by P1N, P2N, P3N, P1S, P2S, and P3S are Plot 1 North, Plot 2 North, Plot 3 North, Plot 1 South, Plot 2 South, and Plot 3 South, respectively (Santoso 2021).

Plot surfaces were cleaned from palm trees, ferns, sedges, and surface litter vegetation, except plot 1 where surface litter vegetation was kept intact (Figure 2b) to obverse its effect on the effectiveness of slash-and-burn ignition. The visual difference from above as shown by Figure 2a is not obvious since the litter vegetation left on Plot 1 have been significantly dried naturally, thus the colour of the vegetation have turned brownish, similar to the surface of dried peat in Plot 2 and Plot 3.

Infrared (IR) images were recorded using a FLIR Duo-R camera, mounted on a crane with an angle-adjustable hand to adjust the field of view of the camera. This crane was mounted on a rail to allow convenient IR image measurement along the plots, on both the north and south sides (Figure 3). Active fire area on the surface was obtained by analysing the acquired IR images. For the analysis of IR images, a similar approach used in (Amin *et al.* 2020) was adopted and a threshold value of camera intensity well above the surrounding area (0.1) was chosen. The images were converted to greyscale and the pixels where the normalized intensity increases above the intensity threshold were marked (subset in Figure 3). The area inside the marked perimeter line was then calculated to be the active fire area. The scaling from pixel dimension to physical length was possible by using a geo-reference plate with a dimension of 0.17 × 0.14 m, also shown in the subset of Figure 3.

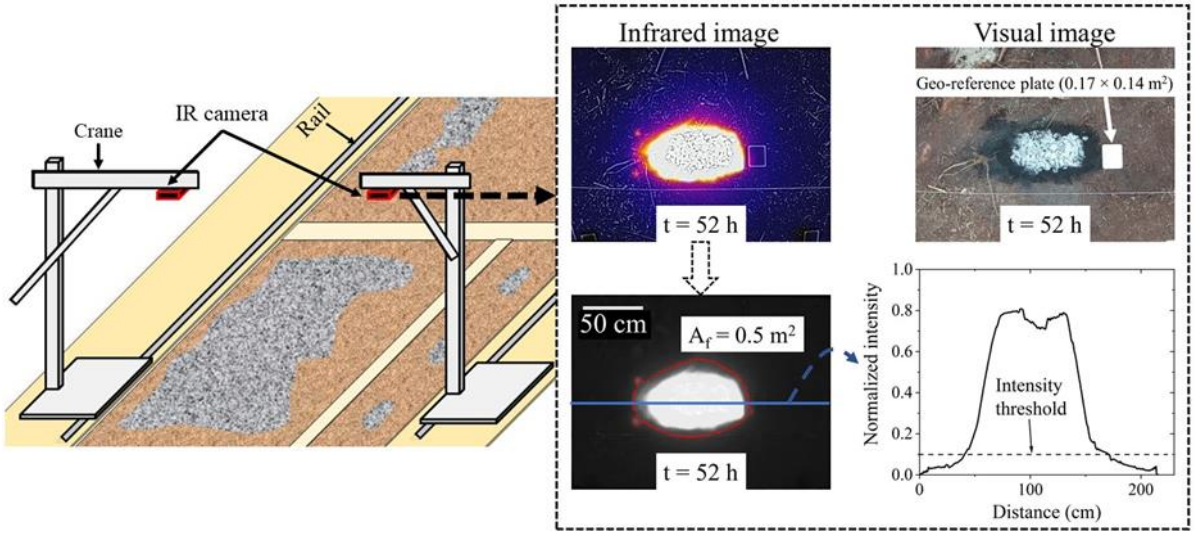

Figure 3. Infrared imaging setup and analysis to measure smouldering spread and area. The normalized pixel intensity threshold is chosen to be 0.1 to represent the point at which the intensity started to steeply increase, indicating the outer perimeter of the peat fire area. A_f and t are the active fire area and time since ignition, respectively (Santoso 2021).

Thermocouples were used to smouldering spread rate at the subsurface level. Due to the uncertain peat fire propagation direction, thermocouples were placed at certain points based on the visual observation and the likelihood of propagation direction. To obtain spread rate data, two thermocouple points were located at a known distance, 15 cm. The spread rate is then calculated from the known distance (15 cm) and the time-lapse of the two consecutive thermocouples reached maximum temperature or 300°C which is above peat char oxidation temperature (230°C). Each thermocouple point contains two K-type thermocouples at 10 cm (shallow layer) with probe diameter of 1.5 mm, and at 30 cm depth (deep layer) with probe diameter of 3 mm. Details of thermocouple placement can be seen in (Santoso 2021). As peat fires progressed and passed a thermocouple point, the thermocouples were then moved to a new location, if the thermocouples were not burnt. Continuous MC measurements were also conducted in P2N fire area by placing module soil moisture sensors at 4 different depths (10, 20, 30, and 40 cm) below the slash-and-burn location (Figure 2b). This live measurement of MC adding to the spread rate measurements by the thermocouples.

3. Results

Figure 4 shows horizontal spread rates analysed from series of infrared images on fires in P1S and P3S. Smouldering spread rate on the surface can be seen to fluctuating during propagation. Rainfalls can also be seen to have minimum impact on both the fluctuations and the average spread rate. In this work, horizontal spread rate measured from infrared images is ranged from 0.1 to 0.5 cm/h. The spread rate in this work is smaller than the values in the literatures (Prat-Guitart *et al.* 2016; Huang *et al.* 2016; Hu *et al.* 2019; Amin *et al.* 2020; Christensen *et al.* 2020), mainly because both the MC and IC in the field here is higher than the soil conditions in the literatures. Figure 5 shows that the spread rate in this work agree with the trend in the literatures, fit within the ranges of high MC and IC soil conditions. No significant difference between horizontal spread rate measured by IR camera (0.3±0.1 cm/h) and subsurface thermocouples (0.8±0.2 cm/h).

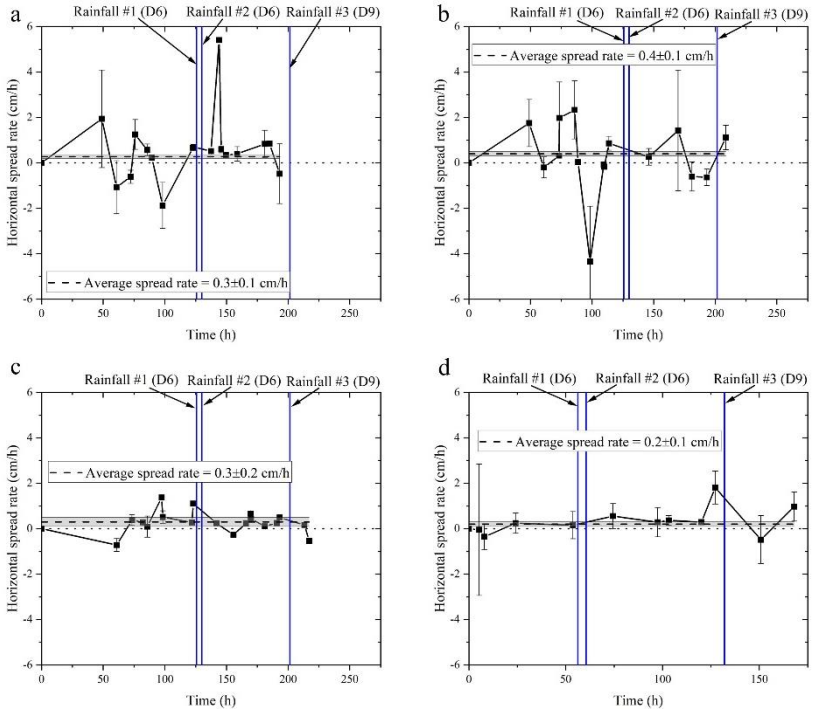

Figure 4- Horizontal spread rate from infrared camera images for a) pit 1 of P1S, b) pit 2 of P1S, c) pit 3 of P1S, d) P3S. The precipitation of the three rainfalls are 4.8 mm in the afternoon of day 6, 1.4 mm in the night of day 6, and 2.5 mm in the night of day 9. Details of weather conditions during GAMBUT can be seen in (Santoso 2021).

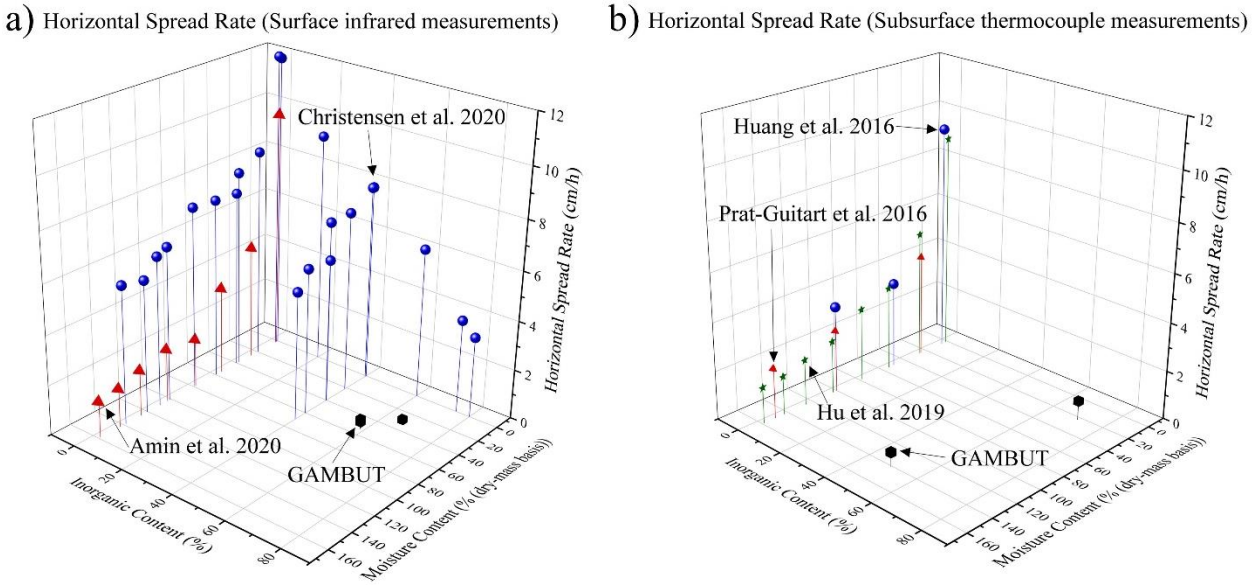

Figure 5- Horizontal spread rates from GAMBUT and literatures (Prat-Guitart et al. 2016; Huang et al. 2016; Hu et al. 2019; Amin et al. 2020; Christensen et al. 2020). a) Horizontal spread rate based on infrared images and b) based on subsurface thermocouple measurement at level more than 2 cm below surface up to 20 cm deep.

4. Conclusions

Here, we report horizontal spread rate measurements from GAMBUT field experiment of peatland wildfires in Sumatra, Indonesia. The smouldering peat fires during this experiment survived up to 10 days against three rainfalls. Horizontal spread rate was measured by using infrared camera and subsurface thermocouple. There is no significant difference between horizontal spread rate observed on the surface by infrared and measured at the subsurface by thermocouples. The spread rate reported here is 0.3±0.1 to 0.8±0.2 cm/h and agree with the laboratory results in the literature, fit within soil conditions with high moisture (MC) and inorganic (IC)

contents, i.e. MC between 23 to 141% and IC between 49 to 72%. The persistent nature of the smouldering observed here also proves that degraded peatlands with high inorganic content are still required to be consistently monitored and mapped for prevention and conservation measures. GAMBUT presents a unique understanding of peatland wildfires at field conditions and aims to contribute to the better monitoring and mitigation acts.

5. Reference

Amin HMF, Hu Y, Rein G (2020) Spatially resolved horizontal spread in smouldering peat combining infrared and visual diagnostics. Combustion and Flame 220, 328–336. doi:https://doi.org/10.1016/j.combustflame.2020.06.039.

Badan Pusat Statistik Kabupaten Rokan Hilir (2015) Rata-Rata Curah Hujan di Kabupaten Rokan Hilir (mm) 2013-2015. https://rohilkab.bps.go.id/subject/151/iklim.html#subjekViewTab3.

Christensen EG, Fernandez-Anez N, Rein G (2020) Influence of soil conditions on the multidimensional spread of smouldering combustion in shallow layers. Combustion and Flame 214, 361–370. doi:10.1016/J.COMBUSTFLAME.2019.11.001.

Hu Y, Christensen EG, Amin HMF, Smith TEL, Rein G (2019) Experimental study of moisture content effects on the transient gas and particle emissions from peat fires. Combustion and Flame 209, 408–417. doi:https://doi.org/10.1016/j.combustflame.2019.07.046.

Huang X, Rein G (2017) Downward spread of smouldering peat fire: the role of moisture, density and oxygen supply. International Journal of Wildland Fire 26, 907–918. https://doi.org/10.1071/WF16198.

Huang X, Restuccia F, Gramola M, Rein G (2016) Experimental study of the formation and collapse of an overhang in the lateral spread of smouldering peat fires. Combustion and Flame 168, 393–402. doi:10.1016/J.COMBUSTFLAME.2016.01.017.

Page SE, Siegert F, Rieley JO, Boehm H-D V, Jaya A, Limin S (2002) The amount of carbon released from peat and forest fires in Indonesia during 1997. Nature 420, 61–65. doi:10.1038/nature01131.

Pastor E, Oliveras I, Urquiaga-Flores E, Quintano-Loayza JA, Manta MI, Planas E (2017) A new method for performing smouldering combustion field experiments in peatlands and rich-organic soils. International Journal of Wildland Fire 26, 1040–1052. https://doi.org/10.1071/WF17033.

Prat-Guitart N, Rein G, Hadden RM, Belcher CM, Yearsley JM (2016) Propagation probability and spread rates of self-sustained smouldering fires under controlled moisture content and bulk density conditions. International Journal of Wildland Fire 25, 456–465. https://doi.org/10.1071/WF15103.

Rein G (2016) Smoldering Combustion. 'SFPE Handb. Fire Prot. Eng.' (Eds MJ Hurley, D Gottuk, JR Hall, K Harada, E Kuligowski, M Puchovsky, J Torero, JM Watts, C Wieczorek) pp. 581–603. (Springer New York: New York, NY) doi:10.1007/978-1-4939-2565-0_19.

Santoso MA (2021) Experimental study of smouldering wildfire mitigation: spread, suppression and transition to flaming. Imperial College London. doi:https://doi.org/10.25560/91115.

See SW, Balasubramanian R, Rianawati E, Karthikeyan S, Streets DG (2007) Characterization and Source Apportionment of Particulate Matter ≤ 2.5 μm in Sumatra, Indonesia, during a Recent Peat Fire Episode. Environmental Science & Technology 41, 3488–3494. doi:10.1021/es061943k.

Simpson J, Wooster M, Smith T, Trivedi M, Vernimmen R, Dedi R, Shakti M, Dinata Y (2016) Tropical Peatland Burn Depth and Combustion Heterogeneity Assessed Using UAV Photogrammetry and Airborne LiDAR. Remote Sensing 8, 1000. doi:10.3390/rs8121000.

Smith TEL, Evers S, Yule CM, Gan JY (2018) In Situ Tropical Peatland Fire Emission Factors and Their Variability, as Determined by Field Measurements in Peninsula Malaysia. Global Biogeochemical Cycles 32, 18–31. doi:https://doi.org/10.1002/2017GB005709.

Usup A, Hashimoto Y, Takahashi H, Hayasaka H (2004) Combustion and thermal characteristic of peat fire in tropical peatland in Central Kalimantan, Indonesia. Tropics 14, 1–19. doi:10.3759/tropics.14.1.

Young AM, Higuera PE, Duffy PA, Hu FS (2016) Climatic thresholds shape northern high-latitude fire regimes and imply vulnerability to future climate change. Ecography 1–12. doi:10.1111/ecog.02205.

Yu ZC (2012) Northern peatland carbon stocks and dynamics: a review. Biogeosciences 9, 4071–4085. doi:10.5194/bg-9-4071-2012.

Identifying the factors affecting the willingness of villagers to participate in forest firefighting in Iran's Zagros forests

Soleyman Ghaderi; Abbas Banj Shafiei*; Hadi beygi heidarlou

Department of Forestry, Natural Resources Faculty, Urmia University, Iran,
{ghaderisoleyman@gmail.com, a.banjshafiei@urmia.ac.ir, hadibeygi@gmail.com}

**Corresponding author*

Keywords

Factor analysis, Firefighting, Forest fire, Sardasht, Participation.

Abstract

One of the environmental factors affecting the forest ecosystem is fire. Local volunteer firefighters are often those who first respond to forest fires. This study was conducted aimed to determine the factors affecting their willingness to participate in firefighting in the northern Zagros forests of Iran (Sardasht County). For this purpose, after extracting Sardasht fire statistics during a 14-year period (2006-2019), the villages with the highest frequency of fires in the above period were selected. Organizing, facilities and equipment, indigenous knowledge and education for firefighting were selected as factors affecting the willingness to participate in firefighting. The research tools were a questionnaire and face-to-face interview. The statistical population included 649 households. According to Morgan's Table, the number of samples required for the distribution of questionnaires was n=242. The questionnaire questions were designed openly and closed with scores based on the Likert scale and the factors affecting villagers' willingness to participate in firefighting were investigated by face-to-face interviews. The results of statistical analysis of data showed that organizing, knowledge and facilities had a significant effect on the participation of respondents. This study showed that for the villagers, organizing was the most effective factor and facilities was the last factor affecting their willingness to participate. Also, a positive and significant relationship was found between the participation and the level of education. Therefore, it is necessary for the promotion department of the Iran's Forests, Range and Watershed management Organization (FRWO), along with the protection unit of the organization, to provide special programs and policies for the organizing of the public, rural and volunteer firefighting forces before the fire spreads to control it in principle.

1. Introduction

According to the statistics published by the Iran's Forests, Rangelands and Watershed management Organization (FRWO), hundreds of fires occur annually in different parts of Iran, which ranks fourth among the countries of the Middle East and North Africa in terms of the amount of forest destruction due to fires (Beygi Heidarlou et al., 2014).

The participation of local people is one of the main factors of the final decision-making and acceptance of ecosystem management practices. Firefighters are the basis of any forest fire prevention and control system in which volunteer firefighters and members of non-governmental organizations play an important role. The success of fire fighting plans or mechanical stress reduction progrmmes may be influenced by how local societies think.

The Zagros forests with an area of about 4,749,000 hectares (Roozitalab et al., 2018) have a special place and importance among the vegetation areas of western Iran. Fires in Zagros are devastating, amounting to 6,500 hectares per year, which mostly are caused by human beings. In order to manage the fire crisis in this vegetation area, it is necessary to know the factors affecting the participation of people and local societies in the fight against fire and how they change in terms of time and place. Specifically in this study, we seek to answer the

following question:

- What are the most important factors affecting the willingness of local societies in Sardasht to participate in firefighting in the Zagros forests?

2. Methods & Materials

2.1. Study area

Sardasht with an area of 138,000 hectares in northwestern Iran has been selected as the study area in this study (Figure 1). According to the latest official statistics (2016), the population of Sardasht is 118,849 people. Sardasht is located between 45°13´48´´ to 45°42´00´´ E longitude and 35°37´36´´ to 36°28´12´´ N latitude. The average height above sea level is 1515 m (Beygi Heidarlou et al., 2020). This area is often covered with dense forests with trees such as Quercus infectoria Oliv, Q. libani, Q. brantii, Vitis vinifera L., Ficus carica and Pyrus glabra. Sardasht forests cover an area of 83,000 hectares (Beygi Heidarlou et al., 2019), Important causes of deforestation in recent decades include cutting down of trees for fuel, frequent fires, pruning to provide fodder, clear-cutting of forests and ploughing of forest soil to agricultural activities and vineyards and the constant presence of livestock, especially goats, in the forests.

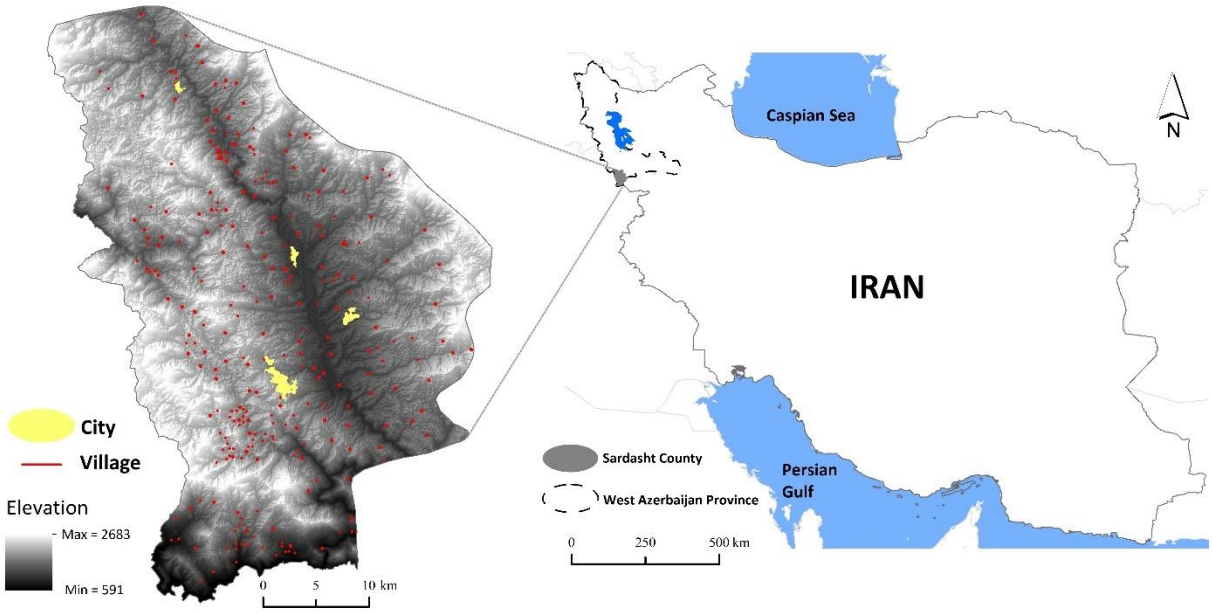

Figure 1. Geogrphical location of study area.

2.2. Research methodology

14 villages with the highest frequency of fires (2006-2019) in their customary system were selected. the present study was conducted by descriptive-survey research method. The study population included 242 residents of the villages who were selected using the Krejcie-Morgan sample size table in 2020 (Table 1).

Table 1. List of villages, number of households and number of measured samples in the study.

Row	Villages name	N of households	Population	N of samples households
1	Molasheikh	56	219	21
2	Gurangan	22	85	8
3	Baskedu	2	6	2
4	Banavile-Hajimine	16	64	6
5	Shalmash	57	201	21
6	Shivashan	9	25	3
7	Niskabad	16	68	6
8	Aghlan	80	307	30
9	Belav	12	61	4
10	Shendre	20	69	7
11	Bizile	39	137	15
12	Torshian	6	19	2
13	Cheku	107	400	40
14	Dolatu	207	834	77
Total	-	649	2505	242

Data were collected using a researcher-made questionnaire. In addition to individual, professional and sociological questions, this questionnaire contained 35 items representing willingness to participate, organizing, facilities and equipment, indigenous knowledge and firefighting training (education) factors provided by literature and Interviews with experts and specialists. The respondents were then asked to determine the effect of each of these factors on their willingness to participate in firefighting on a 5-point Likert scale. The validity of the questionnaire was confirmed using the knowledge of experts and university professors. Cronbach's alpha test was used to investigate the reliability with a coefficient of 0.899, which in social research indicates the appropriate reliability of the measurement tool.

2.3. Statistical analysis

The data obtained from the questionnaires were analyzed by SPSS Windows (version 25). Confirmatory factor analysis (CFA) was used to confirm the classification of factors affecting the willingness to participate in firefighting. The value of Kaiser-Mayer-Olkin (KMO) statistic was 0.867 and the value of Bartlett's Test of Sphericity was 1787.58 (at 0.0001 level), which indicate the appropriateness of the data for factor analysis. Also, in order to increase the interpretability of the items related to the attitude of the respondents, the Varimax method was used and a total of five factors (organizing, willingness to participate, education, indigenous knowledge, and facilities and equipment) were extracted based on eigenvalues and the previous factor criteria. At the next stage, stepwise regression was used to determine the factors affecting the willingness of villagers to participate in firefighting.

3. Results

3.1. Characteristics of the statistical population

The demographic information is presented in Table 2.

Table 2. Results of demographic characteristics of the studied community

Characteristic	Class	Frequency (%)	Characteristic	Class	Frequency (%)
Gender	Female	0.83	Education	Illiterate	18.75
	Male	99.17		High school diploma	47.08
Age (year)	15-20	3.31		Diploma	16.25
	21-30	35.12		Associate degree	3.33
	31-40	33.47		Bachelor’s degree and higher	14.58
	41-50	14.05	Number of livestock available (livestock)	< 25	39.39
	51-60	8.26		26-50	23.23
	61-71	5.79		51-100	17.17
Number of household members (persons)	1-2	8.3		101-150	12.12
	3-4	46.06		> 151	8.08
	5-6	34.44	Marital status	Single	24.79
	7-8	9.54		Married	75.21
	9-10	1.66	Job	Unemployed	4.13
Type of livestock	Goats and sheep	52		Employee	5.49
	Cow	47		Beekeeper, farmer and rancher	45.04
	Other	1		self-employment	45.04
Average monthly income ($)	< $ 55	27.59	Agricultural area (ha)	< 0.5	10.71
	$ 55-110	41.87		0.6-1	28.57
	$ 110-165	14.78		1.1-2	24.49
	> $ 165	15.76		2.1-5	28.57
Participate in training classes	Yes	7.44		> 5	7.65
	No	92.56			

3.2. Factor analysis results

The study result was a reduction in 22 indicators to five factors, which explained about 57% of the variance of participation and indicated the satisfactory factor analysis and indicators used to investigate the dimensions of willingness to participate in this study (Table 3).

Table 3. Variance and igenvalue of factors of people willingness of participation in firefighting programs.

Component	Eigenvalue	Extraction Sums of Squared Loadings			Rotation Sums of Squared Loadings		
		Eigenvalue	% of Variance	Cumulative %	Eigenvalue	% of Variance	Cumulative %
1	6.45	6.45	29.31	29.31	3.73	16.97	16.97
2	2.17	2.17	9.86	39.17	2.63	11.93	28.90
3	1.62	1.62	7.38	46.55	2.19	9.97	38.87
4	1.27	1.27	5.75	52.30	2.15	9.79	48.67
5	1.08	1.08	4.89	57.19	1.88	8.52	57.19

Extraction Method: Principal Component Analysis.

Finally, the last stage is to perform factor analysis, naming the factors that have already been named according to the nature and type of items and indicators of willingness to participate, and according to the expert point of view, the indicators have been named according to their nature. The first, second, third, fourth and fifth factors, which explained about 16.97, 11.93, 9.97, 9.79 and 8.52% of the variance related to factor analysis, respectively, according to the nature of the available variables were named as 1) organizing, 2) willingness to participate, 3) education, 4) indigenous knowledge and 5) facilities and equipment. Factors one to five consist of seven, four, three, four and three variables with the factor loads specified in Table 4, respectively. These variables play a greater role in the total variance of the variable. Also, during factor analysis, variables or questions that have less factor load or correlations i.e. their coefficient of determination (R^2) is less than 0.4, were not included in the analysis.

Table 4. Variables related to each factor and the amount of factor load obtained from the rotated matrix.

Factor	Measuring indices of participation	Factor Load
Organizing	Q6: I am ready to give the necessary training to the villagers in different seasons of the year to prevent fires.	0.572
	Q7: I am willing to participate in firefighting if I pass firefighting training courses and have the equipment.	0.6
	Q8: In the village, one or more responsible and knowledgeable people are needed for the volunteer forces to carry out the orders.	0.765
	Q9: As soon as a fire breaks out, I follow the instructions of the person in charge in the village.	0.75
	Q10: Provide the equipment needed to extinguish the fire before the fire occurs to the people or the village head.	0.566
	Q11: Organizing before putting out a fire will help succeed in putting out the fire.	0.689
	Q12: In organizing, a responsible person must be chosen.	0.56
	Q13: Each organization should be repeated manually in specific time periods.	0.572
Willingness to participate	Q1: I am willing to work with natural resources officers as a volunteer to fight fires.	0.775
	Q2: I am willing to accept responsibility for leading a public firefighting team.	0.542

	Q3: Until the firefighters arrive, we will put out the fire with the help of the villagers.	0.697
	Q5: In the event of a fire, I will try to put it out myself.	0.645
Education	Q29: Teaching how to use devices and equipment is effective in the success of firefighting.	0.72
	Q30: Teaching how to behave and move fire in pastures and forests has an important role in extinguishing fires.	0.822
	Q31: Training should be provided by natural resource experts.	0.597
Indigenous knowledge	Q20: To spread the fire to the top of the hill.	0.736
	Q21: In the event of a small fire, it must be attacked directly.	0.561
	Q23: The rate of fire spread in pastures is higher than in forests.	0.693
	Q24: Relative humidity has the highest correlation with the occurrence and extent of fire spread.	0.654
Facilities and equipment	Q15: Individual facilities and equipment play an important role in firefighting.	0.512
	Q16: Heavy facilities and equipment play an important role in fire fighting.	0.81
	Q17: Motor facilities and equipment play an important role in fire fighting.	0.755

3.3. Stepwise regression test results

The results of factor analysis using stepwise regression showed that organizing, knowledge and facilities factors had a significant effect on the willingness to participate in firefighting. According to the results, three of five predictors in the study were included in the model. The results of the stepwise regression model summary also showed that based on the value of the adjusted R-squared, the three selected predictors had the ability to explain about 45% of the scatter of the dependent variable (participation) (Table 5).

Table 5. Summary of stepwise regression model.

Model	R	R Square	Adjusted R Square	Std. Error of the Estimate
1	0.638[a]	0.407	0.405	2.51
2	0.666[b]	0.443	0.439	2.43
3	0.673[c]	0.453	0.446	2.42

a. Predictors: (Constant), Organizing
b. Predictors: (Constant), Organizing, Indigenous knowledge
c. Predictors: (Constant), Organizing, Indigenous knowledge, Facilities and equipment

Table 6 shows the coefficients of each factor. According to the study results, the factor of organizing with a coefficient of 0.549 played the most important role in participation, followed by knowledge (0.165) and facilities (0.11).

Table 6. Coefficients of stepwise regression model

Model		Unstandardized Coefficients		Standardized Coefficients	t	Sig.	Correlations			Collinearity Statistics	
		B	Std. Error	Beta			Zero-order	Partial	Part	Tolerance	VIF
1	(Constant)	8.889	1.322		6.726	.000					
	Organizing	0.789	0.061	0.638	12.837	.000	0.638	0.638	0.638	1.000	1.000
2	(Constant)	5.943	1.484		4.003	.000					
	Organizing	0.725	0.062	0.586	11.720	.000	0.638	0.604	0.566	0.931	1.074
	Indigenous knowledge	0.263	0.067	0.197	3.947	.000	0.351	0.247	0.190	0.931	1.074
3	(Constant)	4.199	1.715		2.448	.015					
	Organizing	0.679	0.066	0.549	10.336	.000	0.638	0.557	0.496	0.816	1.226
	Indigenous knowledge	0.220	0.069	0.165	3.164	.002	0.351	0.201	0.152	0.843	1.187
	Facilities and equipment	0.129	0.065	0.110	1.994	.047	0.400	0.128	0.096	0.750	1.333

Dependent Variable: participation

The model presented by this regression fit will be as follows:

Participation = 4.199 + 0.549 (Organizing) + 0.165 (Indigenous knowledge) + 0.110 (Facilities and equipment)

4. Discussion

The study results showed that the respondents in this study were willing to fight voluntarily with natural resources officers against fire. Voluntary activities are often carried out in the context of society, with different standards, norms, resources and institutions. By volunteering and willing to participate in solving problems in society, people respond to what they see as social problems in their society, and so social capital increases as encouraging civic and voluntary participation and social trust (creating communication and cooperation between members) (Putnam, 2020). The respondents were also satisfied with accepting responsibility for leading a firefighting team and willing to fight against the fire with the help of villagers until firefighters arrive. The willingness to fight against the fire voluntarily can be done individually or collectively. In collective voluntary activities, the head of groups inspire, and oversee the activities of others (Eckstein, 2001). In the last two decades, the willingness to participate in firefighting voluntarily has been investigated by several researchers (Perkins, 1989, 1990; Perkins and Metz, 1988). Thompson III and Bono (1993) found that the strongest motivation for volunteering as a firefighter was to help society, followed by the will to help contain the fire. Perkins and Metz (1988) argued that firefighting represented powerful sources of solidarity and identity of society.

The respondents believed that facilities and equipment for firefighting play an important role. In the face of forest fires, what is very important is the availability of firefighting equipment and infrastructure (Clément, 2001).

The study results in relation to the native knowledge of the respondents showed that they were relatively aware of the basic principles of firefighting. They believed that: direction of fire spread is to the top of the hill; in the occurrence of a small fire, must be directly attacked; the spread of fire in the rangelands is faster than forests; and Relative humidity has the highest correlation with the occurrence and extent of fire spread, which is

consistent with the results of the Forthofer (2007), Plucinski et al. (2017), Maffei and Menenti (2019) and Ertugrul et al. (2021) studies.

At the pre-fire stage, the human management and firefighting training courses are important for local and national forces (Karimi et al., 2014). The respondents in this study believed that firefighting training and how to use devices and equipment play an important role in firefighting and preventing its spread. Vadrevu et al. (2010) in their study in southern India showed that informing and training the public, publishing risk maps and regional recommendations to authorities have played an important role.

The results of factor analysis using stepwise regression showed that the factors of organizing, knowledge and facilities had a significant effect

($\alpha = 0.01$) on the participation of respondents (Table 6), indicating the importance of these factors. According to the study results, organizing factor had a greatest effect among the other two factors on the participation of respondents, which is contrary to the opinion of officials of the FRWO and Natural Resources Department, which is the main cause of failure due to the lack of facilities. This study showed that for the villagers, organizing was the most effective factor and facilities was the last effective factor on their willingness to participate.

5. Conclusion

The participation of local societies in recent decades as a rational and human necessity is the most important variable of development and protection. In general, in order to promote the willingness for participation of local societies and foresters, it is necessary to organize, train basic measures and use the indigenous knowledge of villagers for firefighting and increase firefighting facilities and equipment in forest areas and natural resources. This will not be possible without considering the various dimensions of the attitude and willingness of villagers and forest dwellers for firefighting and try to improve it. Therefore, the necessary measures to increase the willingness of villagers and foresters for firefighting should not be delayed under the pretext of limited resources to address other dimensions of forest management.

The study results introduced the factor of organizing and knowledge as the first and second factors in terms of importance and the factor of facilities as the third factor for explaining the variance of the willingness for firefighting. Given the current different and opposite attitude towards forest firefighting among most of the top managers in the country, according to the study results, their attitude can be improved.

High efficiency of firefighting, control in a short period of time, quick access to fire extinguishers, professional readiness of local societies to deal with fire, use of firefighting equipment, continuous training classes, constant presence of physical fire control and fighting forces on site and quick access to its location, familiarity with the fastest ways to access the site of the fire, quick and uninterrupted access to individual, collective and motor facilities and equipment, and the presence of one or more local officials to maintain order at times of crisis are very important using different methods of fire control. Therefore, the relevant organizations should organize and train the public forces so that they are ready for firefighting in the event of a fire.

6. References

Amiri, T., Shafiei, A., Erfanian, M., Hosseinzadeh, O., Heidarlou, H., 2018. Locating suitable areas for forest fire fighting stations in Sardasht, NW Iran. Iranian Journal of Forest 10, 319-335.

Beygi Heidarlou, H., Banj Shafiei, A., Erfanian, M., 2014. Forest fire risk mapping using analytical hierarchy process technique and frequency ratio method (case study: Sardasht Forests, NW Iran). Iranian Journal of Forest and Poplar Research 22.

Beygi Heidarlou, H., Banj Shafiei, A., Erfanian, M., Tayyebi, A., Alijanpour, A., 2020. Armed conflict and land-use changes: Insights from Iraq-Iran war in Zagros forests. Forest Policy and Economics 118, 102246.

Beygi Heidarlou, H., Shafiei, A.B., Erfanian, M., Tayyebi, A., Alijanpour, A., 2019. Effects of preservation policy on land use changes in Iranian Northern Zagros forests. Land Use Policy 81, 76-90.

Clément, J., 2001. International Handbook on Forest Fire Protection. FAO Forestry Department Press, 163.

Eckstein, S., 2001. Community as gift-giving: Collectivistic roots of volunteerism. American Sociological Review, 829-851.

Ertugrul, M., Varol, T., Ozel, H.B., Cetin, M., Sevik, H., 2021. Influence of climatic factor of changes in forest fire danger and fire season length in Turkey. Environ. Monit. Assess. 193, 1-17.

Forthofer, J.M., 2007. Modeling wind in complex terrain for use in fire spread prediction. Colorado State University, Fort Collins, CO, p. 123.

Karimi, A., Ebrahimi, A., Asadi, E., Tahmasebi, P., Tavakoli, R., 2014. Investigating the role of management in fire prevention and control in forests and pastures of Chaharmahal and Bakhtiari Province, National Conference on Natural Resources Management, Gonbad Kavus, Iran, p. 7.

Maffei, C., Menenti, M., 2019. Predicting forest fires burned area and rate of spread from pre-fire multispectral satellite measurements. ISPRS Journal of Photogrammetry and Remote Sensing 158, 263-278.

Perkins, K.B., 1989. Volunteer firefighters in the United States: A descriptive study. Nonprofit and Voluntary Sector Quarterly 18, 269-277.

Perkins, K.B., 1990. Volunteer fire and rescue corporations: Structure, process, and survival. Nonprofit and Voluntary Sector Quarterly 19, 359-370.

Perkins, K.B., Metz, C.W., 1988. Note on commitment and community among volunteer firefighters. Soc. Inquiry 58, 117-121.

Plucinski, M., Sullivan, A., Hurley, R., 2017. A methodology for comparing the relative effectiveness of suppressant enhancers designed for the direct attack of wildfires. Fire Saf. J. 87, 71-79.

Putnam, R.D., 2020. "Bowling Alone: America's Declining Social Capital": Journal of Democracy (1995), The City Reader. Routledge, pp. 142-150.

Roozitalab, M.H., Siadat, H., Farshad, A., 2018. The soils of Iran. Springer International Publishing, Switzerland.

Thompson III, A.M., Bono, B.A., 1993. Work without wages; The motivation for valunteer firefighters. American Journal of Economics and Sociology 52, 323-343.

Vadrevu, K.P., Eaturu, A., Badarinath, K., 2010. Fire risk evaluation using multicriteria analysis—a case study. Environ. Monit. Assess. 166, 223-239.

Indirect effects of climate change on forest structure alters fuel availability in wet Eucalypt forests

Tegan P Brown*[1, 2]; Assaf Inbar[3]; Thomas J Duff[4]; Patrick NJ Lane[1]; Gary J Sheridan[1]

[1] School of Ecosystem and Forest Sciences, Faculty of Science, The University of Melbourne, Parkville, VIC, 3010, Australia {tegan.pg.brown@gmail.com}, {patrickl, Sheridan}@unimelb.edu.au
[2] US Forest Service, Rocky Mountain Research Station, Fire Sciences Laboratory, 5775 Highway 10 West, Missoula, MT, 59803, USA
[3] Hawkesbury Institute for the Environment, Western Sydney University, Penrith, NSW, 2753, Australia, {a.inbar@westernsydney.edu.au}
[4] Bushfire Management, Country Fire Authority, Burwood, VIC, 3151, Australia {thomas.duff@cfa.vic.gov.au}

**Corresponding author*

Keywords

Fuel moisture content, fire, forest structure, climate change

Abstract

The direct effects of climate change are increasing the frequency of high-intensity fire events in many ecosystems across the globe, including wet Eucalypt forests of south-eastern (SE) Australia. Recurrent high-intensity fire can alter vegetation structure and composition, and the resultant alternative vegetation states may be more likely (positive feedback) or less likely (negative feedback) to burn again compared to the vegetation community replaced. These indirect effects of climate change have been reported for a range of different ecosystems across the globe. However, a common limitation to many empirical studies is the narrow temporal range of observations, often limited to a single fire season. In turn, this limits our understanding of the potential for vegetation-mediated indirect effects of climate change to generate positive or negative fire feedbacks across the range of climate conditions common to the region.

In wet Eucalypt forests of SE Australia, dead fuel moisture content (FMC) is a key determinant of fire activity and is therefore a useful metric on which to quantify the potential for feedbacks across alternative forest states. To quantify potential for indirect effects of climate change to alter future fire activity, FMC was modelled in the open and at seven alternative forest states to wet Eucalypt forest using a process-based FMC model. The model was run using a long-term climate dataset (1973 – 2020), which were transferred from macro- to microclimate values using forest structural properties derived from lidar. Hourly FMC outputs were summarised to fuel availability (FMC < 16% for at least one hour each day) to understand the potential for positive, negative of no feedbacks on potential fire activity.

The results showed that mean annual FMC was significantly different between alternative forest states across each of the 48 years of climate data – which act as independent replicates for different climate conditions in our experimental design. By quantifying these differences using the metric of fuel availability, we have demonstrated that statistically significant differences in FMC translate into meaningful differences in the context of potential fire activity. Overall, the results show strong positive and negative feedbacks across the alternative forest states compared to the mature wet Eucalypt forest that they replaced, which were greater than age-related differences within the wet Eucalypt forest sites. Overall, our results support the hypothesis that indirect effects of climate change, acting through vegetation conversion to alternative forest states, have a substantial impact on the potential for future fire activity, with important implications for land and fire managers in this region.

1. Introduction

Fire is a critical process in many ecosystems globally that influences the distribution, composition, and successional stage of vegetation communities (Pausas et al., 2017). While fire is important for the maintenance of many ecosystems, altered fire regimes can have negative impacts (Enright et al., 2015). Climate warming is elevating fire danger in many locations across the globe (Abatzoglou et al., 2019; Flannigan et al., 2000; Jolly et al., 2015) and increasing temperatures coinciding with more variable rainfall are expected to increase fire frequency in south-eastern (SE) Australia (Harris and Lucas, 2019). Repeated high-intensity fires can alter the

successional pathways of forest communities by overwhelming the utility of fire adaptive traits (Fairman et al., 2019), which can lead to abrupt shifts in ecosystem composition and forest structural properties (Bowman et al., 2014), in conjunction with an overall shift to forests of a lower age class. This may indirectly affect future fire activity if younger, or alternative forest states create microclimate conditions conducive to increased fire activity (Enright et al., 2015). This phenomenon is commonly referred to as fire-vegetation feedbacks, which can be positive or negative. Positive feedbacks relate to vegetation conditions likely to increase fire activity, while negative feedbacks include vegetation states likely to reduce potential fire activity (Tepley et al., 2018). Positive and negative fire-vegetation feedbacks have been reported across a range of different ecosystems, including in wet Eucalypt forests of SE Australia (Burton et al. 2019). However, a key limitation of these studies is the relatively narrow temporal range of observations – typically one or two seasons, which in turn limits our understanding of the potential for alternative forest states to generate positive or negative feedbacks across the range of climate conditions that are characteristic to the region.

Forests in productive regions can support high biomass loads that reaccumulate quickly after disturbance, so they almost always have enough fuel to sustain large fires (Cawson et al., 2018). Consequently, in these forests it is primarily the fuel moisture content (FMC) that limits fire activity, which is therefore a useful metric for understanding the potential for positive or negative feedbacks. Recurrent high-intensity fires in the dominant mature *Eucalyptus regnans* forests in this region have caused some areas to shift to alternative forest types, that are potentially more adapted to the novel short-interval fire regime (Fairman et al., 2016).

Field studies across a range of alternative forest states and age classes to mature wet Eucalypt forests (Brown et al., 2021; Burton et al., 2019) report both positive and negative feedbacks. However, a key limitation to these studies is that they have a limited timeframe of observation. Consequently, it is difficult to determine whether the feedbacks reported are due to the indirect effects of climate change on vegetation structure and composition, or more strongly related to the specific climate conditions throughout the period of observation. Given these limitations, and the variability in weather and climate conditions in SE Australia (Harris et al., 2019), modelling the potential for fire vegetation feedbacks across alternative forest states across the full range of climate conditions characteristic to the region would enhance our understanding of the potential for indirect effects of climate change to influence future fire activity.

Therefore, the aim of this study is to explore whether observed differences in dead FMC resulting from vegetation-mediated effects of climate change are replicated across the range of climate conditions experienced in the region, and, to evaluate the impact of this on potential fire activity.

2. Methods

To understand the potential for indirect effects of climate change (through changes to forest structure and composition) to influence future fire activity, dead FMC was modelled across seven alternative forest state field sites, and one above canopy open weather station (Figure 1). Dead FMC (represented by automated fuel moisture sticks) was modelled for 48 years using a calibrated process-based model (van der Kamp et al., 2017) that was driven by reconstructed climate data transferred to microclimate values (Brown et al., 2016; Jeffrey et al., 2001). The seven sites cover a range of alternative forest state sites to mature *Eucalyptus regnans* forests in SE Australia (which is assumed to be analogous to 80-year-old *E. regnans* in this study).

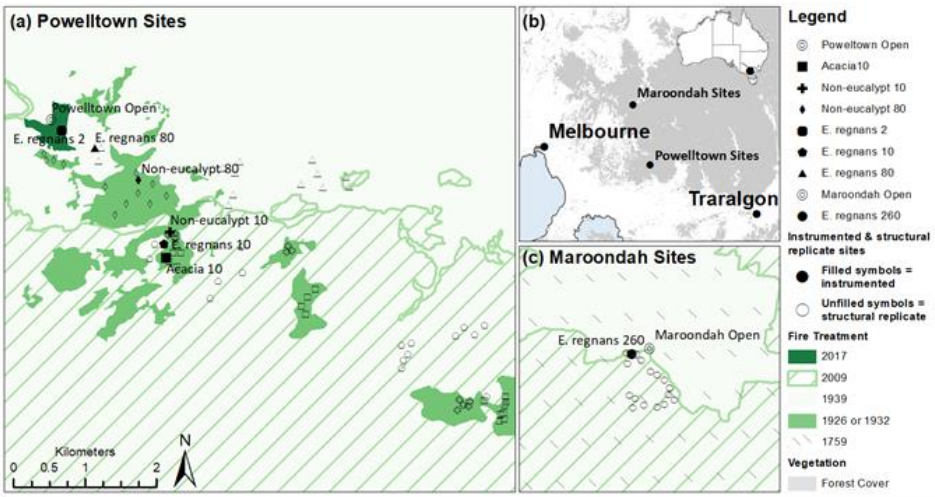

Figure 1. Location of the study areas, including seven instrumented field sites and two open (control) weather stations within the Central Highlands, Victoria, in SE Australia (b). Coloured and dashed areas indicate the fire disturbance conditions, denoting the most recent fires affecting forest structure at the alternative state forest sites. The 1939 fire (light green) affected the entire Powelltown (a) and Maroondah (c) regions.

Table 1. Site information for the open station and seven alternative forest states to wet Eucalypt forest used in this study; including four Eucalypt-dominated sites, one Acacia dealbata site, and two sites dominated by (typically) understorey species (Non-eucalypt).

Site name	Age	Rainfall (mm y^{-1})	Aspect (°)	Elevation (m)
Powelltown Open	-	1495	267	740
$Acacia_{10}$	10	1322	134	558
$Non\text{-}eucalypt_{10}$	10	1344	128	606
$Non\text{-}eucalypt_{80}$	80	1402	166	635
E. regnans$_2$	2	1481	153	735
E. regnans$_{10}$	10	1337	142	588
E. regnans$_{80}$	80	1448	204	672
E. regnans$_{260}$	260	1297	156	727

Hourly FMC data were summarised to mean annual FMC and a simple one-way analysis of variance (ANOVA) and Tukey's Honest Significant Difference (HSD) post-hoc test were conducted to detect statistically significant differences. To understand the importance of differences in FMC in the context of potential fire activity, fuel availability (FA) was assessed following Cawson et al. (2017), where fuels were considered available to burn on a given day if the site minimum modelled FMC is below 16% for at least one hour of that day.

3. Results

FMC modelled at the hourly scale (n=420 767) were summarised at a high level to mean annual FMC (n=48) for each alternative forest state. At this scale, there were significant differences in mean annual FMC ($F_{7,326}$ = 1307.2, $p < 0.001$), with a subsequent post-hoc test between group (alternative forest state) means finding significant differences across all groups at the $p < 0.05$ level. Substantial differences in FA were modelled across the alternative forest states compared to the mature wet Eucalypt forest they replaced. Mean annual days of fuel availability at *E. regnans*$_{80}$ ranged from 0 (1992, 1996, 2011) to 24 days (1976), with 19 days of FA in 2009 – the year of the 'Black Saturday' fires in Victoria, Australia. FA was consistently higher (lower FMC) at $Acacia_{10}$ and $Non\text{-}eucalypt_{10}$ compared to *E. regnans*$_{80}$, peaking at 242 days (1974) at $Non\text{-}eucalypt_{10}$ (Figure 2). In contrast, between 1973 and 2020, FMC did not fall below 16% at the $Non\text{-}eucalypt_{80}$ site, while FA of only 2 days was modelled at the *E. regnans*$_2$ site (1974 and 2009). Modelled FA at the regenerating (*E. regnans*$_{10}$) and multi-cohort (*E. regnans*$_{260}$) were similar to *E. regnans*$_{80}$, with both sites recording years with zero days of fuel availability, and peak years of 16 and 32 days, respectively.

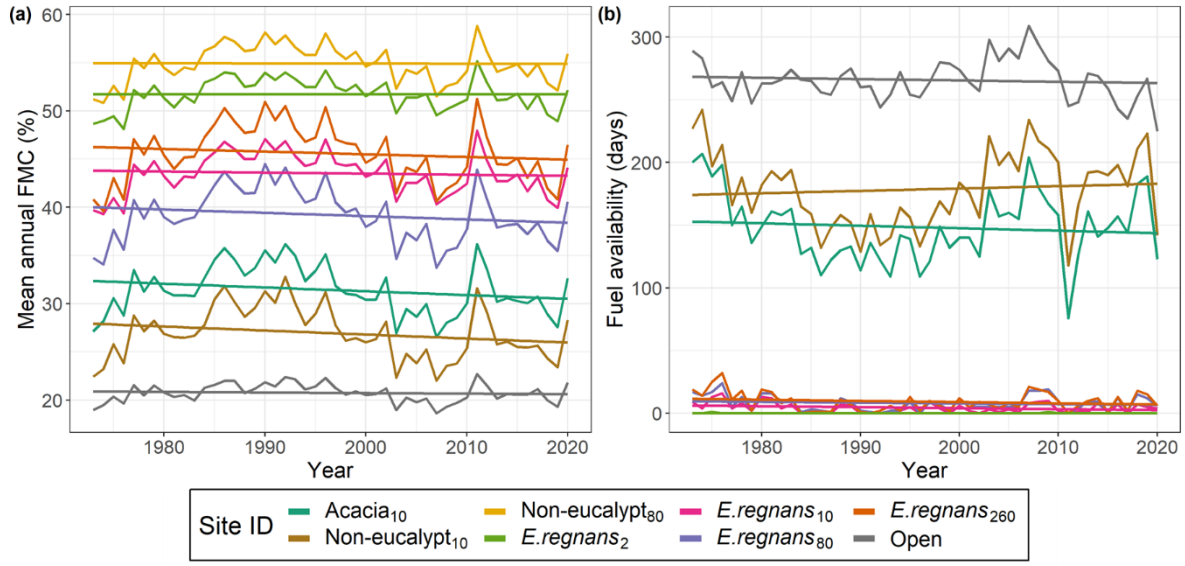

Figure 2. Modelled mean annual fuel moisture content (a) and fuel availability (b) for the alternative forest states between 1973 and 2020. The regression line indicates a simple linear model smoothed across each year of the 48-year climate dataset.

4. Discussion

Our research suggests that the impact of vegetation-mediated indirect effects of climate change on potential fire activity across seven alternative forest states is substantial. Across 48 years of modelled climate data, the results were broadly consistent with single-season observations reported by Burton et al. (2019) and Brown et al. (2021), suggesting that these comparatively shorter studies captured an appropriate range of climatic conditions. Across the 48-years of modelled data, FMC variability within and between the alternative forest states was greater than modelled FMC variability at the open site, suggesting that the indirect effects of climate change (that have altered forest structure and composition) may be more important than the direct effects on FMC in this ecosystem.

Overall, age related differences in dead FMC within E. regnans states were weaker than differences across different alternative forest state vegetation associations, with important implications for land management. We found short-term, positive fire feedbacks related to FMC for non-eucalypt forests in this region, which, as the forest ages, become negative feedbacks. In contrast, our results did not support the existence of positive fire feedbacks related to FMC across different ages of E. regnans forest. Consequently, our findings suggests that the maintenance of a Eucalypt-dominated canopy layer, potentially with patches of older non-eucalypt type forests will provide the most robust vegetation-state related buffer to future fire activity in the Central Highlands regions of SE Australia. Wet Eucalypt forests in SE Australia are a highly valued and contested forest system, and our findings enhance our understanding of ways in which these systems may be vulnerable, or resilient, to future climate change.

5. Conclusion

The indirect effects of climate change, acting through changes to vegetation structure and function, have a significant impact on fuel availability across wet Eucalypt forests in SE Australia. Indirect climate change effects resulted in both positive and negative feedbacks for potential fire activity compared to mature wet Eucalypt forest. Regenerating alternative forest states exhibited strong positive feedbacks, that were consistent across modelled data and observations in the literature. In contrast, feedbacks at *E. regnans* forests between 10-260 years were limited, while juvenile (2-year-old) *E. regnans* forests, and older (80-year-old) alternative state forests exhibited negative vegetation fire feedbacks.

6. Reference List

Abatzoglou, J.T., Williams, A.P., Barbero, R., 2019. Global Emergence of Anthropogenic Climate Change in Fire Weather Indices. Geophys. Res. Lett. 46, 326–336. https://doi.org/10.1029/2018GL080959

Bowman, D.M.J.S., Murphy, B.P., Neyland, D.L.J., Williamson, G.J., Prior, L.D., 2014. Abrupt fire regime change may cause landscape-wide loss of mature obligate seeder forests. Glob. Chang. Biol. 20, 1008–1015. https://doi.org/10.1111/gcb.12433

Brown, T., Mills, G., Harris, S., Podnar, D., Reinbold, H., Fearon, M., 2016. A bias corrected WRF mesoscale fire weather dataset for Victoria, Australia 1972-2012, Journal of Southern Hemisphere Earth Systems Science.

Brown, T.P., Inbar, A., Duff, T.J., Burton, J., Noske, P.J., Lane, P.N.J., Sheridan, G.J., 2021. Forest Structure Drives Fuel Moisture Response across Alternative Forest States. Fire 2021, Vol. 4, Page 48 4, 48. https://doi.org/10.3390/FIRE4030048

Burton, J., Cawson, J., Noske, P., Sheridan, G., 2019. Shifting states, altered fates: Divergent fuel moisture responses after high frequency wildfire in an obligate seeder Eucalypt forest. Forests 10, 436. https://doi.org/10.3390/f10050436

Cawson, J.G., Duff, T.J., Swan, M.H., Penman, T.D., 2018. Wildfire in wet sclerophyll forests: the interplay between disturbances and fuel dynamics. Ecosphere 9, 1–17. https://doi.org/10.1002/ecs2.2211

Cawson, J.G., Duff, T.J., Tolhurst, K.G., Baillie, C.C., Penman, T.D., 2017. Fuel moisture in Mountain Ash forests with contrasting fire histories. For. Ecol. Manage. 400, 568–577. https://doi.org/10.1016/j.foreco.2017.06.046

Enright, N., Fontaine, J.B., Bowman, D.M.J.S., Bradstock, R.A., Williams, R.J., Enright, N.J., Bowman, J.B., Bradstock, D.M., Williams, R.A.&, 2015. Interval squeeze: altered fire regimes and demographic responses interact to threaten woody species persistence as climate changes. Front. Ecol. Environ. 13, 265–272. https://doi.org/10.1890/140231

Fairman, T.A., Bennett, L.T., Nitschke, C.R., 2019. Short-interval wildfires increase likelihood of resprouting failure in fire-tolerant trees. J. Environ. Manage. 231, 59–65. https://doi.org/10.1016/j.jenvman.2018.10.021

Fairman, T.A., Nitschke, C.R., Bennett, L.T., 2016. Too much, too soon? A review of the effects of increasing wildfire frequency on tree mortality and regeneration in temperate eucalypt forests. Int. J. Wildl. Fire 25, 831–848. https://doi.org/10.1071/WF15010

Flannigan, M.D., Stocks, B.J., Wotton, B.M., 2000. Climate change and forest fires. Sci. Total Environ. 262, 221–229. https://doi.org/10.1016/S0048-9697(00)00524-6

Harris, S., Lucas, C., 2019. Understanding the variability of Australian fire weather between 1973 and 2017. PLoS One 14, e0222328. https://doi.org/10.1371/journal.pone.0222328

Harris, S., Nicholls, N., Tapper, N., Mills, G., 2019. The sensitivity of fire activity to interannual climate variability in Victoria, Australia. J. South. Hemisph. Earth Syst. Sci. 69, 146. https://doi.org/10.1071/es19008

Jeffrey, S.J., Carter, J.O., Moodie, K.B., Beswick, A.R., 2001. Using spatial interpolation to construct a comprehensive archive of Australian climate data. Environ. Model. Softw. 16, 309–330. https://doi.org/10.1016/S1364-8152(01)00008-1

Jolly, W.M., Cochrane, M.A., Freeborn, P.H., Holden, Z.A., Brown, T.J., Williamson, G.J., Bowman, D.M.J.S., 2015. Climate-induced variations in global wildfire danger from 1979 to 2013. Nat. Commun. 6. https://doi.org/10.1038/ncomms8537

Pausas, J.G., Keeley, J.E., Schwilk, D.W., 2017. Flammability as an ecological and evolutionary driver. J. Ecol. 105, 289–297. https://doi.org/10.1111/1365-2745.12691

Tepley, A.J., Thomann, E., Veblen, T.T., Perry, G.L.W., Holz, A., Paritsis, J., Kitzberger, T., Anderson-Teixeira, K.J., 2018. Influences of fire–vegetation feedbacks and post-fire recovery rates on forest landscape vulnerability to altered fire regimes. J. Ecol. 106, 1925–1940. https://doi.org/10.1111/1365-2745.12950

van der Kamp, D.W., Moore, R.D., McKendry, I.G., 2017. A model for simulating the moisture content of standardized fuel sticks of various sizes. Agric. For. Meteorol. 236, 123–134. https://doi.org/10.1016/j.agrformet.2017.01.013

Investigating the potential impact of climatic conditions on fire occurrence in Lebanon

George Mitri*; Karen Gebrael

Land and Natural Resources Program, Institute of the Environment, University of Balamand - Kelhat, El Koura, Lebanon, {george.mitri@balamand.edu.lb}

**Corresponding author*

Keywords

Wildfires, climate, drought, high mountains, vulnerable forests

Abstract

As Lebanon has experienced an increasing number of fires, this work aimed at assessing the potential impact of climatic conditions on fire occurrence in the country. The results showed an increasing trend of fire events especially in high altitudinal ranges of vegetation levels. Simultaneously, increasing drought conditions were observed in high mountain lands. The results of this study strongly supported a link between changing climatic conditions and fire occurrence in Lebanon. This has resulted in clear impact on vulnerable forest ecosystems, however, a more detailed analysis about the consequences of frequent and intense fires on both vulnerable community livelihood and the natural environment is yet to be assessed.

1. Introduction

Wildfire intensity, extent and frequency are increasing in the Mediterranean ecosystems, causing major impacts on the ecological, economic, social and health systems (Mitri et al., 2016). Like other Mediterranean countries, Lebanon has increasingly suffered from devastating wildfires across the country during the past two decades. The total burnt area reached 21,674 ha and the minimum total number of fires amounted to 2,249 fires for the period extending from 2008 to 2021 (MOE/UOB, 2021). The average annual burnt area increased to 1,449 ha after it was around 1,000 ha per year before the year 2019.

Intense and large-scale wildfires were major causes of Lebanon's forest severe degradation (El Halabi et al., 2014). Tree growth and survival, yield and quality of wood/non-wood forest products, wildlife habitat, recreational, environmental and cultural value of forests were all affected by wildfires. Additionally, wildfires were linked to human injuries/death and loss of properties (MOE/UOB, 2021). In principle, the main direct causes of fires in Lebanon included cleaning lands using fire, burning waste/agricultural residues, camp fires, fireworks and arson, among others (Mitri et al., 2016). Other indirect causes comprised socio-economic changes, increase in the extent of Wildland Urban Interface (WUI) and land cover/land use changes, among others (Mitri et al., 2016; MOE/UOB, 2021). Climate extremes represented a major wildfire driver. In reference to IPCC (2021) heat wave increase, temperature increase, precipitation decrease (i.e., drought period increase), severe wind storms and heavy rainfall are expected to occur in the Mediterranean region (i.e., including Lebanon), therefore exacerbating the wildfire situation. As Lebanon has observed an increasing number of fire events and unprecedented annual extent of burnt areas, this work aimed at assessing the potential impact of climatic conditions on fire occurrence in the country. The specific objectives were to 1) evaluate trends in fire occurrence over the period 2001 to 2021, 2) assess the relationship between climatic drought conditions and elevation and 3) assess the relationship between fire frequencies and elevation levels.

2. Study area and dataset description

2.1. Study area description

The study area covered the country of Lebanon located on the Eastern Mediterranean. In reference to MOE/UOB (2021), the average start date and end date of the fire season is April 19 and November 6, respectively. The average peak month in number of fire events is August while the average peak month in extent of burnt areas is

the month of September. Lebanon has a Mediterranean climate, with warm dry summers and cool wet winters. Most of the total annual precipitation (i.e., around 90%) occurs between November and March (Mitri et al., 2016; Mitri et al., 2015).

Lebanon is divided into four physiographic regions (i.e. coastal plain, Lebanon mountain range, Beqaa valley, and Anti-Lebanon Mountains). The Lebanon mountain range rises steeply from the coast to mountains reaching 3,088 meters above sea level (masl) and supports most of Lebanon's forests. The forest land and other wooded land in Lebanon cover around 13% and 11% of its territory, respectively (FAO, 2020). The major forest species are *Quercus calliprinos*, *Quercus infectoria*, *Quercus cerris var. pseudo cerris*, *Juniperus excelsa*, *Cedrus libani*, *Abies silicica*, *Pinus pinea*, *Pinus halepensis*, *Pinus brutia*, and *Cupressus sempervirens*. Around 33% of the national territory is classified as moderate to very high fire risk areas (Mitri et al., 2015). The sharp altitudinal gradients of temperature and precipitation lead to the appearance of different climatic zones running along mountain elevations. This explains the presence of five different vegetation levels (Abi-Saleh and Safi, 1998) as shown in **Figure 1**, namely the Thermomediterranean (0-500 m asl), Eumediterranean (500-1000 m asl), Supramediterranean (1000 -1500 m asl), Montanemediterranean (1500-2000 m asl) and Oromediterranean (>2000 m asl).

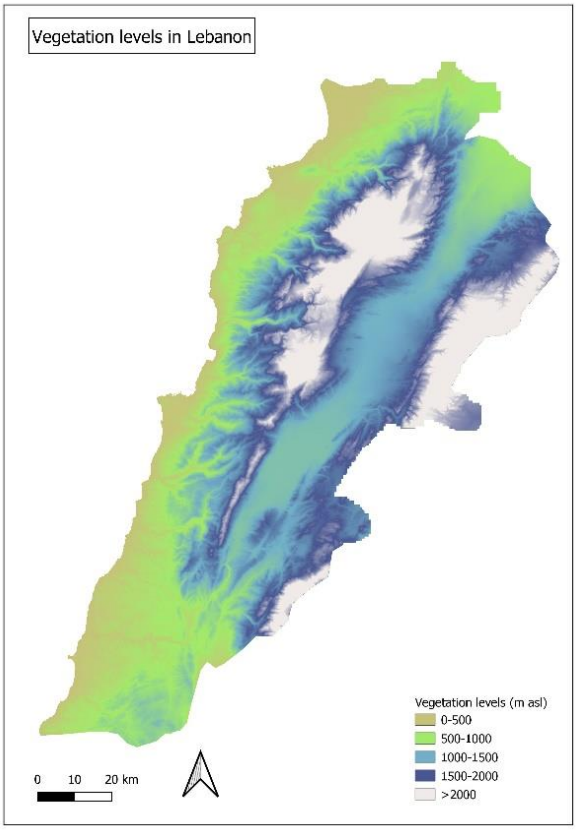

Figure 1. Altitudinal vegetation levels in Lebanon

2.2. Dataset description

Archived fire hotspots in Lebanon for the years 2001 throughout 2021 were collected in form of shapefile using the Fire Information for Resources Management System (FIRMS). Data courses included the J1 VIIRS C1, SUOMI VIIRS C2 and MODIS C6.1. The spatial climatic data needed to calculate the increase in the Keetch-Byram Drought Index (KBDI) between current averages and future averages were mostly obtained from simulated Global Climate Models (GCM). Datasets of historical averages (1950 to 2000) and future 30-year running averages (2010 to 2039) included: monthly maximum temperature, monthly precipitation and mean annual rainfall at 1x1 km of spatial resolution (Mitri et al. 2015). In addition, a Digital Elevation Model (DEM) of 25x25 m resolution and the 2017 land cover-land use map of Lebanon were employed.

3. Methodology

A total of 5095 fires were plotted against their years of occurrence between 2001 and 2021 to evaluate trends in fire events throughout the years. A Pearson correlation test (i.e., linear relationship between data) was performed to assess any significant increase in number of fires in most recent years.

Consequently, the relationship between climatic drought conditions and elevation above sea level was assessed. More specifically, the statistical relationship between increase in KBDI and high country lands was tested using Spearman correlation (i.e., non-linear relationship between data). This eventually helped in evaluating the increase of drought conditions in the range of high altitudinal vegetation levels and its possible relationship with fire occurrence in those areas. The ranges in elevation were chosen according to the categorization of Digital Elevation model (DEM) values into vegetation level zones (**Table 1**). A Pearson correlation test was performed in order to assess the link between fire frequencies and elevation levels. Furthermore, the fire occurrence in high mountain forest ecosystems (e.g., cedar, fir and juniper) was investigated.

Table 1-Vegetation levels (MOE/UNDP, 2011)

Vegetation level	Elevation (m)
Thermomediterranean	[0-500]
Eumediterranean	]500-1000m]
Supramediterranean	]1000-1500m]
Montanemediterranean	]1500-2000m]
Oromediterranean	>2000m

4. Results and discussion

4.1. Trends in fire occurrence (2001-2021)

The total number of fires per year was estimated from 2001 to 2021. **Figure 2** showed that the annual number of fires varied from 4 to 1077 fires, for the assessed period. The highest number of fires was in 2021 and the lowest one was in 2001. Moreover, the performed Pearson correlation test showed that the total number of fires increased significantly throughout years (p value = 0.000084, Pearson correlation coefficient = 0.752).

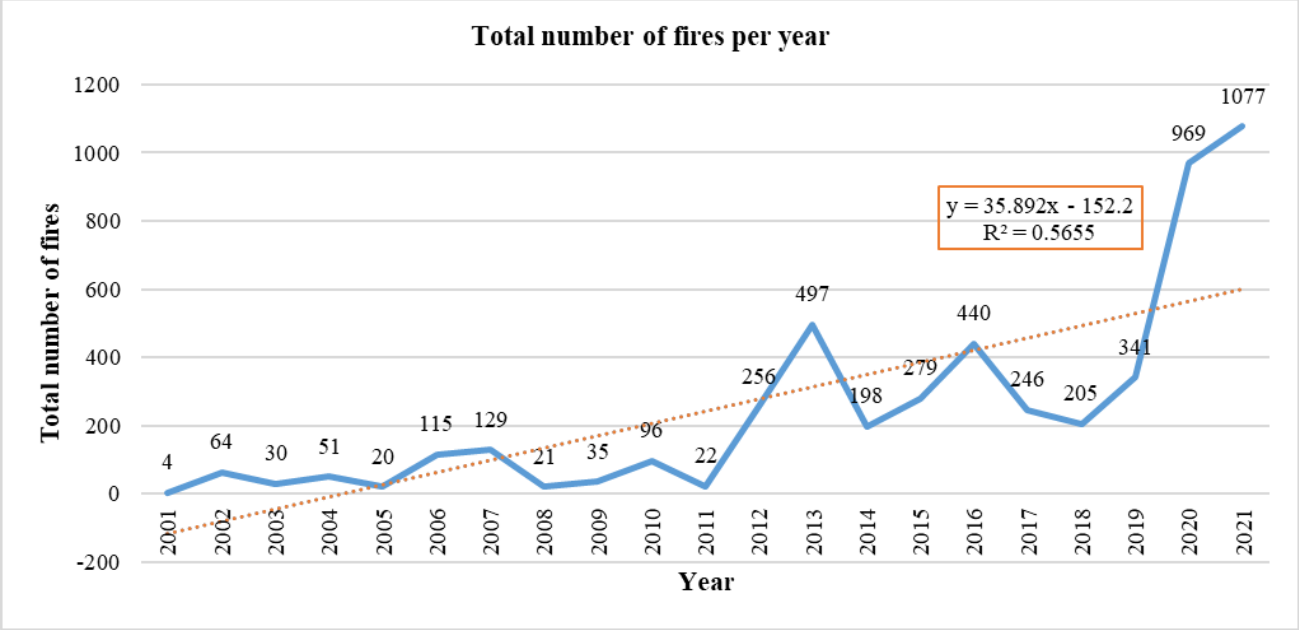

Figure 2-Total number of fires per year in Lebanon

4.2. Climatic drought conditions and elevation

The average KBDI increase varied between 9 (i.e., Supramediterranean level) and 27 (i.e., Oromediterranean level) (**Figure 3**). Moreover, a notable increase in KBDI was remarked in high altitudinal ranges of vegetation levels (i.e., above 1000 m). Accordingly, the relationship between KBDI increase and elevations was evaluated in ranges above 1000 m using the Spearman correlation test. The test showed a significant positive correlation between the 2 variables (p value = 9.182E-17, Spearman correlation coefficient = 0.308). Accordingly, it was assumed that any increase in fire occurrence within high altitudinal ranges of vegetation levels could be linked to increase of drought conditions in those areas.

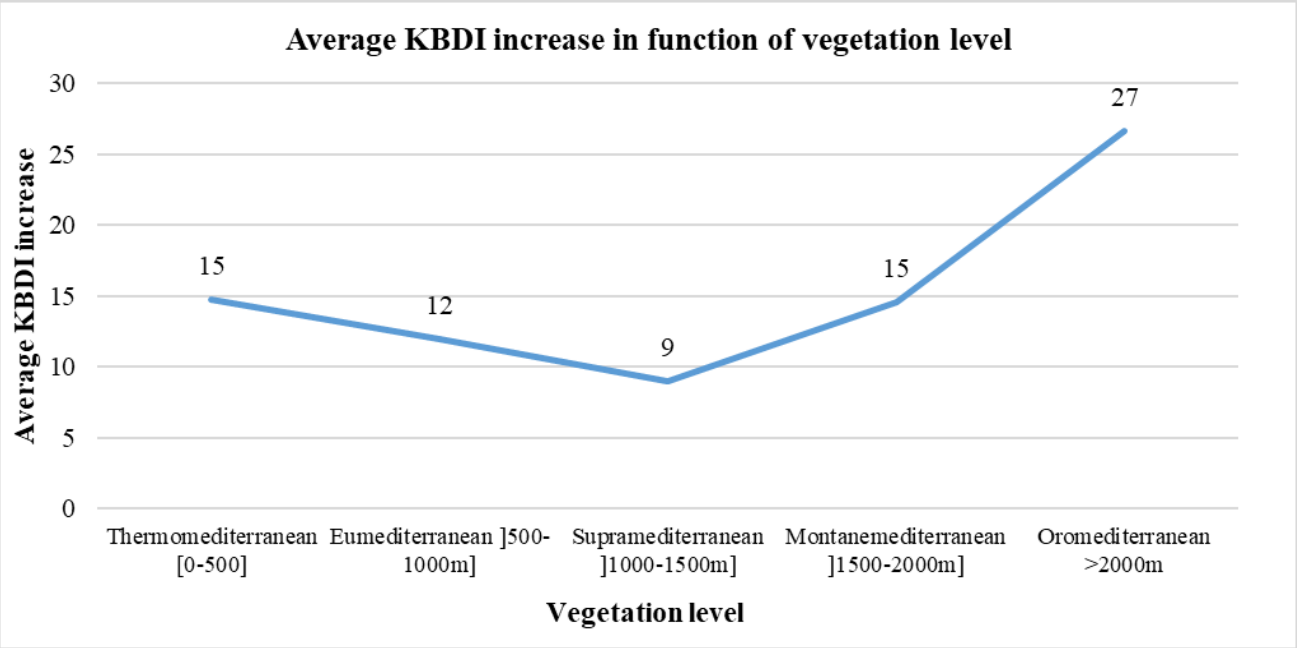

Figure 3-Average KBDI increase variation in function of vegetation levels

4.3. Fire frequencies and elevation levels

The variation in total number of fires in function of vegetation levels was also evaluated for the period extending between 2001 and 2021. **Figure 4** showed that the highest number of fire events occurred in Thermomediterranean level (i.e., 2644 fires) and the lowest number was in Oromediterranean level (i.e., 24 fires). In addition, the statistical analysis showed a negative significant correlation between the total number of fires and elevations (i.e., p value = 5.57 39E-109, Pearson correlation coefficient = - 0.537). These results were expected as high country lands encompass low density vegetation cover therefore lower fire hazard.

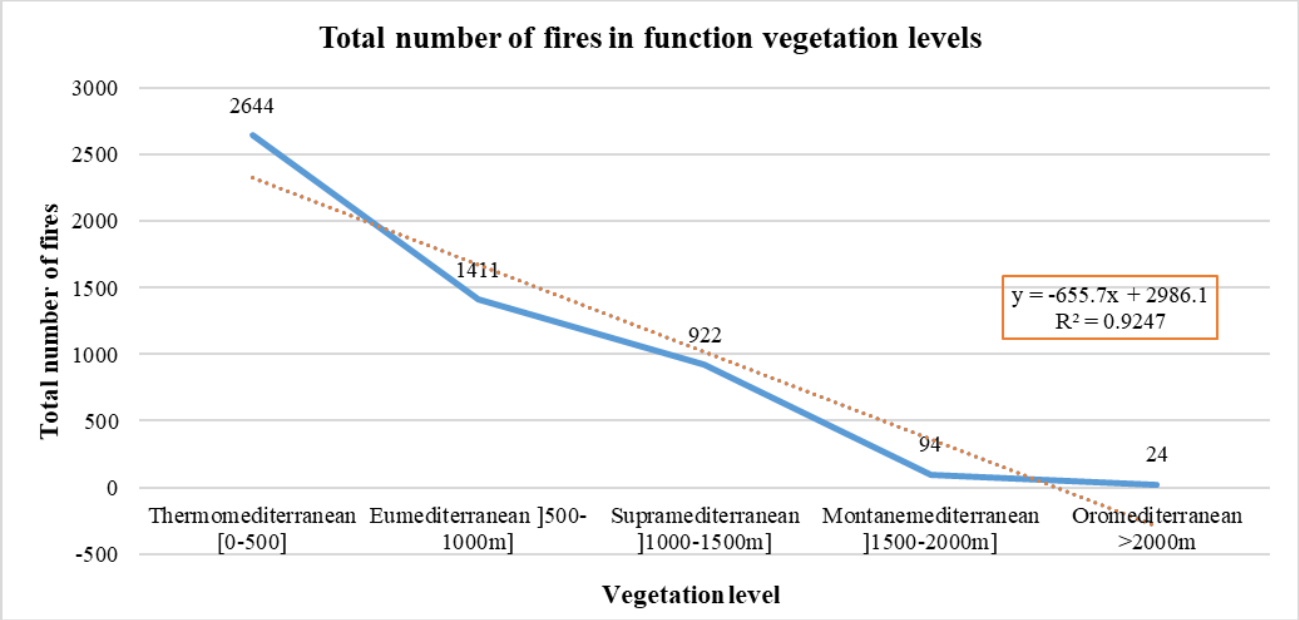

Figure 4-Total number of fires in function of vegetation levels

Yet, the multi-temporal variation in the total number of fires in each vegetation level was further assessed (**Figure 5** – **Figure 9**). The performed statistical analysis showed that the total number of fires increased significantly throughout years, in all vegetation levels. The results were summarized in **Table 2**.

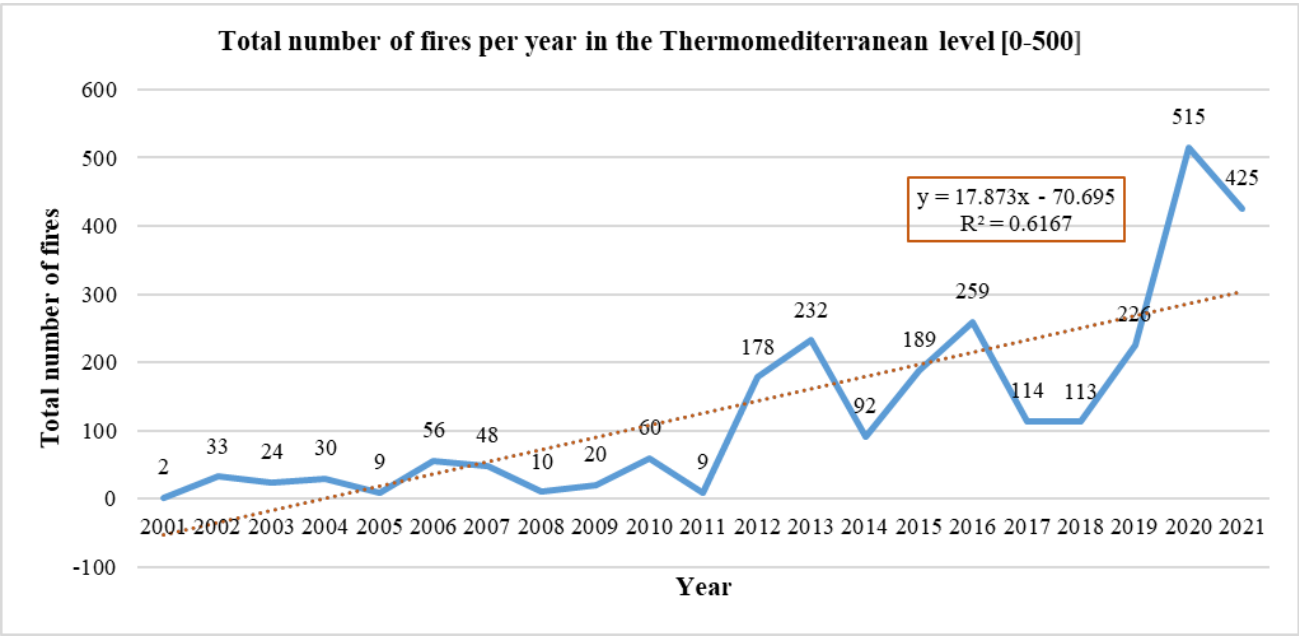

Figure 5-Total number of fires per year in the Thermomediterranean level

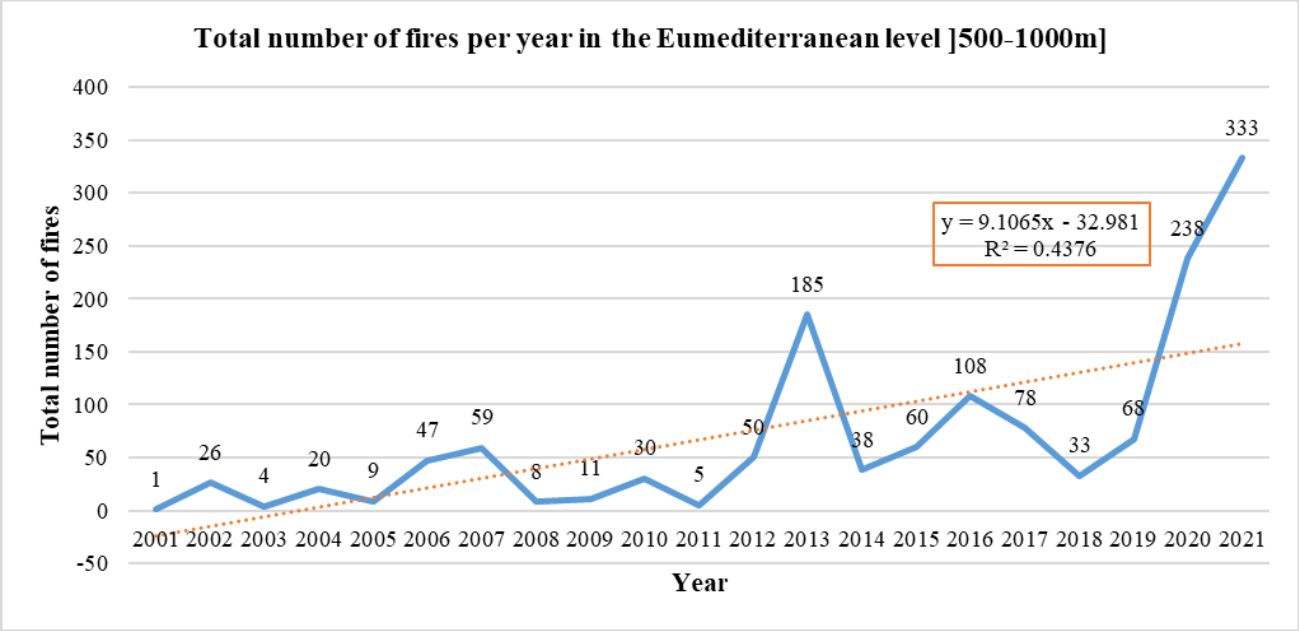

Figure 6-Total number of fires per year in the Eumediterranean level

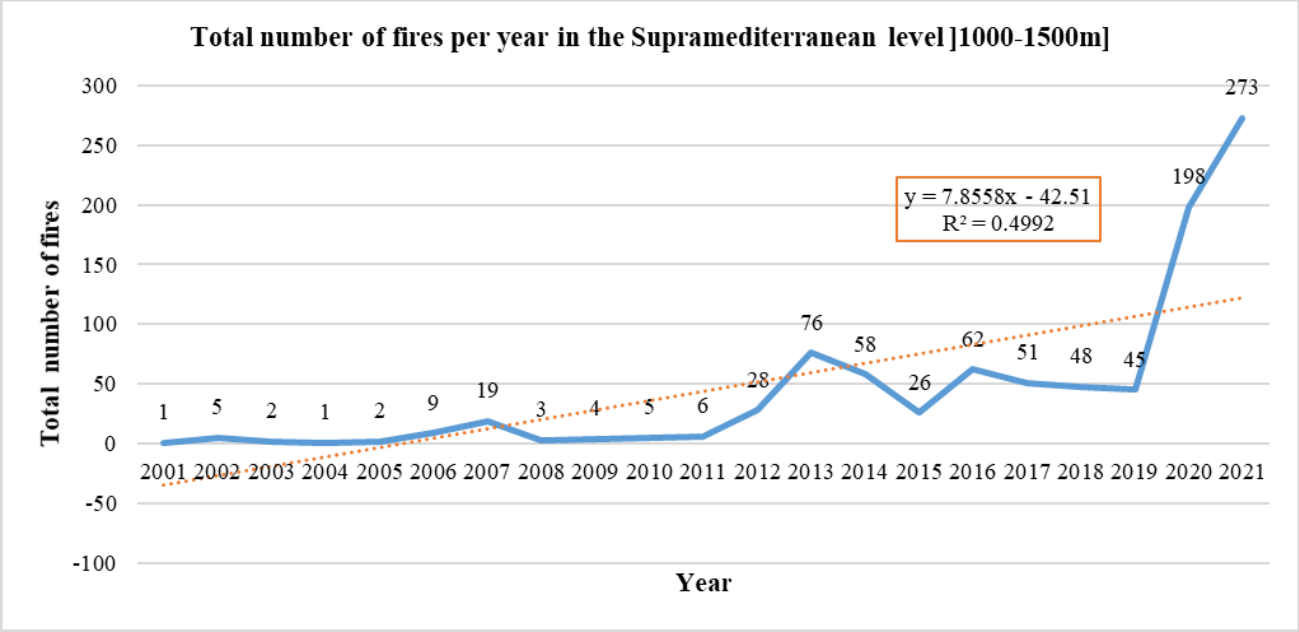

Figure 7-Total number of fires per year in the Supramediterranean level

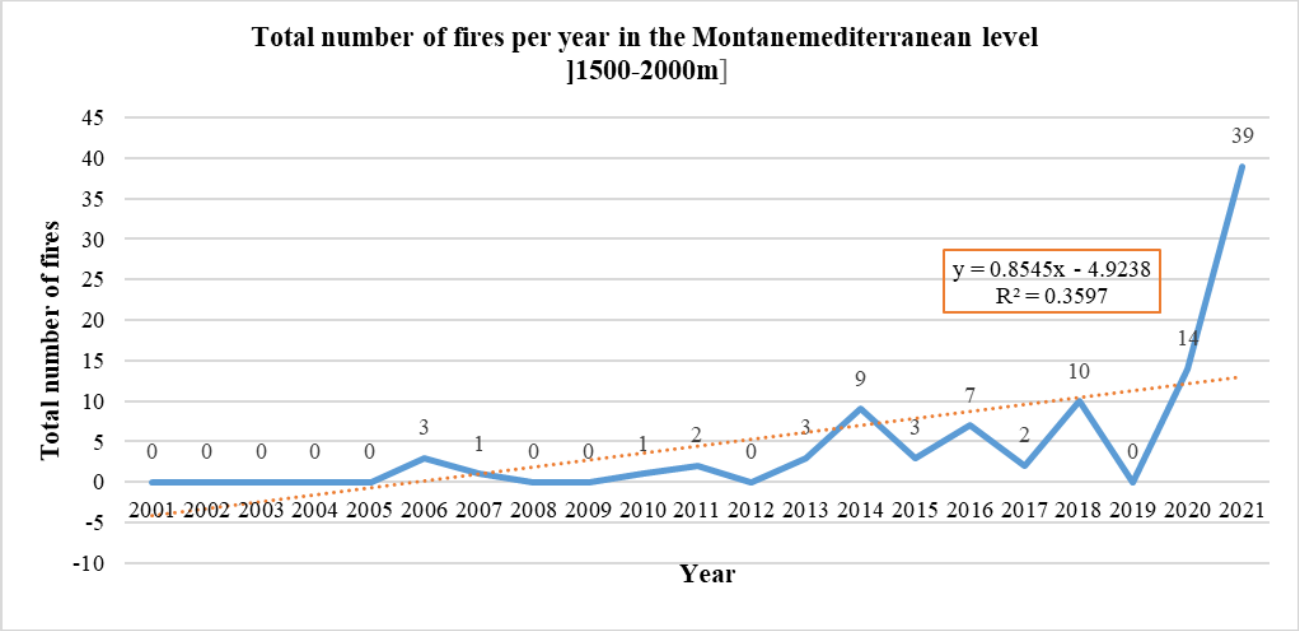

Figure 8-Total number of fires per year in the Montanemediterranean level

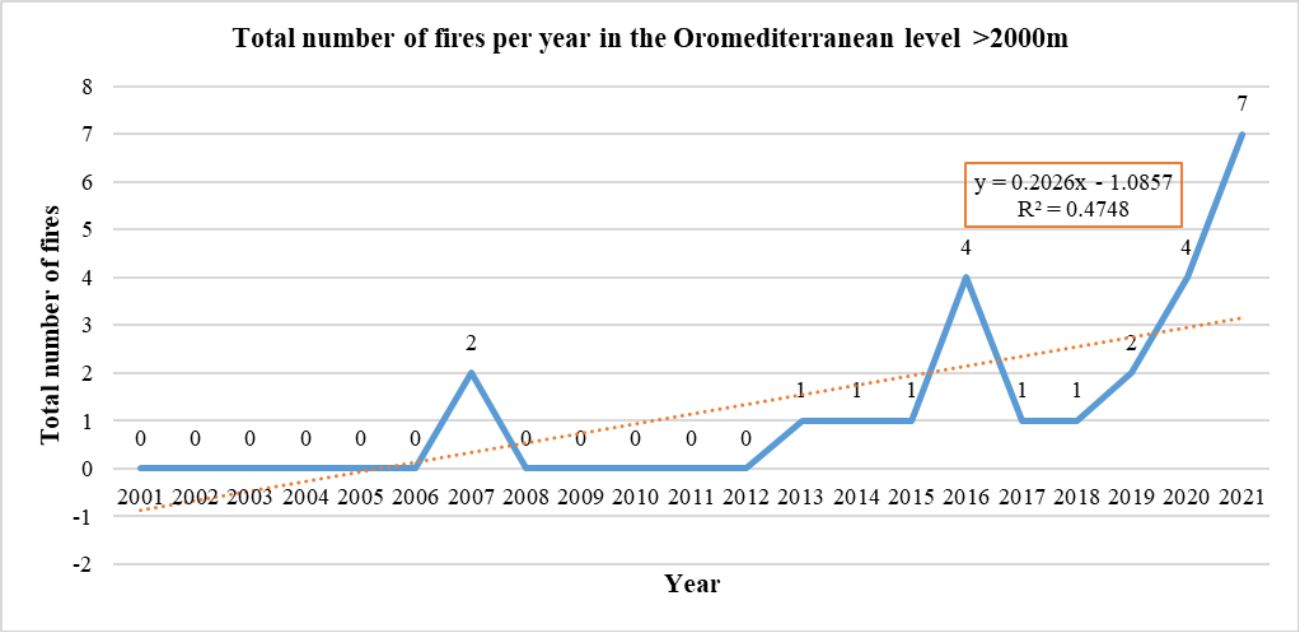

Figure 9-Total number of fires per year in the Oromediterranean level

Table 2-Correlation between total number of fires and years results

Vegetation levels	p value (Correlation between total number of fires and years)
Thermomediterranean [0-500]	p value = 0.000025 (Pearson correlation coefficient = 0.785)
Eumediterranean]500-1000m]	p value = 0.000035 (Spearman correlation coefficient = 0.777)
Supramediterranean]1000-1500m]	p value = 2.2227E-7 (Spearman correlation coefficient = 0.874)
Montanemediterranean]1500-2000m]	p value = 0.00036 (Spearman correlation coefficient = 0.704)
Oromediterranean >2000m	p value = 0.000018 (Spearman correlation coefficient = 0.794)

Overall, the results indicated a significant increase of drought conditions in high mountain lands across the high altitudinal ranges of vegetation levels simultaneously to obvious increase of fire events in those same areas. Accordingly, it was assumed that changing climatic conditions were expected to directly drive the increase of

fire occurrence in high country lands therefore pausing an increasing threat to vulnerable high mountain forest ecosystems such as cedar, fir and juniper forests and other types of natural landscape which comprise very often rare endemic species not adapted to fires. In fact, specific vulnerable mountainous ecosystems (i.e., cedar forests) experienced disastrous fire events for the first time in the recorded history of fires in Lebanon. As shown in **Figure 10**, there was a remarkable increase of fire events in high mountain forest ecosystem especially in the years of 2020 and 2021.

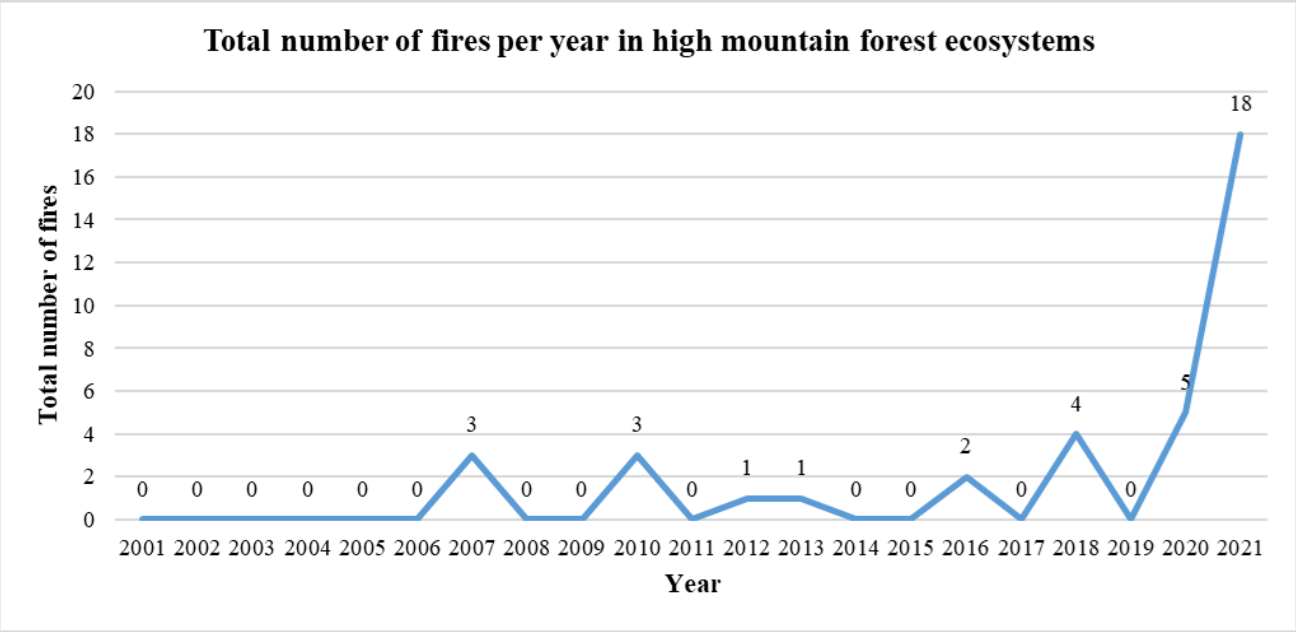

Figure 10-Total number of fires per year in high mountain forest ecosystems

5. Conclusions

As the climate science community sources a suite of global climate models to help decision makers understand the projections of future climate change and related impacts, the Coupled Model Intercomparison Project , Phase 5 (CMIP5) models, as included in the IPCC's Fifth Assessment Report (AR5) showed increase in fire weather conditions throughout the next 30 years with high confidence for the Mediterranean basin. Building on the results of this work, Lebanon is expected to face an increasing risk of fires, whether that's forest fires or grassland fires. More specifically, as the landscape becomes increasingly dry from multiple years of gradual change, an increase in the frequency and intensity of fires is expected. This necessitates developing and implementing all necessary adaptation measures to mitigate the impact of fires on both vulnerable community livelihood and the natural landscape.

6. References

Abi-Saleh, B. and Safi, S. (1998). Carte de la vegetation du Liban (1/500000) + Notice Applicative. Ecologia Mediterranea, XIV (1/2): 123-141.

El Halabi, A., Mitri, G., Jazi, M. (2014). Monitoring post-fire shrub recovery on Pinus brutia burned sites. 20th LAAS International science conference: New frontiers in sciences. March 27-29, 2014, Lebanese University, Lebanon. pp137.

FAO. (2020). Forest and tree resources assessment in Lebanon. FAO, Beirut.

IPCC. (2021). Summary for Policymakers. In: Climate Change 2021: The Physical Science Basis. Contribution of Working Group I to the Sixth Assessment Report of the Intergovernmental Panel on Climate Change [Masson-Delmotte, V., Zhai, P., Pirani, A., Connors, S.L., Péan, C., Berger, S., Caud, N., Chen, Y., Goldfarb, L., Gomis, M.I., Huang, M., Leitzell, K., Lonnoy, E., Matthews, J.B.R., Maycock, T.K., Waterfield, T., Yelekçi, O., Yu, R., Zhou, B. (eds.)]. In Press.

Mitri, G., Jazi, M., McWethy, D. (2015). Assessing Lebanon's wildfire potential in Association with current and future climatic conditions. In: Keane, Robert, E.; Jolly, Matt; Parsons, Russel; Riley, Karin. 2015

Proceedings of the large wildland fires conference; May 19-23, 2014; Missoula, MT. Proc. RMRS-P-73. Fort Collins, CO: U.S. Department of Agriculture (USDA), Forest Service, Rocky Mountain Research Station, pp 318-321.

Mitri, G., Antoun, E., Saba, S., McWethy, D. (2016) Modelling forest fire occurrence in Lebanon using socio-economic and biophysical variables in object-based image analysis. In: GEOBIA 2016: Solutions and Synergies., 14 September 2016 - 16 September 2016, University of Twente Faculty of Geo-Information and Earth Observation (ITC).

MOE/UNDP, 2011. Climate change vulnerability and adaptation of the forestry sector, Lebanon's Second National Communication.

MOE/UOB, 2021. Wildfires in Lebanon 2008-2021 (Mitri, G. Ed.). A joint report of the Ministry of Environment (MOE) and the University of Balamand (UOB), Beirut.

Living with fire in the landscape: uncomfortable adaptation, or border war?

Zoe D'Arcy

RMIT University, 124 La Trobe St, Melbourne VIC 3000, Australia, {s3686427@student.rmit.edu.au}

Keywords

Fire-adaptive communities, more-than-human theory, landscapes, contact zones

Abstract

With anthropogenic climate change already bringing more frequent and more intense wildfires, combined with significant human populations living in wildfire-prone landscapes, there are increased calls for adaptive approaches to fire. There is hope that by doing so, and by moving from a predominantly responsive 'war on wildfire' approach, humans can learn to 'thrive with fire' (Tedim et al. 2020).

Humans around the world have always shared their landscapes with fire – circumstances dictating the degree of comfort. Through these lived experiences, the stories of humans learning to live within their landscapes and therefore with fire have always been – and continue to be – stories of learning and innovation (Bowman et al. 2011; Pyne 2016). These adaptations, however, have been both enabled and constrained by how humans and their institutions have envisioned their relationships with the more-than-human actors and agents that share the landscape with them (Ruane 2018). These actors and agents include, amongst many other things, fire, vegetation and the weather.

There has been a great deal of focus on what can be learnt from Indigenous knowledges about fire on the landscape (i.e. Roos et al. 2016; Steffensen 2020). However, there has been less attention on how complex and often conflicting Western visions of the landscape and therefore of fire have contributed to particular adaptive approaches.

This paper explores how these visions – Aboriginal, as well as colonial, romantic, scientific, national and ecological – are a useful way of examining current narratives and adaptive approaches to fire in an Australian context. Examining these differing visions helps understand the range of fire management adaptions that have emerged in Australia.

Each vision has implications for how 'fire-adaptive' communities might act; what decisions they might make; who might be involved; and the processes that are used to take an adaptive approach to fire. They offer knowledges and practices that could complement the dominant colonial vision of 'war on wildfire', as well as reduce the effects of social and environmental 'slow emergencies' on human and more-than-human vulnerabilities. However, despite knowledge of these alternative visions in governments and communities, they are difficult to incorporate meaningfully into the dominant vision. Adaptive approaches to fire in more-than-human communities will require trade-offs across levels of society, scales of landscapes and of time.

1. Introduction

With anthropogenic climate change already bringing more frequent and more intense wildfires, combined with significant human populations living in wildfire-prone landscapes, there are increased calls for adaptive approaches to fire. There is hope that by doing so, and by moving from a predominantly responsive 'war on wildfire' approach, humans can learn to 'thrive with fire' (Tedim et al. 2020).

Humans around the world have always shared their landscapes with fire. Through these lived experiences, the stories of humans learning to live within their landscapes and therefore with fire have always been – and continue to be – stories of learning and innovation (Bowman et al. 2011; Pyne 2016). These adaptations, however, have been both enabled and constrained by how humans and their institutions have envisioned their relationships with the more-than-human actors and agents that share the landscape with them (Ruane 2018). These actors and agents include, amongst many other things, fire, vegetation and the weather.

There has been a great deal of focus on what can be learnt from Indigenous knowledges about fire on the landscape (i.e. Roos et al. 2016; Steffensen 2020). However, there has been less attention on how complex and often conflicting Western visions of the landscape, and therefore of fire, have contributed to particular adaptive approaches. Colonisation of the Australian landscape, which began in earnest with the establishment of the

British colony of New South Wales in 1788, provides an interesting example of how these Western visions inform narratives about, and therefore adaptions to, wildfire.

2. The Australian landscape: a more-than-human contact zone

When Donna Haraway wrote of contact zones in her book *When Species Meet* (2008), she used the concept to examine how separate species or systems, when 'forcibly brought together in relations of serious inequality' (Haraway and Reti 2007 p.33), can change and innovate through their encounters.

> *Contact zones are where the action is, and current interactions change interactions to follow. Probabilities alter, topologies morph, development is canalised by the fruit of reciprocal induction. Contact zones change the subject – all subjects – in surprising ways (Haraway 2008 p.219).*

Over a period of at least 60,000 years, as people have encountered and learnt about the effects of fire on the Australian continent, they have adapted their relationships with landscapes and fire to meet their needs. Adaptation through the encounters with wildfires – or 'bushfires' as the colonists began calling them – since colonisation has proved uncomfortable and difficult. In contemporary Australia, large populations of people are migrating into bushfire-prone semi-rural and peri-urban areas. Encounters with bushfires are inevitable, and problematic areas have been identified as: not people not 'properly' perceiving the risk that bushfire poses for them (e.g. Eriksen and Prior 2011); people not understanding the need to balance ecological fire with fire risk (e.g. Moskwa et al. 2018); and how negative public perception of prescribed fire puts a stop to prescribed ecological and hazard reduction burning (e.g. Morgan et al. 2020; Pyne 2020).

However, people's individual and collective innovation in fire management has been both aided and constrained by human perceptions, beliefs and values – visions – about their own role within their environment (Ruane 2018). These visions are in turn supported by specific narratives. Narratives are the stories told about humans, creating themes that inform ways of thinking, and therefore policies and actions (Moskwa et al. 2018). Examining and understanding narratives about how people position themselves and others in relation to complex environmental issues complements the modelled 'hard' sciences in developing policies for adaptative approaches regarding the landscape and fire (Bardsley, Wiseman, and Hugo 2016).

Examining these differing visions and narratives helps understand the range of fire management adaptions that have emerged from the human lived experiences of being a part of the contact zone of bushfire-prone landscapes. This in turn may help continue adaptive practices so that people can learn to thrice with fire – rather than simply letting human relationships with fire degenerate into border wars.

3. Envisioning human relationships to the landscape and fire

Several authors have identified a common pattern in how humans relate to the landscape in Australia. These range from an integral, symbiotic Aboriginal vision that was dominant for all but the last 240 years, to exploitative colonial and national development visions, and to more recent sustainable management and ecological visions (i.e. Heathcote 1972; Fien 1988; Ruane 2018). A useful categorisation is provided by geographer R.L. Heathcote (1972). He identifies six ways – visions – in how people perceived their relationships with the Australian landscape. Five of these are Western visions that dominated post-1770 – scientific, romantic, colonial, national, and ecological. He also discusses a sixth vision – Aboriginal, although not with the detail he gives the other visions.

Heathcote presented these visions as roughly sequential, and as arising from different 'eras' of thinking. However, these six visions overlap and aspects of all may be seen as present in the visions of Australians today. Heathcote's categorisations are very anthropocentric, viewing 'the environment' as being without agency and only having value if it is in economic terms for humans. Despite this, his categories offer a valuable way of examining complex more-than-human relationships in a non-binary way – and how they all both inform and contradict one another.

Table 1- Six visions of the Australian landscape that inform current fire narratives and adaptions. Adapted from Heathcote (1972).

Vision	Description
Colonial (dominant)	Survival and domination of the Australian landscape and Aboriginal peoples. Extraction of resources, transformation into a European space
Aboriginal	Cultural and spiritual connection to Country
Scientific	A curiosity about the Australian landscape (including its climate) and its uniqueness. A desire to categorise and therefore to perhaps understand it.
Romantic	Delight in the landscape as an 'untouched' wilderness. A sympathetic view of Aboriginal peoples.
National	Australian identity tied to the bush landscape, and to the hard-working people making a living in rural areas (successfully transforming the landscape with introduced flora and fauna)
Ecological	Concern about the impact that humans are having on the landscape. That European 'improvements'/adaptations have impoverished landscape conditions and facilitated extinctions.

This review of fire adaptive approaches for more-than-human communities contrasts these six visions. It identifies narratives that accompany each of these visions, as well as the fire-adaptive approaches that have arisen in Australia due to them.

3.1. Colonial (dominant) vision: narratives and adaptive approaches

Encounters with bushfires, especially the uncontrollable megafires that started to be experienced by colonists from the 1850s onwards (Morgan et al. 2020), shook perceptions of (white) human dominance, and enforced beliefs that the Australian environment posed a direct threat to European habitation (Collins 2006). The increasing frequency and intensity of megafires within Australia and globally (Morgan et al. 2020) continues to do so. As a result, 'we fear and suppress all of our unplanned fire' (Leonard 2017 p.1). This colonial adaptative approach is deeply entrenched in Australian language, legal system, government policies and practices, and built environment (Howitt 2014).

In Australia, narratives surrounding this colonial vision also take on moral undertones of blame and responsibility. Whittaker and Mercer (2004) point out that the 'aftermath of all major bushfire events in Australia invariably has been the apportioning of blame' (Whittaker and Mercer 2004, p. 263). Australian policy states that managing fire risk and fires as a 'shared responsibility' across governments, organisations and individuals. There is a strong legal framework around who, and under what conditions, can light fires (McLennan and Eburn 2015). Arsonists, people who deliberately light destructive fires, are particularly vilified (Hooper 2018).

Adaptive use of fire is limited to 'hazard reduction' burns that reduce the risk of fire damaging people and built infrastructure (Neale et al. 2019). 'Responsible' human adaptative actions informed by this colonial vision are those that mitigate fire risk (Bosomworth 2018), or plan how to survive a bushfire when it occurs (i.e. NSW Government 2020).

3.2. Aboriginal visions: narratives and adaptive approaches

Australia is one of many countries where colonisation has substantially displaced Indigenous peoples, as well as their fire and land management knowledge and practices (Bowman et al. 2011, Roos et al. 2016). For thousands of years, fire across the Australian continent has been used as a land and animal management tool (Neale et al. 2019, Gammage 2008). This knowledge has often been positioned by white researchers as historical (Eriksen and Hankins 2015), but there is growing contemporary use of Aboriginal fire knowledges – especially in northern Australia – as practice to promote the health and well-being of landscapes and human communities (Neale et al. 2019, McKemey et al. 2020, Russell-Smith et al. 2009). Indigenous writers such as Steffenson (2020) argue that putting cultural fire knowledges into practice on Country are integral to achieving social justice for marginalized peoples who have been enduring colonial rule.

3.3. Scientific vision: narratives and adaptive approaches

A scientific vision was behind the European exploration and colonisation of the Australian continent. The uniqueness of its flora, fauna and Aboriginal peoples were particularly valued, and science attempted to collect, categorise and therefore understand the landscape.

Narratives around fire in this vision are around experts gaining and applying their knowledge. Adaptation tends to be limited to fire management, rather than to local communities (Ruane 2019).

Adaptation is scientific approaches to use of fire – developed firstly through government-controlled forestry research (Pyne 2020). This has contributed enormously to knowledge about fire behaviour, which in turn has improved public safety through changes to building codes, fire danger indexes that create public warnings combining weather, soil and vegetation dryness data .

3.4. Romantic vision: narratives and adaptive approaches

A romantic vision is defined as people living in harmony with nature, and in harmony with diversity including with Aboriginal peoples. It can be linked to the 'co-existing with fire' narrative, which sees humans as a part of nature, and seeks to find a balance between fire and humans as parts of a social-ecological system (Bosomworth 2015).

One key adaptation as a result of this vision is seen in the National Parks in Australia, which are wilderness spaces, where people can only visit for approved recreation purposes. This approach has changed the landscape immeasurably since the 1770s and may have increased probability of fire in some areas. Whittaker and Mercer (2004) identified a 'wise use' narrative being used by timber, farming and mining industries after bushfires in 2003 bushfires to overstate fire risks of parks, and to demand the 'unlocking' of national parks.

3.5. National vision: narratives and adaptive approaches

National vision is defined as a celebration of the transformed bush, where European colonists could live a hard-working life free of the city and the industrial age/conditions. This vision underpins the Australian national identity - 'the bush became the synonym for Australia from the 1880s onwards' (Heathcote 1972, p.93). Its use supports colonial vision of the landscape and fire-suppression.

In national vision narratives, fighting bushfires (as well as the rest of the hostile Australian landscape) is the work of heroes, who work together showing egalitarian 'mateship' (Moore 2015). Arguably this narrative has also come to inform current Australian discourse around how communities do/should 'come together' in times of need, backed up by research into social capital (e.g. Aldrich 2012).

It is also perhaps this national vision which has underpinned recent shifts of populations from cities into bushfire-prone peri-urban and semi-rural landscapes (Eriksen and Prior 2011). In turn, this has meant that the dominant fire emphasis in Australia has to be community safety (Pyne 2020).

3.6. Ecological vision: narratives and adaptive approaches

Heathcote (1972) argues that the ecological vision of the Australian landscape arose from concerns that European 'improvements' to the landscape have actually made the landscape itself vulnerable. Western adaptations have not only limited farming successes, but also facilitated extinctions of native flora and fauna.

Ecological knowledge regarding optimal fire regimes for differing Australian ecologies has been growing (Bradstock 2010), and the narratives around this vision are that fire is natural and inevitable (Whittaker and Mercer 2004). At the same time, there is growing awareness that anthropogenic activities have impacted the Earth's climate, which is impacting the landscape – creating the conditions for more frequent and intense bushfires, as well as for more storms and floods (CSIRO and Bureau of Meteorology 2018).

Adaptation within this vision is about using prescribed fire to promote biodiversity. Some Australian researchers such as Leonard (2017) have suggested use of ecological fire could be 'democratised' out to people living in fire-prone landscapes. It is generally unclear how widespread this practice could be, given the level of bureaucracy that needs to be negotiated to light ecological fires legally.

4. Conclusion

Examining the relationships that Australian people have with their more-than-human communities through the categories of Heathcote's landscape visions exposes a range of narratives about fire. Each of these inform the adaptative approaches that have occurred as human and more-than-human actors/agents encounter one another – with obvious discomfort – in these contact zones.

Howitt (2014) argues that adaptation is not value-neutral, and successful adaptation requires trade-offs across levels of society, scales of landscapes and of time. Looking across these six human visions of the Australian landscape, it is not hard to see why. Which more-than-human actors/agents are the most vulnerable in encounters with which others in their community contact zones? Humans and their built environment encountering wildfire? The entire landscape itself encountering human activities? Marginalised Aboriginal peoples denied access to Country and fire? Ecologies that are no longer being burnt, or are being burnt too much? In the bushfire-prone contact zones, to borrow the words of researcher John Handmer, 'we are all vulnerable' (2003 p.55). The challenge is to identify and enact adaptive approaches to fire that reduce vulnerabilities for many actors/agents, rather than for only a few. Perhaps it is time to re-evaluate human relationships with the landscape and adjust our dominant colonial vision of domination. Perhaps then humans, and the landscapes they live in, can really thrive with fire.

5. Bibliography

Aldrich, D. P. (2012), Building Resilience : Social Capital in Post-Disaster Recovery, Chicago, UNITED STATES: University of Chicago Press.

Bardsley, D. K., Wiseman, N. D., and Hugo, G. J. (2016), "Generating narratives on future risk to inform regional climate change adaptation planning," in Climate Adaptation Governance: Theory, Concepts and Praxis in Cities and Regions, ed. J. Knieling, Chichester: Wiley-Blackwell, pp. 89-111.

Bowman, D. M. J. S., Balch, J., Artaxo, P., Bond, W. J., Cochrane, M. A., D'Antonio, C. M., DeFries, R., Johnston, F. H., Keeley, J. E., Krawchuk, M. A., Kull, C. A., Mack, M., Moritz, M. A., Pyne, S., Roos, C. I., Scott, A. C., Sodhi, N. S., and Swetnam, T. W. (2011), "The human dimension of fire regimes on Earth," Journal of Biogeography, 38 (12), 2223-2236. DOI: 10.1111/j.1365-2699.2011.02595.x.

Collins, P. (2006), Burn: The Epic Story of Bushfire in Australia Allen & Unwin.

CSIRO, and BureauofMeteorology. 2018. State of the Climate 2018. edited by CSIRO and B. o. Meteorology: Australian Government.

Eriksen, C., and Prior, T. (2011), "The art of learning: wildfire, amenity migration and local environmental knowledge," International Journal of Wildland Fire, 20 (4), 612-624.

Fien, J. (1988), "The Australian Environment: Visions, Imperatives and Classroom Realities," Geographical Education, 5 (4), 20-27.

Gammage, B. (2011), The biggest estate on earth: how Aborigines made Australia: Allen & Unwin Sydney.

Griffiths, T. (2001), Forests of Ash: An environmental history: Cambridge University Press.

Handmer, J. (2003), "We are all vulnerable," The Australian Journal of Emergency Management, 18 (3), 55-60.

Haraway, D., and Reti, I. 2007. Edges and Ecotones: Donna Haraway's Worlds at UCSC. eScholarship.

Haraway, D. J. (2008), When Species Meet, Minneapolis: University of Minnesota Press.

Heathcote, R. L. (1972), "The visions of Australia," in Australia as a Human Setting: Approaches to the Designed Environment, ed. A. Rapoport, Sydney: Angus & Robertson.

Hooper, C. (2018), The arsonist: a mind on fire, Australia: Penguin Random House Australia.

Moore, G. (2015), "Home Was Where the Hearth Is: Fire, Destruction, and Displacement in Nineteenth-Century Settler Narratives," Antipodes, 29 (1), 29-42.

Morgan, G. W., Tolhurst, K. G., Poynter, M. W., Cooper, N., McGuffog, T., Ryan, R., Wouters, M. A., Stephens, N., Black, P., Sheehan, D., Leeson, P., Whight, S., and Davey, S. M. (2020), "Prescribed burning in south-eastern Australia: history and future directions," Australian Forestry, 83 (1), 4-28. DOI: 10.1080/00049158.2020.1739883.

Moskwa, E., Bardsley, D. K., Robinson, G. M., and Weber, D. (2018), "Generating narratives on bushfire risk and biodiversity values to inform environmental policy," Environmental Science & Policy, 89, 30-40. DOI: https://doi.org/10.1016/j.envsci.2018.07.001.

Pyne, S. (2020), The Still-Burning Bush : Updated Edition, Brunswick, Victoria, AUSTRALIA: Scribe Publications.

Pyne, S. J. (2016), "Fire in the mind: changing understandings of fire in Western civilization," Philosophical Transactions of the Royal Society B: Biological Sciences, 371 (1696), 20150166. DOI: 10.1098/rstb.2015.0166.

Rolls, E. (1981), A Million Wild Acres: 200 years of man and an Australian forest, Melbourne: Nelson.

Roos, C. I., Scott, A. C., Belcher, C. M., Chaloner, W. G., Aylen, J., Bird, R. B., Coughlan, M. R., Johnson, B. R., Johnston, F. H., McMorrow, J., Steelman, T., and null, n. (2016), "Living on a flammable planet: interdisciplinary, cross-scalar and varied cultural lessons, prospects and challenges," Philosophical Transactions of the Royal Society B: Biological Sciences, 371 (1696), 20150469. DOI: 10.1098/rstb.2015.0469.

Ruane, S. (2018), "Using a worldview lens to examine complex policy issues: a historical review of bushfire management in the South West of Australia," Local Environment, 23 (8), 777-795. DOI: 10.1080/13549839.2018.1467390.

--- (2019), "Applying the principles of adaptive governance to bushfire management: a case study from the South West of Australia," Journal of environmental planning and management, 63 (7), 1-26. DOI: 10.1080/09640568.2019.1648243.

Steffensen, V. (2020), Fire Country: How Indigenous Fire Management Could Help Save Australia: Hardie Grant Publishing.

Tedim, F., McCaffrey, S., Leone, V., Delogu, G. M., Castelnou, M., McGee, T. K., and Aranha, J. (2020), "What can we do differently about the extreme wildfire problem: An overview," in Extreme Wildfire Events and Disasters: Root Causes and New Management Strategies, eds. F. Tedim, V. Leone and T. K. McGee: Elsevier.

Whittaker, J., and Mercer, D. (2004), "The Victorian Bushfires of 2002–03 and the Politics of Blame: a Discourse Analysis," Australian Geographer, 35 (3), 259-287. DOI: 10.1080/0004918042000311313.

Manipulating fire regimes in sensitive ecosystems to adapt to climate change

Adam Leavesley*[1]; Marta Yebra[2,3]; Petter Nyman[4]; Tony Scherl[1]

[1]ACT Parks and Conservation Service. Canberra, ACT, Australia, {adam.leavesley, tony.scherl}@act.gov.au
[2] Fenner School of Environment and Society, Australian National University, Acton, ACT, Australia, {marta.yebra@anu.edu.au}
[3] School of Engineering, Australian National University, Acton, ACT, Australia
[4] Alluvium Consulting, Melbourne, VIC, Australia, {petter.nyman@alluvium.com.au}

**Corresponding author*

Keywords

Climate adaptation, fire regime, prescribed burning, flammability, fuel moisture content

Abstract

Fire regimes in Australian temperate forests have changed with the area burnt by bushfires having increased due to changing climate extremes every decade for the past 40 years. The Australian Capital Territory (ACT) has been heavily impacted with year-since-last-fire in forests being the shortest of all Australian jurisdictions due to large, intense bushfires during the droughts of 2003 and 2020.

The forested landscapes of the ACT are predominantly mountainous and scattered throughout are species and communities which are likely to be disadvantaged by an increase in the frequency of high intensity fire. Examples include alpine bogs, Alpine Ash (*Eucalyptus delegatensis*) and Mountain Plum Pine (*Podocarpus laurencei*). Many of these systems were severely burnt in 2003 and 2020.

Protection of these species and communities from bushfires is a high priority for conservation, but suppression operations are difficult due to inaccessibility and the danger to firefighters. A potential solution is to use prescribed burning to manipulate fire regimes to reduce risk. In this paper, we describe an approach designed to reduce bushfire risk while optimising land management workloads and total area burnt.

The approach has two key components: 1) development of a method for managing landscape bushfire risk in time; and 2) utilisation of landscape flammability mapping to design burn infrastructure to meet ecological objectives.

Bushfire risk planning is focused on space, but risk also changes in time with the effects of drought on fuel moisture accumulating and drying over multiple years. This time-scale offers an opportunity to intervene to reduce bushfire risk in fire sensitive ecosystems and influence fire regimes in favour of those ecosystems using prescribed burning. To do this, bushfire planners need to identify ecosystems at risk and develop burns which are to be implemented contingent on agreed climatic triggers.

Landscape flammability in mountainous landscapes in southeastern Australia during the autumn prescribed burning season is driven by solar radiation with north faces being drier and much more likely to burn than south faces. This imposes a critical constraint on prescribed burn planning. We conducted an assessment of the feasibility of designing burns to protect alpine bogs, Mountain Plum Pine and Alpine Ash. There appears to be some potential for reducing fuels around alpine bogs and good potential for emhancing protection of Mountain Plum Pine. On the other hand Alpine Ash stands largely occur on southern slopes and do not appear to be easily amenable to fire regime manipulation.

1. Changed Forest Fire Regimes

Fire regimes in Australian temperate forests have changed with the area burnt by bushfires having increased due to changing climate extremes every decade for the past 40 years (Canadell et al. 2021). The Australian Capital Territory (ACT) has been heavily impacted with year-since-last-fire in forests being the shortest of all Australian jurisdictions due to large, intense bushfires during the droughts of 2003 and 2020.

The forested landscapes of the ACT are predominantly mountainous and scattered throughout are species and communities which are likely to be disadvantaged by an increase in the frequency of high intensity fires

(Hawkins et al. 2021). Examples include alpine bogs, Alpine Ash (*Eucalyptus delegatensis*) and Mountain Plum Pine (*Podocarpus laurencei*). Alpine bogs are a product of the anaerobic decomposition of vegetation due to saturation in water. Fire is a fundamentally rare event and the ecological impacts of fires on bogs are overwhelmingly negative (DEWHA, 2009). Alpine Ash is a serotinuous species which is killed by high intensity fires and takes >10 years to mature (Doherty et al. 2017). High intensity fires at a frequency of <10 years present a threat to Alpine Ash populations which may be unable to produce seed. Mountain Plum Pine is a slow growing Gondwanan relic which occurs in high rocky mountain tops and is killed by fire of moderate intensity and greater (Tolsma et al. 2004). Discontinuous fuels on rocky mountain tops provide some protection from fire for this species but high intensity bushfires cause mortality (Figure 1). All of these systems were severely burnt in 2003 and 2020.

2. Limitations of Fire Suppression Operations

Protection of these species and communities from bushfires is a high priority for conservation (Hawkins et al. 2021), but suppression operations are difficult due to inaccessibility and the danger to firefighters. Even if suppression operations are technically feasible, for example by deploying helicopter-borne Remote Area Fire Teams (Cooper, 2020) resources must be prioritised to protection of human life and property. During the large fire events which are of most concern for conservation management, conservation-focussed suppression will almost certainly be restricted to small areas of the highest priority.

3. Prescribed Burning in the Australian Capital Territory

The ACT Parks and Conservation Service conducts a prescribed burning program which is evaluated annually using Normalised Burn Ratio (Leavesley et al. 2021). Analysis of the interaction between the Orroral fire in the ACT in 2020 found that burns which were <2 years old halted the spread of the bushfire, reducing its final extent. In addition, a burn which was four years old significantly reduced the severity of the bushfire. Burns which were seven years old were discernible in the landscape but appeared to have a limited effect on bushfire behaviour. The study concluded that the interaction between the burning program and the Orroral fire was positive for conservation and catchment values.

4. Concerns about Prescribed Burning

A criticism of prescribed burning is that in many ecosystems the leverage is low (Price et al. 2015). The leverage number represents the likelihood that a prescribed burn will intersect with a bushfire before fuel accumulates to the point that fire behaviour is affected. For example, in southern Australian forests, the leverage has been calculated to be 0.33 which means that to reduce the annual average area burnt in bushfires from 5 percent to 2.5 percent requires the annual area of prescribed burning to be 7 percent – an overall increase in total area burnt.

But this generalised analysis does not take into account conservation land management objectives or fire response traits of focal species. Species which are tolerant of low or moderate intensity fire but sensitive to high intensity fire can be advantaged by high frequency application of low intensity prescribed burning and this is well documented in ecosystems such as the northern Australian savannahs (Evans and Russell-Smith, 2020).

Similarly, where a species or ecosystem is identified to have exceptional conservation value, managers may make a judgement that a trade-off which advantages a high value ecosystem or species is justified, despite disadvantaging other effected species. To our knowledge, such trade-offs are relatively rare in southern Australian forests where the conservation policy focus is on ensuring that prescribed burning is applied at intervals determined to be consistent with the fire response traits of all of the species in a particular ecosystem or known to be present in a burn block. We suggest, that in the face of changed fire regimes, a greater focus on conservation priorities and a renewed consideration of trade-offs is warranted.

5. How can we adapt?

High-frequency, broad-scale application of low intensity prescribed burning to southern Australian forests is likely to change ecosystems and is difficult and costly to achieve. Can we be more judicious in the use of fire but still reduce the risk to high value species and communities? We think this could be achieved by prescribing burns at times when landscape bushfire risk is elevated and in places most likely to manipulate the conservation outcome positively, should a bushfire subsequently occur.

Our approach has two key components: 1) development of a method for managing landscape bushfire risk in time; and 2) utilisation of landscape flammability mapping to design a burn program to meet ecological objectives.

6. Managing bushfire risk in time

Best practice landscape bushfire risk planning is usually focused on space (eg Gazzard et al. 2020; Penman et al. 2020), but risk also changes in time with the effects of drought on fuel moisture accumulating and drying over multiple years (Nolan et al. 2016). This time-scale offers an opportunity to intervene to reduce bushfire risk to high value conservation assets by conducting burns aimed at manipulating fire regimes in the prescribed burning season, between summer fire seasons, at times when landscape dryness is elevated and the likelihood of large, intense landscape-scale bushfires is consequently also elevated. If applied successfully, the approach would increase the leverage of a burning program because the likelihood of intersection between burns and bushfires is greater. It is worth noting, that operational experience suggests that the risk of prescribed burn escape in the burning season, is not significantly affected by elevated landscape dryness during the burning season.

To be effective in southeastern Australia the approach requires a sound understanding of landscape fuel moisture dynamics and a robust predictive capability for landscape dryness in the coming fire season which exceeds present capability (Vinodkumar *et al*. 2021). The triggering metric would be needed in advance of the peak burning season in March and April, at least seven months before the usual commencement of the fire season on 1 November.

The next stage of the work would be to test some candidate prescriptions in a fire regime simulation. The main aim of the work would be to define a set of parameters which were effective and operationally achievable. If an effective prescription was identified, the results of the simulation would be critical in developing options for stakeholder consideration and ultimately for obtaining a social licence to implement the work.

7. Working with flammability gradients

A critical constraint on the autumn prescribed burning program in southeastern Australian mountain forests is the pattern of landscape flammability (Nyman et al. 2018). In autumn, the landscape transitions from mostly dry enough to burn, to mostly too wet (Nyman 2019). Flammability is driven by solar radiation and during the transition, the north faces are drier and much more likely to burn than south faces.

Prescribed burn planning for high value conservation assets must work within the landscape flammability constraints. Direct manipulation of fire regimes can only occur in the flammable parts of the landscape. Where Alpine Ash stands occurred on northern slopes, fuel could be reduced by low intensity prescribed burning to reduce the risk posed by high intensity bushfire the following summer. Similarly, prescribed burning could be deployed to enhance the topographic protection that Mountain Plum Pine derives from its rocky mountaintop habitat by removing connecting fuels. Alpine bogs present a greater challenge because they cannot be directly fuel-reduced. Nonetheless it may be possible to identify landscapes in which adjacent systems are flammable and which can be burnt to create a protection zone.

Our analyses show that burning to create a protection zone surrounding and directly adjacent the largest alpine bog in the ACT, Ginini Wetland, is not appear likely to be possible due to the large extent of non-flammable terrain adjacent, however an extended area encompassing other ecosystems, might be possible (Figure 2). The second largest alpine bog, Snowy Flat appears to be better situated for creation of a protection zone which is

directly adjacent (Figure 3). Mountain Plum Pine habitat on mountain tops appears to be generally amenable (Figure 4) with an important caveat that operational experience at that altitude is limited. Alpine Ash stands are almost exclusively located on southern slopes and cannot be burnt under prescribed burning conditions (Figure 5). Further thought and planning would be required to manipulate the fire regimes of that community.

8. References

Canadell, JG, Meyer CP, Cook GD, Dowdy A, Briggs PR, Knauer J, Pepler A, Haverd V (2021) Multi-decadal increase of forest burned area in Australia is linked to climate change. *Nat Communications* 12, 6921.

Cooper N (2020) Expert Opinion, In 'Prescribed Burning in Australasia: The Science, Practice and Politics of Burning the Bush'. (Eds A Leavesley, M Wouters, R Thornton R.) pp. 218-223 (AFAC: Melbourne)

DEWHA (2009) Alpine Sphagnum Bogs and Associated Fens: A nationally threatened ecological community. Environment Protection and Biodiversity Conservation Act 1999 Policy Statement 3.16 (Canberra, ACT)

Doherty MD, Gill AM, Cary GJ, Austin M (2017) Seed viability of early maturing alpine ash (*Eucalyptus delegatensis* subsp. *delegatensis*) in the Australian Alps, south-eastern Australia, and its implications for management under changing fire regimes, *Australian Journal of Botany* 65, 517-523.

Evans J, Russell-Smith J (2020) Delivering effective savanna fire management for defined biodiversity conservation outcomes: an Arnhem Land case study, *International Journal of Wildland Fire* 29, 386-400.

Gazzard T, Walshe T, Galvin P, Salkin O, Baker M, Cross B, Ashton P (2020) What is the 'appropriate' fuel management regime for the Otway Ranges. Victoria, Australia? Developing a long term fuel management strategy using structured decision-making framework. *International Journal of Wildland Fire* 29, 354-370.

Hawkins B, Seddon J, Courtney Jones S (2021) Recovery of fire sensitive communities in Namadgi National Park and Tidbinbilla Nature Reserve from the Orroral 2020 bushfire. Conservation Research, ACT Environment, Planning and Sustainable Development Directorate (Canberra, ACT)

Leavesley A, Yebra M, Cooper N, Levine B, Dunne B (2021) Prescribed burning reduced the extent and severity of the Orroral fire in the Australian Capital Territory, January-February 2020. Proceedings of the AFAC Conference, Sydney, 5-7 October.

Nolan RH, de Dios VR, Boer MM, Caccamo G, Goulden ML, Bradstock RA (2016) Predicting dead fine fuel moisture at regional scales using vapour pressure deficit from MODIS and gridded weather data, *Remote Sensing of Environment* 174, 100-108.

Nyman P, Baillie C, Duff T, Sheridan G (2018) Eco-hydrological controls on microclimate and surface fuel evaporation in complex terrain. *Agricultural and Forest Meteorology* 252, 49-61.

Nyman P (2019) Sub-canopy microclimate model for fuel moisture mapping in ACT – data inputs, methods and description of model outputs. Report by Alluvium Consulting to the ACT Government (Melbourne, VIC)

Penman TD, Clarke H, Cirulis B, Boer MM, Price OF, Bradstock RA (2020). Cost-effective prescribed burning solutions vary between landscapes in eastern Australia. *Frontiers in Forests and Global Change* 3, 1-16.

Price OF, Pausas JG, Govender N, Flannigan M, Fernandes PM, Brooks ML & Bird, RB (2015). Global patterns in fire leverage: the response of annual area burnt to previous fire. *International Journal of Wildland Fire* 24, 297-306.

Price OF (2013) Reducing bushfire risk: don't forget the science, *The Conversation*, https://theconversation.com/reducing-bushfire-risk-dont-forget-the-science-19065

Tolsma A, Coates F, Sutter G. (2004) Recovery of Mountain Plum-Pine Shrubland After Wildfire (Cobberas). Arthur Rylah Institute for Environmental Research Technical Series Report No. 153 (Melbourne: VIC)

Vinodkumar V, Dharssi I, Yebra M, Fox-Hughes P (2021) Continental-scale prediction of live fuel moisture content using soil moisture information. Agricultural and Forest Meteorology 301.

Figure 1- Two aerial views of the summit of Mt Murray (1845m) in Namadgi National Park, Australian Capital Territory: green points indicate Mountain Plum Pine records, blue indicates alpine bog and black/white indicates the ACT/NSW border. a) acquired in 2017; and b) acquired in 2020 following the Orroral fire.

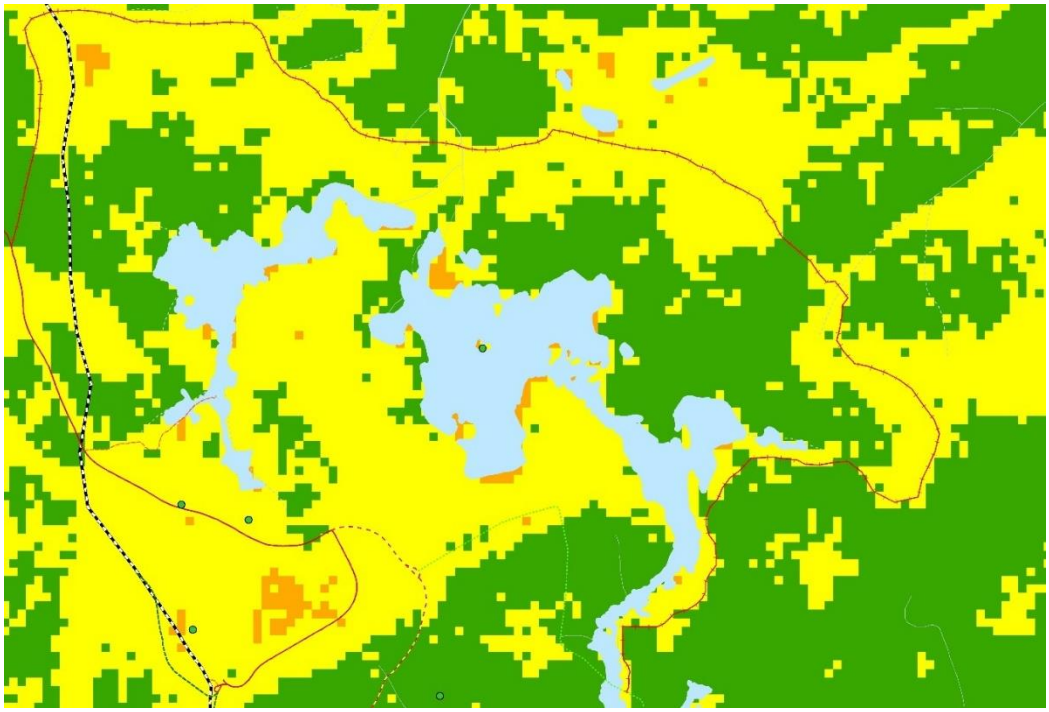

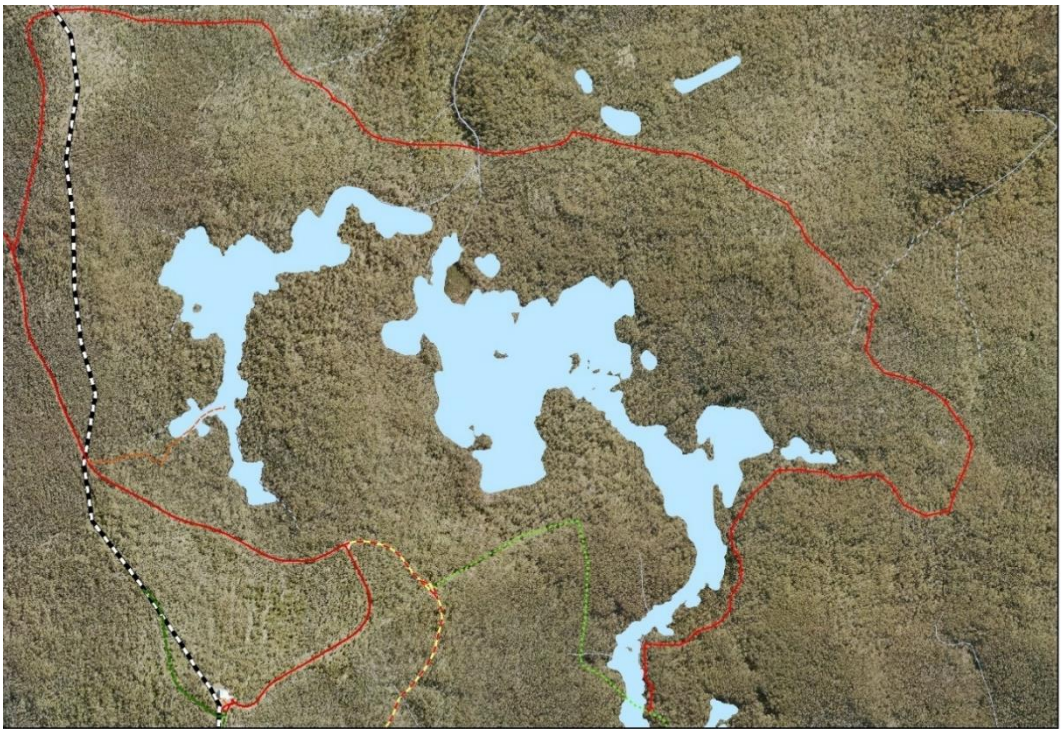

Figure 2- Ginini Wetland, the biggest alpine bog in Namadgi National Park, Australian Capital Territory. Ginini Wetland does not appear to be well situated for creation of a fuel reduced protection zone because a high proportion of the adjacent landscape is predicted to be non-flammable: Blue indicates alpine bog, black/white indicates the ACT/NSW border and other lines indicate roads and tracks required for containment. Top: Flammability mapping: yellow and orange indicates land which is flammable under prescribed burning conditions; green indicates land which is not flammable; and Bottom: aerial image acquired in 2017.

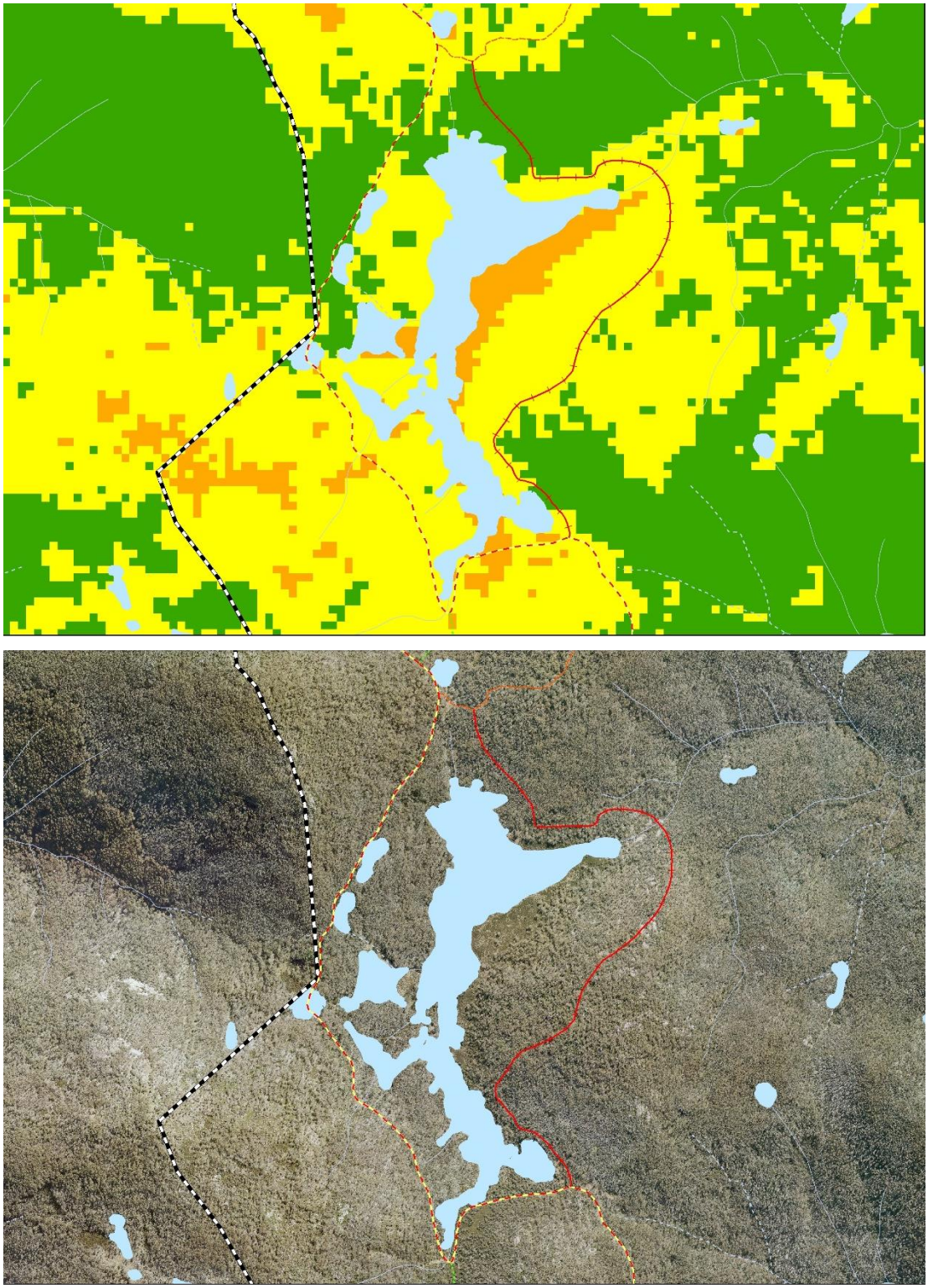

Figure 3- Snowy Flat, the second biggest alpine bog in Namadgi National Park, Australian Capital Territory. Snowy Flat appears well situated for creation of a fuel reduced protection zone because a high proportion of the boundary appears to be flammable under prescribed burning conditions. Blue indicates alpine bog, black/white indicates the ACT/NSW border and other lines indicate roads and tracks required for containment. Top: Flammability mapping: yellow and orange indicates land which is flammable under prescribed burning conditions; green indicates land which is not flammable; and Bottom: aerial image acquired in 2017.

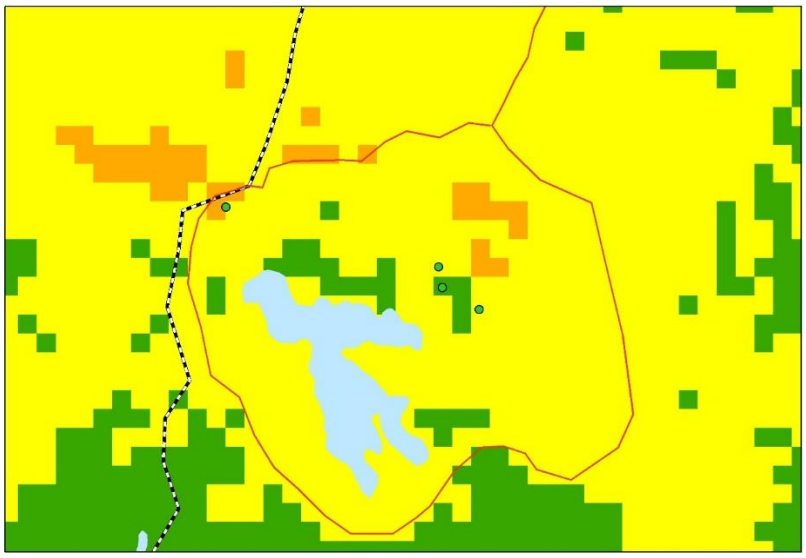

Figure 4- The summit of Mt Murray (1845m) in Namadgi National Park, Australian Capital Territory. The Mountain Plum Pine habitat appears to be flammable in the prescribed burning season which may support creation of a fuel-reduced protection zone for this species. Green points indicate Mountain Plum Pine records, yellow and orange indicates land which is flammable under prescribed burning conditions; green indicates land which is not flammable, blue indicates alpine bog, red line indicates proposed walking track for containment, and black/white indicates the ACT/NSW border.

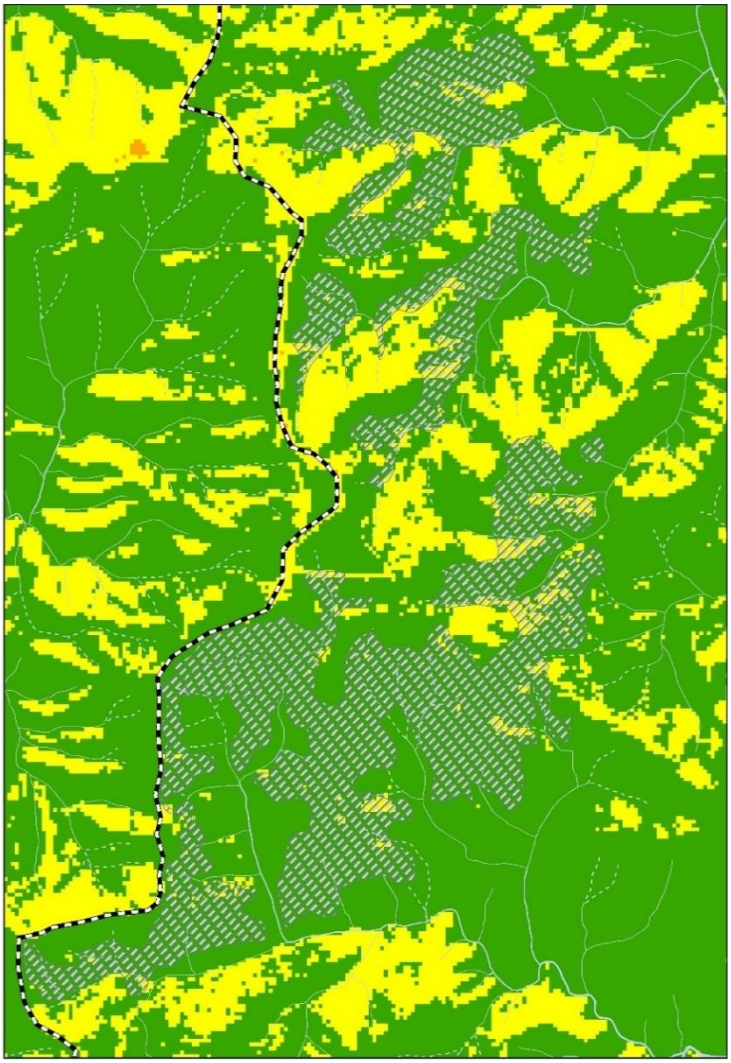

Figure 5- The distribution of Alpine Ash in Namadgi National Park in the Australian Capital Territory, overlayed on a flammability map. Most Alpine Ash occurs in locations which are not flammable in the prescribed burning season. Grey cross-hatching indicates Alpine Ash, yellow and orange indicates land which is flammable under prescribed burning conditions; green indicates land which is not flammable, black/white indicates the ACT/NSW border.

Modelling wildfire effects on the coevolution of soils and flammable temperate forests

Assaf Inbar[1]; Petter Nyman[1,2]; Patrick Lane[1]; Gary Sheridan[1]*

[1]School of Ecosystem and Forest Sciences, the University of Melbourne, Australia, {assaf.inbar, nymanp, patrickl, Sheridan}@unimelb.edu.au
[2]Alluvium Consulting

**Corresponding author*

Keywords

Soil erosion, coevolution, landscape evolution, feedbacks, critical zone

Abstract

Climate drives the coevolution of vegetation and the soil that supports it. Wildfire dramatically affects many key eco-hydro-geomorphic processes, but its potential role in coevolution of soil-forest systems has been largely overlooked. The steep landscapes of southeastern Australia provide an excellent natural laboratory to study the role of fire in the coevolution of soil and forests, as they are characterized by temperate forest types, fire frequencies, and soil depths that vary systematically with aridity. The aims of this study were (i) to test the hypothesis that in Southeastern Australia, fire-related processes are critical to explain the variations in coevolved soil-forest system states across an aridity gradient and (ii) to identify the key processes and feedbacks involved. To achieve these aims, we developed a numerical model that simulates the coevolution of soil-forest systems which employ eco-hydro-geomorphic processes that are typical of the flammable forests of southeastern Australia. A stepwise model evaluation, using measurements and published data, confirms the robustness of the model to simulate eco-hydro-geomorphic processes across the aridity gradient. Simulations that included fire replicated patterns of observed soil depth and forest cover across an aridity gradient, supporting our hypothesis. The contribution of fire to coevolution increased in magnitude with aridity, mainly due to the higher fire frequency and lower post-fire infiltration capacity, increasing the rates of fire-related surface runoff and erosion. Our results show that critical feedbacks between soil depth, vegetation, and fire frequency dictate the trajectory and pace of the coevolution of flammable temperate forests and soils.

1. Introduction

Interactions and feedbacks between soil and vegetation are key factors in controlling catchment ecohydrological behavior (Donohue et al., 2007, 2012; Trancoso et al., 2016; Zhang et al., 2004). Thus, understanding how soil-vegetation systems coevolve can help explain observed variations in catchment responses and enable better predictions of change in response to future climate scenarios (Troch et al., 2015). Coevolution in this context is defined as a climatically driven process in which interactions and feedbacks between vegetation and its supporting soil causes ongoing changes in their properties (Berry et al., 2005; Porder, 2014; Troch et al., 2015; van Breemen, 1993). Due to its interdisciplinarity, complexity, and nonlinearity and because it operates outside of our observational time scales, studying the coevolution of soil-vegetation systems requires models that couple ecological, hydrological, and geomorphological processes and their drivers under one numerical framework (Istanbulluoglu, 2016).

Fire affects both vegetation and soil and is therefore likely to play a role in their coevolution. Fire changes the hydrological properties of the system by removing the canopy cover and changing the properties of the soil surface (DeBano, 2000; Inbar et al., 2014; Shakesby & Doerr, 2006), often making it more conducive to surface runoff (Nyman et al., 2010; Shakesby & Doerr, 2006) and more erodible (Noske et al., 2016; Nyman et al., 2013). These combined transient effects often result in a temporary increase in soil erosion of different magnitudes (Lane et al., 2006; Moody & Martin, 2001; Nyman et al., 2011; Prosser & Williams, 1998). Fire had also been shown to cause transient changes in the water and energy balance by altering the amount of water that infiltrates, is intercepted, and is transpired by the local forested systems (e.g., Nolan et al., 2014).

The role of fire in coevolution had been mainly investigated through its geomorphic effect on landform change (Benda & Dunne, 1997; Gabet & Dunne, 2003; Istanbulluoglu et al., 2004; Istanbulluoglu & Bras, 2005; Orem & Pelletier, 2016; Roering & Gerber, 2005). Here we point to an important feedback that is indirectly related to the geomorphic effects of fire that might have been overlooked. Soil depth holds an important role in controlling vegetation water holding capacity at a point by setting an upper limit to the plant available water capacity (Hahm et al., 2019). This implies that fire-driven erosion processes could potentially push soil-vegetation systems toward an alternative coevolved state by affecting its soil depth, if high fire-frequency is sustained over long time scales. Accounting for the processes that affect fire frequency is therefore necessary to fully untangle the role of fire in the development of the critical zone and landscape evolution.

In the landscape evolution literature, fire is often regarded as a "disturbance" and is modeled stochastically (Gabet & Dunne, 2003; Istanbulluoglu et al., 2004; Istanbulluoglu & Bras, 2005). However, evidence shows that long-term fire frequency depends on processes that control the availability of burnable fuel (Pausas & Bradstock, 2007) and their moisture state (Pausas & Bradstock, 2007; Taufik et al., 2017), making it a dynamic process that is coupled to the ecohydrological state of soil-vegetation systems. This implies that fire is tightly coupled within coevolutionary feedbacks both as a forcing and as a response variable. The modelling of a fire regime that is coupled to the hydrological state of the modeled systems has been explored in some dynamics vegetation models (e.g., Prentice et al., 2011; Thonicke et al., 2010, 2001; Yue et al., 2014). These models, however, do not include the geomorphic effect of fire and its consequences on processes and feedbacks in the coevolution of soil-vegetation systems. The full range of mechanisms by which fire can drive landscape change and coevolution therefore remains unclear. To address this limitation, a model is required that couples fire to both ecohydrological and geomorphic processes and enables the complex coevolution of vegetation and soil to be more robustly investigated.

The central highlands in southeastern (SE) Australia provide an ideal natural laboratory to investigate the role of fire in coevolution of soil-vegetation systems for several reasons: (i) It is home to some of the most flammable forests on earth; (ii) a gradient in temperate climate had resulted in a range of forest types with different fire regime (Cheal, 2010); and (iii) the lack of active uplift (Czarnota et al., 2014; Wellman, 1987) and the lack of glaciation below 1,200melevation during late Pleistocene (Barrows et al., 2001) narrow down the drivers and possible geomorphic processes that might have affected coevolution in the area.

The aims of this study were to (i) test the hypothesis that fire-related processes are critical to explain the variations in coevolved soil-forest systems across an aridity gradient in SE Australia and (ii) to identify key processes and feedbacks involved the coevolution process. To achieve the aims, we developed a numerical model (COevOLution of FLAMmable Systems—CoolFlameS) that simulates the coevolution of soil-forest systems and is underpinned by equations that couple fundamental ecohydrological, vegetation dynamics, and geomorphological processes. CoolFlameS was formulated, parameterized, and calibrated to simulate systems that are typical to SE Australia. The model was evaluated by comparing model outputs of system properties and process rates against observations, measurements, and published data.

2. Method

In systems where nutrient availability is not limiting plant growth, vegetation carrying capacity is driven by the supply and demand for water and the ability of the critical zone to store it (Hahm et al., 2019). While water supply and demand are often affected by climate and topography (Nyman, Sherwin, et al., 2014; Rasmussen et al., 2015), the ability of a system to store water depends on soil properties, primarily depth, but also texture, porosity, and organic matter content (Clapp & Hornberger, 1978; Saxton & Rawls, 2006). CoolFlameS is therefore based on the conceptual model whereby the structure of soil-forest systems at any point in time and space is controlled by the legacy of climatically driven feedbacks between vegetation, fire, and the ability of the system to hold moisture, which is dictated by soil depth (Hahm et al., 2019). In the proposed model (Figure 1a), soil moisture plays a central role in coevolution by controlling evapotranspiration (ET) and primary productivity (Montaldo et al., 2005; Rodriguez- Iturbe, 2000) and by ecohydrological control on the flammability of the system (Krueger et al., 2016). Soil water holding capacity in the model is determined primarily by soil depth and, together with climate (i.e., aridity), limits ET and biomass accumulation (Klein et al., 2015; Milodowski et al., 2015). Fire removes vegetation and causes changes to soil hydraulic properties (Certini, 2005; DeBano, 2000), which temporarily increases erosion potential (Nyman et al., 2013; Wagenbrenner et al., 2010). By this

approach, changes in climate and fire frequency can alter the depth of the soil and its water and biomass holding capacity and thereby drive coevolution.

In order to investigate the role of fire in the coevolution of soil-vegetation systems, it is necessary to couple fire with ecological, ecohydrological, and geomorphic processes. One of CoolFlameS major novelty is that it bridges the gap between landscape evolution, land surface models, and flammability through coupling ecohydrology, vegetation dynamics, and moisture deficits with geomorphic processes that control soil depth. This feature is missing from existing models. For this purpose, we employ a combination of new and well-established generic equations that represent ecohydrological, geomorphological, and forest dynamics processes as defined in existing literature. Moreover, in order to represent SE Australian systems appropriately, CoolFlameS was developed from deep ecohydrological and geomorphic understanding stemming from decades of intensive research and model development. Due to the long time scale and multitude of disciplines and processes involved in the coevolution of soil-vegetation systems, simplicity was prioritized over complexity during model development. To overcome this potential shortcoming, model components (i.e., ecohydrology, geomorphology, and fire) were evaluated by comparing simulation results with measurements and published values.

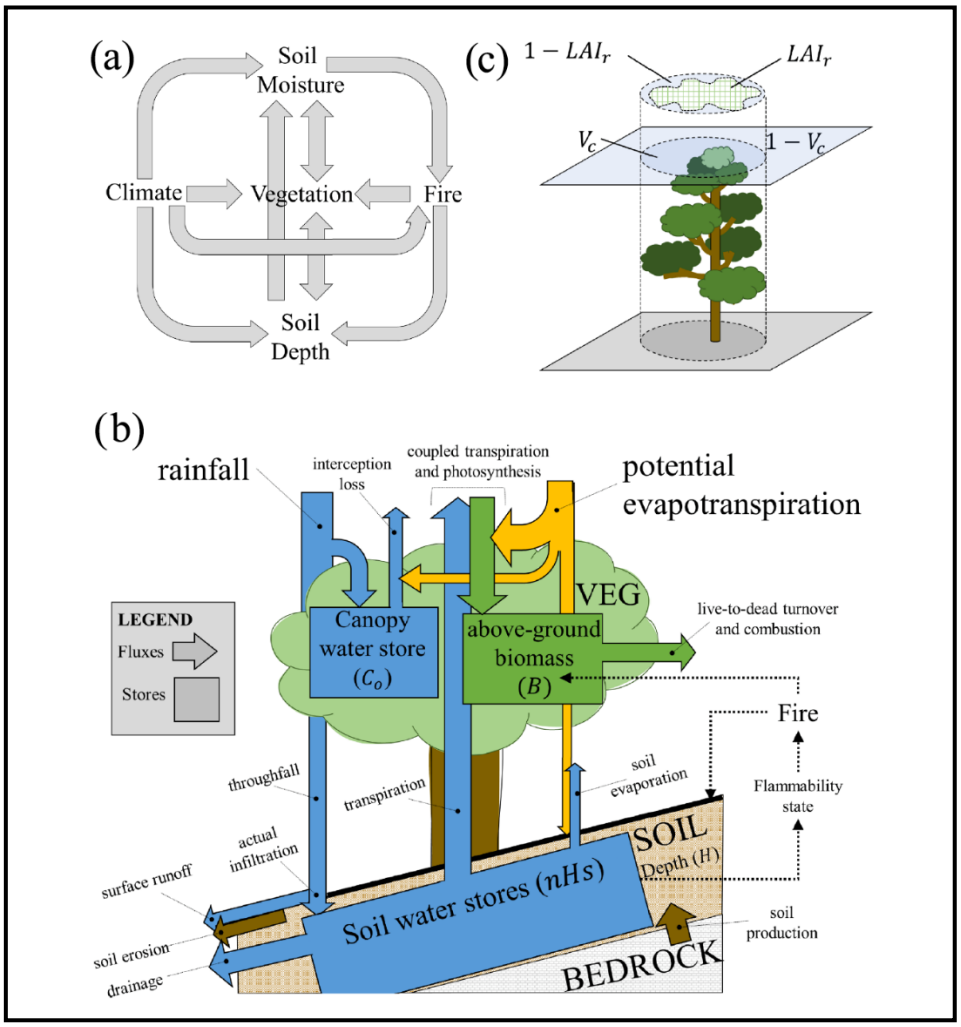

Figure 1-(a) A conceptual model that describes the coevolution of a coupled soil-vegetation system and (b) a schematic representation of what eco-hydrogeomorphic processes represented in CoolFlameS are, and the manner in which they are coupled. The dynamics of soil depth (H), soil moisture (nHs, where s is degree of saturation and n is porosity), and standing biomass (B) are expressed by a set of equations described in Inbar et al. (2020). Thick colored arrows represent fluxes of water (blue), energy (yellow), carbon (green), and minerals (brown). Thin dashed arrows point to the effects of soil moisture on fire and the effect of individual fire on forest cover and soil surface properties. An illustration of the spatial representation of the model system is presented in panel (c). The system surface area is divided horizontally into vegetated (Vc) and bare (1 − Vc) proportions. The vegetated area is further divided into covered (LAIr) and uncovered (1 − LAIr) proportions.

3. Results and Discussion

The performance of the model for the replicating observed patterns in soils, hydrology, fire and vegetation can be found in Inbar et al. (2020). A brief overview of the results and discussion is provided below.

3.1. Experiment 1—The Role of Fire in Coevolution (Evaluating the Hypothesis)

Our initial hypothesis that fire-related processes are critical to explain the variations in coevolved soil-forest system states across an aridity gradient is supported by the results (Figures 2a and 2b) showing that simulations with fire are more consistent with contemporary observation than simulations without fire. Model results show that the relative role of fire increases with aridity (Figures 2a and 2b). This can be explained by the more frequent fires and higher erosion rates as aridity increases. As aridity increases beyond the value of 1, so does the relative contribution of fluvial erosion rates, and this effect is further amplified by fire. The fact that the predicted projected canopy cover (Vc − ss) trends in a similar manner as soil depth (Hss) with respect to aridity can be explained by the change in biomass holding capacity of the soil, caused by the interaction between climate, fire, and the balance between soil production and erosion on soil depth (Hahm et al., 2019). The phenomenon that erosion controls vegetation patterns was observed by Milodowski et al. (2015) in the northern Californian Sierra Nevada, USA, where mean basin slope, a proxy of long term erosion rate, explained 32% of variance in above ground biomass, outweighing the effect of other factors, such as MAP, temperature, and lithology. The authors ascribed this effect to the reduction in water holding capacity due to the limitation dictated by thinner saprolite.

3.2. Experiment 2—The Role of Fire-Related Processes in Coevolution

Results indicates that among the three possible effects of fire that were explored, the role of post-fire reduction in Ic on Hss and Vc − ss was the largest (Figures 2c and 2d). Post-fire reduction in Ic can explain the increasing dominance of fluvial processes at aridity values >1, which result in shallower soils from simulations with fire beyond that point (Figures 2a and 2b). For aridity values <1, post-fire reduction in Ic is not sufficiently large to affect surface runoff. Consequently, on slopes supporting wet forest types, the relative role of diffusive processes is higher compared to that of fluvial processes. Post-fire erosion is often associated with loss of cover, increased hydrophobicity, and reduction in root cohesion (Istanbulluoglu & Bras, 2005). The latter process was not implemented explicitly in CoolFlameS but is implicit within the surface cohesiveness term. Our results indicate that long-term erosion is more sensitive to reduction in Ic (and consequential increase in surface runoff) than to the amount of sediment that is available to be transported after fire (−ΔCO; Figures 2e–2h). This can be explained by the interplay between the transport-limited nature of the non cohesive material and the time it is available for transport (Nyman et al., 2013).

The relative role of post-fire reduction in forest cover (−ΔLAI) was found to be lower than the two other processes examined (Figures 2). This result can be explained by the effect of the interaction between forest cover and infiltration capacity on fluvial erosion across the aridity gradient. At higher aridity values, background forest cover is always relatively low (Figure 2b), and the effect of the short-lived post-fire removal of vegetation cover on fluvial erosion is insignificant compared to the reduction in infiltration capacity during the same period. In wetter climates, vegetation density is higher and the effect of the temporary loss of cover on fluvial erosion rates can be significant. However, this effect is balanced by the high infiltration capacity, which keeps surface runoff rates low even after fire (Noske et al., 2016). These results indirectly suggest that the time to forest canopy recovery that explicitly depend on forest recovery trait has little impact on long-term coevolution of soil depth and vegetation in SE Australia.

In a study aggregating hundreds of post-fire infiltration and runoff measurements, Sheridan et al. (2015) found that post-fire runoff generation was highly correlated with aridity, such that more arid hillslopes, that often have younger and less developed soils, were associated with higher post-fire sediment yields. Our results indicate that the trend of Hss with aridity (Figure 2a) is determined mainly by the amount of surface runoff that is generated (which is controlled by the infiltration capacity) and how it affects post-fire fluvial erosion rates. Our model suggests that in a world without fire, the differences in soil depth and vegetation cover between dry and wet systems would have been significantly smaller to what is currently observed (Figures 2a and 2b). Other theoretical experiments had shown a significant increase in forest cover on the expense of grasslands in a world without fire (Bond et al., 2005). Our results highlight the possible role of fire-related changes in soil depth on global distribution of vegetation.

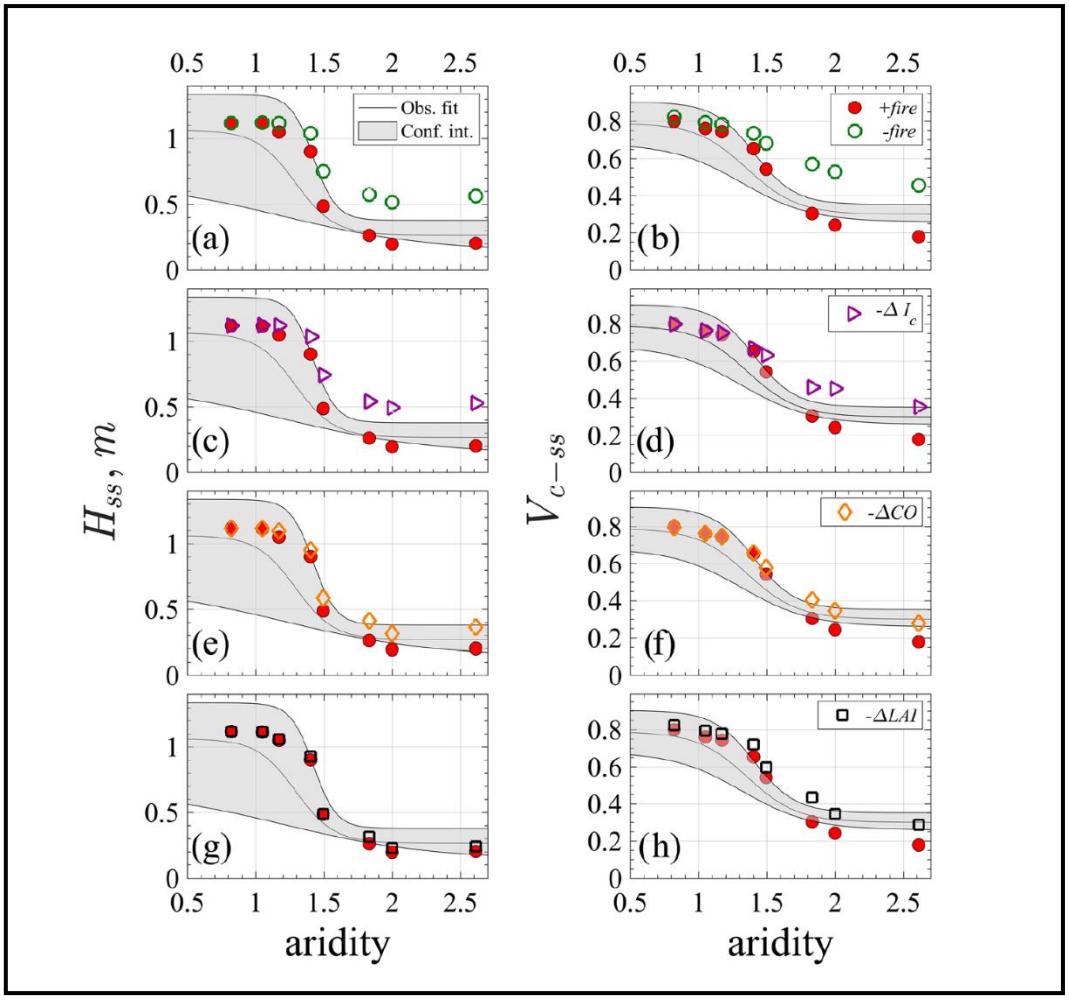

Figure 2-Modeled (Hss and Vc − ss) and observed soil depth and projected vegetation cover as a function of aridity for (a and b) simulations with (+fire) and without fire (−fire) and for simulations with fire but without post-fire changes in (c and d) infiltration capacity (−ΔIc); (e and f) soil cohesiveness (−ΔCO); and (g and h) canopy cover (−ΔLAI). The figure presents results for Experiments 1 (a and b) and 2 (c–h). Hss and Vc − ss values are plotted over functions and 95% confidence interval (gray area) fitted to soil depth measurements (Inbar et al., 2018) and remotely sensed vegetation cover using annual LANDSAT values (Tern AusCover, 2017) for areas near the three steepest sites (Table S5). Confidence interval for vegetation cover was generated for 1,000 randomly sampled values of remotely sensed vegetation cover.

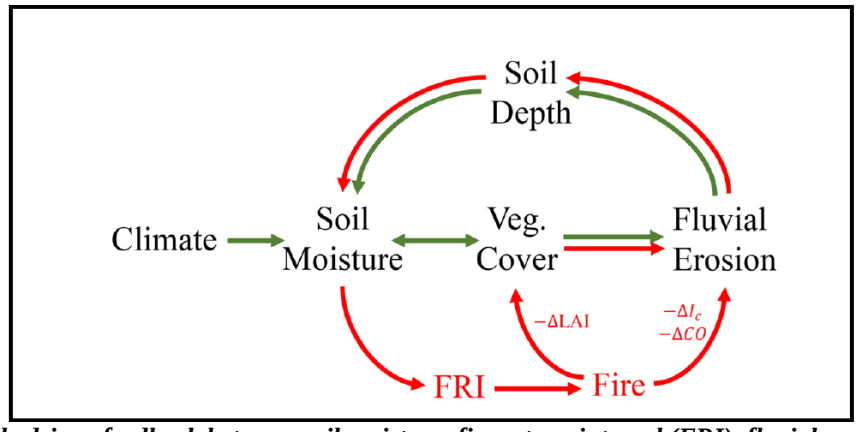

Figure 3-Climatically driven feedback between soil moisture, fire return interval (FRI), fluvial erosion, and soil depth. Red arrows represent effects that are related to fire and green arrows those that are not. In this feedback, long term change in climate affects soil moisture, vegetation cover, and fire frequency. This in-turn forces changes on soil depth and its water holding capacity by altering the rate of fluvial erosion, which feeds back to soil moisture, vegetation cover, and fire frequency. LAI is the leaf area index, Ic is the infiltration capacity of the soil (as affected by fire and water repellence), and CO is soil cohesiveness (altered by fire).

4. Conclusion

We used the flammable landscapes of SE Australia to evaluate the role of fire in the coevolution of soil-forest systems. Using a new numerical model (CoolFlameS) that represents the eco-hydro-geomorphic processes that are typical to SE Australian forests, we (i) tested the hypothesis that fire-related processes are critical to explain the variations in coevolved systems states across an aridity gradient; (ii) identified the dominant fire-related processes and feedbacks involved in the coevolution process. CoolFlameS showed good skill in predicting patterns of soil moisture thresholds ecohydrological partitioning, fire frequency distribution, surface runoff, and erosion and denudation rates across a gradient of aridity when compared to local measurements and published data (see Inbar et al. 20 for details). The validated model was then used to conduct numerical experiments to address the aims. The results showed that (i) the hypothesis was supported and that the relative role of fire in coevolution of soil depth and forests increased with aridity in the study area; (ii) among the three effects of fire examined, the relative role of post-fire reduction in infiltration capacity (and its effects of surface runoff and fluvial erosion rates) on coevolution of soil-vegetation systems was the largest, followed by post-fire reduction in soil cohesiveness and canopy cover; and the trajectory and magnitude of the coevolution of soil-vegetation systems are driven by a climatically driven feedback between soil, vegetation, and fire. For example, under a drying climate, long-term increase in post-fire erosion might contribute to more frequent fires and more erosion. We conclude that incorporating fire-related processes and feedbacks is essential when using models to investigate the critical zone and landscape evolution in fire-prone landscapes.

5. Acknowledgments

This research was funded by the Victorian Department of Environment, Land, Water and Planning (TA37948), Melbourne Water Corporation (TA37690), and the Australian Research Council (LP150100654).

6. References

Barrows, T. T., Stone, J. O., Fifield, L. K., & Cresswell, R. G. (2001). Late Pleistocene glaciation of the Kosciouszko Massif, Snowy Mountains, Australia. *Quaternary Research*, *55*(2), 179–189. https://doi.org/10.1006/qres.2001.2216

Benda, L., & Dunne, T. (1997). Stochastic forcing of sediment routing and storage in channel networks. *Water Resources Research*, *33*(12), 2865–2880. https://doi.org/10.1029/97WR02387

Berry, S. L., Farquhar, G. D., & Roderick, M. L. (2005). Co-evolution of climate, soil and vegetation. In M. G. Anderson (Ed.), *Encyclopedia of hydrological sciences* (Chap. 12, pp. 1–16). Indianapolis: John Wiley And Sons, Ltd. https://doi.org/10.1002/0470848944.hsa011

Bond, W. J., Woodward, F. I., & Midgley, G. F. (2005). The global distribution of ecosystems in a world without fire. *New Phytologist*, *165*(2), 525–538. https://doi.org/10.1111/j.1469-8137.2004.01252.x

Certini, G. (2005). Effects of fire on properties of forest soils: A review. *Oecologia*, *143*(1), 1–10. https://doi.org/10.1007/s00442-004-1788-8

Cheal, D. (2010). Growth stages and tolerable fire intervals for Victoria's native vegetation data sets. Fire and Adaptive Management. Report No. 84.

Clapp, R. B., & Hornberger, G. M. (1978). Empirical equations for some soil hydraulic properties. *Water Resources Research*, *14*(4), 601–604.

DeBano, L. F. (2000). The role of fire and soil heating on water repellency in wildland environments: A review. *Journal of Hydrology*, *231*, 195–206. https://doi.org/10.1016/S0022-1694(00)00194-3

DeBano, L. F. (2000). The role of fire and soil heating on water repellency in wildland environments: A review. *Journal of Hydrology*, *231*, 195–206. https://doi.org/10.1016/S0022-1694(00)00194-3

Donohue, R. J., Roderick, M. L., & McVicar, T. R. (2007). On the importance of including vegetation dynamics in Budyko's hydrological model. *Hydrology and Earth System Sciences*, *11*(2), 983–995. https://doi.org/10.5194/hess-11-983-2007

Donohue, R. J., Roderick, M. L., & McVicar, T. R. (2012). Roots, storms and soil pores: Incorporating key ecohydrological processes into Budyko's hydrological model. *Journal of Hydrology*, *436-437*, 35–50. https://doi.org/10.1016/j.jhydrol.2012.02.033

Gabet, E. J., & Dunne, T. (2003). A stochastic sediment delivery model for a steep Mediterranean landscape. *Water Resources Research*, *39*(9), 1237. https://doi.org/10.1029/2003WR002341

Hahm, W. J., Rempe, D. M., Dralle, D. N., Dawson, T. E., Lovill, S. M., Bryk, A. B., et al. (2019). Lithologically controlled subsurface critical zone thickness and water storage capacity determine regional plant community composition. *Water Resources Research*, *55*, 3028–3055.

Inbar, A., Lado, M., Sternberg, M., Tenau, H., & Ben-Hur, M. (2014). Forest fire effects on soil chemical and physicochemical properties, infiltration, runoff, and erosion in a semiarid Mediterranean region. *Geoderma*, *221-222*, 131–138. https://doi.org/10.1016/j. geoderma.2014.01.015

Inbar, A., Nyman, P., Lane, P.N. and Sheridan, G.J., 2020. The role of fire in the coevolution of soils and temperate forests. *Water Resources Research*, *56*(8), p.e2019WR026005.

Istanbulluoglu, E. (2016). Landscape evolution models and ecohydrologic processes. In E. A. Johnson, & Y. E. Martin (Eds.), *A biogeoscience approach to ecosystems* (pp. 135–179). Cambridge, United Kingdom: Cambridge University Press. https://doi.org/10.1017/ CBO9781107110632.007

Istanbulluoglu, E., & Bras, R. L. (2005). Vegetation-modulated landscape evolution: Effects of vegetation on landscape processes, drainage density, and topography. *Journal of Geophysical Research*, *110*, F02012. https://doi.org/10.1029/2004JF000249

Istanbulluoglu, E., Tarboton, D. G., Pack, R. T., & Luce, C. H. (2004). Modeling of the interactions between forest vegetation, disturbances, and sediment yields. *Journal of Geophysical Research*, *109*, F01009. https://doi.org/10.1029/2003JF000041

Klein, T., Randin, C., & Körner, C. (2015). Water availability predicts forest canopy height at the global scale. *Ecology Letters*, *18*(12), 1311–1320. https://doi.org/10.1111/ele.12525

Krueger, E. S., Ochsner, T. E., Carlson, J. D., Engle, D. M., Twidwell, D., & Fuhlendorf, S. D. (2016). Concurrent and antecedent soil moisture relate positively or negatively to probability of large wildfires depending on season. *International Journal of Wildland Fire*, *25*(6), 657–668. https://doi.org/10.1071/WF15104

Lane, P. N. J., Sheridan, G. J., & Noske, P. J. (2006). Changes in sediment loads and discharge from small mountain catchments following wildfire in south eastern Australia. *Journal of Hydrology*, *331*(3–4), 495–510. https://doi.org/10.1016/j.jhydrol.2006.05.035

Montaldo, N., Rondena, R., Albertson, J. D., & Mancini, M. (2005). Parsimonious modeling of vegetation dynamics for ecohydrologic studies of water-limited ecosystems. *Water Resources Research*, *41*, W10416. https://doi.org/10.1029/2005WR004094

Moody, J. A., & Martin, D. A. (2001). Initial hydrologic and geomorphic response following a wildfire in the Colorado Front Range. *Earth Surface Processes and Landforms*, *26*(10), 1049–1070. https://doi.org/10.1002/esp.253

Nolan, R. H., Lane, P. N. J., Benyon, R. G., Bradstock, R. A., & Mitchell, P. J. (2014). Changes in evapotranspiration following wildfire in resprouting eucalypt forests. *Ecohydrology*, *7*(5), 1363–1377. https://doi.org/10.1002/eco.1463

Noske, P. J., Nyman, P., Lane, P. N. J., & Sheridan, G. J. (2016). Effects of aridity in controlling the magnitude of runoff and erosion after wildfire. *Water Resources Research*, *52*, 4338–4357. https://doi.org/10.1002/2015WR017611

Nyman, P., Sheridan, G. J., Moody, J. A., Smith, H. G., Noske, P. J., & Lane, P. N. J. (2013). Sediment availability on burned hillslopes. *Journal of Geophysical Research: Earth Surface*, *118*, 2451–2467. https://doi.org/10.1002/jgrf.20152

Nyman, P., Sheridan, G. J., Moody, J. A., Smith, H. G., Noske, P. J., & Lane, P. N. J. (2013). Sediment availability on burned hillslopes.

Nyman, P., Sheridan, G. J., Smith, H. G., & Lane, P. N. J. (2011). Evidence of debris flow occurrence after wildfire in upland catchments of south-east Australia. *Geomorphology*, *125*(3), 383–401. https://doi.org/10.1016/j.geomorph.2010.10.016

Nyman, P., Sherwin, C. B., Langhans, C., Sheridan, G. J., & Lane, P. N. J. (2014). Downscaling regional climate data to calculate the radiative index of dryness in complex terrain. *Australian Metrological and Oceanographic Journal*, *64*(2), 109–122. https://doi.org/ 10.22499/2.6402.003

Orem, C. A., & Pelletier, J. D. (2016). The predominance of post-wildfire erosion in the long-term denudation of the Valles Caldera, New Mexico. *Journal of Geophysical Research: Earth Surface*, *121*, 843–864. https://doi.org/10.1002/2015JF003663

Pausas, J. G., & Bradstock, R. A. (2007). Fire persistence traits of plants along a productivity and disturbance gradient in mediterranean shrublands of south-east Australia. *Global Ecology and Biogeography*, *16*(3), 330–340. https://doi.org/10.1111/j.1466-8238.2006.00283.x

Porder, S. (2014). Coevolution of life and landscapes. *Proceedings of the National Academy of Sciences of the United States of America*, *111*(9), 3207–3208. https://doi.org/10.1073/pnas.1400954111

Prentice, I. C., Kelley, D. I., Foster, P. N., Friedlingstein, P., Harrison, S. P., & Bartlein, P. J. (2011). Modeling fire and the terrestrial carbon balance. *Global Biogeochemical Cycles*, *25*, GB3005. https://doi.org/10.1029/2010GB003906

Prosser, I. P., & Williams, L. (1998). The effect of wildfire on runoff and erosion in native Eucalyptus forest. *Hydrological Processes*, *12*(2), 251–265. https://doi.org/10.1002/(SICI)1099-1085(199802)12:2%3C251::AID-HYP574%3E3.0.CO;2-4

Rasmussen, C., Pelletier, J. D., Troch, P. A., Swetnam, T. L., & Chorover, J. (2015). Quantifying topographic and vegetation effects on the transfer of energy and mass to the critical zone. *Vadose Zone Journal*, *14*(11), vzj2014.07.0102. https://doi.org/10.2136/vzj2014.07.0102

Rodriguez-Iturbe, I. (2000). Ecohydrology: A hydrologic perspective of climate-soil-vegetation dynamics. *Water Resources Research*, *36*(1), 3–9. https://doi.org/10.1029/1999WR900210

Roering, J. J., & Gerber, M. (2005). Fire and the evolution of steep, soil-mantled landscapes. *Geology*, *33*(5), 349–352. https://doi.org/ 10.1130/G21260.1

Saxton, K. E., & Rawls, W. J. (2006). Soil water characteristic estimates by texture and organic matter for hydrologic solutions. *Soil Science Society of America Journal*, *70*(5), 1569. https://doi.org/10.2136/sssaj2005.0117

Shakesby, R. A., & Doerr, S. H. (2006). Wildfire as a hydrological and geomorphological agent. *Earth-Science Reviews*, *74*(3–4), 269–307.

Sheridan, G. J., Nyman, P., Langhans, C., Cawson, J., Noske, P. J., Oono, A., et al. (2015). Is aridity a high-order control on the hydro-geomorphic response of burned landscapes? *International Journal of Wildland Fire*, *25*(3), 262–267. https://doi.org/10.1071/ WF14079

Taufik, M., Torfs, P. J. J. F., Uijlenhoet, R., Jones, P. D., Murdiyarso, D., & Van Lanen, H. A. J. (2017). Amplification of wildfire area burnt by hydrological drought in the humid tropics. *Nature Climate Change*, *7*(6), 428–431. https://doi.org/10.1038/nclimate3280

Thonicke, K., Spessa, A., Prentice, I. C., Harrison, S. P., Dong, L., & Carmona-Moreno, C. (2010). The influence of vegetation, fire spread and fire behaviour on biomass burning and trace gas emissions: Results from a process-based model. *Biogeosciences*, *7*(6), 1991–2011. https://doi.org/10.5194/bg-7-1991-2010

Thonicke, K., Venevsky, S., Sitch, S., & Cramer, W. (2001). The role of fire disturbance for global vegetation dynamics: Coupling fire into a dynamic global vegetation model. *Global Ecology and Biogeography*, *10*(6), 661–677. https://doi.org/10.1046/j.1466-822X.2001.00175.x

Trancoso, R., Larsen, J. R., McAlpine, C. A., McVicar, T. R., & Phinn, S. R. (2016). Linking the Budyko framework and the Dunne diagram.

Troch, P. A., Lahmers, T., Meira, A., Mukherjee, R., Pedersen, J. W., Roy, T., & Valdés-Pineda, R. (2015). Catchment coevolution: A useful framework for improving predictions of hydrological change? *Water Resources Research*, *51*, 4903–4922. https://doi.org/10.1002/ 2015WR017032

van Breemen, N. (1993). Soils as biotic constructs favouring net primary productivity. *Geoderma*, *57*(3), 183–211. https://doi.org/10.1016/ 0016-7061(93)90002-3

Wagenbrenner, J. W., Robichaud, P. R., & Elliot, W. J. (2010). Rill erosion in natural and disturbed forests: 2. Modeling approaches. *Water Resources Research*, *46*, W10506. https://doi.org/10.1029/2009WR008314

Wellman, P. (1987). Eastern highlands of Australia; their uplift and erosion. *Journal of Australian Geology & Geophysics*, *10*, 277–286.

Yue, C., Ciais, P., Cadule, P., Thonicke, K., Archibald, S., Poulter, B., et al. (2014). Modelling the role of fires in the terrestrial carbon balance by incorporating SPITFIRE into the global vegetation model ORCHIDEE—Part 1: Simulating historical global burned area and fire regimes. *Geoscientific Model Development*, *7*(6), 2747–2767. https://doi.org/10.5194/gmd-7-2747-2014

Zhang, L., Hickel, K., Dawes, W. R., Chiew, F. H. S., Western, A. W., & Briggs, P. R. (2004). A rational function approach for estimating mean annual evapotranspiration. *Water Resources Research*, *40*, W02502. https://doi.org/10.1029/2003WR002710

Towards rural development and bioeconomy integration into wildfire risk reduction and civil protection strategies

Davide Ascoli[1]; Silvio Oggioni[2]*; Anna Barbati[3]; Antonio Tomao[3;4]; Mario Colonico[3]; Piermaria Corona[3;4]; Francesco Giannino[5]; Mauro Moreno[5]; Gavriil Xanthopoulos[6]; Konstantinos Kaoukis[6]; Miltiadis Athanasiou[6]; Conceição Colaço[7]; Francisco Rego[7]; Ana Catarina Sequeira[7]; Vanda Acácio[7]; Marta Serra[8]; Eduard Plana[8]

[1]*Department of Agriculture, Forest and Food Sciences, University of Torino, Largo Paolo Braccini 2, 10095 Grugliasco, Italy*
[2]*Department of Agricultural and Environmental Sciences, University of Milan, Via Giovanni Celoria 2, 20133 Milano, Italy {silvio.oggioni@gmail.com}*
[3]*Department for Innovation in Biological Agro-Food and Forestry System (DIBAF), University of Tuscia, Via San Camillo De Lellis, SNC, 01100 Viterbo, Italy*
[4]*Council for Agricultural Research and Economics, Research Centre for Forestry and Wood, Viale S. Margherita 80, 52100 Arezzo, Italy*
[5]*Department of Agriculture, University of Naples Federico II, Via Università 100, 80055 Portici, Napoli, Italy*
[6]*Institute of Mediterranean & Forest Ecosystems, Hellenic Agricultural Organization "Demeter", Terma Alkmanos, 11528, Athens, Greece*
[7]*Centre for Applied Ecology 'Prof. Baeta Neves' (CEABN-InBIO), School of Agriculture, University of Lisbon, 1349-017 Lisbon, Portugal*
[8]*Forest Science and Technology Centre of Catalonia, Crta. Sant Llorenç de Morunys, km 2, 25280 Solsona, Lleida, Spain*

**Corresponding author*

Keywords

Wildfire risk prevention, fire resistant and resilient landscapes, fire smart, fuel management, EU Green Deal

Abstract

Pyrosilviculture and understory fuel management to reduce forest stand and landscape flammability represent loss-making interventions from an economic point of view. Consequently, prevention is carried out above all on public property and with public funds (e.g. Rural Development Programs), while the interest of the private individual for prevention interventions on aggregated areas is limited. These shortcomings do not allow to reach the distribution and the quantity of treated surface necessary to modify the fire regime and its impacts.

To solve this problem, we need initiatives that catalyse the interests of multiple stakeholders (economic actors, bodies responsible for territorial management and research, fire-fighter agencies) towards common goals. Moreover, we need to improve the cost-efficiency ratio of prevention through value-chains of products and services generated by preventive measures (e.g. payments for positive externalities and ecosystem services). Within the European project PREVAIL (PREVention Action Increases Large fire response preparedness) we analysed collaborative processes in the Mediterranean Basin between private and public actors that developed "smart solutions". Different sources of funding, including non-specific funds for prevention, offer additional economic resources to support preventive value-chains (e.g. RDP funds for agro-pastoral and forestry development, LIFE funds for habitat conservation, private investments, PES mechanisms). This paper analyses the key elements that characterise smart solutions for wildfire risk prevention in Southern EU: sustainability, cost-benefit ratio, synergies between sources of financing, inter-sectoral cooperation and integration between strategic prevention planning and multiple land governance objectives, innovation and knowledge transfer, and adaptive approach. A selection of solutions documented by the PREVAIL project and replicable in other contests will be presented and discussed.

1. Introduction

In recent decades in Europe there has been an increasing emphasis on multi-objective policies in fire risk management, integrating prevention, preparedness, response and recovery activities (Rego et al., 2010; Bacciu

et al., 2022). This allows for holistic territorial planning (Moreira et al., 2020), working more on the causes and promoting fire-smart territories (FST) (Tedim et al., 2016, Fernandes, 2013).

Fire risk prevention is pursued at European level with several strategies implemented by the European Commission, which contribute widely to building fire-smart territories by converging multiple objectives, e.g. Bioeconomy Strategy, LIFE programme, the EU Climate Change Adaptation Strategy and the Forestry Strategy. All of these are included in the Green Deal objectives, which allows for a synergistic approach to act on fire prevention in multiple aspects. Additional incentives for fire prevention can be provided through the Rural Development Programmes (RDPs). At the same time, active prevention have been promoted by an increasing number of local-scale initiatives especially in southern European countries. These noteworthy initiatives are characterised by the ability to adopt sustainable fuel management programmes and nature-based solution in a smart way, benefiting from policy instruments to functionally act on fire prevention with bottom up projects (Varela et al., 2020; Colonico et al., 2022). In this study, the most relevant initiatives based on management of fire prone territories were identified to define sustainable landscape-scale fuel management models for southern Europe and practical solutions for fire prevention at local level.

2. Selection and description of fire prevention initiatives

Noteworthy fire prevention initiatives were analysed in Greece, Italy, Portugal and Spain, given their particular susceptibility to fire (Moreira et al., 2020) and the high number of forest fire prevention programmes at local and regional scales (Varela et al., 2020). Data were collected through a survey filled in by the managers of the individual initiatives. The initiatives were analysed using five key criteria for the construction of FST (Tedim et al., 2016): (i) sustainability, (ii) cost efficiency in risk reduction, (iii) synergies and cooperation, (iv) knowledge exchange and transfer, and (v) adaptive management. Each initiative was assessed according to its "readiness degree" in the different fields of sustainable fire prevention, considering both its local potential and its ability to create synergies at European level. Finally, on a sub-sample of the initiatives, economic feasibility, stakeholder involvement, the legal framework and social and environmental awareness were assessed, showing strengths and weaknesses through a SWOT analysis.

Thirty-eight initiatives were identified in the four countries under analysis, distributed mainly in Spain (17 initiatives - 45%) and Portugal (11 initiatives - 29%), followed by Italy (7 initiatives - 18%) and Greece (3 initiatives - 8%). Most of these initiatives are implemented by public agencies (60%), financed largely by the Life Programme and Rural Development Programmes (RDPs), followed by initiatives with private investment. Most initiatives are characterised by being mainly related to Direct and Indirect fire prevention, with half of them focusing on Preparedness as an important step in disaster risk management. The initiatives were then evaluated according to their representativeness in each of the 5 evaluation criteria (from "Not at all represented" (0) to "Totally represented" (4)), creating a ranking that allowed for the identification of the most represented criteria and the most comprehensive solutions.

3. The fire-smart solution model

Through the analysed initiatives it is possible to build a general model for the creation of sustainable fire risk prevention programmes in southern European countries, based on some key elements useful for building smart solutions and planning fire resistant and resilient landscapes (Fig. 1).

Some of the fire smart solutions identified are based on the short supply chain as an added value to fire prevention, enhancing products through a label that certifies fire prevention activities. In fact, certification is a powerful tool at local, national and international level to recognise the multiple purposes of these initiatives, maximising cost-efficiency and producing socio-economic services (Varela et al., 2018). Fire prevention must also be recognised as a true ecosystem service, given its multiple roles in different social sectors and the importance of being integrated into territorial governance. Indeed, fire prevention is an essential tool for the creation of resilient and fire-resistant landscapes, which goes hand in hand with biodiversity conservation, water supply, mitigation of other natural hazards, landscape aesthetics, civil protection of infrastructure and local economic development. Another element that contributes to the fire smart solutions definition is the ability to create synergies between local development and international support, giving space for wide-ranging projects

(Proença, 2019). Finally, it is very important to consider the available knowledge on fire risk management at the time of planning functional local activities.

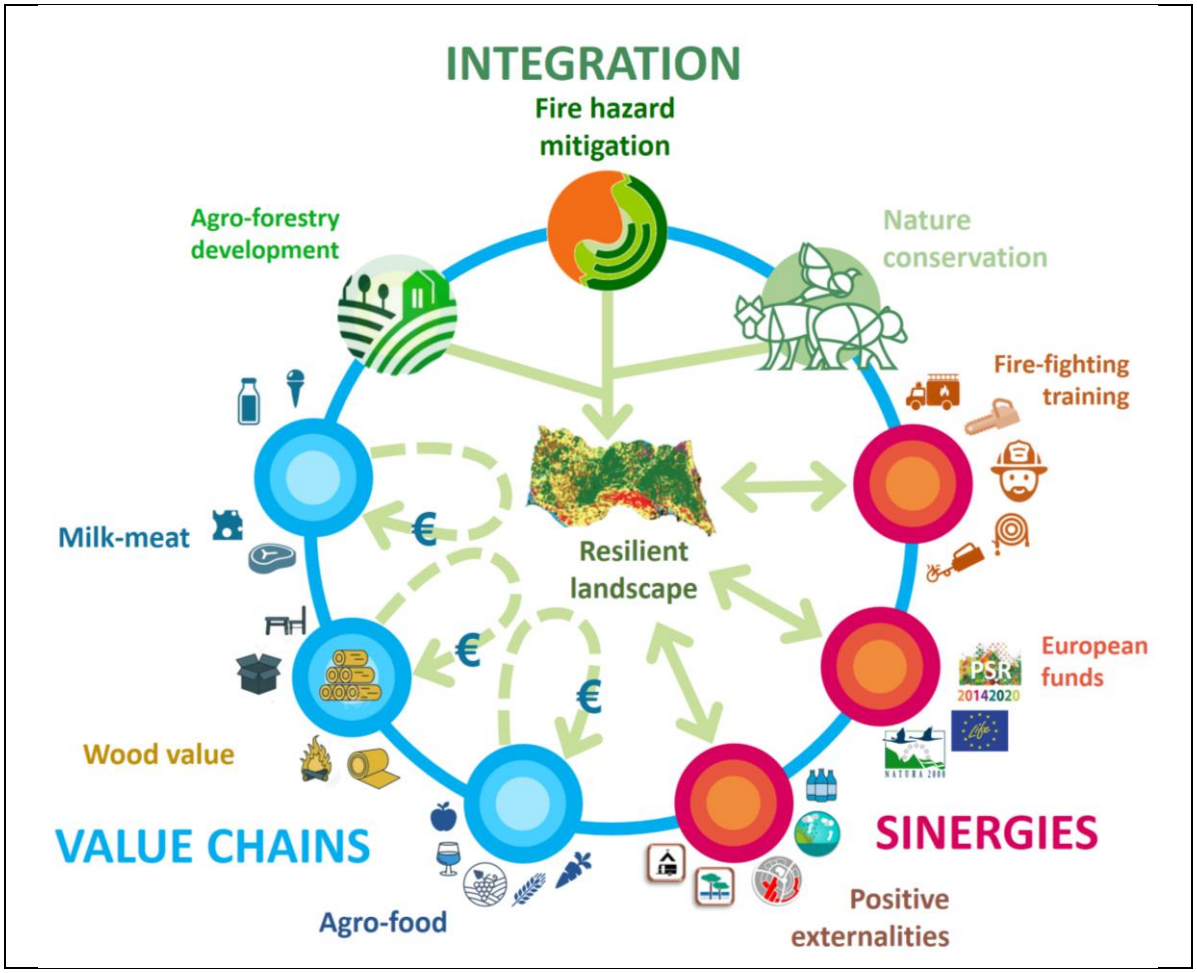

Figure 1 - Key emerging components that characterizes a smart-solution for wildfire risk prevention

4. Prospects for smart solutions replication under the EU Green Deal

The smart-solution model proposed here (Fig. 1) finds with the Green Deal the perfect opportunity to be implemented, acting on forest fire prevention at multiple levels to achieve objectives at the landscape and territory scale. The projects' continuity is also ensured by medium-long term incentives, being able to count on long-lasting projects to manage fire prone landscapes in the future. The ability to involve multiple actors and agencies is a further strength, addressing the European objectives of cooperation and transdisciplinarity and creating local networks essential for managing the territory as a whole (Rego et al., 2018). The fire smart solutions model we propose can also be of inspiration for the creation of calls and projects related to fire prevention funding at European level, being able to identify the key points of local interest, creating per example multi-measure calls for integrated territorial projects in high wildfire risk areas. These types of calls allow the convergence of multiple actors with different goals and objectives, which, with the right policy-management framework, can be able to create complex projects able to manage the territory in a holistic way and include fire risk mitigation.

5. Conclusions

Dealing with extreme fires requires interfacing with many areas simultaneously, such as the environmental and socio-economic factors (Ascoli et al., 2021; Fernandes, 2013; Tedim et al., 2018; Wunder et al., 2021). Indeed, to contain fire effects, it is necessary to adopt multi and transdisciplinary strategies that include the different components at stake (Tedim et al., 2016, Varela et al., 2020).

The smart-solution concept for fire risk management offers a framework to be applied at the local level by being able to take advantage of European tools to achieve its objectives. Their implementation at a local level and replication at a European scale is only possible through close communication between initiatives and institutions involved in fire risk and land management, including communities in a mutual exchange of good practices.

In conclusion, fire smart solutions are a concrete example of implementing the Green Deal locally in disaster risk management. The fundamental criteria of the fire smart solutions presented here derive from a direct exchange with local realities and define the most important aspects to create functional networks for fuel management. These criteria should be considered in the creation of future public funding calls for fire prevention projects, allowing a broad involvement of public and private actors to build solutions adapted to the real needs of marginal territories.

6. References

Ascoli, D., Moris, J.V., Marchetti, M., Sallustio, L., 2021. Land use change towards forests and wooded land correlates with large and frequent wildfires in Italy. Annals of Silvicultural Research 46(2). http://hdl.handle.net/2318/1799361

Bacciu, V., Sirca, C., Spano, D., 2022. Towards a systemic approach to fire risk management. Environmental Science & Policy, 129, 37-44. https://doi.org/10.1016/j.envsci.2021.12.015

Colonico, M., Tomao, A., Ascoli, D., Corona P., Giannino, F., Moris, J., Romano, R., Salvati, L., Barbati, A. (2022). Rural development funding and wildfire prevention: evidences of spatial mismatches with fire activity. Land Use Policy, 117, https://doi.org/10.1016/j.landusepol.2022.106079

Fernandes, P.M., 2013a. Fire-smart management of forest landscapes in the Mediterranean basin under global change. Landscape and Urban Planning 110, 175–182. https://doi.org/10.1016/j.landurbplan.2012.10.014

Moreira, F., Ascoli, D., Safford, H., Adams, M.A., Moreno, J.M., Pereira, J.M.C., Catry, F.X., Armesto, J., Bond, W., González, M.E., Curt, T., Koutsias, N., McCaw, L., Price, O., Pausas, J.G., Rigolot, E., Stephens, S., Tavsanoglu, C., Vallejo, V.R., Van Wilgen, B.W., Xanthopoulos, G., Fernandes, P.M., 2020. Wildfire management in Mediterranean-type regions: Paradigm change needed. Environmental Research Letters 15, 1–6. https://doi.org/10.1088/1748-9326/ab541e

Proença, V., Teixeira, C. M., 2019. Beyond meat: ecological functions of livestock. Science, 366(6468), 962-962. https://doi.org/10.1126/science.aaz7084

Rego, F., Rigolot, E., Fernandes, P., Montiel, C., Silva, J.S., 2010. Towards integrated fire management. European Forest Institute (EFI) 16. https://hal.inrae.fr/hal-02823739

Rego, F.C., Moreno, J.M., Vallejo, V.R., Xanthopoulos, G., 2018. Forest Fires. Sparking firesmart policies in the EU. N. Faivre (editor). European Commission, Directorate-General for Research and Innovation Climate Action and Resource Efficiency. 53. https://doi.org/10.2777/181450

Tedim, F., Leone, V., Amraoui, M., Bouillon, C., Coughlan, M.R., Delogu, G.M., Fernandes, P.M., Ferreira, C., McCaffrey, S., McGee, T.K., Parente, J., Paton, D., Pereira, M.G., Ribeiro, L.M., Viegas, D.X., Xanthopoulos, G., 2018. Defining extreme wildfire events: Difficulties, challenges, and impacts. Fire 1, 1–28. https://doi.org/10.3390/fire1010009

Tedim, F., Leone, V., Xanthopoulos, G., 2016. A wildfire risk management concept based on a social-ecological approach in the European Union: Fire Smart Territory. International Journal of Disaster Risk Reduction 18, 138–153. https://doi.org/10.1016/j.ijdrr.2016.06.005

Varela, E., Górriz-Mifsud, E., Ruiz-Mirazo, J., López-i-Gelats, F., 2018. Payment for targeted grazing: integrating local shepherds into wildfire prevention. Forests, 9(8), 464. https://doi.org/10.3390/f9080464

Varela, E., Pulido, F., Moreno, G., & Zavala, M. Á. 2020. Targeted policy proposals for managing spontaneous forest expansion in the Mediterranean. Journal of Applied Ecology, 57(12), 2373-2380. https://doi.org/10.1111/1365-2664.13779

Wunder, S., Calkin, D. E., Charlton, V., Feder, S., de Arano, I. M., Moore, P., Rodríguez y Silva, F., Tacconi, L., Vega-García, C, 2021. Resilient landscapes to prevent catastrophic forest fires: Socioeconomic insights towards a new paradigm. Forest Policy and Economics 128. https://doi.org/10.1016/j.forpol.2021.102458

Chapter 4:
Risk Assessment

A comparison of four spatial interpolation methods for modeling fine-scale surface fuel load in a mixed conifer forest with complex terrain

Chad M. Hoffman[1]*, Justin P. Ziegler[1], Wade T. Tinkham[1], J. Kevin Hiers[2]; Andrew T. Hudak[3]

[1] *Department of Forest and Rangeland Stewardship, Warner College of Natural Resources, Colorado State University, Fort Collins, CO 80523, USA, {c.hoffman, justin.ziegler, wade.tinkham}@colostate.edu*
[2] *Tall Timbers Research Station, Tallahassee, FL 32312, USA, {jkhiers@talltimbers.org}*
[3] *USDA Forest Service Rocky Mountain Research Station, Moscow, 80521, USA;*

**Corresponding author*

Keywords

Fuel mapping, kriging, regression kriging, Rocky Mountains

Abstract

Forest fuel inventory, monitoring and mapping provide the basis for fuel management activities, including assessing wildfire hazards and risk, prescribed fire planning, designing silvicultural treatments, and predicting fire behaviour and effects at various scales. One of the most significant challenges in developing accurate surface fuel maps is capturing the spatial variability of fuel load within and between different fuel components. In this paper, we compare the performance of four spatial interpolation methods for estimating and mapping fine-scale fuel load in a dry mixed conifer forest in Colorado, USA. The four approaches are: classification, multiple linear regression, ordinary kriging, and regression kriging. We chose these methods because they are commonly used in ecological studies and cover a range of SIM including, non-geostatistical, geostatistical, and hybrid approaches. All SIM methods yielded unbiased fuel load estimates, with mean error within 3% of the observations with MAPE from 100% to 40%, depending on the specific fuel com-ponent and spatial interpolation method. Our results indicate that regression kriging was able to better capture the fine-scale spatial variability in fuel load compared to other spatial interpolation methods.

1. Introduction

Forest fuel inventory and monitoring provide the basis for fuel management activities, including assessing wildfire hazards and risk, prescribed fire planning, designing silvicultural treatments, and predicting fire behaviour and effects at various scales. The most commonly assessed attribute of the fuels complex is the load. Fuel load is a required input to nearly all fire behaviour and effects models and is a critical component of terrestrial carbon inventories and wildlife habitat assessment (Keane et al. 2013). Fuel inventory approaches have traditionally assumed that the spatial variability in fuel load is of little consequence for management decisions and thus focus on providing estimates of spatially averaged values for a given area. Yet, recent studies highlight that fine-scale variability in the fuels complex exerts considerable influence on many ecologically relevant fire behaviour and effects metrics (O'Brien et al. 2016). Directly mapping fine-scale fuel variability is costly and time-consuming, especially across large. To overcome these limitations, it is often necessary to utilize a spatial interpolation method (SIMs) to estimate the fuel load at unsampled locations and generate spatially continuous fuel load maps for wildfire hazard and risk assessments, prescribed fire planning, and silvicultural treatment design.

One of the most significant challenges in developing accurate surface fuel maps is capturing the spatial variability of fuel load within and between different fuel components. This variability arises due to interactions between the physical environment (e.g., climate, soils, and topography) and ecological processes (e.g., productivity, deposition, decomposition, and disturbances) that determine the balance between inputs and outputs of fuel across multiple spatial and temporal scales. One of the most commonly used approaches to capture this variability is to classify an area into unique groups using auxiliary, often remotely sensed data (e.g., vegetation type, topographic data, or land use classes) and then assign a fuel load to all areas of a given class based on the sampled data (e.g., Keane et al. 2013). A drawback of a classification approach is that the variability in the data is reduced to a few unique values. Other researchers have utilized regression-based approaches where the relationship between continuous auxiliary variables and the surface fuel load is used to predict values at

unmeasured locations. Previous studies have weak to nonexistent correlations between the surface fuel load and topographic and forest structural metrics (e.g., Lydersen et al. 2015; Hall et al. 2006) indicating that surface fuel maps developed based on these relationships may have limited accuracy. Recent studies have found that surface fuels exhibit strong fine-scale spatial autocorrelation, which, if taken into account, may increase fuel map accuracy (Keane et al. 2013; Vakili et al. 2016). Although previous research has acknowledged spatial autocorrelation in fuel load, only Pierce et al. (2009) have explicitly assessed the degree to which this improves spatial interpolation. Their results indicate that including spatial autocorrelation did not significantly improve fine-scale predictive accuracy compared to linear regression approaches. However, the scale of analysis used in this study was greater than the inherent spatial scale of surface fuel variability identified by Keane et al. (2013) and Vakili et al. (2016), which may have limited any potential improvements in predictive accuracy.

In this paper, we compare the performance of four SIMs for estimating and mapping fine-scale fuel load in a dry mixed conifer forest in Colorado, USA. The four approaches were: classification, multiple linear regression, ordinary kriging, and regression kriging. We chose these methods because they are commonly used in ecological studies and cover a range of SIM including, non-geostatistical, geostatistical, and hybrid approaches.

2. Methods

2.1. Study Area and Data Collection

We conducted this study on the 17.6-ha Pike Peak Forest Dynamics Plot (PFDP) located within the Pike and San Isabel National Forest of Colorado. PFDP was established in the summer of 2016 as a collaboration between Colorado State University and the USDA Forest Service for long-term forest dynamics monitoring. The PFDP is representative of mixed conifer forests in the southern Rocky Mountains with an elevation range from 2,781 to 2,833 m and a dry, continental climate with 660.7 mm of rain per year and a mean daily temperature ranging from -4.7° C in January to 14.0° C in August. Topographically, the PFDP is shaped by two significant ridges, one oriented west-east in the northern portion of the plot and another oriented northwest-southeast in the southwestern portion, and several smaller secondary ridges protruding from the two main ones. The dominant overstory vegetation for the study site includes ponderosa pine (Pinus ponderosa Lawson & C. Lawson) and quaking aspen (Populus tremuloides Michx.) on southern aspects, and mixtures of Engelmann spruce (Picea engelmannii Parry ex Engelm.), blue spruce (Picea pungens Engelm.), and Douglas-fir (Pseudotsuga menziesii (Mirb.) Franco) on northern aspects. The average density, basal area, and quadratic mean diameter at breast height for the site are 804 trees ha-1, 7.55 m2 ha-1, and 19.0 cm, respectively.

All trees in PFDP at least 1.37 m tall were mapped to the nearest 0.1 m and had their species, diameter at breast height, height, and crown base height recorded. To characterize the surface fuel load across the site, we double sampling procedure to estimate the fuel load of the 1-, 10-, and 100-hr dead down and woody fuels on 437 1-m2 irregularly located plots (Keane and Dickinson 2007, Tinkham et al. 2016). We estimated litter and duff fuel load using the depth-to-load method using locally derived bulk density estimates. Total fuel load was estimated by summing the individual component fuel loads (1- 10-, 100-hr dead, down and woody fuel, and litter and duff).

We used our stem-mapped overstory data along with remote sensing imagery to calculate two overstory (dominate species and basal area) and two topographic (percent slope and Beer's aspect) characteristics that we used as auxiliary information in spatial interpolation. Topographic auxiliary variables were calculated using a 10-m digital elevation model (DEM; available at nationalmap.gov; accessed 20 June 2022).

2.2. Spatial Interpolation Methods and Analysis

We compared the performance of four SIMs for estimating and mapping fine-scale fuel loads: classification (CL), multiple linear regression (LR), ordinary kriging (OK), and regression kriging (RK). For LR and RK, we included local basal area, cover type, aspect, and percent slope as auxiliary variables. The CL model was based solely on the predicted cover type. For OK and RK, we predicted each fuel component separately with fitted auto-semivariograms.

We assessed the comparative performance of each SIM with a k-folds cross-validation approach. We chose the following statistics to assess SIMs' performances: mean error (ME); mean absolute error (MAE); mean absolute percent error (MAPE); and Pearson's correlation coefficient between observed and predicted values.

3. Results and Discussion

All SIM methods yielded reasonably unbiased fuel load estimates, with mean error within 3% of the observations (Table 1, Fig. 1). Except for RK predictions for the total fuel load, all approaches resulted in a slight underprediction bias. Although a minimal bias was associated with all SIM, OK consistently resulted in the greatest bias.

Table 1. Summarization of cross-validation from spatially interpolating surface fuel components' loads in the Pike Forest Dynamics Plot.

Component	Method	ME	MAE	MAPE	$r_{obs,pred}$
1-hour	CL	0.001	0.192	67%	0.36
	LR	0.001	0.193	68%	0.40
	OK	0.007	0.185	65%	0.38
	RK	0.004	0.180	63%	0.44
10-hour	CL	0.001	0.468	70%	0.13
	LR	0.001	0.480	72%	0.11
	OK	0.010	0.451	68%	0.24
	RK	0.004	0.454	68%	0.27
100-hour	CL	0.005	0.963	111%	0.09
	LR	0.005	0.966	111%	0.07
	OK	0.011	0.899	104%	0.23
	RK	0.001	0.894	103%	0.23
Litter	CL	0.000	0.143	50%	0.14
	LR	0.000	0.142	50%	0.15
	OK	0.000	0.134	47%	0.32
	RK	0.000	0.130	45%	0.40
Duff	CL	0.004	1.119	58%	0.55
	LR	0.004	1.082	56%	0.56
	OK	0.022	1.006	52%	0.60
	RK	0.001	0.973	51%	0.63
Total	CL	0.012	2.090	48%	0.43
	LR	0.011	1.830	46%	0.48
	OK	0.061	1.960	49%	0.36
	RK	-0.006	1.740	43%	0.53

The MAPE varied from over 100% to around 40%, depending on the specific fuel component and spatial interpolation method (Table 1). The two Kriging based approaches evaluated produced lower MAPE than either CL or LR, with RK producing the lowest MAPE across all fuel components. However, there were relatively small differences in MAPE among the SIM, with the best-performing SIM reducing MAPE between 2 and 8% compared to the worst-performing SIM. The Pearson Correlation coefficients ranged from 0.07 to 0.63, depending upon the fuel component and SIM. RK resulted in the greatest Pearson correlation coefficient of all SIM tested regardless of the fuel component.

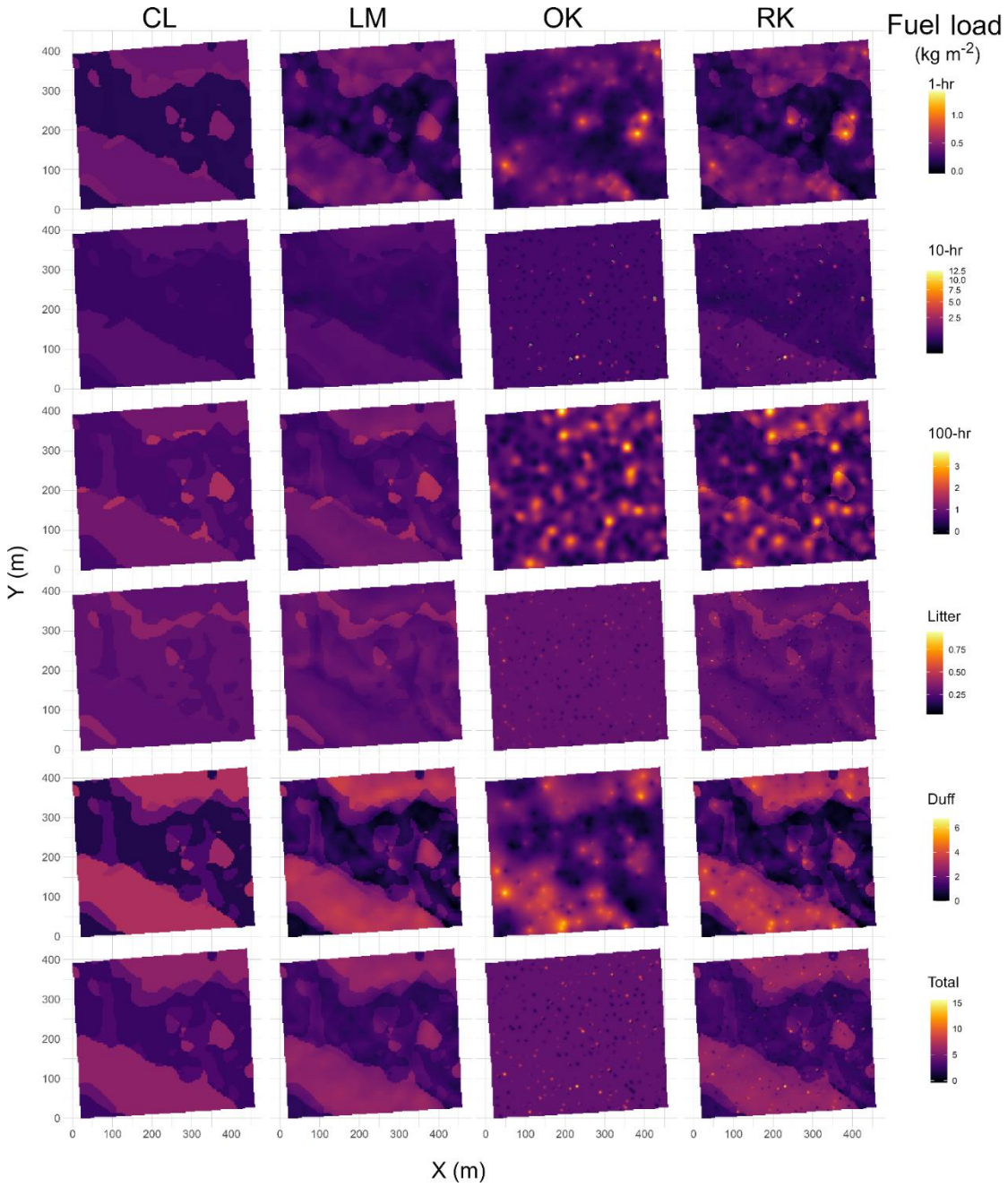

Fig. 1 Fuel load maps predicted in the Pike Forest Dynamics Plot by four spatial interpolation methods of 1-hour, 10-hour, and 100-hour woody fuels, litter, and duff surface fuel components, and total fuel load.

Fuel maps are commonly utilized by fire and land managers across a range of spatial scales to assist with fire suppression planning, locating and designing wildland fuel treatments, evaluating fire hazard and risk. Fine scale variation in fuel characteristics is increasingly recognized as important driver of fire behaviour and effects and as such, there is a growing demand for high-resolution maps of the wildland fuels. Of the four SIM evaluated, regression kriging provided the best overall estimation of surface fuel load for all fuel components. our findings indicate that RK was able to better capture the fine-scale spatial variability in fuel load and therefore is the preferred method to produce spatially interpolated fine-scale fuel maps.

4. References

Keane RE, Dickinson LJ (2007) The photoload sampling technique: from downward-looking photographs of synthetic fuelbeds. USDA For Serv Rocky Mt Res Station Gen Tech Rep RMRS-GTR-190

Keane RE, Herynk JM, Toney C, et al (2013) Evaluating the performance and mapping of three fuel classification systems using Forest Inventory and Analysis surface fuel measurements. For Ecol Manage 305:248–263. https://doi.org/10.1016/j.foreco.2013.06.001

Lydersen JM, Collins BM, Knapp EE, et al (2015) Relating fuel loads to overstorey structure and composition in a fire-excluded Sierra Nevada mixed conifer forest. Int J Wildl Fire 24:484–494. https://doi.org/10.1071/WF13066

O'Brien JJ, Loudermilk EL, Hiers JK, et al (2016) Canopy-Derived Fuels Drive Patterns of In-Fire Energy Release and Understory Plant Mortality in a Longleaf Pine (Pinus palustris) Sandhill in Northwest Florida, USA. Can J Remote Sens 42:489–500. https://doi.org/10.1080/07038992.2016.1199271

Pierce KB, Ohmann JL, Wimberly MC, Gregory, M.J., Fried, J.S. (2009) Mapping wildland fuels and forest structure for land management: A comparison of nearest neighbor imputation and other methods. Can J For Res 39:1901–1916. https://doi.org/10.1139/X09-102

Tinkham WT, Hoffman CM, Canfield JM, et al (2016) Using the photoload technique with double sampling to improve surface fuel loading estimates. Int J Wildl Fire 25:224–228. https://doi.org/10.1071/WF15027

Vakili E, Hoffman CM, Keane RE, et al (2016) Spatial variability of surface fuels in treated and untreated ponderosa pine forests of the southern Rocky Mountains. Int J Wildl Fire. https://doi.org/http://dx.doi.org/10.1071/WF16072

A Knowledge Network dedicated to Advanced Fire Analysis to better intervene

Wilfried Stefic[1*]; Raphaël Supplisson[1]; Mélina Brichler[1]

[1]ENSOSP. 1070 rue Lieutenant Parayre – 13798 Aix-en-Provence, France,
{wilfried.stefic, raphael.supplisson, melina.brichler}@ensosp.fr

**Corresponding author*

Keywords

Knowledge management – prevention – harmonized – fire – analysis.

Abstract

Faced with an increase in risks all over the the planet due to climate change and land management, scientists and operational staff are trying to find answers to adapt to "increased risks". Wildfires are a global problem that impact societies and the environment. Over the past decade, the number of wildfires has been unprecedented, creating great uncertainty for emergency responders.

The results of these events are catastrophic impacts on life, property and the environment, e.g. Portugal 2017, Greece 2018, Spain 2019 in Southern Europe and Sweden 2018, Germany 2019, United Kingdom 2019 in Central and Northern Europe. Science proves that the risk of forest fires is increasing across Europe and that climate change is making the situation worse.

Even countries that have never seen forest fires as a real threat to society and the environment will need to master firefighting. During a fire, European firefighting systems are exposed to demanding situations that help to understand fires and improve firefighting systems. Irrespective of the ability of some European emergency services to transfer acquired knowledge on wildfire management, extracting lessons learned and converting them into applicable knowledge for future events in the same or different countries is not sufficiently taken into consideration.

Some countries have created knowledge networks around fire behavior analysis that operate at regional and national level (e.g. the FAST team in Spain, the Wildfire Tactical Advisor group in the UK and specialist centers in the Council Europe such as the Global Fire Monitoring Center in Germany and the European Forest Fire Center in Greece). A European forest firefighting knowledge sharing network is needed to extend existing regional and national knowledge, translate it with the mission of two-way learning to generate improved overall European emergency response capabilities in case of fire. With expertise in knowledge management (1), ENSOSP has joined forces with other recognized partners to develop a knowledge network (2) specific to forest fires (3).

1. Expertise in knowledge management…

The National School of Fire Officers of France (ENSOSP) has been working for several years to formalize knowledge and skills in the fields of civil security for training, prevention, operational management, feedback … This is part of the development of knowledge management defined as a process that aims to optimize and develop skills by establishing a culture of learning. In other words, it consists of the accumulation and sharing of skills, knowledge resulting from training or experience. Since 2008, ENSOSP has created a platform for sharing knowledge and other resources such as feedback to enable all firefighters in France to optimize their knowledge, which is unified and standardized in order to learn continuously. Thus, PNRS[1] is a free accessible platform with an unprecedented collection and exchange of documents, knowledge and techniques for firefighters in France. This portal has gradually established itself in the civil security ecosystem, increasing from 40,500 visits in 2010 to 586,000 visits in 2021, an increase of 90%.

[1] http://pnrs.ensosp.fr/

2. …faced with the need for the emergence of a knowledge network…

In 2020, the European Commission launched a call[2] for EU proposals in the field of civil protection under the EU Civil Protection Knowledge Network. This call is launched in line with the Annual Work Program 2020. It aims to fund projects that support and enhance EU knowledge building, partnership building and knowledge networking on civil protection. This requires better and faster disaster risk management through consolidated prevention, preparedness and response activities which can only be achieved through enhanced cooperation and better coordination between a wide range of stakeholders across countries. The mission of the UCPM Knowledge Network is to bring together civil protection and disaster management actors and institutions in order to improve the overall knowledge situation and foster the EU's capacity to respond to disasters. The main objectives of the knowledge network are:

- act as a bridge between knowledge holders relevant to the UCPM;
- strengthen coordination, cooperation, compatibility and complementarity between capacities and improve the competence of experts;
- collect and share knowledge, experience, expertise, skills, lessons learned and best practices in close cooperation with civil protection authorities and disaster management authorities and knowledge centres;
- stimulate research and innovation and encourage the introduction and use of new appropriate technologies;
- strengthen links between civil protection and disaster risk management actors and develop a common understanding and culture of prevention, preparedness and response.

3. …at the service of the fight against forest fire.

Drawing on its experience in knowledge management, ENSOSP jointly with the Pau Costa Foundation put together a response to the call for projects by targeting the outcomes relating to the following objectives:

- To support civil protection and disaster risk management actors that promote and facilitate the development, dissemination and exchange of knowledge, good practices and expertise (specific objective n°1).
    - 1.1 Good practices, recommendations, and lessons in prevention, preparedness and response are collected, reviewed, shared and applied during exercises and real-time emergencies.
    - 1.2 Expertise in civil protection and risk disaster management is further developed and shared.
- To support new and consolidate existing partnerships in civil protection and disaster risk management that enhance cooperation and synergies in prevention, preparedness and response. These two objectives will be targeted in a specific operational field, the prevention and fight against fires in natural areas (specific objective n°2).
    - 2.1 Existing structures of relevant civil protection and disaster risk management actors are strengthened and expanded.
    - 2.2 New partnerships are established.

Initiated in January 2021 and ending in June 2022, the European project Advanced Fire Analysis Network (AFAN[3]) co-financed by the European Commission is conceived as the feasibility study of the future global structure, pooling the knowledge generated by the various centers of excellence and networks of existing actors in the analysis of vegetation fires. Forest fires are in fact the area illustrating the development, dissemination and exchange of knowledge, good practices and expertise identified (specific objective no. 1) while relying on existing partnerships, in order to strengthen and make them sustainable (objective no. 2). The consortium has been wisely designed to have complementary skills and geographical reach. For France, the mutual work between Ensosp and the Entente de Valabre makes it possible to combine expertise, training, research and innovation in the field of forest fires with knowledge network projects financed by the EU (DG HOME) such

[2] https://ec.europa.eu/info/funding-tenders/opportunities/portal/screen/opportunities/topic-details/ucpm-2020-kn-ag
[3] https://fireanalysisnetwork.eu/

as the FIRE-IN, MEDEA, Driver+ and other projects. The objective of the AFAN project is to strengthen existing regional, national and international knowledge and capacities, to transfer them with the aim of shared mutual learning and to create the basis of an operational network, based on trust and support to generate an overall improvement of the European Civil Protection Mechanism. This requires the development of a methodology, a process of knowledge capitalization in the field of forest fires, the multiplication and aggregation of partnerships of knowledge networks in the field of forest fires as well as the valuation of the results (experimentation with collaborative platforms and new technologies to prevent and fight forest fires).

Furthermore, the "new" discipline of fire analysis collects information about wildfires and transforms it into knowledge. This knowledge is used during emergencies to provide advice and guidance for decision-making at the strategic, tactical and operational levels of fire management. Six major themes are defined in the analysis of fires, namely, interpreting climate-meteorological data, establishing and monitoring the evolution of the fire, its behavior, the parameters influencing its spread, producing a tactical response and developing a strategic vision of the event.

To fill all these gaps, the AFAN project proposes the drafting of several guidelines[4] on the skills of a fire analyst, on the tools, sciences and good practices used for the analysis. In addition to these guidelines, a map[5] showing the existing expertise capacity across Europe was developed over questionnaire and dissemination during the project. The map, freely accessible on the AFAN website and updated each time a new answer is received, gather 24 structures over Europe. It gives from the address information to the fire analysis profile. To put the expert in touch and facilitate immediate content sharing, AFAN also created a Telegram group where experts could exchange on their situation and share data, information and knowledge.

The AFAN project has also created of a database[6], listing the tools and good practices on which fire analysis relies, depending on the countries of the consortium. The database is currently enriched, it must constantly evolve and it is supported by a guideline describing the different tools. Thus, in addition to being shared in the guidelines, the knowledge is integrated into a database which will eventually make it possible to identify the tools and best practices used by operational staff, by fire experts in Europe, facilitating interoperability between countries in the long term, but also the creation of working groups within the countries that will be most affected by the fires.

4. Conclusion

Through the AFAN project, this document describes how knowledge management can be a factor in improving the prevention and fight against wildfires. The operational network enables the transfer of specialist knowledge between countries, the sharing of experiences, science, new challenges and solutions, offers assessment for emergency management and proposes Europe-wide actions to face future challenges of forest fire fighting. More specifically, AFAN focuses on improving fire analysis skills and capabilities, sharing technological tools, science and best practices available for forest fire management. Finally, it permits to master remote assessment practice to be implemented across Europe and for external operations. Completion of the project would create a coherent network of forest fire analysis capabilities comprising actors from across Europe, with harmonized fire response capabilities and a set of tools (e.g. guidelines, training, tools, reports) for European fire managers and civil protection organizations wishing to strengthen their operational and analytical capacities in the field of forest fire management.

[4] https://fireanalysisnetwork.eu/afan-toolkit-2/
[5] http://umap.openstreetmap.fr/fr/map/afan-map-of-existing-fire-analysis-expertise-and-k_585426#5/49.852/12.656
[6] https://afandatabase.wixsite.com/afandatabase

A Methodology for the Quantitative Risk Analysis of Wildfires in the Wildland-Urban Interface: Application to Electrical Infrastructure

Gonzalo Severino*[1]; Andrés Fuentes[1]; Alejandro Valdivia[2]; Fernando Auat-Cheein[1]; Pedro Reszka[3]

[1]Universidad Técnica Federico Santa María. Avenida España 1680, Valparaíso, Chile, {gonzalo.severino@usm.cl}, {fernando.auat, andres.fuentes}@usm.cl
[2]Chilquinta Distribución S.A. Avenida Argentina N°1, piso 9, Valparaíso, Chile, {avaldivi@chilquinta.cl}
[3]Universidad Adolfo Ibáñez. Diagonal Las Torres 2640, Peñalolén, Chile, {pedro.reszka@uai.cl}

**Corresponding author*

Keywords

Risk, Vulnerability, Consequence, Probit, Wildland-Urban Interface

Abstract

This work describes a methodology to estimate the risk of a wildfire damaging an electrical substation operated by Chilquinta Distribución S.A. (a Chilean utility company) in the Wildland-Urban Interface (WUI) of Valparaiso, Chile. A Wildfire Quantitative Risk Analysis (WFQRA) framework is proposed for this purpose, where risk is defined as the product between the probability of a wildfire reaching the WUI and its consequences. The former is determined with an event tree, a tool where an outcome probability is calculated as the product between the frequency of an initiating event (ignition of a wildland fuel) and the probabilities of passing along a series of intermediate events between the initiating event and the outcome. The intermediate events are burned area > 1 ha, ambient temperature > 22°C, wind velocity > 4 m/s and burn probability > 0.01, for which this event tree anaylsis gives $7.36 \cdot 10^{-5}$ events/year as the probability of a wildfire reaching the WUI. On the other hand, the analysis of consequences requires determining asset vulnerability to a thermal insult, which is the quantitative relationship between thermal exposure of the asset and the damage experienced by it. This vulnerability is assessed by expressing it in terms of a probability of failure (ignition) for different doses of thermal radiation, i.e., a dose-response curve of sigmoid shape. To produce this curve, a probit equation is determined from flammability data of PMMA, a material that served as a proxy for the actual materials within the electrical substation. Thermal exposure of a target within the substation is calculated from fireline intensity and flame length results obtained with FlamMap simulations carried out on a simplified landscape representing the study area along with a simplified model for heat flux from the wildfire front to the target. Ignition probabilities are estimated with this vulnerability model for two wildfire scenarios in the substation. Wildfire risk is thus estimated as 10^{-6} to 10^{-5} events/year, or equivalently, one event every 100,000 to 1,000,000 years.

1. Introduction

Wildfires in Chile have caused significant human, ecological and economic damage to cities, protected areas, and the economy (Reszka and Fuentes 2014; Bowman et al. 2018). Climate change is expected to increase the occurrence and severity of these events (McWethy et al. 2018; Pausas and Keeley 2021; United Nations Environment Programme 2022). A need for tools to address wildfire risk quantitatively has been recognized, to support decision-making for wildfire safety in the Wildland-Urban Interface (WUI) (Finney 2005; Johnston et al. 2020; Miller and Ager 2013; Oliveira et al. 2021), following modern wildfire management paradigms (Moreira et al. 2020).

The goal of this work is to estimate wildfire risk to an electrical substation operated by Chilquinta Distribución S.A., a Chilean utility company. For this purpose, a methodology based on the Quantitative Risk Analysis (QRA) framework (Pasman and Reniers 2014; Center for Chemical Process Safety 2000) is proposed, where risks are defined as the product between the probability of incident outcomes and their consequences. The Wildfire Quantitative Risk Analysis (WFQRA) framework is illustrated in Fig. 1, based on the work by Johnston et al. (2020).

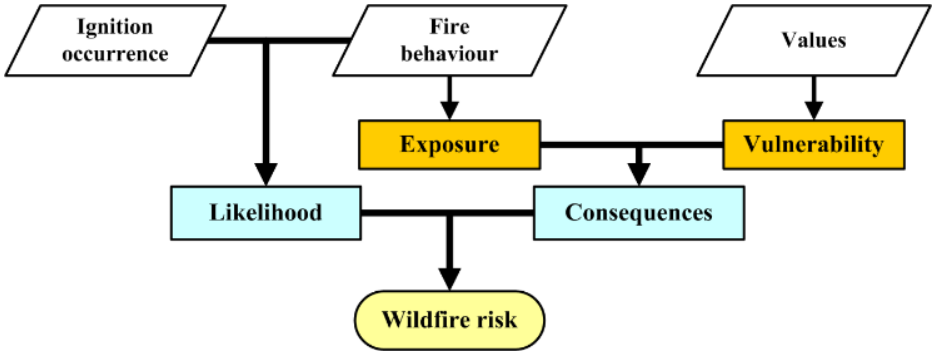

Figure 1- Relations between the definitions adopted for the WFQRA methodology (Johnston et al. 2020).

2. Methodology

The WFQRA can be used to estimate risk at any point of a study area but is used in this work to analyze a small segment of the WUI occupied by the electrical substation. The initiating event of any wildfire is a wildland fuel ignition that develops into sustained combustion of the surrounding fuels. The outcome is the arrival of the wildfire to the WUI. Risk is thus estimated as:

$$R_{x,y} = P_p P_d \tag{1}$$

where P_p is the probability of a wildfire reaching point (x,y), and P_d is the probability of a target sustaining a damage, target ignition in this case.

The electrical substation is in the WUI that surrounds the cities of Valparaíso and Viña del Mar (33°06'30"S, 71°33'32"W; Fig. 2a). Fig. 2b shows a Digital Elevation Model (DEM) of the study area, acquired by the ALOS satellite with resolution of 12.5 m per pixel. Maps for slope and aspect (Figs. 2c and 2d) were produced with this DEM. Fig. 3 shows histograms from hourly data recorded by a weather station located near the study area during the entire year 2020. A survey made by the Chilean Forest Service (CONAF) indicates that *Eucalyptus globulus* plantations are the main fuel in the study area.

Calculating the likelihood of a wildfire reaching the WUI (P_p) requires estimating an historic ignition frequency (f_{ig}), and the conditional probability of a wildfire spreading to the WUI ($P_{p|ig}$), which is predicted with an event tree (Andrews and Dunnett 2000). Therefore:

$$P_p = f_{ig} P_{p|ig} = f_{ig} \prod_{j=1}^{N} P_{p|ig,j} \tag{2}$$

where $P_{p|ig,j}$ is the probability of an intermediate outcome after the j-th node in the event tree, and N is the number of nodes in the branch leading to the outcome of interest.

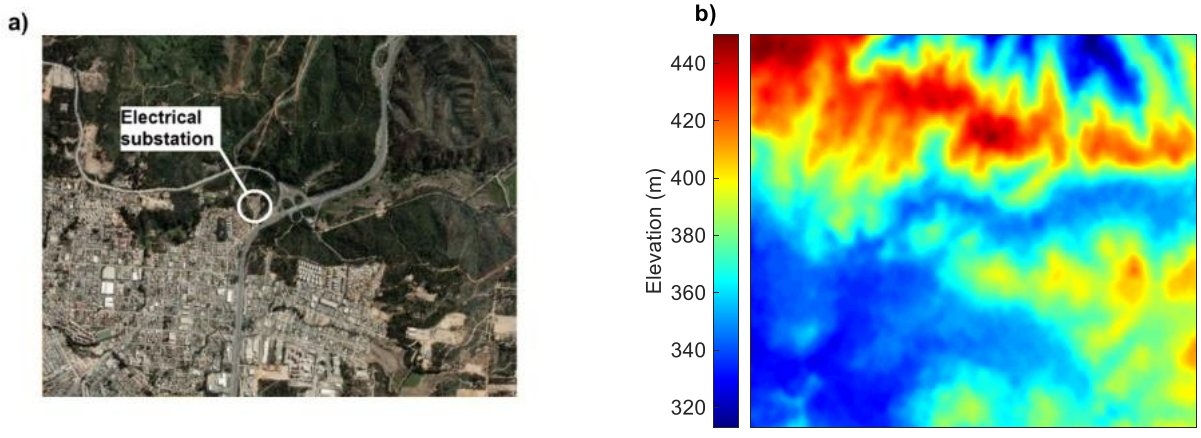

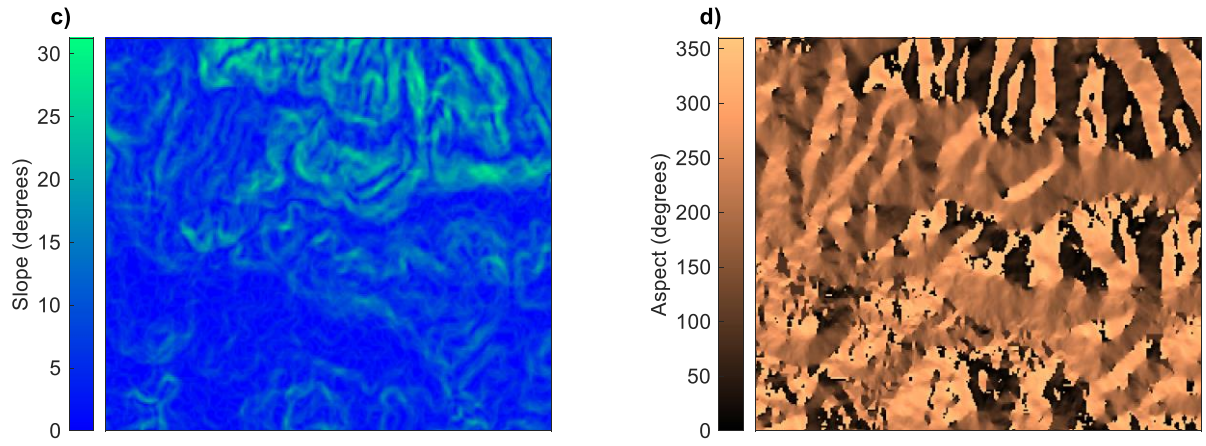

Figure 2- Study area: a) satellite image; b) DEM; c) slope, and; d) aspect map.

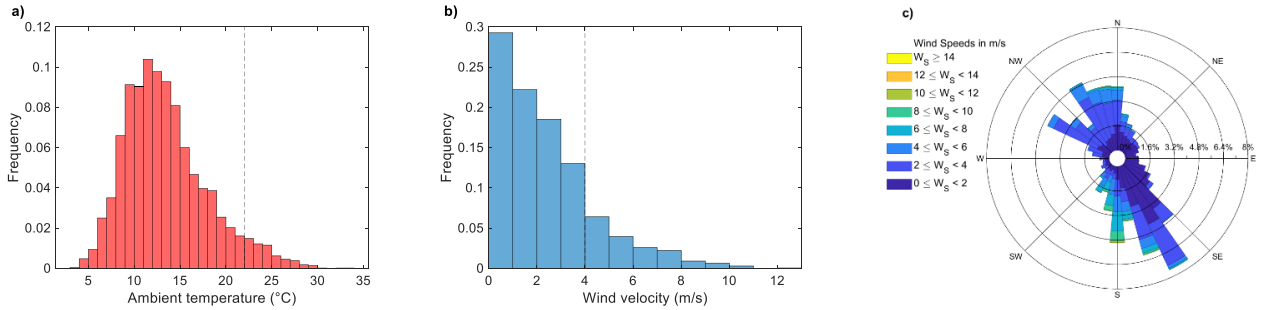

a) ***b)*** ***c)***

Figure 3- Histograms from hourly data recorded by a weather station near the study area during all year 2020: a) temperature; b) wind velocity, and; c) wind rose.

Wildfire consequences depend on both the exposure and the vulnerability of a target to a radiative heat insult. The vulnerability of the target is the quantitative relationship between thermal exposure and target damage. In fires, for damage to occur the target must ignite (a binary response: ignition/no ignition), thus a way of evaluating asset vulnerability is to express it in terms of an ignition probability P_d for different radiant heat fluxes, resulting in a dose-response curve that generally takes a sigmoidal form, which can be converted to a linear function with a probit analysis (Finney 1947). The probit function is the inverse of the cumulative distribution function (CDF) of the standard normal distribution. Therefore, if a dose-response curve is modelled as a normal CDF with mean μ and standard deviation σ, the relation between response P_d and probit variable Y is:

$$P_d(Y) = \frac{1}{\sigma\sqrt{2\pi}} \int_{-\infty}^{Y-5} \exp\left(-u^2/2\right) du \tag{3}$$

where $u = (D-\mu)/\sigma$ and D is a thermal dose. Note that Y is in the upper limit of the integral in the right-hand side of Eq. 3, where 5 is subtracted to Y so that the conversion gives $Y = 5$ when $P_d = 50\%$ (Finney 1947). Since the CDF and its inverse are not available in closed form, computing the probit function requires approximations, e.g.:

$$P_d(Y) = 50\left[1 + \frac{Y-5}{|Y-5|} \cdot \operatorname{erf}\left(\frac{|Y-5|}{\sqrt{2}}\right)\right] \tag{4}$$

By converting the measured cumulative responses into probit variables with Eq. 4, the dose-response curve in terms of the probit variable becomes linearly related to the logarithm of the dose:

$$Y = k_1 + k_2 \cdot \log(D) \tag{5}$$

where k_1 and k_2 are constants from a linear regression. This method is used to evaluate the vulnerability of people (Center for Chemical Process Safety 2000) and vessels (Cozzani et al. 2005) to thermal exposures, and

it is implemented in this work to develop a vulnerability model from flammability data. Considering that electrical equipment is usually manufactured in metallic alloys and polymers, and that the latter are most vulnerable to fires, PMMA is selected as a proxy fuel to develop this model from data available in the literature (Bal and Rein 2011).

For estimating exposure, a configuration consisting of a rectangular solid flame front at some distance from the target within the electrical substation is considered (Fig. 4). Assuming the flame front as a blackbody and neglecting atmospheric transmissivity, radiant heat flux on the target is:

$$\dot{q}_r'' = F\frac{X_r b I_f}{A_f} \tag{6}$$

where F is the view factor between the wildfire front and the target, estimated as described by Morandini et al. (2013), X_r is radiant fraction (assumed equal to 0.3, Pinto et al. 2020), b is rectangle width, H is flame length, A_f is rectangle surface ($A_f = b \cdot H$), and I_f is fireline intensity. Flame length and fireline intensity were determined from FlamMap 6.1 simulations (Finney 2006), using the topography, weather, and fuel models of the study area as inputs. A simplified landscape consisting only of an urban and a wildland area was used for these simulations, with fuel models 91 and 163 from the classification developed by Scott and Burgan (2004) being assigned to these areas. Simulations considered crown fire modeling with constant values for stand height (15 m), canopy base height (1 m) and canopy bulk density (0.2 kg m^{-3}), and a uniform wind field (5 m/s at 150°, cf. Figs. 6d and 3c). Burn probability was also estimated with FlamMap by simulating 1,000 fires ignited at random locations in the study area, considering the same resolution as in the DEM map, crown fire modeling with the same conditions described above, maximum simulation time of 50 min per ignition and spot probability set at 0.5. Although firebrand production is an important pathway for rapid wildfire propagation via spot fires (Fernandez-Pello 2017; Manzello et al. 2020), this phenomenon was not addressed with further detail, since the aim of this work is to demonstrate the usefulness of the WFQRA framework applied to the present case.

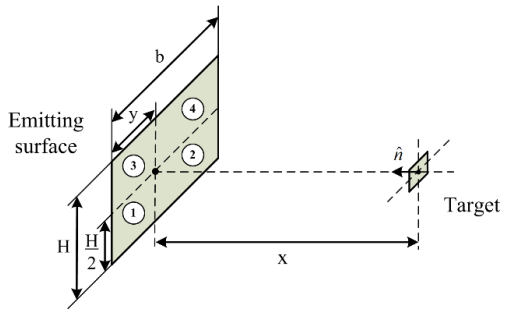

Figure 4- Configuration assumed to determine the view factor between the wildfire front and a differential target.

3. Results

3.1. Likelihood of a wildfire reaching the WUI

Figure 5 shows the event tree proposed to estimate the probability of a wildfire reaching the WUI, which gives P_p = 7.36·10^{-5} events/year. Ignition frequency is estimated at 239 events per year from CONAF historical ignition data circumscribed to the Valparaíso and Viña del Mar municipalities between 2002 and 2019 (Fig. 6a). As this estimation corresponds to the total area of the two cities (52,320 ha), this frequency is scaled down to the study area (996 ha), giving f_{ig} = 239·996/52,320 = 4.55 events per year. Additionally, CONAF has registered the resulting burned areas from these ignitions (Fig. 6b), along with ambient temperature and wind velocity recorded when these ignitions occurred (Figs. 6c and 6d). In the event tree, the probability of a fire resulting in burned area > 1 ha is 0.166 (calculated as 1 – 0.834 = 0.166, where 0.834 is the frequency of burned area between 0 and 1 ha in Fig. 6b), and the probabilities of having representative temperature and wind magnitudes during a wildfire are estimated by selecting their most frequent ranges in the 2002-2019 period (22 to 24°C in Fig. 6c and 4 to 6 m/s in Fig. 6d, respectively), and then summing the frequencies corresponding to temperatures and wind velocities higher than 22°C and 4 m/s in 2020 (Figs. 3a and 3b), giving 0.056 and 0.170, respectively. Figure 7 shows burn probability estimated with FlamMap, from which an average of 0.010 in the substation perimeter is considered for the event tree.

Initiating event	Is burned area > 1 ha	Is ambient temperature > 22°C?	Is wind velocity > 4 m/s?	Burn probability	Outcome
				Yes	Propagation to the WUI
			Yes	0.010	0.0000736
		Yes	0.170	No	No propagation to the WUI
	Yes	0.056		0.990	0.00714
Ignition of a wildland fuel	0.166		No		No propagation to the WUI
4.55			0.830		0.03521
(events/year)		No			No propagation to the WUI
		0.944			0.71239
	No				No propagation to the WUI
	0.834				3.79496

Figure 5- Event tree to estimate the likelihood of a wildfire reaching the WUI.

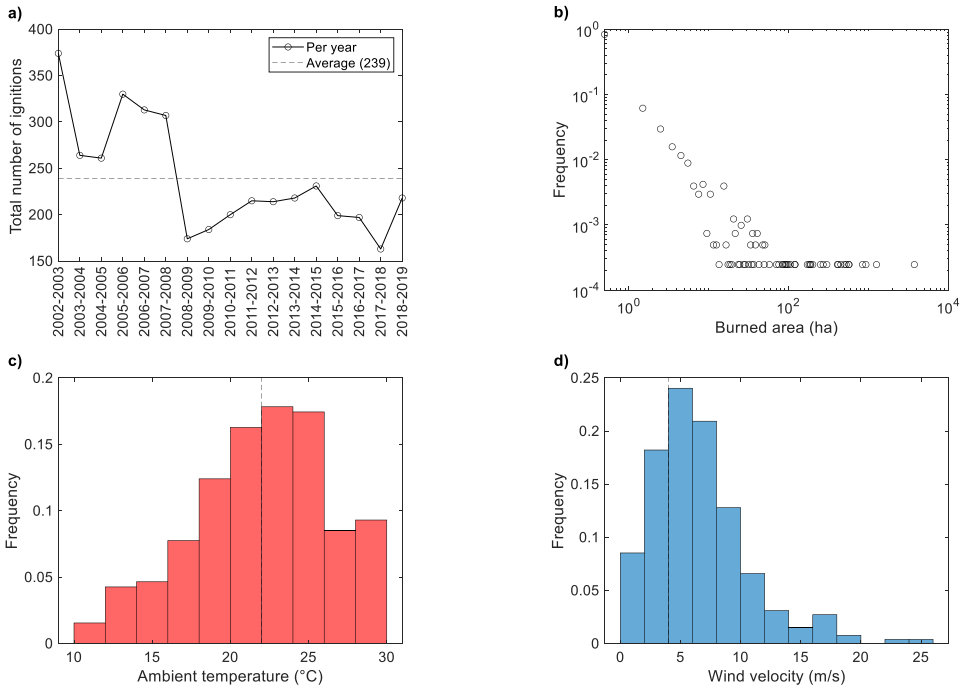

Figure 6- Wildfire data for the Valparaíso and Viña del Mar municipalities between 2002 and 2019: a) ignitions per year (July to June); b) burned area; c) temperature (burned area > 1 ha), and; d) wind velocity (burned area > 1 ha).

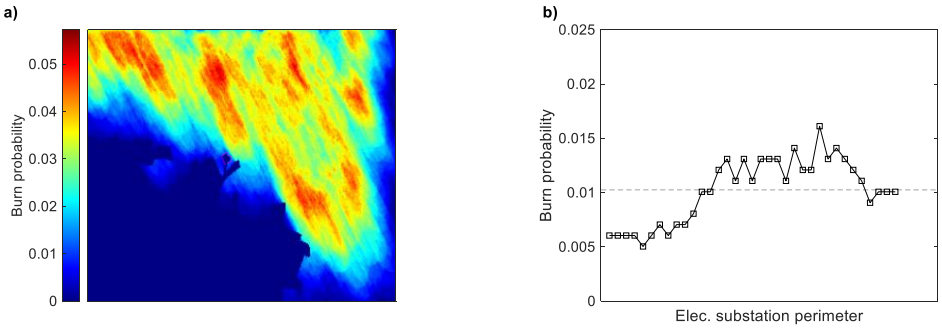

Figure 7- Burn probability: a) map; b) profile in the electrical substation perimeter.

3.2. Vulnerability

A probit equation for the vulnerability of PMMA is determined from the experimental data shown in Fig. 8a (Bal and Rein 2011), where no unique value of a critical heat flux is observed, because these data include results from several authors, heat losses from the specimens induce non-linearities (Sabi et al. 2018, 2021), and a critical heat flux criterion depends on the experimental configuration and procedure (Mindykowski et al. 2011). Instead, there is a transition from a low (~1%) to a high ignition probability (~99%). To estimate the heat fluxes corresponding to these ignition probabilities, it is assumed that data in Fig. 8a is bounded by two curves that tend to these heat fluxes when time to ignition increases:

$$t_{ig,lower} = C_{lower} \cdot (\dot{q}_e'')^{\gamma} \tag{7a}$$

$$t_{ig,upper} = C_{upper} \cdot (\dot{q}_e'')^{\gamma} \tag{7b}$$

where C_{lower} and C_{upper} are two constants, and γ is a common exponent (Sabi et al. 2021). By calculating the logarithm of each side in Eqs. 7a and 7b:

$$\log(t_{ig,lower}) = \log(C_{lower}) + \gamma \cdot \log(\dot{q}_e'') \tag{8a}$$

$$\log(t_{ig,upper}) = \log(C_{upper}) + \gamma \cdot \log(\dot{q}_e'') \tag{8b}$$

Exponent γ is determined with a linear fit to data in Fig. 8b, giving γ = -2.6044. Constants C_{lower} and C_{upper} are estimated by adjusting two bounding curves to the data and determining their intersections with the *y*-axis, giving C_{lower} = exp(12.5) = $2.68 \cdot 10^5$ and C_{upper} = exp(15.3) = $4.41 \cdot 10^6$. With these results, Fig. 8a shows the lower and upper fits to the data expressed by Eqs, 7a and 7b. By setting t_{ig} = 3000 s in Eqs. 7a and 7b, the limiting critical heat fluxes are 5.6 to 16.4 kW/m^2 (dashed lines in Fig. 8a): to the left of this range there is a no-ignition region, and to the right, ignition probability approaches 100%.

Since probit values corresponding to 1% and 99% are 2.67 and 7.33, respectively, a probit equation is obtained by applying a linear fit to these probits as a function of the logarithm of the two limiting heat fluxes (log(5.6) = 1.72 and log(16.4) = 2.80, Fig. 8c), resulting in:

$$Y = -4.8014 + 4.3368 \cdot \log(\dot{q}_e'') \tag{9}$$

Using Eq. 4, Fig. 8d shows ignition probability of PMMA in terms of the logarithm of heat flux.

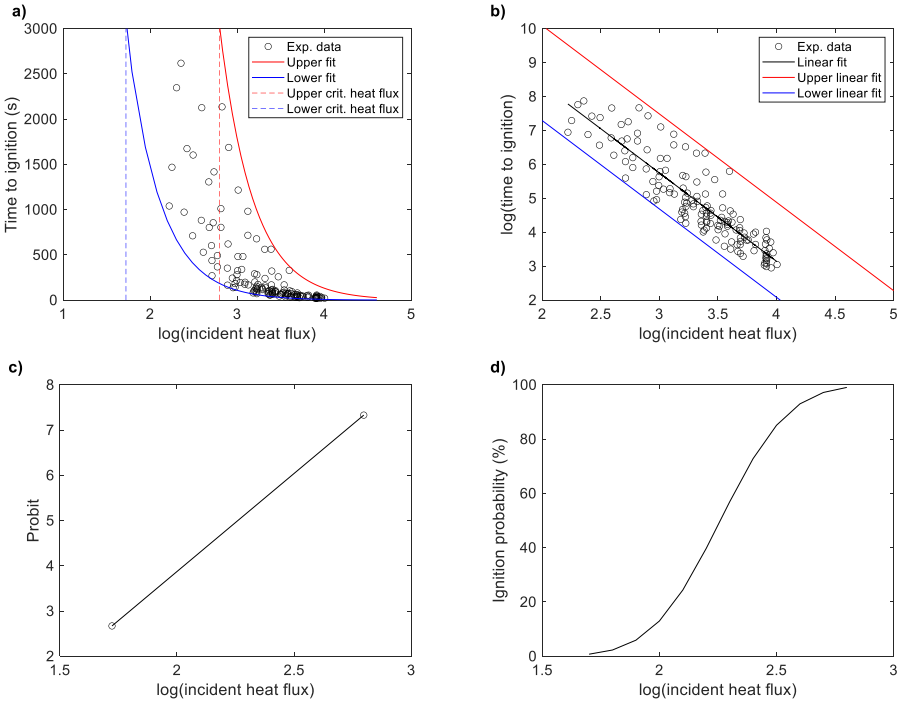

Figure 8- a) Flamambility data used for the PMMA vulnerability model; b) data in log-log scales; c) probit function, and; d) ignition probability.

3.3. Exposure

Fireline intensity and flame length maps from FlamMap simulations are shown in Fig. 9a and 9b. Homogeneous patterns are observed near the WUI, which is attributed to the species uniformity. Fig. 9c and 9d shows fireline intensity and flame length profiles for the substation perimeter, averaging 1832 kW/m and 3.98 m, respectively.

These results represent fire behavior in all the landscape pixels. This is equivalent to a wildfire engulfing the substation perimeter (Fig. 10). A more realistic scenario is a flame front attacking one side of the perimeter at the time. Hence two scenarios are considered (Fig. 10) for estimating view factor and incident heat flux on the target within the substation with Eq. 6, omitting the existence of a wall or fence around it to simplify the problem. Table 1 summarizes these results.

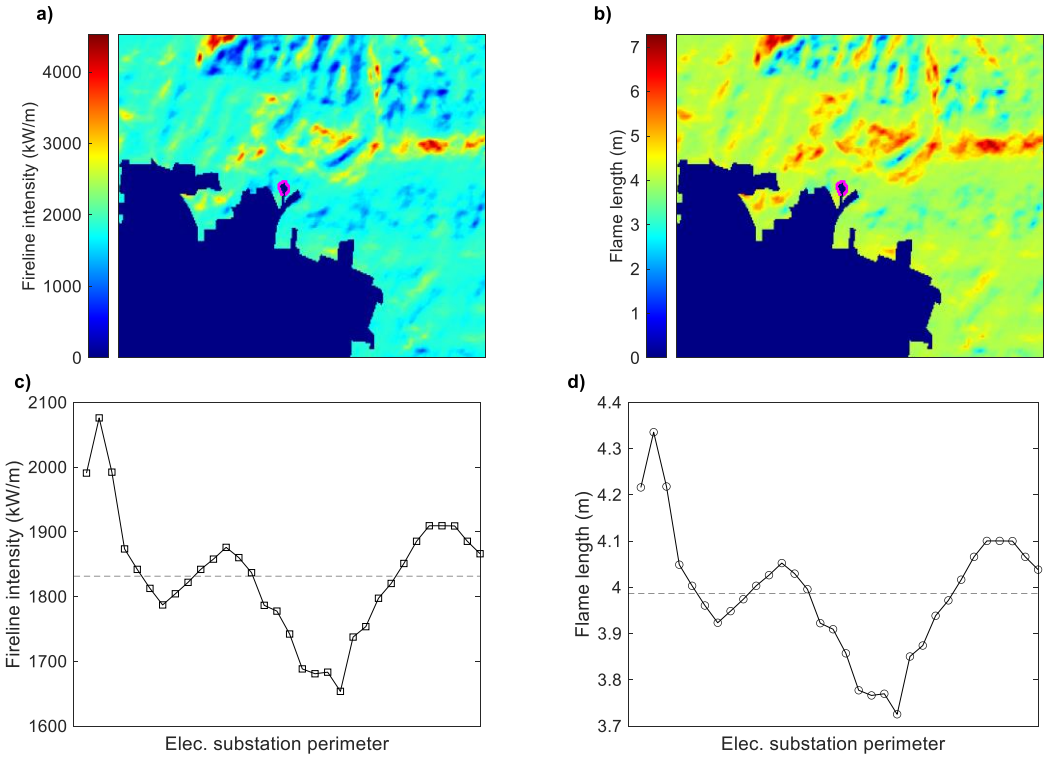

Figure 9- FlamMap outputs: a) fireline intensity; b) flame length; c) fireline intensity profile, and; d) flame length profile.

Figure 10- Scenarios for estimating incident heat flux on a target within the substation. Orange indicates a wildfire engulfing the substation perimeter; yellow rectangles represent the flame fronts considered.

3.4. Wildfire risk

Wildfire risk is calculated with Eq. 1, considering $P_p = 7.36 \cdot 10^{-5}$ events/year (cf. Section 3.1). Probit values are determined with Eq. 9 using the heat fluxes estimated from the fire behavior simulations (cf. Section 3.3), and these probits are used as inputs to Eq. 4 to determine asset ignition probabilities (cf. Table 1). Wildfire risk results are shown in Table 1. Their orders of magnitude are 10^{-6} to 10^{-5} events/year, i.e. one event every 100,000 to 1,000,000 years. It is observed that the probability of a wildfire reaching the electrical substation ($7.36 \cdot 10^{-5}$ events/year) and asset ignition probability (0.03 to 0.3) cannot be used as full risk metrics by themselves only. It is necessary to consider these two components into a wildfire risk estimate, and the definition of wildfire risk proposed in this work is thus more comprehensive than other ones found in the literature (Johnston et al. 2020).

Table 1- Results obtained with the WFQRA for two wildfire scenarios in the electrical substation.

Scenario	A	B
P_p (events/year)	$7.36 \cdot 10^{-5}$	$7.36 \cdot 10^{-5}$
I_f (kW/m)	1832	1832
H (m)	3.98	3.98
b (m)	40	45
A_f (m^2)	159	179
X_r	0.3	0.3
F	0.045	0.060
$\dot{q}_r''$ (kW/m^2)	6.2	8.3
log ($\dot{q}_r''$)	1.82	2.12
Y	3.11	4.38
P_d	0.029	0.269
$R_{x,y}$ (events/year)	$2.2 \cdot 10^{-6}$	$2.0 \cdot 10^{-5}$

4. Discussion

The WFQRA framework presented in this work enables analyzing wildfire risk in a systematic fashion. On one hand, the likelihood of a wildfire reaching the WUI depends on ignition frequency, whose anthropogenic component depends on human behavior and thus could be reduced by educational campaigns, law enforcement or other measures of such nature. This likelihood also depends on burn probability: since a patchy landscape typically hinders wildfire propagation, burn probability could be lowered by treating the wildland fuels and reducing the fuel load near the electrical substation. On the other hand, ignition probability of a target depends mostly on the incident heat flux, which can be lowered by establishing a wide and clear area between the substation and the wildland or blocking radiant heat transfer. Some observations concerning the assumptions, limitations and perspectives of the methodology are:

- Characterizing the study area requires defining a period and spatial delimitation for historical ignition data. Data availability can be an issue because historical records are imperative to estimate ignition frequency. Since climate/weather impacts on the propensity of wildland fuels to ignite, a period of analysis should be clearly and carefully defined so that the estimated ignition frequency be representative of current climatic conditions. Also, the study area may have a particular ignition pattern different to that of the territory in which it is located, hence varying its boundaries for ignition data may also impact on ignition frequency.
- Only two fuel models are considered in this work for simplicity, but a detailed risk analysis requires dividing the study area into several subareas depending on the wildland fuels distribution. This fuel mapping is a challenging task, since it needs a territorial division in terms of plant species, forest type (native or plantation), canopy cover, stand height, fuel load, etc.
- Estimations of flame length and fireline intensity depend on the models incorporated in the fire behavior modeling tool. For example, flame length is usually correlated to fireline intensity via power-law relationships that require two empirical constants, thus flame length might vary one order of magnitude for a given fireline intensity depending on the pair of constants used (Egorova et al. 2022).
- Using a dose-response curve assumes a binary response for the target (ignition/no ignition), in line with a theoretical approach that considers ignition as a phase transition problem where time to ignition either diverges or vanishes according to a universal power-law formula when incident heat flux tends to a critical

value (Sabi et al. 2018, 2021). This approach suits well to understand the sigmoid nature of the dose-response curve for flammability data expressed as ignition probability.

- When the wildfire front arrives to the WUI, firebrands impacting on the target represent a crucial ignition mechanism. Direct thermal radiation and spotting work in parallel, hence the risk posed by them to an asset should be addressed separately, and then summed. Incorporating spotting into the WFQRA framework requires a more extensive database not yet compiled, considering the complex ignition characteristics of structural fuels (Manzello et al. 2020).
- The WFQRA methodology could be used to discriminate between catastrophic and regular wildfires by adding a branch in the event tree to distinguish weather conditions that are prone to extreme fire events from those that are not, leading to two risk estimates, one for regular fires and another for extreme wildfires, which can be directly summed to estimate wildfire risk on the asset.
- In the absence of a tolerability criterion for wildfires, the results obtained with the WFQRA could be compared with risk estimates for other activities. For example, maximum tolerable risks in Canada and the UK are between 10^{-3} and 10^{-6} per year for land-use planning, worker safety and other industries (Muhlbauer 2004).

5. Conclusion

A quantitative methodology for estimating the risk posed by wildfires is proposed and applied to an electrical substation in the WUI of Valparaiso, Chile. Simulations were carried out with FlamMap to estimate burn probability, flame length and fireline intensity in the substation perimeter, but the methodology is independent of the modelling software employed. Wildfire consequences for a proxy fuel within the substation were estimated from a dose-response curve determined with a probit analysis that links incident heat flux on the target with its ignition probability. This comprehensive definition of wildfire risk considers both wildfire occurrence probability (via an event tree analysis) and asset vulnerability, thus potentially enabling a systematic analysis of wildfire risk evolution in time due to climate changes and a quantitative assessment of risk mitigation measures. Due to this, the WFQRA framework is well suited to analyze risk at critical infrastructure located at the WUI.

6. Acknowledgments

This research was jointly funded by ANID SCIA/ANILLO ACT210052 and by Chilquinta Distribución S.A.

7. References

Andrews, J. D., and Dunnett, S. J. (2000). Event-tree analysis using binary decision diagrams. IEEE Transactions on Reliability, 49(2), 230–238. https://doi.org/10.1109/24.877343

Bal, N., and Rein, G. (2011). Numerical investigation of the ignition delay time of a translucent solid at high radiant heat fluxes. Combustion and Flame, 158(6), 1109–1116. https://doi.org/10.1016/J.COMBUSTFLAME.2010.10.014

Bowman, D. M. J. S., Moreira-Muñoz, A., Kolden, C. A., Chávez, R. O., Muñoz, A. A., Salinas, F., González-Reyes, Á., Rocco, R., de la Barrera, F., Williamson, G. J., Borchers, N., Cifuentes, L. A., Abatzoglou, J. T., and Johnston, F. H. (2018). Human–environmental drivers and impacts of the globally extreme 2017 Chilean fires. Ambio, 48(4), 350–362. https://doi.org/10.1007/S13280-018-1084-1

Center for Chemical Process Safety. (2000). Guidelines for Chemical Process Quantitative Risk Analysis (2nd ed.). Wiley-Interscience.

Cozzani, V., Gubinelli, G., Antonioni, G., Spadoni, G., and Zanelli, S. (2005). The assessment of risk caused by domino effect in quantitative area risk analysis. Journal of Hazardous Materials, 127(1–3), 14–30. https://doi.org/10.1016/J.JHAZMAT.2005.07.003

Egorova, V. N., Trucchia, A., and Pagnini, G. (2022). Fire-spotting generated fires. Part II: The role of flame geometry and slope. Applied Mathematical Modelling, 104, 1–20. https://doi.org/10.1016/J.APM.2021.11.010

Fernandez-Pello, A. C. (2017). Wildland fire spot ignition by sparks and firebrands. Fire Safety Journal, 91, 2–10. https://doi.org/10.1016/j.firesaf.2017.04.040

Finney, D. J. (1947). Probit Analysis. Cambridge University Press.

Finney, M. A. (2005). The challenge of quantitative risk analysis for wildland fire. Forest Ecology and Management, 211(1–2), 97–108. https://doi.org/10.1016/j.foreco.2005.02.010

Finney, M. A. (2006). An Overview of FlamMap Fire Modeling Capabilities. In P. L. Andrews and B. W. Butler (Eds.), Fuels Management-How to Measure Success: Conference Proceedings (pp. 213–220). Fort Collins, CO. U.S. Department of Agriculture, Forest Service, Rocky Mountain Research Station.

Johnston, L. M., Wang, X., Erni, S., Taylor, S. W., McFayden, C. B., Oliver, J. A., Stockdale, C., Christianson, A., Boulanger, Y., Gauthier, S., Arseneault, D., Wotton, B. M., Parisien, M. A., and Flannigan, M. D. (2020). Wildland fire risk research in Canada. Environmental Reviews, 28(2), 164–186. https://doi.org/10.1139/er-2019-0046

Manzello, S. L., Suzuki, S., Gollner, M. J., and Fernandez-Pello, A. C. (2020). Role of firebrand combustion in large outdoor fire spread. Progress in Energy and Combustion Science, 76, 100801. https://doi.org/10.1016/j.pecs.2019.100801

McWethy, D. B., Pauchard, A., García, R. A., Holz, A., González, M. E., Veblen, T. T., Stahl, J., and Currey, B. (2018). Landscape drivers of recent fire activity (2001-2017) in south-central Chile. PLOS ONE, 13(8), e0201195. https://doi.org/10.1371/JOURNAL.PONE.0201195

Miller, C., and Ager, A. A. (2013). A review of recent advances in risk analysis for wildfire management. International Journal of Wildland Fire, 22(1), 1–14. https://doi.org/10.1071/WF11114

Mindykowski, P., Fuentes, A., Consalvi, J. L., and Porterie, B. (2011). Piloted ignition of wildland fuels. Fire Safety Journal, 46(1–2), 34–40. https://doi.org/10.1016/j.firesaf.2010.09.003

Morandini, F., Perez-Ramirez, Y., Tihay, V., Santoni, P. A., and Barboni, T. (2013). Radiant, convective and heat release characterization of vegetation fire. International Journal of Thermal Sciences, 70, 83–91. https://doi.org/10.1016/j.ijthermalsci.2013.03.011

Moreira, F., Ascoli, D., Safford, H., Adams, M. A., Moreno, J. M., Pereira, J. M. C., Catry, F. X., Armesto, J., Bond, W., González, M. E., Curt, T., Koutsias, N., McCaw, L., Price, O., Pausas, J. G., Rigolot, E., Stephens, S., Tavsanoglu, C., Vallejo, V. R., Van Wilgen, B. W., Xanthopoulos, G. and Fernandes, P. M. (2020). Wildfire management in Mediterranean-type regions: paradigm change needed. Environmental Research Letters, 15(1), 011001. https://doi.org/10.1088/1748-9326/AB541E

Muhlbauer, W. K. (2004). Pipeline risk management manual: ideas, techniques, and resources (3rd ed.). Elsevier.

Oliveira, S., Rocha, J., and Sá, A. (2021). Wildfire risk modeling. Current Opinion in Environmental Science and Health, 23, 100274. https://doi.org/10.1016/J.COESH.2021.100274

Pasman, H., and Reniers, G. (2014). Past, present and future of Quantitative Risk Assessment (QRA) and the incentive it obtained from Land-Use Planning (LUP). Journal of Loss Prevention in the Process Industries, 28, 2–9. https://doi.org/10.1016/J.JLP.2013.03.004

Pausas, J. G., and Keeley, J. E. (2021). Wildfires and global change. Frontiers in Ecology and the Environment, 19(7), 387–395. https://doi.org/10.1002/FEE.2359

Pinto, P., Cabrera, A., Cruz, J. J., Contreras, J., Severino, G., Demarco, R., Elicer-Cortés, J. C., and Fuentes, A. (2020). Effects of wildland fuel moisture content on radiant heat flux emitted by a laminar non-premixed flame. Applied Thermal Engineering, 181, 115968. https://doi.org/10.1016/j.applthermaleng.2020.115968

Reszka, P., and Fuentes, A. (2014). The Great Valparaiso Fire and Fire Safety Management in Chile. Fire Technology, 51(4), 753–758. https://doi.org/10.1007/S10694-014-0427-0

Sabi, F. Z., Terrah, M. S., Mosbah, O., Dilem, A., Hamamousse, N., Sahila, A., Harrouz, O., Zekri, N., Kaiss, A., Clerc, J.-P., Rahli, O., Giroud, F., and Picard, C. (2018). Ignition/non ignition phase transition. In Advances in Forest Fire Research 2018 (pp. 506–513). Imprensa da Universidade de Coimbra. https://doi.org/10.14195/978-989-26-16-506_55

Sabi, F. Z., Terrah, S. M., Mosbah, O., Dilem, A., Hamamousse, N., Sahila, A., Harrouz, O., Boutchiche, H., Chaib, F., Zekri, N., Kaiss, A., Clerc, J. P., Giroud, F., and Viegas, D. X. (2021). Ignition/non-ignition phase transition: A new critical heat flux estimation method. Fire Safety Journal, 119, 103257. https://doi.org/10.1016/J.FIRESAF.2020.103257

Scott, J. H., and Burgan, R. E. (2005). Standard fire behavior fuel models: a comprehensive set for use with Rothermel's surface fire spread model. U.S. Department of Agriculture, Forest Service, Rocky Mountain Research Station. General Technical Report RMRS-GTR-153. https://doi.org/10.2737/RMRS-GTR-153

United Nations Environment Programme. (2022). Spreading like Wildfire: The Rising Threat of Extraordinary Landscape Fires. A UNEP Rapid Response Assessment.

A statistical model of Fire Radiative Power released by wildfires at the global scale

Carlos C. DaCamara*[1]; José M. C. Pereira[2]; Renata Libonati[3]; Sílvia A. Nunes*[1]

[1]*Instituto Dom Luiz (IDL), Faculdade de Ciências, Universidade de Lisboa, 1749-016 Lisbon, Portugal, {cdcamara, sanunes}@fc.ul.pt*
[2]*Centro de Estudos Florestais, Instituto Superior de Agronomia, Universidade de Lisboa, 1349-017, Lisbon, Portugal {jmcpereira@isa.ulisboa.pt}*
[3]*Departamento de Meteorologia, Universidade Federal do Rio de Janeiro, 21941-916, Rio de Janeiro, RJ, Brasil {renata.libonati@igeo.ufrj.br}*

**Corresponding author*

Keywords

Global fire activity; Fire macroregimes; Fire Radiative Power; Truncated lognormal distribution with generalized Pareto tails

Abstract

Characterization of large-scale fire regimes associated to patterns of fire activity is especially relevant because they reflect the complex interplay of meteorological, landscape, and human factors. We present a statistical model with 8 parameters that adequately describes satellite derived fire radiative power (FRP) at the global scale and over large areas with given fire regimes. The statistical model combines three components, namely a truncated lognormal distribution central body with a lower and an upper tail, both consisting of Generalized Pareto (GP) distributions. The model is fitted to four samples of 1 000 000 values of $\log_{10} FRP$ randomly selected from a dataset consisting of observations by the MODIS instrument on-board Terra and Aqua satellites covering the 19-year period spanning from 4 July 2002 to 3 July 2021. The four samples are extracted from observations worldwide and from regions characterized by three fire macroregimes, respectively Wild, Tamed and Domesticated fires. For all four cases, the very high quality of the fit translates into the agreement between the cumulative distribution function and the respective empirical cumulative distribution function obtained from the sample. When going from the Domesticated fire macroregime to the Tamed and then to the Wild fire macroregimes, there is a progressive displacement towards the right of the respective probability distribution functions that indicates a progressive tendency for the occurrence of extreme events with a high release of radiative power that is associated with a decrease in human actions that translates into lower landscape fragmentation and lower fire suppression. Statistical model of FRP of the type here presented are a useful tool that allows characterizing in an economic way fire behaviour in a given region and monitor changes in time associated to climate change or to changes in landscape or in land occupation.

1. Introduction

The large spatiotemporal patterns of fire activity reflect on the one hand, the control exerted by climate on vegetation productivity and on fuel accumulation and respective moist content (Andela et al., 2019), and on the other hand, the effect of human actions that account for most ignitions in burnable ecosystems as well for the decrease in fire size due to landscape fragmentation and fire suppression (Bowman et al., 2009).

The identification and characterization of the large-scale fire regimes associated to patterns of fire activity as well as of the factors that condition the spatiotemporal variability of fire activity are especially important, not only because fires result from a complex interplay of meteorological, landscape, and human factors, but also because they are a source of greenhouse gases.

The characterization of fire regimes is performed by means of a set of parameters describing which fires occur in each place and time, and Earth Observation by means of satellites plays a crucial role because it represents the only means to get systematic information at the global scale during sufficiently long periods of time. Besides providing the location and date of hotspots, satellites allow estimating fire radiative power (FRP) that is a measure of combustion rate, and therefore of consumed biomass (Wooster et al., 2005).

The aim of this work is to show that satellite derived FRP, at the global scale and over large areas with given fire regimes, can be described by means of a universal statistical model with 8 parameters. This is a useful tool that allows characterizing in an economic way fire behavior in a given region and monitor changes in time associated to climate change or to changes in landscape or in land occupation.

2. Data and Methods

Information about FRP was obtained from NASA's Fire Information for Resource Management System (FIRMS) that provides location, date and hour, FRP estimates and confidence for hotspots detected by the Moderate Resolution Imaging Spectroradiometer (MODIS) on-board Terra and Aqua satellites. Extracted data consist of 85 412 052 estimates of FRP associated to all hotspots (identified as active vegetation fires) during the 19-year period spanning from 4 July 2002 to 3 July 2021. The starting date of the period is that when observations become available for both MODIS instruments on-board Terra and Aqua.

Following Pereira et al. (2022), global fires were stratified into three fire macroregimes that are interpreted according to climate type (Köppen classification) and to ecological patterns created by sustained interactions between ecosytems and humans (anthromes) (Figure 1). The three regimes (each one subdivided into a prototypical and a transitional regime) are as follows; the Wild fire macroregime predominates in cold wildlands, and is characterized by sporadic burning and short fire seasons; the Tamed fire macroregime mostly occurs in rangeland and croplands of dry tropical climate and is characterized by high fire incidence; and the Domesticated fire macroregime that is characteristic of croplands and villages in humid, warm temperate and tropical climates and is characterized by low fire incidence. Results from the stratification into the three fire macroregimes were 67 324 278 Tamed fires, 9 768 127 Domesticated fires, and 8 319 647 Wild fires, respectively representing 79%, 11% and 10% of the active fires observed worldwide.

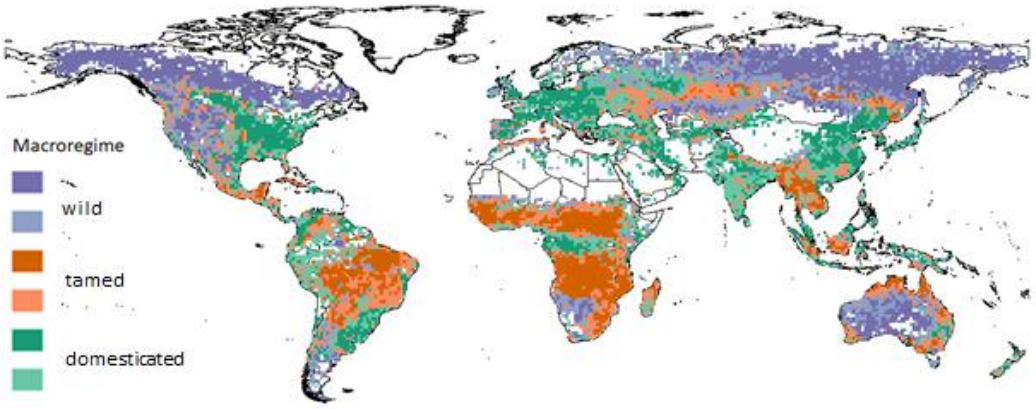

Figure 1- Global distribution of fire macroregimes; wild (violet), tamed (orange) and domesticated (green). For each macroregime, dark and light colors identify subdivision into prototypical and transitional regimes. The map was generated using information from Pereira et al. (2022).

Statistical models used in this study combine three components, namely a truncated lognormal distribution central body, f_b, with a lower and an upper tail, both consisting of Generalized Pareto (GP) distributions, f_l and f_u, respectively. The probability density function (pdf), h, for a generic random variable x is accordingly of the form:

$$h(x;\kappa_l,\sigma_l,x_l,\mu,\sigma_b,\kappa_u,\sigma_u,x_u) = \begin{cases} cbf_l(x;\kappa_l,\sigma_l,x_l), & x < x_l \\ bf_b(x;\mu_b,\sigma_b), & x_l \le x \le x_u \\ abf_u(x;\kappa_u,\sigma_u,x_u), & x > x_u \end{cases} \quad (1)$$

The lower tail GP distribution is:

$$f_l(x;\kappa_l,\sigma_l,x_l) = (1/\sigma_l)[1+\kappa_l\,(x_l-x)/\sigma_l]^{-1-1/\kappa_l}$$

where κ_l and σ_l denote the shape and the scale parameters of f_l, and where x_l is the transition point from the lower tail GP distribution to the truncated lognormal distribution body. When $\kappa_l < 0$, the distribution has a bounded support, $x_{min} < x < x_l$, with $x_{min} = x_l + \sigma_l/\kappa_l$.

The upper tail GP distribution is:

$$f_u(x; \kappa_u, \sigma_u, x_u) = (1/\sigma_u)[1 + \kappa_u\,(x - x_u)/\sigma_u]^{-1-1/\kappa_u}$$

where κ_u and σ_u denote the shape and the scale parameters of f_u, and where x_u is the transition point from the lognormal distribution body to the upper tail GP distribution. When $\kappa_u < 0$, the distribution has a bounded support, $x_u < x < x_{max}$, with $x_{max} = x_u - \sigma_u/\kappa_u$.

Finally, the lognormal distribution central body is:

$$f_b(x; \mu_b, \sigma_b, x_l, x_u) = \exp\left[-\frac{(\ln x - \mu)^2}{2\,(\sigma_b)^2}\right] \Big/ \left[\sqrt{2\pi}\; x\; \sigma\; C(\mu, \sigma_b, x_l, x_u)\right]$$

with

$$C(\mu_b, \sigma_b, x_l, x_u) = \frac{1}{2}\left[\mathrm{erf}\left(\frac{(\ln x_u - \mu_b}{\sqrt{2}\;\sigma_b}\right) - \mathrm{erf}\left(\frac{(\ln x_l - \mu_b}{\sqrt{2}\;\sigma_b}\right)\right]$$

and where μ_b and σ_b are the location and scale parameters of f_b.

Normalization constants a, b, and c in equation (1) must verify the relation:

$$cb + b + ab = 1 \Rightarrow b = (a + c + 1)^{-1}$$

On the other hand, continuity of h at $x = x_l$ and at $x = x_u$ implies that:

$$cbf_l(x_l) = bf_b(x_l) \Rightarrow c = \sigma_l f_b(x_l)$$
$$abf_u(x_u) = bf_b(x_u) \Rightarrow a = \sigma_u f_u(x_u)$$

The eight parameters $(\kappa_l, \sigma_l, x_l, \mu_b, \sigma_b, \kappa_u, \sigma_u, x_u)$ of h in equation (1) are obtained by maximizing the joint log-likelihood of an i.i.d. sample of x. The rationale for the procedure consists of three steps; 1) sample values of $\ln x$ are plotted against a theoretical lognormal distribution, and first guesses of x_l and x_u are obtained by identifying the lower and upper values of x that roughly delimit the inner domain of h, where points closely form a straight line, therefore following a lognormal distribution (Chambers et al., 2017); 2) first guesses of pairs (κ_l, σ_l), (μ_b, σ_b) and (κ_u, σ_u) are then obtained using the maximum likelihood method to fit, respectively, a GP distribution to sampled values $x < x_l$, a truncated lognormal distribution to sampled values $x_l \leq x \leq x_u$, and a GP distribution to sampled values $x > x_u$; 3) finally, first guesses obtained in the previous two steps are used to obtain maximum likelihood estimates of the eight parameters of h.

3. Results and discussion

Since the total number of recorded events is very large (85 412 052 hot spots), a sample of 1 000 000 events was randomly selected, and the statistical model was fitted to the logarithm of FRP (i.e., $x = \log_{10} FRP$) of selected events following the procedure described in the preceding section. Results obtained are presented in Figure 2, and the very high quality of the fit is worth being emphasized; the cumulative distribution function (cdf) virtually coincides with the empirical cumulative distribution function (ecdf) obtained from the sample (Figure 2, left panel) and the probability distribution function (pdf) closely follows the histogram obtained from the sample (Figure 2, right panel).

The same procedure was applied to the recorded events belonging to the three fire macroregimes. Results obtained are presented in Figure 3, and again the very high quality of the fit for each macroregime translates into the agreement between the cdf and the respective ecdf (Figure 3, left panel). It is worth noting that when going from the Domesticated fire macroregime to the Tamed and then to the Wild fire macroregimes, there is a progressive displacement towards the right of the respective pdfs that indicates a progressive tendency for the occurrence of extreme events with a high release of radiative power that is associated with a decrease in human actions that translates into lower landscape fragmentation and lower fire suppression.

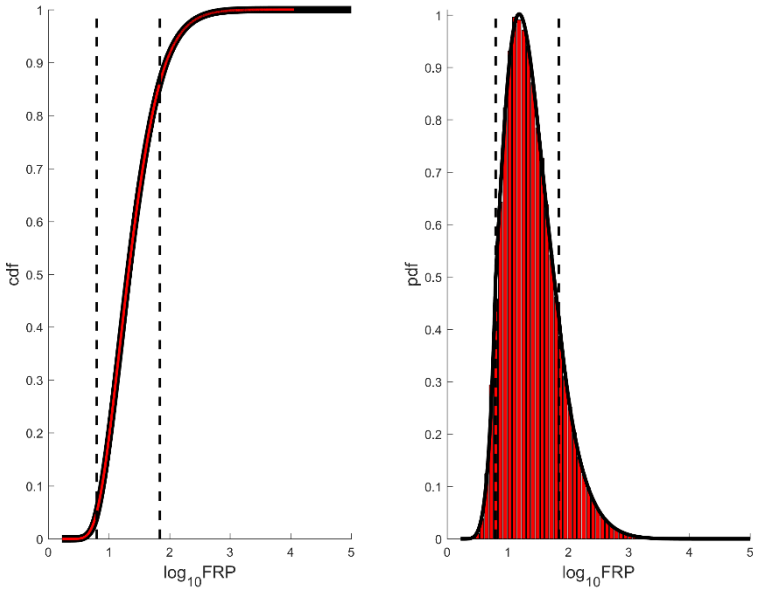

Figure 2 – Distribution of log_{10} FRP as obtained from the randomly selected sample of 1 000 000 hotspots observed worldwide during the period 04/07/2002 – 03/07/2021. Left panel: cumulated distribution function (cdf) of the fitted model (thick black curve) and empirical cumulative distribution function (ecdf) as obtained from the sample (thin red curve); right panel: probability density function (pdf) of the fitted model (thick black curve) and histogram obtained from the sample (red bars)). The two vertical dashed lines delimit the central body of the distribution.

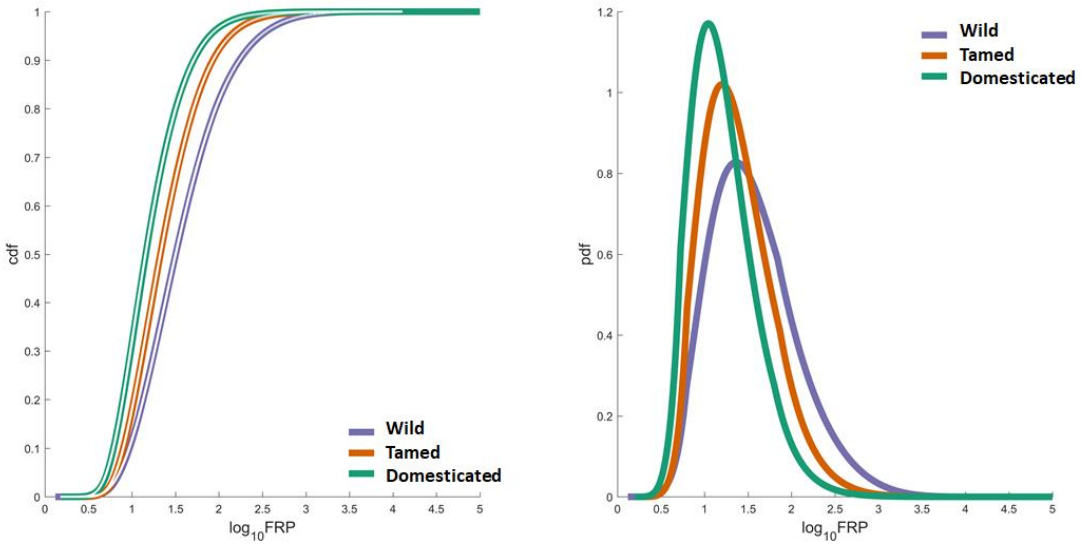

Figure 3 – Distribution of log_{10} FRP as obtained from the randomly selected sample of 1 000 000 hotspots for the Wild (violet), Tamed (orange) and Domesticated fire macroregimes during the period 04/07/2002 – 03/07/2021. Left panel: cumulated distribution function (cdf) of the fitted model (thick colored curves) and empirical cumulative distribution function (ecdf) as obtained from the sample (thin white curves); right panel: probability density function (pdf) of the fitted models.

4. Conclusion

Based on a 19-year record of satellite observations, we showed that the logarithm of FRP released by vegetation fires at the global scale closely follows a two generalized Pareto tail lognormal body distribution. The model showed to be especially useful to characterize fire macroregimes defined according to climate type and ecological patterns created by sustained interactions. Besides condensing information to a reduced number of parameters, models such as those proposed in this study allow comparing fire behavior for different periods and identifying changes in the distribution. Model of this type can be also used to calibrate meteorological indices of fire danger (DaCamara, 2014; Pinto et al. 2018) that provide operational support to decision makers on fire prevention and firefighting of rural and forest fires (DaCamara et al., 2018).

5. Acknowledgents

This work was supported by national funds through FCT (Fundação para a Ciência e a Tecnologia, Portugal) under project FIRECAST (PCIF/GRF/0204/2017), IDL (UIDB/50019/2020) and by EUMETSAT Satellite Application Facility on Land Surface Analysis (LSA SAF).

6. References

Andela, N., D. C. Morton, L. Giglio, R. Paugam, Y. Chen, S. Hantson, G. R. van der Werf, J. T. Randerson, 2019: The Global Fire Atlas of individual fire size, duration, speed and direction, Earth Syst. Sci. Data, 11, 529–552, doi:10.5194/essd-11-529-2019.

Bowman, D. M. J. S., J. K. Balch, P. Artaxo, W. J. Bond, J. M. Carlson, M. A. Cochrane, C. M. D'Antonio, R. S. Defries, J. C. Doyle, S. P. Harrison, F. H. Johnston, J. E. Keeley, M. A. Krawchuk, C. A. Kull, J. B. Marston, M. A. Moritz, I. C. Prentice, C. I. Roos, A. C. Scott, T. W. Swetnam, G. R. van der Werf, S. J. Pyne, 2009: Fire in the Earth system, Science, 324, 481–484, doi:10.1126/science.1163886

Chambers, J. M., W. S. Cleveland, B. Kleiner, P. A. Tukey, 2017: Graphical Methods for Data Analysis, Chapman and Hall/CRC, New York, doi: https://doi.org/10.1201/9781351072304

DaCamara C. C., T. J. Calado, S. L. Ermida, I. F. Trigo, M. Amraoui, K. F. Turkman KF, 2014: Calibration of the Fire Weather Index over Mediterranean Europe based on fire activity retrieved from MSG satellite imagery, Int. J. Wildland Fire, 23(7), 945-958, doi: 10.1071/WF13157

DaCamara C. C., R. M. Trigo, M. M. Pinto, S. A. Nunes, I. F. Trigo, C. M. Gouveia, M. Rainha, 2018: CeaseFire: a website to assist fire managers in Portugal. In "Advances in Forest Fire Research 2018" (D. X. Viegas, ed.), pp. 941-949, Imprensa da Universidade de Coimbra, ISBN 978-989-26-16-506, doi: 10.14195/978-989-26-16-506_103

Pereira, J. M. C., D. Oom, P. C. Silva, A. Benali, 2022: Wild, Tamed, and Domesticated: three fire macroregimes for global pyrogeography in the Anthropocene, Ecological Applications, doi: https://doi.org/10.1002/eap.2588

Pinto M. M., C. C. DaCamara, I. F. Trigo, R. M. Trigo, K. F. Turkman, 2018: Fire danger rating over Mediterranean Europe based on fire radiative power derived from Meteosat. Nat. Hazards Earth Syst. Sci. 18, 515–529, doi:10.5194/nhess-18-515-2018

Wooster, M. J., G. Roberts, G. L. W. Perry, Y. J. Kaufman, 2005: Retrieval of biomass combustion rates and totals from fire radiative power observations: FRP derivation and calibration relationships between biomass consumption and fire radiative energy release, J. Geophys. Res., 110, D24311, doi:10.1029/2005JD006318.

Accounting for the canopy drag effects on wildland fire spread in coupled atmosphere/fire simulations

William P. Antolin[1]; Aurélien Costes[1]; Mélanie C. Rochoux[1;]; Patrick Le Moigne[2]

[1]CECI, Université de Toulouse, CNRS, Cerfacs, 42 Avenue Gaspard Coriolis, 31100 Toulouse, France, {william.antolin, aurelien.costes, melanie.rochoux}@cerfacs.fr
[2] CNRM, Université de Toulouse, Météo-France, CNRS, 42 Avenue Gaspard Coriolis, 31100 Toulouse, France, {patrick.lemoigne@meteo.fr}

**Corresponding author*

Keywords

Wildfire modeling, Meso-NH, BLAZE, SURFEX, LES, drag effects, canopy, turbulence

Abstract (237/500 words)

Since near-surface wind is the main influential parameter governing the rate of fire spread (ROS), its characterization remains key to simulate wildland fire behavior. The correct representation of the intensity and variability of the near-surface wind under complex terrain and vegetation remains an open problem but is essential to make a coupled atmosphere-fire model applicable to actual wildfires. In this work, we study the impact of canopy drag effects on the near-surface flow and the fire behavior simulated by the coupled Meso-NH/BLAZE model in the context of the FireFlux I experimental grass fire for which trees were located upstream and on the flanks. Drag effects can be activated in Meso-NH run in large-eddy simulation (LES) mode following work by Aumond et al. (2013) using SURFEX land surface platform. The drag approach formulation consists of adding drag terms to the momentum equation and subgrid turbulent kinetic energy dissipation as a function of the foliage density. This approach is compared to the standard roughness approach, where a different surface roughness coefficient is applied for the grass and tree areas. Results show the dynamical influence of the surrounding trees on the incoming atmospheric flow that is known to have a significant impact on the fire front propagation in the FireFLux I experiment following work by Costes et al. (2021). Results also indicate that the choice of drag effect parameterization, due to the difference in the represented physics, induces differences on the simulated fire front propagation. This encourages us to explore different options to accurately represent the surface boundary layer in presence of complex vegetation for coupled atmosphere-fire modeling in future work.

1. Introduction

Coupled atmosphere-fire models (Kochanski et al. 2013; Filippi et al. 2018; Costes et al. 2021) are both an efficient and representative way to simulate wildland fire behavior at landscape-to-meteorological scales. They can predict the fire front propagation at the land surface, the fire plume dynamics, and the different interactions they can have. The complex plume dynamics coming from the thermo-convective instability and its retroactive feedback can significantly modify the near-surface wind, enhancing the fire front propagation during a wildland fire event. In coupled atmosphere-fire models, the atmospheric model is run in large- eddy simulation (LES) mode at very high resolution (<100 m) and is coupled with a fire spread model that typically includes a rate of spread (ROS) parameterization and a 2-D front-tracking numerical scheme: see WRF/SFIRE (Mandel et al. 2011), WRF/FIRE (Cohen et al. 2013; Muñoz- Esparza et al. 2018), Meso-NH/FOREFIRE (Filippi et al. 2009) and more recently Meso-NH/Blaze (Costes et al. 2021). In a two-way coupling mode, the fire model requires from the atmospheric model the near-surface wind at a given height to evaluate the ROS and propagate the fire front. In return, it provides surface heat fluxes as surface boundary conditions to the atmospheric model. The counterpart is that parameterization of both the ROS (Rothermel et al. 1972; Balbi et al. 2009) and the surface heat fluxes is required and takes as input a large number of environmental factors related to biomass fuel properties, near-surface wind and terrain slope conditions. These input parameters are partially known (Jimenez et al. 2008) and thereby introduce uncertainties in the coupled model simulations. One way to deal with complex vegetation through these parameters would be either to adopt a stochastic viewpoint (i.e. to run an ensemble of coupled simulations), or to use a land cover database (e.g. ECOCLIMAP, (Masson et al. 2003)) to have a detailed description of the vegetation types and take advantage of the high-resolution simulations. The latter

would allow us to represent both the influence of the vegetation on the wildland fire and on the atmosphere. The main issue addressed in this work is to integrate a land surface modeling approach to the already-existing coupled atmosphere/fire modeling framework so as to represent the dynamical effects of forest canopy on the atmospheric flow and their impacts on wildland fire spread. This is of first importance to extend the applicability of coupled atmosphere/fire models to forest environment and pursue their validation for different types of vegetation.

2. Coupled Atmosphere/Fire Modeling Framework

In the present study, we use the coupled Meso-NH/BLAZE model to simulate the FireFlux I experimental grass fire (Clements et al. 2007). We briefly present Meso-NH/BLAZE in this section. More details can be found in Costes et al. (2021).

2.1. Description of the coupled Meso-NH/Blaze model

Meso-NH (Lac et al. 2018) is a non-hydrostatic anelastic atmospheric model of the French research community, jointly developed by CNRM (Météo-France/CNRS) and Laboratoire d'Aérologie (Université de Toulouse/CNRS). It is used to simulate meso-scale (few kilometers to less than thousand kilometers) up to micro-scale (less than hundred meters) atmospheric flows. For the present wildland fire application, Meso-NH is run in LES mode to simulate the atmospheric flow in the surface layer at decametric horizontal resolution (Δx = 25m resolution in the present study as in Costes et al. (2021)). BLAZE (Costes et al. 2021) is a fire spread model that relies on i) Balbi's ROS parameterization adapted for landscape-scale wildland fires (Santoni et al. 2011); ii) a two-dimensional level-set front-tracking numerical approach to propagate the fire front at the land surface; and iii) surface heat flux parameterization including flaming and smoldering contributions. A subgrid-scale fire front reconstruction is implemented in BLAZE to have a good localization of the surface heat fluxes without significantly constraining the fire model resolution (Δxf = 5m resolution in the present study as in Costes et al. (2021). In a two-way coupling mode, Meso-NH and BLAZE interact as follows: the near-surface wind simulated by Meso-NH at a given reference height (2 m above ground level as in Costes et al. (2021) is interpolated at BLAZE resolution, and is projected along the normal direction to the fire front; it is then given as input to the ROS parameterization. The surface heat fluxes simulated by BLAZE are given as surface boundary conditions to Meso-NH with a vertical distribution following an exponential decay over the first 30 m above the ground level as in Costes et al. (2021).

Figure 1 – Illustration of a coupled Meso-NH/BLAZE simulation of the FireFlux I experiment (without considering the trees near the burn plot).

2.2. Validation of the fire-atmosphere coupled modeling

The FireFlux I experiment (Clements et al. 2007) has been used to provide a first evaluation step of the coupled Meso-NH/BLAZE model. It corresponds to an experimental prescribed burn of 15 min on a flat terrain with tall grass. The burn plot of approximately 30 ha was instrumented with two towers equipped with thermocouples and anemometers at different heights (within the first 50 m above the ground level). In previous work, Costes et al. (2021) have simulated the FireFlux I experiment using the coupled Meso-NH/BLAZE model without considering the trees near the burn plot, i.e. the vegetation was considered as homogeneous tall grass for the whole computational domain and the impact of tall grass on the surrounding atmosphere was represented using the standard roughness approach (Figure 1). Simulation results (in terms of fire front positions and near-surface atmospheric variables such as the horizontal and vertical wind components at different heights) showed good agreement with the experimental measurements. In complement, Costes et al. (2021) have verified the validity of the anelastic approximation by developing a compressible version of Meso-NH to account for the three-dimensional density gradients in the vicinity of the fire front and by comparing results in anelastic and compressible modes for the FireFlux I experiment. Results in the two-way coupled mode have shown that the anelastic approximation for Meso-NH is suitable to represent wildland fire behavior, except for details of the plume if the atmospheric model horizontal resolution is of 10 m or finer. The anelastic approximation is therefore relevant to study canopy drag effects on wildland fire behavior at decametric resolution in the present study. Even though coupled simulations were reduced to a simple flat terrain with uniform vegetation in previous work, Costes et al. (2021) demonstrated the importance of atmospheric variability due to turbulence on the fire front propagation. This is a key result, which motivates the further development of the coupled Meso-NH/BLAZE model towards a more complex representation of the terrain surface and in particular of the vegetation. The objective in the present study is to account for the presence of trees upstream and on the sides of the burn plot (Figure 1), and to evaluate its impact on the near-surface flow and subsequently on the fire front propagation

3. Coupled MesoNH/Blaze/SURFEX simulations including canopy drag effects

To consider a more realistic fuel in the coupled atmosphere/fire simulations, it is of primary importance to have a better representation of the fuel behavior in response to the development of the fire but also of the fuel influence on the atmospheric flow. This implementation will be done via SURFEX (Masson et al. 2013), a surface modeling platform also developed by CNRM (Météo-France/CNRS). This model was originally aimed to better simulate energy and water exchanges between the land surface and the atmosphere to be integrated into Météo-France's operational products. It is also of significant interest in research mode to study surface/atmosphere interactions. In the present study, we mainly use the ISBA (Interaction Soil Biosphere Atmosphere) vegetation scheme (Noilhan et al. 1996; Boone et al. 1999; Decharme et al. 2006) in SURFEX to have a more detailed description of the vegetation (grass and forest areas in the FireFlux I case study). Integrating the ISBA scheme into the already existing coupled atmosphere/fire modeling framework (Figure 2) will allow us to go one step further towards simulating actual cases of large-scale wildfires. To account here for the dynamical effect of the vegetation on the atmospheric flow, we first recreated the immediate vegetation close to the field experiment forming some kind of shelter from the atmospheric flow. We then implemented two different methods to account for the canopy's drag effect on the the fire spread, namely, a roughness approach and a momentum/TKE drag approach.

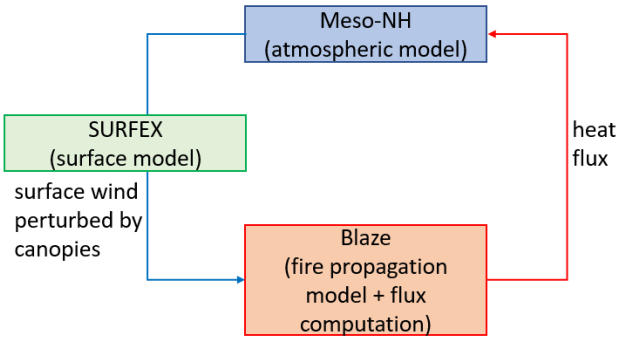

Figure 2 – Schematic of the coupling between Meso-NH, BLAZE and SURFEX with the additional component SURFEX to account for the tree's drag on the the fire spread.

3.1. Classical log-law parameterization

The classical approach, referred to as the standard roughness approach, in large-scale atmospheric models is to have a log-law with characteristics such as roughness length and zero plane displacement that depend on the surface type. This approach, initiated by Von Kármán (1930), revisited by Monin and Obukhov (1954) to take stability into consideration, supposes that the wind profile starts at a given height with a logarithmic profile. However, for LES, the fine horizontal resolution would allow us to represent the wake circulation behind obstacles (a tree barrier for example). Such complex flow feature cannot be fully accounted for using the classical log-law parameterization.

3.2. TKE and conservation of momentum parametrization

To include more physics into the LES, an alternative approach consists in incorporating a drag force directly into the atmospheric model dynamic equations. Using Kanda and Hino's (1994) parameterizations and following Aumond et al. (2013), an additional term is introduced to the momentum equation as follows:

$$\frac{\partial u_i}{\partial t} = A_{dv} + C_{or} + P_{res} + T_{urb}(u_i) - C_d A_f(z) u_i (u_1^2 + u_2^2)^{\frac{1}{2}} \quad i \in \{1,2\} \qquad (1)$$

where (u_1, u_2) corresponds to the two horizontal wind components $[m/s]$, A_{dv} is the advection term, C_{or} is the Coriolis force term, P_{res} is the the pressure gradient term, T_{urb} is the turbulence term, C_d is the canopy drag coefficient [-], and A_f (z) is the canopy area density $[m^{-1}]$ (this is a combination of the leaf area index (LAI), the fraction of vegetation in the grid cell and a function that represents the shape of the trees). To account for the subgrid-scale effect of trees on small-scale turbulence (trees have elements much smaller than the atmospheric grid mesh), additional dissipation is added into the turbulent kinetic energy (TKE) equation:

$$\frac{\partial e}{\partial t} = A_{dv} + D_{ynProd} + T_{hermProd} + T_{urbT}(u_i) - D_{iss-} C_d A_f(z) e (u_1^2 + u_2^2)^{\frac{1}{2}} \qquad (2)$$

where e is the subgrid TKE $[m^2/s^2]$, D_{ynProd} and T_{hermProd} are the dynamic and thermal productions, T_{urbT} denotes the turbulent transport and D_{iss} is the dissipation. This approach, referred to as the TKE/momentum drag approach, is particularly interesting for our wildland fire application since it directly links vegetation parameters, which can be inputs from a database, to drag force through the Cd and Af coefficients.

3.3. Results

We present a first comparison of the coupled Meso-NH/SURFEX simulations of the spin-up step of the FireFlux I case study that account for the forest canopy effect through either the standard roughness approach or the TKE/momentum drag approach (Figure 3). In Figure 3, the dark blue areas correspond to trees, while the rest of the domain is covered by tall grass. The burn plot is delimited by the empty black rectangle. It is worth mentioning that this spin-up step is required prior to the fire ignition to have realistic inflow conditions that correspond to in situ observation measurement statistics (Costes et al. 2021). This is a preliminary step before running the coupled Meso-NH/BLAZE/SURFEX simulations. The two approaches seemed to lead to very similar flow structures at first although the physics involved is very different but several differences can be

spotted. The first main difference is that the momentum/TKE approach dissipates less compared to the standard roughness approach, leading to higher near-surface wind speed. This is of particular interest in the context of wildland fire behavior simulations. The second main difference in the case of the momentum/TKE approach, is the presence of more coherent structures coming from the wake of canopies, possibly due to a slightly better representation of the porosity of the vegetation than in the case of the classical log-law parameterization.

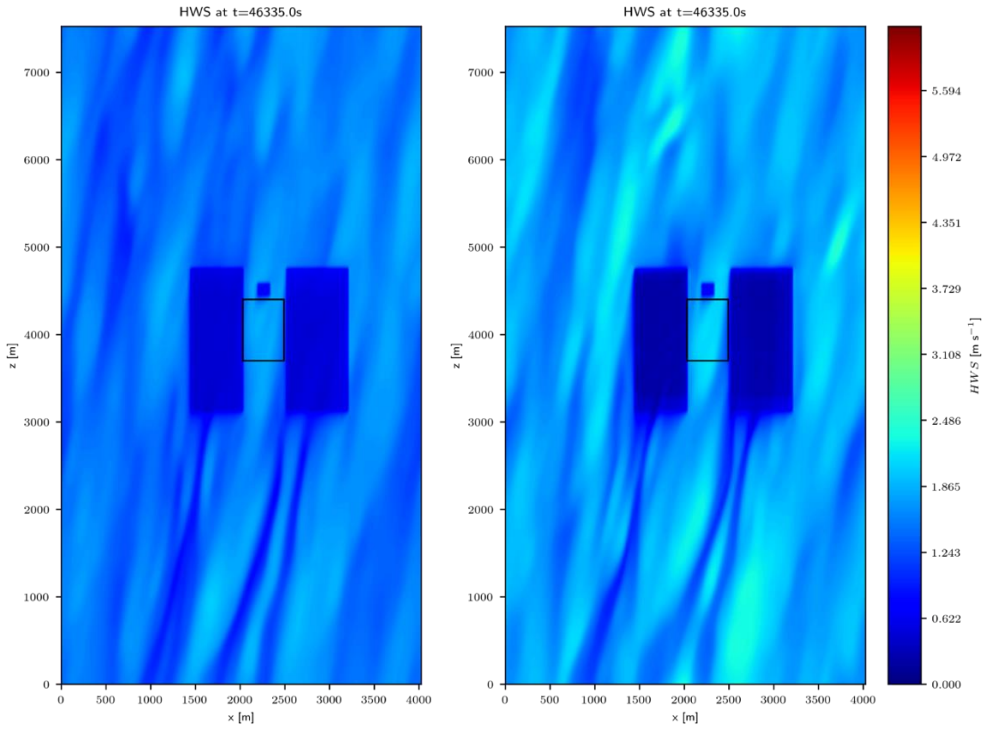

a) Roughness approach (b) Momentum/TKE parametrization

Figure 3 – Simulation of the horizontal wind speed [m/s] for the spin up step of the FireFlux I experimental grass fire, taking into account the immediate tree canopies around the burn plot with the two different approaches: (a) standard roughness approach; and (b) TKE/momentum drag approach. The burn plot is delimited by the black solid lines, and the trees are located in the dark blue areas (the rest of the vegetation, including the burn plot, is set as grass.

4. Conclusions

This study presents a prototype of a coupled atmosphere/fire model based on the coupled Meso-NH/BLAZE/SURFEX system, in which a vegetation scheme capable of representing the drag of forest canopies is integrated through the ISBA scheme of SURFEX. This study assumes that the immediate trees next to the FireFlux I experimental burn plot account for most of the vegetation dynamical influence on the incoming atmospheric flow. The results obtained for the spin-up step of the coupled simulations indicate that the canopy drag affects the overall regime of the atmospheric flow surrounding the burn plot. The canopy drag will therefore have an influence on the fire spread but the choice of parameterization for the turbulent boundary layer may also be decisive. In the short term, future work aims at extending the analysis of the canopy drag effects for the FireFlux I experimental grass fire and at investigating if the sensitivity of the fire spread to the inflow variability is stronger when considering canopy drag effects or not. In the long term, future work aims at enhancing the representation of the wake due to complex vegetation and shifting towards the simulation of large-scale wildland fire in forest environment. Other methods, such as the promising immersed boundary layer (IBM), recently implemented in Meso-NH (Auguste et al. 2019), could also be investigated.

5. References

A.K. Kochanski et al. “Real time simulation of 2007 Santa Ana fires”. In: Forest Ecology and Management 294 (2013), pp. 136–149. doi: 10.1016/j.foreco.2012.12.014.

J.-B. Filippi et al. “Simulation of a large wildfire in a coupled fire-atmosphere model”. In: Atmosphere 9.6 (2018). doi: 10.3390/atmos9060218.

A. Costes et al. “Subgrid-scale fire front reconstruction for ensemble coupled atmosphere-fire simulations of the FireFlux I experiment”. In: Fire Safety Journal 126 (2021), p. 103475. issn: 0379-7112. doi: https://doi.org/10.1016/j.firesaf.2021.103475.

Mandel. “Coupled atmosphere-wildland fire modeling with WRF 3.3 and SFIRE 2011”.

Janice L Coen and Wilfrid Schroeder. “Use of spatially refined satellite remote sensing fire detection data to initialize and evaluate coupled weather-wildfire growth model simulations”. In: Geophysical Research Letters 40.20 (2013), pp. 5536–5541.

Domingo Muñoz-Esparza et al. “An accurate fire-spread algorithm in the Weather Research and Forecasting model using the level-set method”. In: Journal of Advances in Modeling Earth Systems 10.4 (2018), pp. 908–926.

Jean Baptiste Filippi et al. “Numerical experiments using mesonh/forefire coupled Atmospheric- fire model”. In: Eighth Symposium on Fire and Forest Meteorology. 2009, p. 9.

Rothermel; Richard C. A mathematical model for predicting fire spread in wildland fuels. Technical report, Research Paper INT-115. U.S. Department of Agriculture, Forest Service, Ogden, Utah, USA.

J.-H. Balbi et al. “A physical model for wildland fires”. In: Combustion and Flame 156.12 (Dec. 2009), pp. 2217–2230. doi: 10.1016/j.combustflame.2009.07.010. url: https: //hal.archives-ouvertes.fr/hal-00593608.

E. Jimenez; M.Y. Hussaini and S. Goodrick. “Quantifying parametric uncertainty in the Rothermel model”. In: International Journal of Wildland Fire 17.5 (2008), pp. 638–649.

V Masson et al. “ECOCLIMAP, a global database of land surface parameters at 1km res- olution in meteorological and climate models”. In: Fifth International Conference on Urban Climate 1–5 September, 2003 Łódz, Poland: Proceedings. Vol. 2. 2003, p. 393.

C. Lac et al. “Overview of the Meso-NH model version 5.4 and its applications”. In: Geosci- entific Model Development 11.5 (2018), pp. 1929–1969. doi: 10.5194/gmd-11-1929-2018.

P.-A. Santoni et al. “Wildland fire behaviour case studies and fuel models for landscape-scale fire modeling”. In: Journal of Combustion 2011 (2011), p. ID613424. doi: 10.1155/2011/ 613424.

C.B. Clements et al. “Observing the dynamics of wildland grass fires”. In: Bulletin of the American Meteorological Society September (2007). doi: 10.1175/BAMS-88-9-1369.

A. Costes et al. “Effects of high-density gradients on the wildland fire behavior in coupled atmosphere-fire simulations”. In: In review for publication in Journal of Advances in Modeling Earth Systems ().

V Masson et al. “The SURFEXv7. 2 land and ocean surface platform for coupled or offline simulation of earth surface variables and fluxes”. In: Geoscientific Model Development 6.4 (2013), pp. 929–960.

J. Noilhan and J.-F. Mahfouf. “The ISBA land surface parameterisation scheme”. en. In: Global and Planetary Change 13.1-4 (June 1996), pp. 145–159. issn: 09218181. doi: 10 . 1016/0921-8181(95)00043-7. url: https://linkinghub.elsevier.com/retrieve/pii/ 0921818195000437 (visited on 03/22/2022). 5

Aaron Boone, Jean-Christophe Calvet, and Joël Noilhan. “Inclusion of a Third Soil Layer in a Land Surface Scheme Using the Force–Restore Method”. en. In: J. Appl. Meteor. 38.11 (Nov. 1999), pp. 1611–1630. issn: 0894-8763, 1520-0450. doi: 10.1175/1520- 0450(1999) 038<1611:IOATSL>2.0.CO;2. url: http://journals.ametsoc.org/doi/10.1175/1520- 0450(1999)038%3C1611:IOATSL%3E2.0.CO;2.

B Decharme and H Douville. “Introduction of a sub-grid hydrology in the ISBA land surface model”. In: Climate dynamics 26.1 (2006), pp. 65–78.

Th Von Kármán. “Mechanische ahnlichkeit und turbulenz”. In: Math.-Phys. Klasse (1930).

Andreĭ Sergeevich Monin and Aleksandr Mikhaĭlovich Obukhov. “Basic laws of turbulent mixing in the surface layer of the atmosphere”. In: Contrib. Geophys. Inst. Acad. Sci. USSR 151.163 (1954), e187.

Manabu Kanda and Mikio Hino. “Organized structures in developing turbulent flow within and above a plant canopy, using a large eddy simulation”. In: Boundary-Layer Meteorology 68.3 (1994), pp. 237–257.

Pierre Aumond et al. “Including the Drag Effects of Canopies: Real Case Large-Eddy Simula- tion Studies”. en. In: Boundary-Layer Meteorol 146.1 (Jan. 2013), pp. 65–80. issn: 0006-8314, 1573-1472. doi: 10.1007/s10546- 012- 9758- x. url: http://link.springer.com/10. 1007/s10546-012-9758-x.

Franck Auguste et al. “Implementation of an immersed boundary method in the Meso-NH v5.2 model: applications to an idealized urban environment”. In: Geoscientific Model Devel- opment 12.6 (2019). Publisher: Copernicus GmbH, pp. 2607–2633. issn: 1991-959X. doi: 10. 5194/gmd-12-2607-2019. url: https://gmd.copernicus.org/articles/12/2607/2019/.

Advances in burned area detection from remote sensing: The FireCCI products

Emilio Chuvieco[1]; M. Lucrecia Pettinari*[1]; Joshua Lizundia-Loiola[1]; Gonzalo Otón[1]; Amin Khaïroun[1]; Ekhi Roteta[2]; Thomas Storm[3]; Martin Boettcher[3]; Olaf Danne[3]; Carsten Brockmann[3]

[1]Universidad de Alcalá, Environmental Remote Sensing Research Group, Colegios 2, 28801 – Alcalá de Henares, Spain, {emilio.chuvieco; mlucrecia.pettinari; joshua.lizundia; gonzalo.oton; amin.khairoun}@uah.es
[2] Department of Mining and Metallurgical Engineering and Materials Science, School of Engineering of Vitoria-Gasteiz, University of the Basque Country, 01006 Vitoria-Gasteiz, Spain, {ekhi.roteta@gmail.com}
[3] Brockmann Consult GmbH, Chrysanderstr 1, 21029 Hamburg, Germany, {thomas.storm; martin.boettcher; olaf.danne; carsten.brockman}@brockmann-consult.de

**Corresponding author*

Keywords

Wildfire, remote sensing, time series, burned area

Abstract

The FireCCI project has developed, during the last decade, a suite of burned area (BA) products based on remote sensing tailored to the climate researchers and also useful for different fire applications. The different products span from 1982 to 2020, and include global products at coarse spatial resolution (FireCCILT11, at 0.05-degrees) and medium resolution (FireCCI51 and FireCCIS310, at 250 m and 300 m respectively), with derived grid products at 0.25-degree resolution. An additional burned area product at 20 m spatial resolution is also available for Sub-Saharan Africa for the years 2016 and 2019, with an accompanying grid product at 0.05-degrees. All products include ancillary information related to the uncertainty of the detection, the observational limitations, and the land cover burned.

The grid products, in NetCDF format, are specifically developed for climate researchers and those studying global vegetation dynamics, which usually use coarse resolution datasets as input for their models. The pixel products, on the other hand, provide the best possible spatial resolution based on the inputs of the BA algorithms, and are intended for researchers working on fire dynamics, land cover change, or focused on regional study areas, among other applications.

The latest product developed, FireCCIS310, represents the next generation of medium-resolution global burned area products. With an improved algorithm and taking advantage of the SWIR bands of the Sentinel-3 SYN product and the VIIRS active fires, it detected almost 5 Mkm2 of BA during the year 2019. This is expected to result in changes in the global estimation of fire emissions.

1. Remote sensing for burned area detection: FireCCI

Remote sensing data is a widely used and very advantageous source of information for burned area (BA) detection, as it provides global information in a systematic way (Chuvieco et al., 2019). The available sensors deliver images at diverse spatial and temporal resolutions, and in different spectral regions. This makes them suitable for the detection of burned scars with the use of infrared data at different wavelengths (near (NIR), short-wave (SWIR) and thermal).

Within the European Space Agency (ESA) Climate Change Initiative (CCI), the FireCCI project has the objective to develop and validate burned area algorithms to meet, as far as possible, GCOS (Global Climate Observing System) Essential Climate Variable (ECV) requirements for consistent, stable, and error-characterized global satellite data products from multi-sensor data archives. Since the start of the CCI Programme, FireCCI has developed different BA products based on surface reflectance and active fire information from a variety of ESA and NASA sensors.

2. The FireCCI burned area products

The current suite of products obtained from the FireCCI algorithms spans from 1982 to 2020, with plans to expand it to the present and future. These products, apart from providing information on burned area, also include ancillary information related to the uncertainty of the detection, the land cover affected (extracted from the CCI Land Cover product), and the observational limitations of the input data. All products supply information in monthly files, and are delivered at two spatial resolutions: pixel (at the original resolution of the surface reflectance input data) and grid (at a coarser resolution and specifically tailored for climate researchers). Figure 1 shows the total burned area obtained from the aggregation of the monthly grid files of FireCCIS310 for the year 2019.

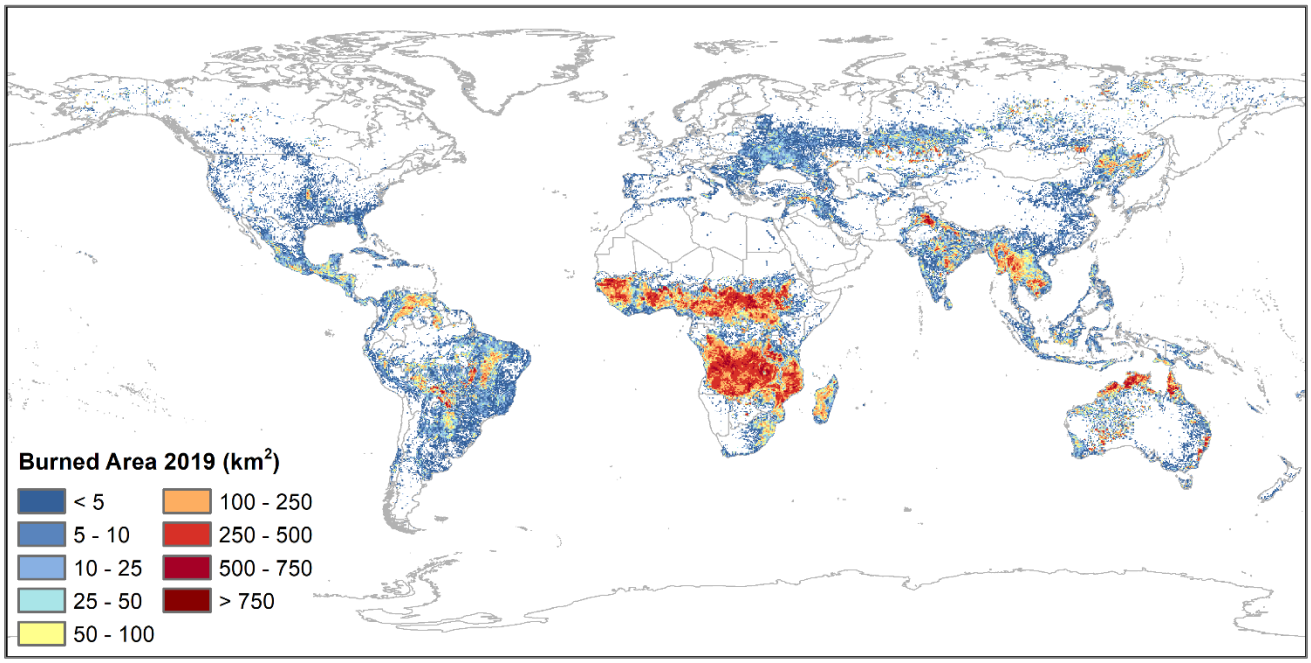

Figure 1- Total burned area of the year 2019 obtained from the FireCCIS310 grid product.

The current products include:

2.1. FireCCILT11

The dataset with the longest time series is the FireCCILT11 product, based on AVHRR information obtained from the Land Long-Term Data Record (LTDR) version 5 (https://ladsweb.modaps.eosdis.nasa.gov/missions-and-measurements/applications/ltdr/#project-documentation, accessed on March 2022), and spanning from 1982 to 2018 at a global scale (Otón et al. 2021). The pixel product has a spatial resolution of 0.05 degrees (approx. 5 km at the Equator), and provides information on the date of the fire detection, the confidence level of that detection, the burned area in each pixel, and an ancillary layer with the number of observations available for the detection. The grid product, at a resolution of 0.25 degrees, summarizes the data of the pixel product for each grid cell, and includes layers corresponding to the sum of burned area, the standard error, and the fraction of burnable area and observed area in each cell. FireCCILT11 is the global BA product with the longest time-series to date, although it presents high uncertainties related to the coarse resolution of input images (0.05 degrees) and stability of the LTDR series. It is especially intended for climate researchers working at global or continental scales and needing long BA time series.

2.2. FireCCI51

Another global product, but with a higher spatial resolution than FireCCILT11, is FireCCI51, whose algorithm uses as input MODIS NIR surface reflectance at 250 m and 1 km-resolution active fires (Lizundia-Loiola et al. 2020). This product covers a 20-year time series (2001 to 2020). It is the product providing global monthly BA information with the highest resolution currently available. The pixel product includes layers corresponding to the date of detection, the confidence level and the land cover burned, while the grid product, at 0.25-degree resolution, contains the same information as FireCCILT11, and also includes layers with the amount of BA for each land cover class.

2.3. FireCCIS310

As part of our effort to extend the BA information into the coming years, the FireCCI project has recently developed a new algorithm to detect BA using the 300 m-resolution SWIR bands of the Sentinel-3 SLSTR (Sea and Land Surface Temperature Radiometer) sensor, extracted from the Synergy (SYN) products developed by ESA (https://sentinels.copernicus.eu/web/sentinel/technical-guides/sentinel-3-synergy, accessed on March 2022). This input is complemented by VIIRS (Visible Infrared Imaging Radiometer Suite) active fire information at 375 m resolution, obtained from the S-NPP (Suomi National Polar-Orbiting Partnership) satellite. The resulting BA product, called FireCCIS310, takes advantage of the improved BA detection capacity of the SWIR bands and the higher resolution of the VIIRS thermal information, apart from including improvements in the detection algorithm. The first assessment of the product for 2019 data shows that it detects more BA than previous global BA datasets (4.99 Mkm^2, 28% more than FireCCI51), and with an increased spatial and temporal accuracy (Lizundia-Loiola et al. 2022). FireCCIS310 supplies the same layers as FireCCI51, but at a spatial resolution of 300 m for the pixel product. This product will continue to be processed for subsequent years.

Figure 2 shows the comparison between the BA detected by FireCCI51, FireCCIS310 and FireCCISFD20 (see section 2.4) in a small region in the border between Tanzania and Mozambique.

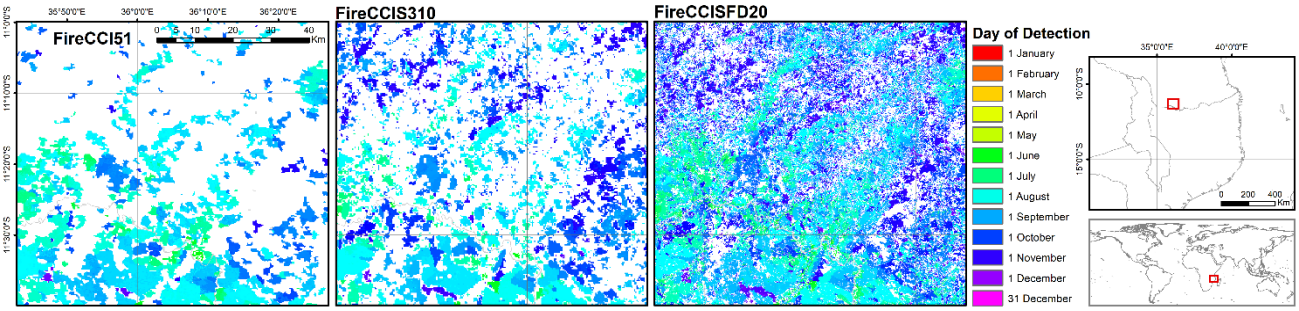

***Figure 2*- Comparison of burned area detection between FireCCI51, FireCCIS310 and FireCCISFD20 during 2019 for a region in Southern Tanzania.**

2.4. FireCCISFD

Finally, a specific dataset has been created for sub-Saharan Africa, where more than 70% of the total global burned area occurs (Chuvieco et al., 2019). This product, called FireCCISFD (SFD comes from Small Fire Dataset), uses surface reflectance from the Sentinel-2 MSI (MultiSpectral Instrument) sensor at 20 m spatial resolution, complemented with active fire information (Roteta et al. 2019). Version 1.1 of this dataset (FireCCISFD11) covers the year 2016 and is based on Sentinel-2A data + MODIS active fires, while the newer version (FireCCISFD20) has been processed for the year 2019, and takes advantage of the additional data provided by Sentinel-2B, duplicating the input data amount and temporal resolution, and the improved spatial resolution of the VIIRS active fire detection (Chuvieco et al. 2022). The grid version of this product has a spatial resolution of 0.05 degrees, as requested by climate researchers. Due to the much higher spatial resolution of the input data (Sentinel-2 MSI versus MODIS or Sentinel-3 SYN), this product detected 58% more BA than FireCCI51 for 2016, and 82% in 2019. The vast majority of this additional BA is due to the improved detection of small burned patches, not detectable with moderate resolution sensors (Ramo et al. 2021, and see also Figure 2). This dataset is especially useful for researchers working at regional level in Africa, and for studies dealing with greenhouse gasses emissions estimations.

2.5. Access to the products

All FireCCI products are available from the CCI Open Data Portal (https://climate.esa.int/en/odp/#/dashboard) and in the CEDA Catalogue (https://catalogue.ceda.ac.uk/uuid/6c3584d985bd484e8beb23ff0df91292), and the documentation of the products can be downloaded from the FireCCI website (https://climate.esa.int/en/projects/fire/about/).

3. References

Chuvieco, E., Mouillot, F., van der Werf, G.R., San Miguel, J., Tanasse, M., Koutsias, N., García, M., Yebra, M., Padilla, M., Gitas, I., Heil, A., Hawbaker, T.J., Giglio, L. (2019). Historical background and current developments for mapping burned area from satellite Earth observation. Remote Sensing of Environment, 225, 45-64.

Chuvieco, E., Roteta, E., Sali, M., Stroppiana, D., Boettcher, M., Kirches, G., Storm, T., Khairoun, A., Pettinari, M.L., Albergel, C. (2022) Building a small fire database for Sub-Saharan Africa from Sentinel-2 high-resolution images. Science of the Total Environment, in press.

Lizundia-Loiola, J., Franquesa, M., Khaïroun, A., Chuvieco, E. (2022). Global burned area mapping from Sentinel-3 Synergy and VIIRS active fires. Remote Sensing of Environment, in review.

Lizundia-Loiola, J., Otón, G., Ramo, R., Chuvieco, E. (2020) A spatio-temporal active-fire clustering approach for global burned area mapping at 250 m from MODIS data. Remote Sensing of Environment 236, 111493, https://doi.org/10.1016/j.rse.2019.111493

Otón, G., Lizundia-Loiola, J., Pettinari, M.L., Chuvieco, E. (2021) Development of a consistent global long-term burned area product (1982–2018) based on AVHRR-LTDR data. International Journal of Applied Earth Observation and Geoinformation 103, 102473. https://doi.org/10.1016/j.jag.2021.102473

Ramo, R., Roteta, E., Bistinas, I., Wees, D., Bastarrika, A., Chuvieco, E. & van de Werf, G. (2021) African burned area and fire carbon emissions are strongly impacted by small fires undetected by coarse resolution satellite data. PNAS 118 (9) e2011160118, https://doi.org/10.1073/pnas.2011160118

Roteta, E., Bastarrika, A., Padilla, M., Storm, T., Chuvieco, E. (2019) Development of a Sentinel-2 burned area algorithm: Generation of a small fire database for sub-Saharan Africa. Remote Sensing of Environment 222, 1-17, https://doi.org/10.1016/j.rse.2018.12.011

Agricultural fires in France: a first national overview from data mining

Lilian Vallet[1] ; Florent Mouillot[1] ; Jean-Marc Ourcival[2]

[1]IRD, UMR CEFE, 1919 route de mende, 34293 Montpellier Cedex 5, France
{lilian.vallet@cefe.cnrs.fr, florent.mouillot@ird.Fr}
[2] CNRS, UMR CEFE, 1919 route de mende, 34293 Montpellier Cedex 5, France
{jean-marc.ourcival@cefe.cnrs.fr}

**Corresponding author*

Keywords

Fire regime; carbon emission; cropland; MODIS; rangeland

Abstract

Introduction
- Even if the agricultural fires can affect a high proportion of burned areas, their inventory is insufficient.
- Considering the importance of agriculture in France, understanding agricultural fire regimes appears to be central to the objective of food security.
- Most cropland or rangeland fires are directly or indirectly related to human activities, facilitating their control.

Material and methods
- A data mining analysis of non-scientific literature was conducted between 2000 and 2021 to study the temporal and spatial evolution of agricultural fires.
- This database is compared to MODIS hotspots in order to validate this active detection method and to define its limits.

Results
- The data mining study allowed the inventory of more than 500 fire events per year.
- The national heterogeneity of agricultural fires is mostly explained by the variation of crop types across the territory as well as by climatic conditions.
- Crop fires occur primarily during the summer months when weather and fuel conditions are most favorable. Pasture fires, mainly prescribed fires, occur before and after winter to limit their spread. Fires in infrastructures occur throughout the year.

Discussion
- This first attempt at inventorying agricultural fires in France allowed us to describe spatial and temporal patterns specific to these types of fires.
- Remote sensing data only partially capture these small fires.
- Carbon emissions from these fires are currently largely underestimated.

1. Introduction

Agricultural fires account for a significant proportion of the annual burned area under temperate and Mediterranean climates (van der Werf et al., 2010).However, these cropland and rangeland fires are generally not included in current fire inventories and their consequences are severely underestimated (Shi et al., 2015). The characterization of these fires in terms of temporal and spatial variability as well as the associated carbon emissions are therefore largely unknown (Hunter and Robles, 2020). This lack of knowledge is partly attributed to the limitation of remote sensing technologies to capture agricultural fires for three main reasons: (1) Many harvested or ploughed croplands have similar spectral characteristics to burned areas. (2) The temporal behavior of harvested or burned cropland is similar to that of grassland fires (sudden decline followed by gradual recovery in NDVI, interannual variation in NBR) (Alonso-Canas and Chuvieco, 2015). (3) Many agricultural fires are human-caused and are generally small and short-lived, making them difficult to capture by satellite sensors (Vilar et al., 2015).

In France, where usable agricultural areas represent 30 million hectares (i.e., 52% of the country), and although croplands and rangelands have relatively lower biomass density than forests, the fire risk of these ecosystems

should not be underestimated ("World development indicators," n.d.). First, current climate change is increasing the number of days when climate-fuel conditions are critical for fire ignition and spread, increasing the vulnerability of these environments (Bowman et al., 2020). Second, because these ecosystems are central to the agri-food production system, the lack of knowledge about the behavior of these fires may pose a threat to food security (O'Mara, 2012). Third, lack of monitoring of these fires can lead to uncontrolled spread of fire to adjacent forests and even to human infrastructure (Dether and Black, 2006).

Most agricultural fires are human-induced, although their ignition may or may not be deliberate. Deliberate fires, called "prescribed fires," are intended to provide many benefits to ecosystems and human society: transforming arable land, cleaning crop residus, providing pasture production, providing habitat for wildlife, reducing hazardous fuels (Hunter and Robles, 2020; McLauchlan et al., 2020; Pausas and Ribeiro, 2017). In order to change land use and improve agricultural production, humans have therefore developed fire control techniques such as "burn-beating" or "stubble burning" approaches (Bowman et al., 2011; Prichard et al., 2017). In contrast, unintentional fires, called "wildfires," are caused by unauthorized ignitions, escaped prescribed fires, arson, or technological malfunctions (McLauchlan et al., 2020). Agricultural fires can also, less frequently, be caused by natural causes such as lightning (Amatulli et al., 2007; Coughlan et al., 2021).

Active detection of thermal anomalies during combustion by remote sensing is the primary source of information used to capture agricultural fire occurrence (Giglio, Louis, 2000), but suffer from a return time interval (6hrs) longer than most small-fire durations. It is therefore essential to assess the accuracy of these hotspots, based on reference data that we performed with datamining in national newspapers.

2. Materiel and Methods

A data mining analysis of the non-scientific literature was carried out for the period 2000-2021 over the whole France. This study was based on a systematic screening of regional and national online newspapers with keywords such as "fire", "agriculture", "fields", "residue", aiming at obtaining an overview of fires occurring on croplands or rangelands. For each fire event, the date and the location of the administrative unit are identified. Depending on the quality of the information source, vegetation type (crop type and status as residue or whole plant) is referenced. Where information is available, the estimated area of pasture or crop burned is recorded. In addition, fires in agricultural storage buildings are also considered, some of which provide a mass of burned dry matter.

This database was then analyzed to describe the temporal evolution, seasonality, and spatial heterogeneity of agricultural fires. This analysis provides an understanding of the spatial and temporal fire patterns associated with cropland and pasture.

This database was then compared with VIIRS-SNPP hotspots (Schroeder et al., 2014) over the 2012-2021 time period. To do this, the VIIRS-SNPP hotspots were filtered out on cropland, grassland and pastures vegetation types (Corine Land Cover), and matched with referenced fires, in order to estimate the accuracy produced by this observation technique, as well identifying potential local or temporal caveats in fire reporting by the litterature. We estimated the fraction of fire events captured by hotspots as a function of fire size, and the relationship between fire events burned area and hotspot numbers. A final model relying hostspots to burned area, and omission errors allowed to provide an objective burned area data base for agricultural fires in France with its associated uncertainty for carbon emission studies.Current results and discussion

The database from the literature review identified 10453 agricultural fire occurrences between 2000 and 2021, i.e. more than 500 per year. These data correspond to 6808 crop fires, 2068 infrastructure fires and 1577 rangeland fires.

2.1. Spatial distribution

Figure 1.1 shows the spatial distribution of agricultural fires, which are present over almost the entire territory, including temperate and mediterranean environments. The least affected regions may correspond to the large French wine-growing regions, whose flammability is very low (Bordeaux, Burgundy and Alsace regions). High altitude regions (Alps) and those largely covered by forests (Landes) seem also less affected by agricultural fires.

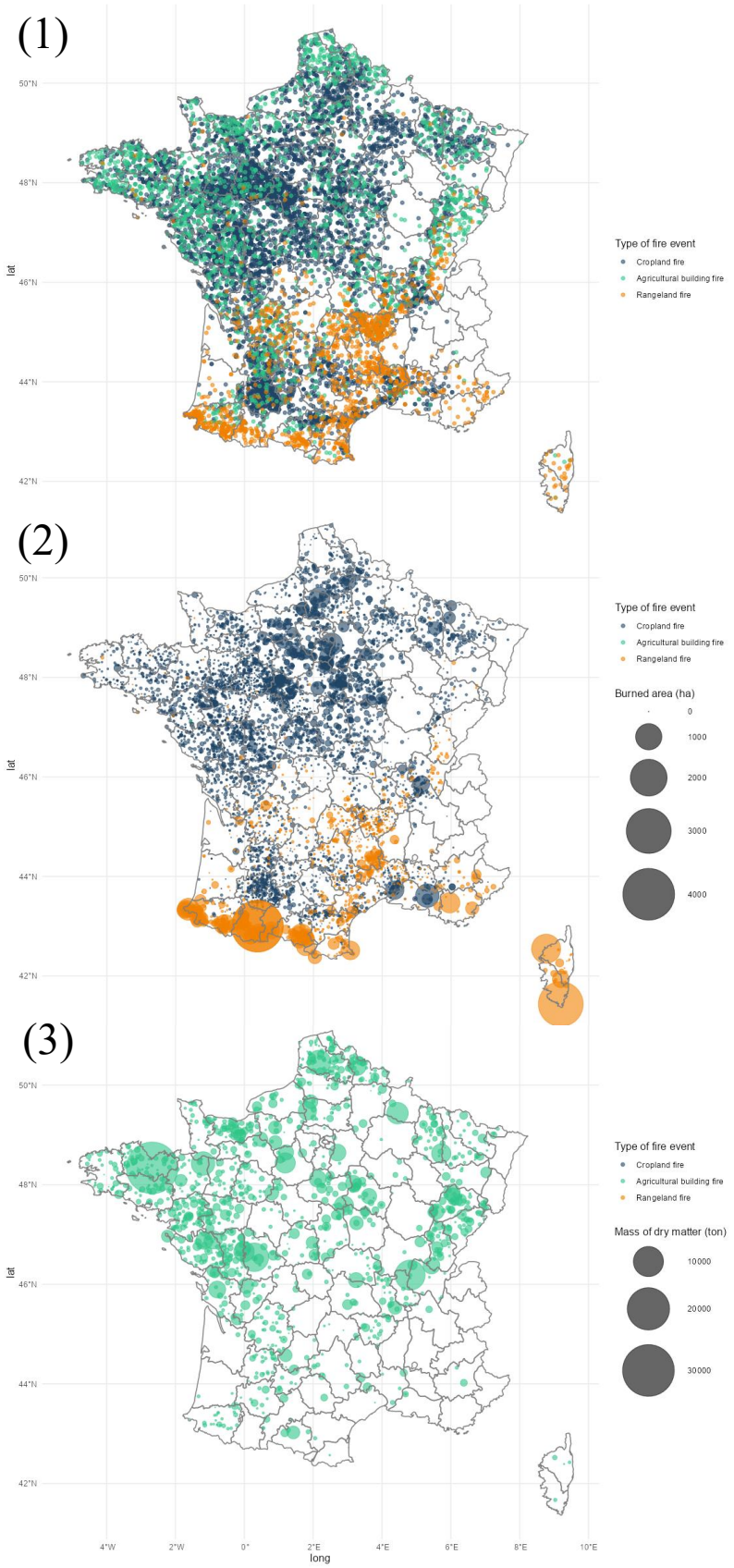

Crop fires seem to be concentrated in the major French rainfed agricultural production areas, namely the Beauce plain south of Paris and Brittany to the west. Fire size (Figure 1.2) appears to be particularly large in the agricultural regions surrounding Paris, mainly composed of large cereal fields.

Fires in agricultural infrastructures largely follow the distribution of crop fires. The mass of dry matter burned seems to be particularly important in the West of France, a region where livestock and therefore fodder storage are important. As storage buildings are generally located close to livestock buildings (e.g. piggeries), these fires can lead to the death of a large part of the livestock and have severe economic consequences.

Rangeland fires particularly affect the high plateaus, especially in the Pyrenees, Corsica and the Massif Central. This distribution corresponds to the continuation of the practice of "stubble burning" in the south of France. This government-regulated practice involves the burning of standing plants to fertilize the soil and facilitate grazing. The fires that are particularly widespread in the Pyrenees are probably mixed fires (partly affecting the forest), probably escaped prescribed fires or involuntary fires.

Figure 1: (1) Distribution of agricultural fire occurrences in France between 2000 and 2021. (2) Spatial variability of cropland and rangeland burned areas (ha). (3) Spatial variability of dry matter mass (ton) burned in agricultural building fires. (Blue = Cropland fire, Green = Agricultural building fire, Orange = Rangeland fire).

2.2. Temporal trend

Figure 2 shows the evolution of agricultural fires over time. There is a strong seasonality and the appearance of particularly extreme years. Specifically, the years 2015 and 2019 for crop fires and the years 2012 and 2019 for rangeland fires show a very high number of fires. These years are characterized by particularly high temperatures related to heat waves early in the season. These climatic conditions lead to early droughts, reducing the moisture content of vegetation and increasing its flammability.

The amount of information available over the study period appears to vary. Indeed, the data available before 2006 do not seem to match the occurrence of agricultural fires in France after this date. The bibliographic review seems to be temporally biased, when there is a strong coverage of fire events by the local media. Our data do not allow us to conclude on a potential increase in agricultural fire events.

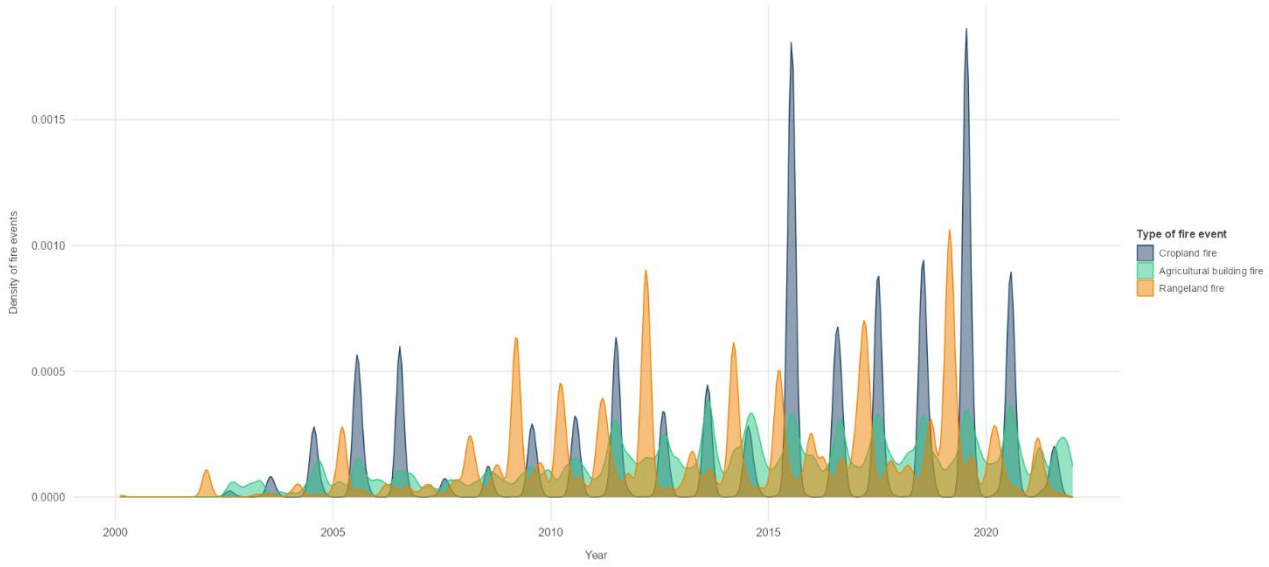

Figure 2 : Temporal evolution of agricultural fire occurrence over the period 2000-2021 in France. (Blue = Cropland fire, Green = Agricultural building fire, Orange = Rangeland fire).

2.3. Seasonality

Agricultural fires are marked by strong seasonality, with the peak occurrence in July with an average of over 200 agricultural fires per month (Figure 3.1). This peak is mainly due to the sharp increase in crop fires from June to August. This period is characterized by a strong increase in temperatures and a decrease in precipitation, particularly around the Mediterranean basin. These climatic conditions favor the burning of plots whose biomass has accumulated since early spring.

Fires in infrastructures occur almost uniformly throughout the year. While climatic conditions may account for their occurrence during the rest of the year, winter building fires can probably be attributed to mechanical and technological malfunctions leading to fire ignition.

The rangeland fires occur particularly in February-March, but also in September-October, especially for the years 2007, 2016, 2018 (Figure 3.2). These fires correspond largely to prescribed fires subject to authorization delivered only during this period when fire weather is less conductive to fire spreading.

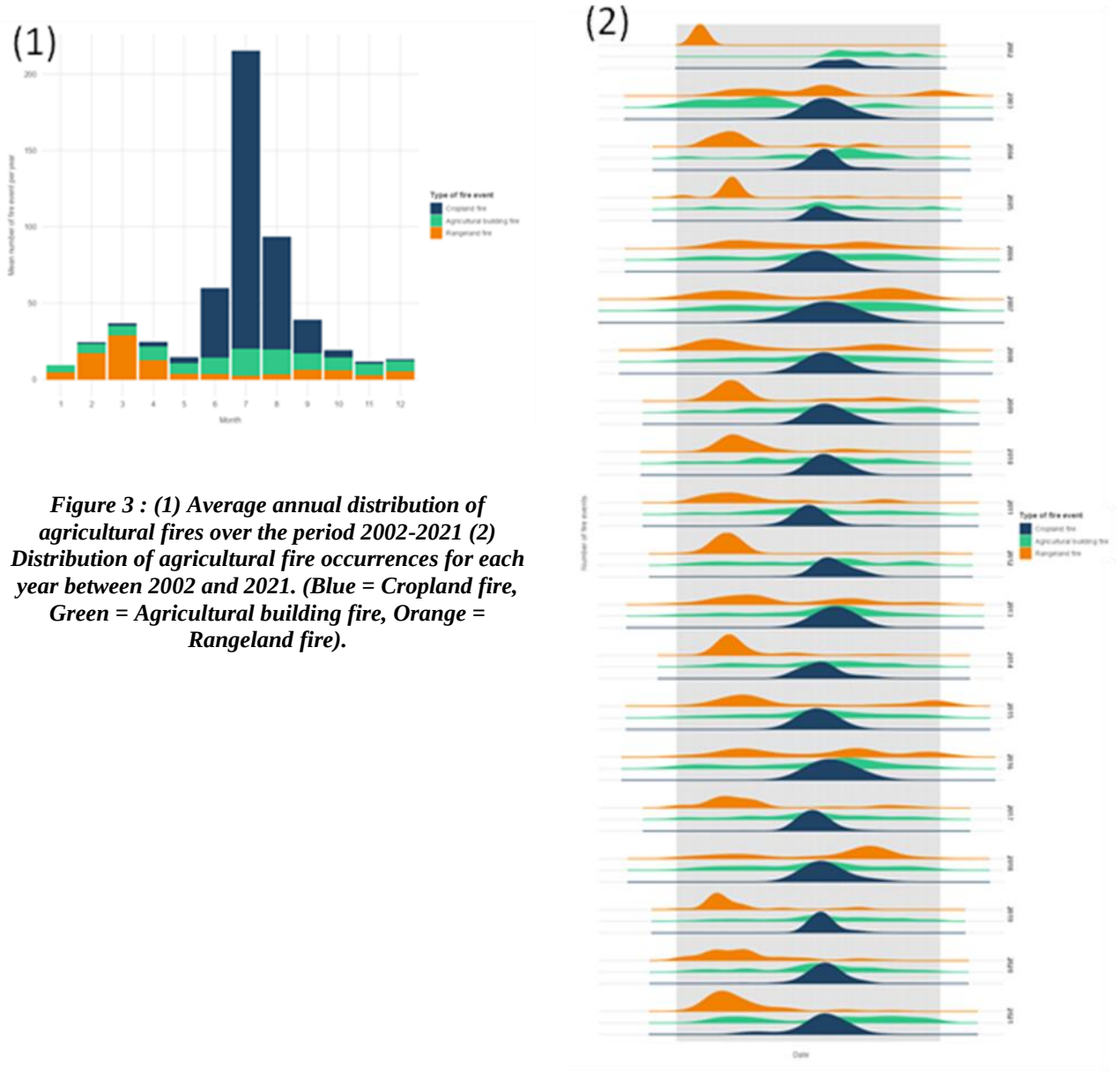

Figure 3 : (1) Average annual distribution of agricultural fires over the period 2002-2021 (2) Distribution of agricultural fire occurrences for each year between 2002 and 2021. (Blue = Cropland fire, Green = Agricultural building fire, Orange = Rangeland fire).

2.4. Remote Sensing

Figure 4 represents the hotspot density map over croplands/pastures in France from VIIRS S-NPP over the 2012-2020 period. We observe a similar national pattern as from datamining, with high fire activity captured where the largest fires are referenced, and the highest fire activity in the southwest mountainous pastures fires. Fires smaller than 100ha and 50ha were however only captured respectively at 50% and 25% (Figure 5), leaving a high uncertainty in small fires detection from remote sensing compared to datamining. The relationship between hotspot number and fire size for each fire event followed a logarithmic increase (figure 6) with remaining high uncertainty in large burned areas estimates (Liu et al., 2019).

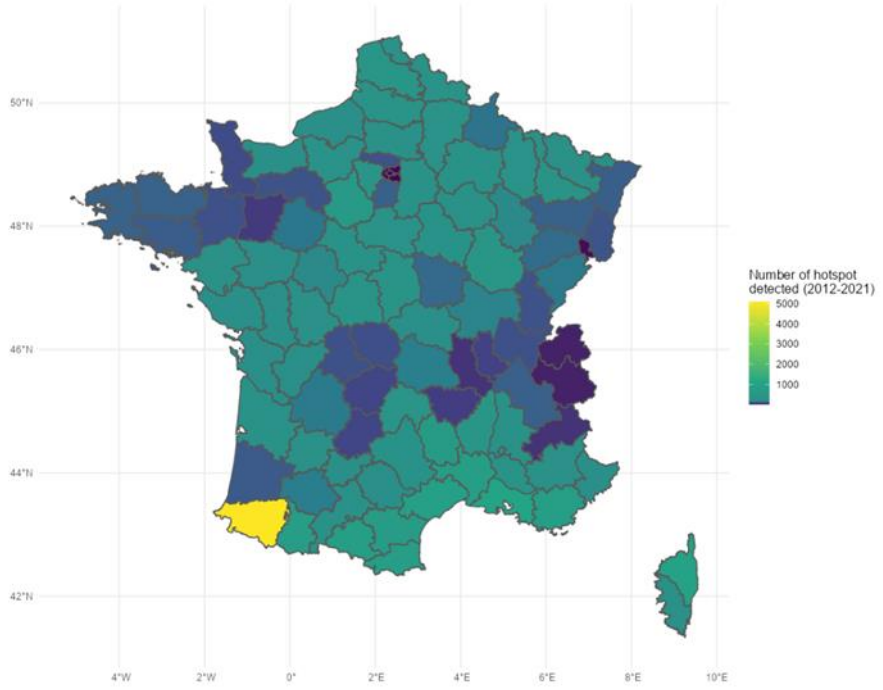

Figure 4 : Number of hotspots detected in croplands by VIIRS Suomi NPP from 2012 to 2021 for each department in France

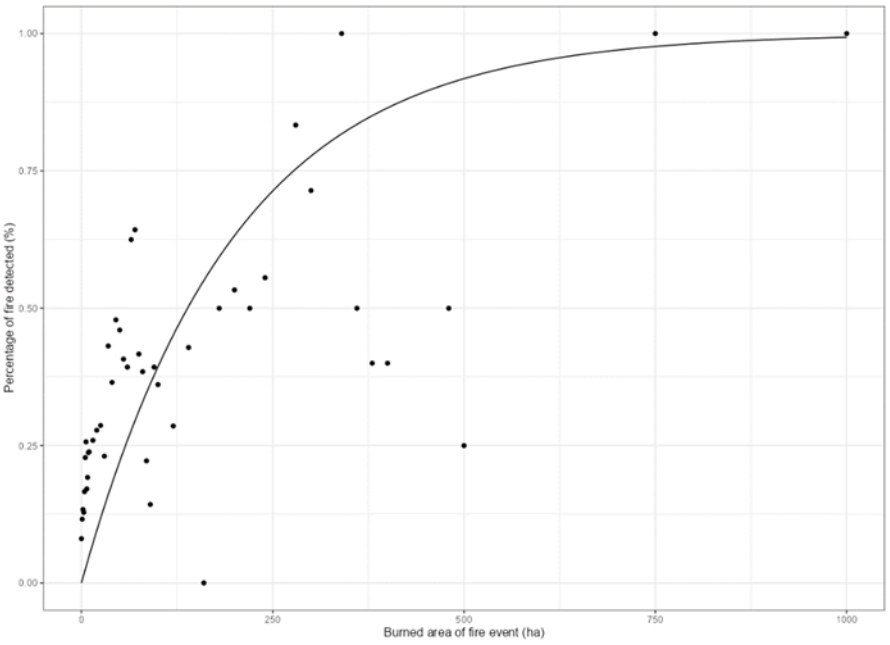

Figure 5 : Fire detection rate (%) with at least one hotspot from VIIRS S-NPP for burned area of fire events (ha) referenced in the datamining References

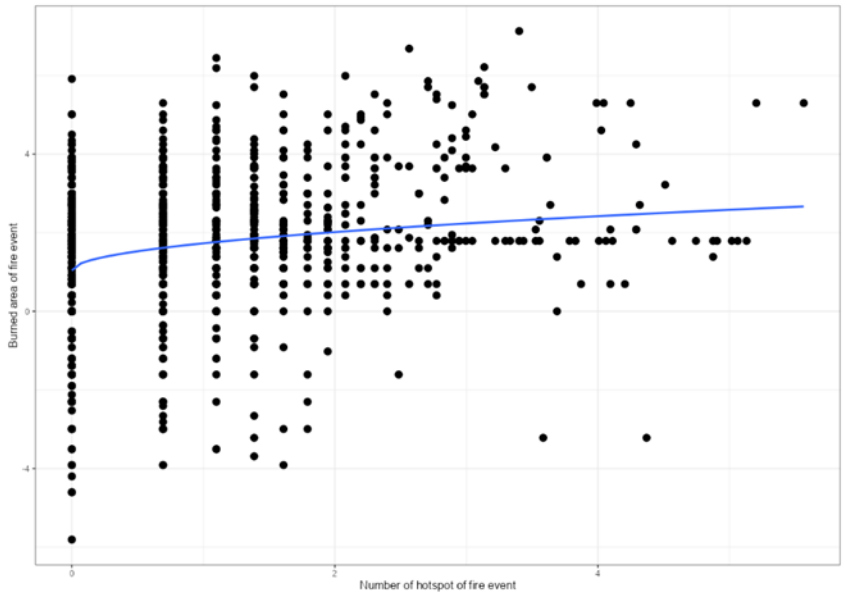

Figure 6 : Relationship between the number of hotspots (log scale) detected and the burned area (log scale) for each fire event (n=1620)

3. Conclusion

This study represents the first attempt to inventory agricultural fires in France. The data mining analysis allowed to highlight spatial and temporal patterns specific to cropland and rangeland fires. Remote sensing data provided a poor improvement for these small, low intensity fires, highlighting the need for better referencing of cropland fires and methodological developments from new sensors (Deshpande et al., 2022).

4. Literature cited

Alonso-Canas, I., Chuvieco, E., 2015. Global burned area mapping from ENVISAT-MERIS and MODIS active fire data. Remote Sens. Environ. 14.

Amatulli, G., Peréz-Cabello, F., de la Riva, J., 2007. Mapping lightning/human-caused wildfires occurrence under ignition point location uncertainty. Ecol. Model. 200, 321–333. https://doi.org/10.1016/j.ecolmodel.2006.08.001

Bowman, D.M.J.S., Balch, J., Artaxo, P., Bond, W.J., Cochrane, M.A., D'Antonio, C.M., DeFries, R., Johnston, F.H., Keeley, J.E., Krawchuk, M.A., Kull, C.A., Mack, M., Moritz, M.A., Pyne, S., Roos, C.I., Scott, A.C., Sodhi, N.S., Swetnam, T.W., 2011. The human dimension of fire regimes on Earth: The human dimension of fire regimes on Earth. J. Biogeogr. 38, 2223–2236. https://doi.org/10.1111/j.1365-2699.2011.02595.x

Bowman, D.M.J.S., Kolden, C.A., Abatzoglou, J.T., Johnston, F.H., van der Werf, G.R., Flannigan, M., 2020. Vegetation fires in the Anthropocene. Nat. Rev. Earth Environ. 1, 500–515. https://doi.org/10.1038/s43017-020-0085-3

Coughlan, R., Di Giuseppe, F., Vitolo, C., Barnard, C., Lopez, P., Drusch, M., 2021. Using machine learning to predict fire-ignition occurrences from lightning forecasts. Meteorol. Appl. 28. https://doi.org/10.1002/met.1973

Deshpande, M.V., Pillai, D., Jain, M., 2022. Detecting and quantifying residue burning in smallholder systems: An integrated approach using Sentinel-2 data. Int. J. Appl. Earth Obs. Geoinformation 108, 102761. https://doi.org/10.1016/j.jag.2022.102761

Dether, D., Black, A., 2006. Learning From Escaped Prescribed Fires – Lessons for High Reliability 66, 7.

Giglio, Louis, 2000. MODIS Thermal Anomalies/Fire Products. https://doi.org/10.5067/FIRMS/MODIS/MCD14ML

Hunter, M.E., Robles, M.D., 2020. Tamm review: The effects of prescribed fire on wildfire regimes and impacts: A framework for comparison. For. Ecol. Manag. 475, 118435. https://doi.org/10.1016/j.foreco.2020.118435

Liu, T., Marlier, M.E., Karambelas, A., Jain, M., Singh, S., Singh, M.K., Gautam, R., DeFries, R.S., 2019. Missing emissions from post-monsoon agricultural fires in northwestern India: regional limitations of

MODIS burned area and active fire products. Environ. Res. Commun. 1, 011007. https://doi.org/10.1088/2515-7620/ab056c

McLauchlan, K.K., Higuera, P.E., Miesel, J., Rogers, B.M., Schweitzer, J., Shuman, J.K., Tepley, A.J., Varner, J.M., Veblen, T.T., Adalsteinsson, S.A., Balch, J.K., Baker, P., Batllori, E., Bigio, E., Brando, P., Cattau, M., Chipman, M.L., Coen, J., Crandall, R., Daniels, L., Enright, N., Gross, W.S., Harvey, B.J., Hatten, J.A., Hermann, S., Hewitt, R.E., Kobziar, L.N., Landesmann, J.B., Loranty, M.M., Maezumi, S.Y., Mearns, L., Moritz, M., Myers, J.A., Pausas, J.G., Pellegrini, A.F.A., Platt, W.J., Roozeboom, J., Safford, H., Santos, F., Scheller, R.M., Sherriff, R.L., Smith, K.G., Smith, M.D., Watts, A.C., 2020. Fire as a fundamental ecological process: Research advances and frontiers. J. Ecol. 108, 2047–2069. https://doi.org/10.1111/1365-2745.13403

O'Mara, F.P., 2012. The role of grasslands in food security and climate change. Ann. Bot. 110, 1263–1270. https://doi.org/10.1093/aob/mcs209

Pausas, J.G., Ribeiro, E., 2017. Fire and plant diversity at the global scale: PAUSAS and RIBEIRO. Glob. Ecol. Biogeogr. 26, 889–897. https://doi.org/10.1111/geb.12596

Prichard, S.J., Stevens-Rumann, C.S., Hessburg, P.F., 2017. Tamm Review: Shifting global fire regimes: Lessons from reburns and research needs. For. Ecol. Manag. 396, 217–233. https://doi.org/10.1016/j.foreco.2017.03.035

Schroeder, W., Oliva, P., Giglio, L., Csiszar, I.A., 2014. The New VIIRS 375 m active fire detection data product: Algorithm description and initial assessment. Remote Sens. Environ. 143, 85–96. https://doi.org/10.1016/j.rse.2013.12.008

Shi, Y., Matsunaga, T., Saito, M., Yamaguchi, Y., Chen, X., 2015. Comparison of global inventories of CO2 emissions from biomass burning during 2002–2011 derived from multiple satellite products. Environ. Pollut. 206, 479–487. https://doi.org/10.1016/j.envpol.2015.08.009

van der Werf, G.R., Randerson, J.T., Giglio, L., Collatz, G.J., Mu, M., Kasibhatla, P.S., Morton, D.C., DeFries, R.S., Jin, Y., van Leeuwen, T.T., 2010. Global fire emissions and the contribution of deforestation, savanna, forest, agricultural, and peat fires (1997–2009). Atmospheric Chem. Phys. 10, 11707–11735. https://doi.org/10.5194/acp-10-11707-2010

Vilar, L., Camia, A., San-Miguel-Ayanz, J., 2015. A comparison of remote sensing products and forest fire statistics for improving fire information in Mediterranean Europe. Eur. J. Remote Sens. 48, 345–364. https://doi.org/10.5721/EuJRS20154820

World development indicators, n.d.

Analysis of the Canadian Fire Weather Index during large fires in Croatian Adriatic

Tomislava Hojsak*; Tomislav Kozarić; Marija Mokorić

Croatian Meteorological and Hydrological Service, Ravnice 48, Zagreb, Croatia,
{tomislava.hojsak, tomislav.kozaric, marija.mokoric}@cirus.dhz.hr

**Corresponding author*

Keywords

Large wildland fires, Fire Weather Index, fire risk assessment

Abstract

Wildland fires, especially the large ones, are becoming a growing problem in the climate-changing world. More frequent and long-lasting drought conditions accompanied by high temperatures and heat waves significantly increase fuel flammability, particularly during summer.

The wildland fire occurrence and behaviour are to a large degree weather driven and thus strongly depend on the meteorological parameters such as humidity, temperature, precipitation, and wind speed as well as on the amount of fuel load. The relationship between weather and fire occurrence and behaviour is included in the Canadian Fire Weather Index System (FWI), which has been used in Croatia for fire risk assessment since 1982.

This paper analyses the characteristics of the Fire Weather Index components for large fires in the Adriatic region of Croatia. Fire weather indices were evaluated for 103 wildland fires with a burned area of over 400 ha that occurred during summer fire seasons from 2003 to 2021. Obtained median values of the moisture indices, as well as the fire behaviour indices (FFMC 93, DMC 139, DC 649, ISI 13, BUI 182 and FWI 45) showed values designated as high and very high in the available literature. Compared to daily frequency distribution of indices for fire seasons from 2003 to 2021, the indices during large fire days belong primarily in their upper percentile categories (>75 percentile).

Climate change will continue to increase the fire risk and thus the possibility of large fires so this analysis can provide a baseline for improvements and recalibration of the fire danger classes in the Adriatic area of Croatia. Along with the improved fire weather warnings, this will give better and more accurate information about the increased wildland fire risk and the possibility of large fires.

1. Introduction

The Mediterranean region is the most prominent climate response hot spot (Giorgi, 2006), and Croatia is no exception. Climate analysis of the last 30 years shows noticeable trends in mean temperature rise and the more frequent occurrence and longer duration of extreme meteorological events such as dry spells and heat waves (Gajić-Čapka et al., 2010). These conditions contribute to the increase of fire risk and lengthening of the fire seasons, which tend to start earlier, in May, and extend until October, sometimes even until November. As a result, meteorological fire weather indices also show a rising trend, indicating a growing risk of large fires.

Weather is one of the main drivers of the wildland fires and the most variable one, both spatially and temporally. Long-lasting droughts and high temperatures provide favourable conditions for ignition by dehydration of fuel, and the wind is one of the main factors of fire propagation. Thus, weather parameters such as temperature, relative humidity, precipitation, and wind speed are considered when assessing the risk and behaviour of wildland fires. The Canadian Fire Weather Index (FWI) and its components - fuel moisture codes (FFMC, DMC and DC) and fire behaviour indices (ISI, BUI) represent the cumulative effect of the weather on fuel and thus allow the assessment of fire risk (Van Wagner, 1987).

For the past 40 years, the Canadian Fire Weather Index System has been used in Croatia for fire risk assessment. The index was calibrated for the Adriatic based on the statistical analysis of the burned area and the number of fires. Also, the fire danger classes were derived through a combination of FWI and BUI (Dimitrov, 1987).

At the peak of the fire season, the fire danger classes are predominantly high and very high. Therefore, they do not provide additional information about the fire risk, especially the conditions favourable for large fires.

2. Method and Data

The study area is the Croatian Adriatic, characterized by the Mediterranean climate. It is covered with agricultural land and Mediterranean vegetation, which are particularly conducive to wildland fires. The area can also be considered the wildland-urban interface zone, with many settlements integrated into the wilderness.

Information on the large fires between 2003 and 2021 was obtained from the Croatian Fire Fighting Association. They contain data about fire location, ignition and extinction date and time, and the total burned area.

In the literature, different thresholds of burned area for large fires can be found. Since the purpose is to evaluate indices for the conditions when the extreme fire spread and erratic fire behaviour were present, the wildland fires with a burned area bigger than 400 ha were referred to as large fires (Heilman and Bian, 2010).

For the analysis, the daily values of the Fire Weather Index components were used, calculated at 12 UTC, for 24 meteorological stations of the Croatian Meteorological and Hydrological Service. The values from the stations closest to the fires were relevant to the investigation and used in the analysis (Figure 1).

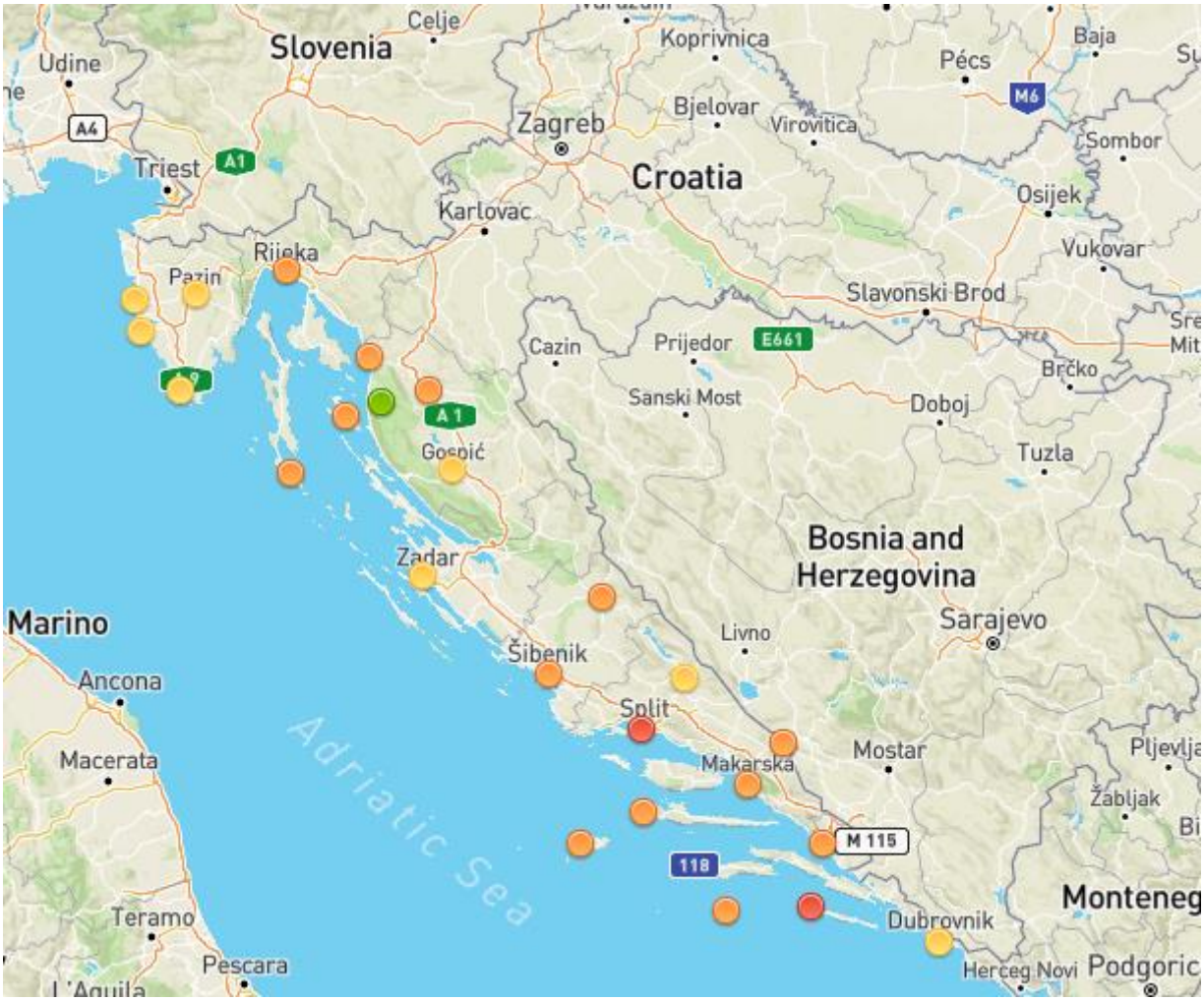

Figure 1 – Location of DHMZ weather stations, source DHMZ.

Empirical cumulative distribution frequency analysis and median and percentile categories were calculated for each FWI component. For comparison, daily distributions of indices for fire seasons (May to September) from 2003 to 2021 were also calculated. The objective of the analysis was to obtain estimates of the index values commonly present during the large wildland fires.

3. Results and Discussion

Statistics for each FWI component is given in Table 1, which summarises the median and percentiles (10, 25, 75 and 90) for FFMC, DMC, DC, BUI, ISI and FWI for days with large fires and fire seasons for a period from 2003 to 2021. Additionally, minimum and maximum values and average and standard deviation are displayed. Related cumulative frequency distributions are shown in Figures 2 to 7.

Table 1 - Statistical values for FWI components (median and percentiles, minimum and maximum value, average and standard deviation) for large fires and daily distribution for fire seasons from 2003 to 2021.

Parameters	Percentiles					Min	Max	Average	Standard deviaton
	10	25	Median	75	90				
FFMC large fires	88	90	93	94	96	73	98	92	3.8
daily distribution	72	85	89	91	93	4.1	98	85	11
DMC large fires	86.4	110	139	184.5	233.2	40	367	150.3	56.4
daily distribution	14.8	28.8	55.8	94.7	143.5	0.4	454.8	70	56.1
DC large fires	487	552.5	649	783.5	874	106	986	662.8	153.2
daily distribution	86.5	174.6	335.7	515.3	681	3.8	1138.7	361	225.1
ISI large fires	6	9	13	19	24.6	1	55	14.6	8.2
daily distribution	1.3	3.9	6.7	10.3	15.2	0	115.2	7.9	6.4
BUI large fires	125	146	182	221.5	262	66	367	187.5	53.2
daily distribution	21.2	40.1	75.5	122.8	176	0.7	454.7	89.2	63.8
FWI large fires	26	34	45	57	67.6	6	108	46	17.2
daily distribution	2.6	10.2	20.7	32.1	44	0	166.5	22.6	16.3

3.1. Fine Fuel Moisture Code – FFMC

The median of FFMC during large fires has a relatively high value of 93, as shown in Table 1. 10-90th percentile interval indicates closely clustered data around the median, with 50% of FFMC values for large fires between 90 and 94, situated above daily frequency median (89).

The FFMC is a numeric rating of the moisture content of fine fuels on forest surface and an indicator of ease of ignition (Van Wagner, 1987). Small spread around the mean as well as the steep slope of both cumulative frequency distributions (Figure 2) point to very low moisture content in fine fuels during most of the days, which can be expected in summer, especially in the environment favourable for large fires. An FFMC of 92 or more points to a high probability of the onset of extreme fire behaviour, depending on the wind and BUI level (Alexander and Cole, 2001). According to the FFMC analysis, these values have been observed in the 50% of large fire data set, and only in 10% of daily distribution (Figure 2).

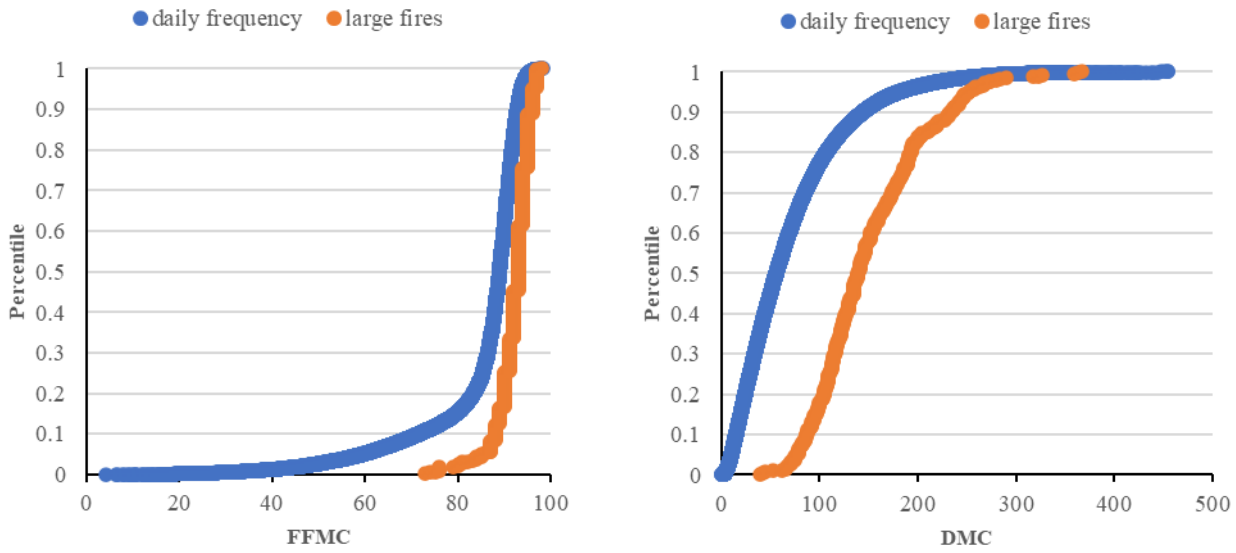

Figure 2 and 3 - Cumulative distribution of Fine Fuel Moisture Code (FFMC) and Duff Moisture Code (DMC) for large fires (red) and daily distribution (blue)

3.2. Duff Moisture Code - DMC

The cumulative frequency analysis for the DMC (Figure 3) shows a median of 139 for large fires and a significantly lower value of 56 for daily distribution (Table 1). Most large fire values are higher than the daily median.

The DMC indicates fuel consumption in moderate duff layers and medium-size woody material, and a value of 150 to 200 indicates that the duff will have lost most of its moisture (Van Wagner, 1987, Canadian Forest Service, 1996). While this is the case in 43% of large fire values, only 10% of daily distribution values indicates moisture loss in duff layers. The DMC analysis could suggest that large wildland fires in the Adriatic occurred even in cases of duff layers not completely dried out.

3.3. Drought Code - DC

According to percentile values (Table 1), for most days with large fires, the DC index was between 487 and 874, with a median of around 650. This value range is situated in the upper 70% of daily distribution values. However, the daily median is much lower, around 335.

The DC index is a numeric rating of the moisture content of a deep layer of organic matter (Van Wagner, 1987) and an indicator of seasonal drought. At a value of 300, the moisture content starts to decrease with depth (De Groot, 1987), so 99% of DC data (Figure 4) show drought conditions were present during large wildland fires, while 55% of daily values were above 300.

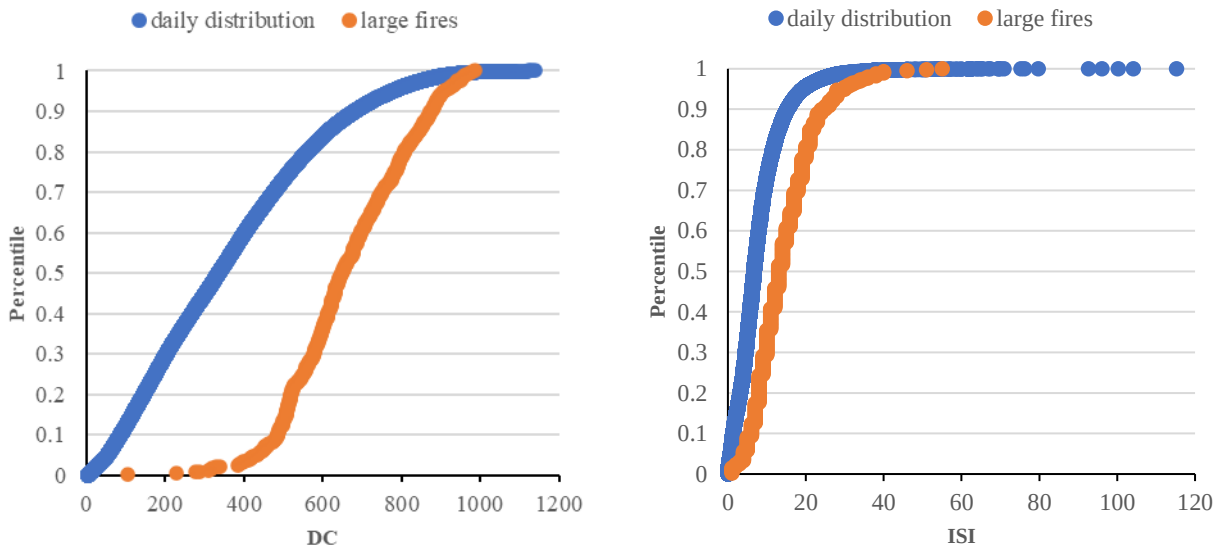

Figure 3 and 4 - Cumulative distribution of Drought Code (DC) and Initial Spread Index (ISI) for large fires (red) and daily distribution (blue)

3.4. Initial Spread Index - ISI

ISI for large fires showed a much larger spread around the median than other indices (Table 1, Figure 4), which is understandable considering its dependence on wind speed. The median for large fires was around 13, with data ranging mostly from 6 to relatively high 25, values that correspond to the 10th and 90th percentile. Compared to daily distribution, about 80% of large fire values were higher than the daily distribution mean. The highest ISI value for large fires was 55, while from 2003 to 2021, values up to 115 were recorded.

Combining the effects of wind and FFMC, the ISI is a numeric rating of the expected rate of fire spread (Van Wagner, 1987). The ISI is used in association with the BUI (or with the degree of curing, in the case of grass fuel types) in the FBP System (Forestry Canada Fire Danger Group 1992) to provide numeric values for fire behaviour for predetermined forest and slash fuel types.

3.5. Buildup Index - BUI

According to the cumulative frequency, BUI mean for large fires (Figure 6, Table 1) is 182, while 90% of the values (125 to 262) are above the 75th percentile of the daily distribution.

The BUI index is a numeric rating of the amount of fuel available for combustion (Van Wagner, 1987) and represents the fire potential. The statistical analysis done by Dimitrov (1987), currently used for fire danger assessment, classified BUI values as very low (0-48), low (49-85), moderate (86-118), high (119-158) and very high (159+). Therefore, around 70% of the large fire values and less than 15% of daily distribution can be placed in very high Dimitrov's class.

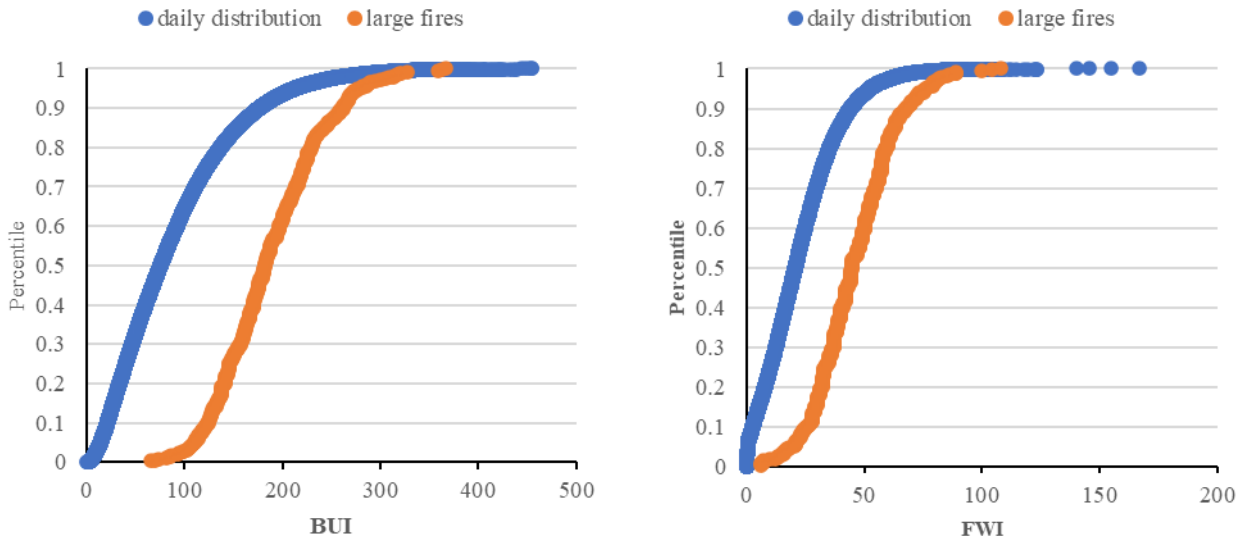

Figure 6 and 7 - Cumulative distribution of Buildup Index (BUI) and Fire Weather Index (FWI) for large fires (red) and daily distribution (blue)

3.6. Fire Weather Index - FWI

Analysis shows that 80% of FWI values for the large fires, ranging between 26 and 68 (Table 1, Figure 7), are situated above the daily frequency median (21). The large fire median of 45 is above the 90th percentile of the daily distribution.

The FWI is a general index of fire danger and a numeric rating of fire intensity calculated from ISI and BUI (Van Wagner, 1987). The FWI values used in Croatia, according to Dimitrov (1987), are considered very low (less than 4), low (5-8), moderate (9-16), high (17-32) and very high (33+). The 25th percentile of the large fire distribution is on the lower boundary of the very high Dimitrov's class, meaning that 75% of FWI data fall in the very high fire danger class.

4. Conclusion

Climate change scenarios suggest extreme weather events such as long dry periods and heatwaves will be more frequent and stronger in the future (Branković et al., 2012). As a result, the conditions conducive to fire will be more common in Croatia, particularly on the Adriatic.

The analysis of the FWI indices during large wildland fires provides an insight into the range of values that typically appear when weather conditions are favourable for extreme fire spread and behaviour. Median values of indices (FFMC 93, DMC 139, DC 649, ISI 13, BUI 182 and FWI 45) showed values designated as high and very high in the cited literature, particularly in Dimitrov (1982), and generally fall in the upper percentile categories (> 75th percentile) of daily frequency distribution for fire seasons from 2003 to 2021. Moreover, 70% of BUI and 75% of FWI fall into the very high Dimitrov's class. So, the median values and upper percentiles, e.g., 90th obtained for large fires and fire weather warnings, can be used as additional information for forecasters and fire managers when assessing the possibility of large fire occurrence.

The climatology of the FWI indices for the Adriatic is long overdue, along with the new calibration of the Index. Dimitrov's fire danger classes have proven inadequate during the peak of fire season when values are predominantly high and very high. However, there are some efforts to calculate the most recent climatology. Results obtained in this paper together with the new FWI climatology could provide a baseline for recalibration of the fire danger classes.

5. References

Alexander, M.E. ; Cole, F.V. 2001. Rating fire danger in Alaska ecosystems: CFFDRS provides an invaluable guide to systematically evaluating burning conditions. USDI Bur. Land Manag., Alaska Fire Serv., Fort Wainwright, AK. Fireline 12(4):2–3

Branković Č., Patarčić M., Güttler I., Srnec L. (2012): Near-future climate change over Europe with focus on Croatia in an ensemble of regional climate model simulations, Climate Research, 52, 227-251, available at https://www.int-res.com/articles/cr_oa/c052p227.pdf

Canadian Forest Service. 1996. Introduction to the Canadian Forest Fire Weather Index System. Nat. Resour. Can., an. For. Serv., and PanVideo Productions, Victoria, BC.

Dimitrov T., 1987: Šumski požari i sistemi procjene opasnosti od požara, in: S. Bertović, T. Dimitrov i dr. (Eds.), Osnove zaštite šuma od požara, Centar za informacije i publicitet, Zagreb, 181-251 (in Croatian)

Gajić-Čapka M., K. Zaninović, K. Cindrić, 2010: Climate Change Impacts and Adaptation Measures – Observed Climate Change in Croatia, Fifth National Communication of the Republic of Croatia under the United Nation Framework Convention on the Climate Change, Ministry of Environmental Protection, Physical Planning and Construction, 137-151. https://unfccc.int/resource/docs/natc/hrv_nc5.pdf

Giorgi, F., 2006: Climate change Hot-spots. *Geophys. Res. Lett*. 33, L08707

Heilman W. E. and X. Bian, 2010: Turbulent kinetic energy during wildfires in the north central and north-eastern US, *International Journal of Wildland Fire*, **19**, 346-363

Van Wagner C.E., 1987: Development and Structure of the Canadian Forest Fire Weather Index System, Canadian Forestry Service, Forestry Technical Report 35

Assessing social vulnerability to wildfires of communities from a relative value approach: a working hypothesis

Daniele Del Bianco[1]; Ramona Velea[1*]; Riccardo Laterza[1]; Olivia Ferrari[1]

[1]ISIG – Institute of International Sociology of Gorizia. Via Mazzini 13, Gorizia, Italy, {delbianco, velea, laterza, ferrari}@isig.it

**Corresponding author*

Keywords

Social vulnerability, Community, Exposure, Sensitivity, Adaptation

Abstract

The present paper provides an overview of the research carried out by the Institute of International Sociology of Gorizia (ISIG) in the framework of three EU funded projects (ECOSTRESS – DG ECHO, RESILOC – H2020, and FirEUrisk – H2020). Throughout these three research projects, a relevant corpus of literature has been analysed and re-elaborated, allowing for the development of methodologies and instruments for the assessment of social vulnerability at a local/community level. This paper provides, first, a theoretical overview on the issue, second, the results and potentialities of such instruments stemming from recent field applications, and third, the potential outline for operational approaches in the field of wildfire resilience-building strategies for local communities.

By addressing the complexity of vulnerability, both as a concept and as a phenomenon, the paper focuses on social vulnerability to wildfire, intended as the magnitude of social impact deriving from wildfires, and the (in)ability of local communities to cope with wildfire as a stressor.

In the absence of standard assessment benchmarks and thresholds for (social) vulnerability, the paper argues for a relative perspective of analysis, within which the 'vulnerability' of a community is analysed in comparison with other similar units of analysis.

Furthermore, the paper argues for participatory approaches towards such assessments, that would allow for an increased level of integration of local knowledge within the analysis. Moreover, building on the results of recent research projects, the paper promotes participatory approaches to vulnerability assessment as a preliminary 'needs assessment' by means of which end users/communities may identify 'areas of vulnerability', as well as well as existing resources/adaptive capacities, to be considered in the elaboration of resilience strengthening strategies or equivalent development/strategic planning processes at local level.

1. Introduction – a research framework for social vulnerability

The paper provides an overview of the research carried out by the Institute of International Sociology of Gorizia (ISIG) in the framework of three EU funded projects[1], namely summarising the relevant corpus of literature that has been analysed and re-elaborated to develop instruments for the assessment of social vulnerability at a local level.

This paper provides a theoretical overview on the issue which could serve as a basis for operational approaches in the field of wildfire resilience-building strategies at local/community level, to be further explored within the framework of FirEUrisk H2020 project.

1.1. Social Vulnerability

[1] ECOSTRESS (DG ECHO): ISIG developed a Relative Social Vulnerability Index and SWOT Analysis of Coastal Case Studies in the Upper Adriatic. RESILOC (H2020): ISIG coordinated the activities related to the analytical framework for the vulnerability analysis at Local Community level. FirEUrisk (H2020): ISIG is coordinating the definition of a methodological framework for wildfire vulnerability assessment, with a specific focus on societal vulnerability.

Vulnerability, both as a concept and as a phenomenon, does not have a univocal definition, nor a unique methodology for its assessment (Füssel, 2007; Fekete & Montz, 2018; Cutter, 2018). It may be broadly understood, however, as the potentiality for loss of a unit/system in the light of stressors. The UNDRR defines vulnerability as "the conditions determined by physical, social, economic and environmental factors or processes which increase the susceptibility of an individual, a community, assets or systems to the impacts of hazards"[2].

Vulnerability is a multifaceted concept: it lacks a definitional unity and clarity (Cutter, 2018) both within, and between, academic research and policy and practitioner driven work (Füssel, 2007; Fekete & Montz, 2018). It is also a dynamic concept, eventually shaped by the recent waves of increased awareness regarding the profound climate change impacts (Hinkel, 2011).

Especially after the 1994 *World Conference on Natural Disaster Reduction* in Yokohama, the concept of vulnerability has become very prominent in the field of risk reduction studies (Cutter, 2018). Vulnerability has been increasingly associated with the term "resilience", whose success was at least partially determined by its positive tone.

There are several elements that are generally acknowledged as being entailed by the concept of vulnerability:

- Exposure: the stress or stresses to which an individual, community, society, ecosystem, structure, etc. are exposed (i.e., they are at risk from a hazard).
- Sensitivity: the extent to which the exposed elements are affected or indeed modified by the stress.
- Adaptive capacity/coping mechanisms: existing or lacking skills, resources, opportunities that allow the exposed/affected elements to survive, absorb the impacts, and manage the adverse outcomes.

Vulnerability studies investigate on different thematic dimensions or types of vulnerability; every dimension has shaped different research perspectives, academic corpuses of knowledge, and consequently different assessment/measurement methods. The MOVE framework (Birkmann et al., 2013) and the 4-dimensional model proposed by Fuchs and Thaler (2018) stand as relevant attempts to systemize different perspectives on the issue of vulnerability under the same framework. The former identifies six dimensions of vulnerability: social, economic, physical, cultural, environmental, and institutional. The latter works on a combination of physical, economic, institutional, and social dimensions of vulnerability.

Within the abovementioned frameworks, social vulnerability describes a state of people, or populations, rather than physical structures, therefore a 'social space' whose boundaries are defined by the "political, economic, and institutional capabilities of people at a specific time and place" (Burton, Rufat, & Tate, 2018, p. 53). Social vulnerability refers to the inability of people, organisations, communities, and societies, to resist adverse impacts from stressors to which they are exposed.

1.2. Social Vulnerability to Wildfires

Social vulnerability to wildfires refers both to the magnitude of social impact deriving from wildfires, and the inability of local society to cope with stressors to which it is exposed. It entails both a structural and a processual dimension. According to the *FAO Strategy on Forest Fight Management*, 90% of wildfires are caused by human activities and behaviours, which are in turn interrelated with meteorological conditions, territorial topography, and fuel availability, following a non-linear and dynamic relationship.

Leone et al. (2003, 2009) proposed a systematisation of the main human-related variables explaining wildfire occurrence, stemming from several previous studies. Martínez et al. (2009) identified seven groups of anthropogenic risk factors associated with wildfires:

- Socio-economic transformations in rural areas.
- Human presence and socio-economic transformations in urban areas.
- Persistence or transformation of traditional activities linked to fire in rural areas.
- Accidental or negligent events related to infrastructures and facilities.
- Landscape structure and housing patterns.

[2] https://www.undrr.org/terminology/vulnerability

- Indirect factors (i.e., regulations and behaviours) of intentional fires.
- (Lack of) forest policy.

These or similar dimensions are used by the authors to identify relevant variables (i.e., indicators) describing exposure and sensitivity associated with fire risk in different geographical contexts (Martínez et al., 2009; Ager, Preisler, Arca, Spano, & Salis, 2014; Vallejo-Villalta et al., 2019; Costafreda-Aumedes et al., 2017).

In the broader framework of human activities, consolidated and/or emerging patterns of territorial development, as well as local policies, play a relevant role in adapting the whole system to wildfire risks, as well as in making available coping mechanisms. Also in this case, relationship between established policies/practices and efficiency and efficacy in fire risk reduction is hard to be traced, for instance in the case of fire management procedures (Fernandes, 2013; Moritz et al., 2014)

Jucker Riva et al. (2018) investigated the impact of land management practices (LMPs) in the enhancement of forests and rangelands resilience vis-à-vis environmental disturbances, including wildfires. They isolated 16 LMPs, clustered in five groups, highlighting that that removal of vegetation was the most beneficial single LMP: clearing of vegetation; managed grazing; planting of shrubs; planting of trees; other practices.

2. Assessing Social Vulnerability: towards a participatory approach

If defining vulnerability is fraught with difficulty, assessing and measuring it is even more difficult. While the notion of measurement refers to the elaboration of specific quantification instruments which can describe the phenomena of vulnerability, the notion of assessment includes a broader spectrum of approaches to identify, investigate, quantify, weight and rank of a set of vulnerabilities.

Various critiques have been voiced at the methodologies of measurement, mainly in relation to the challenges of using indexes, to problems associated with spatial and context differences and assessment of data at various scales of analysis (Barnett, Lambert, & Fry, 2008; Fekete & Montz, 2018). Comparisons have been warned against, on the argument that vulnerability is a context-specific rather than a generic condition (Barnett, Lambert, & Fry, 2008). Also, another critique is focused on the dynamic nature of the vulnerability phenomena (Adger, 2006), which determines shortcomings in the use of static indicators. When considering analysing vulnerability from a community perspective, the dynamic nature of both the phenomenon (i.e., vulnerability) and of the unit of analysis (i.e., the community) plays indeed a fundamental role. Quantitative methods and data can provide for a static picture of a community but limited in the understanding of the real implications and connections of intervening factors at community level, for instance adaptive capacity elements (i.e., skills and resources). Moreover, each community is very different than the other, so in order to be able to grasp fully the interactions and implications of the identified variables with the context itself, there is the need to incorporate in the analysis the local knowledge and awareness. This may be achieved by means of participatory approaches to assess vulnerability.

The understanding of vulnerability and resilience at community level depends on who, what, where, and for whom – all of which are socially constructed and temporally changing (Cutter, 2018). Resilience and vulnerability are embedded in interdependencies between systems, scales, and historical processes. It may be thus challenging to identify thresholds or benchmarks in vulnerability assessments (Fekete, 2019). In a word, vulnerability, as well as resilience, may be approached from a relative perspective rather than in absolute terms (Cutter, 2016; Fekete, 2019). Understanding vulnerability as a relative concept means to consider it in context, so to allow for its observation in comparison with other similar units of analysis, for example neighbouring communities exposed to similar hazards.

Most studies derived from the methodologies devised by Cutter[3] provide a spatial assessment and an empirical ranking. A vulnerability score (a numerical value which aggregates all the operations performed through collecting values for indicators, aggregating them, etc.), is not considered to be high or low *per se*, but by reference (distance) to a mean value, therefore, only by reference to other units of analysis, which compose this mean. Such approach, adopted for the purpose of this paper and of illustrated research projects, enables

[3] See for instance Cutter, Boruff, & Shirley, 2003; Cutter, Burton, & Emrich, 2010; Guillard-Gonçalves, Cutter, Emrich, & Zêzere, 2015.

participatory assessments of vulnerability and resilience of communities, which could allow for a more grounded integration of context knowledge. The later, appears to be key to ensure an accurate analysis/representation of the status quo at community level, that might escape to top-down approaches.

3. Applications of proposed methodology: results and benefits for building targeted resilience strategies at local level

The RESILOC Community Vulnerability Indexes are the result of a participatory process that engaged project end-users (i.e., pilot local communities) in both data collection process and assessment. Starting from a standard set of indicators and related proxies (i.e., quantitative, and qualitative variables), aggregated in five dimensions (social, economic, institutional, human capital, environmental) each pilot Community was requested to select the most relevant ones and to attribute different weights among those considered relevant (i.e., medium and high). The vulnerability relative indexes were then calculated, based on available statistical data, as well as on qualitative variables gathered from end-users. Vulnerability community scores have been calculated for involved pilots (i.e., municipalities) in a relative perspective, against their area of reference (i.e., neighbouring communities).

Ultimately, snapshots of community vulnerability were developed for each pilot, representing an initial 'needs assessment' at local level, enabling the identification of 'vulnerability areas' upon which building a resilience-strengthening strategy perspective. An example of such snapshot is provided in Figure 1, while Figure 2 provides an example of visual representation of a Relative Social Vulnerability Index, performed in more than 300 contiguous communities within the Turin Metropolitan City area (2019, RESBA, Interreg Alcotra Project).

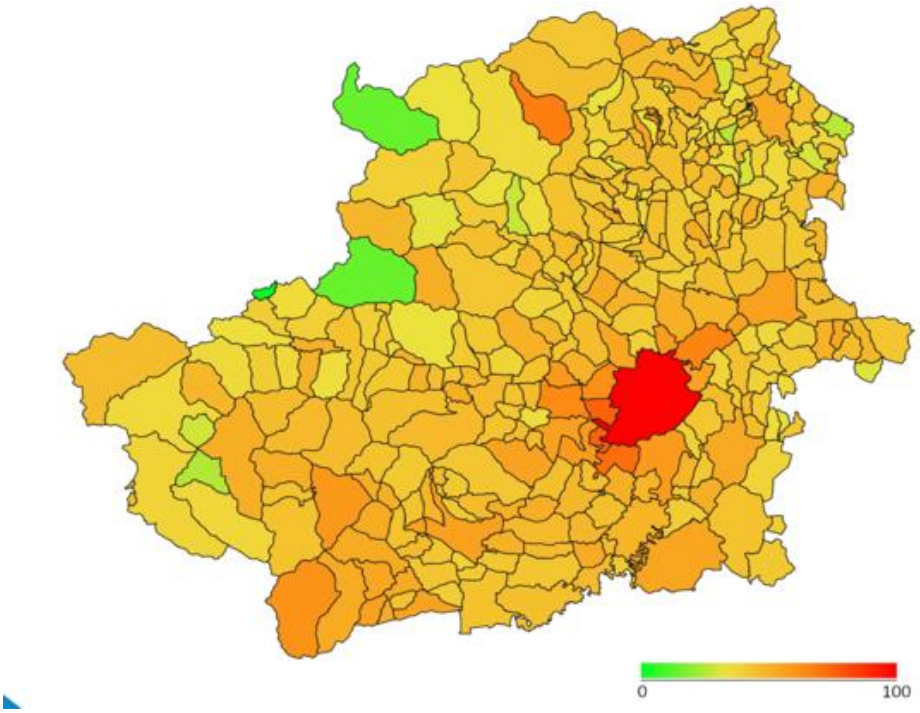

Figure 1 - Example of visual representation of a Relative Social Vulnerability index in contiguous communities, ReSBA Project, Interreg Alcotra, 2019

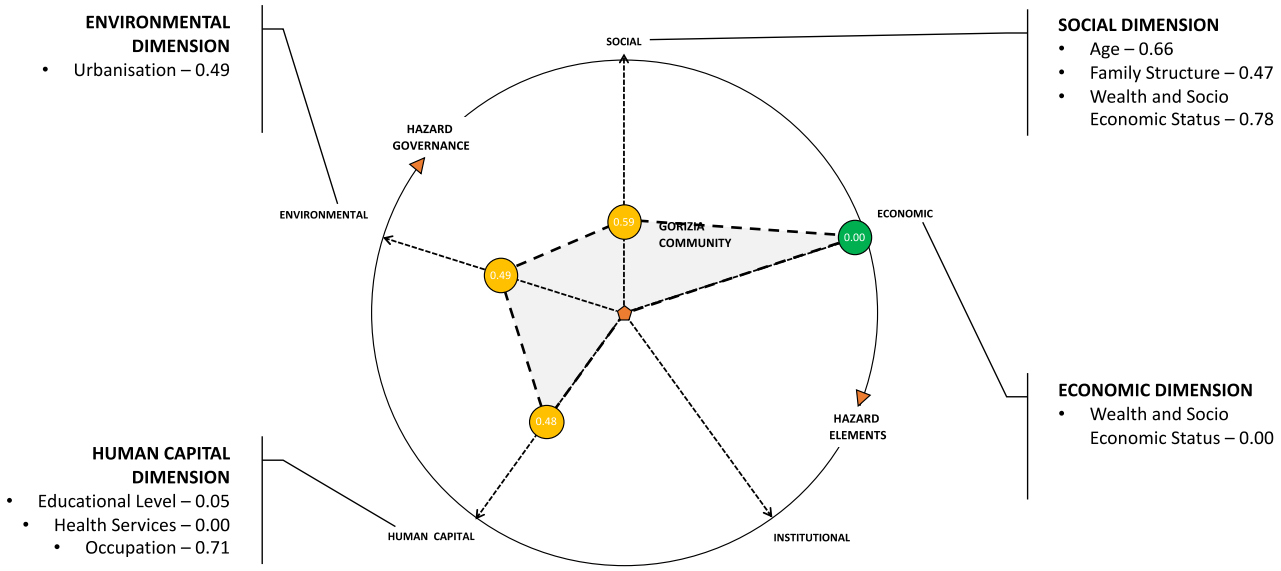

Figure 2 - Example of Vulnerability Snapshot at local level - indication of variables scores per each dimension.

3.1. FirEUrisk Project –relative perspective and participatory approach towards analysing in social vulnerability of communities to wildfire

Building on the previous experiences of constructing relative indexes of vulnerability, within the framework of FirEUrisk project, the direct and indirect effects of fire on people's lives, and more generally, communities, will be analysed based on a methodological framework that:

- Identifies 5 dimension shaping the community and in terms of which vulnerability is assessed.
- Entails a relative approach, in which the 'vulnerability' of a community is analysed in comparison with other similar units of analysis.
- Integrates the role of community experts in the selection of the vulnerability indicators and proxies, as well as in the assessment of their relevance for the specific context.
- Integrates 'local knowledge' and 'context-related' insights within the calculation of the indexes, as variables are weighted according to the assessed level of relevance for the context at stake.
- Indexes allow for depicting the Vulnerability Framework of a Community based on static elements (i.e., statistical data), while expert interviews will allow for the integration of the "dynamic" components of the analysed communities.

Beyond the analysis of susceptibility to fire impacts, the methodology aims to support local communities in analysing their vulnerability to wildfire as a starting point for designing and implementing strategies that aim to strengthen adaptive capacities and overall resilience at the local level.

4. Conclusions

The literature review presented in this paper provides a glance on the extensive, yet diverse, theoretical basis for the definition of wildfire social vulnerability assessment methodologies at a local level. The paper argues that, in order to encompass the complexity of a relative, multi-dimensional, multi-scalar, temporally and spatially dynamic concept such as (social) vulnerability, the assessment processes must be implemented with a great degree of context-awareness, and eventually with the direct involvement of analysed communities.

The issue of vulnerability multi-scalar dimension(s) needs to be further investigated in order to develop effective ways to embed in the same assessment framework qualitative and quantitative information, which very often are collected on different scales and with different granularities (as illustrated in Burton, Rufat, & Tate, 2018).

Moreover, the analysed literature suggests that correlations among different elements characterising "social spaces" in terms of impact on the system exposure, sensitivity and adaptive/coping capacity, play a relevant role in increasing or lowering wildfire social vulnerability. From this perspective, the application of the Forest

Fire Circle model (Tàbara, Saurí, & Cerdan, 2003) might be useful to take into account the relevance of these relationships in wildfire social vulnerability assessment methodologies.

FirEUrisk project provides for the fertile ground in which to further explore the integration of multi-scalar dimension in social vulnerability assessment, as well as for consolidating participatory approaches towards vulnerability assessement across the five projet pilot sites.

5. Disclaimer

This paper is funded by the H2020 Project FirEUrisk (Grant Agreement Number:101003890). Considerations provided are the results of discussions matured between the authors and do not necessarily reflect the point of view of the funder.

6. References

Adger, W. (2006). Vulnerability. Global Environmental Change, 16(3), 268-281.

Ager, A., Preisler, H., Arca, B., Spano, D., & Salis, M. (2014). Wildfire risk estimation in the Mediterranean area. Environmetrics. doi:10.1002/env.2269

Barnett, J., Lambert, S., & Fry, I. (2008). The Hazards of Indicators: Insights from the Environmental Vulnerability Index. Annals of the Association of American Geographers, 98(1), 102-119.

Birkmann, J., Cardona, O., Carreño, M., Barbat, A., Pelling, M., Schneiderbauer, S., . . . Welle, T. (2013). Framing vulnerability, risk and societal responses: The MOVE framework. Natural Hazards, 67(2), 193-211.

Burton, C., Rufat, S., & Tate, E. (2018). Social Vulnerability. In S. Fuchs, & T. Thaler, Vulnerability and Resilience to Natural Hazards (p. 53-81). Cambridge: Cambridge University Press.

Costafreda-Aumedes, S., Comas, C., & Vega-Garcia, C. (2017). Human-caused fire occurrence modelling in perspective: a review. International Journal of Wildland Fire, 26, 983-998. doi:https://doi.org/10.1071/WF17026

Cutter, S. (2016). Resilience to What? Resilience for Whom? The Geographical Journal, 182(2), 110-113.

Cutter, S. (2018). Linkages between Vulnerability and Resilience. In S. Fuchs, & T. Thaler, Vulnerability and resilience to natural hazards (p. 257-270). Cambridge University Press.

Cutter, S., Boruff, B., & Shirley, W. (2003). Social Vulnerability to Environmental Hazards. Social Science Quarterly, 84(2), 242-261.

Cutter, S., Burton, C., & Emrich, C. (2010). Disaster Resilience Indicators for Benchmarking Baseline Conditions. Journal of Homeland Security and Emergency Management, 7(1).

Fekete, A. (2019). Social Vulnerability (Re-)Assessment in Context to Natural Hazards: Review of the Usefulness of the Spatial Indicator Approach and Investigations of Validation Demands. Journal of Disaster Risk Science, 10(2), 220-232.

Fekete, A., & Montz, B. (2018). Vulnerability. In S. Fuchs, & T. Thaler, Vulnerability and Resilience to Natural Hazards (p. 14-31). Cambridge: Cambridge University Press.

Fernandes, P. (2013). Fire-smart management of forest landscapes in the Mediterranean basin under global change. Landscape and Urban Planning, 110, 175-182. doi:http://dx.doi.org/10.1016/j.landurbplan.2012.10.014

Fuchs, S., & Thaler, T. (2018). Vulnerability and resilience to natural hazards. Cambridge University Press.

Füssel, H.-M. (2007). Vulnerability: A generally applicable conceptual framework for climate change research. Global Environmental Change, 17(2), 155-167.

Guillard-Gonçalves, C., Cutter, S., Emrich, C., & Zêzere, J. (2015). Application of Social Vulnerability Index (SoVI) and delineation of natural risk zones in Greater Lisbon, Portugal. Journal of Risk Research, 18(5), 651-674.

Hinkel, J. (2011). Indicators of vulnerability and adaptive capacity: Towards a clarification of the science-policy interface. Global Environmental Change, 21(1), 198-208.

Jucker Riva, M., Baeza, J., Bautista, S., Christoforou, M., Daliakopoulos, I., Hadjimitsis, D., . . . Schwilch, G. (2018). How does land management contribute to the resilience of Mediterranean forests and rangelands? A participatory assessment. Land degradation & development, 29(10), 3721-3735.

Leone, V., Koutsias, N., Martínez, J., Vega-García, C., & Allgöwer, B. (2003). The Human Factor in Fire Danger Assessment. In Wildland fire danger estimation and mapping: the role of remote sensing data (p. 143-196).

Leone, V., Lovreglio, R., Martín, M., Martínez, J., & Vilar, L. (2009). Human factors of fire occurrence in the Mediterranean. In Earth observation of wildland fires in Mediterranean ecosystems (p. 149-170). Berlin: Springer.

Martínez, J., Vega-Garcia, C., & Chuvieco, E. (2009). Human-caused wildfire risk rating for prevention planning in Spain. Journal of Environmental Management(90), 1241-1252. doi:doi:10.1016/j.jenvman.2008.07.005

Moritz, M., Batllori, E., Bradstock, R., Gill, A., Handmer, J., Hessburg, P., . . . Syphard, A. (2014). Learning to coexist with wildfire. Nature, 515, 58-66. doi:doi:10.1038/nature13946

Prior, T., & al. (2017). Risk and Resilience Report. Mapping Social Vulnerability in Switzerland,. Centre for Security Studies.

Tàbara, D., Saurí, D., & Cerdan, R. (2003). Forest Fire Risk Management and Public Participation in Changing Socioenvironmental Conditions: A Case Study in a Mediterranean Region. Risk Analysis, 23(2), 249-260.

Vallejo-Villalta, I., Rodríguez-Navas, E., & Márquez-Pérez, J. (2019). Mapping Forest Fire Risk at a Local Scale—A Case Study in Andalusia (Spain). Environments, 6(30), 1-22. doi:doi:10.3390/environments6030030

Assessing the flammability of *Molinia caerulea* and mosses using a simplified method

Vasileios Koutsomarkos[1]; Rory Hadden*[2];

[1]School of Engineering, The University of Edinburgh. John Muir Building, Colin Maclaurin Road, King's Buildings, Edinburgh EH9 3DW, UK, {v.koutsomarkos@ed.ac.uk}
[2] School of Engineering, The University of Edinburgh. Alexander Graham Bell Building, Thomas Bayes Road, King's Buildings, Edinburgh EH9 3FG, UK, {r.hadden@ed.ac.uk}

**Corresponding author*

Keywords

Flammability assessment, fuel moisture content, ignition, risk assessment

Abstract

An experimental investigation into the impact of moisture content on the flammability of Scottish heathland vegetation has been undertaken in this work. Two different vegetation types are studied; Molinia caerulea and moss. The approach followed in this work consisted of developing an appropriate sample preparation procedure to ensured homogeneous drying in a conditioning chamber and the development of an apparatus to support a consistent ignition procedure. The probability of ignition is evaluated as a function of fuel moisture. For Molinia caerulea, ignition is very likely to occur for a moisture content of less than 75%. For moss, this transition stage revolves around 20% of moisture content. Additionally, drying curves have been drawn for the specific drying conditions (30 ºC and 90% relative humidity), which can provide insight into the rate of drying of organic materials for these given environmental conditions. Finally, a discussion presents the main findings and limitations of this work, while providing insight into possibilities for future research.

1. Introduction

Previous studies (Legg et al., 2007; Nolan et al., 2016) have identified that the fuel moisture content (FMC) of "thin" or "fine" fuel elements responds more rapidly to changes in the environmental conditions than thicker fuel elements. Often fine vegetative matter is the fuel first ignited in wildfire events and therefore understanding the response of these fuels to drying is essential to accurate wildfire risk mitigation (Viegas et al., 1992; Chuvieco et al., 2011; Davies and Legg, 2011). Within the United Kingdom (UK), *Molinia caerulea* and mosses represent two typical fine fuels found on heathlands. This study seeks to develop an understanding on the drying response of these fuels and the conditions required for ignition using a small flame. The likelihood of ignition of a fuel when subjected to small ignition sources is determined. In this study, the probability of ignition is determined as a function of the fuel moisture content. This approach gives an indication of the relationship between fuel moisture content and ignition and can be used to evaluate when different fuels are susceptible to ignition by small sources. The FMC of live and wet dead fuel can be affected differently by environmental conditions, and this work uses only dead Molinia grass which might not be representative of the behaviour of live grass. A separation between live and dead moss was not possible.

Repeatability of results is important, both in the drying behaviour and the flammability response, given the high level of natural variability that exists in wildland fuels. This idea shaped the methodology employed, which was designed to ensure a homogeneous drying of the fuel and consistent flammability responses in a practicable way.

The steps followed throughout this process and the reasoning behind them is presented to ensure clarity, transparency, and highlight the approach's limitations. The methodology section outlines the tools and equipment used to carry out the experimental procedure. Then the results of that procedure are presented, followed by a discussion on the findings. This last section is supplemented by an explicit declaration on the limitations of this approach.

2. Methodology

2.1. Overview

Different preparation and testing methodologies are developed for the grass and moss samples to account for their differing structure. An illustration is presented in Figure 1 that visualises the processes followed for the grass and moss. Blue boxes indicate a process, and green boxes indicate an outcome of the linked process. These are discussed in more detail in the following sections.

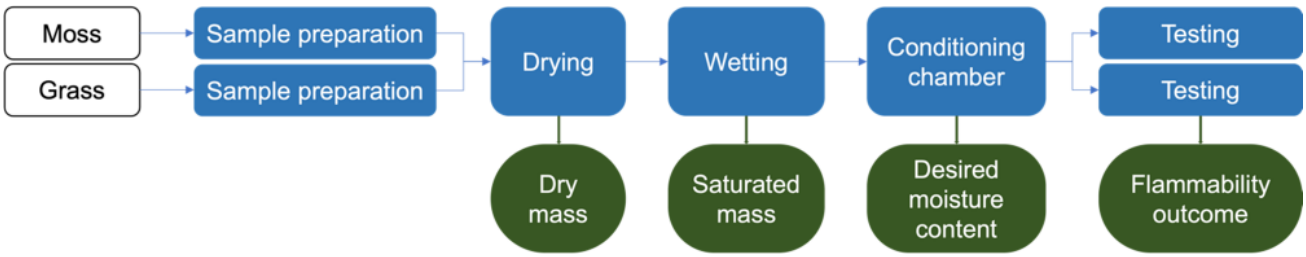

Figure 1. An outline of the process followed for examining relationships between fine fuel moisture (FMC) and flammability

2.2. Sample preparation

2.2.1. Molinia grass

Samples were received in a cured dry condition and required rewetting and drying to obtain the FMC of interest. Repeatable sample preparation was essential to ensure consistent results and homogenous conditioning of the samples. Samples were prepared by attaching a fixed mass of grass to electrical tape. Each sample was of approximately 0.45 g (dry mass). Care was taken to distribute the sample evenly along the tape (Figure 2).

Figure 2. Molinia grass sample prior to testing fixed with electrical tape

2.2.2. Moss

The nature of moss means that it must be supported on a frame prior to testing. A set size of 10 x 10 x 5 cm was chosen for the moss sample holders because this enabled consistency amongst the sample sizes and weights, (Figure 3). Moss samples were prepared by removing grass or other litter to prevent this from impacting on the results. The height of the moss samples was approximately 20 mm.

Figure 3. Moss sample preparation prior to testing

2.2.3. *Drying*

Both Molinia and moss samples were dried straight after preparation in an oven at 60°C to determine their dry mass. The samples remained in the drying oven until their mass remained stable over 4 consecutive hourly measurements. This typically took less than 24 hours. This temperature was chosen to avoid the loss of any volatile organic compounds which can occur in organic fuels when dried at higher temperatures (Samuelsson, Nilsson and Burvall, 2006).

2.2.4. Wetting

After the grass samples were prepared and totally dried, they were placed in groups of 4 in a 500 ml glass beaker of tap water and were left submerged overnight to saturate, covered with aluminium foil.

After the moss samples were prepared and totally dried, they were placed in large tank with tap water and were left submerged overnight to saturate.

2.2.5. Drying for moisture content control

An environmental chamber (TAS ECO MTCL400) was used for the controlled drying of the samples before every experiment. The conditions in the chamber were set at 30°C and 90% relative humidity (RH). These conditions were chosen as suitable for providing a rate of sample drying that allowed for measurements to be taken while maintaining a manageable timeframe of every experimental run. Mass readings were made using a precision balance (Mettler Toledo NewClassic MS), with readability of 0.01 g.

2.2.6. Calculations

The dry basis moisture was used for the calculation of the samples' moisture content, which is defined as the amount of water over the dry sample. This is calculated through the formula:

$$MC = 100\frac{m_w}{m_{ds}}$$

Where:

- MC is the sample's moisture content in percentage form,
- m_w is the mass of the water contained in the sample,
- m_{ds} is the mass of the dry sample.

The drying curves were based on the drying rate normalised per each sample's dry mass, calculated as follows:

$$DR = \frac{m_{i+1} - m_i}{t_{i+1} - t_i}\frac{1}{m_{di}}$$

Where:

- DR is the sample's drying rate normalised to its dry mass,
- m_i is the mass of the sample at a given time t_i,
- t_i is the time of the measurement.

2.2.7. Ignition source

A small flame ignition source was used. This was obtained using a commercially available wax candle. The flame was approximately 15 mm high. This was chosen to give a consistent ignition source both in terms of size and burning duration and seeks to represent a small ignition source. The results presented in this work are strongly dependent on this choice of ignition source.

2.3. Molinia apparatus

For the grass samples, the developed and used apparatus is shown in Figure 4. The sample and sample holder remained in a fixed position while the ignition source could be positioned manually. The vertical orientation of the apparatus was chosen to provide conservative results.

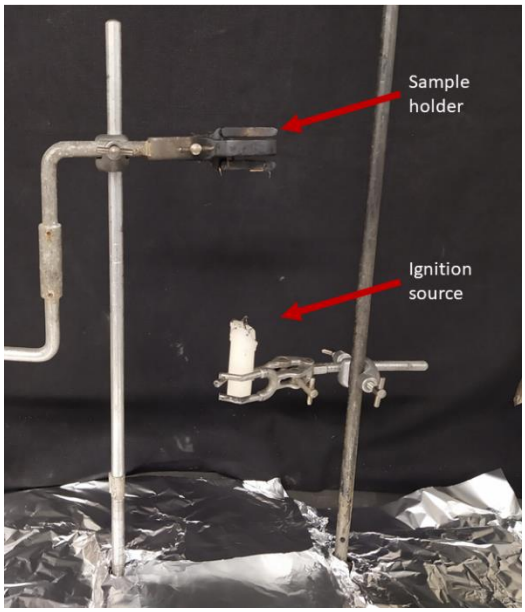

Figure 4. The Molinia grass ignition testing apparatus

2.3.1. Molinia procedure

Once a sample reached the desired moisture content, it was rolled into a clump with diameter of approximately 15 mm at the tied end and placed in the sample holder. This shape was chosen so that the full sample area would be simultaneously exposed to the ignition source, and grass strands would be in such proximity with each other that would be representative of their field condition. The ignition source was placed just below the sample for 5 seconds. Then the ignition source was removed and the resultant burning (or otherwise) of the sample observed.

2.3.2. Moss apparatus

The apparatus used for the moss samples, is shown in Figure 5. The wire mesh was assembled to place the sample holder and ignition source in position. The horizontal orientation of the apparatus was chosen to emulate conditions in which moss is likely to be found.

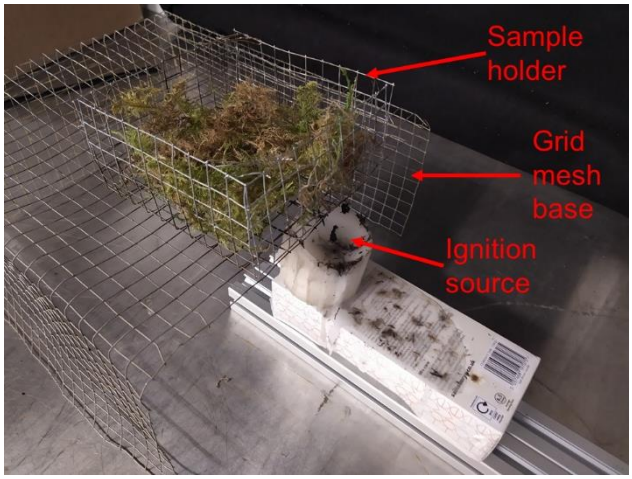

Figure 5. The moss testing apparatus: sample holder, base mesh grid, and ignition source are indicated.

2.3.3. Moss procedure

Once a sample reached the desired moisture content, it was placed on a metal grid above the ignition until the estimation flammability was definitive; either sustained burning or local ignition but no propagation.

2.3.4. Probability of burning

Subjective probabilities were used for the assessment of flammability. This is a type of probability that expresses the observer's belief on a system or outcome, derived from their personal judgment or experience. In this work, these were defined by the amount of fuel consumed by the ignition source alone, and the ability of the sample to sustain burning individually after the ignition source is removed (0 – no fuel consumed, 0.25 – some fuel consumed but no burning, 0.5 – some fuel consumed and some smouldering followed, 0.75 – fuel consumed and some flaming follows, 1 – sample fully consumed in flaming combustion).

3. Results

In this section the results from the measurements and experimental procedure are presented. Initially the indicative moisture loss graphs and the drying curves are presented for Molinia grass and moss, respectively. Following that, the moisture loss graphs up to ignition, and the flammability graphs linking the moisture content with the probability of ignition are provided.

3.1. Moisture loss graphs and drying curves: Molinia

The findings from the 20 indicative samples of grass that were dried from saturation to dryness are presented in the figures below. Figure 6(a) presents the loss of moisture over time. Figure 6(b) also shows the drying curve for these grass samples. The drying curve is characterised by a decreasing drying rate as a function of time. After 60 minutes, the drying rate approaches zero and the samples reach equilibrium with the environmental conditions in the chamber.

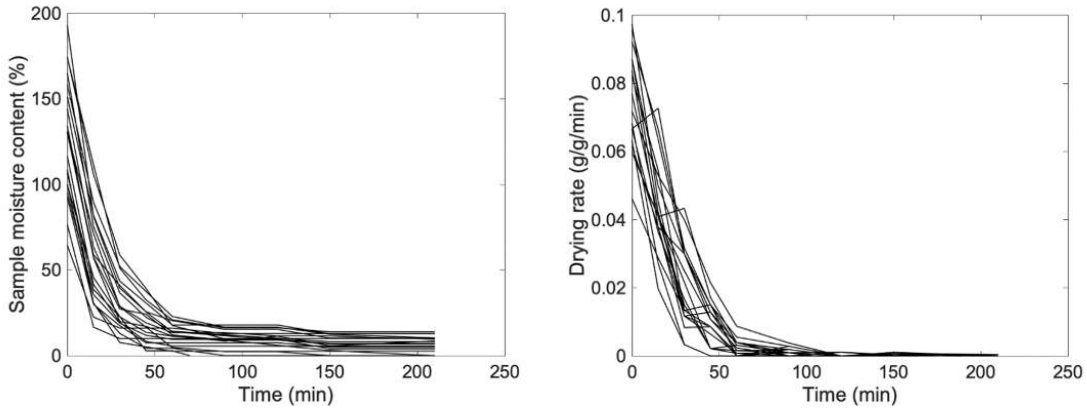

Figure 6. (a) moisture loss, (b) drying curve; for Molinia grass

Change in FMC as a function of time from the 13 indicative samples of moss that were dried from saturation over a period of seven hours are presented in Figure 7(a). Compared to the Molinia samples the characteristic time of the drying is much longer with none of the samples reaching a stable FMC over the time period available. There is a higher degree of variability in these results compared to the Molinia. This is attributed to the differing thickness and more complex structure of the samples compared to the grass. Figure 7(b) below shows the drying curve for these moss samples, which as was presented in the Calculations sub-section, is the drying rate normalised by dry sample mass. Again, given the nature of the fuel structure there is some scatter in the results but for a moss sample in this condition, the drying rate appears to be on the order of 0.01—0.03 g/g/min.

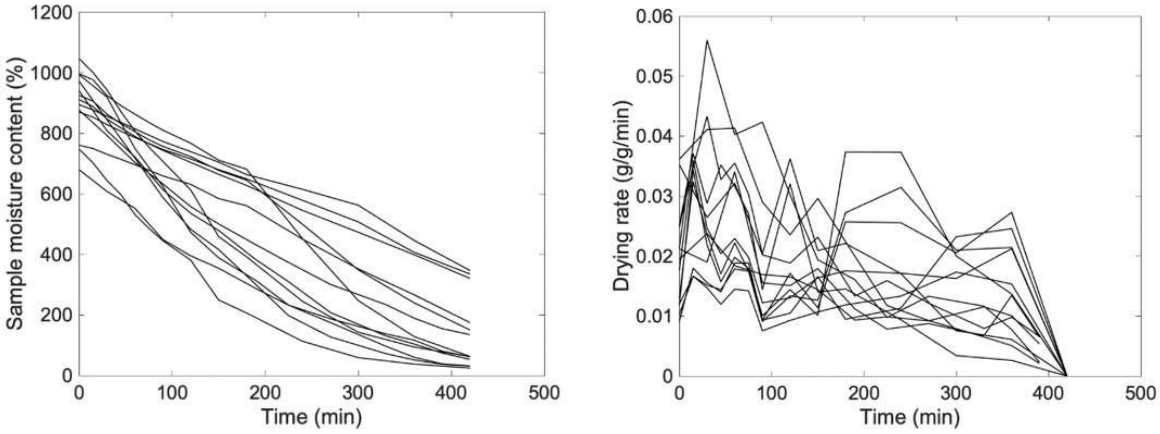

Figure 7. (a) moisture loss, (b) drying curve; for moss

3.2. Flammability graphs

Characterising the drying times allows for target moisture contents to be reached for testing. New samples were prepared, wetted, and dried for a duration required to achieve the desired FMC for testing. Figure 8 shows the resulting probability of ignition for Molinia grass as a function of FMC.

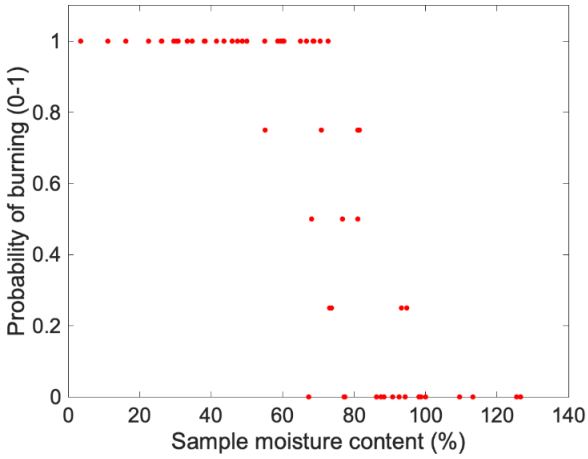

Figure 8. ignition probability as a function of fine fuel moisture content (FMC) for Molinia grass.

From Figure 8 above it can be inferred that there is not a critical FMC at which the behaviour of the fuel changes. Instead, the ignition probability increases from 0 to 1 in the range 85—65% FMC. FMC lower than 65% are almost certain to ignite and burn to completion.

Figure 9 shows the resulting probability of ignition for moss as a function of FMC. Similar to the behaviour of Molinia grass, for this graph too it can be inferred that there is not one point where the behaviour of the fuel immediately changes, but it is rather defined as a region in between 10 and 20% FMC.

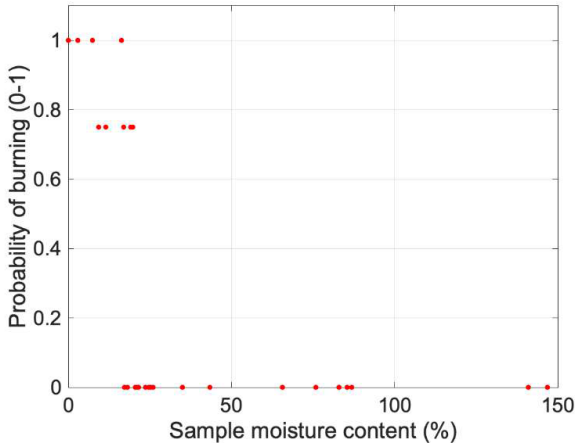

Figure 9. ignition probability as a function of fine fuel moisture content (FMC) for Molinia grass.

4. Conclusions

This study has highlighted the ignition probability for Molinia and moss subject to a small flame source. These fuels were chosen as they are found on the ground where small ignitions sources may arise accidentally e.g. dropped matches, discarded cigarettes. The approach employed in this work is not intended to replace standardised methods of assessing fuel flammability, where a well-defined exposure and combustion environment exists, but provide complementary, easy-to-acquire insights on the behaviour of wildland fuels when exposed to these small ignition sources. These results, however insightful, may not be appropriate as direct inputs in fire models, but the approach could be used as a practical means to provide threshold values in local wildfire risk indices, such as any adaptation to the Canadian Forest Fire Weather Index System, that are relatively easy and quick to produce experimentally.

The Fuel Moisture Content (FMC) for ignition of Molinia grass was found to be in the range below 85%. With a high probability for samples with less than 65% FMC. The ignition of moss was found to occur at FMC below 20% with a high probability at FMC less than 10%. These results serve to calibrate ignition thresholds and to evaluate the relative hazards posed by different fuels. Combining the drying rate data and the ignition probabilities allow an estimation of the timescales required for the different fuels to become ignitable. For Molinia this is on the order of 30 minutes. For the moss, this is on the order of 5 hours. These differing timescales are strong indicators that the hazard associated with different fuel elements requires careful consideration, while acknowledging that they can be affected differently by any wind present and the climatic conditions of the region

When interpreting these results, there are some limitations that should be considered. Firstly, the nature of the ignition source and the duration of the application will have an impact on the results. Particularly it may be possible to ignite samples with FMC outside the ranges quoted here with larger heat sources or longer durations. For example, these results would not be appropriate for determining the ignition arising from discarded barbeques. The variability in the natural structure of the fuel and its impact should be acknowledged. Additionally, qualitative observations suggest that the FMC of the samples after drying was not uniform in some cases, mainly for the moss samples, which would suggest that a thinner sample might be more appropriate. Finally, the extent of burning used to derive probabilities was subjective.

5. Bibliography

C. J. Legg, G. M. Davies, K. Kitchen, and P. Marno, “Developing a Fire Danger Rating System for the UK: FireBeaters Phase I final report. Report to the Scottish Wildfire Forum.,” 2007

R. H. Nolan, M. M. Boer, V. R. de Dios, G. Caccamo, and R. A. Bradstock, “Large-scale, dynamic transformations in fuel moisture drive wildfire activity across southeastern Australia,” Geophysical Research Letters, vol. 43, no. 9, pp. 4229–4238, 2016, doi: 10.1002/2016GL068614

Viegas DX , Viegas MTSP, Ferreira AD (1992) Moisture Content of Fine Forest Fuels and Fire Occurrence in Central Portugal. International Journal of Wildland Fire 2, 69-86

E. Chuvieco, I. Aguado, and A. P. Dimitrakopoulos, "Conversion of fuel moisture content values to ignition potential for integrated fire danger assessment," Canadian Journal of Forest Research, Feb. 2011, doi: 10.1139/x04-101

G. M. Davies and C. J. Legg, "Fuel Moisture Thresholds in the Flammability of Calluna vulgaris," Fire Technol, vol. 47, no. 2, pp. 421–436, Apr. 2011, doi: 10.1007/s10694-010-0162-0

R. Samuelsson, C. Nilsson, and J. Burvall, "Sampling and GC-MS as a method for analysis of volatile organic compounds (VOC) emitted during oven drying of biomass materials," Biomass and Bioenergy, vol. 30, no. 11, pp. 923–928, Nov. 2006, doi: 10.1016/j.biombioe.2006.06.003

Assessing the role played by meteorological conditions on the interannual variability of fire activity in four subregions of Iberia

Sílvia A. Nunes*[1]; Carlos C. DaCamara[1]; José M. C. Pereira[2]; Ricardo M. Trigo[1]

[1]*Instituto Dom Luiz (IDL), Faculdade de Ciências, Universidade de Lisboa, 1749-016 Lisbon, Portugal, {sanunes, cdcamara, rmtrigo}@fc.ul.pt*
[2]*Centro de Estudos Florestais, Instituto Superior de Agronomia, Universidade de Lisboa, 1349-017, Lisbon, Portugal {jmcpereira@isa.ulisboa.pt}*

**Corresponding author*

Keywords

Fire activity; Fire Radiative Power; Two generalized Pareto tail lognormal body distribution; Iberian Peninsula; Fire Weather Index

Abstract

The Iberian Peninsula is recurrently affected by severe wildfires resulting from an interplay of human activities, landscape features, and atmospheric conditions. Here we assess the role played by atmospheric conditions on wildfire activity as measured by Fire Radiative Power (FRP) derived from observations by the MODIS instrument. The study spans the period 2001-2020 and is performed in four pyroregions covering the Iberian Peninsula that have been used in recent years, namely the northwest (NW), southwest (SW), north (N) and east (E). Atmospheric conditions are characterized by means of the Fire Weather Index (FWI), which rates fire intensity. For each pyrogegion, the distribution of $\log_{10} FRP$ is characterized by means of a statistical model that combines a truncated lognormal distribution central body with a lower and an upper tail, both consisting of Generalized Pareto (GP) distributions. The model is then improved by using FWI as a covariate of the parameters of the lognormal and the two GP distributions. Then, for each pyroregion, a set of 100 synthetic time series of total annual FRP is set up using the statistical models with and without FWI as a covariate. The role played by meteorological conditions is finally assessed by comparing the two sets between each other and against the time series of annual FRP derived from observations by the MODIS instrument. Results obtained for region SW show an increase from 90% to 96% of interannual explained variance of FRP when progressing from the model without to the model with FWI as covariate. Increases from 95% to 96%, 84% to 89% and from 79% to 86% were obtained for regions NW, N and E. It is worth stressing that these are conservative estimates of change, since the dependence of number of ignitions on FWI was not taken into account.

1. Introduction

The Iberian Peninsula is recurrently affected by severe wildfires that relate to an increase in fuel availability due to land abandonment and the expansion of forest and shrubland areas (Pausas and Vallejo, 1999; Lloret et al., 2002), as well as to an increase in the occurrence of prolonged droughts and in the number of days with extreme fire weather associated to climate change (Pereira et al., 2005; Trigo et al., 2006; Carvalho et al., 2011; Pereira et al., 2013; Sousa et al., 2015; Pérez-Sánchez et al., 2019; Turco et al., 2019).

The Iberian Peninsula has been affected by large wildfires in the recent decades, and the tragic years of 2003, 2005 and 2017 in Portugal are worth being pointed out. The Iberian Peninsula was struck by a severe heat wave in August 2003 and by two severe heatwaves in 2017 (the first in mid-June and the second in the second week of July), and 2005 and 2017 were affected by two severe droughts, that of 2005 being the most severe in recent times (Garcia-Herrera et al., 2007). Several studies have underlined the critical role played by different meteorological variables, including temperature, humidity and wind on the occurrence of extreme years of fire activity both at shorter (e.g. summer heat waves) and longer (e.g. prolonged droughts) time scales (Ruffault et al., 2020).

The fact that the entire Mediterranean basin, and the Iberian Peninsula in particular, is considered as a hotspot of climate change, increases the likelihood of occurrence of extreme fire weather and of more intense droughts (Turco et al., 2019; Ruffault et al., 2020). This strongly suggests that particular attention should be devoted to the role played by atmospheric conditions on wildfire activity. The aim of this work is to assess the impact of

meteorological conditions on the interannual variability of fire activity in four pyroregions of the Iberian Peninsula (Trigo et al., 2016).

2. Data and Methods

The study area comprises four pyroregions in the Iberia Peninsula (Northwestern, Northern, Southwestern and Eastern) as identified by Trigo, et al. (2016) based on a cluster analysis of monthly burned area (Fig.1).

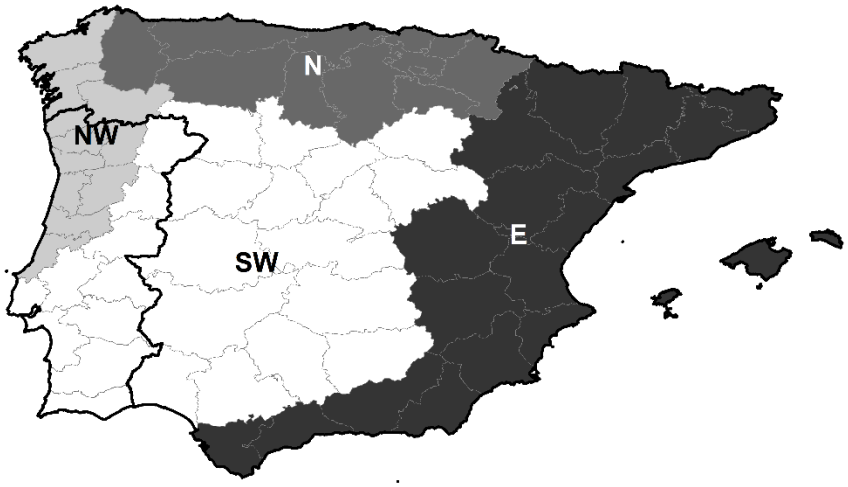

Figure 1- The four pyroregions of the Iberian Peninsula: Northwestern (NW), Northern (N), Southwestern (SW) and Eastern (E). Adapted from Trigo et al. (2016)

Fire activity is measured by the radiative power released by wildfires, as measured by the MODIS instrument on-board Terra and Aqua satellites (Giglio et al., 2020) and meteorological fire danger was rated using the Fire Weather Index (FWI), an index of fire danger that rates fire intensity (Stocks et al., 1989).

Information about Fire Radiative Power (FRP) was obtained from Collection 6 Terra and Aqua MODIS fire product covering the 20-year period from 2001 to 2020 (Giglio et al., 2020). Information about FWI covering the same period was obtained from ECMWF ERA5 reanalysis (CEMS, 2019).

For each pyroregion, a statistical model is adjusted to the distribution of the decimal logarithm of fire radiative power, $\log_{10} FRP$, and the model is then improved by incorporating FWI as a covariate of the model. The statistical models of $\log_{10} FRP$ combine three components, namely a truncated lognormal distribution central body with a lower and an upper tail, both consisting of Generalized Pareto (GP) distributions. For each pyroregion, the eight parameters of the model (namely the two points separating the central body from the tails, the location and dispersion parameters of the central truncated lognormal and the scale and shape parameters of the GP distributions of the tails) are obtained by maximizing the joint log-likelihood of an i.i.d. sample of $\log_{10} FRP$.

Finally, for each pyroregion a set of 100 synthetic time series of annual values of FRP is generated using the statistical model without FWI as covariate according to the following procedure: for each hotspot detected by the MODIS instrument, a random value of probability is generated and the corresponding value of FRP is obtained by inverting the statistical model. A time series of synthetic annual values of FRP is then obtained by adding up the generated values of FRP on a yearly basis. This process is then repeated 100 times. A second set of 100 synthetic time series of annual values of FRP is generated, this time using the model with FWI as covariate. The procedure is identical to the preceding one, with the difference lying in that FRP values are synthesized using a randomly generated probability value, together with the observed FWI value at each hotspot. The role played by meteorological conditions is finally assessed by comparing the two sets between each other and against the time series of annual FRP derived from observations by the MODIS instrument.

3. Results and discussion

Figure 2 provides an overview of results obtained when fitting, for each pyroregion, the statistical models to the samples of observed values of $\log_{10} FRP$ for the period 2001-2020. Cumulative distribution functions of the fitted model closely follow the corresponding empirical cumulative distribution function derived from the samples, and this reflects on Q-Q plots that closely follow the 1:1 straight lines. Pyroregion NW presents the higher probabilities of exceedance for values of $\log_{10} FRP$ between 0.5 and 2 whereas the lower values of exceedance are found in pyroregion E for values of $\log_{10} FRP$ between 0.5 and 1.5 and in pyroregion N for values of $\log_{10} FRP$ between 1.5 and 2.

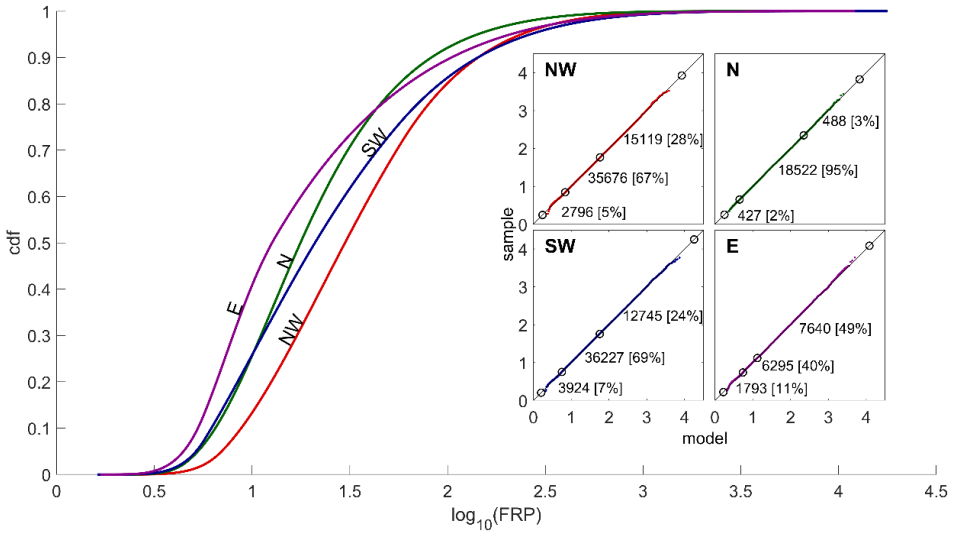

Figure 2 – Cdf curves and Q-Q plots (inside squares) of fitted statistical models of log_10 FRP (in MW) for regions NW (red), N (green) SW (blue), and E (magenta). The open circles in the 1:1 lines of the QQ plots delimit the central body and the upper and lower tails of the distributions, and the small colored dots represent the fire events of the sample. For each pyroregion, the number of events and respective fraction (in brackets) of the sample in the central body and in the lower and upper tails of the distribution are indicated next to the 1:1 line of the respective Q-Q plot

Figure 3 illustrates the results obtained when FWI is added as a covariate of the parameters of the distributions. As might be expected, there is a right displacement of the cumulative distribution functions with increasing FWI, which reflects substantial increases in probability of exceedance of a given threshold of $\log_{10} FRP$.

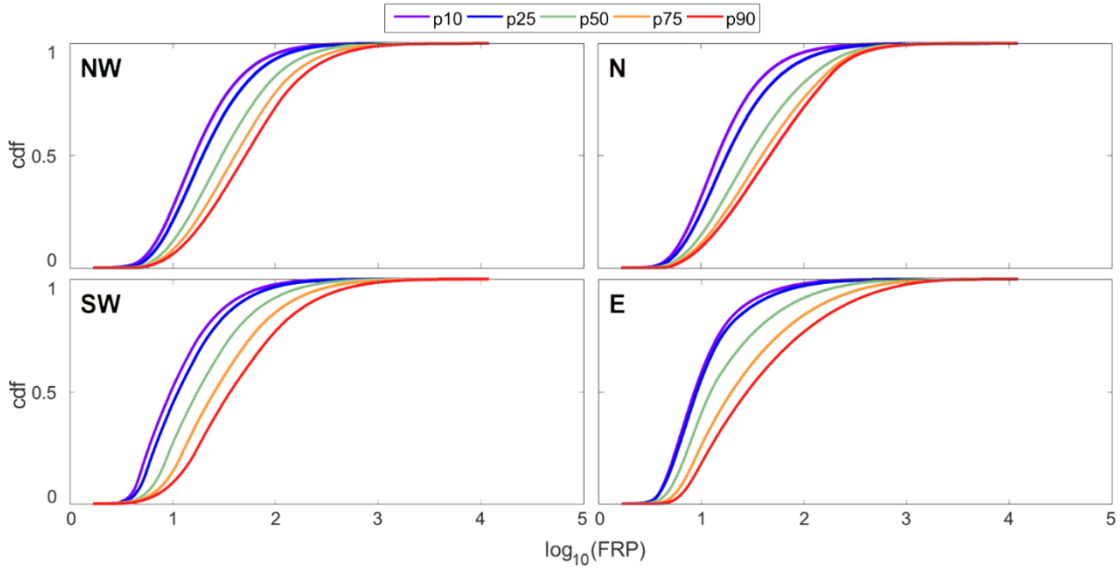

Figure 3 –Sensitivity to FWI of cumulative distribution functions of fitted statistical models of $\log_{10} FRP$ (in MW) for the four subregions. Colors of each curve identify the prescribed value of FWI, respectively percentiles 10 (purple), 25 (blue), 50 (green), 75 (orange) and 90 (red) of the respective samples.

Figure 4 presents, for each ecoregion, the time series of annual FRP as derived from observations by the MODIS instrument (black curves) and the two time series obtained by averaging the two sets of 100 annual values of FRP as derived from the statistical models without (green curve) and with (red curve) FWI as covariate. The interannual variability of the time series generated by the model without FWI as covariate is just due to the interannual variability of hotspots observed by the MODIS instrument, and it is worth noting that some years with large (small) values of total FRP tend to be underestimated (overestimated). The underestimation is conspicuous in 2017 for pyroregions NW and N, in 2003 for pyroregion SW, and in 2012 for pyregion E, whereas the overestimation, although less pronounced, occurs e.g. in 2014 for pyroregion N and in 2007 and 2008 for pyroregion SW. In the case of the time series generated by the model with FWI, an improved behavior is observed that is particularly noticeable for years with large values of total FRP, where synthetic values obtained from the model with FWI are much closer to observed values than synthetic values from the model where meteorological conditions are disregarded.

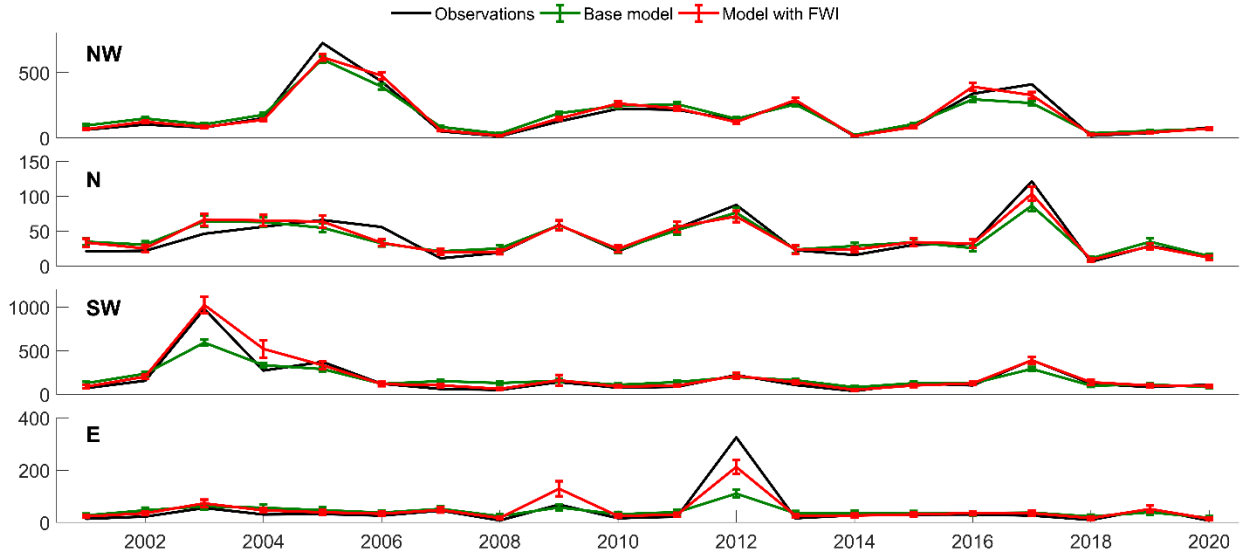

Figure 4 – Time series, for each pyroregion, of annual values of observed (black curves) and of the mean values of the set of synthetically generated annual values of FRP using the statistical models without (green curves) and with (red curves) FWI as covariate. The error bars in the synthetic time series delimit the mean plus/minus one standard deviation.

A quantitative assessment is provided in Table 1, which presents the mean and the standard deviation of the time series of annual FRP derived from MODIS observations and of the annual FRP synthetically generated by the statistical models without and with FWI as covariate. Results indicate that synthetic time series generated by both models are unbiased, the only exception being pyroregion E, where the time series generated by the model with FWI as covariate presents a mean value 12% larger than the mean of time series of observed FRP. Considerable differences do, however, occur with the values of standard deviation, for which time series of synthetically generated FRP present considerably lower values than the corresponding time series of observed FRP. However, time series generated using the model with FWI as covariate systematically display larger variability than the corresponding ones obtained with the model lacking FWI as covariate. For instance, there is an 11% increase (from 21 to 24 GW) for pyroregion N, a 17% increase (from 143 to 167 GW) for pyroregion NW, a 48% increase (from 121 to 179 GW) for pyroregion SW and a 230% increase (from 20 to 46 GW) for pyroregion E. These results indicate that atmospheric conditions are especially important to better reproduce interannual variability in the case of pyroregions E and SW.

Table 1 also presents, for each pyroregion, the explained variance accounted for the synthetic series when they are used to simulate interannual variability. Explained variance was estimated by squaring the linear correlation of the time series of annual observed FRP with the corresponding synthetic time series generated by the statistical models lacking and including FWI as covariate. For all pyroregions there is an increase in explained variance when shifting from synthetic values of annual FRP generated by the models without FWI as covariate to those by the models with FWI. Increases in explained variance are modest for pyroregion NW (95 to 96%),

and are even larger for the other three pyroregions N, SW and E (84 to 89%, 90 to 96% and 79 to 86%, respectively).

Table 1 – Mean value and standard deviation for the period 2001-2020 of time series of annual FRP derived from observations by the MODIS instrument and from the mean of the 100 synthetically generated annual FRP using the statistical models without and with FWI as covariate, and explained variance as obtained by squaring the linear correlation between the observed and each the two synthetic time series of annual FRP.

		NW	N	SW	E
Mean [GW]	Observed	179	40	185	43
	Model without FWI	180	40	184	42
	Model with FWI	179	40	186	47
Standard Deviation [GW]	Observed	181	29	211	68
	Model without FWI	143	21	121	20
	Model with FWI	167	24	179	46
Variance Explained [%]	Model without FWI	95	84	90	79
	Model with FWI	96	89	96	86

4. Conclusion

Results obtained clearly indicate the importance of atmospheric conditions as drivers of interannual variability in fire activity, measured by annual FRP values. This is especially true in pyroregions SW and E, where climate change is expected to have a pronounced impact in terms of increase in frequency both of drought events and of days with extreme fire weather (Sousa et al., 2015).

It is worth pointing out that the assessment performed in this work is likely to be conservative, given that time series of annual FRP were estimated by randomly generating values for all hotspots identified by the MODIS instrument for the study period. Since the number of hotspots strongly depends on the number of large fire events, which in turn depend on atmospheric conditions, the interannual variability of synthetically generated time series of FRP was very likely overestimated when using the model without FWI as covariate. Circumventing this problem would imply modelling the interannual variability of hotspots (with and without FWI as covariate), a task that is well beyond the purpose of the present work.

Models such as the ones proposed in this study provide valuable information about fire activity in the Iberian Peninsula, namely when comparing different scenarios of climate change. On the other hand, following a methodology previously developed by some of the authors (DaCamara et al., 2014; Pinto et al., 2018), the proposed models with FWI can be used to calibrate FWI in four pyroregions of the Iberian Peninsula and then define classes of fire danger that represent an important added value in fire prevention and firefighting of rural and forest fires.

5. Acknowledgments

This work was supported by national funds through FCT (Fundação para a Ciência e a Tecnologia, Portugal) under project FIRECAST (PCIF/GRF/0204/2017), IDL (UIDB/50019/2020) and CEF (UIDB/00239/2020) and by EUMETSAT Satellite Application Facility on Land Surface Analysis (LSA SAF).

6. References

Carvalho AC, Carvalho A, Martins H, Marques C, Rocha A, Borrego C, Viegas DX, Miranda AI. 2011. Fire weather risk assessment under climate change using a dynamical downscaling approach. *Environ. Model. Softw.* **26** (9), 1123–1133. https://doi.org/10.1016/j.envsoft.2011.03.012 Elsevier Ltd.

CEMS. Fire danger indices historical data from the Copernicus Emergency Management Service. 2019. ECMWF https://doi.org/10.24381/cds.0e89c522.

DaCamara CC, Calado TJ, Ermida SL, Trigo IF, Amraoui M, Turkman KF. 2014. Calibration of the Fire Weather Index over Mediterranean Europe based on fire activity retrieved from MSG satellite imagery. *International Journal of Wildland Fire* **23**, 945-958. https://dx.doi.org/10.1071/WF13157.

García-Herrera R, Paredes D, Trigo RM, Trigo IF, Hernández H, Barriopedro D, Mendes MT. 2007. The outstanding 2004–2005 drought in the IberianPeninsula: associated atmospheric circulation. *J. Hydrometeorol.* **8**, 483–498. https://dx.doi.org/10.1175/JHM578.1.

Giglio L, Schroeder W, Hall JV, Justice CO. 2020. MODIS Collection 6 Active Fire Product User's Guide. https://modis-fire.umd.edu/files/MODIS_C6_Fire_User_Guide_C.pdf (Last accessed 29 March 2022).

Lloret F, Calvo E, Pons X, Díaz-Delgado R. 2002. Wildfires and landscape patterns in the Eastern Iberian Peninsula. *Landsc. Ecol*. **17**: 745 – 759. https://doi.org/10.1023/A:1022966930861

Pausas JG, Vallejo R. 1999. The role of fire in European Mediterranean ecosystems. *Remote Sensing of Large Wildfires in the European Mediterranean Basin*, Chuvieco E (ed). Springer-Verlag: Berlin; 3 – 16. https://doi.org/10.1007/978-3-642-60164-4_2

Pereira MG, Trigo RM, DaCamara CC, Pereira JMC, Solange ML. 2005. Synoptic patterns associated with large summer forest fires in Portugal. *Agric. For. Meteorol.* **129**: 11 – 25, https://doi.org/10.1016/j.agrformet.2004.12.007.

Pereira M, Calado TJ, DaCamara CC, Calheiros T. 2013. Effects of regional climate change on rural fires in Portugal. *Clim. Res*. **57** (3), 187–200. https://doi.org/10.3354/cr01176.

Pérez-Sánchez J, Jimeno-Sáez P, Senent-Aparicio J, Díaz-Palmero JM, Cabezas-Cerezo JD. 2019. Evolution of burned area in forest fires under climate change conditions in southern Spain using ANN. *Applied Sciences (Switzerland)* **9** (19). https://doi.org/10.3390/app9194155.

Pinto MM, DaCamara CC, Trigo IF, Trigo RM, Turkman KF. 2018. Fire danger rating over Mediterranean Europe based on fire radiative power derived from Meteosat. *Natural Hazards and Earth System Sciences* **18**, 515-529. doi:10.5194/nhess-18-515-2018.

Ruffault J., Curt T., Moron V., Trigo R.M., Mouillot F., Koutsias N., Pimont F., Martin-StPaul N., Barbero R., Dupuy J.-L., Russo A., Belhadj-Khedher C., (2020) "Increased likelihood of heat-induced large wildfires in the Mediterranean Basin". Scientific Reports, 10, 13790, doi: 10.1038/s41598-020-70069-z

Sousa PM, Trigo RM, Pereira MG, Bedia J, Gutiérrez JM. 2015. Different approaches to model future burnt area in the Iberian Peninsula. *Agric. For. Meteorol*. **202**, 11–25. https://doi.org/10.1016/j.agrformet.2014.11.018.

Stocks BJ, Lawson BD, Alexander ME, Van Wagner CE, McAlpine RS, Lynham TJ, Dubé DE. 1989. The Canadian Forest Fire Danger Rating System: an overview [reprinted from August 1989 issue, 65:258-265, with corrections and new pagination]. *Forestry Chronicle* **65**(6): 450-457.

Trigo RM, Pereira JMC, Pereira MG, Mota B, Calado MT, DaCamara CC, Santo FE. 2006. Atmospheric conditions associated with the exceptional fire season of 2003 in Portugal. *Int. J. Climatol.* **26**(13):1741 – 1757. https://doi.org/10.1002/joc.1333

Trigo RM, Sousa M, Pereira MG, Rasilla D, Gouveia CM. 2016. Modelling wildfire activity in Iberia with different atmospheric circulation weather types. *Int. J. Climatol*. **36**. https://doi.org/10.1002/joc.3749

Turco M, Jerez S, Augusto S, Tarín-Carrasco P, Ratola N, Jiménez-Guerrero P, Trigo RM. 2019. Climate drivers of the 2017 devastating fires in Portugal. *Scientific Reports* **9**, 13886. doi:10.1038/s41598-019-50281-2.

Assessment of forest fire risk perception at the fireshed level

Joseph Bechara*[1]; George Mitri[2]

[1] Lebanon Reforestation Initiative. Jdeideh, Lebanon, {jbechara@lri-lb.org}
2 Institute of the Environment, University of Balamand, Koura, Lebanon, {george.mitri@balamand.edu.lb}

**Corresponding author*

Keywords

Forest Fires, Risk Perception, Fireshed

Abstract

Forest fires are increasingly affecting forest ecosystems, with severe ecological and socio-economic impacts on neighboring communities. In this context, evaluating the risk of fires at the fireshed level is considered a crucial step towards improving knowledge about fire risk management, therefore, minimizing potential damages of wildfires on people, properties, and natural resources. The aim of this study was to assess forest fire risk perception of communities at two firesheds in Lebanon. In-person surveys were conducted in areas of high fire risk within each fireshed. The analyzed data showed variability in opinions and challenges about fire risk management. Most of the provided recommendations included advocating for the increase of awareness about fire risk and safety, inducing training about fire-fighting and creating networks to facilitate communication within communities at risk.

1. Introduction

Forest fires represent an increasing risk not only to forests but also to the livelihood of neighboring communities (Verkerk et al., 2018). Accordingly, forest fire risk assessment is essentially needed to improve management of risk, therefore minimizing potential impacts of fires on vulnerable people, properties, and natural resources (Abedi Gheshlaghis et al., 2019; Çolak and Sunar, 2020). Various studies around the world have been conducted to assess forest fire risk and consequently identify fire susceptible regions (Abedi Gheshlaghi, 2019). This study aimed at assessing forest fire risk perception of communities at two firesheds in Lebanon. In this context, a fireshed takes into account all communities located within a specific watershed. More specifically, a fireshed is "an area where social and ecological concerns regarding wildfire overlap and are intertwined" (GSFFC, 2022).

2. Study area

The study area comprised both the Qadisha-Abu Ali watershed and the Hasbani watershed (Figure 1). All the villages included in the study were selected using a national fire risk assessment report (Mitri et al., 2019) that identified high risk areas and "priority sites" in the respective fireshed.

The Qadisha-Abu Ali fireshed is located in North Lebanon and it is characterized by a Mediterranean landscape with dense mixed forest which is mainly composed of broadleaf and coniferous trees (Figure 1). Its lowest altitude is at sea level and its highest mountain peak reaches 3080 asl. It is composed of 5 vegetation successions within a typical Mediterranean floristic ensemble (Figure 2).

The Hasbani fireshed is located in Southeast Lebanon and it is characterized by a pre-steppic landscape with sparse oak forests dispatched between agricultural lands, rangelands, and urban settlements. Its lowest altitude is 200 m asl and its highest elevation is 2810 m asl. It is composed of four vegetation successions distributed in a typical Mediterranean floristic ensemble (Figure 2). Forests at high risk are scattered in a steppingstone pattern between the urban settlements and the agricultural areas.

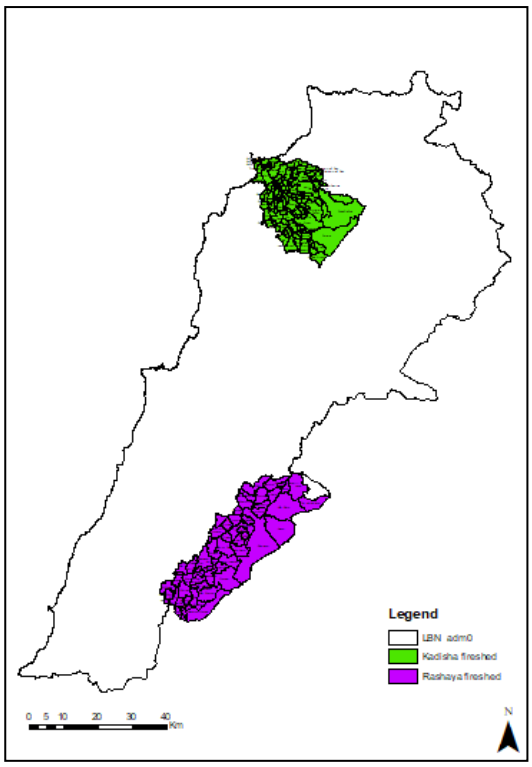

Figure 1: Geographic location of the fireshed

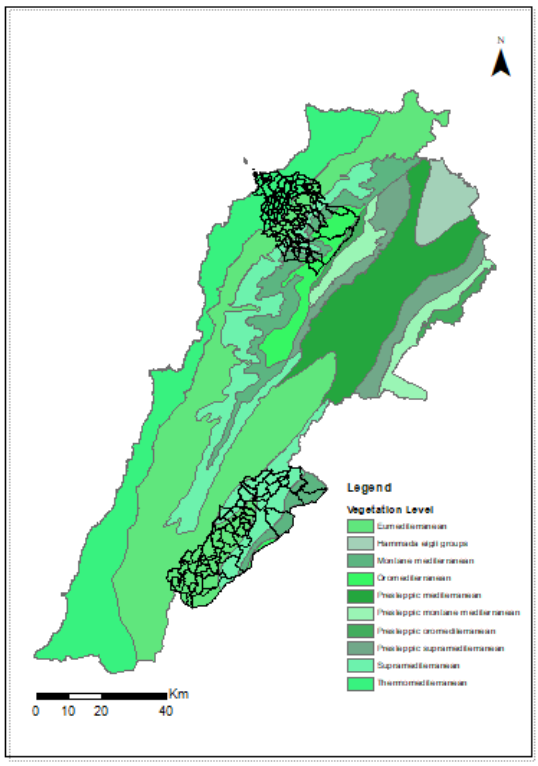

Figure 2: Vegetation levels succession in Lebanon

3. Methodology

Fire risk maps of the two targeted firesheds were generated using the Geographic Object-Based Image Analysis (GEOBIA) approach (Mitri et al., 2015). Fire risk represented the product of hazard and vulnerability. Priority zones of high fire risk villages were identified based on the risk map classes. Accordingly, field surveys were conducted in these priority zones of the two firesheds. A total of 100 participants were selected using a purposive-snowball sampling method while including representatives from local authorities and local community groups. The data was collected through direct interviews using the KOBO application (KOBO, 2020). The questions in the survey aimed to identify the respondent viewpoint on different aspects of fire risk such as causes/origin, damages, responsibilities and cost. The first set of questions aimed at evaluating exposure to fire events. The second set of questions revolved around forestry activity types and associated threats. The third set of questions were designed to recognize stakeholder's engagement towards managing risk. As for responsibilities, the fourth set of questions intended to assess people's judgment on who bears responsibility as well as costs.

4. Results and discussion

4.1. Exposure to fire events

Questions in this category tackled the perceived damage extent of forest fires and respondents' familiarity with the inherent threats and likelihood of fire occurrence.

The majority of respondents (88%) have witnessed at least one fire during the past ten years, and most of them witnessed a number of fire events varying between 1 and 10 fire events (Figure 3).

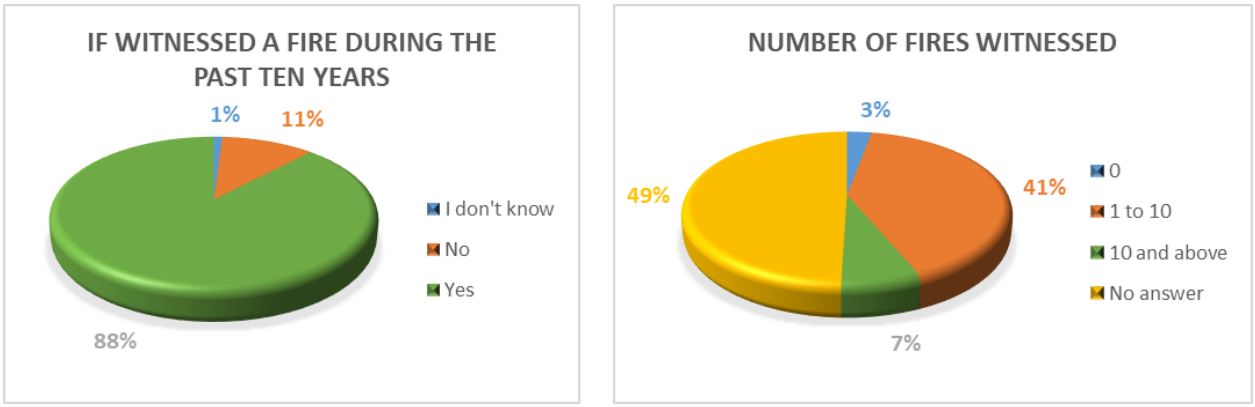

Figure 3. Numbers of fires witnessed by respondents

As for the likelihood of fire occurrence, the respondents' risk perception was very low. Only 10% of respondents indicated a high probability (Figure 4) even though the study was carried out in high-risk zones. This implied a relatively low awareness about fire risk.

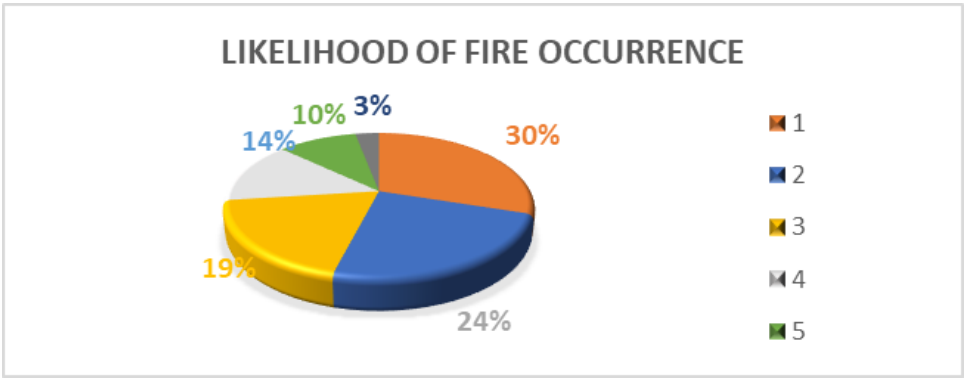

Figure 4. Likelihood of fire occurrence (1 - Not likely - 2 Unlikely - 3 - Neutral - 4 - Likely - 5 - Very likely)

4.2. Types of forest activities

The set of questions in this category revolved around the knowledge of respondents about forest activities usually undertaken to reduce fire risk and familiarity with related threats. To assess the awareness of the respondents about the main forest activities undertaken in their villages, the below matrix was produced crossing mostly identified activities with the type of land ownership. Most of the respondents linked forest activities to private lands (33%).

Table 1. The main forest activities and the type of land ownerships

Activities/Ownership	Mashaa	Government	Private	Waqf
Collection of wood or charcoal making	32	33	37	12
Charcoal making	33	34	38	12
Collection of non-wood forest products	41	42	52	14
Grazing	38	40	39	9
Tourism	38	31	39	9
Hunting	39	40	48	11
Religious ceremonies	16	15	18	9
Conservation/Preservation	34	33	32	10
Beekeeping	41	41	42	9

4.3. Engagement towards managing risk

Respondents were asked to identify measures taken in their villages to reduce fire risk. These mostly included equipping civil defense stations, increasing water sources, increasing firefighters' number, and organizing awareness activities as well as introducing forest management and other fire prevention measures such as roadsides cleaning, firebreaks, and trail opening, among others. Around 29% of the respondents were informed

about activities which were undertaken within their villages to reduce fire risk, while 71% did not refer to any activity of fire prevention (Figure 5). Nevertheless, when asked about their opinion to prioritize specific prevention activities, "awareness raising" came first with 33 answers, "equipping civil defense" followed with 28 answers (Figure 6). Whereas "forest management" came third, therefore entailing the need of creating more awareness about the importance of implementing forest management plans for reducing fire risk.

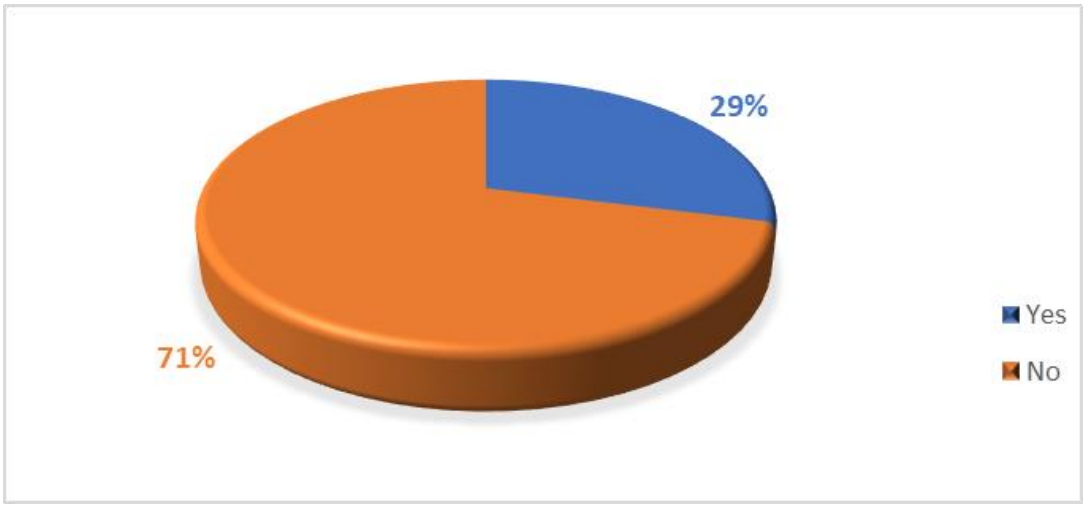

Figure 5. Feedback about fire prevention measures conducted in the respondents' villages

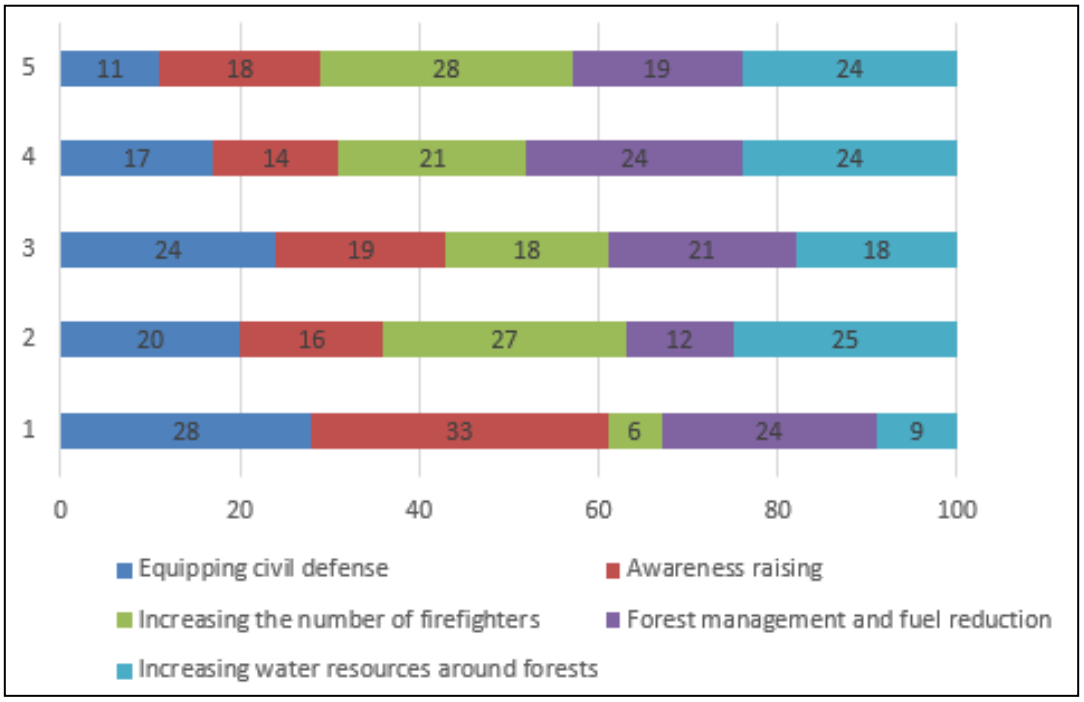

Figure 6. Rank of priorities of fire prevention activities

4.4. Responsibilities and cost

The last set of questions addressed public understanding of responsible bodies for 1) the main damages caused by fire and 2) the main fire-fighting operations. Also, it included inquiries for cost estimation of fire-fighting operations. When asked to estimate a cost of 1-day of fire-fighting in a potential fire incident occurring in their village, 33 % of the respondents were unaware of incurred costs (Table 2). The majority of respondents expressed that local municipalities and civil defense centers were in charge incurred costs.

Table 2. Cost estimation of 1-day of fire-fighting

Cost range	Percentage of answers
Between $2,500 and $5,000	12%
Between $5,000 and $10,000	9%
Between $500 and $2,500	22%
I don't know	33%
Less than $500	9%
More than $10,000	15%
	100%

As for post-fire direct and indirect impacts, responsibilities were mostly misperceived. The respondents did not grasp that such fire incidents were mostly attributed to human impact on nature in addition to environmental changes. Stakeholders and future fire managers could benefit from knowledge about how current actions and choices may influence future events and beliefs instead of focusing on a single solution at a time (Mccafrey, 2013).

5. Conclusions

Understanding key characteristics of the complex social dynamics behind forest fire incidents could greatly facilitate fire management, decrease future risks and dangers, and benefit the ecology of forests. In this study, there seems to be a lack of awareness around the rising issues of climate change and increasing fire risks; nonetheless, the respondents clearly exhibited the willingness to learn more about risks associated with their current activities and choices and how to reduce economic and environmental costs. Most of the recommendations included advocating for increase of awareness about fire risks and safety, induction of training about firefighting, and creation of networks to facilitate communication among the stakeholders. Future studies will target more respondents from different socio-economic backgrounds and different sectors.

6. References

Abedi Gheshlaghi, H., Feizizadeh, B., & Blaschke, T. (2019). GIS-based forest fire risk mapping using the analytical network process and fuzzy logic. Journal of Environmental Planning and Management, 63(3), 481–499. https://doi.org/10.1080/09640568.2019.1594726

Çolak, E., & Sunar, F. (2020). Evaluation of forest fire risk in the Mediterranean Turkish forests: A case study of Menderes region, Izmir. International Journal of Disaster Risk Reduction, 45, 101479. https://doi.org/10.1016/j.ijdrr.2020.101479

GSFFC (2022). What is a fireshed. http://www.santafefireshed.org/. Accessed on 25-3-2022

KOBO (2020). https://kobo.humanitarianresponse.info/#/forms/aVZMrw4usqRUkEQA7XXhZ5/landing

Mccafrey, S. (2013). Social science research related to wildfire management: an overview of recent findings and future research needs, International Journal of Wildland Fire, 22(1) 15-24.

Mitri, G., Jazi, M. & McWethy, D. (2015). Assessment of Wildfire Risk in Lebanon Using Geographic Object-Based Image Analysis. Photogrammetric Engineering and Remote Sensing. 81. 499-506. 10.14358/PERS.81.6.499.

Mitri, G., Bechara, J., Nehme, M. (2019). "Fire risk brief assessment report of the Fireshed of Qadisha/Abu Ali and Hasbani", Lebanon reforestation Initiative – Livelihoods in Forestry (LiF) project.

Verkerk, P. Martinez de Arano, I. and Palahí, M. (2018). The bio-economy as an opportunity to tackle wildfires in Mediterranean forest ecosystems, Forest Policy and Economics, Volume 86, 2018, Pages 1-3, ISSN 1389-9341, https://doi.org/10.1016/j.forpol.2017.10.016.

Biophysical drivers of fire regimes in Central Portugal

Rafaello Bergonse*[1]; Sandra Oliveira[1]; José Luís Zêzere[1]; Francisco Moreira[2,4]; Paulo Flores Ribeiro[3]; Miguel Leal[3,1]; José Manuel Lima e Santos[3]

[1]Centro de Estudos Geográficos, Instituto de Geografia e Ordenamento do Território, Universidade de Lisboa. Laboratório Associado TERRA. Rua Branca Edmée Marques, Cidade Universitária, 1600-276 Lisboa, Portugal, {rafaellobergonse, sandra.oliveira1, zezere}@campus.ul.pt
[2] CIBIO – Research Centre in Biodiversity and Genetic Resources, Universidade do Porto. Campus de Vairão, Rua Padre Armando Quintas, nº 7, 4485-661 Vairão, Portugal, {fmoreira@cibio.up.pt}
[3] Forest Research Centre, Instituto Superior de Agronomia, Universidade de Lisboa. Edifício Prof. Azevedo Gomes, Instituto Superior de Agronomia, Tapada da Ajuda, 1349-017 Lisboa, Portugal. {pfribeiro@isa.ulisboa.pt, mleal@campus.ul.pt, jlsantos@isa.ulisboa.pt}
[4]CIBIO/InBIO, Instituto Superior de Agronomia, Universidade de Lisboa, Tapada da Ajuda, 1349-017 Lisboa, Portugal

**Corresponding author*

Keywords

Fire regime, Biophysical drivers, Classification and regression trees, Central Portugal

Abstract

The spatial and temporal properties of burned areas are a major component of fire regimes. We analyse three parameters related to burned area within central Portugal, and then investigate the degree to which their variation is influenced by a set of biophysical drivers. Using civil parishes as units of analysis, we study three complementary parameters over a reference period of 44 years (1975-2018): cumulative percentage of parish area burned, Gini concentration index of burned area over time, and area-weighted total number of wildfires. Cluster analysis is used to aggregate parishes into groups based on similarities regarding burned area parameters. A classification tree model is then employed to assess the relative capacity of each driver to differentiate between groups of parishes. Drivers included slope, summer temperature and spring rainfall, land use/land cover (LULC) type and patch fragmentation, and net primary productivity. Results allowed to distinguish four parish types in terms of burned area features and show that these can be significantly differentiated by the biophysical drivers, of which LULC, slope and spring rainfall are the most important. Among LULC classes, shrubland and herbaceous vegetation play the foremost role, followed by agriculture. Our results highlight the importance of vegetation type, availability, and rate of regeneration, as well as that of topography, in influencing burned area patterns in the study area, while suggesting that other drivers, likely of a social nature, should also be taken into account.

1. Introduction

Understanding the drivers of fire regimes is highly important due to the damage regularly caused by wildfires. Among the southern European countries, Portugal is one of the most affected despite its relatively small size (San-Miguel-Ayanz et al., 2020). The largest burned areas tend to occur in the forest/shrubland dominated central sector of the country, which has been the subject of several studies (Catry et al., 2010; Maia et al., 2012), and was the most affected by the extreme wildfires occurred in 2017 (Benali et al., 2021).

In a recent work, we employed three complementary variables to express fire regime over a 44-year study period in Central Portugal, and we quantified the influence of a set of 12 biophysical drivers over each fire regime variable using ordinal logistic regression (Bergonse et al., 2022). Drawing upon those results, we intend to differentiate fire regimes in Central Portugal by integrating the three fire regime descriptors, and to characterize their interactions with biophysical conditions.

The study area corresponds to NUTS 2 Centro, comprising 28 199 km^2 within central mainland Portugal (Figure 1). This region is marked by a high variability regarding wildfire hazard and its control factors (Oliveira et al., 2020), with 49.7% of the region classified in the High and Very High hazard classes. The 972 civil parishes

(*freguesias*) of the study area are the spatial units of analysis, which vary in extent between 1.98 km^2 and 373.50 km^2.

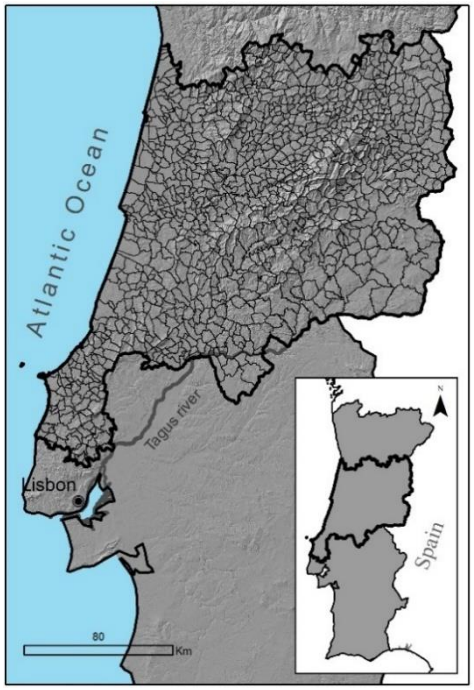

Figure 1 – Location and limits of the study area within mainland Portugal (NUTS 2 Centro), including parish limits. Parish boundaries were extracted from the official administrative map of Portugal (CAOP), produced by the Portuguese Directorate-General of the Territory (DGT).

2. Data and Methods

2.1. Data collection and pre-processing

2.1.1. Fire regime parameters

Fire regime characteristics were described with three parameters for the period 1975-2018 (44 years), following Bergonse et al. (2022). All were obtained from annual burned area maps produced in vector format by the National Forests Service (ICNF). The cumulative percentage of parish area burned (CPAB) was used to measure the propensity of each parish to burn extensively over time. Area-weighted wildfire frequency (AWWF) was calculated as the total number of wildfires recorded within the parish over the study period, divided by its area (km^2). The Gini Concentration Index (GCI) of burned area over time was adopted as an indicator of the temporal concentration of wildfire damage. It was applied to the annual burned areas of each parish over the 44 years and expressed as percentage. Ranging between 0 and 100, the GCI allows to differentiate parishes where most burned area is concentrated in a small number of years (high values), from those where the burned area is more regularly distributed over time (low values), regardless of the extent of that burned area.

Out of the total of 972 parishes, 35 (3.6%) never burned during the study period, having therefore no values in any of the fire regime parameters. These were removed from all analyses.

2.1.2. Biophysical drivers

A set of 12 biophysical drivers was considered (Table 1), which we previously demonstrated to be significantly associated, separately, with the three fire regime parameters under analysis (Bergonse et al., 2022).

Table 1- Description and characteristics of the potential fire regime drivers. Data sources and methods of calculation are described in Bergonse et al. (2022).

Type	Variable code	Variable	Temporal extent	Original spatial Resolution	Units
Topography	**SLO80**	Slope percentile 80	n.a.	25 m	º
Climate	**RFAJ**	Mean cumulative rainfall April-June	1970-2000	Approx. 1000m	mm
	TPJS	Mean monthly temperature July-September			^{0}C
Biomass	**NPP**	Net Primary Productivity	2000-2014	500 m	KgC/m^2
Land use/Land cover (LULC)	**AGR**	% parish area occupied by agriculture	1990-2018	Vector data. Minimum mapped area 1 ha	%
	OAK	% parish area occupied by cork-oak and holm-oak forests			
	EUC	% parish area occupied by eucalyptus forests			
	INV	% parish area occupied by forests of invasive species	1995-2018		
	CON	% parish area occupied by forests of coniferous species other than maritime or stone pine	1990-2018		
	BRD	% parish area occupied by forests of broadleaved species other than eucalyptus, cork-oak and holm-oak			
	SHR	% parish area occupied by brushland and spontaneous herbaceous species			
LULC patch fragmentation	**FRAGF**	Fragmentation of forest patches	1995-2018		centroids/ha of forest

2.2. Statistical techniques

Hierarchical cluster analysis was employed to identify groups of parishes with similar behaviour regarding the fire regime parameters. Clustering was performed using Ward's method, an agglomerative process which begins with as many clusters as cases, successively agglomerating clusters using the solution that minimizes within-cluster variance (Everitt et al., 2011). Prior to inclusion, the three fire regime parameters were converted into z-scores, to ensure an equal contribution regardless of contrasting value ranges (Maroco, 2007).

SPSS's CRT tool was then employed to build a classification tree model with the purpose of assessing the capacity of the biophysical drivers to differentiate between clusters. A 10-fold cross-validation procedure was adopted, with the Gini index being used as criterion of impurity for node splitting.

3. Results and discussion

3.1. Cluster analysis

A four-cluster solution was chosen taking into consideration a preliminary analysis of distances between clusters and the fire characteristics of the clusters identified.

FR1 (includes 450 parishes) is characterized by the lowest CPAB, the highest GCI, and the lowest AWWF values (Fig. 2-A). This fire regime is marked by the lowest extension of burned areas and the lowest wildfire frequency within the study area, with the resulting damage being relatively concentrated over time (corresponding to the highest GCI obtained). Spatially, it occurs mostly along the coastal swath and in the SE extreme of the study area (Figure 2-B).

FR3 (86 parishes) expresses opposite characteristics in relation to FR1. It has the highest CPAB values, as well as the highest AWWF and the lowest GCI. This indicates relatively frequent wildfires, which produce very extensive burned areas over time and result in a temporal dispersion of the damage. It occurs exclusively in the NE and the northern limit of the study area. FR2 (401 parishes) occupies an intermediate position between FR1

and FR3 regarding all three fire regime parameters. Spatially, it concentrates on the central and eastern portions of the study area.

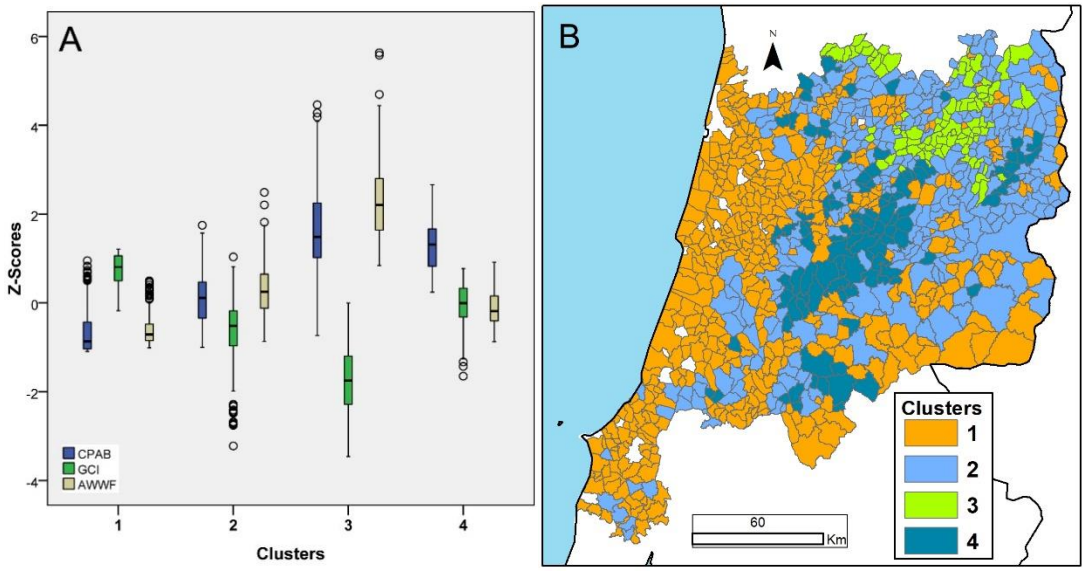

Figure 2 - (A) Box-plots for the values of the three fire regime parameters associated to each cluster/fire regime. Values expressed as z-scores. For each variable, the box includes the 1st and 3rd quartiles as well as the median. The whiskers identify the maximum and minimum values excluding outliers. Outliers (shown as circles) are defined as values between 1.5 times and 3 times the interquartile range, respectively above the 3rd quartile and below the 1st quartile; (B) Spatial distribution of the four clusters/fire regimes.

Finally, FR4 (102 parishes) has the second highest CPAB and the second lowest AWWF, resulting in the second highest temporal concentration of damage (GCI), and indicating relatively extensive but infrequent wildfires. It is mostly concentrated in the central sector of the study area.

3.2. Classification tree model

The CT model correctly classified 72.4% of all parishes, with the accuracy being slightly lower (68.7%) when independently validated using a 10-fold cross-validation process (Table 2). The overall accuracy demonstrates that the biophysical drivers are strongly related to the FRs within the study area. Regarding FR-specific accuracy, results show a notable contrast between the first three FRs (minimum accuracy 69.9%, maximum 82%) and FR4, with only 38.2% of all parishes correctly classified. This indicates that FR4 cannot be adequately discriminated using only the set of biophysical drivers employed in this study. Social variables, such as road or population density, can influence fire regimes, as previously shown in other studies (Pausas & Fernández-Muñoz, 2012; Rogers et al., 2020), and could eventually improve the accuracy of the classification.

Table 2 – Classification accuracy for the final tree model and for the tree models produced in association to the 10-fold cross-validation procedure. FR-specific accuracy values are for the final tree model.

Observed	Predicted				%
	1	2	3	4	Correct
1	369	70	1	10	**82.0**
2	58	209	17	15	**69.9**
3	0	22	61	3	**70.9**
4	17	42	4	39	**38.2**
			Final tree accuracy		**72.4**
			Cross-validated accuracy		**68.7**

All 12 biophysical drivers were integrated into the CT model (Figure 3). The percentage of shrubland and spontaneous herbaceous vegetation (SHR) was the most important driver, closely followed by spring rainfall (RFAJ). Slope (SLO80) and agriculture (AGR) have about half the importance of SHR and RFAJ, whereas eucalyptus forests (EUC), broadleaved species other than eucalyptus, cork oak and holm oak (BRD), and net

primary productivity (NPP) have a relative importance between 40% and 50% of SHR. The remaining drivers vary in relative importance from about 30% down to less than 10%.

To facilitate interpretation of the influences of biophysical drivers, Figure 4 shows the values of each driver in each of the four FRs.

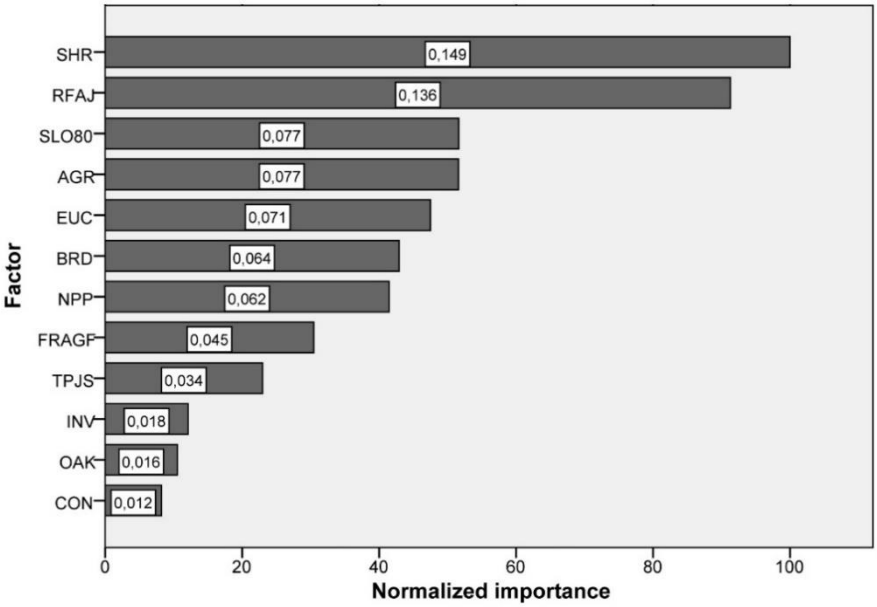

Figure 3 – Importance of each biophysical driver for the classification tree model, shown normalized by the most important driver (SHR).

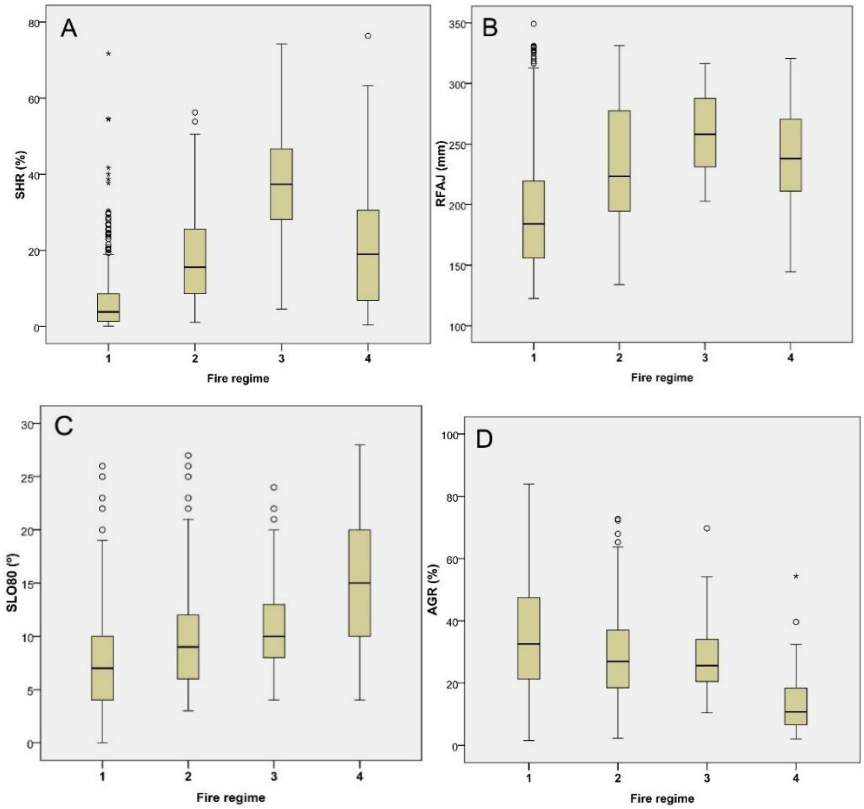

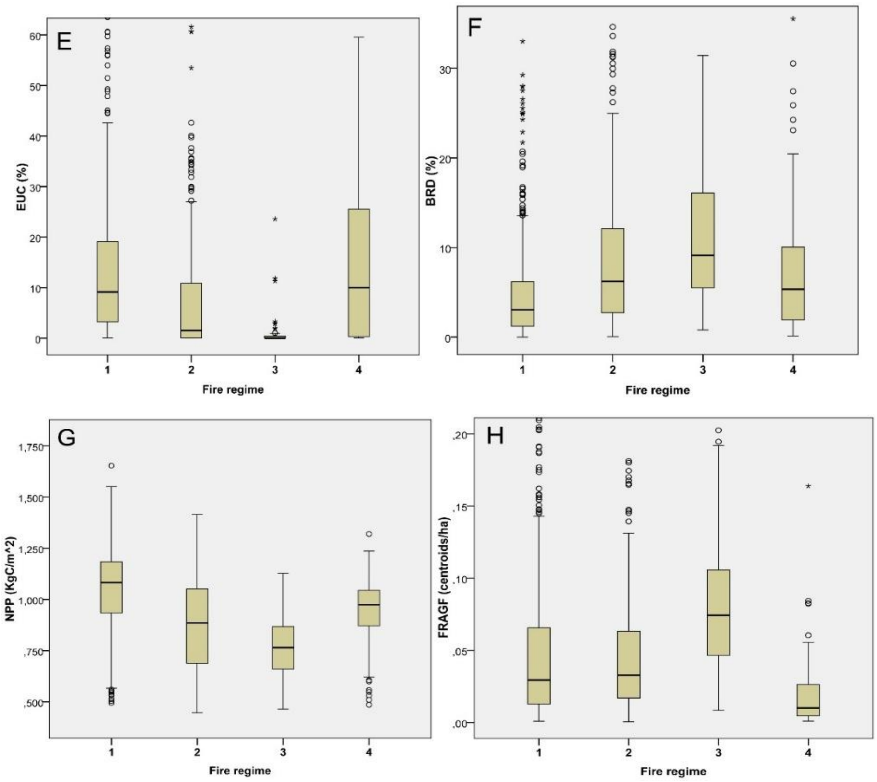

Figure 4 – Boxplots for the values of each biophysical driver in each of the four fire regimes, by decreasing order of importance in the classification tree model. A – SHR; B – RFAJ; C – SLO80; D – AGR; E – EUC; F – BRD; G – NPP; H – FRAGF. The four lowest importance drivers are not shown because their very small values and high level of dispersion in all FRs do not indicate clear patterns. Circles identify potential outliers, defined as situated between 1.5 times and 3 times the interquartile range below the 1st quartile and above the 3rd quartile. Asterisks identify potential extreme outliers, exceeding 3 times the interquartile range below or above the 1st and the 3rd quartile.

FR1 has the lowest percentage of parish area occupied by shrubland, the lowest spring rainfall, the lowest slope and the highest percentage of area occupied by agriculture. These are the four most important variables in the CT model, and their values in FR1 are in accordance with its low CPAB and AWWF. FR1's low shrubland proportion likely contributes to its low cumulative burned area (CPAB) and fire frequency (AWWF), since this landcover type's fire-proneness and quick regeneration promotes extensive and frequent fires (Bergonse et al., 2022; Moreira et al., 2009; Oliveira et al., 2014, 2020), as seen in FR3. Spring rainfall is linked to vegetation growth and thus fuel availability during the warmer summer months, therefore having a positive influence both over AWWF and CPAB (Bergonse et al. 2022), as highlighted by different authors (Oliveira et al., 2012; Xystrakis et al., 2014). Low spring rainfall values will, conversely, be associated with both low wildfire extensiveness and frequency, as seen in FR1. Slope promotes wildfire spread (Marques et al., 2011; Parente & Pereira, 2016), with the lowest slope values in the study area being in accordance with the minimum CPAB values shown by FR1 in relation to all other FRs. Finally, the higher proportion of agricultural land is also expected to contribute to the low CPAB and AWWF of this fire regime, due to its low fire-proneness (Moreira et al., 2009; Oliveira et al., 2014).

FR3 presents opposite characteristics to FR1, showing the maximum percentage of shrubland and the maximum values of spring rainfall, as well as second highest slope values. This fire regime has also the lowest percentage of eucalyptus among all four FRs, which would seem contradictory given the relative fire-proneness of this LULC (Meneses et al., 2018; Xanthopoulos et al., 2012). However, this suggests that the fuel availability behind FR3's high CPAB is mostly dependent on shrubland and its faster response to spring rainfall. This is confirmed by FR3's low Net Productivity Ratio, the lowest among all FRs, which is indicative of a relatively reduced forest cover. Nevertheless, FR3 is marked by the highest incidence of forests of broadleaves other than eucalyptus, cork oak and holm oak of all FRs. As this LULC class has a positive effect over CPAB and AWWF (Bergonse et al., 2022), this suggests that forest-type fuels also have some importance in FR3.This fire regime also shows the greatest burned area extension (CPAB), despite having the highest forest patch fragmentation of all FRs. Although a high level of fragmentation can be expected to constrain extensive wildfires (Gralewicz et

al., 2012; Ryu et al., 2007), the dominant fuel type in FR3 is shrubland; therefore, even if each individual wildfire is constrained in its spread, the quick regeneration of fuels will nonetheless allow for frequent burning, leading to an important accumulation of burned area over time.

FR4 shows a relatively high cumulative burned area (CPAB), which is in accordance with its biophysical characteristics: a relatively high percentage of shrubland, high spring rainfall, the highest slope inclination, and the lowest percentage of agriculture. This fire regime also shows a relatively high percentage of eucalyptus forests. The importance of forest cover in FR4 is indicated by the relatively high Net Productivity Ratio, suggesting that, unlike FR3, this fire regime is more dependent on slowly regenerating forests for fuel instead of shrubland. The high damage concentration over time (GCI) found can be linked to the degree of forest patch fragmentation, the lowest amongst all FRs, indicating the potential influence of fuel and forest continuity to the occurrence of higher damages even when wildfire frequency (AWWF) is low. This suggests the importance of creating fuel discontinuities at the landscape level to prevent large and severe wildfires (Benali et al., 2021).

4. Conclusions

Four distinct fire regimes (FR) can be differentiated within central Portugal. FR1 occurs along the coastal area and in the southeasternmost limit and is marked by the least extensive burned area and the lowest wildfire frequency, as well as the maximum temporal concentration of damage. FR2 occurs in most of the centre and eastern sectors. It is marked by more extensive burned areas and more frequent wildfires than FR1, as well as lower temporal concentration of damage. FRs 3 and 4 are characterized by the most extensive burned areas, and contrast in terms of wildfire frequency and temporal concentration of damage. FR3 occurs mostly in the NE of the study area. It has the most extensive burned area of all, as well as the most frequent wildfires, with burn damage dispersed through time. FR4, occurring mostly in the central sector, has slightly less extensive burned areas, but a much lower wildfire frequency, with the damage being more concentrated in time. LULC, slope and spring rainfall are the most important drivers of these distinct fire regimes. The most relevant LULC classes are shrubland/spontaneous herbaceous vegetation and agriculture, the first due to its fire-proneness and quick regeneration, and the second due to its constraints over wildfire spread. Slope facilitates wildfire spread, whereas spring rainfall promotes fuel availability for burning later in the year. Despite the good discriminating capacity of the classification tree model, other drivers, likely of a social nature, might also influence the fire regimes in the study area.

5. Aknowledgments

This work was financed by national funds through FCT—Portuguese Foundation for Science and Technology, I.P., under the framework of the project “People&Fire: Reducing Risk, Living with Risk” (PCIF/AGT/0136/ 2017), under the programme of ‘Stimulus of Scientific Employment— Individual Support’ (contract 2020.03873.CEECIND), and by the Research Unit UIDB/00295/2020 and UIDP/00295/2020.

6. References

Benali, A., Sá, A. C. L., Pinho, J., Fernandes, P. M., & Pereira, J. M. C. (2021). Understanding the Impact of Different Landscape-Level Fuel Management Strategies on Wildfire Hazard in Central Portugal. Forests, 12(522), 1–22. https://doi.org/10.3390/f12050522

Bergonse, R., Oliveira, S., Zêzere, J. L., Moreira, F., Ribeiro, P. F., Leal, M., & Lima e Santos, J. M. (2022). Biophysical controls over fire regime properties in Central Portugal. Science of The Total Environment, 810, 152314. https://doi.org/10.1016/j.scitotenv.2021.152314

Catry, F. X., Rego, F., Moreira, F., Fernandes, P. M., & Pausas, J. G. (2010). Post-fire tree mortality in mixed forests of central Portugal. Forest Ecology and Management, 260(7), 1184–1192. https://doi.org/10.1016/j.foreco.2010.07.010

Everitt, B. S., Landau, S., Leese, M., & Stahl, D. (2011). Cluster analysis (5th ed.). John Wiley & Sons.

Gralewicz, N. J., Nelson, T. A., & Wulder, M. A. (2012). Factors influencing national scale wildfire susceptibility in Canada. Forest Ecology and Management, 265, 20–29. https://doi.org/10.1016/j.foreco.2011.10.031

Maia, P., Pausas, J. G., Vasques, A., & Keizer, J. J. (2012). Fire severity as a key factor in post-fire regeneration of Pinus pinaster (Ait.) in Central Portugal. Annals of Forest Science, 69(4), 489–498. https://doi.org/10.1007/s13595-012-0203-6

Maroco, J. (2007). Análise Estatística com Utilização do SPSS (3rd ed.)

Marques, S., Borges, J. G., Garcia-Gonzalo, J., Moreira, F., Carreiras, J. M. B., Oliveira, M. M., Cantarinha, A., Botequim, B., & Pereira, J. M. C. (2011). Characterization of wildfires in Portugal. European Journal of Forest Research, 130(5), 775–784. https://doi.org/10.1007/s10342-010-0470-4

Meneses, B. M., Reis, E., & Reis, R. (2018). Assessment of the recurrence interval of wildfires in mainland portugal and the identification of affected luc patterns. Journal of Maps, 14(2), 282–292. https://doi.org/10.1080/17445647.2018.1454351

Moreira, F., Vaz, P., Catry, F., & Silva, J. S. (2009). Regional variations in wildfire susceptibility of land-cover types in Portugal: Implications for landscape management to minimize fire hazard. International Journal of Wildland Fire, 18(5), 563–574. https://doi.org/10.1071/WF07098

Oliveira, S., Gonçalves, A., & Zêzere, J. L. (2020). Reassessing wildfire susceptibility and hazard for mainland Portugal. Science of the Total Environment, 762, 143121. https://doi.org/10.1016/j.scitotenv.2020.143121

Oliveira, S., Moreira, F., Boca, R., San-Miguel-Ayanz, J., & Pereira, J. M. C. (2014). Assessment of fire selectivity in relation to land cover and topography: A comparison between Southern European countries. International Journal of Wildland Fire, 23(5), 620–630. https://doi.org/10.1071/WF12053

Oliveira, S., Oehler, F., San-Miguel-Ayanz, J., Camia, A., & Pereira, J. M. C. (2012). Modeling spatial patterns of fire occurrence in Mediterranean Europe using Multiple Regression and Random Forest. Forest Ecology and Management. https://doi.org/10.1016/j.foreco.2012.03.003

Parente, J., & Pereira, M. G. (2016). Structural fire risk: The case of Portugal. Science of the Total Environment, 573, 883–893. https://doi.org/10.1016/j.scitotenv.2016.08.164

Pausas, J. G., & Fernández-Muñoz, S. (2012). Fire regime changes in the Western Mediterranean Basin: From fuel-limited to drought-driven fire regime. Climatic Change, 110(1–2), 215–226. https://doi.org/10.1007/s10584-011-0060-6

Rogers, B. M., Balch, J. K., Goetz, S. J., Lehmann, C. E. R., & Turetsky, M. (2020). Focus on changing fire regimes: interactions with climate, ecosystems, and society. Environmental Research Letters, 15(3). https://doi.org/10.1088/1748-9326/ab6d3a

Ryu, S. R., Chen, J., Zheng, D., & Lacroix, J. J. (2007). Relating surface fire spread to landscape structure: An application of FARSITE in a managed forest landscape. Landscape and Urban Planning, 83(4), 275–283. https://doi.org/10.1016/j.landurbplan.2007.05.002

Xanthopoulos, G., Calfapietra, C., & Fernandes, P. (2012). Fire hazard and flammability of european forest types. In F. Moreira, M. Arianoutsou, P. Corona, & J. De Las Heras (Eds.), Post-Fire Management and Restoration of Southern European Forests (pp. 79–92). Springer. https://link.springer.com/chapter/10.1007/978-94-007-2208-8_4

Xystrakis, F., Kallimanis, A. S., Dimopoulos, P., Halley, J. M., & Koutsias, N. (2014). Precipitation dominates fire occurrence in Greece (1900-2010): Its dual role in fuel build-up and dryness. Natural Hazards and Earth System Sciences, 14(1), 21–32. https://doi.org/10.5194/nhess-14-21-2014

Burnt area trends in the Middle-East: evidence for the importance of recent conflicts

Georgia Majdalani[1,2]; Nikos Koutsias[3], Jocelyne Adjizian-Gerard [2]; Ghaleb Faour [4]; Florent Mouillot[*5]

[1] UMR CEFE 5175, Centre National de la Recherche Scientifique (CNRS), Université de Montpellier, Département Scientifique Biologie, Écologie, Évolution, Environnement , Sciences Terre et Eau. 1919 route de Mende, 34293 Montpellier CEDEX 5, France, {georgia.majdalani@cefe.cnrs.fr}
[2] CREEMO Laboratory, Geography Department, Saint-Joseph University. Beirut, Lebanon, {jocelyne.gerard@usj.edu.lb}
[3] Department of Environmental Engineering, University of Patras. G. Seferi 2, GR-30100, Greece, {nkoutsia@upatras.gr}
[4] National Center for Remote Sensing, National Council for Scientific Research. Beirut, Lebanon, {gfaour@cnrs.edu.lb}
[5] UMR CEFE 5175, Centre National de la Recherche Scientifique (CNRS), Université de Montpellier, Université Paul-Valéry Montpellier, École Pratique des Hautes Études (EPHE), Institut de Recherche pour le Développement. 1919 route de Mende, 34293 Montpellier CEDEX 5, France, {florent.mouillot@cefe.cnrs.fr}

**Corresponding author*

Keywords

Middle-East, fire history, trend, climate, social conflicts.

Abstract

Fire is a major disturbance affecting Mediterranean ecosystems. Due to a lack of exhaustive fire registration, fire drivers in the Middle East have been hardly investigated. We propose here the analysis of a newly produced fire patch reconstruction from remote sensing over the 1984 – 2020 period in Lebanon and Syria, experiencing peculiar Mediterranean climate and socio-political conflicts. We identified a particular bimodal and late-season fire regimes in the two neighboring countries. Then, taking into account their different socio-political differences since the Syrian civil war in 2011 by using the ICEWS conflict database, we could highlight the dominant role of these conflicts in extreme fire years in the region.

1. Introduction

Wildfire is among the main shaping factors of Mediterranean ecosystems (Paula *et al.*, 2009), affecting yearly about 1 million hectares of Mediterranean forests worldwide (Dimitrakopoulos and Mitsopoulos, 2006). Due to the particularly fire-prone conditions of the Mediterranean climate (Le Houérou, 1973), fires are intrinsic to the functioning of Mediterranean forests. Climate forcings, changes in traditional land use, as well as population movements and lifestyle, lead forest fires to increase after the 1970' in the Mediterranean basin (MB) (Gill *et al.*, 2013; Pausas, 2004; Xanthopoulos and Nikolov, 2019), causing adverse impacts on economic, social and ecological assets (Gill *et al.*, 2013; Xanthopoulos and Nikolov, 2019).

This natural disturbance is mostly being addressed by studies focusing on the European part of the MB where fire events have been registered since the 1970s (San-Miguel-Ayanz *et al.*, 2012). Studies conducted in the Eastern and Southern parts of the basin are more limited and systematic uniform documentation of fires is still lacking (cf. Aini *et al.*, 2019; Belhadj-Khedher *et al.*, 2018; Chergui *et al.*, 2018).

On the Eastern rim of the MB and intermediate between the North ridge where fire activity is driven by summer drought promoting large fires (Turco *et al.*, 2017), and the Southern ridge where fire activity is driven by heat waves during Saharan dry winds (Belhadj-Khedher *et al.*, 2020), Lebanon and Syria lack exhaustive fire registration, an obligate prerequisite for studying fire regimes. In addition, as of 2011, Syria experienced a series

of protests that quickly escalated in 2012 to a full-fledged war (ongoing). Scholars have recently described the effects of war on the fire risk by relying mostly on MODIS global remote sensing data (Schon *et al.*, 2021; Zubkova *et al.*, 2021), over a short period (Mahfoud, 2020; Mohamed *et al.*, 2020) or focusing on agricultural lands (Schon *et al.*, 2021).

In such scarcely documented areas, remote sensing offers the most effective alternative to national statistics, providing global coverage, and multispectral and multitemporal information. Since the late 20th century, satellite imagery has been used to map fires (Xiao-rui *et al.*, 2005), from coarse (Eastwood *et al.*, 1998; Justice *et al.*, 2002; Malingreau, 1990; Pereira, 1999) and medium spatial resolution sensors (Filipponi, 2018; Liew *et al.*, 1998; Wightman, 1973).

The public release of the global historical Landsat archive (1984 – present) by the United States Geological Survey (USGS) in 2008 (Loveland and Dwyer, 2012; Woodcock *et al.*, 2008) initiated the development of automated and semi-automated tools that multi-process long and complete time series of Landsat imagery, resulting in the fast reproduction of fire perimeters over long periods and large surfaces (local to global coverage).

Nevertheless, relying solely on Landsat data can't provide a complete record of past fires and prevents an accurate dating between Landsat's overpasses. Recently, semi- and fully-automated burned area (BA) mapping tools combining Landsat data and daily Moderate Resolution Imaging Spectroradiometer (MODIS) active fire-detection data (hotspots) helped to overcome these limitations (Boschetti *et al.*, 2015; Roteta *et al.*, 2021). Fires detected throughout spectral changes in Landsat data (30 m) are dated using the high temporal resolution MODIS hotspots (1 day) when the two data sets spatially and temporarily coincide, also allowing the visual validation of the burning signal to effectively eliminate commission errors (Chuvieco and Congalton, 1988) and the manual refining of the fire polygons to narrow omission errors (Koutsias and Pleniou, 2021).

Accordingly, the aims of this study were (a) to create a GIS database of wildfire events and spatial extent in Lebanon's and the coast of Syria's wildland vegetation, two neighboring countries with similar climate conditions but contrasted socio-political events, for the last 37 years based on historical satellite archives (1984 – 2020) and MODIS hot-spots data (2001 – 2020), and (b) to provide a description of the fire regime taking into consideration the impacts of the socio-political conflicts on the natural wildfire regime in Syria.

2. Material and Methods

2.1. Study area

The study area includes the wildland areas (forests, shrublands, and grasslands) over Lebanon (between latitudes 33° and 35° N and longitudes 35° and 37° E) and the Syrian coast (between latitudes 32° and 38° N, and longitudes 35° and 43° E) (Figure 1), characterized by a typical Mediterranean climate with hot and dry summers and mild, wet winters (Köppen, 1884).

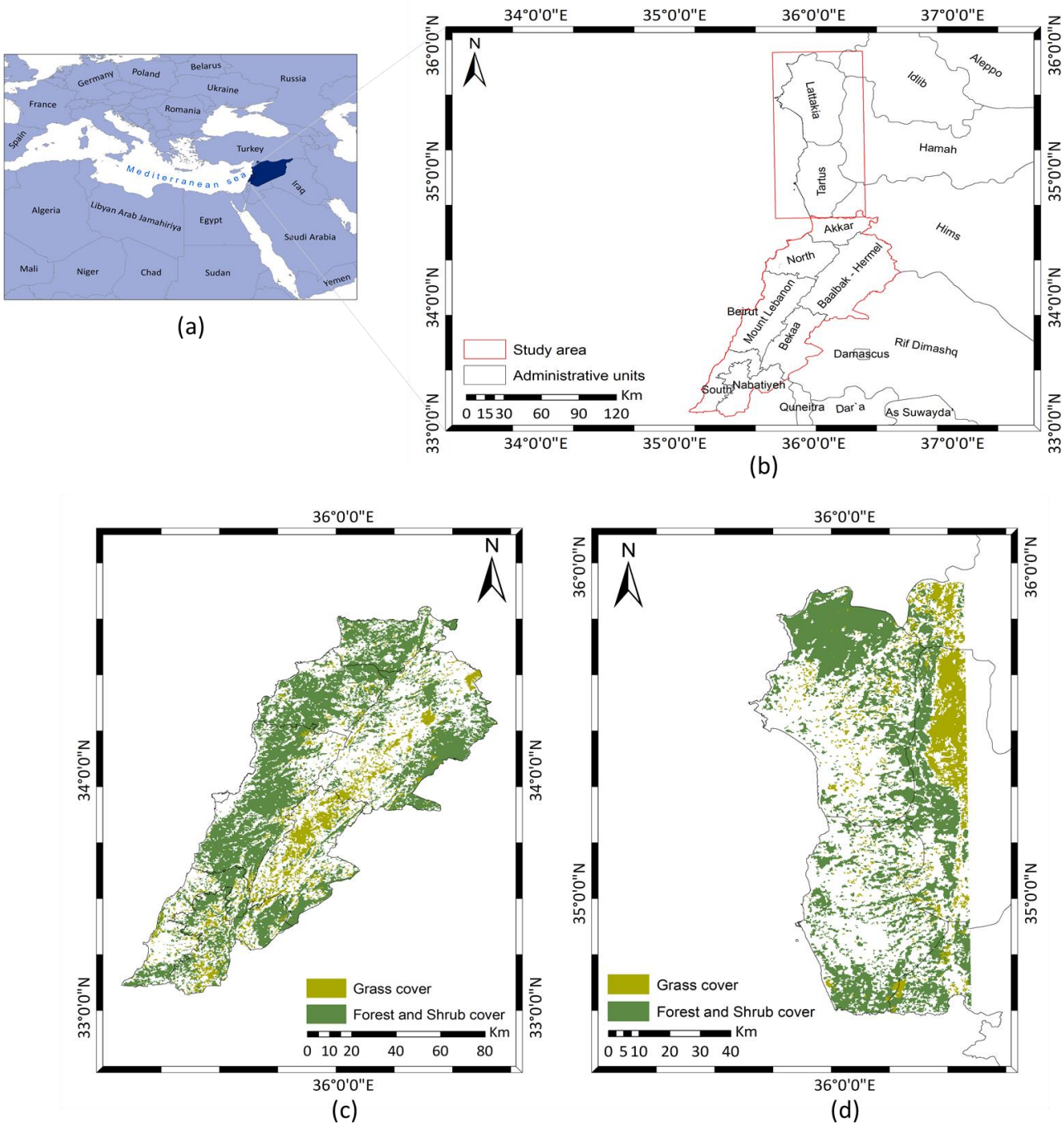

Figure 1- Location of Lebanon and Syria within the Mediterranean basin (a) and administrative units (b) overlayed with the forests/shrub cover (Deep green) and grass cover (light green) in Lebanon (c) and Coastal Syria (d).

The study area is delimited in red.

2.2. Data

2.2.1. Fire data

For the period 2001 – 2020, fire contours were generated over wildlands using the Burned Area Mapping Tools (BAMTs). BAMTs is a semi-automated tool, available on the Google Earth Engine platform (https://github.com/ekhiroteta/BAMT) whereas common spectral indices, used to characterize burnt pixels, are calculated for a pair of Landsat or Sentinel scenes and a random forest classifier algorithm is trained to identify burnt vegetation patches (Roteta *et al.*, 2021).

Fire events were first located and dated based on MODIS MCD14ML hotspots (2001 – 2011) and VIIRS hotspots (2012 – 2020) (available at https://firms.modaps.eosdis.nasa.gov/download/).

Based on the timing and location of each fire hotspot, their contours could be amped by pre and post-fire Landsat time series using BAMTS and visually checked for accuracy.
Due to the lack of hotspots for the period 1984 – 2000 to tackle the location and timing of fire events in BAMTs, a second semi-automated tool relying solely on Landsat data was used to produce the fire contours of 1984 – 2020. The tool, described in Koutsias and Pleniou (2021), is based on a set of valid rules applied to Landsat scene pairs (pre-and post-fire) to identify burnt areas. Fires produced were only yearly dated due to the coarse temporal resolution of Landsat scenes (~ 16 days). Over the period 2001 – 2020, small fires undetected by BAMTs could be identified and added to the database while fires identified from both methods were compared and merged.

Due to the lack of reliable local fire records to filter out commission errors (Faour, 2004; Faour et al., 2006), the accuracy assessment was a visual checking filtering out all detected fires occurring in croplands or with no visual changes in reflectances. Within the red–green–blue (RGB) display, BAs have a very strong spectral signal appearing as a deep red coloring in post-fire scenes (Figure 2), allowing a high accuracy visual assessment (Koutsias and Karteris 2000; Roteta *et al.*, 2019).

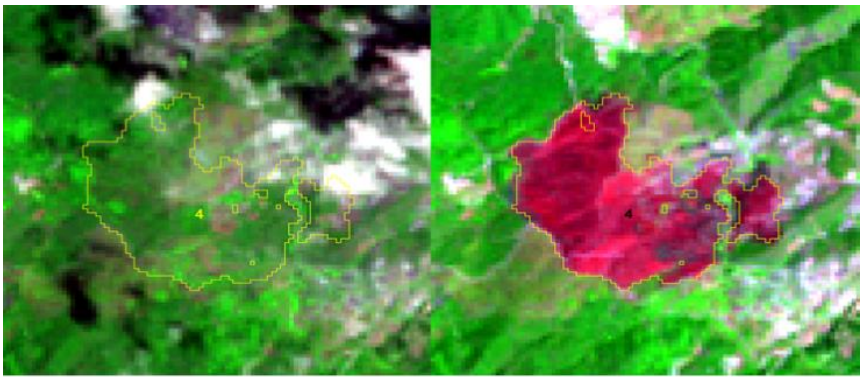

Figure 2 - Pre- (left) and post-fire (right) images showing the burnt signal (red).

2.3. Climatic data

To investigate the climatic control on the seasonal and interannual fire activity, we tested the Fire Weather Index (FWI) (Van Wagner, 1974), previously used in Mediterranean ecosystems (Chelli *et al.*, 2015; Dimitrakopoulos *et al.*, 2011; Moriondo *et al.*, 2006). We computed FWI with the R-cran "*cffdrs*" package and "*fwi*" function based on midday values of temperature (C), wind speed ($km.hr^{-1}$), precipitation (mm), and relative humidity (%) from the ERA5 Land climate database (https://confluence.ecmwf.int/display/CKB/ERA5-Land?src=contextnavpagetreemode) over the cities of Beirut (Lebanon) (33.68°E, 35.5°N) and Lattakia (Syria) (36.0°E, 36.05°N) for the period 1984 – 2020.

2.3.1. Conflict Data

To investigate our hypothesis of the potential impact of conflicts on the wildfire activity in Syria, we used the Integrated Crisis Early Warning System database (ICEWS) (Boschee *et al.*, 2020), previously used in studies about protests, fire, and conflicts driving forces in Syria (Ash and Obradovich, 2020; Linke and Ruether, 2021; Zubkova *et al.*, 2021). ICEWS consists of socio-political conflict and mediation global events identified and extracted automatically from news articles, available from January 1995 until April 2020. For our study, 1,607 violent events taking place in Syria between 1995 and April 2020 (29 out of 290 event types) were retained.

3. Results and Discussion

3.1. General information and Burnt Area database for the period 1984 – 2020

An exhaustive GIS fire database was produced for Lebanon and Mediterranean Syria for the period 1984 – 2020 with a spatial resolution ranging between 20 m (2016 – 2020) and 30 m (1984 – 2015). Each of the fire polygons is associated with a unique identification number, a surface area (ha), and minimum and maximum fire dates based on MCD64ML and VIIRS hotspots.

In Lebanon, a total of 3,232 fires were mapped, affecting a total area of 83,437 ha for the period 1984 – 2020. 0.42% of the wildland was burnt each year (2,255 ha.year^{-1}) with the highest fire years being 2007, 1998, and 1985. The majority of the fires (66.3%) occurred in forests and shrublands. 33.7% of the fires occurred in grasslands (Figure 3).

In Syria, a total of 1,544 fires were mapped, affecting a total area of 106,766 ha for the period 1984 – 2020, 1% of the wildland was burnt each year (2,885 ha.year^{-1}), with the highest fire years being 2020, 2012, and 2015. The majority of the fires (80.6%) occurred in forests and shrublands. 19.4% of the fires occurred in grasslands. (Figure 4).

3.2 Bimodal fire seasonality

In both countries, we observed a particular bimodal distribution of BA over the fire season with a reduced fire activity in August and peaks in the early and late fire seasons (Figure 5). Both the late end of the fire season (October/November) and the reduced fire activity in August are rarely seen in the MB where the fire season usually ends in September (Belhajd Khedher *et al.*, 2018; Ruffault *et al.*, 2020) and the largest BA is observed in August (Aini *et al.*, 2019; Belhadj-Khedher *et al.*, 2018; Chergui *et al.*, 2018; Im *et al.*, 2006). The dry season actually extends from June to early November, quite a long period for the region. During this dry period, we found that air relative humidity (RH) in August doesn't reach the low values observed in the late fire season (October-November in Lebanon; September-October in Syria). In addition, wind speed tends to decline in summer, while the highest temperatures (95% percentile) are stable from May to October leading to higher FWI events in June and September to November (Figure 6).

3.3 Non-climatic abrupt fire regime change in Syria since 2011

While no significant temporal trend of BA is observed for the two countries (Lebanon: p= 0.21, Syria: p= 0.06), contrasting with the general decreasing trends in the European Mediterranean region (Turco *et al.*, 2016), one breakpoint occurs for the year 2011 in Syria with significantly higher BA observed during the period 2012 – 2020 (81,492.5 ha) compared to the whole time series (25,273.5 ha during 1984 - 2011). This abrupt change in the fire regime, usually due to non-climatic factors (Pausas and Keeley, 2017; Syphard *et al.*, 2017), was not observed in neighboring Lebanon (Figure 7).

A higher, yet not significant, correlation was found between the BA and maximum FWI values for Lebanon (r= 0.29) and Syria (r=0.44) than with mean FWI values (Lebanon: r=0.1, Syria: r=0.24). During the pre-conflict period, maximum FWI could detect high fire years in 2010, 2007, 2002, 1994, and 1998 in Lebanon, as well as in 2007, 1986, and 1985 in Syria. We observed that during the conflict period since 2011, the years with high fire activity in Syria (2020, 2012, 2015, and 2013) still experience the highest FWI with the breaking record of 2020, as well as Lebanon for the years 2010, 2013, and 2019 (Figure 8). However, no significant temporal trend of FWI (Lebanon: p = 0.42, Syria: p = 0.09) nor breakpoints were significant in both countries, confirming the poor impact of climate on the BA trend.

When finally considering the ICEWS database, we could find a significant increasing temporal trend in the number of conflict events (p=0.049, slope=4.53) and two breakpoints (2010 and 2016) matching the breakpoint and increase of BA observed during the conflict period in Syria (Figure 9). A highly significant positive correlation between the number of conflict events and BA within each Syrian governorate was also found (p=0.04) (Figure 10).

The poor trend correlation between FWI and BA in Syria, the decorrelation in BA between Lebanon and Syria after 2011 with similar climate while the number of conflicts appeared as a significantly correlated variable suggest that the wildfire trend in Syria has socio-political drivers stronger than climate. Still, extreme fire years, as 2020, remain related to climate with 2020 being the most extreme fire weather since 1984 observed in Syria. The combined effect of climate and social troubles lead to the most extreme fire year observed in the region. In neighboring Lebanon, the social troubles (mostly urban) during the civil war ending in 1990 did not lead to major fire events. However, the political troubles in 2006 might have significantly contributed to the high BA during this year with no extreme fire weather.

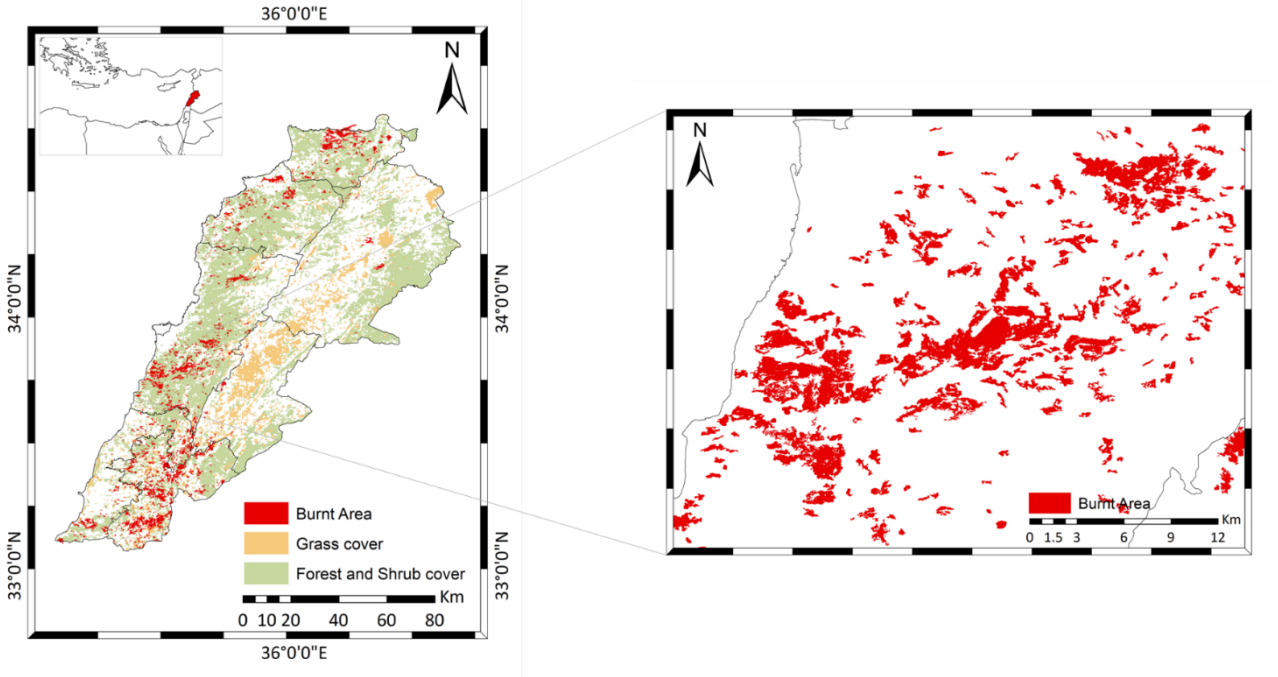

Figure 3 - Location of fire events in Lebanon for the period 1984 – 2020; fire contours (red polygons) and wildland cover (green and yellow polygons).

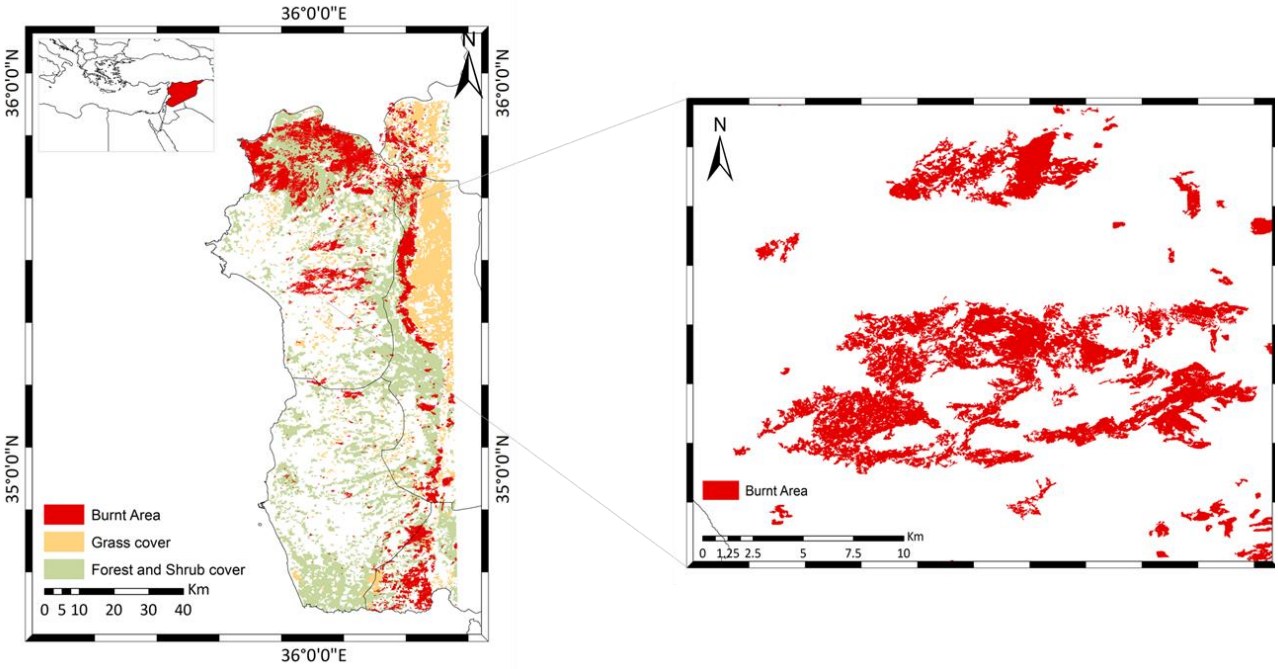

Figure 4 - Location of fire events in Syria for the period 1984 – 2020; fire contours (red polygons) and wildland cover (green and yellow polygons).

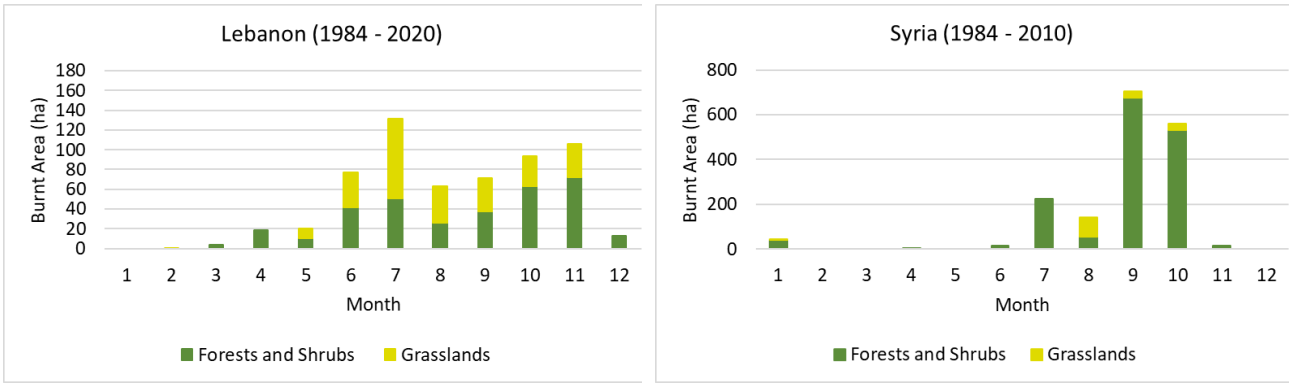

Figure 5- Seasonality of BA in Lebanon (1984 – 2020) (left) and Mediterranean Syria (1984 – 2010) (right).

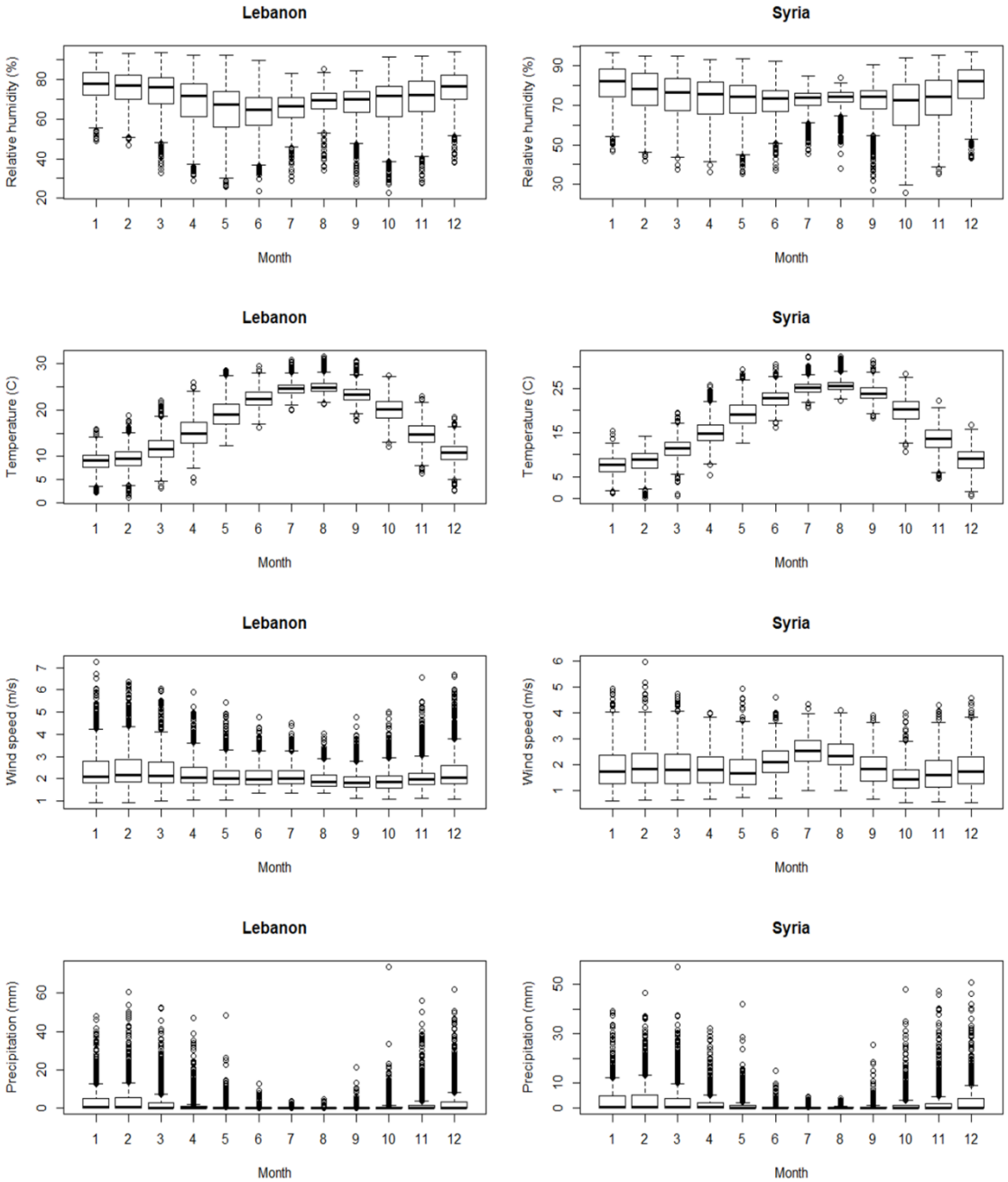

Figure 6 - Median, standard deviation, 95% confidence interval, and outliers of daily values of air Relative Humidity (RH) (%), Temperature (C), Wind Speed (m.s^{-1},) and Precipitation (mm) in Lebanon (left) (1984 – 2020) and Mediterranean Syria (right) (1984 – 2010).

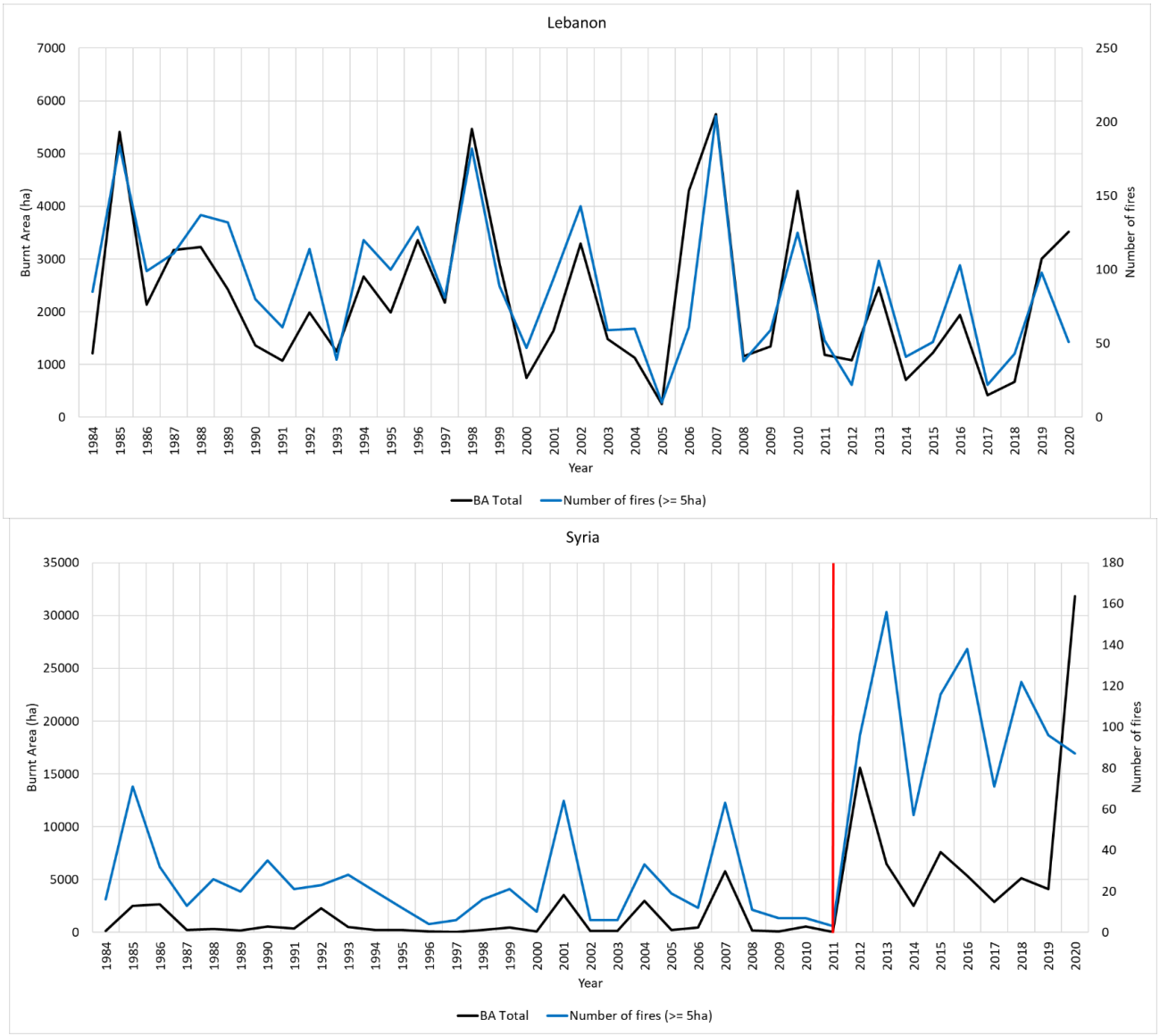

Figure 7 - Interannual variability of BA (black) and number of fires (blue) in Lebanon and Syria for the period 1984 - 2020. Breakpoint in Syria at 2011 (red).

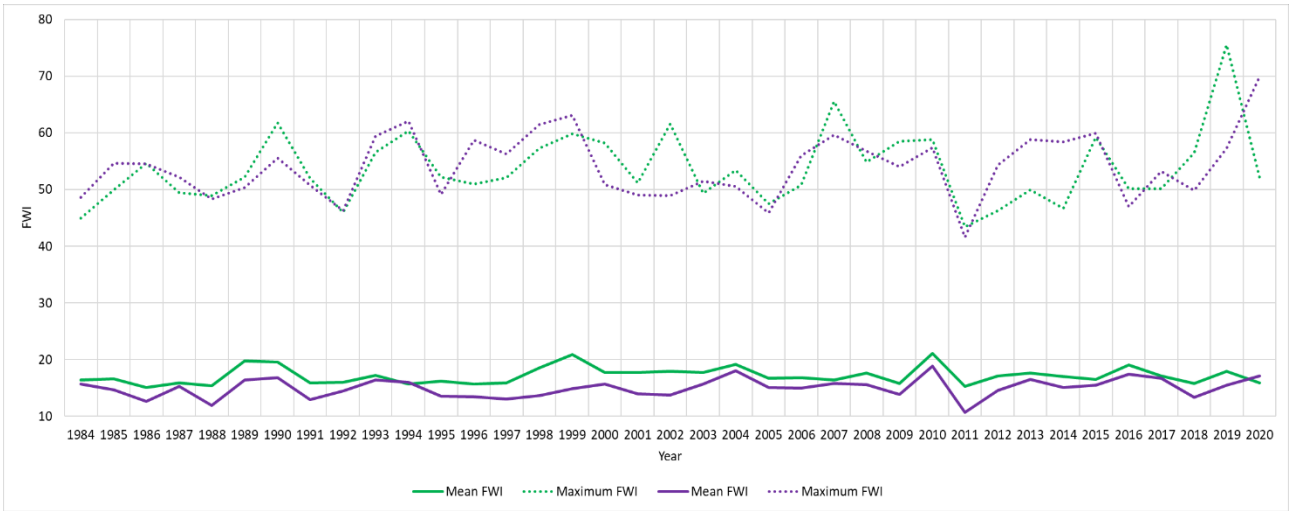

Figure 8 - Interannual variability of FWI values (line) and maximum daily FWI values (dashes) in Lebanon (green) and Syria (purple) for the period 1984 - 2020. The maximum value is the highest data point in the data set excluding outliers.

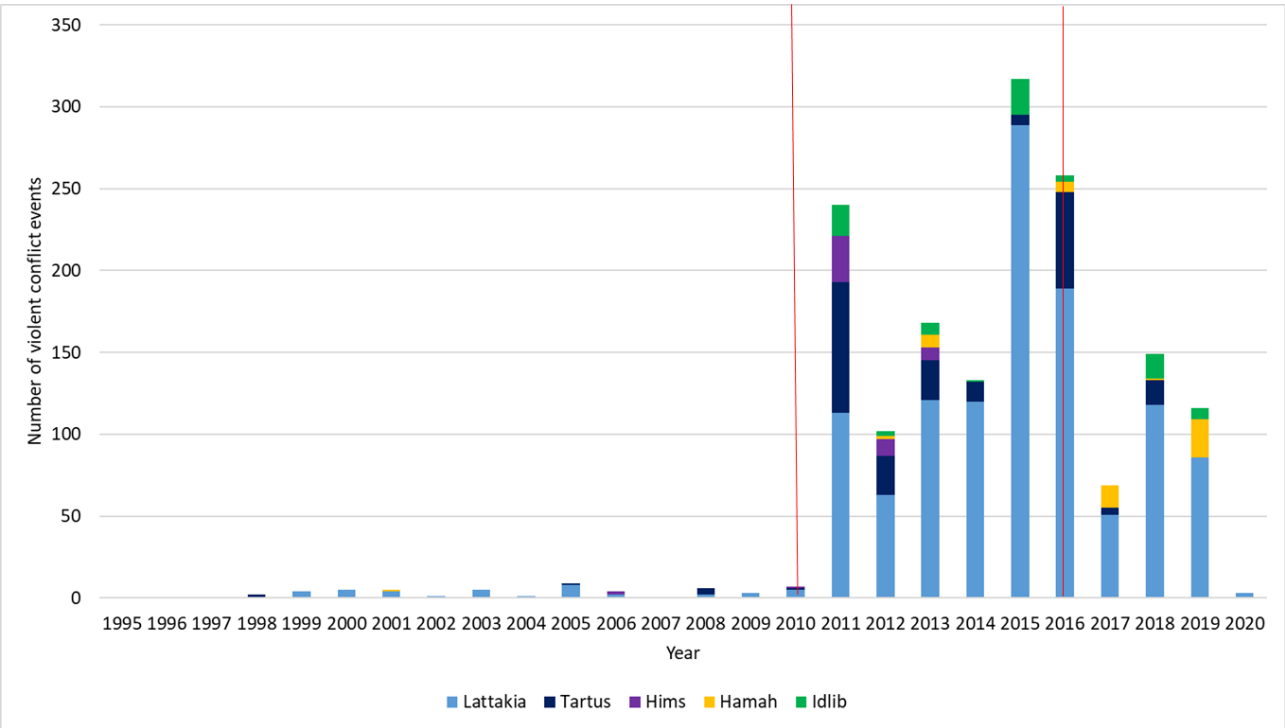

Figure 9 - Breakpoints (red) and interannual variability of the number of violent conflict events per governorate in Syria for the period 1995 - April 2020.

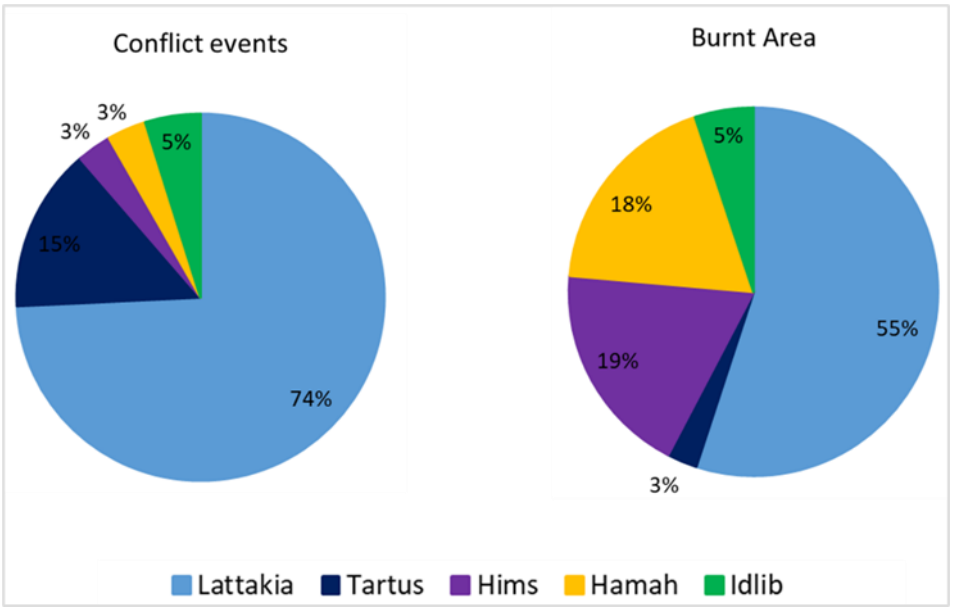

Figure 10 - Conflict events (%) (left) and BA (%) (right) per governorate in Syria for the period 1984 - 2020.

4. Funding

The authors would like to acknowledge the National Council for Scientific Research of Lebanon (CNRS-L) and the University of Montpellier (UM) for granting a doctoral fellowship to Georgia Majdalani.

5. Bibliography

Aini, A., Curt, T., & Bekdouche, F. (2019). Modelling fire hazard in the southern Mediterranean fire rim (Bejaia region, northern Algeria). *Environmental monitoring and assessment*, *191*(12), 1-19.

Ash, K., & Obradovich, N. (2020). Climatic stress, internal migration, and Syrian civil war onset. *Journal of Conflict Resolution*, *64*(1), 3-31.

Belhadj-Khedher, C., El-Melki, T., & Mouillot, F. (2020). Saharan hot and dry Sirocco winds drive extreme fire events in Mediterranean Tunisia (North Africa). *Atmosphere*, 11(6), 590.

Belhadj-Khedher, C., Koutsias, N., Karamitsou, A., EI-Melki, T., Ouelhazi, B., Hamdi, A., ... & Mouillot, F. (2018). A revised historical fire regime analysis in Tunisia (1985–2010) from a critical analysis of the national fire database and remote sensing. *Forests*, *9*(2), 59.

Boschee, E. Lautenschlager, J., O'Brien, S., Shellman, S., Starz, J., Ward, M. (2015). ICEWS Coded Event Data.

Boschetti, L., Roy, D. P., Justice, C. O., & Humber, M. L. (2015). MODIS–Landsat fusion for large area 30 m burned area mapping. *Remote Sensing of Environment*, *161*, 27-42.

Chelli, S., Maponi, P., Campetella, G., Monteverde, P., Foglia, M., Paris, E., ... & Panagopoulos, T. (2015). Adaptation of the Canadian fire weather index to Mediterranean forests. *Natural Hazards*, 75(2), 1795-1810.

Chergui, B., Fahd, S., Santos, X., & Pausas, J. G. (2018). Socioeconomic factors drive fire-regime variability in the Mediterranean Basin. *Ecosystems*, *21*(4), 619-628.

Chuvieco, E., & Congalton, R. G. (1988). Mapping and inventory of forest fires from digital processing of TM data. *Geocarto International*, *3*(4), 41-53.

Dimitrakopoulos, A. P., & Mitsopoulos, I. D. (2006). Global forest resources assessment 2005-report on fires in the Mediterranean region. *Fire Management Working Papers (FAO)*.

Dimitrakopoulos, A. P., Bemmerzouk, A. M., & Mitsopoulos, I. D. (2011). Evaluation of the Canadian fire weather index system in an eastern Mediterranean environment. *Meteorological Applications*, 18(1), 83-93.

Eastwood, J. A., Plummer, S. E., Wyatt, B. K., & Stocks, B. J. (1998). The potential of SPOT-Vegetation data for fire scar detection in boreal forests. *International Journal of Remote Sensing*, *19*(18), 3681-3687.

Faour, G. (2004). Forest fire fighting in Lebanon using remote sensing and GIS.

Faour, G., Kheir, R. B., & Verdeil, E. (2006). Caractérisation sous système d'information géographique des incendies de forêts: l'exemple du Liban. *Forêt méditerranéenne*, 27(4), 339-352.

Filipponi, F. (2018). BAIS2: Burned area index for Sentinel-2. *Multidisciplinary digital publishing institute proceedings*, *2*(7), 364.

Gill, A. M., Stephens, S. L., & Cary, G. J. (2013). The worldwide "wildfire" problem. *Ecological applications*, *23*(2), 438-454.

Im, U., Onay, T., Yeniguin, O., Anteplioglu, U., Incecik, S., Toppu, S., ... & Papadopoulos, A. (2006, July). An overview of forest fires and meteorology in Turkey and Greece. In 2006 *First International Symposium on Environment Identities and Mediterranean Area* (pp. 62-67). IEEE.

Justice, C. O., Giglio, L., Korontzi, S., Owens, J., Morisette, J. T., Roy, D., ... & Kaufman, Y. (2002). The MODIS fire products. *Remote sensing of Environment*, *83*(1-2), 244-262.

Köppen, W. (1884). Die Wärmezonen der Erde, nach der Dauer der heissen, gemässigten und kalten Zeit und nach der Wirkung der Wärme auf die organische Welt betrachtet. *Meteorologische Zeitschrift*, *1*(21), 5-226.

Koutsias, N., & Karteris, M. (2000). Burned area mapping using logistic regression modeling of a single post-fire Landsat-5 Thematic Mapper image. *International Journal of Remote Sensing*, 21(4), 673-687.

Koutsias, N., & Pleniou, M. (2021). A rule-based semi-automatic method to map burned areas in Mediterranean using Landsat images–revisited and improved. *International Journal of Digital Earth*, 14(11), 1602-1623.

Le Houérou, H. N. (1973). *Fire and vegetation in the Mediterranean basin* (pp. 237-277). FAO.

Liew, S. C., Lim, O. K., Kwoh, L. K., & Lim, H. (1998, July). A study of the 1997 forest fires in South East Asia using SPOT quicklook mosaics. In *IGARSS'98. Sensing and Managing the Environment. 1998 IEEE International Geoscience and Remote Sensing. Symposium Proceedings.(Cat. No. 98CH36174)* (Vol. 2, pp. 879-881). IEEE.

Linke, A. M., & Ruether, B. (2021). Weather, wheat, and war: Security implications of climate variability for conflict in Syria. *Journal of Peace Research*, *58*(1), 114-131.

Loveland, T. R., & Dwyer, J. L. (2012). Landsat: Building a strong future. *Remote Sensing of Environment*, *122*, 22-29.

Mahfoud, I. (2020). The Impact of Syrian Crisis on the Forestry Areas in North Latakia Governorate.

Malingreau, J. P. (1990). The contribution of remote sensing to the global monitoring of fires in tropical and subtropical ecosystems. In *Fire in the Tropical Biota* (pp. 337-370). Springer, Berlin, Heidelberg.

Mohamed, M. A., Anders, J., & Schneider, C. (2020). Monitoring of changes in land use/land cover in Syria from 2010 to 2018 using multitemporal landsat imagery and GIS. *Land*, *9*(7), 226.

Moriondo, M.; Good, P.; Durao, R.; Bindi, M.; Giannakopoulos, C.; Corte-Real, J. Potential impact of climate change on fire risk in the Mediterranean area. *Clim. Res*. 2006, 31, 85–95.

Paula, S., Arianoutsou, M., Kazanis, D., Tavsanoglu, Ç., Lloret, F., Buhk, C., ... & Pausas, J. G. (2009). Fire-related traits for plant species of the Mediterranean Basin: Ecological Archives E090-094. *Ecology*, *90*(5), 1420-1420.

Pausas, J. G. (2004). Changes in fire and climate in the eastern Iberian Peninsula (Mediterranean basin). *Climatic change*, *63*(3), 337-350.

Pausas, J. G., & Keeley, J. E. (2017). Epicormic resprouting in fire-prone ecosystems. *Trends in Plant Science*, *22*(12), 1008-1015.

Pereira, J. M. (1999). A comparative evaluation of NOAA/AVHRR vegetation indexes for burned surface detection and mapping. *IEEE transactions on geoscience and remote sensing*, *37*(1), 217-226.

Roteta, E., Bastarrika, A., Franquesa, M., & Chuvieco, E. (2021). Landsat and Sentinel-2 based burned area mapping tools in google earth engine. *Remote Sensing*, *13*(4), 816.

Roteta, E., Bastarrika, A., Padilla, M., Storm, T., & Chuvieco, E. J. R. S. O. E. (2019). Development of a Sentinel-2 burned area algorithm: Generation of a small fire database for sub-Saharan Africa. *Remote sensing of environment*, 222, 1-17.

Ruffault, J., Curt, T., Moron, V., Trigo, R. M., Mouillot, F., Koutsias, N., ... & Belhadj-Khedher, C. (2020). Increased likelihood of heat-induced large wildfires in the Mediterranean Basin. *Scientific reports*, 10(1), 1-9.

San-Miguel-Ayanz, J., Schulte, E., Schmuck, G., Camia, A., Strobl, P., Liberta, G., ... & Amatulli, G. (2012). *Comprehensive monitoring of wildfires in Europe: the European forest fire information system (EFFIS)*. IntechOpen.

Schon, J., Mezuman, K., Heslin, A., Field, R. D., & Puma, M. J. (2021). How fire patterns reveal uneven stabilization at the end of conflict: examining Syria's unusual fire year in 2019. *Environmental Research Letters*, *16*(4), 044046.

Syphard, A. D., Keeley, J. E., Pfaff, A. H., & Ferschweiler, K. (2017). Human presence diminishes the importance of climate in driving fire activity across the United States. *Proceedings of the National Academy of Sciences*, *114*(52), 13750-13755.

Turco, M., Bedia, J., Di Liberto, F., Fiorucci, P., von Hardenberg, J., Koutsias, N., ... & Provenzale, A. (2016). Decreasing fires in mediterranean Europe. *PLoS one*, *11*(3), e0150663.

Turco, M., von Hardenberg, J., AghaKouchak, A., Llasat, M. C., Provenzale, A., & Trigo, R. M. (2017). On the key role of droughts in the dynamics of summer fires in Mediterranean Europe. *Scientific reports*, *7*(1), 1-10.

Wightman, J. M. (1973, January). Detection, mapping and estimation of rate of spread of grass fires from southern african ERTS-1 imagery. In *NASA. Goddard Space Flight Center Symp. on Significant Results obtained from the ERTS-1, Vol. 1, Sect. A and B (SEE N73-28207 19-13)* (No. PAPER-E6).

Woodcock, C. E., Allen, R., Anderson, M., Belward, A., Bindschadler, R., Cohen, W., ... & WULDER, M. A. W. (2008). Free access to Landsat imagery. *SCIENCE VOL 320: 1011*.

Xanthopoulos, G., & Nikolov, N. (2019). Wildfires and fire management in the eastern mediterranean, southeastern Europe, and middle east regions.

Xiao-rui, T., Mcrae, D. J., Li-fu, S., Ming-yu, W., & Hong, L. (2005). Satellite remote-sensing technologies used in forest fire management. *Journal of Forestry Research*, *16*(1), 73-78.

Zubkova, M., Giglio, L., Humber, M. L., Hall, J. V., & Ellicott, E. (2021). Conflict and Climate: Drivers of Fire Activity in Syria in the Twenty-First Century. *Earth Interactions*, *25*(1), 119-135.

Canal Influence on Peat Properties at Different Fire Frequency Areas

Dayang Nur Sakinah Musa [1,2]; Mohd Zahirasri Mohd Tohir [1*]; Luqman Chuah Abdullah [1]; Mohamad Syazaruddin Md Said [1]; Muhammad Firdaus Sulaiman [3]; Xinyan Huang [4]

[1] Department of Environment and Chemical Engineering, Faculty of Engineering, Universiti Putra Malaysia, Malaysia, {zahirasri, chuah, syazaruddin}@upm.edu.my
[2] International Tropical Forestry Programme, Faculty of Tropical Forestry, Universiti Malaysia Sabah, Malaysia, {dns.m@ums.edu.my}
[3]Department of Land Management, Faculty of Agriculture, Universiti Putra Malaysia, Malaysia, {muhdfirdaus@upm.edu.my}
[4] Research Centre for Fire Safety Engineering, Department of Building Environment and Energy Engineering, The Hong Kong Polytechnic University, Hong Kong, {xy.huang@polyu.edu.hk}

**Corresponding author*

Keywords

Peat fire, Peat properties, Fire break canal, Forest reserves

Abstract

Peat in the tropical country was developed from accumulated dead plant materials. Due to frequent fire occurrences, a fire break canal technique is implemented as part of prevention measures to protect the forest reserve from fire spread. Although fire cases in peat swamp forest reserves in Malaysia are minimum, the occurrences can cause changes in the peat properties if they happen frequently. Therefore, this study focuses on determining the peat properties near the fire break canal in low and high fire frequency areas. Peat samples were collected from 0 cm (surface) to 150 cm at 50 cm intervals at 75 m to 300 m from the canal. The findings show that the peat properties were not affected by the presence of fire break canal for porosity (%), moisture content (%), bulk density (g cm3), ash content (%), organic carbon content (%), and organic matter content (%) for both study areas ($p<0.05$). However, peat's lignin and cellulose content from both study areas increased as the distance from the canal increased ($p>0.05$). Other than contributing to vegetation changes in both areas, the peat properties are also different. The High Fire Frequency also shows statistically different properties compared to the Low Fire Frequency area. In summary, fire break canal can reduce the fire spread to forest reserve area and improve the peat properties to protect the land from further degradation.

1. Introduction

Tropical country peat swamps are prone to have poor drainage and water-logging conditions where plant residues usually decay faster (Taufik *et al.* 2019). With the anthropogenic influence nearby the peat swamp area, there is a possibility of fire to spread into the forest reserve and thus may degrade the area. According to the statistics provided by the Annual Report of the Sabah Forestry Department (SFD 2020), it was reported that open burning and arson contributed to the cases of previous fire incidents spread to the forest reserve (FR). In the reports, forest reserves burnt annually for 706 ha (2015), 20,000 ha (2016), 60 ha (2017), 279 ha (2018), 1313 ha (2019), and 556 ha (2020). Additionally, the issue of owners clearing their land by setting it on fire has been the primary threat to the forest (SFD 2019; SFD 2020).

Forest fire in the peat swamp forest is associated with a smouldering fire. Smouldering fire damaged the ecosystem, which caused a slow recovery of the forest (Davies *et al.* 2013). This type of fire is very persistent and may last for a long time (Rein 2013; Rein and Huang 2021). For example, fire incidents that happened in 2016 lasted for six months during the El-Nino phenomenon and lasted for two months without El-Nino influence (SFD 2017; SFD 2020). The government enhanced their fire prevention measures, including constructing a fire break canal in the repeatedly burnt area in Sabah, Malaysia. The fire break canal is meant to reduce the fire spread to the FR and was efficient in Klias FR and then implemented in Binsuluk FR. At this point, it is crucial to observe the properties of peat near the fire break canal at both Klias and Binsuluk FR. Thus, this work studied the fire influence on the peat conditions at Klias and Binsuluk FR near the fire break canal and conveyed the

analysis of the peat properties further from the fire break canal at a different depth to explore if peat fire will influence up to 1.5 m below ground.

2. Methodology

2.1. Sampling method

This research involved two study areas represented the low fire frequency area (LFF), where vegetation is still intact (Klias FR), and the high fire frequency area (HFF), where less vegetation cover presents (Binsuluk FR). The study plots were established at 75 m, 150 m, 225 m, and 300 m from the canal. A total of 192 samples were collected at different levels, i.e. 0 cm, 50 cm, 100 cm, and 150 cm (Figure 1), using a bulk density ring for physical analysis purposes and a peat auger for chemical analysis purposes.

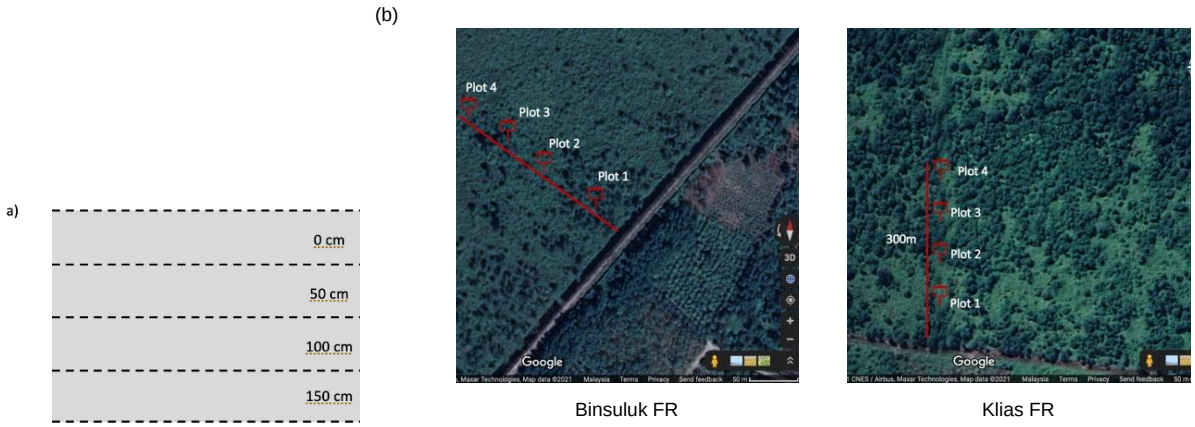

Figure 1- (a) Samples of peat collected at a different level, (b) Plot constructed at both study sites LFF and HFF) for peat samples collections.

2.2. Statistical analysis

The physical and chemical analyses involved are bulk density, moisture, porosity, organic matter, organic carbon, ash, lignin, and cellulose contents. Statistical comparisons between the plots and depths were made by using a two-way analysis of variance (ANOVA) at a 95% confidence level ($p<0.05$). A Pearson-correlation analysis is also done to determine the relationship between the variables.

3. Results and discussion

3.1. Physical properties of HFF and LFF areas

The physical properties studied in this work are bulk density, moisture content, and porosity. In this section, we want to understand how these physical properties were influenced by fire frequency. Also, the relationship between the properties will be presented in Figure 2. Based on analysis of variance analysis (Tukey's test) in the HFF area, peat at 150 m and 300 m further from the canal shows a significant difference in each variable ($p<0.05$) between the depth. In the HFF area, the porosity *has a reasonably strong relationship with bulk density (r=0.988) and a moderate relationship with moisture content (r=0.584). The peat surface has a moisture content of up to 1200% and* low vegetation cover with only tall grass and a few big trees spotted in the study sites. The rain will directly be pouring to the surface of the water. This situation will influence the significantly high moisture content on the surface (0 cm). *However, a fire frequently spreads to the area. A new fire break canal construction does not dry the area to the furthest 300 m from the canal. Because of the frequent fire, the porosity level and moisture content have a moderate relationship (0.584) but still indicate that the three fundamental properties of peat are dependent on each other. However, the higher moisture content on the surface indicates that weak peat can retain the water (Perdana et al. 2018) known as a hydrophobic condition because of a previous fire event.*

The LFF area experienced peat fire, but it was not frequent as the fire break canal was implemented in this area to prevent the fire from spreading. The peat properties in this area were not similar to the HFF area, as the fire

did not change the peat properties too much. The moisture content and porosity have a strong correlation-coefficient of 0.838, or 70% of the moisture content is dependent on the porosity of the peat. Similarly, the peat's bulk density and compaction are 78% dependent on the peat porosity for Klias Forest Reserve. However, the surface moisture content of the peat ranged from 180-400%, which was statistically lower than HFF surface moisture. The highest mean moisture content was 900% at 100-150 cm below the surface. 150 m further from the canal shows a significant difference in variables between the LFF area depth and 225 m further from the canal (p=0.002).

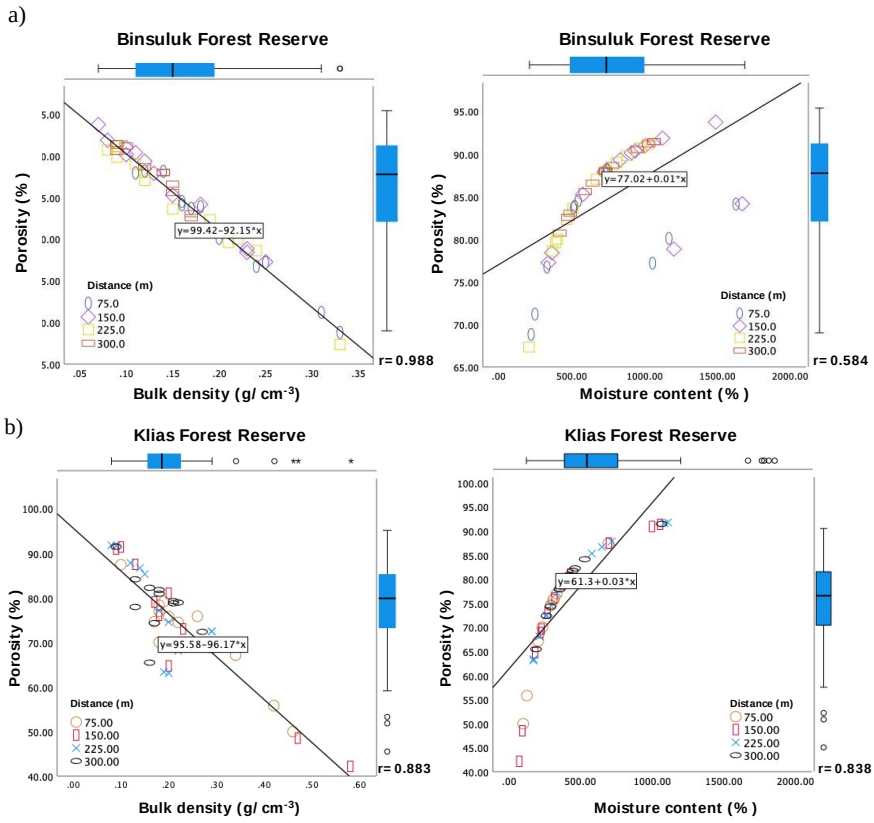

Figure 2- Influence of distance on peat physical properties of porosity (%), bulk density (g/cm3), and moisture content (%) of the a) Binsuluk Forest Reserve (HFF) and b) Klias Forest Reserve (LFF).

3.2. Chemical properties of LFF and HFF areas

The chemical properties studied were organic matter content (OMC), organic carbon content (C_{org}), Ash content, lignin, and cellulose. The analysis of correlation regression (Figure 3) between the chemical content indicates that all variables have a strong correlation for both forest reserves (r=0.998, r=1.000). The findings suggest that all chemical variables are dependent on each other. Ash content studies to identify the area burnt before the show that it was present from 0 cm to 150 cm and up to 300 m further from the canal. Based on the analysis of variance, the significant difference between the depth for the HFF area was shown at 150 m, 225 m, and 300 m further from the fire break canal.

The correlation regression analyses were used to relate each chemical properties studied. The peat's total organic matter content in the HFF area varied from 71.43% to 98.04% at a 75 m distance from the canal, which indicates no significant difference (p>0.05) between the depths. In the Pearson-correlation analysis, the HFF area shows a strong correlation (r=0.998, 0.998, 1.000) for OMC, C_{org}, and Ash content relationship. The findings were similar to LFF, where the variables have a strong (r=1.000) relationship and were expected to have no difference within the depth despite the distance from the canal (p>0.05). The LFF area findings do not influence much of the chemical peat properties on these content, organic carbon content and organic matter content.

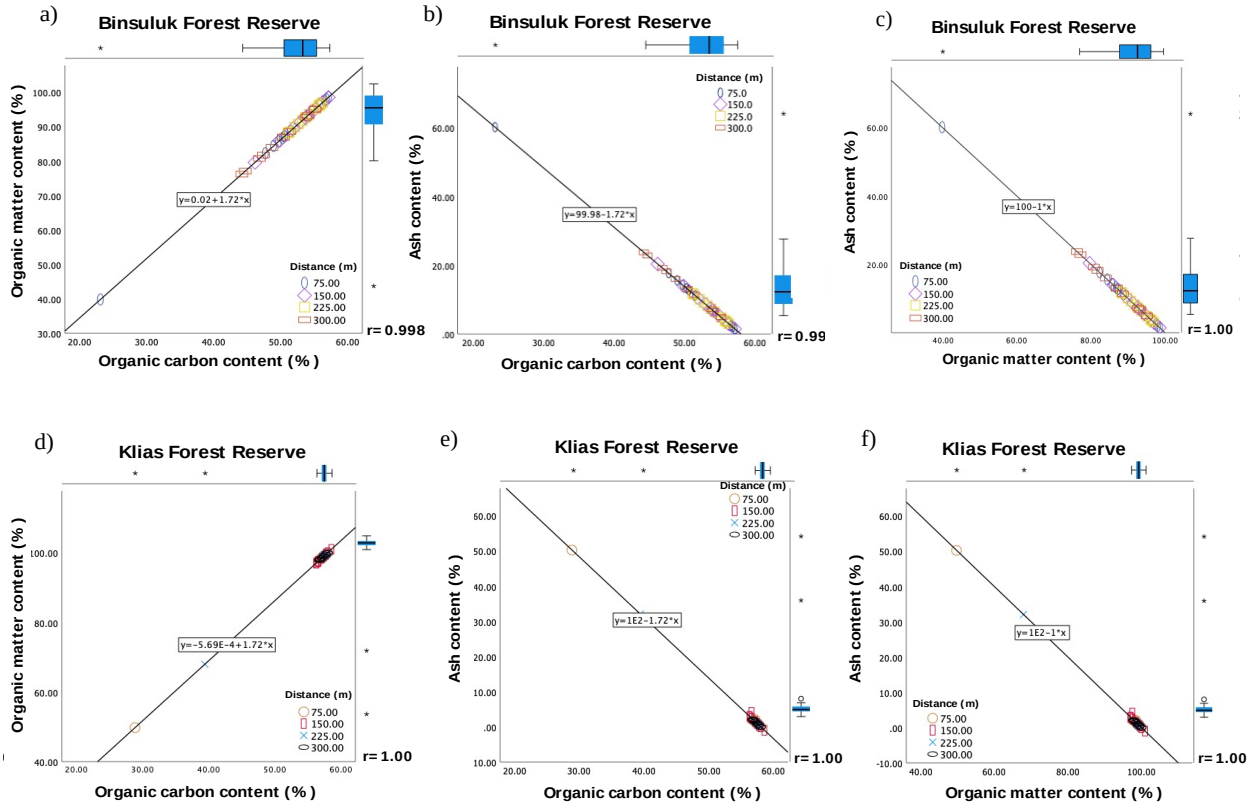

Figure 3- The correlation-regression of the chemical properties of peat-based on the distance from the canal in both Binsuluk Forest Reserve (HFF) - a) OMC (%)-Corg (%); b) Ash content (%)-C_{org} (%); c) Ash content (%)-OMC (%) and Klias Forest Reserve (LFF) - d) OMC (%)-C_{org} (%); e) Ash content (%)-C_{org} content (%); f)Ash content (%)-OMC (%).

The lignin and cellulose content were studied to determine the influence on the moisture content of the LFF and HFF area (Table 1). Based on the findings, the lignin and cellulose content have a significant difference between the plots, where the further the plot from the canal, the higher the cellulose and lignin content ($p<0.05$). The correlation regression analyses were used to relate the lignin and cellulose to moisture content. The findings show that cellulose has a fair relationship with moisture content in the HFF area. Burning the dead material might contribute to these changes as the LFF shows no relationship between the moisture content with lignin and cellulose content.

Table 1 - Pearson-correlation for lignin and cellulose with moisture content

Variable	Moisture content (%)	Lignin (g/kg)	Cellulose (g/kg)
Moisture content (%)	1.000	**-0.280** *0.451*	**-0.062** **0.692*
Lignin (g/kg)		1.000	***0.783** **0.828*
Cellulose (g/kg)			1.000

Note:
*: is used where the relationship between the variable was detected (<0.001, 2-tailed)
Font: Italic is HFF area, Bold is LFF

4. Conclusion

In conclusion, this research focuses on the peat properties nearby the firebreak canal of two other forest reserves and the influence of the canal on the properties. The samples taken were peat from Binsuluk FR, representing the HFF peat, and peat samples from Klias FR, representing the LFF frequency areas. The smouldering fire releases a substantial amount of carbon into the environment to aid the carbon emission in the area (Davies *et al.* 2013). The moisture content was found to be higher in the HFF area and there were ash in each plot indicates

the carbon has been lost during the burning. The repeatedly burnt peat consisted of high lignin and cellulose content, almost similar for 75 m from the canal to 300 m further from the canal. The LFF otherwise have significantly different results between the plots. The further the peat samples from the canal, the higher the cellulose and lignin content. Fire cases is found to influence the fibre content. The changes in peat properties will make it more vulnerable to fire occurrences when the fire from outside spreads to this area.

The importance of this research represents the protected peat swamp forest in Malaysia. This work provides information on soil properties near fire break canals in different hydromorphic settings to identify type-specific threats and derive implications for conservation, cultivation and restoration (e.g. rewetting) (Gabriel *et al.* 2018). When peat is repeatedly burnt, the peat properties will change along with its structure. Therefore, this work could help understand the changes made by a fire outbreak and how the peat will influence the re-occurrences of fire in the future. As a result, this will increase the vulnerability of the land to future fire incidents. The restoration effort and minimum fire incidents might improve the peat properties. Knowing the physical and chemical properties near the fire break canal will provide soil scientists and land managers with important information on these properties of the peat soil.

5. References

Davies GM, Gray A, Rein G, Legg CJ (2013) Peat consumption and carbon loss due to smouldering wildfire in a temperate peatland. Forest Ecology and Management. doi:10.1016/j.foreco.2013.07.051.

Gabriel M, Toader C, Faul F, Roßkopf N, Grundling P, Huyssteen C, Grundling AT, Zeitz J (2018) Physical and hydrological properties of peat as proxies for degradation of south african peatlands: Implications for conservation and restoration. Mires and Peat 21, 1–21. doi:10.19189/MaP.2018.OMB.336.

Perdana LR, Ratnasari NG, Ramadhan ML, Palamba P, Nasruddin, Nugroho YS (2018) Hydrophilic and hydrophobic characteristics of dry peat. IOP Conference Series: Earth and Environmental Science 105, 1–6. doi:10.1088/1755-1315/105/1/012083.

Rein G (2013) Smouldering Fires and Natural Fuels. "Fire Phenomena and the Earth System: An Interdisciplinary Guide to Fire Science." doi:10.1002/9781118529539.ch2.

Rein G, Huang X (2021) Smouldering wildfires in peatlands, forests and the arctic: Challenges and perspectives. Current Opinion in Environmental Science and Health 24, 100296. doi:10.1016/j.coesh.2021.100296.

SFD SFD (2017) "Annual Report 2017." http://www.forest.sabah.gov.my/docs/ar/ar2017.pdf.

SFD SFD (2019) "Annual Report 2019." http://www.forest.sabah.gov.my/docs/ar/SFD.AR2019.pdf.

SFD SFD (2020) "Annual Report 2020." http://www.forest.sabah.gov.my/docs/ar/SFD.AR2018.pdf.

Taufik M, Veldhuizen AA, Wösten JHM, van Lanen HAJ (2019) Exploration of the importance of physical properties of Indonesian peatlands to assess critical groundwater table depths, associated drought and fire hazard. Geoderma 347, 160–169. doi:10.1016/j.geoderma.2019.04.001.

Catastrophic Fire Behaviour in the June 2017 Pedrógão Grande Fire

Domingos X. Viegas*[1]; Miguel Almeida[1]; Paulo Pinto[2]; Luís M. Ribeiro[1]; Carlos Ribeiro[1]; Álvaro Pimpão[2]

[1]Forest Fire Research Centre. Univ Coimbra, ADAI, Department of Mechanical Engineering, Rua Luís Reis Santos, Pólo II, 3030-788 Coimbra, Portugal, {xavier.viegas@dem.uc.pt}; {miguelalmeida, luis.mario, carlos.ribeiro}@adai.pt
[2] Portuguese Institute of the Sea and Atmosphere, Lisbon, Portugal, {paulo.pinto, alvaro.silva}@ipma.pt

**Corresponding author*

Keywords

Fire behaviour, junction fires, thunderstorms, fire and atmosphere interaction

Abstract

Two fires that started near Pedrógão Grande in June 2017 were affected by the presence of a thunderstorm in the region and spread out of control as two initially separate fires. Sometime later these fires merged creating a very intense and fast spreading fire that threatened the lives of hundreds of persons. In a period of around two hours 66 persons were killed by the fire most of them trying to run away in their cars. The physical processes of fires start, interaction with the thunderstorm and merging were studied in detail as well as the circumstances in which the accidents occurred.

1. Introduction

The fires that started in the early afternoon of the 17th June of 2017 near Pedrógão Grande (PG) will be remembered as the worse in record in Portugal as they destroyed around 45000hectares but above all because they caused the death on 66 persons. Several authors analyzed this fire and produced reports studying various aspects of this very complex event, namely Viegas *et al.* (2017), Guerreiro *et al.* (2017), San-Miguel-Ayanz, *et al.* (2020).

The interaction between the thunderstorm, organized as a mesoscale convective system (MCS), and the fire was extensively analyzed in Pinto *et al.* (2022) using weather stations, satellite and radar observation data. The present work complements the previous reference, as the very unusual conditions that resulted from that interaction and produced the catastrophic fire during the late evening of that day are described in detail.

2. Fire ignitions and Spread

The fire of PG occurred in the district of Leiria, in Central Portugal (Figure 1), in a period of drought with air temperatures above 40°C and very low relative humidity. The wind flow in the region was from NW and not very strong. A large MCS developed over central-western Iberian Peninsula and moved towards W-NW causing several fires due to lightning, but at 14.30h (all indicated times are local time which is UTC plus one hour), when the fire of PG started, the more active part of this system was still nearly 100 km far from it and electrical strikes were not registered in the area of the fire until 18.00h (IPMA, 2017).

The fire of PG was actually caused by two ignitions that occurred near Escalos Fundeiros (EF) at 14.30h and near Regadas (RE) at 15.40h (Figure 2). Both ignitions were caused by an electrical line that was touched by tree foliage agitated by the wind that passes by both places which are 3.2km apart.

As there were other fire ignitions in the operational area the firefighting resources were dispersed and were not capable of coping with the very difficult spread of the EF fire which started to spot and threaten houses in the village of EF. When the fire of RE was detected there were not forces to deploy there and the fire was left spreading practically on its own. Between 18.00h and 18.15h a down flow from the MSC, which was not yet over the region of the fire, forced the fire column to tilt towards SW, spreading flames in a wide area and making the control of the fire virtually impossible from that time on (Figure 3). The RE fire which was smaller at that

time started to spread also completely out of control, towards NW forming the right side of a large pincer that was now advancing like a curved fire front more than 20km long, threatening a roughly circular area of 10km diameter (cf. Figure 1).

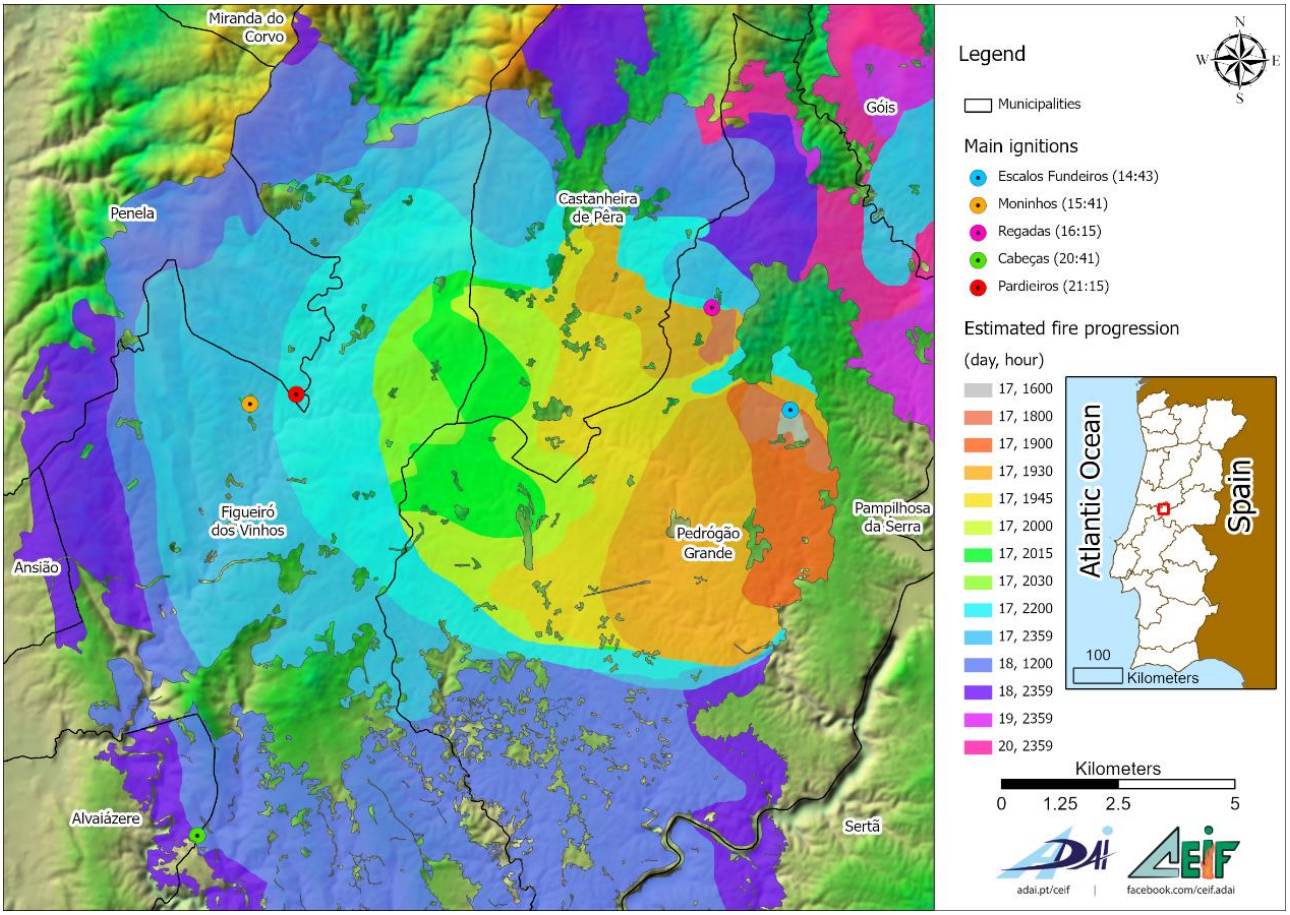

Figure 1 – Map of Portugal and of the area of the fire of Pedrógão Grande with the indication of fire ignition points and the fire spread.

a

b

Figure 2 – Aerial view of the location of the ignition points of (a) Escalos and (b) Regadas.

Figure 3 – Views of the column of the fire of Escalos Fundeiros at 18.00h and at 18.15h, showing the interaction with the down flow produced by the mesoscale convective flow.

3. Merging of the two fires

There is evidence that after 19.30h both fires had their inner flanks very close to each other making a small angle between them, therefore with the ideal conditions to merge as a junction fire that was studied by Raposo, 2012 and Viegas and Raposo 2018. Between 19.30 and 20.30h the process of merging induced very strong winds in the area ahead of the fire. The ROS of the head fire was of the order of 10 km/h. The quick combustion of a very large amount of vegetation produced a convection column that reached 12000 m at 20.10h and remained at that height for several hours. Flames of the order of 50m long and 50 to 100m long separated from the vegetation were registered, creating an environment near the ground like inside a furnace. There are reports of tree stands starting to burn from their tops to the ground (Figure 4). Persons in the area of the fire were under pitch dark and reported that the air was full of fire balls. Besides this there were pieces of wood, branches and bark flying all around, sometimes igniting new fires. In at least two much localized areas wind tornadoes twisted and broke a large number of 20cm diameter trees breaking them as toothpicks. The wind velocity required to cause this effect is estimated to be of the order of 200km/h.

Similar phenomena were observed in the process of merging of the McIntyre and Bendora fires near Canberra on the 18th January 2003, with a very fast spreading fire (27km/h) and a tornado that broke trees trunks larger than 30cm diameter (cf. Doogan (2006)).

The perception of the violence of the fire caused by the noise produced by its very tall and roaring flames, that threatened to destroy everything on their path, caused many citizens to decide to flee from their houses. Some of them took this decision in spite of knowing that their houses would normally sustain the passage of a fire, which most of them did. While running away in their cars many persons, sometimes entire families, were caught

by the smoke, loss of visibility and the flames and lost their lives. Particularly dramatic was the situation of a stretch of 200m of the Road N326-1, between Figueiró dos Vinhos and Castanheira de Pera (Figure 4), in which 30 persons were killed inside or near their cars.

Figure 4 – Some images of fire phenomena during its spread in the late afternoon of the 17th June.

The lack of maintenance of the vegetation - including trees – in the vicinity of the main roads contributed to the lack of survival conditions for the citizens. We identified one particular pine tree that was very close to the road edge and fell with the very strong fire induced wind over the road crossing it from one side to another. This tree and a group of cars that shocked with each other created a trap from which the cars could not drive out. Based on the testimony of survivors and of persons who passed by that road before or during the accident we were able to identify at least 16 persons whose death can be directly attributed to this tree.

The authors performed laboratory experiments at the Combustion Tunnel of the Forest Fire Research Laboratory of the University of Coimbra to simulate the development of the two ignition fires. Starting with the estimated perimeter of the fires at 19.30h with a flow of 2 m/s the merging of the two fires could be observed to follow very approximately the reconstruction that was made on the basis of testimonies and documented events during its spread. The isochrones of the fire spread are shown in Figure 5. It was also shown that the spread of a single fire (either EF or RE) would have been completely different if the other fire was not present, therefore confirming the relevance of the process of merging of the two fires.

The main fire was controlled on the 22nd June by 23.50h after consuming a total area of 45328ha, with the effort of more than 1400 fire fighters and other agents.

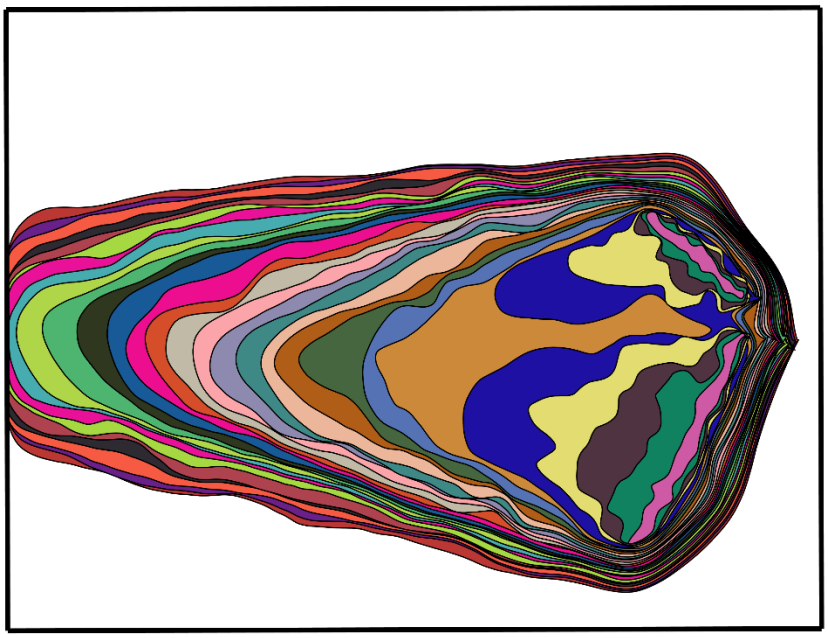

Figure 5 – Map with the isochrones of fire spread of the physical simulation of the two fires in the Combustion Tunnel of the University of Coimbra. The initial position of the fires (pink areas) corresponds at the situation at 19.30h. The time lapse between the lines is 20 seconds.

4. Conclusion

The fire that occurred on the 17th of June of 2017 near Pedrógão Grande covered and area of 45000 hectares resulted in the destruction of more than 1000 houses and structures and caused the death of 66 persons. It's very violent spread was caused by the fact that there were two separate ignitions that started 3km apart, caused by an electric line, and by the interaction of a down flow produced by a thunderstorm that was passing over the fire. The merging of the two fires produced very intense and unusual behaviour of the fire inducing many persons to escape from the fire in their cars.

5. Acknowledgements

This work was funded by the research projects supported by the Portuguese Science and Technology Foundation-FCT: "FireStorm: Meteorology and Fire Storm Behaviour" under the reference PCIF/GFC/0109/2017 and "SmokeStorm: Forecasting and Communicating Wildland Fire Smoke Effects", under the reference PCIF/MPG/0147/2019 and H2020 project "FirEUrisk: Developing a Holistic, Risk-Wise Strategy for European Wildfire Management", under the Grant Agreement Nº 101003890

6. References

Doogan M (2006) 'The Canberra Fire Storm. Inquests and Inquiry into Four Deaths and Four Fires Between 8 and 18 January 2003. Volume 1.' (ACT Coroners Court: Canberra, ACT).

Guerreiro, J., Fonseca, C., Salgueiro, A., Fernandes, P., Lopez, E., de Neufville, R., Mateus, F., Castellnou, M., Silva J. S., Moura, J., Rego, F., Mateus, P. (eds.), 2017, Análise e apuramento dos factos relativos aos incêndios que ocorreram em Pedrógão Grande, Castanheira de Pêra, Ansião, Alvaiázere, Figueiró dos Vinhos, Arganil, Góis, Penela, Pampilhosa da Serra, Oleiros e Sertã entre 17 e 24 de junho de 2017, Comissão Técnica Independente. Assembleia da República, Lisboa.

IPMA (2017). Condições Meteorológicas Associadas ao Incêndio de Pedrógão Grande de 17 de junho 2017. IPMA, Portugal. 2017 (In Portuguese).

Pinto P., Silva Á.P., Viegas D.X., Almeida M., Raposo J., Ribeiro L.M. (2022). Influence of Convectively Driven Flows in the Course of a Large Fire in Portugal: The Case of Pedrógão Grande. Atmosphere. 2022; 13(3):414. https://doi.org/10.3390/atmos13030414

Raposo J.R., Viegas D.X., Xie X., Almeida M., Figueiredo A.R., Porto L., Sharples J. (2018). Analysis of the physical processes associated with junction fires at laboratory and field scales. International Journal of Wildland Fire 27, 52-68. (Doi: 10.1071/WF16173).

San-Miguel-Ayanz, J., Oom, D., Artes, T., Viegas, D.X., Fernandes, P., Faivre, N., Freire, S., Moore, P., Rego, F., Castellnou, M., 'Forest fires in Portugal in 2017', in: Casajus Valles, A., Marin Ferrer, M., Poljanšek, K., Clark, I. (eds.), Science for Disaster Risk Management 2020: acting today, protecting tomorrow, EUR 30183 EN, Publications Office of the European Union, Luxembourg, 2020, ISBN 978-92-76-18182-8, doi:10.2760/571085, JRC114026.

Viegas D.X., Raposo J.R., Davim D., Rossa C.G. (2012). Study of the Jump Fire Produced by the Interaction of Two Oblique Fire Fronts. Part 1: Analytical Model and Validation with No-slope Laboratory Experiments. International Journal of Wildland Fire 21, 843-856. Doi:10.1071/WF10155

Viegas, D.X., Almeida, M.F., Ribeiro, L. M., Raposo, J., Viegas, M.T., Oliveira, R., Alves, D., Pinto, C., Jorge, H., Rodrigues, A., Lucas, D., Lopes, S., Silva, L.F. (2017). O complexo de incêndios de Pedrógão Grande e concelhos limítrofes, iniciado a 17 de junho de 2017, Centro de Estudos sobre Incêndios Florestais, Universidade de Coimbra, Coimbra, 238 p.

.

Characterization of Ecological Vulnerability to Wildfires based on the Fire patterns on a global scale

Fátima Arrogante-Funes*; Inmaculada Aguado; Emilio Chuvieco

Universidad de Alcalá, Facultad de Filosofía y Letras, Departamento de Geografía, Geología y Medio Ambiente, Área de Geografía, GITA, C/Colegios 2, 2881, Alcalá de Henares, Madrid, España, {fatima.arrogante, inmaculada.aguado, Emilio.chuvieco}@uah.es

**Corresponding author*

Keywords

Vulnerability, Wildfires, Ecological Vulnerability to Fire, Global, GIS

Abstract

Fire is a natural phenomenon that has played a critical role in transforming the environment and maintaining biodiversity at a global scale. However, the plants in some habitats have not developed strategies for recovery from fire or have not adapted to the changes taking place in their fire regimes. Maps showing ecological vulnerability to fires could contribute to environmental management policies in the face of global change scenarios. The main objective of this work is to characterize the ecological vulnerability to fires based on how fires occur on a global scale. For this purpose, we are going to create zonal statistics by biome and by vulnerability category, finding out the average data of the different fire variables. For this, we have taken two spatial databases previously developed by us, Ecological Vulnerability to Wildfires and Wildfires Characteristics. Ecological Vulnerability to Wildfires is a global database that categorizes spatial vulnerability by ecoregion. Wildfire Characteristics collects global spatial mean data on recurrence, seasonality, patch size, and interannual variability. The results show that in areas with High/Very High vulnerability of tropical and subtropical biomes, fires are not very intense, with a small patch size and low interannual variability, but are highly recurrent and with extensive seasonality. The most vulnerable areas of the Mediterranean biome have more intense fires, with a considerable patch size and, in addition, they present considerable interannual variability, little recurrence and limited seasonality. Temperate forest biomes present their most vulnerable areas with moderate intensity, patch size and recurrence fires, but with high interannual variability. The most vulnerable areas of the montane grasslands biome show highly recurrent fires, with extensive seasonality, with moderate patch size, intensity, and interannual variability

1. Introduction

Fire is a natural phenomenon that has played an important role in the transformation of the environment and the maintenance of biodiversity on a global scale. It can have numerous positive and negative impacts. Most of the world's terrestrial habitats where fires occur depend on them for ecological sustainability. (Kirkman et al., 2001; Midgley & Bond, 2015). Fire can affect the distribution of habitats, carbon and nutrient fluxes, and the water holding properties of soils (Bowman et al., 2009). In habitats that are adapted to and even dependent on fire exclusion policies, this can result in a decrease in biodiversity (Guyette et al., 2002). In addition, the absence of fire results in increases in fuel loads (Bond et al., 2005), which frequently augment the risk of catastrophic fires over time. Fire has also been and continues to be used by humans as a crucial tool for managing terrestrial ecosystems, producing cultural landscapes that also benefit ecological health (Caprio & Graber, 2000; Guyette et al., 2002).

On the other hand, there are some habitats, such as moist tropical forests, that have never adapted to fires. The introduction of fire by humans can lead to an irreparable loss of their structure and composition (Cochrane & Laurance, 2002). Even in fire-adapted areas such as the Mediterranean ecosystems, recent human and climate related changes in fire regimes are having negative impacts on the functioning of ecosystems (Bajocco et al., 2011; Midgley & Bond, 2015). The increasing frequency and intensity of fires can have negative impacts on forest masses and landscapes, human life, infrastructures and ecosystem services and wildlife; and can cause changes in regeneration dynamics, hydrological regimes and air quality, among other environmental consequences on a global scale (Alcasena et al., 2016; Barrio et al., 2011; Buhk et al., 2007; Díaz-Delgado et al., 2002; Flannigan et al., 2009; Hobson & Schieck, 1999; Moreira et al., 2011; Scott & Van Wyk, 1990). As

a result of this process of change, forest fires have become one of the main environmental problems today at both global and local levels.

This means that fires must be included in global and regional assessments of vulnerability to global change (Houghton et al., 2001; Lindner et al., 2010). Furthermore, fire risk assessment should be carried out spatially in order to design and implement prevention strategies that enable the conservation of the ecological value of ecosystems and landscapes. When fires happen, assessments of this kind can also be useful for implementing post fire strategies to bring about the recovery of pre-fire ecological values and cultural and socioeconomic assets (Aretano et al., 2015; Chuvieco et al., 2010). In terms of natural hazards terminology, spatially measured fire risk is a combination of 'danger' and 'vulnerability'. 'Danger' is defined as the probability of fire occurring in a given place and time, while vulnerability refers to the potential damage that fire could cause to this place (Chuvieco et al., 2007). Vulnerability must include two parts: social and ecological.

There are few attempts to estimate the ecological vulnerability to fire locally or regionally, almost none globally, and none that show how fire occurs in ecosystems that are more or less vulnerable to fires in the world (Turner et al., 2003, Duguy et al., 2012, Aretano et al., 2015, Chuvieco et al., 2010, González, Kolehmainen, & Pukkala, 2007, Duguy & Vallejo, 2008, Giovannini & Lucchesi, 1997, Chuvieco et al. 2014).

In this paper, the main objective of this work is to characterize the ecological vulnerability to fires based on how fires occur on a global scale. This study will be carried out on a global scale so as to enable us to tackle the planetary ecosystem as a whole, unrestricted by governmental or geographic borders. In this way, this research could become an essential tool for decision-making about resource management and nature conservation across the globe.

2. Material and methods

2.1. Study Area

2.1.1. Section 1.1.1

The spatial units used in this study were the terrestrial ecoregions proposed by the World Wildlife Fund (WWF), as corrected in 2017 (Olson et al., 2001). The terrestrial ecoregion concept refers to a land unit large enough to house a set of natural communities composed of different species, dynamics and similar environmental conditions. Thus, ecoregions are a good way to structure ecological and fire information on a global scale, since they are relatively homogeneous in terms of climate and vegetation (Pausas & Ribeiro, 2017). The number of ecorregions and terrestrial biomes were reduced to 554 and 9 (figure 1)in order to exclude lack of data and zones in which forest fire were impossible to occur.

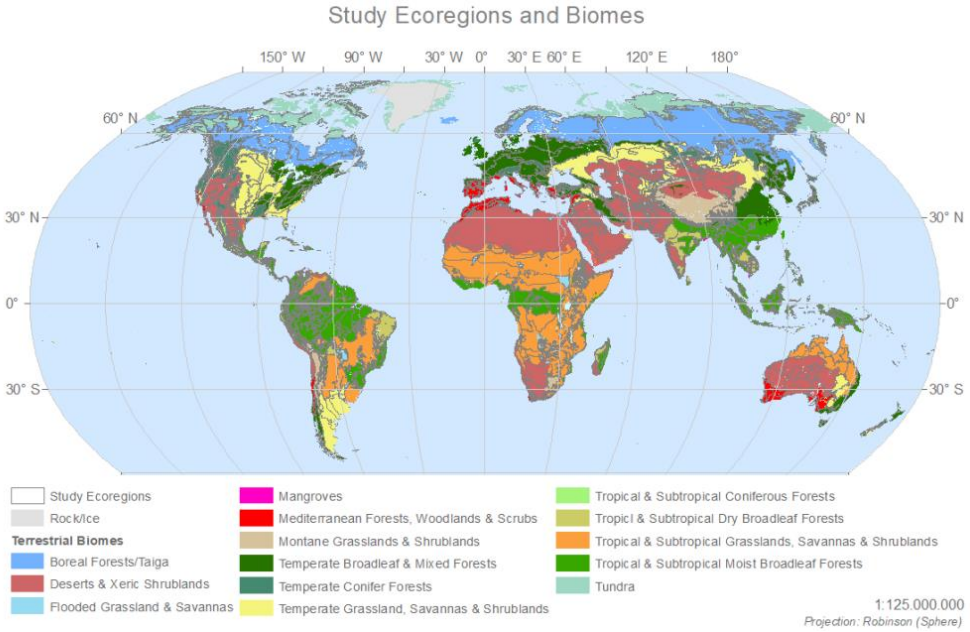

Figure 1. Terrestrial ecorregions within their biome for this study. (Source: The authors).

2.2. Ecological Vulnerability to Wildfires data

Ecological Vulnerability to Wildfire (figure 2) is a categorical spatial database at global scale in which each ecoregion contains a vulnerability category (Arrogante-Funes, F., Aguado, I., & Chuvieco, E. 2021). The categories of ecological vulnerability to fires are: Very High, High, Moderate and Low.

This database keeps in mind two ecological value indices: biological distinction and conservation status. Moreover, for the post-fire regeneration delay index, various factors were taken into account, including the type of fire regime, the increase in the frequency and intensity of forest fires and the potential soil erosion they can cause. These indices were combined by means of a qualitative cross-tabulation to create a new index evaluating Ecological Vulnerability to Wildfire.

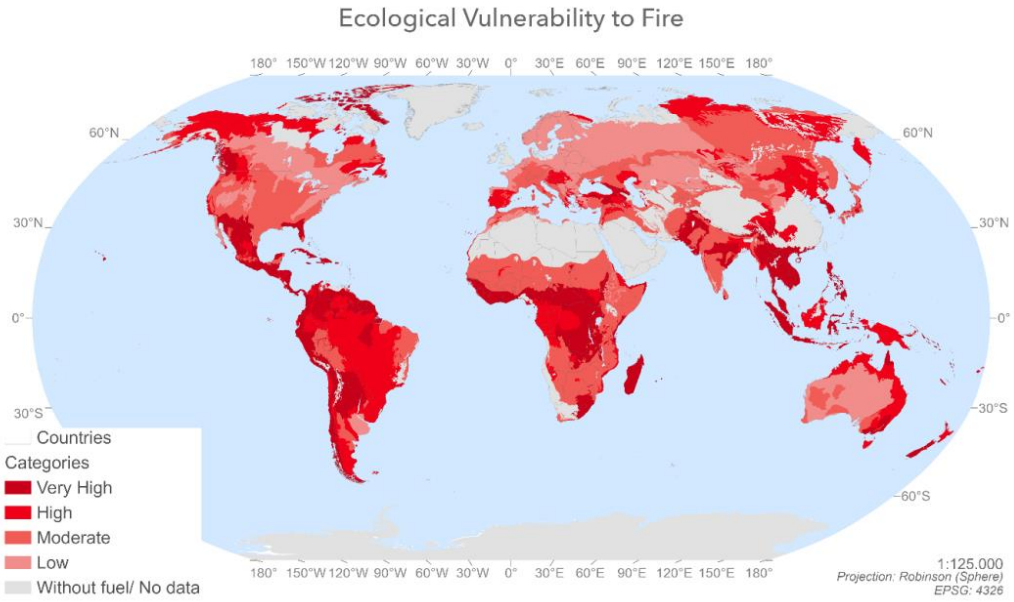

Figure 2- Spatial distribution of the Ecological Vulnerability to Fire.

2.3. Wildfire Characteristics data

Wildfire Characteristic data contain raster information at 0.25 grid for seasonality, recurrence, intensity, interannual variability and patch size, among others (García et al., 2022). This database was developed through the estimation of the mean data for each pixel from the information of remote sensing time series data of the last 20 years.

Seasonality is related to the numbers of months in which there are fire activity. Recurrence variable is the times burn each pixel in wherever part of it. Intensity is relative to the FRP which was estimated in MW through a patch method. Interannual variability measured the variance between patch size for the same zone during the years. Finally, patch size is related to the burned area estimated in km^2. All these variables contain a numeric data base on the mean data for all the time serie.

2.4. Zonal Statistics

Zonal Statistics is an analytical tool specifically for raster datasets used in a several works from different part of the knowledge (Jacox & Samet, 2007). Summarizes the values of a raster within the zones of another dataset and reports the results in a table. It can calculate the mean, median, sum, minimum, maximum, or range in each zone (Theobald, 2005).

Since we wanted to find the fire pattern for each vulnerability category by biome, we were able to use a zonal operation like this one. By using a Wildfire Characteristics raster as its value field, we were able to zone the Ecological Vulnerability to Wildfires categories by biome with the mean function. This process was computed by each fire variables previously cited.

3. Results

The Table 1 shows the results of the tool Zonal Statistics as a table with the mean data of each fire variable by ecological vulnerability to wildfires by biome. Red to green shows from lowest to highest values per column.

The results show that in areas with High/Very High vulnerability of tropical and subtropical biomes, fires have a high recurrence in addition to having an extensive seasonality. On the contrary, in this area the fires present low intensity, patch size and interannual variability.

The most vulnerable areas of the Mediterranean biome have more intense fires, with a considerable patch size and, in addition, they present considerable interannual variability, little recurrence and limited seasonality.

Temperate forest biomes present their most vulnerable areas with moderate intensity, patch size and recurrence fires, but with high interannual variability.

The most vulnerable areas of the montane grasslands biome show highly recurrent fires, with extensive seasonality, with moderate patch size, intensity, and interannual variability.

Table 1. Zonal Statistics as a Table with the mean function by each variables of fire inside the vulnerability categories belong per biome.

Biome	Vulnerability	Intensity (MW)	Patch Size (km2)	Recurence	Seasonality	Interannual Variability
Tropical & Subtropical Moist Broadleaf Forests	Very High	16.75	3981296.70	12	2.28	1.50
	High	21.05	3361362.99	12	2.46	1.44
	Moderate	20.85	4013734.70	11	2.36	1.55
	Low	12.08	4200226.87	14	2.51	1.14
Tropical & Subtropical Dry Broadleaf Forests	Very High	15.43	4522950.77	14	2.56	1.20
	High	22.34	4871753.71	14	2.81	1.35
	Moderate	21.11	4782870.58	11	2.20	1.66
	Low	8.19	2383960.00	8	1.75	1.89
Temperate Broadleaf & Mixed Forests	Very High	29.02	3723493.83	9	1.94	1.91
	High	22.31	5856315.89	10	2.15	1.86
	Moderate	24.29	3611295.52	10	2.12	1.69
	Low	19.09	2723740.31	12	2.43	1.54
Boreal Forests/Taiga	High	40.89	6166993.93	4	1.21	2.83
	Moderate	28.75	6147535.21	7	1.50	2.57
	Low	33.42	4210554.66	6	1.46	2.39
Tropical & Subtropical Grasslands, Savannas & Shrublands	Very High	20.15	8465814.33	17	2.87	0.61
	High	26.91	17008916.42	15	2.90	1.14
	Moderate	20.74	14132522.44	16	2.81	0.85
	Low	34.90	53263661.98	13	2.75	1.42
Temperate Grasslands, Savannas & Shrublands	Very High	34.72	3725854.74	11	2.30	1.56
	High	28.05	11980557.07	11	2.03	1.70
	Moderate	31.01	7567717.30	13	2.45	1.43
	Low	33.02	13497352.38	12	2.60	1.57
Montane Grasslands & Shrublands	Very High	26.73	5511734.67	13	2.82	1.36
	High	21.70	5547367.75	7	1.50	2.35
	Moderate	22.56	6219529.26	12	2.27	1.40
	Low	19.34	5042101.76	13	2.53	1.08
Mediterranean Forests, Woodlands & Scrub	Very High	41.08	5853423.54	11	2.19	1.66
	High	49.90	8364480.94	8	1.78	2.14
	Moderate	32.38	5039767.41	10	2.26	1.74
	Low	39.60	6076207.53	8	1.69	2.08
Deserts & Xeric Shrublands	Very High	21.91	6648254.38	10	2.29	1.67
	High	48.13	29316209.02	9	1.98	1.97
	Moderate	42.79	31419710.55	8	1.82	2.07
	Low	53.21	40374872.73	9	2.09	1.99

4. Discussion

Tropical & Subtropical Dry Broadleaf Forests and Moist Broadleaf Forest are biomes in which the origin of the fire may be due to the human being due to the low values of intensity, patch size and interannual variability, and due to the high values of recurrence and seasonality as in the case of Tropical & Subtropical Grasslands, Savannas & Shrublands (Crochane & Laurance, 2002). In addition, all the categories of ecological vulnerability to fires present similar values.

With Xeric Shrublands, the opposite of the previous case occurs since its origin could be natural and therefore said vegetation coexisted with fire, developing a vegetation with greater adaptation to fire (Moreira et al., 2011).

In the case of the Mediterranean forests, the fires are motivated by the periods of summer drought due to the highest values of intensity and interannual variability of the fire, while it presents lower values in the variables of recurrence and seasonality (Alcasena et al., 2016; Barrio et al., 2011; Bhuk et al., 2007)). In addition, it is more notable in the high and very high categories of the ecological vulnerability index, for which this biome could see its most outstanding ecological values affected (Diaz-Delgado et al., 2002).

In the case of biomes belonging to temperate zones, broadleaf and mixed forests are related to lower values of intensity, patch size, recurrence and seasonality, unlike what occurs in their grasslands, savannas and shrublands zones. This is generalized for all categories of ecological vulnerability to forest fires.

5. Conclusions

This is a first exploratory analysis of fire variables and ecological fire vulnerability categories.

Zonal statistics is a good tool for the spatial data of this work.

There are slight differences between the vulnerability categories within the biome for the various fire variables. The values are homogeneous within the biome.

6. Bibliography

Alcasena, F. J., Salis, M., Nauslar, N. J., Aguinaga, A. E., & Vega-García, C. (2016). Quantifying economic losses from wildfires in black pine afforestations of northern Spain. Forest Policy and Economics, 73, 153–167. https://doi.org/10.1016/j.forpol.2016.09.005

Aretano, R., Semeraro, T., Petrosillo, I., De Marco, A., Pasimeni, M. R., & Zurlini, G. (2015). Mapping ecological vulnerability to fire for effective conservation management of natural protected areas. Ecological Modelling, 295, 163–175. https://doi.org/10.1016/j.ecolmodel.2014.09.017

Arrogante-Funes, F., Aguado, I., & Chuvieco, E. (2021). Global assessment and mapping of ecological vulnerability to wildfires. Natural Hazards and Earth System Sciences Discussions, 1-29.

Bajocco, S., Salvati, L., & Ricotta, C. (2011). Land degradation versus fire: A spiral process? Progress in Physical Geography, 35(1), 3–18. https://doi.org/10.1177/0309133310380768

Barrio, M., Loureiro, M., & Chas, M. L. (2011). Aproximación a las pérdidas económicas ocasionadas a corto plazo por los incendios forestales en Galicia en 2006. Economía Agraria y Recursos Naturales, 7(14), 45. https://doi.org/10.7201/earn.2007.14.03

Buhk, C., Meyn, A., & Jentsch, A. (2007). The challenge of plant regeneration after fire in the Mediterranean Basin: Scientific gaps in our knowledge on plant strategies and evolution of traits. Plant Ecology, 192(1), 1–19. https://doi.org/10.1007/s11258-006-9224-2

Bond, W. J., Woodward, F. I., & Midgley, G. F. (2005). The global distribution of ecosystems in a world without fire. New Phytologist, 165(2), 525–538. https://doi.org/10.1111/j.1469-8137.2004.01252.x

Bowman, D. M. J. S., Balch, J. K., Artaxo, P., Bond, W. J., Carlson, J. M., Cochrane, M. A., D'Antonio, C. M., DeFries, R. S., Doyle, J. C., Harrison, S. P., Johnston, F. H., Keeley, J. E., Krawchuk, M. A., Kull, C. A., Marston, https://doi.org/10.5194/nhess-2021-285 Preprint. Discussion started: 13 October 2021 c Author(s) 2021. CC BY 4.0 License. 22 J. B., Moritz, M. A., Prentice, I. C., Roos, C. I., Scott, A. C., … Pyne, S. J. (2009). Fire in the earth system. Science, 324(5926), 481–484. https://doi.org/10.1126/science.1163886

Caprio, A. C., & Graber, D. M. (2000). Returning fire to the mountains: can we successfully restore the ecological role of pre-Euroamerican fire regimes to the Sierra Nevada (D. Cole, S. McCool, & J. O'Loughlin (eds.)). In Wilderness science in a time of change conference.

Cochrane, M. A., & Laurance, W. F. (2002). Fire as a large-scale edge effect in Amazonian forests. Journal of Tropical Ecology, 18(3), 311–325. https://doi.org/10.1017/S0266467402002237

Chuvieco, E., Aguado, I., Yebra, M., Nieto, H., Salas, J., Martín, M. P., Vilar, L., Martínez, J., Martín, S., Ibarra, P., de la Riva, J., Baeza, J., Rodríguez, F., Molina, J. R., Herrera, M. A., & Zamora, R. (2010). Development of a framework for fire risk assessment using remote sensing and geographic information system technologies. Ecological Modelling, 221(1), 46–58. https://doi.org/10.1016/j.ecolmodel.2008.11.017

Chuvieco, E., Martínez, S., Román, M. V., Hantson, S., & Pettinari, M. L. (2014). Integration of ecological and socio-economic factors to assess global vulnerability to wildfire. Global Ecology and Biogeography, 23(2), 245– 258. https://doi.org/10.1111/geb.12095

Chuvieco, E., Aguado, I., Yebra, M., Nieto, H., Martín, M. P., Vilar, L., Martínez, J., Padrón, D., Martín, S., & Salas, J. (2007). Cartografía del peligro de incendios forestales mediante Teledetección y SIG. Teledetección - Hacia Un Mejor Entendimiento de La Dinámica Global y Regional, January, 19–26.

D. Theobald, GIS Concepts and ArcGIS Methods, 2nd Ed., Conservation Planning Technologies, Inc., 2005.

Díaz-Delgado, R., Lloret, F., Pons, X., & Terradas, J. (2002). Satellite evidence of decreasing resilience in mediterranean plant communities after recurrent wildfires. Ecology, 83(8), 2293–2303. https://doi.org/10.1890/0012-9658(2002)083[2293:SEODRI]2.0.CO;2

Duguy, B., Alloza, J. A., Baeza, M. J., De La Riva, J., Echeverría, M., Ibarra, P., Llovet, J., Cabello, F. P., Rovira, P., & Vallejo, R. V. (2012). Modelling the ecological vulnerability to forest fires in mediterranean ecosystems using geographic information technologies. Environmental Management, 50(6), 1012–1026. https://doi.org/10.1007/s00267-012-9933-3

Duguy, B., & Vallejo, V. R. (2008). Land-use and fire history effects on post-fire vegetation dynamics in eastern Spain. Journal of Vegetation Science, 19(1), 97–108.

E. H. Jacox and H. Samet, "Spatial Join Techniques," ACM Trans. Database Syst., vol. 32, no. 1, p. Article #7, 2007.

Flannigan, M. D., Krawchuk, M. A., De Groot, W. J., Wotton, B. M., & Gowman, L. M. (2009). Implications of changing climate for global wildland fire. International Journal of Wildland Fire, 18(5), 483–507. https://doi.org/10.1071/WF08187

Giovannini, G., & Lucchesi, S. (1997). Modifications induced in soil physico-chemical parameters by experimental fires at different intensities. Soil Science, 162(7), 479–486.

González, J. R., Kolehmainen, O., & Pukkala, T. (2007). Using expert knowledge to model forest stand vulnerability to fire. Computers and Electronics in Agriculture, 55(2), 107–114. https://doi.org/10.1016/j.compag.2006.12.005

Guyette, R. P., Muzika, R. M., & Dey, D. C. (2002). Dynamics of an Anthropogenic Fire Regime. Ecosystems, 6(4), 326–335. https://doi.org/10.1007/s10021-002-0115-7

Hobson, K. A., & Schieck, J. (1999). Changes in bird communities in boreal mixedwood forest: Harvest and wildfire effects over 30 years. Ecological Applications, 9(3), 849–863. https://doi.org/10.1890/1051-0761(1999)009[0849:CIBCIB]2.0.CO;2

Houghton, J. T., Ding, Y. D. J. G., Griggs, D. J., Noguer, M., van der Linden, P. J. Dai, X., & Johnson, C. A. (2001). Climate change 2001: the scientific basis. The Press Syndicate of the University of Cambridge.

Kirkman, L. K., Mitchell, R. J., Helton, R. C., & Drew, M. B. (2001). Productivity and species richness across an environmental gradient in a fire-dependent ecosystem. American Journal of Botany, 88(11), 2119–2128. https://doi.org/10.2307/3558437

Lindner, M., Maroschek, M., Netherer, S., Kremer, A., Barbati, A., Garcia-Gonzalo, J., Seidl, R., Delzon, S., Corona, P., Kolström, M., Lexer, M. J., & Marchetti, M. (2010). Climate change impacts, adaptive capacity, and vulnerability of European forest ecosystems. Forest Ecology and Management, 259(4), 698–709. https://doi.org/10.1016/j.foreco.2009.09.023

Midgley, G. F., & Bond, W. J. (2015). Future of African terrestrial biodiversity and ecosystems under anthropogenic climate change. Nature Climate Change, 5(9), 823–829. https://doi.org/10.1038/nclimate2753

Moreira, F., Viedma, O., Arianoutsou, M., Curt, T., Koutsias, N., Rigolot, E., Barbati, A., Corona, P., Vaz, P., Xanthopoulos, G., Mouillot, F., & Bilgili, E. (2011). Landscape - wildfire interactions in southern Europe: Implications for landscape management. Journal of Environmental Management, 92(10), 2389–2402. https://doi.org/10.1016/j.jenvman.2011.06.028

Olson, D. M., Dinerstein, E., Wikramanayake, E. D., Burgess, N. D., Powell, G. V. N., Underwood, E. C., D'amico, J. A., Itoua, I., Strand, H. E., Morrison, J. C., Loucks, C. J., Allnutt, T. F., Ricketts, T. H., Kura, Y., Lamoreux, J. F., Wettengel, W. W., Hedao, P., & Kassem, K. R. (2001). Terrestrial Ecoregions of the World: A New Map of Life on Earth. BioScience, 51(11), 933. https://doi.org/10.1641/0006-3568(2001)051[0933:teotwa]2.0.co;2

Pausas, J. G., & Ribeiro, E. (2017). Fire and plant diversity at the global scale. Global Ecology and Biogeography, 26(8), 889–897. https://doi.org/10.1111/geb.12596

Scott, D. F., & Van Wyk, D. B. (1990). The effects of wildfire on soil wettability and hydrological behaviour of an afforested catchment. Journal of Hydrology, 121(1–4), 239–256. https://doi.org/10.1016/0022-1694(90)90234-O

Turner, B. L., Kasperson, R. E., Matsone, P. A., McCarthy, J. J., Corell, R. W., Christensene, L., Eckley, N., Kasperson, J. X., Luers, A., Martello, M. L., Polsky, C., Pulsipher, A., & Schiller, A. (2003). A framework for vulnerability analysis in sustainability science. Proceedings of the National Academy of Sciences of the United States of America, 100(14), 8074–8079. https://doi.org/10.1073/pnas.1231335100

Construction and evaluation of Fire Forecasting Model based on IS4FIRES fire information system

Mikhail Sofiev*; Evgeny Kadantsev

Finnish Meteorological Institute, Erik Palmenin Aukio 1, Helsinki 00560, Finland, {Mikhail.Sofiev, Evgeny.Kadantsev}@fmi.fi

**Corresponding author*

Keywords

Fire forecasting, IS4FIRES, Fire radiative power

Abstract

A challenging task of fire forecasting has been approached in climatological mode, i.e. for completely hypothetical meteorological scenarios (or for long meteorological archives) and without any relevant observational information on fires. This challenge has been approached by extending the methodology developed by FMI in collaboration with University of Latvia on the basis of statistical forecasting technique suggested by Main Geophysical Observatory (St. Petersburg). The technique was successfully applied to a wide variety of problems. The essence of the methodology is to establish a "static mapping", i.e. a set of non-linear statistical dependencies between a set of predictors (in the current case, meteorological parameters including cloud-to-ground lightning flash density, and fire danger indices) and the predicted variable - the fire radiative power FRP or its time-integral, fire radiative energy, FRE.

The methodology relies on a thorough investigation of the statistical properties of the data at hand and possible physics-based relations between the parameters. Therefore, the solution to the fire prediction problem started from investigating the statistical properties of the underlying datasets, first of all, MODIS FRP retrievals, which is presently the longest time series of FRP – over 20 years (2000 - present).

1. Introduction

Availability of satellite observations of active fires (Temperature Anomaly, TA, and Fire Radiative Power, FRP) allows for global fire detection in near-real-time. These data however tell very little about the fire pattern in (near) future: extrapolation of the observed patterns even over one day leads to large errors and moreover regional prediction of fire patterns for a few days turned out to be a challenging task (Di Giuseppe et al., 2017, 2016; Partanen and Sofiev, 2022). At the same time, quality and features of fire predictions largely determine the capabilities of downstream applications, such as atmospheric composition and air quality forecasts.

The current paper introduces a new fire prediction model, outlines its key features, and shows the first results.

2. Problem statement

The goal of the study is to construct a statistical model based on machine learning techniques for prediction of daily fire Radiative Power (FRP) released by vegetation fires at regional-to-global scales. The prediction time horizon is unlimited: the model should be able to operate at climate-relevant scales, both in past and future, using only meteorological predictions produced by weather forecasting and climate models.

The system is based on the Integrated System for Wildland Fires IS4FIRES (http://is4fires.fmi.fi, visited 20.08.2022), (Soares et al., 2015; Sofiev et al., 2012, 2009), which uses the FRP retrievals of MODIS instruments onboard of Aqua and Terra satellites and produces time- and space- resolving 4-D emission flux for 21 atmospheric pollutants.

3. Materials and methods

3.1. Input datasets

The detection procedure of Collection 6 of MODIS FRP fire products is based on an algorithm of (Wooster, 2003) that exploits the strong emission of mid-infrared radiation from fires. Details on the way the MODIS FRP is used by IS4FIRES are described in (Soares et al., 2015; Sofiev et al., 2009).

The ERA5 reanalysis (European Reanalysis v.5, https://www.ecmwf.int/en/forecasts/datasets/reanalysis-datasets/era5, visited on 21.08.2022) is a global meteorological dataset, which provides hourly estimates of atmospheric, terrestrial, and oceanic meteorological variables. The data cover the globe with a ~25km grid and resolve the atmosphere with 137 levels from the surface up to a height of ~80km. The current study uses the period 1980-2021.

Another source of meteorological information is ECMWF's Integrated Forecasting System (IFS) global forecast archive, with its advantage of the most recent modelling developments. Since 2018, ECMWF implemented a new lightning parameterization in IFS (Lopez, 2016) predicting total lightning flash density (in flashes km^{-2} day^{-1}). Together with height of convective cloud top and height of zero-degree wet-bulb temperature, it was used to calculate the cloud-to-ground lightning flash density following the approach of Price and Rind (1994). This parameter was used to simulate lightning as a major natural cause of wildland fires (Veraverbeke et al., 2017; Pérez-Invernón et al., 2021). The lightning data are currently available for the period since the lightning parameterization was implemented in IFS (mid-2018 – 2021).

3.2. Statistical procedures

The statistical methodology adapted to fire forecasting has its roots in the ground-setting works of Voeikov Main Geophysical Observatory for urban air pollution (Berlyand, 1991; Genikhovich et al., 2004). This approach has been adapted by the FMI team, in collaboration with University of Latvia, to a variety of tasks (Ritenberga et al., 2017, 2016; Sofiev et al., 2017). However, the statistical features of the fire problem represent an extreme case, which required more complicated arrangements.

Since the prediction of individual fire ignition is meaningless, the problem uses spatial and temporal averaging with adjustable kernels to catch the mean and/or upper percentiles of the fire events.

Apart from non-linear transformations described by Ritenberga et al., (2017, 2016) and Sofiev et al. (2017), the following additional transformation steps were implemented in order to cope with peculiarities of the fire prediction problem:

- MODIS detection limit was parameterized generally following the procedure of (Maier et al., 2013), who estimated it for FRP Collection 5 data in Australia. Modification of that analysis leads to a simple analytical parameterization of MODIS detection limit applicable over the globe.

- SEVIRI-based parameterization of diurnal FRP variation of IS4FIRES v.1.0 has been reviewed by adjusting the day-night spread but keeping the profile shape intact.

- Five popular fire danger indices (FDIs) have been reviewed and their coefficients re-optimized using MODIS fire detections as a fitting target: Fire Weather Index (Van Wagner and Pickett, 1985), Keetch-Byram drought index KBDI (Keeth and Byram, 1968), soil drought index SDI as quoted by (Kumar and Dharssi, 2015), McArthur grass fire danger index as presented by (Schreck et al., 2010).

- Due to episodic character of fires, the normalization step had to be skipped in the pre-processing and replaced with the post-processing alignment of distribution functions. This was realized as a point-by-point rescaling of quantile chart towards the 1:1 relation.

3.3. Input parameters for fire forecasting

The FDIs, both initial and after optimization, were accompanied by a set of basic meteorological variables, which had a theoretical possibility to influence the fire regime:

- temperature at 2m above the ground
- relative humidity at 2m above the ground
- soil skin temperature
- leaf area index for low vegetation

- leaf area index for high vegetation
- soil moisture content
- total cloud cover
- water-equivalent snow depth
- convective rain
- large-scale rain
- windspeed at 10 m above the ground
- day length in hours
- convective available potential energy CAPE
- cloud-to-ground lightning flash density.

All these variables were taken as daily-min, daily-mean and daily-max, while precipitation and lightning data were also used as daily-sum.

4. Results

4.1. Predicted fires and comparison with MODIS

The most-important predicted time series refer to the MODIS observation period, which allows for direct evaluation. For the comparison, the whole period 2000-2020 has been split to training and test subsets of days in proportion 70-30, so that the first 70% of days (approx..14 years) were taken as training and the last 30% of days (approx.. 6 years) were used for testing. This approach was used because: (1) for a global model the "year" term is ambiguous, (2) random split at daily level may facilitate "gap-filling" solutions between neighbouring days instead of time-agnostic predictions,

An example of predicted crop residue fires in Central Europe is shown in Figure 1. Red dots denote the actually observed FRP, blue small dots show the MODIS detection limit for the days when it did not see any fires. The FFM prediction is the brown line. An intriguing feature of these time series is that for the seasons of 2001 and 2002 FFM predicted very low fire intensity. For trees, these were indeed very weak years but for grasses and crop residues the season was among the strongest. The most-plausible explanation was the ignition irregularities: moderate conditions still allow for fires to go if they get ignited. Such sensitivity is characteristic for grass and shrubs fires, whereas forests are more resilient for fires unless conditions are strongly favourable for burning.

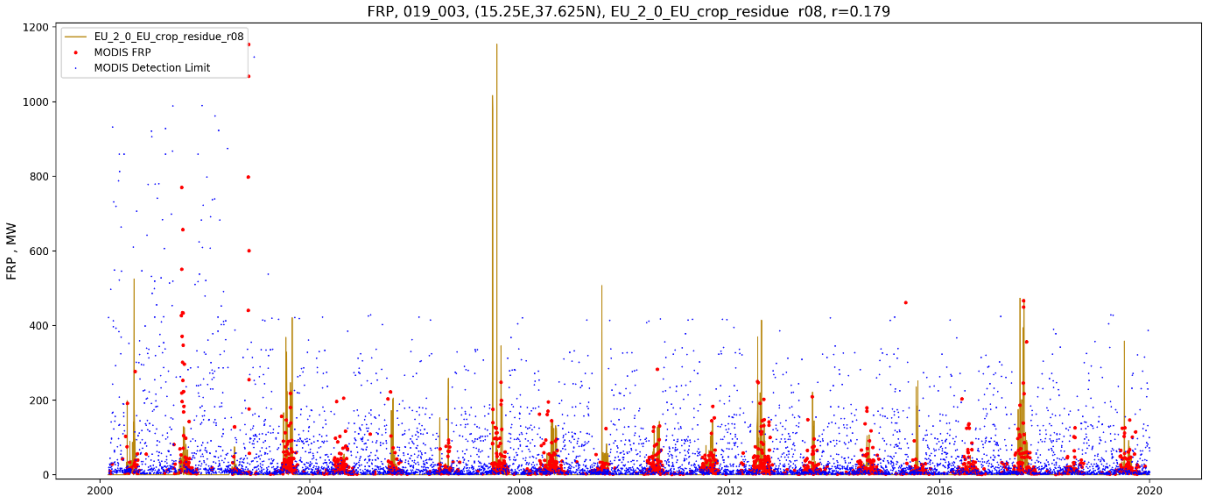

Figure 1. Example of time series for crop residue fires in Central Europe

4.2. Comparison with GFED v.4

Comparison with other fire emission databases is quite difficult because the new dataset has no direct analogies. However, one can compare, e.g., the distribution of total emission of IS4FIRES FFM and GFED v.4 (Figure 2). Since these datasets are based on different input (GFED is based on burnt area observations rather than on the

actual-fire counts), direct comparison of the maps is not very informative due to random fluctuations of the fields. However, the qualitative comparison of the fire patterns reveals both good agreement and striking regional differences.

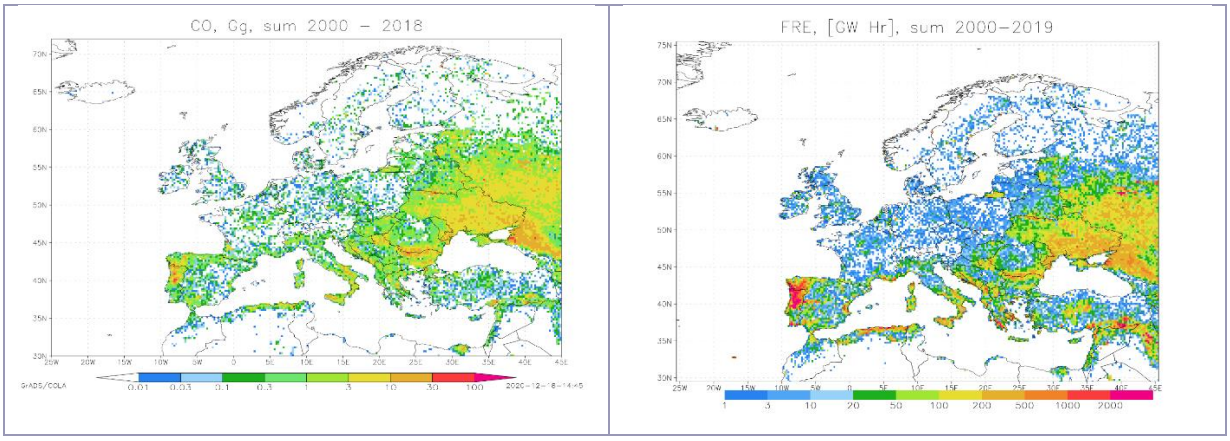

Figure 2. Left: Total CO emission from fires, GFED v.4, sum 2000-2018, Gg CO. Right: A predicted map of total FRE release 2000-2019 in Europe. Grid cell size is 0.25° × 0.25°.

4.3. Model improvements by the inclusion of lightning data

Incorporation of lightning into the list of predictors, on average, increased correlation with MODIS time series for the same region by 2-10% even with the very limited training dataset (2 years of FRP observations). The improvement is spatially distributed (Figure 3) depending on thunderstorm activity, fire frequency, and anthropogenic ignitions. Figure 4 shows an example of the impact of lightning predictor inclusion on the FFM predictions: a few fires in late July 2021 were missed by the original model while the model with the lightning input was able to predict them.

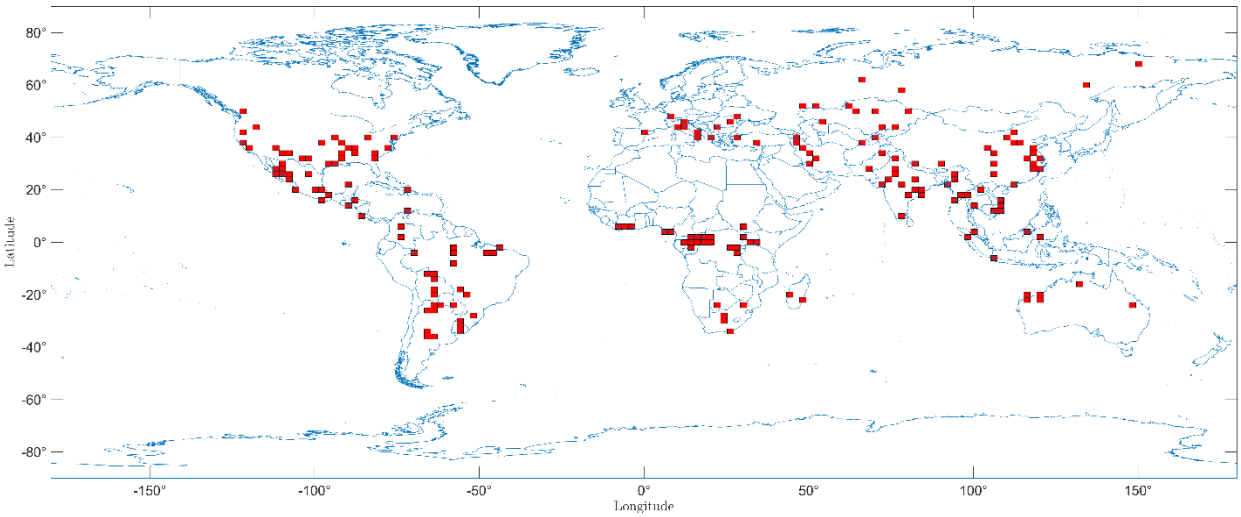

Figure 3. Map of model grid cells with statistically significant contribution of the cloud-to-ground lightning flash density to a predictor. Grid cell size is 2° × 2°.

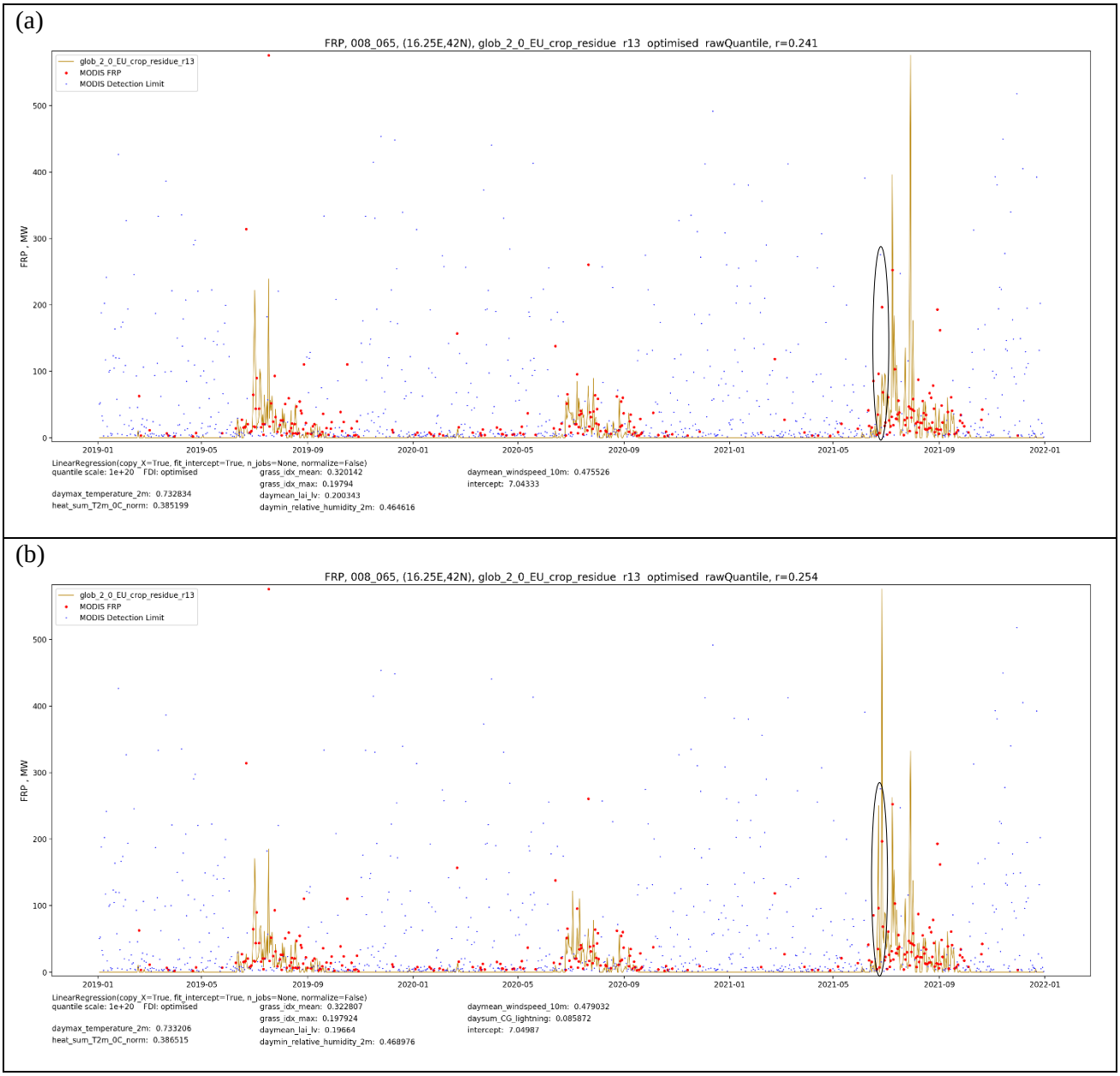

Figure 4. Example of the impact of lightning predictor inclusion on time series for crop residue fires in Central Italy. Panel (a) shows FRP by FFM trained with no lightning data compared to MODIS observations. Panel (b) shows FRP by FFM trained on the same meteorological predictors adding lightning predictions. The black ellipse denotes the area of improvement.

5. Conclusions

The current Fire Forecasting Model version 1.0 is the first practically applicable model capable of reproducing the main features of the fire seasons in Europe and, with some reservations, over the globe. Its time series seem to satisfy the requirements of the climatological-scale applications.

The main unresolved issue refers to handling the strongly non-Gaussian distribution function of FRP. The current approach ensured formal identity of the distribution functions and allowed usage of the data in downstream applications but left the core of the problem unresolved. This topic is closely related to the MODIS detection limit, which is partly behind the unusual features.

6. Acknowledgements

The work has been performed within the scope of H2020 EXHAUSTION (https://www.exhaustion.eu, grant No 820655), FirEUrisk (https://fireurisk.eu/, grant No 101003890), and Academy of Finland HEATCOST (grant No 334798) projects.

7. References

Berlyand, M.E., 1991. Prediction and Regulation of Air Pollution. Springer Netherlands. https://doi.org/10.1007/978-94-011-3768-3

Di Giuseppe, F., Pappenberger, F., Wetterhall, F., Krzeminski, B., Camia, A., Libertá, G., San Miguel, J., 2016. The Potential Predictability of Fire Danger Provided by Numerical Weather Prediction. Journal of Applied Meteorology and Climatology 55, 2469–2491. https://doi.org/10.1175/JAMC-D-15-0297.1

Di Giuseppe, F., Rémy, S., Pappenberger, F., Wetterhall, F., 2017. Improving Forecasts of Biomass Burning Emissions with the Fire Weather Index. Journal of Applied Meteorology and Climatology 56, 2789–2799. https://doi.org/10.1175/JAMC-D-16-0405.1

Genikhovich, E.L., Sonkin, L.R., Kirillova, V.I., 2004. A statistical prognostic model for daily maxima of concentrations of urban air pollutnants, in: 9th Int.Conc. on Harmonisation within Atmospheric Dispersion Modelling for Regulatory Purposes. pp. 34–39

Keeth, J.J., Byram, G.M., 1968. A drought index for forest fire control (No. SE-38), USDA Forest service research paper. USDA - Forest Service Southearstern forest experimental station, Asheville

Kumar, V., Dharssi, I., 2015. Sources of soil dryness measures and forecasts for fire danger rating (No. 009), Bureau Research Report. Australian government Bureau of Meteorology

Lopez, P., 2016. A Lightning Parameterization for the ECMWF Integrated Forecasting System. Monthly Weather Review 144, 9. https://doi.org/10.1175/MWR-D-16-0026.1

Maier, S.W., Russell-Smith, J., Edwards, A.C., Yates, C., 2013. Sensitivity of the MODIS fire detection algorithm (MOD14) in the savanna region of the Northern Territory, Australia. ISPRS Journal of Photogrammetry and Remote Sensing 76, 11–16. https://doi.org/10.1016/j.isprsjprs.2012.11.005

Partanen, T.M., Sofiev, M., 2022. Forecasting the regional fire radiative power for regularly ignited vegetation fires. Nat. Hazards Earth Syst. Sci. 22, 1335–1346. https://doi.org/10.5194/nhess-22-1335-2022

Pérez-Invernón, F. J., Huntrieser, H., Soler, S., Gordillo-Vázquez, F. J., Pineda, N., Navarro-González, J., Reglero, V., Montanyà, J., van der Velde, O., Koutsias, N., 2021. Lightning-ignited wildfires and long continuing current lightning in the Mediterranean Basin: preferential meteorological conditions. Atmospheric Chemistry and Physics 21, 17529–17557. https://doi.org/10.5194/acp-21-17529-2021

Price, C., Rind, D., 1994: Modeling global lightning distributions in a general circulation model. Monthly Weather Review 122, 1930–1939. https://doi.org/10.1175/1520-0493(1994)122<1930:MGLDIA>2.0.CO;2.

Ritenberga, O., Sofiev, M., Kirillova, V., Kalnina, L., Genikhovich, E., 2016. Statistical modelling of non-stationary processes of atmospheric pollution from natural sources: Example of birch pollen. Agricultural and Forest Meteorology 226–227, 96–107. https://doi.org/10.1016/j.agrformet.2016.05.016

Ritenberga, O., Sofiev, M., Siljamo, P., Saarto, A., Dahl, A., Ekebom, A., Sauliene, I., Shalaboda, V., Severova, E., Hoebeke, L., Ramfjord, H., 2017. A statistical model for predicting the inter-annual variability of birch pollen abundance in Northern and North-Eastern Europe. Science of total environment 615, in press. https://doi.org/10.1016/j.scitotenv.2017.09.061

Schreck, M.-B., Howerton, P.J., Cook, K.R., 2010. Adapting Australia's Grassland Fire Danger Index for the United States' Central Plains 19

Soares, J., Sofiev, M., Hakkarainen, J., 2015. Uncertainties of wild-land fi res emission in AQMEII phase 2 case study. Atmospheric Environment. https://doi.org/10.1016/j.atmosenv.2015.01.068

Sofiev, M., Ermakova, T., Vankevich, R., 2012. Evaluation of the smoke-injection height from wild-land fires using remote-sensing data. Atmospheric Chemistry and Physics 12, 1995–2006. https://doi.org/10.5194/acp-12-1995-2012

Sofiev, M., Ritenberga, O., Albertini, R., Arteta, J., Belmonte, J., Bonini, M., Celenk, S., Damialis, A., Douros, J., Elbern, H., Friese, E., Galan, C., Gilles, O., Hrga, I., Kouznetsov, R., Krajsek, K., Plu, M., Prank, M., Robertson, L., Steensen, B.M., Thibaudon, M., Segers, A., Stepanovich, B., Valdebenito, A.M., Vira, J., Vokou, D., 2017. Multi - model ensemble simulations of olive pollen distribution in Europe in 2014 . Atmospheric Chemistry and Physics Discussions. https://doi.org/10.5194/acp-2016-1189

Sofiev, M., Vankevich, R., Lotjonen, M., Prank, M., Petukhov, V., Ermakova, T., Koskinen, J., Kukkonen, J., 2009. An operational system for the assimilation of the satellite information on wild-land fires for the needs of air quality modelling and forecasting. Atmospheric Chemistry and Physics 9, 6833–6847

Van Wagner, C.E., Pickett, T.L., 1985. Equations and FORTRAN program for the Canadian Forest Fire Weather Index System (No. 33), Forestry technical report. Canadian Forestry Service, Ottawa, Canada

Veraverbeke, S., Rogers, B., Goulden, M., Jandt, R., Miller, C., Wiggins, E., Randerson, J., 2017. Lightning as a major driver of recent large fire years in North American boreal forests. Nature Climate Change 7, 529–534. https://doi.org/10.1038/nclimate3329

Wooster, M., 2003. Fire radiative energy for quantitative study of biomass burning: derivation from the BIRD experimental satellite and comparison to MODIS fire products. Remote Sensing of Environment 86, 83–107. https://doi.org/10.1016/S0034-4257(03)00070-1

Clusters analysis applied to drought and forest fires in mainland Portugal (NUT III regions) from 1980 to 2019

Edna Cardoso*[1,2]; Ilda Novo[2]; Nuno Moreira[2]; Pedro Silva[2]; Álvaro Silva[2]; Vanda Pires[2]

[1]*University of Coimbra, FCTUC, Department of Mechanical Engineering. Pólo II Rua Luís Reis Santos, 3030-788 Coimbra,* Portugal, *{uc2004118633@student.uc.pt}*
[2]*IPMA. Rua C do Aeroporto, 1749-077 Lisboa, Portugal, {edna.cardoso, nuno.moreira, ilda.novo, pedro.silva, alvaro.silva, vanda.cabrinha}@ipma.pt*

** Corresponding author*

Keywords

Drought, Forest Fires, Clusters Analysis, NUT III

Abstract

In order to better understand Extreme Fire Event conditions at the regional level in Portugal, a preliminary analysis on drought conditions and forest fires considering NUT III administrative organization was performed and is presented in this work. This analysis will support a more comprehensive study on the relation between weather-climate conditions (drought, heat, wind) and forest fires (occurrences and burned areas). To classify the drought, two drought indices were considered – PDSI (Palmer Drought Severity Index) and SPI (Standardized Precipitation Index), the last one for 3- and 6 months time scales. The computation was based on weather station observations for the period 1981 - 2019 in mainland Portugal, with aggregation in 23 NUT III on a monthly basis. To analyse the forest fires distribution per NUT III a monthly dataset of fire occurrences and burned areas during the period was used. The exploratory analysis was carried out in the STATISTICA software, using two clustering methods (K-Means and tree clustering). Since the results of those methods are subjective, before applying them, in the case of drought, the ideal number of clusters was calculated, making a sensibility analysis using the R tool NbClust. The results from clustering are presented through maps in which the groups of NUT III regions with the same behaviour are identified.

1. Introduction

Droughts are a natural occurring phenomenon, essentially associated with deficient precipitation values, over an extended period of time, resulting in low soil moisture and influencing water resources availability (Riley et al. 2013). Portugal is a country recurrently affected by drought, which has implications in fire occurrences and burned areas, with dry years usually being related with the greatest severity wildfires (Viegas et al. 1999). For a better understanding of the spatial distribution, an exploratory analysis of drought and forest fires was made separately. The final goal of the study is to analyse the regional distribution of the drought and its relation to the fires. The characterization of the droughts for mainland Portugal (in 23 regions of NUT III shown in Figure 1) is done using the Palmer Drought Severity Index (PDSI) and 3- and 6-months Standardized Precipitation Index (IPMA 2021), both presented in Table 1. This data is available on a monthly basis from January 1981 to December 2019. Likewise, for the characterization of the distribution of forest fires for mainland Portugal (in 23 NUT III regions), fires occurrences and burned areas on a monthly basis, from January 1980 to December 2018, were used. The first step was to develop a preliminary analysis of drought conditions calculating frequency and temporal evolution per NUT III. The second step aimed to understand how each NUT III is related to its neighbours considering the drought, through the use of correlation and applying two cluster analysis methods (K-Means clustering and Tree clustering) to identify the spatial drought and spatial distribution of forest fires in NUT III regions. Since this analysis has a subjective nature, to estimate the best number of NUT III clusters according to drought, a sensibility analysis based on the R tool NbClust was performed. The next chapters are organized as follows: i) preliminary analysis of the drought in Portugal, ii) detailed analysis of both drought and forest fires on a NUT III basis, and iii) conclusions drawn from presented data.

Figure 1 – Name of each regional division (NUTS 2013) applied in May 2015 (on the left) (the image is adapted from (INE 2015)) and the respective regional codes (on the right) (the image is adapted from (EUROSTAT 2016)).

Table 1 - PDSI and SPI index category with their respective value ranges and colour code. (the Table is adapted from (Portal do Estado de Ambiente 2021)).

PDSI	Drought classes	SPI
> = 4.00	extremely wet	> = 2.00
3.00 a 3.99	very wet	1.50 a 1.99
2.00 a 2.99	moderately wet	1.00 a 1.49
0.50 a 1.99	slight wet	0.99 a 0.50
0.49 a -0.49	near normal	0.49 a -0.49
-0.50 a -1.99	mild drought	-0.50 a -0.99
-2.00 a -2.99	moderate drought	- 1.00 a -1.49
-3.00 a -3.99	severe drought	- 1.50 a -1.99
< = - 4.00	extreme drought	< = - 2.00

2. Preliminary drought analysis

The first step was a frequency analysis of drought conditions per NUT III (see an example for PDSI in Figure 2). The analysis was followed by an evaluation of the temporal evolution of drought in the period 1981 to 2019, taking into consideration the spatial prevalence of drought on NUT III basis (see an example for PDSI in Figure 3).

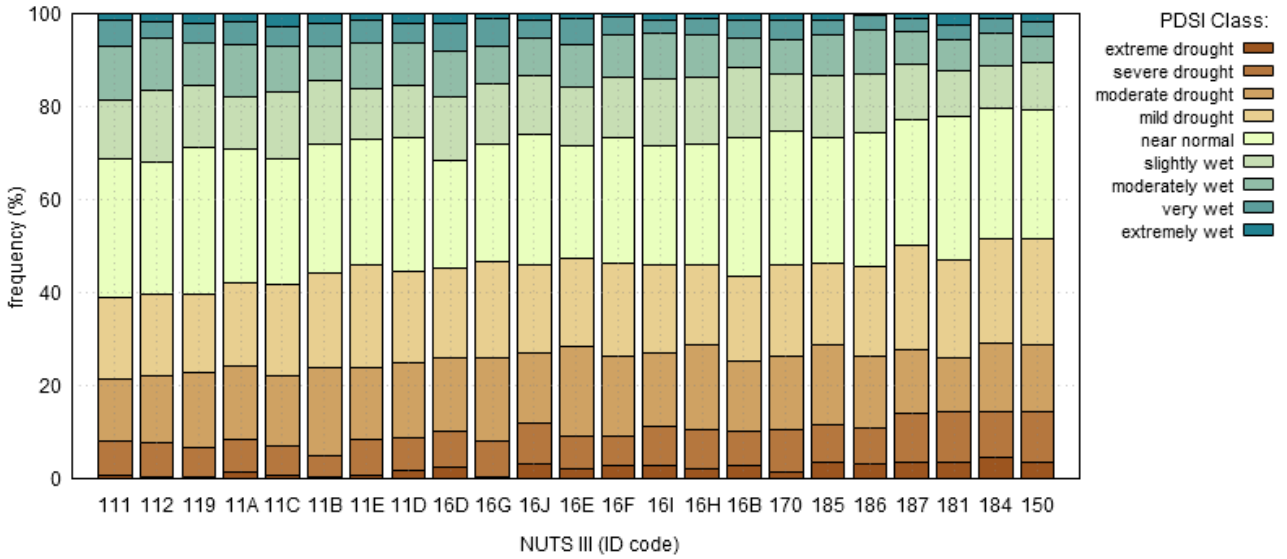

Figure 2 - Frequency of monthly PDSI classes (%) per NUT III in the period 1981-2019 for Portugal.

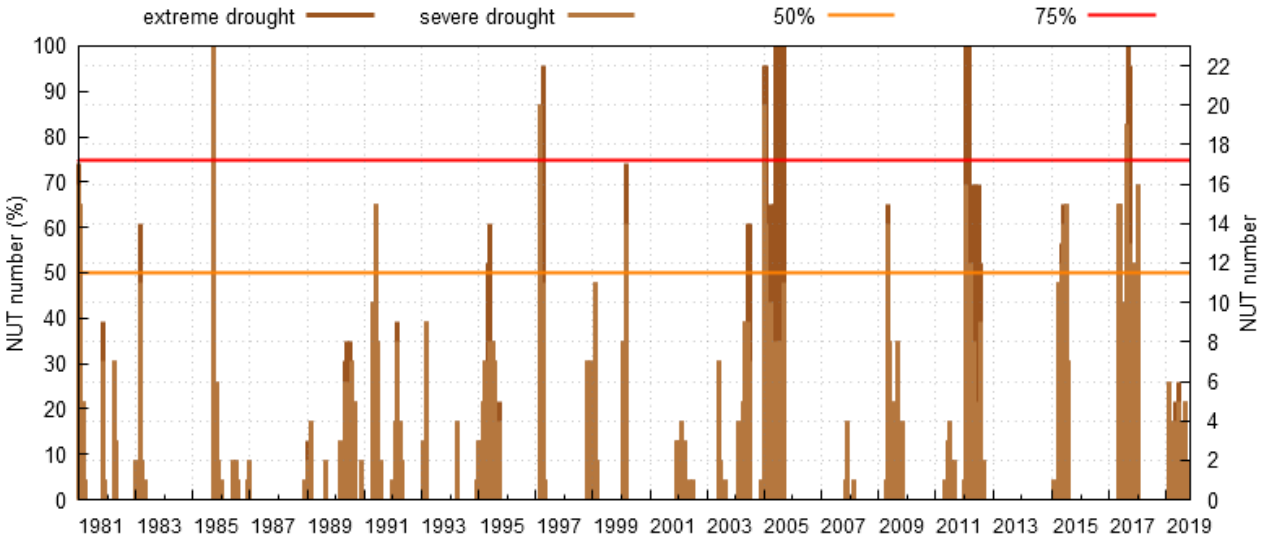

Figure 3 - Number of NUT III (%) in the 2 higher classes of PDSI index (severe and extreme) in the period 1981-2019 for Portugal.

3. Drought on NUT III basis

A second step aimed to understand how each NUT III is linked to its neighbours in relation to drought, through the use of correlation and clustering methods. Regarding correlation, simple correlation matrixes were used for a preliminary inspection of the data (see the example for PDSI considering all months of the year in Table 2).

Table 2 - Correlation matrix for PDSI in NUT III, considering all months within the year, from 1981 to 2019.

	111	112	119	11A	11C	11B	11E	11D	16D	16G	16J	16E	16F	16I	16H	16B	170	185	186	187	181	184	150
111	1,000	0,958	0,930	0,944	0,904	0,908	0,837	0,866	0,872	0,884	0,844	0,888	0,854	0,767	0,767	0,745	0,721	0,696	0,733	0,660	0,599	0,560	0,460
112	0,958	1,000	0,975	0,930	0,892	0,921	0,820	0,866	0,859	0,875	0,846	0,867	0,839	0,765	0,767	0,746	0,708	0,702	0,736	0,661	0,588	0,551	0,438
119	0,930	0,975	1,000	0,924	0,917	0,952	0,819	0,873	0,857	0,867	0,831	0,856	0,829	0,754	0,748	0,737	0,689	0,694	0,724	0,644	0,560	0,516	0,402
11A	0,944	0,930	0,924	1,000	0,966	0,911	0,864	0,891	0,929	0,905	0,853	0,914	0,876	0,774	0,788	0,754	0,718	0,700	0,744	0,657	0,593	0,537	0,423
11C	0,904	0,892	0,917	0,966	1,000	0,909	0,843	0,876	0,885	0,878	0,816	0,869	0,835	0,741	0,749	0,727	0,689	0,684	0,717	0,636	0,565	0,496	0,392
11B	0,908	0,921	0,952	0,911	0,909	1,000	0,910	0,929	0,880	0,904	0,879	0,887	0,873	0,810	0,814	0,801	0,770	0,757	0,785	0,710	0,629	0,583	0,472
11E	0,837	0,820	0,819	0,864	0,843	0,910	1,000	0,941	0,869	0,893	0,906	0,909	0,913	0,868	0,885	0,857	0,843	0,817	0,862	0,792	0,719	0,691	0,576
11D	0,866	0,866	0,873	0,891	0,876	0,929	0,941	1,000	0,893	0,904	0,918	0,914	0,909	0,857	0,874	0,845	0,814	0,811	0,838	0,765	0,684	0,649	0,529
16D	0,872	0,859	0,857	0,929	0,885	0,880	0,869	0,893	1,000	0,902	0,878	0,937	0,905	0,815	0,827	0,795	0,748	0,747	0,779	0,695	0,637	0,587	0,462
16G	0,884	0,875	0,867	0,905	0,878	0,904	0,893	0,904	0,902	1,000	0,931	0,929	0,911	0,857	0,879	0,838	0,808	0,803	0,840	0,768	0,711	0,662	0,568
16J	0,844	0,846	0,831	0,853	0,816	0,879	0,906	0,918	0,878	0,931	1,000	0,919	0,917	0,890	0,935	0,881	0,860	0,854	0,884	0,839	0,779	0,751	0,643
16E	0,888	0,867	0,856	0,914	0,869	0,887	0,909	0,914	0,937	0,929	0,919	1,000	0,983	0,892	0,887	0,854	0,804	0,812	0,851	0,772	0,710	0,676	0,543
16F	0,854	0,839	0,829	0,876	0,835	0,873	0,913	0,909	0,905	0,911	0,917	0,983	1,000	0,948	0,921	0,925	0,865	0,895	0,908	0,844	0,788	0,750	0,618
16I	0,767	0,765	0,754	0,774	0,741	0,810	0,868	0,857	0,815	0,857	0,890	0,892	0,948	1,000	0,937	0,941	0,892	0,935	0,952	0,895	0,838	0,808	0,691
16H	0,767	0,767	0,748	0,788	0,749	0,814	0,885	0,874	0,827	0,879	0,935	0,887	0,921	0,937	1,000	0,922	0,918	0,908	0,950	0,901	0,849	0,816	0,712
16B	0,745	0,746	0,737	0,754	0,727	0,801	0,857	0,845	0,795	0,838	0,881	0,854	0,925	0,941	0,922	1,000	0,949	0,984	0,934	0,924	0,894	0,839	0,738
170	0,721	0,708	0,689	0,718	0,689	0,770	0,843	0,814	0,748	0,808	0,860	0,804	0,865	0,892	0,918	0,949	1,000	0,926	0,923	0,927	0,904	0,856	0,766
185	0,696	0,702	0,694	0,700	0,684	0,757	0,817	0,811	0,747	0,803	0,854	0,812	0,895	0,935	0,908	0,984	0,926	1,000	0,940	0,939	0,907	0,853	0,761
186	0,733	0,736	0,724	0,744	0,717	0,785	0,862	0,838	0,779	0,840	0,884	0,851	0,908	0,952	0,950	0,934	0,923	0,940	1,000	0,957	0,900	0,875	0,773
187	0,660	0,661	0,644	0,657	0,636	0,710	0,792	0,765	0,695	0,768	0,839	0,772	0,844	0,895	0,901	0,924	0,927	0,939	0,957	1,000	0,960	0,946	0,852
181	0,599	0,588	0,560	0,593	0,565	0,629	0,719	0,684	0,637	0,711	0,779	0,710	0,788	0,838	0,849	0,894	0,904	0,907	0,900	0,960	1,000	0,955	0,895
184	0,560	0,551	0,516	0,537	0,496	0,583	0,691	0,649	0,587	0,662	0,751	0,676	0,750	0,808	0,816	0,839	0,856	0,853	0,875	0,946	0,955	1,000	0,925
150	0,460	0,438	0,402	0,423	0,392	0,472	0,576	0,529	0,462	0,568	0,643	0,543	0,618	0,691	0,712	0,738	0,766	0,761	0,773	0,852	0,895	0,925	1,000

In what concerns clustering, two complementary approaches were taken. On one side, a sensibility analysis based on the R tool NbClust (Ghazzali 2014) was performed to find the best number of NUT III clusters according to drought. Most of the aggregation methods indicated 2 or 3 NUT III clusters to be the ideal number of clusters for Portugal, also with a high number of methods to indicate 8 NUT III clusters as ideal (see the example for PDSI considering all months of the year in Table 3).

Table 3 - Number of indexes (per aggregation method and for all methods – last column) that indicate the best number of NUT III clusters, using the R Tool NBClust, for PDSI considering all months.

Number of Clusters	Aggregation Method									All methods
	Ward.D	Ward.D2	Single	Complete	Average	McQuitty	Median	Centroid	Kmeans	
2	6	**11**	**12**	**10**	7	6	8	11	**13**	84
3	**11**	6	8	4	**8**	**11**	2	3	8	61
4	1	1	2	3	2	4	2	**12**	0	27
5	1	1	0	0	1	3	2	0	1	9
6	1	1	0	0	3	0	**12**	0	2	19
7	0	2	2	2	0	0	0	0	0	6
8	4	3	4	6	2	4	1	1	4	29

On the other side, final clustering results were obtained for K-Means (with 3 different initial cluster centers settings, named A (choose observations to maximize initial between-cluster distances), B (sort distances and take observations at constant intervals) and C (choose the first N (number of clusters) observations) and tree clustering methods (Ward's method for 2 metric distances, Euclidean and Pearson r) in STATISTICA software (TIBCO 2022). The example for PDSI considering all months of the year is shown in Figure 4. Four solutions were considered for addressing season sensibility: i) all months of the year; ii) summer months; iii) spring months; iv) non-winter months.

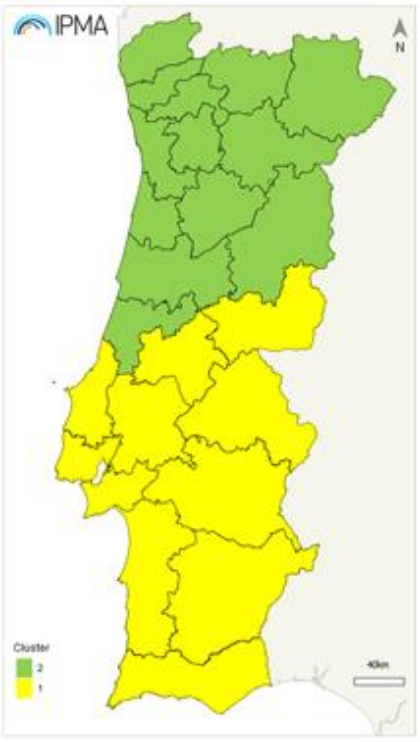

Figure 4 – NUT III aggregation in 2 clusters considering monthly values for 3 considered drought indexes PDSI, SPI3 and SPI6 for all months of the year between January 1981 and December 2019, using 3 different settings for K-Means and 2 metric distances, Euclidean and Pearson r for Ward's method.

4. Preliminary Results for Drought

The results suggest that the longer the period considered throughout the year (inherent to the drought index itself or the number of months considered for drought analysis), the greater the tendency for the drought behaviour to be dominated by the Montejunto-Estrela mountain system. For shorter periods within the year, a finer clustering should be the most appropriate.

Thus, for all months of the year or for the non-winter period (March to November) the drought presents a differentiated behaviour for two main sets of NUTS III (see Figure 4):

- Oeste, Lezíria do Tejo, Médio Tejo, Beira Baixa and other NUT III to the south;
- Região de Coimbra, Região de Leiria, Beiras e Serra da Estrela and remaining NUT III to the north.

In a finer aggregation as a function of drought, the sets of NUT III that show the same behaviour for the meteorological drought are identified below for each of the 4 periods of the year (see Figure 5):

Every month of the year:
- Terras de Trás-os-Montes + Douro;
- Região de Coimbra + Região de Leiria.

Summer:
- Terras de Trás-os-Montes + Douro;
- Região de Coimbra + Região de Leiria;
- Oeste + Lezíria do Tejo.

Spring:
- Terras de Trás-os-Montes + Douro;
- Alto Minho + Cávado;
- Oeste + Lezíria do Tejo.

Non-winter:
- Viseu Dão Lafões + Beiras e Serra da Estrela;
- Região de Coimbra + Região de Leiria;
- Beira Baixa + Alto Alentejo;
- Oeste + Lezíria do Tejo.

In summary, it can be considered that there are 3 sets of NUT III presenting the same behaviour in terms of drought, almost regardless of the period of the year considered:

- **Terras de Trás-os-Montes and Douro**, which just do not belong to the same set in the non-winter period;
- **Região de Coimbra and Região de Leiria**, which do not belong to the same set in the spring period;
- **Oeste and Lezíria do Tejo**, which just do not belong to the same set considering all the months of the year.

There are also other NUT III with drought similarities, but to which this analysis does not allow to attribute the same level of confidence, since there was one combination of drought index (PDSI, SPI3 or SPI6) and a clustering solution (in these cases the solutions "K-Means B", "K-Means C" or "Ward - Pearson") in which aggregation was not verified. In this situation, for 3 of the 4 periods of the year considered, the following sets of NUT III are identified:

Every month of the year:

- Alto Minho and Cávado;
- Viseu Dão Lafões and Beiras e Serra da Estrela;
- Beira Baixa and Alto Alentejo;
- Oeste and Lezíria do Tejo.

Spring:

- Alto Minho, Cávado and Ave;
- Alentejo Litoral and Baixo Alentejo.

Summer:

- Oeste, Área Metropolitana de Lisboa and Lezíria do Tejo.

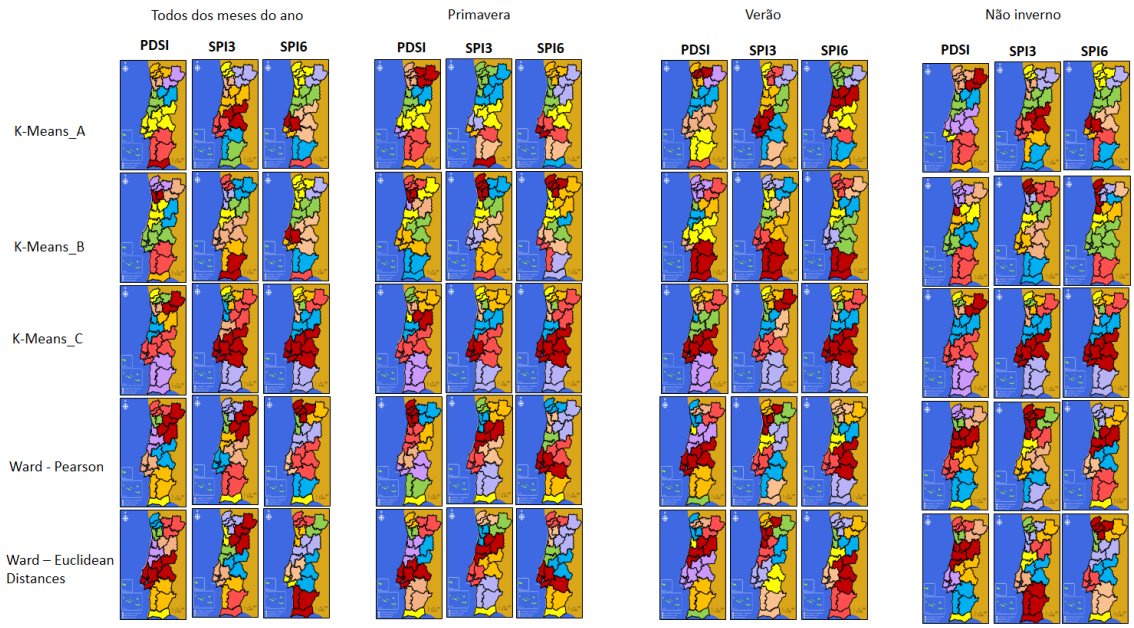

Figure 5 - Spatial aggregation of NUT III into 8 clusters for drought behavior between January 1981 and December 2019 as a function of; i) drought index (PDSI, SPI3 and SPI6); (ii) the time of year (All months of the year, spring, summer and non-winter) and iii) clustering solutions ("K-Means A", "K-Means B", "K-Means C", "Ward – Pearson", "Ward – Euclidean").

5. Forest fires distribution in NUT III

The third step was towards understanding NUT III spatial distribution of fire occurrences number and burned areas, considering both all months of the year (January to December) and forest fire seasons (June to October) for 39 years (1980 to 2018). The results obtained for 8 clusters by applying a tree clustering analysis - Ward's method with Pearson's metric distance r - are shown in the maps in Figure 6. It should be noted that the same results are obtained whether original or normalized data (division by the area of each NUT III) are used.

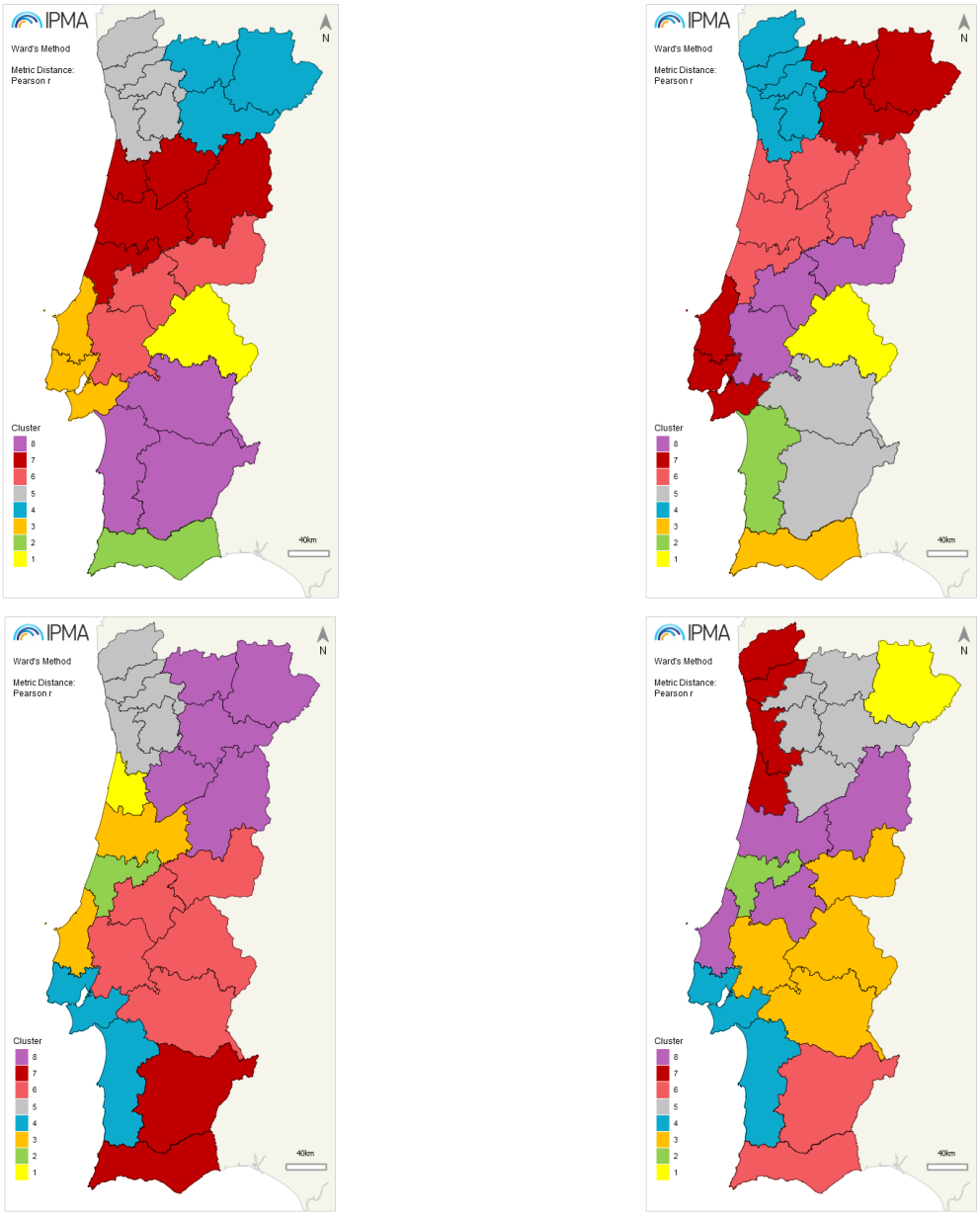

Figure 6 – NUT III aggregation in 8 clusters considering monthly values of fire occurrences (top) and burned areas (bottom) considering all months of the year (in the left) and the fire season months between June and October (in the right), applying a tree clusters analysis with Ward's method using the metric distance of Pearson r. Data from 1980 to 2018.

6. Preliminary Results for Forest Fires

Analysing Figure 6, it can be seen that for the case of forest fire occurrences there is a more homogeneous grouping in terms of NUT III spatial proximity considering both all months of the year and fire season months. The only differences between all months of the year (at the top on the left) and fire season months (at the top on the right) lies in the fact that, in the fire season months the Oeste and Área Metropolitana de Lisboa are in the same cluster as Alto Tâmega, Terra de Trás-os-Montes and Douro, and that there is an individualization of Alentejo Litoral in a single cluster, no longer belonging to Alentejo Central and Baixo Alentejo cluster (as for all months of the year).

The map for burned areas (bottom maps in Figure 6) shows a more homogeneous grouping of NUT III regions in the north and interior of the country, while for the coastal part of the country this is not the case. Anyway, it seems that grouping follows north-south guidance.

Comparing the maps in Figure 6 of the fire occurrences (at the top) with those of the burned areas (at the bottom), it can be seen that in the case of the burned areas there is less spatial consistency distribution of clusters. This suggests that there may be additional factors besides the regional proximity (on NUT III basis) that have to be considered to better understand the regional distribution of burned areas in Portugal.

7. References

Riley, Karin L, John T Abatzoglou, Isaac C Grenfell, Anna E Klene, and Faith Ann Heinsch. 2013. "The Relationship of Large Fire Occurrence with Drought and Fire Danger Indices in the Western USA, 1984 – 2008 : The Role of Temporal Scale," 894–909.

Viegas, D Xavier, Giovanni Bovio, Antonio Nosenzo, and Bernard Sol. 1999. "Comparative Study of Various Methods of Fire Danger Evaluation in Southern Europe" 9 (4): 235–46.

IPMA. 2021. "Definição Dos Índices de Seca Meteorológica." Lisboa. 2021. https://www.ipma.pt/pt/oclima/observatorio.secas/spi/apresentacao/definicao/.

INE. 2015. "NUTS 2013 AS NOVAS UNIDADES TERRITORIAIS PARA FINS ESTATÍSTICOS." 2015.

EUROSTAT. 2016. "NUTS-3-Map-PT." 2016. https://ec.europa.eu/eurostat/documents/345175/7451602/2016-NUTS-3-map-PT.pdf.

Portal do Estado de Ambiente. 2021. "Riscos Ambientais - Seca." 2021. https://rea.apambiente.pt/content/seca.

Ghazzali, Nadia. 2014. "NbClust : An R Package for Determining the Relevant Number of Clusters in a Data Set" 61 (6).

TIBCO. 2022. "Guide of Statistica Software - Data Science Textbook." 2022. https://docs.tibco.com/data-science/GUID-E79CEA1A-02B7-4C9B-9328-980D1DF20FEB.html.

Delivering a New Australian Fire Danger Rating System – Building on decades of research to deliver public safety outcomes

Simon Heemstra*[1]; Stuart Matthews[2]; Fiona Dunstan[3]; Simon Louis; Wayne Kington

[1]AFAC. East Melbourne, VIC, Australia, {simon.heemstra, w.kington}@afac.com.au
[2] NSW Rural Fire Service. Sydney Olympic Park, NSW, Australia, {stuart.matthews@rfs.nsw.gov.au}
[3] Bureau of Meteorology. Melbourne, VIC, Australia, {fiona.dunstan, simon.louis}@bom.gov.au

**Corresponding author*

Keywords

Fire Danger Rating System, Fire Behaviour, AFDRS, Decision Making, Community Messaging

Abstract

The Australian Fire Danger Rating System (AFDRS) was launched on 1 September 2022, bringing a generational change to the way that Australia calculates and communicates fire danger. Its focus is improved public safety and reduced impacts of bushfires through:

- Improving the science behind fire danger predictions.
- Improving the way that fire danger is communicated.
- Providing government and industry with better decision-making tools.
- Reducing future costs associated with bushfire impacts.

The previous fire danger rating system was introduced in the 1960's by Australia's first full-time bushfire researcher, Alan McArthur, based on extensive experimental fires. While useful, the system included only two fire behaviour models (dry sclerophyll forest and grassland), was not easily updateable and fires were being experienced that increasingly exceeded its design parameters.

In July 2014, Senior Officers and Ministers agreed that the development of a new system was a national priority. The new system was developed by the New South Wales Rural Fire Service in collaboration with the Bureau of Meteorology, all Australian states and territories and the Commonwealth government. Program management and system implementation were coordinated by AFAC (Australia's National Council for Fire and Emergency Services).

The new AFDRS uses contemporary fire behaviour science, makes better use of available data and uses software infrastructure that can be continuously improved. The AFDRS starts with eight fire behaviour models representing a range of Australian vegetation types, it captures current fuel information, uses satellite data, integrates weather from the Bureau of Meteorology and calculates fire danger down to a 1.5km by 1.5-kilometer grid. These calculations are linked to tools that assist fire operational decision-making via a Fire Behaviour Index that is calibrated to operational implications for fire management.

A separate arm of the project developed a public-facing Fire Danger Rating framework, guided by one of Australia's largest social research projects. The research found that, while fire danger signage was well recognised, few acted on fire danger ratings to plan their activities. Focus groups and subsequent surveys found that the community preferred a simplified public-facing system where each fire danger rating had a distinct call to action.

The implementation of the new system required an enormous effort from all levels of government across all States and Territories as well as the Commonwealth. It required updates to legislation, policy, procedures, web pages and other IT infrastructure, as well as replacement of physical signage. However, as a result, Australia has a significantly new way of calculating and communicating fire danger, that is continuously improvable and which will bring benefits for decades to come.

1. Introduction

The 2009 Black Saturday fires that devastated the state of Victoria was a watershed moment for Australian bushfire management. It was Australia's highest-ever loss of life from bushfires and many people were left homeless (Parliament of Victoria, 2010). With at least 18 major bushfire inquiries in Australia since 1939, the

Black Saturday fires were by no means the only devastating fires (Parliament of Australia, 2022), nor were they the largest or most recent. The unprecedented fires of the 2019-2020 Black Summer saw over 24 million hectares burnt, 3000 homes destroyed, 33 lives lost, species populations devastated and accrued an estimated financial impact of $10 billion (Commonwealth of Australia, 2020).

But it was the Black Saturday fires of 2009 that galvanised contemporary efforts to improve bushfire management systems in Australia, including the first efforts to review Australia's aging fire danger rating system (Figure 1).

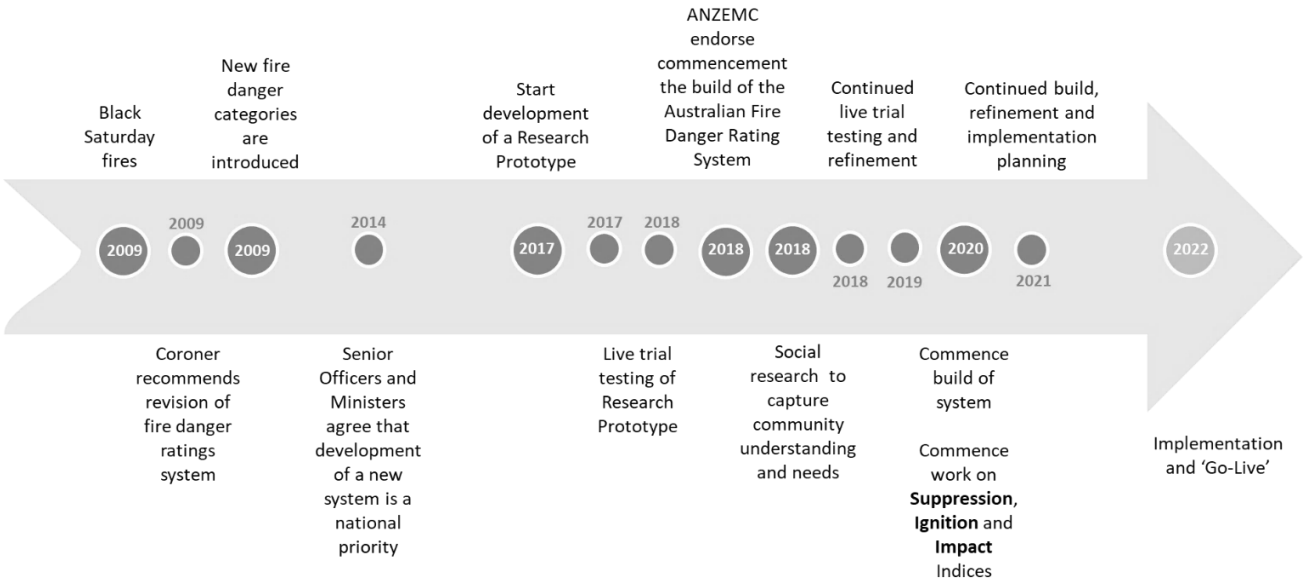

Figure 1- History of the development of the AFDRS

2. Fire Danger Ratings in Australia

Fire danger is a general term representing many factors culminating in a fire environment including ignition potential, fire hazard, risk, rate of spread, difficulty of control, fire impacts and safety. Fire danger rating is a valuable tool in communicating bushfire risk to the community, not only by increasing public awareness but also as a trigger for notification of potential threats. Importantly, because of its foundation in fire weather and behaviour, fire danger rating also provides a tool for decision-making in fire suppression operations and prescribed burning (Matthews *et al.*, 2018).

2.1. The McArthur System

Alan McArthur was the first full-time bushfire scientist in Australia, when he gained a job in 1953 working for the then Commonwealth Forest and Timber Bureau. He was tasked with developing a national fire danger rating system to suit Australian conditions. Alan and his team conducted more than 400 experimental fires that provided data to support fire behaviour models for dry sclerophyll forests, and later, for grassland. This work, together with data from high intensity bushfires, led to McArthur introducing two indices, The Forest Fire Danger Index (FFDI) and the Grassland Fire Danger Index (GFDI). These were aligned to fire danger ratings based on fire suppression difficulty (Cruz et el. 2015).

2.2. Attempts to modify the system

Although the McArthur system served Australia well for many decades, the Black Saturday Fires of 2009 underscored its various weaknesses. The 2009 Victorian Bushfires Royal Commission (Parliament of Victoria, 2010) made several recommendations that led to attempts to modify the system, including a review of the number of fire danger rating categories to provide more definition at higher danger levels, and the additional of a 'catastrophic' ('Code Red' in Victoria) category to capture fires that were increasingly being experienced beyond McArthur's original design parameters (Figure 2).

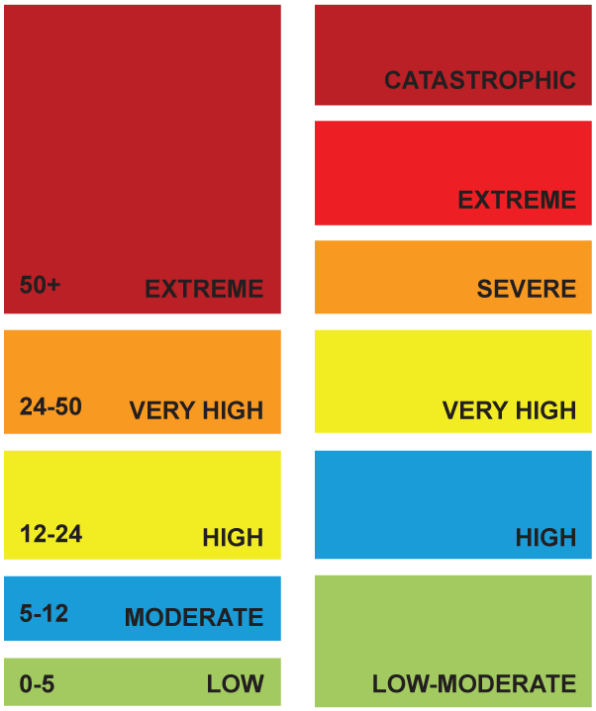

Figure 2- Changes to forest fire danger ratings after 2009

Later, there were also changes made to the ratings for grasslands, causing the GFDI and FFDI to no longer be aligned in terms of the ratings they represent.

2.3. The need for a contemporary system

Decades of research had been carried out since the McArthur system was introduced in the 1960's with countless field-studies leading to new fire behaviour models and a refined understanding of how fire behaves in a variety of fuel types. There had also been research into the impacts of bushfires, and an improved knowledge among practitioners about the implications of fires for prescribed burning, fire suppression and impacts. There had been numerous advances in weather forecasting and an improved understanding about how fire and the atmosphere interact. The quality of fuel data, satellite data and computational software and hardware had also improved (Cube, 2014).

The pressure was mounting on the McArthur system with its various design limitations highlighted (Cube, 2014):

- The design of the McArthur system did not allow for its components to be updated.
- The two fire behaviour models (one for grassland and one for dry sclerophyll forests) were not representative of Australian vegetation types and only accounted for about a third of the continent.
- Fires were being regularly experienced beyond its design considerations.
- It could not account for improved weather inputs from the Bureau of Meteorology.
- It could not account for the decades of improved fire behaviour research.
- It could not account for research into impacts of fire on assets and human lives.
- Decision-makers were forced to rely on a system with well understood flaws.
- The ratings and signage were not consistent from jurisdiction to jurisdiction.
- The system had become confusing for members of the public and did not inspire appropriate action to reduce risk.

The changes made after the 2009 fires only served to highlight the need for a new approach (Cube, 2014). In July 2014, Senior Officers and Ministers agreed that the development of a new National Fire Danger Rating System, based on new computational models, was a national priority (Matthews *et al.*, 2018).

3. The Australia Fire Danger Rating System (AFDRS)

In 2015 a roadmap was identified for the development and implementation of a new system. A national Program Board with jurisdictional and national representation was established in late 2016 to oversee development and implementation.

A key part of the development of the AFDRS was a collaborative approach involving all states and territories and the Commonwealth government. This was a considerable undertaking requiring the attention and commitment of the emergency services industry through the substantial challenges of the Black Summer fires of 2019-2020, the subsequent state and federal inquiries, various flooding events and the ravishes of the covid-19 pandemic.

Fortunately, Australia has a well-established National Council for Fire and Emergency Services (AFAC) with existing cooperative arrangements that proved useful to coordinate the program to develop and implement the AFDRS. Also, the New South Wales Rural Fire Service was well placed to take on the task of leading the science build, with help of the Bureau of Meteorology who built the fire danger calculation engine. Simultaneously, the South Australian Country Fire Service took on the task of leading one of the largest social research projects in Australia, to better understand the community's needs in relation to fire danger ratings.

3.1. The Fire Behaviour Models

Fire behaviour models in Australia are fuel specific, unlike the more unifying approach taken in the US. As fires spread and behave differently in different fuels, specific models have been built for major fuel types; e.g. grasslands, forests and shrublands (Cruz et al., 2015).

The AFDRS makes use of the best fire spread models that are available and ready for application. Table 1 provides an overview of the fire behaviour models used as guided through consultation with experts and by *A Guide to Rate of Fire Spread Models for Australian Vegetation* (Cruz *et el*., 2015).

Table 1 Fire behaviour models used for the AFDRS

Fire behaviour model	Short name	Reference	Fuel type
CSIRO Grassland fire spread meter	Grassland	Cheney et al. (1998) and Cruz et al. (2015b)	Continuous grasslands
CSIRO Grassland for northern Australia	Savanna	Cheney et al. (1998) and Cruz et al. (2015b)	Grassy woodlands and open forests
Desert spinifex model	Spinifex	Burrows et al. (2018)	Hummock grasslands
Buttongrass moorlands model	Buttongrass	Marsden-Smedley and Catchpole (1995b)	Buttongrass moorlands
Dry Eucalypt Forest Fire Model (DEFFM or "Vesta")	Vesta	Cheney et al. (2012)	Shrubby dry eucalypt forests
Mallee heath model	Mallee heath	Cruz et al. (2013)	Semi-arid mallee heath
Heathland model	Shrubland	Anderson et al. (2015)	Temperate shrublands
Adjusted Pine model	Pine	Cruz (pers. comm.)	Pine plantations

3.2. The Fuel Types

A national fuel type layer (Figure 3) consisting of a 1.5 kilometer spatial grid, was developed based on available national, state and territory vegetation mapping. Considerable knowledge and effort was applied to convert vegetation mapping into a fuel type classification useful for application within the AFDRS (Matthews, 2022).

Classification of fuel types was led by the practical need to select an appropriate fire behaviour model, and to capture the range of variation in the fuel parameters that feed the inputs to the models. Fuel types that don't have a specific fire behaviour model (e.g. rainforests, arid shrublands, wetlands, rural and urban areas) have been allocated to the model with the most similar fuel structure (as per Cruz, 2015).

There are often factors limiting the flammability, fuel availability or fuel connectivity in these fuel types. So various modifications to fire behaviour models were made to account for these variations, such as a drying factor or a wind reduction factor. This allowed for calculations of fire danger to be applied across 23 fuel types, allowing more precise results (Matthews, 2022).

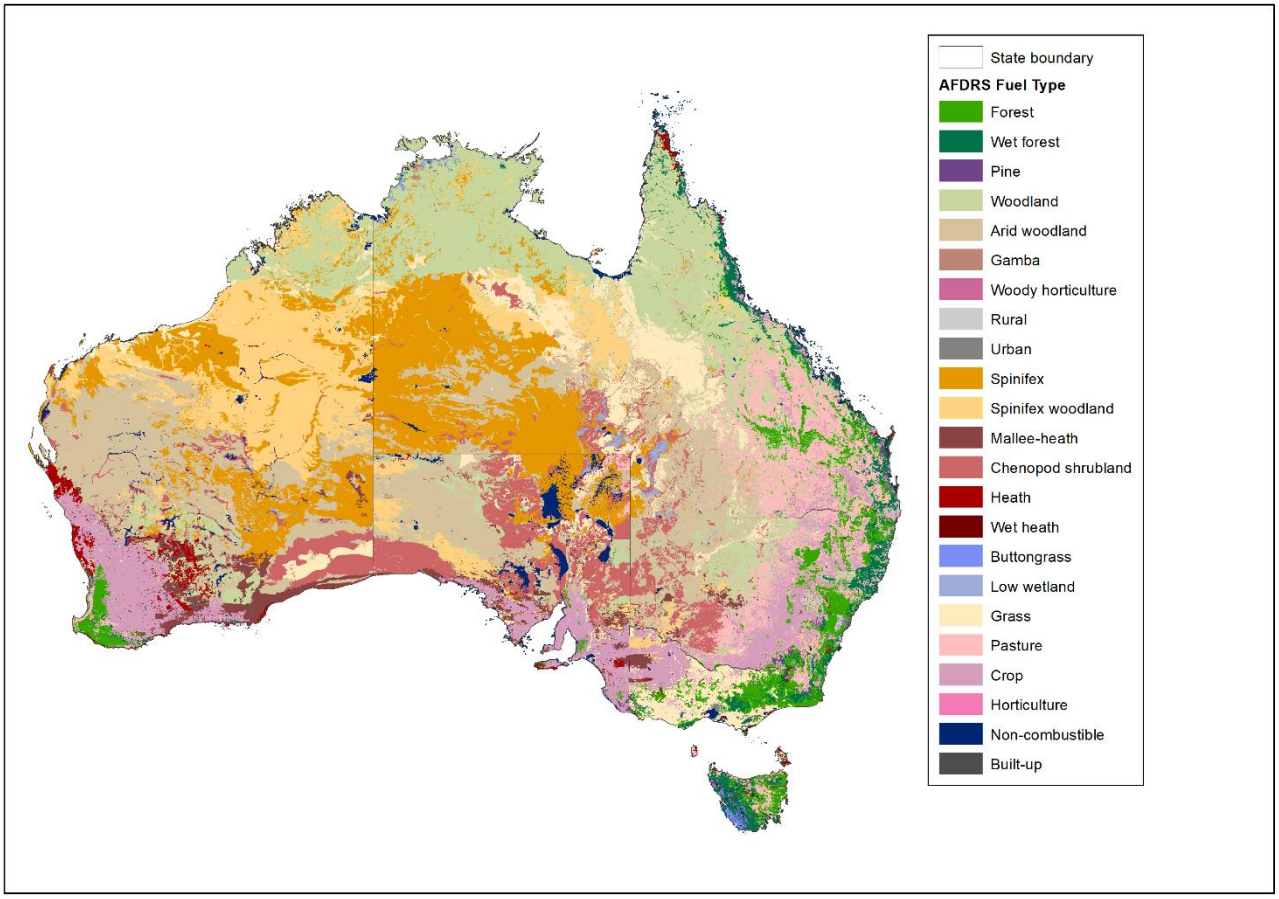

Figure 3 - Map of AFDRS fuel types across Australia

3.3. The Fire Behaviour Index

The Fire Behaviour Index (FBI) is expressed in whole numbers from 0 to 100+. It represents the severity of a fire should one occur under the forecast conditions. The FBI is divided into step-up categories controlled by table definitions (Figure 4 is an example) that represent contemporary understandings of how the underlying fire behaviour transitions create implications for prescribed burning, fire suppression and life and property loss. A step-up in FBI category is triggered by a change in (Matthews, 2022):

- Indicative fire behaviour and fire weather
- Implications for prescribed burning and fire spread
- Implications for suppression and containment
- Implications for potential impacts to life and property.

This, together with various guides produced as part of the FBI, ensures its usefulness as a decision-making tool for operational fire management.

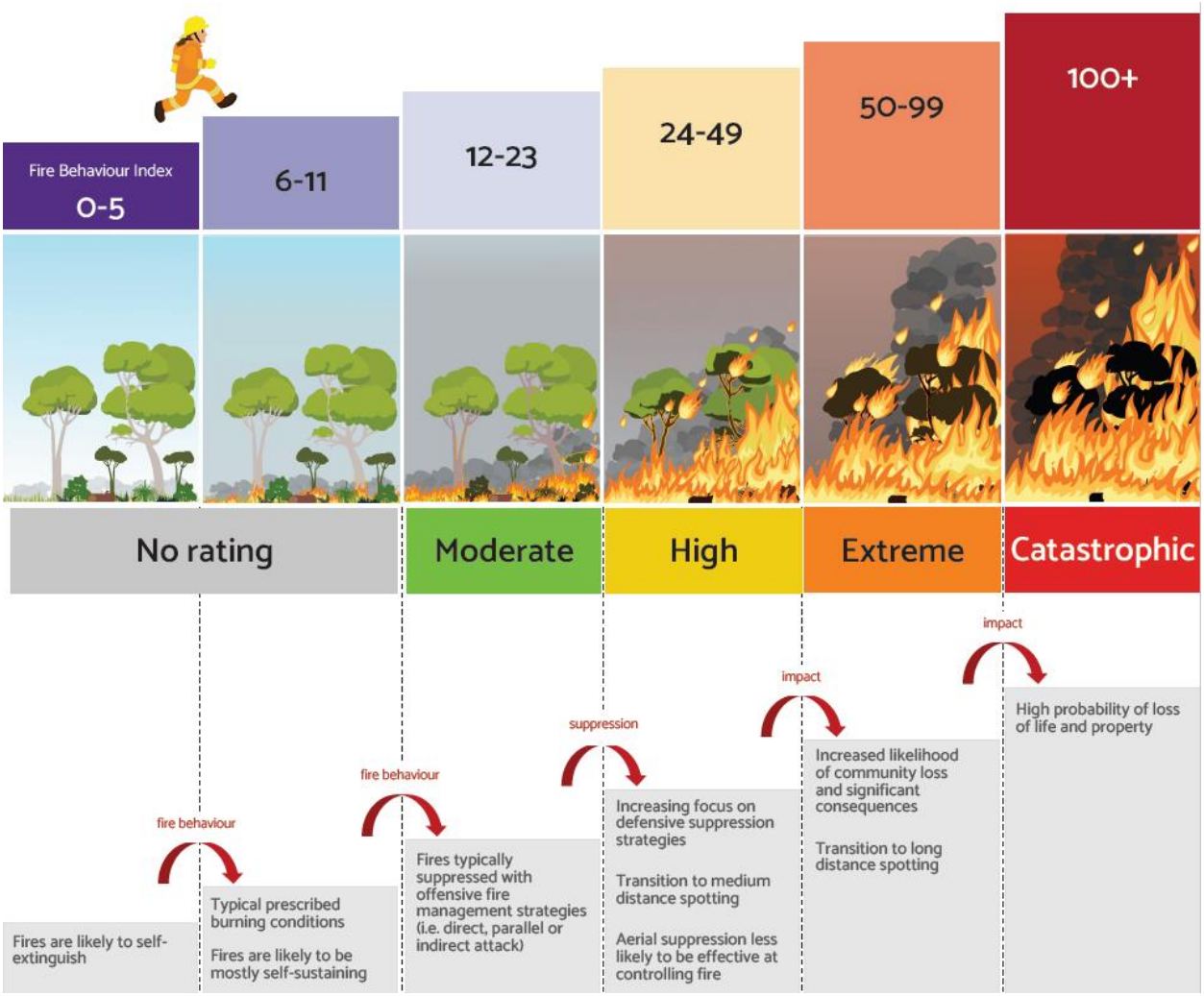

Figure 4 The Fire Behaviour Index for Forest Fuels, broken into steps that are relevant to fire operations

3.4. The Fire Danger Ratings

By contrast, the AFDRS Fire Danger Ratings are purpose built for ease of communication and comprehension for members of the community, so that members of the community are forewarned about fire danger conditions and can take appropriate action to reduce their risk exposure.

The social research conducted on the previous McArthur-based system was influential in the design of the new Fire Danger Ratings. The initial survey was the third largest ever conducted in Australia with 5,430 participants. The key outcomes were (Metrix, 2019):

- Most recognise the Fire Danger Rating system, but many didn't understand it. It was found that 93% had prompted awareness of the system but most thought it predicts how likely a fire is to occur, rather than predicting how dangerous a fire could be if one did occur.
- There is confusion over what action to take when, and it was found that few people would take action below the 'Severe' rating (refer to Figure 2 for the McArthur-based ratings post 2009).
- It was found that while the signage is recognised, most people do not use the system to plan activities and the majority have never taken action relating to fire danger ratings.

Focus groups were conducted with a broad range of communities. Locations encompassed metropolitan and rural areas as well as a variety of low, medium and high-risk bushfire areas (Metrix, 2019): It was found:

- Participants felt that each fire danger rating should be associated with a unique and distinct action-orientated message.

- Participants strongly preferred a three or four-level rating system, with more levels than this seen as confusing and counterproductive.
- Most favoured a four-stage semicircle design with intuitive names and colours.
- A green, yellow, orange and red colour set was preferred.

The finalised public-facing fire danger rating system framework is shown below:

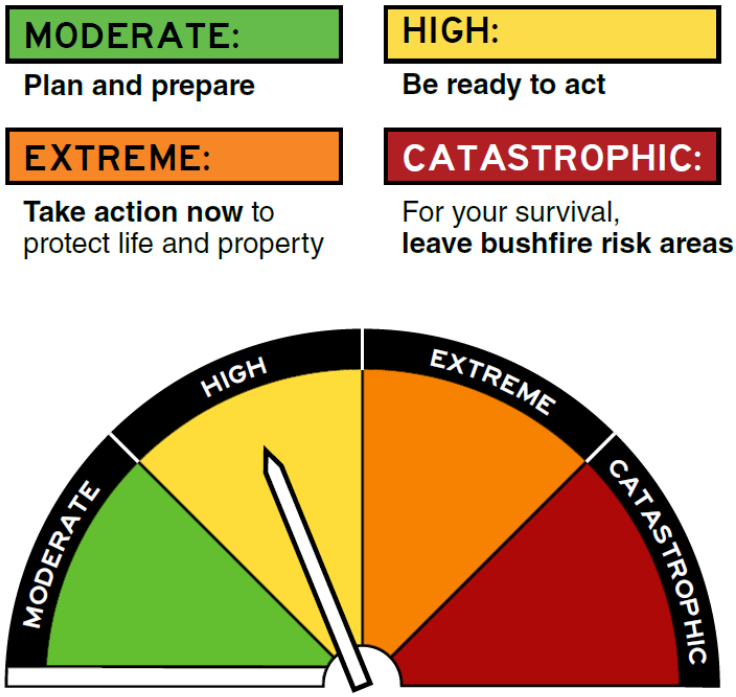

Figure 5 The AFDRS Fire Danger Ratings

The four action-orientated messages are related to underlying transitions in fire behaviour requiring different kinds of actions from members of the community. The fire danger ratings are therefore derived from thresholds in the FBI that encapsulate these transitions. This relationship was shown in Figure 4.

4. References

Commonwealth of Australia, 2020. Royal Commission into National Natural Disaster Arrangements Report. Canberra.

Cruz, M.G., Gould, J.S., Alexander, M.E., Sullivan, A.L., McCaw, W.L., Matthews, S., 2015. A Guide to Rate of Fire Spread Models for Australian Vegetation Revised Edition, CSIRO Land and Water, Canberra, ACT, and AFAC, Melbourne, Vic

Cube Management Solutions (Cube), 2014. Concept Document: Improving our National Fire Danger Rating System. Prodouced for the Bushfire and Natural Hazards Cooperative Research Centre (BNHCRC)., Melbourne.

Parliament of Australia, 2022. https://www.aph.gov.au/Parliamentary_Business/Committees/Senate/Former_Committees/agric/completed_inquiries/2008-10/bushfires/report/c02. {verified, August 2022}.

Parliament of Victoria, 2010. 2009 Victorian Bushfire Royal Commission. Final Report Summary. Government Printer for the State of Victoria. Melbourne.

Matthews, S. 2022. Fire Behaviour Index Technical Guide. NSW Rural Fire Service. Sydney.

Matthews S; Paul Fox-Hughes, Saskia Grootemaat, Simon Heemstra, Jennifer Hollis, Belinda Kenny, Samuel Sauvage, Corey Shackleton, Lew Short, Deb Sparkes, 2018. Building the prototype for a new National Fire Danger Rating System for Australia. **Advances in Forest Fire Research**. DOI:https://doi.org/10.14195/978-989-26-16-506_178

Metrix, 2019. National Fire Danger Rating System Social Research Summary: National Fire Danger Rating System Research Report Stages 1 to 3. Produced for South Australia Country Fire Service. Adelaide.

Demographic processes and fire regimes interact to influence plant population trajectories under changing climates

Sarah McColl-Gausden*[1]; Lauren Bennett[1]; Trent Penman[1]

[1]*School of Ecosystem and Forest Sciences, The University of Melbourne, Melbourne, Victoria, Australia, {mccoll.s, ltb, trent.penman}@unimelb.edu.au*

**Corresponding author*

Keywords

Climate change, fire regime, biodiversity, risk analysis, functional types

Abstract

Fire regimes are changing around the world raising important questions about the risks to biodiversity. Fire seasons are lengthening, high-severity fires are occurring more often and in unexpected places. Extensive research examines some of the fire related risks to life and property. However, in the fire risk research space there is often limited or simplified inclusion of ecological values. Future fire regimes, alongside climatic change, could have profound impacts on biodiversity conservation and ecosystem function. For example, plant population trajectories can be influenced by demographic traits, disturbance regimes and environmental variables such as climate. Climate change can affect all three and is likely to impact on plant populations through altering natural fire regimes as well as influencing species demographic traits. These changes are unlikely to be unidirectional with some plant types benefiting and others being disadvantaged. Here, we examine the impacts of climate change both on the shifts in fire regimes alone and combined with predicted climate-induced demographic shifts. We use two functional plant types (obligate seeder, facultative resprouter) in a number of case-study areas representing woodland-dominated landscapes of south-eastern Australia. We link a fire regime simulation tool with a spatially explicit population viability analysis model. We simulate fire regimes under six different future climates representing different temperature and precipitation shifts, and 16 demographic change scenarios, characterised by changes to individual or multiple plant demographic processes. Obligate seeder species were predicted to be less resilient to changes in demographic parameters. However, both resprouter and seeder species were found to be negatively affected by the combined impacts of changes to multiple demographic parameters or to a combination of a shifting fire regime and changes to demographic traits, particularly through simulated reductions in adult survival. To our knowledge this is the first study to integrate fire regime simulations with spatially explicit population viability analyses. Such an approach significantly increases our ability to identify which functional types are most at risk of population extinction under predicted fire regime and demographic changes. This flexible framework is an important first step in exploring the complex interactions that determine plant viability under a changing climate and will increase our ability to prioritise research and fire management for biodiversity into the future.

1. Introduction

Fire is instrumental in shaping plant community composition (Pausas & Ribeiro, 2017). Many plants are adapted to components of the fire regime (e.g., fire severity, inter-fire interval), through fire-adapted traits, which typically offer two main strategies in the face of fire, survive fire or regenerate following fire (Enright & Goldblum, 1999). Species that rely on one strategy are termed obligate (e.g., an obligate seeder can only regenerate through seeds), and those that are more flexible in their regeneration strategy are termed facultative (e.g., a facultative resprouter can both resprout and produce seeds, Clarke et al., 2015). Resprouting species can survive fire by producing new shoots from meristematic tissues, either above ground from buds on the trunk and branches (epicormic resprouter) or from basal tissues when above-ground tissues are killed or damaged (basal resprouter, Pausas & Keeley, 2014). Groups of species that share fire-adapted traits are often grouped into functional types, which typically describe key processes that contribute to species dynamics (Noble & Slatyer, 1980, Pausas, 1999). Responses of plant populations to fire are thus often described in terms of functional types and associated traits, including whether seeds are stored in the canopy or soil, and whether seed germination is fire cued or can occur without fire (Noble & Slatyer, 1980, Pausas et al., 2004, Pausas & Keeley, 2014).

The interactive effects of a potentially warmer drier climate alongside changes to the fire regime have the potential to increase the extinction risk of plant species through demographic changes (Enright et al., 2015). Plant demographic rates can also vary across climate gradients, with vital rates generally decreasing under warmer conditions (Bowman et al., 2014), and therefore may change as the climate changes. Many demographic traits are directly related to a plant species' fire response. For example, fire-responsive species could be at increased risk of localised extinction if future warmer drier climates decrease growth rates and associated time to maturity (Bowman et al., 2014, Enright et al., 2014, Jump et al., 2006) or decrease seed production and post-fire recruitment (Miller et al., 2019). If fire frequency were to increase alongside demographic changes, the window for population self-replacement may be reduced due to the interacting effects of climate and fire, a phenomenon termed "interval squeeze" (Enright et al., 2015). Improved understanding of the interactions among plant demographic traits, fire regimes, and climate is critical to identifying those species at most risk in fire-prone vegetation communities.

Effective conservation management of any system needs to be based on sound predictions of ecological futures. However, as we move towards the potential for new interactions without historical analogues, we cannot solely rely on past empirical data. As our climate changes and fire regimes change alongside, we need to be able to untangle how variation in plant traits influence the viability of populations. Simulation modelling provides the opportunity to expand the utility of existing empirical data to examine plant population viabilities under various combinations of traits, fires, and climates. In Australia, the empirical, demographic data around fire responsive plant species is substantive, albeit patchy. Initiatives such as Austraits, a database of plants traits from Australian flora (Falster et al., 2021) provide a means for the collation of these into the future. Previous research of fire responsive plant species in Australia has mostly focused on single species where the demographic data are often collected over many years (e.g. Auld, 1986, Ooi et al., 2004, Swab et al., 2012). These investigations are invaluable. However, detailed demographic data for many species of interest are lacking across environmental gradients. Collecting such data and attempting to measure and interpret the relationships among fire, climate, and plant populations would be infeasible for all at-risk vegetation communities.

In this study, we develop a framework for simulating ecological futures, combining a landscape fire regime model with plant demographic data in the form of a spatially explicit population viability analysis. We use this framework to examine how a changing climate might affect demographic processes and fire regimes to influence plant population trajectories.

2. Model framework

Our modelling framework involved six steps:

1. Select study area and species;
2. Create fire raster layers based on six representative climate models;
3. Construct population transition matrices for fire and non-fire years based on demographic change scenarios;
4. Create habitat suitability layers for each selected species;
5. Build population trajectory models for 100-year simulations for each combination of fire regime and demographic change scenario; and
6. Compare outputs across scenarios, functional types, and study areas (Figure 1).

The two simulation programs used in the framework are FROST (Penman et al., 2015) and STEPS (Visintin et al., 2020). FROST (Fire Regimes and Operations Simulation Tool) simulates fire regimes over decades to centuries using a combination of fire event simulation tools (PHOENIX RapidFire: Tolhurst et al., 2008) and Bayesian networks to represent uncertainty. FROST is spatially explicit and produces fire data (cells burnt, intensity, frequency) at a 180 m resolution for each year of a simulation. STEPS (Spatially and Temporally Explicit Population Simulations) is a spatially explicit population dynamics R package (Visintin et al., 2020). It models species populations as a function of species ecological and physiological requirements, and disturbance and landscape dynamics. Spatially explicit FROST outputs of fire occurrence and severity are fed into STEPS to, for example, trigger a germination or resprouting event for a plant species or to trigger mortality within the simulation cell.

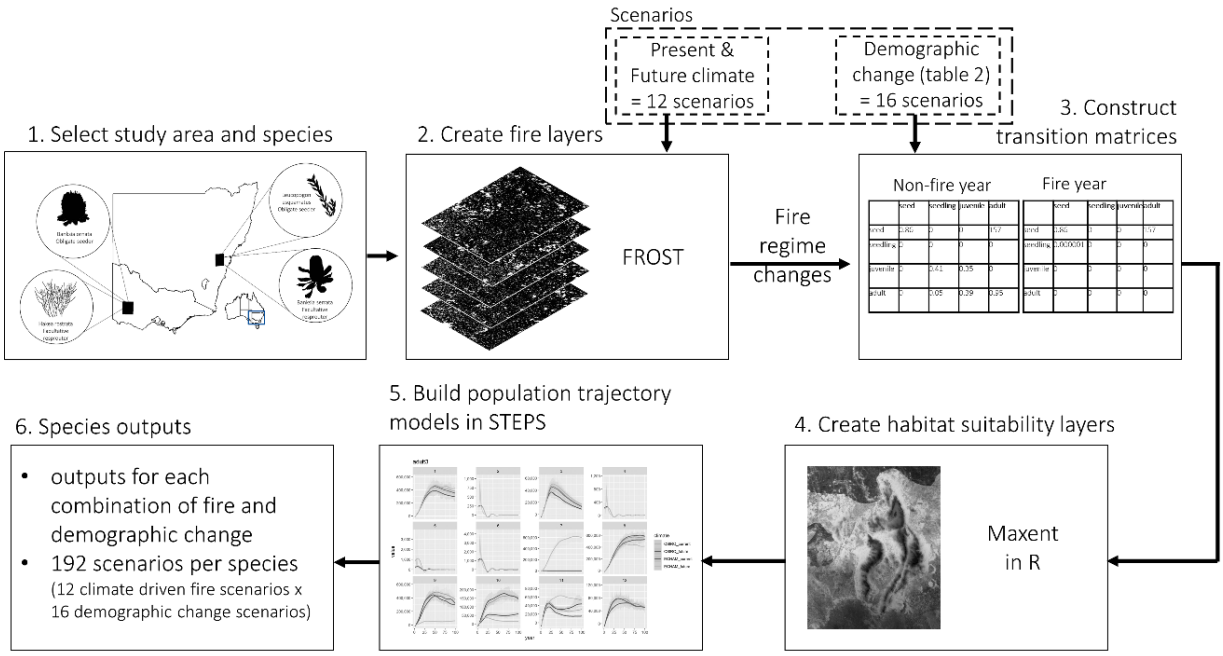

Figure 1 Modelling framework. Step 1: select the study area and species. Step 2: Create fire raster layers using FROST under six predictions of present climate and six predictions of future climate scenarios. Step 3: collate empirical data and expert advice to create population transition matrices for non-fire years and fire years for each species under 16 demographic change scenarios. The transition matrices are used to parametrise the population models with the PVAs. Step 4. Create habitat suitability layers using presence only data with the dismo package in R. Step 5: Build population trajectory models in the STEPS package in R for each combination of fire regime and demographic change scenario. Step 6. Examine species outputs under each combination of fire and demographic change scenario.

3. Implications

Demographic changes on plant population viability far outweighed impacts from a changing fire regime in our simulations. In general, obligate seeder species were predicted to be less resilient to changes in demographic parameters than facultative resprouter species. This introduces considerable challenges for management looking to improve ecological outcomes. The focus needs to shift towards management activities that relate directly to improving demographic outcomes such as protection of adult plants and ensuring adequate seed supply for active restoration. Due to the large number of interconnected mechanisms driving plant viability, there are still significant knowledge gaps that will require research to improve our understanding of how plant communities will respond to fire and demographic shifts.

4. Conclusion

The effects of future climate on biodiversity will be complex. Our study predicts changes in plant population trajectories due to climate effects on demography or climate effects on changing fire regimes and demography. The simulation results suggest we need to understand demography across climate gradients in order to prioritise species conservation. Therefore, field research that gathers demographic data is vital for protecting future ecosystems. Our PVA-fire regime simulation framework can address questions around management intervention through prescribed burning and fire suppression, and identify which demographic shifts an ecosystem may be most sensitive to. However, the importance of demographic shifts in our study emphasises the need for conservation managers to actively understand and appropriately manage at risk ecosystems to improve or promote resilience to future changes in climate.

5. References

Auld TD (1986) Population dynamics of the shrub Acacia suaveolens (Sm.) Willd.: Fire and the transition to seedlings. Australian Journal of Ecology, 11, 373-385.

Bowman DMJS, Williamson GJ, Keenan RJ, Prior LD (2014) A warmer world will reduce tree growth in evergreen broadleaf forests: evidence from Australian temperate and subtropical eucalypt forests. Global Ecology and Biogeography, 23, 925-934.

Clarke PJ, Lawes MJ, Murphy BP et al. (2015) A synthesis of postfire recovery traits of woody plants in Australian ecosystems. Science of The Total Environment, 534, 31-42.

Enright NJ, Fontaine JB, Bowman DM, Bradstock RA, Williams RJ (2015) Interval squeeze: altered fire regimes and demographic responses interact to threaten woody species persistence as climate changes. Frontiers in Ecology and the Environment, 13, 265-272.

Enright NJ, Fontaine JB, Lamont BB, Miller BP, Westcott VC (2014) Resistance and resilience to changing climate and fire regime depend on plant functional traits. Journal of ecology, 102, 1572-1581.

Enright NJ, Goldblum D (1999) Demography of a non-sprouting and resprouting Hakea species (Proteaceae) in fire-prone Eucalyptus woodlands of southeastern Australia in relation to stand age, drought and disease. Plant Ecology, 144, 71-82.

Falster D, Gallagher R, Wenk EH et al. (2021) AusTraits, a curated plant trait database for the Australian flora. Scientific Data, 8, 254.

Jump AS, Hunt JM, Peñuelas J (2006) Rapid climate change-related growth decline at the southern range edge of Fagus sylvatica. Global Change Biology, 12, 2163-2174.

Miller RG, Tangney R, Enright NJ et al. (2019) Mechanisms of Fire Seasonality Effects on Plant Populations. Trends in Ecology & Evolution, 34, 1104-1117.

Noble IR, Slatyer RO (1980) The Use of Vital Attributes to Predict Successional Changes in Plant Communities Subject to Recurrent Disturbances. Vegetatio, 43, 5-21.

Ooi MKJ, Auld TD, Whelan RJ (2004) Delayed post-fire seedling emergence linked to season: a case study with Leucopogon species (Epacridaceae). Plant Ecology, 174, 183-196.

Pausas JG (1999) Mediterranean Vegetation Dynamics: Modelling Problems and Functional Types. Plant Ecology, 140, 27-39.

Pausas JG, Bradstock RA, Keith DA, Keeley JE, The GFN (2004) Plant Functional Traits in Relation to Fire in Crown-Fire Ecosystems. Ecology, 85, 1085-1100.

Pausas JG, Keeley JE (2014) Evolutionary ecology of resprouting and seeding in fire-prone ecosystems. New Phytologist, 204, 55-65.

Pausas JG, Ribeiro E (2017) Fire and plant diversity at the global scale. Global Ecology and Biogeography, 26, 889-897.

Penman TD, Ababei D, Chong DMO, Duff TJ, Tolhurst KG (2015) A fire regime risk management tool In: 21st International Congress on Modelling and Simulation. (ed Sharples J), Gold Coast, Australia.

Swab RM, Regan HM, Keith DA, Regan TJ, Ooi MKJ (2012) Niche models tell half the story: spatial context and life-history traits influence species responses to global change. Journal of biogeography.

Tolhurst K, Shields B, Chong D (2008) Phoenix: Development and Application of a Bushfire Risk Management Tool. The Australian Journal of Emergency Management, 23, 47-54.

Visintin C, Briscoe NJ, Woolley SNC, Lentini PE, Tingley R, Wintle BA, Golding N (2020) steps: Software for spatially and temporally explicit population simulations. Methods in Ecology and Evolution, 11, 596-603.

Developing an Integrated Capitals Approach to Understanding Wildfire Vulnerability: Preliminary Considerations from a Literature Review

Simone Martino[1]*; Michaela Roberts[1]; Tami Wooldridge[1]; Paola Ovando Pol[1;2]; Florent Mouillot[3]; Umberto Pernice[4]; Macarena Ortega[5]; Ramona Velea[6]; Riccardo Laterza[6]; Bruno Moreira[7]

[1]The James Hutton Institute, Craigiebuckler, Aberdeen, AB15 8QH, Scotland, UK {simone.martino@hutton.ac.uk}
[2]Spanish National Research Council (CSIC), Calle Albasanz 26-28. 28037 Madrid, Spain
[3]UMR CEFE, Université de Montpellier, CNRS, EPHE, IRD. 1919 route de Mende, 34293 Montpellier Cedex 5. France
[4]University of Rome 'La Sapienza', Via Salaria 851, 00138, Rome, Italy
5Forest Fire Laboratory (LABIF). Department of Forest Engineering. University of Córdoba (UCO). Edif. Leonardo Da Vinci, Campus de Rabanales, 14071, Córdoba, Spain.
[6]Institute of International Sociology Gorizia, Via Mazzini 13, 34170, Gorizia, Italy
[7]Centro de investigaciones sobre Desertificacion -CIDE- (CSIC/UV/GV), Campus IVIA, Carretera Moncada-Náquera km 4,5 s/n, 46113 Moncada, Valencia, SPAIN.

**Corresponding author*

Keywords

vulnerability, natural capital, social and human capital, socio-economic damage, ecosystem services, impact mitigation and assessment

Abstract

A capitals approach deals with humans' activities and impacts on the environment and their dependencies on stocks of natural, human, social and produced capital to inform decision-making. Traditional assessments focus on one capital at a time such as natural or human capital. Conversely, a multi-capital assessment involves the analysis of more than one relevant capital and presents the results for each capital together. This paper wants to get a step further presenting preliminary findings on developing an Integrated Capitals Approach (ICA) to wildfire vulnerability considering in a holistic way the impacts on natural assets (ecological and economic values), damages on human capital (e.g., health), and the interactions between wildfires and social capital. Although some studies have recently introduced the effect of adaptation to fire, expressed mainly as the institutional capacity of improving fuel management and firefighting, the effect of social bonding and networking on training, capacity building and other actions such as volunteering activities performed at scale of community, as a means of reducing social vulnerability, is not yet thoroughly investigated. We think that it is necessary to extend the current wildfire risk frameworks proposed in the literature by adding social capital in its plurality of forms and by integrating them with the current analysis of natural, human, and economic assets as a tool to mitigate wildfire vulnerability.

1. Introduction

Although an essential disturbance for many ecosystems, wildfires affect 600 to 700 thousand ha of forest per year in Southern Europe, reaching peaks of 1,000,000 ha, and up to 100,000 ha in northern European countries (EC, 2021). These fires cause enormous impacts on socio-economic activities and population wellbeing, and their increase, magnified by climate and land use change (e.g., land abandonment), impairs the efficacy of measures implemented to contain temperature rise and adaptation to climate change. Managing the damages inflicted by wildfires requires an integrated and holistic approach, based on land-management actions such as thinning, prescribed fire and grazing (Kerns et al., 2020), investment in green infrastructures and adoption of adaptive and proactive wildfires risk prevention and management plans (Robinne et al., 2021) that account for interactions between natural and human systems (Kinoshita et al., 2016). To be effective these measures need to assess not only the likelihood that a fire ignites and propagates, but also the human, ecological and economic values potentially affected by it (in other terms, vulnerabilities) (Chuvieco et al., 2010; 2014) as well as the ability to cope with the damage through the implementation of institutional and voluntary initiatives capable of

mitigating environmental and socio-economic impacts. This paper presents a holistic view, developed under the ongoing project H2020 FirEUrisk (Grant agreement 101003890), for the analysis and valuation of vulnerability to wildfires by implementing an Integrated Capitals Approach (ICA) that embraces multiple capitals (natural, human, social, economic, and manufactured) in a common framework (Capital Coalition, 2021).

To achieve this goal, we have carried out a literature review dealing with wildfires and potential assets at risk, from forests and their ecosystem services (e.g., regulating and cultural ones), to semi-natural environments like agricultural ecosystems and wildland-urban interface, but addressing more immaterial values like human life and health, and resilience for both ecosystems and socio-ecological systems. Although institutional mechanisms to cope with wildfires are considered in the recent literature (Oliveira et al., 2018; 2020), only a few papers address human and social capitals and their relations with fire risk reduction, such as the role of information on fire and awareness of correct practices, local training, capacity building, or any volunteer measures (e.g. formalised civic, non-professional initiatives, etc.) able to limit fire vulnerability (Górriz-Mifsud et al., 2019). Analysis of the latter activities remain marginal compared to the relevant literature addressing environmental, socio-economic and health damages. We emphasise this gap and illustrate the need to integrate all the capitals in the wildfire risk analysis framework, to comprehensively assess both exposure and sensitivity and adaptive capacity of local social systems.

2. Methods

We started from a core of 30 papers on risk vulnerability and socio-economic damage proposed by the research team and then we extended our investigation through multiple searches on the online database ISI Web of Science. Search strings used are reported in Table 1. To better characterise our integrated approach to the analysis of wildfire vulnerability, we have searched for economic damage of wildfires to natural capital and socio-economic assets and explored also 1) the impact that fires have on human capital – such as risk to health and lives; 2) the contribution that social and human capitals can bring to mitigate wildfires such as training, participation in volunteer initiatives, such as clearing scrub, and information campaigns to reduce ignition and make humans less vulnerable to fire; and 3) how these themes are considered in wildfire vulnerability and risk framework. Findings from these three points let emerge gaps that need to be addressed in order to build a more comprehensive framework for wildfire risk analysis.

Table 1: List of search strings and results returned from ISI Web of Science considering as cut-off date of publications February 2022.

Search string	**Papers found**
“Forest fire” AND “economic impact assessment”	53
“Economic” AND “damage” AND” wildfire”	235
“Valuation” AND “damage” AND “wildfire”	27
“Valuation” AND “damage” AND “wildfire” AND Ecosystem services”	1
“Forest fire” AND “Willingness to pay” OR “WTP”, “forest fire” AND “choice experiment”, “forest fire” AND “hedonic price method” OR “HPM”, and “forest fire” AND “travel cost”, and “forest fire” AND “replacement cost”,	40
“Forest fire” AND “built capital” OR “manufactured capital”, “forest fire” AND “capacity building”, forest fire” AND “financial capital”, “forest fire” AND “human capital”, forest fire” AND “social capital”,	55

The full dataset of 411 documents was filtered based on the analysis of title, abstract, introduction and methods. We included papers published in English and a limited number (3) in Spanish and Portuguese. Inclusion criteria were the impacts of single and multiple fires on natural capital and human assets (in monetary and non-monetary units), as well as the analysis of vulnerability in wildfire risk framework. We also included papers clearly expressing the benefits of managing fires and dealing with resilience and adaptation to mitigate vulnerabilities. We excluded a few papers proposed in some conference proceedings of difficult availability, particularly those published in Russian, Chinese and Korean.

3. Results

Papers reflecting the inclusion criteria were 187. Notwithstanding the dominance (as expected from the key strings used) of papers addressing socio-economics issues, we found a broader range of themes referring also to Natural Capital and Risk analysis. We decided to cluster these papers in three groups: "Non-economic impacts on Natural Capital" (44 studies), "Natural Capital and ecosystem services valuation and socio-economic impacts" (95 studies), and "Risk Analysis and Vulnerability" (48 papers).

Within the first group of studies focusing on impacts of fire on natural assets, ecological values and ecosystem services, a preeminent role was played by papers addressing damages and disturbances to forest ecosystem dynamics (Wu & Kim, 2013; Aleksić et al., 2009), direct changes to dominant vegetation and biodiversity (Adams, 2013) and indirect shifts caused by grass invasion (Morais et al., 2021; Kerns et al., 2020), higher impacts of pest and diseases on plant survival, variations in traits expression (Lerch et al. 2016; Bélanger et al., 2013; Salazar et al., 2020), and reduction in forest resilience (Wu & Kin, 2013, Mouillot et al., 2005). Less investigated are impacts on water and soils. Wildfire incidents can affect water quality through increased sedimentation and erosion, causing reduction in the supply of potable water (Montagné-Huck & Brunette, 2018), alterations on the hydrology of watersheds through runoff of debris produced in response to storms (Parise & Cannon, 2017), and intensity of rockfalls in the burned area (Sarro et al., 2021). They also alter soil structural properties through mineralogical and biological impacts and their fertility through nutrient volatilization (Certini, 2005).

As regards the second group (see Figure 1), many studies focused on assessing the socio-economic impacts of wildfires on agriculture and agroforestry system by using market approaches (Molina et al., 2011; Stougiannidou et al., 2020; Fagarazzi et al., 2021), but also addressed multiple forest ecosystem services, including timber, carbon and biodiversity (Aleksić et al., 2009; Mueller et al., 2019; Varela et al., 2016), landscape amenities and recreational values (Molina et al., 2019a; Molina et al., 2018) by implementing a mix of stated (contingent valuation and choice experiments) and revealed preference methods (travel cost).

Relevant is the number of papers dedicated to health damage such as respiratory morbidity and cardiovascular diseases caused by haze (Liu et al., 2015), smoke pollutant and contamination rates (Evangeliou et al., 2015), or other physical consequences such as reduced height in adult age (Rosales-Rueda & Triyana, 2018; Sing & Dey, 2021). However, economic estimates remain sparce, focussing on cost of medical treatment and hospital admittance (Stanke et al., 2013), willingness to pay for avoiding respiratory disease (Jones, 2018; Leslie et al., 2013) and mitigating smoke exposure (Heider et al., 2019). We have also found a relevant number of studies addressing the valuation of wildfire prevention policies (categorised as "valuing decision making") (Shrestha et al., 2021; Gorriz-Mifsud et al., 2016; Allo & Loureiro, 2020), and sparse examples of macro-economic analysis of wildfires on employment (Nielsen-Pincus et al., 2014) and on the entire economy of a country (California) (Wang et al. 2021), labelled in Figure 1 as "other socio-economic impacts".

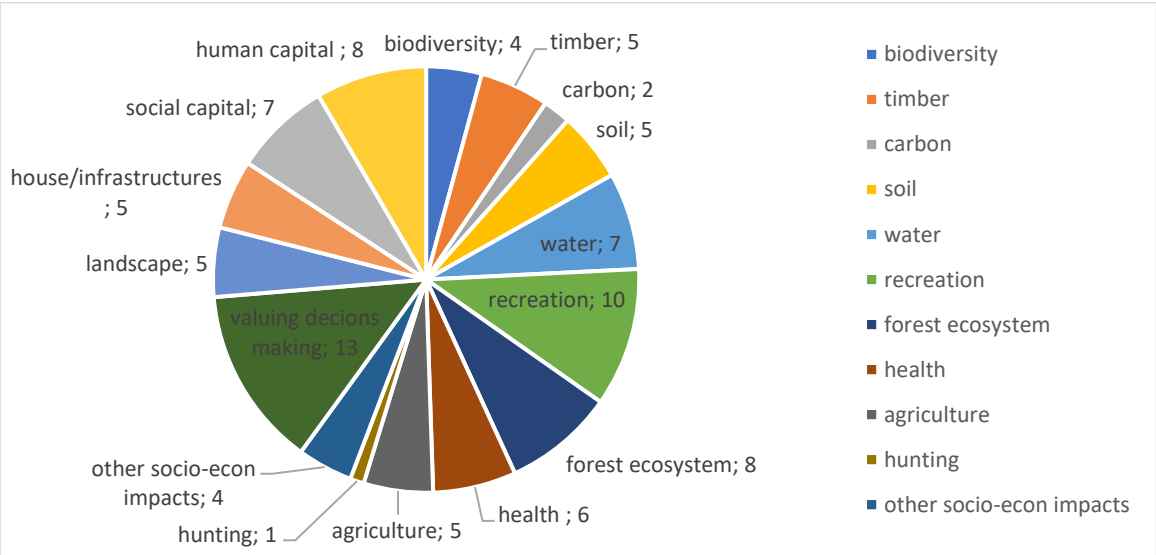

Fig. 1: Types and number of studies addressing impacts to specific ecosystem services, economic sectors and damages caused to social wellbeing and environmental values

We have dedicated attention to the interactions between wildfires and social relations. What is emerging is a limited number of studies that provide evidence of fire as a leverage to increase sound management actions to reduce wildfire risk by promoting community engagement, training and discussions. Examples from the Global South (in countries like Nepal, India, Seychelles and Indonesia – Hiratsuka et al., 2019; Chauhan et al., 2021; Etongo et al., 2021) and Western countries are found to build a stronger nexus between policy makers and scientists (Narayanan et al., 2009; Tabara et al., 2003; Huber-Stearns et al., 2021) by the integration of spatial data and models of wildfire behaviour in decision making. Relevant is the contribution that the impact of wildfires has on strengthening communities with local institutions such as municipalities and fire fighters as evidenced in Australia (Mc Dougall et al., 2014) and in developing countries like Nepal and Indonesia, where collective actions enforced rules for risk mitigation (Sapkota et al., 2015; Jalil et al., 2021). In Mediterranean countries voluntary initiatives at local levels and a series of structural and relational bonding between communities and institutions are found to statistically explain the community's operational capacity and perception of arson level (Górriz-Mifsud et al., 2019).

Finally, our search returned a consistent number of studies (48) referring to the group "Risk Analysis and Vulnerability", addressing:

1. The qualitative analysis of risk by getting information through direct interview on burnt areas, damages, local prevention and suppression techniques (Ribeiro et al., 2015; Appiah et al., 2010; Narayanan et al., 2009);
2. The quantitative analysis of:
    - fire risk by integrating spatial dataset of burnt areas and socioeconomic vulnerabilities of communities such as gender, sex, income, living conditions differences (Grala et al., 2017; Álvarez-Díaz et al., 2015; Barreal et al., 2012; Mallini et al., 2019; Andersen & Sugg, 2019);
    - fire hazard carried out through fire simulation controlling for human, biophysical, meteorological and socioeconomic variables (Guillaume et al., 2019; Molina et al., 2019b; 172- Castillo et al., 2016; Molina et al., 2019c; Castillo-Soto & Rodriguez y Silva, 2015; Rodriguez y Silva & Gonzalez-Caban, 2010; Rodriguez y Silva, 2013);
    - vulnerability as a damage function of socio-economic values (Chuvieco et al. 2010; 2014; Parente et al., 2016), resilience of vegetational types to fire intensity (Molina et al., 2018; Rodriguez y Silva, 2013; Rodriguez y Silva & Gonzalez-Caban, 2010; Chuvieco et al., 2014) and human adaptation (Oliveira et al., 2018; Oliveira et al., 2020).

Institutional aspects of coping capacity such as strengthening firefighters' activities are well reported and included in vulnerability frameworks (Oliveira et al., 2018) as well as the role of evacuation time and distance of wildfire from fire station (Oliveira et al., 2020; Oliveira et al., 2021). However, we think that many more elements making part of social capital can contribute to it and be included in the same framework. The latter can be measured, amongst others, by:

1. voluntary actions supporting fire suppression;
2. educational activities raising awareness of incorrect human behaviours (to reduce ignition causes and minimise extent of fire);
3. implementation of surveillance, patrolling and monitoring measures to reduce fire hazard (by early detection of ignition points);
4. formulation of wildfire prevention and defence plan to better manage fuel through silvicultural treatments, adoption of fire breaks and water pools.

Although recent studies are addressing some of these measures (Górriz-Mifsud et al., 2019; McDougall et al., 2014; Jalil et al., 2021), there is not yet consideration in risk analysis of the importance that training, capacity building and social bonding between citizens and institutions may have to reduce vulnerability. Ways to achieve this integration are under investigation in the FirEUrisk project at the time this paper is proposed. Below we propose an example of integrated framework between capitals, building on the investigated literature (Figure 2).

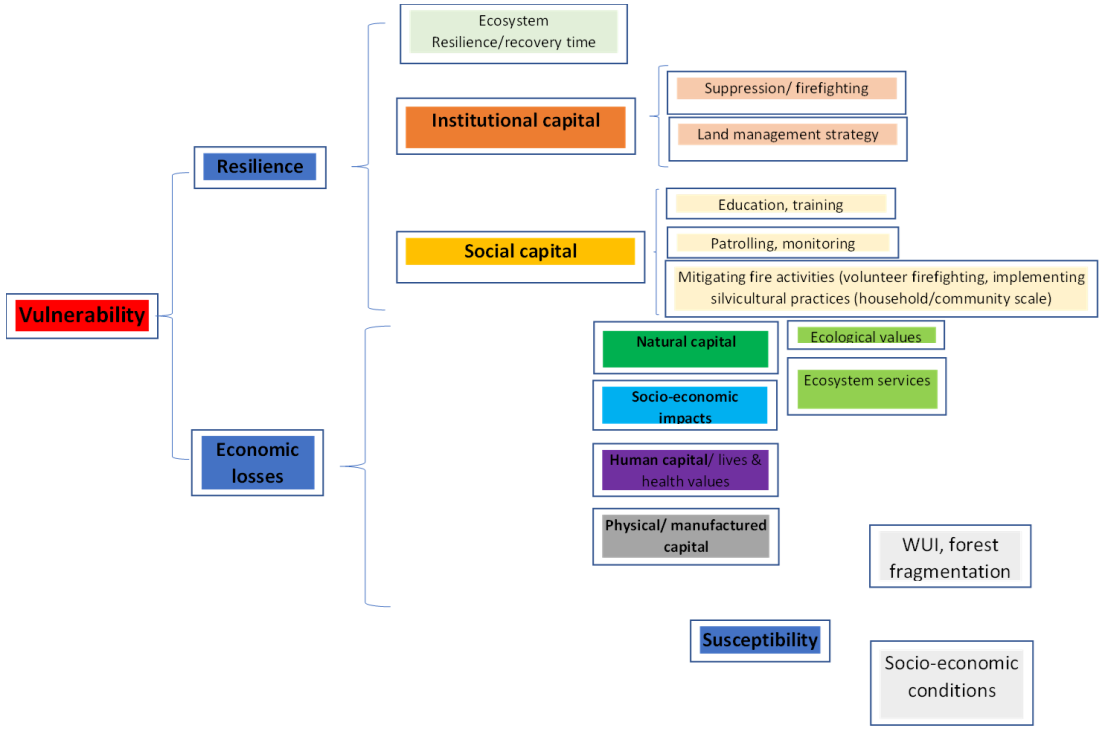

Fig. 2: A preliminary vulnerability framework to wildfires accounting for four types of capital: natural, manufactured, human and social

In the above framework we consider economic losses (as assessed in monetary units) of three different capitals (natural, human, and manufactured) corrected for the resilience of the natural and socio-ecological system. Ecosystems are in fact characterised by resistance and resilience, while societies can change their vulnerability to wildfires through the institutionalization of mechanisms such as strengthening fire suppression and addressing wise land use management strategies. Finally, educating and empowering communities may limit wildfires formation and propagation through actioning preventive measures at household scale, as well as the reduction of landscape fragmentation and other major social challenges (low income, low level of education, etc.) that are all considered relevant to explain wildfire risk.

4. Conclusion

Our preliminary analysis for the development of an integrated capital approach to wildfire vulnerability shows that studies addressing impacts on natural capital, ecosystem services and socio-economic assets are the most represented. We found also human capitals to be well proposed in terms of impacts to human health. However, gaps are evidenced by the limited analysis of social aspects such as role of communities in reducing wildfire risk, as expression of social enfranchisement emerging from the strengthening of relations in communities affected by wildfire. Other frameworks on wildfires vulnerability have introduced the impacts on ecological and economic values (Chuviero et al., 2010), stressing the importance of ecosystem resistance to fire (Parente and Pereira, 2016) and resilience to recover to post-fire conditions (Chiuvieco et al., 2014). More recently, aspects dealing with the capacity of society and communities to cope with wildfires by institutional mechanisms of fire suppression and mitigation by changes in land use management have been proposed (Oliveira et al., 2018; Oliveira et al., 2020). To bridge the gap on the holistic understanding of vulnerability, research and practice should also consider exposure to hazards/stressors, susceptibility of the system/community exposed, and its resilience and adaptive capacity (Birkmann et al., 2013; Burton, Rufat & Tate, 2018). A final consideration can be made on the importance of risk perception and how it influences fire vulnerability: perception acts indeed as a filter through which the different kinds of capital which are at risk assume specific values and/or play different roles in wildfire risk assessment, prevention and management (Paveglio et al., 2009). We consider necessary to investigate in the ongoing steps of the FirEUrisk project the integration of all these aspects in a structured index of vulnerability following the framework suggested in Figure 2.

5. Acknowledgement

This paper is funded by the H2020 Project FirEURisk (Grant Agreement Number:101003890). This research is also supported by the Rural and Environment Science and Analytical Services Division of the Scottish Government through its Strategic Research Programme (2022-2027), project JHI-D5-1 in the Natural resources Theme.

Considerations provided are the results of discussions matured between the authors and other participants of the FireEURisk projects working on the implementation of the ICA approach to wildfire vulnerability and do not necessarily reflect the point of view of the funders.

6. References from the literature review

Adams, M.A. 2013. Mega-fires, tipping points and ecosystem services: Managing forests and woodlands in an uncertain future. Forest Ecology and Management 294, 250-261. **https://doi**.org/10.1016/j.foreco.2012.11.039.

Aleksić, P., Krstic, M., & Janic, G. 2009. Forest fires – ecological and economic problem in Serbia. Botanica Serbia, 33(2): 169-176.

Allo, M., & Loureiro, M.L. 2020. Assessing preferences for wildfire prevention policies in Spain. "Forest Policy and Economics 115, 102145. **https://doi**.org/10.1016/j.forpol.2020.102145.

Álvarez-Díaz, M., Gonzalez-Gomez, M., & Otero-Giraldez M. 2015. Detecting the socioeconomic driving forces of the fire catastrophe in NW Spain. European Journal of Forest Research 134(6), 1087-1094. DOI 10.1007/s10342-015-0911-1.

Andersen, L., & Sugg, M. 2019. Geographic multi-criteria evaluation and validation: A case study of wildfire vulnerability in Western North Carolina, USA following the 2016 wildfires. International Journal of Disaster Risk Reduction Volume 39,101123. **https://doi**.org/10.1016/j.ijdrr.2019.101123.

Appiah, M. Damnyag, L., Blay, D., & Pappinen, A. 2010. Forest and agroecosystem fire management in Ghana. Mitigation and Adaptation Strategies for Global Change 15, 551–570. 10.1007/s11027-010-9236-z.

Barreal, J., Louriero, M., & Picos, J. 2012. The causality of wildfires in Galicia. Economía Agraria y Recursos Naturales – Agricultural and Resource Economics, [S.l.], p. 99-114, **https://doi**.org/10.7201/earn.2012.01.04.

Bélanger, S., Bauce, E., Berthiaume, R., Long, B., Labrie, J., Daigle, L., & Hébert, C. 2013. Effect of Temperature and Tree Species on Damage Progression Caused by Whitespotted Sawyer (Coleoptera: Cerambycidae) Larvae in Recently Burned Logs. Journal of Economic Entomology 106 (3), 1331–1338.

Castillo Soto, M. E., Molina, J.R., Rodriguez y Silva, F., & Alvelar G.H.J. 2013. A territorial fire vulnerability model for Mediterranean ecosystems in South America. Ecological Informatics 13, 106-113. **https://doi**.org/10.1016/j.ecoinf.2012.06.004.

Castillo, M., Molina, J.R., Rodriguez y Silva, F., Chevesich, P.G., & Garfias, R. 2016. A system to evaluate fire impacts from simulated fire behavior in Mediterranean areas of Central Chile. Science of The Total Environment 579, 1410-1418. **https://doi**.org/10.1016/j.scitotenv.2016.11.139.

Castillo-Soto, M., & Rodriguez y Silva, F. 2015. Quantitative analysis of forest fire extinction efficiency. Forest Systems 24(2), e032. DOI: **https://doi**.org/10.5424/fs/2015242-06644.

Chauhan, D.S., Bisht, D.S., Deorai, M., Rawat, D.W., & Sundriyal, R.C. 2021. A sustainable approach for livelihood improvement and integrated natural resource management in Central Himalaya, India. Current Science 120(5), 825-834. DOI:10.18520/cs/v120/i5/825-834.

Chuvieco et al. 2014. Integration of ecological and socio-economic factors to assess global vulnerability to wildfire. Global Ecology and Biogeography 23(2), 245-258. **https://doi**.org/10.1111/geb.12095.

Chuvieco, E., Aguado, I., Yebra, M., Nieto, H., Salas, J., et al. 2010. Development of a framework for fire risk assessment using remote sensing and geographic information system technologies. Ecological Modelling 221, 46–58. **https://doi**.org/10.1016/j.ecolmodel.2008.11.017.

de Oliveira A.S., Raijao, R.G., Soares Filho, B.S., Oliveira, U., Santos, L.R.S, et al. 2018. Economic losses to sustainable timber production by fire in the Brazilian Amazon. The Geographical Journal. **https://doi**.org/10.1111/geoj.12276.

Etongo, D., Barbe, R., Monthy, M., Millet, J., Henriette, E., & Vel, T. 2021. Community engagement in forest rehabilitation within the context of a tropical island: insights from Praslin, Seychelles. Applied Ecology and Environmental Research 19(5), 4185-4217. DOI:10.15666/aeer/1905_41854217.

Fagarazzi, C., Fratini, R., Montanino, M., Viccaro, M., Cozzi, M., Romano, S., & Riccioli, F. 2021. The economic value of fire damages in Tuscan agroforestry areas iForest – Biogeosciences and Forestry 14(1), 41-47. **https://doi**.org/10.3832/ifor3607-013.

Górriz-Mifsud, E., Burns, M., & Marini-Govigli, V. 2019. Civil society engaged in wildfires: Mediterranean forest fire volunteer groupings. Forest Policy and Economics 102, 119-129. **https://doi**.org/10.1016/j.forpol.2019.03.007.

Gorriz-Mifsud, E., Valera, E., Pique, M., & Prokofieva, I. 2016. Demand and supply of ecosystem services in a Mediterranean forest: Computing payment boundaries. Ecosystem Services 17, 53-63. **https://doi**.org/10.1016/j.ecoser.2015.11.006.

Grala, K., Grala, R.K., Hussain, A., Cooke, W.H., & Varner, J.M. 2017. Impact of human factors on wildfire occurrence in Mississippi, United States. Forest Policy and Economics 81, 38-47. **https://doi**.org/10.1016/j.forpol.2017.04.011.

Guillaume, B., Porterie, B., Batista, A., Cottle, P., & Albergel, A. 2019. Improving the uncertainty assessment of economic losses from large destructive wildfires. International Journal of Wildland Fire 28(6), 420-430 **https://doi**.org/10.1071/WF18104.

Haider, W., Knowler, D., Trenholm, R., Bradshaw, P., & Lertzam, K. 2019. Climate change, increasing forest fire incidence, and the value of visibility: evidence from British Columbia, Canada. Canadian Journal of Forest Research 49(10), 19. **https://doi**.org/10.1139/cjfr-2018-0309.

Hiratsuka, M., Nakama, E., Satriadi, T., Fauzi, H., Aryadi, M., & Morikawa, Y. 2019. An approach to achieve sustainable development goals through participatory land and forest conservation: a case study in South Kalimantan Province, Indonesia. Journal of Sustainable Forestry 38 (6), 558-571. **https://doi**.org/10.1080/10549811.2019.1598440.

Huber-Stearns, H., Santo A., Schultz, C.A., & McCaffey, S.M. 2021. Network governance in the use of prescribed fire: roles for bridging organizations and other actors in the Western United State. Regional Environmental Change 21, 118. **https://doi**.org/10.1007/s10113-021-01850-7.

Jalil, A., Yesi, Y., Sugiyanto, S., Puspitaloka, D., & Purnomo, H. 2021. The Role of Social Capital of Riau Women Farmer Groups in Building Collective Action for Tropical Peatland Restoration. Forest and Society 5(2), 341-351. **https://doi**.org/10.24259/fs.v5i2.12089.

Jones, B.A. 2018. Willingness to pay estimates for wildfire smoke health impacts in the US using the life satisfaction approach. Journal of Environmental Economics and Policy 7 (4), 403-419. Doi.org/10.1080/21606544.2018.1463872.

Kerns, B.K., Tortorelli, C., Day, M.A., Nietupski, T., Barros, A.M.G., Kim, J.B., & Krawchuck, M.A. 2020. Invasive grasses: A new perfect storm for forested ecosystems? Forest Ecology and Management 463, 117985. **https://doi**.org/10.1016/j.foreco.2020.117985.

Kinoshita, A.M., Chin, A., Simon, G.L., Briles, C., Hougue, T.S., O'Dowd, A.P., Gerlak, A.K., & Ulbornoz, A.U. 2016. Wildfire, water, and society: Toward integrative research in the Anthropocene, Anthropocene 16, 16-27. **https://doi**.org/10.1016/j.ancene.2016.09.001.

Law, B.E., & Waring, R.H. 2015. Carbon implications of current and future effects of drought, fire and management on Pacific Northwest Forests. Forest Ecology and Management 355, 4-14. **http://dx**.doi.org/10.1016/j.foreco.2014.11.023.

Lerch, A.P., Pfammatter, J.A., Bentz, J. B., & Raffa, F.K. 2016. Mountain Pine Beetle Dynamics and Reproductive Success in Post-Fire Lodgepole and Ponderosa Pine Forests in Northeastern Utah. PloS ONE 11(10), e0164738. Doi:10.1371/journal.pone.0164738.

Leslie, R., Loomis, J., & Champ, P. 2013. Valuing Morbidity from Wildfire Smoke Exposure: A Comparison of Revealed and Stated Preference Techniques. Land Economics 89 (1), 76-100. DOI:10.3368/le.89.1.76

Liu, J.C., Pereira, G., Uhl, S.A., Bravo, M.A., & Bell, M.L. 2015. A systematic review of the physical health impacts from non-occupational exposure to wildfire smoke. Environmental Research 136, 120-132. **https://doi**.org/10.1016/j.envres.2014.10.015.

Mallinis, G, Petrila, M., Mitsopoulos I., Lorent, A., Neagu, S., Apostol, B., Gancz, V., Popa, I., & Goldammer, J.G. 2019. Geospatial Patterns and Drivers of Forest Fire Occurrence in Romania. Applied spatial analysis and policy 12(4), 773-795. 10.1007/s12061-018-9269-3.

Mc Dougall, C., Gibbs, L., & Clark, R. 2014. Community-based preparedness programmes and the 2009 Australian bushfires: policy implications derived from applying theory. Disasters 38(2), 249−266.

Molina, J.R., Machuca, M.H., Diaz, R.Z., Rodriguez y Silva F.R., & Gonzalez-Caban, A. 2011. Economic losses to Iberian swine production from forest fire. Forest Policy and Economics 13(8), 614-621. **https://doi**.org/10.1016/j.forpol.2011.07.011.

Molina, J.R., Rodriguez y Silva, F., & Herrera, M.A. 2017. Economic vulnerability of fire-prone landscapes in protected natural areas: application in a Mediterranean Natural Park. European Journal of Forest Research 136, 609-624. 10.1007/s10342-017-1059-y.

Molina J.R., Moreno, R., Castillo, M., & Rodriguez y Silva, F. 2018. Economic susceptibility of fire-prone landscapes in natural protected areas of the southern Andean Range. Science of The Total Environment 619–620, 1557-1565. **https://doi**.org/10.1016/j.scitotenv.2017.11.233.

Molina, J.R., & Rodriguez y Silva, F. 2019a. Valuation of the economic impact of wildland fires on landscape and recreation resources: a proposal to incorporate them on damages valuation. General Technical Report – Pacific Southwest Research Station, USDA Forest Service **https://www**.fs.usda.gov/treesearch/pubs/57688.

Molina, J.R., Rodriguez y Silva R., & Ruiz, L. 2019b. Integrating teledetection and economic tools in the evaluation of wildfires impacts. The Alhama De Almería fire (Spain) case. Gen. Tech. Rep. PSW-GTR-261 (English). Albany, CA: U.S. Department of Agriculture, Forest Service, Pacific Southwest Research Station: 132-144.

Molina, J.R., Gonzalez-Caban, A., & Rodriguez y Silva, F. 2019c. Potential Effects of Climate Change on Fire Behavior, Economic Susceptibility and Suppression Costs in Mediterranean Ecosystems: Córdoba Province, Spain. Forests 10(8), 679. Doi:10.3390/f10080679.

Montagné-Huck, C., & Brunette, M. 2018. Economic analysis of natural forest disturbances: A century of research. Journal of Forest Economics 32, 42-71. **https://doi**.org/10.1016/j.jfe.2018.03.002.

Morais, M.C., Gonçalves, B., & Cabral J.A. 2021. A Dynamic Modeling Framework to Evaluate the Efficacy of Control Actions for a Woody Invasive Plant, Hakea sericea. Frontiers in Ecology and Evolution. **https://doi**.org/10.3389/fevo.2021.641686.

Mueller, J.M., Soder, A.B., & Springer, A.E. 2019. Valuing attributes of forest restoration in a semi-arid watershed "Landscape and Urban Planning 184 78-87. **https://doi**.org/10.1016/j.landurbplan.2018.12.012.

Narayanan, R., Miller, E., Johnson, S., & Conrad, B. 2009. Wildfires and Invasive Species: Ecology and Environment of the Great Basin Region of the U.S. Bulletin UASVM, nr. 66(1-2)/2009.

Nielsen-Pincus, M., Moseley, C., & Gebert, K. 2014. Job growth and loss across sectors and time in the western US: The impact of large wildfires. Forest Policy and Economics 38, 199-206. **https://doi**.org/10.1016/j.forpol.2013.08.010.

Oliveira, S., Felix, F., Nunes, A., Lourenco, L., Laneve, G., & Sebastian-Lopez, A. 2018. Mapping wildfire vulnerability in Mediterranean Europe. Testing a stepwise approach for operational purposes. Journal of Environmental Management Volume 206, 158-169. **https://doi**.org/10.1016/j.jenvman.2017.10.003.

Oliveira, S., Gonçalves, A., Benali, A., Sa', A., Zezere, J.L., & Pereira, J.M. 2020. Assessing Risk and Prioritizing Safety Interventions in Human Settlements A affected by Large Wildfires. Forests 11(8), 859. Doi:10.3390/f11080859.

Parente, J., & Pereira, M. 2016. Structural fire risk: The case of Portugal. Science of The Total Environment. Volume 573, 15, 883-893. **https://doi**.org/10.1016/j.scitotenv.2016.08.164.

Parise, M., & Cannon, S. 2017. Debris Flow Generation in Burned Catchments. In Mikoš M., Casagli N., Yin Y., Sassa K. (eds) Advancing Culture of Living with Landslides. WLF 2017. Springer, Cham.

Ratknic, T., Milovanovic, J., Sekularac, G., Subic, J., Jelocnik, M., & Poduska, Z. 2017. Analysis of the profitability of the restitution of fire-affected beech forests in Serbia. Applied Ecology and Environmental Research · 15(4), 1999-2010. 10.15666/aeer/1504_19992010.

Ribeiro, C., Valente, S. Coelho, C., & Figueiredo, E. 2015. A look at forest fires in Portugal: technical, institutional, and social perceptions. Scandinavian Journal of Forest Research 30(4), 317-325. **https://doi**.org/10.1080/02827581.2014.987160.

Robinne F.N., Hallema D.W., Bladon K.D., Flanning, M.D., Boisrame', G., et al. 2021. Scientists' warning on extreme wildfire risks to water supply. Hydrological Processes 35(5), e14086. **https://doi**.org/10.1002/hyp.14086.

Rodriguez y Silva, F., & Gonzalez-Caban, A. 2010. 'SINAMI': a tool for the economic evaluation of forest fire management programs in Mediterranean ecosystems. International Journal of Wildland Fire 19, 927–936.

Rodriguez y Silva, F., 2013. VISUAL-SEVEIF, a tool for integrating fire behavior simulation and economic evaluation of the impact of wildfires. In Gonzales-Caban, A. (eds), Proceedings of the Fourth International Symposium on Fire Economics, Planning, and Policy: Climate Change and Wildfires. GENERAL TECHNICAL REPORT PSW-GTR-245.

Rodriguez y Silva, F., Molina J.R., & Castillo Soto, M. 2013. Methodological Approach for Assessing the Economic Impact of Forest Fires Using MODIS Remote Sensing Images. In Gonzales-Caban, A. (eds), Proceedings of the Fourth International Symposium on Fire Economics, Planning, and Policy: Climate Change and Wildfires. GENERAL TECHNICAL REPORT PSW-GTR-245.

Rosales-Rueda, M., & Triyana, M. 2018. The Persistent Effects of Early-Life Exposure to Air Pollution: Evidence from the Indonesian. Journal of Human Resources 0117-8497R1; 10.3368/jhr.54.4.0117.8497R1.

Salazar, N., Meza, C. M., Espelta, J.M., & Armenteras, D. 2020. Post-fire responses of Quercus humboldtii mediated by some functional traits in the forests of the tropical Andes. Global Ecology and Conservation 22, e01021. **https://doi**.org/10.1016/j.gecco.2020.e01021.

Sapkota, L., Shrestha, R.P., Jourdain, D., & Shivakoti, G.P. 2015. Factors Affecting Collective Action for Forest Fire Management: A Comparative Study of Community Forest User Groups in Central Siwalik, Nepal. Environmental Management 55, 171–186. DOI 10.1007/s00267-014-0404-x.

Sarro, R., Perez-Rey, I., Tomas, R., Alejano, L.R., Hernandez-Guitierrez, L.E., & Mateos, R.M. 2021. Effects of Wildfire on Rockfall Occurrence: A Review through Actual Cases in Spain. Applied Science 11(6), 2545. **https://doi**.org/10.3390/app11062545.

Shrestha, A, Grala, R.K., Grado, S.C., Roberts, S.D., Gordon, J.S., & Adhikari, R.K. 2021. Nonindustrial private forest landowner willingness to pay for prescribed burning to lower wildfire hazards . "Forest Policy and Economics 127, 102451. **https://doi**.org/10.1016/j.forpol.2021.102451.

Sing, P, & Dey, S. 2021. Crop burning and forest fires: Long-term effect on adolescent height in India. Resource and Energy Economics 65, 101244.https://doi.org/10.1016/j.reseneeco.2021.101244

Stanke, C., Kerac, M., Prudhomme, C., Medlock, J., & Murray, V. 2013. Health effects of drought: a systematic review of the evidence. PloS Current Disasters 9 (4). 10.1371/currents.dis.7a2cee9e980f91ad7697b570bcc4b004.

Stougiannidou, D., Zafeiriou, E., & Raftoyannis, Y. 2020. Forest Fires in Greece and Their Economic Impacts on Agriculture . KnE Social Sciences, 4(1), 54–70. **https://doi**.org/10.18502/kss.v4i1.5977.

Tabara, D., Sauri', D., & Cerdan, R. 2003. Forest Fire Risk Management and Public Participation in Changing Socioenvironmental Conditions: A Case Study in a Mediterranean Region. Risk Analysis 23(2), 249-60. DOI:10.1111/1539-6924.00305.

Torzhkov I.O., Kushnir, E.A., Konstantinov, A.V., Koroleva, T.S., Efimov, S.V., & Shkolnik, I.M. 2019. Assessment of Future Climate Change Impacts on Forestry in Russia. Russian Meteorology and Hydrology, 2019, Vol. 44 (3), 180–186. 10.3103/S1068373919030038.

Varela, E., Jacobsen, J.B., & Mavsar, R. 2016. Social demand for multiple benefits provided by Aleppo pine forest management in Catalonia, Spain. Regional Environmental Change 17, 539–550. **https://doi.org/10.1007/s10113-016-1038-8**.

Wang, D., Guan, D., Zhu, S., Kinnon, M., Geng, G., Zhang, Q., Zheng, H. et al. 2021. 'Economic Footprint of California Wildfires in 2018'. Nature Sustainability 4, 252–60.

Wu, T., & Kim, Y. 2013. Pricing ecosystem resilience in frequent-fire ponderosa pine forests. Forest Policy and Economics 27, 8-12. **https://doi**.org/10.1016/j.forpol.2012.11.002.

7. Additional references

Birkmann, J., Cardona, O. D., Carreño, M. L., Barbat, A. H., Pelling, M., Schneiderbauer, S., Kienberger, S., Keiler, M., Alexander, D., Zeil, P., & Welle, T. 2013. Framing vulnerability, risk and societal responses: The MOVE framework. Natural Hazards, 193-211.

Burton, C., Rufat, S., & Tate, E. 2018. Social Vulnerability. In S. Fuchs, & T. Thaler, Vulnerability and Resilience to Natural Hazards, 53-81. Cambridge: Cambridge University Press.

Capitals Coalition, 2021. Principles of integrated capitals assessments.

Certini, G. 2005. Effects of fire on properties of forest soils: a review. Oecologia 143, 1–10. https://doi.org/10.1007/s00442-004-1788-8.

EC, 2021. Communication from the Commission to the European Parliament, the Council, the European Economic and Social Committee and the Committee of the Regions — Forging a climate-resilient Europe — The new EU strategy on adaptation to climate change, COM (2021) 82 final.

Evangeliou, N., Balkanski, Y., Cozic, A., Hao, W.M., Mouillot, F., Thonicke, K., Paugam, R., Zibtsev, S., Mousseau, T.A., Wang, R., Poulter, B., Petkov, A., Yue, C., Cadule, P., Koffi, B., Kaiser, J.W., & Moller, A. P. 2015. Fire evolution in the radioactive forests of Ukraine and Belarus: future risks for the population and the environment. Ecological Monographs 85 (1), 49-72. https://doi.org/10.1890/14-1227.1.

Mouillot, F., Ratte, J.P., Joffre, R., Mouillot, D., & Rambal, S. 2005. Long-term forest dynamic after land abandonment in a fire prone Mediterranean landscape (central Corsica, France). Landscape Ecology, 20 (1), 101-112. https://doi.org/10.1007/s10980-004-1297-5.

Oliveira, S., Rocha, J., & Sá, A. 2021. Wildfire risk modeling. Current Opinion in Environmental Science & Health, 23, 100274.

Paveglio, T., Carroll, M., Absher, J., & Norton, T. 2009. Just Blowing Smoke? Residents' Social Construction of Communication about Wildfire. Environmental Communication 3(1), 76-94. doi:10.1080/17524030802704971

Effects of the wildfires of August 2021 in the air quality of Athens through a numerical simulation

Tobias Osswald *[1]; Ana Patrícia Fernandes [1]; Carla Gama [1]; Ana Isabel Miranda [1]

[1] Centre for Environmental and Marine Studies, Department of Environment and Planning, University of Aveiro, Campus Universitário de Santiago, 3810-193 Aveiro, Portugal.
{tobiasosswald, apsfernandes, carlagama, miranda}@ua.pt

**Corresponding author*

Keywords

atmospheric modelling; atmospheric pollution; biomass burning emissions; Greece; wildland urban interface

Abstract

Air quality is significantly deteriorated during wildfire events, which poses a risk for the human health of affected populations. The Mediterranean Basin was strongly impacted by wildfires in the 2021 fire-season, particularly Athens whose numerous inhabitants experienced dangerous levels of air-quality for consecutive days. It is predicted that climate change will lead to a higher frequency of this type of situations over the coming decades.

The numerical modelling system WRF-APIFLAME-CHIMERE, which comprises a meteorological model, a smoke emission model and a chemical transport model, was applied to estimate the impact of 2021 August wildfires in the air quality of Athens. The obtained concentration results were compared with data from air quality monitoring stations with a good agreement between model and measured data. Calculated values indicate concerning levels of air pollution during the days with wildfires close to the city.

1. Introduction

The fire activity around the Mediterranean basin has been increasing over the past years and the burned area in some countries is expected to increase on average by 10% a decade in some countries because of climate change (Dupuy et al., 2021). Allied to this are the lack of adequate forest management, which led during the last decades to the conversion of native oak forests into non-native tree plantations, increasing the risk of large-scale forest fires, and the abandonment of rural areas which may render the situation even worse as fields and forests are left untended, posing a significant fire risk (Corona et al., 2015).

The effects of wildfires are not limited to massive economic and human losses that are caused directly through the action of the flames. Much harm is also done by the unhealthy levels of air-pollutants released in the process such as particulate matter (PM) and carbon monoxide. A study of firefighter health parameters showed how exposure to high levels of air-pollutants released from fires, even for a short term, may lead to dangerous conditions (Miranda et al., 2012).

Greece alongside with other countries around the Mediterranean suffered unusually high levels of fire-activity during the 2021 fire-season. Reports in the media of impressive levels of smoke and ashes are supported by measurements of atmospheric pollutants during that period (Smith, 2021; EEA, 2021). Athens was especially impacted since the city and surrounding urban areas, inhabited by 4 mio people, were surrounded by two large fires in its vicinity during the first week of August.

Previous studies of extreme wildfire events have successfully employed Chemical Transport Models (CTM) and satellite data information to achieve high spatiotemporal resolution fields of species concentrations. This method was used by Péré et al. (2014) in a case-study of an event near Moscow in 2010. They used the Weather Research and Forecasting (WRF) meteorology model coupled with the CHIMERE CTM fed with emissions derived from the Global Fire Assimilation System. The latter uses the satellite derived Fire Radiative Power (FRP) and vegetation maps to estimate emissions. The authors observed a good agreement between satellite observations of Aerosol Optical Depth (AOD) and the model results, whose bias ranged from –40% to 30%. More recently Turquety et al. (2020) used the WRF-CHIMERE system coupled with APIFLAME. This system

showed good results in a case-study of Portugal in the 2016 fire season for which 5% of bias in AOD were estimated. The authors showed how the state-of-the art plume-rise model as well as the detection of small fires were important factors that allowed the reduction of the modelling biases.

This study aims at a better understanding of the emission and dispersion of smoke during extreme wildfire events, including their impacts on air quality (AQ), using the events surrounding Athens as a case study. For this, the biomass burning emissions are estimated based on a top-down methodology (using APIFLAME), and their impact on AQ is assessed based on a modelling approach. The WRF model is used to obtain high spatiotemporal meteorological conditions while CHIMERE simulates the chemical and physical processes that pollutants undergo within the atmosphere.

The validation of the chosen model parameterization and input data was done by comparing results with measurements from AQ monitoring stations from Greece.

In the following chapter the case-study is described followed by a detailed explanation of the model and its parameterization. In section 3 the model results are presented, validated and discussed. The last section deals with the conclusions of this work.

2. Methodology

The APIFLAME model was used for estimating biomass burning emissions, while other emissions, meteorology and chemical transport phenomena were handled by the WRF-CHIMERE model. The system was applied to the case study of Athens during the fires in the beginning of August 2021.

2.1. Case Study

In the beginning of August 2021 fires were detected in the region around Athens in the Terra/MODIS Fire and Thermal Anomalies satellite product (Giglio et al., 2021). The first detection was on the 4th of August due to a wildfire started 100km to the North of the city in Evia Island. The fire continued to burn for six days resulting in 51000ha of burned area (40% of the total during that fire season in Greece) as estimated by the European Forest Fire Information System Burnt Area satellite product (EFFIS, 2021). According to the same sources a wildfire started directly to the Northeast of Athens, in Attica, on the 5th ending on the 6th of August and burning 8400ha. Other significant fires were detected through their FRP signatures in western Greece and in neighbouring countries. During that period residents reported a strong deposition of ashes inside the city and authorities advised the population to stay indoors or use respiratory masks otherwise (Smith, 2021).

2.2. APIFLAME

Biomass burning emissions of trace gases and aerosols during the 2021 Greece wildfires were calculated using the APIFLAMEv2 model (Turquety et al., 2020). The estimates are based on pre-processed satellite imagery in the form of the MODIS burned scars product (MCD64A1) which uses thermal anomalies from active fires and changes in reflectance due to the charring of the vegetation to detect burned regions. This product has a 500m resolution and is released on a monthly basis indicating the estimated day of burning for each detection. For each fire and associated vegetation type, the consumed fuel was calculated, and the corresponding emissions of 46 trace gases and aerosols were derived using a list of emission factors. The module also uses the fire radiative power (FRP) from the MOD14 satellite product, which processes four daily observations at 1km resolution. This is used in the calculation of the injection height. CHIMERE then re-distributes these emissions in the vertical direction according to a plume rise profile that assigns 20% of the emissions below the injection-height and the remainder around that same height.

2.3. WRF-CHIMERE

The impact of the emissions of wildfires on AQ was quantified based on a modelling approach, using the state-of-the-art CHIMERE model (Menut et al., 2021). This model is an open-source multi-scale Eulerian Chemistry Transport Model, which includes detailed gas-, aerosol- and cloud-phase chemistry. The chosen MELCHIOR2 chemistry mechanism takes 49 species and 120 reactions into account. Additionally, 7 aerosol species are subdivided into 10 size bins, whose chemistry is also considered. CHIMERE can run over a range of spatial scales from the hemispheric to the urban scale (up to 1x1km²). It has been widely used for operational forecasts in Europe, which has allowed for extensive testing and validation over this study region (Kukkonen et al., 2012).

In addition to biomass burning, the AQ simulations considered anthropogenic, mineral dust, biogenic and sea salt emissions. Anthropogenic emissions from EMEP (EMEP, 2021) were processed to obtain hourly fluxes for the different model species (associated to the selected chemical mechanism) and the specific simulation grids. Available time profiles for specific countries were used, as well as spatial proxies such as land-use, population density, and road networks density. Desert dust, marine aerosols and biogenic emissions were estimated by the model during the simulations, taking static datasets and meteorological data into account.

The boundary conditions for the WRF meteorology driver were taken from the ERA-5 reanalysis dataset (ECMWF, 2022) with a horizontal resolution of 30km and 37 pressure levels between 1000hPa and 1hPa at six-hour intervals. Once these calculations were performed the higher resolution data was passed on directly to CHIMERE.

The whole system was run between 27-07-2021 and 06-08-2021 thus capturing the period with the highest levels of air-pollution around Athens and providing a seven-day spin-up period to stabilize all simulation variables that may be affected by inaccuracies in the initial conditions. The mesh for Greece was nested inside a larger mesh resulting in two computational domains. The coarser mesh captured phenomena at the level of the Mediterranean Basin with 95x69 cells, while the smaller one was positioned around Greece with 106x81 cells as can be seen in Figure1. The structured hexahedral mesh was created over a lambert conformal map of the computational domain with 24 cells between the surface and 200hPa.

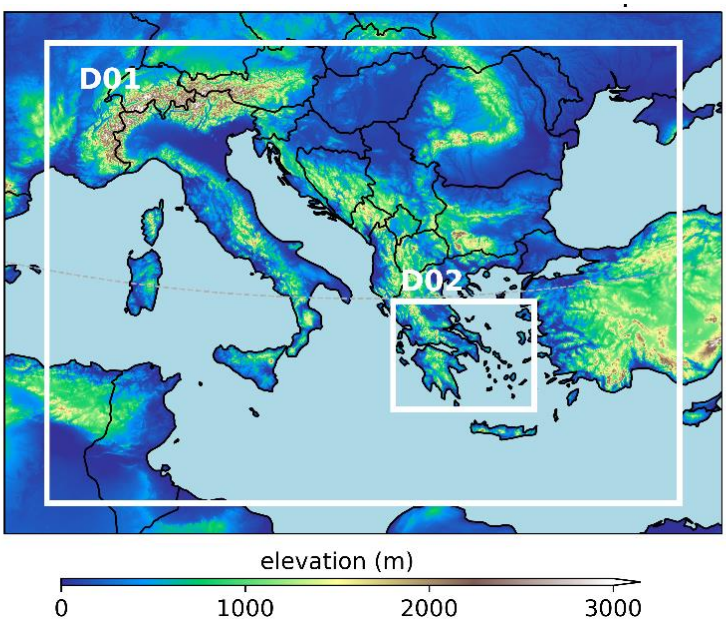

Figure 1 – WRF-CHIMERE nested domains used for the simulations plotted over an elevation map of the Mediterranean Basin. D01: coarse domain with 25km resolution. D02: small domain with 5km resolution.

3. Results

3.1. Validation

The results of the simulations were compared with data from air-quality monitoring stations which were extracted from the AQ database of the European Environmental Agency (EEA, 2021). The goal of this validation is understanding the ability of the system to model smoke emission and dispersion. Since PM and CO are consistently emitted by fires and good tracers of smoke (Schneider, 2021) these two pollutants were considered the most suitable for comparing model results.

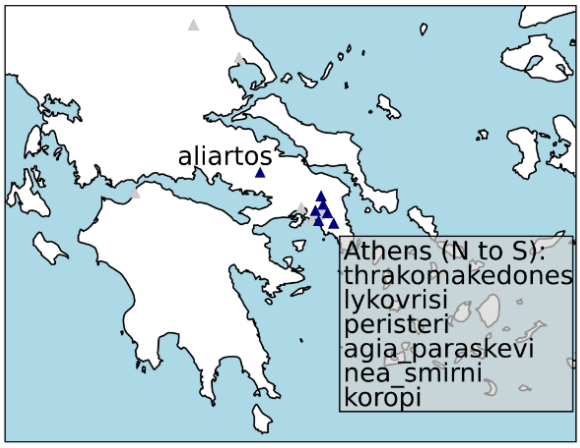

Figure 2 – Location of AQ monitoring stations within D02. Grey locations are not "background" stations and were removed.

Of the 19 available monitoring stations 7 were chosen, with their locations shown in Figure 2. These are classified as "background" stations and are more representative of a larger area around them, as opposed to "traffic" or "industrial" stations which are greatly affected by local phenomena, i.e. sub-grid phenomena for the model.

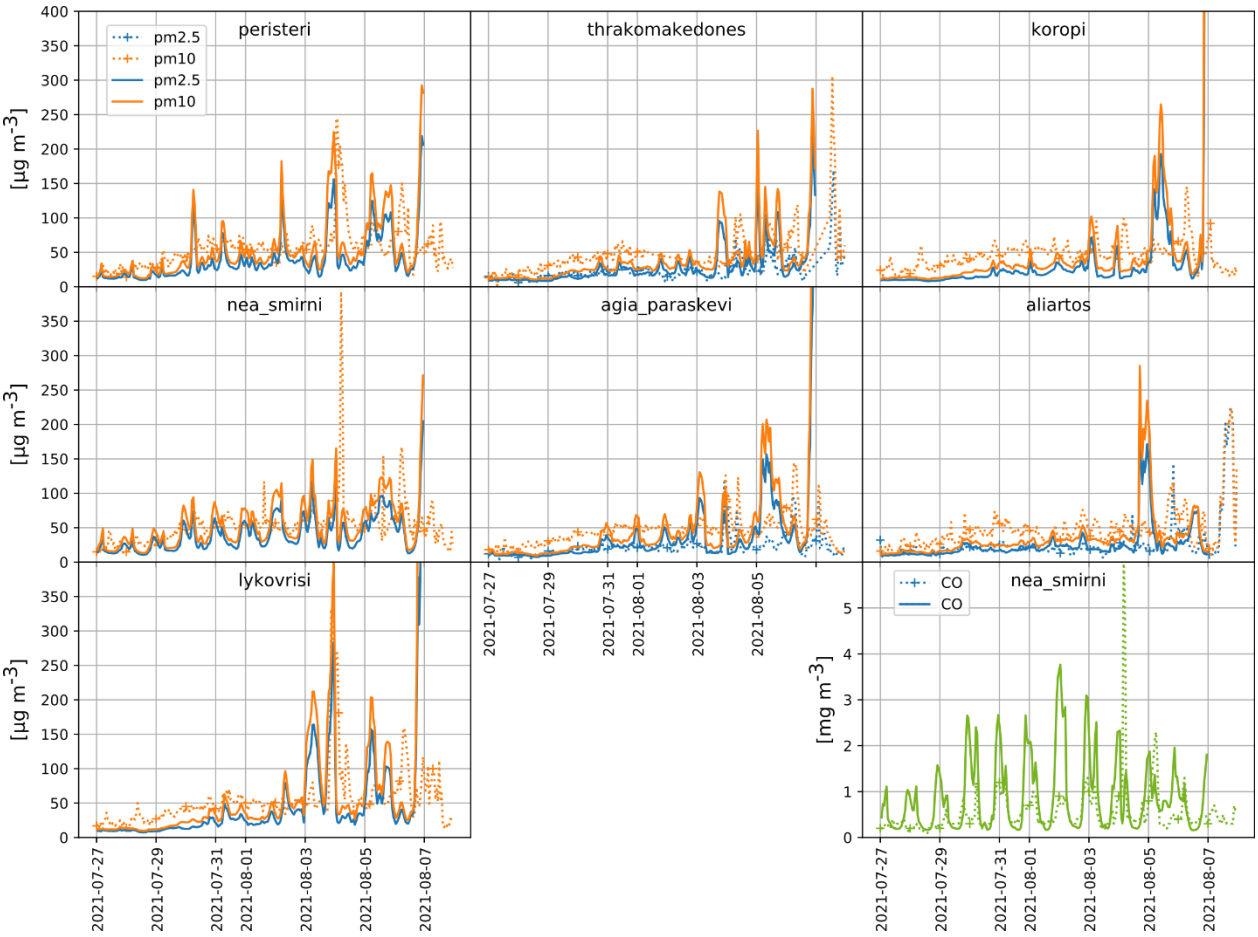

Figure 3 – Measured (dashed) and simulated (continuous) concentrations of CO and PM at the chosen sites.

Once the data was acquired, the AQ monitoring stations were associated to the grid cell of the small domain closest to it and concentration values were compared (Figure 3). Only one station measured CO concentrations, "nea_smirni". The daily fluctuations of this species are slightly underpredicted. PM concentrations, on the other hand, were widely available. Overall, discrepancies become more accentuated during wildfire periods, the

station and model concentrations follow the same trends within the same order of magnitude, and the bias is small.

3.2. Emissions

Figure 4 shows the spatial distribution (5×5 km²) of the atmospheric emissions during the fire events in Greece. It is apparent that the wildfire in Evia Island released the most amount of pollutants, not only due to high emissions by cell, but also the large area. Another four fires in Western Greece evidenced considerable emissions, together with a fire directly East of Athens.

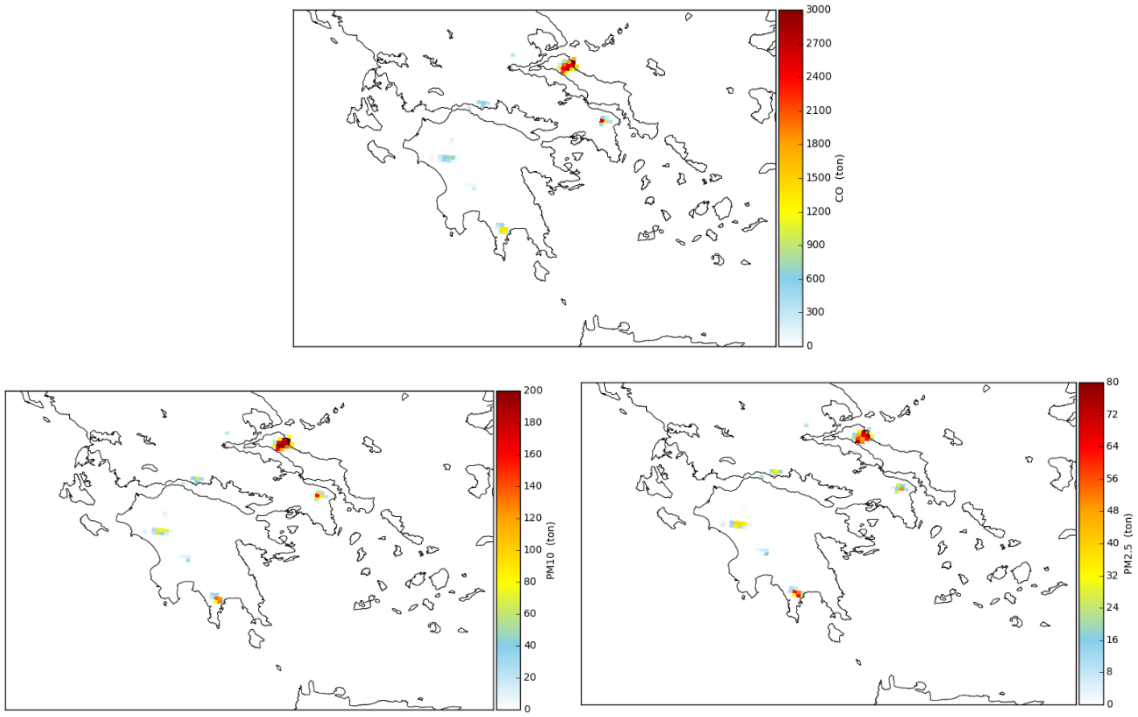

Figure 4 - Spatial distribution of the CO, PM10 and PM2.5 total emissions (ton) between 27th July and 8th August 2021.

3.3. Air Quality

Concentrations of CO and PM at the surface were analyzed through time-series of maps containing the spatial distribution (5×5 km²) of the atmospheric levels. The daily averages for days 4 to 6 are shown in Figure 5. The European Ambient Air Quality Directive (2008/50/EC) sets limits at 25µg/m³ for PM2.5 (annual limit) and 50µg/m³ (daily limit) for PM10 above which considerable health impacts are to be expected.

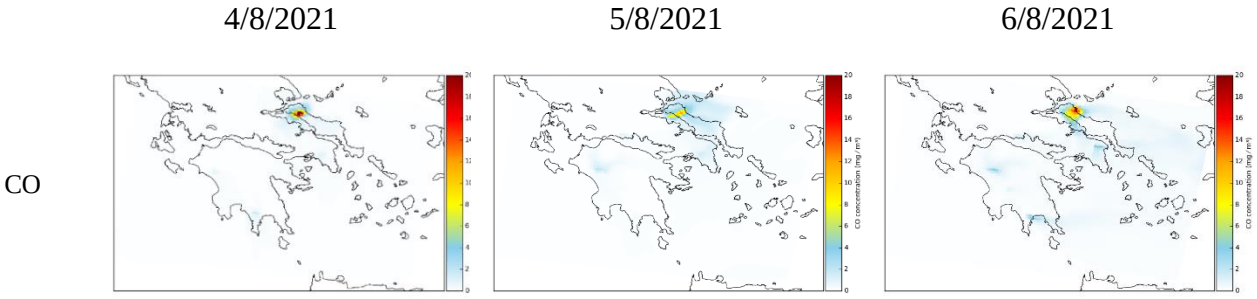

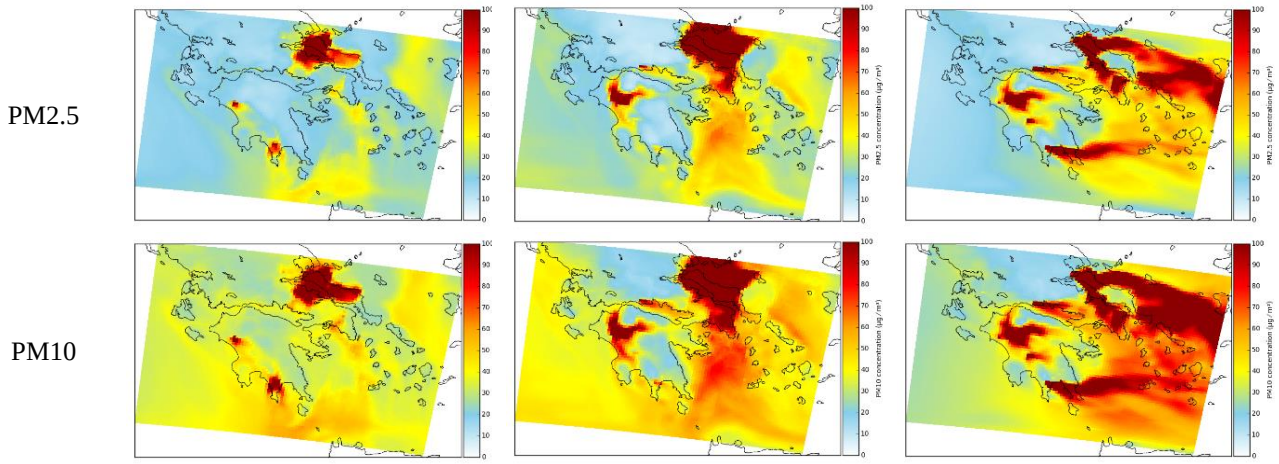

Figure 5 - Spatial distribution of the CO, PM2.5 and PM10 daily mean concentration (µg·m^{-3}) of simulated values at surface level.

On the 4th of August the fire in Evia starts early in the morning and air-pollution in the area increases throughout the day as seen from the plots, however the weak winds near the surface inhibit the dispersion of smoke and Athens is not affected. It is only during the night that PM reach dangerous levels. During the 5th of August PM levels remain high due to the ignition of the fire to the East of Athens. Atmospheric conditions are like the previous day so that PM from Evia is no longer reaching the city. Strong Easterly winds at dusk have a significant impact in cleaning the air-pollutants out of the city. This also advects smoke from fires burning to the East, however the effect on AQ is positive. Throughout the beginning of the 6th of August surface winds remain strong. By veering to the North and loosing much of their strength on the second half of the day, considerable levels of air-pollutants accumulate over Athens.

The simulation results indicate that Athens was experiencing levels of PM above the threshold before the beginning of the fires and days 5 and 6 of August were significantly impacted by the forest-fire smoke. Thus, all three days exceeded the PM thresholds.

4. Conclusions

The high spatiotemporal resolution of the calculated concentrations allowed for a more detailed analysis of the smoke plume dispersion and development, which would be unmanageable with satellite images or local air-quality monitoring stations. The model results showed a good agreement with measurements in general. However, the simulated levels of PM were clearly exaggerated during one of the events of wildfire smoke over Athens. Further analysis of the vertical profiles of the smoke and plume rise models will provide more information on how to improve model predictions during such extreme wildfire events.

8. Acknowledgements

The authors are grateful for the financial support of the Foundation for Science and Technology, I.P., through national funds, under the SmokeStorm project (PCIF/MPG/0147/2019). The authors also acknowledge the financial support of the FirEURisk project. This project has received funding from the European Union's Horizon 2020 research and innovation programme under grant agreement No 101003890. Thanks are due for the financial support to CESAM (UIDB/50017/2020 + UIDP/50017/2020), to FCT/MCTES through national funds.

9. Bibliography

Corona, P., Ascoli, D., Barbati, A., Bovio, G., Colangelo, G., Elia, M., Garfì, V., Iovino, F., Lafortezza, R., Leone, V., Lovreglio, R., Marchetti M., Marchi M., Menguzzato G., Nocentini S., Picchio R., Portoghesi L., Puletti N., Sanesi G. and Chianucci F. (2015). Integrated forest management to prevent wildfires under Mediterranean environments. Annals of Silvicultural Research, 39, 1-22. https://doi.org/10.12899/asr-946

Dupuy, J.L., Fargeon, H., Martin-StPaul, N., Pimont, F., Ruffault, J., Guijarro, M., Hernando, C., Madrigal, J. and Fernandes, P. (2020). Climate change impact on future wildfire danger and activity in southern Europe: a review. Annals of Forest Science, 77(2), 1-24. https://doi.org/10.1007/s13595-020-00933-5

ECMWF: European Centre for Medium-Range Weather Forecast (2022) ERA5 hourly data on pressure levels from 1979 to present. Retrieved March 2022. https://doi.org/10.24381/cds.bd0915c6

EEA: European Environmental Agency (2021). Air quality e-reporting. Retrieved January 2022. https://www.eea.europa.eu/data-and-maps/data/aqereporting-2

EFFIS: European Forest Fire Information System (2022, March). Rapid Damage Assessment – MODIS Burnt Areas. Retrieved March 2022. https://effis.jrc.ec.europa.eu/about-effis/technical-background/rapid-damage-assessment

EMEP/Centre on Emission Inventories and Projections database (2021). EMEP gridding 2021/2019. Retrieved March 2022. https://webdab01.umweltbundesamt.at/download/gridding2021/2019/

Giglio, L., Hall, J. V., Schroeder, W., Justice, C. O. (2021, February 11). MODIS/Terra Thermal Anomalies/Fire 5-Min L2 Swath- 1km. Retrieved March 2021. http://doi.org/10.5067/MODIS/MOD14.NRT.061

Kukkonen, J., Olsson, T., Schultz, D. M., Baklanov, A., Klein, T., Miranda, A. I., Monteiro, A., Hirtl, M., Tarvainen, V., Boy, M., Peuch, V.-H., Poupkou, A., Kioutsioukis, I., Finardi, S., Sofiev, M., Sokhi, R., Lehtinen, K. E. J., Karatzas, K. R., San José, Astitha, M., Kallos, G., Schaap, M., Reimer, E., Jakobs, H. and Eben, K. (2012). A review of operational, regional-scale, chemical weather forecasting models in Europe. Atmospheric Chemistry and Physics, 12(1), 1-87. https://doi.org/10.5194/acp-12-1-2012

Menut, L., Bessagnet, B., Briant, R., Cholakian, A., Couvidat, F., Mailler, S., Pennel, R., Siour, G., Tuccella, P., Turquety, S. and Valari, M. (2021). The CHIMERE v2020r1 online chemistry-transport model. Geoscientific Model Development, 14, 6781-6811. https://doi.org/10.5194/gmd-14-6781-2021

Miranda, A. I., Martins, V., Cascão, P., Amorim, J. H., Valente, J., Borrego, C., Ferreira, A.J., Cordeiro, C.R., Viegas, D.X. and Ottmar, R. (2012). Wildland smoke exposure values and exhaled breath indicators in firefighters. Journal of Toxicology and Environmental Health, Part A, 75(13-15), 831-843. https://doi.org/10.1080/15287394.2012.690686

Péré, J.C., Bessagnet, B., Mallet, M., Waquet, F., Chiapello, I., Minvielle, F., Pont, V. and Menut, L. (2014). Direct radiative effect of the Russian wildfires and its impact on air temperature and atmospheric dynamics during August 2010. Atmospheric Chemistry and Physics, 14(4), 1999-2013. https://doi.org/10.5194/acp-14-1999-2014

Schneider, S. R., Lee, K., Santos, G., & Abbatt, J. P. (2021). Air Quality Data Approach for Defining Wildfire Influence: Impacts on PM2.5, NO_2, CO, and O_3 in Western Canadian Cities. Environmental Science & Technology, 55(20), 13709-13717. https://doi.org/10.1021/acs.est.1c04042

Smith, H. (2021). 'Apocalyptic' scenes hit Greece as Athens besieged by fire (August 2021), https://www.theguardian.com/world/2021/aug/07, accessed 2021-11-09

Turquety, S., Menut, L., Siour, G., Mailler, S., Hadji-Lazaro, J., George, M., Clerbaux, C., Hurtmans, D. and Coheur, P.F. (2020). APIFLAME v2.0 biomass burning emissions model: impact of refined input parameters on atmospheric concentration in Portugal in summer 2016. Geoscientific Model Development, 13(7), 2981-3009. https://doi.org/10.5194/gmd-13-2981-2020

Estimation of biomass consumption coefficients for FRP-based forest fires emission calculations

Patricia Oliva*[1]; Eugenia Espinosa[2]; Idania Briceño[3]

[1] Universidad de Alcalá, Facultad de Filosofía y Letras, Departamento de Geología, Geografía y Medio Ambiente, Grupo de Investigación en Teledetección Ambiental, C/ Colegios 2, 28081, Alcalá de Henares, Madrid, Spain, {patricia.oliva@uah.es}
[2] Magíster en Teledetección, Escuela de Ingeniería Forestal, Facultad de Ciencias, Universidad Mayor, Camino La Pirámide 5750 Huechuraba, Santiago 8580745, {eugenia.espinosa@mayor.cl}
[3] Hémera Centro de Observación de la Tierra, Escuela de Ingeniería Forestal, Facultad de Ciencias, Universidad Mayor, Camino La Pirámide 5750 Huechuraba, Santiago 8580745, Chile, {idania.briceno@umayor.cl}

**Corresponding author*

Keywords

Fire radiative power, active fires, emissions estimation, forest fires, Chilean forest

Abstract

Near real-time emission estimations can be computed based on the fire radiated power (FRP) and the biomass consumption coefficients for each vegetation type. Therefore, the application of the methodology is limited by the knowledge of the biomass consumption (BC) coefficients, as the studies estimating the coefficients offer results on specific vegetation types. This study focuses on calculating biomass consumption coefficients for the most affected vegetation types in the Maule Region (Chile). We needed to estimate the biomass consumption rate to calculate the BC coefficients. Then, we computed the BC rate by estimating the biomass consumed in a specific burn time. We computed the time between VIIRS image acquisitions to assess the burning time. BC coefficients were obtained for four vegetation types: pine plantation, scrub, native oak-hualo forest, and arborescent scrub. In addition, we analyzed the variations of the BC coefficients by computing the BC coefficients on each time frame. Large variations were observed in the oak-hualo and pine plantation, which were related to the greater availability of biomass and variable fire behaviour.

1. Introduction

Forest fires are of great importance in the world because of the high emissions of aerosols and trace gases released into the atmosphere during their occurrence, directly affecting their chemical composition and the climate of the planet (Arora and Boer 2005). The increase in temperatures caused by climate change favours the proliferation of forest fires, being increasingly catastrophic (González et al. 2020). Chile has experienced an extension of the fire season in the last decade, going from 6 to 8 months. This change has produced significant impacts on CO_2 emissions into the atmosphere, biodiversity, and the country's economy (González et al. 2020).

Remote sensing has been widely used to estimate greenhouse gas, particulate matter, and trace gas emissions generated during a fire (Vadrevu and Lasko 2018; Wiedinmyer et al. 2006). These estimates have been obtained from two methods. The first, proposed by Seiler and Crutzen (1980), estimates the emissions by combining the burned area, the biomass available for burning, the consumption efficiency factors, and the emission factors by vegetation type (Oliva et al. 2019; Reid et al. 2009; Van Der Werf et al. 2017). The second method quantifies the biomass burned considering the integration over time of Fire Radiative Power (FRP) to obtain Fire Radiative Energy (FRE) (Vadrevu et al. 2019). The calculation of burned biomass is possible due to the linear relationship between the FRE and the rate of Biomass Consumption (BC) in a fire. The latter method considers within its variables the FRE and the specific biomass consumption coefficient for each type of vegetation (Wooster et al. 2005). The application of this method has shown promising results in southern Brazil (da Costa and da Fonseca 2017) in northern India (Vadrevu and Lasko 2018) and in global estimates (Vermote et al. 2009).

Visible Infrared Imaging Radiometer Suite (VIIRS) sensor provides data on active fires in near real-time thanks to its VNP14 product, which has a nominal spatial resolution of 375 m. Favouring the detection of a greater

number of fires allows a more refined mapping of the largest fires (Schroeder 2018). Therefore, VIIRS has become the new tool to continue working more accurately on emissions estimates (Fu et al. 2020; Li, Zhang, and Kondragunta 2020).

This study proposes a methodology that allows obtaining the biomass consumption (BC) coefficients necessary to estimate biomass burning emissions from the FRP product of active fires of VIIRS. The BC coefficients obtained in this study for the vegetation types of Chile contribute to the use of the VIIRS FRP for the estimation of emissions in future events.

2. Methodology

2.1. Study area

The fire called "Tabunco-El Águila Convenio" located at 35°8,862' S and 71°58,315' W in the commune of Curepto, Maule Region, Chile. We chose this fire because it has crucial characteristics for the application of emissions estimation. Among these characteristics, the presence of endemic native species stands out, such as hazel (Gevuina avellana), peumo (Cryptocarya alba), boldo (Peumus boldus), and litre (Lithraea caustic) (CONAF 2017). The event began on January 25, 2017 and was finally controlled on February 8, 2017. It burnt 4,069.7 hectares, affecting native vegetation, grasslands, thickets, and plantations. This fire also presented a rich diversity of vegetation types and detailed coverage of active fire detections.

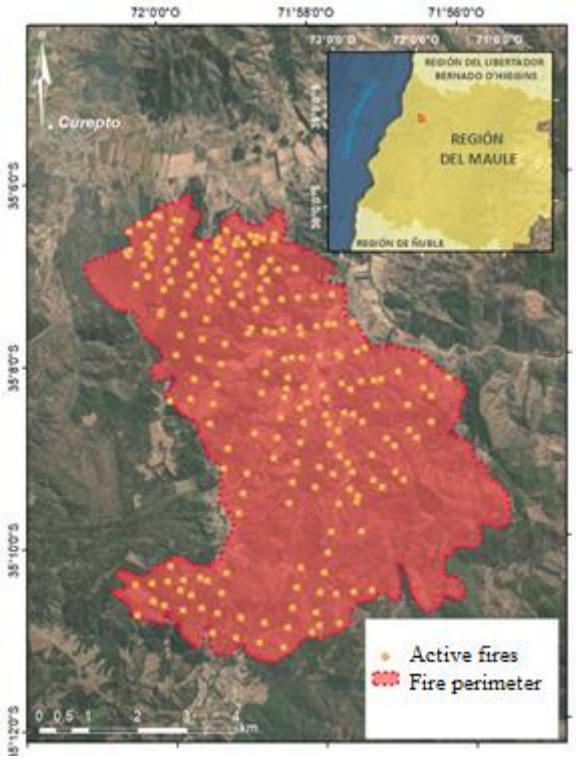

Figure 1- Location and extent of the Tabunco-el Aguila Convenio fire with the distribution of the active fires detected by VIIRS active fire product.

2.2. VIIRS active fire product

In this study we used the VNP14 thermal anomaly product of the NPP-VIIRS sensor. VIIRS active fire product provides detections at least twice a day, crossing the equator at 13:30 PM on the ascending node and at 01:30 AM on the descending node. The download of VIIRS data is done through the Fire Information for Resource Management System (FIRMS) service (https://firms.modaps.eosdis.nasa.gov/download/, last access date on February 27, 2022), from where you can access a global coverage of data from 2012 to date, in different formats.

The VIIRS active fire product provides information regarding fire coordinates, FRP measures (MW), brightness temperature in their respective bands, confidence level, date, time, and sensor characteristics. The time interval

defined for this study was based on the days of higher fire activity, which runs from January 26, 2017, to January 29, 2017.

2.3. Estimation of the biomass consumption rate

We worked over a grid o 375x375m to relate the FRP measurements with the area covered by each vegetation type. The mean FRP values for each date and time of acquisition were assigned to one cell. Subsequently, we calculated the percentages of the area for each type of vegetation, the biomass value, and the burn efficiency factor associated with each cell. The amount of biomass consumption per type of vegetation was obtained for each of the time interval measurements applying equation 1.

$$M=A\times B\times \beta \qquad (1)$$

Where M is the total amount of biomass consumed (kg), A is the total area burned (m^2), B is the dry organic matter by vegetation type (kg m^2), and β is the fuel efficiency (dimensionless).

Next, we applied the equation 2 to estimate the biomass consumption rate.

$$BCR = M / BT \qquad (2)$$

Where BCR is the biomass consumption rate, and BT is the burning time in seconds. We considered as the burning time the time between two consecutive image acquisitions. The time interval considered ranged from January 26, 2017, to January 29, 2017. In that time, eleven VIIRS images were acquired, so we computed the BCR on eleven periods.

2.4. Estimation of the biomass consumption coefficient

Following the methodology of previous studies, we estimated the BC coefficient by vegetation type applying a linear regression equation between the BC rate and the FRP measured at each burning time period. The slope of the liner regression line is assigned as the BC coefficient value. Although a variety of vegetation types were present in the fire, only four vegetation types offered enough data to compute the linear regression line: open shrublands, forested shrublands, pine plantations and native forest oak-hualo.

We also computed the BC coefficients applying the following equation:

$$C_{ex} = BCR / FRP \qquad (3)$$

Where C_{ex} is the BC coefficient by vegetation type x, and FRP the Fire radiative power measured within the burning time of each period (eleven periods considered). We called this BC coefficients, dynamic coefficients as their value change depending on the characteristics of the vegetation and the fire behaviour.

3. Results

The results of the linear regressions by vegetation type indicate that BNRH and open scrub have an R^2 of 0.6 and 0.5, respectively. This indicates that the predicted BC coefficients achieved a better fit, with respect to what is observed in the cases of pine and arborescent scrub plantation with an R^2 of 0.3 and 0.2, respectively. We also analysed the behaviour of the dynamic BC coefficients (see Table 1). We observed that, in certain cases, for the same vegetation type, these BC coefficients have values higher than the observed average. This situation affects BNRH with two high values on the second day, forested shrubs and pine plantation. These higher values are related to higher values of biomass consumption rate.

Table 1. Result of dynamic and static biomass coefficients by vegetation type. BNRH refers to the native oak-hualo forest.

Type of Coefficient	DD-HH code:MM	GNRH	Open Scrub	Shrub Arbolado	Pine Plantation
Dynamic Biomass Coefficient	26-05:31	0.45	0.06	0.21	0.32
	26-17:53	0.04	0.03	0.17	0.11
	26-19:33	1.16	0.11	0.39	0.94
	27-05:13	0.41	0.01	0.40	0.74
	27-06:53	11.33	-	3.02	2.13
	27-17:34	0.0	0.00	0.05	0.07
	27-19:14	17.65	0.00	0.40	0.85
	28-04:54	-	-	0.22	3.07
	28-06:34	-	0.19	0.42	10.28
	28-18:56	-	-	0.05	0.09
	29-18:37	-	-		0.10
Static Biomass Coefficient	-	1.33	0.01	0.07	0.28

4. Conclusions

This study lays the foundation for the application of emissions calculation from FRP measurements of active fires, allowing near real-time estimates. The objective of this study was to obtain the BC coefficients by type of vegetation affected by the fire studied. This was obtained for four of the affected vegetation types. In addition, this study allowed an interesting analysis based on the dynamic BC coefficients. We could then evaluate the error that might be produced by applying the linear regression BC coefficients. The BC coefficients with the most variability was found in the BNRH and in the pine plantation. This result is related to the greater amount of biomass of these vegetation covers and the greater intensity that the fire can reach. Therefore, in those vegetation types, the BC coefficient estimated from the regression analysis does not reflect the natural variation derived from the fire behaviour and the characteristics of the vegetation.

The continuation and extension of this work on other fires and other types of vegetation present in the country are necessary to obtain the biomass coefficients by type of vegetation and use this methodology to estimate fire emissions in almost real-time throughout the country.

5. Acknowledgments

This work could be carried out thanks to the materials provided by Patricia Oliva, which were obtained within the activities of the FONIS SA18I0177 project. The authors of this work thank CONAF for its valuable information regarding the cadaster of vegetation types and the identification of ignition of the event studied.

6. Bibliography

Arora, Vivek K., and George J. Boer (2005). Fire as an Interactive Component of Dynamic Vegetation Models. Journal of Geophysical Research: Biogeosciences 110(G2).

CONAF (2017). Vegetation Cadastre. Retrieved April 28, 2021 (https://www.conaf.cl/nuestros-bosques/bosques-en-chile/catastro-vegetacional/#:~:text=Al year 2017 the area, the forest resources of the country.).

da Costa, Bibiana Salvador Cabral, and Eliana Lima da Fonseca (2017). Uso Da Potencia Radiativa Do Fogo Para Estima o Coefficient de Consumo de Biomassa Em Gramíneas Temperadas No Bioma Mata Atlântica. Revista Brasileira de Meteorologia 32(2):255–60.

Fu, Yuyun, Rui Li, Xuewen Wang, Yves Bergeron, Osvaldo Valeria, Raphaël D. Chavardès, Yipu Wang, and Jiheng Hu (2020). Fire Detection and Fire Radiative Power in Forests and Low-Biomass Lands in Northeast Asia: MODIS versus VIIRS Fire Products. Remote Sensing 12(18):2870.

Giglio, Louis, Jacques Descloitres, Christopher O. Justice, and Yoram J. Kaufman (2003). An Enhanced Contextual Fire Detection Algorithm for MODIS. Remote Sensing of Environment 87(2–3):273–82.

González, M. E., R. Sapiains, S. Gómez-González, R. Garreaud, A. Miranda, M. Galleguillos, M. Jacques, A. Pauchard, J. Hoyos, L. Cordero, F. Vásquez, A. Lara, P. Aldunce, V. Delgado, A.M. Arriagada, Ugarte, A. Sepúlveda, L. Farías, and I. Garcia (2020). Report to La Nación. Fires in Chile: Causes, Impacts and Resilience.

Oliva, Patricia, Leonardo Duran, Alejandro Venegas, Paulina Vidal, and Claudia Montoya (2019). Spatially Refined Biomass and Combustion Efficiency Estimations in Support of Forest Fires Emissions Quantification. International Geoscience and Remote Sensing Symposium (IGARSS) 9420–23.

Reid, Jeffrey S., Douglas L. Westphal, Cynthia A. Curtis, Kim A. Richardson, Edward J. Hyer, Elaine M. Prins, Christopher C. Schmidt, Jay P. Hoffman, Jianglong Zhang, Jun Wang, Sundar A. Christopher, and Daniel P. Eleuterio (2009). Global Monitoring and Forecasting of Biomass-Burning Smoke: Description of and Lessons from the Fire Locating and Modeling of Burning Emissions (FLAMBE) Program. IEEE Journal of Selected Topics in Applied Earth Observations and Remote Sensing 2(3):144–62.

Schroeder, Wilfrid (2018). NASA VIIRS Land Science Investigator Processing System (SIPS) Visible Infrared Imaging Radiometer Suite (VIIRS) 375 m & 750 m Active Fire Products Product User's Guide Version 1.4.

Seiler, W., and P. J. Crutzen (1980). Estimates of Gross and Net Fluxes of Carbon Between. Climatic change. 2(3), 207-247.

Vadrevu, Krishna., and Kristofer. Lasko (2018). Intercomparison of MODIS AQUA and VIIRS I-band Fires and Emissions in an Agricultural Landscape-Implications for Air Pollution Research. Remote Sensing 10(7).

Vadrevu, Krishna Prasad, Kristofer Lasko, Louis Giglio, Wilfrid Schroeder, Sumalika Biswas, and Chris Justice (2019). Trends in Vegetation Fires in South and Southeast Asian Countries. Springer US.

Vermote, Eric, Evan Ellicott, Oleg Dubovik, Tatyana Lapyonok, Mian Chin, Louis Giglio, and Gareth J. Roberts (2009). An Approach to Estimate Global Biomass Burning Emissions of Organic and Black Carbon from MODIS Fire Radiative Power. Journal of Geophysical Research-Atmospheres 114(18):1–22.

Van Der Werf, Guido R., James T. Randerson, Louis Giglio, Thijs T. Van Leeuwen, Yang Chen, Brendan M. Rogers, Mingquan Mu, Margreet J. E. Van Marle, Douglas C. Morton, G. James Collatz, Robert J. Yokelson, and Prasad S. Kasibhatla (2017). Global Fire Emissions Estimates during 1997-2016. Earth System Science Data 9(2):697–720.

Wiedinmyer, Christine, Brad Quayle, Chris Geron, Angie Belote, Don McKenzie, Xiaoyang Zhang, Susan O'Neill, and Kristina Klos Wynne (2006). Estimating Emissions from Fires in North America for Air Quality Modeling. Atmospheric Environment 40(19):3419–32.

Wooster, Martin J., G. Roberts, G. L. W. Perry, and Y. J. Kaufman (2005). Retrieval of Biomass Combustion Rates and Totals from Fire Radiative Power Observations: FRP Derivation and Calibration Relationships between Biomass Consumption and Fire Radiative Energy Release. Journal of Geophysical Research-Atmospheres 110(24):1–24.

Evolution of the annual cycle of Burned Area in Portugal from 1980 to 2018: Implications for fire season management

Pedro Silva*[1]; Miguel Carmo[2]; João Rio[1]; Ilda Novo[1]

[1] *Departamento de Meteorologia e Geofísica, Instituto Português do Mar e da Atmosfera (IPMA, IP). Rua C do Aeroporto, Lisbon 1749-077, Portugal {pedro.silva, joao.rio, ilda.novo}@ipma.pt*
[2] *Institute of Contemporary History, NOVA University. Campus de Campolide, 1099-085 Lisboa, Portugal {miguelcarmo@fcsh.unl.pt}*

**Corresponding author*

Keywords

Fire weather, Wildfire seasonality, Daily Severity Rating, Climate change, Portugal

Abstract

The lengthening of the fire season in Portugal has been understudied although there is evidence of changes in recent decades. In this study, we have focused on the complete annual cycles of fire activity and meteorological fire danger, avoiding any subjective definition of what should mark the beginning and end of the fire season. Based on the daily time series of burned areas and number of active fires collected in mainland Portugal by state services from 1980 to 2018, we have searched for changes in the monthly and daily distributions. In particular, we developed an exceedance date method to determine day-scale trends in the anticipation/prolongation of fire activity in the year. An unequivocal increasing trend in the proportion of annual burned area between January and June was found, compensated by a diminishing trend in the proportion of burned area in the summer months (July to September). Apparently, the known secondary peak of fire activity in March played an important role in these changes that should be clarified in future analyses. Moreover, the daily analysis shows a clear shift of the cumulative burned area curves to the left, which suggests an anticipation of fire activity. The evolution of the 15% exceedance date, the annual date at which the threshold of 15% of the annual burned area is reached, shows a linear variation of -1.34 days per year in 1980-2018. In order to evaluate the meteorological contribution to this found anticipation of fire activity we used the Daily Severity Rating (DSR), from the Canadian Forest Fire Weather Index System, computed from the ECMWF ERA5 reanalysis. The results show a clear earlier growth of the DSR when comparing the averages for the first (1980-1999) and second (2000-2018) halves of the period. This divergence between the two curves rises steadily from the beginning of the second half of April to the end of September. Interestingly, a closer look shows a first increase in the DSR gap in March, which almost disappears in April before steadily increasing again until the beginning of October. Finally, we argue that up-to-date knowledge of interannual and interdecadal changes in the seasonality of both wildfires and fire weather is a decisive (though not the only) aspect for comprehensive fire season management.

1. The seasonality of fire in Portugal: a brief introduction

The incidence of wildfires throughout the year, represented by the number of occurrences and burned areas, shows an uneven pattern that derives from the annual cycles of temperature and precipitation and the corresponding cyclical dynamics of ecosystems (e.g. Kwiecien et al. 2021, Viegas & Viegas 1994). This relationship between climate and fire seasonality is well embodied in the weather fire risk indices – as well exemplified by the FWI and its long memory drought subindices (Van Wagner 1974, Carmo et al. 2021) – and has received renewed attention in recent decades in the context of concomitant changes in climate and fire regimes. The focus on 'the lengthening of the fire season' in a changing climate has in Wotton and Flannigan (1993) one of the first studies and has been increasingly studied in the last few years (Jain et al. 2018, Westerling 2016, Salloum & Mitri 2014, UNEP 2022).

The present study fits these concerns and research framework aiming (i) to identify relevant changes in the annual cycle of fire activity in mainland Portugal, based on the extensive records of fire occurrences in the period 1980-2018 (≥1.0 hectare) and some previous results (cf. Carmo et al. 2021), (ii) to evaluate the meteorological contribution using the Daily Severity Rating (DSR) (Van Wagner 1987) and, finally, (iii) to discuss the interannual and interdecadal variation in wildfire seasonality in the context of fire management and the operational definition of 'fire season'.

On this last point, we must note that contemporary fire regimes are affected by human activities. Fire seasonality is conditioned not only by climatic and ecological forcings, but also by *unnatural* annual cycles of ignitions,

fuel availability, as well as changes in fire suppression approaches and means, which have specific calendars themselves changeable over time. See, for example, the secondary peak of fires in March, identified in northwestern Iberia (da Câmara et al. 2014) and in our nationwide 1980-2018 data (both in number of occurrences and burned areas, data not shown), which is associated with the (inseparable) combination of early spring agricultural practices and a recurrent window of weather conditions conducive to fire spread.

The monthly distribution of the annual burned area in Portugal in the period 1980-2018 shows a broad concentration in July, August and September (which represents on average 82.5% of the total burned area each year) (Figure 1). However, this monthly data also shows an increasing fraction of the annual burned area occurring outside those three summer months (Figure 2). In fact, there is a meaningful increase in the fraction corresponding to the months of January to June, while the fraction of July to September shows a decreasing trend (Mann-Kendall tests with $\rho<0.01$).

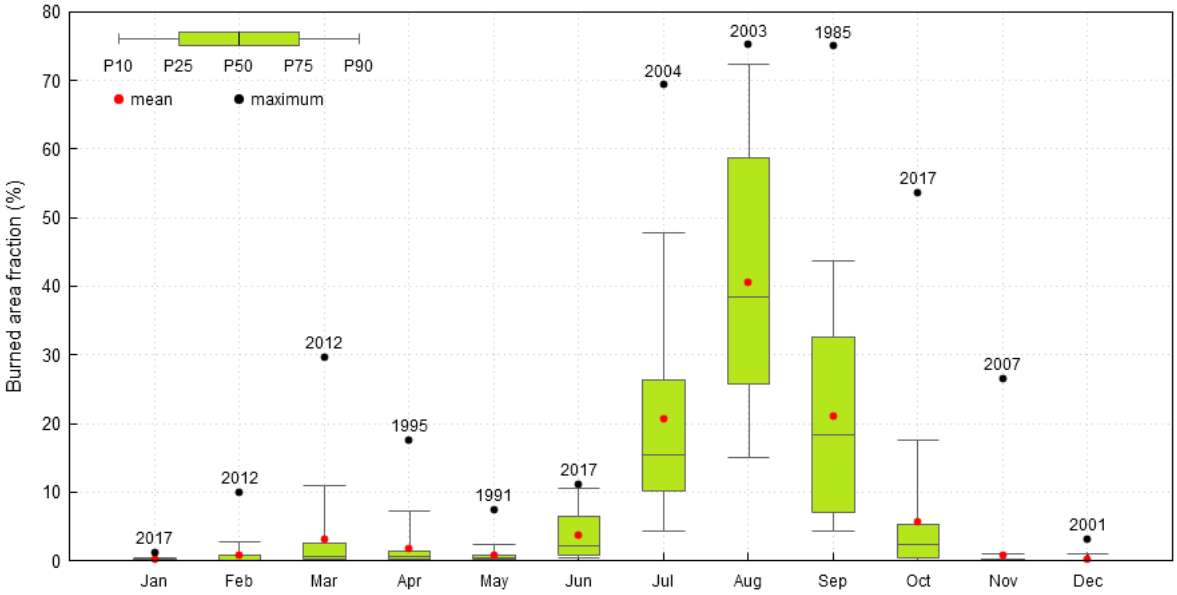

Figure 1: Monthly distribution of the annual burned area in the period 1980 to 2018, indicating the 10th, 25th, 50th, 75th and 90th percentiles (box-and-whisker plot), the mean (red dots) and the maximum monthly values (black dots labeled with the year of occurrence).

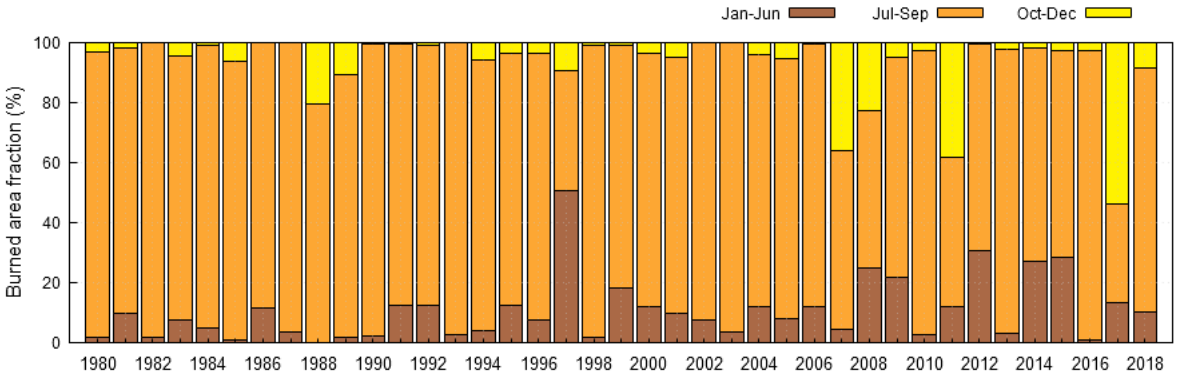

Figure 2: Distribution of the fraction of annual burned area occurred before (Jan-Jun months, brown bars), during (Jul-Set, orange bars), and after (Oct-Dec, yellow bars) the most critical months in wildfires incidence in the period 1980-2018.

2. Evolution of the burned area throughout the year: is the fire season getting longer?

The year 2017 sounded several alarm bells in Portugal: beyond the sad and unprecedented figure of 117 deaths caused by wildfires and a burnt extent never before recorded (about 540,000 ha), the two main fire events occurred before (17-22 June) and after (15-17 October) the official fire season window decreed by the

Portuguese authorities (Turco et al. 2019, Viegas et al. 2017, 2019). In 2017, 67.1% of the burned area did not occur in the three summer months (Jul-Sep, see Figure 2). To better understand the historical evolution of the annual fire cycle, we have used a simple method of determining for each year the dates (annual Julian day) at which the fractions of the annual burned area, in increments of 1%, are reached. This exceedance date method allows us to compute the annual trends for each single fraction and evaluate their statistical significance and as the advantage of being insensitive to the severity of fires in a particular year.

The two-decade averages represented by the color lines in Figure 3 show that, in the last two decades, the fractions of burned area between 1% and close to 30% are being reached earlier in the year. This suggests a widening of the annual cycle with displacement of the left tail of the burned area distribution, as a likely result of the anticipation of fire activity in the year. Trend analysis confirms the significance of early exceedance dates up to the 16% fraction (Mann-Kendall test, $\rho<0.05$). The remaining exceedance dates, including the slowing down phase of the fire cycle in late summer, show no significant trends. There was a 27-day (at the 10% exceedance dates) and 23-day (at the 16% dates) move back comparing the first and the second half-period averages. Considering the 15% fraction as a reasonable indicator of the beginning of the fire season, we obtained an anticipation linear rate of 1.34 days per year (Figure 4).

These results are in line with the expected lengthening of the fire season in Portugal during the 21st century, as detailed in Moriondo et al. (2006) and Carvalho et al. (2010). These two studies also identified a clearer signal in the fire season earliness compared to its extension into autumn. Similar trends have been obtained in the southwestern USA for recent decades, based on both fire activity (Westerling 2016) and fire weather risk (Jain et al. 2018).

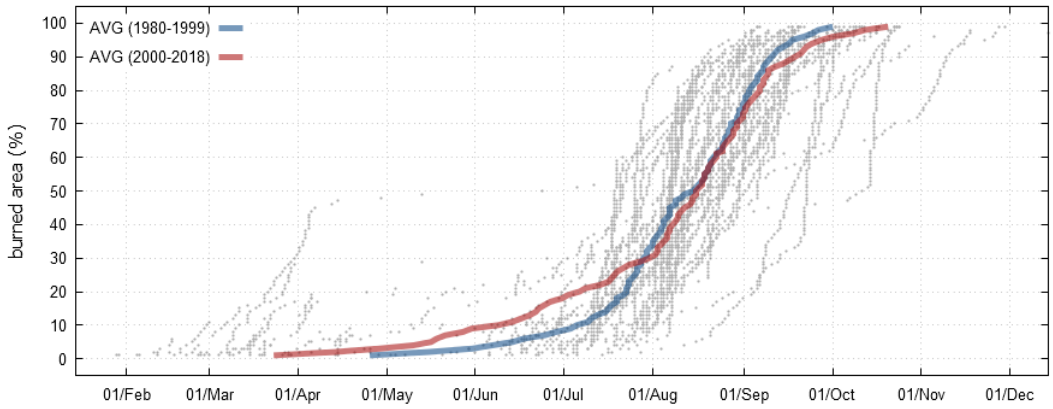

Figure 3: Exceeding dates for successive fractions (1%, …, 99%) of the total annual burned area in each year from 1980 to 2018. The grey dots represent the 39 annual dates for each fraction. The color lines represent the average dates for the first (1980-1999, blue line) and the second half (2000-2018, red line) of the period.

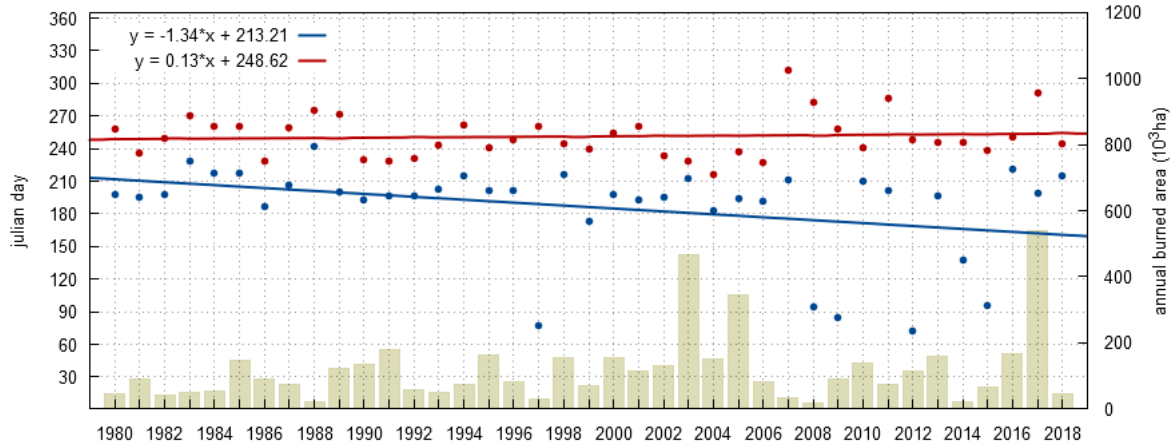

Figure 4: Evolution of the dates on which the 15% (blue points) and 85% (red points) of the total annual burned area are exceeded in the period 1980-2018, and corresponding adjusted linear regressions. The grey bars show the annual burned areas. The correlation between the 15% exceedance dates and the annual burned area is weak (r = 0.18).

3. The meteorological perspective: DSR patterns in the period 1980-2018

Changes in the annual fire cycle are related, in varying ways and intensity, to changes in atmospheric conditions conducive to fire onset and spread (e.g. Flannigan & Wotton 2001, Gouveia et al. 2016, Ruffault et al. 2018). Regarding wildfire seasonality, this relationship can be investigated with the DSR, Daily Severity Rating, which has a regular use in Portugal in the monitoring of the fire weather risk build-up throughout the year. DSR is an extension of the FWI system that transforms daily FWI values through a power expression (higher FWI values are thus emphasised) (Van Wagner 1987). In the present analysis we computed the annual cumulative DSR series, starting on January 1st, with data provided by the ERA5 reanalysis (Vitolo et al. 2020, CEMS 2019) on a grid of 163 points over mainland Portugal for 1980-2018.

Figure 5a shows the two mean cumulative DSR curves for the first (1980-1999) and second (2000-2018) halves of the study period. An increasing departure of the two curves is observed starting around April to the end of September. If we look closely at the difference between the two periods (in Figure 5b), we see a slight growth in the DSR difference as early as March, which then reduces to nearly zero in April before steadily increasing again. Considering the aforementioned secondary peak of fire activity and risk in March, this slight difference may represent a historical accentuation of that peak. In interpreting these results, we must take into account that the DSR is a good indicator of the 'sum' of fire-related weather conditions and that we are comparing average values over Portugal.

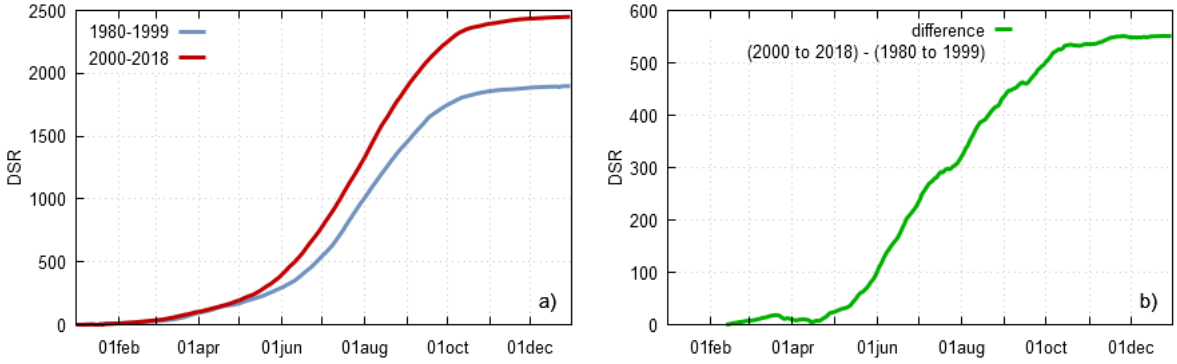

Figure 5: (a) Mean cumulative DSR values in the first (1980-1999, blue curve) and second half (2000-2019, red curve) of the study period. The DSR is cumulated daily from 1 January to 31 December in each year. (b) Daily difference between the two periods average (1980-1999 and 2000-2018); the scale on the Y-axis was changed.

4. Conclusions: Linking fire-weather and fire season management

The results presented show with confidence that the distribution of burned area has been moving progressively out of the critical period from July to September. This change is more evident during the spring period, which may be due to the combination of several factors, such as variations in human activities, in the type of machinery used in fields, in the agricultural and grazing cycles, among others, including necessarily changes in weather conditions on the scale of years and decades. Isolating social, ecological and climatic factors could be an arduous task. A good illustration of the interdependence between these factors is that the annual, operational definition of fire season, based on fire weather indicators, affects the distribution of ignitions by shifting restricted uses of fire and other fire-risk activities to the months preceding the 'season'.

The cumulative DSR showed a faster growth from the end of April when comparing the pre- and post-2000 periods, from which a direct contribution of meteorology can be deduced in the extension of the fire cycle in Portugal since 1980. This early growth must be evaluated in greater detail, both in the temporal and spatial components, in order to assess variations in the frequency of FWI values above specific thresholds and in the regional distribution of fire danger. Furthermore, the effect of March on the early season will need to be clarified, as the burned area series for this month confirms an upward trend (Mann-Kendall, $\rho < 0.01$) that does not occur in neighbouring months.

In 2017, as mentioned, 67.1% of the burned area occurred outside the 'fire season' or 'critical fire period', as legally defined by the Portuguese authorities. The term 'critical period' has gained current use since 2004, when

it replaced in legal framework the 'normal fire season', which had been established in 1981. The legal definition of the season window changed almost every year, recording the earliest beginning on May 1st (e.g. 1995) and latest ending on October 31st (e.g. 1988 and 2011). 2017 has weakened the operational role that the fixed period has had until then, in favour of greater focus on short-term forecasting of weather fire risk. We should note however that the fixed definition of 'season' included since 1981 the possibility of declaring extraordinary periods, 'when meteorological conditions that justify it occur or are expected'. This assessment was at the time based on a daily risk index given by the Angström formula (Fernandes 2015, Lourenço 1988, Decreto Regulamentar n.º 55/1981, Portaria n.º 167/2016, Portaria n.º 195/2017).

From a management point of view the seasonality of fires in mainland Portugal – presenting a well-known interannual and also decadal or climatic variability, as seen in recent decades – must be conciliated with the social and political definition of the fire season, on which numerous activities in rural areas depend.

5. Acknowledgments

Work was developed under the projects FIRESTORM, Weather and Behaviour of Fire Storms (PCIF/GFC/0109/2017) and FIREUSES, A political and environmental history of the large wildfires in Portugal, 1950-2020 (PTDC/HAR-HIS/4425/2021), both funded by FCT/MCTES. The authors thank IPMA colleagues Nuno Moreira and Paulo Pinto and FIREUSES colleagues Ana Queiroz, Joana Sousa, Frederico Ágoas, Marta Silva, and José Ferreira for rich and supportive discussions. We would like to extend a special thanks to ICNF for providing the rural fire records and to IPMA for the weather data and other facilities made available. M.C. is now based at the Institute of Contemporary History (NOVA University), which is funded by FCT/MCTES (UIDB/04209/2020 and UIDP/04209/2020).

6. References

Carmo, M., Ferreira, J., Mendes, M., Silva, Á., Silva, P., Alves, D., Reis, L., Novo, I. & Xavier Viegas, D. (2021). The climatology of extreme wildfires in Portugal, 1980–2018: Contributions to forecasting and preparedness. International Journal of Climatology 1– 24.https://doi.org/10.1002/joc.7411

Carvalho, A., Flannigan, M.D., Logan, K.A., Gowman, L.M., Miranda, A.I. & Borrego, C. (2010). The impact of spatial resolution on area burned and fire occurrence projections in Portugal under climate change. ClimaticChange, 98.1–2: 177–197.https://doi.org/10.1007/s10584-009-9667-2

CEMS (2019). Fire danger indices historical data from the Copernicus Emergency Management Service. ECMWF. https://doi.org/10.24381/cds.0e89c522.

da Câmara, C.C., Trigo, R.M., & Nascimento, M.L. (2014). Characterising the secondary peak of Iberian fires in March. Parte: http://hdl. handle. net/10316.2/34013. In: Viegas, D.X. (Ed.) Advances in ForestFireResearch 2014, Ch. 6. Coimbra: Imprensa da Universidade de Coimbra, pp. 1671–1682.http://dx.doi.org/10.14195/978-989-26-0884-6_184

Decreto Regulamentar n.º 55/1981 de 18 de Dezembro dos Ministérios da Defesa Nacional, da Administração Interna e da Agricultura, Comércio e Pescas. Diário da República: I série, nº 290 (1981), pp. 3299-3307. Available in www.dre.pt.

Fernandes, S. (2015). Incêndios Florestais em Portugal Continental fora do "período crítico". Contributos para o seu conhecimento. Master Thesis. Coimbra: Faculdade de Letras da Universidade de Coimbra

Flannigan, M.D. & Wotton, B.M. (2001). Climate, weather, and area burned. In: Johnson, E.A. and Miyanishi, K. (Eds.) Forest Fires: Behaviour and Ecological Effects, Ch. 10. San Diego, CA: AcademicPress, pp. 351–373.

Gouveia, C.M., Bistinas, I., Liberato, M.L., Bastos, A., Koutsias, N. & Trigo, R. (2016). The outstanding synergy between drought, heatwaves and fuel on the 2007 southern Greece exceptional fire season.Agricultural and Forest Meteorology 218: 135–145.https://doi.org/10.1016/j.agrformet.2015.11.023

Jain, P., Wang, X. & Flannigan, M.D. (2018).Trend analysis of fire season length and extreme fire weather in North America between 1979 and 2015. International Journal of Wildland Fire 26.12: 1009–1020. https://doi.org/10.1071/WF17008

Kwiecien, O., Braun, T., Brunello, C.F., Faulkner, P., Hausmann, N., Helle, G., Hoggarth, J.A., Ionita, M., … & Breitenbach, S.F. (2022). What we talk about when we talk about seasonality – A transdisciplinary review. Earth-Science Reviews 225: 103843. https://doi.org/10.1016/j.earscirev.2021.103843

Lourenço, L. (1988). Tipos de tempo correspondentes aos grandes incêndios florestais ocorridos em 1986 no Centro de Portugal. Finisterra 23.46: 251-270. https://revistas.rcaap.pt/finisterra/article/view/1975/1651

Moriondo, M., Good, P., Durão, R., Bindi, M., Giannakopoulos, C. & Corte-Real, J. (2006), Potential impact of climate change on fire risk in the Mediterranean area. Climate Research, 31(1): 85–95.https://doi.org/10.3354/cr031085

Portaria n.º 167/2016 de 15 de junho do Ministério da Agricultura, Florestas e Desenvolvimento Rural. Diário da República: 1ª série, nº 113 (2016), pp. 1856-1857. Available in www.dre.pt.

Portaria n.º 195/2017 de 22 de junho do Ministério da Agricultura, Florestas e Desenvolvimento Rural. Diário da República: 1ª série, nº 119 (2017), pp. 3163-3164. Available in www.dre.pt.

Ruffault, J., Curt, T., StPaul, N.M., Moron, V. & Trigo, R.M. (2018). Extreme wildfire events are linked to global-change type droughts in the northern Mediterranean. Natural Hazards and Earth System Sciences 18: 847–856. https://doi.org/10.5194/nhess-18-847-2018

Salloum, L., &Mitri, G. (2014). Assessment of the temporal pattern of fire activity and weather variability in Lebanon. International journal of wildland fire 23.4: 503-509. https://doi.org/10.1071/WF12101

Turco, M., Jerez, S., Augusto, S., Tarín-Carrasco, P., Ratola, N., Jiménez-Guerrero, P., &Trigo, R.M. (2019). Climate drivers of the 2017 devastating fires in Portugal. Scientific reports 9(1): 1-8.

United Nations Environment Programme (UNEP) (2022). Spreading like Wildfire – The Rising Threat of Extraordinary Landscape Fires. A UNEP Rapid Response Assessment. Nairobi. https://www.unep.org/resources/report/spreading-wildfire-rising-threat-extraordinary-landscape-fires

Van Wagner, C.E. (1974). Structure of the Canadian Forest Fire Weather Index. Ottawa: Canadian Forestry Service Publications n. 1333.

Van Wagner C.E. (1987). Development and structure of the Canadian Forest Fire Weather Index System.Canadian Forestry Service, Ottawa, ON.Forestry Technical Report 35: 37 p.

Viegas, D.X. &Viegas, M.T. (1994). A relationship between rainfall and burned area for Portugal. International Journal of Wildland Fire, 4.1: 11–16.

Viegas, D.X., Almeida, M.F. and Ribeiro, L.M. (Eds.).(2017) O complexo de incêndios de Pedrogão Grande e concelhos limítrofes, iniciado a 17 de junho de 2017. Centro de Estudos sobre Incêndios Florestais ADAI/LAETA. Coimbra: Universidade de Coimbra.

Viegas, D.X., Almeida, M.F. and Ribeiro, L.M. (Eds.). (2019). Análise dos Incêndios Florestais Ocorridos a 15 de outubro de 2017. Centro de Estudos sobre Incêndios Florestais ADAI/LAETA, Universidade de Coimbra, Coimbra.

Vitolo, C., Di Giuseppe, F., Barnard, C., Coughlan, R., San-Miguel-Ayanz, J., Libertá, G., Krzeminski, B. (2020). ERA5-based global meteorological wildfire danger maps. Sci Data 7, 216. https://doi.org/10.1038/s41597-020-0554-z

Westerling, A.L.R. (2016). Increasing western US forest wildfire activity: sensitivity to changes in the timing of spring. Philosophical Transactions of the Royal Society B: Biological Sciences 371: 20150178. https://doi.org/10.1098/rstb.2015.0178

Wotton, B.M., & Flannigan, M.D. (1993).Length of the fire season in a changing climate.TheForestryChronicle 69.2: 187-192.

Extreme fire spread events and their drivers in the western US

Camille S Stevens-Rumann*[1,2]; Jonathan Coop[3]; Sean Parks[4]; Scott Ritter[1]; Chad Hoffman[2]

[1]Colorado Forest Restoration Institute, Colorado State University 1472 Campus Delivery, Fort Collins, CO, 80521 USA, {c.stevens-rumann, scott.ritter}@colostate.edu
[2] Forest and Rangeland Stewardship, Colorado State University 1472 Campus Delivery, Fort Collins, CO, 80521 USA, {c.stevens-rumann@colostate.edu, chad.hoffman@colostate.edu}
[3] Clark School of Environment and Sustainability, Western Colorado University, Gunnison, Colorado, USA {jcoop@western.edu}
[4]Aldo Leopold Wilderness Research Institute, Rocky Mountain Research Station, USDA Forest Service, Missoula, Montana, USA {sean.parks@usda.gov}

**Corresponding author*

Keywords

Fire spread, drivers of fire spread, climate change, western US

Abstract

Wildfire activity in recent years not only have large total area burned but also large, single-day fire spread events that pose challenges to ecological systems and human communities. Our objective was to better understand the relationships between extreme single-day fire spread events, annual area burned, and fire-season climate, and predict changes under future warming. We employ a satellite-derived dataset of daily fire spread events in the western USA and gridded climate data over this region to assess relationships between extreme single-day fire spread events, annual area burned, and fire-season maximum temperature, climate moisture deficit, and vapor pressure deficit over a time period of 2002-2020. Extreme single-day fire spread events which were classified as single day of burning that burned more than >1100 ha (the top 16%), these could have been a part of multiple days of extreme fire behavior resulting in multiple extreme fire spread events or an isolated day of extreme behavior, regardless days with fire spread >1100ha on a single fire were analyzed separately. We then develop models to predict fire activity under a 2°C warming scenario. These extreme fire spread events accounted for 70% of the cumulative area burned over the period of analysis. Annual area burned was correlated with number and mean size of spread events, and those largest of these large fire spread events. In 2020, wildfires burned over 4 million ha in the US and we identified 441 extreme fire spread events, identified as >1100 ha burned in a single day. These 441 events in 2020, burned 2.2 million ha across our study area. In contrast, the average extreme events between 2002 and 2019 was 168 per year that burned 0.5 million ha. Fire season climate variables correlate strongly with the annual number of extreme events and area burned. Our models predict that the annual number of extreme fire spread events more than doubles under a 2°C warming scenario, with an attendant doubling in area burned. Exceptional fire seasons like 2020 will likely be more common, and wildfire activity under future extremes will likely exceed anything witnessed yet. Safeguarding human communities and supporting resilient ecosystems may require new lines of scientific inquiry, novel land management approaches, and accelerated climate mitigation efforts.

1. Introduction

Recent fire seasons in the western US and elsewhere have been characterized not only by high total area burned, but also periods of extremely rapid fire growth and very large single-day fire spread events. Throughout a fire season, short duration but extreme events may have outsized effects, vastly expanding the area burned in individual fires (i.e. "megafires"; Adams, 2013) and contributing disproportionately to cumulative social and ecological impacts (Duane et al., 2021). As examples, 4 million ha burned in the US in the 2020 fire season, mostly in western states (www.nifc.gov), with many states seeing record-setting fires. In Oregon and Washington, there were multiple days of individual fire growth over 10,000 ha (including one report of 40,000 ha), and a record-setting wildfire in Colorado that burned ca. 1500 ha/hr for >24 hours in October (https://inciweb.nwcg.gov/). Similarly, California reported a record-setting individual fire (the 400,000-ha August Complex) that exhibited extreme fire growth under high winds and low fuel moisture over several days in early September, contributing to record total annual area burned (1.7 million ha; www.fire.ca.gov).

Observations of very large single-day fire runs within the context of recent record-breaking fires and fire seasons raise a suite of research questions and hypotheses (Duane et al., 2021). New methods to calculate daily fire spread from satellite observations have catalyzed the development of datasets of daily fire spread over expanded spatial and temporal scales (Parks, 2014) and are leading to analyses that provide new insights into wildfire activity (Hart & Preston, 2020; Wang et al., 2017). At a foundational level, aggregate fire effects such as area burned represent the accumulation of thousands of single-day fire spread events. Growing evidence suggests that climate change will continue to expand fire activity in coming decades, but with interannual variability (e.g., El Niño Southern Oscillation, Pacific Decadal Oscillation; Crimmins, 2011; Trouet et al., 2009) likely resulting in climatic conditions and patterns in fire spread events outside of those experienced within recent observations. What constitutes an extreme under contemporary climate may change as once rare conditions (such as occurred in 2020) become more common. Thus, we might ask if climate and attendant fire activity in the western US in 2020 could be representative of future norms, and what kind of wildfire activity could occur during future extremes?

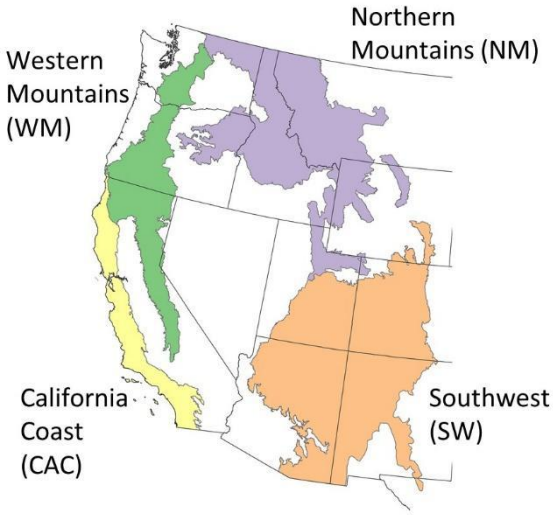

Figure 1- Western US study area, comprising four forested ecoregions.

2. Methods

Our analyses are based on measurements of daily fire spread (ha/day) for individual wildfires. Following the methods of Parks (2014), we developed spatially continuous maps depicting the day-of-burning for all fires whose centroid intersected our western US study area from 2002-2020 (Fig. 1). Briefly, this procedure interpolates VIIRS and MODIS fire detections (from https://firms.modaps.eosdis.nasa.gov/active_fire/) to map the day 1f burning within the entire area of the final fire perimeter at a 30-m resolution. This day-of-burning interpolation technique has been successfully used in several previous fire studies (e.g., Downing et al., 2021; Holsinger et al., 2016; Meigs et al., 2020; Wang et al., 2017). All day-of-burning interpolations were constrained to the final fire perimeters as obtained from national repositories; we obtained 2002-2018 fire perimeters from the Monitoring Trends in Burn Severity (MTBS) program (Picotte et al., 2020). Fire perimeters from 2019 and 2020 were downloaded from the National Interagency Fire Center (Interagency Fire Perimeter History - All Years: available at https://data-nifc.opendata.arcgis.com/datasets/); fires <400 ha were removed to match the MTBS dataset. Given minor differences between the NIFC and MTBS databases, we performed a sensitivity analysis to examine whether or not a bias correction to 2019 and 2020 NIFC fire counts and area burned would influence our findings or interpretations. We found that such a correction led to negligible increases in future projections and thus elected to use the data from NIFC without adjustments, noting that as more and better data become available, more refined future projections may become feasible. Fires with less than 10 fire detections were excluded from the analysis because of uncertainty associated with interpolating small numbers of detections. Fire detections that occurred between 12 am and 6 am were assigned to the previous day. In total, we interpolated day-of-burning for 2391 fires and 20,991 unique fire spread events ranging in size from 25 to 74,509 ha.

3. Results and Discussion

Daily fire spread followed a slightly skewed log-normal distribution, with a median value of 260 ha/day and a mean of 295 ha/day (Fig. 2). Single-day spread events >1100 ha represented the top 16% of events (1 standard deviation from the mean), and accounted for 70% of total area burned. Described another way, the top 10% of fire spread events burned 58% of the total area and just the top 1% of events burned 20% of the total area. Parameters of annual distributions of daily fire spread were closely linked to annual area burned. Number of events (P <0.001), mean event size (P <0.001), and skewness (P = 0.03) were all significant predictors of annual area burned in our best-fitting model (r^2 = 0.90, 15 d.f.). Relative contributions each term were as follows: number of events, 68%; mean event size, 29%; and skewness, 3%.

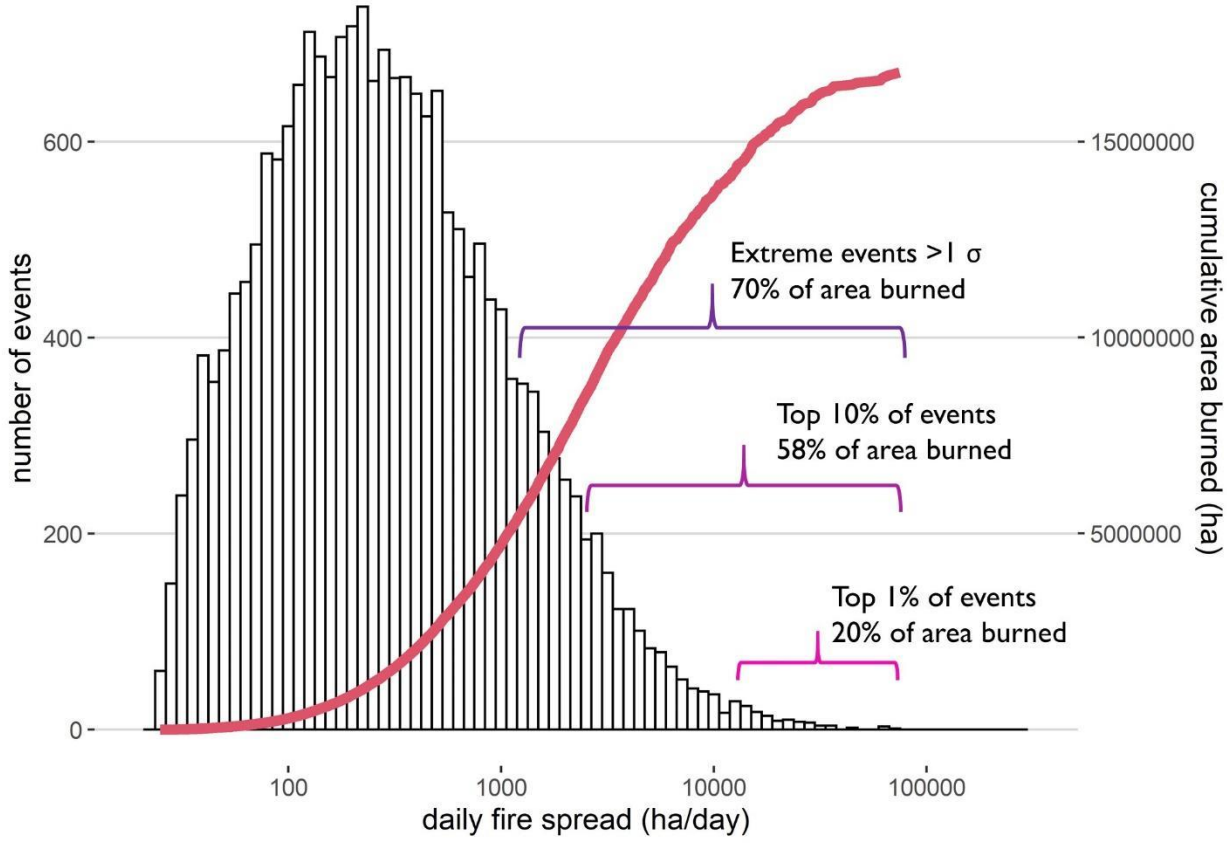

Figure 2- Distribution of daily fire spread events and the cumulative area burned during the 2002-2020 study period. Extreme events ≥1100 ha (the top 16%, 1 standard deviation) account for 70% of area burned).

A generalized linear (negative binomial) model predicting the total count of extreme fire spread events from Aridity provided robust predictions for the entire study area (P<0.001, McFadden's r^2 = 0.42); this model was then employed to predict of the annual number of extreme spread events for a 2°C above pre-industrial warming scenario in contrast to a 1986-2015 reference period, and modeled and observed activity in 2020. This model predicted a mean of 343 extreme spread events per year under the +2°C scenario, ranging from a minimum of 81 to a maximum of 815 events in extreme future years (Fig. 3). In contrast, the mean modeled number of extreme spread events in the reference period was 129, with a range of 32-302. Model predictions for the 2020 fire season climate were 324 extreme spread events; the observed number was 441.

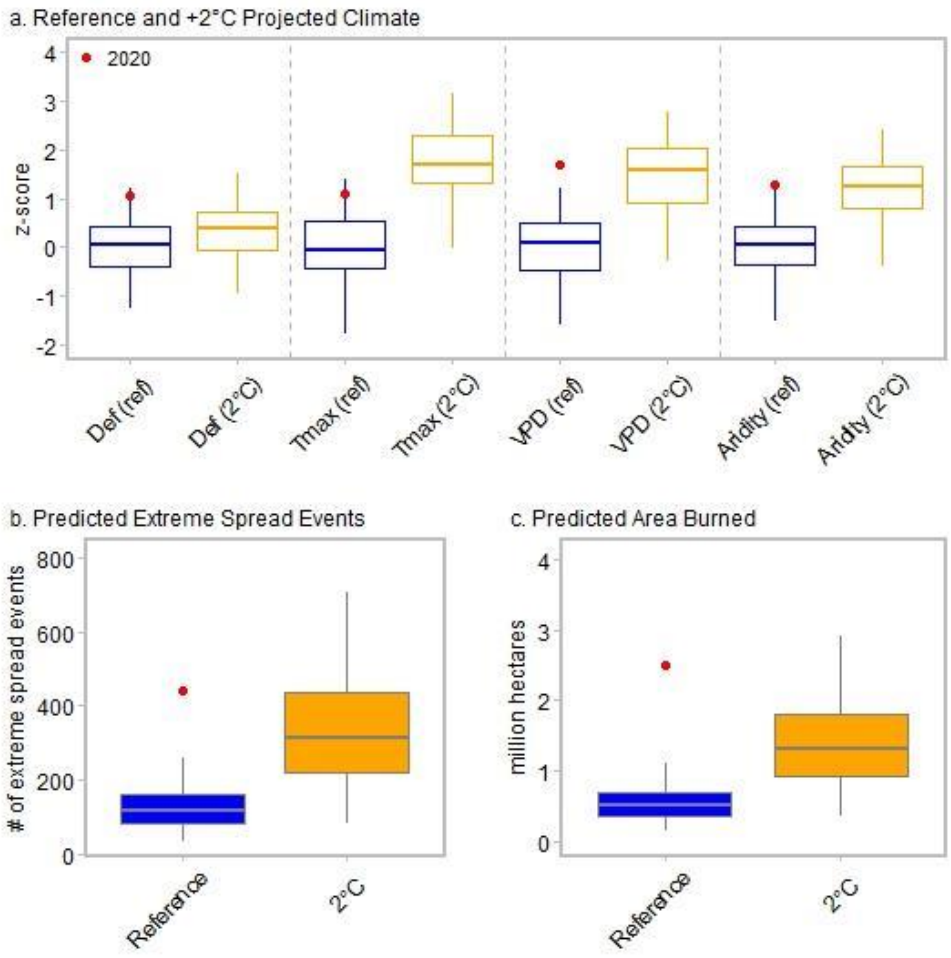

Figure 3- Reference period (1986-2015) vs. future (+2°C) projections (a) for four climate variables, Deficit, Tmax, VPD, and Aridity (defined in the text as the average of the other three variables), (b) predicted number of extreme events >1100 ha/day, and (c) annual area burned. Red dots represent observed climate and fire activity in 2020.

Better understanding the capacity for human activities to modulate the undesirable effects of extreme fire spread is also imperative. Contemporary fire management policies appear to be relatively ineffective in mitigating extreme fire spread events, which are occurring despite recent annual fire suppression expenditures of $1-3 billion in the US (data available from the National Interagency Fire Center, www.nifc.com). Explosive fire growth during extreme fire spread events can severely reduce the efficacy of fire suppression as currently practiced. Extreme burning conditions that facilitate early fire growth allow fires to escape initial attack; as these fires continue to grow, their size and potential to impact communities and other resources can subsequently overwhelm fire management resources. Given the likelihood of increasing societal and ecological exposure to extreme fire spread events, new approaches to fire management and policy may be needed (Cochrane & Bowman, 2021; Moritz et al., 2014; Smith et al., 2016). In some settings, management activities may be directed towards reducing undesirable fire effects, such as by promoting frequent but low-to-moderate severity fire to prevent anomalously severe fire and attendant ecological changes (Walker et al., 2018). In others, higher-severity prescribed fire and managed wildfire might be useful to change fuel types and reduce landscape flammability (e.g., shifts from conifer to broadleaf forest types). Enhancing community preparedness under extreme burning conditions will also be critical to safeguarding human lives and infrastructure.

Writing and conference presentation from Coop J, Parks S, Stevens-Rumann CS, Ritter S, Hoffman C (2022) Extreme fire spread events and area burned under recent and future climate in the western US. Global Ecology and Biogeography 2022: 00:1–11 https://doi.org/10.1111/geb.13496

4. Literature Cited

Adams, M. A. (2013). Mega-fires, tipping points and ecosystem services: Managing forests and woodlands in an uncertain future. *Forest Ecology and Management*, *294*, 250–261. https://doi.org/10.1016/j.foreco.2012.11.039

Cochrane, M. A., & Bowman, D. M. J. S. (2021). Manage fire regimes, not fires. *Nature Geoscience*, *14*(7), 455–457. https://doi.org/10.1038/s41561-021-00791-4

Crimmins, M. A. (2011). Interannual to decadal changes in extreme fire weather event frequencies across the southwestern United States. International Journal of Climatology, 31(11), 1573–1583.

Downing, W. M., Meigs, G. W., Gregory, M. J., & Krawchuk, M. A. (2021). Where and why do conifer forests persist in refugia through multiple fire events? Global Change Biology, 27(15), 3642–3656. https://doi.org/10.1111/gcb.15655

Duane, A., Castellnou, M., & Brotons, L. (2021). Towards a comprehensive look at global drivers of novel extreme wildfire events. Climatic Change, 165(3), 43. https://doi.org/10.1007/s10584-021-03066-4

Hart, S. J., & Preston, D. L. (2020). Fire weather drives daily area burned and observations of fire behavior in mountain pine beetle affected landscapes. Environmental Research Letters, 15(5), 054007. https://doi.org/10.1088/1748-9326/ab7953

Holsinger, L., Parks, S. A., & Miller, C. (2016). Weather, fuels, and topography impede wildland fire spread in western US landscapes. Forest Ecology and Management, 380, 59–69. https://doi.org/10.1016/j.foreco.2016.08.035

Meigs, G. W., Dunn, C. J., Parks, S. A., & Krawchuk, M. A. (2020). Influence of topography and fuels on fire refugia probability under varying fire weather conditions in forests of the Pacific Northwest, USA. Canadian Journal of Forest Research, 50(7), 636–647. https://doi.org/10.1139/cjfr-2019-0406

Moritz, M. A., Batllori, E., Bradstock, R. A., Gill, A. M., Handmer, J., Hessburg, P. F., Leonard, J., McCaffrey, S., Odion, D. C., Schoennagel, T., & Syphard, A. D. (2014). Learning to coexist with wildfire. Nature, 515(7525), 58–66. https://doi.org/10.1038/nature13946

Parks, S. A. (2014). Mapping day-of-burning with coarse-resolution satellite fire-detection data. International Journal of Wildland Fire, 23(2), 215–223. https://doi.org/10.1071/WF13138

Picotte, J. J., Bhattarai, K., Howard, D., Lecker, J., Epting, J., Quayle, B., Benson, N., & Nelson, K. (2020). Changes to the Monitoring Trends in Burn Severity program mapping production procedures and data products. Fire Ecology, 16(1), 16. https://doi.org/10.1186/s42408-020-00076-y

Smith, A. M. S., Kolden, C. A., Paveglio, T. B., Cochrane, M. A., Bowman, D. M., Moritz, M. A., Kliskey, A. D., Alessa, L., Hudak, A. T., Hoffman, C. M., Lutz, J. A., Queen, L. P., Goetz, S. J., Higuera, P. E., Boschetti, L., Flannigan, M., Yedinak, K. M., Watts, A. C., Strand, E. K., … Abatzoglou, J. T. (2016). The Science of Firescapes: Achieving Fire-Resilient Communities. BioScience, 66(2), 130–146. https://doi.org/10.1093/biosci/biv182

Trouet, V., Taylor, A. H., Carleton, A. M., & Skinner, C. N. (2009). Interannual variations in fire weather, fire extent, and synoptic-scale circulation patterns in northern California and Oregon. Theoretical and Applied Climatology, 95(3), 349–360. https://doi.org/10.1007/s00704-008-0012-x

Walker, R. B., Coop, J. D., Parks, S. A., & Trader, L. (2018). Fire regimes approaching historic norms reduce wildfire-facilitated conversion from forest to non-forest. Ecosphere, 9(4), e02182. https://doi.org/10.1002/ecs2.2182

Wang, X., Parisien, M.-A., Taylor, S. W., Candau, J.-N., Stralberg, D., Marshall, G. A., Little, J. M., & Flannigan, M. D. (2017). Projected changes in daily fire spread across Canada over the next century. Environmental Research Letters, 12(2), 025005. https://doi.org/10.1088/1748-9326/aa5835

Fire cause classification of undetermined fires in southeastern France

Christos Bountzouklis*[1]; Dennis Michael Fox[1]; Elena Di Bernardino[2]

[1]Univerisity of Côte d'Azur, UMR CNRS 7300 ESPACE, Nice, 06204, France, {christos.bountzouklis@univ-cotedazur.fr; dennis.fox@univ-cotedazur.fr}
[2] Univerisity of Côte d'Azur, UMR CNRS 7351 LJAD, Nice, 06108, France, {elena.di_bernardino@univ-cotedazur.fr}

**Corresponding author*

Keywords

ignition causes, machine learning, arson fires, southeastern France

Abstract

Knowledge about fire ignition causes and their spatiotemporal patterns can greatly enhance the efficiency of fire management and fire strategies. In France, the majority of forest fire research is based on a 2x2 km gridded database that provides amongst other information, the cause of fire ignition. According to the same database however, approximately 70% of all fires between 1973 and 2020 were recorded without a cause of ignition. Therefore, information on fire causes for a very large part of the fires that were recorded in the last 50 years is not taken into consideration and can potentially provide significant evidence on fire ignition patterns. As arson fires are of particular interest in southeastern France since they are the most frequent and account for the largest volume of burned area, this study aimed to exploit a fire ignition point geodatabase and machine learning methodologies, to create and evaluate a model that can identify whether unknown caused fires can be classified as arson or non-arson fires, based on numerous environmental and anthropogenic factors. The results of the study suggest that cause identification can be adequately accurate using such a model, although a larger fire database would increase overall performance.

1. Introduction

Fire ignition patterns can vary significantly both temporally and spatially depending on the cause of ignition (Curt et al., 2016) and can be impacted by a plethora of environmental and anthropogenic drivers (Catry et al., 2009; Syphard et al., 2008; Syphard and Keeley, 2015). Some studies have demonstrated that arson fires can potentially be predicted both spatially and temporally (Gonzalez-Olabarria et al., 2012; Penman et al., 2013). In SE France, arson (particularly pyromania and conflict/interest) is the most frequent ignition cause for large fires (100>ha) (Ganteaume and Jappiot, 2013). Recording fire causes and studying their spatiotemporal patterns is important for establishing useful fire policies (Rodrigues et al., 2014) since a better understanding can enhance the efficacy of fire prevention measures (Oliveira et al., 2012). In France according to the national fire database (Prométhée) that contains records of fire ignition causes, approximately 70% of all fires between 1973 and 2020 were ignited by an unknown cause. The percentage of non-identified causes is high, and it is an additional constraint to the already limited research conducted on fire ignition causes. As in many other disciplines, applications of machine learning methodologies have seen a significant increase in wildfire science over the past years (Jain et al., 2020). Thus, this study aims to examine whether a fire ignition point dataset coupled with machine learning methods can be used to identify the source (arson or non-arson) of unknown caused fires and evaluate the importance of several environmental and anthropogenic factors in determining the ignition source.

2. Data & Methodology

2.1. Study area

The study area covers the administrative department of "Bouches-du-Rhône", which according to the official forest fire database in France (Prométhée), ranks second in terms of burned area and fire frequency in mainland France (Figure 1, Table 1). The department is characterized by gentle slopes and low to intermediate altitudes that increase when moving eastwards. Population density (388.8 people/km^2) is higher in the eastern half of the department since that is where the second most populated city in France (Marseille) is found and because the

westernmost parts are covered by wetlands and a national park. Therefore, the westernmost section has a low potential for fire ignition and propagation but increases when moving towards the eastern half of the department.

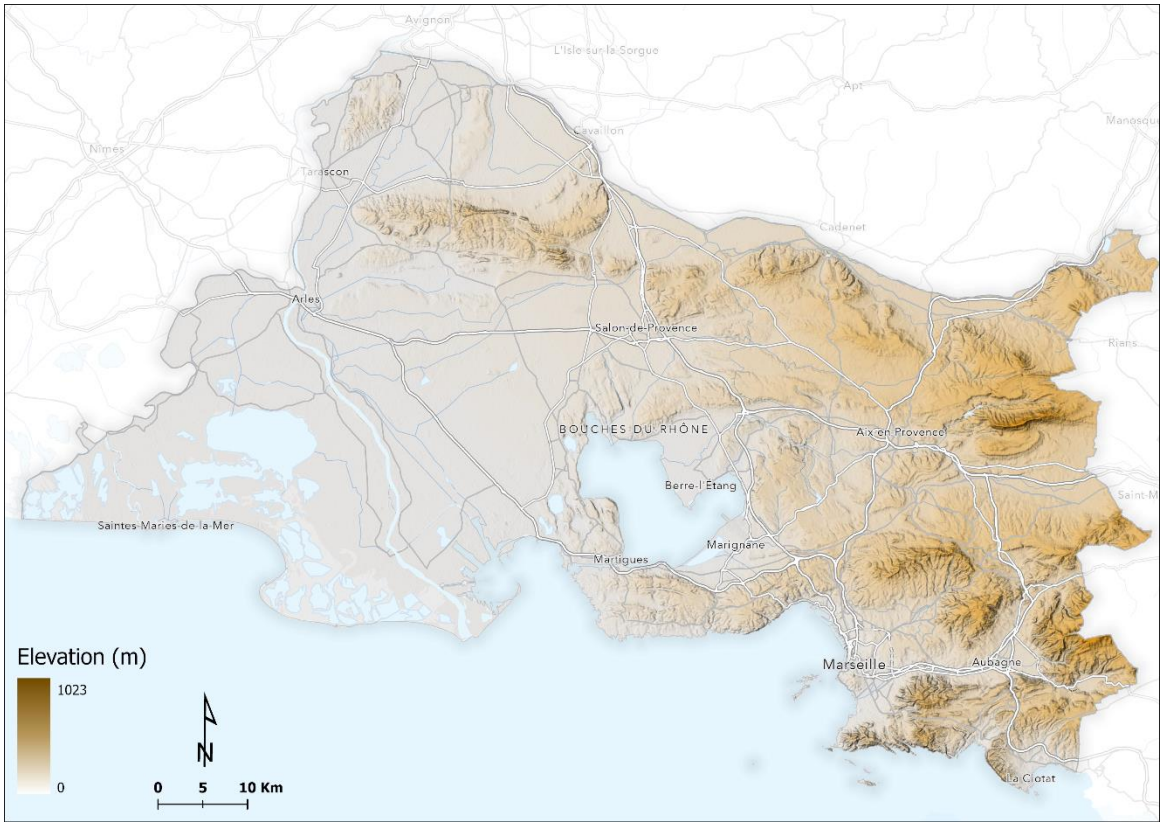

Figure 1 Departmental limits of Bouches-du-Rhônes overlaid on a 25 m Digital Elevation Model.

Table 1 Environmental characteristics of Bouches-du-Rhône.

Total area (km²)	3456
Forested area (km²)	1530
Mean slope (°)	8.8
Median slope (°)	5.7
Mean elevation (m)	142
Median elevation (m)	89

When considering only fires with a known cause, 63 % of the total burned area and approximately half (51 %) of all fire ignitions in the department are due to arson fires, according to Prométhée (Table 2). In addition, most of the large fires (>100 ha) in the study area are caused by arsonists (Figure 2). Even though negligence (professional & personal) is the second most frequent cause of fire ignition, it does not cause a proportionate volume of burned area.

Table 2 Number of fires and volume of burned area per ignition cause from 1973 to 2020 in Bouches-du-Rhônes.

Fire Ignitions (#)	Percentage (%)	Burned Area (ha)	Percentage (%)	Cause
349	3.3	3,020	3.3	Accidental
161	1.5	335	0.4	Natural
1,034	9.7	5,223	5.7	Negligence
1,556	14.7	14,493	15.7	Arson
7,524	70.8	69,105	75	Unknown
10,624	-	92,176	-	Total

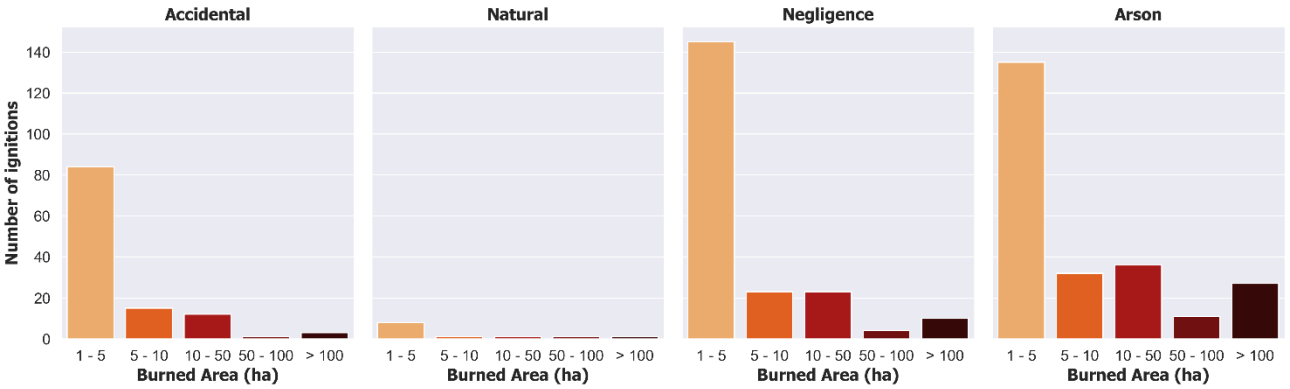

Figure 2 Number of fires per volume category of burned area (> 1ha) and ignition cause from 1973 to 2020.

2.2. Data

2.2.1. Fire database

In France, the majority of forest fire research is based on Prométhée, the national database for forest fires. The specific fire database holds records of fires starting from 1973 and it includes information such as burned area, cause of ignition, date, and approximate location (within a 2x2 km grid) for each fire. In the current study, we used a geographic database that contains exact coordinates of fire ignitions that is provided by the National Forestry Office (Office National des Forêts, ONF), which to the best of our knowledge is the second time being utilized after Ganteaume and Long-Fournel, 2015. The dataset consists of 3,234 fire ignition points ranging from 1960 to 2012, which however does not contain information on the cause of ignition. To enrich the ONF point database with the cause of ignition, two additional databases were used (Figure 3). Information from the Prométhée database was firstly merged with a polygon fire geodatabase that is described in Bountzouklis et al., 2022 and subsequently spatially joined with the point geodatabase resulting in a combined dataset that contains ignition coordinates, burn scars, and cause of ignition.

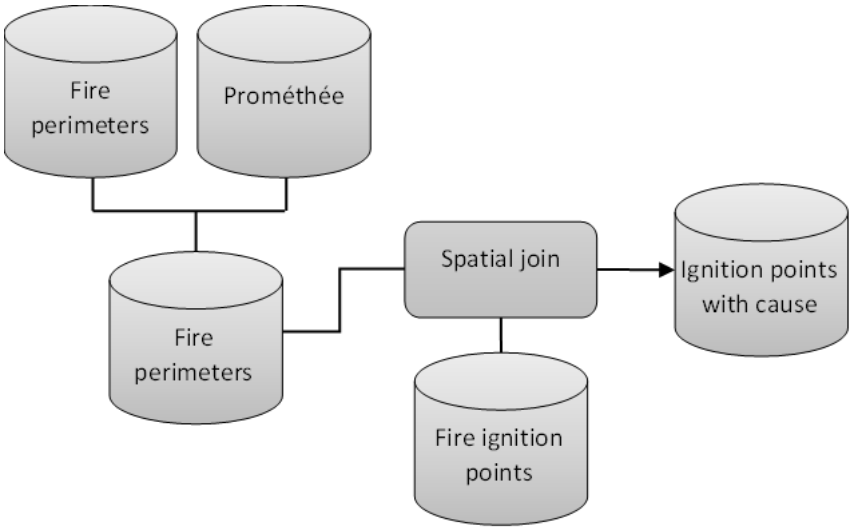

Figure 3Flow chart depicting the processing steps to generate the final dataset.

As earlier records on fire causes are considered less reliable (Ganteaume and Jappiot, 2013) only fires from 1996 to 2012 were considered, resulting in 323 fires (Figure 4). it was deemed best to classify causes into two major categories, arson and non-arson, due to the limited recorded number of fires caused by accident, negligence and lightning strikes but also due to the significance of arson fires in the specific area.

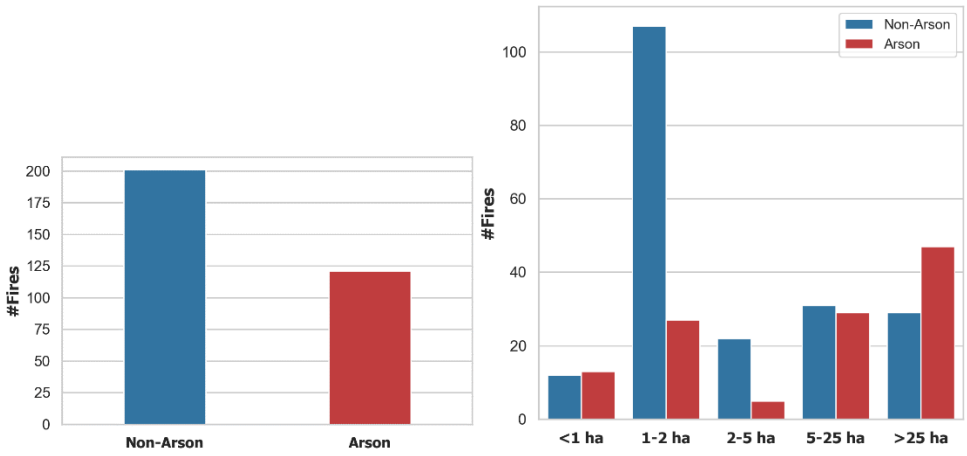

Figure 4 Number of fires per cause and burned area size.

2.2.2. Explanatory variables

Multiple environmental and socioeconomic factors (Table 3 & Figure 5) that are known to be associated with forest fires, were acquired by a combination of European and national databases, in order to train a model that can identify the ignition cause of a fire. To account for any potential geometric errors of the ignition points and more importantly to include contextual geographic information, a circular buffer zone (500 m) was created around each fire ignition point to extract relative information.

Table 3 List of environmental, anthropogenic and spatiotemporal variables considered.

Type	Name	Description	Source
Land Cover	Artificial surfaces	Percentage of cover within each zone	Corine Land Cover - 2006
	Agriculture		
	Vegetation		
	Water/ Wetlands		
Topographic	Slope inclination	Mean inclination (º)	National Geographic Institute - 5 m spatial resolution
	Slope aspect	Percentage of cover within each zone (Flat, N, E, S, W)	
	Elevation	Mean elevation (m) above sea level	
	Topographic wetness index	Topographic-driven control on soil moisture	
Vegetation type	Coniferous	Percentage of cover within each zone	National Geographic Institute - 2006
	Coppice		
	Hardwood		
	Open Forest		
	Shrublands		
Anthropogenic	Population density	Individuals per sq. m.	National Institute of Statistics and Economic Studies - Sub-municipal level - 2006
	Gini index	Inequality index	
	Income	Mean taxable income (€)	
	Unemployment	Unemployment rate (%)	
	Primary road distance	Euclidean distance from fire location (m)	National Geographic Institute - 2008
	Secondary road distance		
	Power pylons distance		
	Railway distance		
	Wildland Urban Interface distance		
	House density	Buildings per sq. m.	
Spatiotemporal characteristics	Season	Winter, spring, summer, autumn	Fire database
	Burned area size	<1 ha, 1-2 ha, 1-2 ha, 2-5 ha, 5-25 ha, >25 ha	
	Coordinates	XY coordinates of each fire	

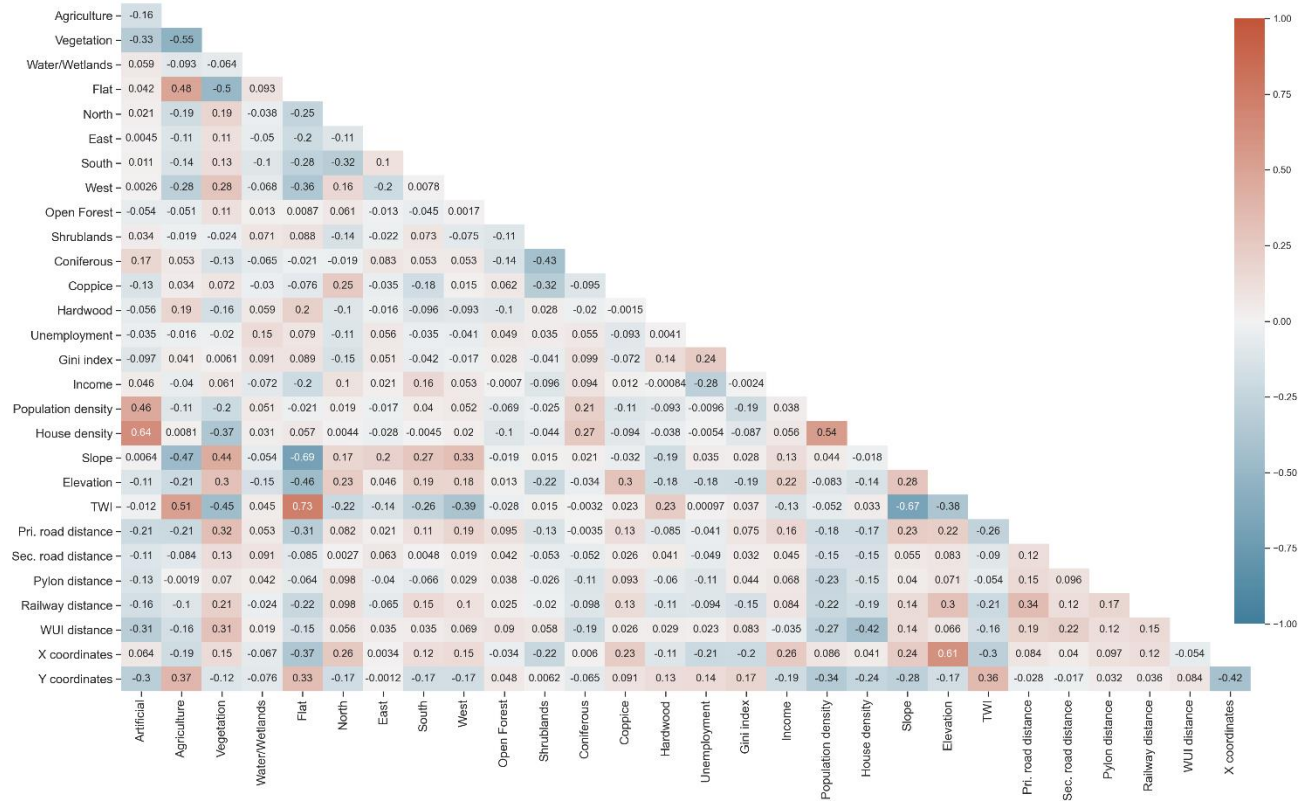

Figure 5 Kendall's Tau rank correlation coefficient heatmap of explanatory variables.

2.3. Methods

The analysis of the data is based on Random Forests (Breiman, 2001), a well-established machine learning algorithm in many disciplines but also in wildfire science (Jain et al., 2020). In order to train the model, 70% of the original dataset was utilized, while the remaining 30% was used for testing the accuracy in predicting the cause of a fire. Due to the limited number of observations, the process of splitting the data (using the same ratio) and executing the model was iterated (n=300) to have a more consistent perception of the accuracy of the model. Additionally, the processing chain included tuning the algorithm's hyperparameters as well as calculating the feature importance score for all variables. Feature importance was based on the Gini impurity method which can be used as a diagnostic which contributes to understanding which variables are driving the results of a model and which ones can be discarded.

3. Results

The accuracy of the model is illustrated in the form of a boxplot (Figure 6) that represents accuracy scores from all iterations of the model. The accuracy of the model to classify unknown caused fires can vary substantially ranging from 56% to 76% (median value 67%), due to the small size of the dataset.

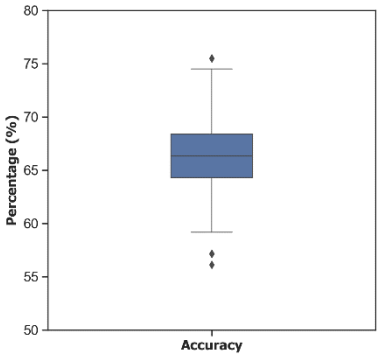

Figure 6 Boxplot representing Random Forest's classification accuracy for all iterations (n=300). (i) Bar within the box is the median value, (ii) bottom part of the box is the first quartile, and (iii) top part of the box is the third quartile. Whiskers represent observations outside the middle 50 % and points represent outliers.

Figure 7 shows the importance values of each explanatory variable used in the model. Overall, anthropogenic features (in blue) appear to surpass in importance the rest. Moreover, topographic factors (in brown) seem to be more important than land cover and vegetation type while spatiotemporal variables except for XY coordinates hold the lowest importance. More specifically, Secondary road distance, Shrublands and Unemployment rate are the three variables displaying the highest importance. Finally, several variables mainly related to spatiotemporal characteristics and others such as certain vegetation types (Hardwood & Coppice) as well as Water can be excluded to decrease model complexity and execution time.

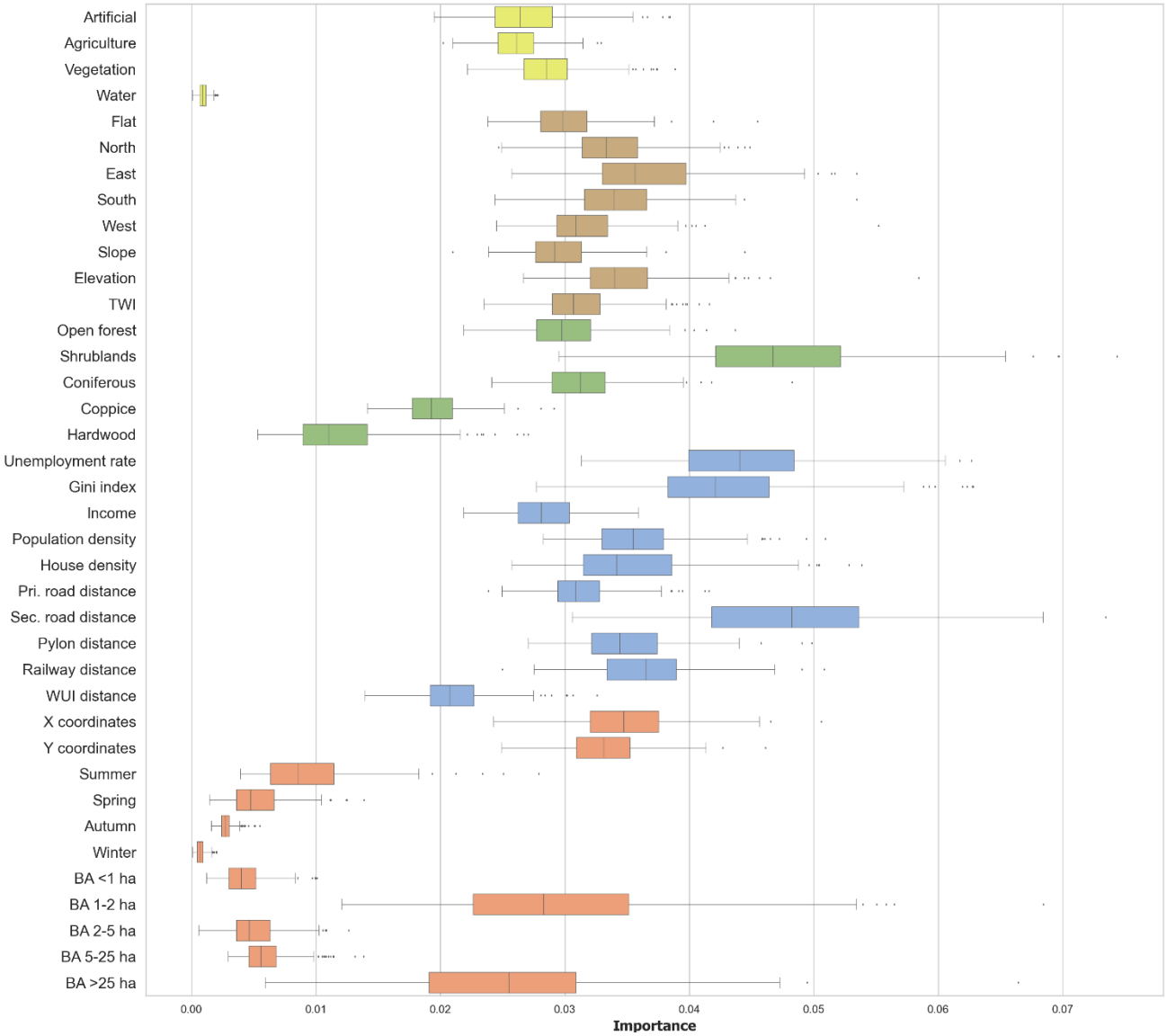

Figure 7 Distribution of the variable importance values for all iterations (n=300).

4. Conclusion

The results of the study suggest that the source of unknown caused fires can be identified at an acceptable level of accuracy even with a limited number of fires. Anthropogenic drivers such as distance to secondary roads and unemployment rate, along with higher volumes of shrublands around ignition points are the most important features in determining the classification of unknown caused fires for the specific area.
Overall performance of such models would most likely greatly benefit from the exploitation of larger datasets as well as from the inclusion of weather-related variables. Finally, as location holds particular importance over certain fire causes, spatial extensions of machine learning algorithms such as Geographic random forests

(Georganos et al., 2021) and Geographically weighted neural networks (Hagenauer and Helbich, 2022) could provide significant enhancements over the original algorithms.

5. References

Bountzouklis, C., Fox, D. M. and Di Bernardino, E.: Environmental factors affecting wildfire-burned areas in southeastern France, 1970–2019, Nat. Hazards Earth Syst. Sci., 22(4), 1181–1200, doi:10.5194/nhess-22-1181-2022, 2022.

Breiman, L.: Random Forests, Mach. Learn., 45, 5–32, doi:https://doi.org/10.1023/A:1010933404324, 2001.

Catry, F. X., Rego, F. C., Bação, F. L. and Moreira, F.: Modeling and mapping wildfire ignition risk in Portugal, Int. J. Wildl. Fire, 18(8), 921–931, doi:10.1071/WF07123, 2009.

Curt, T., Fréjaville, T. and Lahaye, S.: Modelling the spatial patterns of ignition causes and fire regime features in southern France: Implications for fire prevention policy, Int. J. Wildl. Fire, 25(7), 785–796, doi:10.1071/WF15205, 2016.

Ganteaume, A. and Jappiot, M.: What causes large fires in Southern France, For. Ecol. Manage., 294, 76–85, doi:10.1016/j.foreco.2012.06.055, 2013.

Ganteaume, A. and Long-Fournel, M.: Driving factors of fire density can spatially vary at the local scale in south-eastern France, Int. J. Wildl. Fire, 24(5), doi:10.1071/WF13209, 2015.

Georganos, S., Grippa, T., Niang Gadiaga, A., Linard, C., Lennert, M., Vanhuysse, S., Mboga, N., Wolff, E. and Kalogirou, S.: Geographical random forests: a spatial extension of the random forest algorithm to address spatial heterogeneity in remote sensing and population modelling, Geocarto Int., 36(2), 121–136, doi:10.1080/10106049.2019.1595177, 2021.

Gonzalez-Olabarria, J. R., Brotons, L., Gritten, D., Tudela, A. and Teres, J. A.: Identifying location and causality of fire ignition hotspots in a Mediterranean region, Int. J. Wildl. Fire, 21(7), 905, doi:10.1071/WF11039, 2012.

Hagenauer, J. and Helbich, M.: A geographically weighted artificial neural network, Int. J. Geogr. Inf. Sci., 36(2), 215–235, doi:10.1080/13658816.2021.1871618, 2022.

Jain, P., Coogan, S. C. P., Subramanian, S. G., Crowley, M., Taylor, S. and Flannigan, M. D.: A review of machine learning applications in wildfire science and management, , doi:10.1139/er-2020-0019, 2020.

Oliveira, S., Oehler, F., San-Miguel-Ayanz, J., Camia, A. and Pereira, J. M. C.: Modeling spatial patterns of fire occurrence in Mediterranean Europe using Multiple Regression and Random Forest, For. Ecol. Manage., 275, 117–129, doi:10.1016/j.foreco.2012.03.003, 2012.

Penman, T. D., Bradstock, R. A. and Price, O.: Modelling the determinants of ignition in the Sydney Basin, Australia: Implications for future management, Int. J. Wildl. Fire, 22(4), 469–478, doi:10.1071/WF12027, 2013.

Rodrigues, M., de la Riva, J. and Fotheringham, S.: Modeling the spatial variation of the explanatory factors of human-caused wildfires in Spain using geographically weightedlogistic regression, Appl. Geogr., 48, 52–63, doi:10.1016/j.apgeog.2014.01.011, 2014.

Syphard, A. D. and Keeley, J. E.: Location, timing and extent of wildfire vary by cause of ignition, Int. J. Wildl. Fire, 24(1), 37–47, doi:10.1071/WF14024, 2015.

Syphard, A. D., Radeloff, V. C., Keuler, N. S., Taylor, R. S., Hawbaker, T. J., Stewart, S. I. and Clayton, M. K.: Predicting spatial patterns of fire on a southern California landscape, Int. J. Wildl. Fire, 17(5), 602–613, doi:10.1071/WF07087, 2008.

Forest fire history of Poland

Jan Kaczmarowski*[1]; Wojciech Kędziora[2]

[1]General Directorate of State Forests. ul. Grójecka 127, 02-124 Warsaw, Poland, {jan.kaczmarowski@lasy.gov.pl}
[2] Warsaw University of Life Sciences. ul. Nowoursynowska 159, 02-787 Warsaw, Poland, {wojciech_kedziora@sggw.edu.pl}

**Corresponding author*

Keywords

Fire regime, wildfire, fire causes, pyrogeography, forest fire statistics

Abstract

Scots pine (*Pinus sylvestris* L.) covers around 60% of Poland's forests. Pine stands are considered as fire prone, which exposes a large area of forests to the risk of fire ignition and spread. This is confirmed by the statistics, among which Poland belongs to the group of European countries where forest fires occur most often. In addition, the most common cause of fires is deliberate arson. The contemporary fire pattern in lowland forests in Poland is characterised by a large number of fires with a small burnt area.

Understanding historical fire regime is important for the correct assessment of contemporary phenomena. However, compared to boreal or Mediterranean biomes, the characteristics of historical forest fires in Poland are not well researched. To fill this knowledge gap, a review of national thematic literature and historical documents was carried out. There is a limited literature describing a historical fire situation and just few studies have quantified the historical frequency of forest fires. Documentary records are often incomplete, both in time and space. In our research, to better understand the forest fire history paradigm, we took a holistic approach, integrating data from archives, historical sources (research literature and handbooks), press reports, scientific papers, and existing fire databases. An attempt to reconstruct the history of forest fires was carried out for Poland, considering that the modern borders were established in 1945. The reconstruction of fire event chronology and statistics (annual number of fires and burnt area) is presented, which will give a picture of this phenomenon in its various aspects, including periodisation in the decades, with particular emphasis on the 20th and 21st centuries.

This research allowed for the reconstruction of fire statistics in the period from 1920 to the present day. Due to historical conditions, the data for the period 1920-1945 are incomplete, mainly the information on the number of fires is unavailable. The available data show that at least 210,000 ha of forests were burnt during this period. In the years 1946-2020 in Polish forests 342,204 fires occurred, as a result of which 407,093 ha were burnt. The largest number of forest fires (17,088) was recorded in 2003, while the largest area was burnt in 1992 (43,755 ha). On an annual average, in the years 1946-2020 there were 4,562 fires on an area of 5,428 ha, and the area of a single fire was 1.19 ha. In the analysed period, it was observed that the largest number of fires occurred in the decade of 2001-2010 (approx. 9.4 thousand per year), and the largest area of fires in the decade of 1991-2000 (approx. 11 thousand ha per year). The average area of a single fire decreased from 2.35 ha in the decade of 1951-1960 to 0.44 in the last decade.

It is the first such complete study of the history of fires in Poland and it may establish the basis for further work on understanding the fire regime of Central European lowland forests.

1. Introduction

Due to the historical socio-economic transformations and development of silviculture knowledge, as well as climate and soil configuration, Scots pine became the dominant species in the Central European lowlands in the 19th century. This species finds the most suitable growing conditions in Poland. This is the main reason *Pinus sylvestris* is the dominant species in Polish forests and currently covers over 60% of the forest area. Pine stands, because of the high flammability of resins and essential oils, are susceptible to fires, which exposes a large area of forests in Poland to the risk of ignition and their rapid spread – an example of such a devastating fire was the one in 1992, during which almost 10,000 ha were burnt. This means that the species composition of Polish stands is an environment favourable to the growth of fire of considerable size.

The influence of the dominant species on the possibility of fire ignition is confirmed by the statistics, among which Poland belongs to the group of European countries where forest fires occur most often. In addition, the fact that the most common cause of fires is deliberate arson raises the problem to a higher level. Poland, Spain and Italy are the only three European countries where deliberate fires are the most representative cause. In all other European countries, outbreaks of forest fires result from human activity with no intention of causing damage (i.e. accident or neglect).

The contemporary fire pattern in the Central European lowland forests in Poland is characterised by a large number of fires (approx. 7,300 annual average in the last decade) with a small total burnt area (approx. 3,000 ha per year). This translates into low values of the average area of a single fire (0.44 ha). This characteristic places Poland in the top three in terms of the number of fires in Europe but in terms of the area around the 10th place (depending on the year).

Understanding historical fire regimes is of fundamental importance for the correct assessment of contemporary phenomena. Understanding the characteristics of fire history might help in identifying the impacts of climate change, understanding ecosystem processes, and developing fire management principles and objectives. However, compared to boreal or Mediterranean biomes, the historical characteristics of forest fires in Poland are not well researched. To fill this knowledge gap, a review of local thematic works and historical documents was carried out. There is limited literature describing a historical fire situation, and few studies have quantified the historical frequency of forest fires. Documentary records are often incomplete, both in time and space. This situation was influenced by historical events, ranging from the partitions of the country, through the First World War, the incompatibility of various forest management systems in 3 parts of the post-war country, intense warfare during World War II, and the change of the country's borders in 1945. Moreover, during the period 1945-2020, Poland has increased its forest share from 20 to 30%, planting new forests at over 3 million ha. These changes likely affected the pattern of the forest fires as well.

2. Methodology

In this study, to better understand the forest fire history paradigm, a holistic approach was used, integrating data from archives, historical sources, available literature (both scientific and branch textbooks for the forestry sector published during the analysed period), press reports, and existing fire databases.

The collected materials made it possible to systematize the historical data on forest fires in terms of numbers and area burnt, and the following parameters were calculated: **average area of single fire** – determined as the quotient of the annual sum of forest area burned and the number of fires expressed in hectares, which is a measure of the effectiveness of the forest fire protection system, **fire concentration** – the density of the number of fires calculated per 1000 ha of forest, **burnout intensity** – determined as the quotient of the burnt area in a given year and the forest area expressed in hectares per 1000 ha. The last two parameters make it possible to compare the dynamics of changes in the number of fires and the burnt area, taking into account the changes in Poland's forest cover over time.

In addition, the research also focused on the historical background that allows for understanding the context and the changing paradigm of forest fires and their significance in individual decades.

3. Results

The research carried out in this study allowed for the reconstruction of fire statistics for the entire country from 1920 to the present. The analysis of fire data over more than 100 years also provides insight and perspective into the context of changes taking place in Polish society and forest management.

The first Polish archival records referring to the issue of forest fires appear in the "Warcki Statutes" of 1423. The legal provisions contained therein prohibited lighting fires in the forest or in its vicinity under pain of death. Documents drawn up in the following centuries mainly described bans on using fire and the penalties for disobeying them. From the mid-seventeenth century onwards, more detailed instructions on how to protect forest property against fire and how to prevent it began to appear. However, there is no aggregated source material on the extent of forest fire losses in Poland before the second half of the 20th century.

Due to historical conditions, the data for the period 1920-1945 is incomplete, mainly the information on the number of fires is missing. The available data show that at least 210,000 ha of forests were burnt during this period. After World War I and the regaining of independence, Polish forests were devastated by the predatory economy of the occupying powers and as a result of prolonged warfare. The damaged, understocked and grass covered forests often felt victim to fires. However, during the entire inter-war period (1918-1939), forest fires were of little economic importance due to the species composition of forest stands at that time, their geographical location and limited penetration of forests by the public. Losses caused by forest fires in the period of World War II (1939-1945) were estimated at 150,000 burnt hectares.

In the following post-war years (1946-1950), the fire situation remained at a similar, high level. The post-war consequences and causes of the deteriorating forest fire safety situation included: people's disinclination to obey the rules, lowered sense of responsibility and negligence, explosives and mines scattered in the forests as well as partisan units stationed in the forests.

Compared to the first years of post-war history, the situation in the following decade (1951-1960) calms down and the losses caused by forest fires decrease significantly. Forest fire protection becomes a very important issue in the national economy. Between 1961 and 1970, an average of about 1,500 fires occur annually in forests on an area of almost 2,300 ha, deliberate arson is quite rare, sporadic cases have no social significance.

By the end of the 1970s, as a result of post-war afforestation of wasteland and poor agricultural land, the forest cover of the country reached 27% (compared to 20.8% in 1946). Huge forest patches of pine monocultures were created (the share of this species in the forest stand composition reached 70%), which made the Polish woodlands prone to forest fires. In the decade of 1971-1980 almost 1,900 forest fires burning 2,600 ha occurred annually.

Extreme water shortages in the summers of 1982 and 1983 resulted, inter alia, in the first catastrophic (>1000 ha) forest fire after the Second World War. The '80s also showed the beginning of a worrying trend of increasing numbers of fires from arson. It resulted in increased annual number of fires (3300) and area burned (4300 ha).

Industrial pollution contributed to the increase in forest fire danger in the 1990s, damaging, to varying degrees, up to 80% of the country's forest stands. This contributed to the overexposure of stands, the weed infestation of the forest floor, and increase of fuel load. In comparison with the previous decades, there was a clear, dynamic increase in the average annual values characterising the fire seasons. During systemic transformation in Poland (1989-1991), intentional arson became an increasingly important cause of fires. The year 1992 turned out to be disastrous, when 43,755 ha of forest (resulting from 11,858 fires) were burnt. This area represented 9.68% of the total area burnt that year in the forests of Europe. The most tragic fire occurred on 26 August 1992 in Kuźnia Raciborska - it reached in total 9,062 ha. Because of the number of forces involved in its extinguishing and the tragic death of rescuers that fire has remained to this day the most tragic wildfires in the modern history of Poland. The groundbreaking events of 1992 had a huge impact on the directions of improvement of the State Forests fire protection system, the effects of which will be visible in the coming decades. Annually, more than 8,300 forest fires started that damaged over 10,000 ha.

The first decade of the new millennium brought a record annual average number of fires – 9,300 in forests of all ownership forms. This positions Poland in the group of European countries where fires occur most frequently. The largest number of forest fires was reported in 2003, when there were over 17,088 fires in a total area of 21,500 hectares. It was record year by ignition number in Poland's post-war history, which was caused by illegal and uncontrolled agricultural burning. After joining the European Union, the problem lost its importance.

Between 2011 and 2020 there were 72,785 forest fires with a total area of 31,674 ha. This means that in Poland we are dealing with a large number of small incidents. In the last decade, no further upward trend in the number and area of forest fires has been observed, which allows us to conclude that the forecasted upward trend in these characteristics, related to the effects of climate change, has not yet taken place in the area of Poland.

In the years 1946-2020, 342,204 fires occurred in Polish forests, as a result of which 407,093 ha were burnt.

Table 1 - Forest fire statistics in decades from 1951 to 2020

Years	Forest fire no.	Mean	Median	Area burned [ha]	Mean	Median	Single fire avg area	Fire concentration	Burnout intensity
1951-1960	14 998	1 500	1 585	35 294	3 529	3 423	2.35	0.20	0.48
1961-1970	15 134	1 513	958	23 388	2 339	1 607	1.55	0.19	0.29
1971-1980	18 728	1 873	1 765	26 459	2 646	1 990	1.41	0.22	0.31
1981-1990	32 929	3 293	3 431	43 220	4 322	4 085	1.31	0.38	0.50
1991-2000	83 649	8 365	8 172	109 146	10 915	7 652	1.30	0.95	1.24
2001-2010	93 909	9 391	8 979	57 833	5 783	3 572	0.62	1.04	0.64
2011-2020	72 785	7 279	6 882	31 674	3 167	2 793	0.44	0.79	0.34

4. Summary

On an annual average, in the years 1946-2020, there were 4,562 fires on an area of 5,428 ha, and the area of a single fire was 1.19 ha (table 1). In the analyzed period, it was observed that the highest number of fires occurred in the decade of 2001-2010 (approx. 9.4 thousand per year), and the largest area of fires in 1991-2000 (approx. 11 thousand ha per year). The average area of a single fire decreased from 2.35 ha in the 1950s to 0.44 in the last decade. Taking into consideration changes in forest area, fire concentration was stable until 1980s and peaked in 2001-2010, whereas burnout intensity is now very low compared to 1990s.

It is the first such complete study of the history of fires in Poland and it may make up the basis for further work on understanding the fire regime of Central European lowland.

FRISCO: Managing fire-induced risks of water quality contamination

Joana Parente*[1]; João Pedro Nunes[1,2]; Luís Dias[1]; Akli Benali[3]; Marta Marques[4]; Oscar González-Pelayo[5]; Ana Sá[3]; Dina Jahanianfard[3]; Niels Nitzsche[1]; Beatriz Faria[1]; Bruno Aparício[1,3]; Tomás Calheiros[1]; Jinfeng Wu[1]; Jantiene Baartman[2]; Dante Föllmi[2]; Stefan van der Grift[2]; Carlos Brito[4]; Amandine Valérie Pastor[1,6,7]

[1] *cE3c - Center for Ecology, Evolution and Environmental Changes & CHANGE - Global Change and Sustainability Institute, Sciences Faculty, University of Lisbon, Portugal, {joaparente@gmail.com, joao.carvalhonunes@wur.nl, lfdias@fc.ul.pt, Niels.Nitzsche@gmx.de, faribia@gmail.com, amandine.pastor22@gmail.com, bruno.a.aparicio@gmail.com, tlmenezes@fc.ul.pt, jinfengwu2020@163.com}*
[2]*Soil Physics and Land Management Group, Wageningen University & Research, the Netherlands, {jantiene.baartman@wur.nl, dante.follmi@gmail.com}*
[3]*Forest Research Centre (CEF), Instituto Superior de Agronomia, University of Lisbon, Portugal, {aklibenali@gmail.com, anasa30@gmail.com, dinaj@ua.pt}*
[4]*AdP Valor. Portugal, {m.carvalho@ADP.PT, carlos.brito@ADP.PT}*
[5]*Centre of Environmental and Marine Studies (CESAM), University of Aveiro, Portugal, {oscargonzalezpelayo@ua.pt}*
[6]*ITAP, Univ. Montpellier, INRAE, Montpellier SupAgro, Montpellier, France*
[7]*ELSA, Research Group for Environmental Life Cycle Sustainability Assessment, Montpellier France*

**Corresponding author*

Keywords

Fire assessment and modelling; burnt area hydrology; hydrological ecosystem services; water resources management

Abstract

Fires can contaminate streams with fine sediments, nutrients, and ashes, threatening aquatic ecosystems and water supplies. Recent research on sediment and contaminant mobilization processes in burnt areas exists but linking mobilization with water contamination processes at larger scales remains challenging. In the FRISCO project, we argue that recent advances in understanding fire behavior and post-fire landscapes can overcome the major challenges in assessing and managing post-fire contamination risks. Links between fire characteristics and hydrologic impacts can be assessed by combining remote sensing and modeling tools with studies on fire severity and impacts on vegetation and soils. The impacts of fires on contaminant transport pathways can be assessed by combining landscape connectivity and hydrological modeling of burnt areas with field research on contaminant mobilization and transport. Overall, FRISCO researchers want to investigate the vulnerability of Mediterranean streams and water resources to contamination by fires. Our main results include: (i) map of post-fire sediment and ash transport pathways using satellite imagery; and (ii) statistical analysis of relation between fire characteristics (e.g., burnt area and fire severity) and water contaminants. We hope that the results help stakeholders in the development of the best practices for post-fire contamination management.

1. Introduction

Land abandonment in the Mediterranean has led to the combination of fuel build-up with widespread afforestation and an increase in the frequency and severity of wildfires (Moreira et al., 2020). Post-fire processes can contaminate streams with fine sediments, nutrients, and ashes (Verkaik et al., 2013), threatening aquatic ecosystems (Martin, 2016) and water supplies (Shakesby et al., 2016). Recent research focuses on sediment and contaminant mobilization processes in burnt areas (Nunes, Doerr, et al., 2018), but difficulties in linking mobilization with water contamination processes at larger scales persist (Santín et al., 2016).

We argue that recent developments in understanding fire behavior and post-fire landscapes can overcome most of those difficulties (Santín et al., 2016), such as: (i) the relationship between fire spread descriptors and hydrological impacts (Nunes, Doerr, et al., 2018; Sá et al., 2017), using the combination of remote sensing techniques and modeling (Benali et al., 2017; Chafer et al., 2016; Sá et al., 2018) tools with studies on burn severity and impacts on vegetation and soils (Cardil et al., 2019; Keesstra et al., 2018; Moody et al., 2016) to

estimate the hydrological impacts of fires at large scales; and (ii) the impacts of fires on contaminant transport pathways (Martínez-Murillo & López-Vicente, 2018) using the latest methodologies of landscape connectivity (Martínez-Murillo & López-Vicente, 2018; Nunes, Naranjo Quintanilla, et al., 2018) and hydrological modeling of burnt areas (Campos et al., 2016) combined with field research on contaminant mobilization and transport (Hawtree et al., 2014).

The FRISCO project takes advantage of these advances to answer the question: How vulnerable are Mediterranean streams and water resources to contamination by fires? This study aims to present the current developments of the project on developing the information and tools needed to address this question.

2. Data and Methods

The FRISCO project focuses on Portugal as representative of the Mediterranean region. Portugal has an extensive forest cover and has experienced frequent and recurrent forest fires since the 1970s under two distinct fire regimes (Santín et al., 2016). It also has a large and open-access historical water quality database (SNIRH; http://snirh.pt).

This project has 72 main study areas that: (i) represent key water supply sources, e.g., direct water uptake from streams, low-capacity reservoirs, and large volume reservoirs; (ii) represent different fire regimes; and (iii) have available water quality data from the SNIRH network.Currently, we are working on 3 of 5 main tasks of FRISCO:

Task 1 - Characterization of fire impacts on vegetation and soils**:** with the main objective of combining satellite imagery and field data to characterize the fire impacts on vegetation and soils in mainland Portugal, in the last 20 years (2001 to 2020);

Task 2 – Characterization of fire impacts on contaminant mobilization and transport to streams: with the main objective of combining the information produced in task 1 with the new developments in connectivity theory and modelling, to characterize the contaminant mobilization and transport to streams for key water supply sources;

Task 3 - Identification of post-fire contamination episodes in key water supply sources and their main drivers: used historical water quality data and statistical analysis to identify post-fire contamination episodes in the key water supply sources in the last 20 years and assess their main drivers in coordination with water managers.

3. Results and discussion

The results of the 1st stage of FRISCO project show the new state of the art in the study of post-fire water contamination and in the establishment of the relationship between port-fire processes and post-fire hydrology. In particular, (i) the modelling of post-fire sediment and ash transport pathways using satellite imagery datasets; and (ii) the improvement of knowledge on the relations between fire, vegetation, soils, and water, which was done through statistical analysis of relation between fire characteristics (e.g., burnt area and fire severity) and water contaminants.

4. Conclusion

The FRISCO project had advanced the state of the art in the development of new knowledge on the relations between fire, vegetation, soils, and water, overcoming the main limitation for further progress (Santín et al., 2016); help understand and assess the impacts of fire on the provision of hydrological services by forests (Campos et al., 2016); and take fire into account in the assessment of the impacts of climate and land-use changes on water resources, addressing a major uncertainty in adaptation to climate change planning (Santín et al., 2016). As future work, we hope to (i) model a contamination risk index, which will arise to an operational tool that will allow qualitative risk for each water body; and (ii) a combined fire and contamination model that will help to get an operational risk mitigation manual for water managers.

5. Acknowledgements

This work was financed by the project FRISCO - managing Fire-induced RISks of water quality Contamination (PCIF/MPG/0044/2018). This work was also supported by National Funds through FCT - Foundation for Science and Technology under the project UIDB/04033/2020, and funding attributed to the CE3C research center (UIDB/00329/2020).

6. References

Benali, A., Sá, A., Ervilha, A., & Trigo, R. (2017). Fire spread predictions: Sweeping uncertainty under the rug. Science of The Total Environment. https://www.sciencedirect.com/science/article/pii/S0048969717306186?casa_token=Z01yXNxYLnwAAAAA:lX7xh_35dori-Ro8hxF5HpVjs6E2e4Gl4cWJ9qmFNyL4q9fU5XO5pOzOkBt-sMAxkeC2tX4j

Campos, I., Abrantes, N., Keizer, J., & Vale, C. (2016). Major and trace elements in soils and ashes of eucalypt and pine forest plantations in Portugal following a wildfire. Science of The Total Environment. https://www.sciencedirect.com/science/article/pii/S0048969716301863?casa_token=1E3IhltW3FYAAAAA:n90fI1VSYUiv2fP9T2HzgKTmfLAvM3m7FX_csqSpQoaRlthLOG588cAYkur9FGf4qYjpuhZQ

Cardil, A., Mola-Yudego, B., Blázquez-Casado, Á., & González-Olabarria, J. R. (2019). Fire and burn severity assessment: Calibration of Relative Differenced Normalized Burn Ratio (RdNBR) with field data. Journal of Environmental Management, 235, 342–349. https://doi.org/10.1016/j.jenvman.2019.01.077

Chafer, C. J., Santín, C., & Doerr, S. H. (2016). Modelling and quantifying the spatial distribution of post-wildfire ash loads. International Journal of Wildland Fire, 25(2), 249. https://doi.org/10.1071/WF15074

Hawtree, D., Nunes, J. P., Keizer, J. J., Jacinto, R., Santos, J., Rial-Rivas, M. E., Boulet, A.-K., Tavares-Wahren, F., & Feger, K.-H. (2014). Time series analysis of the long-term hydrologic impacts of afforestation in the Águeda watershed of north-central Portugal. Hydrology and Earth System Sciences, 11, 12223–12256. https://doi.org/10.5194/hessd-11-12223-2014

Keesstra, S., Nunes, J. P., Saco, P., Parsons, T., Poeppl, R., Masselink, R., & Cerdà, A. (2018). The way forward: Can connectivity be useful to design better measuring and modelling schemes for water and sediment dynamics? In Science of the Total Environment (Vol. 644, pp. 1557–1572). https://doi.org/10.1016/j.scitotenv.2018.06.342

Martin, D. A. (2016). At the nexus of fire, water and society. Philosophical Transactions of the Royal Society B: Biological Sciences, 371(1696). https://doi.org/10.1098/RSTB.2015.0172

Martínez-Murillo, J. F., & López-Vicente, M. (2018). Effect of Salvage Logging and Check Dams on Simulated Hydrological Connectivity in a Burned Area. Land Degradation and Development, 29(3), 701–712. https://doi.org/10.1002/LDR.2735

Moody, J. A., Ebel, B. A., Nyman, P., Martin, D. A., Stoof, C., & McKinley, R. (2016). Relations between soil hydraulic properties and burn severity. International Journal of Wildland Fire, 25(3), 279. https://doi.org/10.1071/WF14062

Moreira, F., Ascoli, D., Safford, H., Adams, M. A., Moreno, J. M., Pereira, J. M. C., Catry, F. X., Armesto, J., Bond, W., González, M. E., Curt, T., Koutsias, N., McCaw, L., Price, O., Pausas, J. G., Rigolot, E., Stephens, S., Tavsanoglu, C., Vallejo, V. R., … Fernandes, P. M. (2020). Wildfire management in Mediterranean-type regions: paradigm change needed. Environmental Research Letters, 15(1), 011001. https://doi.org/10.1088/1748-9326/ab541e

Nunes, J. P., Doerr, S. H., Sheridan, G., Neris, J., Santín, C., Emelko, M. B., Silins, U., Robichaud, P. R., Elliot, W. J., & Keizer, J. (2018). Assessing water contamination risk from vegetation fires: Challenges, opportunities and a framework for progress. Hydrological Processes, 32(5), 687–694. https://doi.org/10.1002/hyp.11434

Nunes, J. P., Naranjo Quintanilla, P., Santos, J. M., Serpa, D., Carvalho-Santos, C., Rocha, J., Keizer, J. J., & Keesstra, S. D. (2018). Afforestation, Subsequent Forest Fires and Provision of Hydrological Services: A Model-Based Analysis for a Mediterranean Mountainous Catchment. Land Degradation & Development, 29(3), 776–788. https://doi.org/10.1002/ldr.2776

Sá, A., Benali, A., Fernandes, P., & Pinto, R. (2017). Evaluating fire growth simulations using satellite active fire data. Remote Sensing of Environment, 190, 302–317. https://doi.org/10.1016/j.rse.2016.12.023

Sá, A., Turkman, M., & Pereira, J. (2018). Exploring fire incidence in Portugal using generalized additive models for location, scale and shape (GAMLSS). Modeling Earth Systems and Environment, 4(1), 199–220. https://doi.org/10.1007/s40808-017-0409-6

Santín, C., Doerr, S. H., Kane, E. S., Masiello, C. A., Ohlson, M., de la Rosa, J. M., Preston, C. M., & Dittmar, T. (2016). Towards a global assessment of pyrogenic carbon from vegetation fires. Global Change Biology, 22(1), 76–91. https://doi.org/10.1111/gcb.12985

Shakesby, R. A., Moody, J. A., Martin, D. A., & Robichaud, P. R. (2016). Synthesising empirical results to improve predictions of post-wildfire runoff and erosion response. In International Journal of Wildland Fire (Vol. 25, Issue 3, pp. 257–261). https://doi.org/10.1071/WF16021

Verkaik, I., Rieradevall, M., Cooper, S. D., Melack, J. M., Dudley, T. L., & Prat, N. (2013). Fire as a disturbance in mediterranean climate streams. Hydrobiologia, 719(1), 353–382. https://doi.org/10.1007/s10750-013-1463-3

From the probability density function of the rate of spread to that of the corresponding burned area

Alvaro Crespo-Santiago[1,2]; Gianni Pagnini*[1,3]

[1] BCAM. Bilbao, Basque Country, Spain, {gpagnini@bcamath.org , acrespo@bcamath.org}
[2] Stockholm University. Stockholm, Sweden
[3]Ikerbasque. Bilbao, Basque Country, Spain
**Corresponding author*

Keywords

Wild fire, burned area, random area, probability density function, Riemann integral of a random function.

Abstract

We show that the probability density function (PDF) of a burned area enclosed by a random fire-perimeter is driven by the PDF of the bounding-box sides. In particular, the random value of the area emerges to be proportional to the random position of the bounding-box sides times an averaged coefficient dependent on the geometry of the burned area. Therefore, the two PDFs are functionally equal. This means that the PDF of the burned area is driven and functionally equal to the PDF of the position of the head of the fire. The displacement of the head of the fire is given by the rate of spread (ROS), thus the PDF of the burned area results to be driven and equal to the PDF of the ROS. This result holds in general whenever the fire exhibits an advancement along a main direction. The main theoretical result has been tested by different families of stochastic processes. This study can be understood as a start for the development of a theory of stochastic dynamics of wildfire propagation with the aim, for example, to provide physically-grounded initial perturbations of wildfire perimeters for ensemble forecasting.

1. Introduction and Motivation

The determination of the spreading of wildfires is affected by large errors because of such predicting and modelling difficulties. As a consequence of this complexity, the evaluation of fire spreading predictions relies on scoring methods (Filippi 2013, Filippi 2014). Because of such unpredictability, in analogy with the weather forecast, ensemble forecasting has been formulated for wild fires, see, e.g., (Finney 2011, Allaire 2021), together with the application of data assimilation procedure, see, e.g., (Mandel 2008, Rochoux 2014, Rochoux 2015, Ferragut 2015). The idea of ensemble forecasting is based on the concept of stochastic dynamics that describes the evolution of the probability of certain observables. This limit is often associated with the rapid growth of uncertainty originating in the initial conditions; these arise both from imperfect and incomplete observations, and from inaccuracies in the formulation of the model both in terms of its physical processes and its computational representation. Ensemble prediction is a practical method to find a single, deterministic forecast with an estimate of the probability of nearby forecast states. Uncertainties in prediction by fire simulators are statistically related to the simulators' dependence on the required parameters, such that sensitivity analysis is considered for improving the reliability of predictions (Trucchia 2019, Prieto 2015, Asensio 2020) and also on the regional-scale weather prediction. Thus, such uncertainties are covered by probabilistic predictions in terms of ensemble forecasts through a proper distribution of input parameters (Allaire 2018, Allaire 2020, Allaire 2021).

The present research goes in the direction to establish the stochastic dynamics of wild fire spreading. In particular we show that the probability density function (PDF) of a burned area enclosed by a random fire-perimeter is driven by the PDF of the bounding-box sides.

2. Methods

We study the Riemann integral

$$A(t) = \int_0^{a(t)} y(x,t)\, dx,\ y(x,t) \geq 0\ \forall x, \forall t \geq 0$$

when $y(x,t)$ is replaced by a random function and $a(t)$ is replaced by a nondecreasing stochastic process. We show that, under quite general conditions in the random setting, the randomness of the outcome of the integral depends only on the randomness of the upper-bound of the integration interval such that the PDF of the random counter-part of $A(t)$ is ruled by the PDF of the random counter-part of $a(t)$. The same holds for the governing equations of the corresponding PDFs. Hence, we finally provide the PDF of the burned area in terms of the PDF of the ROS with the aim to start the development of a theory for stochastic dynamic predictions of wildfire propagation.

Observable $A(t)$ can be understood as an area that evolves in time and then its interpretation as the burned area of a wildfire is straightforward. In particular, if *x*-axis is aligned with the wind, the point $a(t)$ describes the motion of the head of the fire and then it is driven by the rate of spread. In the context of wildfires, the equation states that the evolution of the statistics of the burned area is determined by the evolution of the head of the fire times the mean value of the function enclosing the area. We report that that the exact shape of the function is not important and we don't account for it in this work. The perimeter of the fire perimeter is assumed to be a noisy ellipse and we use six models of random perturbations in order to capture the stochastic nature of it on each realization. Examples of the random functions enclosing the area for the six models of random perturbations are shown in Figure 1, focusing only on the first quadrant.

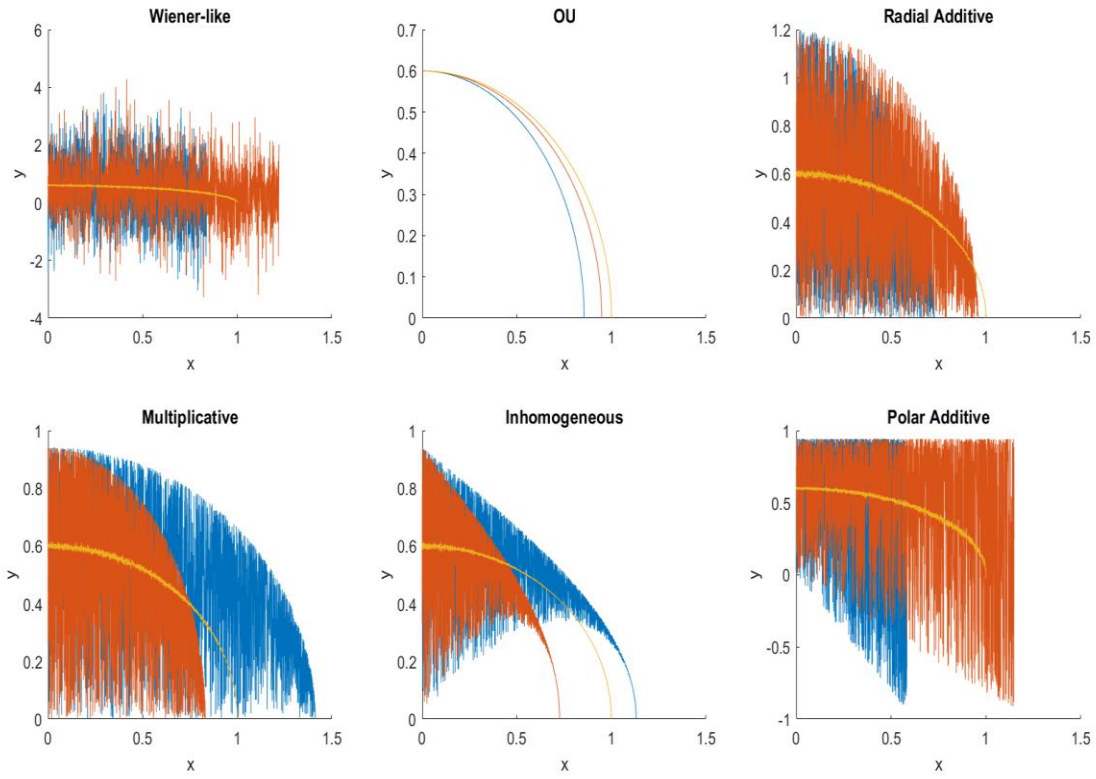

Figure 1 - Two realizations (blue and orange) of the noisy ellipse for the six random perturbations. The mean fire perimeter is also plotted (yellow).

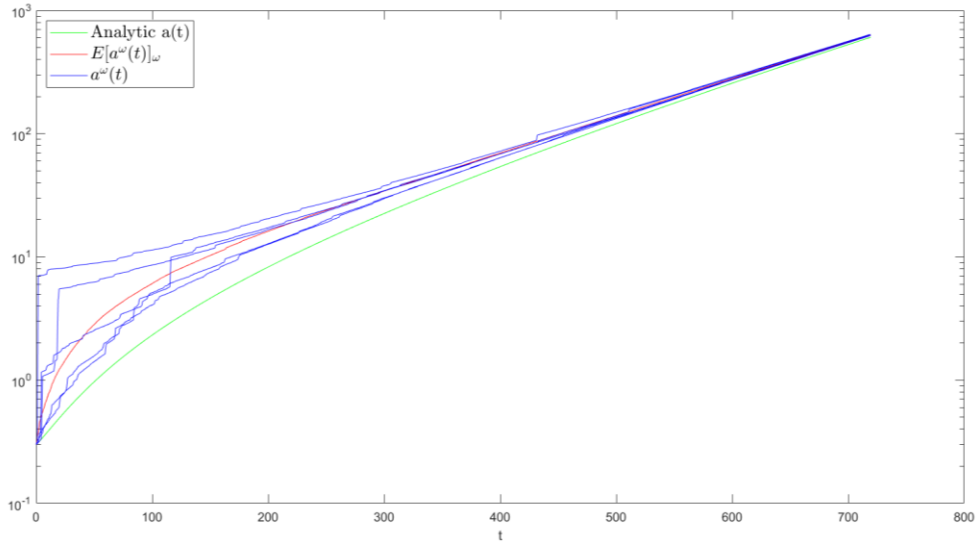

Figure 2 - Five trajectories (blue) of the head of the fire following Viegas' evolution model and lognormal perturbations and the expected value over all the realizations (red). The lowermost line (green) corresponds to the analytic value without noise. Logarithmic y-axis.

The time evolution of the head of the fire is modelized using Viegas' ROS model for eruptive fires (Viegas 2005, Viegas 2006). We use the differential equation and parameters as presented for herbaceous fuel (Viegas 2006), being R the rate of spread. The evolution of the perpendicular direction (the vertical semiaxis in the case of an elliptic-like curve) is taken as propagating with constant ROS. We take a convenient numerical value based on (Rothermel 1972) and (Catchpole 1998). For each realization a perturbation is applied to the analytical value of the head of the fire by using a lognormal PDF. All the realizations are initialized at the same point and we let them evolve as it follows. Some trajectories of the head of the fire are shown in Figure 2 together with the noise-free value and the expected value among all the realizations.

3. Results and Conclusions

We now present and analyse the qualitative results obtained by running simulations as described above and we show that the developed equality holds numerically under different conditions of the random motion of the fire front and for different PDFs of the position of the head of the fire.

First, for the six noisy-model of the front perimeters, we consider and ensemble of realizations of the head of the fire that are distributed according to a Beta distribution $B(2,2)$. In Figure 3 we see that the distribution of the area divided by the mean value of the fire front function clearly follows the distribution of the head of the fire. It can be shown that for every well-behaved PDF mapping the position of the head of the fire, the equality is fulfilled.

In particular, looking at Figure 2, we roughly distinguish three regimes on the evolution curve of the mean head of the fire: An early regime before than $t \approx 15$, a final regime after $t \approx 300$, and the transition between them. Hence, in Figures 4, 5 and 6 we show PDFs of a and $A / \overline{Y}$ for times $t = 10$, $t = 70$ and $t = 700$. We see that both PDFs are equivalent at any time, and for wildfires this shows that the statistical properties of the burned area are driven by the statistics of the position of head of the fire.

The application of this approach to real systems is limited to the existence of a main direction of advancement of the fire that is characterized by large fluctuations among independent realizations, here it is identified by a which corresponds to the head of the fire ruled by the rate of spread, and of a perpendicular direction that is characterized indeed by negligible fluctuations among independent realizations. Actually, this approach is limited, for example, to wind driven fires or fires with similar dynamics.

4. Acknowledgements:

This research has been supported by the Basque Government through the BERC 2022–2025 programme; by the Spanish Ministry of Economy and Competitiveness (MINECO) through the BCAM Severo Ochoa excellence accreditation SEV-2017-0718 and also through the project PID2019-107685RB-I00; and by the European Regional Development Fund (ERDF) and the Department of Education of the regional government, the Junta of Castilla y León (Grant 574 contract SA089P20).

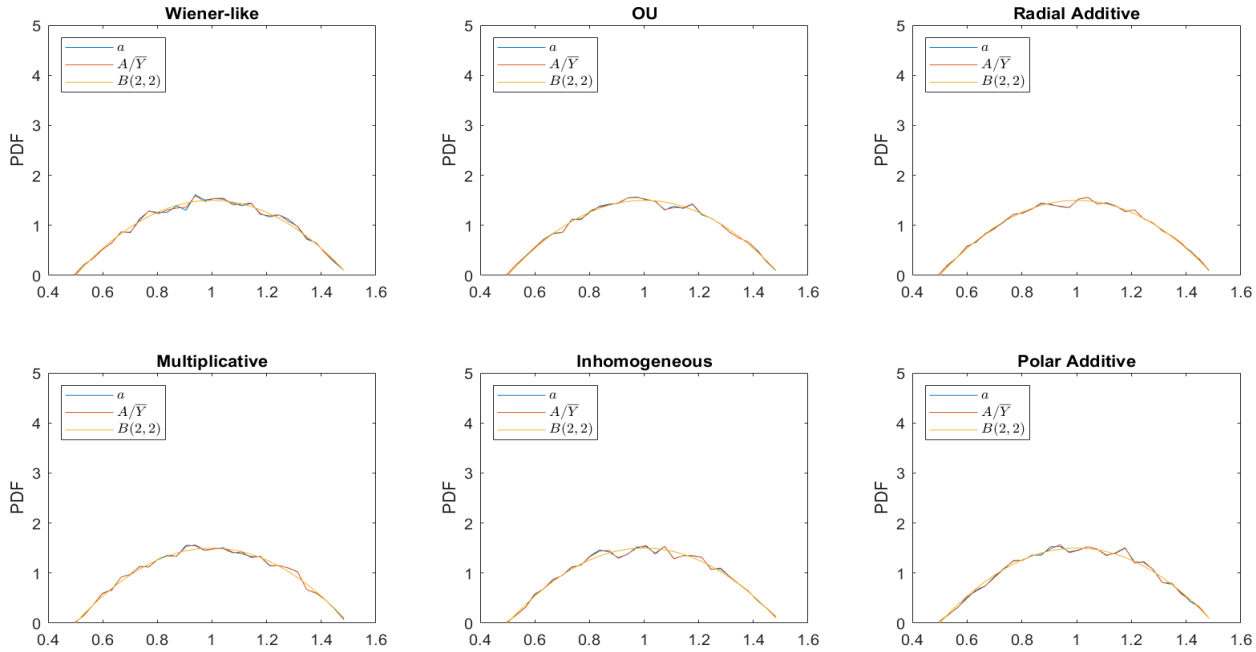

Figure 3 – Probability density functions of a and $A/\overline{Y}$, where $\overline{Y}$ is the mean value of the fire-perimeter y(x), for all the random models of fire front motion and the Beta distribution B(2,2).

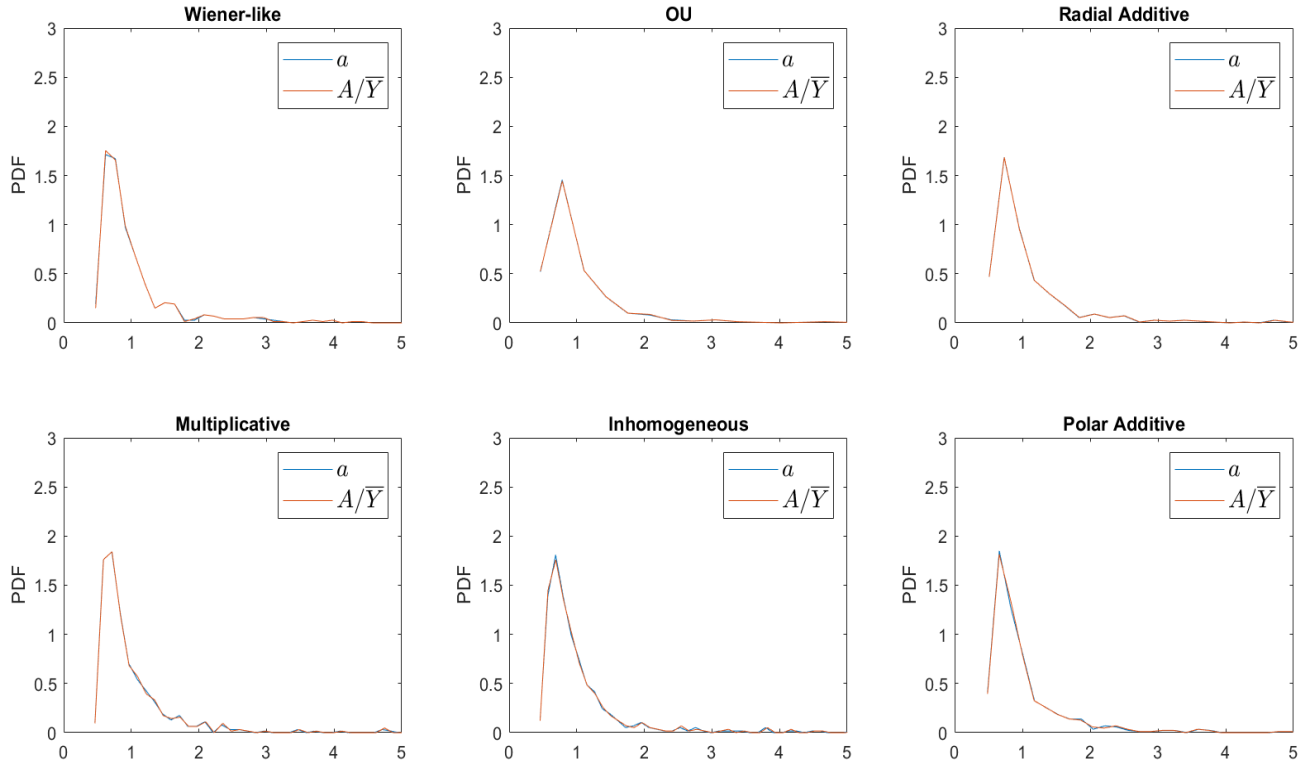

Figure 4 – Probability density functions of the head of the fire a and of the scaled burned are $A / \overline{Y}$ for all the six random models of fire front motion at time $t \approx 10$.

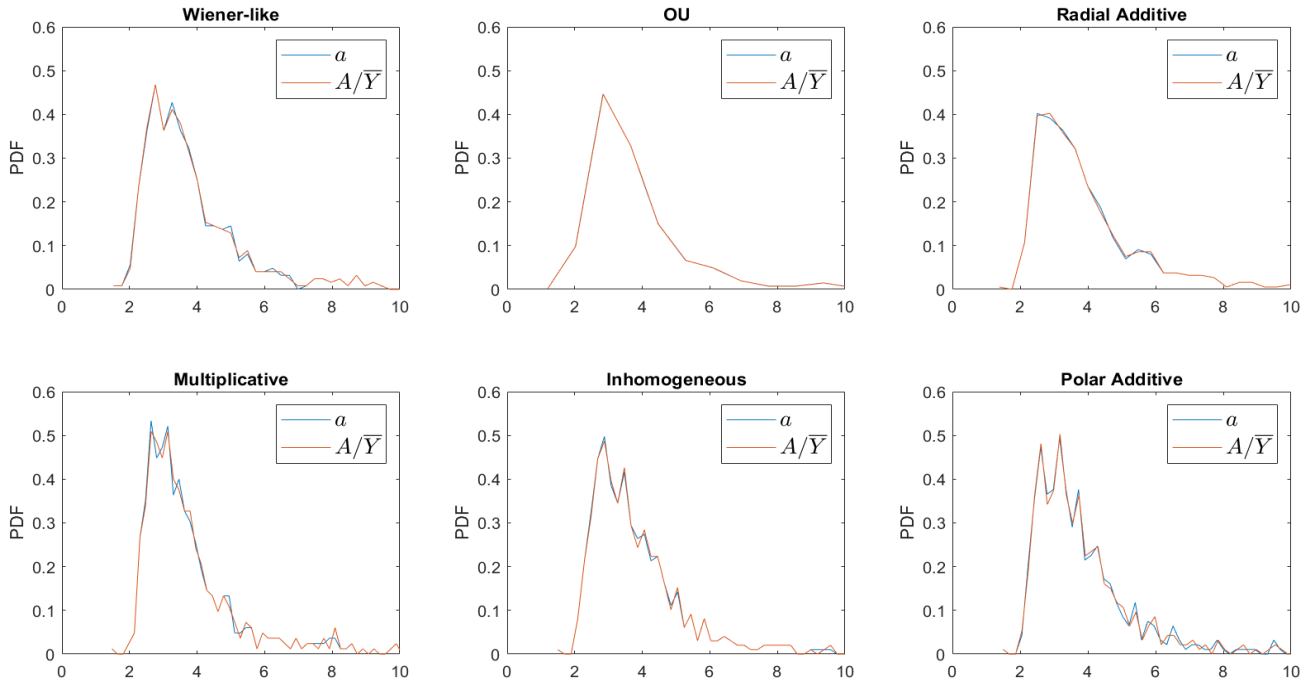

Figure 5 – Probability density functions of the head of the fire a and of the scaled burned are $A / \overline{Y}$ for all the six random fire front models at time $t \approx 70$.

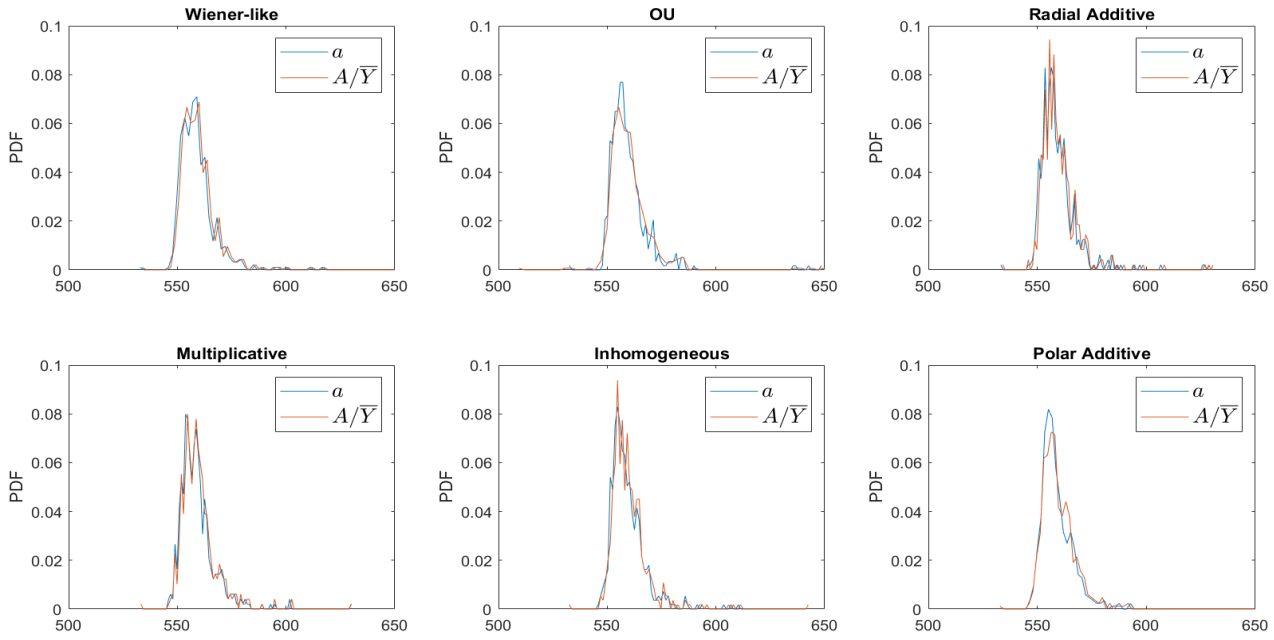

Figure 6 – Probability density functions of the head of the fire a and of the scaled burned area $A/\overline{Y}$ for all the six random fire front models at time $t \approx 700$.

5. References

Allaire F., Filippi J.-B., and Mallet V. (2018). "Generation and evaluation of ensemble simulations of wild fire spread for probabilistic forecast.". Advances in Forest Fire Research, pages 71-80.

Allaire F., Filippi J.-B., and Mallet V. (2020). "Generation and evaluation of an ensemble of wildland fire simulations". Int. J. Wildland Fire., 29:160-173.

Allaire F., Mallet V., and Filippi J.-B. (2021). "Novel method for a posteriori uncertainty quantification in wildland fire spread simulation". Appl. Math. Model., 90:527-546.

Asensio M. I., Santos M. T., Álvarez D., and Ferragut L. (2020). "Global sensitivity analysis of fuel-type-dependent input variables of a simplified physical fire spread model". Math. Comput. Simul., 172:33-44.

Catchpole W.R., Catchpole E.A., Butler B.W., Rothermel R. C., Morris G. A. & Latham D. J. (1998). "Rate of spread of free-burning fires in woody fuels in a wind tunnel". Combustion Science and Technology, 131:1-6, 1-37.

Ferragut L., Asensio M., Cascón J., and Prieto D. (2015). "A wildland fire physical model well suited to data assimilation". Pure Appl. Geophys., 172:121-139.

Filippi J.-B., Mallet V., and Nader B. (2013). "Representation and evaluation of wildfire propagation simulations". Int. J. Wildland Fire, 23:46-57.

Filippi J.-B., Mallet V., and Nader B. (2014). "Evaluation of forest fire models on a large observation database". Nat. Hazards Earth Syst. Sci, 14:3077-3091.

Finney M. A., Grenfell I. C., McHugh C. W., Seli R. C., Trethewey D., Stratton R. D., and Brittain S. (2011). "A method for ensemble wildland fire simulation". Environ. Model. Assess., 16:153-167.

Mandel J., Bennethum L. S., Beezley J. D., Coen J. L., Douglas C. C., Kim K., and Vodacek A. (2008). "A wildland fire model with data assimilation". Math. Comput. Simulat., 79:584-606.

Prieto D., Asensio M. I., Ferragut L., and Cascón J. (2015). "Sensitivity analysis and parameter adjustment in a simplified physical wildland fire model". Adv. Eng. Softw., 90:98-106.

Rochoux M. C., Ricci S., Cuenot B., and Trouvé A. (2014). "Towards predictive data-driven simulations of wild fire spread. Part I: Reduced-cost Ensemble Kalman Filter based on a Polynomial Chaos surrogate model for parameter estimation". Nat. Hazards Earth Syst. Sci., 14:2951-2973.

Rochoux M. C., Emery C., Ricci S., Cuenot B., and Trouvé A. (2015). "Towards predictive data-driven simulations of wild fire spread. Part II: Ensemble Kalman Filter for the state estimation of a front-tracking simulator of wild fire spread". Nat. Hazards Earth Syst. Sci., 15:1721-1739.

Rothermel R. C. (1972). "A mathematical model for predicting fire spread in wildland fuels". UT: U.S. Department of Agriculture, Intermountain Forest and Range Experiment Station.: Res. Pap. INT-115. Ogden, 1972.

Trucchia A., Egorova V. N., Pagnini G., and Rochoux M. C. (2019). "On the merits of sparse surrogates for global sensitivity analysis of multi-scale nonlinear problems: application to turbulence and firespotting model in wildland fire simulators". Commun. Nonlinear Sci. Numer. Simul., 73:120-145.

Viegas D. (2005). "A mathematical model for forest fires blowup". Combustion Science and Technology, 177.

Viegas D. (2006). "Parametric study of an eruptive fire behaviour model". International Journal of Wildland Fire, 15, 169-177.

Generating a framework for fuel inputs to future fire behaviour models: reviews, recommendations and remote sensing

Samuel C Hillman*[1,4]; Luke Wallace[2]; Thomas J Duff[3]; Tegan P Brown[1]; W. Matt Jolly[1]

[1] US Forest Service, Rocky Mountain Research Station, Fire Sciences Laboratory, 5775 Highway 10 West, Missoula, MT, 59803, USA, {samuel.c.hillman@gmail.com, tegan.pg.brown@gmail.com, matt.jolly@usda.gov}
[2] University of Tasmania, School of Geography, Planning and Spatial Sciences, University of Tasmania, Hobart, TAS 7005, Australia, {luke.wallace@utas.edu.au}
[3] Bushfire Management, Country Fire Authority, Burwood, VIC, 3151, Australia {thomas.duff@cfa.vic.gov.au}
[4] Australian-American Fulbright Commission, PO Box 9541, DEAKIN ACT 2600, Australia

**Corresponding author*

Keywords

Fuel, remote sensing, 3D, fire behaviour, modelling

Abstract

Land managers use models to understand potential fire behaviour, which provide insight into the social, economic and environmental implications of fire. Although combustion is a fundamental process, numerous fire behaviour models exist across the world, each with model-specific inputs and outputs. While these are useful for local-level fire management, vegetation- or country-specific fire behaviour models, they do limit knowledge-sharing between jurisdictions – largely because model inputs (particularly fuel arguments) and outputs differ, meaning they cannot be readily compared. At the same time, advancements in remote sensing techniques have resulted in accurate methods to estimate fuel for current fire behaviour models that have not been fully integrated.

This project has two key aims: a) to develop a comprehensive set of model parameters that can be used to universally characterise fuel attributes fundamental to fire behaviour, and b) based on knowledge gaps identified, undertake expert elicitation to identify fuel attributes for fire behaviour not currently utilised in models, and propose methods to estimate these values using remote sensing. To achieve this, we reviewed 25 fire behaviour models to identify similarities and differences in model inputs and outputs. We then subset model inputs to the fuel parameters and linked each to current remote sensing methods. Following the review, and in conjunction with an expert elicitation process, we developed a list of fundamental fuel attributes missing from current fire behaviour models. From this list, we developed novel fuel parameters that fully utilise information contained within remote sending datasets. The final step in this process is to validate the importance of each fuel argument using further expert elicitation and field burning experiments.

We found many common parameters across fire behaviour models. Most models require parameters that describe fuel, short- and long-term fuel moisture, temperature and wind variables, however, the physical fuel parameters are typically where models diverge. Models across the world use fuel inputs that describe the amount, horizontal and vertical arrangement of fuel, bark hazard and the importance of crown fuels. Preliminary expert elicitation identified shared and divergent opinions related to fuel characteristics that drive fire behaviour. While common parameters related to horizontal and vertical arrangement of fuel were important, gaps exist in our capacity to describe ladder fuels. From these results, we have developed novel remote sensing metrics to describe vertical and horizontal connectivity. Throughout 2022, we aim to validate these preliminary results through further expert elicitation and field observations of fire behaviour.

Through this work, we have developed a complete list of fuel parameters for fire behaviour and related these to remote sensing methods. This provides a framework for current models to shift to remotely sensed inputs, and a basis for future fire behaviour models. Overall, we argue that this work provides the foundation for a universal fuel assessment methodology to be developed, that is scalable and captures change over time, that can link physical fuel structure and remote sensing techniques to accurately capture fuel dynamics.

1. Background

In many regions across the globe, fires are becoming increasingly frequent and severe (Pausas & Keeley, 2021). With the effects of climate change likely to continue to amplify this pattern into the future, jurisdictions around the world model fire behaviour to make high-consequence decisions both during the response phase of wildfire management and for the estimation of risk by simulating a set of bushfires across the landscape and observing the associated environmental, economic and social impacts (Gazzard et al., 2020; Kramer et al., 2019; Ladds et al., 2017; Yu et al., 2020). Differences in vegetation across the world have led to independent fire behaviour models being developed (Sullivan, 2009a, 2009b). Consequently, descriptions and systems of measurement for fuel are also unique with the intention to characterise the necessary parameters for the associated model (T. Duff et al., 2017; Keane, 2013). Although this has been useful for local-level fire management, this has limited our capacity to share fire behaviour knowledge across different jurisdictions because the model inputs differ.

Remote sensing products derived from active sensors have been shown to provide an accurate, objective means of measuring fuel attributes. (Gale et al., 2021). Active remote sensing methods utilising LiDAR to measure the 3D structure of fuel have been the focus of the research (Calders et al., 2015; Cooper et al., 2017; Greaves et al., 2015; Kramer et al., 2014; Rowell et al., 2016; Wallace et al., 2016, 2017). A range of platforms have been used to derive measurements including terrestrial, Unoccupied Aircraft Systems (UAS), fixed wing and satellite (García et al., 2011, 2017; Hillman et al., 2021).. Limitations to using these approaches have been highlighted in the ability of these sensors to measure surface fuel characteristics (i.e. vegetation in contact with the ground) (Wallace et al., 2020) due to the inability of sensors to differentiate between ground and surface fuel. Despite this limitation, the information content within remote sensing products provides the ability to describe complex 3D attributes of fuel that are beyond those which are currently utilised in fire behaviour models (Hillman et al., 2021).

2. Knowledge gap

The fuel parameters that are used in current operational fire behaviour models are derived from research at the time of their development. Given advancements in both fire behaviour modelling and remote sensing techniques, there is a clear need for an extensive review of fundamental fuel characteristics that influence fire behaviour, combined with remote sensing techniques that can be employed to assist in the characterisation of complex fuel characteristics.

3. Aims and Objective

This project has two key aims: a) to develop a comprehensive set of model parameters that can be used to universally characterise fuel attributes fundamental to fire behaviour, and b) based on knowledge gaps identified, undertake expert elicitation to identify fuel attributes for fire behaviour not currently utilised in models, and propose methods to estimate these values using remote sensing

4. Methods

To achieve the aims of this project, we firstly reviewed 25 fire behaviour models (empirical, semi-empirical and physical fire behaviour models) across the world. For each model we made note of the input parameters utilised and the outputs derived. For each fuel parameter we identified the scale, units of measure and the minimum levels of precision and accuracy required. Common parameters and outcomes were identified through this process.

Building on the considerable body of work completed by Gale et al. (2021) who reviewed remote sensing research in relation to the fuel attributes that influence fire behaviour, we directly identified the remote sensing research pertinent to each fuel argument identified in part one of this review.

A process of expert elicitation was then undertaken to review the current parameters utilised within fire behaviour models and identify attributes that are fundamental to fire behaviour but not currently measured. Three guiding principles were employed to develop novel metrics that leveraged the full capability of the remote sensing information. Firstly, the attributes had to provide an understanding of the vegetation at the time of

measurement and be able to identify why things are changing over time. This builds on the concepts highlighted by Duff et al. (2012) and Keane et al. (2012). Secondly, a hierarchical system was used to describe the fuel attributes. Wherever possible primary fuel attributes that can be directly linked to fire behaviour were extracted. Thirdly, attributes had to be scalable with the associated remote sensing method able to provide the necessary precision and accuracy. By focussing on developing attributes that can be continuously mapped across the landscape, simulation models should be able to process the values directly.

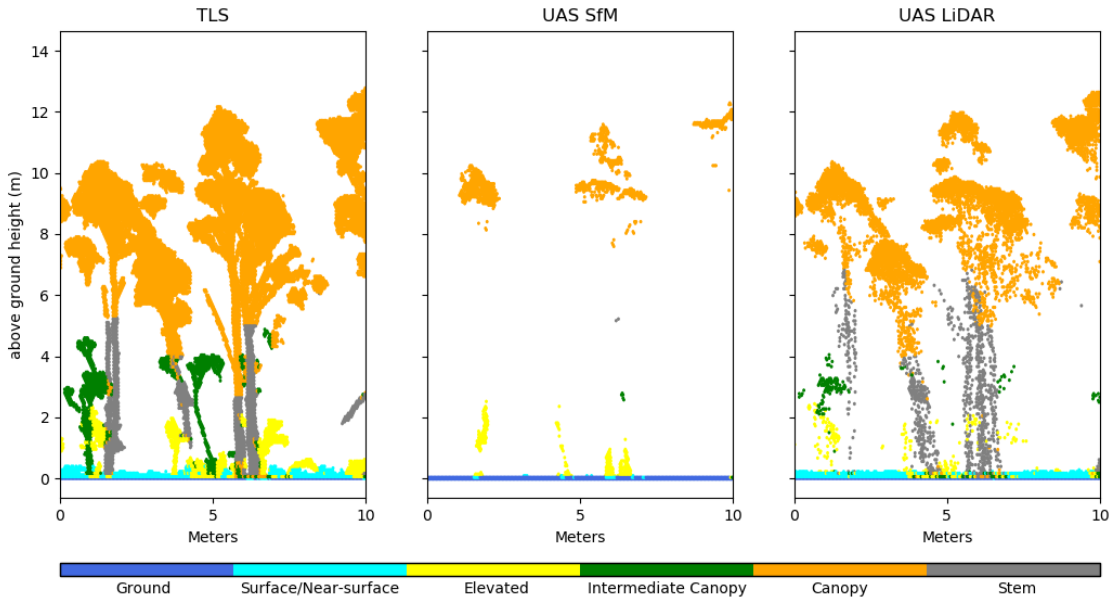

Figure 1. Side view transect through a section of a study area near Hobart, Tasmania demonstrating the capability of 3D remote sensing and novel classification approaches to automatically classify vegetation into canopy, stems intermediate canopy, elevated, surface/near-surface and ground layers (Hillman et al. 2021).

5. Results and Discussion

Preliminary results suggest that broad overlap in the inputs and outputs exist between empirical and semi-empirical fire behaviour models across the world. This is a logical outcome given the fundamental principles of fire behaviour. Most models utilise input arguments describing long term dryness, wind, temperature, short term fuel moisture (as temperature and relative humidity) and a fuel value. The main differences between models can be seen in the fuel parameters. Most models require parameters that describe the horizontal and vertical distribution of fuel at different strata in combination with the amount of fuel. Similar outputs from empirical and semi-empirical models include descriptions of the rate of spread and height, angle and the depth of flames at the head of the fire are observed across fire behaviour models. This contrasts with physical fire behaviour models which enable observations of fire behaviour in greater detail and consequences of multiple fire interactions and connectivity in vegetation to be analysed at the expense of longer running times.

With respect to the alignment of remote sensing literature to describe fuel variables - consistent with previous findings of Gale et al. (2021) most research has focussed on extracting measurements describing overstorey and understorey variables. This suggests that fuel variables at the fuel assemblage scale which are currently utilised in operational fire behaviour models could be measured using remote sensing methods. However, factors which limit wider implementation of such technologies include the inability of active sensors to measure surface fuel properties in contact with the ground and the patchwork nature of these datasets. The incomplete coverage of datasets is also at odds with operational fire behaviour models which need to be run at a regional scale. Potential opportunities to bridge this gap have been demonstrated in recent research which has shown ability to scale up point-based measurements across the landscape (Jenkins et al., 2020; McColl-Gausden et al., 2020). It was also noted through this manuscript that remote sensing derived datasets have the ability to characterise complex 3D fuel attributes (Figure 1).

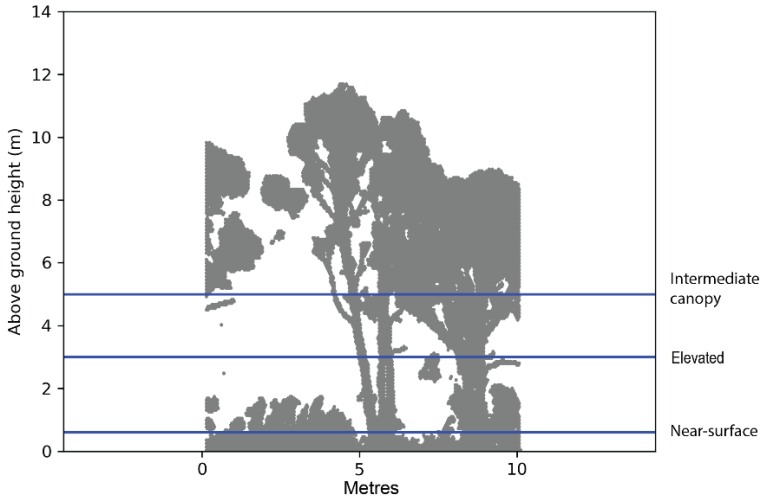

Figure 2. Height thresholds used to extract different fuel strata (based on Hines et al. (2008) and Gould et al. (2012)). Expert elicitation highlighted difficulties in the utilisation of remote sensing to extract vegetation at different strata due to the high variability of vegetation in different areas.

Preliminary results from the expert elicitation process highlighted shared and divergent opinions about the fuel characteristics that drive fire behaviour across the world. Consistent with current fuel inputs used in fire behaviour models, metrics that describe the horizontal and vertical arrangement of fuel are considered important to be measured. In contrast to current fuel hazard measurement systems, there were suggestions to move away from defined strata layers due to the complexities of defining strata using both in-field and remote sensing techniques (Figure 2). Instead, metrics describing the connectedness of fuel across the "ladder" was seen to be an area of opportunity for active 3D remote sensing. Work has begun on developing a metric to describe the vertical and horizontal connectedness of fuel from 3D remote sensing that will also allow changes in the arrangement of fuels to be observed through time. Further metrics of interest derived from the expert elicitation process include the development of an approach that allows for assessment of vulnerability of a site to stand-replacing fire and the fusion of structural and moisture information). Whilst the aforementioned fuel attributes are universal across fuel types, expert elicitation highlighted cases where fuel attributes that influence fire behaviour were unique to the vegetation type. An example of this, is the need to describe canopy fuel properties in coniferous and deciduous trees (e.g. canopy base height, canopy fuel load) which were observed to be of lower relevance in eucalypt dominated systems. Similarly, the properties of different bark types in eucalypt dominated systems were seen to be of great importance to potential fire behaviour and less important in deciduous forests. Future work completed as part of this project will validate the metrics developed through remote sensing with further expert elicitation and field observations of fire behaviour.

6. Conclusions

Overall, we make two key recommendations from this manuscript on the assessment of fuel attributes for fire behaviour in models used across the world. Firstly, we recommended that current operational models (e.g. PHOENIX, RapidFire, and FARSITE) undertake a trial to utilise fuel parameters derived from remote sensing approaches outlined in this manuscript and compare outputs from this approach with current input parameter outputs. Secondly, the complete list of fuel attributes derived from this manuscript are validated in their ability to represent fuel hazard in forest types around the world. This would enable greater confidence in the attributes ability to represent fire behaviour and identify fuel change over time. Overall, we argue that this work provides the foundation for a universal fuel assessment methodology to be developed, that is scalable and captures change over time and can link physical fuel structure and remote sensing techniques to accurately capture fuel dynamics. This work will be undertaken through a Fulbright exchange (Samuel Hillman with Rocky Mountain Research Station, Missoula, Montana).

7. Reference List

Bowman, D. M. J. S., Kolden, C. A., Abatzoglou, J. T., Johnston, F. H., van der Werf, G. R., & Flannigan, M. (2020). Vegetation fires in the Anthropocene. In Nature Reviews Earth and Environment (Vol. 1, Issue 10, pp. 500–515). Springer Nature. https://doi.org/10.1038/s43017-020-0085-3

Bowman, D. M. J. S., Williamson, G. J., Abatzoglou, J. T., Kolden, C. A., Cochrane, M. A., & Smith, A. M. S. (2017). Human exposure and sensitivity to globally extreme wildfire events. Nature Ecology and Evolution, 1(3). https://doi.org/10.1038/s41559-016-0058

Calders, K., Newnham, G., Burt, A., Murphy, S., Raumonen, P., Herold, M., Culvenor, D., Avitabile, V., Disney, M., Armston, J., & Kaasalainen, M. (2015). Nondestructive estimates of above-ground biomass using terrestrial laser scanning. Methods in Ecology and Evolution, 6(2), 198–208. https://doi.org/10.1111/2041-210X.12301

Cooper, S. D., Roy, D. P., Schaaf, C. B., & Paynter, I. (2017). Examination of the potential of terrestrial laser scanning and structure-from-motion photogrammetry for rapid nondestructive field measurement of grass biomass. In Remote Sensing (Vol. 9, Issue 6). https://doi.org/10.3390/rs9060531

Duff, T. J., Bell, T. L., & York, A. (2012). Predicting continuous variation in forest fuel load using biophysical models: A case study in south-eastern Australia. International Journal of Wildland Fire, 22(3), 318–332. https://doi.org/10.1071/WF11087

Duff, T., Keane, R., Penman, T., & Tolhurst, K. (2017). Revisiting Wildland Fire Fuel Quantification Methods: The Challenge of Understanding a Dynamic, Biotic Entity. Forests, 8(9), 351. https://doi.org/10.3390/f8090351

Gale, M. G., Cary, G. J., van Dijk, A. I. J. M., & Yebra, M. (2021). Forest fire fuel through the lens of remote sensing: Review of approaches, challenges and future directions in the remote sensing of biotic determinants of fire behaviour. In Remote Sensing of Environment (Vol. 255). Elsevier Inc. https://doi.org/10.1016/j.rse.2020.112282

García, M., Danson, F. M., Riaño, D., Chuvieco, E., Ramirez, F. A., & Bandugula, V. (2011). Terrestrial laser scanning to estimate plot-level forest canopy fuel properties. International Journal of Applied Earth Observation and Geoinformation, 13(4), 636–645. https://doi.org/10.1016/j.jag.2011.03.006

García, M., Saatchi, S., Casas, A., Koltunov, A., Ustin, S. L., Ramirez, C., & Balzter, H. (2017). Extrapolating forest canopy fuel properties in the California Rim fire by combining airborne LiDAR and landsat OLI data. Remote Sensing, 9(4). https://doi.org/10.3390/rs9040394

Gazzard, T., Walshe, T., Galvin, P., Salkin, O., Baker, M., Cross, B., & Ashton, P. (2020). What is the "appropriate" fuel management regime for the Otway Ranges, Victoria, Australia? Developing a long-term fuel management strategy using the structured decision-making framework. International Journal of Wildland Fire, 29(5), 354–370. https://doi.org/10.1071/WF18131

Greaves, H. E., Vierling, L. A., Eitel, J. U. H., Boelman, N. T., Magney, T. S., Prager, C. M., & Griffin, K. L. (2015). Estimating aboveground biomass and leaf area of low-stature Arctic shrubs with terrestrial LiDAR. Remote Sensing of Environment, 164, 26–35. https://doi.org/10.1016/j.rse.2015.02.023

Hillman, S., Wallace, L., Lucieer, A., Reinke, K., Turner, D., & Jones, S. (2021). A comparison of terrestrial and UAS sensors for measuring fuel hazard in a dry sclerophyll forest. International Journal of Applied Earth Observation and Geoinformation, 95(October 2020), 102261. https://doi.org/10.1016/j.jag.2020.102261

Jenkins, M. E., Bedward, M., Price, O., & Bradstock, R. A. (2020). Modelling Bushfire Fuel Hazard Using Biophysical Parameters.

Jolly, W. M., Cochrane, M. A., Freeborn, P. H., Holden, Z. A., Brown, T. J., Williamson, G. J., & Bowman, D. M. J. S. (2015). Climate-induced variations in global wildfire danger from 1979 to 2013. Nature Communications, 6(1), 1–11.

Keane, R. E. (2013). Describing wildland surface fuel loading for fire management: A review of approaches, methods and systems. In International Journal of Wildland Fire (Vol. 22, Issue 1, pp. 51–62). https://doi.org/10.1071/WF11139

Keane, R. E., Gray, K., & Bacciu, V. (2012). Spatial Variability of Wildland Fuel Characteristics in Northern Rocky Mountain Ecosystems. http://www.fs.fed.us/rm/publications

Kramer, H. A., Collins, B. M., Kelly, M., & Stephens, S. L. (2014). Quantifying ladder fuels: A new approach using LiDAR. Forests, 5(6), 1432–1453. https://doi.org/10.3390/f5061432

Kramer, H. A., Mockrin, M. H., Alexandre, P. M., & Radeloff, V. C. (2019). High wildfire damage in interface communities in California. International Journal of Wildland Fire, 28(9), 641–650. https://doi.org/10.1071/WF18108

Ladds, M., Keating, A., Handmer, J., & Magee, L. (2017). How much do disasters cost? A comparison of disaster cost estimates in Australia. International Journal of Disaster Risk Reduction, 21, 419–429. https://doi.org/10.1016/j.ijdrr.2017.01.004

McColl-Gausden, S. C., Bennett, L. T., Duff, T. J., Cawson, J. G., & Penman, T. D. (2020). Climatic and edaphic gradients predict variation in wildland fuel hazard in south-eastern Australia. Ecography, 43(3), 443–455. https://doi.org/10.1111/ecog.04714

Pausas, J. G., & Keeley, J. E. (2021). Wildfires and global change. Frontiers in Ecology and the Environment, 19(7), 387–395. https://doi.org/10.1002/fee.2359

Rowell, E. M., Seielstad, C. A., & Ottmar, R. D. (2016). Development and validation of fuel height models for terrestrial lidar - RxCADRE 2012. International Journal of Wildland Fire, 25(1), 38–47. https://doi.org/10.1071/WF14170

Sharples, J. J., Cary, G. J., Fox-Hughes, P., Mooney, S., Evans, J. P., Fletcher, M. S., Fromm, M., Grierson, P. F., McRae, R., & Baker, P. (2016). Natural hazards in Australia: extreme bushfire. Climatic Change, 139(1), 85–99. https://doi.org/10.1007/s10584-016-1811-1

Sullivan, A. L. (2009a). Wildland surface fire spread modelling, 1990 - 2007. 1: Physical and quasi-physical models. International Journal of Wildland Fire, 18(4), 349. https://doi.org/10.1071/wf06143

Sullivan, A. L. (2009b). Wildland surface fire spread modelling, 1990-2007. 2: Empirical and quasi-empirical models. International Journal of Wildland Fire, 18, 369–386. https://doi.org/10.1071/WF06142

Tedim, F., Leone, V., Amraoui, M., Bouillon, C., Coughlan, M. R., Delogu, G. M., Fernandes, P. M., Ferreira, C., McCaffrey, S., McGee, T. K., Parente, J., Paton, D., Pereira, M. G., Ribeiro, L. M., Viegas, D. X., & Xanthopoulos, G. (2018). Defining extreme wildfire events: Difficulties, challenges, and impacts. Fire, 1(1), 1–28. https://doi.org/10.3390/fire1010009

Wallace, L., Gupta, V., Reinke, K., & Jones, S. (2016). An assessment of pre- and post fire near surface fuel hazard in an australian dry sclerophyll forest using point cloud data captured using a Terrestrial Laser Scanner. Remote Sensing, 8(8), 1–14. https://doi.org/10.3390/rs8080679

Wallace, L., Hally, B., Hillman, S., Jones, S. D., & Reinke, K. (2020). Terrestrial image-based point clouds for mapping near-ground vegetation structure: Potential and limitations. Fire, 3(4), 1–15. https://doi.org/10.3390/fire3040059

Wallace, L., Hillman, S., Reinke, K., & Hally, B. (2017). Non-destructive estimation of above-ground surface and near-surface biomass using 3D terrestrial remote sensing techniques. Methods in Ecology and Evolution, 38(1), 42–49. https://doi.org/10.1111/2041-210X.12759

Yu, P., Xu, R., Abramson, M. J., Li, S., & Guo, Y. (2020). Bushfires in Australia: a serious health emergency under climate change. In The Lancet Planetary Health (Vol. 4, Issue 1, pp. e7–e8). Elsevier B.V. https://doi.org/10.1016/S2542-5196(19)30267-0

High Resolution Fire Behavior Monitoring and Plume Simulation in the context of Experimental Fire

Ronan Paugam*[1]; William Mell[2]; Jean-Baptiste Filippi[3]; Melanie Rochoux[4]; Martin Wooster[5,6]

[1]Centre for Technological Risk Studies, Department of Chemical Engineering, Universitat Politécnica de Catalunya—BarcelonaTech, Diagonal 647, E-08028 Barcelona, Spain, {ronan.paugam@pm.me}
[2] Wildland Fire Science Lab, USDA Forest Service, 400 N 34th St., Suite 201, Seattle, WA 98103, USA, {william.mell@usda.gov}
[3] Laboratory for the Physical Systems of the Environment, Université de Corse, 20250 Corte, France, {filippi@univ-corse.fr}
[4] CECI, Université de Toulouse, 31100 Toulouse, France, {rochoux@cerfacs.fr}
5 Environmental Monitoring and Modelling Research Group, Department of Geography, King's College London, London WC2R 2LS, UK
6 Leverhulme Centre for Wildfires, Environment and Society, Department of Geography, King's College London, London WC2B 4BG, UK, {martin.wooster@kcl.ac.uk}

**Corresponding author*

Keywords

Plume simulation; fire behavior; airborne observation, Experimental Fire.

Abstract

Coupled fire-atmosphere systems are currently developed to respond to the need of operational system in air quality and fire attack management. This work participates to this effort by proposing a simulation strategy where the plume is simulated using fire observation. Such approach can provide reference test case for more complex coupled fire-atmosphere simulation. Using the Forefire-MesoNH system, we simulate the plume evolution of a landscape scale burn where the fire is not simulated as a spreading front but rather prescribed from multiple fix burners controlled with observation data. The simulation of the plume formed from a 7-hectare savannah fire conducted in Kruger National Park in 2014 is demonstrated using helicopter-borne observations georeferenced at 1-m resolution and post-processed to extract information of heat fluxes at pixel level.

1. Background

Over the past 20 years, the development of earth observation (EO) satellite product enable the observation of wildfire at the global scale and show an increased of fire activity in fire-prone regions such as western USA or eastern Australia (Andela et al., 2017), most probably because of the high population living in Wildand-Urban Interface (WUI) in those regions (Doerr and Santín, 2016). To mitigate wildfire effects, operational forecast systems have been developed with either focus at fire scale for application in fire operational attack like the fire growth model FARSITE (Finney, 1998), or at plume scale for application in air quality like the Smoke Research Forecast (SRF) system BlueSky (Larkin et al., 2009).

More recently, coupled fire-atmospheres systems have been developed to resolve simultaneously the plume updraft/smoke dispersion, the propagation of the fire front, and their mutual interactions. Several coupled systems are now making references: CAWFE (Coen et al 2013), WRF-SFIRE (Mandel et al 2011) and MesoNH-ForeFire (Filippi et al 2013). While still mostly used as research tools, they are intended to become operational (Kochanski et al 2016). They are design to simulate landscape-scale (>100m) propagating fire, and therefore forced to rely on highly parameterized fire model as current computational resources cannot resolve such domain size at the resolution required to capture combustion processes that responsible of the fire front dynamics (<1cm). In atmospheric model grids, fires are set as front lines with associated Rate Of Spread (ROS) and sensible heat flux predicted according to local orography and local modelled atmospheric variables (ie wind speed, humidity).

To the authors knowledges, apart from the recently released Rx-Cadre experiment dataset (Ottmar et al 2016), no other dataset exists that can provide simultaneous information on both the fire and the atmosphere states, and therefore can be used to run detailed validation of coupled fire-atmosphere system. Unfortunately, the prescribed burns of the Rx-Cadre experiment were set in non-homogeneous vegetation and with complex ignition pattern that make them difficult to simulate as detailed vegetation map and fast return observation of the front propagation are then required. Nevertheless, validation exercise against observation already exists for MesoNH-Forefire (Filippi et al. 2013) and WRF-SFIRE (Kochanski et al 2013). They are both based on the simulation of the Fire-Flux field work campaign which took place in 2006 (Clements et al. 2007) in a homogenous grass field in Texas. The fire was set with a single front ignition. However, no comprehensive fire behavior data were collected for this experiment, and the model validations were conducted against turbulent flux measurements acquired with an instrumented mast located along the propagation of the fire front.

2. Objective

To improve the validation of coupled fire-atmosphere system and assess further the impact of the fire model assumption on simulated fire behavior we need validation datasets for scenarios in which the fire induced winds influence fire front behavior (Liu et al 2016) as for example fire front acceleration induced by front merging. In such scenario, plume dynamics point measurement like in Clements et al. 2007 and Clements et al. 2019 are much more difficult to perform due to the more complex predictable location of best measurement point.

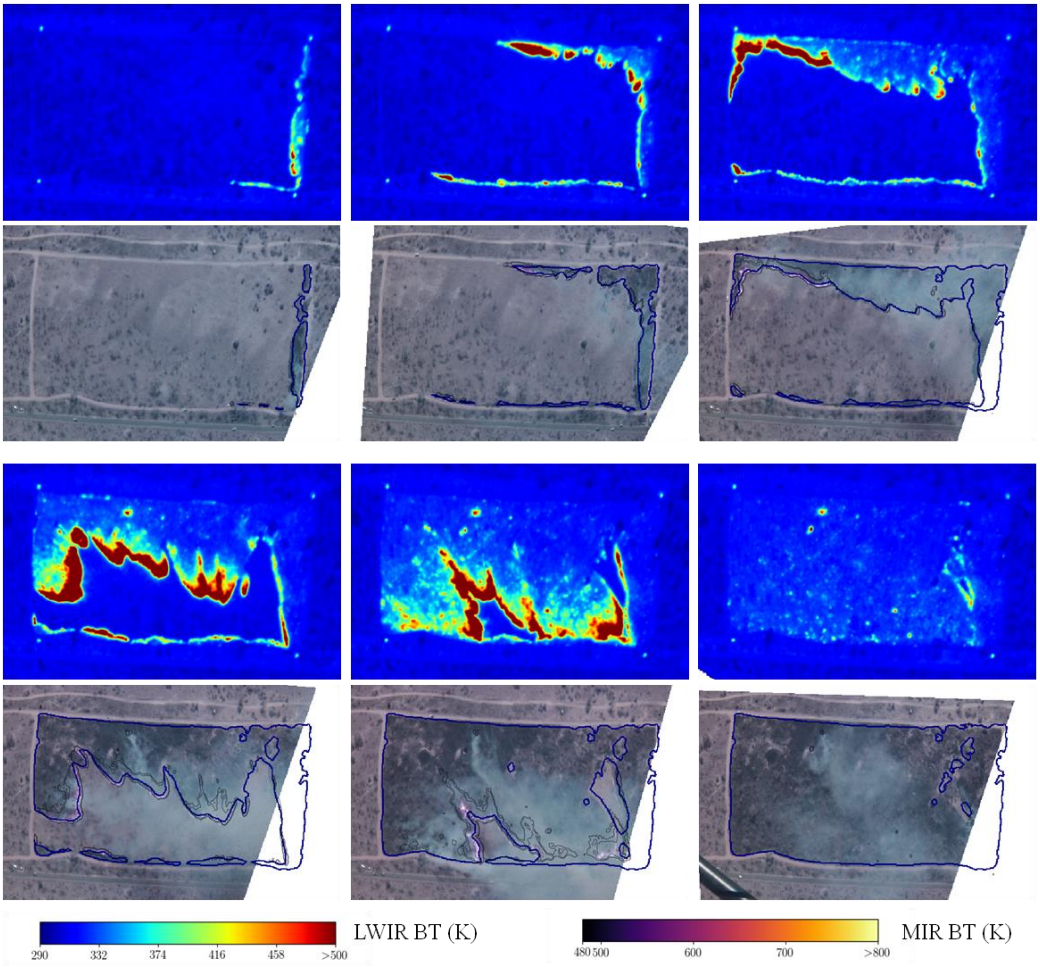

Figure1: Time series of LWIR, and combined MIR/VIS images for 6 times along the 20 minutes of the duration of the Skukuza6 fire conducted on the 26th of June 2014 in Kruger National Park (South Africa). The spatial resolution is 1m for all images. Time after ignition are t=249, 419, 556, 656, 750, 931 s from top left to right bottom. Corner fires are visible on the LWIR images but were not used in the georeferencing. The VIS images show the perimeter of the active fire contour (blue line) as segmented by Convolutional Neural Network trained on the KNP dataset, and the MIR contour plot extracted from the MIR images.

In situation of high variable fire behavior and potential complex front geometry structures, infra-red high temporal and spatial resolution observation have shown capability to capture fire front dynamics (Paugam et al 2021, Paugam et al 2022). To help continuing the development of fire-atmosphere system, we show here the potential such airborne high-resolution observation to force plume simulation.

3. High resolution experimental fire observation

We use here the orthorectified IR image data set of experimental 7-ha savannah fire processed in Paugam et al 2021. The epxeriemtal setup required to produce such data set require to have a set scene (no wildfire), but the common constraint on having bone fires presence on every image is released (Pastor et al 2012, Paugam et al 2013), hence making easier high frequency observation. The set of algorithm developed in Paugam et al 2021 are built on background feature tracking and image to image correlation optimization (Evangelidis and Psarakis 2008) for application on Long Wave Infra-Red (LWIR) and Middle Infra-Red (MIR) images. Orthorectifucation of visible image time serie are also possible if the plume is not too dense.

Results of orthorectified images collected during a fire conducted on the 26th of June 2014 on the KNP plot named Skukuza6 are shown on Fig 1. Hereafter this fire is referenced as Skukuza6. During the KNP fieldwork three cameras were operated simultaneously from a hovering helicopter:

- a visible camera (GOPRO Hero1, 1Hz, 3849x2880 pxs) with its IR filter removed to better capture flame location,
- a Long Wave Infra Red (LWIR) camera (OPTRIS 400, 7-13µm, 1Hz, 382x288 pxs, $T \in [250,1700]$
- and a Middle Infra Red (MIR) camera (FLIR AGEMA 550, 3.9 µm, 3Hz, 320x240pxs, $T \in [473,1073]$.

Fig 1 shows, for 6 times along the 20 minutes of the fire duration, LWIR images together with quasi-simultaneous combined MIR/visible images. The hovering altitude of the helicopter and the sensor resolution of the LWIR and MIR cameras allow a spatial resolution of 1m.

The second step to the image postprocessing tasks is the segmentation of the fire front. Among the 3 cameras available, we decided to base our approach on LWIR images only. This choice is explained by: (a) using only one band avoid potential problem related to time-synchronization, (b) VIS images can be masked by smoke, and (c) the MIR camera used here is not as widespread in the scientific community as the LWIR camera. The LWIR image front segmentation is based on a deep learning approach, it is described in Paugam et al 2022. Using a limited number of manually tagged front, a series of Convolutional Neural Network (CNN) is designed to develop a multiple step learning methodology gradually including information from 4 different burns. Based only on 10 initial manually segmented images, a series of 14 CNN learn front features from each other, using cumulative knowledge and manual annotation adjustment from previous front prediction. Transfer learning techniques are used to improve CNN response when including new burn to reduce overfit inherent to the first learning steps. Results of the final CNN is shown on the visible images of Fig. 1 (see blue line).

4. Plume Simulation

Using previous high-resolution fire front observation, this section intends to simulate the plume triggers by the heat flux and the emissions induced by the spreading fire front and the cooling trail located behind the front. We proposed here to use the MesoNH model (Lafore et al 1998) to simulate the atmosphere above the fire while the fire is simulated as a multitude of fix burner (one per cell of the atmospheric grid) that are switched on and off with a set strength accordingly to the fire observation (Mell and Linn 2017). The fluxes conversion from the observation resolution (1m) to the atmospheric grid (10m) is done via the ForeFire model (Filippi et al 2013). The front spread prediction of ForeFire are not used here, ForeFire control each cell as a burner where the heat flux activation is set using maps of arrival time, time of residence and total energy released. This latter is computed from the measurement of the Fire Radiative Energy (Wooster et al 2005) and an assumed radiation to total energy ratio of 10%. To better model the evolution of the fire spread each burner differentiated the phases of flaming and smoldering, so that a burner is defined with the inputs of arrival time, flaming residence

time, flaming FRE, total burning time and smoldering FRE. See Fig 2 for inputs associated with the Skukuza 6 fire introduced in the previous section.

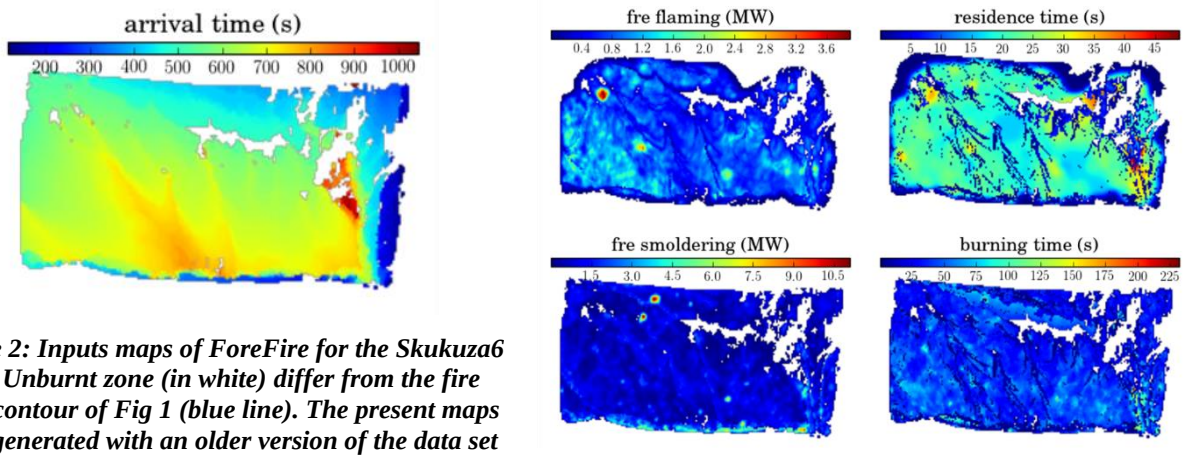

Figure 2: Inputs maps of ForeFire for the Skukuza6 fire. Unburnt zone (in white) differ from the fire front contour of Fig 1 (blue line). The present maps were generated with an older version of the data set presented in Fig 1.

The arrival time map concatenates information from all the fire front CNN prediction to map the time of first appearance of the fire front in a pixel. FRE is computed from the time integration of the Fire Radiative Power that is evaluated using the MIR images following the formulation of Wooster et al 2005. The flaming residence is defined as the time is takes to a pixel ($1m^2$) to cool down below a certain threshold (here we used a MIR brightness temperature of 600K). The total burning time is the time it takes for a pixel to cool down to background temperature.

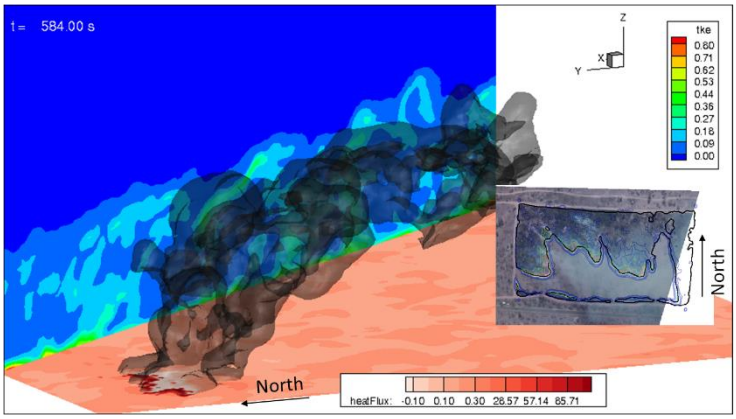

Figure 3: perspective view of the simulated plume of the Skukuza 6 fire a time t=584s after ignition.

Emissions linked to the heat flux is also passed to MesoNH via the FRE formulation (Wooster et al 2005) with a conversion factor of 0.4 (kg/s/MW) and emission factors set for the flaming and the smoldering phases. In this first simulation, only a passive tracer is set. It uses emission factor of 0.05 and 0.01 for flaming and smoldering, respectively.

The MesoNH simulation uses a 10 m spatial resolution and a 4 second time step. It is run in LES mode. The initial condition is set using a radio sounding and a spin-up time of 1500 seconds that was necessary to generate the boundary layer (see tke profile on Fig 3). The radio sounding was generated from a MesoNH simulation using 3 nested models and forced with ERA interim reanalysis data. Fig 3 shows a perspective view of the plume simulated by MesoNH that was induced by fix burners set accordingly to the Skukuza 6 fire observation. The heat flux map generated by ForeFire and pass to MesoNH is seen on the ground level of the MesoNH grid.

Fig 4 shows the 10m wind data from the first level interpolated on the 2m fire data grid for 2 times of the fire evolution: at the start and end of the large ellipsoidal front spreading on the left of the plot. The fire shows a wind dominated dynamics with wind passing through the front (Finney et al 2015, Frangieh et al 2010). The wind field a ground level is significantly alter downwind to the front, see left shift southward of the front at t=600s, or the acceleration in the unburnt area at t=700s. To analyse the impact of the coupling between the fire dynamics and the wind field, Fig 5 shows correlations between the cross product of the ROS and the wind field and (a) the norm of the ROS and, and (b) the Byram's Fire Intensity (FI). FI is computed following the approach of Johnston et al (2017). In the correlation we only select point from the fire front with ROS greater than 0.2m/s to focus on the spreading part of the fronts and remove the back fire and dead front.

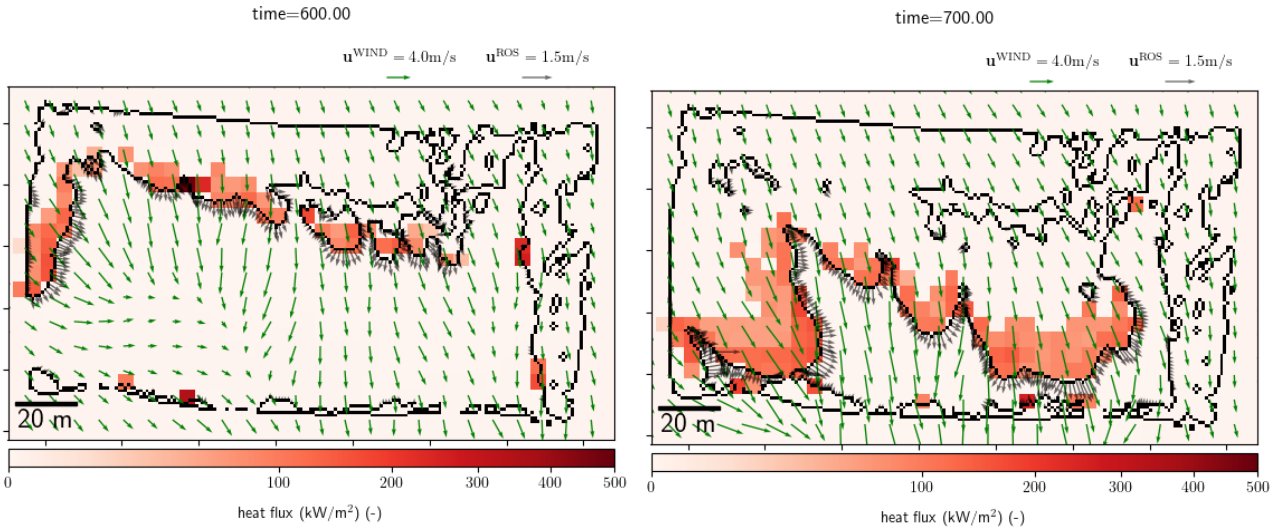

Figure 4: Wind vector field at 5m heigth in green (first MesoNH level) and fire front ROS in grey at 2m resolution for 2 times of the fire evolution: start and end of the main ellipsoidal front spreading on the left of the plot. The black line shows the fire front while the convective heat flux computed by the forefire flux scheme is reported in the background at the 10m MesoNH resolution.

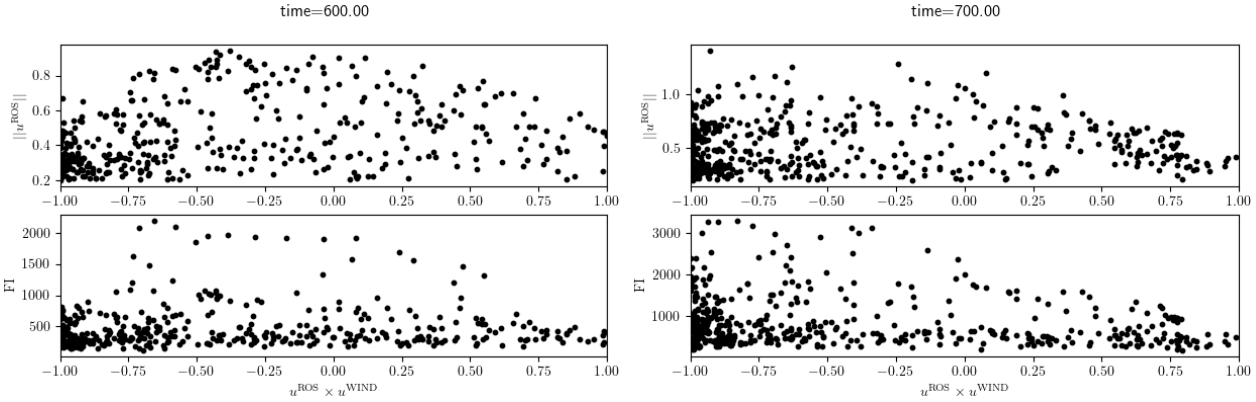

Figure 5: Correlation of the cross product of the ROS vector (uROS) and the wind field (uWIND) with the norm of the ROS (top panels) and the Fire Intensity (FI) for the same two times t (left and right panels) as Figure 4.

No clear correlation appears from Fig 5. The dynamics of the front does not seem to impact the wind speed near the front. This is probably due to the ambient wind direction variability that can be seen in Fig 1, for example at time t=656s, and t=750s. The ambient wind oscilates between west and south during the fire evolution as shown by smoke released by smodlering spots in the back of the fire. This variability is not taken into account in the MesoNH simulation that uses a single radio sounding and a spin-up time to build its boundary layer. As a result the ellipsoidal front spreading from the left of the plot edge is spreading in the MesoNH simulation with a southwards wind (see Fig 4 left panel) when visible image shows a clear eastwards wind at this time. This issue shows also with a right shift of the the wind field from the ROS direction in Fig5, see the large number of negative cross product at t=700s. Improving the ambient wind input will be investigated in future work as well as the impact of the heat release scheme use in forefire. Comparison with the default nominal flux of Filippi et al (2013) will be considered.

5. Conclusion and Perspectives

This work presents the development of a methodology to simulate fire plume from airborne IR observation. Unfortunately, as no atmospheric data or plume sampling were collected during the burn we simulate, no validation of the simulated plume can be run. Furthermore, no details fuel load was performed, hence making fully coupled fire-atmosphere simulation more challenging. This first attempt to simulate a plume from fire

observation is therefore only a proof of concept that emphasize use of airborne IR observation in the on-going effort of the fire community in developing fire-atmosphere coupled models. Details knowledge of plume structure and composition also shows potential application in current effort in 3D radiative transfer simulation in fire scene (Paugam et al 2021b).

6. References:

Andela, N.,et al: A human-driven decline in global burned area, Science, 356, 1356–1362, doi:10.1126/science.aal4108, 2017.

Clements C. B., S. et al: FireFlux A Field Validation Experiment, Bulletin of the Am. Met. Soc. 88 (2007) 1369–1382.

Clements Craig B., et al (2019) The FireFlux II experiment: a model-guided field experiment to improve understanding of fire–atmosphere interactions and fire spread. International Journal of Wildland Fire 28, 308-326.

Coen, J.L. Modeling Wildland Fires: Of the Coupled Atmosphere-Wildland Fire Environment Model (CAWFE); Technical Report, NCAR Technical Note NCAR/TN-500+STR; NCAR: Boulder, CO, USA, 2013.

Doerr SH, Santı´n C. 2016 Global trends in wildfire and its impacts: perceptions versus realities in a changing world. Phil. Trans. R. Soc. B 371: 20150345. http://dx.doi.org/10.1098/rstb.2015.0345

Evangelidis G , Psarakis E . Parametric Image Alignment Using Enhanced CorrelationCoefficient Maximization. IEEE Transactions on Pattern Analysis and Machine Intelligence, Instituteof Electrical and Electronics Engineers, 2008, 30 (10), pp.1858-1865.

Filippi J.-B., et al, Assessment of ForeFire/Meso-NH for wildland fire/atmosphere coupled simulation of the FireFlux experiment, Proceedings of the Combustion Institute 34 (2013) 2633–2640.

Finney, M. A.: FARSITE: Fire Area Simulator-model development and evaluation, Tech. rep., U.S. Department of Agriculture, Forest Service, Rocky Mountain Research Station, Ogden, doi:10.2737/RMRS-RP-4, 1998.

Finney et al, Role of buoyant flame dynamics in wildfire spread, 112 (32) 9833-9838, PNAS, 2015

Frangieh, Accary, Morvan, Méradji, Bessonov, Wildfires front dynamics: 3D structures and intensity at small and large scales, Combustion and Flame, Volume 211, 2020, Pages 54-67,

Johnston, Joshua, Wooster, Martin, Paugam, Ronan, Wang, Xianli, Lynham, Timothy, Johnston, Lynn. (2017). Direct estimation of Byram's fire intensity from infrared remote sensing imagery. International Journal of Wildland Fire. 26. 668-684. 10.1071/WF16178.

Kochanski A. et al, Evaluation of WRF-SFIRE performance with field observations from the FireFlux experiment, Geoscientific Model Development 6 (2013) 1109–1126.

Kochanski A. et al, Toward an integrated system for fire, smoke and air quality simulations, IJW F25 (2016) 534.

Lafore, J. P., et al. The Meso-NH Atmospheric Simulation System. Part I: adiabatic formulation and control simulations, Ann. Geophys., 16, 90–109, 1998.

Larkin, N. K., et al : The BlueSky smoke modeling framework, International Journal of Wildland Fire, 18, 906, doi:10.1071/WF07086, 2009.

Liu Yongqiang, et al. 2017. Fire and Smoke Model Evaluation Experiment (FASMEE): Modeling gaps and data needs. In: Proceedings for the 2nd International Smoke Symposium November; 14-17, 2016, Long Beach, California, USA. Missoula, MT: International Association of Wildland Fire. 13 p.

Mandel, J.; et al.: Coupled atmosphere-wildland fire modeling with WRF 3.3 and SFIRE. Geosci. Model Dev. 2011, 4, 591–610.

Mell, W.E.; Linn, R.R. FIRETEC and WFDS Modeling of Fire Behavior and Smoke in Support of FASMEE—Final Report to the Joint Fire Science Program | FRAMES. 2017.

Ottmar R. D., J. K. Hiers, B. W. Butler, C. B. Clements, M. B. Dickinson, A. T. Hudak, J. J. O'Brien, B. E. Potter, E. M. Rowell, T. M. Strand, T. J. Zajkowski, Measurements, datasets and preliminary results from the RxCADRE project 2008, 2011 and 2012, IJWF 25 (2016) 1.

Pastor E., E. Planas, Infrared imagery on wildfire research. Some examples of sound capabilities and applications, in: 2012 3rd International Conference on Image Processing Theory, Tools and Applications, IPTA 2012, IEEE, 2012, pp. 31–36.

Paugam R., et al, Use of handheld thermal imager data for airborne mapping of fire radiative power and energy and flame front rate of spread, IEEE Transactions on Geoscience and Remote Sensing 51 (2013) 3385–3399.

Paugam, et al 2021b. 3DFireLab: a Virtual Fire Scene Simulator for the Simulation of Infra Red Fire Observation. 13th IAFSS Symposium, Waterloo CA, 26-30 April 2021.

Paugam, R. et al Orthorectification of Helicopter-Borne High Resolution Experimental Burn Observation from Infra Red Handheld Imagers. Remote Sens. 2021, 13

Paugam, R. et al Fire front segmentation and rate of spread estimation from airborne thermal infra red observation using deep learning, Int. J. Wildland Fire, 2022, (submitted in Mars 2022)

Wooster M.et al. Retrieval of biomass combustion rates and totals from fire radiative power observations: FRP derivation and calibration relationships between biomass consumption and fire radiative energy release, Journal of Geophysical Research Atmospheres 110 (2005) 1–24.

High-Resolution Fire Risk Assessment and Management Planning in Peri-urban Areas via Coupling Geoinformatics, Machine-learning and Field Observations. Pilot Application in Attica Region, Greece.

Anastasia Yfantidou*[1,2,3]; Stella Girtsou[1]; Michail-Christos Tsoutsos[1]; Melpomeni Zoka[1]; Martha Kokkalidou[1]; Charalampos Kontoes[1]; Nikolaos Stathopoulos[1]

[1]Institute of Space Applications and Remote Sensing, National Observatory of Athens, I. Metaxa and Vas. Pavlou St, Penteli, Athens 15236, Greece
{yfantidou, sgirtsou, mtsoutsos, zoka, m.kokkalidou, kontoes, n.stathopoulos}@noa.gr
[2] Department of Civil Engineering and Geomatics, Faculty of Engineering and Technology, Cyprus University of Technology, Saripolou 2-8, Limassol 3036, Cyprus
[3] Eratosthenes Centre of Excellence, Saripolou 2-8, Limassol 3036, Cyprus

**Corresponding author*

Keywords

Fire risk assessment, management planning, fire spread, field observations, fire risk forecasting

Abstract

Forest fires are among the most catastrophic natural hazards threatening human lives, properties and infrastructure. In recent years, these events keep rising both in frequency and severity mainly due to climate change, constituting fire risk assessment a critical priority. Scientific and technological bloom, during the last decades, offers the required contemporary tools and data for innovative frameworks on risk assessment leading to operational action-plans for prevention, during-the-event management and post-event mitigation actions. This study illustrates an integrated approach, for high-detail fire risk assessment (at building-block level) and management planning in peri-urban areas that are prone to forest fires, through coupling of geoinformatics, machine learning techniques and field observations. The methodology combines fire hazard modelling, vulnerability and exposure assessment. The fire hazard scenarios refer to spatiotemporal simulations of fire spread (generated by applying the adapted FlamMap model), based on the most probable ignition points for possible fire outbreaks (derived by the BEYOND's daily fire risk forecasting machine learning model modified for seasonal forecasts) and on the analysis of the meteorological regime (wind intensity, directions, frequency) of the area of interest. The vulnerability layer was produced by coupling population (density and age) and building characteristics, based on 2011 census data. The exposure layer refers to land value (€/m2) and works as an indicator for the qualitative estimation of possible economic effects in the study area, in case of a fire event. The high-risk areas resulting from the fire risk map, were visited in-situ for validation and update if/where needed. Throughout the field campaign, important areas and critical points (high-risk buildings, traffic congestion areas, population gathering areas etc.) were recorded and included in the mitigation suggestions and management planning. This integrated and iterative process (office-to-field and field-to-office) forms the basis for the synthesis and recommendation of effective and operational mitigation actions, protective measures and coping/management strategies. The methodological framework is developed by BEYOND Centre of EO Research & Satellite Remote Sensing (National Observatory of Athens) and applied in Vravrona, Chamolia and Porto Rafti settlements (pilots) of the Attica Region in Greece, under the project "Seismic, Fire & Flood Risk Assessment in Attica Region, Greece" funded by Attica Region.

1. Introduction

Climate change has led to increases in the vulnerability of forest ecosystems, as it is a major contributor to the rise of forest fires and tree species' inability to adapt to the intensity and frequency of summer droughts (Prodromou et al., 2020). Peri-urban zones, mainly due to uncontrolled urban-sprawl and lack of proper planning, are more vulnerable to wildfires leaving people's lives and properties, as well as the surrounding natural environment and ecosystem, exposed to increased disaster risk. Attica region, Greece, where the country's capital is located and almost half of the country's population along with critical infrastructure, is characterized by a plethora of peri-urban settlements surrounded by intense morphological relief with steep slopes, and with pine forests being the dominant land cover type. Moreover, the region's rich natural landscape results in the intrusion of dense forest parts inside a significant number of settlements. Fire risk assessments are

necessary to reduce the impact of natural disasters and support decision making (protective measures, mitigation actions, emergency evacuation procedures, etc.). A cornucopia of fire risk assessment methodologies can be found in scientific literature. The Analytic Hierarchy Process (AHP) is highlighted among them and is usually combined with Geographic Information Systems (GIS) (Gheshlaghi et al., 2019). Several studies also used satellite imagery and GIS (Kanga et al., 2014), fuzzy approaches (Erdin and Çağlar., 2014), artificial neural networks (Goldarag et al., 2016) and LIDAR data (González-Olabarria et al., 2012). The methodology presented in this work, is an integrated approach for fire risk assessment and management planning in peri-urban areas that are prone to forest fires, through machine learning techniques, geoinformatics and field observations. It was developed under the umbrella of the national research project "Seismic, Fire & Flood Risk Assessment in Attica Region, Greece", led and coordinated by the National Observatory of Athens (NOA) and specifically the Centre of EO Research & Satellite Remote Sensing – BEYOND, of the Institute for Astronomy, Astrophysics, Space Applications and Remote Sensing (IAASARS).

2. Material and Methods

2.1. Study Area

The study area (Figure 1), concerning the fire risk assessment, includes the settlements of Vravrona, Chamolia and Porto Rafti of the Municipality of Markopoulo Mesogaia. It has an average altitude of 140 m and borders the Athens International Airport, the settlements of Markopoulo Mesogaia, Artemida and Kouvaras in the wider area of Mount Merenda (614 m), while it is limited from the east by the Southern Gulf of Evia. The area is mainly covered by hardwood vegetation and coniferous forest (~ 50% of the total surface), fruit trees, meadows, vineyards and natural pastures (~ 32.5% of the area) and urban fabric, non-irrigated arable land, bare rocks, etc. concerning the 17.5%. It is worth mentioning the cultural and environmental importance of Vravrona as it brings together an archaeological monument and a NATURA region.

Figure 1- Study Area.

2.2. Methodological framework

The approach (Figure 2) is a fusion of the research team's expertise (EMSN041, 2017[20]; EMSN059, 2019[21]; FireHub[22]; (Apostolakis et al. 2021; Girtsou et al. 2021) and of extensive literature review (Darvishi et al. 2020; Gheshlaghi et al. 2019). To assess the fire risk, were taken into account: i. Selected fire hazard scenarios, ii. The composite spatial layer of fire vulnerability and iii. The spatial layer of land values. According to the fire risk assessment map that has been produced, targeted high risk areas were visited for validation/modification purposes and further important observations were recorded for the development of management plans.

Figure 2- Flowchart of the methodology.

3. Fire Hazard

3.1. Analysis of wind characteristics

For the analysis of wind characteristics of the study area, wind velocity and direction data were derived by the ERA-5[23] mission (from 1990 to 2020) as well as by the METEO[24] platform (from 2013 to 2020). The two aforementioned data sources were combined through the "Q-Q plot mapping" methodology so that the gridded ERA-5 data follow the same distribution as the point observations from the meteorological station of Porto Rafti (Figure 3).

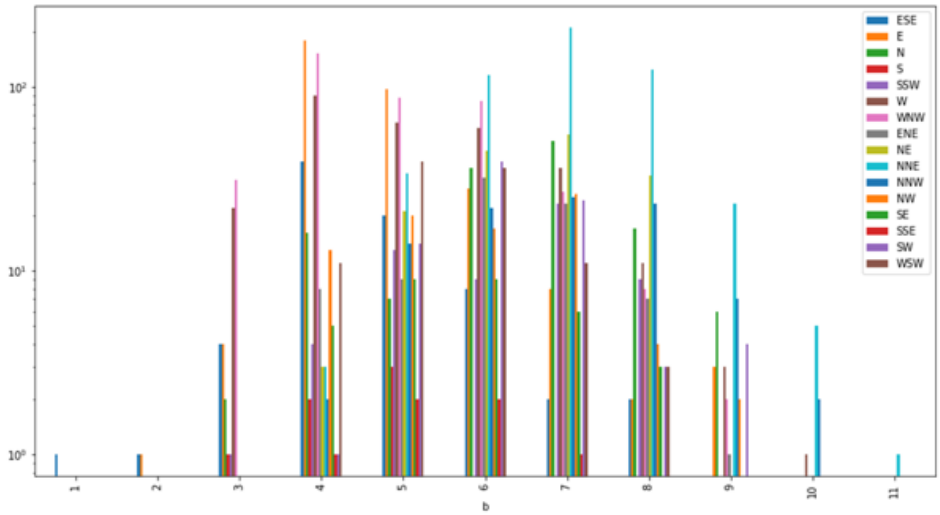

Figure 3- Wind intensity per wind direction in the study area.

[20] https://emergency.copernicus.eu/mapping/list-of-components/EMSN041
[21] https://emergency.copernicus.eu/mapping/list-of-components/EMSN059
[22] http://ocean.space.noa.gr/FireHub
[23] https://climate.copernicus.eu/climate-reanalysis
[24] https://www.meteo.gr/

3.2. Determination of fire ignition points

For the determination of the fire ignition points several datasets have been utilized such as the DEM[25] and its derivatives (aspect, slope), ERA-5 and METEO data related to temperature, wind (velocity, direction), rainfall, along with the adjusted Corine Land Use / Land Cover[26] product and other satellite based spectral indices (e.g. NDVI, EVI). The selection of ignition points is critical to simulate the start and spread of fire scenarios. For this purpose, the Machine Learning model of daily fire risk forecasting, which was developed by the BEYOND Centre, was utilized (Apostolakis et al. 2021). The resulting output (Figure 4) is a set of high fire ignition probability cells (red), based on the model's knowledge gained through the correlations of the input variables with past fire events. Based on these results and the analysis of the worst case wind scenarios in the area, the ignition points were combined with the respective wind intensity and direction that could possibly harm residential areas.

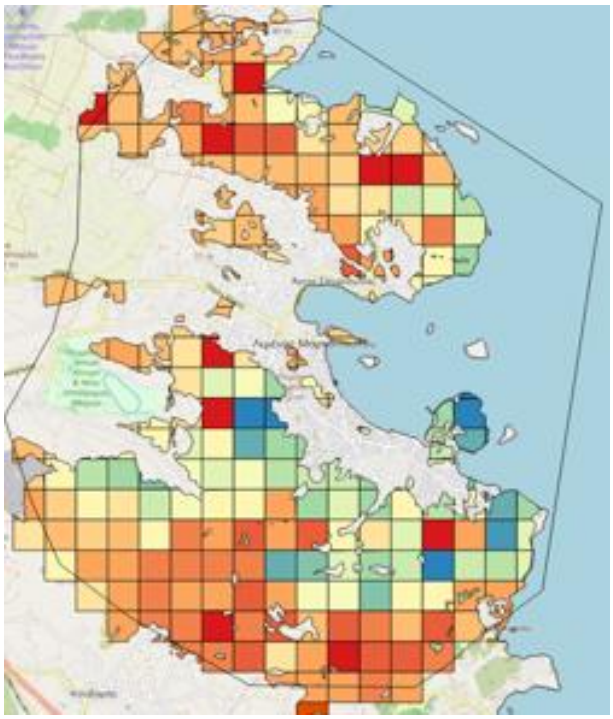

Figure 4- Fire ignition probability cells.

3.3. Fire spread simulations

FlamMap[27] is an open source application that runs in a 64-bit Windows Operating System environment and simulates possible fire behaviour characteristics, such as the rate of spread and its intensity under constant environmental conditions at a given time. By adapting FlamMap in a Linux environment, it was possible to simplify the number of input layers from 8 to 5 as follows: DEM, Aspect, Slope, Fuel and Density. The elevation, the aspect and the slope layers were created through GIS. In this study, the surface fuel, the moisture content of the fuel and the vegetation characteristics of the area, were determined by using an adjusted land use/cover map through GIS, high resolution satellite imagery and photo-interpretation. Each fuel model was assigned to a vegetation type as a combination based on the works of Kalabokidis et al. (2013) and Scott & Burgan (2005). The layer of Density represents the amount of available fuel per unit volume of the surface covered by the canopy space. It is an important factor that affects the probability of starting a fire and the rate of crown fire spread (Johnston, 2012). For the area of interest, this layer was categorized into 4 different classes, concerning the estimated timber volume of the available fuel per m^3.

[25] https://www.ktimatologio.gr/
[26] https://land.copernicus.eu/pan-european/corine-land-cover
[27] https://www.firelab.org/project/flammap

Various hazard scenarios were simulated, based on extensive combinations of ignition points and wind characteristics (direction, speed). Finally, all these scenarios were co-assessed and combined, leading to 4 fire hazard assessments, one per ignition area (ignition areas refer to groups of ignition points depending on their place and impact on the study area).

3.4. Vulnerability

For the estimation of the total vulnerability of the study area, the generation of the population density/age and the building materials datasets from the Hellenic Statistical Authority[28] was a necessary prerequisite. For the generation of the above mentioned datasets, the 2011 Census data were processed along with the support of very high resolution satellite images and orthophoto maps.

3.5. Exposure

The economic exposure layer was generated by using land use and land values data (€ / m^2), very high resolution satellite images and orthophoto maps. These data were obtained from the Ministry of Digital Government[29] and contained polygons with the land value zones. In order to handle areas with no information on land value, polygons of these areas were created and values were manually assigned, through an exhaustive analytical process were the neighbouring land values and the photo-interpretation of high-resolution satellite images and orthophotos were assessed and combined.

3.6. Fire risk

For the risk assessment, the datasets of a) hazard, b) total vulnerability and c) exposure, derived in the previous stages of the methodological approach were fused. Each one of the 4 spatial layers concerning fire hazard were combined with the layer of total vulnerability and economic exposure and the final risk maps were produced for the area of interest.

4. Results

4.1. Fire risk maps

Fire risk maps (e.g. Figures 5, 6) depict the fire risk per building block according to the socio-economic characteristics, the resistance of the buildings and the spatio-temporal spread of fire. Two fire risk maps were produced for each one of the 4 fire ignition areas, with the former presenting the fire risk and the population gathering areas (social and cultural sites, such as schools, museums, etc.), while the latter the fire risk and the essential infrastructure and services of the area (road network, fire brigade, etc.). It is emphasized that building blocks that are shown in red and orange colour are of the utmost importance and priority, as these are of the highest risk during the 1st and the 3rd hour of the fire spread respectively.

[28] https://www.statistics.gr/
[29] https://www.minfin.gr/

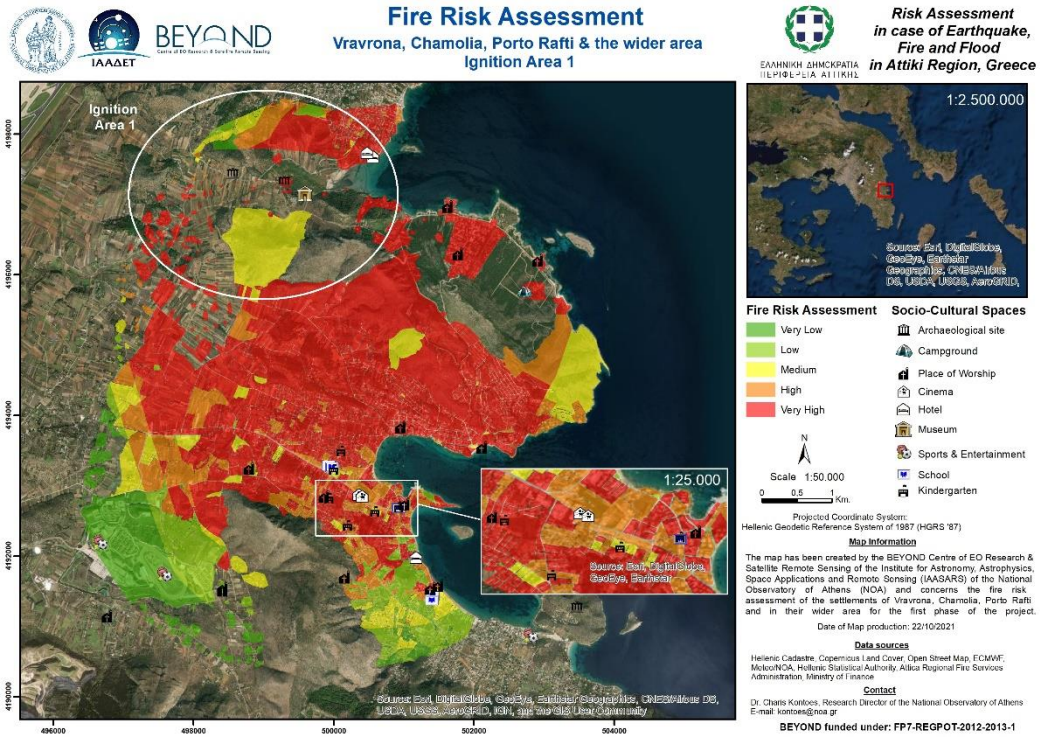

Figure 5- Fire risk assessment for the ignition area 1 (Socio-cultural Places).

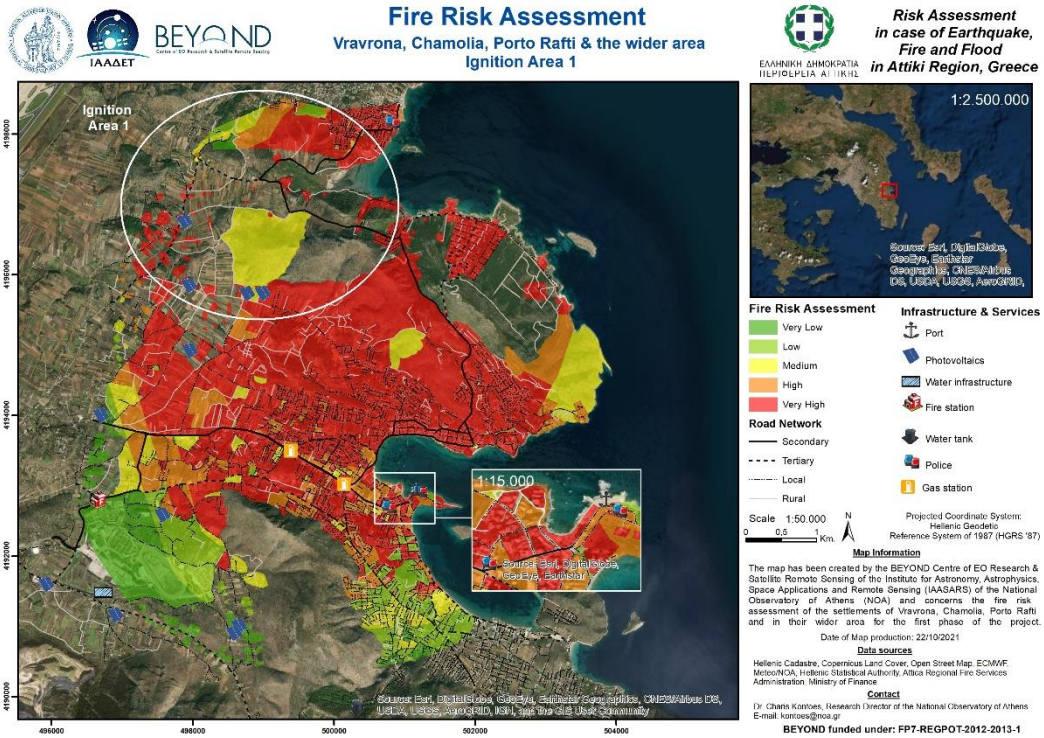

Figure 6- Fire risk assessment for the ignition area 1 (Infrastructure & Services).

4.2. Field observations/Management planning

The study area was divided into sectors for the optimization of field work and the proposed management plans. These sectors were selected according to the produced risk maps and autopsies as the most prone to fire in the area. Priority in each sector was high population gathering areas such as schools, hospitals, nursing homes, etc., as noted in the fire risk maps presented in the previous section. During the field-work, several critical characteristics of the area were recorded like for example road dead ends, high slopes, suitability of roads, possible escape routes, existence of fire protection infrastructure, properties that are surrounded by trees, yards

and roofs covered by pine needles or waste, etc. All these contributed to the creation of evacuation maps (e.g. Figure 7) for the defined ignition areas, with assembly points in case of emergency and escape routes. Moreover, proposed fire protection zones were also mapped as an extra measure of fire protection followed by a list of management suggestions such as the placement of fire alarm and protection systems and cleaning of roads and properties.

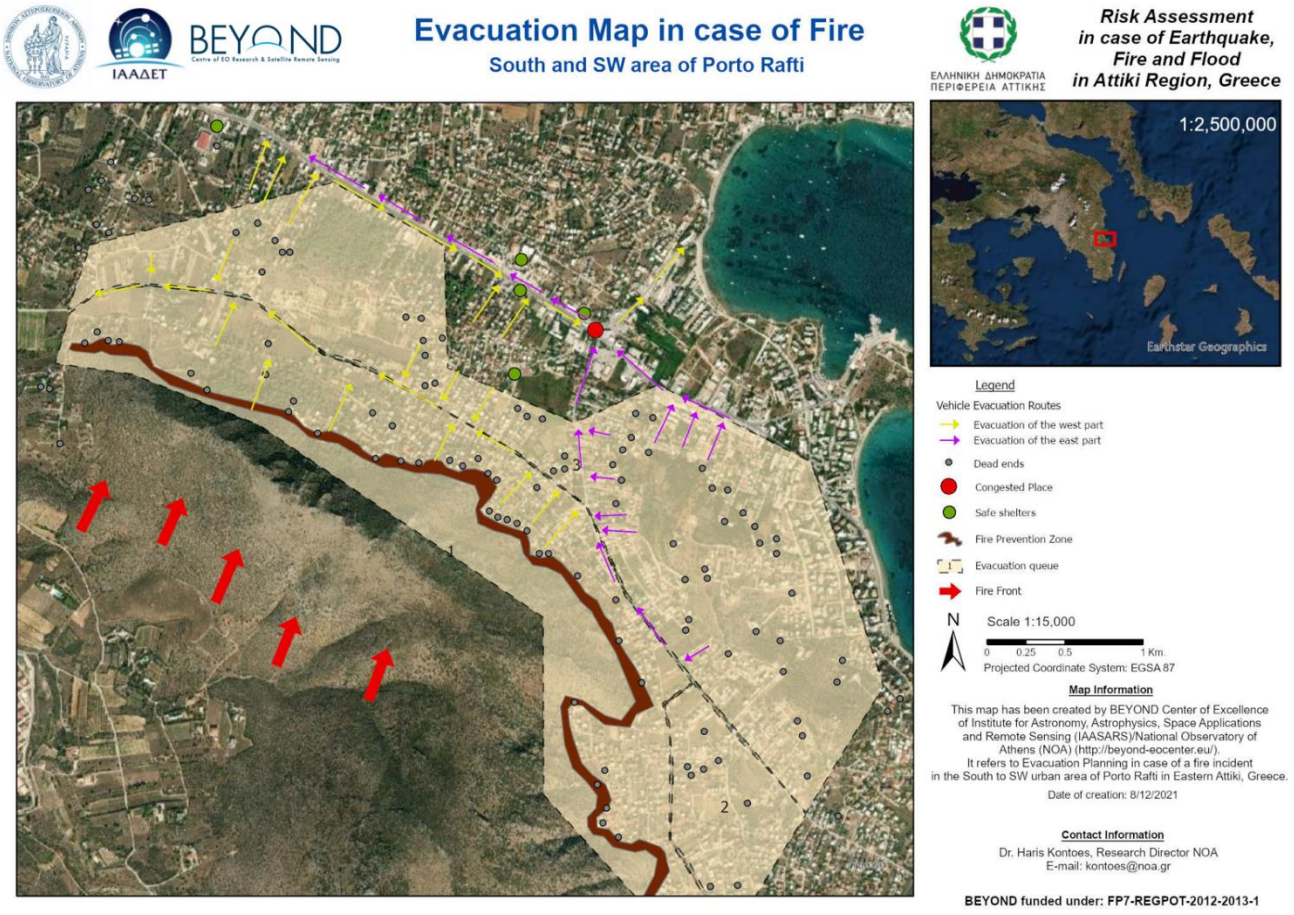

Figure 7. Example of evacuation map.

5. Conclusions

Demographic data, such as population density and age distribution per building block and the buildings' fire resistance characteristics yielded the foundation for a robust approach to estimate the fire vulnerability of each block. In addition, the combination of vulnerability with land values (as a level of economic exposure) composed a comprehensive socio-economic assessment of building-blocks in the event of fire. The combination of the above with the numerous simulations of fire spatio-temporal propagation scenarios led to the overall fire risk assessment of the study area. The two settlements of augmented fire risk, identified through the risk maps and distinguished during the field campaign are the eastern part of the settlement of Hamolia and the settlement of Vravrona (mainly south of Vravronos Avenue on the slopes of the hill). Both of these areas are in direct contact and within the forest, which penetrates into the properties and is adjacent to roofs, power cables, etc. The road network of the areas consists of poor quality roads with significant slopes and many dead ends. In addition, the roads are covered by pine needles, dry side grasses and many of them are used as parking lots. No, or poorly maintained, firefighting and fire protection systems were recorded in those areas. Finally, it is crucial that all civilians take the necessary precautions (e.g. cleaning their roofs and yards from foliage) and follow the instructions of the responsible actors in combination with the development of the appropriate fire preventive measures and fire protection infrastructure.

The presented methodology signifies the importance of coupling innovative technologies (ML modelling, geoinformatics, etc.) and contemporary data (e.g. EO data) with field-work, in service of human life and

infrastructure protection. It is an integrated approach of fire risk assessment and management at a very high-resolution level of analysis (building-block), that is produced for Greece and sets a precedent for the first time.

6. Acknowledgements

This research has been supported by using data and resources from the projects "Seismic, Fire & Flood Risk Assessment in Attica Region, Greece" funded by Attica Region and "CLIMPACT: Flagship Initiative for Climate Change and its Impact by the Hellenic Network of Agencies for Climate Impact Mitigation and Adaptation" funded by the Greek Government – Ministry of Development & Investments.

7. References

Apostolakis, A., Girtsou, S., Kontoes, C., Papoutsis, I., Tsoutsos, M. (2021). Implementation of a Random Forest Classifier to Examine Wildfire Predictive Modelling in Greece Using Diachronically Collected Fire Occurrence and Fire Mapping Data. In: Lokoč J. et al. (eds) MultiMedia Modeling, MMM 2021, Lecture Notes in Computer Science, Vol 12573, Springer, Cham. https://doi.org/10.1007/978-3-030-67835-7_27

Darvishi, L., Daryaei, M. G., Kouchi, A. H. S. (2020). Comparison of Statistical Modeling and AHP Methods in Fire Risk Assessment in Oak Forests of Iran. Fores. Res., Vol 9:229. doi: 10.35248/2168-9776.20.9.229

Erdin, C., Çağlar, M. (2021). Rural Fire Risk Assessment in GIS Environment Using Fuzzy Logic and the AHP Approaches. Polish Journal of Environmental Studies, Vol 30:6, pp 4971-4984. https://doi.org/10.15244/pjoes/136009

Gheshlaghi, H. A., Feizizadeh, B., Blaschke, Th. (2020). GIS-based forest fire risk mapping using the analytical network process and fuzzy logic. Journal of Environmental Planning and Management, Vol 63:3, pp 481-499. doi: 10.1080/09640568.2019.1594726

Girtsou, S., Apostolakis, A., Giannopoulos, G., Kontoes, Ch. (2021). A machine learning methodology for next day wildfire prediction. In IGARSS, 2021

González-Olabarria, J. R., Rodríguez, F. G., Fernández-Landa, A., Mola-Yudego, B. (2012). Mapping fire risk in the Model Forest of Urbión (Spain) based on airborne LiDAR measurements. Forest Ecology and Management, Vol 282, pp 49-156

Jafari-Goldarag, Y., Mohammadzadeh, A., Ardakani, A. (2016). Fire Risk Assessment Using Neural Network and Logistic Regression. Journal of the Indian Society of Remote Sensing, Vol 44, pp 885-894

Johnston, D. (2012). Quantifying the Fuel Load, Fuel Structure and Fire Behaviour of Forested Bogs and Blowdown. Master Thesis, Forestry Faculty of Forestry, University of Toronto, pp 149

Kalabokidis, K., Palaiologou, P., Finney, B. (2013). Fire Behavior Simulation in Mediterranean Forests Using the Minimum Travel Time Algorithm. Proceedings of 4th Fire Behavior and Fuels Conference, July 1 – 4, 2013, St. Petersburg, Russia Published by the International Association of Wildland Fire, Missoula, Montana, USA

Kanga, S., Sharma, L. K., Pandey, P. C., Nathawat, M. S. (2014). GIS Modelling Approach for Forest Fire Risk Assessment and Management. International Journal of Advancement in Remote Sensing, GIS and Geography, Vol 2, pp 30-44

Prodromou, M., Yfantidou, A., Theocharidis, C., Miltiadou, M., Danezis, C. (2020). Analysis of radar and thermal satellite data time-series for understanding the long-term impact of land surface temperature changes on forests. in: EGU General Assembly, Online, 4-8 May 2020. https://doi.org/10.5194/egusphere-egu2020-10582

Scott, J. H., Burgan, R. E. (2005). Standard fire behavior fuel models: a comprehensive set for use with Rothermel's surface fire spread model. Gen. Tech. Rep. RMRS-GTR-153. Fort Collins, CO: U.S. Department of Agriculture, Forest Service, Rocky Mountain Research Station, pp 72

Implementing a probabilistic fire modeling system at the pan-European level

Fermín Alcasena*[1]; Marcos Rodrigues[2]; Michele Salis[3]; Víctor Resco[4]; Palaiologos Palaiologou[5]; Alan Ager[6]; Adrián Jiménez-Ruano[2]; Liliana Del Giudice[3]; Pere Gelabert[1]; Àngel Cunill[4]; Cristina Vega[1]

[1]Department of Agricultural and Forest Engineering, University of Lleida, Spain, {fermin.alcasena, perejoan.gelabert, cristina.vega}@udl.cat
[2]Department of Geography, University of Zaragoza, Zaragoza, Spain, {rmarcos, jimenez}@unizar.es
[3]National Research Council of Italy, Institute of BioEconomy (CNR IBE), Sassari, Italy, {michele.salis, liliana.delgiudice}@ibe.cnr.it
[4]Department of Crop and Forest Sciences, University of Lleida, Lleida, Spain, {victor.resco, angel.cunill}@udl.cat
[5]Department of Forestry and Natural Environment Management, Agricultural University of Athens, Karpenisi, Greece, {palaiologou@aua.gr}
[6]Missoula Fire Sciences Laboratory, Rocky Mountain Research Station, USDA Forest Service, Missoula, USA, {alan.ager@usda.gov}

**Corresponding author*

Keywords

Fire modeling, burn probability, extreme fires, wildfire risk, Europe

Abstract

This research shows the potential use of cross-boundary fire modeling systems at the pan-European level. Despite the growing interest in building fire-resilient cultural landscapes, European Union (EU) level efforts have been reactive and focused on early detection, fire propagation monitoring, and perimeter mapping rather than predicting where the disaster can potentially occur to develop a comprehensive wildfire management strategy. We propose a modeling system that integrates wildfire occurrence models and observed fire-weather scenarios with a fire spread model to generate the probabilistic risk components, i.e., wildfire likelihood and hazard estimates. We selected four NUTS-2 level administrative division pilot sites from different fire-prone countries to implement the modeling system. The European-level pyromes were first delineated based on ecoregions and historical wildfire activity. We then generated human and lightning wildfire occurrence models to display the ignition points. Remote sensing products were used to derive fire spread modeling spatial input data such as surface fuels and canopy metrics. Global atmospheric products were used to calculate the fuel moisture content with physical models and determine the most frequent wind scenarios for each pyrome. We then used the Minimum Travel Time algorithm to model the fire footprints that correspond to 10,000 years or synthetic iterations. This modeling approach accounted for the spatial variation of ignition locations and the changing weather conditions across the different pyromes within each pilot site. The modeling results include the annual burn probability and fire intensity rasters, and fire perimeter vector outputs. Modeled burn patterns showed a close agreement with observed fire size distributions. We compared this modeling system with previous works to explain why stochastic fire modeling is essential to assess wildfire exposure of natural values at risk and human communities. Our results may help predict future catastrophic fires and provide quantitative estimates to identify high-priority management areas within vast regions. The probabilistic predictions generated in this work represent the foundation for developing long-term adaptation strategies to better coexist with fire. This work is also a demonstration of how this modeling system is replicable in any European country.

1. Introduction

In the European Union (EU), some 72,500 fires burned about 450,000 ha annually from 1990 to 2019, and Mediterranean countries alone (i.e., Portugal, Spain, France, Italy, and Greece) accounted for 86% of the total burned area (San-Miguel-Ayanz et al., 2021). Despite the high effectiveness in suppressing most ignitions, the few extreme fires escaping initial attack overwhelm firefighting efforts and burn vast areas (Rodrigues et al.,

2019a). These wildfire events show very high spread rates, exhibit extreme behavior and produce massive amounts of embers showered at long distances (Tedim et al., 2018). The 2007 fire season in Portugal and the Greek fires of 2021 (e.g., a single mega-fire burned 45,000 ha) are the most recent extreme wildfire manifestations (Ribeiro et al., 2020). Increasing fuel loads in cultural landscapes and more frequent severe droughts are the main factors explaining the increase of severe wildfire episodes in Mediterranean areas. As a result, the European Commission promoted the development of early detection and fire risk monitoring systems that facilitate a coordinated emergency response among the EU members. However, as the fire exclusion policy fails to protect socioeconomic and natural values at risk, wildfire managers request a paradigm shift towards a management-oriented, more preemptive strategy (Wunder et al., 2021).

The wildfire risk assessment integrates burn probability estimates with fire effects at different fire intensity levels (Finney, 2005). On the other hand, the wildfire exposure analysis describes burn probability and fire intensity but ignores potential effects. Fire intensity and burn probability show complex patterns across landscapes due to the interaction between fire spread direction, weather scenarios, topography, and heterogeneous fuels. Moreover, a given location will show a variable fire intensity depending on the changing interactions between the previously mentioned factors. Therefore, understanding wildfire exposure and spatial risk patterns is paramount for strategic management in extensive areas (Palaiologou et al., 2022).

Fire simulation modeling is essential to generate a large sample of fires, reduce uncertainty, and capture the stochastic variation in fire ignition location and changing weather conditions (Finney et al., 2011). Observed extreme fires are rare episodes, rearrange fuels over large areas, and represent a far too limited sample of the potential burn patterns. Modeling the fire footprints for thousands of years or iterations from a sufficiently large set of plausible scenarios allows for describing the magnitude of the next "black swan" event. In this line, recent fire modeling studies showed strong capabilities for predicting catastrophic wildfires (Ager et al., 2021).

In this study, we generated the spatial dataset of probabilistic wildfire risk components for three NUTS-2 level fire-prone administrative units from different EU countries. Our previous works implemented fire modeling systems in Mediterranean areas at regional and national levels (Alcasena et al., 2021; Palaiologou et al., 2021; Salis et al., 2021). We demonstrate in this work how probabilistic modeling systems can be replicated at the pan-European level using a harmonized set of input data. The outcomes showed a high potential to allocate management efforts efficiently at the continental level from science-based consistent fire exposure and risk metrics.

2. Material and methods

2.1. General framework

This modeling system parallels previous works conducted in the US (Finney et al., 2011; Short, 2017). The system includes a wildfire occurrence module to predict lightning and human ignitions across the landscape, and weather conditions are sampled from the most frequent observed scenarios during the wildfire season (Fig. 1). The landscape file contains spatial data for fuels and terrain. The outputs include the annual burn probability, flame length probabilities, and modeled fire perimeters for the NUTS-2 fire-prone selected sites.

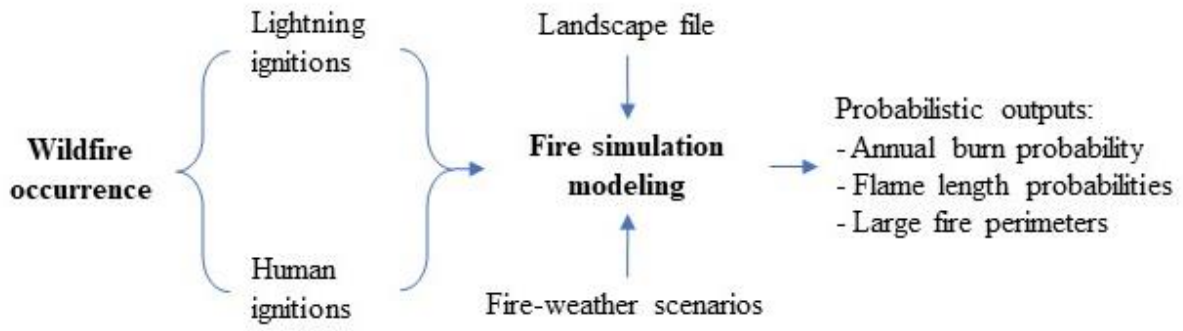

Figure 1: General flowchart of the modeling system.

2.2. Pyrome delineation

We used clustering techniques to delineate the pyromes within the EU ecoregions based on historic wildfire activity (i.e., annual burned area) and large fire weather typologies (Rodrigues et al., 2020). The ecoregions describe the areas with similar ecosystems resulting from edaphoclimatic conditions and dominant vegetation types. The burned area was calculated for a 100-km^2 grid using remote sensing global products. The pyromes were 2,500 to 5,000 km^2 cross-boundary blocks nested within the ecoregion map.

2.3. Pilot site selection

The pilot sites were selected from the NUTS-2 level EU administrative division considering the annually burned area. The burned areas were calculated using remote sensing data and available wildfire records from the last 25 years. We selected four administrative units from different fire-prone Mediterranean countries (Portugal, Spain, Italy, and Greece).

2.4. Input data

2.4.1. Wildfire occurrence

We generated different wildfire occurrence models to predict human and lightning ignition locations. The models were built with machine learning techniques using European-level geospatial data extracted from ignition point locations (Rodrigues and De la Riva, 2014). The number of available years varied between countries but were sufficient to enable us to extract a large data sample to build the models. The fire modeling input data were presented as 100 m resolution ignition probability grids for lightning and human ignitions.

2.4.2. Landscape file

The landscape (LCP) spatial data grids include terrain (aspect, elevation, slope), surface fuels, and canopy metrics. First, we associated a standard fuel model to each land cover class from the 2018 Corine land cover grid to generate the fuel model map (EEA, 2018; Scott and Burgan, 2005). Next, the canopy metrics were **Fire-weather scenarios**

We characterized the most frequent fire-weather scenarios for each pyrome. The winds (speed, direction, and probability) were derived from atmospheric circulation patterns (Rodrigues et al., 2019b), and the fuel moisture content was calculated at 500 m resolution for different percentile values (e.g., 50, 85, 90 and 97th percentiles) with physical models from global products (Resco de Dios et al., 2021).

2.5. Fire simulation modeling

We used the minimum travel time algorithm (MTT) to model fire spread (Finney, 2002). The MTT has been widely used in fire-prone areas to model fire footprints for thousands of synthetic years (Alcasena et al., 2021; Salis et al., 2021). First, the fire spread model was calibrated to replicate the observed fire size distributions. Then, we modeled 10,000 years or iterations at 100 m resolution. Lightning and human fires were separately modeled considering different fire-weather percentile thresholds and frequencies calculated from observed burned areas.

3. Expected results

The expected dataset of probabilistic fire risk components for the three fire-prone NUTS-2 pilot sites will contain the annual burn probability (number of times a pixel burns divided by the modeled years), flame length probability grids (burn probabilities for 20-bin 0.5 m flame length levels), and fire perimeters polygons.

4. References

Ager, A.A., Day, M.A., Alcasena, F.J., Evers, C.R., Short, K.C., Grenfell, I., 2021. Predicting Paradise: Modeling future wildfire disasters in the western US. Sci Total Environ 784, 147057.

Alcasena, F., Ager, A., Le Page, Y., Bessa, P., Loureiro, C., Oliveira, T., 2021. Assessing wildfire exposure to communities and protected areas in Portugal. Fire 4, 82.

EC, 2018. Tree cover density. Copernicus Emergency Management Service., in: JRC), E.C.J.R.C.E. (Ed.).

EEA, 2018. Corine Land Cover (CLC) 2018, Version 2020_20u1, 12 July 2013 ed.

Finney, M.A., 2002. Fire growth using minimum travel time methods. Can J For Res 32, 1420-1424.

Finney, M.A., 2005. The challenge of quantitative risk analysis for wildland fire. For Ecol Manag 211, 97-108.

Finney, M.A., McHugh, C.W., Grenfell, I.C., Riley, K.L., Short, K.C., 2011. A simulation of probabilistic wildfire risk components for the continental United States. Stoch Env Res Ris A 25, 973–1000.

Palaiologou, P., Kalabokidis, K., Ager, A.A., Galatsidas, S., Papalampros, L., Day, M.A., 2021. Spatial optimization and tradeoffs of alternative forest management scenarios in Macedonia, Greece, Forests, p. 697.

Palaiologou, P., Kalabokidis, K., Day, M., Ager, A., Galatsidas, S., Papalampros, L., 2022. Modelling fire behavior to assess community exposure in Europe: combining open data and geospatial analysis. International Journal of Geo-Information 11.

Potapov, P., Li, X., Hernandez-Serna, A., Tyukavina, A., Hansen, M.C., Kommareddy, A., Pickens, A., Turubanova, S., Tang, H., Silva, C.E., Armston, J., Dubayah, R., Blair, J.B., Hofton, M., 2021. Mapping global forest canopy height through integration of GEDI and Landsat data. Remote Sens Environ 253, 112165.

Resco de Dios, V., Cunill Camprubí, À., Pérez-Zanón, N., Peña, J.C., Martínez del Castillo, E., Rodrigues, M., Yao, Y., Yebra, M., Vega-García, C., Boer, M.M., 2021. Convergence in critical fuel moisture and fire weather thresholds associated with fire activity in the pyroregions of Mediterranean Europe. Sci Total Environ, 151462.

Ribeiro, L.M., Rodrigues, A., Lucas, D., Viegas, D.X., 2020. The impact on structures of the Pedrógão Grande Fire Complex in June 2017 (Portugal), Fire, p. 57.

Rodrigues, M., Alcasena, F., Vega-García, C., 2019a. Modeling initial attack success of wildfire suppression in Catalonia, Spain. Sci Total Environ 666, 915–927.

Rodrigues, M., De la Riva, J., 2014. An insight into machine-learning algorithms to model human-caused wildfire occurrence. Environ Modell Softw 57, 192-201.

Rodrigues, M., González-Hidalgo, J.C., Peña-Angulo, D., Juménez-Ruano, A., 2019b. Identifying wildfire-prone atmospheric circulation weather types on mainland Spain. Agric For Meteorol 265, 92-103.

Rodrigues, M., Trigo, R.M., Vega-García, C., Cardil, A., 2020. Identifying large fire weather typologies in the Iberian Peninsula. Agric For Meteorol 280, 107789.

Salis, M., Arca, B., Del Giudice, L., Palaiologou, P., Alcasena-Urdiroz, F., Ager, A., Fiori, M., Pellizzaro, G., Scarpa, C., Schirru, M., Ventura, A., Casula, M., Duce, P., 2021. Application of simulation modeling for wildfire exposure and transmission assessment in Sardinia, Italy. International Journal of Disaster Risk Reduction 58, 102189.

San-Miguel-Ayanz, J., Durrant, T., Boca, R., Maianti, P., Liberta, G., Artes-Vivancos, T., Oom, D., Branco, A., de Rigo, D., Ferrari, D., Pfeiffer, H., Grecchi, R., Nuijten, D., Onida, M., Loffler, P., 2021. Forest Fires in Europe, Middle East and North Africa 2020, Publications Office of the European Union, Luxemburg, p. 169.

Scott, J.H., Burgan, R.E., 2005. Standard fire behavior fuel models: a comprehensive set for use with Rothermel's surface fire spread model. USDA Forest Service, Rocky Mountain Research Station, Fort Collins, CO, p. 72.

Short, K.C., 2017. Spatial wildfire occurrence data for the United States, 1992-2015 [FPA_FOD_20170508]. (4th Edition). USDA Forest Service, Rocky Mountain Research Station.

Tedim, F., Leone, V., Amraoui, M., Bouillon, C., Coughlan, M.R., Delogu, G.M., Fernandes, P., Ferreira, C., McCaffrey, S., McGee, T.K., Parente, J., Paton, D., Pereira, M.G., Ribeiro, L.M., Viegas, D.X., Xanthopoulos, G., 2018. Defining extreme wildfire events: Difficulties, challenges, and impacts, Fire, p. 9.

Wunder, S., Calkin, D.E., Charlton, V., Feder, S., Martínez de Arano, I., Moore, P., Rodríguez y Silva, F., Tacconi, L., Vega-García, C., 2021. Resilient landscapes to prevent catastrophic forest fires: Socioeconomic insights towards a new paradigm. Forest Policy Econ 128, 102458.

Increasing potential wildfire energy flux from climate-driven mortality and fuel aridity

Matthew D. Hurteau*[1]; Marissa G. Goodwin[1]; Harold S.J. Zald[2]; Malcolm P. North[3]

[1]*Department of Biology, University of New Mexico, USA, {mhurteau, mjgoodwin}@unm.edu*
[2] *Pacific Northwest Research Station, US Forest Service, USA, {harold.zald@usda.gov}*
[3] *Pacific Southwest Research Station, US Forest Service, USA, {mnorth@ucdavis.edu}*

**Corresponding author*

Keywords

Climate change; coarse wood; fuel; energy

Abstract

Moisture stored in live and dead vegetation acts as a regulator on fire behaviour and area burned. Climate change is altering the distribution of live and dead fuels in forests through drought and insect-induced mortality and simultaneously making dead fuels more flammable because of decreasing fuel moisture. These system changes, both of which are driven by increasing temperature, have the potential to increase the heat flux from combustion, contributing to an increased risk of fires in affected areas becoming plume-dominated. In the southern Sierra Nevada of California and the Rocky Mountains in Colorado, drought and insect outbreaks have increased tree mortality rates, increasing the proportion of biomass that is in dead versus live fuel pools. We sought to determine the contribution that high rates of mortality could have on potential changes in energy release (energy release component and fire radiant energy) for mixed-conifer forests in the southern Sierra Nevada and lodgepole pine forests in the Colorado Rocky Mountains, the site of two large wildfires during the 2020 fire season. We found substantial increases in dead fuels and substantial decreases in fuel moisture during 2020, which increased the potential fire radiative energy. Our results demonstrate that climate-driven tree mortality and increasing temperatures that lead to lower fuel moisture are increasing the amount of energy stored in biomass that is available for combustion.

1. Introduction and Methods

1.1. Introduction

Fuel moisture content (FMC) helps regulate the amount of fuel available for combustion during wildfire (Brown and Davis 1973, Rothermel 1972). Climate warming is increasing atmospheric water demand and early season temperature increases are causing forest fuel FMC to decrease earlier in the fire season (Abatzoglou and Williams 2016, Westerling 2016). Ecosystem drying from increased warming is also increasing rates of tree mortality globally, which has the potential to increase the proportion of biomass within a forest that is more responsive to temperature effects on FMC (Allen et al. 2015, Goodwin et al. 2021).

Drought and insect-induced mortality events increase the total biomass in the dead fuel pool (Goodwin et al. 2020). The primary fuel for wildfire ignition and spread, fine fuels (litter, 1-, 10-, 100-hour), are available to burn for the duration of fire season in dry conifer forests (Rothermel 1972). While fire season length has increased with increasing temperature, it has not influenced the proportion of these quick drying fuels that are available to burn. However, large fuels (1000-hour +) dry out over longer time scales and are typically unavailable to burn during a sizable fraction of the fire season. Climate change may be increasing the availability of these larger fuels because of the increasing aridity that results from increasing temperature (Abatzoglou and Williams 2016).

Two large fire events during the 2020 fire season, the Creek Fire in the southern Sierra Nevada and the Cameron Peak Fire in the Colorado Rocky Mountains, burned through forests that had been heavily impacted by drought and insect-mortality (Meddens and Hicke 2014, Pile et al. 2019). The 153,738 ha Creek Fire began September 4, 2020 and burned through an area where severe drought from 2012-2016 had caused as much as 90% overstory tree mortality. The 84,443 ha Cameron Peak Fire began August 13, 2020 and burned through an area that had extensive mortality from a bark beetle outbreak that peaked from 2007-2009. Here we use forest inventory data

from these two fire footprints to estimate the potential increase in fire radiative energy (FRE) as a function of mortality, temperature, and fuel moisture.

1.2. Methods

We used US Forest Service Forest Inventory and Analysis (FIA) plot data to estimate increases in dead tree basal area before and after drought/insect mortality in the forest types in which these fires burned. Our selection procedure for plots that were measured both before and after disturbance and included the target tree species resulted in a sample size of 118 plots in the Sierra Nevada and 173 plots in the Rocky Mountains. We used changes in dead biomass following drought/insect mortality to calculate changes in fuel availability and FRE.

To quantify changes in 1000-hour FMC and ERC over the past three decades, we used daily maximum temperature, 1000-hour fuel moisture, and ERC data from GRIDMET (Abatzoglou 2013). We also used 1000-hour fuel moisture data for the southern Sierra Nevada from the Wildland Fire Assessment System (WFAS) and temperature data from the Remote Automatic Weather Station (RAWS) Climate Archive to develop monthly fuel moisture and temperature averages for 1998-2002, 2012-2016, and 2020. For the Colorado Rocky Mountains, we used 1000-hr and lodgepole pine (*Pinus contorta v. contorta)* fuel moisture data from WFAS and corresponding RAWS temperature data for 2006-2010 and 2016-2020. We converted FMC to water content to calculate FRE and biomass consumed using the equations outlined in Smith et al. (2013).

2. Results and Discussion

2.1. Results

Drought and insect mortality within these forest types caused a substantial increase in dead basal area when we compared pre/post-drought inventory data (Figure 1). Hotter temperatures during the 2020 fire season decreased 1000-hour fuel moisture and increased energy release component (ERC) over previous seasonal averages (Figure 2). In both the Creek Fire and Cameron Peak Fire footprints, the proportion of 1000-hour fuels available to burn because they fell below the 30% moisture threshold increased during the 2020 fire season, with approximately greater than 80% of the fuel available by the start of the Creek Fire in July in the Sierra Nevada. Similarly, data from the Cameron Peak Fire in the Colorado Rocky Mountains indicate that a 5% reduction in fuel moisture increases dead fuel availability by 7%.

2.2. Discussion

Our results indicate that as climate change interacts with agents of tree mortality such as insects and drought, the amount of dead tree biomass will substantially increase and hotter temperatures can make that biomass more available to burn. Globally, tree mortality is increasing, and this suggests that as ecosystems come into alignment with changing climatic conditions, we can expect an increase in the amount of dead fuel, which is more responsive to changes in temperature and precipitation (Allen et al. 2015, Goodwin et al. 2020). Understanding how this additional stored energy will influence fire behaviour and ecosystem effects are important areas of investigation that requires further investment.

3. References

Abatzoglou, JT, 2013. Development of gridded surface meteorological data for ecological applications and modelling. International Journal of Climatology 33:121-131.

Abatzoglou, JT, AP Williams. 2016. Impact of anthropogenic climate change on wildfire across western US forests. Proceedings of the National Academy of Sciences of the United States of America 113:11770-11775.

Allen, CD, DD Breshears, NG McDowell. 2015. On underestimation of global vulnerability to tree mortality and forest die-off from hotter drought in the Anthropocene. Ecosphere 6:1-55.

Brown, AA, KP Davis. 1973. Forest fire: Control and use (2nd ed). McGraw-Hill Book Company.

Goodwin, MJ, MP North, HSJ Zald, MD Hurteau. 2020. Changing climate reallocates the carbon debt of frequent-fire forests. Global Change Biology 26:6180-6189.

Goodwin, MJ, HSJ Zald, MP North, MD Hurteau. 2021. Climate-driven tree mortality and fuel aridity increase wildfire's potential heat flux. Geophysical Research Letters 48:e2021GL094954.

Meddens, AJH, JA Hicke. 2014. Spatial and temporal patterns of Landsat-based detection of tree mortality caused by a mountain pine beetle outbreak in Colorado, USA. Forest Ecology and Management 322:78-88.

Pile, LS, MD Meyer, R Rojas, O Roe, MT Smith. 2019. Drought impacts and compounding mortality on forest trees in the southern Sierra Nevada. Forests 10:237.

Rothermel, RC. 1972. A mathematical model for predicting fire spread in wildland fuels. USDA Forest Service, Intermountain Forest and Range Experiment Station.

Smith, AMS, WT Tinkham, DP Roy, L Boschettie, RL Kremens, SS Kumar, AM Sparks, MJ Falkowski. 2013. Quantification of fuel moisture effects on biomass consumed derived from fire radiate energy retrievals. Geophysical Research Letters 40:6298-6302

Westerling, AL. 2016. Increasing western US forest wildfire activity: sensitivity to changes in the timing of spring. Philosophical Transactions of the Royal Society B 371: 20150178.

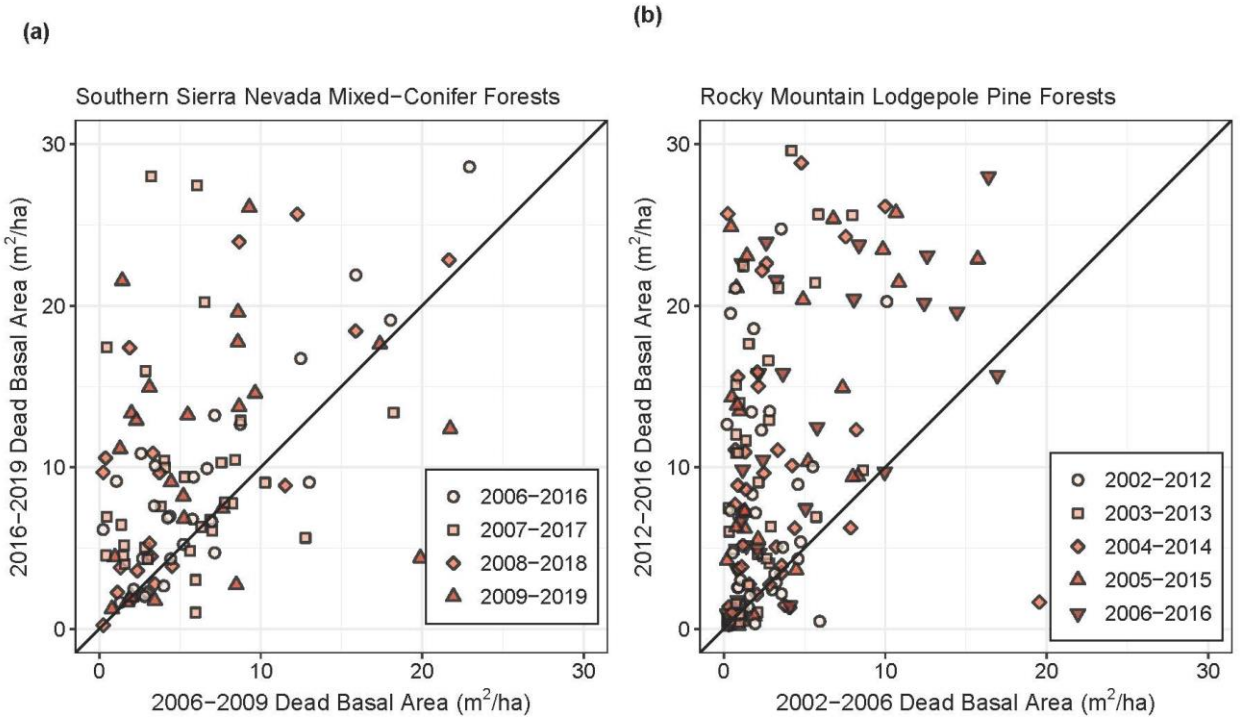

Figure 1: Increases in dead tree basal area (m^2 ha^{-1}) following disturbance events. The 1:1 trend line represents no change in dead tree basal area before and after the disturbance. Plots with the same color/symbol are grouped by 10-year measurement period. Points represent FIA plots measured: A.) Before and after the 2012-2016 California drought. Points represent mixed-conifer FIA plots in the southern Sierra Nevada. B.) Before and after peak Mountain Pine Beetle mortality in the Colorado Rocky Mountains (2007-2009). Points represent lodgepole -pine FIA plots in Colorado. Figure from Goodwin et al. (2021)

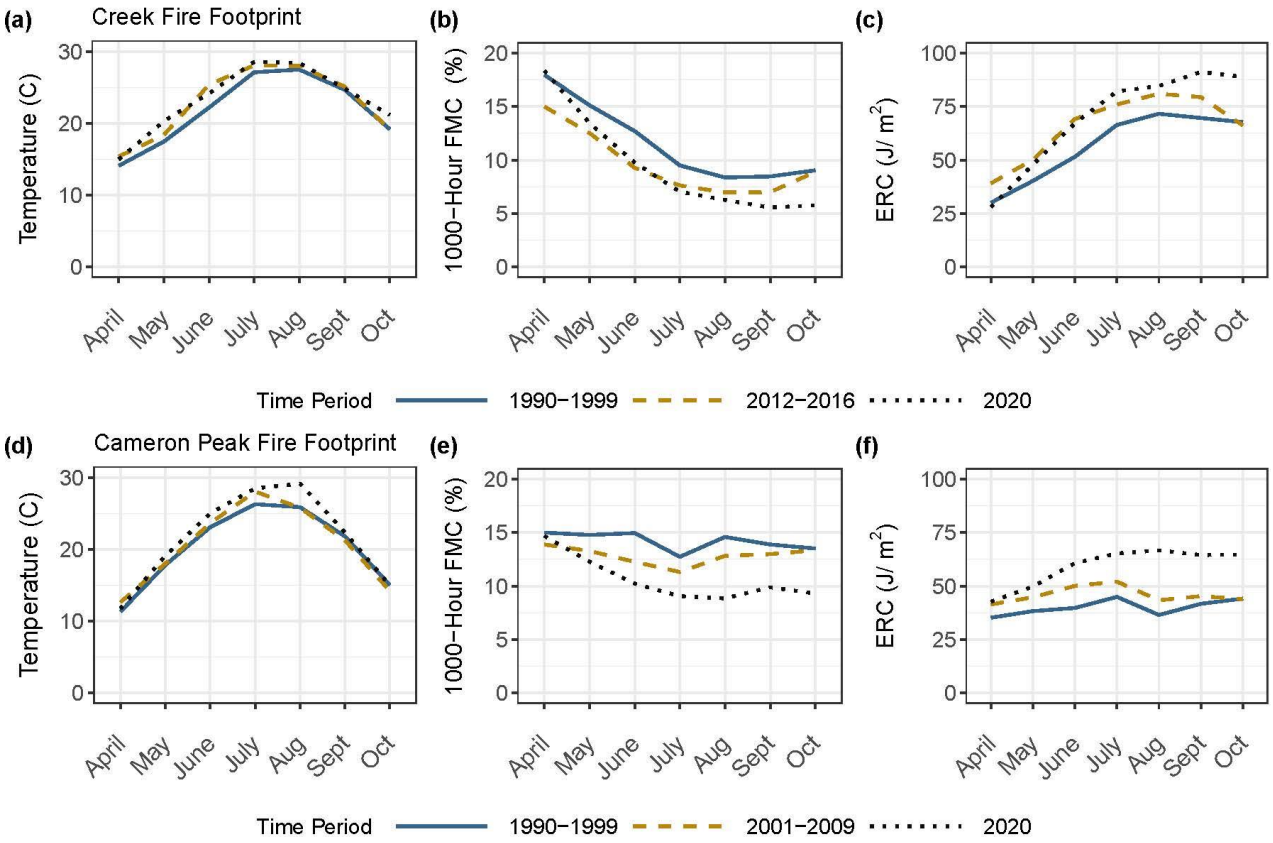

Figure 2: Average monthly temperature maximums (C), average 1000-hr fuel moisture content (FMC), and average energy release component (ERC) for the footprints of the Creek Fire (a-c) and Cameron Peak Fire (d-f) based on GRIDMET data. Time series for each site include 1990-1999, 2012-2016 or 2001-2009 (the respective drought periods for each site) and 2020. Figure from Goodwin et al. (2021).

Influence of tree species on surface fuel structure in Swedish forests

Frida Vermina Plathner*[1]; Johan Sjöström[1]; Anders Granström[2]

[1] Department of Fire Technology, RISE Research Institutes of Sweden, Box 857, 501 15 Borås, Sweden, {frida.vermina.plathner, johan.sjostrom}@ri.se
[2] Department of Forest Ecology and Management, Swedish University of Agricultural Sciences, 901 83, Umeå, Sweden, {anders.granstrom@slu.se}

**Corresponding author*

Keywords

Fuel depth; tree species; fuel bed; boreal; fuel load; BEHAVE

Abstract

The highly managed forests of Fennoscandia are dominated by coniferous (Scots pine and Norway spruce) stands with occasional inclusion of deciduous trees (Betula spp, Populus tremula, Quercus robur). Without active pre-commercial thinning, broadleaved deciduous trees would be more common and it is often assumed this would reduce flammability. Generally, there is little information on surface fuel structure in Fennoscandia and its relation to the dominant tree species. We therefore evaluated fuel characteristics in 153 plots from 82 mature, closed-canopy forest stands dominated by Pinus sylvestris (23), Picea abies (20), Quercus robur (20), Betula pendula (14), Populus tremula (5).

Stand properties (tree species and basal area) were measured on site and fuel bed composition was determined by destructive sampling of two 0.25 m2 plots per stand (species, fuel bed depth, weight, %-coverage). Dry weight per fuel category was measured in the laboratory. The measured parameters were used as input to the BEHAVE wildfire model, to assess relative fire behaviour for these different fuel assemblies.

The results show that the moss/litter layer (sometimes including lichens) was thicker and had a larger dry weight under pure pine stands compared to that under spruce stands. BEHAVE modelling suggested both fireline intensity and rate-of-spread to be substantially higher for pine stands. As for the broadleaved deciduous tree species, even a small inclusion in the coniferous stands severely affected the moss/litter layer. Leaf litter formed horizontal, multi-layered packs that replaced the porous structure and high surface-to-volume ratio of the moss/litter with a more compacted pure litter layer, resulting in reduced flammability.

The BEHAVE models presented here are available at https://www.ri.se/sites/default/files/2021-12/SwedishForestFuels_0.zip.

1. Introduction

Of the three main driving factors for wildfire spread and intensity – weather, terrain, and fuel – it is only the fuel that can be modified to reduce risk (Skowronski & Gallagher 2018). For tactical fire suppression it is also essential to characterize various biotopes from a fuel quality perspective, e.g. in the form of standardized fuel maps (Fernandes, 2009).

As for boreal regions it is often assumed that the fuel situation is relatively uniform, with a conifer canopy above moss/litter surface fuels. There are, however, surprisingly few quantitative analyses to illustrate this (but see Brown, 1974; McRae, 1979). The Fennoscandian boreal region, comprising Sweden, Finland and part of Norway is dominated by two conifer tree species, *Pinus sylvestris* and *Picea abies*, but there is also a high potential for broadleaved deciduous trees, primarily *Betula* spp and *Populus tremula*, which often outcompete the conifers unless culled by pre-commercial thinning (Andersson, 1993).

Experimental burns (Granström & Schimmel, 1998; Tanskanen, 2005) as well as empirical evidence from large fires (Nilsson et al., 2014; Granström, 2020) suggest that fires in Fennoscandia most often burn as surface fires, consuming mainly the moss/litter layer including lichens on the forest floor. Crown fires are rare and when they occur usually cover only minor parts of the burnt area.

Although the tree canopy seldom becomes involved in the fire directly (i.e. crowning), the stand type and structure will have an indirect effect through the litter composition and quantity, as well as by affecting both the vascular and non-vascular flora on the forest floor. For instance, leaf size affects both the litter characteristics and the extent of shadowing by the sub-canopy layer (Kauf et al., 2018; Dickinson et al., 2013). These stand-type to surface fuel relationships are not yet well established in Fennoscandia. Here we aim to relate stand properties to the surface fuel characteristics for five homogenous stand types and to provide indications of how deciduous tree inclusion in coniferous stands alter the surface fuel structure.

Wildfire modelling has several important uses, for instance as an operational tool during large incidents, and in preventive planning, to identify areas with an elevated hazard. In models such as BEHAVE, the fuel composition is accounted for using so called "fuel models". There are 53 predefined fuel models for the BEHAVE software, based on extensive field sampling of biotopes in the U.S. (Burgan & Rothemel, 1984; Scott & Burgan, 2005), which also form the basis for their national fuel map. None of these models apply *a priori* to boreal forests with moss/litter as the main fuel component. Thus, a secondary aim of this study was to build fuel models for wildfire modelling based on the quantitative fuel distributions we obtained.

2. Methods

2.1. Selected sites

Fuel characteristics were recorded for 153 sample plots under 82 mature stands of *Pinus sylvestris* (pine) (23), *Picea abies* (spruce) (20), *Betula pendula* (birch) (14), *Populus tremulus* (aspen) (5) and *Quercus robur* (oak) (20). Stands were sampled from the 55th to the 64th parallel for most species (Fig 1). Homogeneous oak stands, however, occur predominantly in the south-eastern Sweden and thus, geographically restricted the sampling.

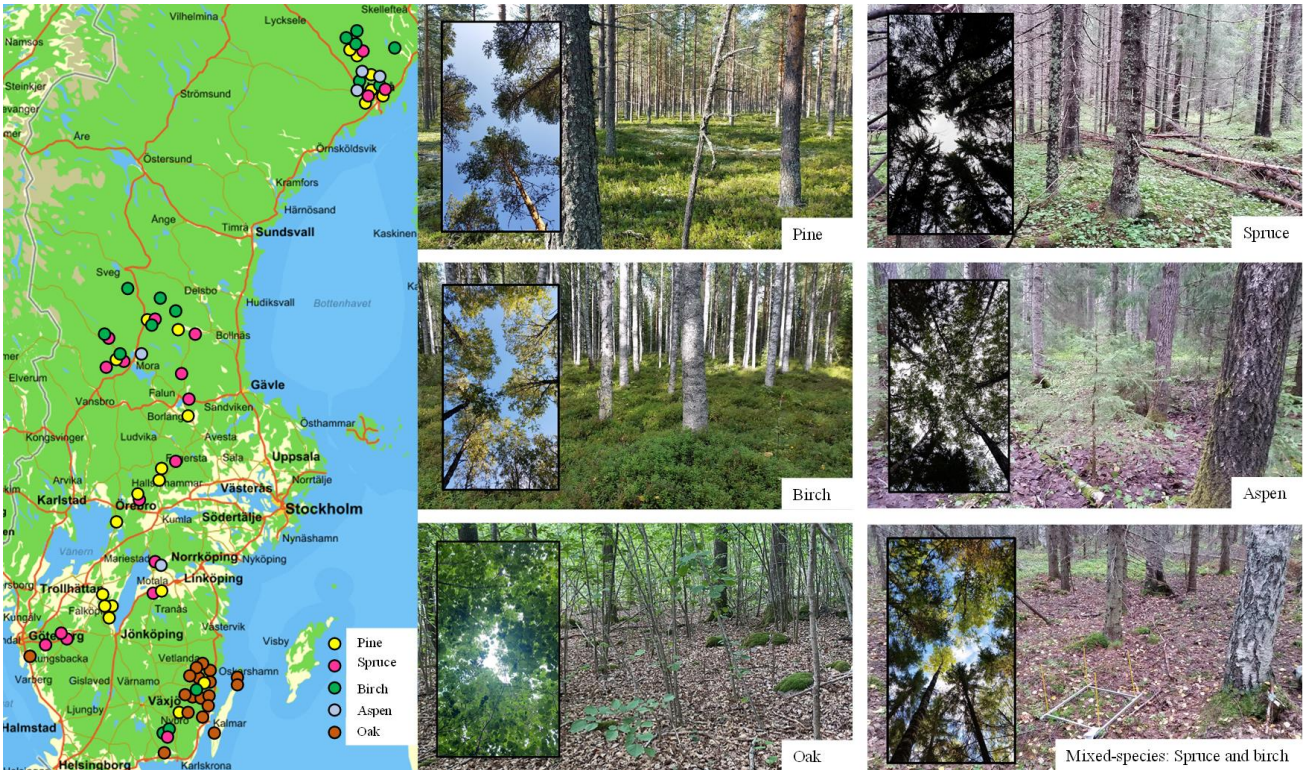

Figure 1. Geographical locations of stands and examples of selected stand types.

The study was delimited by selecting stands that were on dry or mesic soils according to the SLU site index estimation (Hägglund & Lundmark 1977), lacked large stone blocks, had a closed canopy with homogenous stand properties (except mixed stands) and were not in the first cycle of forest on abandoned farmland. Most Swedish forests are production forests where occasional thinning takes place. Thinning will add branch litter and impact surface fuels. We therefore omitted any stand with thinning operations less than 10 year before sampling.

2.2. Field data collection

Stand height and basal area of all tree species in each stand was determined using a relascope and hypsometer. Surface fuel was destructively sampled on two representative 0.25 m^2 plots in each stand (Fig 2). Cover of field layer species (mostly ericaceous shrubs e.g. *Vaccinium* spp or *Calluna vulgaris*) was visually assessed and their respective height measured. They were then cut at the top of the moss layer and brought to lab for obtaining dry weight after drying at 95℃. Similarly, the surface cover of moss/litter layer was assessed per species and litter type (leaves, needles etc.).

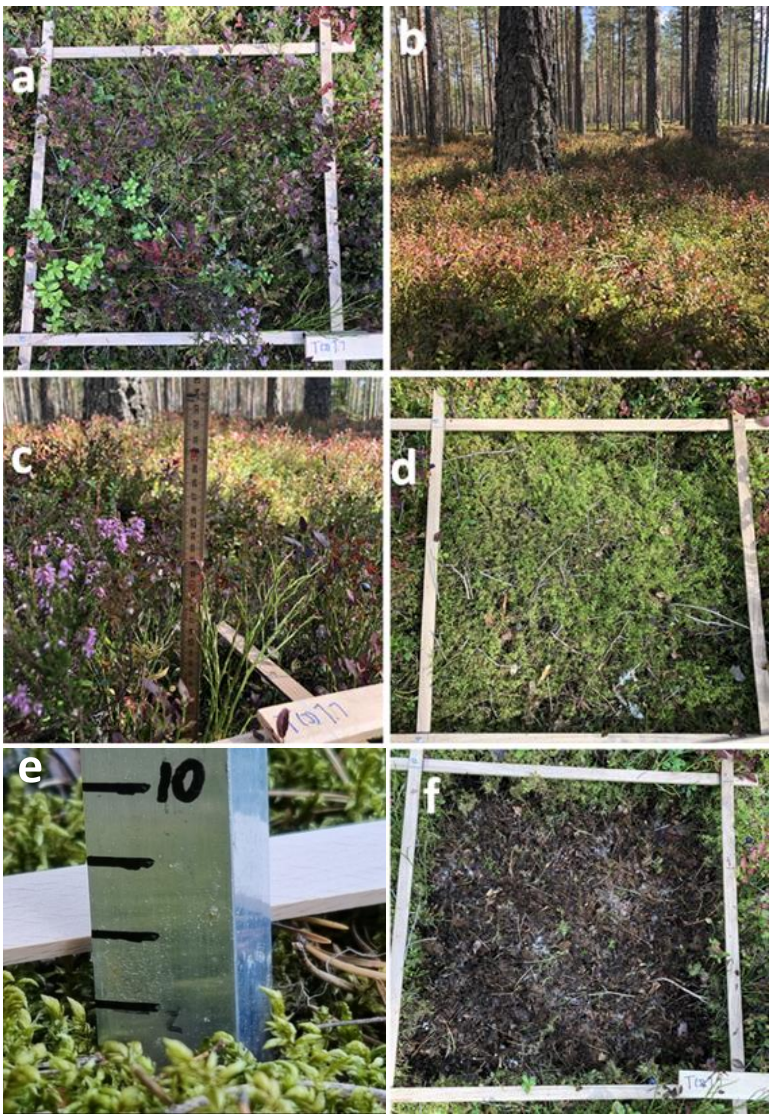

Figure 2. Progressive steps for quantifying the fuel structure: (a) Estimating surface cover of different shrub species; (b) Photographing stand characteristics and performing relascope measurements; (c) Defining shrub height and harvesting for dry weight determination; (d) Estimating surface cover of litter and moss species; (e) Defining depth of moss litter layer by several pressure probe measurements; (f) Harvesting moss/litter layer for dry weight specification and determining humus depth.

Surface fuel depth was determined using the penetration depth of a 2 cm sided L-shaped aluminium probe with a 15 N downward force. This is related to previous observations of what is typically consumed by flaming fire and defines the depth of the moss/litter-layer, a very loosely packed fuelbed of moss/lichen intermixed with tree litter (leaves, needles and other small litter) (Fig 2). The moss/litter layer was thereafter collected to the depth defined by the probe and brought to lab where easily defined litter (dead tree-branches, bark flakes and cones) were separated from the litter/moss-layer, sorted in different size classes (1-h, 10-h and 100-h) (Fosberg, 1971) and dry weight determined. The remaining *Vaccinium/Calluna* stems penetrating the moss layer were also

collected separately. Finally, the humus layer was cut through with a knife and its thickness measured with a ruler, down to the underlying mineral soil.

2.3. Modelling

Results from the field work were used to create five 'custom fuel models' for each fuel type in BEHAVE. BEHAVE divides fuels into different size classes, as well as into a 'live' or 'dead' class. Three modelling parameters; the dead fuel moisture of extinction (25%), the surface area to volume ratio (SA/V) of moss, and other 1-, 10- and 100-h fuels as well as their heat content were extracted from literature (Schimmel & Granström, 1997), Table 1. Finally, all input parameters were weighted based on their average fraction of the dry weight of the fuel package within each size class, Table 2.

Table 1. Fuel parameters taken from Schimmel and Granström (1997)

Modelling parameter	**SA/V** (cm^{-1})	**Heat content** (kJ/kg)
1-h (moss)	115	18700
1-h (needles, bark, dwarf shrub litter etc)	45	18700
10-h	3	18700
Ericaceous shrub	80	21000
Grass and herbs	115	18700

Table 2. Modelling parameters based on the field work

Modelling parameter	**Pine**	**Spruce**	**Birch**	**Aspen**	**Oak**
1-h fuel load (g/m^2)	963	643	396	342	406
10-h fuel load (g/m^2)	40	11	47	47	124
100-h fuel load (g/m^2)	0	3.3	1.3	0	15
Live herbaceous fuel load (g/m^2)	6	6	28	6	8
Live woody fuel load (g/m^2)	192	39	101	63	3
1-h fuel SA/V (cm^{-1})	108.2	107.4	93.8	97.8	97.4
Fuel bed depth (cm)	9.1	5.6	5.5	4.5	2.8
Live fuel heat content (kJ/kg)	20929	20693	20501	19327	19327

These fuel models were run in two different weather situations, (1) a "mild" weather/fuel moisture scenario: 11% m.c. of the dead fine fuel, 170% m.c. of live herbaceous fuel and 100% m.c. of the live woody fuel, and (2) a "severe" weather/fuel moisture scenario (8%, 120% and 90% m.c. respectively). For both scenarios we employed midflame wind speeds ranging between 0-3 m/s and no slope.

Rate of spread (RoS) (m/min), flame length (m) and fireline intensity (kW/m) were obtained for the different type of tree stands as an indication of relative fire hazard.

3. Results and discussion

3.1. Fuel characteristics

The conifer stands, together with birch, had the most developed field-layer (Fig 3). Lingonberry was far more common under pine stands compared to other tree-species. The forest floor in coniferous stands was almost completely covered with moss/lichen while under the deciduous trees the mosses were much reduced, apparently smothered by the leaf-litter. Live herbaceous plants on the other hand, were more abundant under the deciduous stands (Fig 3).

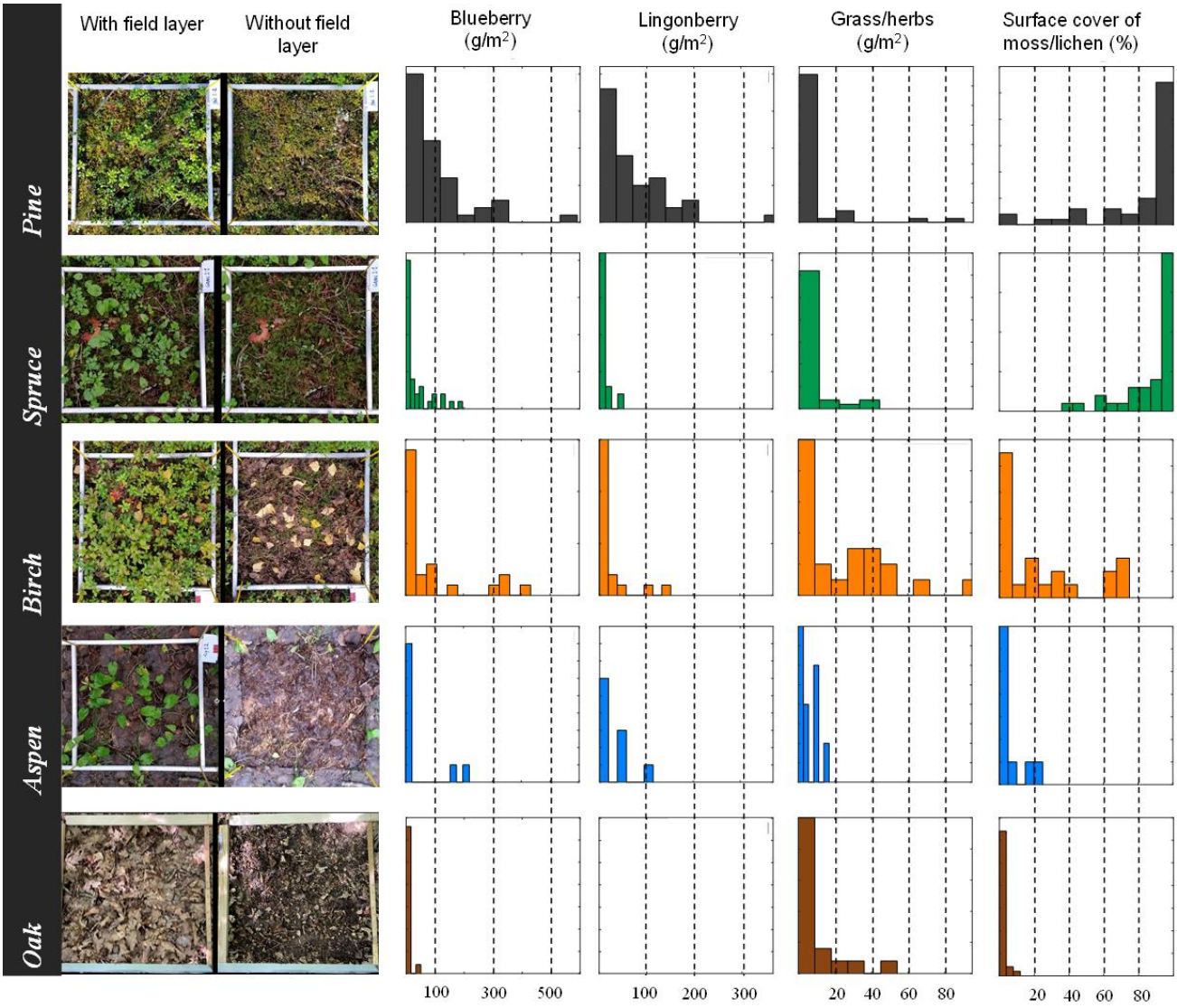

Figure 3. Distributions of measured field-layer fuel parameters and the estimated moss/litter layer surface cover for the five stand types. Photos exemplify the field layer for each stand type before and after removal of the field layer (pine, spruce, birch) and before and after removal of herbaceous species and the litter layer (aspen, oak).

Histograms for the moss/litter layer fuel bed depth and dry-weight show that most coniferous stands had deeper and more massive litter/moss-layers (mean values of 7.6 and 5.2 cm for pine and spruce stands respectively, as opposed to 2-3 cm for deciduous species) (Fig 4). The occurrence of other 1-h fuels and larger-sized litter varied less between stand types except that 10-h fuels were less common in spruce stands and more common in oak stands (Fig 4).

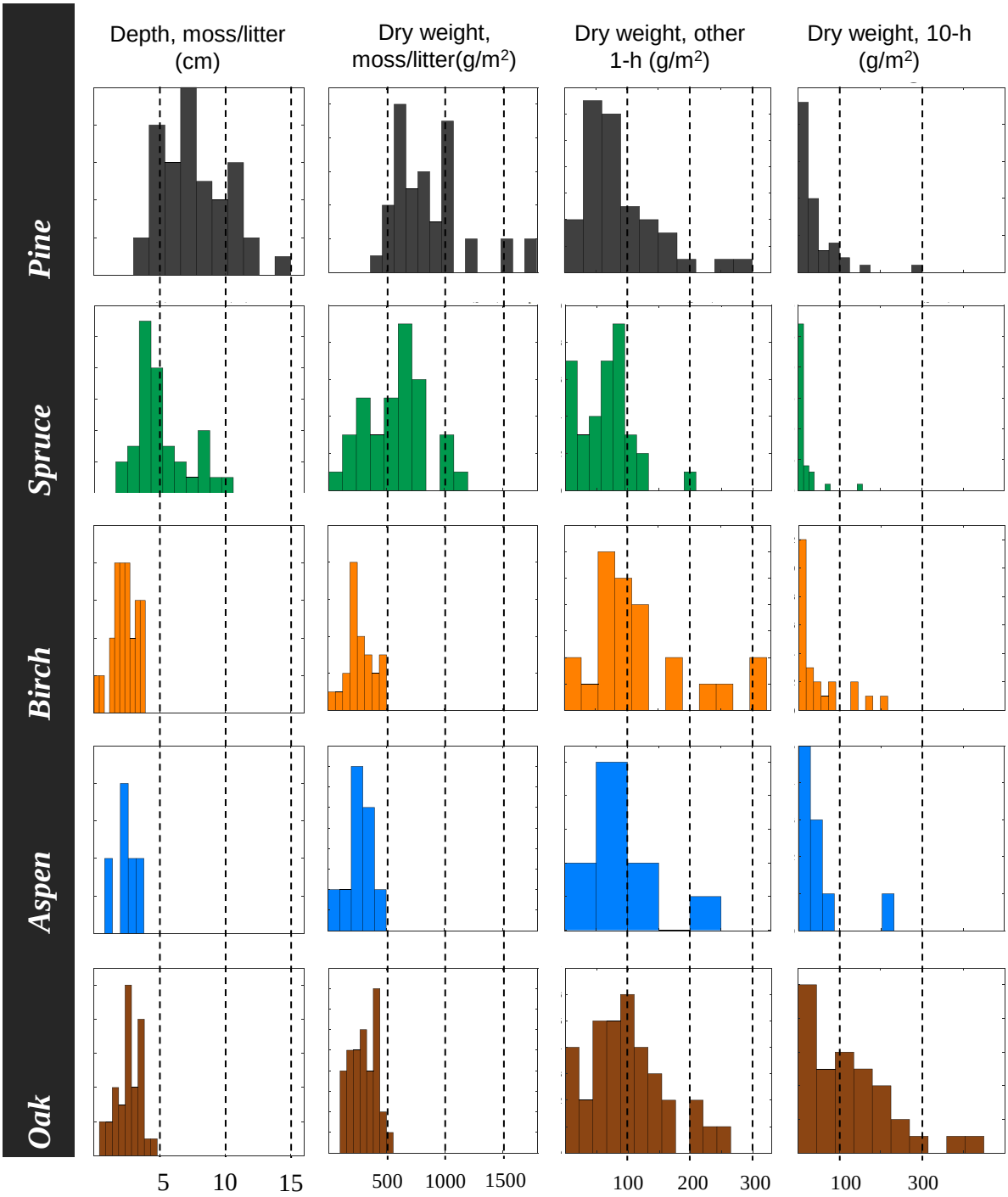

Figure 4. Distributions of measured moss/litter layer fuel parameters for the five stand types. Other 1-h fuels include e.g. easily separated dead tree-branches, twigs and bark flakes.

3.2. Mixed species stands

Sampling of mixed-species stands indicate that even a minor inclusion of broad-leaved trees affected the fuel bed substantially (Fig 5a). The surface cover of moss/lichens was also reduced monotonically with increasing deciduous component (Fig 5b). Moreover, the dry weight of the moss/litter layer decreased with the inclusion of just a few deciduous trees, from 750(±140) g/m^2 for pure conifer stands to an average of around 200 g/m^2 for stands with basal area of birch/aspen trees ≥4 m^2/ha (Fig 5c). No clear effect on the amount of Ericaceous shrubs was found (Fig 5d).

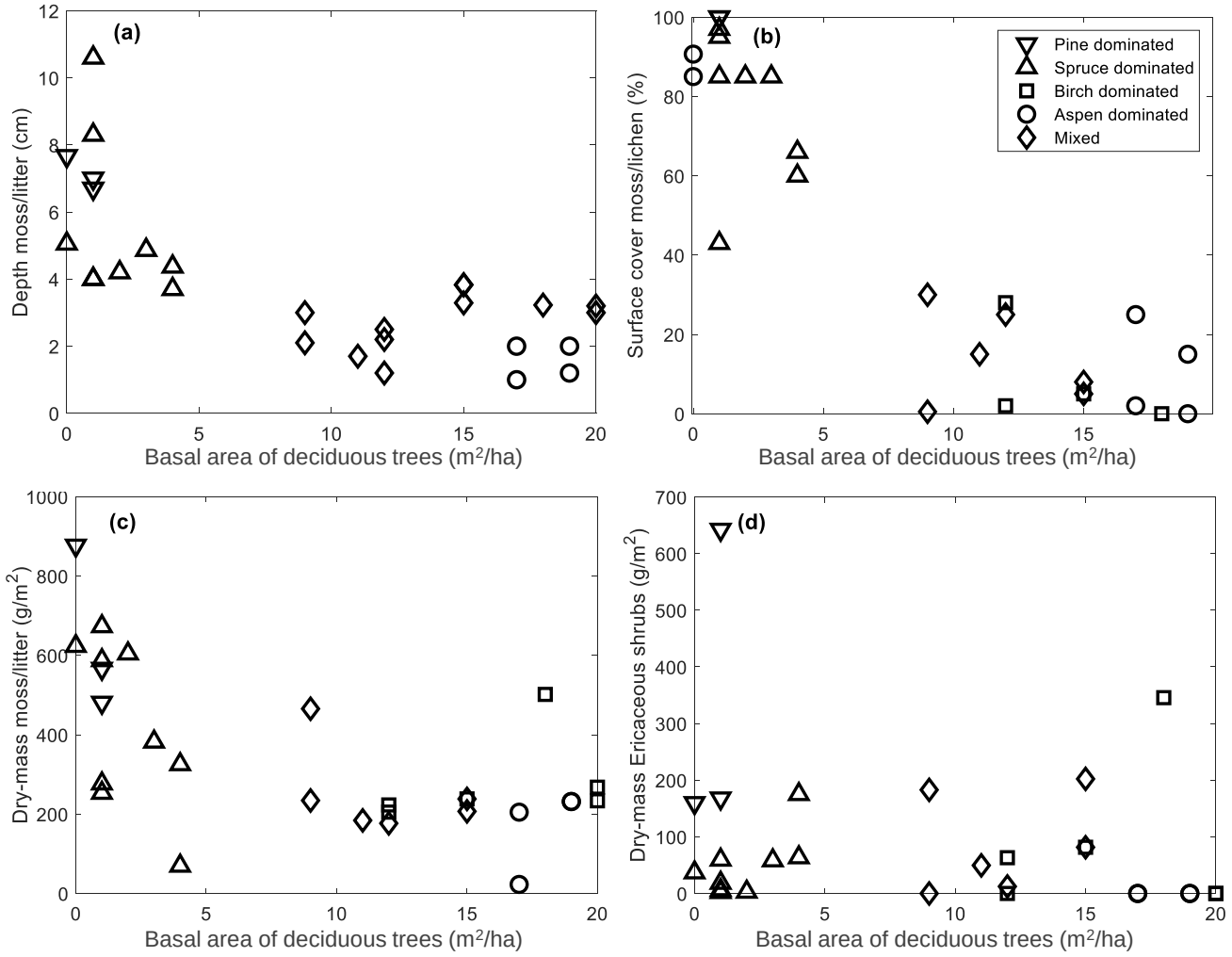

Figure 5. Effect of basal area of deciduous trees (i.e. number of trees in the relascope measurement) on (a) moss/litter depth; moss/lichen surface cover (b); moss/litter weight (c); Ericaceous shrubs weight (d).

3.3. Relative fire behaviour in BEHAVE

For both weather scenarios, pine generated the most severe fire behaviour, followed by spruce, birch, aspen and oak (Fig 6). This relationship holds regardless of wind speed and moisture content and can therefore be normalized to obtain relative behaviour (Fig 7). One can expect the RoS to increase by 50% and 200% when a surface fire enters a pine stand from a spruce or deciduous stand, respectively.

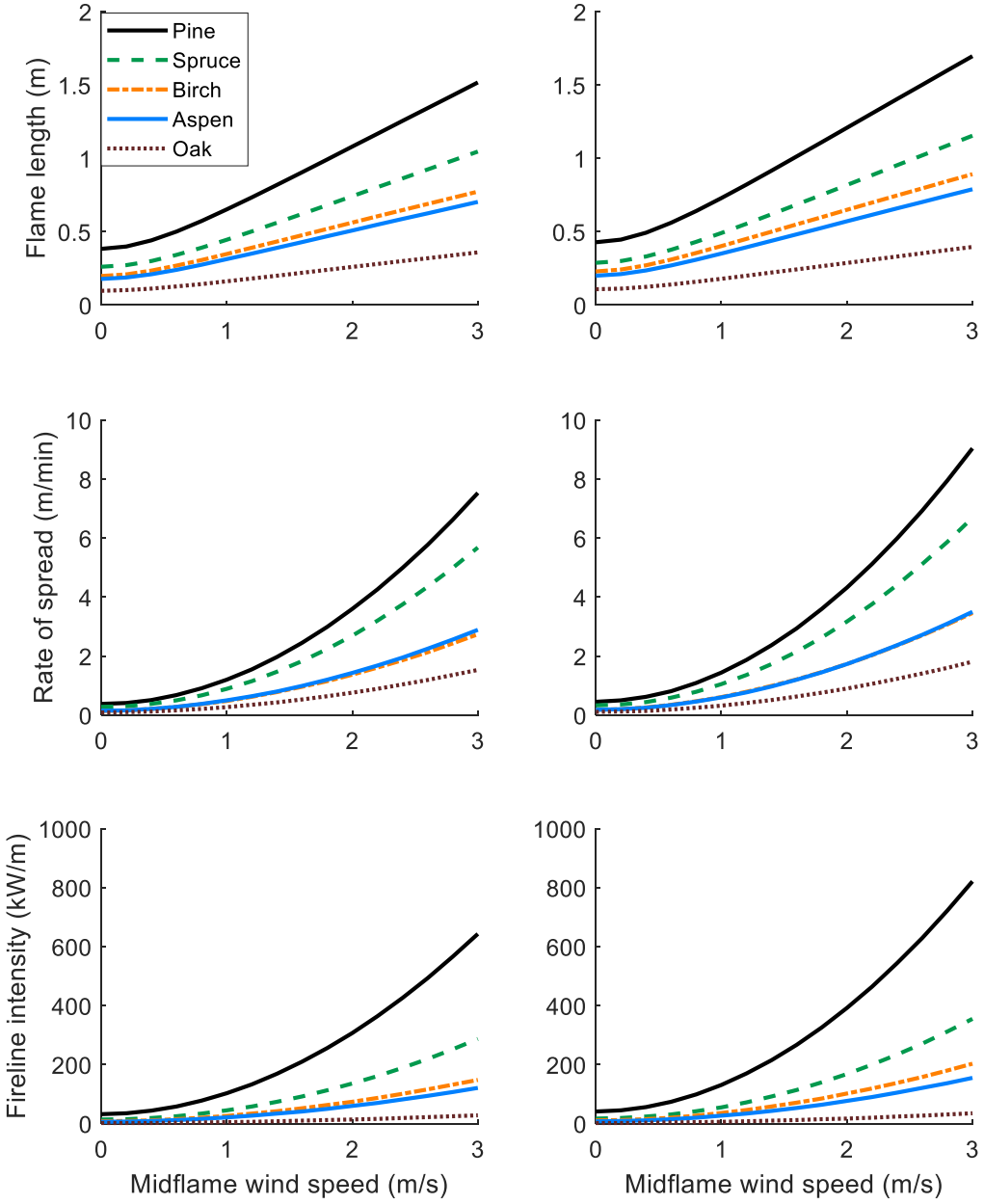

Figure 6. Modelling results for the two weather scenarios: Flame length, rate of spread and fireline intensity

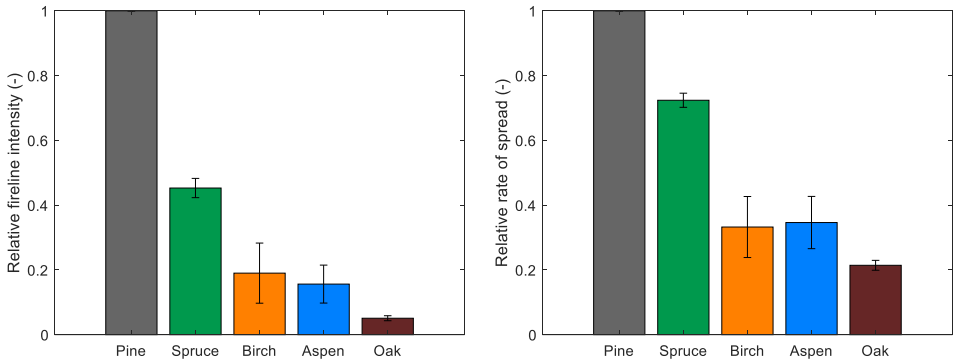

Figure 7. Relative fire behaviour between the different stand types

4. Discussion and conclusions

This study describes the surface fuel characteristics under typical north European closed-canopy stands of five different tree species. It shows that the flat leaves from birch and aspen can smother moss growth and thereby decrease the surface-layer depth and dry weight by more 50%. The porous structure and high surface-to-volume ratio of the moss/lichen under coniferous stands are transformed to a more compact layer of horizontally arranged leaf litter, which likely has a negative effect for both fire rate-of-spread and intensity.

Even a small portion of deciduous trees in a conifer stand has a significant effect on the forest floor fuel structure and as little as 20 % of deciduous trees in a coniferous stand makes the surface fuel structure essentially "leaf-dominated".

In the BEHAVE simulations we found a significant difference in intensity and rate-of-spread between pure pine and spruce stands, mainly due to differences in the depth of the moss/litter-layer. This is possibly related to the higher light availability in pine stands, but also due to structural differences in needles between the two conifers, pine having paired longer needles that add to the loose structure of the moss. According to the BEHAVE modelling this effect results in a 50% and 25% reduction of the fireline intensity and rate-of-spread, respectively, for both normal and extreme summer drought conditions. Relative to pine, broadleaved stands have the potential to reduce both fireline intensity and RoS in a progressing fire front by a factor of 1/5 and 1/3, respectively.

Models are available at https://www.ri.se/sites/default/files/2021-12/SwedishForestFuels_0.zip

5. Acknowledgements

This work was funded by the Swedish Civil Contingency Agency (MSB), under grant numbers 2337461 and 2021-14648.

6. References

Andersson, B. (1993). The influence of broad-leaved trees on survival, height and diameter of small Scots pine (Pinus sylvestris L.) trees (Report 36). Department of Silviculture, University of Agricultural Sciences: Umeå, Sweden.

Brown, J.K. (1974). Handbook for inventorying downed woody material (Report INT-16). US Department of Agriculture, Forest Service, Intermountain Forest and Range Experiment Station: Ogden, UT.

Burgan, R.E. & Rothermel, R.C. (1984). Behave: fire behavior prediction and fuel modeling system, fuel subsystem (Report INT-167). US Department of Agriculture, Forest Service, Intermountain Forest and Range Experiment Station: Ogden, UT.

Dickinson, M., Johnson, E., & Artiaga, R. (2013). Fire spread probabilities for experimental beds composed of mixedwood boreal forest fuels. Canadian Journal of Forest Research, 43(999), 321-330.

Fernandes, P. (2009). Combining forest structure data and fuel modelling to classify fire hazard in Portugal, Annals of Forest Science, 66(4), 415.

Fosberg, M.A. (1971). Climatological influence on moisture characteristics of dead fuel, theroretical analysis. Forest Science, 17(1), 64-72.

Granström, A. (2020). Brandsommaren 2018 – Vad hände och varför? (Report MSB1496). Swedish Civil Contingency Agency: Karlstad, Sweden.

Granström, A. & Schimmel, J. (1998). Assessment of the Canadian forest fire danger rating system for Swedish fuel conditions (Report P21–244/98). Räddningsverket: Karlstad, Sweden.

Hägglund, B. & Lundmark, J-E. (1977). Site index estimation by means of site properties. Scots pine and Norway spruce in Sweden. Studia Forestalia Suecica, 138. Swedish College of Forestry: Stockholm, Sweden.

Kauf, Z., Damsohn, W. & Fangmeier, A. (2018). Do relationships between leaf traits and fire behaviour of leaf litter beds persist in time? PLOS ONE 13:e0209780.

McRae, D.J., Alexander, M.E., & Stocks, B.J. (1979). Measurement and description of fuels and fire behavior on prescribed burns: a handbook (Report O-X-287). Department of the Environment, Canadian Forestry Service, Great Lakes Forest Research Centre: Sault Ste. Marie, ON.

Nilsson, B., Tyboni, M., Pettersson, A., Granström, A., & Olsson, H. (2014). Punktgittertolkning av brandområdet i Västmanland (Report 413 2014). Department of Forest Resource Management, University of Agricultural Sciences: Umeå, Sweden.

Schimmel, J. & Granström, A. (1997). Fuel succession and fire behavior in the Swedish boreal forest. Canadian Journal of Forest Research, 27, 1207–1216.

Scott, J.H. & Burgan, R.E. (2005). Standard fire behavior fuel models: a comprehensive set for use with Rothermel's surface fire spread model (Report RMRS-GTR-153). Rocky Mountain Research Station, Forest Service, US Department of Agriculture: Fort Collins, CO.

Skowronski, N. & Gallagher, M. (2018). Fuels Characterization Techniques. In S.L. Manzello (Ed.), Encyclopedia of Wildfires and Wildland-Urban Interface (WUI) Fires. (pp.1-10). Springer: Switzerland.

Tanskanen, H. Venäläinen, A. Puttonen, P. & Granström, A. (2005). Impact of stand structure on surface fire ignition potential in Picea abies and Pinus sylvestris forests in southern Finland. Canadian Journal of Forest Research, 35(2), 410–420.

Initial Assessment of Fire Response Time Between Different Category of Fire Station

Wan Nursheila Wan Jusoh*[1]; Ahmad Faiz Tharima[2]; Wahyunah Ghani[1]; Nur Kamarulzaman Malik Abdullah[2]; Hafizah Mohammad Lukman[2]; Sunthaar Visvasathan[2] ; Mohd Hafizi Shamsudin[1]; Nurul Zuhairah Mahmud Zuhudi[1]; Nurhayati Mohd Nur[1]

[1]Aerospace Section, Malaysian Institute of Aviation Technology, Universiti Kuala Lumpur, Jalan Jenderam Hulu, 43800 Dengkil, Selangor, Malaysia,
{wannursheila, wahyunah, mdhafizi, zuhairah,, nurhayatimn}@unikl.edu.my
[2]Planning and Research Division, Fire and Rescue Department of Malaysia, Lengkok Teknologi, Kawasan Perindustrian Enstek, 71760 Nilai, Negeri Sembilan, Malaysia,
{ahmad.faiz, kamarulzaman, hafizah_lukman, sunthaar}@bomba.gov.my

**Corresponding author*

Keywords

Fire, response time, fire station, ANOVA, demand zone,

Abstract

Response time is an important indicator in fire operations. A continuous assessment of the response time is crucial for monitoring the firefighter's performance level. An initial assessment of fire response time was conducted on selected category A–D fire stations throughout Malaysia from 2018 until 2020. In this study, the mean response time and distance travelled for the selected fire stations were calculated. To measure the fire station's performance, a 10-min standard response time was used as a benchmark. A one-way ANOVA is also applied to determine statistically any significant differences between the mean response time and mean distance travelled. Category C and D fire stations recorded high mean distances travelled and mean response times within the four categories. Most of the fire stations in this category travelled approximately 14 km with a mean response time of 18 mins. A new risk profiling for minimising fire risk stemming from constant development in these areas might be necessary for future improvement

1. Introduction

Fire departments are constantly working with numerous measurements to improve their performance and effectiveness. An essential indicator in the management of any emergency call is the response time. A prompt response by the fire department to the fire scene is crucial for minimising the damage a fire can cause to a structure and public safety. Suppressing a fire before the flashover will reduce the ability of the fire to grow and spread to adjacent areas. A large amount of heat and smoke is generated during flashover, reducing the chances of saving occupants.

The total response time calculation is the period calculated from the receipt of the alarm until the arrival of the first responder team at the scene to initiate action or control the incident. Nonetheless, response times are frequently determined with different measures by firefighters and reported to the public using different approaches (NFPA 1710,2010).

Claridge and Spearpoint (2013) studied the New Zealand Fire Service response time. The response time analysis was established based on topographic conditions and divided into urban and rural area approaches. The response time for the permanent fire station was 90% achievement at 7 min 30 sec while that for volunteer-based fire stations was 90% at 10 min. The United Kingdom regulations for fire are divided into four risk categories (A, B, C, and D), with response times of 5, 8, 10, and 20 min, respectively (Institution, 2019).

Several studies have investigated the response time for monitoring the service performance and capability of fire organisations. Nonetheless, the response requirements vary greatly between countries. The standard response time of the Fire and Rescue Department of Malaysia (FRDM) is 10 min without any classification of demand zone. There have been limited studies on FRDM response times in recent years, but only focused on specific districts or states (Sardi & Razak, 2019; Subramaniam et al., 2012; Tamat et al., 2014). This study

conducted an initial assessment of the response time across different fire station categories and states in Malaysia. In addition, the distribution of Malaysian fire station categories was identified and the mean response times compared using analysis of variance (ANOVA).

2. Methodology

2.1. Data Collection

The fire response time data from 2018 to 2020 were obtained from FRDM. The data were based on fire stations under four categories in five states (Johor, Kedah, Pahang, Selangor and Sarawak). Each state represents a specific Malaysian geographical region, namely East Coast, Northern, Southern, and West Coast Peninsular Malaysia, and East Malaysia. Each state represents a specific Malaysian geographical region. The initial data comprised of fire and rescue incidents, including special tasks assigned such as support to other government agencies on natural disaster relief and handling wildlife. For this study, only fire incidents data recorded from 2018 to 2020 are selected for further analysis.

The State Operations Management Centre or fire station control room involved in the fire incident logs the response time data in the Malaysian Emergency Response Services (MERS) 999 system. The control room duty officer records the interval directly in the MERS 999 system.

The FDRM emergency response time was calculated as follows:

Response time = time of arrival at the scene – time of the alarm is acknowledged at fire station control room

2.2. One-way Analysis of Variance (ANOVA)

Several organisations publish a considerable quantity of statistical data on fires via annual reports on fires and fire departments. Unfortunately, the actual firefighter performance or the relationship between firefighting operations are not included in most statistics (Sardqvist & Holmstedt, 2000).

This study used one-way ANOVA to determine statistically significant differences between the mean response time and mean distance travelled. The first stage of the ANOVA involved constructing a hypothesis statement set consisting of a null hypothesis (H0, all means are equal) and an alternative hypothesis (at least one mean is not equal).

3. Results and Discussion

3.1. Data Description

Currently, there are 324 fire stations in Malaysia and are categorised under A, B, C, D, and E. Nationwide, 52.8% (n = 171) of fire stations fall under category C, indicating moderate-fire risk locations, 25.3% (n = 82) of fire stations are category B, indicating high-risk locations, followed by 11.7% (38) under category A for very high-risk areas. Category E fire stations were excluded from this study as the category encompassed very few fire stations. Figure 1 illustrates the distribution of fire stations in Malaysia according to category.

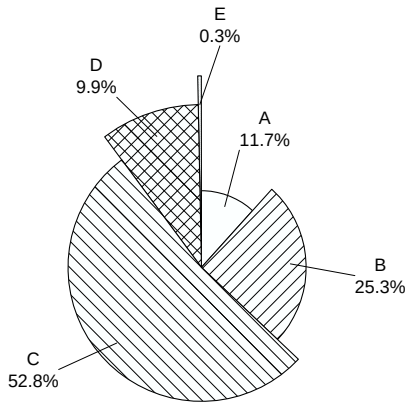

Figure 1. Fire station category in Malaysia

3.2. Fire Incidents of the Selected Stations

Total of 20 fire stations included in this study as listed in Table 1 with 10 233 fire incidents were recorded. Some of the recorded data yielded a negative value due to system error and were excluded from the analysis.

State	Fire Stations			
Johor	Larkin	Kota Tinggi	Pekan Nenas	Yong Peng
Kedah	Alor Setar	Kulim	Pokok Sena	Sungai Petani
Pahang	Bukit Angin	Kuantan	Ringlet	Taman Tas
Sarawak	Kanowit	Limbang	Petra Jaya	Tanjung Manis
Kuala Lumpur	Seputeh	Jalan Hang Tuah	Setapak	Sungai Besi

Table 1. The fire stations included in this study

Figure 2 illustrates the mean fire incidents for 2018–2020 according to category. The mean fire incidents were highest in category A locations, which recorded 50% more fire incidents compared to the other categories. In 2020, there were 15 393 reported fire incidents nationwide from March 18 to August 31. During the same period in 2018 and 2019, 19 165 and 23 094 fire incidents were reported, respectively (Mohammad, 2020). Similar trends were observed for the data from the selected fire stations, where reported cases decreased in 2020. This finding could be related to the issuance of the first Movement Control Order (MCO) beginning 18 March 2020 in response to the COVID-19 pandemic in the country. Over the three consecutive years, the fire incidents reported for all categories was highest for 2019. In the next section, fire station comparisons within a similar category yielded an excellent basis for assessing the response time.

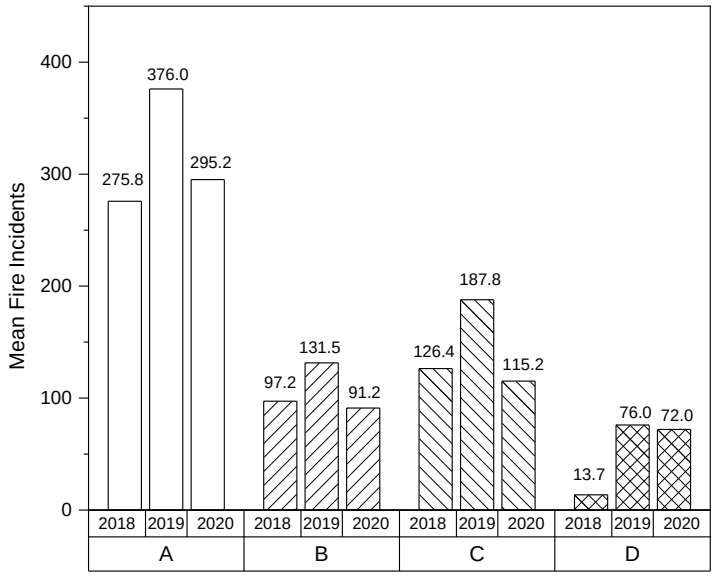

Figure 2. Mean fire incidents reported from 2018 to 2020 for selected fire station for all category

3.3. Mean Response Time from 2018 to 2020

Figure 3 demonstrates that most of the selected fire stations recorded a mean response time of > 10 min between 2018 and 2020. It is worth noting that the mean response time for category A, C, and D fire stations improved, while category B fire stations maintained the same mean response time of 14 min. In 2020, category A and D fire stations met the 10-min standard response time with mean response times of 7.96 and 8.90 min, respectively. The MCO had reduced traffic density significantly, which aided the reduction of the rescue team's delay in arriving at fire incidents as compared to that in 2019, as supported by Chen et al. (2021).

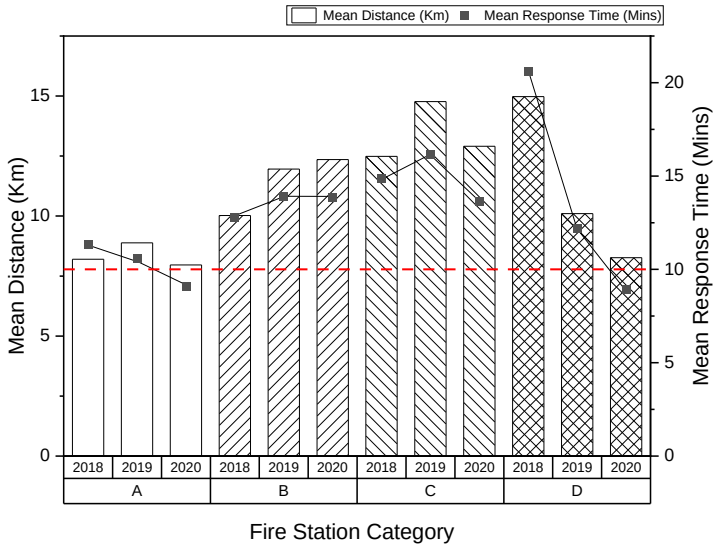

Figure 3. Mean distances travelled against mean response times by fire stations category

The shorter mean distance travelled for category D fire stations could be an important factor for the significant reduction in response time in 2020. Yung (2008), Tómasson et al. (2008), and Claridge and Spearpoint (2013) reported that one of the main factors influencing the response time was the distance travelled, where the city centre recorded average speeds of approximately 20 km/h for a short distance compared to 70 km/h on state highways for longer distances.

This main factor was proven with Pearson's correlation value between response time and distance travelled based on fire station category.

Table 2. Summary of Pearson's correlation analysis

Station category	**A**	**B**	**C**	**D**
Pearson correlation	0.39	0.89	0.76	0.86

Table 2 demonstrates exhibits a strong positive correlation between response time and distance travelled for category B, C, and D fire stations where the values lies between 0.5 and 1. The highest Pearson correlation value was for category B with 0.899, followed by 0.859 and 0.764 for category D and C. This positive value indicates that the response time may increase with distance. Category A fire stations recorded a medium positive correlation (0.387), as the value was < 0.5.

Figure 4 depicts the mean distances travelled and mean response times of the category A fire stations. The highest mean distance travelled and mean response time was recorded for the fire station in Kuantan, a city on the Peninsular Malaysia east coast. East Coast cities are moderately less dense than cities in west or south Peninsular Malaysia. In 2019, Kuantan firefighters travelled a mean 11.76 km to fire incident locations. Meanwhile, from 2018 to 2020, the Kuantan fire station recorded a mean distance travelled of 10.72 km with a mean response time of 13.9 min. The Larkin fire station recorded improved mean response times each year, with a response time of 7.45 min in 2020. The clearer traffic in 2020 could be one of the primary factors for the better response time by the category A fire stations.

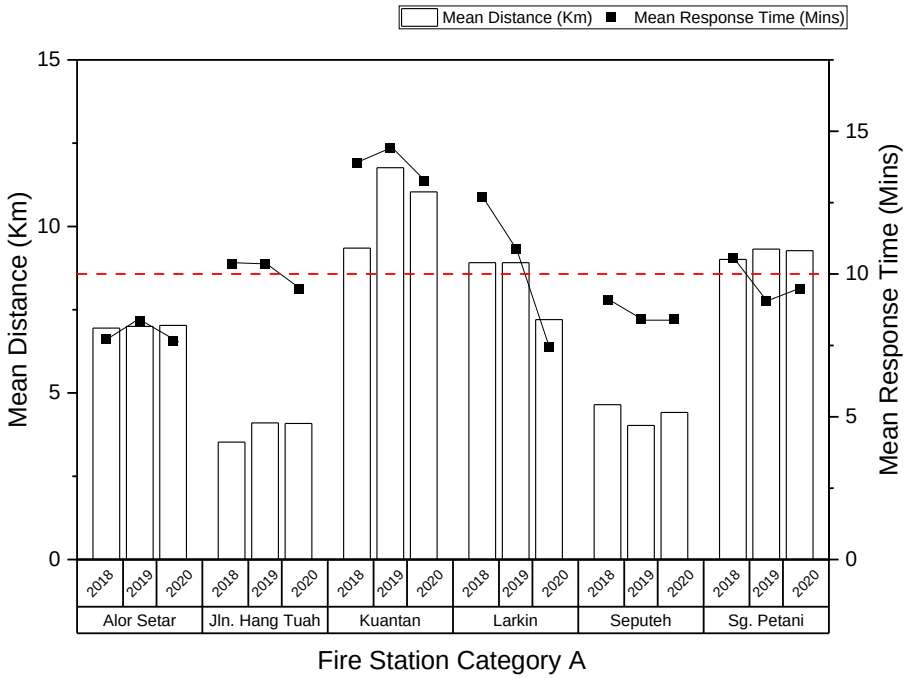

Figure 4. The mean distance and mean response time for category A fire stations

The high response time of the Kuantan fire station might be due to its bigger coverage, as the overall mean distance travelled was 10.88 km. The population and industry distribution in this area are quite distant from each other. A New York study reported that travel time increased linearly with the square root of the distance travelled for short distances and proportionally with the distance travelled for long distances (Kolesar & Walker, 1974).

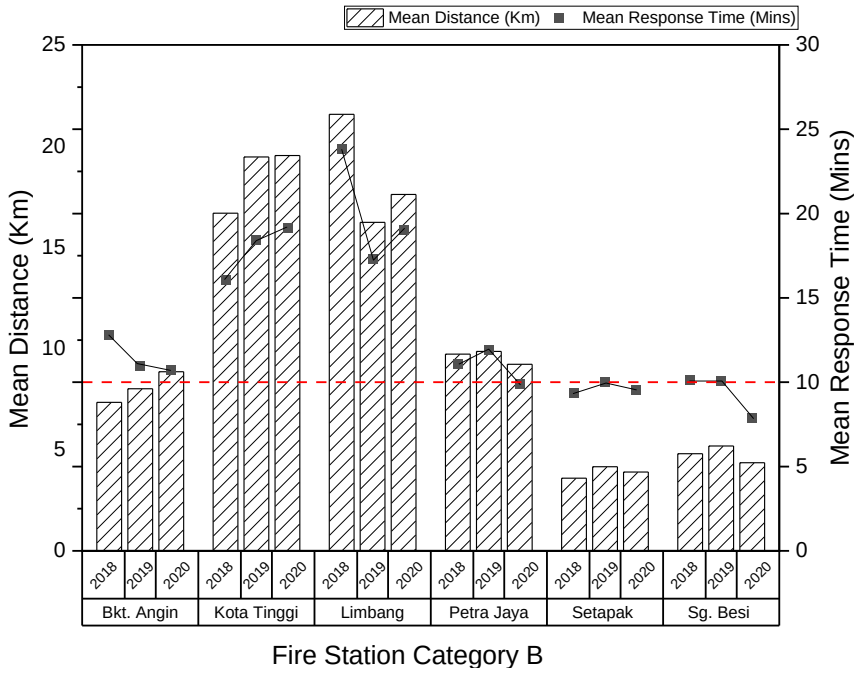

Figure 5. Mean distances travelled and mean response times recorded by category B fire stations

Figure 5 demonstrates that under category B, the Kota Tinggi and Limbang fire stations recorded the highest mean distances travelled and mean response times from 2018 to 2020. The mean distance travelled and mean response times of the Kota Tinggi and Limbang fire stations were 18.6 km and 17.9 mins and 18.5 km and 20.0 mins, respectively. The two fire stations also recorded a slight increment in mean response times for 2019 and

2020. The Setapak and Sungai Besi fire stations recorded consistent mean response times. These two stations experience slower traffic movement during peak hours (to and from the office).

Category C is the largest category of Malaysian fire stations. Figure 6 demonstrates that all fire station except for Kulim fire station did not meet the standard response times in 2019 and 2020. Kulim is a district in Kedah, a northern Peninsular Malaysian state known for its growing industrial area. Kulim firefighters travelled a mean distance of only 8.6 km for three years compared to the 20.1 km by Kanowit firefighters. Kanowit is a Sarawak district with a less dense population and development than other fire stations. This could contribute to larger coverage of Kanowit fire station compare to other areas. The Taman Tas, Yong Peng, and Pekan Nenas fire stations recorded mean distances travelled of < 17 km and decreased mean response times in 2020. The lower traffic density during the MCO could be the main reason for the reduced response times.

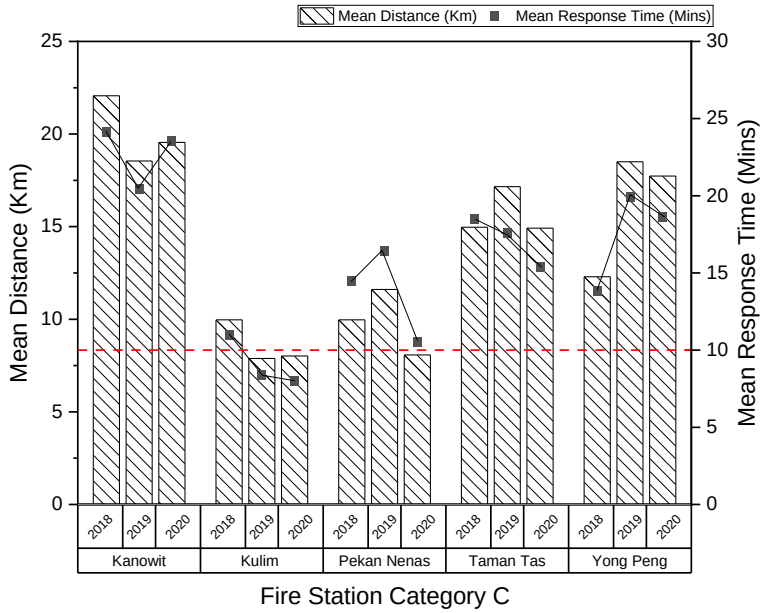

Figure 6. Mean distances travelled and mean response times recorded by category C fire stations

The areas in which category D fire stations are located are considered semi-rural. The low density of these areas results in the fire stations servicing a greater coverage area, as illustrated in Figure 7 for the Ringlet and Tanjung Manis fire stations. Both fire stations recorded a mean distance travelled of approximately 14 km and a mean response time of 18 min.

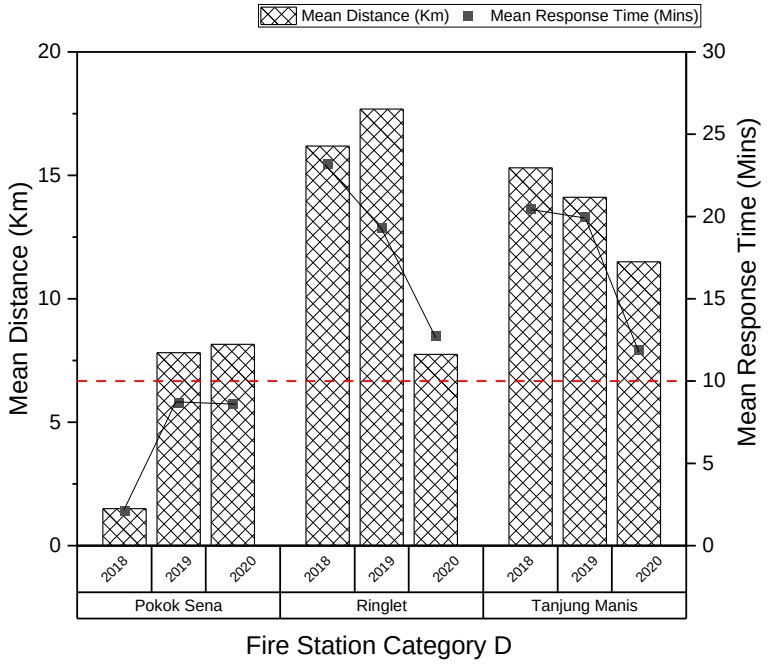

Figure 7. Mean distances travelled and mean response times recorded by category D fire stations

Based on the study conducted by (Tharima, 2010), most fire incidents that happened in semi-rural or rural areas are mainly on houses made of wood. This flammable building material is possible to create a flashover of less than 10 mins. As reported by Zikmund (2001), the flashover can occur from three to eight minutes while Wrack (2010) claims that flashover incidents happen from four to six minutes.

4. Conclusion

The initial assessment demonstrated that, regardless of category, most of the fire station response times recorded an improvement trend from 2018 to 2020. Besides, more than half of the category C and D fire stations recorded shorter mean response times in 2019, whereas fire stations in the other categories demonstrated no significant changes.

The distance travelled demonstrated a directly proportional relationship with the response time, as illustrated by the graphs that supported the Pearson correlations of > 0.7 for category B, C, and D. The findings indicated that new fire station developments are inevitable for reducing the fire incident response time in Malaysia. Developing new fire stations in strategic locations based on the risk profiling schedule and analysing urban planning, particularly in semi-urban areas, would ensure a fast response from firefighters.

5. References

Chen, Y., Qin, R., Zhang, G., & Albanwan, H. (2021). Spatial temporal analysis of traffic patterns during the covid-19 epidemic by vehicle detection using planet remote-sensing satellite images. Remote Sensing, 13(2), 1–18. https://doi.org/10.3390/rs13020208

Claridge, E., & Spearpoint, M. (2013). New Zealand fire service response times to structure fires. Procedia Engineering, 62, 1063–1072. https://doi.org/10.1016/j.proeng.2013.08.162

Institution, B. S. (2019). BS 7974:2019 Application of Fire Safety Engineering Principles to the Design of Buildings - Code of Practice. In British Standards Institution (Vol. 1, Issue 1).

Kolesar, P., & Walker, W. (1974). Measuring the Travel Characteristics of New York City's Fire Companies (p. 47).

Mohammad, N. H. (2020). Firefighters dealt with more fires in first MCO. The Star, 1–8. https://www.thestar.com.my/news/nation/2020/12/12/firefighters-deal-with-more-fires-in-first-mco

NFPA1710. (2010). Standard for the Organization and Deployment of Fire Suppression Operations , Emergency Medical Operations , and Special Operations to the Public by Career Fire Departments 2010 Edition D84FF70F-EFFC-49AE-B078-BDDCCBF519A1.

Sardi, M. F., & Razak, K. A. (2019). Assessment of effectiveness of emergency response time during landslide event in Malaysia. ASM Science Journal, 12. https://doi.org/10.32802/ASMSCJ.2019.360

Subramaniam, C., Ali, H., & Shamsudin, F. M. (2012). Initial emergency response performance of fire fighters in Malaysia. International Journal of Public Sector Management, 25(1), 64–73. https://doi.org/10.1108/09513551211200294

Tamat, A., Pawanchik, S., Kamil, A. A., Halmi, M. F., Lateh, H. H., Hasan, M. Z., Ferdushi, K. F., & Hossain, M. K. (2014). Analysis of Variation in ToT and Response in Penang. In Journal of Environmental Science and Technology (Vol. 7, Issue 4, pp. 200–208).

Tharima, A. F. (2010). Determination The Cause Of Structural Fire By Electrical Failure In Dwelling. University Malaysia Pahang.

Tómasson, B., Bengtsson, J., Thorsteinsson, D., & Karlsson, B. (2008). A probabilistic risk analysis methodology for high-rise buildings taking into account fire department intervention time. Fire Safety Science, January 2009, 957–968. https://doi.org/10.3801/IAFSS.FSS.9-957

Wrack, M. (2010). It ' s About Time : Why emergency response times matter to firefighters and the public. The Fire Brigade Union, 49(8), 798–799.

Yung, D. (2008). Principles of Fire Risk Assessment in Buildings. Wiley.

Zikmund, Nyle R. (2001). Response Research Indicates Time for a Change. Americal Fire Journal, 30-32

Introducing LPJ-GUESS-SPITFIRE: a coupled global fire-vegetation model

Matthew Forrest*[1]; Thomas Hickler [1,2]

[1] Senckenberg Biodiversity and Climate Research Centre (SBiK-F). Senckenberganlage 25 D-60325 Frankfurt am Main, Germany, {matthew.forrest@senckenberg.de}
[2] Department of Physical Geography at Goethe-University Frankfurt. Altenhoeferallee 1 D-60438 Frankfurt am Main, Germany, {thomas.hickler@senckenberg.de}

**Corresponding author*

Keywords

Global fire model, LPJ-GUESS-SPITFIRE, DGVM, vegetation-fire interactions

Abstract

Fire-enabled dynamic global vegetation models (DGVMs) provide modelling frameworks for integrating many drivers of fire regimes and simulating feedbacks between fire and vegetation. They can then be used to investigate fire-vegetation dynamics and project fire activity into future or past scenarios. Here we present the fire-enabled DGVM LPJ-GUESS-SPITFIRE which combines the widely used LPJ-GUESS DGVM with the SPITFIRE global fire model. We also evaluate the model simulation against burnt area and fire speed Earth observation datasets. We find that the model reproduces the global burnt area patterns with reasonable skill and improves on a previous model version. However there are some regions where model performance is lacking, and through the comparison with fire speed we diagnose some possible causes and suggest potential ways to improve model performance. Despite this, we conclude that overall model performance is sufficient for global scale studies.

1. Introduction

Fire activity is determined by both meteorological conditions and fuel availability and flammability (Bradstock, 2010). Thus, to project future fire regimes under global change, methods must capture not only how fire behaviour responds to changing meteorological conditions (direct effects of climate change), but also how they respond to changing fuel properties. These arise from vegetation responses to climate change, which can include alterations to vegetation structure, species composition and overall biomass productivity, and have consequences for fuel availability, flammability and continuity (both horizontally and vertically). Further to this, human-driven factors, both direct (such as changing ignitions patterns and suppression efforts) and indirect (such as land use change and landscape fragmentation), will also affect future fire regimes (Bowman et al., 2011).

One possible means to integrate all these factors is to combine a dynamic global vegetation model (DGVM) with a global fire model. These models are designed to be applied to the full gamut of global vegetation (and so feature rather generalised representations of fire processes) and operate over gridded domains at comparatively coarse scales (typically 50km or larger). In such model frameworks, the DGVM dynamically simulates the ecosystem state using mechanistic representations of many ecosystem and plant physiological processes such as: photosynthesis; autotrophic respiration; biomass allocation; competition for resources; biomass turnover (i.e. litter production); heterotrophic respiration; and nutrient and water cycling (Prentice et al., 2007). DGVMs may also simulate human land use, such as pasture, cropland and managed forest areas. The simulated ecosystem state is used to derive the fuel properties which are used by the global fire model to simulate fire occurrence and behaviour. The fire activity simulated by the fire model then induces biomass combustion and post-fire mortality in the DGVM's vegetation state, thus representing the bidirectional effects and feedbacks between vegetation and fire.

Global fire models vary widely in their complexity, both in terms of the processes represented and calculated fire properties (Hantson et al., 2016; Rabin et al., 2017). The earliest and simplest models only derived burnt area and applied fixed mortality rates and combustion fractions based on vegetation type (e.g. GlobFIRM,

Thonicke et al., 2001). However global fire models have become increasingly complex over the last two decades and now include representations of fire properties such as number of successful ignitions, rate of spread, intensity, combustion completeness and size-dependent mortality. Here we present the coupled global fire-vegetation LPJ-GUESS-SPITFIRE, which comprises the LPJ-GUESS DGVM (Smith et al., 2001, 2014) and the SPITFIRE global fire model (Thonicke et al., 2010).

2. Materials and Methods

2.1. The LPJ-GUESS DGVM

LPJ-GUESS builds on the biogeography and biogeochemical cycling of the LPJ DGVM (Sitch et al., 2003) by including a forest gap model of vegetation dynamics through the General Ecosystem Simulator (GUESS) (Smith et al., 2001). In this model, vegetation dynamics are represented through competing cohorts of identical woody individuals over a layer of herbaceous vegetation. In the global version used here, 10 different plant functional types (PFTs) are used to represent the global diversity of tree types (for example "boreal needle-leaved evergreen tree"). For the herbaceous layer two grass types are distinguished, a temperate/boreal type which uses C_3 photosynthesis and tropical grass type which uses C_4 photosynthesis. The dynamics of the woody cohorts are driven by establishment and mortality processes and by generic patch destroying disturbance events, here occurring with a mean return interval of 100 years. These processes are implemented stochastically and so a number of replicate "patches" (typically 15-100, in this study 20) are simulated and averaged to smooth out the resultant stochastic variability.

The version of the model used here (v4.1) also includes nitrogen cycling and limitation on photosynthesis (Smith et al., 2014); representation of human land use through croplands, pasture (Lindeskog et al., 2013; Olin et al., 2015) and forest management (Lindeskog et al., 2021); methane emissions from arctic wetlands and permafrost dynamics (Miller & Smith, 2012); emissions of biogenic volatile organic compounds (Arneth, Miller, et al., 2007; Arneth, Niinemets, et al., 2007)**.**

2.2. The SPITFIRE global fire model

SPITFIRE is one of the more complex global fire models. For a full description of the initial implementation see Thonicke et al., 2010, and for details of an earlier version of LPJ-GUESS-SPITFIRE see Rabin et al., 2017. We briefly summarise the main SPITFIRE model structure and logic here. Individual fires are resolved by calculating successful fire starts from potential ignitions from humans and lightning flashes as modified by a flammability index based on fuel moisture. This fuel moisture is based on the Nesterov fire danger index (Nesterov, 1949) and an exponential decay function with smaller coefficients (hence slower fuel drying) for the larger fuel classes. Fire size is modelled as an ellipse with the major axis dependent on rate of spread (which is calculated using the equations of Rothermel 1972) and fire duration (dependent on flammability index with a maximum of 4 hours in the initial formulation). The length-to-breadth ratio of the ellipse is determined by wind speed, and the number of daily fire starts multiplied by the size of each fire gives the daily burned area. Slope is not currently considered in the model as it acts on a landscape scale which is much finer than the coarse continental-to-global spatial scale for which LPJ-GUESS-SPITFIRE is designed.

Combustion completeness, derived from fuel moisture, is used to determine biomass burnt, and trace gas emissions are calculated from biomass burnt using PFT-specific emission factors. Post-fire mortality occurs by two mechanisms, crown scorch and cambial kill. Crown scorch mortality considers the fraction of an individual's crown which is affected by flame height (which is derived from Byram's fire intensity), and a PFT-specific parameter to account for species specific fire resistance. Cambial kill depends on calculated fire residence time (Peterson and Ryan) and bark thickness, with thicker bark providing increased survivorship. Bark thickness is determined based on PFT-specific allometric relationships between bark thickness and diameter at breast height.

Further to this initial implementation described above, the version of SPITFIRE presented here includes a number of modifications. Whilst the original model did not consider burning in agricultural lands, this implementation burns pastures (with the same formulation as natural area) but not croplands. Further, cropland fraction is used to reduce fire size in *adjacent* areas of natural and pasture lands (i.e. in the same gridcell) to represent the effects of landscape fragmentation on fire size. Fire duration has been modified from a maximum of 4 hours to a maximum of 12 hours, but with an additional reduction factor based on human population density

to represent human suppression following Hantson et al. (2015). To integrate SPITFIRE into LPJ-GUESS's replicate patches approach, fire behaviour is calculated separately for each patch and, for the application of post-fire mortality and combustion, burnt area is interpreted probabilistically (ie. each day the patch may burn with probability equal to the daily burnt area) and, if it burns, the combustion effects are applied to the entire patch.

2.3. Simulation set up

For the simulations used here we applied the standard LPJ-GUESS global settings and parameters (Smith et al., 2014). The input datasets required for LPJ-GUESS (climate, atmospheric CO2 concentration, nitrogen deposition and land use data) followed the TRENDY 2019 protocol (Friedlingstein et al., 2019). The TRENDY project coordinates an ensemble of DGVMs for estimation of the land carbon fluxes used in the Global Carbon Budget[30] on an annual basis and so the TRENDY protocol specifies state-of-the-art DGVM input datasets. To provide SPITFIRE with the additional information required for ignitions, the WGLC (Kaplan & Lau, 2019) lightning flash density and HYDE3.2 population density (Klein Goldewijk et al., 2017) datasets were used. The simulations followed the standard LPJ-GUESS spinup procedure whereby the first 30 years of the climate dataset (1901-1930) are detrended and repeated for 500 years to allow the vegetation and soil carbon pools to reach equilibrium. Following this, the full transient climate time series (1901-2018) was used.

2.4. Comparison data sets

To assess overall model performance, simulated burnt area was compared to the observed ESA FireCCI51 burnt area data set (Lizundia-Loiola et al., 2020). Both the observations and model output were summed to annual totals which were then averaged across the years 2001 to 2018. We also compare the daily simulated fire speed to mean fire speed from the Global Fire Atlas (GFA, Andela et al., 2019). SPITFIRE does not explicitly simulate mean daily fire speed, but it can be derived by dividing the length of the major ellipse in the fire size calculation by the duration of the observation period (in this case one day, matching the GFA units of fire speed and observation interval). This "macroscopic" fire speed depends on rate of spread and fire duration (in this case the duration of fire propagation within one day), and so comparing this to observations allows a first-order check of the combined effects of these two simulated properties. In order to examine fire behaviour at the peak of the fire season where the bulk of burning occurs, we compared the maximum of the mean monthly fire speeds.

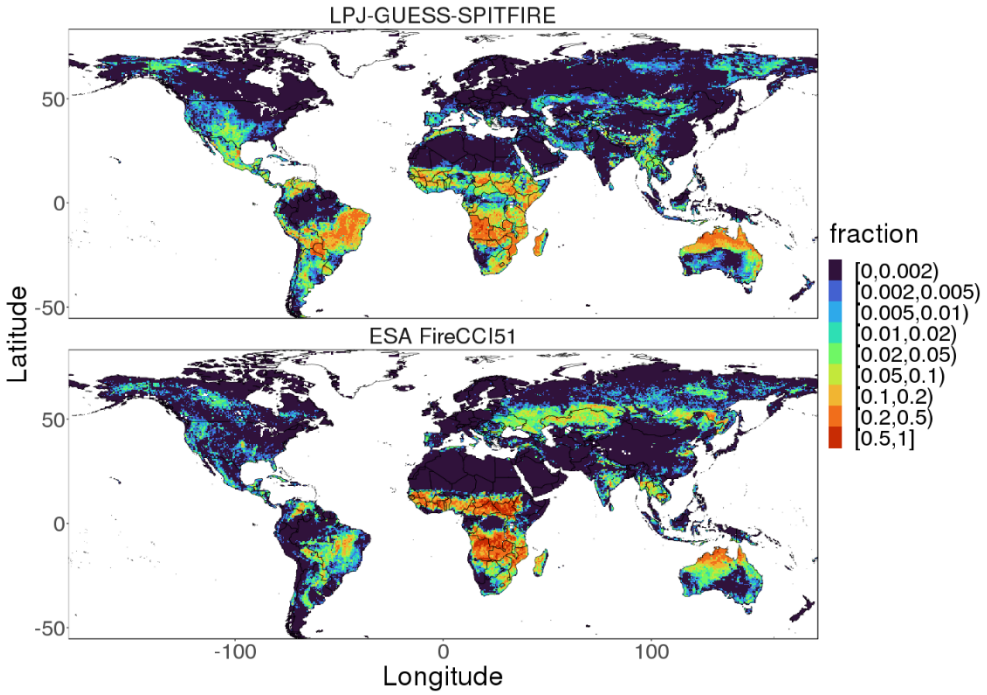

[30] https://www.globalcarbonproject.org/

Figure 1- Annual fractional burnt area from the LPJ-GUESS-SPITFIRE simulation and the ESA FireCCI51 dataset (mean 2001-2018).

3. Results

LPJ-GUESS-SPITFIRE reproduced the global patterns of burnt area reasonably well (Fig. 1), with the largest burnt area simulated in the tropical savanna and dry forest regions. It also correctly simulated little or no burning in areas which are too arid (ie too dry to allow sufficient accumulation of fuel), humid or cold to burn and a modest amount of burning in the temperate and boreal zones. There were, however, some sizable regional discrepancies and, in some cases, opposite tendencies can be observed in the same climate zones but different continents. In the dry tropics fire activity was overestimated in South America but underestimated in Africa. Burnt area was overestimated in the continental interior of the US, but underestimated in the interior of Eurasia. The model simulated well the extent of burning in the warm temperate coastal and mediterranean regions (e.g. the Pacific coast and South East in the US, southern Australia, around the Mediterranean and across the Cape region in South Africa) with some small regional mismatches. In the boreal zone a reasonable amount of fire was simulated, but there were significant spatial mismatches between the modelled burnt area and the observed data.

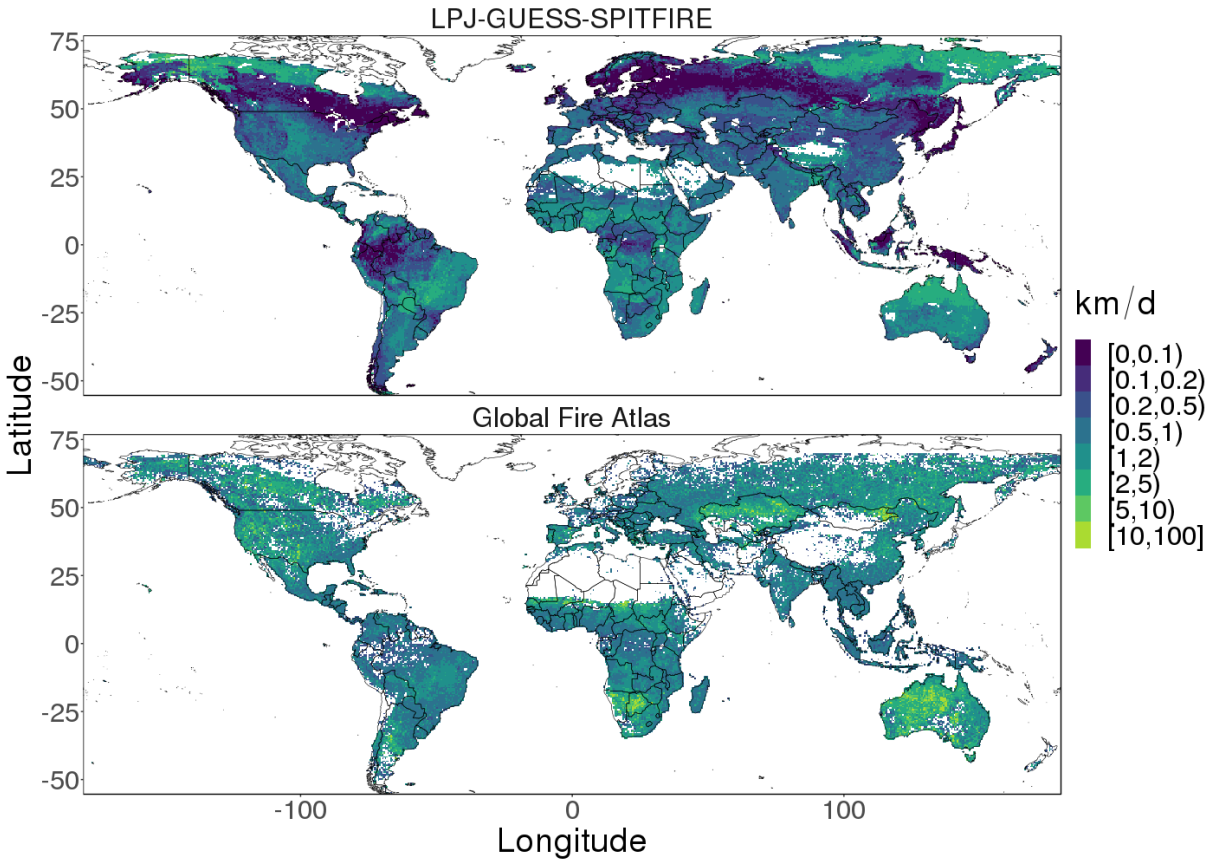

Figure 2 - Maximum of mean monthly fire speed from the LPJ-GUESS-SPITFIRE simulation and Global Fire Atlas dataset (mean 2001-2015).

The comparison of the maximum of mean monthly fire speeds (Fig. 2) gives some indication of what may be driving some of the discrepancies in burnt area. Whilst there was fairly good correspondence in the tropics and much of the temperate zone, there were considerable mismatches elsewhere. In central Eurasia, peak fire speed was underestimated and this corresponds with the region of underestimated burnt area (Fig. 1). Across the boreal forest fire speed was extremely low in LPJ-GUESS-SPITFIRE compared to the GFA observations and at very high latitudes (beyond the simulated tree line) it was very large, even in areas where no fires are observed.

4. Discussion

Compared to a simulation performed by a previous version of LPJ-GUESS-SPITFIRE used in the Fire Model Intercomparison Project (FireMIP, Rabin et al., 2017; Hantson et al., 2020), the simulation presented here showed a tangible improvement, as evidenced by a reduction of normalised mean error (NME, Kelley et al., 2013) from 0.96 (Hantson et al., 2020) to 0.77 (this study). This is similar to the other models from the FireMIP ensemble. However, given the importance of understanding and forecasting fire activity, it is a clear and present priority for the community to reduce this error and improve the skill of global fire models. In the

case of LPJ-GUESS-SPITFIRE, we can identify the boreal and arctic zones as areas for improvement. Our investigation of fire speed indicates that in the arctic region fire speed is too high which can only be a consequence of an over-simulation of fuel load and flammability. A cursory consideration of LPJ-GUESS's global PFTs reveals that there are no tundra shrubs included in the global setup. Instead, the C_3 grass PFT is the only viable vegetation type beyond the tree line, thus an overproduction of highly flammable fuel is simulated.

The underestimation of burnt area in the boreal forest is harder to diagnose. However, corresponding underestimation of fire speed indicates the simulated fuel characteristics are at least partly the issue, giving a definite direction for model improvement.

5. Conclusions

Here we have presented LPJ-GUESS-SPITFIRE, a coupled global fire-vegetation model, and some basic model evaluation. The model shows some regional discrepancies in spatial burnt area patterns, particularly at the higher latitudes, and we suggest some ways forward. However, the model does capture the global distribution of burnt area reasonably well and demonstrates similar model skill to other models in a recent model intercomparison project. We therefore consider it suitable for examining fire and vegetation interactions at global scope.

6. References

Andela, N., Morton, D. C., Giglio, L., Paugam, R., Chen, Y., Hantson, S., Werf, G. R. van der, & Randerson, J. T. (2019). The Global Fire Atlas of individual fire size, duration, speed and direction. *Earth System Science Data*, *11*(2), 529–552. https://doi.org/10.5194/essd-11-529-2019

Arneth, A., Miller, P. A., Scholze, M., Hickler, T., Schurgers, G., Smith, B., & Prentice, I. C. (2007). CO2 inhibition of global terrestrial isoprene emissions: Potential implications for atmospheric chemistry. *Geophysical Research Letters*, *34*(18), L18813. https://doi.org/10.1029/2007GL030615

Arneth, A., Niinemets, U., Pressley, S., Bäck, J., Hari, P., Karl, T., Noe, S., Prentice, I. C., Serça, D., Hickler, T., Wolf, A., & Smith, B. (2007). Process-based estimates of terrestrial ecosystem isoprene emissions: Incorporating the effects of a direct CO2-isoprene interaction. *Atmos. Chem. Phys.*, *7*(1), 31–53. https://doi.org/10.5194/acp-7-31-2007

Bowman, D. M. J. S., Balch, J., Artaxo, P., Bond, W. J., Cochrane, M. A., D'Antonio, C. M., DeFries, R., Johnston, F. H., Keeley, J. E., Krawchuk, M. A., Kull, C. A., Mack, M., Moritz, M. A., Pyne, S., Roos, C. I., Scott, A. C., Sodhi, N. S., & Swetnam, T. W. (2011). The human dimension of fire regimes on Earth. *Journal of Biogeography*, *38*(12), 2223–2236. https://doi.org/10.1111/j.1365-2699.2011.02595.x

Bradstock, R. A. (2010). A biogeographic model of fire regimes in Australia: Current and future implications. *Global Ecology and Biogeography*, *19*(2), 145–158. https://doi.org/10.1111/j.1466-8238.2009.00512.x

Friedlingstein, P., Jones, M. W., O'Sullivan, M., Andrew, R. M., Hauck, J., Peters, G. P., Peters, W., Pongratz, J., Sitch, S., Le Quéré, C., Bakker, D. C. E., Canadell, J. G., Ciais, P., Jackson, R. B., Anthoni, P., Barbero, L., Bastos, A., Bastrikov, V., Becker, M., … Zaehle, S. (2019). Global Carbon Budget 2019. *Earth System Science Data*, *11*(4), 1783–1838. https://doi.org/10.5194/essd-11-1783-2019

Hantson, S., Arneth, A., Harrison, S. P., Kelley, D. I., Prentice, I. C., Rabin, S. S., Archibald, S., Mouillot, F., Arnold, S. R., Artaxo, P., Bachelet, D., Ciais, P., Forrest, M., Friedlingstein, P., Hickler, T., Kaplan, J. O., Kloster, S., Knorr, W., Lasslop, G., … Yue, C. (2016). The status and challenge of global fire modelling. *Biogeosciences*, *13*(11), 3359–3375. https://doi.org/10.5194/bg-13-3359-2016

Hantson, S., Kelley, D. I., Arneth, A., Harrison, S. P., Archibald, S., Bachelet, D., Forrest, M., Hickler, T., Lasslop, G., Li, F., Mangeon, S., Melton, J. R., Nieradzik, L., Rabin, S. S., Prentice, I. C., Sheehan, T., Sitch, S., Teckentrup, L., Voulgarakis, A., & Yue, C. (2020). Quantitative assessment of fire and vegetation

properties in simulations with fire-enabled vegetation models from the Fire Model Intercomparison Project. *Geoscientific Model Development*, *13*(7), 3299–3318. https://doi.org/10.5194/gmd-13-3299-2020

Hantson, S., Lasslop, G., Kloster, S., & Chuvieco, E. (2015). Anthropogenic effects on global mean fire size. *International Journal of Wildland Fire*, *24*(5), 589–596. https://doi.org/10.1071/WF14208

Kaplan, J. O., & Lau, H.-K. (2019). *The WGLC global gridded monthly lightning stroke density and climatology* [Data set]. PANGAEA. https://doi.org/10.1594/PANGAEA.904253

Kelley, D. I., Prentice, I. C., Harrison, S. P., Wang, H., Simard, M., Fisher, J. B., & Willis, K. O. (2013). A comprehensive benchmarking system for evaluating global vegetation models. *Biogeosciences*, *10*(5), 3313–3340. https://doi.org/10.5194/bg-10-3313-2013

Klein Goldewijk, K., Beusen, A., Doelman, J., & Stehfest, E. (2017). Anthropogenic land use estimates for the Holocene – HYDE 3.2. *Earth System Science Data*, *9*(2), 927–953. https://doi.org/10.5194/essd-9-927-2017

Lindeskog, M., Arneth, A., Bondeau, A., Waha, K., Seaquist, J., Olin, S., & Smith, B. (2013). Implications of accounting for land use in simulations of ecosystem carbon cycling in Africa. *Earth Syst. Dynam.*, *4*(2), 385–407. https://doi.org/10.5194/esd-4-385-2013

Lindeskog, M., Smith, B., Lagergren, F., Sycheva, E., Ficko, A., Pretzsch, H., & Rammig, A. (2021). Accounting for forest management in the estimation of forest carbon balance using the dynamic vegetation model LPJ-GUESS (v4.0, r9710): Implementation and evaluation of simulations for Europe. *Geoscientific Model Development*, *14*(10), 6071–6112. https://doi.org/10.5194/gmd-14-6071-2021

Lizundia-Loiola, J., Otón, G., Ramo, R., & Chuvieco, E. (2020). A spatio-temporal active-fire clustering approach for global burned area mapping at 250 m from MODIS data. *Remote Sensing of Environment*, *236*, 111493. https://doi.org/10.1016/j.rse.2019.111493

Miller, P. A., & Smith, B. (2012). Modelling Tundra Vegetation Response to Recent Arctic Warming. *AMBIO*, *41*(3), 281–291. https://doi.org/10.1007/s13280-012-0306-1

Nesterov, V. G. (1949). Gorimost' lesa i metody eio opredelenia. *Gosles-Bumaga, Moscow*.

Olin, S., Lindeskog, M., Pugh, T. a. M., Schurgers, G., Wårlind, D., Mishurov, M., Zaehle, S., Stocker, B. D., Smith, B., & Arneth, A. (2015). Soil carbon management in large-scale Earth system modelling: Implications for crop yields and nitrogen leaching. *Earth System Dynamics*, *6*(2), 745–768. https://doi.org/10.5194/esd-6-745-2015

Prentice, I. C., Bondeau, A., Cramer, W., Harrison, S. P., Hickler, T., Lucht, W., Sitch, S., Smith, B., & Sykes, M. T. (2007). Dynamic Global Vegetation Modeling: Quantifying Terrestrial Ecosystem Responses to Large-Scale Environmental Change. In J. G. Canadell, D. E. Pataki, & L. F. Pitelka (Eds.), *Terrestrial Ecosystems in a Changing World* (pp. 175–192). Springer. https://doi.org/10.1007/978-3-540-32730-1_15

Rabin, S. S., Melton, J. R., Lasslop, G., Bachelet, D., Forrest, M., Hantson, S., Kaplan, J. O., Li, F., Mangeon, S., Ward, D. S., Yue, C., Arora, V. K., Hickler, T., Kloster, S., Knorr, W., Nieradzik, L., Spessa, A., Folberth, G. A., Sheehan, T., … Arneth, A. (2017). The Fire Modeling Intercomparison Project (FireMIP), phase 1: Experimental and analytical protocols with detailed model descriptions. *Geosci. Model Dev.*, *10*(3), 1175–1197. https://doi.org/10.5194/gmd-10-1175-2017

Rothermel, R. C. (1972). A mathematical model for predicting fire spread in wildland fuels. *A Mathematical Model for Predicting Fire Spread in Wildland Fuels., No. INT-115*. https://www.cabdirect.org/cabdirect/abstract/19730605850

Sitch, S., Smith, B., Prentice, I. C., Arneth, A., Bondeau, A., Cramer, W., Kaplan, J. O., Levis, S., Lucht, W., Sykes, M. T., Thonicke, K., & Venevsky, S. (2003). Evaluation of ecosystem dynamics, plant geography and terrestrial carbon cycling in the LPJ dynamic global vegetation model. *Global Change Biology*, *9*(2), 161–185. https://doi.org/10.1046/j.1365-2486.2003.00569.x

Smith, B., Prentice, I. C., & Sykes, M. T. (2001). Representation of vegetation dynamics in the modelling of terrestrial ecosystems: Comparing two contrasting approaches within European climate space. *Global Ecology and Biogeography*, *10*(6), 621–637. https://doi.org/10.1046/j.1466-822X.2001.t01-1-00256.x

Smith, B., Wårlind, D., Arneth, A., Hickler, T., Leadley, P., Siltberg, J., & Zaehle, S. (2014). Implications of incorporating N cycling and N limitations on primary production in an individual-based dynamic vegetation model. *Biogeosciences*, *11*(7), 2027–2054. https://doi.org/10.5194/bg-11-2027-2014

Thonicke, K., Spessa, A., Prentice, I. C., Harrison, S. P., Dong, L., & Carmona-Moreno, C. (2010). The influence of vegetation, fire spread and fire behaviour on biomass burning and trace gas emissions: Results from a process-based model. *Biogeosciences*, *7*(6), 1991–2011. https://doi.org/10.5194/bg-7-1991-2010

Thonicke, K., Venevsky, S., Sitch, S., & Cramer, W. (2001). The role of fire disturbance for global vegetation dynamics: Coupling fire into a Dynamic Global Vegetation Model. *Global Ecology and Biogeography*, *10*(6), 661–677. https://doi.org/10.1046/j.1466-822X.2001.00175.x

Joint Drought-Temperature conditions as factors contributing to the occurrence of forest fires in Portugal: a NUT III clustering perspective in a monthly/seasonal time scale

Nuno Moreira*[1]; Ilda Novo[1]; Pedro Silva[1], Edna Cardoso[1,2]; Álvaro Silva[1]; João Ferreira[1]; Ricardo Ramos[1]

[1]*IPMA. Rua C do Aeroporto 1749-077 Lisboa, Portugal*
{nuno.moreira, ilda.novo, pedro.silva, alvaro.silva, joao.ferreira, ricardo.ramos}@ipma.pt
[2]*University of Coimbra, FCTUC, Department of Mechanical Engineering. Pólo II*
Rua Luís Reis Santos, 3030-788 Coimbra, Portugal, *{uc2004118633@student.uc.pt}*

**Corresponding author*

Keywords

Drought, Temperature, Forest Fires, Clustering, NUT III

Abstract

The objective of the present work is to find a joint relation of drought and temperature regimes as factors contributing to the occurrence and severity of forest fires in the period 1981-2018 in mainland Portugal. To meet this goal PDSI drought data in NUT III regions from automatic weather stations were matched with temperature regimes obtained from a 3 km downscaling using WRF model and ERA5 reanalysis as forcing data. Clustering analysis was used to aggregate seasons from June to October, according to the weather-climate conditions provided together by drought and temperature regimes. The proposed scheme may be used to compare a seasonal forecast with this database and find a better match in order to support seasonal forestry and forest fire management policies. An additional analysis, also with SPI3 and SPI6 drought indices, was carried out to evaluate the influence of pre-season drought/wet conditions on the forest fire season.

1. Introduction

To better understand Extreme Fire Event conditions at a regional level in Portugal in the scope of the FIRESTORM project a preliminary independent analysis on drought conditions and on forest fires was performed in NUT III administrative organization in the period 1980-2019 (Cardoso *et al*, 2022). This analysis supports a more comprehensive study on the regional level on the relation between weather-climate conditions (drought, temperature, wind) and forest fires (occurrences, burned areas). In the current work the weather-climate conditions are focused on drought and temperature.

2. Data

To classify drought, two indexes were considered – PDSI (Palmer Drought Severity Index) and SPI (Standardized Precipitation Index), the last one for 3 and 6 months configurations (see e.g. Pires *et al.*, 2010, Silva *et al.*, 2014 and Pires *et al.*, 2019). The computation was based on weather station observations in mainland Portugal, with aggregation in 23 NUT III regions on a monthly basis. To classify the temperature regime a 3 km downscaling using the Weather Research and Forecasting (WRF) model and the fifth generation of European ReAnalysis (ERA5) as forcing data were used. Namely, monthly means of maximum temperature were considered over mainland Portugal grid points, that is, a mask was used to exclude grid points over the ocean and Spain. Drought and temperature data were analysed in the period 1981-2018. For the analysis of forest fires, data on occurrences and burned areas, both on a daily and monthly basis, were compiled from the Portuguese records of fire occurrence for the same period (ICNF, 2020).

3. Joint relation scheme of drought and temperature – a seasonal approach

A first step to see how the years could be clustered regarding drought and temperature was to set the most critical months for forest fires in Portugal. These months were set to be the ones between June and October, considering the number of occurrences per month in the dataset (see Figure 1). In this work, these 5 months together are considered a season. For this purpose, each month between June and October in mainland Portugal was reclassified regarding drought index into 4 classes: i) very dry, ii) dry, iii) normal, iv) wet or very wet - depending on the number of NUT III regions and their drought PDSI classification (extreme drought, severe drought, moderate drought, mild drought, near normal, slightly wet, moderately wet, very wet, extremely wet). The reclassification is described in Table 1. A season classification (also with 4 classes) is consequently computed from monthly drought reclassifications, using the percentiles 40, 60 and 90, as described in Table 2.

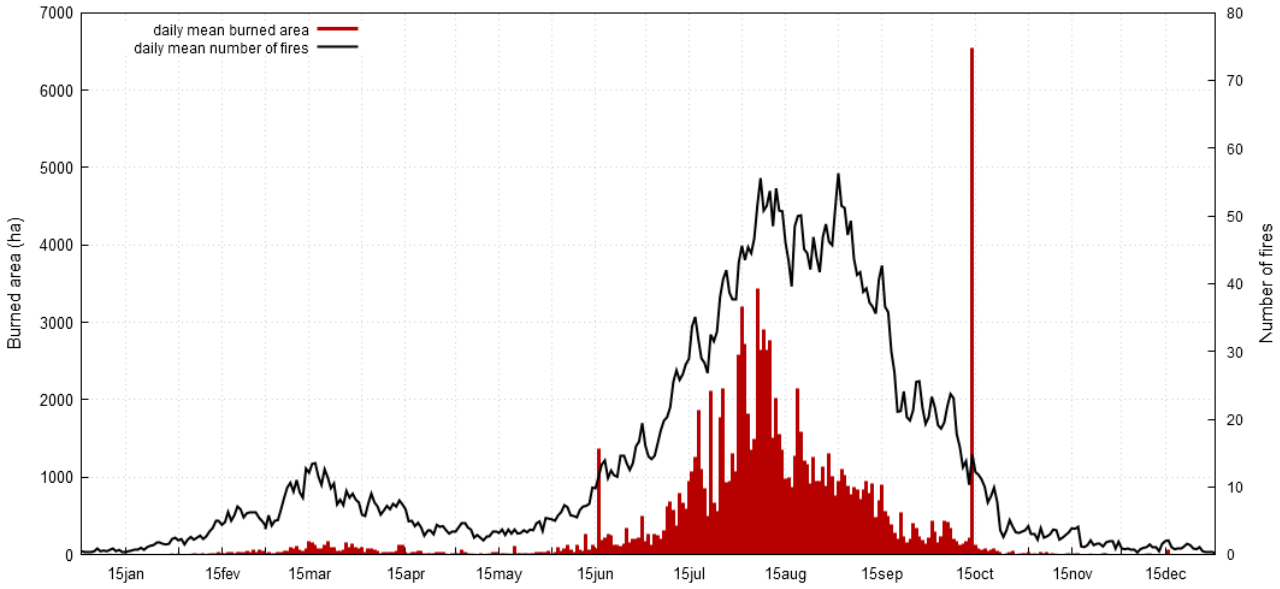

Figure 1- Daily mean values of burned area and number of fires (>1 ha), between 1980 and 2018, retrieved from the Portuguese records of fire occurrence (ICNF, 2020).

Table 1 – Reclassification of drought for a particular month between June and October in mainland Portugal according to the NUT III PDSI drought classification.

Monthly reclassification		Criteria	
1	Very Wet	At least 12 NUT III very or extremely wet PDSI (> 50 %)	At least 18 NUT III in any PDSI wet class (> 75 %)
	Wet	At least 12 NUT III moderately or slightly wet PDSI (> 50 %)	At least 18 NUT III in any PDSI wet class (> 75 %)
2	Normal	If the criteria are not met for very dry, dry, wet or very wet	
3	Dry	At least 12 NUT III in moderate or mild drought PDSI (> 50 %)	At least 18 NUT III in any PDSI drought class (> 75 %)
4	Very dry	At least 12 NUT III in extreme or severe drought PDSI (> 50 %)	At least 18 NUT III in any PDSI drought class (> 75 %)

Table 2 – Season (June to October) classification for drought in mainland Portugal based on monthly reclassifications as described in Table 1.

Season classification (June to October)	Sum of monthly drought reclassification (1 to 4) between June and October from Table 1	Corresponding percentile
Wet	< 10	< 40
Normal	≥ 10 and < 11	≥ 40 and < 60
Dry	≥ 11 and < 16	≥ 60 and < 90
Very Dry	≥ 16	≥ 90

On the other hand, each month between June and October in mainland Portugal was also classified regarding temperature in 4 classes – cold, normal, hot and very hot – depending on the maximum temperature monthly mean percentile over the whole territory in that period of the year. This classification is described in Table 3. Like for drought, a season temperature classification in 4 classes is consequently computed from monthly temperature classifications using the percentiles 40, 60 and 90, as described in Table 4.

Table 3 – Classification of Temperature of a particular month between June and October in mainland Portugal according to maximum temperature monthly mean percentile over the whole territory (also in the period from June to October).

		Maximum temperature monthly mean percentile in period June to October
1	Cold	< 40
2	Normal	≥ 40 and < 60
3	Hot	≥ 60 and < 90
4	Very Hot	≥ 90

Table 4 – Season (June to October) classification for temperature in mainland Portugal based on monthly classifications as described in Table 3.

Season classification (June to October)	Sum of monthly temperature classification (1 to 4) between June and October from Table 3	Corresponding percentile
Cold	< 9	< 40
Normal	≥ 9 and < 11	≥ 40 and < 60
Hot	≥ 11 and < 14	≥ 60 and < 90
Very Hot	≥ 14	≥ 90

4. Results on joint drought - temperature conditions

A joint season classification of drought and temperature was therefore set for the seasons between 1981 and 2018, with a clustering analysis being applied using both K-Means and Generalized EM (Expectation Maximization) with similar results. The results for Generalized EM are plotted in Figure 2 confirming the adequacy of season categorization for drought and temperature. Cluster 1 represents wet to normal and cold to normal seasons, corresponding to seasons that are less likely to originate extreme forest fire occurrences. On the other side of the spectrum lies cluster 2, with hot or very hot and dry or very dry seasons, with a clear signal for 2005 and 2017 on the top right corner of the diagram. Clusters 3 and 4 represent a mix of conditions pulling

in opposite directions in terms of conditions favouring forest fire occurrences. Therefore, cluster 3 aggregates dry or very dry seasons that are somehow compensated by cold to normal temperature regimes. On the other hand, cluster 4 aggregates hot to very hot seasons that are somehow compensated by wet to normal drought contexts.

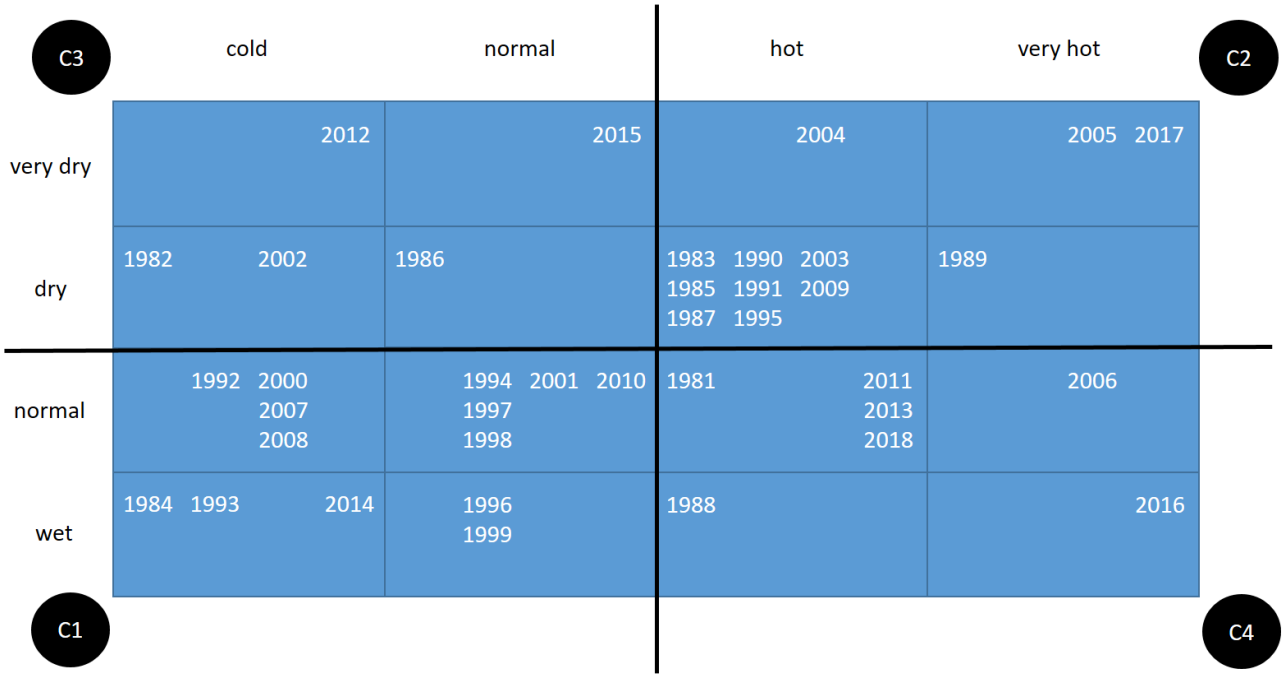

Figure 2 – June to October season clusters (1 to 4) in the period 1981-2018 for a joint drought-temperature classification according to the scheme proposed by Tables 1 to 4 for mainland Portugal.

5. Forest fire severity and pre-season drought conditions – a monthly approach

Despite the benefits of a seasonal analysis for drought and temperature for characterizing the fire season, it was found that seasonal forest fire indicators (occurrences and burned areas) were poorly correlated with pre-season drought indices (PDSI, SPI3 and SPI6) monthly values. Therefore, an additional lagged correlation analysis for NUT III was computed, but considering monthly forest fire indicators between June and October. For each NUT III, these monthly indicators were correlated with the monthly drought indices back to January, considering the 38 years of the dataset (1981-2018). A zero-lag correlation was also computed for determining the baseline.

6. Results on the relation between forest fire severity and drought

Figure 3 shows the baseline zero-lag correlation coefficient between monthly forest fire occurrences and monthly SPI3, PDSI and SPI6 drought indices from June to October at a NUT III level. Note that as drought is defined as negative in the drought indices, drought influence on forest fires will be defined as a negative correlation. The maps in Figure 3 show that, although drought conditions are important to characterize forest fire occurrences and burned areas, clearly other factors have to be taken into account. For example, even for SPI3 - the index that shows better zero-lag correlation results, along with higher statistical significance - the strongest negative correlation index was -0.739 (significant at 99% level) for *Beira Baixa* in June, which means that 54.7% (approximately half) of the variance in the number of occurrences in June is explained by the SPI3 drought index in June. For the majority of NUT III areas, the number of occurrences is generally more negatively correlated with drought indices in June, followed by October and then July. The stronger negative correlations (between -0.4 and -0.6, significant at least at 95% level) are essentially found in NUT III in the North and Centre of Portugal, showing that for these cases only 15 to 35% of the variance on the number of occurrences is explained by drought. Weaker negative (or even positive) correlations happen for August and September, meaning that the number of occurrences in those months shall be accounted for, in a larger proportion, by other

factors. Similar patterns occur if burned areas are considered, but generally with lower and less significant correlations, nevertheless with PDSI and SPI3 indices performing better.

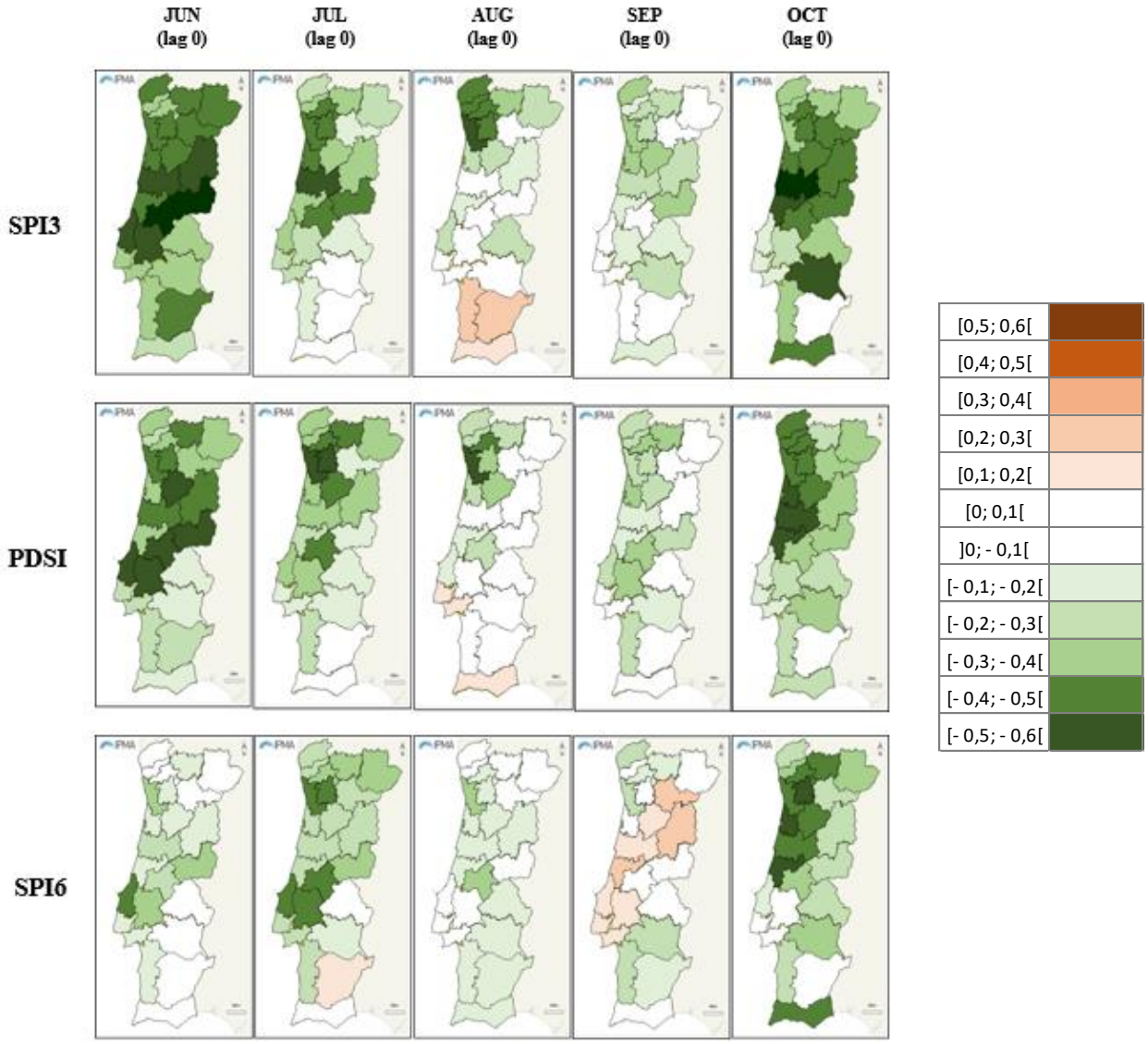

Figure 3 - Correlation coefficient between monthly forest fire occurrences and monthly SPI3 (upper row), PDSI (middle row) and SPI6 (lower row) drought indices from June (on the left) to October (on the right) at a NUT III level. Negative correlation in greenish shades and positive correlation in brownish shades.

It is clear that the negative correlation rapidly gets weaker with lags of 1, 2 or 3 months, even for the cases with stronger negative zero-lag correlation of drought with occurrences and burned areas (see Figure 4 for the case of July). Generally, correlations are not even significant at a 90% level with lags of 2 months or more. For lagged correlation SPI3 now seems to retain a weaker lagged correlation than PDSI (unlike zero-lag correlation). On the other hand, SPI3 seems to retain a higher lagged correlation than SPI6 for forest fire indicators in October, while the opposite happens for July, August and September.

Figure 4 shows that occurrences (also burned areas, not shown) in July for NUT III in the North and Centre of Portugal keep negative correlations of -0.3 to -0.5 (significant at least at a 90 % level) with the 3 drought indices in June and May, the signal being stronger for PDSI and SPI6. Even the strongest negative correlation with SPI6 in April (3 months' lag) for *Oeste* is only of -0.44 (20% of explained variance).

Figure 4 – Lagged correlation coefficient between forest fire occurrences in July and monthly SPI3 (upper row), PDSI (middle row) and SPI6 (lower row) drought indices from January (lag -6, on the left) to July (lag 0, on the right) at a NUT III level. Negative correlation in greenish shades and positive correlation in brownish shades.

Another relevant aspect is the relation between forest fires and wet pre-season regimes (positive values in drought indices) for some areas in the south of Portugal. Forest fire occurrences in *Alto Alentejo*, *Alentejo Central* or *Baixo Alentejo* in June and July (and also burned areas in June) are reasonably correlated with PDSI precipitation regimes in March, with correlation coefficients varying between +0.3 and +0.5 (10 to 25% of explained variance), significant at 90 or 95% level. For SPI3 and SPI6 correlations are lower and less significant, as partly showed in Figure 4 for July. In October, and also in *Alentejo Litoral*, occurrences and burned areas have correlation coefficients, statistically significant at 90 or 95%, between +0.27 and +0.45 (that is, at most 20% of explained variance), with wet regimes in months from January to July (not shown).

7. Final Remarks

Drought-Temperature data for mainland Portugal were jointly analysed in the period 1981-2018, both in a NUT III administrative aggregation and on grid point means. Results show seasons from June to October can be clustered in 4 groups according to monthly drought and temperature regimes. The proposed scheme may be used to compare a seasonal forecast with this database and find a better match in order to support seasonal forestry and forest fire management policies. The current study shows also that, regarding the relation between drought and the forest fire season, occurrences correlate better with drought than burned areas do. Zero-lag correlations are stronger (coefficient correlations of -0.4 to -0.6) in June and October, and in the North and Centre of Portugal, suggesting that other factors (such as the temperature/wind regime or human activity) have to be considered in the other months, namely August and September, and for the south of Portugal. Even for the cases of stronger correlation, pre-season drought conditions do not seem so preponderant, as monthly forest fire activity already has a lower correlation with drought conditions in the previous month, with no statistically significant correlation for more than the 2 previous months, at the most. On the other hand, for the south of Portugal wet regimes in March do explain up to 25% of the variance in forest fire occurrences in June and July (that is, 3 to 4 months ahead), while wet regimes between January and July also seem to explain up to 20% of the variance on forest fire occurrences in October. Finally, it should be noted that this study is based on a NUT

III administrative aggregation, which is in line with the 5 regional administrative domains currently considered in mainland Portugal for managing forest fire prevention and combat.

8. References

Cardoso, E., Moreira, N., Novo, I., Silva, P., Silva, P., Pires, V., 2022: Clusters analysis applied to drought and forest fires in mainland Portugal (NUT III) from 1980 to 2019. Submitted to the IX International Conference on Forest Fire Research, D. X. Viegas (Ed.).

ICNF, 2020: Incêndios Rurais – Estatísticas. Instituto da Conservação da Natureza e das Florestas (ICNF). Fire occurrence database. Available at: http://www2.icnf.pt/portal/florestas/dfci/inc/estat-sgif. [Accessed 26th March 2020].

Pires, V., Silva, A., Mendes, L., 2010: Drought Risk in Mainland Portugal. Rev. Territorium, 17(17):27-34., DOI:10.14195/1647-7723_17_3.

Pires, V., Cota, T., Silva, A., Santo, F., 2019: Drought Monitoring and Analysis in Mainland Portugal. Geophysical Research Abstracts, Vol 21. EGU General Assembly.

Silva, A.; De Lima, M.I. P., Espírito Santo, F., Pires, V., 2014: Assessing changes in drought/wetness episodes in drainage basins using the SPI. Die Bodenkultur - Journal for Land Management, Food and Environment; 12/2014; 65(3-4):31-37.

Large Fires in Portugal and Synoptic Circulation Patterns: Meteorological parameters and fire danger indices associated to Critical Weather Types

Ilda Novo*[1], João Ferreira[1], Pedro Silva[1], Jorge Ponte[1], Nuno Moreira[1],
Ricardo Ramos[1], João Rio[1], Edna Cardoso [1,2]

[1]IPMA. Rua C do Aeroporto 1749-077 Lisboa, Portugal,
{ilda.novo, joao.ferreira pedro.silva, jorge.ponte, nuno.moreira, ricardo.ramos, joao.rio}@pma.pt
[2]University of Coimbra, FCTUC, Department of Mechanical Engineering. Pólo II
Rua Luís Reis Santos, 3030-788 Coimbra, Portugal, {uc2004118633@student.uc.pt}

**Corresponding author*

Keywords :

Circulation Weather Types (WT), Critical Days, Critical Weather Type, Large Fires, NUT III

Abstract

Large fires in Portugal, with a daily burned area equal to or greater than 3000 ha for the entire territory, tend to occur under specific circulation patterns. The severity of the meteorological conditions, expressed by the magnitude of the meteorological parameters anomaly and fire danger indices, associated with these patterns, could be an important tool to enable earlier forecast of fire weather conditions, being a useful support for decision making. However, there are some regional differences that we intend to analyze at NUT III level, contributing to a forecast with greater detail and oriented to support the fight and prevention of forest fires in Portugal. At NUT III level, we considered as Large Fires the 97th percentile of mean burned area of all NUT III, corresponding more or less to 300 ha of daily burned area. To link the synoptic circulation patterns with Large Fires, ten groups or clusters of NUT III were considered and four classes of normalized daily burned area in each NUT III or cluster of NUT III were considered. The six critical Weather Types (WTs) identified (North-easterly, Easterly, Anticyclonic Easterly Quadrant, Cyclonic Easterly, Quadrant, Northerly and Anticyclonic) exhibit distinctive circulation characteristics and mean values and anomalies of the meteorological parameters. The spatial distribution of Large Fires showed preferred regions for some of these WTs. The mean value of the Fire Weather Index (FWI) was computed for each WTs and for Critical Days (days with burned area equal or greater than 300 ha in each NUT III), using the WRF (Weather Research and Forecasting) mesoscale model. The mean value of FWI for each NUT III or cluster of NUT III, showed a few differences according to the WT and region. These values, can thus be taken as historical indicators at regional level of the likelihood of a large fire occurring.

1. Introduction

Large fires are responsible for very significant percentages of burned area every year. In Portugal 92% of the annual burned area is on average consumed during the period June to October, especially in July to September (82%) (Carmo *et al*, 2021). However, even during the fire season, most of the burned area occurs within a few days, these days designated as spread-event days (Lagerquist *et al* (2017), Flanning *et al* (2000), Flanning *et al* 2013). Several studies have pointed out the occurrence of these days associated to specific circulation patterns and associated to weather conditions (Crimmins (2006), Skinner *et al* (2002), Pereira et al (2005), Calheiros *et al* (2020), Duane *et al* (2018), (Dimitrakopoulos *et al* 2011). In the framework of the FireStorm project, a methodology based on circulation weather patterns (Trigo *et al*., 2000) was applied to provide a detailed description of the meteorological conditions during these events in Portugal. This methodology has already been applied to the entire Portuguese territory (Carmo *et al*, 2021). However, some differences amongst the regions of mainland Portugal are expected which can be more significant in certain synoptic patterns and regions. In the present study our goal is to use this methodology to obtain a finer analysis at the regional level of the administrative regions known as NUT III or aggregations of NUT III. Although circulation patterns describe synoptic-scale meteorological phenomena, they imply differences at smaller scales which are associated with fire spread and fire behaviour. The goal of this work is to relate the large fires at the regional level, with the synoptic circulation patterns and search for regional thresholds on the anomalies of the most relevant meteorological parameters and on the values of the Fire Weather index (FWI) and corresponding sub-indices

of the Canadian System. Those thresholds could be good tools to establish a warning system that enable an earlier forecast of fire weather.

2. Large Fires in Portugal and Circulation patterns

2.1. Methodology and Data

To determine the relationship between synoptic circulation patterns and large fires, four classes of daily burned area were established, with the burned area being normalized by each NUT III area, whose distribution in each class was based on the daily time series of burned areas above 1 ha, in Portugal mainland from 1980 to 2018 (Table 1). The cases of fires in the class of burned area equal to or greater than 300 ha were considered as LF. These cases correspond to the 99th percentile if the normalized area is considered or the 97th percentile if the average of the burned area in all NUTS III is considered**.** The days with burned area equal to or greater than 300 ha in each NUT III are critical days and each event is associated with a circulation synoptic pattern.

These cases have been associated to mean values and anomalies, of the meteorological parameters, computed using ERA 5 (fifth generation ECMWF Reanalysis) or with the numerical weather prediction model, WRF (Weather Research and Forecasting). The Fire data was obtained from ICNF (2020) and adapted by (Carmo *et al* 2021).

Table 1 – Daily classification according to burned area.

Class ID	Burned area class (ha)	Number of Cases	Number of Cases (%)
1	< 100	45278	95.5
2	[100, 300 [	1434	3.0
3	[300, 1000 [	524	1.1
4	> 1000	194	0.4

2.2. Weather Types and daily burned area classes

The Weather Types (WTs) were built using the methodology of Circulation Weather Pattern (Trigo *et al*, 2000) which is based on computation of a set of indices of the direction and vorticity of geostrophic flow, either pure or hybrid. Here we used a version with 18 weather types: i) 8 directional ii) 2 pure rotational (anticyclonic and cyclonic) and iii) 8 hybrid (4 anticyclonic and 4 Cyclonic). The distribution of the 18 WT shows high frequency of directional WT (56.6%), with NE being the most frequent (20%). The anticyclonic weather types have 32.2%, with the pure anticyclonic WT A the most frequent (17.7%). The cyclonic weather types have a frequency of 11.2%.

2.3. Critical Days and Critical Weather Types

In the fire data series under study (1980-2018), 409 critical days were found throughout the territory, with a much higher frequency (43%) associated with the WT NE, which is one of the most frequent during summer in Portugal. To find out the statistical significance of the predominance of a given WT on critical days, the Chi-square test between observed and expected days within each WT was computed. Three WTs with more significance (p-value< 0.001) and with more cases observed than expected at national level were confirmed: CQE, E, NE (Table 2).

Table 2 – Chi square tests between observed and expected critical days for 9 weather types. In bold p-values (<0.001) and underlined WTs with more critical days than would be expected by chance alone.

Weather Types	**NE**	**E**	**CQE**	**A**	**N**
Summer days **(Critical days)**	1191 **(176)**	247 **(48)**	103 **(19)**	1057 **(31)**	960 **(46)**
χ^2	**< 0.001**	**< 0.001**	**< 0.001**	**< 0.001**	**< 0.001**
	AQE	**AQN**	**CQN**	**C**	
Summer days **(Critical days)**	114 **(11)**	544 **(22)**	96 **(4)**	385 **(24)**	
χ^2	0.25	0.009	0.3	0.6	

This methodology was applied to the Portuguese administrative regions at NUT III level. In order to obtain groups of NUTs III with similar large fire regime, cluster analysis was used for the daily classes of burned area.

The K-means cluster analysis was used, but considering a subjective adjustment to ensure geographic consistency. Ten clusters of NUT III were taken (Table 3*)*.

Table 3 - NUT III Clusters.

	Cluster 1	**Cluster 2**	**Cluster 3**	**Cluster 4**	**Cluster 5**
NUT III	Minho (111) Cávado (112)	Ave (119) Alto Tâmega (11B)	A.M. Porto (11A) Tâmega Sousa (11C)	Trás-os-Montes (11E) Douro (11D)	Aveiro (16D) Viseu D. L. (16G)
	Cluster 6	**Cluster 7**	**Cluster 8**	**Cluster 9**	**Cluster 10**
NUT III	S. Estrela (16J) Beira Baixa (16H)	Coimbra (16E) Leiria (16F) Médio Tejo (16I)	Oeste (16B) A.M. Lisboa (170)	Lezíria Tejo (185) Alto Alentejo (186) Alentejo Centr (187)	Alentejo Lit.(181) Bx. Alentejo (184) Algarve (150)

2.4. Description of the Critical Weather Types

In Figure 1 the most relevant synoptic patterns related with large fires in Portugal are presented. Figure 1and Table 4, highlight the main meteorological characteristics associated with the aforementioned synoptic circulation patterns. These patterns jointly with Iberian thermal low (TL) and the adjustment to local and regional factors, create the weather conditions that can lead to the occurrence of large fires.

The North-easterly flow WT (NE): it is identified by a high pressure system over Atlantic, located at northwest of Coruña (The North Atlantic Block, Kautz *et al*, 2021), extending in ridge to the western Mediterranean, and the TL centered in southwestern Iberia, defining a northeast flow with a warm and dry air mass over mainland Portugal.

The Easterly flow WT (E): this WT results from a block settled over Western Europe with the Azores high located north of Iberia. In low level, the Morocco´s TL, extending to north over southwestern Iberia defining an east flow with a warm and very dry air mass over the Portuguese territory. This WT, together with AQE (Anticyclonic Easterly Quadrant flow), have the highest, warmest and driest air mass in low and middle troposphere, followed by NE (Table 4).

The Northerly flow WT (N): it is identified by the Azores high located over Azores Islands and the TL located in central part of Spain. In this WT the influence of the sea breeze is well marked. This WT has the coldest and wet air mass, among these six WT, followed by CQE (Table 4).

The Cyclonic Easterly Quadrant flow WT (CQE): it is identified by a high north of Azores and a low system located southeast, breaking the zonal flow (cut-off). At low levels, a low is centered south/southwest of Algarve, defining an east quadrant flow with a warm and slightly wetter air mass over Portugal (Table 4).

The Anticyclonic Easterly Quadrant flow WT (AQE): It is very similar to E, but with the high located a little further south (over western Bay Biscay) resulting in a greater pressure gradient over Portugal.

The Anticyclonic WT (A), "The Sub- tropical Ridge"**:** it is identified by a high over the Azores - Madeira region, extending to northwestern Iberia and a low system over Greenland and UK, defining a zonal flow to the north of Iberia. This pattern, combined with TL, defines a northwest flow over Portugal. This WT exhibits average properties close to the normal Portuguese summer (Table 4).

The southerly or southeasterly patterns with intrusion of Saharan air over Iberia, are very adverse patterns for wildfires, but they are very rare (about 2%) in the Portuguese summer.

Table 4 – Meteorological parameters of critical weather types: ERA 5 mean values at 12 UTC of geopotential height at 500 hPa (Z500), temperature and relative humidity at 850 hPa (T850 and HR850). WRF data, mean monthly anomalies (June to October), 2 m minimum temperature (Tm), 2m maximum temperature (Tx), and 2 m minimum relative humidity (HRm).

Data	Parameter	Critical weather types					
		NE	E	CQE	AQE	N	A
Mean Values (ERA5)	Z500 (m)	5849	5886	5844	5887	5808	5854
	T850 (°C)	17	18	17	17	14	14
	HR 850 (%)	45	39	48	39	54	49
Anomalies (WRF)	Tm (°C)	0.9	2.1	2.1	1.1	-0.9	-0.9
	Tx (°C)	2.4	4.4	3.5	3.3	-1.5	-0.6
	HRm (%)	-9.0	-15.0	-8.0	-13.0	3.0	0.0

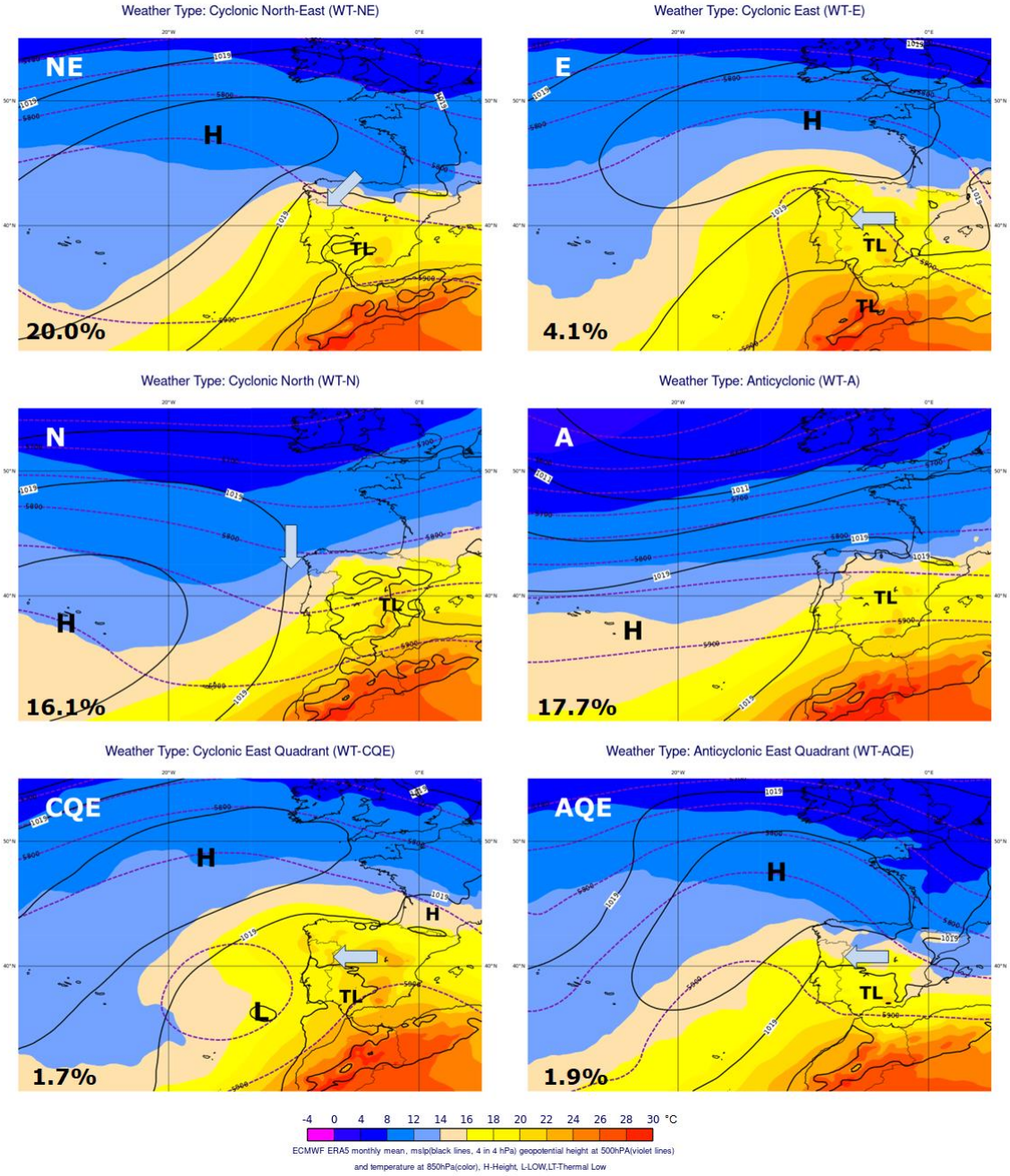

Figure 1- Monthly mean summer (June to October) weather types circulation pattern, from ECMWF ERA5 at 12 UTC in period 1981-2010 and its frequency. NE (Top left), E (top right), N (in middle left), A (in middle right), CQE (bottom, left AQE (bottom right). Mean sea level pressure (mslp, black lines, 4 in 4 hPa), geopotential height at 500

hPa (Z500, lines in violet, 50 in 50 m), temperature at 850 hPa (T850, colour, °C). H – Height, L - Low, TL - Thermal Low, blue arrow - flow direction. WT frequencies (%), June to October, in the bottom left corner.

3. Spatial Fire distribution and Weather Types Frequency

The Figures 2, 3 and 4 shows for each of the ten clusters of NUT III defined in Table 3, the spatial fire distribution for each burned area class in period of 1980-2018, by the six WTs mentioned in chapter 2.2 and 2.3 and three more - AQN, CQN, C - that presented some incidence in large fires in some NUT III. In tables 5, 6 and 7, the frequency of LF in each WT and the respective mean value of Fire Weather Index (FWI) in each of the ten clusters of NUT III is shown.

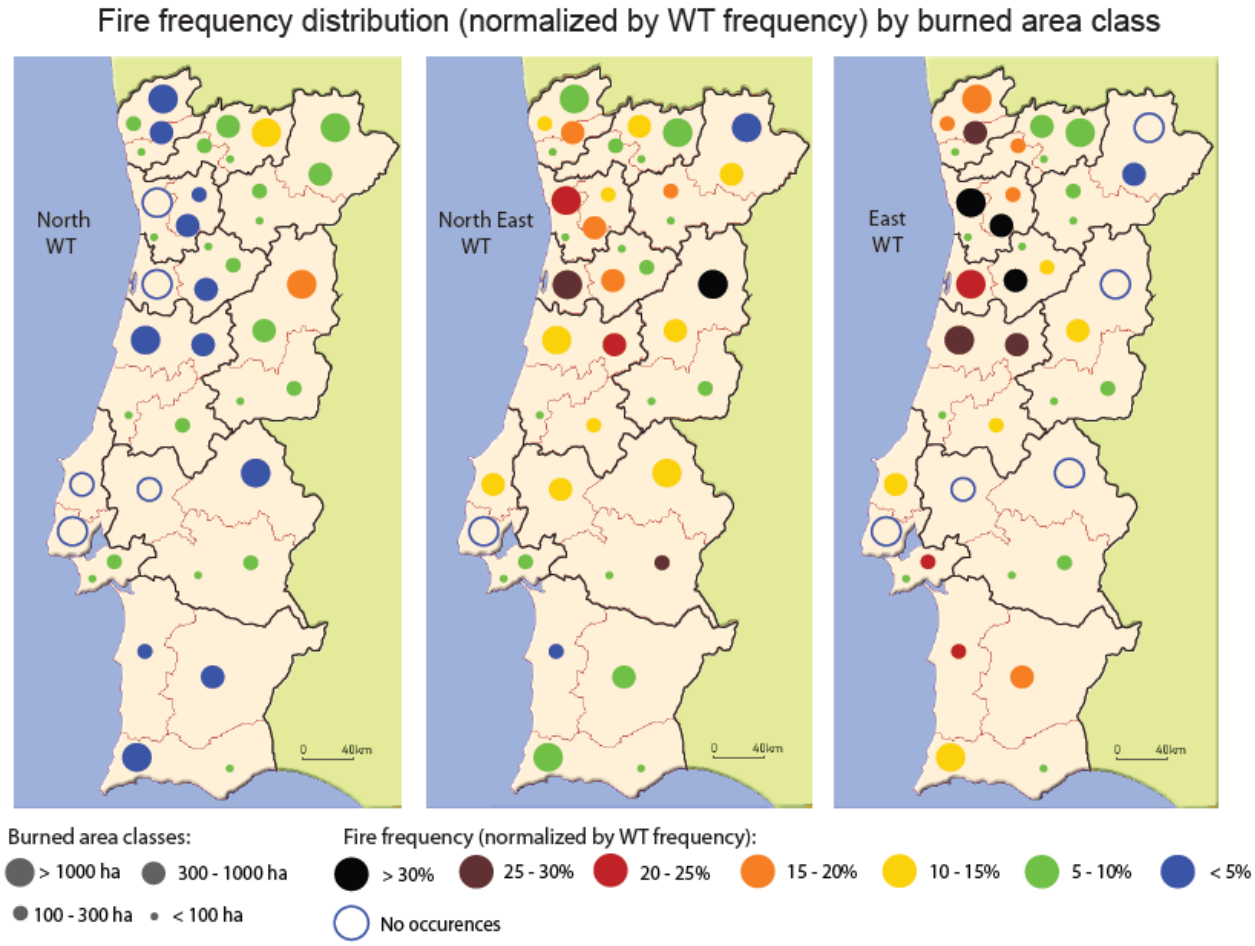

Figure 2 - Spatial Fire Distribution and frequency for each Weather Type in ten clusters of NUT III in Portugal, 1980-2018: N (Left), NE (middle) and E (right).

Table 5 - Fires distribution (%) for the ten clusters of NUT III and for the Weather Types N, NE and E. FWI mean value in NUT III cluster for critical WT and critical days. In bold: Frequency > 25% and FWI > 70.

WT and Burned Area class (normalized daily BA)		**Cl1**	**Cl2**	**Cl3**	**Cl4**	**Cl5**	**Cl6**	**Cl7**	**Cl8**	**Cl9**	**Cl10**
N [BA] ≥ 300ha] (%)		2.6	7.5	0.8	8.0	2.3	7.4	3.7	0.0	2.8	2.5
NE [BA ≥ 300ha] (%)		13.7	10.9	17.9	10.4	20.6	14.8	16.9	8.5	12.5	6.7
E [BA ≥ 300ha] (%)		22.3	7.1	**35.9**	3.0	**29.7**	12.3	**26.4**	9.4	0.0	13.3
FWI	**WT-N**	35.7	38.1	37.4	44.2	39.1	48.8	43.9	43.7	57.5	53.8
	WT-NE	48.4	49.9	51.1	55.9	53.3	60.4	57.2	56.4	63.8	64.6
	WT-E	59.3	63.1	65.6	69.0	68.0	**71.8**	**70.6**	**70.8**	**77.9**	**75.9**

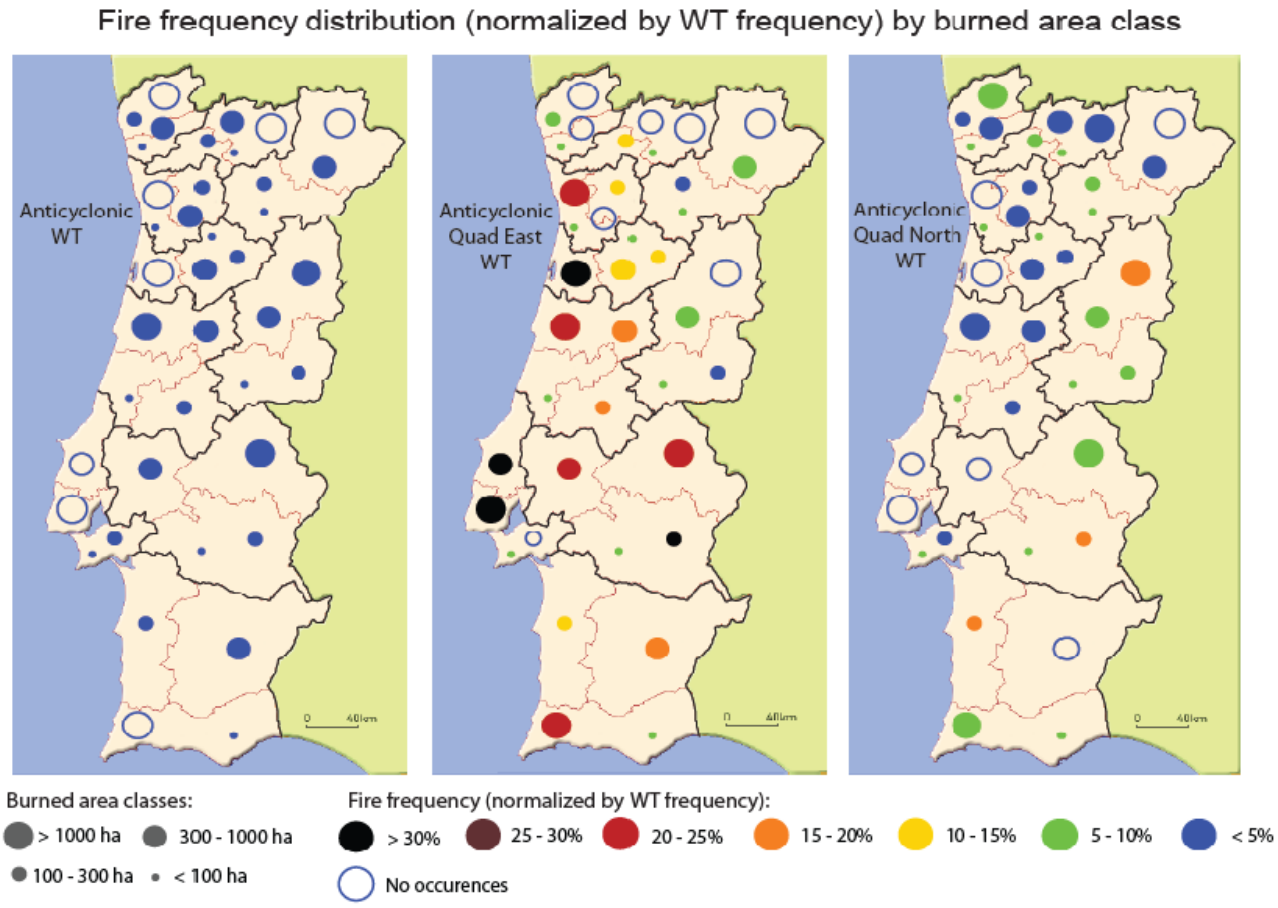

Figure 3 - Spatial Fire Distribution and frequency for each Weather Type in ten clusters of NUT III in Portugal, 1980-2018: A (Left), AQE (middle) and AQN (right).

Table 6 - Fires distribution (%) for the ten clusters of NUT III and for the Weather Types A, AQE and AN). FWI mean value in NUT III cluster for critical WT and critical days. In bold: Frequency > 25% and FWI > 70.

WT and Burned Area class (normalized daily BA)		**Cl1**	**Cl2**	**Cl3**	**Cl4**	**Cl5**	**Cl6**	**Cl7**	**Cl8**	**Cl9**	**Cl10**
A [BA] ≥ 300ha] (%)		0.9	2.0	1.0	1.0	0.7	1.9	1.6	0.0	2.2	0.5
AQE [BA ≥ 300ha] (%)		0.0	0.0	3.3	6.5	17.2	8.6	21.1	**76.0**	**31.6**	**29.3**
AQN [BA ≥ 300ha] (%)		4.0	4.1	0.8	1.4	3.6	9.7	2.0	0.0	6.1	3.0
FWI	**WT-A**	10.1	14.0	12.5	23.7	15.3	27.4	20.6	22.2	30.3	33.0
	WT-AQE	59.0	61.1	62.3	67.3	65.0	73.3	69.7	**70.9**	**75.3**	**80.1**
	WT-AQN	9.1	9.9	11.2	13.5	12.0	14.7	15.6	16.1	20.2	25.5

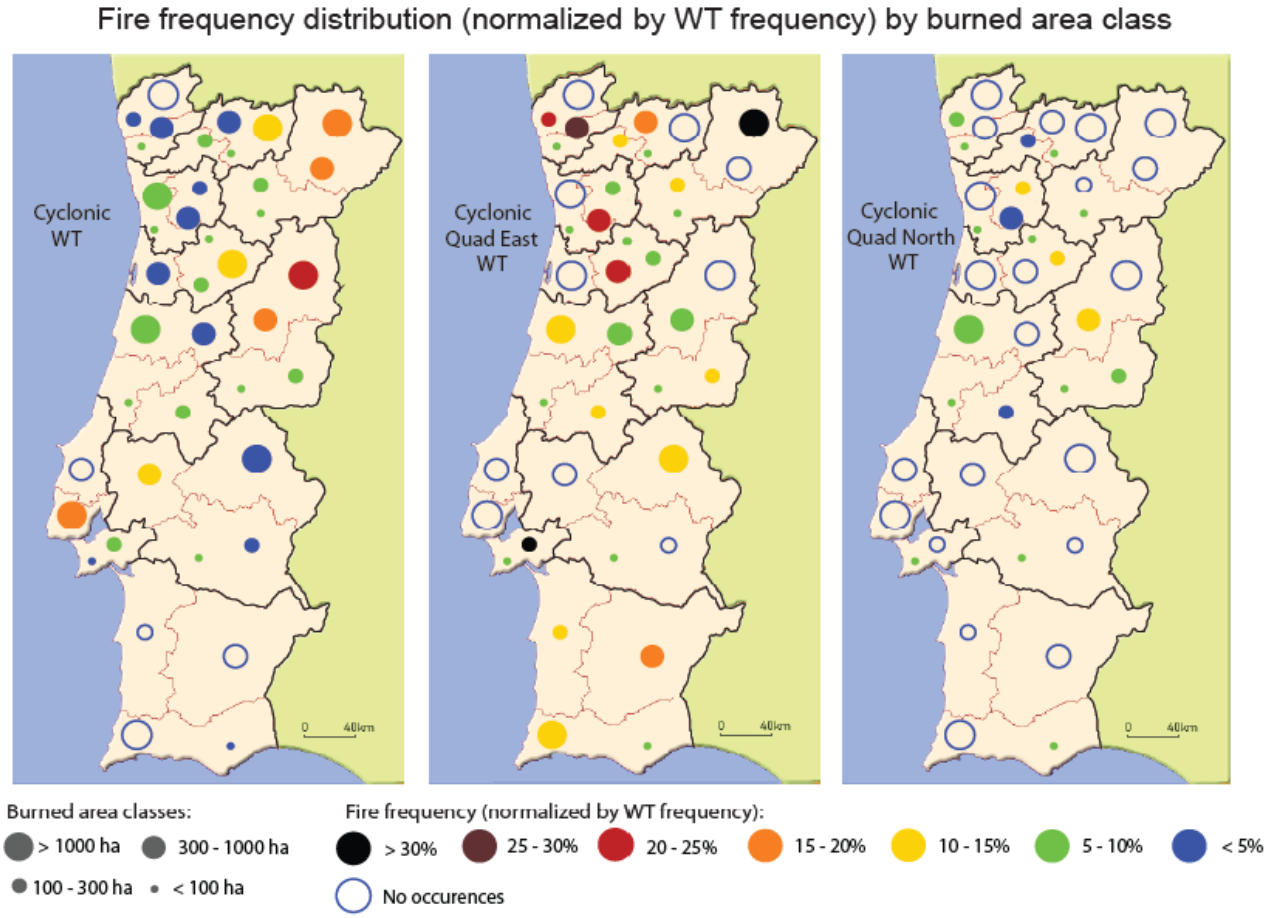

Figure 4 - Spatial Fire Distribution and frequency for each Weather Type in ten clusters of NUT III in Portugal, 1980-2018: C (Left), CQE (middle) and CQN (right).

Table 7 - Fires distribution (%) for the ten clusters of NUT III and for the Weather Types C, CQE and CQN. FWI mean value in NUT III cluster for critical WT and critical day. In bold: Frequency > 25% and FWI > 70.

WT and Burned Area class (normalized daily BA)		Cl1	Cl2	Cl3	Cl4	Cl5	Cl6	Cl7	Cl8	Cl9	Cl10
C [BA] ≥ 300ha] (%)		2.5	5.2	5.2	17.6	5.1	16.2	4.3	6.1	6.4	0.0
CQE [BA ≥ 300ha] (%)		16.3	14.5	19.4	17.1	16.4	8.3	9.2	0.0	8.4	15.7
CQN [BA ≥ 300ha] (%)		0.0	0.0	4.0	0.0	0.0	10.2	3.7	0.0	0.0	0.0
FWI	**C**	52.7	52.6	58.5	53.9	61.2	56.8	53.2	61.8	62.2	62.2
	CQE	62.9	64.8	68.5	65.0	69.7	68.2	65.5	**72.1**	**72.9**	**72.9**
	CQN	9.1	9.3	12.0	9.9	12.9	12.2	12.4	15.0	18.4	18.4

A detailed analysis of fires distribution based on Figures 2, 3, 4 and on tables 5, 6 and 7, is presented below:

- Fires in the two lowest daily burned area classes occur with high frequency (about 70%), mean value for all NUT III, in these critical weather types (NE, E, CQE, AQE, A, N), distributed throughout the territory, especially in the north and centre of the territory, with a higher frequency (60'%) in NE WT and for WTs with an eastern component
- Fires in the two highest daily burned area classes showed a high frequency (about 70%), mean value for all NUT III in NE, E, AQE, CQE and C WTs, being about 90% in NUT III near the coast (clusters l, 3, 5, 7 and 8). Considering only the E WT, there is a high concentration of LF (about 30%) in clusters

l, 3, 5 and 7. On the contrary, in clusters 4 and 9 the E WT has low frequency (< 5%). These cases are associated to high values of mean FWI in each cluster of NUT III, in the order of 60 and 75;

- **N WT** shows some LF distributed throughout the territory, with high frequency (5-10%) in clusters 2, 4 and 6 (far north and eastern territory). The mean value of FWI shows moderate values, in the order of 35 and 45, and above 50 in southern;
- **A WT** shows some LF (< 2%) fires distributed throughout the territory, especially in the North and Central regions and no LF occurrences in NUTIII near the coast. The mean value of FWI shows low values, in the order of 20-30, being below 15 in clusters 1, 2 and 3 and above 50 in the south of Portugal;
- **AQE WT** shows the highest concentration (>35%) of LF in the clusters 8 and 9 and in clusters 10. In the cluster 8, most LF (79%) occurred with this WT. The mean value of FWI shows the highest value of 80 in cluster 10 and values above 60 in all clusters, except in cluster 1, that is 59;
- **C and CQE WTs**, these WTs, especially the C, show LF with higher frequency of about 15% in cluster 4 and 6 (the most eastern part of territory), being more frequent (> 15%) the CQE WT, near the coast and in south (Clusters 1, 2, 3, 5 and 10). These WTs, during summer season, are associated to atmospheric instability under warm and wet air conditions. The mean value of FWI shows high values between 50 and 70.
- **AQN and CQN WTs** show a few cases of LF (< 5%) they are concentrated in most eastern part of territory, especially in cluster 6 (*Serra da Estrela and Beira Baixa*) where these WTs showed a frequency of about 20%. The FWI shows the lowest mean values, in the order of 10 to 25 in most of the territory, being below 10 in most northwestern territory. These WTs are associated to cold air mass and for the CQN precipitation is likely.

4. Final remarks:

This study confirmed that large fires (LF) in Portugal are associated with certain synoptic patterns of circulation. The patterns with flow from the east quadrant are the ones with the highest frequency (> 70%), corresponding to most cases of LF in the NUT III, located in the most western part of territory. In this study, the set of critical Weather Types (WTs) are well identified, as well as the differences in the regional distribution of the LF according to these WTS.

The mean value of FWI in each NUT III or cluster of NUT III, showed large differences, according to the WT and region. The highest mean FWI reaches the maximum value of 80 for AQE WT in cluster 10. Nevertheless, the mean values of FWI for A WT are moderate or low (<25) in most NUT III and the north component hybrid WTs (AQN and CQN) exhibit the lowest FWI, below 20 in most NUT III and below 10 in cluster 1 and 2. These values can thus be taken as historical indicators at regional level of the likelihood of a large fire occurring.

The high frequency of directional or hybrid WTs show the importance of wind-driven fires in LF in Portugal. Additionally, orographic effects have to be considered as they can intensify the large-scale flow characteristics. Ultimately, it will be this combined effect that will support a better relation between the synoptic pattern, described by the Weather Types, and the Large Fires regime.

5. References

Lagerquist, R., Flanning, M. D., Xianli W., and Marsha, G., A. (2017). Automated prediction of extreme fire weather from Synoptic patterns in northern Alberta, Canada, Can. J. For.Res.47: 1175-1183.

Flanning, M.,D., Stocks, B.J., Wotton, B., M., (2000).Climate change and forest fire Sci, Total Environ, 262, 221-229.

Flannigan M., D., Cantin, A.,S., De Groot, W., J., Wotton, M., Newbery, A., Gowman, L.,M. (2013). Global wildland fire season severity in the 21st century. Forest Ecology and Management 294: 54-61.

Crimmins M., A. (2006). Synoptic climatology of extreme fire-weather conditions across the Southwest United States. International Journal of Climatology 26(8): 1001-1016.

Skinner, W., R., Flanning, M., D., Stocks, B., J., Martell, D., L., Wotton, B., M., Todd J., B.,

Mason, K., A., Bosch, E. M. (2002). Theoretical and Applied Climatology, 71, 157-169.

Pereira, M., G., Trigo, R.,M., DaCâmara, C., C., Pereira, J., M.,C., Leite, S., M. (2005). Synotic patterns associated with large summer forest fire in Portugal. Agriculture and Forest Meteorology 129 11-25.

Calheiros T., Nunes, J., P., Pereira, M., G. (2020). Recent Evolution of spatial and temporal patterns of burnt areas and fire weather risk In the Iberian Peninsula, Agriculture and Forest Meteorology 287,107923.

Duane A., Brotons L. (2018). Synoptic weather conditions and changing fire regimes in a

Mediterranean environment, Agricultural and Forest Meteorology 253: 190-202.

Dimitrakopoulos A., Gogi, C., Stamatelos, G., Mitsopoulos I., (2011). Statisyical Analysis of the Fire Environment of Large Forest Fires (>1000 ha) in Greece, Polish J.of Environ.Stud.Vol.20, Nº2, 327-332.

FireStorm Project (Weather and Behaviour of Fire Storms), Project Reference PCIF/GFC/0109/2017- FCT

Trigo, R., M. and DaCâmara, C.C., (2000); Circulation Weather Types and their influence on the precipitation regime in Portugal. International Journal of Climatology, 20 (13), 1559-1581.

Carmo, M., Ferreira, J., Mendes, M., Silva, Á., Silva, P., Alves, D., Reis, L., Novo, I., Xavier Viegas, D. (2021). The climatology of extreme wildfires in Portugal, 1980–2018: Contributions to forecasting and preparedness. International Journal of Climatology 1– 24. https://doi.org/10.1002/joc.7411

ICNF (2020), Instituto da Conservação da Natureza. Fire occurence data base. http://www2.icnf.pt/portal/florestas/dfci/inc/estat-sgif.

Kautz, L., A., Martius,O.,Pinto, J., G., Ramos, A., M., Sousa, P., Woolings, T., (2021). Atmospheric Blocking and Weather Extremes over Euro- Atlantic Sector- A Review, Weather and Climate Dynamics, EGU, https://doi.org/10.5194/wcd-2021-56

Lengthening, expansion and intensification of future fire activities in South-Eastern France

François Pimont*[1]; Julien Ruffault[1]; Thomas Opitz[2]; Hélène Fargeon[1]; Jorge Castel-Clavera[1]; Nicolas Martin-StPaul[1]; Eric Rigolot[1]; Renaud Barbero[3]; Jean-Luc Dupuy[1]

[1]URFM INRAe. Avignon 84914 France, {françois.pimont, julien.ruffault, jorge.castel-clavera, nicolas.martin, eric.rigolot, jean-luc.dupuy}@inrae.fr, {helene.fargeon@gmail.com}
[2] BioSP INRAe. Avignon 84914 France, {thomas.opitz@inrae.fr}
[3] RECOVER INRAe. Aix-en-Provence, {renaud.barbero@inrae.fr}

**Corresponding author*

Keywords

Firelihood; Fire risk severity; fire season length; Mediterranean; projections; climate change;

Abstract

Anticipating future fire activity at global and regional scales is critical in a changing climate. Indeed, fire seasons are expected to lengthen and fire prone areas are expected to expand, but the magnitude, location and timing of such increases remain uncertain. Moreover, an intensification is expected during the core of the fire season of already fire-prone regions. However, quantifying seasonal and spatial impacts of climate change on fire activity is challenging. Here, we projected future fire activities in Southern France using the Firelihood model. This Bayesian probabilistic model operates on a daily basis in 8-km pixels, allowing to analyze both seasonal and spatial distributions of fire activities in a framework integrating stochasticity. Projections were computed for 13 GCM-RCM couples under two RCP scenarios (4.5 and 8.5), assuming that the only factor of change in future fire activity was the daily fire weather. The fire season was defined as the period with fire-activity level higher than the level of the 15th of July of the present period. The fire-prone region corresponded to locations with fire-activity levels higher than the 2nd level of a 5-level fire-activity scale derived from numbers of fires larger than 1ha, 100ha (N1ha and N100ha) and burnt areas (BA).

Simulations under RCP8.5 show that large increases in fire activity should be expected from the mid-century and that the rate of increase should then accelerate, leading to more than three-fold increases for number of fires larger than 100ha by the end of the century. In particular, all metrics except N1ha increased faster than the mean FWI and even the mean DSR. Such increases were partly caused by a massive seasonal lengthening from 42-43 days to up to 100 days, almost equally distributed between spring and autumn. However, the intensification during the present fire season was found to contribute slightly more to the overall increase than the lengthening itself. For example, for N100ha, the intensification would represent a 200 % increase in fire activity with respect to the present seasonal reference, whereas the lengthening outside of the present season would represent +190%. The fire prone area would increase by 140%, shifting from 28 to 67% of the regional total area. However, the intensification inside the already fire-prone region was found to contribute more to the increase than to the spatial expansion. For example, for N100ha, the intensification would represent a 183% increase with respect to the present fire-prone regional reference, whereas the expansion outside of this area would represent +101%.

These drastic increases provide a good indication of the potential lengthening of the fire season, spatial expansion and intensification of future fire activities under RCP 8.5, all three being importantly concerned, but dominated by intensification. Expanding and lengthening suppression policies may allow to mitigate projected increases, but the intensification of fire activity during the core of the fire season overwhelm current fire suppression capacities.

1. Introduction

Anticipating future fire activity at global and regional scales is critical in a changing climate. Indeed, burnt areas have already increased across parts of the globe over the last decades and are expected to keep growing over the century (Abatzoglou and Williams 2016; Amatulli et al. 2013), as the potential for large fires (Barbero et al. 2015; Ruffault et al. 2020). Fire seasons are expected to lengthen and fire prone areas are expected to expand (Flannigan et al. 2013), but the magnitude, location and timing of such increases remain uncertain, especially in the Mediterranean area. Moreover, an intensification is expected during the core of the fire season of already

fire-prone regions, which should become more severe (Dong et al. 2022; Senande-Rivera et al. 2022). Quantifying those changes remain challenging at the regional scale, because of the complex interactions between climate, meteorology, vegetation, humans, and fires. In particular, disentangling seasonal lengthening and spatial expansion from intensification has been seldom addressed.

Here, we estimated future fire activities in Southern France with climatic projections of simulations of the *Firelihood* model. This region has already showed an increase in fire danger mostly attributed to anthropogenic climate change, resulting in drastic increase in the frequency of heat waves, as observed in 2003 (Barbero et al. 2020). The Bayesian probabilistic model allowed to analyze both future seasonal and spatial distributions of fire activities in a framework accounting for stochasticity. Thanks to 300 replications of potential future activities, fire activity metrics were used to compute the expansion, the lengthening and the intensification of future fire activities under two RCP scenarios (4.5 and 8.5).

2. Methods

Fire activity were simulated with *Firelihood*, a probabilistic Bayesian framework designed and validated for stochastic modeling of summer fire activity (number and size) in southeastern France (Pimont et al. 2021). The occurrence of escaped fires (i.e. number of fires larger than 1ha) is modelled through a space-time Poisson process simulating the number of fires occurring in each 8km-pixel and day of year. For each fire, its burnt area (fire size in ha) is assigned by sampling from the estimated distribution of burnt area in each pixel and day. Explanatory variables are the FWI, which summarizes the influence of fire weather on daily fire danger, and the Forest area as a landscape factor representing exposition to wildfire danger. Here, the fire size model was slightly improved, thanks to the inclusion of spatial effects operating at NUTS3 level, to improve the accuracy of spatial predictions.

Present and future FWI were estimated from weather data derived from 13 climate models of the EURO-CORDEX initiative for RCPs 4.5 and 8.5, which were developed for IPCC Assessment Reports and representative of the currently most-likely radiative forcing trajectories. For each of the 26 FWI simulations, Firelihood was used repeatedly by sampling from the posterior distribution of the Bayesian model to provide 300 replications of fire activity, which represent both the distributional uncertainty associated with stochastic processes and the statistical uncertainty from the estimation of model parameters. Such replications allow to compute fire occurrences and sizes in each pixel × day through different fire metrics of numbers of fire larger than certain thresholds (N1ha, N10ha, N100ha, N1000ha) and burnt areas (BA).

To analyse seasonal variations, fire metrics were aggregated by day of year and the fire season was computed for the whole area for three periods (2000-2019, 2040-2059 and 2080-2099). We selected the 15th of July (day of year 196) as the reference date of the present period (2000-2019), as it corresponds to the beginning of the fire season in agreement with considerations of operational services. This reference date was used to identify a reference level for each fire activity metric, which was subsequently used for determining the end of the fire season of the present period, as well as future fire-prone periods. Intensification and lengthening were quantified as the percentages of additional future fire activities with respect to those of the present fire season, occurring respectively inside and outside of the present season.

To analyse spatial variations, fire metrics were aggregated by pixels to determine the fire distributions for three periods (2000-2019, 2040-2059 and 2080-2099) on a yearly basis. In order to facilitate interpretation, fire activity metrics (N1ha, N100ha and BA) were classified according to three different levels corresponding to low, moderate, high, very high and extreme fire activities, by means of "k-means" clustering. We defined the present extent of the present fire-prone region as regions where the fire activity level is at least moderate, so that the expansion corresponds to pixels that would shift from low to moderate levels. The intensification and expansion were quantified as the percentages of additional future fire activities with respect to those of the already fire-prone region, occurring respectively inside and outside of this region.

3. Results and discussion

Firelihood allowed to distinguish the effects of projected climate on several fire metrics, as represented in Figure 1. For RCP 4.5, the increase factor remained limited to 1.6 folds, with a saturation after 2040. Similar results

were observed for RCP8.5.5 until 2040, but the increase factor reached between 2.1 and 3.4 folds for respectively 1 ha and 100 ha fires near the end of the century. 1000 ha fires and burnt areas increased slightly slower than 100 ha-fires, which is explained by a steeper response to FWI for 100 ha than for larger fire size, especially in the 20-35 range (Pimont et al. 2021; Fig. 3b). This could reflect that landscape factors, such as fuel continuity or natural barriers (Mediterranean Sea, riparian zones) induce a constraint on the development of very large fires. Another explanation could be some limitations in the FWI for rating consistently the fire danger in Southern France, as already pointed out in Pimont et al. (2021). For all fire activity metrics, the increase was faster than the one of the mean FWI (1.76 folds) and even DSR (2.2), except for 1ha fires which increased slower than the DSR. This is an important result, as the mean DSR -also called SSR- is often used to estimate the difficulty to control fires and seasonal length (Flannigan et al. 2013).

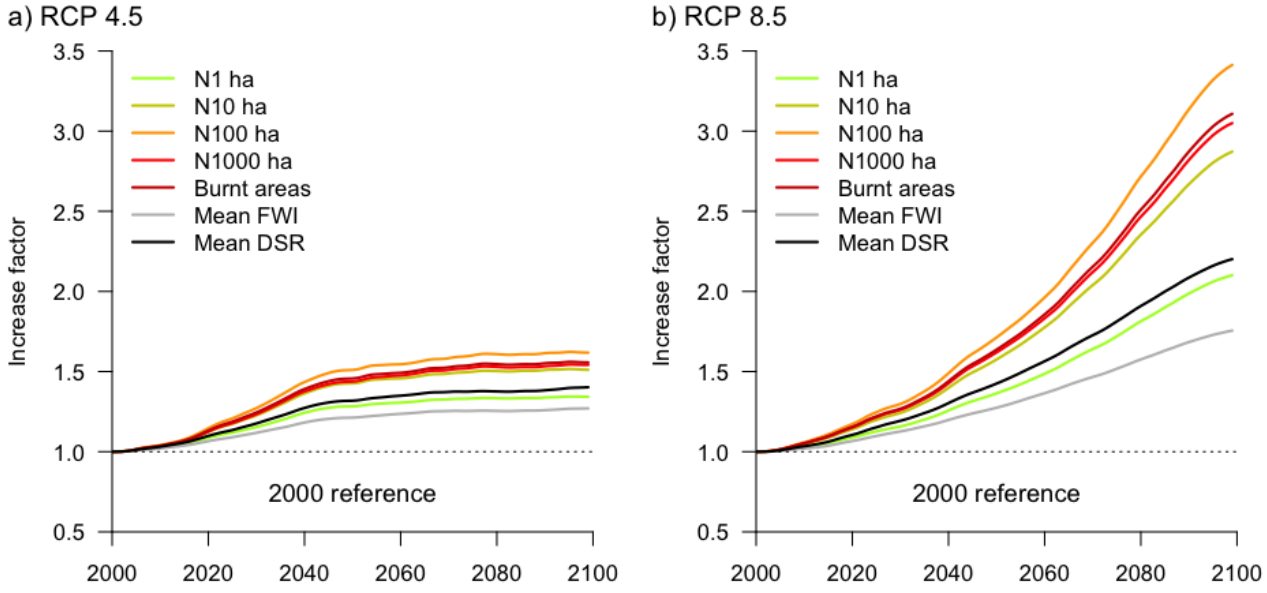

Figure 1- Trends in fire activity metrics under a) RCP 4.5 and b) RCP 8.5

Future expected fire activity increased for all days of the warm season (between day 148 and 309, Fig. 2), with a greater absolute increase in summer than in spring and fall. These increases translate into the lengthening of the fire season, as well as into the intensification of the fire activities during the present fire season. The lengthening was roughly equally distributed between spring and fall, differing by only a few days. Such a symmetric lengthening is expected in other temperate ecoregions, contrary to other regions where the fire season typically ends with the arrival of monsoonal precipitation (Barbero et al. 2015; Dong et al. 2022). The worse increases (RCP8.5 in 2090) were observed for N100ha and BA, showing +56 days by the end of the century. With respect to fire activities occurring during the present fire season, an increase by roughly 180-200% should be expected from intensification for N100ha and BA. With respect to the same reference, an increase by 180-190% is expected for new fire activity occurring during the lengthening period. The intensification in N1ha was slightly smaller than lengthening.

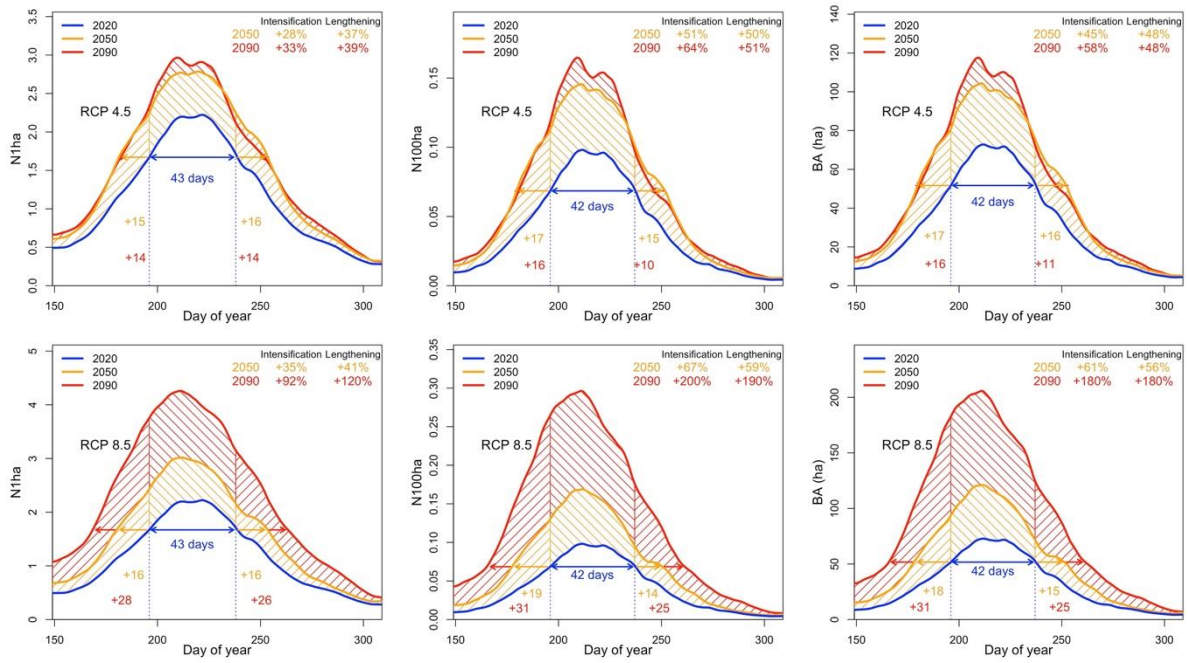

Figure 2- Seasonal lengthening and intensification for 1ha fires (N1ha), 100ha fires (N100ha) and burnt areas (BA) for RCP 4.5 (up) and 8.5 (down). Downward and upward hatches correspond to respectively the intensification and the lengthening of the fire season. There are expressed in percentages of the metric sum with respect to the present fire season.

Fire activity maps derived from the five levels are plotted in Fig. 3 for the three different periods and scenario RCP 4.5 and 8.5. The fire prone region should expand from 28% to 45% and 67% of the region of interest, with a strong expansion in the western part of the region. A potential expansion in Corsica and eastern parts was apparently more limited, probably because of mountainous barriers. As a result, the major part of expected increase was related to intensification in fire prone areas, which was roughly twice as large as the part related to expansion, despite of the large spatial expansion (Table 1). These spatial projections of fire activity were consistent with expected trends in FWI in France, which anticipate a strong heat-induced increase in fire danger in the French already fire-prone region (Fargeon et al. 2020).

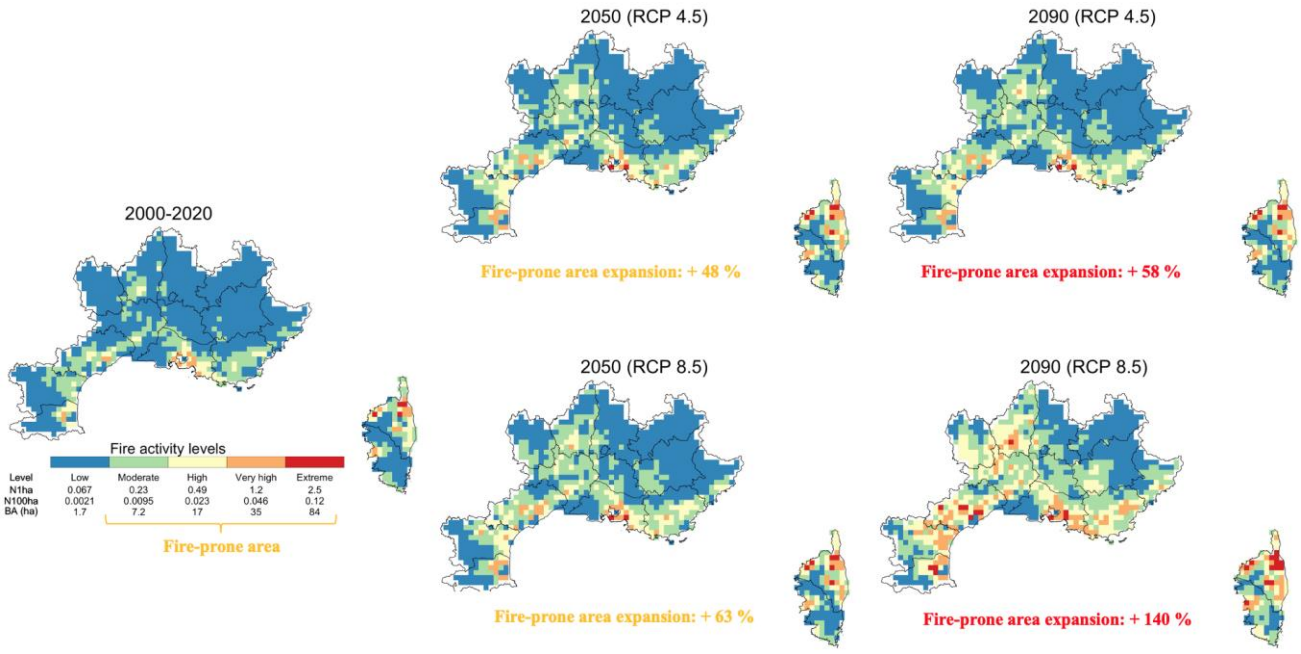

Figure 3- Fire activity level maps (Fire prone area expansion corresponds to pixels that should turn from low to moderate level).

Table 1- Percent fire activity changes due to the intensification and the expansion (Expressed in percentages of the metric sum over the fire-prone area for the present period).

RCP	Period	Fire metric	Intensification	Expansion
4.5	2050	N1	+30%	+14%
		N100	+54%	+21%
		BA	+48%	+20%
	2090	N1	+32%	+17%
		N100	+58%	+26%
		BA	+52%	+25%
8.5	2050	N1	+34%	+18%
		N100	+64%	+29%
		BA	+57%	+27%
	2090	N1	+90%	+52%
		N100	+183%	+101%
		BA	+162%	+93%

This study assumed that everything but climate remained equal, an assumption common to many projection studies, but which becomes questionable facing such large changes and long-term perspective. Land use and land cover could be included in the modelling framework of Firelihood (Castel-Clavera et al. 2022), but projecting future values for these variables remains challenging even if scenarios are becoming available. Moreover, even if fire return intervals remained quite large in 8-km pixels, local reburns can be frequent (Ganteaume and Barbero 2019), so that the increasing impact of fire-activity on fuel structure should be accounted. Finally, the expansion, lengthening and intensification were estimated assuming that suppression and prevention will remain identical. Expanding and lengthening management may allow to mitigate projected increases, at the cost of significant expansion of these policies. The intensification could be even more problematic, as suppression might be more frequently overflowed by simultaneous escaped fires (N1ha) and large fire events (N100ha).

4. Conclusion

These drastic increases provide a good indication of the potential lengthening of the fire season, spatial expansion and intensification of future fire activities under RCP 8.5, all three being importantly concerned, but dominated by the intensification in the case the spatial expansion. Lengthening and expansion might be mitigated by an expansion of the fire prevention and suppression policies, but the intensification might raise most operational concerns.

5. References

Abatzoglou JT and Williams AP (2016) Impact of anthropogenic climate change on wildfire across western US forests PNAS 113 11770–5

Amatulli G et al. (2013) Estimating future burned areas under changing climate in the EU-Mediterranean countries Science of The Total Environment 450–451 209–22

Barbero R et al. (2015) Climate change presents increased potential for very large fires in the contiguous United States. International Journal of Wildland Fire 24, 892

Barbero R et al. (2020) Attributing Increases in Fire Weather to Anthropogenic Climate Change Over France. Frontiers in Earth Science 8, 104

Castel-Clavera et al. (2022) Modelling the influence of regional drivers on spatio-temporal patterns of wildfire activity. IX International Conference on Forest Fire Research

Dong C et al. (2022) The season for large fires in Southern California is projected to lengthen in a changing climate. Commun Earth Environ 3, 22

Dupuy J et al. (2020) Climate change impact on future wildfire danger and activity in southern Europe: a review Annals of Forest Science 77 35

Fargeon H et al. (2020) Projections of fire danger under climate change over France: where do the greatest uncertainties lie? Climatic Change 160 479–93

Flannigan M et al. (2013) Global wildland fire season severity in the 21st century. For Ecol Manag 294:54–61
Ganteaume A and Barbero R (2019) Contrasting large fire activity in the French Mediterranean. Natural Hazards and Earth System Sciences 19, 1055–1066
Pimont F et al. (2021) Prediction of regional wildfire activity in the probabilistic Bayesian framework of Firelihood. Ecological Applications 31 e02316
Ruffault J et al. (2020) Increased likelihood of heat-induced large wildfires in the Mediterranean Basin. Scientific Reports 10, 13790
Senande-Rivera M et al. (2022) Spatial and temporal expansion of global wildland fire activity in response to climate change. Nature Communications 13, 1208

Long-term erosion and the impact of wildfires: two different approaches

Joana Parente*[1]; João Pedro Nunes[1,2]; Jantiene Baartman[2]; Dante Föllmi[2]

[1] cE3c - Center for Ecology, Evolution and Environmental Changes & CHANGE - Global Change and Sustainability Institute, Sciences Faculty, University of Lisbon, Portugal {joaparente@gmail.com; joao.carvalhonunes@wur.nl}
[2]Soil Physics and Land Management Group, Wageningen University & Research, the Netherlands, {jantiene.baartman@wur.nl; dante.follmi@gmail.com}

**Corresponding author*

Keywords

Erosion; Sediment connectivity; post-fire; index of connectivity; modelling approach

Abstract

Rivers act as a network of channels that carry water, sediment, and energy downstream. On the heterogeneous area of the watershed, some areas might be responsive to disturbance (e.g., wildfires and droughts), while others may be resistant to the change. As a disturbance, fire is usually regarded as a key agent of soil erosion and land degradation. Fires are thought to be responsible for: (i) overland flow and reduction of the capacity of infiltration; (ii) increase of the availability of ash and debris and disruption of the soil nutrient cycle; and (iii) increase of connectivity across the watershed. The potential fire effects on soils and aquatic resources have created a strong demand for a post-fire sediment loss prediction tool. Taking this in mind, this study aims to assess post-fire soil erosion patterns at the decadal scale comparing different approaches. The methodology comprises (i) a process-based model that is able to investigate long-term and large-scale spatial landscape evolution, LAPSUS model; (ii) an index that represents a connectivity assessment based on local landscape information, the Borselli Index of Connectivity (IC); and (iii) and the sediment export that represents the sediment eroded that actually reaches the stream based on local landscape information, combining the IC with the Revised Universal Soil Loss Equation (RUSLE) model. Results include a comparison between the approaches used in the context of specific fire events between 1979 and 2020 for the Agueda watershed in central Portugal. The authors believe that assessing the spatial-temporal evolution of connectivity in the actual landscape with the appropriate tool is extremely important to estimate the probability that a given part of the landscape transfers its sediments downstream.

1. Introduction

Rivers act as a network of channels that carry water, sediment, and energy downstream (1). On the heterogeneous area of the watershed, some areas might be responsive to disturbance events (e.g., wildfires and droughts), while others may be resistant to the change (Khan et al., 2021).

Fire disturbance is usually regarded as a key agent of soil erosion and land degradation (Shakesby, 2011). Fire is pointed as responsible for: (i) overland flow and reduction of the capacity of infiltration (Basso et al., 2021; Fernández et al., 2010); (ii) increase of the availability of ash and debris and disruption of the soil nutrient cycle (Basso et al., 2021); and (iv) increase of connectivity across the watershed (van der Grift, 2021). The potential fire effects on soils and aquatic resources have created a strong demand for a post-fire sediment loss prediction tool (Fernández et al., 2010; Larsen & MacDonald, 2007; Vieira et al., 2014).

It is then important to have a working connectivity definition and usable indices and models to assess its spatial and temporal distribution. In this study, the authors work with the sediment connectivity definition recognized by the scientific community: the capacity of sediment to move through the watershed (Bracken & Croke, 2007; Crema & Cavalli, 2018; Hooke, 2003). To assess sediment connectivity spatial and temporal distribution the authors use three different approaches based on information available in a GIS environment: the Index of Connectivity (IC)(Borselli et al., 2008), the long-term landscape evolution model LAPSUS (Landscape Process Modelling at Multi-Dimensions and Scales) (Baartman et al., 2010; Temme et al., 2011), and the Sediment Export (SE) approach (Sharp et al., 2020).

This study seeks to answer the specific research questions: (i) "What aspect of connectivity do the different indexes and models measure?"; and (ii) "How these approaches are related?".

2. Data and Methods

This study focused on the Águeda watershed located in the central area of mainland Portugal. This watershed is a representative region where different agents contribute to landscape evolution/modification, and where sediment connectivity should consider the contribution of such agents to erosion and transport and their influence on the morphological settings that control sediment conveyance (Cavalli et al., 2013).

To assess sediment connectivity the authors used IC, LAPSUS, and SE for different soil burn severity scenarios for 1979-2020. These approaches need as inputs: (i) fire severity, (ii) land use information, (iii) USLE-C factor values; and (iv) annual soil parameters (P-factor, LS-factor, K-factor, and R-factor). To test independence and find interactions between the three approaches the authors used contingency tables, accuracy metrics and statistical measures of association.

3. Results and discussion

Results include the connectivity description and the comparison between the approaches in the context of specific fire events between 1979 and 2020. The three approaches take different times to be computed, due to the necessity of LAPSUS need to be calibrated. From the 3 approaches, LAPSUS needs more inputs and IC fewer inputs. The relation is better between LAPSUS and SE than between LAPSUS and IC. In addition, this relation between LAPSUS and the other approaches depends on the target year and/or fire characteristics.

4. Conclusion

This study presents 3 different approaches to assess sediment connectivity which lead to the identification of potential sources of ash and post-fire contaminants. The authors believe the results of this study are extremely important to estimate the probability that a given part of the landscape transfers its downstream.

5. Acknowledgements

This work was financed by the project FRISCO - managing Fire-induced RISks of water quality Contamination (PCIF/MPG/0044/2018) and supported by National Funds through FCT - Foundation for Science and Technology under the project UIDB/04033/2020, and funding attributed to the CE3C research center (UIDB/00329/2020).

6. References

Baartman, J. E. M., Schoorl, J. M., Veldkamp, T. A., & Ritsema, C. J. (2010). Erosion in a landscape evolution context : LISEM and LAPSUS. Library.Wur.Nl, 12(March), 3480. https://library.wur.nl/WebQuery/wurpubs/fulltext/14381

Basso, M., Mateus, M., Ramos, T. B., & Vieira, D. C. S. (2021). Potential Post-Fire Impacts on a Water Supply Reservoir: An Integrated Watershed-Reservoir Approach. Frontiers in Environmental Science, 9, 201. https://doi.org/10.3389/fenvs.2021.684703

Borselli, L., Cassi, P., & Torri, D. (2008). Prolegomena to sediment and flow connectivity in the landscape: A GIS and field numerical assessment. Catena, 75(3), 268–277. https://doi.org/10.1016/j.catena.2008.07.006

Bracken, L. J., & Croke, J. (2007). The concept of hydrological connectivity and its contribution to understanding runoff-dominated geomorphic systems. Hydrological Processes, 21(13), 1749–1763. https://doi.org/10.1002/HYP.6313

Cavalli, M., Trevisani, S., Comiti, F., & Marchi, L. (2013). Geomorphometric assessment of spatial sediment connectivity in small Alpine catchments. Geomorphology, 188, 31–41. https://doi.org/10.1016/j.geomorph.2012.05.007

Crema, S., & Cavalli, M. (2018). SedInConnect: a stand-alone, free and open source tool for the assessment of sediment connectivity. Computers and Geosciences, 111, 39–45. https://doi.org/10.1016/j.cageo.2017.10.009

Fernández, C., Vega, J. A., & Vieira, D. C. S. (2010). Assessing soil erosion after fire and rehabilitation treatments in NW Spain: Performance of rusle and revised Morgan-Morgan-Finney models. Land Degradation and Development, 21(1), 58–67. https://doi.org/10.1002/ldr.965

Hooke, J. (2003). Coarse sediment connectivity in river channel systems: A conceptual framework and methodology. Geomorphology, 56(1–2), 79–94. https://doi.org/10.1016/S0169-555X(03)00047-3

Khan, S., Fryirs, K., & Bizzi, S. (2021). Modelling sediment (dis)connectivity across a river network to understand locational-transmission-filter sensitivity for identifying hotspots of potential geomorphic adjustment. Earth Surface Processes and Landforms. https://doi.org/10.1002/ESP.5213/FORMAT/PDF

Larsen, I. J., & MacDonald, L. H. (2007). Predicting postfire sediment yields at the hillslope scale: Testing RUSLE and Disturbed WEPP. Water Resources Research, 43(11). https://doi.org/10.1029/2006WR005560/FORMAT/PDF

Shakesby, R. A. (2011). Post-wildfire soil erosion in the Mediterranean: Review and future research directions. Earth-Science Reviews, 105(3–4), 71–100. https://doi.org/10.1016/J.EARSCIREV.2011.01.001

Sharp, R., Douglass, J., Wolny, S., Arkema, K., Bernhardt, J., Bierbower, W., Chaumont, N., Denu, D., Fisher, D., Glowinski, K., Griffin, R., Guannel, G., Guerry, A., Johnson, J., Hamel, P., Kennedy, C., Kim, C. K., Lacayo, M., Lonsdorf, E., … Wyatt, K. (2020). SDR: Sediment Delivery Ratio — InVEST documentation. In R. Sharp, J. Douglass, & S. Wolny (Eds.), InVEST 3.10.2.post63+ug.ga451015 User's Guide. The Natural Capital Project, Stanford University, University of Minnesota, The Nature Conservancy, and World Wildlife Fund. https://storage.googleapis.com/releases.naturalcapitalproject.org/invest-userguide/latest/sdr.html?highlight=rainfall%20erosivity%20index

Temme, A. J. A. M., Claessens, L., Veldkamp, A., & Schoorl, J. M. (2011). Evaluating choices in multi-process landscape evolution models. Geomorphology, 125(2), 271–281. https://doi.org/10.1016/j.geomorph.2010.10.007

van der Grift, S. (2021). The effect of wildfires on sediment connectivity using the AIC method - Long term analysis for the Águeda catchment in Portugal from 1979 until 2019. Wageningen University.

Vieira, D. C. S., Prats, S. A., Nunes, J. P., Shakesby, R. A., Coelho, C. O. A., & Keizer, J. J. (2014). Modelling runoff and erosion, and their mitigation, in burned Portuguese forest using the revised Morgan-Morgan-Finney model. Forest Ecology and Management, 314, 150–165. https://doi.org/10.1016/j.foreco.2013.12.006

Mediterranean fire danger classes based on the Canadian Forest Fire Weather Index System, taking into account the Fire Radiative Power products from SEVIRI/MSG satellite

Mafalda Silva[1]; Rita Durão[1,2]; Catarina Alonso[1]; Célia Gouveia[1,3]

[1] Instituto Português do Mar e da Atmosfera (IPMA), Portugal.
[2] Centro de Recursos Naturais e Ambiente, Instituto Superior Técnico, Universidade de Lisboa
[3] Instituto Dom Luiz, Faculdade de Ciências da Universidade de Lisboa, Portugal,
{ana.silva, rita.durão, catarina.alonso, celia.gouveia}@ipma.pt
**Corresponding author*

Keywords

Canadian Forest Fire Weather Index System, Fire Radiative Power, Fire Danger Thresholds, SEVIRI/MSG satellite data, Mediterranean

Abstract

Fire danger rating systems (FDRS) are widely used across the world for many purposes, from planning for the daily deployment of fire suppression resources to the evaluation of fire management strategies. FDRS can also be incorporated into different types of models and regions to assess the short and long-term effects of specific fire regimes and fire management policies. The Canadian Forest Fire Weather Index System (FWIS) is a widely known FDR system, being extensively applied for fire danger early warning in several regions around the world, namely in Europe. The FWIS includes a set of six sub-indices, based on meteorological data, to predict fire weather danger and fire behavior over regions under study. In order to have a reliable assessment of the fire danger based on the FWIS, it is essential to define the most suitable threshold values for each danger class of the FWIS sub-indices over different regions. To establish those limit values for each class of the FWIS sub-indices, historical percentiles were computed for the period understudy, taking into account the occurred fire events (hotspots), despite the lack of information regarding fire events history and its relation to FWIS sub-indices. To accomplish the proposed validation, our approach is based on Fire Radiative Energy (FRE) released by each fire event that occurred in the Mediterranean region, over the study period. The FRE is computed from Fire Radiative Power (FRP) product as obtained from MSG/SEVIRI, generated and disseminated in near real-time by EUMETSAT in the framework of Land Surface Analysis Satellite Applications Facility (LSA SAF). Since FRP estimates the radiative power emitted by a given fire, it can be linked to local fuel burned amounts and be used as a proxy of fire intensity. By integrating FRP measures emitted during the lifetime of the fires that occurred over the regions under study, an estimate of the total FRE released can be easily obtained for each event. To obtain the FRE data for this work, it was considered the period of available FRP/SEVIRI data, from March 2010 to October 2021. Threshold values of each defined danger class for the FWI, FFMC, and ISI indices were calculated considering the total FRE hotspots registered, in agreement with the different fire regimes of the Mediterranean region. Since extreme wildfire patterns in Southern Mediterranean countries have been increasing over the last years, FRP/FRE products are a key tool to monitor and improve fire managing activities, preparedness-including planning for deployment of fire suppression resources, over affected regions.

1. Introduction

To establish fire danger conditions in a given location or region, a fire danger rating system (FDRS) or a model should be able to reproduce short and long-term variations of temperature, relative humidity, precipitation, and wind intensity, in the variation of fuel humidity, that can be used to forecast fire occurrence and it (Di Giuseppe et al., 2016, 2020; Stocks et al., 1989). FDRS are often included or linked to different types of models to assess the long-term effects of fire regimes and specific fire management policies (Dacamara et al., 2014; Durão et al., 2010; Flannigan et al., 2001; Pereira et al., 2011; 7. San-Miguel-Ayanz et a., 2012, 2013; Sousa et al., 2015). FDRS like the Canadian Forest Fire Weather Index System (FWIS) transforms daily meteorological observations into relatively simple indices that can be used to forecast fire weather danger, the dead fuel moisture content and consequentially fire behavior, and impacts; being widely used for a fire danger early warning in several regions around the world, namely in Europe (Stocks et al., 1989; Van Wagner, 1987). To obtain a reliable assessment of the fire danger based on the FWIS it is crucial to determine the limit values for

each fire danger class of the FWIS sub-indices for a given region and day. One of the simplest methods to define the fire danger classes is to compute daily percentiles based on historical data, but this method lacks information regarding wildfire history and its relation to FWIS sub-indices. In order to overcome this lack of information, the Fire Radiative Power products, generated and disseminated in near real-time by EUMETSAT Land Surface Analysis Satellite Applications Facility, were used in this validation work. Since FRP consists of estimates of the radiative power emitted by fires it can be directly linked to the amount of fuel burned and smoke production (Wooster et al., 2005), being used as a proxy of fireline intensity helping to develop and improve suppression and mitigation strategies (Johnston et al., 2017; Smith and Wooster, 2005). Namely, in Mediterranean countries, the use of this type of FRP product is very useful, since extreme fires have been increasing in the last years, presenting an eruptive or erratic behavior pattern, running out the responsiveness and suppression capacities of local authorities (Dacamara et al., 2019; Evin et al., 2018; Fernandes et al., 2016; Pinto et al., 2020; San-Miguel-Ayanz et al., 2018).

2. Materials and Methods

2.1. Study Area

The study area of this work comprises the countries of the Mediterranean basin, accordingly to figure 1.

To be easier to evaluate and compare the local fire danger thresholds, the Mediterranean area was split into small areas of interest: Portugal (PT), Iberian Peninsula (IP), North Africa 1 (NA1), North Africa 2 (NA2), Southern France (SF), Italy (IT), Greece, Turkey and Cyprus (GTC), as can be seen in Fig 1 and Table 1.

2.2. Fire Radiative Energy

The analysis of the fire severity is based on the Fire Radiative Energy (FRE) released by each fire, computed as a daily accumulation of Fire Radiative Power (FRP) delivered by the Land Surface Analysis Satellite Applications Facility (LSA-SAF) from EUMETSAT (Trigo et al., 2011; Wooster et al., 2005). The FRP (Heward et al., 2013), registers data on the position, timing, and fire radiative power (in MWatts) output per pixel of fire events detected every 15 minutes. FRP is disseminated for the full spatio-temporal resolution of SEVIRI (*Spinning Enhanced Visible and Infrared Imager*) imager on board the Meteosat Second Generation (MSG) series of EUMETSAT geostationary satellites (Wooster et al., 2015), provided for the whole MSG disk (up to 72◦ view zenith angle), where each active-fire position is represented at the center of the SEVIRI pixel, with a 3 km spatial sampling distance at sub-satellite point (decreasing away from the West African sub-satellite point). Since FRP estimates the radiative power emitted by fire events, integrating it over the length of a fire event, an estimation of the total Fire Radiative Energy (FRE) emitted by each one can be computed. By definition, the daily FRE is the energy released by a fire at a given pixel, by the integration of the 15-minute FRP records, accordingly to Pinto *et al* (Pinto et al., 2018a, 2018b)' formula:

$$E_{pd} = 0.9 \times \left(\sum_{k=1}^{96} \mathrm{FRP}_{kp}\right)_d,$$

where k is the daily sequence of 15-minutes, FRP_{kp} is the fire radiative power (in megawatts) in a given pixel p of image k, and the 0.9 factor converts the obtained result into gigajoules units (GJ). In addition, the FRE can be defined as the emitted radiant energy released during biomass combustion, being proportional to the total amount of biomass burned during a given fire (Pinto et al., 2018a, 2018b).
The FRE values were computed for all the fire events that occurred over the period under study, as can be seen in Table1.

2.3. Meteorological Fire danger

Briefly, the FWIS consists of six sub-indices that account for the effects of fuel moisture and weather conditions on fire behavior, by providing numeric ratings of relative potential for wildfire occurrence (Stocks et al., 1989; Van Wagner, 1987; Wotton, 2009). The first three indices of FWIS (FFMC, DMC, and DC) are the fuel moisture codes, which are numeric ratings of the moisture content of litter and other fine fuels, and the average moisture content of deep and compact organic layers. The remaining FWIS indices (ISI, BUI, and FWI) are fire behavior indices, which represent the rate of fire spread, the fuel available for combustion, the frontal fire intensity, or the fire weather index. The values of these behavior indices increase as the fire danger increases (Stocks et al.,

1989; Van Wagner, 1987; Wotton, 2009). The previous indices selected to perform this validation are the Fire Weather Index (FWI), the Fine Fuel Moisture Code (FFMC), and the Initial Spread Index (ISI).

FWI is defined as a numerical rating of the potential frontal fire intensity, that indicates fire intensity by combining the rate of fire spread given by the Initial Spread Index (ISI), with the amount of fuel being consumed given by the Build-Up Index (BUI). FFMC is defined as an indicator of the moisture content in litter and other fine fuels less than 1 cm in diameter (needles, mosses, twigs), being representative of the top litter layer less than 1-2 cm deep. FFMC values change rapidly because of a high surface area to volume ratio, and direct exposure to changing environmental conditions (Van Wagner, 1974, 1987; Van Wagner et al., 1985; Wotton, 2009). ISI is defined as the numeric rating of the expected rate of fire spread. It is based on wind speed and FFMC. Like the rest of the FWI system components, ISI does not take fuel type into account. Actual spread rates vary between fuel types at the same ISI.

The indices of the Canadian Forest Fire Weather Index System (FWIS) are computed based on the meteorological parameters (temperature at 2 m, relative humidity, wind speed at 10 m, and accumulated precipitation in 24 h) of the short-term forecasts of the numerical forecast models delivered by the European Center for Medium-Range Weather Forecasts, ECMWF. Then, FWIS data delivered by the ECMWF are interpolated into the MSG grid, generated, and distributed as layers of the Fire Risk Map (FRM) product of the LSA-SAF under the framework of the Land Surface Analysis Satellite Applications Facility (LSA SAF) project.

2.4. Methodology

The proposed calibration is based on two main steps: firstly the Fire Radiative Energy (FRE) emitted by the fires was computed as a daily accumulation of the Fire Radiative Power (FRP) from MSG/SEVIRI, over the period 2010-2021; secondly, the fire weather danger percentiles of the FWI, FFMC, and ISI indices were extracted for the areas of interest, to assess local fire weather conditions and the different fire Mediterranean regimes.

Considering the study period from March 2010 to October 2021, the P_k percentiles were extracted for the FWI, FFMC, and ISI indices, namely percentiles P25, P50, P60, P65, P70, P75, P80, P85, P90, P95, P98, and P99, considering the total number of hotspots occurred over the study areas.

Additionally, since 2000 GJ is the typical daily amount of the energy released by a severe fire and very difficult to suppress (Pinto et al., 2018), this calibration analysis was performed in two steps - without considering any FRE threshold (FRE > 0 GJ) and considering an FRE severity threshold of 1500 GJ (FRE > 1500 GJ). The rationale is to identify the Mediterranean areas with the most severe wildfires.

3. Results and Discussion

The number of the total events registered, without considering any FRE threshold (FRE ≥ 0 GJ), is 246444 over almost 12 years of the study period. The number of events registered considering the threshold of FRE >1500 GJ is 16366, which represents 6.6% of the total events, as can be seen in Table1.

Results show that a major part of the fire events considering FRE ≥ 0 GJ, occurs in Greece, Turkey, and Cyprus (GTC) region with approximately 35% of the total hotspots since this area spans most of the Mediterranean basin. Conversely, considering the 1500 GJ threshold, the Iberian Peninsula (IP) stands out with approximately 51% of the total hotspots, followed by Italy (IT) (18,3%), North Africa 2 (NA2) (18,1%), Greece, Turkey, and Cyprus (GTC) (16%), North Africa 1 (NA1) (3,2%), and finally South France (SF) (2,8%). However, it should be noted that some selected areas are overlaid.

To compare and validate the results, we consider the European thresholds of the European Forest Fire Information System (EFFIS), established by the European Commission for supporting the services in charge of the protection of forests against fires in the EU and neighboring countries (http://effis.jrc.ec.europa.eu).

The EFFIS network adopted, as well, the Canadian Forest Fire Weather Index system with the main goal of providing a harmonized picture of the spatial distribution of fire danger levels throughout Europe, the Middle East, and North Africa (https://effis.jrc.ec.europa.eu/about-effis/technical-background/fire-danger-forecast). Currently, FWI is classified into seven classes [Very Low, Low, Moderate, High, Very High, Extreme, and

Very Extreme] accordingly to the update of the last fire season whereas; FFMC and ISI are still classified in five classes (see Table 2.).

The obtained FWI percentiles (P50, P75, P85, P95, P99), considering FRE >1500 GJ, for the seven areas of interest, are presented in Table 3. It can be seen, that 50% of the fire events that occurred in the Mediterranean basin and all areas, belong to the four last fire danger classes: High, Very High, Extreme, and Very Extreme, accordingly to EFFIS classification (see Table 2).

Histograms for the FWI were computed for the Mediterranean basin and the Portuguese hotspots (Figures 2 and 3, respectively). Regarding both figures, where percentiles P50, P75, P85, P95, and P99 are marked, it is clear the increment of the FWI values, when the more severe fires are considered, namely when FRE>1500GJ. It is also noted the large number of hotspots related to low danger classes, and, therefore, lower fire intensity, concurrently to more severe fires.

Taking a closer look at Portuguese FWI values in Table 3, it can be seen that 50% of the fire events are classified in the last three classes: Very High, Extreme, and Very Extreme. Moreover, this pattern indicates that Portugal itself or considering the Iberian Peninsula, has more fire events, with more severe behavior and intensity than the remaining Mediterranean interest areas under study.

4. Conclusion

Results highlight the robustness of the proposed methodology that will also be applied to FFMC and ISI indices. Therefore, an overall discussion of the fire danger thresholds would be very fruitful and will be done in further work. However, these first results regarding the FWI clearly show already the differences in the fire regimes and fire intensity for the Mediterranean basin countries. They also reveal that all the fire-related activities of local authorities, such as fire danger assessment, monitoring, planning, and mitigation activities should be adopted or taken accordingly to these local patterns.

5. Figures

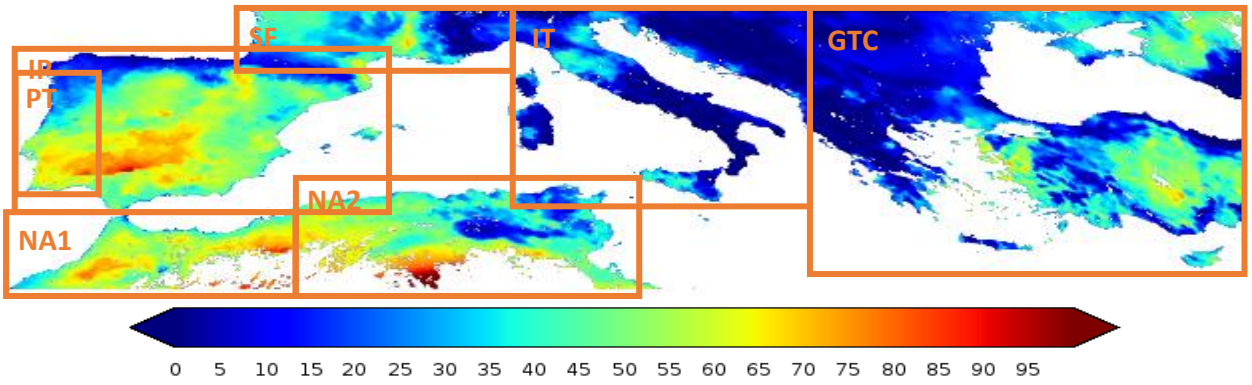

Figure 1: Fire Weather Index (FWI) for 5th August 2018 on the Mediterranean basin and selected study areas. IP – Iberian Peninsula, PT- Portugal, NA1 – North Africa 1, NA2 – North Africa 2, SF – Southern France, IT- Italy, GTC – Greece, Turkey, and Cyprus.

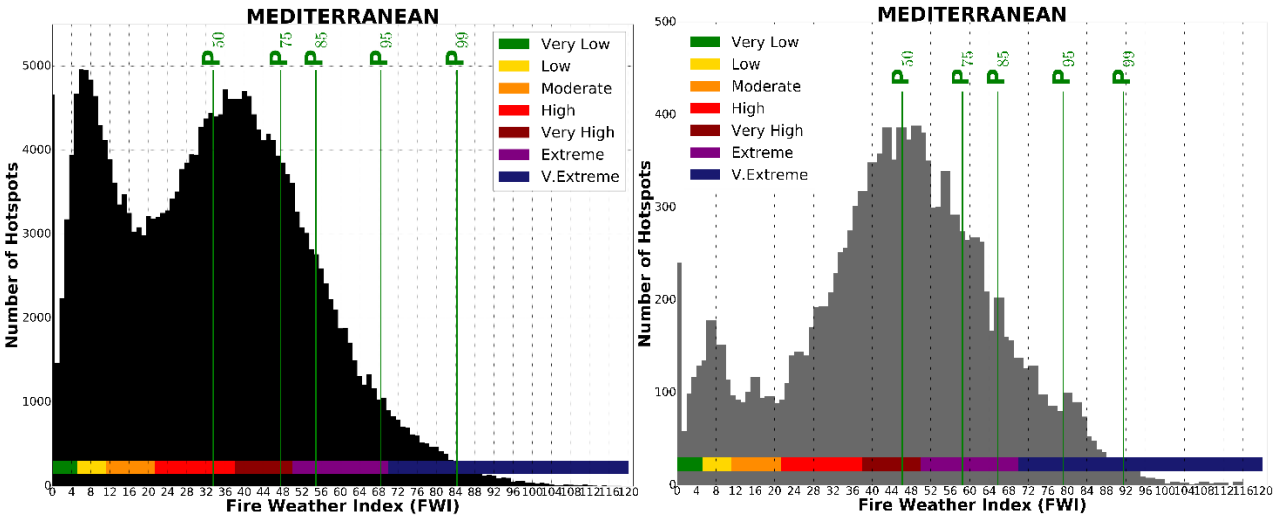

Figure 2: FWI histogram for Mediterranean basin hotspots with FRE≥0 GJ (left) and the selected threshold of FRE≥1500 GJ (right). Percentiles 50, 75, 85, 95, and 99 are marked with green lines.

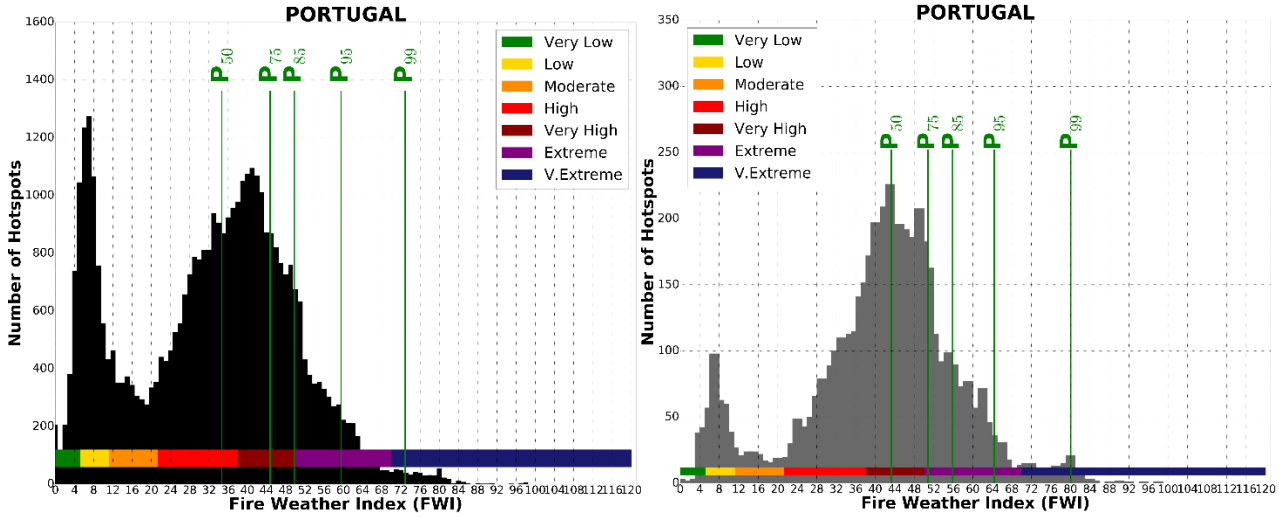

Figure 3: FWI histogram for Portuguese hotspots with FRE≥0 GJ (left) and the selected threshold of FRE≥1500 GJ (right). Percentiles 50, 75, 85, 95, and 99 are marked with green lines.

6. Tables

Table 1. The number of hotspots registered over the study area with FRE ≥ 0 GJ and the selected threshold of 1500 GJ.

Region	Hotspots			
	FRE≥0		FRE≥1500	
	#	%	#	%
Mediterranean Basin	**246444**	**100**	**16366**	**100**
Greece, Turkey and Cyprus (GTC)	87157	35,4	2710	16,6
Iberian Peninsula (IP)	73533	29,8	8310	50,8
Italy (IT)	51916	21,1	2992	18,3
Portugal (PT)	39636	16,1	5595	34,2
North Africa 2 (NA2)	36582	14,8	2963	18,1
Southern France (SF)	9652	3,9	464	2,8
North Africa 1 (NA1)	6779	2,8	519	3,2

Table 2. Fire Danger Classes of FWI, FFMC, and ISI accordingly to the European Fire Forecast Information System (EFFIS, http://effis.jrc.ec.europa.eu/).

Fire Danger Classes	FWI	FFMC	ISI
Very Low	FWI < 5,2	FFMC < 82,7	ISI < 3,2
Low	5,2 ≤ FWI < 11,2	82,7 ≤ FFMC < 86,1	3,2 ≤ ISI < 5,0
Moderate	11,2 ≤ FWI < 21,3	86,1 ≤ FFMC < 89,2	5,0 ≤ ISI < 7,5
High	21,3 ≤ FWI < 38,0	89,2 ≤ FFMC < 93	7,5 ≤ ISI < 13,4
Very High	38,0 ≤ FWI < 50,0	FFMC ≥ 93,0	ISI ≥ 13,4
Extreme	50,0 ≤ FWI < 70,0		
Very Extreme	FWI ≥ 70,0		

Table 3. FWI percentiles, considering the FRE severity threshold of 1500 GJ (FRE > 1500 GJ).

FWI					
P_k	P_{50}	P_{75}	P_{85}	P_{95}	P_{99}
Region	**FRE≥1500**	**FRE≥1500**	**FRE≥1500**	**FRE≥1500**	**FRE≥1500**
Medit.	**46,19**	**58,48**	**65,71**	**79,16**	**91,47**
IP	43,85	53,50	59,66	70,53	81,01
PT	43,27	50,78	55,83	64,38	80,07
NA[1]	50,34	57,77	63,03	74,87	106,9
NA[2]	59,03	69,58	76,27	84,32	95,52
SF	42,18	61,43	69,12	93,25	106,69
IT	40,29	57,21	65,18	77,73	86,99
GTC	48,70	64,82	72,33	85,71	96,56

7. Acknowledgments

This study was performed within the framework of the LSA-SAF, co-funded by EUMETSAT and was partially supported by national funds through FCT (Fundação para a Ciência e a Tecnologia, Portugal) under project FIRECAST (PCIF/GRF/0204/2017) and by the 2021 FirEUrisk project funded by European Union's Horizon 2020 research and innovation programme under the Grant Agreement no. 101003890).

8. References

Dacamara C C, Calado T J, Ermida S L, Trigo I F, Amraoui M and Turkman K F 2014 Calibration of the fire weather index over Mediterranean Europe based on fire activity retrieved from MSG satellite imagery Int. J. Wildland Fire 23 945–58

Dacamara C C, Libonati R, Pinto M M and Hurduc A. 2019 Nearand middle-infrared monitoring of burned areas from space Satellite Information Classification and Interpretation ed R B Rustamov (Rijeka: IntechOpen) ch 8

Di Giuseppe, F., Pappenberger, F., Wetterhall, F., Krzeminski, B., Camia, A., Libertá, G., and San Miguel, J.: The potential predictability of fire danger provided by numerical weather prediction, Journal of Applied Meteorology and Climatology, 55, 2469–2491, 2016

Di Giuseppe, F., Vitolo, C., Krzeminski, B., Barnard, C., Maciel, P., and San-Miguel, J.: Fire Weather Index: the skill provided by the European Centre for Medium-Range Weather Forecasts ensemble prediction system, Nat. Hazards Earth Syst. Sci., 20, 2365–2378, https://doi.org/10.5194/nhess-20-2365-2020, 2020.

Durão R. M., Pereira M.J., Branquinho C., Soares A. (2010): Assessing Spatial Uncertainty of the Portuguese Fire Risk through Direct Sequential Simulation. Ecological Modelling - 221(1): 27-33. https://doi.org/10.1016/j.ecolmodel.2009.09.004

Evin, G., Curt, T., and Eckert, N.: Has fire policy decreased the return period of the largest wildfire events in France? A Bayesian assessment based on extreme value theory, Nat. Hazards Earth Syst. Sci., 18, 2641–2651, https://doi.org/10.5194/nhess-18-2641-2018, 2018.

Fernandes, P. M., Barros, A. M. G., Pinto, A., and Santos, J. A.: Characteristics and controls of extremely large wildfires in the western Mediterranean Basin,. Geophys. Res.-Biogeo., 121, 2141–2157, https://doi.org/10.1002/2016JG003389, 2016

Flannigan, M. D. and Wotton, B. M.: Climate, weather, and area burned, For. Fires Behav. Ecol. Eff., 351–373, https://doi.org/10.1016/B978-012386660-8/50012-X, 2001.

Heward H, Smith A M S, Roy D P, Tinkham W T, Hoffman, C M, Morgan P, Lannom K O. 2013. Is burn severity related to fire intensity? Observations from landscape scale remote sensing. International Journal of Wildland Fire, 22(7), 910, doi:10.1071/wf12087

Johnston, J. M., Wooster, M. J., Paugam, R., Wang, X., Lynham, T. J., and Johnston, L. M.: Direct estimation of Byram's fire intensity from infrared remote sensing imagery, Int. J. Wildland Fire, 26, 668–684, https://doi.org/10.1071/WF16178, 2017.

Pereira M G, Malamud B D, Trigo R M and Alves P I 2011 The history and characteristics of the 1980–2005 Portuguese rural fire database Nat. Hazards Earth Syst. Sci. 11 3343–58

Pinto M M, Dacamara C C, Trigo I F, Trigo R M and Turkman K F 2018a Fire danger rating over Mediterranean Europe based on fire radiative power derived from Meteosat Nat. Hazards Earth Syst. Sci. 18 515–29. https://doi.org/10.5194/nhess-18-515-2018.

Pinto M M, Hurduc A, Trigo R M, Trigo I F and Dacamara C C 2018b The extreme weather conditions behind the destructive fires of June and October 2017 in Portugal Advances in Forest Fire Research 2018 (Coimbra: Imprensa da Universidade de) pp 138–45

Pinto M M, Dacamara C C, Hurduc A, Trigo R M, Trigo I F. 2020. Enhancing the Fire Weather Index with atmospheric instability information. Environmental Research Letters, doi:10.1088/1748-9326/ab9e22;

San-Miguel-Ayanz J et al 2012 Comprehensive monitoring of wildfires in Europe: the European forest fire information system (EFFIS) Approaches to Managing Disaster-Assessing Hazards, Emergencies and Disaster Impacts ed J Tiefenbacher (Rijeka: IntechOpen) ch 5

San-Miguel-Ayanz J, Moreno J, Camia A. Analysis of large fires in European Mediterranean landscapes: Lessons learned and perspectives. FOREST ECOLOGY AND MANAGEMENT 294; 2013. p. 11-22. JRC85949

San-Miguel-Ayanz J., Durrant T., Boca R., Libertà G., Branco A., de Rigo D., Ferrari D., Maianti P., Vivancos T.A., Costa H., et al. (2018). Forest Fires in Europe, Middle East and North Africa 2017; EUR 29318 EN; Joint Research Centre: Ispra, Italy, ISBN 978-92-79-92831-4. 6.

Smith, A. M. S. and Wooster, M.J. 2005. Remote classification of head and backfire types from MODIS fire radiative power and smoke plume observations, Int.J.Wildland Fire, 14, 249–254, https://doi.org/10.1071/WF05012, 2005.

Sousa, P. M., Trigo, R. M., Pereira, M. G., Bedia, J., and Gutiérrez, J. M.: Different approaches to model future burnt area in the Iberian Peninsula, Agr. Forest Meteorol., 202, 11–25, https://doi.org/10.1016/j.agrformet.2014.11.018, 2015.

Stocks B.J., Lawson B.D., Alexander M.E., Van Wagner C.E., McAlpine R.S., Lynham T.J., Dube D.E. (1989). Canadian Forest Fire Danger Rating System: an overview. The Forest Chronicle, 65, pp. 258-265

Trigo, I.F., Dacamara, C.C., Viterbo, P., Roujean, J.L., Olesen, F., Barroso, C., Camacho-DeCoca, F., Carrer, D., Freitas, S.C., García-Haroj, J., Geiger, B., Gellens-Meulenberghs, F., Ghilain, N., Meliá, J., Pessanha, L., Siljamo, N., Arboleda, A., 2011. The satellite application facility for land surface analysis. Int. J. Remote Sens. 32, 2725–2744. https://doi.org/10.1080/01431161003743199

Van Wagner, CE (1974) Structure of the Canadian Forest Fire Weather Index. Can. Forestry Serv., Publication 1333, Ottawa, Ontari, pp. 49.

an Wagner, C., Pickett, T., et al.: Equations and FORTRAN program for the Canadian forest fire weather index system, vol. 33, Canadian Forestry Service, Headquarters, Ottawa, 1985.

Van Wagner, C. et al.: Development and structure of the Canadian forest fire weather index system, vol. 35, Canadian Forestry Service, Headquarters, Ottawa, 1987.

Wooster, M. J., Roberts, G., Perry, G., and Kaufman, Y.: Retrieval of biomass combustion rates and totals from fire radiative power observations: FRP derivation and calibration relationships between biomass consumption and fire radiative energy release, Journal of Geophysical 405 Research: Atmospheres (1984–2012), 110, 2005.

Wooster M J, Roberts G, Freeborn P H, Xu W, Govaerts Y, Beeby R, He J, Lattanzio A, Fisher D, Mullen, R. 2015. LSA SAF Meteosat FRP products–Part 1: Algorithms, product contents, and analysis. Atmos. Chem. Phys. 15, 13217-13239. https://doi.org/10.5194/acp-15-13217-2015.

Wotton, B.M. Interpreting and using outputs from the Canadian Forest Fire Danger Rating System in research applications. Environ Ecol Stat 16, 107–131 (2009). https://doi.org/10.1007/s10651-007-0084-2

Modeling daily natural-caused ignition probability in the Iberian Peninsula

Adrián Jiménez-Ruano[1]*; Pere Joan Gelabert[2]; Victor Resco de Dios[2]; Cristina Vega-García[2]; Luis Torres[3]; Jaime Ribalaygua[3]; Marcos Rodrigues[1*]

[1]Department of Geography and Land Management, University of Zaragoza. Pedro Cerbuna 12,5009, Zaragoza, Spain, {jimenez, rmarcos}@unizar.es
[2] Department of Agriculture and Forest Engineering, University of Lleida. Alcalde Rovira Roure 191, 25198, Lleida, Spain, {perejoan.gelabert, victor.resco, cristina.vega}@udl.cat
3 MeteoGRID SL., Almansa 88, Madrid, Spain, {luis, jrb}@meteogrid.com

**Corresponding author*

Keywords

Lightning, wildfires, machine learning, fire probability, Iberian Peninsula

Abstract

In the European Mediterranean region natural-caused wildfires are a small fraction of total ignitions. Lightning strikes are the most common source of non-human fires, being strongly tied to specific synoptic conditions and patterns associated with atmospheric instability, such as dry thunderstorms. Likewise, lightning-related ignitions often associate with dry fuels and dense vegetation layers. In the case of Iberian Peninsula, the confluence of these factors favors recurrent lightning fires in the eastern Mediterranean mountain ranges, the western region of "El Bierzo" and central Portugal. However, under appropriate conditions lightning fires can start elsewhere, holding the potential to propagate over vast distances.

In this work, we assessed the likelihood of ignition leveraging a large dataset of lightning strikes and historical fires available in Spain. We trained and tested a machine learning model to evaluate the probability of ignition provided that a lightning strikes the ground. Our model was calibrated in the period 2009-2015 using data for mainland Spain plus the Balearic Islands. To build the binary response variable we classified lightning strikes between that triggered a fire event. For each lightning strike we extracted a set of covariates relating fuel moisture conditions, the presence and density of the vegetation layer and the shape of the relief.

The final model was subsequently applied to forecast daily probabilities at 1x1 km resolution for the entire Iberian Peninsula. Although the model was originally calibrated in Spain, we extended the predictions to the entire Iberian Peninsula. By doing so we were able to validate in the future our outputs against the Portuguese dataset of recent natural-caused fires (bigger than 1 ha) from 2001 to 2021. Overall, the model attained a great predictive performance with a median AUC of 0.82. Natural-caused ignitions triggered mainly in low dead (dFMC <8%) and moderate alive (DC > 250) fuel moisture conditions. Lightning strikes with negative polarity seem to trigger fires more frequently when the mean density of discharger was greater than 5. Finally, natural wildfires usually started at higher elevations (above 500 m.a.s.l.).

1. Introduction

In Europe, natural-caused fires represent a small percentage of the total number of fires. In contrast to anthropogenic fires, which are arranged in a spatial pattern close to the human footprint, the spatial location of natural fires is often clustered in specific hot spots of intense lightning occurrence and fuel availability. Recent studies warn of the likely increase in fire frequency and size linked to climate warming and global change. Most climate predictions envisage a decrease in fuel moisture content while fuel accumulation due to land abandonment is creating the perfect conditions for larger and more extreme fires. Although further research is needed, there is already evidence of an increase in the occurrence of natural fires related to the increased frequency of dry storms and heat waves (Li et al. 2020; Coogan et al. 2020). Lightning fires start more frequently in distant and remote regions, which pose an additional layer of difficulty to suppression, potentially growing into large fire events when fuel and relief conditions facilitate fire spread.

The Iberian Peninsula is one of the main hotspots of forest fire activity in Europe and the western Mediterranean basin. Numerous studies have focused on addressing the probability of fires caused by lightning, by man or by

both. Understanding the linkages and feedbacks between environmental and atmospheric conditions that ultimately relate to lightning-caused fires is relevant. Most studies dealing with natural fires are based on historical compilations of natural fires coupled to environmental and climatic variables (Rodríguez-Pérez et al. 2020) or on meteorological data to determine the atmospheric conditions conducive to lightning fires (Soler et al. 2021; Pérez-Invernón et al. 2021; Pineda et al. 2022). Other works, like the one by Couto et al. (2020), investigated the interactions between atmospheric models and the rate of spread of wildfires. However, there is still a lack of homogeneity in the methods, variables, and protocols to predict, and therefore anticipate, the occurrence of natural wildfires. We advocate an approach that decouples the conditions that favor lightning strikes from the environments that favor ignition.

The present work is developed within the framework of the H2020 project FireEUrisk, aimed at understanding, modeling, and predicting fire risk conditions by addressing the main risk components (hazard, exposure, and vulnerability) and mitigation steps (prevention, planning and adaptation) at the European scale. The main objective of this work is to predict the probability of ignition of natural forest fires using lightning records in the period 2009-2015. For this purpose, we analyzed a large lightning strike dataset (more than 17 million) to ascertain the conditions under which a lightning strike will trigger an ignition, i.e., the probability of ignition conditional on the occurrence of the lightning strike itself. The model was initially trained and validated using data covering all peninsular Spain plus the Balearic Islands, subsequently investigating its ability to predict ignitions in Portugal. Several variables related to fuel moisture content and vegetation structure, topography, as well as some factors related to polarity, intensity and density of impacts were used. The methodology is based on Random Forest modeling and other related techniques to assess the accuracy of the probability obtained. In this way, a daily and high-resolution lightning ignition prediction for the whole Iberian Peninsula has been elaborated.

2. Material and methods

The study area encompasses the whole Iberian Peninsula, i.e., mainland Spain and Portugal plus the Balearic Islands, covering a surface circa 588,000 km2 (Figure 1).

Figure 1- Digital elevation model and rivers network of mainland Spain plus Balearic Islands and Portugal.

2.1. Dependent variable: lightning strikes and fire ignitions

The core of our approach leverages a large and comprehensive dataset of cloud-to-ground lightning strikes recorded in the period 2009-2015. The dataset was provided by Meteogrid S.L.. It consists of more than 17 mill records reporting the intensity (and polarity) and density of flashes. Information about fire ignitions (location, date, cause, and size) was retrieved from the Spanish (EGIF) and Portuguese (DECIF) databases. The Spanish dataset was used to identify those lightning strikes that started a fire while the Portuguese records were retained to evaluate the applicability of the model to the specific conditions of Portugal.

The response variable was extracted from ignitions in Spain consisted in 11,000 fires. Approximately 2,500 fires were matched to a lightnings strike (i.e., occurring within 1,000 meters and no more than 3 days holdover

period respect to the ignition date). Upon this information we built a binary response variable combining lightnings that triggered a fire (1 or presence) with lightning not related to a fire (0 or absence). We implemented a stratified sampling procedure to prevent undesired effects from the largely unbalanced response (more 0 than 1) and minimize spatial autocorrelation.

2.2. Independent variables

To predict the probability of fires, we employed 7 factors related to vegetation state, topography and others directly linked to sparks' discharges (Figure 2). Firstly, we retrieved both the daily dead fuel (FM; calculated as described in Resco de Dios et al. (2015) and live fuel moisture content (using the Drought Code -DC- as proxy) at 11 km of spatial resolution. Secondly, elevation (*elev*) and relief curvature (*curvG*) were selected to depict the influence exerted by the terrain in the ignition of natural-cause fires. In turn, we included the vegetation height (hveg) as a proxy of the vegetation structure. The model also accounts for lightning-related features, such as strike intensity (mxi) and density (nse). To perform model predictions the latter two were set as constant figures equal to their average value over the study area (-10 of intensity and 5 discharges, respectively). All variables (aside FM and DC) were retrieved at 30x30 meters of resolution and later resampled at 1x1 km.

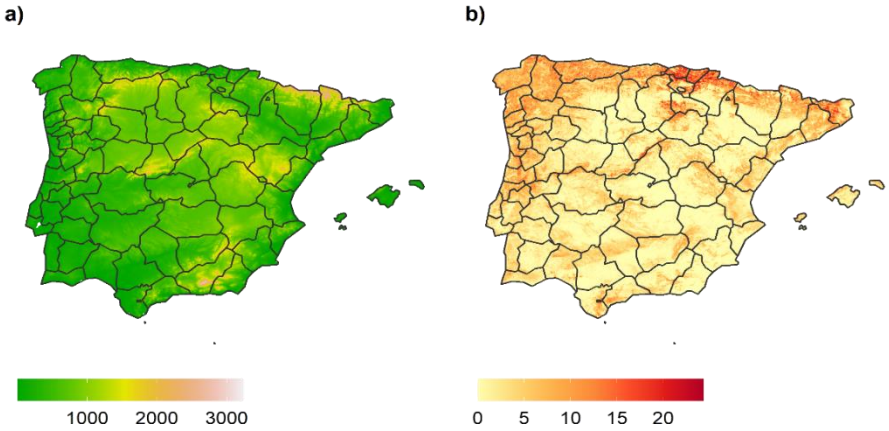

Figure 2- A) Digital elevation model (meters) and, B) height of vegetation (meters) in mainland Spain plus Balearic Islands and Portugal.

2.3. Model calibration with random forest

The model was trained using the random forest algorithm (Breiman 2001). We trained a total of 100 models exploring different realizations of the response variable. For each realization we extracted a balanced sample of 1-presence (flashes igniting a fire) and 0-absence (lightnings non-conducive to fire). The process was stratified using a 100x100 km grid so that at each grid cell we extracted an even sample of 1-presence and 0-absence. In turn, the absence observation pool included the same number of records in days experiencing fires and days not experiencing a fire. It must be noted that we only analyzed the April-to-October period, since natural fires seldom occur outside that season.

Model calibration was conducted using the caret package (Kuhn 2008) in the R environment for statistical computing (R Core Team, 2021). For each model realization we implemented a 5-fold repeated (3 repetitions) cross-validation, optimizing model parameters: number of trees (ntree) and number of variables to use at each split (mtry). We evaluated the importance of each co-variate using the Mean Decrease in the Gini index and the overall performance of each model via AUC. Out of the set of 100 models we selected the one attaining the average prediction performance (AUC=0.828) as candidate model to forecast and map the daily evolution of lightning-related ignition probability. The model was subsequently evaluated calculating the AUC from the Portuguese fire data, which consisted in 105 lightning fires (>1ha) in the period 2009-2015.

3. Results

In general terms, the Random Forest models attained a high AUC value (average AUC=0.828; Figure 3). The most relevant factor was fuel moisture content (DC and FM), followed by elevation, density of strikes, relief curvature, intensity/polarity and vegetation height. The response to fuel moisture content was the most

remarkable linkage found (Figure 4). In the case of DC (i.e., live fuel moisture content), the response curve showed an increase in ignition likelihood peaking around the 300 mark, remaining constant afterwards. In turn, dead fuel moisture content (FM) related to higher ignition likelihood below 10% moisture content. Likewise, probability peaked at above 20 of strikes density up yo 1,500 m.a.s.l. According to the spatial distribution of daily natural-caused probability, the highest values were often in the inner mountain ranges of the Iberian Peninsula, especially in the south-eastern half (see Figure 5). Locally, the likelihood of lightning fires is more common in the forested areas of medium elevations, thus usually excluding the lowest and altitudes but also the agricultural areas.

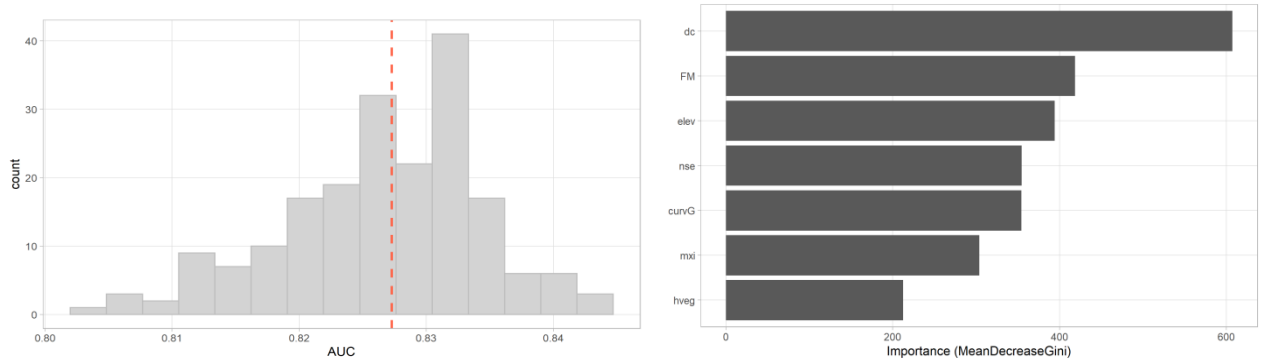

Figure 3- Model accuracy according to Area Under the Curve (left) and Random Forest variable importance (right).

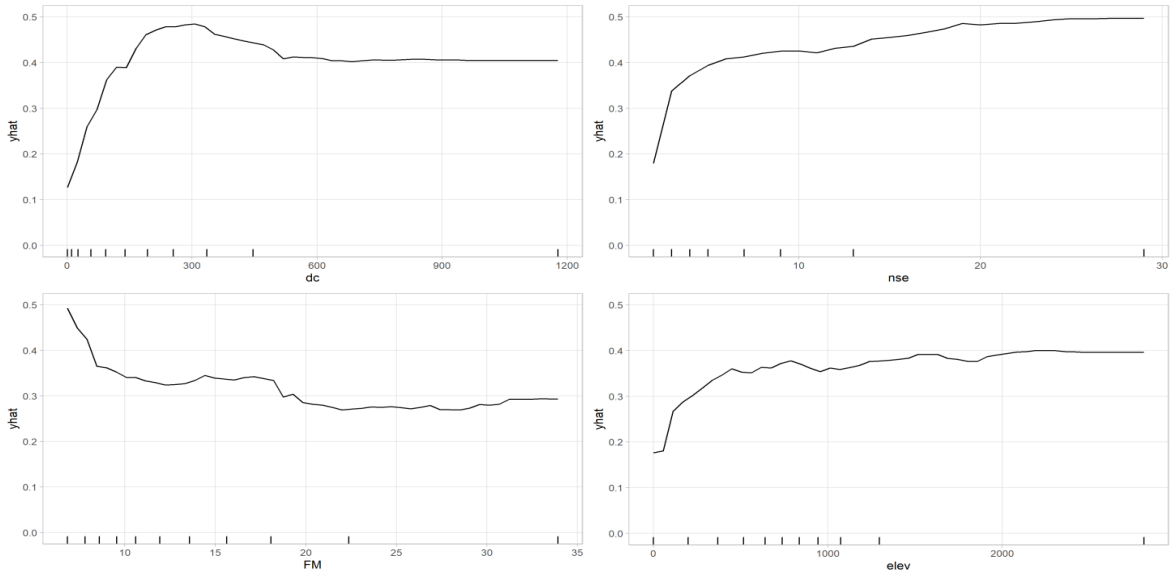

Figure 4- Partial effects plots for the most important variables included in the Random Forest model built to predict the natural-caused probability.

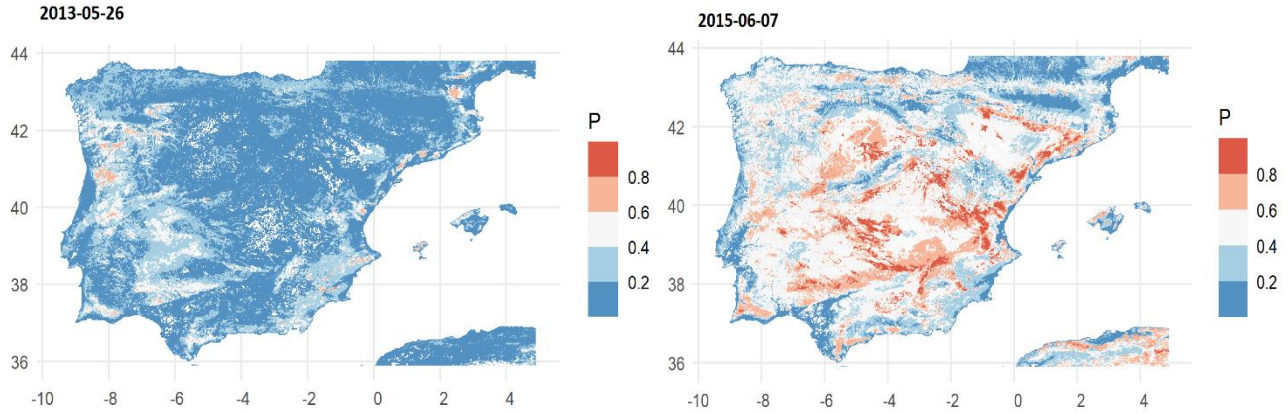

Figure 5- Daily lightning wildfire predictions examples for four specific days in the Iberian Peninsula and Balearic Islands.

4. Discussion

In this work we produced a daily forecast of natural-caused wildfire ignition probability over the whole Iberian Peninsula plus the Balearic Islands. We followed a novel method based mainly on lightning strikes, opposite to fire-based approaches. The model holds a good predictive accuracy (around 0.82 AUC), which is noteworthy given the rare nature of thunderstorm-driven fires (Fernandes et al., 2021). In turn, the future calibration of our fitted model in Portugal shows the feasibility of extending the model to regions like Spain. The observed relationships between ignition drivers and predicted likelihood are in line with the expected behavior, i.e., fuel moisture as the most influential factor modulating ignition followed by topography. The important role of the moisture of the live/dead fuels causing the ignition and propagation of new fire events have been documented in many works previously (Baranovskiy & Kirienko, 2022; Resco de Dios et al., 2021, 2022; Rodrigues et al., 2021). However, our findings were non-conclusive in terms of the role of the characteristics of the fire-prone flash. We did not find a strong signal in terms of intensity nor polarity, though an increased density of strikes did increase the chance of ignition.

In terms of risk assessment, we believe that the strategy of breaking down ignition likelihood and the probability of lightning occurrence offers several advantages. Decoupling both phenomena allow us to better understand their relative importance while enabling embedding different models for lightning or thunderstorm forecast, or even real observations of lightning flashes. That is particularly important for short-term predictions. In turn, long-term modeling would also benefit for such approach. Our ignition forecast requires few weather-related factors (the same necessary for the calculation of the FWI), thus their prediction under climate scenarios (SSP or RCP) is already feasible. In the same line, several models are available to forecast lightning strikes (Woodard et al., 2014), hence, being possible to combine them with the ignition component. Our next steps include extending the temporal span of calibration and, more important, modeling the phenomena in other locations, preferably in northern latitudes. Furthermore, we need to investigate the performance of the model outside the calibration time frame, both forward and backward in time.

5. Conclusions

In this work we produced a daily forecast of the probability of natural wildfires in the Iberian Peninsula and the Balearic Islands. We combined lightning and wildfire data with environmental variables to train and test a binary Random Forest model. Our results revealed the major role played by fuel moisture content, the most sensitive factor to climate warming in the coming decades. This highlights the need for further research and consideration of natural ignitions in hazard mitigation plans, even though their contribution to fire activity is currently moderate.

6. References

Baranovskiy, Nikolay Viktorovich, and Viktoriya Andreevna Kirienko. 2022. “Forest Fuel Drying, Pyrolysis and Ignition Processes during Forest Fire: A Review.” Processes. MDPI. https://doi.org/10.3390/pr10010089.

Breiman, L. 2001. “Random Forests.” Machine Learning 45 (1): 5–32. https://doi.org/https://doi.org/10.1023/A:1010933404324.

Coogan, Sean C.P., Xinli Cai, Piyush Jain, and Mike D. Flannigan. 2020. “Seasonality and Trends in Human-A Nd Lightning-Caused Wildfires ≥ 2 Ha in Canada, 1959-2018.” International Journal of Wildland Fire 29 (6): 473–85. https://doi.org/10.1071/WF19129.

Couto, Flavio Tiago, Maksim Iakunin, Rui Salgado, Paulo Pinto, Tânia Viegas, and Jean Pierre Pinty. 2020. “Lightning Modelling for the Research of Forest Fire Ignition in Portugal.” Atmospheric Research 242 (September). https://doi.org/10.1016/j.atmosres.2020.104993.

Fernandes, Paulo M., João A. Santos, Fernando Castedo-dorado, and Rui Almeida. 2021. “Fire from the Sky in the Anthropocene.” Fire 4 (1). https://doi.org/10.3390/fire4010013.

Kuhn, Max. 2008. “Building Predictive Models in R Using the Caret Package.” Journal of Statistical Software, Articles 28 (5): 1–26. https://doi.org/10.18637/jss.v028.i05.

Li, Yang, Loretta J. Mickley, Pengfei Liu, and Jed O. Kaplan. 2020. "Trends and Spatial Shifts in Lightning Fires and Smoke Concentrations in Response to 21st Century Climate over the National Forests and Parks of the Western United States." Atmospheric Chemistry and Physics 20 (14): 8827–38. https://doi.org/10.5194/acp-20-8827-2020.

Pérez-Invernón, Francisco J., Heidi Huntrieser, Sergio Soler, Francisco J. Gordillo-Vázquez, Nicolau Pineda, Javier Navarro-González, Víctor Reglero, Joan Montanyà, Oscar Van Der Velde, and Nikos Koutsias. 2021. "Lightning-Ignited Wildfires and Long Continuing Current Lightning in the Mediterranean Basin: Preferential Meteorological Conditions." Atmospheric Chemistry and Physics 21 (23): 17529–57. https://doi.org/10.5194/acp-21-17529-2021.

Pineda, Nicolau, Patricia Altube, Fermín J Alcasena, Enric Casellas, Helen San Segundo, and Joan Montanyà. 2022. "Characterizing the Holdover Phase of Lightning-Ignited Wildfires in Catalonia." Agricultural and Forest Meteorology. https://ssrn.com/abstract=4022142.

R Core Team. 2021. "R: A Language and Environment for Statistical Computing." Vienna: R Foundation for Statistical Computing. https://www.r-project.org/.

Resco de Dios, Víctor, Àngel Cunill Camprubí, Núria Pérez-Zanón, Juan Carlos Peña, Edurne Martínez del Castillo, Marcos Rodrigues, Yinan Yao, Marta Yebra, Cristina Vega-García, and Matthias M. Boer. 2022. "Convergence in Critical Fuel Moisture and Fire Weather Thresholds Associated with Fire Activity in the Pyroregions of Mediterranean Europe." Science of the Total Environment 806 (February). https://doi.org/10.1016/j.scitotenv.2021.151462.

Resco de Dios, Víctor, Aaron W. Fellows, Rachael H. Nolan, Matthias M. Boer, Ross A. Bradstock, Francisco Domingo, and Michael L. Goulden. 2015. "A Semi-Mechanistic Model for Predicting the Moisture Content of Fine Litter." Agricultural and Forest Meteorology 203 (April): 64–73. https://doi.org/10.1016/j.agrformet.2015.01.002.

Resco de Dios, Víctor, Javier Hedo, Àngel Cunill Camprubí, Prakash Thapa, Edurne Martínez del Castillo, Juan Martínez de Aragón, José Antonio Bonet, et al. 2021. "Climate Change Induced Declines in Fuel Moisture May Turn Currently Fire-Free Pyrenean Mountain Forests into Fire-Prone Ecosystems." Science of the Total Environment 797 (November). https://doi.org/10.1016/j.scitotenv.2021.149104.

Rodrigues, Marcos, Michela Mariani, Ana Russo, Michele Salis, Luiz Felipe Galizia, and Adrian Cardil. 2021. "Spatio-Temporal Domains of Wildfire-Prone Teleconnection Patterns in the Western Mediterranean Basin." Geophysical Research Letters 48 (19). https://doi.org/10.1029/2021GL094238.

Rodríguez-Pérez, José Ramón, Celestino Ordóñez, Javier Roca-Pardiñas, Daniel Vecín-Arias, and Fernando Castedo-Dorado. 2020. "Evaluating Lightning-Caused Fire Occurrence Using Spatial Generalized Additive Models: A Case Study in Central Spain." Risk Analysis 40 (7): 1418–37. https://doi.org/https://doi.org/10.1111/risa.13488.

Soler, Anna, Nicolau Pineda, Helen San Segundo, Joan Bech, and Joan Montanyà. 2021. "Characterisation of Thunderstorms That Caused Lightning-Ignited Wildfires." International Journal of Wildland Fire 30 (12): 954–70. https://doi.org/10.1071/WF21076.

Woodard, Stella C., Yair Rosenthal, Kenneth G. Miller, James D. Wright, Beverly K. Chiu, and Kira T. Lawrence. 2014. "Antarctic Role in Northern Hemisphere Glaciation." Science 346 (6211): 847–51. https://doi.org/10.1126/science.1255586.

Modelling sorption processes of 10-hour dead Pinus pinaster branches

Sérgio Lopes*[1,2]; Paulo Pinho[2]; Sandra Santos[1]; Nuno Rodrigues[2]; Jorge Raposo[1]; Domingos Viegas[1]

[1]CEIF/ADAI/LAETA, Association for the Development of Industrial Aerodynamics, Rua Pedro Hispano, 12, PT-3030-289 Coimbra, Portugal, {rafahunstman@hotmail.com}, {xavier.viegas@dem.uc.pt}
[2] CISeD, Research Centre in Digital Services, Polytechnic Institute of Viseu, Avenida Coronel José Maria Vale de Andrade, Campus Politécnico, 3504-510 Viseu – Portugal, {slopes, ppaulo, Miguel}@estgv.ipv.pt, {marinasantos02@sapo.pt}

**Corresponding author*

Keywords

Moisture content, 10-hour fuels, EMC, Timelag

Abstract

Forest fuel moisture content is an important parameter that determines fire risk and fire behaviour. An accurate prediction of moisture content is therefore of great importance in fire management. In the fire risk period, dead forest fuel moisture content changes mainly by water vapour sorption processes so its knowledge enables the development of predictive fire risk models.

In the present work, the adsorption and desorption processes and equilibrium moisture content of 10-hour dead Pinus pinaster branches (diameter between 0.6 cm and 2.5 cm) were described in order to develop a moisture content prediction model for this type of fuels.

Laboratorial tests were used to determine sorption curves, timelag and equilibrium moisture content for different sets of air temperature (range between 20°C and 40°C) and relative humidity (range between 10% and 90%). The sorption curves and equilibrium moisture were also modelled with forest fuels and agricultural and food products existing models.

Field tests were used to evaluate the sorption and equilibrium moisture content models performance. Dead Pinus pinaster branches were collected in central Portugal through the year 2020 and 2021 on the Portuguese fire risk period (15th May to 15th October) between 12:00h and 13:00h LST. Samples with 0.6 cm to 2.5 cm diameter were collected and transported to laboratory to determine moisture content.

The laboratorial drying and wetting curves of dead Pinus pinaster branches (0.6 cm to 2.5 cm diameter) show that they are not pure exponential functions, but with different timelag values until equilibrium is reached. Additionally, the results suggest no significant relationship of the timelag periods with air relative humidity but a dependence with air temperature, showing an increase in the sorption rates with temperature. In terms of sorption curves, Modified Henderson and Pabis model provide the best fitting.

For this type of fuels, the representation of EMC values as a function of air relative humidity at constant temperature allowed to obtain a typical sigmoid curve. The EMC values obtained were higher for desorption process than for adsorption process, indicated the typical hysteresis effect in these processes. It was found that, besides the models used in forest fires, other EMC models are also suitable to predict fuel moisture content of dead Pinus pinaster branches, as the ones used in agricultural and food analysis.

1. Introduction

Forest fuel moisture content (FFMC) has a considerable influence on many aspects of forest fire behaviour, including rate of fire spread, ignition probability, flame dimensions and fuel consumption (Rothermel 1983; Viegas et al. 1992), however, its accurate prediction is difficult due to its interactions with weather conditions, topography and vegetation (Matthews 2014).

In the absence of rainfall, dead forest fuels respond to changes in meteorological conditions by sorption processes where it dominates water transfer mechanisms below the fiber saturation point. In these conditions, and at constant air temperature and relative humidity, the FFMC changes (increases or decreases) until it reaches a constant value designated equilibrium moisture content (EMC) (e.g. Catchpole et al. 2001; Viney and

Catchpole 1991). These moisture sorption processes are also characterized by a response time or log drying rate or timelag (τ) that is the time required for the fraction of evaporable water remaining in the forest fuel to decrease from 1 to 0.368 (Byram, 1963). Timelag is on the basis of forest fuels classification into four categories (1-hour, 10-hour, 100-hour and 1000-hour fuels) (Bradshaw et al. 1983).

In the present work, the adsorption and desorption processes and EMC of 10-hour dead *Pinus pinaster* branches (diameter between 0.6 cm and 2.5 cm) were determined in order to develop a moisture content prediction model for this type of fuels.

2. Methods

Laboratorial tests were used to determine sorption curves, timelag and EMC of dead *Pinus pinaster* branches (0.6 cm to 2.5 cm diameter) for different sets of air temperature (range between 20°C and 40°C) and relative humidity (range between 10% and 90%). Samples were placed inside a climatic chamber (Aralab Fitoclima 300) equipped with an analytical balance (precision of 0.001g). Continuous weighing was recorded until it reached constant weight, determining dead *Pinus pinaster* branches moisture content evolution and showing the changing rates at which equilibrium approaches.

In terms of mathematical modelling, sorption processes were modelled using the exponential equation described by Byram (1963) (equation 1), Page (1949) (equation 2), Henderson and Pabis (1961) (equation 3), two-term (Henderson 1974) (equation 4) and Modified Henderson and Pabis (Karathanos, 1999) (equation 5).

$$\mathrm{E(t)}_1 = \exp\left(\frac{-\mathrm{t}}{\tau}\right) = \exp(-\mathrm{k}_1\mathrm{t}) \tag{1}$$

$$\mathrm{E(t)}_2 = e^{-k_1 t^n} \tag{2}$$

$$\mathrm{E(t)}_3 = a_1 e^{-k_1 t} \tag{3}$$

$$\mathrm{E(t)}_4 = a_1 e^{(-k_1 t)} + a_2 e^{(-k_2 t)} \tag{4}$$

$$\mathrm{E(t)}_5 = a_1 e^{(-k_1 t)} + a_2 e^{(-k_2 t)} + a_3 e^{(-k_3 t)} \tag{5}$$

where τ is the timelag (h), t is time (h), k_1, k_2 and k_3 are the drying constants (h^{-1}) and n, a_1, a_2 and a_3 are empirical dimensionless constants. The fraction of evaporable water remaining in the fuel at time t, E(t), was calculated using equation 6. Model parameters and constants were obtained from laboratory data

$$\mathrm{E(t)} = \frac{\mathrm{m_{(t)}} - \mathrm{m_e}}{\mathrm{m_0} - \mathrm{m_e}} \tag{6}$$

where m(t) is the fuel average moisture content at time t, m_0 is the value of m at t = 0, m_e is the value of m as t approaches infinite (m_e approaches EMC).

To assess the relationship between EMC of dead *Pinus pinaster* branches and air temperature and relative humidity were used semi-empirical and empirical models such as Van Wagner (Van Wagner, 1987) (equation 7), Modified Halsey (Iglesias and Chirife 1976) (equation 8), Modified Oswin (Chen 1990) (equation 9), Nelson (Nelson, 1984) (equation 10) and Modified Chung-Pfost (Pfost et al. 1976) (equation 11).

$$EMC = \frac{1}{100}\left[a(100RH)^b + ce^{(100RH-100)/d} + e(21.1 - T)(1 - e^{100fRH})\right] \tag{7}$$

$$EMC = \left[\frac{e^{(a-bT)}}{-ln(RH)}\right]^{1/c} \tag{8}$$

$$EMC = (\mathrm{a} - \mathrm{bT})\left[\frac{RH}{(1-RH)}\right]^c \tag{9}$$

$$EMC = \frac{1}{a} ln\left(-\frac{RT_K}{Me^b} ln\left(\frac{RH}{100}\right)\right) \quad (10)$$

$$EMC = -\frac{1}{a} ln\left[-\frac{(T+b)}{c} \ln(RH)\right] \quad (11)$$

where a, b, c, d, e and f are coefficients specific to individual equations, RH is the relative humidity, T (°C) and T_k (K) are the temperatures, R is the universal gas constant (1.987 cal.mol^{-1}K^{-1}) and M is the molecular weight of water (18 gmol^{-1}). Model constants were obtained from laboratory data.

In the field tests, used to evaluate the sorption and EMC models performance, dead *Pinus pinaster* branches were collected from *Pinus pinaster* forest stands in Viseu (40°42'30.02"N, 7°54'8.96"W) in central Portugal through the year 2020 and 2021. Field sampling was performed on the Portuguese fire risk period (15th May to 15th October) between 12:00h and 13:00h LST. Samples with 0.6 cm to 2.5 cm diameter were collected and transported to laboratory in an isothermal bag to avoid moisture changes. Here, samples were weighted and then oven-dried at 105°C for 24 h, until constant weight, to obtain its dry weight and therefore the dry basis moisture content.

Hourly meteorological conditions (air temperature, relative humidity, wind and rainfall) from a weather station located approximately at 10 km south of the sampling site, were used to characterise weather conditions during field tests.

To assess the model fitting quality some statistical parameters were calculated namely the mean absolute error (MAE), the mean absolute percentage error (MAPE), the root mean squared error (RMSE) and the determination coefficient (R^2). RMSE and MAPE show the accuracy of model fitting, MAE measures the bias of the model and the R^2 measure how well observed values are replicated by the model. Usually, higher values of R^2 and lower values of MAE, MAPE and RMSE, associated with randomly distributed residuals indicate a good fit.

3. Results

Figure 1 shows the drying and wetting curves of dead *Pinus pinaster* branches represented by the evaporable water fraction (E), described in equation 6, as function of time for air temperatures of 20°C, 30°C and 40°C in a range of relative humidity between 10% and 90%. The drying and wetting curves show a deviation from pure exponential behaviour, which means that other functions should be considered as well to represent these processes. Additionally, these curves show some fluctuations, particularly in the late stages of the experiment mainly caused by temperature and relative humidity oscillations inside the climatic chamber.

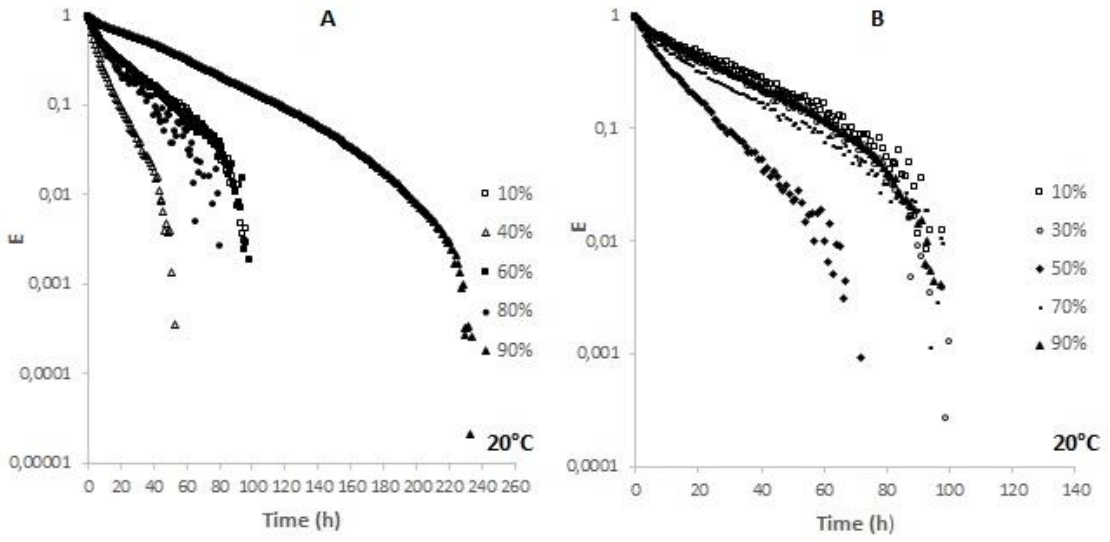

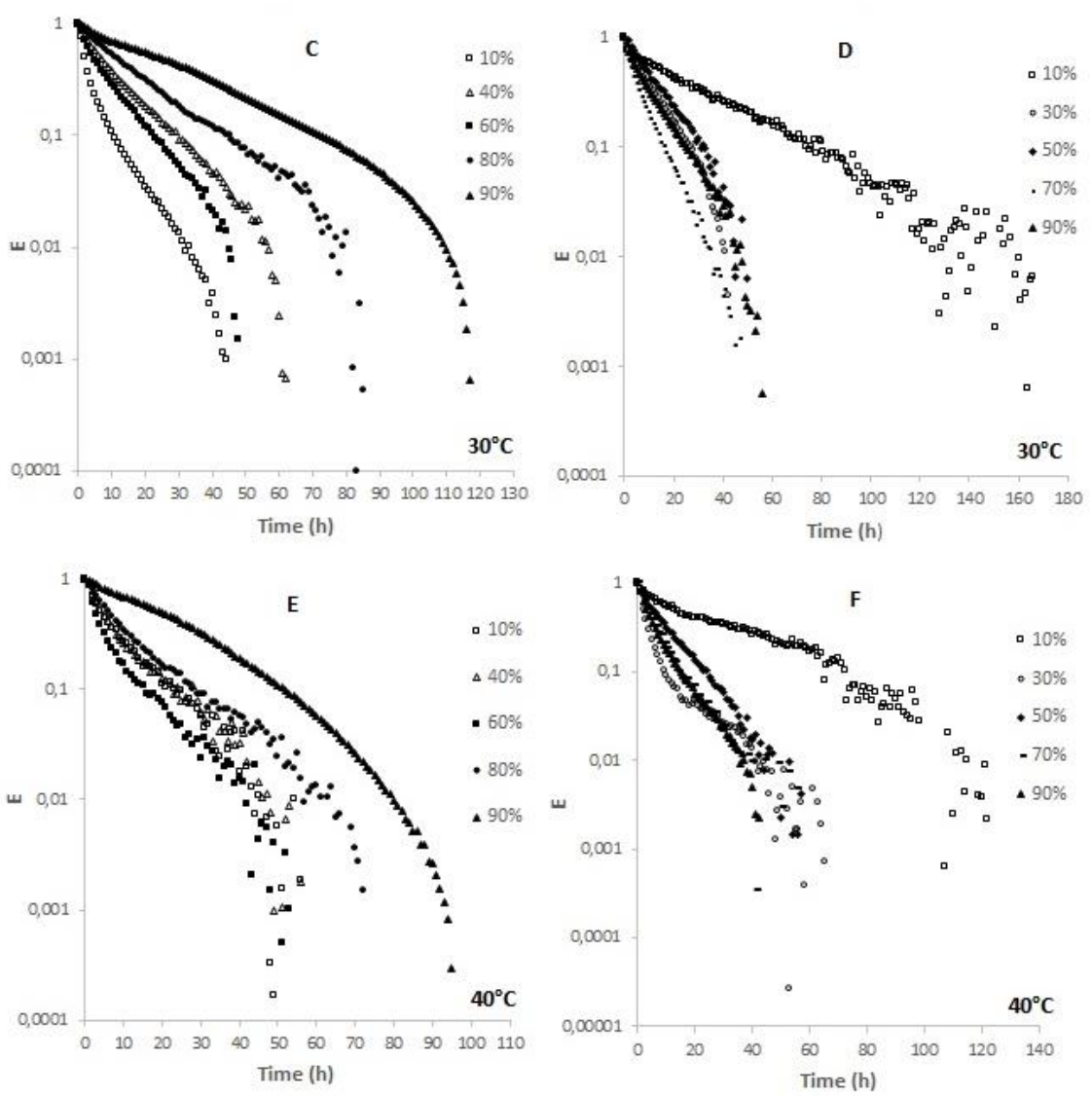

Figure 1- Semi-log graphs of desorption tests (A, C, E) and adsorption tests (B, D, F)

Breaking the drying and wetting curves in four periods and assuming a constant rate as fuel approaches EMC in each step, it was calculated the four timelag values. Table 1 shows the average timelag periods obtained in the laboratorial tests. No significant relationship of the four timelag periods with air relative humidity was found therefore an average value is presented. However, a dependence of the four timelag periods with air temperature was observed.

Table 1- Average timelag periods obtained in order of air temperature

Process	Temperature (°C)	First timelag (h)		Second timelag (h)		Third timelag (h)		Fourth timelag (h)	
		Average	s.d.	Average	s.d.	Average	s.d.	Average	s.d.
Desorption	20	20,99	14,04	26,46	11,38	19,89	11,50	16,76	6,09
	30	8,12	6,46	12,85	5,80	9,65	5,10	7,86	4,49
	40	8,23	6,43	9,96	4,24	9,60	4,02	7,37	2,62
Adsorption	20	19,02	7,60	23,32	8,25	22,38	9,98	13,71	10,48
	30	9,31	5,50	11,65	5,04	9,09	4,19	6,97	5,10
	40	6,29	3,40	12,09	11,29	8,89	4,44	6,65	3,20

Table 2 shows the estimated parameters for sorption processes based on the laboratorial tests for the models described from equation 1 to equation 5. As it can be seen, drying and wetting experimental curves are best

fitted by the Modified Henderson with a R^2 of 0.694 and 0.749 and a RMSE of 0.134 and 0.116 for desorption and adsorption processes, respectively.

Table 2- Model parameters for the sorption processes

Equation			Byram	Page	Henderson and Pabis	Two-term	Modified Henderson and Pabis
Model parameters	K_1	Desorption	0.072	0.257	0.051	0.011	0.398
		Adsorption	0.073	0.269	0.047	0.014	0.171
	n	Desorption	-	0.533	-	-	-
		Adsorption	-	0.515	-	-	-
	a_1	Desorption	-	-	0.779	0.267	0.257
		Adsorption	-	-	0.753	0.323	0.622
	k_2	Desorption	-	-	-	0.160	0.106
		Adsorption	-	-	-	0.189	0.809
	a_2	Desorption	-	-	-	0.718	0.544
		Adsorption	-	-	-	0.666	0.071
	a_3	Desorption	-	-	-	-	0.007
		Adsorption	-	-	-	-	0.312
	k_3	Desorption	-	-	-	-	0.215
		Adsorption	-	-	-	-	0.014
Statistical parameters	R^2	Desorption	0.542	0.673	0.595	0.692	0.694
		Adsorption	0.565	0.730	0.636	0.748	0.749
	MAE	Desorption	0.129	0.107	0.124	0.104	0.103
		Adsorption	0.131	0.098	0.123	0.093	0.093
	RMSE	Desorption	0.163	0.138	0.154	0.137	0.134
		Adsorption	0.153	0.121	0.140	0.117	0.116

Laboratorial EMC values of *Pinus pinaster* branches obtained in both adsorption and desorption tests in a range of relative humidity between 10% and 90% for three air temperatures 20°C, 30°C and 40°C are shown in Table 3 and plotted in Figure 2. These results were fitted to five EMC models and Table 4 shows the EMC model parameter estimation obtained for the desorption and adsorption processes described in equation 7 to equation 11. As an example, the estimation by the Van Wagner model is also shown in Figure 2.

As can be seen, for a wide range of temperature and relative humidity values all sorption models show good fitting ability with the laboratory results however the Van Wagner model presented the best fit for both adsorption and desorption processes. This model gives the higher R^2 of 0.991 and 0.984, the lowest MAE of 0.428 and 0.453 and the lowest RMSE of 0.514 and 0.584 for desorption and adsorption processes, respectively. The residual distribution was also analysed and showed that all adsorption and desorption models presented a random residual distribution indicating good fitting ability and only Halsey model presented a systematic residual distribution.

The EMC values obtained were higher for the desorption process than for the adsorption process, presenting the typical hysteresis effect.

Table 3- EMC of dead Pinus pinaster branches for the tested air temperature and relative humidity conditions

Relative Humidity (%)	$EMC_{adsorption}$ (%)			$EMC_{desorption}$ (%)		
	T=20ºC	T=30ºC	T=40ºC	T=20ºC	T=30ºC	T=40ºC
10	2.1	2.3	1.8	5.7	5.5	4.5
20	3.7	2.7	3.7	7.5	6.9	6.4
30	5.0	4.1	4.7	9.0	8.3	7.8
40	8.6	6.9	5.7	11.2	10.0	9.4
50	10.9	7.9	7.1	11.7	1.1	10.5
60	11.1	9.8	8.9	13.7	12.9	12.6
70	13.1	12.4	11.3	-	-	-
80	14.5	12.9	13.8	16.8	17.0	15.9
90	18.0	17.6	17.0	23.0	24.0	21.1

Table 4- EMC model parameters estimation for the sorption processes

Equation			Van Wagner	Halsey	Oswin	Nelson	Chung-Pfost
Model parameters	a	Desorption	1.473	5.767	12.653	-0.183	0.183
		Adsorption	0.218	4.232	9.409	-0.193	0.193
	b	Desorption	0.531	0.012	0.053	5.236	57.182
		Adsorption	0.958	0.014	0.052	4.714	40.913
	c	Desorption	24.304	2.45	0.321	-	489.918
		Adsorption	68.193	2.07	0.390	-	236.158
	d	Desorption	8.442	-	-	-	-
		Adsorption	2.863	-	-	-	-
	e	Desorption	-389.814	-	-	-	-
		Adsorption	0.094	-	-	-	-
	f	Desorption	2.742×10^{-6}	-	-	-	-
		Adsorption	-0.042	-	-	-	-
Statistical parameters	R^2	Desorption	0.991	0.977	0.989	0.979	0.984
		Adsorption	0.984	0.903	0.944	0.968	0.977
	MAE	Desorption	0.428	0.702	0.384	0.579	0.421
		Adsorption	0.514	1.328	0.989	0.630	0.610
	RMSE	Desorption	0.514	0.818	0.563	0.776	0.681
		Adsorption	0.622	1.530	1.159	0.873	0.744
Residual distribution		Desorption	Random	Systematic	Random	Random	Random
		Adsorption	Random	Systematic	Random	Random	Random

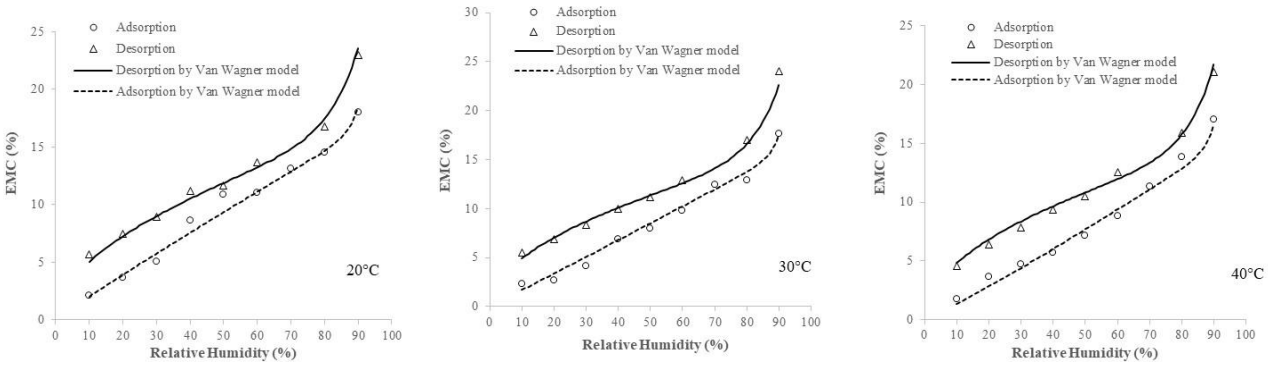

Figure 2- EMC of Pinus pinaster branches in both the adsorption and desorption processes. Estimates obtained by Van Wagner model.

In terms of model validation, Figure 3 shows the comparison between the predicted (line) and the observed (dots) FMC of *Pinus pinaster* branches. Predicted values result from the Modified Henderson and Pabis model for the drying and wetting curves and the Van Wagner model for EMC, both with empirical parameters estimated in the present work. The observed FMC values were obtained in the field tests. FMC values corresponding to rainfall events were excluded from the model validation.

Comparing the predicted and the observed FMC values, in terms of MAE, MAPE and RMSE, the results show a high prediction ability, with a MAE equal to 1.83%, a MAPE equal to 19.34% and a RMSE equal to 2.11.

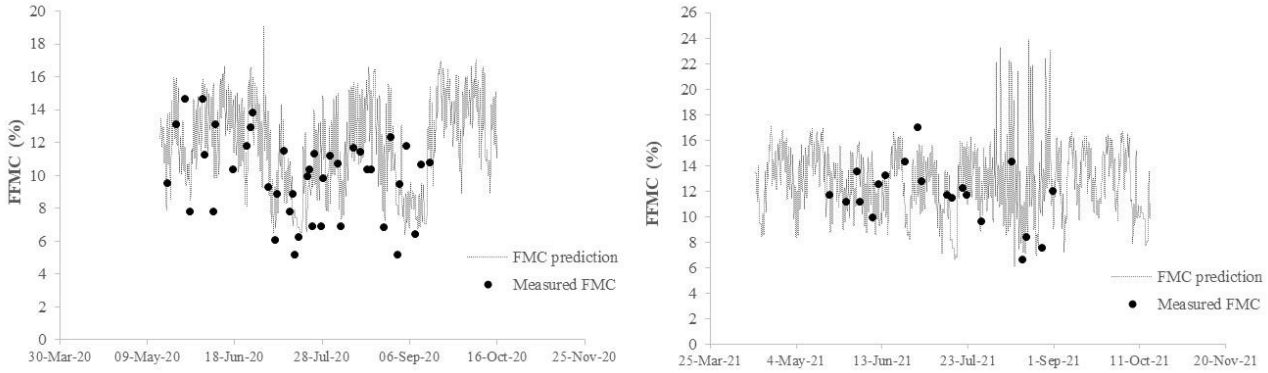

Figure 3- Comparison between the predicted (line) and the observed (dots) FMC of Pinus pinaster branches during 2020 and 2021 (15th May to 15th October). Predicted values result from the Modified Henderson and Pabis model for the drying and wetting curves and the Van Wagner model for EMC.

4. Discussion and Conclusion

The drying and wetting curves of dead *Pinus pinaster* branches (0.6 cm to 2.5 cm diameter) show that they are not pure exponential functions, but with different timelag values until equilibrium is reached. Additionally, the results suggest no significant relationship of the timelag periods with air relative humidity but a dependence with air temperature. An increase in the sorption rates with temperature is observed in this study that is in agreement with the results reported by Byram (1963). However, the pure exponential equation of Byram (1963), that is usually used in forest fire research, does not represent well the drying and wetting curves of dead *Pinus pinaster* branches. Modified Henderson and Pabis model provide the best fitting.

For this type of fuels, the representation of EMC values as a function of air relative humidity at constant temperature allowed to obtain a typical sigmoid curve. The EMC values obtained were higher for desorption process than for adsorption process, indicated the typical hysteresis effect in these processes.

It was found that, besides the models used in forest fires, other EMC models are also suitable to predict fuel moisture content of dead *Pinus pinaster* branches, as the ones used in agricultural and food analysis.

Comparing the predicted and the observed FMC of *Pinus pinaster* branches, the results show a high prediction ability of the best models, with a MAE equal to 1.83%, a MAPE equal to 19.34% and a RMSE equal to 2.11. Lee et al. (2020) and Dios et al. (2015) obtained similar results using other models type with this type of forest fuel (10h-fuels).

5. Acknowledgements

This work was financially supported by the Portuguese Foundation for Science and Technology through project MCFire-PCIF/MPG/0108/2017.

6. References

Bradshaw LS, Deeming JE, Burgan RE, Cohen JD (1983) The 1978 National Fire-Danger Rating System: technical documentation. United States Department of Agriculture, Forest Service, General Technical Report INT-169. Intermountain Research Station, Ogden, Utah. 44 pages

Byram GM (1963) An analysis of the drying process in forest fuel material. USDA Forest Service, Fire Sciences Laboratory, Rocky Mountain Research Station, Report. (Missoula, MT)

Catchpole E A, Catchpole WR, Viney NR, McCaw WL, Marsden-Smedley JB (2001) Estimating fuel response time and predicting fuel moisture content from field data. International Journal of Wildland Fire 10, 215-222 https://doi.org/10.1071/WF01011

Dios VR, Fellows AW, Nolan RH, Boer MM, Bradstock RA, Domingo F, Goulden ML (2015) A semi-mechanistic model for predicting the moisture content of fine litter. Agricultural and Forest Meteorology 203, 64-73.

Chen CC (1990) Modification of Oswin EMC/ERH equation. Chinese Agricultural Research 39(4), 367–376.

Henderson SM (1974) Progress in developing the thin layer drying equation. Transactions of the ASAE. American Society of Agricultural Engineers 17, 1167–1168. doi:10.13031/2013.37052

Henderson SM, Pabis S (1961) Grain drying theory I: temperature effect on drying coefficient. Journal of Agricultural Engineering Research 6, 169–174.

Iglesias HA, Chirife J (1976) Prediction of the effect of temperature on water sorption isotherms of food materials. Journal of Food Technology 11, 109–116. doi:10.1111/J.1365-2621.1976.TB00707.X

Karathanos VT (1999) Determination of water content of dried fruits by drying kinetics. Journal of Food Engineering 39, 337–344. doi:10.1016/S0260-8774(98)00132-0

Lee HT, Won M, Yoon S, Jang K (2020) Estimation of 10-hour fuel moisture content using meteorological data: A model inter-comparation study. Forests 11, 982. Doi:10.3390/f11090982

Matthews S (2014) Dead fuel moisture research: 1991–2012. International Journal of Wildland Fire 23, 78–92 doi:10.1071/WF13005

Nelson, RM (1969) Some factors affecting the moisture timelags of woody materials. USDA For. Serv. Southeast. For. Exp. Stn. Res. Pap. SE-44

Page GE (1949) Factors influencing the maximum rate of air drying shelled corn in thin-layers. MSc thesis, Purdue University, West Lafayette, IN.

Pfost HB, Maurer SG, Chung DS, Milliken GA (1976) Summarizing and reporting equilibrium moisture data for grains, ASAE paper number 76–3520. (St Joseph, MI)

Rothermel RC (1983) How to predict the spread and intensity of forest and range fires. Gen. Tech. Rep. INT-143. Ogden, UT: U.S. Department of Agriculture, Forest Service, Intermountain Forest and Range Experiment Station. 161 p.

Van Wagner, CE (1987) Development and Structure of the Canadian Forest Fire Weather Index System. Canadian Forestry Service, Petawawa National Forestry Institute, Forestry Technical Report 35 (Chalk River, ON)

Viegas DX, Viegas MT, Ferreira AD (1992) Moisture contente od fine forest fuels and fire occurrence in Central Portugal. International Journal of Wildland Fire 2 (4), 69-86.

Viney, NR, & Catchpole EA (1991) Estimating fuel moisture response times from field observations. International Journal of Wildland Fire, 1, 211-214

Modelling the influence of regional landscape drivers on spatio-temporal patterns of wildfire activity

Jorge Castel-Clavera*[1] ; François Pimont[1] ; Thomas Opitz[2] ; Julien Ruffault[1] ; Jean-Luc Dupuy[1]

[1]URFM INRAE, France, {jorge.castel-clavera, françois.pimont, julien.ruffault, jean-luc.dupuy}@inrae.fr
[2] BioSP INRAE, France, {thomas.opitz@inrae.fr}

**Corresponding author*

Keywords

Firelihood; Wildfire activity; Risk management; Modelling; Bayesian; Mediterranean France

Abstract

Identifying the drivers of fire activity's spatio-temporal variability is challenging in densely populated and fire prone landscapes. Human usage and climate affect the local fire regime in contrasting ways. The identification of these drivers is further complicated due to the stochastic nature of fire activity. Fire regimes in Mediterranean France show contrasted spatial patterns and temporal changes at decadal scales. While overall, the number of fires decreased over the last thirty years, certain zones suffered local increases in fire activity. To describe and understand the drivers of those changes and the spatial variability, we introduced several improvements in the *Firelihood* model - a probabilistic framework capable of prediction fire occurrence of >1ha fires, and exceedance probabilities of 10 and 100 ha thresholds - by incorporating Land-Use Land-Cover (LULC) explanatory variables, as well as by enhancing its spatio-temporal components to account for unexplained variability in models. The novel model - fitted on a 2km-pixel grid, but relying on variables aggregated at various spatial aggregations (2, 4, 8 and 16km) - is used to explain the observed spatial patterns of fire activity during the last 27 years, as well as the regional and local changes observed between two decades with contrasted fire activities by running counterfactual scenarios.

LULC variables, including road density, wildland-urban interface, or expert-based fuel type rating explain a significant part (as much as fire-weather) of the variability in fire occurrence (>1ha), thereby reducing the effect of unexplained spatial variability. The selected occurrence model uses only 2km-resolution variables, as local factors have a high influence on fire ignition and initial spread. The occurrence of larger fire (>10 ha or >100 ha) is largely driven by fire-weather, followed by unexplained spatial variability; selected models for larger fires uses a few LULC variables aggregated at 4, 8 and/or 16 km. This indicates the influence of surrounding factors on fire size extension. The spatial effect for fire occurrence presents contrasted hot and cold-spots throughout the area, while it has a clear east to west decreasing trend for fire size.

Regarding temporal changes in fire activity between the two decades, changes in fire weather induced a strong increase in fire probability in many hot spots throughout the region, but this effect was overcompensated by a negative trend associated with unexplained temporal factors (and of larger magnitude than fire weather). LULC variables had negligible effect on the fire regime's temporal trends. Moreover, an east-to-west gradient appears for the spatial trends of the larger fires, and for the temporal trends in all sizes, highlighting the increase in fire activity in the western side of the region. Those results suggest that observed temporal changes in fire activity are the result of a changing socio-economic or policy frame, probably related to reinforced suppression policies following the year 2003, and the increasing agricultural abandonment.

1. Introduction

In south-eastern France, the Mediterranean climate creates fire-prone fuel moisture conditions and regional winds often trigger large fire events (Ruffault et al. 2017). The climatic and land characteristics of the region (Fréjaville and Curt 2015; Barbero et al. 2019) shape the spatial patterns of fire activity: highest burnt area in fire-prone populated areas, with high exposure of human settlements to fire, and in hinterland and inland mountains lower summer fire activity, despite local "hot-spots" (Figure 1A).

Fire-weather largely drives seasonal and interannual variations in fire activity in south-eastern France (Pimont et al. 2021), and it has increased in the last decades, suggesting a rise of potential fire risk (Fréjaville and Curt 2015; Barbero et al. 2020), yet the translation of this potential to realized fire risk remains unknown. Fire records

show a decrease in fire activity in the last 40 years which makes the assessment of the weather effects more difficult. To understand past changes in fire regimes and risk, and anticipate future scenarios, it is necessary to disentangle how climate, landscape and human factors affected spatio-temporal dynamics of fires.

Several studies aimed to explain different aspects of fire activity in south-eastern France and how it varies in time and space (e.g., Ruffault et al. 2017, Pimont et al. 2021). However, there are still many uncertainties about the role of human and biophysical factors in the spatial and temporal trends in this region. Here we improved the *Firelihood* probabilistic fire activity model (Pimont et al. 2021) to quantify how much of the observed changes in fire activities can be attributed to these factors and how these temporal changes are distributed at the regional scale. This second goal is not only important in the context of retrospective analysis of changes in fire activity, but also in the context of anticipation of the near future.

2. Materials and methods

Firelihood (FL) is a Bayesian probabilistic framework accounting for the stochastic nature of fire activities with several statistical components that model daily occurrence and size of wildfires as a marked point process parametrized with several explanatory variables (Pimont et al. 2021). FL models the occurrence of fire larger than 1ha (escaped fires) as a Poisson process and the size of these fires as a combination of exceedance threshold probability and piecewise size distributions. FL includes spatio-temporal effects to account for limitations in explanatory variables. Effects are adjusted with the R-INLA package, which implements the Integrated Nested Laplace Approximation and allows spatial effects with Matérn covariance function represented through the Stochastic Partial Differential Equation (SPDE) approach.

The first developments (in the following FL1) included FWI and Forest Area as explanatory variables and spatio-temporal effects of the occurrence component were seasonal, spatial and annual, with a shift following the 2003 heat wave. The estimation was done in 8-km pixels (Pimont et al. 2021). In FL1, spatio-temporal effects were critical to mitigate the impact of large unexplained effects which can induce confusion between factors and limit the accuracy of estimated effects of explanatory variables. Moreover, they allow a realistic representation of processes involved in fire activities, so that simulations can be used to carry out spatio-temporal analyses, despites of the stochasticity in fire observations.

FL1 was limited for detailed analyses of the evolution of spatio-temporal patterns of fire activity. We develop an extension of FL1, referred as FL2, which includes additional LULC at 2-km resolution and refined spatio-temporal effects. The occurrence component of FL2 includes a yearly effect and a spatial effect for temporal trends (equation 1). Size exceedance models for 10 and 100 ha include a yearly effect and spatial effects for Sylvo-Eco Regions exhibiting similar characteristics (equation 2).

$$\log N_{i,d}^{1ha} \sim \beta_0 + \underbrace{f_{FWI}(FWI_{i,d}) + f_{WEEK}(WEEK_{i,d})}_{FL1} + \beta(WAp_{i,y}) + \sum_{LULC} f_{LULC}(LULC_{i,y}) + f_{X,Y}(X_i, Y_i) + \underbrace{f_{YEAR}(y) + f'_{X,Y}(X_i, Y_i)(y - 1992)}_{Spatio-temporal\ trends} \quad (1)$$

$$log\,\frac{p_{i,d}^{u}}{1-p_{i,d}^{u}} = \beta_0^{p,u} + f_{FWI}^{p,u}(FWI_{i,d}) + \sum_{LULC} f_{LULC}^{p,u}(LULC_{i,y}) + f_{YEAR}^{p,u}(y) + f_{BESAG}^{p,u}(SER) \quad U = [10,100] \quad (2)$$

Simulations with FL2 (Figure 1B) allowed to (i) quantify the relative contributions of the different variables to spatial patterns thanks to a partition of variance; (ii) predict the evolution of fire activities from the 1993-2002 decade, to which would have occurred during the 2009-2018 decade if only climate, LULC or unexplained factors had changed at a time, allowing to attribute observed changes to the different explanatory variables.

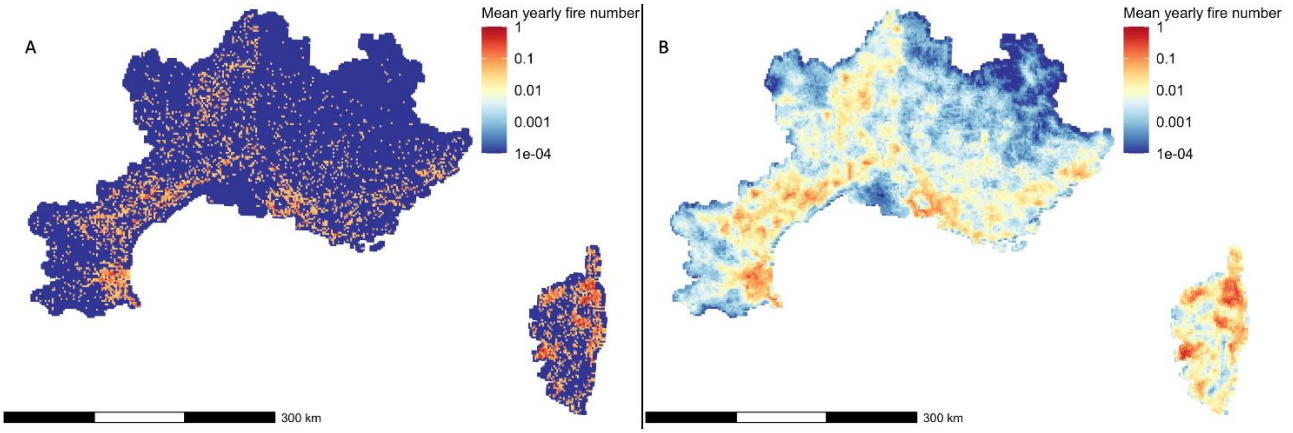

Figure 1. Fire occurrence over the study period expressed as the mean number of fires larger than 1ha per year in each 2km pixel: (A) Observed; (B) Simulated.

3. Results and discussion

3.1. Variable selection and model performance

Variable selection based on DIC and AUC led to FL2, summarized in Table 1. Significant improvements were obtained with the inclusion of LULC. The coarser scales of spatial aggregation (4, 8 and 16km) underperformed to explain occurrence, so that only finer predictors (2km) were retained. This highlights that occurrence patterns were better explained by fine scale landscape factors, contrary to size models for which 4km and even 8 and 16km were sometimes better predictors.

The effects of the occurrence model components were consistent, showing increases associated with FWI (Figure 2B), fuel type rating (Figure 2C), wildland area (Figure 2A), road length and population (not shown). Inverted U-shape responses associated with wildland area, slope, aspect or wildland urban interface were explained by reverse effects of these factors on ignition and initial spread, as already observed for wildland area in Pimont et al. (2021). Road length and population are among the most influential variables, confirming the key role of accessibility to forest areas found in other regions of Europe and the influence of human activities (e.g. Costafreda et al. 2017).

The yearly effect (Figure 2D) confirmed the huge decay in fire activity observed after the 2003 crisis. The negative values of the spatial effect (Figure 3A) corresponds to areas where explanatory factors tend to overestimate the observed activity. The spatial distribution of annual trends (Figure 3B) was contrasted from west to east, with positive trends to the west and negative to the east. In a context where unexplained factors depending on the local conditions are very important, this approach allowed accurate estimations of the effect of explanatory variables and of residual unexplained spatio-temporal random effects.

The partial effects of both size models were similar (100ha in Figure 2), with monotonic responses. Exceedance probabilities increased with FWI (Figure 2F), fuel type rating (Figure 2G), wildland (Figure 2E), shrubland and coniferous areas and slope, and decreased with broadleaved and agricultural areas, and population (not shown). Upper ranges were generally associated with saturations. The yearly effect for the 100ha threshold decreased - except the 2003 peak-, but with a non-significant trend as current trends (blue dashed line) were inside the credible interval of early years (Figure 3H. The spatio-temporal effects here are less sophisticated because the datasets for fires above 100 ha were too small to afford the approach described above for occurrence. The temporal effects allowed potential yearly changes and spatial effects into SylvoEcoRegions and proved to enhance the predictive ability of the model. The spatial effect (Figure 3C) shows a west-east gradient with increased probability in the eastern part and in mountainous regions, possibly explained by operational constraints in suppression policies in remote mountainous regions.

Table 1. Variable selection of the occurrence model (OCCURRENCE) and size models for the 10 ha (SIZE 10) and the 100ha (SIZE100) exceedance thresholds. The distance indicated in parenthesis refers to the spatial aggregation used for a given variable (by default is 2km).

Model	Variables	DIC	AUC (training)	AUC (validation)
OCCURRENCE	Intercept + WAp + Fuel + WA + Aspect + Slp + WUI + Pop + Agri + Roads + SPDE + Sp_temp + Years	50131,24	0,877	0,827
SIZE 10	Intercept + FWI + WA(4km) + Agri (4km) + Con + Brl + Shr + Pop + Slp + Mxf (8km) + Fuel + Besag + Years	5646,03	0,71	0,66
SIZE 100	Intercept + FWI + WA(4km) + Agri (4km) + Con + Brl + Shr (4km) + Pop + Slp (16km) + Fuel + Besag + Years	2002,53	0,79	0,78

Where: : **WAp** – Wildland area presence, **Fuel** – ONF's fuel rating, **WA** – Wildland area, **Aspect –** Aspect of the pixel, **Slp** – Slope, **WUI** – Wildland to Urban interface, **Pop** – Population per pixel, **Agri** – Agricultureal area, **Roads** – Road length, **Con** – Coniferous forest area, **FWI** – Fire Weather Index, **Brl** – Broadleaved forest area, **Shr** – Shrublkand area, **Mxf** – Mixed forest area, **SPDE** – Spatialmodel, **Sp_temp** – spatio-temporal model, **Besag** – Spatial model based on the SER. DIC and AUC are the criterion for the model evaluation," fit" and "pred" Make refference to the training and validation data respectively.

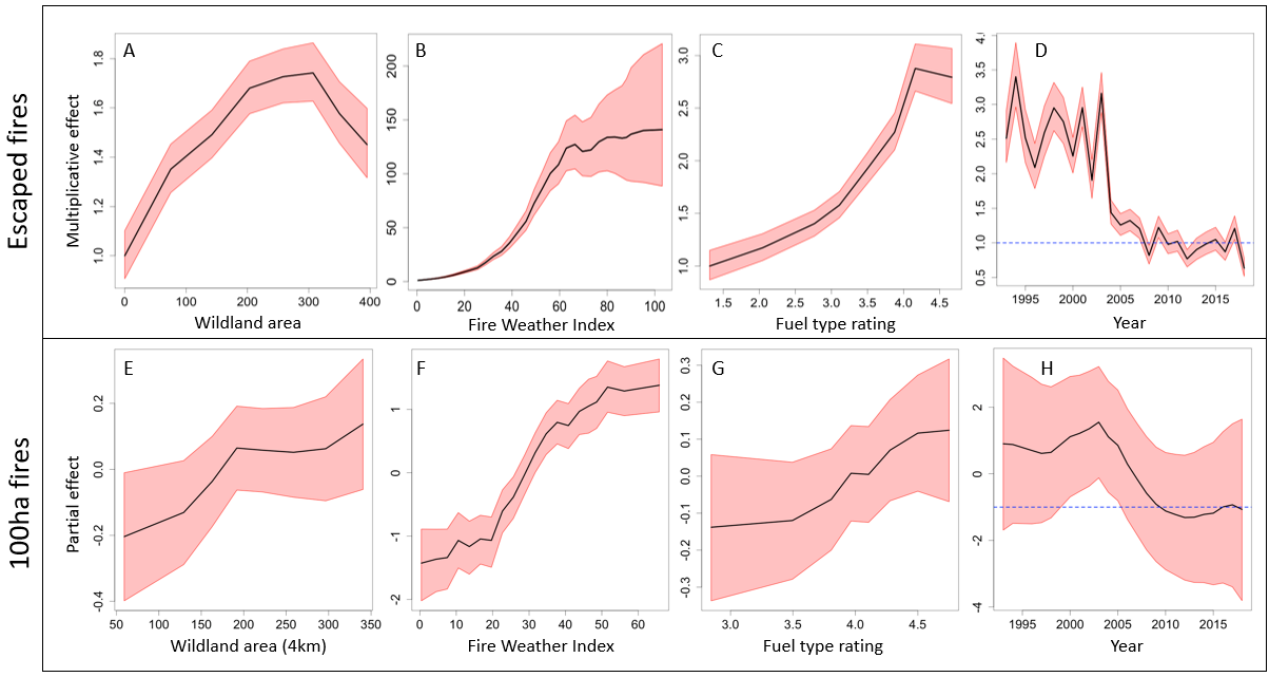

Figure 2. Examples of: (A-D) multiplicative effects for the predictor variables of the occurrence model (escaped fires) with confidence intervals; (E-H) partial effects (E-H) of the predictor variables for the 100ha exceedance probability models.

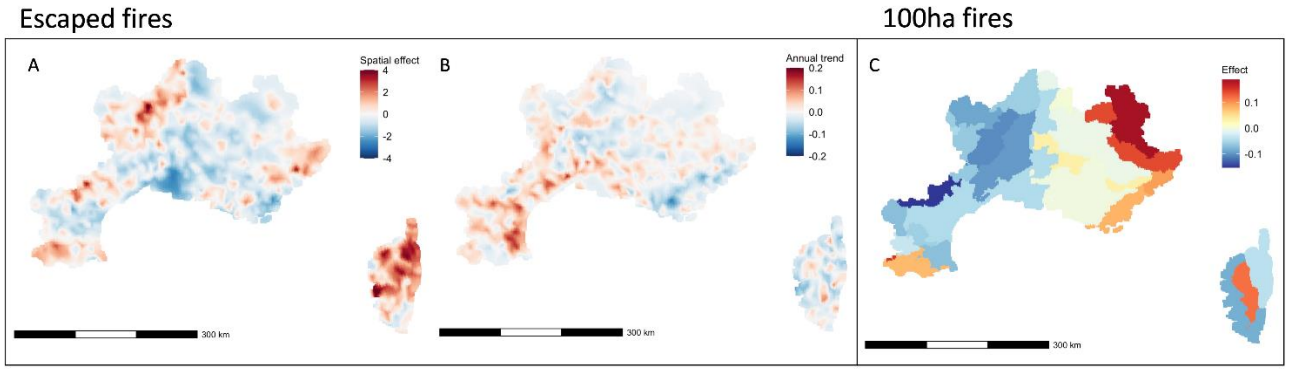

Figure 3. Spatial effect of the occurrence model from SPDE (A); spatial trends of the occurrence model (B); Spatial effect from the "Besag" component of the 100ha exceedance model (C). The effect's magnitude is drawn in a color coding in each pixel, the labels inside each polygon (thin black lines) corresponds to the code of the SylvoEcoRegions.

3.2. Factors explaining spatial distributions and their changes

The partition of fire activity variance allowed to attribute the spatial variability to three types of effects (Fire-weather, LULC and unexplained) over the whole period. The spatial effect had the biggest contribution to 1ha-number simulations (40%), while LULC and fire-weather explained one fourth of the total variance each. The "temporal effect" in spatial patterns - associated with spatial trends- was less important. For larger fire numbers (N10 and N100), the fire weather explained the biggest part of spatial variance (~50%), followed by the spatial effect (~25%), while LULC were around 17-20%. The temporal effect was marginal. Therefore, fire-weather and LULC together explained roughly 50% of spatial distribution of 1ha fires and up to 70% for larger fires (N10 and N100).

The next analysis aimed at determining whether the changes in spatial distribution between 1993-2002 and 2009-2018 could be explained by these variables. The comparison between decades for the actual evolution of variables confirmed a decrease in fire numbers for all sizes, ranging between -50 and -60%. When considering changes in factors one at a time, simulations for the recent decade were more contrasted. The "Fire-weather-change" scenario shows an increase in fire events while the "LULC-change" scenario did not affect the fire number. The "other-temporal-change" scenario showed a decrease in fire number, but with bigger magnitude than the "actual" simulations. The potential increase caused by fire-weather change was overcompensated by temporal changes which were not explained by LULC variables. It is very likely that suppression fire policy strongly reduced the number of escaped fires in part of the region.

We then investigated the spatial distributions of these changes by mapping anomalies between the reference period and recent scenarios (Figure 4). The spatial distributions were similar throughout the three fire sizes. Both the real-present and the other-temporal-changes (Figure 4A,D) scenarios showed a widespread decrease over the eastern regions and sharp local increases in the western regions, revealing that the overall trend was very heterogeneous over the territory. Fire-weather change (Figure 4B) induced scattered increases in a few "hot spots", in locations where the effect on activity should have increased the most, without other changes. Finally, changes in LULC (Figure 4C) produced marginal changes, clearly not explaining any of the recent fire regime change.

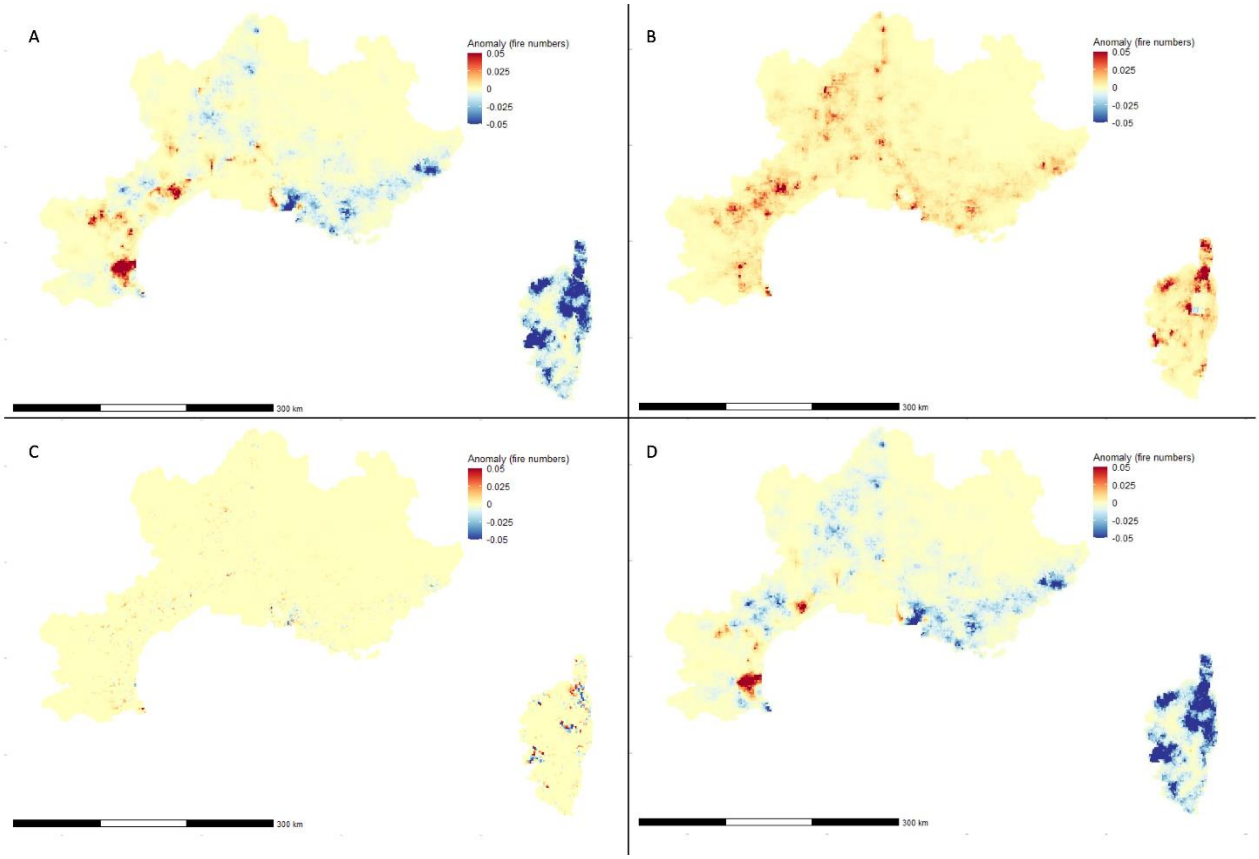

Figure 4. Spatial distribution of anomalies between the 1993-2002 and 2009-2018 decades for 1ha fire numbers. A: Real present. B: Fire-weather. C: LULC. D: Other temporal changes.

4. Conclusion

Analyzing factors of fire activities at regional scales is highly challenging. Our modeling framework and the simulation plan allowed to quantify important changes in fire activity and their drivers. We showed that usual explanatory variables (fire-weather, LULC) failed to explain the main temporal changes observed over recent decades, because of large unexplained factors. Among these unexplained factors, prevention and suppression policies affect the fire regime. Our study reveals that, if very significant reductions occurred after the 2003 heat wave on the number of escaped fires (1ha fires), no significant reduction could be detected over the last decade, neither on the ability of escaped fires to turn into large fires. Finally, spatial patterns of these changes were very contrasted from west to east, suggesting that significant reductions could be reached. Our framework might be extended to future scenarios involving climate, vegetation or human drivers

5. References

Barbero, R., Curt, T., Ganteaume, A., Maillé, E., Jappiot, M., and Bellet, A.(2019) Simulating the effects of weather and climate on large wildfires in France, Nat. Hazards Earth Syst. Sci., 19, 441–454.

Barbero R et al. (2020) Attributing Increases in Fire Weather to Anthropogenic Climate Change Over France. Frontiers in Earth Science 8, 104

Fréjaville T, Curt T (2015) Spatiotemporal patterns of changes in fire regime and climate: defining the pyroclimates of south-eastern France (Mediterranean Basin). Climatic Change 129, 239–251. doi:10.1007/s10584-015-1332-3.

Pimont F et al. (2021) Prediction of regional wildfire activity in the probabilistic Bayesian framework of Firelihood. Ecological Applications 31.

Ruffault J, Moron V, Trigo RM, Curt T (2017) Daily synoptic conditions associated with large fire occurrence in Mediterranean France: evidence for a wind-driven fire regime: DAILY SYNOPTIC CONDITIONS ASSOCIATED WITH LARGE FIRE OCCURRENCE. *International Journal of Climatology* **37**, 524–533.

Mulching treatments favour the recovery of ecosystem multifunctionality after a large wildfire in Northwest Spain

Elena Marcos*[1]; Sara Huerta[1]; Víctor Fernández-García[1]; Iván Prieto[1]; Rayo Pinto[1]; Gemma Ansola[1]; Luis Saénz de Miera[2]; Leonor Calvo[1]

[1] Area of Ecology. Faculty of Biological and Environmental Sciences. University of León, 24071 León, Spain
[2] Area of Genetics. Faculty of Biological and Environmental Sciences. University of León, 24071 León, Spain, {elena.marcos, shueg, vferg, ipria, rpinp, gemma.ansola, luis.saenzdemiera, leonor.calvo}@unileon.es

**Corresponding author*

Keywords

Ecosystem multifunctionality, high severity, Mediterranean ecosystems, post-fire treatments, wildfires

Abstract

Wildfires are a widespread phenomenon in forests across the Mediterranean Basin but have increased in risk and severity in recent decades. Post-fire treatments are measures that help recover burned vegetation and their functionality but to what extent they also help recover soil functionality is currently unknown. The main objective of this study was to assess the effect of post-fire treatments on ecosystem multifunctionality after a large wildfire in the Cabrera mountain range in 2017 (NW Spain) where close to 10000 Ha of forest were burnt. At the end of 2017 and during 2018, the administration applied different post-fire treatments in high fire severity affected areas: i) straw mulching, ii) woody debris and iii) subsoiling and iv) mechanical hole afforestation. In each treatment, we established ten 2 x 2 m plots and ten adjacent untreated burned plots and collected a composite soil sample from each plot four years after the fire (2021). We calculated regulating services as the standardized mean of total soil organic C (climate regulation), soil water repellence (water regulation) and soil aggregation (soil protection). Supporting services were measured as the standardized mean of mineral N-NH4+ and N-NO3- and available P (soil fertility), β-glucosidase, urease and acid phosphatase (nutrient cycling) and microbial biomass (soil quality). Ecosystem multifunctionality was measured as the standardized mean of all functions measured. Application of straw mulch and woody debris increased regulating ecosystem services in relation to burned control plots. Afforestation with holes had no impact but subsoiling decreased regulating ecosystem services in relation to burned control plots. Post-fire treatments did not have any effect on supporting services. Straw mulch, Woody debris and afforestation with holes improved ecosystem multifunctionality when compared with subsoiling methods. These results show that post-fire stabilisation treatments, in particular straw mulching have a significant positive impact on regulating services and are effective measures in restoring the ecosystem multifunctionality, helping develop effective management based-decisions for the recovery of ecosystem services and functioning after large wildfires.

1. Introduction

Wildfires are a very common phenomenon in the Mediterranean Basin and have increased in severity in recent decades, a rise that is likely to continue in the future (Wagenbrenner et al., 2021). This is not only because of increased temperatures and drought with climate change (IPCC 2021) that is exacerbating wildfire conditions, but also because of socio-economic factors such as land use change and urban expansion that are also considered main drivers of increased fire severity and surface (Pausas et al., 2008). Increase fire severity is not only affecting vegetation composition and growth but also lead to the appearance of serious impacts on forest soils such as loss of soil quality, increased runoff, flooding and/or erosion (Fernández-García et al., 2021). All these changes are associated with a loss of important ecosystems functions and services that not only have a negative impact on rural populations but also for society as a whole. These has resulted in both the scientific community and government administrations being increasingly worried in evaluating and implementing measures that help mitigate wildfire impacts. In recent years, effective post-fire measures have been developed focusing on stabilising the burnt area to prevent further additional damage to essential resources such as water supply systems or human infrastructures and critical habitats for protected species (e.g. straw mulching to prevent soil

erosion). These measures need to be implemented as soon as possible after the fire to avoid potential damaging effects of rain events as their effectiveness in preventing soil erosion is high (Fernández and Vega, 2016). In other cases, post-fire treatments are implemented to assist and facilitate the recovery of the damaged ecosystem after the wildfire (e.g. vegetation afforestation). This type of treatments is usually applied in areas degraded by repeated fires that prevent the natural regeneration of vegetation (García-Matallana et al., 2022).

Many studies have evaluated the effectiveness of these practices on individual ecosystem properties in soil (erosion, runoff…) (Gómez-Rey et al., 2013; Prats et al., 2021) and vegetation (species richness, vegetation cover...) (Duniway et al., 2015; García-Matallana et al., 2022) but ecosystems provide multiple functions and services at the same time (ecosystem multifunctionality *sensu* Garland et al., 2020). Ecosystem multifunctionality could be considered as the ability of an ecosystem to supply multiple ecosystem functions and services increasing the benefits that societies can be obtain from an ecosystem (Hölting et al., 2019; Liu et al., 2021). However, the influence of these post-fire treatments on the provision of multiple ecosystem services and the recovery of the ecosystem multifunctionality (EMF) has not, to our knowledge, yet been analyzed (Taboada et al., 2021). As a soil contribute to a range of ecosystem services, in this study we focused on a set of ecosystem indicators that are relevant to a successful recovery and functioning of the ecosystem. Soil plays an important role as a carbon sink helping to favour infiltration and mitigate erosion and contributing to the development to microbial community. Therefore, our main objective was to evaluate the medium-term impact of four post-fire treatments (straw mulching, woody debris, afforestation with mechanical hole and afforestation with subsoiling) on ecosystem services and ecosystem multifunctionality after a large wildfire in Northwest Spain

2. Material and methods

The study area is located in the Cabrera mountain range, León province (NW Spain) where a large wildfire burned close to 10000 Ha of forests and scrub dominated areas in 2017 (Fig. 1). The burnt area was dominated by *Quercus pyrenaica* Willd forests and *Pinus sylvestris* L. afforestations (3480 Ha), different scrub formations dominated by *Genista hystrix* Lange, *Erica australis* L., and *Cytisus scoparius* (L.) Link (5440 Ha) and Mediterranean grasslands (580 Ha). The fire was intentionally set and the adverse weather conditions at the time, with maximum temperatures of 35ºC, a 35% relative humidity in combination with two months of drought prior to the fire increased its virulence and facilitated its spread. The climate in the area is Mediterranean with dry temperate summers with mean annual temperatures of 9ºC and mean annual precipitation of 700-800 mm (Iberian Climate Atlas, 2011) The orography is heterogeneous with altitudes ranging from 836 to 1938 m.a.s.l. Soils are acidic (pH ~5), with slates, sandstones, and quartzites from the Ordovician period as the predominant type of rocks (Huerta et al., 2020).

At the end of 2017 and during 2018, the regional government administration implemented a series of post-fire actions aimed at protecting the soil in the most affected and steeper areas and facilitate the recovery of vegetation. These included: (1) addition of straw mulching and (2) woody debris with the aim to protect soil and, (3) subsoiling and (4) mechanical hole afforestation in the steeper areas (Fig.1). In each treatment, ten 2 x 2 m plots and ten adjacent untreated burned plots were established during 2018. In summer 2021, we collected 4 randomly selected soil samples within the 2 x 2 m plots using an auger (7 cm diameter x 3 cm depth) that were pooled together in a composite sample for each plot. Half of the sample was air dried and sieved (<2 mm) to analyse chemical and physical properties and half frozen (-18ºC) to determine soil $N\text{-}NO^{-3}$ and $N\text{-}NH^{+4}$ and microbial biomass an activity. Total organic carbon (TOC) was determined following the combustion method (Dumas 1831), using a EuroVector EA3000 elemental analyser and available P was measured at 882 nm wavelength after digestion with HClO4 (Olsen et al. 1954). We measured weight diameter (MWD) to determine the average size of stable aggregates (Kemper and Rosenau 1986) and we used the water drop penetration test (WDPT) was used to determine soil water repellency (WR) (Doerr, 1998). Ammonium (N-NH4+) and nitrate (N-NO3-) were extracted with 2M KCl at a 1:10 soil-extractant ratio (Keeney and Nelson 1982) and measured by distillation with an automatic micro-Kjeldhal analyzer (Bremner 1965). β-glucosidase (β-D-glucoside glucohydrolase) and acid phosphatase (phosphate-monoester phosphohydrolase) activities were analysed following Tabatabai (1994) and urease (urea amidohydrolase) activity following Kandeler and Gerber (1988). Microbial biomass C was determined by the fumigation-extraction method (Vance et al., 1987).

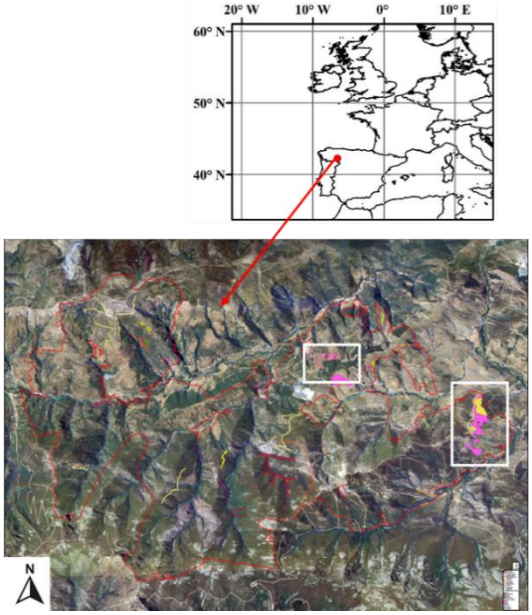

Figure 1- Post-fire treatments (yellow and pink) within the perimeter (red) of Cabrera wildfire which occurred in 2017.

Each of these variables was assigned to a regulating or supporting ecosystem service following Gardlan et al (2020). Regulating ecosystem services indicators were TOC for climate regulation, soil water repellence for water regulation and MWD for erosion protection. Supporting ecosystem services indicators were $N\text{-}NH_4^+$ and $N\text{-}NO_3^-$ for soil fertility, β-glucosidase, urease and acid phosphatase for nutrient cycling and microbial C biomass for soil quality. We then calculated a standardized value of regulating and supporting services as the average value of the standardized (between 0-1) corresponding variables. Similarly, ecosystem multifunctionality was calculated as the average standardized values of regulating and supporting ecosystem services.

In order to test differences in provisioning of regulating and supporting ecosystem services between post-fire treatments and unburned controls we used one-way analysis of variance (ANOVA) or nonparametric Kruskal-Wallis test when assumptions for ANOVA were not met. One-way ANOVA was used to compare differences in the recovering of ecosystem multifunctionality between post-fire treatments. Analyses were performed with PAST 4.01 (Hammer et al., 2001).

3. Results and discussion

Post-fire treatments aimed at protecting soil (straw mulch and woody debris) improved the ability of the soil to provision regulating ecosystem services (Fig 2). After a high severity fire, high temperatures in the soil reduced soil organic matter content affecting other related properties such as soil aggregate stability (Fernández-García et al., 2019) and water repellence (Marcos et al., 2018). In our study, both straw mulching and addition of woody debris increased TOC and improved the soil structure by increasing the size of the aggregates in the mid-term whereas soil water repellence was only improved where woody debris was added. Short-term studies found no effect of similar stabilisation treatments on soil quality after 16 weeks (Díaz-Raviña et al. 2012) but our results indicate that they can have an impact in the mid-long term. On the other hand, subsoiling afforestation did not have this beneficial effect in regulating ecosystem services although, individually, it reduced soil water repellence. When afforestation was done mechanically with a hole, the impact in regulating ecosystem services was negative because it did not improve any of the indicators analysed. Similar results were found by Mongil Manso and Bengoa Martínez de Mandojana (1997) that found 20% greater soil moisture in plots that were subsoiled than in plots that had been hollowed, as subsoiling favours soil physical properties related with hydrological processes (Fig. 2).

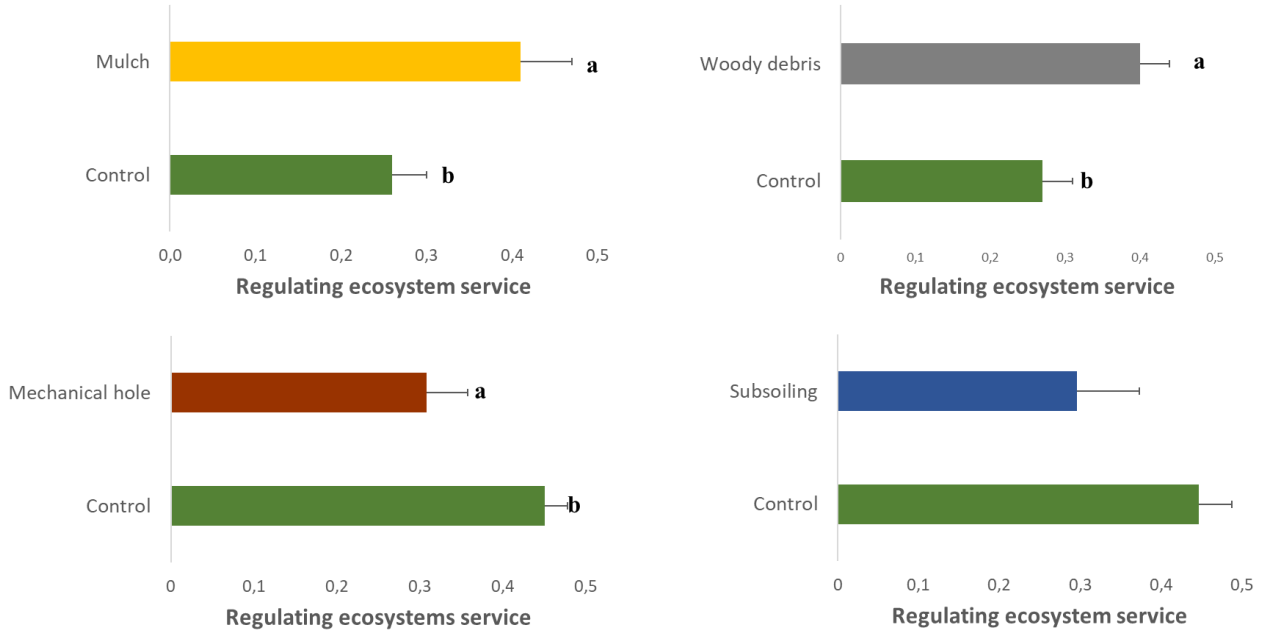

Figure 2. Regulating ecosystem services (Mean and standard error) for post-fire treatments (mulch, woody debris, mechanical hole and subsoiling) and their respective burned controls. Different letters show significant differences at $p < 0.05$.

Supporting ecosystem services were not significantly affected by post-fire treatments and only a slight tendency to improve this service was observed when straw mulching was applied (0.38 in treated plots vs. 0.29 in control plots). Straw mulching tends to improve soil nutrient concentrations (P and N), microbial C biomass and increased enzymatic activities, while in the other post-fire treatments results were not as consistent (e.g. enzyme activities were increased with addition of woody debris and soil microbial C biomass was increased under mechanical hole and subsoiling afforestation treatments). If we compare all treatments together, we observed that those aimed at protecting soil in the short-term were the most effective in facilitating the recovery of the multifunctionality of ecosystems in the mid-term (Fig.3).

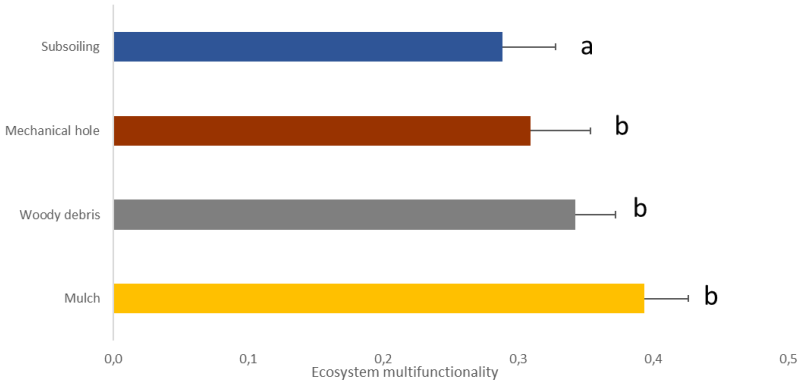

Figure 3. Average value and standard error of ecosystem multifunctionality for each post-fire treatment: mulch, woody debris, mechanical hole and subsoiling. Different letters show the presence of significant differences ($p < 0.05$) among post-fire treatments.

4. Conclusions

This study shows that post-fire stabilisation treatments, and in particular straw mulching, are effective in restoring ecosystem multifunctionality (EMF). These treatments had a significant positive impact on regulating services which may help reduce local and global impacts after a wildfire. However, afforestation with subsoiling or mechanical hole had a negative effect on the recovery of ecosystems functions so these measures are not

recommended with we aim at recovering ecosystem functionality. This type of studies is essential in order to make decisions focused on the recovery of functions and services that are strongly impacted by large wildfires.

5. Acknowledgements

This research was financially supported by the Spanish Ministry of Economy and Competitiveness in the framework of the FIRESEVES (AGL2017-86075-C2-1-R) project, and by the Regional Government of Castilla and León in the framework of the WUIFIRECYL (LE005P20) project.

6. References

Bremner, J.M., Mulvaney, C.S., 1982. Nitrogen total. In: Page, A.L., Miller, R.H., Keeney, D.R. (Eds.), Methods of Soil Analysis. Part 2: Chemical and Microbiological Properties, second ed. ASA, Madison, Wisconsin, USA, pp. 595–624.

Díaz-Raviña, M., Martín, A., Barreiro, A., Lombao, A., Iglesias, L., Díaz-Fierros, F., Carballas, T., 2012. Mulching and seeding treatments for post-fire soil stabilisation in NW Spain: Short-term effects and effectiveness. *Geoderma* 191: 31-39.

Doerr, S.H. 1998. On standardizing the 'water drop penetration time' and the 'molarity of an ethanol droplet'techniques to classify soil hydrophobicity: A case study using medium textured soils. *Earth Surf. Process. Landf.* 23, 663–668.

Dumas, J.B.A., 1831. Procedes de l'analyse Organic. *Ann. Chem. Phys.* 247, 198–213.

Duniway, M.C., Palmquist, E., Miller, M.E., 2015. Evaluating rehabilitation efforts following the Milford Flat Fire: successes, failures, and controlling factors. *Ecosphere* 6(5): 1-33.

Fernández-García, V., Marcos, E., Huerta, S., Calvo, L., 2021. Soil-vegetation relationships in Mediterranean forests after fire. *For. Ecosyst.* 8: 18.

Fernández-García, V., Marcos, E., Fernández-Guisuraga, J.M., Taboada, A., Suárez-Seoane, S., Calvo, L., 2019. Impact of burn severity on soil properties in a Pinus pinaster ecosystem immediately after fire. *Int. J. Wildland Fire* 28, 354–364

Fernández, C., Vega, J.A., 2016. Effects of mulching and post-fire salvage logging on soil erosion and vegetative regrowth in NW Spain. *For. Ecol. Manag.* 375: 46-54.

García Matallana, R., Lucas-Borja, M.E., Gómez –Sánchez, M.E., Mijan Uddin, S.M., Zema, D.A., 2022. Post-fire restoration effectiveness using two soil preparation techniques and different shrubs species in pine forests of South-Eastern Spain. *Ecol. Eng.* 178: 106579.

Garland, G., Banerjee, S., Edlinger, A., Miranda Oliveira, E., Herzog, C., Wittwer, R., Philippot, L., Maestre, F.T., van der Heijden, M.G.A., 2021. A closer look at the functions behind ecosystem multifunctionality: A review. *J. Ecol.* 109, 600-613

Gómez-Rey, M.X., Couto-Vázquez, A., García-Marco, A.S., González-Prieto, S.J., 2013. Impact of fire and post-fire management techniques on soil chemical properties. *Geoderma* 195-196: 155-164.

Hammer, Ø., Harper, D.A.T., Ryan, P.D. 2001. PAST: Paleontological statistics software package for education and data analysis. *Palaeontologia Electronica* 4(1): 9pp. http://palaeo-electronica.org/2001_1/past/issue1_01.htm

Hölting, L., Beckmann, M., Volk, M., Cord, A.F., 2019. Multifunctionality assessments – More than assessing multiple ecosystem functions and services? A quantitative literature review. *Ecol. Indic.* 103: 226-235.

Huerta, S., Fernández-García, V., Calvo, L., Marcos, E., 2020. Soil resistance to burn severity in different forest ecosystems in the framework of a wildfire. *Forests* 11, 773.

Iberian Climate Atlas. Air Temperature and Precipitation (1971–2000), 2011. Agencia Estatal de Meteorología, Ministerio de Medio Ambiente y Medio Rural y Marino; Instituto de Meteorologia de Portugal: Lisbon, Portugal, pp. 1–80. ISBN 978-84-7837-079-5.

IPCC, 2021: Climate Change 2021: The Physical Science Basis. Contribution of Working Group I to the Sixth Assessment Report of the Intergovernmental Panel on Climate Change [Masson-Delmotte, V., P. Zhai, A. Pirani, S.L. Connors, C. Péan, S. Berger, N. Caud, Y. Chen, L. Goldfarb, M.I. Gomis, M. Huang, K. Leitzell, E. Lonnoy, J.B.R. Matthews, T.K. Maycock, T. Waterfield, O. Yelekçi, R. Yu, and B. Zhou (eds.)]. Cambridge University Press. In Press.

Kandeler, E., Gerber, H., 1988. Short-term assay of soil urease activity using colorimetric determination of ammonium. *Biol. Fertil. Soils* 6, 68–72.

Keeney, D.R., Nelson, D.W., 1982. Nitrogen-inorganic forms. In: Page, A.L., Miller, R.H., Keeney, D.R. (Eds.), Methods of Soil Analysis, Part 2: Chemical and Microbiological Properties. ASA, Madison, USA, pp. 643-698.

Kemper, W.D.; Rosenau, R.C. Aggregate stability and size distribution. In Methods of Soil Analysis, Part 1; American Society of Agronomy: Madison, WI, USA, 1986; pp. 425–442.

Liu, C., Yang, M., Houa, Y., Xuea, X., 2021. Ecosystem service multifunctionality assessment and coupling coordination analysis with land use and land cover change in China's coastal zones. *Sci. Total Environ*. 797: 149033

Marcos, E., Fernández-García, V., Fernández-Manso, A., Quintano, C., Valbuena, L., Tárrega, R., Luis-Calabuig, E., Calvo, L., 2018. Evaluation of Composite Burn Index and Land Surface Temperature for Assessing Soil Burn Severity in Mediterranean Fire-Prone Pine Ecosystems. *Forests* 9:494

Mongil Manso, J., Bengoa Martínez de Mandojana, J.L., 1997. Seguimiento del contenido de humedad del suelo en distintos métodos de preparación del suelo para repoblaciones forestales (ahoyado mecanizado y subsolado lineal a nivel). II Congreso Forestal Español, 3: 419-424.

Olsen, S.R., Cole, C.V., Frank, S.W., Dean, L.A., 1954. USDA Circular No. 939. In: Estimation of Available Phosphorus in Soils by Extraction with Sodium Bicarbonate. US Government Printing office, Washington, USA, pp. 19.

Pausas, J.G., Llovet, J., Rodrigo, A., Vallejo, R., 2008. Are wildfires a disaster in the Mediterranean Basin? A review. *Int. J. Wildland Fire* 17, 713–723.

Tabatabai, M.A., 1994. Soil enzymes. In: Weaver, R.W., Angle, J.S., Bottomley, P.J., Bezdicek, D.F., Smith, S., Tabatabai, M.A., Wollum, A.G. (Eds.), Methods of Soil Analysis. Part 2: Microbial and Biochemical Properties. ASA and SSSA, Madison, USA, pp. 775–833.

Taboada A., García-Llamas, P., Fernández-Guisuraga, J.M., Calvo, L. 2021. Wildfires impact on ecosystem service delivery in fire-prone maritime pine-dominated forests. *Ecosyst. Serv.* 50: 101334

Vance, E.D., Brookes, P.C., Jenkinson, D.S., 1987. An extraction method for measuring soil microbial biomass C. *Soil Biol. Biochem*. 19: 703–707.

Wagenbrenner, J.W., Ebel, B.A., Bladon, K.D., Kinoshita, A.M., 2021. Post-wildfire hydrologic recovery in Mediterranean climates: A systematic review and case study to identify current knowledge and opportunities. *J. Hydrology* 602: 126772

Observation of Horizontal Smouldering Spread on Layer Thickness of Tropical Peat

Hafizha Mulyasih; Randitia Andika Putra; Bintang Farhan Muhammad[1]; Ridho Irwansyah[1]; Yulianto Sulistyo Nugroho*[1]

Department of Mechanical Engineering, Universitas Indonesia, Kampus UI Depok 16424, Indonesia
{hafizha.mulyasih, bintang.farhan, ridho.irwansyah04, yulianto.nugroho}@ui.ac.id,
{randitia.andika@alumni.ui.ac.id}

**Corresponding author*

Keywords

Smouldering; peat fires; layer thickness; tropical peat; horizontal spread

Abstract

Smouldering spread of peat fires has been studied by numerous researchers. Experimental work was performed to study the impact of peat layer thickness on horizontal smouldering spread behaviour. The thickness of the peat layer was varied 2 cm, 3 cm, and 4 cm peat thickness. A 3 cm-long coil heater was placed in the centre of the base. For ignition protocol, the coil heater was powered with 100 W of electricity for the first 60 minutes. Smouldering behaviour was observed by the temperature data, that measured using thermocouples and a thermal camera. The thickness of the peat layer and bulk density play important roles in the horizontal spread probability, as it changes the heat balance between the heat generation at the reaction zone and heat loss to the environment. Higher peak temperature was observed for peat 4 cm depth and then decreased by the thickness. The smoldering spread rate increases by peat thickness from 2.01 cm/h to 2.21 cm/h and then reach an asymptotic level. Extinction corresponds to a negative energy balance observed in thickness 2 cm of peat. A self-sustained smoldering front could not be maintained after the igniter was turned off.

1. Introduction

Peat fires remain a serious environmental problem on a global scale (Stracher *et al*. 2015). It releases a large amount of carbon into the atmosphere and causes significant damage to peatland ecology and the landscape (Usup *et al.* 2004). When ignited, peat fires can produce a thick smoke that reduces visibility and causes several health problems. Reduction of peat fire probability has been a high priority through peatland restoration and better early warning systems for the development of fire hotspots.

Peat is a transitional organic soil from plant matter to coal with a high carbon content (Roy *et al.* 1983), consisting of a porous structure that causes smouldering combustion dominated when it burns (Rein 2009). Smouldering combustion is a phenomenon with low temperature and slow propagation characteristics. Ohlemiller (2002) and Rein *et al.* (2009) explained in general that smouldering has four stages while it is spreading: the preheat zone, the evaporation zone, the decomposition zone, and the char-oxidation zone. Zanoni et al. (2018) pointed out that all phenomena in smouldering combustion affect the burning object's energy balance, suggesting a local and global energy balance (Zanoni *et al.* 2018). For the smouldering experiment, the energy balance could be represented by the flow of $\dot{E}in$ as the energy provided by the heater; $\dot{E}oxid$ as the energy released by the oxidation process; $\dot{E}pyr$ as the energy absorbed by the pyrolysis process; $\dot{E}evp$ as the energy absorbed by the water evaporation process; $\dot{E}out$ as the energy removed by the convective gas flow out; and, $\dot{E}loss$ as the energy removed by radial heat loss. Therefore, the net energy rate is:

$$\dot{E}net = \dot{E}in + \dot{E}oxid + \dot{E}pyr + \dot{E}evp + \dot{E}out + \dot{E}loss \quad (1)$$

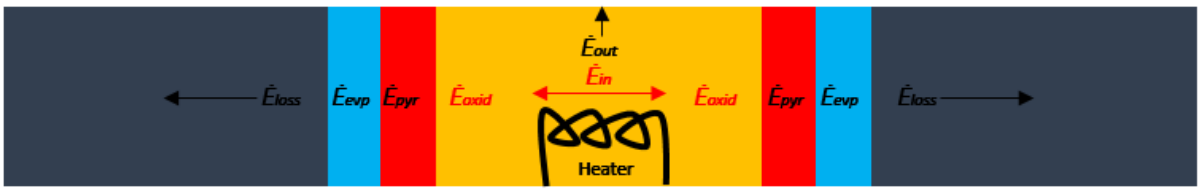

Figure 1- Conceptual model of Horizontal Smouldering Spread

Several studies have been reported before, that includes the upward and downward peat smouldering (Huang and Rein 2018) and the investigation of smouldering combustion propagation of dried peat (Palamba *et al.* 2017). In another work, the results of a modelling work by Huang and Rein (Huang and Rein 2015) reveal that smouldering combustion can spread over peat layers with very high moisture content (>250%) if the layer is thin and located below a thick drier layer. Christensen et al. (Christensen *et al.* 2020) was conducted a novel approach combining lateral and in-depth spread rates as vector components. The questions arise regarding the influence of peat layer thickness from one area to another. This is a challenge whether ignition can occur on peat with different thicknesses. In its natural stage, even though the peat layer is deep and covered by water, as soon as the rainy season is over, the draining process in the upper layer of the peat (1-5 cm) may create a dry surface that is vulnerable to catch fire. In addition, it is still rarely found research that discusses the spread that occurs horizontally on thin layers of tropical peat. This study extends earlier work on the horizontal smouldering spread of a peat sample from Papua, Indonesia (Putra *et al*. 2020). Samples and methods were changed so that the impact of density and peat structure on the phenomenon could be better explained.

2. Experimental Methods

2.1. Peat sample preparations

The peat samples came from the Palangka Raya, Indonesia, with coordinates N: 02°17'21.5412"; E: 114°1'58.492", and called PKY. The results of the Proximate and Ultimate (Table 1), are used to find out the difference in the physical characteristics and chemical components that affect the combustion process. Higher volatile matter, oxygen concentration, and lower bulk density could accelerate the smouldering spread, while ash content and moisture content tend to slow down the smouldering spread. A higher calorific value could produce greater heat energy when the sample is burned.

The PKY was dried in an electric oven at 100 ℃ within 24 hours until the peat samples' moisture was ~ 8%. Scanning electron microscope tests are also carried out to determine the structure and pore sizes of the peat samples. Figure 2b shows that the pore size for PKY is approximately 2.5 μm. This porosity value can affect the drying and combustion reaction processes.

Table 1- Proximate and Ultimate Analysis of Peat Samples

Proximate Analysis		Ultimate Analysis	
Initial Moisture (%)	69.20	C (%)	57.43
Moisture in as-dry based (%)	8.20	H (%)	4.80
Ash (%)	7.50	N (%)	1.10
Volatile Matter (%)	49.80	O (%)	29.01
Fixed Carbon (%)	34.50	Total Sulphur (%)	0.10
Gross Calorific Value (MJ/kg)	4930	Bulk Density (kg/m^3)	360

(a) (b)

Figure 2- (a) PKY before the combustion process, (b) Scanning electron microscope result of PKY.

2.2. Smouldering experiments procedure

The adjustable reactor was developed to conduct the smouldering experiment. It is made of stainless steel measuring 40 × 40 cm isolated by 10 mm thick calcium-silicate board insulation around the reactor side and on the bottom of the reactor. The reactor was designed with an adjustable base so that it can be used for a variety of peat thicknesses. This work investigated the horizontal spread on 4 cm, 3 cm, and 2 cm peat layer thickness. For the ignition protocol, a three cm-long coil heat igniter was placed at the centre of the base and was powered with 100 W of electricity for 60 min. This ignition protocol follows previous work (Putra *et al*. 2020). After the igniter was turned off, the combustion process was self-sustaining smouldering. The seventeen thermocouples (Figure 3b) were inserted from the bottom side and measured using a Graphtec GL840 data logger. The thermocouple tip was located at a depth of 1 cm from the reactor base. The peat samples' mass was weighed before and after the experiment to determine the mass reduction caused by combustion. The experiments were repeated twice on each peat thickness.

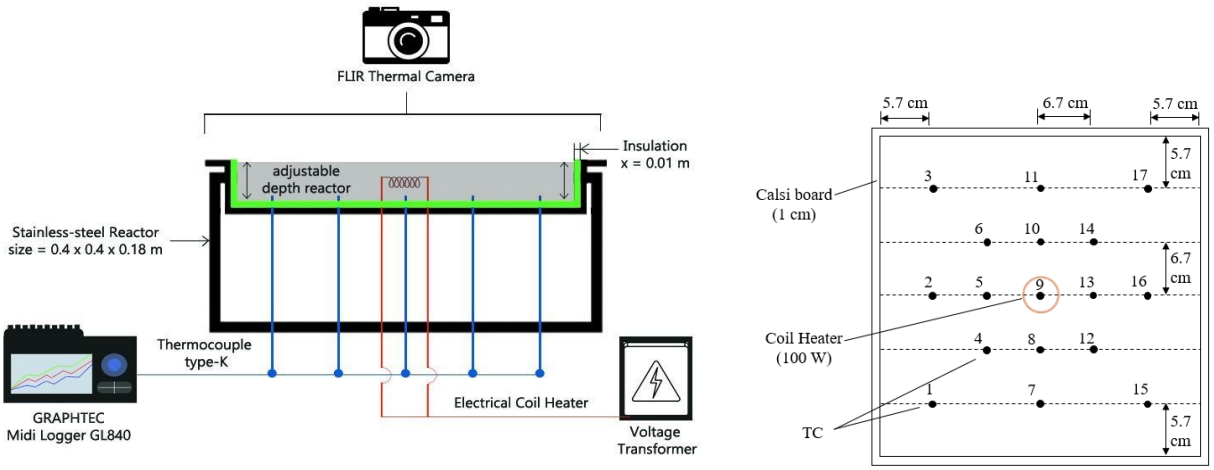

(a) (b)

Figure 3- Experimental setup. (a) Device arrangement, (b) Thermocouple arrays.

2.3. Image Analysis Tools

The thermal camera used in this experiment was a FLIR A35x with a resolution of 320 x 256 pixels, temperature range from 50 ˚C to 550 ˚C with accuracy ± 5 ˚C or 5% of reading. The images were taken every 10 minutes after the ignition started. The infrared camera was placed at a distance of 100 cm with angles of 20˚ from the

peat surface to avoid getting too hot from the burning peat. The images obtained from thermal cameras represented the temperature that occurred on the peat surface. In general, every image consists of RGB colour in its pixels. These three colour component combinations will create a specific colour for its pixel. To determine the value of spread rate, two pictures with different time taken were compared. To do this image processing needs to be done on thermal images. Many authors have suggested this method for different scales of application (Stracher *et al.* 2015, Putra *et al.* 2020, Burke *et al*. 2019, Bhattacharjee *et al.* 2017, Christensen *et al.* 2018).

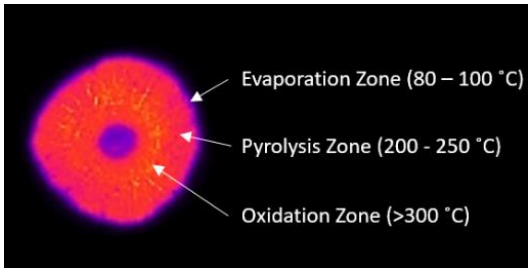

Figure 4- Different zones when the peat combustion process occurs

3. Results and Discussion

3.1. Infrared Images Results

Smouldering on peat with a thickness of 4 cm and 3 cm managed to spread to the side of the reactor, while peat with a thickness of 2 cm failed to sustained-smouldering because it went out shortly after the igniter was turned off. Smouldering fire on peat with a thickness of 4 cm has high sustainability. These caused by the heat generated by the peat fire is higher than heat loss to the environment and to the peat itself for the drying process and pyrolysis process. Therefore the smouldering process will continue until the heat generated could not equilibrate the heat loss. On the thinner thickness of 2 cm on PKY shown in Figure 5c, the smouldering fire did not sustain after the igniter was turned off. This proves that the heat generated by the peat is smaller than the heat loss to the environment (Huang and Rein 2018). This process also happened on Papua peat with a thickness of 2 cm from previous work (Putra *et al.* 2020).

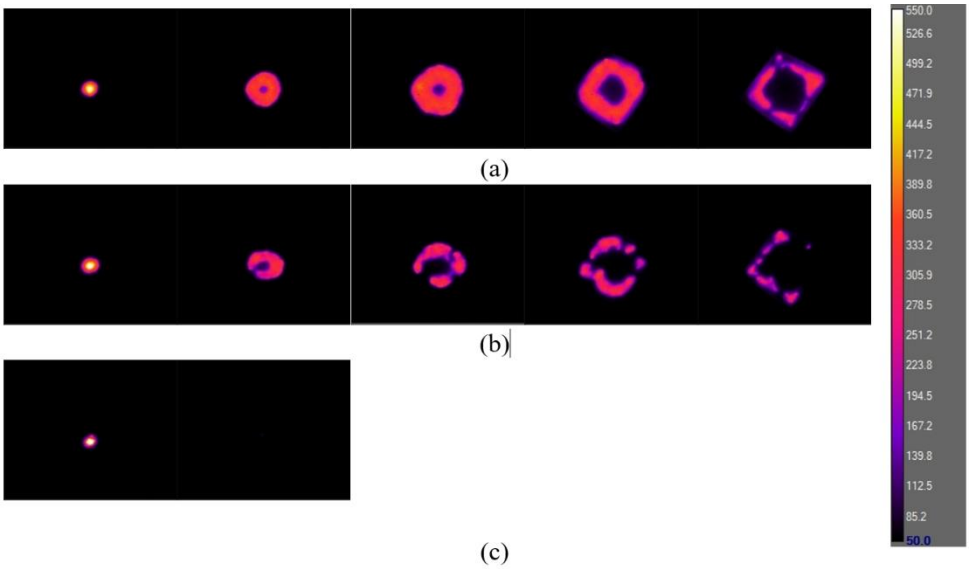

Figure 5- Horizontal Smouldering Spread from PKY Peat: (a) 4 cm thickness, (b) 3 cm thickness, (c) 2 cm thickness. The time between each picture is 2 hours.

3.2. Temperature Profile of Smouldering Peat

Differences were also found in the results of temperature measurements obtained from thermocouple measurements (Figure 6). Moreover, the difference in bulk density and homogeneity can be explained by Figure 7. In this case, peat samples were sieved using a 6 mm wire mesh size. With the sieving process, it is expected that peat approaches closer to more homogeneous conditions in terms of peat grain size. The first sieved peat

shows a more regular temperature pattern compared to the un-sieved one. The regularity of this pattern is also seen in images captured by infrared cameras (Figure 8), where the sieved peat has better homogeneity so that the distribution of heat also occurs more evenly. Different peat grain sizes cause cavities in several areas in the reactor, making a difference in oxygen supply so that the spread becomes less consistent. Whereas on peat that is not sieved, its distribution is often irregular. Sometimes, it suddenly experiences a drastic increase in temperature while in an area with a better fuel and oxygen supply mixture. Peak temperature also differs between sieved and un-sieved peat samples. This is due to the sieved peat sample having a higher bulk density so that the surface area of the peat that experiences a combustion reaction is also greater, causing a higher peak temperature. Table 4 shows the bulk density values of the sieved and un-sieved peat samples used in this study. There are significant differences in the bulk density values of the two peat samples. For un-sieved peat samples, the average bulk density used for the experiment is 278.79 ± 1.4 kg/m^3. After the sieving process, the average bulk density was increased to 299 ± 4.4 kg/m^3. The difference in bulk density values can be seen visibly from peat after being drained, whereas the un-sieved peat tends to be more porous compared to the sieved peat. Lower bulk density causes a faster spread of horizontal smouldering. The cavity between macros between one and another provides a pathway for oxygen to enter, thus accelerating the combustion reaction rate.

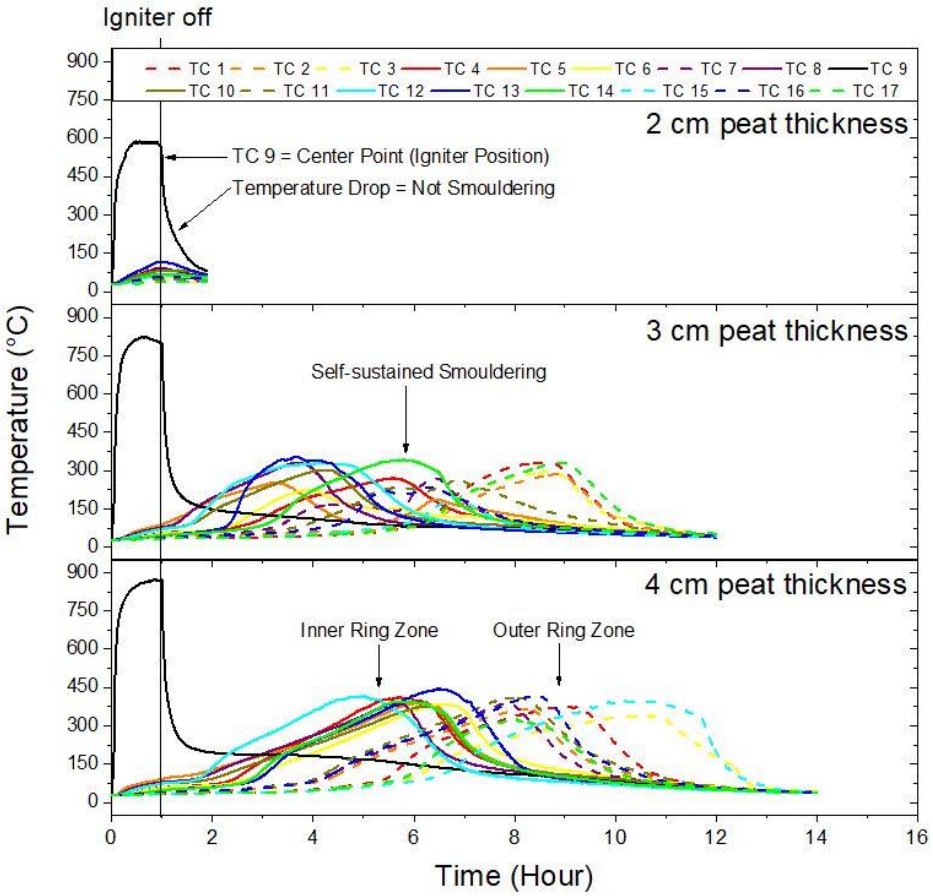

Figure 6- Temperature Measurements from Thermocouples from several Peat Layer Thickness PKY Peat

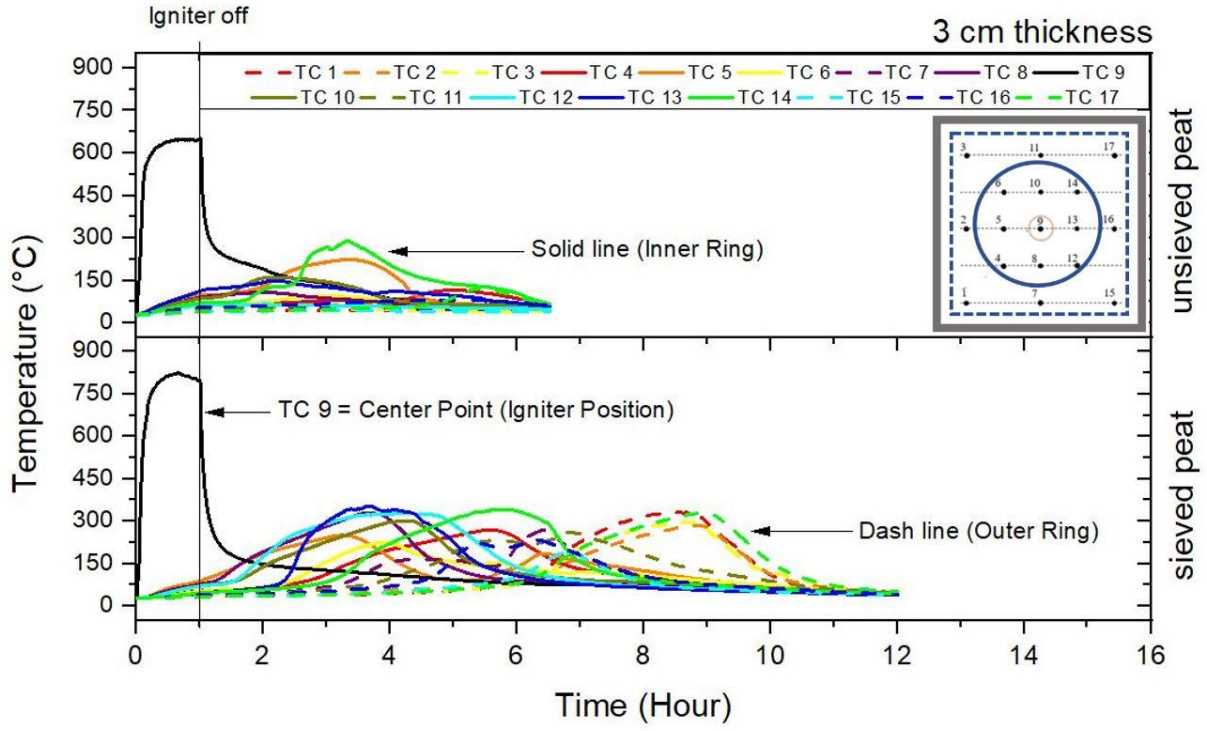

(a)

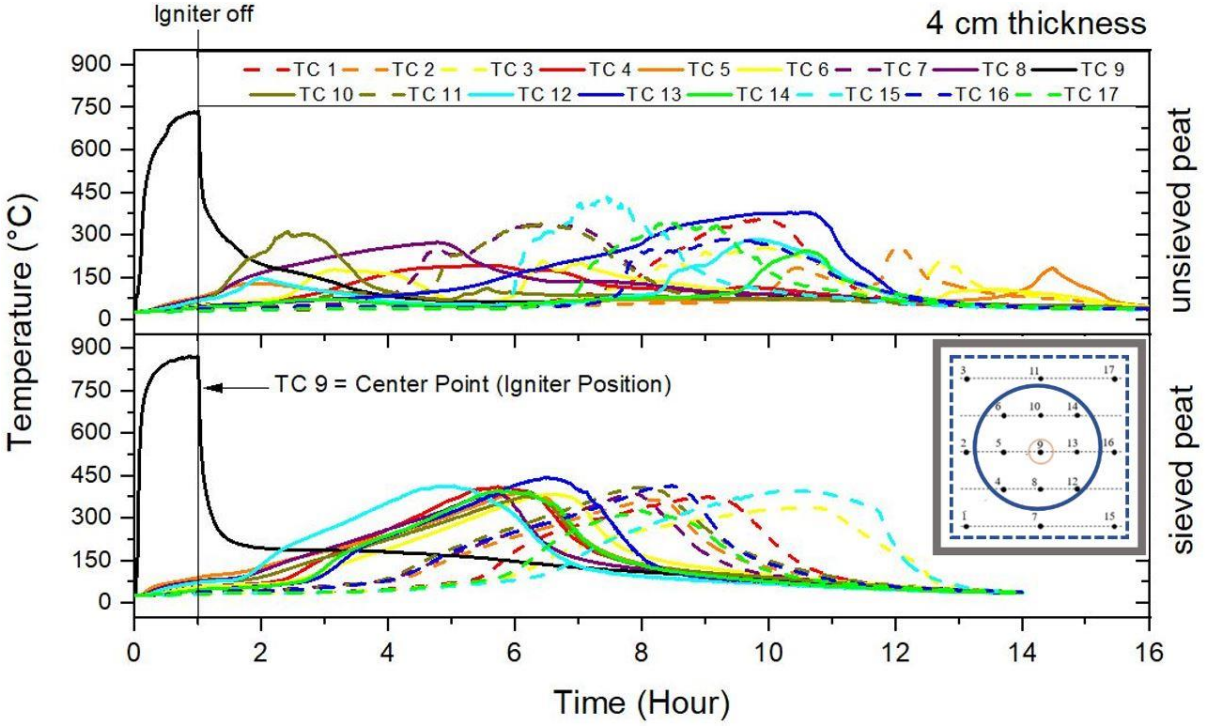

(b)

Figure 7- The difference in temperature readings between sieved and un-sieved on peat thickness (a) 3 cm, (b) 4 cm

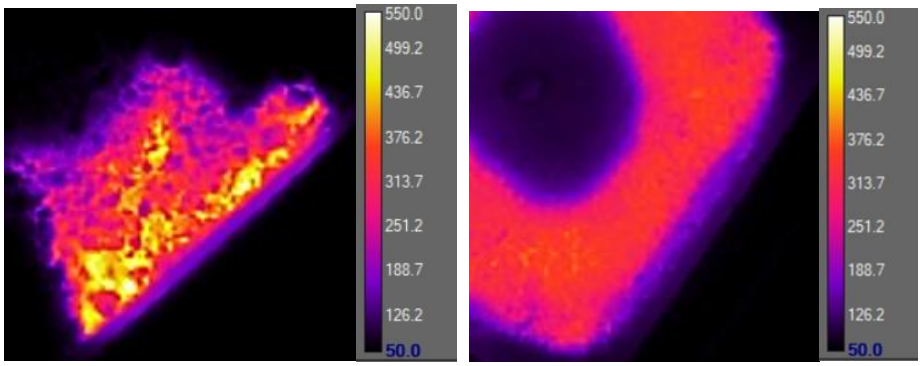

(a) (b)

Figure 8- Differences in visualization results from surface textures captured by infrared cameras, (a) un-sieved peat samples, (b) sieved peat samples

Table 2- Bulk Density difference between sieved and un-sieved peat

Peat Sample	Preparation	Bulk Density (kg/m^3)
PKY	Un-sieved	278.79 ± 1.4
	Sieved	299 ± 4.4

3.3. Spread Analysis

The smouldering spread from PKY on each thickness can be seen in Figure 9. It can be seen that an increase in the speed of smouldering spreads with increasing thickness of the layer, but the increment is slowly decreasing when a certain thickness level. As the thickness of the peat layer decreases, it increases the surface to volume ratio (Rein 2009). Thus, in a negative energy balance, the heat generated by the combustion process cannot overcome the heat loss released to the environment. This causes the peat to burn to the extinction process. Smouldering combustion fails to survive on peat with layer thickness as thick as 2 cm where the spread of smouldering only lasts shortly after the heater is turned off. The heterogeneous nature of peat causes its smouldering speed to vary. The average smouldering spread rate for PKY includes 2.01 cm/h for 3 cm thick peat and 2.21 cm/h for 4 cm thick peat. In separate experiments, the horizontal smouldering spread rate was found to be about 2.82 cm/h using a 10 cm depth reactor and 2.91 cm/h using an 18 cm depth reactor (Putra *et al.* 2020).

$$v_r = \frac{s_{0\to n}}{\Delta t_{0\to n}} \quad (2)$$

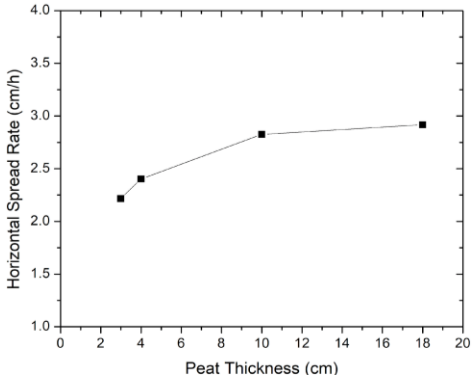

Figure 9- Horizontal spread rate of PKY Peat

4. Conclusion

Self-sustained smouldering depends on a positive energy balance between heat generation due to oxidation reaction and heat loss to the environment. The adjustable reactor used in this experiment was varied to represent 4 cm, 3 cm, and 2 cm peat layer thickness. The thickness and the bulk density of the peat layer play important

roles on the horizontal spread probability, as it changes the heat balance between the heat generation at the reaction zone and heat loss to the environment. The smouldering spread rate increases by peat thickness from 2.01 cm/h to 2.21 cm/h and then reaches an asymptotic level. Extinction corresponds to a negative energy balance that was observed in 2 cm peat layer thickness in which a self-sustained smouldering front could not be maintained after the igniter was turned off.

5. Acknowledgement

The authors would like to thank Universitas Indonesia for the financial assistance through Hibah Publikasi Terindeks Internasional (PUTI) Q1 2022 funding scheme managed by the Directorate for Research and Public Services (DRPM) Universitas Indonesia. Ms. Hafizha Mulyasih thanks to Directorate of Higher Education of Republic of Indonesia for financial support through the PMDSU scholarship funding scheme with a contract number: NKB-352/UN2.RST/HKP.05.00/2021.

6. References

Bhattacharjee, S., Carmignani, L., Celniker, G., & Rhoades, B. (2017). *Measurement of instantaneous flame spread rate over solid fuels using image analysis*. Fire Safety Journal, 91, 123–129.

Burke, Claire., Serge Wich, Kitso Kusin, Owen McAree, Mark E. Harrison, Bernat Ripoll, Yunsiska Ermiasi, Margarita Mulero-Pázmány, and Steve Longmore, Thermal-Drones as a Safe and Reliable *Method for Detecting Subterranean Peat Fires*, Drones 2019, 3(1), 23; https://doi.org/10.3390/drones3010023

Christensen, E. G., Fernandez-Anez, N., & Rein, G. (2020). *Influence of soil conditions on the multidimensional spread of smouldering combustion in shallow layers*. Combustion and Flame, 214, 361-370.

Christensen, E., Hu, Y., F. Restuccia, M. A. Santoso, X. Huang, G. Rein, 2018, *Experimental Methods and Scales in Smouldering Wildfires. Chapter 19 in: 'Fire effects on soils: State of the Art and Methods'*, Commonwealth Scientific and Industrial Research organisation (CSIRO), Australia

Glenn B. Stracher, Anupma Prakash, Guillermo Rein, *Coal and Peat Fire: A Global Perspective Volume 4: Peat-Geology*, Combustion, and Case Studies, Elsevier, 2015.

Huang, X. and Rein, G. *Computational study of critical moisture and depth of burn in peat fires*. Int. J. Wildland Fire 2015, doi:10.1071/WF14178.

Huang, X., and Rein, G. *Upward-and-downward spread of smoldering peat fire*, Proceedings of the Combustion Institute (2018), https://doi.org/10.1016/j.proci.2018.05.125

Ohlemiller, T.J., *SFPE Fire Protection Handbook, chapter 2-10: Smouldering Combustion*, pp. 2–201–2–210. National Fire Protection Association, Quincy, MA 02269, 3rd edition, 2002.

Palamba, Pither. Ramadhan, Mohamad. Imran, Fahri Ali. Kosasih, Engkos. S. Nugroho, Y. (2017). *Investigation of smoldering combustion propagation of dried peat*. AIP Conference Proceedings. 1826. 020017. 10.1063/1.4979233.

Putra, R. A., Akbar, L. A., Hatmojo, R. B. D., Mulyasih, H., & Nugroho, Y. S. (2020, September). *Smoldering combustion spread on a thin layer of Papuan peat*. In AIP Conference Proceedings (Vol. 2255, No. 1, p. 070007). AIP Publishing LLC.

Rein, G. (2009). *Smouldering Combustion Phenomena in Science Technology*. University of Edinburgh. United Kingdom.

Rein, G., Cohen, S., Simeoni, A. *Carbon emissions from smouldering peat in shallow and strong fronts*, Proc. Combust. Inst. 32 (2) (2009) 2489–2496. http://dx.doi.org/10.1016/j.proci.2008.07.008.

Roy, C., E. Chornet, and C. H. Fuchsman. The pyrolysis of peat: a comprehensive review of the literature. Journal of Analytical and Applied Pyrolysis, 5:263-332,1983.

Usup, A., Hashimoto, Y., Takahashi, H., & Hayasaka, H. (2004). Combustion and thermal characteristics of peat fire in tropical peatland in Central Kalimantan, Indonesia. Tropics, 14(1), 1–19.

Zanoni, M.A.B. et al., Determining the conditions that lead to self-sustained smouldering combustion by means of numerical modelling, Proceedings of the Combustion Institute (2018), https://doi.org/10.1016/j.proci.2018.07.108

Observed Wind Vector Change Across New Zealand's National Network of Fire-Weather Stations in Predicting Fire Risk

Siena Brody-Heine*; Marwan Katurji; Jiawei Zhang

[1]*University of Canterbury. 20 Kirkwood Avenue, Upper Riccarton, Christchurch 8041, New Zealand. {sbr153@uclive.ac.nz}, {marwan.katurji, jiawei.zhang}@canterbury.ac.nz*

**Corresponding author*

Keywords

Extreme fire behaviour, vector wind change, complex terrain, fire weather index

Abstract

Wildfire spread is influenced significantly by weather fluctuations. Specifically, wind speed and direction change can drastically alter fire intensity and spread. Vector wind change can result from synoptic or mesoscale weather systems and small-scale meteorological processes, such as thermal circulations and low-level wind shear in complex terrain. These small-scale processes are usually underrepresented in numerical weather forecasting models, usually needing to be resolved by more expensive sub-kilometre grid resolution simulations. Recent New Zealand wildfires, such as 2017 Port Hills and 2019 Pigeon Valley wildfires, experienced wind change due to local sea breezes and strong nocturnal downslopes flows, exacerbating fire behaviour.

The aim of this research is to investigate if vector wind change (VWC) can be a metric to better represent the effect of mesoscale and microscale weather and the subsequent impact in extreme fire behavior. This was achieved utilizing hourly VWC, or the difference in magnitude of the hourly wind vectors, from the Fire and Emergency New Zealand (FENZ) national network of more than 200 weather monitoring stations. An additional variable, wind direction change (WDC), was also calculated to include the degree change of wind direction.

To identify high-risk stations, the top 20% of stations for VWC and WDC were calculated and investigated spatially across the New Zealand landscape. The high-risk stations are located primarily on the South Island, inland and in areas of complex terrain. There is little to no variation of these stations when mapped in each synoptic type, suggesting that the main factor in determining high VWC and WDC is meso and microscale terrain driven meteorology as opposed to larger synoptic regimes. Critically, the current fire risk metric, the Fire Weather Index, does not include wind direction changes at high windspeeds. Therefore, the inclusion of VWC and WDC as additional metrics in fire risk calculations could increase operational understanding of high-risk locations and terrain impacts on extreme and unpredictable fire behavior.

1. Introduction

1.1. Critical Fire Weather

Wildfire behavior is highly dependent on near-surface meteorological conditions such as …"the atmospheric conditions that encourage extreme fire behavior resulting in large and destructive wildland fires." (Werth et al., 2016). Wildfire danger increases with low atmospheric humidity, strong winds, drought, and unstable air conditions (Mills et al., 2020) (Harris et al., 2017). These elements are not simply a sum—they are intertwined and dependent on the other and have a significant impact on extreme and unpredictable fire behavior.

In complex terrain, wildfire behavior can be influenced by dynamically and thermally driven wind systems (Werth et al., 2016). A dynamically driven wind is channeled, directed and amplified by the topography, while thermally driven wind systems are driven by differences in heat flux. New Zealand's complex terrain, including mountain ranges, valley systems and the complex coastal topography, means that near-surface wind systems are a critical variable to understand to better predict wildfire danger (Hilton et al., 2015; Dong et al., 2021).

1.2. Wildfire in New Zealand

Until the last 5 years, large scale wildfires were an infrequent occurrence in New Zealand. However, like many countries around the world, wildfires are increasing in size and frequency with warmer and drier weather

(Langer & Wegner, 2018). These fires are also increasingly encroaching on urban spaces. This trend is illustrated in the recent 2017 Port Hills fire, 2019 Pigeon Valley and the 2020 Ohau fire in New Zealand. All three fires prompted evacuations of residents for multiple days and destroyed residential structures (AFAC, 2017, 2019; Foley, 2020)

To predict fire risk around New Zealand, Fire and Emergency New Zealand (FENZ) and the National Institute of Water and Atmospheric Research (NIWA) collect hourly weather data from over 250 stations. From this weather station data, the Fire Weather Index (FWI) is calculated based on fuel type, temperature, relative humidity, windspeed and precipitation (Mandal et al., 2021; Van Wagner, 1987). The FWI combines individual markers of fire risk, including the Initial Index Spread and Buildup Index, which are combined to give a more comprehensive evaluation of fire risk (Van Wagner, 1987).

1.3. Vector Wind Change

Wind change is an important variable in fire behavior and can drastically alter the fire direction and intensity (Mills et al., 2020). Wind change can occur at time scales of minutes to hours. Many firefighter entrapments are caused by sudden wind changes, happening within a few minutes, and is defined by the metric Vector Wind Change (VWC), or the difference in magnitude of the hourly wind vectors. Two recent wildfires in New Zealand illustrate the significance of understanding VWC for fire behavior; the 2017 Port Hills and 2019 Pigeon Valley experienced a wind direction change due to local sea breezes and strong nocturnal downslopes flows that exacerbated unpredictable fire behavior (Pretorius et al., 2020). Critically, the current fire risk prediction tool the FWI, does not account for wind direction changes and therefore misses critical meteorological and climatological information for predicting and understanding wildfire danger across complex terrain. This research presents an investigation into VWC in New Zealand, and how VWC can be utilized as an additional metric for predicting wildfire risk.

2. Methods

Observations from the Fire Emergency New Zealand (FENZ) weather stations were gathered using the open access data from the Envlib Modeling Consortium using the Tethysis API in Python (Kitteridge, 2021; New Zealand Modeling Consortium Open Environmental Digital Library, 2021). Stations with a complete time series between November 28th 2020 - November 28th 2021 (130 stations) were included. Meteorological data was logged as sub-hourly intervals, between 10 and 50 minutes, but are presented as hourly averages in the database. Vector Wind Change (VWC) was calculated using the hourly wind vector observations. While VWC does account for impact from both windspeed and wind direction changes, it does not clarify the change in wind direction measured in degrees. Therefore, an additional metric, hourly Wind Direction Change (WDC), was compiled for each station to give a more complete understanding of the wind changes at each of the 130 stations. WDC was calculated hourly using the modified degree range of -180 to 180 degrees. VWC is then averaged for each station over the yearlong period. For wind direction change, the kurtosis of the distribution is calculated to quantify the differences between the tails of distribution amongst stations the data. A high kurtosis value corresponds to light tails, indicating small hourly wind direction change.

To determine the highest risk stations, the top 20% of stations for VWC and WDC were identified, and stations present in both the top VWC and WDC were labeled as “high risk”. Stations were also analyzed with Kidson synoptic regime classifications, are based on the original 12 Kidson regimes, which are further split into three main groups based on overall pressure systems: Trough, Zonal, and Blocking. and are labeled with letters describing the pressure system and location (Kidson, 1999). VWC and WDC are further investigated within each synoptic regime in the year of data (Renwick, 2021). The Fire Weather Index (FWI) is calculated daily using the wind speed, temperature, relative humidity and precipitation at each of the 130 stations with a complete year of data. The FWI value was then averaged for each station over the same yearlong period as the VWC.

3. Results and Discussion

3.1. VWC and WDC for a Canterbury Case Study

In the Canterbury region, and out of the 130 stations, the Hakatere station had the highest values for both VWC and WDC indicating that there are both high windspeeds as well as significant wind direction change at high

windspeed (Figure 1A). Given that critical fire weather conditions become more important for both high windspeeds as well as frequent wind direction changes, this suggests that the region around the Hakatere station is likely to experience more wildfire behavior unpredictability in the event of wildfire than the other station locations in Canterbury. In comparison, Godley Head has a low WDC at high windspeed, and therefore experiences more consistent winds, with low hourly changes and a predictable direction. This is likely due to the graduation change of the sea breeze cycle at the coastal location, as compared with the complex topographic influenced meteorology at the Hakatere location (Figure 1B).

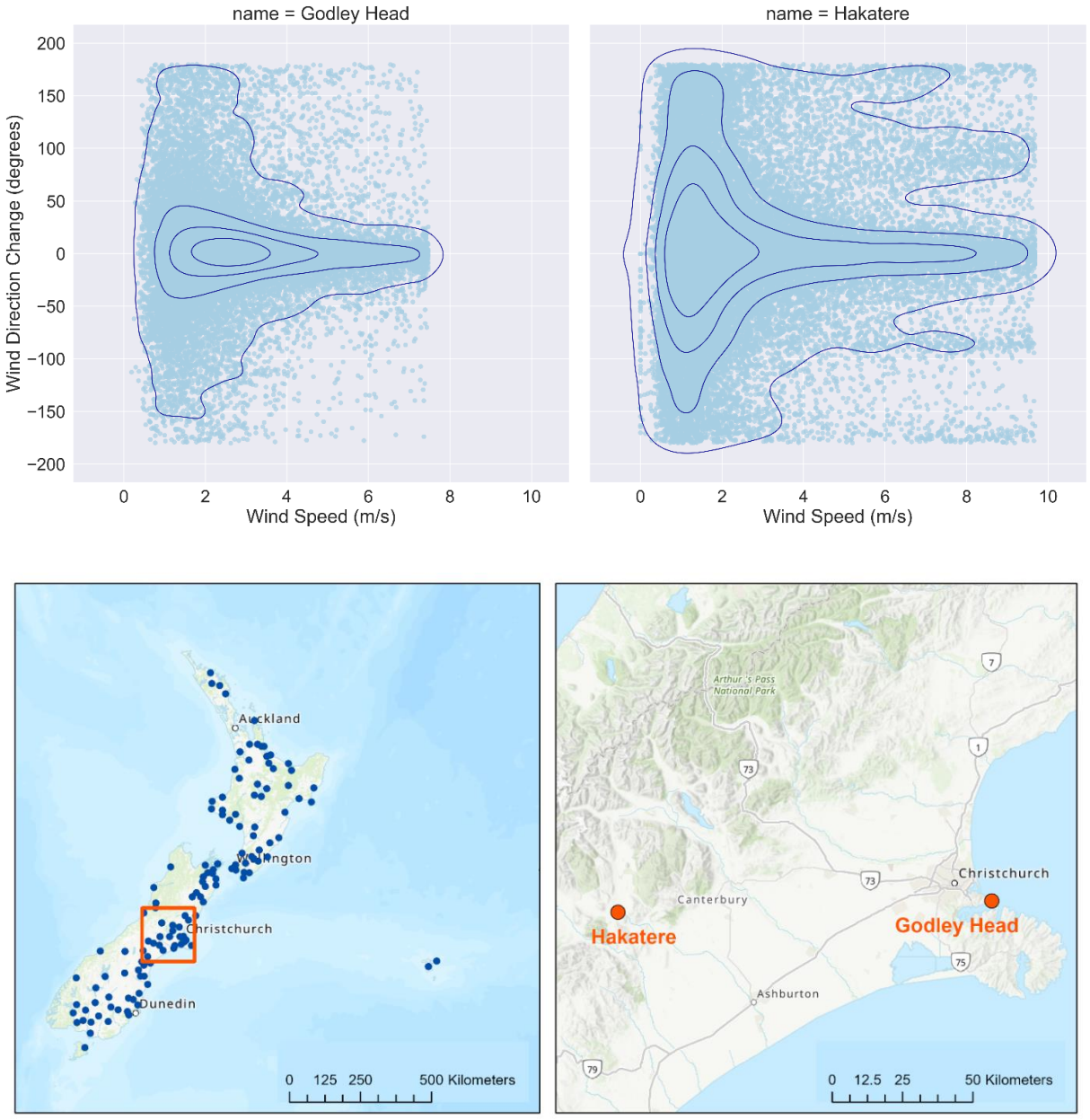

Figure 1- A) Highest and lowest windspeed kurtosis stations in Canterbury, with hourly wind speed plotted against wind direction change. B) Location of national stations, and Hakatere & Godley Head in Canterbury.

3.2. Nationwide wind change distributions

A nationwide analysis of stations shows distinct regional and topographic trends. High-risk stations (Figure 2, red) are located almost exclusively on the South Island, with one exception north of Wellington. Furthermore, all of these stations are located in areas of complex terrain and are not coastal. Similar to the trend in the Canterbury stations, stations in locations of complex terrain, such as the Southern Alps, have high VWC and WDC. This suggests that in New Zealand, there is a correlation between terrain complexity and wind vector

and direction change, and therefore a potential trend to better predict fire spread. The locations with high VWC and low WDC (Figure 2, orange) are still a high risk for critical fire weather with high windspeeds, however do not exhibit as significant wind changes at high speeds. The stations with both low VWC and low WDC (Figure 2, green) are located on the North Island and the Chatham Islands. This suggests costal stations and stations on flat terrain exhibit more consistent wind and wind direction leading to lower VWC and WDC. This is likely due to the more predictable sea breeze cycle.

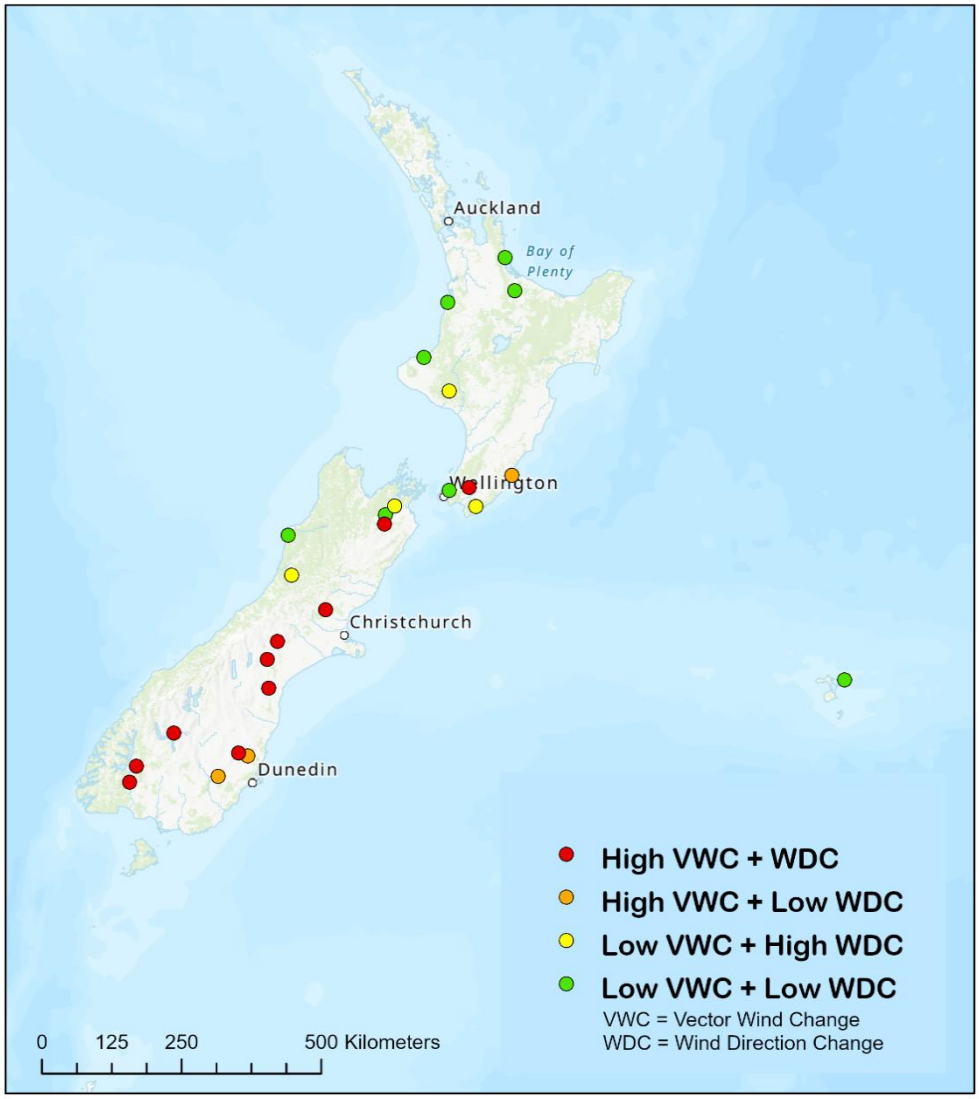

Figure 2- National Stations, highest or lowest 20% of VWC or WDC (based on mean and kurtosis respectively).

3.3. Synoptic Type Impact on Wind Change

In order to better understand the variables affecting VWC and WDC across New Zealand, a synoptic regime analysis was applied to investigate spatial pattern changes of high-risk stations in regard to weather systems. There is some variation between synoptic regimes in the stations identified, however the overall trend is consistent. High-risk stations appear almost exclusively on the South Island, except for a station near Wellington and one in the Central North Island (Figure 3). There are several stations that appear in almost all synoptic types, located in Fiordland, mountainous Canterbury and the top of the South Island. This uniformity in stations with VWC and WDC across synoptic types can suggest that the primary factor in these variables is terrain, not synoptic weather. Therefore, it is likely that some locations in New Zealand are at a higher risk of extreme fire behavior regardless of synoptic type due primarily to location and proximity to complex terrain.

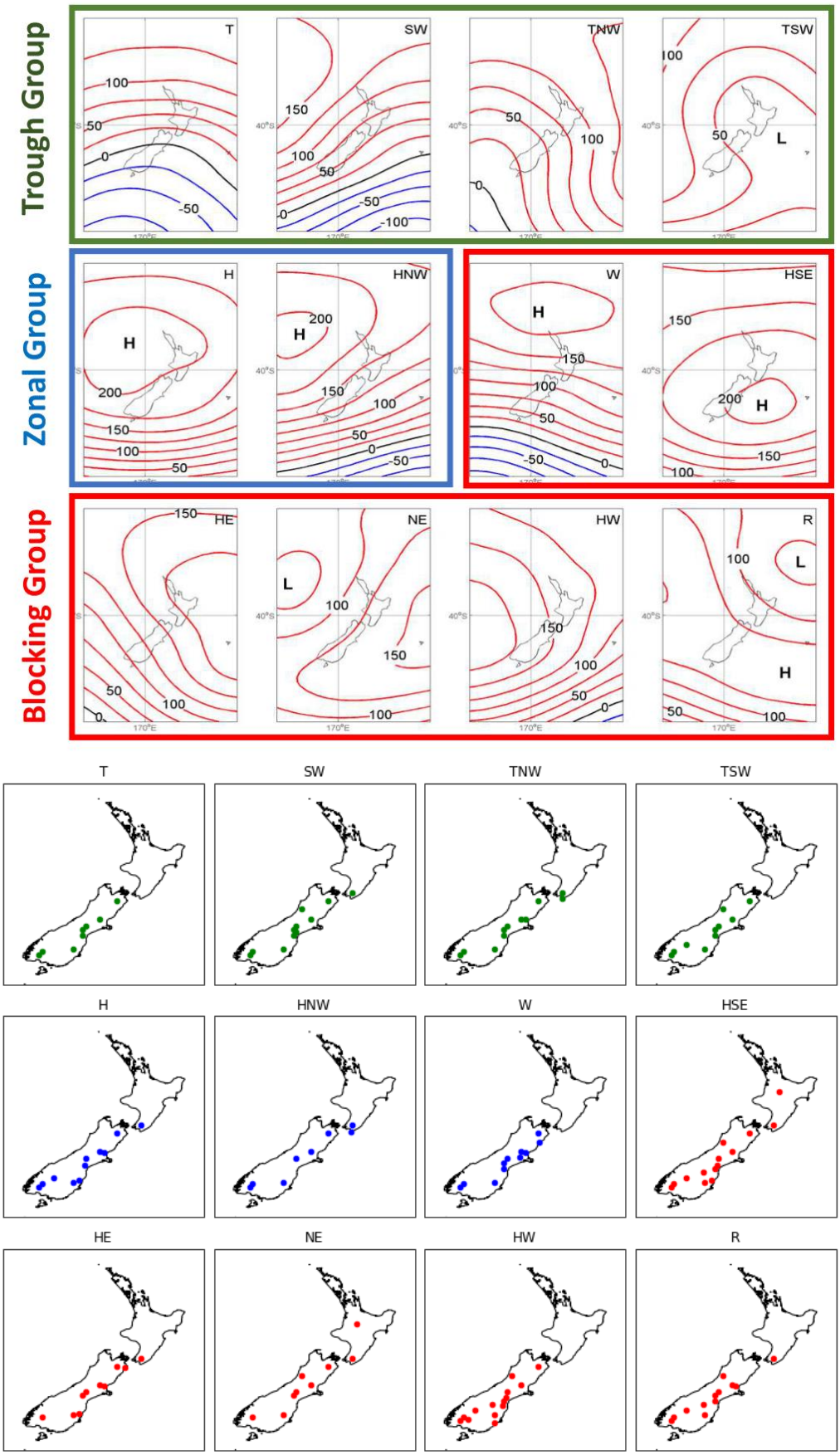

Figure 3- A) Synoptic Regimes in New Zealand (Kidson, 1999; Renwick, 2021). B) High Risk (Top 20% of Vector Wind Change and Lowest 20% Kurtosis) within each Synoptic Type, November 2020-2021.

3.4. Vector Wind Change and Fire Weather Index

The FWI was calculated for the 130 national FENZ weather stations at a daily time scale and averaged over the same period year long period as the VWC. The top 20% FWI stations were then mapped (Figure 4) to compare to the top 20% of the VWC and WDC stations. Interestingly, the same spatial trends appear in the high FWI stations as the high-risk stations, with most of the stations on the South Island. In contrast to the VWC stations, however, high FWI stations are found both coastal and inland. Out of the ten high VWC and WDC stations, four of them also appeared in the high FWI stations. The overlap in stations suggests that VWC and WDC could be useful additional parameters to FWI calculations around New Zealand to provide FENZ with additional information relating to microclimates in complex terrain to better inform fire risk and extreme fire behavior.

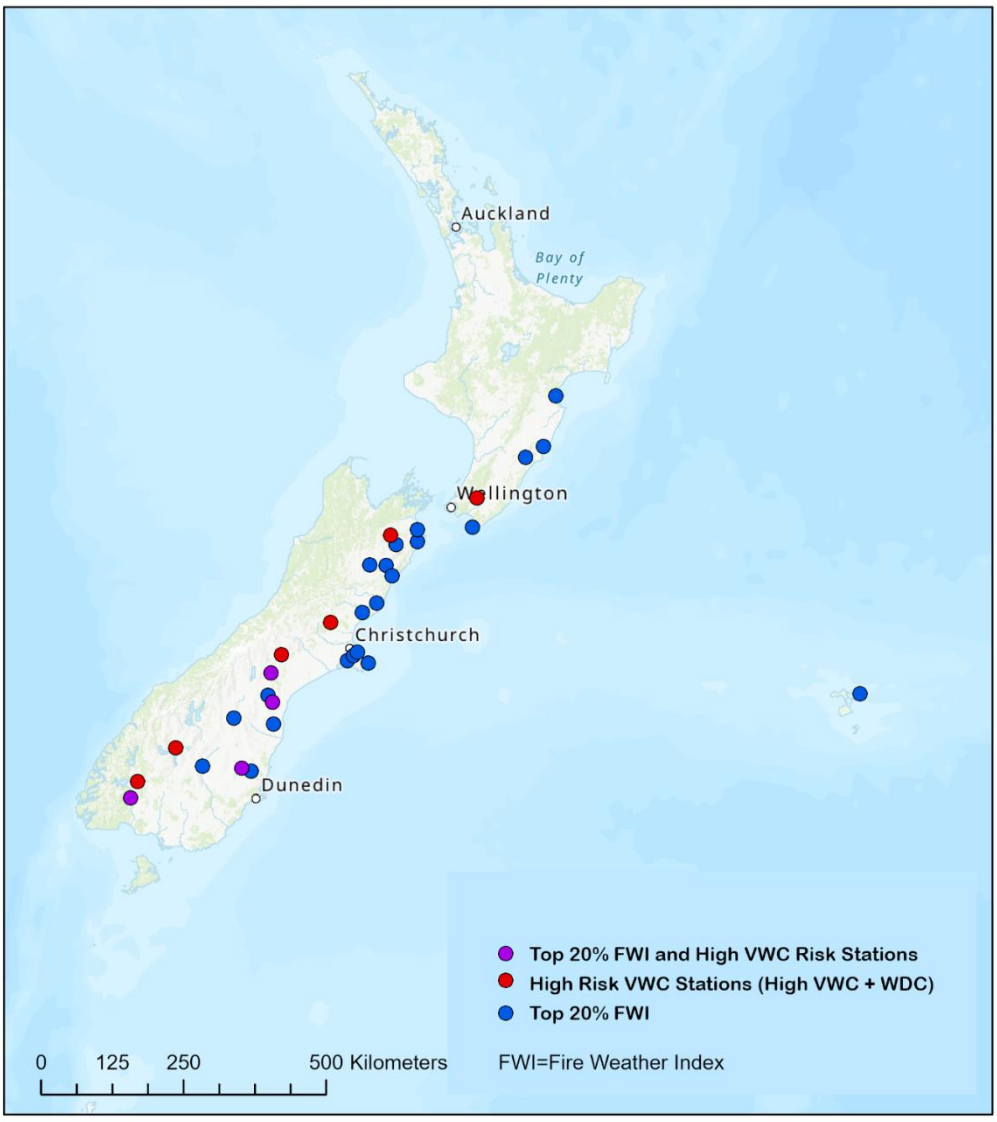

Figure 4- Top 20% VWC and Top 20% FWI Stations around New Zealand, for November 2020-2021.

4. Conclusions

Vector Wind Change, as well as Wind Direction Change, are useful near-surface variables for understanding potential wildfire occurrence conditions and its severity around New Zealand. These metrics are primarily forced by the impact of complex terrain on wind speed and direction and can be studied at the micro- and/or mesoscales and provide insight to the hourly wind changes across New Zealand. Given the importance of windspeed and direction on fire spread as well as extreme fire behavior, VWC and WDC could be important

additional metrics in analyzing fire risk in New Zealand. When combined with Fire Weather Index data, VWC and WDC may provide additional information in predicting extreme fire weather and risk of unpredictable fire behavior. The next step for this project is to complete a comprehensive analysis of New Zealand meteorology using gridded weather data from numerical weather simulations providing 20 years of data to calculate the FWI, VWC and WDC, and analyze the trends spatially and temporally, across both an individual fire season as well as larger inter-annual trends. These trends will be explored further in an upcoming publication.

5. References

AFAC. (2017). Independent Operational Review Port Hills Fires February 2017.

AFAC. (2019). A review of the management of the Tasman fires of February 2019.

Dong, L., Leung, L. R., Qian, Y., Zou, Y., Song, F., & Chen, X. (2021). Meteorological Environments Associated With California Wildfires and Their Potential Roles in Wildfire Changes During 1984– 2017. Journal of Geophysical Research: Atmospheres, 126(5). https://doi.org/10.1029/2020jd033180

Foley, J. (2020). Fire and Emergency New Zealand Wildfire Investigation Report Lake Ohau.

Harris, S., Mills, G., & Brown, T. (2017). Variability and drivers of extreme fire weather in fire-prone areas of south-eastern Australia. International Journal of Wildland Fire, 26(3). https://doi.org/10.1071/wf16118

Hilton, J. E., Miller, C., Sullivan, A. L., & Rucinski, C. (2015). Effects of spatial and temporal variation in environmental conditions on simulation of wildfire spread. Environmental Modelling & Software, 67, 118-127. https://doi.org/10.1016/j.envsoft.2015.01.015

Kidson, J. W. (1999). An Analsysis of New Zealand Synoptic Types and Their Use in Defining Weather Regimes. International Journal of Climatology, 20, 299-316.

Kitteridge, M. (2021). Tethysts. In https://tethysts.readthedocs.io/en/latest/license-terms.html

Langer, E. R. L., & Wegner, S. (2018). Wildfire risk awareness, perception and preparedness in the urban fringe in Aotearoa/New Zealand: Public responses to the 2017 Port Hills wildfire. Australasian Journal of Disaster and Trauma Studies, 22: Port Hills Wildfire Special Issue.

Mandal, A., Nykiel, G., Strzyzewski, T., Kochanski, A., Wrońska, W., Gruszczynska, M., & Figurski, M. (2021). High-resolution fire danger forecast for Poland based on the Weather Research and Forecasting Model. International Journal of Wildland Fire, 31(2), 149-162. https://doi.org/10.1071/wf21106

Mills, G., Harris, S., Brown, T., & Chen, A. (2020). Climatology of wind changes and elevated fire danger over Victoria, Australia. Journal of Southern Hemisphere Earth Systems Science, 70(1). https://doi.org/10.1071/es19043

New Zealand Modeling Consortium Open Environmental Digital Library. (2021). https://www.envlib.org/#Data_access_updated

Pretorius, I., Sturman, A., Strand, T., Katurji, M., & Pearce, G. (2020). A Meteorological Study of the Port Hills Fire, Christchurch, New Zealand. Journal of Applied Meteorology and Climatology, 59(2), 263-280. https://doi.org/10.1175/jamc-d-19-0223.1

Renwick, J. (2021). Kidson Type Time Series New Zealand 1948-2021.

Van Wagner, C. E. (1987). Development and structure of the canadian forest fire weather index system. Canadian Forest Service.

Werth, P. A. P., Brian E.; Alexander, Martin E.; Clements, Craig B.; Cruz,, Miguel G.; Finney, M. A. F., Jason. M.; Goodrick, Scott L.; Hoffman,, Chad; Jolly, W. M. M., Sara S.; Ottmar, Roger D.; Parsons, Russell, & A. (2016). Synthesis of Knowledge of Extreme Fire Behavior: volume 2 for fire behavior specialists, researchers, and meteorologists.

On the vertical profiles of temperature, relative humidity and wind in the nighttime period in central mainland Portugal

João Rio*; Manuel Lopes; Pedro Silva; Ilda Novo; Maria Monteiro

Instituto Português do Mar e da Atmosfera (IPMA, I.P.), Portugal,
{joao.rio, manuel.lopes, pedro.silva, ilda.novo, maria.monteiro}@ipma.pt

**Corresponding author*

Keywords

FireStorm, weather stations, temperature inversions, downslope windstorms, vertical profile

Abstract

In the framework of the FireStorm project, four portable weather stations were installed in the Lousã/Estrela mountain range. The data observed with this equipment, along with two other stations from the Portuguese Institute for Sea and Atmosphere's network of surface weather stations, allows the monitoring of the vertical profile of temperature, relative humidity and wind in the region. Many forest fires in mainland Portugal affect areas with complex terrain, with hills or mountains in the 400-1200 m asl range, where weather conditions strongly influence the fire propagation and lifetime. Therefore, it becomes even more pertinent to study the vertical profiles of temperature, humidity and wind as they often exhibit large variability, namely in the nighttime period. This paper provides an overall assessment of the weather conditions in the nighttime period in selected events in which significant temperature inversions or downslope windstorms were observed. The forecast skill of the two operational numerical weather prediction models used at IPMA is also provided and highlights the challenges of weather forecasting in areas with complex terrain.

1. Introduction

Most of the major forest fires in mainland Portugal occur in the summer period and are located north of river Tagus, in areas with complex terrain, typically with hills or mountains in the range 400-1200 m asl. Often it is considered that in the nighttime period lighter winds, lower temperatures and the recovery of the relative humidity contributes to lower rates of fire spread and reduced fire intensity (Potter, 2012). Although this behaviour is commonly observed close to the surface over plains or plateaus, it is not necessarily the case in complex terrain. Additionally, the effects of complex terrain on the flow must be addressed, particularly in the case of dynamically driven winds, as these tend to be stronger (Sharples, 2009; Werth *et al.*, 2011). Well known effects include flow over mountains with speeding/blocked flow, gap or corner winds, mountain wakes and channelling effects.

Recent work suggests that fire intensity in the nighttime has increased globally, which is linked to warmer and drier nights (Balch, 2022). This suggests that it is highly recommended to carefully monitor the variability of the weather conditions during nighttime, particularly in areas that are prone to large wildfires and where extreme fire behaviour is likely to play a relevant role. In the framework of the FireStorm project, four portable weather stations were installed in the north-western slope of the Lousã/Estrela mountain range. This region has benefits such as the easy access, it is in the middle of the area where most of the forest fires occur and it spans a wide range in altitudes. Additionally, the network of surface weather stations of the Portuguese Institute for Sea and Atmosphere (IPMA) has data at two other locations in the area, which ultimately allows a higher spatial resolution.

In Rio *et al.* (2022) an overview of the weather conditions in the summer 2021 and in the winter 2021/22 was given, with insight into the differences that are observed in the daily cycle of the stations within the slope. An evaluation of the observed weather conditions allowed the identification of significant weather events, such as frequent surface inversions in the valley stations, sharp inversions aloft due to warm air advection or large-scale subsidence and downslope windstorms.

This paper presents further results from the observed data in the Lousã/Seia region. In this paper the overall forecast skill of numerical weather forecasts (NWP) is provided. The forecasts used in this study are from the two operational NWP models used at IPMA. This paper also presents three events, in which significant temperature inversions or downslope windstorms were detected in the area.

2. Location and data availability

Figure 1 shows the area being monitored in this study, with a total of six weather stations. Two of them are from the surface network from IPMA and the other four are the new portable weather stations installed in the Lousã and Seia regions. The location of the new portable weather stations was chosen considering the availability of two other stations from IPMA and the need to monitor the slope in a range of altitudes as wide as possible. Tables 1 and 2 provide details about the weather stations used, respectively, in the Seia and Lousã regions.

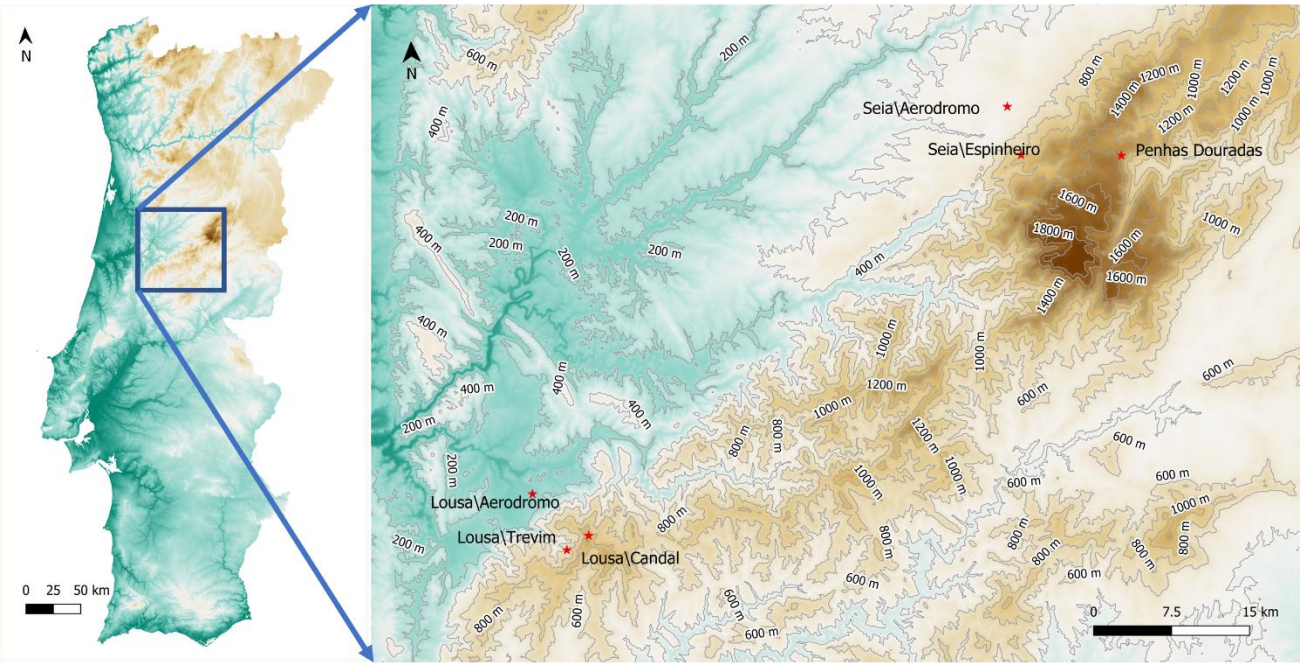

Figure 1 – Location of the weather stations used in this study.

Table 1 – Identification of the weather station in the Seia region.

Station name (short name)	Latitude	Longitude	Altitude [m]	Source	Available since
Penhas Douradas	40.41°N	7.56°W	1380	IPMA	---
Seia-Espinheiro (Espinheiro)	40.41°N	7.67°W	995	IPMA/FireStorm	03.2020
Seia-Aeródromo (Seia-Aero)	40.46°N	7.69°W	438	IPMA/FireStorm	03.2020

Table 2 – Identification of the weather station in the Lousã region.

Station name (short name)	Latitude	Longitude	Altitude [m]	Source	Available since
Lousã-Trevim (Trevim)	40.09°N	8.18°W	1167	IPMA/FireStorm	02.2021
Lousã-Candal (Candal)	40.08°N	8.20°W	621	IPMA/FireStorm	02.2021
Lousã-Aeródromo (Lousã-Aero)	40.13°N	8.24°W	195	IPMA	---

The weather stations in the Seia region were installed in March 2020. In Lousã it was only possible to install the equipment in October 2020, namely due to the pandemic restrictions. Additional unexpected issues with the

power supply and communication systems caused further delays, hence full availability of data from the weather stations in Lousã started only in February 2021.

The station of Penhas Douradas is the historical reference for Serra da Estrela, as it stands nearly at 1400 m asl. The station of Trevim is located at the top of Serra da Lousã, at 1167 m asl, with excellent exposure to the flow. The station of Espinheiro also has very good exposure, but is installed slightly below 1000 m asl. The weather stations of Seia-Aero and Lousã-Aero are both located in the valley (or slightly above it in the latter), in the aerodromes of each city. The station of Candal is installed in a narrow valley with a north-west/southeast orientation.

The data from IPMA's surface weather stations is observed at default heights (wind at 10 m, temperature and relative humidity at 2 m), but in the portable weather stations all the variables are observed at 2 m. To make the wind speed observations comparable, the 2 m data was extrapolated to the 10 m level using a logarithmic profile with a conservative value (0.1). This study only considers hourly data.

3. Forecast verification

The forecast verification shown here uses data from the operational versions of the NWP models used at IPMA. The high-resolution forecasts are from the AROME model (Seity *et al.*, 2011; Termonia *et al.*, 2018), which is run at IPMA four times a day (00, 06, 12 and 18 UTC) with a forecast range of 48 hours. This is a convective-scale limited-area model and is run with a horizontal resolution of 2.5 km. The second set of forecasts is from the global IFS/ECMWF model, namely the high-resolution (ECMWF-HRES), with a horizontal resolution of 9 km. The data used in this study is from the 00 UTC run and it considers hourly short-term forecasts (H+6 to H+30). The results shown here are a broad view of the forecast skill, as it provides only a score for the whole period. The metrics used here are the root mean square error (RMSE) and the bias (BIAS). The meteorological variables are the 10 m wind speed and the 2 m temperature and relative humidity. For conciseness only results for the summer of 2021 are shown (Table 3).

Table 3 – Forecast verification in the Lousã/Seia region, in the summer of 2021.

Station name	2 m temperature				2 m relative humidity				10 m wind speed			
	ECMWF		AROME		ECMWF		AROME		ECMWF		AROME	
	RMSE	BIAS	RMSE	BIAS	RMSE	BIAS	RMSE	BIAS	RMSE	BIAS	RMSE	BIAS
Penhas Douradas	**2,14**	**-0,27**	**1,99**	**0,10**	**17,89**	**-1,08**	**11,91**	**-3,68**	**2,76**	**-1,71**	**2,00**	**-1,21**
Trevim	**3,45**	**-0,78**	**2,39**	**0,24**	**25,08**	**-1,48**	**14,29**	**0,97**	**1,76**	**-0,73**	**1,72**	**0,83**
Candal	**1,84**	**-0,30**	**1,70**	**-0,81**	**15,09**	**0,19**	**9,77**	**0,04**	**1,93**	**1,46**	**1,72**	**0,83**
Lousã-Aero	**1,91**	**-0,47**	**1,47**	**-0,33**	**11,46**	**-6,14**	**10,17**	**-5,93**	**1,20**	**0,73**	**0,94**	**0,26**
Seia-Aero	**3,07**	**2,08**	**2,73**	**1,59**	**14,11**	**-10,95**	**15,39**	**-8,98**	**1,38**	**0,83**	**1,29**	**0,59**
Espinheiro	**1,74**	**-0,25**	**2,05**	**0,41**	**12,19**	**-2,17**	**11,91**	**-3,68**	**1,23**	**-0,17**	**1,22**	**-0,36**

The results show that the RMSE in these stations is larger than what is usually computed in low lying regions in mainland Portugal. The large errors in Seia-Aero, with a strong positive bias in temperature and large negative bias in relative humidity, is mainly due to the fact that in this location the cold-pool effect is very effective in the nighttime period. The highest errors in the 2m relative humidity are in the high slope (above 1000 m asl), which is likely due to the large variability of this variable. For the 10 m wind speed, while there is a negative bias in the locations at higher altitudes, in the valley stations the forecasts over-estimate the observed values. Finally, it should be stressed that these results are only valid for the stations and period in study.

4. Case studies

Since the spring of 2021 several events with large temperature inversions or downslope windstorms have been observed in the nighttime period. In the three events shown below, observed and short-term forecast data is shown only in the nighttime, which is defined as the period between 00 and 06 UTC.

4.1. Temperature inversion in August 2021

On August 5/6th, 2021, an event of strong temperature inversion enhanced by large scale subsidence was observed. Figure 2 shows the ECMWF-HRES analysis of the geopotential, temperature and wind at the 850 hPa, valid at 00 UTC, on August 6th. The Azores high extended a ridge towards the east-southeast, which lead to large-scale subsidence, dry and stable conditions in mainland Portugal. At the 850 hPa level the flow was moderate or strong from the west-northwest.

Figure 3 shows the cross-section of the wind (parallel) and relative humidity over Serra da Estrela, using the H+6 ECMWF-HRES forecast, valid at 06 UTC, on August 6th. This plot shows a strong gradient of relative humidity, over the orographic ridge and on the leeside of the mountain, associated with downward motion of very dry air. At the 860 hPa level, around the real altitude of Penhas Douradas, the relative humidity had values around 15-20%. At the same time, the vertical profile in Lousã-Aero (Figure 4) shows an inversion layer between 800 m and 2200 m asl, where the temperature increases around 5ºC and the humidity decreases around 75%. The downward motion is strongest between 1800 m and 2000 m asl, with vertical speeds around -0.8 m/s. Figure 5 shows the time series of the observed 2 m relative humidity. This suggests that the base of the "real" inversion should be located above and close to the height of Trevim (1167 m asl). Also, the difference between the observed relative humidity in Trevim and Penhas Douradas is larger than the difference of the corresponding forecasted relative humidity, which suggests a stronger inversion in this layer. In fact, at 06 UTC the temperature in Penhas Douradas was 6.4ºC higher than the one observed in Trevim (not shown), while the 2 m relative humidity were, respectively, 13% and 100%.

Figures 6 and 7 show that this event was very challenging for NWP models, even in the case of the high-resolution AROME. While in Penhas Douradas both models suggested dry air reaching the station, they over-estimated the 2 m relative humidity values by around 20%, with AROME in closer agreement with the observations. In Trevim, none of the models suggested the values of 20-30% during the nighttime on August 5th.

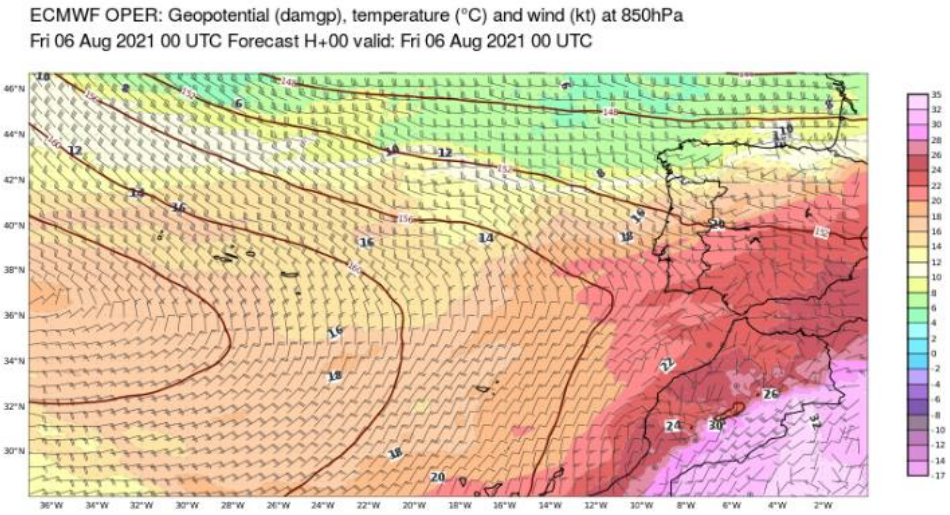

Figure 2 – ECMWF-HRES analysis of the geopotencial height, temperature and wind at the 850 hPa level, valid on August 6th, 2021, at 00 UTC.

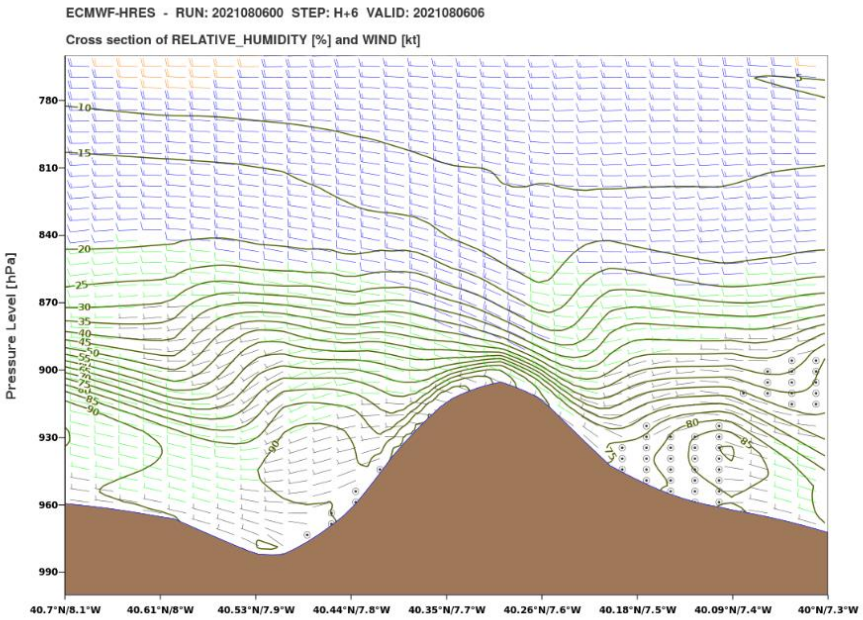

Figure 3 – Cross-section (orientation NW-SE) of relative humidity and wind (parallel) over Serra da Estrela, from a short-term ECMWF-HRES forecast, valid on August 6th, 2021, at 06 UTC.

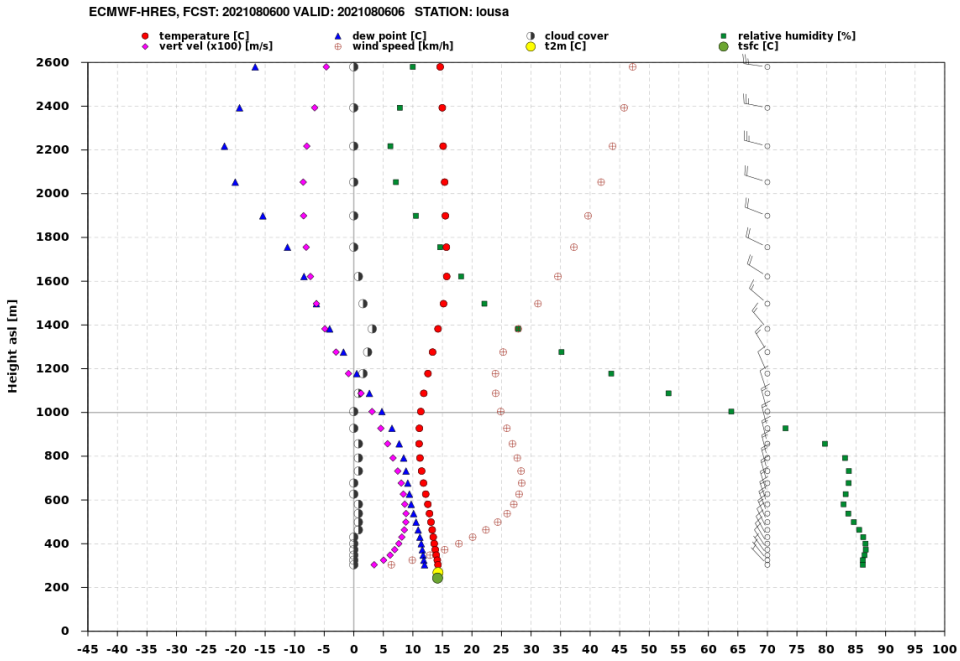

Figure 4 – ECMWF-HRES profile for Lousã-Aero, valid on August 6th, 2021, at 06 UTC.

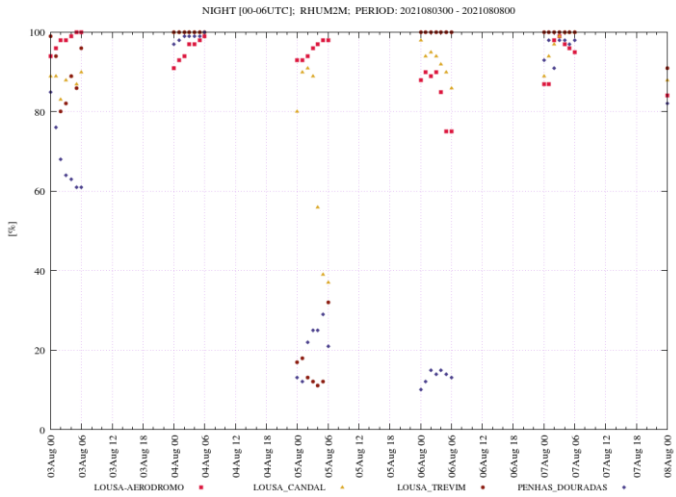

Figure 5 – Time series of the observed 2m relative humidity, in the weather stations located in the Lousã region and Penhas Douradas. Data in the period August 3rd – 8th, 2021.

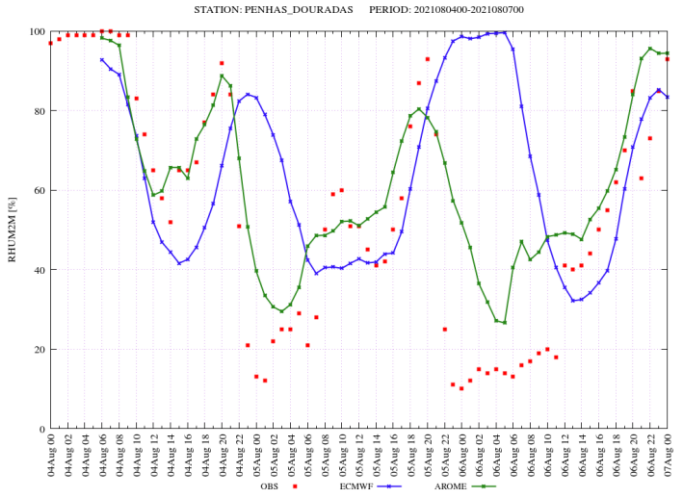

Figure 6 – Time series of observed and forecast (ECMWF-HRES and AROME) 2m relative humidity in Penhas Douradas, on August 4th – 7th, 2021.

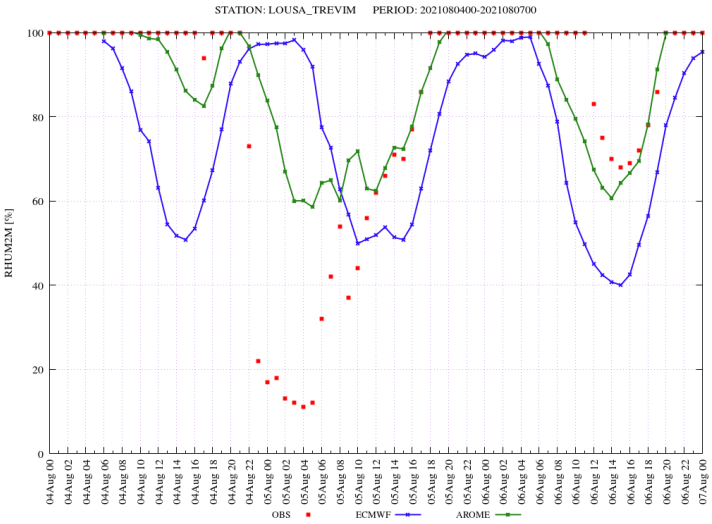

Figure 7 – Time series of observed and forecast (ECMWF-HRES and AROME) 2m relative humidity in Trevim, on August 4th – 7th, 2021.

4.2. Downslope windstorms

The two downslope windstorms briefly described in this paper were observed on March 31st, 2021, and March 28th, 2022. Figures 7a and 9a show the 00 UTC analysis of the geopotential, temperature and wind at the 850 hPa. Figures 7b and 9b show the cross section of the wind and relative humidity over Serra da Estrela, with a NW-SE orientation, using short-term ECMWF-HRES forecasts (H+6), valid at 06 UTC in each event. Figures 8 and 10 show the AROME forecasts of the 3 hour maximum 10 m wind gust and the 2 m temperature, valid at 03 UTC on each date.

In both events, a low pressure system was centred southwest of Iberia, close to Madeira, which originated a moderate or strong south-easterly flow. The cross sections show that the short-term ECMWF-HRES forecast was able to provide guidance into the strong downslope wind. In both cases, this model suggested much lighter wind speeds close to the valley. The AROME forecasts suggested south-east winds (not shown), with wind gusts in the 70-80 km/h range in the north-western slopes of the mountain range. The observed 2 m temperatures (not shown) were much higher than expected for the time of the year, mainly on the event in March 2022.

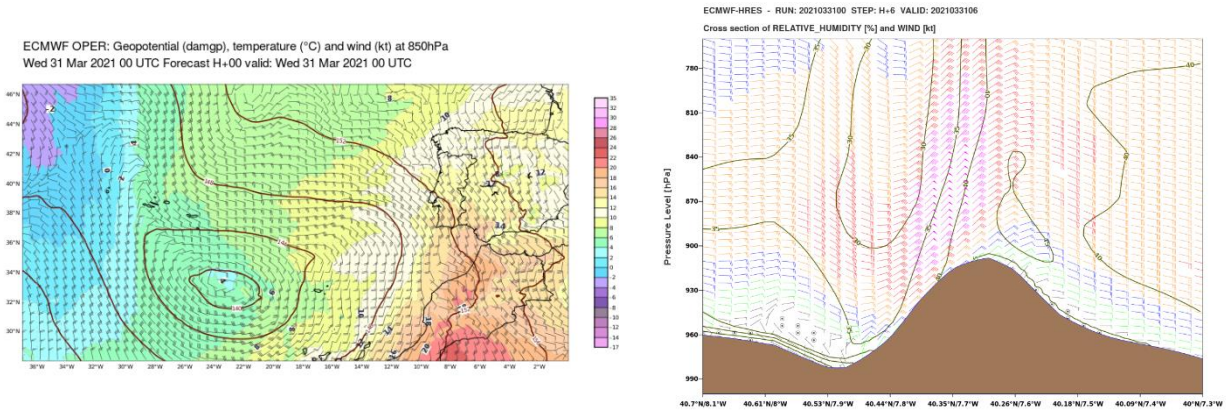

Figure 7 – ECMWF-HRES analysis of the geopotencial height, temperature and wind at the 850 hPa level, valid on March 31st, 2021, at 00 UTC (left). Cross-section (orientation NW-SE) over Serra da Estrela, from a short-term ECMWF-HRES forecast, valid on March 31st, 2021, at 06 UTC (right).

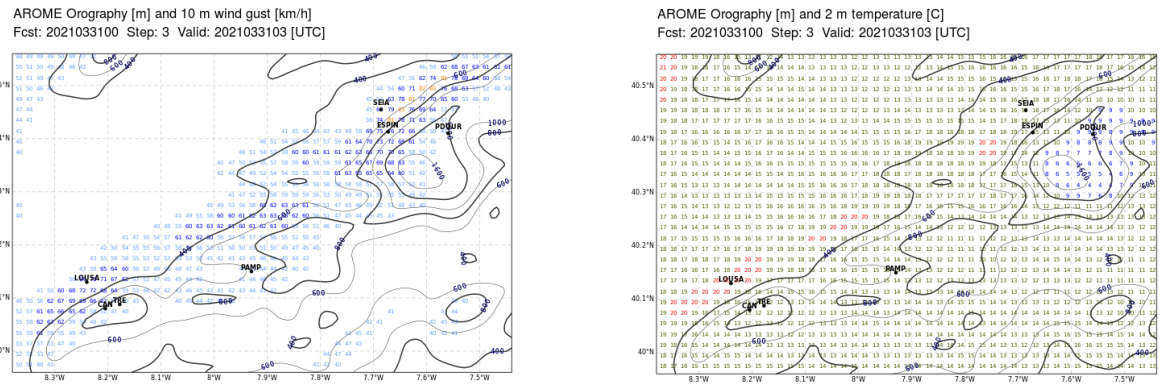

Figure 8 – AROME forecasts (H+3) of the 3 hour maximum 10 m wind gust (left) and 2 m temperature(right), valid on March 31st, 2021, at 03UTC.

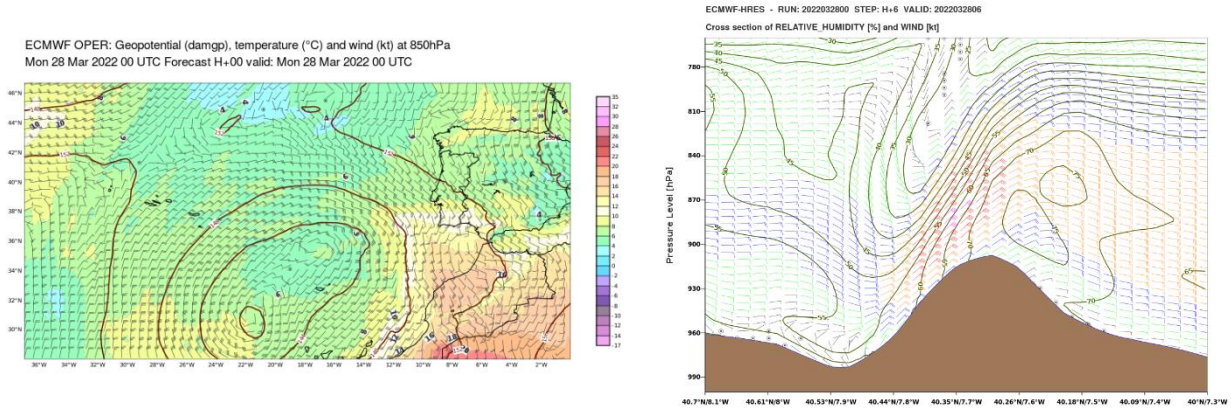

Figure 9 – (a) ECMWF-HRES analysis of the geopotencial height, temperature and wind at the 850 hPa level, valid on March 28th, 2022, at 00 UTC. (b) Cross-section (orientation NW-SE) over Serra da Estrela, from a short-term ECMWF-HRES forecast, valid on March 28th, 2022, at 06 UTC.

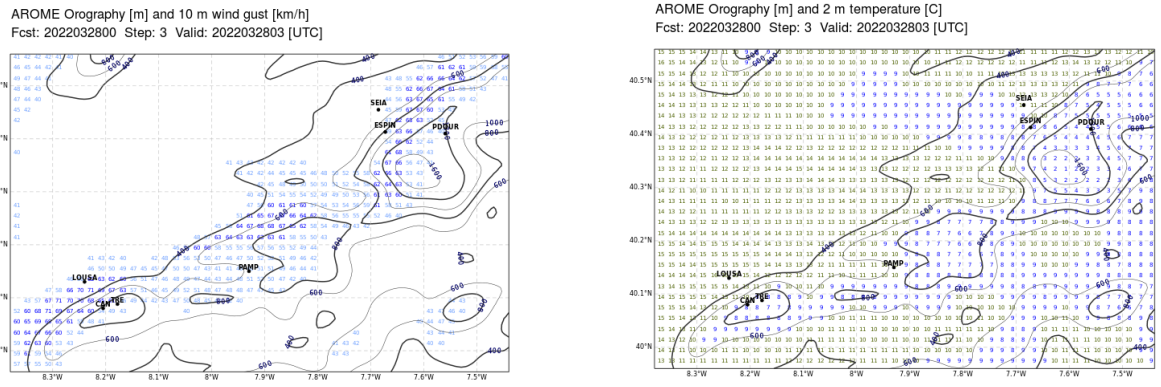

Figure 10 – AROME forecasts (H+3) of the 3 hour maximum 10 m wind gust (left) and 2 m temperature(right), valid on March 28th, 2022, at 03UTC.

The discussion above on downslope windstorms shows that ECMWF and AROME forecasts provide useful guidance in the broad features of these events, at least in the Lousã/Estrela mountain range. However, it must be stressed that these circulations are extremely challenging for NWP models (Haraldur *et al.*, 2021), as they are very sensitive to the initial conditions, namely the wind profile, atmospheric stability, direction of the flow into the mountain range and model horizontal resolution. Additionally, as turbulence plays a key role in these circulations, extreme caution is advisable if NWP direct model output is to be used operationally, as large differences between forecast and observations at specific locations are most likely to occur.

5. Final remarks

The results shown in this study highlight the challenges of weather forecasting in complex terrain. Even though NWP data provides useful guidance on the broad features of many events, comparing forecasts and observations clearly shows that large difference are very common. Therefore, these results show that extreme caution is advisable when direct model output of NWP data is used as a guidance for the weather data at a specific site.

6. Acknowledgments

The work was only possible in the framework of the FireStorm Project (Weather and Behaviour of Fire Storms), Project Reference PCIF/GFC/0109/2017- FCT. The installation of the portable weather stations was only possible with a very close and fruitful cooperation between IPMA (Jorge Neto, João Rio, Ilda Novo), ADAI (Luís Reis, Daniela Alves and Professor Domingos Xavier) and the Municipalities of Lousã and Seia.

7. References

Balch, J.K.; Abatzoglou, J.T.; Joseph, M.B. *et al.* (2022). Warming weakens the night-time barrier to global fire. *Nature*, 602, 442–448.

Haraldur, O. and Bao, J.W. (2021). Uncertainties in numerical weather prediction, 1st ed. Elsevier, 2021, 364 pp.

Potter, Brian (2012). Atmospheric interactions with wildland fire behaviour - I. Basic surface interactions, vertical profiles and synoptic structures. International Journal of Wildland Fire 21(7):779-801.

Rio, J., Lopes, M., Silva. P. *et al.* (2022). First assessment of the observed meteorological data in the Lousã/Seia region, in the framework of the FireStorm project. Atmosphere (*submitted*).

Seity, Y., Brousseau, P., Malardel, S. *et al.* (2011). The AROME-France Convective-Scale Operational Model, *Monthly Weather Review, 139*(3), 976-991.

Sharples, J.J. (2009). An overview of mountain meteorological effects relevant to fire behaviour and bushfire risk. *Int. J. Wildland Fire*.

Termonia, P., Fischer, C., Bazile, E. *et al.* (2018). The ALADIN System and its canonical model configurations AROME CY41T1 and ALARO CY40T1, Geosci. Model Dev., 11, 257–281, https://doi.org/10.5194/gmd-11-257-2018, 2018.

Werth, P. A.; Potter, B. E.; Clements, C. B. *et al.* (2011). Synthesis of knowledge of extreme fire behavior: volume I for fire managers. Gen. Tech. Rep. PNW-GTR-854. Portland, OR: U.S. Department of Agriculture, Forest Service, Pacific Northwest Research Station. 2011, 144 p.

Pan-European Wildfire Risk Assessment- preliminary version

Duarte Oom[1]*; Daniele de Rigo[2,3]; Hans Pfeiffer[4]; Alfredo Branco[2]; Davide Ferrari[4]; Rosana Grecchi[2]; Tomás Artes-Vivancos[1]; Tracy Houston Durrant[4]; Roberto Boca[2]; Pieralberto Maianti[2]; Giorgio Liberta[1] and Jesús San-Miguel-Ayanz[1]

[1]European Commission, Joint Research Centre (JRC), Ispra, Italy,
{Duarte.Oom, Tomas.Artes-Vivancos, Giorgio.Liberta, Jesus.San-Miguel}@ec.europa.eu
[2] ARCADIA SIT s.r.l, Vigevano (PV), Italy {Daniele.De-Rigo,
Alfredo.Branco, Rosana.Grecchi, Roberto.Boca, Pieralberto.Maianti}@ext.ec.europa.eu
[3] Maieutike Research Initiative, Milano, Italy
[4] Engineering Ingegneria Informatica S.p.A., Roma, Italy
{Hans.Pfeiffer, Davide.Ferrari, Tracy.Durrant}@ext.ec.europa.eu

**Corresponding author*

Keywords

Wildfire, Risk, index, EFFIS, Pan-European

Abstract

Wildfire, as a global phenomenon, is an integral part of the Earth system that affects different regions in diverse ways resulting in variable levels of long-lasting impacts to environmental, social, and economic systems. In a context where extreme and high severity events are becoming more frequent, it is crucial to respond with a more robust preparedness and planning, identifying the risks posed by wildland fires, fostering better fire management policy tools, and developing mitigation strategies accordingly. However, scope and methods for wildfire risk assessment vary widely among countries leading to different regional/national approaches not always comparable, although wildfires are often transborder events and may affect several countries simultaneously. The elaborateness of these assessments is often related to the impact of fires in the corresponding regions, with countries more often confronted with wildfires being more prepared by having more elaborated and detailed wildfire risk maps at country/regional level, although based on the specificities of each country. To integrate currently incompatible approaches, harmonised procedures for wildfire risk assessment are needed at the pan-European scale, enhancing planning and coordination of prevention, preparedness, and cross-border firefighting actions to mitigate the damaging effects of wildfires. The development of a pan-European approach follows from a series of European Union (EU) regulations requiring the European Commission (EC) to have a wide overview of the wildfire risk in Europe, to support the actions of its Member States and to ensure compliance in the implementation of EU regulations related to wildfires. The conceptualization of the European Wildfire Risk Assessment (WRA) as the combined impact of wildfire hazard on people, ecosystems, and goods exposed in vulnerable areas, explicitly accounts for the multiplicity of risk dimensions and sources of uncertainty. Already serving as an integrated framework for gathering the European countries' experience on fire management and risk, it will support the inter-comparison of WRA among countries, with the aim to complement existing national WRA with a simpler, but harmonised, methodology. A semi-quantitative approach, designed to be robust to uncertainty and flexible in ingesting new components, is currently under development in close cooperation with the EC Joint Research Center (JRC), other Commission services, and the Commission Expert Group on Forest Fires which is now composed of fire management representatives from 43 countries in the region. Additionally, the harmonised framework can serve as a first approach to assess wildfire risk in those countries that have not yet performed a national WRA, and as a guideline for extending the approach to larger areas, where data coverage may be scarcer and more uncertain.

1. Introduction

Given the projected increase of fire risk in the Mediterranean-type climate regions due to climate change (Pechony et al., 2010), wildfire risk assessment is fundamental for developing prevention, mitigation and preparedness plans, but also as a key element to disentangle the complex relationships between fire occurrence, drivers, and impacts caused by fires at different levels (Oliveira et., 2021; Moreira et al., 2020). Many countries have customized approaches to assess wildfire risk, widely varying based on different variables and methodologies (San-Miguel-Ayanz et al., 2003, 2017). Usually, these different approaches are not only related to the frequency/impact of fires, level of preparedness, and data availability, but also to how risk components

are incorporated in the decision-making processes at different levels, such as landscape management or risk governance. Hence, this process repeated at multiple scales, for very different territories and specific purposes has led to different regional/national approaches, difficult to compare at the European scale, although wildfires are often transborder events and may affect several countries simultaneously. Fire-risk terminology is far from standardized, and even the concept itself is subject to several (sometimes incompatible) definitions (Hardy et al., 2005). A noticeable share of published fire risk systems only considers wildfire likelihood and behaviour, usually ignoring the damage caused by fire impacts in operational fire danger assessment systems (San-Miguel-Ayanz et al., 2003). Some other systems integrate fire danger and vulnerability, as two essential risk components (Calkin et al., 2010; Chuvieco et al., 2010, 2012; Tutsch et al., 2010; Thompson et al., 2011; Oliveira et al.,2020). However, much work is still needed to converge on a clear and concise terminology and harmonise quantitative risk analysis in the context of wildland fire management and of disaster risk management (Bachmann et al., 2001). The main goal of this work is to describe the development of a pan-European wildfire risk assessment (WRA) based on the definition of risk adopted by UNISDR (2009) which was also followed by the European Commission (EC) Joint Research Centre (JRC) reports (San-Miguel-Ayanz et al., 2017, 2019; Oom et al., 2021) by presenting a first set of data that would enable the implementation of the proposed assessment. Quantitatively, wildfire risk is defined as the product of the probability of wildfire occurrence/propagation (hazard) and the damage potentially caused (exposure and vulnerability) (Finney, 2005; Scott et al., 2013). This involves three main fire research areas: fire ignition/occurrence, fire behaviour/propagation, and fire effects (exposure and potential loss of assets/resources in vulnerable wildfire-prone areas). The harmonised WRA will support the inter-comparison of methods and needs among countries and be complementary to existing national WRA. Additionally, it can serve as a first approach to assess wildfire risk in those countries that have not yet performed a national WRA.

1.1. Pan-European risk assessment in the context of EFFIS

The development of the pan-European approach follows from a series of EU regulations that require the EC to have a wide overview of the wildfire risk in the European region, to support the actions of its Member States and to ensure compliance in the implementation of EU regulations related to wildfires. The process is closely linked with the Expert Group on Forest Fires (EGFF), composed of fire management representatives from 43 countries in the region and part of the European Forest Fire Information System (EFFIS) which was established jointly by the EC services (DG ENV and JRC) and the relevant fire services from the EU Member States, other non-EU European countries and Middle East and North African countries (Figure 1).

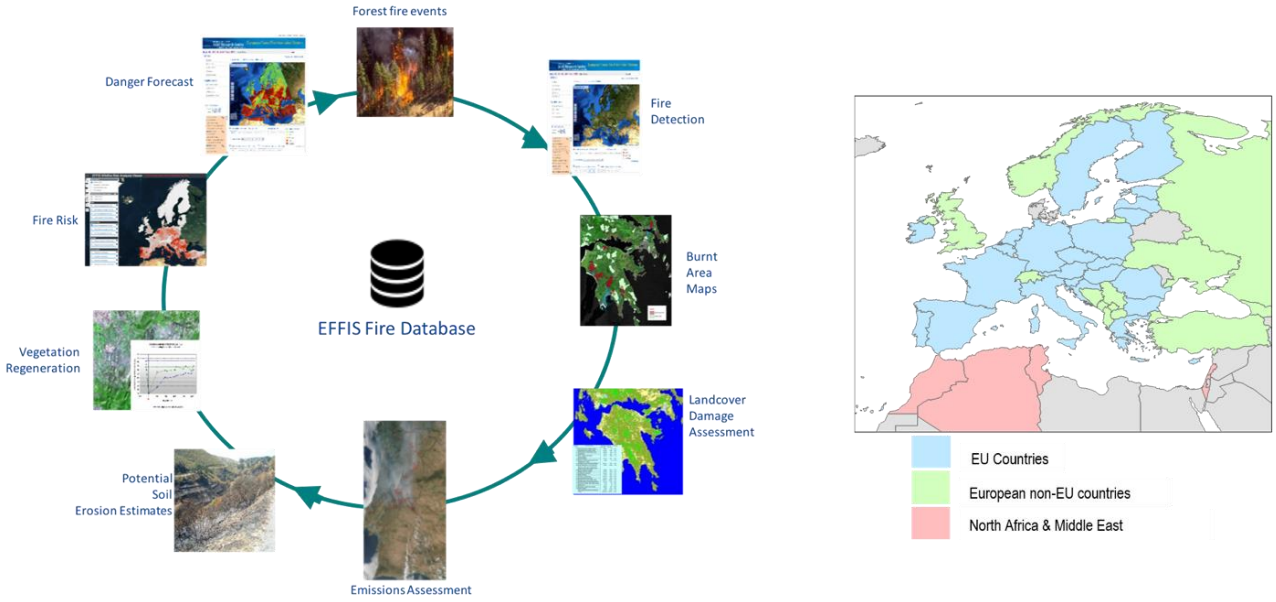

Figure 1- European Forest Fire Information System (EFFIS) services (left); map of countries that are currently part of the Expert Group on Forest Fires (EGFF) (right).

1.2. Wildfire risk scheme

An integrated framework of interconnected components associated with the fire process (Chuvieco et al., 2012; Xi et al., 2019) should support risk modelling to provide an integrated view of both fire likelihood and consequences (Dunn et al., 2020). Figure 2 illustrates the WRA scheme here proposed, designed to be scale-independent and easily applicable to local, regional, and global scale. Two main groups of components are defined by considering the fire danger (or hazard) and the vulnerability on three categories: people, ecological, and economic values exposed in vulnerable areas.

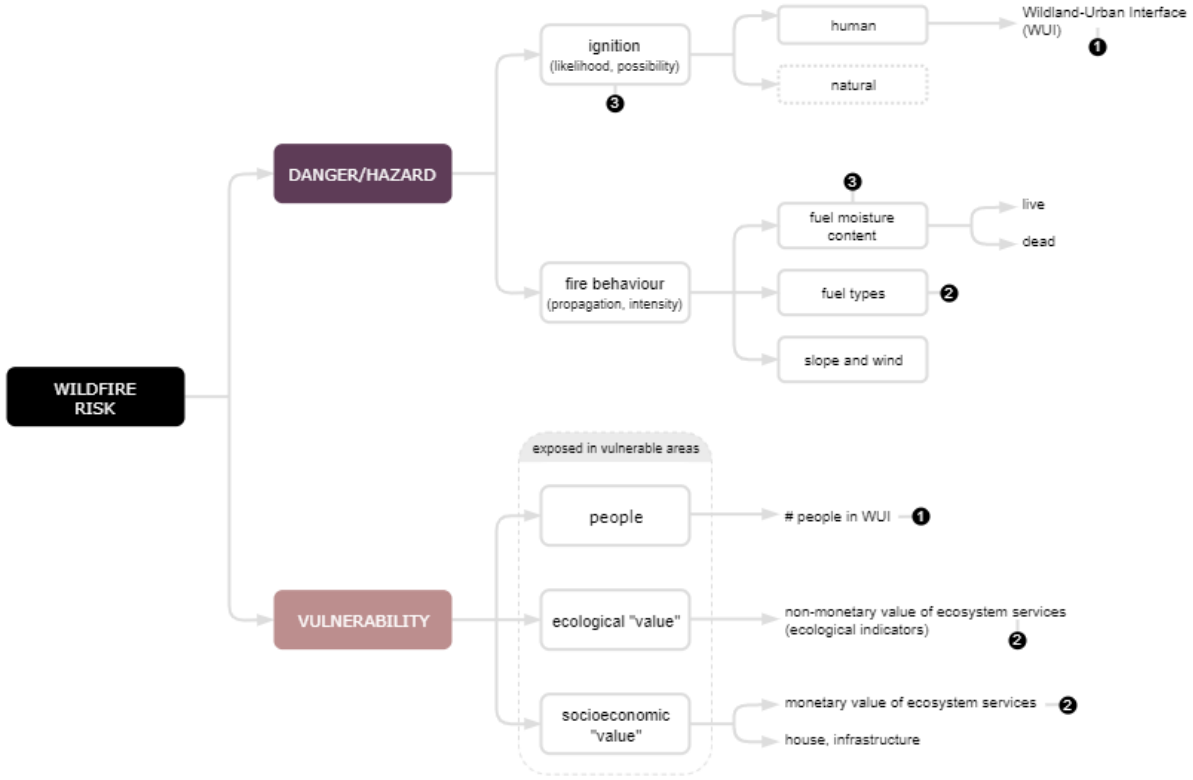

Figure 2- Basic components of the Pan-European Wildfire Risk Assessment scheme (from Oom et al., 2021).

The scheme follows a classic quantification of "risk", based on the probability or possibility (*P*) of negative outcomes (damage, *D*)

$$R = P \times D \quad (1)$$

The probability for a fire to start at a given location and time (*P*,fire danger/fire hazard) depends on the likelihood for ignition sources and local conditions to start and spread a fire (fire behaviour), namely it depends on the fuel availability, type and pre-conditions of the fuel, the prevalent meteorological conditions, and on the presence of an event triggering the initial ignition. In Europe, the vast majority of wildfires is linked to human causes, either deliberate or due to accident/negligence (de Rigo et al., 2017). Therefore, *P* is not only a function of fuel and weather, but prominently also of human behaviour *P*(*fuel*, *weather*, *human*). The expected outcomes/impacts on people, landscape/ecosystems, assets exposed in vulnerable areas (*D*, vulnerability) refer to the susceptibility to suffer damage by fire: "the conditions determined by physical, social, economic and environmental factors or processes which increase the susceptibility of an individual, a community, assets or systems to the impacts of hazards" (UNISDR, 2009). Vulnerability, which is also associated with exposure (people, ecosystems, goods *exposed* in *vulnerable* areas, so that in the following the two entwined concepts are referred to as the overall "vulnerability" component of wildfire risk), should be assessed based on relevant proxy indicators and data. The impact of wildfire hazard on vulnerability is typically estimated as a *structural* assessment, also known as *climatological* risk (San-Miguel-Ayanz et al., 2017) and should explicitly consider the variability and uncertainty of the conditions historically observed. Given that even the damage by fire is a key function of human behaviour (fire prevention, firefighting, post-fire recovery policies) and depends prominently on policy, economic, social and cultural aspects, then even the second component of eq. 1 is a

function of human factors for which there is an overwhelming lack of data. Therefore, *P* and *D* cannot be fully estimated "probabilistically", but they might with a simpler semi-quantitative risk ranking (where *P* is a simpler fuzzy possibility subject to uncertainty analysis).

2. Data

The development of an operational fire risk assessment system for the pan-European scale requires the generation of multiple datasets for each component, and a method to integrate them into a risk ranking. Table 1 describes the datasets for each component in the WRA.

Table 1- Datasets for the components of the fire risk assessment system (grey boxes are variables that are not yet operational, being still the object of exploratory research)

Risk components		Components detail	Variables used	Source
DANGER /HAZARD	Ignition	Human cause	Historical fire data	EFFIS burned area (2003-2020)[1] MODIS thermal anomalies (2003-2020)[2] Corine Land cover[3]
		Natural cause	lightning	
	Fire behavior	Fuel moisture content	Live Fuel Moisture Content (LFMC)	[4]
			Dead Fuel Moisture Content (DFMC)	Fire Weather Index system[5,6,7]
		Fuel types	vegetation types	Corine Land Cover[3] Fuel Map of Europe[8]
		Climatic conditions	- wind, humidity, precipitation and temperature	Fire Weather Index system[5,6,7]
		Terrain	slope, aspect	Elevation data[9]
VULNERABILITY	People	# People in WUI	wildland–urban interface (WUI)[10]	Population density[11,12] Built-up areas[13]
	Ecological "value"	Ecological indicators	- irreplaceability score[14] - protected area - potential burnable land	Nature 2000[15] Protected area[16]
	Socioeconomic "value"	Monetary value of land cover and vegetation	Wildfire-damage restoration costs [17,18,19]	Corine Land Cover[3], vegetation age (restoration time) [17,18,19] restoration costs [17,18,19]
		House, infrastructure		

[1] European Forest Fire Information System (EFFIS), https://effis.jrc.ec.europa.eu
[2] Fire Information for Resource Management System (FIRMS), https://firms.modaps.eosdis.nasa.gov/active_fire/
[3] Corine Land Cover (CLC), https://land.copernicus.eu/pan-european/corine-land-cover
[4] Yebra et al., 2013
[5] CEMS, 2019
[6] Vitolo et al., 2020
[7] Herbach et al., 2018
[8] EFFIS, 2017
9 Amatulli et al., 2020
[10] Costa et al., 2020
[11] Freire et al., 2016
[12] Schiavina et al., 2019
[13] Corbane et al., 2018
[14] LE Saout et al., 2013
[15] The European network of protected sites, Natura 2000, https://www.eea.europa.eu/data-and-maps/data/natura-12
[16] The World Database on Protected Areas (WDPA), https://www.protectedplanet.net/en/thematic-areas/wdpa?tab=WDPA
[17] Mavsar et al., 2011
[18] camia et al., 2017
[19] Oehler et al., 2012

3. Methodology

To identify areas where vegetation fires could occur, a high-resolution mask was developed ("Potential Burnable Area", PBA) (Figure 3) acting as a filter to avoid false alarms, avoiding observations that do not correspond to vegetation fires. The Global Human Settlement Layer (GHSL) built-up product (Corbane et al., 2018) jointly with the JRC's Global Water Layer (Pekel et al., 2016)[1] and PROBA-V 333m Difference Vegetation Index (NDVI) product generated by the Global Land Service of Copernicus[2] were used as input. The data processing was implemented with spatial resolution of ~30 meters, and then aggregated at the spatial resolution of the WCRP[3].

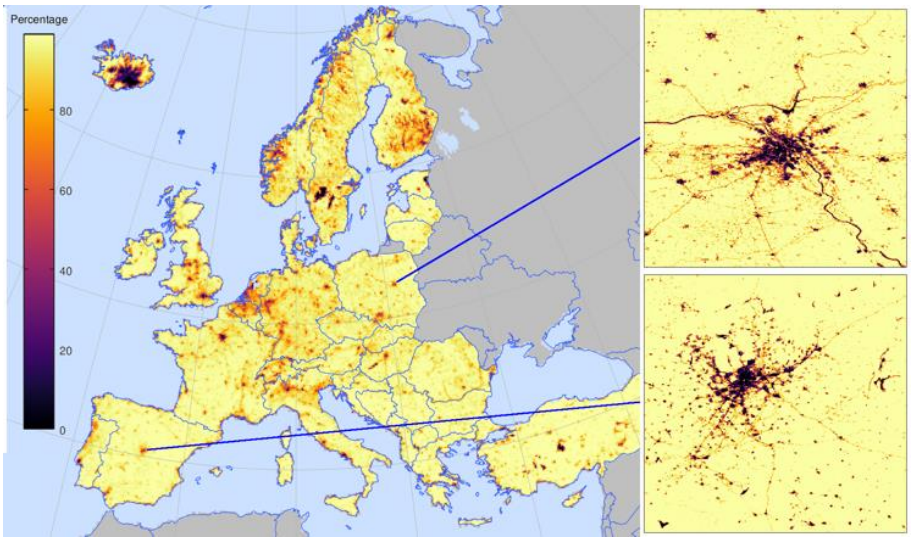

Figure 3- Potential Burnable Area proportion (0-100%) in each 12.5 km cell. Right inside are examples of the cities of Madrid and Warsaw.

The WRA was assessed through a semi-quantitative approach by using the available quantitative data presented in Section 2, as proxy information for the wildfire danger and vulnerability components, along with a qualitative aggregation of them in classes of importance (from low to high importance).

Virtually all the layers discussed above (Table 1) as components of the fire risk are associated with an intrinsic uncertainty, so that their non-linear integration (Figure 2) to estimate the final risk magnifies the cumulative aggregated uncertainty.

Therefore, this structural uncertainty is at the basis of a *robust* method for identifying the areas to prioritise, where the estimated risk is consistently higher than in other areas. This robust risk assessment is computed by considering multiple simulations of the uncertainty – as explored in a corresponding set of multiple model instances (where each instance is a bootstrap statistical resampling repeated for all the uncertain components). The degree of agreement between model instances can be easily estimated, thereby identifying the *high-priority areas* where most instances agree on these areas being at high risk. Analogously, areas with relatively low risk (*lower priority areas*) can also be identified, where most instances agree on the same low-risk classification. Not always the model instances agree, because in some areas the extent of bootstrap uncertainty might generate a higher noise in the model instances. In the worst case (*un-assessable areas*), the risk level in some areas may be too uncertain to assess: this happens if the model instances classify these areas with contradictory levels of risk. This risk-level ranking yields a robust method for integrating the *noisy signal* provided by the various

[1] https://global-surface-water.appspot.com/
[2] https://land.copernicus.eu/global/products/ndvi
[3] European grid of the Coordinated Regional Climate Downscaling Experiment (CORDEX) by World Climate Research Programme (WCRP). Archived at https://tinyurl.com/y85nxfdw. The standard grid EUR-11 is used (grid cell resolution of approximately 0.11 degrees, or about 12.5 km).

components considered in the wildfire risk assessment, offering users a robust estimation of the WRA stability (or conversely its potential fragility) in each area.

However, it should be underlined how the proxy layers available in a harmonised way at the European scale forcefully supply less detailed and accurate information compared with that available only at the national or sub-national scale. Therefore, a trade-off exists between the aim of offering a European-wide harmonised WRA, and its potential degree of fitness for many specific purposes at national/sub-national level. Although some of the available European-wide components do not provide a proper assessment on their uncertainty, a distribution of equi-possible instances of each of the uncertainty-aware components can be modelled. This is the case of data displaying a marked variability in different years. Examples are weather data, and their derivative estimates of fire danger by weather, the fire weather index (De Groot at al., 1987; Wan Wagner et al., 1987; Vitolo et al., 2020) and the observed historical fire activity including large fires mapped in EFFIS (Sedano et al., 2012, 2013) and MODIS thermal anomalies (Giglio et al., 2020).

Wildfire risk may be assessed by considering the vulnerable areas where people, ecological, and socioeconomic values are exposed to fire danger. An aggregated wildfire risk index is proposed, which prioritizes the risk for human lives, while also considering ecological and socioeconomic aspects. This is done by ranking as high-risk areas those where people may be exposed to wildfires, and secondarily other areas where ecological and socioeconomic aspects are at stake. The mathematical mechanism for this ranking relies on standard long-established lexicographic sorting algorithms (Fishburn et al., 1974; Ben-Tal, 1980; Weber et al., 2002).

Looking at Figure 2, in some branches of the WRA tree graphical representation, proceeding from right to left, more than one input component needs to be aggregated into a single output. In these cases, a classical Pareto ranking aggregation (Ben-Tal, 1980; Fonseca et al., 1993; Tracey et al., 2018) is used, so that a semi-quantitative prioritisation can be derived, irrespective of any particular preference on how input components could be weighted[4]. Pareto ranking is a standard methodology to derive a robust ranking (invariant for *any* monotonic transformation of the input components) where the Pareto frontier between the values in each area of two or more components defines higher priority areas, and iteratively the Pareto frontier of the remaining areas defines progressively lower priority areas. For example, aggregating the danger components from (a) the observed historical fire activity, and (b) the monitored fire danger by weather, a Pareto ranking would de-prioritise areas where negligible or no fire activity was historically observed, *and* a time series of fire danger by weather was locally monitored verifying it to be much lower compared with the danger by weather in other regions. Overall, the proposed WRA approach is designed to respect the semantics of the arrays of proxy data sources and their inherent uncertainty (Figure 2, Table 1) through their intermediate data-transformations, up to aggregate them in a final risk-class ranking. The robust semi-quantitative modelling integration is based on the semantic array programming paradigm (deRigo et al., 2012, 2015) and explicitly designed to ease the support for a future climate change analysis (de Rigo et al., 2017; Costa et al., 2020).

4. Preliminary results

A wildfire risk map was generated as an index to summarize the combined effect of wildfire danger and vulnerability. The format of the risk map allows risk classes (from low to high risk) to be identified, with a simple score ranging from 0 % to 100 %, which could then be aggregated in three levels of risk: low, medium and high (Figure 4). High risk may be expected where high wildfire danger affects the most critical areas for people, and secondarily for the other ecological and socioeconomic aspects.

[4] as this may subjectively vary depending on political and society values which are inherently non-technical and cannot be delegated to others than policy makers – with decision makers in different countries and sub-national regions being able to display a very diverse range of preferences.

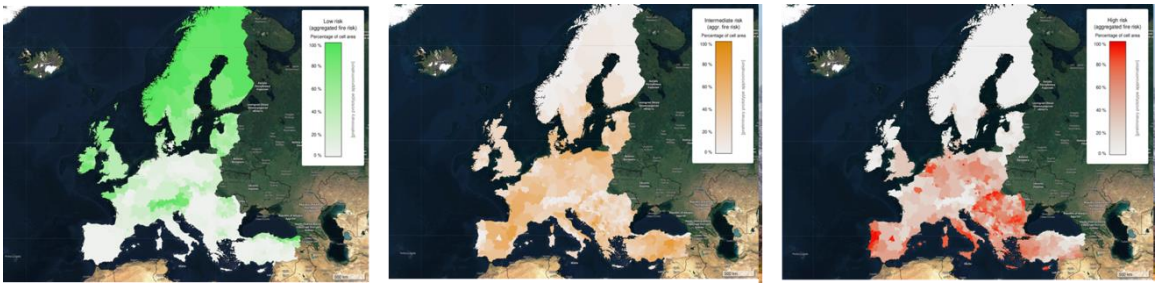

Figure 4- Final aggregated wildfire risk by administrative units. Prevalence of the lower-risk class (left); intermediate-risk class (centre); and higher-risk class (right) in each EURO-CORDEX spatial cell. Percentage based on the risk classification in each EURO-CORDEX cell of 100 equi-possible model runs, to integrate the uncertainty sources. Average aggregation by administrative units, expressing the prevalence of each risk class at the administrative level.

A preliminary version of the pan-European Wildfire risk map viewer was built to include all the input data and the final risk on a pixel (circa 12.5 km) and administrative level basis. This version is displayed in Figure 5 with two examples of the layers included in the viewer.

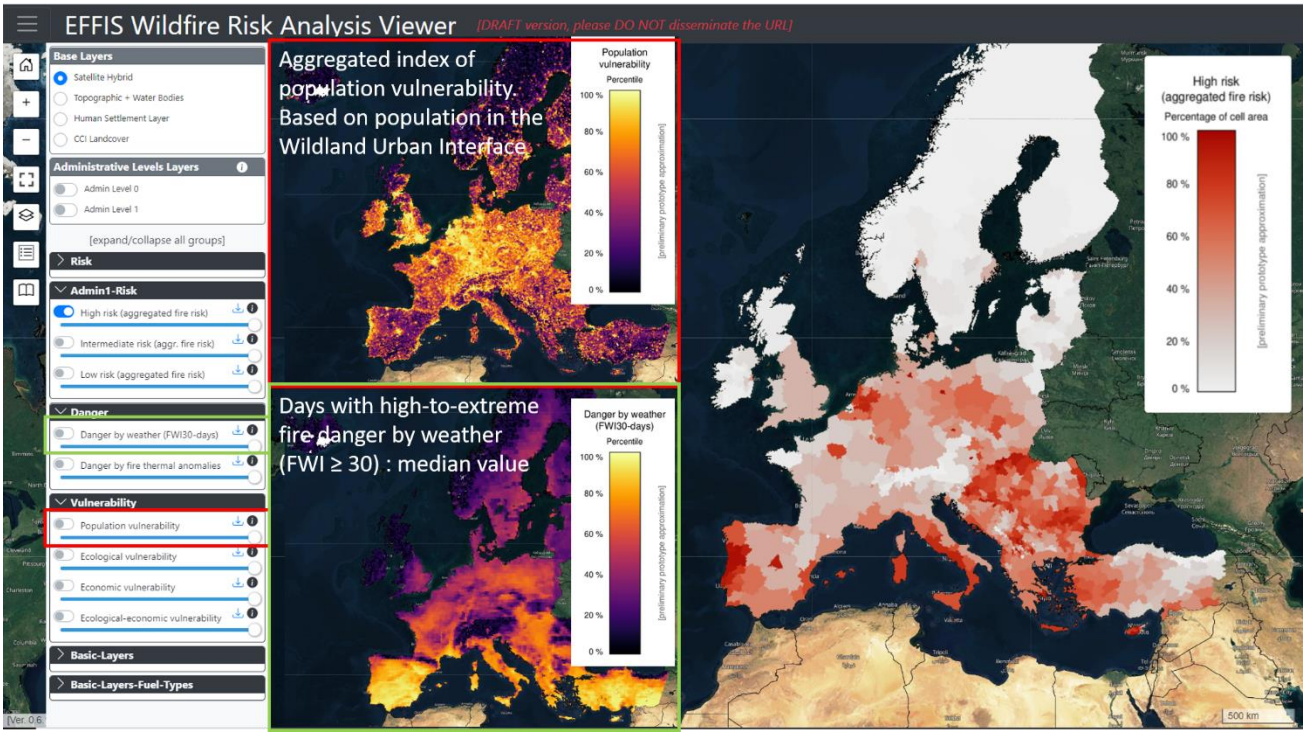

Figure 5- EFFIS Wildfire Risk Viewer (preliminary version). Values displayed in the map correspond to the high-risk class at administrative levels, based on GADM (https://gadm.org/index.html). As an example of some of the layers included on the viewer, the inside boxes display the Danger by Weather (green) and the aggregated index of population vulnerability (red). On the left panel are displayed the layers available in the viewer and on the right inside the legend for the two examples aforementioned.

5. Ongoing research

The above sections set the input data and the basic criteria for the WRA. Also, lessons learned from previous critical fires must be taken into consideration (San-Miguel-Ayanz et al., 2013), as these are becoming more frequent in Europe and worldwide. Next steps foresee testing and validating the WRA and will be undertaken in close collaboration with the EGFF. At the same time, research is ongoing on both deriving enhanced datasets and methods such as fuel classification, socio-economic components, or live fuel moisture content.

6. References

Amatulli, G., McInerney, D., Sethi, T., Strobl, P., & Domisch, S., 2020. Geomorpho90m, empirical evaluation and accuracy assessment of global high-resolution geomorphometric layers. Scientific Data, 7(1), 1-18. https://doi.org/10.6084/m9.figshare.12145791

Bachmann A, Allgo¨ wer B, 2001. A consistent wildland fire risk terminology is needed! Fire Management Today 61, 28–33. https://doi.org/10.1071/WF12052

Ben-Tal, A., 1980. Characterization of Pareto and lexicographic optimal solutions. In: Fandel, G., Gal, T. (Eds.), Multiple Criteria Decision Making Theory and Application. Springer, Berlin, Heidelberg, pp. 1–11. https://doi.org/10.1007/978-3-642-48782-8_1

Calkin, D. E., Ager, A. A., Gilbertson-Day, J., 2010. Wildfire risk and hazard: procedures for the first approximation. Gen. Tech. Rep. RMRS-GTR-235. Fort Collins, CO: US Department of Agriculture, Forest Service, Rocky Mountain Research Station. 62 p., 235. https://doi.org/10.2737/RMRS-GTR-235

Camia, A., Libertà, G., San-Miguel-Ayanz, J., 2017. Modeling the impacts of climate change on forest fire danger in Europe: sectorial results of the PESETA II Project. Publications Office of the European Union, Luxembourg, 24 pp. ISBN: 978-92-79-66259-1, https://doi.org/10.2760/768481

Chuvieco E, Aguado I, Yebra M, Nieto H, Salas J, Martín P, Vilar L, Martinez J, Martín S, Ibarra P, de la Riva J, Baeza J, Rodríguez F, Molina JR, Herrera MA, Zamora R., 2010. Development of a framework for fire risk assessment using remote sensing and geographic information system technologies. Ecological Modelling 221, 46–58. https://doi.org/:10.1016/J.ECOLMODEL.2008.11.017

Chuvieco E., Aguado I., Jurdao S., Pettinari M. L., Yebra M., Salas J., Hantson S., de la Riva J., Ibarra P., Rodrigues M., Echeverría M., Azqueta D., Román M. V., Bastarrika A., Martínez S., Recondo C., Zapico E., Martínez-Vega F. J., 2012. Integrating geospatial information into fire risk assessment. International Journal of Wildland Fire 23 (5), 606-619. https://doi.org/10.1071/WF12052

Copernicus Emergency Management Service, 2019. Fire danger indices historical data from the Copernicus Emergency Management Service. Copernicus Climate Change Service (C3S) Climate Data Store (CDS). https://doi.org/10.24381/cds.0e89c522

Corbane, C., Florczyk, A., Pesaresi, M., Politis, P., Syrris, V., 2018. GHS built-up grid, derived from Landsat, multitemporal (1975-1990-2000-2014), R2018A. European Commission, Joint Research Centre (JRC). http://data.europa.eu/89h/jrc-ghsl-10007

Costa H., de Rigo, D., Liberta, G., Houston Durrant, T., San-Miguel-Ayanz, J., 2020. European wildfire danger and vulnerability in a changing climate: towards integrating risk dimensions. Publications Office of the European Union, Luxembourg, 59 pp. ISBN: 978-92-76-16898-0, https://doi.org/10.2760/46951

De Groot, W.J., 1987. Interpreting the Canadian Forest Fire Weather Index (FWI) System, in: Fourth Central Regional Fire Weather Committee Scientific and Technical Seminar, Proceedings. Winnipeg, Manitoba, Canada, pp. 3–14. https://tinyurl.com/y38mgoxr

de Rigo, D., 2012. Semantic Array Programming for environmental modelling: application of the Mastrave library. In: Seppelt, R., Voinov, A.A., Lange, S., Bankamp, D. (Eds.), International Environmental Modelling and Software Society (IEMSs) 2012 International Congress on Environmental Modelling and Software - Managing Resources of a Limited Planet: Pathways and Visions under Uncertainty, Sixth Biennial Meeting. pp. 1167–1176. https://scholarsarchive.byu.edu/iemssconference/2012/Stream-B/69/

de Rigo, D., 2015. Study of a collaborative repository of semantic metadata and models for regional environmental datasets' multivariate transformations. Ph.D. thesis, Politecnico di Milano, Milano, Italy.

de Rigo, D., Libertà, G., Houston Durrant, T., Artés Vivancos, T., San-Miguel-Ayanz, J., 2017. Forest fire danger extremes in Europe under climate change: variability and uncertainty. Publications Office of the European Union, Luxembourg, 71 pp. ISBN:978-92-79-77046-3, https://doi.org/10.2760/13180

Dunn, C. J., D O'Connor, C., Abrams, J., Thompson, M. P., Calkin, D. E., Johnston, J. D., Stratton, R., Gilbertson-Day, J., 2020. Wildfire risk science facilitates adaptation of fire-prone social-ecological systems to the new fire reality. Environmental Research Letters, 15(2), 025001. https://doi.org/10.1088/1748-9326/ab6498

European Forest Fire Information System, 2017. European Fuel Map, 2017, based on JRC Contract Number 384347 on the "Development of a European Fuel Map". European Commission, Joint Research Centre (JRC)

Finney, M. A. (2005). The challenge of quantitative risk analysis for wildland fire. Forest ecology and management, 211(1-2), 97-108. https://doi.org/10.1016/j.foreco.2005.02.010

Fishburn, P.C., 1974. Exceptional paper - Lexicographic orders, utilities and decision rules: a survey. Management Science 20, 1442–1471. https://doi.org/10.1287/mnsc.20.11.1442

Fonseca, C.M., Fleming, P.J., 1993. Genetic algorithms for multiobjective optimization: formulation, discussion and generalization, in: Forrest, S. (Ed.), Proceedings of the 5th International Conference on Genetic Algorithms. Morgan Kaufmann Publishers Inc., San Francisco, CA, USA, pp. 416–423.

Freire, S., MacManus, K., Pesaresi, M., Doxsey-Whitfield, E., Mills, J., 2016. Development of new open and free multi-temporal global population grids at 250 m resolution. In: Proceedings of the 19th AGILE International Conference on Geographic Information Science

Giglio, L., Schroeder, W., Hall, J.V., Justic, C.O., 2020. MODIS Collection 6 active fire product user's guide-Revision C. NASA. https://tinyurl.com/ysjtrycf

Hardy, C. C., 2005. Wildland fire hazard and risk: Problems, definitions, and context. Forest ecology and management, 211(1-2), 73-82. https://doi.org/10.1016/j.foreco.2005.01.029

Hersbach, H., Bell, B., Berrisford, P., Biavati, G., Horányi, A., Muñoz Sabater, J., Nicolas, J., Peubey, C., Radu, R., Rozum, I., Schepers, D., Simmons, A., Soci, C., Dee, D., Thépaut, J-N., 2018. ERA5 hourly data on single levels from 1979 to present. Copernicus Climate Change Service (C3S) Climate Data Store (CDS). https://doi.org/10.24381/cds.adbb2d47

Le Saout, S., Hoffmann, M., Shi, Y., Hughes, A., Bernard, C., Brooks, T.M., Bertzky, B., Butchart, S.H.M., Stuart, S.N., Badman, T., Rodrigues A.S.L., 2013. Protected areas and effective biodiversity conservation. Science 342 (6160), 803-805. https://doi.org/10.1126/science.1239268

Mavsar, R., Pettenella, D., San-Miguel-Ayanz, J., Camia, A., 2011. Development of a methodology for the analysis of socio-economic impact of forest fires in Europe. Presented at the 5th International Wildland Fire Conference, Sun City, South Africa. https://tinyurl.com/yerb8ewe

Moreira, F., Ascoli, D., Safford, H., Adams, M.A., Moreno, J. M., Pereira, J. M.C., Catry, F.X., Armesto, J., Bond, W., González, M.E., Curt, T., Koutsias, N., McCaw, L., Price, O., Pausas, J.G., Rigolot, E., Stephens, S., Tavsanoglu, C., Vallejo, V.R., Wilgen, B.W.V., Xanthopoulos, G., Fernandes, P.M., 2020. Wildfire management in Mediterranean-type regions: paradigm change needed. Environmental Research Letters 15 (1), 011001+. https://doi.org/10.1088/1748-9326/ab541e

Oehler, F., Oliveira, S., Barredo, J.I., Camia, A., San-Miguel-Ayanz, J., Pettenella, D., Mavsar, R., 2012. Assessing European wild fire vulnerability. Geophysical Research Abstracts 14, 9452

Oliveira, S., Gonçalves, A., Benali, A., Sá, A., Zêzere, J. L., Pereira, J. M., 2020. Assessing risk and prioritizing safety interventions in human settlements affected by large wildfires. Forests, 11 (8), 859+. https://doi.org/10.3390/f11080859

Oliveira, S., Rocha, J., Sá, A.,2021. Wildfire risk modeling. Current Opinion in Environmental Science & Health 23, 100274+. https://doi.org/10.1016/j.coesh.2021.100274

Oom, D., de Rigo, D., San-Miguel-Ayanz, J., Artes-Vivancos, T., Boca, R., Branco, A., Campanharo, W., Grecchi, R., Durrant, T., Ferrari, D., Liberta, G., Maianti, P., Pfieffer, H., 2021, Wildfires. In: Poljansek, K., Valles, A.C., Ferrer, M.M. (Eds). Recommendations for national risk assessment for disaster risk management in EU: where science and policy meet, Version 1, pp. 93–105. Publications Office of the European Union, Luxembourg. ISBN 978-92-76-30256-8, https://doi.org/10.5281/zenodo.6045338

Pechony, O., Shindell, D.T., 2010. Driving forces of global wildfires over the past millennium and the forthcoming century. Proceedings of the National Academy of Sciences 107 (45), 19167–19170 https://doi.org/10.1073/pnas.1003669107.

Pekel, J. F., Cottam, A., Gorelick, N., & Belward, A. S., 2016. High-resolution mapping of global surface water and its long-term changes. Nature, 540(7633), 418-422. https://doi.org/10.1038/nature20584

San-Miguel-Ayanz, J., Carlson, J. D., Alexander, M., Tolhurst, K., Morgan, G., Sneeuwjagt, R., Dudley, M., 2003. Current methods to assess fire danger potential. In: Wildland Fire Danger Estimation and Mapping. Vol. 4 of Series in Remote Sensing, World Scientific, pp. 21-61. https://doi.org/10.1142/9789812791177_0002

San-Miguel-Ayanz, J., Chuvieco, E., Handmer, J., Moffat, A., Montiel-Molina, C., Sandahl, L., Viegas, D., 2017. Climatological risk: wildfires. In: Poljanšek, K., Marín Ferrer, M., De Groeve, T., Clark, I. (Eds.), Science for disaster risk management 2017: knowing better and losing less. Publications Office of the European Union, Luxembourg, pp. 294-305. ISBN: 978-92-79-60679-3

San-Miguel-Ayanz, J., Costa, H., de Rigo, D., Libertà, G., Artés Vivancos, T., Houston Durrant, T., Nuijten, D., Löffler, P., Moore, P., Baetens, J., Konstantinov, V., Duche, Y., Joannelle, P., Debreceni, P., Nagy, D., Zaken, A.B., Mitri, G., Assali, F., Alaoui, H.M., Piwnicki, J., Szczygieł, R., Almeida, R., Mara, S., Eritsov,

A., Sandahl, L., Moffat, A., Gazzard, R., 2019. Basic criteria to assess wildfire risk at the pan-European level. Publications Office of the European Union, Luxembourg. ISBN:978-92-79-98200-2, https://doi.org/10.2760/052345

San-Miguel-Ayanz, J., Moreno, J. M., Camia, A., 2013. Analysis of large fires in European Mediterranean landscapes: lessons learned and perspectives. Forest Ecology and Management 294, 11-22. https://doi.org/10.1016/j.foreco.2012.10.050

Schiavina, M., Freire, S., MacManus, K., 2019. GHS population grid multitemporal (1975, 1990, 2000, 2015) R2019A. European Commission, Joint Research Centre (JRC). http://data.europa.eu/89h/0c6b9751-a71f-4062-830b-43c9f432370f

Scott, Joe H.; Thompson, Matthew P.; and Calkin, David E., 2013. A Wildfire Risk Assessment Framework for Land and Resource Management. USDA Forest Service / UNL Faculty Publications. 328. https://digitalcommons.unl.edu/usdafsfacpub/328

Sedano, F., Kempeneers, P., San-Miguel-Ayanz, J., Strobl, P., Vogt, P., 2013. Towards a pan-European burnt scar mapping methodology based on single date medium resolution optical remote sensing data. International Journal of Applied Earth Observation and Geoinformation 20, 52–59. https://doi.org/10.1016/j.jag.2011.08.003

Sedano, F., Kempeneers, P., Strobl, P., McInerney, D., San-Miguel-Ayanz, J., 2012. Increasing spatial detail of burned scar maps using IRS-AWiFS data for Mediterranean Europe. Remote Sensing 4, 726–744. https://doi.org/10.3390/rs4030726

Thompson, M. P., Calkin, D. E., Finney, M. A., Ager, A. A., Gilbertson-Day, J. W., 2011. Integrated national-scale assessment of wildfire risk to human and ecological values. Stochastic Environmental Research and Risk Assessment, 25(6), 761-780. https://doi.org/10.1007/s00477-011-0461-0

Tracey, J.A., Rochester, C.J., Hathaway, S.A., Preston, K.L., Syphard, A.D., Vandergast, A.G., Diffendorfer, J.E., Franklin, J., MacKenzie, J.B., Oberbauer, T.A., Tremor, S., Winchell, C.S., Fisher, R.N., 2018. Prioritizing conserved areas threatened by wildfire and fragmentation for monitoring and management. PLOS ONE 13, e0200203+. https://doi.org/10.1371/journal.pone.0200203

Tutsch, M., Haider, W., Beardmore, B., Lertzman, K., Cooper, A. B., Walker, R. C., 2010. Estimating the consequences of wildfire for wildfire risk assessment, a case study in the southern Gulf Islands, British Columbia, Canada. Canadian Journal of Forest Research, 40 (11), 2104-2114. https://doi.org/10.1139/X10-159

United Nations International Strategy for Disaster Reduction (UNISDR), 2009. Terminology on disaster risk reduction. Geneva, Switzerland.

Van Wagner, C.E., 1987. Development and structure of the Canadian Forest Fire Weather Index System, Forestry Technical Report. Canadian Forestry Service, Ottawa, Canada. https://tinyurl.com/y5d5bxx2

Vitolo, C., Di Giuseppe, F., Barnard, C., Coughlan, R., San-Miguel-Ayanz, J., Libertá, G., Krzeminski, B., 2020. ERA5-based global meteorological wildfire danger maps. Scientific Data 7, 216+. https://doi.org/10.1038/s41597-020-0554-z

Weber, E., Soncini-Sessa, R., Castelletti, A., 2002. Lexicographic optimisation for water resources planning: the case of Lake Verbano, Italy. In: Rizzoli, A.-E., Jakeman, A.J. (Eds.), Proceedings of the IEMSs First Biennial Meeting: Integrated Assessment and Decision Support. International Environmental Modelling and Software Society (iEMSs), pp. 235–240. https://scholarsarchive.byu.edu/iemssconference/2002/all/44/

Xi, D. D., Taylor, S. W., Woolford, D. G., & Dean, C. B., 2019. Statistical models of key components of wildfire risk. Annual review of statistics and its application, 6, 197-222. https://doi.org/10.1146/annurev-statistics-031017-100450

Yebra, M., Dennison, P. E., Chuvieco, E., Riano, D., Zylstra, P., Hunt Jr, E. R., Danson F. M., Jurdao, S., 2013. A global review of remote sensing of live fuel moisture content for fire danger assessment: moving towards operational products. Remote Sensing of Environment 136, 455-468. https://doi.org/10.1016/j.rse.2013.05.029

Persistent Underground Smouldering Fire in Deep Peat Layer

Yunzhu Qin[1]; Dayang Nur Sakinah Musa[3,4]; Shaorun Lin[1,2]*; Xinyan Huang[1,]*

[1]Research Centre for Fire Safety Engineering, The Hong Kong Polytechnic University, Hong Kong
[2]The Hong Kong Polytechnic University Shenzhen Research Institute, Shenzhen, China.
{flynn.lin@connect.polyu.hk}, {xy.huang@polyu.edu.hk}
[3]Department of Chemical and Environmental Engineering, Faculty of Engineering, Universiti Putra Malaysia, 43400 UPM Serdang, Selangor, Malaysia
[4]International Tropical Forestry Programme, Faculty of Tropical Forestry, Universiti Malaysia Sabah, Malaysia

**Corresponding authors*

Keywords

Smouldering; peat fire; underground fire; wildland fire; fire spread

Abstract

Peatlands are essential terrestrial carbon pools. Due to climate change and human activities, peatlands are more prone to large-scale fires than ever, especially deep underground fires. However, most current smouldering researches focus on small-scale smouldering behaviour in relatively shallow layers, posing a research gap. This work explores in-depth (up to 60 cm) smouldering behaviour, such as persistence, propagation and emission. The commercial organic peat soil from Netherland was chosen for lab experiments. Reactors with good thermal insulation conditions were built to simulate the natural smouldering environment. Experimental results demonstrate that smouldering underground fires can sustain in deep soil layers for more than a week without any additional oxygen supply. Because of the competition of oxygen supply and heat losses, a critical depth of 55 cm for smouldering propagation was obtained, below which smouldering cannot self-sustained propagate. This work will help connect lab-scale experiments with natural underground smouldering peat fires and understand smouldering dynamics in deep soil layers.

1. Introduction

Peatland, as a type of wetland, accumulates a considerable amount of organic matter decomposed from vegetation material (Hugron et al. 2013). Peatlands are essential terrestrial carbon pools, storing one-third of the world's soil carbon (500-600 Gt C), as much carbon as surface vegetation globally, and may be of similar magnitude to the atmospheric carbon pool (~850 Gt C) (Ballhorn et al. 2009; Turetsky et al. 2015).

Due to climate change and human activities, peatlands are more prone to large-scale fires than ever before (Jolly et al. 2015; Lin et al. 2021a). Especially, at certain times and in certain areas, such as hot, dry summers and regions with a high diversity of plants, the fire risk is significantly increased (Evtyugina et al. 2013). Frequent peat fires have caused serious ecological and climatic damage, as well as significant economic losses. For example, in 2019, the slash-and-burn activities in southeast Asia (Goldstein et al. 2020) resulted in mega-scale peatland wildfires that burned for several months, leading to severe air pollution and causing many health issues to residents (Normile 2019). Peat fires are started by flaming fires in forests, lightning strikes, and human activities and are dominated by smouldering combustion. Smouldering wildfire requires less ignition energy than flaming combustion and can persist in wetter and lower oxygen conditions. Once ignited, smouldering can propagate vertically and horizontally in a deep and wide soil layer, thus sustaining the largest and most persistent fire on Earth (shown in Fig. 1). For such underground fires, it's challenging to detect and extinguish them. Even though fires on the soil surface was extinguished, hidden underground smouldering fire may spread at a very low propagation rate and re-spreading to the surface in some conditions (Rein 2013). However, this kind of in-depth smouldering behaviour is poorly understood. Smouldering wildfire and the relevant ecological problems have attracted much research attention. Still, most of them focus on smouldering propagation in relatively shallow soil layers in terms of smouldering ignition, propagation (Huang and Rein 2017, 2019), extinction (Lin

and Huang 2021; Lin et al. 2021b), and firefighting (Ramadhan et al. 2017; Santoso et al. 2021). So far, there is a lack of both lab-scale and field-scale smouldering research to reveal the in-depth smouldering propagation behaviour, thus bringing a considerable knowledge gap.

This study aims to conduct a lab-scale series of in-depth smouldering experiments to understand the deep-layer smouldering propagation behaviour. This work will help better connect small-scale laboratory experiments with natural underground smouldering peat fires.

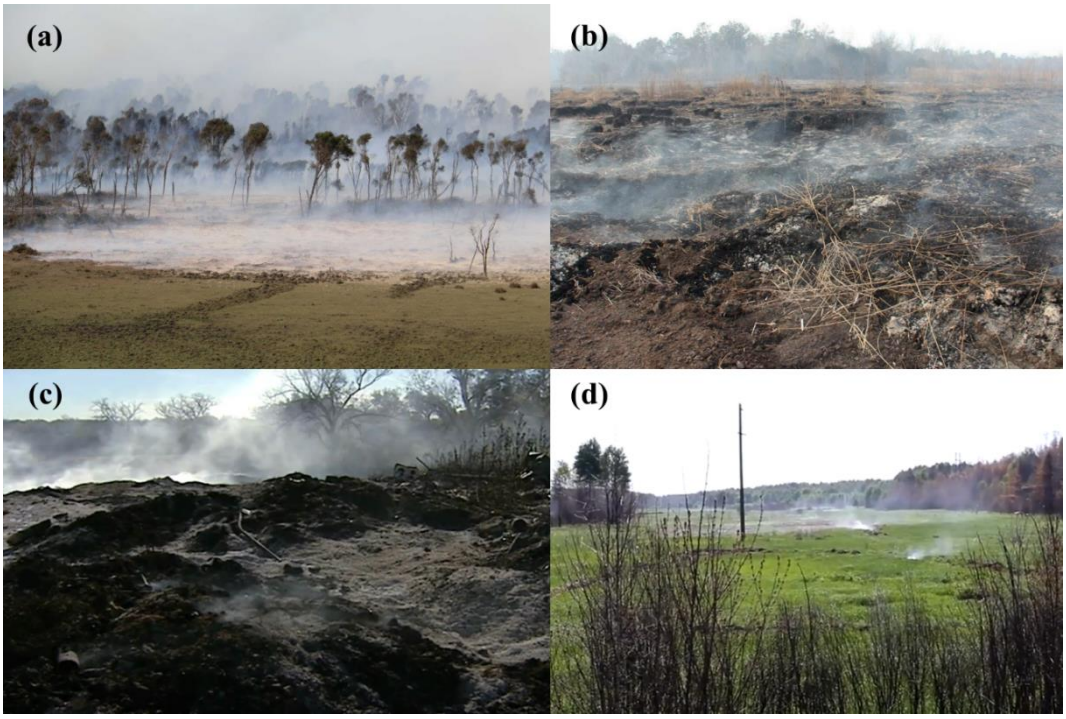

Figure 1- Underground smouldering fire in (a-b) Southeast Asia, (c) North America, and (d) Eastern Europe

2. Methodology

2.1. Peat sample

The commercial moss peat sample from Estonia with high organic content (~97%), uniform density, and homogenous particle size was chosen in this study. Before the tests, the peat soil was first oven-dried at 90 ^{o}C for 48 h to reach an equilibrium with the air of MC = 10% (Huang and Rein, 2017). The measured peat bulk density and porosity were 145 ± 10 kg/m^3 and 0.90 ± 0.01. Elemental analysis shows that its mass fraction of C/H/O/N/S is 45.6/6.0/48.0/0.5/0.3%, respectively.

2.2. Experimental setup and procedure

Fig. 2 shows the schematic diagram of the experimental setup for the peat fire initiation and spread. In order to simulate a natural peat underground fire, the smouldering reactor needs to have good insulation. The smouldering reactor in this study was built of 1 cm-thick insulation ceramic fibreboards to contain the peat sample and had different heights (30 cm – 60 cm). The aluminium foil was attached to the outer surface of the insulation board to reduce the radiative heat loss. The top of the reactor was open to supply oxygen and release emissions. An array of K-type thermocouples with an interval of 3cm was inserted into the reactor to record the temperature history at a different height. The coil ignitor inserted into the sample was used to initiate the smouldering combustion.

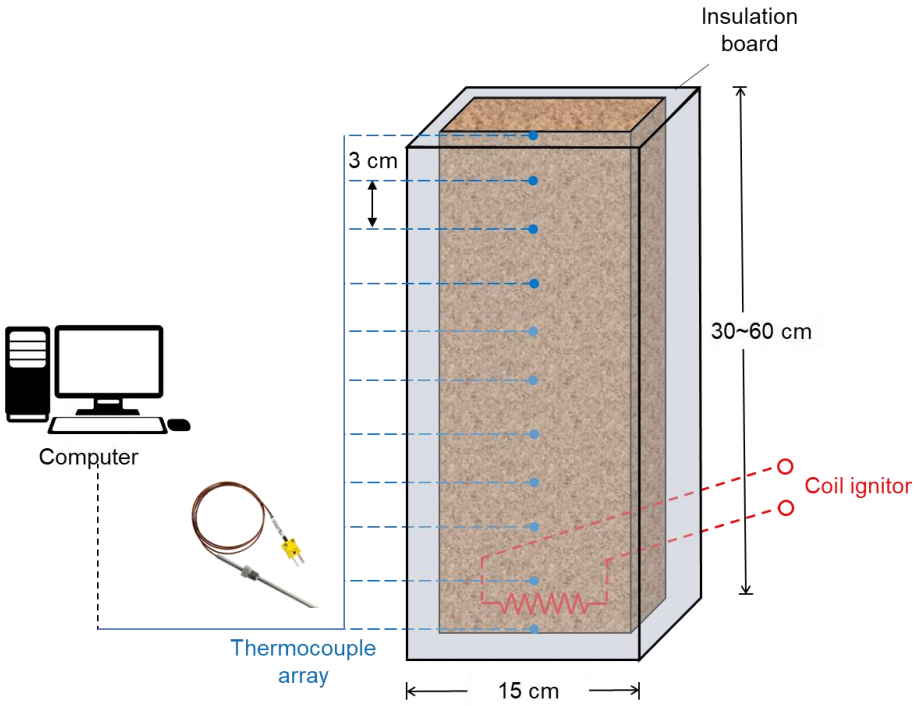

Figure 2- Experimental setup for in-depth smouldering peat fire

In order to initiate the peat and form a robust smouldering front, the ignition protocol was fixed at 100 W for 60 min. The tests are stopped until all peat has returned to room temperature for 2 hours, which indicates the end of smouldering. The test started with ignition at the bottom. Subsequently, tests with different reactor heights were conducted, and all the tests were repeated at least twice to ensure repeatability.

3. Results and Discussion

3.1. Smouldering phenomenon and critical depth

Fig. 3 shows the thermocouple measurements of (a) smouldering propagation and (b) no propagation in reactors with different depths of 50 cm and 60 cm, respectively. Taking (a) as an example, the ignition was started from the bottom (-50 cm). After 60-min heating, the temperature at the corresponding height exceeds 250 ºC, which is the minimum smouldering temperature and suggests a robust smouldering front formation. Afterward, it shows that smouldering propagated upward with a very low propagation rate (~4 mm/h). A noticeable change occurred after 3.5 days. Smouldering no longer continued to propagate upward but instead propagated downward with a similar propagation speed and higher smouldering temperature (> 400 ºC). Then the smouldering fluctuated around the bottom before final extinction. Notably, a peat layer of 50-cm depth maintained continuous smouldering combustion for about a week.

A completely different phenomenon occurs if the depth is increased to 60 cm (Fig. 3 (b)). The temperature near the bottom (-60 cm) still exceeded 250 ºC after 60 min heating, but no smouldering propagation was observed. Even though a few thermocouples near the bottom showed a short-term temperature increase, this is probably the effect of heat transfer since the duration was short and the temperature was low. Repeated tests have demonstrated that at this depth, even if the ignition power is further increased or the ignition time is extended, no smouldering propagation can be observed.

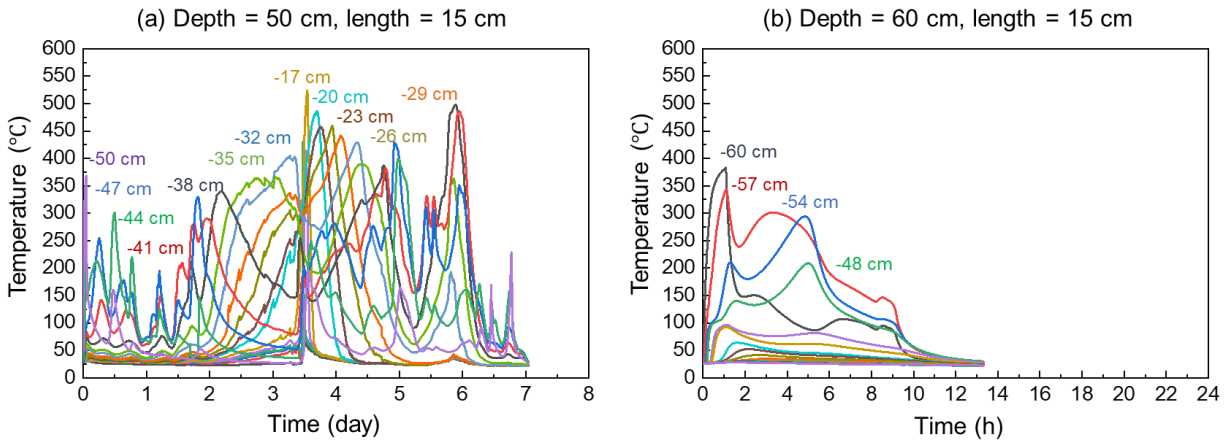

Figure 3- Thermocouple profiles in different depths. (a) shows a typical smouldering phenomenon while (b) indicates no smouldering propagation after ignition (The negative sign means that the thermocouple is below the reactor's top free surface).

3.2. Critical depth

Experimental results show that at this reactor size (length = 15 cm), smouldering can only propagate when the depth is less than 50 cm. Continue to deepen the depth, even if smouldering is still able to be ignited under a strong ignition, it cannot self-sustained propagate. Thus, the critical smouldering depth for this reactor size is 55 cm.

Critical depth exists due to the limitation of the oxygen conditions. Oxygen can only be provided by diffusion into the deep peat layers, and it may not be sufficient to support the oxidation processes necessary for smouldering below the critical depth. According to Darcy's law,

$$q = \frac{k}{\mu L}\Delta p \qquad \text{(Eq. 1)}$$

where q is airflow flux (or the air supply per unit area) in (m/s), k is the permeability of the porous medium in m^2, μ is the dynamic viscosity of the fluid in (Pa·s), and Δp is the pressure drop in (Pa) over a given distance L (m). Thus, given a heat transfer condition and minimum oxygen supply for the oxidation process of smouldering, the critical depth for smouldering can be determined. Future research could explore the critical smouldering depth in different insulation conditions or even smouldering in field-scale.

4. Conclusions

In this work, we conducted a series of lab-scale experiments to investigate the in-depth smouldering peat fire. We experimentally demonstrated that smouldering underground fires could sustain in deep soil layers for more than a week without any additional oxygen supply. In the current experimental setup, a critical depth of 55 cm for smouldering propagation was obtained, below which smouldering cannot self-sustained propagate. However, reducing heat loss, such as using a reactor of a larger size, will make smouldering sustain in a deeper peat layer. This work will help better connect small-scale laboratory experiments with natural underground smouldering peat fires and understand smouldering behaviour in deep layers.

5. Acknowledgements

This work is funded by the National Natural Science Foundation of China (No. 51876183) and the Society of Fire Protection Engineers (SFPE) Educational & Scientific Foundation.

6. References

Ballhorn U, Siegert F, Mason M, Limin S., Limin S (2009) Derivation of burn scar depths and estimation of carbon emissions with LIDAR in Indonesian peatlands. Proceedings of the National Academy of Sciences 106, 21213–21218. doi:10.1073/pnas.0906457106.

Evtyugina M, Calvo AI, Nunes T, Alves C, Fernandes AP, Tarelho L, Vicente A, Pio C (2013) VOC emissions of smouldering combustion from Mediterranean wildfires in central Portugal. Atmospheric Environment 64, 339–348. doi:10.1016/j.atmosenv.2012.10.001.

Goldstein JE, Graham L, Ansori S, Vetrita Y, Thomas A, Applegate G, Vayda AP, Saharjo BH, Cochrane MA (2020) Beyond slash-and-burn: The roles of human activities, altered hydrology and fuels in peat fires in Central Kalimantan, Indonesia. Singapore Journal of Tropical Geography 1–19. doi:10.1111/sjtg.12319.

Huang X, Rein G (2017) Downward spread of smouldering peat fire: The role of moisture, density and oxygen supply. International Journal of Wildland Fire 26, 907–918. doi:10.1071/WF16198.

Huang X, Rein G (2019) Upward-and-downward spread of smoldering peat fire. Proceedings of the Combustion Institute 37, 4025–4033. doi:10.1016/j.proci.2018.05.125.

Hugron S, Bussières J, Rochefort L (2013) 'Tree plantations within the context of ecological restoration of peatlands: practical guide.'

Jolly WM, Cochrane MA, Freeborn PH, Holden ZA, Brown TJ, Williamson GJ, Bowman DMJS (2015) Climate-induced variations in global wildfire danger from 1979 to 2013. Nature Communications 6, 1–11. doi:10.1038/ncomms8537.

Lin S, Huang X (2021) Quenching of smoldering: Effect of wall cooling on extinction. Proceedings of the Combustion Institute 38, 5015–5022. doi:10.1016/j.proci.2020.05.017.

Lin S, Liu Y, Huang X (2021a) Climate-induced Arctic-boreal peatland fire and carbon loss in the 21st century. Science of the Total Environment 796, 148924. doi:10.1016/j.scitotenv.2021.148924.

Lin S, Liu Y, Huang X (2021b) How to build a firebreak to stop smouldering peat fire: Insights from a laboratory-scale study. International Journal of Wildland Fire 30, 454–461. doi:10.1071/WF20155.

Normile D (2019) Indonesia's fires are bad, but new measures prevented them from becoming worse. Science. doi:10.1126/science.aaz7020.

Ramadhan ML, Palamba P, Imran FA, Kosasih EA, Nugroho YS (2017) Experimental study of the effect of water spray on the spread of smoldering in Indonesian peat fires. Fire Safety Journal 91, 671–679. doi:10.1016/j.firesaf.2017.04.012.

Rein G (2013) Smouldering Fires and Natural Fuels. 'Fire Phenomena in the Earth System'. (Ed Claire M. Belcher) pp. 15–34. (John Wiley & Sons, Ltd.: New York) doi:10.1002/9781118529539.ch2.

Santoso MA, Cui W, Amin HMF, Christensen EG, Nugroho YS, Rein G (2021) Laboratory study on the suppression of smouldering peat wildfires: effects of flow rate and wetting agent. International Journal of Wildland Fire 30, 378–390. doi:10.1071/WF20117.

Turetsky MR, Benscoter B, Page S, Rein G, Van Der Werf GR, Watts A (2015) Global vulnerability of peatlands to fire and carbon loss. Nature Geoscience 8, 11–14. doi:10.1038/ngeo2325.

Present and future fire risk changes in Central Europe

Maik Billing[1]; Christopher Marrs[2]; Matthias Forkel[2]; Eike Sebode[3]; Kirsten Thonicke[1,3]*

[1] *Research Department "Earth System Analysis", Potsdam Institute for Climate Impact Research (PIK). Telegrafenberg A31, D-14473 Potsdam, Germany, {Maik.Billing, Kirsten.Thonicke}@pik-potsdam.de*
[2] *Institute for Photogrammetry and Remote Sensing, TU Dresden. 01062 Dresden, Germany {christopher.marrs, matthias.forkel}@tu-dresden.de*
[3]*Institute for Environmental Science and Geography, University of Potsdam, Germany.*

**Corresponding author*

Keywords

Future fire risk, climate change, Fire Weather Index, Central Europe, Wildland-Urban Interface

Abstract

Fire risk is projected to increase under future climate change. Most projections focus on fire-prone regions, such as the Mediterranean-type ecosystems, whereas little attention has been paid to regions of low fire risk such as Central Europe. Here, future projections of fire risk which are tailor-made for its specific conditions are scarce. With our study we aim to fill this gap. We use meteorological station data and interpolated climate datasets to compute future fire risk for Central Europe (covering Germany, Poland and the Czech Republic) using the Fire Weather Index. In a next step, we analyse the spatial distribution of reported fire ignitions to identify additional drivers that can explain the spatial pattern of fire ignition and risk, or accelerate fire risk under climate extremes (drought or extreme heat). We analyse how transport infrastructure and proximity to settlements have influenced fire ignition in Central Europe and compare it against relationships known from fire-prone regions. We aim to build on recent adjustments of the FWI to account for respective increased fire risk and apply it to our study area.

In a next step, downscaled future climate scenarios (CMIP6) are applied to compute changes in future fire risk for the entire study area as well as selected sites in Central Europe. Uncertainty ranges of future fire risk projections will be covered by using several climate scenarios for the entire study region.

1. Introduction

Central Europe is until now characterized by relatively low fire risk. Fire occurrence is rare and most fires remain small. For example, the mean annual total burned area in Germany was around 800 ha in 1991-2019 (European Forest Fire Information System). Fires occur mainly in dry lowland pine forests in eastern Germany and in Poland, especially in young to medium forest stands (< 40 years) (Müller 2019). The low level of fire occurrence is caused by the temperate climate conditions and by the development of various forest fire protection measures over the past century. Fire monitoring and forest fire protection has a long tradition in those regions (König 2007). For example, the first fire lookout tower was invented and patented in eastern Germany in 1902. Several forest management practices, forest fire protection measures and public education initiatives were introduced during the 1970s and 1980s that resulted in a general public awareness about forest fire risks and ultimately in a decline in fire occurrence (König 2007). Many past forest fires were caused by military activities and the occurrence of such fires dropped after 1990 (Müller 2019). As most of the pine forests are now in older age classes and thus have less ladder fuels, the occurrence of large devasting crown fires was declining further. Given those developments in forest management and fire protection, societies and foresters are rarely confronted with forest fires in Central Europe.

Despite those past developments, unexpected large fires occurred in Germany during the drought of 2018, which had similar burned area like fires back in the 1970s. Although the dry and hot conditions promoted those recent fires, the large burned area is explained with the impossibility to fight those fires because they occurred at areas contaminated with old ammunition (Müller 2019). However, those recent fires demonstrate that extreme dry and hot weather conditions can suddenly increase fire risks also in forests of Central Europe and that fire occurrence at former military sites or close to public infrastructures are indeed a risk to society and a challenge for fire fighters. We assume that fire risks will increase in future in central Europe because regional climate warming and a possible increased occurrence of droughts will increase fire danger conditions. Currently, there

is no recent assessment of fire risks in Central Europe that accounts for the specific regional patterns and developments of forest fire protection and for future climate change conditions. Here we aim to develop a comprehensive assessment of present and future fire risks in Central Europe (Germany, Poland, Czechia).

2. Analysis of fire risk under current climate

The fire season in Central Europe is characterized by short dry and hot spells in the order of a few days during the summer months. Plant productivity (via phenology) is limited by temperature and light, making the growing season to last from spring (April) through early autumn (September). Therefore, enough fuel is available throughout the fire season, while the fire risk is limited by climatic conditions. Due to its continental climate, sandy soils and fire-prone pine forests, fire risk is slightly elevated in eastern Germany and in Poland or in some lowland sites in Czechia, while the mountain sites in those countries generally experience less fires because of the colder and moister site conditions that are largely dominated by spruce forests. Interannual climate variability is relatively low compared to Mediterranean or semi-arid regions and lightning is in most cases associated with storms and rain. Hence almost all fires in Central Europe are human-caused and occur in a managed agricultural and forestry landscapes. An analysis of the drivers determining these ignitions is important to manage future fire risks.

2.1. Analysis of settlements and transport infrastructure on current fire risk

We use data on reported fire events to analyse the spatial structure of observed ignitions in the study area and relate them to fire risk under current climate conditions. To achieve this objective, we compute the Fire Weather Index using data from meteorological stations as well as interpolated climate data sets, e.g. climate re-analysis data from GLDAS. We analyse differences obtained from both data sets to verify possible error propagation. We then compare the spatial pattern of observed ignitions against climate and land-cover data to determine their importance in explaining observed pattern using spatial statistical methods. Recently, the FWI was extended to account for risk stemming from urban areas. Since the extension was developed for fire-prone Sardinia, we analyse how the modelled influence of proximity to urban areas can be applied to the central European fire regimes under temperate climate conditions. Fire fighters in Central Europe recently reported that forest fires were caused by forest machinery, an effect which was also investigated for Sweden (Sjöström et al. 2019). In a next step we analyse the implication for fire risk.

3. Towards improved estimates of future fire risks

Changes in future fire risk are usually quantified based on fire weather indcies such as FWI using seasonal forecast and future climate scenario data. In EFFIS, the respective risk is computed for the EU member states and is reported regularly. However, such approaches do not account for changes in vegetation types, fuel loads or socieconomic effects. At continental to global scales, fire-enabled Dynamic Global Vegetation Models (DGVMs) can be used to assess the effects of climate change and vegetation dynamics on climatic fire risk, ignitions, spread and effects of fire. DGVMs simulate the composition, amount and characteristics of live and dead fuel and form the input to the fire module. Similarly, fire effects, including combusted dead and alive biomass and post-fire mortality, affect the regeneration of the simulated vegetation. Composition and dynamics of the vegetation, including fuel composition and fuel load, depend on the fire sensitivity of the affected vegetation and resulting vegetation productivity. Therefore, bi-directional feedbacks establish between fire and vegetation in the model.

However, because of the low fire risk in Central Europe, model quality of fire-enabled DGVMs to match observed spatio-temporal pattern of fire occurrence has been rarely assessed. Building on the data analysis and application of the FWI for present fire risks, we will evaluate model simulations and analyse uncertain model functions to suggest ways of improving respective model components. Specifically, we will apply the LPJmL-SPITFIRE model (Thonicke et al. 2010, Drüke et al. 2019) with downscaled climate input data (9 km resolution). We will compare the simulated climatic fire danger and fire ignitions against the FWI computations in the study area. Spatial and temporal patterns will be analysed using respective statistical methods to quantify model error and benchmarking techniques.

We will analyse how the adjusted ignition component in the FWI calculation is changing under projected changes in land cover in the study area. We conduct a factorial analysis to identify the influence of land-cover change against climate change on fire ignition. We will attribute the influence of a changing fire season, which is expected to increase in length and/or intensity under high fire risk, against the influence of land-cover change on potential human-caused ignitions. We will compare changes in spatiotemporal pattern against contemporary pattern and identify areas of increased high fire risk and actual ignitions.

In a second step, projected changes in climatic fire danger and fire ignitions applying the improved LPJmL-SPITFIRE model will be analysed. We will compare the influence of changes in vegetation dynamics on future fire risk and fire ignitions using LPJmL-SPITFIRE against FWI computations. Finally, the maps of future fire risks will be used as updated input to the mapping of fire risk areas at the wildland-urban interface.

4. References

Drüke, M., Forkel, M., von Bloh, W., Sakschewski, B., Cardoso, M., Bustamante, M., and Thonicke, K.: Improving the LPJmL4-SPITFIRE vegetation-fire model for South America using satellite data, 2019.

König, H. C.: Waldbrandschutz: Kompendium für Forst und Feuerwehr, 1., Edition., Fachverlag Grimm, Berlin, 200 pp., 2007.

Müller, M.: Waldbrände in Deutschland, Teil 1, 18/2019, 27–31, 2019.

Müller, M.: Waldbrände in Deutschland, Teil 1, AFZ- Der Wald 18/2019, 27–31, 2019.

Sjöström, J., Plathner, F. V., and Granström, A.: Wildfire ignition from forestry machines in boreal Sweden, Int. J. Wildland Fire, 28, 666, https://doi.org/10.1071/WF18229, 2019.

Thonicke, K., Spessa, A., Prentice, I. C., Harrison, S. P., Dong, L., and Carmona-Moreno, C.: The influence of vegetation, fire spread and fire behaviour on biomass burning and trace gas emissions: results from a process-based model, Biogeosciences, 7, 1991-2011, 10.5194/bg-7-1991-2010, 2010.

Quick assessment of burn area and burn severity on black locust stands using Sentinel 2 imagery in South-West Romania

Adrian Lorenț[1,2]; Marius Petrila[1]; Vladimir Gancz[1]; Florin Capalb[1,2]; Bogdan Apostol[1]; Nicolae-Ovidiu Badea[1,2]

[1]National Institute for Research and Development in Forestry (INCDS), "Marin Drăcea". Bulevardul Eroilor nr. 128, 077190 Voluntari, Ilfov, Romania, {adrian.lorent, marius.petrila, vladimir.gancz, bogdan.apostol}@icas.ro, {florin.capalb@yahoo.com}, {ovidiu.badea63@gmail.com}
[2]Faculty of Silviculture and Forest Engineering, "Transilvania" University of Braşov. Str. Sirul Beethoven, nr. 1, 500123 Brașov, Romania

**Corresponding author*

Keywords

Forest fires, black locust, burn severity, dNBR, Sentinel 2

Abstract

In Romania forest fires have a strong annual and seasonal variability, having a distribution pattern correlated with human activities like stubble burning practices. The most fire affected region is located in the southwest of Romania, in the counties of Mehedinți and Gorj with a mosaic landscape of forests with agricultural land and human settlements. Although the year 2021 was generally a mild fire season at national level, almost 60% of the forests burned area occurred in Mehedinți, county whose surface covers 2.06% of the national territory. The reported affected area is determined by measurements with GPS receivers or by an approximate estimate of the percentage of affected area in a forest parcel. The accuracy of those determinations is not being verified through other procedures like remote sensing-based methods, thus there is a need for independent evaluation of the reported fire impact. The aim of this research is to perform a quick robust enough assessment of the areas affected by forest fires in August 2021 and their severity in a forested area covered mostly by black locust (Robinia pseudoacacia), located in the southwestern part of Mehedinți county, using Sentinel 2 imagery and in field validation. In order to assess the degree of damage of the forest stands, Sentinel 2 satellite images were used, before, during and after the fire events. Additionally, official RGB and CIR aerial orthophoto images with a spatial resolution of 0.5 m from 2015 were used together with ultra-high resolution orthoimages obtained by processing RGB aerial photographs taken post-fire event with an UAV. Several remote sensing-based indices mostly used in forest fire-science literature were tested in order to extract the affected burn area and burn severity, among which the difference Normalized Burn Ratio (dNBR) proved to give the best estimates. A field inspection was carried out in order to verify whether the burn severity classes are corresponding to the ground truth impact of the fires. By comparing the dNBR mapping with terrain observations, we found that burn severity is corelated with canopy cover and height of the trees, at least in black locust stands, who naturally have lower canopy cover than other deciduous tree species. The correlation between dNBR and the canopy cover is negative, that means low canopy cover shows a false high severity on dNBR map and vice versa because the burnt grass and understory layer is more visible from above and denser in sparse forest stands. Also, low height of the trees induces high severity on the dNBR, the flames and heat produced by the burnt understory reaching easily to the canopy level. These observations were afterwards used to adjust the burn severity map.

1. Introduction

According to the last national disasters risk assessment (IGSU, 2016), forest fires in Romania have a low impact in terms of physical, economic and psychosocial consequences and a high probability of occurrence. In the last 65 years, Romania has recorded an average of 176 forest fires per year, with an average area of 917 ha per year and 5.2 ha per forest fire. However, since 2000 there was a significant increase in manifestation of this hazard, both in term of frequency and affected surface. The average number of forest fires per year increased to 319, while the affected area averaged 1867 ha. Since 2010 there was an appreciable increase in forest fires that affected areas over 25 ha. Most forest fires occur due to human activities, such as uncontrolled burning of stubble and dry grass in the fall and spring, on agricultural land in the forest neighborhood.

In Romania forest fires have a strong annual and seasonal variability, revealing that the distribution pattern correlates with human activities that are the predominant cause, while also influenced by prolonged periods of droughts which induces reduced combustible humidity (Lorent et al, 2018).

The most fire affected region is located in the southwest of Romania, in the counties of Mehedinți and Gorj, a region with a climate with Mediterranean influences, with mosaic landscapes of forests with agricultural land and human settlements. Although the year 2021 was below average in terms of the number of fires recorded at national level and the affected surface, out of a total of 278 forest fires which affected a surface of 2101.14 ha, 71 of them covering a surface of 1238.81 ha occurred in Mehedinți county, whose surface covers 2.06% of the national territory.

Even though Mehedinți is known as a fire prone area, 2021 was an exceptional year in terms of vegetation fires, which occurred with an unprecedented frequency, amid a period of drought and strong winds, coupled with the local practices of burning stubble and dry grass for clearing the land. According to the Inspectorate for Emergency Situations of Mehedinți county, between 1st of July and 30th of September 2021, there were 852 fires that started from brambles, shoots and dry vegetation, of which 35 fires occurred in the forests. Out of the 35 fires, 24 were surface fires and 11 damaged forest plantations. Practically, in July and August (and to some extent in September), military firefighters intervened daily to extinguish vegetation fires, which endangered community areas and even spread to several households.

After each forest fire intervention, a report is drawn up by the military firefighters and the forestry personnel in which the area affected and the damages caused are evaluated. The affected area is determined by measurements with GPS receivers or by an approximate estimate of the percentage of affected area in a forest parcel. The accuracy of those determinations is not being verified through other procedures like remote sensing-based methods, thus there is a need for independent evaluation of the reported fire impacts.

The aim of this research is to perform a quick and robust enough assessment of the areas affected by forest fires in August 2021and their severity in a forested area covered mostly by black locust trees (*Robinia pseudoacacia*), located in the southwestern part of Mehedinți county, using Sentinel 2 imagery and in field validation.

2. Materials and methods

2.1. Study area

The study area is located in Southwestern Romania, in Mehedinți county (Figure 1), being covered mainly by black locust forests installed on the river dunes in the high terrace of the Danube, where the forests are interspersed with cultivated or uncultivated agricultural land. The obligation to demonstrate that the agricultural lands are being cultivated (for obtaining subsidies in agriculture) makes the local practice, such as cleaning of dry grass and vegetable waste (after harvesting cereals) to be often based on the burning of stubble and of the uncultivated land. In conditions of prolonged drought and strong wind, during August – September 2021, these repeated fires led to the spread of dry vegetation fires in the forest stands, resulting in thousands of hectares of burned agricultural fields and forests, with varying degrees of damage.

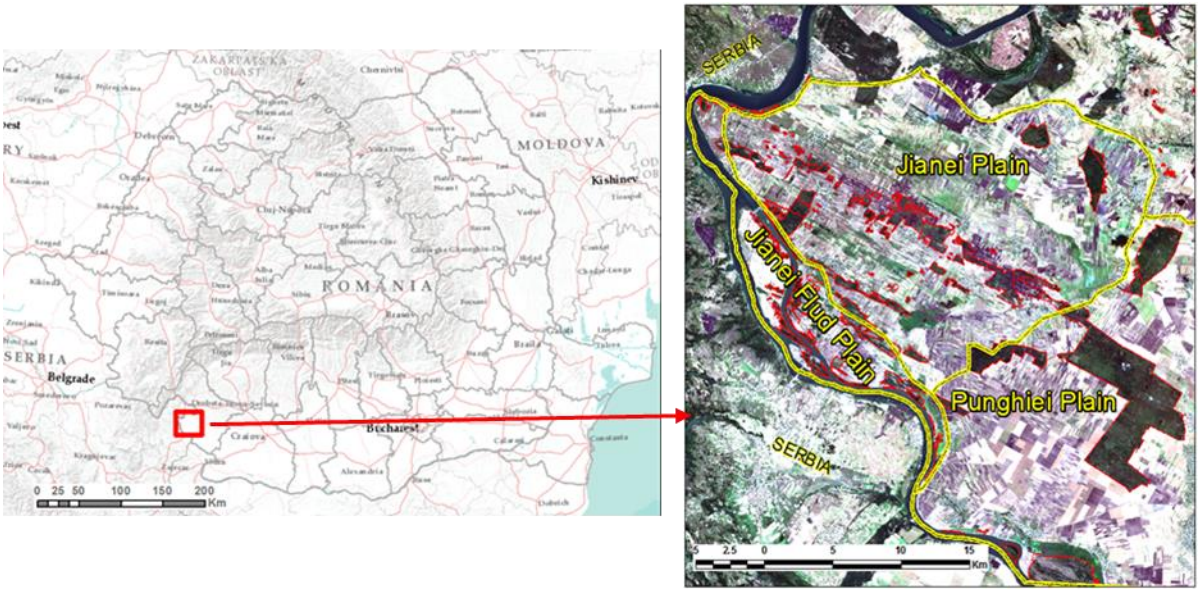

Figure 1 - Location of the study area

2.2. Materials

In order to assess the degree of damage of the forest stands, a methodology for estimating the severity of the forest fires was adopted, using Sentinel 2 satellite images recorded before, during and after the fire events. Additionally, official RGB and CIR aerial orthophoto, captured in 2015 with a ADS80 camera, with a spatial resolution of 0.5 m, were used together with ultra-high resolution orthoimages obtained by processing RGB aerial imagery taken with a DJI Mavic 2 Enterprise Dual drone about a month after the fire events.

Sentinel 2 satellite imagery were downloaded from Copernicus Open Access Hub (https://scihub.copernicus.eu/dhus/#/home). A total of 9 images of 2A processing level (bottom-of-atmosphere reflectance ortho-image product) have been found and used within the study, covering the period between 1st of August and 8th of September 2021, in which most of the forest fires occured. All imagery was stacked by bands (except B1, B9 and B10), clipped for study area and re-projected into Stereografic 1970 *(*national Romanian cartographic projection). For rapid evaluation were picked up two images, one before fire (2021-08-01) and another one after fire was finished (2021-08-11). In Figure 2 is displayed a representative detail from study area on both images.

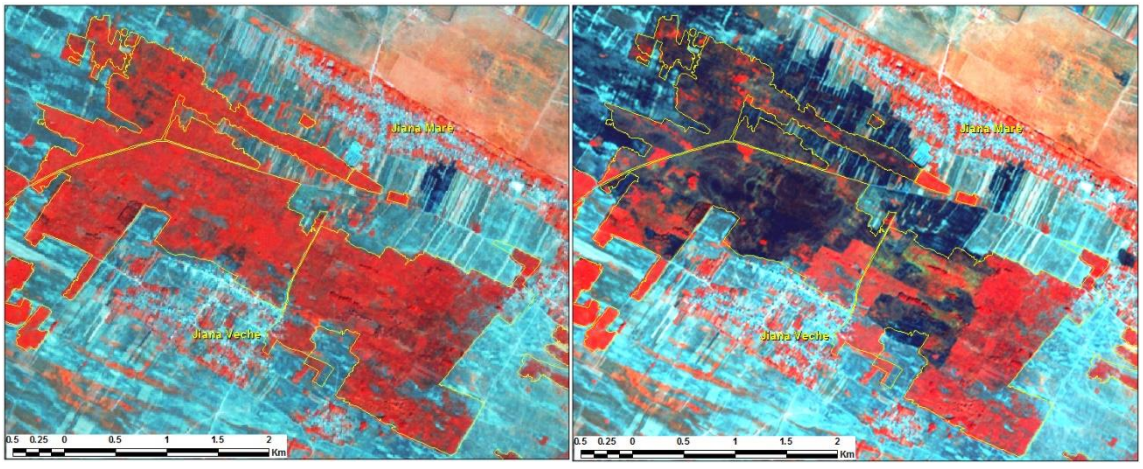

Figure 2 - Sentinel 2 images from study areas: 2021-08-01 (left – before the fire events), 2021-08-11 (right – after the fire events). Color combination: RGB = B8, B3, B2. Yellow line – forest limits

Forest fires incidents reports, containing detailed information about the fire events reported by the forest districts, were obtained from the Ministry of Environment, Waters and Forests. In total there were 8 forest fire events in August 2021 for the study area, totalizing 518.8 hectares of fire affected forests.

Forest management maps and plans were used to inform about the stand characteristics and to delineate the managed forest area within the study site.

2.3. Field data collection

After mapping the severity of forest fires based on satellite images, a field inspection was carried out in order to verify whether the burn severity classes are corresponding to the ground truth impact of the fires. For this purpose, several stands with different degrees of severity and with different characteristics in terms of height and canopy cover were identified on the map of severity degree obtained. The categories of land without forest vegetation, plantations, young, short trees, with height of up to 10 meters and mature trees with a height of over 10 meters, all with low, medium and high densities, were taken into account. They were then visited in the field to estimate of the actual degree of damage. The filed data collection was carried out in October 2021, one month after the forest fires took place.

In order to establish the degree of damage to the stand, a severity scale was developed to systematize and standardize the way it is evaluated according to the visible effects on the ground and on aerial images on the stand, broken down by the size of the stand (correlated with age) and stand density. The burn severity represents the degree or extent of the change in the environment caused by the fire. The change can be represented by simple or multiple biophysical variables on a continuous scale from no change to major changes. No universal standards are defined for describing the severity from an ecological point of view, although there are attempts to structure it in accordance with estimation based on remote sensing methods. For the field estimation of severity, 5 severity classes, similar to Key C.H and Benson N.C., 2006, were considered: unburned, low, moderate-low, moderate-high and high. The severity of fire was visually assed in the field for the four strata: substrate, herbs and low shrubs, tall shrubs and low trees and tall trees assigning a value ranging from 0 (unburned) to 4 (high severity). In total, 40 field plots with a surface of 20X20 meters were established. The classes were adapted to the specifics of the black locust stands from the study region and presented in Table 1.

Table 1 – Synthetic criteria for assessing forest fire severity in the field

Severity class	**Field classification criteria – synthetic description**
unburned	• The soil and the vegetation strata are unaffected by fire Substrates—Inert surface materials of soil, duff, litter, and downed woody fuels.
low	• duff is unaffected • burnt litter and herbs layer, shrub layer and seedling up to 1m high are partially affected • seemingly unaffected plantations • short (young) trees with unaffected foliage • tall (mature) tree with blackened trunks up to 0.5 m
moderate-low	• duff layer is partially affected • burnt litter and herbs layer, shrub layer and seedling are heavily affected • plantations are visibly affected • short (young) trees with the foliage partially dry • tall (mature) tree with blackened trunks up to 1 m
moderate-high	• the organic soil is charred • burnt litter and herbs layer, shrub layer and seedling are charred • the plantations are charred, return possible only after the cutting above the collar • short (young) shrub with crown affected by scorch or girdle • tall (mature) shrub with blackened trunks up to 2 m, the lower part of the crowns affected by scorch or girdle
high	• the soil organic layer is transformed into ash • litter and herbs layer, shrub layer and seedling are transformed into ash • plantations are torched, the stems are consumed by fire • short (young) shrub with crown affected by scorch or girdle, the stems are carbonized • tall (mature) shrub with blackened trunks over 2 m, more than 50% dry or burnt foliage in the upper part of the crown

Representative areas were aerial photographed with a DJI Mavic 2 Enterprise Dual UAV system at the same time with the field sampling campaign and high resolution (i.e., 40 cm) orthoimages were derived. The field observations were used afterwards to adjust the predefined burn severity classes according to the severity classes depicted in the field.

2.4. Image processing

First step was to calculate several remote sensing-based indices recommended by forest fire-science literature using formulas adapted for Sentinel 2 (Mallinis et all, 2018) such as: NBR, NDVI, GNDVI, NBRn, NDVIRE1, NDVIRE1n, CIRE1, MSRRE1, MSR, RE1n and PCA (PC1) for each of both images and, also bitemporal indexes: dNBR, RdNBR, RBR, dNBRn and dNDVI, dPC1. Each result was studied visually, by comparing between them and the satellite imagine from 2021-08-11. Visual inspection of the results indicated that the differenced Normalized Burn Ratio (dNBR) index showed the best results in estimating the fires severity for the study area. The dNBR severity classes were firstly classified according to Key and Benson (2006) thresholds. In Figure 3 the burn severity classes derived from the dNBR index are showed for one of the area most affected by fire.

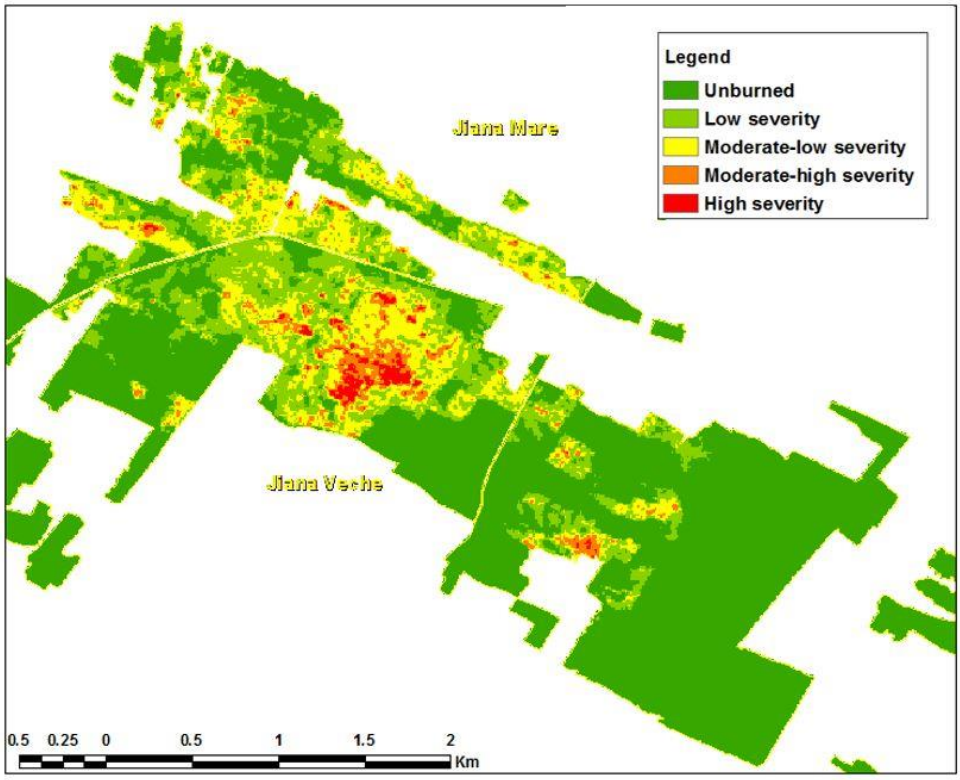

Figure 3 - dNBR: images S2 2021-08-01 (before), 2021-08-11 (post). Yellow line – forest limits

After a detailed visual inspection in accordance with S2 image from 2021-08-11 it was observed that the dNBR thresholds of Key and Benson (2006) are not very appropriate for this area. Consequently, using data collected from the field, the thresholds were adjusted to fit as best as possible the severity classes depicted in the field. In the Table 2 are shown the thresholds used in this study compared with the Key and Benson's thresholds.

Table 2 – The dNBR fire severity thresholds

Key and Benson's thresholds	Thresholds used in this study	Severity class
-0,360 – 0,100	-0,364 – 0,139	Unburned
0,100 – 0,269	0,139 – 0,319	Low severity
0,269 – 0,439	0,319 – 0,456	Moderate – low severity
0,439 – 0,659	0,456 – 0,568	Moderate – high severity
0, 659 – 0,999	0,568 – 0,999	High severity

In figure 4 is presented a detail of the severity map adjusted with the terrain.

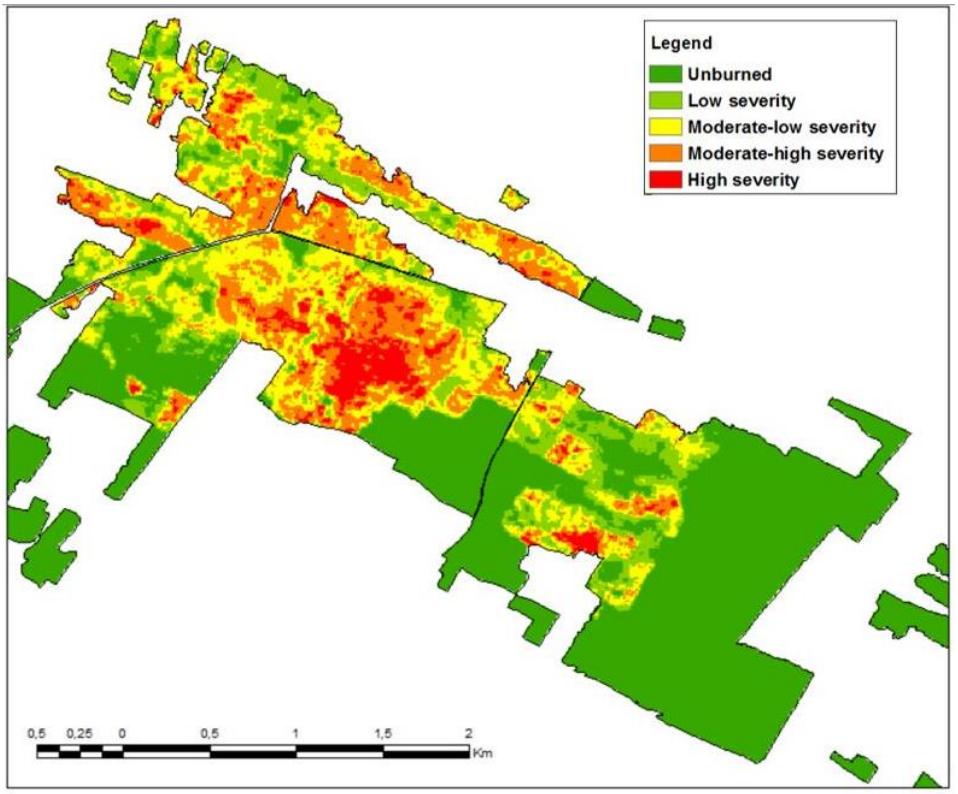

Figure 4 – dNBR: Result of using the adjusted thresholds.Images S2 2021-08-01 (before), 2021-08-11 (post). Black line – forest limits.

First visual inspection of the result, by comparing with S2 image before the fire (see figure 2) and then a field inspection was carried out in order to verify whether the burn severity classes are corresponding to the ground truth impact of the fires, we found that burn severity is in accordance with canopy cover and height of the trees, at least in black locust stands, who naturally have lower canopy cover than other deciduous tree species. The correlation between dNBR and the canopy cover is negative, that means low canopy cover shows a false high severity on dNBR map and vice versa because the burnt grass and understory layer is more visible from above and denser in sparse forest stands. Also, low height of the trees induces high severity on the dNBR, the flames and heat produced by the burnt understory reaching easily to the canopy level.

In order to increase the accuracy of the fire effects map, based on dNBR, a digital map of canopy closure and height of the trees was produced, within GIS environment, based on the aerial, colour infrared (CIR) of 0.5 m spatial resolution captured in 2015. The classes were delineated through manual vectorization and the canopy closure and height classes were visually established through photo-interpretation.

For the height of the trees, three classes were considered, namely plantations (artificial culture of young trees, with the canopy not yet developed), short trees (height below 10 m), tall trees (height over 10 m). The classes were established after it was found in the field that the vulnerability to the fires was inversely proportional to height of the trees. For canopy closure four categories were established: without canopy, low 0.1-0.3, medium 0.4-0.6 and high de 0.7-1.0. The stands with low canopy closure appear to be more severely affected than in reality on satellite images.

It has to be mentioned that for the studied area are not any managements plans and maps to provide such information. Beside this, in the management plans, the canopy cover and height of the trees are given as an average for the entire parcel or subparcel which is not useful for the study. Within figure 5 an example on an aerial CIR image is presented.

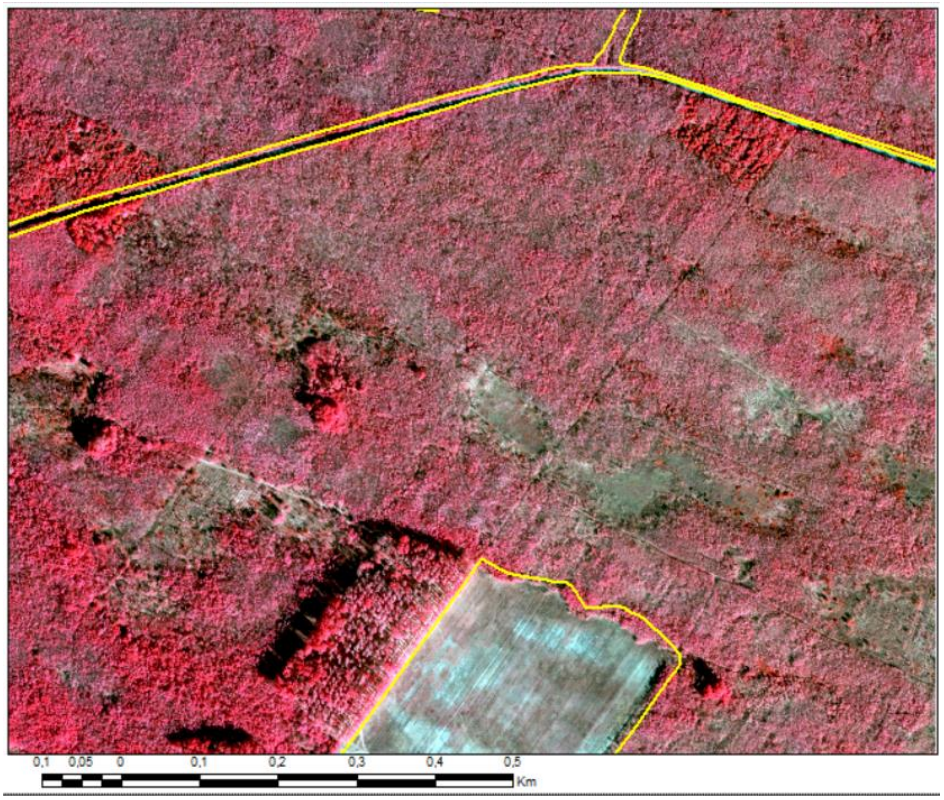

Figure 5 – Aerial image (CIR), 0.5 m, within the area (detail) showing high inhomogeneity of the canopy cover and trees height. Yellow line – forest limits

Moreover, it was found that in the young black locust stands (young trees were considered to be those with a height of up to 10 m, this being the approximate limit to which the heat released by surface fires affects the foliage) are most affected by surface fires (fed by tall, dry grass, litter and sometimes shrub state). Shrubs with an average height of more than 10 m were the least affected, as the thicker bark and the height of the canopy make them less vulnerable. Estimation of severity on images tends to be overestimated in the case of low stands and underestimated in the case of tall stands compared to that estimated in the field. In the stands with a lower canopy closure (as is the case with black locust), the grass developed more, providing more fuel for burning, being seconded by a higher visibility from the air / space of the burned soil. In dense trees, which cover the ground well (in the case of trees with oak species), grass and shrubs do not grow, so the surface fire is fed only by litter and the green canopy can hide the real severity. The estimation of severity on images tends to be exaggerated in the case of rare trees and underestimated in the case of dense trees, compared to that estimated in the field. A special case is the one of the plantations, which are very vulnerable due to their small age (and size), large amounts of fuel (tall, dry grass), which have no canopy and in which the soil is exposed. This is the case where the estimated severity on aerial or satellite images is usually underestimated, as they can be severely affected even by low-intensity surface fires. The presence or absence of fire-affected foliage is the factor that makes the estimation of severity based on aerial / satellite images different from the ground truth severity. This makes the estimate closer to reality in the case of deciduous trees and in leaf-off periods. A key proposal for correcting the estimated severity on aerial / satellite imagery based on the criteria set out above is presented in Table 3.

Table 3. Key for correcting the estimated severity derived from Sentinel 2 imagery (the dNBR index)

Sentinel 2 severity Based on dNBR index	**Plantation**	**Real ground severity correction**					
		Short stand (tree heights ≤ 10 m)			**Tall stand (tree heights >10 m)**		
		canopy cover			**canopy cover**		
		low 0,1-0,3	medium 0,4-0,6	high 0,7-1,0	low 0,1-0,3	medium 0,4-0,6	high 0,7-1,0
1 unburned	unburned	unburned	unburned	unburned/ low severity ↑	unburned	unburned	unburned / low severity ↑
2 low severity	moderate – low severity↑	low severity	low severity	low severity	low severity	low severity	moderate – low severity ↑
3 moderate–low severity	moderate – high severity↑	low severity ↓	moderate -low severity	moderate – low severity	low severity ↓	moderate – low severity	moderate-high severity ↑
4 moderate–high severity	high severity↑	moderate – low severity↓	moderate – high severity	moderate – high severity	moderate – low severity↓	moderate-high severity	high severity ↑
5 high severity	high severity	moderate – high severity↓	high severity	high severity	moderate – high severity↓	high severity	high severity

The dNBR raster map of was converted into a vectorial map of severity (5 classes). This strata was afterwards intersected with the layer representing the canopy cover and the trees height classes. The severity classes were adjusted according to the correction key from Table 3. Within figure 6 it is shown a detail of the new severity map, thus obtained.

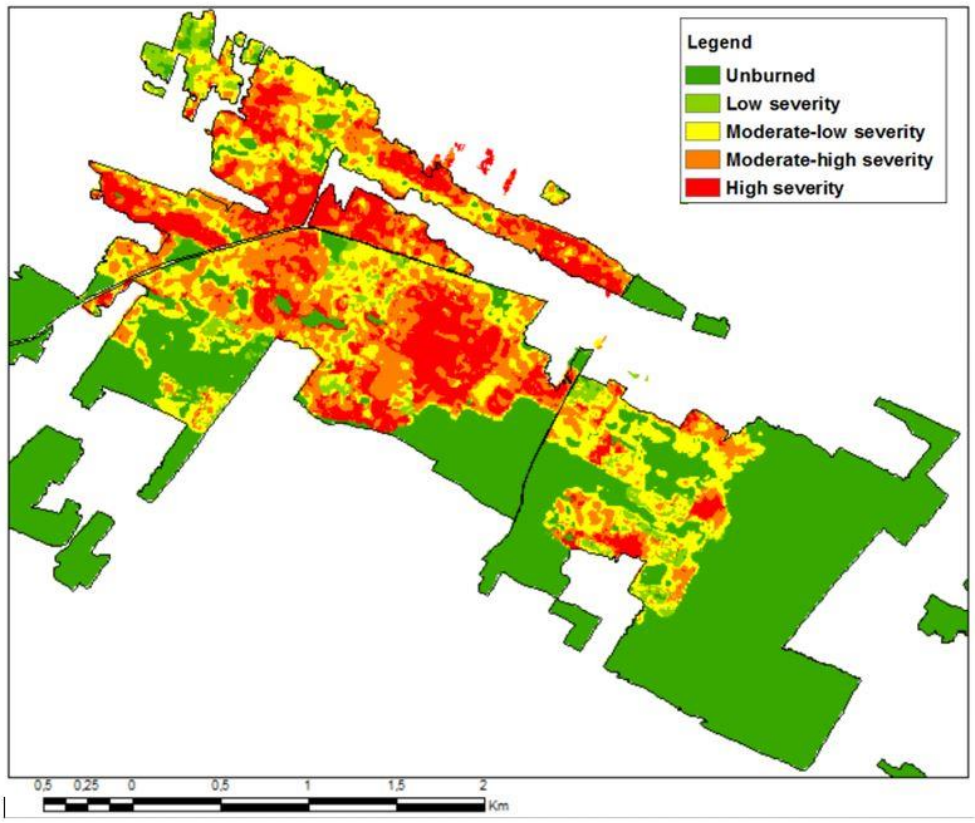

Figure 6 – The new severity map corrected based on canopy cover-trees height map. Black line – forest limits

The final adjusted severity map shows that the severity was lowered in the case of stand with low stand canopy cover considering the fact that the dNBR tends to amplify the severity because the pixels receive much of the signal from the ground level and higher in case of dense and tall stands.

3. Results and discussion

The analysis of different indices found in specialty literature (Llorens, R. et al. 2021, Mallinis G. et al. 2018, Llorens, R. et al. 2021) showed that the dNBR index was the most suitable for burn severity estimation, showing more accurate results, at least for our study area.

The dNBR map shows a severity distribution apparently close to the severity visually estimated on Sentinel 2 image from 2021-08-11 date. A more detailed analyze showed that burn severity depends on the canopy cover and height of the trees, at least in black locust stands, who naturally have lower canopy cover and subsequently canopy density than other deciduous species. This was first observed on Sentinel 2 imagery before fire (2021-08-01), on the aerial imagery (2015-05-30) and also was confirmed in the field. The relation between dNBR and canopy cover confirm that low canopy cover shows a false high severity on dNBR map and vice-versa, due to the burnt grass and understory layer is more visible from above and denser in sparse forest stands. Also, low height of the trees induces high severity on the dNBR, the flames and heat produced by the burnt understory reaching easily to the canopy level. This observation had to be used to adjust the burn severity map. The stands with low canopy cover, but high trees, could have in reality lower severity resulting from dNBR because if only surface fuel is burned and the trees are not really affected, on the imagery the signal coming from ground will be dominant for this spatial resolution and dNBR will be high. Into the dense and taller stands, with the same surface burned severity, the signal will be dominated by canopy, which is less affected. These stands could show on dNBR "unburned severity level", even the real severity could be different (from "low" to "medium-low" or even higher), if the upper canopy was not affected. Concerning low height forest stands with, the situation will be different even if density is high or low, because the tree crowns could be highly damaged by surface fire and the severity could be high, which is not the case of high trees stands. In the case of other tree species from the area, like Scots pine (*Pinus sylvestris*), the effect was more serious, stands were burned up to the top and severity put into evidence by dNBR was closer to the reality. Gibson et al. (2020) also found, using Sentinel imagery to evaluate the fire severity in eastern Australia that higher canopy cover and higher topographic complexity was associated with a higher rate of under-prediction, due to the limitations of viewing the burnt understorey of low severity classes. In terms of the fire affected area, we found that the affected area reported by the forestry districts was close to that obtained from Sentinel 2 imagery.

Concerning the forest surface affected by fires, a total of 8 fire incidents were reported by the forestry districts for the study area between the period of 04-11 August 2021 with a total forest affected surface of 518.8 ha. Our satellite imagery analysis showed that in total there were affected 756,3 ha, thus resulting an underreported surface of 237.5 ha. A one-to-one evaluation comparison of each forest fire incident in terms of affected area could not be carried out due to the relatively low temporal resolution of the Sentinel imagery (i.e., 5-day revisit time) and because it was hard to distinguish on imagery with high confidence what was the surface affected by each fire because some of the fire merged together in a single, bigger one.

4. Conclusions

Sentinel 2 imagery can by successfully used to estimate the burned area and the burn severity in stands dominated by black locust. For a more accurate estimation of burn severity levels for black locust stands more situations need to be considered in terms of density cover and height of the trees. Moreover, the study reveals only a first step for the assessment of the areas affected by fires, presenting a quick and robust enough assessment method.

5. Acknowledgements

This research was funded partially by Romanian Ministry of Research, Innovation and Digitization and Innovation, within the Nucleu BIOSERV National Programme (Contract No. 12N/2019), Project ID PN 19070108 and the H2020 project FirEURisk.

6. References

Delcourt, C. J. F., Combee, A., Izbicki, B., Mack, M. C., Maximov, T., Petrov, R., Rogers B.M., Scholten R.C., Shestakova T.A., Wees, Dave van, Veraverbeke, S. (2021). Evaluating the differenced normalized burn ratio for assessing fire severity using sentinel-2 imagery in northeast siberian larch forests. Remote Sensing, 13(12), 1–20. https://doi.org/10.3390/rs13122311

Gibson, R., Danaher, T., Hehir, W., & Collins, L. (2020). A remote sensing approach to mapping fire severity in south-eastern Australia using sentinel 2 and random forest. Remote Sensing of Environment, 240(September 2019), 111702. https://doi.org/10.1016/j.rse.2020.111702

IGSU, (2016) Country report, 5.1 Conditionality, Romania (Raport de țară, Condiționalitatea 5.1, România). https://www.igsu.ro/Resources/COJ/RapoarteStudii/Raport_Final_de_tara%20pt%20Condit%20ex-ante%202016.pdf

Key, H.C., Benson, N (2006). Landscape Assessment: Ground measure of severity, the Composite Burn Index; and Remote sensing of severity, the Normalized Burn Ratio. In book: FIREMON: Fire Effects Monitoring and Inventory System. Edition: RMRS-GTR-164. Publisher: USDA Forest Service, Rocky Mountain Research Station, Ogden, UT

Llorens, R., Sobrino, J. A., Fernández, C., Fernández-Alonso, J. M., & Vega, J. A. (2021). A methodology to estimate forest fires burned areas and burn severity degrees using Sentinel-2 data. Application to the October 2017 fires in the Iberian Peninsula. International Journal of Applied Earth Observation and Geoinformation. https://doi.org/10.1016/j.jag.2020.102243

Lorenţ, A., Neagu, Ș., Petrila, M., Apostol, B., Gancz, V., Mitsopoulos, I., Mallinis, G., 2018. Evaluarea hazardului la incendii de pădure la nivel de unitate administrativ-teritorială în perioada 2006-2015. [*Forest fire hazard assessment at territorial administrative unit level during 2006-2015 period*]. Revista Pădurilor nr. 4/2018, ISSN print 1583-7890, ISSN online: 2067-196. p. 37-58.

Mallinis G., Mitsopoulos I., Chrysafi I. (2018). Evaluating and comparing Sentinel 2A and Landsat-8 Operational Land Imager (OLI) spectral indices for estimating fire severity in a Mediterranean pine ecosystem of Greece, GIScience & Remote Sensing, 55:1, 1-18, DOI: 10.1080/15481603.2017.1354803

Contrasting two alternative models for rate of fire spread in a dynamic global vegetation model

Jessica Hetzer[1]*; Matthew Forrest [1]; Thomas Hickler[1,2]

[1] Senckenberg Biodiversity and Climate Research Centre (SBiK-F). Senckenberganlage 25 D-60325 Frankfurt am Main, Germany, {jessica.hetzer, matthew.forrest}@senckenberg.de
[2] Department of Physical Geography at Goethe-University Frankfurt. Altenhoeferallee 1 D-60438 Frankfurt am Main, Germany, {thomas.hickler@senckenberg.de}

**Corresponding author*

Keywords

Rate of spread, DGVM, fuel characteristics, Europe, forests

Abstract

Rate of spread (RoS) is a key determinant of a fire regime and rate of spread models have a long tradition in fire research. Initially they were used to assess fire risk on a local to regional scale. Latest approaches combine them with scalable models to investigate fire risk globally. However, correctly simulating RoS across large spatial extents requires good knowledge of how fuel characteristics vary across the region of interest. For this purpose, both observed fuel characteristics and effective model representation of the characteristics are indispensable. To facilitate investigation of RoS dynamics and fuel characteristics, dynamic global vegetation models (DGVMs) can link vegetation characteristics (e.g., biomass composition, vegetation type) to fuel characteristics and simulate rate of spread over various spatial and temporal scales. Earlier studies compared rate of spread models for various sites of different biomes. Insights in site specific performance thereby supported decision-making regarding the choice of the model. Here, we address this issue for modelled forest types and biomes across Europe incorporating fire-vegetation interaction by a DGVM. We investigate two common rate of spread models: The widely used Rothermel rate of spread model (Rothermel, 1972) as well as a related modified approach proposed by Wilson (1990). Using the global dynamic vegetation model LPJ-GUESS with the fire module SPITFIRE, we show that the two RoS models lead to substantially different rates of spread and area burned in some parts of Europe, while the differences are small in other parts. After further evaluation, such results might guide the choice of RoS model for different regions.

1. Rate of spread models

The study investigates two rate of spread (RoS) models: The Rothermel's Rate of Spread model (Rothermel, 1972) and the related modified approach proposed by Wilson, (1990). In both models, the rate of spread is represented by ratio of the heat received by unburned fuel from the flame (power density of propagation flux) to the heat required to ignite the unburned fuel (Rothermel (1972); Wilson (1990)). More specifically, the rate is calculated by the reaction intensity I_R times the propagation flux ratio ξ, divided by the overdry bulk density ρ_b, the effective heating number ε and the heat of ignition multiplied by a term that includes the wind factor ϕ_W and a slope factor ϕ_S. Both lead to a higher rate of spread in steep terrain where fuel in the upper part is more exposed to flames from further below, as well as forest fires that propagate rate of spread based on flame-exposing down winds.

$$RoS = \frac{I_R \cdot \xi \cdot (1 + \phi_W + \phi_S)}{\rho_b \cdot \varepsilon \cdot Q_{ig}}$$

While the overall equation structure seems quite similar between the Rothermel and Wilson formulations, the rate of spread models differ in the definition and interpretation of the parameters listed above. Main differences can be found in the reaction intensity, propagation flux ratio, and heat of ignition (Weise & Biging, 1997; Wilson, 1990).

The reaction intensity I_R is a measure of energy release per unit area within the combustion zone (Rothermel, 1972; Wilson, 1990). Rothermel interprets this variable as the rate of change of organic matter from a solid to a gas. The approach of Wilson narrows this term focusing on the energy release of the flames driven by

pyrolyzed gases only (explicitly excluding energy release from burning char). Minor additional changes of Wilson are the exclusion of the optimal packing ratio in the reaction velocity. Furthermore, fuel moisture is no longer included in the reaction intensity as a source of fire extinction. Instead it affects the rate of spread as a separate term by a probability function.

The propagation flux ratio ξ represents the proportion of the fires power that drives the fire (Rothermel, 1972; Wilson, 1990). Both approaches, Rothermel's and Wilson's, are based on fitted equations, related to field data of surface to volume ratio σ and the packing ratio (measure of how dense fuel is spatially distributed). The equation provided by Rothermel is mainly dependent on σ, as it is considered as a nonlinear driver in multiple equation terms. Wilson aims to simplify that equation based on physical principals of energy transport.

Originally, Rothermel relates the heat of ignition Q_{ig} to the change in specific heat from ambient to ignition temperature and the observed latent heat of vaporization of the moisture (Rothermel, 1972). In turn, Wilson approximates this heat dependent on observations of heat for pyrolysis and heat of vaporization measured in the field (Wilson, 1990).

2. Modelling concept and simulation setup

In this study we use the dynamic global vegetation model LPJ-GUESS, which integrates eco-physiological processes, such as photosynthesis, autotrophic and heterotrophic respiration, and plant growth with individual-based tree population dynamics and biome biogeography (Smith, Prentice, & Sykes, 2001; Smith et al., 2014). The detailed representation of vegetation dynamics enables insights in local forest ecosystem composition as well as large scale spatial trends of vegetation - bridging the gap from stand level to continental scale.

The rate of spread equations are implemented in the fire-enabling module SPITFIRE (SPread and InTensity of FIRE, (Thonicke et al., 2010)). The process-based fire model explicitly considers fuel characteristics by combining environmental fire drivers and linking vegetation traits to fuel class characteristics (fuel classes are live grass and dead 1hr, 10hr, 100hr fuels). SPITFIRE has been proven to be a useful tool to explore fire regimes explaining broad geographic patterns of annual fractional burnt area. For instance, in combination with the LPJ DGVM, the fire regime of boreal forests could be investigated in more detail (Thonicke et al., 2010). The SPITFIRE fire modelling approach has been adopted by several DGVMs, e.g. Yue et al. (2018). Most recently, SPITFIRE has been integrated in LPJ-GUESS (Smith et al. 2014, Forrest et al., (in prep.)), which has been used here. The model was run without land use, i.e. the potential natural vegetation was simulated.

The model setup includes global plant functional types (PFTs) simulated across Europe from 1700 to 2018. While fire processes in LPJ-GUESS SPITFIRE are simulated daily, vegetation dynamics are updated annually. Climate forcing was provided by the daily CRU-JRA data at a 0.5° resolution. This dataset includes monthly maximum and minimum air temperature, precipitation, wet days, wind, and cloud cover from the CRU database (Harris, 2019) merged with a reanalysis product (Harada et al., 2016; Kobayashi et al., 2015), which provides the sub-monthly temporal disaggregation. Slope was not considered.

3. Simulated fire patterns

In this study we compared the rate of spread based on Rothermel (RoS_R) and on Wilson (RoS_W) simulated by LPJ-GUESS. Overall, the RoS_W was higher than RoS_R (Fig. 1), but the differences were generally low between 45 and 55 degrees north. Deviations regarding the underlying calculation increased from Central to Northern Europe. In Southern regions (e.g., Portugal, Western Spain and Greece) comparison also showed spatial clusters in which RoS_R was higher (Fig. 1).

Similarly, to the rate of spread, the fraction of burned area of Wilson was higher than that by Rothermel (Fig. 2). The general pattern of burned area in Europe (with most fires in Mediterranean areas (Chuvieco et al., 2018)) was reproduced by both approaches, but there also exists clear discrepancies between the satellite-derived estimates and the model results. For example, the Rothermel approach has resulted in too sparse burning in Eastern Europe (Fig. 2). In turn, the mountain regions in northern Italy and Sweden are much more pronounced.

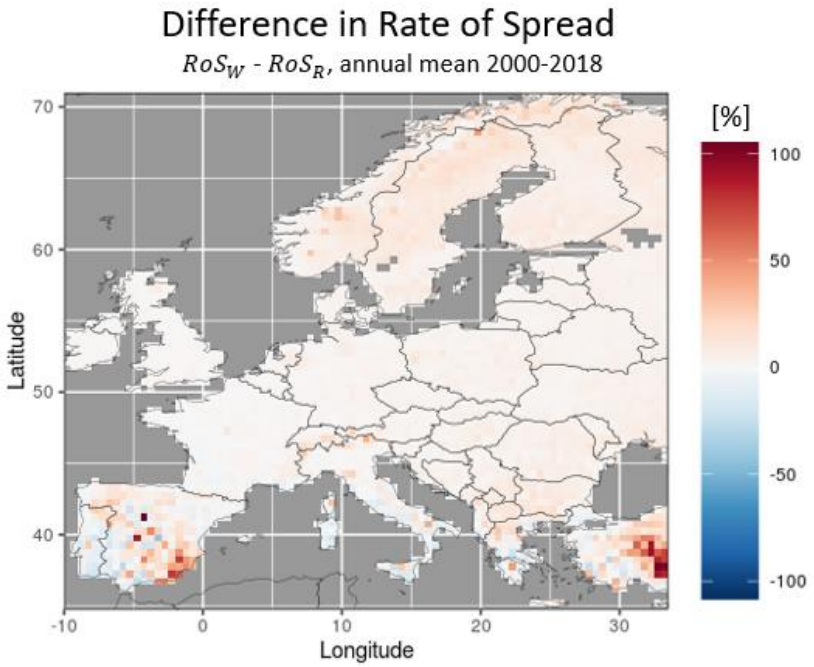

Figure 1- Percentage difference in mean annual rate of spread. Red pixels indicate a higher rate of spread for the Wilson approach than for Rothermel's, blue pixels indicate a lower one.

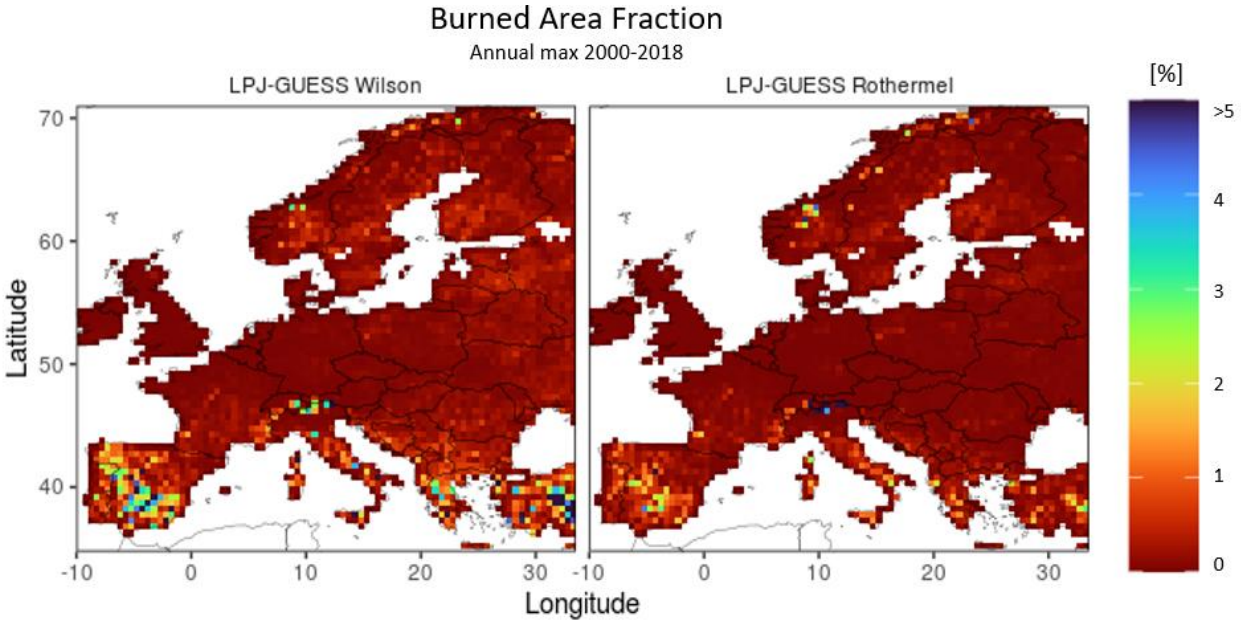

Figure 2- Simulated burned area fraction.

4. Discussion

When embedded in the LPJ-GUESS DGVM, the two RoS models lead to substantial differences in terms of RoS and area burned in some parts of Europe, while the differences were minor at intermediate latitudes. Where the differences are large, the choice of RoS model becomes more crucial. Further evaluation of model results will be necessary to derive suggestions for which model should be used were.

To use the full potential of the coupled vegetation-fire modelling approach, another important next step will be to use the vegetation model with a more regional vegetation representation of Europe (e.g. Hickler et al., 2012)

and land use. Only with the actual vegetation in the vegetation model, a detailed evaluation, e.g. of the area burned presented here in Fig. 2, makes sense.

The choice of the RoS model should also depend on regional data to parameterize the RoS model. The equations of Wilson (1990) were parameterised about two decades after Rothermel's first calculations (1972), with more data points included by that time. Therefore, Wilson's function coefficients might have a higher accuracy for the region where the model has been parameterized. However, since the Rothermel model has a long tradition in forest fire research, many observational data are still tailored for the original Rothermel approach.

5. References

Chuvieco, E., Lizundia-Loiola, J., Pettinari, M. L., Ramo, R., Padilla, M., Tansey, K., . . . Plummer, S. (2018). Generation and analysis of a new global burned area product based on MODIS 250 m reflectance bands and thermal anomalies. *Earth Syst. Sci. Data, 10*(4), 2015-2031. doi:10.5194/essd-10-2015-2018

Harada, Y., Kamahori, H., Kobayashi, C., Endo, H., Kobayashi, S., Ota, Y., . . . Takahashi, K. (2016). The JRA-55 Reanalysis: Representation of Atmospheric Circulation and Climate Variability. *Journal of the Meteorological Society of Japan. Ser. II, 94*(3), 269-302. doi:10.2151/jmsj.2016-015

Harris, I. C. (2019). *CRU JRA v1.1: A forcings dataset of gridded land surface blend of Climatic Research Unit (CRU) and Japanese reanalysis (JRA) data*. Retrieved from: http://dx.doi.org/10.5285/13f3635174794bb98cf8ac4b0ee8f4ed

Hickler, T., Vohland, K., Feehan, J., Miller, P. A., Smith, B., Costa, L., . . . Sykes, M. T. (2012). Projecting the future distribution of European potential natural vegetation zones with a generalized, tree species-based dynamic vegetation model. *Global Ecology and Biogeography, 21*(1), 50-63. doi:10.1111/j.1466-8238.2010.00613.x

Kobayashi, S., Ota, Y., Harada, Y., Ebita, A., Moriya, M., Onoda, H., . . . Takahashi, K. (2015). The JRA-55 Reanalysis: General Specifications and Basic Characteristics. *Journal of the Meteorological Society of Japan. Ser. II, 93*(1), 5-48. doi:10.2151/jmsj.2015-001

Rothermel, R. C. (1972). A mathematical model for predicting fire spread in wildland fuels. *USDA Forest Service, 115*.

Smith, B., Prentice, I. C., & Sykes, M. T. (2001). Representation of vegetation dynamics in the modelling of terrestrial ecosystems: comparing two contrasting approaches within European climate space. *Global Ecology and Biogeography, 10*, 621-637.

Smith, B., Warlind, D., Arneth, A., Hickler, T., Leadley, P., Siltberg, J., & Zaehle, S. (2014). Implications of incorporating N cycling and N limitations on primary production in an individual-based dynamic vegetation model. *Biogeosciences, 11*(7), 2027-2054. doi:10.5194/bg-11-2027-2014

Thonicke, K., Spessa, A., Prentice, I. C., Harrison, S. P., Dong, L., & Carmona-Moreno, C. (2010). The influence of vegetation, fire spread and fire behaviour on biomass burning and trace gas emissions: results from a process-based model. *Biogeosciences, 7*(6), 1991-2011. doi:10.5194/bg-7-1991-2010

Weise, D. R., & Biging, G. S. (1997). A Qualitative Comparison of Fire Spread Models Incorporating Wind and Slope Effects. *Forest Science, 43*(2), 170-180. doi:10.1093/forestscience/43.2.170

Wilson, R. A. (1990). Reexamination of Rothermel's Fire Spread Equations in No-wind and No-slope Conditions. *United States Department of Agriculture*.

Yue, C., Ciais, P., Luyssaert, S., Li, W., McGrath, M. J., Chang, J. F., & Peng, S. S. (2018). Representing anthropogenic gross land use change, wood harvest, and forest age dynamics in a global vegetation model ORCHIDEE-MICT v8.4.2. *Geoscientific Model Development, 11*(1), 409-428. doi:10.5194/gmd-11-409-2018

Spatial estimates of fire risk in Victoria, Australia considering ignition likelihood and containment probability through Bayesian Network Analysis

Erica Marshall*; Trent Penman

School of Ecosystem and Forest Sciences, The University of Melbourne, Melbourne, Victoria, Australia, {erica.marshall, trent.penman}@unimelb.edu.au

**Corresponding author*

Keywords

Fire risk, Bayesian network analysis, Ignition likelihood, Containment probability, Fire impacts

Abstract

Accounting for multiple changing systems in environmental decision making is challenging and requires balancing several competing priorities. In fire risk, one approach which is increasingly used to capture uncertainty within multiple systems and to prioritise management efforts is Bayesian Network (BN) analysis. Here, we have used a BN to understand the interactions between ignition likelihood, containment probability, fire behaviour, and fire weather, alongside the subsequent risks to people and property. We developed, populated and tested a BN which classifies the likelihood of outcomes for each of these systems. We then apply this BN to grid of 72,000 potential ignition locations accross Victoria to predict house and life loss values under conditions capturing the top ten worst ranked weather days in the history of each location. We use Phoenix fire behaviour simulations and landscape scale raster data to populate the parent nodes for each ignition and extract the expected values for predicted nodes under different weather scenarios and varying levels of suppression. We found values predicted by the BN broadly matched the spatial patterns of risk produced in Phoenix i.e., areas where risk was highest and lowest in terms of fire area and house loss aligned. However, the values are rescaled by the BN as it takes into account the influence of ignition likelihood and containment probability on risk estimates. The BN is also able to capture uncertainty around the values presented from across the top ten Phoenix simulations, so the recorded values represent the likely outcome for each node given the range of potential weather conditions in those scenarios. We show that BNs can be a useful management tool for estimating fire risks across a range of weather scenarios and locations while still considering ignition likelihood and suppression effectiveness.

1. Introduction

Fire is a globally significant environmental disturbance which increasingly presents risk to people, property, infrastructure, and biodiversity (Banks et al. 2011; Moritz et al. 2014; Filkov et al. 2020; Borchers Arriagada et al. 2020; Higuera and Abatzoglou 2021). Managing wildfire risks is complicated as decision makers need to account for several interacting systems which may vary spatially and temporally (Thompson and Calkin 2011; Penman et al. 2020).

Weather conditions conducive to ignition and spread, as measured by both temperature and the forest fire danger index (FFDI; Noble et al., 1980), are expected to increase under climate change (Olson et al. 2016; Clarke and Evans 2019). Therefore, improved understanding of ignition likelihood will provide managers with some of information about where and when potential wildfire risk is highest. Additionally, understanding the factors that contribute to containment probability is also essential as suppression efforts play a critical role in limiting wildfire spread and reducing risk to people and assets (Penman et al. 2015; Dunn et al. 2017). The likelihood of ignition and containment both intersect to influence how a fire spreads and the potential risk it poses to lives, infrastructure, property, and biodiversity.

Current wildfire management frameworks in Australia generally only consider containment probability and ignition likelihood in isolation and do not account for interactions between them. This makes it difficult for managers to prioritise areas of highest concern for different fire weather or environmental conditions. One tool that is increasingly being used to support environmental decision-making within multiple systems is Bayesian Network Analysis (Penman et al. 2011, 2014, 2020; Hradsky et al. 2017; Marcot and Penman 2019). Bayesian Networks (BNs) are statistical tools uniquely capable of managing the suite of uncertainties which arise in complex environmental systems, making them ideal for risk analysis research (Pollino et al. 2007; Dlamini

2010; Johnson et al. 2010; Johnson and Mengersen 2012; Kelly et al. 2013). A major advantage of using a BN in structured decision making is that it allows the use of data from multiple sources on different scales (Pollino et al. 2007; Penman et al. 2014; Marcot and Penman 2019). They can also be applied at various spatial resolutions which is an important aspect of managing risk, particularly for disturbances such as fire which impact both local and landscape scales.

Here, we aimed to understand how ignition likelihood, containment probability and subsequent fire behaviour impacts the distribution of wildfire risks across the state of Victoria, Australia. We build, parameterise, and test a Bayesian Network to answer two questions 1) how are the risks to people and property distributed across the state given a range of weather scenarios? and 2) how do ignition likelihood and containment probability influence the distribution of these risks for a range of weather scenarios? We combine our Bayesian Network with PHEONIX Rapidfire (hereafter Phoenix; Tolhurst et al. 2008) fire behaviour simulations. Phoenix is an application which simulates one or more fires using a characterisation model to capture the details of fire spread such as flame height, rate of spread and ember production etc. Here we use Phoenix simulations to generate fire impacts for ignitions across the landscape and to compare current risk estimates, which do not consider the likelihood of ignition or containment, with our estimates of risk from a Bayesian approach.

2. Model framework

Our modelling framework involved three key stages. First, we developed a conceptual model combining ignition likelihood, containment probability and fire weather to predict risk to houses and lives accross a range of scenarios and landscapes. This conceptual model (Figure 1) includes two random forest models fit to state wide datasets of historical ignition events and suppression efforts in Victoria. We took the top six most important variables from each of these models to include in our Bayesian Network. The second stage of our modelling framework expands the conceptual model into an influence diagram capturing the variables important to each of our sub-models, and from our Phoenix fire behaviour simulations, as nodes in our network. Lastly, we populated the conditional probability tables within the model using real data to learn the relationships between nodes through Bayesian inference (Korb and Nicholson 2010).

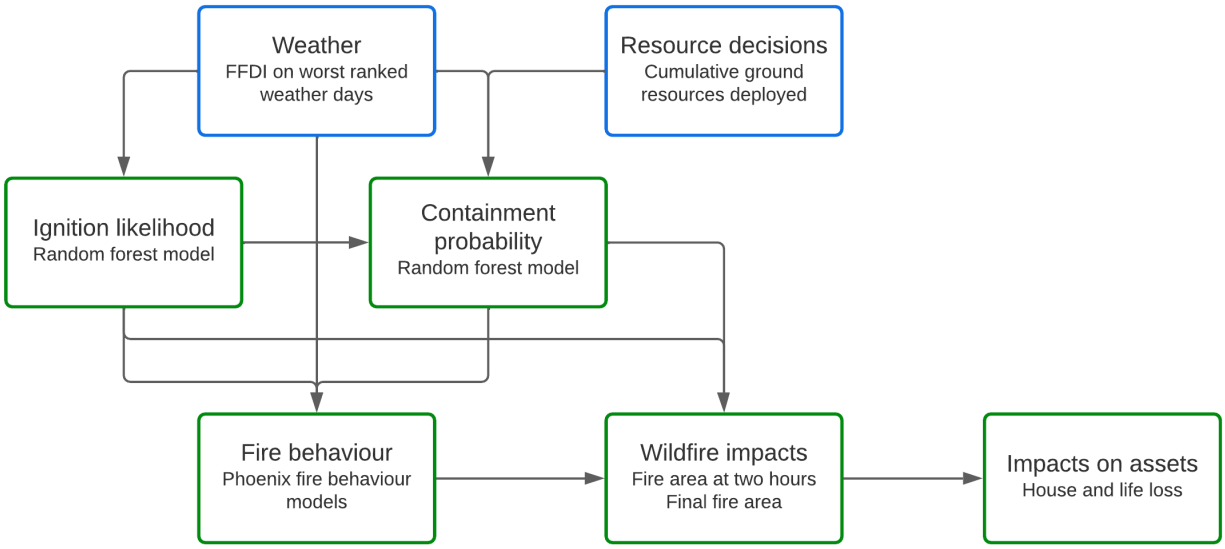

Figure 1: Conceptual model underlying the final Bayesian Network used in this study. Green boxes show sub-models and output nodes in the network. Blue boxes show decision nodes in the network.

We applied the network in R (version 3.6.2) to 71808 ignition locations across Victoria. Data on the top 50 FFDI values in history observed at each ignition location was provided by the Victorian State Government's Department of Environment, Land, Water and Planning (DELWP), who also provided us with Phoenix fire simulations under the top ten of these 50 FFDI values. To apply the BN to these locations we cycle through all locations individually. Using the FFDI values, and ten example Phoenix runs, we set the probabilities of getting each FFDI, fire area, fire area at two hours, and house loss value at that location. For each location we extract the predicted ignition likelihood, and containment probability, alongside the rescaled fire area at two hours, final fire area, house, and life loss. We compare the outputs from our BN to those

produced by Pheonix runs to determine whether accounting for containment probability and ignition likelihood, as well as the range of possible phoenix outcomes, influences the predictions of risk.

3. Results and implications

The estimates of fire risk produced by Phoenix and those predicted by the BN are spatially consistent. The ignitions with the largest predicted fire area tend to occur in the same locations in both methods and therefore hotspots are easily identified using either approach. However, the BN produced rescaled values when considering the likelihood of ignition and probability of containment in its risk estimates for some areas. The fire area values, as well as the predicted house loss and life loss were far lower in the BN as compared to Phoenix. The extent to which values were rescaled also varied across the state (Figure 2). When considering ignition likelihood and containment probability the greatest reductions in fire area occurred in the north west and eastern parts of Victoria (Figure 2; A). Probably because ignition likelihood is lower in these areas as they are less populated and prone to human ignitions. Comparatively, house loss declined most in the central areas of Victoria close to the major settlements of Melbourne and Geelong (Figure 2: B). This is probably because ignition likelihood is lower than expected by Phoenix and suppression efforts are most targeted and effective in these areas. Areas with little change in house loss indicate either low predicted values using both methods or little effect of ignition likelihood or suppression on outcomes. This could provide managers with a useful tool for prioritising allocation of suppression resources to these areas.

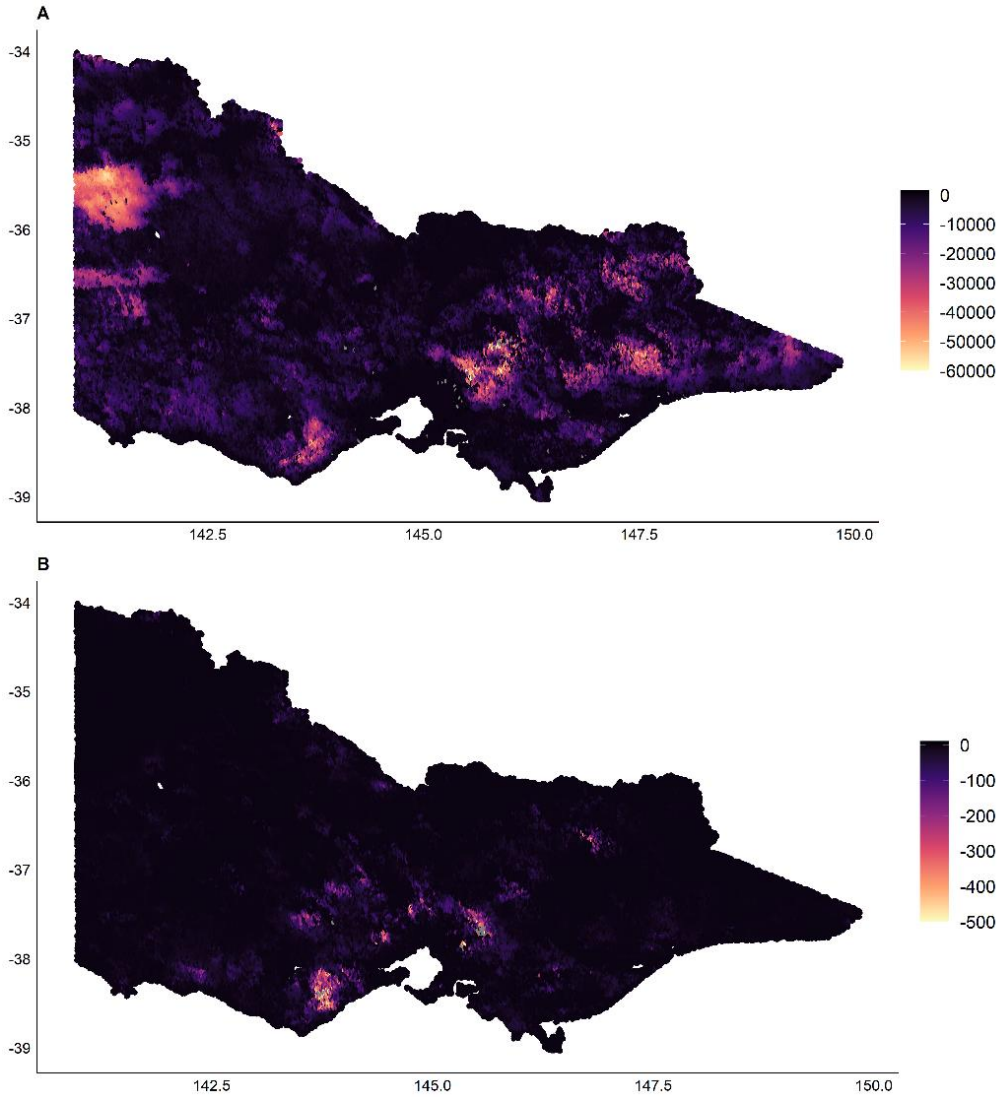

Figure2: Maps showing where the values predicted by Phoenix were different compared to those predicted by the BN for Final fire area (A) and house loss (B) nodes. Negative values indicate the Phoenix predicted values were higher than those predicted by the BN. The colours indicate the extent of these differences accross the state with dark purple indicating no or little change and light yellow showing the maximum predicted change.

4. Conclusions

Our results highlight the importance of considering multiple systems in fire risk analysis. Ignition likelihood and containment probability, as well as the environmental variables and management decisions which may influence these systems, provide essential insight into where in the landscape fires may be most impactful. While the results of our BN broadly matched the spatial patterns produce by Phoenix, the rescaled values, and the spatial differences in where rescaling was most pronounced, may offer managers nuanced insights into where resources may be most needed or most effective. This approach is also able to better account for uncertainty in multiple competing systems and can be applied to a wide range of weather scenarios and management decisions. Applying a more holistic approach to fire risk analysis will be required in the future as climate mediated shifts in ignition likelihood and fire behaviour change the patterns of fire risk to people and property. Understanding these changes will allow managers to better allocate resources to fuel management and suppression efforts.

5. References

Banks SC, Knight EJ, McBurney L, Blair D, Lindenmayer DB (2011) The effects of wildfire on mortality and resources for an arboreal marsupial: Resilience to fire events but susceptibility to fire regime change. PLoS ONE 6,. doi:10.1371/journal.pone.0022952.

Borchers Arriagada N, Palmer AJ, Bowman DMJS, Morgan GG, Jalaludin BB, Johnston FH (2020) Unprecedented smoke-related health burden associated with the 2019–20 bushfires in eastern Australia. Medical Journal of Australia 213, 282–283. doi:10.5694/mja2.50545.

Clarke H, Evans JP (2019) Exploring the future change space for fire weather in southeast Australia. Theoretical and Applied Climatology 136, 513–527. doi:10.1007/s00704-018-2507-4.

Dlamini WM (2010) A Bayesian belief network analysis of factors influencing wildfire occurrence in Swaziland. Environmental Modelling and Software 25, 199–208. doi:10.1016/j.envsoft.2009.08.002.

Dunn CJ, Thompson MP, Calkin DE (2017) A framework for developing safe and effective large-fire response in a new fire management paradigm. Forest Ecology and Management 404, 184–196. doi:10.1016/j.foreco.2017.08.039.

Filkov AI, Ngo T, Matthews S, Telfer S, Penman TD (2020) Impact of Australia's catastrophic 2019/20 bushfire season on communities and environment. Retrospective analysis and current trends. Journal of Safety Science and Resilience 1, 44–56. doi:10.1016/j.jnlssr.2020.06.009.

Higuera PE, Abatzoglou JT (2021) Record-setting climate enabled the extraordinary 2020 fire season in the western United States. Global Change Biology 27, 1–2. doi:10.1111/gcb.15388.

Hradsky BA, Penman TD, Ababei D, Hanea A, Ritchie EG, York A, di Stefano J (2017) Bayesian networks elucidate interactions between fire and other drivers of terrestrial fauna distributions. Ecosphere 8,. doi:10.1002/ecs2.1926.

Johnson S, Mengersen K (2012) Integrated Bayesian network framework for modeling complex ecological issues. Integrated Environmental Assessment and Management 8, 480–490. doi:10.1002/ieam.274.

Johnson S, Mengersen K, de Waal A, Marnewick K, Cilliers D, Houser AM, Boast L (2010) Modelling cheetah relocation success in southern Africa using an Iterative Bayesian Network Development Cycle. Ecological Modelling 221, 641–651. doi:10.1016/j.ecolmodel.2009.11.012.

Kelly RA, Jakeman AJ, Barreteau O, Borsuk ME, ElSawah S, Hamilton SH, Henriksen HJ, Kuikka S, Maier HR, Rizzoli AE, van Delden H, Voinov AA (2013) Selecting among five common modelling approaches for integrated environmental assessment and management. Environmental Modelling and Software 47, 159–181. doi:10.1016/j.envsoft.2013.05.005.

Korb KB, Nicholson AE (2010) "Bayeisan Artifical Intelligence." (CRC Press)

Marcot BG, Penman TD (2019) Advances in Bayesian network modelling: Integration of modelling technologies. Environmental Modelling and Software 111, 386–393. doi:10.1016/j.envsoft.2018.09.016.

Moritz MA, Batllori E, Bradstock RA, Gill AM, Handmer J, Hessburg PF, Leonard J, McCaffrey S, Odion DC, Schoennagel T, Syphard AD (2014) Learning to coexist with wildfire. Nature 515, 58–66. doi:10.1038/nature13946.

Noble IR, Bary GA v, Gill AM (1980) McArthur's fire-danger meters expressed as equations.

Olson R, Evans JP, di Luca A, Argüeso D (2016) The NARCliM project: Model agreement and significance of climate projections. Climate Research 69, 209–227. doi:10.3354/cr01403.

Penman TD, Bradstock RA, Price OF (2014) Reducing wildfire risk to urban developments: Simulation of cost-effective fuel treatment solutions in south eastern Australia. Environmental Modelling and Software 52, 166–175. doi:10.1016/j.envsoft.2013.09.030.

Penman TD, Cirulis B, Marcot BG (2020) Bayesian decision network modeling for environmental risk management: A wildfire case study. Journal of Environmental Management 270,. doi:10.1016/j.jenvman.2020.110735.

Penman TD, Nicholson AE, Bradstock RA, Collins L, Penman SH, Price OF (2015) Reducing the risk of house loss due to wildfires. Environmental Modelling and Software 67, 12–25. doi:10.1016/j.envsoft.2014.12.020.

Penman TD, Price O, Bradstock RA (2011) Bayes Nets as a method for analysing the influence of management actions in fire planning. International Journal of Wildland Fire 20, 909–920. doi:10.1071/WF10076.

Pollino CA, Woodberry O, Nicholson A, Korb K, Hart BT (2007) Parameterisation and evaluation of a Bayesian network for use in an ecological risk assessment. Environmental Modelling and Software 22, 1140–1152. doi:10.1016/j.envsoft.2006.03.006.

Tolhurst K, Shields B, Chong D (2008) Phoenix: Development and application of a bushfire risk management tool. The Australian Journal of Emergency Managemen 23,.

Thompson MP, Calkin DE (2011) Uncertainty and risk in wildland fire management: A review. Journal of Environmental Management 92, 1895–1909. doi:10.1016/j.jenvman.2011.03.015.

Spatial predictions of human and natural-caused wildfire likelihood across Montana (USA)

Adrián Jiménez-Ruano*[1]; W.Matt Jolly[2]; Patrick Freeborn[2]; Daniel José Vega-Nieva[3]; Norma Angélica Monjarás-Vega[3]; Carlos Iván Briones-Herrera[3]; Marcos Rodrigues[1]

[1]Department of Geography and Land Management, University of Zaragoza. Pedro Cerbuna, 12, 50009, Zaragoza, Spain, {jimenez, rmarcos}@unizar.es
[2] Missoula Fire Sciences Laboratory, Rocky Mountain Research Station, USDA Forest Service. 5775 Hwy 10W, Missoula, MT 59808, US {matt.jolly, patrick.h.freeborn}@usda.gov
[3] Faculty of Forestry Sciences, University of Juarez of the State of Durango. Río Papaloapan y Blvd, Durango S/N Col. Valle del Sur, 34120 Durango, Mexico, {danieljvn, normonjaras, briones.ipi}@gmail.com

**Corresponding author*

Keywords

Wildfire occurrence; fire danger; Spatial GAM; BAM; Montana

Abstract

Spatial wildfire ignition predictions are needed to ensure efficient and effective wildfire response but robust methods for modelling wildfire occurrence have not been fully evaluated. Here we leverage high resolution, static spatial data to predict the ignition locations of human and naturally-caused wildfires across the state of Montana (USA). We leveraged a 25-year historical wildfire dataset (1992-2017) and four high resolution spatial variables that capture fuel availability, topography, geographic location and human transport infrastructure. We combined these data to train spatial logistic regression Generalized Additive Models (GAM) designed for big datasets (BAM) for both human and natural ignitions and we tested the efficacy of incremental changes in model complexity. Results showed that the best human and natural-caused ignition models were highly capable of distinguishing locations with and without new wildfire occurrences statewide (AUC = 0.89 and 0.84 respectively). Natural-caused ignitions were strongly influenced by slope and location, while human-caused fires were best predicted by distance to roads as well as terrain and fuel availability. Finally, these spatial fire occurrence models can be combined with temporally-variant data to predict the spatial and temporal distribution of wildfires across the state with the view that these methods can be used to develop predictive models at larger scales.

1. Introduction

Wildfires are present in all vegetated environments worldwide (Krawchuk et al. 2009; 2011; Archibald et al. 2013), where they would otherwise be beneficial, are suppressed to limit or prevent immediate human-related loss (Riley et al. 2018). Although effective wildfire planning requires early information about where new ignitions are likely to start (Belval, Stonesifer, and Calkin 2020), this information is generally not available at high spatial resolution.

New wildfires start when there is an ignition source, sufficient fuel and suitable weather conditions. Natural ignitions are mainly caused by cloud-to-ground lightning strikes and depend on the timing and lightning characteristics in relation to fuel condition (Mitchener and Parker 2005; Schultz et al. 2019). Negligence causes are the most common ones (Prestemon et al. 2013) being favored by road networks (Faivre et al. 2014; Benefield and Chen 2022). Therefore, differentiating the spatial distributions of wildfire ignitions is crucial to designing and implementing source-specific prevention and mitigation strategies.

Wildfire ignition likelihood may be modelled if proxies are included to represent the fuels, weather, topography and human presence that control their spatial distribution (Barreto and Armenteras 2020). Although fuels are seasonally dynamic, static factors such as loading and continuity may limit the wildfire location where insufficient fuels prevent propagation (Briones-Herrera et al. 2019). Road networks affect fire activity in two

ways: first, making wildlands accessible to humans, thus promoting anthropogenic wildfire ignitions (A. Syphard et al. 2007; Narayanaraj and Wimberly 2012); and second, roads enable ground-based firefighting resources to quickly respond to new events (Thompson, Gannon, and Caggiano 2021). Thus, if ignition sources are differentiated and adequate spatial biophysical-demographic drivers are identified, wildland fire ignition likelihoods could be modeled, mapped and predicted across large areas.

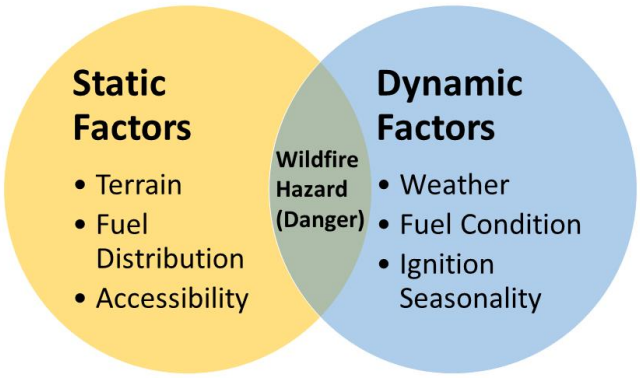

Figure 1. Conceptual scheme of the dual component of wildfire hazard or danger: the static factors and the dynamic factors.

In this study, we develop and evaluate several spatial models of wildfire occurrences to predict ignition likelihood across the state of Montana (US). To do this, we focus solely on constructing static ignition models by combining fire records with a suite of temporally invariant factors (Figure 1). We evaluate the efficacy of increasingly more complex models to map human and natural ignition probabilities. Our main objectives are: a.) to evaluate the contribution of different environmental-human factors considered crucial to wildfire ignition, b.) select the best predictive models' parameters configuration, and c.) map static human-natural wildfire ignition likelihood.

2. Material and Methods

2.1. Study area

Montana covers an area of 376,962 km^2 and it is characterized by west-to-east gradients in climate, topography, vegetation cover and wildfire causality (Figure 2).

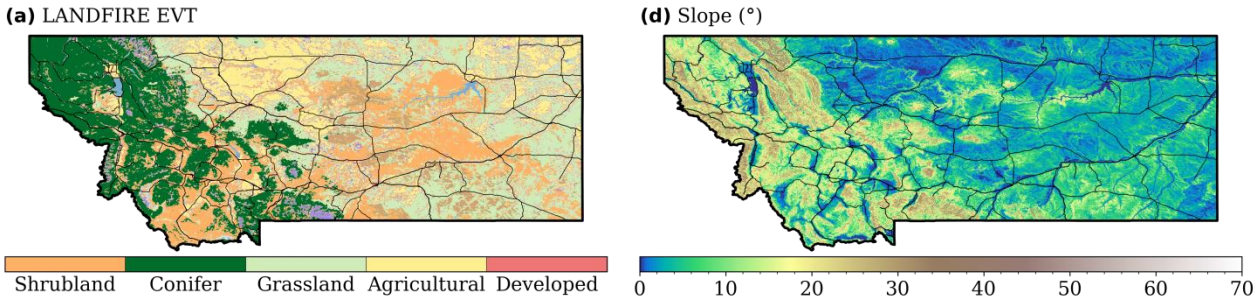

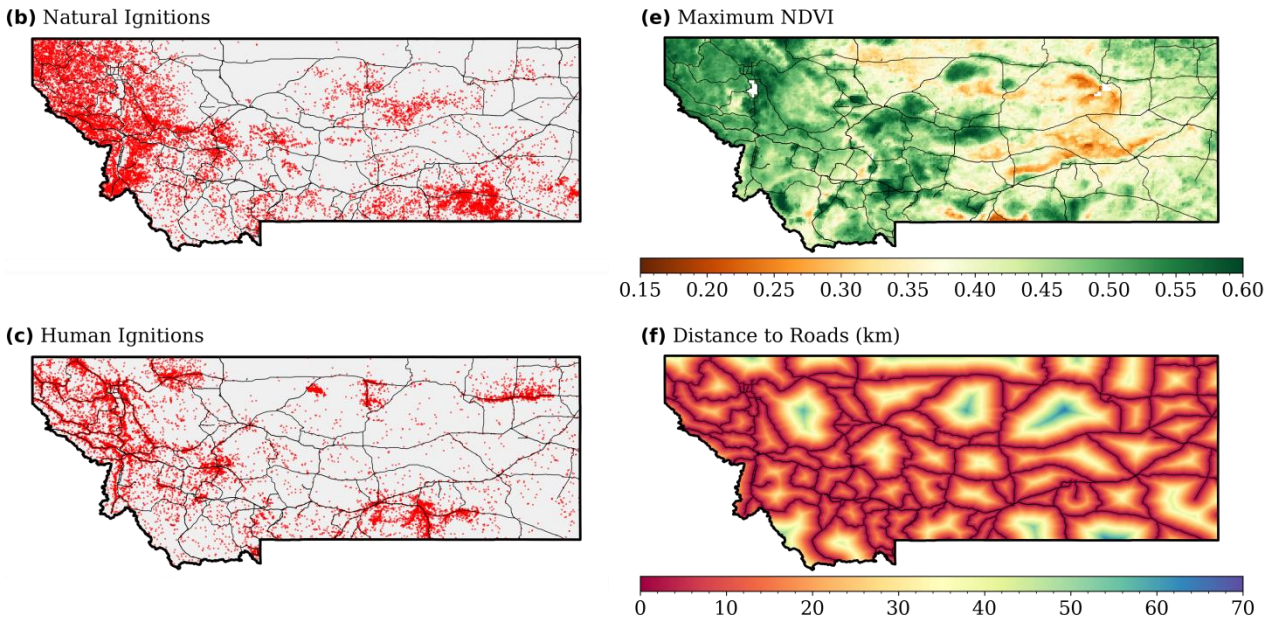

Figure 2. Maps of Montana shown with the road network. (a) Existing Vegetation Type (EVT). (b) and (c) Locations of natural and human ignitions (1992-2017). (d) Slope. (e) Maximum NDVI (1996-2017). (f) Distance to roads.

2.2. Data preparation

Wildfire point records from 1992-2017 were obtained from the Fire Program Analysis Fire-Occurrence Database (Short 2014), containing geographic coordinates of the origin, discovery date, ignition cause and final fire size. Wildfires were partitioned according to their causality (natural or human, excluding the unknown). The dependent variable (presence-absence) was obtained from the 30m binary masks of new wildfire reports. Several static potential covariates were explored (Figures 2d - 2f). To represent fuel availability, smoothed rasters of NDVI were retrieved from the Blended Vegetation Health Product (Kogan 2001; Yang, Kogan, and Guo 2020). Maximum-NDVI was chosen to capture the peak amount of above ground live biomass (Xu et al. 2012). Topography was represented by slope, obtained from the 30m resolution Digital Elevation Model (Rollins 2009). Distance from roads was used to represent accessibility, by downloading a road shapefile from the United States Census Bureau (US Census Bureau 2015), and creating a raster of distance to roads at 30m resolution.

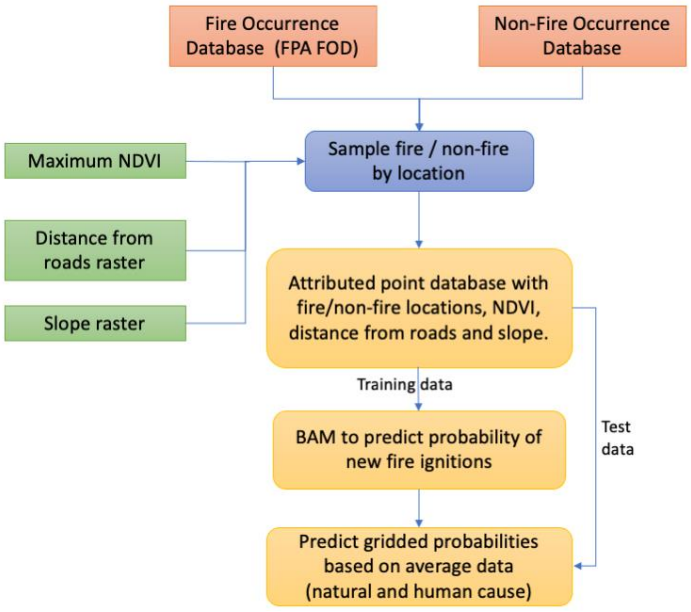

Figure 3. General workflow for model building and evaluation including inputs, sampling of wildfire presence-absence, extraction of covariates, creation of a point wildfire database, model fitting, and the final spatial predictions of wildfire ignition probabilities.

The datasets used were derived from the presence/absence masks of wildfires and the covariables' rasters (Figure 3). First, presence only datasets were created by using the grid cells containing a new wildfire report. This produced two presence only datasets (one for cause), together with their associated value for slope, maximum-NDVI, distance to roads and longitude-latitude. The presence only datasets were then split into training (70%) and testing (30%) datasets. Absence only datasets were created by randomly selecting grid cells from the binary masks at locations without any wildfire recorded. To provide balanced datasets, the number of absence grid cells was equal to the number of presence ones. After using the absence grid cells to extract the covariates, the absence only datasets were themselves spit again into training and testing datasets. Combining the presence and absence datasets for each ignition source yielded four datasets: the natural-caused training and test datasets, and the human-caused training and test datasets.

2.3. Model construction and evaluation

We included Generalized Additive Models (GAMs) (A.D. Syphard et al. 2008; Bar Massada et al. 2012) apart from Generalised Linear Model (GLMs), since the former overcomes the apriori assumption of linearity by replacing the linear terms with smoothed (Vilar et al. 2010). In this work, a suite of logistic-GLMs/GAMs were built in R (R Core Team 2021), starting with simple logistic-GLMs/GAMs to examine the isolated effects, using slope, maximum-NDVI and distance-to-roads as the sole explanatory variables. Then covariates were procedurally added using the default basis dimension (k = 10) to create increasingly more complex models with the goal of achieving the best fit with the fewest explanatory variables necessary. Additional variables were retained if they were statistically significant and if the percent deviance explained increased by more than 0.1%. Once added, the basis dimension in the spatial-GAM were iteratively increased to ensure that the smoothed terms had sufficient degrees of freedom without being overly complicated or computationally intractable. After fitting the models, each one was applied to the held back testing datasets to predict the natural and human-caused wildfire probabilities. Receiver operating characteristic (ROC) curves (Bradley 1997) and the area under the ROC Curve (AUC) were used to assess the models accuracy.

3. Results

Simple logistic-GLMs/GAMs built with one covariate illustrate the isolated effects of slope, maximum-NDVI and distance-to-roads on the probability of a new wildfire ignition (Figure 4). In contrast to the GLMs, the GAMs capture nonlinearities in the response, particularly at the lower and upper limits of slope and maximum-NDVI. Although there are strong differences between the GLM and GAM fits at the extremes, only a small fraction (5%) of the natural and human-caused ignitions in the training data had a slope >30º or a maximum-NDVI > 0.56. Moreover, both (GLM and GAM) fits exhibit monotonic behaviour over most of the range of the covariates, thus obtaining similar AUCs.

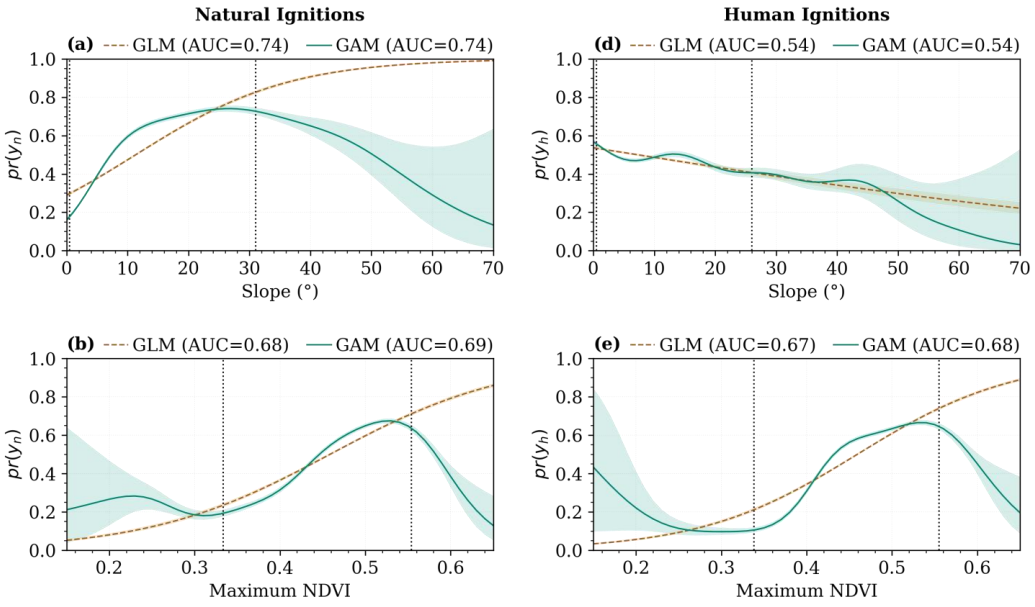

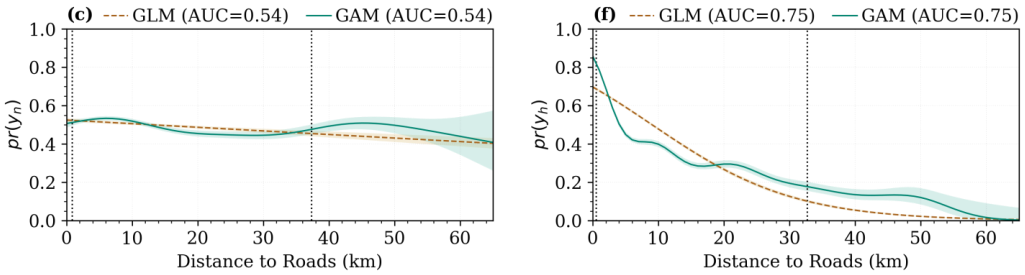

Figure 4. Simple General Linear Models (GLMs) and simple General Additive Models (GAMs) built with one covariate to predict the probability of natural ignitions (left column), and human ignitions (right column). The dotted vertical lines indicate the 5th and 95th percentiles of the covariates and capture 90% of the training data.

In the simplest version, all covariates were statistically significant ($p \leq 0.01$) and the percent deviance explained increased when spatial coordinates were added. However, whereas all variables were significant in the spatial-GAM of human-caused ignition probability, distance-to-roads was not significant in the spatial-GAM of natural ignition probability and was therefore excluded (Table 1). Initiating spatial-GAMs, the basis dimensions (k) were iteratively increased for all the smoothed terms. However, for slope, maximum-NDVI and distance to roads this had little effect on the percent deviance explained compared to the values of k for the geographic coordinates. Ultimately, the basis dimension for the smoothe geographic coordinates was increased until k = 50 and k = 35 for the natural and human-caused ignition models, respectively.

Table 1. Development from the General Linear Model (GLM) to the General Additive Model (GAM) and spatial-GAM. Formulas are presented, where α is the intercept, υ1= slope, υ2= maximum-NDVI, υ3 = distance to roads, x = longitude and y = latitude. The "s()" functions indicate the smoothed terms in the GAMs.

Version	*Cause*	*Formula*	*AUC*
GLM	Natural	$pr(y_n) = \alpha + \upsilon1 + \upsilon2 + \upsilon3$	0.75
	Human	$pr(y_h) = \alpha + \upsilon1 + \upsilon2 + \upsilon3$	0.77
GAM	Natural	$pr(y_n) = \alpha + s(\upsilon1) + s(\upsilon2) + s(\upsilon3)$	0.76
	Human	$pr(y_h) = \alpha + s(\upsilon1) + s(\upsilon2) + s(\upsilon3)$	0.80
Spatial GAM	Natural	$pr(y_n) = \alpha + s(\upsilon1) + s(\upsilon2) + s(x,y)$	0.84
	Human	$pr(y_n) = \alpha + s(\upsilon1) + s(\upsilon2) + s(\upsilon3) + s(x,y)$	0.89

According to the held-back testing (Figures 5 and 6), the logistic-GLMs exhibited the most uniform probability distributions and the greatest overlap between the presence-absence probabilities. In turn, the logistic-GAMs shifted the probability distributions towards higher values for the presence locations and towards lower values for the absence locations, indicating better differentiation. Overall, the spatial-GAMs (with geographic coordinates and optimized k values) yielded the greatest separation between the probability distributions. For the spatial-GAMs, half of the locations with a natural and human ignition had a predicted probability >76% and >80%, respectively; and half of the locations without a natural and human ignition had a predicted probability <25% and <18%, respectively. Consequently the spatial-GAMs offered the best performance, with AUC = 0.84 (natural-cause) and AUC = 0.89 (human-cause).

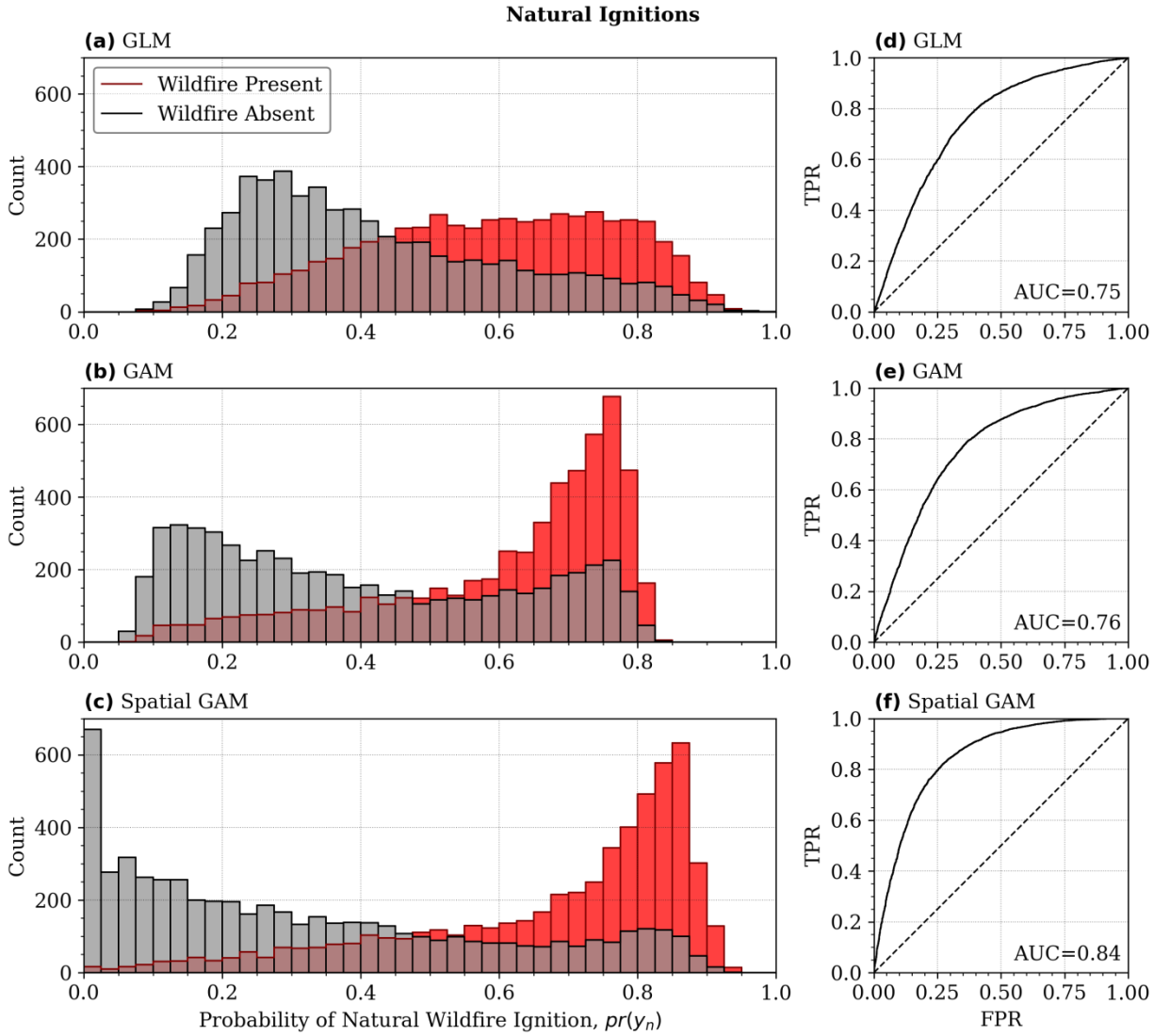

Figure 5. Evaluation of the General Linear Models (GLMs), General Additive Models (GAMs) and spatial-GAM used to model the probability of natural wildfire ignitions. Each model was applied to the held back testing datasets and the frequency distributions shown in (a)-(c) indicate the count of presence (red) and absence (black) grid cells according to their predicted probability.

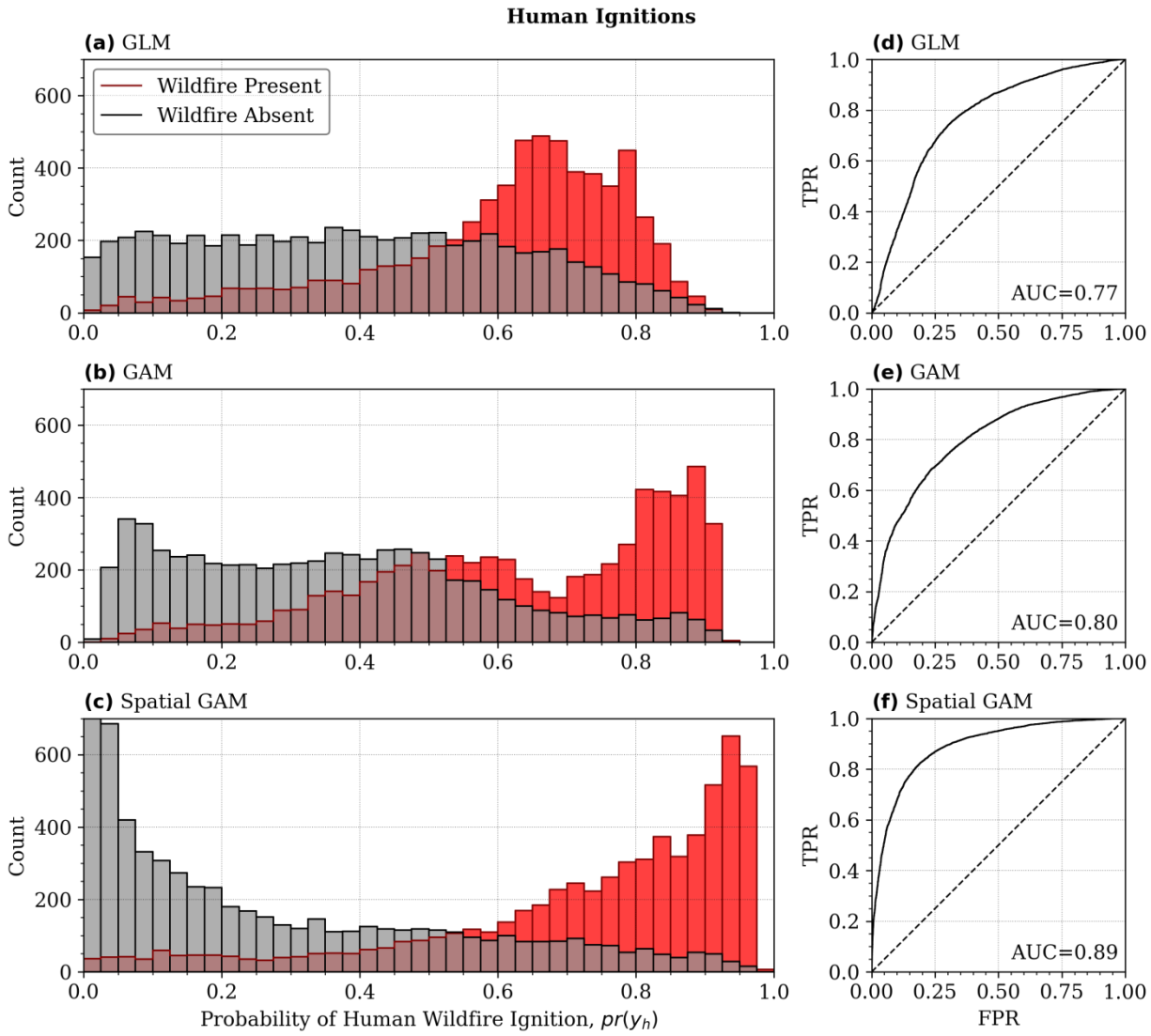

Figure 6. Same as Figure 5, but for human wildfire ignitions.

For natural ignitions, the response to slope (Figure 7a) shows a likelihood increase up to ~30º and decreasing thereafter with a greater predictive uncertainty due to fewer training data. In turn, the likelihood of a new wildfire was relatively insensitive to maximum-NDVI until a value of ~0.5 and then decreased. The geographic coordinates in the logistic-GAM imparted a spatial smoother, with locations in the Northern Rocky Mountains and south-eastern MT, exhibiting the highest probabilities. For human ignitions, the response of the spatial-GAMs to slope and distance to roads was similar to GAMs with the exception that, again, of maximum-NDVI. Here, distance to roads played a prominent role in the spatial-GAM of human-caused ignitions (50% of the grid cells containing a human caused wildfire located < 2,500 meters of a road). The spatial smoother revealed similar though slightly different patterns, most noticeably in northern MT along the Canadian border.

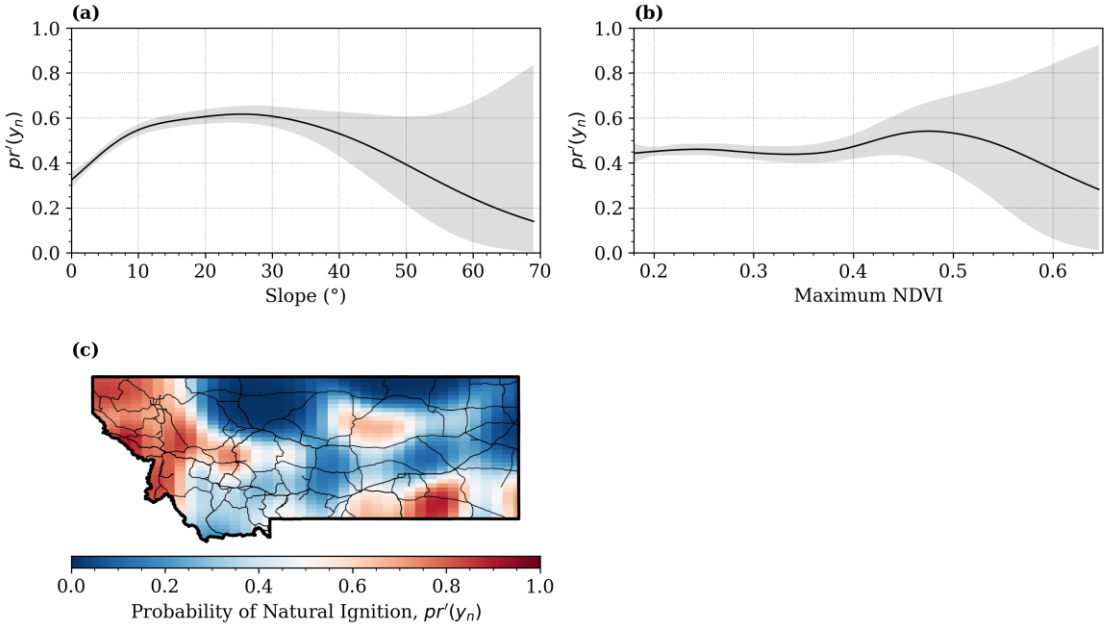

Figure 7. Partial effects plots for all smoothed variables in the spatial-GAM built to predict the probability of a natural wildfires.

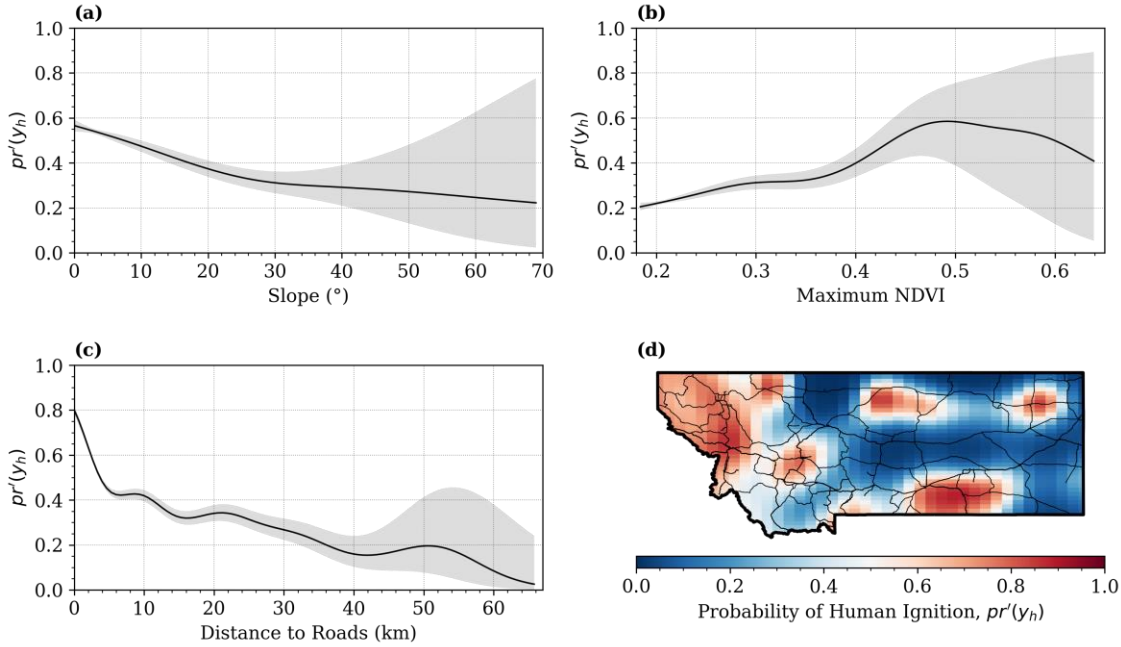

Figure 8. Same as Figure 7, but for human-caused wildfires.

Generally, the 30m static probability maps were broadly influenced by the spatial smoothers (Figures 9a and 9c versus Figures 7c and 8d) and locally modulated by slope, maximum-NDVI and distance to roads. This is most evident in the spatial-GAM of natural ignitions where probabilities are lower in the valley bottoms and nearby shallower slopes, and in the spatial-GAM of human-caused ignitions where probabilities are highest along the road network. In fact, both spatial-GAMs predicted large areas with low probabilities of wildfire ignition (50% of the territory have <23% and <15% chances of a natural and human-caused ignition, respectively). Conversely, locations with a high predicted probability of a new wildfire are rare (~2% of the state had >90% of ignition chance).

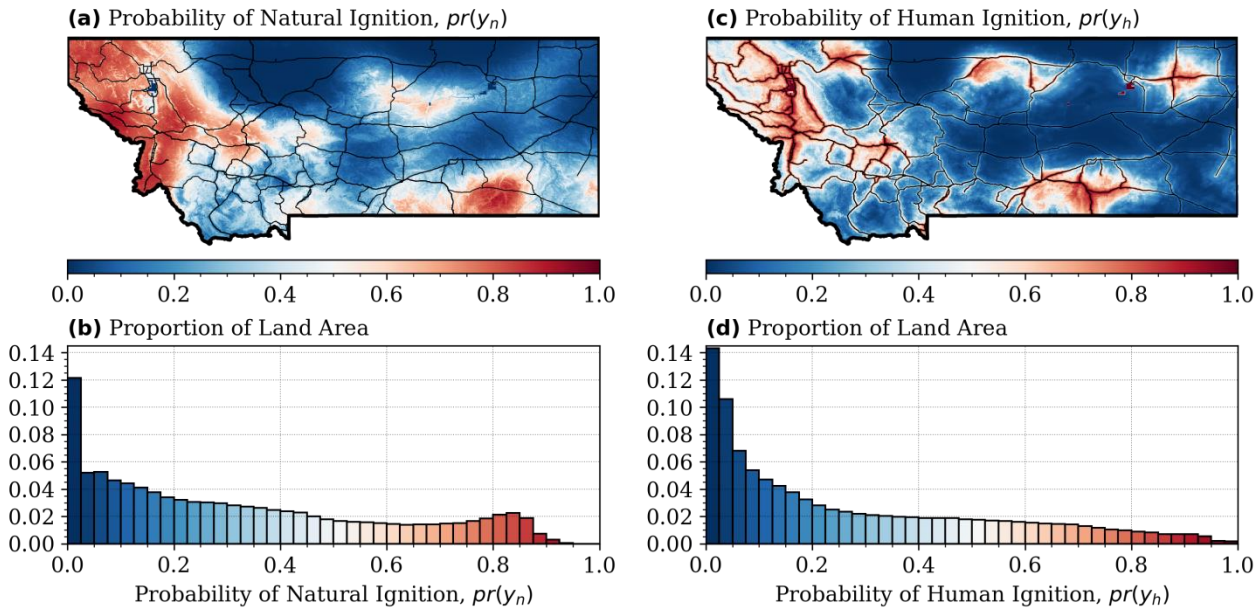

Figure 9. Maps of (a) the probability of a natural wildfire, and (b) the probability of a human wildfire obtained from the spatial-GAMs. Distributions of the land area proportion as functions of both causes are shown in (b) and (d), respectively.

4. Conclusions

In this study we have tested two different spatial-GAMs models using a daily wildfire database and drivers through a 25-year time span. Spatially, human model produced the highest wildfire probabilities, although the homogeneity of its greatest values were very clustered in particular areas. The inclusion of environment-human variables allowed us to forecast static wildfire probability in areas with a high wildfire activity and, thus, a future danger is expected. In addition to the advantage of easily updating the models as new available wildfire data, we find the selection of these basic variables to be practical.

5. References

Archibald, Sally, Caroline E R Lehmann, Jose L Gómez-dans, and Ross A Bradstock. 2013. "Defining Pyromes and Global Syndromes of Fire Regimes." Proceedings of the National Academy of Sciences of the United States of America 110 (16): 6445–47. https://doi.org/10.1073/pnas.1211466110/-/DCSupplemental.www.pnas.org/cgi/doi/10.1073/pnas.1211466110.

Balch, Jennifer K., Bethany A. Bradley, John T. Abatzoglou, R. Chelsea Nagy, Emily J. Fusco, and Adam L. Mahood. 2017. "Human-Started Wildfires Expand the Fire Niche across the United States." Proceedings of the National Academy of Sciences of the United States of America 114 (11): 2946–51. https://doi.org/10.1073/pnas.1617394114.

Bar Massada, A., A.D. Syphard, S. Stewart, and V.C. Radeloff. 2012. "Wildfire Ignition-Distribution Modelling : A Comparative Study in the Huron – Manistee National Forest , Michigan, USA." International Journal of Wildland Fire 22: 174–183. https://doi.org/https://doi.org/http://dx.doi.org/10.1071/WF11178.

Barreto, Joan Sebastian, and Dolors Armenteras. 2020. "Open Data and Machine Learning to Model the Occurrence of Fire in the Ecoregion of 'Llanos Colombo–Venezolanos.'" Remote Sensing 12 (3921): 1–18. https://doi.org/10.3390/rs12233921.

Belval, Erin J., Crystal S. Stonesifer, and David E. Calkin. 2020. "Fire Suppression Resource Scarcity: Current Metrics and Future Performance Indicators." Forests 11 (2). https://doi.org/10.3390/f11020217.

Benefield, A., and J. Chen. 2022. "Examining the Influence of Outdoor Recreation on Anthropogenic Wildfire Regime of the Southern Rocky Mountains." Natural Hazards 111: 523–45. https://doi.org/10.1007/s11069-021-05065-1.

Bradley, Andrew P. 1997. "The Use of the Area Under the ROC Curve in the Evaluation of Machine Learning Algorithms." Pattern Recogn. 30 (7): 1145–59. https://doi.org/10.1016/S0031-3203(96)00142-2.

Briones-Herrera, Carlos Ivan, Daniel José Vega-Nieva, Norma Angélica Monjarás-Vega, Favian Flores-Medina, Pablito Marcelo Lopez-Serrano, José Javier Corral-Rivas, Artemio Carrillo-Parra, et al. 2019. "Modeling and Mapping Forest Fire Occurrence from Aboveground Carbon Density in Mexico." Forests 10 (5): 1–19. https://doi.org/10.3390/f10050402.

Faivre, Nicolas, Yufang Jin, Michael L. Goulden, and James T. Randerson. 2014. "Controls on the Spatial Pattern of Wildfire Ignitions in Southern California." International Journal of Wildland Fire 23 (6): 799–811. https://doi.org/10.1071/WF13136.

Kogan, Felix N. 2001. "Operational Space Technology for Global Vegetation Assessment." Bulletin of the American Meteorological Society 82 (9): 1949–64. https://doi.org/10.1175/1520-0477(2001)082<1949:OSTFGV>2.3.CO;2.

Krawchuk, Meg A., Max A. Moritz, Marc André Parisien, Jeff Van Dorn, and Katharine Hayhoe. 2009. "Global Pyrogeography: The Current and Future Distribution of Wildfire." PLoS ONE 4 (4). https://doi.org/10.1371/journal.pone.0005102.

Krawchuk, Meg A, Max A Moritz, Meg A Krawchuk, and Max A Moritz. 2011. "Constraints on Global Fire Activity Vary across a Resource Gradient." Ecology 92 (1): 121–32. https://www.jstor.org/stable/29779580.

Mitchener, Lori Jean, and Albert J. Parker. 2005. "Climate, Lightning, and Wildfire in the National Forests of the Southeastern United States: 1989-1998." Physical Geography 26: 147–62. https://doi.org/https://doi.org/10.2747/0272-3646.26.2.147.

Narayanaraj, Ganapathy, and Michael C. Wimberly. 2012. "Influences of Forest Roads on the Spatial Patterns of Human- and Lightning-Caused Wildfire Ignitions." Applied Geography 32 (2): 878–88. https://doi.org/10.1016/j.apgeog.2011.09.004.

Prestemon, J.P., T.J. Hawbaker, M. Bowden, J. Carpenter, M.T. Brooks, K.L. Abt, R. Sutphen, and S. Scranton. 2013. "Wildfire Ignitions : A Review of the Science and Recommendations for Empirical Modeling," 20.

R Core Team. 2021. "R: A Language and Environment for Statistical Computing." Vienna: R Foundation for Statistical Computing. https://www.r-project.org/.

Riley, Karin L., Matthew P. Thompson, Joe H. Scott, and Julie W. Gilbertson-Day. 2018. "A Model-Based Framework to Evaluate Alternative Wildfire Suppression Strategies." Resources 7 (1): 1–26. https://doi.org/10.3390/resources7010004.

Rollins, Matthew G. 2009. "LANDFIRE: A Nationally Consistent Vegetation, Wildland Fire, and Fuel Assessment." International Journal of Wildland Fire 18 (3): 235–49. https://doi.org/10.1071/WF08088.

Schultz, Christopher J., Nicholas J. Nauslar, J. Brent Wachter, Christopher R. Hain, and Jordan R. Bell. 2019. "Spatial, Temporal and Electrical Characteristics of Lightning in Reported Lightning-Initiated Wildfire Events." Fire 2 (2): 1–15. https://doi.org/10.3390/fire2020018.

Short, K. C. 2014. "A Spatial Database of Wildfires in the United States, 1992-2011." Earth System Science Data 6 (1): 1–27. https://doi.org/10.5194/essd-6-1-2014.

Syphard, A.D., Volker C. Radeloff, Nicholas S. Keuler, Robert S. Taylor, Todd J. Hawbaker, Susan I. Stewart, and Murray K. Clayton. 2008. "Predicting Spatial Patterns of Fire on a Southern California Landscape." International Journal of Wildland Fire 17 (5): 602–13. https://doi.org/10.1071/WF07087.

Syphard, AD, VC Radeloff, JE Keeley, TJ Hawbaker, MK Clayton, SI Stewart, and RB Hammer. 2007. "Human Influences on California Fire Regimes." Ecological Applications 17 (5): 1388–1402. https://doi.org/10.1890/06-1128.1.

Thompson, Matthew P., Benjamin M. Gannon, and Michael D. Caggiano. 2021. "Forest Roads and Operational Wildfire Response Planning." Forests 12 (2): 1–11. https://doi.org/10.3390/f12020110.

US Census Bureau. 2015. "TIGER/ Line Shapefiles."

Vilar, Lara, Douglas G. Woolford, David L. Martell, and M. Pilar Martn. 2010. "A Model for Predicting Human-Caused Wildfire Occurrence in the Region of Madrid, Spain." International Journal of Wildland Fire 19 (3): 325–37. https://doi.org/10.1071/WF09030.

Xu, Chi, Yutong Li, Jian Hu, Xuejiao Yang, Sheng Sheng, and Maosong Liu. 2012. "Evaluating the Difference between the Normalized Difference Vegetation Index and Net Primary Productivity as the Indicators of Vegetation Vigor Assessment at Landscape Scale." Environmental Monitoring and Assessment 184 (3): 1275–86. https://doi.org/10.1007/s10661-011-2039-1.

Yang, Wenze, Felix Kogan, and Wei Guo. 2020. "An Ongoing Blended Long-Term Vegetation Health Product for Monitoring Global Food Security." Agronomy 10 (12). https://doi.org/10.3390/agronomy10121936.

Spatial wildfire hazard patterns in the Eastern Mediterranean: perspectives from a harmonised approach

Andrea Trucchia*[1]; Giorgio Meschi[1]; Paolo Fiorucci[1]; Antonello Provenzale[2]; Marj Tonini[3]; Umberto Pernice[4,1]

[1] CIMA Research Foundation, I-17100 Savona, Italy, {andrea.trucchia, giorgio.meschi, paolo.fiorucci}@cimafoundation.org
[2] Istituto di Geoscienze e Georisorse del CNR, Via Moruzzi 1, 56124 Pisa, Italy {antonello.provenzale@cnr.it}
[3] Institute of Earth Surface Dynamics, Faculty of Geosciences and Environment, University of Lausanne, CH-1015 Lausanne, Switzerland, {marj.tonini@unil.ch}
[4] University of Rome 'La Sapienza', Scuola di Ingegneria Aerospaziale, Via Salaria 851, 00138, Rome, Italy, {umberto.pernice@uniroma1.it}

**Corresponding author*

Keywords

Hazard Mapping – Susceptibility mapping – Risk Management - Machine Learning

Abstract

Wildfires are a menace which is growing in intensity and spreading in range across all planet's ecosystems causing devastation on the environment, wildlife, human health, and infrastructure. Most of the damage caused by forest fires is related to extreme wildfire events (EWEs). To foster prevention activities, a thorough understanding of territorial features determining EWEs is crucial in Civil Protection and fire management activities. An approach which learns from past wildfire events providing susceptibility, intensity and hazard maps is presented. This mapping approach leads to the individuation of the main drivers of EWEs and in the zonation of the areas more prone to hazardous and impactful wildfire events. The case study where the mapping approach is applied encompasses thirteen countries of the Eastern Mediterranean and Southern Black Sea basins. The presented results focus on wildfire susceptibility. A Machine Learning approach is pursued, by adopting open data layers as both predisposing factors and past wildfire events.

1. Introduction

Fire trends from the '70s up to now show on the average a decrease in burned area and number of fires, after the large impacts of the '80s wildfire seasons, in most of the Southern European countries, as demonstrated by (Turco et al. 2016). This can be mainly considered as the results of increasing firefighting capacities and awareness thanks to improved forecasting. However, impacts of climate change, coupled with the drastic modifications in land use and socio-economic conditions, occurred in the same period, have triggered a potential increase in frequency, extent and severity of wildfires worldwide (Doerr and Santín, 2016). Wildfires are growing in intensity and spreading in range across all planet's ecosystems, causing devastation on the environment, wildlife, human health, and infrastructures (UNEP, 2022). In highly densely populated areas, recent studies indicate that most of the damage caused by forest fires is related to extreme wildfire events (EWEs) which represent less than 2% of the total number of fires (Catry et al., 2009; Tedim et al., 2013). Despite huge investments in fire suppression, firefighting activities cannot effectively cope with EWEs, even in cases of massive resource deployment (Fernandes et al., 2016).

The impacts of the recent and recurrent EWEs in the Mediterranean highlight that societies are facing an increasing fire risk due to the combination of climate conditions and landscape-scale accumulation of fuel because of the almost complete abandon of rural activities.

Recently, EWEs characterized the 2021 wildfire summer season, where Greece, Italy, Algeria and Turkey experienced a large number of severe wildfire events burning more than 630,000 ha (San-Miguel-Ayanz, 2022). The 2021 Algerian wildfires killed at least 90 people (ReliefWeb, 2021) resulting in the deadliest fires of the recent times after the EWEs in Portugal (2017) and in Mathi, Greece (2018).

It is evident that there is an urgent need to shift from suppression to prevention and risk mitigation in order to reduce such impacts. A limitation to this shift is represented by the absence of a collective and pervasive understanding of the conditions related with EWEs beyond both the sole cause of ignition and the effect of weather, which are the main uncontrollable aspects of EWEs. The fatalist approach which blames only ignition patterns and weather effects neglects that there is still plenty of room for knowledge improvement leading to the identification of priorities for effective wildfire prevention. Such knowledge begins with susceptibility, hazard and risk mapping, including the characterization of the exposed elements in terms of their value and vulnerability, and ultimately leads to the identification of the areas where EWEs can happen with more severe impacts.

To foster prevention activities, a thorough understanding of the features of the territory determining EWEs is of crucial help in Civil Protection and fire management activities. From a technological point of view, there is plenty of data, tools and models which can be applied to this issue.

A harmonized mapping methodology is needed to be applied at different scales. Synoptic time series of burned area a significant help to learn from the past, bringing useful knowledge to present wildfire management, determining the principal drivers of catastrophic wildfires. However, those time series may be not long enough locally to reach these goals. To circumvent this problem, a more vast and diverse area can be studied, to infer wildfire drivers in different climates, topographic and anthropogenic conditions. This is achieved using wildfire susceptibility, hazard, and risk maps, which can help decision makers and practitioners in wildfire management and long-term landscape management, strengthening proactive prevention activities adapted to local environmental and socio-economic contexts. The objective of such maps may range from the static assessment (hazard) to the dynamic one (danger).

This is in line with the recent IPAFF European program, which targets Western Balkans (Albania, Kosovo*[1], Montenegro, Serbia, North Macedonia, Bosnia-Herzegovina) and Turkey to empower capacities in forest fire risk assessment and mapping, considering static hazard and risk mapping across boundaries.

The Authors with the presented work continue a research framework started at the local level (Tonini et al., 2020) and recently expanded at the national scale (Trucchia et al., 2022). The described work is one of the first attempts (up to the Authors' knowledge), to model wildfire hazard at the supernational scale, where useful information can be drawn in view of cross-border wildfire management, supporting also the European Civil Protection Mechanism.

1.1. The proposed framework to wildfire hazard assessment and mapping

The proposed approach combines multi-source data gathering, model / expert-based processes and Machine Learning (ML) analyses.

This preliminary work, undertaken for a large set of countries in the Eastern Mediterranean and Southern Black Sea region, tries to get the most from the available global data sets, using only open data. The main steps are summarised below:

1. Susceptibility mapping - wildfire susceptibility is defined as the static probability of experiencing wildfire in a certain area, depending on the intrinsic characteristics of the terrain. This can be achieved with several approaches, ranging from the statistical hierarchical ones to the ML driven ones.
2. Intensity mapping - wildfire intensity is defined as the rate of heat energy released by the fire. At this stage, the areas where severe wildfires can develop owing to the fuel cover and other features of the terrain are detected. This can be done with expert-based classification of fuel cover or via empirical models.
3. Hazard mapping – wildfire hazard is the spatial distribution of the areas where a severe wildfire is likely to occur. This can be done merging the outputs of the two previous steps.

In this short abstract, the results obtained for Steps 1-2-3 are described.

[1] This designation is without prejudice to positions on status, and is in line with UNSCR 1244 and the ICJ Opinion on the Kosovo declaration of independence.

2. Materials and Methods

2.1. Study Area

The considered countries are the following: Italy, Slovenia, Croatia, Western Balkans (Albania, Bosnia and Herzegovina, North Macedonia, Montenegro, Kosovo* and Serbia), Greece, Cyprus, Bulgaria, and Turkey. They constitute a vast area (more than 1,600,000 km2) characterized by a high number of biogeographical regions: Mediterranean, Continental, Alpine, Anatolian, Pannonian, and Black Sea biogeographical region (European Environment Agency, 2002).

2.2. Methodology

The proposed methodology for susceptibility mapping is based on a ML model (Trucchia et al., 2022), structured as a classification task. It uses a Random Forest Classifier (RF) as an algorithm, to find a functional relation between the dependent variable (the label, that is, wildfire occurrences) and the independent variables (that is, the predisposing factors). As per the predisposing factors, geographic data (elevation, slope, aspect, land cover/fuel cover), climatic data (Köppen-Geiger climate classes, mean precipitation, mean temperature) and anthropogenic data (distance from settlements and crops) are considered. The input layers are summarised in Table 3. The main data source used for computing vegetation cover variables is CORINE Land Cover 2018 (CLC2018). The obtained raster, containing the CORINE code for the pixels, then has been processed to obtain the neighbouring vegetation variables, which express the vegetation continuity over the analysed landscape. Those extra variables are used to associate with any pixel information on the surrounding vegetation. This is useful to identify homogeneity in vegetation, or to spot the interface between two main vegetation covers. For any pixel, a Moore neighbourhood of order 2 (the 24 surrounding pixels) has been evaluated (see Figure 1). The frequency of appearance of the several vegetation types has been computed. For instance, in case of a pixel is totally surrounded by CLC2018 code “311”, that is, broadleaves, the variable “neighbouring_311” will be set to 1 while all the other "neighbouring_XXX" variables will be set to 0.

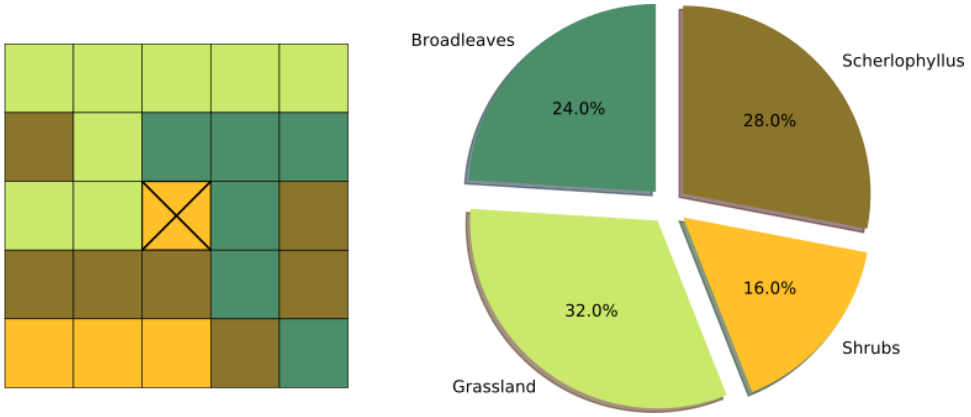

Figure 1- A representation of a Moore Neighbourhood and the obtained “neighbourhood percentages” of vegetation classes (vegetation continuity) is portrayed. Any other neighbour vegetation type not represented in the image is set to 0%.

As per the observed data, the EFFIS database of 10,118 burned polygons (more than 2,922,500 burned hectares), retrieved from 2008 to 2019 is considered.

All inputs and outputs are rescaled to the working resolution of 500m.

For any of the considered countries, 10% of their burned pixels is retrieved and their predisposing factors collected, as well as an equal number of non-burned pixels with their geoclimatic and anthropogenic factors. This allowed building a balanced dataset. The contribution of each country is merged in the total dataset. Such database was split between the training ones (75 percent of the entries) and the test ones (the remaining 25% of the database). The RF model has been trained on the training dataset and evaluated over the test pixel, to compute performance indicators. In this work, the Area under the ROC Curve (AUC) and the Mean Square Error (MSE) are considered and reported in Table 4.

The input features then are ranked by their relevance using the measure given by the Gini impurity to spot the main drivers of wildfire occurrence in the study area.

While the susceptibility layer raw values ranging from 0 to 1 have been used to compute the performance indicators, the values have been also aggregated into percentile classes (see Figure 2).

In order to have a layer accounting for wildfire intensity, the CLC2018 land cover has been processed aggregating the CLC2018 classes into four different intensity classes, as reported in Table 1.

Having for every pixel of the study area a class for potential intensity and a class for wildfire susceptibility, a simple expert-based contingency matrix for hazard assessment has been developed. Such matrix is reported in Table 2.

Table 1- Fire behaviour / fire intensity classification. Thanks to this classification a land cover map can be converted to a fire intensity map, to be used as input for the hazard mapping.

Intensity classes	Description	Vegetation cover
1	Surface fire – low intensity	crops, grasslands
2	Surface fire – medium intensity	broadleaves, agroforest
3	Surface fire – high intensity	Sclerophyllus, shrubs
4	Crown fires – very high intensity	Conifers, mixed forest

Table 2- The contingency matrix for the Hazard is portrayed. It combines the input classes of susceptibility (rows) and intensity (columns). Every entry of the matrix is the hazard level (from one to six: very low, low, medium, high, very high, extreme hazard) related to a specific combination of susceptibility and intensity levels.

Susceptibility / Fire Intensity	Low Intensity	Medium Int.	High Int.	Very High Int.
Low Susceptibility	1	2	3	4
Medium Susc.	2	3	4	5
High Susc.	3	4	5	6

3. Results

The first results for the susceptibility mapping of the study area are here listed. In Figure 2, the susceptibility distribution is portrayed after aggregating via percentile classes. In Figure 3, the Hazard Map for the reported area is portrayed.

The performance indicators are resumed in Table 4, with promising and consistent results for the AUC score.

Interesting insights are also given by the ranking of the predisposing factors in Table 5: the importance of vegetation continuity when compared to single pixel vegetation is an evident result of the analysis, with climatic and topographic classes which cannot be neglected for a good classification of the study area. This is in line with the more consolidated results from the recent work at the national scale in Italy (Trucchia et al., 2022).

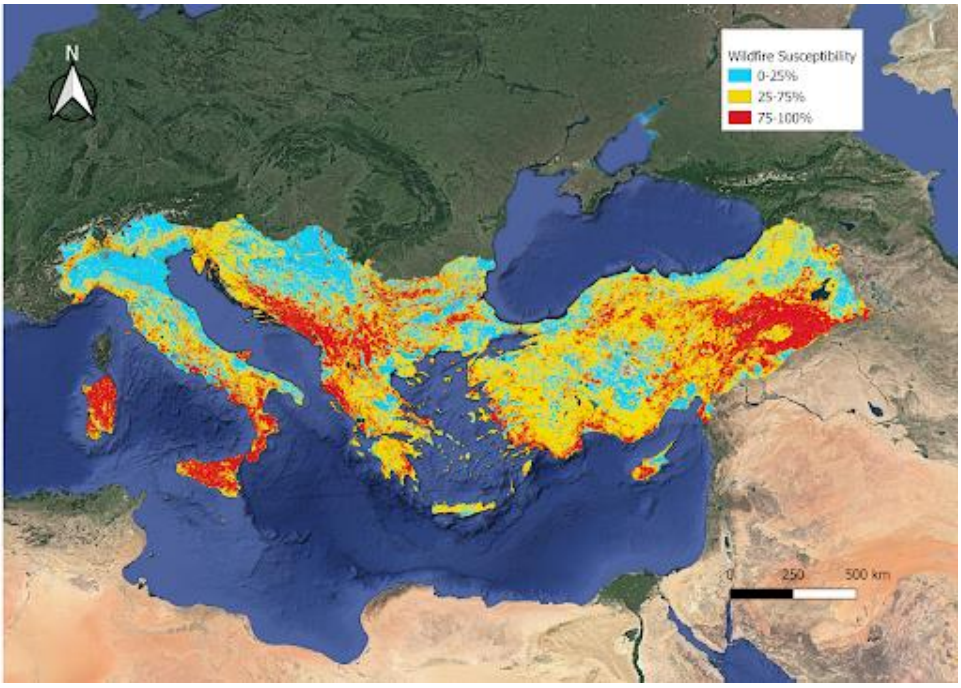

Figure 2: Susceptibility map of the study area, coloured by percentiles: 0-25% (low susceptibility), 25-75% (medium susceptibility), 75-100% (high susceptibility).

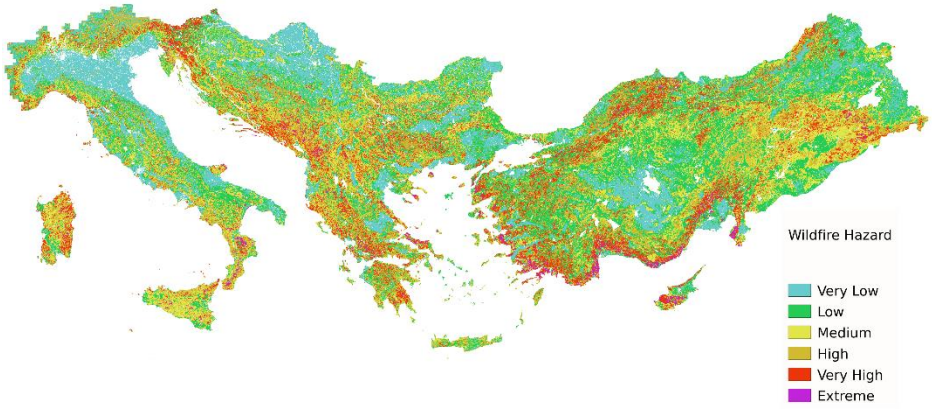

Figure 3: Wildfire Hazard map of the study area, coloured by the hazard classes of Table 2, taking as inputs the susceptibility classes (Figure 2) and the fire intensity category (Table 1)

4. Discussion and Conclusions

Promising results showing the most wildfire prone areas achieved through ML in step 1 supported the work in step 2 and 3 of the proposed approach. The susceptibility map produced at this stage of the implementation evidenced the importance of vegetation continuity in susceptibility assessment. At the scale of the presented analysis of course climatic information is a good asset for discriminating between different species of vegetation that belong to the same CORINE class. On the other hand, vegetation continuity covers at least two roles: firstly, high flammability fuels continuity is the main responsible of EWEs; secondly, continuity of native broadleaved forests may limit the propagation of EWEs. The adopted strategy for fire behaviour/intensity mapping and Hazard mapping are an example of how to make use of open data and informed decisions to perform hazard mapping at the supernational level. There exist of course plenty of different modelling choices, but the Authors tried to stick to the most straightforward one to highlight the solidity of the proposed framework. For instance, a modelling approach relying to worst-case scenarios for wind and moisture conditions could have been employed for intensity mapping (Trucchia et al. 2022 b). These preliminary results open the right path to

restoration and adaptation strategies, fostering the objectives of EU Biodiversity Strategy for 2030. This initial susceptibility mapping is currently under refinement by implementing ad-hoc spatial validation procedures, and a more thorough factor importance analysis, with a special focus on the impact of the different vegetation types.

Table 3- Input data for the susceptibility mapping

Input data	**Source**	**Description**
CORINE land cover	Copernicus[2]	Land cover raster file of the Corine 2018 at 100 m resolution
Copernicus tree cover density (TCD)	Copernicus[3]	Density of the forestry areas at European level at100 m resolution
Digital Elevation Model (DEM)	JAXA's Global ALOS 3D World (Takaku et al. 2020)	Raster file related to the elevation in meter for the study area
Köppen-Geiger - climate	Open data repository (Beck et al. 2018)	Raster layer of the Köppen-Geiger climate classification at 1-km resolution
Mean Precipitation	ERA5 data (ECMWF reanalysis) of the 1991-2020 time window from Climate Change Knowledge Portal (CCKP) of World Bank Group [4]	Average of yearly accumulated precipitation [mm]
Mean Temperature		Average mean temperature [°C]
Burned areas	EFFIS[5]	Historical burned areas retrieved from EFFIS (data ranging from 2008 to 2019)

Table 4- Performance indicators of the training dataset for the susceptibility ML model.

AUC	**MSE**
0.77	0.192

Table 5- Importance ranking of the input factor of the ML model. Importance of factors belonging to same category have been summed up.

Predisposing Factor (feature)	**Gini based Importance**
Climate variables	0.279
Vegetation continuity (sum of all Gini importances)	0.265
Topography	0.235
Anthropic	0.141
Tree Cover Density	0.045
Vegetation (value for single pixel)	0.03

5. Acknowledgments

A.P. acknowledges support from the EU H2020 project FirEUrisk, Grant Agreement Number 101003890. P.F., U.P., G.M., A.T. acknowledge support from the DG ECHO project IPA Floods and FIres "EU Support to Flood Prevention and Forest Fires Risk Management in the Western Balkans and Turkey". P.F., G.M., A.T. acknowledge support from EU-funded programme "Prevention, Preparedness and Response to natural and man-made disasters in Eastern Partnership countries – phase 3 (PPRD East 3)"

6. Bibliography

Beck, H.E., N.E. Zimmermann, T.R. McVicar, N. Vergopolan, A. Berg, E.F. Wood: Present and future Köppen-Geiger climate classification maps at 1-km resolution, Nature Scientific Data, 2018.

Catry, F. X., Rego, F. C., Bação, F. L., & Moreira, F. (2009). Modeling and mapping wildfire ignition risk in Portugal. International Journal of Wildland Fire, 18(8), 921-931. https://doi.org/10.1071/WF07123

Doerr, S.H.; Santín, C. Global trends in wildfire and its impacts: perceptions versus realities in a changing world. Phil. Trans. R. Soc. B 2016, 371, 20150345.

European Environment Agency, Europe's biodiversity – biogeographical regions and seas. Biogeographical regions in Europe. Introduction. EEA Report No 1/2002, 2002, https://www.eea.europa.eu/publications/report_2002_0524_154909

Fernandes P. M., Pacheco A.P., Almeida R. and Claro J., 2016 The role of fire-suppression force in limiting the spread of extremely large forest fires in Portugal Eur. J. For. Res. 135 253–62

ReliefWeb, 2021. Algeria: Forest Wildfires - Emergency Appeal №: MDRDZ007, Posted: 2 Nov 2021, Originally published 30 Oct 2021, https://reliefweb.int/report/algeria/algeria-forest-wildfires-emergency-appeal-mdrdz007

San-Miguel-Ayanz, J., Durrant, T., Boca, R., Maianti, P., Libertá, G., Artés-Vivancos, T., Oom, D., Branco, A., de Rigo, D., Ferrari, D., Pfeiffer, H., Grecchi, R., Nuijten, D. 2022. Advance Report on Forest Fires in Europe, Middle East and North Africa 2021, EUR 31028 EN, Publications Office of the European Union, Luxembourg, 2022, ISBN 978-92-76-49633-5, doi:10.2760/039729, JRC128678.

Takaku, J. andT. Tadono, M. Doutsu, F. Ohgushi, and H. Kai, "Updates of 'AW3D30' ALOS Global Digital Surface Model with Other Open Access Datasets", The International Archives of the Photogrammetry, Remote Sensing and Spatial Information Sciences, ISPRS, Vol.XLIII-B4-2020, pp.183–189, 2020.

Tedim F, Remelgado R, Borges C, Carvalho S and Martins J, 2013. Exploring the occurrence of mega-fires in Portugal Forest Ecol. Manage. 294 86–96

Tonini, Marj, Mirko D'Andrea, Guido Biondi, Silvia Degli Esposti, Andrea Trucchia, and Paolo Fiorucci. 2020. "A Machine Learning-Based Approach for Wildfire Susceptibility Mapping. The Case Study of the Liguria Region in Italy" *Geosciences* 10, no. 3: 105. https://doi.org/10.3390/geosciences10030105

Trucchia, Andrea, Giorgio Meschi, Paolo Fiorucci, Andrea Gollini, and Dario Negro. 2022. "Defining Wildfire Susceptibility Maps in Italy for Understanding Seasonal Wildfire Regimes at the National Level" Fire 5, no. 1: 30. https://doi.org/10.3390/fire5010030

Trucchia, Andrea; Fiorucci, Paolo; Massabò, Marco; Zegeye, Abiy; Soltesova, Katarina M; Yasin, Nesibu; Debele, Chali; Abebe, Adugna (2022b) A multi-agency Forest Fire Early Warning System for environment and biodiversity preservation in Ethiopia. Abstract id 3624013. Presented at XV WORLD FORESTRY CONGRESS, 2–6 May 2022, Coex, Seoul, Republic of Korea

Turco M, Bedia J, Di Liberto F, Fiorucci P, von Hardenberg J, Koutsias N, et al. (2016) Decreasing Fires in Mediterranean Europe. PLoS ONE 11(3): e0150663. https://doi.org/10.1371/journal.pone.0150663

UNEP, 2022 United Nations Environment Programme (2022). Spreading like Wildfire – The Rising Threat of Extraordinary Landscape Fires. A UNEP Rapid Response Assessment. Nairobi.

SurEau-Ecos-FMC: mechanistic modelling of fuel moisture content (FMC) at leaf and canopy scale under extreme drought

Julien Ruffault*[1]; Jean-Marc Limousin[2]; François Pimont[1]; Jean-Luc Dupuy[1]; Hervé Cochard[3]; Nicolas Martin-StPaul[1]

[1]URFM, INRAE, 84000 Avignon, France
{julien.ruff@gmail.com}, {francois.pimont, jean-luc.dupuy, nicolas.martin}@inrae.fr
[2]CEFE, CNRS, 34000 Montpellier, France, {jean-marc.limousin@cefe.cnrs.fr}
[3] Université Clermont Auvergne, INRAE, PIAF, 63000 Clermont-Ferrand, France, {herve.cochard@inrae.fr}

**Corresponding author*

Keywords

Forest flammability, plant-water relations, fuel modeling, fire-vegetation interactions

Abstract

Understanding and predicting fuel moisture content (FMC) is a crucial prerequisite to increase our knowledge of forest's vulnerability to fires in a changing climate. While live fuel moisture content (LFMC) is a main driver of fire behavior and activity in crown fires in forests and shrublands, it remains poorly understood and predicted, especially under extreme drought. A major reason for that is that LFMC sensitivity to climate is mediated by a range of location-specific factors, including soil characteristics and plant response to drought. Another reason is that LFMC is often simulated at the leaf scale while, from a fire danger perspective, canopy scale fuel moisture content (CFMC) is more relevant.

Here we introduced a FMC module in the plant-hydraulic SurEau-Ecos model to simulate the dynamics of both LFMC and CFMC as a function of leaf water potential (ψ_{Leaf}). CFMC integrates the impacts on moisture content of foliage mortality that can occur under extreme drought because of leaf embolism. SurEau-Ecos-FMC relies on two main mechanisms. The relationship between ψ_{Leaf} and leaf relative water content of the symplasm is modeled through pressure volume curves. Percent loss of leaf conductance (PLC) is derived from ψ_{Leaf} through vulnerability curves to cavitation and affects the dynamics of fuel moisture content in two different ways. At the leaf level, PLC dictates the dynamics of the leaf apoplasmic reservoir. At the canopy level, PLC drives the proportion of dead fuel within the canopy.

SurEau-Ecos-FMC accurately reproduced the temporal dynamics of LFMC in a Quercus ilex stand at the Puéchabon site over a three-years period. The model explained 69 % (RMSE = 4.27) and 74 % (RMSE = 4.92) of the variance in the minimum and maximum daily observed LFMC, respectively. The model was also able to capture the dynamics in CFMC resulting from leaf mortality during the summer drought. The years when SurEau-Ecos-FMC predicted leaf mortality were also the ones with the highest anomaly in NDVI. Multi-model projections of fire danger indices based on CFMC showed a general increase of fire danger over the next century. Under RCP8.5, the averaged minimum CFMC reached during the year is expected to decrease from 65 % to 32 % and the fire season length (number of day when CFMC<67%) is expected to increase from 15 to 120 days per year.

SurEau-Ecos-FMC offer new opportunities to improve our comprehension of LFMC's sensitivity to climate and we show that plant embolism might be a growing cause of FMC decrease in a drier climate. We also encourage the use of SurEau-Ecos-FMC to inform fire models in order to increase our understanding of the FMC's effect on fire behavior and activity.

1. Introduction

Fuel moisture content (*FMC*), the ratio of water mass to dry mass of vegetation, governs the amount of time and energy needed to vaporize fuel moisture before ignition can occur. *FMC* is usually separated into dead (*DFMC*) and live (*LFMC*). Declining *LFMC* was associated with an increase in area burned (Pimont *et al.* 2019a), extreme wildfires (Ruffault *et al.* 2018a) and increased fire behavior (Pimont *et al.* 2019b).

Despite its importance, LFMC remains poorly understood and predicted for two main reasons. First, unlike DFMC, the effect of climate on LFMC is regulated by a range of location-specific factors, including plant traits

and soil characteristics (Ruffault et al. 2018b, Nolan et al. 2020). As a result, models based on meteorological drought indices do not accurately predict LFMC (Ruffault *et al.* 2018b). Second, canopy level moisture content (CFMC) is more relevant for wildfire danger (Rossa and Fernandes 2018) but predicting CFMC requires to take into account the mechanisms that lead to leaf mortality under severe to extreme drought.

Recent advances in our physiological understanding of plant response to drought have led new opportunities to improve our comprehension of leaf-level and canopy-scale FMC sensitivity to climate (see Figure 1). A first theoretical framework, derived from pressure volume (p-v) curves, states that the response of symplasmic water content to leaf water potential essentially depends on cell wall elasticity (ε) and leaf osmotic potential (π_0). Such relationships have recently been adapted to model leaf-level LFMC (Nolan *et al.* 2020). A second framework, inherited from plant hydraulic, allow to derive the water content of the apoplasmic tissue and the ratio of dead to live fuels within the canopy from the percent loss of conductance (PLC).

Understanding and anticipating fire hazard requires to improve our current knowledge of fuel moisture response to climate. As compound dry and hot events become more frequent and intense (Ruffault et al. 2020), drought-induced plant defoliation and mortality that affect CFMC are likely to increase in many ecosystems (Allen et al., 2015). Here we developed a FMC module in the plant-hydraulic SurEau-Ecos model (Ruffault et al., 2022) to simulate the dynamics of LFMC and CFMC and compared them with field measurements. We then explored the impact on future climate changes on wildfire danger.

2. Methods

2.1. SurEau-Ecos-FMC

We implemented a fuel moisture content (*FMC*) module into *SurEau-Ecos* to simulate *FMC* dynamics of fine canopy fuels (shoot and leaves), both at the leaf and canopy levels. *SurEau-Ecos* is a plant-hydraulic model that simulates plant water status and fluxes between the soil, plant and the atmosphere. *SurEau-Ecos* draws on the mechanisms developed in *SurEau* (Cochard *et al.* 2021) and an ecosystem-level water balance model (Ruffault *et al.* 2013). It predicts hourly plant water potentials as function of soil properties, plant hydraulic traits, stand structure and daily climatic variables (see a full description in Ruffault *et al.* 2022).

SurEau-Ecos-FMC relies on two main mechanisms (Figure 1). The relationship between ψ_{Leaf} and leaf relative water content of the symplasm is modeled through pressure volume curves. Percent loss of leaf conductance (PLC) is derived from ψ_{Leaf} through vulnerability curves to cavitation and affects the dynamics of fuel moisture content in two different ways. At the leaf level, PLC dictates the dynamics of the leaf apoplasmic reservoir. At the canopy level, PLC drives the proportion of dead fuel within the canopy (α_{Dead}). Dead leaves are assumed to stay on plant until the end of the year.

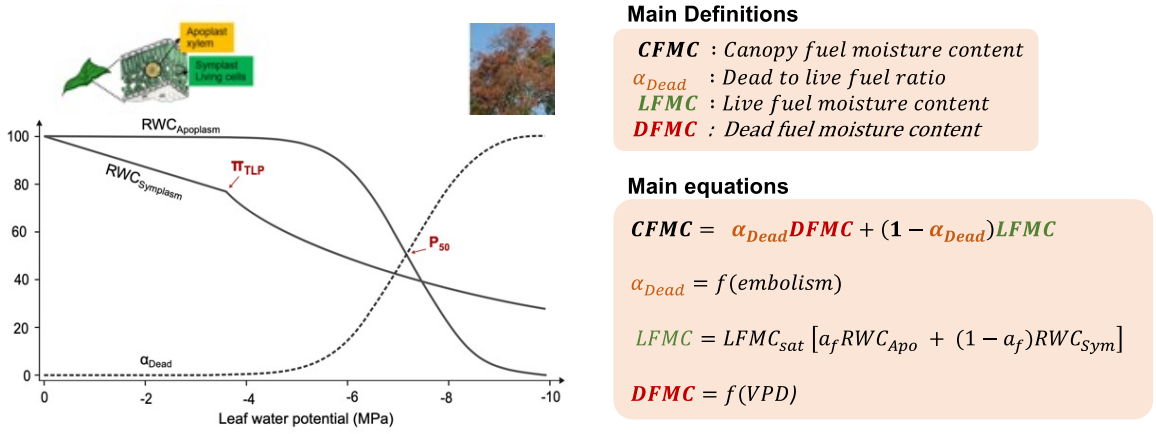

Figure 1- Schematic representation of the main processes and equations involved in the dynamics of live fuel moisture content (LFMC) and canopy moisture content (CFMC) in the plant-hydraulic model SurEau-Ecos-FMC.

2.2. Validation datasets

SurEau-Ecos-FMC estimations of ψ_{Leaf}, LFMC and *CFMC* were compared to measurements made on a *Quercus ilex* Mediterranean forest for the period 2016-2018. The study site is located at the Puéchabon forest at 35 *km* north-west of Montpellier (southern France; 270 m ASL). ψ_{Leaf} and *LFMC* were measured at predawn and at midday for five trees during the summer drought (May to October) approximatively once per 3 weeks each year. As a proxy of leaf mortality, we used the Normalized Difference Vegetation Index (NDVI). Continuous NDVI measurements were made using a sensor positioned above the canopy. We computed an index of foliage change during the summer drought as the relative variation in NDVI between leaf maturity (around early July) and the end of the summer.

2.3. Projections of fuel moisture content

Projections of climate variables for the future climate period (2005-2100) and historical periods used as input in FMC projections (section 2.3.5) were obtained from the climate simulation program involved in the 5th phase of the Coupled Model Intercomparison Project (CMIP5) produced as part of the EURO-CORDEX initiative. 13 GCM-RCM couples were selected and extracted for the historical (1990–2005) and future (2006–2099) periods for the RCP4.5 and RCP8.5 scenarios. Model outputs were bias-corrected by a multivariate correction approach (*MBCn*, Cannon, 2018).

3. Results and Discussion

SurEau-Ecos-FMC captured well the variations in predawn (ψ_{pd}) and midday (ψ_{md}) leaf water potentials measured at the Puéchabon site over the three studied years (Figure 2A), explaining 98 % (RMSE = 0.27) and 87 % (RMSE = 0.45) of their variance, respectively. *SurEau-Ecos-FMC* also captured relatively well the temporal dynamics of leaf level LFMC (Figure 2B). The model explained 69 % (RMSE = 4.27) and 74 % (RMSE = 4.92) of the variance in the minimum and maximum daily observed LFMC, respectively. This provides further evidence of the relevancy of p-v curves to estimate LFMC from leaf water potential. However, model performance was lower than that obtained for ψ_{pd} and ψ_{md}. A potential gain of performance in LFMC predictions could be attained by taking into account year-to year osmotic adjustments.

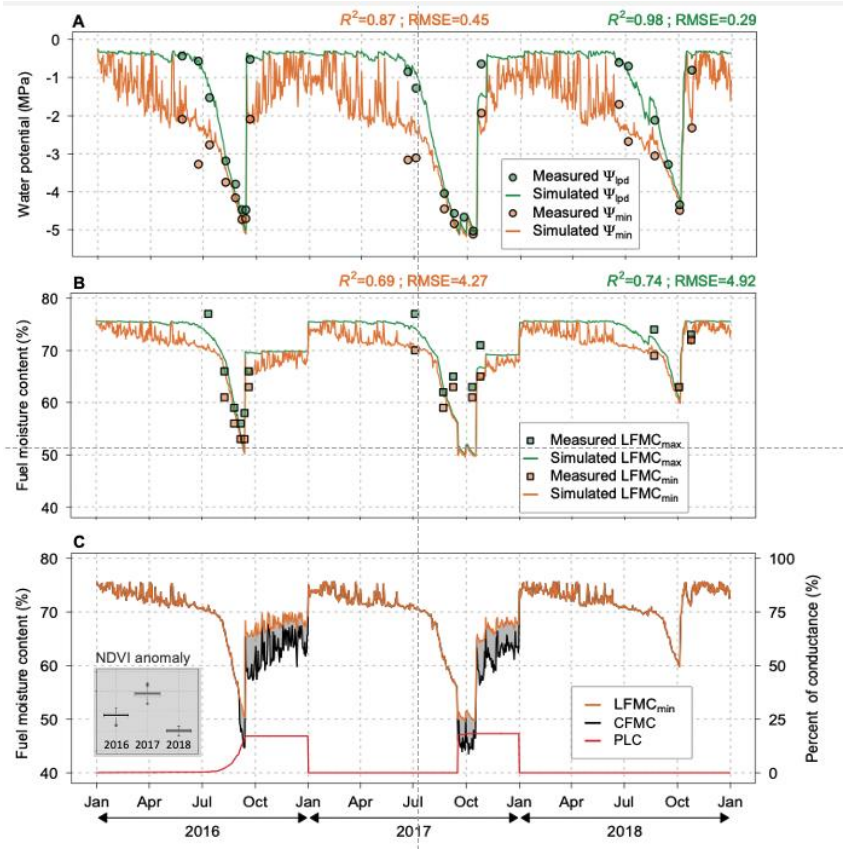

Figure 2- Dynamics of simulated and observed (A) leaf water potential, (B) live fuel moisture content (LFMC) and (C) canopy fuel moisture content (CFMC) for the three studied years. The insert panel in (C) shows the standardized anomaly in NDVI

Our model showed that the conditions observed during the 2016 and 2017 summer droughts (Figure 2C) led to a 20% rate of leaf embolism. This in turn led to a decrease in *CFMC* compared to what was observed at the leaf level. These results are consistent with a higher relative change in NDVI during the year 2016 and 2017 compared to 2018 (insert panel in Figure 2C).

Our projections of fire danger indices based on *CFMC* showed a general increase of fire danger over the next century but with major differences according to the emission scenario (Figure 3A and 3B). $CFMC_{min}$ decreased from 65% to the 62% for end of the century under RCP4.5 but down to 32% under RCP8.5. Similarly, FSL increased from 15 to 20 days per year under RCP4.5 but up to 120 day per year under RCP8.5. A significant part of these trends was due to the increase in drought-induced leaf embolism (Figure 3C) that contribute to decrease LFMC and increase dead to live ratio of foliage in the canopy. More research is need to assess how long do dead leaves might stay on the trees. Plants are also likely to adapt to drier conditions by a series of mechanisms, including long-term reductions in leaf are index, that were not included in the present simulations, but might be explored in future work.

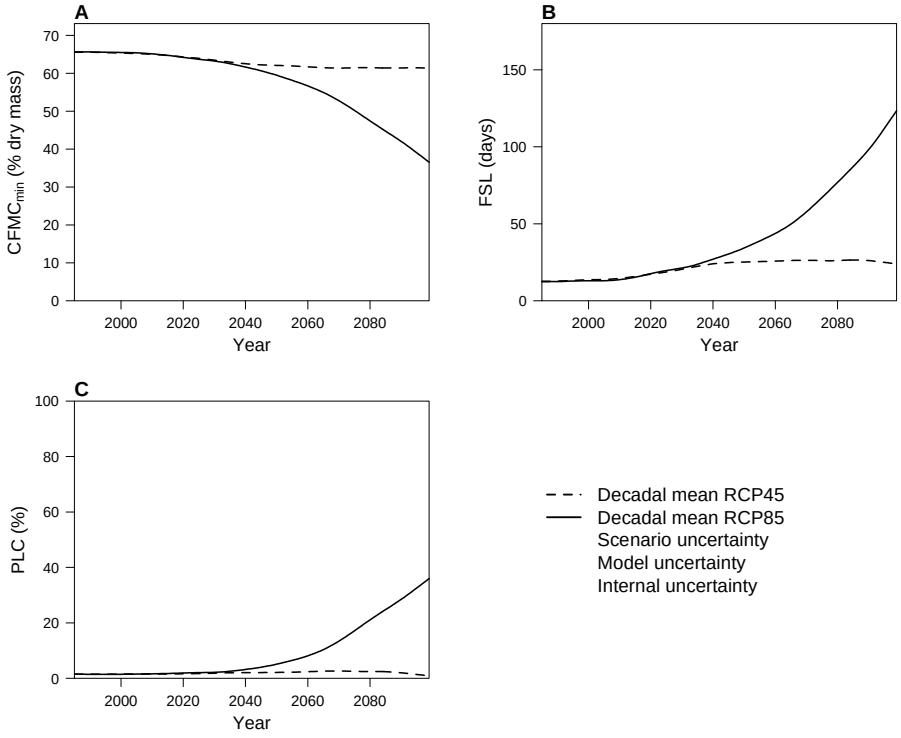

Figure 3- Multi-model projections of fire danger indices and plant cavitation for Quercus ilex at the Puéchabon study site for two emission scenarios (RCP4.5 and RCP8.5). $CFMC_{min}$ is the minimum canopy moisture content reached during the year; FSL is the fire season length, defined as the number of days when CFMC is below the 67% critical threshold.

4. Conclusion

Understanding and predicting FMC is an important prerequisite to increase our knowledge of forest's vulnerability to fires in a changing climate. Here, we developed and validated *SurEau-Ecos-FMC* a mechanistic model predicting *LFMC* and *CFMC* based on plant-hydraulics. We show that leaf embolism might be a growing cause of FMC decrease in a drier climate. We encourage the use of *SurEau-Ecos-FMC* to inform fire models and increase our understanding of the FMC's effect on fire behavior and activity.

5. References

Allen CD et al. (2015). On underestimation of global vulnerability to tree mortality and forest die-off from hotter drought in the Anthropocene. *Ecosphere*, *6*(8), 1-55.

Cochard H et al. (2021). SurEau: a mechanistic model of plant water relations under extreme drought. *Annals of Forest Science*, *78*(2), 1-23.

Nolan RH et al. (2020). Linking forest flammability and plant vulnerability to drought. *Forests*, *11*(7), 779.

Pimont F et al. (2019a). A cautionary note regarding the use of cumulative burnt areas for the determination of fire danger index breakpoints. *International journal of wildland fire*, *28*(3), 254-258.

Pimont F et al. (2019b). Why is the effect of live fuel moisture content on fire rate of spread underestimated in field experiments in shrublands? *International journal of wildland fire*, *28*(2), 127-137.

Rossa CG and Fernandes PM (2018) Short communication: On the effect of live fuel moisture content on fire-spread rate. *Forest Systems* **26**, eSC08.

Ruffault J et al. (2013). Differential regional responses in drought length, intensity and timing to recent climate changes in a Mediterranean forested ecosystem. *Climatic Change*, *117*(1), 103-117.

Ruffault J et al. (2018a). Extreme wildfire events are linked to global-change-type droughts in the northern Mediterranean. *Natural Hazards and Earth System Sciences*, *18*(3), 847-856.

Ruffault J et al. (2018b). How well do meteorological drought indices predict live fuel moisture content (LFMC)? An assessment for wildfire research and operations in Mediterranean ecosystems. *Agricultural and Forest Meteorology*, *262*, 391-401.

Ruffault J et al. (2020). Increased likelihood of heat-induced large wildfires in the Mediterranean Basin. *Scientific reports*, *10*(1), 1-9.

Ruffault J et al. (2022). SurEau-Ecos v2. 0: A trait-based plant hydraulics model for simulations of plant water status and drought-induced mortality at the ecosystem level. *Geoscientific Model Development Discussions*, 1-47.

The effects of fuel moisture on fire spread in shrub vegetation typical of upland heath systems in northern latitudes

Rory M. Hadden*[1]; Zakary Campbell-Lochrie[1]; Vasileios Koutsomarkos[1]; Carlos Walker-Ravena[1]; Eric V. Mueller[1]; Andy F. S. Taylor[2]; I. Jason Owen[2]

[1]School of Engineering, University of Edinburgh, Edinburgh, UK, {r.hadden, Z.Campbell.Lochrie, V.Koutsomarkos, c.walkerravena}@ed.ac.uk,{ericvmueller@gmail.com}
[2]James Hutton Institute, Aberdeen, UK, {andy.taylor, jason.owen}@hutton.ac.uk

**Corresponding author*

Keywords

Heathlands, Fire spread, Fuel moisture content, Energy release, Heat flux, Fuel structure

Abstract

Shrubs are the dominant fuel for wildfires which occur in heathland systems however, there are relatively few studies which explore the processes of flame spread in shrub fuels. A series of laboratory flame spread experiments are used to identify the relationships between the fuel moisture content of the fuel components of heather (Calluna vulgaris) shrubs and the resulting fire spread dynamics. Measurements of energy release, flame spread rate and mass loss are made to characterise the burning of 2 m × 0.75 m fuel beds, and heat flux measurements are made to record the magnitude of the propagating fluxes. Fuel moisture thresholds for fine and coarse fuel elements required for fire spread are identified, and the magnitude of the in-bed heat fluxes are reported. From the observations, it is suggested that the leading edge of the flame front is driven by the moisture content of the fine dead material suspended in the heather canopy while the trailing edge is dominated by the burning of coarser fuels which supports the burning of fine green fuels. These findings allow further targeted experimental study and can be used to aid determination of fire effects.

1. Introduction

Heathlands represent a major fire hazard in many parts of the world. For example, in the UK, 94% of wildfires fires occurred on heathlands (Taylor et al., 2021). The primary vegetation structures on UK heathlands are shrubs (e.g., *Calluna vulgaris, Ulex minor*), mosses and litter. There are also significant areas of upland heaths in the UK with underlying organic peat soils which, if ignited, can result in large release of carbon dioxide to the atmosphere. Despite the significance of these systems globally, there remains relatively little understanding of the drivers of fire spread in these systems. Fires are common in these systems through natural ignitions or through traditional land management practices (Davies et al., 2008). However, climate and land use changes are predicted to alter the intensity, and frequency of fires in these systems and therefore it is necessary to develop a detailed understanding of the mechanisms of fire spread in shrub fuels. This will allow improved fire risk prediction in these systems.

This work seeks to develop a process-based understanding of the fire spread in shrub fuels. Laboratory experiments are used to study the burning of *Calluna vulgaris*-dominated systems under quiescent conditions to identify the drivers of fire spread.

2. Methods

Experiments were carried out in the Rushbrook Fire Laboratory at the University of Edinburgh. Experiments were performed by constructing fuel beds with a nominal area of 2 m × 0.75 m using vegetation harvested locally.

2.1. Fuels: collection and conditioning

The structure of the *Calluna vulgaris* (heather) plant is given in Figure 1. There are three parts of note in the heather plant, older leafy growth which typically comprises fine dead (brown) leaves; younger growth which is

characterised by green leafy growth and flowers; and coarse stems. In addition to the heather, heathlands have a moss and litter layer on the soils.

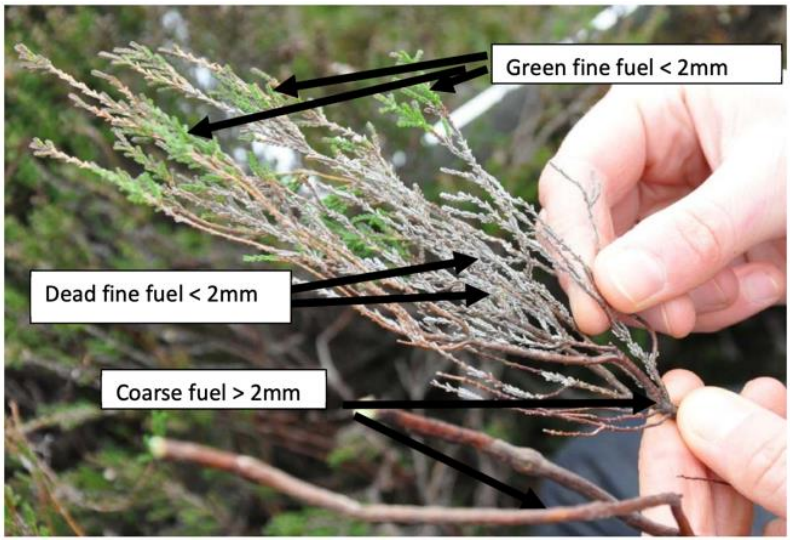

Figure 1 The different fuel types on heather (from Taylor et al., 2021)

Fuels were collected from the Pentland Hills Regional Park near Edinburgh, UK. Fuel samples comprised heather shrubs and the underlying moss and litter. Fuels were harvested in plots of approximate dimensions similar to those of the experimental fuel bed area (2 m × 0.75 m). After harvesting, fuels were stored under laboratory conditions until they were burnt. Prior to each experiment three samples of each of the fine green, fine brown, coarse stems and moss were collected. These were dried in an oven at 80°C for 48 hours to determine the fuel moisture content.

2.2. Experimental procedure

Immediately prior to burning, the fuel beds were assembled on a mineral wool substrate. The moss was distributed uniformly over the fuel bed area and the stems of the heather were pierced through the mineral wool. Care was taken to ensure consistent fuel bed heights and uniform distribution of stems across the area. A length of cotton rope (~0.8 m long) soaked in acetone and laid at the base of the heather was used as the ignition source. This is a strong, repeatable ignition source ensuring even ignition along the full 0.75 m short edge of the fuel bed. After ignition, the fire was allowed to spread (or not) and the test was terminated after flaming combustion had stopped or, if there was significant smouldering of course material, after this had stopped.

2.3. Measurements

Global and local fire behaviour measurements were made to characterise the flame spread and burning of the fuel bed. The whole fuel bed was supported on a load cell to obtain mass loss, total mass lost, and mass loss rate measurements. Heat release was measured by oxygen consumption calorimetry. Visual recordings of the flame spread were used to calculate the flame spread rate.

Local measurements of heat flux were made in three locations: at 2/3 fuel height facing the spreading flame; flush with the surface of the moss, and flush with the surface of the mineral wool substrate. Measurements were made using water cooled heat flux gauges (Huskeflux SBG01). These measurements allow analysis of the magnitude and duration of heating and help guide analysis of dominant heat transfer processes.

3. Results and discussion

An overview of the experimental conditions is given in Table 1. Sixteen experiments were conducted in total. These fall into two categories: experiments 2—7 with reduced measurement and instrumentation and variation in fuel loading and fuel moisture treatments. Experiments 8—17 were carried out with a more consistent fuel loading and fuel moisture treatment regime and also include the heat flux measurements. The fuel loadings are given on a wet basis.

Table 1 The experimental conditions, mass loss, and spread rate

Exp.	Fuel loading, kg/m^2				Fuel moisture content, %				Mass consumed, %	Spread rate, cm/s
	Moss	Heather	Total	Post burn	Fine green	Fine dead	Coarse	Moss/ Litter		
1	--	--	--	--	--			--	--	--
2	1.22	2.24	3.46	1.96	1 day lab conditioned			Dry	43.43	--
3	1.31	3.59	4.90	0.71	2-day lab conditioned			Dry	85.48	1.295
4	0.27	4.97	5.24	0.10	3-day lab conditioned			Dry	98.17	1.622
5	0.75	6.18	6.93	4.80	5-day dry, then wetted (200 g water/kg heather)			Dry	30.79	--
6	0.22	1.84	2.06	--	5-day dry, then wetted (200 g water/kg heather)			Dry	--	--
7	2.57	4.20	6.77	1.78	6-day lab conditioned			Wetted	73.65	1.139
8	0.39	3.11	3.50	3.34	73.69	43.73	77.71	135.26	4.40	--
9	0.39	3.26	3.65	3.57	73.69	43.73	77.71	135.26	2.40	--
10	0.39	29.27	3.06	0.54	23.97	22.17	43.92	23.04	82.20	1.268
11	0.24	3.52	3.75	3.70	112.62	45.88	87.18	222.81	1.55	--
12	0.24	35.78	3.10	1.51	43.95	26.49	53.92	84.39	51.29	0.741
13	0.33	3.50	3.83	3.77	65.32	33.18	59.70	180.17	1.51	--
14	0.33	3.44	3.76	3.52	65.32	33.18	59.70	180.17	6.55	--
15	0.36	3.09	3.46	0.88	41.46	23.77	60.63	48.18	74.64	1.277
16	0.14	2.81	2.95	1.09	70.14	27.26	72.24	27.27	63.01	0.664
17	0.29	2.89	3.18	0.28	46.54	12.54	36.39	66.55	91.23	1.714

Figure 2 shows a composite image of the 16 experiments taken 60 s after ignition to give an indication of the typical behaviours observed. The leading edge of the flame front in experiments 2, 3, 4, 7, 12, 15, 16 and 17 has propagated away from the ignition source and it is assumed that there is no longer an influence of this on the fire spread. Flame heights in these experiments are in excess of 2 m and the flame front has a depth approaching 1 m, indicating a significant degree of combustion behind the leading edge of the flame front. Experiments 5 and 6 remain in the location of the ignition source and flame heights in these cases are approximately 1.5 m. The flame in experiments 8, 9, and 14 are both discontinuous and less than 0.5 m in height. The flames in experiments 11 and 13 have quenched at this time with only residual burning near the ignition source apparent.

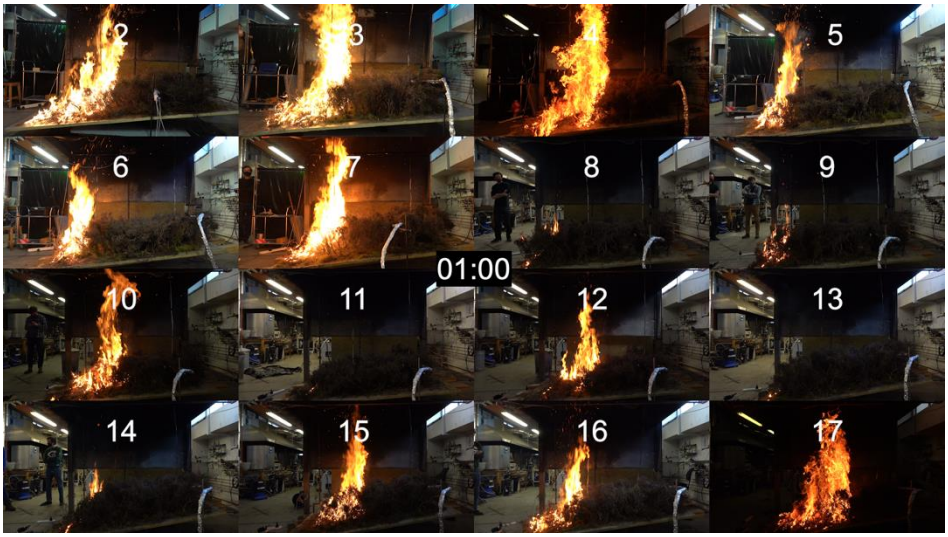

Figure 2 Composite image of laboratory flame spread experiments 60 s after ignition

3.1. Spread rate

The average rate of spread is measured by evaluating the time taken from ignition required for the flame to traverse the entire length of the fuel bed. Flame spread data are only reported when the flame traversed the entirety of the fuel bed. Flame spread rates ranging from 0.66 to 1.71 cm/s were recorded.

The spread rate is shown as a function of the fuel moisture content (FMC) of the different fuel elements in Figure 3. These data indicate that the flame spread rate has a strong dependence on the FMC of the fine dead fuels. The FMC of the fine green and coarse fuel elements also show an increasing trend in spread rate with decreasing FMC. The FMC of the moss does not appear to have a strong influence on the spread rate. It should be noted that in performing this analysis the assumption that the variations in fuel loading between experiments is not significant has to be made.

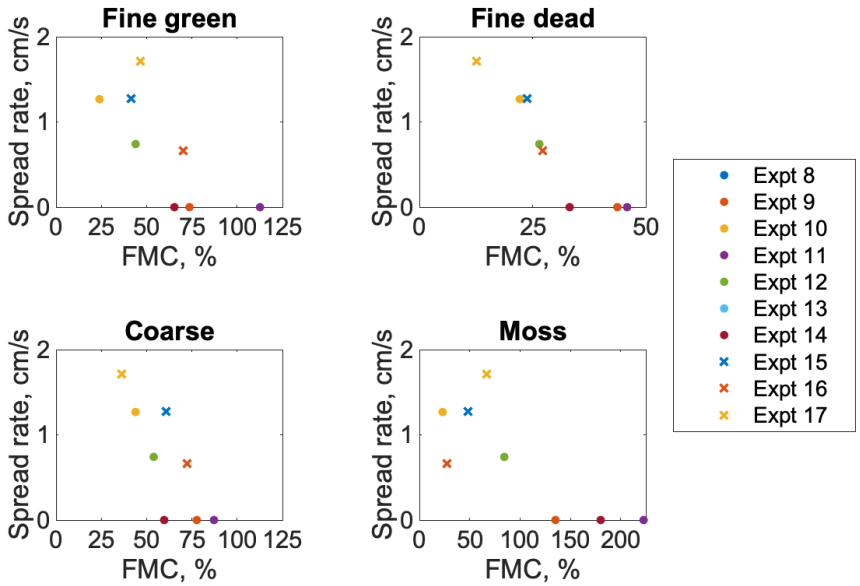

Figure 3 Flame spread rate as a function of the FMC of different fuel elements. Note the different ranges on the x axes.

These data also allow some thresholds for fire spread to be identified by evaluating the lowest FMC at which the fire did not spread and the highest FMC at which the fire did spread for each of the fuel classes to be identified. These are summarised in Table 2.

Table 2 Fuel element FMC thresholds for fire spread

Fuel element	**FMC threshold for spread, %**
Fine green	47—65
Fine dead	26—33
Coarse	54—60
Moss	84—135

3.2. Mass consumed

The total mass lost was recorded using measurements of the total mass of fuel in the fuel bed before ignition and at the end of the experiment. The mass loss ranged from 2 to 98%. Low mass losses were attributed to cases where the fire did not spread beyond the ignition source. For the cases which were identified as spreading through the whole fuel bed, the mass lost ranged from 51 to 98%.

The mass lost is shown as a function of the FMC of the different fuel elements in Figure 4. The total mass lost is again shown to be a function of the FMC for the different fuel elements. Again, there is a strong correlation with the FMC of the fine dead fuel. These data may suggest a stronger relationship between the FMC of the

coarse fuels and the total mass lost compared to the spread rate, however this should be treated with caution due to the interactions between spread rate and heat release rate.

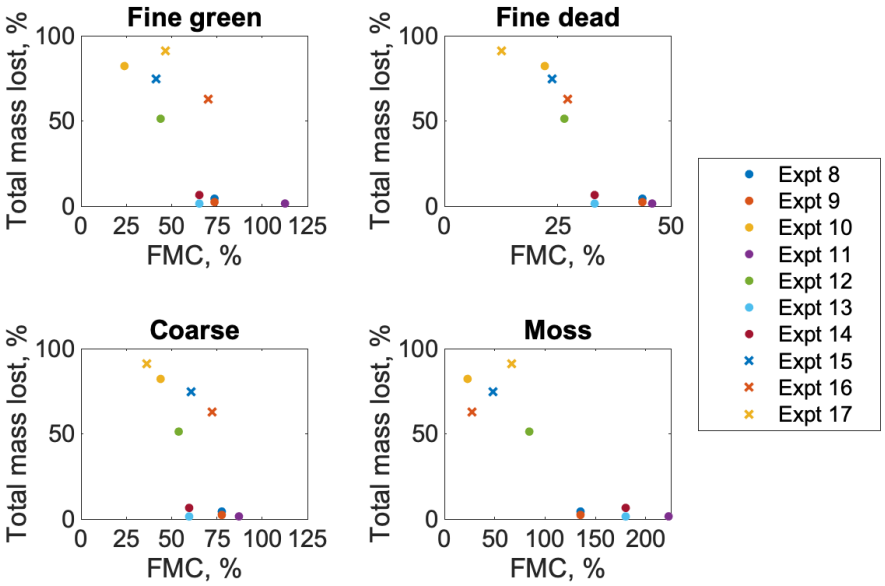

Figure 4 Total mass lost as a function of the FMC of different fuel elements. Note the different values on the x axes.

3.3. Energy release

The observations made until now can be subjected to independent verification using the energy release as measured by oxygen consumption calorimetry. This is shown for experiments 2—7 in Figure 5. The highest energy release exceeded 600 kW for experiment 4. This experiment also had the highest mass consumption (98%). This is due to these fuels having been dried for 3 days in the laboratory. Experiment 3 which also had a high mass consumption (85%) and had been dried for 2 days showed a lower peak energy release with a maximum in the range 400 kW. Similarly experiment 7 with 6 days conditioned dry heather and wetted moss, had a similar peak heat release rate (400 kW). However, this experiment took longer to reach the peak compared to experiment 3 indicating that the combustion of the moss layer, while not significant in determining the overall energy (due to the relatively small mass), may play a role in determining the total energy release under some conditions.

In experiments 2, 5 and 6, the flame did not spread on the full length of the fuel bed. In experiment 2 and 5, 43 and 31% of the mass was consumed indicating partial spread. No measurements of mass lost are available for experiment 6. Consequently, the measured energy release is low for these experiments. The peak in energy release in experiment 6 at around 120 s is attributed to uneven application of water while wetting the heather. These interpretations are confirmed by visual observations.

The energy release data for experiments 10, 12, 15, 16, 17 are shown in Figure 6 (data for experiments 8, 9, 11, 13 and 14 are omitted as no fire spread beyond the point of ignition was observed). These data indicate that there are two clusters: a high energy release cluster with experiments 10, 15 and 17 and a lower energy release grouping with experiments 12 and 16. This is reflected in the spread rate measurements where the spread rates in experiments 10, 15 and 17 were in excess of 1.20 cm/s but for experiments 12 and 16 the rates of spread were 0.74 and 0.66 cm/s, respectively. The higher spread rate in experiment 12 is attributed to the combination of lower moisture content of the coarse and fine green fuel elements compared to experiment 16. The coarse FMC was between 36 and 61% in experiments 10, 15 and 17 meanwhile for experiments 12 and 16 the coarse FMC was 54 and 72%. Likewise, the fine green FMC was between 24 and 47% for experiments 10, 15 and 17 and between 44 and 70% for experiments 12 and 16. For context, should be noted that in field experiments the FMC of the live coarse fuels was approximately 70—80% (Taylor et al., 2021).

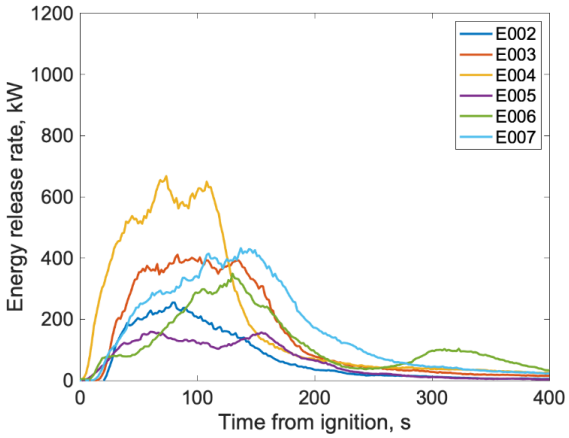

Figure 5 Energy release as a function of time for experiments 2—7.

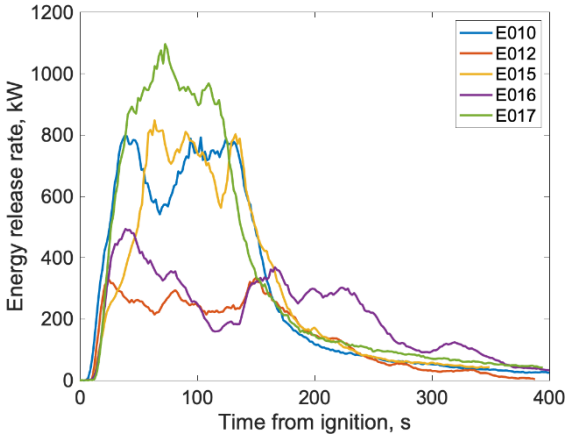

Figure 6 Energy release as a function of time for experiments 10, 12 15, 16, 17.

3.4. Heat fluxes.

The heat fluxes to the mid height of the heather canopy are shown in Figure 7. Only data for experiments in which flame spread was observed to occur on the whole length of the fuel bed are reported. The data show that the heat fluxes through the heather canopy exceed 100 kW/m^2 where there are large flames and significant burning behind the leading edge of the flame e.g., experiments 4, 10 and 17. For experiments with smaller flames with less burning behind the leading edge (e.g., experiment 16), lower heat fluxes are recorded but for extended durations. In cases where the flame thickness is lower (e.g., experiments 7 and 12), the heat flux was between 50 and 100 kW/m^2. Finally, in cases where the flame spread is characterised by a thin flame front, the heat fluxes is around 30kW/m^2. This highlights the importance of the burning behind the leading edge of the flame front in driving the fire spread processes.

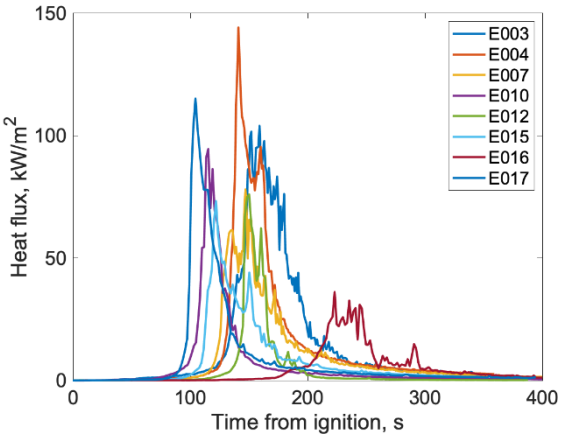

Figure 7 Heat fluxes to the heather canopy as a function of time from ignition.

4. Conclusions

Using laboratory scale experiments, we have observed the effects of different fuel elements on the likelihood for fire spread in *Calluna vulgaris*-dominated systems. These results apply only to laboratory conditions and should not be applied directly to fire danger assessments. The results indicate that the fire spread in heather under these conditions is a complex process in which the interaction between the different components of the fuel structure determines the fire spread characteristics. It seems that the fine brown fuels dominate the leading edge of the fire spread and that radiation from the trailing edge where the coarse fuels are burning supports combustion of fine green fuels. Heat fluxes greater than 100 kW/m^2 are measured from the combustion zone to the heather ahead however the heating lengths are very short. These insights will help develop models for flame spread in shrub fuels, in the development of fire danger systems and in the evaluation of fire impacts.

5. References

Matt G. Davies, Alan Gray, Alistair Hamilton & Colin J. Legg (2008) The future of fire management in the British uplands, The International Journal of Biodiversity Science and Management, 4:3, 127-147, doi: 10.3843/Biodiv.4.3:1

Taylor AFS, Bruce M, Britton AJ, Owen IJ, Gagkas Z, Pohle I, Fielding D, Hadden R (2021) Fire Danger Rating System (FDRS) Report, Available at https://www.hutton.ac.uk/research/projects/scottish-fire-danger-rating-system-sfdrs

The firefighters on the frontline of forest fires – preliminary characterization of Bio4FOX study population

Filipa Esteves[1, 2, 3, 4]*; Joana Madureira[1, 2, 3]; João Paulo Teixeira[1, 2, 3]; Solange Costa[1, 2, 3]

[1]Environmental Health Department, National Institute of Health. Rua Alexandre Herculano, 321, 4000-055 Porto, Portugal, {filipa.esteves, joana.madureira, joao.teixeira, solange.costa}@insa.min-saude.pt
[2]EPIUnit – Instituto de Saúde Pública, Universidade do Porto (ISPUP). Rua das Taipas 135, 4050-600 Porto, Portugal, {filipa.esteves3@hotmail.com},{jvmadureira; jpft12; solange.costa2}@gmail.com
[3]Laboratório para a Investigação Integrativa e Translacional em Saúde Populacional (ITR), Universidade do Porto. Rua das Taipas 135, 4050-600 Porto, Portugal
[4]Department of Public Health and Forensic Sciences, and Medical School, Faculty of Medicine, University of Porto. Alameda Prof. Hernâni Monteiro, 4200-072 Porto, Portugal, {up201406771@up.pt}

Corresponding author

Keywords

Wildland firefighters; Occupational exposure; Health effects; Biomonitoring; Public Health

Abstract

The increased frequency and intensity of forest fires have been concerning populations particularly in countries typically affected by this natural disaster. Portugal has been harshly afflicted by wildfires specially in the north and central regions. In the frontline of forest fire combat there is one of the riskiest occupations in the world – firefighters. Firefighting involves high physical and psychological demanding activities typically performed in hostile environments. The proximity to fire exposes them not only to high temperatures but also to high concentrations of hazardous pollutants, most of which are listed as probable or known carcinogens. Given the above, IARC classified occupational firefighting activity as possibly carcinogenic to humans. However, it is still among the least studied occupations, existing very little information on exposure induced mechanisms that lead to health diseases. Thus, the general aim of Bio4FOX study is to identify a set of (bio)markers for the surveillance of Portuguese Wildland firefighters' occupational exposure during three phases, pre-, during and post- fire season. Here, we aim to describe the preliminary data on sociodemographic and occupational context of the Bio4Fox study population in the pre-fire season.

For the 1st phase of the study were enrolled around 175 wildland firefighters from 14 fire stations located in the northern region of Portugal. Information on sociodemographic data, health status, lifestyle and occupational exposure were obtained via a comprehensive questionnaire. The study group was composed by 143 men and 32 women; the mean age of the group was 37.46±10.85. Most of the firefighters reported to be voluntary (88%; n=155) beginning their activities at young ages; more than half (n=92) started within 17 - 22 years old and 15% (n=26) of the individuals attended firefighters' activities at earlier ages (12-16 years old). The average length of service as firefighter was 15.94±10.23 years. Around 45% (n=79) claimed to spend more than 10 hours in their duties, while 35% (n=62) and 13% (n=22) spend 8-9hours and < 8 hours, respectively. Concerning their risk perception related to exposure to occupational hazards, 80% (n=140) believed to be exposed to smoke, gases, and/or particles and 19% (n=33) to solvents (e.g., combustible). Self-reported symptoms (of last 30 days, not related with cold/flu) were: expectoration (14%; n=24), tiredness (13%; n=22), breath difficulty (9%; n=16), cough (7%; n=13) and wheezing (6%; n=10).

Our preliminary data describes the sociodemographic factors and occupational activities of a group of Portuguese firefighters before the fire-season. This data will be integrated together with the biological and environmental findings collected over different time points of a wildfire season. Bio4FOX will contribute to the establishment of recommendations/good practices to improve firefighters' working conditions, as well support the definition of better policies/prevention strategies highly needed in this sector.

1. Introduction

Portugal is a Mediterranean country extremely prone to forest fires (Schmuck et al., 2014). Unmanaged forest lands with extent fuel loads, high number of unwanted fire ignitions and the hot season periods characterized by dry weather contribute for the incidence and escalation of wildfires. Worryingly, the risk of fire is expected to worsen in the upcoming years and decades fuelled by climate changes through rising temperatures and low

humidity and precipitation levels (Flannigan et al., 2006). The frequency, extent and severity of wildfires, brings an urgent need to focus among a crucial human resource in fire management: wildland firefighters.

Firefighters are the backbone of any firefighting system. In Portugal the number of firefighters (both volunteer and professional) have been decreasing through the years requiring more efforts/longer periods of work from those on service. Firefighting is a physically and psychologically demanding activity and a potentially hazardous occupation (Naeher et al., 2007). During their activities wildland firefighters typically experience long work shifts (up to 24 hours), sleep deprivation, heat stress, exhausting hiking, and exposure to smoke via different routes of exposure (i.e., inhalation, dermal absorption and ingestion) (IARC, 2010). Smoke is a complex mixture that includes several hazardous combustion byproducts, including particulate matter, nitrogen dioxide, carbon monoxide, and volatile organic compounds (VOCs) such as polycyclic aromatic hydrocarbons (PAHs), formaldehyde, toluene, acrolein, xylene. But firefighters are not only exposed during wildfire combat. Their exposure continues long after a fire is extinguished, mainly from contaminated equipment/vehicles. Some of the symptoms reported include eye and respiratory irritation, shortness of breath, nausea, headaches, and dizziness (Reinhardt, 2000). It is known that many of the combustion by-products are associated to adverse health effects (Manisalidis et al., 2020) being some of these compounds classified as potentially/possibly carcinogenic to humans by the International Agency for Research on Cancer (IARC) (IARC, 2010). Several epidemiological studies have described an elevated risk of cardiorespiratory diseases/outcomes (Reinhardt, 2000; Gaughan et al., 2008; Navarro et al., 2019) as well as different types of cancers (e.g., prostate, testicular, non-Hodgkin's lymphoma) (LeMasters et al., 2006). Given the above, IARC has classified occupational firefighting activity as possibly carcinogenic to humans (IARC, 2010). However, firefighter is still among the least studied occupations concerning the exposure-induced mechanisms that lead to adverse health effects. The existing research gaps limits the ability to develop effective measures to protect the health of these workers. The timely occupational risk assessment is utmost importance for early interventions such the suggestion of preventive measures to mitigate the risk of possible adverse health outcomes in firefighters.

Different factors that may modify the relationship between health effects and pollutants exposure must be considered such individual characteristics (e.g., age, body mass index, health status, lifestyle) and other contextual factors such occupational-related variables (e.g., type/frequency of occupational exposures, use of personal protective equipment (PPE), tasks performed, etc.). The application of questionnaires is among the most used methods to collect relevant information in epidemiological studies. Questionnaires is a non-expensive tool that can provide useful information on the duration (past, recent or current) and frequency of certain exposures providing an overview of different risk factors. In combination with other exposure assessment methods such biological and environmental monitoring may provide a comprehensive characterization of firefighters' occupational risks.

Bio4FOX project is an ongoing study that aims to identify a set of appropriate biomarkers for the surveillance of Portuguese wildland firefighters' occupational exposure, evaluating the biological impact of different time-points of exposure through a longitudinal approach (pre-, during and post- fire season). Here, we aim to describe the preliminary data concerning the Bio4Fox study population characterization - sociodemographic and occupational related - in the pre-fire season. Preliminary data collected via self-administered questionnaires will be further used to perform a comprehensive assessment of firefighters' occupational exposure and related health impacts.

2. Methods

Around 175 wildland northern Portuguese firefighters, from 14 fire stations, were involved in this study. Participants were initially fully informed about the nature and the study – in a face-to-face approach - stressing the possibility of stop at any time. In case of acceptance, individuals were asked to sign an informed consent approved by the University of Porto Ethic Committee. The individual characteristics of the participants were collected through a comprehensive questionnaire that was applied in the first phase of the study (pre-exposure; 2021) comprising questions on sociodemographic factors, lifestyle, health status, occupational history (as firefighter or/and other profession) and environmental exposures.

Preliminary data related with the sociodemographic and occupational context are here described through means, standard deviation, percentages, and frequencies. Reported height and weight was used to calculate Body Mass Index (BMI - kg/m^2).

3. Results/Discussion

We present preliminary data collected from 175 professionally active firefighters - 143 males and 32 females. A greater proportion of men performing firefighting activities is part of the Portuguese reality; in 2016 there were about 28308 firefighters, being 5119 woman and 23189 men (INE, 2016). The mean age of participants was 37.88±11.03 and 35.62±9.99 for men and woman, respectively. BMI of this group of firefighters was 27.35±4.08kg/m2. According to World Health Organization criteria only 27% (n=48) were in the category of normal weight (range, 18.5–24.9 kg/m2) with the remainder, 41% (n=73) and 24% (n=43), being either pre-obese (range, 25.0–29.9 kg/m2) and obese (≥ 30.0 kg/m2) correspondingly. Previous studies also found higher rates of overweight levels (BMI ≥ 25 kg/m2) in firefighters when compared with the general population (Poston et al., 2011; Soteriades et al., 2011).

A total of 56% (n=98) reported to have accomplished the 12th grade, 24% (n=43) claimed to have the 9th grade or less and only 13% (n=23) declared to have completed university education. The majority of the participants (88%; n=155) reported to be voluntary firefighters, a common trend verified in the Portuguese firefighting system. The average length of service in firefighting activities was 15.94±10.23 years indicating a considerable life period of firefighting exposures. In fact, data shows that around 15% (n=26) of the individuals began their firefighters' activities (i.e., learning/training) between 12 – 16 years old, whereas more than a half (52%; n=92) started their activities within 17 and 22 years old. Around 26% (n=46) of individuals only started after turning 23 years old.

Regarding functions performed in firefighter activity, 30% (n=53) reported to have driver functions, 27% (n=47) indicated to provide support to emergency services, 26% (n=46) incorporate the permanent intervention team (EIP), 10% (n=18) mentioned to be telephone operator, 7% (n=12) to perform rescue activities, 7% (n=12) reported to have command activities and 1% (n=2) declared to have administrative functions. Concerning the mean time/day spend in some of the referred activities, long periods of work were reported: the most of firefighters (45%; n=79) spend more than 10 hours in their duties, while 35% (n=62) and 13% (n=22) spend 8-9hours and less than 8hours, respectively.

Firefighters are exposed to different hazards in their occupational context. Figure 1 presents an overview of the occupational exposures that were referred by the participants.

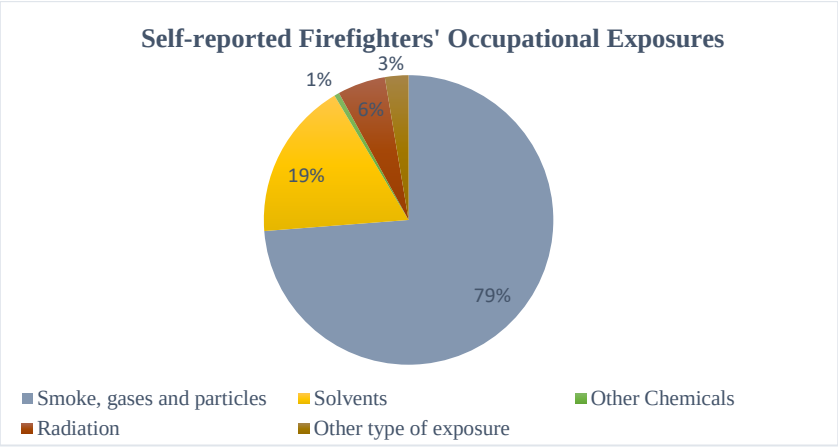

Figure 1 - Percentage of individuals that reported to be exposed to different hazards.

Data indicates that firefighters are mostly exposed (according to their risk perception) to smoke, gases and particles in their activities. Indeed, firefighters may be required to participate in firefighting activities (e.g., fire suppression, fuel management) with a certain regularity. As example, around 15% (n=27) of individuals reported to be exposed to fire in the week before, indicating a mean period of exposure of 2.08±6.66 hours/week.

Although in fewer proportions, firefighters also stated to be exposure to solvents (e.g., combustible), radiation and other type of exposures/chemicals.

When asked about the use of PPE during participation on firefighting activities, most individuals (97%; n=170) reported to use PPE, such protective clothes, boots, respiratory protection, gloves, protective glasses and helmet. PPE to be used by firefighters during their activities is regulated (Despacho nº3974, 2013) however, there is a general reluctance to wear protection since it adds physiological demands and heat stress upon the user (IARC, 2010) and the respiratory protection typically used is not ideal to effectively protect firefighters in wildfires context (Austin, 2008).

Concerning the health problems, 3% (n=6) of the individuals reported having diagnosed respiratory problems and 2% (n=3) heart disease. Figure 2 shows the felt symptomology in the last month (non-related with colds/flu).

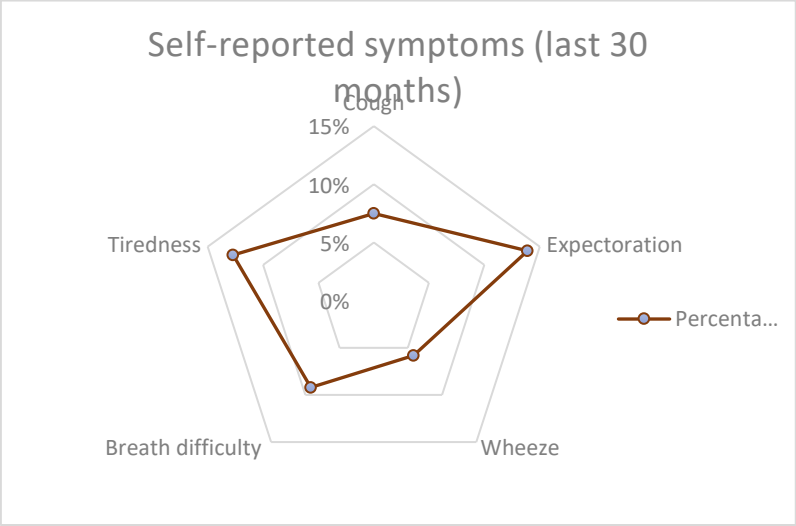

Figure 2 – Percentage of self-reported symptoms in the last 30 days among study group.

Expectoration (14%; n=24) and tiredness (13%; n=22) were the most common symptoms reported, followed by breath difficulty (9%; n=16), cough (7%; n=13) and wheezing (6%; n=10).

Regarding some aspects of their lifestyle, 31% (n=55) declared drinking alcohol regularly; 18% (n=31) have a daily consumption of wine whereas 23% (n=41) have a daily consumption of beer. In this group, thirty-eight percent (n=67) of individuals never smoked, 22% (n=38) were former smokers and 37% (n=65) current smokers (mean of 15 cigarettes/day).

4. Conclusions and future perspectives

There are no doubts that firefighters have one of the most dangerous and demanding occupations in the world being exposed to a variety of hazards. In the present study, we observed a high percentage of firefighters that indeed assumed to be exposed to particles, smoke and gases in their occupational context. This finding is particularly concerning due the long periods of work and the length of service that were described. Firefighters may have different physical and psychological demanding tasks that are many times accompanied by dangerous exposures. The stressful nature of this occupation may be related with some individual behaviours (e.g., smoking habits, alcohol consumption, high BMI) that were here observed.

Overall, present findings offer a glimpse of Bio4Fox study population. The characterization of population is a very important step to have a broad perspective of the relevant factors that must be considered in further analysis.

This ongoing study is expected to contribute for a comprehensive risk assessment of firefighting occupational exposure and for the establishment of recommendations/good practices to improve firefighters' working conditions as well as for the definition of policies and prevention strategies highly needed in this sector. The characterization of Portuguese firefighters' occupational exposure and potential health risks is particularly relevant because Portugal is one of the European countries more highly affected by forest fires. Finally, it is also essential to promote a wise fuel management in forests, because reducing the amount of fuel or changing

its arrangement before a wildfire can prevent or attenuate severe fire behaviors as well its impacts on human health.

5. Ackowlegments

This work received financial support by the project PCIF/SSO/0017/2018 by the Fundação para a Ciência e a Tecnologia (FCT), Ministério da Ciência, Tecnologia e Ensino Superior (MCTES) through national funds. Filipa Esteves, recipient of PhD grant UI/BD/150783/2020, is supported by FCT and by the European Social Fund (ESF). Joana Madureira, under the grant SFRH/BPD/115112/2016, is supported by FCT and by ESF, through Programa Operacional Capital Humano (POCH). The authors also acknowledge the ISPUP (UIDB/04750/2020) and ITR (LA/P/0064/2020).

6. References

Austin, C. (2008). Wildland Firefighter Health Risks and Respiratory Protection (Report R-572). Montreal, Quebec, Canada: IRSST (Institut de recherche Robert-Sauvé en santé et en sécurité du travail).

Flannigan, M. D., Amiro, B. D., Logan, K. A., Stocks, B. J., & Wotton, B. M. (2006). Forest Fires and Climate Change in the 21ST Century. Mitigation and adaptation strategies for global change, 11(4), 847-859. doi:10.1007/s11027-005-9020-7.

Gaughan, D. M., Cox-Ganser, J. M., Enright, P. L., Castellan, R. M., Wagner, G. R., Hobbs, G. R., Bledsoe, T. A., Siegel, P. D., Kreiss, K., & Weissman, D. N. (2008). Acute upper and lower respiratory effects in wildland firefighters. Journal of occupational and environmental medicine, 50(9), 1019-1028.

IARC. (2010). Painting, firefighting, and shiftwork (Vol. 98): IARC Press, International Agency for Research on Cancer.

INE, I.P., (2016). Inquérito às entidades detentoras de corpos de bombeiros.

LeMasters, G. K., Genaidy, A. M., Succop, P., Deddens, J., Sobeih, T., Barriera-Viruet, H., Dunning, K., & Lockey, J. (2006). Cancer risk among firefighters: a review and meta-analysis of 32 studies. Journal of occupational and environmental medicine, 48(11), 1189-1202.

Manisalidis, I., Stavropoulou, E., Stavropoulos, A., & Bezirtzoglou, E. (2020). Environmental and health impacts of air pollution: a review. Frontiers in public health, 8.

Naeher, L. P., Brauer, M., Lipsett, M., Zelikoff, J. T., Simpson, C. D., Koenig, J. Q., & Smith, K. R. (2007). Woodsmoke health effects: a review. Inhalation toxicology, 19(1), 67-106.

Navarro, K. M., Kleinman, M. T., Mackay, C. E., Reinhardt, T. E., Balmes, J. R., Broyles, G. A., Ottmar, R. D., Naher, L. P., & Domitrovich, J. W. (2019). Wildland firefighter smoke exposure and risk of lung cancer and cardiovascular disease mortality. Environmental Research, 173, 462-468.

Poston, W. S., Haddock, C. K., Jahnke, S. A., Jitnarin, N., Tuley, B. C., & Kales, S. N. (2011). The prevalence of overweight, obesity, and substandard fitness in a population-based firefighter cohort. Journal of occupational and environmental medicine, 53(3), 266.

Reinhardt, T. E. (2000). Smoke exposure at western wildfires (Vol. 525): US Department of Agriculture, Forest Service, Pacific Northwest Research Station.

Soteriades, E. S., Smith, D. L., Tsismenakis, A. J., Baur, D. M., & Kales, S. N. (2011). Cardiovascular disease in US firefighters: a systematic review. Cardiology in review, 19(4), 202-215.

Schmuck, G., San-Miguel-Ayanz, J., Camia, A., Durrant, T., Boca, R., Liberta`, G., Petroliagkis, T., Di Leo, M., Rodriguez Aseretto, R., Boccacci, F., Schulte, E. (2014). Forest Fires in Europe, Middle East and North Africa 2013. Retrieved from https://publications.jrc.ec.europa.eu/repository/handle/JRC91373.

The Flames Catalogue: an engineering tool to predict flame geometry

Juan Antonio Muñoz[1]; Elsa Pastor*[1]; Paulo M. Fernandes[2]; Miguel Cruz[3]; Eulàlia Planas[1]

[1] Centre for Technological Risk Studies (CERTEC), Universitat Politècnica de Catalunya. Avinguda Eduard Maristany 16, 08019, Barcelona, Spain {juan.antonio.munoz, elsa.pastor, eulalia.planas}@upc.edu
[2] Centro de Investigação e Tecnologias Agroambientais e Biológicas, Universidade de Trás-os-Montes and Alto Douro. Quinta de Prados, 5000–801 Vila Real, Portugal, {pfern@utad.pt}
[3] Commonwealth Scientific and Industrial Research Organisation. GPO Box 1700, Canberra, ACT 2601, Australia, {miguel.cruz@csiro.au}

**Corresponding author*

Keywords

Flame length; Flame angle; Fire safety

Abstract

Flames can be geometrically described from a simplified perspective by means of their length (or height), angle and depth. These parameters are key for fire safety calculations, to prevent injuries during entrapments or to design preventive infrastructures. Most methods to estimate flame geometry require information on fire behaviour (e.g. rate of spread or fireline intensity), which are not always available or straightforward. Within this context, we are developing a tool to estimate flame geometry only from environmental parameters (fuel, weather and terrain) and without the need of fire behaviour predictions beforehand. To achieve this, we have gathered data on field-scale fires and used them to fit binary logistic regressions, to obtain the probability of occurrence of a certain flame geometry for specific fuel structures. We have already modelled flame length probability from fine fuel load, moisture content and wind speed in different fuel structures and flame angle probability from fine fuel load and wind speed in grasslands. We are currently working to extend the dataset and cover a wider range of fuel structures and conditions.

1. Introduction

Wildfire flames are a complex and transient phenomenon, but can be geometrically described from a simplified perspective by means of their length (or height), angle, depth (Figure 1) and residence time.

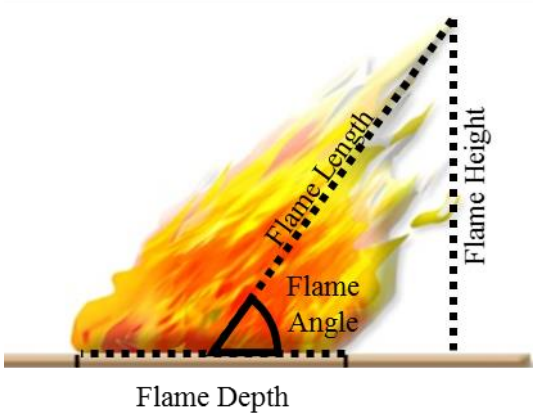

Figure 1- Flame geometry sketch.

Flame geometry is key for fire safety calculations involving radiative energy transfer, such as to estimate firefighter safety and survival zones (Page & Butler, 2017; Butler, 2014) or as input to solid flame models (*e.g.* Eisenberg *et al.*, 1975) to design preventive infrastructures by comparing the radiation profile with the resistance threshold of the elements to protect (*e.g.* Ricci *et al.*, 2021; Standards Australia, 2009). Several works attempted to estimate flame geometry from empirical and physical models (*e.g.* Alexander & Cruz, 2012; Nelson *et al.*,

2012; Anderson *et al.*, 2006), an approach that requires information on fire behaviour beforehand, namely rate of spread and intensity.

To overcome the need of *a-priori* fire behaviour predictions, our aim is to build a "Flames Catalogue" to estimate flame geometry for particular sets of environmental conditions (fuel, weather and terrain). The catalogue will consist on typical scenarios of interest for fire management linked to the range of expected flame geometries. In this short paper we present the current status of this tool and its potential to predict flame geometry in different fuel structures.

2. Methodology

2.1. Data gathering

We have gathered data from field-scale fires. These data consisted of environmental parameters (weather, terrain and fuel) and flame geometries (flame length and angle) from observations and measurements during wildfires and field experiments. We have excluded data from indoor experiments, wind-tunnel experiments and prescribed burnings, in which the aim of the burn constrains the free spread of the flame front. The sources of the data were the BONFIRE (Fernandes et al., 2020), Anderson et al. (2006) and CERTEC (unpublished) databases.

In this communication, environmental parameters refer to weather (wind speed) and fuel (Fine fuel load and moisture content of the dead fraction). We grouped the data in three fuel structures: open grasslands, open shrublands and undercanopy fuels (a mixture of litter, grasslands and shrublands). Flame geometries refer to flame length and flame angle, expressed in accordance with Figure 1.

2.2. Data modelling

We used these data to fit binary logistic regressions and estimate the likelihood of occurrence of certain flame length and flame angle at a given set of environmental parameters. Binary logistic regressions have the form of Eq. 1, with a logit of the form of Eq. 2:

$$P(Y = 1|X) = \frac{e^{f(x)}}{1 + e^{f(x)}} \quad \text{Eq. 1}$$

$$f(x) = \beta_0 + \sum_{i=1}^{i=n} \beta_i Var_i \quad \text{Eq. 2}$$

Where $P(Y = 1|X)$ is the probability of occurrence of an event under certain conditions (*e.g.* the probability of flames being smaller than 3 meters when fire burns dry grasslands with a fine fuel load of 1 kg/m^2 in still air). β_0 is a constant parameter and β_i are coefficients for the different independent variables (Var_i), namely fine fuel load (ffl), wind speed measured at a height of 2 (U_2) or 10 meters (U_{10}) and fuel moisture content of the dead fraction (FMC_d). The relation between an event and a predictor is expressed by means of its odds ratio; odds ratios greater than 1 indicate that the event is more likely to occur as the predictor increases, while odds ratios lower than 1 indicate that the event is less likely to occur as the predictor increases.

3. The Flames Catalogue

3.1. Flame length

Flame length results from the equilibrium between the release of pyrolysis gases, the diffusion of oxygen and the transmission of heat, among other factors involving combustion (Finney *et al.*, 2021). Generally, greater fuel loads (especially fine fuels) are a sign of a greater release of pyrolysis gases and hence larger flame lengths. Most models developed to predict flame length require fire behaviour predictions (*e.g.* Alexander & Cruz, 2012). Our approach dismisses fire behaviour predictions and relies exclusively on environmental parameters to predict flame length, which makes it easier to use for fire managers. To fit the binary logistic regressions, we used ffl for shrublands, ffl and U_2 for understory fuels and ffl, U_2 and FMC_d for grasslands. Table 1 shows the constant parameters and coefficients to fit Eq. 2 and Figure 2 computes Eqs. 1 and 2 to show the probability of having flames smaller than a certain length as a function of the expected variables. Data used to fit the model

covered up to 3 kg/m², 1.2 kg/m² and 1.5 kg/m² of fine fuels in shrublands, grasslands and understory fuels respectively, 25 % of moisture content in grasslands and 25 km/h of wind speed.

Table 1- Constant parameters and coefficients for logistic regressions to estimate flame length probability from fine fuel load (ffl), wind speed at 2 meters above the ground (U_2) and fuel moisture content of dead fuels (FMC_d). "FL" stands for Flame Length (m). Underlined values indicate p<0.05 in Pearson goodness of fit test.

		FL ≤ 0.5	FL ≤ 1	FL ≤ 2	FL ≤ 3	FL ≤ 4	FL ≤ 6	Odds ratio
Shrubland	β_0	3.10	3.88	3.68	4.79	4.57	4.91	-
(n = 117)	β_{ffl}	– 6.22	– 5.74	– 3.72	– 3.34	– 2.32	– 1.80	0.05±0.06
Grassland	β_0	0.96	2.10	2.78	4.06	5.64	-	-
(n = 173)	β_{ffl}	– 5.87	– 5.52	– 5.05	– 5.23	– 5.00	-	0.01±0.002
	β_{U_2}	0.08	0.06	0.05	0.08	0.07	-	1.07±0.01
	β_{FMC_d}	– 0.11	– 0.14	– 0.09	– 0.08	– 0.15	-	0.89±0.02
Understory	β_0	1.42	2.15	4.49	6.66	8.98	-	-
(n = 395)	β_{ffl}	– 1.94	– 0.99	– 1.51	– 2.11	– 2.51	-	0.18±0.11
	β_{U_2}	– 0.36	– 0.30	– 0.41	– 0.51	– 0.66	-	0.64±0.09

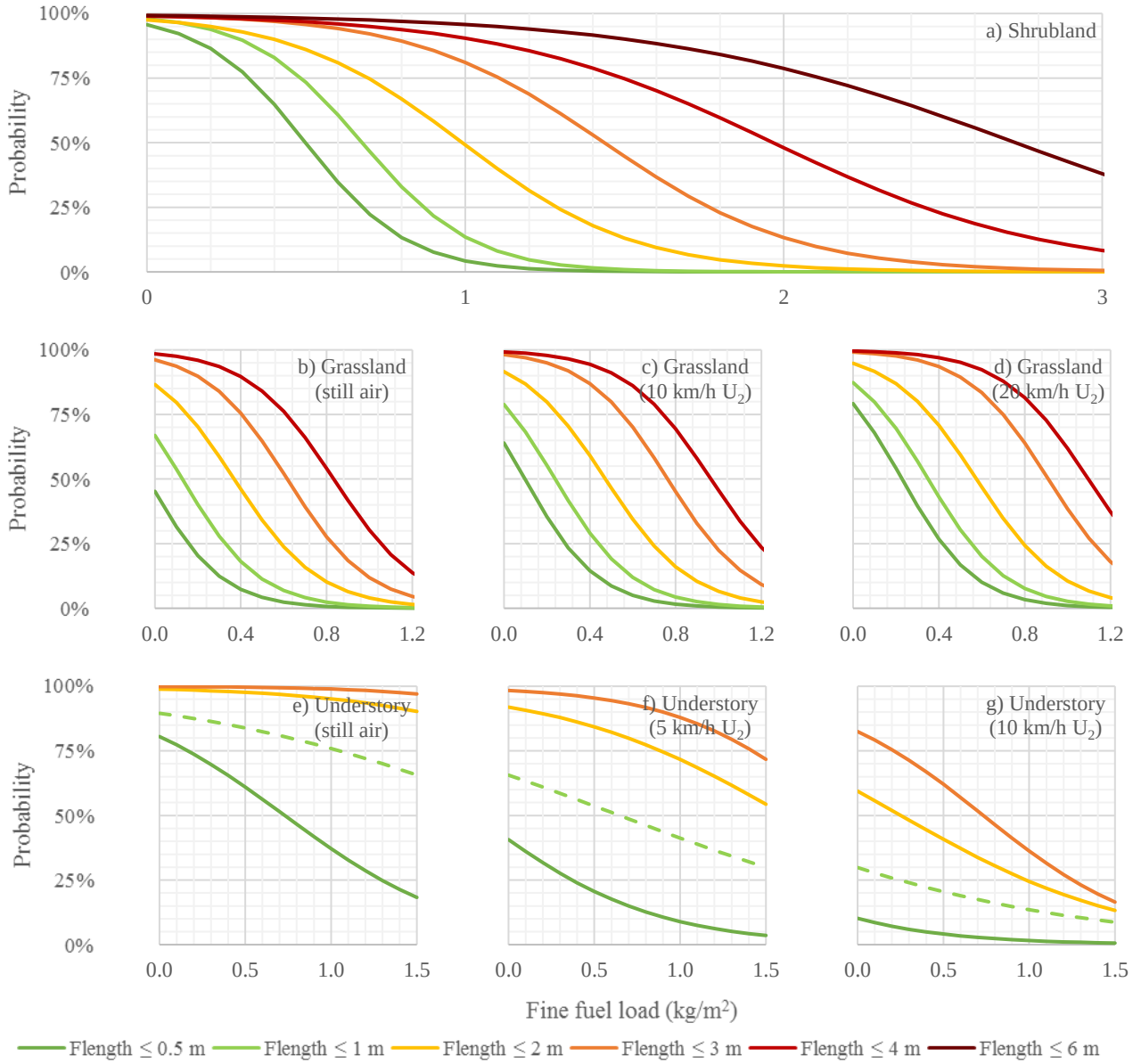

Figure 2- Logistic regressions to estimate flame length probability (y-axis) from the variables in Table 1. Dashed lines indicate p<0.05 in Pearson goodness of fit test.

3.2. Flame tilt angle

Flame tilt angle results from the equilibrium between buoyancy forces, that raise the fire plume, and wind, that pushes the flame forward (Finney *et al.*, 2021). Most models developed to predict flame angle require fire behaviour predictions (*e.g.* Nelson *et al.*, 2012). Our approach uses fine fuel load (ffl) as a proxy for buoyancy forces and wind speed at 10 meters above the ground (U_{10}), dismissing fire behaviour predictions and making it easier to use for fire managers.

Table 2 shows the constant parameters and coefficients to fit Eq. 2 and Figure 3 uses Eqs. 1 and 2 to show the probability of having flames with a certain angle from grassfires. Data used to fit the model covered up to 1 kg/m^2 of fine fuel load and 35 km/h of wind speed.

Table 2- Constant parameters and coefficients for logistic regressions of flame angle in grasslands.

		α < 80	**α < 60**	**α < 45**	**Odds ratio**
Grasslands	β_0	0.601	– 0.787	– 1.85	-
(n = 211)	β_{ffc}	– 2.311	–1.867	– 2.970	0.10±0.05
	$\beta_{U_{10}}$	0.235	0.152	0.105	1.18±0.08

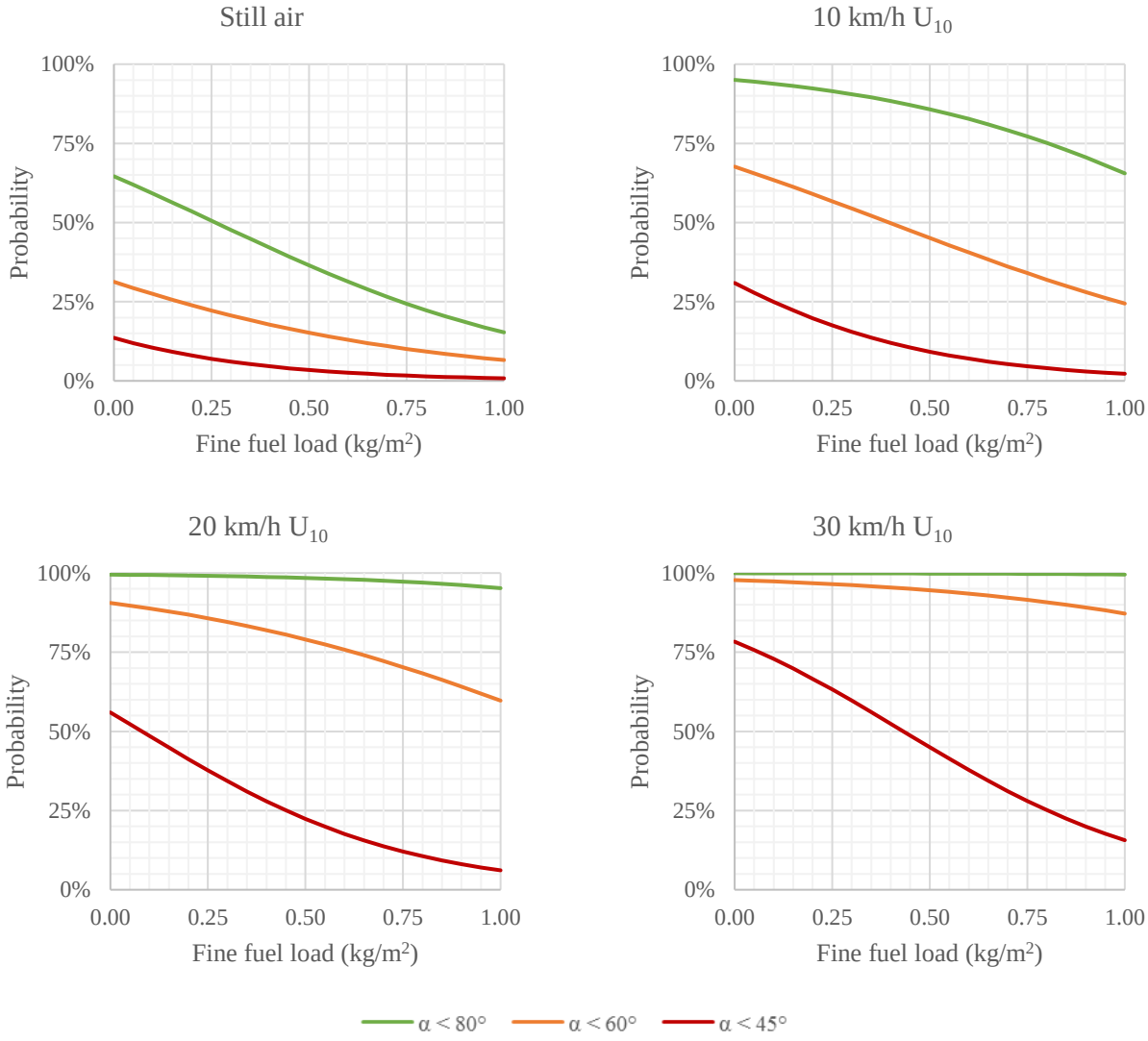

Figure 3- Logistic regressions to estimate flame angle in grasslands.

3.3. Study case

As part of the fire prevention program, the Fire Service is building safety areas for sheltering in a firebreak network. This firebreak network is surrounded by shrublands, with a fine fuel load of 1 kg/m^2. These safety

areas have been dimensioned for flames of 6 meters, at most. The Fire Service aims to outline their validity, with an acceptance threshold of 95% probability. Using Eqs. 1 and 2 and data in Table 1 for shrublands, the probability of flames equal or smaller than 6 meters is 96%, which is acceptable.

4. Conclusions

We have presented a novel approach to predict flame geometry from environmental parameters and fuel consumption, independent of *a priori* fire behaviour knowledge. With it, it is possible to manage fire prevention from a small number of inputs, easily measurable in the field. This Flames Catalogue does not intend to substitute empirical and physical approaches to estimate fire geometry, but to serve as a complementary tool for fire managers.

Prior to develop a definitive tool, the dataset should be extended to cover existing gaps, like the prediction of flame angles with fuel structures other than grasslands, or introducing slope values in the logit functions for flame length. Some obstacles to reach this goal are the lack of common criteria to measure flame geometry among the various existing studies and the difficulty to perform accurate measurements during large experiments and wildfires. The Flames Catalogue is aimed to include other important parameters such as flame depth or residence time.

5. Acknowledgements

This research was funded by the project PID2020-114766RB-100 of MCIN/ AEI /10.13039/501100011033. The first author acknowledges the Spanish Ministry of Universities for the funds from the FPU program.

6. References

Alexander, M. E. & Cruz, M. G. (2012). Interdependencies between flame length and fireline intensity in predicting crown fire initiation and crown scorch height. *International Journal of Wildland Fire*, 21(2), 95-113.

Anderson, W., Pastor, E., Butler, B., Catchpole, E., Dupuy, J. L., Fernandes, P., Guijarro, M., Mendes-Lopez, J. M. & Ventura, J. (2006). Evaluating models to estimate flame characteristics for free-burning fires using laboratory and field data. *Forest Ecology and Management*, (234), S77.

Arnaldos, J., Giménez, A., Navalón, X., Pastor, E., Planas, E. & Zárate, L. (2003). Manual d'enginyeria per a la prevenció i extinció d'incendis forestals. Centre d'Estudis del Risc Tecnològic: Barcelona, Spain.

Butler, B. W. (2014). Wildland firefighter safety zones: a review of past science and summary of future needs. *International Journal of Wildland Fire*, *23*(3), 295-308.

Eisenberg, N. A., Lynch, C. J., & Breeding, R. J. (1975). *Vulnerability model. A simulation system for assessing damage resulting from marine spills*. Enviro control inc rockville md.

Fernandes, P. M., Sil, A., Rossa, C. G., Ascoli, D., Cruz, M. G., Alexander, M. E. (2020). Characterizing fire behavior across the globe. In: Hood, S., Drury, S., Steelman, T., Steffens, R. (tech. eds), The Fire Continuum—Preparing for the Future of Wildland Fire: Proceedings of the Fire Continuum Conference. 21-24 May 2018, Missoula, MT. Proc. RMRS-P-78. Fort Collins, CO: U.S. Department of Agriculture, Forest Service, Rocky Mountain Research Station. pp. 258-263.

Finney, M. A., McAllister, S. S., Forthofer, J. M., & Grumstrup, T. P. (2021). *Wildland Fire Behaviour: Dynamics, Principles and Processes*. CSIRO publishing.

Nelson, R. M., Butler, B. W. & Weise, D. R. (2012). Entrainment regimes and flame characteristics of wildland fires. *International Journal of Wildland Fire*, *21*(2), 127-140.

Page, W. G., & Butler, B. W. (2017). An empirically based approach to defining wildland firefighter safety and survival zone separation distances. *International Journal of Wildland Fire*, *26*(8), 655-667.

Ricci, F., Scarponi, G. E., Pastor, E., Planas, E., & Cozzani, V. (2021). Safety distances for storage tanks to prevent fire damage in Wildland-Industrial Interface. *Process Safety and Environmental Protection*, 147, 693-702.

Standards Australia, A. S. 3959-2009: Construction of Buildings in Bush Fire Prone Areas.

Wotton, B. M., Gould, J. S., McCaw, W. L., Cheney, N. P. & Taylor, S. W. (2011). Flame temperature and residence time of fires in dry eucalypt forest. *International Journal of Wildland Fire*, *21*(3), 270-281.

The influence of packing ratio on forest fuel fire spread on a laboratory scale: no wind, no slope

Hanane Boutchiche[1]; Adel Sahila[1]; Luís Reis[2]; Domingos Xavier Viegas[2]; Nouredine Zekri*[1]

[1]Université des Sciences et de la Technologie d'Oran, LEPM BP 1505 El Mnaouer Oran, Algeria, {hananelimang@gmail.com, sahilaadel@yahoo.fr, nzekri@univ-usto.dz}
[2] Association for the Development of Industrial Aerodynamics, Forest Fire Research Center, University of Coimbra, Portugal, {luis.reis, xavier.viegas}@dem.uc.pt

**Corresponding author*

Keywords

Packing ratio, rate of spread, optical length, flame height, mass-loss rate.

Abstract

The influence of Pinus Pinaster needles packing ratio on fire spread at laboratory scale is investigated experimentally and compared to other wildland fuels. The packing ratio was varied from up to 10% by changing the fuel bed load and thickness. An optimum ratio of 5.5% is obtained corresponding to a maximum rate of spread. This optimum ratio is close to that found by Rothermel for crib fuels. However, the rate of spread increases again for higher porosity, which suggests the existence of a second optimum ratio. Two optimum ratios were also observed by Rothermel for excelsior fuels and recently by He et al for experiments using laser-cut cardboard. Recently, two optimum ratios corresponding to a minimum ignition time were observed using Pinus Halepensis needles. The minimum ignition time for spreading fuels correspond to a maximum rate of spread. These ratios have been attributed to a maximum heat flux absorption by the fuel. The heat flux absorption effect on the rate of spread is discussed by using the fuel optical length. The obtained optimum ratio corresponds to a small optical length ($12\ mm$), which means that the heat flux is absorbed by the surface of the fuel bed. The second optimum ratio may correspond to an optical length much larger than the fuel bed thickness (around $50\ mm$). This corresponds to a bulk absorption of the heat flux. Further analyses of the mass-loss rate are provided to discuss thermochemical effects.

1. Introduction

Forest fire behavior is still far to be understood, due to the large variety of wildland fuels and their complex structure and composition. Burning conditions may vary significantly from one region to another because of the fuel spatial distribution induced by their moisture, density, surface-to-volume ratio, and packing ratio. The packing ratio has been found to influence directly the fire propagation (Z. Campbell-Lochrie et al, 2021), and the observed optimum ratio has been attributed to thermochemical effects (Rothermel, 1972). Further investigations suggest that the packing ratio directly affects radiative heat transfer to the fuel bed surface (Simeoni et al, 2011). A recent experimental study on a discrete fuel bed composed of laser-cut cardboards found that internal heat transfer affects the rate of spread (ROS) in the case of dense fuel (He et al, 2021). Heat transfer has been found recently to be the main cause of the non-monotonic behavior of ignition time as a function of packing ratio (Boutchiche et al, submitted). This work aims to highlight the relation between ROS behavior and absorbed heat flux at different packing ratios.

2. Experimental setup

Pinus Pinaster needles dried naturally with a moisture content of about 10% are used in this work. The vegetation is weighed and spread out on a square table of $0.8 \times 0.8\ m^2$ size that is placed on a digital balance A&D HW-100KGL with a resolution of $10\ g$ and a recording frequency of $1\ Hz$. The weight is recorded on a computer through a data acquisition software RSKey v.1.40 see Fig.1. To follow the variation of the height of the flame an optical video camera Sony FDR-AX53 and an infrared camera SC660 from FLIR were placed on the front of the table while a second optical video camera Sony HXR-NX30E was placed laterally to the table. The resulting videos were converted into images, and the flame height was manually measured against a vertical scale placed close to the sample.

Figure 1: The experimental setup at the Fire Laboratory of ADAI (Coimbra).

The samples are ignited at one side, and the variation with time of the front position was recorded to estimate the ROS. The fuel bed packing ratio $\boldsymbol{\varphi}$ is varied by varying its mass ($\boldsymbol{m}$) and height ($\boldsymbol{e_b}$) according to the following equation:

$$\boldsymbol{\varphi} = \frac{\boldsymbol{m}}{\boldsymbol{S.e_b.\rho}} \qquad (1)$$

where $\boldsymbol{\rho}$ is the fuel particles density. The porosity measures the proportion of air in the fuel bed $\mathbf{1} - \boldsymbol{\varphi}$.

3. Results and discussion

The influence of compactness on rate of spread of the above described *Pinus Pinaster* is compared in Fig.2a to *excelsior* and ¼ inch *cribs* fuels (Rothermel, 1972) and laser-cut cardboards (He et al, 2021). The ROS behavior shows at least an optimum ratio for all presented fuels for $\varphi < 10$ %. An optimum ratio is observed for *Pinus Pinaster* (PP) needles around 5.5% close to that found by Rothermel for *cribs* fuels, but the ROS of PP needles increases again for smaller ratios as if they have another optimum packing ratio. Two optimum ratios have been observed also for excelsior fuels (Rothermel, 1972) and cardboards (He et al, 2021), and have been attributed to thermochemical effects. However, heat transfer has been found to be the main cause of non-monotonic ignition time (Boutchiche et al, submitted). As the ROS corresponds to the ignition time of the nearest fuels of the flame, absorption heat transfer might be also the cause of the optimum ratios observed for the rate of spread. Ignition and combustion are influenced also by surface-to-volume ratio SVR. The optical length of radiation heat transfer is related to these quantities by

$$\boldsymbol{\delta} = \frac{\mathbf{4}}{\boldsymbol{\varphi \times SVR}} \qquad (2)$$

In Fig.2b, the ROS is presented as a function of the optical length. The absorption probability decreases exponentially with with the fuel thickness ($e^{-e/\delta}$) (Boutchiche et al, submitted). As the optical length at the optimum ratio of PP needles is around $12\ mm$, much smaller than the fuel bed thickness which varies from $e = 40$ to $e = 70\ mm$, the maximum ROS is characterized by a surface absorption of the heat flux similar to that of the *excelsior* fuel bed (around $20\ mm$) (Rothermel, 1972). As mentioned above, the ROS seems to increase again for larger lengths which corresponds to the existence of a second optimum ratio. This optimum ratio seems to corresponds to an optical length much larger than the fuel bed thickness, which means that the heat flux is absorbed by the whole fuel bed. A similar absorption behaviour occurs for *cribs* (Rothermel, 1972) and cardboards (He et al, 2021).

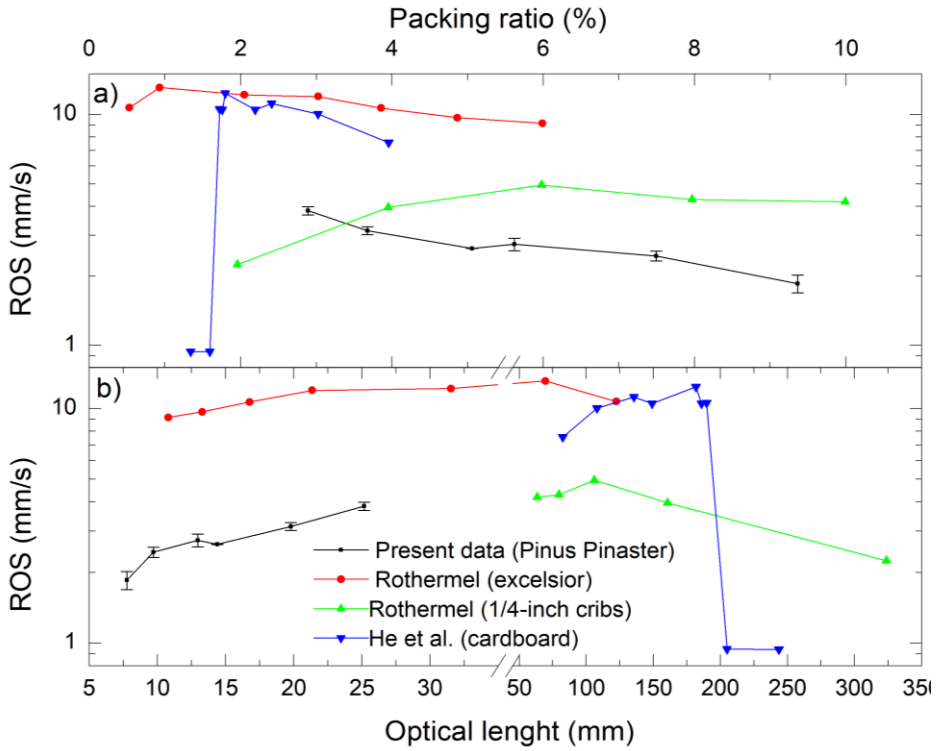

Figure 2: Rate of spread as a function of a) packing ratio, b) Optical length

Now let us examine the thermochemical effects through the mass-loss rate of the fuelbed during spread, which is proportional to the potential reaction velocity according to equation (35) of (Rothermel, 1972). Since internal combustion is involved during spread, the mass-loss rate corresponds to the emitted flammable gas, and is thus expected to vary with porosity. In Fig.3a the mass-loss rate evolution during fire spread is presented for an example configuration of fuel bed. Here, the contribution of glowing embers that remain in the burned area, and the pre-heating contribution of the foreward area are neglected compared to that of the burning area. After ignition, the burning rate seems to increase linearly with time during spread, and decreases when the forward front reaches the end of table. The increase of the burning rate may be explained by the increase of the burning area of the fuel as fire spreads. Indeed, at ignition, the front is a straight line, but becomes curved as the front advances due to the edge effects (see Fig.3b). At the edges, fire spreads slowly compared to the center because of the lack of nearest burning fuels contribution. Assuming the burning rate homogeneous, the increase of the curvature of the front during spread corresponds to an increase of the burning area, and thus to the increase of the total mass-loss rate. Therefore, the slope in Fig.3a may depend on the rate of spread. It is thus burning rate is the minimum for the initial line front,

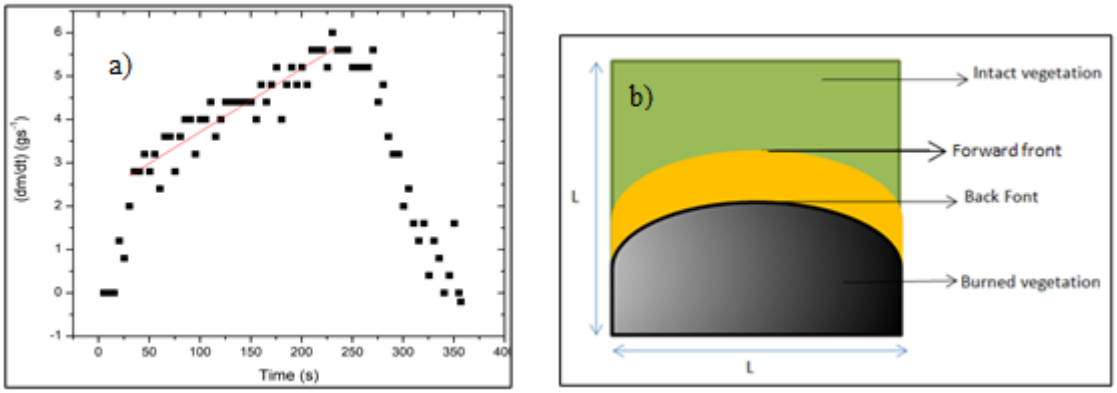

Figure 3: a) The mass-loss rate as a function of time of selected sample $m = 1.2\ kg$; $e = 5.5\ cm$ b) schematic view of the front during spread.

To examine the influence of the optimum packing ratio on potential reaction velocity, it is convenient to consider the minimum mass loss rate corresponding to the initial fire line. This avoids the contribution of the rate of spread on the burning rate. In Fig.4 the minimum mass-loss rate seems to be independent of the packing ratio within errors in the range of φ up to 10 %. Therefore, the optimum ratio observed for *Pinus Pinaster* in Fig.2 seems to not be caused by the burning rate (or reaction velocity (Rothermel, 1972)). The heat transfer mechanism may be the main cause of this non-monotonic behavior as found for ignition (Boutchiche et al, submitted).

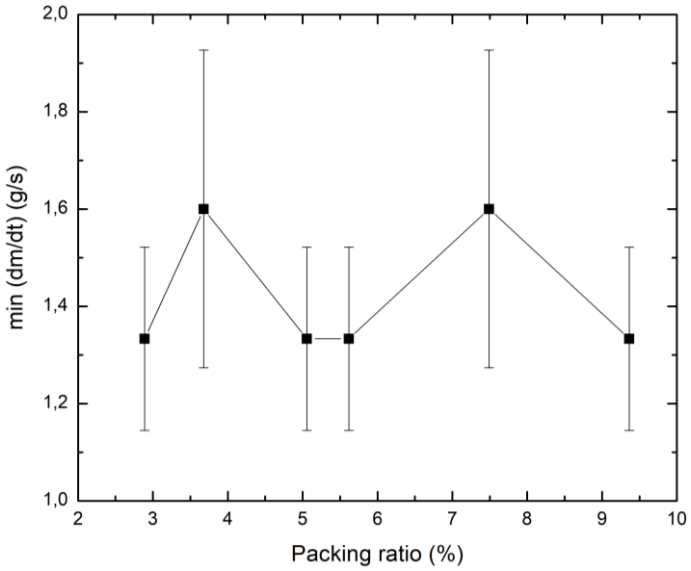

Figure 3: The mass-loss rate as a function of the packing ratio.

The flame height seems to follow the same trend as ignition time by varying the packing ratio. The flame heigh is not shown to avoid clutter.

4. Conclusion:

The effect of the packing ratio and optical length on the rate of spread of *Pinus Pinaster* fuels is examined and compared to those of other fuels in litterature. An optimum packing ratio corresponding to a maximum rate of spread is found for a ratio of 5.5 %, and the trend indicates the existence of another maximum rate of spread for a much smaller packing ratio. By using the optical length, the maximum rate of spread occurs at an optical length of about 12 *mm* much smaller than the fuel bed thickness, which corresponds to a maximum surface absorption. While the other maximum rate of spread is expected to occur at an optical length much larger than the fuel bed thickness, which means a bulk absorption of heat flux. Although an internal combustion occurs during spread, the mass loss rate seems to be independent of the packing ratio in the range of ratios considered.

5. References:

Z. Campbell-Lochrie, C. Walker-Ravena, M. Gallagher, N. Skowronski, E. V. Mueller, R.M. Hadden, Investigation of the role of bulk properties and in-bed structure in the flow regime of buoyancy-dominated flame spread in porous fuel beds, Fire Saf. J. 120 (2021) 103035, https://doi.org/10.1016/j. firesaf.2020.103035.

R.C.Rothermel, A mathematical model for predicting fire spread in wildland fuels. USDA, 1972. For.Serv.Res. Pap. INT-115. 40.

A. Simeoni, P. Bartoli, J.L. Torero, P.-A. Santoni, On the role of bulk properties and fuel species on the burning dynamics of pine forest litters, in: Proceedings of the 10th IAFSS Symposium, University of Maryland, USA, 2011, https://doi.org/ 10.3801/IAFSS.FSS.10-1401

Q.He, N.Liu, X.Xie, L.Zhang, Y.Zhang, W.Yan, Experimental study on fire spread over discrete fuel bed-Part I: Effects of packing ratio, Fire Safety Journal 126 (2021) 103470: 1-8, https://doi.org/10.1016/j.firesaf.2021.103470.

H.Boutchiche, O.Mosbah, A.Sahila, J. Raposo, L. Reis, D.X.Viegas, N.Zekri, Influence of fuel porosity on the flammability properties of forest fuels, Fire Safety Journal submitted.

M. El Houssami, J.C. Thomas, A. Lamorlette, D. Morvan, M. Chaos, R.M. Hadden, A. Simeoni, Experimental and numerical studies characterizing the burning dynamics of wildland fuels, Combust. Flame 168 (2016) 113–126, http://dx.doi.org/10.1016/j.combustflame.2016.04.004.

The loss of ecosystem multifunctionality in Pinus pinaster forests as one of the main footprints of large wildfires

Leonor Calvo*[1]; Sara Huerta[1]; Víctor Fernández-García[1]; José Manuel Fernández-Guisuraga[1]; Paula Monte[1]; Reyes Tárrega[1]; Luz Valbuena[1]; Ángela Taboada[1]; Sara Turiel[1]; Elena Marcos[1]; Susana Suárez-Seoane[2]

[1] Area of Ecology. Faculty of Biological and Environmental Sciences. University of León, 24071 Leó, Spain, {leonor.calvo, shueg, vferg, jofeg}@unileon.es, {pmonts02@estudiantes.unileon.es}, {r.tarrega, luz.valbuena, angela.taboada, sturs, elena.marcos@unileon.es}
[2] Department of Organisms and Systems Biology (Ecology Unit) and Research Unit of Biodiversity (IMIB; UO-CSIC-PA), University of Oviedo, Oviedo, Mieres, Spain {s.seoane@uniovi.es}

**Corresponding author*

Keywords

Megafires, recurrence, severity, *Pinus pinaster*, ecosystem services.

Abstract

The main objective of this study was to analyse the effect of recurrence and burn severity on ecosystem multifunctionality in Pinus pinaster forests. We selected a large wildfire that occurred in the Sierra del Teleno in 2012 (NW Spain), where we differentiated two recurrences and two burn severity situations. As a result, four scenarios were identified: low recurrence plus low severity, low recurrence plus high severity, high recurrence plus low severity, high recurrence plus high severity. In each one, a number of 1 m x 1 m plots proportional to the burned area were established. Three years after the wildfire we evaluated in each plot: (1) percentage of covered soil, (2) total percentage cover of herbaceous species, (3) percentage cover of each woody species, (4) total plant species richness. Also, a composite soil sample was collected from each plot. Chemical (total organic carbon, total nitrogen and available phosphorus) and microbiological (microbial biomass carbon) properties were analysed in each soil sample. The following variables were used as indicators of ecosystem functions: percentage of covered soil, total cover of herbaceous species, Pinus pinaster cover, total plant richness, total organic carbon, total soil nitrogen, available phosphorus and microbial biomass carbon. Another indicator of ecosystem functions was calculated: floral colours of shrub species diversity using the Shannon index. The values of each ecosystem function indicator were standardized. The indicators/functions of regulating ecosystem services were: Climate regulation (indicator: total % of organic soil carbon) and Erosion protection (indicator: covered soil %). The functions/ indicators of supporting ecosystem services were: soil fertility (indicator: total nitrogen and available phosphorous) and soil quality (indicator: microbial biomass C). The indicators/functions of cultural ecosystem services were: species diversity (indicator: plant species richness) and aesthetic value (indicator: the Shannon index of floral colours). The functions/indicators of provisioning ecosystem services were: grass for livestock (indicator: % cover of herbaceous species) and timber production (indicator: % cover of Pinus pinaster). The results indicated that all scenarios apart from low recurrence plus low severity negatively affected the multifunctionality of the ecosystems.

1. Introduction

In the Mediterranean Basin dramatic shifts in fire regime have been detected during recent decades, driving an increase in large and severe wildfires, with significant consequences on ecosystems and societies at different scales (Singleton et al., 2019). Impacts include loss of lives and infrastructures, alterations in functional processes (e.g. erosion, vegetation dynamics or carbon cycle) and reduction in ecosystem service provision (e.g. food, timber or fresh water stocks) (Taboada et al., 2021). In general, these alteration of the ecosystem services are related not only to fire severity but also to fire recurrence that modify ecosystem resilience, due to damage to vegetation and soil characteristics.

In recent decades, rural depopulation and agricultural land abandonment have favoured the expansion of shrublands and forests to the detriment of open areas such as pasturelands and croplands. Consequently, fuel amount and its connectedness increase, leading to a simplification of the landscape mosaic associated with an increase in the risk of extreme wildfires that are more dangerous to people and ecosystems. In this context,

increase in drought periods and thermal anomalies associated with climate change are favouring fuel ignition (Stephens et al., 2014). Indeed, according to global change predictions, Spain will be included in a primary climate change hotspot, where warming will be above the global average. Both changes in climatic conditions and land use contribute to the increase in new wildfire regimes, with more frequent catastrophic fires causing abrupt changes in the functioning of ecosystems and in the delivery of ecosystem services to society. In general, ecosystem functioning is inherently multidimensional and so, multifunctionality measures can summarise the ability of an ecosystem to deliver multiple functions or services simultaneously (Manning et al., 2018).

Mediterranean ecosystems largely affected by megafires are those dominated by *Pinus pinaster*, which provide relevant provisioning, regulating, cultural and supporting ecosystem services. A new and innovative approach to evaluate the status of the forest ecosystem and interruption of multifunctionality by fire is currently being implemented. This approach of studying the modifications in biotic and abiotic processes that determine the provision of ecosystem services in *Pine* forest, represent an integrated analysis of the footprints of large recurrent and severe wildfires. Thus, the knowledge acquired in this integrated analysis would help in the implementation of novel solutions to promote landscapes and socio-ecological contexts less susceptible and more resilient to recurrent high burn severity wildfires (Moreira et al., 2020).

The main objective of this work was to analyse the effect of recurrence and burn severity on ecosystem multifunctionality in *Pinus pinaster* forests in Northwest Spain.

2. Material and methods

The study area (Figure 1) is located in Sierra del Teleno (NW Spain), within the perimeter of a megafire (11,600 ha) that occurred in August 2012, affecting a forest dominated by *Pinus pinaster*, with the understorey community dominated by *Pterospartum tridentatum* (L.) Willk., *Halimium lasianthum* (Lam.) Spach and *Erica australis* L. (Calvo et al., 2008). The climate in this region is temperate with dry warm summers. The orography is heterogeneous, ranging from flat to mountainous areas. Soils are developed over siliceous lithologies.

Prior to the fire in 2012, the area had suffered another large fire in 1998 of around 3000 ha. Therefore, within the perimeter of the 2012 fire, we defined two recurrent scenarios: low recurrence (a single fire in the last 15 years) and high recurrence (two fires in the last 15 years). Additionally, based on a dNBR (differenced Normalized Burn Ratio) index derived from Landsat pre-fire and post-fire images (September 20th, 2011 - September 6th, 2012) and CBI (Composite Burn Index) field measured values (Key and Benson, 2006), we established two severity scenarios within the perimeter of the 2012 fire: low severity (dNBR between 220-550) and high severity (dNBR between 550-1400). Overlaying the recurrence and severity classes, we identified four scenarios (low recurrence-low severity (LR-LS), low recurrence-high severity (LR-HS), high recurrence-low severity (HR-LS) and high recurrence-high severity (HR-HS). Within the fire perimeter, we selected a 3000 ha study framework where the four scenarios of recurrence and severity were represented (Figure 1) to collect field data. A total of 88 1 m x 1 m plots were established: 20 in LR-LS, 20 in LR-HS, 20 in HR-LS and 28 in HR-HS. Three years post-fire, we evaluated in each plot the visual percentage cover of each plant species and the bare soil. In addition, a composite soil sample (consisting of 4 subsamples) was collected from each plot. Chemical (total organic C, total N and available P) and microbiological (microbial biomass carbon) properties were analysed in each soil sample.

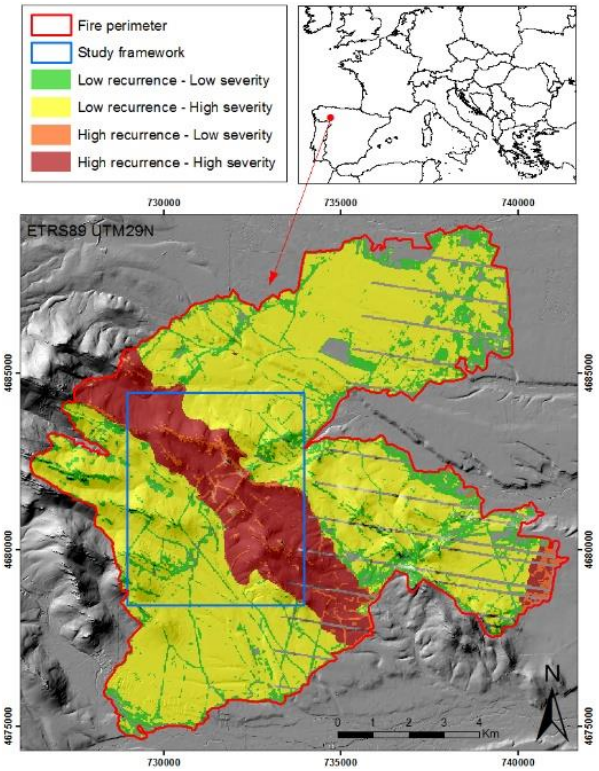

Figure 1- Study framework within the perimeter of the Sierra del Teleno megafire which occurred in 2012, and the considered recurrence-severity scenarios

Soil organic C was obtained by Walkley-Black dichromate oxidation (Nelson and Sommers, 1982). Total N was determined by the Kjeldahl method (Bremner and Mulvaney, 1982) and available P was analysed following the Olsen *et al.* (1954) procedure. Microbial biomass C was determined by the fumigation-extraction method (Vance *et al.*, 1987).

The variables used as indicators of ecosystem functions were (Table 1): percentage of covered soil, total cover of herbaceous species, *Pinus pinaster* cover, total plant richness, total organic carbon, total soil nitrogen, available phosphorus, microbial biomass carbon and % of floral colours of shrub species diversity using the Shannon index (Shannon, 1948). The values of each ecosystem function indicator were standardised according to the following procedure: Standardized value = (Unstandardized value – Minimum value) / (Maximum value – Minimum value).

Minimum and maximum values correspond to the lowest and highest unstandardized values of each indicator, respectively. Consequently, a set of standardized data was obtained for each indicator, ranging from 0 (minimum value) to 1 (maximum value).

The indicators of regulating ecosystem services were: climate regulation (indicator: total % of organic soil carbon) and erosion protection (indicator: covered soil %). The indicators of supporting ecosystem services were: soil fertility (indicator: total N and available P) and soil quality (indicator: microbial biomass C). The indicators of cultural ecosystem services were: species diversity (indicator: plant species richness) and aesthetic value (indicator: Shannon index of floral colours). The indicators of provisioning ecosystem services were: grass for livestock (indicator: % cover of herbaceous species) and timber production (indicator: *Pinus pinaster* percentage cover).

In the soil fertility function, in which we used more than one indicator, the average value of these indicators was calculated. In the same way, ecosystem multifunctionality was calculated by averaging the values of regulating, supporting, cultural and provisioning ecosystem services.

Generalized linear models (GLMs), with a quasi-Poisson error distribution (log link function) to account for overdispersion, were applied to evaluate the effects of recurrence and burn severity on ecosystem functions, services, and multifunctionality. Data analyses were carried out with R (R Core Team, 2021).

Table 1. List of functions for regulating, supporting, cultural, and provisioning ecosystem services, and indicators used to define these functions.

Ecosystem functions		Function indicators
Regulating ecosystem service		
Climate regulation	Carbon sequestration	Total organic soil C (%)
Erosion protection		Covered soil (%)
Supporting ecosystem service		
Soil fertility	Soil nutrient storage capacity	Total N (mg kg-1) Available P (mg kg-1)
Soil quality		Microbial biomass C (µg C g^{-1} dw soil)
Cultural ecosystem service		
Species diversity		Plant species richness
Aesthetic value		Shannon index of floral colours of shrub species
Provisioning ecosystem service		
Grass for livestock		Total cover of herbaceous species (%)
Timber production		Total cover of *Pinus pinaster* (%)

3. Results and discussion

The significant negative effects of recurrence and burn severity in the regulation of ecosystem services, even three years after wildfire (Figure 2), are a consequence of the impact on climate regulation and erosion protection functions. Recurrent and severe fires are characterized by the elimination of vegetation cover and therefore, the soil is non-protected, and could be affected by erosion processes after rain events. However, in low recurrent plus low severe fire scenarios, a higher level of survival of vegetation, which facilitates the protection of the soil, is observed. Another ecosystem service negatively affected by burn severity is provisioning (Figure 2), as grass for livestock and timber production functions had higher values in low recurrent and severe scenarios, decreasing with increased severity or recurrence. González-De Vega et al. (2018) also observed a lower presence of herbaceous species with increasing burn severity. In the same way, high recurrence and severity affect reducing the probability of regeneration of *Pinus pinaster* (Fernández-García et al., 2019).

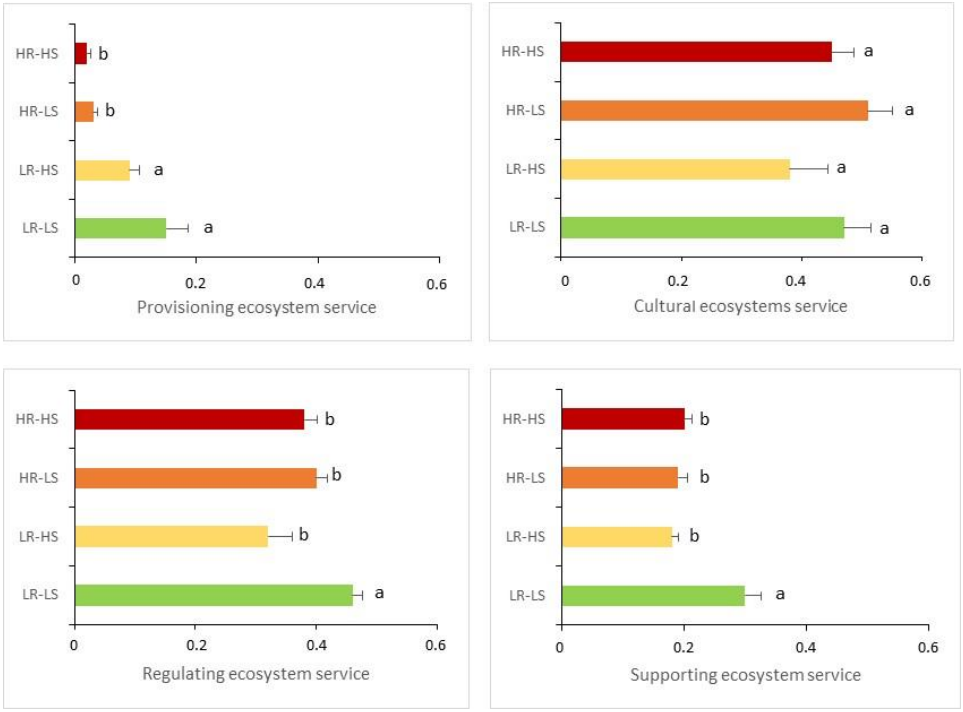

Figure 2. Average value and standard error of provisioning, cultural, regulating and supporting ecosystem services for each scenario: Low recurrence and low severity (LR-LS), low recurrence and high severity (LR-HS), high recurrence and low severity (HR-LS) and high recurrence and high severity (HR-HS). Different letters indicate significant differences ($p < 0.05$) between scenarios.

High recurrence and/or high severity negatively modify nutrient availability due to the reduction in soil organic matter content (Hedo et al., 2015). These patterns determine the reduction in supporting ecosystem services observed in these scenarios of high recurrence plus low and high severity (Figure 2).

Three years after fire, we only detected a significant decrease in plant richness after high recurrence and burn severity. However, the recovery of woody species with different flower colours showed an opposite pattern, as the elimination of the dominant tree species favoured colonization by other understory shrub species. These two opposing patterns mean that the cultural ecosystem services do not show significant effects among recurrence and burn severity scenarios.

As a result of the effects of fire recurrence and severity on plant community and soil properties, which act as indicators of functions, and modulate post-fire ecosystem multifunctionality (Lucas-Borja et al., 2021), showed a clear reduction in those scenarios different to low recurrence plus low severity (Figure 3).

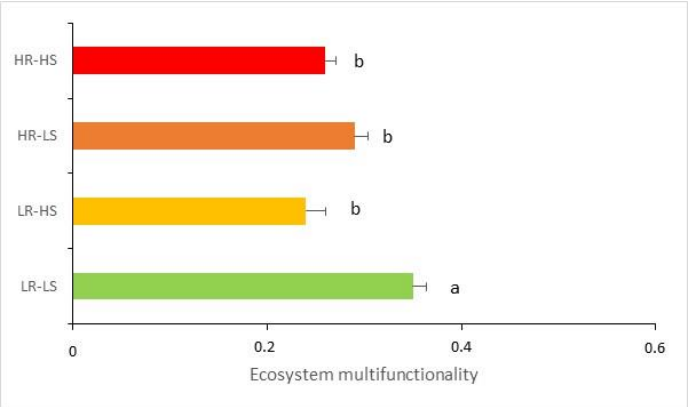

Figure 3. Average value and standard error of ecosystem multifunctionality for each scenario (Low recurrence and low severity (LR-LS), low recurrence and high severity (LR-HS), high recurrence and low severity (HR-LS) and high recurrence and high severity (HR-HS). Different letters show the presence of significant differences (p < 0.05) between burn severity categories.

4. Conclusions

The footprint of a megafire, three years after, is very evident through the reduction of ecosystem multifunctionality under those scenarios of high recurrence plus low or high burn severity. This integrated approach to the study of the effects of large wildfires on the functioning and provisioning of ecosystem services in fire prone ecosystems represents an outstanding advance in the design of adequate post-fire recovery strategies to minimise the impact and accelerate the recovery of the vegetation and soil.

5. Acknowledgements

This study was financially supported by the Spanish Ministry of Economy and Competitiveness, and the European Regional Development Fund (ERDF), in the framework of the FIRESEVES (AGL2017-86075-C2-1-R) project; and by the Regional Government of Castilla and León in the framework of the WUIFIRECYL (LE005P20) project.

6. References

Calvo, L.; Santalla, S.; Valbuena, L.; Marcos, E.; Tárrega, R.; Luis, E. 2008. Post-fire natural regeneration of Pinus pinaster forest in NW of Spain. *Plant Ecol*. 197: 81-90.

Fernández-García, V., Marcos, E., Fernández-Guisuraga, J.M., Taboada, A., Suárez-Seoane, S., Calvo, L., 2019. Impact of burn severity on soil properties in a *Pinus pinaster* ecosystem immediately after fire. *Int. J. of Wildland Fire* 28: 354-364.

González-De Vega, S., De las Heras, J., Moya, D., 2018. Post-fire regeneration and diversity response to burn severity in *Pinus halepensis* Mill. forests. *Forests* 9: 299

Hedo, J., Lucas-Borja, M.E., Wic, C., Andrés-Abellán, M., de Las Heras, J., 2015. Soil microbiological properties and enzymatic activities of long-term post-fire recovery in dry and semiarid Aleppo pine (*Pinus halepensis* M.) forest stands. *Solid Earth* 6: 243–252.

Key C.H., Benson N.C. 2006. Landscape assessment (LA) sampling and analysis methods. USDA Forest Service General Technical Report, RMRS-GTR-164-CD. Fort Collins, CO, United States of America.

Lucas-Borja, M.E., Delgado-Baquerizo, M., Muñoz-Rojas, M., Plaza-Álvarez, P.A., Gómez-Sanchez, M.E., González-Romero, J., Peña-Molina, E., Moya, D., de las Heras, J., 2021. Changes in ecosystem properties after post-fire management strategies in wildfire-affected Mediterranean forests. *J. Appl. Ecol.* 58: 836-846.

Manning, P., van der Plas, F., Soliveres, S., Allan, E., Maestre, F. T., Mace, G., Fischer, M. 2018. Redefining ecosystem multifunctionality. *Nature Ecol. & Evol.* 2(3): 427-436.

Moreira, F., Ascoli, D. Safford, H., *et al* 2020. Wildfire management in Mediterranean-type regions: paradigm change needed. *Environ. Res. Lett.* 15 011001

Nelson D.W., Sommers L.E. 1982. Total carbon, organic carbon and organic matter. In: Page A.L., Miller, R.H., Keeney, D.R. (Eds.), Methods of Soil Analysis Part 2: Chemical and Microbiological Properties. 539-579. ASA: Madison, WI, United States of America.

Olsen, S.R., Cole, C.V., Frank, S.W., Dean, L.A., 1954. USDA Circular No. 939. In: Estimation of Available Phosphorus in Soils by Extraction with Sodium Bicarbonate. US Government Printing office, Washington, USA, pp. 19.

R Core Team 2021. R: A language and environment for statistical computing. R Foundation for Statistical Computing, Vienna, Austria. URL https://www.R-project.org/.

Shannon, C. E., 1948. A mathematical theory of communication. *Bell Syst. Tech.* J., 27: 379-423.

Singleton, M.P., Thode, A.E., Sánchez Meador, A., Iniguez, J.M. 2019. Increasing trends in high-severity fire in the southwestern USA from 1984 to 2015. *For. Ecol. Manag.*, 433: 709-719.

Stephens, S. L.; Burrows, N.; Buyantuyev, A.; Gray, R. W.; Keane, R. E.; Kubian, R.; Liu, S.; Seijo, F.; Shu, L.; Tolhurst, K.G.; van Wagtendonk, J. W. 2014. Temperate and boreal forest mega-fires: characteristics and challenges. *Front. Ecol. Environ.* 12: 115-122.

Taboada A., García-Llamas, P., Fernández-Guisuraga, J.M., Calvo, L. 2021. Wildfires impact on ecosystem service delivery in fire-prone maritime pine-dominated forests. *Ecosyst. Serv.* 50: 101334

Vance, E.D., Brookes, P.C., Jenkinson, D.S., 1987. An extraction method for measuring soil microbial biomass C. *Soil Biol. Biochem.* 19: 703–707.

The role of the fuel moisture content on the prediction of large wildfires using the Fire Weather Index system

Daniela Alves*[1]; Domingos Viegas[1,2]; Miguel Almeida[1]; Luís Reis[1,2]; Jorge Raposo[2]; Carlos Ribeiro[1]

[1]Association for the Development of Industrial Aerodynamics, Forest Fire Research Center, University of Coimbra, Coimbra, Portugal, {danielaalves, miguelalmeida, carlos.ribeiro}@adai.pt
[2] Department of Mechanical Engineering, Faculty of Sciences and Technology, University of Coimbra, Coimbra, Portugal, {xavier.viegas, luis.reis@dem.uc.pt, jorge.raposo}@dem.uc.pt

**Corresponding author*

Keywords

Wildfires, Fuel moisture content, fire danger, FWI, prediction

Abstract

Fuel moisture content is one of the fundamental parameters in forest fire research and management given its implications for many aspects of fire danger systems. In Portugal, such as in many other countries, to classify the days with more favourable conditions for wildfires it is common to use the Canadian Forest Fire Weather Index System (CFFWIS) which is based on the estimation of moisture content of several fuel components. The mathematical structure of CFFWIS requires as input the daily meteorological parameters which are used to estimate the moisture content of the soil for different layers that are the primary outputs of the system – the fire moisture codes. The final output parameter of the system is the Fire Weather Index (FWI) which represents a measure of the fire danger due to meteorological conditions.

The temporal scale of the study is from 2018 and 2021 and the study area is in Lousã, a central region of Portugal. In this work, in addition to the meteorological data, we will use as input the direct measurements of dead fuels in the CFFWIS and analyse its influence on the FWI. The fuel moisture content (m_f) is determined through the sample collection of dead pine needles in Lousã. For this temporal scale, m_f by sampling is significantly lower than the modelled m_f using meteorological parameters. An advantage of using the m_f measurements is to increase the range of FWI variation, giving a higher sensitivity to the index to more easily discriminate the days with high fire danger and large burned areas. Two methods are addressed: "FWI a" which represents the traditionally FWI determined only by meteorological parameters, and the "FWI b" which is determined with fuel moisture content measurements and with meteorological data for the days that we did not have measurements.

The original FWI, based only meteorological parameters, is compared with the FWI determined using m_f measurements. The different methods will be related with the number of fires and burned area to analyse their performance. The results show a good fit between m_f and FWI for days with extreme weather conditions (m_f<5%).

1. Introduction

Fuel moisture content is determinant in the extension of the burned area (Lopes, 2013; Viegas et al., 2017) being a fundamental parameter in wildfire research and management given its implications for many aspects of fire danger. Recent work found that high values of the Fine Fuel Moisture Code (FFMC) may determine when large fires can occur, supporting close relationships between moisture thresholds and fire behaviour (Carmo et al., 2021). The assessment of fuel moisture content reveals to be crucial for the characterization of extreme fire events allowing the improvement of early warning systems over extreme weather conditions.

Traditional fire danger systems rely on meteorological indices, based on variables that are routinely measured on weather stations (Chuvieco et al., 2010). To estimate the fire danger in Portugal, as in Europe (Viegas et al. 1999), it is common to use the Canadian Forest Fire Weather Index System (CFFWIS) developed by Van Wagner (1987). The CFFWIS produces the Fire Weather Index (FWI) which is a composite index that represents the meteorological conditions and gives an indication of the expected fire intensity (Van Wagner 1987). The structure of CFFWIS is presented in Figure 1.

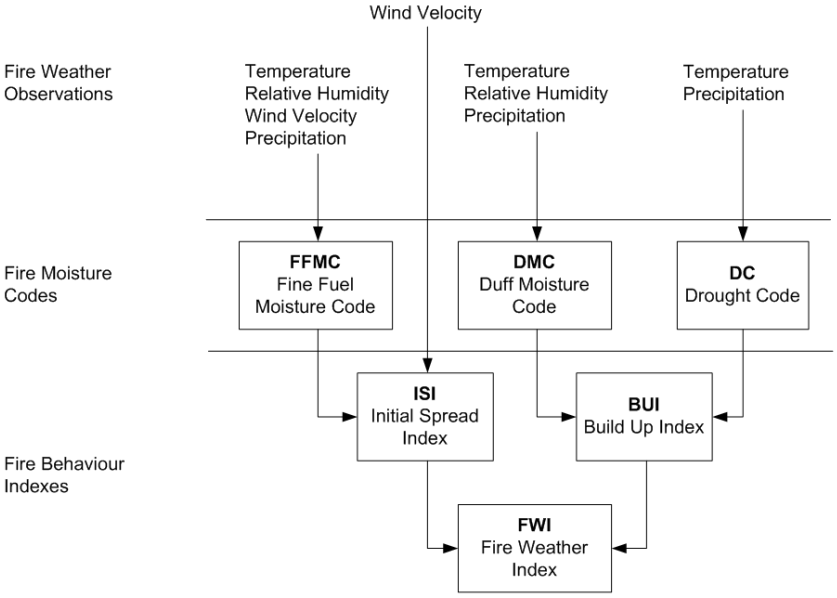

Figure 1 - Structure of CFFWIS by Van Wagner 1987.

The basis of this system is the prediction of dead fuel moisture content based on a set of physical equations calculated through meteorological data that are the input parameters (see Figure 1). The intermediate outputs are respective to fire moisture codes: Fine Fuel Moisture Code (FFMC) is associated to the surface litter, the Duff Moisture Code (DMC) is associated to the duff layers about 7cm deep, and the Drought Code (DC) is associated to the soil layers about 18cm deep and is well correlated with live moisture content (Viegas et al., 2001). The intermediate outputs of the system are the fire behaviour indices: Initial Spread Index (ISI) and Build-Up Index (BUI) giving a relative indication of the initial fire spread after the ignition and of the availability of the fuel to participate in fire propagation, respectively. These indices are combined to provide the final output parameter of the system – the Fire Weather Index (FWI), which represents the expected intensity of a spreading fire. The indices are cumulative as they take into consideration the effect of weather conditions in the previous days. The increase in each of these components corresponds to an increase of fire danger. These meteorological indices have some limitations when applied to other regions than that led to its formulation, namely they do not provide a real quantitative assessment of fuel moisture content value and therefore need to be validated with local data.

Based on the model used to calculate the CFFWIS, an approach to analyse the role of fuel moisture content on large wildfire occurrences will be addressed. We intend to analyse how FFMC changes when it is determined through direct measurements of fuel moisture content (m_f) and, consequently, how FWI changes.

The study is based on m_f measured in Lousã, a central region of Portugal. The analysis focuses exclusively on dead fine fuels, leaving aside the dynamics of live fuel with fire. In this paper the time period from 2018 to 2021 (4 years) is considered.

2. Methodology

2.1. Determination of the m_f

The fuel moisture content is determined by sample collection of several species in a field plot located in Lousã near the Forest Fire Research Laboratory (LEIF) – Figure 2.

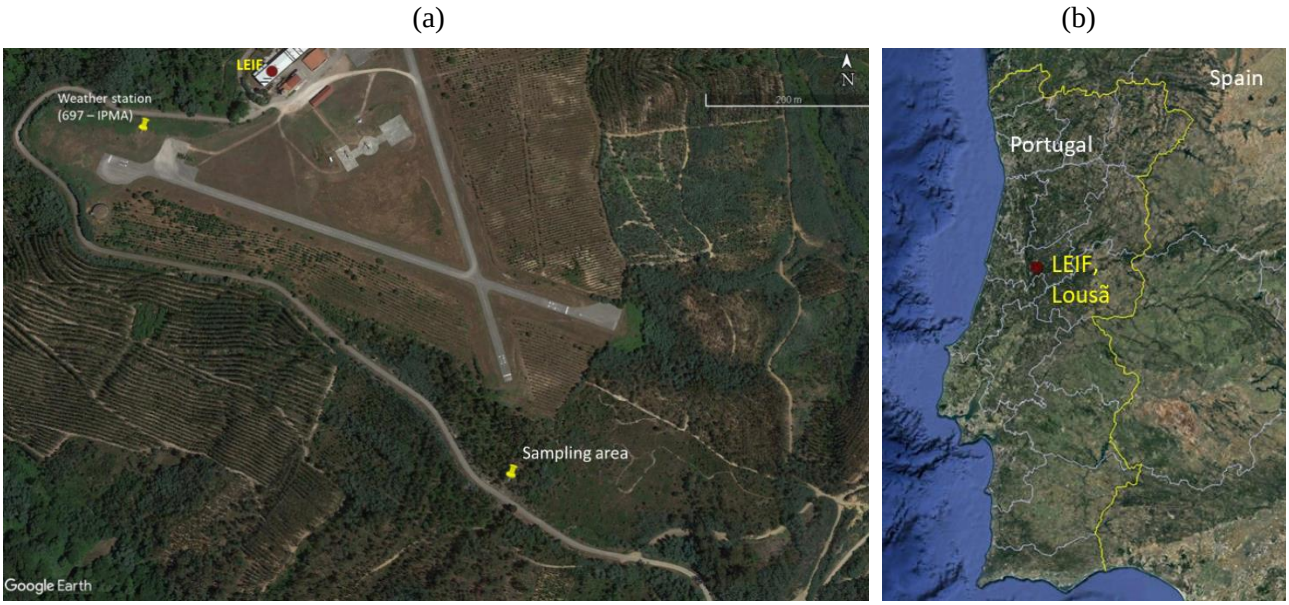

Figure 2 – (a) Local of the sampling area, Forest Fire Research Laboratory (LEIF), weather station and (b) their position in the Portuguese territory.

In LEIF, the samples are weighed with 5g each (initial mass: m_i), they are dried in an oven (24h and 105ºC) and their dry mass: m_d is determined. Fuel moisture content, $m_{f_{sampling}}$, in a dry basis is determined by Equation 1.

$$m_{f_{sampling}} = \frac{m_i - m_d}{m_d} \quad (1)$$

For this analysis, the m_f measurements of pine needles of *Pinus Pinaster* are used.

Figure 3a presents the relation of the m_f modelled in the CFFWIS ($m_{f_{meteo}}$) and the m_f observed ($m_{f_{sampling}}$) for all data (450 days). Figure 3b) presents the distribution of both m_f (modelled and observed) among the study period.

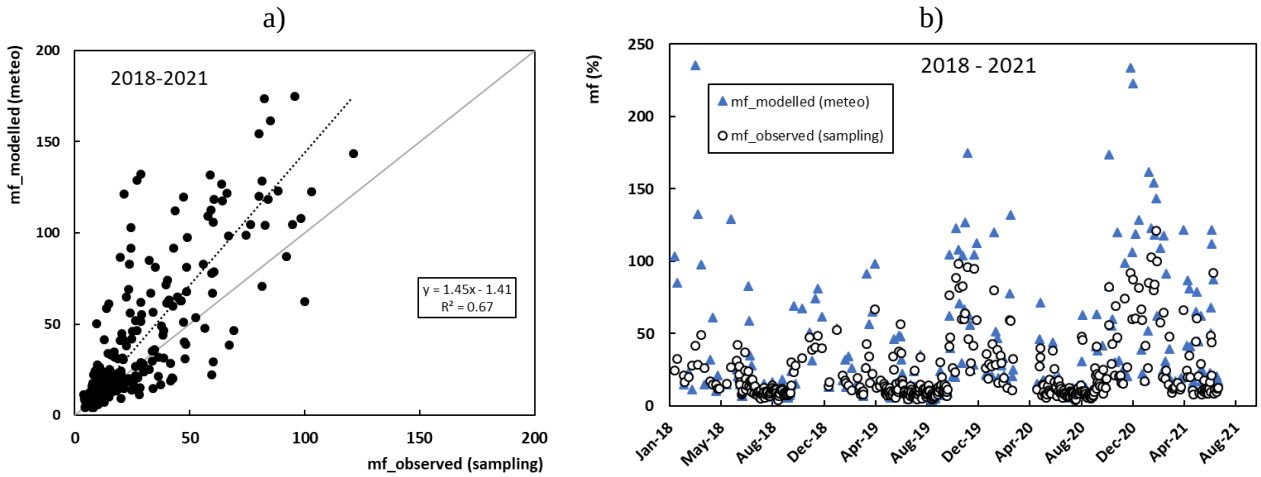

Figure 3 – a) Relation of the $m_{f_{meteo}}$ proposed by Van Wagner (1987) with the observed $m_{f_{sampling}}$ in Lousã; b) Distribution of the $m_{f_{meteo}}$ and the o $m_{f_{sampling}}$ per day.

Both figures show that the range of values for observed m_f is lower than the range values for modelled m_f.

Between 2018 and 2021 and considering all data (n=450), the sample mean for $m_{f_{sampling}}$ and $m_{f_{meteo}}$ was 20.47% and 28.36%, respectively. A "T-test for Equality of Means" was done using the statistical software

SPPS (28) to verify if the $m_{f\ sampling}$ is significantly lower than the $m_{f\ meteo}$. The following test hypothesis were done:

- H0: $m_{f\ sampling}$ mean = $m_{f\ meteo}$ mean;
- H1: $m_{f\ sampling}$ mean < $m_{f\ meteo}$ mean.

Output of the test is presented in Figure 4.

Independent Samples Test

		t-test for Equality of Means							
				Significance				95% Confidence Interval of the Difference	
		t	df	One-Sided p	Two-Sided p	Mean Difference	Std. Error Difference	Lower	Upper
mf	Equal variances not assumed	4,09	708,88	<,001	<,001	7,88	1,93	4,10	11,67

Figure 4 – Output of the "T-test for Equality of Means" between two independent variables: $m_{f\ sampling}$ and $m_{f\ meteo}$.

The test has a p-value <0.001, so for any usual significance level ($0.01 < \alpha < 0.1$) we reject the null hypothesis (H0) and we keep the one-sided alternative hypothesis (H1). The $m_{f\ sampling}$ is significantly lower than the modelled $m_{f\ meteo}$. An advantage of using the m_f measurements, since they have lower values, is to increase the range of FWI variation, giving a higher sensitivity to the index to more easily discriminate the days with high fire danger and large burned areas.

2.2. Determination of the FFMC

The function defined by Van Wagner (1987) relating FFMC with the moisture content of the surface fuels is presented in Equation 2. In this equation $m_{f\ meteo}$ is estimated by meteorological data.

$$FFMC = 59{,}5 \times \frac{250 - m_{f\ meteo}}{147 + m_{f\ meteo}} \tag{2}$$

Viegas et al. (2004) have developed a calibration function that uses FFMC to estimate the m_f (Equation 3) for dead fuels in the Portuguese forests.

$$m_f = 9 \times 10^9 \times FFMC^{-4.56} \tag{3}$$

In Figure 5 data of m_f obtained in the study period is plotted as function of FFMC measured at Lousã. The curves corresponding to equations 2 and 3 are plotted in the Figure 5.

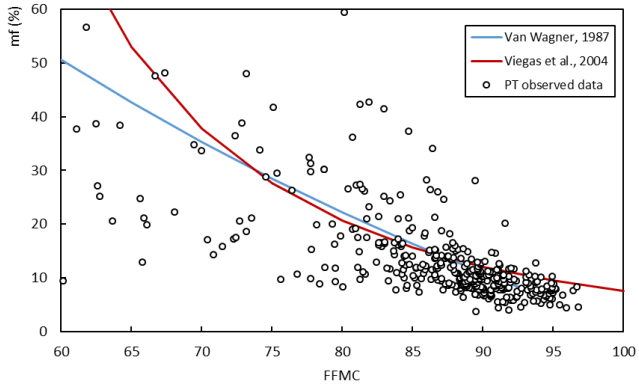

Figure 5 – Relation between m_f and the FFMC in Lousã – PT observed data. Functions proposed by Van Wagner, 1987 and Viegas et al., 2004.

The m_f measurements to be used in this study are distributed according to both models.

Figure 6 presents the relation of the m_f determined for each model (Van Wagner (1987) and Viegas et. al. (2004) with m_f measurements in Lousã (observed data) for values of mf<30% (335 days).

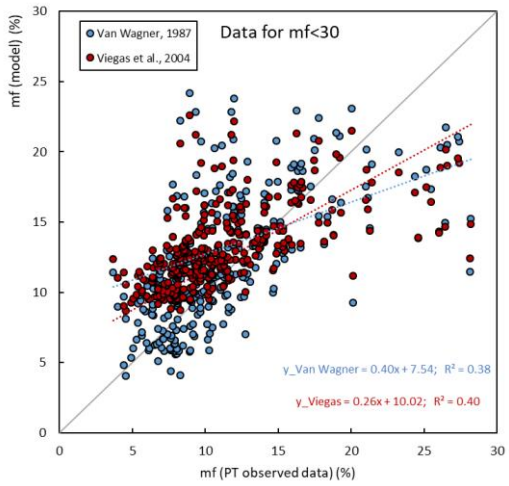

Figure 6 – Relation of the m_f proposed by Van Wagner (1987) and Viegas et al. (2004) with the m_f measurements in Lousã (observed data).

Both models have a similar relation with the observed data and similar coefficients correlation. We will maintain the Equation 2 to determine FFMC since its validity was verified for the Portuguese data and it is the original equation of the FWI system.

2.3. Determination of the FWI

Two methods are addressed to determine the FWI value:

a) FWI calculated as defined in Van Wagner, 1987 (only meteorological data).
b) FWI calculated with m_f measurements - m_f is used as input parameter in the FFMC calculation through Equation 2; the remaining moisture content codes (DMC and DC) are determined using meteorological data as defined by Van Wagner. After this step the system runs according with Van Wagner equations giving the final output – FWI.

2.4. Relation of the results with the number of fires and burned area

In order to calibrate the different methods (***FWI a*** and ***FWI b***) in terms of number of fires (NF) and burned area (BA) we used the fire history of the municipalities surrounding Lousã (Coimbra, Miranda do Corvo, Penacova, Góis, Penela, Vila Nova de Poiares, Arganil e Pampilhosa da Serra) as presented in Table 1.

Table 1 – Municipalities surrounding Lousã considered to calibrate the methodology regarding the number of fires (NF) and burned area (BA) between 2018 and 2021. Source: NF and BA provided by ICNF.

Municipality (area)	NF (2018-2021)	BA (ha) (2018-2021)
Lousã (138.40 km²)	32	11.6
Coimbra (319.40 km²)	159	21.0
Miranda do Corvo (126.38 km²)	44	570.4
Penacova (216.73 km²)	5	1.5
Góis (263.30 km²)	27	2.8
Penela (132.49 km²)	35	5.8
Vila Nova de Poiares (84.4 km²)	9	0.9
Arganil (332.84 km²)	36	5.1
Pampilhosa da Serra (396.46 km²)	22	26.8

We followed the methodology proposed in Viegas et al. (2004) and replicated in Alves et al. (2018, 2021) that requires the following parameters:

- Daily FWI values;
- Daily NF, and
- Daily BA.

A new field called Probability (P) was determined (Equation 4). This field reflects the weight that a given day (and its respective FWI) has in respect to the total number of days. The higher the FWI, the higher the "incremental day" and the higher the respective "probability" of occurrence of values of FWI.

$$P = \frac{Incremental\ day}{Incremental\ day\ total} \tag{4}$$

After the ***P*** calculation we need to categorize the probability into classes which is equivalent to splitting the results by percentiles. For each one was calculated: maximum FWI value that limits the class, average FWI value, average of number of fires and average of burned area.

NF and BA, in terms of average values, were related with the original FWI (***FWI a***) and with the FWI calculated with m_f measurements (***FWI b***).

3. Results and discussion

In Figure 7 the relationship between the ***FWI a*** and ***FWI b*** is presented**,** as well as the respective correlation coefficient (R^2).

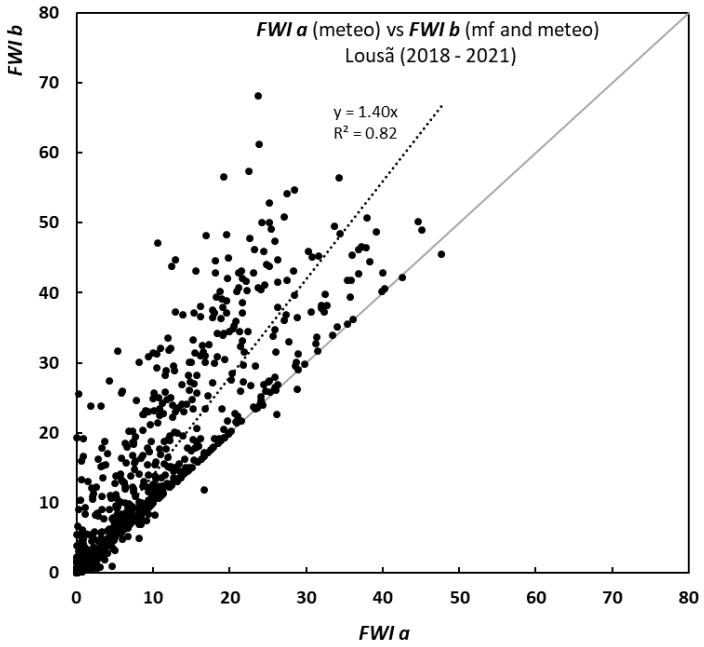

Figure 7 – Function of the original FWI calculated (FWI a) and FWI with m_f measurements (FWI b)

In Figure 7, the results show a good relationship between the two methods since the linearity is evident (high correlation coefficient) but the ***FWI b*** has higher values than the ***FWI a***.

Figure 8 presents an example of the values obtained for the two methods (***FWI a*** and ***FWI b***) for the main season in 2020 (15 May – 30 September). Also presents the values of m_f measurements in the secondary axis for the same period.

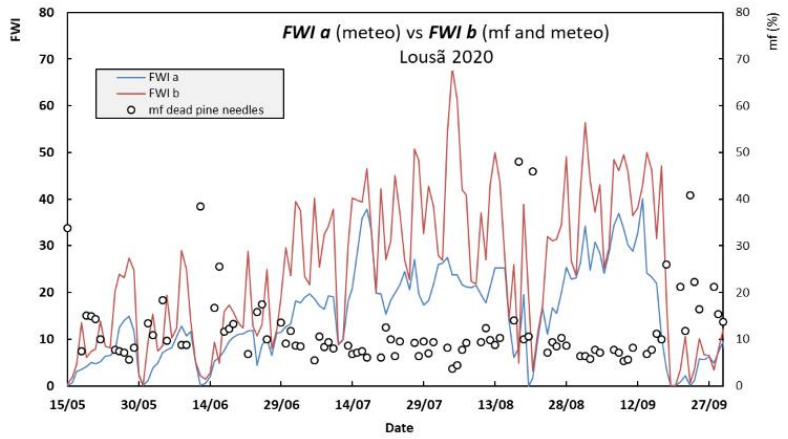

Figure 8 – Original FWI (FWI a) and FWI with m_f measurements (FWI b) – principal axis; m_f measurements – secondary axis.

The results show some differences between the two methods. FWI determined with direct m_f measurements were higher for days considered with "extreme conditions" since the m_f in Lousã was lower than 5% (Viegas et al., 2017). For example, on 4th of August, the m_f was 3.68% and for that day ***FWI a*** was 24 (high level according with Viegas et al., 2004 and EFFIS-JRC, 2022) while the ***FWI b*** was 70 (extreme level according with the same studies).

In Figure 9 is presented the average values of FWI determined for each percentile and the threshold for each danger class: low, moderate, high, very high and maximum.

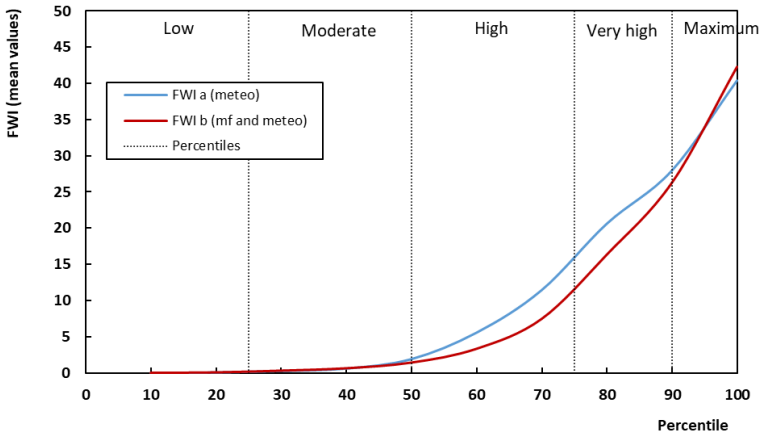

Figure 9 – Mean values of "FWI a" and mean values of "FWI b" calculated for each percentile. The vertical dotted lines define the threshold for each danger class: low, moderate, high, very high and maximum. "FWI a" is the FWI original calculated; and "FWI b" in the FWI with mf measurements.

The distribution of the two methods is similar in the begin, but from P50 to P90 the FWI ***a*** is higher than the ***FWI b***. Around P95 the ***FWI b*** presents higher values which highlights the importance that direct *mf* measurements can have for the maximum fire danger classes. The measurements can have a higher effect on the numerical value of the FWI but this effect is "hidden" with the other codes (DMC and DC) that do not consider the real m_f measurements. As a future work, we propose the measurement of soil moisture at different depths and its inclusion in the calculation of DMC and DC.

Figure 10a) presents the relation of the two methods (***FWI a*** and ***FWI b***) with the number of fires and Figure 10b) presents the relation with the burned area. In both figures, the solid lines represent the real data and the dotted lines represent the correlation equation.

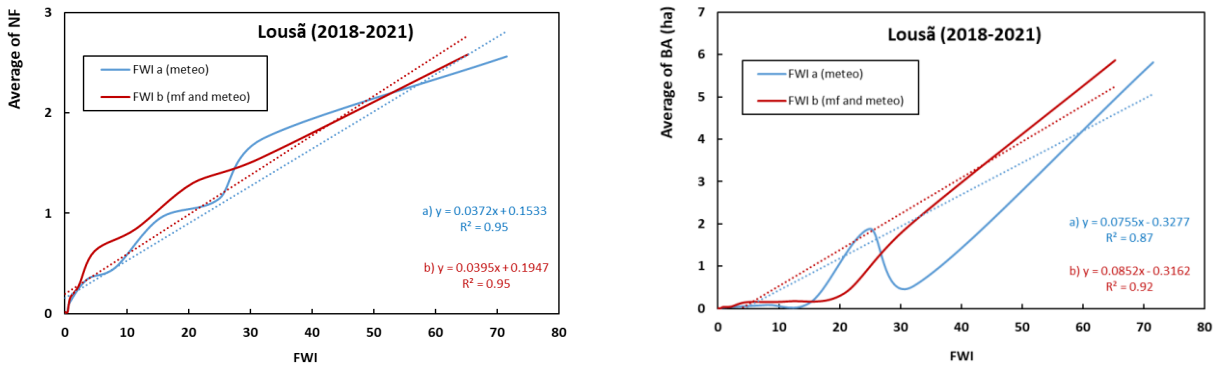

(a) (b)

Figure 10 – a) Relationship between FWI and the number of fires (NF); b) relationship between FWI and the burned area (BA).

The methods (***FWI a*** and ***FWI b***) have a similar behaviour for the NF (Figure 10a)), but for the BA the method considering m_f (***FWI b***) has a higher correlation coefficient than the method using only meteorological data (***FWIa***). In Figure 10b) it is verified that for FWI < 10 ***FWI a*** and ***FWI b*** are similar, but for high values of FWI, the ***FWI b*** crosses the ***FWI a*** curve and starts to represent larger burned areas, demonstrating the potentiality of using real measurements to represent the fire danger in terms of BA.

Figure 10 is an example for the calibration results that is typically made for this data, but we only considered the municipalities surrounding Lousã for 2018-2021.

4. Conclusion

Fuel moisture content is determinant in the extension of the burned area being a fundamental parameter in many aspects of fire danger.

The fire danger system used in Portugal – the Fire Weather Index (FWI), considers moisture indices or codes in their mathematical routine but estimates them through meteorological data. We presented a methodology to study the role that direct measurements of fuel moisture content can have in the FWI and its potentialities to predict large wildfires. Two methods were addressed: "***FWI a***" which represents the traditionally FWI determined only by meteorological parameters, and the "***FWI b***" which was determined with fuel moisture content measurements and with meteorological data for the days that we did not have measurements.

The fuel moisture content measurements, m_f, of dead pine needles collected in Lousã were used between 2018 and 2021. The preliminary results show that measurements can improve the FWI system to days with extreme weather (m_f<5%) since the FWI achieve higher values for lower m_f values. Also, the correlation between FWI considering m_f and burned area contributes to increase the correlation between the variables. Regarding the relation with number of fires seems to have not much differences between using only meteorological data or considering real measurements.

We will consider in future studies the extension of the temporal scale and the analysis of the dead eucalyptus leaves since they are also represent the dead blanket of Portuguese forests.

5. References

Alves, D., Ribeiro, L. M. and Viegas, D. X. 2017. Calibration of the Canadian FWI System for the Territory of Europe, Forest Fire Research Centre, In Advances in forest fire research 2018, Chapter 1, 33-43. Imprensa da Universidade de Coimbra doi: https://doi.org/10.14195/978-989-26-16-506_3

Alves, D., Almeida, M., Viegas, D.X., Novo, I. and Luna, M.Y. Fire Danger Harmonization Based on the Fire Weather Index for Transboundary Events between Portugal and Spain. Atmosphere 2021, 12, 1087. doi: https://doi.org/10.3390/atmos12091087

Carmo, M., Ferreira, J., Mendes, M., Silva, A., Silva, P., Alves, D., Reis, L., Novo, I. and Viegas D.X. 2021. The climatology of extreme wildfires in Portugal, 1980–2018: Contributions to forecasting and preparedness. International Journal of Climatology, 1-24. doi: https://doi.org/10.1002/joc.7411

Chuvieco, E., Aguado, I., Yebra, M., Nieto, H., Salas, J., Martín, M.P., Vilar, L., Martínez, J., Martín, S., Ibarra, P., Riva, J., Baeza, J., Rodríguez, F., Molina, J.R., Herrera, M.A., Zamora, R. (2010). Development of a framework for fire risk assessment using remote sensing and geographic information system technologies. Universidad de Alcalá, Spain. https://doi.org/10.1016/j.ecolmodel.2008.11.017.

EFFIS-JRC (2022). Fire Danger Forecast. https://effis.jrc.ec.europa.eu/about-effis/technical-background/fire-danger-forecast (Accessed on 26 March, 2022).

ICNF (Instituto da Conservação da Natureza e das Florestas). 2021. SGIF (Sistema de Gestão de Informação de Incêndios Florestais. Retrieved from https://fogos.icnf.pt/sgif2010/InformacaoPublicalist.asp (Accessed on 26 March, 2022).

Lopes S. 2013. Modelos de Previsão do Teor de Humidade de Combustíveis Florestais. Doctoral Thesis. University of Coimbra. Retrieved from https://estudogeral.sib.uc.pt/handle/10316/23786 (Accessed on 26 March, 2022).

Van Wagner, C. 1987. Development and structure of the Canadian Forest Fire Weather Index System. Otawa: Canadian Forestry Service, Forestry Technical Report 35. Retrieved from https://cfs.nrcan.gc.ca/publications?id=19927 (Accessed on 26 March, 2022).

Viegas, D. X., Bovio, G., Ferreira, A., Nosenzo, A., & Sol, B. (1999). Comparative study of various methods of fire danger evaluation in Southern Europe. 9(4)(235-246). doi: https://doi.org/10.1071/wf00015

Viegas, D.X., Piñol, J., Viegas, M.T., Ogaya, R., 2001. Estimating live fine fuels moisture content using meteorologically-based indices. International Journal of Wildland Fire 10(2): 223-240.

Viegas, D. X., Reis, R. M., Cruz, M. G., Viegas, M. T., 2004. Calibração do Sistema Canadiano de Perigo de Incêndio para Aplicação em Portugal. 77-94. EFN, Lisboa: Silva Lusitana.

Viegas, D. X., Almeida, M. F., Ribeiro, L. M., Raposo, J., Viegas, M. T., Oliveira, R., Alves, D., Pinto, C., Jorge, H., Rodrigues, A., Lucas, D., Lopes, S. and Silva, L. F. 2017. O complexo de incêndios de Pedrógão Grande e concelhos limítrofes, iniciado a 17 de junho de 2017. Coimbra, Portugal: Centro de Estudos sobre Incêndios Florestais (CEIF/ADAI/LAETA). Retrieved from https://www.portugal.gov.pt/pt/gc21/comunicacao/documento?i=o-complexo-de-incendios-de-pedrogao-grande-e-concelhos-limitrofes-iniciado-a-17-de-junho-de-2017 (Accessed on 26 March, 2022).

Tree geometrical attributes measurement using UAV-born laser scanning

Babak Chehreh*[1]; Carlos Viegas[1]; Alexandra Moutinho[2]

[1] Univ Coimbra, ADAI, Department of Mechanical Engineering, Coimbra, Portugal, {babak@adai.pt, carlos.viegas@uc.pt}
[2]IDMEC, Instituto Superior Técnico, Universidade de Lisboa, Lisbon, Portugal {alexandra.moutinho@tecnico.ulisboa.pt}

**Corresponding author*

Keywords

UAV; Tree; LiDAR; Canopy Height Model, Tree Height

Abstract

Forestry is the science and craft of creating, managing, using, conserving and repairing forests, woodlands, and associated resources for human and environmental benefits. Forest management as one of the categories of forestry, is essential to exploit forest's full economic and environmental value while ensuring the safety and resilience of the territory against natural or anthropogenic threats such as wildfires. UAV-based remote sensing is a powerful tool for forestry related tasks and measurements. Various studies and experiments have been conducted by different teams all around the world; proving the effectiveness and efficiency of this remote sensing platform and the machine learning techniques used for the analysis of the acquired data. In this study a multirotor UAV equipped with a LiDAR sensor payload is used to produce a high density point cloud of a forested area in Coimbra, Portugal. The acquired data is then used to produce point cloud-driven digital models for various forestry tasks including individual tree detection and total height. The calculated results are then validated by comparing them to the field data. The proposed methodology has potential applications for the detailed mapping of forest and wildland urban interface environments using autonomous, time and cost-effective means, towards proper forest land management for profitability and wildfire risk assessment.

1. Introduction

With the ever-increasing numbers of wildfires all over the world, as a result of human activity and climate change, now more than ever, forest management towards fire risk reduction has become a critical mission (Almeida et al., 2017), (Viegas et al., 2017). Deep knowledge about forest characteristics, more specifically vegetation parameters, is required for proper management. The trees' geometrical attributes are among the most important ones in terms of potential bio fuels for wildfires, as they govern the fire propagation through mechanisms such as crown and spot fires. Traditionally, fieldwork is required to obtain local vegetation and topography data. The extent and quality of the acquired data directly depends on the management and fire prevention plan for each municipality, and the experience of the landowner/service provider. It is also limited by its high logistic cost, in terms of time, money, and site access (Hernandez-Santin et al., 2019), often leading to insufficient or inadequate temporal and spatial data resolution.

Remote sensing, the process of obtaining information about an object or an area by measuring the radiation emitted by it from a distance (typically through airborne or spaceborne sensors), is a very useful technique to perform land mapping tasks and is a rapidly growing technology for forest monitoring (Adão et al., 2017; Müllerová et al., 2017; Nex & Remondino, 2014; Siebert & Teizer, 2014; Todoroff & Kemp, 2016). Many of these applications require individual tree detection (ITD), measuring their dimensions, state and assessing other relevant parameters.

Remote sensing can be divided into two general categories: data acquisition and data analysis. Data acquisition itself consists of two parts: remote sensing platforms (satellites, manned airplanes, high altitude balloons, unmanned aerial vehicles (UAVs) and terrestrial sensors) and sensor type. Satellites have allowed to monitor the entire world surface for different purposes (Tucker & Choudhury, 1987), (Tucker et al., 1984) and much of this data is freely available (www.copernicus.eu/en/access-data), but have coarse spatial and temporal resolutions. Aircraft systems offer increased spatial resolution, but at higher costs, often exceeding $20,000 per flight (Vandapel et al., 2004). Terrestrial delivery methods, such as handheld laser scanning devices or cameras mounted on tripods, offer high spatial resolution, but are limited in spatial extent and site accessibility.

With the need of a high spatial resolution and on-demand data, the use and development of UAVs have increased. Despite their shortcomings, which include low flight autonomy and payload capabilities, these platforms offer a complementary solution that is significantly better in terms of resolution and accuracy compared to satellites, costs less than aircraft systems and can be as precise as terrestrial delivery methods (Scholten et al., 2019). These set of advantages i.e., on demand data acquisition, high spatial and temporal resolution and relatively lower cost make UAVs very popular for forestry applications.

2. State of the art

Four types of sensors are commonly used with UAV platforms in Forestry applications; RGB cameras, Multispectral cameras, Hyperspectral cameras and LiDAR (Light Detection And Ranging) sensors. In case of the first three, the output is an image in the format of a multi-layered tensor, each layer representing a certain spectral band (3 for RGB, normally between 4 to 15 for multispectral and between 100 to 200 for hyperspectral). In case of laser scanners, the output is a point cloud; a set of data points in three-dimensional space that beside the cartesian coordinates each point can have various attributes that are built into the data structure (timestamps, labels, etc.). These datasets are pre-processed to perform various measurement, segmentation and classification tasks.

In the field of forest remote sensing, one of the most widely used models is the Canopy Height Model (CHM) (Gu et al., 2020; Ma et al., 2022; Miraki et al., 2021). This model consists of a digital surface constructed by rasterization of a point cloud set. First, the Digital Elevation Model (DEM) and Digital Terrain Model (DTM) are created; DEM and DTM are raster grids referenced to a vertical datum, DEM represents the whole scenery (ground and any observed object) while DTM only represents bare-ground; the subtraction of the two is the CHM (Figure 1). The CHM is the basis for various tree attributes measurements such as Diameter at Breast Height (DBH), Above Ground Biomass (AGB) (Wang et al., 2017) and Height Percentiles (Puliti et al., 2020).In this study a multirotor UAV platform equipped with a LiDAR payload is used to generate high density point cloud of a forested environment. This point cloud is then used to create DEM, DTM and CHM. Based on the CHM, ITD and individual tree height measurement tasks are done. The obtained data has multiple applications, including forest biomass monitoring and management for profitability and wildfire risk assessment.

3. Materials and Methods

3.1. Study area description

The study site is located in the city of Coimbra, Portugal. The area is at an elevation of 40 m above sea level, cantered at a western latitude of 40° 11' 05.8" and a northern longitude of -8° 24' 54.9" (see Figure). The climate is classified as Mediterranean climate according to Köppen climate classification (Beck et al., 2020). In the region, the dominant tree species are *Eucalyptus Globulus* and *Pinus Pinaster*, but the trees existing in the study site are *Olea europaea*. The study site is a flat ground with spaced trees and has an area of $4{,}900\ m^2$ which makes it ideal for validating the capability of the UAV payload for mapping trees.

3.2. Data Acquisition

3.2.1. Ground level measurements

Manual ground level measurements were conducted to obtain the tree height and record their location with a GPS locator. A total of 8 randomly selected trees were measured using a *Nikon® Forestry Pro* hypsometer, to serve as the ground truth. This hypsometer has an accuracy of $\pm 0.3\ m$ for distance measurement and 0.1° for angle measurement when the target object's distance is shorter than 1,000 meters, therefore height measurement accuracy is $\pm 5.2 \times 10^{-4}\ m$ (www.nikon.com).

3.2.2. UAV Data Acquisition

The UAV platform used in this study is a DJI Matrice 600 pro, a Hexacopter UAV with the payload capacity of up to 6 kg. This battery powered UAV has a triple redundant positioning system which makes it ideal for topography and mapping applications. The flight took place in June 2022.

The LiDAR sensor payload used in the study is a multisensory payload developed at Carnegie Mellon University's Robotics Institute and consists of a LiDAR scanner (*Velodyne® Puck lite*, this scanner has 16 channels, vertical and horizontal field of view of 30° and 360° respectively and vertical and horizontal angular resolution of 2.0° and 0.1° – 0.4° respectively), an IMU unit (*XSENS® MTi-30, a 9 axis high performance IMU*), and a computer (CPU: *Intel® core™ i7 8th generation*, Motherboard: *Mini-ITX Gigabyte Z390 I Aorus Pro WiFi*, RAM:*16 GB DDR3*) that does onboard data processing, producing high density point clouds that are noise filtered and down-sampled. Figure shows the hardware that was used. The point cloud's mean surface density is 45 p/m^2.

Figure 1- Satellite image of the area (40° 11' 05.8", -8° 24' 54.9")

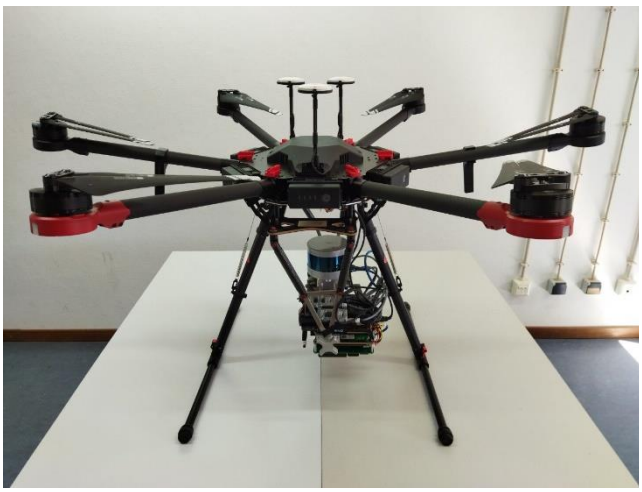

(a)

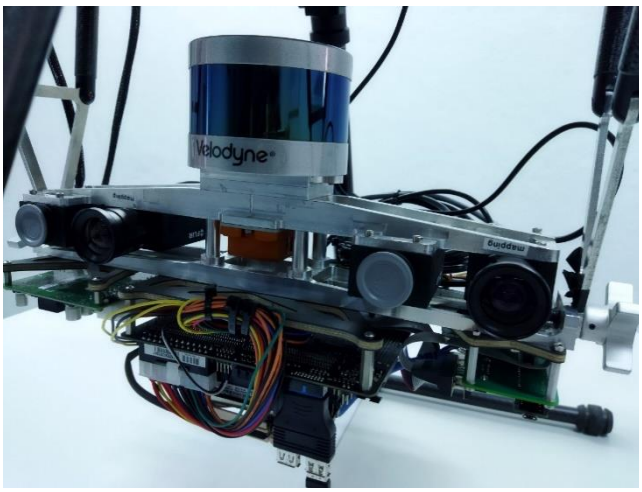

(b)

(c)

Figure 2- (a) Matrice 600 pro drone, (b) Sensor Payload, (c) Drone and the payload attached to it mid-operation

4. Results

4.1. Data pre-processing

The acquired point cloud map is shown in Figure . An open-source point cloud processing software (Cloud Compare, v 2.11.3) was used for point cloud filtering and rasterization.

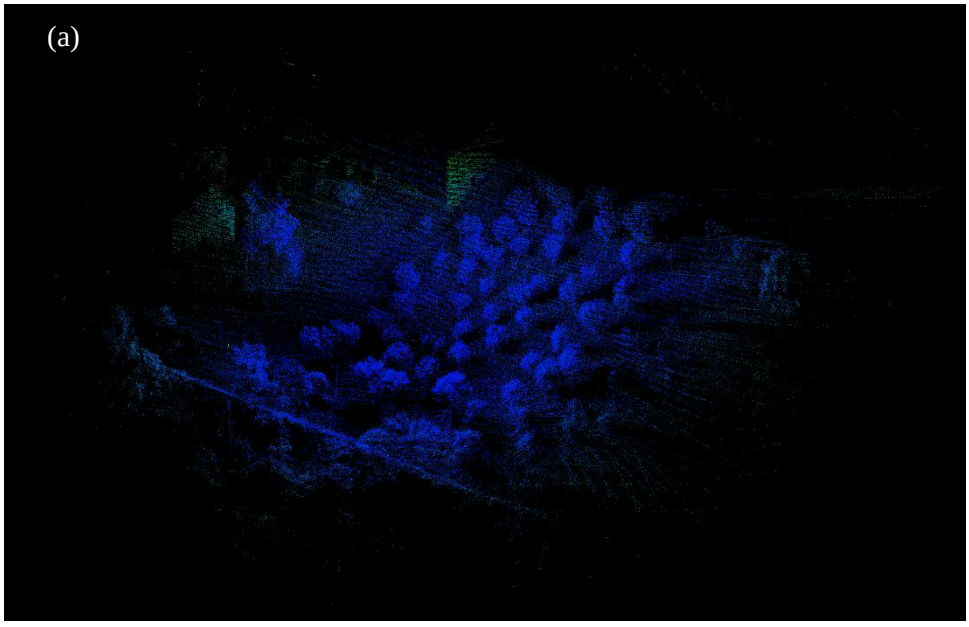

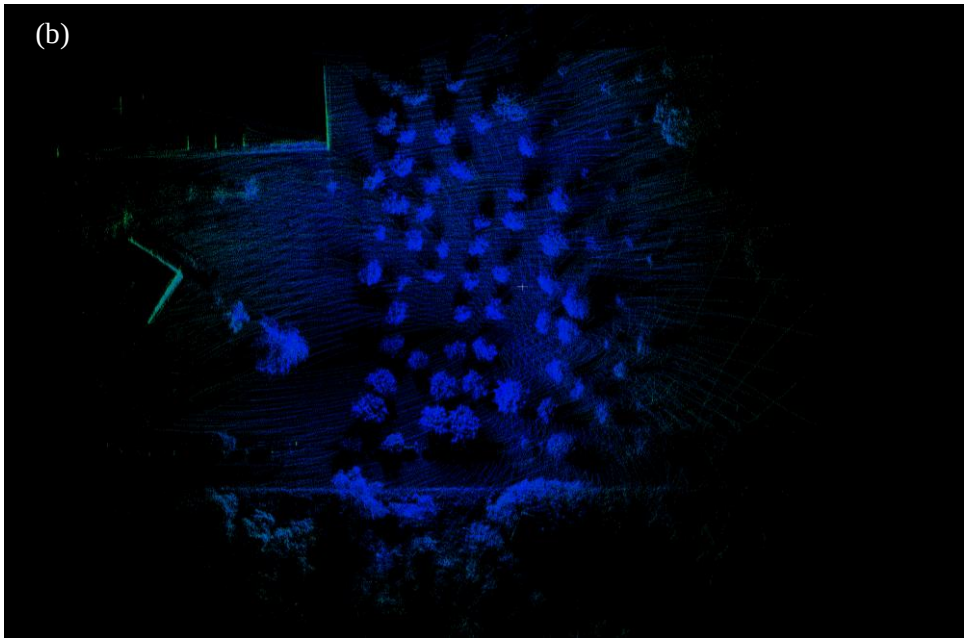

Figure 3 - Point cloud data of the study area (a) Isometric view and (b) Top view

First, the acquired point cloud map was pre-processed. The pre-processing included the following stages: 1- a noise filtering algorithm (Statistical Outlier Filter or SOR) was applied to the point cloud data to remove the points that were too far away from their neighboring point clusters. 2- After trimming the data to achieve the area of interest (AOI), a second filtering algorithm was applied on the data called Cloth Simulation Filter (CSF) to separate the ground points and above-ground points. This filter creates a mesh based on extrapolation of ground points to simulate the ground (see *Figure*). For more details about the algorithm please refer to (Zhang et al., 2016).

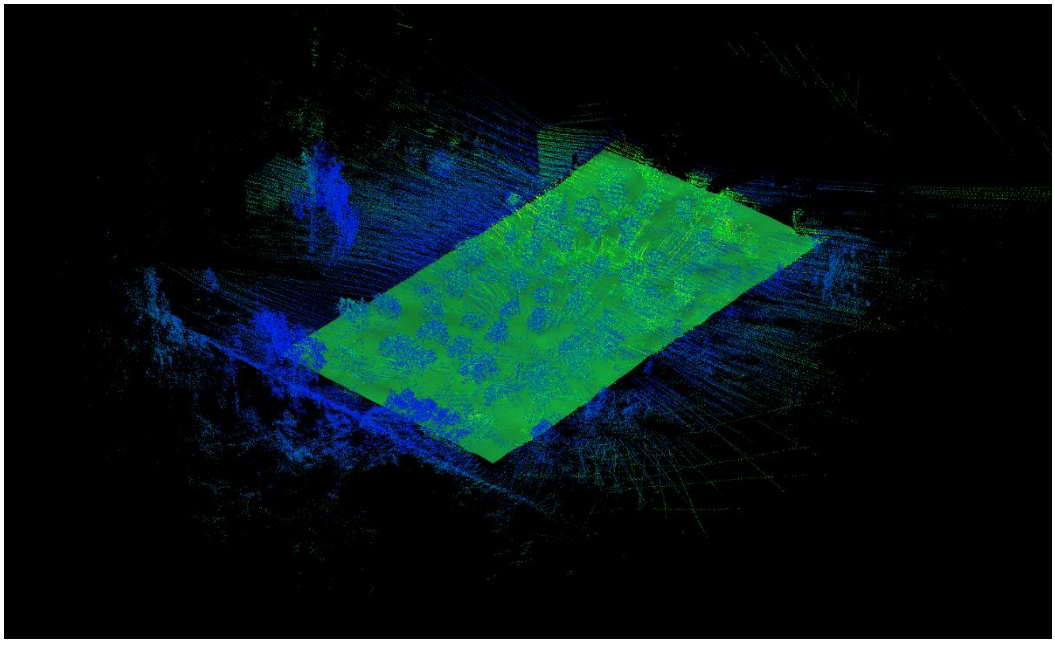

Figure 4- Generated mesh representing the ground, using CSF algorithm

The generated mesh serves as the simulation of the ground (DEM) and is used as the reference for measuring above ground points' elevation (*Figure*).

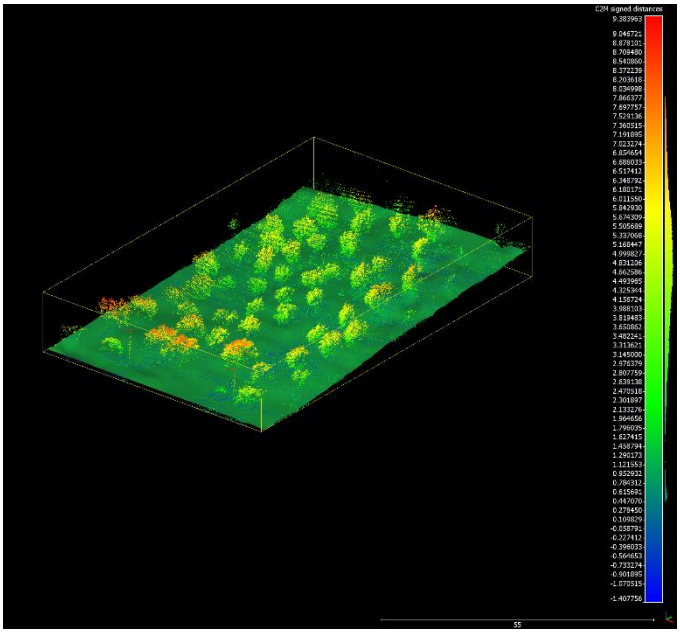

Figure 5- Pre-processed point cloud (colors indicate distance from ground)

4.2. Data Processing

After the above-ground points were annotated with their elevation relative to the ground, the point cloud was rasterized, resulting in the CHM of area (Figure).

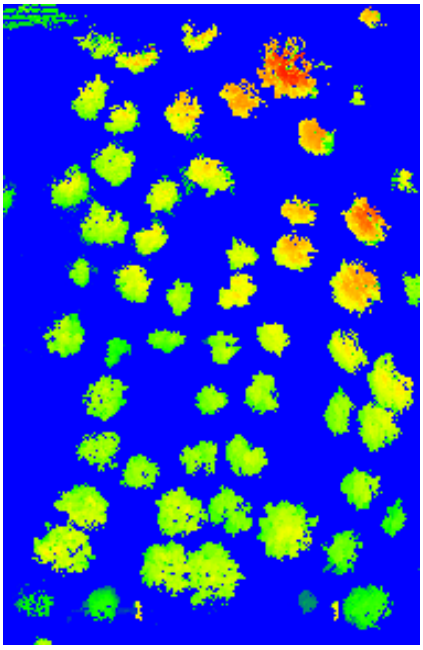

Figure 6- Canopy Height Model of the area

(R -v 4.2.0, 2021) was used for processing the CHM. To count the trees in CHM, a local maxima algorithm was used. The result is shown in Figure . Resulting height from this procedure is compared with the ground level measurements, obtained by the hypsometer, and shown in Table . The root mean square deviation (RMSD) from the height estimation is 0.11 m, demonstrating that this method is a viable solution to automatically measure tree geometrical attributes using UA 0V-born laser scanning.

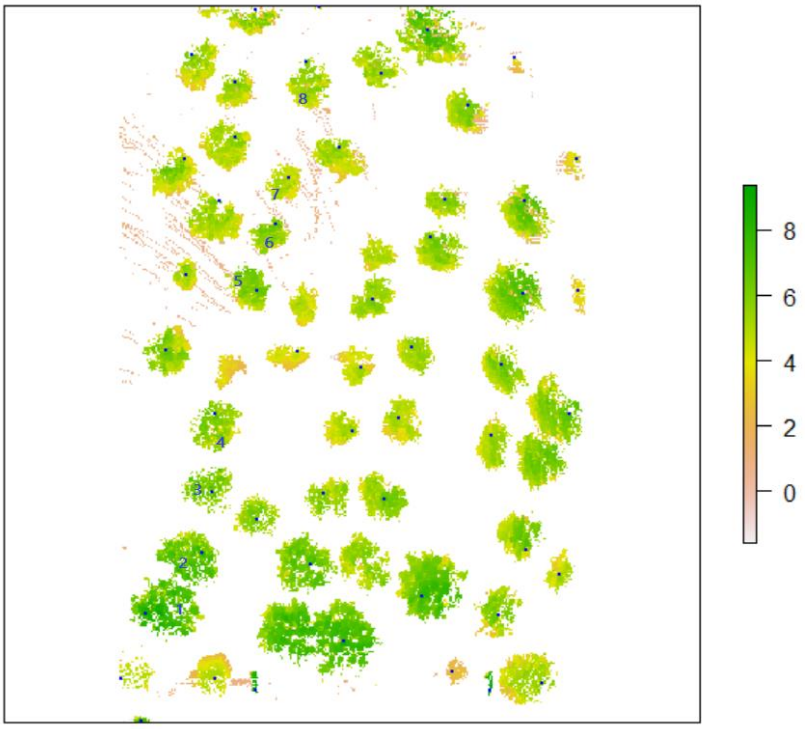

Figure 7- Tree Identification using local maxima filter

Table 1- Height measurement comparison

Tree Tag	Ground truth height (m)	Estimated height (m)
1	8.2	8.23
2	7.7	7.81
3	6.3	6.32
4	6.6	6.50
5	7.8	7.70
6	6.4	6.50
7	5.2	5.00
8	6.0	6.13
RMSD = 0.11 m		

5. Conclusion and Remarks

The comparison between the results from the UAV-born LiDAR scan processed data and the ground measurements reveal that UAV data is in good agreement with ground measurements, therefore the proposed system in this study can be used as a robust measurement tool for forestry applications. A few highlights of this study are listed as follows:

Down-sampling algorithm (point accumulation methodology) is a critical factor, density of point clusters has a direct effect on the quality of simulation of Object of Interest (OBI).

Flight and scanning scenario are the other deciding factors on the quality of obtained result. Depending on the defined task (specific forestry parameters to be measured), scan scenarios must be defined in terms of observed scenery, point density, energy and resources allocation.

The conducted flight and scan scenario is sufficient for an area with the similar characteristics as the one in this study. Denser and more complex environments require deeper and more complex scan scenarios.

A comparison between the manual field measurements time and drone flight is a good indicator of the efficiency of the proposed system; it took about 45 minutes to measure the heights of 8 trees (3 times each, for redundancy

and error reduction), while the flying time was about 8 minutes (capturing more than 50 trees in the area, not to mention part of the scanned area was trimmed and ignored).

Manual measurement time per tree: 5.5 min

UAV-born measurement time per tree: 0.16 min

Therefore, the proposed system is more than 30 times faster than manual field measurement.

6. Acknowledgments

This work was supported by project SAFEFOREST - Semi-Autonomous Robotic System for Forest Cleaning and Fire Prevention, ref. CENTRO-01-0247-FEDER-045931, partially funded by national funds through FEDER and Portugal2020, and through IDMEC under LAETA, project UIDB/50022/2020.

7. Bibliography

Adão, T., Hruška, J., Pádua, L., Bessa, J., Peres, E., Morais, R., & Sousa, J. (2017). Hyperspectral Imaging: A Review on UAV-Based Sensors, Data Processing and Applications for Agriculture and Forestry. Remote Sensing, 9(11), 1110. https://doi.org/10.3390/rs9111110

Almeida, M., Azinheira, J. R., Barata, J., Bousson, K., Ervilha, R., Martins, M., Moutinho, A., Pereira, J. C., Pinto, J. C., Ribeiro, L. M., Silva, J., & Viegas, D. X. (2017). Analysis of Fire Hazard in Campsite Areas. Fire Technology, 53(2), 553–575. https://doi.org/10.1007/s10694-016-0591-5

Beck, H. E., Zimmermann, N. E., McVicar, T. R., Vergopolan, N., Berg, A., & Wood, E. F. (2020). Publisher Correction: Present and future Köppen-Geiger climate classification maps at 1-km resolution. Scientific Data, 7(1), 274. https://doi.org/10.1038/s41597-020-00616-w

Gu, J., Grybas, H., & Congalton, R. G. (2020). A Comparison of Forest Tree Crown Delineation from Unmanned Aerial Imagery Using Canopy Height Models vs. Spectral Lightness. Forests, 11(6), 605. https://doi.org/10.3390/f11060605

Hernandez-Santin, L., Rudge, M. L., Bartolo, R. E., & Erskine, P. D. (2019). Identifying Species and Monitoring Understorey from UAS-Derived Data: A Literature Review and Future Directions. Drones, 3(1), 9. https://doi.org/10.3390/drones3010009

Ma, K., Chen, Z., Fu, L., Tian, W., Jiang, F., Yi, J., Du, Z., & Sun, H. (2022). Performance and Sensitivity of Individual Tree Segmentation Methods for UAV-LiDAR in Multiple Forest Types. Remote Sensing, 14(2), 298. https://doi.org/10.3390/rs14020298

Miraki, M., Sohrabi, H., Fatehi, P., & Kneubuehler, M. (2021). Individual tree crown delineation from high-resolution UAV images in broadleaf forest. Ecological Informatics, 61(November 2020), 101207. https://doi.org/10.1016/j.ecoinf.2020.101207

Müllerová, J., Bartaloš, T., Brůna, J., Dvořák, P., & Vítková, M. (2017). Unmanned aircraft in nature conservation: an example from plant invasions. International Journal of Remote Sensing, 38(8–10), 2177–2198. https://doi.org/10.1080/01431161.2016.1275059

Nex, F., & Remondino, F. (2014). UAV for 3D mapping applications: A review. Applied Geomatics, 6(1), 1–15. https://doi.org/10.1007/s12518-013-0120-x

Puliti, S., Breidenbach, J., & Astrup, R. (2020). Estimation of Forest Growing Stock Volume with UAV Laser Scanning Data: Can It Be Done without Field Data? Remote Sensing, 12(8), 1245. https://doi.org/10.3390/rs12081245

Scholten, C. N., Kamphuis, A. J., Vredevoogd, K. J., Lee-Strydhorst, K. G., Atma, J. L., Shea, C. B., Lamberg, O. N., & Proppe, D. S. (2019). Real-time thermal imagery from an unmanned aerial vehicle can locate ground nests of a grassland songbird at rates similar to traditional methods. Biological Conservation, 233(March), 241–246. https://doi.org/10.1016/j.biocon.2019.03.001

Siebert, S., & Teizer, J. (2014). Mobile 3D mapping for surveying earthwork projects using an Unmanned Aerial Vehicle (UAV) system. Automation in Construction, 41, 1–14. https://doi.org/10.1016/j.autcon.2014.01.004

Todoroff, P., & Kemp, J. (2016). Contribution of Remote Sensing to Crop Monitoring in Tropical Zones. Land Surface Remote Sensing in Agriculture and Forest, 179–220. https://doi.org/10.1016/B978-1-78548-103-1.50005-4

Tucker, C. J., & Choudhury, B. J. (1987). Satellite remote sensing of drought conditions. Remote Sensing of Environment, 23(2), 243–251. https://doi.org/10.1016/0034-4257(87)90040-X

Tucker, C. J., Holben, B. N., & Goff, T. E. (1984). Intensive forest clearing in Rondonia, Brazil, as detected by satellite remote sensing. Remote Sensing of Environment, 15(3), 255–261. https://doi.org/10.1016/0034-4257(84)90035-X

Vandapel, N., Huber, D. F., Kapuria, A., & Hebert, M. (2004). Natural terrain classification using 3-D ladar data. Proceedings - IEEE International Conference on Robotics and Automation, 2004(5), 5117–5122. https://doi.org/10.1109/robot.2004.1302529

Viegas, X., Almeida, M. F., Ribeiro, L. M., Raposo, J., Viegas, M. T., Oliveira, R., Alves, D., Pinto, C., Humberto, J., Rodrigues, A., Lucas, D., Lopes, S., & Silva, L. F. (2017). O Complexo De Incêndios De Pedrógão Grande E Concelhos Limítrofes, Iniciado a 17 De Junho De 2017. 238. https://www.portugal.gov.pt/download-ficheiros/ficheiro.aspx?v=3bb9773b-59fb-4099-9de5-a22fdcad1e3b

Wang, D., Xin, X., Shao, Q., Brolly, M., Zhu, Z., & Chen, J. (2017). Modeling Aboveground Biomass in Hulunber Grassland Ecosystem by Using Unmanned Aerial Vehicle Discrete Lidar. Sensors, 17(12), 180. https://doi.org/10.3390/s17010180

Zhang, W., Qi, J., Wan, P., Wang, H., Xie, D., Wang, X., & Yan, G. (2016). An easy-to-use airborne LiDAR data filtering method based on cloth simulation. Remote Sensing, 8(6), 1–22. https://doi.org/10.3390/rs8060501

R Core Team (2021). R: A Language and Environment for Statistical Computing. R Foundation for Statistical385 Computing Vienna, Austria. URL: https://www.R-project.org/

Using simulation and deep learning to derive synthetic high resolution daily fire danger maps

Jean-Baptiste Filippi[1*]; Frédéric Allaire[1]; Florence Vaysse [,3]

[1] Centre National de la Recherche Scientifique (CNRS), Sciences Pour l'Environnement – Unite ì Mixte de Recherche 6134, Università di Corsica, Campus Grossetti, Corte, France. {filippi_j@univ-corse.fr}
[2] Météo-France, Centre régional Sud-Est, 2 bd Château Double, Aix-en-Provence, France.

**Corresponding author*

Keywords

wildfire simulation, deep learning, fire danger, potential fire size, fire weather, probability distributions

Abstract

Diagnostic of next day wildfire danger typically relies on computation of meteorological indices, usually derived from weather forecast. These indices may represent the danger of ignition, potential rate of spread or droughts, and while it takes into account the vegetation state it does not represent exactly how it will burn, as this is dependent of the fuel distribution and landscape at a scale much finer than weather model allows. On the other hand, overall landscape danger is more and more often evaluated statistically using mass simulation, with a very large number of fires simulated over a variety of weather situation to estimate effective fire area burned (in Ha), reaching a very fine scale at a cost of a computational time too long for next day forecast. Deep learning and model emulation can be used to overcome this computational problem and compute this next day fire size distribution a very high temporal and spatial resolution. Nevertheless, such simulation still comes at a cost, the amount of generated data is large and challenges on how to create a synthesis that may actually be helpful and insightful in operations. In this study, several approaches are proposed to analyze results and provide new range of fire danger maps and ratings, it is applied to the real forecasts of 13 relatively large fires that occurred in Corsica and compared to corresponding forecasts using standard fire danger index used in operational conditions.

1. Introduction

Diagnostic of wildfire danger for the next day typically relies on computation of meteorological indices, usually derived from weather forecast. These indices may represent the danger of ignition, potential rate of spread or droughts. Fire danger rating systems include assessment and forecast of one or several discrete indices, rated from "low" to "extreme", but the notion of "rating" may also refer to scalar values composing the system. These indices relate to the proneness for ignition, spread and/or intensity of a wildfire according to the state of vegetation and its environment at a given time. Well known examples are The Canadian Forest Fire Danger Rating System (CFFDRS, cf. Lawson and Armitage (2008)) and the National Fire Danger Rating System (NFDRS, cf. Bradshaw et al. (1984)). Fire danger maps may be available among other data via internet-based information systems; for instance, covering the US as part of the Wildland Fire Assessment System (WFAS, cf. Burgan et al. (1997)). While these systems take into account the vegetation state it does not represent exactly how it will burn, as this is dependent of the fuel distribution and landscape at a scale much finer than weather model allows. On the other hand, overall landscape danger is more and more often evaluated statistically using mass simulation, with a very large number of fires simulated over a variety of weather situation to estimate effective fire area burned (in Ha), reaching a very fine scale at a cost of long computational time. The strategy to rely on fire spread simulations is common to Burn Probability modelling (e.g., Parisien et al. (2005), Finney et al. (2011), Parisien et al. (2019)) although the goal here is to provide a fire danger index focusing on potential for fire spread, instead of potential for a location to burn.

We have recently introduced a method to overcome the computational problem and pinpoint where and when the most critical situation of next day may occurs. DeepFire (Allaire et al. (2022)), based on deep learning emulation of wildfire simulation, to compute this next day fire size distribution at a very high temporal and spatial resolution. Nevertheless, this simulation comes at a cost, the amount of generated data is large and pose the challenge of creating a synthesis that may actually be helpful in operations. In this study, several approaches

are proposed to analyze results and provide fire danger maps and ratings using this new simulation-based prediction system, it is applied to forecasts for 13 relatively large fires that occurred in Corsica and compared to corresponding forecasts using another fire danger index used in operational conditions.

2. Methodology

The new approach proposed to quantify fire danger consists in predicting, for a given time and location, the size of the burned surface that would result from one hour of free wildfire spread after an early stage where the fire has already ignited and spread over about one acre. Ignition probability is assumed homogeneous, except for locations without vegetation where it is considered null. A duration of one hour is generally more than the time necessary for the first attack on the fire to be carried out, even more so if one assumes that the fire has been detected in the early stage. These simplifying assumptions imply that fire danger mostly expresses potential for fire spread if it is not attacked rather than potential for ignition. The overall approach has already been presented in Allaire et al. (2022), tested and compared to the French IEP (Indice éclosion-Propagation, similar to the ISI Initial Spread Index) that range from low to severe in 5 classes. As DeepFire computes effective area burnt in one hour, there has been matched to fire size classes as in Table 1.

Table 1: Values of fire sizes used to determine a class of fire danger. The fire size classes follow the US classification and a correspondence of fire danger classes was made between DeepFire and IEP in the present study

Fire size (ha)	< 0.1	[0.1, 4.0[	[4.0, 40.5[	[40.5, 121.4[	[121.4, 404.7[	[404.7, 2023.4[	≥ 2023.4
Category	A	B	C	D	E	F	G
Corresponding IEP	None	very low (1)	low (2)	moderate (3)	severe (4)	very severe (5)	very severe (5)

3. Results

In Allaire et al. (2022), it has been shown that if the focus is on the vicinity of the ignition location, DeepFire predictions proved to be better (less false-positive area), or on par with standard index, with the added advantage of providing a quantifiable output. For the fire cases studied, we knew what were the when and where to focus on because the information was known a posteriori. However, in practice, information on the fires is not known before making fire danger predictions, and area of interest must be investigated on a full 24 hours ensemble simulation dataset that consists of 10.000 members (slightly different runs), 240 time steps on a 80m resolution grid. Computation is possible in 2 hours' time, but the analysis of this entire dataset is unrealistic in operational context unless it is guided with synthetic maps.

All these deepfires computations takes as input high resolution (600 m resolution) weather forecast initialized from the French Arome model. These computations are initiated at midnight (T0 here) and available at T6 (6:00UTC) all the evaluated forecasts are between T6 and T30 (6:00 of the first day to 6:00 on the next day).

These maps have been designed to attempt to address specific questions. First, what are the locations and time where/when fire danger is highest for the day to come? (cf. deterministic: Figure 1 & 2, and probabilistic: Figure 3 & 4) Then, starting from when and for how long is there high fire danger? (cf. Figure 5 and Figure 6.) Regarding these aspects, the question of uncertainty in the prediction is also addressed to some extent by comparing the deterministic maps to their probabilistic counterparts.

A focus on one small fire, Calenzana 2017

From the deterministic prediction of either DeepFire or IEP, the maximum value over the day can be computed easily for each location. The maps of the maximum between T+6 and T+30 of DeepFire (resp., IEP) and of the associated time of maximum are shown in Figure 1 (resp., Figure 2). On this fire day, a relatively strong south-westerly wind was definitely the driving factor, but this wind also brought some humidity, leaving area of high danger either where a downslope effect was strong. By looking at the time of the maximum of DeepFire on the right of Figure 1 it can be seen that although there is a high danger potential (some areas in red in map on the left), there is actually much contrast regarding time of highest danger in the area of Calvi, suggesting that if there is an event, a detailed local analysis is required. On the IEP map in Figure 2 such requirement is less

obvious, with large areas marked in orange and less contrast, indicating a dangerous but more general situation (less discriminant) with an event having strong probabilities of occurring in the morning.

If the maximum is obtained at several forecast times (T, with T+6), we show the earliest one. Because the IEP has only 5 categories, the maximum value will most likely be predicted at several times. Figure 2 shows that the time of maximum is T+6 for most locations, making it hard to tell when fire danger is highest. In practice, this issue can be avoided by identifying the time of maximum of another a continuous quantity, such as the FFMC which is one of the two components of IEP. In Figure 1, although the maximum is represented by a categorical color scale, it corresponds to a continuous index, so this issue does not occur. The time of maximum for DeepFire predictions is between T+8 and T+18 on the majority of the island, but for some locations (even among these predicted in class F) the time of maximum is after T+18, notably around the ignition location where the fire occurred at T+16 while the maximum is more around T+22.

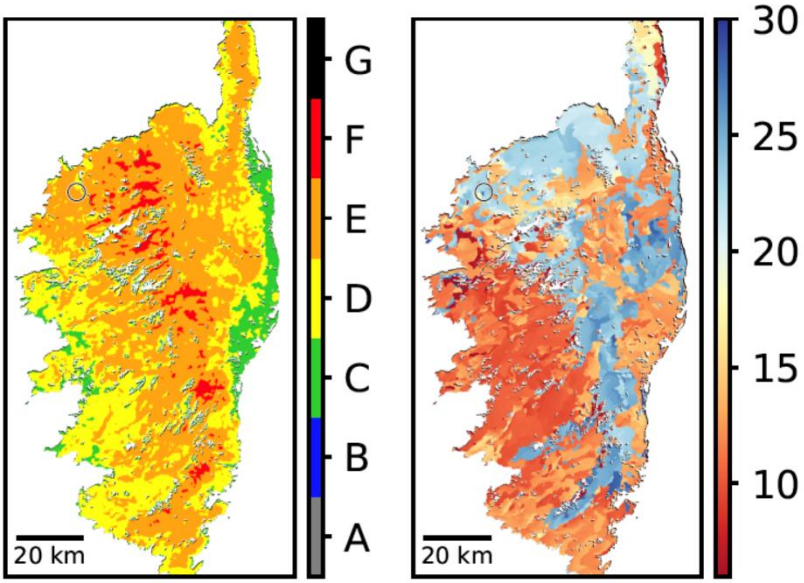

Figure 1: Maximum over the forecast between T+6 and T+30 (left) and time thereof (right) of the DeepFire prediction, location of actual fire in circle.

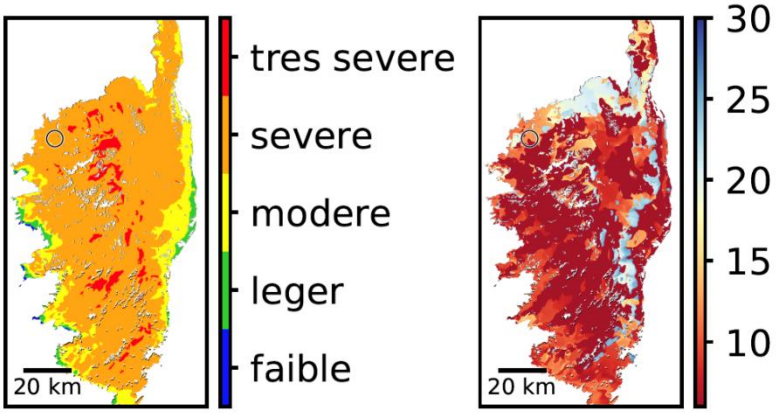

Figure 2: Same as Figure 1 but for IEP prediction

From the probabilistic forecast of DeepFire, the computation of a counterpart to Figure 1 is less direct. The ensemble can be summarized by a statistic such as the mean or a quantile. For either statistic, it makes more sense to first compute it for all locations and forecast times, then to identify the time of maximum. In the case of a quantile, for instance, the time of maximum can therefore be interpreted to that of a more or less optimistic predicted scenario. In Figure 3, the quantile for probability 0.8 was chosen. According to the Prométhée database, about 80% of the fires in Corsica have a final burned surface of 1 ha or less, which is quite low

considering the range of DeepFire predictions. Although it is untuitive to define quantile from a meaningful fire size derived from a database of observations, it does not seem relevant here, and it makes more sense to interpret the chosen quantile as a quantity that represents a quite "pessimistic" scenario. However, as can be seen in Figure 3 (middle map) there are still many locations where fire danger is at least in class D. It might be possible to make a distinction among the high-danger areas by looking at the less intuitive continuous value (left map). Regarding the time of maximum, it is similar to that of the deterministic counterpart in Figure 1.

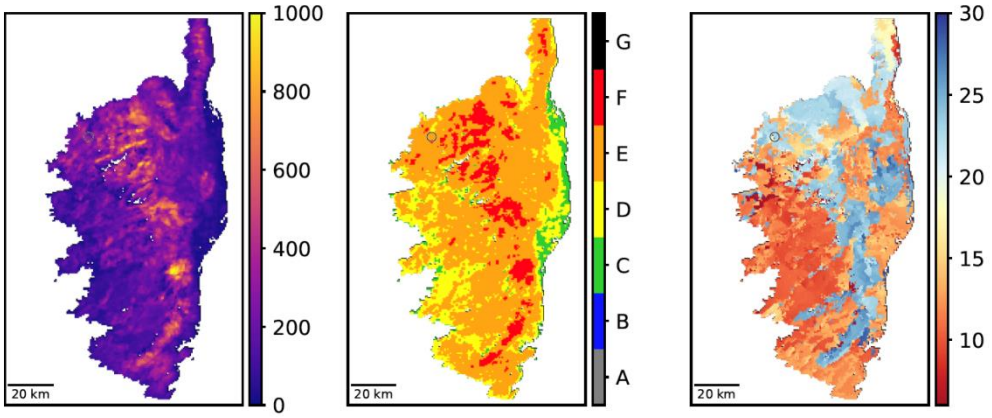

Figure 3: Maximum over the forecast between T+6 and T+30 of the quantile for probability 0.8 in the ensemble of DeepFire predictions. From left to right: continuous scale; categorical scale; time of the maximum.

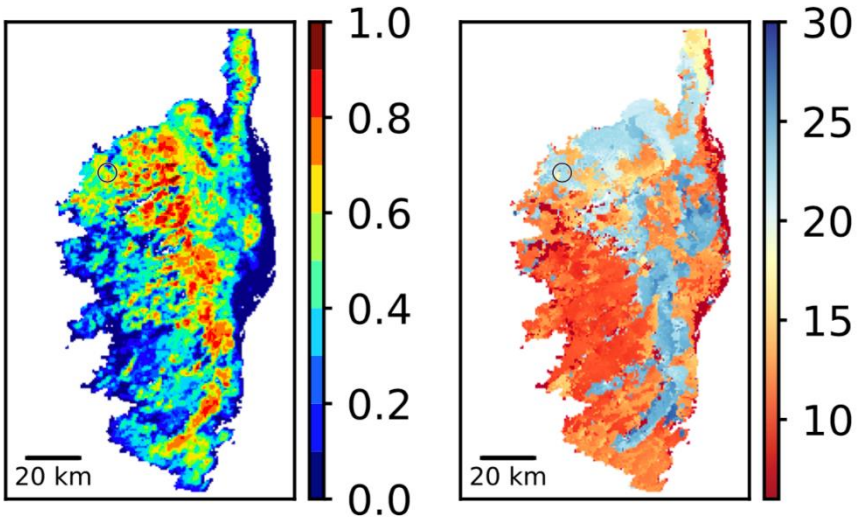

Figure 4: Maximum over the forecast between T+6 and T+30 of the probability of being into class E or higher (left) and time thereof (right).

Overview of the predictions for 12 fires

A number of numerical quantities that could serve as a daily indicator were proposed. Due to its ability to discriminate between locations with high fire danger in the cal_2017 fire case, the maximum over the forecast between T+6 and T+30 of the probability of being into class E or higher is chosen as a daily fire danger map for the 12 other fire cases. This map is shown for all 12 cases in Figure 5, together with the evolution of the proportion in the island of each class for both DeepFire and IEP according to the deterministic prediction to have an idea of how the overall spatial distribution of fire danger evolves over time.

Overall there is a general agreement in variations between T+6 and T+30 between IEP and DeepFire, with a general trend of more "contrasted" DeepFire predictions, indicating a better ability to pinpoint high danger locations (i.e. it is more discriminant). Alternatively, one may consider another maximum over time: that of the

probability (based on the ensemble) of being into class E or higher. The resulting map for cal_2017 fire case is shown in Figure 4 together with the associated time of maximum. Compared to Figure 3, the maximum probability seems better suited to discriminate among locations with high fire danger during the day, whereas the time of maximum appears similar overall, except for some locations where the predicted probability is 0 over all 24 hours, resulting in a time of maximum at the value of T+6 by default.

In terms of danger, Figure 5 has been separated into two main classes that corresponds to winter and summer fires. More than the season, a difference that can be observes is that for most summer fires, the peak in fire danger corresponds to noon (or the solar maximum), does not stay very long in peak value and overall, a situation that is bad over a large area. In winter, peaks do not have a clear time, with situation prone to large fires for a longer period. Moreover, for winter fire, there is a strong contrast between areas upwind and downwind, each of the winter situations happened in very strong winds.

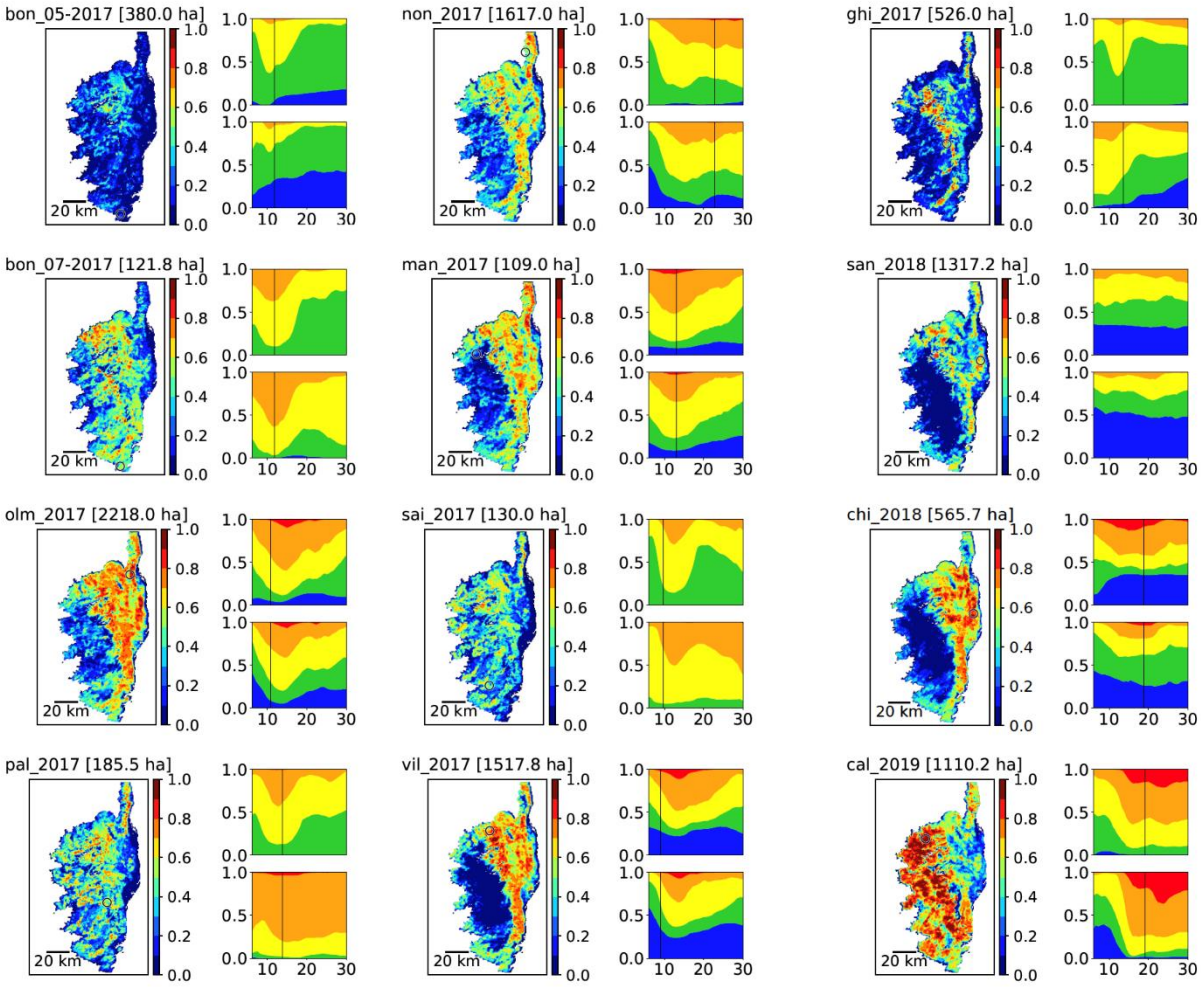

Figure 5: For all 12 complementary fire cases: maximum between T+6 and T+30 of the probability of being into class E or higher (left, cf. Figure 4), together with the evolution of the proportions over the island of DeepFire (top right) and IEP (bottom right) classes. First two columns: summer fires; last column: winter fires.

4. Conclusions

This works presents some insights on how to represent a synthesis of the large amount of data that results from fire danger predictions of potential fire size using DeepFire fire behaviour emulation.

Arguably, a daily rating of fire danger based on DeepFire should be computed on a relatively large area, at the sub-regional level for Corsica Island and the maximum value over the day can be considered. At this spatial scale, a representative fire danger rating could be the one associated to the DeepFire value that separates the 80% lower values from the 20% highest in a given area. As a complement to fire danger ratings, that are

associated to a low spatial resolution, it only makes sense to use these predictions with high spatial resolution and high frequency weather predictions to analyze the situation in more detail.

A major strength of the prediction using DeepFire seems to be its spatial granularity allowing to be more discriminant. Compared to traditional fire danger indices that mostly rely on weather forecasts, the potential fire size estimated by DeepFire accounts for the influence of terrain on fire spread at via the variability over space in type of vegetation, presence of non-burnable areas, and slope. The high-resolution maps could be used as complement of fire danger ratings, that generally attribute a single value to a large area, for better anticipation but potentially to help to decide firefighting actions after a fire has started spreading. For instance, the maps can be used to finely identify locations that, if reached at some point, the fire will spread even faster and become harder to control. Moreover, another strength regarding its design, compared to other fire danger rating systems, is that it is not based on empirical knowledge, except for the actual choices of fire size for each class, these results are not based on experience of past fires, nor on expert analysis.

Current work is focused towards removing a simplification. Separation in fire categories based on a size factor poses the problem of defining these classes. As a first guess, defining this threshold based on observed fire sizes seems a logical answer, but it may not be that representative. In Corsica and Europe, a vast majority of fires are attacked early enough and do not spread far, even when fire danger is high. It may make more sense to reanalyze the situation of a high number of days (e.g., a hundred) and provide a "reference" fire danger category, regardless of whether a fire occurred or not. Then, the thresholds could be adjusted so as to optimize the match between reference and predicted values of fire danger. Information on the intermediate sizes of the fires, rather than that of final burned surfaces, would be most relevant for evaluating the prediction performance of DeepFire, but most of the time the fire is stopped early and, otherwise, the 1-hour fire size is difficult to measure. This feedback would be very valuable to adjust the thresholds, but also to evaluate the usefulness of such a prediction system for operational use. Overall, the amount of information and complexity is increasing with the increase in resolution of most of the forecasting systems, and performing a synthesis that can leverage the advances offered by such systems is a major concern for any operational research.

5. Acknowledgments

This research is funded by the European Union through the European H2020 FIRE-RES (GA: 101037419), and also by national funds through- ANR-16-CE04-0006 FIRECASTER

6. References

Allaire F, Filippi JB, Mallet V (2022) Simulation-based high resolution fire danger mapping using deep learning. International Journal of Wildland Fire p. Just accepted, https://doi.org/10.1071/WF21143

Bradshaw LS, Deeming JE, Burgan RE, Cohen JD (1984) The 1978 National Fire-Danger Rating System: technical documentation. Gen. Tech. Rep. INT-169. Ogden, UT: U.S. Department of Agriculture, Forest Service, Intermountain Forest and Range Experiment Station. 44 pp.

Burgan RE, Andrews PL, Bradshaw LS, Chase CH, Hartford RA, Latham DJ (1997) Current status of the wildland fire assessment system (WFAS). Fire Management Notes 57, 14–17

Finney MA, McHugh CW, Grenfell IC, Riley KL, Short KC (2011) A simulation of probabilistic wildfire risk components for the continental United States. Stochastic Environmental Research and Risk Assessment 25, 973–1000, https://doi.org/10.1007/s00477-011-0462-z

Lawson B, Armitage O (2008) Weather Guide for the Canadian Forest Fire Danger Rating System. Natural Resources Canada, Canadian Forest Service, Northern Forestry Centre, Edmonton, Alberta. 84 p.

Parisien M, Kafka V, Hirsch K, Todd J, Lavoie S, Maczek P (2005) Mapping Wildfire Susceptibility with the BURN-P3 Simulation Model. Natural Resources Canada, Information Report NOR-X-405, Canadian Forest Service, Northern Forestry Centre, Edmonton, Alberta.

Parisien MA, Dawe DA, Miller C, Stockdale CA, Armitage OB (2019) Applications of simulation-based burn probability modelling: a review. International Journal of Wildland Fire 28, 913–926, 10.1071/wf19069

Wildfire rate of spread according to fire isochrones and wind direction in four of the 2019-2020 Black Summer Fires in Australia

Andrea Duane[1,2]*; Mercedes Bachfisher[3]; Lluís Brotons[4]; Marc Castellnou[5]

[1]Department of Agriculture and Forest Engineering (EAGROF), University of Lleida, Av. Alcalde Rovira Roure 191, 25198 Lleida, Spain. {andreaduane@gmail.com}
[2] Forest Science Centre of Catalonia (CTFC), Carretera vella de Sant Llorenç de Morunys km 2, 25280 Solsona, Lleida, Spain
[3] The Emergency Program, Calle Ignasi Barraquer Nº4, 08460, Santa Maria de Palautordera, Barcelona, Spain. {mercedes.bachfischer@gmail.com}
[4] CREAF, Edifici C. Autonomous University of Barcelona. 08193 Bellaterra, Barcelona, Spain.{lluis.brotons@gmail.com}
[5] GRAF division, Catalan Fire and Rescue Service, Carretera Unversitat Autonoma s/n, 08290 Cerdanyola del Vallès, Spain. {incendi@yahoo.es}

**Corresponding author*

Keywords

Rate of spread, algorithm, extreme fire behavior, isochrones, wind direction

Abstract

Wildfires of recent years are unprecedented in terms of fire behavior and impacts all around the world. The wildfire community still needs to better comprehend the physics behind the phenomenon to reduce uncertainty and increase the response capacity during emergencies. Studying past fires becomes crucial for predicting future fire behaviors. However, often the description of fire behavior in past fires has been associated with a high degree of subjectivity according to responders' description. Here, we offer a new tool that enables the user to calculate the maximum rate of spread of wildfires according to an isochrones map of the fire. In addition, it includes the possibility to calculate this maximum rate of spread according to wind direction. We apply it to a set of four fires that occurred between the 29 and 31st December 2019 in Australia. We believe this can be a very useful tool for fire analysts to compare and analyze past fires and increase our global understanding of fire behavior.

1. Introduction

Wildfires of recent years are unprecedented in terms of fire behavior and impacts all around the world (Duane, Castellnou, and Brotons 2021). The wildfire community still needs to better comprehend the physics behind the phenomenon to reduce uncertainty and increase the response capacity during emergencies (Castellnou et al. 2019). Studying past fires is a crucial step for evaluating wildfire behavior, understanding the mechanisms and providing new theories for fire spread.

Current fire behavior research is based both on mathematical spread models and on witnessed evidence on wildfire spread. While the first one has a wide range of possibilities for analyzing fires, the latter has been mostly based on laboratory experiments. However, the observations in wildland fires differ far away from what has been traditionally observed during wildfires.

Reports on wildfires have always informed very important data about fire behavior, but that has been difficult to systematically collect, or liable to a high degree of subjectivity. Many studies and reports have published values for rate of spread, one of the most important variables that explain fire behavior. These values, although useful, become difficult to compare because of a lack of an objective method to calculate it. Although the literature has reported a rate of spread of about 33 km/h in grassland fires (Cruz et al. 2015), fires spreading at a 1 km/h are already above the suppression capacity for firefighters. The limit of 3 km/h has been proposed to define an extreme wildfire event (Scott and Burgan 2005; Tedim et al. 2018).

In this study, we present an algorithm that allows the user to calculate the maximum rate of spread of a wildland fire according to a map of isochrones of wildfire growth. With this new tool, we allow the scientific community to objectively compare the observed fire behavior of different fires and relate such information with the appropriate data to derive new knowledge on fire mechanisms.

More specifically, we apply the tool to a set of wildfires that occurred during the black summer 2019-2020 season in Australia.

2. Methods

2.1. Algorithm

The algorithm presented here is currently in the publication process. However, we provide some general traits that can help to understand the potentiality of the tool.

The goal of the algorithm is to provide a maximum distance run by the fire in a certain period according to wildfire isochrones. However, the potential also relies on the fact that this distance can be calculated according to the shape of the isochrones exclusively, or by following wind direction (+-5º) at the moment of the fire interval period. In case the polygon of a fire return interval contains unburnt areas in that fire interval period (i.e. "holes"), the algorithm assumes that the fire has had the capability to jump these areas in its maximum run.

The basic information required to run the algorithm are the isochron map (polygon file type) and a wind direction table associated with each interval. The algorithm is built in R (R Core Team 2021).

2.2. Selection of fires

We selected four that fires occurred in the region between Victoria and New South Wales on the days 29-30 and 31 December 2019 (Table 1). They all occurred in similar weather and drought conditions, and they affected areas with similar vegetation types.

Table 1- Characteristics of selected fires

Fire	Country	Region	Initial Date	Final Date (imagery based)	Total Burnt Area (ha)
1- Green Valley Talmalmo	Australia	NSW	31/12/2019	15/01/2020	471,398
2- Wadbilliga	Australia	NSW	29/12/2019	05/02/2020	373,246
3- East Gippsland – Goongerah	Australia	Victoria	30/12/2019	07/02/2020	645,618
4- East Gippsland – Mallacoota	Australia	Victoria	30/12/2019	07/02/2020	363,233

It is important to notice that the two Gippsland fires shared boundaries after a while of their beginning. However, since we aim at studying the behavior of fire and thus capturing the direction is important, we have considered both fires distinct fires four our propagation analysis.

2.3. Isochrones

We positioned fire fronts (isochrones) for each fire according to the hotspots reported by the VIIRS and MODIS sensors (Schroeder et al. 2014), building a VIIRS fire perimeter (polygon) using a minimum bounding geometry. We supported such polygons with Sentinel-2 and Landsat 5,6,7, and 8 images (we used whatever image was available for each fire interval period. The goal of these supporting images was to check the consistency of the delimitation made by the VIIRS sensor). The fire interval periods lasted between 11 and 13 hours, according to the VIIRS revisit time.

2.4. Weather data

We used hourly weather data provided by the Copernicus Data Store, specifically the reanalysis ERA5 hourly pressure dataset downscaled at 0.25º resolution. Data included the two components of wind (U,V) at 10 meters, from which we calculated wind direction.

3. Results

We calculated maximum runs according to the shape of the isochrones (Figure 1) and according to the wind direction and the shape of the isochrones (Figure 2).

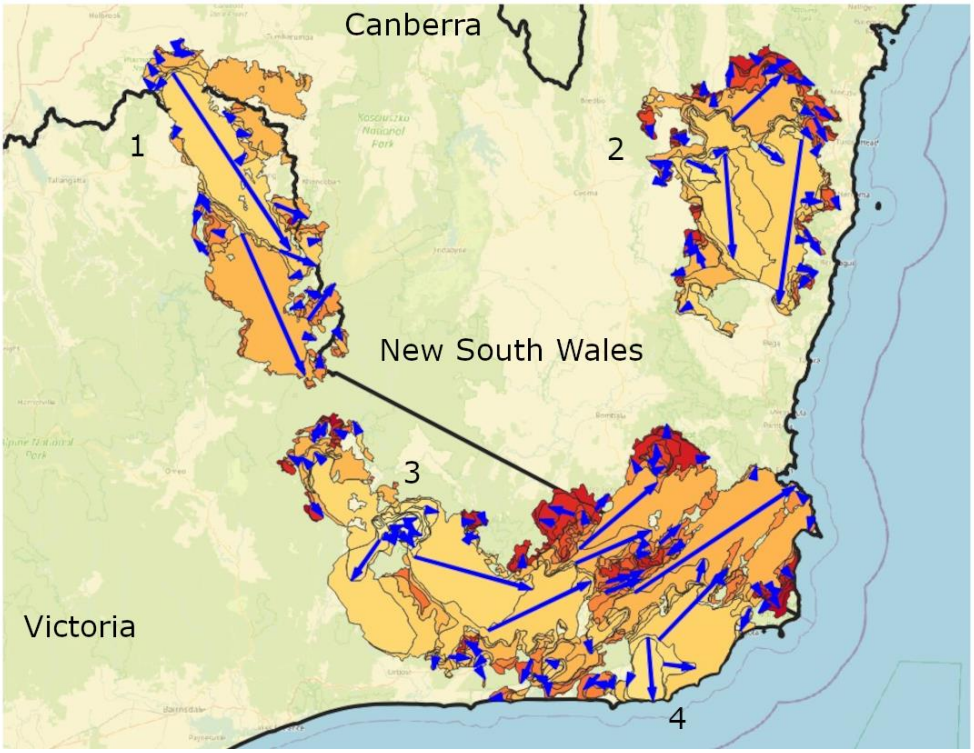

Figure 1. Maximum fire runs (blue arrows) according to the isochrone shape in the four major fires analyzed in Southeastern Australia. The Goongerah and Mallacota fires seem a single one because they share boundaries, but they are considered two different starting ignitions.

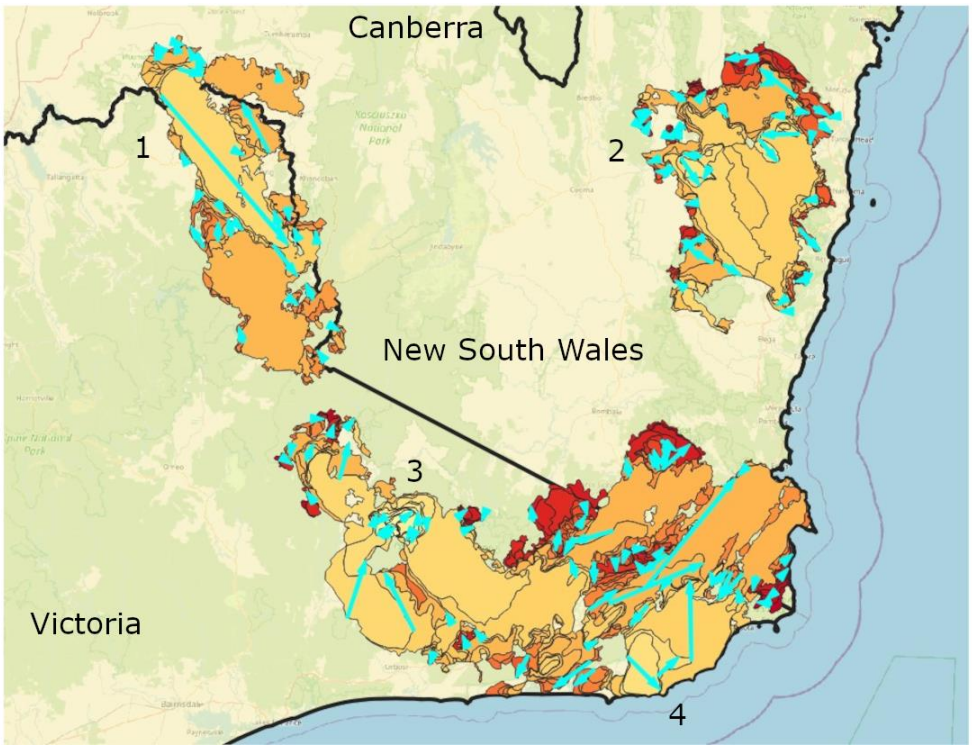

Figure 2. Maximum fire runs (light blue arrows) according to the wind direction and the isochrone shape in the four major fires analyzed in Southeastern Australia. The Goongerah and Mallacota fires seem a single one because they share boundaries, but they are considered two different starting ignitions.

We found that the most rapid fire runs where usually detected using only the shape of the isochrones (Figure 3). Maximum runs were calculated at around 6 km/h, being the fastest run in this analysis a run that took place in the Talmalmo fire on the 31st of December 2019 at 01:00 am, running at 6.535 km/h. However, when considering the total amount of runs, the average was usually higher when using the shape of the isochrones together with wind direction, although the differences where not significant (Figure 3). However, a paired analysis has not been considered in the present paper. Importantly, although the average speed was not very high when considering all runs (around 0.65 km/h), there were 21 runs exceeding the 1 km/h threshold, which can be considered a limit in fire suppression capacity. In addition, these 21 runs occurred mostly between the 31st of December 2019 and 5th of January 2020 and occurred in the four analyzed wildfires.

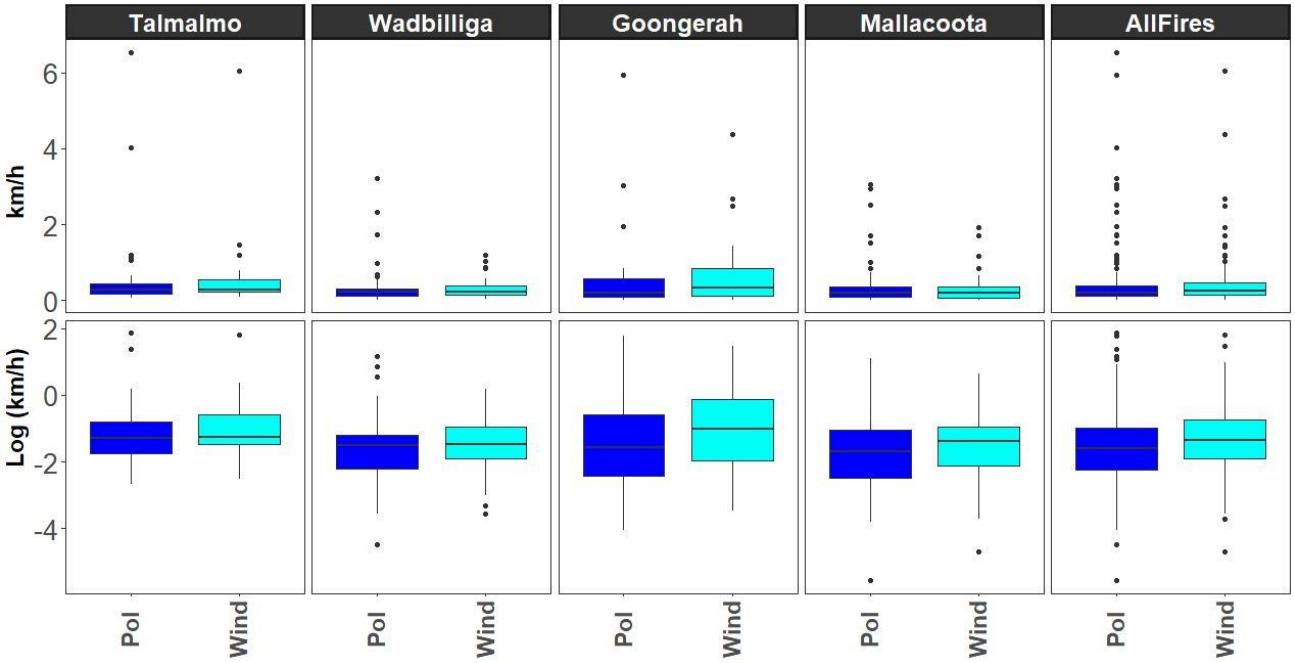

Figure 3. Maximum fire runs in each fire and considering all fires together. The upper panels show the actual values, whereas the lower panel show the logarithmic transformation to better appreciate the bulk of the data. Dark blue boxplots represent runs according to the shape of the isochrones ("pol"), whereas light blue boxplots according to the wind direction and the isochrone shape ("wind").

4. Discussions

We present the application of a new algorithm in a set of four wildfires that occurred in Australia during the black summer 2019-2020 season. The algorithm provided insightful results about fire rate of spread in these extreme fires. First of all, we detected very fast runs in the four fires: the maximum run reached 6.5 km/h in the Talmalmo fire. This is a very fast run for a forest fire: while in grass fires some rates of spread have been monitored at more than 30 km/h (Cruz et al 2015), in forest fires few runs exceed the 6 km/h threshold, only few of them in Eucalypt forests of Australia (Cruz et al 2020). Alexander and Cruz 2006 reported a 6.42 km/h fire in coniferous forests of Canada. We also obtained that a number of fire runs spread at more than 3 km/h (threshold to considered extreme), and several spread at more than 1 km/h, the limit of direct fire suppression. This indicates that the episode lived in Australia during the occurrence of these four fires was of extreme gravity given the fire behavior reported.

Our algorithm was able to calculate two different rates of spread for the same fire interval: according to the shape of the isochrones and according to the wind direction. In Figure 3 we compared both sets of results and we could see that there are not big differences between both ways of calculating rate of spread: while the major runs where always reported when considering only the shape of the isochrones, the average was higher when considering the wind direction. However, differences were not significative. It is important no notice that a "per pair" analyses would allow to obtain if per each run, the wind direction calculation gives larger or smaller rates of spread, because having all runs together does not allow to differentiate per each run.

Having a standard and homogenous way to report fire of spread opens the possibility to develop more in deep science about the factors behind fire behavior in a more general and objective way. We believe this is a simple exercise but can have a great potentially in applying it at different fires in which the progression of the fire is available.

The algorithm does not inform about the possible path of the fire inside the fire interval period, as this information is not derivative from the isochrones. The fire can change its direction because of wind direction changes in that time span, new slopes in different directions, interaction between wind and topography (Sharples et al. 2011), erratic atmospheric winds due to unstable atmospheres, fire suppression forces re-adjustments (back-fire), etc. But our analysis considers only straightforward runs as they represent the minimum distance travelled by the fire at least in that time (it might have gone faster, but we have no evidence). However, including wind direction in its calculation is an added value that can help to understand observed rate of spread and explain some of the behaviors that firefighters often report but that until now were not objectively measurable.

In this study, neither the fuel type, amount nor humidity, have been included. Although the objective was not to predict rate of spread rather than calculate the observations, we believe that mixing this type of data with other explanatory variables could increase the understanding of fire spread. By the obtainment of the rate of spread of past fires one can also analyze the spatio-temporal patterns of extreme runs around the world. For instance, the moment of the maximum rate of spread. It is commonly assumed that maximum rate of spread happens at the beginning of the afternoon, when temperature is maximum, relative humidity is minimum, and local winds and breezes achieve their maximum speed (van Wagner 1987). But recent extreme fires put into question this pattern: the Pedrogao Grande Fire occurred in June 2017 in Portugal reported an extreme run of 5.7 km/h at 20:00 hour local time (CTI 2017) generating a very serious civil entrapment with 64 fatalities. In the black summer season 2019-2020 in Australia, many of the pyrocumulonimbus events and their massive spread were reported at night (Peterson et al. 2021). At the same time, this analysis can help to disentangle the relation between fire spread direction, fire front, general wind, and many other spatial patterns of the fire.

Having an objective way of calculating rate of spread will likely help to understand wildfire behavior around the globe. This will ultimately help to develop appropriate prevention measures to diminish fire of spread and the negative impacts of wildfires.

5. References

Alexander, M. E., & Cruz, M. G. (2006). Evaluating a model for predicting active crown fire rate of spread using wildfire observations. Canadian Journal of Forest Research, 36(11), 3015–3028. https://doi.org/10.1139/X06-174

Castellnou, Marc, Núria Prat-Guitart, Etel Arilla, Asier Larrañaga, Edgar Nebot, Xavier Castellarnau, Jordi Vendrell, et al. 2019. “Empowering Strategic Decision-Making for Wildfire Management: Avoiding the Fear Trap and Creating a Resilient Landscape.” Fire Ecology 15 (1). https://doi.org/10.1186/s42408-019-0048-6.

Cruz, M. G., James S. Gould, M.E. Alexander, Andrew L Sullivan, W Lachlan McCaw, and Stuart Matthews. 2015. A Guide to Rate of Fire Spread Models for Australian Vegetation. Canberra, ACT, Australia: Australasian Fire and Emergency Service Authorities Council Ltd. and Commonwealth Scientific and Industrial Research Organisation.

Cruz, M. G., Hurley, R. J., Bessell, R., & Sullivan, A. L. (2020). Fire behaviour in wheat crops-effect of fuel structure on rate of fire spread. International Journal of Wildland Fire, 29(3), 258–271. https://doi.org/10.1071/WF19139

CTI. 2017. “Análise e Apuramento Dos Factos Relativos Aos Incêndios Que Ocorreram Em Pedrogão Grande, Castanheira de Pera, Ansião, Alvaiázere, Figueiró Dos Vinhos, Arganil, Góis, Penela, Pampilhosa Da Serra, Oleiros e Sertã, Entre 17 e 24 de Junho de 2017.” https://www.parlamento.pt/Documents/2017/Outubro/RelatórioCTI_VF .pdf.

Duane, Andrea, Marc Castellnou, and Lluís Brotons. 2021. “Towards a Comprehensive Look at Global Drivers of Novel Extreme Wildfire Events.” Climatic Change 165 (3–4): 1–21. https://doi.org/10.1007/s10584-021-03066-4.

Peterson, David A, Michael D Fromm, Richard H D Mcrae, James R Campbell, Edward J Hyer, Christopher P Camacho, George P Kablick Iii, Chris C Schmidt, and Matthew T Deland. 2021. “Australia ’ s Black Summer

Pyrocumulonimbus Super Outbreak Reveals Potential for Increasingly Extreme Stratospheric Smoke Events." Npj Climate and Atmospheric Science 38: 1–16. https://doi.org/10.1038/s41612-021-00192-9.

R Core Team. 2021. R: A Language and Environment for Statistical Computing. Vienna, Austria: R Foundation for Statistical Computing.

Schroeder, Wilfrid, Patricia Oliva, Louis Giglio, and Ivan A. Csiszar. 2014. "The New VIIRS 375m Active Fire Detection Data Product: Algorithm Description and Initial Assessment." Remote Sensing of Environment 143 (October 2018): 85–96. https://doi.org/10.1016/j.rse.2013.12.008.

Scott, Joe H., and Robert E. Burgan. 2005. "Standard Fire Behavior Fuel Models: A Comprehensive Set for Use with Rothermel's Surface Fire Spread Model." USDA Forest Service - General Technical Report RMRS-GTR, no. 153 RMRS-GTR: 1–76. https://doi.org/10.2737/RMRS-GTR-153.

Sharples, JJ, D.X. Viegas, R H D Mcrae, J.R.N. Raposo, and H.A.S Farinha. 2011. "Lateral Bushfire Propagation Driven by the Interaction of Wind, Terrain and Fire." In 19th International Congress on Modelling and Simulation, 235–41. Perth, Australia.

Tedim, Fantina, Vittorio Leone, Malik Amraoui, Christophe Bouillon, Michael Coughlan, Giuseppe Delogu, Paulo Fernandes, et al. 2018. "Defining Extreme Wildfire Events: Difficulties, Challenges, and Impacts." Fire 1 (1): 9. https://doi.org/10.3390/fire1010009.

Wagner, C. E. van. 1987. "Development and Structure of the Canadian Forest Fire Weather Index System." Canadian Forestry Service. Ottawa, Ontario. https://doi.org/19927.

Chapter 5:
Risk Reduction

A spatially explicit model of litter accumulation in fire maintained longleaf pine forest ecosystems of the Southeastern USA

Nuria Sánchez-López *[1]; Andrew T. Hudak[2]; Luigi Boschetti [1] ; Carlos A. Silva[3]; Benjamin C. Bright [2]; E Louise Loudermilk [4]

[1] University of Idaho, Dept of forest, rangeland and fire sciences, College of Natural Resources, USA
[2] USDA Forest Service, Rocky Mountain Research Station, Forestry Sciences Laboratory, USA, {nsanchezlopez@uidaho.edu}
[3] University of Florida, School of Forest Resources and Conservation, USA
[4] USDA Forest Service, Southern Research Station, Center for Forest Disturbance Science, USA

**Corresponding author **

Keywords

Litter production, litter accumulation, years since fire, tree crown, ALS

Abstract

The continuity and depth of the surface litter and duff layers are major drivers of fire spread and fuel consumption. Nevertheless, its spatially explicit quantification over relatively large areas remains unresolved: local fuel heterogeneity introduces large uncertainties in estimates derived from field-based models and sparse data samples. Besides that, the sensitivity of remote sensors to surface litter loads is limited, particularly under canopy cover. In fire-maintained pine forests of the Southeastern US, surface fuel accumulation and its distribution over the forest floor are mainly driven by vegetation productivity, decomposition, and years since fire (YSF). Traditional ecological and stand-level models provide a means to equilibrate between opposing rates of deposition and decomposition as a function of YSF at the landscape level but don't account for spatial heterogeneity.

We developed a top-down, object-based approach for wall-to-wall estimation of surface litter loads using TSF records, the ecologically based Olson model, and tree crown objects derived from airborne laser scanning (ALS) data. The approach involves, first, the spatially explicit estimation of litter production through a tree crown production model. This model is driven by tree crown attributes extracted from the ALS point clouds, and it is informed by tree inventory data and allometric equations, including vegetation leaf turnover rates. Second, litter accumulation is estimated using the fire-driven Olson equation, which models accumulation progressively with time until decomposition balances deposition and a steady state of accumulation is reached. The methodology is demonstrated at several fire-maintained longleaf pine forest management units in southeastern USA, where tree inventory data, surface litter loads, prescribed fire records, and ALS data are available for testing and validation of the methodology. Comparison between modeled estimates and observed litter loads shows a relatively good agreement (RMSD=0.24 [kg m-2]; BIAS 0.004 [kg m-2]). This suggests that the proposed approach to indirectly map patterns of litter production and litter accumulation can provide a realistic means to map the continuity of the litter layer, thus overcoming the limitation of traditional ecological landscape models to account for spatial heterogeneity. This high-resolution map of litter loads will be further valuable as input to physics-based fire behavior and spread models and to improve the spatially explicit characterization of the duff layer.

1. Background and goals

High spatial resolution maps of surface fuels are critically needed by the carbon and fire communities, being especially relevant for forest managers that operationally use prescribed fires to maintain forest health and wildlife habitat in the longleaf pine forests of the southeastern US. Unfortunately, such maps are missing for most forested sites: the sensitivity of remote sensors to surface litter loads is limited, particularly under canopy cover, and the high heterogeneity of surface fine fuels and the lack of enough reference data (i.e., field measurements) limits the scope of data-driven modelling techniques (Keane, 2015; Keane et al., 2001).

In these longleaf pine forests, surface fuel accumulation and its distribution over the forest floor are mainly driven by vegetation productivity, decomposition, and years since fire (YSF) (López-Senespleda et al., 2021; Prescott, 2002; Zazali et al., 2020). Traditional ecological models such as the Olson model (Olson, 1963)

provide a means to equilibrate between opposing rates of deposition and decomposition as a function of TSF at the landscape level but generally don't account for spatial heterogeneity.

In the absence of disturbances at a specific location (e.g., under a specific tree crown), litter accumulates proportionally to the foliage biomass (FB) produced aboveground and deposited on the ground as litterfall until it decomposes into duff (Zazali et al., 2020). Therefore, characterizing the spatial variability of FB driven by the forest canopy would provide a means to describe surface fuel dynamics at the tree-level scale. Nowadays, remote sensing, and particularly airborne laser scanning (ALS) data, provides the most practical means to characterize tree aboveground biomass across entire forest landscapes at high spatial resolution, as shown in the many studies on tree detection and crown delineation, and on modelling tree attributes including height, volume, and/or biomass (e.g, Chen et al., 2007; Hudak et al., 2008; Jakubowski et al., 2013; Li et al., 2012; Roussel et al., 2020; Silva et al., 2016; Wan Mohd Jaafar et al., 2018).

In this study, we propose an object-based approach to map litter loads at high spatial resolution by mapping patterns of tree leaf litter production (i.e., litterfall) and quantifying litter accumulation through time with a spatially explicit implementation of the Olson model. This approach assumes that, locally, the amount and distribution of litter over the forest floor are mainly driven by litter production, i.e., by aboveground biomass and canopy characteristics (López-Senespleda et al., 2021; Prescott, 2002), and that due to the overstory inputs, litter loads are higher under trees than in gaps and edges.

2. Materials

The methodology was tested in three forest management units (i.e., 608A, 703C, L2F) at Eglin Air Force Base (AFB) in the panhandle of Florida (Figure 1). These sites undergo frequent prescribed burning that serves to maintain the native wildlife of the predominant longleaf pine ecosystem and facilitate military training.

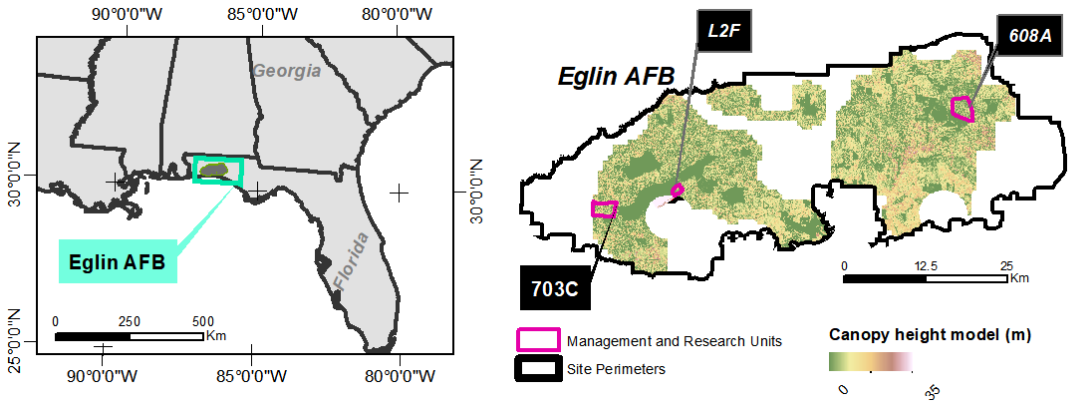

Figure 1. Location of the L2F, 608A, and 703C management units at Eglin Air Force Base (AFB). The canopy height model derived from airborne laser scanning (ALS) is displayed as background where ALS data is available.

ALS data were acquired in 2018 and points clouds were delivered by the provider in binary format (.las) with ground points labeled. The point cloud was normalized, converting points to height above ground, and a canopy height model (1-meter spatial resolution) was created.

A total of 166 litter biomass samples within the three management units were collected over square litter clip plots (0.25-1 m^2) in the framework of the RXCADRE project (2008-2012) (Ottmar et al., 2015) (Table 1, Figure 2). These data were used for accuracy assessment of the proposed methodology.

Table 1. Number of field clip plots, and minimum, mean, maximum, and standard deviation of the litter biomass (LB) [kg m^{-2}]. YSF: years since fire in the management unit at the time of the data collection.

Units	Sampling Year	YSF	# samples	Min LB [kg m^{-2}]	Mean LB [kg m^{-2}]	Max LB [kg m^{-2}]	Std Dev. [kg m^{-2}]
L2F	2012	3	66	0.04	0.48	1.27	0.31
608A	2011	2	60	0.05	0.34	0.75	0.15
703C	2011	2	40	0.07	0.33	0.72	0.16

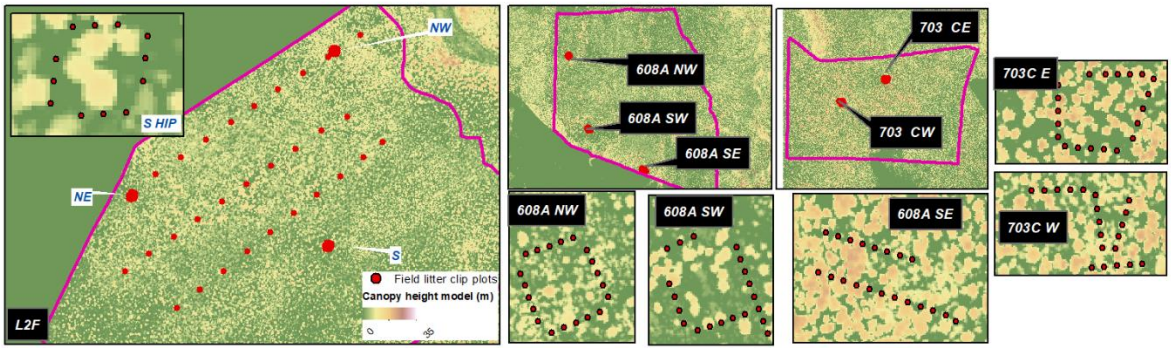

Figure 2. Location of the 166 litter clip plots established in 2011 and 2012 within the L2F, 608A, and 703C units at Eglin AFB.

3. Methods

Our proposed methodology involves the spatially explicit estimation of annual litter production following a biomass abundace approach in which littefall is proportionally estimated from tree FB. FB is modelled at the crown level from ALS data and random forest (RF) modelling, and informed by tree inventory data. Litter production maps are rasterized (5 m) and used, together with decomposition rates, to quantify litter accumulation after fire with a spatially explicit implementation of the Olson model (Figure 3).

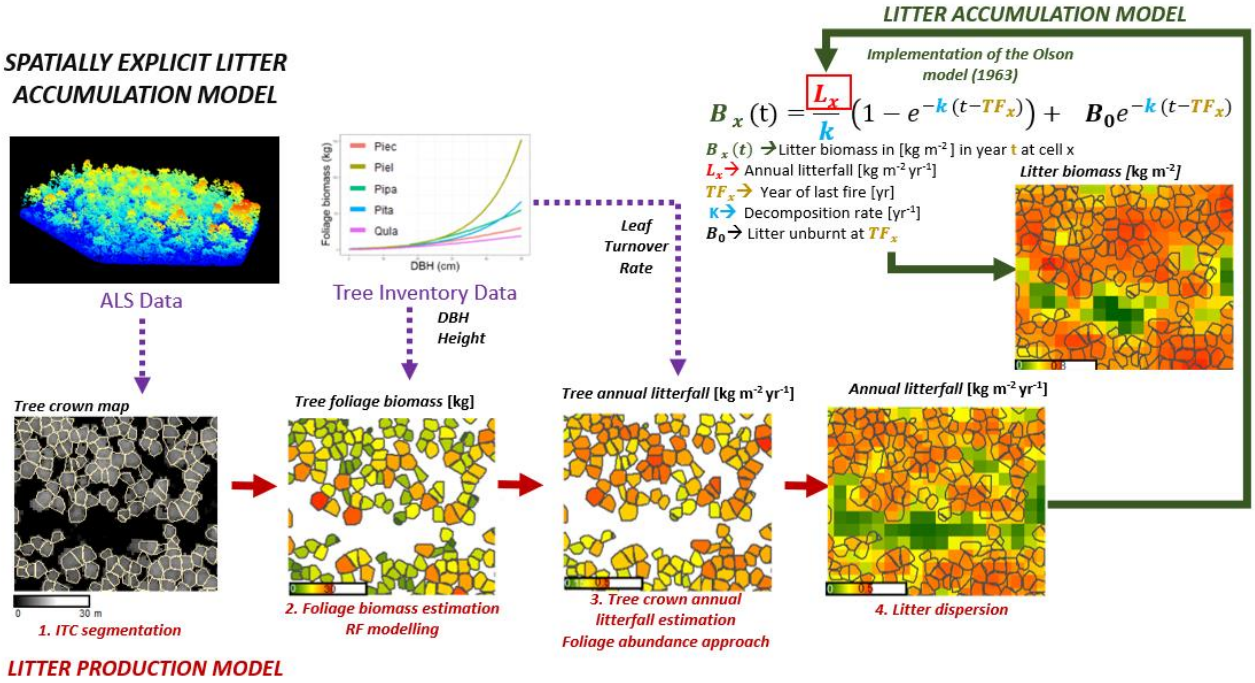

Figure 3. Workflow of the spatially explicit model of litter accumulation based on a tree crown-level litter production model.

3.1. Litter Production model

The spatially explicit estimation of litter production involves four processing steps: (1) generation of a tree crown map through segmentation of the ALS data, and computation of tree crown attributes also from the ALS data; (2) estimation of the total foliar biomass of each tree crown, by applying a RF model; (3) estimation of annual litterfall at the crown level following a FB abundance approach; and (4) annual litterfall distribution over the forest floor using a convolution filter (Figure 3).

Individual tree crown delineation was performed on the ALS canopy height model applying Silva's tree segmentation algorithm (Silva et al., 2016). A set of attributes was obtained for each crown from the 3D point cloud, and a RF model (Breiman, 2001) was calibrated to estimate crown FB. We used tree field inventory data

to determine FB from dbh-height allometric equations. These FB estimates were used as the response variable in the RF model, and the corresponding crown attributes were used as the predictor variables.

Once FB was estimated at the crown level, litterfall was proportionally estimated from tree FB applying leaf turnover rates that were based on leaf longevity of the dominant species observed in the study area (Neumann et al., 2018; White et al., 2000). Estimates of litterfall from tree crowns were rasterized and mapped at 5 m spatial resolution which approximates the size of the dominant tree crown in this ecosystem. Finally, to consider a dispersion rate of litterfall from the tree driven by external factors such as topography or weather, a convolution filter was applied.

3.2. Litter Accumulation

Total litter accumulation after fire was calculated through a spatially explicit implementation of the Olson model (Eq. 1):

$$B_x\,(t) = \frac{L_x}{k}\left(1 - e^{-k_x\,(t-TF_x)}\right) + B_0 e^{-k_x\,(t-TF_x)} \qquad (Eq.\,1)$$

where $B_x\,(t)$ [kg m^{-2}] is litter biomass accumulated in a cell x in year t; L_x is the steady annual accumulation rate, i.e., annual litter production or litterfall [kg m^{-2} yr^{-1}]; TF_x is the year of the last fire in a cell x; k is the decomposition rate in a cell x [yr^{-1}]; and B_0 is litter remaining after the previous burn [kg m^{-2}]. Based on the post fire litter samples collected at Eglin AFB, B_0 was established at 0.04 [kg m^{-2}] (Ottmar et al., 2015).

Climate and litter quality (e.g., percentage of lignin) and litter traits (e.g., leaf area) are main drivers of decomposition (Berg, 2014; Gholz et al., 2000; Meentemeyer, 1978). The dominant species on the study sites was longleaf pine. Accordingly, decomposition was calculated applying the single regression model calibrated for pine needles as part of the Long-term Intersite Decomposition Experiment (LIDET) that uses actual evapotranspiration (AET) as the only predictor variable. AET was obtained from the Moderate Resolution Imaging Spectroradiometer (MODIS) derived product available at https://earlywarning.usgs.gov (accessed on 9th of September 2021) (Senay et al., 2013).

The model was run for 2 YSF at the 703C and 608 A units, and for 3 YSF at the L2F unit, with YSF calculated at the time of the field data collection (Table 1).

3.3. Model assessment

Accuracy assessment was performed by comparing the litter loads observed at each of the 166 litter clip plots (Figure 2) with the predicted litter loads on the litter accumulation map. Model accuracy was evaluated using Root Mean Square Difference (RMSD) and BIAS statistics:

$$RMSD = \sqrt{\frac{\sum_{i=1}^{n}(\hat{Y}_i - Y_i)^2}{n}} \qquad (Eq.\,2)$$

$$BIAS = \frac{1}{n}\sum_{i=1}^{n}\left(\hat{Y}_i - Y_i\right) \qquad (Eq.\,3)$$

where n is the number of field litter clip plots, Y_i is the observed litter biomass for a given clip plot *i*, and $\hat{Y}_i$ is the predicted litter biomass corresponding with the cell value spatially intersecting the center of the field litter clip plot.

4. Results

The average litter production at the 608A, 703C, and L2F units was 0.13, 0.18, and 0.17 [kg m^{-2} yr^{-1}] respectively (Figure 4).

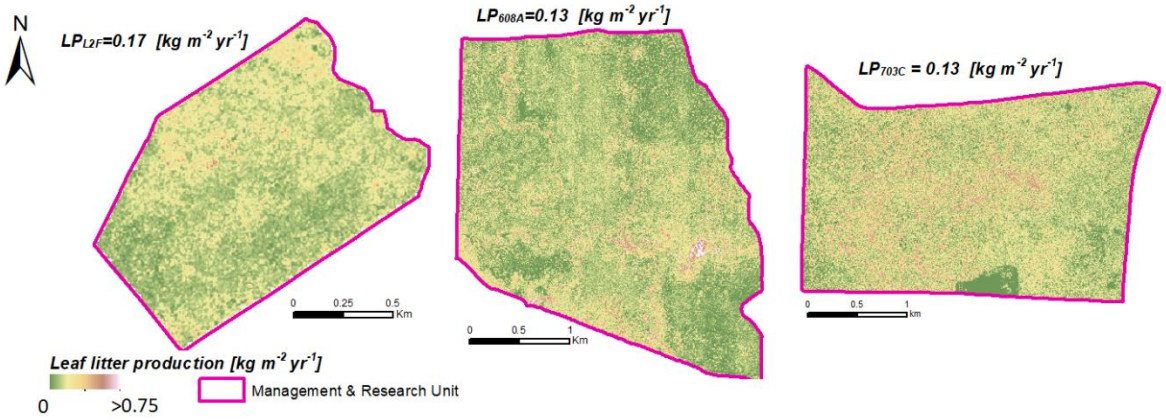

Figure 4. Annual litterfall [kg m^{-2} yr^{-1}] at the L2F, 608A, and 703C management units.

Average actual evapotranspiration within Eglin AFB was 714 mm, and the average decomposition rate was 0.13 [kg yr^{-1}]; therefore, the expected time necessary to reach 90% of the accumulation based on the Olson model was ~17 years. Average estimated litter loads at the L2F unit after 3 YSF was 0.38 [kg m^{-2}], and 0.26 and 0.35 [kg m^{-2}] at the 608A and 703C units after 2 YSF (Figure 5).

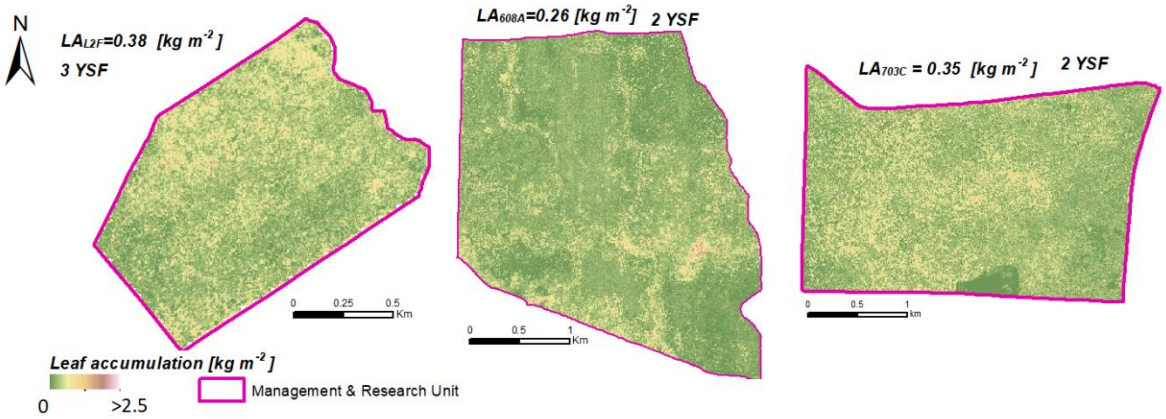

Figure 5. Litter loads at the 608A and 703C management units after 2 years since fire and after 3 years at L2F unit.

Table 2. R Pearson's correlation (R), RMSD, and BIAS of the litter biomass observed (Y_i) in the clip plots (0.25-1 m^2) sampled pre-fire at the L2F, 608A, and 603C units and the estimated ($\hat{Y}_i$) litter biomass corresponding with the cell value spatially intersecting the center of the field litter clip plot (0.25-1 m^2); n indicates the number of clip plot measurements evaluated at each time

Unit	n	$\frac{1}{n}\sum_{i=1}^{n}(Y_i)$ [kg m^{-2}]	$\frac{1}{n}\sum_{i=1}^{n}(\hat{Y}_i)$ [kg m^{-2}]	R	RMSD [kg m^{-2}]	BIAS [kg m^{-2}]
L2F	66	0.48	0.43	0.58	0.27	-0.05
608A	60	0.34	0.35	0.63	0.20	0.01
703C	40	0.33	0.42	0.32	0.24	0.09

Overal RMSD and BIAS were 0.24 and 0.004 [kg m^{-2}]. By unit, RMSD and BIAS were 0.27 and -0.05 [kg m^{-2}] at the L2F unit, 0.20 and 0.01 [kg m^{-2}] at the 608A unit, and 0.24 and 0.09 [kg m^{-2}] at the 703C unit. Accuracy assessment revealed a moderate R Pearson correlation between predicted ($\hat{Y}_i$) and observed (Y_i) litter loads (R=0.52) (Figure 6), which was expected given the large variability observed on the field data (Table 1). The correlation was higher at the L2F and 608A units (R=0.63, and 0.58) compared to the 703C (R=0.32), where the number of field samples was lower (n=40) (Table 2).

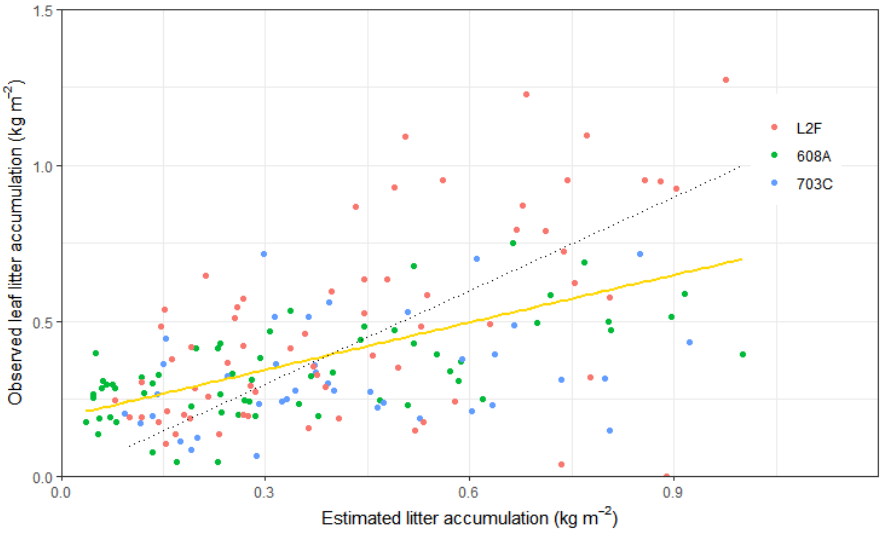

Figure 6. Litter biomass observed on the 166 litter clip plots (0.25-1 m^2) sampled pre-fire at Eglin AFB (y axis) and estimated litter biomass corresponding with the cell value of the litter accumulation map (25 m^2) spatially intersecting the center of the field litter clip plot (x axis). In each case, the spatially explicit implementation of the Olson's model was run for the same YSF observed on the units at the time of the data collection. The yellow line represents the best fit of the linear model between estimated and observed values, and the grey dashed line represents the 1:1 relationship.

5. Discussion

We mapped litter accumulation at high spatial resolution (5 m), developing a conceptual approach to estimate annual litterfall patterns at the tree level using 3D remotely sensed data and using the fire-driven Olson accumulation model to subsequently estimate litter loads. Our results support our initial hypothesis that, on these frequently burned forest ecosystems and up to 3 YSF, tree leaf litter accumulation and its distribution over the forest floor are mainly driven by tree foliar biomass and YSF, as indicated by the relatively good agreement between predicted and observed accumulated litter loads (R=0.52) (Figure 6). While it is a moderate correlation, it is relevant considering the large heterogeneity of litter loads observed over the forest floor at the local scale (Table 1), and the difference in size of the litter clip plots (0.25-1 m^2) and the pixel size of the leaf litter map (25 m^2).

The methodology can be transferred to other study sites and ecological regions where ALS data and the time since fire are known. Nevertheless, further research is needed to assess the performance on the model over a longer term (> 3 YSF). Our methods provide a realistic means to map the continuity of the litter layer conditioned on overstory tree crowns, thus overcoming the limitation of traditional ecological landscape models to account for spatial heterogeneity. This high-resolution map of litter loads will have further value as input to physics-based fire behavior and spread models and to improve the spatially explicit characterization of the duff layer.

6. Bibliography

Berg, B., 2014. Decomposition patterns for foliar litter–a theory for influencing factors. Soil Biol. Biochem. 78, 222–232.

Breiman, L., 2001. Random forests. Mach. Learn. 45, 5–32.

Chen, Q., Gong, P., Baldocchi, D., Tian, Y.Q., 2007. Estimating basal area and stem volume for individual trees from lidar data. Photogramm. Eng. Remote Sens. 73, 1355.

Gholz, H.L., Wedin, D.A., Smitherman, S.M., Harmon, M.E., Parton, W.J., 2000. Long-term dynamics of pine and hardwood litter in contrasting environments: toward a global model of decomposition. Glob. Change Biol. 6, 751–765.

Hudak, A.T., Crookston, N.L., Evans, J.S., Hall, D.E., Falkowski, M.J., 2008. Nearest neighbor imputation of species-level, plot-scale forest structure attributes from LiDAR data. Remote Sens. Environ. 112, 2232–2245. https://doi.org/10.1016/j.rse.2007.10.009

Jakubowski, M.K., Li, W., Guo, Q., Kelly, M., 2013. Delineating Individual Trees from Lidar Data: A Comparison of Vector- and Raster-based Segmentation Approaches. Remote Sens. 5, 4163–4186. https://doi.org/10.3390/rs5094163

Keane, R.E., 2015. Wildland fuel fundamentals and applications. Springer.

Keane, R.E., Burgan, R., van Wagtendonk, J., 2001. Mapping wildland fuels for fire management across multiple scales: Integrating remote sensing, GIS, and biophysical modeling. Int. J. Wildland Fire 10, 301–319.

Li, W., Guo, Q., Jakubowski, M.K., Kelly, M., 2012. A new method for segmenting individual trees from the lidar point cloud. Photogramm. Eng. Remote Sens. 78, 75–84.

López-Senespleda, E., Calama, R., Ruiz-Peinado, R., 2021. Estimating forest floor carbon stocks in woodland formations in Spain. Sci. Total Environ. 788, 147734.

Meentemeyer, V., 1978. Macroclimate and lignin control of litter decomposition rates. Ecology 59, 465–472.

Neumann, M., Ukonmaanaho, L., Johnson, J., Benham, S., Vesterdal, L., Novotný, R., Verstraeten, A., Lundin, L., Thimonier, A., Michopoulos, P., Hasenauer, H., 2018. Quantifying Carbon and Nutrient Input From Litterfall in European Forests Using Field Observations and Modeling. Glob. Biogeochem. Cycles 32, 784–798. https://doi.org/10.1029/2017GB005825

Olson, J.S., 1963. Energy storage and the balance of producers and decomposers in ecological systems. Ecology 44, 322–331.

Prescott, C.E., 2002. The influence of the forest canopy on nutrient cycling. Tree Physiol. 22, 1193–1200. https://doi.org/10.1093/treephys/22.15-16.1193

Roussel, J.-R., Auty, D., Coops, N.C., Tompalski, P., Goodbody, T.R., Meador, A.S., Bourdon, J.-F., de Boissieu, F., Achim, A., 2020. lidR: An R package for analysis of Airborne Laser Scanning (ALS) data. Remote Sens. Environ. 251, 112061.

Silva, C.A., Hudak, A.T., Vierling, L.A., Loudermilk, E.L., O'Brien, J.J., Hiers, J.K., Jack, S.B., Gonzalez-Benecke, C., Lee, H., Falkowski, M.J., 2016. Imputation of individual longleaf pine (Pinus palustris Mill.) tree attributes from field and LiDAR data. Can. J. Remote Sens. 42, 554–573.

Wan Mohd Jaafar, W.S., Woodhouse, I.H., Silva, C.A., Omar, H., Abdul Maulud, K.N., Hudak, A.T., Klauberg, C., Cardil, A., Mohan, M., 2018. Improving individual tree crown delineation and attributes estimation of tropical forests using airborne LiDAR data. Forests 9, 759.

White, M.A., Thornton, P.E., Running, S.W., Nemani, R.R., 2000. Parameterization and sensitivity analysis of the BIOME–BGC terrestrial ecosystem model: Net primary production controls. Earth Interact. 4, 1–85.

Zazali, H.H., Towers, I.N., Sharples, J.J., 2020. A critical review of fuel accumulation models used in Australian fire management. Int. J. Wildland Fire.

Assessing the benefits of a national fuel break network to reduce wildfire exposure and risk in Portugal

Bruno A. Aparício[1,2]*; Fermín Alcasena[3], Alan Ager[4]; Woodam Chung[2]; José M.C. Pereira[1]; Ana C.L. Sá[1]

[1]Forest Research Centre, School of Agriculture, University of Lisbon, Portugal, {Bruno.a.aparicio@gmail.com, jmcpereira@isa.ulisboa.pt, anasa30@gmail.com}
[2] Department of Forest Engineering, Resources and Management, Oregon State University, Peavy Hall, Corvallis, OR 97331, USA {Bruno.aparicio@oregonstate.edu, Woodam.Chung@oregonstate.edu}
[3] Department of Agricultural and Forest Engineering, Universitat de Lleida, Lleida 25003, Spain {fermin.alcasena@udl.cat}
[4] USDA Forest Service, Rocky Mountain Research Station, Missoula Fire Sciences Laboratory, 5775 US Highway 10W, Missoula, MT 59808, USA {alan.ager@usda.gov}

**Corresponding author*

Keywords

Fuel break networks, Mediterranean wildfires, wildfire simulation

Abstract

The impact of rural fires in the Mediterranean Basin is rapidly increasing as extreme fire seasons become the new norm. Following the catastrophic 2017 fire season in Portugal, a national-scale fuel break network (FBN) was designed by the Rural Fire Management Agency (AGIF), and the implementation of fuel treatments along the fuel break network was initiated. Despite growing interest in developing extensive fuel treatment programs to prevent catastrophic wildfires and reduce exposure and risk in the Mediterranean region, there is still little information on the effectiveness of such programs. The Portuguese nation-wide FBN is part of the fuel management plan aiming to prevent loss of lives, reduce large fires (> 500 ha) and decrease annual burned area is under implementation. In this study, we used Monte Carlo methods and mechanistic wildfire spread modeling to simulate plausible wildfire events in Portugal. The modeling system was calibrated to local fuels and weather at monthly time steps. We then examined how the proposed fuel break network was intersected by simulated fires and the effectiveness in terms of protecting residential buildings and designated protected areas. The fuel breaks burn over percentage, i.e. the percentage of fires that are not contained by the FBN was modeled as a function of pre-defined flame length thresholds for individual FBN segments. From these outputs, we were able to compare priorities as determined from the simulation system to the FBN implementation plan by AGIF. Our results show that the full implementation of FBN can provide tactical opportunities for rural fire suppression and containment. The FBN has the potential to reduce up to 1) 13% in the annual burned area due to large fires; 2) 8% in the annual number of residential buildings exposed, and 3) 14% in the annual burned area in protected areas. However, the results also reveal that in many cases the FBN intersects fires after they have grown to over 500 ha, hence representing minimal potential in preventing large fires. The expected burn-over percentage was highly variable among the segments. An overall average decrease of 40% of the total benefits was estimated, with the most important fuel breaks typically showing a high percentage of fire burn over. Our results suggest that additional landscape-scale fuel reduction strategies are required to meet short-term national wildfire management objectives.

1. Background

Recent extreme wildfire events marked a turning point for Portuguese society and motivated a coordinated national response aimed at preventing catastrophic wildfires. The 2017 fire season was particularly harsh, with a record-breaking area burned of 557 thousand ha, 119 fatalities, thousands of structures destroyed, and over 1456 million euros in economic losses (Castellnou and et. al., 2018; Guerreiro et al., 2018). After this disaster, the Portuguese authorities were widely criticized for their lack of response and initiatives to reduce the potential for future catastrophic wildfires (Guerreiro et al., 2018). These and other factors led to the development of a new 10-year fuel management plan to reduce national wildfire risk (AGIF, 2020). The plan proposed three strategic targets: 1) the loss of lives in rural fires is reduced to a rare event; 2) the percentage of fires larger than 500 ha is reduced below 0.3 % of the total number of fires; and 3) the cumulative burned area over a period of

a decade is less than 660,000 ha. To achieve these, the plan proposes (among other fuel reduction actions) the implementation of a nation-wide fuel break network (FBN).

Fuel breaks are defined as "a strategically located wide block, or strip, on which a cover of dense, heavy, or flammable vegetation has been permanently changed to one of lower fuel volume or reduced flammability" (Green, 1977). Ultimately, fuel breaks are expected to facilitate fire containment and consequently decrease burned area, by providing safe conditions to engage in firefighting (Syphard et al., 2011a, 2011b).

In this study, we used simulation modelling and scenario analyses to evaluate the effectiveness of the Portuguese national 125-meter-wide FBN in terms of potential reduction burned area and in exposure of communities and protected areas to rural fires. We further quantified the probability of failure in containing the fire for each FBN segments based on the estimated flame lengths in the adjacent vegetation areas. We also added a simulation scenario we prioritized the implementation of the FBN over a period of five years according to estimated effectiveness of each FBN segment.

2. Methods

We used wildfire simulation data from Alcasena et al. (2021), representing 10,000 simulated fire seasons comprising a total of 1,654,448 simulated fires for mainland Portugal. The corresponding fire perimeters were intersected with the FBN to quantify the avoided burned area, reduced exposure of communities and avoided burned area in protected areas under the assumption of fire containment. Given the effectiveness of each FBN segment, we created a 5-year plan of FBN implementation for each objective, where the scheduling of the implementation of FBN segments follows their importance. We created two scenarios of FBN effectiveness: i) we assumed that fire spread stops at the FBN due to the full readiness of fire brigades; ii) we complemented this analysis by estimating the burn over percentage of each FBN segment, i.e., the percentage of times that each FBN segment may not allow for safe firefighting, failing to stop the fire spread. The burn over percentage was estimated using the simulated Flame Length Probability (FLP). We considered flame lengths longer than 2.5 m to represent surface fires likely to generate torching and crown fires, which are extremely difficult to suppress, and that have high spotting activity and spotting distances may be longer than 100 m (FBN is 125 meter wide). Hence, high intensity fires can decrease opportunities for fire control and originate embers that cross the FBN segment, reducing the effectiveness of the FBN.

3. Results and discussion

Our results showed that assuming maximum effectiveness of the FBN (i.e., fire containment) the full implementation of the Portuguese FBN could make a significant contribution to all fire management objectives of the country, with 13 % reduction in annual burned area due to large fires, 8 % reduction in the annual number of residential building exposure, and a reduction of 14 % in annual burned area in the protected areas. Nevertheless, the effect of the FBN in reducing large fires (> 500 ha) was minimal.

When the implementation of the FBN is scheduled following the prioritization given one of the three objectives cited above, its effectiveness showed an inverse exponential curve for all objectives with a sharp increase in the early years of implementation. The objectives of avoiding burned area due to large fires and avoiding exposure of residential buildings were more dependent on the complete implementation of the FBN. This reflects the known widespread risk of large fires and fire exposure of residential buildings across the country. Our analysis also revealed that the effect of the FBN segments already implemented is not different from a scenario of random scheduling (Figure 1).

In this study, we also identified the FBN segments with high burn over percentage caused by extreme fire behavior. Extreme fire behavior (as indicated by the burn over percentage) can jeopardize the safety of firefighters and ignite new fires over the FBN through intense crowning and long-distance spotting events (Alexander and Cruz, 2018; Alexander and Lanoville, 1989; Tedim et al., 2018). When assessing the effectiveness of FBN while acknowledging the possibility of burn over, the benefits of the FBN were dropped by almost 40 % on average for the three objectives studied, even assuming full readiness of fire suppression operations (Figure 1, dashed line).

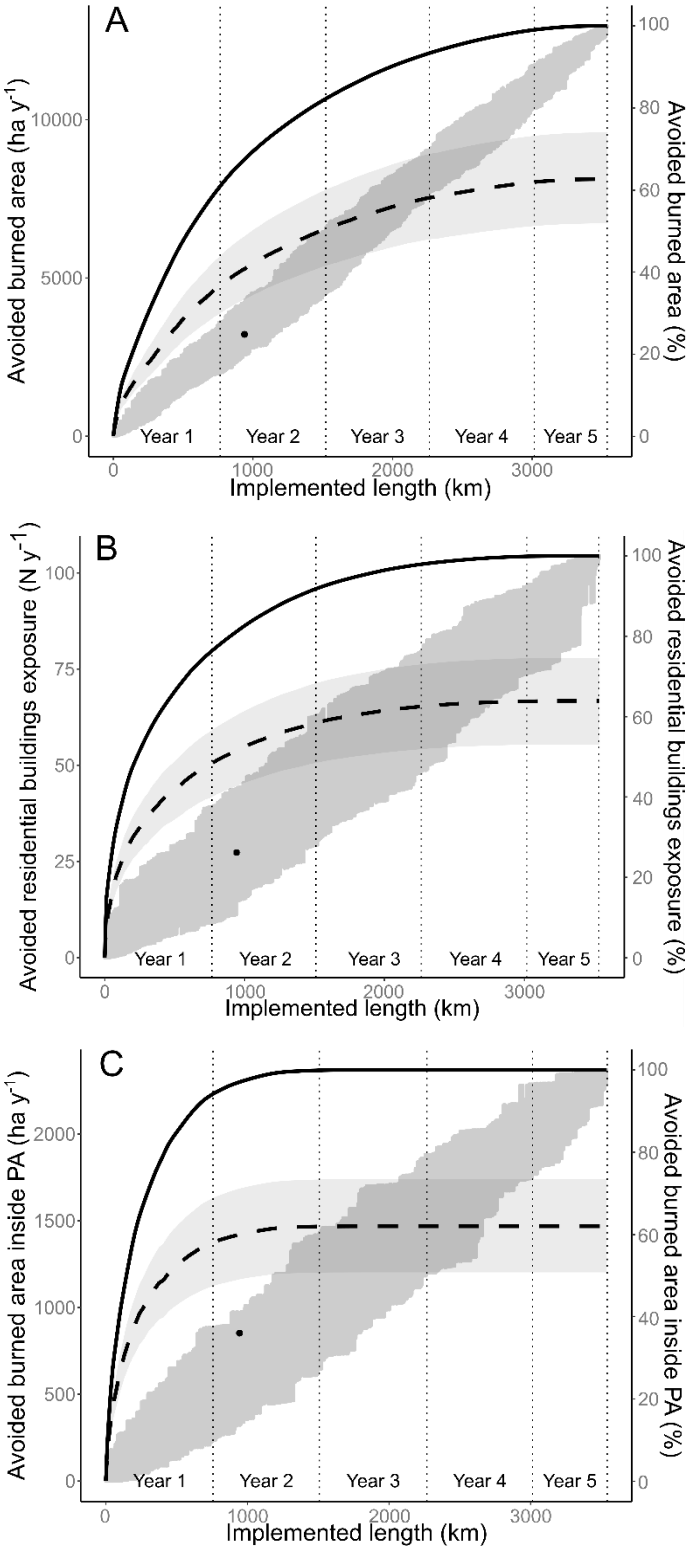

Figure 1. Cumulative annual effect of FBN implementation for avoided burned area due to large fires (A), avoided exposure of residential buildings (B) and avoided burned area inside protected areas (PA) (C). The solid line represents the optimal implementation scenario for each criterion; the dark grey area represents 100 random scenarios of implementation; and the solid dot represents the current stage of FBN implementation (identified in Figure 1). The dashed line represents the optimal scenario of implementation after adjusting the effectiveness of each FBN segment given the fire behavior and spotting distance in its surroundings (i.e. burn over percentage); the light grey area following the dashed line represents the 95% confidence envelope.

Finally, we show that a small portion of the FBN is responsible for great contributions to reduce the wildfire risk and exposure. This highlights the importance of strategically prioritize the FBN segments. These highly importance segments should also be monitored regularly to avoid fuel build-up, as they often have high values of burn over percentage. The widespread high burn over percentages indicates that the FBN itself may not be sufficient to substantially reduce large fires and wildfire risk. This, there is a clear need to integrate ecological restoration treatments in key areas close and adjacent to the FBN. We suggest that prescribed burning and preventive silviculture should be implemented in a synchronized way with the FBN to decrease fire spread and intensity, enhancing the safety of fire suppression operations (Alcasena et al., 2018). We further advocate that the afforestation of the areas surrounding the FBN with fire prone tree species that are either ignited by embers must be avoided (Viegas et al., 2014). We demonstrate how this framework can be used to design, evaluate, and implement future national fuel break programs in any fire-prone region.

4. References

AGIF, 2020. National Plan for Integrated Wildfire Management 2020–2030. Lisbon, Portugal.

Alcasena, F., Ager, A., Le Page, Y., Bessa, P., Loureiro, C., Oliveira, T., 2021. Assessing Wildfire Exposure to Communities and Protected Areas in Portugal. Fire . https://doi.org/10.3390/fire4040082

Alcasena, F.J., Ager, A.A., Salis, M., Day, M.A., Vega-Garcia, C., 2018. Optimizing prescribed fire allocation for managing fire risk in central Catalonia. Sci. Total Environ. 621, 872–885. https://doi.org/https://doi.org/10.1016/j.scitotenv.2017.11.297

Alexander, M.E., Cruz, M.G., 2018. Fireline intensity, in: Manzello, S.L. (Ed.), Encyclopedia of Wildfires and Wildland-Urban Interface (WUI) Fires. Springer International Publishing, Cham, pp. 1–8. https://doi.org/https://doi.org/10.1007/978-3-319-51727-8

Alexander, M. E, Lanoville, R.A., 1989. Predicting fire behavior in the black spruce-lichen woodland fuel type of Western and Northern Canada. For. Can., North. For. Cent., Edmonton, Alberta, and Gov. Northwest Territ., Dep. Renewable Resour., Territ. For. Fire Cent., Fort Smith, Northwest Territories. Poster

Castellnou, M., Guiomar, N., Rego, F., Fernandes, P., 2018. Fire growth patterns in the 2017 mega fire episode of October 15, central Portugal. Adv. For. fire Res. 2018 447–453. https://doi.org/10.14195/978-989-26-16-506_48

Green, L., 1977. Fuelbreaks and other fuel modification for wildland fire control, Washington, DC: US Department of Agriculture, Forest Service, Agricultural Handbook.

Guerreiro, J., Fonseca, C., Salgueiro, A., Fernandes, P., Lopez, I.E., de Neufville, R., Mateus, F., Castellnou, R.M., Sande, S.J., Moura, J.M., Castro, N., Rego, F., Caldeira, D., 2018. Avaliação dos Incêndios Ocorridos Entre 14 e 16 de Outubro de 2017 em Portugal Continental. Relatório Final. Lisboa, Portugal.

Syphard, A.D., Keeley, J.E., Brennan, T.J., 2011a. Factors affecting fuel break effectiveness in the control of large fires on the Los Padres National Forest, California. Int. J. Wildl. Fire 20, 764–775.

Syphard, A.D., Keeley, J.E., Brennan, T.J., 2011b. Comparing the role of fuel breaks across southern California national forests. For. Ecol. Manage. 261, 2038–2048. https://doi.org/https://doi.org/10.1016/j.foreco.2011.02.030

Tedim, F., Leone, V., Amraoui, M., Bouillon, C., Coughlan, M.R., Delogu, G.M., Fernandes, P.M., Ferreira, C., McCaffrey, S., McGee, T.K., Parente, J., Paton, D., Pereira, M.G., Ribeiro, L.M., Viegas, D.X., Xanthopoulos, G., 2018. Defining Extreme Wildfire Events: Difficulties, Challenges, and Impacts. Fire. https://doi.org/10.3390/fire1010009

Viegas, D.X., Almeida, M., Raposo, J., Oliveira, R., Viegas, C.X., 2014. Ignition of Mediterranean Fuel Beds by Several Types of Firebrands. Fire Technol. 50, 61–77. https://doi.org/10.1007/s10694-012-0267-8

Assessment of micro-combined heat and power system based on an organic Rankine Cycle coupled to a boiler for residual biomass valorization

Christian Di Stasi*; Yarima Torreiro; Ángela Rodríguez-Abalde

EnergyLab, Edificio CITEXVI, Fonte das Abelleiras, s/n, Campus Universitario de Vigo, 36310 Vigo, Spain, {christian.distasi, yarima.torreiro, angela.rodriguez}@energylab.es

**Corresponding author*

Keywords

Forestry biomass; combustion; microcogeneration

Abstract

Energy from biomass obtained in rural areas provides a sustainable alternative for heat and power production. In particular, the combustion of biomass in boilers represents the most widely used valorization route for the production of thermal energy. Furthermore, cogeneration has proven to be an efficient and clean way of simultaneous production of electricity and useful heat in the place of consumption, with the consequent saving of primary energy and emissions.

The specific aim of this experimental work is to study the feasibility of employing forestry wastes as feedstock for microcogeneration (electrical power <15 kW) processes for small scale (residential and commercial level) applications in order to avoid problems associated to their accumulation, mainly risk of fire.

Three forestry biomasses (Pinus pinaster, Eucalyptus globulus, and Acacia melanoxylon) abundant in Galicia, north of Spain, were selected as fuels to be used in the above-mentioned processes. An organic rankine cycle (ORC) coupled to a biomass boiler (60 kWt) were used to carry out the experiments. Cogeneration yields (thermal + electrical), as a function of temperature difference between cold and hot focus, were studied.

1. Introduction

Among all the countries of the European Union, Spain and Portugal are two of the most vulnerable against the climate change. In fact, in the last 30 years, both countries have suffered numerous wildfires which destroyed a large fraction of the local vegetation. In this context, the FIREPOCTEP project aims to: 1) Identify strategic management areas to minimize the risk and impact of large fires throughout an integral management of the landscape in relation to global climate change; 2) Promote public and private investment through pilot experiences in the framework of Green Circular Economy and investigation of new market opportunities; 3) Educate the permanent and occasional rural population about the risk of large forest fires, preventive practices and self-protection.

One of the main causes of these fires is the accumulation of forestry biomass derived from tree-pruning operations, due to the large quantities of dry material that can is left in-situ. Therefore, research on alternative uses of forestry wastes is mandatory to prevent beforementioned risks.

One alternative is represented by the biomass cogeneration, which allows the simultaneous production of electricity and useful heat in the place of consumption, with consequent saving of primary energy (up to 40%) and emissions into the atmosphere. In fact, cogeneration is considered as the main option for the replacement of traditional energy systems (D'Accadia, 2003). Taking this into account, microcogeneration (referred to small power equipment, less than 50 kW) is emerging as a suitable alternative in the aforementioned small-scale applications (Fenercom, 2012). One of the most promising techniques for electrical energy obtention through biomass is the so-called organic rankine cycle (ORC) (Qiu, 2012). The ORC follows the same principles as the traditional steam Rankine cycle used in most thermal power plants to produce electricity but uses an organic fluid instead of water. This fluid (generally a fluorocarbon) has a high molecular weight and a boiling point below 100°C, which allows to considerably simplify the traditional process in terms of complexity and cost.

In this work, carried out in the framework of the FIREPOCTEP project, the potential of three forestry biomasses (*Pinus pinaster, Eucalyptus globulus* and *Acacia melanoxylon*) as fuels for energy recovery through

microgeneration was investigated. This was done employing those biomasses in a pilot ORC module coupled to a boiler in order to determine microcogeneration feasibility in terms of global efficiency.

2. Materials and methods

To demonstrate the feasibility of the use of microcogeneration as a system for energy recovery of the biomass previously presented, a pilot plant was used with the main following elements:

- A 60-kW multi-fuel boiler (hot source) equipped with a caterpillar burner, fed by a hopper and responsible for generating the thermal energy needed to produce electricity in the ORC (provided by hot water up to 90°C).
- An ORC module thermal machine based on an organic Rankine cycle with a maximum power of 4 electric kW and designed for the use of heat at low temperature (up to 100°C in water) by its conversion into electricity. This system employs an organic refrigerant fluid (R245fa).

Despite being a plant for cogeneration, the experimental system has an aerorefrigerator (cold source) to evacuate the heat from the condenser through a water circuit. This equipment is an air/water heat exchanger that drives air by forced convection to cool the incoming water. The system also has a heatsink in the form of resistors to prevent the injection of electricity generated by the grid. Finally, the plant has a data control and visualization system where all parameters relevant to the operation of the plant are displayed and recorded.

Figure 1 shows the scheme of the ORC module employed.

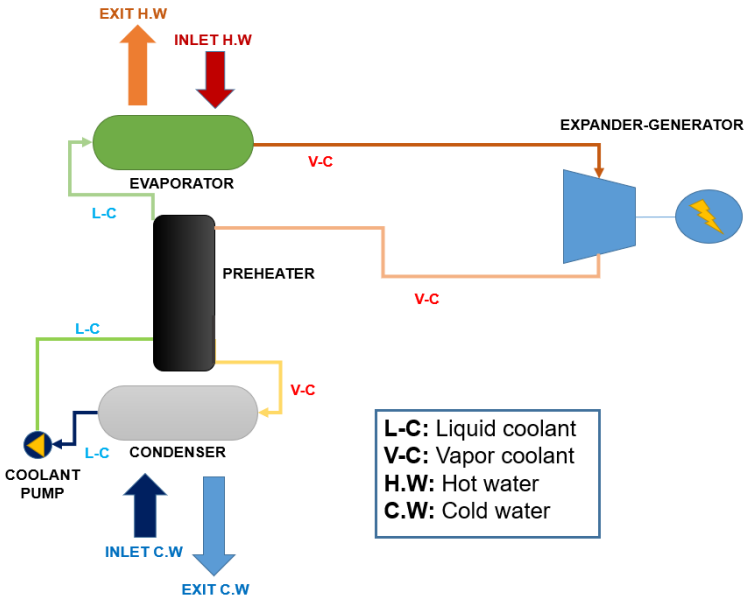

Figure 1- ORC.

As it can be observed in Figure 1, once preheated, the liquid refrigerant is conducted to the evaporator where it changes its state to the vapor phase. It is then led to an expander on whose axis mechanical work is generated. That expander is coupled by a mechanical transmission to an asynchronous generator, producing electrical energy. Once the fluid leaves the expander, already with a reduced pressure, it gives part of the heat in the regenerator or preheater and then goes to a condenser where the vapor – liquid phase change occurs and the cycle can start again in the coolant pump.

Microcogeneration performance is assessed based on the global efficiency obtained (electrical plus thermal). Equations (1) and (2) show the electrical and thermal efficiency calculation.

η_{el}= electrical power on terminals generator (kWe)/thermal power apported by the evaporator (kWt) (1)

η_t = heat provided by the condensator (kWt)/heat captured by the evaporator (kWt) (2)

3. Results

As confirmed by other authors (Peris, 2015), the greater the temperature difference between the hot and the cold source, the greater the electrical power generated by the module studied. This behaviour was also observed for the generated power.

In the tests conducted, values around 4 kW were obtained in all evaluated cases. Using the ORC module used in the present investigation, cogeneration efficiencies close to 97% can be achieved, demonstrating its suitability for energy recovery with the forestry biomasses studied.

4. Conclusions

The results obtained during the preliminary microcogeneration tests show that it is feasible to valorize the selected biomasses (*Pinus pinaster, Eucalyptus globulus* and *Acacia melanoxylon*). The tests carried out make it possible to determine that the temperature differences between the hot and the cold source had a significant influence on the results obtained. In the conditions used in this work, cogeneration yields close to 97% can be obtained (around 9% net electric yield and around 88% thermal yield). Those results are highly promising as micro-cogeneration allows simultaneous heat and electricity production, which opens the door to an interesting way to use forestry wastes for energy production instead of its accumulation and the risk of fire associated.

5. References

D'Accadia, M. D., Sasso, M., Sibilio, S., & Vanoli, L. (2003). Micro-combined heat and power in residential and light commercial applications. Applied Thermal Engineering, 23(10), 1247-1259.

Fenercom (2012). Guía básica de microcogeneración. https://www.fenercom.com/publicacion/guia-basica-de-microcogeneracion-2012/.

Qiu, G., Shao, Y., Li, J., Liu, H., & Riffat, S. B. (2012). Experimental investigation of a biomass-fired ORC-based micro-CHP for domestic applications. Fuel, 96, 374-382.

Peris, B., Navarro-Esbrí, J., Molés, F., Collado, R., & Mota-Babiloni, A. (2015). Performance evaluation of an Organic Rankine Cycle (ORC) for power applications from low grade heat sources. Applied Thermal Engineering, 75, 763-769.

Atmospheric turbulent structures during shrub fires and implications for flaming zone behavior

Marwan Katurji*[1]; Bob Noonan[1]; Jiawei Zhang[1,3]; Andres Valencia[2]; Benjamin Shumcher[1]; Jessica Kerr[3]; Tara Strand[3]; Grant Pearce[3,4]; Peyman Zawar-Reza[1]

[1]School of Earth and Environment, University of Canterbury, New Zealand, {marwan.katurji@canterbury.ac.nz}
[2]Dept. Of Civil and Natural Resources Engineering, University of Canterbury, New Zealand
[3]New Zealand Forest Research Institute, Scion, New Zealand
[4]Fire Emergency New Zealand- FENZ

**Corresponding author*

Keywords

Atmosphere, turbulence, fire observations, flaming zone

Abstract

Wildfires propagate across vegetated canopies exhibiting complex spread patterns. Wind gusts at the fire-front extend/intensify flames and direct convective heating towards unburnt fuels resulting in rapid acceleration of spread. This behavior could be modulated by ambient atmospheric boundary layer wind turbulence. Our aim is to characterize ambient turbulence over gorse shrub experimental burns and explore how this contributes to fire behavior. Developing coupled fire-atmosphere numerical models capable of resolving most turbulent energy scales is important for understanding rapid and small-scale dynamics. However, it is equally as important to design fire-burn experiments that allow for simultaneous measurements of fire behavior and atmospheric turbulence covering a range of the turbulent spectra. We have completed six experimental burns (24-hectares) in Rakaia, New Zealand under varying wind speed and direction and atmospheric stability regimes. The ignition process ensured a fire-line propagating through dense gorse bush (1m high). Two 30m high sonic anemometer towers measured turbulent wind velocity (20Hz) at six different height levels. Visible imagery was captured for all burns by cameras mounted on Un-crewed Aerial Vehicles (UAV) at 200m AGL. Using wavelet decomposition, we identified different turbulent scales that varied relative to height above vegetation and boundary layer thermal regimes. Quadrant analysis identified statistical distribution of atmospheric sweeps (downbursts of turbulence towards vegetation) and ejections (detachment of turbulence from vegetation). Discrete analysis of sweep/ejection events revealed their temporal and spatial scales and tracked their progression as the flaming zone approached the towers. Undergoing work aims to discern these interactions with observed fire sweeps from aerial imagery by applying image velocimetry techniques and sweep structure tracking.

1. Introduction

Turbulence is a ubiquitous property of the Atmospheric Boundary Layer (ABL) that extends up to 1 or 2km above ground level. ABL turbulence modulates how the near-surface atmosphere interacts with the anomalous/introduced energy perturbations caused by wildfires over timescales of minutes to hours (Stull, 1988). Closer to the surface, turbulent processes control heat, momentum and moisture transport between vegetated surfaces and the overlying Atmospheric Surface Layer (ASL) that extends between 100 and 200m above the surface and strongly influenced by wind shear or mechanically induced turbulence (LeMone et al. 2018). Wildfires produce positively buoyant turbulent motion that can lead to significant downward surges of momentum, interacting with ASL turbulence and potentially modulating a fire's rate of spread over short periods of time. (Heilman et al. 2019; Cunningham & Linn, 2007; Sun et al. 2009). Identifying these processes and studying their characteristics under environmental conditions can lead to better understanding erratic fire behavior.

Experimental field scale fires designed to measure turbulent flux at the fire-atmosphere interface can provide insights into the atmospheric processes controlling fire behavior. These experiments include in-situ tower-mounted sonic anemometer measurements from spreading fires in low grass to higher canopy fuels (Clements

et al., 2006, 2007, 2008; Heilman et al. 2019). Sonic anemometry allows for the ability of measuring 3-dimensional wind velocity, air temperature and humidity at high sampling rate, and quantifying momentum and moisture fluxes between the fire and the integral atmospheric scales measured across an averaging interval. Conclusions are then made regarding the amount of energy exchanged between the fire and the overlying atmosphere, the role of near-surface environmental shear and static stability on fire behavior (Potter, 2012). Other studies (Heilman et al., 2015, 2019) carried out measurements of vertically distributed turbulent heat and momentum flux during a surface fire progressing under 23m high pine trees. Their results confirmed that the largest enhancement of vertical turbulent flux happens at or above canopy levels. Spectral analysis of momentum and heat flux suggested that fire-atmosphere interactions can happen across a wide range of frequencies and further studies are needed to assess how those fluxes feedback into fire behavior. Complex vegetation cover, including spatial density variations, forest gaps and edges, and steep topography will produce spatially complex turbulent interactions. The presence of dense vegetation acts to increase wind shear and the production of turbulent kinetic energy, reduce the mean wind speed and increase gusts, and enhance vertical motion allowing for enhanced downward momentum transfer from the atmospheric surface layer (Kiefer et al. 2018; Schlegel et al. 2012, 2015).

The impact of atmosphere driven momentum surges on fire behavior has not been extensively studied. For grass fires, we now can hypothesize that convective heating pulses originating from the flaming zones are responsible for fuel heating and could play a large role in fire spread in any direction along the fire line (Cunningham & Linn, 2007). These processes have been (Cunningham & Linn, 2007) modelled by couple LES atmospheric-fire models like FIRETEC and observed in laboratory experiments (Finney et al., 2015; Tang et al., 2019). Turbulent flaming zone dynamics can now be observed using thermal image velocimetry techniques for real landscape scale experiments (Katurji et al., 2021), and have been shown to be related to overlying wind turbulence spectra. However, the role of atmospheric source momentum downward surges and their associated turbulence structures have not been studied in relation to fire horizontal convective heating dynamics. In this paper we present observations of characterized atmospheric turbulence strictures over a fast-spreading shrub fire and discuss their implication on fie behavior.

2. Methodology

2.1. Experimental Burn Design

The experimental burn layout is shown in Figure 1 and included 4 burn blocks hereafter referred to as plots P1, P2, P3, and P4. The experiments were carried out on the 2nd and 6th of March 2020 in the Rakaia Valley in New Zealand. Plots 3 and 4 were instrumented with a 30m sonic anemometer tower shown in Figure 1 and instrument setup details are shown in Table 1. The two towers were nearly centered in the burn blocks while the fire line and flaming zone passed across the towers.

Table 1. Observational systems and corresponding measurement parameters and specifications

Observational System	**Instrument**	**Accuracy, range (sensitivity, resolution)**	**Measured variable**	**Installation details**
Nadir visible video acquisition	Video camera (DJI Ltd.12MP RGB)	100m AGL 1920 x 1080 pixels Spatial resolution (pixels/m)	Visible video at 30fps	On Un-crewed Aerial Vehicle (UAV)
In-fire wind turbulence tower	Applied Technologies, Inc. 3-dimensional ultrasonic anemometer – SATI/3(K) series, Campbell Scientific CR6 datalogger	K-probe - 150 mm vertical and horizontal measurement path length. Sampling frequency 20Hz	U (+ve towards east), V (+ve towards north), W (+ve vertically upwards) [ms^{-1}]	1.6m (6h, 6.4h), 5m (18.9h, 20h), and 10m (37.7h, 40h) AGL and perpendicular to fire line

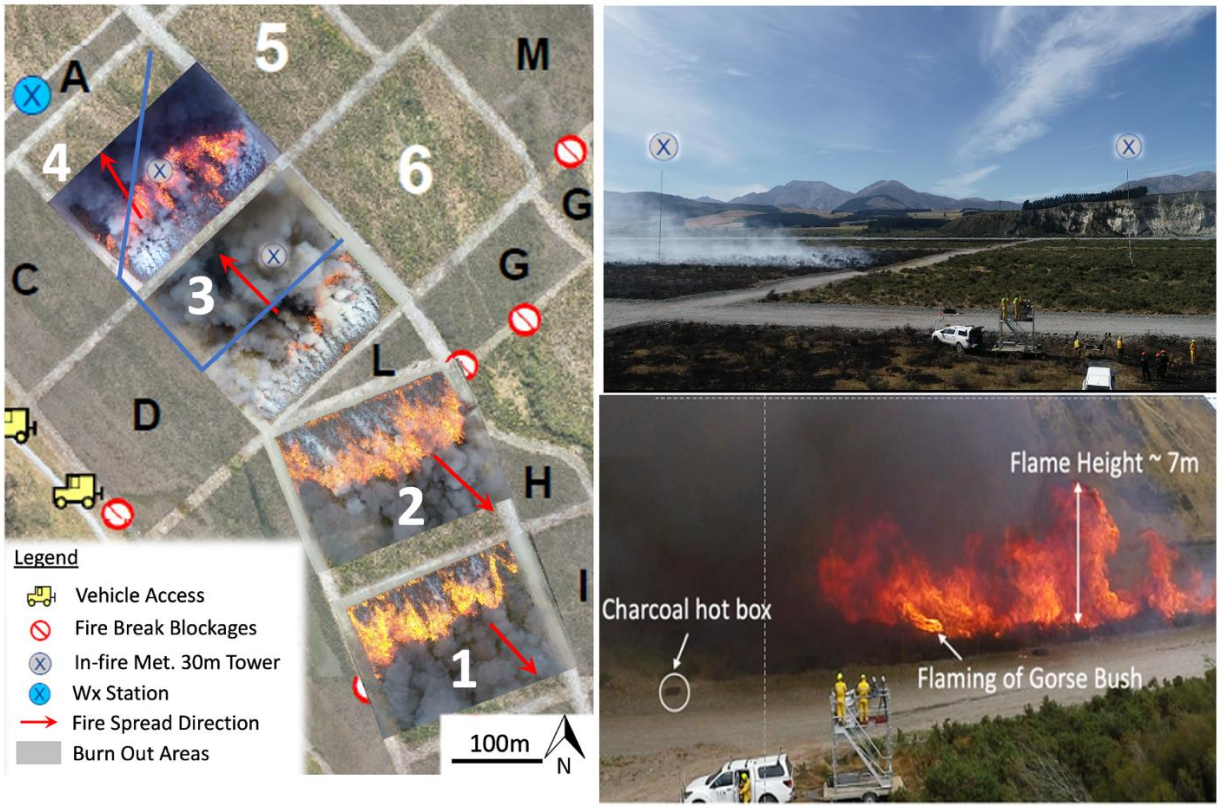

Figure 1- Experimental burn layout showing plot layout, fire spread direction and some site pictures The top view pictures of the flaming zone were taken from a UAV and overlaid on the map at the 2-minute point after the ignition of each plot

2.2. Data Processing

Data de-spiking, sonic tilt and orientation corrections were carried out on the sonic anemometer data – as in Katurji et al. (2021). The streamwise (U), velocity component was then geometrically projected to align with the mean wind direction for all the plots. Aerial video data was collected from nearly 200m above the plots.

2.3. Atmospheric Turbulence Analysis

2.3.1. Wavelet Transform

This study used the python package PYCWT to calculate the wavelet transform for time frequency analysis. Unlike Fourier transform, wavelet transform reserves the temporal information alongside the frequency information and is more suitable to look at the temporal variations of coherent structures in the turbulence time series from the streamwise and vertical wind velocity.

2.3.2. Quadrant Analysis

Wavelet transform can give temporal coherency information at difference frequency scales, but the method cannot distinguish different types of turbulent coherent structures. These involve “ejection motion” associated with turbulent eruption of low momentum streaks away from the surface; “sweep motion” or deceleration of the flow caused by the turbulent motion towards the surface; “outward motion” associated with the acceleration of the flow away from the surface due to low-level convergence; and “inward motions” associated with deceleration of the flow moving towards the surface due to low-level divergence (Christen et al., 2007; Li & Bou-Zeid, 2011; Wallace, 2016). The quadrant analysis in this study uses the instantaneous product of the streamwise (u′) and vertical velocity (w′) perturbations. For momentum flux, if we plot the velocity component pair (u′w′) into the Cartesian plane (abscissa for w′ and ordinate for u′), the first (I) quadrant (+w′-u′) will be outward quadrant while II, III and IV would be sweep, inward and ejection respectively (a sample from the tower data shown in Figure 2.

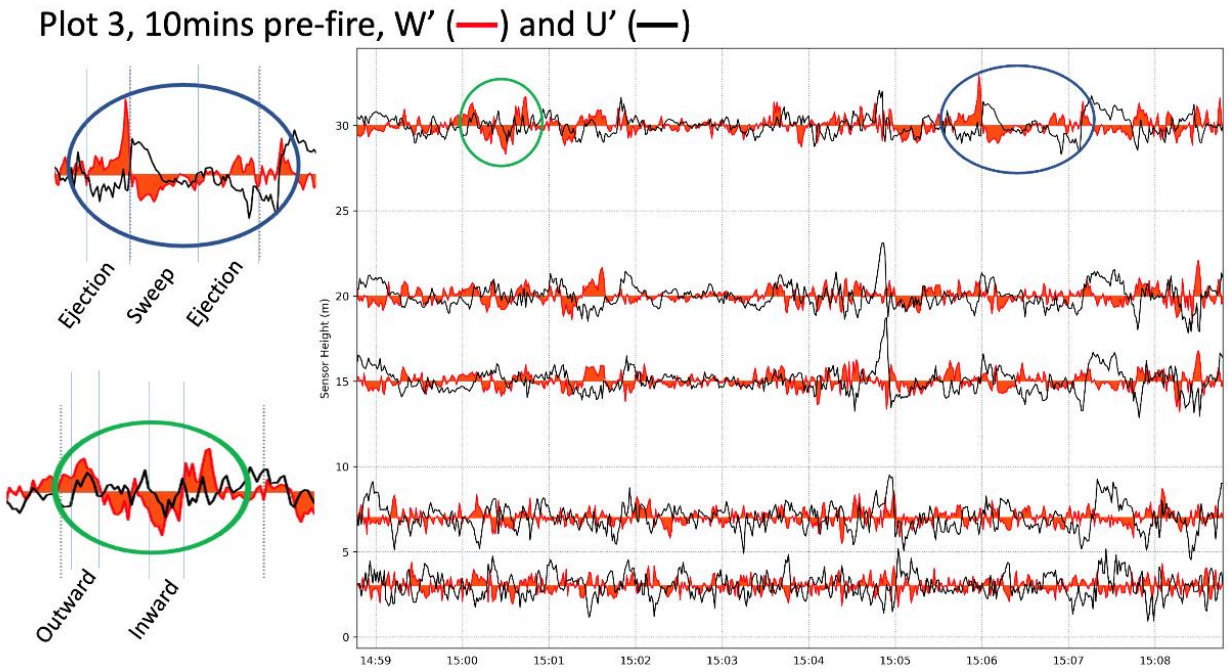

Figure 2- Vertical (streamwise) velocity perturbations from the 30m tower in plot 3. 20Hz perturbations were calculated from a 1-min rolling average window then subsampled with a 1s window average. Examples of sweep, ejection, inward, and outward motions are extracted in the left panel.

2.4. Flaming Zone Observation and Image Velocimetry

Image Velocimetry (IV) (Katurji et al. 2021) was applied on UAV overhead fire videos in order to derive and map the displacement of flame structures shown later in Figure 7. These structures manifest as diverging flame streaks that ignite fuel (example shown in Figure 3b, c). It was found that first-order physical characteristics of the observed fire sweeps, namely divergent fire flow from a near static center, were successfully captured and represented using IV. The ability of image velocimetry to capture physical characteristics of the fire sweeps was leveraged to develop a methodology capable of identifying fire sweeps from overhead UAV videos. This methodology applies a 2D convolution on the displacement vector field, and uses a kernel carefully designed to highlight the characteristics of fire sweeps spatially and temporally. The resultant scalar field represents a 2D map of the likelihood of occurrence of fire sweep, which is mainly limited by the size of the kernel and by the difficulty to calibrate it other than by visual inspection.

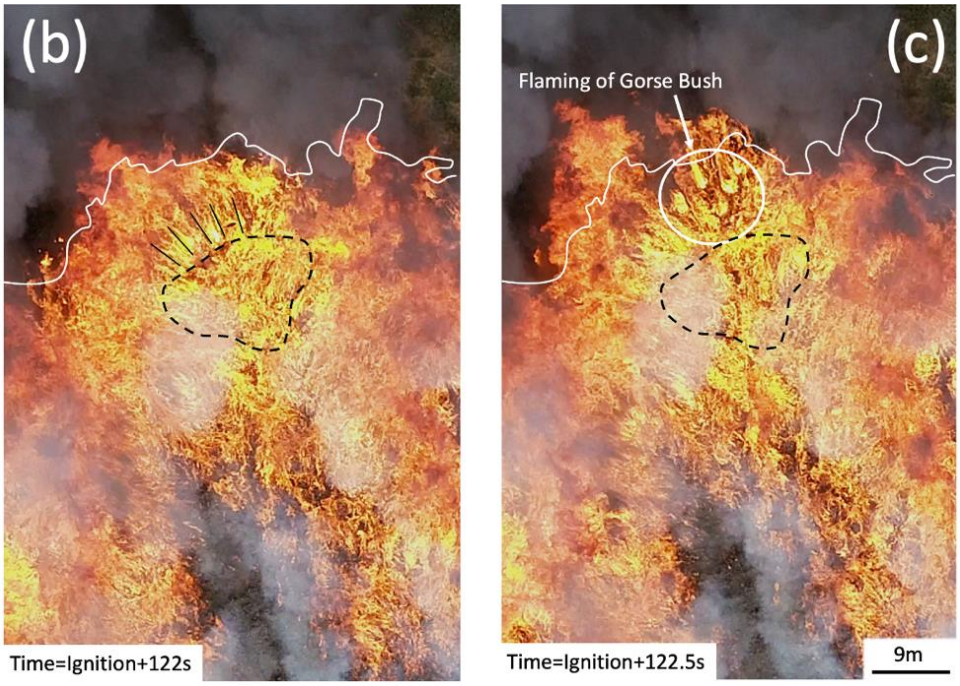

Figure 3- Observed flaming zone from nearly 200m AGL using a UAV. The black dotted outline in (b) and (c) shows the area of a fire "sweep" and its impact on vegetation ignition.

3. Results and Discussion

3.1. Meteorological and Burn Conditions

Burn events for plots 3 and 4 were associated with a typical up-valley afternoon air flow up to 1.5 ºC fluctuations in air temperature associate with the convective boundary layer (see third panel of Figure 4). Plots 1 and 2 were conducted under a synoptically driven nor-wester wind regime that produced orographically channeled down-valley winds, and warmer and drier air conditions as the airflow descended from the New Zealand Southern Alps towards the Rakaia valley. The burn time for all plots varied between 3 and 5 mins with an initial straight-line ignition and a wind driven flaming process.

Table 2. Fire behavior, and meteorological conditions (averaged over duration of burns) recorded at from the weather station tower marked by a blue circled "x" in Figure 1

Plot	Ignition time (plot edge reached) [NZDT]	Tair [°C] (RH) [%]	Wind speed [ms^{-1}] (direction) [°]	Mean gorse height [m]	Pre-burn gorse (grass, litter, debris) fuel load [kg m^{-2}]	Total fuel consumption [kg m^{-2}]	Rate of spread [m/s]	Flame height [m]
P1	02/03/2020, 10:10 (10:14)	20.7, (36)	8.27 (310)	0.83	1.8 (0.1,0.7,0.8)	2.5	0.89	4.9
P2	02/03/2020, 12:11 (12:14)	22.9, (33)	9.8 (311)	1.10	4.1 (0.3,1.3,1.7)	6.7	0.92	3.7
P3	06/03/2020, 15:08 (15:12)	21.6, (41)	6.8 (146)	0.84	2.2 (0.2,0.6,0.4)	2.4	0.9	5.4
P4	06/03/2020, 13:31 (13:36)	20.0, (43)	5.0 (142)	0.85	2.5 (0.7,0.7,1.0)	3.4	0.75	5.6

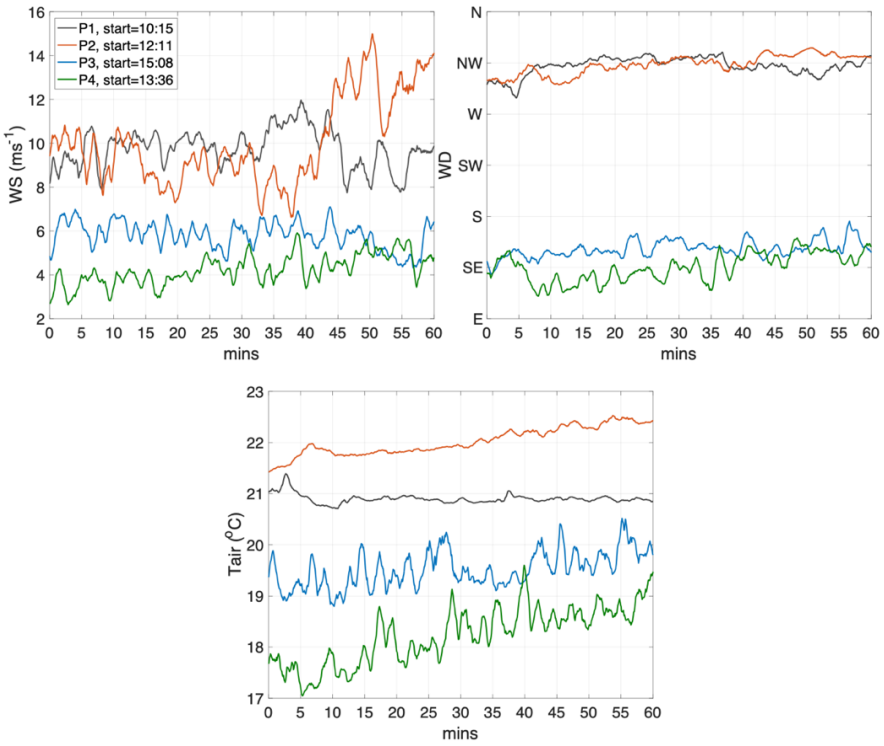

Figure 4- Time series of wind speed (WS), direction (WD), and air temperature (Tair) for 1-hour pre-fire at 30m AGL and 1min average interval. Plots 1 (P1), P2, P3, and P4 are shown indifferent colors with the start time hh:mm in NZDT indicated for each

3.2. Wind Turbulence Spectra

For all the plots, the integral time scales (usually detected when a power peak is evident) of turbulent wind velocity appear to get shorter as the measurement gets closer to the canopy (Figure 5), which is in accordance with boundary-layer turbulence theory. For heights less than 15m, where the observed flame heights (Table 2) occurred between 3 and 6 m, the results suggest that the energetic turbulent motion along the streamwise wind direction can occur between 2 and 32s. These results also show that the turbulent time scales vary between the atmospheric stability regimes of plots P1 and P2 compared to P3 and P4. Results from the vertical wind spectra, not shown in this extended abstract, reveal much shorter integral time scales for P1 and P2 (around 1 s) compared to P3 and P4 (between 3 and 5 s) when atmospheric turbulence was largely dominated by a thermal regime as opposed to the wind shear dominated regime of P1 and P2.

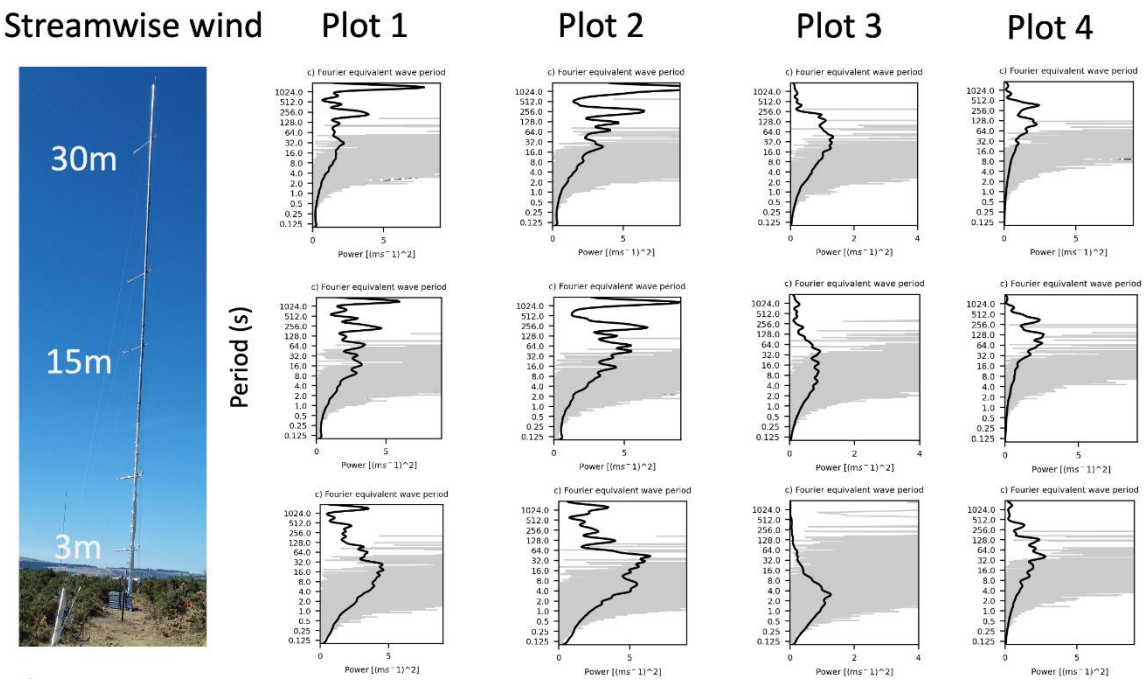

Figure 5- Black line shows the time integrated spectra across the wavelet time frequency decomposition showing the integral time scales (period on the y-axis) versus spectral power (on x-axis) for plots 1, 2, 3, and 4 and for three selected height levels on the tower (3, 15, and 30m). The gray line shows the Fast Fourier decomposition inserted for reference but not used in the analysis.

3.3. Atmospheric Sweep, Ejection, Inward and Outward Motions

Atmospheric turbulent structures plotted against time for all the plots (Figure 6) show more sweep and ejection events than inward and outward events. It has been previously suggested that coherent sweep (gust) and ejection (burst) motions dominate near-surface momentum and scalar fluxes(Li & Bou-Zeid, 2011). The reduction of the number of inward and outward motions for P1 and P2 compared to P3 and P4 does support the earlier findings of the integral time scale difference between the shear driven surface layer condition of P1 and P2 and the thermally driven surface layer turbulent motion of P3 and P4. Forward slanting coherence of sweep and ejection structures (highlighted in yellow - Figure 6) across the 30m tower height suggest that events can originate from within the surface layer (above the observed 30m roughness boundary layer) and impinge on the surface. These types of interactions will have a time scale associated with them (the width of the black boxes) and are being investigated as part of the ongoing work for this research. These events can be significant as it is our hypothesis that fire "sweeps", explained in the following section, can be impacted by these atmospheric turbulent structures by prolonging their duration and/or expanding the flame-vegetation interaction zone.

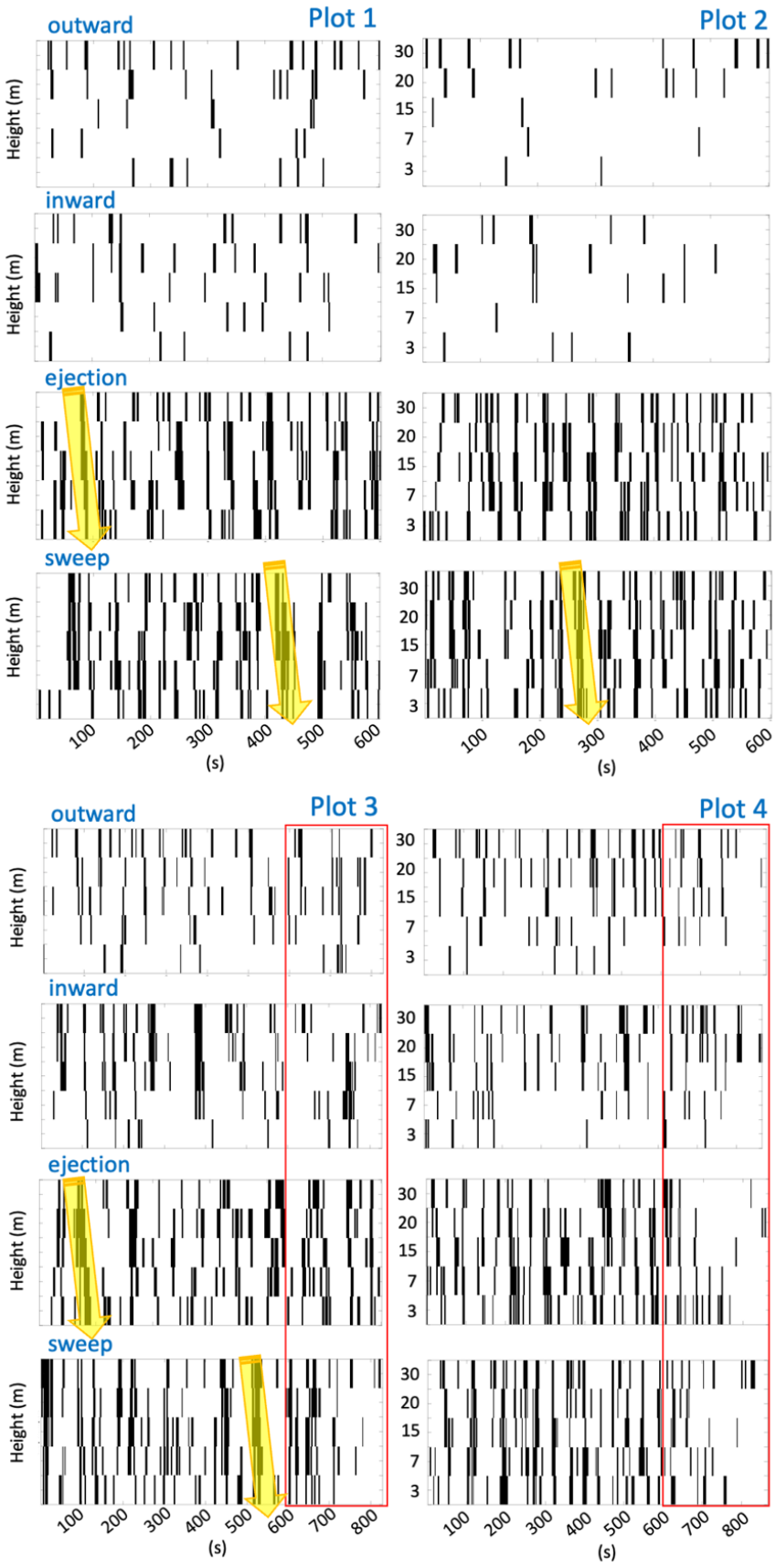

Figure 6- Sweep, ejection, inward and outward events detected at all the 5 height levels of the in-situ tower for plots 1, 2, 3 and 4. The red outlined box shows the period when the fire was progressing through plots 3 and 4. The yellow arrows show examples of downwards propagating structures

3.4. Flaming Zone and Fire Sweep Observations

UAV overhead visible video of the gorse vegetation fire carried out in P2 were selected for this preliminary analysis. Figure 7 highlights the observable flaming zone and some of its main features during the steady-state phase of the fire spread. The flaming zone dynamics was characterized by intermittent "fire bursts" in which clusters of unburned fuel were covered by the fire and ignited. Fire bursts were typically accompanied by strong tilting of the flame front inducing, in most of the cases, direct flame impingement.

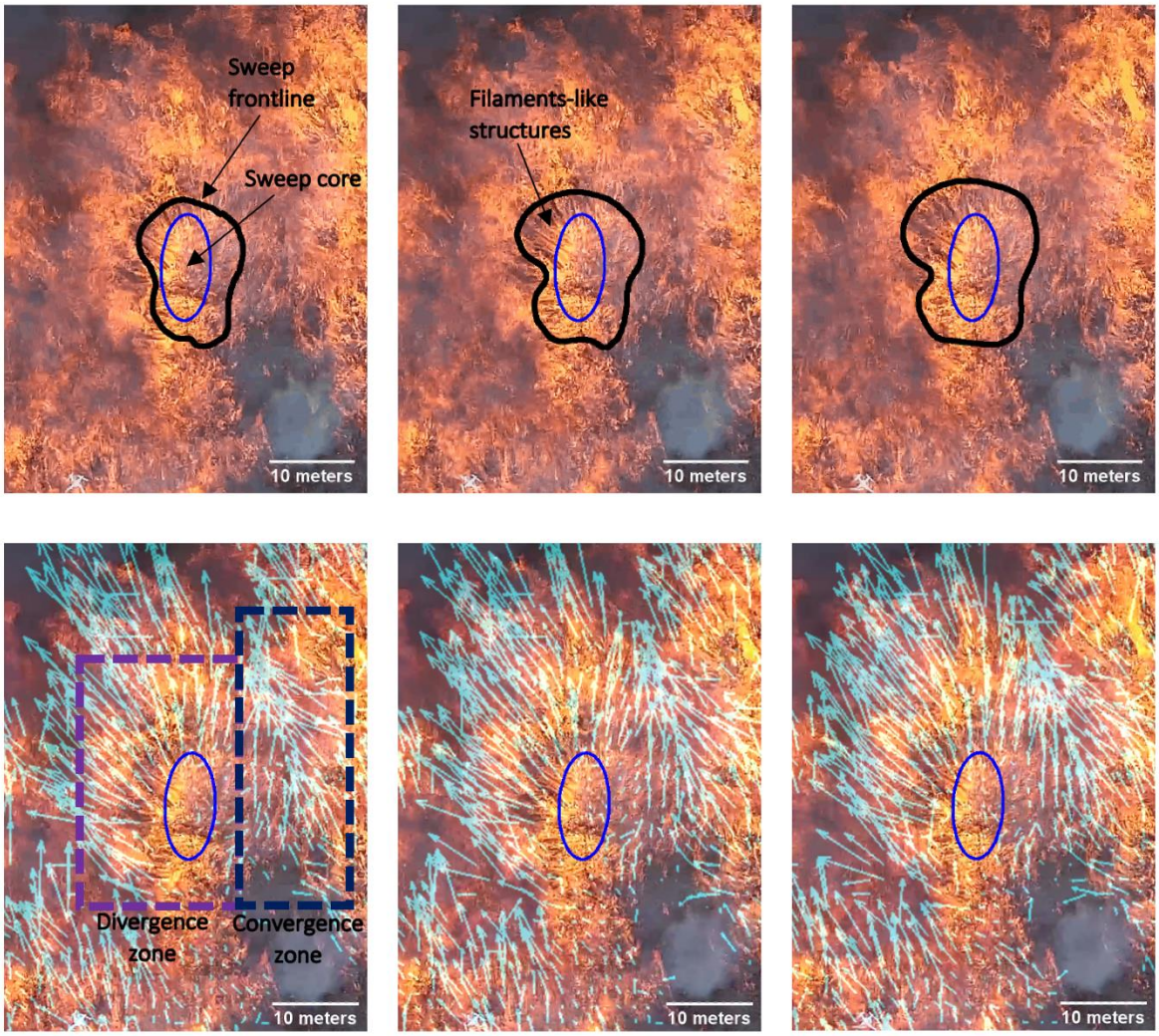

Figure 7- Time sequenced (at 1/30 s interval) frames extracted from the UAV video recorded during the P2 burn and an example of the resulting image velocimetry of identified fire sweep" events"

The structures in Figure 7, are referred to as *fire sweeps*, and are characterized by divergent motion of fire (or *fire sweep frontline*, black line) from a nearly static luminous region (or *fire sweep core*, region inside blue line). Structures with these characteristics were identified sporadically at multiple locations into the flaming zone. Generally, they were found to have a characteristic length of ~ 10 m during the incipient stage up to ~20-30 m during its peak. High luminosity inside the core region of the fire sweeps can last several seconds, and is recurrently accompanied with filament-like fire structures located around the it, which are characterized by divergent motion of the fire with higher spatiotemporal frequency. Inspection of side-view UAV footage (not shown here) suggests that tilted flames from individual bushes located near the core region are at the origin of these structures. Preliminary results from 2D convolution approach was used to track individual fire sweeps and estimate their duration. Two main groups of fire sweeps were identified. The first group is characterized by short-duration structures (< 1 s), generally quickly appearing and disappearing sporadically with short displacement through the flaming zone. Fire sweeps of the second group presented longer durations (up to 4 s) and were observed to move across the flaming zone, some of them from the back to the head of the fire.

4. Conclusion and Ongoing Work

Experimental fire observations included turbulent wind velocity measurements from a 30m tower and UAV-based video in nadir from nearly 200m above the flaming zone. The methods focussed on characterizing the overlying atmospheric turbulence strutcure, Image Velocitmetry (IV) and feature tracking of *fire sweeps*. More IV is planned and will be used to derive and map the displacement of *fire sweeps* and their durations and will be compared with statistical distribution of atmospheric turbulent motions and their durations.

The observations from the gorse aerial imaging of the flaming zone and some of the *fire sweep* processes are similar to the results of the numerical modelling of a spreading fire using FireTec (Cunningham & Linn, 2007). Their simulations included wind speed ranges similar to the conditions of the gorse fire experiment but without atmospheric boundary layer turbulence. The fire produced a series of regular streamwise vortices with flame buoyancy lifting air along the updraft lines and descending between two flaming corridors causing a *fire sweep*. The scale of one of the fire sweep in the Firetec simulations was between 10 and 20m, which is not very dissimilar to the scales we analyzed in this study.

5. Acknowledgements

We would like to give a special thanks to all field support teams including technical and general staff. We also thank landowner for their various contributions leading to the success of the field campaigns. University of Canterbury atmospheric research team would like to acknowledge the very thoughtful, well organized, and proactive support we have received from all the volunteering firefighting crew. The success of our experiments and the safety of our science crew can only be partially attributed to our design but greatly attributed to the safe and well-executed plan from the volunteer crew. A special thanks to the Scion UAV crew: Robin Hartley and Peter Massam. This research was co-funded by Ministry of Business, Innovation and Employment (MBIE), New Zealand, grant number C04X1603 and C04X2103.

6. References

Christen, A., Gorsel, E. van, & Vogt, R. (2007). Coherent structures in urban roughness sublayer turbulence. *International Journal of Climatology*, *27*(14), 1955–1968. https://doi.org/10.1002/joc.1625

Cunningham, P., & Linn, R. R. (2007). Numerical simulations of grass fires using a coupled atmosphere-fire model: Dynamics of fire spread. *Journal of Geophysical Research: Atmospheres (1984–2012)*, *112*(D5). https://doi.org/10.1029/2006jd007638

Finney, M. A., Cohen, J. D., Forthofer, J. M., McAllister, S. S., Gollner, M. J., Gorham, D. J., et al. (2015). Role of buoyant flame dynamics in wildfire spread. *Proceedings of the National Academy of Sciences*, *112*(32), 9833–9838. https://doi.org/10.1073/pnas.1504498112

Heilman, W. E., Bian, X., Clark, K. L., & Zhong, S. (2019). Observations of Turbulent Heat and Momentum Fluxes During Wildland Fires in Forested Environments Observations of Turbulent Heat and Momentum Fluxes During Wildland Fires in Forested Environments. *Journal of Applied Meteorology and Climatology*. https://doi.org/10.1175/jamc-d-18-0199.1

Hunt, K. M. R., Zaz, S. N., & Romshoo, S. A. (2021). Linking the North Atlantic Oscillation to winter precipitation over the Western Himalaya through disturbances of the subtropical jet. *Earth and Space Science Open Archive*, 13. https://doi.org/10.1002/essoar.10508131.1

Heilman, W. E., Clements, C. B., Seto, D., Bian, X., Clark, K. L., Skowronski, N. S., & Hom, J. L. (2015). Observations of fire-induced turbulence regimes during low-intensity wildland fires in forested environments: implications for smoke dispersion. *Atmospheric Science Letters*, *16*(4), 453–460. https://doi.org/10.1002/asl.581

Katurji, M., Zhang, J., Satinsky, A., McNair, H., Schumacher, B., Strand, T., et al. (2021). Turbulent Thermal Image Velocimetry at the Immediate Fire and Atmospheric Interface. *Journal of Geophysical Research: Atmospheres*, 126(24). https://doi.org/10.1029/2021jd035393

Kiefer, M. T., Heilman, W. E., Zhong, S., Charney, J. J., & Bian, X. (2016). A study of the influence of forest gaps on fire-atmosphere interactions. *Atmospheric Chemistry and Physics Discussions*, 1–23. https://doi.org/10.5194/acp-2015-933

Kiefer, M. T., Zhong, S., Heilman, W. E., Charney, J. J., & Bian, X. (2018). A Numerical Study of Atmospheric Perturbations Induced by Heat From a Wildland Fire: Sensitivity to Vertical Canopy Structure and Heat Source Strength. *Journal of Geophysical Research: Atmospheres*. https://doi.org/10.1002/2017jd027904

LeMone, M. A., Angevine, W. M., Bretherton, C. S., Chen, F., Dudhia, J., Fedorovich, E., et al. (2018). 100 Years of Progress in Boundary Layer Meteorology. *Meteorological Monographs, 59*, 9.1-9.85. https://doi.org/10.1175/amsmonographs-d-18-0013.1

Li, D., & Bou-Zeid, E. (2011). Coherent Structures and the Dissimilarity of Turbulent Transport of Momentum and Scalars in the Unstable Atmospheric Surface Layer. *Boundary-Layer Meteorology*, *140*(2), 243–262. https://doi.org/10.1007/s10546-011-9613-5

Potter, B. E. (2012). Atmospheric interactions with wildland fire behavior – I. Basic surface interactions, vertical profiles and synoptic structures. International Journal of Wildland Fire, 21(7), 779–801. https://doi.org/10.1071/WF11128

Sun, R., Krueger, S. K., Jenkins, M. A., Zulauf, M. A., & Charney, J. J. (2009). The importance of fire–atmosphere coupling and boundary-layer turbulence to wildfire spread. International Journal of Wildland Fire, 18(1), 50–60. https://doi.org/10.1071/wf07072

Tang, W., Finney, M., McAllister, S., & Gollner, M. (2019). An Experimental Study of Intermittent Heating Frequencies From Wind-Driven Flames. *Frontiers in Mechanical Engineering*, *5*, 34. https://doi.org/10.3389/fmech.2019.00034

Wallace, J. M. (2016). Quadrant Analysis in Turbulence Research: History and Evolution. *Annual Review of Fluid Mechanics*, *48*(1), 131–158. https://doi.org/10.1146/annurev-fluid-122414-034550

Autonomous wildfire containment tool

Martin Hofmann*[1]; David Zenz[1]

[1]*HoZe Solutions GmbH, Bergisch Gladbach, Germany, {info@hoze-solutions.com}*

**Corresponding author*

Keywords

Autonomous, containment, resource efficiency, safety

Abstract

Go-to strategies to contain advancing wildfires with water as an extinguishing agent can be differentiated in ground- and air-based techniques. Ground-based techniques rely on man-held nozzles connected to a water reservoir such as the water tank on a fire truck. This approach can only be used for fires with intensities below 2000kW/m above which it is deemed unsafe. For higher intensity water is dropped ahead or on top of burning materials. Recent studies have unveiled how inefficient these approaches can be. Studies characterising aerial drops make use of water rigs fitted with nozzles. We propose to scale up such mimicking devices to a novel type of appliance which can be used to contain a fire front of several hundreds of meters length. We show the typical wetting pattern obtained as well as the effective containment of fires reaching intensities above 2500 kW/m.

1. Aerial drop characterisation

Above a certain wildfire intensity, ground-based operations involving personel presence in proximity of the fire front can not be carried out. Aerial support from planes and helicopters are required. The desired effect of aerial water drops is a reduction in the fire intensity to reach levels allowing for ground crews to intervene. The efficiency of such drops on reduction of fire intensity has become the subject of critical review. Indeed, studies show that such operations are effective in only 30% of the cases.[1] Reasons for this inefficiency can be the poor control over the water distribution on the ground and the "shadowing" effect of leaf cover not allowing for the water to reach the ground with the fire progressing in still dry vegetation. A further aspect which has not been fully investigated is the turbulence occurring around an aerial drop, which can fan the wind and thus be enitrely counter-productive.

Setups have been devised to characterise aerial drops. Arrays of cups have been placed on an airstrip to obtain the wetting pattern of a certain aerial mean. This obviously has been carried out at ideal dropping heights in absence of strong wind, which can make the relationship between these idealised wetting patterns and real wetting patterns in proximity of a wildfire difficult. Models have been proposed in order to provide a basis for water distribution in fire management tools.[2] Linking the water distribution to effective containment can be achieved empirically, highlighting the critical aspect of homogeneous water distribution.[3] Indeed patches which receive less than a critical amount of water still allow for fire progression.

The critical amount of water remains surprisingly an elusive parameter. Little research has been carried out on the critical apparent fuel moisture content required to inhibit fire progression. Lab-scale experiments provide hints at certain species requiring a higher exposure to water before reaching pyrolysis temperature.[4]

[1] Aerial Firefighting Use and Effectiveness (AFUE) Report
[2] Amorim, J. H. "Numerical modelling of the aerial drop of firefighting agents by fixed-wing aircraft. Part II: model validation." *International Journal of Wildland Fire* 20.3 (2011): 394-406.
[3] Plucinski M., Gould J., McCarthy G., Hollis J. (2007) The Effectiveness and Efficiency of Aerial Firefighting in Australia, Part 1.Bushfire Cooperative Research Centre,Australia. Report A.07.01.
[4] *Stechishen* E (1970) Measurement of the effectiveness of water as a fire suppressant

2. Wetting pattern characterisation in wind tunnel

We take inspiration of such experimental rigs with nozzles to propose a novel containment tool in itself. Such a construction can provide with well-controlled water distribution. With a given flow rate, the running time is the only parameter controlling the amount of water spent on the surrounding vegetation. Knowing the fuel type and density it should be possible to estimate the critical amount of water and thus the required running time of the system.

We carry out similar experiments to the aerial drop characterisation by arranging an array of plastic containers in a wind tunnel. A nozzle is placed laterally to the array and exposed to various wind patterns mimicking real conditions to characterise its wetting pattern on the ground. The nozzle is optimised so as to allow for a homogeneous distribution even in presence of the strongest wind attainable in the facility (3 m/s). Details of the wetting pattern are kept confidential.

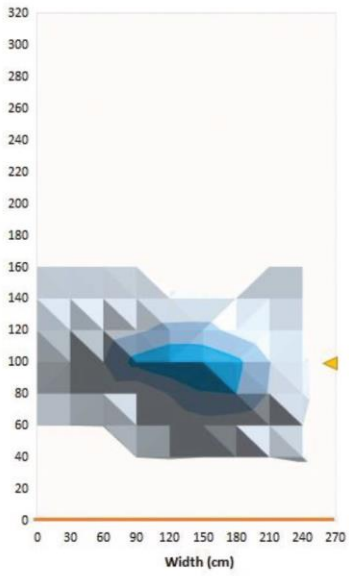

Figure 1: Wetting pattern of nozzle (triangle) over plastic container array in absence of wind.

The droplet dimension distribution is chosen so as to allow for both a wetting of the surrounding vegetation as well as to produce wind-entrained droplets of smaller diameter. This combination will allow the effective wetting of the vegetation, avoiding the "shadowing" effect. Similarly, the entrainment of droplets will allow them to wet vegetation in the general spread direction of the fire and will therefore not be wasted. The effect of increased humidity levels obtained on the extinguishment of flying embers remains to be studied. More detailed PIV analysis in presence of surface-tension modifying agents is also under progress.

3. Effective fire containment in field experiments

A series of selected nozzles is connected by the means of firefighting hoses, forming a closed loop with the single opening being connected to the water reservoir of a fire truck. The hose loop is placed in the top third of a plot of 25meters width and 50 meters length and dubbed Papageno system for the remainder. Water is then pumped at standard operational pressure. After a wetting time of 60 minutes a fire is ignited at the lower section and left to progress towards the system. Infrared images allow for the determination of the rate of spread. Similarly the flame length is recorded. Both indicators (flame lenght of 7 meters and derived fireline intensity of 2500kW/m) place the fire in an intensity regime too high to be safely contained using ground-based approaches. Upon approaching the Papageno system, the fire intensity drops and eventually is contained at the height of the system. The exact dynamics of intensity drop upon approach are still under investigation.

Figure 2: Effective fire containment using the Papageno system

4. Conclusion and outlook

We propose a novel fire containment tool consisting of a hose lenght with bespoke nozzles at regular intervals. The autonomous system allows for the safe retreat of practitioners outside of the danger zone, can operate at night and in presence of strong winds and allows for resource-efficient operations. Further field tests are required to characterise the operating windows of the system. Similarly we strongly recommend to pursue studies allowing for an effective understanding of critical amount of water as a function of fire intensity, which in turn is dictated by fuel type and density.

BRIDGE – a participatory-action research project for community engagement in forest fire risk prevention

Maria Rosario Partidario[1]; Guilherme Ximenes[1]; Margarida Monteiro[1]; Rute Martins[1]; Isabel Loupa Ramos[1]; Joana Dias[2]; Maria de Belém Freitas[2]; Carla Maria Antunes[2]; Miguel Teixeira[2]; Henrique Ribeiro[3]; Delta Silva[3]; Margarida Rebelo[3]; Marta Vicente[3;] Afonso Marques[3]; Anastasiya Felenchak[3]

[1] Instituto Superior Técnico. Campus Alameda, 1049-001, Lisboa, Portugal
{mariapartidario, guilherme.saad, margarida.monteiro, rutemartins, isabel.ramos, joanafmdias}@tecnico.ulisboa.pt
[2] Universidade do Algarve. Campus da Penha, 8005-139, Faro, Portugal,
{mbfreitas, cmantunes, a65890, a62984}@ualg.pt
[3] Laboratório Nacional de Engenharia Civil. LNEC, 1700-075, Lisboa, Portugal
{delta, mrebelo, magvicente, aamarques, afelenchak}@lnec.pt

**Corresponding author*

Keywords

Community-based approach, participatory action research, capacity-building, participatory mapping, forest fire risk reduction

Abstract

This brief introduces the BRIDGE research project, its core objectives and the main activities that are being developed in view of stimulating local action for forest fires risk reduction. BRIDGE is a participatory action research project (PCIF/AGT/0072/2019) that aims to develop an integrative approach to different forms of knowledge and action, linking science and local communities, to reduce the vulnerability and enhance strategies for forest fire risk reduction, mainly through collective and preventive action. It was initiated in March 2021 as a consortium coordinated by the Instituto Superior Técnico, Universidade de Lisboa, also including the Laboratório Nacional de Engenharia Civil and the Universidade of Algarve. BRIDGE adopted the Monchique municipality (southern Portugal, Algarve region) as a case study, but aims to develop knowledge, tools and experiences that can be shared with other forest fire risk prone regions in Portugal and elsewhere.

An Innovation Laboratory (InnoLab) is central in BRIDGE as a privileged space aiming to promote dialogue and knowledge sharing between local communities, science and organizations involved in forest fire risk reduction, in this case in the Monchique municipality. The main objective of the InnoLab is to bring together all relevant multiple actors that act, directly or indirectly, in the management of forest territories to promote social learning about forest wildfire risk, strengthening networks and building skills and capacities, both socially and institutionally, to foster participatory processes focused on forest fire risk reduction. A Participatory Mapping method was adopted in InnoLab involving the local community, in particular landowners of Monchique, placing them at the centre of the process of identification, analysis and management of forest fire risks, valuing local knowledge and experiences to reduce vulnerabilities and strengthen adaptive capacities from the perspective of local resilience.

This brief will share achieved outcomes with the participatory mapping involving local landowners of Monchique. It represented an important social practice to foster capacity-building and collaborative actions to forest fire prevention. It also represented an opportunity to promote social learning to better understand forest territories focusing on key issues in forest fire prevention, local vulnerabilities and adaptive capacities, to trigger a Community-based Disaster Risk Reduction (CBDRR) process in Monchique.

1. The BRIDGE Project

This brief introduces the BRIDGE research project, its core objectives and the main activities that are being developed in view of stimulating local action for forest fire prevention. BRIDGE is a participatory action research project (PCIF/AGT/0072/2019) about the development of strategies for forest fire risk reduction, mainly through preventive action. It builds upon scientific and local knowledge and engages local community

action. BRIDGE means linking science and local communities to reduce the vulnerability to forest fires risk. It was initiated in March 2021, with the Instituto Superior Técnico, Universidade de Lisboa coordinating a consortium that includes the Laboratório Nacional de Engenharia Civil and the Universidade of Algarve.

BRIDGE main objective is to integrate different forms of knowledge, explore the nexus society-science-policy to contribute to stimulate forms of local action that build upon communities improved capacities of self-protection and management of local territories and ecologies. BRIDGE builds upon bottom-up approaches but also on top-down approaches, to connect to relevant policies and management orientations that are established at national and European levels. BRIDGE adopted the Monchique municipality (southern Portugal, Algarve region) as a case study, but aims to develop knowledge, tools and experiences that can be shared with other forest fire risk prone regions in Portugal and elsewhere.

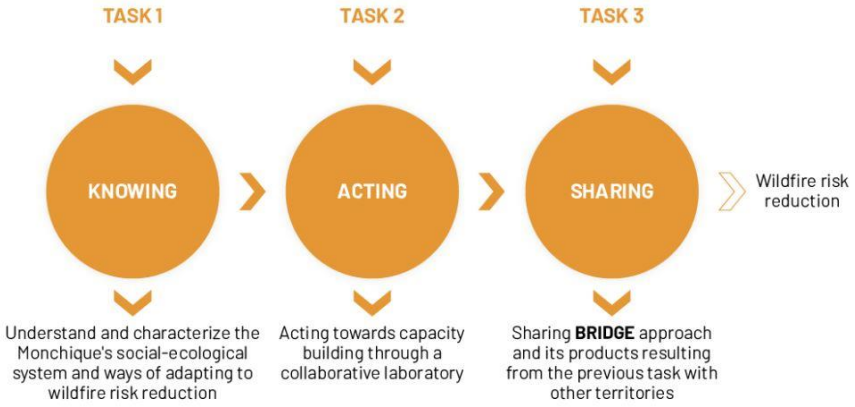

Figure 1. Main tasks of BRIDGE Project (own authors)

BRIDGE is structured in three main tasks (**Figure 1**). The first task is dedicated to improve our project team knowledge on the socio-ecological systems in Monchique and what have been forms of human adaptation to fire risk. The second task is the essence of the participatory action research during which, through the development of a collaborative innovation laboratory (InnoLab), the project aims to improve local capacities and promote dialogues that enable collective learning and sharing of knowledge and experiences on forms of reducing forest fire risks and local vulnerability. The third task aims to share with the outside communities and other territories prone to forest fire risk, what have been learnings and progresses achieved with the local community in Monchique.

In this brief we introduce our conceptualisation of the InnoLab where those collective debates are being and will be further promoted, and also share achieved outcomes from participatory mapping methodology applied in InnoLab meetings involving local landowners of Monchique. These meetings represented an important social practice to foster capacity-building and collaborative actions in view of forest fire prevention and an opportunity to promote social learning on key issues in forest fire prevention and adaptive capacities that can lead to better local resilience.

2. InnoLab: conceptualisation

An Innovation Laboratory (InnoLab) is central in BRIDGE as a privileged space aiming to promote dialogue and knowledge sharing between local communities, science and organizations involved in forest fire risk reduction. The main objective of the InnoLab in Monchique is to bring together all relevant actors that act, directly or indirectly, in the management of forest territories, promoting social learning about forest fire risk, strengthening actors' networks, building skills and capacities, both socially and institutionally, and fostering participatory processes focused on forest fire risk reduction. The ideation of the InnoLab is anchored in the support to create a common purpose of sharing knowledge and experiences and build together multiple forms of collaboration that can stimulate and promote a community-based disaster risk reduction (CBDRR).

Participatory mapping has been widely used in processes of CBDRR (e.g., Gaillard and Maceda, 2009), promoting knowledge exchange among various actors (Rizzi and Porebska, 2020). The use of this methodology

allows visual expressions of the realities perceived by the community, realities expressed through 'filtered' characteristics of the territory (Bartolucci et al., 2022). It contributes to the interpretation of risk areas, local vulnerabilities, allowing the identification of critical issues for a successful disaster risk management and to direct desired and useful risk reduction measures for the community (Cadag and Gaillard, 2012).

In March and April 2022, BRIDGE developed a participatory mapping methodology in InnoLab meetings with local landowners in Monchique, placing them at the centre of the process of identification and analysis of forest fire risk, valuing local knowledge and experiences to strengthen adaptive capacities from the perspective of self-organisation and local resilience (**Figure 2**). In total 30 landowners were involved in the participatory mapping, as members representing one of the followung organisations: Association of Forest Producers of Barlavento Algarvio (Aspaflobal) and/or Agricultural Cooperative of Monchique (Coopachique), A Nossa Terra Environmental Association and Monchique Alerta Association, the last formed by local landowners directly affected by the 2018 forest fire in Monchique.

Figure 2. Participatory Mapping with landowners of Monchique (BRIDGE)

An interesting aspect observed in the participatory mapping involving landowners in Monchique are the different local visions and interests related to forest territories. While some see the forest resources as a source of income based on forest production (in general Portuguese landowners and members of Aspaflobal and/or Coopachique), others focus on the valorisation of forest resources from the perspective of the landscape and local biodiversity (mainly in foreign landowners and members of the associations Nossa Terra and Monchique Alerta). However, even with different interests, visions and expectations, an interesting result of the participatory mapping was the convergent local knowledge of different groups of landowners about the current fire-prone areas, the main factors of forest fire risk and the local vulnerabilities of Monchique's forest territories.

The participatory mapping resulted in an important and valuable georeferenced database (GIS), elaborated on the basis of the perceptions of Monchique's community of landowners and the knowledge of local actors who act directly in the management of Monchique's forest territories. The GIS database resulted in the Integrated Map (Figure 3) containing information such as: location of participants' properties and/or houses, commonly used local access routes, forest areas of relevance and interest to participants, identification of vulnerable residents in the context of forest fires (children, the elderly, people with special needs, etc.), currently fire prone areas, main risk factors and local vulnerabilities in Monchique.

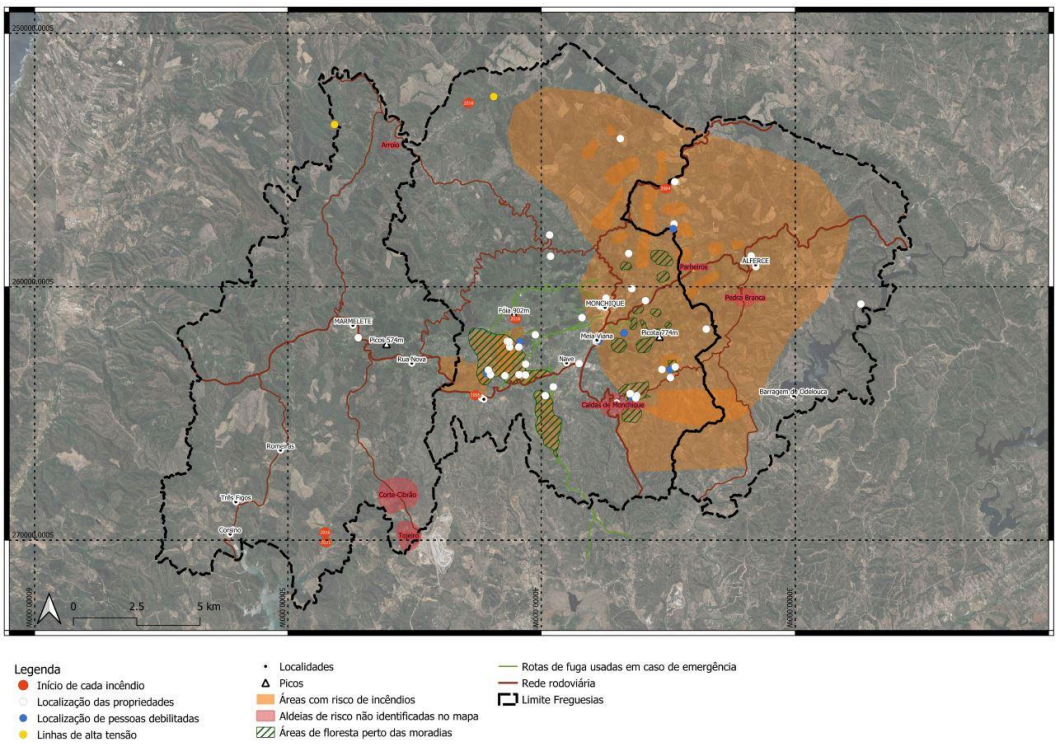

Figure 3. Participatory Map with landowners of Monchique (BRIDGE)

This GIS database, and the respective information that resulted from the debate and collective reflections involving the community of landowners, can contribute to (re)orient strategies for forest fire prevention with a bottom-up perspective, based on local knowledge and expectations. It can also contribute to (re)direct plans, programmes and policies (PPP) tailored to the local reality and specificities of Monchique, for example, the review of the Municipal Forest Defence and Fire Fighting Plan (PMDFCI) and the review of territorial development plans (e.g. Municipal Master Plan, Landscape Management and Recovery Plan, among others).

In line with scholars' suggestions in the literature, the participatory mapping also represent the opportunity for a collective debate on key issues in disaster risk management, promoting a fair and balanced dialogue (Kurastmoko et al., 2017), as well as better understanding of the territory through a social learning process (Kienberger, 2014; Wolf, 2021). In BRIDGE it is emphasized that beyond an important database that integrates diverse views, experiences, and local knowledge, the participatory mapping represents an important social practice to extend adaptive capacities to disasters (Haworth et al., 2016).

The participatory mapping developed in the BRIDGE InnoLab represent, therefore, an opportunity to involve landowners of Monchique in a social learning process on key issues in forest fire risk and prevention. Thus, it contributes to increase the understanding of forest territories, with a potential to reduce vulnerabilities and strengthening adaptive capacities to forest fire risk from the perspective of self-organization and local resilience, as well as to trigger a community-based disaster risk reduction (CBDRR) process in Monchique.

3. Bibliography

Cadag, J. & Gaillard, J. (2012). Integrating Knowledge and Actions in Disaster Risk Reduction: The Contribution of Participatory Mapping. Area. 44(1): 100-109. DOI: 10.1111/j.1475-4762.2011.01065.x

Gaillard, J. & Maceda, E. (2009). Participatory three-dimensional mapping for disaster risk reduction. In Participatory Learning and Action: Community-based adaptation to climate. URL: https://bit.ly/3NktK7o

Haworth, B., Whittaker, J., & Bruce, E. (2016). Assessing the application and value of participatory mapping for community bushfire preparation. Environmental Management. 69(4): 115-127. DOI: 10.1007/s00267-021-01582-8

Kienberger, S. (2014). Participatory mapping of flood hazard risk in Munamicua, District of Búzi, Mozambique. Journal of Maps. 10(2): 269-275. DOI: 10.1080/17445647.2014.891265

Kurastmoko, E., Wibowo, A., Cholid, S. & Tjiong, G. (2017). Participatory three dimensional mapping for the preparation of landslide disaster risk reduction program. AIP Conference Proceedings. 1857(1). DOI 10.1063/1.4987120

Rizzi, P. & Porębska, A. (2020). Towards a Revised Framework for Participatory Planning in the Context of Risk. Sustainability. 12(14): 5539. DOI: 10.3390/su12145539

Tebbutt, C., Devisscher, T., Obando Cabrera, L., Gutiérrez García, G., Meza Elizalde, M., Armenteras, D. & Oliveras, I. (2021). Participatory mapping reveals socioeconomic drivers of forest fires in protected areas of the post-conflict Colombian Amazon. People and Nature. 3(10): 811-826. DOI: 10.1002/pan3.10222

Wolf, E. (2021). The promise of "people-centred" approach to floods: Types of participation in the global literature of citizen science and community-based flood risk reduction in the context of the Sendai Framework. Progress in Disaster Science. 10 (100171). DOI: 10.1016/j.pdisas.2021.100171

Canopy fuel modelling in Mediterranean forest stands with airborne LiDAR data at regional scale: preliminary results

Eva Marino*; Stefano Arellano-Pérez; Santiago Martín-Alcón, José Luis Tomé

AGRESTA Sociedad Cooperativa. C/Duque de Fernán Núñez 2, 28012 Madrid, Spain
{emarino, sarellano, smalcon, jltome}@agresta.org

**Corresponding author*

Keywords

Canopy base height, canopy fuel load, canopy bulk density, airborne laser scanning, fuel maps

Abstract

Canopy fuel characterization is highly relevant for wildfire prevention, especially in the context of extreme events involving crown fires. Airborne laser scanning has been proven very useful to retrieve 3D forest structure at large scales, becoming freely available in many countries in the recent years which provide an opportunity to map fuel parameters that are critical for fire behaviour simulation. Previous studies on canopy fuel modelling predict canopy base height (CBH), fuel load (CFL) and bulk density (CBD) mainly in tree species from temperate conifer forests, with specific models still lacking for the main Mediterranean forest stands and especially deciduous species. This work presents first results of models obtained from low density airborne LiDAR data (1.5 p/m2) for canopy fuel characterization of critical structural variables (CBH, CFL and CBD) in the main Mediterranean forest stands existing in Andalusia region, including Pinus sp, Quercus sp and Eucalyptus sp tree species. The study is part of an ongoing project that include field inventory in 750 plots to characterize canopy fuels in 15 different forest stands representative of Mediterranean tree species, with a samplig design that consider structural heterogeneity in a wide study area (29000 km2). Different modelling techniques (linear regression and random foresst) were tested to assess the best formulation and input LiDAR metrics to be included in the models for each fuel parameter estimation, that will be used to generate high resolution maps of canopy fuels at regional scale. Preliminary models obtained from a set of 170 field plots in pure stands of Quercus ilex, Quercus suber, Pinus halepensis, Pinus pinea and Eucaliptus sp show promising results for canopy fuel characterization from low density airborne LiDAR data in these widely distributed species. However, our results also highlight a significant effect of the different modelling tecniques on the input metrics and accuracy of the models.

1. Introduction

Canopy fuel characterization is highly relevant for wildfire prevention and management, especially regarding potential extreme fire behaviour involving crown fires. Canopy base height (CBH), fuel load (CFL) and bulk density (CBD) are the main canopy structure variables conditioning fire initiation and spread rate in the transition of flames from surface fuels to canopy fuels (Van Wagner, 1977; Cruz et al., 2003; Molina et al., 2014). Fire simulation software can be used to predict fire behaviour but requires high resolution fuel maps of both surface and canopy fuels. Fire managers are increasingly using this kind of simulation programs for operational use, fuel treatment planning and fire severity assessment, demanding updated fuel cartography at regional scales.

LiDAR (Laser Imaging Detection and Ranging) technology has been proven very useful to characterize 3D forest structure, including canopy fuels (Riaño et al. 2003; Andersen 2005; Hudak et al. 2008). Free LiDAR data from airborne platforms are becoming available in more countries in the recent year (e.g. Spain, Finland, Slovenia or France), being a revolution on data gathering for forest monitoring at large scales. For example, the Spanish National Plan for Aerial Orthophotography (PNOA) is providing the second nation-wide coverage of LiDAR data at low pulse density in Spain and already planning the third coverage to start next year. Hence, airborne LiDAR data give an opportunity to get spatially-explicit information to map fuel parameters that are critical for fire behaviour simulation.

Previous studies on canopy fuel modelling with airborne LiDAR include CBH, CFL and CBD models, showing different success depending on the fuel parameter and laser pulse density used. The main tree species assessed include North-American and European conifers, mostly typical of temperate forests (Andersen et al. 2005,

Riaño et al. 2003; González-Olabarria et al, 2012; Gonzalez-Ferreiro et al. 2014, 2017; Alonso-Rego et al., 2021), and some studies for Mediterranean tree species but fitted with field data from small areas with limited transferability (Botequim et al, 2019; Ferrer Palomino y Rodriguez y Silva, 2021). Specific models are needed to get reliable estimation of canopy fuels at regional scale, but information is still lacking for many Mediterranean forest stands, especially deciduous species.

The aim of the present study is to explore different modelling techniques to obtain models for canopy fuel varaibles (CBH, CFL and CBD) from low density airborne LiDAR data for the main Mediterranean forest stands, including *Pinus sp*, *Quercus sp* and *Eucalyptus sp* tree species, and considering the structural heterogeneity from a wide study area. The work is part of a wider project on forest fuel characterization in Andalusia region that is currently ongoing. The best models obtained will be used to generate high resolution maps of canopy fuels at a regional scale.

2. Methods

2.1. Study area and field data

The study area includes the forest stands located in the Andalusia region, in the south of Spain (Figure 1). Most of them are located within the High Wildfire Risk areas ("Zonas de Alto Riesgo de incendio forestal", ZAR) which cover 58% of the whole Andalusian territory, e.i. more than 29000 km^2. The most representative forest stands in terms of area covered and potential fire risk were selected for canopy fuel characterization in the field, resulting in 15 different forest ecosystems (Table 1). Tree species composition was derived from a detailed vegetation map (1:10000 scale) available for Andalusia region. Selected forest ecosystems included pure stands (one dominant tree species) and mixed stands (minimum of 25% of relative canopy cover of the secondary tree species), covering 85% of the forest areas in the region.

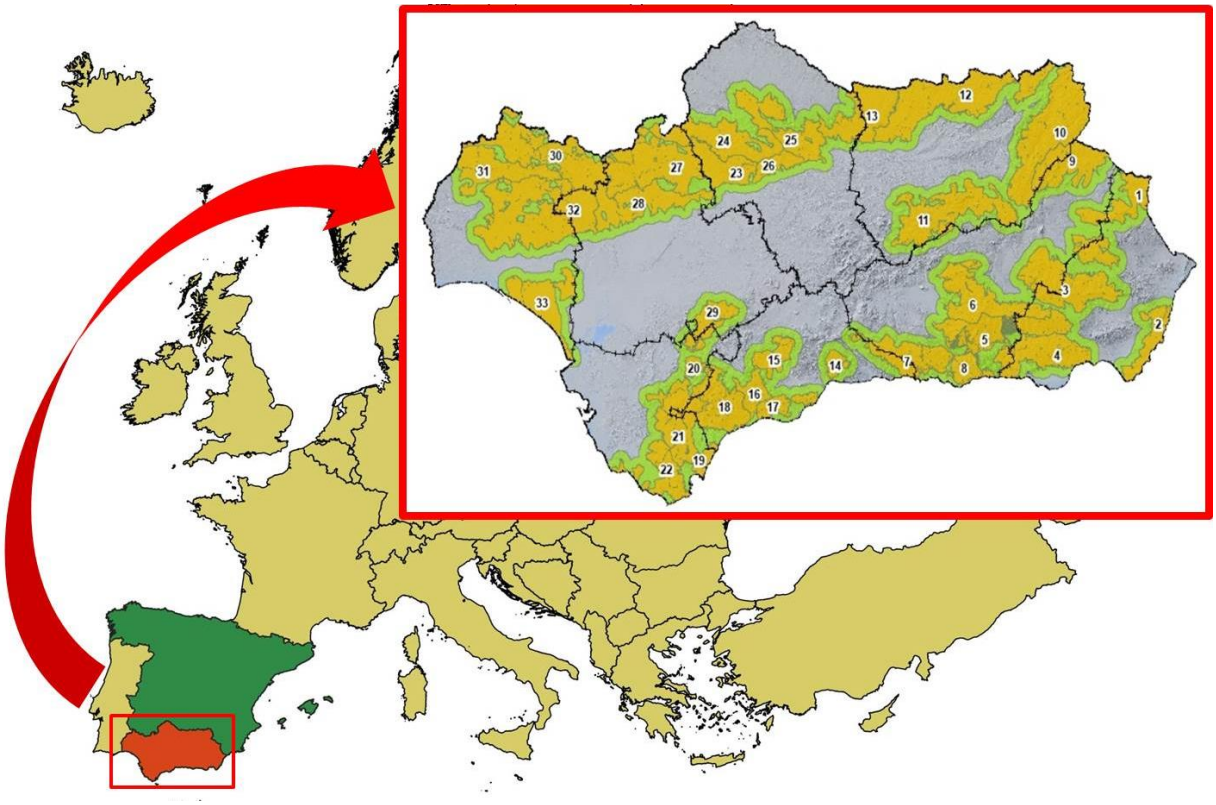

Figure 1- Study area, with detail of the High Wildfire Risk areas (ZAR) in Andalusia (orange) and a 5-km buffer included (green)

A total of 750 field plots will be placed in the selected forest stands including the main Mediterranean tree species. According to the area covered by each forest ecosystem in the study region, between 30 to 90 circular plots will be measured to retrieve canopy fuel data for each forest stand type. Plot locations are chosen in order

to cover the range of structural variability according to the Spanish National Forest Inventory IFN3 (MARM, 2008) and LiDAR data, considering metrics related to fractional canopy cover (FCC), height (H) and canopy relief ratio (CRR) to identify structural heterogeneity in each forest ecosystem (Parker and Russ, 2004).

A GPS providing sub-metre accuracy is used to registered plot centre coordinates for proper LiDAR data comparison in the modelling process. Field measurements are performed in 11.3-m-radius circular plots, equivalent to the 20-m-pixel canopy fuel maps to be generated for the study area. In each plot, diameter at breast height (DBH) of trees thicker than 7.5 cm is measured and used to calculate crown foliar biomass from previous allometric equations developed for each species (Montero et al. 2005). Available canopy fuel load at plot level (CFL) is calculated as the foliar biomass in the stand (kg/m^2).Tree height and crown base height are registered in 4 representative trees per plot, selecting one tree within each quarter section of the circular plot to characterize the mean stand height and canopy base height (CBH). Canopy bulk density (CBD) is calculated from CFL and mean canopy length at plot level, the latter being obtained as H minus CBH.

Table 1- Selected forest stands for canopy fuel modelling at regional scale. *P: pure stands; M: mixed stands; P & M: pure and mixed stands

Forest stand	**Area (ha)**	**Stand type***
Quercus ilex	1218082	P
Pinus halepensis	241798	P
Pinus pinea	206213	P
Quercus suber	190698	P
Eucalyptus sp	138373	P
Olea europaea var. sylvestris	138334	P & M
Pinus pinaster	116117	P
Pinus nigra	61436	P
Quercus ilex & Pinus halepensis	47254	M
Pinus sylvestris	28766	P
Pinus pinaster & Quercus ilex / Quercus suber	27535	M
Quercus faginea / Quercus pyrenaica & Quercus ilex / Quercus suber	18934	P & M
Pinus pinea & Quercus ilex / Quercus suber	19370	M
Quercus suber & other Quercus sp	17460	P & M
Eucalyptus sp & Pinus sp	10510	M
TOTAL	**2480268**	

2.2. LIDAR data

The LiDAR data used in this study correspond to the 2nd regional cover of Spanish PNOA in Andalusia, acquired between 2020 and 2021 at a pulse density of 1.5 p/m^2. Point cloud files were provided in LAZ format and processed using R software (R Development Core Team, 2014) with lidR package (Roussel *et al*. 2020) and QGIS software (QGIS Development Team, 2014). Points classified as soil returns were used to generate a digital terrain model (DTM) at 2m resolution. Points classified as vegetation returns were normalized with DTM to retrieve heights to soil level. LiDAR metrics were extracted from point clouds at plot level to compare with field measurements (Figure 2). Two different thresholds, 2 m and 4 m, were used to get LiDAR metrics from canopy returns in order to considered the heterogeneity of Mediterranean vegetation (Table 2).

Selected LiDAR metrics were also extracted in a 20m grid for the whole study area to characterized the structure of forest stands prior to field measurement (see details in section 2.1), in order to assess FCC (percentage of first returns above 2m), H (percentile 95% of vegetation returns) and CRR (canopy relief ratio). Once the LiDAR models for each canopy fuel variable (CBH, CFL and CBD) and forest type (Table 1) will be fitted and validated with field data, selected input metrics included in the final models will be also obtained as 20m raster files to generate high resolution wall-to-wall canopy fuel maps of the study area.

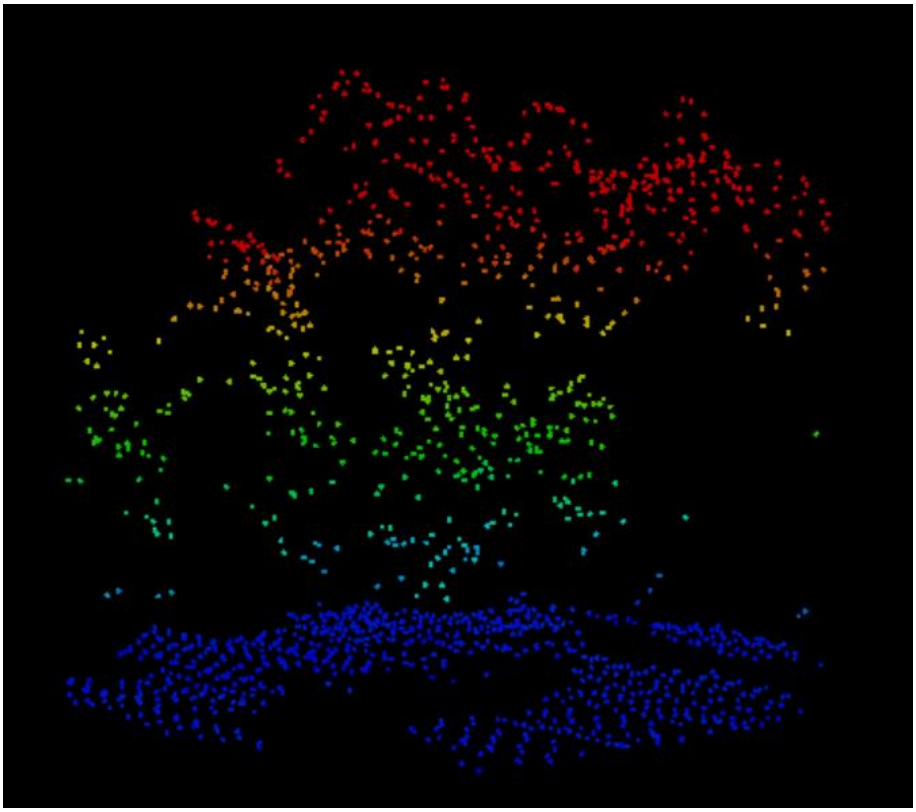

Figure 1- Example of LiDAR point cloud (1.5 p/m2) extracted in a field plot

Table 2- LiDAR metrics used as potential explanatory variables. All metric were extracted and tested at both threshold levels: 2m and 4m

Metric	**Description**
zmax	Maximum return height
zmean	Mean return height
zvar	Variance of return heights
zsd	Standard deviation of return heights
zcv	Coefficient of variation of return heights
ziq	Interquartile range of return heights
zskew	Skewness of return heights
zkurt	Kurtosis of return heights
pzabove	Percentage of first returns above threshold
pzabovezmean	Percentage of first returns above mean height
crr	Canopy relief ratio
p_i	Percentile *i* of return heights (5,10,20,25,30,40,50,60,70,75,80,90,95,99)

2.3. Statistical analysis

Parametric and non-parametric regression methods were used to model canopy fuels with LiDAR data. Different modelling techniques including linear regression and random forests were tested in order to compare the performance of different models. Models were fitted in R software, using crossvalidation for final model selection based on minimum root mean squared error (RMSE) and maximum variability explained.

3. Preliminary results

The field inventory is ongoing, and most of the plots in the main ecosystems are expected to be finished during the summer 2022. At present, there were more than 300 plots available out of 750 planned in the 15 forest types

included in the study. However, here we are presenting preliminary results retrieved from only 170 plots in five pure stands, including *Quercus ilex* (n=41), *Quercus suber* (n=16), *Pinus halepensis* (n=18), *Pinus pinea* (n=44) *and Eucaliptus sp* (n=51), where at the time of writing this communication there were enough field data to perform the statistical analysis. Main statistics describing canopy parameters in each forest stand are summarized in Table 3.

Table 3- Summary of the canopy fuel characteristics of the selected pure forest stands. H = Stand height, CBH = canopy base height, CFL = canopy fuel load, CBD = canopy bulk density, s.d. = = standard deviation

Forest species (field plots)	H (m)		CBH (m)		CFL (kg/m^2)		CBD (kg/m^3)	
	mean (range)	s.d.	mean (range)	s.d.	mean (range)	s.d.	mean (range)	s.d.
Quercus ilex (n=41)	7.27 (3.53-11.48)	1.69	2.08 (0.67-3.7)	0.53	0.20 (0.04-0.76)	0.15	0.04 (0.01-0.14)	0.03
Quercus suber (n=16)	8.60 (5.30-14.65)	2.26	2.58 (2.10-3.7)	0.50	0.04 (0.01-0.08)	0.02	0.01 (0.003-0.01)	0.003
Pinus halepensis (n=18)	9.48 (5.15-17.63)	3.22	3.43 (0.10-9.4)	2.52	0.28 (0.07-0.59)	0.14	0.05 (0.01-0.13)	0.03
Pinus pinea (n=44)	10.71 (5.28-21.30)	3.62	5.85 (1.45-13.0)	3.12	0.61 (0.17-2.19)	0.37	0.14 (0.04-0.59)	0.11
Eucalyptus sp (n=41)	12.56 (5.75-19.98)	3.04	6.17 (2.15-14.2)	2.66	0.66 (0.02-3.02)	0.49	0.12 (0.003-0.88)	0.13

In general, first results showed better models for *Pinus sp* than *Quercus sp* and *Eucalytus sp* stands (Table 4). CBD was the canopy fuel parameter more difficult to estimate, with even unsuccessful model fitting in some cases. Comparing parametric and non-parametric modelling techniques, linear regression generally provided better goodness-of-fit than random forest. In terms of LiDAR metrics, we also observed and effect of the different modelling techniques on the input variables selected as predictors in the models.

When field inventory would be completed, further analysis will be performed to improve these models and to include the rest of selected forest stands. Additional LiDAR metrics (e.g. percentage of returns normalized by height strata) and statistical methods (e.g. non-linear formulations) will be also tested. The final models fitted will allow retrieving predictions of CBH (m), CFL (kg/m^2) and CBD (kg/m^3) based on low-density LiDAR data (1.5 p/m^2) to obtain high spatial resolution canopy fuel maps of the study area adapted to the particularities of the main forest ecosystem in Andalusia. These results could be also applied to get canopy fuel maps from LiDAR data available in other forest stands in the Mediterranean region, as the selected species are very representative not only of the Iberian Peninsula but also of other South-European forest ecosystems, e.g. autochthonous stand composed by the main *Pinus sp* and *Quercus sp* as well as *Eucalyptus sp* plantations (Table 1).

Results from this study are expected to provide relevant information to improve fuel mapping in forest stands for enhance wildfire prevention and management, especially with regard to most conifer and deciduous tree species that are commonly involved in large wildfires in the Mediterranean region but are currently lacking specific LiDAR models for canopy fuel characterization.

Table 4- Statistics of the preliminary models fitted to estimate canopy fuel characteristics in the selected pure forest stands from LiDAR data. CBH = canopy base height, CFL = canopy fuel load, CBD = canopy bulk density, R^2_{adj} = adjusted R^2, R^2_{ps} = pseudo-R^2, RMSE = root mean square error, n.a. = not applicable (unsuccessful model fitting)

Forest species	Lineal regression		Random Forest	
	R^2_{adj}	RMSE (%)	R^2_{ps}	RMSE (%)
Quercus ilex (n=41)				
CBH (m)	0.30	0.432 (20.6 %)	0.19	0.478 (23.0 %)
CFL (kg/m^2)	0.38	0.076 (37.2 %)	0.37	0.121 (59.6 %)
CBD (kg/m^3)	0.34	0.018 (43.1 %)	0.43	0.021 (51.5 %)
Quercus suber (n=16)				
CBH (m)	0.52	0.326 (12.6 %)	0.55	0.328 (12.7 %)
CFL (kg/m^2)	n.a.	n.a.	0.43	0.013 (31.2 %)

CBD (kg/m^3)	0.38	0.002 (28.6 %)	n.a.	n.a.
Pinus halepensis (n=18)				
CBH (m)	0.88	0.774 (22.6 %)	0.75	1.188 (34.6 %)
CFL (kg/m^2)	0.85	0.051 (18.2 %)	0.49	0.098 (35.1 %)
CBD (kg/m^3)	0.63	0.025 (50.0 %)	0.31	0.026 (52.3 %)
Pinus pinea (n=44)				
CBH (m)	0.92	0.892 (15.2 %)	0.88	1.063 (18.2 %)
CFL (kg/m^2)	0.51	0.192 (31.5 %)	0.23	0.322 (52.8 %)
CBD (kg/m^3)	n.a.	n.a.	0.09	0.105 (75.1 %)
Eucalyptus sp (n=41)				
CBH (m)	0.44	1.952 (31.6 %)	0.42	2.023 (32.8 %)
CFL (kg/m^2)	0.75	0.179 (27.1 %)	0.41	0.379 (57.4 %)
CBD (kg/m^3)	n.a.	n.a.	0.23	0.115 (95.8 %)

4. Acknowledgements

This study is part of a broader work performed within the frame of CILIFO Project (Iberian Centre for Research and Forest Firefighting) co-funded by the EU through the Cross-Border Cooperation Programme INTERREG VA Spain-Portugal (POCTEP) 2014-2020 from the European Regional Development Fund (ERDF) and the Regional Government of Andalucía (Junta de Andalucía). The authors thank Francisco Senra and Fran Castelló from INFOCA, and Juan José Vales and Yolanda Gil from REDIAM.

5. References

Alonso-Rego, C., Arellano-Pérez, S., Guerra-Hernández, J., Molina-Valero, J. A., Martínez-Calvo, A., Pérez-Cruzado, C., … Ruiz-González, A. D. (2021). Estimating Stand and Fire-Related Surface and Canopy Fuel Variables in Pine Stands Using Low-Density Airborne and Single-Scan Terrestrial Laser Scanning Data. Remote Sensing, 13, 5170.

Andersen, H.E., McGaughey, R.J., Reutebuch, S.E. (2005). Estimating forest canopy fuel parameters using LIDAR data. Remote Sens. Environ. 94, 441–449.

Botequim, B.; Fernandes, P. M.; Borges, J. G.; González-Ferreiro, E.; Guerra-Hernández, J. (2019). Improving silvicultural practices for Mediterranean forests through fire behaviour modelling using LiDAR-derived canopy fuel characteristics. International Journal of Wildland Fire, 28(11), 823–839.

Cruz, M. G., Alexander, M. E., & Wakimoto, R. H. (2003). Assessing canopy fuel stratum characteristics in crown fire prone fuel types of western North America. International Journal of Wildland Fire, 12(1), 39–50.

Ferrer Palomino, A., & Rodríguez y Silva, F. (2021). Fuel Modelling Characterisation Using Low - Density LiDAR in the Mediterranean: An Application to a Natural Protected Area. Forests, 12(1011).

González-Ferreiro, E.; Diéguez-Aranda, U.; Crecente-Campo, F.; Barreiro-Fernández, L.; Miranda, D.; Castedo-Dorado, F.; 2014. Modelling canopy fuel variables for Pinus radiata D. Don in NW Spain with low-density LiDAR data. Int. J. Wildland Fire 23, 350–362.

González-Ferreiro, E., Arellano-Pérez, S., Castedo-Dorado, F., Hevia, A., Vega, J. A., Vega-Nieva, D., Ruiz-González, A. D.; 2017. Modelling the vertical distribution of canopy fuel load using national forest inventory and low-density airbone laser scanning data. PLoS ONE, 12(4), 1–21.

González-Olabarría, J.R., Rodríguez, F., Fernández-Landa, A., Mola-Yudego, B., 2012. Mapping fire risk in the model forest of Urbión (Spain) based on airborne LiDAR measurements. For. Ecol. Manag. 282, 149–156.

Hudak, A.T.; Crookston, N.L.; Evans, J.S.; Hall, D.E.; Falkowski, M.J.; 2008. Nearest neighbor imputation of species-level, plot-scale forest structure attributes from LiDAR data. Remote Sensing of Environment 112, 2232–2245.

MARM (2008). Tercer Inventario Forestal Nacional (IFN3) 1997-2007. Andalucía. Ministerio de Medio Ambiente. Madrid.

Molina, J. R., Rodríguez y Silva, F., Mérida, E., & Herrera, M. Á. (2014). Modelling available crown fuel for Pinus pinaster Ait . stands in the " Cazorla , Segura and Las Villas Natural Park " (Spain). Journal of Environmental Management, 144, 26–33.

Montero G., Ruiz-Peinado R., Muñoz M. (2005) Producción de biomasa y fijación de CO2 por los bosques españolesMonografía INIA, serie forestal nº13.

Parker, G.G. & Russ, M.E. (2004) The canopy surface and stand development: assessing forest canopy structure and complexity with near-surface altimetry. Forest Ecology and Management, 189, 307– 315.

QGIS Development Team (2014). Quantum GIS Geographic Information System. Open Source Geospatial Foundation Project. URL: http://qgis.osgeo.org/.

R Development Core Team (2014). R: A language and environment for statistical computing. R Foundation for Statistical Computing, Vienna, Austria.

Riaño, D., Meier, E., Allgöwer, B., Chuvieco, E., Ustin, S.L. (2003). Modelling airborne laser scanning data for the spatial generation of critical forest parameters in fire behaviour modelling. Remote Sensing of Environment 86 (2), 177-186.

Roussel, J.R., Auty, D., Coops, N. C., Tompalski, P., Goodbody, T. R. H., Sánchez Meador, A., Bourdon, J.F., De Boissieu, F., Achim, A. (2020). lidR: An R package for analysis of Airborne Laser Scanning (ALS) data. Remote Sensing of Environment 251, 112061.

Van Wagner, C. E. (1977). Conditions for the start and spread of crown fire. Canadian Journal of Forest Research, 7(1), 23–34.

Characterising and managing fire risks to plantations under changing climates

Kate Parkins*; Brett Cirulis; Lauren Bennett; Trent Penman

The University of Melbourne, FLARE Wildfire Research Group, Faculty of Science, School of Ecosystem and Forest Sciences. 4 Water Street, Creswick, Victoria, Australia, 3363.
{kate.parkins, brett.cirulis, mccoll.s, ltb, trent.penman}@unimelb.edu.au

**Corresponding author*

Keywords

Risk reduction, fuel modelling, plantations, future fire, climate change

Abstract

Wildfires are a common threat to the sustainability of commercial plantations in fire-prone regions. Large losses of plantations from wildfires can lead to the disruption of forest yield, with flow-on impacts to downstream industries, resulting in significant social and economic impacts to local communities. Future climate projections indicate an increase in wildfire activity, including increases in fire extent, severity or frequency in many fire-prone ecosystems. Land and fire management agencies around the world invest significant resources to reduce the likelihood and impact of future fires and increase the capacity for fire suppression. However, we currently know very little about how commercial plantations will be impacted by fire as the climate changes, or if strategic management can mitigate some of these risks into the future.

In this study we sought to 1) quantify fire risks to plantations and nearby community assets under current and changing climates; and 2) evaluate the effectiveness of management options for mitigating some of these risks under changing climates. This research included the customisation of a fire simulation tool (PHOENIX RapidFire) for use in plantation landscapes by developing plantation-specific fuel functions (derived from field-sampling in hardwood and softwood plantations around Australia) that were integrated into fire spread models. To quantify longer-term risks, these advancements were also integrated into a stochastic fire regime simulator (FROST– Fire Regimes and Operation Simulation Tool). Fire risks to both environmental and community assets were evaluated under current and changing climates to support evidence-based management to help guide investment, insurance negotiations, and fire mitigation in the plantation sector. The fire regime simulator (FROST) was also used to evaluate a range of different management options for reducing risk as a basis for efficient allocation of fire prevention and response resources both by plantation growers and by broader fire management agencies.

We found that reducing suppression response times (to 15 minutes or less for all ignitions) and the current approach to management (a construction rate of 2km/h for suppression and 15-minute response times, with 4000ha/year of prescribed burning) were consistently the best management strategies for reducing fire risks to plantations and adjacent communities, regardless of the climate model used. These strategies offer the greatest scope for reducing future wildfire risks to plantation assets and adjacent communities as the climate changes. High pruning in strategic locations may also be worthy of future investment but should be considered in combination with more rapid suppression and prescribed burning. Plantation owners currently have little influence over the amount and location of prescribed burning adjacent to plantations, and fuel reduction burning is not regularly undertaken in Australian plantations. Therefore, rapid suppression response times was found to be the single best investment for minimising impact to plantation assets under a hotter or drier climate.

1. Background & Introduction

Wildfires are a common threat to the sustainability of commercial plantations in fire prone regions. Wildfire is considered one of the main threats to plantations in many countries including Australia, Brazil, Indonesia, Chile and Portugal (Matthews et al. 2012; Booth 2013; Galizia & Rodrigues 2019), with an increased frequency of incidents in recent years (Bartlett 2012). In Australia, vast areas of hardwood and softwood plantations were burnt by the devastating 2019/2020 Black Summer wildfires, with more than a quarter (26%) of commercial plantations burnt in New South Wales alone (Cruz, Alexander & Plucinski 2017). The growth characteristics of plantations can be highly flammable, especially at key stages in their growth cycle. Severe wildfires may result

in high economic losses if burnt trees are not salvageable due to their age profile, or when high-severity fire results in whole-of-stand losses. Wildfires that impact plantations can have flow-on effects for other parts of the wood products industry, potentially resulting in significant negative economic and social impacts to regional communities (Cruz, Alexander & Plucinski 2017). Understanding changes in fire regimes and the associated impacts in plantation landscapes will be key to adequately managing risks to both plantation and community assets in coming decades.

Future climate projections indicate an increase in wildfire activity, including increases in fire extent, severity or frequency in many fire-prone ecosystems (Bowman et al. 2009; Flannigan et al. 2009). Land and fire management agencies around the world invest significant resources to reduce the likelihood and impact of future fires and increase the capacity for fire suppression (Calkin et al. 2005; Berry, Donovan & Hesseln 2006). However, we currently know very little about how commercial plantations will fare as the climate changes, nor how management may be able to mitigate some of these risks into the future. Plantation forestry involves relatively long time scales, with 30-year rotations common. Therefore, improved prediction of fire risk over decade long time-scales is crucial to the industries sustainability.

Fuel management is the primary means for land and fire managers to reduce the occurrence, size and severity of future fires while also having the co-benefit of increasing the capacity for suppression during an active fire (Agee & Skinner 2005; Wilson & Wiitala 2005; Finney, Grenfell & McHugh 2009; Penman et al. 2011). Fuel management in and around plantations is regarded as being important for reducing the likelihood of future impacts from wildfires. Fuel management within plantations primarily focuses on modifying or reducing the amount of fuel in key strata. The modification or removal of surface fuel and increasing the gap between the canopy base height and the ground (through removal of elevated fuels) is known to reduce the overall flammability (Burrows et al. 1989; Agee & Skinner 2005; Johnson & Peterson 2005; Fernandes et al. 2008). However, the effectiveness of different types of management under a changing climate is not yet well understood.

In this study, fire risks to both environmental and community assets were evaluated under current and changing climates to support evidence-based management to help guide investment, insurance negotiations, and fire mitigation in the plantation sector. A fire regime simulator (FROST - Fire Regimes and Operation Simulation Tool) was also used to evaluate a range of different management options for reducing risk as a basis for efficient allocation of fire prevention and response resources both by plantation growers and by fire management agencies.

This research had two key objectives:

1. To quantify fire risks to plantations and nearby community assets under current and changing climates;
2. To evaluate the effectiveness of management options for mitigating fire risks to plantations and nearby community assets under changing climates.

2. Approach

This research included the customisation of a fire simulation tool (PHOENIX RapidFire) for use in plantation landscapes by developing plantation-specific fuel functions (derived from field-sampling in hardwood and softwood plantations around Australia, see Figure 1A) that were integrated into fire spread models. To quantify longer-term risks, these advancements were also integrated into a stochastic fire regime simulator - FROST, that is proposed for future use in operational risk assessments.

2.1. Quantifying fuel accumulation in plantations over time

Prior to this study, plantation fuels were represented in fire-behaviour simulators by Olson fuel accumulation curves based on native vegetation. These curves are characterised by a rapid and steady increase in fuel load in young age classes (~5 to 8 years) followed by a progressive stabilisation to loads of ~16 Mg ha^{-1} in the surface/near-surface stratum and 2 Mg ha^{-1} in the elevated stratum. However, the accuracy of these fuel functions for plantations has not been fully assessed. As a result, fuel hazard has been poorly estimated in plantations, resulting in sub-optimal predictions of fire behaviour and risk in plantation areas.

To address this, we undertook a series of field-based vegetation surveys, to quantify how fuel accumulates over time in hardwood and softwood plantations. The project involved six study landscapes (each roughly 80 km^2) across Australia (Figure 1A). In each study landscape a series of field-based fuel accumulation surveys were conducted. *Sampling of surface, near-surface, elevated and ladder fuels occurred across five different plantation species from immediately post-harvesting (0 years) through to just prior to harvesting (~30 years). These data were used to develop fuel accumulation curves for each species, per region.* Polynomial regression analyses were used to fit functions to the fuel load by age data, using an iterative approach that increased the order of the polynomial to optimise R-squared values.

2.2. Fire regime modelling

The newly developed fuel accumulation curves were integrated into a stochastic fire regime simulator – FROST. FROST is an innovative model that uses available environmental data to spatially and temporally predict current and future trends in fire regimes and can simulate fire regimes over decades and centuries (Penman et al. 2015). It uses PHOENIX RapidFire as the fire behaviour simulator, and uses empirical ignition and fuel models based on biophysical data to allow for realistic estimates of future fire risk. FROST also uses Bayesian Networks to capture uncertainties in risk estimates and produces reliable simulations by integrating dynamic relationships associated with past fires (Penman et al. 2015).

The major components of FROST are termed 'machines'. The primary machines include a weather machine, an ignition machine and a fuel machine. These machines provide the input data for the fire behaviour simulator (in this case PHOENIX RapidFire) to run fires for each day. FROST also includes a fuel treatment manager, a disruption machine and a suppression machine. These machines allow the user to test various operational scenarios and can be used to simulate management strategies and their impact on fire behaviour. These machines were used to evaluate management options for mitigating fire risks to plantations and nearby community assets under changing climates.

2.3. Scenario modelling

The FROST simulation modelling tested the effects of climate change on the fire regime across the six study landscapes. We selected two global climate models:

1. ECHAM5 (*hotter*), submodel 1 – characterised by a relatively large increase in annual temperature over south-eastern Australia (of about 2.5 ^oC) with little change in annual precipitation (0%), and,
2. CSIRO Mk3 (*drier*), submodel 1 – characterised by an increase in average annual temperatures over south-eastern Australia (of about 1.6 ^oC) and a decrease in average annual precipitation (-7%).

We ran simulations for current (1990-2009) and far-future (2060-2079) climate epochs. Planning for a changing climate with associated higher future fire risk will enable plantation owners to assess and undertake management options that will have the greatest reduction in risk under a changing climate. The 20 years of climate data were looped five times to allow the fire regime to play out over 100 years. Each scenario was replicated 25 times to cover variation in the runs given that many of the conditions are probabilistic.

2.4. Management strategies

In consultation with plantation owners from the six study landscapes, a series of potential management strategies were identified. Management strategies were designed around the themes of fire preparedness, fire response or fire prevention. A set of four potential management scenarios were defined for each region. These scenarios were compared to a 'current management' option and a 'no-management' option. Current management reflected a construction rate of 2 km/h and response time of between 15-45 mins for all ignitions, depending on the region, with prescribed burning (outside of plantations) set at a 5-year interval within Strategic Fire Advantage Zones and at minimum tolerable fire intervals based on the native vegetation in landscape burning areas. Each of these scenarios were explored for current (1990-2009) and far-future (2060-2079) epochs, and using the two global climate models (ECHAM5 and CSIRO Mk3).

3. Key findings & recommendations

3.1. Fuel curves for plantations

3.1.1. Softwood plantations (Pinus radiata)

We found that fuel curves derived from field data collected in plantations around Australia (hereafter termed 'new plantation' fuels) were much more nuanced than the 'traditional' fuel curves. Surface/near-surface fuel loads were consistently higher in the new plantation fuel curves (particularly in the first year or two of a rotation) suggesting that traditional fuel curves used in Phoenix may be under-predicting fuel accumulation, and therefore fire risk in plantations.

New plantation fuels for softwood plantations indicated that combined surface/near-surface fuel loads peak at age 0 at around 25 Mg ha^{-1}. This was followed by a sharp decrease to a low point of 5 Mg ha^{-1} at 5 years, followed by a near-linear growth until 14 years (to 15 Mg ha^{-1}) and a decrease in load until 24 years (12 Mg ha^{-1}). When compared to the traditional fuel function currently implemented in PHOENIX this translates to an increase in surface/near-surface fuels load under 5 years, and lower or similar loads from 5-30 years.

Elevated fuel loads for *P. radiata* peaked at 2.5 Mg ha^{-1} at around 8 years in the new plantation curve, followed by a steady decrease to approximately 0.5 Mg ha^{-1} at 20 years. While fuel loads are in the same range as the traditional fuel curve, the new plantation fuels were found to predict higher elevated fuel loads at younger ages than the traditional fuels, which predict a maximum of 1.8t/ha at approximately 15 years.

3.1.2. Hardwood plantations (Eucalyptus globulus)

Similar to the softwood plantation fuel curves, we found that fuel accumulation curves in hardwood plantations also differed from the traditional fuel curves, indicating more variability in the curves than previously suggested. For hardwood plantations, the new plantation fuel curves demonstrated that the combined surface/near-surface fuels started at ~6 Mg ha^{-1} and remained relatively stable until 10 years, before reaching a peak of 16 Mg ha^{-1} at 18 years. These values were higher than the traditional fuel curve which starts at 1.7 Mg ha^{-1} before reaching a maximum of 13.9 Mg ha^{-1} at 15 years.

Elevated fuels in the new plantation curves for *E. globulus* were found to be very low immediately post-harvest before reaching a peak of ~2.5 Mg ha^{-1} at 3 years. This was followed by a decrease to almost 0 Mg ha^{-1} from 7 years from which point fuel loads remained largely stable at less than 1 Mg ha^{-1}.

The new field-derived plantation fuel accumulation curves demonstrated that fuel loads in hardwood plantations were considerably higher than previously indicated by traditional Olson curves, especially in the surface/near-surface stratum between 0-7 years from planting.

Information about when fuel loads are at their highest will be important for plantation owners. This knowledge may help guide fuel management within plantations in an attempt to reduce future fire risk to their assets.

3.2. Fire risk profiles

Overall, impacts were greatest under the hotter (ECHAM5) climate prediction. Annual area burnt, annual area burnt by high intensity fire, and burn frequency were consistently higher under this model, and these effects were more pronounced in the northern study landscapes. This indicates that future climate predictions that are characterised by a larger increase in temperatures (i.e. >2.5 ^{o}C) with little change in annual precipitation, are likely to result in higher future fire risks for both plantation and other human assets.

In terms of the best management scenarios for reducing risks to plantation assets and adjacent communities, our results were largely consistent across the study landscapes. Increased suppression effectiveness (characterised by early detection and a response time of <15 minutes for all ignitions) and the current approach to management (a construction rate of 2km/h for suppression and 15-minute response times, with 4000ha/year of prescribed burning) were consistently the best management strategies (Figure 1B). Our results indicate that improving suppression response times and continuing the current rate of fuel management outside of plantations will offer the greatest scope for reducing future wildfire risks to plantation assets and adjacent communities. High pruning in strategic locations may also be worthy of future investment but should be considered in combination with more rapid suppression and prescribed burning.

4. Conclusions

In this study we found that fuel curves derived from field data collected in plantations around Australia were much more nuanced than traditional fuel curves. Surface/near-surface fuel loads were consistently higher in the new plantation fuel curves (particularly in the first few years of a rotation) indicating that traditional fuel curves used in PHOENIX may be under-predicting fuel accumulation, and therefore fire risk in plantations. We therefore recommend that the traditional Olson curves be replaced with the new plantation fuel curves for future fire risk modelling where plantations are present in the landscape of interest.

We found that future climate predictions characterised by larger increases in annual average temperatures with little change in annual precipitation were more likely to result in increased fire risks for both plantation and other human assets. This knowledge, combined with a new understanding of how fuel accumulates in plantations over time will help guide strategic fuel management in plantations.

Regarding the best use of resources for reducing fire risk to plantations under a changing climate, we found that increasing suppression response times and continuing the current approach to fuel management outside of plantations were the best strategies for reducing future impacts to plantations, regardless of the climate model used. Therefore, additional suppression resources and strategic positioning of these resources throughout the landscape (i.e. based on burn frequency maps and areas of high-risk plantations) will be an important area for future investment. Focusing on increasing early detection may also help reduce the risk of future losses. Plantation owners currently have little influence over the amount and location of prescribed burning adjacent to plantations, and fuel reduction burning is not regularly undertaken in Australian plantations. Therefore, rapid suppression response times is the single best investment for minimising impact to plantation assets under a hotter or drier climate.

A)

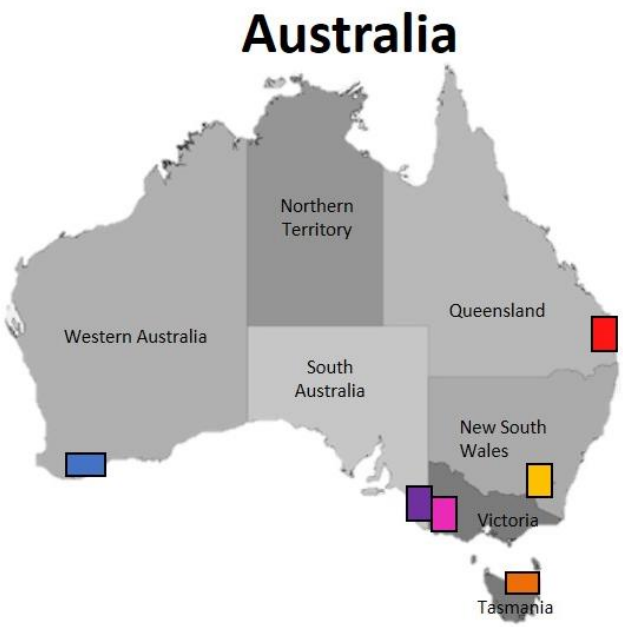

B)

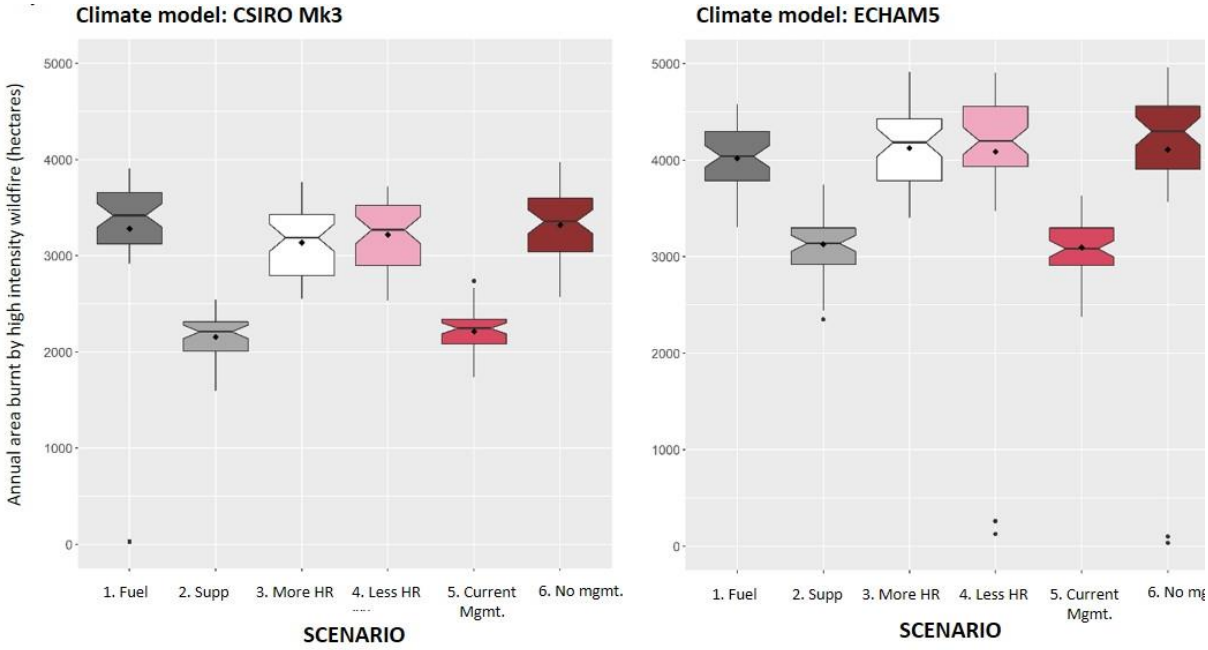

Figure 1- A) Map of Australia with the six study regions indicated by coloured boxes. B) Simulated future annual area burnt by high-intensity wildfire by management scenario and under two climate models (CSIRO Mk3 left; ECHAM5 right). Values are based on 25 replications over a 100-year simulation period and are presented as notched box plots with the mid-line indicating the median and non-overlapping notches indicating significant differences. Modelled scenarios were: 1. Fuel – surface/near-surface fuel loads reduced to 10t/ha throughout rotation and elevated fuels reduced within 1km of towns to reflect high pruning practices. 2. Reducing suppression response time (to an average of 10 minutes throughout each plantation region). 3. Increasing the amount of annual area burnt by prescribed fire outside of plantations (from 4000ha/year to 6000ha/year). 4. Reducing the amount of annual area burnt by prescribed burning outside of plantations (from 4000ha/year to 2000ha/year). 5. Current management approach (suppression resources set to reflect a construction rate of 2km/h and response time of 15 minutes for all ignitions, and prescribed fire outside of plantations at 4000ha/year). 6. No management – a 'do-nothing' approach (no fuel management within or outside of plantations).

5. References

Agee, J.K. & Skinner, C.N. (2005) Basic principles of forest fuel reduction treatments. Forest Ecology and Management, 211, 83-96.

Bartlett, A.J.A.f. (2012) Fire management strategies for Pinus radiata plantations near urban areas. Australian Forestry, 75, 43-53.

Berry, A.H., Donovan, G. & Hesseln, H. (2006) Prescribed burning costs and the WUI: economic effects in the Pacific Northwest. Western Journal of Applied Forestry, 21, 72-78.

Booth, T.H. (2013) Eucalypt plantations and climate change. Forest Ecology & Management, 301, 28-34.

Bowman, D.M., Balch, J.K., Artaxo, P., Bond, W.J., Carlson, J.M., Cochrane, M.A., D'Antonio, C.M., Defries, R.S., Doyle, J.C., Harrison, S.P., Johnston, F.H., Keeley, J.E., Krawchuk, M.A., Kull, C.A., Marston, J.B., Moritz, M.A., Prentice, I.C., Roos, C.I., Scott, A.C., Swetnam, T.W., van der Werf, G.R. & Pyne, S.J. (2009) Fire in the Earth system. Science, 324, 481-484.

Burrows, N., Woods, Y., Ward, B. & Robinson, A. (1989) Prescribing low intensity fire to kill wildings in Pinus radiata plantations in Western Australia. Australian Forestry, 52, 45-52.

Calkin, D.E., Gebert, K.M., Jones, J.G. & Neilson, R.P. (2005) Forest Service Large Fire Area Burned and Suppression Expenditure Trends, 1970-2002. Journal of Forestry, 103, 179-183.

Cruz, M.G., Alexander, M.E. & Plucinski, M.P. (2017) The effect of silvicultural treatments on fire behaviour potential in radiata pine plantations of South Australia. Forest Ecology and Management, 397, 27-38.

Fernandes, P.M., Vega, J.A., Jimenez, E. & Rigolot, E. (2008) Fire resistance of European pines. Forest Ecology & Management, 256, 246-255.

Finney, M., Grenfell, I.C. & McHugh, C.W. (2009) Modeling containment of large wildfires using generalized linear mixed-model analysis. Forest Science, 55, 249-255.

Flannigan, M.D., Krawchuk, M.A., de Groot, W.J., Wotton, B.M. & Gowman, L.M. (2009) Implications of changing climate for global wildland fire. International Journal of Wildland Fire, 18, 483-507.

Galizia, L.F.d.C. & Rodrigues, M. (2019) Modeling the influence of eucalypt plantation on wildfire occurrence in the Brazilian savanna biome. Forests, 10, 844.

Johnson, M.C. & Peterson, D.L. (2005) Forest fuel treatments in western North America: merging silviculture and fire management. The Bark Beetles, Fuels, Fire Bibliography, 126.

Matthews, S., Sullivan, A.L., Watson, P. & Williams, R.J. (2012) Climate change, fuel and fire behaviour in a eucalypt forest. Global Change Biology, 18, 3212-3223.

Penman, T., Ababei, D., Chong, D., Duff, T. & Tolhurst, K. (2015) A fire regime risk management tool. 21st International Congress on Modelling and Simulation. Gold Coast, Australia, pp. 270-276.

Penman, T., Christie, F., Andersen, A., Bradstock, R., Cary, G., Henderson, M., Price, O., Tran, C., Wardle, G., Williams, R. & York, A. (2011) Prescribed burning: how can it work to conserve the things we value? International Journal of Wildland Fire, 20, 721-733.

Wilson, A.E. & Wiitala, M.R. (2005) An empirically based model for estimating wildfire suppression resource response times. System analysis in forest resources: proceedings of the 2003 symposium. (eds M. Bevers & T.M. Barrett), pp. 189-194. U.S. Department of Agriculture, Forest Stevenson, WA.

Comprehensive Characterization of Pyrolysis and Combustion of Genista Salzmannii Needles (GSN) for Fire Hazard Analysis

Yassine Rahib*; Valérie Leroy-Cancellieri; Dominique Cancellieri; Carmen Awad ; Jean-Louis Rossi

SPE Laboratory, UMR-CNRS 6134, Campus Grimaldi, University of Corsica, BP 52, 20250 Corte, France
{rahib_y, leroy_v, cancellieri_d,_awad_c, rossi_j}@univ-corse.fr

**Corresponding author*

Keywords

Forest fuel, TGA-FTIR, Heating rate, Combustion indices, Kinetic analysis

Abstract

This article presents a first attempt of implementation of a lab-scale methodology proposed to describe the thermal decomposition behavior, and evolved volatile analysis of vegetative fuels using the TG-FTIR technique. Experiments within this method include testing the usual grinded form of samples compared to the intact form, which can render reliable and useful information to improve the understanding of the ignitability and combustibility of forest fuels. Moreover, slow (20 and 40 °C/min) and quasi-fast (60, 80 and 100 °C/min) heating rates were chosen to get close from the actual conditions of wildland fires (preheating/smoldering and flame region, respectively). In this work, we report the thermal decomposition behavior under inert (N2) and oxidative (air) atmospheres of Genista Salzmannii Needles (GSN) involved in high-intensity fires of Mediterranean forests. The results showed that the intact GSN were characterized by a higher mass loss rate compared to the grinded GSN. Furthermore, TG analyses were performed to assess thermal reactivity and combustion indices (ignition, devolatilization, combustion and burnout indices) of grinded and cut GSN samples at fives heating rates. The used set of the thermal indices are important properties to be determined when talking about efficient wildland fire management. As the heating rate increases, reactivity and combustion indices increase linearly. At low heating rates (20 and 40 °C/min), these parameters were quite similar for both samples, while the gap becomes more and more significant at elevated heating rates (60, 80 and 100 °C/min). High correlation coefficients (R2 > 0.96) were obtained, which indicate a good degree of fitting reliability between combustion characteristics and the tested heating rates. The determined slope can be used to compare and classify ignitability and combustibility of vegetative fuels related to fire risk potential. Based on the 3D-FTIR spectra, the dominant gases released during pyrolysis were CO2, C=O bond, C-H and C-O bond and H2O, while during combustion, CO2 and H2O were the major products. For kinetic investigations, activation energy (Ea) was calculated by means of two iso-conversional methods. The variation of Ea with the conversion rate has exhibited a quite similar behavior during the whole pyrolysis and combustion process. Char formation, at the end of an intense devolatilization, was the most complex process. The oxidation of the remaining char was characterized by a significant decrease of Ea and thus it was not considered as a major event in the combustion process.

1. Introduction

Due to the worrying climatic conditions and the high sensitivity of Mediterranean forests to fires, the evaluation of fuel hazard and fire risk gets more and more attention. The thermal decomposition of forest fuels is considered as the initial step of the forest fire process. Moreover, the determination of kinetic parameters of thermal degradation provides the necessary data for the development of realistic models *(Cancellieri et al. 2013)*. In studying forest fires, thermogravimetric analysis (TGA) was commonly used to investigate the thermal behavior and kinetics data of the decomposition process of vegetative fuels *(Leroy et al. 2006, 2010)*. Moreover, *Shu et al. (2021)* analyzed the combustibility and pyrolysis kinetics of forest combustibles and demonstrated their importance for fuels managing and forest fires prediction. However, few reliable experimental and modelling studies have examined the effect of different heating rate and sample sizes on the pyrolytic and combustion behavior and kinetics of forest fuels using TG-FTIR.

Genista Salzmannii is considered as an important vegetative fuel involved in fires of Mediterranean forests. This species is characterized by a very strong homogeneity and a 90% cover (Leroy-Cancellieri, 2014). Moreover, in a recent paper focus on an experimental and numerical investigation of prescribed fire on *Genista*

salzmannii, Fayad et al. (2022) highlight the high-intensity of wildland fire generate by this vegetation specie. As it has been demonstrated that only small fuel particles with diameter less than 6 mm, were supposed to contribute actively to fire spread *(Burrows, 2001)*, this study is focused on *Genista Salzmannii* Needles (GSN) which constitute the most of this plant.

So far, to authors knowledge, there has been no detailed investigation on the solid-phase thermal degradation behavior and kinetic analysis of GSN to support wildland fire research. This work is in this purpose. It was first focused on the investigation of thermal decomposition behavior and the evolved gas component during pyrolysis and combustion by TG-FTIR. Both grinded and cut GSN were investigated, and the effect of heating rate on thermal reactivity and combustion indices (ignition, devolatilization, combustion and burnout indices) was studied. Then, kinetic analyses were performed using two model-free methods at five heating rates of 20, 40, 60, 80 and 100 °C/min. Finally, the followed methodology and the obtained data were used to establish a database of forest fuels and will provide basic information for forest fuels management and fire modellings.

1.1. Test sample

The plant material under study, representing *Genista salzmannii*, was collected from the mountain forest in Letia region, France. The raw *Genista Salzmannii Needles* (GSN) were prepared (cut and grinded samples, see Figure 1) and dried in a forced air convection oven with a temperature of 60 °C to remove the external moisture part before the thermogravimetric tests. The grinded sample (< 600 µm) was selected for proximate analysis. Moisture (M), volatile matter (VM) and ash (A) content were determined according to EN14774-3:2009: E, EN15148:2009: E and EN14775:2009: E standards, respectively. The fixed carbon content was calculated by difference: FC (%) = 100% - (M+A+VM). The moisture content was 1.28 and 5.7% for grinded and cut sample, respectively. The result of proximate analysis, on a dry basis, was volatile (77.95%), fixed carbon (20.11) and ash (1.94%). The GSN has lower moisture and higher content of VM. The flaming zone could be the major step during combustion process. In addition, the ash content of GSN was very low. Ash in vegetative fuels retards flaming combustion and reduces the rate of VM release, which result in poor combustion performance and enhanced fire resistance *(Cai et al. 2017)*.

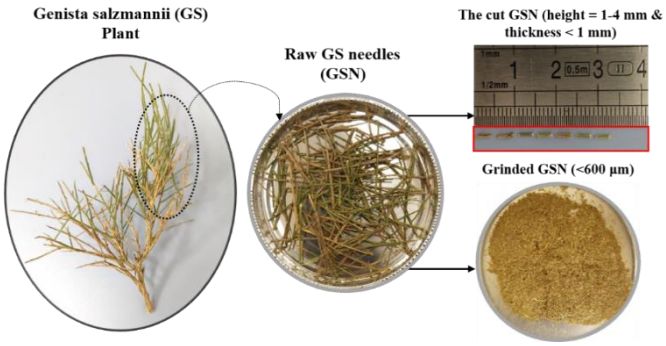

Figure 1- Grinded and cut GSN samples.

1.2. TG-FTIR analysis

Thermal decomposition behavior of grinded (< 600 µm) and cut (3-4 mm) samples of GSN was investigated by using a Perkin Elmer TGA 8000 analyzer. Air and N_2 atmospheres were used as the carrier gas with a flow rate of 30 ml/min. The gases evolved during pyrolysis and combustion were qualitatively monitored in real-time by coupling the TG instruments with a Fourier Transform Infrared (FTIR) spectrometer (Frontier, PerkinElmer, USA). The non-isothermal TG experiments with mass of about 15 ± 0.5 mg, placed in a ceramic crucible, were conducted from 35 to 1200 °C at different heating rates of 20, 40, 60, 80, 100 °C/min. During wildland fires, slow pyrolysis exists during preheating and/or smoldering combustion of vegetative fuels, while fast pyrolysis occurs in the flame zone. The selected heating rates conform to those adopted in the slow (20 and 40 °/min) and fast (60, 80 and 100 °C/min) pyrolysis *(Safdari et al. 2019)*.

1.3. Combustion characteristic indices

On the basis of TG-DTG data, characteristic parameters of thermal decomposition of vegetative fuel including the initial decomposition temperature (T_{id}), the ignition temperature (T_{ig}), the maximum mass loss rate temperature ($T_{DTG-max}$), the burnout temperature (T_b), their corresponding time (t_{id}, t_{ig}, $t_{DTG-max}$ and t_b,

respectively), the maximum and average mass loss rate (DTG_{max} and DTG_{mean}), and temperature and time interval at the half value of DTG_{max} in the descending and the rising part of the peak (ΔT and Δt, respectively) were determined. These parameters can be used to quantitatively evaluate the thermal reactivity (R) and combustion indices namely ignition characteristic index (ICI), devolatilization index (DI), combustion characteristic index (CCI) and burnout characteristic index (BCI) *(Xie et al. 2020; Liu et al. 2021; Wnorowska et al. 2021)*. The used equations were listed in Table. 1.

Table. 1-Thermal reactivity and combustion indices formulas.

$R = 100 * \sum \frac{\|DTG_{max}\|}{T_{DTG_{max}}}$	$ICI = \frac{\|DTG_{max}\|}{t_{peak} * t_{DTG_{max}}}$	$DI = \frac{\|DTG_{max}\| * \|DTG_{mean}\|}{T_{DTG_{max}} * T_i * \Delta T_{1/2}}$
$CCI = \frac{\|DTG_{max}\| * \|DTG_{mean}\|}{T_i^{\,2} * T_b}$	$BCI = \frac{\|DTG_{max}\|}{\Delta t_{1/2} * t_{DTG_{max}} * t_b}$	

1.4. Kinetic theory

The kinetic parameters provide required information to better understand the mechanisms controlling the thermal decomposition of vegetative fuels and for fire risk assessment. The kinetic analysis of GSN was carried out by using non-isothermal iso-conversional methods *(Álvarez et al. 2016)*. According to Arrhenius theory, the rate equation in terms of conversion (α) was represented as:

$$\frac{d\alpha}{dt} = Ae^{\frac{-E_a}{R.T}} f(\alpha)$$

where, α is the conversion degree ($\alpha = (m_0 - m_t)/(m_0 - m_f)$), A is the pre-exponential factor, E_a is the activation energy and f(α) is the reaction model. The model-free method as Flynn-Wall-Ozawa (FWO) was used to estimate the activation energy as follows:

$$\ln(\beta) = \ln\left(\frac{A.E_a}{R.G(\alpha)}\right) - 5.331 - 1.052\left(\frac{E_a}{R.T}\right)$$

A straight line was obtained by plotting log(β) versus 1/T and E_a can be estimated from the slope for each conversion $\left(slope = -1.052\left(\frac{E_a}{R.T}\right)\right)$. Another iso-conversional integral model-free method is Kissinger-Akahira-Sunose (KAS), which gives more accuracy or gives exact values of activation energy as compared with FWO. It was represented as follows.

$$\ln\left(\frac{\beta}{T^2}\right) = \ln\left(\frac{A.R}{E_a.G(\alpha)}\right) - \left(\frac{E_a}{R.T}\right)$$

Here, E_a can be estimated by plotting $\log(\beta/T^2)$ versus 1/T.

2. Results and discussion

2.1. Thermal decomposition of GSN

Figure 2 and 3 shows the TG-DTG profiles and a typical 3D-FTIR spectra of gas products from pyrolysis and combustion of grinded (a, b) and cut (c, d) GSN at different heating rates. It can be seen that pyrolysis process of both sizes can be divided into three stages constituting two peaks and one flat line. The first stage (< 180°C), corresponds to GSN self-rehydration and the release of light volatiles. The second stage (major mass loss) include the next peak (200-600 °C) was dominated by the degradation of hemicellulose, cellulose and partly by that of lignin (rapid pyrolysis). The last stage (> 600 °C) indicates the carbonization, where a small quantity of char (unreacted fixed carbon and ash particles) was remaining. Based on the different peaks wavenumbers, the prominent pyrolytic products were CO_2, carbonyl groups (C=O), aromatic rings (C=C), H_2O, CH_4, and C-H or C-O bond contained organics. The evolved gases were principally emitted between 200 and 600 °C, which was in agreement with TG data. In case of combustion, it was observed that after residual moisture removal the mass loss takes place in two steps: the first one corresponds to the devolatilization (oxidative pyrolysis), and the second one relates to the oxidation of char. The dominant gases released during oxidative pyrolysis zone (100-

400 °C) were CO_2, C=O, H_2O and C=C. The peak of aliphatic C-H was very low. At higher temperature (above 550 °C), char oxidation produces a large amount of CO_2 while the absorbance bands of C=O and C=C decreased. In addition, the absorbance peak of CH_4 appeared at 500 °C while the saturated C-H declined gradually. Overall, the char combustion process produces CO_2, H_2O, CH_4 and a small amount of CO.

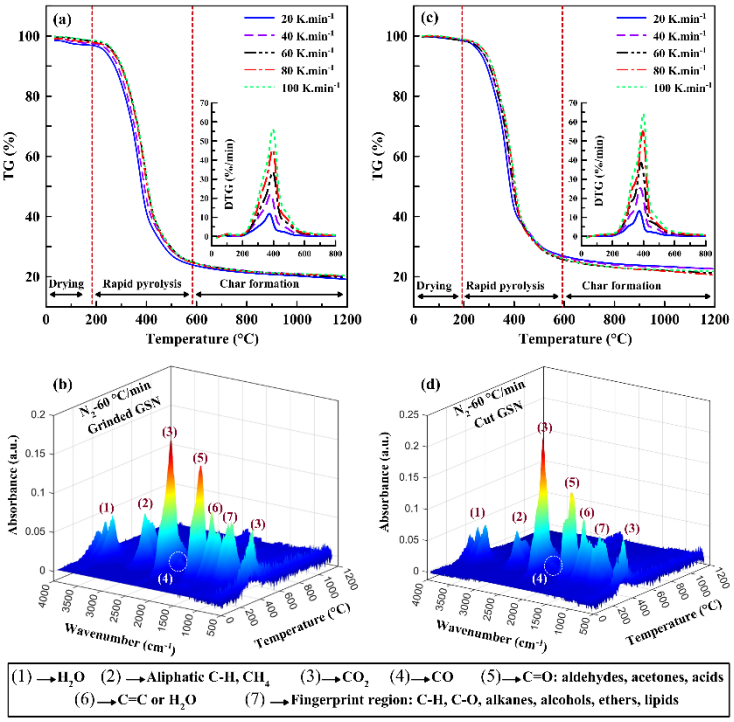

Figure 2-TG-DTG profiles and typical 3D-FTIR spectrum of the evolved volatile products from the pyrolysis of grinded (a, b) and cut (c, d) GSN.

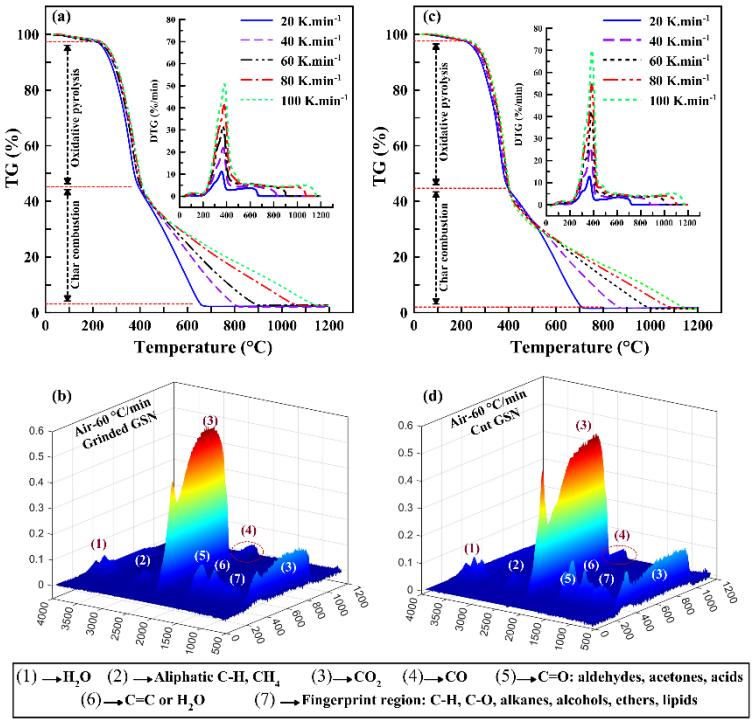

Figure 3- TG-DTG profiles and typical 3D-FTIR spectrum of the evolved volatile products from the combustion of grinded (a, b) and cut (c, d) GSN.

When the heating rate increased, the TG curves move towards high temperature region because of the limited heat transfer throughout and between particles *(Parthasarathy et al. 2021)*. Moreover, it can be observed from

the DTG curves that the width and the height of peaks were increasing with increasing heating rate. On the other hand, the observed thermal behavior of grinded and cut samples of GSN was compared. The difference of DTG peaks between grinded and cut samples was increasing with increasing heating rate. This can be explained by the control of heat and mass transfer limitations, which leads to improving the weight loss rate of cut samples. Moreover, the residence time of combustion at high heating rate was short, which often leads to ineffective heat and mass transfer within and among particles. Furthermore, the rapid pyrolysis zone of both samples become more homogenous at height heating rates (80 and 100 °C/min) because of the simultaneous degradation of some components, which effecting an overlapping of peaks/shoulders.

Figure 4 demonstrates the evolution of thermal reactivity (R) and the four combustion parameters (ICI, DI, CCI and BCI) as a function of heating rates. Correlation coefficients (R^2) were all greater than 0.96, indicating a high degree of fitting reliability between combustion parameters and the tested heating rates for grinded and cut samples of GSN. As the heating rate increases, all the calculated parameters increase linearly. At low heating rates (20 and 40 °C/min), the combustion indices values for grinded and cut GSN were quite similar. The gap becomes more and more significant at high heating rates (60, 80 and 100 °C/min). This can be explained by the fact that during the heating of the cut GSN (at higher heating rate), the limitations of heat transfer leads to inefficient heat flux transmission within the sample, and thus their accumulation on the open surfaces of the sample. This leads in turns to a very short ignition and combustion times, which improves ignition and combustion indices compared to grinded GSN.

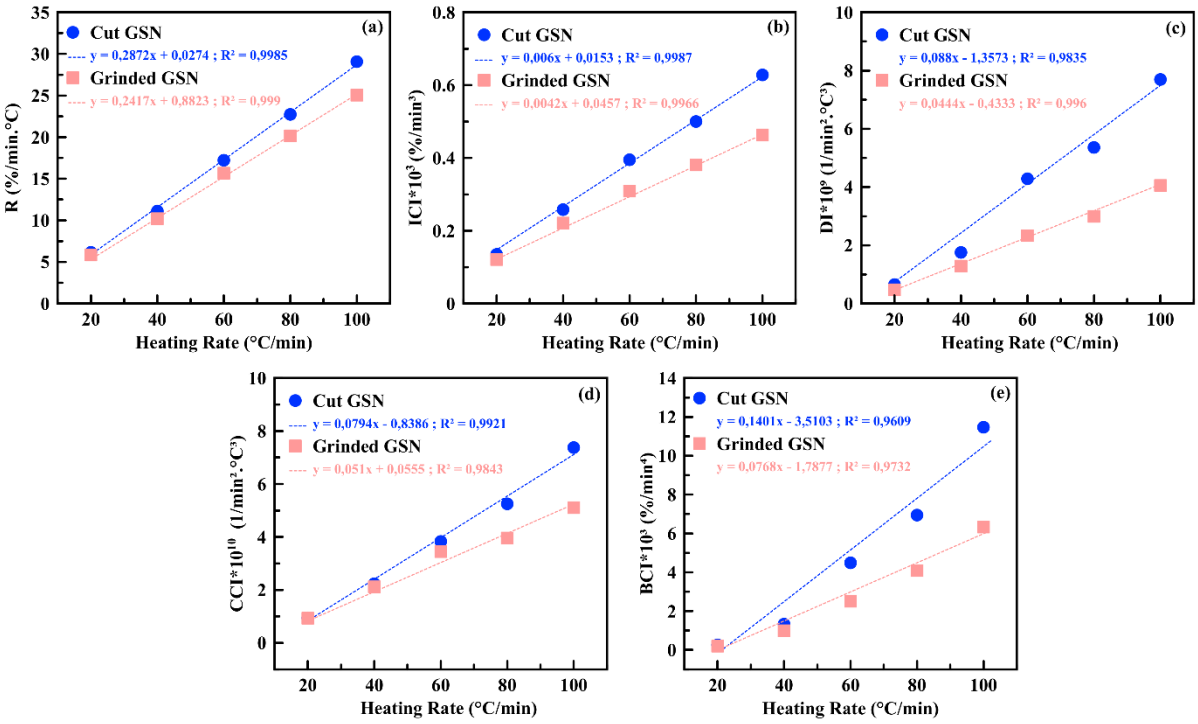

Figure 4- The relationship between R (a) ICI (b), DI (c), CCI (d) and BCI (e) and heating rates.

2.2. Kinetic analysis by model free methods

Understanding the thermal behavior and kinetics of vegetative fuels is very important for managing these resource materials and predicting forest fires. In the present study, the FWO and KAS models were used to evaluate the apparent activation energy (E_a) during pyrolysis and combustion of grinded and cut GSN samples at five heating rates. Figure 5 exhibits the E_a values for pyrolysis (a, b) and combustion (c, d) at different conversion degree. During pyrolysis (Figure 5a-b), it was observed that the E_a values for the cut GSN samples were higher as compared with grinded samples. The increased E_a in the conversion range of 0.05-0.35 was mainly caused by the hemicellulose decomposition. At $\alpha = 0.35$, the E_a values show a slight change until $\alpha = 0.75$ and represent the degradation of active cellulose. It is likely that pyrolysis reaction at $0.35<\alpha<0.75$ follow the same mechanism. Thereafter, a significant increase in the E_a values (especially for cut sample) was observed at the high conversion rate (0.8-0.9), followed by a rapid decrease at $\alpha = 0.95$. This can be explained by the fact that after the rapid pyrolysis reaction, solid char was formed gradually. A further volatilization of this material

(with low reaction activity) resulted in a remarkable activation energy increase (Chen et al. 2013). Moreover, the differences in the inherent structures of the produced char of grinded and cut GSN possibly account for the different pyrolysis behaviors at high conversion rates ($\alpha > 0.8$). Figure 5c shows the same behavior of E_a values at $0.05 < \alpha < 0.65$ during combustion of the grinded sample. A significant decrease of E_a at $\alpha > 0.65$ was due to the oxidation of remaining char, which was not considered as a major event (Rahib et al. 2020). Combustion of the cut sample (Figure 5d) at $0.55 < \alpha < 0.75$ displays a complex mechanism with negative E_a values, which indicates that devolatilization process was completed and the char was formed (Bhattacharyya et al. 2021). The reason behind this fact was probably due to the slow rate of degradation taking place at this juncture as indicated by the change of the TG curves slope in Figure 5d (see also Figure 3c). Moreover, the calculated correlation coefficients (R^2) at this region were very low, which means that the obtained E_a values were not reliable.

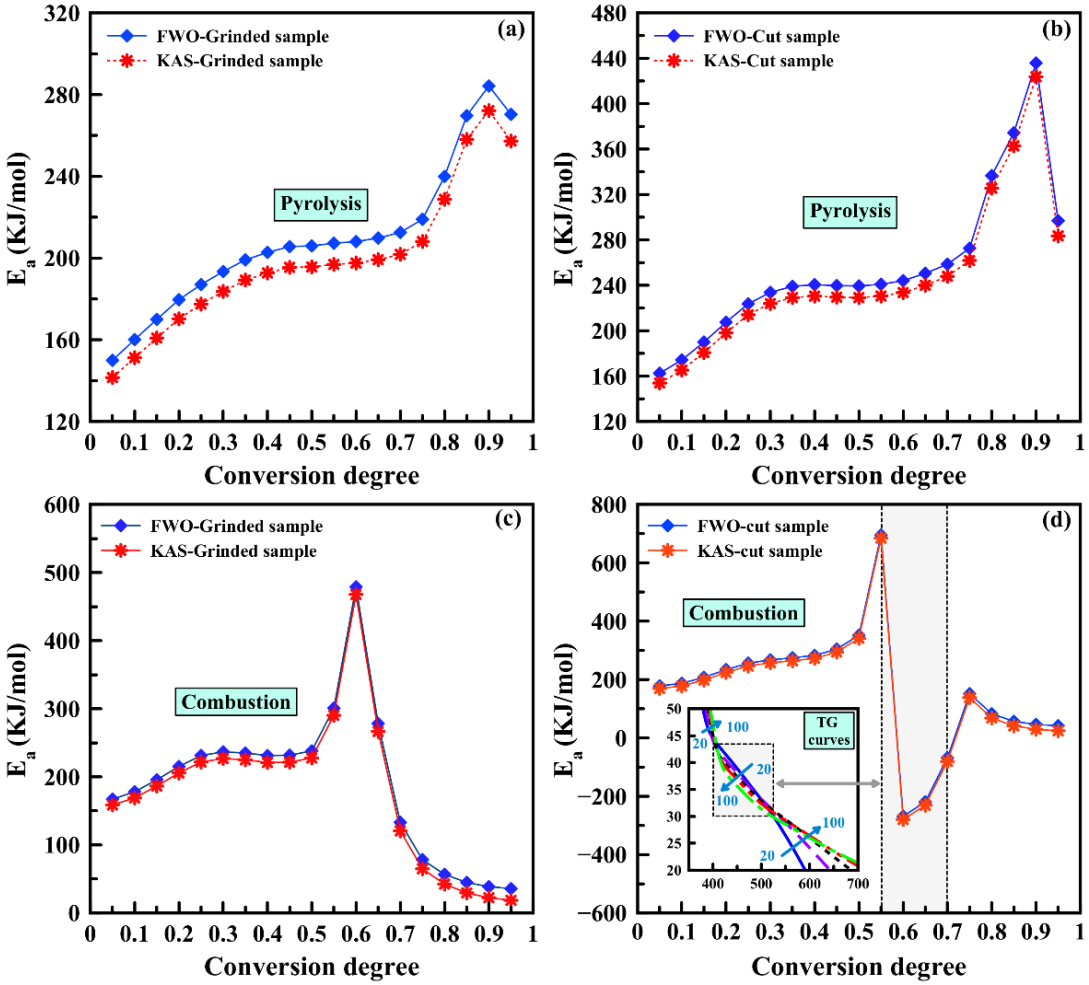

Figure 5- Estimation of E_a values according to FWO and KAS methods.

Generally, the verification of the whole chemical kinetics, controlling the thermal decomposition of forest fuel, is critical to ensure that the obtained parameters can be used in modelling the wildfire behavior. In perspective, the activation energy boundary obtained in this study by FWO and KAS methods will be compared with that obtained by model-fitting method to predict the most probable reaction mechanism. To go further into the improvement of kinetics analysis, a numerical optimization procedure will be applied in order to determine the adequate kinetic triplet.

3. References

Álvarez A, Pizarro C, García R, Bueno JL, Lavín AG (2016) Determination of kinetic parameters for biomass combustion. Bioresource Technology 216, 36–43. doi:10.1016/j.biortech.2016.05.039.

Bhattacharyya M, Shadangi KP, Mahanta P, Mohanty K (2021) Co-pyrolysis of coal-biomass: study on reaction kinetics and thermodynamics. Biofuels, Bioproducts and Biorefining 1–18. doi:10.1002/bbb.2333.

Burrows N.D. (2001) Flame residence times and rates of weight loss of eucalypt forest fuel particles. Int. J. Wildland Fire 10, 137–143, doi:10.1071/WF01005, 2001.

Cai J, He Y, Yu X, Banks SW, Yang Y, Zhang X, Yu Y, Liu R, Bridgwater A V. (2017) Review of physicochemical properties and analytical characterization of lignocellulosic biomass. Renewable and Sustainable Energy Reviews 76, 309–322. doi:10.1016/j.rser.2017.03.072.

Cancellieri D, Innocenti E, Leroy-Cancellieri V (2013) WinGPYRO: A software platform for kinetic study of forest fuels. Fire Safety Journal 58, 103–111. doi:10.1016/j.firesaf.2013.01.005.

Chen D, Zheng Y, Zhu X (2013) In-depth investigation on the pyrolysis kinetics of raw biomass. Part I: Kinetic analysis for the drying and devolatilization stages. Bioresource Technology 131, 40–46. doi:10.1016/j.biortech.2012.12.136.

Fayad J, Rossi L, Frangieh N, Awad C, Accary G, Chatelon F-J, Morandini F, Marcelli T, Cancellieri V, Cancellieri D, Morvan D, Pieri A, Planelles G, Costantini R, Meradji S, Rossi J-L (2022) Numerical study of an experimental high-intensity prescribed fire across Corsican Genista salzmannii vegetation. Fire Safety Journal 131, 103600. doi:10.1016/j.firesaf.2022.103600.

Leroy V, Augustin P, Filippi JB, Mari C, Fourmentin M, Bosseur F, Morandini F, Delbarre H (2014) Evaluation of wildland fire smoke plume dynamics and aerosol load using UV scanning lidar and fire-atmosphere modelling during the Mediterranean Letia 2010 experiment. Natural Hazards and Earth System Sciences 14, 509–523. doi:10.5194/nhess-14-509-2014.

Leroy V, Cancellieri D, Leoni E (2006) Thermal degradation of ligno-cellulosic fuels: DSC and TGA studies. Thermochimica Acta 451, 131–138. doi:10.1016/j.tca.2006.09.017.

Leroy V, Cancellieri D, Leoni E, Rossi JL (2010) Kinetic study of forest fuels by TGA: Model-free kinetic approach for the prediction of phenomena. Thermochimica Acta 497, 1–6. doi:10.1016/j.tca.2009.08.001.

Liu L, Pang Y, Lv D, Wang K, Wang Y (2021) Thermal and kinetic analyzing of pyrolysis and combustion of self-heating biomass particles. Process Safety and Environmental Protection 151, 39–50. doi:10.1016/j.psep.2021.05.011.

Parthasarathy P, Al-Ansari T, Mackey HR, McKay G (2021) Effect of heating rate on the pyrolysis of camel manure. Biomass Conversion and Biorefinery. doi:10.1007/s13399-021-01531-9.

Rahib Y, Sarh B, Bostyn S, Bonnamy S, Boushaki T, Chaoufi J (2020) Non-isothermal kinetic analysis of the combustion of argan shell biomass. Mater. Today Proc. 11–16. doi:10.1016/j.matpr.2019.07.437.

Safdari MS, Amini E, Weise DR, Fletcher TH (2019) Heating rate and temperature effects on pyrolysis products from live wildland fuels. Fuel 242, 295–304. doi:10.1016/j.fuel.2019.01.040.

Shu Y, Zhang J, Li W, Zhao P, Zhang Q, Zhou M (2021) Thermogravimetric analysis of the pyrolysis and combustion kinetics of surface dead combustibles in the Daxing'an Mountains. PLoS ONE 16, 1–16. doi:10.1371/journal.pone.0260790.

Wnorowska J, Ciukaj S, Kalisz S (2021) Thermogravimetric analysis of solid biofuels with additive under air atmosphere. Energies 14, 2257. doi:10.3390/en14082257.

Xie T, Wei R, Wang Z, Wang J (2020) Comparative analysis of thermal oxidative decomposition and fire characteristics for different straw powders via thermogravimetry and cone calorimetry. Process Safety and Environmental Protection 134, 121–130. doi:10.1016/j.psep.2019.11.028.

Designing an effective risk communication plan as a tool to reduce the risk associated with traditional burning practices in Portugal

Mayara Emilia Barbosa Souza*[1]; Abílio Pereira Pacheco[2,1]; Jorge Grenha Teixeira[1]; José Miguel Cardoso Pereira[3]

[1] INESC TEC and Faculty of Engineering of the University of Porto. Rua Dr. Roberto Fria, 378, 4200-465, Porto, Portugal, {msouza, app, jteixeira}@fe.up.pt
[2] ForestWISE, Collaborative Laboratory for Integrated Forest & Fire Management. Quinta de Prados, Campus da UTAD, 5001-801, Vila Real, Portugal, {abilio.p.pacheco@gmail.com}
[3] Forest Research Centre, School of Agriculture, University of Lisbon. Tapada da Ajuda, 1349-017, Lisbon, Portugal, {jmcpereira@isa.ulisboa.pt}

**Corresponding author*

Keywords

Rural fires, risk communication, traditional burning practices, mental models

Abstract

Climate change increases the average temperature and reduces precipitation, leading to an increased risk of rural fires around the world, but mainly in regions with a Mediterranean climate, such as Portugal. Despite the high risk of rural fires, fire is still a traditional land management practice. Beyond fire misused risk, the accumulation of fuel loads, due to the high population dispersion and lower interaction of communities with the land, also drives rural fires risks. Thus, researchers have sought to understand the key features of communication practices to achieve the most desired natural risk management results in relation to rural fires. According to the Committee on Risk Perception and Communication, in 1989, risk communication is defined as "an interactive process of exchanging information and opinions between individuals, groups, and institutions". However, there is a need for dialogue between the responsible for communication and relevant stakeholders. The Carnegie Mellon mental-models approach encompasses participatory processes to translate the nature and magnitude of the risk, allowing for a deeper understanding of what can be done to mitigate social and environmental impacts in the future.

Considering rural fires risks and risk communication challenges, this study aims to design an effective risk communication plan oriented to the rural population, in the context of rural fires. For this objective to be achieved, the mental models approach was developed, exploring the underlying reasons for resistance to behavioral change and defining guidelines to support the design of new risk communication strategies, including the dissemination of new behaviors and practices that mitigate the ignition of rural fires.

This systemic approach has been applied and tested in the rePLANT project, whose purpose is the development of research activities, innovation and transfer of knowledge and technology, to increase sustainable forest management, the competitiveness of the Portuguese forestry sector and reduce the impact of rural fires. Preliminary findings show what must be communicated about rural fires risk, how must be communicated, target audiences' profiles, the role of actors for effective risk communication on rural fires, attributes of good risk communication on rural fires, evaluation of the risk communication results.

Finally, it is expected that this research provides guidelines to help decision-makers and stakeholders to design an effective risk communication plan oriented to prevent traditional burning practices, as well as to mitigate socioeconomic and environmental impacts in the future. This approach also highlights the importance of exploring the underlying reasons for resistance to behavioral change and defining guidelines to support the design of new risk communication strategies.

1. Introduction

Climate change has been affecting society and nature in an intense and progressive way over the last few years (Shukla et al. 2019). The increase in the average temperature and the significant reduction in precipitation led to an increased risk of rural fires around the world, but mainly in regions with a Mediterranean climate, such as Portugal (Nunes et al. 2021). Despite the high risk of rural fires, fire is still a traditional land management tool,

used for the elimination of residual materials from agricultural and forestry activities, and cleaning method to eliminate of excess biomass in the control of invasive species (Nunes et al. 2021; Meira Castro et al. 2020; Pereira et al. 2013). Beyond the risk of fire misuse, the accumulation of fuel loads, due to the high population dispersion and lower interaction of communities with the land, also contribute to increase the rural fires risks.

These challenges motivated the launch of a set of legislative measures that seek to promote the management, cleaning, and control of these species (Nunes et al. 2021), such as Decree-Law 14/2019 which make burning prior communication and authorization mandatory. Although the efforts, the risk of rural fires stems in part from the absence of effective management policies aimed at rural areas (Coelho et al., 2020). Still, implementing risk-based long-term planning improve fire management efforts (Turco et al., 2019).

Thus, researchers have sought to understand the key features of best communication practices to achieve the most desired natural risk management results in relation to wildfires (Steelman and McCaffrey, 2013). In the past, the term "risk communication" was considered a one-way process of disclosing messages in which experts assumed the role of transmitters and, in turn, laypeople assumed the role of recipients of messages. However, this unidirectional character of messages within the scope of risk communication began to be understood as too limiting. According to this perspective, the Committee on Risk Perception and Communication, in 1989, presents a distinction between the terms "risk messages" and "risk communication", exposing this the latter as "an interactive process of exchanging information and opinions between individuals, groups and institutions" (Committee on Risk Perception and Communication, 1989, p. 2).

Morgan et al. (2002) retrieve Fischhoff (1990), Gibson (1985), Gow and Orway (1990) to define the concept of risk communication, considering it as the communication whose purpose is to provide lay individuals with the information necessary for them to be capable of making independent and informed decisions about risks in the field of health, safety and the environment. However, there is a need for dialogue between the responsible for communication and the set of stakeholders (Palenchar, 2005). Stakeholder participation in the risk assessment and management process can enable not only improve the quality of decision-making, but it can also avoid harmful confrontations between the entities and the community (Renn, 2010). Mental models approach encompasses participatory processes to translate the nature and magnitude of the risk, allowing for a deeper understanding of what can be done (Morgan et al. 2002) to mitigate social and environmental impacts in the future.

Considering the rural fires risks and risk communication challenges, this study aims to design an effective risk communication plan oriented to the rural population, in the context of rural fires. For the objective to be achieved, a systemic approach was developed, exploring the underlying reasons for resistance to behavioral change and defining guidelines to support the design of new risk communication strategies, including the dissemination of new behaviors and practices that mitigate the ignition of rural fires.

2. Method

According to Fraser and Gondim (2004) "in the qualitative approach, what is intended, in addition to knowing the people's opinions on a given topic, is to understand the motivations, meanings and values that support opinions and worldviews. In other words, it is giving voice to the other and understanding from what perspective does he speak". In this sense, the qualitative research approach is predominantly present in this study, combining participatory processes (such as interviews, dynamic interactions to build mental models, focus groups) and ethnographic (such as on-site visits and observations) to design an effective risk communication plan oriented to prevent rural fires in Portugal. Additionally, the quantitative approach was employed in the mapping and definition of lay sampling zones, through the application of Non-Parametric Multi-Criteria Analysis (Vego et al. 2008).

This systemic approach is divided into three main stages: understanding the expert perspective, understanding the context, and designing the solution, and six milestones, as shown in Figure 1. The research design involved mapping and defining the sample, identifying potential participants to be interviewed (including actors from industries, public entities, academics, the third sector, and society), developing the data collection instrument (semi-structured interview scripts), systematizing data collection with different actors (mental models development in a digital visual collaboration platform) on the risk of rural fires.

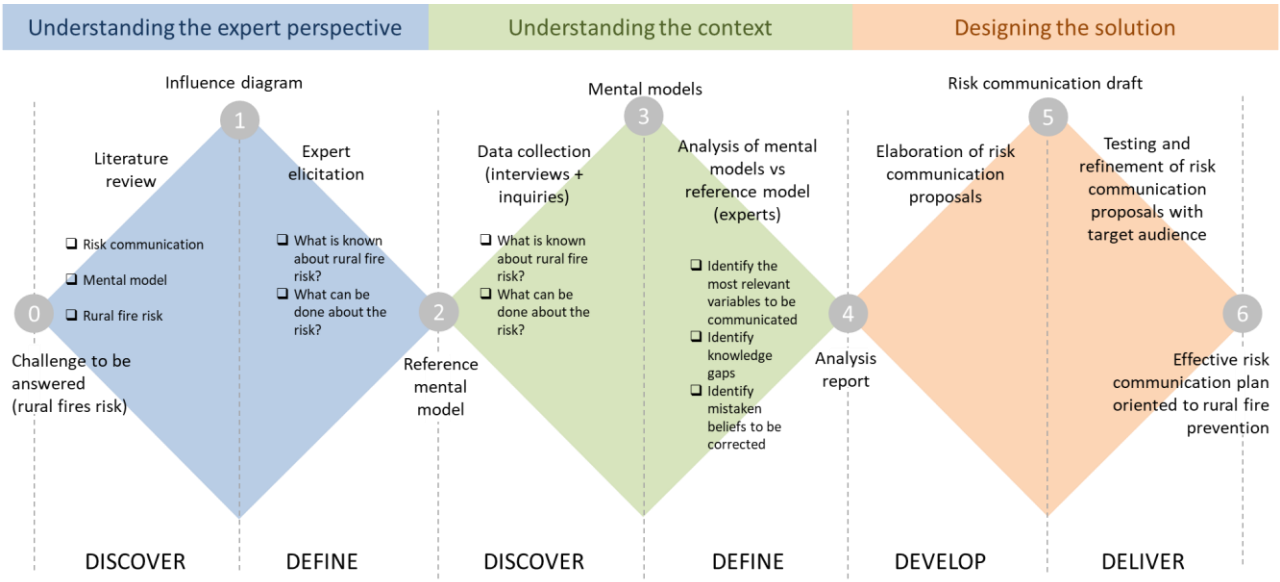

Figure 1- Systemic approach to design an effective risk communication plan oriented to mitigate the impact of traditional burning practices in rural fires

Overall, understanding the expert perspective stage included the literature review and expert elicitation to build the reference mental model. Literature review encompasses topics on risk communication, mental models and rural fires that enable in-deep understanding of the topics, especially regarding the best practices of risk communication, crucial tasks to develop an effective mental model and associated factors of rural fires risk, including risky behaviors and practices. Additionally, the bibliographic review established methodological premises to study development, being the first one is the mental model's elaboration, commonly represented by an influence diagram (Morgan et al. 2002).

Part of the expert elicitation consists of experts giving their contributions and comments regarding the mental model under construction. The experts' contributions are periodically validated by the research team and incremented in the reference mental model to translate the aggregated knowledge of the expert community regarding rural fires risk, behaviors, and practices to mitigate the ignition of rural fires.

Once concluded the reference mental model, Non-Parametric Multi-Criteria Analysis (Vego et al. 2008) was employed to map and define the lay sampling zones, as previously said. In this mapping, criteria were used, such as: Municipalities Council involved in the Forest Intervention Zones of Vale do Sousa; respective municipalities, districts, codes, terrain typologies and demographic data; analysis of occurrences associated with burning - last 3 to 5 years; construction of indicators for sample selection.

The understanding of the context stage begins with the data collection in the field through interviews with rural residents to understand their beliefs and perception about the impact of traditional burning practices in rural fires hazard, expressed in their own terms. Interview protocol was shaped by the expert mental model, so it allows for the expression of correct and incorrect beliefs (Morgan et al. 2002). However, to enrich the research at the beginning of this stage, participatory components such as focus groups and on-site visits and observations were added to compose the original Carnegie Mellon mental-models approach that we have been followed.

The data collected was transcribed, coded, and analyzed following a thematic analysis approach. We use software to support this process, NVivo. Once the results are summarized, the responses from interviews with rural residents will be analyzed in term of how well these mental models correspond to the expert model captured in the influence diagram (identify the most relevant variables to be communicated, identify knowledge gaps, identify mistaken beliefs to be corrected).

In addition, it will be applied inquiries to groups sampled from the intended audience to validate the mental model final analyses. This confirmatory questionnaire includes items captured about the beliefs expressed in the open-ended interviews and experts' model. The main purpose of this step is to estimate the population prevalence of these beliefs (Morgan et al. 2002).

Finally, the design solution stage encompasses three steps: elaboration of risk communication proposals which are presented as a risk communication draft, after the testing and refinement of risk communication proposals with the target audience, an effective risk communication plan oriented to rural fire prevention is concluded.

3. **Preliminary findings and work in progress**

We sought to present the systemic approach designed to build an effective risk communication plan to prevent traditional burning practices in Portugal. This systemic approach has been applied and tested in the first major project of initiative and operationalization of the ForestWISE Collaborative Laboratory – Collaborative Laboratory for Integrated Forest and Fire Management, called rePLANT, whose purpose is the development of research activities, innovation and transfer of knowledge and technology, to increase sustainable forest management, the competitiveness of the Portuguese forestry sector and reduce the impact of rural fires.

However, it is important to emphasize the original Carnegie Mellon mental-models approach have been amplified in this study, with the employment of participatory components (focus groups and on-site visits and observations), and quantitative elements (Non-Parametric Multi-Criteria Analysis), which supported deepening the knowledge of underlying reasons for resistance to behavioral change and defining guidelines to support the design of new risk communication strategies.

Preliminary findings show some themes resulted from the data analysis, between them: what must be communicated about rural fires risk, how must be communicated and attributes of good risk communication on rural fires, target audiences' profiles, the role of actors for effective risk communication on rural fires, evaluation of the risk communication results. Table 1 shows these themes and some respective quotes.

Table 1 - Preliminary findings (themes resulted from the data analysis and quotes)

What must be communicated about rural fires risk	*(…) "if I'm going to communicate, I have to tell people what depends on them so that things go well. They cannot change the day, they cannot change the temperature of the day, they cannot change humidity, they cannot stop the wind. But they can make strips, they can put little vegetation so they don't burn too hard. That's why I would say that here in a communication strategy, the person has to be responsible for what he has control over and he has to pay attention to what he has no control over. And in risk communication, I think this is very important, making people realize that they have to act on the factors over which they have control".* (Regional Coordinator at a public institute that seeks to increase the protection of people, their property and reduce the impact of rural fires)
How to communicate and attributes of good risk communication on rural fires	*" I think proximity, because this works better if it is done locally, by local people, with local bodies, because obviously a massive campaign, as Portugal now calls it, obviously affects a part of the population that does these practices, it touches in some points, but I think it doesn't reach everyone, it's not like that, so accurate for this type of... or rather, a solution for this type of target audiences. I think this has to be much more worked on locally, with the action of local producers, with the association of farmers, with the parish councils, with the councils, it has more to be with this type of local solutions".* (Wood Regulation & Sustainability Manager at one of the main producers of wood-based panels in the world)
Target audience profiles	*"There are several target audiences, not everything is the same, the message should not be the same for everyone".* (Lieutenant Colonel at a security force of a military nature from Portugal) *"Communication must not only respond to this aging process, but at a later stage, it must respond to those who will succeed them".* (Executive Director at Forestry Association of Portugal)
The role of actors for effective risk communication on rural fires	*"We contribute to, we are not the entity that generates awareness-raising actions, but we contribute to. AGIF does it in terms of general communication, in strategic terms, it gives the guidelines, because in the past it was the ICNF that was the responsible entity. All entities carry out awareness-raising actions at their various levels. We also do it,*

	and this is important because we reach the population, the municipality, the parish and explain to the elderly, how it should be done, the risks they have, the impact they may have on these burnings". (Lieutenant Colonel at a security force of a military nature from Portugal) *"The presidents of the Municipality Council, in regions like ours, have a preponderant role in the transmission of this type of messages, even the priest, so it ends up being.... Then obviously, as the message passes, the more informal spaces such as cafes and communities turn out to be good places to spread the word, and people pass on this message of responsibility for the use of fire and the need to communicate its use".* (Forestry Technician at a consulting and technical support company, investment management and the execution of agroforestry work) *"And that's another issue that we're really bad at, and that's alignment. it's like saying "Okay, there is all this, and we have to give all this to people so they can understand in 360 degrees the problem. And how do I have to do it?" And that too fails. And then each authority, each technician who is responsible for a given matter, always thinks that his or her own will definitely contribute to the solution of the problem, and is unable to bridge the gap with the other. I make a parenthesis again, that I think this is changing, but it is changing very slowly, that should have changed a long time ago".* (Executive Director at Forestry Association of Portugal)
Evaluation of the risk communication results	*"You have to listen the person on the other side, he has to say what he perceived from the message and what he really understands from this message, if he agrees, if he does not agree, if he thinks it should be different, if there was another way to do it".* (Head Forestry Innovation and Development at a Portuguese pulp and paper company) *"(...) very little has been done to evaluate the results of the many information campaigns that have been carried out. And one thing is done, which in my view is profoundly wrong, and that is to measure the success of a campaign by counting how many tens of thousands of pamphlets have been distributed. And that's the effort made, and how much money was spent. This is the effort made, this is the cost. What was the benefit? What has been gained? To what extent have behaviors changed? Very little is known. And this is a fundamental aspect".* (Full Professor and Ph.D. Natural Resources) *"The truth is that the number of fires in Portugal has decreased a lot, the number of ignitions has decreased. I mean, today it's a third of what it was 20 years ago. Now... as there are no studies on this, we don't know if this is behavior change, per se, that is, more care, more prevention, more awareness-raising results, or prevention results, or campaigns, we don't know if that's it. , or if it's simply changes in, say, lifestyle".* (Associate Professor and Ph.D. Forest Sciences)

We are currently in the context understanding phase, which we have already been carried out two focus groups sessions and also on-site visits and observations. These activities are the firsts steps to start collecting data in the field, that precede the interviews with rural residents to understand their beliefs about the impact of traditional burning practices on rural fire risk, expressed in their own terms.

Finally, it is expected with this research to provide guidelines of a systemic approach to help decision-makers and stakeholders to design an effective risk communication plans oriented to prevent burning practices, as well as socioeconomic and environmental impacts in the future. This approach also highlights the importance of exploring the underlying reasons for resistance to behavioral change and defining guidelines to support the design of new risk communication strategies, including the dissemination of new behaviors and practices that mitigate human caused rural fires.

4. References

Coelho, Sílvia, Sandra Rafael, Miguel Coutinho, Alexandra Monteiro, João Medina, Susana Figueiredo, Sofia Cunha, Myriam Lopes, Ana Isabel Miranda, and Carlos Borrego. 2020. "Climate-Change Adaptation Framework for Multiple Urban Areas in Northern Portugal." Environmental Management 66 (3): 395–406. https://doi.org/10.1007/s00267-020-01313-5.

Fraser, M. T. D.; Gondim, S. M. G. Da fala do outro ao texto negociado: discussões sobre a entrevista na pesquisa qualitativa. Paidéia, v. 14, n. 28, p. 139-152, 2004.

Meira Castro, Ana C., Adélia Nunes, António Sousa, and Luciano Lourenço. 2020. "Mapping the Causes of Forest Fires in Portugal by Clustering Analysis." Geosciences 10 (2): 53. https://doi.org/10.3390/geosciences10020053.

Morgan MG, Fischhoff B, Bostrom A, Atman CJ. Risk Communication: A Mental Models Approach. Cambridge, MA: Cambridge University Press, 2002.

National Research Council, Committee on Risk Perception and Communication. 1989.Improving risk communication. National Academy Press, Washington, DC.

Nunes, L.J.R.; Raposo, M.A.M.; Pinto Gomes, C.J. A Historical Perspective of Landscape and Human Population Dynamics in Guimarães (Northern Portugal): Possible Implications of Rural Fire Risk in a Changing Environment. Fire 2021, 4, 49. https://doi.org/10.3390/fire4030049

Palenchar, M. J., Heath, R. L., & Orberton, E. M. (2005). Terrorism and industrial chemical production: A new era of risk communication. Communication Research Reports, 22(1), 59-67.

Pereira, Mg, Tj Calado, Cc DaCamara, and T Calheiros. 2013. "Effects of Regional Climate Change on RuralFires in Portugal." Climate Research 57 (3): 187–200. https://doi.org/10.3354/cr01176.

Renn, O. (2010). The contribution of different types of knowledge towards understanding, sharing and communication risk concepts. Catalan Journal of Communication & Cultural Studies, 2(2), 177-195.

Shukla, P. R. ; Skeg, J. ; Calvo Buendia, E. ; Masson-Delmotte, V. ; Pörtner, H.-O. ; Roberts, D. C. ; Zhai, P. ; Slade, R. ; Connors, S. ; van Diemen, S. ; Ferrat, M. ; Haughey, E. ; Luz, S. ; Pathak, M. ; Petzold, J. ; Portugal Pereira, J. ; Vyas, P. ; Huntley, E. ; Kissick, K. ; Belkacemi, M. & Malley, J. (eds.) (2019). Climate Change and Land: an IPCC special report on climate change, desertification, land degradation, sustainable land management, food security, and greenhouse gas fluxes in terrestrial ecosystems.

Steelman, T. A., & McCaffrey, S. (2013). Best practices in risk and crisis communication: Implications for natural hazards management. Natural hazards, 65(1), 683-705.

Turco, Marco, Sonia Jerez, Sofia Augusto, Patricia Tarín-Carrasco, Nuno Ratola, Pedro Jiménez-Guerrero, and Ricardo M. Trigo. 2019. "Climate Drivers of the 2017 Devastating Fires in Portugal." Scientific Reports 9 (1): 13886. https://doi.org/10.1038/s41598-019-50281-2.

Vego, G., Kučar-Dragičević, S., & Koprivanac, N. (2008). Application of multi-criteria decision-making on strategic municipal solid waste management in Dalmatia, Croatia. Waste management, 28(11), 2192-2201.

Effect of Fuel Bed Structure on the Controlling Heat Transfer Mechanisms in Quiescent Porous Flame Spread

Zakary Campbell-Lochrie*[1]; Carlos Walker-Ravena[1]; Michael Gallagher[2]; Nicholas Skowronski[3]; Eric V. Mueller[1]; Rory M. Hadden[1]

[1]The University of Edinburgh. Edinburgh, UK,
{z.campbell.lochrie, c.walkerravena, R.Hadden}@ed.ac.uk, {ericvmueller@gmail.com}
[2]Northern Research Station. USDA Forest Service. New Lisbon, NJ, USA {Michael.r.gallagher@usda.gov}
[3]Northern Research Station. USDA Forest Service. Morgantown, WV, USA
{Nicholas.s.skowronski@usda.gov}

**Corresponding author*

Keywords

Flame spread, fuel structure, heat transfer, fire modelling, thermal model

Abstract

The increasing importance of prescribed fire use has led to an increased focus on the development of modelling tools suited to conditions typical of prescribed fire scenarios. An improved understanding of flame spread through porous surface fuels represents an important part of these efforts. In the lower wind speed conditions typical of many prescribed burns, the role of fuel structure may be of greater importance than in highly wind-aided flame spread scenarios. The porous nature of wildland fuel beds complicates efforts to apply existing, solid surface theories for flame spread in low or quiescent wind conditions as radiation, convection and conduction may all occur within the porous fuel in addition to flame heating. An important first step in the development of any flame spread theory is the identification of the dominant heat transfer mechanisms but for wildland fuels the effect of fuel structure on the relative importance of different heating mechanisms must be considered. To investigate the role of fuel structure we therefore present a series of laboratory-based flame spread experiments conducted in pine needle fuel beds with various structural properties. The fuel loading and bulk density were independently varied by controlling fuel bed height with water-cooled heat flux gauges used to measure the (radiant and total) heat flux from both the above-bed flame and the in-bed combustion region. A single dimensionless parameter ($\alpha\sigma\delta$), incorporating the fuel bed porosity (α), fuel element surface-to-volume ratio (σ), and fuel bed height (δ), was used to describe the overall fuel bed structure. The heat flux measurements highlighted the dominant role of in-bed heating across all of the studied fuel conditions although the magnitude of above-bed flame heating increased with increasing fuel loading. Heat fluxes from the in-bed combustion region exceeded those from the above-bed flame region with the magnitude of the peak (radiant and total) heat flux at each measurement location generally increasing with increasing $\alpha\sigma\delta$ across the studied range ($\alpha\sigma\delta = 49\ to\ 399$). However, the effect of fuel loading was also apparent with a positive relationship also observed between fuel loading and flame height. The experimentally observed effective heating distances also varied with bulk density and fuel loading and were used to evaluate the use of a thermal modelling approach incorporating the bulk structural properties of the porous fuel bed. Comparison with experimental observations of spread rate indicated a maximum variation in predicted spread rate of 29 % where only radiative transfer from the in-bed combustion region was considered, with closer agreement at lower ασδ values. Where the contributions of both the in-bed and above-bed heat transfer mechanisms were considered, the need to incorporate additional heat loss terms into this thermal model were apparent. This study therefore emphasises the important role of porous fuel structure on the in-bed heat transfer and assesses suitable, physically meaningful structural descriptors. The experiments presented in this study will also provide a valuable dataset for future model development efforts incorporating measurements of fire behaviour and underlying physical phenomena across a wide range of structural conditions.

1. Introduction

Flame spread dynamics in quiescent/low-wind conditions typical of many prescribed fire scenarios differ compared to wind-driven wildfires particularly as the dominant heat transfer modes may change, altering the pre-heating of fuels ahead of the flame front. Differences in fire behaviour challenge existing model tools (Hiers *et al.*, 2020) and have motivated recent physics-based model development efforts (Gallagher *et al.*, 2021). However, semi-empirical models (e.g. Rothermel's model) underpin many simulation models (Andrews, 2018).

Rothermel's model (Rothermel, 1972) involves application of the energy conservation principle to a unit volume of fuel ahead of the flame front. This results in an expression for the rate of spread equal to the ratio between the propagating heat flux and the net heat required for ignition of the fuel. In the development of the Rothermel model, an analytical solution of this energy balance could not be made as the heat transfer mechanisms associated with these heat flux terms was unknown therefore the development of empirical terms was required for model closure.

Identification of the dominant heat transfer mechanism(s) is an important first step in the development of any flame spread theory (Williams, 1977). The porous structure of wildland fuels allows radiative and convective heat transfer to occur within the fuel bed. Appropriate descriptors of porous fuel bed structure which can be related to variations in both above-bed and in-bed heat transfer processes are therefore required. Several studies have measured heat fluxes in/near wildland fuels however analysis of the relative importance of heat transfer mechanisms and the effect of fuel structure is restricted by the wide variety of measurement types and locations limiting inter-study comparisons (Frankman *et al.*, 2010).

In the present study, heat transfer in pine needle fuel beds (heat fluxes from both from the trailing combustion region and the overhead flame) were investigated experimentally. Fuel loading and bulk density were independently varied by controlling the fuel bed height with fuel bed structure also described by the dimensionless parameter $\alpha\sigma\delta$ which incorporates porosity (α), surface-to-volume ratio (σ), and fuel height (δ) (Campbell-Lochrie *et al*, 2021). A simple thermal modelling approach, incorporating the experimentally measured heat fluxes and heating distances, is used to explore the relative importance of different heating sources.

2. Methods

Experiments involved a flame spread table (1.5 m by 0.67 m) with vermiculite substrate and insulated sidewalls (extending 0.03 m above fuel height). Gas phase temperature measurements (0.25 mm dia. K-Type thermocouples) and video analysis enabled characterisation of fire behaviour (spread rate, flame height). Heat Release Rate (HRR) was calculated using oxygen consumption calorimetry. 10 ml of acetone, distributed equally over a 0.67 m length of alumina-silica fibre, provided a line ignition source.

Heat fluxes from the flame and the in-bed combustion region were measured using water-cooled heat flux gauges (calibrated up to 100 kW/m^2). Windowed (sapphire lens with spectral transmission range of 0.2 – 5.5 µm) and exposed gauges were co-located to measure radiant and total heat flux respectively. Two different experimental setups were employed (as shown in Figure 1) allowing measurement of both horizontal heat flux through the fuel bed and vertical heat fluxes to/through the fuel bed.

The first series involved four heat flux gauges (two pairs of co-located windowed and exposed gauges) positioned vertically (sensor face parallel to fuel bed surfaces) at a horizontal distance of 1.3 m from the ignition line (0.2 m from the end of the fuel bed). One pair was positioned flush to the table surface (exposed to above-bed flame heating) while the second pair was positioned flush with the fuel bed surface (exposed to both above-bed and in-bed heating). In-bed thermocouples were positioned at a distance of 0.3 m, 0.6 m and 0.9 m from the ignition line.

In the second series, two heat flux gauges (windowed and exposed pair) were used. Gauges were positioned to measure the horizontal heat flux (sensor face perpendicular to fuel bed surfaces) and located within the fuel bed (midpoint of the gauge at a height of 12.7 mm above the table surface). Gauges primarily measured heat fluxes from the in-bed combustion region transferred horizontally through the fuel bed. Gauges were located at a horizontal distance of 0.9 m from the ignition line (0.6 m from the end of the fuel bed). Above-bed thermocouples were positioned at distances of 0.6 m, 0.8 m, 0.85 m and 0.9 m from the ignition line.

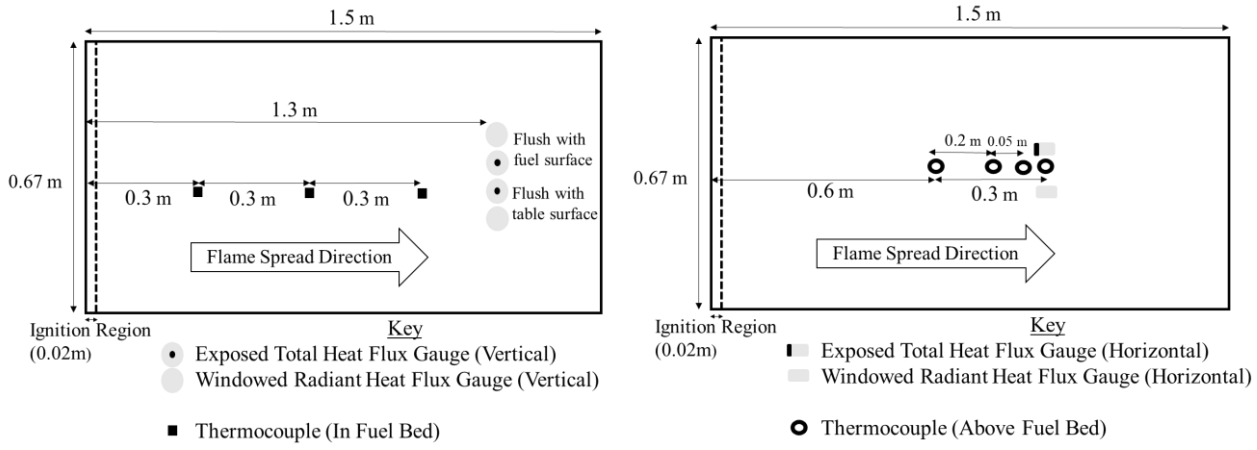

Figure 1. (left) 1st experimental setup involving four vertical heat flux gauges [sensor faces parallel to fuel bed surfaces] (right) 2nd experimental setup involving two horizontally-oriented heat flux gauges [sensor faces perpendicular to fuel bed surfaces]

Fuel beds (1.5 m by 0.67 m) were composed of pitch pine *(Pinus rigida* Mill.) needles (density = 706 ± 71 kg/m^3, surface-to-volume ratio = 5063 ± 640 m^{-1}) collected in the New Jersey Pinelands National Reserve. The dead needles had an average Fuel Moisture Content (FMC) of 13.2 % ± 4.6 %. Fuel bed structure was varied by altering fuel loading (0.2 to 1.6 kg/m^2), bulk density (10 to 40 kg/m^3), and fuel height (10 to 80 mm).

3. Results & Discussion

3.1. Overall Observations

A positive correlation between spread rate and fuel loading, and a negative correlation between spread rate and bulk density were observed, as shown in Table 1. Positive relationships between spread rate and $\alpha\sigma\delta$ ($R^2 = 0.91$) and between flame height and spread rate ($R^2 = 0.86$) were also observed.

Table 1. Summary of fire behaviour observations

Fuel Loading [kg/m^2]	**Bulk Density** [kg/m^3]	α	δ [mm]	$\alpha\sigma\delta$	**N**	**Flame Spread Rate** [mm/min ± Max/Min]	**Flame Height** [m ± 0.05 m]	**Peak HRR** [kW ± Max/Min]
0.2	20	0.972	10	49	2	82 ± 17	0.05	4.5 ± 2.4
0.4	10	0.986	40	200	2	168 ± 16	0.23	24.5 ± 5.0
0.4	20	0.972	20	98	4	114 ± 24	0.13	15.6 ± 1.7
0.6	20	0.972	30	148	2	139 ± 20	0.29	19.5 ± 5.0
0.8	10	0.986	80	399	4	195 ± 37	0.55	38.3 ± 1.0
0.8	20	0.972	40	197	5	149 ± 30	0.36	31.7 ± 1.8
0.8	40	0.943	20	96	4	122 ± 47	0.34	20.7 ± 1.0
1.2	20	0.972	60	295	2	198 ± 18	0.55	69.2 ± 6.9
1.6	20	0.972	80	394	4	206 ± 67	0.74	120.3 ± 12.3

3.2. Heat Fluxes

As shown in Figure 2, except where negligible heat flux was measured, heat flux profiles typically consisted of an initial steady growth period followed by a sharp rate of increase prior to a period of peak-decay behaviour.

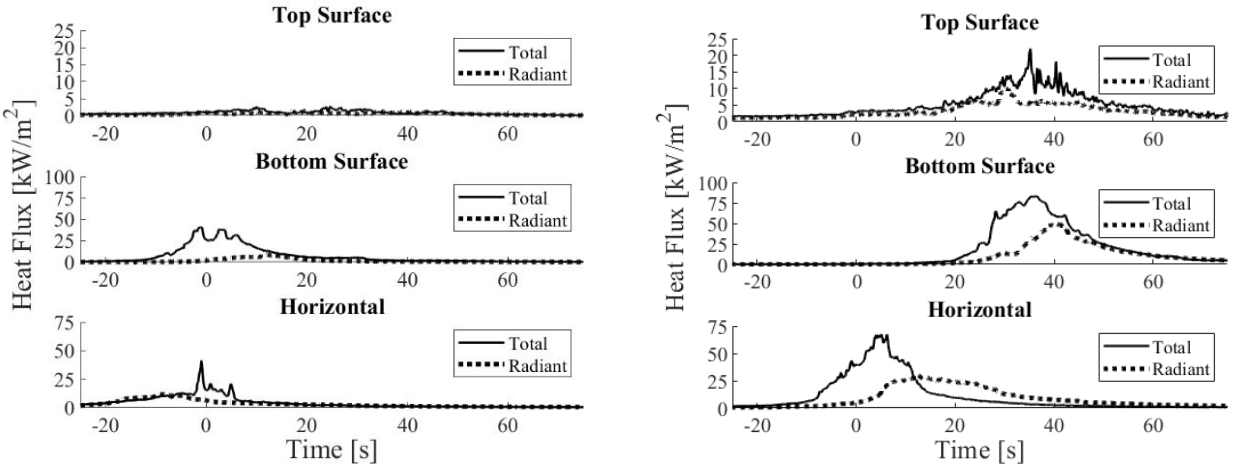

Figure 2. Characteristic total heat flux profiles at each gauge location for fuel beds of (left) $\alpha\sigma\delta = 98$ and (right) $\alpha\sigma\delta = 197$

Across all fuel conditions, heat transfer from the in-bed combustion region was the dominant heat transfer path in this flame spread scenario (compare top surface with bottom surface and horizontal measurements in Figure 2). In the first experimental series, the ratio of peak total heat flux measured at the bottom surface to that measured at the top fuel bed surface, ranged from 2.2 to 14 across the studied conditions. In-bed heating as measured by the horizontal gauges (heat transferred horizontally through the fuel bed from the combustion region) exceeded flame heating from the above-bed flame (measured at the top surface of the fuel bed), as shown in Figure 3.

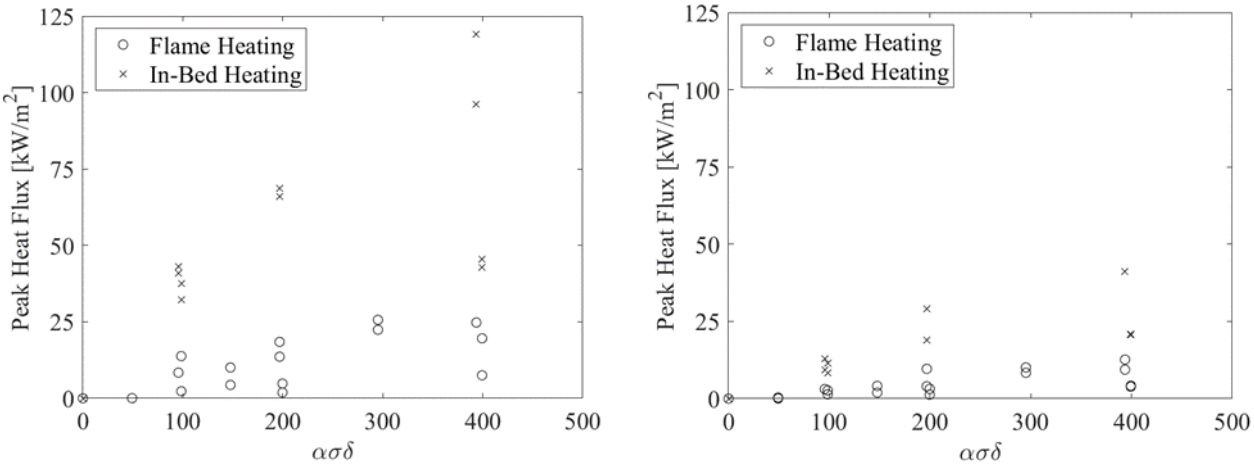

Figure 3. Comparison of peak (left) total and (right) radiant heat flux from the above-bed flame (flame heating) with horizontal heat flux through fuel beds (in-bed heating) of various structures

As shown in Figure 3, heat fluxes varied between fuel beds of different fuel structure ($\alpha\sigma\delta$). Generally, higher peak fluxes (radiant and total) occurred in fuel beds of higher $\alpha\sigma\delta$ values. However, the importance of fuel loading at similar ασδ values is observed in the two highest ασδ cases (ασδ=394 and ασδ=399), with significant variation in heat flux magnitudes occurring between these cases. The heat flux from the overhead flame increased with fuel loading which is in line with the positive relationship observed between fuel loading and flame height. Effective heating distance through the fuel bed is dependent upon porosity and attenuation characteristics of the fuel bed and varied with fuel loading and bulk density.

3.3. Thermal Model

A thermal model was constructed based on assumed bulk fuel bed properties, following an energy conservation approach similar to those previously described for porous fuel beds (Frandsen, 1971) and thermally thin solids (Quintiere, 2006). A control volume was defined within the fuel bed and fixed to the pyrolysis front position (x_p) as shown in Figure 4 with the flame spread rate described by:

$$v_p = \frac{\int_{x_p}^{\infty} \dot{q}_p^{"}(x)\,dx + \int_{x_p}^{\infty} \dot{q}_f^{"}(x)\,dx}{\rho c_p \delta (T_{ig} - T_s)}$$

where $\dot{q}_p^{"}$ is the heat flux into the control volume from the combustion region (integrated across the effective heating length), $\dot{q}_f^{"}$ is the heat flux from the above-bed flame, T_{ig} and T_s are the ignition and initial fuel temperatures respectively, and δ is the fuel height. Bulk fuel bed properties were based upon volume-averaged air and needle properties (density (ρ) and specific heat capacity (c_p)). Both $\dot{q}_p^{"}$ and $\dot{q}_f^{"}$ were integrated across their respective effective heating distances which were determined experimentally based upon the time between onset of heating at the heat flux gauge (0.5 kW/m^2 threshold) and the time of peak heat flux. Similarly, heat flux magnitude is based on experimental values, with 1 s moving average applied.

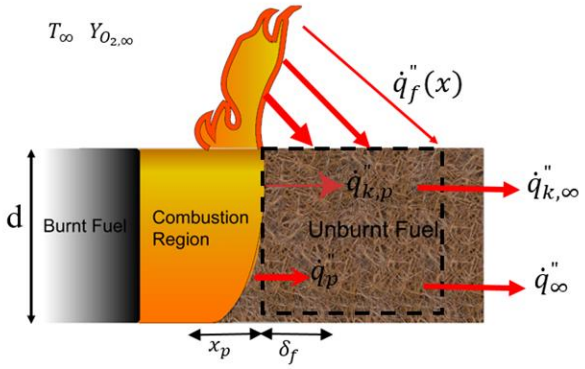

Figure 4. Schematic of control volume for flame spread model

Considering only radiative heat flux from the combustion region results in similar predicted Rate of Spread (ROS) values to those observed experimentally. A maximum variation between the predicted ROS and the experimentally measured ROS of 29 % was observed, with closer agreement for fuel beds of lower ασδ values, as shown in Figure 5. Given the greater HRR values in fuel beds of higher ασδ values, it may be that greater entrainment increases the convective cooling, with these heat losses not accounted for in this model.

Considering instead heat transfer only from the flame results in an underestimation of the ROS, particularly in fuel beds of lower ασδ values. This suggests that the dominance of the heat transfer from the combustion region increases at lower ασδ values. The predicted ROS is also shown where both the combustion region and flame heat transfer are included in the thermal model. This tends to overestimate the ROS, compared to experimental observations, however the effect of convective cooling (or radiative losses) is not considered and therefore this over-estimate is not unexpected and is in line with previous studies (De Mestre *et al.*, 1989).

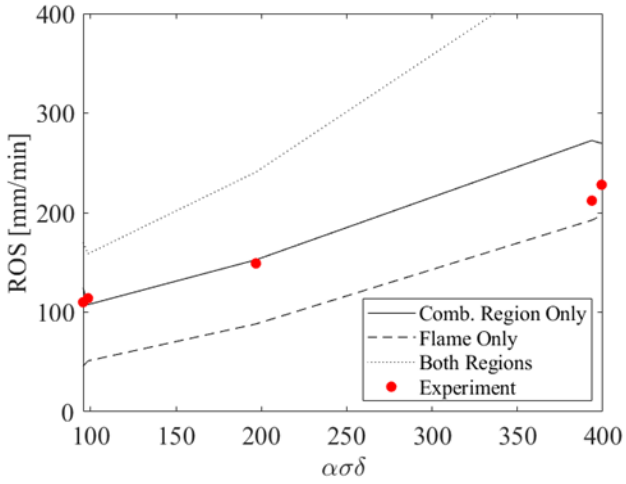

Figure 5. Comparison of avg. experimental Rate of Spread (ROS) values and thermal model ROS predictions for cases considering radiant heat flux from combustion Region only, flame region only, and both regions

4. Conclusions

By varying the structure of porous fuel beds (fuel loading, bulk density, fuel bed height), fuel loading and bulk density were observed to independently influence flame spread rate and fire behaviour (flame height, heat release rate). The effect of fuel structure on flame spread rate was well-described by the parameter $\alpha\sigma\delta$. Examining further the underlying physical mechanisms controlling the flame spread process highlighted the dominant role of in-bed heat transfer (from the combustion region in the fuel bed) across the range of fuel beds studied ($\alpha\sigma\delta$ = 49 to $\alpha\sigma\delta$ = 399). The significance of heat transfer contributions from the overhead flame generally increased with increasing $\alpha\sigma\delta$ value of the fuel bed, in contrast with some past predictions regarding heat transfer mechanisms in shallow fuel beds. Direct measurement of heat flux and effective heating distance, allowed development of a simple thermal model considering only radiative heating contributions. Comparison with experimental observations of spread rate indicated a maximum variation in predicted ROS of 29 % where only radiative transfer from the in-bed combustion region was considered, with closer agreement at lower $\alpha\sigma\delta$ values. Where the contributions of both the in-bed and above-bed heat transfer mechanisms were considered, the need to incorporate appropriate heat loss terms into this thermal model was apparent.

5. References

Andrews, P.L. (2018) The rothermel surface fire spread model and associated developments: A comprehensive explanation. U.S. Forest Service. Rocky Mountain Research Station. General Technical Report RMRS-GTR-371.

Campbell-Lochrie, Z., Walker-Ravena, C., Gallagher, M., Skowronski, N., Mueller, E.V., Hadden, R.M. Investigation of the role of bulk properties and in-bed structure in the flow regime of buoyancy-dominated flame spread in porous fuel beds, Fire Saf. J. (2021). doi:10.1016/j.firesaf.2020.103035.

De Mestre, N.J., Catchpole, E.A., Anderson, D.H., Rothermel, R.C. Uniform Propagation of a Planar Fire front Without Wind, Combust. Sci. Technol. 65 (1989) 231–244. doi:10.1080/00102208908924051.

Frandsen, W. H. (1971). Fire spread through porous fuels from the conservation of energy. Combustion and Flame, 16(1), 9-16.

Frankman, D., Webb, B.W., Butler, B.W., Time-resolved radiation and convection heat transfer in combusting discontinuous fuel beds, Combust. Sci. Technol. 182 (2010) 1391–1412. doi:10.1080/00102202.2010.486388.

Gallagher, MR., Cope, Z., Giron, D.R., Skowronski, N.S., Raynor, T., Gerber, T., Linn, R.R., Hiers, J.K., Reconstruction of the Spring Hill Wildfire and Exploration of Alternate Management Scenarios Using QUIC-Fire. Fire. 2021; 4(4):72. https://doi.org/10.3390/fire4040072

Hiers, J.K., O'Brien, J.J., Varner, J.M., Butler, B.W., Dickinson, M., Furman, J., Gallagher, M., Godwin, D., Goodrick, S.L., Hood, S.M. Prescribed fire science: the case for a refined research agenda. Fire Ecology, 16(1), 1-15 (2020). https://doi.org/10.1186/s42408-020-0070-8

Rothermel, R. C. (1972). A mathematical model for predicting fire spread in wildland fuels (Vol. 115). Intermountain Forest & Range Experiment Station, Forest Service, US Department of Agriculture.

Quintiere, J.G. Fundamentals of Fire Phenomena, 2006. doi:10.1002/0470091150

Williams, F.A. Mechanisms of fire spread, Symp. Combust. 16 (1977) 1281–1294. doi:10.1016/S0082-0784(77)80415-3.

Effect of Spatiotemporally Varying Fuel Moisture Content on Turbulence Statistics During Fire Propagation

Ritambhara Dubey; Neda Yaghoobian*

Florida State University, FAMU-FSU College of Engineering, Department of Mechanical Engineering, Tallahassee, FL, USA. {rrd20z@my.fsu.edu, nyaghoobian@eng.famu.fsu.edu}

**Corresponding author*

Keywords

Fuel moisture content, Prescribed burns, Turbulence statistics, WFDS

Abstract

Prescribed burns are valuable tools utilized for land management. They serve the purpose of reducing the risk of wildfires by lowering the build-up of dry fuels, improving forest health, and controlling the growth of plants and insects. One of the crucial components that affects the execution of prescribed burns and controls the fire behaviour and smoke dispersal thereafter is the fuel moisture content, which needs to be considered when planning prescribed burns. The fuel moisture content variation is dependent on the meteorological variables, fuel properties, and the local turbulent fire dynamics, and so varies spatially and temporally over the land area before and during the fire advancement. In previous studies, the fuel moisture content was treated based on average properties, independent of the effect of local turbulence. In this study, the spatiotemporally varying fuel moisture content is obtained by a physics-based model that considers the coupled energy and moisture balance dynamics inside the fuel layers. This moisture model is implemented into the Wildland-urban Interface Fire Dynamics Simulator (WFDS) by means of a two-way coupling. Along with the local fuel properties, the model uses the instantaneous solar radiation and relative humidity, together with the instantaneous turbulent wind velocity and ambient air temperature at the boundary of each fuel sub-surface (grid) in the simulation domain. The coupled model is employed to study the effect of the dynamic variations of the fuel moisture on the turbulent evolution of the fire plume during a line fire propagation over a flat grassland. The findings of the study will provide insights into the effect of the fuel moisture content on the plume dynamics and smoke dispersal during prescribed burns and will assist in planning these burns.

1. Introduction

Prescribed fires, also known as controlled burns, are planned and controlled applications of moderate to low intensity fires under specific atmospheric conditions. In addition to mitigating wildfires, prescribed fires are essential for maintaining the health of fire-dependent ecosystems. In fire-dependent ecosystems, prescribed fires serve the purpose of: (1) regulating the buildup of dry fuel, (2) controlling the growth of plant species, insects, and parasites, and (3) improving the health of the soil (Heinselman and Wright, 1973). In addition, prescribed fires help with training firefighters and prepare them for the required actions during wildfires. The smoke from prescribed fires, however, may be troublesome for the neighboring communities. It may substantially impact the air quality and increase the risk of road accidents. When the plumes from prescribed fires penetrate the troposphere, they add smoke aloft, which impacts regional as well as global scale climate for instance by reducing insolation and altering the cloud microphysics (Lareau and Clements, 2017). Contradictory to this, when the plumes remain restricted to the atmospheric boundary layer, they affect the local population by posing health hazards in the nearby communities. These near-field plumes bring about persistent temperature inversions, unanticipated patterns of smoke transport, and could pose a travel risk by reducing visibility.

An important factor that influences the fire plume dynamics, as well as the fuel flammability, fire propagation behavior, and the burn plan is the fuel moisture content (FMC). FMC is influenced by the vegetation characteristics, the background atmospheric conditions, and the local fire-induced turbulent airflow and temperature during the fire. Therefore, as a result of the instantaneous variations in solar radiation, relative humidity, and the local turbulent wind velocity and air temperature the FMC varies both spatially and temporally at the fuel boundary. While there are studies that investigate temporal variations of the FMC using empirical models (Alves, 2009; Slijepcevic, 2013) and physics-based models (Wittich, 2005; Matthews, 2006), an

understanding of the spatiotemporal turbulent variations of the FMC at the fuel boundary during fire events is missing. In this study, we aim to examine the effects of the dynamically varying FMC on the turbulence statistics of the flow and plume dynamics during a line fire using a coupled fire-atmospheric interaction model that considers the spatiotemporal variations of the fuel moisture content.

2. Model Description and Simulation Setup

The change in the FMC is modelled by utilizing a physics-based FMC variation model (Matthews, 2006). The model represents the transfer of energy and water and their two-way interactions in a fuel bed, which is bounded between the atmosphere and soil surface. The fuel bed is comprised of multiple layers of fuel and each layer is made up of three components of the fuel solid, air, and free liquid water. The model is controlled by precipitation, diurnal solar radiation, the local wind speed and ambient air temperature, relative humidity, and the physical properties of the fuel (e.g., the surface to volume ratio, packing ratio, and height of the fuel bed). The energy and moisture balance equations (Eq. 1 and 2, respectively) are solved inside each layer in a coupled way to obtain the FMC (m).

$$C_{h,m}\frac{\partial T_m}{\partial t} = \frac{1}{V_m}\left(\frac{\partial R_{net}}{\partial z} + \frac{\partial H_C}{\partial z}\right) - \mu_{m,a}H_{ma} - \mu_{m,a}\lambda E_{ma} - \mu_{m,l}H_{ml} \quad (1)$$

$$\rho_{air}\frac{\partial m}{\partial t} = -\mu_{m,a}E_{ma} - \mu_{m,l}E_{ml} \quad (2)$$

Here, the energy budget equation (Eq. 1) models the variations of the fuel temperature (T_m) with time. In these equations, $C_{h,m}(Jm^{-3}K^{-1})$ and $V_m(m^3m^{-3})$ are the volumetric heat capacity and volume fraction of the fuel solid. $\mu_{m,a}(m^{-1})$ and $\mu_{m,l}$ (m^{-1}) are, respectively, the surface area-to-volume ratio at the interface between the fuel solid and air and at the interface between the fuel solid and the intercepted liquid water. λ (Jkg^{-1}) and ρ_{air} (kgm^{-3}) are the latent heat of vaporization of water and density of air. R_{net} (Wm^{-2}) is the net radiative heat flux, H_C (Wm^{-2}) is the heat flux due to conduction, H_{ma} (Wm^{-2}) is the sensible heat flux at the fuel boundary, E_{ma} $(kgm^{-2}s^{-1})$ is the moisture flux between the litter solid and air, H_{ml} (Wm^{-2}) is the heat flux between the fuel solid and the intercepted liquid water, and E_{ml} $(kgm^{-2}s^{-1})$ is the moisture flux between the fuel solid and the intercepted liquid water.

The FMC model is coupled with the Wildland-urban interface Fire Dynamics Simulator (WFDS) in a two-way manner to allow for the investigation of the FMC variation effects on the fire and plume dynamics. WFDS is a large-eddy simulation (LES)-based model that simulates the fire-atmospher interactions. In the two-way coupling, the FMC model utilizes the instantaneous information of the meteorological conditions and the fire-induced flow from WFDS and provides the instantaneous fuel moisture content to WFDS at each timestep.

In this study, the coupled model is used to investigate how the instantaneous changes of the fuel moisture due to the turbulent interactions at the fuel boundary affect the fire and plume behavior in a case of a line fire in a flat grassland. The domain size and grid resolutions are found through sensitivity analyses and the first and second-order turbulence characteristics of the flow and plume dynamics, as well as the fire propagation behaviour under the effect of dynamic FMC change is investigated. The results are also compared against cases with constant FMC and with no fuel moisture. Findings of this study provides a better understanding of the role of fuel moisture in fire behavior and near-field plume structure and dynamics.

3. References

MVG Alves et al. “Fuel moisture sampling and modeling in Pinus elliottii Engelm. plantations based on weather conditions in Paran´a-Brazil”. In: iForest-Biogeosciences and Forestry 2.3 (2009), p. 99.

Heilman, W. E., Banerjee, T., Clements, C. B., Clark, K. L., Zhong, S., & Bian, X. (2021). Observations of Sweep–Ejection Dynamics for Heat and Momentum Fluxes during Wildland Fires in Forested and Grassland Environments. Journal of Applied Meteorology and Climatology, 60(2), 185-199.

Heilman, W. E., Bian, X., Clark, K. L., Skowronski, N. S., Hom, J. L., & Gallagher, M. R. (2017). Atmospheric turbulence observations in the vicinity of surface fires in forested environments. Journal of Applied Meteorology and Climatology, 56(12), 3133-3150.

Heinselman, M. L., & Wright, H. E. (1973). The ecological role of fire in natural conifer forests of western and northern North America. Quaternary Research, 3(3), 317-318.

Lareau, N. P., & Clements, C. B. (2017). The mean and turbulent properties of a wildfire convective plume. Journal of Applied Meteorology and Climatology, 56(8), 2289-2299.

Matthews, S. (2006). A process-based model of fine fuel moisture. International Journal of Wildland Fire, 15(2), 155-168.

Mell, W., Charney, J., Jenkins, M. A., Cheney, P., & Gould, J. (2013). Numerical simulations of grassland fire behavior from the LANL-FIRETEC and NIST-WFDS models. In Remote Sensing and Modeling Applications to Wildland Fires (pp. 209-225). Springer, Berlin, Heidelberg.

Seto, D., Clements, C. B., & Heilman, W. E. (2013). Turbulence spectra measured during fire front passage. Agricultural and forest meteorology, 169, 195-210.

Slijepcevic, A., Anderson, W. R., & Matthews, S. (2013). Testing existing models for predicting hourly variation in fine fuel moisture in eucalypt forests. Forest Ecology and Management, 306, 202-215.

Wittich KP (2005). A single-layer litter-moisture model for estimating forest-fire danger. Meteorologische Zeitschrift, 14, 157–164.

Emergency Alerting Technologies Relevant to Forest Fires

Frank W. Bell

Kybernetix LLC, Clifton NJ, USA, {fbell@kynx.us}

Keywords

Fire fatalities, Mobile, WEA, SMS Broadcast, Broadcast digital radio, Broadcast television, Alerting

Abstract

California wild and forest fires in 2017 resulted in over 100 fatalities. While WEA alerts were transmitted to mobiles in selected areas, the power and network outages limited their delivery. WEA is similar to the SMS Broadcast system used elsewhere. It does not require subscription, and can be geotargeted, usually by map polygon. There are already available and in development other alerting technologies. The Emergency Alert System on radio and TV in the U.S. has been in use for many years. It is a broadcast break-in system the overrides program content. This was used in one location for the wildfires, but not elsewhere as geotargeting is not possible with this system. It is and analog broadcast technology architecture. AM and FM Broadcast in the U.S. now has HD Radio that is mixed analog and digital. A limited data message can be carried and used for selective delivery of messages. DAB, DAB+ and DRM also can carry a message payload, which can be used for a selective delivery mechanism when the receiver has location position. This may be in a vehicle radio/navigation system. The current digital television system in the U.S. and some other countries is now being replaced by ATSC 3.0. This provided a superior modulation format, Layered Division Multiplexing (LDM) for delivery of program content and alerts to suitable mobiles. An IC for UHF reception and prototype mobiles have been developed. No external antenna is required. Bothe of these new technologies are tested as delivering alerts independently of the mobile network. Within the limitations of radio and TV propagation, such capabilities would provide technology redundancy. The television signal propagation may be limited in rural areas, but ATSC 3.0 is capable of having on frequency repeaters to make a single frequency network for improved coverage of program content and alerting. Multilingual alerts based on the CAP Event Terms list with Message Formats are being provided for.

1. The Lifesaving Value of Alerting

Some comparisons are made between disasters that are unalerted and others which have alerts beforehand.

1.1. Samoa and American Samoa Tsunami 2009

1.1.1. Fatalities comparison

In the 2009 earthquake and subsequent tsunami, there were 22 confirmed fatalities in American Samoa and 147 in Samoa. While the tsunami in American Samoa was 4.6 to 6 m high the Samoan landing was 6.1 to 9 m high. This explains in part the difference in fatalities

1.1.2. Benefit of Alerting Comparison

The fatality ratio is 22 to 147. The height ratio is 6 to 9. Compensating for the height, the ratio is 1 to 4.45. In American Samoa the radio station operator, DJ Ms Lupe Lohman, initiated a tsunami alert. http://news.bbc.co.uk/2/hi/asia-pacific/8282741.stm. This was relayed by criers, church bells and other means. In Samoa, no alerting was recorded, and the radio station had no Emergency Alert System. At the NAB Trade show in 2017, I spoke with the representatives of Triveni (a Viavi division) who stated that it was one of their products that was used. Samoa at that time was a protectorate of New Zealand. Such equipment is not in use in New Zealand, but SMS Broadcast is now in use to mobiles.

1.2. Indian Ocean 2004 and Tohoku, Japan 2011

1.2.1. Fatalities Comparison

In the 2004 Indian Ocean earthquake and tsunami, there were an estimated 227 898 fatalities and in Japan there were 22 303 fatalities and missing. While the tsunami height in Indonesia was 30 m for a 9.3 magnitude quake, the 2011 earthquake and tsunami in Tohoku had a 40.5 m height for 9.1 magnitude.

1.2.2. Benefit of Alerting Comparison

The fatality ratio is 22 303 to 227 898. Whie the height and earthquake magnitude differ; they somewhat cancel each other at a 40.5 m and 9.1 magnitude in Japan versus 30 m and 9.3 in Indonesia. Compensating for the differences the benefit ratio is 1 to 13.5. This is much higher than for Samoa, however in Japan there were many more mitigation measures implemented beyond alerting. The cost of the alerting system has not been obtained in writing. It is worth noting that this system was installed in 2009 and is considered to have delivered sufficient benefit to pay for that investment in two years.

While this analysis of only two examples is unsatisfactory for assessing a standard deviation of results or of differences with control examples, the problem is the lack of comparable examples. As an illustration, compare the Haiti earthquake 2010 magnitude 7.0 with 300,000 fatalities and Christchurch New Zealand 2010 magnitude 7.1, or 2011 magnitude 6.1 or 2016 magnitude 5.7 with considerable damage in the latter but with two noted fatalities and 100 injuries in 2010, 185 deaths in 2011. None of the events included alerting the public. It may be possible to use factor analysis to extract some factors relevant to the alerting question, but that requires a large amount of related set data. Such a set of data does not appear to be available. One would hope that future researchers are able to improve on this with future data after some more implementation of alerting in the future.

1.3. Evaluation of Wild and Forest Fire Fatalities in the U.S.

1.3.1. Los Angeles Times 2018-12-03

This is a newspaper report copied and is in the appendix as an attachment. In one of the fires there were 88 fatalities in Butte County. The headline noted that more than one third of the cellular recipients did not receive alerts. A subscription alerting service was used.

1.3.2. Cellular at risk of wildfires

This is an engineering evaluation of cellular or mobile base stations and the risk of fires at their locations, which may be on high land. It is in the appendix. No discussion of fatalities is included.

1.3.3. Gatlinburg 2016 Nov 28 firestorm

This report is applying to Gatlinburg, Tennessee and is in the appendix as an attachment. While there were a limited number of fatalities, being 14, this is included because the Emergency Management Office lost its communications and was unable to initiate an Emergency Alert to mobiles or broadcasters. While satellite or amateur radio hypothetically could have been technologies to use in such a situation, the lack of landline and internet phone were also rendered inoperative. This highlights the importance of redundant technologies.

1.3.4. NBNCBC Telecommunications Outage Report 2017 Firestorm

This report applies to wild and forest fires in California in 2017 and is in the appendix as an attachment. Napa, Sonoma and Mendicino Counties were affected with 44 lives lost.

2. The Importance of Redundancy for Emergency Alerting, Including Technologies

2.1. The Fatalities noted in 1.3 total 132.

This is a situation where one single or few technologies were used. The Emergency Alert System using broadcast radio and television was only used in one alert, and no fatalities in that area were noted. It is also worth noting that broadcast coverage areas are normally much larger than forest fire areas. This technology at that time would have alerted large numbers of recipients for whom the alert was irrelevant. The lack of selection of alert delivery as a polygon on a map is highly desirable. Alerting delivery presently has the potential to give rise to large numbers of people evacuating, with a potential for traffic congestion that could have been a serious hindrance to firefighting, police and ambulance crews. There is no suggestion that this is an advisable course of action for alerting should such problems arise.

If an appropriate area could be selected, given the conservative benefit of alerting noted in 1.1.2 as being 4.7, the fatalities could have been reduced to 28, saving 105 lives compared with using a single technology. The results for Japan in 2011 suggest that more technologies produce better results.

3. An Outline of Broadcast Alerting Developments.

3.1. HD Radio, DAB, DAB+ and DRM.

In the U.S. there is AM and FM digital broadcasting added to the analog carrier. It is possible to replace the analog carrier with digital only. On FM there is a 200 kHz station spacing and this allows for digital carriers alongside the analog signal. There is a limited data rate available for alerting messages, which may include a map polygon, jurisdiction or receiver type for selectivity. A receiver may obtain the current location from the navigation system or via Bluetooth from a mobile. AM HD Radio has very limited alert data capacity, but this has potential. Selectivity may be implemented by selecting between the alert audio and the program audio. On FM there are up to 3 digital programs, of which one is replicating the analog signal. In a region, one may be a news, alert and weather program with lower data rate. This may be possible on DRM, but research is needed.

DAB and DAB+ are multi-station and digital only. It may be possible to designate one as a news, alert and weather program with lower data rate. The alert message data would provide the selection criteria for program or alert audio selection. This would only require software added to the consumer receiver and a means of determining the location, e.g., vehicle navigation or Bluetooth to a mobile.

3.2. ATSC 3.0 “nextgenTV” and DVB.

The ATSC 3.0 or nextgenTV system included alerting audio+data (as A/331) and video as separate from the TV program, which may be 4K or UHD with High Dynamic Range and Wide Colour Gamut. It is a transport technology that may be used for new technologies in the future as a complement to the present internet. The audio may be immersive. Other HD or SD TV channels may be included, or UHD when a 7 or 8 MHz bandwidth is available. The video is HTML5, not an inflexible format. The modulation is Layered Division Multiplexing (LDM). There is a QPSK high power and low data rate layer, and a selectable constellation lower power high data rate component. The alerting and a Standard Definition video with stereo plus the alerting data is in the QPSK. This UHF band signal may be received by a little antenna in a suitable mobile. Protypes have been demonstrated. While this expands the potential audience to such mobiles, the importance here is the delivery of alerts. This system is broadcast in South Korea and USA currently. India, Brazil, Jamaica have announced, and Canada and Japan are expected to replace their digital TV system with ATSC 3.0. It can carry European SD and HD video. It addition to cinema quality video and audio, it is also IP based. Enabling delivery via the air, satellite, or cable as well as the internet. China is participating also. The importance here is the better delivery of alerts than possible with DVB to mobiles. In order to reach more remote areas, it is possible to replace TV translators with Single Frequency Networks (SFN) for wider coverage without additional spectrum required. U.S. broadcasters have released considerable spectrum to the mobile providers.

3.3. Cable, fibre and telco TV.

The various systems all have low bandwidth data delivery possible. When the Set Top Box has its location data by one of various means, the selective alert delivery can be implemented. This is anticipated development work. The distribution of these fixed line systems in rural areas is not expected to be high, but they are important for urban areas.

3.4. Satellite TV and radio.

In the U.S. this is DirecTV, Dish Network and SiriusXM. These all provide alerting currently, but with better alerting technology, these distributions can be improved. Other countries have various systems which are likely to be amenable to better alert delivery. Satellite delivery for Earthquake Early warning has an added delay that becomes significant.

3.5. Internet alerting.

There are many forms of internet alerting. A distribution to broadcasters is via the internet. Then there is Federation of Internet Alerts, Google Alerts and more including subscription services.

3.6. Message content.

The OASIS-Open Emergency Management Technical Committee has developed an Event Terms list which is now a committee note for the Common Alert Protocol standard x.1303 of itu.int. This standard is adopted by over 70% of the world, including much of Europe. Each term may have a detailed spectra which is not defined. Based on this Committee Note, a collection of historical alerts, various lists from many sources and other

research a list of Message Formats {currently 427} these include many for fire alerts and fire risk messages. A tab for wildfire messaging is in the spreadsheet. The Message Formats have been translated into a first draft for many languages. The intent is to enable multilingual alert generation by Emergency Managers who only know one language. Also, using this message added data and the codes, alerts in neighbouring countries for emergencies that are cross-border can reasonably easily be made. Information from previous work has been incorporated. The intent is to have a level playing field for consumer electronics manufacturers to be able to implement one version of software to be able to process alerts in any country. English, Spanish, French and Portuguese are some of the languages translated.

3.7. WEA and SMS Broadcast to Mobiles.

Currently many mobiles receive alerts from WEA (in the U.S.) or SMS Broadcast (many countries) and other SMS or subscription services. In the U.S., authorized Emergency Managers using Alert Origination Software may send alerts to the FEMA IPAWS system to various recipients including mobile service providers and broadcasters. With the anticipated implementation of ATSC 3 or nextgenTV to mobiles, there is the likelihood of the mobile receiving multiple alerts from one origination message. Identification of this to reduce alert fatigue by the public is designed into the complete system. Between the various sources, the technology redundancy should provide much improved reliability of distribution. Intelligent Highway Signs, loudspeaker systems and other technologies may also be incorporated.

3.8. Systems Interoperability Standards and some applications.

Alerting Protocols; Common Alert Protocol (CAP) with Event Terms list expanded as core protocol. This may be translated to Emergency Alert System (EAS) based on FCC Part 11 rules for analog and legacy television and analog radio. Improved EAS adapted for HD Radio, DAB, DAB+ and perhaps DRM. DVB Alerting distribution where applicable. CAP based messages on ATSC 3 in HTML5 which can be translated to CAP if needed. Others may be adapted e.g., for Japan.

Earthquake Early Warning using an appropriate version of CAP with delivery optimized for speed. If possible, within 3 seconds of detection.

Healthcare; EDXL-HAVE, HL7 and others

Other Emergency Management; EDXL-DE, EDXL-RM. EDXL-TEP, EDXL-TEC, EDXL-SITREP, XchangeCore. Google Earth, Esri, NAVTEX, https://www.g2.com/categories/emergency-management atsc3advocate.com. https://onemediallc.com/resources/

4. Conclusions.

4.1. Audience Relevance.

This is always important with any media content distribution. The audience of an alert should as much as is reasonably practicable, be those for whom the alert is intended. That audience of this paper is gathered to address Forest Fires. Consequently, while much more could be stated on these subjects, those things are considered not as relevant. A public opinion survey regarding alerting is attached as Research_Study. Questions are welcome to fbell@kynx.us

4.2. Anticipated Costs and Benefits.

The major expense for such improvements is for improved software for the consumer receivers where that is practicable. Vehicle digital or satellite radio receivers may have their software upgraded as part of the dealer maintenance. Older vehicles may be replaced with newer ones which may already have the software from the factory. Some devices can have software downloaded to a USB for vehicle upgrade or directly to the device. Once developed, the cost is the time and effort including informing the users. Other consumer electronics like radios have new replacements in time. The cost of the infrastructure for alerting delivery is significant, and the cost of developing that is also significant. The benefit of lives saved is considerably more significant. In “Risk and Reason” by Cass Sunstein, the value of a life for public policy purposes in the U.S. when written was in the range of $US 1 M to $10 M. Other countries may have such assessments made. An honest assessment of this aspect is helpful for making economic decisions. Disasters and wars may be made lesser problems by such considerations.

A desirable capability is that of delivering alerts to mobiles. ATSC 3.0 or nextgenTV has this capability designed in and is also designed to be significantly better to deliver such alerts to mobiles than previous digital TV systems. Much of the world is using DVB or ISDB which have been improved. DVB-H was a commercial failure, and probably a poorer performer with a limited range. DVB-NGH has been developed as a successor, but the implementation commercially has been limited by the range. That is primarily arising from the type of modulation ATSC 3.0 uses LDH which has a high power low data rate component for inherently greater range. Future mobiles providing for this and DVB-NGH would require development. A Mark One nextgenTV evaluation model has been produced but is not yet publicly available. While there is much progress, this particular aspect has remaining significant work to be done, and the benefit is not at present apparent to the public if this cost is to be recouped by a full increase in product price.

Experimental and numerical characterisation of the smouldering combustion of peat

Raquel S.P. Hakes[1]; Hamish Allan[2]; Da Ke[2]; Sara S. McAllister[3]; Matthew W. Kury[1]; Sarah N. Scott[1]; Rory M. Hadden[2*]

[1]Sandia National Laboratories[1], Livermore, California, USA, {rshakes, mwkury, snscott}@sandia.gov
[2]University of Edinburgh, Edinburgh EH9 3JL, UK, {r.hadden@ed.ac.uk}
[3]United States Forest Service, Missoula, Montana, USA, {sara.mcallister@usda.gov}

**Corresponding author*

Keywords

Smouldering; peat; pyrolysis; char oxidation; burning rate

Abstract

Smouldering peat fires are a major source of greenhouse gas emissions. As the climate warms, the frequency and severity of peat fires will continue to increase, with a single large fire event contributing as much CO2 to the atmosphere per day as an industrialized country. Estimates of the amount of CO2 released by peat fires contain large uncertainties, driven by overwhelming uncertainty in the mass of peat consumed in these fires. The present work addresses uncertainties in peat fire dynamics and smouldering through an iterative experimental and modelling process. Presented here is a first step towards predicting greenhouse gas emissions. Experiments focus on capturing the mass burnt in a smouldering peat fire and describing the smouldering—pyrolysis and oxidation—process. Mass loss rate is found to vary as a sample is tested in lateral spread vs downward spread configurations. A one-dimensional model of peat smouldering is implemented, with initial qualitative results presented here, showing the drying of wet peat and the pyrolysis front. These results represent the current work in progress on this effort. Further work will compare experimental and simulation results for additional parameters of interest, and simulations will be used to inform which soil parameters to explore experimentally.

1. Introduction

The smouldering of organic soils is a key wildfire hazard across the globe with peat fires burning primarily in boreal regions in the northern hemisphere (e.g., Siberia, Canada, Alaska) and tropical regions (e.g., Southeast Asia). Boreal peat (at northern latitudes from Europe to the Arctic) stores over 400 Gt of carbon (Beaulne *et al.* 2021), which can be released to the atmosphere if the peat is ignited. As the climate warms, the frequency and severity of peat fires will continue to increase. The timescales of this release (days) compared to the timescales for the formation of peat (millennia) mean it has a significant potential to drive climate change. Estimates of the amount of greenhouse gases (GHGs) released by peat fires contain large uncertainties, driven by overwhelming uncertainty in the mass of peat consumed in these fires (Rodríguez Vásquez *et al.* 2021).

Sustained smouldering is dominated by two processes: pyrolysis and oxidation. The pyrolysis process is controlled by heat transfer through the soil and is therefore influenced by its moisture content (MC), the composition of the peat (specifically the quantity of inert material/inorganic content (IC)), and the heat losses to the environment. The oxidation process is governed by the diffusion of oxygen through pyrolyzed soil regions. These two processes produce different carbon-based emissions. Therefore, to elucidate the contribution of peat fires to GHG emissions, we must (1) be able to predict the mass of peat consumed, and (2) have detailed knowledge of the processes and dynamics of the smouldering combustion.

[1] Sandia National Laboratories is a multimission laboratory managed and operated by National Technology and Engineering Solutions of Sandia, LLC., a wholly owned subsidiary of Honeywell International, Inc., for the U.S. Department of Energy National Nuclear Security Administration under contract DE-NA0003525. SAND2022-3524 C.

Recent efforts have been made to understand the process of smouldering combustion to better understand the hazards posed by this wildfire process. Previous work on peat fires has used commercial peat to analyze gas emissions (Hu *et al.* 2020) and the chemical reactions involved in the ignition and spread of smoulder (Hadden *et al.* 2013) in the laboratory. The influences of MC (Amin *et al.* 2020; Huang and Rein 2017; Lin *et al.* 2020), wind and slope (Christensen *et al.* 2020), density (Krieger Filho *et al.* 2020), and depth of peat (Lin *et al.* 2021) on spread rate have been studied. A one-dimensional (1-D) model has been developed (Huang and Rein 2015; Huang and Rein 2019; Huang *et al.* 2015) and used to understand the relationship between depth of smouldering and MC. This model has been used to explore the effects of MC, IC, and peat properties on critical ignition conditions (Huang and Rein 2015; Huang *et al.* 2015). Limited work has been done in the laboratory using natural peat as the medium under investigation, though work has been done with peat from near Edinburgh, Scotland (Rein *et al.* 2009).

Here, we present initial steps towards providing more accurate estimates of GHG emissions from peat fires. The experiments explore key 3-D effects, such as specimen size and orientation. Initial results are presented from quasi-1D simulations, based on the model created by Huang and Rein. As part of an iterative experimental and modelling process, the experiments will be used to validate the model and expand it to 2-D and 3-D, while the model will be used for physics elucidation and to explore the experimental parameter space to inform which experiments to perform.

2. Experimental set up

To explore the competing effects of heat transfer and oxygen diffusion on peat smouldering, a series of one-dimensional opposed flow smouldering experiments were undertaken in the laboratory. Two cuboidal peat sample sizes of cross-sectional area 625 and 2,500 mm^2 (25- and 50-mm side lengths) and total length of 300 mm were studied in the vertical downward and lateral orientations, as shown in Figure 1 below. An open boundary condition was used in all cases to allow the free flow of oxidiser into the reaction zone by constructing sample holders from woven stainless-steel mesh with hole size of 0.96 mm (~46% open area). An electrical nichrome coil was used for ignition, supplying a power of 50 W for 5 min. Commercially harvested sphagnum moss peat was used as the feedstock. Prior to testing, the peat was dried in batches for at least 48 hours at 80°C. The bulk density of peat was fixed at 350-400 kg/m^3. The approximate mass of peat for the three sample sizes tested is 50 and 200 g.

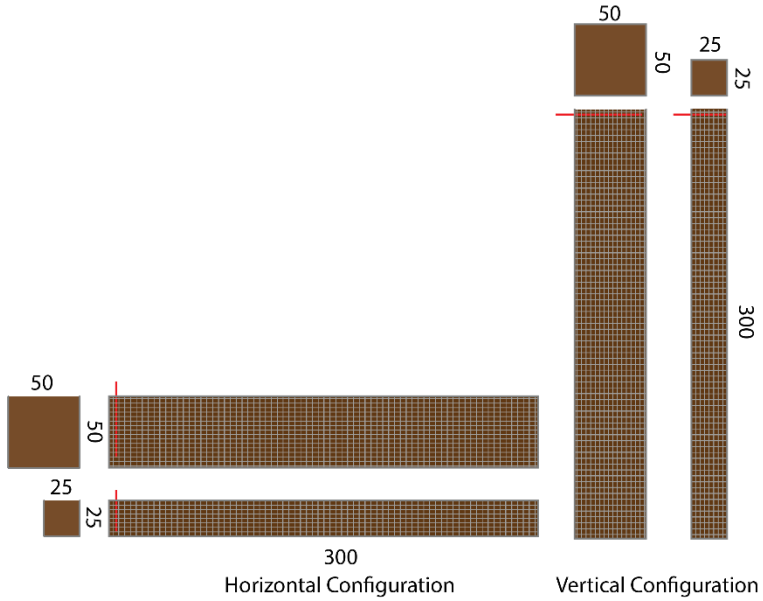

Figure 1- Schematic of experimental setup for lateral (horizontal configuration) and downward (vertical configuration) spread experiments for both sample sizes. All dimensions are in mm. The red line represents the ignition location.

Real time mass measurements were made during the experiment and the mass loss rate (MLR) was calculated and smoothed using a 51-point Savitsky-Golay filter with a second order polynomial. Temperature

measurements were made at the centreline of the sample using 0.25 mm diameter K-type thermocouples. These are used to track the position of the pyrolysis and smouldering fronts as a function of time. The propagation rate was recorded using time-lapse imagery which was processed computationally.

3. Experimental results and analysis

The smouldering process is characterised using the mass and MLR data, which can capture the effects of both pyrolysis and oxidation. Propagation rate data and temperature data will be included subsequently to elucidate the smouldering front characteristics.

3.1. Experimental mass and mass loss rate data

The mass of the sample as a function of time is presented in Figure 2a. As the sample dimension increases, so does the duration of the smouldering, as the mass of peat has also increased. Orientation of the specimen impacts the duration of the smouldering process for a given propagation direction. The smouldering propagation direction also appears to change the smouldering dynamics. Vertical downwards smouldering is characterised by a period of relatedly high MLR per unit cross section (Figure 2b) after ignition (25-100 minutes) and then a period of lower MLR (100-150 minutes), which is anticipated to represent the transition from primarily pyrolysis to long-time oxidation. The longitudinal smouldering, on the other hand, is characterised by a quasi-steady MLR, suggesting that steady state propagation has been achieved.

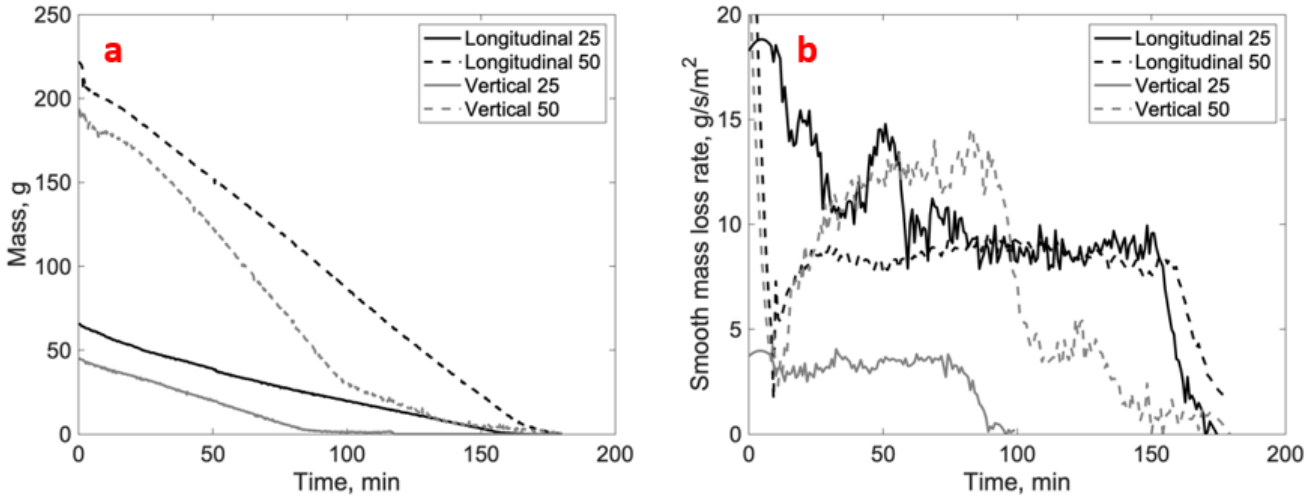

Figure 2- Sample mass (left) and mass loss rates (right) as a function of time for cuboidal samples with 25- and 50-mm sides.

4. Computational modelling

The quasi-1-D model used here is based on the work of Huang *et al.* (2015) and Huang and Rein (2015), in which a 1-D model of peat smouldering was developed in GPyro. A version of their model has been implemented in Sierra Thermal/Fluids: Aria, a generalized Galerkin finite element method code (Notz *et al.* 2016). The governing equations are solved both in the solid phase and in the gas phase for continuity, continuity of species, and enthalpy. We use Darcy's law for flow through a porous media to calculate the gas phase velocity. The ignition source is modelled as a constant 800°C temperature on the top end of the peat column. Boundary conditions on the cool end assume convective and radiative heating to an ambient environment. Material properties of the solid phase species were taken from Huang and Rein (2015). A 5-step reaction mechanism, developed in Huang and Rein (2014), is used to describe the peat smouldering process, with kinetic parameters for each reaction taken from Huang and Rein (2015). To account for the experimentally observed collapse when a peat column burns, the model solves the quasi-static conservation of momentum.

The model is run for 30,000 s on a lateral column of peat 400 mm long and 100 mm x 100 mm square. A 1-D problem is approximated in Aria by creating a mesh with elements in only one direction (i.e., a stack of blocks).

The element edge length along the column of the peat is 2 mm. Time is advanced implicitly using adaptive time stepping based on problem difficulty and error control, with a minimum of 1^{-9} s and a maximum of 1 s.

Initial modelling results, presented in Figure 3, show notional agreement with lateral spread experiments. A snapshot of one of the experiments shows black char and ash behind the smouldering front. Modelling results show the drying front (in red) and leading edge of the pyrolysis front (in blue). Experiments and simulations are compared at an arbitrary time. While further work is required to verify and validate the model, initial results are promising.

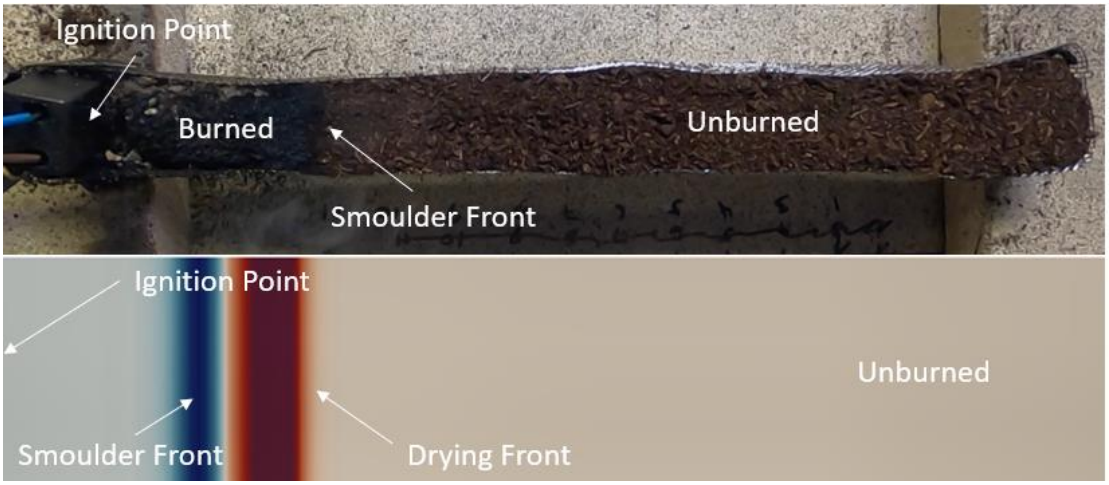

Figure 3- Top: Lateral peat spread experiment, smouldering direction left to right; Bottom: simulated peat smouldering, where red represents the drying front and blue represents the pyrolyzing front

5. Conclusions and application

The present work shows the first steps of an iterative modelling and experimental process aimed at ultimately predicting GHG emissions from smouldering peat fires. The experimental MLR results show areas of pyrolysis versus oxidation, correlating with expected carbon emissions. More detailed modelling results will be presented after verification with literature and validations with the experiments has been completed. A limitation of this model is the 1-D assumption as peat smouldering, particularly in field environments, is spatially heterogeneous. While the current computational model is 1-D, the code base is fully 3-D, allowing for easy expansion to higher dimensions in future work. Further work will include the iterative experimental/computational design process described.

6. Acknowledgements

The authors would like to acknowledge Sagar Gautam, Mark Lara, and Umakant Mishra for our discussions on this work. HA and DK acknowledge the financial support of the School of Engineering, University of Edinburgh. Funding for the modeling portion of this work was provided by the Sandia LDRD program. This paper describes objective technical results and analysis. Any subjective views or opinions that might be expressed in the paper do not necessarily represent the views of the U.S. Department of Energy or the United States Government.

7. References

Amin, H.M.F., Hu, Y., Rein, G. (2020) Spatially resolved horizontal spread in smouldering peat combining infrared and visual diagnostics. *Combustion and Flame* 220: 328-336.

Beaulne, J., Garneau, M., Magnan, G., Boucher, É. (2021) Peat deposits store more carbon than trees in forested peatlands of the boreal biome. *Scientific Reports* 11, 2657.

Christensen, E.G., Hu, Y., Purnomo, D.M.J., Rein, G. (2021) Influence of wind and slope on multidimensional smouldering peat fires. *Proceedings of the Combustion Institute* 38(3): 5033-5041.

Hadden, R.M., Rein, G., Belcher, C.M. (2013) Study of the competing chemical reactions in the initiation and spread of smouldering combustion in peat. *Proceedings of the Combustion Institute* 34(2): 2547-2553.

Hu, Y., Cui, W., Rein, G. (2020) Haze emissions from smouldering peat: The roles of inorganic content and bulk density. *Fire Safety Journal* 113, 102940.

Huang, X., Rein, G. (2014) Smoldering combustion of peat in wildfires: Inverse modelling of the drying and the thermal and oxidative decomposition kinetics. *Combustion and Flame* 161: 1633-1644.

Huang, X., Rein, G., Chen, H. (2015) Computational smoldering combustion: Predicting the roles of moisture and inert contents in peat wildfires. *Proceedings of the Combustion Institute* 35: 2673-2681.

Huang, X., Rein, G. (2015) Computational study of critical moisture and depth of burn in peat fires. *International Journal of Wildland Fire* 24: 798-808.

Huang, X., Rein, G. (2017) Downward spread of smouldering peat fire: the role of moisture, density and oxygen supply. *International Journal of Wildland Fire* 26(11): 907-918.

Huang, X., Rein, G. (2019) Upward-and-downward spread of smoldering peat fire. *Proceedings of the Combustion Institute* 37(3): 4025-4033.

Krieger Filho, G.C., Bufacci, P., Costa, F., Cortez, E.V., Andrade, J.C., Riberiro, K., Costa, F.D.S. (2021) Smoldering characteristics of high bulk density peat. *Proceedings of the Combustion Institute* 38(3): 5053-5062.

Lin, S., Cheung, Y.K., Xiao, Y., Huang, X. (2020) Can rain suppress smoldering peat fire? *Science of the Total Environment* 727, 138468.

Lin, S., Liu, Y., Huang, X. (2021) How to build a firebreak to stop smouldering peat fire: insights from a laboratory-scale study. *International Journal of Wildland Fire* 30(6): 454-461.

Notz, P.K., *et al*. (2016) *SIERRA Multimechanics Module: Aria User Manual*. Tech. rep. Albuquerque, NM: Sandia National Laboratories.

Rein, G., Cohen, S., Simeoni, A. (2009) Carbon emissions from smouldering peat in shallow and strong fronts. *Proceedings of the Combustion Institute* 32(2): 2489-2496.

Rodríguez Vásquez, M.J., Benoist, A., Roda, J.-M., Fortin, M. (2021). Estimating Greenhouse Gas Emissions From Peat Combustion in Wildfires on Indonesian Peatlands, and Their Uncertainty. *Global Biogeochemical Cycles* 35(2).

Yang, J., Chen, H., Liu, N. (2016), Modeling of Two-Dimensional Natural Downward Smoldering of Peat. *Energy & Fuels* 30(10): 8765-8775.

Experimental evaluation of bench-scale flammability of Ulex europaeus using a cone calorimeter

Katharine O. Melnik*[1]; Andres Valencia[1]; Dennis Pau[1]; Andy Park[2]; Marwan Katurji[3]; Daniel Nilsson[1]; Greg Baker[4]; Oleg M. Melnik[5]; Grant Pearce[6]; Tara Strand[7]

[1]*Department of Civil and Natural Resources Engineering, University of Canterbury, Christchurch, New Zealand, {kme96@uclive.ac.nz}*
[2]*School of Product Design, University of Canterbury, Christchurch, New Zealand*
[3]*School of Earth and Environment, University of Canterbury, Christchurch, New Zealand*
[4]*Fire Research Group Ltd, Wellington, New Zealand*
[5]*Forest Management Division, Department of Environment and Natural Resources, Government of the Northwest Territories, Fort Smith, Canada*
[6]*Fire and Emergency New Zealand, Christchurch, New Zealand*
[7]*New Zealand Forest Research Institute (Scion), Christchurch, New Zealand*

**Corresponding author*

Keywords

Gorse, oxygen consumption, TGA/DSC, heat release rate, burning behaviour

Abstract

Wildfires have been causing considerable damage worldwide, and improving the ability to predict wildfire behaviour will ensure effective emergency response and keep ecosystems and communities safe. Increasing the understanding of factors affecting vegetation flammability is necessary for improving fire behaviour prediction models. This work investigates the influence of moisture content on the flammability of live and dead needles (0-3mm), twigs (3.1-6mm) and stems (6.1-10mm) of gorse (Ulex europaeus L.). Gorse is a shrub invasive in New Zealand, Chile and Western United States. In these countries, gorse poses a fire risk to nearby communities, as it contains flammable volatile resins, accumulates a substantial amount of elevated dead material, and grows in large masses, all of which promote fire ignition and growth. Gorse flammability was quantified with a bench-scale oxygen consumption calorimeter (cone calorimeter) with a focus on heat release rate. Supporting tests were performed on small sub-samples using simultaneous thermogravimetric analysis (TGA) and differential scanning calorimetry (DSC) to assess material-scale pyrolysis dynamics, providing fine scale information on the thermal degradation of each tissue type at the particle level.

The experimental methodology included investigation of the maximum moisture content at which each tissue type can ignite at 50 kW/m2, which is a reasonable approximation of the heat flux at the vegetation surface during fire front arrival in a shrub fire. Six moisture content levels from zero to the highest ignitable moisture content were then selected, and samples were conditioned in a climate chamber until the desired moisture content was reached. Three replicates of each tissue type were tested in a cone calorimeter at each moisture content. Flammability was assessed based on the heat release rate, total heat release, effective heat of combustion, residual mass fraction, time to ignition and combustion duration. Additionally, a small sub-sample of fresh live and dead needles, twigs and stems was analysed in the TGA/DSC apparatus. TGA/DSC results showed a different thermal degradation mechanism between live and dead fuel, with live tissue undergoing pyrolysis at a lower temperature than dead. However, the pyrolysis dynamics were not substantially different between needles, twigs, and stems, suggesting that the differences in their flammability attributes measured in the cone calorimeter are likely driven by physical characteristics such as surface-area-to-volume ratio rather than chemical composition. The results of this work contribute to the understanding of gorse flammability and the effect of moisture content and fuel structure on fire behaviour.

1. Introduction

In recent years, wildfires around the world have been increasing in frequency, intensity and duration (Jolly et al., 2015), leading to the loss of lives and property, and the destruction of ecologically important areas. Simultaneously with changes to the wildfire regime, a growing number of people are living in the wildland-urban interface (WUI) – the interface between the urban setting and the rural landscape such as lifestyle blocks (Andrew & Dymond, 2013), significantly increasing the potential damage from wildfires due to the proximity

of people and property to large vegetated areas. More wildfires are entering the urban environment from the natural surroundings, such as the 2018 Carr Fire in Northern California (Lareau et al., 2018) and the 2017 Port Hills Fire in Christchurch, New Zealand (Pearce, 2018). In order to protect the growing WUI and make communities more resilient to future wildfire events, it is vital to understand fire behaviour and the complex interactions between fire, fuel (vegetation), weather and terrain in these environments. The current knowledge of how vegetation characteristics such as species, size, chemical composition and physiological properties affect wildfire behaviour (e.g. heat production, rate of spread, thermal radiation, etc.) is limited, and there is a need to increase our understanding of the physical and chemical dynamics of vegetative fuels commonly found in the WUI.

Gorse (*Ulex europaeus* L.) is a shrub native to Western Europe that has been introduced to other parts of the world (Kariyawasam and Ratnayake 2019), and is a prolific invasive species in some places such as New Zealand, Chile, and Western United States. Gorse poses a serious problem not only from a land management perspective, but also for wildfire management, as it occupies vast areas, often near populated centres (Figure 1), and burns readily. The flammability attributes of gorse and how they are affected by plant characteristics have not been extensively studied in the literature. Previous studies show that moisture content and surface-area-to-volume ratio are among the most important variables dictating plant flammability (White & Zipperer, 2010, Fares et al., 2017, Etlinger & Beall, 2004), and both of these characteristics vary spatially and temporally.

Figure 1 – Gorse shrubland on a hillside overlooking Christchurch, New Zealand

The flammability of vegetation is a complex phenomenon that encompasses attributes of the fuel's ability to initiate and propagate combustion. There are four main components of vegetation flammability: ignitibility, or the ease with which the fuel ignites; combustibility, or the rate at which combustion occurs; consumability, or the proportion of biomass that gets consumed; and sustainability, or the ability of the fuel to maintain combustion and produce energy (Anderson, 1970; Martin, 1994; White & Zipperer, 2010).

On one hand, oxygen consumption calorimetry is a relatively direct method for quantifying heat release rate (HRR) by measuring the amount of oxygen consumed per unit mass of fuel during the combustion of the sample. A cone calorimeter (Huggett 1980, Janssens 2002) is a bench-scale oxygen consumption calorimeter that creates a nearly uniform heat flux at the surface of a 10×10 cm^2 sample with a conical heating coil. A cone calorimeter measures all four flammability components: ignitibility as the time to sustained ignition, combustibility as the averaged and maximum heat release rate, consumability as the mass loss rate, and sustainability as the duration of heat release. Although all these components are considered in this study, emphasis was placed on the heat release rate, as it is considered to be the main attribute for describing fuel flammability (Babrauskas & Peacock, 1992; Madrigal et al., 2012), and can be used to indicate the extent of damage caused to the environment as well as the amount of energy available for igniting subsequent fuel and propagating the fire.

On the other hand, simultaneous thermogravimetric analysis (TGA) and differential scanning calorimetry (DSC) is a method that can give insight into the small-scale flammability dynamics of a solid fuel, tracking the mass loss rate of a small (~15 mg) sample in pure nitrogen while the temperature is increased at a consistent rate. Unlike with the cone calorimeter, measurements at this small scale provide insights into flammability characteristics that fundamentally affect fire behaviour. More specifically, variables such as particle size and moisture content are explicitly disregarded in the context of TGA/DSC measurements, so the results can be

directly tied to other attributes such as live/dead condition of the sample. This technique is used in this study to complement and reinforce the analysis emerging from the cone calorimetry results.

The objectives of this research are to evaluate the effect of moisture content on gorse flammability, and to investigate the effect of condition (live and dead) and tissue diameter (needles, twigs and stems) of gorse on its flammability. These objectives are achieved by quantifying the heat release rate, effective heat of combustion, residual mass fraction, time to ignition and combustion duration of live and dead needles, twigs and stems at a range of moisture contents. Because of word-limit constraints, we only report cone calorimeter test results for a single moisture content of 7%, and results from TGA/DSC for a single heating rate of 20°C/min.

2. Materials and methods

2.1. Sample collection and classification

The flammability of six gorse tissue types was investigated, namely dead and live needles, twigs and stems using the cone calorimeter and the TGA/DSC apparatus. The samples were collected from a research site (43.461°S, 172.353°E) along the Waimakariri river, north of West Melton, New Zealand. The predominant vegetation at the site is gorse, with plant heights ranging from 40 to 200 cm. Plant material up to one centimetre in diameter was collected and separated into needles, twigs and stems based on diameter, with particles up to 3 mm classified as needles, material from 3.1 to 6 mm classified as twigs, and material from 6.1 to 10 mm classified as stems. The groups were further separated into live and dead condition based on the colour and general appearance of the material (Figure 3).

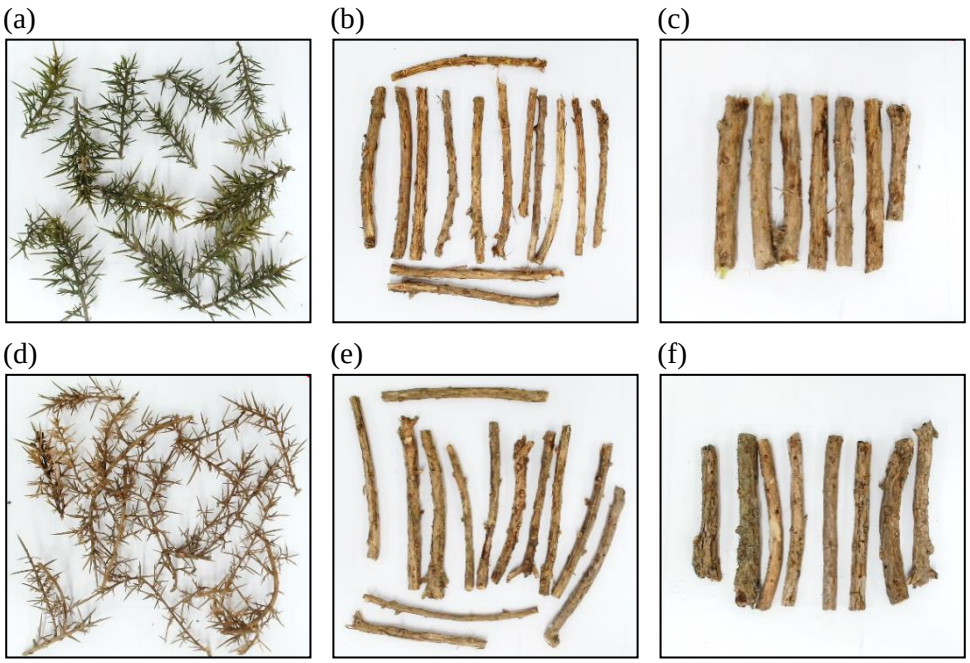

Figure 2 – Examples of six tissue types tested in the cone calorimeter and the TGA/DSC apparatus: live needles (a), live twigs (b), live stems (c), dead needles (d), dead twigs (e), and dead stems (f). The samples shown were prepared for testing in the cone calorimeter, and all have the apparent surface area of 70 cm^2.

2.2. Cone calorimetry

The collected plant material was trimmed to 10 cm lengths to fit into the 10×10 cm^2 sample holder of the cone calorimeter. Some material of each tissue type was placed into an environmental chamber to obtain a range of moisture contents, and ignition tests were performed on each tissue type to determine the maximum moisture content at which piloted ignition can occur at 50 kW/m^2. The heat flux of 50 kW/m^2 was chosen for ignition testing and cone calorimetry experiments because it is representative of the radiative heat flux at the vegetation surface at the time of fire front arrival in a shrub fire (Morandini & Silvani, 2010). Following the ignition tests, six moisture content treatment levels were selected to span the range from 0% up to the maximum ignitable moisture content, and three replicates of each tissue type at each moisture content were prepared for testing in

the cone calorimeter, ensuring that the apparent surface area (the surface area of the sample exposed to the radiative heat flux from the cone heater) is consistent between samples.

Table 1 – Experimental design for the cone calorimetry tests and TGA/DSC tests, with 7% tissue moisture content for cone colometry samples, and variable moisture content representative of field conditions for TGA/DSC samples

3 tissue sizes		2 conditions		2 experiments		1 or 3 replicates
Needles Twigs Stems	×	Live Dead	×	Cone calorimetry	×	Rep 1 Rep 2 Rep 3
				TGA/DSC	×	Rep 1

The samples were tested in the cone calorimeter at 50 kW/m^2 in accordance with the ISO 5660-1 standard (ISO 5660-1, 2002), with the exception that a porous 10×10×2 cm^2 wire frame sample holder (Barboni et al. 2017) was used to ensure that testing conditions are representative of field conditions. The surface area exposed to the cone heater element was kept at 70 cm^{-2} for all tissue types to ensure similar heating and ignition conditions. Because of word-limit constraints, we only report results from cone calorimeter test for a moisture content of 7%. Mass of the samples varied between the experiments as follows: 3.05 to 4.5g for needles, 12.9 to 15.7g for twigs, and 25.2 to 31g for stems.

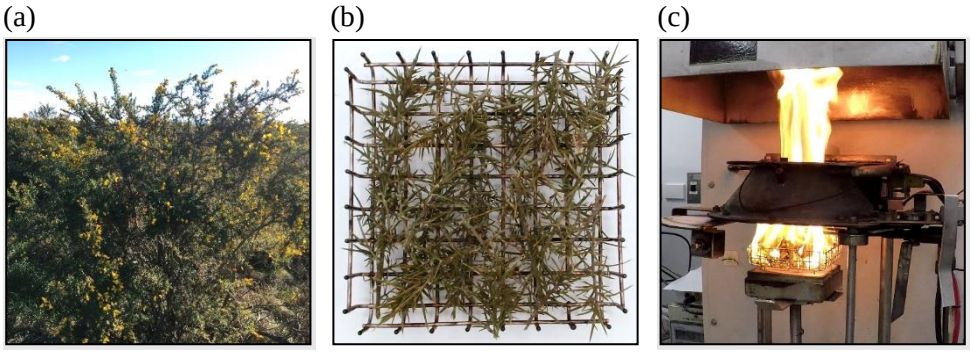

Figure 3 – Gorse plant at the field site (a), gorse needles in a sample holder prepared for the test in the cone calorimeter (b), and gorse needles during the test (c)

2.3. Simultaneous differential scanning calorimetry and thermogravimetry

SDT Q600 manufactured by TA Instruments was used to investigate the thermal decomposition behaviour of gorse needles under nitrogen environment. The equipment was calibrated following manufacturer's instructions for weight, temperature and heat flow at the tested heating rate. Fresh gorse samples were ground using a sample grinder and sealed in air-tight plastic containers for testing within 24 hours. Approximately 15 mg of ground sample was placed inside a 90 µL alumina cup, applying a dynamic heating mechanism from 20 to 1200°C at 20°C/min. The relative sample weight was calculated by dividing the raw weight by the weight of the sample at 185°C once all the cellular water evaporated and the mass loss rate stabilized.

3. Results

The heat release rate curves measured with the cone calorimeter for the six tissue types at 7% moisture content are presented in Figure 4. The pattern of heat release rate varies between tissue types, providing a good basis for comparing their overall flammability. Tissues of smaller diameter ignited faster and burned more vigorously, reaching their peak heat release rate faster than larger size classes, while larger particle sizes were associated with delayed ignition, longer burning and decay stages of combustion, and greater total energy production.

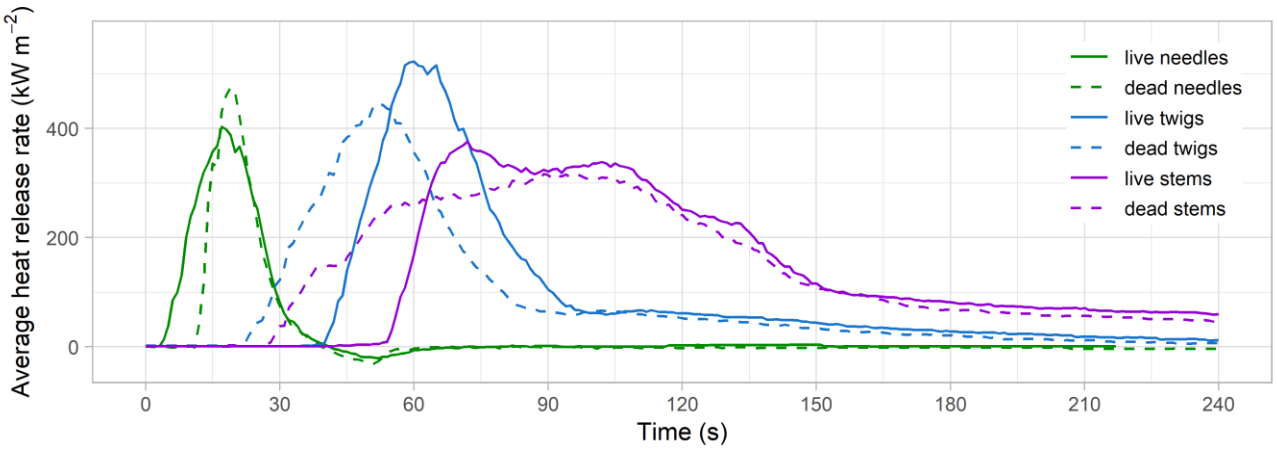

Figure 4 – Heat release rate for gorse needles with 7% moisture content as a function of time since the start of exposure to the radiative heat flux of 50 kW m^{-2}. Three replicates of each tissue type were tested, and their results were averaged into one curve for readability.

Flammability attributes derived from the heat release rate data are summarised in the top row of Figure 5, and attributes manually measured in the lab during testing are shown in the bottom row of the figure. Total heat release ranged from 50.6 kJ to 502 kJ for all tissue types at the studied moisture content. The effective heat of combustion ranged from 13.7 to 18.1 kJ g^{-1}, which is similar to the 12 to 17 kJ g^{-1} range observed for Douglas fir (*Pseudotsuga menziesii* (Mirb.) Franco) trees with 5 to 15% moisture content (Babrauskas, 2006). Peak heat release rate, a measure of combustibility, increased with decreasing particle size, and ranged from 318 to 613 kW m^{-2} across tissue types. This is similar to values found in literature for different species such as 400 kW m^{-2} for dead litter of *Pinus pinaster* (Madrigal et al., 2011) obtained using mass loss calorimetry, and 550 to 1050 kW m^{-2} for dead leaves and twigs of *Cistus monspeliensis* 0.75 to 3mm in diameter (Barboni et al., 2017) obtained with a cone calorimeter. Time to ignition, a measure of ignitibility, and combustion duration, a measure of sustainability, increased with increasing particle size. Time to ignition ranged from 8 to 59 seconds, while combustion duration ranged from 10 to161 seconds respectively. Time to ignition for individual tissue types was comparable to values found in literature. For instance, time to ignition for live and dead twigs measured in this study was between 23 and 51 seconds, while the time to ignition for oven-dried leaves and twigs of Montpellier cistus (*Cistus Monspeliensis* L) from existing literature was 35.7 ± 5.8 seconds. Residual mass fraction ranged from 0.0236 to 0.077 g g^{-1}, and was considerably higher for dead tissue compared to live tissue. Further experiments are required to gain insights into this trend.

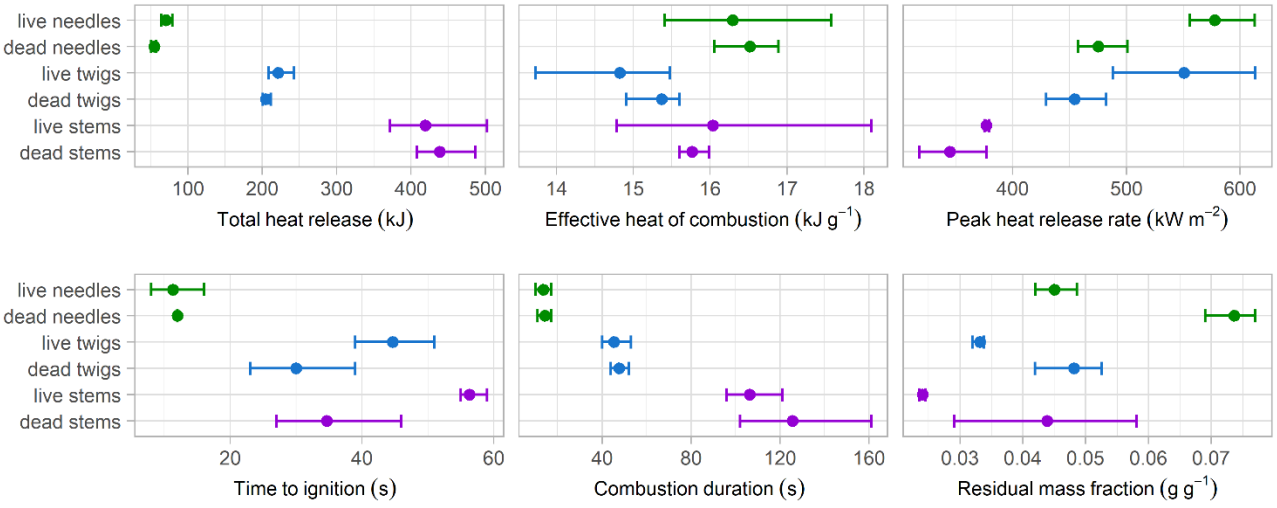

Figure 4 – The mean and range of flammability attributes measured with the cone calorimeter. The whiskers indicate the minimum and maximum values measured for the three replicates, and the point indicates the mean

The mass loss rate of small (~15 mg) ground samples of the six tissue types measured in the TGA/DSC apparatus is presented in Figure 6. The peak mass loss was greater for the live needles, twigs and stems (1.14, 1.02 and

0.904 % °C^{-1} respectively) compared to the dead needles, twigs and stems (0.61, 0.78 and 0.74 % °C^{-1} respectively). The peak mass loss also generally occurred at a lower temperature for the live needles, twigs and stems (93, 356 and 350 °C respectively) than for the dead needles, twigs and stems (366, 371 and 348 °C respectively). The varying slope before the decomposition peak and the subsequent plateau and perturbations after the decomposition peak for all tissue types indicate that gorse tissues consist of multiple material components, which thermally decompose across overlapping temperature range.

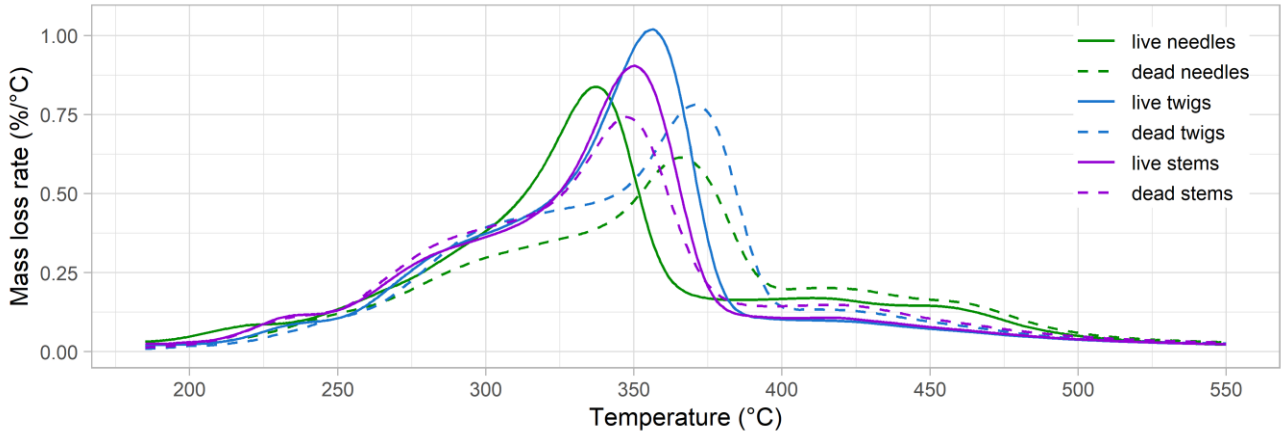

Figure 6 – TGA/DSC results: mass loss rate as a function of temperature at the heating rate of 20 °C/min

The pyrolysis dynamics were not substantially affected by particle size for live material, as the degradation rate and temperature peaks were around 350°C, suggesting that the differences in flammability attributes measured in the cone calorimeter are likely driven by physical characteristics such as surface-area-to-volume ratio rather than chemical composition. Generally, dead material showed higher peak temperature, suggesting lower flammability potential, which can be associated with the differences in the volatiles content.

4. Acknowledgements

The authors thank Grant Dunlop, Logan Cooper and Milap Dhakal for assistance with experimental tests, and Environment Canterbury for providing access to the research site. This research was co-funded by Ministry of Business, Innovation and Employment (MBIE), New Zealand (grant number C04X2103 “Extreme wildfire, our new reality, are we ready?”), the Royal Society of New Zealand (grant number RDF-UOC1701), and the University of Canterbury College of Engineering.

5. References

Anderson, H. E. (1970). Forest fuel ignitibility. *Fire Technology*, *6*(4), 312–319. https://doi.org/10.1007/BF02588932

Babrauskas, V., & Peacock, R. D. (1992). Heat release rate: the single most important variable in fire hazard. In *Fire Safety Journal* (pp. 255–272). https://doi.org/10.1007/978-3-319-52090-2_68

Babrauskas, V. (2006). Effective heat of combustion for flaming combustion of conifers. *Canadian Journal of Forest Research*, *36*(3), 659–663. https://doi.org/10.1139/x05-253

Barboni, T., Leonelli, L., Santoni, P.-A., & Tihay-Felicelli, V. (2017). Influence of particle size on the heat release rate and smoke opacity during the burning of dead Cistus leaves and twigs. *Journal of Fire Sciences*, *35*(4), 259–283. https://doi.org/10.1177/0734904117709964

Beltrán, V., Martínez, L. V., López, A., & Gómez, M. F. (2019). Kinetic analysis of Wood residues and Gorse (Ulex europaeus) pyrolysis under non-isothermal conditions: A case of study in Bogotá, Colombia. *E3S Web of Conferences*, *103*, 1–6. https://doi.org/10.1051/e3sconf/201910302004

Huggett, C. (1980). Estimation of rate of heat release by means of oxygen consumption measurements. *Fire and Materials*, *4*(2), 61–65. https://doi.org/10.1002/fam.810040202

ISO 5660-1. (2002). Reaction-to-fire tests-Heat release, smoke production and mass loss rate-Part 1: heat release rate (cone calorimeter method).

Janssens M (2002) Chapter 3-2: Calorimetry. In 'The SFPE handbook of fire protection engineering'. 3rd edn. (Eds PJ DiNenno, WD Walton) pp. 3-38–3-62. (National Fire Protection Association: Quincy, MA)

Jolly, W. M., Cochrane, M. A., Freeborn, P. H., Holden, Z. A., Brown, T. J., Williamson, G. J., & Bowman, D. M. J. S. (2015). Climate-induced variations in global wildfire danger from 1979 to 2013. *Nature Communications*, *6*(May), 1–11. https://doi.org/10.1038/ncomms8537

Kariyawasam, C., & Ratnayake, S. (2019). Reproductive biology of gorse, Ulex europaeus (Fabaceae) in the Mount Lofty Ranges of South Australia and Sri Lanka. *The International Journal of Plant Reproductive Biology*, *11*(2), 145–152. https://doi.org/10.14787/ijprb.2019

Lareau, N. P., Nauslar, N. J., & Abatzoglou, J. T. (2018). The Carr Fire Vortex: A Case of Pyrotornadogenesis? *Geophysical Research Letters*, *45*(23), 13,107-13,115. https://doi.org/10.1029/2018GL080667

Madrigal, J., Guijarro, M., Hernando, C., Díez, C., & Marino, E. (2011). Effective Heat of Combustion for Flaming Combustion of Mediterranean Forest Fuels. *Fire Technology*, *47*(2), 461–474. https://doi.org/10.1007/s10694-010-0165-x

Madrigal, J., Marino, E., Guijarro, M., Hernando, C., & Díez, C. (2012). Evaluation of the flammability of gorse (Ulex europaeus L.) managed by prescribed burning. *Annals of Forest Science*, *69(3)*, 387–397. https://doi.org/10.1007/s13595-011-0165-0

Martin, R. (1994). Assessing the flammability of domestic and wildland vegetation. *12th Conference on Fire and Forest Meteorology, At Jekyll Island, GA, USA, Volume: Pages 26-28, November*, 26–28. https://doi.org/10.13140/RG.2.1.3999.3680

Morandini, F., & Silvani, X. (2010). Experimental investigation of the physical mechanisms governing the spread of wildfires. *International Journal of Wildland Fire*, *19*(5), 570–582. https://doi.org/10.1071/WF08113

Pearce, H. G. (2018). The 2017 port hills wildfires-a window into New Zealand's fire future? *Australasian Journal of Disaster and Trauma Studies*, *22*(Special Issue), 35–50.

Weise, D. R., White, R. H., Beall, F. C., & Etlinger, M. (2005). Use of the cone calorimeter to detect seasonal differences in selected combustion characteristics of ornamental vegetation. *International Journal of Wildland Fire*, *14*(3), 321–338. https://doi.org/10.1071/WF04035

White, R. H., & Zipperer, W. C. (2010). Testing and classification of individual plants for fire behaviour: Plant selection for the wildlandurban interface. *International Journal of Wildland Fire*, *19*(2), 213–227. https://doi.org/10.1071/WF07128

Flame spread and combustion dynamics in pine litter under unsteady wind conditions

Eric V Mueller*[1]; Zakary Campbell-Lochrie[2]; Carlos Walker-Ravena[2]; Matt Patterson[3]; Jason Cole[3]; Michael R Gallagher[3]; Kenneth L Clark[3]; Nicholas S Skowronski[3]; Rory M Hadden[2]

[1] National Institute of Standards and Technology. Gaithersburg, MD, USA, {eric.mueller@nist.gov}
[2] University of Edinburgh. Edinburgh, UK, {Z.Campbell.Lochrie, c.walkerravena, r.hadden@ed.ac.uk}
[3] USDA Forest Service Northern Research Station. Morgantown WV, Syracuse NY, and New Lisbon NJ, USA, {matthew.m.patterson, jason.cole2, michael.r.gallagher, kenneth.clark, nicholas.s.skowronski}@usda.gov

**Corresponding author*

Keywords

Flame spread, combustion dynamics, prescribed fire, field experiment, pine litter

Abstract

Understanding flame spread and combustion dynamics in surface fuels is important for both planning and evaluating the impact of prescribed fires. However, prescribed fires tend to be conducted under light and unsteady wind conditions as compared with those which have been well studied for wildfire scenarios. To improve this understanding and provide data for next-generation fire models, it is necessary to collect detailed time-resolved observations of these processes. To accomplish this, a series of small-scale field experiments was conducted in pine needle litter. 10 m x 10 m plots were constructed with fuel loads of either 0.5 kg/m2, 1.0 kg/m2, or 1.5 kg/m2. Wind was measured with an array of 17 anemometers and flame spread and combustion mode were monitored with an overhead infrared camera and thermocouple arrays. The light and gusty wind conditions resulted in unsteady fire behavior and a single relationship between wind speed and spread rate is unable to capture the range of behavior observed. A novel technique is introduced for identifying regions of flaming versus smoldering combustion in the infrared imagery. This approach indicates that flaming and smoldering times can be related directly to fuel loads, rather than wind conditions, though more work is required to link these times to burning rates. The implication is that dynamic flame spread in these conditions is difficult to predict without models that account for fire-atmosphere interactions. However, fuel consumption, and therefore prescribed fire effects, may be more straightforward to predict. This work has also resulted in a uniquely detailed dataset for testing fire models.

1. Introduction

Understanding and predicting fire behavior in relatively light and unsteady wind conditions is important in the context of prescribed fire. A quantitative approach to both planning these activities and evaluating their effectiveness relies on such an understanding (Hiers et al., 2020). For example, modelling the spread rate of fires can help practitioners plan specific burns to optimize desired objectives. However, unlike fires under strong wind conditions (typical of wildfires) and steady or zero wind conditions (typical of laboratory studies), realistic burning conditions during prescribed fires often involve light, dynamic winds where fire-induced buoyant flows may become dominant. In order to investigate the effect of these conditions, and to provide detailed data for modeling efforts, a series of field experiments was conducted in pine needle litter. The aim of this work is to analyze highly-resolved measurements of flame spread and combustion to determine the relative roles of fuel structure and wind at fine scale, under conditions relevant to prescribed burning.

2. Methods

Experiments were carried out on a 10 m x 10 m plot (see Figure 1) within a pitch pine/loblolly pine plantation in the Pinelands National Reserve of New Jersey. A total of 35 experiments were conducted under various fuel and weather conditions; however, this analysis focuses on a subset of 19 of these for which fire spread

successfully across the plot and the measurements made were consistent. The fuel beds consisted of pitch pine (*Pinus rigida* Mill.) needles or an equal mix of pitch pine needles and oak (predominantly *Quercus montana Willd.*) leaves from local sources. The beds were manufactured to achieve average loadings of nominally 0.5 kg/m^2, 1.0 kg/m^2, or 1.5 kg/m^2, in order to represent different prescribed fire return intervals. Burns were carried out in ambient temperatures between 17 °C and 31 °C, relative humidity between 22 % and 66 %, and fuel moisture contents between 5.9 % and 14.4 %.

2.1. Wind measurement

Wind was measured with an array of 17 3D sonic anemometers (Figure 1). One of these was located at the plot center at a height of 10 m Above Ground Level (AGL), while the remaining 16 were in a 4x4 grid at nominally 3.0 m AGL. All anemometers were sampled at a frequency of 10 Hz.

For this analysis, a characteristic time-dependent horizontal wind vector was determined for each experiment. All anemometers were used for this calculation, to give an indication of the average wind across the experimental area. Previous measurements of ambient wind in the plantation indicated low sensitivity to height between the 2.5 m and 10 m levels (both are in the open sub-canopy space). Measurements of *u* and *v* velocity components were averaged independently, using 10-second moving average. Readings where the anemometer recorded a temperature in excess of 50 °C were rejected from this process, as they were within the fire plume and outside the operating range of the anemometer.

The spatial averaging procedure removes any localized features of the wind field, over the plot area, but allows for the fact that at any given moment, individual sensors may be impacted by the fire and not produce reliable data. The temporal averaging procedure removes some high frequency components of the signal in order to focus on the dominant behavior. The choice of a 10-second window was guided by the fact that mean winds were on the order of 1 m/s and the plot length was 10 m.

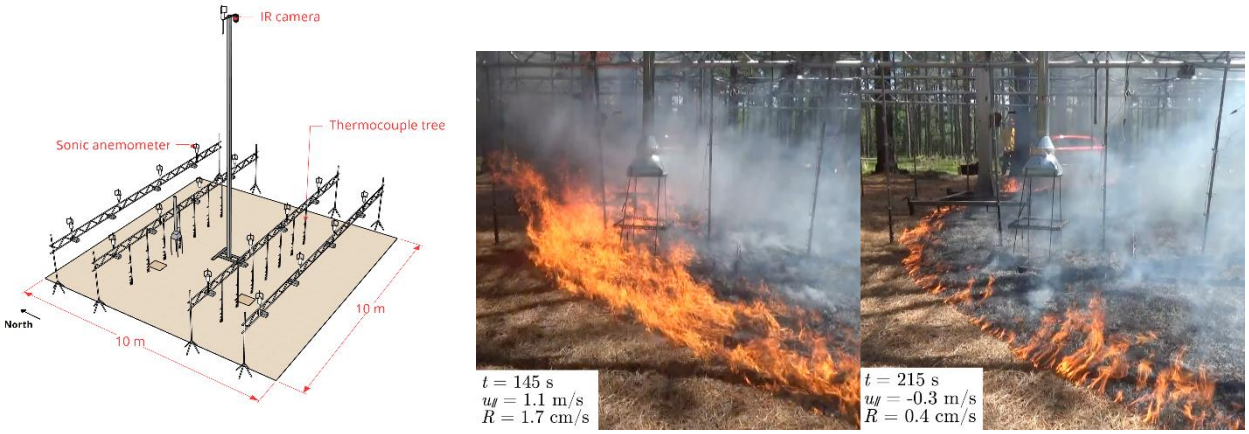

Figure 1- (left) Schematic of experimental plots; (right) example of fire spread during heading and backing conditions in a single experiment.

2.2. Flame spread

Infrared (IR) images were captured from a downward-facing IR camera placed at the center of the plot (Figure 1). The camera had a frame rate of nominally 25 Hz and provided a resolution of ~5 cm^2/pixel. True temperature measurement of the fuel bed is complicated by several factors (including unknown emissivity and possible emission and absorption by combustion products). However, the data are still valuable in a comparative sense, as described below, and temperatures are referred to as 'pixel' temperature rather than solid or gas phase.

The IR data were used to determine the progression of the leading edge of the flame front as a function of time. For each pixel, the arrival time of the flame front was determined by the corresponding temperature first exceeding 200 °C for a continuous period at least 1 second. The exact location of the flame front is sensitive to these criteria, but the advancement of the front is much less so.

Masks were applied to remove regions of spurious data where objects (e.g., camera support tower, instrumentation trusses, trees) obscure the view of the camera. Images were post processed and projected onto a Cartesian coordinate system. The spread rate, *R*, was calculated by taking the inverse of the gradient of the

arrival time matrix using and applying filtering and spatial averaging techniques to create a continuous spread map over the entire plot area (including masked regions).

Spread vectors with relevant corresponding arrival times were averaged to create a plot-average magnitude and direction of spread, excluding 1 meter of data on either flanking edge of the fire (dependent on the ignition edge). This approach allows the wind to be decomposed into the component in the direction of spread at a given moment, $u_{/\!/}$, and the component perpendicular, $u_{\perp}$, and the influence of wind could be analyzed independent of the compass direction at a given moment.

2.3. Combustion mode

An assessment of the combustion dynamics was conducted by estimating the duration of flaming and smoldering combustion for a given experiment. Separating these different combustion modes can prove quite difficult, particularly in the field. Visual assessment can be complicated by the obscuring presence of smoke and by the fact that the occurrence of smoldering combustion can be difficult to observe.

The IR imagery offers a solution to both problems; however, there is still a challenge in identifying the different regimes in the temperature signal for a given pixel. Both flaming and smoldering combustion may be associated with high temperatures in overlapping ranges, so it is not enough to simply apply thresholds. Further, the long-wave spectral range of the IR camera used here is poorly suited to observing emission from the flames.

Despite these challenges, visual inspection of the IR imagery shows that some presence of the flaming region can be detected. Because the flaming combustion zone is strongly affected by turbulence, we hypothesize that the ability to observe this region in the IR footage is a function of the rapid fluctuation in the temperature signal, rather than its absolute value. Therefore, we classified the combustion modes by analyzing these fluctuations.

A short-time Fast Fourier Transform was computed on the pixel noise, taken as the difference between the 25 Hz signal and a 1 Hz moving average. The average power at high frequency (> 4 Hz) was then computed. The maximum power was identified for each pixel, and the point at which the transient power falls below 5% of this value was taken as the threshold between flaming and smoldering. The onset of flaming was taken as the first point the 1-second moving average of temperature exceeds 200 °C, and the end of smoldering was taken as the final point above 200 °C. The resulting image of combustion times was then subjected to the same projection and spatial averaging as the spread rate map. This approach relies on user-selected thresholds for both the magnitude of the temperature and the magnitude of the signal noise. However, the calculation of flaming time was consistent with measurements made with thermocouples positioned at the top of the fuel bed (see Figure 1).

3. Results and discussion

3.1. Flame spread

Mean wind speeds were in the range of 0.5 m/s to 1.5 m/s, with relative standard deviations between 0.17 and 0.61. This gives an indication of the light and unsteady conditions; however, it does not account for shifts in wind direction which contribute to the dynamic fire behavior. Mean spread rates were in the range of 0.2 cm/s to 5.0 cm/s, with relative standard deviations between 0.26 and 1.73. To demonstrate the dynamic nature of individual burns, an example of the flame spread and wind calculation is shown in Figure 2. When the spread vector and the horizontal wind are not aligned there is necessarily a reduction in the magnitude of wind speed in the direction of spread ($u_{/\!/} \leq U$). An evaluation of the correlation between mean wind and spread, using Spearman's rank coefficient, yields a value of 0.22 (probability, p = 0.37) when using overall magnitude (U) and 0.53 (p = 0.02) when using magnitude in the direction of spread ($u_{/\!/}$). This points to the importance of capturing the dynamic wind in gusty conditions, rather than an average horizontal magnitude.

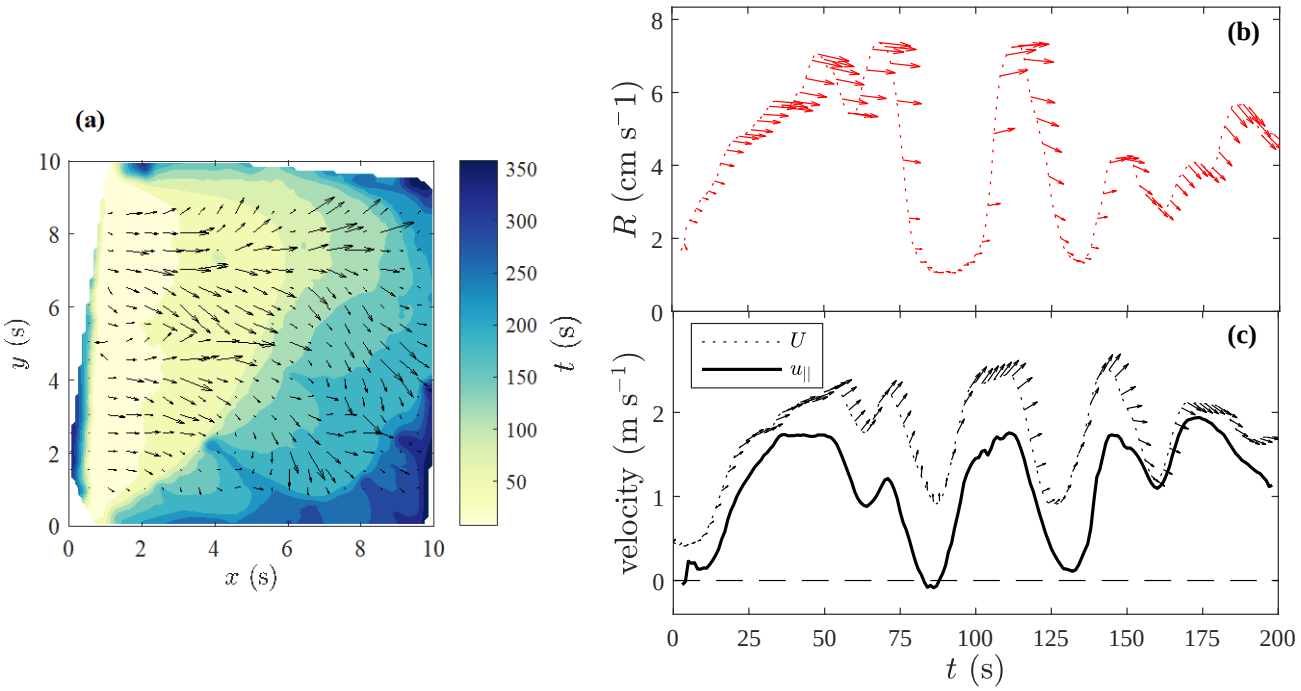

Figure 2- Example of fire spread analysis for one burn, ignited from the west (x = 0 m) with a fuel load of 0.5 kg/m². (a) The computed vectors of spread rate, overlaid on a contour plot of arrival time. (b) The time history of plot-average spread vectors. (c) The average wind vectors with the total magnitude (U), and wind magnitude in the direction of average spread ($u_{\parallel}$).

The analysis of spread rate and wind speed for all burns indicates a large scatter which cannot be accounted for with other environmental variables (fuel load, fuel moisture, relative humidity, ambient temperature). This is demonstrated by normalizing the spread by its value with no-wind, as shown in Figure 3. Large deviations occur when fitting to possible simple models for wind speed dependence. In fact, a hysteresis was observed in temporally resolved relationships of spread rate and wind. An assessment of Byram's convective number (Nelson, 1993) indicates the significant feedback between wind speed and spread rate is linked to the marginal conditions – fires are neither consistently plume dominated nor wind driven.

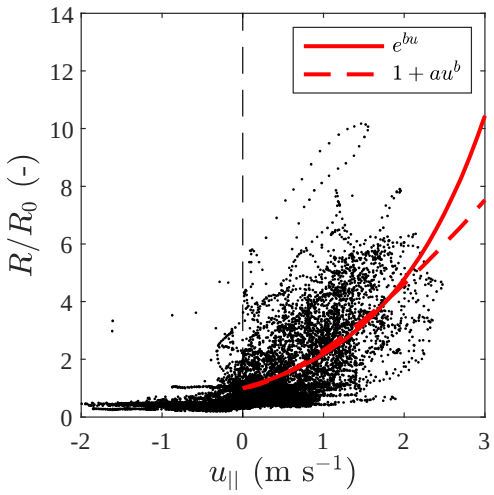

Figure 3- Relationship between instantaneous wind and spread rate. Spread rate is normalized against the average no-wind ($|u_{\parallel}|$<0.2 m/s) value for a given burn. Red lines are fits to common functions (Sullivan, 2009).

3.2. Combustion mode

An example of the analysis of flaming versus smoldering time is shown in Figure 4. The thermocouple and IR pixel temperature increase dramatically at the same time, indicating arrival of the fire front. Both maintain an elevated temperature for roughly 40 s, at which point the thermocouple temperature drops rapidly while the pixel temperature remains elevated. The power in the high-frequency noise in pixel temperature drops dramatically at the same time the flaming period ends, thus all remaining time at elevated temperature can be classified as smoldering.

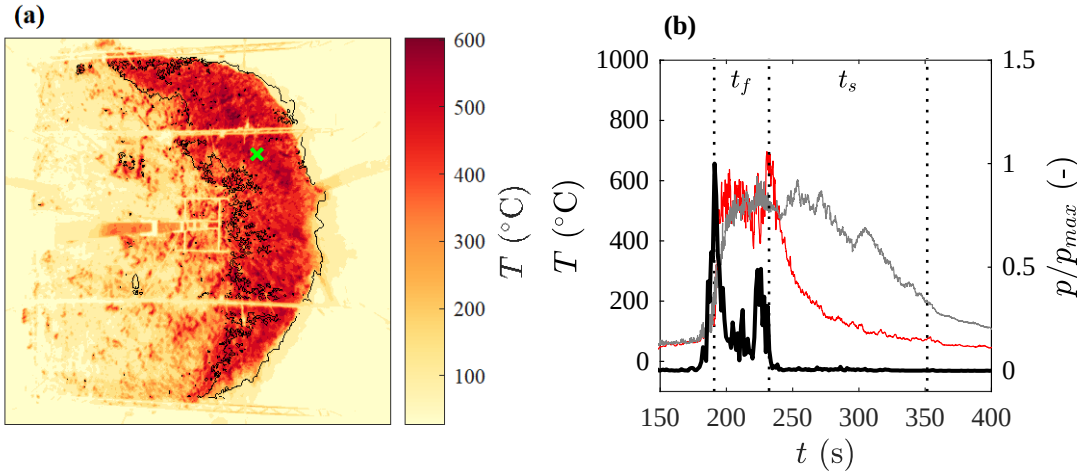

Figure 4- Example of fire spread analysis for one burn, ignited from the west (x = 0 m) with a fuel load of 1.5 kg/m^2. (a) Single frame of IR footage with sample point at the base of a thermocouple array shown as a green x. The region of active flaming is shown by the black contour line. (b) Time history at the sample point in (a): thermocouple temperature (red), pixel temperature (grey), and normalized power of noise (black). Duration of flaming (t_f) and smoldering (t_s) are shown by vertical lines.

The mean and standard deviations of both flaming and smoldering time are shown for each relevant burn in Figure 5. The duration of both combustion modes increases with fuel load, but the ratio may not be constant and requires more analysis. Preliminary results also indicate that wind speed is a less significant factor than fuel load under these conditions.

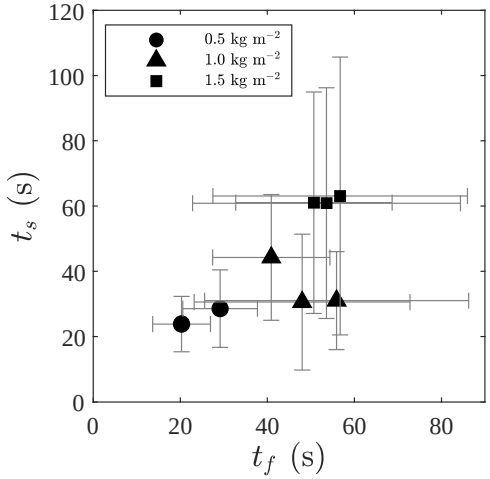

Figure 5- Average flaming time (t_f) and smoldering time (t_s) for all relevant pixels in each of the 8 burns. Error bars represent one standard deviation.

4. Conclusions

We observed a dynamic relationship between flame spread and ambient wind in conditions typical of prescribed burns. This is not fully captured by simple relationships which do not consider fire-atmosphere feedback. The experimental data can help to provide uncertainty bounds to these simple relationships. They can also act as test cases for more complex models which attempt to resolve such interactions and therefore require data with greater spatial and temporal resolution than is often available.

The combustion analysis provides a novel method for obtaining maps of flaming and smoldering times, though there are some limitations associated with this approach. The time of transition between flaming and smoldering can be evaluated against thermocouple data, but sensitivity to the noise threshold requires further examination. The optimal criteria to identify the end of smoldering using these diagnostics is also unknown. Further analysis may be able to identify combustion behavior specific to certain periods of fire behavior (e.g., heading or backing fire) or as a function of spatial fuel distribution. The inclusion of detailed fuel consumption information could also aid in estimating mass loss rates. The current analysis also has implications for understanding emissions and smoke plume development, as a function of the mode and distribution of energy release. Here again, there is also significant value for testing models of fire-atmosphere interactions. Such models either require a parameterization of energy release or endeavor to resolve it directly, but in either case a better understanding of combustion in field conditions is essential.

5. References

Hiers, J. K., O'Brien, J. J., Varner, J. M., Butler, B. W., Dickinson, M., Furman, J., Gallagher, M., Godwin, D., Goodrick, S. L., Hood, S. M., Hudak, A., Kobziar, L. N., Linn, R., Loudermilk, E. L., McCaffrey, S., Robertson, K., Rowell, E. M., Skowronski, N., Watts, A. C., & Yedinak, K. M. (2020). Prescribed fire science: the case for a refined research agenda. Fire Ecology, 16(1). DOI: 10.1186/s42408-020-0070-8

Nelson Jr, R. M. (1993). Byram derivation of the energy criterion for forest and wildland fires. International Journal of Wildland Fire, 3(3), 131–138. DOI: 10.1071/WF9930131

Sullivan, A. L. (2009). Wildland surface fire spread modelling, 1990–2007. 2: Empirical and quasi-empirical models. International Journal of Wildland Fire, 18(4), 369–386. DOI: 10.1071/WF06144

Impact of prescribed burning on soil organism communities in a *Pinus laricio* forest.

Pauline Longeard*[1]; Pauline Belliard[1]; Sugahendni Nadarajah[1]; Antonella Massaiu[2]; Antoine Pieri[1]; Frederic Morandini[1]; Marie-Cécile Andrei-Ruiz[3]; Lila Ferrat[1]

[1] *University of Corsica, UMR CNRS 6134, Sciences Pour l'Environnement, BP 52, 20250 Corte, France, {longeard_p, belliard_p, nadarajah_s, Pieri_a, morandini_f, ferrat_l}@univ-corse.fr*
[2] *Office National des Forêts – U DFCI, 20250 Corte, France, {antonella.massaiu@onf.fr}*
[3] *Office de l'Environnement de la Corse – Observatoire, Conservatoire des Insectes de Corse, F-20250 Corte, France, {Marie-Cecile.Ruiz@oec.fr}*

**Corresponding author*

Keywords

Prescribed burning, heat transfer, *Pinus laricio* forest, soil macrofauna, soil mesofauna

Abstract

The objective of this preliminary study is to highlight the potential impacts of prescribed fire on soil organism communities in Pinus laricio forests, a species endemic to Corsica. For this purpose, a control plot, and a plot burned on 10th November 2020, were delimited in Bavella (South Corsica). The intensity of the burning was characterized using K-Type thermocouples at different depths in the soil. Soil organisms were collected with pitfall trap and Berlèse method, then identified to the order. Results show a decrease of all orders on the burned plot, with important potential of survival of the organisms in the soil, since heat transfer is weak (+10°C max at 3cm depth) and the burned surfaces heterogeneous. A rapid recolonization is indeed observed in the spring. The contribution of organic matter, minerals, and free ecological niches could encourage this phenomenon.

In order to better understand the heterogeneity of the plots and to highlight the specificities of Pinus laricio forests, a study at the sub-plot level is in progress, as well as an identification of organisms up to the family level.

1. Introduction

In the Mediterranean Basin, forest fires are a recurrent problem. Pines are particularly affected by wildfires, they account for a large proportion (> 2/3) of the total burned areas (Pausas and Vallejo 1999; Quézel and Médail 2003). In Corsica, the most represented pine species is *Pinus nigra* subsp. *laricio* (Poir.) Maire var. *corsicana* (Loudon) Hyl. The development of these ecosystems takes place between 900m and 1800m altitude (Gamisans, 1999); hard to reach and steeply sloping terrain make it difficult to manage and protect these sensitive habitats using mechanical methods. Reintroducing fire into ecosystems through prescribed burning (Fernández et al. 2013) is time saving and allows to circumvent logistical and cost constraints. It removes hazardous understory flammable materials and creates more spatial variability in the structure of the forest (Fulé et al. 2004). Some studies have provided answers on the resistance of *Pinus laricio* to prescribed burning (Cannac et al. 2007, Ferrat et al, 2021). However, the effects of these prevention techniques on the ecology of a forest soil have been little studied.

A cascade of trophic interactions between microorganisms, detritivores and predators (Hunter et al. 2003; Santonja et al. 2015) allows the decomposition of organic matter (Aubert et al. 2010), soil regeneration, and nutrient recycling.

Fire can change the physical nature of the soil (grain size, permeability), but also its chemical quality through ash input (mineralization of organic matter, nitrogen input, pH change ; Shakesby et al. 2015). These modifications can destabilize the balance of the environment, and influence the recovery of the communities of organisms living in the soil (Wikars and Schimmel, 2001).

This study has several objectives:

- A preliminary characterization of the soil organism communities in a *Pinus laricio* forest, little studied so far, under different types of micro-habitats.
- Characterization of prescribed burns intensity and heat transfer in the soil
- Highlight the potential impacts of prescribed burns on the soil fauna

2. Material and methods

The study was carried out in a pure stand of *Pinus laricio* located in Bavella, South Corsica, France (9.224334740328 ; 41.791482512769) at 1218 m above sea level. This forest, managed by the French Forest Office, has been thinned and pruned, leaving an important and heterogeneous amount of branches and trunks on the soil, with a consistent needle litter. Trees are about 30 years old, the average tree height and DBH are 12.72m and 18.12cm respectively. The understory is absent, the herbaceous layer is mostly represented by *Brachypodium pinnatum* (L.) P. Beauv. and the moss is present discontinuously. The slope is about 20% with a west aspect. The site is submitted to supramediterranean climate, with hot summers and mild winters (mean annual temperature : 10,1°C ; min : -7°C ; max : 26°C, 620 mm total precipitation in 2020).

The stand is divided into both 25 m² control (CP) and burned (BP) plots. Each plot is subdivided into 16 subplots of about 6.25 m².

The prescribed burning was carried out on 10th november 2020 by trained forest managers. Temperature measurements were performed for different fuel configuration (litter, branches and trunk from thinning residues) at the surface and at various depths (under litter and – 3 cm) in the soil using K-type thermocouples. Measurements of the different fuel biomass and surface (grass, litter and thinning residues) was realized before and after burning.

Soil fauna was sampled prior to burning, then one week and 4 months after burning, using pitfall traps positioned on all subplots. Pitfall traps allow the study of all organisms present in the litter and humus (macrofauna and mesofauna). Spot corings (5cm*5cm*5cm) in different micro-habitats (moss, moss + litter, litter) followed by extraction with Berlèse (Berlèse, 1905) were also performed just before, and after burning, then one month post-burning, in order to study the mesofauna of humus and soil. Collected organisms are quantified and identified to order.

3. Results

The maximum temperatures were recorded at the litter surface (674–1007 °C), and the average flame residence time (duration of exposure to temperatures > 300 °C) was in the range of 25–173 s. The heat was very little transferred from the litter to the humus (+ 10.08 °C maximum). A typical example of temperature evolution is presented in Figure 1 for litter and branches configurations.

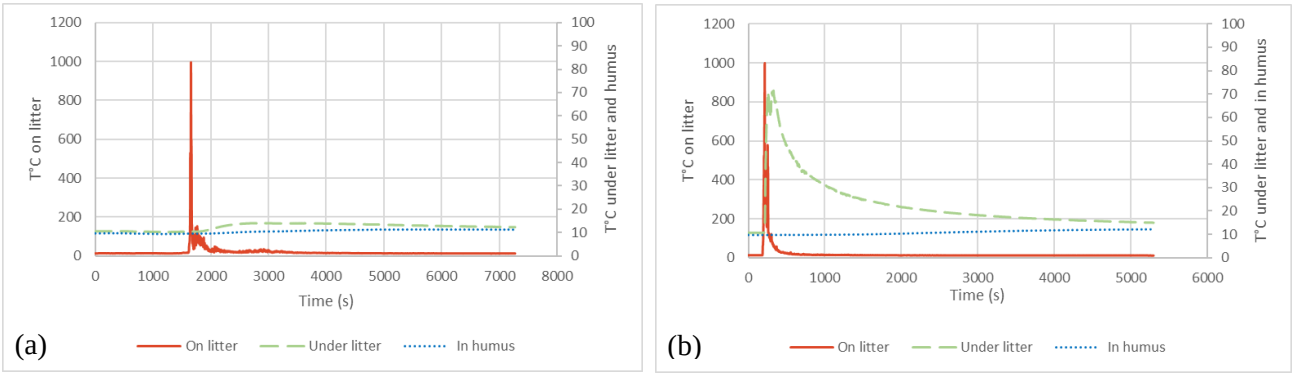

Figure 1- Temperature monitoring at different depths during prescribed burning, (a) under litter and (b) under a pile of branches.

90% of the litter, and particles smaller than 3mm (branches, herbaceous stratum) were heterogeneously removed by the burning. In contrast, larger diameter particles were not removed (Figure 2).

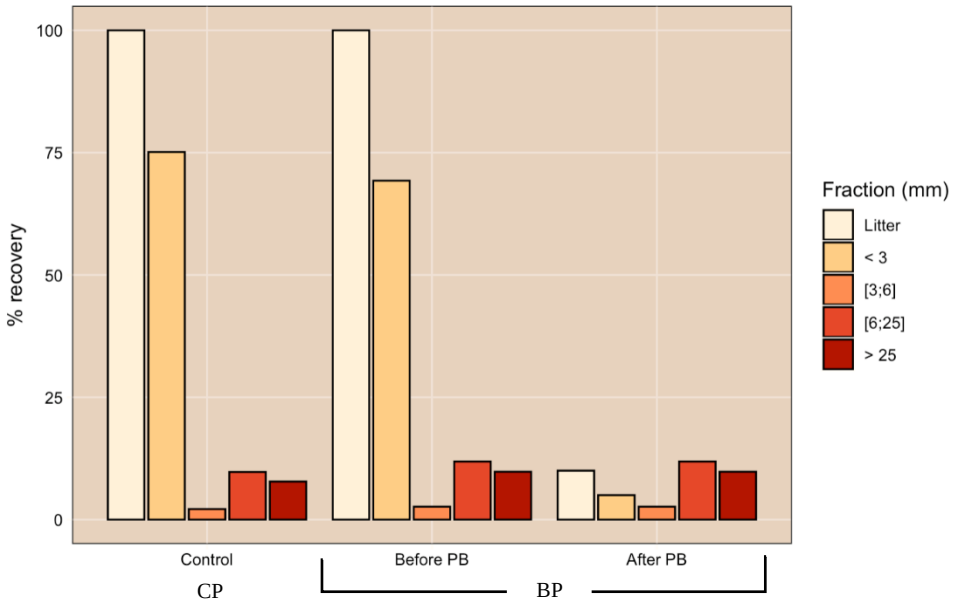

Figure 2- % plot coverage by fuel type (<3: particles less than 3mm in diameter; [3;6]: particles between 3mm and 6mm in diameter; [6;25]: particles between 6mm and 25mm in diameter; >25: particles greater than 25mm in diameter), before and after burning

20 different orders were identified within pitfall traps, all periods and all plots combined. Whatever the plot, Acari, Collembola, Diptera and Coleoptera always represented more than 80% of the total number of organisms (Figure 3). The Shannon index (Shannon & Weaver, 1949) was initially 2.15 for BP and 2.46 for CP. Abundance in the subplots was highly variable, from from 56 to 283 organisms for BP and 30 to 144 organisms for CP.

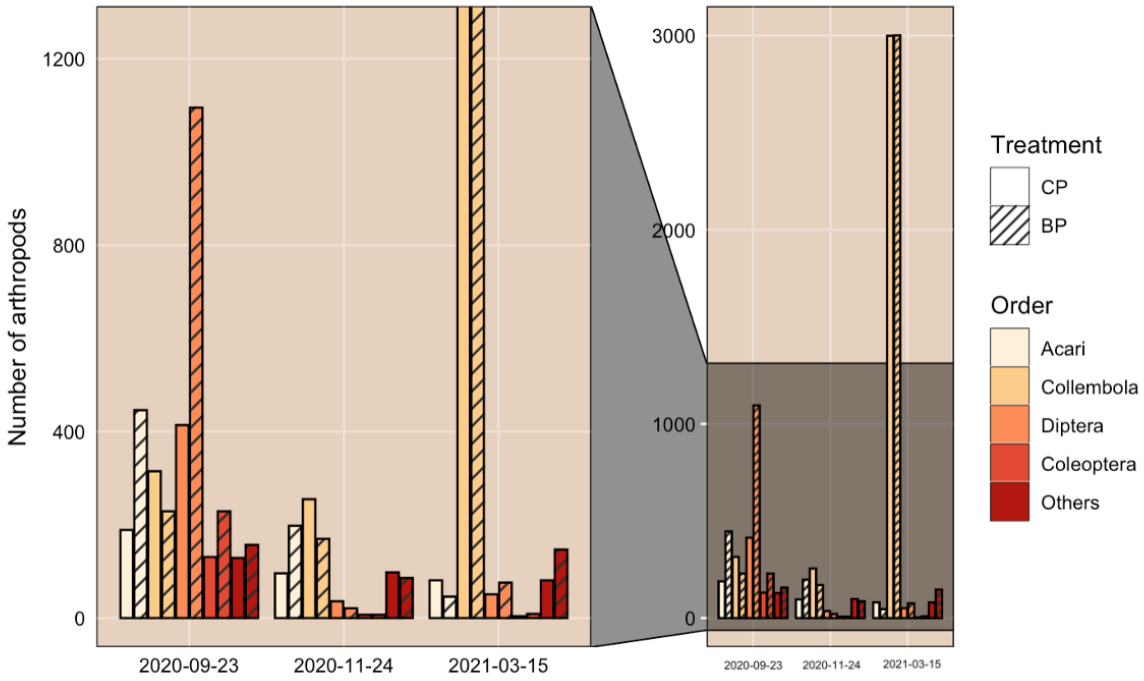

Figure 3- Total count for each order at different dates, collected by Pitfall traps (16 orders with less than 5% total count on all plots, all dates combined, were grouped in "Others")

On 09/23/2020, BP counted 2156 organisms, against only 1178 for CP. This difference can mainly explained by the abundance of diptera and acari, which are 1095 and 446 respectively for BP, and 414 and 189 for CP.

Organisms decreased by 78% after the prescribed burning in BP (482 organisms on 11/24/2020), and only by 58% in CP plot.

In spring, both plots had a similar population of organisms (3279 for BP and 3216 for CP), with a very low diversity (Shannon index of 0.64 for BP and 0.54 for CP).

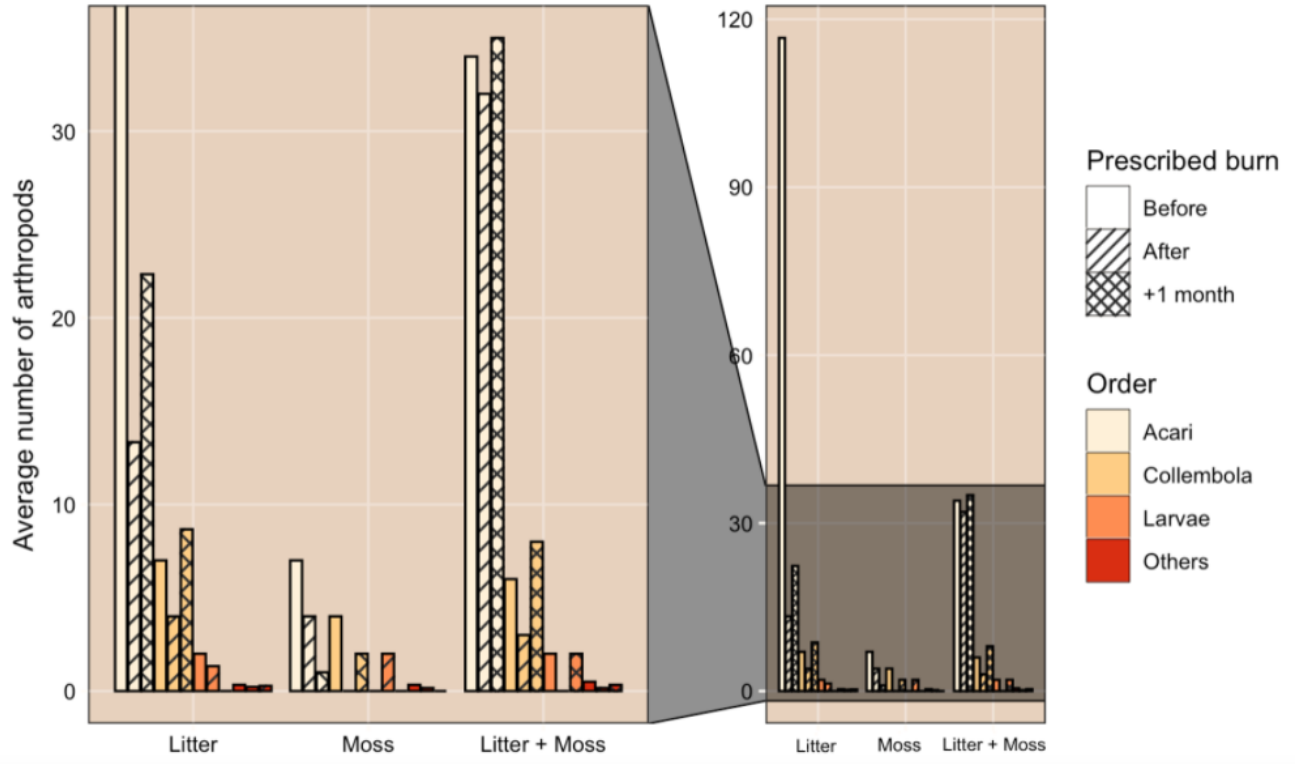

Figure 4- Distribution of mesofauna in the soil of Pinus nigra laricio ecosystems, according to microhabitat type, before and after prescribed burning.

Berlese sampling allowed to highlight the presence of 8 orders in the soil, all types of micro-habitat included. Litter had the highest total population, with an average of 130 organisms, compared to 45 in litter+moss, and 13 in moss, before burning.

Acari were in the majority, representing between 91% (litter) and 54% (moss) of the population in the samples (Figure 4). Next came the Collembola, representing between 5% (litter) and 31% of the total population. The remaining orders were very poorly represented (araneae, coleoptera, thysanoptera, hymenoptera, hemiptera and myriapoda).

The average population of the litter micro-habitat showed a decrease of 84% just after the burn. This decrease was mainly due to the loss of acaris, whose population decreased by 89%. The other orders weree present in too small numbers to show a difference in abundance.

The litter+moss microhabitat showed only a slight decrease of 20% in abundance after the burn. Moss was the poorest environment, with a very low number of organisms before the burn (13 organisms). This number decreased by 46% after the burn.

No difference in the distribution of organisms between the control and burned plots were noted. Pitfall traps and Berlèse samples showed the same trends: a decrease in total abundance after burning.

4. Discussion

Pinus laricio is a Corsican endemic species, its ecosystem is very poorly characterized.

The two types of trapping used in this study provide a preliminary overview of the communities of organisms living in these forests. The orders identified seem to fit very well with the descriptions given for the Mediterranean forests (Mantoni et al. 2020; Samain et al. 2019).

Precribed fire seems to cause a significant decrease in the population of organisms (78% for pitfall traps and 50% for Berlèse). This decrease is much greater than the one observed in the control plot (CP), which is only due to a seasonal effect. As a matter of fact, the average temperatures of November did not exceed 9°C on the pass of Bavella, which slows down biological activites (Mòron-Rios et al. 2010).

Thus, fire does not eliminate all organisms, either locally or at the plot level. Temperature measurements may partially explain these results. Indeed, the surface temperature during burning reached a maximum of 1007°C, which is totally incompatible with the survival of litter organisms. Heat transfer to the soil remained very low, since no more than a 10°C increase was measured. This demonstrates the insulating and protective power of the soil for organisms that live deeper than 3cm, which is the case for many species (acari, collembola, larvae of few Diptera and Coleoptera). Moreover, soil microarthropods can resist temperatures up to 40°C (Malmstrom, 2008) thanks to their cuticule (Moretti et al., 2006). Our finding follows the results of Uotila and Levula, 2011, who showed that the impact of fire on soil is relatively low due to its high insulating capacity.

The study of Berlèse, sampled in entirely burned areas, shows that not all microhabitats react in the same way to the passage of fire. Acari decreased in numbers under the "litter" habitat, composed of combustible pine needles. This could be explained by the fact that soil-dwelling organisms tend to occupy the surface layers of the environment. However, several studies have demonstrated the ability of microarthropods to escape deep into the soil (Certini, 2005; Gongalsky et al., 2012). The remaining organisms may have used this ability to protect themselves from the heat stress of passing through the burn. The low impact on other microhabitats (moss and moss + litter) could be explained by stronger insulation in these areas, it may be interesting to confirm this hypothesis with additional sampling.

Another important aspect of this study, which must be taken into account in the analysis of soil populations, is the evidence that BP did not burn completely during prescribed burning. The plot had about 10% unburned area. Auclerc et al. (2019), demonstrated the importance of both endogenous (i.e., surviving species) and exogenous species in recolonizing the disturbed environment. In this study, the heterogeneity of burning (a mosaïc of burned and unburned areas) could allow a very rapid recolonization of fire-affected areas, which happen to be an available ecological niche, and a source of organic matter and minerals of interest for organisms.

This recolonization is already evidenced by the spring samples (+680% in BP), wich is similar to the seasonal increase of CP (due to the recovery of biological activity, especially for springtails, whose number goes up to 3000). It must be noted that BP had almost twice the number of CP in the initial state and that this level has not yet been found.

This preliminary study clearly shows the difficulty of highlighting the effect of a prescribed burning on the dynamics of soil arthropod populations, as the heterogeneity of the plots and the conduct of a fire are important. A further study at the scale of subplots will allow to better define the heterogeneity of the plots. An identification of the organisms to the family will also highlight the specificities of *Pinus laricio* forests. Finally, to complete the study, sampling of different soil strata, treated with the Berlèse instrument, could allow a better understanding of the degree to which they are impacted by heat transfer.

5. Bibliography

Aubert M., Margerie P., Trap J., et Bureau F. (2010). « Aboveground–Belowground Relationships in Temperate Forests: Plant Litter Composes and Microbiota Orchestrates » Forest Ecology and Management 259 (3): 563-72.

Auclerc A., Le Moine J. M., Hatton P.-J., Bird J. A., & Nadelhoffer K. J. (2019). « Decadal post-fire succession of soil invertebrate communities is dependent on the soil surface properties in a northern temperate forest. » Science of The Total Environment, 647, 1058-1068.

Aupic-Samain A., Baldy V., Lecareux C., Fernandez C., Santonja M. (2019). « Tree litter identity and predator density control prey and predator demographic parameters in a Mediterranean litter-based multi-trophic system. » Pedobiologia, Journal of Soil Ecology, 73, 1–9.

Berlese, A. (1905). « Apparecchio per raccogliere presto ed in gran numero piccoli arthropodi. » Redia. pp. 85-89.

Cannac M.C., Pasqualini V., Greff S., Fernandez C., Ferrat L. (2007). « Characterization of Phenolic Compounds in *Pinus laricio* Needles and Their Responses to Prescribed Burnings. » Molecules, 12, 8. 1614-1622.

Certini, G. (2005). « Effects of fire on properties of forest soils: a review. » Oecologia 143, 1–10.

Fernandes P. M. (2018). « Scientific support to prescribed underburning in southern Europe: What do we know? » Science of The Total Environment, 630 , 340-348.

Ferrat L., Morandini F., Lapa G. (2021). « Influence of Prescribed Burning on a *Pinus nigra* subsp. *Laricio* Forest: Heat Transfer and Tree Vitality. » *Forests* 2021, *12*(7), 915.

Gamisans J. (1999). « La végétation de la Corse. » Aix-en-Provence : Edisud, ISBN 978-2-7449-0083-9.

Gongalsky K.B., Malmström A., Zaitsev A.S., Shakhab S.V., Bengtsson J., Persson T. (2012). « Do burned areas recover from inside? An experiment with soil fauna in a heterogeneous landscape » Appl. Soil Ecol., 59, 73-86.

Hunter M.D., Adl S., Pringle C.M., Coleman D.C. (2003). « Relative Effects of Macroinvertebrates and Habitat on the Chemistry of Litter during Decomposition » Pedobiologia 47 : 101-15.

Kendra L.L., Wise D.H. (2004). « Unexpected Indirect Effect of Spiders on the Rate of Litter Disappearance in a Deciduous Forest » Pedobiologia 48 (2): 149-57.

Mantoni M., Di Musciano M., Fattorini S. (2020). « Use of microarthropods to evaluate the impact of fire on soil biological quality. » Journal of Environmental Management, 266, 110624.

Malmström, A. (2008). « Temperature tolerance in soil microarthropods: Simulation of forest-fire heating in the laboratory. » Pedobiologia 51, 419–426.

Moretti M., Duelli P., Obrist M.K. (2006). « Biodiversity and resilience of arthropod communities after fire disturbance in temperate forests. » Oecologia, 149, 312-327.

Morón-Ríos A., Rodríguez M.A., Pérez-Camacho L., Rebollo S. (2010). « Effects of seasonal grazing and precipitation regime on the soil macroinvertebrates of a Mediterranean old-field. » European Journal of Soil Biology, 46, 91-96.

Pimont F., Prodon R., Rigolot E. (2011) « Comparison of postfire mortality in endemic Corsican black pine (*Pinus nigra* ssp.) and its direct competitor (Pinus pinaster) » Annals of Forest Science, 68, 2 : 425-432.

Santonja, M., Fernandez C., Gauquelin T., et Baldy V. (2015). « Climate Change Effects on Litter Decomposition: Intensive Drought Leads to a Strong Decrease of Litter Mixture Interactions. » Plant and Soil 393 (1-2): 69-82.

Shakesbya R.A., Bento C.P.M., Ferreira C.S.S., Ferreira A.J.D., Stoof C. R., Urbaneka E., Walsha R.P.D. (2015). « Impacts of prescribed fire on soil loss and soil quality: An assessment based on an experimentally-burned catchment in central Portugal » CATENA 128, 278-293.

Shannon C. E., Weaver W. (1949). « The mathematical theory of communication. » Illinois: University of Illinois Press.

Uotila A., Levula J.. (2012). « Soil Temperatures during prescribed burning and the occurrence of Rhizina undulata Fr. » Journal of Agricultural Extension and Rural Development, 4(9), 207-210.

Wikars L.O., Schimmel J.. (2001). « Immediate effects of fire-severity on soil invertebrates in cut and uncut pine forests. » For. Ecol. Manage., 141, 189-200.

Influence of Fuel Structure on Gorse Fire Behaviour

Andres Valencia*[1]; Katharine Melnik[1]; Nick Sanders[1]; Adam Sew Hoy[1]; Mozhi Yan[1]; Marwan Katurji[2]; Jiawei Zhang,[3,2]; Benjamin Schumacher[2]; Robin Hartley[3]; Samuel Aguilar-Arguello[3]; Grant Pearce[3,4]; Mark Finney[5]; Veronica Clifford[3]; Tara Strand[3]

[1]Department of Civil and Natural Resources Engineering, University of Canterbury, Christchurch 8140, New Zealand, {andres.valencia, katharine.melnik}@pg.canterbury.ac.nz
[2] University Center for Atmospheric Research, School of Earth and Environment, University of Canterbury, New Zealand {marwan.katurji, benjamin.schumacher}@pg.canterbury.ac.nz
[3] New Zealand Forest Research Institute, Scion, New Zealand {jiawei.zhang, robin.hartley, tara.strand, samuel.aguilar}@scionresearch.com
[4]Fire Emergency New Zealand {grant.pearce2@fireandemergency.nz}
[5]Forest Service, Missoula Fire Science Laboratory, United States of America {mark.finney@usda.gov)

** Corresponding author*

Keywords

Fire behaviour, wildfires, lidar, UAV, Image velocimetry

Abstract

Complex interactions between fuel structure and fire highly affects the fire spread efficiency and localized behaviour. Heterogeneous arrangement of the fuel coupled with variability in fuel characteristics can strengthen or hinder heat transfer efficiency, preheating of unburned fuel and consecutive ignition. In this study, we leverage recently developed non-intrusive unmanned aerial vehicle-based (UAV) methods to spatially resolved field-scale fire behaviour properties and compare them with the Canopy Height Model (CHM) derived from pre-burn lidar measurements. Rate of spread and flaming residence time are calculated and mapped from high-resolution overhead visible footages acquired during a four-hectare prescribed gorse fire. The proposed method allows for quantification of the influence of fuel structure spatial variation on fire behaviour properties by capturing localized fire front and burning time variations associated with negative ("gaps") and positive ("bumps") changes in canopy height. These findings are supported by results obtained from a novel fire flow visualization method based upon image velocimetry, described here for the first time. Complex fire flow is synthetised via 2D time-averaged motion streamlines and compared with CHM fuel structure. Results suggest that localized fire behaviour changes may be related to flow channelling effects induced by the presence of gaps, enhancing fire flow contact and overall heat transfer efficiency.

1. Introduction

Fire behaviour is driven by complex interactions between fire energy exchanges, fuel load and structure, and atmospheric processes (Clements et al., 2007; Dahale et al., 2013; Finney et al., 2015; Sullivan, 2017; Katurji et al., 2021). Understanding these interactions is essential for several critical aspects of wildfire sciences and for informed firefighting operations (Beer, 1991; Page and Butler, 2017), building design in the Wildland Urban Interface (WUI) (Penney, Habibi and Cattani, 2020; Penney et al., 2022) and development of wildfire simulation models (Mell et al., 2007, 2011; Morvan, 2011; Hoffman et al., 2016). Field-scale fire behaviour has primarily been characterised through experimental and analytical properties describing the overall behaviour of the fire (e.g. average rate of spread, residence time and fire intensity) generally accounting for first-order mechanisms. Although this practical approach is deemed reasonable for numerous applications, it falls short of the required level of detail necessary to progress the current knowledge on fire spread mechanisms (Martins Fernandes, 2001; Santoni et al., 2006; Cruz et al., 2013) and to assess the ability of the physics-based models (e.g. WFDS and FireTEC) to predict fire behaviour, among others.

Several efforts have been made to develop deployable techniques able to accurately characterize spatial and transient fire behaviour and their interactions with fuel and overlying atmosphere at field scale. Rossi et al. (2010) developed a 3D imaging technique capable of measuring morphological characteristics of the fire and estimate ROS of complex fire fronts. This technique has been expanded to include UAV technology (Ciullo,

Rossi and Pieri, 2020) aiming to enhance spatial coverage and fire geometry definition, as well as exploring fuel/fire interactions. Recently, Katurji et al. (2021) developed a novel velocimetry technique based upon high-resolution infrared images suitable for understanding fire/atmospheric interactions between the flaming zone and the overlying atmospheric turbulent boundary layer. The technique was tested during stubble wheat prescribed fires and validated with in-field instrumentation.

These aforementioned capabilities are examples of a new generation of experimental techniques capable of capturing complex wildfire interactions at field scale, and they will contribute to further characterising the dynamics of the flaming zone which is essential for the development of future fire spread models. In this context, we present an experimental study of spatially-resolved fire behaviour properties at field scale linked to high fidelity fuel structure derived from pre-burn UAV lidar (ULS) measurements. We leverage on recently developed non-intrusive UAV-based methods to study the influence of fuel structure (canopy height and spatial arrangement) from pre-burn ULS on fire behaviour (rate of spread and flaming residence time) derived high-resolution overhead RGB videos during a four-hectare prescribed gorse fire. Because of word-limit constraints, we only summarize the non-intrusive experimental methods used in this research (Section 2) and we present and comment the derived maps Rate of Spread (ROS) and Flaming Residence Time (FRT) (section 3) in this short paper.

2. Experiments and Methods

2.1. Site description and burning conditions

The research site is located at -43.409, 171.568, 15 km south of the Rakaia Gorge in Mid-South Canterbury, New Zealand. A 200 m × 200 m burn plot was established on flat ground (a dry riverbed with slight undulations), ensuring that it aligns with the prevailing wind directions. The overstory was made up of gorse (*Ulex europaeus* L.) with a small component of matagouri (*Discaria toumatou* Raoul), and the understory consisted of mostly grasses with a component of rose (*Rosa* sp.), California thistle (*Cirsium arvense* (L.) Scop) and Russell lupin (*Lupinus polyphyllus* Lindl). Gorse height ranged from 0.2 m to 2.0 m, and its density and distribution was heterogeneous across the site, with some areas containing tall dense vegetation, and other areas being relatively open with short clumps of gorse interspersed with grassy patches.

The burn was ignited on 2nd March 2020 at 12:11pm and lasted 5 minutes. The mean temperature was 22.9 °C, mean relative humidity was 33.2%, mean wind direction was 311.2° and mean wind speed was 9.8 m/s (35.28 km/hr) as recorded by the on-site 10-meter weather station.

2.2. UAV and lidar Acquisition

UAVs capabilities were used for two different purposes: to record nadir RGB videos of the flaming zone and to obtain a pre-burn high-density point cloud from a ULS. In advance of any flight operations, an extensive set of ground control points (GCPs) was established throughout the study site. Eight ground control points evenly distributed across the study area ensured a suitable level of accuracy of the ULS data. Furthermore, 36 ground control points were established around the individual research burn blocks to be used during the georectification of the acquired frames from the visual imagery and the alignment of the two data streams.

Aerial video data of the flame zone was captured using a DJI Zenmuse XT2 dual thermal RGB sensor with integrated 1/17 inch 12MP RGB camera (DJI Ltd., Shenzhen, China), mounted on a DJI Matrice 210 UAV (DJI Ltd., Shenzhen, China). Video was captured in MP4 format at a framerate of 30 fps. Pre-burn ULS data was captured with a LidarUSA Snoopy V-series system (Fagerman Technologies, INC., Somerville, AL, USA), that incorporates a Riegl MiniVUX-1 UAV scanner (Riegl, Horn, Austria). This sensor was attached to a DJI Matrice 600 Pro UAV (DJI Ltd., Shenzhen, China).

Figure 1. Pilot taking off Matrice 210 with DJI XT2 camera prior to burn commencing; b. Setting up Matrice 210 UAV; c. DJI Matrice 600 craft taking off, carrying MiniVUX lidar sensor as payload.

Processing of the raw point cloud from Lidar was then carried out using two pieces of software. First, the point cloud was tiled and had basic noise filtering applied using the LasTools software version 210,418 (Isenburg, 2014). The tiles output from LasTools were then imported into the R statistical software version 4.0.4 (R Core Team, 2020) and processed using a data processing pipeline developed using the LidR library (Roussel et al., 2018). First ground points were classified and then a digital terrain model (DTM) with a resolution of 1 m was derived from these points. The point cloud was then height-normalised using the DTM, more noise filtering was applied to remove spurious points, and finally a pit-free canopy height model (CHM) with a resolution of 0.25 m was calculated.

3. Description of Techniques

3.1. Flame Residence Time and Fire Perimeter Tracking

In order to calculate the residence time and the pixel-wise rate of spread (ROS) of the fire, the Fire Perimeter Tracking algorithm (Melnik 2021, Schumacher et al. 2021) was used. First, each frame of the stabilized RGB videos was analysed to identify which pixels contain active flames. This was done by manually identifying colour thresholds in the hue, saturation and value (HSV) colour space that indicate the presence of flames in a given pixel. Using the location of active flaming in each video frame, two two-dimensional arrays were created: (1) the ignition array, each pixel of which contained the first timestamp of active flaming in the given pixel of the burn plot, and (2) the extinction array, each pixel of which contained the last timestamp of active flaming. The ignition array was subtracted from the extinction array in order to create the flame residence time array, which contained the burning duration of each pixel across the burn plot.

In order to calculate the pixel-wise rate of fire spread, a 41×41 pixel moving window was established across the ignition array, with every pixel of the ignition array taking its turn to serve as the centre pixel of the moving window. Within the moving window, only timestamps immediately preceding or following the timestamp of the central pixel were retained. Vectors going from the preceding-timestamp pixels to the central pixel, and advancing from the central pixel to the following-timestamp pixels were calculated, and these vectors were averaged to obtain the rate and direction of spread of the central pixel. The window then moved over and the process was repeated for the next pixel in the ignition array to serve as the centre pixel. The resulting array contained the computed rate and direction of fire perimeter spread for each pixel in the burn plot.

3.2. Fire Flow Streamlines visualization and Image Velocimetry

Image Velocimetry was used to derive and map the displacement of fire features from consecutive RGB frames. The method (Schumacher et al. 2021), which has originally been developed for flow velocimetry estimations from infrared image analysis, has been successfully applied in this work to visualise gorse fire flow from RGB images, and to compare it with fuel structure. The technique uses greyscale image processing to estimate direction and magnitude of the displacement of the observed fire features between two consecutive frames (1/30

s). The resulting vectorial field was then derived to calculate the corresponding flow streamlines and visualize the fire flow.

4. Results

4.1. Description of Fuel Structure and Fire Behaviour

Figure 2a shows an image of the fire extracted from the RGB UAV footage ~1 min after ignition. The figure highlights the observable flaming zone and fire front once the acceleration phase is ended. The length of the observable fire in the streamwise direction $y+$, or flaming zone depth, was found to variate across the width of the plot, ranging from ~10 m in regions of low canopy height to ~50 m in regions of high canopy height. Fire spread was characterized by quick progressions of the fire front involving intermittent coverage and subsequent ignition of immediate preheated unburned fuel, resulting in localized progression in short periods of time.

Figure 2b shows the pre-burn CHM obtained from ULS data. The plot was heterogeneous involving interspersed zones of high and low canopy height, with and averaged CHM of 0.75 m and a high standard deviation of ± 0.56, representing 75% of the average value. The right side of the plot was mostly composed of low height fuel with sporadic sectors of high fuel (e.g. dotted line), whereas the opposite occurred in most of the left side of the plot (e.g. dashed line).

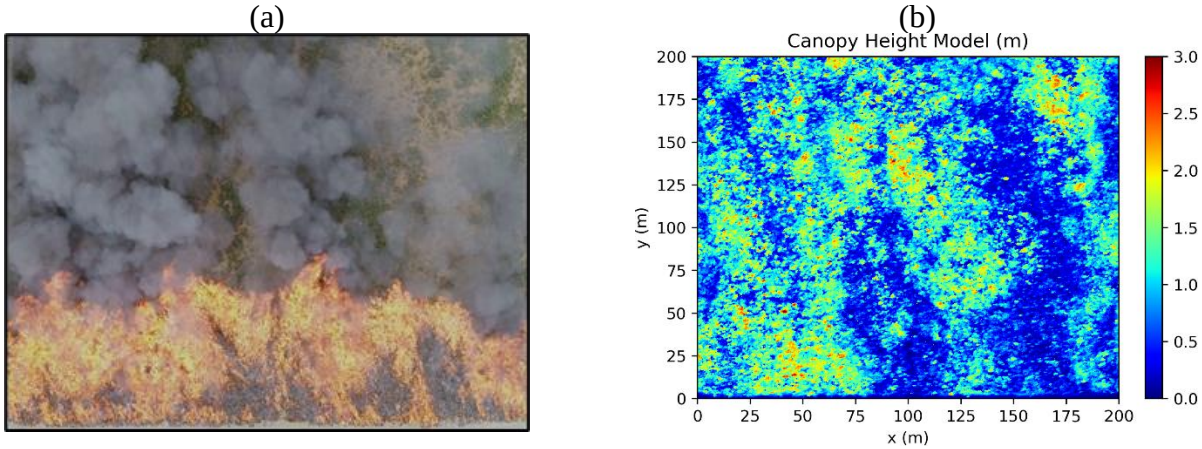

Figure 2. Collected datasets of the burn plot where the ignition took place along the bottom of the x-axis, with the x-axis showing plot width in meters, the y-axis showing the plot length in meters, and the value corresponding to (a) the colour sensed with the UAV-mounted RGB videos, plan view, (b) the height of the vegetation canopy obtained from ULS data. The resolution of the CHM is $7.8 \cdot 10^{-2}$ m/pixel

Figure 3a and Figure 3b show the fire behaviour properties estimated in this study. FRT, shown in Figure 3a, ranged between approximately 10 s to 1.5 min with very high values at the plot edges where liquid fuel was used for ignition purposes. Through qualitative comparison with CHM, FRT seems to present longer flaming combustion in regions of high canopy height. For instance, this pattern can be observed in the bottom-left (x = 50 m y = 25 m) and bottom-right (x = 175 m y = 25 m) sections of the maps. We hypothesize this behaviour results from high canopy height locations linked with high biofuel content participating in the combustion, relationship confirmed through analysis of pre-burn destructive samples. ROS, presented in Figure 3b, was found to be low during the first approximate 20 m where the fire was transitioning from an accelerating fire front with a small flaming zone to the established quasi-steady fire shown in Figure 2a. The ROS map captured the previously described quick progressions of the fire front as localized high ROS values. We hypothesize this could be explained by the presence of greater flame heights and longer fire activity in regions with higher canopy height, most likely associated with higher fuel load.

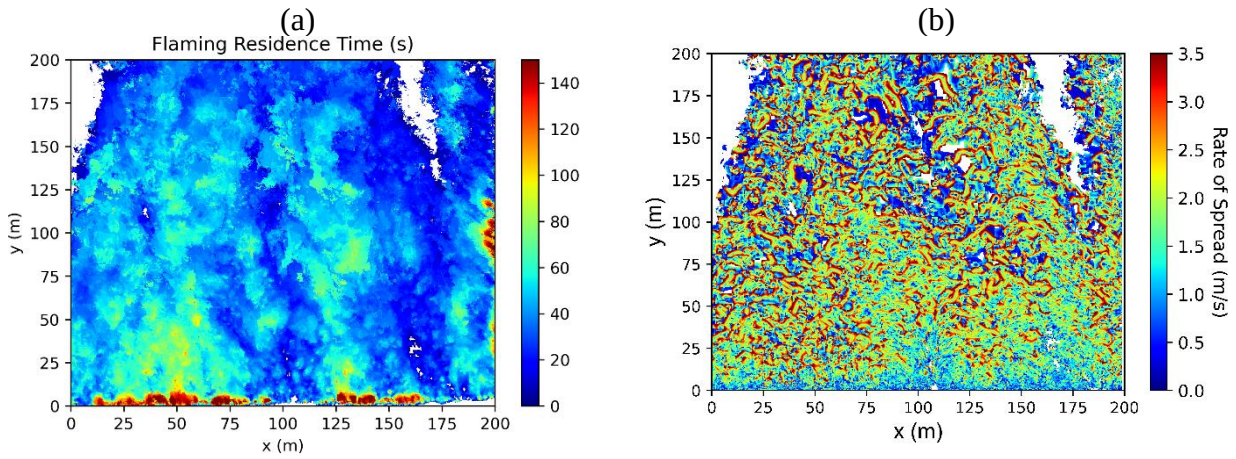

Figure 3. Derived datasets of the burn plot where the ignition took place along the bottom of the x-axis, with the x-axis showing plot width in meters, the y-axis showing the plot length in meters, and the value corresponding to (c) the rate of fire spread derived from the video footage, and (d) flame residence time also derived from the footage. The resolution of both maps is $7.8 \cdot 10^{-2}$ m/pixel

5. Acknowledgments, Samples, and Data

We would like to give a special thanks to all field support teams including technical and general staff. We also thank landowner for their various contributions leading to the success of the field campaigns. University of Canterbury research team would like to acknowledge the very thoughtful, well organized, and proactive support we have received from all the volunteering firefighting crew. The success of our experiments and the safety of our science crew can only be partially attributed to our design but greatly attributed to the safe and well-executed plan from the volunteer crew. A special thanks to the Scion field crew: David Glogoski, Max Novoselov, Richard Parker, Brooke O'Connor, Emma Percy, and Ilze Pretorius. We would also like to acknowledge Peter Massam from Scion's UAV team for assistance with UAV data capture and processing. This research was co-funded by Ministry of Business, Innovation and Employment (MBIE), New Zealand, grant number C04X1603 entitled "Preparing New Zealand for Extreme Fire" and grant number C04X2103 "Extreme wildfire: Our new reality - are we ready?"

6. References

Beer, T. (1991) 'Bushfire rate-of-spread forecasting: Deterministic and statistical approaches to fire modelling', Journal of Forecasting, 10(3), pp. 301–317. doi:10.1002/for.3980100306.

Clements, C.B. et al. (2007) 'OBSERVING THE DYNAMICS OF WILDLAND GRASS FIRES', Bulletin of the American Meteorological Society, 99(7), pp. 1369–1382.

Cruz, M.G. et al. (2013) 'Fire behaviour modelling in semi-arid mallee-heath shrublands of southern Australia', Environmental Modelling and Software, 40, pp. 21–34. doi:10.1016/j.envsoft.2012.07.003.

Dahale, A. et al. (2013) 'Effects of distribution of bulk density and moisture content on shrub fires', International Journal of Wildland Fire, 22(5), pp. 625–641. doi:10.1071/WF12040.

Finney, M.A. et al. (2015) 'Role of buoyant flame dynamics in wildfire spread', Proceedings of the National Academy of Sciences of the United States of America, 112(32), pp. 9833–9838. doi:10.1073/pnas.1504498112.

Hoffman, C.M. et al. (2016) 'Evaluating Crown Fire Rate of Spread Predictions from Physics-Based Models', Fire Technology, 52(1), pp. 221–237. doi:10.1007/s10694-015-0500-3.

Isenburg, M. (2014) 'LAStools-efficient LiDAR processing software', Available online: lastools. org (accessed on 10 October 2017) [Preprint].

Katurji, M. et al. (2021) 'Turbulent Thermal Image Velocimetry at the Immediate Fire and Atmospheric Interface', Journal of Geophysical Research: Atmospheres, 126(24), pp. 1–14. doi:10.1029/2021JD035393.

Martins Fernandes, P.A. (2001) 'Fire spread prediction in shrub fuels in Portugal', Forest Ecology and Management, 144(1–3), pp. 67–74. doi:10.1016/S0378-1127(00)00363-7.

Mell, W. et al. (2007) 'A physics-based approach to modelling grassland fires', International Journal of Wildland Fire, 16(1), pp. 1–22. doi:10.1071/WF06002.

Morvan, D. (2011) 'Physical Phenomena and Length Scales Governing the Behaviour of Wildfires: A Case for Physical Modelling', Fire Technology, 47(2), pp. 437–460. doi:10.1007/s10694-010-0160-2.

Page, W.G. and Butler, B.W. (2017) 'An empirically based approach to defining wildland firefighter safety and survival zone separation distances', International Journal of Wildland Fire, 26(8), pp. 655–667. doi:10.1071/WF16213.

Penney, G. et al. (2022) 'The CAED Framework for the Development of Performance-Based Design at the Wildland–Urban Interface', Fire, 5(2), pp. 1–19. doi:10.3390/fire5020054.

Penney, G., Habibi, D. and Cattani, M. (2020) A handbook of wildfire engineering: guidance for wildfire suppression and resilient urban designHabibi, Daryoush Cattani, Marcus, Bushfire and Natural Hazards CRC. Edited by B. CRC and N. Hazards. Melbourne. Available at: https://www.bnhcrc.com.au/publications/handbook-of-wildfire-engineering.

Rossi, L. et al. (2010) 'A 3D vision system for the measurement of the rate of spread and the height of fire fronts', Measurement Science and Technology, 21(10). doi:10.1088/0957-0233/21/10/105501.

Roussel, J.-R. et al. (2018) 'lidR: Airborne LiDAR data manipulation and visualization for forestry applications', R package version, 1(1).

Santoni, P.A. et al. (2006) 'Instrumentation of wildland fire: Characterisation of a fire spreading through a Mediterranean shrub', Fire Safety Journal, 41(3), pp. 171–184. doi:10.1016/j.firesaf.2005.11.010.

Schumacher, B. et al. (2022) 'Rate of spread and flaming zone velocities of surface fires from visible and thermal image processing', International Journal of Wildland Fire (in press) [Preprint].

Sullivan, A.L. (2017) 'Inside the Inferno: Fundamental Processes of Wildland Fire Behaviour: Part 2: Heat Transfer and Interactions', Current Forestry Reports, 3(2), pp. 150–171. doi:10.1007/s40725-017-0058-z.

Vacca, P. et al. (2020) 'WUI fire risk mitigation in Europe: A performance-based design approach at home-owner level', Journal of Safety Science and Resilience, 1(2), pp. 97–105. doi:10.1016/j.jnlssr.2020.08.001.

Introducing the use of fire for wildfire prevention in Greece: pilot application of prescribed burning in Chios island

Miltiadis Athanasiou*[1]; Triantafyllos Bouchounas[2]; Evangelia Korakaki[3]; Elias Tziritis[4]
Gavriil Xanthopoulos[3]; Stamatia Sitara[5]

*[*1] Wildfire Management Consulting and Training. 8 Thoma Paleologou st., 13673, Athens, Greece, {info@m-athanasiou.gr}*
[2] Gigonis Ecospatial Services, 20, 28th of October st. 57500, Epanomi, Greece, {info@gigonis.gr}
[3] Hellenic Agricultural Organization "Demeter". Institute of Mediterranean Forest Ecosystems. Terma Alkmanos, Ilisia, 11528, Athens, Greece, {e.korakaki, gxnrtc}@fria.gr
[4] WWF Greece {e.tziritis@wwf.gr}
[5] Agriculturist / Volunteer Firefighter, Chios Voluntary Action Team - OMIKRON, Chios, Vrontados, Peripheral Road, 82150, Greece {info@omikron.org.gr}

**Corresponding author*

Keywords

Prescribed fire; Controlled burn; Fuel management; Fire prevention; Landscape resilience; Greece

Abstract

This paper presents the first steps of a 2-year pilot project on prescribed burning (PB) in Greece. To re-introduce the use of fire in wildfire prevention in the country, as an accurate and effective management tool, more research is needed. Hence, we will conduct planned field PB experiments which will provide us sound knowledge about fire behaviour matched with the fire impact on soil properties, the effects on trees and the plant biodiversity. The experimental fires can serve as an excellent training tool, also, for some of the participants (firefighters, land managers and researchers).

The first efforts to introduce and utilize the PB in Greece begun in the 1970s, when members of the Greek forest scientific community and the Hellenic Forest Service applied PB experimentally, analysed data and drew some preliminary conclusions. They made some steps to document the use of fire and study its impacts before introducing PB as a tool to prevent forest fires. Unfortunately, without constant funding, legal support, logistics, continuous scientific guidance and clear objectives, those sporadic attempts did not tie bonds with the forest and fire management community and the endeavour was soon abandoned. Almost half a century later, fire is still not used in fuel management and fire prevention and there is no institutional framework for the implementation of PB.

Inspired by those first efforts in applying PB in Greece and guided by the fire science and the best practices for wildfire prevention, a core team of researchers and practitioners from WWF Greece, the Institute of Mediterranean Forest Ecosystems of ELGO "DIMITRA", the Forest Directorate of Chios Island, and the Voluntary Action Team "OMIKRON" started in 2021 a pilot project on the implementation of the PB on the island of Chios. Fire Service of Chios Island and Municipality of Chios support the pilot project by supplying water trucks and personnel during the burns. The Project is sponsored by Procter and Gamble corporation.

The project aims to introduce PB as a tool for forest fuel management, increase social– ecological resilience to wildfire and contribute to a climate – resilient future. More specifically, the project is expected:

i. to develop the standards and procedures, through applied research, for the use of the prescribed fire in Greece,
ii. to be a successful paradigm of fuel management,
iii. to strengthen the role of the forest service in fuel management and build the capacity of local stakeholders on potential contribution,
iv. to strengthen the horizontal cooperation among agencies, by introducing compatible methods and techniques,
v. to build the capacity of the volunteer firefighters' teams on issues related to the wildfire prevention and fuel management,
vi. to increase knowledge and improve experience on the fire behaviour,
vii. to further strengthen, improve and expand local alliances in Chios Island
viii. to improve landscape resilience and prevent forest fires.

1. Introduction

Prescribed burning (PB) is a fuel management (FM) method which can be either used alone or in combination with grazing and mechanical treatment (Stephens et al 2012), depending on many factors such as fire management objectives, forest types, location, fire regime (Jain et al 2012, Moghaddas et al. 2010), possible restrictions and on the different spatial and temporal scales at which FM is applied, fine and broad. It improves fire resilience over a particular landscape, reduces the probability of fire ignition, affects fire behaviour (Samara et al. 2018), making firefighting easier and safer, mitigates fire severity and reduces fire damages. PB is both science and technique and it can be a very accurate management tool.

Although increased PB is needed to provide a diversity of public benefits, including wildfire hazard reduction, improved forest resilience, and biodiversity conservation (Varner et al. 2021), there is practically no PB in many parts of Europe (Rego et al. 2010) and progress in adopting the method across the continent remains relatively limited. Only in Portugal, Spain, and south France, PB is practiced quite often, mainly for fuel reduction.

An evidence-based, and flexible approach to prescribed burning with emphasis to the biology and ecology of species and habitats, is needed (Fernandes et al 2013). A shift to 'knowledge' (Castellnou et al 2010) with improved reporting practices to invigorate PB science and suggest minimum reporting standards for future PB experiments, will facilitate future research syntheses, and foster actionable science (Bonner et al 2021). Unfortunately, planned field PB experiments are infrequent in Mediterranean ecosystems up to now, although they can provide sound knowledge about fire impact on soil properties and effects on trees.

In Greece there is no PB application for fuel management and wildfire prevention. In March 2022, Greek Parliament approved a law, making it legal for the firefighters to use backfire and burnout techniques for fire suppression and in June 2022, the government published the technical aspects on how to use them.

The first efforts to introduce and utilize the PB in Greece had begun in the 1970s, when members of the Greek forest scientific community and the Hellenic Forest Service applied PB experimentally, analyzed data and drew some preliminary conclusions. They made some steps to document the use of fire and study its impacts before introducing PB as a tool to prevent forest fires.

In Thasos, an island situated in the northern Aegean Sea, there was periodic application (every 3 years with some repetition i.e., 1974, 1977, etc.) of experimental prescribed burns in plots in mature *Pinus brutia* stands (Papanastasis 1977). Since at those years, there was lack of data and research findings derived from Greece, regarding the use of the fire, the foresters who applied the PB in Greece had followed some U.S. standards. They had met in scientific meetings and workshops, had demonstrated how to use the fire, discussing also ecological and managerial issues as well as its potential combination with grazing and mechanical treatments (Tsiouvaras et al. 1987, Nastis 1989). Unfortunately, without constant funding, legal support, logistics, continuous scientific guidance, and clear objectives, those sporadic attempts did not tie bonds with the forest and fire management community and the endeavour was soon abandoned. In 1980s, according to the legislation, safety standards for the application of the fire, were occasionally defined by the Forestry Administration and the applicant had to file an impact assessment study, including techniques, a time plan, safety precautions and measures during and after the use of fire and attach a plat (contour plan), also.

Almost half a century later, fire is still not used in fuel management in Greece and fire prevention, and there is no institutional framework for the implementation of PB. Inspired by those first efforts in applying PB in Greece and guided by the fire science and the best practices for wildfire prevention, a core team of researchers and practitioners from WWF Greece, the Institute of Mediterranean Forest Ecosystems of ELGO "DIMITRA", the Forest Directorate of Chios Island, and the Voluntary Action Team "OMIKRON" started in mid-2021 a 2-year pilot project on the implementation of the PB on the island of Chios. Fire Service of Chios Island and Municipality of Chios support the pilot project by supplying water trucks and personnel during the burns. The General Directorate for Forests and Forest Environment of Ministry of Environment and Energy provided all necessary permits for the implementation of pilot application of PB in Chios.

The project aims to introduce PB as a tool for forest fuel management, increase social– ecological resilience to wildfire and contribute to a climate – resilient future.

The wildfire problem in Chios is significant, often threatening human lives, disturbing biodiversity and affecting or burning mastic and olive groves. Chios, is the fifth largest of the Greek islands, located in the northern Aegean

Sea and was chosen for two reasons: i) it hosts a variety of Mediterranean forest types with typical characteristics i.e., phrygana, maquis, and thermophilic conifers, so the research findings can be utilized across the country and because ii) of the achieved alliance (Figure 6) and cooperation among the stakeholders, agencies, and the volunteers.

The Chios Voluntary Action Team – Omikron was created in 1999. It is based on Chios Island; operates across the entire island and potentially in the Prefecture of Northern Aegean, and is quite active in wildfire suppression, in prevention [construction of fuel breaks (Athanasiou 2016, 2018, Figure 1), population awareness raising] as well as in restoration and reforestation activities (such as planting seedlings for reestablishing forest vegetation in desertified areas).

Figure 1 Omikron volunteers constructing a fuel break in Chios Island, in 2012 (Photo: Apostolos Flioukas)

2. Methods

The 2-year project started in summer of 2021, and it is to be implemented in at least 4 PB campaigns. Since data-driven decision making is the key to providing effective and efficient wildfire protection (Hogland et al. 2021), we carefully chose 16 plots for the PB application (Table 1, Figure 2). Unfortunately, due to the adverse weather conditions in the 2021-2022 winter in Greece, there were no weather windows for PB application in Chios in the fall of 2021, so we ran two campaigns, in February (Figure 4) and April 2022, and there will be at least two more, in November 2022 and February 2023.

A series of parameters are monitored, measured, and recorded before, during and after the implementation of PB in some of the selected plots:

i. soil infiltration (mm),
ii. soil temperature (ºC) in various depths,
iii. erodibility,
iv. soil texture, nutrients and carbon in the soil,
v. soil respiration,
vi. organic matter decomposition,

vii. soil enzyme and microbial activity,
viii. plant biodiversity,
ix. sap flow ($cm \cdot h^{-1}$),
x. water potential (MPa),
xi. fireline construction rate ($m \cdot h^{-1}$) along the plot perimeter, by mowing and using various hand tools,
xii. surface fuel loading ($kg \cdot m^{-2}$), cover (dimensionless), height (cm) and fuel moisture content (%) through destructive sampling (Figure 3), to describe the fuel situations and complexes before the burn,
xiii. meteorological conditions,
xiv. fire behaviour that is rate of fire spread (ROS, $m \cdot min^{-1}$) and flame lengths (FL, m).

Table 1 16 plots for the PB application in Chios island

ID	Protected Area	Forest type	Area (m^2)	Ownership / Notes
Π3Σ24	No	Maquis, phrygana	3,099	Municipal
Π4Σ12α	No	Maquis	1,528	National
Π4Σ12β	No	Maquis	2,167	National
Π7Σ1	No	Grass, pine litter	5,741	National
Π8Σ30	SPA	Phrygana, pines' regeneration	2,750	Municipal / Fire break maintainance
Π9Σ56	Wildlife Refuge	Phrygana	2,900	National / Shaded fuel break maintainance
Π10Σ57α	Wildlife Refuge	Phrygana, grass	6,812	Glebe / Shaded fuel break
Π10Σ57β	Wildlife Refuge	Phrygana, grass	4,578	Glebe / Shaded fuel break
Π11Σ54	No	Pine litter	10,641	National Public
Π12Σ50	SCI SPA	Phrygana, grass	9,573	Municipal / Fire break maintainance
Π13Σ38α	SCI SPA Wildlife Refuge	Phrygana	1,172	National Public
Π13Σ38β	SCI SPA Wildlife Refuge	Phrygana	294	National Public
Π13Σ38γ	SCI SPA Wildlife Refuge	Phrygana	388	National Public
Π13Σ40α	SCI SPA Wildlife Refuge	Phrygana	1,491	National Public
Π13Σ40β	SCI SPA Wildlife Refuge	Phrygana	1,584	National Public
Π14Σ100	SCI SPA Wildlife Refuge	Broadleaf litter (oak)	1,031	Private
Total area			55,749	

Recording includes ground and aerial photographs. Regarding the aerial perspective, the use of unmanned aerial vehicles (UAVs) provided highly detailed mosaics pre- and post-PB (Figure 5). Fine resolution 3D models were generated by applying low altitude and slow velocity grid flights.

The predefined dimensions of the test areas instructed the use of a versatile, yet robust multirotor UAV, with sophisticated camera load. DJI Phantom 4 Pro was selected as an ideal combination, since it provides wind resistance up to 10 m/sec, more than 20 minutes of autonomous flight per battery and carries an 1'' CMOS, 20Mp sensor, with FOV 84° 8.8 mm/24 mm (35 mm format equivalent) f/2.8 - f/11 auto focus at 1 m - ∞ lens and mechanical/electronic shutter speed of 8 - 1/2000 sec. Images were created in a 3:2 JPEG format of 5472 × 3648 aspect ratio.

Each grid flight was predesigned in Pix4dCapture application, respecting the National Cadastre Digital Elevation Model (2007-2009) and neighbouring obstacles. Data processing (mosaic and dsm/dtm creation) was completed in Pix4d Mapper software.

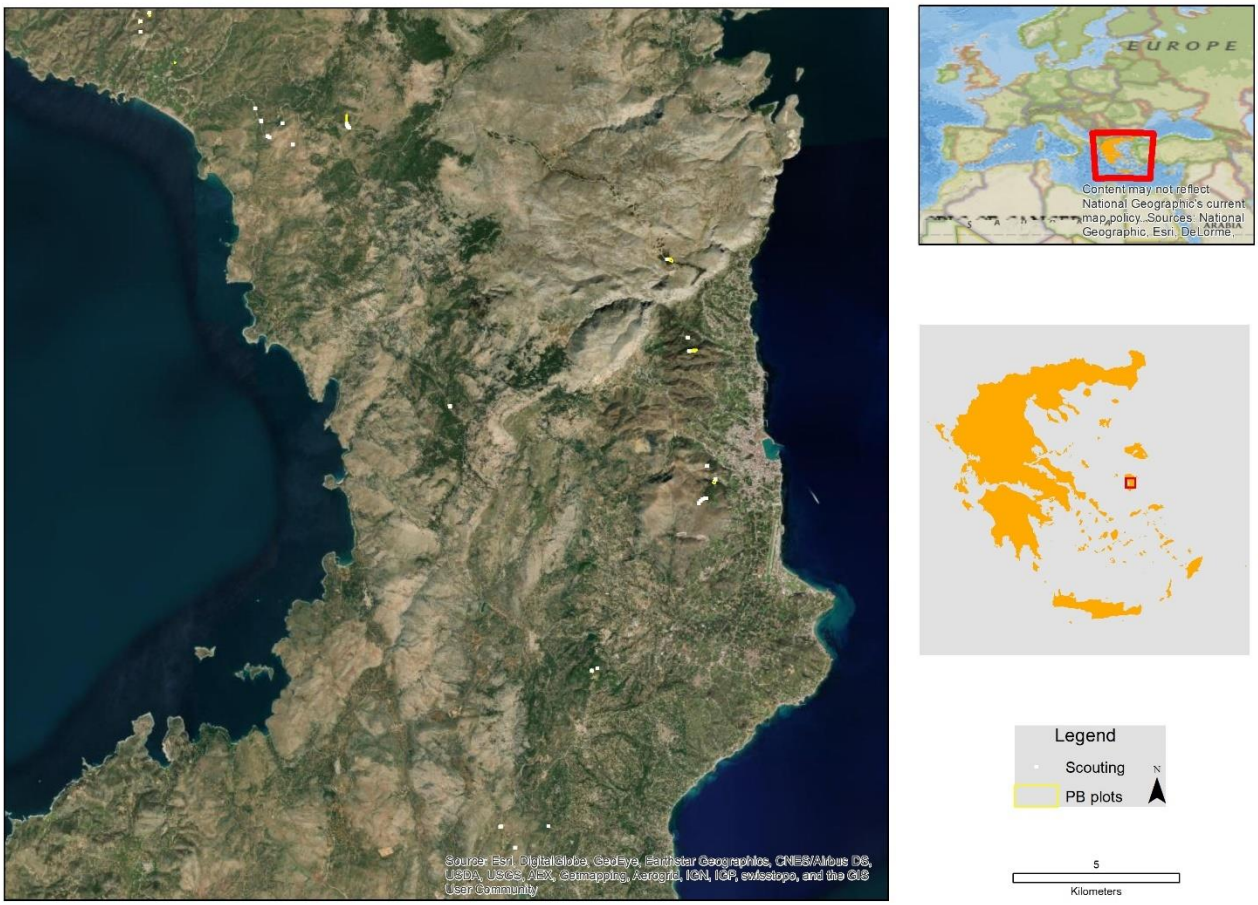

Figure 2 - 16 plots for the PB application in Chios island

Figure 3 - Training Omikron volunteers in destructive sampling of surface fuels

Figure 4 - PB application in one of the plots, in February 2022. The upper left photo is taken in July 2021

3. Discussion – conclusions

This pilot project is expected to be the starting point for the application of PB in Greece, using specific standards. More specifically, the project is expected:

i. to develop the standards and procedures, through applied research, for the use of the prescribed fire in Greece,
ii. to be a successful paradigm of fuel management,
iii. to strengthen the role of the forest service in fuel management and build the capacity of local stakeholders on potential contribution,
iv. to strengthen the horizontal cooperation among agencies, by introducing compatible methods and techniques,
v. to build the capacity of the volunteer firefighters' teams on issues related to the wildfire prevention and fuel management,
vi. to increase knowledge and improve experience on the fire behaviour,
vii. to further strengthen, improve and expand local alliances in Chios Island,
viii. to improve landscape resilience and prevent forest fires.

Figure 5 - A post-PB highly detailed mosaic

Figure 6 - The stakeholders showed interest in the kick off meeting of the project, in Chios island, October 2021 which included a training seminar and initial briefing.

Thus, through this effort we expect, in the long run, PB to be institutionalized in Greece, and assimilated by competent services and local communities, as a tool for fuel management and consequently forest fire prevention through documented policy proposals that will be based on the results of this pilot implementation.

4. Bibliography

Athanasiou M. 2016. Forest fires: management, characteristics and prediction. Monograph for the Intensive Workshop "Analysis and Management of Anthropogenic Natural Hazards and Disasters, Faculty of Geology and Geoenvironment, National and Kapodistrian University of Athens, Naxos, Erasmus+ project: McAgenda, 29/08/2016 – 11/09/2016. 36 p.

Athanasiou M. 2018. Guidebook for Civil Protection volunteers' safety in wildfire prevention and post-fire restoration activities. NSEA, eOUTLAND, Interreg V-A "Greece-Bulgaria 2014-2020" Cooperation Programme, 40 p.

Bonner SR, Hoffman CM, Kane JM, Varner JM, Hiers JK, O'Brien JJ, Rickard HD, Tinkham WT, Linn RR, Skowronski N, Parsons RA and Sieg CH (2021) Invigorating Prescribed Fire Science Through Improved Reporting Practices. Front. For. Glob. Change 4:750699. doi: 10.3389/ffgc.2021.750699

Espinosa, J.; Martin-Benito, D.; Rodriguez de Rivera, Ó.; Hernando, C.; Guijarro, M.; Madrigal, J. Tree Growth Response to Low-Intensity Prescribed Burning in Pinus nigra Stands: Effects of Burn Season and Fire Severity. Appl. Sci. 2021, 11, 7462. https://doi.org/10.3390/app11167462

Hogland, J.; Dunn, C.J.; Johnston, J.D. 21st Century Planning Techniques for Creating Fire-Resilient Forests in the AmericanWest. Forests 2021, 12, 1084. https://doi.org/10.3390/f12081084

Papanastasis V. P., 1977. Report on the seminar results, held in Thasos, for the improvement of *Pinus brutia* timber stands, by using the prescribed burning method. Thasos island, Greece, March 10-11, 1977. Forestry Chronicle, 19 (4-5): 98-102.

Paulo M Fernandes, G Matt Davies, Davide Ascoli, Cristina Fernandez, Francisco Moreira, et al.. Prescribed burning in southern Europe: developing fire management in a dynamic landscape. Frontiers in Ecology and the Environment, Ecological Society of America, 2013, 11 (1), pp. e4-e14. 10.1890/120298. hal-02650706

Steel ZL, Collins BM, Sapsis DB, Stephens SL. 2021 Quantifying pyrodiversity and its drivers. Proc. R. Soc. B 288: 20203202. https://doi.org/10.1098/rspb.2020.3202

Tsiouvaras C.N., Papanastasis V. Nastis A., L. Liakos. 1987. Understory post logging regeneration and growth in a Pinus brutia stand after slash burning. p. 73-94 In proceedings of the scientific workshop, September 30 - October 2, 1987, Chalkida, Euboea, Greece. Hellenic Forestry Society. (in Greek)

Varner, J.M.; Hiers, J.K.; Wheeler, S.B.; McGuire, J.; Quinn-Davidson, L.; Palmer, W.E.; Fowler, L. Increasing Pace and Scale of Prescribed Fire via Catastrophe Funds for Liability Relief. Fire 2021, 4, 77. https://doi.org/10.3390/fire4040077

Castellnou M., Kraus D., Miralles M. 2010 - Prescribed burning and suppression fire techniques: from fuel to landscape management. In: Montiel C., Kraus D. (Eds) - Best practices of fire use – prescribed burning and suppression fire programmes in selected case-study Regions in Europe. European Forest Institute Research Report 24: 3-16.

J.R. Molina, M. Ortega, F. Rodríguez y Silva. 2022. Fire ignition patterns to manage prescribed fire behavior: Application to Mediterranean pine forests, Journal of Environmental Management, Volume 302, Part A, 114052, ISSN 0301-4797, https://doi.org/10.1016/j.jenvman.2021.114052.

Nastis A., 1989. Control of forest fires in Mediterranean region by use of prescribed burning and grazing: Effect on forest ecosystem, CEE EV4V 0095 – GR (TT), Progress report of the year 1989.

Moisture content of live forest fuel of Holm oak (Quercus ilex L.) related with forest fires in Mediterranean part of Croatia

Roman Rosavec*; Damir Barčić; Stjepan Mikac; Damir Ugarković

University of Zagreb, Faculty of Forestry and Wood Technology, Svetošimunska 23, Zagreb, Croatia, {rrosavec, dbarcic, smikac, dugarkovic}@sumfak.hr

**Corresponding author*

Keywords

Moisture content, live forest fuel, Holm oak, Mediterranean

Abstract

Due to its biological diversity and preservation, the Mediterranean area is an extremely valuable area on Earth. In recent years, the Mediterranean region has been frequently affected by fires. An increasing number of fires are certainly degrading the Mediterranean ecosystem and disrupting its stability, leading to a reduction in biodiversity and an increase in devastated areas. In addition to understanding and knowing the biological and ecological consequences of forest fires and methods of remediation and restoration of burned areas, knowledge of factors that cause forest fires and factors that cause the initial spread of fire is important to reduce burned areas and prepare and conduct preventive activities. The moisture content of living forest fuel is an extremely important factor for the spread of forest fires. It is a factor that is very sensitive and depends on local micrometeorological conditions. The practice is that some very significant variables for forest fires, such as the moisture content of potential fuels, are sought to be obtained by applying various models, although it is known that these models cannot determine the true values of required variables unlike actual, empirical research. The most important meteorological factors that are taken into account when it comes to forest fires are temperature and humidity or water (precipitation). It is a climazonal species in the forest ecosystems of the Mediterranean part of Croatia. The research was conducted at two locations; the island of Rab and Makarska. The results show differences in the influence of meteorological conditions depending on the location of the research. The obtained results confirm that the understanding of meteorological conditions and vegetation characteristics in terms of moisture content of living fuels and their relationship can contribute to improving knowledge about firefighting issues and identify critical periods of high risk of forest fires.

1. Introduction

Due to its biological diversity and preservation, the Mediterranean area is an extremely valuable area on Earth. In recent years, the Mediterranean region has been frequently affected by fires. An increasing number of fires are certainly degrading the Mediterranean ecosystem and disrupting its stability, leading to a reduction in biodiversity and an increase in devastated areas. At the same time, there are high costs of reconstruction that last for decades, there are landscape changes, socio-economic turmoil and conflicts of interest. Among the most important natural destabilizers that cause change are forest fires (Trabaud, 1980; Casal, 1987; Naveh, 1999). When it comes to the factors of occurrence and spread of forest fires, vegetation characteristics, ie combustible material and meteorological factors are the most decisive and most important factors of natural origin and spread of forest fires. Vegetation elements are based on vegetation cover, type, moisture content and availability of combustible material (Pyne *et al.*, 1996; Pellizzaro *et al.*, 2007). Meteorological parameters have a great impact on fires. Thus Viegas *et al.* (1999), Skinner *et al.* (1999), Viegas *et al.* (2004) and Pereira et al. (2005) point out that weather and climate play a key role in determining the fire regime of an area, and the fire regime in turn is very close to climate change. Topographic elements are an important factor influencing the formation and spread of forest fires. Different landforms can be natural barriers or conveniences for forest fires. Slope is a factor on which the spread of forest fires depends. On steep slopes, forest fires spread much faster than on flat terrain. If a forest fire develops uphill, in the direction of rising hot air, it will develop faster, and the rate of spread can further regulate the influence of the wind. At higher altitudes, the temperature is lower, and therefore the intensity of fires is lower. When it comes to the initial occurrence of forest fires, in terms of forest fuels, dead forest fuel plays a key role in the occurrence of fires. It is a fuel that participates in the initial ignition and further flare-up of the fire element, and when a fire develops, in addition to the role of dead fuel, living forest fuel, its

condition and quantity are important for its further progress. The objectives of this study are to determine the moisture content of live holm oak (*Qurcus ilex* L.) for the Adriatic area in Croatia and to analyze the impact of meteorological factors (temperature, humidity and precipitation) on the moisture content of live fuel of this species.

2. Material and methods

2.1. Research area

The island of Rab is located on the northern Croatian coast, and Makarska on the southern Croatian coast. On the island of Rab, research was conducted at the Teaching Experimental Forest Facility Rab, Faculty of Forestry and Wood Technology, University of Zagreb. In Makarska, the research was conducted in an experimental laboratory located within the main meteorological station Makarska.

2.2. Research methods

For two years, once a month, tests were performed at each location. The meteorological data used for the analyzes were taken from the State Hydrometeorological Institute, and were measured at the meteorological station Rab and the main meteorological station Makarska. The moisture content of the tested samples was obtained using a standardized equation for determining the moisture content (percentage of dry weight) by the method of drying in an oven.

The equation is:

$$LFMC = ((FW - DW) / DW) * 100$$

Where is:

LFMC – moisture content of the tested sample

FW – mass of fresh sample

DW – mass of dry sample

3. Results

Table 1. Moisture content of live fuel Holm oak (Quercus ilex L.)

Species	Moisture content of live fuel LFMC (%)	
	Makarska	**Rab**
Holm oak (Quercus ilex L.)	48.99-91.37	66.36-102.86

The moisture content of live holm oak (*Quercus ilex* L.) fuel is higher on the island of Rab than in Makarska. The obtained results indicate that although it is the same type, the moisture content of live fuel is lower on the island of Rab, which belongs to the northern Croatian coast.

Table 2 - Linear correlation of live fuel moisture content (LFMC) for holm oak (Quercus ilex L.) on the island of Rab and in Makarska

Variable	Correlations (Alepski bor – *P. halepensis* Mill. – DI); Marked correlations are significant at p<.05000; N=25					
	LFMC	Mean monthly air humidity	Mean monthly air temperature	Mean monthly maximum air temperature	Mean monthly minimum air temperature	Mean monthly precipitation
Rab – LFMC	1.00	-0.02	-0.44	-0.44	-0.44	-0.43
Makarska – LFMC	1.00	-0.10	0.14	0.14	0.15	0.22

The correlation between LFMC and mean monthly precipitation (0.43 *) is positive, statistically significant and mean, while the correlations are mean monthly air temperature (-0.44 *), mean monthly maximum air temperature (-0.44 *), mean monthly minimum air temperatures (-0.44 *) statistically significant, negative and moderate. In Makarska, the LFMC of holm oak (*Quercus ilex* L.) does not show a statistically significant correlation with the variables used (Table 2.). Makarska belongs to the southern Croatian coast and the role of meteorological factors describing the climate impact is not statistically significant as it is on the island of Rab.

4. Concluding discussion

Fuel moisture content has been identified as one of the most critical factors influencing the occurrence and spread of fires (Van Wagner, 1977; Viegas *et al.*, 1992; Andre *et al.*, 1992; Viegas *et al.*, 1998; Carlson and Burgan, 2003; Chuvieco *et al.*, 2004). Cappelli *et al.* (1983) and Dimitrakopoulos and Papaioannou (2001) found that there is a great connection between the flammability of Mediterranean species and the moisture content in them. The increase or decrease in moisture content of the fuel is the result of weather conditions (Simard, 1968) and depends on the physiological and chemical characteristics of the fuel (Castro *et al.* 2003; Aguado *et al.*, 2007). However, Sun *et al.* (2006) point out that Mediterranean vegetation has structural, morphological and phenological characteristics suitable for the formation and spread of fire in conditions when the amount of available fuel and meteorological conditions are not critical. Therefore, a better understanding of meteorological conditions and vegetation characteristics in terms of flammability and moisture content of fuels and their relationship can contribute to improving knowledge about firefighting issues and identify critical periods of high risk of forest fires. Changes in moisture content are related to meteorological conditions and available soil moisture on the one hand, and the ecophysical characteristics of the species on the other, but also to living conditions in the past (Alessio *et al.*, 2008). Low fuel moisture content is the main reason for the occurrence of fires in early autumn due to drying of fuel during the summer and in the spring before the new leaf mass begins its activities (Rothermel, 1972). According to Pompe and Vines (1966), the occurrence of fires with catastrophic consequences arising in arid conditions is due to the stronger impact of reduced moisture content than high air temperatures. The significant impact of moisture content on fuel flammability can be demonstrated through the evaporation and exclusion of oxygen from the combustion zone (Brown and Davis, 1973). Apparently, the ignition energy is lower with a higher moisture content. On the other hand, the moisture content affects the behavior of the fire, because when combustion is reduced due to fuel humidity and further ignition is limited.

5. References

Trabaud, L. (1980): Impact biologique et écologique des feux de végétation sur l'organisation, la structure et l'évolution de la végétation des garrigues du Bas-Languedoc. Thèse Doct. Etat Univ. Sci. Tech. Languedoc, Montpellier, France.

Casal, M. (1987): Post-fire dynamics of shrublands dominated by Papilionaceae plants. Influence of fire on the stability of Mediterranean forest ecosystems. Ecología Mediterránea XIII (4), 87–98.

Naveh, Z. (1999): The role of fire as an evolutionary and ecological factor on the landscapes and vegetation of Mt. Carmel. Journal of Mediterranean Ecology 1, 11–25.

Pyne, S. J., *et al*. (1996): Introduction to Wildland Fire 2nd edition, John Wiley and Sons, Inc, NY, 769 pp.

Pellizzaro, G. *et al*. (2007): Seasonal variations of live moisture content nad ignitability in shrubs of the Mediterranean Basin. Int. J. Wild. Fire 16, 633-641.

Viegas, D. X. *et al*. (1999): Comparative study of various methods of fire danger. Int. J. Wild. Fire 9 (4), 235-246.

Skinner, W. B. *et al*. (1999): The association between circulation anomalies in the mid-troposphere and area burned by wildland fire in Canada. Theor. Appl. Climatol. 63, 89-105.

Viegas, D. X. *et al*. (2004): Calibracao do Sistema Canadiano de Perigo de Incendio para Aplicacao em Portugal (Canadian Fire Weather Risk System Calibration for aplication in Portugal). Silva Lusitana 12 (1), 77-93.

Pereira, M. G. *et al*. (2005): Synoptic patterns associated with large summer forest fires in Portugal. Agricultural and Forest Meteorology 129, 11-25.

Van Wagner, C. E. (1977): Conditions for the start and spread of crown fires. Can. J. For. Res. 7, 23-34.

Viegas, D. X. *et al*. (1992): Moisture content of fine forest fuels and fire occurrence in Central Portugal. Int. J. Wild. Fire 2, 69-86.

Andre, J. C. S. *et al*. (1992): Caderno Científico sobre Incêndios Florestais, Grupo de Mecânica dos Fluidos, Universidade de Coimbra.

Viegas, D. X. *et al*. (1998): Moisture content of living forest fuels and their relationship with meteorological indicces in the Iberian Peninsula. U: VIEGAS, D. X. (ur.): Proceedings Of III. International Conference On Forest Fire Research/14th Conference On Fire And Forest Meteorology. ADAI, University of Coimbra, Vol. I: 1029-1046.

Carlson, J. D., Burgan, R. E. (2003): Review of users' needs in operational fire danger estimation: The Oklahoma example. Int. J. Rem. Sens. 24, 1601-1620.

Chuvieco, E. *et al*. (2004): Conversion of fuel moisture content values to ignition potential for integrated fire danger assessment. Can. J. For. Res. 34, 2284-2293.

Cappelli, M. *et al*. (1983): Sul Grado d Infiammabilita di Alcune Specie Della Macchia Mediterranea. Collana Verde, Vol 62, 1-52.

Dimitrakopoulos, A. P., Papaioannou, K. K. (2001): Flammability Assessment of Mediterranean Forest Fuels. Fire Technol. 37, 143-152.

Simard, A. J. (1968): The mositure content of forest fuels – a review of the basic concepts. Forest Fire Research Institute, FF-X-14.

Castro, F. X. *et al*. (2003): Modeling moisture content in shrubs to predict fire risk in Catalonia (Spain). Agricultural and Forest Meteorology 116, 49-59.

Aguado, I., E. *et al*. (2007): Estimation of dead fuel moisture content from meteorological data in Mediterranean areas. Applications in fire danger assessment. Int. J. Wild. Fire 16, 390-397.

Sun, L. *et al*. (2006): Comparison of burning characteristics of live and dead chaparral fuels. Comb. Flame. 144, 349-359.

Alessio, G. A. *et al*. (2008): Implications of foliar terpene content and hydration on leaf flammability of *Quercus ilex* and *Pinus halepensis* plant. Ecology 10, 123–128.

Rothermel, R. C. (1972): A mathematical model for predicting fire spread in wildland fuels. USDA, Forest Service, Research Paper INT-115. (Ogden, UT).

Pompe, V., Vines, R. G. (1966): The influence of moisture on the Comustion of leaves. Aust. For. 30: 231-241.

Brown, A. A., Davis, K. J. (1973): Forest fires: Control and use, New York: Academic press.

Numerical Investigation of Crown Fuels Arrangements on Wildfire Behavior Following Fuels Treatments

Justin Paul Ziegler[1]∗; Chad M. Hoffman[1]; Russel A. Parsons[2]; Morris Johnson[3]; James Menakis[4]

[1]Department of Forest & Rangeland Stewardship, Colorado State University, Fort Collins, CO 80523, USA, {c.hoffman@colostate.edu}
[2]Fire Sciences Laboratory Forest Service, Rocky Mountain Research Station, US Forest Service, Missoula, MT, USA, {russell.a.parsons@usda.gov}
[3]Pacific Northwest Research Station, US Forest Service, Seattle, WA, USA, {morris.c.johnson@usda.gov}
[4]Washington Office Fire & Aviation Management, US Forest Service, Washington, DC, USA, {james.menakis@usda.gov}

**Corresponding author*

Keywords

Physics-based fire model; structural complexity; forest restoration; Pinus ponderosa; spatial heterogeneity

Abstract

Conventional fuels treatments often simplify forest structure by spacing residual trees and thinning from below to optimize fire hazard reduction. Conversely, restoration treatments, aimed at achieving ecological multiple objectives in addition to fire hazard reduction, purposefully retain heterogeneous forest structures. The retention of tree groups and small trees following restoration may however limit reductions in fire behavior. To quantify this potential trade-off, we performed a suite of simulations with the Wildland-urban interface Fire Dynamics Simulator to compare stand-level fire behavior between silvicultural cuttings that either emphasized or reduced forest heterogeneous structure under a range of residual basal areas, surface fuel loads, and burning conditions. These cuttings included distance-based retention, variable retention, and random cuttings, optionally with thinning from below. While all treatments reduced fire behavior, differences between cutting scenarios emerged at low levels of residual basal area. Rate of spread did increase under more severe burning conditions, and slightly increased after thinning from below or after variable retention cuttings due to higher wind speeds associated with the creation of openings. Canopy consumption was lowest when thinning from below and highest after variable retention. The differences we observed support the advantage of using fuels treatments that preferentially space residual trees and remove small trees where fire hazard reduction is of primary importance. Additionally, the effects of residual basal area, surface fuel load, and burning conditions highlight the multivariate considerations required when planning fuels treatments and assessing performance at stand scales.

1. Introduction

Mechanical fuels treatments are a primary tool in forests to reduce the likelihood of undesirable fire behavior and post fire effects at the stand scale (Reinhardt et al., 2008; Stephens et al., 2021). At a minimum, fuels treatments are oriented around four principles (Agee and Skinner, 2005): reduce surface and canopy fuel loads, increase canopy base height, and preserve larger fire-resistant trees. These principles are often implemented silviculturally by removing small trees and leaving widely spaced large trees (Larson and Churchill, 2012; Stephens et al., 2021).

There is a desire in many forests globally however to use silvicultural practices which emphasize the creation of heterogeneous forest structures (Fahey et al., 2018; Puettmann, 2011; Zenner and Hibbs, 2000; Ziegler et al., 2017). For example, dry forest stands of the western USA, for example, were composed of fine-scale (sub-ha) mixtures of openings, isolated trees and tree groups prior to EuroAmerican settlement (Clyatt et al., 2016; Larson and Churchill, 2012). In these forests, restoration treatments aim to dually achieve both ecological and fire hazard objectives. Restoration-based silvicultural practices permit variable tree spacing rather than distance-based minima (Churchill et al., 2013), and shift from a size-centric focus geared towards lifting the canopy to a free thinning approach (Addington et al., 2018; Tuten et al., 2015; Underhill et al., 2014).

Restoration treatments are generally seen as compatible with reducing fire hazard (Addington et al., 2018; Stephens et al., 2021). The long-term persistence of heterogeneously structured forests, historically sparser than their modern counterparts, suggests these forests have been resilient (Larson and Churchill, 2012). In addition, Koontz et al. (2020) found that sparse and heterogeneous forest structures experienced low severity fire effects following wildfires. Further, fire simulation studies confirm heterogeneous restoration treatments reduce fire behavior relative to their state pre-treatment (Ziegler et al., 2017). However, it is suggested that fire behavior reduction may be hindered after restoration relative to homogenizing conventional fuels treatments, implying restoration treatments carry tradeoffs (Addington et al., 2018; Larson and Churchill, 2012; Stephens et al., 2021; Ziegler et al., 2017). These remarks cite the potential for surface-crown transitions facilitated by residual ladder fuels and local crown fire spread within tree groups (Larson and Churchill, 2012; Stephens et al., 2021). Further, the openings created by restoration treatments can increase within-stand wind speeds, exacerbating fire rate of spread and fireline intensity (Linn et al., 2013; Ziegler et al., 2017).

We conducted a systematic study of simulated fire behavior under hypothetical cutting alternatives using data measured in real-world dry forests in the intermountain West, USA. We developed five hypothetical cutting scenarios to manipulate the horizontal and/or vertical arrangements of tree crowns. We implemented cutting scenarios to various levels of residual basal areas. Then we simulated fire using a three-dimensional, physics-based fire model across a range of surface fuel loads and burning conditions. Last, we compared measures of fire behavior and severity between cutting scenarios at each level of residual basal area.

2. Materials and Methods

2.1. Design of Fire Simulations

We planned our experiment to simulate the effects of cutting scenarios on potential fire behavior and severity across a range of burning conditions. With the Wildland urban interface Fire Dynamics Simulator (WFDS) (Mell et al., 2007; Mueller et al., 2014), we simulated fire before and following virtual cuttings on five stem-mapped 4-ha sites. These sites are located within ponderosa pine (*Pinus ponderosa* Lawson)-dominated forests in Colorado and Arizona, USA (Ziegler et al., 2017). Cuttings included: random, distance-based, with or without thinning from below, and variable retention, with or without thinning from below. Each cutting operated by sequentially removing, or retaining, trees until a basal area target of either 5, 10 or 15 m^2 ha^{-1} was met. The random cutting equally sampled trees. The distance-based cutting removed trees nearest to another tree. Our variable retention cuttings used an algorithm previously described by Tinkham et al. (2017) to retain groups of trees. For each WFDS simulation, we populated three-dimensional domains with the residual trees for a given site, its respective cutting scenario at each residual basal area. Our parameterization mimicked related WFDS studies, e.g. Ziegler et al., (2021, 2020, 2017). Table 1 details the forest structure following each cutting scenario.

Table 1- Spatial and aspatial summary of forest structure following hypothetical cuttings, averaged (std. error) across five 4-ha sites.

Cutting scenario	Trees ha^{-1}	QMD	Mean trees $group^{-1}$	Mean opening size (m^2)	Mean nearest neighbor (m)
Pre-cutting	687 (88)	22.8 (2)	10.1 (2.2)	16 (6)	1.6 (0.1)
Residual basal area: 15 m^2 ha^{-1}					
Random	403 (56)	23 (2)	4.1 (0.6)	37 (13)	2.2 (0.2)
Distance-based	292 (46)	27 (2)	2.4 (0.4)	29 (11)	3.6 (0.4)
Variable-retention	386 (60)	23 (2)	4.3 (0.7)	62 (14.4)	2.1 (0.2)
Distance-based w/ thin-from-below	118 (23)	43 (5)	1.1 (0.0)	105 (34)	6.3 (0.7)
Variable-retention w/ thin-from-below	153 (28)	38 (4)	1.6 (0.1)	117 (29)	4.1 (0.4)
Residual basal area: 10 m^2 ha^{-1}					
Random	265 (37)	23 (2)	2.7 (0.2)	68 (19)	2.7 (0.2)
Distance-based	178 (28)	28 (3)	1.3 (0.1)	56 (19)	5.0 (0.5)
Variable-retention	269 (36)	22 (2)	3.1 (0.3)	117 (16)	2.2 (0.2)
Distance-based w/ thin-from-below	62 (12)	49 (6)	1.0 (0.0)	189 (38)	9.0 (1.0)

Variable-retention w/ thin-from-below	83 (15)	42 (5)	1.3 (0.0)	194 (30)	5.6 (0.6)
Residual basal area: 5 m^2 ha^{-1}					
Random	132 (22)	23 (2)	1.7 (0.1)	139 (28)	4.2 (0.4)
Distance-based	82 (13)	29 (2)	1.0 (0.0)	141 (26)	7.9 (0.8)
Variable-retention	144 (18)	22 (2)	2.7 (0.3)	215 (8)	2.6 (0.2)
Distance-based w/ thin-from-below	24 (5)	56 (7)	1.0 (0.0)	312 (21)	15.9 (1.9)
Variable-retention w/ thin-from-below	32 (7)	48 (6)	1.1 (0.0)	304 (22)	9.5 (1.2)

We varied additional parameters in WFDS simulations to capture a range of fire behavior outcomes from moderate to extreme. Our experimental design varied the open wind speed (5, 10, or 15 m s^{-1} at 20-m AGL), surface fuel loading, and surface fuel moisture (5%, 8%, or 11%) to generate a range of burning condition severities. Median surface fuel loads were 0.4, 0.8 or 1.2 kg m^{-2}. We distributed surface fuel loads heterogeneously to reflect the influence that canopy cover has on the composition of the surface fuelbed locally (Figure 1) (Banwell and Varner, 2014; Matonis and Binkley, 2018). First, we calculated the distances from any location to a tree, then inverted these distances, and last re-scaled these distances to fuel load using a triangular distribution with a minimum of 0.2, maximum of 3.0, and median of either 0.4, 0.8, or 1.2. Where the surface fuel load was 0.2 kg m^{-2}, we assigned a fuel bulk density of 2 kg m^{-3}. For each surface fuel load increase of 1 kg m^{-2}, we increased fuel bulk density by 6.25 kg m^{-3}.

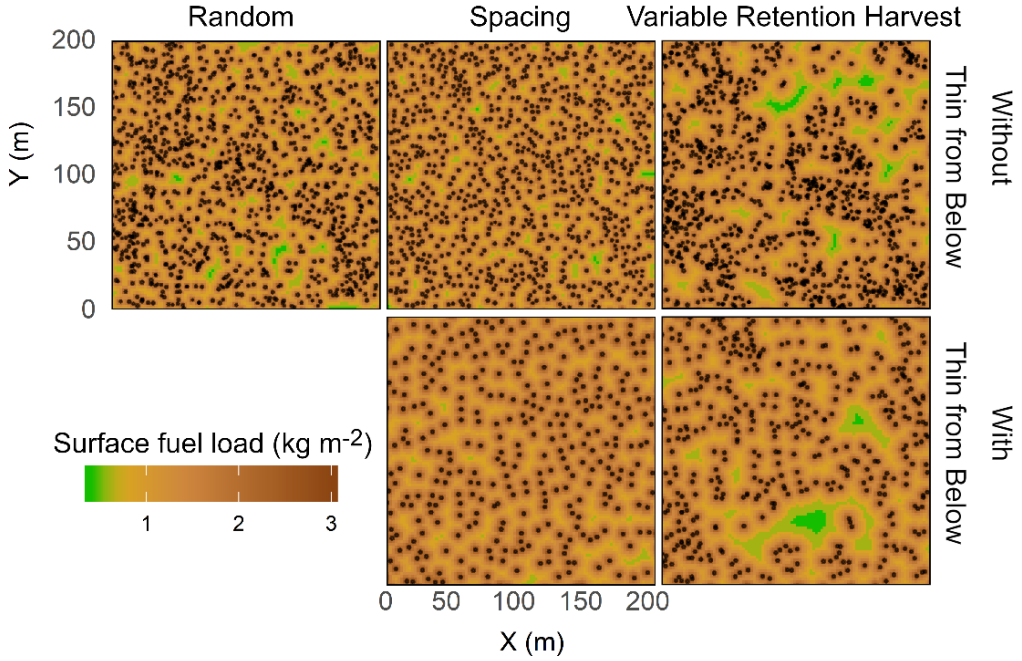

Figure 1- Example of simulated cuttings on one site, Long John, mapping the locations of residual trees (black dots) given a target basal area of 10 m^2 ha^{-1}, and the arrangement of surface fuel loads, given a spatial median of 1.2 kg $^{-2}$

2.2. Experimental Design & Analysis

We performed 200 simulations of fire behavior after cutting. We used an implementation of C-optimized Fedorov's exchange algorithm (Atkinson and Donev, 1992) as implemented by the AlgDesign v1.2.0 package (Wheeler, 2019) in R to choose a subset of simulations to run among a full factorial candidate list. We also simulated fire behavior a total of 40 times across sites pre-cutting across all variables, again using C-optimized Fedorov's exchange algorithm.

We measured mean rate of spread and logit-transformed percent canopy consumption for each WFDS simulation. First, we used linear mixed-effects regressions, with nlme v.3-1-152 (Pinheiro et al., 2021) in R, to measure the estimators for each variable, using the form (Eq. 1):

$$\{ROS, CC\} = U_{10} + SFL + SFM + BA + Cutting + BA \times Cutting + Plot, \quad (1)$$

which includes fire rate of spread (ROS), percent canopy consumption (CC), open wind speed (U_{10}) measured at 10 m above the ground, surface fuel load (SFL), surface fuel moisture (SFM), residual basal area (BA), cutting scenario, and plot as the single random variable. Second, we then applied a subsequent analysis of deviance test to assess statistical significance of variables, using an α of 0.05 for all hypothesis tests in this study.

3. Results

Fire rate of spread (ROS) was lower after all cutting scenarios relative to pre-cutting (Dunnett's test, all *p*-values < 0.002). ROS averaged 0.67 m s^{-1} before cutting, and from 0.48 m s^{-1} to 0.53 m s^{-1} across cutting scenarios. There was a significant main effect between cuttings (Analysis of deviance, $\chi^2(df = 5) = 24.6$, $p < .001$). Further, while there was no trend with respect to residual basal area (Analysis of deviance, $\chi^2(df = 1) = 3.4$, $p = .064$), we found that the differences between cuttings increased with lower residual basal area (Analysis of deviance, $\chi^2(df = 5) = 13.9$, $p = .016$; Figure 2a). At the highest basal area, pairwise comparisons tests showed that ROS was not different between cutting scenarios, averaging 0.51 m s^{-1}. But when thinning to 5 m^2 ha^{-1}, ROS decreased to 0.47 m s^{-1} within distance-based and random cuttings. Meanwhile, ROS increased to 0.54 m s^{-1} after variable retention.

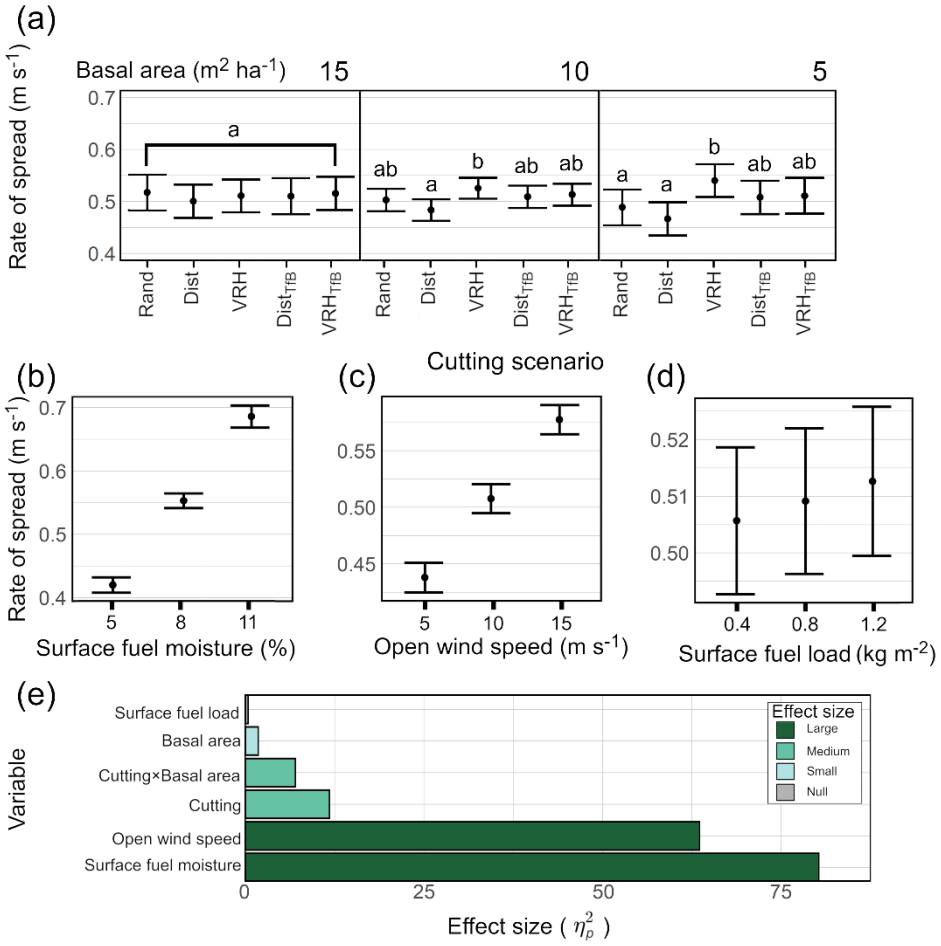

Figure 2- Marginal effects of a) cutting scenario × basal area, b) surface fuel moisture, c) open wind speed, and d) surface fuel load following mixed effects modelling on rate of spread, and e) effect size of variables. Letters indicate significant differences between cuttings using pairwise comparison procedures.

Among the other independent variables, surface fuel moisture most explained ROS (Analysis of deviance, $\chi^2(df = 1) = 759.9$, $p < .001$; Figure 2e), with 0.42 m s^{-1} ROS at 11% surface fuel moisture to 0.69 m s^{-1} ROS at 5% surface fuel moisture (Figure 2b). Meanwhile, ROS ranged from 0.44 to 0.58 m s^{-1} as open wind speed increased from 5 to 15 m s^{-1} (Analysis of deviance, $\chi^2(df = 1) = 323.1$, $p < .001$; Figure 2c). Surface fuel load was the only variable which did not explain variability in ROS (Analysis of deviance, $\chi^2(df = 1) = 0.8$, $p = .381$; Figure 2d).

The percent canopy consumption (CC) averaged 73% before cuttings and significantly dropped to 43% to 54% across cuttings (Dunnett's test, all *p*-values < 0.001). CC did vary between cutting scenarios (Analysis of deviance, χ^2(df = 5) = 65.6, $p < .001$) and explained the most variance alone of any variable (Figure 3a, e). In general, we found that the cuttings including thinning from below had lower CC than those cuttings without any thinning from below; of the latter scenarios, variable retention harvests were the highest. While CC diminished with lower residual basal areas (Analysis of deviance, χ^2(df = 1) = 34.5, $p < .001$), we identified an interaction with cutting scenarios. Specifically, the spread in CC between cutting scenarios was greater with less residual basal area (Analysis of deviance, χ^2(df = 5) = 23.3, $p < .001$).

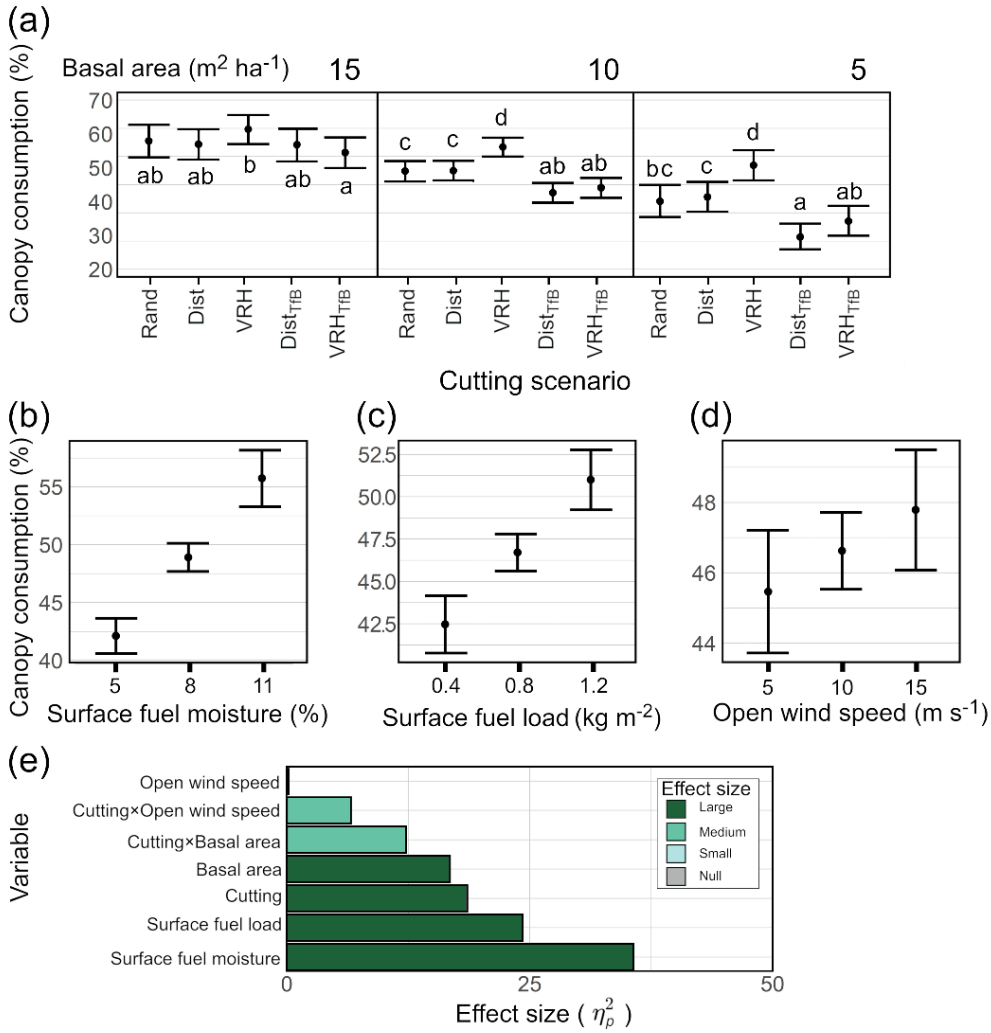

Figure 3- Marginal effects of a) cutting scenario × basal area, b) surface fuel moisture, c) surface fuel load, and d) open wind speed following mixed effects modelling on canopy consumption, and e) effect size of variables. Letters indicate significant differences between cuttings using pairwise comparison procedures.

Surface fuel moisture was the second most important variable (Analysis of deviance, χ^2(df = 1) = 95.7, $p < .001$) as CC rose from 42% to 56% while surface fuel dried (Figure 3b). As surface fuel loads increased from 0.4 to 1.2 kg m^{-2}, CC rose from 42% to 51% (Analysis of deviance, χ^2(df = 1) = 56.4, $p < .001$; Figure 3c). Open wind speed was a significant predictor of CC (Analysis of deviance, χ^2(df = 1) = 4.0, p = .045; Figure 3d), but had only a small effect size (Figure 3e).

4. Discussion

Most notably we found that all cuttings reduced fire behavior relative to pre-cutting scenarios, at all residual basal areas and burning conditions. This gives silviculturalists and fuels managers more opportunity to decide how remnant trees are arranged to realize other objectives. Where forest managers seek to maximize every

potential gain in fire haz-ard reduction with few other considerations, our results validate the use of conventional fuels treatments which combine distance-based specifications with thinning from below (Addington et al., 2018; Stephens et al., 2021). We found lower rates of canopy consumption because isolated trees experience greater convective cooling (Ritter et al., 2020) and lower heat fluxes between tree crowns (Contreras et al., 2012) (Figure 4). In contrast, restoration treatments which create both vertical and horizontal heterogeneity in forest structure were less effective at reducing fire behavior; wind entrained in openings pushing fire rate of spread higher, and the retention of both small trees and grouped trees allowed for instances of group torching, resulting in higher canopy consumption (Figure 4). This affirms a trade-off between retention of heterogeneous forest structure and fire hazard reduction (Stephens et al., 2021).

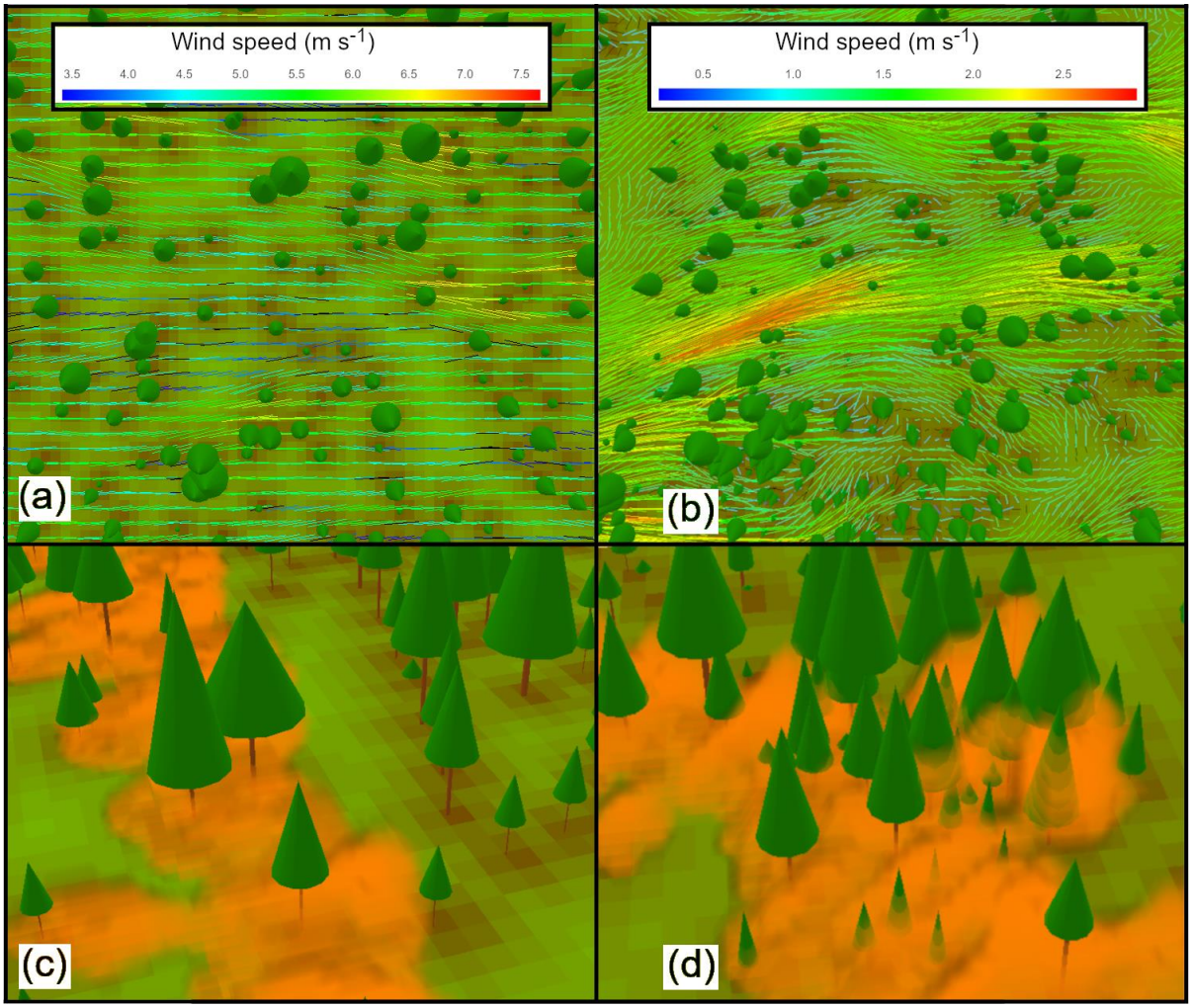

Figure 4- Demonstration of regimes of pre-fire (a) laminar flow with distance-based cuttings and (b) entrainment of wind following variable retention harvest, with wind vectors at 2 m above ground level flowing from left to right. During fire spread, (c) fire passed under large trees after distance-based cutting, while (d) groups torched after variable retention harvest.

Forest managers can close the spread between conventional fuels cuttings and forest restoration. Firstly, silviculturalists can undertake more aggressive reductions in basal area. As reported by Underhill et al. (2014) and Ziegler et al. (2017), recent implementations of restoration treatments in the forests simulated by this study have been retaining a basal area of 10 to 20 m^2 ha^{-1}. In contrast, these forests historically had an average basal area of 6.3 and density of 97 trees ha^{-1} (Battaglia et al., 2018). Forest managers have an opportunity to further reduce residual stocking and potential fire behavior without deviating outside of the range of natural variability and impairing ecosystem functioning. Secondly, some removal of small trees can increase fire behavior reduction; specifically, retaining tree groups without ladder fuels (Churchill et al., 2013) while preserving clusters of smaller, regenerating tree groups (Addington et al., 2018) can reduce the potential for surface-crown fire transition while maintaining younger cohorts of trees.

5. References

Addington, R., Aplet, G., Battaglia, M., Briggs, J., Brown, P., Cheng, A., Dickinson, Y., Feinstein, J.A., Pelz, K., Regan, C., Thinnes, J., Truex, R., Paula, J., Gannon, B., Julian, C., Underhill, J., Wolk, B., 2018. Principles and practices for the restoration of ponderosa pine and dry mixed-conifer forests of the Colorado Front Range. Gen. Tech. Report, RMRS-GTR-373, USDA For. Serv. Rocky Mt. Res. Station. Fort Collins, CO. 121. https://doi.org/10.1093/acprof:oso/9780195310139.003.0002

Agee, J.K., Skinner, C.N., 2005. Basic principles of forest fuel reduction treatments. For. Ecol. Manage. 211, 83–96. https://doi.org/10.1016/j.foreco.2005.01.034

Atkinson, A.C., Donev, A.N., 1992. Optimum Experimental Designs. Oxford University Press.

Banwell, E.M., Varner, J.M., 2014. Structure and composition of forest floor fuels in long-unburned Jeffrey pine-white fir forests of the Lake Tahoe Basin, USA. Int. J. Wildl. Fire 23, 363–372. https://doi.org/10.1071/WF13025

Battaglia, M.A., Gannon, B., Brown, P.M., Fornwalt, P.J., Cheng, A.S., Huckaby, L.S., 2018. Changes in forest structure since 1860 in ponderosa pine dominated forests in the Colorado and Wyoming Front Range, USA. For. Ecol. Manage. 422, 147–160. https://doi.org/10.1016/j.foreco.2018.04.010

Churchill, D.J., Larson, A.J., Dahlgreen, M.C., Franklin, J.F., Hessburg, P.F., Lutz, J.A., 2013. Restoring forest resilience: From reference spatial patterns to silvicultural prescriptions and monitoring. For. Ecol. Manage. 291, 442–457.

Clyatt, K.A., Crotteau, J.S., Schaedel, M.S., Wiggins, H.L., Kelley, H., Churchill, D.J., Larson, A.J., 2016. Historical spatial patterns and contemporary tree mortality in dry mixed-conifer forests. For. Ecol. Manage. 361, 23–37. https://doi.org/10.1016/j.foreco.2015.10.049

Contreras, M.A., Parsons, R.A., Chung, W., 2012. Modeling tree-level fuel connectivity to evaluate the effectiveness of thinning treatments for reducing crown fire potential. For. Ecol. Manage. 264, 134–149. https://doi.org/10.1016/j.foreco.2011.10.001

Fahey, R.T., Alveshere, B.C., Burton, J.I., D'Amato, A.W., Dickinson, Y.L., Keeton, W.S., Kern, C.C., Larson, A.J., Palik, B.J., Puettmann, K.J., Saunders, M.R., Webster, C.R., Atkins, J.W., Gough, C.M., Hardiman, B.S., 2018. Shifting conceptions of complexity in forest management and silviculture. For. Ecol. Manage. 421, 59–71. https://doi.org/10.1016/j.foreco.2018.01.011

Koontz, M.J., North, M.P., Werner, C.M., Fick, S.E., Latimer, A.M., 2020. Local forest structure variability increases resilience to wildfire in dry western U.S. coniferous forests. Ecol. Lett. 23, 483–494. https://doi.org/10.1111/ele.13447

Larson, A.J., Churchill, D., 2012. Tree spatial patterns in fire-frequent forests of western North America, including mechanisms of pattern formation and implications for designing fuel reduction and restoration treatments. For. Ecol. Manage. 267, 74–92. https://doi.org/10.1016/j.foreco.2011.11.038

Linn, R.R., Sieg, C.H., Hoffman, C.M., Winterkamp, J.L., McMillin, J.D., 2013. Modeling wind fields and fire propagation following bark beetle outbreaks in spatially-heterogeneous pinyon-juniper woodland fuel complexes. Agric. For. Meteorol. 173, 139–153. https://doi.org/10.1016/j.agrformet.2012.11.007

Matonis, M.S., Binkley, D., 2018. Not just about the trees: Key role of mosaic-meadows in restoration of ponderosa pine ecosystems. For. Ecol. Manage. 411, 120–131. https://doi.org/10.1016/j.foreco.2018.01.019

Mell, W., Jenkins, M.A., Gould, J., Cheney, P., A, W.M., B, M.A.J., C, J.G., C, P.C., 2007. A physics-based approach to modelling grassland fires. Int. J. Wildl. Fire 16, 1–22. https://doi.org/10.1071/WF06002

Mueller, E., Mell, W., Simeoni, A., 2014. Large eddy simulation of forest canopy flow for wildland fire modeling. Can. J. For. Res. 44, 1534–1544. https://doi.org/10.1139/cjfr-2014-0184

Pinheiro, J., Bates, D., DebRoy, S., Sarkar, D., Team, R.C., 2021. {nlme}: Linear and Nonlinear Mixed Effects Models.

Puettmann, K.J., 2011. Approaches, silvicultural challenges and options in the context of global change: "Simple" fixes and opportunities for new management. J. For. https://doi.org/10.3928/01477447-20080901-33

Reinhardt, E.D., Keane, R.E., Calkin, D.E., Cohen, J.D., 2008. Objectives and considerations for wildland fuel treatment in forested ecosystems of the interior western United States. For. Ecol. Manage. 256, 1997–2006. https://doi.org/10.1016/j.foreco.2008.09.016

Ritter, S.M., Hoffman, C.M., Battaglia, M.A., Stevens-Rumann, C.S., Mell, W.E., 2020. Fine-scale fire patterns mediate forest structure in frequent-fire ecosystems. Ecosphere 11, 1–17. https://doi.org/10.1002/ecs2.3177

Stephens, S.L., Battaglia, M.A., Churchill, D.J., Collins, B.M., Coppoletta, M., Hoffman, C.M., Lydersen, J.M., North, M.P., Parsons, R.A., Ritter, S.M., Stevens, J.T., 2021. Forest restoration and fuels reduction: Convergent or divergent? Bioscience 71, 85–101. https://doi.org/10.1093/biosci/biaa134

Tinkham, W.T., Dickinson, Y., Hoffman, C.M., Battaglia, M.A., Ex, S., Underhill, J., 2017. Visualization of heterogeneous forest structures following treatment in the Southern Rocky Mountains. Gen. Tech. Report, RMRS-GTR-365, USDA For. Serv. Rocky Mt. Res. Station. Fort Collins, CO.

Tuten, M.C., Sánchez Meador, A., Fulé, P.Z., 2015. Ecological restoration and fine-scale forest structure regulation in southwestern ponderosa pine forests. For. Ecol. Manage. 348, 57–67. https://doi.org/10.1016/j.foreco.2015.03.032

Underhill, J.L., Dickinson, Y., Rudney, A., Thinnes, J., 2014. Silviculture of the Colorado Front Range Landscape Restoration Initiative. J. For. 112, 484–493. https://doi.org/10.5849/jof.13-092

Wheeler, B., 2019. AlgDesign: Algorithmic Experimental Design.

Zenner, E.K., Hibbs, D.E., 2000. A new method for modeling the heterogeneity of forest structure. For. Ecol. Manage. 129, 75–87.

Ziegler, J.P., Hoffman, C., Battaglia, M., Mell, W., 2017. Spatially explicit measurements of forest structure and fire behavior following restoration treatments in dry forests. For. Ecol. Manage. 386, 1–12. https://doi.org/10.1016/j.foreco.2016.12.002

Ziegler, J.P., Hoffman, C.M., Collins, B.M., Knapp, E.E., Mell, W., 2021. Pyric tree spatial patterning interactions in historical and contemporary mixed conifer forests, California, USA. Ecol. Evol. 11, 820–834. https://doi.org/10.1002/ece3.7084

Ziegler, J.P., Hoffman, C.M., Collins, B.M., Long, J.W., Dagley, C.M., Mell, W., 2020. Simulated fire behavior and fine-scale forest structure following conifer removal in aspen-conifer forests in the Lake Tahoe Basin, USA. Fire 3, 1–16. https://doi.org/10.3390/fire3030051

Preventing wildfires through smart management and valorisation of residual forest biomass into biochar: experiences from the BioValChar project

Flávio C. Silva*; Márcia Santos; Jéssica Moura; Ana C. Vilas Boas; Manuel A. Matos; Luís A.C. Tarelho

[1]University of Aveiro, Department of Environment and Planning, CESAM – Centre for Environmental and Marine Studies, Campus Santiago, 3810-193 Aveiro, Portugal
{flavio.silva, marciasantos, jessica.moura, catarina.vilas.boas, amatos, ltarelho}@ua.pt

**Corresponding author*

Keywords

Residual biomass; pyrolysis; biochar; forest cleaning

Abstract

Forest management operations adequately integrated in the forestry value-chain are the gold standard in wildfire prevention. However, these operations generate considerable amounts of residual forest biomass (RFB) that cannot be legally disposed in land and further require suitable management. Residual biomass also includes highly flammable plants existing in the Portuguese forest such as gorse, broom, giant reed and acacia. Quite often wildfires in Portugal are linked with spreading of this residual biomass that promotes fuel accumulation. Besides deleterious impacts on rural and forestry economy, wildfires are also a driver for desertification and soil degradation.

Alternative uses for this residual biomass to promote its valorisation and enable proper models of management of forest areas are needed, thus providing economic and environmental benefits towards decreasing of the fuel load. Though this biomass has reasonable carbon content and heating value, they also present inorganic composition (e.g. Na, K, Cl) that promotes operating problems in thermochemical conversion processes as combustion and gasification for useful energy production because of ash related problems (e.g., sintering/fouling), thus restricting their use in such applications.

As such, biochar production by pyrolysis is a potential alternative to generate added-value. During pyrolysis the volatile matter of biomass is released to the gaseous phase, resulting a solid product, biochar, which is carbon-rich and contains most of the inorganics (nutrients) of the raw biomass. Exposure of biomass inorganics as free ashes is prevented in this process, and hence pyrolysis mitigates their negative effects. Nonetheless, the efficient pyrolysis of these types of biomass requires development of novel solutions optimized for energy and environmental performance. Enhancing of the energetic sustainability of the process and minimizing of the environmental impacts associated to the emission of gaseous pollutants are aspects of major relevance. Additionally, the biochar quality depends on biomass type, technology and operating conditions used.

The BioValChar project (https://biovalchar.web.ua.pt/en/) seeks to answer these challenges related to valorisation of low-quality residual biomass through production of biochar by pyrolysis, which can return back to forest and rural soils. This approach will provide both carbon/nutrient cycling and synergies within forestry management, wildfire prevention, improvement of soil quality and rural development, under the circular economy principle. The research focus valorisation of residual forest biomass in full-control pyrolytic batch and continuous (auger-type reactor) processes, and testing of the resulting biochar performance as soil amendment. Moreover, a prototype of an integrated mobile unit for auto-thermal and continuous biochar production by pyrolysis of biomass is also being developed, by using the pyrolysis gases to provide the energetic needs of the process. Here we present the project overview, as well as some preliminary results on pyrolytic valorisation of one selected biomass (acacia) into biochar through distinct operating modes and conditions.

1. Context

Portugal territory has a significant fraction of forest supporting economic activity. However, as a result of improper forestry management, forest and rural areas have been subjected to strong pressure from wildfires, with negative impacts on natural resources (ecosystem degradation) and human life (socio-economic threats). The Portuguese Government launched a commitment program to develop Scientific and Technological

Research (S&TR) related to forest management and valorisation and prevention of forest fires (Conselho de Ministros, 2017), in line with the National Strategy for Forest (Conselho de Ministros, 2015). The goal is to generate applied knowledge to integrate perspectives of management and valorisation of forest resources, and underlying prevention to forest fires. Valorisation of residual biomass in rural areas is of the most relevant topics requiring applied S&TR.

Previous studies have identified distinct types of residual biomass from forestry operations with potential to be valorised to energy (Lopes *et al.*, 2013). In turn, forest cleaning for wildfires prevention also results in significant amounts of residual biomass without quality enough to be valorised into energy. This includes shrubs (acacia, gorse, broom, giant reed), which inorganic contents (e.g. K, Cl, Na) and resulting ash pose operating problems during combustion or gasification (van Loo and Koppejan, 2008; Niu *et al.*, 2016). These shrubs are highly flammable and have been identified recently as drivers for wildfire propagation in Portugal, as the Independent Technical Commission that investigated the wildfires that occurred in 2017 recommend their proper management towards wildfire prevention (Comissão Técnica Independente, 2017).

Since some of this residual biomass has considerable carbon content and heating value (van Loo and Koppejan, 2008), alternative valorisation must be developed. Biochar production by pyrolysis is an option. The pyrolysis process allows generation of distinct products, namely gases, liquids (bio-oils) and solids (biochar), with relative yields and composition depending on biomass type, pyrolysis reactor and operating conditions (Neves *et al.*, 2011). During pyrolysis the volatile matter of the biomass is released to the gas phase, thus remaining a solid fraction (biochar) where most of the inorganic content (ash constituents) of the raw biomass is embedded onto a carbon-rich matrix (Neves *et al.*, 2011; Neves *et al.*, 2017; Tarelho *et al.*, 2020), thus minimizing ash related problems that otherwise would be experienced during combustion or gasification.

The appropriate process for biochar production is slow pyrolysis (or carbonization), and several technologies have been referred as applicable, yet most of them derive from those applied to charcoal production from woody biomass (Neves *et al.*, 2011; Tarelho *et al.*, 2020) to be used as fuel. These technologies are mostly of type batch operated, large size, with low energy efficiency and high environmental impact. Considering the characteristics of residual biomass, more appropriate reactor configurations need development (Qureshi *et al.*, 2018) by addressing fuel flexibility, continuous operation, energy efficiency, portability/mobility, and this is a major challenge since existing information on technologies for biochar production relies on conventional configurations. New standards of product quality and energy efficiency can only be achieved with high level of process integration, e.g. by using the pyrolysis gas as fuel to satisfy the process energy needs (Salgado *et al.*, 2020; European Biochar Certificate, 2022). As such, these subjects require further applied research and technological development (R&TD), as most of the knowledge on biochar production concerns laboratorial small-scale.

Biochar produced from this low-grade residual biomass has no interest as fuel (charcoal) in typical energy applications due to its inorganics content and particle size, so alternative applications to boost its added-value have been suggested (Qureshi *et al.*, 2018; Salgado *et al.*, 2020; European Biochar Certificate, 2022; Lehmann and Joseph, 2015) yet lacking of technical evaluation and scale-up. The pyrolysis variables (e.g. feedstock, reactor type, heating rate, peak temperature, residence time) should be defined in order to obtain biochar with suitable characteristics (e.g. surface area, porosity and chemical composition) for specific applications and with economic profits, and that depends on biomass and pyrolysis conditions (Tarelho *et al.*, 2020; Salgado *et al.*, 2020; Lehmann and Joseph, 2015). As a way of improve physico-chemical and biological properties of soils, it has been shown that biochar significantly increases soil water holding capacity (Qian *et al.*, 2015; Verheijen *et al*., 2019), while increased infiltration in Mediterranean soil can increase available soil moisture during dry periods (Abrol *et al.*, 2016). Biochar in soil contributes to carbon sequestration and nutrient recycling (European Biochar Certificate, 2022; Lehmann and Joseph, 2015). Biochar contains (in)organic forms of N and P that can improve the nutrient use efficiency in plant-soil systems. This feature can provide N/P recycling and enhanced crop nutrition and yield, thus decreasing the application of inorganic fertilisers (Gul and Whalen, 2013) with associated environmental and economic gains. However, besides soil type, the agronomic value of biochar also relies on its redox chemistry that rules nutrient dynamics (Gul and Whalen, 2013; Palansooriya *et al.*, 2019), which in turn strongly depends on feedstock and process conditions. Therefore, trade-offs between pyrolysis conditions, biochar characteristics and impact on soil nutrient pools of specific agro-ecosystems require deeper research to boost the agronomic value of biochar.

Applied knowledge on biochar production from pyrolysis of residual biomass in a decentralised (in-situ) and energy sustainable process, and its valorisation in soil, is a key subject requiring innovative R&TD to support proper management and valorisation of residual biomass in rural areas. Demonstration of this integrated approach will both assist wildfires prevention and enable business models based on circular economy.

2. Project objectives and overview

The BioValChar project is public-funded and aims at valorisation of low-grade residual forest biomass (RFB) resulting from forestry maintenance operations for wildfire prevention. The valorisation process involves biochar production by pyrolysis, followed by biochar use as soil amendment and demonstration of the economic gains of the process towards development of sustainable business models. The methodology gathers scientific competences related to thermochemical conversion processes of biomass to energy vectors and organic products, waste management, biochar application, restoration of soil functions and energy/engineering economics, as well as collaborating companies. Furthermore, project demonstration targets two contrasting edaphoclimatic study areas in Portugal (north-central coast and central inland) in which wildfires often occur and where one of the partner companies has on-going forestry cleaning activities. This way the project outputs and impacts become validated to possibly apply to other countries experiencing wildfire issues.

The BioValChar research is being developed over four integrated axes:

1) Development and characterisation of the pyrolysis process at bench-scale under batch (fixed-bed reactors) and continuous (auger-type reactor) modes of operation. It will allow evaluate the influence of processes conditions (e.g. peak temperature, heating rate and soak time) in the yields and properties of each of the products (biochar, bio-oil and gas). Both fixed-bed and auger-type reactors were designed and developed at the University of Aveiro.
2) Design and construction of a prototype of a mobile integrated pyrolysis unit with a biomass processing capacity up to 10 kg h^{-1}, including a continuous pyrolysis reactor integrated with a combustion reactor to deliver heat for the pyrolysis process. It will be optimised for considering energy efficiency and environment performance. This will advance significant innovation and scientific knowledge on energy efficiency and mitigation of emission of air pollutants during biochar production in integrated pyrolysis-combustion systems, in order to suppress the existing knowledge gaps in this field.
3) Valorisation of the biochar produced by studying its performance as soil amendment at bench- and field-scale. This will allow obtaining dose-response curves in several variables (e.g. pH, CEC, organic matter/carbon/nutrient contents, geochemical reactive content, respiration, biomass productivity, among others), aiming at determining and demonstrating the biochar agronomic value. Ultimately it will help to close the loop between biomass pyrolysis and return of carbon and nutrients to soil.
4) Techno-economic analysis of the several operations (e.g., biomass collection and processing, pyrolysis unit construction and operation, biochar application costs, and greenhouse gas offset) involved in the solution proposed towards establishment of feasible business models applied to the forestry sector. It will also comprise field-scale demonstration activities to stakeholders to upscale and transfer of the key-results.

3. Preliminary results

Since most of the work packages are currently still on-going, we present here an example of results obtained during the work progress in Axis 1 (bench-scale pyrolysis) applied to one of the selected biomass species (acacia). Biomass was collected from a coastal pine forest in north-central Portugal, as a result from forest cleaning operations for wildfires prevention. It was further chopped till a maximum particle size of c.a. 1 cm, and characterised for proximate and elemental analysis.

Pyrolysis experiments took place in both batch and continuous modes with full control and monitoring of the operating variables. For the batch experiments, a fixed-bed tubular quartz reactor with 20 mm internal diameter, 23 mm outer diameter and 350 mm length, and a tubular furnace with 25 mm internal diameter and 300 mm length was used. The tubular furnace is operated by means of a control and data acquisition electronic system that allows the definition of heating rate and peak temperature of the tubular quartz reactor. For the continuous experiments, an auger reactor was used. The experimental facility is composed of a biomass silo, a screw-type

reactor made in stainless steel with 0.05 m internal diameter and an overall length of 2 m (including biomass feeding section, pyrolysis section and biochar discharge). The reactor comprises three sections, namely biomass feeding section, pyrolysis section, and biochar and gas discharge section. The biochar is discharged by means of a continuous screw feeder, and the pyrolysis gas produced is burned in a downstream combustion reactor.

Two peak temperatures were tested (450 and 550 ºC). In the batch process, soaking time and heating rate were set it 30 min and 20 ºC min^{-1}, respectively. In the continuous process, residence time (in the pyrolysis section) was set in 5 min. Biochar yields and proximate analysis are presented in Figure 1.

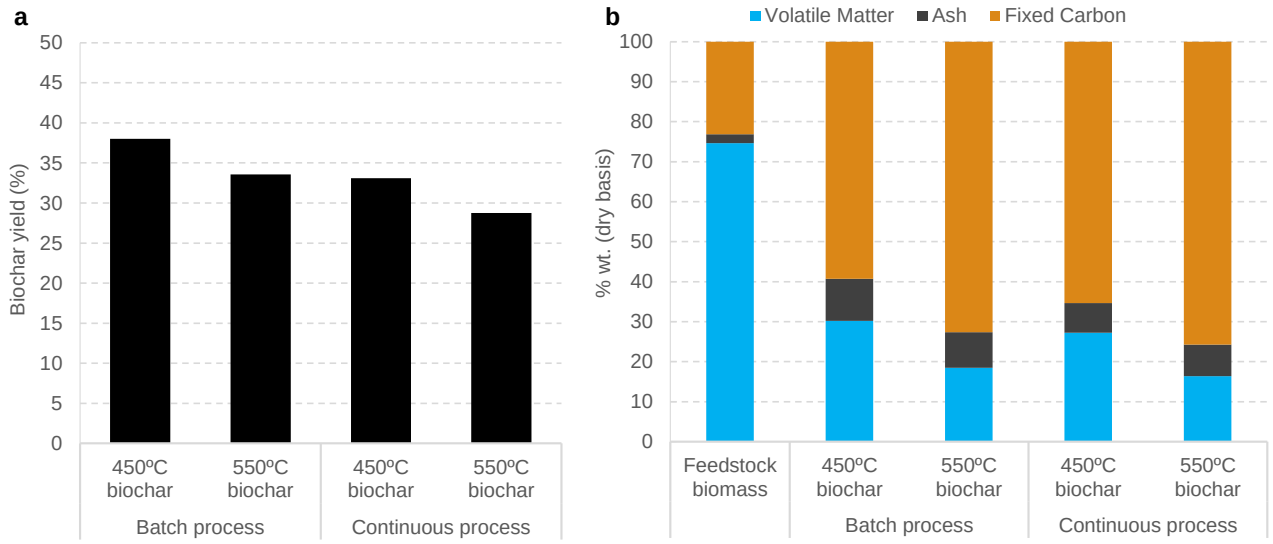

Figure 1- Biochar yield and properties, from batch and continuous pyrolysis of acacia: (a) biochar yield; (b) biochar proximate analysis

Biochar yields over the tested conditions and processes varied in the range 29 to 38%wt (Figure 1a). The biochar yield was influenced by both temperature and process mode. Peak temperatures of 450 ºC yielded 13 to 15% more biochar than 550 ºC peak temperatures, regardless of the process type. In turn, when reproducing pyrolysis batch processes in the auger reactor, a 13 to 14% drop in biochar yield was observed, regardless of the process temperature tested. The reasoning for this effect is under study, and its understanding is of upmost relevance to consider when designing scale-up of pyrolysis processes.

Regarding biochar proximate analysis (Figure 1b), similar trends are observed regardless of the pyrolysis operation mode. In both cases, the fraction of fixed carbon is substantially higher in the highest process temperature (73 to 76%wt) when compared to the lowest process temperature (59 to 65%wt), with the opposite trend observed in the volatile matter content. When comparing the process mode, continuous pyrolysis resulted in biochar with 4 to 10% higher fixed carbon content and 10 to 12% lower volatile matter than in the batch processes.

The ash content is systematically greater in the biochar resulting from the batch processes (9 to 11%wt) when compared to that produced through continuous processes (7 to 8%wt). When comparing process temperature, the increasing of 450 to 550 ºC resulted in a 15% decrease in the biochar ash content produced through batch pyrolysis. In turn, the same temperature shift in the continuous process resulted in a slight increase (5%) of the biochar ash content.

These preliminary results highlight the influence of the pyrolysis conditions and parameters in the key characteristics of the resulting biochar, and hence its further behaviour and feasibility as an added-value product in selected applications. Therefore, ensuring of a full control of the pyrolysis process, not only at prototype-scale, but especially considering upscaling scenarios, is of major importance to effectively provide a strategy to manage and valorise residual forest biomass, and thus enabling both wildfires prevention and profitable business models in the forestry sector. Moreover, the scope and outcomes of the BioValChar project are expected to provide a comprehensive basis towards replication of the models for management of residual forest biomass.

Its valorisation into biochar that can be applied to increase soil quality is of most relevance in ecosystems affected by recurrent wildfires and soil quality issues, such as the Mediterranean region.

4. Acknowledgements

BioValChar project "Sustainable valorization of residual biomass for biochar" (PCIF-GVB-0034-2019) is funded within the scope of the Scientific Research and Technological Development Project Call on Prevention and Fighting of Forest Fires - 2019, of the Fundação para a Ciência e a Tecnologia (FCT), being financed exclusively by national funds. F.C. Silva acknowledges national funds (OE) under the contract framework foreseen in art. 23º DL57/2016 (nº 4, 5, 6) August 29th, amended by DL57/2017 July 19th. It is also acknowledged the financial support to CESAM by FCT/MCTES (UIDP/50017/2020+UIDB/50017/2020+ LA/P/0094/2020), through national funds.

5. Bibliographic references

Abrol V, Ben-Hur M, Verheijen FGA, Keizer JJ, Martins MAS, Tenaw H, Tchehansky L, Graber ER. 2016. Biochar effects on soil water infiltration and erosion under seal formation conditions: rainfall simulation experiment. Journal of Soils and Sediments; 16(12):2709—2719.

Comissão Técnica Independente (CTI) Report on analysis of facts concerning wildfires that occurred [in Central Portugal] between 17 and 24 June 2017. 2017. Assembleia da República. Portuguese Government.

Conselho de Ministros, Resolução n.° 159/2017, Diário da República n.° 209/2017, Série I de 2017-10-30. Portuguese Law about the development of activities of Scientific and Technological Research related to the prevention and combat of forest fires.

Conselho de Ministros, Resolução n.° 6-B/2015, Diário da República n.° 24/2015, 1° Suplemento, Série I de 2015-02-04. Portuguese Law about the National Strategy for Forests.

European Biochar Certificate. 2022. https://www.european-biochar.org/en

Gul S, Whalen JK. Biochemical cycling of nitrogen and phosphorus in biochar-amended soils. 2013. Soil Biology & Biochemistry; 103:1-15.

Lehmann J, Joseph S (Editors). 2015. Biochar for Environmental Management: Science, Technology and Implementation. 2nd Edition, ISBN: 978-0-203-76226-4. Roufledge.

Lopes M, Tarelho L, Ribeiro I, Monteiro A, Martins H, Rafael S, Miranda A, Borrego C (Editors). 2013. Impacts of biomass to energy chain on air quality and Portuguese climate policy (Biogair Project). CESAM — Centre for Environmental and Marine Studies, University of Aveiro. ISBN: 978-989-98673-2-1.

Neves D, Matos A, Tarelho L, Thunman H, Larsson A, Seemann MC. 2017. Volatile gases from biomass pyrolysis under conditions relevant for fluidized bed gasifiers. Journal of Analytical and Applied Pyrolysis; 127:57-67.

Neves D, Thunman H, Matos A, Tarelho L, Barea AG. 2011. Characterization and prediction of biomass pyrolysis products. Progress in Energy and Combustion Science; 37:611-630.

Niu Y, Tan H, Hui S. 2016. Ash-related issues during biomass combustion: Alkali-induced slagging, silicate melt-induced slagging (ash fusion), agglomeration, corrosion, ash utilization, and related countermeasures. Progress in Energy and Combustion Science; 52:1-61.

Palansooriya KN, 0k YS, Awad YM, Lee SS, Sung JK, Koutsospyros A, Moon DH. 2019. Impacts of biochar application on upland agriculture: a review. Journal of Environmental Management; 234:52-64.

Qian K, Kumar A, Zhang H, Bellmer D, Huhnke R. 2015. Recent advances in utilization of biochar. Renewable and Sustainable Energy Reviews; 42:1055-1064.

Qureshi KM, Lup ANK, Khan S, Abnisa F, Daud WMAW. 2018. A technical review on semi-continuous and continuous pyrolysis process of biomass to bio-oil. Journal of Analytical and Applied Pyrolysis; 18:52-75.

Salgado MAH, Tarelho LAC, Matos MAA. 2020. Analysis of combined biochar and torrified biomass fuel production as alternative for residual biomass valorization generated in small-scale palm oil mills. Waste and Biomass Valorization; 11:343-356.

Tarelho, L.A.C., Hauschild, T., Vilas-Boas, A.C.M., Silva, D.F.R., Matos, M.A.A. 2020. Biochar from pyrolysis of biological sludge from wastewater treatment. Energy Reports; 6:757-763.

van Loo S, Koppejan J. (Editors). 2008. Handbook of biomass combustion and co-firing, 2nd Ed., Earthscan, London, UK.

Verheijen, F.G.A., Zhuravel, A., Silva, F.C., Amaro, A., Ben-Hur, M., Keizer, J.J. 2019. The influence of biochar particle size and concentration on bulk density and maximum water holding capacity of sandy vs sandy loam soil in a column experiment. Geoderma; 347:194-202.

Regeneration of quaking aspen (*Populus tremuloides*) after fire risk reduction treatments

Allison Trudgeon*; Kristin Nesbit; Larissa Yocom; R. Justin DeRose

[1]*Utah State University, Department of Wildland Resources and Ecology Center. 5200 Old Main Hill, Logan UT, 84322, USA, {allison.trudgeon, kristin.nesbit, larissa.yocom, justin.derose}@usu.edu*

**Corresponding author*

Keywords

Forest management; Fuel reduction treatment; Mechanical disturbance; Regeneration; Silvicultural treatment

Abstract

Quaking aspen (*Populus tremuloides* Michx.) is a keystone species in the western US, and readily regenerates following high-severity disturbance (historically stand-replacing fire). Aspen forests are thought to be in decline as a result of fire suppression, herbivory, and drought, such that restoration has become a priority. Typically, restoration involves prescribed fire or harvest to regenerate aspen, but these methods are not applicable everywhere, due to heavy coarse fuel loads that make prescribed fire risky and harvesting challenging. The need for alternative, stand-replacing treatment methods that regenerate aspen has led to the development of a mechanical method, termed 'roller-felling'. Like fire or harvest, roller-felling can reset succession and rearrange fuel loading in late-seral stage, conifer-dominated aspen communities. We examined the ecological impact of roller-felling by investigating factors that contributed to post-treatment aspen regeneration, in a replicated experimental design containing variable levels of post-treatment cleanup (i.e., residual slash amount). Prior to treatment, we collected stand structural and compositional characteristics from 5 plots per unit to allow for post-treatment comparison. One year after treatment, we quantified aspen regeneration stem densities. We also assessed possible factors that could have influenced aspen regeneration, including herbivore browsing pressure, topography, and pre-treatment composition. Additionally, we determined the impact this treatment had on vegetative ground covering. Post-treatment aspen stem density varied from 0 to 237,000 stems/ha across 30 plots among all treatment areas. There were significant differences in post-treatment stocking among cleanup levels, with full cleanup densities averaging ~100,000 stems/ha, while partial cleanup densities averaged ~23,000 stems/ha. Cleanup level and topography (i.e., slope) best predicted aspen densities post-treatment, and pre-treatment aspen composition had less effect on regeneration than predicted. Approximately 44% of aspen regeneration stems were browsed by herbivores one year after treatment. While the long-term effects of this method have yet to be quantified, the one-year results in this study lay the groundwork for longer-term monitoring of roller-felling treatment outcomes and their application to forest and fire management regionally, where goals are to reduce fire risk and maintain aspen communities across the western US.

1. Introduction

Quaking aspen (*Populus tremuloides* Michx.) is North America's most widespread broadleaf tree species, valued for providing many ecosystem services, such as increased biodiversity, making management of these communities a priority across the western US. (Little, 1971; Kuhn et al., 2011; Long and Mock, 2012). As an early successional species, aspen require disturbance to persist, establishing in high densities post-disturbance. Aboveground stem removal stimulates aspen's primary reproduction strategy of suckering, or establishment of a genetically identical ramet (i.e., sucker) from a root, which is initiated by interruption of auxin transport from leaves to roots (Frey et al., 2011; Wan et al., 2006). Within seral aspen forest types, conifers establish under mature aspen and dominate the canopy in later succession. When they burn, late-seral aspen communities are susceptible to high-severity fires due to high fuel loading (Shinneman et al., 2013). Stand-replacing fires historically reduced fuel loading and promoted aspen regeneration, but have become increasingly rare due to fire suppression efforts (DeByle and Winokur, 1985). Currently, prescribed fire and harvesting are the most feasible stand-replacing treatments in practice but can be difficult to implement with weather or infrastructure limitations. The need for alternative treatments that regenerate aspen and reduce fire risk by resetting succession has led to the development of roller-felling. This treatment method involves pulling a large barrel attached via cable between two bulldozers (Fig. 1) to restart succession within aging aspen communities. Recently, roller-

felling has been implemented in late- stage, mixed aspen-conifer stands, however, treatment efficacy (i.e., aspen regeneration) and associated impacts have yet to be quantified.

Prolific aspen regeneration via suckering is expected after treatment, as aspen preferentially establish in disturbed areas with high light (DeByle and Winokur, 1985). However, various factors influence aspen regeneration densities, such as aspen composition pre-disturbance, amount of residual coarse woody debris (CWD) post-disturbance, topography, and herbivore pressure. Because regeneration is primarily via suckering, larger proportions of pre-disturbance aspen correlate with greater regeneration, and were predicted in this study (Graham et al., 1963; Frey et al., 2011). Conversely, higher pre-treatment conifer proportions were expected to decrease aspen regeneration (Smith et al., 2011; Margolis and Farris, 2014). Pre-treatment understory advance regeneration (<10 cm diameter) was predicted to increase regeneration (Britton et al., 2016). Greater amounts of CWD can increase shading and decrease surface area, which has been correlated to lower regeneration (Doucet, 1989; Sheppard 1996, 2001). Lower aspen densities were expected with increased CWD, or slash retention. Additionally, the role of CWD as refugia from herbivory is well-documented (Grisez, 1960; Rumble et al., 1996; Ripple and Larsen, 2001), and a lower percentage of aspen stems browsed, primarily by elk (*Cervus elaphus* L.), were expected with increased slash retention. The objective of this study was to determine the regeneration response of aspen to roller-felling and then assess the impact of (1) pre-treatment stand conditions, (2) the amount of slash retention, (3) topography, and (4) herbivory on aspen stem densities. Better understanding of the efficacy and impacts of this treatment will set the baseline for long-term monitoring of treated sites, with possible application to regional forest and fire management.

2. Methodology

2.1. Study area

Treatment areas were on private property in Utah, USA, and were split into 3 experimental units with similar edaphic, climactic, and elevational characteristics. Prior to roller-felling, stands were characterized as mixed-conifer, primarily subalpine fir (*Abies lasiocarpa*). Pre-treatment basal area varied minimally by unit, averaging 30 m^2/ha, while aspen comprised 29% to 63% basal area. Units differed moderately in potential productivity (aspen site indices 44 to 52) and were characterized by very high woody surface fuel loadings (26.9-46.3 Mg/ha across all size classes).

2.2. Study design

We applied a replicated, variable treatment design at 3 experimental units, totaling 18 treated hectares. Each 6-hectare unit contained 3 adjacent blocks (i.e., cleanup levels) approximately 2 hectares in area, containing a gradient of residual slash densities, and an untreated control (Fig. 2). These cleanup levels were: 1) all slash pushed into burn pile (full), 2) moderate residual densities of slash, with most slash pushed into pile (partial), and 3) no slash pushed into piles (none). Woody surface fuel loadings (i.e., residual slash) outside of piles in full cleanup averaged ~ 8 Mg/ha, 37 Mg/ha in partial cleanup, and 174 Mg/ha in no cleanup areas.

Prior to treatment, 60 variable radius plots were sampled using a 4m basal area prism to quantify stand structure and composition. At each plot, we measured diameter at breast height (DBH) and species of every overstory tree (>10 cm DBH) and the height of every other tree; the tallest tree was cored for site index determination. Fixed-area, 1/1000th (1.78 m radius) hectare plots were measured to determine understory (<10 cm DBH) advance regeneration. Woody fuel loads were quantified by diameter classes on two transects using protocols outlined in Brown (1974), and 1 m^2 quadrats were surveyed along these transects to quantify ground covering by functional group (delineated by biotic: forb, shrub, grass, tree, and abiotic: CWD, bare soil, etc.). After treatment, five, 1/1000th hectare regeneration plots were sampled within full cleanup, partial cleanup, and untreated control areas, totaling 45 plots (direct sampling in no cleanup areas was omitted as high slash restricted access; Fig. 2). We identified seedlings and suckers to species, delineated stems by height class, and noted apical meristem as browsed or unbrowsed. Measurements were taken along two transects to determine ground covering and residual slash/fuel loading. Twenty-seven ungulate exclosures (1.2m^2 x 1.22m height) were constructed, with 3 in each cleanup level and control area (again, omitting no cleanup), and sampled identically to regeneration plots (Fig. 3).

2.3. Analytical Approach

Linear regression was used to explore relationships between predictor variables (percentage and absolute aspen basal area, advance regeneration, conifer composition, topography, residual slash) and post-treatment aspen regeneration densities. Percentages of browsed stems were also compared across cleanup levels and units with linear regression and analysis of variance. Analysis of variance was used to compare differences between units. T- and F- tests were used to determined differences in densities between cleanup levels and ground covering percentages before and after treatment.

3. Results

Aspen regenerated in high densities after roller-felling. Stem densities were significantly higher and more variable (P-values <0.0001) in full cleanup compared partial cleanup areas, where densities averaged ~102,000 stems/ha and ~23,000 stems/ha, respectively (Fig. 4). Pre-treatment composition was not highly predictive of post-treatment density (P-value = 0.18) and higher proportions of both advance regeneration and overstory aspen pre-treatment did not predict of greater post-treatment densities when analyzed independently ($r^2 \leq 0.15$). Collectively, cleanup level, slope, and pre-treatment composition were highly predictive of aspen regeneration densities ($r^2 = 0.71$). When cleanup areas were analyzed independently, pre-treatment variables became more predictive in full cleanup areas. Additionally, in full cleanup areas, steeper slopes were associated with lower stem densities, however, densities remained constant across the same slope gradient in partial cleanup areas.

After roller-felling, the percentage of ground occupied by bare soil changed significantly (P-value < 0.0001) from a pre-treatment average of 2% to ~30%. Proportions of bare soil and CWD varied significantly between the two cleanup levels (all P-values <0.0001). Partial cleanup contained less bare soil (14%) and greater CWD (38%) than full cleanup, in which bare soil occupied 42% of ground covering and CWD only 9%. Full cleanup areas generally had slightly greater biotic ground covering. Partial cleanup areas had significantly greater residual slash than full cleanup areas, with all CWD diameter classes of greater densities (P-value <0.0001); however, this did not deter herbivory, as percentages of observed browse on aspen stems remained similar between full and partial cleanup areas (42% and 46%, respectively). Browse percentages were relatively uniform across units and cleanup levels with no significant differences observed. Aspen stems within exclosures were significantly greater in height, but not density, in contrast to unfenced, browsed stems (Fig. 3).

4. Discussion and Conclusion

4.1. Discussion

Many outcomes of roller-felling were consistent with our predicted hypotheses. Generally, the response of aspen to treatment was suckering in high densities, as expected, but thresholds indicating 'successful' regeneration vary in the literature (e.g., Kitchen et al., 2019). A regional, applicable regeneration threshold of 2500 stems/ha was met one year after treatment, with 93% of plots meeting this objective (Kitchen et al., 2019). Furthermore, a predictable, negative relationship between residual slash and regeneration was observed: increased CWD post-treatment resulted in decreased aspen density. Greater proportions of CWD and lower proportions of bare soil within partial cleanup areas resulted in less area for unobstructed sucker establishment, increased shade, and consequentially lower stem densities. Increased slash did not deter ungulate browse; this could be due to low (<1m) pile heights observed after roller-felling, as debris piles reducing browse are typically >1m (Ripple and Larsen, 2001; Nichols, 2005).

Ungulate herbivory of young aspen can alter regeneration dynamics, and high amounts of browse can stunt growth and promote unhealthy growth structure (i.e., bush-like); insufficient aspen recruitment is a common result of repeated browse (Baker, 1918, 1925; Bartos and Campbell, 1998). Taller aspen stems within exclosures confirm a negative impact of browse on regeneration. A sustainable, 30% maximum threshold of repeated browse allows for long-term, healthy stand structure and development (Olmsted, 1979). In the first growing season, roughly 45% of all aspen stems were browsed. By this metric, browse levels immediately violated sustainable thresholds. However, this was not strong enough to denote *absolute* levels of unsuccessful regeneration (i.e., 10,000 stems/ha at 45% browse still provides 5,500 stems/ha). Nevertheless, if browsing pressure remains constant (or even moderately declining) and compounded across future growing seasons,

regeneration will be insufficient, failing to reach 2500 stems/ha. High levels of observed browse in this short-term study are concerning from the standpoint of long-term stand health and development.

Some well-established, pre-treatment factors we hypothesized as predictors of aspen regeneration were not strongly correlative in this study. Prior to treatment, units varied significantly in both aspen percent of total basal area and absolute aspen basal area, ranging from 4 m^2/ha to 20 m^2/ha. Many metrics quantifying pre-disturbance aspen composition have been linked to greater regeneration, such as increased "vigor", greater height and DBH of overstory aspen (Worrall et al., 2008, 2010; King and Landhäusser, 2018; Jean et al., 2019), and advance regeneration (Britton et al., 2016). However, these pre-treatment variables were weakly correlated to greater one-year, post-treatment regeneration densities unless other variables were added.

While many biotic, pre-treatment variables were not predictive, cleanup level (i.e., amount of residual slash) and slope were more strongly correlated to increased aspen densities. We presume that residual slash mitigated the negative effect of slope in full cleanup areas because increased slash provided soil stability and decreased erosion potential. This finding has notable implication on management: if roller-felling is to be considered, leaving residual CWD on steeper slopes may increase regeneration and promote soil stability. Overall, lack of overt correlation between pre-treatment aspen and regeneration also has interesting management implications (i.e., pre-treatment aspen composition alone has little effect on regeneration, allowing for application in later-stage stands with little aspen).

4.2. Conclusion

The short-term, regeneration response of aspen to roller-felling generally mimics conditions of a stand-replacing disturbance by restarting succession and reducing fuel loading. Topography and residual slash strongly influenced regeneration densities, highlighting the importance of context within management application. Importantly, this study assessed the impact of roller-felling one-year following treatment, but long-term impacts warrant further study. The groundwork set by this study will further the understanding of aspen regeneration dynamics, which will apply to forest and fire management regionally, where goals are to reduce fire risk and maintain aspen communities.

Fig. 1. Roller-felling barrel situated centrally between two cables and dragged between a pair of bulldozers. The cable fells trees, while the large barrel drum keeps the cable roughly >1m above the ground surface, providing necessary leverage to pull over trees. Once felled, variable amounts of slash can be retained, while remaining debris is pushed into a pile and burned at a later time. Inset photo for scale.

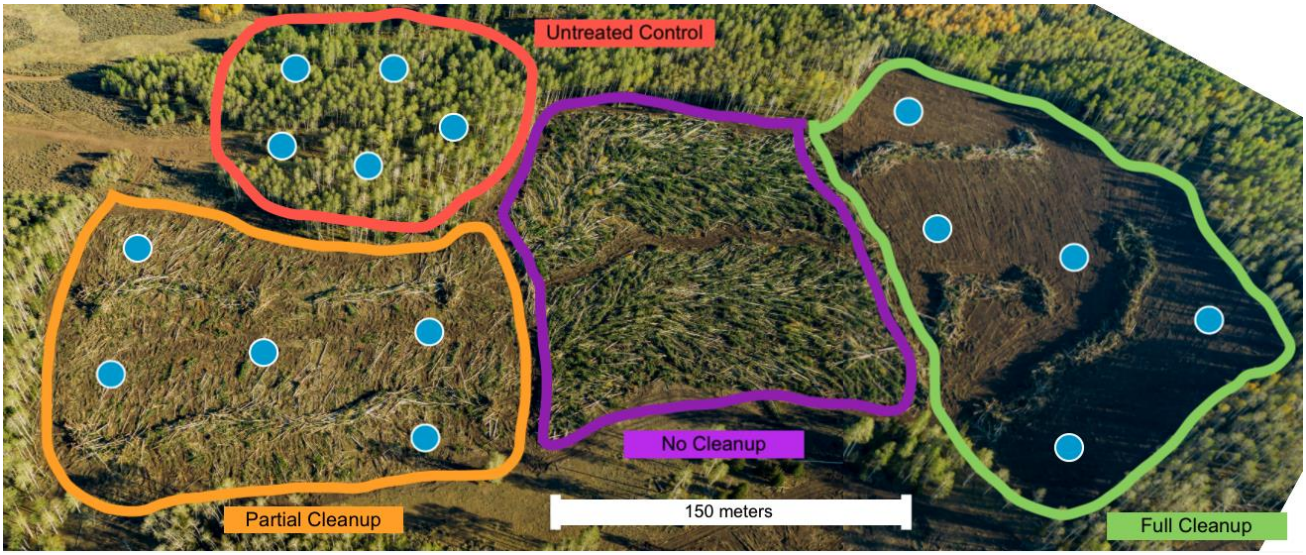

Fig. 2. Study design of variable treatment cleanup levels within experimental unit. Left to right: partial cleanup (orange), no cleanup (purple), and full cleanup (green). An adjacent, untreated control area above the treatment areas and shown in red. Sampling plots, shown in blue, are independent, spaced at a minimum of 45 meters apart, and do not intersect with slash piles. No plots were established in the no cleanup treatment, as slash levels restricted sampling.

Fig. 3. Contrasting aspen regeneration within fenced exclosure and browsed stems outside of exclosure in partial cleanup treatment area (photo taken one year after treatment). Inset: completed exclosure in partial treatment area, constructed prior to aspen regeneration emergence.

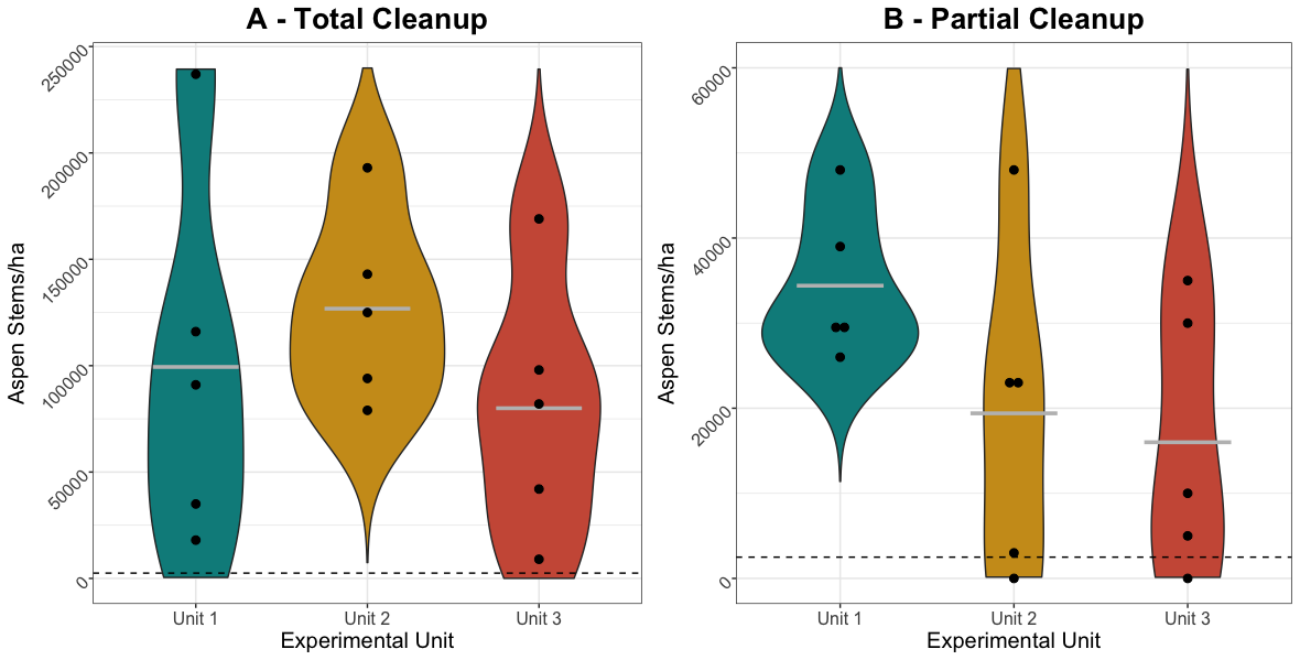

Fig. 4. Post-treatment aspen regeneration stems per hectare, delineated by (A) total and (B) partial cleanup treatment areas. Note different scales for stems per hectare on y-axis. The three experimental unit areas are indicated by different colors. The dashed line (near x-axis) indicates the 2500 stems/ha objective. Black points indicate stem densities at 5 plots within each treatment area. Gray bars denote stem density averages of each respective unit. Total cleanup (A) vastly exceeds this objective, while partial cleanup (B) stem densities largely meet this objective. Two individual sampling points within partial cleanup areas fell below the 2500 stems/ha objective, indicating insufficient regeneration.

5. References

Baker, F.S. 1918. Aspen reproduction in relation to management. Journal of Forestry, 16, 389–398.

Baker, F.S. 1925. Aspen in the central Rocky Mountain region. United States Department of Agriculture Bulletin Number 1291.

Bartos, D.L. and Campbell, R.B. 1998. Decline of quaking aspen in the Interior West- examples from Utah. Rangelands 20(1), 17–24.

Britton, J. M., DeRose, R. J., Mock, K. E., and Long, J. N. 2016. Herbivory and advance reproduction influence quaking aspen regeneration response to management in southern Utah, USA. Canadian Journal of Forest Research, 46(5), 674–682.

Brown, J.K. 1974. Handbook for inventorying downed woody material. General Technical Report INT-16. United States Department of Agriculture, Forest Service, Intermountain Forest and Range Experiment Station, Ogden, UT.

DeByle, N.V. and Winokur, R.P. 1985. Introduction. Page 1 in: N.V. DeByle & R.P. Winokur (eds.). Aspen: Ecology and Management in the Western United States (RM-GTR-119). U.S. Department of Agriculture, Forest Service, Rocky Mountain Forest and Range Experiment Station, Fort Collins, CO. p. 7-38

Doucet, R. 1989. Regeneration silviculture of aspen. Forestry Chronicle, 65(1), 23–27.

Frey, B. R., Lieffers, V. J., Landhäusser, S. M., Comeau, P. G., and Greenway, K. J. 2011. An analysis of sucker regeneration of trembling aspen. Canadian Journal of Forest Research, 33(7), 1169–1179.

Grisez, T.J. 1960. Slash helps protect seedlings from deer browsing. Journal of Forestry, 58(5):385–387.

Graham, S.A., Harrison, R.P., and Westell, C.E. 1963. Aspens: Phoenix trees of the Great Lakes Region. 272 p. University of Michigan Press, Ann Arbor.

Jean, S. A., Pinno, B. D., and Nielsen, S. E. 2019. Trembling aspen root suckering and stump sprouting response to above ground disturbance on a reclaimed boreal oil sands site in Alberta, Canada. New Forests, 50(5), 771–784.

Kitchen, S. G., Behrens, P. N., Goodrich, S. K., Green, A., Guyon, J., O'Brien, M., and Tart, D. 2019. Guidelines for aspen restoration in Utah with applicability to the intermountain west. United States Department of

Agriculture, Forest Service, General Technical Report, Rocky Mountain Forest and Range Experiment Station 2019 (390), 1–55.

King, C. M. and Landhäusser, S. M. 2018. Regeneration dynamics of planted seedling-origin aspen (*Populus tremuloides* Michx.). New Forests, 49(2), 215–229.

Kuhn, T. J., Safford, H. D., Jones, B. E., and Tate, K. W. 2011. Aspen (*Populus tremuloides*) stands and their contribution to plant diversity in a semiarid coniferous landscape. Plant Ecology, 212(9), 1451–1463.

Little, E.L. 1971. Atlas of the United States trees. Volume 1. Conifers and important hardwoods. Miscellaneous Publication 1146. Washington, DC: United States Department of Agriculture, Forest Service. 320 p. 1462

Long, J. N. and Mock, K. 2012. Changing perspectives on regeneration ecology and genetic diversity in western quaking aspen: Implications for silviculture. Canadian Journal of Forest Research, 42(12), 2011–2021.

Margolis, E. Q. and Farris, C. A. 2014. Quaking aspen regeneration following prescribed fire in Lassen Volcanic National Park, California, USA. Fire Ecology, 10(3), 14–26.

Nichols, T.F. 2005. Aspen coppice with coarse woody debris: A silvicultural system for interior Alaska moose browse production. MS thesis, University of Alaska–Fairbanks, Fairbanks, AK. 92 p.

Olmsted, C.E. 1979. The ecology of aspen with reference to utilization by large herbivores in Rocky Mountain National Park. In: Boyce, M.S. and Hayden Wing, L.D. North American elk: ecology, behavior, and management, pp. 89–97. University of Wyoming, Laramie, WY, US.

Ripple, W.J., and Larsen, E.J. 2001. The Role of Postfire Coarse Woody Debris in Aspen Regeneration. Western Journal of Applied Forestry, 16, 61–64.

Rumble, M. A., Pella, T., Sharps, J. C., Carter, A. V, and Parrish, J. B. 1996. Effects of Logging Slash on Aspen Regeneration in Grazed Clearcuts. The Prairie Naturalist, 28(4), 199.

Shepperd, W.D. 1996. Response of Aspen Root Suckers to Regeneration Methods and Post-Harvest Protection. Research Paper RM-RP-324. Fort Collins, CO: United States Department of Agriculture, Forest Service, Rocky Mountain Forest and Range Experiment Station. 8 p.

Shepperd, W.D. 2001. Manipulations to regenerate aspen ecosystems. In: Sustaining Aspen in Western Landscapes: Symposium Proceedings. pp. 355–365.

Shinneman, D. J., Baker, W. L., Rogers, P. C., and Kulakowski, D. 2013. Fire regimes of quaking aspen in the Mountain West. Forest Ecology and Management, 299, 22–34.

Smith, E. A., O'Loughlin, D., Buck, J. R., and St. Clair, S. B. 2011. The influences of conifer succession, physiographic conditions and herbivory on quaking aspen regeneration after fire. Forest Ecology and Management, 262(3), 325–330.

Worrall, J.J., Egeland, L., Eager, T., Mask, R.A., Johnson, E.W., Kemp, P. A., and Shepperd, W.D., 2008. Rapid mortality of *Populus tremuloides* in southwestern Colorado, USA. Forest Ecology and Management, 255, 686–696.

Worrall, J.J., Marchetti, S.B., Egeland, L., Mask, R.A., Eager, T., and Howell, B. 2010. Effects and etiology of sudden aspen decline in southwestern Colorado, USA. Forest Ecology and Management, 26, 638–648.

Systematizing experts' risk perception on rural fires resulting from traditional burnings in Portugal: A Mental Model approach

Mayara Emilia Barbosa Souza*[1]; Abílio Pereira Pacheco[2,1]; Jorge Grenha Teixeira[1]

[1] INESC TEC and Faculty of Engineering of the University of Porto. Rua Dr. Roberto Fria, 378, 4200-465, Porto, Portugal, {msouza, app, jteixeira}@fe.up.pt
[2] ForestWISE, Collaborative Laboratory for Integrated Forest & Fire Management. Quinta de Prados, Campus da UTAD, 5001-801, Vila Real, Portugal, {abilio.p.pacheco@gmail.com}

**Corresponding author*

Keywords

Risk communication, mental model, rural fires, burning

Abstract

Fire is a traditional method used for the elimination of residual materials from agricultural and forestry activities, but its improper and negligent use increases the risk to cause significant social, economic, and environmental impacts. Translating the nature and magnitude of the risk, a mental model approach has been used for a deeper understanding of what can be done to reduce future socioeconomic and environmental impacts. Considering the rural fire risk context, in this study we applied the mental model approach to (1) systematize the aggregated knowledge of experts on rural fire risks, focusing on the burning problem, and (2) explore the different perspectives of experts on the subject. Experts are actors with in-depth involvement and experience in fire and forest management in Portugal, including actors from industry, academics, third sector, and public entities. Semi-structured interviews that included real-time interactions with the proposed mental model on the MURAL platform were remotely conducted with twenty-eight experts. The contributions were periodically validated by the research team and included in the reference mental model to translate the aggregated knowledge of the expert community. The data collected was transcribed, coded, and analyzed following a thematic analysis approach with NVivo software support. After nine iterations, the expert's mental model was concluded encompassing the burning motivators, alternative solutions, associated risks before and during the burning, underlying causes, natural elements and factors, and impacts.

Overall, the study provides an in-depth and holistic understanding of rural fire risks, focusing on burning, which is essential for identifying incorrect beliefs and existing risk factors that are often neglected. The participatory and dynamic process of actors' knowledge systematization on burning risks through a mental model allowed the identification of divergent perspectives between expert groups, especially concerning the effectiveness of the current legislation on the use of fire, indicating the need to improve the dialogue between experts. Moreover, the study shows how risk communication campaigns do not replace technical monitoring closer to the population, given that the diversity of people inhabiting fire-prone areas in peri-urban landscapes (that holds widely varying experiences, beliefs, attitudes, and values relating to fire) can influence people's understanding and interpretation of risk messages. Thus, it is recognized the importance and need of sensitization and communication actions to disseminate adequate and safer burning practices and available alternatives. Still, it indicates that alternative solutions of burning (such as on-site pellet processing, local micro-plants for heat production, community initiatives of composting, as well as crushing and distribution of crushed material to be incorporated into the soil) may be achieved with strong local and sectoral involvement. Finally, this research provides a baseline to help decision-makers and stakeholders identify the relevant associated risks before and during the burning practice, which can support the design of effective risk communications strategies and mitigate social and environmental impacts in the future.

1. Introduction

Ignitions from human activity are responsible for 98% of all fire incidents in Portugal (SGIF, 2020). The improper use of fire corresponds to more than half of the 41% of fires attributed to negligent causes in 2020, according to presented data by the Institute for the Conservation of Nature and the Forest (ICNF), which increase the risk to cause significant social, economic, and environmental impacts. However, fire is a traditional method used for the elimination of residual materials from agricultural and forestry activities, it is also commonly used as a cleaning method to eliminate of excess biomass in the control of invasive species, and its misuse causes the

positions it as the main cause among the rural fires that occurred in Portugal (Nunes et al. 2021; Meira Castro et al. 2020; Pereira et al. 2013)

Most fires start in the proximity of agricultural areas and at the interface of urban spaces (Pacheco et al. 2020). The proximity of forest and agricultural spaces to the urban context and the accumulation of variables linked to climate change, namely, the increase in average temperatures, the reduction of precipitation and relative humidity of the air, justify the recurrence of rural fires (Nunes et al. 2021). In addition, high temperature and drought, acting as important drivers for the burned area in Portugal (Turco et al. 2019), the risk of rural fires can be aggravated due to the accumulation of fuel load. Despite efforts to improve fire management, as Decree-Law 14/2019 that make burning prior communication and authorization mandatory, the risk of rural fires stems in part from the absence of effective management policies aimed at rural areas (Coelho et al., 2020). Furthermore, some studies point out that implementing risk-based long-term planning would improve fire management efforts (Turco et al., 2019). But governmental efforts to reduce wildfire risk are not enough on their own, and it is recommended that risk mitigation strategies be a joint effort between public agencies and private landowners (Doerr et al. 2013). A current poor translation of risk information materials into mitigation actions may be attributed to the diversity of people inhabiting fire-prone areas in peri-urban landscapes. The widely varying experiences, beliefs, attitudes, and values relate to fire can influence people's understanding and interpretation of risk messages and constrain their actions (Eriksen and Prior 2011).

Resorting to the literature on risk communication and wildfire (Steelman and McCaffrey 2013), we came across studies that address "mental models" approach. That approach has been used to translate the nature and magnitude of the risk, allowing for a deeper understanding of what can be done (Morgan et al. 2002) to mitigate social and environmental impacts in the future.

The mental model's concept was originally defined as "small-scale models" of reality that [the mind] uses to anticipate events, to reason, and to underlie explanation' (Craik, 1943), being essential to choose safe alternatives in critical situations, highlighting its relevance in risk communication. The application of mental models in studies of communication and risk perception aims to identify specific information needs (e.g., gaps in knowledge, misunderstandings, questions, concerns about terminologies and beliefs of the population) for decision by contrasting the mental models of specialists and lay people concerning a specific risk (Morgan et al., 2002). Therefore, it is a method that continues to receive attention in different contexts and fields of study, for example: to capture and compare the mental models of those conducting restoration activities to inform potential policy changes (Walpole et al. 2020), to investigate perceptions of risk and mitigation of employees (Stege et al., 2019), to compare perspectives of government agencies, academic experts, and suppliers on providing risk information (Aliperti et al., 2020).

According to Zaksek and Arvai (2004), risk management information and topics vary considerably between experts, actors from different stakeholder groups, and laypeople. In addition, groups may have different windows of knowledge about a particular risk, leading to an agreement between groups and management decisions that are not aligned with the most current scientific knowledge. The fundamental notions about risk, its characteristics, impacts, and forms of control are always necessary, so the level of understanding of the target group adjusts with the new information (Breakwell, 2001).

As such, in this study, we use a mental model approach to (1) systematize the aggregated knowledge of experts on rural fire risks, focusing on the burning problem, and (2) explore the different perspectives of experts on the subject. Based on scientific data about rural fire risks and the aggregated knowledge of the expert community, a mental model was built that encompasses the motivators, alternative solutions, associated risks, underlying causes, natural elements and factors, and impacts about burning. An in-depth and holistic understanding of rural fire risks, focusing on burning, is essential for maintaining cohesion between actors and building effective risk communications strategies to mitigate social and environmental impacts in the future.

2. Method

Based on the literature review, the methodological premises for the development of the study were established; the first one was the mental model's elaboration, commonly represented by an influence diagram. The research design involved the development of the data collection instrument (semi-structured interview scripts), the

systematization of data collection with different stakeholders (mental model development in a digital visual collaboration platform, called MURAL) on the risk of rural fires, focusing on the burning problem. Interviews were conducted virtually (by Zoom), and each interview took, on average, 1h30min. To gather a richer understanding of the expert's perspective, this study involved a comprehensive sample, that included experts from academia (7), industry (5), public entities (9), and third sector (7), accounting for 28 interviews, as shown in table 1.

Table 1 - Sample description

Experts	Number of participants (% sample)	Role
Industry	5 experts (18%)	Executive Director, Head of Department, Directors, and Manager
Academy	7 experts (25%)	Ph.D. and Associate Professors
Third sector	7 experts (25%)	Executive Director, Chairman of the Board, Engineers and Technical consultant
Public entity	9 experts (32%)	Cavalry Colonel, Commanders, Operations Deputy, Engineers, Landscape architect
	N = 28 experts	

Between the entities, we had representants from National Military Security Force, Volunteer Firefighters, National Emergency and Civil Protection Authority, National Guard, Agency for the Integrated Management of Rural Fires; National Institute for the Management and Conservation of Nature and Forests, forestry companies, electricity, and natural gas transport industries, multinationals that operate in telecommunications and other segments, associations, universities.

Following ethical standards, the interviewed participants consented to record the interviews for further analysis, accounting for approximately 39 hours of recorded data.

The experts' contributions were periodically validated by the research team and incremented in the reference mental model to translate the aggregated knowledge of the expert community. The data collected were transcribed, coded, and analyzed following a thematic analysis approach with NVivo software support.

3. Findings

Given the focus of the mental model on the practice of burning and in order to explore the risks, associated variables, and mitigation modes in-depth, we set three periods (before, during, and after) to delimit the burning process from start to finish. After nine interactions of contributions validation, the expert's mental model was concluded. In total, 170 changes were counted in the mental model (including node description changes; adding, relocation, and removing nodes; adding, relocation, and removing edges). Between changes made to the mental model, 50% were made by actors from public entities, 18% by actors from academia, 23% by actors from the third sector, and 9% by actors from the industry, as shown in table 2.

	Before burning		**During burning**		**After burning**		**Total**	
Public entity	*50*	*59%*	*23*	*27%*	*12*	*14%*	*85*	*50%*
Academy	*19*	*61%*	*7*	*23%*	*5*	*16%*	*31*	*18%*
Third sector	*24*	*62%*	*10*	*26%*	*5*	*13%*	*39*	*23%*
Industry	*13*	*87%*	*2*	*13%*	*0*	*0%*	*15*	*9%*
Total	**106**	*62%*	**42**	*25%*	**22**	*13%*	**170**	***100%***

Table 2 - Changes made in the mental model by experts' group

The expert's mental model encompasses eight main blocks (Figure 1), such as motivators to burning, alternative solutions, associated risks before and during the burning practice, underlying causes and natural elements that can increase the burning risk, and potential impacts.

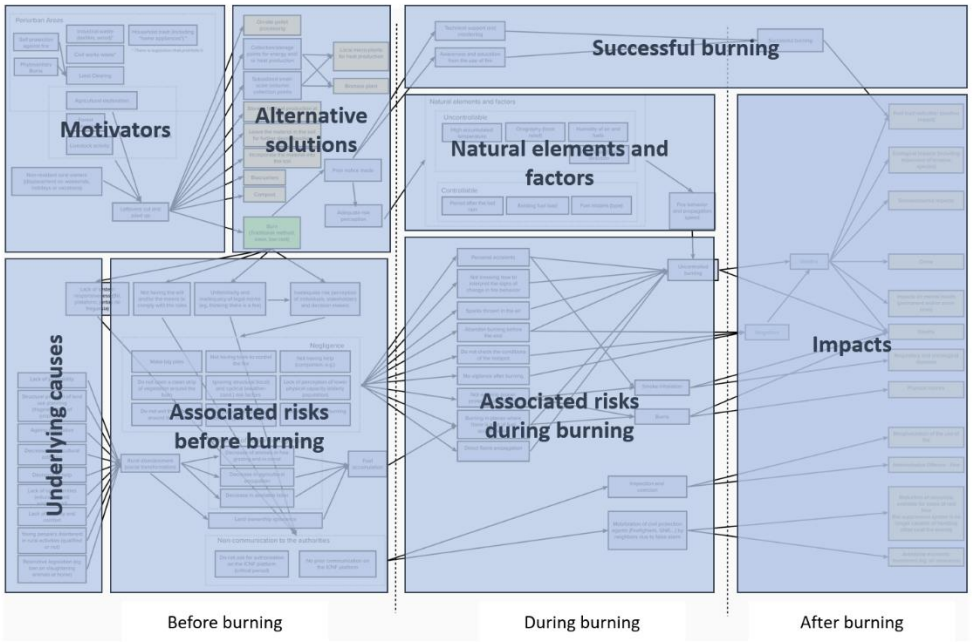

Figure 1- Expert mental model in main blocks

Before burning, the mental model shows burning motivators in peri-urban and rural areas, such as land clearing to self-protection against fire or phytosanitary burns, agricultural and forest exploration, etc.; in addition to considering the non-resident rural owners (displacement on weekends, holidays, or vacations).

Associated risks before burning block listed several risk factors and aspects that precede the practice of burning that often lead to neglect action, such as inadequate risk perception of individuals (e.g., not having a companion, ignoring structural (local) and cyclical (weather-cond.) risk factors, etc.), stakeholders, and decision-makers; unfamiliarity and inadequacy of legal norms (e.g., thinking there is a fee regarding the request for authorization to conduct a burning); lack of system responsiveness from Voluntary Fire Service, platform, Municipal Councils; or simply not having the will and/or the means to comply with the rules, leading to no prior burning communication to the authorities, thus not complying with the Portuguese Decree-Law 14/2019. Tied to this, underlying causes block describe rural abandonment causes represents indirect factors that contribute to increasing rural fire risks (e.g., lack of profitability, aging population, decrease in agricultural activities, structural problem of land use planning (fragmentation of properties), etc.), because of the absence of active management and fuel accumulation.

In contrast, alternative solutions include crushing, on-site pellet processing, leaving the material in the soil for further decomposition or incorporation to improve the structure and quality of the soil, collection/storage to use for biomass, composting, energy production, at small or large scale.

During the burning,natural elements and factors block include controllable (e.g., existing fuel load and fuel models) and uncontrollable (e.g., the humidity of air and fuels, orography, wind speed, and direction) elements that can potentially impact fire behavior and propagation speed. Associated risk block encompasses risk factors such as, not knowing how to interpret the signs of change in fire behavior, abandoning burning before the end, not wearing proper protective equipment, sparks thrown in the air, and other risk factors that can cause an uncontrolled burning or their reignition.

After burning, the mental model included twenty variables of impact, beyond the social, environmental, and economic impacts, we can mention for instance the fuel load reduction, which represents a positive impact and the reduction of resources available if there is a mobilization to false alarm of fires, which could be an avoidable investment. Lastly, successful burning block highlight actions to mitigate the risk, such as technical support and monitoring, awareness, and education from the use of fire.

4. Implications and conclusion

The findings indicate three preliminary theoretical and practical implications. First, there is a need to improve the dialogue between experts, which corroborates other research in which the mental model's approach was applied (Aliperti et al., 2020). This dialogue should focus on the perception of the administrations and decision-makers risk in the practice of burning and its relationship with the effectiveness of the current legislation on the use of fire, as some specialists have the perception of the imposition of punitive law, of repression, which leads to marginality and the illegal practice of burning. Still, many actors see the beneficial ecological role of fire, especially about reducing accumulated fuel and consequent mitigation of large fires, while other actors simply fail to identify any positive impact in this issue.

Second, alternative solutions of burning (such as on-site pellet processing, local micro-plants for heat production, community initiatives of composting, as well as crushing and distribution of crushed material to be incorporated into the soil) may be achieved with strong local and sectoral involvement. Experts agree that biomass plants are viable in some regions, where there is a market logic, the volume of material, and the plants are close for supply, making the market economically sustainable. However, this does not happen in regions where the land is fragmented, as there is no supply of material in the necessary volume, and in some cases the plants are far away, not compensating for the cost of transport, as it is a material of low value. Therefore, micro-biomass plants are identified as a relevant solution to reduce the risk of burning. Still, on this topic, specialists also state that the incentive to disseminate the use of biomass would potentially originate from public policies (e.g., percentage of energy sources must be renewable, and another percentage must contribute to the active management of fuels, in the latter case the use of biomass for home heating), what does not exempt the local and sectoral actors' involvement.

Finally, understanding that risk communication campaigns do not replace technical monitoring closer to the population. Experts believe closer technical monitoring is the main factor to contribute to rural fires risk mitigation, but given the limited operational capacity in relation to demand, they recognize the importance and need of sensitization and communication actions to disseminate adequate and safer burning practices and available alternatives.

Most effective communication practices are associated with flexible fire management and interactive communication (before and during the event), that strives to address local contextual concerns, explain actions, and provide honest, timely, accurate, and reliable information while leveraging local relationships (Steelman and McCaffrey 2013). As such, by understanding relevant actors' perception about traditional burnings, a mental model approach can support an effective risk communication strategy.

5. References

Aliperti, G., Nagai, H., & Cruz, A. M. (2020). Communicating risk to tourists: A mental models approach to identifying gaps and misperceptions. Tourism Management Perspectives, 33, 100615.

Breakwell, G. M. 2001. Mental models and social representations of hazards: the significance of identity processes. Journal of Risk Research 4:341-351.

Craik, K. J. W. 1943. The nature of explanation. Cambridge University Press, Cambridge, UK.

Coelho, Sílvia, Sandra Rafael, Miguel Coutinho, Alexandra Monteiro, João Medina, Susana Figueiredo, Sofia Cunha, Myriam Lopes, Ana Isabel Miranda, and Carlos Borrego. 2020. "Climate-Change Adaptation Framework for Multiple Urban Areas in Northern Portugal." Environmental Management 66 (3): 395–406. https://doi.org/10.1007/s00267-020-01313-5.

Divisão de apoio à Gestão de Fogos Rurais/DGFR (2020). 8.º RELATÓRIO PROVISÓRIO DE INCÊNDIOS RURAIS DE 2020. ICNF – SGIF/Sistema de Gestão de Informação de Incêndios Florestais

Doerr, S.H., Cristina Santín, Trevor Maynard, Neil Smith, and Sandra Gonzalez. 2013. Wildfire: A Burning Issue for Insurers? https://doi.org/10.13140/2.1.2551.9681.

Eriksen, Christine, and Timothy Prior. 2011. "The Art of Learning: Wildfire, Amenity Migration and Local Environmental Knowledge." International Journal of Wildland Fire 20 (4): 612–24. https://doi.org/10.1071/WF10018.

Meira Castro, Ana C., Adélia Nunes, António Sousa, and Luciano Lourenço. 2020. "Mapping the Causes of Forest Fires in Portugal by Clustering Analysis." Geosciences 10 (2): 53. https://doi.org/10.3390/geosciences10020053.

Morgan MG, Fischhoff B, Bostrom A, Atman CJ. Risk Communication: A Mental Models Approach. Cambridge, MA: Cambridge University Press, 2002.

Nunes, L.J.R.; Raposo, M.A.M.; Pinto Gomes, C.J. A Historical Perspective of Landscape and Human Population Dynamics in Guimarães (Northern Portugal): Possible Implications of Rural Fire Risk in a Changing Environment. Fire 2021, 4, 49. https://doi.org/10.3390/fire4030049

Pacheco, A. P, Guiomar, N., Abreu, P. T. & Rodrigues, J. C. (2020) Monitorização 2019 – Campanha de incêndios rurais de 2019. AGIF 2019-2020

Pereira, Mg, Tj Calado, Cc DaCamara, and T Calheiros. 2013. "Effects of Regional Climate Change on RuralFires in Portugal." Climate Research 57 (3): 187–200. https://doi.org/10.3354/cr01176.

Steelman, T. A., & McCaffrey, S. (2013). Best practices in risk and crisis communication: Implications for natural hazards management. Natural hazards, 65(1), 683-705.

Stege, T. A. M., Bolte, J. F. B., Claassen, L., & Timmermans, D. R. M. (2019). Particulate matter exposure in roadwork companies: a mental models study on work safety. Safety Science, 120, 137-145.

Turco, Marco, Sonia Jerez, Sofia Augusto, Patricia Tarín-Carrasco, Nuno Ratola, Pedro Jiménez-Guerrero, and Ricardo M. Trigo. 2019. "Climate Drivers of the 2017 Devastating Fires in Portugal." Scientific Reports 9 (1): 13886. https://doi.org/10.1038/s41598-019-50281-2.

Walpole, E.H., Toman, E., Stidham, M. et al (2020). The science and practice of ecological restoration: a mental models analysis of restoration practitioners. Environ Syst Decis 40, 588–604.

Zaksek, Melissa, and Joseph L. Arvai. 2004. "Toward Improved Communication about Wildland Fire: Mental Models Research to Identify Information Needs for Natural Resource Management." Risk Analysis 24 (6): 1503–14. https://doi.org/10.1111/j.0272-4332.2004.00545.x.

TGA/TDA and Analytical Pyrolysis (Py/GC-MS) of Two Mediterranean Forest Species with Distinctive Flammability Characteristics: *Cupressus sempervirens L.* and *Quercus suber L.*

Rawaa Jamaladdeen*[1]; Imene BenBelkacem[2]; Bruno Coudour[1]; Laurent Lemée[3]; Christelle Roudaut[3]; Aicha Bouhafsoun[2]; Abderrezak Djabeur[2]; Hui-Ying Wang[1]; Jean-Pierre Garo[1]

[1] Institut P', ENSMA ISAE, Université de Poitiers, Chasseneuil-du-Poitou, France, {rawaa.jamaladdeen, bruno.coudour, hui-ying.wang, jean-pierre.garo}@ensma.fr
[2] Laboratoire de Production et valorisation végétale et microbienne, Université des Sciences et Technologie Mohamed Boudiaf (USTO-MB), Oran 31000, Algérie, {imenoo13@hotmail.com}, {abouhafsoun@gmail.com}, {sidjabeur@yahoo.fr}
[3] IC2MP - UMR CNRS 7285, Université de Poitiers, Poitiers Cedex, France {christelle.roudaut, laurent.lemee}@univ-poitiers.fr

**Corresponding author*

Keywords

TGA/TDA, Py/GC-MS, Cupressus sempervirens L., Quercus suber L., wildfires, silviculture measure

Abstract

The frequencies of wildfires in the Mediterranean climate regions (MCRs) have amplified due to the increased temperatures and drought periods resulting from climate change. Vast areas of forests are consumed by wildfires and certain species are threatened by extinction due to their high flammability and weak thermotolerance to climate change whereas, other species with high thermotolerance are exploited as silviculture measures in forest management strategies. Canopy and litter foliage are the first ignitable structures in a forest fire. In this context, the foliar flammability characteristics of two fire resilient Mediterranean forest species are tested and compared on a laboratory scale; Quercus suber L. (Q.s.L.) and Cupressus sempervirens L (C.s.L). Thermo gravimetric/thermo differential analysis (TGA/TDA) and low- to high- temperature analytical pyrolysis tests and gas chromatography-mass spectrometry (GC-MS) were conducted on live and dry foliar samples of Lebanese C.s.L and Algerian Q.s.L. Branch and cork samples of Q.s.L were also pyrolyzed (Py/GC-MS) for their volatile content. The hemicellulose/cellulose degradation temperatures of C.s.L. were in the order of 30 to 50°C more than those of Q.s.L. Lignin degradation started later in the Q.s.L. and took place at temperatures higher than those of C.s.L. (≥30°C), while the heat release rates (HRR) were greater for the latter than the former in both degradation phases. The pyrolysis tests showed higher volatile content of C.s.L compared to Q.s.L. The high thermotolerance characteristic of C.s.L may be referred to its high terpene content which was negligible in Q.s.L given the fact that it is a non-monoterpene emitter oak species with no terpene storage compartments. The use of C.s.L as a fire barrier could be justified given their thermotolerance characteristic. Q.s.L. fire resilience is justified for their bark characteristics however; their foliage fire resilience should be further experimented.

1. Introduction

Climate change with increased temperatures and prolonged drought periods promote a positive trend in the frequency of wildfires in the Mediterranean climate. The Mediterranean vegetation is adapted to natural wildfires but is vulnerable to the abiotic stresses brought by the prolonged dry and hot summer seasons which is suspected to affect their BVOCs (biogenic volatile organic compounds) reserves. Therefore, an accurate determination of the flammability characteristics of the Mediterranean vegetation is needed in order to implement effective forest management strategies. Flammability descriptors define the vegetation ignitability, combustibility, consumability, and sustainability. However, the methods for evaluating these descriptors have not yet been standardized but are strongly linked to their BVOC reserves at the event of the wildfire. Cork oak or Quercus suber L. (Q.s.L.) and Cupressus sempervirens L. (C.s.L.) are abundant Mediterranean forest species with distinctive morphological characteristics. C.s.L. species which possess foliar monoterpene storage compartments (resin ducts) (Hamidpour et a. 2011) are recognized for their high thermotolerance characteristics and are being considered in silviculture measures as green barriers against wildfires (Della Rocca et al. 2015).

A cypress plantation in Spain (Valencia), was slightly affected by a wildfire that burnt all trees arounds whereas only 12.7% of the cypress trees were burned, 37.1% were dehydrated and 61.6% were not affected (Della Rocca et al. 2015). Although, this same species is dangerous as a house hedge because when it is regularly cut to form a clean hedge, dead fuel accumulates inside the trees. This dead fuel constitutes a powerful source of radiation once a fire reaches it. On the other hand, Q.s.L. found abundantly in countries of the Mediterranean basin and in Portugal, are considered non-monoterpene emitters because they are incapable of endogenous monoterpene production (Loreto 2002) and their photosynthesis is inhibited at temperatures >30°C (Delfine et al. 2000). Therefore, they possess the lowest thermotolerance levels amongst other Mediterranean forest species and are largely consumed in wildfires. The flammability and thermotolerance characteristics of the two species were investigated by undergoing thermogravimetric/differential thermal analysis (TGA/DTA) and low- to high-temperature pyrolysis testing (Py/GCMS) on foliar live and dry samples of the Lebanese Cupressus sempervirens L. and Algerian Quercus suber L. The TGA/DTA and Py/GC-MS tests were conducted in the IC2MP laboratories of the University of Poitiers, France.

2. Materials and Methods

2.1. TGA/DTA:

The device used is SDT Q600 (DSC-TGA) equipped with a horizontal dual-balance mechanism which provides a high level of accuracy in the measurements of weight and temperature differentials. 20 mg of live and dry foliar samples of the two species: Cupressus sempervirens L. and Quercus suber L. were tested in an air medium with a flow rate of 50 $mL.min^{-1}$ at a temperature range from 20 to 900°C with a ramp of 10°C/min. The same method was used to analyze branches and cork of Q.s.L., and compare seasonal (winter and summer) dry foliar samples of C.s.L.

2.2. PY/GC-MS

The pyrolyzer is a Frontier Lab EGA 2020 pyrolyzer equipped with an AS-1020E auto-shot sampler coupled with a GCMS (Shimadzu QP 2010 Ultra). GC separations were done using a SLB-5MS (Supelco) capillary column (30 m long, 0.25 mm i.d, 0.25 μm phase thickness). Low- to high- temperature pyrolysis experiments were done on seasonal live and dry foliar samples of Cupressus sempervirens L. and live and dry foliar samples in addition to branches and cork samples of Quercus suber L. The designated pyrolysis temperatures were correlated to the TGA/DTA results which defined the different degradation temperatures of the cellulose, hemicellulose and lignin of the vegetation species. Also we were interested to simulate the effects of the thermal stresses of the fire-front approaching the vegetation in an open forest fire. The program of the pyrolysis tests is shown in Table1.

Table1. Pyrolysis program and designated temperatures of the experiments

	Cupressus sempervirens L. (Foliar samples)	**Quercus suber L. (Foliar, wooden, cork)**
Single Shot	50 - 80 - 120 - 180	800
Double Shot	350 - 550	350 - 550
Triple Shot	120 - 350 - 550	

2.3. Materials

Dry foliar samples of C.s.L. were collected and transported by airplane from a Lebanese forest in the summer season in August with an average ambient temperature high at 28/30°C, and in the winter season in January with an average temperature low at 5/10°C and annual rainfall of 700 to 1000 mm. Live foliar samples were obtained from irrigated cut branches of the same tree in both seasons and brought to France to be experimented in 3 days period. The Q.s.L dry foliar samples branches and cork were collected randomly from a mature Quercus forest in M'sila, Algeria by our collaborated research team of the University of Oran, Algeria. The live foliar of Q.s.L. were taken from a 1year old Quercus tree planted in Algeria and transported to France and were cut at the day of experimenting. All specimens were stored in the lab freezer at temperatures (-21±1°C) prior and during the experiments. The experiments showed similar fuel moisture content between the dry and live samples of the two species.

3. Results

The TGA/DTA (Figures 1&2) provided the temperature evolution of the specimen degradation phases that are likely to occur in an open fire for each of the two species. First trough indicating the endothermic thermal dehydration (distillation/drying) followed by the first peak signaling the exothermic ignition of the semi volatiles resulting from the degradation of cellulose/hemicellulose. The second peak at the higher temperature ranges is due to the combustion of the partially charred biomass and the aromatics released from the degraded lignin. The temperature ranges for each of the processes allowed us to correlate them to their flammability descriptors: ignitability and combustibility.

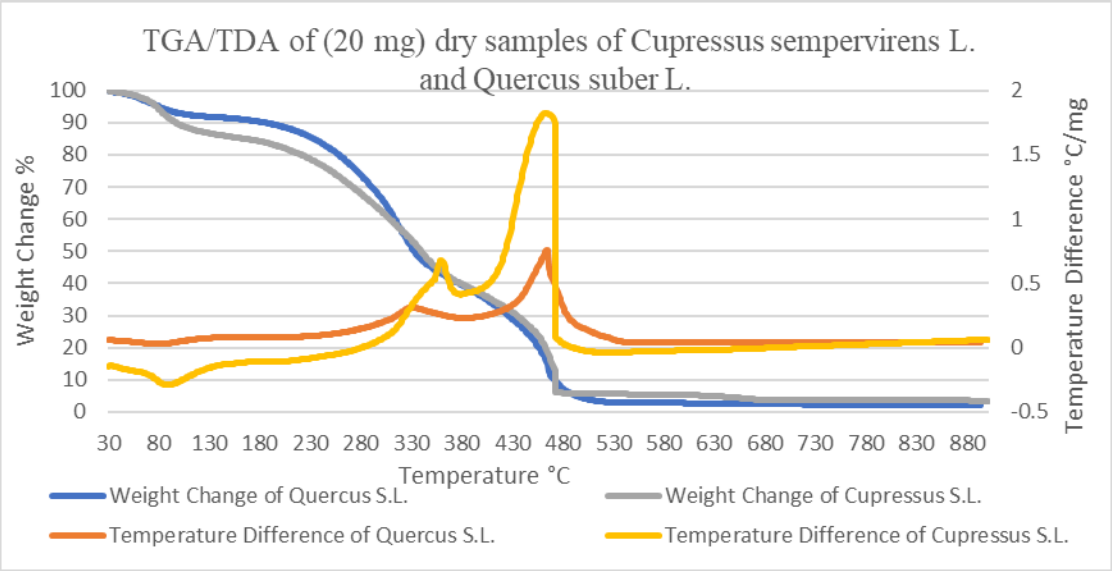

Figure 1- TGA/TDA of foliar dry samples of Cupressus sempervirens L. vs Quercus suber L.

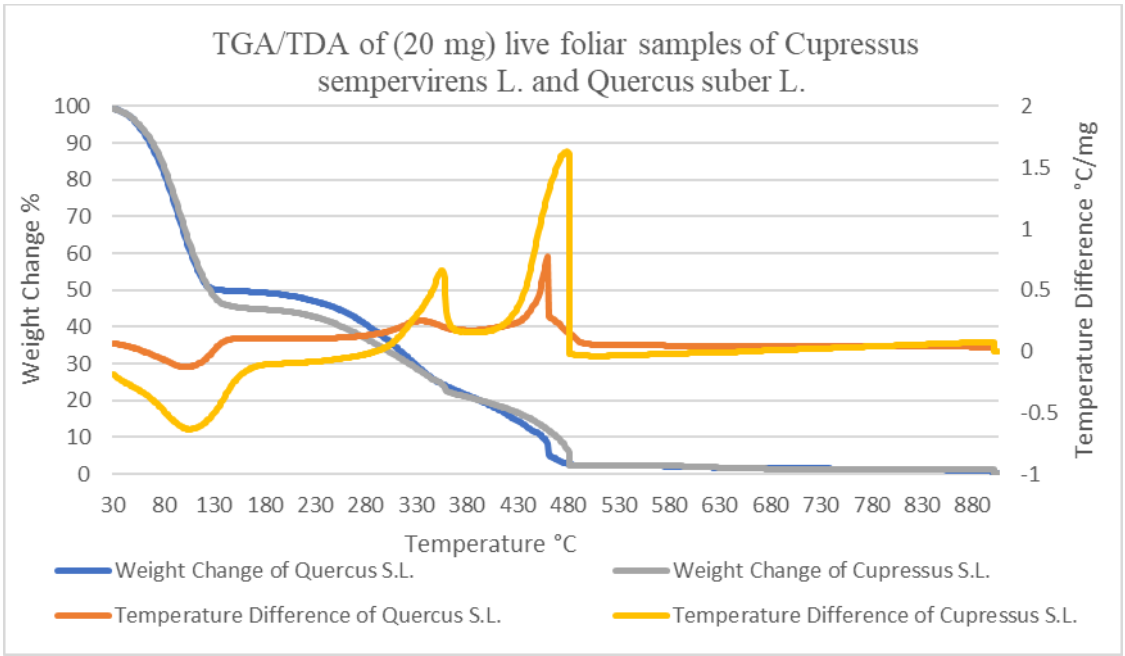

Figure 2- TGA/TDA of foliar live samples of Cupressus sempervirens L. vs Quercus suber L.

The time to ignition (TTI) (Dehane et al. 2017) or the ease to ignite (Fernandes et al. 2012) described vegetation ignitability. The combustibility is measured by HRR, and the consumability depends on the burnt mass residue. TGA/TDA of dry and live foliar C.s.L and Q.s.L. (Figure 1&2), showed cellulose degradation (first peaks) of C.s.L. at higher temperatures than those of Q.s.L and the inverse for lignin degradation (second peaks). The HRR in both degradation phases was higher C.s.L. compared to Q.s.L. Therefore, we can argue about the better combustibility of C.s.L. probably due to its larger volatile content. We were also able to compare the thermal

degradation profiles of seasonal (summer and winter) dry foliar of C.s.L. (Figure 3). The thermotolerance of summer foliar C.s.L. is clearly greater than that of winter C.s.L., and the (HRRs) of the former were higher than the latter probably due to higher volatile reserves; a characteristic of resinous conifers.

Table 2. Temperature profiles of each degradation phase from the TGA/TDA of live and dry foliar samples of C.s.L. and Q.s.L.

	Vegetation Species	Approximate Temperature range °C		
		Thermal Dehydration	Hemicellulose/Cellulose Degradation	Lignin Degradation
Dry Foliar	Cupressus sempervirens L.	80 - 130	330 - 380	400 - 480
	Quercus suber L.	75 - 80	280 - 330	430 - 500
Live Foliar	Cupressus sempervirens L.	80 - 180	330 - 380	400 - 480
	Quercus suber L.	75 - 130	300 - 330	430 -50

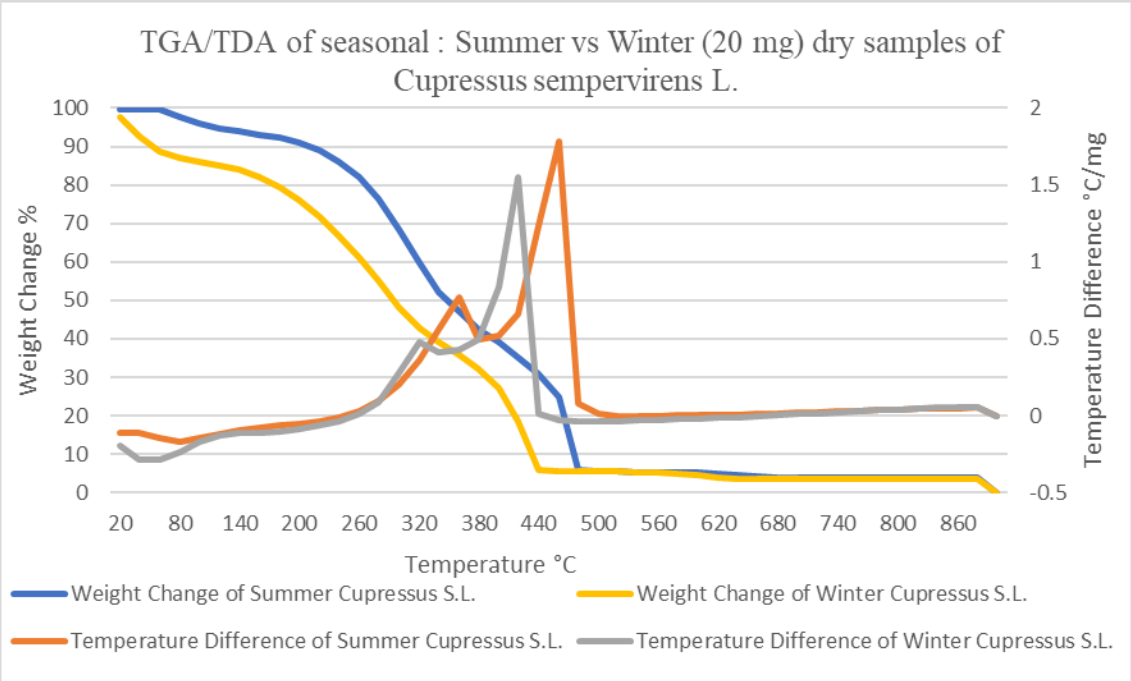

Figure 3- TGA/TDA of seasonal (summer & winter) foliar dry samples of Cupressus sempervirens L.

The Py-GC-MS experiments were conducted on the dry foliar samples of the two species. The pyrolysis products were identified on the basis of their GC retention times and by comparison of their mass spectra with those of standards and library data (NIST), (Figure 4). We identified terpene reserves (monoterpenes, sesquiterpenes, diterpenes) in the C.s.L. samples and none in the Q.s.L. (non -endogenous monoterpene emitter). Pyrolysis of Quercus cork released phenols of guaiacyl-type and syringyl type while the acetic acid indicated the thermal degradation of suberinic acids.

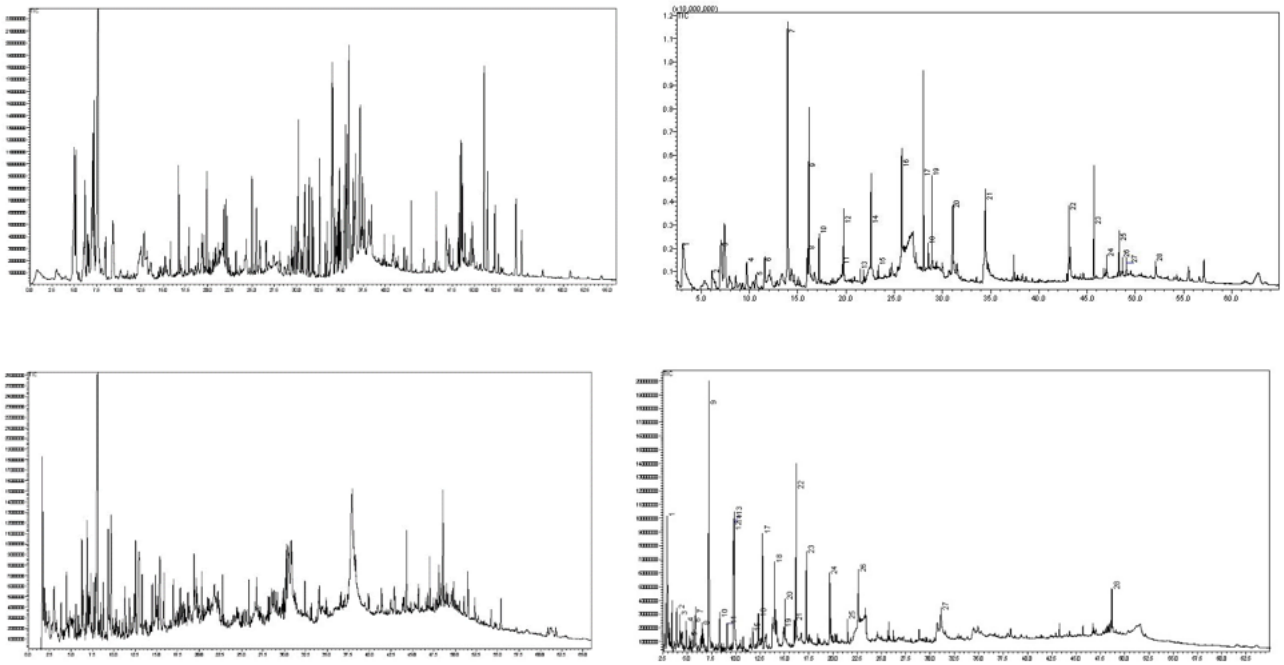

Figure 4- Pyrograms of dry C.s.L. (left) and dry Q.s.L. (right): up at 350°C, below at 550°C.

The aromatization of Q.s.L. to produce phenol and phenol homologues (i.e., methoxyphenol, dimethyl phenol, vinyl methoxyphenol, …) was remarkable at 350°C due to the degradation of lignin in dry foliar, branches and cork of with percentages of 51%, 71%, and 36%, respectively. These percentages increased remarkably at 550°C to 81%, 67% and 47%, respectively. The yield of suberin (insulation characteristic of Quercus suber) from cork pyrolysis was null at 350°C, 45% at 550°C, and 22,8% at 800°C. Phenol-derived compounds emerged humbly from C.s.L. dry foliar pyrolysis at 350°C while furanics (furfural, furan) of cellulosic origin and terpenes (mono, sesqui and di) were still dominant. Remarkably, sesquiterpenes were still identified from C.s.L. pyrolysis at 550°C and the percentages of mono aromatics (toluene), phenolics (phenol, methoxy-phenol, benzenediol) increased remarkably. Comparison between the pyrolysis products from dry foliar C.s.L. showed bigger reserves of VOCs in summer versus winter samples. Unlike the case of C.s.L., the degradation of Q.s.L. foliar lignin at 350°C (a temperature easily reached in wildfires), with the release of phenols and aromatics would accelerate flame propagation in wildfires hitting Quercus suber L. forests. The complete analysis of the experimental pyrolysis results will be presented in detail in the full paper edition.

4. References

Dehane, B., Hernando, C., Guijarro, M. and Madrigal, J., 2017. Flammability of some companion species in cork oak (Quercus suber L.) forests. *Annals of Forest Science*, *74*(3), pp.1-10.

Delfine, S., Csiky, O., Seufert, G. and Loreto, F., 2000. Fumigation with exogenous monoterpenes of a non-isoprenoid-emitting oak (Quercus suber): monoterpene acquisition, translocation, and effect on the photosynthetic properties at high temperatures. *The New Phytologist*, *146*(1), pp.27-36.

Della Rocca, G., Hernando, C., Madrigal, J., Danti, R., Moya, J., Guijarro, M., Pecchioli, A. and Moya, B., 2015. Possible land management uses of common cypress to reduce wildfire initiation risk: a laboratory study. *Journal of environmental management*, *159*, pp.68-77

Fernandes, P.M. and Cruz, M.G., 2012. Plant flammability experiments offer limited insight into vegetation–fire dynamics interactions. *New Phytologist*, *194*(3), pp.606-609.

Hamidpour, A., Radjabian, T., Charlotte, D. and Zarei, M., 2011. Leaf anatomical investigation of Cupressaceae and Taxaceae in Iran. *Wulfenia*, (18).

Loreto, F., 2002. Distribution of isoprenoid emitters in the Quercus genus around the world: chemo-taxonomical implications and evolutionary considerations based on the ecological function of the trait. *Perspectives in Plant Ecology, Evolution and Systematics*, *5*(3), pp.185-192.

The application of a genetic algorithm to estimate fuel bed properties from bench-scale testing

Carlos Walker-Ravena*[1]; Zakary Campbell-Lochrie[1]; Michael R. Gallagher[2]; Nicholas S. Skowronski[3]; Eric V. Mueller[1]; Rory M. Hadden[1]

[1]The University of Edinburgh. Edinburgh, UK,
{C.WalkerRavena, Z.Cambell.Lochrie, R.Hadden}@ed.ac.uk, {EricVMueller@gmail.com}
[3]Northern Research Station. USDA Forest Service. New Lisbon, NJ, USA
{Michael.R.Gallagher@usda.gov}
[4]Northern Research Station. USDA Forest Service. Morgantown, WV, USA
{Nicholas.S.Skowronski@usda.gov}

**Corresponding author*

Keywords

Ignition, Flammability, Porous fuels, Genetic algorithm,

Abstract

A methodology based on an automated optimisation technique is applied to interrogate the relationship between fuel bed structure and effective heat transfer properties. The methodology uses optimisation of the heat equation to resolve the temperature of the fuel bed upon exposure to an external heat flux and is coupled with thermogravimetric data to generate data on mass loss rate. The experimental mass data are provided by undertaking ignition experiments conducted on Pinus rigida Mill. fuel beds in the Fire Propagation Apparatus. Fuel solid fractions ranging from 0.03 to 0.51 are used. The fuel bed structure is represented by the solid fraction and the effective fuel bed properties (conductivity, convective heat loss coefficient and absorptivity) are posed as a function of the fuel bed structure. Each property is considered individually and the relationship between the property and the fuel structure is optimised using a genetic algorithm. In this way a methodology for interrogating the relationship between the fuel bed structure and the effective properties is presented.

1. Introduction

Wildfires are a natural phenomenon but can occur, and be exacerbated, due to human activity. Regardless of origin an uncontrolled fire poses a potential risk to life, property and environment. Nevertheless, the risk is difficult to define if wildfires are not fully understood. By understanding the processes that control the evolution of a wildfire it is possible to define the risk for different situations and a strategy for tackling the risk can be developed. Furthermore, by intervening with measures that alter the processes underpinning a wildfire the risk can be reduced. There are many parameters that affect the processes that control a wildfire including weather, topology and fuel. In this work we focus on the role of the fuel structure on the processes that underpin ignition.

One of the major challenges in understanding wildfire behaviour is defining the structure of the fuels and how this impacts the burning behaviour. Wildland fuels are defined by their thermophysical and thermochemical properties, and their structure (i.e. arrangement of the fuel elements). The thermochemical properties affect the combustion processes whereas the changes in fuel bed structure lead to changes in the heat and mass transfer mechanisms in the fuel bed. Describing the fuel bed structure in a way that is appropriate to resolve the heat and mass transfer processes remains largely elusive. Therefore, an approach to explore how different fuel bed structures affect the heat transfer mechanisms during ignition of porous fuel beds is presented.

This work develops flammability studies previously undertaken to capture the response of wildland fuels at different fuel bed conditions (Schemel, 2008; Mindykowski, 2011; Simeoni, 2012; Houssami, 2016; Jervis, 2016; Thomas, 2017; Walker-Ravena, 2019). Experiments have been conducted on fuel beds of *Pinus rigida* Mill. needles over a range of solid mass fractions (0.03-0.51) to determine the mass loss (and mass loss rate) before ignition as a function of the fuel solid mass fraction. This approach allows the effects of fuel structure to be studied independently of the species-dependent thermochemical properties.

The porous structure of wildfire fuel beds means that classical ignition theory, in which ignition is defined as a surface temperature (Torero, 2016), is unlikely to apply. Instead, a finite thickness of fuel will be heated and will undergo pyrolysis prior to ignition (an 'active region'). This has been observed previously (Thomas, 2017). Modelling ignition therefore requires that the temperature distribution inside the fuel be modelled, in order that a pyrolyzing region can be identified. This requires knowledge of the effective thermal properties as a function of the fuel solid mass fraction.

To address this issue, Genetic Algorithms (Launtenberger, 2006) are used to identify the relationship between the fuel bed effective properties and the fuel bed solid fraction by simultaneously optimising against experimental data of ignition of a range of fuel bed structures of the same material. The assumed relationship between the effective fuel bed properties and the fuel bed structure is varied until the best agreement between the numerical and experimental results is obtained.

Due to the challenges associated with measuring temperatures in porous media, the numerical and experimental results are compared on the basis of mass loss. Modelled temperatures are used to identify the mass loss using data from thermogravimetric analysis of the fuels. In this way the changes in the heating response are modelled to be due to relationship between the fuel bed effective properties and the fuel bed structure.

2. Methods

2.1. Sample preparation

To manufacture the different fuel beds, individual needles were cut to predefined lengths as shown in Figure and Table 1. The needle size determines the packing efficiency of the fuel bed and hence the solid fraction. Six different types of sample were prepared: two using full length needles with different masses, and four samples with needles cut to different lengths (3-4 cm, 1-1.25 cm, <1.5 cm) and one sample was manufactured by grinding the needles to a powder. The solid fraction was calculated by dividing the mass by product of the volume of the sample basket (diameter = 128 mm, depth = 30 mm) and the density of a single pine needle (density = 607 kg/m^3) (Houssami, 2016).

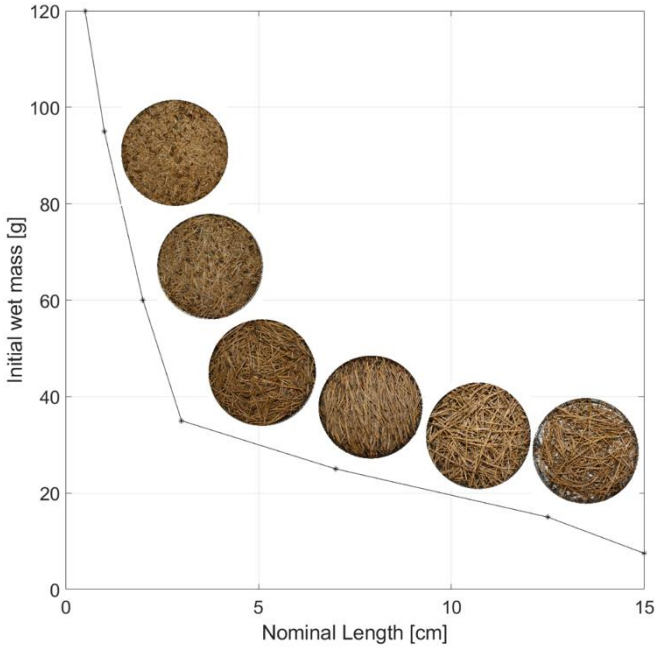

Figure 1 – Initial wet mass of fuel bed as a function of the approximate cut length of the Pinus Rigida needle

Table 1 - Manufactured fuel beds

Sample Preparation	Wet Mass [g]	Solid Fraction [-]
None	7.5	0.03
None	15	0.06
3-4cm	35	0.15
1-2.5cm	60	0.26
<1.5cm	90	0.38
Powder	120	0.51

2.2. Fire Propagation Apparatus

Samples were prepared in closed circular baskets. Closed baskets are used to minimise the contribution of the convective flow. Samples were conditioned by drying in an oven at 60°C for 24 hrs before testing. The preconditioned average fuel moisture content was ~8% whilst the conditioned fuel was <1% (Walker-Ravena, 2019).

Samples were exposed to heating of 25 kW/m^2 using the Fire Propagation Apparatus. The pilot flame was positioned 20 mm above the sample. The sample mass was recorded up to ignition. Repeat tests were averaged at each time-step to compute an average pre-ignition mass loss for each fuel bed.

2.3. Thermogravimetric Analysis

Thermogravimetric analysis (TGA) was carried out in air with a heating rate of 5 K/min for the *Pinus rigida* Mill. needle samples. Needles were ground and put in alumina crucibles. A representative TGA curve was generated by averaging repeat experiments, as shown in Figure 2b. The TGA data are used with the solution of the heat diffusion equation to generate mass data. The temperature at each depth is modelled and the normalised mass, for that temperature, is defined using the TGA data. This is illustrated in Figure 2a and the mapping shown in Figure 2b.

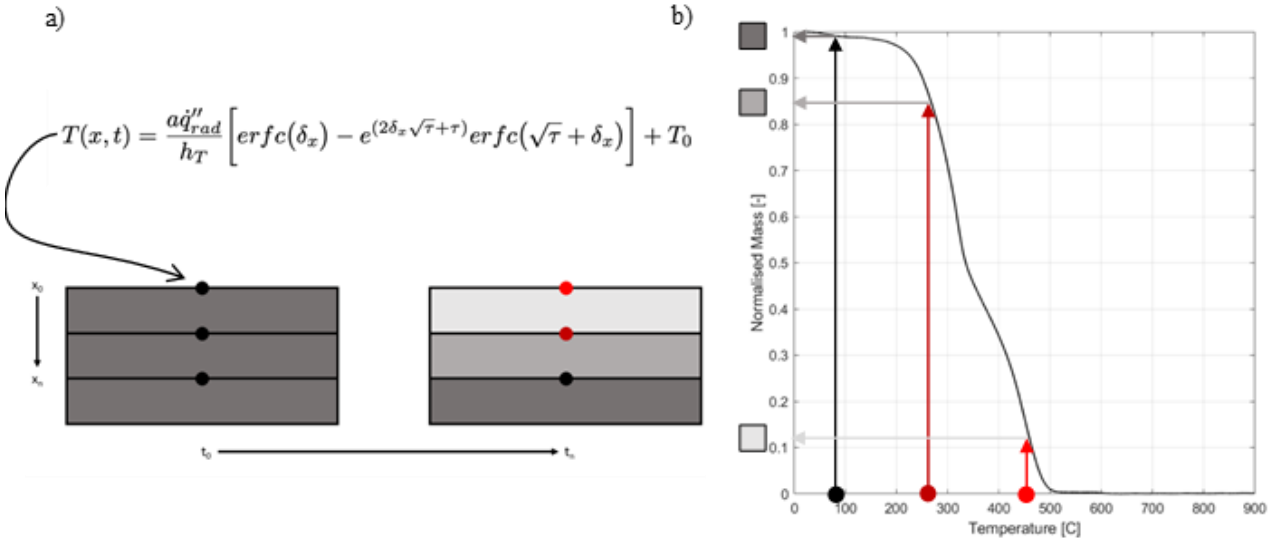

Figure 2 – a) Illustration of heat transfer model at t=0 and t=t_n. Red nodes indicate higher temperature and lighter shades of grey indicate increased mass loss b) TGA experimental data used as a look-up table

2.4. Genetic Algorithm

Genetic algorithms have been used to find material properties from bench-scale experiments (Launtenberger, 2006). A similar approach is followed here whereby optimisation of the model to the experimental data is conducted through minimising an objective function.

The solution to the heat diffusion equation (Torero, 2016), as presented in Figure 2a, is used to determine the temperature distribution in the solid phase. The mass loss rate is computed using the TGA data as indicated on Figure 2b. The objective function quantifies the difference between the model and the experimental data. In this work the relationship between the effective fuel bed properties and the fuel bed structure is sought. As such the different conditions are considered simultaneously by summing the value over each experimental condition as well as each time-step. The objective function is split into two parts so that both the mass and mass loss rate are used to compare the model and the experimental data.

$$R_1 = \sum^{\text{exp.}} \frac{\sum^{\text{t}} (m_{exp} - m_{mean})^2 - \sum (m_{exp} - m_{model})^2}{\sum (m_{exp} - m_{mean})^2}$$

$$R_2 = \sum^{\text{exp.}} \frac{\sum^{\text{t}} (\Delta m_{exp} - \Delta m_{mean})^2 - \sum (\Delta m_{exp} - \Delta m_{model})^2}{\sum_{\text{t}} (\Delta m_{exp} - \Delta m_{mean})^2}$$

$$R = R_1 + 0.5 R_2$$

Equation 1 - Objective functions minimised in genetic algorithm optimisation.

2.5. Effective Fuel Bed properties

The effective fuel bed properties (conductivity, convective heat loss coefficient and absorptivity) were assigned by assuming they are a function of the solid fraction of the fuel bed. This represents how the fuel bed properties are different to the material properties. In Equation 2 the material property is represented by *A* subscript whilst *B* represents the deviation due to the solid fraction. Moreover by assuming a continuous function the number of variables that need to be optimised is reduced.

$$k = k_A + k_B e(m)$$
$$H = H_A + H_B e(m)$$
$$a = a_A + a_B e(m)$$

Equation 2 – Assumed relationships between the heat transfer properties (k is conductivity; H is convective heat loss coefficient and a is absorptivity). Where e(m) is the solid fraction as a function of mass.

3. Results and Discussion

A series of images showing the process of piloted ignition, burning and extinction of a sample is shown in Figure 3. The pyrolysis gases are clearly visible before ignition.

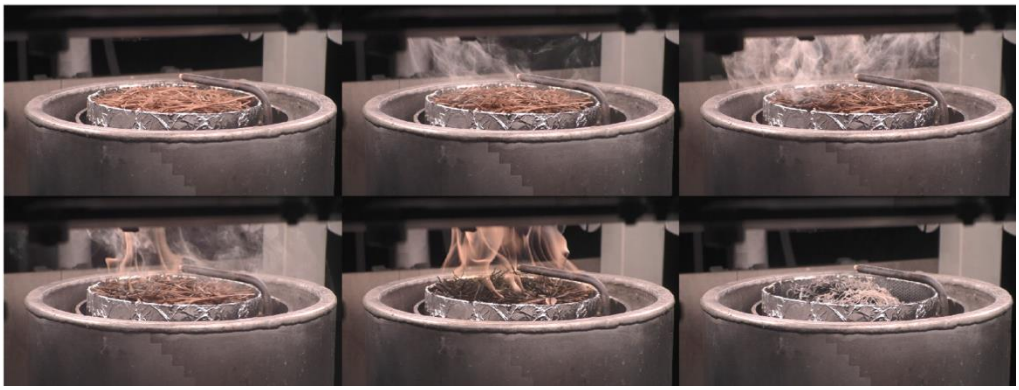

Figure 3 - Collage of 15g subjected to25 kW/m^2. Chronological order from left to right and top to bottom.

3.1. Experimental results

The experimental results shown in Figure 3 show that the mass lost at ignition and time to ignition are non-monotonic functions of the solid fraction. A minimum is observed at a solid fraction 0.15. Changes in the solid mass loss rate will lead to changes in time to form this gas mixture and therefore changes to the time to ignition. A higher mass loss rate indicates that the gas phase environment is such that it is harder to obtain a flammable mixture e.g. it is subject to higher levels of dilution or heat losses.

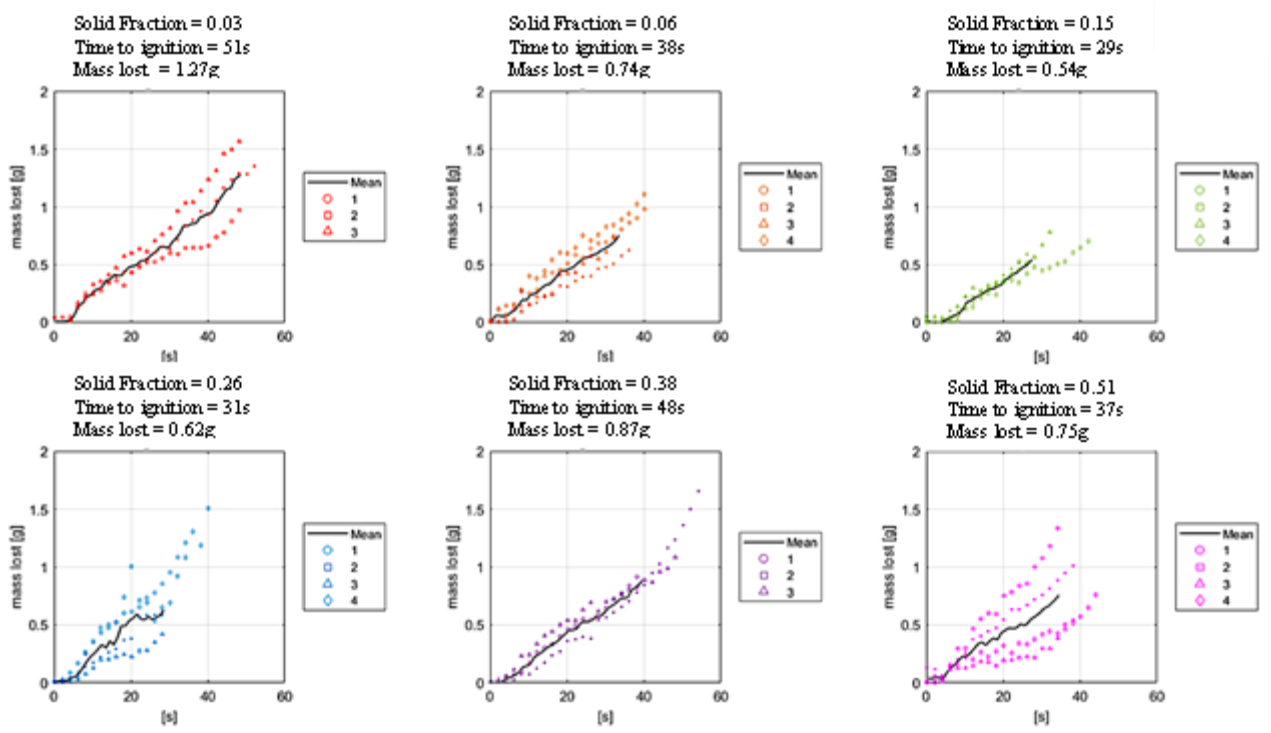

Figure 3 - Pre-ignition data for bench-scale testing conducted in the FPA. Markers represent individual tests whereas the black line is the experimental average. The values above are the experimental averages.

3.2. Genetic Algorithm

The changes in the fuel structure will be affect the conductivity, absorptivity and convection. To determine which is the most sensitive to the changes in fuel structure they are considered on a case-by-case basis. These cases are positive linear conduction, positive linear absorptivity and negative linear convection. These respectively represent the assumed trends of an increase in heat transfer through the bed due to an increase in needles connectivity; an increase in heat absorbed at the upper surfaces due to an increase in needle density per depth and decrease in convective heat loss due to a decrease in the fuel bed permeability causing lower fluid flows. The effective fuel bed properties are compared to literature values (Houssami, 2016).

3.2.1. Positive Linear Conductivity

The first case is positive linear conductivity as a function of the fuel solid fraction. The intention here was to represent the increase in conductivity that is assumed to occur with a decrease in the porosity of the fuel bed. That is to say smaller spacing between needles is assumed to lead to an increased effective thermal conductivity due to increased particle to particle contact. An increase in conductivity may also represent the heat transferred through the fuel bed due to needle-to-needle radiation (Simeoni, 2012). Optimisation gave the values for k_A and k_B as 2.41×10^{-6} W/mmK and 8.96×10^{-5} W/mmK, respectively.

Nevertheless, the output values did not capture the experimental behaviours appropriately. The lowest solid fractions showed similar behaviours but the mass loss at the high fuel loads were over estimated. In the low solid fractions it is expected that radiation penetration into the depth of the fuel bed is significant resulting in higher in depth temperatures.

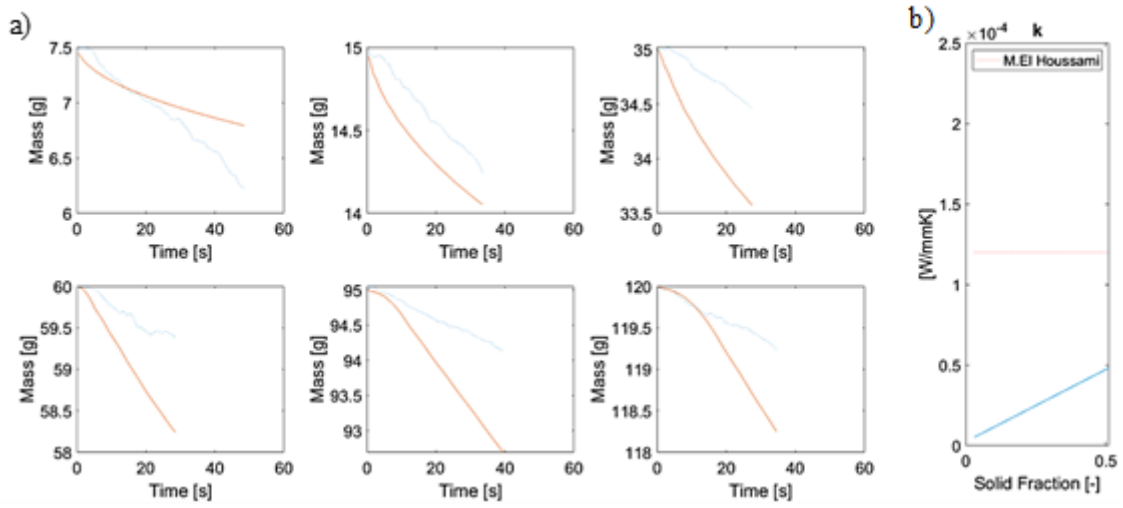

Figure 5 - Positive Linear Conductivity model outputs. Blue line shows experimental mean whilst red line shows the model output. Clockwise from top left, the fuel loads shown are 7.5g, 15g, 35g, 60g, 95g, 120g. b) Conductive coefficient as a function of solid fraction.

3.2.2. Positive Linear Absorptivity

The next case is positive linear absorptivity. Here the intention is to represent the increase in heat absorbed at the upper surfaces of the fuel bed due to there being a greater amount of exposed surface area due to increase in needle density. Optimisation gave the values for a_A and a_B as 0.46 and 0.56 respectively.

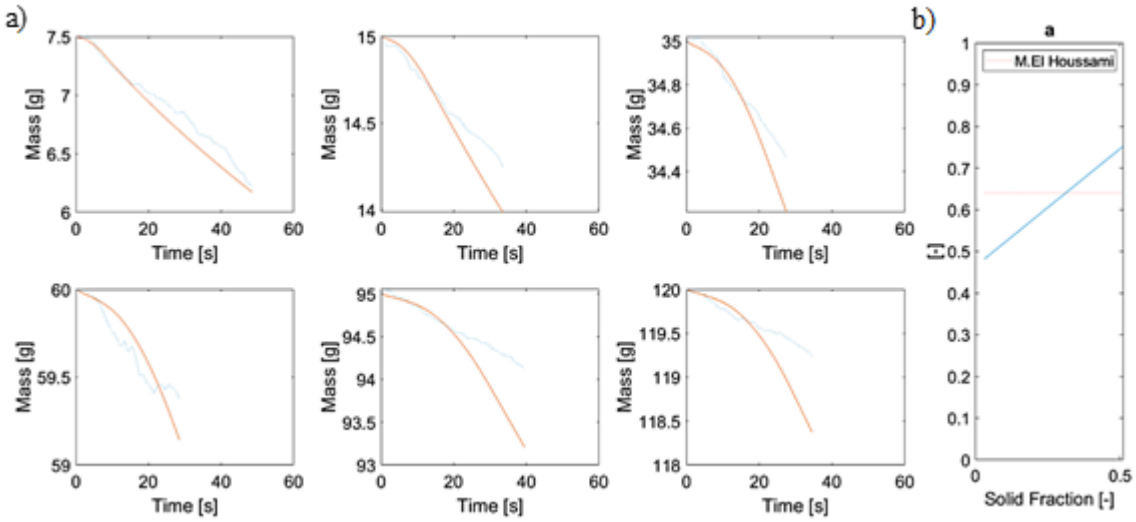

Figure 6 - Positive Linear Absorptivity model outputs. Blue line shows experimental mean whilst red line shows the model output. Clockwise from top left, the fuel loads shown are 7.5g, 15g, 35g, 60g, 95g, 120g. b) Absorptivity coefficient as a function of solid fraction.

These conditions seem to capture the behaviours at low fuel loads well however the high fuel loads are seen to overestimate the mass loss rate at longer times. This indicates that the temperature in the system is too high. This suggests that, the effects of fuel structure are not represented by the change in the absorptivity alone.

3.2.3. Negative Linear Convection

The next case is negative linear convection. This intention here is to represent the increase in convective heat loss that is assumed to occur as the bed becomes more porous. The increase in the porosity of fuel bed leads to an increase in its permeability and so the fuel bed is more susceptible to fluid flows and therefore convective losses (Simeoni, 2012). Optimisation gave the values for H_A and H_B as 3.35e-5 W/mm^{2}K and -8.54e-6 W/mm^{2}K respectively.

The output leads to improved representation of the experimental results in both the low and high fuel load cases. Although the lines do not overlap in the high fuel cases, a similar gradient is found at long time. This indicates that the rates of degradation are similar and as such some of the experiment physics are being captured.

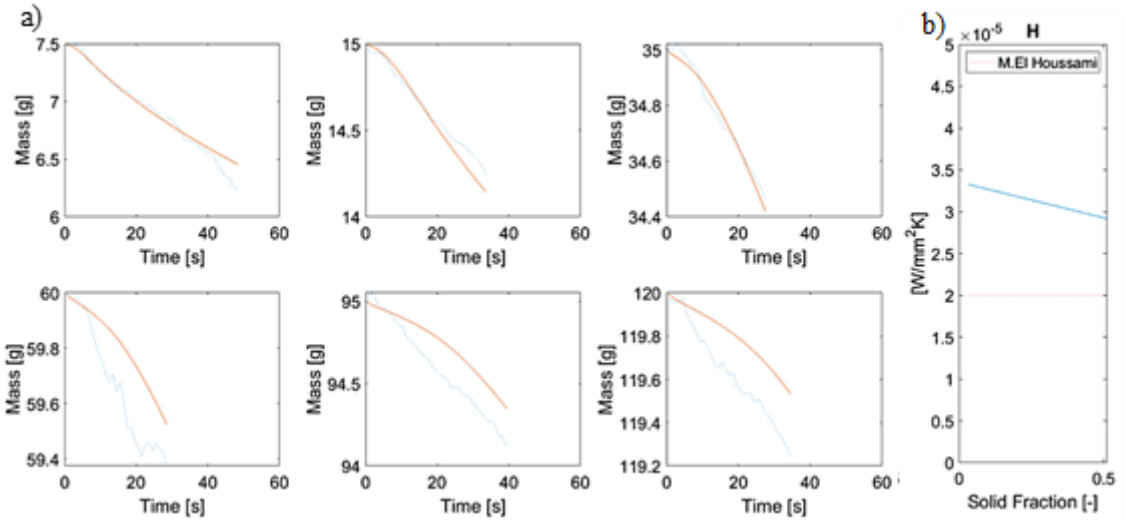

Figure 7 – a) Negative Linear Convection model outputs. Blue line shows experimental mean whilst red line shows the model output. Clockwise from top left, the fuel loads shown are 7.5g, 15g, 35g, 60g, 95g, 120g. b) Convective coefficient as a function of solid fraction.

4. Conclusion

This study has explored the effect of fuel solid fraction on the ignition of fuel beds. Experimentally the mass lost from the fuel bed before ignition and the time to ignition is shown to vary as a function of the fuel solid fraction. This indicates that the structure of the fuel bed and the heat transfer within the fuel bed play a key role in determining the ignition characteristics. Using a simple genetic algorithm approach, we show that the absorption of radiation and the heat losses of the system play a governing role in these experiments. The study also showed that the convective flow through a porous fuel has a large impact on determining the flammability due to convective cooling of fine elements air. This finding is important for the design of future studies of the burning of wildland fuels as the fuel bed structure is generally not considered beyond the level of fuel loading or bulk density. This approach also results in the need to move away from a surface temperature condition for ignition of porous fuel beds to one that considers the temperature distribution through the porous media.

5. References

C. Lautenberger, G. Rein, and C. Fernandez-Pello, “The application of a genetic algorithm to estimate material properties for fire modeling from bench-scale fire test data,” Fire Safety Journal, vol. 41, no. 3, pp. 204–214, 2006.

C. F. Schemel, A. Simeoni, H. Biteau, J. D. Rivera, and J. L. Torero, “A calorimetric study of wildland fuels,” Experimental Thermal and Fluid Science, vol. 32, no. 7, pp. 1381–1389, 2008.

J. L. Torero and A. Simeoni, “Heat and Mass Transfer in Fires: Scaling Laws, Ignition of Solid Fuels and Application to Forest Fires,” The Open Thermodynamics Journal, vol. 4, no. 1, pp. 145–155, 2010. [Online]. Available: http://benthamopen.com/ABSTRACT/TOTHERJ-4-145

P. Mindykowski, A. Fuentes, J. L. Consalvi, and B. Porterie, “Piloted ignition of wildland fuels,” Fire Safety Journal, vol. 46, no. 1-2, pp. 34–40, 2011. [Online]. Available: http://dx.doi.org/10.1016/j.firesaf.2010.09.003

A. Simeoni, J. C. Thomas, P. Bartoli, P. Borowieck, P. Reszka, F. Colella, P. A. Santoni, and J. L. Torero, “Flammability studies for wildland and wildland-urban interface fires applied to pine needles and solid polymers,” Fire Safety Journal, vol. 54, pp. 203–217, 2012. [Online]. Available: http://dx.doi.org/10.1016/j.firesaf.2012.08.005

F. X. Jervis and G. Rein, "Experimental study on the burning behaviour of Pinus halepensis needles using small-scale fire calorimetry of live, aged and dead samples," Fire and Materials, vol. 40, no. 3, pp. 385–395, apr 2016. [Online]. Available: http://doi.wiley.com/10.1002/fam.2293

Torero J., Flaming Ignition of Solid Fuels. In: Hurley M.J. et al. (eds) SFPE Handbook of Fire Protection Engineering. Springer, New York, NY, 2016. https://doi.org/10.1007/978-1-4939-2565-0_21

M. El Houssami, J. C. Thomas, A. Lamorlette, D. Morvan, M. Chaos, R. Hadden, and A. Simeoni, "Experimental and numerical studies characterizing the burning dynamics of wildland fuels," Combustion and Flame, vol. 168, pp. 113–126, 2016. J. C. Thomas, R. M. Hadden, and A. Simeoni, "Experimental investigation of the impact of oxygen flux on the burning dynamics of forest fuel beds," Fire Safety Journal, vol. 91, no. February, pp. 855–863, 2017. [Online]. Available: http://dx.doi.org/10.1016/j.firesaf.2017.03.086

J. C. Thomas, "Improving the understanding of fundamental mechanisms that influence ignition and burning behavior of porous wildland fuel beds," Ph.D. dissertation, University of Edinburgh, 2017

J. C. Thomas, R. M. Hadden, and A. Simeoni, "Experimental investigation of the impact of oxy- gen flux on the burning dynamics of forest fuel beds," Fire Safety Journal, vol. 91, no. February, pp. 855–863, 2017. [Online]. Available: http://dx.doi.org/10.1016/j.firesaf.2017.03.086

C. Walker-Ravena, Z. Campbell-Lochrie, and R. M. Hadden, "The influence of structure on the flammability of wildland fuels under radiative heating," in 6th Int. Fire Behavior and Fuels Conference, 2019.

The role of helicity and fire-atmosphere turbulent energy transfer on potential wildfire behavior

Jiawei Zhang*[1;2]; Marwan Katurji[2]; Peyman Zawar-Reza[2]; Tara Strand[1]

[1] *New Zealand Forest Research Institute, Scion, New Zealand, {jiawei.zhang@scionresearch.com}*
[2] *School of Earth and Environment, University of Canterbury, New Zealand,*

**Corresponding author*

Keywords

Fire-atmosphere interaction, Turbulence, Energy transport, Large eddy simulation

Abstract

Understanding near surface fire-atmosphere interactions at turbulence scale is fundamental for predicting fire spread behavior. This study investigated the fire-atmosphere interaction and the accompanying energy transport processes within the convective boundary layer. Three groups of large eddy simulations (LES) representing common ranges of convective boundary layer conditions (resulting from land surface heat flux ranging from 120 to 360W/m2) and fire intensities (50 to 150kW/m2) were used to examine how ambient buoyancy-induced atmospheric turbulence can impact fire region heat and momentum transport.

In a relatively weak convective boundary layer, the change of near-surface atmospheric turbulence caused by the buoyancy force from the fire heat release is substantial and can cause an anticorrelation of the helicity between the ambient atmosphere and the fire-induced flow. Fire-induced impact becomes much smaller in a relatively strong convective environment with ambient atmospheric flow maintaining coherent structures including vortices across the fire heating region. The helicity also shows strong correlation between the ambient atmosphere and the fire-induced flow. A further energy transport efficiency analysis shows a narrow heat transport zone above the fire line for the weak convective boundary layer scenario. This indicates confined heat release and stronger fire-induced buoyancy force. The high-efficiency heat transport zone becomes much wider in a stronger convective boundary layer which leads to a wider distribution of heat released from fire, the weaker fire-induced buoyancy force and causes less fire-induced flow-field change. The work also found counter-gradient transport zones of both momentum and heat in fire cases in the weak convective boundary layer group. The counter-gradient transport might indicate the existence of strong buoyancy-induced mixing processes.

1. Introduction

Atmospheric motions vary in scale from thousands of kilometers (planetary circulations) to sub-meter turbulence eddies (Orlanski, 1975). These atmospheric motions can interact and influence fire behavior at different scales and aspects (Potter, 2002). The thermal internal boundary layer caused by localized heating of fire, and the atmospheric boundary layer (ABL) that envelops it, develop at integral time scales spanning from seconds to tens of minutes (Stull, 2012). Within this fire turbulence environment (hereafter referred to as the FTE, Figure 1), atmospheric turbulence plays an important part in energy transfer between the fire and the surrounding atmosphere ((Dickinson et al., 2021; Finney et al., 2015; Kremens et al., 2012; Sullivan, 2017).

Quantifying turbulent heat and momentum fluxes is important to better describe the coupled processes within the FTE which can lead to spatial and temporal variation in fire behavior. This work aims to describe the role of the background atmospheric flow in fire-atmosphere interactions and discuss the physical mechanisms driving these interactions. The main objective is to understand processes that control the spatial and temporal development of turbulent heat and momentum transport under different convective boundary layer (CBL) turbulence intensities.

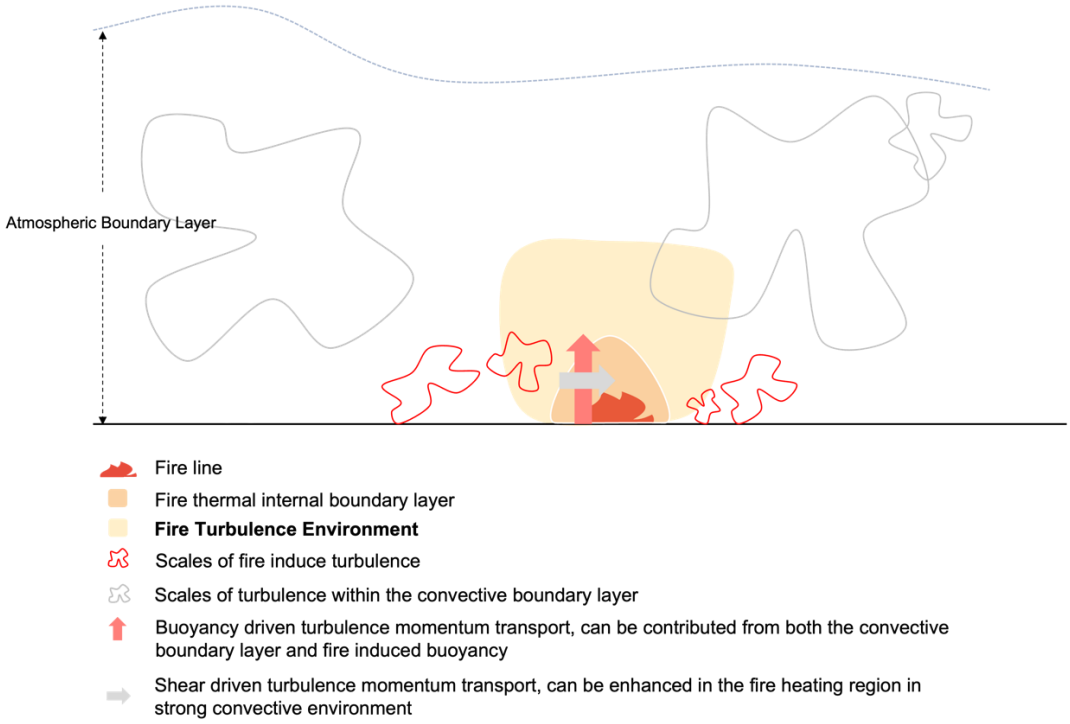

Figure 1- Conceptual diagram showing the fire turbulence environment (FTE).

The impact of different fire intensities for each turbulence regime is also considered using a 2D hot patch with different fixed heat flux intensities. The novel quantitative partitioning of heat and momentum flux using spatially distributed energy partitioning (referred to as spatial quadrant analysis) allowed the definition of spatial energy transfer zones that define the scales and intensities of these interactions. Finally, and by calculating the helicity above the fire region influenced by atmospheric motion, the potential for fire behavior influenced by atmospheric turbulence is discussed in relation to fire and atmospheric turbulence intensity levels.

2. Methods

2.1. Model description and set-up

The PArallelized LES Model (PALM) model (Maronga et al., 2015; Raasch & Schröter, 2001) is the model employed here . A matrix of simulations was carried out with three ambient land surface heat fluxes and three fire intensities (Table 1). A base case, with no simulated fire, was also run for every ambient land surface heat flux group to represent the ambient atmospheric flow field. In all cases, three nested domains with one-way nesting were used, downscaling from 32m to 4m grid resolution (Figure 2). A 12m wide 2D hot patch with different heat fluxes was placed in the center of the inner-most domain (D3) to represent fire with different intensities for the fire cases.

Table 1- Simulation naming convention including a total of 12 simulations. Note the difference in magnitude between the land surface heat flux and the fire intensities.

Group	**Land Surface Heat Flux**	**Fire Intensity**			
		Base	Low	Med	High
C1	120 $W\ m^{-2}$	No Fire	50 $kW\ m^{-2}$	100 $kW\ m^{-2}$	150 $kW\ m^{-2}$
C2	240 $W\ m^{-2}$				
C3	360 $W\ m^{-2}$				

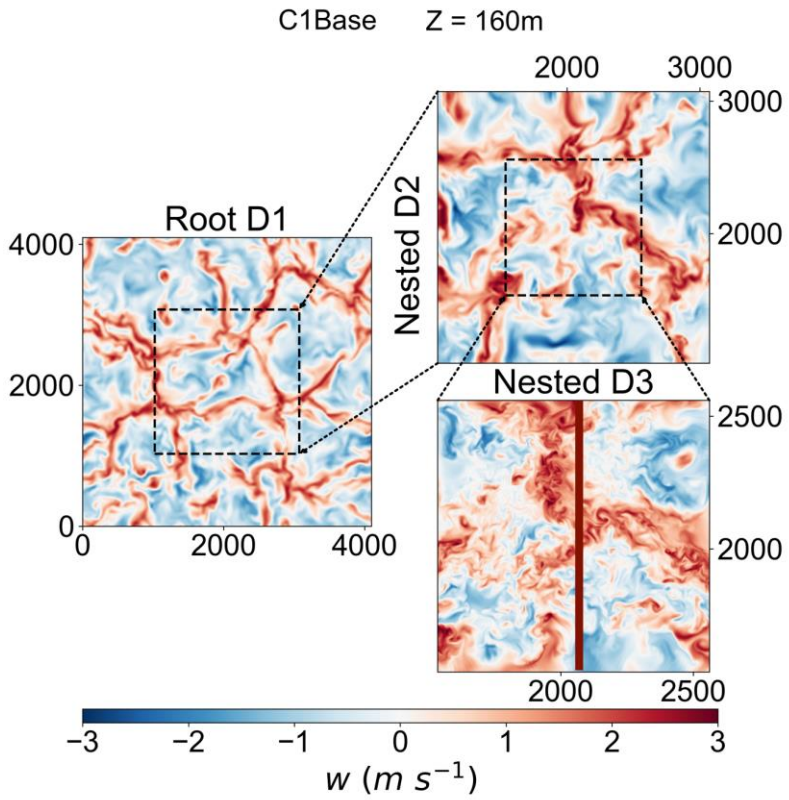

Figure 2. Instantaneous horizontal cross-section of vertical velocity at 160m above ground level (AGL) (z=160m) from one of the simulations (C1Base). D1, D2, D3 are for the nested Domains 1 (root or outermost domain), 2 and 3 (innermost domain). The red line in the D3 domain illustrates the hot patch location which was only set up at the surface of the fire cases after 03:30:00 simulation time.

The same initial profiles were used for all the simulations. For the potential temperature profile, constant potential temperature of 293K is used from the surface up to 1km with an inversion then applied. The initial wind speed is set to be 0m/s at all locations. All cases were run for 4 hours with the first 3 hours as spin up period and the fire set up after 3.5 hours.

2.2. Helicity

Helicity is used to explore the changes or transfer of vorticity caused by the interaction between the fire-induced buoyancy and the ambient atmospheric flow. The helicity is calculated using the non-integral form (Equation 1). To better quantify the domain-wide helicity, the averaged magnitude of the vertical helicity component is calculated from the horizontal cross-section of the innermost (D3) domain.

$$H = (\nabla \times \vec{v}) \cdot \vec{v} \quad (1)$$

where $\vec{v}$ is the velocity vector and $\nabla \times \vec{v}$ is the vorticity vector $\vec{\omega}$.

2.3. Quadrant analysis

In any point location, the time series of instantaneous vertical transfer of horizontal momentum (w'u') and kinematic heat flux (w'θ') can be drawn in the Cartesian coordinate system with w' and the respective perturbation variable as the coordinates (Figure 3; Shaw et al., 1983). Each quadrant in the coordinate system has different physical interpretation.

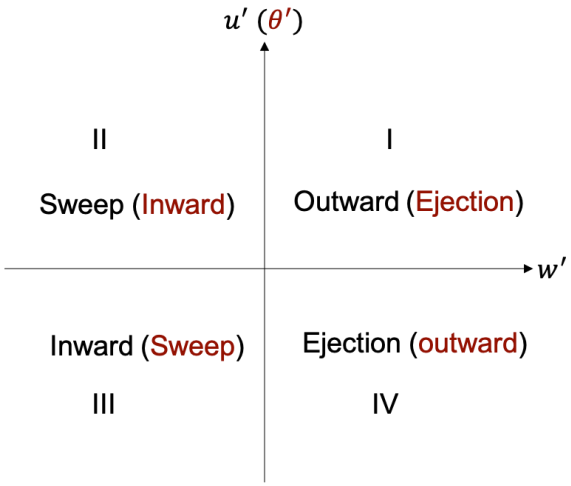

Figure 3. The terminology and convention used for the quadrant analysis. A time series of w'u' (or w'θ') can be classified into each quadrant. For the momentum flux (w'u'), quadrants I and III represent the outward and inward motions which account for counter-gradient momentum transport. Quadrants II and IV represent the sweep and ejection motions and contribute to downgradient momentum transport. For the instantaneous kinematic heat flux (w'θ'), the sweep/ejection and outward/inward quadrants are reversed and illustrated using the red color.

Based on quadrant analysis, Wyngaard and Moeng (1992) implemented the concept of energy transport efficiency, which was defined as the ratio of downgradient flux to total flux. The mathematical form of energy transport efficiency is further discussed by Li and Bou-Zeid (2011) and is shown below,

$$\eta = \frac{F_{\text{total}}}{F_{\text{downgradient}}} = \frac{\overline{w'c'}}{\overline{w'c'}_{\text{ejections}} + \overline{w'c'}_{\text{sweeps}}} \tag{2}$$

where c represents variables like velocity, temperature or other scalars. The flux in each quadrant is calculated using the equation below,

$$\overline{w'c'}_i = \frac{1}{t}\sum_{j=t_0}^{t} w_j{}' \, c_j{}' I_{ij} \tag{3}$$

where I_j is defined as,

$$I_{ij} = \begin{cases} 1 & \text{if } w_j{}' c_j{}' \text{ is in quadrant } i \\ 0 & \text{otherwise} \end{cases} \tag{4}$$

From the above definition, the transport efficiency (η) is positive when the F_{total} and $F_{downgradient}$ have the same sign. This means the down-gradient transport is dominating the energy transport process and the turbulence is mainly shear driven. On the other hand, when the counter-gradient transport component is strong enough to counteract the down-gradient transport, the transport efficiency can be very small and even negative. To obtain spatial information about the momentum and heat transport within the FTE, the work extended the transport efficiency to the spatial modelling data.

3. Results

3.1. General flow patterns

Figure 4 shows the horizontal cross-section of the 1-minute averaged u velocity component at 10m above ground level (AGL) after the fire had been set up for 20 minutes. In the C1 group, a clear fire-induced convergence zone is formed across all fire cases while no such zone exists in the base case. In the C2 group, vortex structures can be found in both the ambient atmosphere (represented by the base case) and the fire cases. These vortex structures remain and are strengthened with the addition of the simulated fire. All C3 group cases show similar flow patterns with predominant negative values in the center of the domain and positive values at the edge.

Although not shown here, the fire cases in the C2 and C3 group maintain similar flow patterns of all velocity components to the respective base case up until 20 minutes after the fire line set-up.

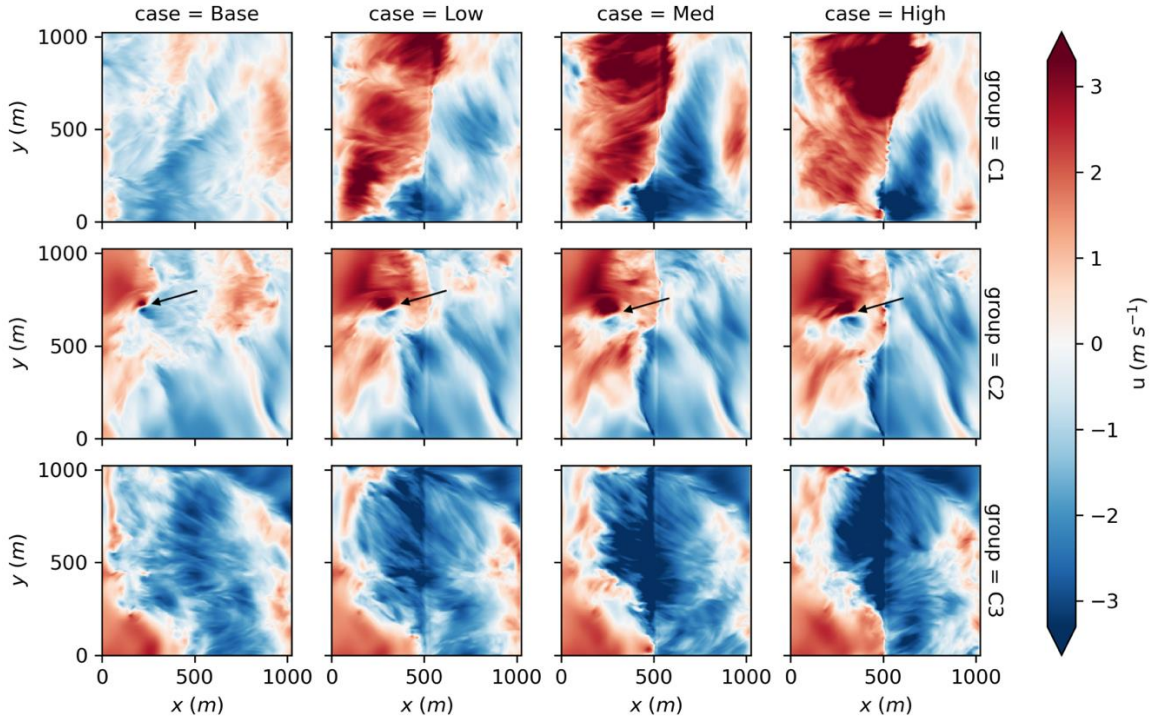

Figure 4. Horizontal cross-section (10m AGL) of 1-minute averaged horizontal u-velocity component 20 minutes after the fire lines were set up). Each row represents simulation groups with different ambient land surface heat flux (120W/m² for the C1 group, 240W/m² for the C2 group and 360W/m² for the C3 group). From left to right, each column represents the fire line intensity (heat flux) (no fire for the base case, 50kW/m² for the low intensity fire scenario, 100kW/m² for the medium intensity scenario and 150kW/m² for the high intensity scenario).

The temperature anomaly caused by fire also shows distinctive characteristics between C1 and the two other groups. Even 10 minutes after the fire line is set up, the high temperature zone caused by the fire maintains a relatively straight and narrow line at 10m AGL in all fire cases in the C1 group (Figure 5). Conversely, the high temperature anomaly in the fire cases in the C2 and C3 groups show much wider horizontal extent. From the vertical cross-section (not shown here), this is caused by tilting of the hot plume.

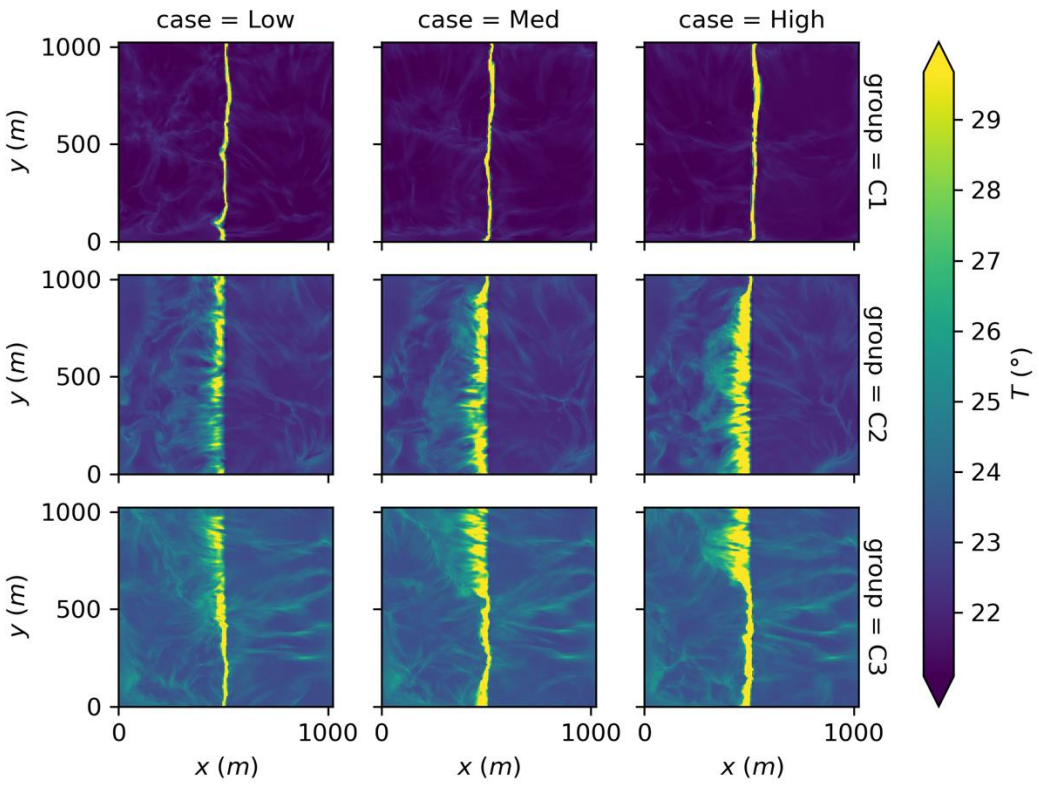

Figure 5. Horizontal cross-section (10m AGL) of 1-minute averaged air temperature after 20 minutes of the fire lines being set up). Each row represents simulation groups with different ambient land surface heat flux (120W/m^2 for the C1 group, 240W/m^2 for the C2 group and 360W/m^2 for the C3 group). From left to right, each column represents the fire line intensity (heat flux) (50kW/m^2 for the low intensity fire scenario, 100kW/m^2 for the medium intensity scenario and 150kW/m^2 for the high intensity scenario).

3.2. Helicity

The magnitude of the domain average vertical helicity component ($|H_z|$) is much lower in the base case in the C1 group (Table 2a) while the magnitude is higher in the base cases in the C2 and C3 groups. In all groups, fire cases have higher $|H_z|$ which might be caused by the reorganizing and tilting of the ambient vortices from the fire-induced buoyancy. This aligns with the framework suggested by Potter et al. (2012).

Table 2a- Average magnitude of the vertical helicity component $|H_z|$ at 10m AGL.

$\|H_z\|$	Base	Low	Med	High
C1 group	0.009	0.018	0.026	0.030
C2 group	0.015	0.023	0.028	0.031
C3 group	0.019	0.026	0.030	0.033

Table 2b- Correlation coefficient (r) of the vertical helicity magnitude $|H_z|$ time series (domain averaged at 10m height) between fire cases and the base (no fire) case from the same group.

r	Base	Low	Med	High
C1 group	N/A	-0.74	-0.76	-0.77
C2 group	N/A	0.69	0.55	0.60
C3 group	N/A	0.86	0.90	0.87

Time series of $|H_z|$ show some similarity between the fire cases and the base case, especially in the C2 and C3 groups (Figure 6). The similarity can be confirmed by the correlation coefficient (Table 2b). In general, fire cases and the ambient atmospheric flow represented by respective base cases have high correlation coefficients up to 0.9 in the C2 and C3 groups. The high correlation coefficients indicate that ambient atmospheric flow can maintain its coherent turbulent flow structures and impact fire behaviors under the convective boundary layer conditions similar to the C2 and C3 groups. On the other hand, strong anticorrelation can be found between the fire cases and the base case in the C1 group which means an increase of $|H_z|$ in the fire cases corresponds to a decrease of the $|H_z|$ in the ambient atmosphere. This indicates that fire-induced processes like vortex stretching/tilting might be dominating and changing the rotational flow field in a relatively weak convective boundary layer.

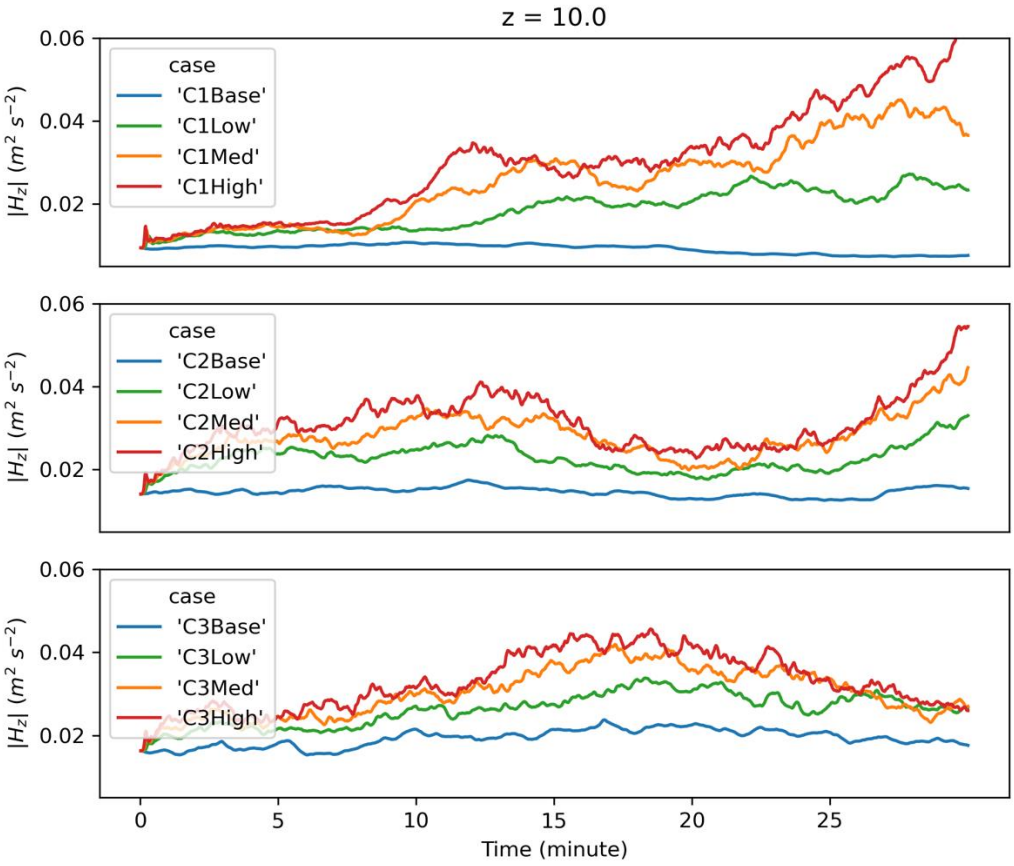

Figure 6. Time series of the vertical helicity magnitude (domain averaged at 10m AGL) from each case in each simulation group from the moment fire was set up. (a), (b), (c) show results in the C1, C2 and C3 groups respectively while blue, green, orange, and red lines represent base (no fire), low, medium, and high intensity fire case in each group respectively.

3.3. Energy transport efficiency

While the above analysis has shown evidence of different fire-atmosphere interaction under different CBL conditions, to understand the physical processes behind these results, the turbulent transport efficiency is further investigated.

Horizontal and vertical cross-sections of the vertical heat transport efficiency ($\eta_{w'\theta'}$) from all cases are shown in Figures 7 and 8. From both horizontal and vertical cross-sections, a much narrower and more distinctive high-efficiency transport zone can be found in the C1 group compared to other groups. In both the C1 and C2 groups, counter-gradient heat transport zone (negative values) can be found.

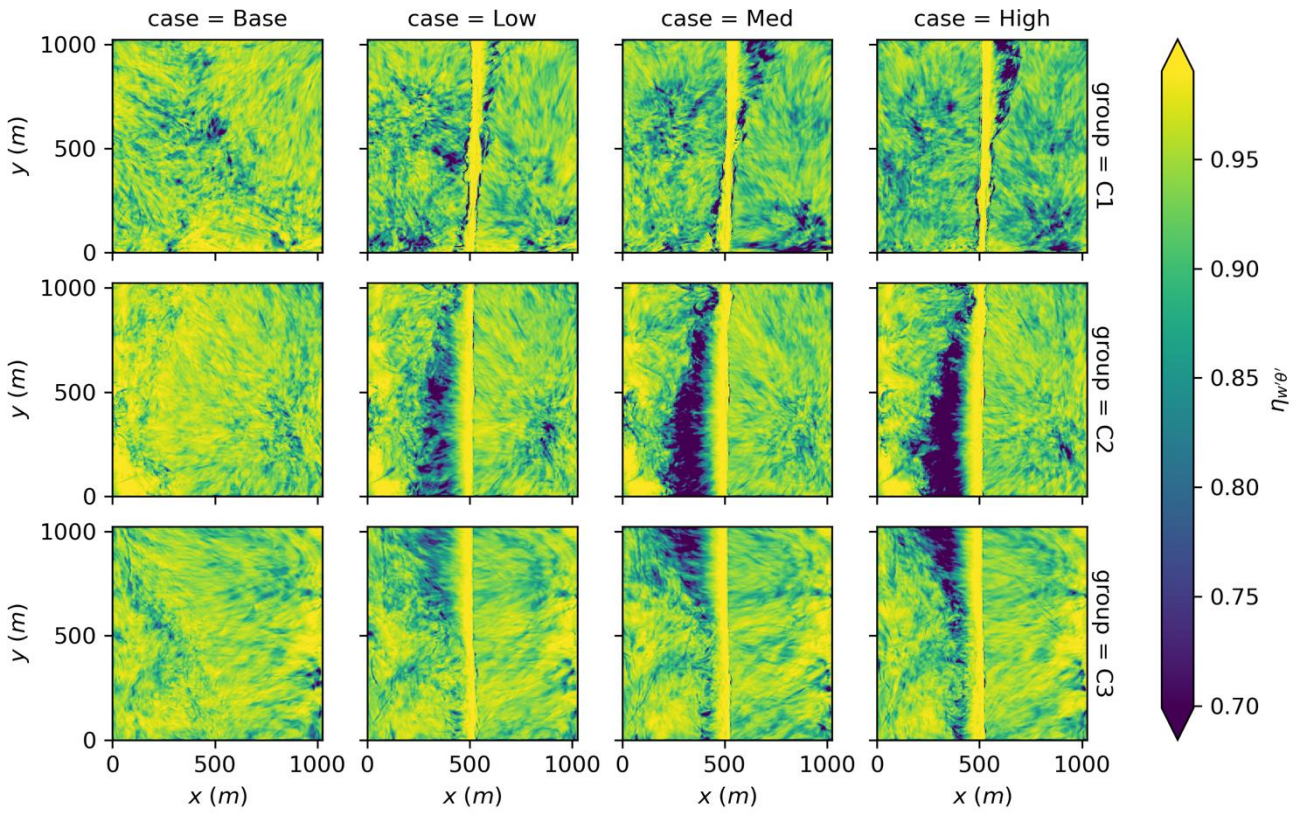

Figure 7. Horizontal cross-section of heat transport efficiency $\eta_{w'\theta'}$ at 10m above the surface from all cases during the first 15 minutes of the fire being set up. Each row represents different groups while each column represents either the base cases or the cases with the different fire intensities.

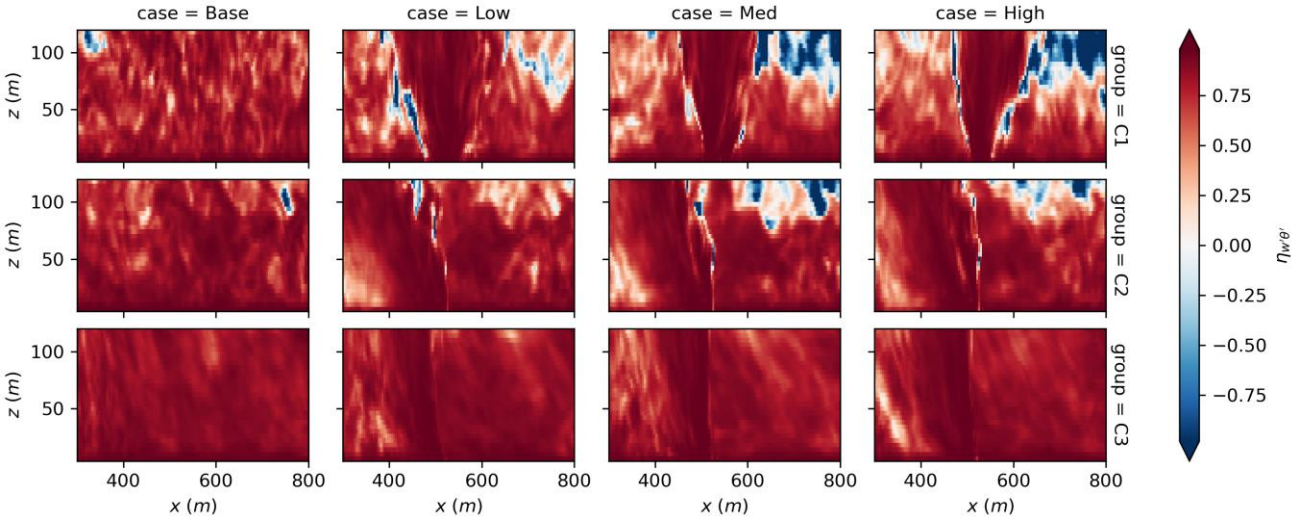

Figure 8. xz cross-section of heat transport efficiency $\eta_{w'\theta'}$ at the center of the domain from all cases during the first 15 minutes of the fire being set up. Each row represents different groups while each column represents either the base cases or the cases with the different fire intensities.

From both the horizontal and vertical cross-sections of the momentum transport efficiency ($\eta_{w'u'}$) (Figures 9 and 10), a new counter-gradient (negative values) momentum transport zone can also be found in the fire cases in the C1 group. This is in consistent with the analysis above and might be caused by the strong fire-induced buoyancy.

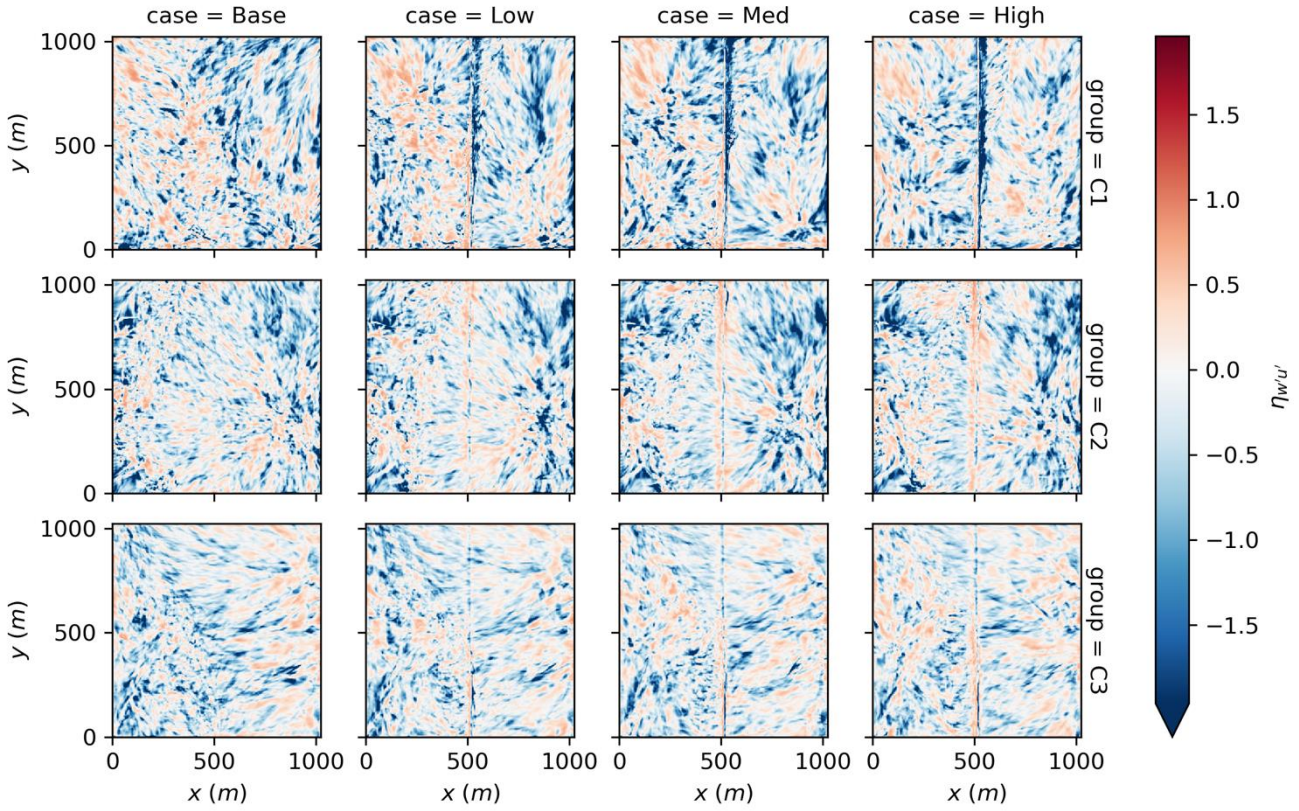

Figure 9. Horizontal cross-section of momentum transport efficiency $\eta_{w'u'}$ at 10m above the surface from all cases during the first 15 minutes of the fire being set up. Each row represents different groups while each column represents either the base cases or the cases with the different fire intensities.

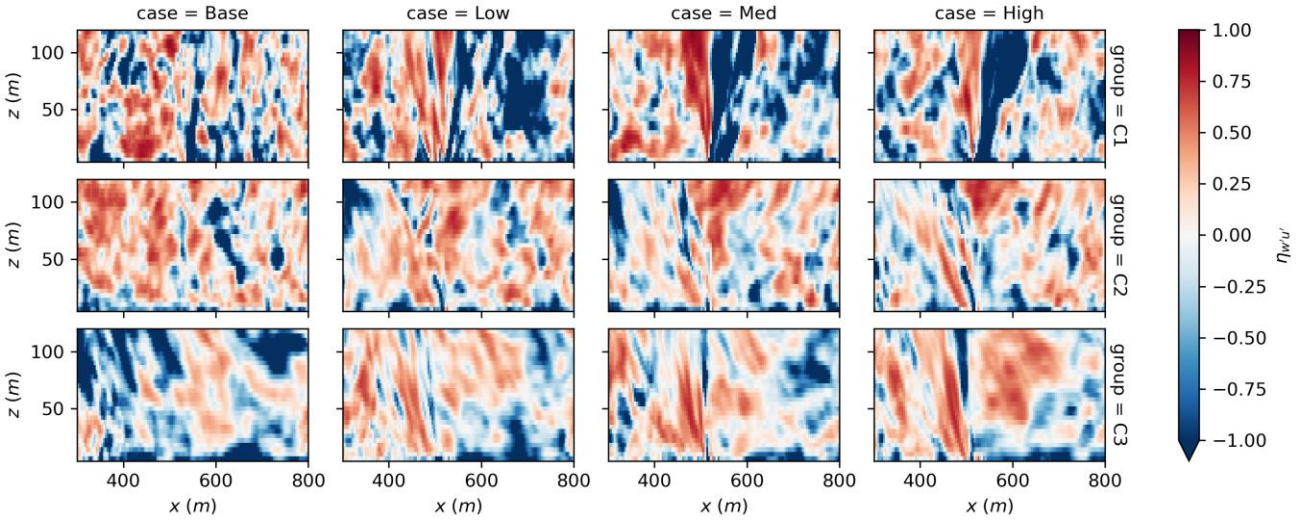

Figure 10. xz cross-section of momentum transport efficiency $\eta_{w'u'}$ at the center of the domain from all cases during the first 15 minutes of the fire being set up. Each row represents different groups while each column represents either the base cases or the cases with the different fire intensities.

4. Discussion and conclusion

The study found that different convective boundary layer conditions will have different impacts in the fire-atmosphere interaction process. In a relatively weak atmospheric CBL (C1 group), our results have shown that the near-surface flow field changed substantially due to the fire-induced flow in all fire cases. The helicity analysis shows an anticorrelation between the ambient atmosphere and the fire-induced flow. The fire-induced temperature anomaly in all cases is spatially confined with a relatively narrower horizontal span compared to

other groups. The horizontal span of the anomaly is consistent with the narrow fire-induced high-efficiency heat transport zone and counter-gradient momentum transport zone. The influence of the fire-induced flow change in heat and momentum transport is extended beyond these zones to the entire near-surface region. This further suggests that fire-induced flow can be substantial in the ambient flow field and reach a large spatial extent. As a result, it would be difficult to predict fire behavior in this scenario without information about fire fuel.

On the other hand, in a stronger buoyancy driven CBL turbulence environment like the C2 and C3 groups, which represent conditions closer to typical midaltitude midday, the ambient flow field remains largely unchanged after the fire initiation. This suggests that, in an ABL with stronger buoyancy driven turbulence, the ambient atmospheric flow can play an important role in fire behavior while fire-induced flow change can be very limited. The strengthening of the vortex structures in the fire cases in the C2 group might also indicate that the ambient vortex structures could contribute to the fire whirl generation process. The fire-induced high-efficiency heat transport zone has a much wider spatial extent which is consistent with the wider extent of the temperature anomaly. The wider heat transport also leads to a weaker buoyancy flow. Unlike in the weak atmospheric CBL, there is no clear buoyancy induced counter-gradient momentum transport zone.

The results might provide guidelines to determine whether ambient atmosphere could play an important role in fire region energy transport and subsequently influence short-term fire behaviors. Future work is needed using either field campaigns or coupled fire-atmosphere models, including detailed physical and chemical processes of fire combustion and spread, to verify our results with moving fire at similar ranges of intensity.

5. Acknowledgement

The work used computational resources from both the high-performance computational center in University of Canterbury and the New Zealand eScience Infrastructure (NeSI), We would like to thank technical team from School of Earth and Environment, University of Canterbury for their technical support to this work. The work is co-funded by University of Canterbury through the Doctoral Scholarship, Ministry of Business, Innovation and Employment (MBIE), New Zealand (Grant No. C04X1603 - “Preparing New Zealand for Extreme Fire” and C04X2103 – “Extreme wildfire: Our new reality – are we ready?”) and the Royal Society of New Zealand (Grant No. RDF-UOC1701).

6. Bibliography

Dickinson, M. B., Wold, C. E., Butler, B. W., Kremens, R. L., Jimenez, D., Sopko, P., & O’Brien, J. J. (2021). The Wildland Fire Heat Budget—Using Bi-Directional Probes to Measure Sensible Heat Flux and Energy in Surface Fires. Sensors, 21(6), 2135. https://doi.org/10.3390/s21062135

Finney, M., Cohen, J. D., Forthofer, J. M., McAllister, S. S., Gollner, M. J., Gorham, D. J., et al. (2015). Role of buoyant flame dynamics in wildfire spread. Proceedings of the National Academy of Sciences, 112(32), 9833–9838. https://doi.org/10.1073/pnas.1504498112

Kremens, R. L., Dickinson, M. B., Bova, A. S., Kremens, R. L., Dickinson, M. B., & Bova, A. S. (2012). Radiant flux density, energy density and fuel consumption in mixed-oak forest surface fires. International Journal of Wildland Fire, 21(6), 722–730. https://doi.org/10.1071/WF10143

LeMone, M. A., Grossman, R. L., Coulter, R. L., Wesley, M. L., Klazura, G. E., PouIos, G. S., et al. (2000). Land–Atmosphere Interaction Research, Early Results, and Opportunities in the Walnut River Watershed in Southeast Kansas: CASES and ABLE. Bulletin of the American Meteorological Society, 81(4), 757–780. https://doi.org/10.1175/1520-0477(2000)081<0757:LIRERA>2.3.CO;2

Li, D., & Bou-Zeid, E. (2011). Coherent Structures and the Dissimilarity of Turbulent Transport of Momentum and Scalars in the Unstable Atmospheric Surface Layer. Boundary-Layer Meteorology, 140(2), 243–262. https://doi.org/10.1007/s10546-011-9613-5

Potter, B. E. (2012). Atmospheric interactions with wildland fire behaviour - II. Plume and vortex dynamics. International Journal of Wildland Fire, 21(7), 802. https://doi.org/10.1071/WF11129

Rizza, U., Miglietta, M. M., Degrazia, G. A., Acevedo, O. C., & Marques Filho, E. P. (2013). Sunset decay of the convective turbulence with Large-Eddy Simulation under realistic conditions. Physica A: Statistical Mechanics and Its Applications, 392(19), 4481–4490. https://doi.org/10.1016/j.physa.2013.05.009

Sullivan, A. L. (2017). Inside the Inferno: Fundamental Processes of Wildland Fire Behaviour: Part 2: Heat Transfer and Interactions. Current Forestry Reports, 3(2), 150–171. https://doi.org/10.1007/s40725-017-0058-z

Wallace, J. M. (2016). Quadrant Analysis in Turbulence Research: History and Evolution. Annual Review of Fluid Mechanics, 48(1), 131–158. https://doi.org/10.1146/annurev-fluid-122414-034550

Wyngaard, J. C., & Moeng, C.-H. (1992). Parameterizing turbulent diffusion through the joint probability density. Boundary-Layer Meteorology, 60(1–2), 1–13. https://doi.org/10.1007/BF00122059

Yates, D. N., Chen, F., LeMone, M. A., Qualls, R., Oncley, S. P., Grossman, R. L., & Brandes, E. A. (2001). A Cooperative Atmosphere–Surface Exchange Study (CASES) Dataset for Analyzing and Parameterizing the Effects of Land Surface Heterogeneity on Area-Averaged Surface Heat Fluxes. Journal of Applied Meteorology, 40(5), 921–937. https://doi.org/10.1175/1520-0450(2001)040<0921:ACASES>2.0.CO;2

Chapter 6: Wildfire Management and safety

A comparative study of the combustion dynamics and flame properties of dead forest fuels

Adel Sahila[1]; Hanane Boutchiche[1]; Domingos Xavier Viegas[2]; Luis Reis[2]; Nouredine Zekri*[1]

[1]Université des Sciences et de la Technologie d'Oran, LEPM BP 1505 El Mnaouer Oran, Algeria, {adel.sahila@univ-usto.dz}, {hananelimang@gmail.com}, {nzekri@yahoo.com}
[2] Association for the Development of Industrial Aerodynamics, Forest Fire Research Center, University of Coimbra, Portugal, {xavier.viegas, luis.reis}@dem.uc.pt

**Corresponding author*

Keywords

Forest fires, Flame height, Burning rate, Flame temperature, Air velocity profile.

Abstract

The combustion properties of several dead Mediterranean forest fuels were investigated experimentally. Samples of *straw*, *eucalyptus*, *shrubs*, and *Pinus Pinaster* with the same load were placed in cylindrical containers of the same size and were ignited from the perimeter of the container's bottom. A pitot tube and a thermocouple are placed one meter above the fuel surface to measure the airflow induced by the flame and the flame temperature. The main combustion parameters (mass-loss rate, flame height and temperature, and the induced air velocity) seem to evolve according to the same trend regardless of the fuel type. They increase rapidly in the growth phase of the flame then they decrease over a relatively long period characterizing the decay phase. In the crossover period between these two burning phases, the flame is fully developed with a maximum height and burning rate. The time required for the burning rate to attain its maximum value seems to vary only slightly with the fuel type. The maximum flame height and burning rate are found to be the largest for *shrubs* and the lowest for *straw*. The flame temperature and airflow are found to depend on the position in the flame with maximum values near the continuous zone of the flame.

1. Introduction

The increasing number of forest fires around the globe represents a major concern because it endangers seriously the ecosystem by affecting the flora, fauna, the environment, and even human life (Pausas et al. 2008; Vilén and Fernandes 2011). Therefore, a deeper understanding of the combustion dynamics of forest fuels and a better estimation of their combustion characteristics and their correlations are necessary. Many works were already devoted to examining the behavior of these parameters in the case of pool fires (Zabetakis and Burgess 1961; Tarifa 1967; Kung and Stavrianidis 1982; Babrauskas 1983; Koseki and Yumoto 1988; Koseki 1989; Klassen and Gore 1994; Chatris et al. 2001), fire whirls (Martin et al. 1976; Lei et al. 2011; Pinto et al. 2017), and natural fires (Thomas 1963; Dupuy et al. 2003; Sun et al. 2006; Weise et al. 2005).

In this work, an experimental study of the burning characteristics of several Mediterranean forest fuels is realized where the turbulent diffusion flame is subjected only to buoyancy forces. Samples of dead *shrubs*, *Pinus Pinaster*, *eucalyptus*, and *straw* are placed in cylindrical baskets of the same size and ignited to study the effect of the fuel type on fire behavior. The time evolution of the mass-loss rate, flame's height, temperature, and upward air velocity are examined during all the phases of fire development. A systematic comparison between the combustion characteristics and flame properties of these fuels is realized to study their correlations and their role in the flaming combustion behavior.

2. Experimental setup

The samples with the same fuel load (M_f) and initial height ($34\ cm$) are placed in cylindrical containers (with a fixed diameter $d_c = 0.5m$) made of a metallic grid and open on the top. Before each burning experiment, the fuel moisture content is estimated by using a moisture analyzer A&D MX-50 with a resolution of $0.01\ g$. The relative humidity of air and ambient temperature are measured by a thermo-hygrometer. A thermocouple and a Pitot tube are placed one meter above the fuel surface to determine the flame temperature and air velocity at this height respectively (see Fig.1).

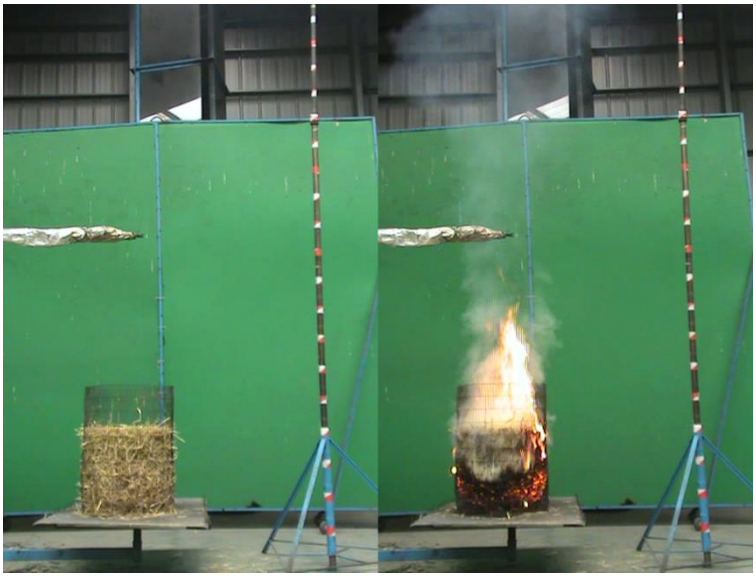

Figure 1. Experimental setup for a straw burning experiment at the Fire Lab of ADAI (Coimbra).

These samples are ignited from the perimeter of the container's bottom under free burning conditions. Three experiments were realized for each fuel to ensure the repeatability of the tests. Each experiment is recorded by an optical video camera Sony FDR-AX53 and a digital camera Canon EOS 550D. The videos are segmented into images by using a Video to JPG Converter software allowing the estimation of the flame heights during the entire duration of flaming combustion. A vertical scale was placed near the container to allow a proper scaling of the flame height values. A digital balance A&D HW-100KGL (10 g resolution) with a frequency of 1 Hz was used to measure the mass evolution of the fuels during their combustion, and its values are recorded on a computer by an RSKey v.1.40 software.

3. Results and discussion

The time evolution of the normalized fuel mass (M_f/M_0, M_0 being the initial mass of the fuel) is shown in Fig.2 for all the fuels considered. The fuel mass decreases towards an asymptotic minimal value M_{fmin}. These curves can be described by the following equation (Drysdal 2011):

$$\frac{\mathrm{d}M_f}{\mathrm{dt}} = -\mathrm{K(T)}.M_f \qquad (1)$$

Where K(T) obeys the Arrhenius law K(T) $\propto$ exp $(-E_A/\mathrm{RT})$. E_A is the activation energy (J/mol) and R the universal gas constant (8.314J /K.mol). This formula is very simple because it accounts only for the water evaporation accompanied by volatiles emission during the pyrolysis of the fuel. It does not take into consideration other mechanisms such as the scission and formation of molecules (David 1975). Equation (1) is also a relaxation equation that leads to an exponential relaxation if the temperature is constant. The curves shown in Fig.2 seem to exhibit two distinct relaxation regimes. For short times, the fuel mass relaxes very rapidly through time and characterizes the growth phase of the fire. Relaxation becomes anomalously slower during the decay phase of the flame (long times). The crossover between these two processes occurs when the flame is fully developed. Moreover, this tendency to equilibrium seems to depend on the fuel type, it is faster for *shrubs* than for *Pinus Pinaster* needles, *straw*, and *eucalyptus* leaves.

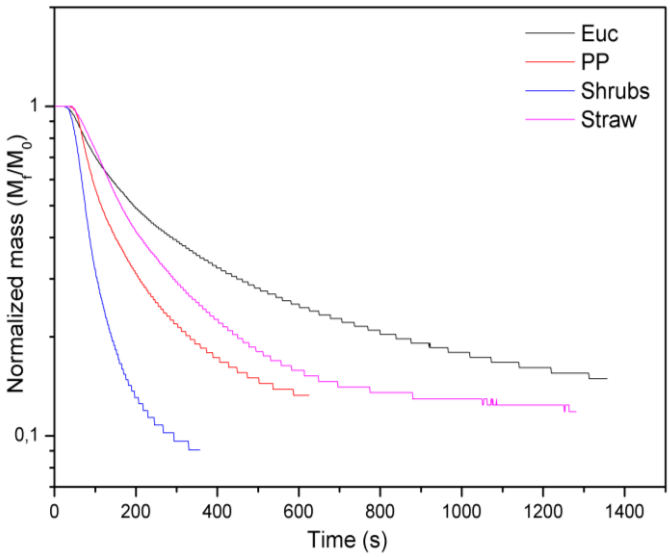

Figure 2. Temporal evolution of the normalized fuel mass for several dead forest fuels.

The mass-loss rate $\dot{M}_f$ is a measure of the rate at which the fuel is consumed, and is a key element to understanding the combustion dynamics. It is deducted from the balance data and its averaged values are estimated at regular intervals (five seconds). The results illustrated in Figs.3 show the same temporal trend for the mass-loss rate, the flame's height, temperature, and the flame-induced air velocity. Fire development is as follows: after ignition, the flame spreads vertically very rapidly along the lateral fuel surface, where a consistent flame begins to form accompanied by a horizontal spread of the flame through the upper surface of the fuel. Afterward, the growth phase begins where the mass loss rate, flame's height, temperature, and upward air velocity increase continuously and the fire uses the available combustible and oxygen to grow until it attains its peak. Then, the flame becomes fully developed and its height is maximum l_{max}. This is followed by a decay of the flame height and mass-loss rate over a relatively long period that characterizes the decay phase. As the thermocouple and pitot tube are placed at the same position to the initial fuel surface, the flame temperature and the vertical motion of gas particles are measured at different relative positions of the flame. Indeed, according to McCaffrey, the flame is subdivided into three regions (McCaffrey 1979):

- The continuous zone that begins at the fuel surface and where the velocity of gas particles increases with height ($v \propto \sqrt{z}$) and the temperature is constant ($T \propto z^0$).
- The intermittent region (the pulsating part of the flame that begins at the end of the first zone) where v is approximately invariant and the flame temperature decreases inversely with height ($T \propto z^{-1}$),
- The thermal plume (situated above the flame) where the gas velocity begins decreasing with height ($v \propto z^{-1/3}$) and the smoke temperature continues falling with height at a faster rate ($T \propto z^{-5/3}$)

Hence, the flame temperature and gas velocity reach their maximum values when the flame is fully developed because they are measured at the closest position to the continuous zone of the flame (see Fig.3a where $l_{max} > 1m$ is much higher than the thermocouple position for all the fuels studied). Since $l < 1m$ in the first part of the growth stage and the last part of the decay phase, the temperatures and velocities measured in these periods are those of the thermal plume and not the flame itself. Therefore, the convection coefficient, which is related to air velocity varies with the vertical position in the flame.

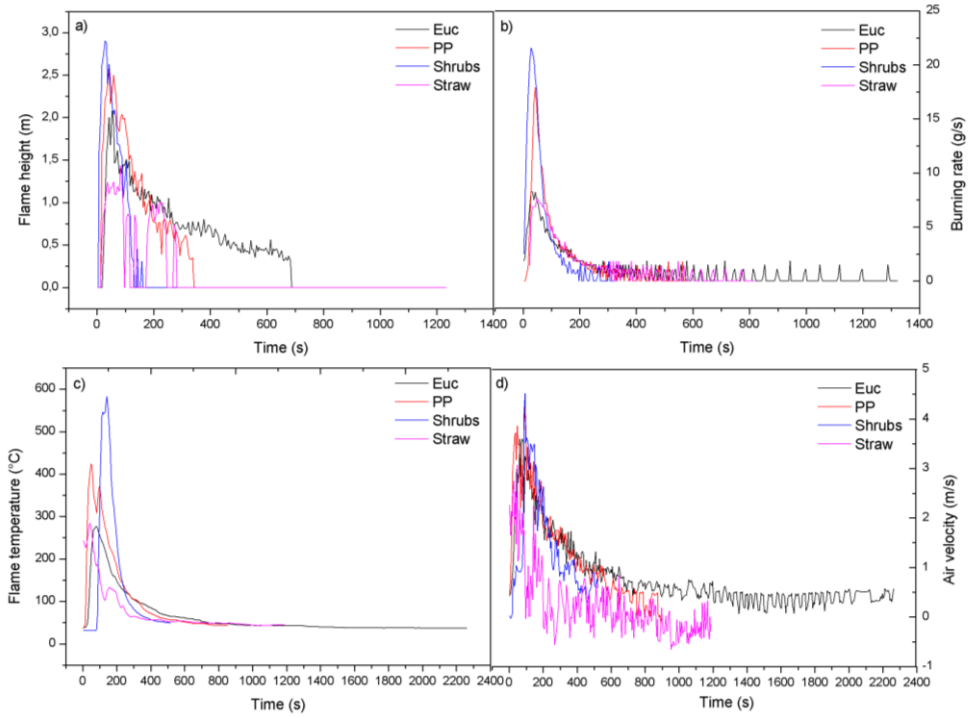

Figure 3. Temporal evolution of: a) flame height (m), b) mass loss rate (kg/s), c) flame temperature (°C), d) air velocity (m/s).

The time t_{max} required for the mass-loss rate to attain its maximum seems to be independent of the fuels $t_{max} = (32.5 \pm 10)$s.There is a time delay Δt between the time at which the burning rate is maximum ($\dot{M}_{fmax}$) and that at which the flame height is maximum (l_{max}). This delay has been found to depend linearly on the fuel moisture content (Sun et al. 2006). The moisture content may not be the only cause of delay since even for completely dried fuels, Δt would still not vanish because of the time required for gas molecules to diffuse through the porous fuel before contributing to the flame. In this work, the moisture content of the samples is around $8 - 10\%$ for all experiments, Δt seems to not change significantly (within statistical errors) for the dead fuels considered (besides a slight increase for straw) as shown in Table 1 where he maximal values of the flame's geometrical and physical characteristics are summarized. The maximum flame height and mass-loss rate are the largest for *shrubs* and the lowest for *straw*. This may be due to the heat flux absorption of the fuel which is related to its optical length, and thus to its packing ratio and surface-to-volume ratio. An extensive analysis of the heat transfer mechanism through the fuels considered is necessary.

Fuel type	Heat of Combustion (kJ/g) [13]	Maximum flame height (m)	Maximum mass loss rate (g/s)	Maximum temperature (°C)	Maximum air velocity (m/s)	Residence time (s)	Δt (s)
Eucalyptus	22.5	1.9 ± 0.3	10 ± 2	292 ± 30	3.9 ± 0.4	845 ± 260	7 ± 6
Pinus Pinaster	13.5	2.5 ± 0.3	18 ± 1	397 ± 19	4.2 ± 0.2	242 ± 83	8 ± 8
Shrubs	16.9	2.9 ± 0.1	24 ± 2	488 ± 78	4.9 ± 0.4	148 ± 35	13 ± 8
Straw	11.7	1.5 ± 0.3	7 ± 1	334 ± 34	3.3 ± 0.4	296 ± 67	25 ± 7

Table 1. Maximum values of some burning characteristics of various forest fuels.

The flaming combustion duration defines the residence time of the flame t_{res}. In Table 1, the maximum flame height (and maximum mass-loss rate) decreases as the residence time t_{res} increases for the fuels considered with a saturation tendency for *Eucalyptus* and *straw*. This is in qualitative agreement with the experimental results found in the case of fire whirls (Pinto et al. 2017). Note the very large residence time of *Eucalyptus*,

which is also characterized by a large heat of combustion. Therefore, the total heat released is much larger for *Eucalyptus* leaves despite their heat release rate being smaller than that of *Shrubs*.

4. Conclusion

An experimental study of the burning characteristics of several dead forest fuels was realized. Samples of dead *Eucalyptus, Pinus Pinaster, straw,* and *shrubs* with the same fuel load were placed in cylindrical baskets and ignited from the bottom. Time evolution of the combustion parameters was found to follow the same trend for all the fuels considered. In the growth phase of the flame, the fuel mass-loss rate, flame's height, temperature, and upward air velocity increase rapidly, then they decrease over a relatively long period characterizing the decay phase. The crossover between these two processes occurs when the flame is fully developed, and the time required for the burning rate to attain its maximal value was found to be the same for all the used fuels. The flame heights and mass loss rate are the largest for *shrubs* and lowest for *straw*. The flame temperature and air velocity seem to depend on the position in the flame, which implies that the heat transfer mechanism varies in the flame.

5. References

Babrauskas V (1983) Estimating large pool fire burning rates. *Fire Technology* **19**, 251-261. https://doi.org/10.1007/BF02380810

Chatris JM, Quintela J, Folch J, Planas E, Arnaldos J, Casal J (2001) Experimental study of burning rate in hydrocarbon pool fires. *Combustion and Flame* **126**, 1373-1383. https://doi.org/10.1016/S0010-2180(01)00262-0

David C (1975) Thermal degradation of polymers. In 'Comprehensive Chemical Kinetics'.

(Eds. Bamford CH, Tipper FH) pp. 1-173. (Elsevier: Amsterdam). https://doi.org/10.1016/S0069-8040(08)70333-9

Drysdale D (Ed) (2011) An Introduction to Fire Dynamics. (A John Wiley & Sons, Ltd).

Dupuy JL, Maréchal J, Morvan D (2003) Fires from a cylindrical forest fuel burner: combustion dynamics and flame properties. *Combustion and Flame* **135**, 65–76. https://doi.org/10.1016/S0010-2180(03)00147-0

Klassen ME, Gore JP (1994) Structure and Radiation Properties of Pool Fires. National Institute of Standards and Technology, Gaithersburg. Final Report, in NISTGCR, 94-651.

Koseki H, Yumoto T (1988) Air entrainment and thermal radiation from heptane pool fires. *Fire Technology* **24**, 33–47. https://doi.org/10.1007/BF01039639

Koseki H (1989) Combustion properties of large liquid pool fires. *Fire Technology* **25**, 241–255. https://doi.org/10.1007/BF01039781

Kung HC, Stavrianidis P (1982) Buoyant plumes of large-scale pool fires. *Symposium (International) on Combustion* **19**, 905–912. https://doi.org/10.1016/S0082-0784(82)80266-X

Lei J, Liu N, Zhang L, Chen H, Shu L, Chen P, Deng Z, Zhu J, Satoh K, De Ris JL (2011) Experimental research on combustion dynamics of medium-scale fire whirl. *Proceedings of the Combustion Institute* **33**, 2407–2415. https://doi:10.1016/j.proci.2010.06.009

Martin RE, Pendleton DW, Burgess W (1976) Effect of fire whirlwind formation on solid fuel burning rates. *Fire Technology* **12,** 33–40. https://doi.org/10.1007/BF02629468

McCaffrey BJ (1979) Purely Buoyant Diffusion Flames: Some Experimental Results. Center for Fire Research National Engineering Laboratory National Bureau of Standards Washington, D.C. NBSIR 79-1910, 20234.

Pausas JG, Llovet J, Rodrigo A, Vallejo R (2008) "Are wildfires a disaster in the Mediterranean basin? - A review". *International Journal of Wildland Fire* **17**, 713–723. https://doi.org/10.1071/WF07151

Pinto C, Viegas D, Almeida M, Raposo J (2017) Fire whirls in forest fires: An experimental analysis. *Fire Safety Journal* **87,** 37–48. http://dx.doi.org/10.1016/j.firesaf.2016.11.004

Sun L, Zhou X, Mahalingam S, Weise DR (2006) Comparison of burning characteristics of live and dead chaparral fuels. *Combustion and Flame* **144**, 349–359. https://doi:10.1016/j.combustflame.2005.08.008

Tarifa CS (1967) Open fires; Transport and combustion of firebrands. Instituto Nacional de Tecnica Aerospacial Esteban Teradas.

Thomas PH (1963) The size of flames from natural fires. *International Symposium on Combustion* **9**, 844-859. https://doi.org/10.1016/S0082-0784(63)80091-0

Vilén T, Fernandes PM (2011) Forest fires in Mediterranean countries: CO2 emissions and mitigation possibilities through prescribed burning. *Environmental Management* **48**, 558-567. https://doi.org/10.1007/s00267-011-9681-9

Weise DR, Fletcher T, Smith S, Mahalingam S, Zhou X and Sun L (2005), Correlation of mass loss rate and flame height for live fuels. In 'Proceedings of the Sixth Symposium',

(Fire and Forest Meteorology, Canada).

Zabetakis MG, Burgess DS (1961) Research on the Hazards Associated with the Production and Handling of Liquid Hydrogen. Bureau of Mines BM-RI-5707. https://doi.org/10.2172/5206437

A multimodal approach to understand and improve cognitive decision-making during firefighting

Ana Dionísio[#1]; Isabel Catarina Duarte[#1]; Rita Correia[1]; Joana Oliveira[1]; Marco Simões[1;2]; João Redondo[3]; Salomé Caldeira[3]; João Castelhano[1]; Miguel Castelo-Branco*[1]

[1]Coimbra Institute for Biomedical Imaging and Translational Research/Institute of Nuclear Sciences Applied to Health, University of Coimbra, Coimbra, Portugal, {adionisio@uc.pt, catarinaduarte86@gmail.com, ana.correia@icnas.uc.pt, jfoliveira@icnas.uc.pt, msimoes@dei.uc.pt, joaocastelhano@uc.pt, mcbranco@fmed.uc.pt}
[2]Centre for Informatics and Systems, University of Coimbra, Coimbra, Portugal {msimoes@dei.uc.pt}
[3]Department of Psychiatry, Coimbra Hospital and University Centre, Coimbra, Portugal, {armejoao@gmail.com, mscaldeira@gmail.com}

**Corresponding author*
[#]AD and ICD contributed equally to this work

Keywords

Decision-making; Stress; Training; Biosignals; fMRI

Abstract

Day-to-day we have to make choices. When it comes to critical decisions which may lead to impactful and irreversible consequences, the understanding of the decision-making process is highly relevant but scarcely explored. In the present project, we aim to understand decision-making in the context of firefighting and to study how neurocognitive control and stress management strategies affect decision-making, while also addressing coping responses.

We present here the preliminary results from a cohort of 13 firefighters. We used a functional magnetic resonance brain imaging coupled with biosensors while firefighters played a dilemmatic decision-making task of structural firefighting.

We found brain regions, including the ventromedial and dorsolateral prefrontal cortices and angular gyrus, showing a parametric pattern of activation during the decision phase, i.e. the lower the risk of house collapsing, the higher the neural activity in these areas. This suggests that these regions are processing that risk information and signalling the chances of being successful in the rescue phase. We also found that the power in high frequencies of the pulse rate variability was higher when they decided to enter for the rescue. It is suggestive that deciding not to enter for rescue causes an increase in arousal, which may be related to the expectation about the victims' survival. Concerning coping strategies, we found that active coping used in personal context was significantly correlated with the age and the years of experience of firefighters.

We aim to understand if this pattern of brain activity reflects the coping strategies and if, in turn, it is reflected in the physiological signals we measure. Our results provide here preliminary evidence for a role of specific brain regions in decision-making under critical conditions, with concurrent physiological responses. In the future, we will investigate whether the decision processes in firefighters are different from non-firefighters, and we will address if post-traumatic stress disorder impairs decision-making in this context. Biosignals will also be used in a second phase of the project to inform virtual reality training systems. This may help developing optimal neurocognitive control and better coping strategies to deal with stress.

1. Background

Decision-making implicates making choices based on the balance between associated risks and possible rewards(Shad et al.,2011). This higher order cognition skill involves a complex set of processes that includes different steps of building preferences, choosing behaviours, performing actions and evaluating the outcomes(Ernst&Paulus,2005).

Previous research from our group has pointed out the importance of optimising decision-making and controlling emotions effectively during intensely stressful experiences(Almeida et al.,2015;Banca et al.,2015). This holds particular pertinence in the context of firefighting, wherein poor decisions can bring devastating consequences.

Studies on decision-making during firefighting are scarce despite their potential relevance, mainly in which concerns optimal neurocognitive control and stress management. While some manage to properly deal with these experiences, others adopt maladaptive responses and are at a high risk of developing stress-related disorders and other complications(Sindhu et al.,2020). Dysfunctional coping patterns of response are associated with higher levels of stress and trauma(Fonseca et al.,2020;Skeffington et al.,2017).

Stressful events that are perceived as potential threats can trigger not only emotional but also physiological responses that can be measured by biosensors and functional magnetic resonance imaging (fMRI, an approach that measures in an indirect way the neural activity)(Lee et al.,2022).

It is our goal to study decision-making and stress responses under extreme scenarios of uncertainty in firefighting. We developed a dilemmatic task in the context of strategic decisions considering fire management/victim rescue and self-protection, involving decisions that encompass rational reasoning, risk perception and emotional control. We therefore used fMRI to investigate the neural correlates underlying the decision process and error monitoring in firefighting. Further, we coupled biosensors to measure physiological stress aiming at understanding how different variables influence physiological responses and how they relate with the emotional perception of the firefighter.

We hypothesize that the process of decision in firefighters is associated with specific brain activation patterns and with changes in biophysiological responses to stress, including in pulse rate variability. A further question of our interest is the firefighters' use of coping responses to better understand their resource availability, the level of risk and protection, and the main strategies adopted by these professionals in unpredicted critical scenarios in which immediate decisions and prompt actions are needed.

Here, we provide some preliminary data of our ongoing Project.

2. Methods

This study was approved by the Ethics Committees of the Faculty of Medicine of the University of Coimbra, of the Coimbra Hospital and University Center (CHUC) and of the Regional Health Administration (ARS Centro), and was conducted according with the Declaration of Helsinki. All subjects gave written informed consent.

2.1 Sample characterization

We included a total of 13 right-handed(Espírito-Santo et al.,2017) firefighters (10 males, 3 females), with a mean age of 35.92±9.16 years. Inclusion criteria comprised (1) age between 18 and 75 years and (2) active participation in firefighting. We excluded participants with (1) diagnosed neurological or psychiatric disease, (2) visual or auditory impairments that compromised tasks performance, (3) substance (drugs or alcohol) dependence and (4) contraindications to magnetic resonance imaging. None of the participants reached the cut-off in the Portuguese version of PTSD Checklist for DSM-5 [PCL-5;(Ferreira et al.,2016a)], based on events (identified using Ferreira et al.,2016b;Maia et al.,2016) which ruled out the presence of post-traumatic stress disorder (PTSD). Nine firefighters were volunteer workers and four were professionals, ranging in years of experience from two to 34 years as a firefighter. Our sample worked a mean of 25.15 weekly hours in firefighting activity (ranged from six to 52 hours).

2.2 Coping strategies

The Portuguese version of Brief Coping Orientations to Problems Experienced Inventory [Brief-COPE;(Pais Ribeiro&Rodrigues,2004)] was applied to address dispositional coping strategies to stressful events and problems that occurred, separately, in personal life and during firefighting activity. Scores were obtained with a 4-point Likert scale, ranging from 0 to 3 points in each item, corresponding to lower or higher frequency of actions. In this work, we sought to analyze three distinct coping strategies (subscales Active, Planning and Behavioral disengagement) and three patterns of coping styles [Problem-focused, Emotion-focused and Dysfunctional (Cooper et al.,2008)].

2.3 Functional imaging and biosignals

Magnetic resonance imaging was performed on a 3T Siemens MAGNETOM Prisma Fit scanner (Siemens, Erlangen), equipped with a 64-channel birdcage head coil. Structural images of the brain were obtained with

the Magnetization-Prepared two Rapid Gradient Echo (MP2RAGE) sequence [voxel size=1×1×1mm3; FOV (field-of-view)=256×256mm2; 192 slices]. We acquired three fMRI runs using a multi-band accelerated echo planar imaging (MB-EPI) sequence [multi-band acceleration factor 6; phase encoding: anterior-posterior; TR=1000ms; TE=37ms; FA=68°; voxel size=2×2×2mm3; FOV=200×200mm2; 72 axial slices].

During fMRI, participants were performing a decision-making task following an experimental paradigm with mixed block event-related design [as in Banca et al.(2015)]. An initial scenario (Fig.1) was presented with a burning house, indicating the number of people that were inside the house [1 adult or 1 family], the risk (%) of the house to collapse and the probability (%) of victims saving themselves without external help. Firefighters had to decide, based on these data, if they would enter to try saving the victims, knowing that if unsuccessful, they could also "die". After each decision, the outcome was presented showing what happened to the victims, the firefighter and the house. The stimuli were presented on an LCD monitor and participants selected responses with a Hybridmojo MR-compatible joystick. This was repeated for 20 trials in each of the 3 runs.

Figure 1- Initial scenario of the fMRI trials.

Pulse Rate Variability (PRV) was computed from the blood volume photoplethysmography (PPG) recordings acquired through the Physiological Measurement Unit (PMU) of the MRI scanner with a sampling rate of 400Hz. To reduce noise contamination, the PPG signal was bandpass filtered using a 6^{th} order Butterworth filter with a lower and higher cut-off frequencies of 0.5Hz and 20Hz. The clean PPG signal was then used to compute the PRV by first identifying the PPG pulse peaks, computing the interbeat intervals (IBI), and using a cubic spline interpolation to obtain a uniformly sampled time series with a new sampling frequency of 4Hz. The PRV from each run was then divided into 8s segments, comprising the entry/no entry decision block of the task, and the relative power in the High Frequency (HF) band (0.15–0.4Hz) of the PRV was extracted as a marker for each of the segments using the Fast Fourier Transform algorithm.

2.4 Data analysis

A significance level of 0.05 was adopted in all statistical tests. We did not correct for multiple comparisons due to the preliminary and exploratory nature of these analyses.

Statistical analyses were performed using the IBM SPSS statistics software (v.27). The sociodemographic variables were explored through descriptive analyses. We used Wilcoxon test to investigate within-group differences in coping strategies in life versus firefighting contexts. The correlations between age, years of firefighter activities and workload (hours per week) and coping strategies (used in both personal and firefighting activity contexts) were analysed with Kendall rank correlation coefficient.

FMRI data analyses were fully conducted in the BrainVoyager 22.0 software (Brain Innovation, Maastricht, the Netherlands). We applied pre-processing steps (slices-scan time correction, 3D head-motion correction, temporal high-pass filtering and geometrical distortions correction) and normalized the data to Montreal Neurological Institute (MNI) space. We performed General Linear Model (GLM) analysis for obtaining whole-brain statistical maps at the group level (cluster threshold=20 voxels).

PRV data were analyzed in Matlab (R2021a, MathWorks, USA). Observations were split into enter or not enter, and the balance of the sample sizes was obtained through random elimination of samples belonging to the bigger group. The two conditions were tested against each other using the Wilcoxon signed-rank test.

3. Results and Discussion

We started by evaluating whether the coping style was different comparing firefighters' strategies used in personal contexts and during the activity as a firefighter and found no significant differences ($p>0.05$, $n=12$). Active coping strategies used in personal context were significantly correlated with age ($\tau=0.568$; $p=0.016$, $n=12$) and years of experience as firefighters ($\tau=0.493$; $p=0.034$, $n=12$) (Fig.2). Active coping involves the ability to take active actions to suppress the stressor or to minimize or remediate these effects(Carver et al.,1989). We suggest that older individuals accumulated learning to improve mechanisms of adaptive coping to deal with stress, using active coping as a dispositional tendency in their lives. Concerning coping strategies related to firefighting activity, we did not find any correlation with age or years of firefighting ($p>0.05$). Firefighters are trained to take immediate actions and decisions early in their activities. We hypothesize this growth ability may be transposed to personal events later in life. Also, existing literature suggests the protective effect of resilience in firefighters and experience of personal growth following stress-related events(Sattler et al.,2014).

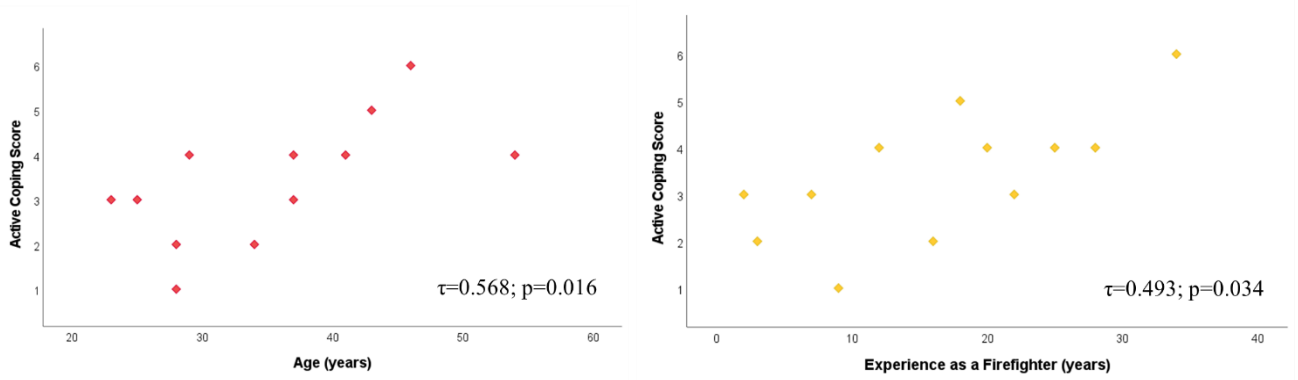

Figure 2- Correlations between active coping score and age (left) and years of experience in firefighting (right).

We studied, with an fMRI task, which brain regions are involved in the decision-making process under the context of firefighting. In Fig. 3 we present brain activity patterns during the decision phase. A parametric analysis showed that the lower the probability of the house collapsing, the higher the activity in the ventromedial prefrontal cortex (vmPFC) ($p<0.05$). We suggest that the activation of vmPFC was related to risk perception, given its association with valuation and risk assessment(Spaniol et al.,2019). The right dorsolateral prefrontal cortex (dlPFC) also showed a significantly greater activation for more favorable probabilities ($p<0.05$), which might possibly be explained by greater risk-taking behavior that was found in the literature to be associated with an increase in the activity of dlPFC(Leota et al.,2021). A role of angular gyrus (AG) in both decision-making, visuospatial attention(Studer et al.,2014) and number processing(Seghier,2013) has been recognized. In this work, the right AG was significantly more active when the risk was smaller ($p<0.05$). We hypothesize that when firefighters have more chances of being successful, they spend more efforts in deciding if they will take the risk.

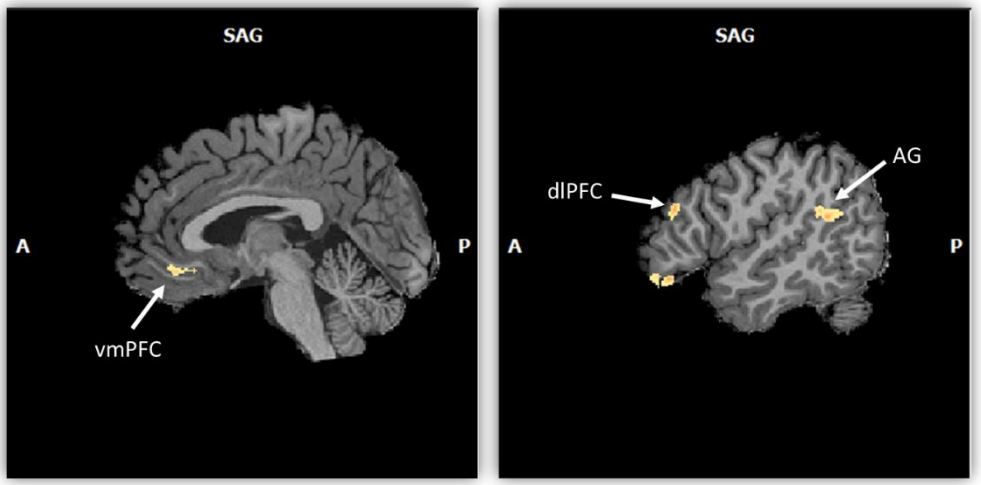

Figure 3- FMRI images showing brain parametric activation associated with lower probability of house collapsing (p<0.05).

The preliminary analysis of the PRV of the participating group of firefighters revealed a significant higher value for the relative power in the HF band of the PRV for the entry decision (median=0.38) compared to the no entry decision (median=0.35), Z=2.59, p<0.01. The distribution of values for this marker for both conditions is represented in Fig. 4.

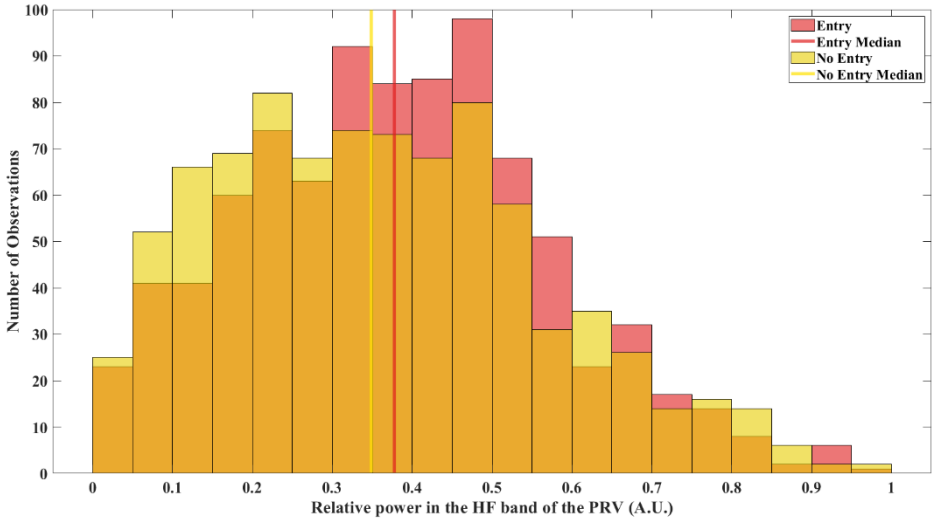

Figure 4- Distribution of values for the relative power in the HF band of the PRV for the entry decision (in red) and no entry decision (in yellow) (p<0.01).

States of stress and anxiety seem to be accompanied by a decrease in HF power(Shaffer&Ginsberg,2017). The lower values found for the HF marker for the no entry decision hint at a decrease in parasympathetic activation and are potentially related to an increase in physiological arousal. A possible interpretation is that choosing not to endanger his/her own life causes a greater expectation in the firefighter to know whether the victims survived or not. Another interpretation, falling in line with Fooken and Schaffner's(2016) suggestion, is that risk aversion in dilemmatic situations is associated with higher arousal, while risk-taking is accompanied by moderate physiological responses. This could suggest that less emotionally involved individuals are prone to taking more risks when confronted with a dilemma.

These results may have potential implications for understanding critical decision processes in firefighters, more directly in structural firefighting contexts. Our findings encourage future works addressing decision-making in different scenarios, such as wildland firefighting.

4. Conclusions

Our results support the relevance of studying decision-making in extreme conditions such as firefighting, from a multimodal approach. These preliminary data suggest an involvement of specific frontal brain regions, that can also be translated into physiological stress and coping strategies. In a future work, we will investigate whether decision processes in firefighters are different from the global community and address if post-traumatic stress disorder impairs effective decision-making. Biosignals will also be used in a second phase of the project to inform virtual reality training systems about the physiological state of the firefighter during firefighting simulation.

5. Funding

This work was funded by the Foundation for Science and Technology (projects PCIF/SSO/0082/2018 and FCT/UIDP/2020).

6. References

Almeida, I., Soares, S. C., CasteloBranco, M. (2015). The Distinct Role of the Amygdala, Superior Colliculus and Pulvinar in Processing of Central and Peripheral Snakes. PLoS ONE. 10(6):e0129949. https://doi.org/10.1371/journal.pone.0129949

Banca, P., Vestergaard, M. D., Rankov, V., Baek, K., Mitchell, S., Lapa, T., Castelo-Branco, M., Voon, V. (2015). Evidence Accumulation in Obsessive-Compulsive Disorder: the Role of Uncertainty and Monetary Reward on Perceptual Decision-Making Thresholds. Neuropsychopharmacology, 40(5), 1192–1202. https://doi.org/10.1038/npp.2014.303

Carver, C. S., Scheier, M. F., Weintraub, J. K. (1989). Assessing coping strategies: A theoretically based approach. Journal of Personality and Social Psychology, 56(2), 267-283. https://doi.org/10.1037/0022-3514.56.2.267

Cooper, C., Katona, C., Livingston, G. (2008). Validity and reliability of the Brief COPE in carers of people with dementia: the LASER-AD Study. The Journal of Nervous and Mental Disease, 196(11), 838–843. https://doi.org/10.1097/NMD.0b013e31818b504c

Ernst, M., Paulus, M. P. (2005). Neurobiology of decision making: a selective review from a neurocognitive and clinical perspective. Biological Psychiatry, 58, 597–604.https://doi.org/10.1016/J.BIOPSYCH.2005.06.004

Espírito-Santo, H., Pires, C. F., Garcia, I. Q., Daniel, F., Silva, A. G., Fazio, R. L. (2017) Preliminary validation of the Portuguese Edinburgh Handedness Inventory in an adult sample. Applied Neuropsychology Adult, 24(3), 275-287. https://doi.org/10.1080/23279095.2017.1290636 [Portuguese version]. Original version: Oldfield, R. C. (1971). The assessment and analysis of handedness: The Edinburgh Inventory. Neuropsychologia, 9(1), 97–113. https://doi.org/10.1016/0028-3932(71)90067-4

Ferreira, R., Ribeiro, L., Santos, P., Maia, A. (2016a). The PTSD Checklist for DSM-5 (PCL-5) Portuguese version [Portuguese version]. Original version: Weathers, F.W., Litz, B.T., Keane, T.M., Palmieri, P.A., Marx, B.P., Schnurr, P.P. (2013). The PTSD Checklist for DSM-5 (PCL-5). Scale available from the National Center for PTSD at www.ptsd.va.gov.

Ferreira, R., Ribeiro, L., Santos, P., Maia, A. (2016b). The Life Events Checklist for DSM-5 (LEC-5) Portuguese version [Portuguese version]. Original version: Weathers, F.W., Blake, D.D., Schnurr, P.P., Kaloupek, D.G., Marx, B.P., Keane, T.M. (2013). The Life Events Checklist for DSM-5 (LEC-5). Instrument available from the National Center for PTSD at www.ptsd.va.gov

Fonseca, S. M., Cunha, S., Campos, R., Queirós, C. (2020). Stress e trauma na emergência médica pré-hospitalar: Coping disfuncional como mediador. Psicologia, Saúde & Doenças, 21(1), 176-182. http://dx.doi.org/10.15309/20psd210126

Fooken, J., Schaffner, M. (2016). The role of psychological and physiological factors in decision making under risk and in a dilemma. Frontiers in Behavioral Neuroscience, 10:2, 1–10. https://doi.org/10.3389/fnbeh.2016.00002

Lee, D., Lee, J.E., Lee, J., Kim, C., Jung, Y-C. (2022) Insular activation and functional connectivity in firefighters with post-traumatic stress disorder. BJPsych open, 8(2):e69. https://doi.org/10.1192/bjo.2022.32

Leota, J., Kleinert, T., Tran, A., Nash, K. (2021). Neural signatures of heterogeneity in risk-taking and strategic consistency. European Journal of Neuroscience, 54(9), 7214–7230.https://doi.org/10.1111/EJN.15476

Maia, A., Carvalho, Lopes, R. (2016). Questionário de Exposição e Perturbação dos Acontecimentos Traumáticos (QEPAT)

Pais Ribeiro, J. L., Rodrigues, A. P. (2004). Questões acerca do coping: A propósito do estudo de adaptação do Brief Cope. Psicologia, Saúde & Doenças, 5(1), 3-15 [Portuguese version]. Original version: Carver, C. S. (1997). You want to measure coping but your protocol's too long: Consider the Brief COPE. International Journal of Behavioral Medicine, 4(1), 92–100. https://doi.org/10.1207/s15327558ijbm0401_6

Sattler, D. N., Boyd, B., Kirsch, J. (2014). Trauma-exposed firefighters: relationships among posttraumatic growth, posttraumatic stress, resource availability, coping and critical incident stress debriefing experience. Stress and Health, 30(5), 356–365. https://doi.org/10.1002/smi.2608

Seghier, M. L. (2013). The angular gyrus: multiple functions and multiple subdivisions. The Neuroscientist, 19(1), 43–61. https://doi.org/10.1177/1073858412440596

Shad, M. U., Bidesi, A. P., Chen, L., Ernst, M., Rao, U. (2011). Neurobiology of decision making in depressed adolescents: a functional magnetic resonance imaging study. Journal of the American Academy of Child & Adolescent Psychiatry, 50(6), 612-621. https://doi.org/10.1016/J.JAAC.2011.03.011

Shaffer, F., Ginsberg, J. P. (2017). An Overview of Heart Rate Variability Metrics and Norms. Frontiers in Public Health, 5:258, 1–17. https://doi.org/10.3389/fpubh.2017.00258

Sindhu, B., Banerjee, P., Sindhu, N., Navya, N., Ola, M. (2020). Mental health issues of fire personnel: An exploratory study. Journal of Psychology and Clinical Psychiatry, 11(1), 1-5.

Skeffington, P. M., Rees, C. S., Mazzucchelli, T. (2017). Trauma exposure and post-traumatic stress disorder within fire and emergency services in Western Australia. Australian Journal of Psychology, 69(1), 20-28. https://doi.org/10.1111/ajpy.12120

Spaniol, J., Di Muro, F., Ciaramelli, E. (2019). Differential impact of ventromedial prefrontal cortex damage on "hot" and "cold" decisions under risk. Cognitive, Affective & Behavioral Neuroscience, 19(3), 477–489. https://doi.org/10.3758/S13415-018-00680-1

Studer, B., Cen, D., Walsh, V. (2014). The angular gyrus and visuospatial attention in decision-making under risk. NeuroImage, 103, 75–80. https://doi.org/10.1016/J.NEUROIMAGE.2014.09.003

A study of fire and plume dynamics for static pool fires and their interaction with vegetation

Navya Muniraj; Weixuan Gong; Muthu Kumaran Selvaraj; Albert Simeoni*

Worcester Polytechnic Institute, Worcester, Massachusetts 01609, USA,
{nmuniraj, wgong, mselvaraj, asimeoni}@wpi.edu

**Corresponding author*

Keywords

Pool fire, Fire Plume, Vegetation, Prescribed burns

Abstract

Prescribed burns are an essential tool of fire management to reduce the impact and occurrence of wildfires. While managing prescribed burns, the smoke trajectory and downwind exposure to smoke are intimately coupled with the smoke production dynamics and the development of the fire plume in the vicinity of the fire front. In turn, the fire plume development is strongly coupled to fire behavior and the flow environment near the fire. This work aims at understanding fire behavior and plume development while interacting with vegetation at the large laboratory scale through experiments and modeling. In order to investigate these coupled processes, initially, flame and plume behavior from a static fire source was characterized. A rectangular pool fire fueled by diesel was used and point measurements of flow, temperature, and heat flux have been recorded. The mass burning rate was measured using a load cell. K-type thermocouples and bi-directional pressure probes have been used for measuring the velocity and temperature, respectively in the flame and plume zones. These data are used for validating a numerical model, the Fire Dynamics Simulator (FDS), for simulating pool fires and the model is subsequently used for predicting the plume interaction with vegetation. A Douglas fir tree, whose properties are well defined in literature, was used as vegetation. The Lagrangian particle model available in FDS was used to model the tree, which was represented with regular shape and size. It had foliage and different classes of wood split based on typical size (diameter) range. The bulk density of the tree was varied to replicate the systematic and controlled variation of the flow obstruction encountered by the plume and to provide realistic predictions of velocity, temperature, and heat flux within the vegetation. In the future, experiments with vegetation located in the plume region will be conducted to validate the numerical predictions.

1. Introduction

Prescribed burns are one of the commonly used fire management tools to reduce the impact and occurrence of wildfires. During prescribed burns, the fire and plume generated from the combustion of the surface fuel (such as pine needles) interacts with the raised vegetation. The fire and plume behavior are influenced by the non-burning raised vegetation through drag and heat transfer and they also have an impact on the raised vegetation when heating it. Similarly, the variability in vegetation also affects the flow, fire, and plume dynamics. In order to analyze such complex phenomena, the fire, which is the source of the plume, must be well characterized. Pool fires were chosen for study as they mimic the fire environment in prescribed burns and are relatively easy to control, while avoiding additional complexities due to fire spread. Generating a volume of smoke at the laboratory scale that is relevant to the field scale requires the use of medium and large-scale pool fires. Several works have been reported earlier on small scale pool fires (Prasad et al., 1999; Attar et al., 2013; Wu et al., 2020), which are typically less than 0.3 m in diameter. However, only limited research has been conducted on medium and large-scale pool fires (Wen et al., 2007; Sudheer et al., 2013; Xin et al., 2005; Wahlqvist et al., 2016; Stewart et al., 2021). These fires fall either in the transition or turbulent regime and are dominated by radiative heat transfer. Wen et al. (2007) conducted experimental and numerical study on medium-scale methanol pool fires. Temperature and velocity measurements were used to validate a numerical model available in FDS. (Sudheer et al., 2013) analyzed the temperature distribution and emissivity of gasoline pool fires with varying pool diameters (0.3 - 1 m). FDS was able to accurately predict the centerline temperature distribution and heat flux measurements for all the cases. Wahlqvist & van Hees (2016) used FDS to predict the mass loss rate of heptane pool fires with the inclusion of heat feedback from external sources, such as walls, and the oxygen concentration near the pool. Stewart et al. (2021) numerically investigated the ability of FDS to predict

medium and large-scale open pool fires of several hydrocarbon fuels including gasoline and diesel. Results showed that FDS predicted the three-step transient burning pattern of: fire growth, quasi-steady burning, and extinction, as observed in the experiments. However, for higher order hydrocarbon fuels such as diesel, when the pan is fully covered with flame, the model overpredicted the burning rate.

It is clear that there is a significant gap in reporting the flame characteristics and dynamics of medium and large-scale pool fires. The transient nature of the flame affects the plume dynamics, entrainment, and mass burning rate. Therefore, it is essential to characterize the pool fires before investigating their interaction with vegetation. Furthermore, the interaction of vegetation with the plume and its impact on the fire environment have not been investigated yet. In this work, point measurements of flow, temperature, and heat flux at various locations in the plume and flame zones were carried out to validate a numerical model for predicting the dynamics of the flame and buoyant plume over a static pool fire. The validated model was then used with raised vegetation to analyze its influence on flow and plume dynamics relevant to a prescribed burn scenario.

2. Experimental methodology

A rectangular pan having a dimension of 68 cm × 63 cm × 6.3 cm was used to generate a diesel pool fire. Diesel flames are highly sooty, and it facilitates the visualization of plume during its interaction with the raised vegetation in the lab and field scale experiments. The rectangular shape has been chosen to allow creating larger fires in the future, by attaching multiple pans together. Figure 1 presents a schematic of the experimental setup. The pan was filled with 2 gallons (7.56 liters) of fuel to provide a steady burning time of 8 to 9 min. The pan was placed over a load cell with an accuracy of 0.1 g for measuring the mass loss rate of the burning fuel. K-type thermocouple with a bead diameter of 0.5 mm were used for measuring the temperature in the flame and plume zones. Velocity measurements were carried out using bi-directional pressure probe. Heat flux sensors (both convective and radiative) were used for measuring the convective and radiative heat flux from the flame. The center of the pool surface was taken as origin. The thermocouples and bi-directional pressure probes were located along the vertical direction (z-axis) 0.5 m from the pool surface and in arrays up to 3.5 m (see Fig. 1.a), while the heat flux sensors were located at 1, 2 and 3 m from the fuel surface and were offset by 1 m in the y-direction (not shown on Fig. 1.a). In the horizontal plane (x-axis), four arrays of thermocouples (a total of seven thermocouples spaced by 15 cm in each array) were fixed at heights of 1, 2, 3, and 3.5 m from the pool surface. Similarly, two bi-directional pressure probes were located on each horizontal plane (8 in total) spaced 15 cm apart from either side of the central probe. Since the boiling point of diesel quite high, a small amount (100 ml) of gasoline was added to the pool prior to ignition in order to facilitate the process. The pool ignited within two seconds when using a propane torch. Figure 1.b shows a flame photographed during the steady burning regime.

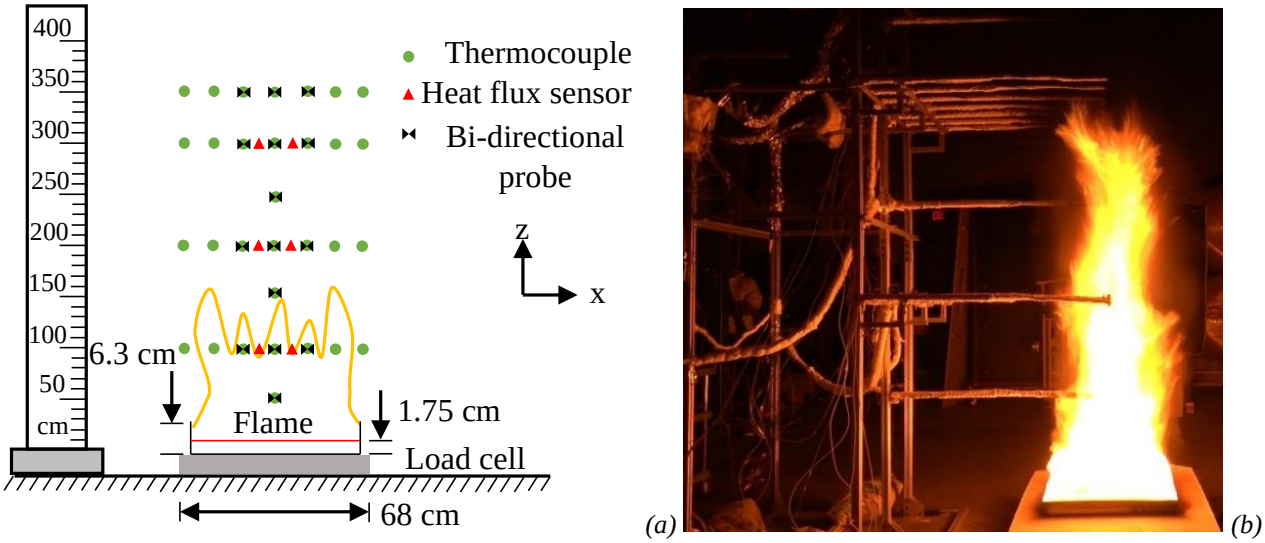

Figure 1- (a) Schematic of the experimental setup (b) flame photograph during steady state burning

3. Numerical approach

3.1. Computational domain

Numerical simulations were carried out using Fire Dynamics Simulator (FDS v6.7.7). Figure 2 shows a schematic of the computational domain used in the simulations. The dimensions of the domain were 6 m × 6 m × 8 m. The bottom boundary was taken as an adiabatic wall. All other boundaries were open to atmosphere. In case of a reverse flow, ambient air (O_2 - N_2: 23.3% - 76.7%, by mass) at a temperature of 20ºC entered the domain through the open boundaries. Dodecane, a surrogate of diesel was used as the fuel. The properties of diesel, adapted from Stewart et al., (2021) were used in the simulations. For simulations with vegetation (Fig. 2.b), the geometrical and thermo-physical properties of Douglas fir tree reported in Mell et al. (2009) were used. The domain was split into several multi-block meshes with uniform grid spacing in the z-direction (within each block). The total number of cells in the domain was around 2.8 million. Numerically, the pool was ignited by giving a constant heat flux of 300 kW/m^2 at the fuel surface to replicate the ignition time observed in the experiments. With this heat flux value, the pool ignited within 3 s.

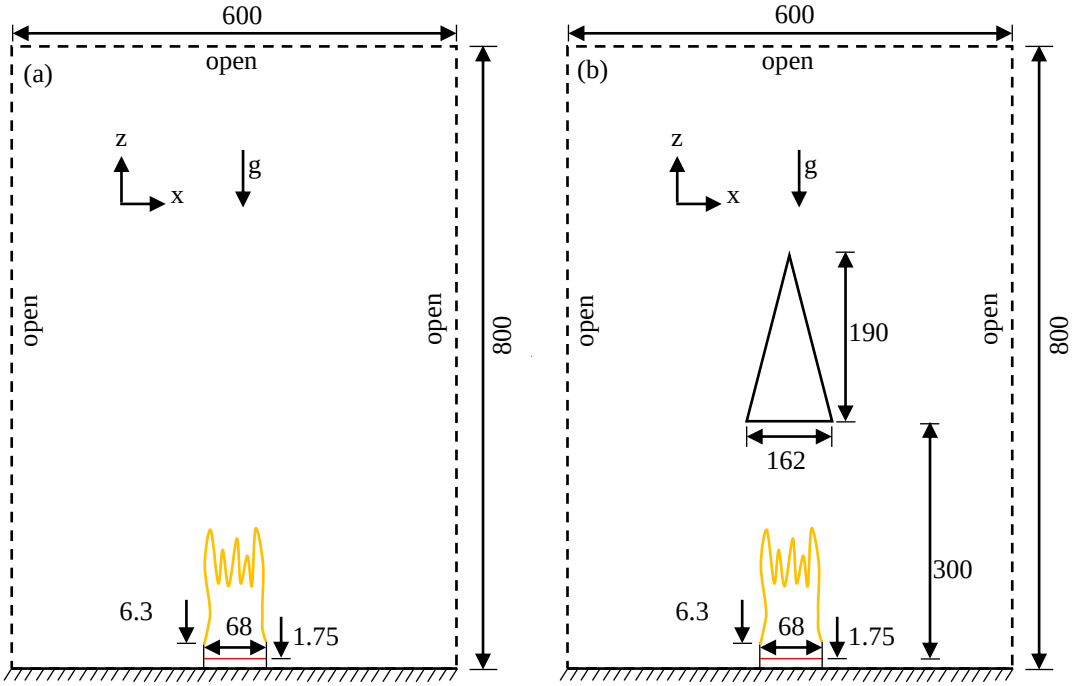

Figure 2- Schematic of the computational domain with (a) a diesel pool fire and (b) a Douglas fir tree located above the pool fire (the trunk was not represented) – Dimensions are in cm

4. Results and Discussion

Figure 3 presents the comparison of the predicted mass loss rate and temperature profiles with the experimental values, along the centerline at different heights above the fuel surface. In the experiments, first gasoline at the surface of the pool ignites and preheats the diesel pool to the boiling temperature. The flame height is low during this stage and the experimental mass burning rate (Fig. 3.a) gradually increases to an average steady state value of around 0.011 kg/s. It takes around 60 s to achieve steady state burning from the start of ignition (t = 0 s) and the average mass burning rate remains constant at 0.011 kg/s during the steady burning regime. It lasts from t = 60 s to t = 580 s, for around 9 min. The burning rate then decreases and the flame extinguishes 2 min after the end of the steady burning regime.

In the simulations, the pool is ignited 3 s after ignition and the mass burning rate quickly reaches steady state (average around 0.0115 kg/s). Then, it slowly increases to 0.013 kg/s with a further increase in time (300 s). After t=300 s, the burning rate rapidly increases to 0.02 kg/s and then steeply decreases until flame extinction. The difference between the experimental and predicted mass burning rate is due to (1) the difference in the ignition process, (2) the difference in fuel properties used in the experiments and in the model (as reported in Stewart et al., 2021), (3) the neglection of internal convection within the pool in the model, while it can be quite

significant in this case because of the adiabatic boundary. The model underpredicts the temperature profiles at z = 0.5 m, however, the experimental trend is captured (see Fig. 3.b). The model accurately predicts the temperature in the flame zone (z = 1 m) and overpredicts it in the intermittent (z = 1.5 m), and plume zones (z = 2.0 and 3.5 m).

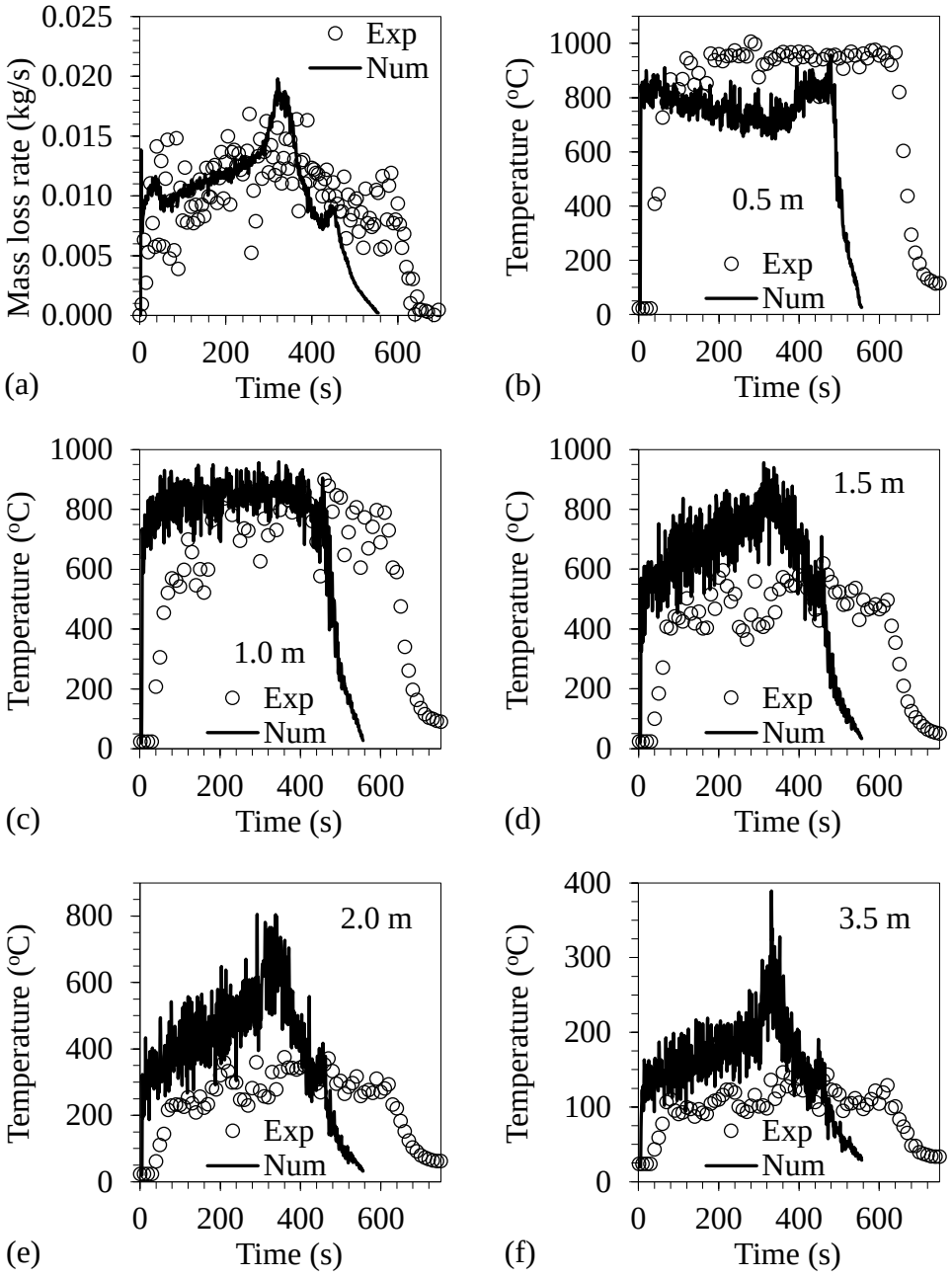

Figure 3- Comparison of predicted (a) mass loss rate and temperature profiles at (b) z=0.5 m, (c) z=1.0 m, (d) z=1.5 m, (e) z=2.0 m, (f) z=3.5 m to experimental data

Figures 4.a and 4.b show the comparison of temperature and water vapor mass fraction contours for cases with pool fire and pool fire with tree. The contours are plotted at 200 s after the start of simulation. The temperature in the flame zone is almost the same in both cases. However, there is a significant difference in the plume temperature above 2.5 m. For the case without tree, the plume temperature reduces to 100ºC - 150ºC above 4 m due to air entrainment and diffusion. On the other hand, for the case with tree, the temperature within the tree is around 250ºC – 350ºC. This results in moisture evaporation (and subsequent pyrolysis of vegetation) as indicated by higher values of water vapor mass fraction contours within the tree (0.02). Figures 4.c and 4.d show the velocity vectors and contours of dodecane and the oxygen mass fraction for these cases. The air entrainment and the acceleration of product gases due to buoyancy in the flame zone are clearly visible. In the vicinity of

the tree, a significant portion of the plume with sufficiently high velocity passes through the tree. Then, the flow velocity reduces due to drag by the fuel particles. Near the edge of the tree (base of the cone), a small portion of the plume is deflected away (as for a flow around an obstacle). However, the drag resulting from this behavior will strongly depend on the packing ratio inside the tree. The oxygen mass fraction within the tree is in the range of 0.16 - 0.23. The oxygen mixes with the pyrolysis gases but will not ignite the tree since the temperatures are not high enough. This justifies the distance chosen for locating the tree above the pool fire, which in this case is 3 m, as the objective of prescribed burns is to avoid burning or harming the trees.

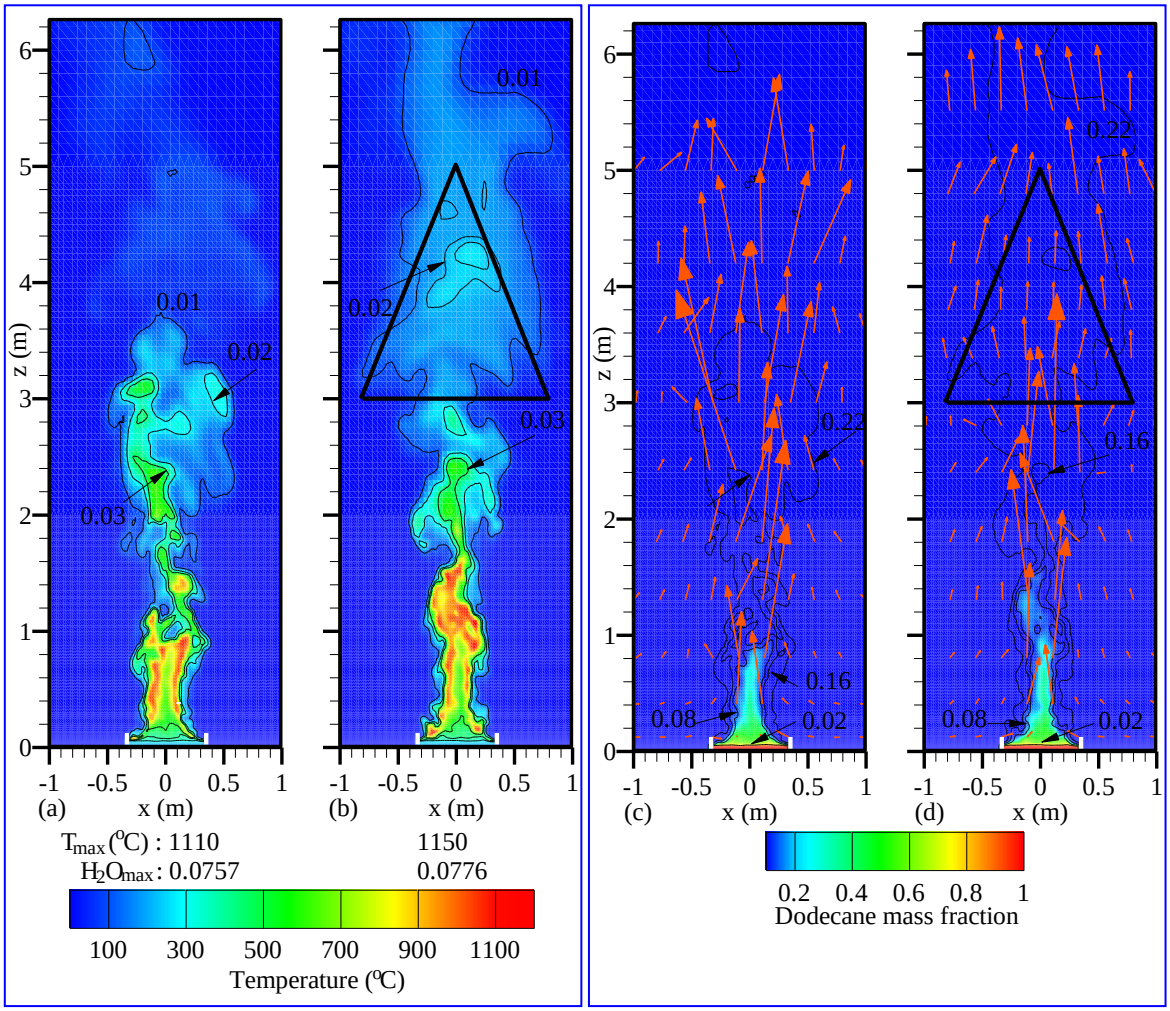

Figure 4 - (a), (b) Contours of temperature (colored) and water vapor mass fraction (lines) (c), (d) Contours of dodecane mass fraction (colored) and oxygen mass fraction (lines) with velocity vectors. The white lines represent the boundaries of the pan, and the triangle represents the Douglas fir tree.

5. Conclusions

An experimental and numerical study has been conducted as the first step of a larger study of the interaction between plume and vegetation during prescribed burns. The predicted mass burning rate and temperature were compared with measurements in a diesel pool fire. The model predicts a higher mass burning rate due to (1) the difference in ignition process, (2) the difference in fuel properties of diesel used in the experiments and that reported in the literature, which was subsequently used in the model, and (3) absence of sub-models to simulate convective heat transfer within the pool. The temperature is overpredicted in the intermittent and plume zones. Even though discrepancies exist, the model reveals some of the key processes such as moisture release within the vegetation which could be difficult to measure due to the presence of water vapor in the plume.

In the future, trees of various size and shape will be placed over the pool fire and point measurements of temperature, velocity, and heat flux will be recorded to model the drag and heat transfer within the vegetation. These sub-models will be included to validate and improve the accuracy of the numerical model.

6. Acknowledgement

The authors thank Abhinandan Singh for his help with the experiments.

7. References

Attar, A.A., Pourmahdian, M., Anvaripour, B. (2013). Experimental Study and CFD Simulation of Pool Fires, International Journal of computer applications, 70(11), 9-15. 10.5120/12004-5790

Fire Dynamics Simulator, User Guide, FDS v6.7.7. https://tsapps.nist.gov/publication/get_pdf.cfm?pub_id=913619

Mell, W., Maranghides, A., McDermott, R., Manzello, S. (2009). Numerical simulation and experiments of burning Douglas fir trees. Combustion and Flame, 156, 2023-2041. https://doi.org/10.1016/j.combustflame.2009.06.015

Prasad, K., Li, C., Kailasanath, K., Ndubizu, C., Ananth, R., Tatem, P.A. (1999). Numerical modelling of methanol pool fires, Combustion Theory and Modelling, 3, 743-768. https://doi.org/10.1088/1364-7830/3/4/308

Stewart, J.R., Phylaktou, H.N., Andrews, G.E., Burns, A.D. (2021). Evaluation of CFD simulations of transient pool fire burning rates, Journal of Loss Prevention in the Process Industries, 71, 104495, https://doi.org/10.1016/j.jlp.2021.104495

Sudheer, S., Saumil, D., Prabhu, S.V. (2013). Physical experiments and Fire Dynamics Simulator simulations on gasoline pool fires, Journal of Fire Sciences, 31(4), 309-329. https://doi.org/10.1177/0734904112472953

Wahlqvist, J., van Hees, P. (2016). Implementation and validation of an environmental feedback pool fire model based on oxygen depletion and radiative feedback in FDS, Fire Safety Journal, 85, 35-40. https://doi.org/10.1016/j.firesaf.2016.08.003

Wen, J.X., Kang, K., Donchev, T., Karwatzki, J.M. (2007). Validation of FDS for medium-scale pool fires, Fire Safety Journal, 42, 127-138. https://doi.org/10.1016/j.firesaf.2006.08.007

Wu, B., Roy, S.P., Zhao, X. (2020). Detailed modeling of a small-scale turbulent pool fire, Combustion and Flame, 214, 224-237. DOI:10.1016/j.combustflame.2019.12.034

Xin, Y., Gore, J.P, McGrattan, K.B., Rehm, R.G., Baum, H.R. (2005). Fire dynamics simulation of a turbulent buoyant flame using a mixture-fraction-based combustion model, Combustion and Flame, 141, 329-335. https://doi.org/10.1016/j.combustflame.2004.07.001

A systematic study of the reliability of fire pattern indicators used in wildland fire investigation

Juan I. Cuevas*[1]; Michael R. Gallagher[2]; Jason Cole[3]; Matthew Patterson[4]; Nicholas S. Skowronski[4]; Albert Simeoni[1]

[1]*Department of Fire Protection Engineering, Worcester Polytechnic Institute, MA 01605, USA, {jcuevas, asimeoni}@wpi.edu*
[2] *USDA Forest Service, Northern Research Station, New Lisbon, NJ 08064, USA, {michael.r.gallagher@usda.gov}*
[3] *USDA Forest Service, Northern Research Station, Syracuse, NY 13210, USA, {jason.cole2@usda.gov}*
[4] *USDA Forest Service, Northern Research Station, Morgantown, WV 26505, USA, {matthew.m.patterson, nicholas.s.skowronski}@usda.gov*

**Corresponding author*

Keywords

Fire pattern indicator, Fire investigation, Prescribed burn, Wildfire, Field experiments, Reliability

Abstract

This work presents the preliminary results obtained from the first set of six field experiments conducted within the scope of a project focused on systematically evaluating the reliability of fire pattern indicators used in wildland fire investigation. The field experiments were conducted in the Pinelands National Reserve (NJ, USA) during the conduction of prescribed burns. This allowed studying the generation of fire pattern indicators in a realistic scenario and under controlled conditions. During the experiments, a series of sensors were used to determine the heat exposure that induces the appearance of fire pattern indicators over planted supporting elements. The preliminary results suggest that fire pattern indicators are a valuable and valid tool for the determination of the area of origin of a fire if they are used holistically. Further results and analysis to be presented in the full version of this work include fire spread and the characterization of the heat exposure that generates the fire pattern indicators observed in the complete experimental campaign.

1. Background and Motivation

The increased frequency of catastrophic wildfire events is projected to continue over the next century causing dramatic impacts to human and ecological systems (e.g., loss of life, health impacts, property, and economic losses, lost ecological function, and resilience) (NIFC, 2022; Sample et al., 2022). The rapid expansion of the wildland-urban interface and the effects of climate change have increased the frequency and intensity of these events, highlighting a specific need for fire behavior and effects research, where human and ecological systems intersect to understand anthropogenic roles in unwanted wildland fire ignitions (Maranghides & Mell, 2013; Hammer et al., 2007). Scientific gaps in the basis for standard approaches used for studying ignitions in the field limit our understanding of the reliability and scientific integrity of these approaches and justify a need for new science to either support existing methods or guide improvements.

Field studies of unwanted wildland fire ignitions focus on identifying and evaluating physical fire pattern indicators (FPIs) within a fire's footprint as a forensic means of locating a fire's exact point of origin and ignition source. From this perspective, ensuring the accurate determination of the origin and causes of wildland fires is paramount, and thus standardized methods are provided to fire investigators. In the United States and worldwide, the National Fire Protection Association's Guide for Fire and Explosion Investigations (NFPA, 2021) and the Guide to Wildland Fire Origin and Cause Determination of the National Wildfire Coordinating Group (NWCG, 2016) are the primary documents that provide a systematic method for the conduction of this type of investigation and rely on fire pattern indicators. As per this guide, indicators are commonly divided into two classes: macroscale and microscale FPIs (NWCG, 2016). Macroscale FPIs are associated with large objects and are easily noticeable, for example, the angle of the charring displayed by a tree trunk. On the other hand, microscale FPIs are only observable by getting up close to an object, such as the protection shown behind a

pinecone. The interpretation of microscale FPIs typically becomes more important as investigators work closer to the area of ignition.

Very few scientific studies have attempted to assess the reliability of FPIs systematically, despite their primary importance in fire investigations (Simeoni et al., 2017). To begin addressing this gap, we present a project to develop a novel experiment-based dataset that will be used to assess the reliability of FPIs related to fire behavior and local fire conditions.

To generate a statistically robust dataset, experiments will be conducted in two different settings: field and laboratory. In the field, prescribed burns will be used to study the creation of FPIs in realistic but controlled fire conditions (Mueller et al., 2017). In this setting, it will be possible to observe the generation of most indicators, paying attention to the macroscale FPIs that appear on vegetation and landscape features. Furthermore, microscale FPIs will be identified, and the thermal exposure conditions needed to produce them will be quantified. After the field experiments, laboratory experiments will be conducted using the information gathered in the field. A wind tunnel will be used to study the effects of wind, slope, and vegetation layout on the creation and reliability of FPIs. The combination of the experiments conducted in these two settings will establish a robust and statistically representative dataset centered on the reliability of FPIs within the range of the tested conditions.

The work presented herein showcases the approach and preliminary results obtained from the first set of six field experiments conducted within the scope of this project.

2. Methodology

2.1. Study site and burn plot characteristics

The field experiments were conducted in March 2022 at the Pineland National Reserve (PNR), located in New Jersey, United States. The PNR comprehends an area of ~ 445,000 ha, composed mainly of upland and wetland forests. The basic geography of the area is a relatively flat coastal plain with low-angle slopes and a maximum elevation of 63.5 m, with well-drained sandy loam as the primary soil type (Clark et al., 2015).

As presented by Clark et al. (Clark et al., 2015), the upland forests represent roughly 60% of the forested areas in the PNR, with many closed-canopy stands of approximately 60–90 years of age. In general terms, it is composed of the following three major communities: oak-pine, pine-oak, and pine-scrub oak (Skowronski et al., 2007). For all communities, understory vegetation comprises mainly Scrub oaks and Ericaceous shrubs such as huckleberry and blueberry.

The experiments reported here were conducted in small plots of ~0.5 ha, with low-intensity fires that replicate the conditions near the point of origin of a fire. Supporting elements to study the generation of FPIs were planted in clusters of ~9 m^2 to study the generation of micro-scale FPIs.

To replicate the initial conditions of a fire incident as close as possible, single-point ignition was conducted using a typical isobutane lighter. The location of the point of ignition was varied according to the fire spread scenario to be represented and current wind conditions.

2.2. Diagnostics

2.2.1. Fuel characterization

Vegetation samples were collected from randomly-sampled 1 m^2 destructive harvest subplot areas within each burn unit. As prescribed fires rarely reach the more highly decomposed organic layers of the ground, a collection depth that reaches the litter layer of the forest floor was sufficient (Clark et al., 2015).

The material collected was sorted in-situ as detritus and vegetative material. These materials were then dried for a minimum of 48 hours at 70°C and sorted into fuel particle and time-lag components (e.g., downed wood, stems, fine fuels; 1-, 10-, 100- hour time-lag classes).

Terrestrial laser scans (TLS) were conducted at each plot before and after the fire to obtain a 3D survey of the vegetation, indicators, and equipment to estimate the initial and final vegetation bulk density and fuel consumption.

2.2.2. Fire spread

Protected conventional cameras mounted at elevated positions inside and in the vicinity of the fire perimeter were used to capture the fire spread from different angles and visualize the fire behavior near the indicators. In addition to these cameras, a weather station and 3D sonic anemometers placed outside the perimeter of the burn plot were used to characterize the environmental and air entrainment conditions before, during, and after the fire.

2.2.3. Generation of fire pattern indicators

Following the approach presented by Simeoni et al. (Simeoni et al., 2017), supporting elements that allow the appearance of microscale fire pattern indicators were used. Fig. 1(a) shows an example of the supporting elements used by Simeoni et al. in the past. As previously mentioned, the supporting elements were planted in clusters comprising an area of approximately 9 m^2 dispersed throughout the burn plot, as shown in Fig. 1(b). The clusters were distributed in the burn plot in a way that allowed to capture head, flank, and backing fire-induced fire pattern indicators.

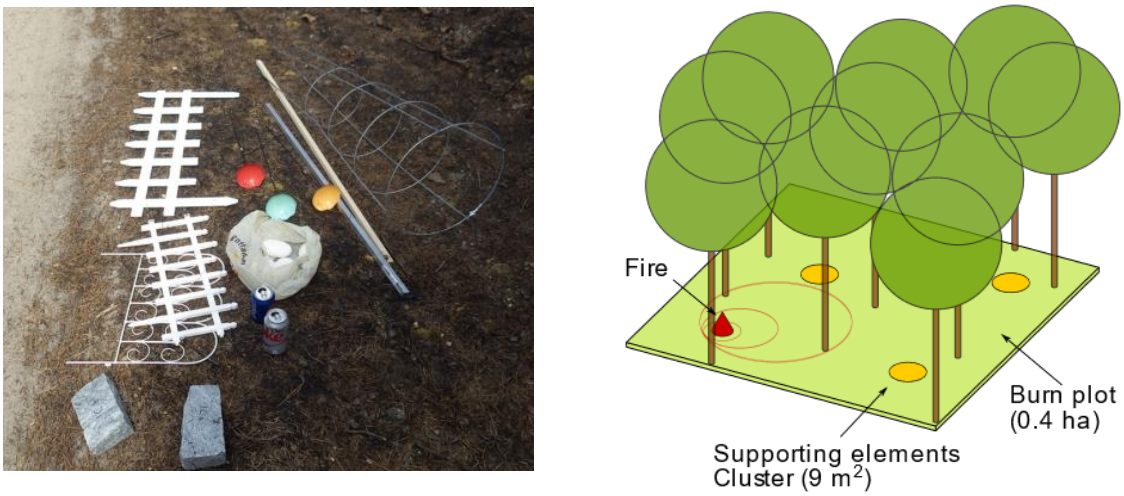

(a) *(b)*

Figure 1: Supporting items for the generation of micro-scale FPIs. (a) Example of the items used by Simeoni et al., (b) Positioning of the clusters of supporting elements within a burn plot.

Through close post-fire inspection of the supporting elements, the micro-scale FPIs generated were registered. Furthermore, to understand the generation of micro-scale indicators, the heat exposure over the supporting elements was characterized through the following instruments (Fig. 2(a)):

A set of four 1.5 mm-diameter type-K thermocouples (TC) and four thin-skin calorimeters (TSC) were placed near selected supporting elements in different cluster regions. Even though this number of TC+TSC pairs is insufficient to characterize the heat exposure over every planted element accurately, it does allow for an estimate of the time-resolved average effect of the fire within the cluster.

A set of three bi-directional velocity probes and differential pressure transducers were placed at the center of the cluster to register the average 3D wind and gas velocity within the cluster. Additionally, two protected conventional cameras were placed outside the cluster to record the progression of the fire front at perpendicular angles, as shown in Fig. 2(b). The objective of these cameras was to provide a detailed visual record of the fire progression and its effect on the supporting elements.

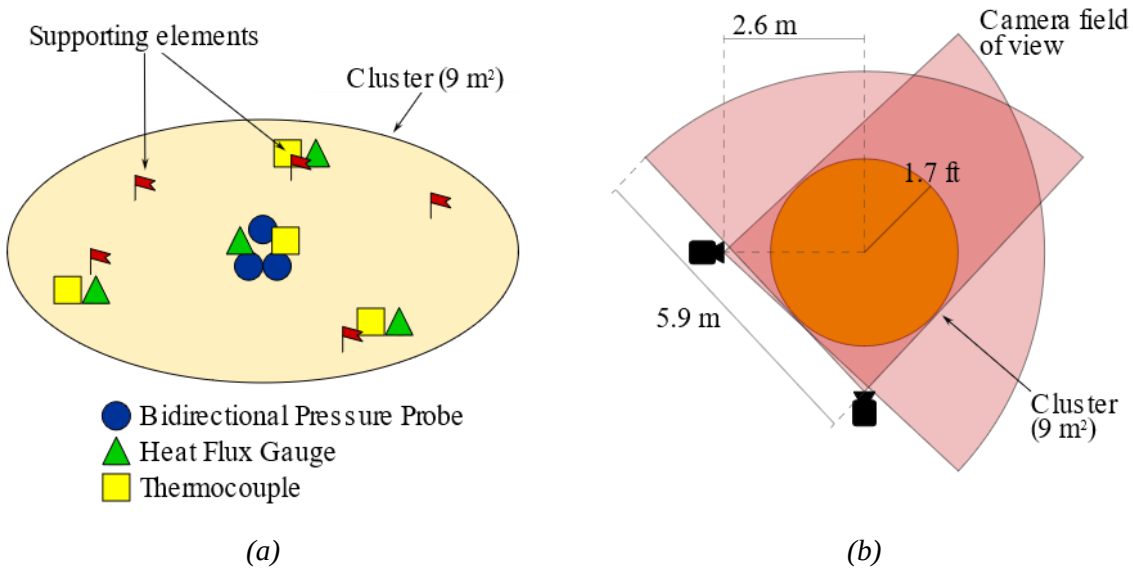

Figure 2: Instrumentation placing within a cluster of supporting elements. (a) Thermal exposure sensors placing, (b) near-cluster camera positioning.

Finally, the generation of macro-scale FPIs was evaluated through visual identification and documentation. Whenever possible, key elements within the burn plot (such as trees or shrubs) were targeted, and a detailed pre- and post-fire analysis (including ground-based LiDAR scanning) was conducted. By using the results obtained from this analysis along with the fire-spread footage registered, it is possible to identify the thermal exposure conditions that lead to the generation of the macro-scale fire pattern indicators observed in these key elements.

3. Results and Discussion

The preliminary results of some experiments are presented to illustrate the approach in practice. Pre- and post-burn TLS scans highlight the ability qualitatively evaluate fuel consumption within the plot as a first step in the approach (Figure 3). In addition to collecting fuel information, this step records the locations of the FPI materials while sonic anemometers collect data from outside the plot (idealized representation in Figure 4(a)). Figures 4(b) and (c) provide a before-and-after comparison of some of the planted elements to provide an example of the FPIs collected; mainly soot deposition and charring. Figure 4(d) displays the overall propagation of the fire derived from visual observations (red contour lines) as well as the propagation direction derived by the individual interpretation of the microscale FPIs (black arrows).

For three of the eight supporting elements, it was impossible to derive a fire propagation direction based on the damage displayed by the supporting element. It is also interesting to notice the apparent contradiction in the propagation direction derived from the FPIs displayed by the two top-most supporting elements, one of them being the galvanized steel cylinder shown in Fig. 4(b). This contradiction was caused by the collapse and the eventual burning of the branch where the supporting element was installed. These preliminary findings support those of Simeoni et al. (Simeoni et al., 2017); the consideration of a single fire pattern indicator can provide insufficient or potentially incorrect information regarding the evolution of a fire. To infer the real behavior of the fire, the information provided by all FPIs identified must be analyzed holistically.

4. Conclusions

The current work presents and demonstrates an approach for systematic studies of fire pattern indicator reliability in wildland fire investigations. The results of this demonstration support the existing idea that fire pattern indicators are a valuable and valid tool for the determination of the area of origin of a fire, but only when they are used holistically. Further results and analysis to be presented in the full version of this work include

fire spread and the characterization of the heat exposure that generates the fire pattern indicators observed in the complete experimental campaign.

(a)

(b)

Figure 3: Example of the LiDAR scans conducted close to a cluster of planted elements (in red circles) in Experiment 6, (a) pre-burn scan, (b) post-burn scan.

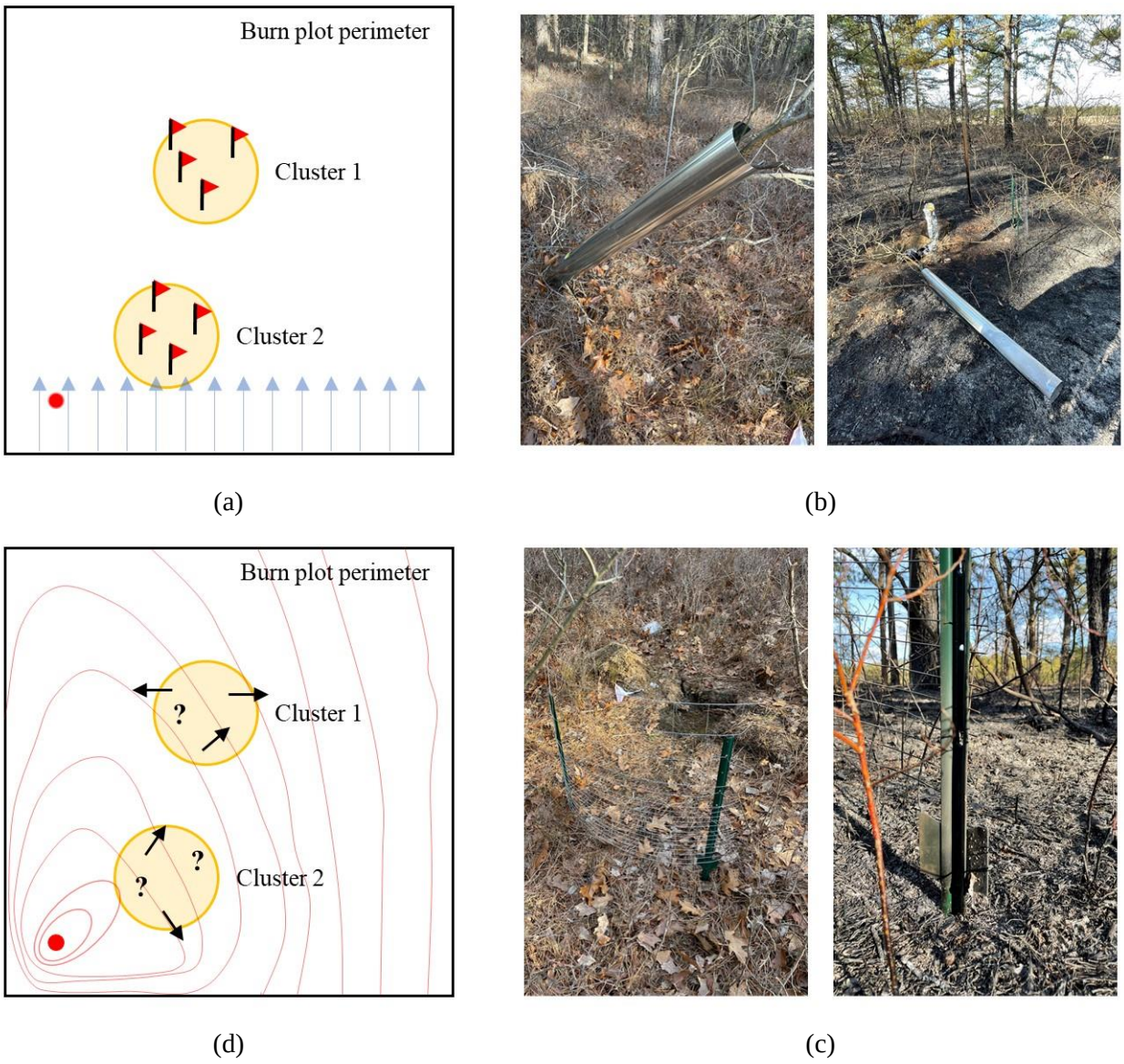

Figure 4: Generation of FPIs, (a) Placements of the clusters within the burn plot, wind direction, and point of ignition, (b) Damage generated by the fire in a supporting element of cluster 1, (c) fire damage over a supporting element of cluster 2, (d) fire spread derived from visual observation, and propagation direction indicated by the individual FPIs.

5. References

Clark, K. L., Skowronski, N., & Gallagher, M. (2015). Fire Management and Carbon Sequestration in Pine Barren Forests. Journal of Sustainable Forestry, 34(1–2), 125–146. https://doi.org/10.1080/10549811.2014.973607

Hammer, R. B., Radeloff, V. C., Fried, J. S., & Stewart, S. I. (2007). Wildland-urban interface housing growth during the 1990s in California, Oregon, and Washington. International Journal of Wildland Fire, 16(3), 255–265. https://doi.org/10.1071/WF05077

Maranghides, A., & Mell, W. (2013). Framework for Addressing the National Wildland Urban Interface Fire Problem- Determining Fire and Ember Exposure Zones using a WUI Hazard Scale. NIST Technical Note 1748.

Mueller, E. V., Skowronski, N., Clark, K., Gallagher, M., Kremens, R., Thomas, J. C., … Simeoni, A. (2017). Utilization of remote sensing techniques for the quantification of fire behavior in two pine stands. Fire Safety Journal, 91(February), 845–854. https://doi.org/10.1016/j.firesaf.2017.03.076

NFPA. NFPA 921: Guide for Fire and Explosion Investigations. , (2016).

NIFC. (2022). Statistics. Retrieved May 5, 2022, from https://www.nifc.gov/fire-information/statistics

NWCG. (2016). Guide to wildland fire origin and cause determination, PMS 412. National Wildlife Coordinating Group.

Sample, M., Thode, A. E., Peterson, C., Gallagher, M. R., Flatley, W., Friggens, M., … Swanston, C. (2022). Adaptation Strategies and Approaches for Managing Fire in a Changing Climate. Climate, 10(4), 58. https://doi.org/10.3390/cli10040058

Simeoni, A., Owens, Z. C., Christiansen, E. W., Kemal, A., Gallagher, M., Clark, K. L., … Hadden, R. M. (2017). A preliminary study of wildland fire pattern indicator reliability following an experimental fire. Journal of Fire Sciences, 35(5), 359–378. https://doi.org/10.1177/0734904117720674

Skowronski, N., Clark, K., Nelson, R., Hom, J., & Patterson, M. (2007). Remotely sensed measurements of forest structure and fuel loads in the Pinelands of New Jersey. Remote Sensing of Environment, 108(2), 123–129. https://doi.org/10.1016/j.rse.2006.09.032

Analysis of thermal behaviour of merging fire fronts in crop field experiments

Alexander Filkov*; Brett Cirulis; Brendan Holyland; Trent Penman

University of Melbourne. VIC 3363 Australia,
{alexander.filkov, brett.cirulis, b.holyland, trent.penman}@unimelb.edu.au

**Corresponding author*

Keywords

Junction forward and backward fires, coalescence fires, parallel fire fronts

Abstract

Merging fires are known as destructive fires resulting in loss of life and houses. Despite growing efforts in the past decade to understand merging fires, there are still many knowledge gaps about their behaviour, especially at the field scale. In this study, we conducted experimental harvested crop burns in Victoria, Australia, in March and April 2021 to better understand thermal behaviour of merging fire fronts. UAVs with visual and thermal cameras were used to capture high-resolution fire propagation and the combustion process of merging fires. During experiments 50 junction fire fronts (32 forward and 18 backward) and 24 coalescence fire fronts were studied. For thermal analysis, 15 forward and 4 backward junction fire fronts, 6 coalescence fire fronts, and 10 parallel fire fronts were considered. Special methods were developed to process IR footages and compare the combustion process of merging fires and linear fire fronts (head and back fires). To do this, regions of interest (ROIs) containing the merging fire and linear fire front were selected in each frame using FLIR Research Studio. The ROIs were then exported using as bitmask images together with radiometric JPEG image containing both fires. Using the R programming platform, we determined the length and shape of the perimeter of fires for each JPEG image and defined buffer zones within the fire perimeter inside the ROI for each fire for further pixel temperature analysis. Thermal analysis showed that for forward junction fires the median temperature of head linear fire fronts was higher than forward junction fires except towards the end of merging. While in backward junction fires, the proportion of pixels with high temperature was much higher than in back linear fire fronts, indicating much larger burning areas. The temperature distributions of coalescence and parallel fires showed a decrease in the number of high-temperature pixels toward the end of the merge for coalescence and throughout for parallel fires. The fire behaviour observed in the field experiments demonstrates the necessity for better understanding of merging of fire fronts and the relationship between fuel, weather and fire line interaction.

1. Introduction

Over the past decade, extreme wildfires have occurred around the world with significant social, economic, and environmental consequences. They threaten the lives of many people and cause billions of dollars in damage. Climate change is further worsening fire seasons by increasing the number of dry and hot days (Bradstock 2010; Parente et al. 2018; Halofsky et al. 2020; Vilà-Vilardell et al. 2020). Longer fire seasons are expected to lead to more frequent and severe fires (Matthews et al. 2012; Di Virgilio et al. 2019). Such predictions were observed during the 2019/20 bushfire season in Australia (Filkov et al. 2020b).

These consequences are mainly the result of dynamic fire behaviours (DFBs) (Werth et al. 2011; Filkov et al. 2018; Tedim et al. 2018; Filkov et al. 2020a), which can lead to rapid increases in fire intensity and rate of spread (Hilton et al. 2017). Merging fires (Viegas 2012; Viegas et al. 2013; Thomas et al. 2017; Hilton et al. 2018; Raposo et al. 2018) is one of them. The convergence of separate individual fires into larger fires is called coalescence, and the merging of two lines of fire intersecting at an oblique angle is termed junction fire or junction fire fronts (Viegas 2012). Fire coalescence, junction and parallel fire fronts are all examples of merging fire fronts.

Most of experimental studies of merging fires have been conducted in the laboratory (Viegas et al. 2013; Oliveira et al. 2014; Sullivan et al. 2019), and only a few in the field (Raposo et al. 2018). Filkov et al. (2021) have demonstrated that the fire behaviour associated with merging fires in the field can be different and there remain ‘scale-gaps’ in the experimental data used to inform model development. Moreover, information about

thermal behaviour of merging fires and burning depth is unknown. Therefore, the aim of this study was to develop materials that provide a better understanding of the dynamic nature of fire line merging.

1.1. Methods

Two experimental burns (Shelford and Lake Burrumbeet) on harvested wheat fields were conducted in Victoria, Australia, in March and April 2021. During experiments, junction fires, spot fire coalescence and parallel fire fronts were investigated.

Automatic Weather Station (AWS, 30 min temporal resolution) was used for air temperature and relative humidity measurements. Davis cup anemometer sensor in the Shelford burn (ICT International) and 2-dimentional DS-2 sonic sensors in the Lake Burrumbeet burn (Decagon Devices, Inc., Pullman, USA) with one min temporal resolution were used for wind direction and speed measurements. The terrain in both burns was relatively flat with minimal undulations. Fuel properties and weather condition are presented in Table 1.

Table 1- Fuel properties and weather characteristics

Burn name	Fuel height, cm	Fuel load, kg/m^2	MC, %	Wind speed, m/s	T, C	RH, %
Shelford	18.6±3.8	0.11±0.03	36±3	3.4±1.1.	27.4	44
Lake Burrumbeet	51.4±2.6	0.65±0.12	17±4.5	5.4±1.2	16	62

MC is the fine fuel moisture content (wet basis), T is the air temperature at 15:00, RH is the relative humidity at 15:00, ± is the standard deviation

Two UAVs, a DJI Mavic Pro (Shelford burn) and DJI Matrice 210 (Lake Burrumbeet burn) were used to capture high-definition video imagery of fire propagation. DJI Mavic Pro is equipped with visual camera (3840×2160 pixels, 30 Hz). The camera model used with the DJI Matrice 210 was the XT2 payload with dual visual (3840×2160 pixels, 30 Hz) and thermal (640x512 pixels, 30 Hz) video capability. XT2 payload allows to film simultaneously both visual and thermal (radiometric) videos. The post processing phase was completed for each separate visual and thermal video and metadata file using the Full Motion Video (FMV) toolbox within the ArcGIS Pro 2.8.0 software (Macdonald 2017). The result is a video file with each frame georeferenced. The multiplexed video file was then used to identify and spatially define fire fronts at set time intervals.

After starting the ignition line, the fire front produced fire tongues. When the fire lines of two neighbouring tongues naturally merged together, we identified it as junction fire fronts (forward junction fire fronts) and the angle between them as an initial angle. If the junction fire fronts were spreading opposite to the direction of the head linear fire front, we identified them as the backward junction fire fronts. Two spot fires spreading toward each other were identified as coalescence fires. Two fire fronts burning parallel to each other and propagating towards each other were identified as inward parallel fire fronts. We measured travelling distance of the merging fire fronts every 2-5 seconds to calculate ROS. To estimate the effect of merging fire fronts on fire propagation we compared them with head and back linear fire fronts. The ROS of the linear fire front was measured in the vicinity to each merging fire front for their entire duration.

To analyse the effect of merging fire fronts on fire behaviour and thermal energy release, we compared the temperatures above 200 °C on thermal images of merging fires and linear fire fronts. Since the junction and linear fire fronts are very different in length and shape of the fire perimeter, we required a method for their relative comparison. To do this, we compared the temperature of pixels inside the buffer zones for each fire. In order to define them, we had to delineate linear and junction fires and determine their perimeters on thermal images. This process is different for each type of merging fires. For junction fires, we first manually created two regions of interest (ROIs) containing a junction fire and a section of a linear fire front on the thermal video (head and back linear fire fronts for forward and backwards junction fire fronts, respectively) using FLIR Research Studio 2.0.0. For parallel fire fronts and coalescence fires, we created one ROI containing both parallel fire fronts (their sections) and coalescence fires (complete fires).

The ROIs were then exported using FLIR Research Studio 2.0.0 as bitmask images together with radiometric JPEG image containing both fires. All images were exported at 2-, 4- or 5-second intervals, starting from the formation of the merging fire to its transition to a linear fire front for junction fires (180-degree junction angle) or to the moment of joining parallel or coalescence fires. Using the R programming platform 4.1.0 (R Core

Team 2021), we determined the length and shape of the perimeter of the merging and linear fires for each JPEG image. Using this information and the st_buffer function in R (sf package), we defined buffer zones within the fire perimeter inside the ROI for each fire for further analysis. We then analysed the temperatures of pixels, after which we calculated the temperature distributions for each time step. Due to different time duration of each merging fire, we converted time steps to percentages of final time.

2. Results and discussion

The use of a drone with a dual visual and thermal camera showed that the thermal camera was able to detect all active hot spots and fire fronts even through dense smoke, which was a significant constraint in our previous study (Filkov et al. 2021).

Thirty-four videos were filmed and multiplexed. Seventy-four merging fire fronts (42 in Shelford and 32 in Lake Burrumbeet burn) were identified: 50 junction fire fronts (32 forward and 18 backward) and 24 coalescence fire fronts. For thermal analysis, 15 forward and 4 backward junction fire fronts, 6 coalescence fire fronts, and 10 parallel fire fronts were considered since the amount of available thermal video footage was limited.

The combined ROS of forward, backward and head linear fire fronts had the highest median ROS for forward junction fires (2.02 m/s), followed by head linear and backward ROS, 0.67 m/s and 0.18 m/s, respectively. The ROS of the head linear fire fronts changed mostly in the range 0.1-2 m/s during the lifetime of the merging fires. A comparison of the median ROS values for forward junction fires and head linear fire fronts between the two burns showed that the difference was very consistent. Forward junction fires were 3 times faster than head linear fire fronts, 3.02 and 3.11 times faster for the Shelford and Lake Burrumbeet burns, respectively. The ROS of backward fire fronts is consistent between the two burns, 0.17-0.2 m/s. Although the average ROS of forward junction fires was 3 times that of head linear fire fronts, it was up to 18 times higher than head linear fire fronts in some cases.

The pixel temperature distribution within the buffer zones for merging fires is presented on Fig. 1. Data analysis for forward junction fires showed that the median temperature of head linear fire fronts was higher than forward junction fires except towards the end of merging (Fig. 1a). In backward junction fires, the proportion of pixels with high temperature was much higher than in back linear fire fronts (Fig. 1b). For example, the difference in median temperature between the two ranged from 100 to 200 °C, indicating much larger burning areas in the backward junction fires. Non overlapping notches in all groups indicate with a 95% confidence level that the temperature medians for junction fires and linear fire fronts are different.

Analysis of temperatures above 500 ºC in forward junction fires, representing flaming combustion in wildfires (Wotton et al. 2011), showed that the density of high-temperature pixels (above 500 °C) increases, and the temperature peak shifts toward higher temperatures during the merging process. Whereas for head linear fire fronts, the temperature density and its peak remain practically unchanged. It was expected that the density of "hot" pixels should be higher for forward junction fires compared to head linear fire fronts during the merging process. Higher ROS should have resulted in more fuel burning simultaneously and larger "deep flaming" areas. However, we found that only in the last stage of merging (75% and 100% time) was the median temperature and temperature range higher and larger. It is assumed that the “deep flaming” is a consequence of the forward junction fires and not a mechanism of their propagation. Liu et al. (2021) in their literature review discuss potential mechanisms of fire merging and point to interacting air entrainment fields and enhanced heat feedback to fuels. In our study, we did not have the opportunity to study convection, but it will be addressed in future studies.

Unexpected results were also received for coalescence fires (Fig. 1c). Although, the ROS increases over time, its value decreases as the distance between two spot fires decreases. At this point, we have no explanation for these results. The temperature distribution also showed a decrease in the number of high-temperature pixels toward the end of coalescence. One possible explanation for this is that in our analysis we assumed that the end of coalescence is the time when the two fires joined together, but not the time when they completely merged to form one fire. Additional experiments and analysis are needed to explain the above results.

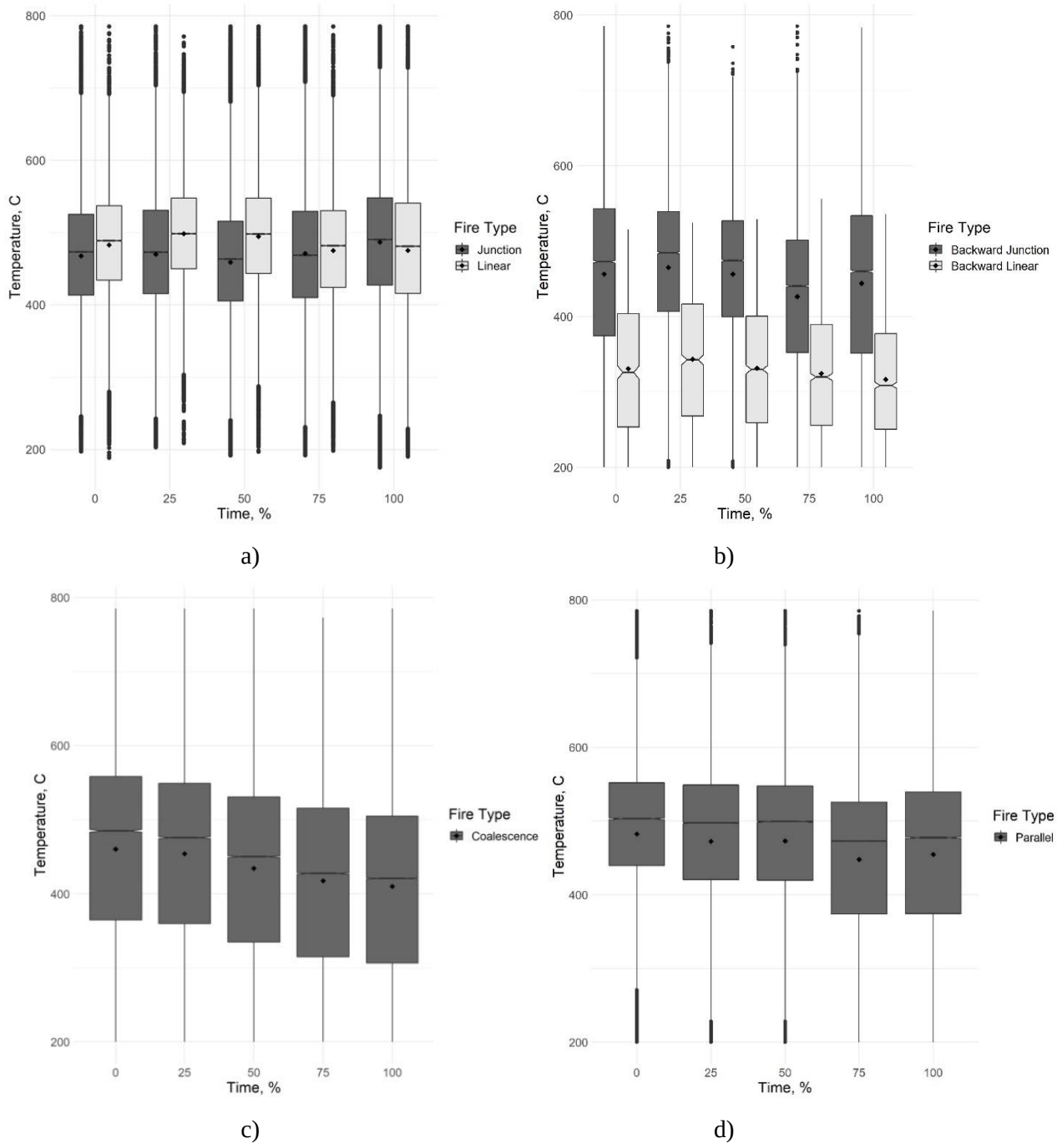

Figure 1- A notched box plot of the distribution of pixel temperature in the buffer zone of the merging fires: a) the forward junction fire (Junction) and head linear fire front (Linear) for the duration of forward junction fire; b) the backward junction fire (Backward junction) and back linear fire front (Back linear) for the duration of backward junction fire; c) the coalescence fires; d) the parallel fires. Time is dimensionless. Zero percent is the moment of formation of the merging fire, 100% is the moment of transition to the linear fire front (180-degree junction angle) or to the moment of joining parallel or coalescence fires. Boxes contain 50% of data. Dots represent outliers. Line is the median and rhombus is the mean.

Parallel fire, opposite to forward junction fires, had a decrease in the number of high-temperature pixels by the end of merging.

Our study has a few limitations. The drone thermal camera is factory calibrated to 550 °C. Values above this value are extrapolations in the FLIR software. They should be analysed with caution. In our future study we are going to use a thermal filter to extend the temperature range. Also, comparing thermal pixels within buffer zones of merging fires and linear fire fronts may not be the best option.

3. Conclusion

Conducted field experiments have confirmed that merging fires behave differently than regular fires (linear fire fronts), and standard operational models will underestimate fire behaviour when merging occurs. In some cases, the forward ROS of forward junction fires can be up to 18 times higher than the head linear ROS. Analysis of the thermal footages revealed that a greater number of pixels with higher temperatures were observed at the end of fires merging in forward junction fires and during the entire merging time in backward junction fires compared to linear fire fronts. These results indicate the danger that junction fires can pose to firefighters and communities and the need to incorporate them into fire behaviour models. Further research is needed to better understand the unexpected temperature behaviour of coalescence and parallel fires.

4. References

Bradstock, RA (2010) A biogeographic model of fire regimes in Australia: current and future implications. Global Ecology and Biogeography 19, 145-158.

Di Virgilio, G, Evans, JP, Blake, SAP, Armstrong, M, Dowdy, AJ, Sharples, J, McRae, R (2019) Climate Change Increases the Potential for Extreme Wildfires. Geophysical Research Letters 46, 8517-8526.

Filkov, A, Cirulis, B, Penman, T (2021) Quantifying merging fire behaviour phenomena using unmanned aerial vehicle technology. International Journal of Wildland Fire 30, 197-214.

Filkov, AI, Duff, TJ, Penman, TD (2018) Improving fire behaviour data obtained from wildfires. Forests 9, 1-21.

Filkov, AI, Duff, TJ, Penman, TD (2020a) Frequency of Dynamic Fire Behaviours in Australian Forest Environments. Fire 3, 1-19.

Filkov, AI, Ngo, T, Matthews, S, Telfer, S, Penman, TD (2020b) Impact of Australia's catastrophic 2019/20 bushfire season on communities and environment. Retrospective analysis and current trends. Journal of Safety Science and Resilience 1, 44-56.

Halofsky, JE, Peterson, DL, Harvey, BJ (2020) Changing wildfire, changing forests: the effects of climate change on fire regimes and vegetation in the Pacific Northwest, USA. Fire Ecology 16,

Hilton, J, Sharples, J, Sullivan, A, Swedosh, W, 2017. Simulation of spot fire coalescence with dynamic feedback. 22nd International Congress on Modelling and Simulation, Hobart, Tasmania, Australia, 3 to 8 December 2017. 1111-1117.

Hilton, JE, Sullivan, AL, Swedosh, W, Sharples, J, Thomas, C (2018) Incorporating convective feedback in wildfire simulations using pyrogenic potential. Environmental Modelling and Software 107, 12-24.

Liu, N, Lei, J, Gao, W, Chen, H, Xie, X (2021) Combustion dynamics of large-scale wildfires. Proceedings of the Combustion Institute 38, 157-198.

Macdonald, O (2017) Getting to know ArcGIS Pro. Cartographic Journal 54, 284-285.

Matthews, S, Sullivan, AL, Watson, P, Williams, RJ (2012) Climate change, fuel and fire behaviour in a eucalypt forest. Global Change Biology 18, 3212-3223.

Oliveira, LA, Lopes, AG, Baliga, BR, Almeida, M, Viegas, DX (2014) Numerical prediction of size, mass, temperature and trajectory of cylindrical wind-driven firebrands. International Journal of Wildland Fire 23, 698-708.

Parente, J, Pereira, MG, Amraoui, M, Fischer, EM (2018) Heat waves in Portugal: Current regime, changes in future climate and impacts on extreme wildfires. Science of the Total Environment 631-632, 534-549.

R Core Team (2021) 'R: A language and environment for statistical computing. R Foundation for Statistical Computing.' Vienna, Austria)

Raposo, JR, Viegas, DX, Xie, X, Almeida, M, Figueiredo, AR, Porto, L, Sharples, J (2018) Analysis of the physical processes associated with junction fires at laboratory and field scales. International Journal of Wildland Fire 27, 52-68.

Sullivan, AL, Swedosh, W, Hurley, RJ, Sharples, JJ, Hilton, JE (2019) Investigation of the effects of interactions of intersecting oblique fire lines with and without wind in a combustion wind tunnel. International Journal of Wildland Fire 28, 704-719.

Tedim, F, Leone, V, Amraoui, M, Bouillon, C, Coughlan, RM, Delogu, MG, Fernandes, MP, Ferreira, C, McCaffrey, S, McGee, KT, Parente, J, Paton, D, Pereira, GM, Ribeiro, ML, Viegas, DX, Xanthopoulos, G (2018) Defining Extreme Wildfire Events: Difficulties, Challenges, and Impacts. Fire 1, 1-28.

Thomas, CM, Sharples, JJ, Evans, JP (2017) Modelling the dynamic behaviour of junction fires with a coupled atmosphere-fire model. International Journal of Wildland Fire 26, 331-344.

Viegas, DX, 2012. Extreme Fire Behaviour. Forest Management: Technology, Practices and Impact. Nova Science Publishers, Inc., 1-56.

Viegas, DX, Raposo, J, Figueiredo, A (2013) Preliminary analysis of slope and fuel bed effect on jump behavior in forest fires. Procedia Engineering 62, 1032-1039.

Vilà-Vilardell, L, Keeton, WS, Thom, D, Gyeltshen, C, Tshering, K, Gratzer, G (2020) Climate change effects on wildfire hazards in the wildland-urban-interface – Blue pine forests of Bhutan. Forest Ecology and Management 461, 117927.

Werth, PA, Potter, BE, Clements, CB, Finney, MA, Goodrick, SL, Alexander, ME, Cruz, MG, Forthofer, JA, McAllister, SS (2011) Synthesis of knowledge of extreme fire behavior: Volume I for fire management. US Department of Agriculture, Forest Service, Pacific Northwest Research Station No. Gen. Tech. Rep. PNW-GTR-854, Portland, OR.

Wotton, BM, Gould, JS, McCaw, WL, Cheney, NP, Taylor, SW, Wotton, BM, Gould, JS, McCaw, WL, Cheney, NP, Taylor, SW (2011) Flame temperature and residence time of fires in dry eucalypt forest. International Journal of Wildland Fire 21, 270-281.

Assessing Potential Safety Zone Suitability using the Safe Separation Distance Evaluator (SSDE)

Daniel Jimenez[1]; Michael Campbell*[2]; Philip Dennison[2]; Matthew Thompson[3]; Bret Butler[1]

[1]Fire Science Laboratory, Rocky Mountain Research Station, USDA Forest Service, Missoula Montana, USA, {dan.jimenez@usda.gov}
[2]Department of Geography, University of Utah, Salt Lake City, UT, USA, {mickey.campbell57@gmail.com, dennison@geog.utah.edu}
[3]Rocky Mountain Research Station, USDA Forest Service, Fort Collins, CO, USA, {matthew.p.thompson@usda.gov}

**Corresponding author*

Keywords

Safety Zone, Safe Separation Distance, Radiant Heat Flux, Convective Heat Flux, Entrapment, Burnover

Abstract

Safety zones are fundamental tools that can be used by wildland firefighters to avoid injury or fatality when engaging in wildland fire operations. The National Wildfire Coordinating Group (NWCG) recommends that a safety zone be defined as a pre-planned area of sufficient size and suitable location that is expected to prevent injury to fire personnel from known hazards without using fire shelters. Currently, safety zones are primarily designated by fireline personnel as part of daily fire management operations. Though critical to safety zone assessment, the effectiveness of this approach is inherently limited by the individual's ability to accurately and consistently interpret vegetation conditions, topography, burning conditions and spatial characteristics of potential safety zones (e.g., area and geometry of a forest clearing). Regardless, effective safety zones provide safe separation distance (SSD) from surrounding flames, ensuring that the surrounding heat cannot cause burn injury. We introduce a new online tool for mapping SSD based on vegetation height, terrain, wind speed, and burning conditions: the Safe Separation Distance Evaluator (SSDE). The new tool allows users to draw a potential safety zone polygon and estimate SSD and the extent to which that safety zone polygon may be suitable, given the local landscape, weather, and fire conditions. The SSDE tools calculates separation distance based on vegetation height, wind and slope adjustment factors and burning conditions. Fuels layers are imported for LANDFIRE Existing Vegetation Height. Slope is calculated from the Shuttle Radar Topography Mission (STRM) digital elevation model. Winds are derived from the local fire weather forecast. Burning conditions are based on fuel moisture, relative humidity, and temperature. The Safe Separation Distance Evaluator (SSDE) algorithm is built and applied in Google Earth Engine (GEE), a cloud-based platform for processing and analyzing GIS and remotely sensed data, using JavaScript application programming interface. SSDE is a tool that can provide valuable safety information to wildland fire personnel who are charged with the critical responsibility of protecting the public and landscapes from increasingly intense and frequent fires in a changing climate.

1. Introduction

Wildland firefighters are tasked with a wide variety of fire management duties, many of which place them in close proximity to flames. One of the primary tasks is the removal of fuels and construction of containment lines to limit the potential damage to lives, property, and other critical resources (Wei, 2019; Silva, 2020; Connor, 2017). Particularly when engaged in a direct attack, whereby firefighters may be working within a few meters or less of that flaming zone, the potential risk for safety incidents is elevated (Cheney, 2001). Sudden or unexpected changes in fire behaviour can have devastating effects to vulnerable fireline personnel on the ground (Page, 2017). Events such as the Yarnell Hill fire in 2013, which claimed the lives of 19 firefighters and the South Canyon fire, which resulted in 14 firefighter fatalities, demonstrate the tragedy that can occur in the wildland fire profession (Arizona State Forestry Division, 2022; Butler, 1998; Alexander, 2015). Beyond these well-known, high-fatality events, there is an additional and significant background level of mortality that occurs among on-duty wildland firefighters (Butler, 2017). The causes of death are varied, and include heart attacks, vehicular and aircraft accidents, falling trees, and smoke inhalation, to name a few. Between 1990 and 2020, there were 525 documented wildland firefighter fatalities in the United States (National Interagency Fire Centre,

Wildfire Today). The causes of fatalities vary greatly (Figure 1), with nearly one fifth (19%) of which were due to burnovers or entrapments. This category is the direct result of fatal exposure to excessive heat, fire, and/or smoke. Burnover results from fire rapidly overtaking firefighting personnel before they can move to a safe area, and entrapment indicates that firefighters' ability to move to a safe area is compromised (National Wildfire Coordinating Group, 2017). As wildland fires increase in frequency, extent, and intensity, wildland firefighters may be put at heightened risk while working in the increasingly complex fire environment (Abatzoglou, 2016; Abatzoglou, 2021; Dennison, 2014; Balch, 2017; Westerling, 2016).

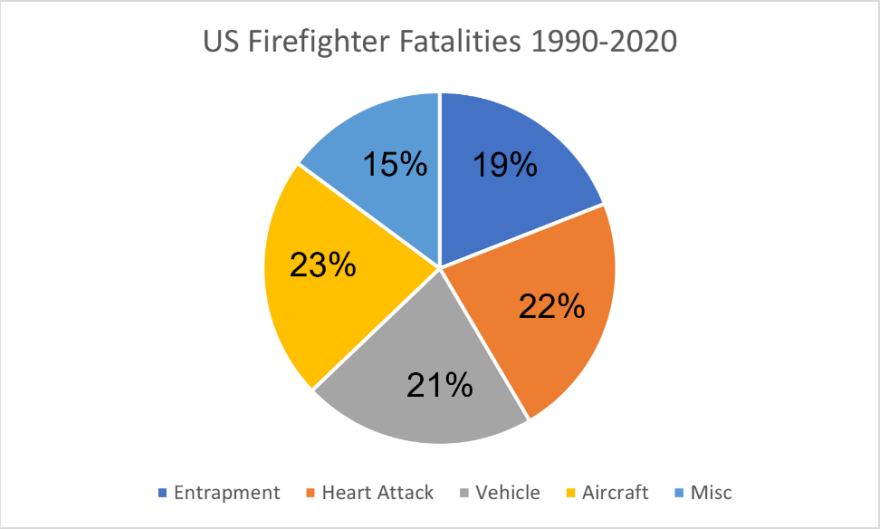

Figure 1- Firefighter fatalities by category from 1990-2020. Total wildland fire fatalities during that time span were 525.

Gleason (1991) proposed a system of interdependent safety measure to reduce firefighter risk of burnover and entrapment: lookouts, communications, escape routes, and safety zones (LCES). Safety zones are a critical component of this system, essentially areas large enough to allow firefighters to escape the harmful effects of fire (Beighley, 1995). Safety zones must be large enough to hold firefighting personnel and equipment and should provide a safe separation distance (SSD) between vegetation and these assets (Figure 2). The SSD must be large enough that heat from the wildfire is reduced to the point that a fire shelter is not necessary to prevent firefighter injury.

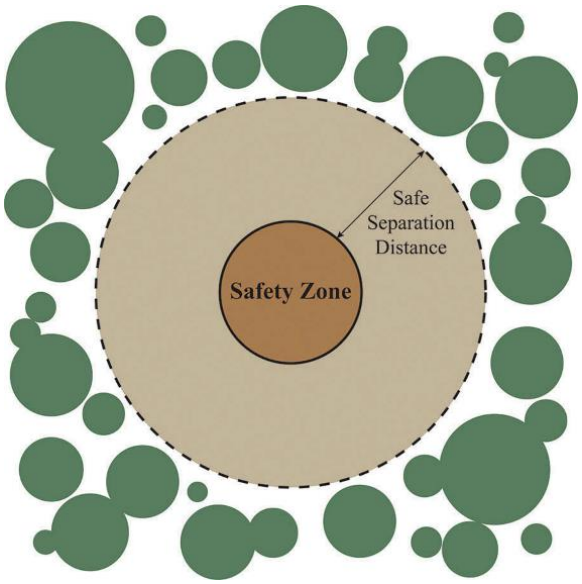

Figure 2 – Basic safety zone example diagram depicting Safe Separation Distance (SSD)

The current NWCG guideline for estimating SSD comes from Butler and Cohen (1998a), who determined, based on radiant heat modelling, that SSD should be equal to or greater than four times flame height. This

guideline assumes flat terrain and does not account for convective heat transfer, which can strongly contribute to firefighter heat exposure (Butler, 2014). Although this guideline has since been widely adopted (National Wildfire Coordinating Group, 2022), the research that underlies it is based solely on one heat transfer mechanism: radiation. Heat transfer by convection is also a major—sometimes dominant—force, particularly in the presence of steep slopes and high winds (Dupuy, 2011; Frankman, 2013; Parsons, 2014). In the presence of such convective heat, particularly if a fire crew is upslope and/or downwind of flames, SSD will increase (Page, 2017, Butler, 2014). Thus, the four times flame height rule is likely insufficient in these conditions. Recent work by Butler et al. (Butler, 2017) has sought to update this guideline with the inclusion of a "slope-wind factor", which adds a multiplicative term to the SSD equation to account for the effects of convective heat transfer (Page, 2017, Butler, 2014; Parsons, 2014; Page, 2018, Campbell, 2022). In addition, given that safety zones should be designated prior to, rather than during, the presence of flames, the four times flame height rule requires firefighters to predict how tall the flames might eventually be, which is a challenging endeavour. Accordingly, the newly proposed guidelines assume that, in a crown fire, flame height is approximately equal to twice the vegetation height (Campbell, 2022). As a result, the new SSD equation is defined as:

$$\mathbf{SSD = 8 \times VH \times \Delta,}$$

where VH is vegetation height and Δ is the slope-wind factor. Butler recently defined these slope-wind factors seen in Table 1, based not only on slope and wind speeds, but also on the burning conditions, as dictated by fuel conditions (e.g., moisture) and weather (e.g., relative humidity) (Campbell, 2022).

Table 1. Slope-wind factors (Δ) from Butler, coloured on a scale from blue (low Δ) to while (moderate Δ) to red (high Δ) (Campbell, 2022).

		Slope				
		Flat (0–7.5%)	Low (7.6–22.5%)	Moderate (22.6–40%)	Steep (>40%)	
Wind Speed	Light (0–4.5 m/s)	0.8	1	1	2	Low
		1	1	1.5	2	Moderate
		1	1.5	1.5	3	Extreme
	Moderate (4.6–8.9 m/s)	1.5	2	3	4	Low
		2	2	4	6	Moderate
		2	2.5	5	6	Extreme
	High (>8.9 m/s)	2.5	3	4	6	Low
		3	3	5	7	Moderate
		3	4	5	10	Extreme

Burning Condition

Although guidelines for use on the ground are valuable, they still require the firefighters themselves to make the calculation of SSD on the ground while engaged in other fire management activities. This requires the ability to accurately estimate vegetation height and terrain slope and anticipate wind speed and fire intensity. Moreover, even if these difficult interpretations and predictions can be made, an even more challenging endeavour is to identify an area on the ground cleared of vegetation that provides the calculated SSD in all directions.

To resolve these limitations and improve wildland firefighter safety, we introduce a new, interactive, web-based, open-access mapping tool for estimating SSD and evaluating potential safety zone effectiveness through geospatial analysis. The Safe Separation Distance Evaluator (SSDE) tool uses LANDFIRE Existing Vegetation Height data, which is both nationally available in the contiguous US and is updated every few years. Additionally, instead of only assessing SSD-driven suitability on clearings that already exist, this tool allows users to draw their own safety zone polygon to evaluate the potential suitability of a safety zone in any environment (Figure 3). The SSDE algorithm is built and applied in Google Earth Engine (GEE), a cloud-based platform for processing and analyzing GIS and remotely sensed data, using the JavaScript application programming interface (Gorelick, 2017).

2. Methods

2.1. Algorithm Description

The Safe Separation Distance Evaluator (SSDE) algorithm is built and applied in Google Earth Engine (GEE), a cloud-based platform for processing and analyzing GIS and remotely sensed data, using the JavaScript application programming interface (Campbell, 2022). GEE was selected a for few reasons: (1) it enables the

production of user-facing applications that can be widely accessed by anyone with an internet connection; (2) it hosts an immense catalog of geospatial data, including datasets necessary for the analysis of SZ suitability; (3) its cloud computing capabilities provide for rapid execution of complex geospatial functions, allowing users to quickly assess SZ suitability.

SSDE evaluates SSD through the analysis of proportional SSD (pSSD) within potential SZ polygons (Figure 3). pSSD quantifies the extent to which a potential SZ polygon provides SSD from surrounding vegetation/flames, considering the average per pixel SSD contained within a series of segments (or clusters of contiguous pixels) around the SZ polygon. Measured in percent, a pSSD of 100% or greater for a given pixel would mean that, factoring in vegetation height surrounding the polygon, slope, wind speed, and burn condition, the pixel's location should provide sufficient SSD, should fire personnel opt to use this location as a SZ. Conversely, a pixel with a pSSD of less than 100% would indicate that firefighters located within that pixel may risk injury from burning vegetation outside the boundary of the polygon.

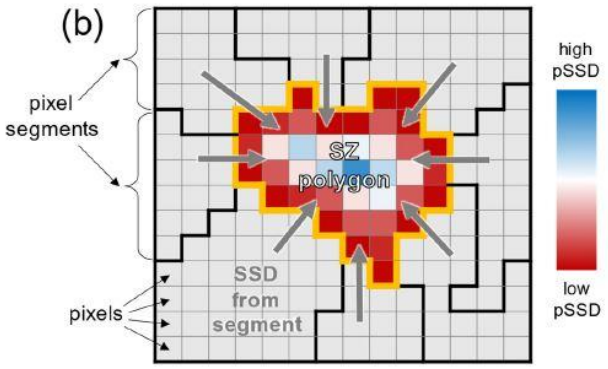

Figure 3: Conceptual depiction of that SSDE calculates SSD within a safety zone (SZ) polygon.

To calculate pSSD at the SZ polygon level, the user can define a potential SZ using the polygon drawing tools in SSDE, guided by the conditions both within the polygon and surrounding the polygon. The best SZs are those that contain no flammable material within, naturally or otherwise, so ideally this SZ polygon would be drawn in an area with low fuel loading, such as short or sparse grasses or litter. Alternatively, a SZ polygon could also be drawn in an area that has recently burned, or an area that would be targeted for fuel removal to create a SZ.

pSSD within a SZ is dependent upon the slope and vegetation height of the surrounding landscape. As discussed in the introduction, heat transfer from flames generally increases with increasing vegetation height and terrain slope. Accordingly, a SZ in the midst of steep terrain and tall vegetation will require a larger SSD than a SZ in the midst of flat terrain and short vegetation. If we assume that the SZ itself contains little or no flammable material, then the primary concern for SZ evaluation is the area surrounding the SZ. Accordingly, to calculate pSSD within the SZ polygon, slope and vegetation height need to be evaluated within a "buffer" surrounding a SZ (Campbell, 2017; Dennison, 2014).

3. Results and Discussion

The SSDE was developed in GEE and a free, open-access, web-based application can be viewed at https://firesafetygis.users.earthengine.app/view/ssde. The full publication can be viewed at https://www.mdpi.com/2571-6255/5/1/5/htm.

We envision the SSDE being of broad interest to the wildland fire community, from fire scientists to incident management personnel to wildland firefighters. Its open-access nature allows anyone to explore, examine, and interact with the concepts of SZs and SSD. Even if not used in an operational context, there is great value in being able to quickly and easily examine the conditions that define potential SZ suitability on a broad spatial scale. Wildland firefighters designate SZs on a daily basis as a part of their fire management

duties. Built into this designation process is an inherent degree of subjectivity that can result in differences in the interpretation of SZ suitability between and among crews. By using an objective tool for SZ suitability analysis that can be broadly applied in the US, fire crews across the country can increase the consistency and

reliability of the SZ evaluation process. However, given that this is a web-based platform requiring an internet connection, that also does not translate well to a mobile environment, we do not envision this as a real-time decision-making tool that firefighters could use on the ground. Instead, operational use of SSDE could be at the incident command level, for daily or more frequent evaluation of potential SZs for crews working on a fire. Given the dynamic and fast-paced nature of fire management, it is essential to be able to make rapid assessments of SZ suitability, particularly as fire conditions change. For example, cross-referencing near-real time data representing the current fire perimeter with SSDE can enable the evaluation of whether or not previously burned areas can provide SSD from nearby unburned fuel. Additionally, our SZ suitability driver analysis revealed the strong influence of wind on maximum within-SZ pSSD. This highlights the need to continually re-evaluate SZ suitability not only as the fire evolves, but as local weather conditions change as well.

4. References

Abatzoglou, J.T.; Williams, A.P. Impact of Anthropogenic Climate Change on Wildfire across Western US Forests. Proc. Natl. Acad. Sci. USA 2016, 113, 11770–11775.

Abatzoglou, J.T.; Battisti, D.S.; Williams, A.P.; Hansen,W.D.; Harvey, B.J.; Kolden, C.A. Projected Increases in Western US Forest Fire despite Growing Fuel Constraints. Commun. Earth Environ. 2021, 2, 227.

Alexander, M.E.; Taylor, S.W.; Page, W.G. Wildland firefighter safety and fire behaviour prediction on the fireline. In Proceedings of the 13th International Wildland Fire Safety Summit & 4th Human Dimensions Wildland Fire Conference, Boise, ID, USA, 20–24 April 2015; pp. 20–24.

Arizona State Forestry Division. Yarnell Hill Fire: Serious Accident Investigation Report. 2013. Available online: **https://dffm.az**. gov/sites/default/files/YHR_Data_092813_0.pdf (accessed on 3 January 2022).

Balch, J.K.; Bradley, B.A.; Abatzoglou, J.T.; Nagy, R.C.; Fusco, E.J.; Mahood, A.L. Human-Started Wildfires Expand the Fire Niche across the United States. Proc. Natl. Acad. Sci. USA 2017, 114, 2946–2951.

Beighley, M., 1995. Beyond the safety zone: creating a margin of safety. Fire Management Notes, 55 (4), 22–24.

Butler, B.W.; Bartlette, R.A.; Bradshaw, L.S.; Cohen, J.D.; Andrews, P.L.; Putnam, T.; Mangan, R.J. Fire Behaviour Associated with the 1994 South Canyon Fire on Storm King Mountain, Colorado; Research Paper RMRS-RP-9; U.S. Department of Agriculture, Forest Service, Rocky Mountain Research Station: Ogden, UT, USA, 1998; 82p.

Butler, B.W., 2014. Wildland firefighter safety zones: a review of past science and summary of future needs. International Journal of Wildland Fire, 23, 295–308. doi:10.1071/WF13021

Butler, C.; Marsh, S.; Domitrovich, J.W.; Helmkamp, J.Wildland Firefighter Deaths in the United States: A Comparison of Existing Surveillance Systems. J. Occup. Environ. Hyg. 2017, 14, 258–270.

Campbell, Michael J., Philip E. Dennison, and Bret W. Butler. "Safe separation distance score: a new metric for evaluating wildland firefighter safety zones using lidar." International Journal of Geographical Information Science 31.7 (2017): 1448-1466.

Campbell, Michael J., Philip E. Dennison, Matthew P. Thompson, and Bret W. Butler. "Assessing potential safety zone suitability using a new online mapping tool." *Fire* 5, no. 1 (2022): 5.

Cheney, P.; Gould, J.; McCaw, L. The Dead-Man Zone—A Neglected Area of Firefighter Safety. Aust. For. 2001, 64, 45–50.

Connor, C.D.O.; Calkin, D.E.; Thompson, M.P. An Empirical Machine Learning Method for Predicting Potential Fire Control Locations for Pre-Fire Planning and Operational Fire Management. Int. J. Wildland Fire 2017, 26, 587–597.

Dennison, P.E.; Brewer, S.C.; Arnold, J.D.; Moritz, M.A. Large Wildfire Trends in the Western United States, 1984–2011. Geophys. Res. Lett. 2014, 41, 2928–2933.

Dennison, Philip E., Gregory K. Fryer, and Thomas J. Cova. "Identification of firefighter safety zones using lidar." Environmental Modelling & Software 59 (2014): 91-97.

Dupuy, J.-L.; Maréchal, J. Slope Effect on Laboratory Fire Spread: Contribution of Radiation and Convection to Fuel Bed Preheating. Int. J. Wildland Fire 2011, 20, 289–307.

Frankman, D.; Webb, B.W.; Butler, B.W.; Jimenez, D.; Forthofer, J.M.; Sopko, P.; Shannon, K.S.; Hiers, J.K.; Ottmar, R.D. Measurements of Convective and Radiative Heating in Wildland Fires. Int. J. Wildland Fire 2013, 22, 157–167.

Gorelick, N.; Hancher, M.; Dixon, M.; Ilyushchenko, S.; Thau, D.; Moore, R. Google Earth Engine: Planetary-Scale Geospatial Analysis for Everyone. Remote Sens. Environ. 2017, 202, 18–27.

National Wildfire Coordinating Group Glossary A-Z|NWCG. Available online: https://www.nwcg.gov/glossary/a-z (accessed on 17 February 2017).

National Wildfire Coordinating Group. Incident Response Pocket Guide. 2014. Available online: https://www.nwcg.gov/sites/default/files/publications/pms461.pdf (accessed on 3 January 2022).

Page,W.G.; Butler, B.W. An Empirically Based Approach to Defining Wildland Firefighter Safety and Survival Zone Separation Distances. Int. J. Wildland Fire 2017, 26, 655–667.

Page, W.G.; Butler, B.W. Fuel and Topographic Influences on Wildland Firefighter Burnover Fatalities in Southern California. Int. J. Wildland Fire 2018, 27, 141–154.

Parsons, R.; Butler, B.; Mell,W. "Ruddy" Safety Zones and Convective Heat: Numerical Simulation of Potential Burn Injury from Heat Sources Influenced by Slopes and Winds; Imprensa da Universidade de Coimbra: Coimbra, Portugal, 2014; ISBN 978-989-26-0884-6.

Silva, F.R.Y.; O'Connor, C.D.; Thompson, M.P.; Martínez, J.R.M.; Calkin, D.E. Modelling Suppression Difficulty: Current and Future Applications. Int. J. Wildland Fire 2020, 29, 739–751.

Wei, Y.; Thompson, M.P.; Scott, J.H.; O'Connor, C.D.; Dunn, C.J. Designing Operationally Relevant Daily Large Fire Containment Strategies Using Risk Assessment Results. Forests 2019, 10, 311. [CrossRef]

Westerling, A.L. Increasing Western US Forest Wildfire Activity: Sensitivity to Changes in the Timing of Spring. Phil. Trans. R. Soc. B 2016, 371, 20150178.

Characteristics of surface litter fires: A systematic experimental study

Christos N. Pallikarakis; Dionysios I. Kolaitis*; Maria A. Founti

Fire Engineering Unit, Laboratory of Heterogeneous Mixtures and Combustion Systems,
School of Mechanical Engineering, National Technical University of Athens,
Heroon Polytechneiou 9, Zografou 15780, Greece.
{pallik@mail.ntua.gr}, {dkol, mfou}@central.ntua.gr

**Corresponding author*

Keywords

Wildland fires, litter fires, measurements, Rate of Spread, Heat Release Rate

Abstract

This work presents the results of laboratory experiments, focused on the characterization of surface wildland fires propagating in a litter fuel bed. A series of fire tests are conducted using an inclinable combustion table, measuring 2 m x 2 m, aiming to identify the effects of several important operational parameters on the characteristics of the developing fire. The parameters studied are the slope angle and the fuel load. A broad sensor network is installed, including 52 thermocouples, 3 bi-directional velocity probes, 2 heat flux sensors, a weighing system, 2 optical cameras and a real-time gas analyser. The obtained measurements are used to determine the time evolution of several characteristic parameters, such as position of the flame front (that yields the mean rate of spread), heat release rate, heat flux, axial velocity, as well as the mass loss. The construction of a 2D temperature field from the thermocouples that rest on a plane parallel to the propagation axis, illustrates several interesting flame characteristics. It is found that the rate of spread increases with slope angle and fuel load, whereas the heat release rate increases with slope and, dramatically, with fuel load.

1. Introduction

Wildland fires draw a large attention from multiple fields of science and engineering, due to the broad range of interacting physical and chemical phenomena that develop in multiple temporal and spatial scales. Understanding the wildland fire behaviour aims in acquiring in-depth scientific knowledge that will enable to adequately predict several key characteristics, such as flame rate of spread. The main parameters affecting the behaviour of wildland fires are the characteristics of the flora fuel, the atmospheric conditions, and the local topography.

Laboratory experimentation on wildland fires is broadly used to investigate various aspects of their characteristic behaviour (Rothermel and Anderson, 1966; Viegas and Pita, 2004). Although laboratory-scale experiments cannot incorporate the full spectrum of length scales observed in real-scale wildland fires, they still offer some significant advantages, since they facilitate controllability, repeatability and instrumentation management. In this context, small-scale fire tests may provide significant insight to the spread rate of surface wildland fires, thus providing valuable information to further understand and analyse more complicated wildland fire scenarios, e.g., crown fires (Scott et al., 2014).

A broad range of physical quantities has been proposed to describe the behaviour of a wildland fire. Undoubtedly, the most widely studied quantity, of both academic and practical value, is the Rate of Spread (ROS); knowledge of a wildland fire's spatio-temporal evolution is required to effectively coordinate fire suppression and civilian evacuation activities. In terms of the fire's combustion characteristics, the Heat Release Rate (HRR) is the most common quantity used to describe the thermal power and, thus, the severity of the fire; estimation of the HRR is usually performed in a laboratory environment by means of the oxygen consumption calorimetry method.Other measured quantities like the fuel mass loss rate, the radiative heat flux and the temperatures inside and above the fuel bed, can potentially reveal significant information regarding the underlying phenomena (e.g. convection, radiation) that affect the fire behaviour. .

In this work, a series of surface (litter) fire tests are performed on an inclinable combustion table, aiming to investigate the impact of several operational parameters on certain significant quantities that describe the fire behaviour. The investigated parameters are the fuel bed slope and the fuel load, and the measured properties are the mean Rate Of Spread (ROS), the Heat Release Rate (HRR), the mass loss rate, the heat flux, the axial velocity profile as well as the temperature spatial distribution, above and "inside" the fuel bed.

2. Experimental apparatus and experimental method

The experimental apparatus used is an inclinable combustion table, where fuel beds of Pinus Halepensis needles are evenly distributed. The table has an area of 2 m x 2 m and it can change its slope angle from 0 to 30 degrees (c.f. Figure 1). The table is located under an exhaust hood, which is used to collect the combustion product gases; a continuous gas analyser is employed to estimate the instantaneous HRR, using the oxygen consumption calorimetry method (Thornton, 1917; Janssen, 1991). The combustion table is equipped with a broad network of measuring instruments, i.e., a grid of 52 thermocouples distributed on a vertical plane along the direction of fire spread, near the middle of the fuel bed's width (y = 40 mm); 3 bi-directional velocity probes and 2 heat flux meters (one located vertically, at the downstream end, and the other located horizontally, at the level of the fuel bed surface) are also installed. To measure mass loss, the inclinable table rests upon three load cells. The positions of the instruments on the table are presented in Figure 2.

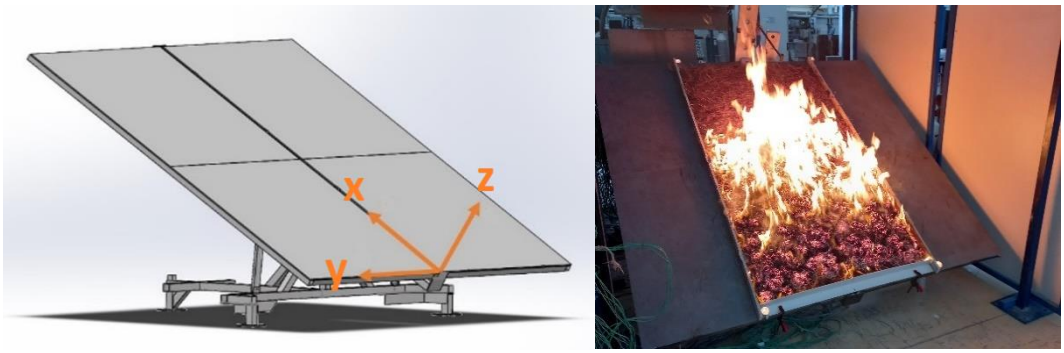

Figure 1: Model representation of the combustion table and its coordinate system (left) and indicative view of the experimental apparatus during a fire test (right).

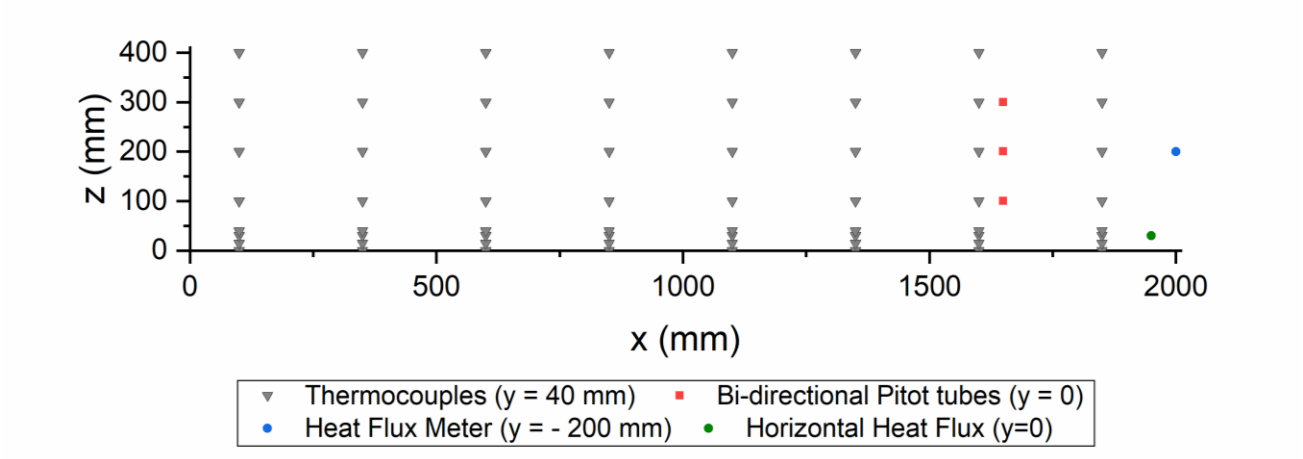

Figure 2: Locations of the measurment sensors (the coordinate system is defined in Figure 1).

The performed parametric study investigated the impact of two operational parameters, which are known to affect the characteristics of the developing fire, i.e., the fuel load and the slope angle. The specific characteristics of the 5 experimental test cases are presented in Table 1. For all the fire tests conducted, the fuel bed dimensions were 1.0 m (width) x 1.9 m (length). The Fuel Moisture Content was measured with a moisture analyser, yielding for all the experiment a value around 9% (in dry basis). The fire was linearly ignited at the upstream edge of the fuel bed (x = 50 mm) with the help of a paper string soaked in ethanol. Each test case was repeated 3 times; the presented results are averaged values.

Table 1- Characteristic parameters, and results of the 5 investigated test cases.

Test case	Slope angle, S (deg)	Fuel load (wet basis), m'' (kg/m^2)	Fuel bed height, δ (mm)	Rate of Spread, R (mm/s)	Fire duration, t_{end} (s)	Peak HRR, HRR_{max} (kW)
S00-M0_50	0	0.50	30	3.7	515	31
S00-M0_25	0	0.25	15	3.0	627	17
S20-M0_50	20	0.50	30	9.8	194	69
S30-M0_50	30	0.50	30	40	48	205
S00-M0_25	30	0.25	15	36	53	126

The ROS was estimated using temperature measurements from thermocouples located at the top surface of the fuel bed. More specifically, the first time that the second derivative of the temporal temperature recording was zero was assumed to be the time that the flame front reached that specific thermocouple. The rate of spread, R (mm/s), was estimated via linear interpolation of the resulting points of time and x position for the eight thermocouples in the array. The time the fire front required to reach the end of the fuel bed, t_{end} (s), was calculated by dividing the length of the fuel bed with the respective R; this value was used in each test case to define a dimensionless "flame propagation time", $\tau = t / t_{end}$, which is used in subsequent plots, allowing better comparison of the temporal evolution of the measured properties.

3. Results and Discussion

The temporal evolution of the flame front position is presented in Figure 3; the respective mean ROS values are given in Table 1. The ROS is found to increase with increasing slope as well as with increasing fuel load, in agreement with the existing literature (e.g. Tihay et al., 2014; Campbell-Lochrie et al., 2020). It is interesting to note that for the cases of 30° slope, there is a rapid increase of ROS. For all test cases, the instantaneous R appears to be relatively constant, thus suggesting the establishment of "steady-state" fire spreading conditions.

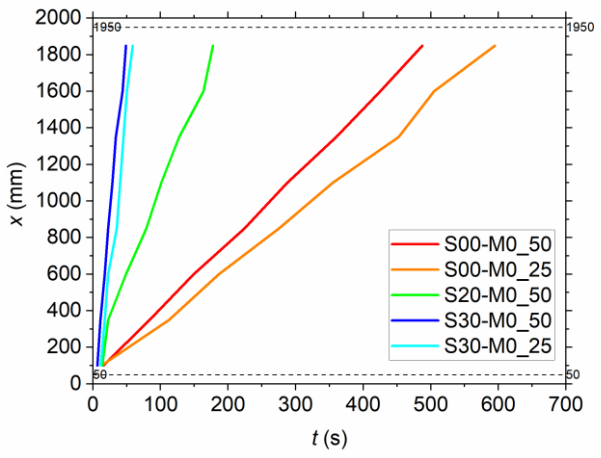

Figure 3 – Estimated temporal evolution of the flame front position.

The temporal evolution of the estimated HRR and the dimensionless mass loss are illustrated in Figure 4. Regarding the HRR (Figure 4, left), a similar trend to the temporal evolution of ROS is observed; more specifically, the HRR is found to increase with increasing slope and fuel load (Tihay et al., 2014). The effect of fuel loading seems to be stronger for the HRR, compared to that observed for the ROS, which is not surprising, since an increase in the fuel load results in a corresponding increase in the total amount of energy available for combustion. As far as the HRR temporal profile is concerned, it appears to reach a prolonged "plateau", for the test cases where the slope was less than 30 degrees. On the contrary, for the S30 test cases, the HRR exhibited a dramatic increase, showing a rather instantaneous "peak" before decreasing again. For all test cases, the HRR started to decrease roughly at $\tau = 1$. From that point on, it seems that the higher the peak value (HRR_{max}, c.f. Table 1), the longer the combustion processes continued to evolve behind the flame front. The continuation of the combustion process after $\tau = 1$ is also evident by the temporal evolution of the dimensionless mass loss

(Figure 4, right), where the mass continues to decrease for test cases S20 and S30, whereas it essentially ceases for test cases S00. Additionally, it is noted that with increasing the slope and the fuel load (while keeping the bulk density, $\rho_b = m''/\delta$, constant) the remaining fuel mass increases. This is mainly owed to the non optimal ventilation of the lower part of the fuel bed when its depth is increased as a consequence of the fuel load increase; in addition, the high ROS values observed with increasing slope, lead to reduced flame front residence times over the fuel bed, thus resulting in a prolonged combustion process.

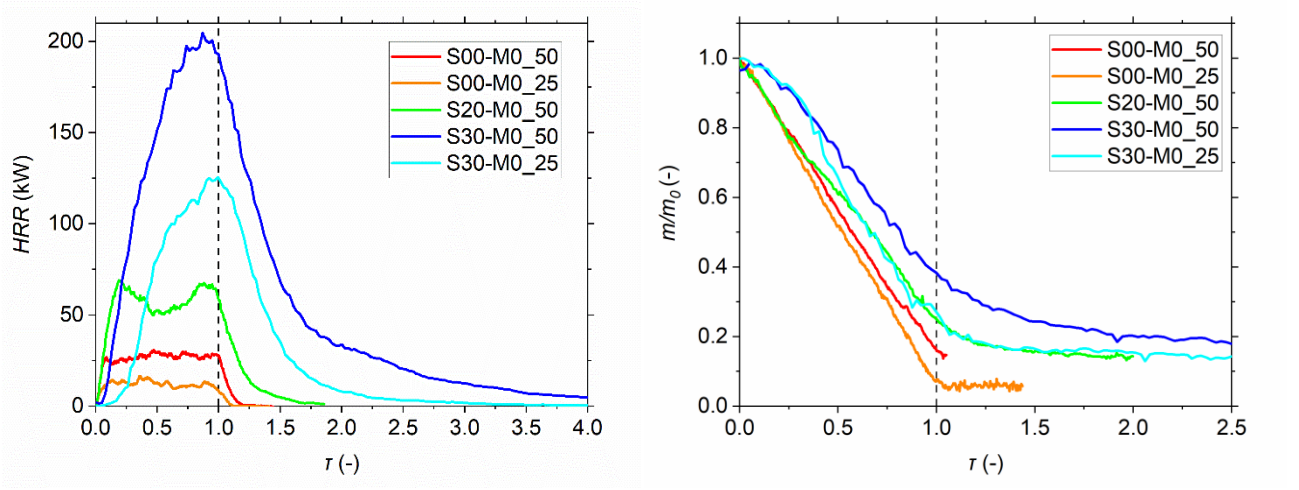

Figure 4 – HRR (left) and "normalised" mass loss (right) as a function of dimensionless time, τ.

The developing temperature fields above and inside (the dashed line corresponds to the fuel bed thickness, δ), the fuel bed, at three characteristic dimensionless times (0.25, 0.50 and 0.75) are presented in Figure 5 for all test cases. Increasing the slope results in a general increase of the temperature of the flame front, in agreement with relevant observations in the literature (Morandini et al., 2001); the same trend is observed when the fuel load is increased. The inclination angle of the flame toward the plane of propagation is increased with increasing slope angle. In addition, as the slope angle increases the flame front "depth" increases as well.

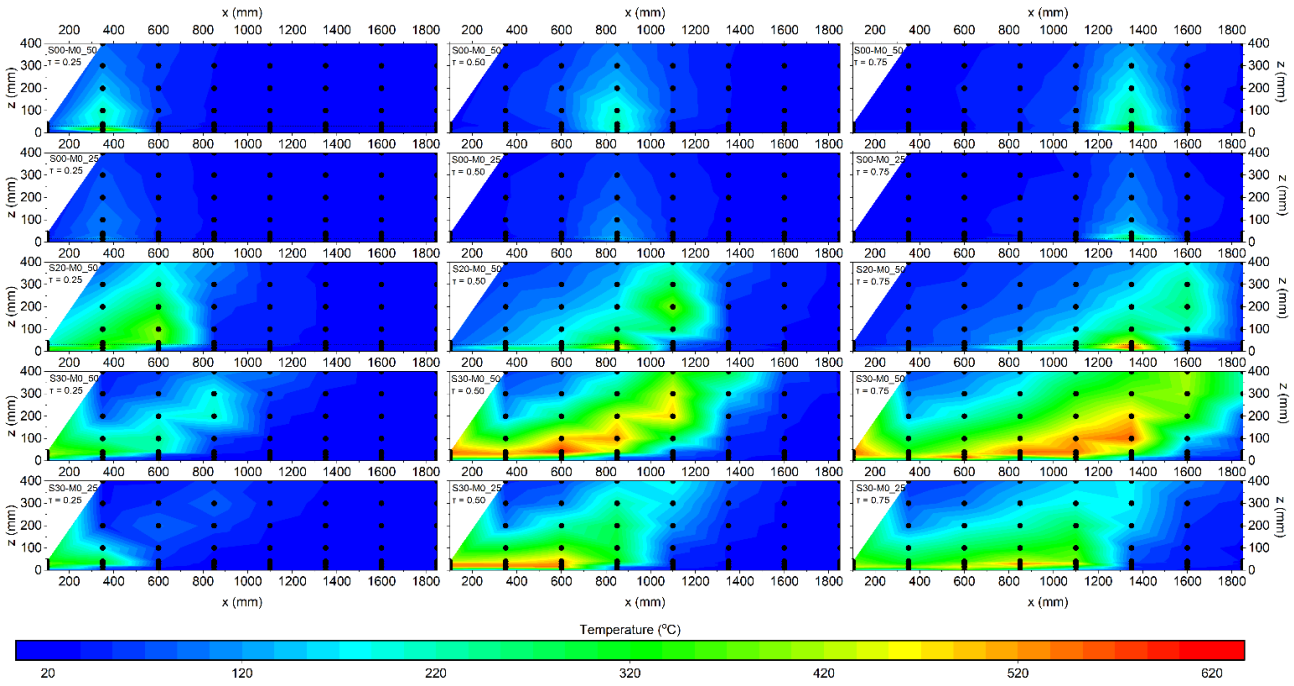

Figure 5 - Temperature contour plots for all test cases, at three characteristic dimensionless time values.

The temporal evolution of the horizontal heat flux at the downstream end of the fuel bed is presented in Figure 6. Again, increasing the slope and the fuel load result in an increase of the heat flux from the flame front. This is due to the fact that increasing the fuel load results in an increase of the flame height, while increasing the

slope decreases the flame tilt angle (the angle between the flame front and the combustion table). Both trends results in an increase of the radiative view factor which enhances the measured radiative heat flux. The latter is additionally enhanced by increased temperatures (as a result of increasing fuel load), as well as by increased emissivity (due to the increase of the flame depth).

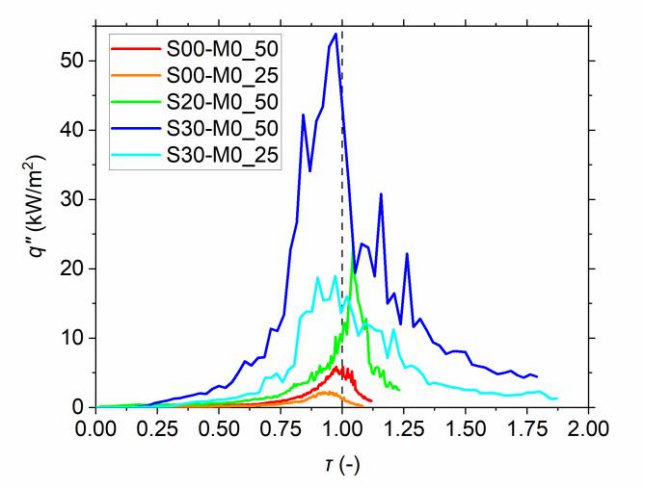

Figure 6: Temporal evolution of horizontal heat flux at the downstream end of the fuel bed.

The temporal evolution of the axial velocities near the downstream end of the fuel bed (x = 1650 mm) at three different heights (z = 100, 200 and 300 mm) are presented in Figure 7. At the height of 100 mm, close to the fuel bed surface, the negative velocities prior to the flame front's arrival indicate a downstream entrainment of air. After the passing of the flame front the axial velocities turn positive with a trend to increase with increasing slope. The magnitude of that upstream velocity seems to be unaffected by the fuel load (test cases M0_50 and M0_25), in contrast to the downstream velocity. At higher levels (200 mm and 300 mm), downstream air entrainment appears mainly in the non-sloped test cases (S00); additionally, the effect of fuel load seems to be stronger for test cases S30. As expected, the axial velocity magnitude decreases with increasing height.

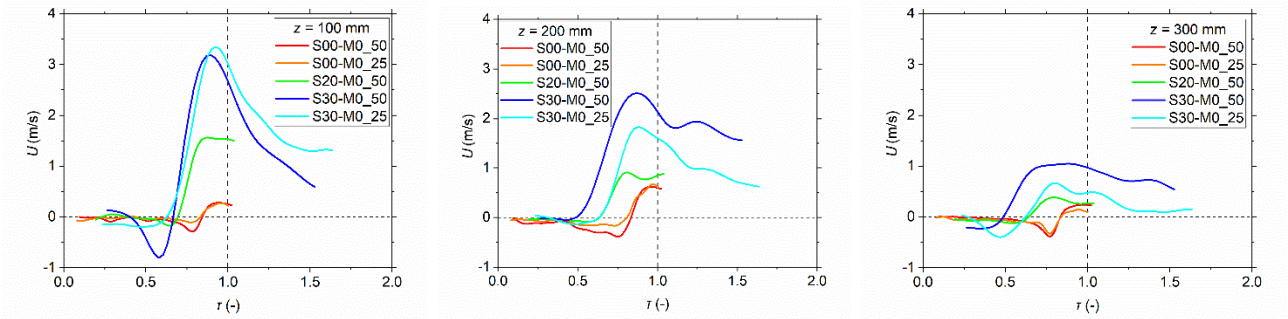

Figure 7: Axial velocity measurements at z = 100 mm (left), 200 mm (middle) and 300 mm (right).

4. Concluding Remarks

A parametric investigation regarding the effects of slope angle and fuel load on the characteristics of surface wildland fires has been conducted on a laboratory-scale combustion table. The trends observed are generally in agreement with respective findings reported in the literature. ROS increases with increasing slope angle and fuel load; a rapid increase is observed for a 30º slope angle. HRR follows a similar trend; the fuel load has a stronger influence on HRR compared to ROS. After ignition, the HRR seems to reach a plateau for all test cases, except those with a 30º slope, where HRR exhibits a continuous increase until a peak value is reached and then a gradual decrease. The remaining fuel mass increases with increasing slope, due to the appearance of incomplete combustion conditions at the lower parts of the fuel bed. The spatio-temporal evolution of gas temperatures reveals that the flame depth increases with increasing slope and fuel load, while the flame tilt angle is decreased. Moreover, increasing fuel load and slope result in increased flame front temperatures; the same observations appears to be true also for the heat flux. Finally, axial velocity measurements reveal the magnitude

and the direction of the upstream and downstream air entrainment flows and how they change with slope and fuel load.

5. References

Campbell-Lochrie Z., Walker-Raver C., Gallagher M., Skowronsiki N., Mueller E.V., Hadden R.M., Investigation of the role of bulk properties and in-bed structure in the flow regime of buoyancy-dominated flame spread in porous fuel beds, Fire Safety Journal 120 (2020) 103035.

Morandini F., Santoni P. A., Balbi J. H., The contribution of radiant heat transfer to laboratory-scale fire spread under the influences of wind and slope, Fire Safety Journal 36 (2001) 519-543.

Rothermel R. C., Anderson H. E., Fire Spread Characteristics determined in the Laboratory, (1966), U.S. Forest Service, Research Paper INT-30, Intermountain Forest & Range Experiment Station, U. S. Department of Agriculture, Ogden, Utah.

Scott A. C., Bowman D. M. J. S., Bond W. Pyne J., S. J., Alexander M. E. (2014), Fire on Earth: An Introduction, Wiley Blackwell, West Sussex, UK.

Thornton W.M., The Relation of Oxygen to the Heat of Combustion of Organic Compounds, The London, Edinburg and Dublin Philosophical Magazine and Journal of Science 33 (194) (1917) 196-203.

Janssens M. L., Measuring Rate of Heat Release by Oxygen Consumption, Fire Technology 27 (1991) 234-249.

Tihay V., Morandini F., Santoni P.-A., Perez-Ramirez Y., Barboni T., Combustion of forest litters under slope conditions: Burning rate, heat release rate, convective and radiant fractions for different loads, Combust. Flame 161 (2014) 3237-3248.

Viegas D. X., Pita L. P., Fire Spread in Canyons, Int. J. Wildland Fire 13 (2004) 253-274.

Clean Forest – Project concept and preliminary results

João Gomes*[1;2]; Jaime Puna[1;2]; António; Marques[1]; Jorge Gominho[3]; Ana Lourenço[3]; Rui Galhano[2]; Sila Ozkan[2]

[1] Departamento de Engª Química, Instituto Superior de Engenharia de Lisboa, R. Conselheiro Emídio Navarro, 1, 1959-007 Lisboa, Portugal. {jgomes@deq.isel.ipl.pt}
[2] CERENA – Centro de Ambiente e Recursos Naturais, Instituto Superior Técnico, Universidade de Lisboa, Av. Rovisco Pais, 1, 1049-001 Lisboa,Portugal
[3] Instituto Superior de Agronomia, Universidade de Lisboa, Tapada da Ajuda, 1349-017 Lisboa, Portugal

**Corresponding author*

Keywords

Forest waste valorization; Generation of synthesis gas; Biofuels

Abstract

The aim of this project is to valorize forest biomass wastes (and then prevent their occurrence as a fuel source in forests) into bioenergy, more precisely, production of 2nd generation synthetic biofuels, such as biogas, biomethanol, bio-DME, etc., depending on the process operating conditions, such as pressure, temperature, and type of solid catalyst used. The valorization of potential forest waste biomass enhances the reduction of the probability of occurrence of forest fires and presents a major value for local communities, especially, in rural populations. Biogas produced can be burned as biofuel to produce heat and/or electricity, for instance, in cogeneration engines applied for domestic/industrial purposes. After the removal of forest wastes from the forest territory, this biomass is dried, grounded to reduce its granulometry, and liquified at temperatures between 100-200 ºC. Then, using the electrocracking technology, this liquified biomass is mixed with an alkaline aqueous electrolyte located in an electrolyzer (electrochemical reactor which performs an electrolysis process), using a potential catalyst, in order to produce syngas (fuel gas, mainly composed of CO, H2, and CO2). In a second reaction step, the syngas produced can be valorized in the production of synthetic biofuels, in a tubular catalytic reactor. The whole process is easy to implement and energetically, shows significative fewer costs than the conventional process of syngas gasification, as the energy input in the conventional pyrolysis/gasification process is higher than 500 ºC, with higher pressures, while, in the electrochemical process, applied in this project, the temperatures are not higher than 70 ºC, with 4 bars of pressure, at maximum. Besides that, the input of energy necessary to promote the electrolysis process can be achieved with solar energy, using a photovoltaic panel. In the production of biogas in the catalytic reactor, there is another major value from this process, which is the co-production of water, as Sabatier reaction converts CO2 and H2 into biomethane (CH4) and steam water, at atmospheric pressure, with 300 ºC of temperature, maximum, with a high selective solid catalyst. Finally, it is expected to produce a new bio-oil from this kind of biomass, with properties closer to a fossil fuel than wood bio-oils, which can be used as a fuel or as a diolefins/olefins source and, also, to produce, from forest biomass wastes, pyrolytic bio-oils with complementary properties and valorized characteristics. This can be used in the wood treatment or as a phenol source, for several industrial applications. A new and valorized application can be found for forest biomass wastes, which can be incorporated into the biorefinery concept.

1. Project background

Over the past years, Portugal has been affected by wildfires resulting in the degradation of natural resources and human life. The increased agriculture and forest lands that are unmanaged are one of the main contributions to wildfires. The present project intends to contribute to the reduction of wildfires by collection and valorization of the forest biomass growing in lands of higher wildfire susceptibility. The first step for biomass valorization passes through a detailed characterization (anatomical, chemical, physical and thermal properties) in order to establish the best platform for their transformation into energy or chemicals. Liquefaction and syngas production are two processes where the biomasses can be transformed into added-value products. Biomass liquefaction is a recent method that converts biomass into bio-oil. In the last years, there was an increase in the number of published works related to this technology (Huang, 2017), in particular, using forest biomasses (e.g. eucalypt, cork residues) (Mateus, 2016). Generally, this process has three main steps: depolymerization, decomposition, and recombination of biomass compounds at higher temperatures. The biomass is decomposed into bio-oil,

solid, and small gas components. The critical process parameters, such as temperature, residence time, repolymerization process, condensation, and compound decomposition of the different phases can change (Gollakota, 2018). The biomass liquefaction was applied first by Mateus et. al. (2016), using cork dust from the cork stoppers rectification process. The dust was dried at 120 ºC, and mixed under a glass reactor, with a mixture of organic solvents, and an acid catalyst at 160 ºC (90 min). The bio-oil was recovered after a purification process and, the solid waste obtained was dried. Hydrogen can be produced by water electrolysis, an electrochemical process, where it's needed to supply energy, from an electric source, producing also, oxygen, half the quantity of hydrogen (Carmo et al., 2013). It uses electric current through two electrodes: the anode (oxygen production) and the cathode (hydrogen production) (Guerra, 2015).

The natural gas, coal, and biomass can be converted into biofuels and chemical products, like biodiesel by the Fischer-Tropsch process, methanol/DME, hydrogen, and ammonia, all of them used as raw-material, syngas, depending on their quality, operating conditions, etc., through thermochemical processes, like, reforming, pyrolysis, partial oxidation, and gasification. Due to the higher energetic input costs, these processes are only economically feasible at large scales (Venvik, 2017). Besides that, it's possible to produce syngas ($CO/CO_2/H_2$), by water co-electrolysis with a carbon source. Today, syngas is indispensable in the chemical industry, crude oil, and energy industries. It is considered an attractive raw material in the chemical synthesis, as well, as in the production of clean fuels, like biofuels (biogas, methanol, DME) (Nguyen, 2015) (Khodakov, 2007). The main production processes result from the reforming process, especially used in the crude oil and petrochemical industries. The methanation reaction is called the Sabatier process. Recently, the methanation of carbon dioxide gained interest due to its application in the Power-to-Gas technology, as well, as the biogas upgrading, into natural gas. Hydrogen reacts with carbon monoxide and carbon dioxide and they are transformed into methane and, water as co-product. The methanation of carbon monoxide/dioxide is an overall exothermic chemical process (Stangeland et al., 2017).

The GreenSynFuel technology, patented by GSYF, a small Portuguese company that has been working with ISEL and IST-ID partners, with the purpose of producing syngas in only one reaction step, through an innovative electrochemical process of water alkaline electrolysis, using graphite as electrodes and, with electricity supply. The design of the electrolyzer used in this project is a quite differentiating point since the produced gas isn´t separated, as there is not a physical separation of the hydrogen and oxygen gases. This electrolyzer presents a significant reduction in costs, from the conventional electrolyzer technology (alkaline, PEM, and SOEC). This process can be used to produce renewable synthetic biofuels, as alternatively to fossil fuels. Biofuels obtained from forest biomass, are considered environmentally friendly and sustainable ones, if the electric source is a renewable one, like solar or wind energy (Guerra et. al, 2015) (Guerra et. al., 2018a) (Guerra et. al., 2018b). GSyF technology belongs to this category. The production and utilization of these biofuels will play an important role in the decarbonization of the energy mix, maximizing the utilization of renewable sources, like the forest biomass, going to meet the Energy Roadmap 2050 objectives of the EU, also defined in the National Script of Low Carbon.

A preliminary step, already performed at ISEL, was the built-up of a lab prototype, to test/validate this technology. Then, it was possible to build a pilot plant of this electrolyzer (with modules of 1 kW power) applied to produce syngas, with posterior production of biomethane and biomethanol, through water electrolysis with steel electrodes and liquified biomass, as the renewable carbon source. The valorization of biogas produced can be used, also, to produce heat/electricity, for the off-grid market, with special emphasis on the rural electrification. After technology validation, it's our purpose to perform the scale-up for modules with more power (megawatts), where the potential clients are the network management of low voltage, storage of renewable electric energy, and production of synthetic fuels. In this project, the main purpose is to produce biogas with this renewable process, valorizing the liquified biomass from the forest wastes, to prevent the probability of occurrence of wildfires.

2. Project preliminary results

2.1. Sampling and fractionation

Residues from *Acacia melanoxylon* were collected with the cooperation of Parques de Sintra - Monte da Lua, in Sintra, Portugal. Three types of residues were collected: i) chips (composed of wood and bark); ii) Crown

residues (composed of branches and leaves); and iii) a Mixture of the first two types of residues (chips and crown residues). The samples were air-dried in the laboratory for 1 month and then milled in a Retsch SM 2000 knife mill, sieved in a Retsch ISO 9001 vibratory screen, and the 40-60 mesh fraction was used for chemical analysis.

2.2. Chemical analysis

Forest residues from *Acacia melanoxylon* (chips – wood and bark; crown residues – leaves and branches; a mixture of both) were collected and characterized by pyrolysis analysis (PY-GC/MS). The extractive-free samples were milled to a fine powder and around 0.10mg pyrolyzed at 550ºC for 1 min. The content in carbohydrates ranged from 42.6% (crown) to 52.4% (mixture), while lignin ranged from 19.6% (mixture) and 24.0% (chips). The monomeric lignin composition was similar between the samples, with a predominance of syringyl units (S, 15.2%, 11.1%, and 12.6%), followed by guaiacyl units (G, 7.8%, 7.1%, and 5.5%), and a minor percentage of *p*-hydroxyphenyl units (H, 0.3%, 0.7%, and 0.3%). This agrees with the literature since the Acacia species belongs to hardwoods, and in this group, the S and G-units prevail.

2.3. Bio-oils production and characterization

Several materials were used as feedstock for theprocess, such as heartwood, sapwood, bark, and branches from the burnt remains of a tree caught in the fires in Leiria national park, and pinewood sawdust was used as the standard feedstock material. Besides the shredding of some of the samples, such as the heartwood, sapwood, and bark samples, to increase the contact surface area between the solvent and the feedstock, no further treatments were done to the feedstocks. The standard chemical used as a solvent in the process was 2-Ethylhexanol, but studies were done utilizing pork lard (PL) and glycerol carbonate(GC). Regarding the catalyst, it was used p-Toluenesulfonic acid (PTSA) primarily, although some tests were done using sulfuric acid (SA). Also, a liquefaction procedure was tried which consisted of a moderate acid-catalyzed liquefaction process. The liquefaction of lignocellulosic material occurs through a solvolytic reaction under acid catalysts to form smaller fragments, with the further possibility that these fragments continue reacting with either themselves or with the solvent to form higher molecular fragments or solvent-derived compounds. The types of biomass used in the liquefaction processes were tested to find out their water and ash content, and the elemental analysis as well.

The studies performed on the solvent showcased the problem of using either PL or GC as a solvent, with the first producing low conversion rates and the second-highest viscosityproducts that are difficult to work with at an industrial scale. As for studies done about the catalyst and temperature, the best results using PTSA were produced when it was fed in higher amounts to the reactor, and whilst the SFA showed better conversion yields for reaction temperatures below 170 ºC, as the temperature increased the conversion gap between the two catalysts tested decreased. Some of the lignocellulosic samples, heartwood, and sapwood, produced consistently higher conversion yields for the type of feedstock used, showcasing similar behavior. At the same time, the reaction times increased, with thestandard pine trailing behind them. As for the bark and branches samples, their conversionrates were mostly lower than those of other samples, similar to the increasing liquefaction time. Some bio-oil samples, produced from heartwood,sapwood, and bark, had their excessive solvent removed and their TAN and OHN calculated through titration, with both of those values following opposite trends to the ones expected by the literary research. The OHN of the samples was also mostly lower than the lowest limit necessary for rigid and semi-rigid polyurethane production. As a whole, the tests conducted showed that the samplesfrom burned wood, especially samples of heartwood andsapwood, can be used in liquefaction processes and produce high conversion yields that originate in final products, such asbio-oils, that have a higher HHV and can be used in several industrial processes as fuels. This indicates that liquefaction is a possible way to somewhat reduce the economic impact felt by landowners who suffered due to the fires that raged through the country last summer and autumn, by using the valueless waste resulting from the burnt wood and creating a value-added product that can be used as fuel.

Also, bio-oil production was performed by the thermochemical liquefaction method. Different species of woody biomass such as burnt pine heartwood, Acacia Melanoxylon bark wood; 2-Ethylhexanol was used as a solvent and p-Toluenesulfonic acid was used as a catalyst. The procedure consisted of a moderately acid-catalyzed liquefaction process., and it was applied under different conditions in accordance with MODDE 12.1 Pro® software program to obtain the model. After numerous trials, optimal results showed a bio-oil yield of 86.03% at 160 ºC for 180 mins of reaction time and by using 5.5% p-TSA catalyst concentration overall mass and an HHV of 36.41 MJ/kg, energy densification ratio of 1.96 times greater than the HHV of burnt pine heartwood.

In addition, the liquefaction conversion of the bio-oil from acacia bark wood was 83.29% at 170 ºC for 30 mins of reaction time and by using 10% p-TSA catalyst concentration overall mass. A reaction surface methodology (Box-Behnken design) was applied for liquefaction reaction optimization. The obtained model for the liquefaction of Burnt Pine heartwood offers an ideal correlation with the experimental data as R^2= 0.988. The model predicts accurate responses with a probability of 98.8%. Furthermore, the software offers relatively more accurate responses with a probability of 99.8% (R^2=0.998). In the proposed model for Burnt pine heartwood, the most effective coefficient was temperature, while the most effective was the catalyst concentration for acacia bark wood. The liquefied products were characterized by Fourier Transformed Infrared (FTIR) and thermogravimetric analysis (TGA); Scanning electron microscopy (SEM) was also performed to confirm the effect of the morphological changes on the surface area of the solid samples.

3. Acknowledgments

This project is partially financed by Fundação da Ciência e Tecnologia, through grant ref. PCIF/GVB/0167/2018.

4. References

Carmo, C. (2013). A comprehensive review on PEM water electrolysis. Journal of Hydrogen Energy, 8 (12), 4901-4934.

Gollakota, A.; Kishore, N.; Gu, S. (2018). A review on hydrothermal liquefaction of biomass. Renewable and Sustainable Energy Reviews, 81 (Part 1), 1378-1392.

Guerra, L,; Gomes, J.; Puna, J.; Rodrigues, J. (2015) Preliminary study of synthesis gas production from water electrolysis, using the ELECTROFUEL concept. Energy, 89, 1050-56.

Guerra, L.; Rossi, S.; Rodrigues, J.; Gomes, J.; Puna, J.; Santos, M. (2018) Methane production by a combined Sabatier reaction/water electrolysis process. Journal of Environmental Chemical Engineering, 6, 671-76.

Guerra, L.; Moura, K.; Rodrigues, J., Gomes, J.; Puna, J.; Santos, T. (2018) Synthesis gas production from water electrolysis using the Electrocracking concept. Journal of Environmental Chemical Engineering, 6, 604-09.

Huang, H.; Yuan, X. (2015). Recent progress in the direct liquefaction of typical biomass. Progress in Energy and Combustion Science, 49, 59-80.

Khodakov, A.; Shu, W.; Fongarland, P. (2017). Advances in the development of novel cobalt Fischer-Tropsch catalysts for synthesis of Long-Chain hydrocarbons and Clean Fuels, Chemical Reviews, 7, 1692-1744.

Mateus, M.; Bordado, J. C.; Santos, R. G. (2016). Potential biofuel from liquefied cork – Higher heating value comparison. Fuel, 174, 114-117.

Stangeland, K.; Kalai, D.; Li, H.; Yu, A. (2017). CO_2 Methanation: The Effect of Catalysts and Reaction Conditions. Energy Procedia, 105, 2022-2027.

Venvik, H.; Yang, J. (2017). Catalysis in microstructured reactors: short review on small-scale syngas production and further conversion into methanol, DME and Fischer-Tropsch products. Catalysis Today, 285, 135-146.

Climate adjustment of the physical parametrization for the fire-spotting

Vera N. Egorova*[1]; Gianni Pagnini[2,3]

[1]Depto. De Matemática aplicada y Ciencias de la Computación, Universidad de Cantabria, Av. De los Castros s/n, 39005, Santander, Spain, {vera.egorova@unican.es}
[2] BCAM–Basque Center for Applied Mathematics, Alameda de Mazarredo 14, 48009, Bilbao, Basque Country, Spain, {gpagnini@bcamath.org}
[3] Ikerbasque–Basque Foundation for Science, Plaza Euskadi 5, 48009, Bilbao, Basque Country, Spain.

**Corresponding author*

Keywords

Fire-spotting, Flame geometry, Atmospheric stability, Climate classification, Climate change

Abstract

The aim of the present study is to provide a simple yet complete addition to operational fire spread models for representing the random behavior of fire-spotting in various climate classes through simple inputs related to the wildfires. Results from different test cases highlight the sensitivity of the proposed simple physical parametrization in simulating different scenarios of the generation of secondary fires by fire-spotting under different climatic conditions. Since climate change may cause extreme conditions that contribute to the high fire intensity and larger wildfires, the parametrization here proposed allows us to model the fire-spotting process in various climatic zones and to adjust the existing operational model to the climatic changes.

Fire-spotting involves aspects among scales: from the combustion chemistry in microscale, to fire-atmosphere interaction in macroscale. At the meso-scale level, fire-spotting is affected by the mean wind and fireline intensity, which is found to be in a strong interaction with the surrounding factors, such as fuel and local orography. At the macroscopic level, the atmospheric stability conditions impact the fire-spotting pattern. Both, meso- and macro-scale factors are taken into consideration in the proposed probabilistic model devised to provide a physical meaning to the spread of fire by virtue of firebrands, which allows the integration of the diversity of all these parameters into a few differentiable regions. For this purpose, the classification based on the Köppen-Geiger map is considered, as it is done in the study of complex natural systems in a broad range of topics in hydrology, agriculture, biology, and many others.

Preliminary studies show as well that fire-spotting is a vegetation-dependent phenomena, since not all types of vegetation can generate sufficient combustion energy or produce the firebrands. In order to represent the vegetation component of the fire-spotting generation, the biome world map is incorporated, resulting in the integrated climate-biome classification for the fire-spotting generated fires.

1. Introduction

In present study we are aimed to integrate the diversity of climate-dependent parameters of the fire-spotting into a few differentiable regions basing on an integrated climate-biome classification. For that purpose, ***RandomFront2.3*** routine described in Truccia et al. (2019) is considered to perform the calibration of the fire-spotting parameters to different climate classes by applying the statistical study and simulations. In the considered approach, the effect of the fire-spotting is incorporated into the main fire-front model by adding features related to the statistical description of the firebrands transport, which depends on flame structure and local weather, aerodynamics around firebrands, combustion and heat transfer of firebrands during flight. Since ignition of the fuel at the landing position involves heat exchange over a sufficient period, a delay effect due to "heating-before-burning" is taken into account by the model proposed in Trucchia et al. (2019).

The proposed multi-scale physical parametrization for the fire-spotting phenomena points out the impact of atmospheric stability and fuel moisture on the fire-spotting. This fact motivates us to improve the probabilistic model by including the local climate characteristics. Moreover, since climate change may cause extreme conditions that contribute to the high fire intensity and larger wildfires, the proposed parametrization allows for modelling fire-spotting phenomenon in various geographical zones and adjustment of the existing model to the

climate changes. Thus, we focus on the calibration of the fire-spotting parameters to different climate classes by applying the statistical study and simulations.

2. Integrated climate-biome classification

Despite a growing body of literature that recognizes the interaction between climate and wildfires, much less is known about the climate impact on fire-spotting. However, the amount and bark type of fuel determine the energy available for combustion, while wind and hot air are the primary drivers of the fire-spotting. Locality of these factors cause the possible geographical variations of the fire-spotting patterns. Previous studies reported different spotting distributions, number and distances of the secondary fires in various geographical zones, see Storey et al. (2020).

In present research, we integrate the diversity of climate-dependent parameters of the fire propagation into a few differentiable regions basing on climate-biome classification. For the biome, the Walter's vegetation classification by Breckle (2002) is considered, while for the climate the Köppen-Geiger climate classification by Peel et al. (2007) has been applied. This classification distinguishes five climate groups, depending on seasonal precipitation and air temperature and their seasonality. These groups are:

A: Tropical, that is characterized by average temperature ≥ 18◦C with significant precipitation.

B: Arid, where the average temperature is around 20◦C with little precipitation.

C: Temperate, that has the coldest month averaging between 0◦C and 18◦C and at least one month averaging above 10◦C.

D: Cold (continental), where at least one month averaging ≤ 0 ◦C and at least one month averaging ≥ 10◦C.

E: Polar, that includes tundra and ice cap, and characterized by every month average temperature ≤ 10◦C.

Hence, there have been chosen several climate classes with the parameters given in Table 1. The integrated climate-biome parametrization is incorporated to the operational code LSFire+ via ***RandomFront2.3*** post-processing routine, see Trucchia et al. (2019). In the considered probabilistic model, depending on the climate class the ambient temperature, the ABL height and mean biomass are chosen. Rest of parameters are fixed in order to emphasize the impact of the climatic factors. Table 1 connects and systematizes various classifications, such as Köppen-Geiger climate classes, biomes and NFFL fuel models. The flame geometry is found to be proportional to the mean biomass. It is important to notice that the parameters may vary within the same climate class due to season and location.

Table 1. Climate dependent parameters for the wildfire propagation modelling

Climate Class	Biome	Mean biomass, tons/ha	NFFL Model	H_{ABL}	Localization
Af	Tropical rainforest	500	6	1200 / 350	South America, Amazonia
BSh	Savanna	27	3	3500 / 2500	South-East Australia
BWh	Desert	4	1	2700 / 550	South-East Australia
Cfb	Temperate forests	370	7	3500 / 2500	South-East Australia
Csa	Mediterranean vegetation	410	2	3500 / 400	Mediterranean Area
Dfb	Temperate broad leaf forests	400	9	1500 / 400	Eastern Europe, Northern Rockies (USA)
Dfc	Taiga	260	9	1500 / 500	Canada, Finland

In present study, for the simulation of the fire front propagation, we use the NFFL fuel model Scott and Burgan (2005), which allows the consideration of the fuel characteristics in accordance with the chosen climate class. Thus, the climate characteristics are incorporated not only through the parameters of the fire-spotting distribution but also through the parameters of the underlying fire-spread model. Moreover, one of the key vegetation characteristics, net primary productivity, impacts through the fire intensity on the flame length and the maximum loftable height.

3. Multiscale parametrization

The described above climate-biome parameters are incorporated into the fire-spotting probabilistic model of Trucchia et al. (2019). The firebrand landing distribution $q(\ell)$ is here assumed to be lognormal distributed following

$$q(\ell) = \frac{1}{\sqrt{2\pi}\sigma\ell} e^{-\frac{\left(\ln\frac{\ell}{\mu}\right)^2}{2\sigma^2}}, \tag{1}$$

with median μ and mode $\mu e^{-\sigma^2}$.
At the macroscopic scale, fire-spotting is affected by atmospheric conditions. In particular, we plug the depth of the atmospheric boundary layer (ABL), that is related to the atmospheric stability, into the estimation of the smoke-injection height including the uplift against the atmospheric stratification and the plume widening due to entrainment of the surrounding air. Then, it holds

$$\mu = H_{max}\sqrt{\frac{3\,\rho\,C_d}{2\,\rho_f}},$$

where H_{max} is the maximum loftable height, ρ is the air density, ρ_f is the fuel density and C_d is the drag coefficient. In fact, H_{max} depends on the fire intensity and atmospheric stability, the detailed study of this parameter and the impact of the atmospheric stability conditions are provided in Egorova et al. (2020).

The parameter σ is defined in Egorova et al. (2022) as follows

$$\sigma = \frac{1}{z_p}\ln\left(\sqrt{Fr} + \beta\sqrt{\frac{2\,\rho_f U^2}{3\rho C_d g\,L_f}}\right),$$

where Fr is the Froude number, $\beta = 0.945$ is a correcting factor, g is the gravitational acceleration, and L_f is the flame length written in terms of the fireline intensity I_f and some surrounding factors as follows

$$L_f = \beta_0 I_f^{2/3} = \frac{I_f^{2/3}}{\cos\theta\,\left(2g\left(\rho c_p T_a\right)^2\right)^{1/3}},$$

where c_p is the specific heat of air at constant pressure, T_a is the air temperature and θ is the tilting angle in the simplified model of the flame geometry presented in Figure 1.

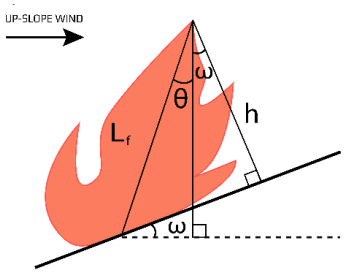

Figure 1: Flame geometry

Considered parametrization of the downwind landing distribution admits the consideration of climatic factors and their impact on fire-spotting, and, consequently, on the fire front propagation, which will be discussed further.

4. Simulations

The simulations show that by using the considered physical parametrization of the fire-spotting distribution different fire-front patterns can be obtained. We focus mainly on the climate classes with registered fire-spotting events, such as South-Eeastern Australia (BSh and BWh classes) and Mediterranean zone (Csa class).

For BSh and BWh climate classes (see Table 1), which can be considered as a pattern for the South-East Australia, as well as Csa class (Mediterranean class), the stable and unstable atmospheric conditions are considered to compare the fire-spotting patterns not only between the classes but also within the chosen class. The simulated fire fronts are plotted in Figures 2, 3 and 4, respectively.

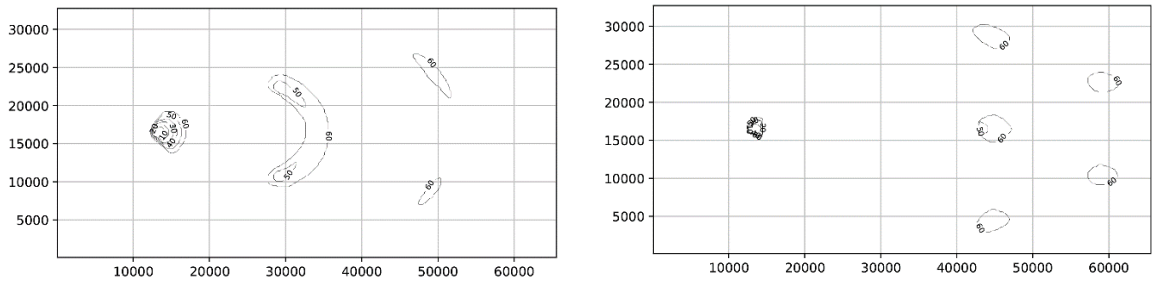

Figure 2: Fire-spotting pattern in the BSh climate class (South-Eastern Australia) during the unstable (left) and stable (right) atmospheric conditions

In the case of BSh, the fire-spotting is observed in both modes: unstable and stable atmospheric conditions. However, with unstable atmosphere, which corresponds to the daylight period, the secondary fires merge, while during the stable conditions the fire-spotting pattern is characterized by longer travel distance of the fire brands and higher number of new independent ignitions.

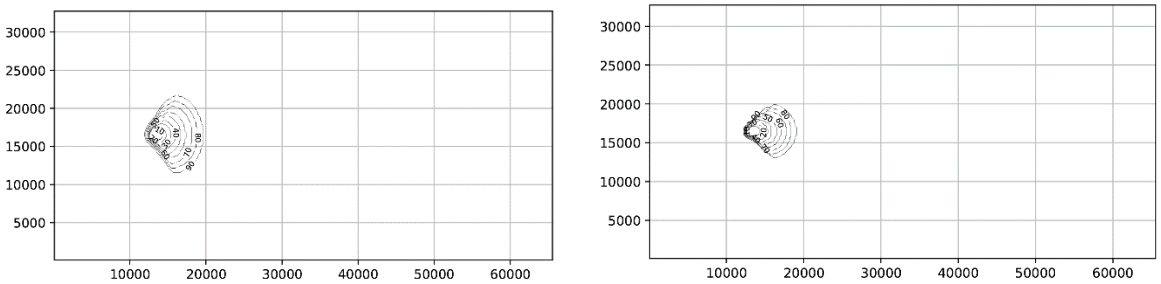

Figure 3: Fire front without fire-spotting in the BWh climate class (deserts in South-Eastern Australia) during the unstable (left) and stable (right) atmospheric conditions.

In contrast, for the BWh class, which represents deserts located in the South-Eastern Australia, fire-spotting is not observed, exposing the effect of the climate factors of the model. Moreover, the main front under the unstable atmospheric conditions is larger due to the turbulence effect, see Egorova et al. (2020) for details.

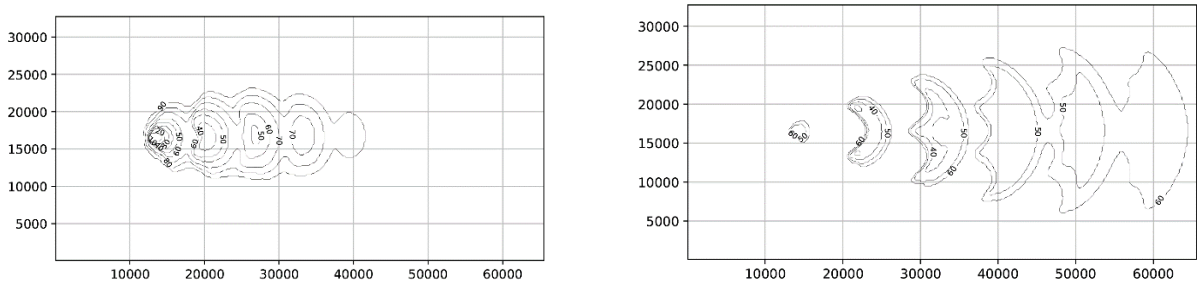

Figure 4: Fire-spotting patterns for the Csa climate class (Mediterranean Area) during the unstable (left) and stable (right) atmospheric conditions

Slightly different patterns can be obtained for the Mediterranean climate class Csa in Figure 4: during unstable conditions fast merging leads to one large fire, while during the stable atmosphere several spotting fires can be observed. Hence, the structure is like for BSh class, but the form of the fire front is completely different.

The performed simulations reflect qualitatively the reality: in different climate classes different fire-spotting patterns are observed. Unfortunately, validation though the comparison with historical data is not feasible. In fact, we cannot get sufficient statistical information about fire-spotting generated fires from wildfires worldwide from satellites' data collected using NASA Fire Information for Resource Management System (FIRMS).

Actually, data are taken from two satellites: MODIS with resolution 1 km and VIIRS with resolution 375 m, which means that VIIRS can capture smaller fires.

The observation horizon is chosen from 2012-01-20 to 2021-08-31. The data were collected for BSh and Csa climatic zones, BWh class is omitted since there is no fire-spotting. Due to this lack of data, we oversimplify the framework by assuming that fires captured by MODIS are primary fires, while the rest "small" ones could be secondary, or spot fires. The results for various climate classes are reported in Table 2. Thus, in order to estimate the proportion of the fire-spotting generated fires, we calculate the percentage of these larger fires and then estimate the number of possible secondary fires for one primary fire.

Table 2. Approximate number of small independent fires for one large fire in various climate classes.

	BSh class	***Csa class***
Total	3.77	4.31
Day fires	2.69	2.19
Night fires	6.50	12.31

The proposed model of fire-spotting with integrated climate-biome classification reflects qualitatively real patterns: during the night the number of small independent fires is higher. In the case of BSh climate class the number of small fires is doubled, see Figure 2, which agrees with the performed simulations where the doubled number of secondary fires is observed during the stable atmosphere conditions comparing to the unstable ones. For Csa class the difference between patterns in unstable and stable atmospheric conditions is rather significant, see Figure 4, which is also reflected by the simulations. Beside these, we remind the case of the BWh class where actually, for the corresponding set of the parameters, no fire-spotting generated fires appear consistently with the property of the class: these also can be considered as a kind of first validation test of the model since simulations reflect the fact that in desert there is no fire-spotting, see Figure 3.

5. Conclusions

In this study, we propose a multi-scale physical parametrization for the fire-spotting phenomena, which includes such climate-dependent factors as atmospheric boundary layer, fuel type, vegetation, in order to adjust the existing model to the changing conditions. Analyzing the different parameters, the integrated climate-biome classification has been proposed for the various climatic zones. The simulations show that by using the proposed parametrization of the fire-spotting distribution different fire-front patterns can be obtained. We focus mainly on the climate classes with registered fire-spotting events, such as South-Eastern Australia, and Mediterranean zone. The South-Eastern Australia is represented by two climate classes with completely different fire-spotting patterns: in the case of desert, the fire-spotting is not observing in the simulations, which agrees with reality. This fact shows the sensibility of the proposed classification for the probabilistic fire-spotting model.

The adjustment of the fire-spread model to the climate class becomes more and more urgent due to the climate change. In other words, the prediction of the wildfire propagation may vary not only in space but also in time. Some parameters, mainly climatic, which are usually considered as constant for a given location may change and the fire will propagate in different manner.

6. Acknowledgments

This research has been supported by the Basque Government through the BERC 2022–2025 program; by the Spanish Ministry of Economy and Competitiveness (MINECO) through the BCAM Severo Ochoa excellence accreditation SEV-2017-0718 and also through the project PID2019-107685RB-I00; and by the European Regional Development Fund (ERDF) and the Department of Education of the regional government, the Junta of Castilla y León (Grant 574 contract SA089P20).

7. References

Trucchia, A., Egorova, V., Butenko, A., Kaur, I., Pagnini, G. (2019) RandomFront 2.3: a physical parametrisation of fire spotting for operational fire spread models - implementation in WRF-SFIRE and response analysis with LSFire+, Geoscientific Model Development, 12, 69–87.

Storey, M. A., Price, O. F., Sharples, J. J., Bradstock, R. A. (2020) Drivers of long-distance spotting during wildfires in South-Eeastern Australia, International Journal of Wildland Fire, 29, 459–472.

Breckle, S.-W. (2002) Walter's Vegetation of the Earth: The Ecological Systems of the Geo-Biosphere. Springer-Verlag.

Peel, M. C., Finlayson, B. L., McMahon, T. A. (2007) Updated world map of the Köppen-Geiger climate classification, Hydrology and Earth System Sciences, 11, 1633–1644.

Scott, J. H., Burgan, R. E. (2005) Standard fire behavior fuel models: A comprehensive set for use with Rothermel's surface fire spread model.

Egorova, V.N., Trucchia, A., Pagnini, G. (2020) Fire-spotting generated fires. Part I: The role of atmospheric stability, Applied Mathematical Modelling, 84, 590 – 609.

Egorova, V.N., Trucchia, A., Pagnini, G. (2022) Fire-spotting generated fires. Part II: The role of flame geometry and slope, Applied Mathematical Modelling, 104, 1–20.

Critical heat flux for ignition of dead and live *Pinus halepensis* needles. Influence of moisture content

Fatima Z. Sabi[1]; Nouredine Zekri*[1]; Sidi M. Terrah[2]; Omar Mosbah[1] ; Hanane Boutchiche[1]; Ahmed Kaiss[3]

[1]Université des Sciences et de la Technologie d'Oran, LEPM BP 1505 El Mnaouer Oran, Algeria, {sabi.fatimazohra@yahoo.fr, nzekri@yahoo.com, mosbah31omar@yahoo.fr, hananelimang@gmail.com}
[2]Ecole supérieure de génie électrique et énergétique d'Oran, B.P 64 CH2 Achaba Hanifi, USTO, Oran, Algeria, {t_mohamed31@yahoo.fr}
[3]Aix Marseille Université, IUSTI, Technopôle Château Gombert 5 Rue E. Fermi, 13453 Marseille Cedex13 {ahmed.kaiss@amu-univ.fr}
**Corresponding author*

Keywords

Critical heat flux for ignition, dead fuel, live fuel, moisture content, *Pinus halepensis* needles.

Abstract

Wildland fire spread has been shown to exhibit unexpected behaviors depending on the fuel roughness, wind and land topography. Fire outbreak has attracted for a long time both wildland fire scientists and operational. The critical heat flux for ignition is one of the most important parameters used in fire safety. For example, it may be used for the fuel breaks estimation at Wildland Urban Interface. The critical heat flux for ignition of dead and live Pinus Halepensis needles (moist and dry) is investigated using a cone calorimeter. It is determined by using a recently developed method based on the phase transition theory where ignition time behaves according to a power-law trend near threshold. Compared to the usual deterministic methods, this method accounts for the probabilistic ignition behavior observed for porous fuels. The determined critical heat flux for ignition seems to be independent of the state of the fuel (live or dead) and of its moisture content within the errors. A heat transfer analysis is realized using the steady temperature which is related to the absorbed incident heat flux. From this analysis it is concluded that surface temperature at ignition does not change for fresh or dry live and dead fuels.

1. Introduction

Every year, a very large number of wildfires raged across the globe (Martin et al.2016), causing human misery and damage to properties. In the last decade, wildland fires become more intense and prolonged in time. The wildland fire safety has drawn the interest of scientists and operational in the effort to overcome fire outbreak and spread. Wildland management and Wildland Urban Interface (WUI) are among the main topics requiring fire risk reduction. This may be realized either by including fire breaks or by planting less flammable fuels. The critical heat flux for ignition is the parameter investigated for this end. Usually, the critical heat flux for ignition has been estimated by deterministic methods like ASTM 1534 standards (ASTM, 2017). However, such methods do not account for the probabilistic behavior of ignition that occurs near the critical heat flux. Recently, a new method based on phase transition theory (Stanley, 1971; Yeomans, 1992) has been proposed for the estimation of the critical heat flux for ignition applied to porous fuels (Sabi et al., 2021). The critical heat flux obtained by this method appears much smaller than those using deterministic ones. This is due to the probabilistic behavior occurring at lower heat flux intensities. Phase transitions are ubiquitous in nature, they can be observed in various fields like conductor/insulator or percolation (Stauffer and Aharony, 1992), liquid/gas (Blundell and Blundell, 2006), paramagnetic/ferromagnetic transitions (Stanley, 1971), etc.

The flame is a gas phase phenomenon (Drysdale, 2011), and emitted volatiles can be either in the flame state if ignition occurs, or remain in gaseous state if ignition does not. Ignition/non-ignition phase transition is referred to the different states of the gas phase: flame (ignitable) or gas (non-ignitable) (Sabi et al. 2021). Sabi et al. (2021) have studied analytically the ignition time behavior using a simple model based on conservation energy, where ignition temperature was the only ignition criterion. This analysis led to a logarithmic divergence of ignition time while this divergence has been found experimentally to be power-law. The power-law divergence has been recovered by considering the critical rate of flammable gas emission. The critical heat flux for ignition may depend on various fuel parameters like moisture content, porosity, and its live or dead state. Terrah et al.

(2020) have found that there is no critical moisture for ignition; they suggested that for any moisture content there is a critical flux for ignition because of the difficulty igniting of fresh live fuel. Jervis and Rein (2015) have shown that the most flammable fuels are fresh dead and aged needles followed by dry live needles, the least flammable are the fresh live needles. Recently, it was found that the rate of spread is higher for dried live *Pinus Halepensis* needles (with maximum flame height) than for fresh live ones (with smaller flame heigh) which indicates the existence of moisture threshold for fire spread (Aizeti, 2021). According to such a flammability difference, it is expected that the more the fuel is flammable, the more its critical heat flux for ignition is smaller. For instance, it can be reasonably thought that a moist fuel has a larger critical heat flux than a dry one. In this work, the influence of the state of the fuel (dead or live) and moisture content on the critical heat flux for ignition of *Pinus Halepensis* needles is investigated using a cone calorimeter.

2. Experimental setup and sample preparation

The ignition process is realized through a cone calorimeter with an electrical resistance of a power of $3000\ W$ used as a heat source. The heat source provides to the sample an incident radiation heat flux of magnitude ranging from 5 to $25\ \mathrm{kW/m^2}$. The received heat flux is varied by changing the distance of the top surface of the sample to bottom of the cone calorimeter. The heat flux at the top surface position of the sample is calibrated by using a water-cooled heat flux sensor of type Hukseflux SBG 01 working in the range 0-200kW/m². The experimental setup and calibration are shown in Fig.1. The ignition is controlled by a pilot flame located *2 cm* above the sample top surface. Although the distance to pilot is slightly greater than the $1\ cm$ required by ASTM 1354 standards (ASTM 2017), it allows avoiding the contact of needles with the pilot. The cone calorimeter is further equipped with a K-type thermocouple measuring surface temperature (placed perpendicular to the needles at the top surface of the sample). The time evolution of temperatures provided by the K-type thermocouples is recorded via a data acquisition station Graphtec midi-LOGGER GL 840 connected to a personal computer. The steady temperature is realized by exposing the samples to a sufficiently low heat flux to avoid ignition. In this case, both surface and gas temperatures become nearly constant at a maximum value within a steady period (around 50 min). As will be shown below, the maximum steady temperatures are related to the absorbed incident heat flux.

Pinus halepensis needles are harvested from the Campus of USTO University. The fuel is in three (3) states: dead, fresh live and dried live. The live fuel is completely dried using a micro-wave oven for $3\ min$. This device allows a short drying time to maintain the fuel it is live state before ignition. The micro-wave oven provides the same drying quality as the other devices (Terrah et al, 2020). Live fuels of $10\ g$ mass are either ignited directly (moist fuels) or completely dried (moisture content of 50% in wet basis) before ignition. Dead fuels of $5.5\ g$ mass (moisture content of 10% in wet basis) are considered for ignition. The samples are placed in a cylindrical holder of $10\ cm$ diameter of a mesh shape. The mass was weighted using a Kern PCB 350 balance with $1\ mg$ resolution. The ignition test is considered as succeeded and recorded if the flame persistence time is greater than $4\ s$ (sustained ignition). It is considered as failed if smoldering combustion is observed instead of flaming, with complete oxidation of the fuel in its solid phase (Rein, 2016).

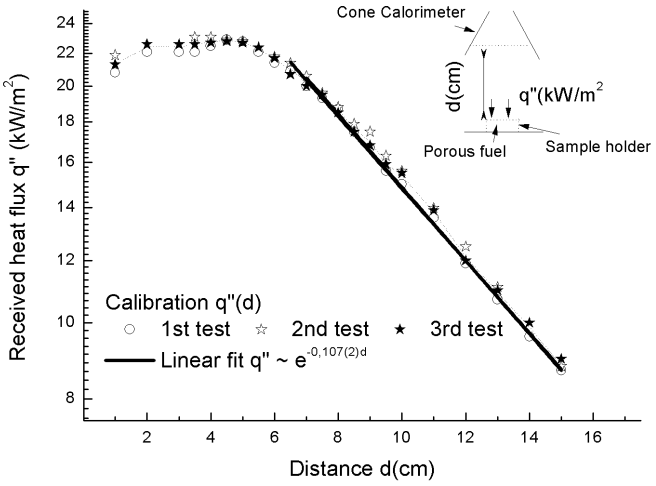

Figure 1- A schematic representation of the calibration flux and the experimental setup

3. Results and discussion

As mentioned above, recently a new method based on phase transition theory (Yeomans, 1992; Stanley, 1971) has been proposed to estimate the critical heat flux for ignition of porous fuel (Sabi et al. 2021). Compared to the usual methods, this method has been shown to account for the ignition probabilistic behavior occurring near the region of the critical heat flux for ignition. Sabi et al. (2021) have shown that ignition time t_{ign} diverges as a power-law as $q"_{inc} - q"_c$ as

$$t_{ign} \sim (q"_{inc} - q"_c)^{-\gamma} \quad (1)$$

The critical exponent γ is related to the kind of ignition. The estimation of the critical heat flux consists in varying $q"_c$ until the power-law trend appears of t_{ign} as a function of $q"_{inc} - q"_c$ (i.e. until the best linear fit of the plot in logarithmic scale is obtained).

Fig. 2 shows ignition time as a function of $q"_{inc} - q"_c$ in logarithmic scale for the 3 states of *Pinus Halepensis* needles (fresh live, dry live and dead). The critical heat flux for ignition $q"_c$ is obtained as to have the best linear fit. The uncertainty is estimated by estimating the critical flux within 5 % reduced correlation coefficient. It is found that the critical heat flux for ignition is the identical within uncertainties for the 3 states (dead fuel, fresh live fuel and dried live fuel), despite that the ignition process takes a longer time for moist live fuels than dried ones or dead fuels. The critical heat flux for ignition is independent of moisture content contrary to Terrah's suggestion (Terrah et al. 2020). The lines representing the three states of the fuel in Fig.2 (logarithmic scale) appear nearly parallel, corresponding to nearly constant a critical exponents. This suggests that ignition process is similar for the three states of the fuel.

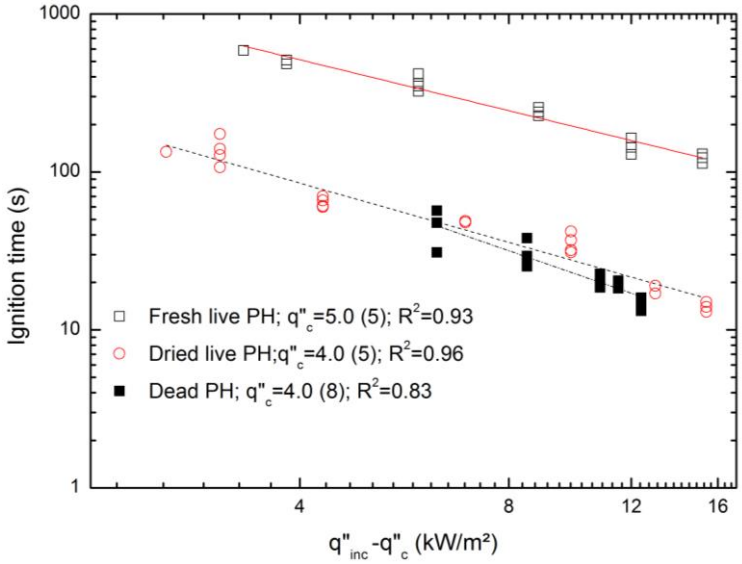

Figure 2: Ignition time vs. $q"_{inc} - q"_c$ for dead and live fresh and dried live fuls

To interpret this result let us analyze the heat transfer mechanism involved in ignition process. When the fuel bed of mass $m = m_{dry} + m_w$ is submitted to an incident heat flux $q"_{inc}$, it is heated to a temperature T, and the net absorbed heat flux by the fuel $q"_{net}$ is related to the absorbed incident heat flux $aq"_{inc}$ and the lost flux. Neglecting conduction heat transfer, and vapors emission, this is described by the following equation:

$$q"_{net} = aq"_{inc} - h(T - T_0) + \sigma\varepsilon\left(T^4 - {T_0}^4\right) = \left(m_{dry}{c_p}^f + m_w{c_p}^w\right)\frac{dT}{dt} \qquad (2)$$

Here h is the convection coefficient, σ is the Stefan Boltzmann constant, ε is the emissivity of the fuel, T_0 the ambient temperature, and ${c_p}^f$ (${c_p}^w$) is the specific heat of fuel (water). As surface temperature T increases with time, the lost heat flux increases, which decreases the net absorbed heat flux until it vanishes asymptotically (for a sufficiently low heat flux with no ignition), leading to a steady (maximum) temperature T_{max}. Therefore, the absorbed incident heat flux is related to the maximum temperature as:

$$aq"_{inc} = h(T_{max}-T_0) + \sigma\varepsilon\left({T_{max}}^4-{T_0}^4\right) \qquad (3)$$

In Fig.3 time evolution of temperature is presented for the parameters of moist and dry *Pinus Halepensis needles* used in (Sabi et al., 2021). The maximum temperatures seem to fluctuate within $10° C$. Within this temperature interval, both moist and dry fuels maximum temperatures seem to collapse. At the critical heat flux for ignition, the maximum temperature coincides with ignition temperature. This means that the fuel bed surface temperature reaches ignition (T_{ign}) asymptotically at $t \to \infty$. Replacing T_{ign} in equation (3) The critical heat flux for ignition reads thus:

$$aq"_c = h\left(T_{ign}-T_0\right) + \sigma\varepsilon\left({T_{ign}}^4-{T_0}^4\right) \qquad (4)$$

As a consequence of the results shown in Fig.2, it appears that ignition temperature does not vary with moisture content, and is identical for dead and live fuels within the uncertainty.

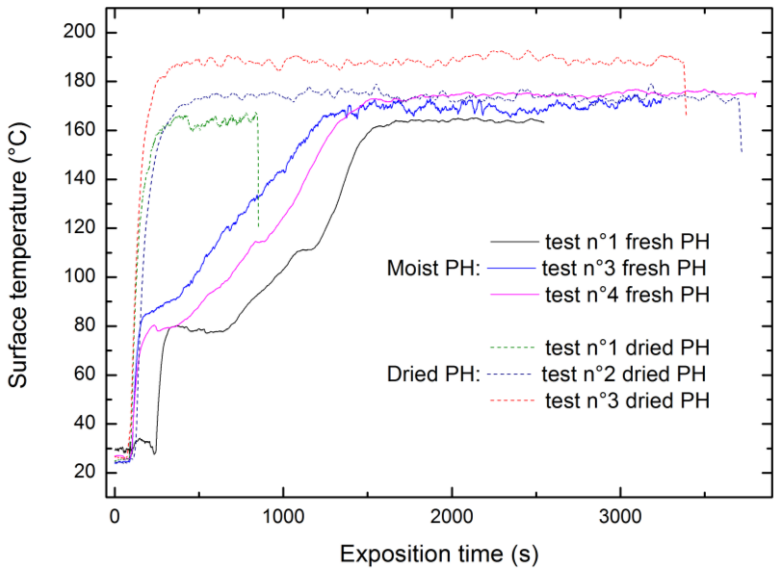

Figure 3: Steady surface temperature as a function of exposition time for moist and dried Pinus Halepensis

4. Conclusion

The estimation of the critical heat flux for ignition based on phase transition theory is used to compare the ignition for three states of *Pinus Halepensis* needles: dead, live fresh and live dried. The critical heat flux for ignition seems identical for the three states, although ignition time is very different for each state. A heat transfer analysis led us to conclude that surface temperature at ignition is identical for these states of the fuel bed within statistical errors.

5. References

Aizeti, A. (2021), Etude de l'effet de la teneur en eau sur la propagation du feu de végétation ; Détermination de la teneur en eau critique de propagation, Master in physics, Université des sciences et de la technologie d'Oran, Algeria.

ASTM (2017), International, Designation E 1354-17, Standard Test Method for Heat and Visible Smoke Release Rates for Materials and Products Using an Oxygen Consumption Calorimeter

Blundell, S.J., Blundell, K.M. (2006), Concepts in Thermal Physics, Oxford: Oxford University Press.

Drysdale, D. (2011), An Introduction to Fire Dynamics, Chichester: John Wiley & Sons, 3rd ed.

Jervis F.X., Rein G, (2015) Experimental study on the burning behavior of pinus halepensis needles using small-scale fire calorimetry of live, aged and dead samples, Fire Mater. 40, 385–395, https://doi.org/10.1002/fam.2293

Martin D., Tomida, M., Meacham, B., (2016). Environmental impact of fire, Fire Science Reviews. 5:5 DOI 10.1186/s40038-016-0014-1.

Rein, G. (2016). Smoldering combustion, in: M.J.Hurley (Ed), SFPE Handbook of fire protection engineering, chap.19. Heidelberg :Springer pp. 581-603.

Sabi, F.Z., Terrah, S.M., Mosbah, O., Dilem, A., Hamamousse, N., Sahila, A., Harrouz, O., Boutchiche, H., Chaib, F., Zekri, N., Kaiss, A., Clerc, J.P., Giroud, F., Viegas, D.X. (2021). Ignition/non-ignition phase transition: A new critical heat flux estimation method, Fire Safety Journal 119 (2021) 103257, https://doi.org/10.1016/j.firesaf.2020.103257

Stanley, H.E. (1971). Introduction to phase transitions and critical phenomena. Oxford: Clarendon Press.

Stauffer, D., Aharony, A. (1992), Introduction to Percolation Theory, London : Taylor and Francis.

Terrah, S.M., Sabi, F.Z., Mosbah, O., Dilem, A., Hamamousse, N., Sahila, A., Harrouz, O., Boutchiche, H., Chaib, F., Zekri, N., Kaiss, A., Clerc, J.P., Giroud, F., Viegas, D.X. (2020). Nonexistence of critical fuel moisture content for flammability, Fire Saf. J. 111, 102928, doi :10.1016/j.firesaf.2019.102928.

Yeomans J.M. (1992), Statistical mechanics of phase transitions. Oxford : Clarendon Press.

Drone swarm technology as a competitive alternative to traditional aerial firefighting

Ágoston Restás

University of Public Service, Institute of Disaster Management. 1101 Budapest, Hungary, krt. 9-11., {restas.agoston@uni-nke.hu}

Keywords

Aerial firefighting, drone, swarm, effectiveness, water flow

Abstract

Aerial firefighting is effective however very expensive solution to suppress forest fires. Drone application as a most developing branch of the aviation industry can be a complement, or perhaps even a competitive solution with the traditional aerial firefighting. Based on the input data drone swarm technology can be not just an effective but also an efficient solution suppressing forest fires. In this study author used both practical and theoretical approach to investigate the possibility of drone usage delivering suppressant to fire front. Firstly, the required width of wetting strip and the required amount of water per unique area were investigated; practical experience shows that based on the flame length first responders can estimate both the effective width of the fire brake and the amount of water required per a unique area. As a second part of this paper, the transport capability of a drone was investigated during its life cycle that is specially optimized for firefighting. In the example author took a 100 kg transport capacity that is easy to transfer to other drone design; in case of 0.3 MWm-1 fire intensity 100 kg water is enough to make 100 m long fire brake, in case of 3.4 MWm-1 fire intensity 100 kg water enough to create only 2.5 m fire brake. Even if this latest results can be seen a bit short we have to take into account the swarm technology. In 10 km distance 30 drones can built a 5 m long fire brake per a minute that means 300 m per hour. This result is no worse than what large or very large air tankers can built averagely in this fire intensity. Expecting the technological development in the near future the length of the fire brake will raise drastically meaning that drone swarm technology will be not a complement but a competitive solution to the traditional aerial firefighting.

1. Introduction

Due to climate change, forest fires are an increasingly serious problem in the developed world. Fires will become more frequent, more widespread, and more difficult moreover the suppression costs are raising very dynamically. One of the most effective, but certainly the most expensive ways to suppress fires is by using aircraft. In doing so, planes or helicopters release various extinguishing agents, especially water or retardants, at the burning front line. Drone applications, as the most dynamically developing branch of aviation (Tsiamis et al. 2019) raises the question of whether the use of drones makes sense, has a professional or an economic advantage in firefighting tactics. Attempts have been made to use drones for fire detection (Yandouzi 2022), surveillance (Alexis 2009, Kumar 2011), and even to ignite controlled fires (Goldammer et al. 2012), but the possibility of extinguishing large-scale front lines has been investigated very limited (Ghamry et al. 2017; Ausonio et al. 2021).

There are more and more literatures dealing with drone technology (Tsiamis et al. 2019) moreover the latest time appeared even videos and reports, mostly in the social media, presenting the possibility of drone technology in the fight with different kind of fires (Gabbert 2019; Steffen 2020; Tech Insider 2021; Aydin et al. 2019). Forest fire requires much more extinguishing material than closed area fires so the drone technology due to its limited transport capacity seems to be not reasonable for this purpose. However, the swarm technology might compensate the limited transport capacity of single drones. As an example, a large air tanker (LAT) carrying 12,000 litres suppressant to 100 kilometres and it can takes 2 circles per hour means that the flow rate is 400 litres per minute at the fire front. The distance that is 100 kilometres seems to be long in normal case however this value is normal in case of LAT service. The flow rate can be the same if a fire engine with 12,000 litres capacity transports water for 10 kilometres distance with 2 circles per hour frequency. The fire does not mind about how far the water comes from or how it gets there, the main condition for extinguishing the fire is the amount of water flow. At the current level of technology, one drone is assumed not to be able to provide an efficient flow of water, but with their mass application, that is swarm technology, this might be ensured even today. The purpose of this paper is to investigate the possibilities of drone swarm technology to suppress fires.

2. Methods

The author used the relevant literatures dealing with drone swarm technology and firefighting however there are only some that focusing specially on this topic (Ghamry et al. 2017; Ausonio et al. 2021). Therefore, this study uses some assumptions that is adapted basically from other technology and practical experiences however the data regarding forest fires calculating with comes from the practice that confirmed by literatures as fundamentals (Byram 1959; Bel 1986/87). The author used in this research even his practical experience in both the application of drones and the extinguishing of forest fires, and he used also simple mathematical methods and logical conclusions to present the results.

3. Results

Knowing or estimating the intensity of a fire is important to be able to calculate how much suppressant we need to extinguish it. Low fire intensities can be extinguished with fewer extinguishing agents, while in the case of a higher fire intensity, the maximum amount of suppressant that can be used is not enough. The minimum and maximum amount of extinguishing agent required for successful suppression is known from laboratory measurements and practical experiences. The minimum effective amount may vary depending on the literature, usually between 0.2 and 0.5 kgm^{-2}; in this study, the author calculates a value of 0.5 kgm^{-2}. The maximum amount of suppressant does not exceed 5 kgm^{-2}, even in a mature forest. Knowing the length of the flame is needed to determine the width of wetted strip in front of the front line. Based on practical experience, a wetted strip of 2 to 2.5 times the flame length effectively counteracts the thru-burn, i.e., it prevents the spread of fire. The lower width value is sufficient at lower fire intensities, the higher value is at higher fire intensities. In the study, the author calculates a 2-fold value.

Based on the above, we have to choose the amount of extinguishing agent required per unit area by the intensity of the fire or by the height of the flame. The minimum effective amount of water is 0.5 kgm^{-2} and the maximum is 5 kgm^{-2}. In the study, the amount of water that the author assumed is delivered to the fire front with the drone was 100 kg. Figure 1 shows the amount of water that is sufficient to wet this area as a function of fire intensity.

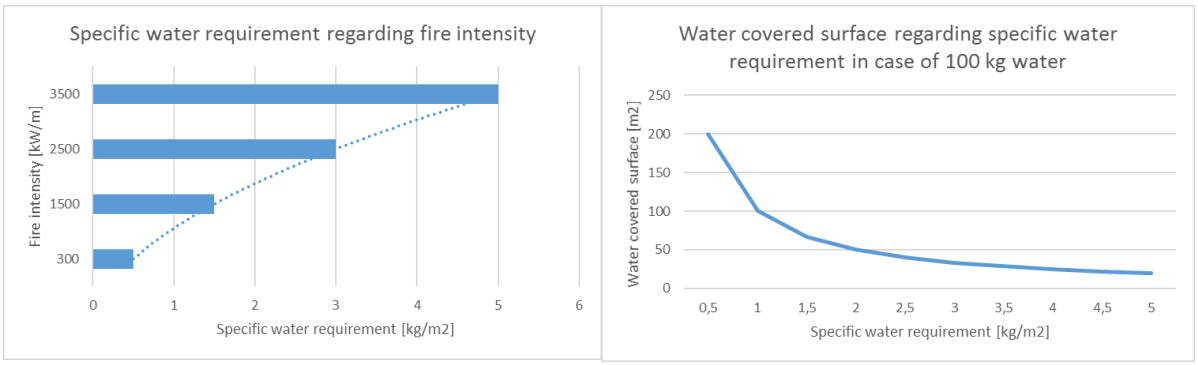

Figure 1. The amount of water that is sufficient to wet the area as a function of fire intensity (left) and the water covered surface depending on the specific water requirement (right)

The author assumed that the average life cycle of a drone optimized for firefighting is about 2,000 hours. It is possible if we count with the life cycles of brush less electric engines (Brando et al. 2022), that is a main critical part of the drone. The average speed during the service life is calculated with 80 kmh^{-1}, so the distance covered during the life cycle is about 160,000 km, in one half of which it carries a fire suppression materials to the fire front that can be water, short or long term retardants. In the other half of life cycle drone flies back to the charging station empty. The shape of the drone is aerodynamically optimized due to continuous long-range flights, so it also produces buoyancy with its surface design. This allows the specific energy consumption to be lower than e.g. at spray drones of the same power. When flying back, the weight of the drone is significantly less, so its flight speed can be higher than average, which can result in time savings that compensate for the loss of time caused by charging at the base and releasing time at the fire front. Using the above assumptions, the life cycle time is halved, so the transport time of the suppressants, as well as the return time is 1,000 to 1,000 hours. Besides the flight hours the time of suppressant release at the fire front and the refuelling time at the base site is considered negligible.

The load capacity of a drone developed for firefighting is assumed 100 kg. Based on this, the transport capacity of the drone is 8,000,000 kg.km (1000 h x 80 $km.h^{-1}$ x 100 kg) during its life cycle. This can be modified in the same way as the other data, following the logical principle of the calculations to obtain the efficiency characteristics for the given values.

Based on the first assumption (A), the distance between the refuelling base and the front line of the fire is taken to be 10 km on average. In this case, the drone can make 4 turns in 1 hour, so the delivered quantity is 400 kg. The distance and the delivered quantity are inversely proportional, i.e. the smaller the distance, the more the delivered quantity, and vice versa. Assuming individual cases, as the distance increases, the quantity that can be delivered decreases (200 kg per hour for 20 km) and increases as the distance decreases (800 kg per hour for 5 km). During the life cycle of the drone, that is about 2,000 hours, and taking four missions per hour cycle, 800,000 kg of suppressant can be applied at a distance of 10 km (2,000 h x 4 mission per hour x100 kg per mission). With this process at a distance of 5 km carried 1,600,000 kg water, at a distance of 1 km carried 8,000,000 kg water by only one drone. Based on the above we can multiply the transported value of the water depending on the number of the drones included in the swarm.

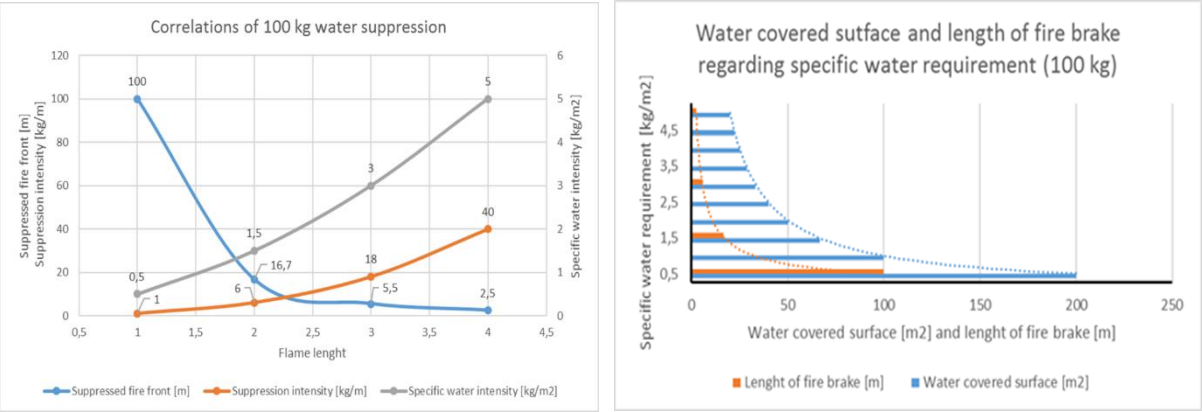

Figure 2. Different calculations of effectiveness with 100 kg water delivered by drone

4. Conclusions

Aerial firefighting is effective however very expensive solution to suppress forest fires. Drone application as a most developing branch of the aviation industry can be a complement, or perhaps even a competitive solution with the traditional aerial firefighting. Based on the input data drone swarm technology can be not just an effective but also an efficient solution suppressing forest fires. In the example author took a 100 kg transport capacity that is easy to transfer to other drone design; in case of 0.3 MWm^{-1} fire intensity 100 kg water is enough to make 100 m long fire brake, in case of 3.4 MWm^{-1} fire intensity 100 kg water enough to create only 2.5 m fire brake. Even if this latest results can be seen a bit short we have to take into account the swarm technology. In 10 km distance 30 drones can built a 5 m long fire brake per a minute, that means 300 m per hour. This result is no worse than what large or very large air tankers can built averagely in this fire intensity.

5. References

Alexis K, Nikolakopoulos G, Tzes A, Dritsas L, (2009) Coordination of Helicopter UAVs for Aerial Forest-Fire Surveillance. Applications of Intelligent Control to Engineering Systems, https://doi:10.1007/978-90-481-3018-4_7

Ausonio E, Bagnerini P, Ghio M, (2021) Drone Swarms in Fire Suppression Activities: A Conceptual Framework. *Drones*, **5** (1) 17 https://doi.org/10.3390/drones5010017

Aydin B, Selvi E, Tao J, Starek J.M, (2019) Use of Fire-Extinguishing Balls for a Conceptual System of Drone-Assisted Wildfire Fighting. *Drones*, **3** (1), 17; https://doi.org/10.3390/drones3010017

Bell A, (1986/87) Water bombing of fires: no magic solution. Ecos 50 Summer, available online on 04.03.2022 http://www.ecosmagazine.com/ ?act=view_file&file_id=EC50p18.pdf

Brando G, Dannier A, Del Pizzo A, (2022) Efficiency Analytical Characterization for Brushless Electric Drives. *Energies*, **15** 2963. https://doi.org/10.3390/en15082963

Byram G.M., (1959) Combustion of Forest Fuels. In Forest Fire: Control and Use; McGraw-Hill: New York, NY, USA, 61–89.

Gabbert B, (2019) Spanish company developing firefighting drones. Fire Aviation, available online on 04.04.2022 https://fireaviation.com/2019/01/03/spanish-company-developing-firefighting-drones/

Ghamry A.K, Kamel A.M, Zhang Y, (2017) Multiple UAVs in Forest Fire Fighting Mission Using Particle Swarm Optimization. International Conference on Unmanned Aircraft Systems (ICUAS), Miami, FL, USA

Goldammer J.G, Brunn E, Held A, Johst A, Kathke S, Meyer F, PahlK, Restas A, Schulz J, (2012) Kontrolliertes Brennen zur Pflege von Zwergstrauchheiden (Calluna vulgaris) auf munitionsbelasteten Flächen. Erhaltung von Offenlandlebensräumen auf aktiven und ehemaligen militärischen Übungsflächen. *Naturschutz und Biologische* **127** 65 – 95.

Kumar M, Cohen K, HomChaudhuri B, (2011) Cooperative control of multiple uninhabited aerial vehicles for monitoring and fighting wildfires. *Journal of Aerospace Computing, Information, and Communication*, **8** (1) 1–16

Steffen L, (2020) Autonomous Firefighting Drone For High-Rise Fires in China. *Intelligent Living*, Report, available online on 20.03.2022 https://www.intelligentliving.co/autonomous-fire-fighting-drone/

Tech Insider, (2021) Drone Could Help Firefighters By Putting Out Fires. Report, avialable online on 15.04.2022 https://www.youtube.com/watch?v=Bm2BVTTir4c

Tsiamis N, Efthymiou L, Tsagarakis P.K, (2019) A Comparative Analysis of the Legislation Evolution for Drone Use in OECD Countries. *Drones*, **3** (75) https://doi:10.3390/drones3040075

Yandouzi M, Grari M, Idrissi I, Moussaoui O, Azizi M, Ghoumid K, Elmiad A.K, (2022) Review on forest fires detection and prediction using deep learning and drones. *Journal of Theoretical and Applied Information Technology*.**100** (12) 4565-4576

Experimental studies on the fire behaviour and smoke toxicity of German pine vegetation (*Pinus sylvestris*)

Lukas Heydick*[1]; Kira Piechnik*[1]; Florian Köhler[1,2]; Andrea Klippel[1]

[1]*Otto-von-Guericke-University Magdeburg, Universitätsplatz 2, 39106 Magdeburg, Germany*
[2] *Fire Department of Verbandsgemeinde Flechtingen, Lindenplatz 11-15, 39345 Flechtingen, Germany*
{lukas.heydick, kira.piechnik, florian.koehler, andrea.klippel}@ovgu.de

**Corresponding authors*

Keywords

Pine forest, Ignition Characteristics, Fire spread, Smoke Toxicity, Smouldering (FT-IR)

Abstract

The mechanisms of fire and smoke spread in forest and vegetation fires have not been fully investigated. Most numerical models often only consider the topography of the area and climatic influences such as wind and temperature. There is a need to understand the fire behaviour of specific vegetation in order to predict how the fire and smoke will spread during a fire incident. Understanding the mechanisms and behaviour of fire is therefore important for both, preventing and fighting fires. The European research project DRYADS and the associated German pilot project "Fire research in forest fires and derivation of safety measures" deal with these problems. Therefore, several measurement campaigns were carried out to study safety-relevant parameters, fire behaviour, fire spread and spontaneous combustion processes of specific German vegetation and soil samples. The research objectives of the studies focused on the characterisation of fire development and spread as well as smoke composition.

1. Introduction

Common pine vegetation (Pinus sylvestris) is involved in approximately 75% of wildfires in Germany. Over the past five years, the German regions of Saxony-Anhalt and Brandenburg have been particularly affected, with an increase in the number, severity and area affected by fires. It is essential to understand the mechanisms of vegetation-specific fire behaviour and smoke production in order to develop effective fire fighting measures. To achieve this, fire experiments are conducted on 0.25 m² soil samples to characterize the ignition proteries and fire spread in ground fires. In addition, self-ignition amd smouldering tests of the local soil and vegetation samples were conducted in a DIN tube furnace and the resulting smoke gases were measured and analysed by FT-IR spectrometry. Furthermore, the self-ignition behavior of soil samples was investigated by thermal storage tests, performed in the SEDEX-oven. Also here the smoke gases were measured by FT-IR. The results provide an comprehensive overview of typcial fire behavior and smoke compositions and characterize essential factors influencing ground fires.

Previous studies (Huand & Rein, 2014; Morandi & Silvani, 2010; Martin et al, 1993; Tihay et al, 2016) (selection) already show characteristic processes of fire spread in forest soils; the present series of experiments is intended to determine regional characteristics. In addition the results provide the basis for large-scale tests and numerical simulations within the DRYADS-project.

2. Small-Scale Fire Tests

2.1. Experimental Setup

The small scale (real scale) fire experiments were conducted in 25 x 50 x 50 cm plexiglass boxes outdoors. Samples were taken from natural vegetation (52°23'04.8"N, 11°14'11.8"E) and dried under ambient conditions, to obtain low moisture levels. The ignition was performed by placing a heat-conditioned metal cylinder (approximately 650°C, pre-heated in the Muffeloven) on the dry litter layer of organic material. Temperatures were measured at different locations and depths of the sample to characterize the intensity of the ground fires. The fire spread was recorded with a thermal imaging camera, and mass loss was tracked using a burn scale. To

measure the temperatures, thermocouples were mounted at a depth of 5 cm (TC 2 to 10) and 10 cm (TC 11 to 14). As the intensity of the fire tests was significantly influenced by the wind, the prevailing wind speeds were recorded with a weather station.

Figure 1 – Burning Soil Sample

2.2. Results

Due to the high dryness (soil moisture <15%), the organic litter layer ignited when the cylinder was placed on top. The dry components of the upper layer burned with the appearance of flames. After 5 minutes, a smouldering fire is established on the entire surface of the specimens. Horizontal and vertical heating of the entire sample occurs. Selected measured temperatures and the mass lass of one specimen are shown in Figure 2.

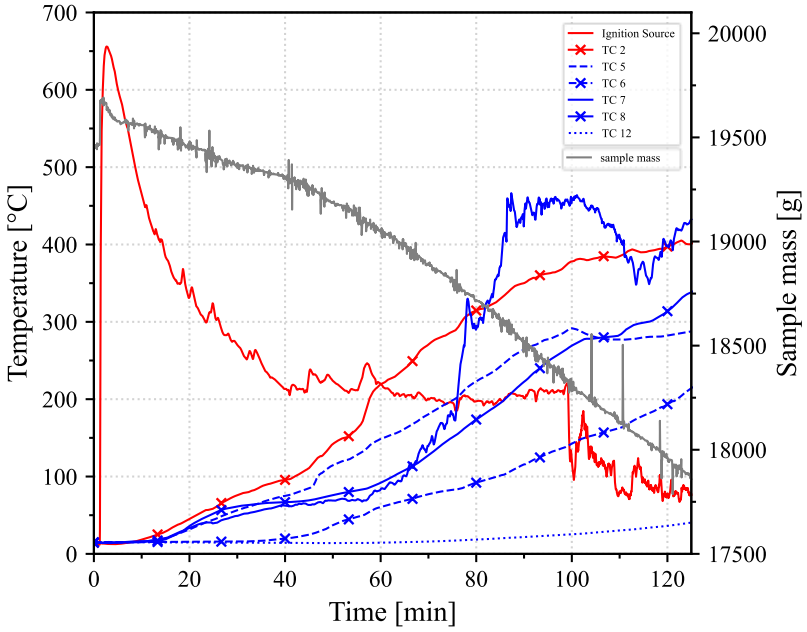

Figure 2 - Temperature curves and mass decrease of pine soil sample

The smouldering fire led to the slow combustion of the organic material of the soil, also recognizable by a steady mass decrease. Furthermore, the classical combustion processes of forest soil (preheating, drying, pyrolysis, oxidation), as described by Huang & Rein (2013) among others, could be observed. The smouldering fire is

maintained by the heat generated in the reaction zone. It also provides energy to fuel the drying, preheating and pyrolysis processes. It was also shown that previously ignition-resistant components (e.g. mosses) could be thermally conditioned by the addition of heat, and if sufficient pyrolysis gases were produced, flaming combustion could be initiated at a later stage. The heat of the metal cylinder just only delivers the initial energy, to start the tests. The thermocouple (TC 1) under the metal shows a constant temperature after about 40 minutes, so it could be stated, that from this point on the combustion is no longer influenced by the energy of the ignition source.

The studies show that all of the ground fires investigated spread independently and persistently after initial ignition. All tests showed fully developed smoldering fires, which constantly heated the soil samples to over 300°C (also up to 400°C) after two hours. Figure 3 shows typical temperature curves (measurement 5 cm below litter layer) of different soil samples. It can be seen that the samples from the coniferous forests show a much faster and significantly more severe temperature rise over the experimental time.

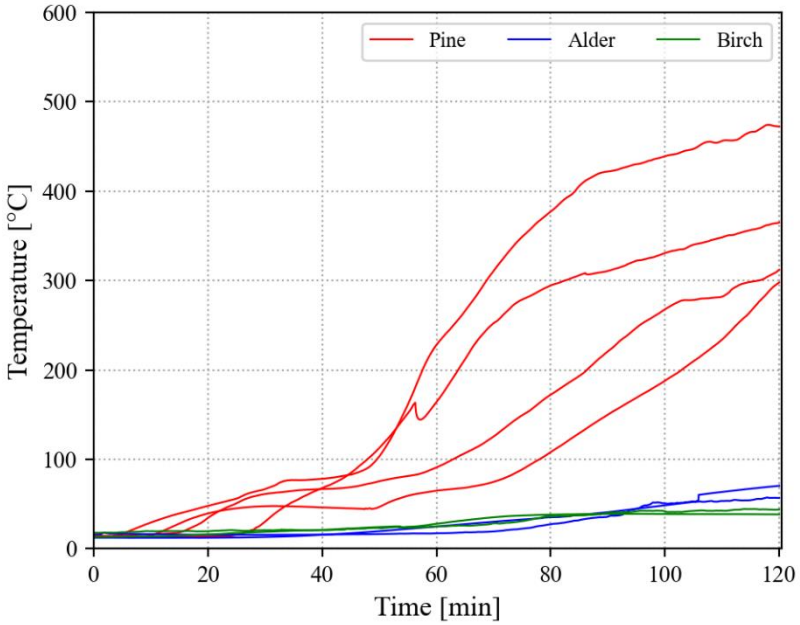

Figure 3 - Comparison of maximum soil temperatures of different samples

The intensity of the fires varied with the composition and moisture of the soils, the possibility of air entry into the soil layer and the duration of the tests. In general, the test stand is very suitable for investigating the characteristic fire behaviour of certain soil samples and the inter-soil fire spread. It should be noted that as the scale is increased, the influence of fire thermic increases (e.g. radiant heat, greater turbulence) and affects aboveground fire behaviour. The experiments show the danger of the rapid horizontal fire spread and the intensive heating of the soil layers, which pose major challenges for the firefighters during large-scale forest fires and can irreversibly damage the vegetation.

3. Experiments on Smoke Toxicity

3.1. Experimental Setup

The DIN tube furnace is suitable for creating optimal and reproducible smouldering conditions. This is to be understood as thermal oxidative decomposition without flame formation. For the tests in the DIN tube components (5g each) of the organic litter layer were taken. In another test series a thermal storage furnace (SEDEX-oven) was used to study spontaneous ignition behaviour. Heterogenous samples of soil (100g) were heated until the pre-set maximum temperature was reached. By measuring the temperature with a thermocouple, it is possible to detect any spontaneous ignition.

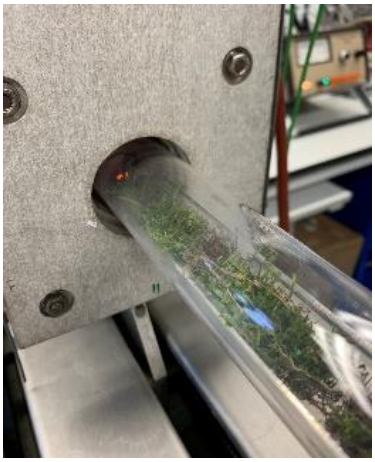

Figure 4 – DIN tube furnace with 5g soil sample

Figure 5 – SEDEX-Oven with 100g soil sample

Both, the DIN tube furnace and the SEDEX-oven were coupled with an FT-IR spectrometer to determine combustion products of the smouldering fires. The FT-IR were calibrated to different typical smoke components, which can be identified and quantified in respect to their concentration. By this determination, approaches to the evaluation of the hazard from smoke in regional ground fires should be made.

3.2. Results

3.2.1. Smouldering Test in the DIN Tube Furnace

In the comprehensive series of experiments, samples of moss, leaves, needles, bark, branches, soil, wood fragments, sand and pine cones in different compositions were investigated. Due to the heterogeneity of the samples, the composition of the smoke gases also varied.

The displayed sample in figure 4 contained small branches, as well as a proportion of sand, moss, needles and bark. Figure 6 and 7 show typical measured concentrations of this specimen 1.1 of hydrogen cyanide and sulfur dioxide, which are classified as toxic gases. The black line shows the medium concentration of two trials of a measurement series while the red line shows the average concentration during the whole experiments.

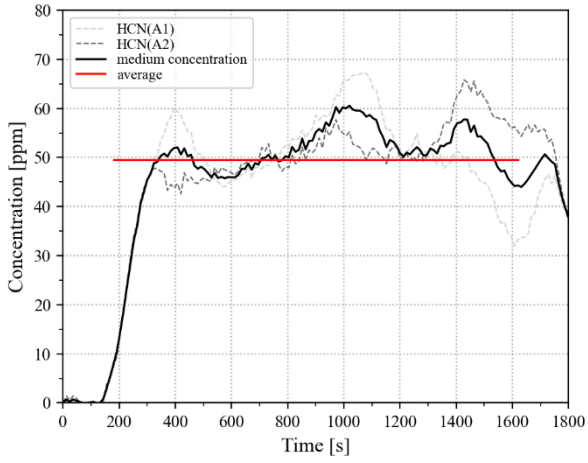

Figure 6 - Concentration of hydrogen cyanide (sample 1)

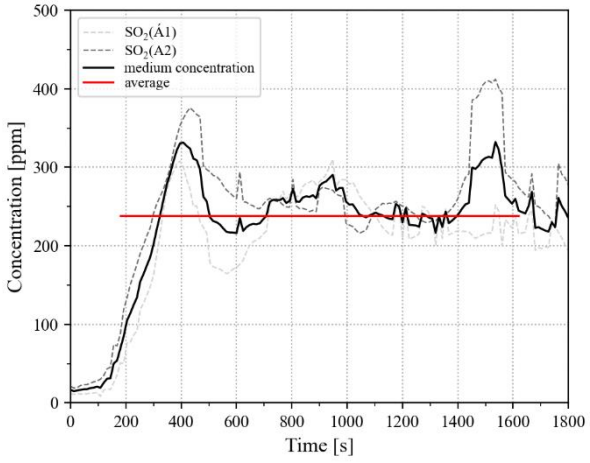

Figure 7 - Concentration of sulfur dioxide (sample 1)

The graphs rise continuously at the beginning when the heating ring of the DIN tube furnace initiates smouldering. During the course of the experiment, a relatively constant release of the toxic gases is established. The averaged released values are 50 ppm for HCN and 240 ppm for SO_2. The following table presents the average concentrations of typical measured product from different experiments.

Table 1 – Average concentrations (medium of two tests each) of different samples in [ppm]

SOIL SAMPLE	HCN	SO_2	C_3H_4O	C_2H_6O	CO	NH_3	CH_4
A	48	236	24	77	2940	13	640
B	45	276	29	79	3095	22	958
C	99	217	9	58	4280	25	545
D	36	301	54	86	5818	16	1064
E*	21	417	120	364	4316	10	4524

*(only needles)

The comparison shows the similar magnitudes of concentrations for different samples. The experimental setup makes it possible to measure the different components of the smoke gases. In additional experiments, the concentrations will be further quantified and the sources of the hazardous combustion substances can be determined by specific analyses.

3.2.2. Self-Ignition test in the SEDEX-oven

The samples in the SEDEX furnace were heated up to 400°C for 24 hours. Typically, spontaneous combustion occurred after 9-10 hours at temperatures of 180°C. The self-ignition of the organic material leads to a sudden increase of the temperature up to 440°C and initiates a burning process inside the oven.

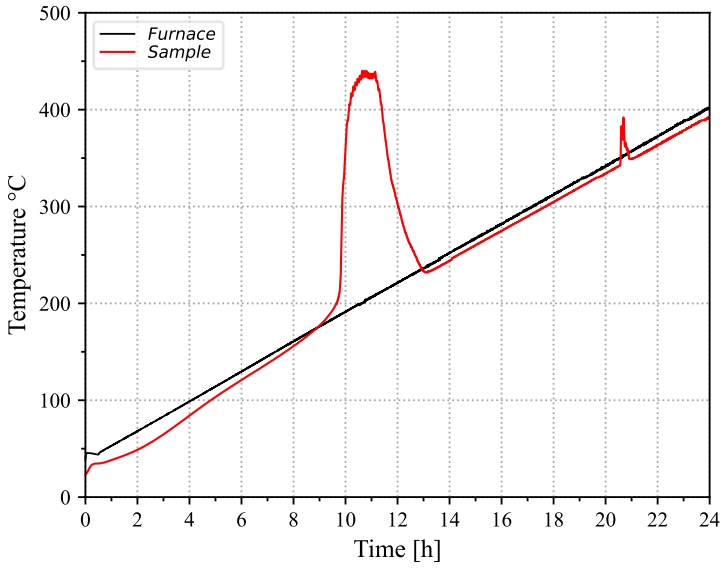

Figure 8 – Self-Ignition of sample from organic pine vegetation

During the experiments, analogous to the smoldering tests, the composition of the smoke was analyzed. The combustion products in the smoke are the similar to those of the other determination. The emissions of the

By the end of the self-ignition tests, complete combustion of the organic material can be assumed, leaving behind non-combustible components, such as heavy metals. Both the amount of mass loss and the level of concentrations of smoke depend on the composition of the sample. Due to the heterogeneity of the samples, further test series will be carried out to compare the values in order to determine a generally valid quantification of the hazards.

3.3. Evaluation of the smouldering tests

The inhalation of the harmful substances contained in the fire smoke can represent a not inconsiderable health hazard for people at the appropriate concentration. The experimental setup offers the possibility to determine the smoke compositions of different samples and to quantify them by comparison. The experiments provide knowledge in the area of basic research on the concentration of pollutants in fire smoke under smoldering conditions typically encountered in ground fires. The study of local vegetation provides specific insights into hazards from fire smoke, which must be considered in terms of fire suppression.

4. Conclusions

The fire tests and smoldering experiments are to be used to investigate the vegetation-specific fire behavior of local forest soils. The measured temperatures in the soil und the detected smoke compositions show the possible, high damaging effects of soil fires. Furthermore, the rapid and extensive spread of fire can spread to above-ground vegetation and lead to severe fires. The experiments will be expanded to include other vegetation types and in number to provide quantitative information on specific hazards.

Small and medium scale experiments are the basis to develop a numerical model capable of predicting the fire propagation. The combination of experiments and numerical investigation allows a quantitative assessment of the influence of the different heat transfer modes and therefore will significantly improve the understanding of fire propagation in these fires. In addition, by analyzing possible combustion products in the smoke, hazards for first responders and further, for the civil population can be determined and protective measures can be derived.

5. Acknowledgments

DRYADS project has received funding from the European Union's Horizon 2020 research & innovation programme under grant agreement No 101036926. Content reflects only the authors' view and European Commission is not responsible for any use that may be made of the information it contains.

6. References

F. Morandi and X. Silvani. Experimental investigation of the physical mechanisms governing the spread of wildfires. *International Journal of Wildland Fire Vol. 19 (p. 570-582), 2010.* DOI: 10.1071/WF08113.

R. Martin, D. Gordon, M. Gutierrez (et al). Assessing the flammability of domestic and wildland vegetation. *12th Conference on Fire and Forest Meterology, (p. 130-137), 1993.* DOI: 10.13140/RG.2.1.3999.3680

V. Tihay-Felicelli, P. Santoni, T. Barboni and L.Leonelli: "Autoignition of Dead Shrub Twigs: Influence of Diameter on Ignition." *Fire Technology Vol. 52 (p. 897–929), 2016*, DOI: 10.1007/s10694-015-0514-x

X. Huang und G. Rein: Smouldering combustion of peat in wildfires: Inverse modelling of the drying and the thermal and oxidative decomposition kinetics. *Combustion and Flame Vol. 161 (p. 1633-1644), 2014*. DOI: 10.1016/j.combustflame.2013.12.013

Firefighters' leadership and well-being in rural fires: study in virtual reality environments

Raquel Pinheiro*[1]; Vítor Reis [2]; Luis Curral [3]; Maria José Chambel[4]

[1 2] Escola Nacional de Bombeiros, Portugal, {raquel.pinheiro, vitor.reis}@enb.pt
[3 4]CicPsi, Faculdade de Psicologia da Universidade de Lisboa, Portugal, {lcurral, mjchambel}@psicologia.ulisboa.pt

**Corresponding author*

Keywords

Firefighters; leadership; well-being; rural fires; virtual reality.

Abstract

In this study, we analysed the effects of team leadership style on the well-being of firefighter teams operating under conditions of a simulated rural fire. Twenty teams of firefighters (composed of five elements each) took part in a computer-based fire-fighting simulation task and were randomly assigned to one of two conditions (leadership style: directive vs. empowering). Our results showed that directive leadership style was negatively associated with team members levels of stress and anxiety, while an empowering leadership style did not have a significant effect on team members levels of stress and anxiety. The distinct effects of team leadership style remain unchanged when we controlled for the levels of stress and anxiety before the simulation. Through moderated regression analyses we observed that the effect of directive leadership styles in reducing stress and anxiety was stronger for participants with higher levels of previous stress and anxiety. Implications for theory and practice are discussed.

1. Leadership and well-being among firefighters

Firefighters have a high-strain occupation, since physical danger and psychological stress are part of their daily lives (Prati, Pietrantoni, & Cicognani, 2010). In this study, we draw from the theory of leadership, defined as a social influence process where leadership behaviors affect followers' outcomes, to build an understanding of the different ways firefighters react to the constant disruption and ongoing strain involved in their work, focusing specifically on responses that lead to positively adaptive outcomes. We have considered leadership a contextual variable that can explain this positive result because leaders have the potential to be a buffer against work stressors (Harms, Credé, Tynan, Leon & Jeung, 2016), thus we expect to contribute to the literature, by empirically investigating leadership behaviors that explain when and how firefighters positively adapt to stressful situations.

2. Virtual reality

The development of virtual environments and computer game technologies made it possible to create scenarios in 3D graphic environments and new learning contexts based on virtual simulation tools for the training of incident commanders (Wijkmark & Heldal, 2020). The scenarios can have different levels of complexity and firefighters can move and interact in the virtual environment, make decisions, and observe the consequences of decisions taken.

Virtual reality scenarios challenge firefighters and make them feel involved and react as if they were in real events (Reis & Neves, 2019). Virtual reality simulation enables to create large-scale events that would be extremely difficult and even dangerous to recreate in a live exercise (Boosman, Lamb & Verhoef, 2015).

3. Hypothesis

In this study, we wanted to verify which leadership style contributed better to the well-being of subordinates, and therefore raised the following hypotheses:

1) the empowering leadership style is negatively associated with stress and anxiety levels during intervention action in a simulated rural fire situation.

2) the directive leadership style is positively associated with stress and anxiety levels during an intervention in a simulated rural fire situation;

3) the effect of the empowering style (3.a) and the directive style (3.b) is stronger in relation to firefighters who at the beginning of the intervention had higher levels of stress and anxiety when compared to those who at the beginning of the intervention had lower levels of stress and anxiety.

4. Procedure and sample

Twenty teams of firefighters (composed of five elements each) participated in the simulation exercise where they hat to confront a simulated rural fire scenario. Simulation studies enable us to manipulate contextual conditions difficult to access in real environments (*e.g.* extreme conditions in a rural fire) and to measure their impact on the deployment of participants well-being.

We used a simulation exercise similar to the ones used in firefighters' training and participants were randomly assigned to teams of five individuals to fight a massive extent rural fire. Teams were also randomly distributed through 2 experimental conditions in which leadership style [i.e. empowering leadership; directive leadership] was manipulated.

To induce a high-demand situation, we presented participants with disruptive conditions in the scenario. To manipulate leadership behavior, participants in each team answered a questionnaire to measure their style as leaders (empowering vs. directive), and the participant with the higher score on either empowering or directive style was assigned the leading role (team leader). Next, the leader was given a script with the behaviors considered to be the most effective according to the condition he was assigned to (directive or empowering). Each team was assigned to one of the two leadership style conditions.

Pre and post simulation stress and anxiety were measure with 6 and 5 items, respectively, from the Portuguese version (EADS-21; Pais-Ribeiro, Honrado & Leal, 2004) of the Depression Anxiety Stress Scales (Lovibond & Lovibond, 1995).

5. Results

To test our hypothesis that directive and empowering leadership have a different impact on subordinates' levels of stress and anxiety in a firefighting situation, we conducted a regression analysis. In addition, to test the hypothesis that the behavior of the leader has more impact when subordinate levels of anxiety and stress before the situation were high, we conducted a moderated regression.

Table 1. Direct and interaction effects of leadership style and previous stress and anxiety levels on stress and anxiety after the simulated firefighting episode.

Variable	Model 1 Stress as outcome	Model 2 Anxiety as outcome
Empowering leadership	.278	.394
Directive leadership	-.494*	-.578**
Previous stress	.251*	
Previous anxiety		.417**
Directive leader X Previous stress	-.258**	
Directive leader X Previous anxiety		-.234*
R2	.170**	.277**

* $p < .05$; ** $p < .01$

As we can see in Table 1. team leader's directive leadership style had a significant direct negative effect on subordinates' levels of stress and anxiety after the simulated firefighting episode. A directive leadership style

seems to be associated with reduced levels of stress and anxiety in subordinates, measured immediately after they engaged in firefighting simulated with a VRX simulator used to train firefighters. Opposite to our expectations, team leaders empowering leadership style did not have a significant effect on the levels of stress and anxiety of individuals after the simulated firefighting episode.

In Figure 1. we plotted the interaction between team leader's directive leadership style and subordinates stress levels measured before the episode of simulated firefighting. As shown in Figure 3, individuals led by a directive leader exhibited lower levels of stress after the performance than they reported before. Moreover, this stress-reducing effect was stronger for subordinates with higher stress levels in the beginning, thus supporting Hypotheses X.

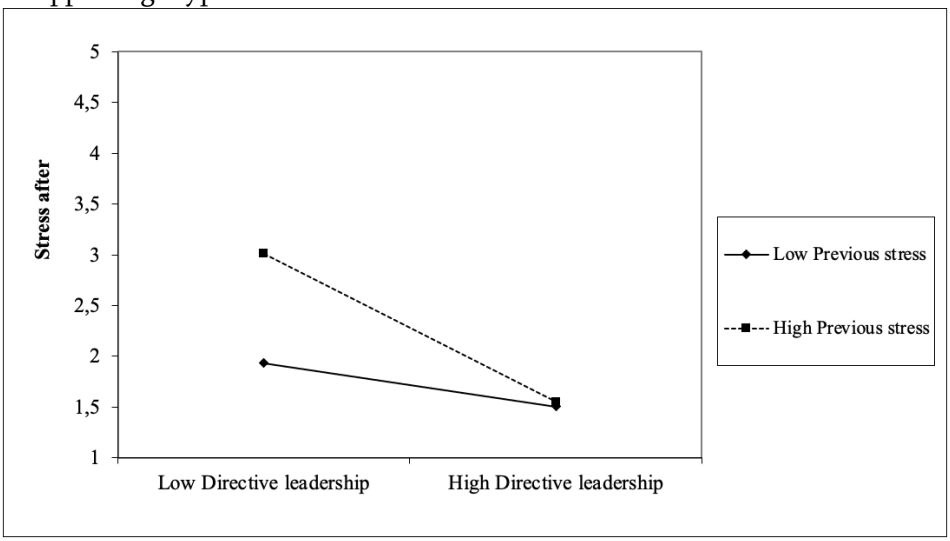

Figure 1. Interactive influence of previous stress and directive leadership style on stress after the firefight.

In Figure 2. we plotted the interaction between team leader's directive leadership style and subordinates' anxiety levels measured before the episode of simulated firefighting. As shown in Figure 3, individuals led by a directive leader exhibited lower levels of anxiety after performance than they reported before. Moreover, this anxiety reducing effect was stronger for subordinates with higher anxiety levels in the beginning, thus supporting Hypotheses X.

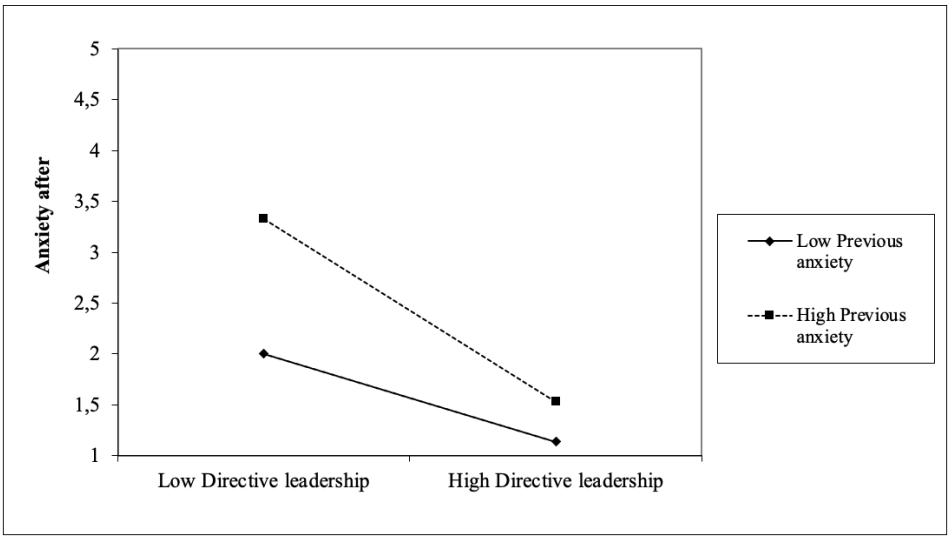

Figure 2. Interactive influence of previous anxiety and directive leadership style on anxiety after the firefighting episode.

6. Discussion

Directive leadership is associated with a leader's positional power and is characterized by behaviors aimed at actively structuring subordinates´ work by providing clear directions and expectations regarding compliance with instructions (Somech, 2006). Directive leaders help followers resolve task and role ambiguity and provide external monitoring and feedback on their performance, reducing process loss and allowing the team to execute decisions more quickly (Lorinkova et al. 2013; Sagie, 1996).

Empowering leadership, on the other hand, involves sharing power with subordinates and raising their level of autonomy and responsibility, and it manifests through behaviors like encouraging team members to express opinions and ideas, promoting collaborative decision-making and information sharing (Arnold et al., 2000; Yun et al., 2005). Although empowering leadership tends to enhance team efficacy and commitment through psychological ownership of the task and improved coordination and teamwork (Zaccaro et al., 2001) in extreme situations where lives are at risk and good decisions must be made rapidly assigning tasks and providing clear directions seems to work better to solve the problem and consequently reducing the levels of anxiety and stress triggered by an extreme situation like a fire.

Previous research has confirmed the positive influence of empowering leadership on individual performance (Zhang & Bartol, 2010) and on the development of project and action teams (Kozlowisky et al., 1999). However, other studies have demonstrated that empowering leadership comes at an initial performance cost, showing to be more effective in later developmental phases, mainly through learning about their task environment and each other's areas of expertise to develop team mental models of how to integrate their efforts, gain collective efficacy and commitment through psychological empowerment, and foster routines to coordinate their behaviors (Lorinkova et al., 2013; Kozlowski et al., 1999; Sharma & Kirkman, 2015).

Although an empowering leadership style may be more appropriate for development of shared mental models and routines for coordination and learning necessary to adapt to complex and changing environments, the consequent team development and readiness requires time (Lorinkova et al., 2013). For teams with short-term or emergent engagements and teams facing emergency situations (e.g., surgical, police, military, and firefighter teams), a directive style may be most appropriate, as teams must be able to immediately perform at a high level and cannot afford the performance delays learning errors associated with empowered teams (Sims et al., 2009; Yun et al., 2005).

7. References

Arnold, J. A., Arad, S., Rhoades, J. A., & Drasgow, F. (2000). The empowering leadership questionnaire: The construction and validation of a new scale for measuring leader behaviors. *Journal of Organizational Behavior, 21*, 249-269.

Boosman, M., Lamb, K., & Verhoef, I. (2015). Why Simulation is Key for Maintaining Fire Incident Preparedness. *Fire Protection Engineering*, 2nd Quarter, 46-56.

Deppa, K.F. & Saltzberg, J. (2016). Resilience Training for Firefighters: An approach to prevent behavioral health problems. College Park: SpringerBriefs in Fire. http://www.springer.com/gp/book/9783319387789

Harms, P.D., Credé, M., Tynan, M., Leon, M. & Jeung, W. (2016). Leadership and stress: A meta-analytic review. *The Leadership Quarterly*, Volume 28, Issue 1, 178-194.

Kozlowski, S. W. J., Gully, S. M., Salas, E., Cannon-Bowers, J. A. (1996). 1996. Team leadership and development: Theory, principles, and guidelines for training leaders and teams. In M. M. Beyerlein, D. Johnson, & S. T. Beyerlein (Eds.), Interdisciplinary studies of work teams (pp. 253-291). JAI.

José L. Pais-Ribeiro, J. L., Honrado, A., & Leal, I. (2004). Contribuição para o estudo da adaptação portuguesa das escalas de ansiedade, depressão e stress (EADS) de 21 itens de Lovibond e Lovibond. Psicologia, Saúde & Doenças, 5(1), 229-239

Lorinkova, N. M., Pearsall, M. J., & Sims, H. P. (2013). Examining the differential longitudinal performance of directive versus empowering leadership in teams. *Academy of Management Journal, 56*(2), 573-596.

Lovibond, P., & Lovibond, S. (1995). The structure of negative emotional states: Comparison of the depression anxiety stress scales (DASS) with the Beck Depression and Anxiety Inventories. Behaviour Research and Therapy, 33(3), 335-343.

Prati, G., Pietrantoni, L., & Cicognani, E. (2010). Self-efficacy moderates the relationship between stress appraisal and quality of life among rescue workers. *Anxiety, Stress, and Coping*, *23*(2), 463-470. https://www.ncbi.nlm.nih.gov/pubmed/19937503

Reis, V., & Neves, C. (2019, November). Application of virtual reality simulation in firefighter training for the development of decision-making competences. In *2019 International Symposium on Computers in Education (SIIE)* (pp. 1-6). IEEE.

Sagie, A. (1996). Effects of leader's communication style and participative goal setting on performance and attitudes. *Human Performance, 9*(1), 51-64.

Sharma, P. N., & Kirkman, B. L. (2015). Leveraging leaders: A literature review and future lines of inquiry for empowering leadership research. *Group & Organization Management, 40*, 193-237.

Sims, H. P., Faraj, S., & Yun, S. 2009. When should a leader be directive or empowering? How to develop your own situational theory of leadership. *Business Horizons, 52*(2): 149-158.

Wijkmark, C. H., Heldal, I., Fankvist, S., & Metallinou, M. M. (2020). Remote Virtual Simulation for Incident Commanders: Opportunities and Possibilities. In *2020 11th IEEE International Conference on Cognitive Infocommunications (CogInfoCom)* (pp. 000445-000452). IEEE.

Yun, S., Faraj, S., & Sims, H. P. (2005). Contingent leadership and effectiveness of trauma resuscitation teams. *Journal of Applied Psychology, 90*(6), 1288-1296.

Zaccaro, S. J., Rittman, A. L., & Marks, M. A. (2001). Team leadership. *Leadership Quarterly, 12*(4), 451-483.

Zhang, X., & Bartol, K. M. (2010). Linking empowering leadership and employee creativity: The influence of psychological empowerment, intrinsic motivation, and creative process engagement. *Academy of Management Journal, 53*(1), 107-128.

Firefighting: Challenges of Smart PPE

Gilda Santos*[1]; Rita Marques[1]; J. Ribeiro[2]; A. Moreira [2]; P. Fernandes[2]; Margarida Silva[3,4]; André Fonseca[3,4]; João M. Miranda[3,4]; João B. L. M. Campos[3,4]; Soraia F. Neves[3,4]

[1]CITEVE - Technological Centre for the Textile and Clothing Industries of Portugal, V. N. Famalicão, Portugal, {gsantos, rmarques}@citeve.pt
[2]CeNTI - Centre for Nanotechnology and Smart Materials, V. N. Famalicão, Portugal, {jpribeiro, amoreira, pfernandes}@centi.pt
[3] CEFT - Transport Phenomena Research Center, Department of Chemical Engineering, Faculty of Engineering, University of Porto, s/n Rua Dr. Roberto Frias 4200-465 Porto, Portugal, {up201909589@up.pt}, {eq10026, jmiranda, jmc, sfneves}@fe.up.pt
[4]ALiCE - Associate Laboratory in Chemical Engineering, Faculty of Engineering, University of Porto, Rua Dr. Roberto Frias, 4200-465 Porto, Portugal

**Corresponding author*

Keywords

Fire Protection, Smart PPE, Phase Change Materials, Normative Requirements, Care and Maintenance

Abstract

The continuous research and development regarding firefighters' personal protective equipment (PPE) has led to significant improvements in recent decades. The findings that contributed the most to the firefighters' protective clothing evolution, increasing the protection, were the use of high-performance fibers, flame-retardant polymer fibers and the changes on clothing structure namely the incorporation of a multi-layer system. Despite the evolution of firefighters PPE, every year an undesirable number of firefighters are seriously burned during firefighting operations with some of them eventually losing their life. Therefore, the need to proceed the research and development regarding thermal protective clothing arises, to increase firefighters' protection and consequently minimize firefighters' heat load and skin burn. Firefighters' protection can be further increased with the incorporation of smart textiles in the personal protective equipment, such as integrated sensors to monitor parameters such as heart rate, oxygen saturation, carbon dioxide detector and setting real-time communication with a command post. In addition to the wearable electronics, regarding smart textiles alternatives for firefighters PPE, several studies have been conducted to incorporate phase change materials (PCM) in firefighters thermal protective clothing with satisfactory results. These advanced materials will absorb the heat from the fire leading to a reduction of the amount of heat to which firefighters are exposed to and an increase of the time that firefighters can be exposed to heat. The evolution of firefighters PPE has been followed by an evolution and update of the international and national standards that specify performance requirements for firefighters' protective clothing for structural and wildland firefighting as well as technical rescue. In respect to structural firefighting, the applicable European standard is EN 469:2020: Protective clothing for firefighters – Performance requirements for protective clothing for firefighters' activities and regarding the wildland firefighting, the international standard prevailing is EN ISO 15384:2020: Protective clothing for firefighters – Laboratory test methods and performance requirements for wildland firefighting clothing. For technical rescue the applicable European standard is EN 16689: 2017: Protective clothing for firefighters – Performance requirements for protective clothing for technical rescue. Given the growing trend towards the incorporation of smart materials in firefighters PPE is important to study and develop new standards to certify these innovative protective clothing for firefighters, regardless the efforts being done within CEN / TC 248/WG 31 - Smart Textiles. To preserve the protection of firefighters protective clothing there are some actions that must be taken during the protective garments' life cycle. Therefore, recently was developed a technical report, a CEN/ TR1760:2021 that describes the guidelines for selection use, care and maintenance of smart garments protecting against heat and flame. This study will focus on the analysis of firefighters protective clothing evolution regarding the use and integration of advanced smart materials, namely phase change materials, taking in consideration the evolution and requirements of international and European standards as well as national legislation for firefighters' protective clothing.

1. Introduction

Firefighters are often exposed to high temperatures and heat-fluxes due to high radiation produced by fire during fire extinguish operations. Therefore, personal protective equipment is of extreme importance for firefighters to

ensure their protection during firefighting activities. Due to the importance of firefighters' protective clothing, over time several research and development studies were taken leading to a continuous evolution of firefighters PPE. Currently, the emergence of smart textiles opened a wide range of opportunities to increase the level of protection of firefighters' protective clothing.

1.1. Firefighters PPE evolution

The scientific developments that led to the introduction of high-performance fibers have been the first major contribution for the increase of the firefighters' personal protective equipment level of protection, however, the biggest revolution regarding firefighters' protection was the use of flame-retardant polymer fibers, namely aromatic polyamides (aramids) and polybenzimidazole (PBI). Nowadays meta-aramids and para-aramids are widely used in firefighters' PPE due to their good thermal tolerance and long-time stability at high temperatures (Hertleer et al., 2013). Alongside the research and development of innovative fibers for firefighters' PPE, the major finding that contributed to increasing firefighters' PPE level of protection, resulting from studies regarding the clothing structure, was the introduction of a multi-layer system, used currently for structural firefighting. Three layers compose this multilayer system: outer shell (flame retardant fabric), vapor barrier, and thermal barrier. The design of the multilayer system allows the wearer to be firstly protected from heat and flame but also against moisture.

1.2. Smart firefighters PPE

The research and development carried out in the field of firefighters' PPE increasingly encompasses advanced materials and/or electronic components. From the combination of these smart materials with conventional PPE appears a new typology of PPE for firefighters. Regarding the development of garments with wearable electronic technologies, many include the integration of sensors for vital function and location monitoring in textiles, communication interface and energy supply with the purpose of increase functionality and protection of firefighters clothing (Mäkinen, 2008). On the other hand, the evolution in the field of advanced materials led to the emergence of new materials which can improve firefighter' clothing functionality. Currently, the development of new materials with adaptive function, such as phase change materials (PCM) has been the subject of interest to the researchers.

1.2.1. Phase change materials

Phase change materials are substances that can absorb and release energy in form of latent heat during a phase transition (Fonseca et al., 2018). These materials are commonly used to improve thermal comfort, however, when applied in smart firefighters' PPE they can be additionally used to improve the heat protection due to its high thermal storage capacities. An extensive spectrum of PCM for textile application is available with different heat storage capacities and melting points. Since PCM becomes liquid when exposed to heat, when integrated into textiles they should be confined to a container. To avoid this problem, PCM can be encapsulated in a polymeric structure(Zhu et al., 2015). Several recent studies have shown that the addiction of PCM layer into a conventional firefighter suit can be used to mitigate severe burns, increasing the time to second burns (Zhang et al., 2021).

1.3. Standardization and Certification

Due to the nature of their job, firefighters require the use of the most suitable PPE available, to be protected from the risks inherent to their activities. Therefore, is of most importance to ensure a high quality of PPE that is assessed through compliance with standards. International and European standards specify the performance requirements for firefighters' protective clothing. Regarding wildland firefighting prevails the international standard EN ISO 15384:2020: Protective clothing for firefighters – Laboratory test methods and performance requirements for wildland firefighting clothing. On the other hand, the requirements for structural firefighting protective clothing are defined in the European standard EN 469:2020: Protective clothing for firefighters – Performance requirements for protective clothing for firefighters' activities. As for technical rescue the applicable European standard is EN 16689: 2017: Protective clothing for firefighters – Performance requirements for protective clothing for technical rescue. Although PPE sector benefits from an abundance of standards, regarding smart PPE there is still a gap in the standardization. Currently an important study is being conducted concerning the requirements and testing procedures for innovative smart protective garments within CEN / TC 248/WG 31 - Smart Textiles. In fact, a new European standard named FprEN 17673 Protective clothing - Protection against heat and flame - Requirements and test methods for garments with integrated smart

textiles and non-textile elements is now at a final stage of approval. At the same time, there have been an evolution regarding the guidelines for selection, use, care, and maintenance (SUCAM) of garments protecting against heat and flame. In this field, a new technical report (CEN/ TR1760:2021) was developed that includes guidelines regarding smart personal protective clothing.

2. Methods

The purpose of this study involves the analysis of the major differences between the structural and wildfire firefighting protective clothing as well as a comparison of the prevailing standards for both firefighting protective clothing and further examination of the alterations done to the previous standards. This study is important to define and understand the prevailing performance requirements for each type of firefighting protective clothing, being the starting point for the development of innovative smart firefighters' PPE.

In addition, the study concerning possible ways to integrate phase change materials into a firefighter protective clothing, to enhance heat protection, was approached, creating a smart PPE. The integration methods study has considered the technical report (CEN/ TR1760:2021) which presents a section dedicated to smart garments with PCM. Besides the best practices mentioned by SUCAM the integration study took in consideration also circular economy and sustainable principles using techniques as eco-design.

3. Results

The purpose of the phase change materials integration is to improve heat protection. Thus, this study will focus on protective clothing for structural and wildland firefighting and will not analyse the protective clothing for technical rescue that is only applied for protection against limited heat and flame.

According to Portuguese firefighters' legislation (dispatch 7316/2016) and accomplishing the respective standards the following figure presents the current personal protective clothing for structural and wildland firefighting.

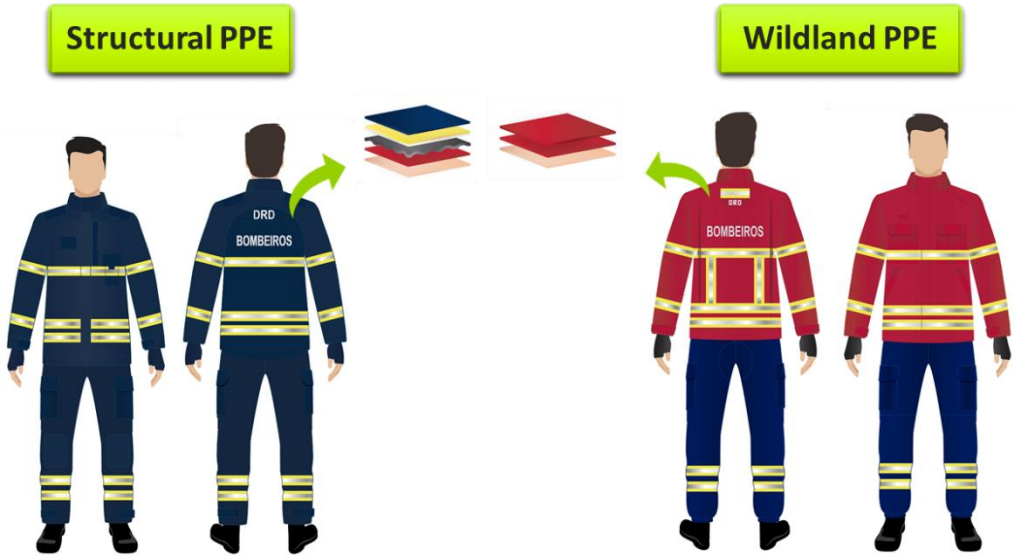

Figure 1. Structural and wildland PPE according to dispatch 7316/2016

The protective clothing suit for structural firefighting consists in a multilayer system composed by three layers with different functions as described in section 1, to be worn over the undergarment. In contrast, the wildland firefighting protective clothing suit has only one layer, outer shell, to provide protection against heat and flame, and must be worn over a long sleeve shirt.

The standards for structural and wildland firefighters' protective clothing (EN 469 and EN ISO 15384) define the performance requirements that must be accomplished. The focus of this study will be in thermal, mechanical and comfort performance requirements. The following table comprises a comparison regarding minimum

compliance values for test methods used both in structural and wildland firefighting protective clothing standards.

Table 1. Comparison between the minimum compliance values for wildland and structural firefighting protective clothing for the same test methods

Protective Clothing Standard	Standard	Description	Minimum compliance values	
EN 469:2020	EN ISO 15025	Flame spread test	A1 or A2	
EN ISO 15384:2020			A1 and A2	
EN 469:2020	ISO 6942	Heat transfer (radiation)	Level 1: $RHTI_{24}$≥10,0s $RHTI_{24}$-$RHTI_{12}$≥3,0s	Level 2: $RHTI_{24}$≥18,0s $RHTI_{24}$-$RHTI_{12}$≥4,0s
EN ISO 15384:2020			$RHTI_{24}$≥11,0s $RHTI_{24}$-$RHTI_{12}$≥4,0s	
EN 469:2020	ISO 13935-2	Main seam strength	≥ 300 N	
EN ISO 15384:2020				
EN 469:2020	ISO 13937-2	Tear strength	≥ 30 N	
EN ISO 15384::2020			≥ 25 N	
EN 469:2020	ISO 13934-1	Residual tensile strength	≥ 450 N	
EN ISO 15384:2020			≥ 600 N	
EN 469:2020	EN 31092	Water vapor resistance (Ret) / Thermal resistance (Rct)	Level 1: Ret>30 m^2Pa/W	Level 2: Ret≤30 m^2Pa/W
EN ISO 15384:2020			Ret ≤ 10 m^2Pa/W Rct ≤ 0,055 m^2K/W	
EN 469:2020	ISO 17493	Heat resistance	180°C	
EN ISO 15384:2020			260°C	
EN 469:2020	ISO 5077	Dimensional change	≤3% woven fabrics ≤5% non-woven and knitted fabrics	
EN ISO 15384:2020				

The comparison presented in table 1 allows to conclude that despite both standards use the same test methods, the minimum compliance values change for several tests. In addition to the test methods described in table 1, structural protective clothing has some specific required tests, presented in table 2.

Table 2. Specific required tests and minimum compliance values for structural firefighting protective clothing

Standard	Description	Minimum compliance values	
ISO 9151	Heat transfer (flame)	Level 1: HTI_{24}≥9,0s HTI_{24}-HTI_{12}≥3,0s	Level 2: HTI_{24}≥13,0s HTI_{24}-HTI_{12}≥4,0s
EN 20811	Water penetration	Level 1: >20kPa	Level 2: ≥20 kPa
EN 6530	Resistance to chemical penetration	No penetration to innermost surface; Index of repellence ≥80%	
EN ISO 12127-1	Contact heat test	Level 1: -	Level 2: 250 °C (10s)

Regarding test methods to evaluate performance requirements, the update of the standard for structural firefighting protective clothing in 2020, introduced the contact heat test and reduced the number of chemicals that are used in resistance to chemical penetration test. In addition, flame testing of hardware like labels (≥10 cm^2), badge and retroreflective materials as well as the moisture barrier shall be tested as part of the assembly. For the wildland firefighting, EN 15614 was superseded by EN ISO 15384 demanding now slightly higher values for the mechanical parameters and a higher temperature (260 °C) for the heat resistance of the materials.

The PCM integration in firefighters' protective clothing have considered the guidelines present in CEN/ TR1760:2021. This technical report defines guidelines regarding selection, use care and maintenance of smart garments protecting against heat and flame. The following figure presents the main topics within each step of PPE life cycle.

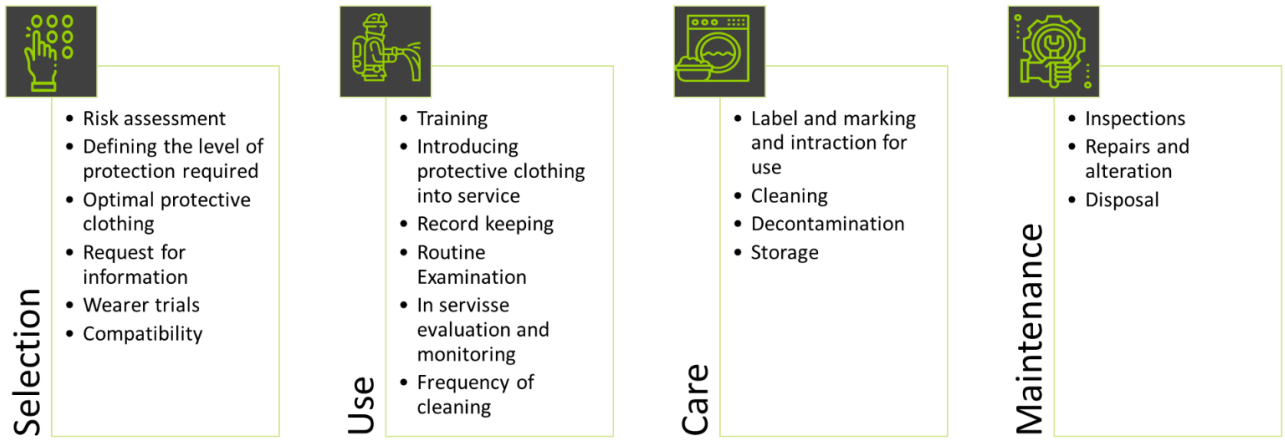

Figure 2. Main topics approached in SUCAM guideline

In addition to the generic guidelines concerning protective clothing on use, care and maintenance up to and including the disposal of the protective gear, this document provides examples of the scenarios and SUCAM procedures, being garments with PCM packages one of the given examples.

PCM packages must be selected considering the melting temperature more suitable for the exposure needs that vary with different parameters: activity level (heat produced by the body), climatic conditions, exposure length and logistical opportunities or limitations, for instance the possibility to replace the PCM packages during the mission.

Regarding cleaning and decontamination of garments with PCM, the PCM packages must be withdraw from the garment, and be cleaned according to manufacturer's instructions, and wiped with a soap solution. Garments with PCM packages must be stored horizontally during the solidification process to avoid material accumulation at the lower end of the package, and consequently, uneven cooling effect, reduced protection and potential tactile discomfort during next use. If noticing any problems during care and maintenance procedures such as PCM substance leaking or if any package has not melted even if being above the melting temperature, the situation must be reported.

Concerning the inspection of PCM packages on regular basis the user must inspect the packages according to the figure 3 and at least once a year verify if PCM will melt at their melting point. The disposal of broken packages must be according to manufacturer's instructions.

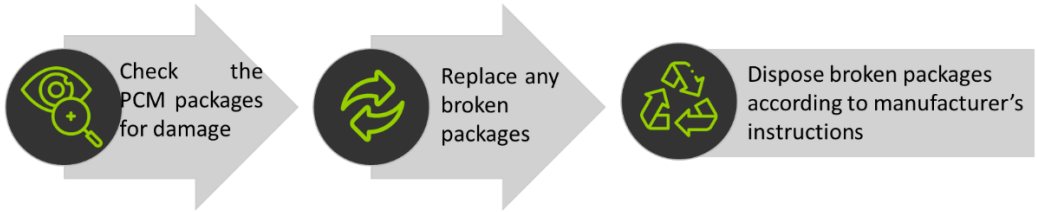

Figure 3. Inspection and disposable procedure for PCM packages

Considering that recent studies in which was found that the optimum position for the PCM layer is the closest to the external heat, PCM packages are being integrated into a vest to be worn over a conventional firefighter PPE, creating a smart protective clothing system. The design of the vest was studied to protect mainly the torso of the firefighter preserving ergonomics. However, after some firefighters feedback a second version was developed to enhance the protection of the upper limbs, Figure 4.

Figure 4. Study of PCM vest design: ergonomic (left) and enhanced protection (right)

The distribution of PCM packages in the vest took in consideration different variables namely the amount of PCM in each package, and the size and the amount of the PCM packages to achieve a commitment between heat management and breathability.

Considering SUCAM guidelines for garments with PCM packages and the different parameters concerning PCM packages distribution in the vest, the integration of PCM packages is described schematically on Figure 5.

Figure 5. Study of the integration of PCM packages in the vest

As evidenced in Figure 5, PCM packages were integrated in a matrix composed by two layers, an insulation material and a flame retardance fabric. The introduction of the PCM packages through laser cut openings makes routine inspections and cleaning procedures described in SUCAM easy and allows the replacement of broken packages. Afterwards, this matrix was inserted into the vest main structure creating a PCM vest. In addition to making SUCAM procedure easier, the design of the vest considered also circular economy principles, since this removable system allows the separation of all the components of the vest making possible to recycle them.

4. Conclusions

The use of smart textiles, and in this specific case textiles with PCM integrated, combined with conventional PPE can play an important role towards the increase of firefighter's heat protection.

Having in mind a modular approach that could fit both, wildland and structural firefighters, the analysis of the major differences between the respective protective clothing as well as a comparison of the prevailing standards and legislation was performed.

A first architecture of a PCM vest to be worn over the conventional protective clothing was designed based on the integration study done aiming at protecting mainly the torso to preserve ergonomics. Protective standards

requirements, best practices mentioned by SUCAM and also circular economy and sustainable principles using techniques as eco-design were taken into account.

The study will proceed with testing and simulation measurements in straight collaboration with ENB (Portuguese national firefighters' school), towards the solution improvement.

5. Acknowledgements

This work was financially supported by LA/P/0045/2020 (ALiCE), UIDB/00532/2020 and UIDP/00532/2020 (CEFT), and by PCIF/SSO/0106/2018 - Project for "Development of an innovative firefighter's jacket", funded by national funds through FCT/MCTES (PIDDAC).

6. Bibliography

Hertleer, C. (2013). Smart Textiles for Protection. Protective clothing for firefighters and rescue workers. 338–363. doi:10.1533/9780857097620.2.338

Mäkinen, H. (2008). Firefighters' protective clothing. Advances in Fire Retardant Materials, 467–491. https://doi.org/10.1533/9781845694701.3.467

Fonseca, A., Mayor, T. S., & Campos, J. B. L. M. (2018). Guidelines for the specification of a PCM layer in firefighting protective clothing ensembles. *Applied Thermal Engineering*, 133, 81–96.

Zhu, F., Feng, Q. Q., Liu, R., Yu, B., & Zhou, Y. (2015). Enhancing the thermal protective performance of firefighters' protective fabrics by incorporating phase change materials. Fibres and Textiles in Eastern Europe, 23(2), 68–73.

Zhang, H., Liu, X., Song, G., & Yang, H. (2021). Effects of microencapsulated phase change materials on the thermal behavior of multilayer thermal protective clothing. Journal of the Textile Institute, 112(6), 1004–1013. https://doi.org/10.1080/00405000.2020.1832363

Fire-smart management as nature-based solution to extreme wildfires in abandoned rural landscapes of Southern Europe

Silvana Pais[1,2,3]*; João Campos[1]; Judit Lecina[4]; Adrián Regos[1,5,6]

[1] CIBIO, Centro de Investigação em Biodiversidade e Recursos Genéticos, InBIO Laboratório Associado, Campus de Vairão, Universidade do Porto. 4485-661 Vairão, Portugal, {silvana10pais@gmail.com, jc_campos@cibio.up.pt, adrian.regos@usc.es}
[2] Departamento de Biologia, Faculdade de Ciências, Universidade do Porto. 4099-002 Porto, Portugal
[3] BIOPOLIS Program in Genomics, Biodiversity and Land Planning, CIBIO, Campus de Vairão. 4485-661 Vairão, Portugal
[4] Technical University of Munich, Germany; TUM School of Life Sciences; Ecosystem Dynamics and Forest Management Group. Hans-Carl-von-Carlowitz-Platz 2, 85354, Freising, Germany, {judit.lecina.diaz@gmail.com}
[5] Forest Science Center of Catalonia. Crta. Antiga St Llorenç de Morunys km 2, 25280 Solsona, Catalonia, Spain
[6] Departamento de Zooloxía, Xenética e Antropoloxía Física, Universidade de Santiago de Compostela. 15782 Santiago de Compostela, Spain

**Corresponding author*

Keywords

Ecosystem Services; Fire-Smart; Nature Conservation; Stakeholders; Wildfires

Abstract

In Mediterranean regions worldwide, climate and landscape change increased the occurrence and the risk of (very) large and intense fires, which override the current firefighting capacity. Fire management policies, largely focused on fighting at the expense of prevention, have proven inadequate to address this challenge. Agricultural abandonment has shaped rural mountain areas in many parts of Southern Europe since the last century, owing to diverse socio-economic and biophysical constraints such as reduced job opportunities, poor generational renewal, low accessibility and soil productivity. The cessation of traditional livestock and agricultural practices caused by rural exodus has favoured more homogeneous and flammable landscapes —with strong side-effects on fire regime, ecosystem services and biodiversity.

In fact, the challenge for managers and policy makers is no longer simply how to reduce wildfire impacts but how to reconcile socio-economic impacts of fires with their ecological benefits. Fire-smart management would clearly enable a more balanced integration of positive (reducing species competition, diseases and pests or fire intensity, and increase fire protection in wildland-urban interfaces) and negative contributions of fire to human well-being, which would inform better decision making in fire management policy and land-use planning. In practice, fire-smart landscapes can be obtained by fuel-reduction treatments and by fuel type conversion, rather than by fuel isolation. From this perspective, proactive management should therefore focus on reshaping vegetation (fuel) configuration to foster more fire-resistant and/or fire-resilient landscapes while simultaneously ensuring the long-term supply of ecosystem services and biodiversity conservation. In contrast, rewilding has been proposed as an opportunity for biodiversity conservation in abandoned landscapes. However, rewilding is challenged by the increasing fire risk associated with more flammable landscapes, and the loss of open-habitat specialist species.

Here we present three complementary studies carried out in the frame of the FirESmart project (https://firesmartproject.wordpress.com) focusing on two contrasting land-use policy scenarios (Rewilding vs High Nature Value farmlands) based on stakeholders' perception of fire-landscape dynamics, and their potential impacts on biodiversity conservation and ecosystem services. Our studies were implemented in a transboundary protected area, the Gerês-Xurés Biosphere Reserve, where we predicted the potential impacts in terms of fire regime change, species conservation and carbon sequestration.

Our studies contribute to the increasing evidence of agricultural policies as essential tools to ensure biodiversity while reducing fire hazard, an aspect that has been frequently neglected when assessing the beneficial effects of agricultural policies. Also, our findings suggest using fire to enhance rewilding as an alternative management strategy in our study area — an issue that decision makers and managers should consider when implementing rewilding initiatives in other fire-prone regions. These studies represent the needs of local communities in these mountainous areas, which are heavily

affected by rural abandonment, fire regimes, and loss of natural resources. These rural communities try to keep alive the few and scarce agricultural activities and manage the mountain landscapes. However, the reduced investment and financial support of these isolated communities has led to the decline of these traditional fuel and habitat management tools.

1. Introduction

Wildfires are a major component of disturbance regimes worldwide (Keeley et al., 2012). Despite the increasing amount of resources invested in fire suppression, the number of extreme fire events has largely increased over the last decades in southern Europe, overriding current fire-suppression systems (San-Miguel-Ayanz et al., 2013). Agricultural abandonment has shaped rural mountain areas in many parts of the Mediterranean Europe since the last century, owing to diverse socio-economic and biophysical constraints such as reduced job opportunities, poor generational renewal, low accessibility and soil productivity (Cerqueira et al., 2010; MacDonald et al., 2000).

Society has co-evolved with fire over centuries (Pausas & Keeley, 2019). In rural areas, fire was also used as a tool for land management (e.g., clearing land for pastures Chas-Amil et al., 2015; Tedim et al., 2016), which resulted in a large number of low-intensity and small-sized fires (Chas-Amil et al., 2010). At the same time, fire has been perceived by society as a damaging hazard with only negative impacts, which reinforced fire exclusion and suppression policies. In the last decades, as a result of both agricultural abandonment and fire exclusion policy, Mediterranean landscapes have become more homogeneous and flammable (Moreira et al., 2011) and therefore more susceptible and vulnerable to forest fires.

The interactions between fire and landscape dynamics in these complex socio-ecological systems hinder how to efficiently treat landscapes in terms of spatial configuration and density of treatments (Alcasena et al., 2018; Oliveira et al., 2016; Thompson et al., 2017). In protected areas, landscape management becomes more complex because legislation regulates management, which together with land ownership constraints, complicates treatment allocation (Alcasena et al., 2018). Therefore, treatment strategies must consider multiple objectives and should involve the needs and views of stakeholders in relation to fire and landscape management. In particular, fire management strategies in these areas have been directed towards promotion of agro-pastoral activities, total or partial removal of the fuel in strategic areas, and use of prescribed burning.

More recently, fire-smart management (defined as “an integrated approach primarily based on fuel treatments through which the socio-economic impacts of fire are minimized while its ecological benefits are maximized”; Hirsch et al., 2001) has been proposed as an alternative including fire as a socio-ecological process while balancing the benefits and drawbacks of fire to human well-being (Fernandes, 2013).

On the contrary, land abandonment in rural landscapes is one of the most important drivers of regional land-use change (Estoque et al., 2019), and has been suggested as an opportunity for biodiversity conservation and the reinstatement of natural ecological processes (Queiroz et al., 2014). However, rewilding holds some constraints that may limit its successful implementation. The inherent homogenization of rewilded landscapes leads to loss and fragmentation of open habitats, mainly due to shrub encroachment and forest expansion (Moreira et al., 2011). Studies also indicated that the gradual cessation of traditional farming areas, many of which known to support “High Nature Value farmlands” (hereafter HNVf), is a major cause of local biodiversity losses, accelerating population declines of species adapted to wet grasslands, pastures and other extensive agricultural areas (Franks et al., 2018; Ribeiro et al., 2014). The intricate links between land abandonment and fire regimes complexify the selection of appropriate alternative scenarios, and subsequently decision-making in fire management and planning (McLauchlan et al., 2020).

In this new era of megafires, the question is how landscape management could integrate social and ecological perspectives to solve the growing problem of forest fires. Possibly, the most effective way to integrate both dimensions of this societal challenge in fire-prone regions is mainstreaming fire-smart management as Nature-based Solution (hereafter NbS).

1.1. Aims

These studies have sought to address several important issues in landscape and fire regime management, nature conservation, and the inclusion of local stakeholders in the understanding of these complex processes.

Firstly, we analysed stakeholders' perceptions about wildfire-landscape interactions in abandoned rural landscapes of Southern Europe, and how fire and the territory should be managed to reduce wildfire hazard and ensure the long-term supply of ecosystem services. To do so, we have used a structured online questionnaire that was sent to stakeholders. We also analysed the differences in the stakeholders' perceptions among sectors and we also explore to what extent fire management strategies can be considered Nature-based Solutions using the IUCN standard.

The second study aimed to identify 'win-win' situations to reduce the impact of wildfires and maximize the provision of carbon storage and sequestration and biodiversity conservation in fire-prone regions affected by rural abandonment. We assessed the potential trade-offs between wildfire mitigation (measured through total burned and suppressed area), climate regulation ecosystem services (i.e., carbon storage and sequestration) and biodiversity conservation under fire-smart management scenarios.

Lastly, we assessed the impacts of alternative landscape trajectories and fire suppression management strategies on future fire regimes and on biodiversity conservation. We focused on changes in burned and suppressed areas and habitat availability for 211 vertebrate species. We aimed to answer the following questions: 1) How would different land-use and fire suppression management scenarios contribute to future fire mitigation (i.e. fewer areas burned associated with higher suppression efficiency)?, 2) How would those scenarios affect biodiversity?; 3) Which is the best management scenario for promoting fire mitigation and biodiversity conservation?; and 4) With agricultural policies failing to cope with rural abandonment, could a rewilding trajectory integrated with fire suppression policies contribute to enhance biodiversity conservation?

2. Methodology

2.1. Study area

These studies were conducted in the Transboundary Biosphere Reserve Gerês-Xurés (ca. 276,000 ha, of which 71% in Portugal and the remaining 29% in Spain), a representative mountain landscape of NW Iberian Peninsula. The region is located at the transition between the Mediterranean and Eurosiberian (Temperate) biogeographic zones, close to the Atlantic coast. The study area includes the entire reserve, encompassing three EU Natura 2000 sites besides two nationally designated protected areas, the Peneda-Gerês National Park in Portugal and the Baixa Limia - Serra do Xurés Natural Park in Spain. Although our study is conducted in the entire Biosphere Reserve, we intend to discern the management impacts both within and outside protected areas, given the differences between both areas in terms of socio-economic values and protection measures, which would influence how the different management strategies could be implemented.

2.2. Local stakeholders' perception and scenarios design

The questionnaire was conducted based on an online questionnaire structured in four sections related to: 1) fire; 2) landscape; 3) and potential impacts of fire management strategies on fire regime, and ecosystem services; (see details in Lecina et al. *under review*).

2.3. Modelling framework

We used a spatially explicit process-based model (REMAINS) that integrates the main factors driving fire-landscape dynamics (Pais et al., 2020). The model allows investigating how the spatiotemporal interactions between fire-vegetation dynamics, fire management and land-use changes affect fire regime at short- and medium-timescales. The REMAINS model reproduces fire-landscape dynamics according to pre-designed scenario storylines (Pais et al., 2020). In particular, the model simulates wildfires (including fire ignition, spread, burning and extinction), vegetation dynamics (natural succession), land-use changes (agriculture abandonment or intensification) and forest management.

We combined fire-landscape model simulations with species distribution models to identify the best strategies for wildfires prevention and bird conservation (between 1990 to 2050). This model was calibrated using historical fire statistics and landscape change analysis based on remote sensing information. We run fire-simulated fire-landscape dynamics under scenarios with different land-use and fire management policies, based on four storylines (Figure 1) (Pais et al., 2020).

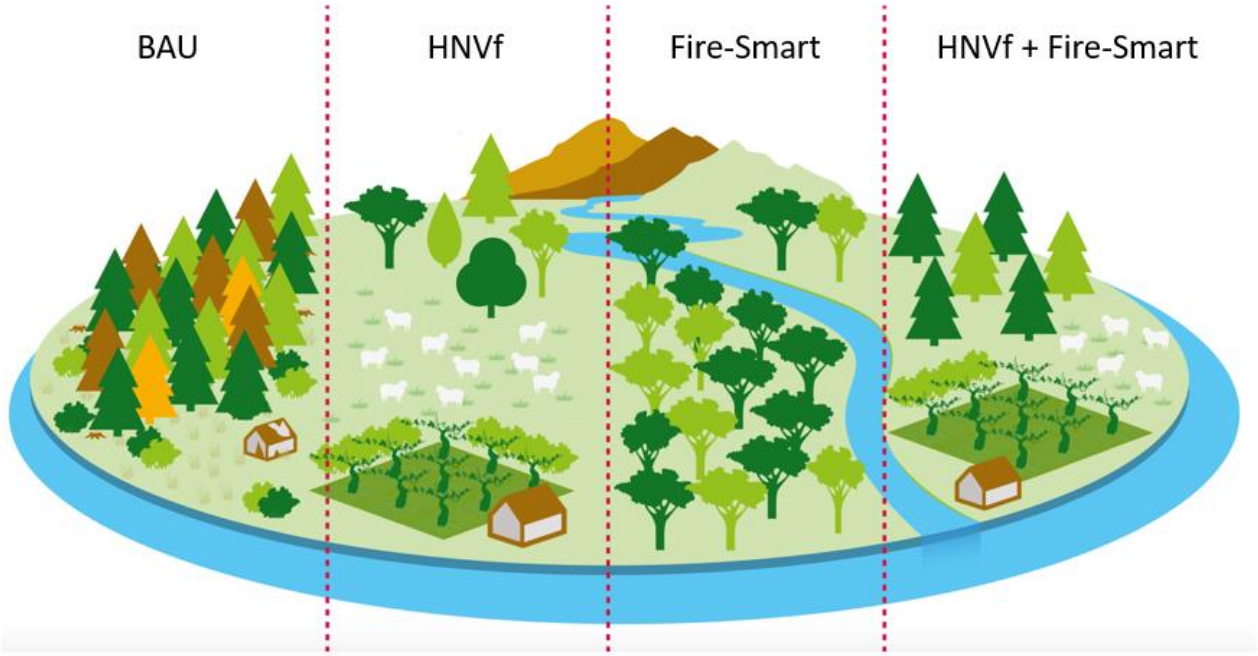

Figure 1 - Storylines: Business-as-usual scenario (BAU) describes the current trend of land abandonment; High Nature Value Farmland (HNVf) represents a policy promoting traditional agricultural activities. Fire-smart scenarios aims to create landscapes more resistant to wildfires. HNVf plus Fire-smart combines these two policies (see details in Pais et al., 2020) (extracted fr om Hernández, 2021).

To predict biodiversity distribution, we used species data from atlases and fire-landscape model simulations under the 4 most extreme scenarios. We applied an ensemble modelling approach from different modelling techniques for these species, to account for the uncertainty related to the modelling technique (see Pais et al., 2020). We conducted a biophysical assessment of the climate regulation ecosystem service (hereafter CRES) based on the carbon sequestration ecosystem function, by applying the InVEST (Integrated Valuation of Ecosystem Services and Tradeoffs) model. We evaluated the impact of fire and land-use management scenarios on this ecosystem service over a period of 63 years (1987–2050) (see Campos et al., 2021).

3. Results and conclusions

The first step showed stakeholders' perceptions about fire, its impacts on the landscape, and the fire management opportunities. Overall, there is a general agreement among stakeholders across sectors and study areas. They state that fire must be managed and support fire prevention rather than suppression policies. They also perceived that rural abandonment is the main cause of large wildfires, with more high-intensity fires impacting the study regions than in the last 30 years, a situation that they expect to continue in the future in the absence of management. Regarding fuel management, all strategies except using chemical methods were accepted by the stakeholders who perceive more positive than negative effects of fire management on forest ecosystem services. In particular, promoting agricultural and livestock uses, modifying forest species composition to increase fire resistance, and introducing large herbivores have potential to become effective Nature-based Solutions in the regions. Nevertheless, additional studies are needed to engage the stakeholders more actively in the management of these areas, as well as to evaluate the cost-effectiveness of fire management strategies. This study is a first-step analysis for the co-design and co-implementation of these fire management strategies as NbS, which will guarantee its successful application in solving the societal challenges and contributing to the sustainable development of the areas.

Our findings also found the benefits of integrating proactive land-use policies and fire-smart management strategies at the regional scale to promote sustainable solutions to the forest fires problem in abandoned mountain landscapes of Southern Europe. Overall, our results highlight that land-use policies aimed at promoting farmland areas would provide fire-suppression opportunities while simultaneously ensuring biodiversity conservation within (and around) protected areas. Our results confirm the urgent need for policies

promoting farmland areas, both in terms of future fire-suppression opportunities and biodiversity conservation. A large amount of strategically allocated cropland areas (at least 1,200 ha per year) should be gradually incorporated to the landscape along the next decades to significantly affect fire regime in the medium term. These policies would be also positive for conservation objectives since most of the species would benefit for the recovery of habitats associated with agricultural activities. In terms of long-term supply of the climate regulation ecosystem service (through carbon sequestration), our models predicted the best outcomes under large-scale fire-smart forest conversion. However, the integration of this fire-smart landscape conversion would be only acceptable for biodiversity conservation and fire prevention if embedded in landscape matrix characterized by increasing agricultural areas over the next decades.

The last study contributes to the increasing evidence of agricultural policies as essential tools to ensure biodiversity while reducing fire hazard, an aspect that has been frequently neglected when assessing the beneficial effects of agricultural policies. Also, this study suggests using fire to enhance rewilding as an alternative management strategy in our study area — an issue that decision makers and managers should consider when implementing rewilding initiatives in other fire-prone regions. Additionally, our study highlights the need for renewed political and socio-economic efforts exploring different solutions to economic incentives and/or management strategies integrating both rewilding and HNVf. In this context, our study demonstrates how an effective implementation of European agricultural policies could benefit biodiversity (through the creation of new open habitats for endangered species) while providing further fire-suppression opportunities. Our study also shows how fire suppression policies can help the implementation of rewilding initiatives in other abandoned, fire-prone mountain areas across Southern Europe (see dissemination video at https://youtu.be/x7ouTIBp__E).

4. References

Alcasena, F. J., Ager, A. A., Salis, M., Day, M. A., & Vega-Garcia, C. (2018). Optimizing prescribed fire allocation for managing fire risk in central Catalonia. Science of The Total Environment, 621, 872–885. https://doi.org/10.1016/j.scitotenv.2017.11.297

Campos, J. C., Bernhardt, J., Aquilué, N., Brotons, L., Domínguez, J., Lomba, Â., Marcos, B., Martínez-Freiría, F., Moreira, F., Pais, S., Honrado, J. P., & Regos, A. (2021). Using fire to enhance rewilding when agricultural policies fail. Science of The Total Environment, 755, 142897. https://doi.org/10.1016/j.scitotenv.2020.142897

Cerqueira, Y., Araújo, C., Vicente, J., Pereira, H. M., & Honrado, J. (2010). Ecological and Cultural Consequences of Agricultural Abandonment in the Peneda-Gerês National Park (Portugal). In Natural Heritage from East to West (pp. 175–183). Springer Berlin Heidelberg. https://doi.org/10.1007/978-3-642-01577-9_22

Chas-Amil, M. L., Prestemon, J. P., McClean, C. J., & Touza, J. (2015). Human-ignited wildfire patterns and responses to policy shifts. Applied Geography, 56, 164–176. https://doi.org/10.1016/j.apgeog.2014.11.025

Chas-Amil, M. L., Touza, J., & Prestemon, J. P. (2010). Spatial distribution of human-caused forest fires in Galicia (NW Spain). In G. Perona & C. A. Brebbia (Eds.), Modelling, Monitoring and Management of Forest Fires II (pp. 247–258).

Estoque, R. C., Gomi, K., Togawa, T., Ooba, M., Hijioka, Y., Akiyama, C. M., Nakamura, S., Yoshioka, A., & Kuroda, K. (2019). Scenario-based land abandonment projections: Method, application and implications. Science of The Total Environment, 692, 903–916. https://doi.org/10.1016/j.scitotenv.2019.07.204

Fernandes, P. M. (2013). Fire-smart management of forest landscapes in the Mediterranean basin under global change. In Landscape and Urban Planning (Vol. 110, Issue 1, pp. 175–182). Elsevier. https://doi.org/10.1016/j.landurbplan.2012.10.014

Franks, S. E., Roodbergen, M., Teunissen, W., Carrington Cotton, A., & Pearce-Higgins, J. W. (2018). Evaluating the effectiveness of conservation measures for European grassland-breeding waders. Ecology and Evolution, 8(21), 10555–10568. https://doi.org/10.1002/ece3.4532

Hernández, L. y cols. (2021). Paisagens corta-fogos. Proposta da ANP|WWF e WWF Espanha para um território ibérico adaptado aos incêndios. www.natureza-portugal.org

Hirsch, K., Kafka, V., Tymstra, C., McAlpine, R., Hawkes, B., Stegehuis, H., Quintilio, S., Gauthier, S., & Peck, K. (2001). Fire-smart forest management: A pragmatic approach to sustainable forest management in fire-dominated ecosystems. Forestry Chronicle, 77(2), 357–363. https://doi.org/10.5558/tfc77357-2

Keeley, J., Bond, W., Bradstock, R., Pausas, J., & Rundel, P. (2012). Fire in mediterranean ecosystems: ecology, evolution and management.

MacDonald, D., Crabtree, J. ., Wiesinger, G., Dax, T., Stamou, N., Fleury, P., Gutierrez Lazpita, J., & Gibon, A. (2000). Agricultural abandonment in mountain areas of Europe: Environmental consequences and policy response. Journal of Environmental Management, 59(1), 47–69. https://doi.org/10.1006/jema.1999.0335

McLauchlan, K. K., Higuera, P. E., Miesel, J., Rogers, B. M., Schweitzer, J., Shuman, J. K., Tepley, A. J., Varner, J. M., Veblen, T. T., Adalsteinsson, S. A., Balch, J. K., Baker, P., Batllori, E., Bigio, E., Brando, P., Cattau, M., Chipman, M. L., Coen, J., Crandall, R., … Watts, A. C. (2020). Fire as a fundamental ecological process: Research advances and frontiers. Journal of Ecology, 108(5), 2047–2069. https://doi.org/10.1111/1365-2745.13403

Moreira, F., Viedma, O., Arianoutsou, M., Curt, T., Koutsias, N., Rigolot, E., Barbati, A., Corona, P., Vaz, P., Xanthopoulos, G., Mouillot, F., & Bilgili, E. (2011). Landscape – wildfire interactions in southern Europe: Implications for landscape management. Journal of Environmental Management, 92(10), 2389–2402. https://doi.org/10.1016/j.jenvman.2011.06.028

Oliveira, T. M., Barros, A. M. G., Ager, A. A., & Fernandes, P. M. (2016). Assessing the effect of a fuel break network to reduce burnt area and wildfire risk transmission. International Journal of Wildland Fire, 25(6), 619. https://doi.org/10.1071/WF15146

Pais, S., Aquilué, N., Campos, J., Sil, Â., Marcos, B., Martínez-Freiría, F., Domínguez, J., Brotons, L., Honrado, J. P., & Regos, A. (2020). Mountain farmland protection and fire-smart management jointly reduce fire hazard and enhance biodiversity and carbon sequestration. Ecosystem Services, 44, 101143. https://doi.org/10.1016/j.ecoser.2020.101143

Pausas, J. G., & Keeley, J. E. (2019). Wildfires as an ecosystem service. Frontiers in Ecology and the Environment, 17(5), 289–295. https://doi.org/10.1002/fee.2044

Queiroz, C., Beilin, R., Folke, C., & Lindborg, R. (2014). Farmland abandonment: threat or opportunity for biodiversity conservation? A global review. Frontiers in Ecology and the Environment, 12(5), 288–296. https://doi.org/10.1890/120348

Ribeiro, P. F., Santos, J. L., Bugalho, M. N., Santana, J., Reino, L., Beja, P., & Moreira, F. (2014). Modelling farming system dynamics in High Nature Value Farmland under policy change. Agriculture, Ecosystems and Environment, 183, 138–144. https://doi.org/10.1016/j.agee.2013.11.002

San-Miguel-Ayanz, J., Moreno, J. M., & Camia, A. (2013). Analysis of large fires in European Mediterranean landscapes: Lessons learned and perspectives. Forest Ecology and Management, 294, 11–22. https://doi.org/10.1016/j.foreco.2012.10.050

Tedim, F., Leone, V., & Xanthopoulos, G. (2016). A wildfire risk management concept based on a social-ecological approach in the European Union: Fire Smart Territory. International Journal of Disaster Risk Reduction, 18, 138–153. https://doi.org/10.1016/j.ijdrr.2016.06.005

Thompson, M. P., Rodríguez y Silva, F., Calkin, D. E., & Hand, M. S. (2017). A review of challenges to determining and demonstrating efficiency of large fire management. International Journal of Wildland Fire, 26(7), 562. https://doi.org/10.1071/WF16137

Flame Length of Wildland Fires: Effect of Flame Zone Depth

Mark A. Finney*[1]; Torben P. Grumstrup[1]

[1]*USDA Forest Service Missoula Fire Sciences Laboratory, 5775 Highway 10 West, Missoula MT 59808, USA, {mark.finney, torben.p.grumstup}@usda.gov*

**Corresponding author*

Keywords

Flame length, fireline intensity, flame zone depth

Abstract

Correlations of flame length $\boldsymbol{L}$ with fireline intensity $\boldsymbol{I_B}$, based on theory and data by Thomas (1963), showed that flame zone depth $\boldsymbol{D}$ of a line fire could be neglected if $\boldsymbol{L}$ was much greater than $\boldsymbol{D}$. This has not been verified for wildland fires where $\boldsymbol{D}$ is typically a non-negligible proportion of $\boldsymbol{L}$ (*i.e.*, roughly $\boldsymbol{L/D} < \sim 2$). Here we report on experiments with line-source fires from a gas burner where $\boldsymbol{I_B}$ and $\boldsymbol{D}$ were controlled independently ($0.15 \leq \boldsymbol{L/D} \leq 13.6$). The resulting correlation showed $\boldsymbol{D}$ significantly reduced $\boldsymbol{L}$ for a given $\boldsymbol{I_B}$ over the entire range of observations and was in accord with independent data from spreading fires. Flame length is reduced because the horizontal extent of deep flame zones entrains more air for combustion than assumed by theory involving only the vertical flame profile. Fire behavior modeling that relies on correlations of $\boldsymbol{L}$ with $\boldsymbol{I_B}$ for scaling of heat transfer processes would likely benefit by including the effects of $\boldsymbol{D}$.

1. Introduction

Flame length $\boldsymbol{L}$ (m) of wildland fires is used for modelling heat transfer by radiation (for determining view factor and emissivity) and convection (for determining flame velocity and temperature profiles). It also has practical utility for wildland firefighters as a visual proxy for intensity.

Many empirical studies have shown that $\boldsymbol{L}$ is a power function of Byram's (1959) fireline intensity $\boldsymbol{I_B}$ (kW/m) from linear fire sources such that $\boldsymbol{L \propto c I_B^{\,n}}$. The coefficient $\boldsymbol{c}$ and exponent $\boldsymbol{n}$ in the line fire correlations vary considerably for wildland fires, leading some to suspect the $\boldsymbol{L}$-$\boldsymbol{I_B}$ relationships cannot be compared among fuel types, for example grass vs. shrubland (Alexander 1982; Alexander and Cruz 2012). Importantly, some of the variation in $\boldsymbol{I_B}$ derives from how it is estimated based on Byram's (1959) formula ($\boldsymbol{I_B = H m'' R}$) for spreading fires because of uncertainty in heat yield of the fuel ($\boldsymbol{H}$, kJ/kg), overestimation of fuel mass consumed in flaming per unit area ($\boldsymbol{m''}$, kg/m^2), and sometimes unsteady spread rate $\boldsymbol{R}$ (m/s). Differences have also been attributed to variations in the geometry of the fuel source, fuel material (Steward 1964, Quintiere and Grove 1998) (natural biomass, different hydrocarbon gas, or liquid fuels for example), and the difficulty with obtaining consistent measurements of fluctuating flame length (Zukoski et al. 1986; Newman and Wieczorek 2004).

Data and theory by Thomas (1960, 1963) supported the reasoning that effects of flame zone depth $\boldsymbol{D}$ (m) would become negligible as $\boldsymbol{L}$ greatly exceeded $\boldsymbol{D}$. This paper describes an experiment to test that assumption. We employed a laboratory sand-burner apparatus that allows precise independent control of the gas flow rate and magnitude of flame zone depth $\boldsymbol{D}$.

2. Methods

A propane-fuelled sand burner was constructed at the US Forest Service, Missoula Fire Sciences Laboratory for the purpose of studying flame structure and heat transfer from stationary flame zones (Figure 1). This sand burner is similar to the one described by Finney et al. (2020) but double the size, having rectangular dimensions of the burner box of 1.22 m × 3.66 m. The sand box is 0.15 m deep with 8 perforated tubes running the long axis (3.66 m) along the inside bottom surface under the sand. The burner box is mounted on a tilting platform 3.66 × 7.3 m in size with 4.8 m uphill decking made of flame-resistant Super Fire Temp board 2.54 cm thick.

The downhill decking is 1.2 m (Figure 1) in length. Each tube is controlled separately for gas flowing from a common manifold so that any combination of tubes can be fired with a controlled rate of propane. Gas flow is regulated by an Alicat ® mass flow controller capable of flowing up to 1500 standard liters per minute (SLPM).

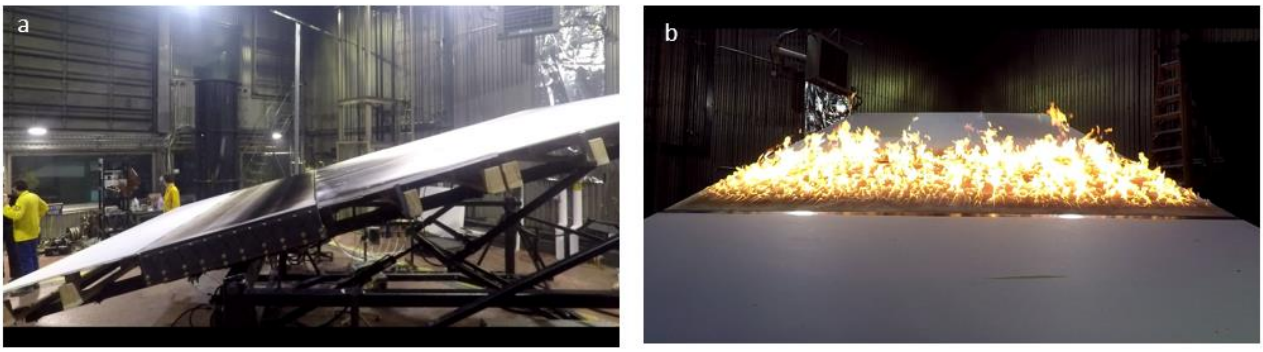

Figure 1- Pictures of propane-fuelled sand burner on a) tilting platform and b) with flames issuing from sandbox.

These experiments were conducted with the platform oriented horizontally so that length of diffusion flames could be measured in the pure vertical dimension. This flame source can be considered buoyancy dominated because the vertical velocity of the propane is so low. Two vertical graduated poles were placed at the foreground edge of the long dimension of the burner in full view of a high-speed camera (Figure 2). The long dimension was chosen because it could more directly incorporate the spatially variable peak and trough structure of line-source flames (Finney et al. 2015) and the non-steady and pulsatile dynamics happening at any given location along a linear flame front (Cetegen et al. 1998). The camera was adjusted to the approximate height of the flames at each setting of propane mass flow rate – 300, 600, 900, 1200, and 1500 SLPM with field of view extending the full 3.66 m width of the burner. For all flow rates, 1-8 burner tubes were opened for 10 seconds of filming.

Video was recorded at 240 frames per second (fps) to minimize smearing from flame movement in each frame. Video was processed to discriminate flaming from non-flaming in each frame using a cut-off brightness value of 90%. Individual binary images were then added to form a probability field for each intensity-flame depth combination and overlayed with a rasterized height gradient determined by the graduated reference poles (Figure 2b). A visual comparison of the video with the probability image suggested that impressions of flame height coincided with the 20% probability contour. For each pixel between the height poles in the image, we obtained the raster height value intersected by the 20% flame presence contour, the mean value of which was an estimate of $\boldsymbol{L}$ (Figure 2c).

Flame length correlations from the gas burner were compared with data from 100 laboratory fires spreading through laser-cut cardboard fuel beds in wind and on a sloping surface (Finney et al. 2013, 2015). Fire spread rate was obtained using thermocouple arrays, flame depth was measured from digital video cameras, and flame length was estimated ocularly. Fireline intensity was calculated from the fuel loading and measured spread rate.

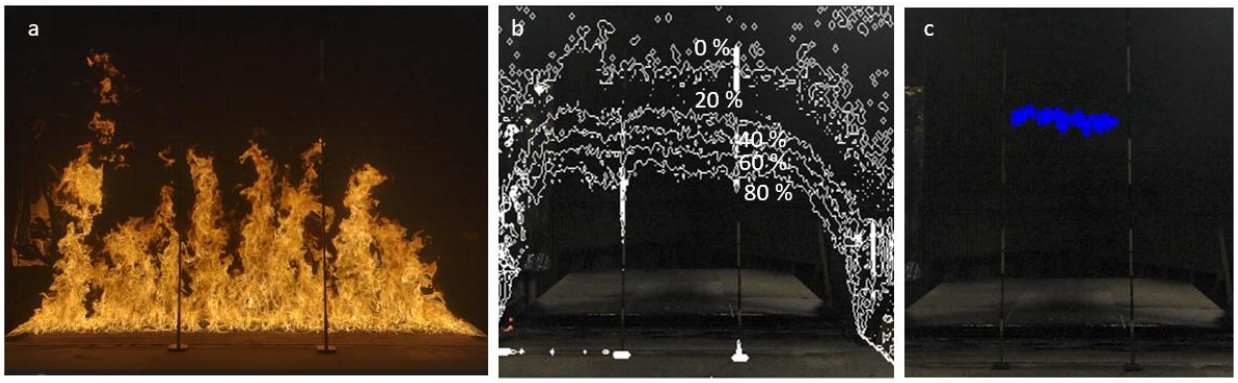

Figure 2 - Image processing of flames is illustrated for a 1200 SLPM gas flow rate with 0.3m flame zone depth D for a) single image of flames from video taken at 240 frames per second showing graduated height poles in the foreground, b) contours of flame presence from 10 seconds of video, and c) points along 20% contour corresponding to an average of $L = 1.55$ m tall (L/D=5.40).

3. Results

The gas burner experiment produced flame length data from a total of 40 combinations of total gas flow rates to the burner (i.e., fireline intensity $\boldsymbol{I_B}$) and number of burner tubes (i.e., flame zone depth $\boldsymbol{D}$) (Table 1). Ratios of $\boldsymbol{L/D}$ ranged from 0.15 to 13.6.

Table 1. Ratios of L/D resulting from experimental combinations of fireline intensity and flame zone depth.

Flame Length/Flame Depth (L/D)								
I_B	**Flame Zone Depth *D* (m)**							
(kW/m)	**0.15**	**0.30**	**0.46**	**0.61**	**0.76**	**0.91**	**1.07**	**1.22**
123	3.20	1.50	0.87	0.60	0.36	0.27	0.20	0.15
246	5.60	2.70	1.73	1.25	0.84	0.67	0.54	0.43
369	9.00	4.30	2.73	1.95	1.40	1.13	0.91	0.78
492	11.20	5.40	3.33	2.40	1.84	1.50	1.23	1.05
615	13.60	6.60	4.27	3.00	2.32	1.80	1.51	1.28

Trends of $\boldsymbol{L}$ as a function of $\boldsymbol{I_B}$ for the gas burner data (thin black curves in Figure 3a) had slopes more like Thomas' (1963) correlation than Byram's (1959). Most importantly, the data showed a strong negative effect of $\boldsymbol{D}$ on the relation of $\boldsymbol{L}$ and $\boldsymbol{I_B}$ for the entire range of variables tested. This is explained using the dimensionless expression of Thomas (1963, eq. 4*ii*):

$$L/D = f(Q'^2/gD^3)^n \quad [1]$$

where $\boldsymbol{Q'}$ is the volumetric flow rate of gas (m^3/s per meter of flame front). Because $\boldsymbol{Q' = I_B/(\rho H)}$, eq. [1] can be rewritten in terms of $\boldsymbol{I_B}$ and absorb the constants into a single coefficient. Using the sand burner data, the empirical coefficient and exponent for the reformulated equation were found by applying nonlinear regression to the experimental data (Figure 3b):

$$L/D = 0.01051\left(I_B^2/D^3\right)^{0.3867} \quad [2]$$

which simplifies to illustrate the significant effect of $\boldsymbol{D}$ on $\boldsymbol{L}$ for the gas burner data:

$$L = 0.01051\left(I_B^{0.774}/D^{0.161}\right) \quad [3]$$

A plot of the burner data shows $\boldsymbol{L}$ was closely predicted by eq. [3] (Figure 3c). Independent data from spreading laboratory fires (Finney et al. 2013, 2015) in Figure 4a showed that when only a function of $\boldsymbol{I_B}$, $\boldsymbol{L}$ was generally overpredicted by Thomas' (1963) correlation and underpredicted by Byram's (1959) at higher intensities. The data trend was well approximated by the correlation from Eq. [3], where $\boldsymbol{L}$ is a function of both $\boldsymbol{I_B}$ and $\boldsymbol{D}$ (Figure 4b).

4. Discussion and Conclusions

The gas burner apparatus allowed precise control over intensity independent of flame source dimensions and revealed the important role of $\boldsymbol{D}$ in determining $\boldsymbol{L}$ in these line-source fires. This result contrasts with Thomas' (1963) data for a similar range ($\boldsymbol{L/D}$ <7) where the exponent for the fitted correlation in eq. [2] (Figure 3b) was found to be 1/3 for $\boldsymbol{L/D}$ > 3 and thus, cancelled the influence of $\boldsymbol{D}$. Steward (1964) also established the theoretical exponent of 1/3 for line fires but experimentally obtained a larger exponent of 0.363 by analysis of a variety of fuel sources for which $\boldsymbol{2 < L/D < 11}$. The flame length data assembled by Quintiere and Grove (1998) largely conform to the 1/3 exponent, but only for $\boldsymbol{L/D > \sim 10}$. Such tall flames with narrow bases are unrealistic for spreading fires in the field and laboratory, suggesting the 1/3 exponent in eq. [2] is not applicable to flames for which $\boldsymbol{L/D < \sim 10}$. Indeed, the following shows that the underlying theory leads one to *expect* an exponent greater than 1/3 for such fires.

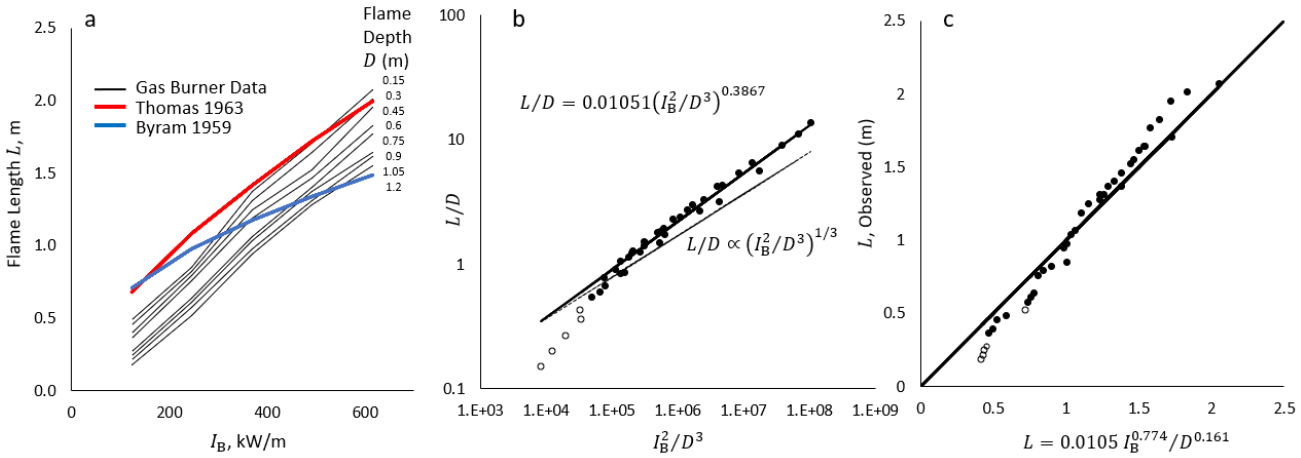

Figure 3. Results of gas burner data a) for flame length L in relation to fireline intensity I_B compared with correlations by Byram (1959) (eq. [1]) and Thomas (1963) (eq. [5]), b) the statistical fit of L/D data compared with Thomas' correlation and c) L observed vs. predicted by eq. [3]. Open circles are observations where L/D<0.52 and flames would likely not form a single plume (Heskestad 1991).

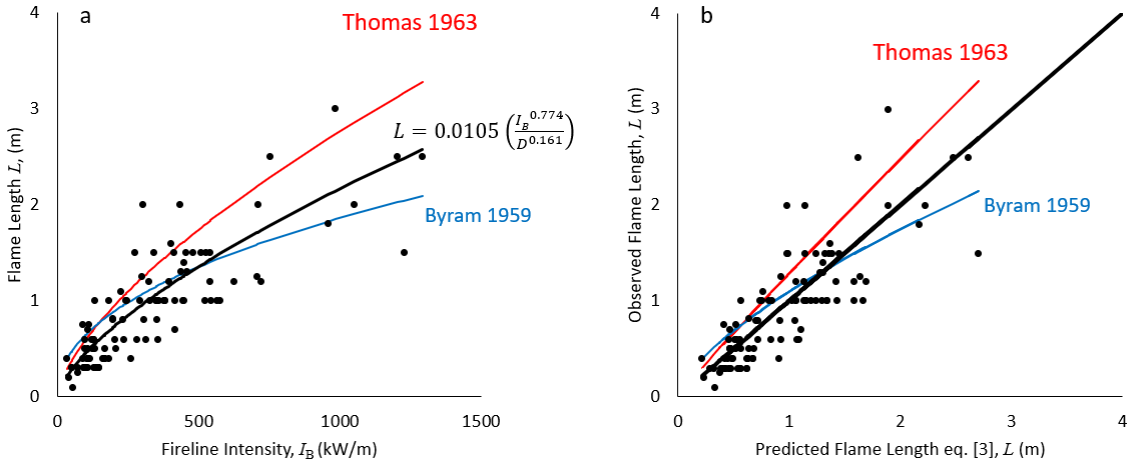

Figure 4. Data from 100 laboratory fires spreading with wind or slope show a) L as a power-function of I_B is generrally overpredicted by the relations of Thomas (1963) (RMSE=0.469) and underpredicted by Byram (1959) at higher intensities (RMSE=0.349), but b) stronger agreement with flame length predicted by eq.[3] (RMSE=0.337).

The roles of $\boldsymbol{I_B}$ and $\boldsymbol{D}$ on $\boldsymbol{L}$ are dependent upon how air is entrained into a turbulent flame. Turbulent entrainment supplies air required for combustion of fuel gases emitted near the ground. Taller flames result from higher fuel flow rates because gases must travel further before adequate mixing allows combustion. Flame length theories have relied upon two principal assumptions. First, air entrainment takes place entirely along the vertical profile of the flame (Thomas 1960, 1963, Steward 1964, Grove and Quintiere 2002, and Nelson et al. 2012). Second, the exterior surface area of the flame profile subjected to air entrainment has been assumed to be linearly proportional to the flame depth and length as would be found if the flames were triangular, rectangular, or trapezoidal. With these assumptions, Thomas (1963) showed that the exponent in equation [1] has the expected value of 1/3, cancelling the effect of $\boldsymbol{D}$ as shown in Figure 3b. This assumption has been assumed to hold where $\boldsymbol{L}$ is much greater than $\boldsymbol{D}$ (Thomas 1963, 1967).

The data in our study clearly contravened the above assumptions because $\boldsymbol{D}$ significantly reduced $\boldsymbol{L}$ in the range $\boldsymbol{0.15 \leq L/D \leq 13.6}$ which is entirely common for spreading wildfires. Published data sets showed median $\boldsymbol{L/D}$ ratios for heading fires of 1.6 (Finney et al. 2013, 2015); 1.4 (Nelson and Adkins 1986, 1988); 0.55 (Catchpole et al. 1998); 1.67 (Sneeuwjagt and Frandsen 1977); and 1.7 (Nelson et al. 2012). However, backing and no-wind fires had greater $\boldsymbol{L/D}$ ratios of 1.81 (Catchpole et al. 1998) and 2.48 (Wilson 1990). All such fires produce inwardly curved flame profiles (Figure 5) that increase entrainment and combustion along much of the horizontal surface in proportion to $\boldsymbol{D}$. Thus, deeper flame zones experience greater combustion of flame gases

traveling along the horizontal fuel bed than allowed by traditional entrainment theory (Thomas 1960, 1963, Steward 1964, Grove and Quintiere 2002, and Nelson et al. 2012) and consequently produce shorter flames for a given intensity. Thomas' (1963) original scaling in equation [1] reflects the increased entrainment with an exponent greater than 1/3, meaning that $\boldsymbol{L}$ depends both on $\boldsymbol{I_B}$ and $\boldsymbol{D}$.

The effect of $\boldsymbol{D}$ on $\boldsymbol{L}$ suggests an important but undescribed negative feedback mechanism that would serve in limiting the spread rate of wildfires. Negative feedbacks are clearly involved in limiting fire spread rate because immediate acceleration of spread and intensity after ignition ultimately gives way to reasonably steady spread. We had earlier reported on the role of $\boldsymbol{D}$ in reducing convective heating through its reduction in the gas temperature profile adjacent to the flaming edge (Finney et al. 2020). A similar effect of $\boldsymbol{D}$ on $\boldsymbol{L}$ would decrease radiation view factor and reduce scaling of convective processes dependent upon flame size, including flame velocity. Both effects of $\boldsymbol{D}$ would work together to dynamically limit fire spread rate as the flame zone depth expands in a spreading fire.

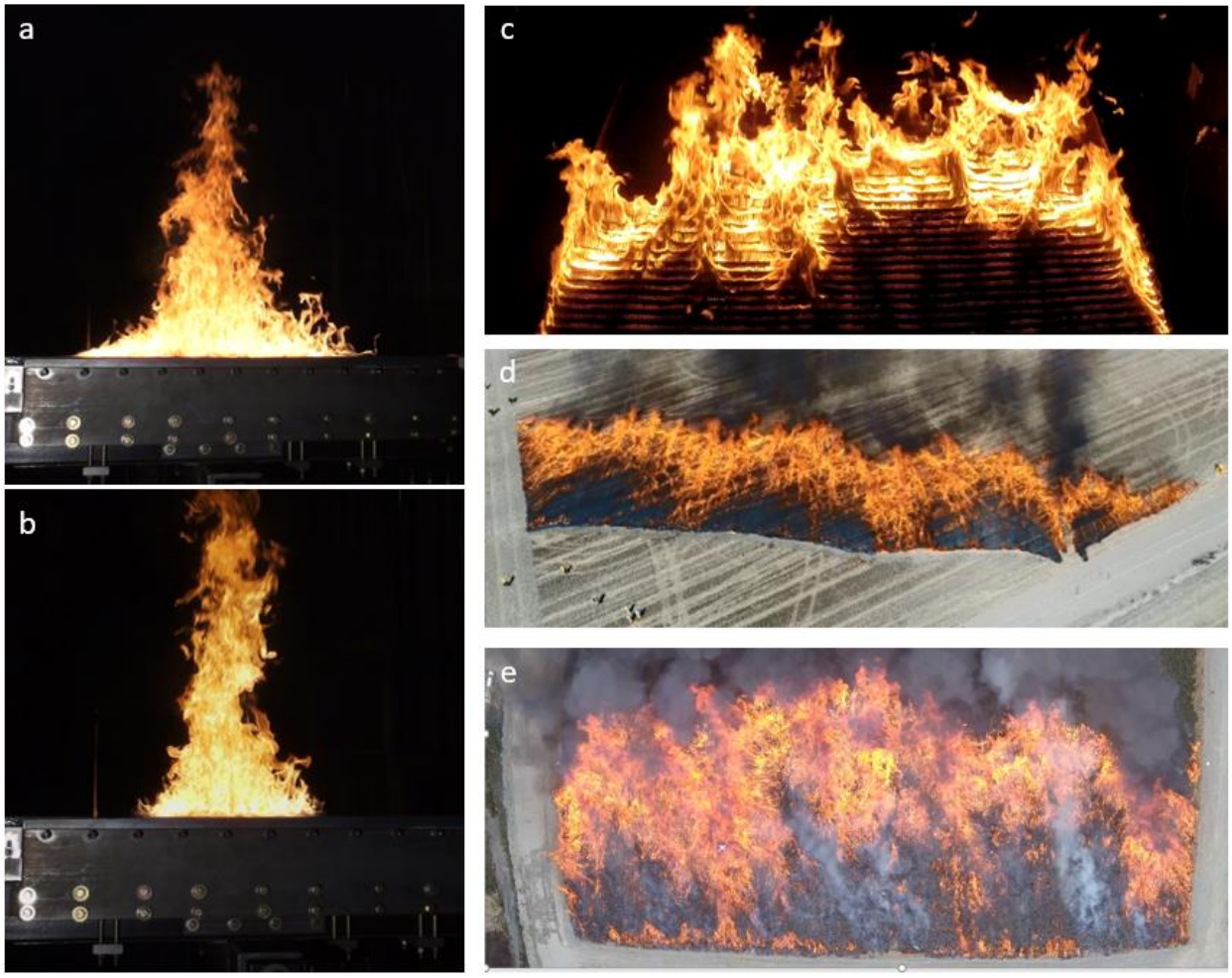

Figure 5. Images of curved flame profiles from gas burner flames a) I_B=205 kW/m; D=0.91m, b) I_B=205 kW/m; D=0.46m. Oblique overhead images of heading fires showing concave flame circulations within flame zones of c) a laboratory fire in laser-cut cardboard (L=0.4m; D=0.4m; $\underline{L/D \cong 1}$; Finney et al. 2015), d) crop stubble fire (L~5m; D~10m; $L/D \cong 0.5$), and e) gorse brush fire in New Zealand (L~15m; D~30m; $L/D \cong 0.5$).

5. Acknowledgements

Research was supported by the USFS, Rocky Mountain Research Station, National Fire Decision Support Centre. The authors thank Jon Bergroos, Ian Grob, and Isaac Grenfell for their assistance with this work.

6. References

Alexander, M.E., 1982. Calculating and interpreting forest fire intensities. *Canadian Journal of Botany*, 60(4), pp.349-357.

Alexander, M.E. and Cruz, M.G., 2012. Interdependencies between flame length and fireline intensity in predicting crown fire initiation and crown scorch height. *International Journal of Wildland Fire*, 21(2), pp.95-113.

Byram, G.M., 1959. Combustion of forest fuels. *Forest fire: control and use*, pp.61-89.

Catchpole, W.R., Catchpole, E.A., Butler, B.W., Rothermel, R.C., Morris, G.A. and Latham, D.J., 1998. Rate of spread of free-burning fires in woody fuels in a wind tunnel. *Combustion Science and Technology*, 131(1-6), pp.1-37.

Cetegen, B.M., Dong, Y. and Soteriou, M.C., 1998. Experiments on stability and oscillatory behavior of planar buoyant plumes. *Physics of Fluids*, *10*(7), pp.1658-1665.

Finney, M.A., Forthofer, J., Grenfell, I.C., Adam, B.A., Akafuah, N.K. and Saito, K., 2013. A study of flame spread in engineered cardboard fuelbeds: Part I: Correlations and observations. In *In: Seventh Intl Symp on Scale Modeling (ISSM-7); Hirosaki, Japan; 6-9 August, 2013. Intl Scale Modeling Committee. 10 p*.

Finney, M.A., Cohen, J.D., Forthofer, J.M., McAllister, S.S., Gollner, M.J., Gorham, D.J., Saito, K., Akafuah, N.K., Adam, B.A. and English, J.D., 2015. Role of buoyant flame dynamics in wildfire spread. *Proceedings of the National Academy of Sciences*, *112*(32), pp.9833-9838.

Finney, M.A., Grumstrup, T.P. and Grenfell, I., 2020. Flame Characteristics Adjacent to a Stationary Line Fire. *Combustion Science and Technology*, pp.1-21.

Finney, M.A., McAllister, S.S., Grumstrup, T.P. and Forthofer, J.M., 2021. Wildland Fire Behaviour: Dynamics, Principles and Processes. CSIRO Publishing, Clayton South, Victoria, Australia, 360 pp.

Grove, B.S. and Quintiere, J.G., 2002. Calculating entrainment and flame height in fire plumes of axisymmetric and infinite line geometries. *Journal of Fire Protection Engineering*, 12(3), pp.117-137.

Heskestad, G., 1991. A reduced-scale mass fire experiment. *Combustion and Flame*, 83(3-4), pp.293-301.

Nelson Jr, R.M. and Adkins, C.W., 1986. Flame characteristics of wind-driven surface fires. *Canadian Journal of Forest Research*, *16*(6), pp.1293-1300.

Nelson Jr, R.M. and Adkins, C.W., 1988. A dimensionless correlation for the spread of wind-driven fires. *Canadian Journal of Forest Research*, *18*(4), pp.391-397.

Nelson, R.M., Butler, B.W. and Weise, D.R., 2012. Entrainment regimes and flame characteristics of wildland fires. *International Journal of Wildland Fire*, *21*(2), pp.127-140.

Newman, J.S. and Wieczorek, C.J., 2004. Chemical flame heights. *Fire safety journal*, 39(5), pp.375-382.

Quintiere, J.G. and Grove, B.S., 1998, January. A unified analysis for fire plumes. In *Symposium (International) on Combustion* 27(2): 2757-2766.

Thomas, P.H., 1960. Buoyant diffusion flames. *Combustion and Flame*, *4*, pp.381-382.

Thomas, P.H., 1963, January. The size of flames from natural fires. In *Symposium (International) on Combustion* (Vol. 9, No. 1, pp. 844-859). Elsevier.

Thomas, P.H., 1967. Some aspects of the growth and spread of fire in the open. *Forestry: An International Journal of Forest Research*, *40*(2), pp.139-164.

Thomas, P.H., Pickard, R.W. and Wraight, H.G., 1963. On the size and orientation of buoyant diffusion flames and the effect of wind. *Fire Safety Science*, *516*, pp.1-1.

Steward, F.R., 1964. Linear flame heights for various fuels. *Combustion and Flame*, 8(3), pp.171-178.

Zukoski, E.E., Cetegen, B.M. and Kubota, T., 1985, January. Visible structure of buoyant diffusion flames. In *Symposium (International) on Combustion* 20(1):361-366.

Ground water as water source opportunity at the fire front – case study at Bács-Kiskun County, Hungary

Ágoston Restás*[1]; András Kristóf[2]; László Bodnár[3]

[1, 3] University of Public Service, Institute of Disaster Management. 1101 Budapest, Hungary, krt. 9-11., {restas.agoston, bodnar.laszlo}@uni-nke.hu
[2] Municipality Fire Brigade. 6080 Szabadszállás, Kálvin tér 6. {kandre770811@gmail.com}

**Corresponding author*

Keywords

Ground water, well drilling, logistics, water flow, effectiveness

Abstract

Almost without exceptions, in case of long time wildfires, the continuous water supply is always a logistic problem. One of the several reasons is obviously that most of the wildfires occur during droughts, when there is no rainfall and the natural water sources have low flows. Another problem with the water supply is that the frontline of fire and the water source are usually quite far apart from each other. In this case, firefighters are facing a logistical problem, where not only the limited number of fire trucks, but also the slow movement of these vehicles or even blocks have to be taken into account. The Hungarian example presented in the paper shows the use of local opportunities, just as the imaginative use of groundwater can provide a suitable water source at the fire site. With regard to the effective water transport, the question arises as to whether the average water flow that can be provided during a conventional long-distance water transport can also be provided by the water flow of wells drilled on the fire site. The research shows that, under certain conditions, the groundwater provided by drilled wells can be an alternative solution to the logistical difficulties of long-distance water transport.

1. Introduction

The generation of wildfires can be traced back to human negligence (Chas-Amilm 2010, Teknős and Debreceni 2022). In order to save human life and property, firefighters use several tactics to fight against wildfires (Restás 2003). They can use so-called hand tools for firefighting purposes, ground power machines, aircrafts for aerial firefighting or counter fire, but the most common solution is to extinguish the frontline of fire with water. One of the characteristics of wildfires is that forests ignite when the availability of water sources in wildland is already limited, i.e. during droughts (Bodnár et. al. 2019). In this case, the water required for firefighting can be replaced with artificial water sources. For this purpose, based on plans, we create artificial reservoirs, which we maintain and provide the right amount of water in them. The disadvantage of artificial water sources is that their construction and maintenance costs are high and their efficiency will only prevail if there is a wildfire nearby and they need to be used. Until they are used, the costs so far may seem unnecessary. Another characteristic of wildfires is that the frontlines are often far from the forest roads that can be used by heavy fire trucks, therefore the so-called long-distance water transport is also difficult (Bodnár 2016). On the one hand, traffic on dirt roads is rather slow, and on the other hand, the soil in the observation plot in the paper is rather sandy. As a result of this, heavy, water-filled fire trucks simply sank in the sand. The above mentioned problems can be justified by a number of examples, so it is clear that effective firefighting requires either a different firefighting method or a new solution to the water supply problem. Based on the above, the authors aimed how to provide the amount of water needed for firefighting in the most flammable area of Hungary (Bacs-Kiskun County) at the same time.

2. Methods

Authors have examined and analysed the relevant literatures focusing on the logistic problems of the firefighting and water supply. In addition, authors conducted discussions with the local firefighting experts on the subject. Case studies, made after the latest fires in the Bacs-Kiskun County, have also analysed focusing on the problem

of water supply. Moreover, authors made a real experience in well drilling at a random place at the county and measured the water capacity of the well (flow rate) with using a simple water pump.

3. Results

The authors were able to prove that the area is high vulnerable with the help of previous case studies on large wildfires in Bács-Kiskun County (Gyapjas 2007). During firefighting, natural water sources are only available to a limited extent (Farkasinszky 2007a and 2007b) the so-called long-distance water transport is difficult and slow on dirt roads (Árpás 2007) and the risk of blocks are high. Study area is highly threatened by the climate change so suppressing fires in this area seems to be more and more difficult in the future (Teknős 2019, Kovács and Jakab 2021).

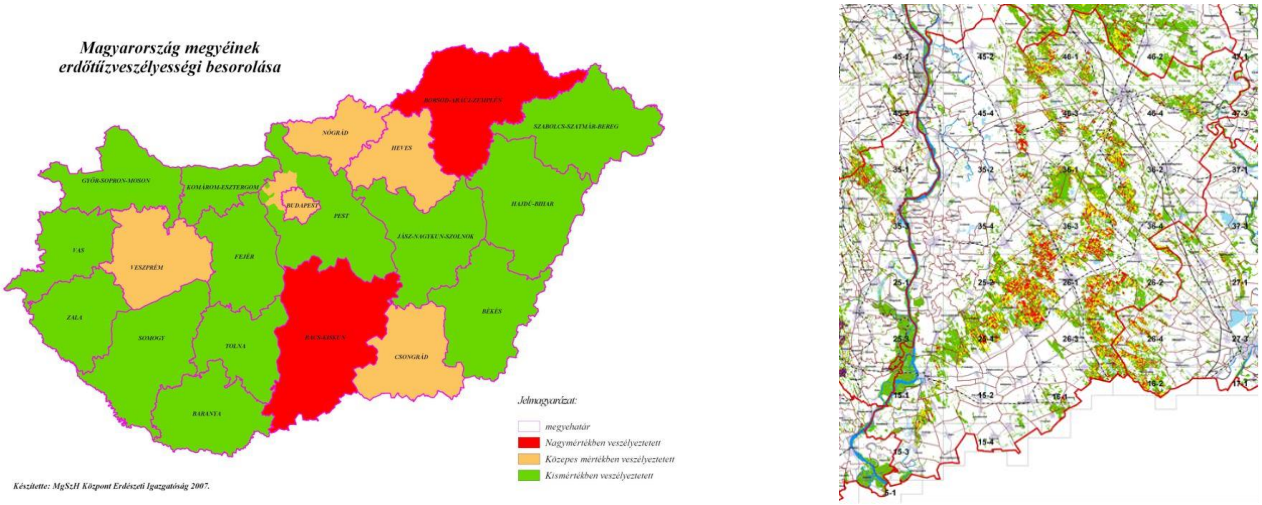

Figure 1. Fire danger classification of counties in Hungary (left) and the fire danger classification of forests at Bacs-Kiskun County (right) (Gyapjas 2007)

Figure 2. Water transport vehicles trapped in sandy dirt road (Gyapjas 2007).

Based on the geographical analysis, it can be stated that Bacs-Kiskun County is basically a flat area (plain), without significant prominence, but the surface is covered with sand in many places. During the search for water sources, local firefighters suggested that wells used for irrigation of agricultural land should also be considered as potential water sources. Based on experience, these simple wells can be created in a short time, and their water flow appears to be relatively stable even at the order of a few hundred litres per minute (Higuera 2015). Based on the above, the authors first reviewed the area of the observation plot and then the whole country in terms of groundwater availability. For this purpose, the official groundwater map of Hungary (MBFSz maps 2022) and other relevant literatures were analysed (Grundwaters in Hungary 2006; Kovács and Jakab 2021). According to it, there is a water layer a few meters below the wildland area of Bács-Kiskun County, which can

be easily reached with the help of a well drilled, due to the sandy soil (Fig. 3). Based on it, the authors conducted an experiment to drill a well at a random selected spot in the county.

The experiment had several purposes.

- First, the authors wanted to prove that the well could be drilled easily and quickly on the soil that characterized the county.
- Another objective of the experiment was for the authors to be able to demonstrate that the water flow provided by the well is stable, so it can provide the same amount of water for at least 24 hours.
- Third objective of the study was to create graphics on which we can find the tipping points where drilled well able to supply as much water as tradition solution.

Figure 3. Ground water level in Hungary below the surface (left) (MBFSZ maps) and measuring the water flow after drilling (archive of authors).

The authors involved in the experiment the Municipality Fire Brigade of Szabadszállás and a well drill master. The well drilling master did the professional part of the work (well drilling), the firefighters helped with the preparation and setup of the pump after drilling. During the experiment, the water layer was available in less than 2 hours, slightly deeper than expected, at approximately 5 metres deep. The preparation of the well with 60 mm diameter of well tube, the setting of the pump and the further preparatory works took an additional 1 hour. The water flow, which was then measured for 1 hour, reached 400 $lmin^{-1}$, which appeared to be completely stable. Drilling master stated also that drilled wells can produce stable water amounts after about 1 hour usage. It is proved on the selected place drilling wells can supply firefighters with stable water flow. Based on the results of the experiment, authors calculated the assumption that in case of drilling 2 wells after professional preparation, firefighters can be able to provide a water flow of 800 $lmin^{-1}$ after 3 hours of the arrival of the fire forces. The authors went on to find out whether this amount of water (from the well) competes with the amount that can be provided by long-distance water transport.

In case of long-distance water transport, the following can be expected: the average speed of the water transporter is considered to be 30 kmh^{-1}. Based on it, the vehicle travels a distance of 5 km in 10 minutes and returns in another 10 minutes, thus making a total of 10 km in 20 minutes in both directions. As a result of it, the average flow rate of a 10,000 litre tank is 250 $lmin^{-1}$ (Fig. 4 left). The maximum value of the water flow is obtained when the vehicle is not moving, so it is filled and then emptied locally. In this case, the water flow is maximum (500 $lmin^{-1}$). The water flow increases in a straight line with increasing the average speed, while it is inversely proportional to the distance (Fig. 4 right).

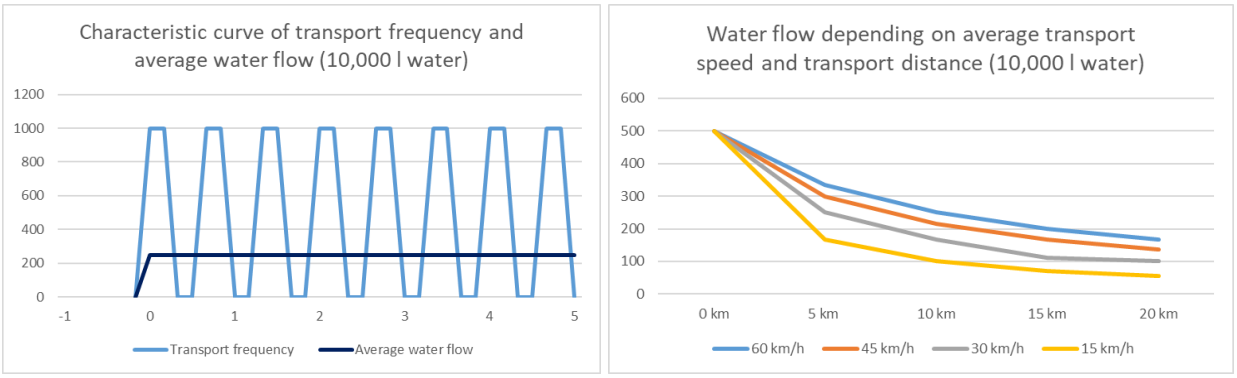

Figure 4. Characteristic curve depending on transport frequency and average water flow in case of 30 kmh^{-1} average transport speed and 5 km transport distance (left) and water flow rate depending on average transport speed and transport distance in case of 10,000 l water capacity (right).

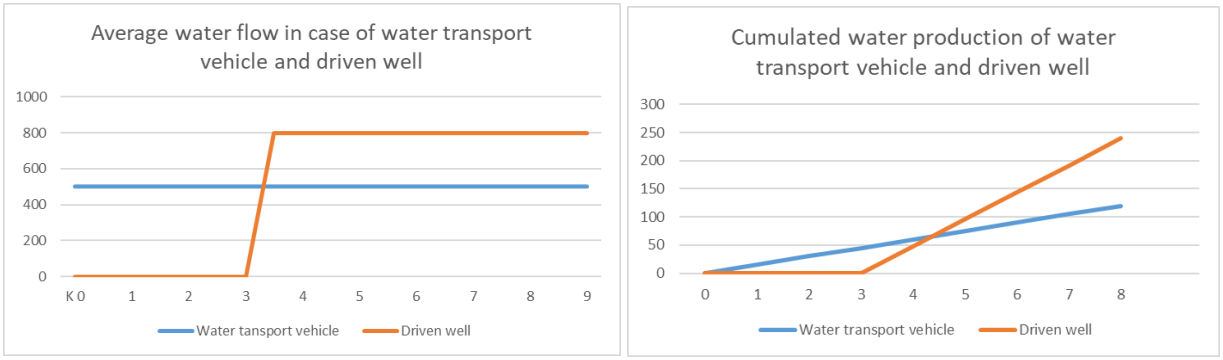

Figure 5. Average water flow in case of water transport vehicle and driven well (left) and cumulated water production of water transport vehicle and driven well in optimal cases (0 km) (right).

4. Conclusion

The results show that water transporters can be replaced by drilled wells after about 3 hours. The results also show that the farther the water has to be transported, the more difficult it is to transport the water, and the more difficult (slower) is the fire site to approach. The diagrams also show when the cumulative amount of water in drilled wells with higher water flows reaches or exceeds the amount of water provided by water transporters. According to the above, authors considering that during a long firefighting, water transporters can also be replaced or their capability can complete by drilled wells, depending on the given conditions. The authors suggest further research into the international applicability of this method. Example, based on the ground water map of Europe (GWM of Europe 2022) the fire departments could measure their responsible area where ground water can be acceptable by reasonable efforts especially focusing on the forest fire threatened areas, like Mediterranean region. Even if the study area has a good capacity using ground water for supporting firefighters, as a new method it can be an option in other places too. In order to compare the efficiency of the two methods from an economic point of view further research is also required.

5. References

Árpás M, (2007) Protection of forests against forest fires in Bács-Kiskun County in 2007. https://slideplayer.hu/slide/2170835/ download: 26.03.2022.

Bodnár L, (2016) Logistic problems of fighting forest fires based on case studies from Hungary. In: Proceedings of the 8th International Scientific Conference Wood and Fire Safety, 23-32.

Bodnár L, Pántya P, (2019) The Threat of Forest and Vegetation Fires and the Possibilities of Intervention in Hungary. In: *Academic And Applied Research In Military And Public Management Science*, **18** (3) 21-31.

Chas-Amilm L, Touza J, Prestemon J.P, (2010) Spatial distribution of human-caused forest fires in Galicia (NW Spain). *WIT Transactions on Ecology and the Environment*, **137**, 247 – 258.

Farkasinszky L, (2007a) Summit of forest fire happened in Nyarlorinc, July, 2007. Report, Disaster Management Headqarter of Bacs-Kiskun County, Kecskemet, Hungary

Farkasinszky L, (2007b) Summit of forest fire happened in Kunfeherto – Keleshalom July, 2007, Report, Disaster Management Headqarter of Bacs-Kiskun County, Kecskemet, Hungary.

Groundwaters in Hungary (2006) Guide. Ministry of Environment and Water, Budapest, Hungary, ISBN 963037675X

GWM of Europe, (2022) Groundwater map of Europe, available on-line (15.05.2022): https://i.imgur.com/4pNOUC0.png

Gyapjas J, (2007) Case study of fires in Bacs-Kiskun county happened in July of 2007. Report, Disaster Management Headqarter of Bacs-Kiskun County, Kecskemet, Hungary.

Higuera P, (2015) Taking time to consider the causes and consequences of large wildfires. *Proceedings of the National Academy of Sciences*, **112** (43) 13137–13138

Kovács A, Jakab A, (2021) Modelling the Impacts of Climate Change on Shallow Broundwater Conditions in Hungary. *Water,* **13** (5) 668 doi: 10.3390/w13050668

MBFSZ maps (2022) Mining and Geological Survay of Hungary, available (25.06.2022): https://map.mbfsz.gov.hu/tvz/

Restás Á, (2003) Logistics basics of the activity of fire departments. *Katonai logisztika*, **11** (4) 147-158.

Teknős L, (2019) Current Issues in Disaster Management Aspects of Global Climate Change. In: Földi L, (ed.) Effects of Global Climate Change and Improvement of Adaptation Especially in the Public Service Area, Hungary, 145-162.

Teknős L, Debreceni K, (2022) Disaster Management Aspects of Global Climate Change. In: Molnár A, Wenczel D, (ed.) Third International Conference on Effective Response: Conference Proceedings, Hungarian Red Cross, Budapest, 45-55

High Resolution Wildfire Fuel Mapping for Community Directed Forest Management Planning

Patrick Robinson*; Che Elkin; Scott Green

University of Northern British Columbia. Prince George, BC, Canada,
{robinsonp, che.elkin, scott.green}@unbc.ca

**Corresponding author*

Keywords

Wildfire; Mapping; ALS; First Nations; Forestry

Abstract

Climate change and institutional forest management practices have lead to more frequent and severe wildfire events around the world, a trend that is projected to increase in coming years. Wildfire plays an important role in maintaining ecological systems, but wildfires also pose threats to health, safety, infrastructure, and ecosystem services. Reactionary response to these threats has predominantly informed management decisions in recent decades and greater focus on mitigation and adaptation is needed. Through a community-directed consultation process, the goal of this work has been to provide direct, operational information to aid in local management decision making for a First Nations community in British Columbia, Canada. Using a combination of field sampling and high-resolution Airborne Laser Scanning (ALS) data, we assessed vertical and horizontal fuel loading at fine resolution. Our analysis found a high degree of fuel loading heterogeneity in areas characterized as homogeneous using coarser fuel layers and provided a means of identifying high fire risk areas that may be targeted for ecosystem rehabilitation aimed at reducing current and future fire risk. We discuss how this spatially explicit data can be used to evaluate feedback between forest dynamics and fuel loading, information critical for managing forests for multiple objectives into the future. Following our analysis, we compiled our results into an interactive decision support web mapping platform designed with the goal of providing a user friendly, accessible land management planning tool for the community.

1. Introduction

Wildfire is an integral part of natural forest dynamics across a range of different forest types globally (Moritz et al., 2014). In many areas, fire serves an important role in maintaining forest ecosystem functioning by rejuvenating plant health, creating animal habitat and forage, and mitigating the risk of large scale destructive stand-replacing wildfire events (Driscoll et al., 2010). In addition, wildfires also account for significant contributions to the global carbon budget (Driscoll et al., 2010; Ager et al., 2010). Although wildfire plays an important role in maintaining ecological systems, management objectives relating to wildfire are most often directed at mitigating the near term and immediate threats it poses to society (Duff et al., 2017). The negative impacts of wildfires on human health and safety, values and infrastructure, and ecosystem services cannot be ignored. However there is room for more attention to be paid towards managing wildfires to promote the positive impacts they can have in forest ecosystem dynamics. Understanding how wildfire will interact with a given landscape and forest ecosystem requires information about the three most influential factors for fire behavior: weather, topography, and fuels. Of these three elements, the only one manageable on an attainable scale is fuels. Having the ability to meausre fuel load and structure at scale across forest ecosystems is critical to understanding how to better manage wildfires overall. In addition, the ability to include and prioritize local community knowlegde and input in forest management planning can greatly enhance the positive impact of managment actions.

2. Project Overview

This project is part of a multi-year collaboration between a First Nations community in southwestern British Columbia and University of Northern British Columbia researchers Patrick Robinson, Dr. Scott Green, and Dr. Che Elkin, with support from the Pacific Institute of Climate Solutions. This project is a community-directed initiative, with the aim of assessing how high resolution aerial laser scanning (ALS) data can best be used to

evaluate and quantify forest fuels, and directly aid in fire risk mitigation, forest ecosystem restoration, and climate adaptation planning efforts at local and regional scales. The project is guided by the shared goal of promoting the re-establishment of traditional management principles and practices, which pre-date modern intitutional mangement and have been around since time immemorial. In collaboration with the community, the goal is to provide information relating to wildfire fuel load distributions with local context that is directly applicable and immediately useful to the community's unique forest management planning and ecosystem restoration objectives. Additionally, the results of the analysis are intended to contribute to and support general wildfire fuel mapping efforts around the province and amongst the broader scientific community.

Previous work and existing data have established that the community is facing significant risk of catastrophic stand replacing wildfire. To address this risk effectively, the spatial distribution and connectivity of hazard fuels types is required in greater detail than previously existed. High resolution data provided by ALS has the potential to describe fuel structure and distribution with the detail required to enable tangible and prioritized management throughout the study area. This work probes beyond fuel mapping alone, taking into consideration community objectives and First Nations Traditional Ecological Knowledge in the process of determining how wildfire and fuels distribution, both past and present, play a role in the restoration and responsible future management of forests for multiple values. In addition, there is interest in the identification of areas potentially suitable for the integration of prescribed burning practices in support of landscape-level wildfire resilience and risk mitigation, as well as the cultural revitalization of traditional burning practices.

3. Study Area

The study area is located in southwestern British Columbia, Canada, east of Lillooet in the Pavilion Ranges Ecosection (Figure 1). In the past, the area has experienced a relatively frequent fire return interval (6.6 to 11.6 years over the last 500 years), of regular low-intensity surface fire within fire resilient, open forest areas of Douglas Fir and Ponderosa Pine stands, and less frequent fire occurrence in higher elevation stands comprised of Montane Spruce and Lodgepole Pine (Gray et al., 2002). Over the past 100 years, largely as a result of aggressive fire suppression, the forests throughout the area have become less fire resilient with increased hazardous fuel load build-up, resulting in an altered fire regime of less frequent and more severe fires. In response to the increased fire risk, several areas throughout the territory have undergone fuel treatments, fire-smarting, and ecosystem restoration initiatives, including thinning and pruning, with a particular focus placed around community areas and recreation sites (Diver, 2016).

Figure 1- Map of Southwestern British Columbia, indicating the general location of the study area in red.

4. ALS Data

Airbourne laser scanning (ALS) data was collected for the entire study area at approximately 15 points per square meter. ALS can be used to model forest biophysical structure and inventory variables at a fine grain (plot level) over a large landscape extent (Hayashiet al., 2016; Hummel et al., 2011; Treitz et al., 2012; White et al., 2016). Forest structural characteristics are critical for develping forest fuel load maps, which classify fuel attributes relevant for the evaluation of fuel treatments, risk mitigation and other related planning activities (Chen et al., 2016; Hayashi et al., 2016; Peterson et al., 2015; Pimont et al., 2016). ALS data has the capacity to significantly enhance the current spatial understanding of forest fuels by providing detailed three-dimensional forest structural characteristics (fuel metrics) for entire landscapes (Ahmed et al., 2015; Coops et al., 2016; Filotas et al., 2014; Gao et al., 2014). Improving the spatial resolution of the fuel mapping enables more confidence in fire and forest management planning and promotes more informed decision-making for ecosystem restoration and general management objectives.

Forest fuels can be considered as a physical complex composed of surface fuels, understory fuels, ladder fuels and canopy fuels. Some of the key metrics used to describe these structural attributes include total tree/canopy biomass, canopy bulk density, canopy base height, canopy fuel loading, stems per hectare, ladder fuel load, understory fuel load, and basic surface classification (fuel/non-fuel) (Jakubowksi et al., 2013; Zhao et al., 2011; Reinhardt, 2006). We acknowledge the importance of understanding ground fuels as a fundamental component of fire risk mapping, however this study focuses on above-ground forest fuel structure. Considering that these above ground metrics all relate to structural components of the forest, ALS data is well suited to provide this type of data.

5. Empirical Data

Empirical forest and fuel data were collected in the form of field plots throughout the study area and used to calculate various forest fuel load metrics. To develop the models responsible for deriving the fuel metrics from the ALS point cloud, empirical field data is required to train and calibrate the models (Andersen et al., 2005; Zellweger et al., 2014). The empirical field data in this application was collected in the form of forest plots designed to capture relevant structural characteristics of the various forest types in the study area, pertinent to fuel load calculation (Andersen et al., 2005; Price & Gordon, 2016). The forest sample plot characteristics have been informed by reference to the literature and reliance on the best practices described by White et al., (2013). A random stratified sampling framework was used to ensure a representative sample set across the complete range of forest type diversity.

6. Modelling and Analysis

We used a machine learning framework to develop predictive models for several important forest fuel characteristics in common forest types of interior southwestern BC with the goal to determine how forest structure differs across the landscape and how those differences are reflected in ALS derived fuel metrics. The following objectives guided this work:

- Being able to accurately evaluate the distribution of metrics for describing fuel load throughout the study area (i.e., Canopy Bulk Density, Canopy Base Height, Ladder Fuel Density, Understory Fuel Density) across multiple forest strata in a way that enables the community to easily target focal areas for restoration and treatment;
- Assess the variation in fuel loading components within the standard Canadian Forest Fire Danger Rating System Fire Behaviour Prediction system fuel types categories, and to test if emergent clusters of fuel loading classes can be used to better classify fire risk across the landscape; and
- Analyze how historic management practices and recent forest ecosystem restoration activities have altered fuel loading.

Random Forest (RF) was used to model the fuel metrics by identifying statistical relationships between the ALS data and the empirical data.

7. Results

The landscape level fuel load distribution map products produced from the process described above have proven effective in their ability to accuratley describe fuel struture throughout the study area, and have produced relatively high R^2 values (Table 1). As expected with ALS derived data, the model confidence is lower in the fuel metrics that describe fuel attributes for lower elements of the vertical forest/vegetation profile (i.e., Ladder Fuel Density and Understory Density). This is largely due to the effect of the upper canopy components shading out the lower components during the ALS data collection, however preliminary field validation excercises have helped to validate the accuracy of these lower level metrics as seen in the ladder fuel density image displayed in Figure 2.

Fuel Metric/Response Variable	R^2 Value
Tree Height	0.90
Canopy Bulk Density	0.86
Canopy Fuel Load	0.84
Canopy Base Height	0.89
Ladder Fuel Density	0.33
Understory Density	0.38
Total Biomass	0.95

Table 1- R^2 values for the model results, produced for the k-fold cross validation.

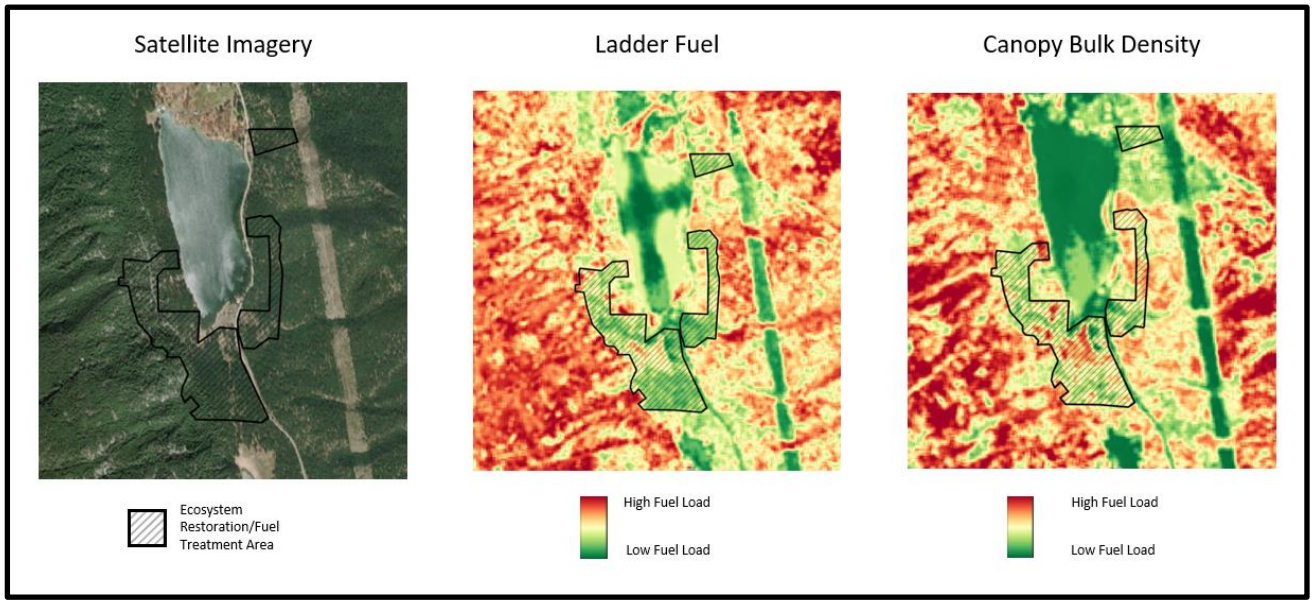

Figure 2- Comparison of modelled fuel metric products for a known fuel treatment site in the study area. All three maps display the same area with the black hashed boundary indicating an area that has been thinned and pruned for fire risk reduction. The map on the left indicates the inability to differentiate the treated area from the untreated areas in the satellite imagery, whereas the Ladder Fuel and Canopy Bulk Density maps indicate the subsequent ability to distinguish the areas of increased and decreased fuel load (i.e., treated vs. untreated) with the ALS derived products.

8. Web Mapping Platform

One of the main priorities of this work has been to promote community capacity building by providing information accessibility, research methods transparency, and direct collaboration. With that in mind, a suite of web mapping tools have been developed to provide a comprehensive GIS decision support platform to the community. The platform provides user-friendly access to important spatial data visualizations, enables community-directed management planning, and facilitates co-development of management solutions.It

encourages discourse regarding management objectives by providing a means for translating technical data directly to the solution seeker in a way that is accessible and useful. The web map tool is essentially a multi-part story map, made in Arc GIS online that functions as both as a data sharing outlet/communication network and a decision support platform for fire risk mitigation and general forest management planning.

9. Conclusion

Ongoing work continues with the community to utilize the results of the ALS fuel modelling and integrate them into current and future management planning. In addition, further development and design refinement of the web mapping platform continues in collaboration with the community to continually improve the ability to leverage the results of this study towards tangible managment objectives, as well as build the internal capacity of the community.

10. References

Ager, A. A., Finney, M. A., McMahan, A., & Carthcart, J. (2010). Measuring the effect of fuel treatments on forest carbon using landscape risk analysis. Natural Hazards and Earth System Sciences. 10: 1-12, 10, 1-12.

Ahmed, O. S., Franklin, S. E., Wulder, M. A., & White, J. C. (2015). Characterizing stand-level forest canopy cover and height using Landsat time series, samples of airborne LiDAR, and the Random Forest algorithm. ISPRS Journal of Photogrammetry and Remote Sensing, 101, 89-101.

Andersen, H. E., McGaughey, R. J., & Reutebuch, S. E. (2005). Estimating forest canopy fuel parameters using LIDAR data. Remote sensing of Environment, 94(4), 441-449.

Chen, Y., Zhu, X., Yebra, M., Harris, S., & Tapper, N. (2016). Strata-based forest fuel classification for wild fire hazard assessment using terrestrial LiDAR. Journal of Applied Remote Sensing, 10(4), 046025.

Coops, N. C., Tompaski, P., Nijland, W., Rickbeil, G. J., Nielsen, S. E., Bater, C. W., & Stadt, J. J. (2016). A forest structure habitat index based on airborne laser scanning data. Ecological indicators, 67, 346-357.

Diver, S. (2016). Community voices: The making and meaning of the xaxli'p community forest.

Driscoll, D. A., Lindenmayer, D. B., Bennett, A. F., Bode, M., Bradstock, R. A., Cary, G. J., ... & Gill, M. (2010). Fire management for biodiversity conservation: key research questions and our capacity to answer them. Biological conservation, 143(9), 1928-1939.

Duff, T. J., Keane, R. E., Penman, T. D., & Tolhurst, K. G. (2017). Revisiting wildland fire fuel quantification methods: the challenge of understanding a dynamic, biotic entity. Forests, 8(9), 351

Filotas, E., Parrott, L., Burton, P. J., Chazdon, R. L., Coates, K. D., Coll, L., ... & Putz, F. E. (2014). Viewing forests through the lens of complex systems science. Ecosphere, 5(1), 1-23.

Gao, T., Hedblom, M., Emilsson, T., & Nielsen, A. B. (2014). The role of forest stand structure as biodiversity indicator. Forest Ecology and Management, 330, 82-93.

Gray, R. W., Andrew, B., Blackwell, A., Needoba, A., & Steele, F. (2002). The Effect of Physiography and Topography on Fire Regimes and Forest Communities [Draft]. Retrieved from Habitat Conservation Trust Fund website: https://www.for.gov.bc.ca/hfd/library/FIA/2002/FIA2002MR009.pdf

Hayashi, R., Weiskittel, A., & Kershaw, J. A. (2016). Influence of Prediction Cell Size on LiDAR- Derived Area-Based Estimates of Total Volume in Mixed-Species and Multicohort Forests in Northeastern North America. Canadian Journal of Remote Sensing, 42(5), 473–488. doi: 10.1080/07038992.2016.1229597

Hummel, S., Hudak, A. T., Uebler, E. H., Falkowski, M. J., & Megown, K. A. (2011). A comparison of accuracy and cost of LiDAR versus stand exam data for landscape management on the Malheur National Forest. Journal of forestry, 109(5), 267-273.

Jakubowksi, M. K., Guo, Q., Collins, B., Stephens, S., & Kelly, M. (2013). Predicting surface fuel models and fuel metrics using Lidar and CIR imagery in a dense, mountainous forest. Photogrammetric Engineering & Remote Sensing, 79(1), 37-49.

Moritz, M. A., Batllori, E., Bradstock, R. A., Gill, A. M., Handmer, J., Hessburg, P. F., ... & Syphard, A. D. (2014). Learning to coexist with wildfire. Nature, 515(7525), 58-66.

Peterson, B., Nelson, K. J., Seielstad, C., Stoker, J., Jolly, W. M., & Parsons, R. (2015). Automated integration of lidar into the LANDFIRE product suite. Remote sensing letters, 6(3), 247- 256.

Pimont, F., Dupuy, J. L., Rigolot, E., Prat, V., & Piboule, A. (2016) A. Correction: Estimating leaf bulk density distribution in a tree canopy using terrestrial LiDAR and a straightforward calibration procedure.

Price, O. F., & Gordon, C. E. (2016). The potential for LiDAR technology to map fire fuel hazard over large areas of Australian forest. Journal of environmental management, 181, 663-673.

Reinhardt, E., Scott, J., Gray, K., & Keane, R. (2006). Estimating canopy fuel characteristics in five conifer stands in the western United States using tree and stand measurements. Canadian Journal of Forest Research, 36(11), 2803-2814.

Treitz, P., Lim, K., Woods, M., Pitt, D., Nesbitt, D., & Etheridge, D. (2012). LiDAR Sampling Density for Forest Resource Inventories in Ontario, Canada. Remote Sensing, 4(4), 830–848. doi: 10.3390/rs4040830

White, J.C., Coops, N.C., Wulder, M.A., Vastaranta, M., Hilker, T., Tompalski, P., 2016. Remote Sensing Technologies for Enhancing Forest Inventories: A Review. Can. J. Remote Sens. 42, 619–641. doi:10.1080/07038992.2016.1207484

White, J. C., Wulder, M. A., Varhola, A., Vastaranta, M., Coops, N. C., Cook, B. D., ... & Woods, M. (2013). A best practices guide for generating forest inventory attributes from airborne laser scanning data using an area-based approach. The Forestry Chronicle, 89(6), 722-723.

Zellweger, F., Morsdorf, F., Purves, R. S., Braunisch, V., & Bollmann, K. (2014). Improved methods for measuring forest landscape structure: LiDAR complements field-based habitat assessment. Biodiversity and conservation, 23(2), 289-307.

Zhao, K., Popescu, S., Meng, X., Pang, Y., & Agca, M. (2011). Characterizing forest canopy structure with lidar composite metrics and machine learning. Remote Sensing of Environment, 115(8), 1978-1996.

Impact of the bulk density on fire spread through a homogenous vegetation layer

Carmen Awad *[1]; Jacky Fayad [1]; Nicolas Frangieh [1]; Frédéric Morandini [1]; Jean Louis Rossi [1] ; François Joseph Chatelon [1]; Thierry Marcelli [1]; Dominique Morvan [2] ; Gilbert Accary [3]

[1]UMR CNRS SPE 6134, Université de Corse, 20250 Corte, France, {awad_c, fayad_j, frangiyeh_n, morandini_f, rossi_j, marcelli_t, chatelon_j}@univ-corse.fr
[2]Aix Marseille Université, CNRS, Centrale Marseille, M2P2, Marseille, France, {dominique.morvan@univ-amu.fr}
[3]Scientific Research Center in Engineering, Lebanese University, Lebanon, {gaccary@ul.edu.lb}

** Corresponding author*

Keywords

Fire spread modelling; fuel properties; numerical simulations; fire behavior and dynamics; laboratory experiment

Abstract

The bulk density as definition represents the ratio between the packing ratio and the density of the vegetation. Therefore, it is directly related to the fuel load, the height and to the porosity of the vegetation. In fact, the bulk density plays an important role in fire propagation and behavior. Due to its dependence on the fuel porosity, the bulk density influences heat transfers inside the fuel bed, so, it can affect directly the rate of spread. Or, the bulk density influences also the fire intensity and flame characteristics (residence time, height and depth) due to its dependence of the fuel load and fuel bed height. However, despite the important influence of the bulk density on fire propagation, the literature does not clarify its impact on fire behavior, different points of view can be exanimated.

So, the aim of this study is to investigate the role played by the bulk density upon both propagation parameters and heat transfer of a surface fire through a homogeneous vegetation layer. Investigations were conducted numerically using "FireStar2D", a complete physical model based on multiphase formulation. Also, experimentally, tests were constructed at the university of Corsica at laboratory scale under no wind and no slope condition. In order to study the elementary effect of the bulk density on fire behavior, three different cases were evaluated: (a) variable fuel load with a constant bulk density, (b) variable fuel load and variable bulk density, (c) variable bulk density with a constant fuel load.

Case (a) was only studied numerically, the obtained results are in agreement with the literature: the rate of spread increases with the fuel load until a specific value where the ROS becomes independent of it. Case (b) was evaluated numerically and experimentally using a fix fuel bed height. The numerical and the experimental results showed that the ROS is barely affected by both fuel load and bulk density. Finally, the results of the last case, with a constant fuel load, showed numerically the same tendency proposed by Rothermel: the rate of spread reaches a maximum value at an optimal packing ratio that depends of the surface-volume ratio of the vegetation. Or, experimentally the ROS decreases with the increase of the bulk density. Different variables such as the optical thickness, the fire intensity, the residence time, the radiation and convection heat fluxes have been analyzed.

1. Introduction

Surface fire spread behavior is always related to the vegetation complex structure (Rothermel and Anderson 1966; Balbi et al. 2010; Rossa 2017), described by the properties of the fuel particles (fuel moisture content, density, surface to volume ratio, fuel load, bulk density, fuel bed depth, and packing ratio). Each one of these properties has its own effect on fire propagation. For instance, several studies have showed that the rate of spread decreases with the increase of fuel moisture content (Morvan 2013; Awad et al. 2021). Others showed that the rate of spread increases with the fuel bed height, and the fuel load (Morvan and Dupuy 2004; Rossa and Fernandes 2018; Awad et al. 2020). However, the effect of the vegetation bulk density and packing ratio on fire behavior has always been an examination subject due to the different point of views of its impact listed in the literature (Morvan and Dupuy 2004; Rossa and Fernandes 2018; Awad et al. 2020). In fact, as mentioned, the bulk density is directly dependent on the vegetation fuel load, height and porosity which can have opposite effects on fire behavior. Several studies noted a decrease of the rate of spread with the bulk density or the packing ratio (Rothermel and Anderson 1966; Catchpole et al. 1998). Several explanations of this tendency

were proposed: a large bulk density, therefore a large packing ratio and a low porosity leads to less diffusion of oxygen inside the fuel bed. Also, the radiation from burning fuel particles, heated by the flame base, impinges on the unburnt fuel on a distance equal to the extinction depth δ (Balbi et al. 2007) (equation 1) that is inversely proportional to the bulk density.

$$\delta = 4/\beta s \quad (1)$$

Where, β is the packing ratio and s is the surface to volume ratio.

However, other studies showed another tendency. Rothermel (Rothermel and Anderson 1966) performed several experiments using fuel beds of excelsior and sticks, showed that the ROS reaches a peak under an optimal packing ratio. For $\beta \leq \beta_{opt}$, the heat loss between fuel particles was important, it was explained by the increase of the air cooling effect inside the fuel bed with higher porosity. Or, for $\beta \geq \beta_{opt}$, the porosity decreases and the ratio of air fuel decreases. Qianqian He et al 2022 (He et al. 2022) showed that the surface heat transfer increases under lower packing ratios which increases the rate of spread (ROS). Or, under higher packing ratios, the surface heat transfer does not vary significantly, and, the ROS reduction in this case is attributed mainly to the internal heat transfer dominated by radiation.

The main purpose of this is to determine the elementary effect of the bulk density of fire behavior. Therefore, three different cases were evaluated: (a) variable fuel load with a constant bulk density, (b) variable fuel load and variable bulk density, and finally (c) variable bulk density with a constant fuel load. Several numerical simulations and experimental tests were conducted. Fire propagation parameters have been analyzed as the rate of spread, the fire intensity, the radiative and the convective heat transfer, and the residence time.

2. Study case (a): Variable fuel load with a constant bulk density

Previous studies showed that the fuel load has impact on fire behaviour, especially on the rate of spread and on fire intensity (Rothermel 1972; Morvan and Dupuy 2001; Weise David R., Zhou Xiangyang, Sun Lulu 2005; Zhou et al. 2005). Morvan and Dupuy (Morvan and Dupuy 2004) have demonstrated that the fuel load with a constant bulk density is a factor that determines the mode (thin or thick) of the porous medium where the fire front propagates. They found out that the rate of spread increases with fuel load until a specific value where it becomes independent. This behaviour can be explained by introducing a critical optical thickness τ_{opt} related to the fuel extinction length δ and to fuel height that determines if the vegetation medium is considered to be thick or thin.

$$\tau_{opt} = \frac{s\beta}{4}.e \quad (2)$$

In fact, if $\tau_{opt} < 1$ the porous medium is considered as a thin and all the vegetation depth participates to the fire front propagation. And, if $\tau_{opt} > 1$ only a depth equal to the extinction length δ that participates to the fire front propagation.

In order to study the influence of the fuel load on fire behavior with a constant bulk density, simulations were performed using fireStar2D, in a 2D domain, 170 m long and 35 m height. A homogenous layer of Australian grassland, whose physical properties are described in Table 1, lied between x = 20 m and x = 170 m. Different fuel loads are considered in this study by changing the fuel height between 0.3 and 1 m and maintaining the same fuel density and packing ratio.

Figure 1 shows that ROS increases with the fuel load (up to 0.5 kg/m^2) until reaching a value beyond which the dependence of the fuel load becomes relatively weak. This tendency can be related to the fire propagation mode in the porous medium.

Table 1- Vegetation characteristics

Fuel density (Kg/m^3)	500
Surface to volume ratio S/V (m^{-1})	4000
Packing ratio	0.002
Fuel load (Kg/m^2)	0.3-1
Height (m)	0.3-1

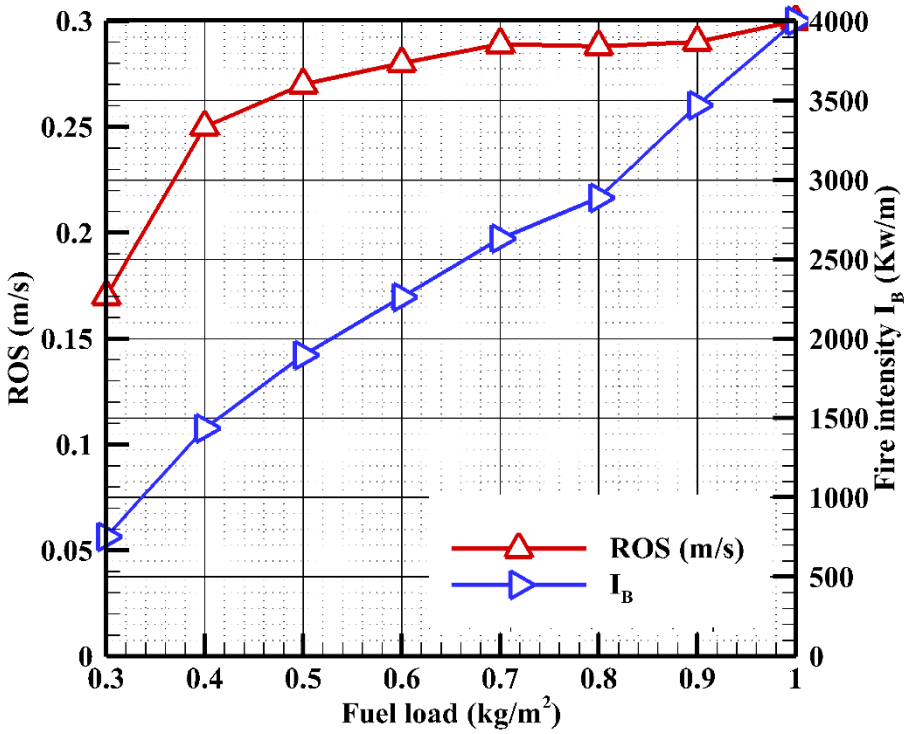

Figure 1- The rate of spread and Fire intensity evaluated for the grass for different fuel load with a constant bulk density under no slope no wind condition using FireStar2D

For a relatively thin vegetation medium ($\tau_{opt} < 1$) obtained for e < 0.5 m all the fuel-bed depth participates to the fire propagation. Therefore, the ROS increases with the fuel load. But, for a thicker vegetation medium, δ > e, radiative heat transfer does not penetrate the entire depth of the fuel bed. The lower fuel bed layers are not heated enough to participate to fire front propagation.

In another hand the fire intensity continues to increases with fuel load, as shown in figure 1. In fact, fire intensity depends directly of mass degradation rate and of the heat of combustion of the vegetation:

$$I = \dot{m} \, . \, \Delta H_c \qquad (3)$$

Where $\dot{m}$ (kg m^{-1}s^{-1}) is the vegetation degradation rate evaluated by the summation of mass losses due to pyrolysis and charcoal combustion producing CO and CO_2 gases.

3. Study case (b): variable fuel load and variable bulk density

3.1. Numerical tests

In this paragraph the fuel bed height remains constant or the fuel load and the bulk density (packing ratio) are variables. Simulation were conducted using the grassland (table 1) under no wind and no slope conditions. The different configurations are represented in table 2.

Table 2- Different configurations of grassland evaluated with Firestar2D

Packing ratio	0.0014-0.0032
Fuel load (Kg/m^2)	0.49-1.12
Height (m)	0.7

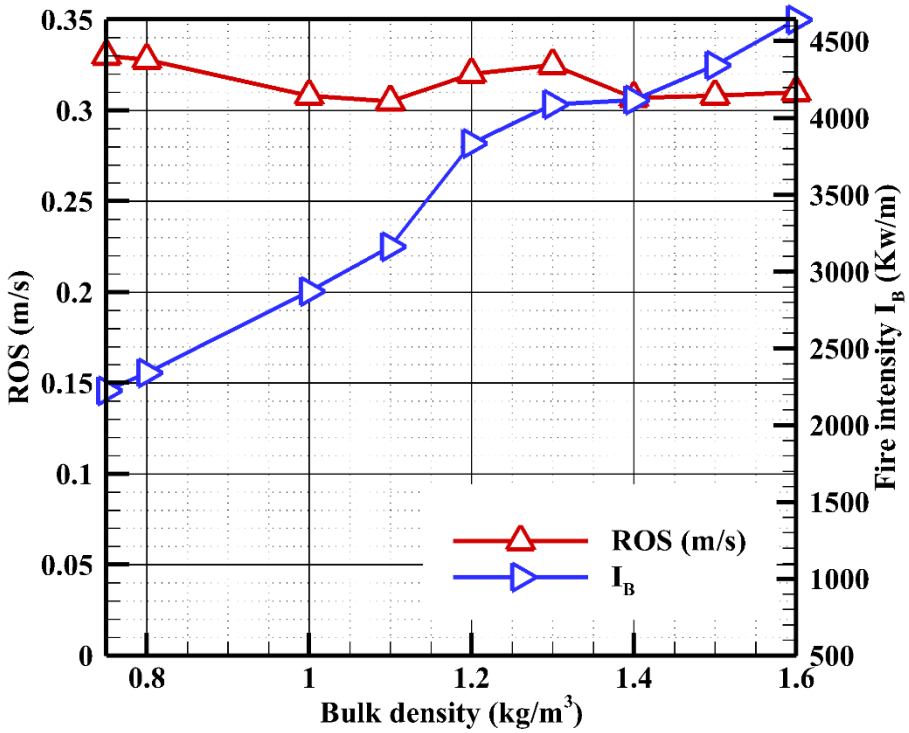

Figure 2- ROS and the Fire intensity variation in function of the bulk density for a constant fuel bed height 0.7 m evaluated using FireStar2D

Figure 2 shows that for a constant fuel bed height, with variable packing ratio and fuel load, the variation of the ROS is barely dependent on either bulk density or fuel load. In fact for the different configurations, the optical thickness τ is higher than 1 ; so the fire propagates in a thick medium where the extinction length δ is always less than the fuel bed height. Or, δ is inversely proportional to the packing ratio, therefore the depth of the vegetation that really participates to the fire propagation decreases with the increase of the packing ratio. This tendency is in agreement with the experimental results showed by Campell Lochrie (Campbell-Lochrie et al. 2021).

3.2. Experimental tests

Twelve tests were conducted at the laboratory of the university of Corsica with the excelsior in order to evaluate the influence of the bulk density and the fuel load when the fuel bed height remains constant.

Four different bulk densities were evaluated. The properties of the fuel are listed in the table 3.

Table 3- Excelsior characteristics

Fuel density (Kg/m^3)	780
Packing ratio	0.0023-0.0035-0.0046-0.0058
Fuel load (Kg/m^2)	0.2-0.3-0.4-0.5
Height (m)	0.11

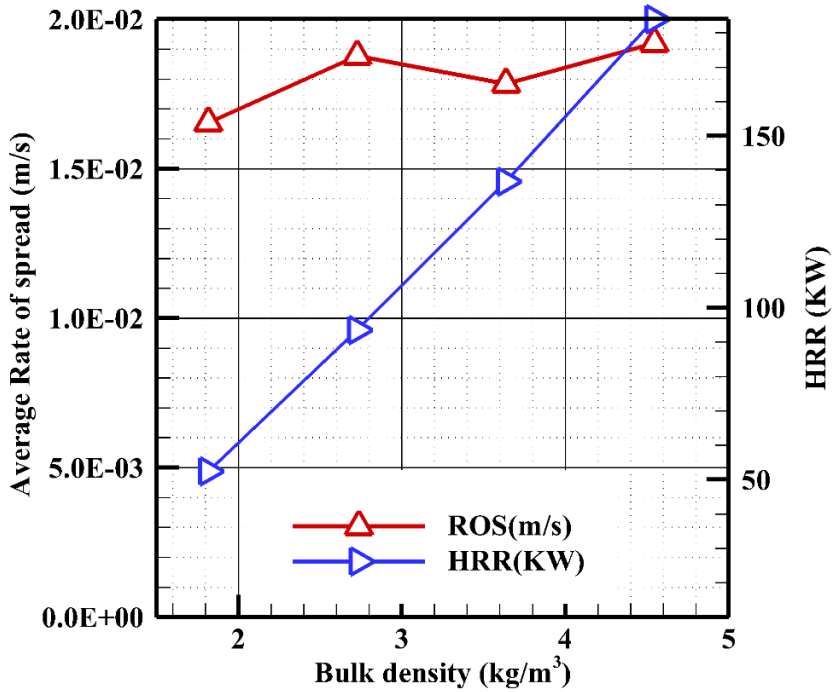

Figure 3- ROS and HRR variation in function of the bulk density for a constant fuel bed height 11 cm evaluated experimentally

The results of experimental tests are in agreement with the numerical results (Figure 3): the rate of spread barely depends of the bulk density or the fuel load when the fuel bed height remains constant. However, the fire intensity and the residence time increases with the bulk density (Figure 4).

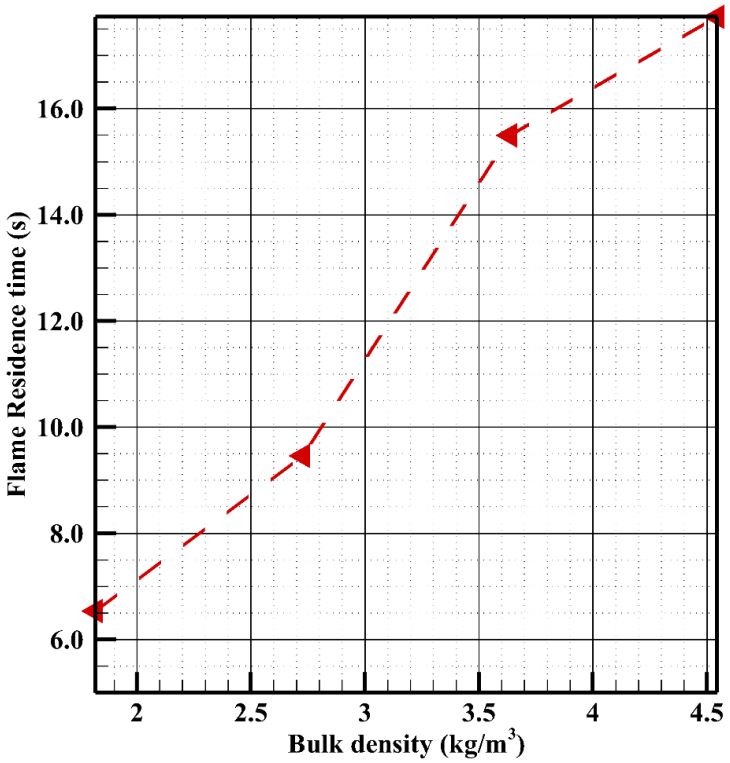

Figure 4- Flame residence time variation evaluated experimentally in function of the bulk density for a constant fuel bed height 11 cm

4. Study case (c): variable bulk density with a constant fuel load

4.1. Numerical tests

In this paragraph the fuel load remains constant or the bed height and the bulk density (packing ratio) are variables. Simulations were conducted using the grassland (table 1) under no wind no slope condition. The different configurations are represented in table 4.

Table 4 - Different configuration of grassland evaluated with Firestar2D

Packing ratio	**0.0014-0.0035**
Fuel load (Kg/m^2)	0.7
Height (m)	0.3-1

Numerical results shown is figure 4 are in agreement with the tendency proposed by Rothermel [2]: the ROS reaches a maximum for an optimal bulk density (Figure 5).

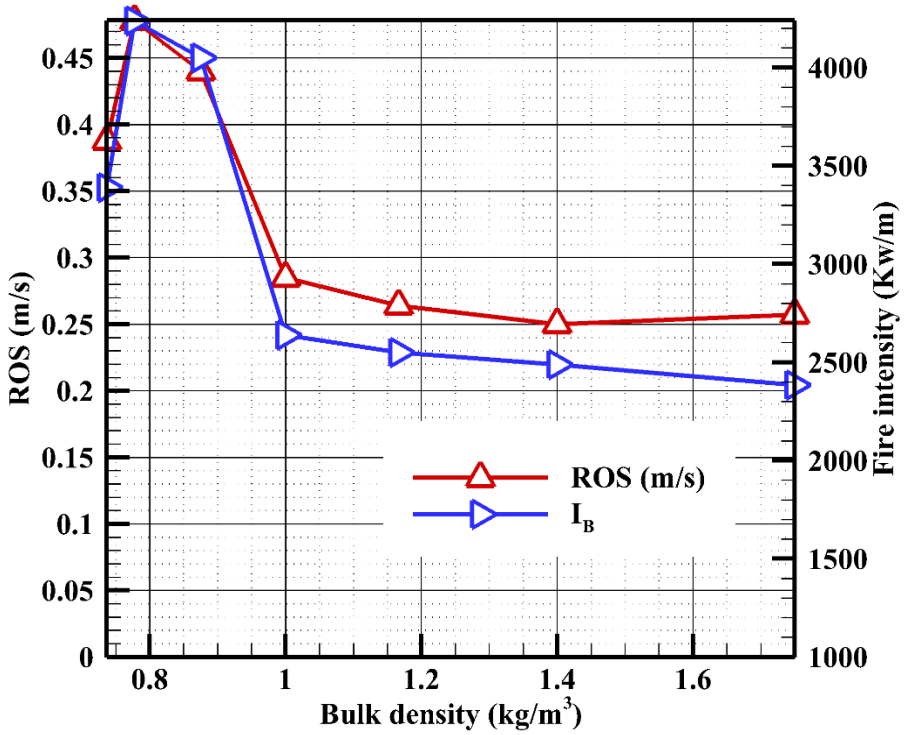

Figure 5- ROS and fire intensity variation in function of the bulk density for a constant fuel load evaluated numerically for the grass

4.2. Experimental tests

3 tests were conducted experimentally at the laboratory of the university of Corsica using the excelsior with a constant fuel load. The different configurations are represented in table 4.

Table 4- Different configuration of excelsior evaluated experimentally

Packing ratio	0.0039-0.0064-0.0017
Fuel load (Kg/m^2)	0.4
Height (m)	0.13-0.08-0.03

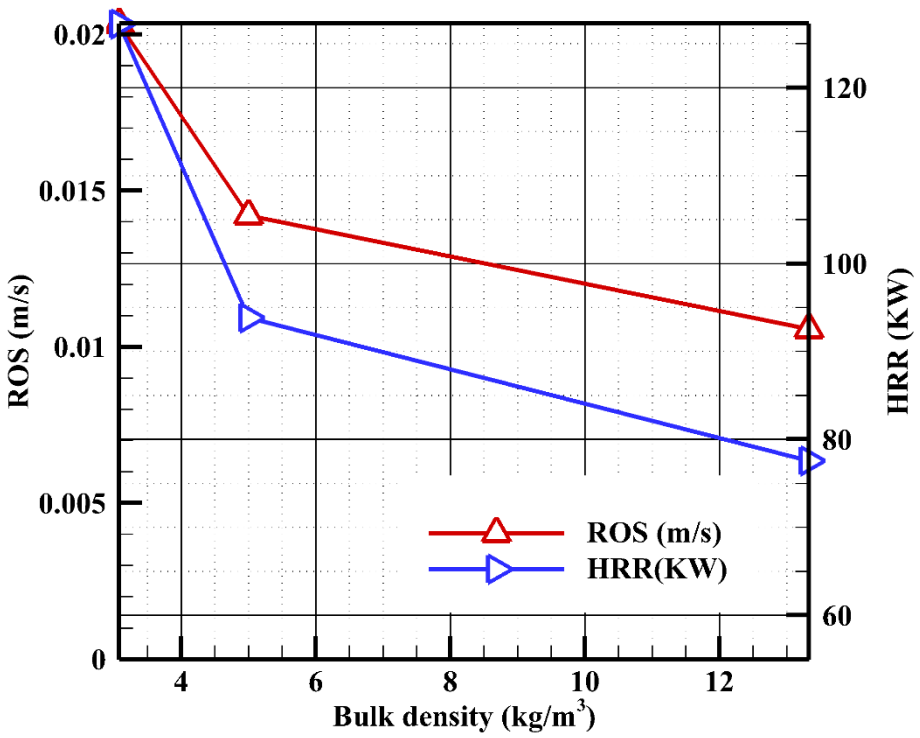

Figure 6- ROS and HRR variation in function of the bulk density for a constant fuel load evaluated experimentally for the excelsior

Figure 6 shows that the ROS and the HRR decreases with the increase of the packing ratio. In fact, this result can be explained by the fact that the packing ratio increased, the porosity of the fuel bed decreases therefore the inlet of the oxygen inside of the fuel bed also decreases. In another hand the increase of the packing ratio decreases the extinction length and therefore the total depth of the vegetation participating to the fire front propagation which explains the decrease of the HRR.

5. Conclusion

The effect of the bulk density on fire behavior is related directly to the fuel bed height and to the fuel load. For this reason, three different cases were evaluated numerically and experimentally:

(a) variable fuel load with a constant bulk density: the rate of spread increases with the fuel load or height until a specific value where it becomes independent of it; or the fire intensity increases with the increase of the fuel load.

(b) variable fuel load and variable bulk density: with a constant fuel bed height, the rate of spread is barely dependent of the fuel load or the bulk density, However the fire intensity increases with fuel load.

(c) variable bulk density with a constant fuel load: the rate of spread reaches a maximum value for an optimal packing ratio depending on the surface to volume ratio of the vegetation; the same tendency was found for the fire intensity.

6. Bibliography

Awad C, Frangieh N, Marcelli T, Accary G, Morvan D, Meradji S, Chatelon F-J, Rossi J-L (2021) Numerical study of the moisture content threshold under prescribed burning conditions. Fire Safety Journal 122, In Press. doi:https://doi.org/10.1016/j.firesaf.2021.103324.

Awad C, Morvan D, Rossi J-L, Marcelli T, Chatelon FJ, Morandini F, Balbi J-H (2020) Fuel moisture content threshold leading to fire extinction under marginal conditions. Fire Safety Journal 118, 11. doi:10.1016/j.firesaf.2020.103226.

Balbi J-H, Rossi J-L, Marcelli T, Chatelon F-J (2010) Physical Modeling of Surface Fire Under Nonparallel Wind and Slope Conditions. Combustion Science and Technology 182, 922–939. http://www.tandfonline.com/doi/abs/10.1080/00102200903485178.

Balbi J-H, Rossi J-L, Marcelli T, Santoni P-A (2007) A 3D Physical Real-Time Model of Surface Fires Across Fuel Beds. Combustion Science and Technology 179, 2511–2537. http://dx.doi.org/10.1080/00102200701484449 http://www.tandfonline.com/doi/pdf/10.1080/00102200701484449.

Campbell-Lochrie Z, Walker-Ravena C, Gallagher M, Skowronski N, Mueller E V., Hadden RM (2021) Investigation of the role of bulk properties and in-bed structure in the flow regime of buoyancy-dominated flame spread in porous fuel beds. Fire Safety Journal 120, 9. doi:10.1016/j.firesaf.2020.103035.

Catchpole WR, Catchpole EA, Butler BW, Rothermel RC, Morris GA, Latham DJ (1998) Rate of Spread of Free-Burning Fires in Woody Fuels in a Wind Tunnel. Combustion Science and Technology 131, 1–37. doi:10.1080/00102209808935753.

He Q, Liu N, Xie X, Zhang L, Lei J, Zhang Y, Wu D (2022) Experimental study on fire spread over discrete fuel bed-Part II: Combined effects of wind and packing ratio. Fire Safety Journal 103520. doi:10.1016/j.firesaf.2021.103520.

Morvan D (2013) Numerical study of the effect of fuel moisture content (FMC) upon the propagation of a surface fire on a flat terrain. Fire Safety Journal 58, 121–131. doi:10.1016/j.firesaf.2013.01.010.

Morvan D, Dupuy JL (2001) Modeling of fire spread through a forest fuel bed using a multiphase formulation. Combustion and Flame 127, 1981–1994. doi:10.1016/S0010-2180(01)00302-9.

Morvan D, Dupuy JL (2004) Modeling the propagation of a wildfire through a Mediterranean shrub using a multiphase formulation. Combustion and Flame 138, 199–210. doi:10.1016/j.combustflame.2004.05.001.

Rossa CG (2017) The effect of fuel moisture content on the spread rate of forest fires in the absence of wind or slope. International Journal of Wildland Fire 26, 24–31. doi:10.1071/WF16049.

Rossa CG, Fernandes PM (2018) An Empirical Model for the Effect of Wind on Fire Spread Rate. Fire 2018, Vol 1, Page 31 1, 31. doi:10.3390/FIRE1020031.

Rothermel RC (1972) A mathematical model for predicting fire spread in wildland fuels. (USDA Forest Service, Research Paper INT-115, Intermountain Forest and Range Experiment Station, Ogden, Utah) doi:http://www.snap.uaf.edu/webshared/JenNorthway/AKFireModelingWorkshop/AKFireModelingWkshp/FSPro Analysis Guide References/Rothermel 1972 INT-115.pdf.

Rothermel RC, Anderson HE (1966) Fire spread characteristics determined in the laboratory. (USDA Forest Service, Research Paper INT-30, Intermountain Forest and Range Experiment Station, Ogden, Utah)

Weise David R., Zhou Xiangyang, Sun Lulu MS (2005) Fire spread in chaparral - 'go or no-go?' International Journal of Wildland Fire 14, 99–106. doi:https://doi.org/10.1071/WF04049.

Zhou X, Weise D, Mahalingam S (2005) Experimental measurements and numerical modeling of marginal burning in live chaparral fuel beds. Proceedings of the Combustion Institute 30, 2287–2294. doi:10.1016/j.proci.2004.08.022.

Influence of combined hydric and thermal stresses on Rosmarinus officinalis and *Cistus albidus*

Rawaa Jamaladdeen [1]; Bruno Coudour *[1]; Fabienne Dédaldéchamp [2]; Laurent Lemée [3]; Jean-Pierre Garo[1]; Hui-Ying Wang [1]

[1]Institut P' - UPR 3346 CNRS, ENSMA, Univ. Poitiers, Futuroscope Chasseneuil, France, {rawaa.jamaladdeen, bruno.coudour, jean-pierre.garo, hui-ying.wang}@ensma.fr
[2] Unités Mixtes de Recherche, Ecologie et Biologie des Interactions, Université of Poitiers/Centre National de la Recherche Scientifique, Poitiers, France, {fabienne.dedaldechamp@univ-poitiers.fr}
[3] IC2MP - UMR CNRS 7285, Universite´ de Poitiers, Poitiers Cedex, France, {laurent.lemee@univ-poitiers.fr}

**Corresponding author*

Keywords

Combined thermal and hydric stresses, leaf and plant emissions, physiology analyses, *Rosmarinus officinalis* and *Cistus albidus*, adsorbent tubes, TD-GC-MS

Abstract

Wildfires are a growing threat, especially in Mediterranean climate areas during periods of drought. Wildfire research community continues to investigate propagation mechanisms on a large scale considering the thermal and fluid mechanics effects, or the main fire emissions (CO, CO2, H2O, H2, CH4). However, research on the effect of abiotic stresses on the plant emission during wildfires remains lacking, despite the fact that Mediterranean are considered important volatile essence emitting and storing species. This article addresses the effect of combined hydric and thermal stresses on physiology and emissions of two important Mediterranean shrub species; Rosmarinus officinalis and Cistus albidus that are largely consumed in wildfires. Different levels of hydric stress were applied on plants of the two species in a greenhouse. Thermal stress was executed by placing the water stressed plants inside a hermetic enclosure equipped with a radiant panel of maximal radiant heat flux of 84kW.m-2 and a fire-resistant glazed window for visualisation. The gaseous emissions of the plants under thermal stresses were collected and analysed by two complementary devices: an instantaneous gas analyser for CO, CO2, H2 and CH4, and adsorbent tubes by using the techniques of adsorption and desorption (by pyrolysis) for emission collection and analyses, respectively. Simultaneous pyrolyses experiments were realised on a foliar scale of the water stressed plants. Gases of pyrolyses separated with gas chromatography and identified using mass spectrometry. The heating tests showed a good reproducibility for pyrolyses of leaf samples and interesting variations between the monoterpene emissions of stressed and unstressed plants. At plant scale, number of tests for each plant species at a given hydric stress level were insufficient to give trends and strong results because of some imposed technical problems and the constraints of public health crisis. However, these tests allowed us to adapt experimental protocols and devices for further testing such as: plant location and fixation, heat flux ramp, sampling location, use of adsorbent tubes, hydric stress duration and normalisation of measured concentrations according to the plant size.

1. Context and objectives

1.1. Context

Wildfires are a growing issue, especially in Mediterranean climate areas during periods of drought where more and more uncontrollable fires are observed such as: megafires, too large and strong to be confined, and eruptive fires, too fast and unpredictable to be able to fight. These last years have been particularly disastrous with worldwide mediatised megafires (Fernando et al. 2022). As to eruptive fires, these are sudden and impressive wildfire accelerations occurring without wind, or moderate one, which have already caused more than 150 fatalities so far [2-8], mainly among firefighters involved in the extinguishing operations.

According to Schneider et al. (2021) "there is a strong need to increase the basic understanding of the propagation mechanisms of wildfires to improve the scientific tools needed for firefighting and fire prevention". Classical propagation of a wildfire is mainly due to two correlated mechanisms: important heat transfers

(energy) and formation of flammable mixtures ahead of the fire front (gases). Heat is transmitted principally by thermal radiation and convection. Flammable mixtures are formed from the only available fuel (vegetation) while it is heated, pyrolysed, and burnt. Wildfire research community continues investigating propagation mechanisms of the fire front such as thermal radiation (Frangieh et al. 2020) or buoyant flame dynamics (Finney et al. 2015). Research on eruptive fires issue are also focusing on airflow considerations (Viegas et al. 2009, Chatelon et al. 2014) such as induced wind, flame attachment, inclination angle, etc. Mentioned studies on wildfire propagation take into account large scale mechanisms such as thermal and fluid mechanics ones, or take into account the main chemical compounds resulting from degradation and combustion (CO, CO_2, H_2O, H_2, CH_4). However, there is a lack of investigation on the role of plants (Fernando et al. 2022) and the large range of molecules released during wildfires at the fire front knowing that Mediterranean plants are particularly rich in volatile essences (Owen et al. 2001). Hydric and thermal stresses have been studied independently showing influence on plant emissions (Barboni 2006, Chetehouna et al. 2014, Ormeño et al. 2007, Lavoir 2010, Ciccioli et al. 2014, Courty et al. 2014, Lemoine et al. 2013) but to our knowledge there is no study on combination of these wildfire stresses. This project intends to better understand the biological and thermochemical aspects of wildfire propagation taking into account a wider range of molecules involved in it and the role of two combined wildfire stresses.

1.2. Objectives

Experiments consisted of submitting two plant species (*Rosmarinus officinalis* and *Cistus albidus*) to different levels of hydric stress first, and then to a thermal stress similar than the one of the arrival of a wildfire. During these tests, we studied plant behaviour by analysing their physiology and their emissions (composition and concentration) at leaf and plant scale.

1.3. Team and funding

This study was conducted in the mark of Rawaa Jamaladdeen's thesis from P' Institute and in collaboration with Associate Professor Fabienne Dédaldéchamp from the laboratory EBI (Ecology and Biology of Interactions, SEVE team) and Engineer Researcher Laurent Lemée from IC2MP (Institute of Chemistry of Environments and Materials of Poitiers), as part of two Master internship grants from Labex Interactifs (Ms. Kenza Ait Ali Yahia) and EUR-InTREE which is a new training about Interfaces from a physico-chemical aspect in Poitiers (M. Axel Rigoulet), and a grant from P' Institute.

Associate Professor Fabienne Dédaldéchamp brought her expertise in biology [17] during plant conditioning to hydric stress and plant physiology analyses and issues. We co-supervised with her and Rawaa Jamaladdeen Ms. Kenza Ait Ali Yahia, a second year Master student in Green Chemistry, Catalysis and Environment (CVCE, University of Poitiers). She helped us during hydric stress conditioning, physiology analyses at EBI laboratory and thermal stress tests at P' Institute. Engineer Researcher Laurent Lemée brought his chemistry expertise for accurate chemical analyses by thermodesorption of adsorbent tubes. We co-supervised Mrs. Axel Rigoulet a first year Master student (EUR-CVCE). He helped us on leaf pyrolyses and adsorbent tubes analyses at IC2MP.

2. Material and methods

2.1. Plant conditioning to hydric stress

For this part, we benefitted from the greenhouse equipment of EBI laboratory. *Rosmarinus officinalis* and *Cistus albidus* were chosen to be Mediterranean plants typically concerned by documented eruptive fires (Courty et al. 2014) but also to be physiologically different (Ormeño et al 2007). 20 plants of each species were correctly watered, 20 others were submitted to hydric stress. The end of the hydric stress was decided according to physiology analyses made in EBI laboratory to keep plants alive for heating tests: plant soil moisture, leaf water amount and chlorophyll concentration. Hydric stress conditioning required about two to three weeks depending on the weather (sunny/cloudy, humid/dry). Other microscopic and macroscopic analyses were done to get more data on the influence of hydric stress. Analysed parameters included stomatal conductance, osmotic pressure and water status of leaves which are directly related to the plant emissions (Ormeño et al 2007, Lavoir 2010). Pictures of the plants were done and analysed with image based software in order to normalise emission quantification according to plant sizes during thermal tests. For each of the two species, we got physiological

observations during hydric stress and a normalisation method for emission quantification according to plant size.

Watered and non-watered plants were then submitted to thermal stress (cf. below).

2.2. Heating tests at plant scale

2.2.1. Material

For this part, we benefitted from a compartment of 1 m^3 equipped with a radiant panel lent by PRISME laboratory (Fig. 1). The latter can provide a maximum of 84 $kW.m^{-2}$ of radiative flux and is made with a fire resistant glazed window for plant surveillance. It was instrumented with thermocouples, fluxmeters and a cooled scale (Fig. 1 left).

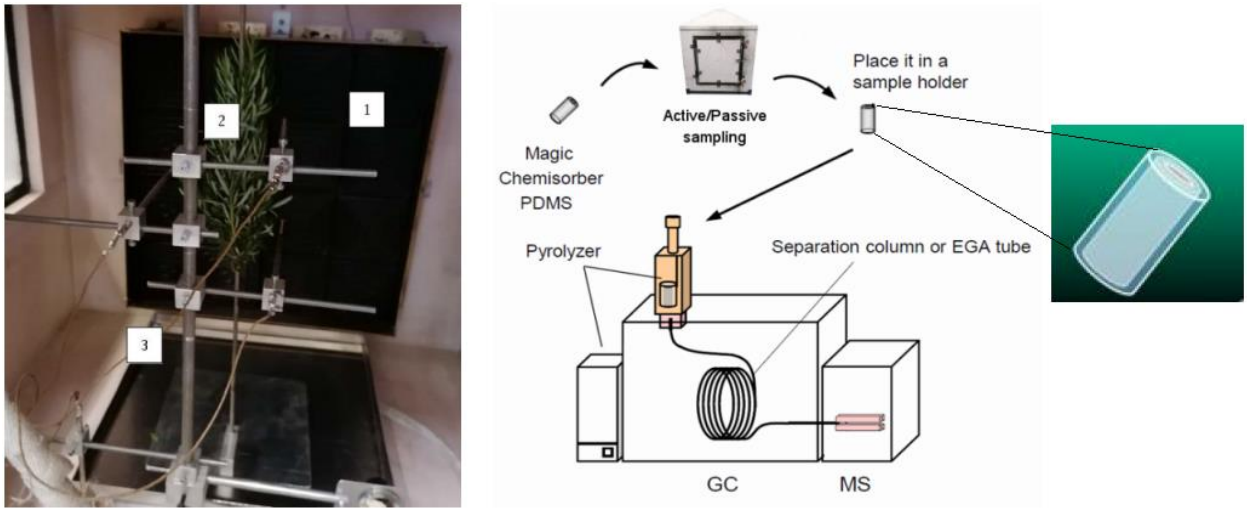

Fig. 1. On the left: photograph of Rosmarinus plant (2) submitted to thermal stress inside a 1m³ compartment equipped with radiant panel (1) and lent by PRISME laboratory (Bourges). On the right: method of analysis with adsorbent tubes

Two complementary gas analysis devices were used during tests: a mobile analyser introduced from the top of the compartment to quantify continuously O_2, CO, CO_2, H_2 and CH_4; and adsorbent tubes to identify VOCs (Volatile Organic Compounds) by trapping them *in-situ*. Trapped compounds were identified by TD-GC-MS (Fig. 1 right), i.e. they were thermally desorbed (TD), separated with gas chromatography (GC) and identified using mass spectrometry (MS). The pyrolysis products were identified by comparison of their mass spectra with NIST (National Institute of Standards and Technology) mass spectral library and thanks to their retention times. The adsorbent tubes, also known as SPEE (solid phase extraction elements), are titanium tubes coated with polydimethylsiloxane (PDMS). For each test, an adsorbent tube was placed into the heating compartment at the ground level and another one was placed inside an active sampling composed from a pump and a flexible connecting the pump to the compartment. It allowed us to compare the gas composition at different heights knowing that density is very variable between e.g. isoprene and sesquiterpenes.

2.2.2. Protocol

At the end of hydric stress conditioning, plants were retrieved from the greenhouse and introduced one by one inside the compartment. Plants were cut at their basis and depending on their size, one, or two superimposed plants, were attached to a stand close to the radiant panel (see Fig. 1 left). Consequently to preliminary tests, we chose to impose a temperature/heat flux ramp of 30 minutes not to exceed 200°C at the plant level in order to avoid hemicellulose degradation and study only vegetation emissions. After each heating test, we retrieved data of temperature, heat flux, light gases concentration over time (continuous analyser), and the two adsorbent tubes for analyses by TD-GC-MS desorb, separate, identify and quantify the VOC emission. Thermodesorption of of adsorbed compounds was performed from 150°C to 280°C with a heating rate of 500°C/min and 1 min at final temperature.

2.3. Heating tests at leaf scale

Leaf samples were cut from plants during the hydric stress conditioning and pyrolysed at IC2MP. The pyrolyser was a Multi-shot Pyrolyzer EGA/PY-3030-D which was coupled with a GCMS-QP2010 Ultra Gas Chromatograph-Mass spectrometer. The pyrolysis products were carried by a helium gas flow to the GC column and separated on a TR5-MS capillary column (dimensions: 30.0 m, 0.25 mm i.D, 0.25 µm phase thickness). The injector was a split/splitless. The MS device was a quadrupole analyser, the ionization mode was electron impact (70 eV).

Around 15 mg of not lyophilized leaves (equivalent to one rosemary leaf or a piece of cistus leaf) were placed into an inox cup and the pyrolysis was carried out in the isothermal mode at 180°C (temperature of maximal emissions of plants (Barboni 2006, Chetehouna et al. 2014, Courty et al. 2014) for 1 minute. When cut leaves needed to be stored for later experiments, they were conserved inside glass tubes covered with aluminium foil in a freezer at a temperature of -21±1°C.

3. Results

The physiological analyses show clearly the influence of the hydric stress at microscopic scale (Fig. 2) with a decrease in vacuole volume and an increase in secondary metabolite synthesis for stressed plants. For *Rosmarinus officinalis*, we also observed dead cells (Dc) (Fig. 2.d) indicating that hydric stress was worse than for *Cistus albidus*. The heating tests showed a good reproducibility for pyrolyses of leaf samples and interesting variations between stressed and unstressed plants regarding monoterpenes and fatty acids (Fig. 3). At plant scale, number of tests for each plant species at a given hydric stress level were insufficient to give trends and strong results because of technical problems, sanitary restrictions and specificity of each plant. However these tests allowed us to adapt experimental protocols and devices for further testing such as: plant location and fixation, heat flux ramp, sampling location, use of adsorbent tubes, hydric stress duration and normalisation of measured concentrations according to the plant size.

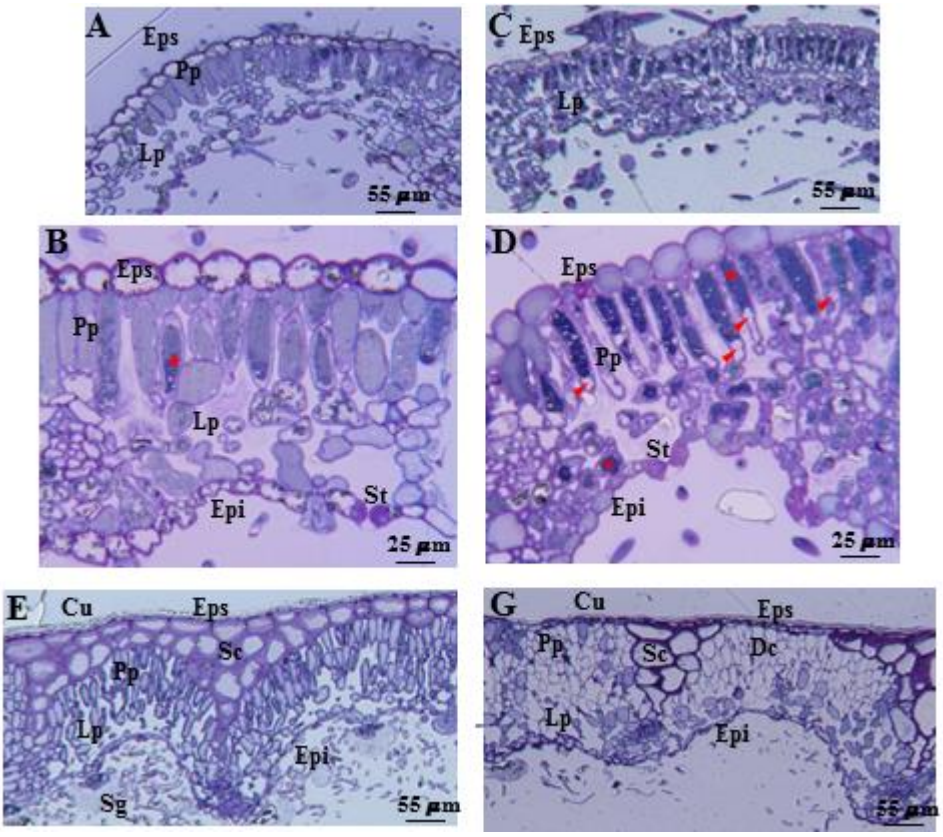

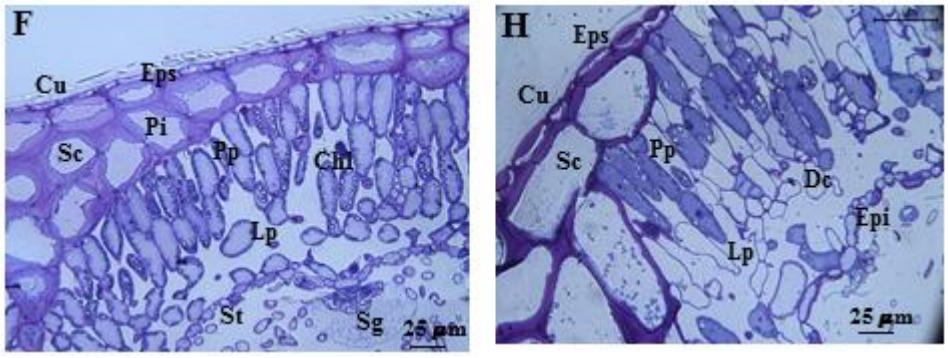

Figure 2: Cross section of Cistus albidus (A,B,C,D) and Rosmarinus officinalis (E,F,G,H) leaves, Plants growing condition: well-watered (A,B,E,F) and without water supply for 16 days (C,D,G,H). Cu, cuticle; Eps, superior epidermis (adaxial); Epi, inferior epidermis (abaxial); Sc, Sclerenchyma; Pi, pit; Pp,: Palisade parenchyma; Lp, lacunar parenchyma; Chl, Chloroplast; Sg, Secretory gland; Dc: Dead cell; St: Stomata. Tannins (asterisk): Cell plasmolysis (arrow). Semithin section, toluidine blue staining, optic microscopy.

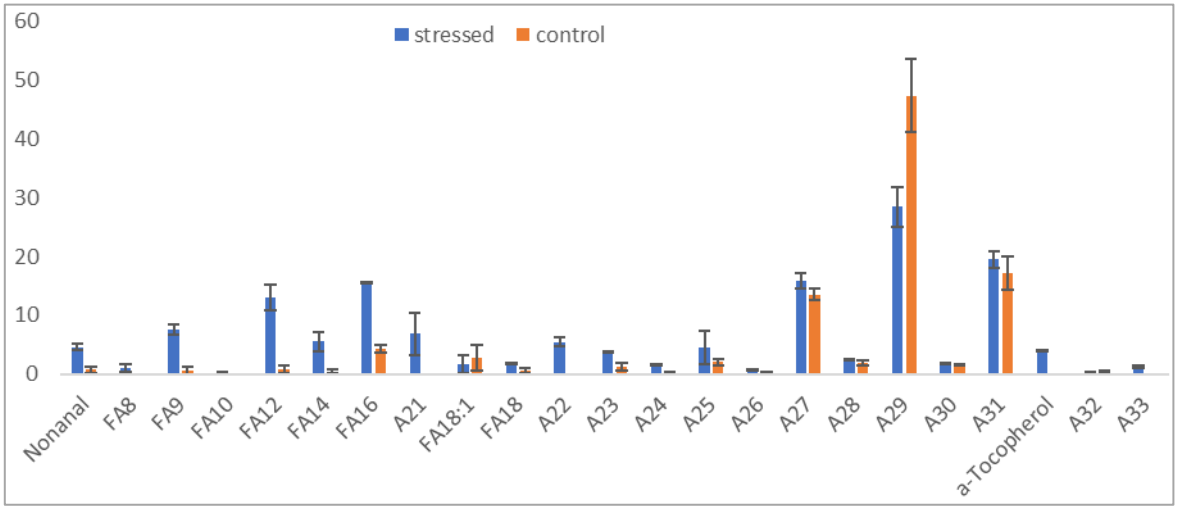

Fig. 3. Pyrolysis products (180°C for 1 minute) of control and hydrically stressed Cistus albidus (A_n: alcane C_n ; Fa_n : fatty acid C_n)

4. Acknowledgement

We acknowledge Labex Interactifs of P' Institute which allowed us working on the biological part with the Master student Ms. Kenza Ait Ali Yahia and we acknowledge EUR-InTREE which is a new training about Interfaces from a physico-chemical aspect in Poitiers which allowed us working on the chemical part with Master student M. Axel Rigoulet. The authors would like to thank Vincent Lebeurre for plant production. We also acknowledge Khaled Chetehouna from PRISME laboratory (Bourges-France) to have lent us the heating compartment equipped with a radiant panel.

5. Bibliography

Barboni (2006). Caractérisation chimique d'un hybride de clémentine et du myrte commun. Etude de cas d'embrasement généralisé éclair par la détermination des COVb. Analyse des fumées issues de la combustion des végétaux. Thèse de doctorat de l'Université de Corse.

Carbonell et al. (2005). Embrasement Généralisé Éclair (EGE) lors de feux de forêt. Face au risque n° 410.

Chatelon et al. (2014). Generalized Blaze Flash, a "Flashover. Behavior for Forest Fires—Analysis from the Firefighter's Point of View. Open Journal of Forestry, 4, 547-557.

Chetehouna et al. (2014). Volatile Organic Compounds: Emission, Pollution and Control. Nova Science Publishers.

Ciccioli P. et al. (2014). Biogenic volatile organic compound emissions from vegetation fires. Plant. Cell and Environment 37, 1810–1825.

Coudour et al. (2016). Experimental and numerical investigation of the geometry influence on gas accumulation using a V-shape forest model, Atmospheric Environment, 141, 67–79.

Courty et al. (2014). Biogenic volatile organic compounds emissions at high temperatures of common plants from Mediterranean regions affected by forest fires. Journal of Fire Sciences, 32(5), 459-479.

Fernando A.O. et al. (2022). Fire and vegetation: Introduction to the special issue, Flora, Volume 286.

Finney et al. (2015). Role of buoyant flame dynamics in wildfire spread. Proceedings of the National Academy of Sciences (doi.org/10.1073/pnas.1504498112)

Frangieh et al. (2020). Wildfires front dynamics: 3D structures and intensity at small and large scales. Combustion and Flame, 211, 54-67.

Lahaye S. (2018). Comprendre les grands feux de forêt pour lutter en sécurité. Thesis of Paris Sciences et Lettres Research University

Lavoir (2010). Comment le stress hydrique influence les COV biogéniques ? Cas des émissions de monoterpènes chez le chêne vert (Quercul ilex). Editions Universitaires Européennes.

Lemoine R, La Caméra S., Atanassova R., Dédaldéchamp F. et al. (2013). Source-to-sink transport of sugar and regulation by environmental factors. Frontiers in Plant Science.

Ormeño E., J.P. Mévy, B. Vila, et al. (2007) Water deficit stress induces different monoterpene and sesquiterpene emission changes in Mediterranean species. Relationship between terpene emissions and plant water potential, Chemosphere, 67, Issue 2, 276-284.

Owen et al. (2001). Volatile organic compounds (VOCs) emitted from 40 Mediterranean plant species: VOC speciation and extrapolation to habitat scale, Atmospheric Environment. 35, pp. 5393-5409.

Schneider L. et al. (2021). Experimental study of fire spread through discontinuous fuels without flame contact. Fire Safety Journal, Volume 120, 103066, ISSN 0379-7112.

Viegas D.X., Caballero D. (2009). Recent forest fire accidents in Europe, Viegas (ed.).

Influence of fuel load on the flammability of live *Pinus Halepensis* needles

O. Mosbah[1]; F. Z. Sabi[1] ; S.M. Terrah[1,2] ; H. Boutchiche[1]; N.Hamamousse; A.Sahila; A. Kaiss[3]*; N. Zekri[1]

[1]Université des Sciences et de la Technologie d'Oran, LEPM BP 1505 El Mnaouer Oran, Algeria, {mosbah31omar@yahoo.fr, sabi.fatimazohra@yahoo.fr, hananelimang@gmaik.com, nadjet.hamamousse@gmail.com, sahilaadel@yahoo.fr, Ahmed.Kaiss@amu-univ.fr, nzekri@yahoo.com}
[2]Ecole supérieure de génie électrique et énergétique d'Oran, B.P 64 CH2 Achaba Hanifi, USTO, Oran, Algeria, {t_mohamed31@yahoo.fr}
[3] Aix Marseille Université, IUSTI, Technopôle Chateau Gomber, 5, rue E. Fermi, 13453, Marseille Cedex 13

**Corresponding author*

Keywords

Load, incident flux, volatile organic compounds, *Pinus Halepensis* needles.

Abstract

The fuel flammability, combustibility, and fire spread properties depend on several parameters, such as the heat flux, moisture content, wind, and the fuel load. Flammable ignition occurs when the emitted organic volatile components flow mixed with air reaches a minimum rate corresponding to the lower flammability limit. The gas flow of these components depends on the fuel quantity (load) and its temperature. Therefore, ignition time depends on the fuel load.

In this work, the effect of the load on ignition time of live *Pinus Halepensis* needles is investigated using a cone calorimeter (providing three incident heat flux intensities). The average fuel moisture content is around 50% on a wet basis. Ignition time exhibits an exponential trend for all the incident heat flux intensities considered with a correlation coefficient $R^2 > 0.96$. The exponent corresponds to a characteristic load $\bar{m}_0$ around 1 kg/m^2 slightly dependent on the incident flux within statistical errors. For very small loads compared to $\bar{m}_0$ ignition time is nearly independent of the load because the time required for water evaporation is neglected compared to that required for a volatile mixture with air to reach the lower flammability limit. For larger loads (in the range of 0.38 kg/m^2 to 1.27 kg/m^2), the time required for water evaporation introduces a shift in ignition time which increases linearly with the load. Finally, for large loads compared to $\bar{m}_0$, the fuel bed thickness becomes larger than the optical length, and only its top layer is heated, transmitting thus heat to the internal layers by conduction. Therefore, the internal layers evaporate water and cool the upper one, leading to the exponential ignition time with the load. For dry fuels, ignition time appears independent of the load.

1. Introduction

Fires are considered in ecology as one of the most important and traumatic disturbances. Mediterranean ecosystems are particularly sensitive to conditions favoring fires: repeated climatic droughts, strong and frequent winds, accumulation of combustible biomass resulting from forest plantations, the abundance of rural areas, and the low exploitation of the forest (Di Castri, 1981). During the period from 1985 to 2006, a total burned area of 779,872.11 ha was recorded for 32,354 fires. *Pinus Halepensis* and *Cork Oak* forests fuels paid the heaviest price. Based on these statistics, we choose to study *Pinus Halepensis* needles. Ignition conditions depend on several parameters such as the heat flux, water content, wind, load, etc. Regarding the first parameter, there is a critical heat flux for flammability (Terrah et al, 2018; Sabi et al, 2018; Mindykowski et al, 2008). Concerning the second parameter, it has recently been shown that there is no critical water content for flammability, but for each moisture, there is a sufficient heat flow to allow ignition (Terrah et al, 2018). During the exposition of the fuel to a heat source, its temperature rises, and flammable volatiles is emitted and mixed with air. The composition of gas in the air increases with temperature and reaches a critical concentration allowing ignition under a critical temperature. The time for gas flow to reach the critical composition (lower flammability limit depends also on the load). Ignition time dependence on the load is investigated here for different incident flux intensities.

2. Heat transfer and experimental setup

The *Pinus Halpensis* needles with an average moisture content of 50% (on a wet basis) are harvested the same day to ensure their live character. The sample is placed in a cylindrical holder with a diameter of $0.1\ m$, and exposed to thermal radiation flows ranging from 10 to 21 kW/m^2 provided by a cone calorimeter (Fig.1a) equipped with an electrical resistance of 3000W. The calibration of the heat flux is realized by using a heat flux sensor Hukseflux SBG01 working in the range from 0 to 200 kW/m^2. The desired heat flux intensities are obtained by varying the distance between the sample and the cone calorimeter (Fig.1b). Vegetation ignition is controlled by a pilot flame located 1cm above the sample. Ignition is considered successful if the flame persists for a time longer than 4s, and ignition time is recorded.

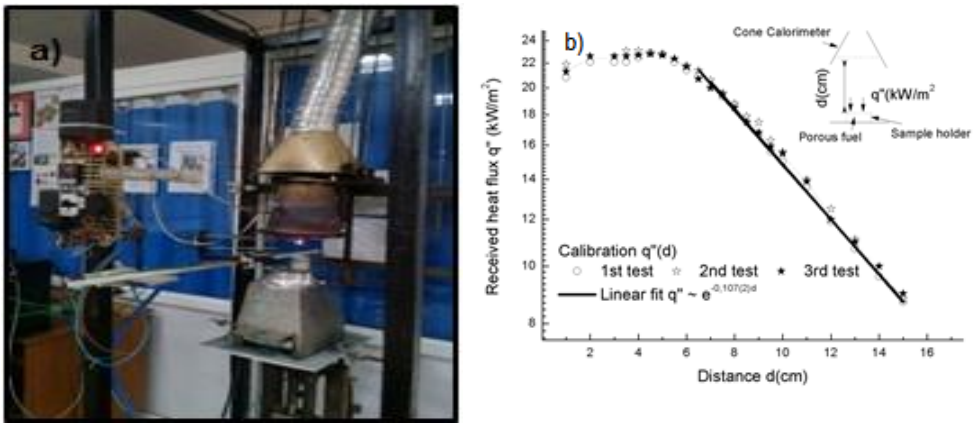

Figure1: a) the experimental setup, b) a schematic representation of the heat flux calibration

The net absorbed heat flux by the fuel $q"_{net}$ is related to the absorbed incident heat flux and that lost by the fuel bed. Neglecting conduction heat transfer, the net heat flux reads:

$$q"_{net} = aq"_{inc} - h(T - T_0) + \sigma\varepsilon\left(T^4 - {T_0}^4\right) \quad (1)$$

Here h is the convection coefficient, σ is the Stefan Boltzmann constant, ε is the emissivity of the fuel, and T_0 the ambient temperature. The samples were prepared with caution to keep similar arrangements of the species as far as possible. As the fuel bed is porous, the heat transfer mechanism involves the packing ratio φ which measures the average volume proportion of fuel in the sample:

$$\varphi = \frac{4\,m}{S \times e \times \rho} \quad (2)$$

Where m is the sample mass, S its surface, e its thickness, and $\boldsymbol{\rho}$ the particle density. The porosity (proportion of air in the bed) is directly related to the packing ratio $(1 - \varphi)$. The surface-to-volume ratio SVR was also found to influence the ignition and combustion properties of the fuel bed (Schemel et al, 2008; Santoni et al, 2014). Flammability properties might be influenced by the optical length δ of radiation that corresponds to the extinction coefficient defined as CFR (1981):

$$\frac{1}{\delta} = \frac{\varphi \times SVR}{4} \quad (3)$$

This quantity is an important optical parameter of porous material, and allows the determination of the absorption probability a, which is related to the thickness e as Callister & Rethwisch (2914):

$$a\ \alpha\left(1 - e^{-e/\delta}\right) \quad (4)$$

The replacing (2) in (3), this quantity is related to the fuel load ($\bar{m} = m/S$) as:

$$\frac{e}{\delta} = \bar{m}\frac{SVR}{\rho} \quad (5)$$

Since the fuel considered is the same (same $\boldsymbol{SVR}$ and density), ignition time (t_{ign}) is related to the load $\bar{\boldsymbol{m}}$.

3. Results and discussion

Fig.2 shows the variations of ignition time with the load $\bar{m}$ for three heat flux intensities ($17\ kW/m^2$, $13.83\ kW/m^2$, and $10.93\ kW/m^2$). The load is changed by varying the mass of the fuel bed, the area S of the sample holder being constant. Note here that the depth of the fuel bed may change from one sample to another depending on the packing ratio from equation (2). From (5) the fuel bed thickness (e) varies linearly with the optical length (δ) for the same load. From this figure (presented on the semi-logarithmic scale) ignition time seems to increase exponentially with the load for all the heat flux intensities considered with a correlation coefficient larger than 0.96 as:

$$\left(t_{ign} \propto e^{\bar{m}/\bar{m}_0}\right) \tag{6}$$

The growth exponents determined from the fitting slopes in Fig.2, correspond to characteristic loads $\bar{m}_0$. The exponential trend appearing in Fig.2 involves a characteristic quantity as in other fields (like the relaxation time in charge or discharge of a condenser). The characteristic load seems to depend only slightly on the incident heat flux: $\bar{m}_0 \approx 1.05 \pm 0.05\ kg/m^2$ for an incident heat flux of $17\ kW/m^2$, $0.99 \pm 0.03\ kg/m^2$ for $13.83\ kW/m^2$ and $1.14 \pm 0.02\ kg/m^2$ for $10.93\ kW/m^2$). For small loads ($\bar{m} \ll \bar{m}_0$) ignition time is nearly constant. Indeed, as the load is sufficiently small, the whole surface of the sample will be heated at the same time, and the time for water to be evaporated is neglected compared to that of volatiles and their mixture with air to reach the lower flammability limit. For loads in the range $0.38 < \bar{m} < 1.27\ kg/m^2$ (i.e close to $\bar{m}_0$) ignition time increases linearly with the load (the time of water evaporation induces a delay before ignition).

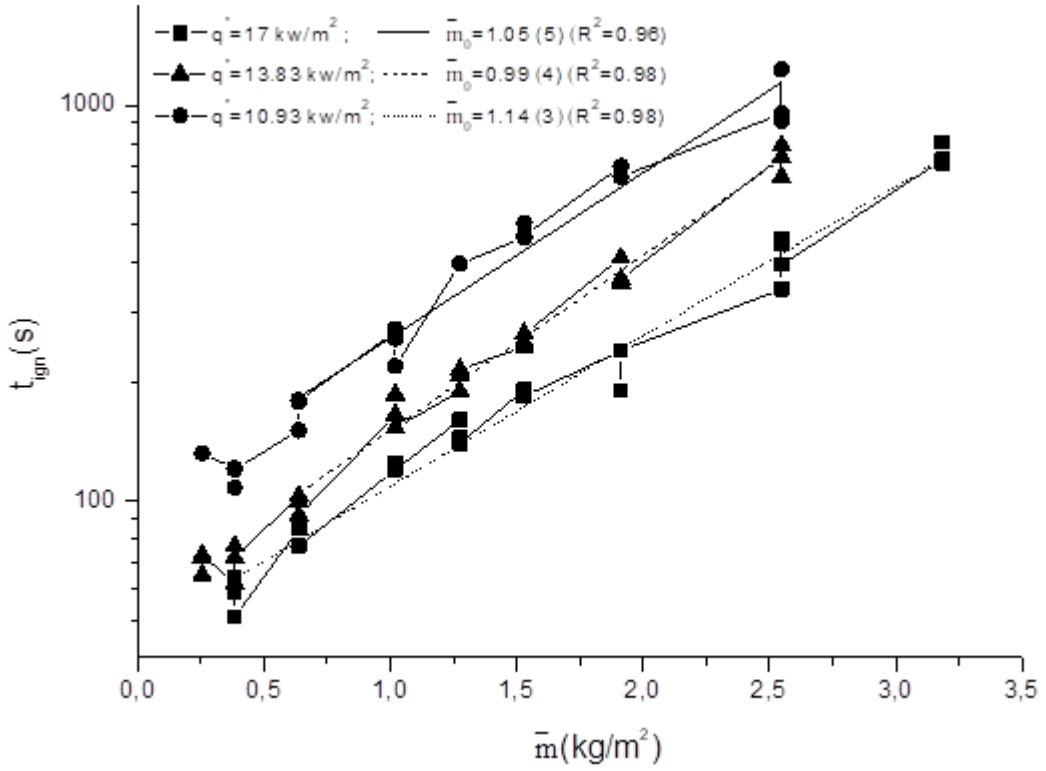

Figure2: Variation of ignition times vs. the load ($\bar{m}$) for the three different heat flux intensities: 17 kW/m², 13.83 kW/m² and 10,93 kW/m². The lines represent the exponential fits, and the characteristic loads are estimated from the fit slopes.

For larger loads ($\bar{m} > 1.27\ kg/m^2$) the trend of ignition time becomes exponential. The exponential trend is explained by the fact that the fuel bed thickness becomes much larger than the optical length, and the heat flow heats only the top layer of the fuel bed, which heats the internal layers by thermal conduction. The water evaporated from these inner layers cools the top layer which delays their ignition (Drysdale, 2011). This transition from a constant ignition time to an exponential increase with the fuel bed load can be explained by the transition from thermally thin to thermally thick fuel beds If the fuel bed itself is thermally thin, there is no temperature gradient, and all the water will be evaporated before ignition. If the fuel bed is thermally

thick, there is a temperature gradient so the deeper layers of fuel could still be cool enough to be evaporating water (and diluting the pyrolyzed). Hence, the characteristic load ($\overline{m}_0$) corresponds to a crossover fuel bed thickness separating the thermally thin and thermally thick regions.

4. Conclusion

In this work, we studied experimentally the effect of the fuel load on ignition time using a cone calorimeter delivering three different heat flux intensities. An exponential trend of ignition time is observed for all heat fluxes, with the corresponding characteristic load of around 1 kg/m^2 slightly dependent on the heat flux. The exponential trend is explained for large loads ($\overline{m} > 1.27\ kg/m^2$) by a complex heat transfer process due to the large fuel bed, thickness compared to the optical length. Only a top layer of the sample is heated and heats the internal layers. Water evaporation of the inner layers cools the top layer and therefore delays ignition.

5. Reference

DI CASTRI F. Mediterranean-type shrublands of the world. In: DiCastri F., Goodall D., Specht(1981).

Terrah SM, Sabi F. Z, Mosbah O, Dilem A, Hamamousse N, Sahila A, Harrouz O, Zekri N; Kaiss A, Clerc J-P, Rahli O, Giroud F, Picard C., (2018), "Is there a critical fuel moisture content for flammability?", In *Advances in Forest Fire Research 2018,* ed *D.X Viegas* (ADAI/CEIF Coimbra), pp 522-528

Sabi F.Z, Terrah SM, Mosbah O, Dilem A, Hamamousse N, Sahila A, Harrouz O, Zekri N; Kaiss A, Clerc J-P, Rahli O, Giroud F, Picard C., (2018), "Ignition/non-ignition phase transition", In *Advances in Forest Fire Research,* ed *D.X Viegas* (ADAI/CEIF Coimbra 2018), pp 506-513.

Mindykowski P, Fuentes P, Consalvi JL, Porterie B (2011), "Piloted Ignition of Wildland Fuels", *Fire Safety Journal* **46** (1-2), 34-40.

C.F. Schemel, A. Simeoni, H. Biteau, J.D. Rivera, J.L. Torero, A calorimetric study of wildland fuels, Experimental Thermal and Fluid Science 32 (2008) 1381–1389, https://doi.org/10.1016/j.expthermflusci.2007.11.011.

P.A.Santoni, P.Bartoli, A.Simeoni and J.L.Torero, Bulk and particle properties of pine needle fuel beds – influence on combustion, Int. J. Wild. Fire **23** (2014) 1076-1086, https://doi.org/10.1071/WF13079.

Committee on Fire Research Publ. 949, U.S. Nat. Acad. Sci. Res. Counc. 1961.

W.D. Callister Jr and D.G.Rethwisch, Materials Science and Engineering. An introduction, 9th Edition, Wiley Danvers 2014, pp. 838-852.

Drysdale D (2011), An Introduction to Fire Dynamics, (3rd Ed. John Wiley and Sons, Chichester).

Innovative Fire Fighting Strategy

Joseph Perry

Private R&D Consultant. 15 Habanim st., Ramat-Hasharon, Israel, {josephperry@bezeqint.net}

Keywords

Fire Fighting "Tank", Fire Fighting Bombs, Firefighting robot, Advanced Firefighting Technology gun

Abstract

Recent developments in heavy weapon design can be applied to fighting forest fires since both situations involve hazardous environments that present a high risk of damage to physical assets and extreme danger to human participants.

In military applications, heavy armored or robotic systems are designed to match the task at hand. For example, tanks are used to break out a fortified area, robots are used to clear mines and obstacles, and aerial or artillery bombing precedes every ground attack. Similarly, the proposed Fire Fighting Tank & Robots (FFTR) and Fire Fighting Bombs (FFB) would be designed to meet the rough duty of forest fire suppression. The FFTR crew (4) will carry out their firefighting activity without leaving the vehicle, exactly like the crew of a main battle tank during a military operation.

The advantages of using a FFTR include: the ability of operating within the fire itself (FF robots), the ability to clear its own path or to create firebreaks, and continuous operation in cooperation with chemical airdrops or other firefighting techniques, without the need to withdraw or protect human firefighters.

Furthermore, the proposed FFTR concept includes a unique liquid fire-suppressant delivery system, a “gun” that applies liquid and gas mixing technology developed for use in rocket technology thus having a firefighting capability of almost 10 times that of conventional fireman's hose. The same technology of liquid and gas mixing is used with the FFB to intensify the aerial firefight eight folds as compared to present methods. This means that a medium category, low cost, firefighting aircraft (Air-Crane helicopter) will be practically converted into a super heavy category aircraft (747-400 Supertanker), which is very expensive and difficult to operate.

To shorten the R&D stage, existing components and technologies will be used.

1. Introduction

Recent developments in heavy weapon design can be applied to fighting forest fires since both situations involve hazardous environments that present a high risk of damage to physical assets and extreme danger to human participants. In military applications, heavy armored or robotic systems are designed to match the task at hand (Sapaty, 2015). For example, robots are used to clear mines and obstacles, and aerial or artillery bombing precedes every ground attack. Similarly, the proposed Fire Fighting "Tank" & Robots (FFTR) and Fire Fighting Bombs (FFB) would be designed to meet the rough duty of forest fire suppression. Furthermore, the proposed FFTR concept includes an Advanced Firefighting technology (AFT) gun (AFT, 2022) that applies liquid and gas mixing technology developed for use in rocket technology thus having a firefighting capability of almost 10 times that of conventional monitors.

The FFTR will be operated by a crew of 4 firefighters: the commanding officer, the driver and two FF robots operators. The advantages of using a FFTR include: the ability of operating within the fire itself (FF robots), the ability to clear its own path or to create firebreaks, and continuous operation in cooperation with chemical airdrops or other firefighting techniques, without the need to withdraw or protect human firefighters.

To retard wildland fires, fire-retarding material is typically dropped into, or in front of the advancing fire from aircraft such as helicopters or airplanes. To be effective, the conventional Aerial Firefighting dropping must be performed from an altitude no higher than 60 m above the treetops (Lovellette, 2000). But such low flights are extremely difficult and dangerous, particularly at night. The FFB will be dropped from any appropriate altitude and be activated at the most effective distance above the fire.

The basic Fire Fighting Bomb structure will be similar to the conventional aerial bomb. The explosive fill will be replaced by a solid propellant (Sodium-azide) and a bulk of water. The heavy high fragmentation steel body

will be replaced by biodegradable material or aluminum shell. Once the requisite threshold has been reached or exceeded, the FFB fuse ignites the solid propellant resulting in a gas bursts into the water tank that forces the bomb shell to open. The opened FFB will release a huge fire-retarding aerosol cone precisely at an optimal level above the fire, resulting in effective rapid extinguishing as compared to conventional methods. This means that a medium category, low cost, firefighting aircraft will be virtually converted into a super heavy category aircraft, which is very expensive and difficult to operate.

To shorten the R&D stage, existing components and technologies will be used.

2. Fire Fighting Tank & Robots (FFTR)

2.1. The FFTR system

The FFTR system (see Fig. 1) will include the following components:

- Firefighting vehicle
- AFT main gun
- Two firefighting robots
- Camera drone

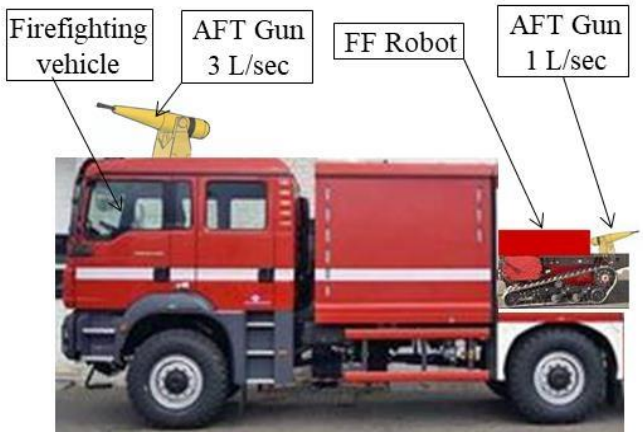

Fig. 1 Fire Fighting Tank & Robots (FFTR)

The FFTR will be operated by a crew of 4 firefighters: the commanding officer, the driver and two FF robots operators. The commanding officer will operate the main AFT gun and the camera drone.

2.2. Firefighting vehicle

The FFTR can be based on MAN TGM 4x4 fire truck, a Volvo FMX, a Mercedes Benz Actros and many other vehicles.

The chassis and the outer shape of the cabin will remain the original one, but all the other parts will be modified to fit the FFTR tasks.

The cabin interior will be fitted for the 4 crew members (instead of the original 6) and the rest of the space will be used for computers and control panels.

The cabin will be sealed against the chemical and biological contaminations and will have a Temperature and Humidity Control (THC) that maintains environmental conditions so that the firefighters can comfortably work in.

The estimated total FFTR weight will be 15000 kg (33070 lb.). Special design efforts will be made to develop a Rapid Deployment (RD) FFTR, weighting only 10,000 kg (22,050 lb.) that will be air transportable by helicopter.

2.3. The main AFT gun

The major innovation of the FFTR firefighting system is based on the Advanced Firefighting technology (AFT) gun (see Fig. 2), which is based on rocket technology and its application to liquid and gas mixtures (AFT, 2022).

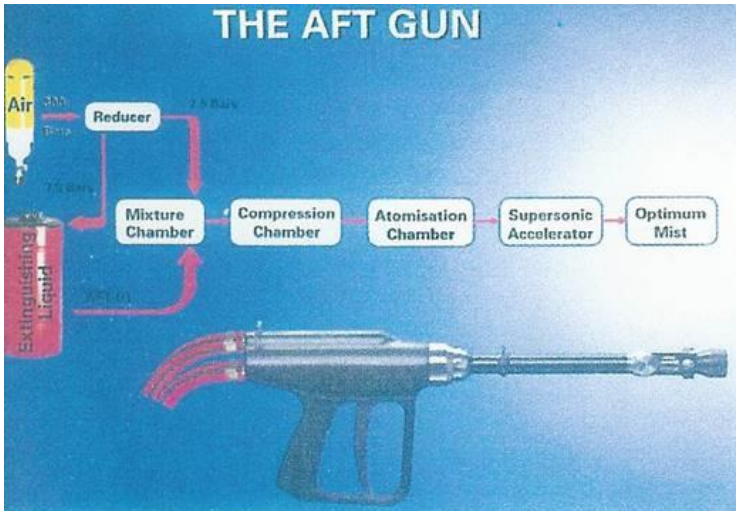

Fig. 2 The advanced firefighting gun

The AFT Gun technology creates a narrow distribution of an ultra-fine water mist (100-150 μm) that covers much larger surface area as compared to the conventional water monitor (almost 50 times). This results in rapid cooling of the burning area, due to extensive heat absorption by water evaporation. The combined effect of cooling and blanketing, results in effective rapid extinguishing of the fire. The AFT gun uses significantly less water (almost 10 times) as compared to conventional systems, hence reducing the total FFTR weight and extending time between resupplies.

The AFT gun generates a lot of steam that endangers the fire-fighters in their direct fire extinguishing actions. Operating from the protected FFTR and using the FF robots, solves this problem in a very effective way.

The roof mounted main AFT gun will be developed similar to the existing one, but with larger flow rate and lancing distance.

The main AFT gun will be mounted on a special, remotely controlled weapon station, similar to the medium caliber weapons installed on any type of military vehicles.

2.4. Firefighting robot

To shorten the R&D stage, an existing robotic platform can be used such as the TC800 FF Colossus, among others (see Fig. 3).

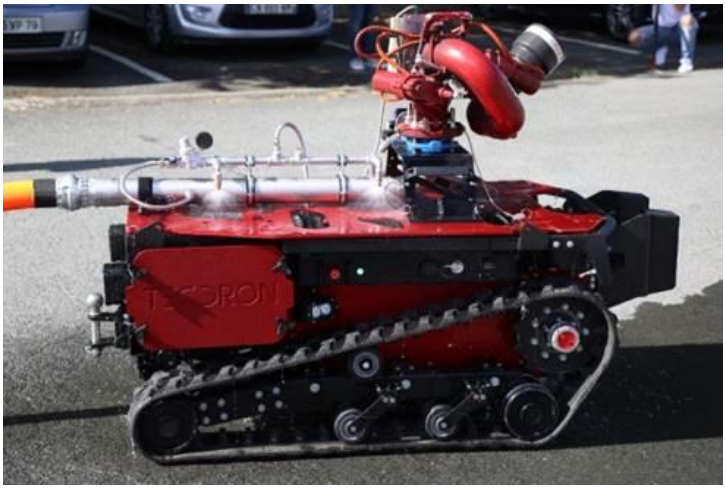

Fig. 3 Firefighting robot TC800 FF Colossus

TC800 FF is a remotely operated robot with autonomous navigation capabilities designed to assist fire-fighters during operations.

The FF robot's upper deck will be used for the installation of the existing AFT gun, a water tank and pump.

Most of the firefighting robots in development or being used today are tethered by a fire hose which supplies water, allowing continuous operation with a running time of 2-4 hours (see Fig. 4).

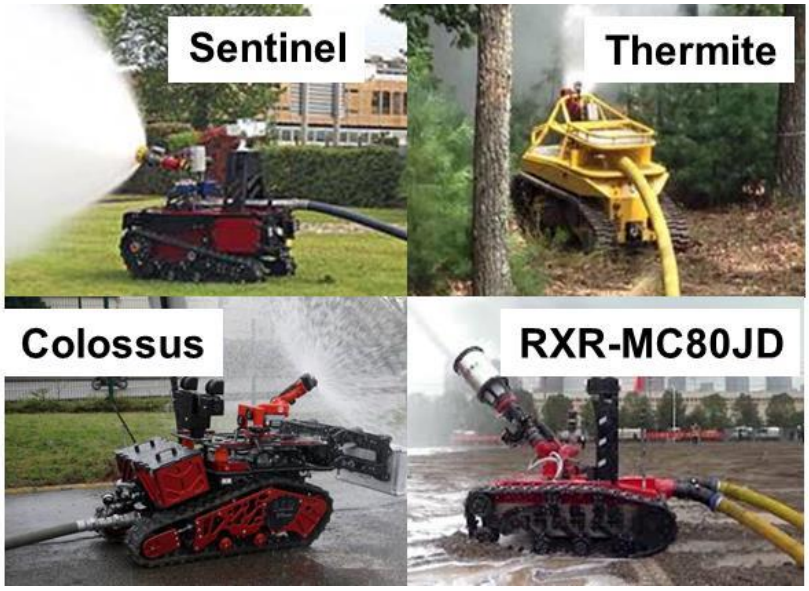

Fig. 4 Firefighting robots tethered by a fire hose

This heavy and relatively rigid hose disrupts the robot's maneuvering to overcome obstacles, especially in forested area.

One of the few water-autonomous firefighting robots is the MVF-5 U3 Multifunctional Remote Controlled Robotic System. It is equipped with 2500 l water tank but weights as much as 16000 kg and is very robust and slow.

The proposed firefighting robot will be equipped with AFT gun which uses significantly less water (almost 10 times) as compared to conventional systems. For example, the proposed robot equipped with 250 l will have the same firefighting capability as the MVF-5 U3 Robotic System but weighting only 1300 kg.

This unique quality enables the robot to be air-transportable taking its place immediately with the first attack, which is the most important to prevent fire expansion.

The FF robot will be equipped with special tools to cut trees and bushes for fire lane formation and FFTR's pass-way clearance similar to these installed on Russian Uran-6 (see Fig. 5).

Fig. 5 Uran-6 unmanned multifunctional demining system (Army 2021)

At the front of the Uran-6, there is one bulldozer blade and standard Flail tool, the heavy metal parts (chains and balls) of which will be replaced by a flexible part of the fire bat.

3. The Fire Fighting Bomb (FFB)

3.1. Hybrid Fire Extinguishing Systems (HFES)

Hybrid media is a combination of inert gas, typically nitrogen, and atomized water that creates an atmosphere that does not support combustion (Raia 2014). The inert gas is used to atomize the water into small, 250 µm (10 µinch) droplets. The atomized water droplets provide a large available surface area for heat absorption, and are easily converted to steam to provide cooling and oxygen dilution.

Fig. 6 Hybrid fire extinguishing nozzle discharging

The hybrid media discharge is regulated by nozzles operating at a controlled nitrogen pressure that controls the discharge rate. Water is delivered to each nozzle at a controlled flow rate, mixed with the nitrogen, and atomized into small droplets (see Fig. 6). The longer suspension time, and the nitrogen, makes Hybrid Fire Extinguishing Systems effective on concealed or shielded fires. In many instances, these fires would not be reached by larger droplets that tend to fall directly to the ground. The cooling effect of water mist takes place when the water mist droplets absorb the heat radiation from the fire. Nozzles discharge fine water mist at high velocity wetting the fuel and the area around the fire. The pressure employed in the water mist fire protection system is a key aspect in the fire extinguishing quality of water mist. Oxygen displacement happens at the heart of the fire when the water mist droplets turn into vapor and take oxygen from the fire.

The nitrogen is stored in high pressure canisters but can be also generated by Sodium-azide reaction. Sodium-azide is the gas-forming (nitrogen) component in many car airbag systems. Once the requisite threshold has been reached or exceeded, the airbag control unit will trigger the ignition of a gas generator propellant to rapidly inflate a fabric bag.

These beneficial water mist attributions were used for Fire-Fighting Bomb (FFB) development.

3.2. Fire Fighting Bombs (FFB)

The combination of climate changes and the expanding human development in the wildland-urban interface create devastating fires that are burning and spreading more quickly than they did 20 years ago. To retard those fires, fire-retarding material is typically dropped into, or in front of the advancing fire from aircraft such as helicopters or airplanes.

The basic Air Fire Fighting Bomb (AFFB) structure is depicted on figure 7.

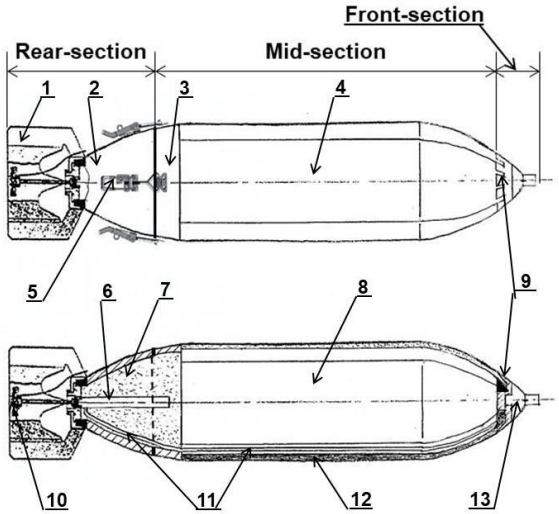

Fig. 7 The Fire Fighting Bomb basic structure

The explosive fill will be replaced by the Sodium-azide propellant and a bulk of water. The heavy high fragmentation steel body will be replaced by biodegradable or aluminum parts.

Once the required gas pressure is exceeded, the FFB case disintegrates, creating an ultra-fine water mist similar to the HFES nozzle (see Fig. 6). Exactly as the AFT technology this water mist will cover an enlarged surface area as compared to the conventional aerial firefighting resulting in effective rapid extinguishing using significantly less water as compared to conventional methods.

To be effective, the conventional Aerial Firefighting dropping must be performed from an altitude no higher than 60 m (200 ft.) above the treetops. But such low flights are extremely difficult and dangerous, particularly at night. Most of the aviation-related wild-land firefighting fatalities results from failure to maintain clearance from terrain, water, or objects. The FFB can be dropped from any appropriate altitude and be activated at the most effective distance above the fire (see Fig. 8). This will eliminate completely the aerosol losses and will increase the fire extinguishing efficiency. In case of unexploded FF bomb, there will be no human casualties due to the fact that FF robots will operate on the ground.

Fig. 8 FFBs opens on an optimal level above the fire

To demonstrate the FFB fire extinguishing efficiency we compare it to Erickson S-64 Air-Crane fire-fighting helicopter. The Air-crane can be fitted with a 2,650-gallon (~10,000 liter) retardant material tank to assist in the control of bush and forest fires.

Let's take as an example a 200 L (66 gallon) FF bomb. The estimated weight of the external body and the propellant will be approximately 50 kg (110 lb.), so the total weight will be 250 kg (551 lb.). The Erickson S-64 Air-Crane helicopter can carry 40 of such bombs at 10,000 kg (22,050 lb.) total weight.

The FFB efficiency will be similar to that of the AFT gun (10 times higher) but to be on a safe side, let us assume a lower value of 8. The outcome of this assumption is that the fire-fighting capability of 200 L FF bomb will be equal to 1600 L of the conventional water dropping. If we multiply this water volume by the FFB number (40) we get 64000 L, which is similar to water carrying capacity of 747-400 Supertanker.

This means that a medium category, low cost, firefighting aircraft has been virtually converted into a super heavy category aircraft, which is very expensive and difficult to operate.

4. References

AFT, 2022, https://aftwatermist.com/technology-2

Army Recognition Group, 2021, "Uran-6 unmanned multifunctional demining system". https://www.armyrecognition.com/

Lovellette Greg, 2000, "Safe Drop Height for Fixed-Wing Air Tankers", USDA Forest Service, http://fsweb.mtdc.wo.fs.fed.us

Raia P, Gollner M, 2014, "Literature Review on Hybrid Fire Suppression Systems", University of Maryland, Fire Protection Research Foundation, One Batterymarch Park Quincy, Massachusetts, U.S.A. Web: www.nfpa.org/foundation

Sapaty Peter, 2015, "Military Robotics: Latest Trends and Spatial Grasp Solutions", International Journal of Advanced Research in Artificial Intelligence 4(4). DOI:10.14569/IJARAI.2015.040402

Lessons from the 2021 Fire Season: An Opportunity for Greece to Reform its Wildfire Risk Governance

Palaiologos Palaiologou*[1]; Kostas Kalabokidis[2]

[1]*Department of Forestry and Natural Environment Management, Agricultural University of Athens. Karpenisi, 36100, Greece, {palaiologou@aua.gr}*
[2]*Department of Geography, University of the Aegean. Mytilene, 81100, Greece, {kalabokidis@aegean.gr}*

**Corresponding author*

Keywords

Large-scale fires; fuel management; wildfire resilience; climate change adaptation; settlement protection.

Abstract

The 2021fire season in Greece was disastrous in terms of area burned (140,000 ha), from six large-scale events (>10,000 ha) and one mega-fire in Evia Island (46,000 ha). These fires burned under extreme drought conditions and paradoxically, with moderate to low wind speeds, mostly inside low elevation conifer forests (*Pinus halepensis*) and shrublands. The concurrent burst and propagation of several large-scale events lead, once again, to the collapse of the firefighting mechanism, like what happened during the 2007 fire season when more than 260,000 ha burned. As a result, wildfires of 2021 were extinguished only when they reached the sea (Evia) or previously burned areas (western Attica), with firefighting forces completely unable to successfully contain them for weeks. The large number of reinforcements from other countries helped the government officials to understand and clarify (after debriefing) that with the current firefighting operational philosophy of the Greek Fire Service, it is impossible to contain large-scale wildfires. They detected several issues, including the total dependence on airborne firefighting means (Greece had during 2021 one of the largest aerial fleets in Europe), the inability of firefighters to operate inside forested areas, the prohibition of backfires, the slow creation rates, or complete lack, of vegetation clearings for creating new fuel breaks during firefighting, and the lack of appropriately previously treated areas. This sparked a debate among political parties and the society of what can Greece do from now on to prevent future mega-fires that can have devastating economic effects not only to the local population (e.g., northern Evia, an island that has based its local economy to forest products and recreational tourism), but also to the country's economy (>4 billion euros in 2021). Another important issue is the environmental impact caused by the loss of forest carbon pools, soil loss and erosion, increased water runoff and degradation of the aesthetic quality, all having a long-lasting effect on the affected areas. The above lead the Greek Government to take a series of measures that were proposed, including legislation changes, administrative organization reforms and adaptation of firefighting operational tactics. A breakthrough is considered the re-creation of six special forest fire operation crews (a total of 500 people) following the standards of the US smokejumpers or hotshots' crews. These crews are foreseen to be allowed to use backfires, after a necessary planned legislation reform. Another important legislation change was the simplification of bureaucracy that will enable landowners outside city limits to easily perform mild fuel reduction operations inside their property, currently illegal without permission. Despite these changes, an important component of improved fire risk governance is still missing. Fuel reduction is applied at the wrong scale, with inappropriate treatment methods, without proper planning and measurable outcomes and to landscape parts that can hardly influence fire propagation and intensity. In this work, we provide the context and a set of proposals and measures for fuel management that we believe are missing and if applied, can enhance prevention, and improve the firefighting effectiveness, considering ecological, economic, and operational issues.

1. Introduction

The importance of forest management in mitigating large forest fires risk for the protection of human lives and the wildland-urban interface (WUI) is increasingly emphasized. It is a fact that Mediterranean climate regions experience an ever-increasing trend for creating new and/or expand existing human settlements inside or close to natural areas which, in turn, cause pressures on the environment with the introduction of alien to native vegetation species, deforestation and human activities in wildlife areas that increase the fire risk (Moreira et al. 2011). As a result, the mixing of natural and human systems has created densely populated landscapes with large amounts of fuel that will certainly be affected by difficult to suppress near-future large-scale wildfires. The combination of forest cover increase, reduction of the annual recoverable timber and the consequent

accumulation of dead and live biomass (Figure 1) indicates the need to increase the annually managed area to reduce the rate of spread and fire intensity in locations where wildfires can damage residential areas, cultural monuments, ecological sites and values, and ecosystem services.

Figure 1: Typical conditions of unmanaged low-elevation coniferous forests in Greece, having large quantity and continuity of dead and live fuels

The recent extreme wildfire season of 2021 has prompted forest management authorities and policy makers of Greece to reconsider the existing policies regarding fire risk governance. Of all the measures proposed and implemented so far by the Greek Government and other public agencies, the least emphasis has been given to the fuel reduction efforts and especially, how they should be applied to achieve a change in future fire behavior that can be utilized to improve the efficiency of firefighting. Recently, the Greek Government announced a 50-million-euro program that will fund fuel reduction and fire protection projects, but it is still unclear how these projects will be allocated on the landscape, what will be their size and arrangement, what forested ecosystems are eligible to receive these projects, what is their expected and measurable impact on the behavior of future wildfires, who will apply them and with what management methods.

With this work, we attempt to advice and guide the Greek Government's effort to plan and fund these projects and avoid pitfalls that will result in reduced effectiveness, rare or no encounter with future fires, and failure to protect settlements and other values-at-risk. In addition, we will start by describing the main lessons learned during and after the 2021 fire season and describe how they guided so far, and how they will, government efforts to improve fire risk governance and implement changes to established outdated forest (and fire) management policies of 50 years ago.

2. Lessons learned from forest fires of 2021

The most valuable lesson learned, especially for the cases when large-scale wildfires were approaching or burning inside the WUI, was that the existing firefighting tactics of waiting along the roadside, avoid getting into forested areas away from the road network, and spraying parts of the fire front or flanks with water, is a failed strategy. Not only it cannot contain or stop a typical raging large-scale wildfire with flame lengths of up to 50 m and spread rates of up to 10 km/h, but it keeps an important number of firefighting forces occupied to a lost cause. In addition, by giving emphasis to a passive and narrow scale strategy to protect homes and properties instead of an active that involves operational planning at a landscape level and inside forested areas, it gives space and time to the wildfire to escape or surpass the still suppression units. When this happens, firefighting forces start chasing the fire or desperately call for aerial support. The large dependence of ground

forces on aerial support to achieve alteration in fire behavior leads to requests that not only do not ensure airborne means are necessary but also are not in clear alignment with a wildfire's incident strategy and with agency and interagency general fire management goals and objectives (Stonesifer et al. 2021), increasing aircraft and personnel fatigue. As a result, the Greek Government decided to create a special firefighting unit with 500 persons divided into six crews, with training in the US to learn modern firefighting tactics, including the backfire technique (currently prohibited, but soon to be legalized).

Before the 2021 fire season, when homeowners and landowners wanted to protect their property from wildfires with preventive fuel treatments, they were required to either request a permission from the Urban Planning Agency, if their property was within urban area limits, or from the Greek Forest Service (GFS) if it was outside. For both cases, the owners were obliged to file a technical study with the trees that needed to be cut and then, after a time-consuming process (bureaucracy and corruption were the two reasons for multi-year delays in granting those permissions), get the permission; otherwise, they could have serious legal issues. Owners were reluctant to go through that process since it required both time and money and as a result, they let their property without any fuel treatment. The simplification of bureaucracy that enables landowners outside city limits to easily perform mild fuel reduction operations is an important legislation reform.

Finally, evacuation of settlements has become the mainstream policy of the Greek Civil Protection agencies. To avoid fatalities from wildfires approaching the WUI or urban boundaries, as was the case of the 2018 small scale event (1,300 ha) of Mati at the outskirts of Athens that killed more than 100 people, large-scale evacuations happen even in cases where there is low or no probability of the fire to enter the settlement.

3. How fuel treatments should be applied in Greece to improve their efficiency?

The three pillars for the suppression of large-scale wildfires are (Figure 2): 1) the combined suppression from ground forces and airborne means, 2) in areas with previously implemented fuel management, and 3) by applying passive fire suppression and indirect firefighting, such as the backfire technique. Prerequisite for the above is the existence of strategically allocated fuel treatment units, with adequate extent and treatment intensity. As the international experience shows, areas receiving fuel management must be able to drastically reduce the fire rate of spread even without fire suppression. To achieve this, a series of conditions must be met.

First, local government agencies have neither the planning expertise nor the technical skills to perform fuel treatments. We propose the entire fuel treatment funding to be transferred to the GFS, an agency with the necessary skills to accomplish this task, after a substantial increase from 25 million euros per year to at least 50 million euros. The GFS should oversee the application of the planned fuel treatments on all lands, even without the consent of the landowners. To allow this, a legislation reform is required. This is necessary because the fragmented landscape among multiple owners does not leave much space for consensus and collaboration; and as a result, the planned projects can be cancelled. The planning of project allocation should be done by considering (Palaiologou et al. 2021): a) the dominant weather patterns of each area, b) the vegetation and fuel conditions, c) the possibility of encountering a future wildfire, and d) their estimated impact on fire spread and intensity. This can be accomplished only if stochastic fire behavior modelling is applied. By simulating thousands of wildfires, we can account for different ignition locations and weather scenarios, and reveal hidden trends and patterns on the landscape from fires that have not happened yet but are highly possible to occur in the near future.

After the best candidate sites are found, it is necessary to consider the scale and arrangement of the applied projects and also, the fuel treatment methods applied to maximize their efficiency. Small scale or isolated projects should be avoided, and the treated area should be large enough to counter the scale of a large wildfire. Projects should form a network or create a protective "umbrella" around values-at-risk or settlements if this is the fuel treatment priority (Ager et al. 2013). One of the most important challenges for forest managers is to consider and decide between competing landscape management priorities, and such a challenge creates a complex spatial trade-off problem (Ager et al. 2017). Developing a broader set of forest management priorities tailored to specific areas should be based on fire regimes, human values, and land uses. Different arrangement and scale of fuel treatments and management methods are required when the priority is settlement protection vs. strategic containment vs. ecological restoration of forested ecosystems vs. timber production (Ager et al. 2013).

Regarding the fuel treatment methods, the combination of mechanical treatments, mostly thinning, pile burning, and grazing is a promising choice that does not require legislative reforms. Ideally, prescribed fire can further reduce implementation costs, but it is currently illegal. To avoid hazardous fuel accumulation, logging residuals should be either lopped and scattered or piled to be burned when conditions allow it. Also, pruning of trees that are left after thinning is suggested to break the continuity of the ladder fuels. Finally, the forests most in need to receive fuel treatments are the low elevation conifer forests (*Pinus halepensis* and *P. brutia*), especially those mixed with shrubs in the understory. In addition, cold tolerant species such as fir (*Abies* spp.) on higher elevations present an aggressive expansion against other forested ecosystems. Combined with climate alterations and severe droughts, these young coniferous forests present an ever-increasing fire risk. Fuel management is required there as well to restore the ecological balance (these ecosystems were intensively treated up to the 1980s with traditional agroforestry practices, including the use of fire to clean the forest understory).

Figure 2: Combined suppression from ground forces and airborne means near roads and fuel breaks

4. Conclusion

The main problem is that Greece perceives wildfires as a suppression problem rather than a forest management one. Instead of covering fire suppression with a "veil" of heroism that expects from the "heroes" to enter the fire like ancient warriors in battles, we propose the use of improved firefighting tactics and combine them with preventive forest management. Claims that the problem of mega-fires and their transmission into settlements will be solved by hiring more firefighters or by purchasing additional aerial firefighting equipment, unfortunately, do not recognize the nature and ecology of wildfires, nor are they aware of the latest scientific data. Wildfires are a complex problem and require the synergy of many actors, methodologies and practices to mitigate their dire effects, and only partially. It is considered *a priori* knowledge that there is no way to eliminate fires from the fire-adapted ecosystems of Greece, and they will continue to manifest no matter how many measures are taken. It is impossible to deal with each ignition, or with simultaneous high-intensity wildfires, regardless of how many firefighters and aircraft the country possesses. Therefore, fuel management with proper application is crucial to improve the chances of successful containment of large-scale wildfires.

5. References

Ager, A.A., Vaillant, N.M. and McMahan, A., 2013. Restoration of fire in managed forests: a model to prioritize landscapes and analyze tradeoffs. *Ecosphere*, 4(2), pp.1-19.

Ager, A.A., Vogler, K.C., Day, M.A. and Bailey, J.D., 2017. Economic opportunities and trade-offs in collaborative forest landscape restoration. *Ecological Economics*, **136**, pp.226-239.

Moreira, F., Viedma, O., Arianoutsou, M., Curt, T., Koutsias, N., Rigolot, E., Barbati, A., Corona, P., Vaz, P., Xanthopoulos, G. and Mouillot, F., 2011. Landscape–wildfire interactions in southern Europe: implications for landscape management. *Journal of environmental management*, **92**(10), pp.2389-2402.

Palaiologou, P., Kalabokidis, K., Ager, A.A., Galatsidas, S., Papalampros, L. and Day, M.A., 2021. Spatial optimization and tradeoffs of alternative forest management scenarios in Macedonia, Greece. *Forests*, 12(6), p.697.

Stonesifer, C.S., Calkin, D.E., Thompson, M.P. and Belval, E.J., 2021. Is This Flight Necessary? The Aviation Use Summary (AUS): A Framework for Strategic, Risk-Informed Aviation Decision Support. *Forests*, **12**(8), p.1078.

Local population safety challenges and property self-protection issues during the mega-fire of 2021 in North Euboea, Greece

George Eftychidis*; Vassiliki Varela

KEMEA 4, P. Kanellopoulou str. Athens GR-101 77 Greece,
{g.eftychidis, v.varela}@kemea-research.gr

**Corresponding author*

Keywords

North Euboea fire, property safety, self-protection

Abstract

The fire in North Euboea in August 2021 was burning continuously for two weeks and destroyed an area greater than fifty thousand hectares, Greece's biggest ever from a single fire. The response planning of the Greek Civil Protection and the public fire management mechanism urged for preventive evacuation even in cases the fire front was tens of kilometers away from the villages requested to be evacuated. This was dictated by the loss of hundred two people in the fire of Mati three years ago (2018). The locals criticize that the government's decision left firefighters without permission to fight the flames even in the case where lives weren't threatened. The ad-hoc reaction of the local rural population, who self-organized themselves and substituted the absence of the public fire services, saved several houses and properties that would be condemned to be burned due to the diehard evacuation planning. Analysis of the information gathered from local authorities and citizens who participated in these ad-hoc response teams proves the potential of involving the local population as first responders in large wildfires and fire emergencies in the wildland-urban interface and rural areas.

1. Introduction

Wildfires severely affect the communities and the properties developed in the wildland-urban interface (WUI). Thus, these communities, whose living is directly linked with the natural landscape and the surrounding forest, must become more resilient and proactive about fires. A sound way to achieve this is to develop a Fire-Adapted Community, meaning a community that can deal with a wildfire with little or no assistance from firefighters (Ingram, 2015).

Local communities can be adapted to wildfires in different ways. On many occasions, the response of the firefighting mechanism focuses strictly on protecting structures and houses, which allows a significant growth of the firefront, developing heat loads beyond any control and causing substantial human lives and property losses. On other occasions, social power, environmental resilience, and fire management can be combined to improve the situation (Marey-Perez et al., 2021; Moritz, M.A et al., 2014; Twidwell et al., 2019).

Fire spread by a combination of a moving firefront and airborne burning and glowing embers. Building losses during wildfires occur because of structure ignition and exposure due to embers (called firebrands), radiant heat, and direct flame contact. Embers are light enough to be blown through the air and can result in the rapid spread of wildfire by spotting (Quarles L.C. et al., 2010, CALFIRE,n.d.), in which case the embers are blown ahead of the active firefront, starting new fires). In the case of villages and settlements where the peripheral buildings create a wall to the rapid fire propagation, the structures in the perimeter are exposed to radiant heat and flame contact. There it is usually concentrated, the firefighting effort. However, spotting embers may travel, land, ignite vegetation or accumulated debris inside the village or settlement, or even enter the home or attic through openings or vents, igniting furnishing or combustible debris in those locations. The roof is considered the most vulnerable design element, and the construction material is a critical factor in the structure's resilience. Houses with wood or shingle roofs are at high risk of being destroyed during a wildfire. Vents create openings for flying embers, while windows often break even before the home is on fire due to the flames' heat. The presence of homeowners can prevent the ignition or extinguish spot fires that cross over the fire defense line at the initial

stage. This opportunity is lost in case a flat evacuation order is issued. The above is empirical knowledge broadly available in the communities thriving in mountainous areas and near the forest.

In Australia, the "Prepare, Stay and Defend or Leave Early" policy emphasizes that in the case of bushfires, it is often the safest option for people to remain in their homes in case they are caught in the path of a bushfire. They are thus protected from the radiant heat of the oncoming fire and can take measures to protect their homes from being destroyed by the fire. (Loh, 2007)

Recent major wildfire disasters in Europe reveal that government authorities and civil society, notably rural communities, are not sufficiently prepared and coordinated to prevent and reduce the risk of wildfires. Such coordination is necessary to defend local communities and rural assets at stake against the adverse direct and indirect impacts and consequences of wildfires.

A degree of self-government is a characteristic of many such communities, expressed in the form of rejection of interference from outside, represented by externally generated rules and regulations. This stems from the fact that the population in rural and working landscape areas has developed the ability to be sufficient in self-protecting their villages due to their lifestyle. These communities conceptualize trust differently as well. In some cases, they may have minimal political confidence in government agencies but relatively high social confidence in local authorities, volunteer groups, or their neighbors. (Billings,2021)

1.1. The North Euboea fire event

Fires are not uncommon in the pine forests of Euboea Island, but they swelled to massive proportions in the summer of 2021. Forests cover 23% of Evia, with 33% of this land burned (8% of the island's 'area) and approximately 10% of this area being agricultural land. The fire weather conditions were characterized by an extreme heatwave affecting Greece, Turkey, and the southern Balkan peninsula, lasting from the last days of July until the first ten days of August 2021. The heatwave was the worst recorded in the past 30 years.

The fire started in the afternoon of 03/08/202 and raged for two weeks, burning tens of thousands of hectares before it was contained and secured on the 17th of August. Despite low winds, due to the accumulated forest fuel loads developed because of the inadequate management in most of the forests in the area, flames wound their way up and down mountains and around villages, devouring one-third of the island's ' pine forests and olive groves. As a result, Evia's’ wildfire is the country's most significant ever single fire. The total burned area was 51245 ha, and the affected area comprised two municipalities: Istiaia-Aidipsos & Mantoudi-Limni-AgiaAnna.

The fire extensively consumed the area's primary production, including timber, honey, resin, olives, and figs, and destroyed several assets, infrastructures, and touristic investments. However, the fire's extent, the size of the burned area, the number of the burned houses (150), and the burning of their surroundings were limited.

The result is quite attractive since it was achieved despite the policy adopted in 2021 by the General Secretariat of Civil Protection and the Hellenic Fire Service to evacuate several villages consistently in the vicinity of an active fire. The purpose of this policy is to avoid fatalities at any expense. The emphasis on evacuation resulted from heated political clashes in the aftermath of the East Attica fire of July 23, 2018, in the settlements of Neos Voutzas and Mati, which had caused 102 fatalities (Xanthopoulos G., Athanasiou M., and K.Kaoukis, 2022).

Due to the previous fatal fire in Mati (2018), with a hundred two lives lost, the government prioritized evacuations over the preservation of land. This was partly successful since only two fire-related deaths were reported in Euboea. However, multiple reports show that this diehard decision of the government left firefighters without permission to fight the flames even in case human lives weren't explicitly in danger. The General Secretariat of Civil Protection gave frequent orders to evacuate villages via 112 service messages during the fire. However, many residents ignored the alerts and stayed in their villages to defend their homes and properties. Their decision limited the damages to the houses and structures and contributed to the effectiveness of response at the local scale during the fire.

Several people from the villages challenged by the flames of the Euboea fire and stayed to defend their town, when interviewed by the media, claimed that if they had evacuated their villages, as the civil protection recommended, everything would have been burnt down to ashes perhaps even two days sooner. (Frost-Euronews, 2021).

During the fire and after its suppression, many residents and local citizens criticized the government's ineffective and passive reaction, which they consider to be the main reason for the unprecedented disaster. They experienced a situation where instead of the public firefighting service, volunteer fire corps and locals who defied evacuation orders and remained behind, fighting the fires with tree branches, garden hoses, and any means they had to ferry water have saved hundreds of houses and thousands of hectares from being burned. (Schmitz- DW, 2021; Frost-Euronews, 2021)

2. Methodology

The methodology used for gathering information and processing data to extract relevant knowledge comprised of the following techniques:

- Desk-based research from public sources, news press, and electronic media, including websites, online videos, and social media.
- Earth Observation data during and after the fire, including satellite imagery and information from relative data services.
- Collection and analysis of UAV recordings from villages within the fire perimeter, having more than one house burned, and representing various types of landscape and vegetation forms and
- Extended field visits focused on collecting testimonial information and recital of events from more than 45 residents who experienced the fire crisis in their villages. Open-ended questions were used in an interview format also linked with contextual discussions. The information regarding the exposure of the burned houses, the features (vulnerabilities) of the surrounding environment, and the fire proneness of the landscape on the broader area was recorded on-site, post-processed, and analyzed.

In addition, information on fire behavior and propagation characteristics were collected based on the observations of the personnel from local authorities and volunteer firefighters who substituted the firefighting mechanism inside the villages during the fire.

The analysis aimed to gain, as extensively as possible, an understanding of the fire conditions to which the properties and their owners were exposed, the safety challenges they faced, and their assessment of the situation. Organizational prerequisites, societal and solidarity aspects, good practices for self-protection, and interaction with the local authorities were elaborated with the residents of the villages in the context of locally organized open discussions.

3. Results

The local population of the North Euboea's villages is familiar with living in a forest and agricultural region and forest fires. Due to their professional activity and relation with the forest and rural environment, they have local knowledge of the forest. They have the skills required for addressing an active fire situation. They own and can use agricultural machinery, pumps, small tanks, etc., which help protect properties and infrastructure without public services. The protection of the houses was facilitated by the fact that most of the dwellings and structures in the area were made of concrete, although they may also have some wooden elements. The information analysis showed that several isolated properties (mainly villas or farms) exist in the vicinity or inside the forest in this type of rural landscape. The mainland areas fall in the classic Mediterranean villages, with dense construction elements developed around a central "village square." The outer area of these villages is surrounded by pine forests (Pinus brutia) and patches of olive trees. In the coastal areas of the North Euboea, like in most of the touristic regions in Greece, the WUI is similar but has a linear than circular development with the forest surrounding the built part from one side.

Based on the information gathered, the damage caused by the fire around many settlements and other points of economic activity (e.g., orchards with houses or other buildings, farms, etc.) was limited compared to the fire consequences to their surroundings (Figure 1). This mainly concerns settlements and places reached by the fire after the second day. In this case, the residents had the time to organize themselves and respond to the fire almost exclusively on their own.

In most cases, especially after the second day, the residents did not follow the warnings and prompts for evacuating their places and were self-organized, deciding to remain in their villages. This spontaneous reaction, supported by the capabilities of the rural population, led to saving many houses and properties. Self-organization in ad-hoc groups of volunteers and solidarity with neighbors' property was proven the critical success factor for protecting homes and properties.

Several houses were protected this way by these self-organized ad-hoc citizen groups. As a result, they experienced no damage, even if placed in the middle of burning dense and high vegetation. On the contrary, uninhabited or evacuated houses within the boundaries of the settlements or located in remote forest areas suffered significant damage (Figure 2).

For safety reasons, camps and touristic resorts inside the forest were evacuated immediately following the official warning for an urgent evacuation order. All assets falling in this category were utterly burned down to ashes.

Figure 1. Houses with minor damages due to the construction material and existence of defensible space

Figure 2. Houses with significant damage due to pure or aged construction materials

4. Discussion

The involvement of local communities in forest fire management, the use of their skills, and capabilities, such as the contribution of their resources to protect properties and infrastructures in the absence of public civil protection services, need to be considered within the wildfire management organization. However, this can be

an efficient strategy, particularly in the case of villages and settlements whose populations thrive and work in the forest.

Homeowners and the local populations are the first responders and the critical stakeholders for addressing the lack or the inefficiency of the public firefighting and civil protection organization. In light of the ongoing climate change and global warming, it is imperative to invest in the knowledge, skills, and capabilities of the local communities, as a complementary resource, in managing large-scale wildfire events. Civil protection organizations must integrate the local society into the fire management cycle by exploiting all existing capabilities and human resources in holistic fire protection and resilience plan.

Moreover, wildfire management regarding the security and protection of local communities needs to be addressed mainly at the local level. The community needs to be prepared and ready before the fire occurrence to manage the fire threat efficiently and effectively. Adequate maps per community/settlement need to be developed, prioritizing the protection need of the municipalities in the broader region. Assets at risk, location of vulnerable populations, and in-place sheltering possibilities need to be identified and communicated to the community and local authorities. Self-protection of villages entails the preparation of simple plans depicting who will stay on-site in case an evacuation is issued due to the fire and what they must do. Similarly, the plan needs to foresee who will evacuate and how. Such plans need to be updated, discussed, and shared within the community and with all stakeholders involved in fire management every year.

5. Acknowledgment

This research has been performed in the context of the European Research projects FIREURISK (https://fireurisk.eu) and RISKPACC (https://www.riskpacc.eu). These projects have received funding from the European Commission's Horizon 2020 research and innovation program under the Grant agreements No. 101003890 and No. 101019707, respectively.

6. References

Billings, Mark C.; Caroll, Matthew B; Paveglio, Travis B. (2021)." The "Strings Att "ched" to Community Difference and Potential Pathways to Fire Adaptiveness in the Wildland Urban Interface, Journal of Forestry, Volume 119, Issue 1, January 2021, Pages 13–27, https://doi.org/10.1093/jofore/fvaa042

CALFIRE (n.d.) Prepare for wildfire. Available at: ***https://www.readyforwildfire.org/prepare-for-wildfire/get-ready/hardening-your-home/***

Frost, R. Euronews (2021). Watch as people in Greece resist evacuation to battle widespread wildfires. Available at: https://www.euronews.com/green/2021/08/11/watch-as-people-in-greece-resist-evacuation-to-battle-widespread-wildfires

Goldammer, J.G., Mitsopoulos, I., Byambasuren, O., and Sheldon, P. (2013). Defence of villages, farms and other rural assets against wildfires: guidelines for rural populations, local communities and municipality leaders in the Balkan region. Published by the Global Fire Monitoring Center (GFMC) on behalf of the European and Mediterranean Major Hazards Agreement (EUR-OPA) Council of Europe. Available at: http://www.fire.uni-freiburg.de/Manag/Village-RuralAssets-Wildfire-Defense-Guidelines-2013-ENG-web.pdf

Ingram, Kim, (2015). Becoming a fire-adapted community. Available at: https://ucanr.edu/blogs/blogcore/postdetail.cfm?postnum=17201

Loh, E, (2017). "What does'the 'Prepare, Stay and Defend or Early policy mean for me?". Legal liabilities of emergency workers and emergency-service organisations in South Australia Bushfire Cooperative Research Centre.

Marey-Perez, M.; Loureiro, X.; Corbelle-Rico, E.J.; Fernández-Filgueira, C.(2021) Different Strategies for Resilience to Wildfires: The Experience of Collective Land Ownership in Galicia (Northwest Spain). Sustainability 2021, 13, 4761. https://doi.org/10.3390/su13094761

Moritz, M.A.; Batllori, E.; Bradstock, R.A.; Gill, A.M.; Handmer, J.; Hessburg, P.F.; Leonard, J.; McCaffrey, S.; Odion, D.C.; Schoennagel, T.; et al. (2014) Learning to coexist with wildfire. Nature 2014, 515, 58–66.

Twidwell, Dirac Wonkka, Carissa L.; Wang, Hsiao-Hsuan; Grant, William E.; Allen, Craig R.; Fuhlendorf, Samuel D.; Garmestani, Ahjond S.; Angeler, David G.; Taylor, Charles A.; Kreuter, Urs P.; Rogers, William

E. (2019) Coerced resilience in fire management, Journal of Environmental Management, Volume 240, Pages 368-373, ISSN 0301-4797, https://doi.org/10.1016/j.jenvman.2019.02.073. (https://www.sciencedirect.com/science/article/pii/S0301479719302245)

Quarles S.C., Valachovic Y., Nakamura M.G., Nader A.G, De Lasaux, (2010). Home Survival in Wildfire-Prone Areas: Building Materials and Design Considerations. University of California. Agriculture and Natural Resources Communication Services. Publication 8393, May 2010. ISBN-13: 978-1-60107-693-9

Schmitz, Florian/ DW (2021). Greece: Abandoned to the flames on Evia. https://www.dw.com/en/greece-abandoned-to-the-flames-on-evia/a-58860740

Xanthopoulos G., Athanasiou M.; and K.Kaoukis, (2022). Suppression versus Prevention: The disastrous forest fire season of 2021 in Greece. International Journal of Wildfire Magazine, Quarter 2, 2022, pp. 18-24.

Logistics challenges of approaching the wildfires with different fire vehicles

László Bodnár

Assistant lecturer, University of Public Service, Faculty of Law Enforcement, Institute of Disaster Management. 1101 Budapest, Hungary, krt. 9-11, {bodnar.laszlo@uni-nke.hu}

Keywords

Logistic, forest roads, fire trucks, tipping point, fire frontline, tools

Abstract

In order to protect human life, property and the environment from wildfires, professional and voluntary fire departments are the first interveners in Hungary. One of the major challenges of firefighting against wildfires is the logistics. Such a logistic challenge is the migration to the fire site with different fire vehicles. The logistic challenges of wildfires usually developed in rural areas, on dirt roads of the forest, away from the residential areas. These areas are difficult to approach with some fire trucks that are not specifically designed for these purposes. These difficulties affect the efficiency of firefighting. In the paper, the Author draw conclusions from the logistical difficulties of firefighting against wildfires that are suitable for proving the time loss of migration and to determine how the time loss affects the spread of a fire and the effectiveness of firefighting. The Author shows how the frontline ($T_{frontline}$) of a fire can change due to time loss (Δt) at 1 m/min, 5 m/min and 9 m/min fire propagation ($V_{fire\ propagation}$). By using a formula, the Author also calculate the size of frontline fire. As a result of the paper he determines the amount of time loss with a new method, which is related to the increase of fire frontline.

1. Introduction

According to The Global Risks Report 2022 created by the World Economic Forum, for the next five years, respondents again signal societal and environmental risks as the most concerning. However, over a 10-year horizon, the health of he planet dominates concerns: environmental risks are perceived to be the five most critical long-term threats to the world as well as the most potentially damaging to people and planet, with "climate action failure", "extreme weather", and "biodiversity loss" ranking as the top three most severe. (WEF 2022). Climate change is a challenge in many areas of science, society and life, so it also has an impact on the disaster management. The above mentioned climate change factors provide a greater opportunity to ignite the combustible fuel, which increases the risk of wildfires. The wildland as a natural area carries many social values in itself, so we protect it from fires (Almeida 2021).

Firefighting is often a long and complex process (Figueras 2015), the main stages of it is to stop the fire spread, to eliminate the flames and to supress the fire. In the process, firefighters face a huge number of logistical challenges (Jain 2020). Several researchers have investigated the logistic difficulties of firefighting. (Rácz, 2016), (Bodnár, 2016). The first deep investigation in the topic was carried out by (Restás 2003) in Hungary, who examined the effectiveness of increasing the number of firefighting interventions with a value - time function, but he also analysed the time elapsed during the steps of firefighting, the network of logistics bases and their distance. Other research focuses on threat of forest and vegetation fires and the possibilities of intervention (Bodnár 2019), and the forest fire detection (Bodnár 2018).

2. Methods

In order to achieve the research objectives, I studied the most important national and international literatures focusing on the topic of the logistics of firefighting. In addition, I have had personal consultations with various experts and participated in international scientific conferences and study tours. I presented my logical conclusions and results using histograms and diagrams. In illustrating the logistics problems, I made schematic diagrams and explanatory drawings, the analysis of it helped me to understand the mathematical foundations of

my efficiency analysis. During the logistic challenges of firefighting, I examined the effects of time loss caused by migration on poor quality roads. I also took pictures of poor quality roads on my observation plot (Figure 1).

Figure 1- Poor quality dirt roads in the forest, nearby a water source in Hungary.

In addition, I examined the extent and impact of time loss, caused by migration to the fire site on poor quality dirt roads. For my research, I edited a conceptual Figure (Figure 2) which shows how far a fire truck can travel on different types of roads in a given amount of time. I did not simply characterize the problem of time loss during marching, but I first related it to the increase in length of the burnt fire frontline.

To investigate the approach of fire site, I established my assumptions based on the experiences of drivers of fire trucks. According to drivers and relevant national legislations, a fire truck has an average speed of 60 km /h on driveway and an average speed of 20 km/h on dirt roads (Decree, 2011). The average speed of 20 km / h on dirt road is a third of the speed on a driveway, so there is a logical proportionality between the two values. Consequently, I consider the two values to be acceptable and authoritative during the research. After determining the speed of the fire trucks, I also have to assume a migration time. The average time to approach a fire site with fire trucks is 15 minutes in the European Union is (Müller, 2020). Based on my own analysis, the Hungarian fire brigades cannot yet fulfilling this in all cases, so during my research (schematic figure) I expect an intervention time of 20 minutes. Areas in literatures refer to so-called white spots as areas that are not approachable from a professional fire brigade during the specified 25-minute migration period (Berczi and Papp 2017). This time is an upper limit, so I consider the 20-minute long marching time I have chosen to be logically acceptable.

For my research, I edited a schematic figure (Figure 2), which shows how far a fire truck can travel on different types of roads. In the figure, the vertical axis indicates each route possibilities and how many km the fire truck can travel on a driveway. The horizontal axis shows the travel on dirt roads for the remaining time. The green line indicates the distances reached within 20 minutes (reality). The red line indicates the distance of 20 km (goal). The area between the green and red lines gives the difference in efficiency (Time loss).

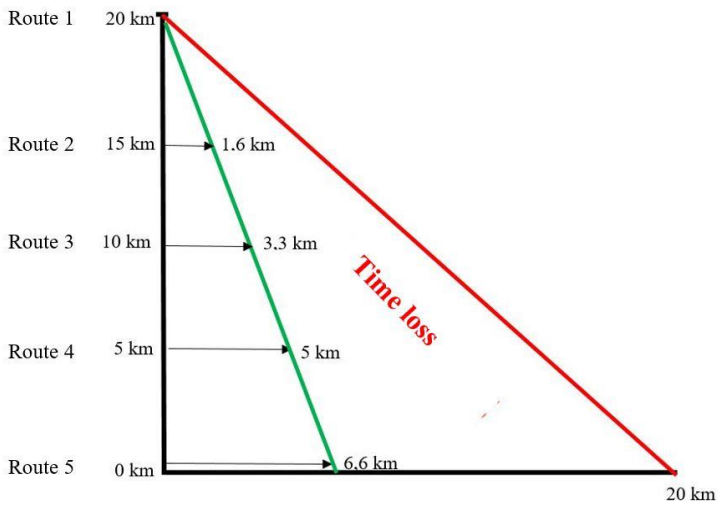

Figure 2- Schematic figure of different migration route combinations.

On *Route 1*, the approach of fire site is entirely on driveway with a speed of 60 km / h (in 20 minutes), so the maximum distance that a fire truck can be covered is 20 km. I consider it to be the most favorable condition. On *Route 5*, fire truck travels along the dirt road (with a speed of 20 km / h), so it cannot cover the distance of 20 km, only a fraction of it, which is 6.6 km. I consider it to be the most unfavorable condition. Of course this case is only a logical assumption, as all fire stations are located so as to be approach on driveways. The Figure also proves the logical conclusion that the more a fire truck travels on a dirt road, the less distance it takes in 20 minutes. I have plotted five different hypothetical route options.

I have already analyzed the best and the worst route options (Route 1 and 5), for the other routes traveled the distances change as follows. In Route 2, site approach will take place on a 15 km driveway and then on a 1.6 km dirt road (which would be 5 km on a driveway). This ratio is already 10 km - 3.3 km in Route 3 and 5 km - 5 km in Route 4. Figure 2 demonstrate my logical assumption that the site approach on a dirt road results in a significant time loss, which affects the effectiveness of firefighting. Table 1 illustrates the traveled distance in km (in 20 minutes) in six routes options. In addition, I also calculated the average speed of the fire truck on the different route options.

Table 1 - Approach to the fire site on different types of routes. Created by the author.

Approach to the fire site on different types of routes			
Routes	**Traveled distance (km)**	**Average speed**	**Elapsed time**
1.	20	60 km/h	20 min
2.	16,6	50 km/h	20 min
3.	13,3	40 km/h	20 min
4.	10	30 km/h	20 min
5.	6,6	20 km/h	20 min

In case of wildfires, fire trucks sometimes travel long distances on narrow dirt roads in order to approach a fire site, which is a significant time loss in terms of firefighting. This happened in Hungary in case of large fires in the Southern Great Plain (Kaskantyú, Törtel). Case studies have also been prepared on this topic (Bodnar, 2017). In the next chapter I will examine how much the length of the frontline fire increases as a result of the time loss.

3. Results

After the analysis of the site approach, I calculated (Table 2) how the frontline ($T_{frontline}$) of a fire can change due to time loss (Δt) at 1 m/min, 5 m/min and 9 m/min fire propagation ($V_{fire\ propagation}$). By using the bottom formula, I also calculate the size of frontline fire (conditions: homogeneous wildland fuel, calm wind, flat terrain).

$$T_{frontline} = 2x\Delta t x\, v_{fire\ propagation}\, x\, \pi \quad (1)$$

Table 2 - Changes in the frontline of fire during different fire propagations.

Changes in the frontline of fire during different fire propagations					
Time loss (min)	0	10	20	30	40
1 m/min	0	63	126	188	251
5 m/min	0	314	628	942	1 256
9 m/min	0	556	1 130	1 696	2 261

I would like to note that, from the modelling point of view of, fire propagation can only be characterized by a circular shape on flat terrain in case of homogeneous fuel and calm winds, in all other cases the ellipse shape should be considered as dominant (Rothermel, 1972). However, at ellipse, the increase in circumference is not linear but larger than in case of circle, so this proves my conclusion. In Table 2 I rounded my results for a more comprehensible illustration. As a result of Table 2, I conclude that, on the one hand, the longer the travelled distance decreases in 20 minutes, the more time loss will be (it makes sense). On the other hand, the more is time loss, the longer the length of the fire frontline will be. To illustrate my conclusion, I created Figure 3, where I illustrate the relationship between time loss and the increase in fire frontline at the fire propagation speeds (1 m/min, 5 m/min, 9 m/min) examined above. It is clear from the graph that as the lower velocity section increases, the length of the unnecessarily increasing frontline changes linearly.

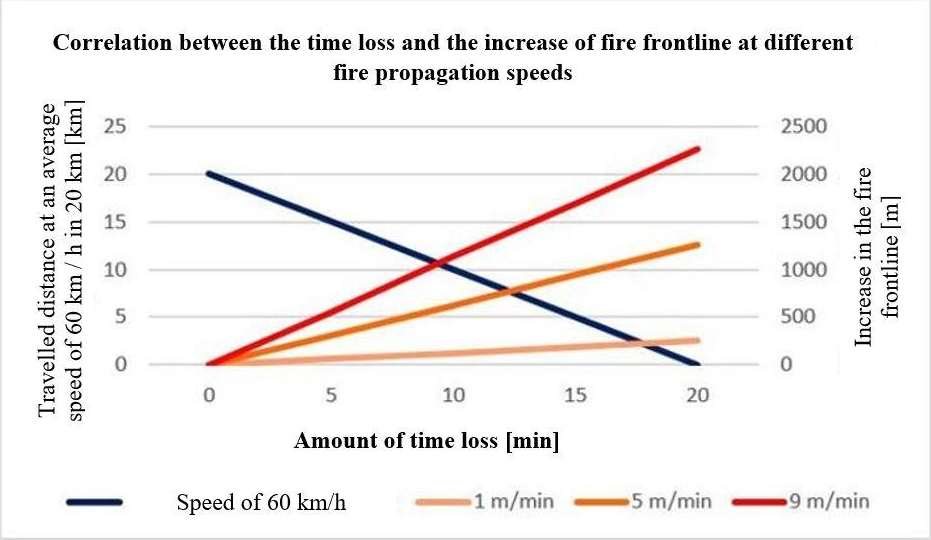

Figure 3 - Correlation between the time loss and the increase of fire frontline at different fire propagation speeds. Created by the Author.

Poor terrain conditions reduce the effectiveness of firefighting not only during site approach but also later during the constant water supply. However, this condition also helps the fire to spread further. In order to protect the built environment and residential areas it is unavoidable to move fire trucks in the field. In addition, I analysed the pros and cons of the use of an Extinguisher water backpack, an All-terrain vehicle (ATV), a Pick up and a Fire truck during the firefighting. By comparing the effectiveness of vehicles, I determined what types of interventions they could be used efficiency. I based my analysis on the approach to fire site, on the following types of routes: paved road, good quality dirt road, poor quality dirt road, forest path, forest trail, forest.

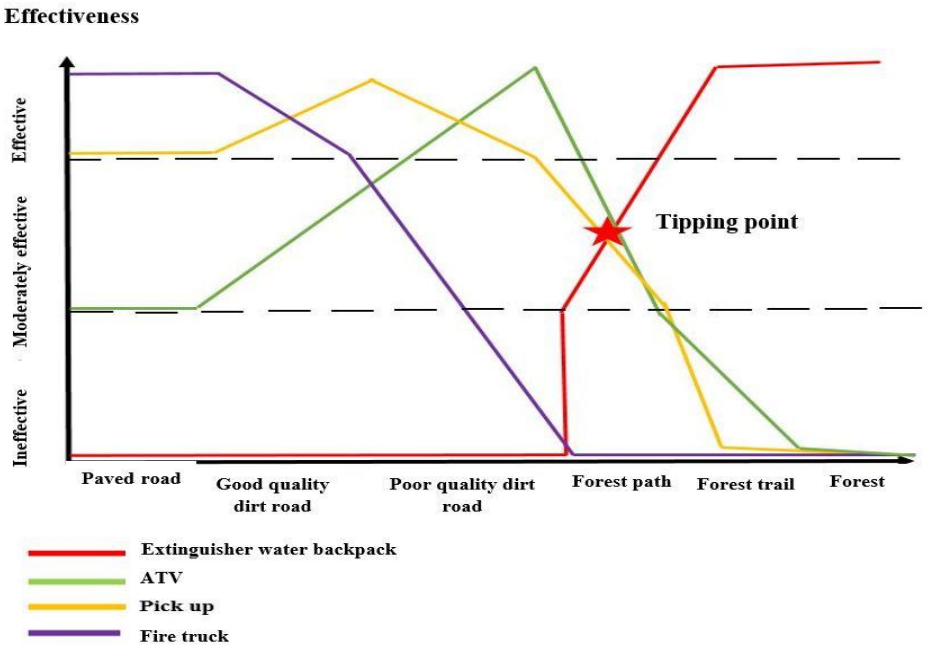

Figure 4- Illustration of logistical efficiency of vehicles and equipment on different types of roads.

Based on Figure 4, I found that as long as we can approach the fire site easily, the use of fire trucks is effective. However, this is changing as we move towards into the interior of wildland, where smaller vehicles like Pick up and ATV are a more effective solution, mainly because of their good off-road capability. I considered forest path to be tipping points in the efficiency of site approach, as this is the point where use of large fire trucks is no longer effective. On these types of routes, smaller firefighting vehicles are more effective.

4. Conclusion

As a result of my analysis of route combinations, I came to the conclusion that site approach on the dirt road results in time loss. As a result of it, interveners start firefighting at the fire site late. This also affects the lengths of the fire frontline, making the efficient firefighting more difficult. Intervention in time will also help save lives, and amount of damage will be less due to the shorter migration time. After examining the approach problem of fire site, my logical conclusion is that a calculation of time loss of migration should be made. In addition, it would be useful to widen and improve the quality of several dirt roads in the forest, in order to make these routes more walkable in case of a wildfire, thus reducing time loss. In many cases, fire site is covered with a large amount of reeds or grass, so much of the burned area can only be approached with the help of local people. Orientation can also be made with geographic information system (GIS), but in many cases this is not real-time and needs to be regularly updated (Burrough; Mc Donnel, 1998).

From logistical difficulties of fighting against wildfires, I drew conclusions that are suitable for detecting the time loss of migration and for establishing new methods and tools. Within this framework, I have dealt with effects of time loss caused by migration on poor quality roads. I not only characterized the problem of late arrival with time, but I related it to the increase in length of the fire frontline. To understand and illustrate this problem, I created a self-edited figure. Next, I analyzed advantages and disadvantages of an extinguisher water backpack, a firefighting ATV, a pick up, and a fire truck during the firefighting. By comparing the efficiency of vehicles, I determined what types of interventions they can be used efficiency. This was based on one of the most important factors in efficiency of vehicles, which is the approach to fire site. Consequently, I have concluded that, as long as we can approach the fire site easily, the use of large and high-capacity vehicles is effective. However, this changes as we move towards into the interior of the forest, the smaller vehicles are more effective because of their good off-road capability. I consider the forest path as a tipping point in the application efficiency between large and small vehicles.

5. References

Almeida M., Porto L., Viegas X. D 82021). Characterization of Firebrands Released From Different Burning Tree Species. Frontiers in Mechanical Engineering **7**: Article: 651135. 1-17.

Bérczi L., Papp C., (2013). Dislocation of fire stations as a function of the so-called white spots (A mentő tűzvédelem diszlokációja a valóságos fehér foltok függvényében). Védelem katasztrófa - és Tűzvédelmi Szemle, 20 (2). 9-12.

Bodnár L. (2016). Logistic problems of fighting forest fires based on case studies from Hungary. In: Proceedings of the 8th International Scientific Conference Wood and Fire Safety 2016. 23-32.

Bodnár L. (2017) Case study of "Hortobagy" and "Kunfeherto" fires, Hungary: disaster in costs of their elimination's view. Ecoterra- Journal of Environmental Research and Protection, **14**, (1) 40-46.

Bodnár L., Restás Á., (2018). Examination of the forest fires detection: the relationship between the fire and the detection. In: Viegas, Domingos Xavier (ed.) Advances in forest fire research 2018. Imprensa da Universidade de Coimbra (2018) 995-1001.

Bodnár L., Pántya P., (2019). The Threat of Forest and Vegetation Fires and the Possibilities of Intervention in Hungary. Academic And Applied Research In Military And Public Management Science, **18** (3) 21-31.

Burrough P., McDonnel R. (1998). Principles of Geographical Information Systems (Spatial Information Systems). Oxford: Oxford University Press. ISBN 0-19-823366-3 Appendix I. Glossary, p. 301.

Decree No. 48/2011. (IX. 15.) on the minimum number of employees of the municipal fire station, the minimum quantity and quality of its facilities and equipment and the service. https://net.jogtar.hu/jogszabaly?docid=a1100048.bm download: 10.05.2022.

Figueras J., Montero J., Crespo J.S., Casanovas J., Verdaguer P. Fire Fighting by Optimization of Ground Logistics (FireFIGHT). Available: https://inlab.fib.upc.edu/en/fire-fighting-optimization-ground-logistics-firefight download: 22.03.2022

Finney A. M., McAllister S.,. Grumstrup, T.P.,, Forthofer J. 82021). Wildland Fire Behaviour: Dynamics, Principles and Processes. CSIRO. 2021. Clayton South. Australia.

Jain P.,. Coogan S. C. P.,, Subramanian S.G, Crowley M., Taylor S., and M. D. Flannigan (2020). A review of machine learning applications in wildfire science and management. Environmental Reviews, **28** (3) Available at: https://www.nrcresearchpress.com/doi/10.1139/er-2020-0019#.X1jbKtNKhTY download: 18.03.2022.

Rácz S 82016). Focusing on the problems of extinguishing large scale storage fires. Ecoterra: Journal of Environmental Research and Protection **13** (4) 19-25.

Restás Á (2003). Logistics basics of the activity of fire departments. (A tűzoltóság tevékenységének logisztikai alapjai). Katonai logisztika, **11** (4) pp. 147-158.

https://drive.google.com/file/d/0B2IT5sLzLGdDT2VZRHhDY1NEbUE/view?resourcekey=0-wymGJF5o78Xdp_g3D8gBPg download: 18.03.2022.

Rothermel R. (1972). A mathematical model for predicting fire spread in wildland fuels. U.S. Department of Agriculture, Intermountain Forest and Range Experiment Station. Ogden: 1972.

World Economic Forum: The Global Risk Report 2022. World Economic Forum. Geneva, Switzerland. 2022. https://www.weforum.org/reports/global-risks-report-2022/in-full download: 18.03.2022.

B. Müller T.: Fire stations and voluntary fire departments. (Tűzoltóságok és önkéntes tűzoltó egyesületek). https://www.parlament.hu/documents/10181/303867/Infojegyzet_2015_46_tuzoltosag.pdf/a8697359-85f0-428a-86af-2dedbc7238e3 Download: 16.04.2020.

Low cost protection system of infrastructures against forest fires

Gilberto Vaz*[1,2]; Jorge Raposo[1,2]; Luís Reis[2]; Pedro Monteiro[2]; Domingos Xavier Viegas[2]

[1] *Coimbra Polytechnic - ISEC. Coimbra, Portugal, {gcvaz@isec.pt}*
[2] *Univ Coimbra, ADAI, Department of Mechanical Engineering, Rua Luís Reis Santos, Pólo II, 3030-788 Coimbra, Portugal {jorge.raposo, luis.reis, xavier.viegas}@dem.uc.pt, {pedro.mj.monteiro@gmail.com}*

**Corresponding author*

Keywords

Forest fires, Fire protection, Telecommunication stations, Rigid panels, Wildland-urban interface

Abstract

Forest fires are one of the main disasters that devastate many countries every year. The destruction caused by these phenomena generates social impacts putting at risk the population lives, environmental impacts due to the extreme deforestation and the high number of pollutants that are released to the atmosphere but also extremely important economic impacts caused by the destruction of a wide range of infrastructures and essential goods. Therefore, as it is impossible to remove all the infrastructures from the forest and from the wildland-urban interface, the development and installation of protection systems is essential. The main objective of this work is the development of a low cost protection system, with rigid panels, requiring a simple and easy installation, to protect outdoor infrastructures such as telecommunications stations, shelters, roadside enclosures, power cabinets, and other structures. A study was carried out on panels that could be used for the protection in order to determine whether the protective material would be more appropriate. Taking into account the fire resistance behaviour, thermal and structural properties and cost, the panels selected were the magnesium oxide fibreglass reinforced. The protection was constructed, installed on a telecommunication cabinet and experimentally laboratory tested in a wind combustion tunnel. To collect the data Infrared and video cameras, heat flux sensors and sheathed thermocouples were used to determine the fire propagation, heat flux and temperatures, respectively. The data obtained in the experimental tests show clearly that the simple low cost protection is effective for the protection of telecommunication cabinets and other similar infrastructures against forest fires.

1. Introduction

Forest fires are one of the main disasters that devastate many countries every year. The destruction caused by these phenomena generates impacts at several levels, whether social by putting at risk the population lives, whether economic through the destruction of a wide range of infrastructures and essential goods, or the environment. The forest fires that have been occurring in Portugal, and especially those in 2017, have highlighted the importance of infrastructures protection. In 2017, until October, 356 large forest fires (burned are larger than 1000ha) were recorded with an estimated burned area of 520,515 hectares (ANACOM, 2017). It was also in this year that the Pedrógão Grande fire occurred and it is known as one of the worst fires in Portugal and Europe. This terrible catastrophe took the lives of dozens of people, injured hundreds and caused a wave of destruction. During this fire, a lot of infrastructures were destroyed, including telecommunications stations, poles, copper and fiber optic cables, leading to numerous communication problems. “The failure of the communications system may have contributed to the lack of coordination of combat and rescue services, to the difficulty of people asking for help and to the worsening of the consequences of the fire” (Xavier et al., 2017). In the context of the high risk of forest fires in Portugal, a work has emerged whose objective is to develop a protection system applicable to infrastructures that are inserted in forest areas and that can be affected by forest fires.

According to (Andrade & Souza, 2015) the materials used for fire protection can be classified into three major groups: rigid and semi-rigid materials; intumescent paints; sprayed materials. (Takahashi, 2019) showed that the use of protective blankets made up of multiple layers of fibers allows the protection of infrastructures against fire. However, the application of this type of protection only becomes viable when the exposure time is relatively short, since for longer exposures, deterioration of the protection becomes evident. The work developed emerges

as a continuation of previous studies (Brinca, 2020), in which a fiberglass blanket coated with aluminium was used in order to protect a telecommunications cabinet. This protection, in addition to being effective in protecting against fire, also showed that the temperature inside the cabinet increased even when there was no exposure to fire. Thus, the author left open the possibility of using another type of protection. As forest fires are transient phenomena, thermal inertia of the protection is important to reduce the temperature increase of the protection and air inside the cabinets or enclosures. So, in this work, rigid panels will be used and applied to cabinet stations to test the fire resistance, in adverse conditions.

2. Experimental methodology

The first step of the work was the study and selection of the most appropriate material panel for the protection. The panels to be used in the protection must be impact resistant, fire resistant, resistant to climatic adversities and must have low thermal conductivity and high thermal inertia to withstand outdoor ambient conditions and forest fire transient effects. Several panels were identified and compared as shown in Table 1. The selected panel was the MAGOOX Board panel with 9mm thickness (MGOBoard, 2020) since that the boards are produced with thicknesses of 4 to 18mm being the thickness of 9mm an average value that does not turn the protection into a heavy structure. This material meets all the requirements for the protection material and it is non-toxic, has a low environmental impact and low price. The current approximate European price of the selected panel is 12€/m^2. This panel is composed of fiberglass reinforced magnesium oxide and has a fire resistance of 60 to 90 minutes. Generally, forest fire fronts have a residence time of no more than 15 to 20 minutes and they can reach very high propagation speeds (Raposo et al., 2018).

Table 1 – Commercial panels identified for the study.

Commercial name	DuraSteel	Promatec-XW	WeatherKem	SpeedPanel	MAGOOX Board	TriplacM
Composition	2 perforated steel plates and fiber reinforced cement core	Gypsum board with mat reinforcement	Mixture of cement, cellulose fibers and silicon-based binders	Cement core and galvanized steel cladding	Magnesium oxide reinforced with fiberglass mesh	Magnesium, fiber reinforced and other refractory materials
Thickness [mm]	9,5	15	6-18	51; 64; 78;	4-18	24-30
Fire resistance [min]	240	≤ 60	are completely non-combustible	Varies with thickness (60; 90; 120)	60-90	180-240
Resistance to climatic adversities	Yes	Yes	Yes	Yes	Yes	Yes
Impact resistance	Yes	Yes	Yes	Yes	Yes	Yes
Thermal conductivity (20ºC aprox.) [W/m.K]	0.55	0.264	0.24	Varies with cement densities	0.213	0.29

The protection was constructed and installed on a telecommunication cabinet as shown in Figure 1.

Figure 1- a) Telecommunication cabinet; b) Protected telecommunication cabinet.

To study the thermal behaviour of the cabinet and its protection, they were subjected to a series of tests carried out at the LEIF-ADAI facilities using the Combustion Tunnel 3 (CT3), which has two 35kW fans that can generate air speeds of up to 8m/s. This tunnel has dimensions of 8m length, 6m width and sidewalls of 2m height. The experimental apparatus is shown in Figure 2. The fuel bed area was defined by fixed length and width of 4m, corresponding to the 16m^2, with a fuel load of 1.5kg.m^{-2} of typical Mediterranean shrubs composed by a mixture of *Erica umbelatta*, *Erica australis*, *Ulex minor* and *Chamaespartium tridentatum*.

Figure 2- a) Combustion tunnel CT3; b) General view of the tests.

The existence or not of protection and the existence of side walls (which avoid lateral air entrainment promoting the arrival of a structured front, without edge effect) were tested. The list of tests performed and the respective variables are presented in Table 2 and they were performed in random order.

Table 2 – Conditions of the experimental tests performed.

Ref.	Wind speed (U [m/s])	Protection	Side walls
01	0	Yes	No
02	1	Yes	No
03	3	Yes	No
04	0	Yes	Yes
05	1	Yes	Yes
06	3	Yes	Yes
07	0	No	No
08	1	No	No
09	0	No	Yes
10	1	No	Yes
11	3	No	Yes

In the tests it was used an InfraRed FLIR Camera SC660, a heat flux sensor (Hukseflux sensor IHF01) and five sheathed K-type thermocouples of inconel with 1mm diameter. The referred equipment was used to determine the fire propagation, heat flux and temperatures. Additionally, at all the tests, two optical video cameras were used. One (Sony FDR-AX53) placed in a lift platform and the other (Sony HXR-NX30E) at ground level. Experimental setup is shown in Figure 3.

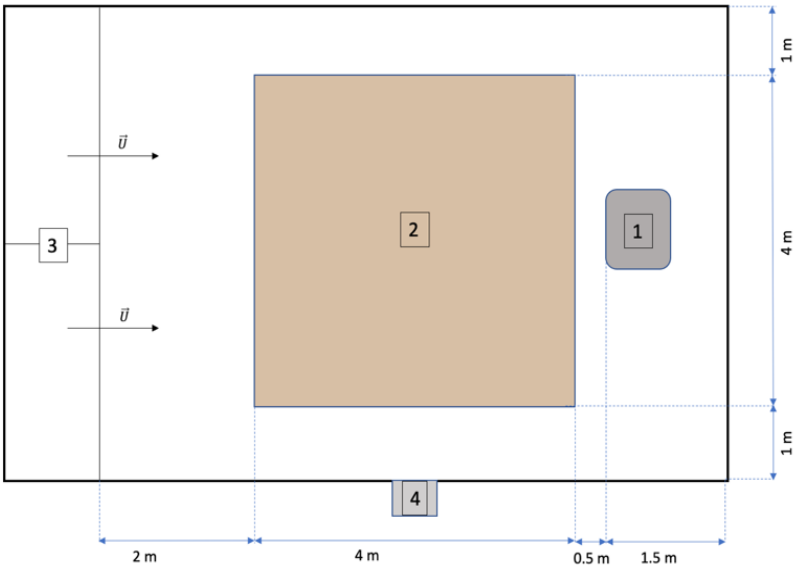

Figure 3- Experimental setup

(1 - Telecommunication cabinet, 2- fuel bed, 3- wind tunnel fans, 4- infrared and video cameras).

For the installation of thermocouples and heat flux sensor in the cabinet and respective protection, an acquisition board NI chassis cDaq 9174, a thermocouple board 9213, a voltage board 9211 and a computer with the *signalExpress* program with an acquisition frequency of 1Hz were used. The thermocouples and heat flux sensor were installed in the following positions:

Thermocouple 1(T_1): placed inside the cabinet (roughly in the center, about 1.30m from the ground) ;

Thermocouple 2 (T_2): placed on the inner front surface of the protection (about 1.30m from the ground) and in the tests carried out without protection, this was placed on the side of the cabinet;

Thermocouple 3 (T_3): placed on the outer front surface of the protection or cabinet (in absence of the protection), at about 1.30m from the ground;

Thermocouple 4 (T_4): placed behind the cabinet about 1m away in order to be able to assess the downstream air temperature;

Thermocouple 5 (T_5): placed on the sidewalls (when applicable);

Heat flux sensor: placed on the outer front surface of the protection (or of the cabinet, respectively, if testing with or without protection), approximately 1.30m from the ground. The flux and temperature values at the various points of the shield protection and cabinet were taken directly from the thermocouple data and converted into Microsoft Excel®.

3. Analysis and discussion of results

Figure 4 and 5 shows the temperature evolution in two tests performed with the protection applied to the telecommunications cabinet and 3m/s wind speed (highest wind tunnel speed which is the most critical situation tested and corresponding to the typical wind speeds of intense forest fires). Regarding the temperature inside the cabinet, it is possible to verify that the maximum temperatures do not exceed 30ºC, proving that the use of the protection under study is capable of protecting the cabinet against the high temperatures and heat fluxes of a forest fire.

Figure 6 shows the temperature evolution in the test performed without protection applied to the telecommunications cabinet and 3m/s wind speed. For this case, the evolution of temperatures is quite similar to that observed previously. However, there is a considerable difference with regard to the maximum temperature registered inside the cabinet, reaching a value above 60ºC. This value is considered critical for the normal operations of communication equipment.

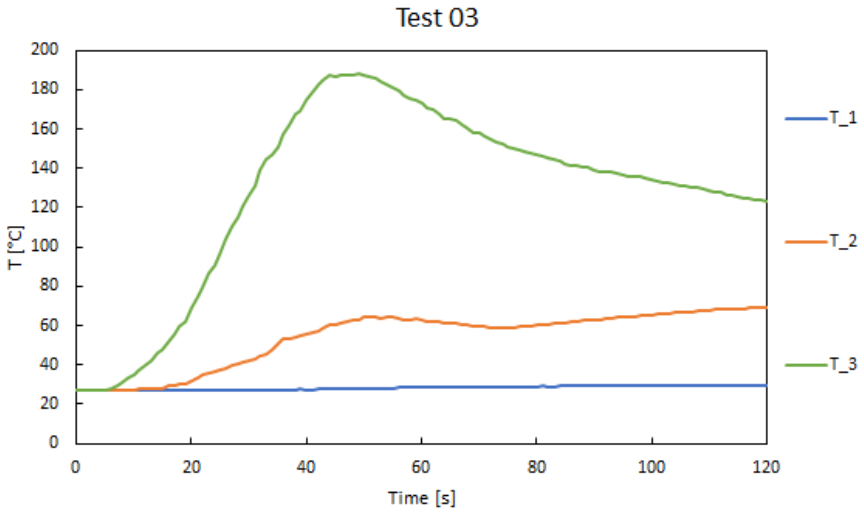

Figure 4- Evolution of temperatures in Test 03.

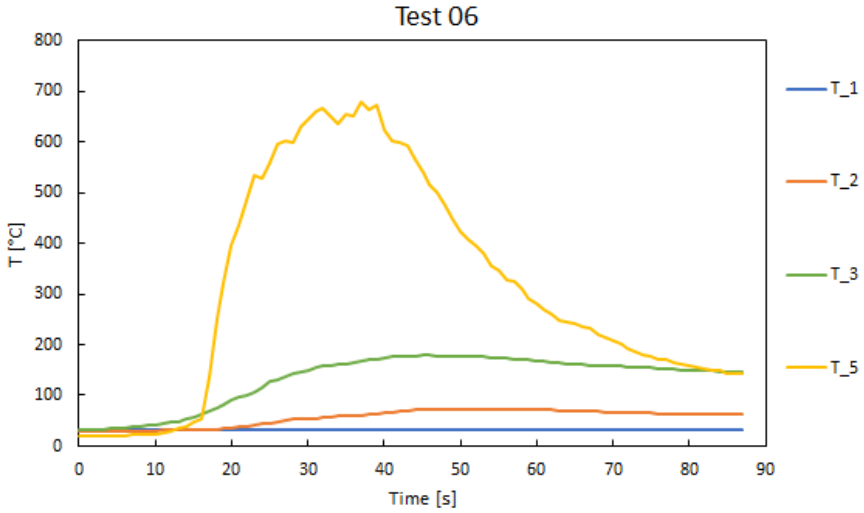

Figure 5- Evolution of temperatures in Test 06.

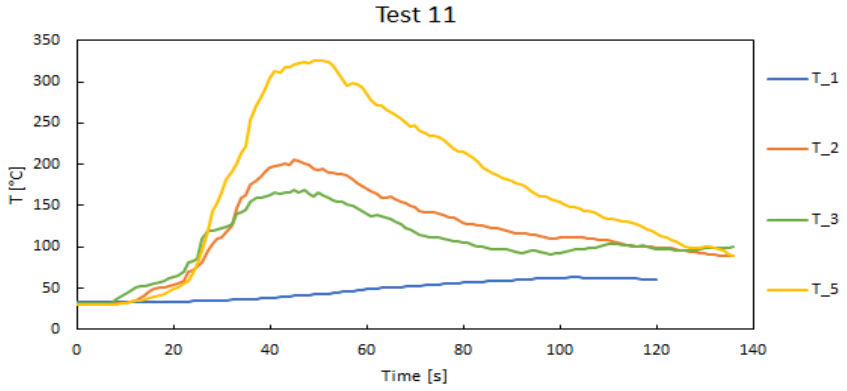

Figure 6- Evolution of temperatures in Test 11.

Table 3 presents a summary of the experimental results and it can be easily concluded that the protection system is effective as the maximum temperature inside the cabinet remains below 30°C, even with high fireline intensities.

Table 3 – Main results of the tests performed.

Test Reference	Protection	Wind speed [m/s]	Side walls	Max dimensionless rate of spread	Maximum fireline intensity [MW/m]	Maximum external surface temperature [ºC]	Maximum temperature inside cabinet [ºC]	Max Heat Flux [kW/m^2]
01	Yes	0	No	1.95	0.59	90.63	24.10	1.85
02	Yes	1	No	7.73	2.34	158.90	26.97	5.87
03	Yes	3	No	18.10	5.48	188.63	29.72	10.07
04	Yes	0	Yes	1.68	0.51	61.87	26.37	2.14
05	Yes	1	Yes	5.71	1.73	144.86	29.02	3.79
06	Yes	3	Yes	14.96	4.53	179.24	33.72	10.12
07	No	0	No	1.65	0.50	113.51	30.20	2.43
08	No	1	No	6.80	2.06	70.37	33.46	1.31
09	No	0	Yes	1.63	0.49	108.89	34.60	2.54
10	No	1	Yes	4.56	1.38	196.22	42.64	1.34
11	No	3	Yes	19.85	6.01	168.67	63.03	10.16

4. Conclusions

The data obtained in the experimental tests show that the simple low cost protection is effective to the protection of telecommunication cabinets and other similar infrastructures against forest fires. The protection avoided the high temperatures in the cabinet. The temperature obtained inside the cabinet, without protection, reached a value above 60ºC. This value is considered critical for the normal operations of communication equipment. Another great advantage of this protection is its low cost of material and labour for installation. In this case, the protection was built and installed at a cost of approximately 150 euros, increasing the protection of an asset that costs thousands of euros. Installing this type of protection does not compromise system operations at all. The access for maintenance or repairing is maintained since the plates are integrated in the movement of the openings of the cabinet.

5. References

ANACOM. (2017). Incêndios Florestais-Medidas de Proteção e Resiliência de Infraestruturas de Comunicações Eletrónicas.

Andrade, C. C., & Souza, J. C. (2015). Projeto de arquitetura-proteção contra incêndio em elementos estruturais de aço. 2, 49–68. https://periodicos.unifap.br/index.php/estacao.

Brinca, A. C. (2020). Protection of telecommunications stations against forest fires. CIFFC. (2021). Canadian Wildland Fire Glossary.

MGOBoard. (2020). Placa MAGOXX. https://mgoboard.pt/fichastecnicas/Ficha-Técnica-Placa-MAGOXX-9mm-Março-2020.pdf

Raposo, J. R., Viegas, D. X., Xie, X., Almeida, M., Figueiredo, A. R., Porto, L., & Sharples, J. (2018). Analysis of the physical processes associated with junction fires at laboratory and field scales. International Journal of Wildland Fire, 27(1). https://doi.org/10.1071/WF16173.

Takahashi, F. (2019). Whole-House Fire Blanket Protection From Wildland-Urban Interface Fires. Frontiers in Mechanical Engineering, 5. https://doi.org/10.3389/fmech.2019.00060.

Viegas, D.X., Almeida, M., Ribeiro, L. M., Raposo, J., Viegas, M. T., Oliveira, R., Alves, D., Pinto, C., Jorge, H., Rodrigues, A., Lucas, D., Lopes, S. (2017). O complexo de incêndios de Pedrógão Grande e concelhos limítrofes, iniciado a 17 de Junho de 2017. ADAI-UC.https://www.portugal.gov.pt/pt/gc21/comunicacao/documento?i=o-complexo-de-incendios-de-pedrogao-grande-e-concelhos-limitrofes-iniciado-a-17-de-junho-de-2017-extrato-do-capitulo-6-de-acordo-com-a-deliberacao-da-cnpd

Low-cost solution for forest fire detection using surveillance camera

Ágoston Restás*[1]; Valentin Virovácz[2]; Sándor Rácz[3]; László Bodnár[4]

[1,3,4] University of Public Service, Institute of Disaster Management. 1101 Budapest, Hungary, krt. 9-11., {restas.agoston, racz.sandor, bodnar.laszlo}@uni-nke.hu}
[2]Professional Fire Brigade, 7630 Pécs, Engel József street 1. {virovacz.valentin@gmail.com}

**Corresponding author*

Keywords

Remote sensing, active fire detection, surveillance camera, efficiency, cost-effectiveness

Abstract

Nowadays climate change is one of the biggest challenges in the entire world. The average temperature on Earth is constantly increasing, and the distribution of seasonal precipitation is extreme. These factors together result in large fires and the new challenges require new solutions. The paper discusses the possibilities of developing the detection of outdoor fires with a camera. One of the objectives of the research is to prove the existence of a detection system by examining the detection conditions of outdoor fires and supporting them with practical examples. The research was determined to keep the costs of the examined developments below the value of properties they saved, so authors consider it a realistic aim to apply them in practice. Another objective was to demonstrate the time gain of the detection of remote sensing. In each case, the comparative analyzes of the authors show that citizen reports, i.e. the current, traditional solution, allow for a later alert than it would have been possible by using remote sensing. In the paper, wildfires were analyzed that were randomly recorded by video cameras. Authors have collected data on the specific fire from various official databases of the Hungarian Disaster Management. Taking into account the speed of fire propagation, it was determined that the burned area and perimeter of the fire are much smaller than the early detection when the firefighters arrive to the site. It shortens the length of the frontline to be extinguished. This predisposes to a lower force requirement for elimination and also significantly reduces the use of intervening forces along with the need for the used extinguishing agent. Overall, the intervention can be made more effective.

1. Introduction

In Europe, wildfires are most common during the summer fire season, due to the high average temperature and the quantitative distribution of precipitation. As a result of climate change, droughts have become common in the summer. In this case, no open flame is needed to ignite the dry fuel, a spark bursting from a machine can also do it. Combustion of accumulated combustible fuel releases enough thermal energy to cause even crown fire. Outdoor fires cause enormous damage to animals and wildland vegetation that can only be recovered in decades. By outdoor fires authors mean fires in the forest, wildlands, agricultural lands, grass, shrubs, forest litters, so they are talking about a collective concept.

The problems associated with fighting against forest fires are also very diverse, and their solution requires different tactics. If a fire already develops, it is important for everyone to put it out quickly and professionally with the least possible effort. Therefore, fast and accurate fire detection is very important for the efficiency. It is a negligent behaviour to rely solely on passive detection in case of outdoor fires. The later we become aware of fires in our environment, the more tools and forces we need to extinguish them successfully. The most effective solution for monitoring large areas is remote sensing. Nowadays, the presence of cameras is already common, it is no longer a big challenge for modern technology to produce devices suitable for high-quality images at minimal cost. All people have smartphones in their pockets whose cameras can take clear pictures. If the presence of cameras is so much part of our everyday lives, its benefits could also be used to support disaster management operations.

There are many papers focusing on camera based fire detection, some of them give a review of the technology (Alkhatib 2014, Mathi and Latha 2015, Yandouzi et al. 2022), others focus on the option of autonomous detection (Breejen et al. 1998, Liyang 2005, Saponora et al. 2018), the network system (Benzekril et al. 2020, Muhammad et al. 2018), the machine learning technology (Byongjun 2019, Xu et al. 2021) or the optimization of the detection (Restas et al. 2014, Quttineh et al. 2022).

The purpose of this study is to analyse the low-cost webcam videos of the locations where the fire occurred and then present the time difference between the occurrence of the fire alarm and the optional fire detection. Authors intend to demonstrate

even the difference between both the sizes of burnt areas and the lengths of perimeters in cases of active and passive detection.

2. Methods

We have examined and analysed the relevant literatures on the topic as well as the results of other authors. Part of the secondary research was the analysis of reports, data and webcam recordings of outdoor fires. The data on the alarm sheet provided by the fire service were studied and compared with the remote sensed recordings provided by the webcams. Using the timestamp of the recordings and the data on the alarm sheet, authors performed basic calculations from which comparisons were made and logical conclusions were drawn. In addition, authors analysed figures, signalling dates and damage descriptions through the statistical service of one of the online interfaces of the Hungarian Disaster Management. In addition to the practical experience of the authors, they received information about related examples during consultations with firefighting colleagues and experts, for which a remote sensing would have been very helpful.

3. Results

In this study 9 rural fires were analysed, all of them can be found in the 2021 year database of the Hungarian Fire Service. These fires were marked with A, B and C with 1 – 3. Authors summarized the data of these fires in the Table 1, where the time of fire alarm (T_p – passive fire "detection" that is reported by civilians), the time when fire could have been detected by the webcam video (T_C – optional detection time) and the time of the beginnings of the suppression (T_A – arrival time of the fire service) were provided. Based on these data authors could calculate the time of the free escalation of the fires (t_{dfree}), the time of marching of the firefighters (t_m), the fire development time of the fire supposed in case of webcam analysis (t_{dcam}) and the obtained time in case of camera based detection (t_w). In this study 1 minute was added to the cases of camera based fire detection as processing time. Based on the above data authors calculated the rate of fire propagation in all cases of passive detection (v_{tp}) and took also an average rate of spread for the further calculation (v_f).

Table 1. Data of fires analysed in this study.

	A/1	**A/2**	**A/3**	**B/1**	**B/2**	**B/3**	**C/1**	**C/2**	**C/3**
T_P	18:55	16:33	14:20	15:13	13:56	17:04	15:49	14:41	15:37
T_C	18:45	15:34	14:09	14:05	12:44	16:50	15:18	14:36	15:25
T_A	19:19	16:51	14:47	15:47	14:13	17:24	16:14	14:50	16:18
t_{dfree} [min]	24	77	38	103	89	34	56	14	54
t_m [min]	14	18	27	34	17	20	25	9	41
t_p [min]	1	1	1	1	1	1	1	1	1
t_{dcam} [min]	15	19	28	35	18	21	26	10	42
t_w [min]	9	58	10	68	73	13	30	4	11
v_f [$mmin^{-1}$]	2.2	2.2	2.2	2.2	2.2	2.2	2.2	2.2	2.2
v_{tp} [$mmin^{-1}$]	3.3	2	1.8	0.7	2.45	1.65	1.78	4	1.8
A_p [m^2]	20,000	80,000	15,000	20,000	150,000	10,000	30,000	10,000	30,000
R_p [m]	79.8	159.6	68.1	79.8	218.5	56.4	97.7	56.4	97.7
K_p [m]	501	1,003	434	501	1,373	354	614	354	614
A_A [m^2]	10,747	5,489	11,921	18,626	4,926	6,705	18,626	1,520	26,822
R_A [m]	33	42	62	42	40	46	77	22	92
K_A [m]	207	262,6	387	483	248,8	290,3	483,8	138,2	580
K_d [m]	294	740	47	18	1,124	64	130	216	34
T_d [m^2]	9,253	74,510	3,079	1,374	148,876	3,295	11,374	8,480	3,178

Legend:

T_P : passive fire detection (fires, reported by civilians)	**v_{fp}:** assumed rate of fire spread based on passive detection
T_C: active fire detection (fires, can be seen on webcam)	**A_P :** burnt area at arrival in case of passive detection
T_A: arrival time of the first responders	**R_p:** the radius of the fire at arrival (passive detection)
t_{dfree} : time of fire escalation at real intervention	**K_p :** the perimeter of fire at arrival (passive detection)
t_m: marching time of first responders	**A_a :** burnt area at arrival (active detection)
t_p : assumed processing time of the automatic signal	**R_a :** the radius of the fire at arrival (active detection)
t_{dcam} : time of fire escalation according to the camera signal	**K_a :** the perimeter of fire at arrival (active detection)
t_w : time obtained by using automatic detection	**K_d :** the difference in the perimeter of fire
v_f : supposed rate of fire propagation	**T_d :** the difference in the area of fire

Database contains even the size of the burnt area reported officially by the firefighters after arriving to the fire front (A_P), and based on these the study calculated the radius (R_P) and the perimeter (K_P) of each fire. The authors also provided these data for webcam based active detections (A_A, R_A, K_A) and calculated the differences of the perimeter and the burnt area in case of each fire. The rate of the burnt areas in case of passive and assumed active detections presented in the Figure 1 as well as the time benefit between the passive and active detection.

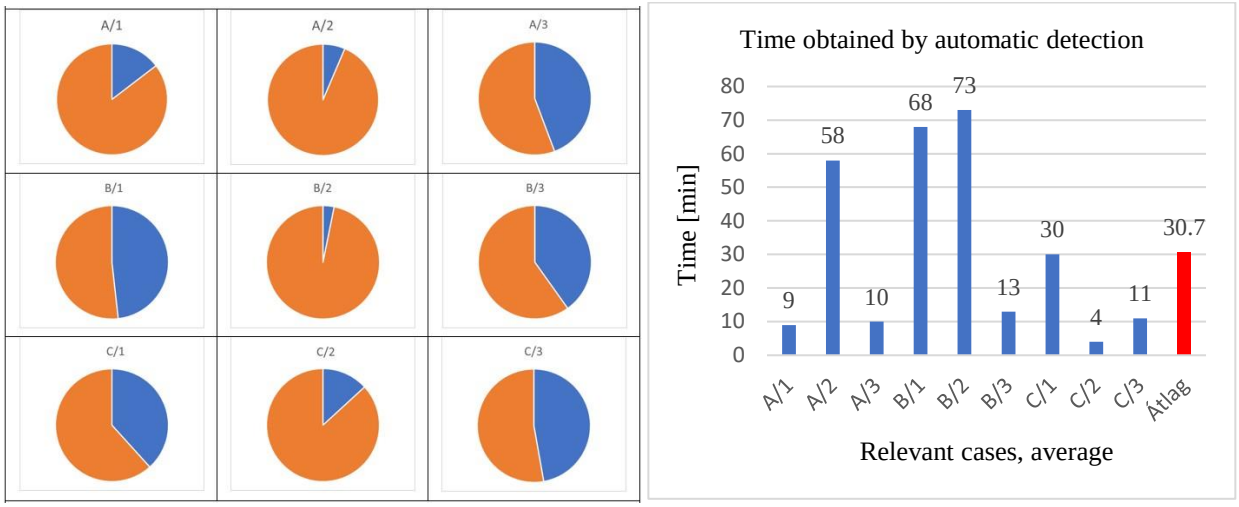

Fig. 1. The rate of the burnt areas in case of passive (orange) and active detections (blue) (left) and the time benefit between the passive and active detection (blue) with the average time benefit (red) (right). Created by authors.

Results show that in all cases using active detection firefighters would have had time gain, 4 minutes in the worst case (C/2) and 73 minutes in the best case (B/2), averagely more than 30 minutes (30.7 min). The burnt area would have been also smaller, with 1,374 m^2 in the worst case (B/1) and almost with 15 hectares in the best case (B/2), without the best case, averagely almost 1.5 hectares per fire. The perimeter, which is the fire front that firefighters have to suppress would have been shorter with 18 meters in the worst case (B/1) and more than 1 km in the best case (B/2), averagely 193 meters without the best case. Based on the above, authors state that the active fire detection can be effective even if fire service uses only the low-cost webcam solution for it.

4. Conclusions

It is very difficult to predict precociously the advantages of any early warning systems and camera based fire detection systems belongs to it too. Therefore, researches focusing on it have to take some simplifications and standard assumptions. This study generated by a random fire detection, however, authors could collect nine other cases to base the results. Even if this research focused on the saved area that can be achieved by the time difference between the traditional (reported by civilians) and camera based fire detection, authors found even some other results. One of these is, there was no fire to be reported earlier than staff could have been detected by cameras. All fires could be seen earlier by cameras than the fires was reported by civilians, averagely cameras could detect fire about 30 min earlier. The other is the standard deviation of the fire propagation is not essential in firefighters view; firefighters can calculate with 2.2 m/min fire propagation. Using surveillance cameras for fire detection can be a good opportunity in the future however more research is required to optimize its capability besides remaining even the original function. Summarizing the results, research demonstrates that, we can gain advantages even with a cheap and existing surveillance camera systems to reduce the burnt area.

5. References

Alkhatib A. A, (2014) A Review on Forest Fire Detection Techniques. International Journal of distributed sensor networks.

Benzekri1 W, Moussati A. E, Berrajaa M, (2020) Early Forest Fire Detection System using Wireless Sensor Network and Deep Learning. International Journal of Advanced Computer Science and Applications, 11 (5) 496 – 503.

Breejen E, Breuers M, Cremer F, Kemp R, Roos M, Schutte K; Vries J, (1998) Autonomous forest fire detection. Presentation, 3rd International Conference on Forest Fire Research, Luso, Portugal

Byoungjun K, Lee J, (2019) A Video-Based Fire Detection Using Deep Learning Models. Applied Sciences. 9 (14) 2862

Liyang Y, (2005) Real-time Forest Fire Detection with Wireless Sensor. Retrieved from IEEE: (available online 15.03.2022) https://ieeexplore.ieee.org/stamp/stamp.jsp?tp=&arnumber=1544272

Mathi P.T, Latha L, (2015) A survey on forest fire detection. Elk Asia Pacific Journal of Computer Science and Information Systems, 1 (2) 32-41

Muhammad K, Ahmad J, Mehmood I, Rho S, Baik S.W, (2018) Convolutional neural networks based fire detection in surveillance videos. IEEE Access, 6, doi: 10.1109/ACCESS.2018.2812835

Quttineh N.H, Olsson P.M, Larsson T, Lindell H, (2022) An optimization approach to the design of outdoor thermal fire detection systems. Fire Safety Journal, 129103548 doi: 10.1016/j.firesaf.2022.103548

Restás Á, Hinkley E, Ambrosia V, (2014) An approach for measuring the effectiveness of fire detection systems in different dimensions. Bolyai Szemle, 23 (3) 283-296.

Saponara S, Elhanashi A, Gagliardi A, (2021) Real-time video fire/smoke detection based on CNN in antifire surveillance systems. J Real-Time Image Proc 18, 889–900 (2021).

Xu R, Lin H, Lu K, Cao L, Liu Y, (2021) A Forest Fire Detection System Based on Ensemble Learning. Forests, 12 (217). doi: 10.3390/f12020217

Yandouzi M, Mounir G, Idrissi I, Moussaoui O, Azizi M, Ghoumid K, Elimiad A.K, (2022) Review on forest fires detection and prediction using deep learning and drones. Journal of Theoretical and Applied Information Technology, 100 (12) 4565-4576

Mitigating rural fires through transformative service research: value cocreation with forest-related rural communities

Mayara Emilia Barbosa Souza*[1]; Jorge Grenha Teixeira[1]; Abílio Pereira Pacheco[2,1]

[1] INESC TEC and Faculty of Engineering of the University of Porto. Rua Dr. Roberto Fria, 378, 4200-465, Porto, Portugal, {msouza, jteixeira}@fe.up.pt
[2] ForestWISE, Collaborative Laboratory for Integrated Forest & Fire Management. Quinta de Prados, Campus da UTAD, 5001-801, Vila Real, Portugal, {abilio.p.pacheco@gmail.com}

**Corresponding author*

Keywords

Rural fires, transformative service research, value cocreation, wellbeing

Abstract

Socioeconomic changes have caused profound transformations in forest landscapes and increased abandonment of rural areas, leading to fuel accumulation and higher landscape homogeneity, and consequently, raising the rural fires risk. Rural fires risk is also fueled by climate change, due to heat waves and lack of precipitation. In this context, rural communities inhabiting forest areas are those who suffer the most, because rural fires, land degradation and climate change can disturb their food and economic strategy. These communities already suffer from underdeveloped rural infrastructure, and services, lack of labor and education opportunities, that trigger poverty and migration. Given this accelerating pace of change and increasing uncertainty, many fields of knowledge have been dedicated to contributing towards a more sustainable and inclusive future. In service research, transformative service research (TSR) literature plays a central role on understanding problems and finding solutions that improve well-being and create uplifting change through services. Similarly, the fire research field highlights the need for an integrated perspective to analyze all the aspects involved in rural fires occurrence, whether they are of an environmental or economic nature, or a sociological or demographic nature.

This study aims to explore transformative services oriented to cocreate value with forest-related rural communities, thus helping to manage forest areas and mitigate rural fires risks. A qualitative methodology was employed involving 28 participants related to fire management and forest areas and communities, including actors from industries, public entities, academics, the third sector. The data collected through individual interviews was transcribed, coded, and analyzed following a thematic analysis approach, with NVivo software support.

Overall, the study emphasizes the need for an endogenous and adapted set of services to cocreate value with vulnerable communities in forest areas, which consequently enable rural fires mitigation. Given the high level of land abandonment and accumulation of residual materials that increases the risk of rural fires, the development of valuing and recovery solutions is a priority. Finally, this research can also help decision-makers and stakeholders to generate and support services that cocreate value with rural communities to a sustainable, safe and inclusive future.

1. Introduction

Socioeconomic changes have caused profound transformations in forest landscapes and increased abandonment of rural areas since the 19th century. Land abandonment led to fuel accumulation and higher landscape homogeneity, and both contribute to raised rural fires risk (Mantero et al. 2020); also fueled by climate change, due to heat waves and lack of precipitation (Nunes et al. 2021). In this context, rural communities inhabiting forest areas are those who suffer the most, since they are especially vulnerable to land degradation and climate change (Shukla et al. 2019), which can disturb their food and economic strategy, exposing them to new social vulnerabilities and inequities (Miller and Mach 2022). These communities also suffer from the underdeveloped rural infrastructure, and services, lack of labor and education opportunities, that trigger poverty and migration (Lazarte 2017). So, increasing the land abandonment and rural fires risk, in a cyclical transformation of an ecosystem in increasingly poor health.

Given this accelerating pace of change and increasing uncertainty, many fields of knowledge have been dedicated to contributing towards a more sustainable and inclusive future. In service research, transformative

service research (TSR) literature plays a central role on understanding problems and finding solutions that improve well-being and create uplifting change through services (Anderson et al. 2013; Ostrom et al. 2021) in an inclusive way (Boenigk et al. 2021). Addressing how different stakeholders can share resources to achieve common goals (Ostrom et al., 2021) and how sustainability efforts require the active involvement of stakeholders throughout the service ecosystem (Field et al. 2021). Similarly, forest fire research field highlights the need for an integrated perspective to analyze all the aspects involved in rural fires occurrence, whether they are of an environmental or economic nature, or a sociological or demographic nature (Nunes et al. 2021). The increased risk of rural fires, due accumulation of biomass fuels in forests, motivated the launch of a set of legislative measures that seek to promote the management, cleaning, and control of these species. At the same time, it stimulates the study and research for more efficient and viable recovery alternatives, which allow the creation of value for these residual materials and the promotion of their sustainable management, thus mitigating the risk of rural fires. An example of this is the energy recovery of these species in local, small-scale processes, that is, increasing the value through planned actions (Nunes et al. 2021)

Considering the challenges presented, this article is bridging the service research field, namely, transformative service research (TSR) literature, with the forest fire research, through endogenous and adapted services that cocreate value with forest-related rural communities, mitigating rural fires risks. These services can foster value cocreation with the endogenous forest resources for commercial and non-commercial purposes, such as exploitation of natural resources (timber, pine resin, mushrooms, bee hives, etc), human nutrition, cultural and experience services. It can potentially contribute to the generation of jobs and income in rural areas (Weiss et al. 2020), as well as create more efficient and viable recovery alternatives for residual materials and promote their sustainable management, thus mitigating the risk of rural fires (Nunes et al. 2021). Thus, transformative services do not directly lead to well-being but serve as a mediating construct to promote greater well-being among individuals and collectives (Blocker and Barrios 2015).

Based on TSR approach in the improvement of individuals and ecosystems well-being and create uplifting change through services, this research aims to explore services to cocreate value with forest-related rural communities to mitigate rural fires risks. The following sections describe the method employed to answer this objective, as well as characterize main findings, discussion, and conclusions of this study.

2. Method

A qualitative methodology was undertaken to gain an in-depth understanding of how transformative service research can contribute to mitigating rural fires risks and increasing the well-being forest-related rural communities, through services. To ensure the holistic perspective of the research topic, 28 stakeholders with in-depth involvement and experience in Portugal forest-related areas and communities, and fire management, were individually interviewed. The sample included representatives from industries, public entities, academics, the third sector, from National Military Security Force, Volunteer Firefighters, National Emergency and Civil Protection Authority, National Guard, Agency for the Integrated Management of Rural Fires; National Institute for the Management and Conservation of Nature and Forests, forestry companies, electricity, and natural gas transport industries, multinationals that operate in telecommunications and other industries, associations, universities.

The data collected was transcribed, coded, and analyzed following a thematic analysis approach, with NVivo software support. Data analysis followed the Gioia approach (Gioia, Corley, and Hamilton 2013). Firstly, the interviews were initially coded following open coding procedures, in first-order codes, where the concepts were initially identified, and the properties and dimensions of these concepts were discovered in the data.

Afterwards, the codes were grouped, with continuous analysis of their subcategories, allowing the emergence of preliminary themes (second-order codes). These set of concepts were refined into “aggregate dimension”, that we named services to cocreate value with rural communities and mitigate rural fire risk, described in the following section.

3. Findings

From the data analysis a set of adapted services were identified with potential features to cocreate transformative value with rural communities and mitigate rural fires risk (Figure 1), such as associative and collaborative

services, ecosystem services remuneration, mentoring for smart use of land and management of its resources, rural industries and training and education services, as well as rural marketing and advertisement. Each identified service according to the stakeholders perspective will be reported in the following paragraphs.

Associative and collaborative services describe the collaborative effort to develop and protect local interests to overcome challenges of territory fragmentation, land abandonment, lack of land management and cleaning that increase the rural fires risk.

Ecosystem services remuneration consist of the landowner continually payment in exchange for guaranteeing the flow of ecosystem services, which is provided by nature and essential to survival, quality of life and well-being of society. These payments for ecosystem services can have different objectives and characteristics (e.g. payment for conservation, for active management of the landscape) and may favor a specific service (e.g. carbon sequestration), or a set of services provided by ecosystems (e.g. fertility of the soil, erosion control, hydrological regulation).

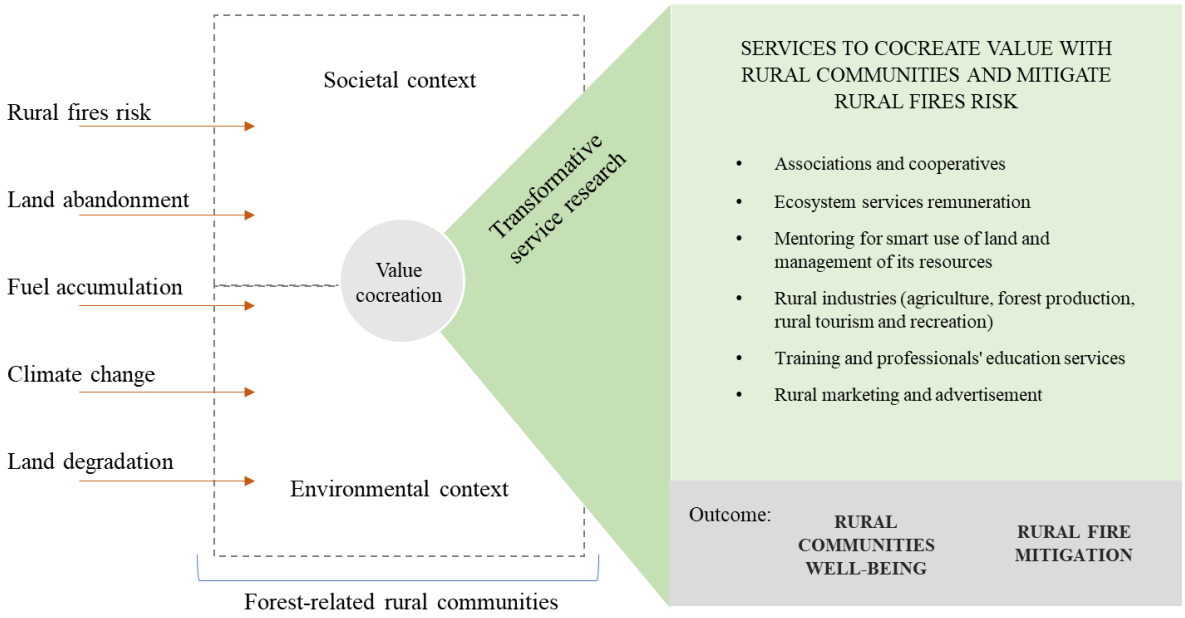

Figure 1- Services to cocreate value with rural communities and mitigate rural fires risk

Mentoring for smart use of land and management of its resources includes services oriented to active landscape management, sustainable manners to manage and promote the land and the resources, such as valuing residual biomass to energy recovery in local or small-scale processes, or recovery alternatives for residual materials. Rural industries encompass industries that run in rural areas, based on the utilization of local available resources, including agriculture, forest production, rural tourism and recreation.

Training and education services describe services to leverage knowledge in technical training in sustainable management of the land (suitable plant species to specific areas, valorization of natural materials, agrosilvopastoral system), and the professionalization of technicians in the forest clearing and safe fire use. These training and education services could be planned according to forest-related rural communities' profiles, such as local residents or technicians. And if oriented to young people, it can also contribute to attract them to rural areas. Lastly, rural marketing and advertisement services refers to foster and generate new social and economic dynamics to rural development through advertisement.

4. Discussion and conclusion

Rural communities' well-being in forest areas is linked to the recognition of the value of resources and the active and significant contribution of these territories to the mitigation of current challenges, such as rural fires (Nunes et al. 2021), land abandonment (Mantero et al. 2020), climate change (Nunes et al. 2021; Shukla et al. 2019), land degradation (Shukla et al. 2019) - that cannot be done without caring for the well-being of forest-related

rural communities. In other words, society needs rural areas and communities and the enhancement of the resources to face current global social and environmental challenges.

Moreover, the study demonstrates how transformative service research (TSR) favored forest fire research avenue, namely, to fire risk management with rural fires prevention, through a set of adapted services oriented to cocreate value with forest-related rural communities.

These services can improve the wellbeing of rural communities and, at the same time, foster active fuel management, promote the local economy and engagement of the community. Thus, mentioned services can foster value cocreation with the endogenous forest resources for commercial and non-commercial purposes (Weiss et al. 2020), contributing to sustainable land management and resources promotion, such as the possibility of valuing residual biomass (Nunes et al. 2021), generating new social and economic dynamics to rural development, such as jobs opportunities, income to local markets, and so avoiding land abandonment and encouraging the active land management. In a broader perspective, transformative services oriented to value cocreation with forest-related rural communities can also contribute substantially to poverty alleviation and the transition towards low-carbon and green economies. As previously said, transformative services do not directly lead to well-being but serve as a mediating construct to promote greater well-being among individuals and collectives (Blocker and Barrios 2015).

This study introduces an alternative lens to address the rural fires issue with a call for endogenous and adapted services oriented to value cocreation with vulnerable communities in forest areas. Given the high level of land abandonment and accumulation of residual materials that increase the risk of rural fires, the development of valuing and recovery solutions is a priority. Lastly, this research may inspire decision-makers and stakeholders to foster transformative services for a sustainable, safe, and inclusive future.

5. References

Anderson, Laurel, Amy L. Ostrom, Canan Corus, Raymond P. Fisk, Andrew S. Gallan, Mario Giraldo, Martin Mende, et al. 2013. “Transformative Service Research: An Agenda for the Future.” Journal of Business Research 66 (8): 1203–10. https://doi.org/10.1016/j.jbusres.2012.08.013.

Blocker, Christopher P., and Andrés Barrios. 2015. “The Transformative Value of a Service Experience.” Journal of Service Research 18 (3): 265–83. https://doi.org/10.1177/1094670515583064.

Boenigk, Silke, Aaron A. Kreimer, Annika Becker, Linda Alkire, Raymond P. Fisk, and Sertan Kabadayi. 2021. “Transformative Service Initiatives: Enabling Access and Overcoming Barriers for People Experiencing Vulnerability.” Journal of Service Research 24 (4): 542–62. https://doi.org/10.1177/10946705211013386.

Field, Joy M., Darima Fotheringham, Mahesh Subramony, Anders Gustafsson, Amy L. Ostrom, Katherine N. Lemon, Ming-Hui Huang, and Janet R. McColl-Kennedy. 2021. “Service Research Priorities: Designing Sustainable Service Ecosystems.” Journal of Service Research, September, 109467052110313. https://doi.org/10.1177/10946705211031302.

Gioia, Dennis A., Kevin G. Corley, and Aimee L. Hamilton. "Seeking qualitative rigor in inductive research: Notes on the Gioia methodology." Organizational research methods 16.1 (2013): 15-31.

Lazarte, Alfredo. 2017. “Understanding the Drivers of Rural Vulnerability.” Understanding the Drivers of Rural Vulnerability. 2017.

Mantero, G., Morresi, D., Marzano, R. et al. The influence of land abandonment on forest disturbance regimes: a global review. Landscape Ecol 35, 2723–2744 (2020). https://doi.org/10.1007/s10980-020-01147-w

Miller Rebecca K., Mach Katharine J. (2022) Roles and experiences of non-governmental organisations in wildfire response and recovery. International Journal of Wildland Fire 31, 46-55. https://doi.org/10.1071/WF21080

Nunes, Leonel J.R., Mauro A.M. Raposo, Catarina I.R. Meireles, Carlos J.P. Gomes, and Nuno M.C.A. Ribeiro. 2021. "Energy Recovery of Shrub Species as a Path to Reduce the Risk of Occurrence of Rural Fires: A Case Study in Serra da Estrela Natural Park (Portugal)" Fire 4, no. 3: 33. https://doi.org/10.3390/fire4030033

Nunes, L.J.R.; Raposo, M.A.M.; Pinto Gomes, C.J. A Historical Perspective of Landscape and Human Population Dynamics in Guimarães (Northern Portugal): Possible Implications of Rural Fire Risk in a Changing Environment. Fire 2021, 4, 49. https://doi.org/10.3390/fire4030049

Ostrom, Amy L., Joy M. Field, Darima Fotheringham, Mahesh Subramony, Anders Gustafsson, Katherine N. Lemon, Ming-Hui Huang, and Janet R. McColl-Kennedy. 2021. “Service Research Priorities: Managing and

Delivering Service in Turbulent Times." Journal of Service Research 24 (3): 329–53. https://doi.org/10.1177/10946705211021915.

Shukla, P. R. ; Skeg, J. ; Calvo Buendia, E. ; Masson-Delmotte, V. ; Pörtner, H.-O. ; Roberts, D. C. ; Zhai, P. ; Slade, R. ; Connors, S. ; van Diemen, S. ; Ferrat, M. ; Haughey, E. ; Luz, S. ; Pathak, M. ; Petzold, J. ; Portugal Pereira, J. ; Vyas, P. ; Huntley, E. ; Kissick, K. ; Belkacemi, M. & Malley, J. (eds.) (2019). Climate Change and Land: an IPCC special report on climate change, desertification, land degradation, sustainable land management, food security, and greenhouse gas fluxes in terrestrial ecosystems.

Weiss, Gerhard, Marla R. Emery, Giulia Corradini, and Ivana Živojinović. 2020. "New Values of Non-Wood Forest Products." Forests 11 (2): 165. https://doi.org/10.3390/f11020165.

Modeling wind adjustment factor in Mediterranean stands of Southern Europe

Juan Ramón Molina*[1]; Macarena Ortega[1]; Juan Antonio Navarro[2]; Francisco Rodríguez y Silva[1];

[1] University of Cordoba. Forest Fire Laboratory. Edificio Leonardo da Vinci. Campus de Rabanales, Córdoba, Spain, {jrmolina, macarena.ortega, ir1rosif}@uco.es
[2] Universitat Politècnica de Catalunya. Centre d´Estudis del Risc Tecnològic. Barcelona, Spain, {juan.antonio.munoz@upc.edu}

**Corresponding author*

Keywords

Wind speed; drag coeffcient; midflame wind; fire behavior; forest characterization

Abstract

Wind speed, that is strongly affected by terrain and vegetation, is one of the most important factors on fire spread. Fire simulators calculate wind speed as open 10-m wind speed multiplied by the wind adjustment factor (WAF). In forested sites, the sub-canopy wind speed plays a keystone role in low intensity fire or prescribed burn, and therefore, in prescribed burn plan. This research aims to estimate a WAF model based on in-stand wind speed at 2-m above ground and forests characteristics. Different sampling sites were established for WAF training and test. WAF range from 0.03 and 0.84, showing significant differences due to stand characteristics. Our findings showed canopy cover as the most influenced variable in WAF. On the one hand, the non-linear WAF model reached a coefficient of determination of 87.4%, including a second variable: the vertical distance between surface vegetation and the canopy base height. This approach proposes a novel method for the identification of WAF for prescribed fire implementation without the source of error could be generated using fixed WAF for each fuel model. The proposed model can be used to simulate different canopy management alternatives both fuel treatments and timber harvesting.

1. Introduction

Wind is affected by terrain, vegetation and the heigh above the ground (Andrews, 2012). The wind adjustment factor (WAF) has been widely used to identify a midflame wind from the 20-ft wind speed (Andrews, 2012). The midflame wind, which is used by several fire simulators, such as Behave Plus and FlamMap, is calculated as the product between 20-ft wind speed ("free wind") and WAF. In the case of Europe, weather station observations at 10-m height, clear ground, are used in opposition to 20-ft height following meteorological standards of the World Meteorological Organization (Brock, 2001). However, WAF depends on the vegetation characteristics and roughness (Mueller et al., 2014). The WAF, which is dimensionless (< 1), is reduced based on forest canopy and roughness (Albini and Baughman, 1979).

WindNinja software models wind speed according to terrain exposure and vegetation type. Other computational fluid dynamics (CFD) approaches, such as FIRETEC (Pimont et al., 2011) and WFDS (Mueller et al., 2014), can modify the wind speed based on fluid physical analysis. Although wind simulation using fluid dynamics is very realistic, a great time is required to run. Some approaches have been developed to simplify WAF calculation and to minimize the running time. Firstly, Deeming et al. (1977) assigned a mean WAF for each fuel model according to free wind at 20-ft height. Albini and Baughman (1979) proposed two mathematical models based on sheltered and unsheltered vegetation from the wind. Subsequently, Baughman and Albini (1980) modified the initial WAF for each fuel. Finney et al. (2011) proposed a WAF based on surface fuel bed depth.

Although wind speed profile is adjusted as a logarithmic function in open areas (Andrews, 2012), a complex wind profile is shown in forested areas due to the vegetation height, canopy cover and plant are density profile (Queck et al., 2010, 2012). Some authors (Gillies et al., 2002) have even proposed differences between species, but they suggested that is not be large enough to have a practical implication. However, a simplified wind profile simulation assumes a constant sub-canopy WAF when canopy gaps and topographical position could increase

wind speed due to Venturi effect (Molina et al., 2022). Therefore, WAF could be also affected by wind speed (Moon et al., 2019). All the above antecedents, subcanopy WAF plays a keystone role in surface fire spread in low intensity fires and prescribed fires, but a source of error could be generated using fixed WAFs for each fuel model.

This research aims to propose a mean wind adjustment factor (WAF) at 2-m above ground based on canopy characteristics. We attempt to find the relationship between reference wind (open area) and wind speed at 2-m height with different forests characteristics. In this sense, the identification of canopy characteristics that can affect wind speed and, therefore, fire intensity is essential for improving fire behavior models and prescribed burn plans.

2. Material and methods

2.1. Study area

Different forested sites were selected across southern Spain, covering two administrative regions (Andalusia and Castilla la Mancha) (Figure 1). Forested areas were dominated by *Pinus* species with and without understory. While 53.66% of the sampling sites were sheltered sites, 46.34% of the sampling sites were in unsheltered sites. One hundred meters was established as threshold to compare open wind speed and in-stand wind speed.

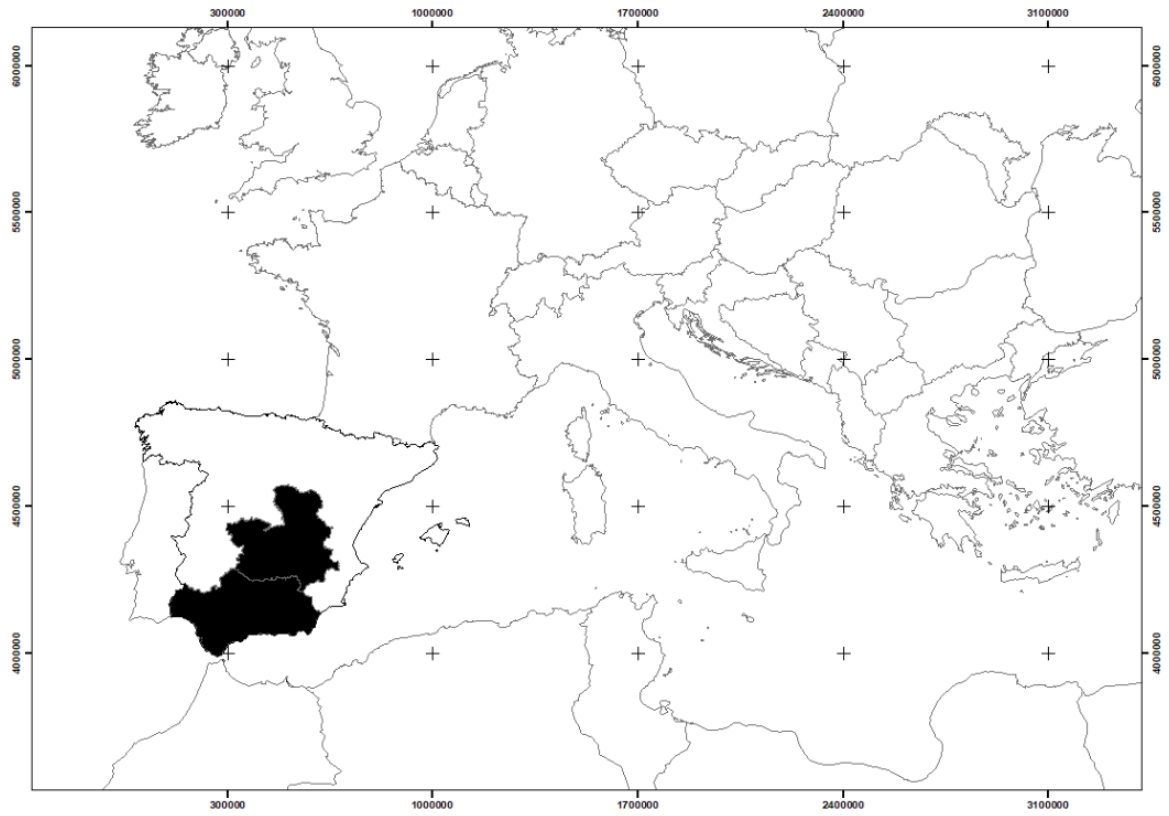

Figure 1- Study area location

Vegetation data was collected using circular plots of 20 m de radius. The vegetation inventory included variables such as stand density, stand height, canopy base height (live branch and dead branch), diameter at breast height, crown diameter and understory height. Basal area was calculated based on diameter at breast height and stand density. Canopy cover was estimated using the sum of tree crown vertical projection divided by the total area. The range of the vegetation characteristics was defined in Table 1.

Table 1. Range of the dependent and independent variables

Variable	Range
Wind adjustment factor	0.03 – 0.89
Wind speed (km/h)	0 – 47.2
Canopy cover (%)	10 – 100
Stand density (trees/ha)	10 – 1,205
Diameter at breast height (cm)	14 – 38.56
Stand height (m)	4.5 – 14.40
Basal area (m^2/ha)	13 – 65.53
Canopy base height (m)	4.5 – 15.3
Canopy dead base height (m)	0.1 – 71.91
Crown length (m)	0.44 – 7.57
Crown ratio	0.44 – 6.00
Undergrowth height (m)	1.10 – 9.01
Vertical distance between surface vegetation and the canopy base height (m)	0 – 7.57
Vertical distance between surface vegetation and the canopy dead base height (m)	0 – 5.63
Topographical stand position (unsheltered and sheltered stand)	1 = stand on flat or near base of mountain 2 = stand on high ridges

2.2. Wind speed measurements

Wind speed measurements were carried out from 2014 to 2020 using a meteorological vehicle and ThiesClima weather stations at open-canopy sites and guyed-mast with SkyWatch weather stations at sub-canopy wind speed (Figure 2). Wind speed was measured at height of 2 and 6 m (sub-canopy sites) and 10 m (reference open sites). Although the weather stations recorded data each ten seconds, the data were analyzed as ten minutes averaging interval to reduce effects of canopy cover. Our research has the limitations of the use of cup anemometer in-stand measures with turbulence patterns.

Figure 2- Weather stations used in this approach

2.3. WAF calculation

Although WAF can be modified by wind speed, this research identified an average WAF for a wide range of wind speed due to the reduced wind speed traditionally used for prescribed burns. WAF is calculated as the ratio between in-stand wind speed at 2-m of height (U_c) and open wind speed at 10 m above ground (U_o) (Equation 1).

$$WAF = U_c / U_o \quad \text{Equation 1}$$

2.4. Statistical analysis

Some statistical tests were performed using SPSS© software. Multi-linear and non-lineal models were tested to identify the best adjustment for WAF based on forest characteristics. A subsample of 70% of the dataset was

used for model training and 30% of the dataset for model test. The coefficient of determination, the mean absolute error (MAE), and the root mean square error (RMSE) were used to select the best model. Finally, a Wilcoxon test was used to identify significant differences in WAF based on canopy cover and unsheltered and sheltered fuels (< or > 50% of canopy cover).

3. Results

The wind adjustment factor (WAF) ranged from 0.01 to 0.84 for the different sampled sites. Canopy cover (CC) was the most related variable for WAF. Although basal area and stand density were the most important variables immediately following CC, they were strongly correlated with CC. The proposed model included two independent variables: canopy cover and the distance between surface vegetation and the canopy dead base height (z) (Table 2). While CC was negatively related to WAF, z was positively related to WAF. The coefficient of determination reached a value of 0.780 with only one variable. RMSE ranged from 1.21 m to 4.94 m and MAE was between 1.39 m and 5.85 m based on the training and test dataset, respectively.

Table 2. WAF model based on vegetation characteristics

Model	Parameter	Estimation	R^2	RMSE	MAE
WAF = a*FCC + EXP (b*CC)	a	2.594	0.780	0.29	0.11
	b	-0.033			

Note: FCC is the canopy cover (%) and CC is the canopy cover (%)

4. Discussion

Drag coefficient depends on wind speed, air density and contact area (Queck et al., 2010). Our findings observed higher WAF with light winds than heavy winds due to higher contact area like other studies (Queck et al., 2012). Considerable heterogeneity was found in vertical wind profiles based on vegetation structure and characteristics (Cassiani et al., 2008). Our findings showed canopy cover as the most influenced variable in WAF, like other approaches (Pimond et al., 2011). While some authors (Mueller et al., 2014) showed WAF range in canopies between 0.15 and 0.37, other studies (Moon et al., 2019) showed a wide WAF variation between open woodlands and dense forests. In our study area, WAF ranged from 0.03 to 0.89, showing differences more than nine times in dense stands than in open woodlands. Pimont et al. (2011) identified significant differences in treated areas with canopy cover lower than 25%, but they did not find significant differences with cover higher than 50%. We found significant differences with canopy cover lower than 30% and higher than 50%. Further studies would focus on the WAF adjustment based on the canopy fuel load.

There was a significant variation in the range of the WAF when they are compared to reference values or fuel model values used by fire simulators. We wonder that the limited sampling could be an issue here as possibly the adjustment could be different in different regions. BehavePlus offers the possibility to consider unsheltered o sheltered fuel models (Andrews, 2012). While fully sheltered WAF from BehavePlus varied from 0.1 (dense stands) to 0.2 (open stands), unsheltered WAF ranged from 0.3 to 0.4 from timber-understory and timber-litter fuel models. The reference WAF for canopy cover higher than 50% is like our WAF for very dense stands (cover higher than 90%) and other values found in literature from sheltered stands (Queck et al., 2012). Finally, although Baughman and Albini (1980) and NWCG (2006) performed significant WAF differences between shade-intolerant and shade-tolerant species, in our study are they were did not found due to the usual presence of Mediterranean mixed stands.

Wind speed at low canopy layer plays a keystone role in prescribed fire implementation. Canopy cover can be estimated by satellite images, hyperspectral images, and LIDAR data to improve economically the cartography required by WAF and fire simulation. With the help of LIDAR data and Geographic Information System, we performed WAF for different prescribed burns based on our test model. WAF variation implies a change in fire behavior, mainly in spread rate, flame length and fire-line intensity. A change in rate of spread and flame length would promote a higher fire-line intensity (Byram, 1959), and therefore, a higher scorch height and damages to trees (Molina et al., 2022). The wind speed modeling is a very complex phenomenon (Moon et al., 2019). Although computational fluid dynamics can precisely model the air flow (Pimont et al., 2011), forest managers

demand easy tools for use "in situ" or "on the fireline" for supporting changes in fire-ignition patterns of prescribed burns. The proposed model can be used to simulate different management alternatives and for discerning the most appropriate canopy cover to the achieve the trade-off between canopy fuel load and wind speed.

5. Acknowledgements

This research was supported by the following projects: VIS4FIRE (RTA2017-00042-C05-01), ENFIRES (PID2020-116494RR-C44) from Spanish Ministry of Science and Innovation; CILIFO (POCTEP-0753_CILIFO_5_E) and FIREPOCTEP (POCTEP-0756_FIREPOCTEP_6_E) from the European Union; and Regional FEDER 2014-2020 project (Tool for the efficiency and sustainable management of the Mediterranean forest landscape against forest fires.

6. References

Albini F.A., Baughman R.G., 1979. Estimating windspeeds for predicting wildland fire behavior. Research Paper INT-221. U.S. Department of Agriculture. Forest Service. Intermountain Forest and Range Experiment. Ogden, 92 p.

Andrews P., 2012. Modeling wind adjustment factor and midflame wind speed for Rothermel's surface fire spread model. General Technical Report RMRS-GTR-266. Department of Agriculture, Forest Service. United States. Rocky Mountain Research Station, 39 p.

Baughman R.G., Albini F.A., 1980. Estimating midflame windspeeds. In: Society of American Foresters. Proceedings of the Sixth Conference of Fire and Forest Meteorology. Seatle. USA. 88-92.

Brock F.V., Richardson S.J., 2001. Meteorological measurement systems. Oxford University Press. New York.

Byram, G.M., 1959. Combustion of forest fuels. In: Davis, K.P. (Ed.), Forest Fire: Control and Use. McGraw-Hill, New York, NY, pp. 61–89, 554–555.

Cassiani M., Katul G.G., Albertson J.D., 2008. The effects of canopy leaf area index on airflow across forest edges: large-eddy simulation and analytical results. Boundary-Layer Meteorology 126(3), 433-460.

Deeeming J.E., Burgan R.E., Cohen J.D., 1977. The National Fire-Danger Rating System-1978. General technical Report INT-39. U.S. Department of Agriculture. Forest Service. Intermountain Forest and Range Experiment Station. Ogden, 63 p.

Finney M., 1998 [revised 2011]. FARSITE. Fire Area Simulator-model development and evaluation. Research Paper RMRS-RP-4. U.S. Department of Agriculture. Forest Service. Rocky Mountain Research Station. Ogden, 47 pp.

Gillies J.A., Nickling W.G., King J., 2002. Drag coefficient and plant form response to wind speed in three plant species: Burning Bush (*Euonymus alatus*), Colorado Blue Spruce (*Picea pungens* glauca.), and Fountain Grass (*Pennisetum setaceum*). Journal of Geophysical Research 107(24), 10-15.

Molina J.R., Ortega M., Rodríguez y Silva F., 2022. Scorch height and volume modeling in prescribed fires: Effects of canopy gaps in *Pinus pinaster* stands in Southern Europe. Forest Ecology and Management 506, 119979.

Moon K., Duff T.J., Tolhurst K.G., 2019. Sub-canopy forest winds: understanding wind profiles for fire behaviour simulation. Fire Safety Journal 105, 320-329.

Mueller E., Mell W., Simeoni A., 2014. Large eddy simulation of forest canopy flow for wildland fire modeling. Canadian Journal of Forest Research 44, 1534-1544.

NWCG, 2006. NFCW fire-line handbook Appendix B: fire behavior. PMS 410-2/NFES 2165. National Interagency Fire Center. Boise, 124 pp.

Pimont F., Dupu J.L., Linn R., Dupont S., 2011. Impacts of tree canopy structure on wind flows and fire propagation simulated with FIRETEC. Annals of Forest Science 68, 523-530.

Queck R., Bienert A., Maas H.G., Harmansa S., Goldberg V., Bernhofer C., 2012. Wind fields in heterogeneous conifer canopies: parameterization of momentum absorption using high-resolution 3D vegetation scans. European Journal of Forest Research 131, 165-176.

Queck R., Bernhofer C., 2010. Constructing wind profiles in forests from limited measurements of wind and vegetation structure. Agriculture and Forest Meteorology 150, 724-735.

Numerical simulation of the aerial drops of the Canadair CL-415 and the Dash-8 airtankers

Corentin Calbrix[1,2]; Alexei Stoukov[1]; Axelle Cadière[2]; Benoit Roig[2]; Dominique Legendre[1,*]

[1]*Institut de Mécanique des Fluides de Toulouse (IMFT) - Université de Toulouse, CNRS-INPT-UPS, 31400 Toulouse, France, {corentin.calbrix@toulouse-inp.fr}, {stoukov, Legendre}@imft.fr*
[2]*Université de Nîmes ; Laboratoire CHROME. 7 Place Gabriel Péri, France, {axelle.cadiere, benoit.roig}@unimes.fr*

** Corresponding author*

Keywords

Airtanker, Aerial drop, Numerical simulation, Fluid mechanic, Liquid atomization

Abstract

Fighting wildland fires is a major issue for the protection of populations and environment with a need of more efficient means to fight fires. Airtankers are able to drop volumes of liquid (water or fire retardant) varying from less than 1m3 to several tens of m3, directly on fire or with the objective to form barriers of retardant to stop or reduce the fire propagation. However, the dynamics of a liquid dropped from an airplane has received few attentions in the scientific community, and related studies have mostly focused on Newtonian liquid jets injection in cross flow from millimetric injectors for combustion applications. For firefighting purpose, the liquid can be a retardant (a non Newtonian fluid) and the characteristic size of the delivery systems is of the order of a meter. The objective of this work is to demonstrate that Computational Fluid Dynamics (CFD) can be used to provide a deep understanding of the liquid fragmentation and dispersion when dropped from an aircraft. A numerical investigation is proposed for the analysis of airtanker performance and applied here to the biggest airtankers used in Europe: the Canadair CL-415 and the Dash-8. A numerical approach based on the Volume of Fluid method (VoF) is used to provide an accurate description of the tank discharge as well as to study the liquid ejection, fragmentation and atomization in air. The 3D unsteady resolution of the Navier-Stokes equations for both the liquid and the air allows us to provide a description of the main characteristics of the resulting liquid cloud, characterized by the vertical penetration of the liquid, its lateral expansion and the process of atomization.

1. . Introduction

Airtanker performances are usually tested with the cup & grid method (Suter 2000) developed by the USDA Forest service in USA and by the CEREN in France. Depending on drop conditions and systems, the resulting liquid deposit can present some irregularities resulting in zones of large concentration of product separated by zones of lower concentration offering a lower protection against fire (Plucinski *et al.* 2007). However, the dynamics of a fluid dropped from an airplane has received few attentions in the scientific literature with the development of simplified modelling (Amorim 2011; Legendre *et al*. 2014; Qureshi and Altman 2018), experiments in wind tunnel (Ito *et al*. 2010;) or numerical simulation (Rimbert 2003; Zhao *et al*. 2018). When considering airtanker the size of the delivery system doors is of the order of a meter, thus 3 orders of magnitude larger than millimetric injectors in combustion applications extensively investigated (Broumand and Birouk 2016), resulting in fragmentation and atomisation over a larger range of spatial scales making the experimental investigation more challenging. For that purpose, the use of Computational Fluid Dynamics (CFD) that allows to solve the liquid evolution after its exit from the tank can offer a promising tool. Indeed, all the information of the fluid evolution both in time and in space are available for a deep investigation. The objective of this work is to introduce the numerical approach proposed for the analysis of airtanker performance.

This study considers the aerial fleet of the French Civil Protection, more specifically the Canadair CL-415 and the Dash-8. These two airtankers are using different delivery systems. The Canadair CL-415 is made of two tanks incorporate in its fuselage and can drop a maximum of 6000 L of liquid. It has scoops on its belly, and can slide along a water surface to fill its tanks. The Canadair CL-415 is mostly used for a direct attack of the fire with water. The Dash8 is a fret plane reconverted with a tank attached under its belly and can drop a maximum of 10,000 L of liquid. Its tank is filled on the tarmac and this airtanker is used to provide line of

retardant in coordination with ground operations. A numerical approach based on CFD is used here to describe the liquid drop and atomization in air.

The paper is organized as follows. In section 2, the numerical method used for this study is presented. The liquid atomization and dispersion in air is then described in section 3.

2. Numerical methods

In this first approach we consider a Newtonian fluid (water) of density ρ_L and viscosity μ_L released at velocity U_L in air of density ρ_G, viscosity μ_G and relative velocity U_G. For that purpose, we solve the 3D unsteady Navier-Stokes equations for two incompressible and immiscible Newtonian fluids. Considering the Volume of Fluid (VoF) approach, the interface between the two fluids is obtained by solving the transport equation of the VoF function (or liquid volume fraction) α ($0 \leq \alpha \leq 1$):

$$\frac{\partial \alpha}{\partial t} + \nabla . \alpha v = 0 \quad (1)$$

The evolution of the fluids velocity v and pressure P are given by the conservation of mass and momentum

$$\nabla . v = 0 \quad (1)$$

$$\frac{\partial \rho v}{\partial t} + \nabla . (\rho v v) = -gradP + \nabla . \bar{\bar{T}} + \rho g \quad (2)$$

where t is the time, $\rho = \alpha \rho_L + (1-\alpha) \rho_G$ is the one-fluid density, $\bar{\bar{T}}$ is the viscous stress tensor expressed using the one-fluid viscosity $\mu = \alpha \mu_L + (1-\alpha) \mu_G$ and g is the gravity. The numerical solver of Star CCM++ has been used and turbulence has been modeled with a standard k-ε model. The meshes built for the simulations are described in the following sections. For each case, at least two meshes of different resolution have been considered in order to test the effect of the grid resolution on the results. The simulations have been performed on the regional Super computer CALMIP based in Toulouse.

The proposed numerical approach has two steps. First, CFD is used to describe the respective tank discharge in order to provide an accurate description of the discharge flow rate. For that purpose, the tank geometries of the CL-415 and Dash-8 have been designed and meshed. For the geometry of the Canadair's tank, a trimmed cell mesher has been used. The number of cells is around 810 000 and their size ranges from 1.10^{-2} m at the center of the tank to 5.10^{-6} m at the walls. For the geometry of the Dash tank, a polyhedral mesher has been used. The number of cells is around 1.9 millions, and their size ranges from 2.10^{-2} m at the center of the tank to 5.10^{-6} m at the walls. The resulting time evolution of the liquid velocity U_L(t) at the exit of the two tanks has recorder. The maximum velocity observed after 0.5s for the two tanks is around 6 m/s for the Canadair and 4.8m/s for the Dash8. The time to discharge the Canadair tank is around 1s while it is around 4s for the Dash8. This information is then considered for the second step to study the liquid drop and atomization in air. U_L(t) is imposed as inlet condition as described in the next section.

3. Liquid drop from Canadair CL-415 and Dash8

3.1. Domains and meshes

The second objective of the numerical approach is to simulate the dynamics of the liquid ejection, fragmentation and dispersion in air. The simulations are conducted in the frame of reference moving with the airplane. For each case, the air flow velocity is imposed at U_G=50 m/s at the domain inlet, which corresponds approximately to an operational speed for these aircrafts. Each belly of the studied airplanes has been meshed in an adapted domain. The domain is selected in order to observe the liquid fragmentation during its evolution in air while minimizing the size of the computational domain to reduce the number of cells. Several domain shapes have been tested and the selected ones are shown in Fig. 1 for the Canadair and the Dash-8.

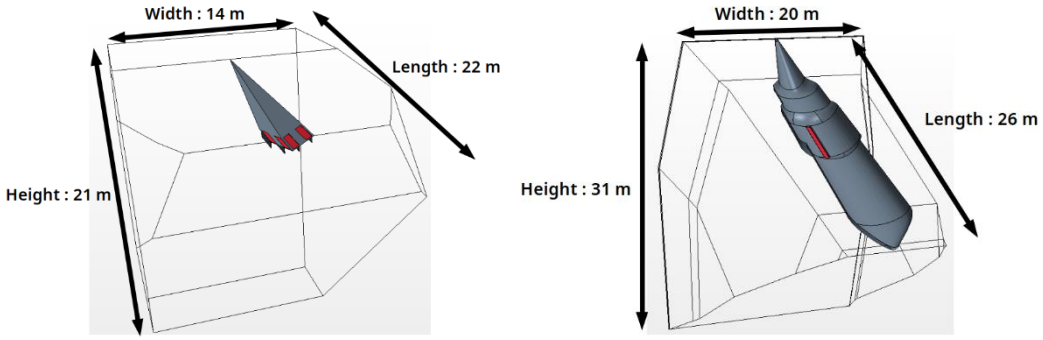

Figure 1 - Dimensions of the numerical domain. (left) under a Canadair belly with the four exits in red. (right) under a Dash8 belly with the exit in red.

Due to the complex geometry of the belly and the sharp angles on the corner of the domains, we have chosen in both cases a polyhedral mesher. The grid size ranges from 8.10^{-6}m at the walls to 8.10^{-2}m in the center of the domain. The total number of cells are 6.9 millions and 10.9 millions for the Canadair and Dash8, respectively. Parallel simulations made use of 180 and 720 processors, with computation CPU time of 18h and 40h, respectively. The liquid evolution in air is described in the following by considering its vertical penetration, lateral expansion and atomization. The liquid interface being tracked with the VoF model, we are able to select different values for the liquid volume fraction α for the liquid cloud inspection. "The liquid core" corresponds to $0.9 \leq \alpha \leq 1$, while the envelop of the liquid cloud can be described by considering $0.001 \leq \alpha \leq 1$.

3.2. Liquid vertical penetration

The liquid vertical penetration is defined as the evolution of the vertical distance *z* of the front of the liquid surface as a function of the streamwise distance *y*, red and black arrows in Fig 2, respectively. The shape of the corresponding curve indicates how the liquid front is deformed by the impact of the relative air flow. The liquid penetration *z* is compared for the Canadair and Dash8 in Fig. 2 at *t*=0.5s. As shown the penetration of the Dash8 and the Canadair are very close because the liquid velocity is of the same order of magnitude at *t*=0.5s. This confirm results observed for millimetric liquid jets where the penetration is controlled by the momentum ratio $q = \rho_L U_L^2 / \rho_G U_G^2$. Then the liquid penetration for the Canadair rapidly decreases and becomes less important than observed for the Dash-8.

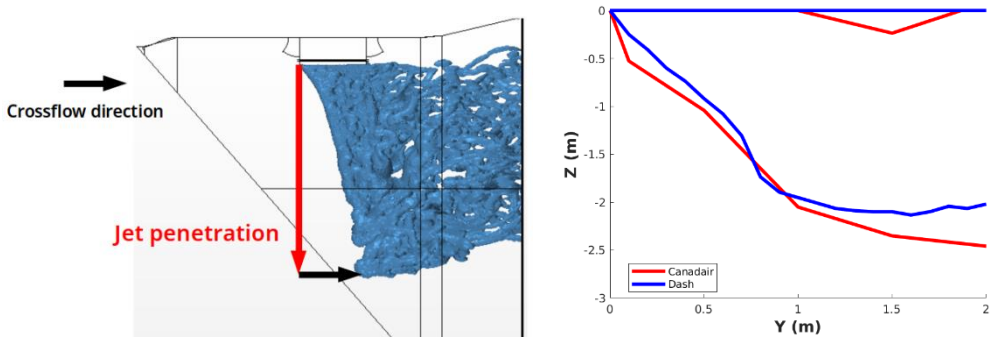

Figure 2 – Liquid penetration. (left) Visualization of the iso-surface of a=0.001 for the Dash8 at t=1s. (right) Comparison at t=0.5s of the liquid vertical penetration z as a function of the streamwise distance y for a Canadair (red) and a Dash8 (blue).

3.3. Liquid lateral expansion

The lateral (or transverse) expansion *x* is defined as the maximum width of the dispersed liquid as shown in figure 3. This parameter is important because its evolution controls the final width of the liquid deposit on ground. As shown in the figure, the lateral expansion is reduced for the Dash-8 compared to the Canadair, resulting in a more narrow liquid deposit on ground, and thus a higher liquid concentration.

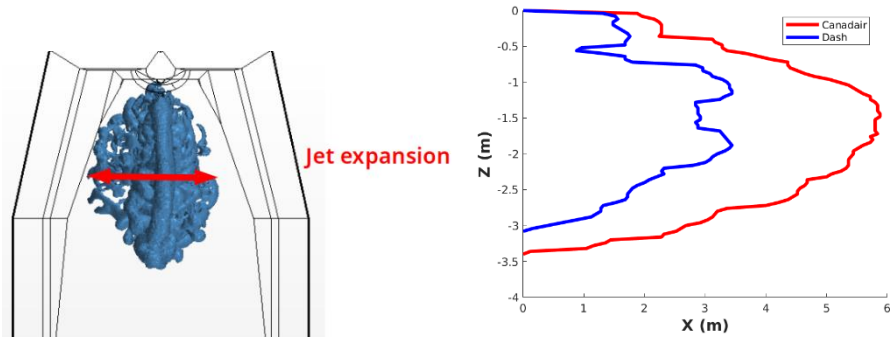

Figure 3 – Liquid lateral expansion. (left) Visualization of the iso-surface of a=0.001 for the Dash-8 at t=0.5s. (right) Comparison of the liquid lateral expansion x as a function of the streamwise distance y for a Canadair (red) and a Dash8 (blue).

3.4. Liquid atomization in air

One important aspect of the liquid evolution in air is related to the liquid fragmentation and dispersion. The objective is to finally obtain on ground a uniform liquid deposit. We consider here the evolution of the number and the size of produced droplets as illustrated by figure 4 with the observation of the formation of ligaments and droplets of large volume (several tens of cm). The shear stress from the air at the liquid surface tear off liquid ligaments, which are then fragmented into liquid volumes of different size. Their following dynamics may differ and result in different contributions to the ground pattern.

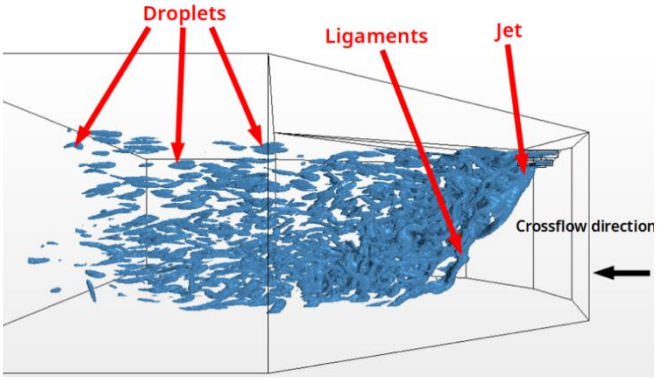

Figure 4 – Liquid atomization process for a Canadair CL-415 drop at t=1s. The iso-surface of the volume fraction is a =0.001.

A Matlab code has been developed to reconstruct the 3D liquid structures at each instant, to characterize their respective velocities and sizes. Figure 5 (left) reports the time evolution of the number of the identified liquid structures for the Canadair CL-415 for two thresholds for the detection: $\alpha \geq 0.9$ and $\alpha \geq 0.1$. The first one identifies droplets while the second one identifies volume of fragmented liquid in a more important number. Figure 5 (right) shows the distribution of droplets with their respective velocities for three different classes of size. The velocity components v_Z, v_Y and v_X, for the vertical, streamwise and transverse components, respectively, are reported. As shown the streamwise velocity is much larger because imposed by the relative airflow (50m/s), and the vertical velocity of lower magnitude is controlled by the velocity at ejection. The order of magnitude of the transverse velocity is around 1m/s, showing a significant liquid dispersion in the transverse direction.

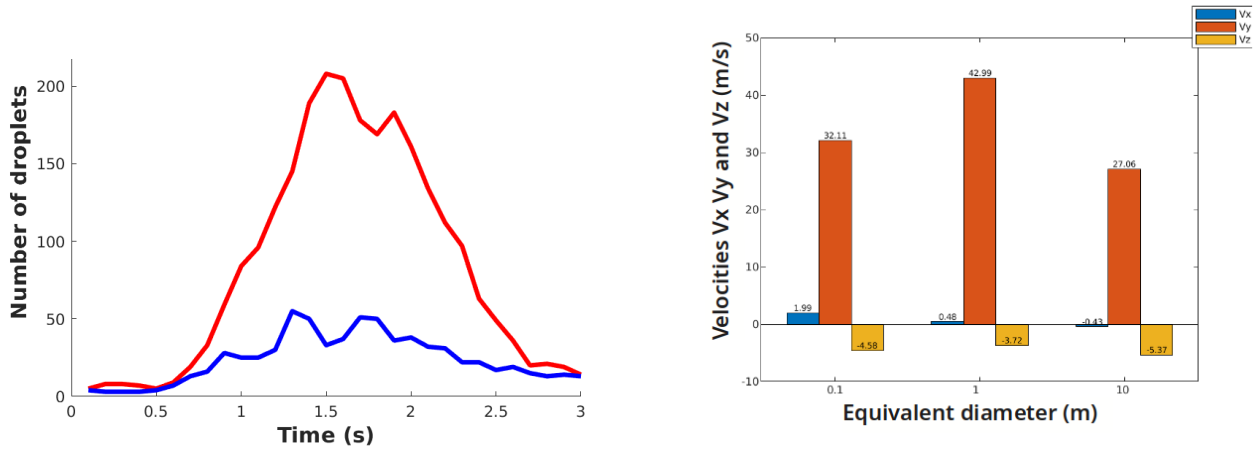

Figure 5 – Liquid fragmentation for the Canadair CL-415. (left) Time evolution of the number of identified fluid structures. Comparison for a detection using a liquid volume fraction a between 0.1 and 1 (red), and 0.9 and 1 (blue). (right) Repartition of the droplets with their respective velocities and size at t=1s for a detection with a volume fraction a between 0.1 and 1.

4. Conclusion

In this work, a numerical strategy has been proposed to deeply investigate the drop of a liquid from an airtanker. For this study, we have considered water drop from the Canadair CL-415 and the Dash-8. The 3D unsteady resolution of the liquid motion for both the liquid and the air allows us to provide a description of the main characteristics of the resulting liquid cloud. These liquid drops have been characterized through three main parameters: the vertical penetration, the lateral expansion and the structure of the liquid cloud during the atomization process. The next step will consist in extrapolating from these simulations the resulting liquid deposit on ground in order to make possible a direct comparison with the real tests performed using the cup & grid method.

5. Acknowledgments

This project is funded by Nîmes Métropole. It also benefited computation resources on the super computer CALMIP under the allowance 2020 – P20015.

6. References

Amorim J. H. (2011) Numerical modelling of the aerial drop of firefighting agents by fixed-wing aircraft. Part I: model development, *International Journal of Wildland Fire*, **20**, 384–393.

Broumand M, Birouk M (2016) Liquid jet in a subsonic gaseous crossflow: Recent progress and remaining challenges Progress, *Energy and Combustion Science*, **57**, 1–29.

Ito T, Kato H, Goda Y, Tagawa S, Negishi E (2010) Water-dropping aerodynamics for fire-fighting amphibian, 27th International congress of the aeronautical science (ICAS2010).

Legendre D, Becker R, Alméras E, Chassagne A (2014) Air tanker drop patterns, *International Journal of Wildland Fire*, **23**(2), 272-280.

Plucinski M, Gould J, Mccarthy G, Hollis J (2007) The effectiveness and efficiency of aerial firefighting in Australia, Part 1, Bushfire CRC Technical Report n°A0701, Australia. Www.bushfirecrc.com/sites/default/files/managed/resource/aerial_suppression_report_final_web_0.pdf

Qureshi S, Altman A, (2018) Studying fluid breakup and dispersion to predict aerial firefighting ground drop patterns, AIAA Aerospace Sciences Meeting.

Rimbert N (2003) Contribution à l'étude de la pulvérisation et de la dispersion dans l'air de fluides newtoniens et non-newtoniens. Application au largage aérien d'eau et de mélanges retardants, PhD thesis, Institut National Polytechnique de Lorraine, Nancy, France.

Suter A (2000) Drop testing airtankers: a discussion of the cup-and-grid method, USDA Forest Service, Missoula Technology and Development Center, Technical Report 0057-2868-MTDC.

Zhao X, Zhou P, Yan X, Weng Y, Yang X-L (2018) Numerical simulation of the aerial drop of water for fixed-wing airtankers, 31st International congress of the aeronautical science (ICAS2018).

Numerical study of high intensity experimental field fires across Corsican shrubland vegetation

Jacky Fayad[1]*; Lucile Rossi[1]; Nicolas Frangieh[1]; Carmen Awad[1]; Gilbert Accary[2]; François-Joseph Chatelon[1]; Frédéric Morandini[1]; Thierry Marcelli[1]; Valérie Cancellieri[1]; Dominique Cancellieri[1]; Dominique Morvan[3]; Antoine Pieri[1]; Gilles Planelles[5;6]; René Costantini[5]; Patrice Briot[7]; Sofiane Meradji[4]; Jean-Louis Rossi[1]

[1] *UMR CNRS SPE 6134, Université de Corse - CNRS, 20250 Corte, France, {fayad_j@univ-corse.fr}*
[2] *Scientific Research Center in Engineering, Lebanese University, Beirut, Lebanon*
[3] *Aix-Marseille Univ, CNRS, Centrale Marseille, M2P2, Marseille, France*
[4] *IMATH laboratory, EA 2134, Toulon University, 83160 Toulon, France*
[5] *SIS2B, Centre Administratif du Fango, 20200 Bastia, France*
[6] *Office National des Forêt – Corse - Unité Production Travaux - Responsable UP*
[7] *Service régional ingénierie DFCI FORSAP de la collectivité de Corse*

**Corresponding author*

Keywords

Winter wildfires; field experiment; fire behaviour; physical fire model

Abstract

Field-scale experiments have been conducted on steep sloped terrains in Speluncatu and Letia, north-western and southern regions of Corsica. This work lies within the GOLIAT project framework and it was provided by the Fire and Rescue Service of North Corsica and the Corsican DFCI (Défense de la Forêt Contre l'Incendie) Group. This work reported high intensity fires propagating through shrub vegetation areas (*Genista Salzmannii*) lying between 60 cm and 85 cm. These sites were selected because of the density of the vegetation, the high slope angle values with a wind direction aligned with the main slope, which can generate a fire close to wildfire behaviour. A detailed experimental protocol is used in order to determine the propagation conditions and the fire behaviour using UAV cameras and heat flux gauges. In order to investigate the different phenomena encountered in these types of fires, numerical simulations were conducted using a complete physical fire model, based on multiphase formulation, namely FireStar2D. Numerical predictions were used to examine the fire front dynamics related to the fire's rate of spread and fireline intensity. Despite the unfavourable wind and humidity conditions, experimental results analysis showed that the fireline intensity was higher than 7 MW/m, which means that these fires fall into the category of the very high fire severity. Numerical results predicting the fire's rate of spread, fireline intensity and fire impact were in good agreement with the experimental data.

1. Introduction

Wildfires represent one of the main causes of the natural capital damage in the regions characterized by the Mediterranean climate like the Mediterranean basin, Chile, California, South Africa, and South and South-West of Australia. The Mediterranean climate is characterized by a high seasonality that can be summarized as hot, dry summers, and mild wet winters (di Castri 1981). Changes in climatic and weather conditions in these regions are one of the major reasons for the increase in wildfire risk, where they tend to be warmer and drier with more frequent heat waves (Benson et al. 2008; Sommers et al. 2011). Thus, in the presence of flammable vegetation, these climate conditions are prone to fire ignition and propagation. The real problem is that the Mediterranean region is witnessing a new wildfire context characterized by high intensity dangerous fires that present a real threat where their behaviour is unpredictable and uncontrollable.

In general, extreme fires are characterized by a high fireline intensity, and a high rate of spread, with the possibility of spotting or suddenly changing the fire behaviour (Alexander 1982). Firefighters know that beyond a threshold of 10 000 kW/m, a fire becomes erratic and incontrollable (Tedim et al. 2018). Indeed, fireline intensity has become one of the standard criteria by which firefighters estimate the difficulty of controlling a wildfire, and also the most appropriate descriptor of immediate fire effect on vegetation. The real problem is that extreme wildfire events tend to overwhelm suppression efforts, and cause lots of humans and economical

losses (Tedim et al. 2018; European Science & Technology Advisory Group 2020). This new context requires adapted policies to shift the focus from suppression to prevention that requires a good knowledge of the physical mechanisms governing fire behaviour like ignition, fire spread and fire impact. Many experimental fires have been conducted at the field scale (Cheney et al. 1993; Cheney and Gould 1995; Marsden-Smedley and Catchpole 1995; Vega et al. 1998; Viegas et al. 2002; Morandini et al. 2006; Mueller et al. 2018), but there are only few data for high intensity fires. Therefore, relevant experimental data on high-intensity wildfires is of paramount interest and experiments at the field-scale are highly valuable. Such fires are often subject to the vagaries of the weather and variations in the vegetation and land topography (Mulvaney et al. 2016). The interaction of these, and even with the fire itself, can result in seemingly capricious behaviour.

In this context the main purpose of this work is to present experimental data of the fires carried out at large scale fields, having important slopes, resulting in high fire intensities. This field-scale experiments have been conducted in two different regions of Corsica in March 2021 and 2022 and October 2021. In order to understand and investigate the different phenomena encountered in this type of fires, the experimental results are compared to the prediction provided by a complete physical model, namely FireStar2D (Morvan et al. 2009). In the next section the experimental method is described, followed by the modelling approach that was used. Finally, an analysis and a discussion of the relevance and the significance of the results are presented.

2. Experimental method

2.1. Site description and experimental protocol

Experimental sites were selected because of the structural homogeneity of the *Genista Salzmanni* vegetation with a coverage > 90%, and also because of the steep slopes that can generate high intensity fires. Slope values are obtained by measuring the coordinates of four poles positions as shown in Figure 1, using *a high-precision Global Navigation Satellite System (GNSS).* Concerning the experimental protocol, measuring devices were deployed in the field: Heat flux sensors and thermocouples were placed in the vegetation free area, video cameras were located on the sides of the plot, wind properties and ambient conditions were recorded using a weather station and fire propagation was recorded from above using a drone-mounted Visible-IR camera.

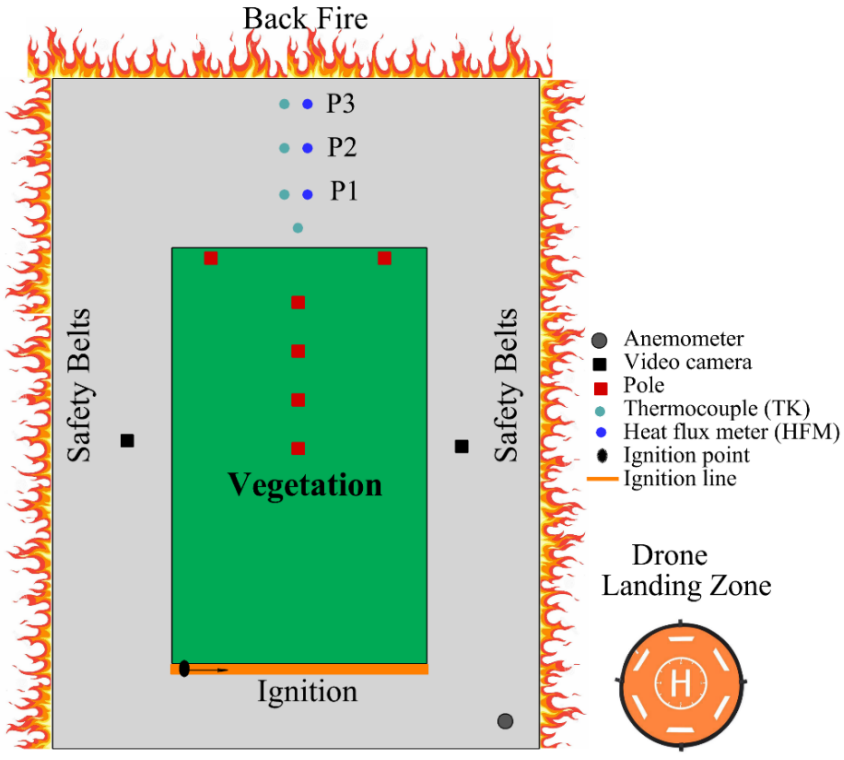

Figure 1- Schematic view of the experimental plot and the location of the measuring devices.

2.2. Characterization of the vegetation and meteorology

Physical properties of the vegetation are specific to the geographic area. Table 1 contains the main characteristics of the vegetation and meteorological conditions during the two burn campaigns. Fuel moisture content was evaluated after oven-drying fuel samples of dead and live fuel elements with diameter less than 6 mm at 60° for 48h (Awad et al. 2020). Fuel height was obtained after averaging 20 different measurements of the distance between the ground and the top of the vegetation. Ambient weather conditions were obtained less than 50 m away from the centreline of the plot, were a two-dimensional ultrasonic anemometer located at 3m above the ground recorder wind velocity and direction.

Table 1- Main average properties of Genista salzmannii vegetation and meteorological conditions

	Speluncatu March (2021)	**Speluncatu October (2021)**	**Letia March (2022)**
	Fuel Characteristics		
Fuel moisture content, FMC (%)	65	56	51
Fuel bed depth, e (m)	0.6	0.85	0.68
Fuel load, σ (kg/m^2)	1.8	1.79	2.67
Volume fraction, β	0.0031	0.0021	0.004
Surface-area to volume ratio, s (m^{-1})	3100		
Particle density, ρ_v (kg/m^3)	970		
Thermal capacity, Cp (J/kg/K)	1648		
Yield heat, ΔH_c (J/kg)	1.8620×10^7		
Thermal emissivity, ε	1		
Vegetation family shape	Cylindrical		
	Meteorological and topography conditions		
Average wind speed U_3 (m/s)	1.67	1.3	1.3
Ambient temperature T (°c)	6	18	15
Relative humidity RH (%)	82	53	36
Terrain slope value (°)	28	21.6	15.6

2.3. Experimental evaluation of fire parameters

2.3.1.ROS

The ROS represents one of the main parameters that characterize wildland fire behaviour. Fire front propagation is recorded using a drone located at a height of about 100 m, in order to determine the time needed by the fire to cross between the prefixed poles placed in the field. This allowed the evaluation of the ROS when the fire reaches a steady state propagation as shown in Figure 2.

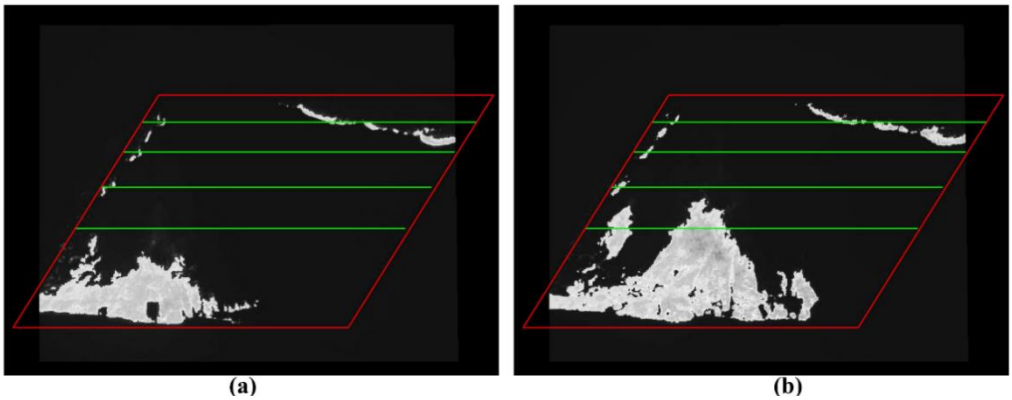

(a) **(b)**

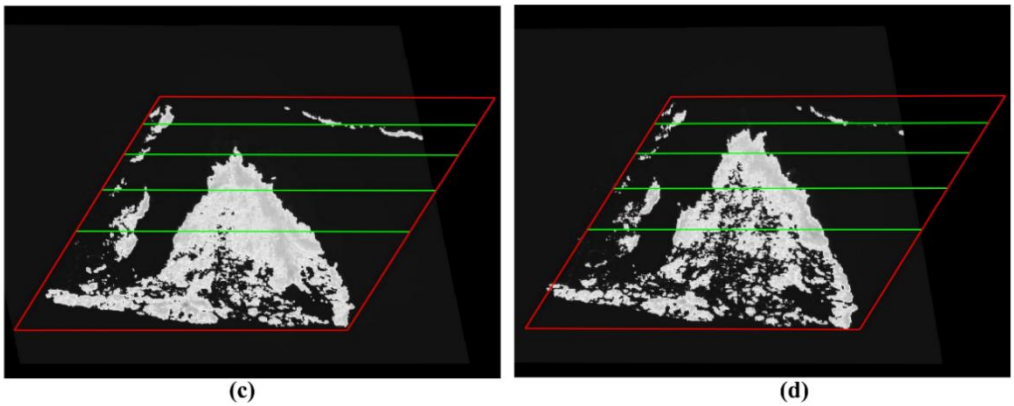

Figure 2- Infrared images of the fire front travel between equidistant positions (the green lines passing through prefixed poles) at different times.

2.3.2. Fireline intensity

Fireline intensity is estimated experimentally based on the Byram formulation: $I_{BExp} = \Delta H_c . w_a . ROS$, where $w_a = \mu\ \sigma$, with μ the percentage of the fuel weight actually consumed in the active flaming front and effectively contributed to fire propagation and ΔH_c represents the vegetation heat yield. This experimental method is often inaccurate because it is based on visual estimation of the burned vegetation during the fire (Alexander and Cruz 2020).

2.3.3. Heat fluxes

Concerning the fire impact evaluation, total and radiant heat fluxes were measured using three transducers (Figure 3) calibrated by the manufacturer in the range 0-200 kW/m^2, fixed on 0.5 m high supporting rods located at different positions from the upper limit of the vegetation plot.

Figure 3- Radiant and total heat flux sensors and thermocouple fixed on supporting rod and protected by aluminum foils.

3. Numerical method

3.1. Numerical modelling

Numerical simulations were conducted using a fully physical model, based on multiphase formulation, namely FireStar2D (Morvan and Dupuy 2001, 2004; Morvan et al. 2008, 2009; Morvan 2013; Awad et al. 2021). This model was validated from calculations carried out different scales and compared with experimental results, so it appears to be suitable for operational works since it provides valuable results and requires less simulation time compared to the 3D models. The main parameters of the computational domain and the vegetation layer is given in Figure 4. Both the solid-phase and the fluid-phase grids were characterized by cells sizes below the

radiation extinction length scale (Morvan 2011; Morvan et al. 2013) given by $4/s\beta$, in order to avoid fire extinction especially in the case of radiation-dominated fire propagation. Simulations were carried out for a 10 m open wind speed U_{10} by assuming a one-seventh power wind velocity profile. The domain inclination angle was specified through two non-zero components of gravitational acceleration: $g_x = -g\sin(\alpha)$ and $g_z = -g\cos(\alpha)$, where $g = 9.81$ m/s^2 is Earth gravity.

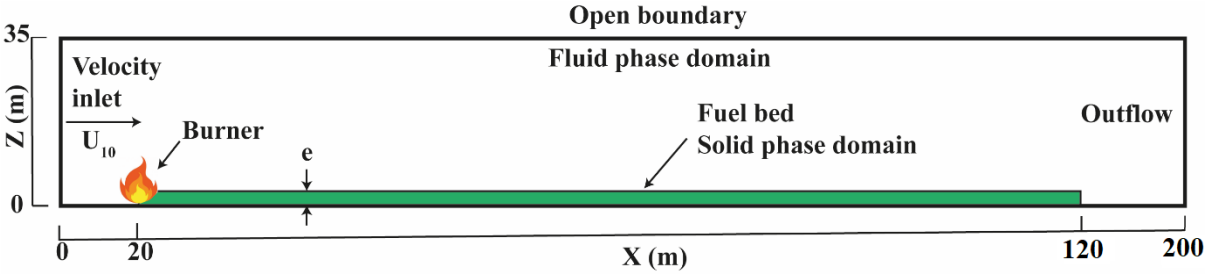

Figure 4- Computational domain and boundary conditions used in the 2D simulation of the experimental fire.

3.2. Numerical evaluation of fire parameters

3.2.1. ROS

Numerical prediction of the ROS using FireStar2D is obtained from the position of the pyrolysis front at the fuel-bed surface. It is the slope of the curve shown in Figure 5, once fire propagation had become steady.

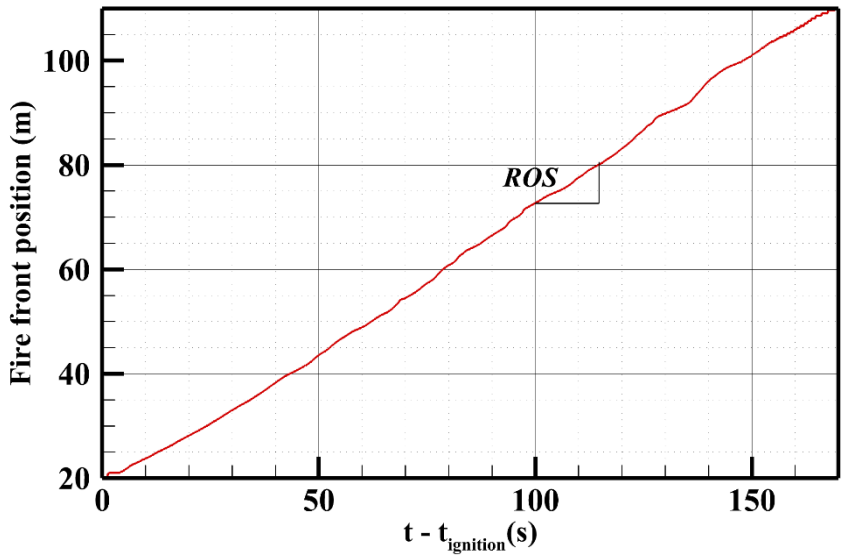

Figure 5- Position versus time of the furthermost point of the pyrolysis front at the fuel-bed surface obtained by FireStar2D after ignition at t = 30 s.

3.2.2. Fireline intensity

Numerical evaluation of fireline intensity is based on the following formulation: $I_{BNum} = \dot{m}\,.\,\Delta H_c$. Numerically, there is no difficulties to evaluate the vegetation degradation rate $\dot{m}$ as in the experimental method, where it is evaluated in this case by doing the summation of mass losses due to pyrolysis and charcoal combustion.

3.2.3. Heat fluxes

FireStar2D allows the evaluation of radiative and convective heat fluxes received by the targets, and assesses the heat fluxes recorded by the flux meters located ahead of the fire front. Convective heat flux is evaluated using Newton's law of cooling (Owen 2009), given by the following equation: $Q_{conv} = h_{\text{conv}}(T_0 - T_a)$, where $(T_0 - T_a)$ represents the difference between the gas mixture temperature and the target temperature (assumed to be the ambient temperature) and h_{conv} is the convective heat transfer coefficient.

4. Results and discussion

In this section, the results of the burns campaigns of Speluncatu and Letia will be presented. In this context, a comparison between experimental and numerical results concerning the ROS, and fireline intensity are shown in Table 2. Radiant and total heat fluxes received by the transducers located ahead of the vegetation area were registered when the fire front reached the end of the plot. During the burn campaign in October, backfires conducted by the firefighters to protect the burning zone were so close to the sensors, which have affected the measurements during fire. In this case, only heat flux measurements during March (2021) in Speluncatu and March 2022 in Letia were investigated, and compared with numerical predictions. Thus, time-averaged ratios (experimental and numerical) of the radiative heat fluxes to the total heat fluxes (i.e., convective and radiative), evaluated for the three flux meters are shown in table 3.

Table 2- Experimental and numerical results for the two burns campaigns in March and October.

	Speluncatu March (2021)		**Speluncatu October (2021)**		**Letia March (2022)**	
	Experimental	**Numerical**	**Experimental**	**Numerical**	**Experimental**	**Numerical**
ROS (m/s)	0.45	0.5	0.38	0.47	0.21	0.29
Fireline intensity (MW/m)	10.5	7.7	10.8	9.9	10.44	9.5

Table 3- Time-averaged ratio of the radiative heat flux to the total one evaluated experimentally in March, and with FireStar2D at the different target positions.

	Speluncatu March (2021)		**Letia March (2022)**	
Position	**Q_{rad}/Q_{tot} FireStar2D**	**Q_{rad}/Q_{tot} Experiment**	**Q_{rad}/Q_{tot} FireStar2D**	**Q_{rad}/Q_{tot} Experiment**
1	0.796	0.845	0.91	0.94
2	0.993	0.971	0.95	0.99
3	0.961	0.93		

Concerning the rate of spread, results show an agreement between experimental and numerical evaluations with a certain difference may be due to numerical considerations: (1) numerically, a homogeneous fuel bed is considered; (2) in 2D simulations, the fire front is considered as a uniform thermal barrier, while the fire front is in reality structured as a succession of peaks and troughs, allowing for the air flow to find a way across it (Frangieh et al. 2020). Concerning heat fluxes evaluation, both numerical and experimental heat fluxes reported in Table 3, show the same order of magnitude for the calculated ratios and they both reveal the dominance of the radiation heat transfer contribution at different targets positions.

Concerning fireline intensities, results show that these fires conducted in winter and autumn are high intensity fires where fireline intensities (numerical and experimental) exceeds the value of 7 MW/m, despite the unfavorable conditions (low wind speeds, high FMC and RH). Knowing that the fireline intensity is an index to characterize fire severity rating, the considered fires fall then into the "very high" fire severity (Cheney 1981). Fire severity also depends on fire residence time (Cruz et al. 2013) related to the ROS. In general, due to the important slope, fire moves fast, and the residence time becomes relatively small, which does not allow reaching a high percentage of fuel consumption, especially for high fuel moisture content (>40%) (Dahale et al. 2013). These three experiments confirm the fact that a fire can exhibit a dangerous behavior of a high intensity fire, even in winter, because it occurs along a steep slope, and for a high fuel load especially for Letia experiment. The presence of a slope induces a pressure gradient between the burned and the unburned zone due to the changes in the capacity of air entrainment. The Coanda effect is a reaction to this pressure difference (Sharples et al. 2010), where the fluid flow tends to be attached to the propagation surface. Due to the important slope, the Coanda effect is reinforced by a component of the buoyancy force acting in the x-direction, g_x. Consequently, the flame becomes more inclined toward the ground, which increases the heat transfer between the hot gases and the unburned vegetation, resulting in a fire acceleration and higher intensity fire (Sharples et al. 2010; Sánchez-Monroy et al. 2019). In addition, fireline intensity estimation is directly related to fuel load that contributes to the fire front propagation. Thus, important values of slope angles and fuel loads can explain the high intensity fires obtained during these different campaigns despite the unfavorable propagation conditions.

5. References

Alexander ME (1982) Calculating and interpreting forest fire intensities. Canadian Journal of Botany 60, 349–357. doi:10.1139/b82-048.

Alexander ME, Cruz MG (2020) Fireline Intensity (SL Manzello, Ed.). Encycl. Wildfires Wildland-Urban Interface Fires 453–460. doi:10.1007/978-3-319-52090-2_52.

Awad C, Frangieh N, Marcelli T, Accary G, Morvan D, Meradji S, Chatelon F-J, Rossi J-L (2021) Numerical study of the moisture content threshold under prescribed burning conditions. Fire Safety Journal 122, In Press. doi:https://doi.org/10.1016/j.firesaf.2021.103324.

Awad C, Morvan D, Rossi J-L, Marcelli T, Chatelon FJ, Morandini F, Balbi J-H (2020) Fuel moisture content threshold leading to fire extinction under marginal conditions. Fire Safety Journal 118, 11. doi:10.1016/j.firesaf.2020.103226.

Benson RP, Roads JO, Weise DR (2008) Chapter 2 Climatic and Weather Factors Affecting Fire Occurrence and Behavior. 'Dev. Environ. Sci.' (Eds A Bytnerowicz, MJ Arbaugh, AR Riebau, C Andersen) pp. 37–59. (Elsevier) doi:10.1016/S1474-8177(08)00002-8.

di Castri F (1981) 'Mediterranean-type shrublands of the world.' (R Specht, Ed.). (Elsevier: Amsterdam)

Cheney PN (1981) Fire behaviour. InGill A, Grooves R, Noble I (eds) 'Fire Aust. Biota', Canberra, ACT. 151–175. (Australian Academy of Science: Canberra, ACT)

Cheney N, Gould J (1995) Fire Growth in Grassland Fuels. International Journal of Wildland Fire 5, 237–247. doi:https://doi.org/10.1071/WF9950237.

Cheney NP, Gould JS, Catchpole WR (1993) The Influence Of Fuel, Weather And Fire Shape Variables On Fire-Spread In Grasslands. International Journal of Wildland Fire 3, 31–44. doi:10.1071/WF9930031.

Cruz MG, Alexander ME (2013) Uncertainty associated with model predictions of surface and crown fire rates of spread. Environmental Modelling and Software 47, 16–28. doi:10.1016/j.envsoft.2013.04.004.

Dahale A, Ferguson S, Shotorban B, Mahalingam S (2013) Effects of distribution of bulk density and moisture content on shrub fires. International Journal of Wildland Fire 22, 625–641. doi:10.1071/wf12040.

European Science & Technology Advisory Group (2020) Evolving Risk of Wildfires in Europe - The changing nature of wildfire risk calls for a shift in policy focus from suppression to prevention. (Brussels, Belgium) https://www.undrr.org/publication/evolving-risk-wildfires-europe-thematic-paper-european-science-technology-advisory.

Frangieh N, Accary G, Morvan D, Méradji S, Bessonov O (2020) Wildfires front dynamics: 3D structures and intensity at small and large scales. Combustion and Flame 211, 54–67. doi:10.1016/j.combustflame.2019.09.017.

Marsden-Smedley JB, Catchpole WR (1995) Fire behaviour modelling in tasmanian buttongrass moorlands. I. Fuel characteristics. International Journal of Wildland Fire 5, 203–214. doi:10.1071/WF9950203.

Morandini F, Silvani X, Rossi L, Santoni PA, Simeoni A, Balbi JH, Louis Rossi J, Marcelli T (2006) Fire spread experiment across Mediterranean shrub: Influence of wind on flame front properties. Fire Safety Journal 41, 229–235. doi:10.1016/j.firesaf.2006.01.006.

Morvan D (2011) Physical Phenomena and Length Scales Governing the Behaviour of Wildfires: A Case for Physical Modelling. Fire Technology 47, 437–460. doi:10.1007/s10694-010-0160-2.

Morvan D (2013) Numerical study of the effect of fuel moisture content (FMC) upon the propagation of a surface fire on a flat terrain. Fire Safety Journal 58, 121–131. doi:10.1016/j.firesaf.2013.01.010.

Morvan D, Dupuy JL (2001) Modeling of fire spread through a forest fuel bed using a multiphase formulation. Combustion and Flame 127, 1981–1994. doi:10.1016/S0010-2180(01)00302-9.

Morvan D, Dupuy JL (2004) Modeling the propagation of a wildfire through a Mediterranean shrub using a multiphase formulation. Combustion and Flame 138, 199–210. doi:10.1016/j.combustflame.2004.05.001.

Morvan D, Meradji S, Accary G (2008) Wildfire behavior study in a mediterranean pine stand using a physically based model. Combustion Science and Technology 180, 230–248. doi:10.1080/00102200701600978.

Morvan D, Méradji S, Accary G (2009) Physical modelling of fire spread in Grasslands. Fire Safety Journal 44, 50–61. doi:10.1016/j.firesaf.2008.03.004.

Morvan D, Meradji S, Mell W (2013) Interaction between head fire and backfire in grasslands. Fire Safety Journal 58, 195–203. doi:10.1016/j.firesaf.2013.01.027.

Mueller E V., Skowronski N, Thomas JC, Clark K, Gallagher MR, Hadden R, Mell W, Simeoni A (2018) Local measurements of wildland fire dynamics in a field-scale experiment. Combustion and Flame 194, 452–463. doi:10.1016/j.combustflame.2018.05.028.

Mulvaney JJ, Sullivan AL, Cary GJ, Bishop GR (2016) Repeatability of free-burning fire experiments using heterogeneous forest fuel beds in a combustion wind tunnel. International Journal of Wildland Fire 25, 445–455. doi:10.1071/WF15068.

Owen MS (2009) '2009 ASHRAE Handbook: Fundamentals.' (American Society of Heating, Refrigeration and Air-Conditioning Engineers)

Sánchez-Monroy X, Mell W, Torres-Arenas J, Butler BW (2019) Fire spread upslope: Numerical simulation of laboratory experiments. Fire Safety Journal 108, 13. doi:10.1016/j.firesaf.2019.102844.

Sharples J, Gill A, Dold J (2010) The Trench Effect and Eruptive Wildfires: Lessons from the King's Cross Underground Disaster. In 'Aust. Fire Emerg. Serv. Authorities Counc. 2010 Conf.', Darwin.(Darwin)

Sommers WT, Coloff SG, Conard SG (2011) Synthesis of Knowledge: Fire History and Climate Change. http://www.firescience.gov/JFSP_fire_history.cfm.

Tedim F, Leone V, Amraoui M, Bouillon C, Coughlan M, Delogu G, Fernandes P, Ferreira C, McCaffrey S, McGee T, Parente J, Paton D, Pereira M, Ribeiro L, Viegas D, Xanthopoulos G (2018) Defining Extreme Wildfire Events: Difficulties, Challenges, and Impacts. Fire 1, 9. doi:10.3390/fire1010009.

Vega JA, Cuinas P, Fonturbel T, Perez-Gorostiaga P, Fernandez C (1998) Predicting fire behavior in Galician (NW Spain) shrubland fuel complexes. InViegas DX (ed) '3rd Int. Conf. For. Fire Res. 14th Conf. Fire For. Meteorol.', Luso-Coimbra, Portugal. 713–728. (ADAI, Univsersity of Coimbra: Luso-Coimbra, Portugal)

Viegas DX, Cruz MG, Ribeiro LM, Silva AJ, Ollero A, Arrue B, Dios R, Gómez-Rodríguez F, Merino L, Miranda AI, Santos P (2002) Gestosa fire spread experiments. In 'For. fire Res. Wildl. fire Saf. Proc. IV Int. Conf. For. Fire Res. 2002 Wildl. Fire Saf. Summit, Luso, Coimbra, Port. 18-23 Novemb. 2002',(Millpress Science Publishers)

Perception of wildfire behaviour and fire suppression tactics among Swedish incident commanders

Johan Sjöström*[1]; Anders Granström[2]; Lotta Vylund[1]

[1] RISE Research institutes of Sweden, Box 857, 501 15 Borås, Sweden, {johan.sjostrom, lotta.vylund}@ri.se
[2] Department of Forest ecology and management, Swedish university of agricultural sciences, 901 83 Umeå, Sweden, {anders.granstrom@slu.se}

**Corresponding author*

Keywords

Wildfire; Tactics; Perception; Incident commanders; Fire-fighting

Abstract

Unlike most regions with high-intensity wildfire potential, Sweden lacks specialized wildfire suppression organization. Instead, wildfire suppression is handled by highly decentralized and multitask municipal rescue services. This prompts the question how the incident commanders (ICs) perceive and interpret variation in fire behaviour and how they respond to wildfire incidents with regard to dispatching for initial attack and selecting tactics. To elucidate this, we exposed a spectrum of Swedish ICs to a questionnaire and round-table-exercises of different fire scenarios.

The informants had on average 13 years of experience as incident commanders and had on average managed 6 wildfires over the last 5 years. Despite minimal formal wildfire training the respondents showed reasonable consensus in rating of fire behaviour in response to fuels and weather, suggesting that their knowledge was built on personal and group experience. Likewise, they gave estimates on rate of production of hose-lays similar to published expert assessments from Canada. When exposed to a spectrum of fire scenarios, resource dimensioning by ICs was linearly related to the Canadian FWI-index, although most organizations did not have any preordained schemas or rules of initial dispatching resources to guide them.

Tactics employed were based mainly on accessing the fire from the nearest road and using direct attack with hose-line laid from the engine and water ferried on trucks. In a scenario where initial attack failed, suppression crews typically fell back on roads, which however would be breached by intense fire, and which also exposed the operation to risk of being outflanked. This response was in fact similar to that employed during a 2014 catastrophic wildfire in central Sweden and may indicate a fundamental flaw in tactics employed for large and intense fires.

The present structure of the Swedish wildfire suppression system developed during the second half of the 1900s and depends on rapid access to the fire by a relatively small number of firefighters. The study suggests a relatively high capacity for suppressing forest fires, despite that the organization is primarily rigged for other purposes and that ICs have minimal formal training in this area. Climate change-scenarios suggest longer fire season and more risk days in parts of the country, but the future wildfire scene may be even more sensitive to de-population and diminishing economic resources in heavily forested regions of the country.

1. Introduction

Swedish wildfires are handled by multipurpose rescue services organized at municipal level having extensive autonomy and no legally binding targets regarding resource levels or formal training of staff. Instead, the 290 municipalities (median population 16 300) are obliged to organize and pay for their fire protection, which should be capable of dealing with hazards based on a local risk assessment.

Wildfires constitute only a fraction of rescue services workload, the bulk being car accidents and structural fires. Most wildfires are easily contained, but some escape initial attack (annually 270 forest fires >0.5 ha and since 1996 a handful larger than 1000 ha (Sjöström & Granström, 2020). Fires are suppressed free of charge, but mop-up is the responsibility of the landowner.

Scandinavian climate-projections suggest increasing frequency of high-risk days (Yang *et al*, 2015). Future outcome will however depend also on preparedness and capacity of response organizations. Due to municipal

autonomy, no national wildfire-fighting doctrine or detailed tactics manual existed at the time of the study although a national guidance document was published in 2020 (Hansen *et al*, 2020). Here we elucidate perceptions of wildfire behaviour and tactics among Swedish ICs by interviewing and performing round-table-exercises of four wildfire scenarios from alarm to extinguishment.

Incident commanding typically evolve by deliberation/discussion/testing, but we focus on initial response and perceptions. Expert opinion has earlier been used to estimate fire-fighting variables e.g. situation-specific hose-lay production rates (Parker *et al*, 2007). The round-table-exercise scenarios presented operation pictures reflecting what an incident commander (IC) can encounter following an alarm call, and through this semi-realistic approach we elucidate normally concealed questions: Do ICs distinguish complexity levels regarding weather and other initial factors and does this reflect initial deployment? What tactics are employed, related to available resources and likely fire behaviour?

2. Methods

We interviewed 20 trained ICs with wildfire commanding experience from 8 municipalities (1-3 participants each). They were questioned regarding fire behaviour and suppression, e.g. estimated rates-of-spread (ROS) in two fuel-types given detailed weather (Figure 1) and hose-lay production rates, with/without simultaneous watering as well as individual experience/training and their organization's deployment capacity.

Scenarios spanned from simple (easily controllable) to complex (certainly escaping initial attack), based on weather, position, wind and access roads, containing at least one additional challenge (Table 1).

Table 1- Scenario weather and CFFWIS (Taylor et al., 1997) indices (ordered by increasing FWI-value, #-numbers refer to game chronology).

Case	**#3**	**#2**	**#1**	**#4**
RH (%)	48	42	33	31
Temperature (°C)	18	25	21	18
Windspeed (m/s)	1	2	3	6.5
FD-class	Moderate	Moderate	Very high	Extreme
FWI-value	11.4	16.4	22.4	35.3
DMC-BUI-DC	33-55-437	40–56–228	47–68–317	43–54–177
FFMC-ISI	88-3.9	89.9–6.1	91–8.0	92–18.6
Challenges	Poor road access	Steep slope impacts ROS/direction	Possible new head if flank not secured	Extreme conditions

Initial information offered: ignition time and point (on topographic maps), daily fire-danger (FD-) class (grouping FWI-values into e.g. *Moderate*=7-17; *High*=17-22; *Very high*=22-28 and *Extreme*>28) plus current weather (windspeed/direction, RH, temperature). Once the initial response crew arrived (30 minutes travel to nearest accessible road) burnt length/width and flame lengths was communicated and photos from real equivalent fires were presented, showing vegetation, smoke, flames etc. Fire behaviour was extracted from the Canadian FBP system (Taylor *et al*, 1997) using fuel type C-3 surrogating for *Pinus sylvestris*-dominated forests and S-1 for clear-felled areas.

Figure 1- Left: forest scenes (1-2) presented for grading potential fire-behaviour. Right: fire scenes (head - scene 1, backing – scene 2) for assessing ROS.

Informant knew they could ask for information they normally obtain from headquarters, such as CFFWIS indices or weather variables. CFFWIS was nationally employed 1996, but without nation-wide supplementary training efforts.

All scenarios occurred on forest-company land. If called for, companies could send a mop-up crew of six with basic equipment (shovels, pump, 500m hose) within 2 hours.

All decisions/actions were logged including respondents' comments. Tactical decisions (attack routes, water-sources, and hose-lays/crews/vehicles) were noted on maps. Scenarios were sequentially run as semi-directed interviews (Huntington, 2000) with follow-up questions upon ambiguities. E.g., if ICs asked headquarters for current weather prognosis, the facilitator first asked for which variables before delivering.

3. Results

3.1. Training

IC experience averaged at 12.6 years and 5.8 wildfire deployments last five years. Their average wildfire training during initial schooling was 4.6/2.4 days of theory/practice, without live fire-training in field. 44% had follow-up training averaging <1 day over five years. One informant had participated in prescribed burning.

3.2. Perceptions of fire behaviour and production rates

Respondents overestimated ROS in both fire scenes (Figure 1, A-B) while underestimating potential ROS in forests under given weather-scenarios (Forests 1-2) (Table 2). When asked in which forest (Figure 1-left) fire would spread the fastest, all identified Forest 1 and highlighted differences in fuel structure as main cause. Some specifically commented on structure and species ("*more lichens"*, "*Calluna dwarf shrubs"*, "*dead branches lower to the ground*").

Table 2- Informants answers concerning ROS and hose-line construction.

Question	**Respondent's average (range/σ)**	**Reference answer**
ROS: Fire scene A	5.4m/min (1-15)	2-3m/min (observed)
ROS: Fire scene B	1.7m/min (0.5-5)	~0.5m/min (observed)
Most fire intensity potential (1/2), Figure 1	Forest 1 (everyone)	1
ROS[1]: Forest 1 (RH=30%, Wind=5m/s)	12.7m/min (2-25)	25m/min (FBP C-4)
ROS[1]: Forest 2 (RH=30%, Wind=5m/s)	4.9m/min (1-15)	15m/min (FBP C-3)
Advance rate: 5-person crew laying a 500m 42mm hose-line, from engine, without watering.	24.9m/min (σ=12.3)	
As above including watering of hose	13.1m/min (σ=6.8)	
Advance rate: additional extension of 500m without ATV	8.6m/min (σ=5.5)	
Secure duration: wet-line a hot, windy day	1.6hrs (σ=0.7)	
Advance rate: re-wetting 500m	17.8m/min (σ=15.5)	
Advance rate: 2-person crew mop-up 5m wide belt	5.6m/min (σ=5.8)	

[1] After two precipitation-free summer weeks.

Production rates constructing hose-lays were relatively consistently estimated, ~25 min for 500m from the engine without watering and twice the time if watering. A wet-line was considered secure for nearly 2h (1-3h) on hot-windy days. Mop-up of a 5m belt along established hose-line: ~6m/min after prolonged drought (Table 2).

3.3. Deployment vs fire-danger

Initial deployment varied with fire-danger (indices/weather) and almost linearly with FWI-values (Figure 2). Typically, minimum 2 "units" (2 officer + 8 firefighters) from two different stations were deployed, each travelling with one engine (~3m^3, one pump and 500m hose), one tanker (8-10 m^3) and IC riding a separate vehicle. For severe cases, 1-2 ATVs were brought on trailers.

This basic initial deployment was increased by adding units. Initial deployment varied between respondents but even for the most severe scenario 45% initially deployed only two units, immediately requesting substantially larger forces once shown pictures of the smoke column.

Upon alarm, station officers contacted landowners and surveyed available helicopters. For case #4, helicopters were called early on and 1/3rd requested 40-50 people from the military. One informant had a local system how to mix these (1+1) with professional fire-fighters.

Generally, deployment sizes relied on IC judgement, based on FD-class or windspeed but two different municipalities had independently developed their own rule-based dispatching schema using FD-class for initial crew sizes.

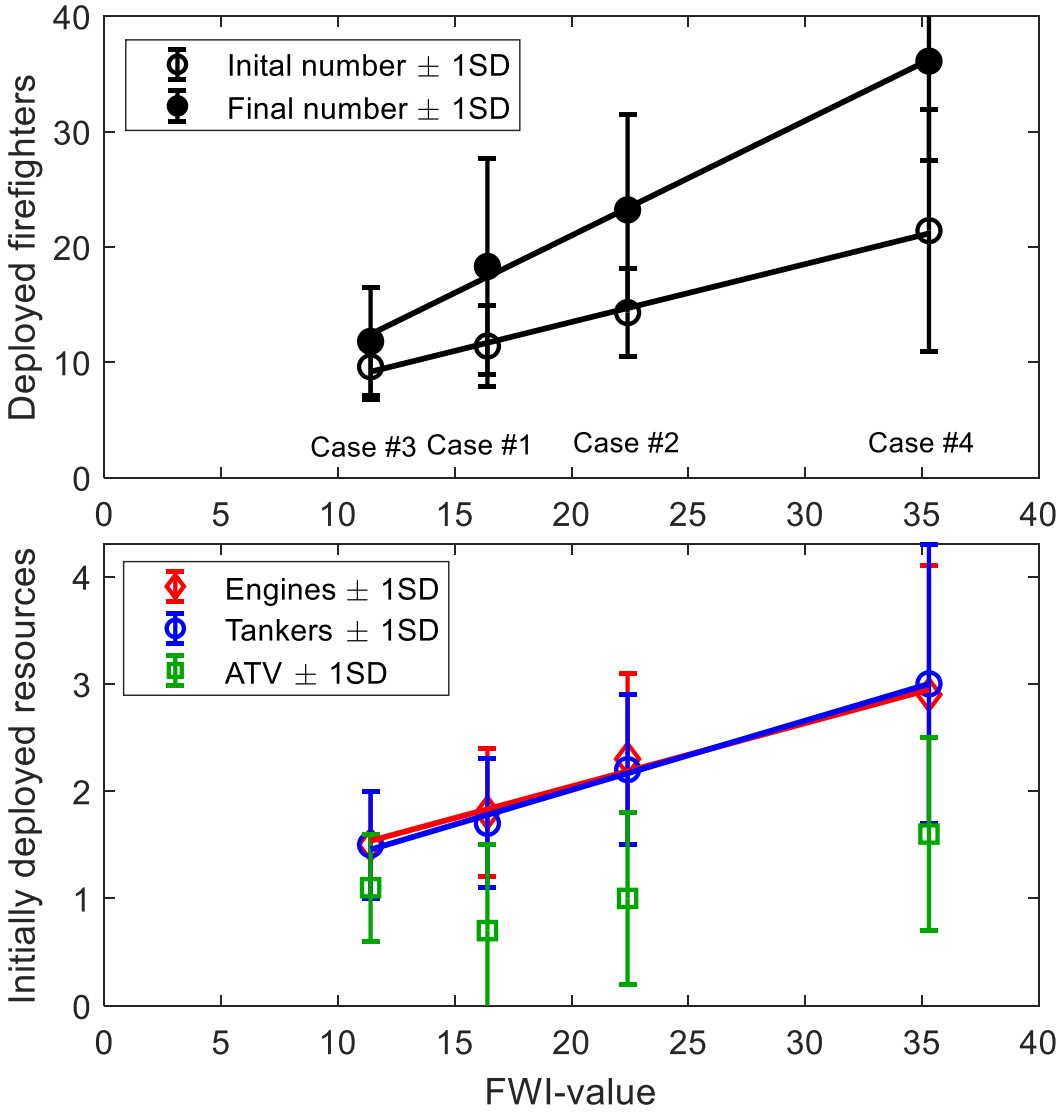

Figure 2- Initial resource deployment against scenario FWI-value (average ±1 standard deviation).

3.4. Suppression tactics

Standard procedure was driving to closest road position, sending 1-2 foot-scouts (sometimes with a drone), and start hose-laying from the engine once the fire location was verified (first 76-63mm hoses, transitioning to 42-38mm). Frequently, informants kept one unit at a distant staging point until engaging them from another direction. When fire was far from road access (2km, case#3), ATVs were often used for situational awareness and material transport. Hose-lay water supply was typically ferried by tankers from nearby accessible lakes, but occasionally smaller pumps were placed in nearby streams/lakes to feed hose-lines locally. Only two respondents used swatters/brooms on low-intensity backing and flanking flames. Landowner crews were not involved in the suppression stage.

Most respondents recognized/noted challenges such as slope-influence on ROS, or the danger of not controlling a flank early, allowing flames to circumvent a lake forming a high-intensity head fire. However, for the most severe scenario (#4), most respondents concentrated on the fire head, without securing the flanks from an anchor point. On this fire several respondents also worked exclusively along roads with hose-lays/watering from vehicles, setting up control lines far from the fire perimeter, thus adding risks in case of wind-shifts. As the high-intensity head reached the prepared lines, only two informants acted to control spot-fires. Two informants discussed expanding fire breaks using burn-out operations, but only one had relevant prior experience.

Mop-up time varied significantly, between 1-12h (case#1), after which landowner crews continued. Typically, hose-lines, pumps were precautiously left on site.

4. Discussion

Even in structured, hierarchical systems as in USA, variations occur among IC's risk perception (and McBride, 2013) but in decentralized Swedish organizations the competence is highly depending on individual- and group- field experience, developed through local rather than national organizational cultures. Most ICs had only a few days of formal theoretical/practical wildfire suppression instructions. Parallel to collective fire-knowledge in regions of active fire-use in land management (Johansson *et al*, 2012) the respondents did, however, exhibit considerable consensus in perception and judgement, suggesting reasonable degrees of field knowledge.

Initial deployments were rarely rule-based but depended on intuitive scaling of resources according to perceived fire behaviour, but with a two-units-minimum deployment. Most likely, ICs primarily based decisions on the 6-grade FD-class since few referred to FWI-values or its subcomponents. However, windspeed was also considered a separate risk factor and, on site, the colour and size of smoke columns were important signals.

Due to budget constraints, initial resources are weighed against the perceived risk of escaping initial attack (Lee *et al*, 2013), particularly so for helicopters, primarily called from the private sector (military helicopters are occasionally available at no cost for municipalities). Already, rescue service costs are 4X higher per capita in rural compared to urban regions (Anon., 2014). Another factor mentioned was resource conservation, to buffer for additional emergencies within the municipality.

Line construction rates have never been issued or discussed among Sweden's fire-fighting community, but our estimates were on par with previous Canadian results (Hirsh *et al*, 1998; 2004) and therefore one-crew hose-laying at 17m/min is a reasonable estimate for operational guidelines and modelling (Duff and Tolhurst, 2015). Reliable rates for hose-laying and re-wetting are important particularly as these often become limiting factors when fires escape.

The standard tactic of ferrying water by tanker is potentially vulnerable. First, the typical 76mm hose-lay from an engine means that its $3m^3$ capacity is emptied already by filling the first 660m. Then, to supply four nozzles implies one tanker (~$10m^3$) arriving each 30 minutes. Thus, one stationary engine and two rotating tankers can feed a hose-lay continuously but, will tie-up at least half of two-unit crew of 10.

Once fires were reached, the crews mostly proceeded to circle them close to the perimeter but sometimes well ahead of the fire, most evident for the worst-case scenario with high ROS and elongated perimeter. Here, no flanks were secured from safe anchor points, inviting outflanking risks. Further, strategies for controlling spot-fires were not planned-for. In fact, this scenario was based on a disastrous fire 2014 with similar response (Anon., 2015), suggesting results are indicative of typical response in case of fast-spreading and intense fires.

Time-to-initial-attack (median 25 minutes, 75% <30 minutes) vary greatly with population density within Sweden, and directly relate to likelihood of escape (Sjöström and Granström, 2020). The present-day system with few professional fire-fighters relies on Sweden's dense forest-road network (average distance <500m (1990), (Anon., 1991)). Road density correlates positively with fire occurrence and negatively with burnt area (Pinto *et al*, 2020). Median driving distance is 15 minutes and with 500m hose-lay within 20 minutes two standard 1+4-units may in fact be adequate for suppressing most low-intensity fires.

Though mostly adequate (89% of forest fires <0.5ha (Sjöström and Granström, 2020)), high-ROS or intense fires can quickly overwhelm such small forces. Even with helicopters, substantial ground crews are needed to secure perimeters. There are few stand-by firefighters in rural regions (Lindblad *et al*, 2015) and a deployment of as few as 40 fire-fighters (Case#4) drains resources over a large area. Additionally, tactics are vulnerable, e.g. relying on roads as fire breaks without burning off fuels ahead. This is, however, expected given that ICs seldom have been trained for or experienced complex wildfire scenarios.

5. Acknowledgements

We thank respondents for participation and MSB for funding

6. Literature

Anonymus. 1991. Vägplan 90. Skogsvägnätets tillstånd och standard 1990 samt behov av utbyggnad och förbättring. Skogsstyrelsen, Jönköping.

Anonymus. 2014. Räddningstjänst i siffror 2014. MSB. Swedish civil contingencies agency. ISBN: 978-91-7383-576-3.

Anonymus. 2015. Observatörsrapport. Skogsbranden i Västmanland 2014. MSB. Swedish civil contingencies agency. ISBN: 978-91-7383-527-5.

Black, A. E., and McBride, B. B. 2013. Safety climate in the US federal wildland fire management community: influences of organisational, environmental, group and individual characteristics. International Journal of Wildland Fire 22:850-861.

Duff, T. J., and Tolhurst, K. G.. 2015. Operational wildfire suppression modelling: a review evaluating development, state of the art and future directions. International Journal of Wildland Fire 24:735-748.

Hansen, R., Nordlund, A., Ekström, L., Edlund, F., Sundberg, A. Montan, A. and Wahlström, J. 2020. Vägledning i skogsbrandsläckning 2:a utgåvan, MSB1366. Swedish Civil Contingency Agency, Karlstad, ISBN: 978-91-7927-038-4. (in Swedish)

Hirsch, K. G., Corey, P. N. and Martell, D. L. 1998. Using expert judgment to model initial attack fire crew effectiveness. Forest Science 44:539-549.

Hirsch, K. G., Podur, J. J, Janser, R. F., McAlpine, R. S., and Martell, D. .. 2004. Productivity of Ontario initial-attack fire crews: results of an expert-judgement elicitation study. Canadian Journal of Forest Research-Revue Canadienne De Recherche Forestiere 34:705-715.

Huntington, H. P. 2000. Using Traditional Ecological Knowledge in science: Methods and applications. Ecological Applications 10:1270-1274.

Johansson, M. U., Fetene, M., Malmer, A. and Granström, A. 2012. Tending for Cattle: Traditional Fire Management in Ethiopian Montane Heathlands. Ecology and Society 17:19.

Lee, Y., Fried, J. S., Albers, H. J. and Haight, R. G. 2013. Deploying initial attack resources for wildfire suppression: spatial coordination, budget constraints, and capacity constraints. Canadian Journal of Forest Research-Revue Canadienne De Recherche Forestiere 43:56-65.

Lindblad, S., Tynelius, U., Danell, T., Pichler., W., and Anderstig, C. 2015. Demografins regionala utmaningar. Bilaga 7 till Långtidsutredningen 2015. Statens offentliga utredningar 2015:101.

Parker, R., Ashby, L., Pearce, G. and Riley, D. 2007. Review of methods and data on rural fire suppression resource productivity and effectiveness. Ensis Client report No 12337.

Pinto, G., Rousseu, F., Niklasson, M. and Drobyshev, I. 2020. Effects of human-related and biotic landscape features on the occurrence and size of modern forest fires in Sweden, Agricultural and Forest Meteorology 291, 108084

Sjöström, J., and Granström. A. 2020. Wildfires in Sweden - trends and patterns during recent decades, MSB1536. Swedish Civil Contingency Agency, Karlstad, ISBN: 978-91-7927-032-2. (in Swedish)

Taylor, S. W., Pike, R. G. and Alexander, M. E.. 1997. Field guide to the Canadian forest fire behavior prediction (FBP) system. Natural Resources Canada, Canadian Forest Service.

Yang, W., Gardelin, M., Olsson, J. and Bosshard, T. 2015. Multi-variable bias correction: application of forest fire risk in present and future climate in Sweden. Natural Hazards and Earth System Sciences 15:2037-2057.

Physical modelling of fires spreading upslope, involved in fire eruption triggering

François Joseph Chatelon*[1]; Jacques-Henri Balbi[1]; Jacky Fayad[1]; Jean-Louis Rossi[1]; Dominique Morvan[2]; Thierry Marcelli[1]; Nicolas Frangieh[1]; Carmen Awad[1]; Gilbert Accary[3]; Sofiane Meradji[4]

[1]UMR SPE 6134. University of Corsica, 20250 Corte, France, {chatelon_j, fayad_j, rossi_j, marcelli_t, Frangieh_n, awad_c}@univ-corse.fr
[2]Aix Marseille Université, CNRS, Centrale Marseille, M2P2, Marseille, France, {dominique.morvan@univ-amu.fr}
[3]Scientific Research Center in Engineering, Lebanese University, Lebanon, {gaccary@ul.edu.lb}
[4]IMATH laboratory, EA 2134, Toulon University. 83160 Toulon, France {sofiane.meradji@univ-tln.fr}

**Corresponding author*

Keywords

Eruptive fire; physical model; fire induced wind;

Abstract

Eruptive fires are one category of extreme fire behaviour. They are characterized by a sudden and unpredictable change in the fire behaviour which represents an extreme danger for people involved in firefighting. The major point is about the mechanism that turns a usual fire behaviour into an eruptive fire behaviour. Among the different explanations found in the literature, the pioneering interpretation consisting in a feedback effect caused by the convective flow induced by the fire under wind and/or slope conditions, has never been disproved with an example of fire accident. The main goal of this work lies in proposing a physical modelling of this fire induced wind. This modelling attempt is derived from the brand-new version of the Balbi model, which is a simplified physical model for surface fires at the field scale that explicitly depends on the triangle of fire (fuel bed, wind and slope). This work is a first step to the modelling of fire eruption. The model tries to represent accurately the acceleration of the fire rate of spread propagating on different sloped terrain under no-wind or weak wind conditions. It is tested against three sets of experiments carried out at the laboratory scale without external wind and against a high intensity experimental fire spreading on a steep sloped terrain and conducted under weak wind conditions in the north-western of Corsica. Some statistical tools are used to compare predicted and observed rate of spread (NMSE, Normalized Mean Square Error and MAPE, Mean Absolute Percentage Error) and to understand the model's under-predictions or over-predictions trends (FB, Fractional Bias).

1. Introduction

A small part of wildfires (less than 2 per cent) (European Science & Technology Advisory Group 2020) has the most significant ecological and socio-economic impacts. These so-called extreme wildfire events ((Tedim *et al.* 2018) are characterized by very high fire intensities which lead to ineffective suppression capabilities. Eruptive fires are part of these extreme fire behaviours. If those eruptive fires are also known in the literature as flashover (in enclosed spaces, NFPA 921, 2011), blow-up (Butler *et al*. 1998) or generalized blaze flash (Chatelon *et al*. 2014), some slight differences remain between each definition. The definition of fire eruption has been proposed and characterized by Viegas (2004). It describes a fire with a sudden acceleration of the head fire rate of spread (ROS) in a very short time lapse with or without any changes in the topography, in the environmental conditions or in the vegetal stratum characteristics.

This phenomenon is very dangerous for firefighters and civilians because of its difficulty to be predicted and anticipated. Viegas and Simeoni (2008) reviewed the major mechanisms supposed to be the cause of a fire eruption triggering. For instance, from the firefighters point of view, an important release of VOCs (volatile organic compounds) is the main reason for a fire to erupt. Indeed, when a fuel is severely stressed, it releases VOCs that ignite a a lower temperature than the usual ignition temperature. The VOC's theory consists in assuming that a fire eruption is mainly caused by this gas release and is widely used in the literature (Chetehouna *et al*. 2014, Courty 2012). But the example of the Kornati fire accident (Viegas *et al*. 2008) refute this argument with a fire spreading across a grass fuel bed.

The pioneering interpretation proposed by Viegas (2004) consists in the presence of an air flow created by the fire itself which may significantly lead to a change in the fire behaviour, particularly for fires spreading upslope. The role of this induced convective flow is to bring fresh air and then oxygen to the flame in order to support the combustion. Viegas and Pita (2004) observed the importance of this air movement on the behaviour of fire spreads in canyons (at the laboratory scale and also during the field scale Gestosa fire experiments) and the accident occurred in Freixo de Espada-a-cinta (Viegas 2004) also support this interpretation.

So, a good modelling of the fire induced wind is the first step before trying to give a fire eruption physical model. In this work, the explanation provided by Viegas is selected and a first attempt of a physical modelling of this induced wind is proposed. It is based on a brand-new Balbi model formulation derived from (Chatelon *et al*. 2022) tested against more than 300 shrubland and grassland fires at the field scale with a very good agreement. This induced wind modelling is supposed to provide a good representation of a fire spreading upslope without wind (or with weak wind conditions). The model gives a new expression of the ROS that takes into account the pronounced acceleration of the fire spread with the increasing slope. It is tested against three different series of laboratory fire experiments (Butler *et al*. 2007, Liu *et al.* 2014, Liu *et al.* 2022) conducted without wind and in which the terrain slope angle varies ranges from 0 to 35° and against a field scale experimental fire conducted in Corsica across shrub species under weak wind and steep slope conditions (28°).

2. Physical modelling of the fire induced wind

2.1. Main equations of the new Balbi model

The Balbi model presented by Chatelon *et al.* (2022) calculates the ROS as the sum of three components (see fig. 1): (1) the radiation from the free flame F1 on the unburnt fuel (R_r), (2) the radiation from the flame base (the fuel burning particles area, R_b) and (3) the convection inside the vegetal stratum (R_c). The main equation of the model is the following:

$$R = R_b + R_c + R_r \tag{1}$$

The flame F2 is due to the flame base radiative and convective heat fluxes. All details and nomenclature can be found in (Chatelon *et al.* 2022).

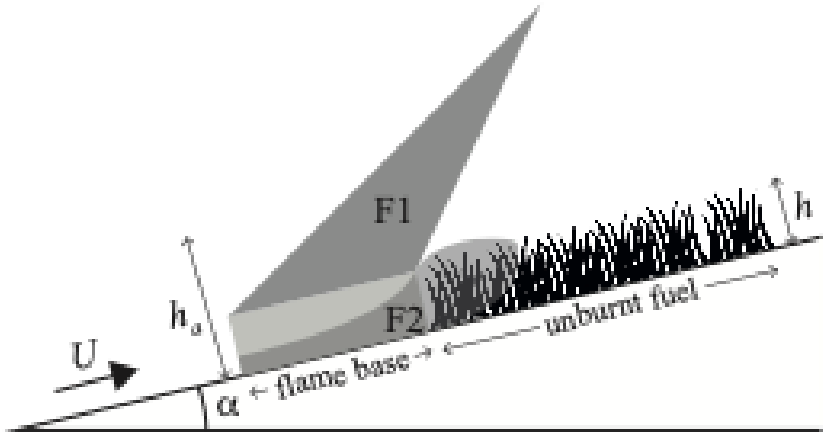

Figure 1- An idealized representation of the flaming zone combustion profile

As the convective and free flame radiative contributions to the ROS (R_c and R_r, see eq. 1) depend on the ROS, an iterative method is necessary to obtain the ROS. So, in order to obtain a formulation which is easier to implement into real time decision making tools, a new version of the Balbi model is developed in order to avoid the use of iterative methods for the calculus of the ROS. This new version is also presented in this IX ICFFR conference. In brief, the main equation (1) is replaced with the following:

$$R = \max(R_b + R_c\ ;\ R_r) \tag{2}$$

Where the component of the ROS due to the flame base radiative heat flux (R_b) is still defined thanks to a Stefan-Boltzman Modelling:

$$R_b = \min\left(\frac{S_t}{\pi}, 1\right)\frac{BT^4}{\beta\rho_v q} \quad (3)$$

And where the two other components are the following:

$$R_c = \min\left(\sqrt{\frac{b\,U}{K}}, b\,U\right) \quad (4)$$

$$R_r = s\,\frac{r_{00}}{u_0}\,(2A-1)(U-\,U_r) \quad (5)$$

If the drag forces law (K) is still a linear function of the packing ratio (β), the modelling of the radiative coefficient (A) and the upward gas velocity (u_0) are multiplied by a term τ_b which represents the fuel burning rate:

$$A = \min\left(\frac{S}{2\pi}; 1\right)\frac{\chi_0\Delta H}{4q}\,\tau_b \quad (6)$$

$$u_0 = 2\frac{(s_t+1)}{\tau_0}\,\frac{\rho_v}{\rho_a}\,\frac{T}{T_a}\min(S, 2\pi)\,\tau_b \quad (7)$$

Finally, the convective coefficient b is modelled as follows:

$$b = a\frac{\Delta H}{q\,\tau_0}\sqrt{\frac{s}{\beta}} \quad (8)$$

2.2. Modelling of the fire induced wind

As the flame needs fresh air for the combustion, it is assumed that this fresh air enters into the flame on a given height (denoted by h_a, see fig. 1). So, a simplified mass balance leads to:

$$\rho_a\,h_a\,U = s_t\,L\,\dot{\sigma} \quad (9)$$

After some simplifications, eq. 8 yields the expression of the fire induced wind:

$$U\ = \frac{R}{p} \quad (10)$$

Where p denotes the term:

$$p\ = h_0\,\frac{h_a\,h\sqrt{\beta}}{s_t\,\tau} \quad (11)$$

When the packing ratio β increases, there is less and less fresh air that could enter the flame base and then the given height h_a needs to increase. Thus, it is assumed that the given height is proportional to the square root of the packing ratio and the fuel height (h):

$$h_a\ = h_0\,h\,\sqrt{\beta} \quad (12)$$

Where h_0 is a scaling factor.

Finally, using eq. 12, the coefficient p is defined as follows:

$$p\ = h_0\,\frac{\rho_a}{\rho_v}\,\frac{1}{\sqrt{\beta}} \quad (13)$$

This modelling is possible thanks to the new formulation of the Balbi model whose main equation is defined by eq. (2).

2.3. The coupled model

Note that under zero wind conditions or when the ambient wind is not strong enough, the external wind U in eqs 2—8 is replaced by the fire induced wind.

When the slope angle (α) increases, the induced wind U increases as well and then the flame base cools. Consequently, the upward gas velocity u_0 decreases and the flame tilt angle γ increases. It therefore leads to a decrease in the vertical heat losses of the convective flow and to an increasing convective coefficient b through

the scaling factor *a* (see eq. 8). From a physical point of view, it means that the free flame F1 flattens the flame F2. So it is assumed that the scaling factor *a* linearly depends on the terrain slope angle α.

As the combustion rate τ_b decreases, the radiative coefficient *A* decreases as well and turns smaller than ½. Therefore, the free flame radiation can be neglected and $R_r = 0$. Finally, eq. 2 yields:

$$R = R_b + R_c \tag{14}$$

The expression of the ROS can be expanded according to two different induced wind regimes:

(1) For low induced wind values, $R_c = b\,U$ and using eq. 10:

$$R = R_b + b\,U = R_b + b\,\frac{R}{p} \tag{15}$$

Eq. 15 allows the characterisation of the ROS *R*:

$$R = \frac{R_b}{1-\frac{b}{p}} = \frac{R_b}{1-\frac{\alpha}{\alpha_\infty}} \tag{16}$$

Where α_∞ is a critical slope angle related to some fuel characteristics and model parameters:

$$\alpha_\infty = h_0\,\frac{\rho_a}{\rho_v}\,\frac{1}{\sqrt{s}}\,\frac{q\,\tau_0}{a_0\,\Delta H} \tag{17}$$

(2) For high induced wind values,

$$R = R_b + \sqrt{\frac{b\,U}{K}} = R_b + \sqrt{\frac{b}{p}\,\frac{R}{K}} \tag{18}$$

After some calculations, eq. 18 yields:

$$R = \frac{\alpha}{\alpha_\infty\,K} \tag{19}$$

The final expression of the ROS is obtained in merging eqs. 16 and 19:

$$R = \begin{cases} \frac{R_b}{1-\frac{\alpha}{\alpha_\infty}} \;if\; \alpha < \alpha_\infty \\ \frac{\alpha}{\alpha_\infty\,K} \;if\; \alpha \geq \alpha_\infty \end{cases} \tag{20}$$

3. Numerical results and discussion

The model given by eq. 20 is tested against three sets of laboratory experiments conducted under zero-wind conditions. The set of experiments conducted by Butler *et al*. (2007) aims at studying the fire spread on slope. An excelsior fuel bed with three different heights (and packing ratios) and six different slope angles ranging from -17° to 43° were set. The second set of experiments was performed by Liu *et al*. (2014). Fires spreading on 10 different values of the slope angle (from 0 to 32°) across a dead pine needles fuel bed were monitored. The last set of laboratory experiments carried out with the same pine needles fuel bed is composed of four series of fires spreading upslope (slope angle ranging from 0 to 40°). Each series differs from another by the dimensions (the height) of the lateral walls of the bench.

All the ROS measurements in the three sets of experiments suggest two different types of fire behaviour. Up to a specific value of the slope angle (which is different from one experiment to another), the fire growths slowly with a very low to moderate ROS. Beyond this threshold value, a dramatic acceleration of the ROS is observed.

The numerical results obtained by the proposed model against the experiments performed by Butler *et al.* (2007), and by Liu *et al.* (2014, 2022) are plotted in figs. 2 and 3, respectively. Note that Butler and his co-authors (2007) calculated the normalized ROS (ratio between ROS and ROS0, obtained for zero-wind and zero-slope) in all their set of experiments.

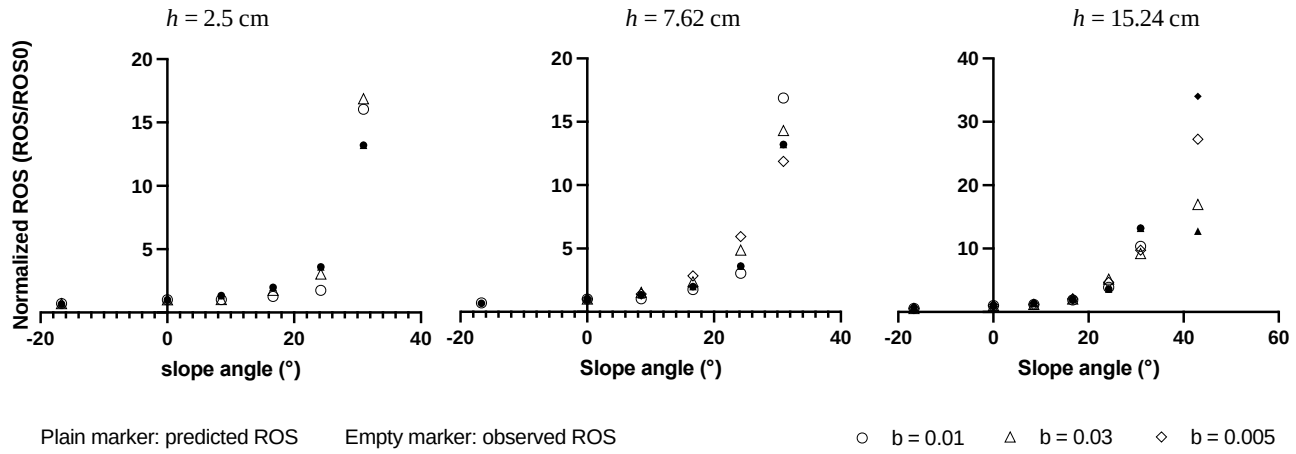

Figure 2 – Comparison between observed ROS (empty markers) and predicted ROS (plain markers) for three different fuel heights (2.5, 7.62 and 15.24 cm) and three different packing ratios (0.01, 0.03 and 0.005) in the set of experiments carried out by Butler et al. (2007)

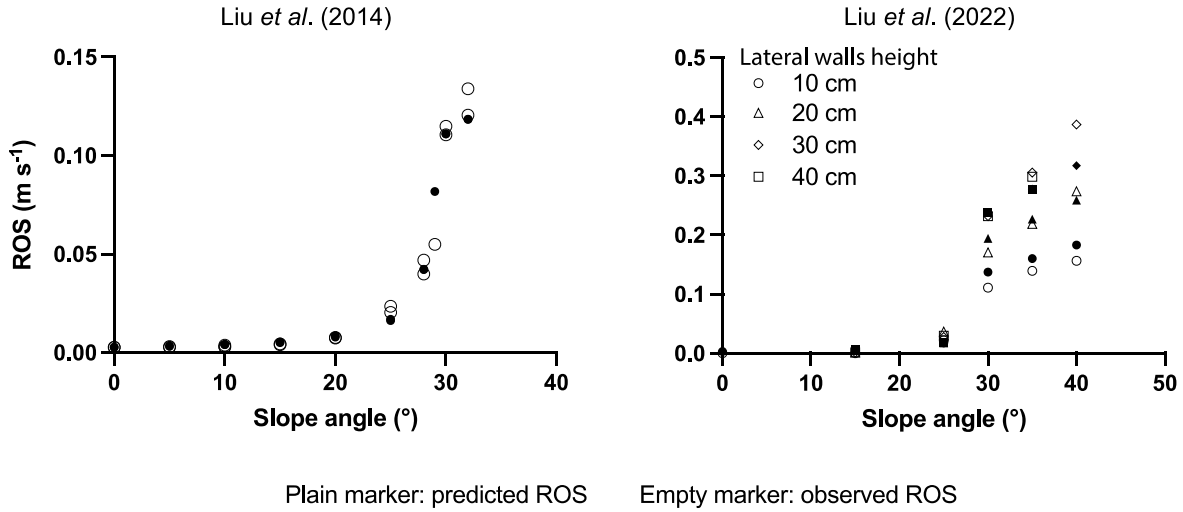

Figure 3 – Comparison between predicted ROS (plain markers) and observed ROS (empty markers) in the set of fire experiments conducted by Liu et al. (2014) (left plot) and by Liu et al. (2022) (right plot). Liu et al. (2022) measured several propagations with only a change in the height of the lateral walls of their experimental bench.

The agreement between observed and predicted rate of spread is assessed using three statistical tools whose results are presented in table 1. Both Normalized Mean Square Error (NMSE) and Mean Absolute Percentage Error (MAPE) are useful for estimating the overall deviations and the Fractional Bias (FB) allows to understand if a model shows under-predictions or over-predictions. An ideal model is obtained for a zero NMSE, MAPE and FB.

Table 1- Agreement between observed and predicted rate of spread estimated with three statistical tools (NMSE, Normalized Mean Square Error, MAPE, Mean Absolute Percentage Error and FB, Fractional Bias)

Set of experiments	*NMSE*	*MAPE*	*FB*
Butler *et al*. (2007)	0.25	18%	0.08
Liu *et al*. (2014)	0.04	16%	0.07
Liu *et al*. (2022)	0.02	58%	0.29
Winter high intensity fire (unpublished)	0.03	20%	0.18

According to figs. 2 and 3, the ROS predicted by the proposed model seems to match well the trends of the ROS against slope angle. The slow increasing of the ROS for small values of the slope angle and the ROS acceleration

are correctly reproduced. This visual impression is confirmed by the error results (table 1) with low NMSE and MAPE, except for the last set of laboratory experiments. Indeed, 58% is a quite high value for the MAPE but this result is mainly due to the two first values (where the slope angle is equal to 0° and 15°) with a practically zero ROS (order of magnitude smaller than a millimetre per second). If these two first values are removed from the calculation, the MAPE falls to a value of 17%.

The model has also been tested against an experimental shrubland fire conducted in the north-western of Corsica in march, 2021. The plot was approximately 150 m (length) x 30 m (width) and was burnt on a steep sloped terrain (slope angle ~ 28°) upon winter environmental conditions (ambient temperature ~ 6°C, weak wind velocity ~ 1.3 m s^{-1}). This fire fell into the very high fire severity (Cheney, 1981) with a fireline intensity close to 10 MW m^{-1} and a very fast ROS (0.45 m s^{-1}). As the Balbi model (Chatelon *et al.* 2022) does not include any fire induced wind sub-model, it provides poor results with a predicted ROS equal to 0.1 m s^{-1}. The ROS calculated with the proposed induced wind model (eq. 20) is equal to 0.54 m s^{-1} and is clearly a good approximation of the observed ROS. Indeed table 1 provides small errors (NMSE = 0.03 and MAPE = 20%).

The three sets of laboratory experiments exhibit the same ROS behaviour, consisting in a very slow increase of the ROS up to a threshold value of the terrain slope angle. Below this threshold value, without external wind, the fire spreads as on flat terrain, where the main heat transfer mechanism is the radiation from the fuel burning particles area. Beyond this value, the ROS highly accelerates in an exponential way for Liu *et al.* (2014) and Butler *et al.* (2007) or in a quite linear way in the experiments carried out by Liu *et al.* (2022). The slope angle threshold value seems to be different for each fire experiments series but approximately ranges from 20° to 30°. For these steep slopes, the flame is more tilted on the ground and creates a convective airflow in order to compensate the draft caused by the hot gases moving upwards. This feedback accelerates the ROS and in certain cases, an equilibrium is not obtained, causing a fire eruption. The proposed model (eq. 20) suggests two different behaviours splitted by a threshold slope angle calculated with the model. The numerical results shows a quite good agreement for these sets of laboratory experiments and for the winter fire at the field scale.

4. Conclusion

An accurate modelling of the convective flow induced by a fire spreading on a steep sloped terrain is the first step towards the modelling of eruptive fires. This work is a first attempt to give a physical formulation to this fire induced wind phenomenon. If the tests against three sets of laboratory experiments and against a field scale shrubland fire are very encouraging (with quite small deviations), the proposed model needs to be confronted to much more laboratory and field experiments in order to improve the physical formulation.

5. References

Butler, B. W., Bartlette, R. A., Bradshaw, L. S., Cohen, J. D., Andrews, P. L., Putnam, T., & Mangan, R. J. (1998). *Fire Behavior Associated with the 1994 South Canyon Fire on Storm King Mountain, Colorado*. Research Paper RMRS-RP-9, Ogden, UT, USDA, Forest Service, Rocky Mountain Research Station, 82 p.

Butler B.W., Anderson W.R., Catchpole E.A. (2007) Influence of Slope on Fire Spread Rate, In Butler, Bret W.; Cook, Wayne, comps. 2007. The fire environment—innovations, management and policy; conference proceedings. 26-30 March 2007; Destin, FL. Proceedings RMRS-P-46CD. Fort Collins, CO: U.S. Department of Agriculture, Forest Service, Rocky Mountain Research Station. 662p.

Chatelon, F.-J., Sauvagnargues, S., Dusserre, G., & Balbi, J.-H. (2014). Generalized Blaze Flash, a "Flashover" Behavior for Forest Fires—Analysis from the Firefighter's Point of View. *Open Journal of Forestry, 4*, 547-557. http://dx.doi.org/10.4236/ojf.2014.45059

Chatelon, F.-J., Balbi, J.-H., Cruz, M.G., Morvan D., Rossi J.L., Awad C., Frangieh N., Fayad J., Marcelli T. (2022) Extension of the Balbi fire spread model to include the field scale conditions of shrubland fires, *International Journal of Wildland Fire*, **31(2)**, 176-192, http://dx.doi.org/10.1071/WF21082.

Cheney, P.N. (1981) Fire behaviour, in: A. Gill, R. Grooves, I. Noble (Eds.), Fire Aust. Biota, Australian Academy of Science, Canberra, ACT, pp. 151–175.

Chetehouna K., Courty L., Garo J.P., Viegas D.X., Fernandez-Pello A.C. (2014) Flammability limits of biogenic compounds emitted by fire-heated vegetation (Rosmarinus officinalis) and their potential link with

accelerating forest fires in canyons: A Froude-scaling approach, *Journal of Fire Sciences*, **32(4)**, 316-327, http://dx.doi.org/10.1177/0734904113514810.

Courty L. (2012) Etude de l'émission et des propriétés de combustion des composés organiques volatils potentiellement impliqués dans les feux de forêts accélérés, Thèse pour l'obtention du grade de Docteur de l'école nationale supérieure de mécanique et d'aéronautique.

European Science & Technology Advisory Group (2020) Evolving risk of wildfires in Europe – the changing nature of wildfire risk calls for a shift in policy focus from suppression to prevention. Brussels, Belgium. https:// www.undrr.org/publication/evolving-risk-wildfires-europe-thematic- paper-european-science-technology-advisory.

Liu N., Wu J., Chen H., Xie X., Zhang L., Yao B., Zhu J., Shan Y. (2014) Effect of slope on spread of a linear flame front over a pine needle fuel bed: experiments and modelling, *International Journal of Wildland Fire*, **23**, 1087-1096.

Liu N., Yuan X., Xie X., Lei J., Gao W., Chen H., Zhang L., Li H., He Q., Korobeinichev O. (2022) An experimental study on mechanism of eruptive fire, *Combustion Science and Technology*, doi:10.1080/00102202.2021.2019240

National Fire Protection Association: NFPA (2011). Guide for Fire and Explosion Investigations, NFPA 921.

Tedim, F.; Leone, V.; Amraoui, M.; Bouillon, C.; Coughlan, M.R.; Delogu, G.M.; Fernandes, P.M.; Ferreira, C.; McCaffrey, S.; McGee, T.K.; Parente, J.; Paton, D.; Pereira, M.G.; Ribeiro, L.M.; Viegas, D.X.; Xanthopoulos, G. (2018) Defining Extreme Wildfire Events: Difficulties, Challenges, and Impacts. *Fire*, *1*, 9. https://doi.org/10.3390/fire1010009

Viegas, D. X. (2004). A Mathematical Model for Forest Fire Blowup. *Combustion Science and Technology*, *177*, 27-51. http://dx.doi.org/10.1080/00102200590883624

Viegas, D. X., & Pita, L. P. (2004). Fire Spread in Canyons. *International Journal of Wildland Fire*, *13*, 253-274. http://dx.doi.org/10.1071/WF03050

Viegas D.X., Stipanicev D., Ribeiro L., Pita L.P., Rossa C. (2008) The Kornati fire accident – eruptive fire in relatively low fuel load herbaceous fuel conditions, In 'Modelling, Monitoring and Management of forest fires' (Ed. WitPress) Vol. **I**, pp 365-375.

Viegas D.X., Simeoni A. (2010) Eruptive behaviour of forest fires, *Fire Technology*, **47(2)**, 303-320, http://dx.doi.org/10.1007/s10694-010-0193-6.

Post–fire management for improving soil quality and hydrological process: a case study in a Mediterranean Croatia

Domina Delač*[1]; Ivica Kisić[1]; Paulo Pereira[2]

[1]*University of Zagreb, Faculty of Agriculture, Croatia, {ddelac, ikisisc}@agr.hr*
[2]*Mykolas Romeris University, Environmental Management Laboratory, Latvia, {pereiraub@gmail.com}*

**Corresponding author*

Keywords

Mulching, on-site, soil quality, runoff, nutrients

Abstract

Wildfires in Mediterranean Croatia have increased in recent decades, raising concerns about the adverse effects of fire and the rate of soil and water degradation. Post-fire management techniques, such as mulch application, are commonly used after high to moderate wildfire severity. Local, site-specific solutions are needed to mitigate wildfire effects in this context. This research aims to study the effect of mulches (from on-site sources) on soil and hydrological properties. We hypothesised that mulch application would increase soil quality and reduce erosion and runoff yield. During July 2019, about 900 ha of *Pinus halepensins* Mil. forest, abandoned grazing and agricultural olive groves (*Olea europea* L.) were affected by a moderate to high wildfire in the hinterland of Šibenik City (Croatia, 43°45'N 15°56'E, 105 m a.s.l.). Twenty-five days after the wildfire occurrence, unmulched (UM, control) and two mulch treatments (*Olea europea* leaves (OM) and *Pinus halepensis* needles (PM) were applied for post-fire stabilisation on *Cambisols*. One treatment covered an ~10 m^2 area with 0.5. kg m^2 mulch application which was measured on the experimental plots. Prior to mulch application, 15 (5 per treatment) metal rings (0.2 m^2) with connected plastic collectors were set up on sloped terrain (~9°) to monitor erosion and runoff yield. Soil samples were collected every three months, and erosion and runoff yield after major precipitation events during two years. The studied soil properties were: soil water repetency (SWR), soil hydraulic conductivity (SHC), mean weight diameter (MWD), water stability of aggregates (WSA), soil organic matter (SOM), total carbon (TC), total nitrogen (TN), extractable potassium (K_2O), and available (P_2O_5). Our results showed that both mulch treatments reduce runoff generation in addition to UM treatment. The erosion yield was not occurred due to natural soil conditions. A linear decreasing trend was noted for SWR in all treatments. Overall, PM was showed higher efficiency in increasing soil aggregate stability (MWD and WSA), SHC SOM, and TC. OM has mostly increased soil nutrients such as TN, P_2O_5, and K_2O. Bot mulch treatment increased soil quality, but the effect was variable due to the different chemical compositions of the material. The use of native mulch can be recommended because it improves soil quality and reduces runoff ratio. However, consideration should be given to whether they are available in the areas affected by wildfire.

1. Introduction

Wildfire is a common phenomenon and part of the Mediterranean ecosystem. However, in recent decades, the number and intensity of wildfires over the entire Mediterranean area have increased related to the long drought periods and intense high temperatures (Pausas et al., 2008). In addition, land abandonment, depopulation of rural areas, reduction of pastures, accumulations of flammable vegetation contribute to the spared of wildfires frequency and magnitude (Moreira et al., 2011; Pausas and Keeley, 2009). In the Mediterranean Croatia, such cases are often pronounced in the hinterland of large cities, especially in areas where landscape management and land use are not properly implemented (Delač et al., 2020, 2021). One of the main consequences of wildfires is the complete removal of vegetation and litter, which exposes topsoil to the risk of erosion and degradation of soil's physical and chemical properties. Soil affected by wildfire will experience degradation of primary functions, at least for some time (Certini, 2005; Pereira et al., 2019). The post-fire management is often implemented in the wildfire affected area to rehabilitate and stabilise the upper soil profile. Very often, mulch is applied to burned areas during post-fire restoration (Díaz-Raviña et al., 2012). Mulch is a common technique to inhibit soil erosion and encourage faster soil recovery after the passage of fire. Moreover, these treatments, known as emergency rehabilitation treatments, reduce rainwater's impact, favour the infiltration process, mitigate soil degradation, and prevent runoff and soil sediment removal after a wildfire. Moreover, mulching

with organic plant residues has improved the soil structure, mainly due to an increase in stability of soil aggregates, soil porosity, and improvement in soil hydraulic conductivity (De la Rosa et al., 2019). Although depending on the fire severity, soil organic matter (SOM), total carbon (TC), total nitrogen (TN) and available and extractable nutrients such as phosphorus (P) and potassium (K) can increase, decrease or remain unchanged. (Caon et al., 2014). The mulch addition and the compounds that have not been volatilised in the form of ash and charred residues are incorporated into soil increasing nutrients content (Caon et al., 2014). However, there is a lack of research about their manner after applying different types of mulch materials. In addition, there is a need to observe runoff and erosion behaviour after application on native mulch materials. This research aims to study the effect of Pinus halepensis and Olea europea mulches (from on-site sources) on soil and hydrological properties. We hypothesised that mulch application would increase soil quality and reduce erosion and runoff yield.

2. Material and method

The study was carried out in the Dalmatia region on the Adriatic coast (Croatia) in a hinterland of Šibenik City, (5 km from the Coast, 43°45'06.0"N 15°56'02.9"E.; Fig.1.). Elevation ranges between 50 and 200 m a.s.l. and the aspect is NE. According to Köppen classification, the study area's climate is Mediterranean Csa (warm temperatures with dry and warm summers). The mean annual temperature is 15.8 °C, and the annual precipitation is 800 mm (Šibenik meteorological station) (Kottek et al., 2006). The soil type is classified as *Cambisol*. Vegetation belongs mainly to *Pinus halepensis* Mil., forest and cultivated olive groves (*Olea europaea* L.) and fig tress (*Ficus carica* L.). In the study area, the wildfire occurred on 28 July 2019 and affected an area of about 900 ha (Delač et al., 2020, 2021) and it lasted three days until local firefighters stopped the fire. The first intervention to the burned area was 25 days after wildfire occurrence due to safety reasons and recommendations from local firefighters. The severity of wildfire was moderate to high, which was evident in partially burned canopy places. The area provided natural organic materials for usage and implementation. For covering burned soil surface, two different mulch treatments were applied. One was composited of *Pinus halepensis* needles (PM) the other one of mulch of *Olea europaea* leaves (OM). These mulched were used due to on-site availability and the valuable input of native plants on the soil. The mulches were applied in 0.5 kg m^2 on 10 m^2 each treatment. The erosion equipment to measure runoff and sediment yield were set-up on the same treatments. The studied soil properties were: soil water repetency (SWR), soil hydraulic conductivity (SHC), mean weight diameter (MWD), water stability of aggregates (WSA), soil organic matter (SOM), total carbon (TC), total nitrogen (TN), extractable potassium (K_2O), and available (P_2O_5). The effect of wildfire without any human intervention (unmulched, UM) was monitored next to mulch treatments to assess the impact of both mulches. The soil sampling campaign was conducted during two years: 25 days after fire (DAF), 3 months after fire (MAF), 6, 9, 12, 15, and 24 MAF. Soil samples (0–3 cm) were collected in each treatment in 5 repetitions after litter removal (105 in total). The runoff and erosion yield were collected after major precipitation events.

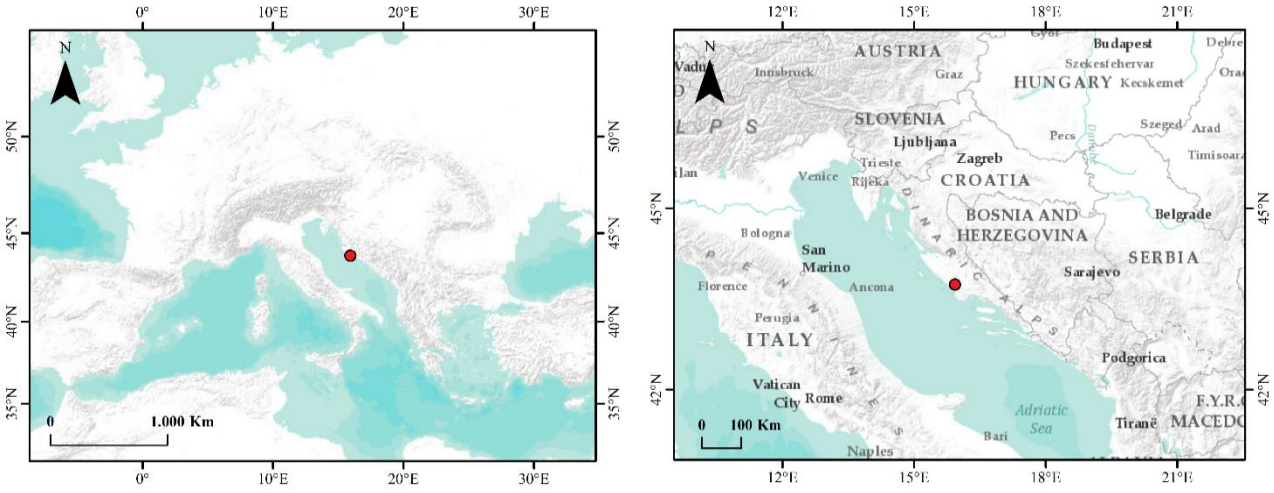

Figure 1. Study area (red dot shows experimental location)

3. Results and conclusions

Post-fire management is typically a trade-off between the cost and potential effectiveness of applied treatment and the potential damage to valuable resources from unmitigated erosion. Mulching is a technique that belongs to emergency stabilisation techniques, as it immediately stabilises the soil of the burned area and reduces additional damage to the fragile bare soil which confirmed our results. After a wildfire, there is a mosaic of low, moderate, and high soil burn severity conditions, but the cost of mulch material and the energy required to apply it must be considered. Preference should be given to local and available on-site material. Our results showed that both mulch treatments reduce runoff generation in addition to UM treatment. The erosion yield was not occurred due to natural soil conditions. A linear decreasing trend was noted for SWR in all treatments. Overall, PM was showed higher efficiency in increasing soil aggregate stability (MWD and WSA), SHC SOM, and TC. OM was mostly increased soil nutrients such as TN, P_2O_5, and K_2O. Bot mulch treatment increased soil quality, but the effect was variable due to the different chemical compositions of the material. The use of native mulch can be recommended because of its effect on improving soil quality and reducing runoff ratio, however consideration should be given to whether they are available in the areas affected by wildfire.

4. Acknowledgements

The work was supported by Croatian Science Foundation under the project “Influence of Summer Fire on Soil and Water Quality” (IP-2018-01-1645).

5. References

Certini, 2005. Effects of fire on properties of forest soils: a review. Oecologia, 143, 1–10. https://doi.org/10.1007/s00442-004-1788-8

Caon, L. Ramón Vallejo, V. Coen, E. J. Geissen V. Earth-Science Reviews, 139, 47–58. http://dx.doi.org/10.1016/j.earscirev.2014.09.001

De la Rosa, J.M., Jiménez-Morillo, N.T., González-Pérez, J.A., Almendros, G., Vieira, D., Knicker, H.E. & Keizer, J. 2019. Mulching-induced preservation of soil organic matter quality in a burnt eucalypt plantation in central Portugal. Journal of Environmental Management, 231, 1135–1144. https://doi.org/10.1016/j.jenvman.2018.10.114

Delač, D., Pereira, P. & Kisić, I. 2020. The effects of mulch (Olea europea and Pinus halepensis) on burned soils: A preliminary study in Adriatic Coast (Croatia). EGU General Assembly 2020. https://doi.org/10.5194/egusphere-egu2020-1295

Delač, D., Pereira, P. & Kisić, I. 2021. Impact of post-wildfire stabilisation treatments on major and minor topsoil elements in a Mediterranean environment (Croatia): first- year study. EGU General Assembly 2021. https://doi.org/10.5194/egusphere-egu21-648

Díaz-Raviña, M., Martín, A., Barreiro, A., Lombao, A., Iglesias, L., Díaz-Fierros, F. & Carballas, T. 2012. Mulching and seeding treatments for post-fire soil stabilisation in NW Spain: Short-term effects and effectiveness. Geoderma, 191, 31–39. https://doi.org/10.1016/j.geoderma.2012.01.003

Moreira et al., 201 Moreira, F., Viedma, O., Arianoutsou, M., Curt, T., Koutsias, N., Rigolot, E., Barbati, A., Corona, P., Vaz, P., Xanthopoulos, G., Mouillot, F. & Bilgili, E. 2011. Landscape - wildfire interactions in southern Europe: Implications for landscape management. Journal of Environmental Management, 92, 2389–2402. https://doi.org/10.1016/j.jenvman.2011.06.028

Pausas, J.G. & Keeley, J.E. 2009. A burning story: The role of fire in the history of life. BioScience, 59, 593–601. https://doi.org/10.1525/bio.2009.59.7.10

Pausas, J.G., Llovet, J., Rodrigo, A. & Vallejo, R. 2008. Are wildfires a disaster in the Mediterranean basin? A review. International Journal of Wildland Fire, 17, 713–723. https://doi.org/10.1071/WF07151

Pereira, P., Martínez-Murillo., J. F., Francos M. 2019. Environments affected by fire. In book: Advances in Chemical Pollution, Environmental Management and Protection, 4, 119–155. https://doi.org/10.1016/bs.apmp.2019.09.001

Pre-standardization activity on wildfire tactical situation symbology: The SITAC CEN/CENELEC workshop agreement

Ilias Gkotsis[1]*; George Eftychidis[1]; Leonidas Perlepes[1]; Dimitris Diagourtas[1]; Gianfilippo Micillo[2]; Giovanni Fresu[2]; Philippe Meresse[3]; Cristina Popa[4]

[1]SATWAYS. 15, M.Konstantinou, 14122 Irakleio, Greece
{i.gkotsis, g.eftychidis, l.perlepes, d.diagourtas}@satways.net
[2] CNVVF. Corpo Nazionale dei Vigili del Fuoco. Via Cavour 5 – 00128 Roma, Italy
{gianfilippo.micillo, giovanni.fresu}@vigilfuoco.it
[3] EPLFM. Domain de Valabre – 13120 Gardanne, France {p.meresse@valabre.com}
[4] ASRO. Str. Mihai Eminescu nr. 238, 020085 Bucharest, Romania {cristina.popa@asro.ro}

**Corresponding author*

Keywords

Standardization, symbology, wildfire, tactical, mapping

Abstract

During the onset of a crisis, a wide range of local, regional, national and sometimes international authorities generate maps using proper symbols to support coordination and communication during a potential disaster, such as a large forest fire. In this context, it is essential that all stakeholders can readily understand the information shown on these maps to respond in a prompt and adequate manner. The standardization of a set of symbols, which could facilitate the efficiency of the operations in the field and at the same time optimize the coordination between all the command chain levels during the fire crisis, is conducted in context of the European research project STRATEGY, which aims to build and implement a Pan-European pre-standardisation framework for improving the interoperability of crisis management solutions.

The pre-requisite for standardization is a concrete pre-standardization activity aiming to describe and document the subject of the standardization as well as the purpose and the context of use. This is achieved through a properly organized pre-standardization procedure known as CEN/CENELEC Workshop Agreement (CWA), with the active involvement of interested organizations. In the envisaged case of wildfires, the organization is represented by the entities involved in the fire operations and the service provided is firefighting. In this direction, the relative pre-standardization initiative further described in this paper, aims to introduce a standardized set of tactical symbols that can be used by the responsible public safety agencies across EU and worldwide for the graphical presentation of mission critical operational information, based on SITAC approach. SITAC is a set of tactical symbols for wildfire managers, initially developed by the French Fire Service, used since 2000, further adopted and operationally used by the Fire Services in Italy and other EU Member States. SITAC, consists of tactical symbols, displaying graphic and textual information about an object at a single geographic position at a particular point in time.

The SITAC CWA shall deliver clear, concrete, and adequate instructions and guidelines for the visual description of the field operations during forest fire incidents in a predefined, formal way. Information related to the characteristics of the affected area, the evolution of the fire, the intervention measures as well as current or planned actions, are encompassed by the proposed symbology. This will play an important role during large and very large fire events where several organizations and actors need to cooperate and exchange information in common, such as incident commanders, fire officers, forest managers, personnel of the civil protection agencies and emergency services. Furthermore, in the case of cross-border incidents the use of a standardized symbology, familiar and known to international firefighting teams and modules, will facilitate to overcome the language barrier and to optimize the response to the crisis. Finally, such standardization will push the EU security industry, dealing with the development and deployment of related Command & Control systems and solutions, to follow formal visual communication guidelines, enhancing the communication and cooperation of the organizations in charge of managing wildfires and the organizations supporting the field operations.

1. Introduction

Conveying spatial information plays a very important role in efficient emergency response where maps are the most solid basis for direct representation of this spatial information. During the onset of a crisis, a wide range

of local, regional, and national authorities need to generate maps using proper symbols to help communicate information, respond to, and recover from a potential disaster such as a large forest fire. In this context, it is essential that all stakeholders (national and potentially international according to the incident) can readily understand the information shown on these maps to respond in a prompt and adequate manner. In this regard, a concrete symbology, in the sense of a visual language displayed on the map, is needed to share the operational message in a concise and clear way to all responsible decision makers.

The standardization of a set of symbols, which could facilitate the efficiency of the operations in the field and at the same time optimize the coordination between all the command chain levels during the fire crisis situation, is conducted in context of the European research project STRATEGY (https://strategy-project.eu/). STRATEGY aims to build and implement a Pan-European pre-standardisation framework to improve the interoperability of crisis management solutions, based on a gap analysis initially implemented within the project, given the expertise of involved end-users.

Base on the gaps identified, a standardized approach for visually communicating operational messages, using a commonly agreed and understood symbology among the actors of wildfire management is currently missing. This fact limits the effectiveness of coordinating the response effort of the resources involved in the incident. Having each organization in the various EU member states to use diverse processes, procedures, and symbols for communicating situational information during large fire incidents and crisis management operations can't be effective. This is more evident in case of cross-border crises where such peculiarities and differences may cause confusion among the first responders, often wasting the assistance offered between the Union's Member States. More specifically, in the case of large-scale forest fires in a cross-border context and with multiple authorities and modules from foreign countries engaged, the sharing of operational information and the common understanding of the situation becomes crucial. Therefore, establishing a common symbology which can be used by the fire services and the public safety agencies involved in wildfire management, is essential for the efficient and effective management of situations as mentioned before.

2. Methodology

2.1. Standardization and CWA

Standardization is a framework of agreements to which all relevant parties in an industry or organization must adhere to ensure that all processes associated with the creation of a good or performance of a service are performed within set guidelines. In the envisaged case of wildfires, the organization is represented by the entities involved in the fire operations and the service provided is firefighting. The pre-requisite for standardization is a concrete pre-standardization activity aiming to describe and document the subject of the standardization as well as the purpose and the context of use. This is achieved through a properly organized pre-standardization procedure known as CEN/CENELEC Workshop Agreement (CWA).

A CEN/CENELEC Workshop is considered as a body with a short-term task specified in its project plan. If the proposed scope calls for a long-term activity, the possibility to propose a Technical Committee should be explored. A CWA is a deliverable, which may take various forms such as text file or computer code, developed and agreed by the participants in a temporary working group (CEN/CENELEC Workshop). It is designed to meet an immediate need, can be quickly developed and can be used as fast track to future standardization activities. The stakeholder involvement is limited to those directly interested in the subject. The direct participation of interested parties, the possibility to indicate the participants and their organizations in the foreword and the rapid development process offered by a CWA, are particularly attractive for European research and innovation projects, which must deliver results within the limited duration of their project lifetimes.

In the case of the CWA presented in this paper, which concern the pre-standardization of the wildfire management symbology for mapping purposes during large scale fire crises the participants comprise representatives from fire and forest organizations, industry, research and technology organizations and standardization bodies. The standardization community is represented in the SITAC workshop by the National Romanian Standardization Organization (ASRO), which acts as the link with the European Standardization Committees and Technical Groups.

2.2. SITAC CWA

The CWA mentioned in this paper refers to SITAC (Standardization of Firefighting Tactical Situation Management), a set of tactical symbols for wildfire managers, initially developed by the French Fire Service (Sapeur Pompiers) being in use since 2000. The set of symbols that was originally developed included all type of hazards. SITAC literally stands for SITuation TACtique, an acronym corresponding to a schematic representation of an intervention of the Fire Brigades. It is part of the Operational Management and Command tools, which are implemented during a disaster to best organize the return to initial conditions or in a preeminent situation, a way out of the crisis.

The last decade, the original set was adopted by the "Corpo Nazionale dei Vigili del Fuoco (CNVVF)" in Italy and several other fire service agencies in EU Member States and the part of the symbology related to exclusively to wildfire management was marked out to be used operationally. This specific set is the focus of the respective CWA mentioned in this paper.

SITAC, as any set of tactical symbols, can be used by the respective agencies across EU and worldwide for the graphical presentation of mission critical operational information during operational missions. A tactical symbol displays graphic and textual information about an object at a single geographic position at a particular point in time. The graphic displayed is typically a screen icon with supplemental text and graphics surrounding the icon. In general, the graphic displayed depends on the symbology set a tactical symbol belongs to. Information related to the characteristics of the affected area, the evolution of the fire, the intervention measures as well as current or planned actions, are encompassed by the proposed symbology.

The CWA focuses on a specific set of symbols that can be used by public safety agencies for the depiction of operational information against a cartographic background during forest fires incidents. In this context, information related to (among others) the characteristics of the affected area, the advancement of the fire, the intervention measures / available equipment and actions that need to be taken, will be encompassed by the proposed set of symbols. Given its simplicity, its operational maturity and its acceptance in several EU countries, the SITAC set of symbols (known as) sets the basis for delivering a standardized way to share forest fire management information in paper and electronic maps during fire response operations. Its use in training sessions can further facilitate familiarization and efficiency during real operations.

The use of the graphics makes it possible to schematize using a normalized code, the main operational information related to an ongoing crisis. The objective is to facilitate the collection, transmission and understanding of information exchanged by the different levels of the command chain. Saving time and being aware of the real operational situation is essential for the wildfire managers when lives or property are threatened by an active fire. In addition, the standardization of means and actions considerably reduces the risk of misunderstanding and improves the accuracy of actions.

This paper presents the approach and the expected results of the standardization of the SITAC set of symbols, incorporating the feedback on several countries approaches deriving from the CWA members, to generalize its use by the EU public safety agencies for depicting operational information against a cartographic background (either digital or paper based) during forest fires incidents. The SITAC CWA aims to gain consensus from many of the EU wildfire management organizations for using a common approach to graphically symbolize the elements (means, operations, assets) of wildfire management operations, in an agreed manner building on the SITAC approach. It should be kept in mind that firefighting is a particular case of operations, where a variety of organizations are involved (not exclusively the fire brigade but forest services and forest fire fighting organizations as well). Due to the large extent of the incidents and the large number of the organizations involved (services and agencies), specific equipment and operations are used, and the coordination is often challenging. In case of large wildfires, it is a common practice that civil protection modules are deployed from one EU country to another. In such case the use of standardized symbols for planning, monitoring, and coordinating cross-border operations in the field will be even more beneficial for the effectiveness of the coordination.

Hence, this document is intended to benefit the cooperation among the EU and global wildfire management community, comprising incident commanders, fire officers, forest managers, personnel of the civil protection agencies and Emergency services. At the same time such standardization will push the EU safety and security industry dealing with the development and deployment of related Command & Control systems and solutions.

In this direction, the document will provide formal visual communication guidelines to support the communication and cooperation of the organizations in charge of managing wildfires and the organizations supporting the field operations (e.g., police, ambulance services, coast guard, etc.).

The SITAC symbology organizes the information to be shared in several groups depicting a. the environment i.e., the wind, the vegetation type and the slope b. the fire i.e. the type of the fire and its current and expected progression c. the operating area i.e. landscape type and infrastructures such as lifelines, water sources, helispots d. fire operations (ground, aerial and special e.g. backburn) and the forces (ground and aerial) deployed or planned to be in the field.

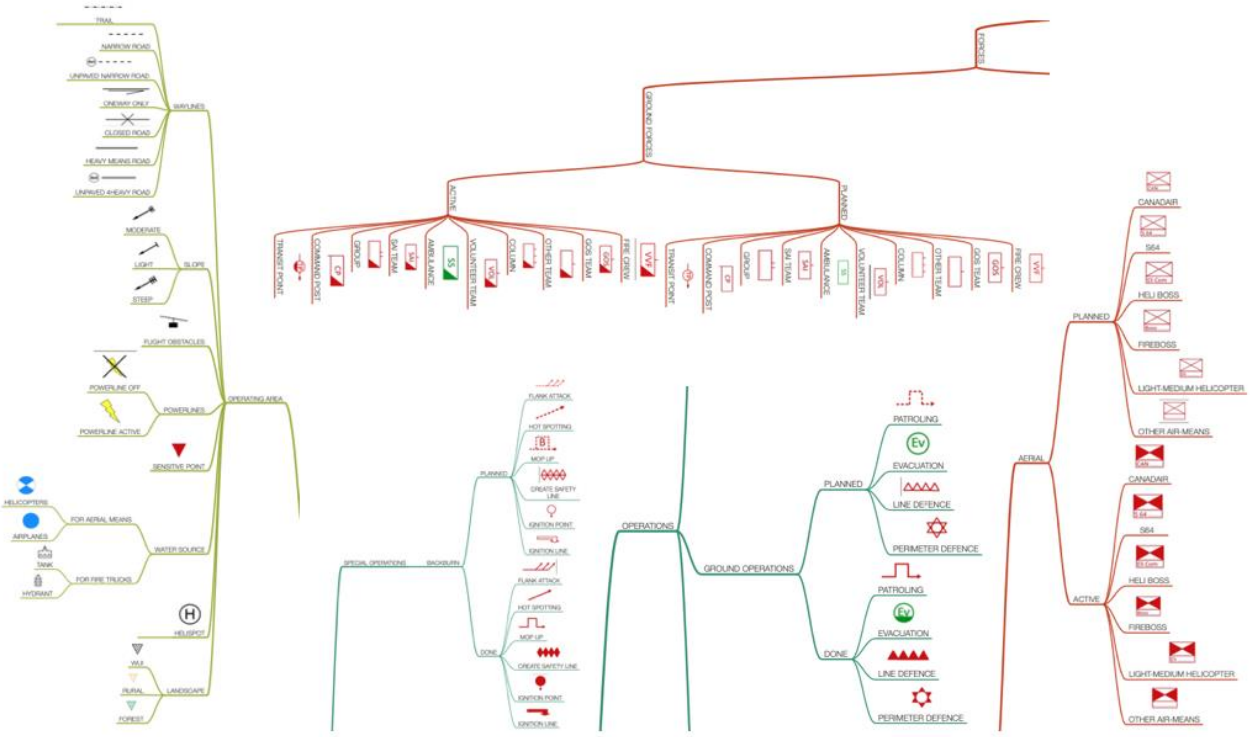

Figure 1- Groups of SITAC symbols for wildfire management information sharing

The SITAC symbols are kept simple to be easily drawn on paper maps in the field while semantic to be easily perceived and interpreted in the command post.

3. Results

The SITAC CWA shall deliver clear, concrete, and adequate instructions and guidelines for the visual description of the field operations during forest fire incidents in a predefined, formal way. This will allow to organize efficient and effective information sharing among all the operational actors involved in the fire management command chain. This will be important during large and very large fire events where several organizations need to cooperate and exchange information in common. Furthermore, in the case of cross-border incidents the use of a standardized symbology, familiar and known to international firefighting teams and modules will facilitate to overcome the language barrier and to optimize the response to the crisis.

4. Discussion

The outcome of the work presented here shall benefit the cooperation among the EU and global wildfire management community, comprising incident commanders, fire officers, forest managers, personnel of the civil protection agencies and Emergency services. At the same time such standardization will push the EU security

industry, dealing with the development and deployment of related Command & Control systems and solutions, to follow formal visual communication guidelines, enhancing the communication and cooperation of the organizations in charge of managing wildfires and the organizations supporting the field operations.

5. Acknowledgments

The aforementioned pre-standardization activity is currently performed within STRATEGY project that has received funding from the European Union's Horizon 2020 Research and Innovation programme under Grant agreement No 883520. Please see https://strategy-project.eu for more information.

6. References

STRATEGY project (H2020 GA 883520): Facilitating EU pre-Standardization process Through stReamlining and vAlidating inTeroperability in systems and procEdures involved in the crisis manaGement cYcle (https://strategy-project.eu).

CEN-CENELEC Guide 29. CEN/CENELEC Workshop Agreements – A rapid way to standardization. Edition 2, October 2020. CEN/BT Decision C168/2020 and CENELEC BT Decision D166/C082.

NASA World Wind. Tactical symbols (https://worldwind.arc.nasa.gov/java/tutorials/adding-new-tactical-symbols/)

Yann Kacenelen, CartoSITAC v2.2.: Facilitating EU pre-Standardization process Through stReamlining and vAlidating inTeroperability in systems and procEdures involved in the crisis manaGement cYcle, July 2002.

A. Kuveždić Divjak, B. Pribičević, and A. Đapo, 2019. Comparative Analysis Of Taxonomy, Standardisation And Availability Of Cartographic Symbol Sets For Crisis Mapping. The International Archives of the Photogrammetry, Remote Sensing and Spatial Information Sciences, Volume XLII-3/W8, 2019 Gi4DM 2019 – GeoInformation for Disaster Management, 3–6 September 2019, Prague, Czech Republic

Pyrocumulonimbus Firepower Threshold: Selected learnings from the 'Black Summer' real-time trial.

Kevin Tory*; Mika Peace

Bureau of Meteorology. GPO Box 1289 Melbourne Vic Australia 3001,
{kevin.tory, mika.peace}@bom.gov.au

**Corresponding author*

Keywords

Pyrocumulonimbus, Fire-generated thunderstorms, Fire-weather prediction

Abstract

Pyrocumulonimbus (pyroCb) clouds are difficult to predict and can produce extreme and unexpected wildfire behavior that can be hazardous to fire crews. Many forecasters modify conventional thunderstorm diagnostics to predict pyroCb potential, by adding temperature and moisture increments to represent smoke plume thermodynamics near the expected plume condensation level. An alternative approach is to anticipate the minimum firepower required to generate pyroCb for a given atmospheric environment.This concept, termed the pyroCb firepower threshold (PFT), requires only atmospheric information, removing the need for subjective estimates of the fire contribution. A simple approach to calculating PFT was presented by Tory and Kepert (2021) that incorporates only basic plume-rise physics, and yields an analytic solution for the minimum heat flux required to enter the base of the plume for pyroCb to form. This version takes into consideration the magnitude of any inversion or stable layer the smoke plume must penetrate, the height the smoke plume must rise before sufficiently buoyant cumulus clouds form in the smoke plume, and it incorporates the impact of wind on plume rise via the Briggs plume-rise model. This PFT also offers important insight into plume behavior and pyroCb formation.

Many assumptions are made to close the equations and to maximise simplicity. Two of these assumptions are questioned in this paper following the investigation of two deep, moist pyro-convection cases that occurred during 'Black Summer' (southern Australia, September 2019—March 2020). The first assumption, consistent with many thunderstorm diagnostics, is that the moist (cloudy) plume is non-entraining, and the second assumption is that the plume is positively buoyant when it saturates and remains buoyant until it rises beyond the -20 ℃ level of the atmosphere. The first assumption underpredicts the fire-power required and the second assumption can overpredict the necessary firepower, since a vigorous plume may have sufficient kinetic energy to penetrate stable layers or capping inversions. Procedures are introduced to address these limitations.

1. Introduction

When intense smoke plumes develop on wildfires, the so-called plume-dominated fires, fire behaviour can become erratic, unpredictable and the fire ground can become highly dangerous for fire fighters. Strong updrafts can transport burning embers downwind, amplifying firespread through the ignition of spotfires ahead of the fire front. The formation of deep cumulus clouds with strong vertical motion in these plumes may amplify the dangerous fire behaviour, and introduce additional hazards separate to the fire such as extreme winds from evaporative downbursts, and tornadic-strength vortices. When conditions are favourable the fire-induced deep, moist convection can produce lightning with the potential to ignite more fires. These fire-generated thunderstorms (FGT) are also known as pyrocumulonimbus (pyroCb).

A procedure for identifying atmospheric conditions that favour deep, moist plume growth in wildfire smoke plumes, termed the Pyrocumulonimbus Firepower Threshold (PFT, Tory and Kepert 2021) was tested in a real-time trial (Tory 2020) during Australia's 'Black Summer' (southern Australia, September 2019—March 2020). The procedure estimates a theoretical minimum heat flux (or firepower) required for deep, moist plume growth. This version of the PFT (hereafter PFT1) takes into consideration the magnitude of any inversion or stable layer the smoke plume must penetrate, the height the smoke plume must rise before sufficiently buoyant cumulus clouds form in the smoke plume, and it incorporates the impact of wind on plume rise via the Briggs plume-rise model (e.g., Briggs 1984). Below the condensation height it is assumed that the smoke plume can be described

by a Briggs plume rising through a neutrally stable layer of constant background wind. Above the condensation height, it is assumed the rising moist plume can be described by simple parcel theory (non-entraining, as applied to common thunderstorm forecast products such as Convective Available Potential Energy, CAPE).

During the real-time trial PFT1 forecast maps provided excellent guidance for predicting deep, moist pyro-convection (hereafter DMPC). A selection of interesting DMPC cases were investigated in detail, using a manual PFT1 analysis method applied to thermodynamic diagrams, yielding important insight into plume behaviour, which has inspired further development and tuning of PFT products. In this short paper, two such cases are presented.

2. PFT

The full PFT1 derivation is provided in Tory and Kepert (2021), as well as an approximated form designed for estimating and visualising PFT1 manually on a thermodynamic diagram,

$$PFT1 \sim 0.3 \times \left(z_{fc}\right)^2 \times U \times \Delta\theta_{fc}. \qquad 1.$$

Here z_{fc} is the free-convection height in units of km (the minimum height the plume must rise to initiate deep moist pyro-convection), U is the average velocity magnitude of the mixed layer horizontal wind, units ms^{-1}, and $\Delta\theta_{fc}$ represents how much warmer the plume needs to be than the mixed-layer potential temperature, units ℃ (or K). These units yield PFT1 in GW. An example from the evening of the disastrous Black Saturday fires of 2009 is shown in Fig. 1. The mixed-layer potential temperature (thick red line) and specific humidity (thick cyan line) represent the average thermodynamic properties of air entrained into the plume. The saturation point curve is approximated by a straight line representing a 15:1 ratio of temperature to moisture increments (units $K/g\ kg^{-1}$, blue line) produced by the fire (Luderer et al. 2009, Tory et al. 2018). It represents a range of possible positions on the diagram where the plume can reach saturation. The minimum-buoyancy plume-path that freely convects to a level cooler than -20 ℃ is indicated by the gold curve. The free-convection height (z_{fc}) is the height at the base of the gold curve. Here the plume must be at least $\Delta\theta_{fc}$ warmer than the mixed-layer potential temperature (thick red line), and the average mixed-layer wind, U, can be estimated from the wind barbs highlighted in green.

In theory, the fire must be able to produce enough firepower for the plume to rise to at least a height of z_{fc}, while maintaining an average plume temperature of at least $\Delta\theta_{fc}$ warmer than the mixed-layer potential temperature, while battling the wind, U, which inhibits the plume rise by stretching the plume out downwind and exposing it to more dilution from entrainment.

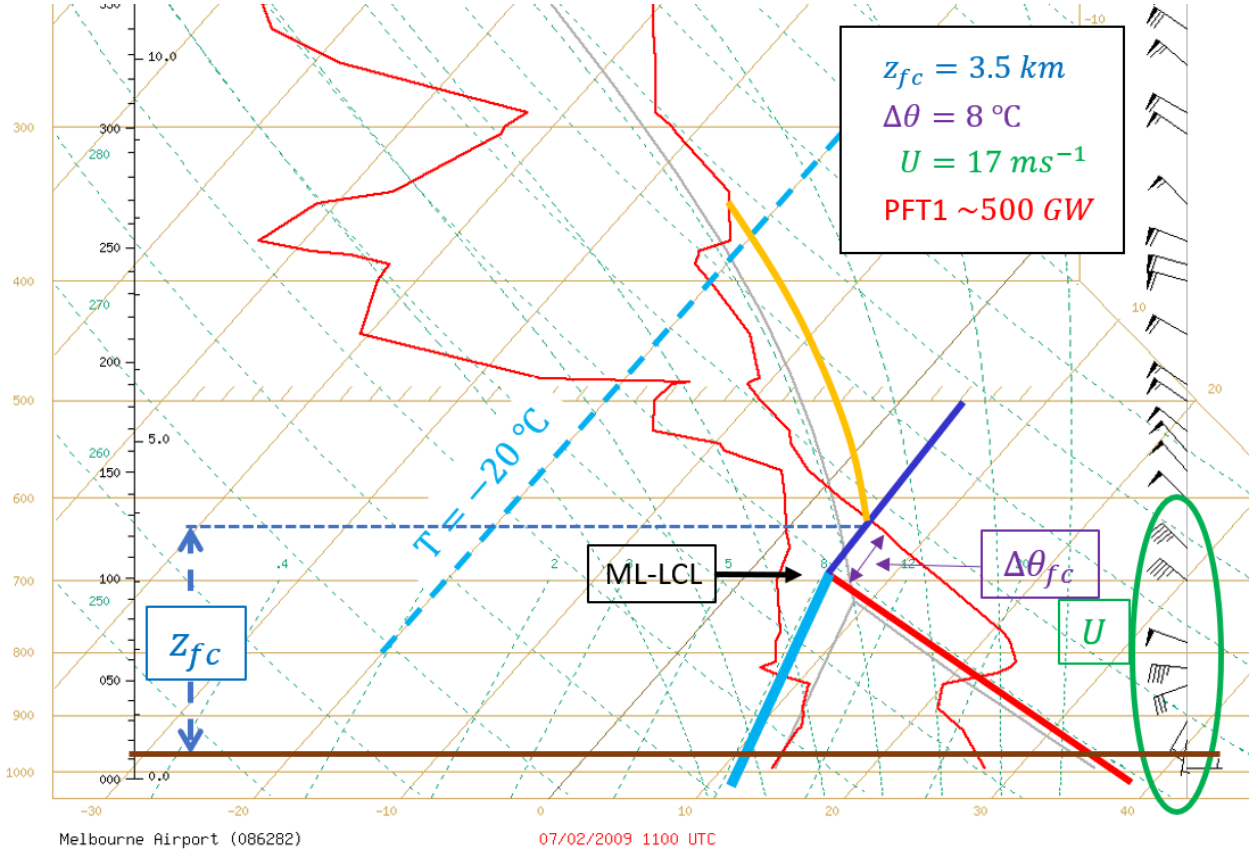

Figure 1- Melbourne Airport sounding 1100 UTC, 7 February 2009 (10 PM local time), with markers used in the manual PFT calculation (Eq. 1). Thick red and cyan lines represent the mixed-layer potential temperature and specific humidity respectively, with the mixed-layer lifting condensation level (ML-LCL) marked at the apex of these two lines. The saturation point (SP) curve (approximated by the blue line) identifies the potential plume condensation positions. The minimum-buoyancy plume-path is indicated by the gold curve. The free-convection height (z_{fc}) is the height at the base of the gold curve. The plume must be at least $\Delta\theta_{fc}$ warmer than the mixed-layer potential temperature (thick red line), and the average mixed-layer wind term (U) can be estimated from the wind barbs highlighted in green.

3. Case study events

One focus of forecasters during the trial was the prediction of lightning in DMPC because lightning is generally well observed and offers a clear distinction between towering pyrocumulus and pyrocumulonimbus clouds. Cloud-top temperature (CTT) observations from satellites are readily available that enable near-real-time assessment of DMPC maturity, and an indication of when the convection has penetrated the typical charge separation layer (-15 to -25 ℃) above which lightning might be expected to develop. However, it was common for DMPC to develop with CTT much cooler than -25 ℃ without lightning. Then on Sunday 2 Feb 2020 forecasters were confounded by lightning that developed in DMPC when the CTT only reached -15 ℃. This was unexpected, especially given that on the previous day DMPC with CTT of -45 ℃ developed on a fire nearby, with no lightning.

To try and understand these differences, a PFT1 analysis was performed for each case, with both identifying scenarios where assumptions used to simplify PFT1 need to be reconsidered. The first of these simplifying assumptions is that a rising plume-parcel is always buoyant, i.e., it is assumed a parcel cannot penetrate a capping inversion unless it is warmer than that inversion. The second simplifying assumption is that the moist plume is non-entraining, i.e., it does not lose buoyancy from dilution and cloud moisture evaporation when cooler drier air is mixed into the plume from outside.

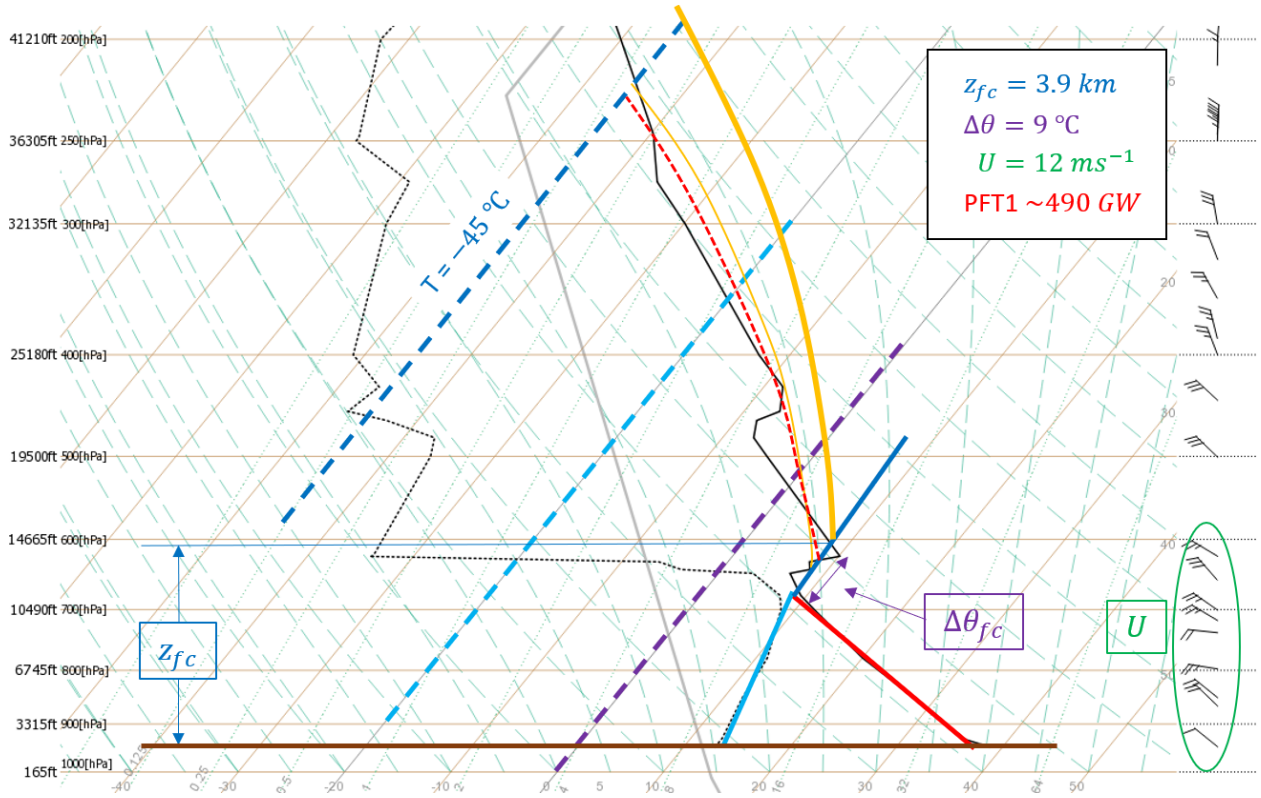

Figure 2- Canberra sounding 1 PM local time (0200 UTC) Saturday 1 Feb. The solid and dotted black lines represent temperature and dewpoint temperature respectively. The 0, -20 and -45 ℃ temperature lines are indicated by purple, cyan and blue dashed lines respectively. The solid red and cyan lines show a mixed layer temperature and dewpoint temperature of constant potential temperature and specific humidity that represent the average quantities entrained into a hypothetical plume rising through the mixed layer. The solid blue line is an approximate Saturation Point curve. The gold lines are moist parcel paths emerging from the SP curve, one with minimum buoyancy just able to breach the capping inversion and exceed the -20 ℃ level (thick, used in PFT1), and the other (thin) represents a non-entraining parcel path corresponding to the observed cloud-top temperature of -45 ℃. The red dashed line is a hypothetical parcel path that reaches the observed cloud top temperature with some overshooting, takes into account buoyancy losses associated with entrainment, and assumes sufficient vertical kinetic energy to penetrate the lower temperature inversion (between 650 and 610 hPa). The three ingredients for a manual PFT1 calculation are illustrated, and their estimated values shown in the legend.

The PFT1 analyses used to explore the two events are presented in Figs 2 and 3 respectively. Dark blue dashed lines corresponding to the observed CTT, and corresponding non-entraining moist-plume parcel paths (thin gold lines) have been added to highlight the discrepancy between the observed, and minimum-predicted equilibrium levels. On both days the minimum-predicted equilibrium level (top of the thick gold line) is much colder (-60 ℃ and -50 ℃ respectively) than the observed CTTs (-45 ℃ and -15 ℃ respectively). However, the zero-entrainment parcel paths matching the observed CTTs (thin gold lines) both have regions of negative buoyancy, which is counter to the PFT1 assumption of positive buoyancy everywhere.

In the first case (Fig. 2), negative buoyancy is encountered when the thin gold line penetrates the capping inversion near 600 hPa, and it also approaches zero buoyancy near 450 hPa. If this parcel path is realistic, it implies that the plume had sufficient kinetic energy to penetrate the capping inversion.

A theoretical kinetic energy can be calculated from the Briggs plume-rise equations, which, with a few simplifications (not shown), becomes,

$$E_k \sim 4.3 \times \Delta\theta_{SP} \times z_{SP}. \qquad 2.$$

Here E_k is the vertical kinetic energy of a plume parcel in units of Jkg^{-1}, the subscript SP refers to a point on the SP curve (blue solid line), and $\Delta\theta_{SP}$ and z_{SP} are analogous to $\Delta\theta_{fc}$ and z_{fc} (same units). Importantly, Eq. 2 shows that the larger $\Delta\theta_{SP}$ and z_{SP}, the larger the plume kinetic energy.

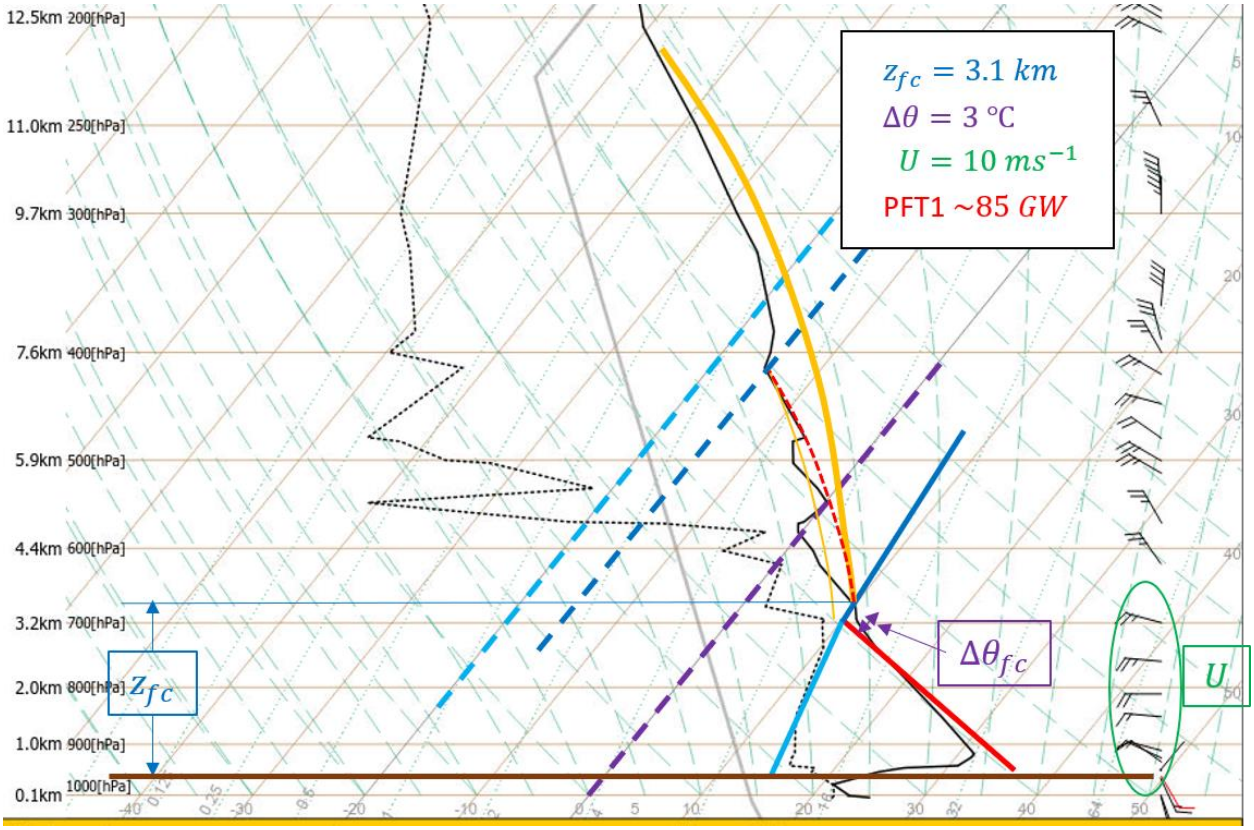

Figure 2- As in Fig. 2 but for the Sydney sounding 2 PM local time (0300 UTC) Sunday 2 Feb. Observations from a PAWS (RF55) located at Faulconbridge (elevation 410m, 20 km north of the fire) were used to estimate the actual conditions below 1.0 km.

In the second case (Fig. 3), the negative buoyancy regions encountered by a parcel on the thin gold line are more substantial than the first case. These include a stable layer just above the ML-LCL and two inversions near 550 and 470 hPa. Furthermore, the corresponding $\Delta\theta_{SP}$ would be close to zero or even negative, suggesting any plume elements at the base of the thin yellow line would not only have negative buoyancy, but no vertical kinetic energy prior to plume condensation. It follows that the real plume parcel paths must have had $\Delta\theta_{SP} \geq 2$ to have reached the observed CTT (assuming the temperature trace represents the fire environment), which implies they would have had vertical momentum at saturation, and were probably buoyant too. However, any non-entraining parcel paths (moist adiabats) matching these $\Delta\theta_{SP}$ values would rise well beyond the observed CTT levels. It follows that any plume parcel with $\Delta\theta_{SP} \geq 2$ that reaches equilibrium at -15 ℃ must have lost buoyancy while ascending. The most likely cause of buoyancy loss is entrainment of cooler and drier air. The warmer plume is diluted by the cooler entrained air, and the evaporation of cloud water by the entrained dry air further cools the plume.

Hypothetical entraining-plume paths, are included in Figs 2 and 3 (red dashed lines). Entrainment is often expressed as a dilution fraction per km of ascent. While the entraining interface between the plume and environment is more turbulent in rapidly rising plumes (which enhances entrainment), plume elements spend less time ascending and hence less time entraining, with the net effect that rapidly rising plumes experience less total entrainment than slower rising plumes (e.g., Gregory 2001). It follows that as a general rule, larger (smaller) $\Delta\theta_{SP}$ would relate to greater (smaller) ascent rates and thus smaller (larger) entrainment rates.

On both days very dry air was located above about 600 hPa, indicating entrainment would be particularly detrimental to plume buoyancy. However, the $\Delta\theta_{SP}$ values corresponding to the hypothetical entraining plume paths (difference in potential temperature between the SP and mixed-layer value) are about 7 ℃ (Fig. 2) and 3 ℃ (Fig. 3) respectively, suggesting the former would have ascended more rapidly and thus experienced less entrainment than the latter. Furthermore, it suggests entrainment may only be significant for cases with relatively small $\Delta\theta_{SP}$.

4. Summary and Discussion

The two cases presented suggest the PFT1 assumptions of non-entraining moist plume paths that are everywhere buoyant from condensation to the -20 ℃ isotherm (thick gold lines in Figs 2 and 3), may not always be reasonable. Plumes with non-trivial $\Delta\theta_{SP}$ are likely to have sufficient vertical kinetic energy to penetrate some stable layers and inversions, and plumes with smaller $\Delta\theta_{SP}$ will likely experience greater buoyancy losses from entrainment. However, the associated errors from ignoring these effects will partly cancel, since the plume-kinetic-energy omission yields a PFT1 over-prediction and the entrainment omission yields a PFT1 under-prediction.

A manual procedure for estimating the minimum $\Delta\theta_{SP}$ of a plume capable of penetrating a stable layer is under development. The plume kinetic energy is estimated using Eq. 2, and the integrated buoyancy force it will encounter is estimated from the area between the parcel path and the environment temperature trace, similar to the calculation of convective inhibition (CIN) used in CAPE calculations. Where the E_k and CIN balance, the plume is deemed to just have sufficient kinetic energy to penetrate the stable layer. Estimating entrainment rates is considerably more complex. It may be necessary to add 1—3 ℃ to $\Delta\theta_{SP}$ to account for buoyancy losses due to entrainment, with a larger increment added if the initial $\Delta\theta_{SP}$ is relatively small and a smaller increment if it is relatively large (suitable increments are yet to be determined). Finally, the updated $\Delta\theta_{SP}$ along with a matching z_{SP} can be fed into Eq. 1 to calculate an improved PFT. There will be many cases in which these modifications will have no or negligible impact on the PFT result. It is anticipated that users will soon identify environments in which taking these additional steps will yield improved PFT estimates.

5. Acknowledgements

Thanks to Zach Porter and David Wilke for providing soundings and plume-behaviour descriptions for the Bees Nest, Orroral/Clear Range and Erskine Creek fires.

6. References

Briggs, G. A., 1984: Plume rise and buoyancy effects. Atmospheric Science and Power Production, D. Randerson, Ed., U.S. Dept. of Energy DOE/TIC-27601, available from NTIS as DE84005177, 327—366.

Gregory, D., 2001: Estimation of entrainment rate in simple models of convective clouds. Quart. J. Roy. Meteor. Soc., 127, 53—72, https://doi.org/10.1002/qj.49712757104.

Luderer, G., J. Trentmann and M. O. Andreae, 2009: A new look at the role of fire released moisture on the dynamics of atmospheric pyro-convection. Int. J. Wild. Fire, 18, 554—562.

Tory, K. J., W. Thurston and J. D. Kepert, 2018: Thermodynamics of pyrocumulus: A conceptual study. Mon. Wea. Rev., 146, 2579—2598. DOI: 10.1175/MWR-D-17-0377.1

Tory, K. J., 2020: The real-time trial of the pyrocumulonimbus firepower threshold. Southern Australia 2019/2020 fire season. https://www.bnhcrc.com.au/sites/default/files/managed/downloads/the_real-time_trial_of_the_pyrocumulonimbus_firepower_threshold_0.pdf

Tory, K. J., and J. D. Kepert, 2021: Pyrocumulonimbus Firepower Threshold: Assessing the atmospheric potential for pyroCb. Weather and Forecasting, 36, 439—456. https://doi.org/10.1175/WAF-D-20-0027.1

Research on Application of Forest Fire GS Mark III (Patent Pending) for Peat Fires Extinguishment Methods: A Field Experiment

Ahmad Faiz Tharima*[1]; Nur Hafizah Mohamad Lukman[1]; Kamarulzaman Malik Abdullah[1]; Azfarizal Mukhtar[2]; Mohd Adib Mohammad Razi[3]; Wan Nursheila Wan Jusoh[4]

[1]Planning and Research Division, Fire and Rescue Department of Malaysia, Lengkok Teknologi, Kawasan Perindustrian Enstek, 71760 Nilai, Negeri Sembilan, Malaysia, {ahmad.faiz, hafizah_lukman, kamarulzaman}@bomba.gov.my
[2] Department of Mechanical Engineering, Universiti Tenaga Nasional (UNITEN), Putrajaya Campus, Jalan IKRAM-UNITEN, 43000 Kajang, SelangorDarul Ehsan, Malaysia, {azfarizal@uniten.edu.my}
[3] Eco Hydrology Technology Research Centre (Eco-Hytech), Faculty of Civil Engineering & Built Environment, Universiti Tun Hussein Onn Malaysia, 86400 Parit Raja, Batu Pahat, Johor, Malaysia, {adib@uthm.edu.my}
[4]Aerospace Section, Malaysian Institute of Aviation Technology, Universiti Kuala Lumpur, Jalan Jenderam Hulu, 43800 Dengkil, Selangor, Malaysia, {wannursheila@unikl.edu.my}

**Corresponding author*

Keywords

Peat Fires, Forest Fire GS Mark III, Spray length, Pressure. Fire suppression

Abstract

Anthropogenic interventions and global warming are normally the cause of Malaysian peat fires. Fire suppression methods and techniques have garnered the attention of innovators. In the current study, a series of field experiments were undertaken to quantify the effectiveness of an invention of fire-fighting equipment called Forest Fire GS Mark III (patent pending). A number of hoses and water pumps, as well as accessories, are also integrated into the GS Mark III configuration. The installation of equipment only considers single hoses line with several lengths from an open water source. This involved three field tests using a single pump, an end-to-end pump, and series pumps. Both the end-to-end pump and the serial water pump were found to have significant performance with longer spray length and consistent water pressure. Further, according to the present invention, the area covered during extinguishment is about 18,000m^2 or 4.45 acres or 1.8 hectares within 50 minutes by mains off the end-to-end pump or serial pump installation. Conversely, the pressure and length decreased when the number of hoses increased. This study makes a good contribution to the firefighter community by providing the initial design of fire extinguishment methods under better conditions.

1. Introduction

Forests are extremely valuable because of their ability to trap rainwater, produce oxygen, store carbon, and provide habitat for a wide variety of animals. Haze is commonly caused by major forest fires, which can spread significant distances and blanket extensive areas. People's respiratory systems, health, livelihoods, and lifestyles can all be negatively impacted by air pollution, and in extreme circumstances, the pollution can even force schools and airports to close. Firefighter put their lives on the line in order to extingto fires.

The use of fire retardants, fire barriers, rewetting peatland, water bombing, and cloud seeding are s the strategies that are now being utilized to stop forest fires. However, these approaches can be risky, expensive, time-consuming, depending on the weather, and ineffectual geographically remote and inaccessible areas. A significant amount of study has been carried to cut carbon emissions, respiratory health problems, and economic loss brought on by forest fires and the smoke hat they produce.

In the earlier studies, fire suppression models (Duff and Tolhurst, 2015), stochastic fire simulation model (Riley et al., 2018) and the species, momentum, and energy conservation equations (Huang et al., 2015) have been used to model the decision-making process for a significant portion of fire costs and for a large portion of

impacts to describe drying, thermal, and oxidative degradation during the smouldering combustion in previous studies. However, these models have significant drawbacks when it comes to simulating the spread of a fire.

The other solution was also proposed by the previous researchers to overcome the suppression method. Suppression chemicals which proposed by Plucinski, (2019) is not a promising alternative since the scale and purpose that they are considered. Kalabokidis, (2000) also reported that the chemical usage showed major impacts, on the environment, which may be through the adverse effects on water quality, and subsequently to aquatic ecosystems.

On wildfire suppression equipment, only a small amount of research and development work has been done. In 2018, Bartenev et al. developed a combined machine for putting out forest fires and using soil to create fire-break makers. This machine works by removing the upper fire-hazardous cover, which is made up of plant residues. Drapalyuk et al., 2019 proposed fire-fighting soil-thrower machine which provide better preventive and fireproof work in conditions of heavy soils, saturated with roots of the tree. Kasymov et al., (2017) have been presented backpack motorized fire extinguisher too minimizes the damage caused to the environment but limited for extinguishing low and medium intensity forest fires. However, the aforementioned machine do not extinguish for large fire especially involving ground or peat fire where the thickness of the burned layer is should taken into account. In addition, when a layer of organic soil ignites, it burns steadily without flaming and eventually spreads through the soil (Rein et al., 2008). Smouldering in peat soil can go days undetected Zaccone et al., 2014). During a peat fire, the temperature at ground level can reach 400 degrees Celsius, while temperatures 5, 10, 20, 30, and 40 centimetres below ground level can reach 200 degrees Celsius, 90 degrees Celsius, 50 degrees Celsius, and 45 degrees Celsius, respectively (Rinaldi et al 2019). Since peat soil has high water content, it is hard for firefighters to walk on it. Efforts to extinguish fires on peatlands is strenuous, wildly if the fire has penetrated the deep layer of peat, only heavy rain can effectively extinguish it (Rosita, 2018). In this regards, this paper intends to propose new suppression equipment for forest fire particularly peat fire which merge three suppression techniques ; direct attack and fire break, and total flooding.

2. Methodology

2.1. Forest Fire GS Mark III,

The Forest Fire GS Mark III (patent pending) comprise a sprinkler; connect to the 1¼ ” upper pipe; and it is attached to stop valves to allow and close the water flow to the sprinkler. The upper pipe are mounted to the Cross tees – four - steam divider. On the bottom of the cross tees divider, a ½” stop valve will be mounted to allow and close the underground water flow. An underground pipe ½” in size will be attached and a ½” round cap is fix at the end of the underground pipe as pipe cover. (The detailed of the aforementioned equipments is patent pending).

The Forest Fire GS Mark III as claimed in previous pragraph characterized in that a male coupling and female coupling which working as a connector to the hose, will connected on the left and right side of the cross tees four steam divider. Water supply will flow over to the upper pipe for water spraying and lower pipe for total flooding.

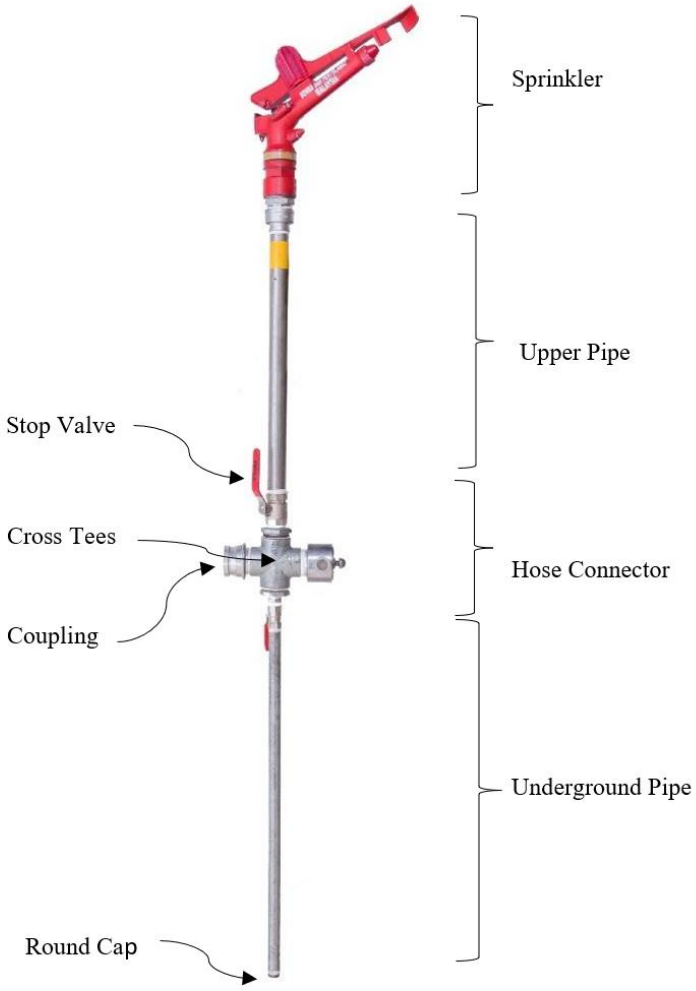

Figure 1: Forest Fire G.S Mark III

The Forest Fire G.S Mark III testing were conducted in an open area. Table 1 shows the apparatus needed in this study.

Apparatus	**Utilization**
Forest Fire GS Mark III	Water outlet
Water pump	Pump water to hose
Collecting Breeching	two water feed hoses supplying one outlet
2 ½ inches hose	Deliver water to outlets
Flowmeter	measuring nonlinear or linear flow rate
Wajex Hose c/w nozzle	Water outlet

Table 1: List of apparatus and its utilization

2.2. Experimental Set Up

The Forest Fire GS Mark III comprises a sprinkler, an upper pipe, a hose connector, and an underground pipe. The total length is 90 inches and weighs 9 kilogrammes. The diameter of the upper pipe is 1 1/4 inches, whereas the diameter of the underground pipe is 1/2 inches. The size of the discharged outlet at the sprinkler and the underground pipe is different. The discharge outlet of a sprinkler, which is regulated by a nozzle tip, is adequate for 10mm particles. In addition, the subsurface pipe initially consisted of four 4.6mm outlets. The stop valves are fitted on both the above- and below-ground pipes. During a fire suppression operation, these functions are employed to shut off a water supply for maintenance i an emergency.

In order to run the Forest Fire G.S Mark III, a water pump is equipped and positioned near water sources such as rivers, temporary ponds, and lakes. For water supply, hard suction hoses are laid from the water source to the water pump. The delivery hoses are fitted every 30 or 60 metres using Forest Fire G.S Mark III from the water

pump. With these two installation alternatives, firefighters can make choices based on the severity of the fire. In the event of a peat fire, the installation of G.S. Mark III equipment at a distance of 30 metres is necessary to raise the groundwater level more quickly, which is equivalent to the technique of total flooding. Moreover, the distance of water spray radius covered between adjacent G.S Mark III. In cases other than peat fires, it is recommended to install G.S Mark III equipment every 60 metres because water spray can reach to a 30-meter radius around the fire.

Currently, the spray type of the Forest Fire GS Mark III sprinkler can be selected using either a static or rotating technique. With the rotating option, the sprinkler's water spray can be changed to 180 degrees or 360 degrees, depending on the fire suppression strategy and local fire scenario. In reality, the installation of Forest Fire GS Mark III along the hoses created a fire break zone to prevent the impacted fire area from spreading to the adjacent region.

2.3. Experimental Configuration

2.3.1. Single Pump Approach

Knowledge of the Forest Fire G.S Mark III in the performance of the water pumping sprinkler systems is important to maximize its effectiveness in extinguishing the peat fire. Forest Fire G.S Mark III is the latest design from its model. The design concept is similar to the sprinklers

There are two designs conducted for a single pump approach. The **first** type of test utilized six Forest Fire GS Mark III while for the **second** design, three Forest Fire G.S Mark III and three Wajex hoses were employed. The field test conducted was to evaluate every design performance base on the pump's pressure. Flowmeters were placed in each test designs.

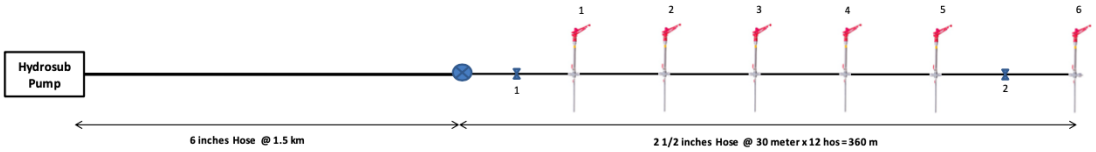

Figure 2: First design

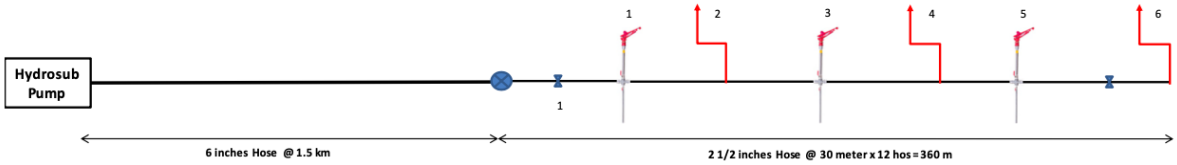

Figure 3: Second design

2.3.2. End-to-End Approach

The test were carried out in a real peat fire test in Tanjung Sepat, Kuala Langat Selangor on 6th March 2021 during the drought season.

The hoses were connected to two portable water pumps between end to end from a different water source. So, the water is put under pressure along the hoses. This test involved laying approximatle of 300m hoses or 10 rolls of delivery hoses. Every 30m, Forest Fire GS Mark III and Forest Fire GS Mark II were installed alternately.

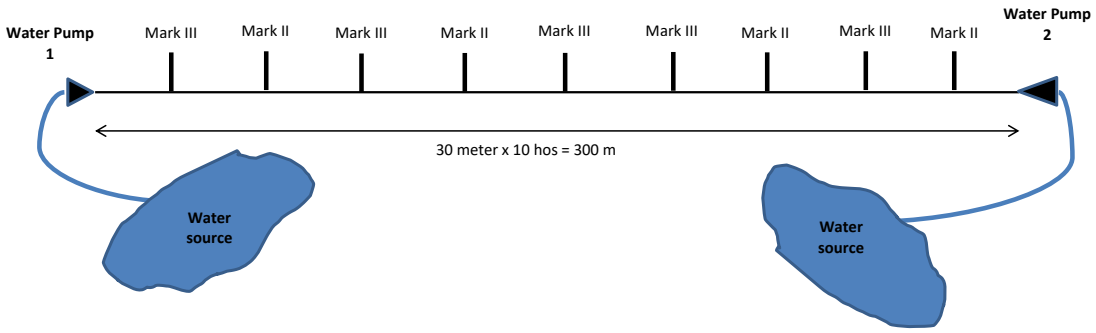

Figure 4: End-to-end pump

2.3.3. Serial Pump Approach

The first rule that should be applied in serial pump approach is the pressure at the second pump should be lower than the first pump. In the same way, the GS Mark III installed before a second pump should not have a pressure drop. Pressure is considered dropped as a spray length at that point is lower than spray length at the next point.

To execute the serial pump approach, a water pump, 16 hoses (480 meters) and 8 units of Forest Fire GS Mark III were set up. Two hoses from the water pump were connected to the hose line using a collecting breaching.

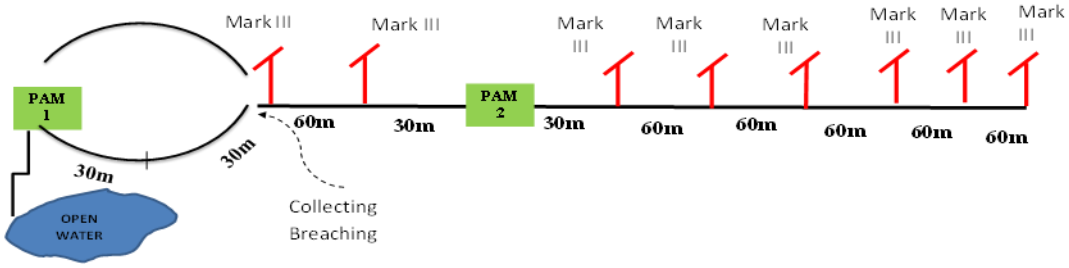

Figure 5: Serial pump arrangement

3. Results and Discussion

3.1. Single Pump Approach

During the test, the environment condition where the test is taken place is very important to get accurate data. This test was conducted place in the open environment, and the weather is not windy. The following table present data from the test conducted to test the performance of Forest Fire G.S Mark III. The result of test 1 and test 2 are as follow:

Table 2: Result for 1st Design

Hydrosub pump pressure (Bar)	Flowmeter 1		GS Mark III					Flowmeter 2		GS Mark III
			1	2	3	4	5			6
	Pressure (Bar)	Flowrate (L/Min)	Spray Length (Meter)					Pressure	Flowrate (L/Min)	Length
5	5.01	1070	24.19	17.17	10.9	6.28	5.09	0.43	80	4.23
7	6.1	1210	28.87	23.93	18.45	9.42	7.83	0.62	110	7.5
9	7.72	1370	29.41	19.93	19.26	11.96	11.11	0.84	130	8.69
11	8.35	***1440***	31.9	28.86	23.91	17.22	13.43	0.99	147	12.08

Table 3: Result for 2nd Design

Hydrosub pump pressure (Bar)	Flowmeter		GS Mark III + Wajex Hose					Flowmeter		Wajex Hose
			1	w	3	w	5			W
	Pressure (Bar)	Flowrate (L/Min)	Spray legth (Meter)					Pressure (Bar)	Flowrate (L/Min)	Length
5	3.86	850	22.3	13.88	8	6.58	5.5	0.15	12	2.6
7	5.55	1100	28.89	17.43	10.66	8.34	8.18	0.84	70	4.26
9	7.3	1300	30.75	23.19	16.45	14.13	14.95	1.02	117	10.99
11	9.03	1440	29.46	20.56	19.56	17.76	15.92	1.34	128	12.69

The data of design 1, and 2, show that increasing the hydrosub pump pressure increase the flow rate and the spray length. The pressure reduction from the first output station to the last output station. The length of spray also reduces from every output station to output stations.

3.2. End-to-End Approach

The installation of the equipment took about one hour. The area covered during extinguishment about 18, 000m2 or 4.45 acres or 1.8 hectares within 50 minutes.

3.3. Serial Pump Approach

The result of testing is elaborated as follows:

Table 4: Result for Serial pump

Field Test	Pump 1	Spray Length		Pump 2	Spray Length					
	Pressure (Bar)	GS Mark III	GS Mark III	Pressure (Bar)	GS Mark III	GS Mark III	GS Mark III	GS Mark III	GS Mark III	GS Mark III
		1	2		3	4	5	6	7	8
Test 4	7 bar	19.62	19.96	5 bar	21.92	21.24	19.26	17.65	17.54	17.20

The test performance showed the spray length remained nearly similar even though the hose line increased to 480 meters. Using a collecting breaching technique, the water flow rates remain maintained along the hose line. For a longer hose line, a powerful water pump should be used to get a longer spray length and keep the flow rate along the hose line. The performance also showed that any Forest Fire GS Mark III could be changed to be an attack hose (with nozzle) for direct attack purposes.

4. Conclusion

To extinguish traditional forest fires, the Forest Fire G.S Mark III is also designed to extinguish peatland fires where the source of the flame is buried deep underground. The most successful and capable means of extinguishing a peat forest fire, according to the experienced firefighters involved in peat forest fire operations, is watering or flooding the area until the underground water layer is raised. Using Forest Fire G.S Mark III equipment, the spray of water flowing out of the underground pipe can permeate the peat soil's pores, flooding the peat layer under the surface. In addition, spraying on the higher pipe and rotating sprinklers assist in saturating the upper and lower soil surface layers.

With the development of G.S Mark III technology, extinguishing operations can be conducted constantly for 24 hours (including at night). Firefighters need just monitor the portable water pump at the fire scene. The method and application of G.S Mark III equipment are highly effective at preventing the spread of fires, hence avoiding considerable forest destruction and losses for all parties. In addition, firefighters are protected from a variety of perils, including pit falls, wild and toxic animals, and even pre-war munitions. This method of extinguishment can also restrict the exposure of firefighters to harmful plants, water-borne infections, and mosquito-borne disorders.

Further, according to the present invention, the area covered during extinguishment about 18,000m^2 or 4.45 acres or 1.8 hectares within 50 minutes by mains off end to end pump or serial pump installation.

5. References

Duff, T. J., & Tolhurst, K. G. (2015). Operational wildfire suppression modelling: a review evaluating development, state of the art and future directions. International Journal of Wildland Fire, 24(6), 735-748.

Riley, K. L., Thompson, M. P., Scott, J. H., & Gilbertson-Day, J. W. (2018). A model-based framework to evaluate alternative wildfire suppression strategies. Resources, 7(1), 4.

Huang, X., Rein, G., & Chen, H. (2015). Computational smoldering combustion: Predicting the roles of moisture and inert contents in peat wildfires. Proceedings of the Combustion Institute, 35(3), 2673-2681.

Plucinski, M. P. (2019). Fighting flames and forging firelines: Wildfire suppression effectiveness at the fire edge. Current Forestry Reports, 5(1), 1-19.

Kalabokidis, K. D. (2000). Effects of wildfire suppression chemicals on people and the environment—a review. Global Nest: The International Journal, 2(2), 129-137.

Bartenev, I. M., Malyukov, S. V., Gnusov, M. A., Stupnikov, D. S., & Platonov, A. D. (2018, December). Modern designs of forest fires machines for soil extinguishment of fire. In International Symposium" Engineering and Earth Sciences: Applied and Fundamental Research"(ISEES 2018) (pp. 48-53). Atlantis Press.

Drapalyuk, M., Stupnikov, D., Druchinin, D., & Pozdnyakov, E. (2019). Forest fires: methods and means for their suppression. In IOP Conference Series: Earth and Environmental Science (Vol. 226, No. 1, p. 012061). IOP Publishing.

Kasymov, D. P., Fateyev, V. N., & Zima, V. P. (2017, November). Methods and devices used in the wildfire localization for the protection of forest ecosystems. In 23rd International Symposium on Atmospheric and Ocean Optics: Atmospheric Physics (Vol. 10466, pp. 1316-1319). SPIE.

D. Rosita, Kedudukan Kejaksaan Sebagai Pelaksana Kekuasaan Negara Di Bidang Penuntutan Dalam Struktur Ketatanegaraan Indonesia, vol. 3, no. 1. 2018.

G. Rein, N. Cleaver, C. Ashton, P. Pironi, and J. L. Torero, "The severity of smouldering peat fires and damage to the forest soil," Catena, vol. 74, no. 3, pp. 304–309, 2008.

C. Zaccone, G. Rein, V. D'Orazio, R. M. Hadden, C. M. Belcher, and T. M. Miano, "Smouldering fire signatures in peat and their implications for palaeoenvironmental reconstructions," Geochim. Cosmochim. Acta, vol. 137, pp. 134–146, 2014.

P. S. Rinaldi et al., "Physical and Chemical Analysis of Land in Forest Peat Swamp in Resort Pondok soar, Tanjung Puting National Park, Central Kalimantan," IOP Conf. Ser. Earth Environ. Sci., vol. 394, no. 1, 2019.

Slope effect on Junction Fire with Two Non-symmetric Fire Fronts.

Carlos Ribeiro[1*]; Domingos Viegas[1;2]; Jorge Raposo[1;2]; Luís Reis[1]; Jason Sharples[3;4]

[1] Association for the Development of Industrial Aerodynamics (ADAI)/Associated Laboratory on Energy, Transportation and Aeronautics (LAETA), University of Coimbra, Coimbra 3030-289, Portugal, {carlos.ribeiro, jorge.raposo, luis.reis}@adai.pt
[2] Department of Mechanical Engineering, University of Coimbra, Coimbra 3030-788, Portugal, {xavier.viegas@dem.uc.pt}
[3] School of Science, University of New South Wales (UNSW), Canberra, ACT, Australia, {j.sharples@adfa.edu.au}
[4] Bushfire and Natural Hazards Cooperative Research Centre, East Melbourne, VIC, Australia {j.sharples@adfa.edu.au}

**Corresponding author*

Keywords

Junction Fires; Fire behaviour; Extreme Fire Behaviour; Merging Fires; Dynamic Fire behaviour

Abstract

The merging of two linear forest fire fronts that intersect at a small angle creates an accelerating fire in a relatively short time. In the majority of cases during the interaction, the fire fronts are non-symmetric. In Pedrogão Grande on the 17th June 2017, two-fire front merged and the propagation of the fire was influenced by the interaction of these two non-symmetric fire fronts. This forest fire motivates us to study the Junction Fire with two non-symmetrical fire fronts. The analysis of the interaction of two fire fronts and the angle between the bisector of the fire lines and the maximum ROS (γ) is of particular relevance. We found that with these preliminary laboratory tests, the non-ROS of intersection fire fronts for small rotation angles (δ) depends on the slope angle (α) and the initial angle between fire fronts. For the higher slope angles, the non-ROS is the highest influence by the convection process, and the angle γ where the maximum ROS occurred, increases when δ increases. However, for the lowest slope angles, the radiation process is dominant and influences the non-ROS. For these cases, the angle γ is near to the bisector of the fire lines.

1. Introduction

The merging of two fire fronts that intersect at a small angle induced very high values of the Rate of Spread (ROS) and fire intensity of their intersection point, and followed a gradual velocity decrease in the course of the time when the angle between fire fronts increases. This problem was studied in the past by Viegas et al. 2012, initially described this phenomenon as a Jump Fire, and developed a conceptual analytical model for the vertex "V" ROS. After the initial project, numerous research works experimental, analytical, and numerical simulation were followed (Viegas et al. 2013; Raposo et al. 2015, 2018; Sharples et al. 2013; Hilton et al. 2016; Thomas et al. 2017; Sullivan et al. 2019; Filkov et al. 2020). The fire fronts were always symmetrical in relation to the vertex "V" and there was no fuel bed to burn outside of linear straight fire lines. The results showed that the ROS of the vertex "V" has a great relationship in which the initial angle between the merging fire fronts and the ROS increases sudden zero to values of the order of one hundred times the basic ROS. A real fire situation occurred in the merging of two large fires: one near Canberra on the 18th January 2003 and, more recently, in Pedrogão Grande on the 17th June 2017.

On 17th June of 2017, the Pedrogão Grande fire starts at Escalos Fundeiros by 14:30h, and there was a second ignition in Regadas by 16:00h, local time, according to Viegas et al. 2017. The distances between those two ignitions were 2.6km and at 19:30h the two-fire front merged and the propagation of the fire was influenced by the interaction of these two non-symmetric fire fronts. This forest fire motivates us to study the Junction Fire with two non-symmetrical fire fronts.

2. Physical Problem

In the present study, it is assumed that two straight fire lines intersect at point ***A*** with an initial angle θ_0 between them and spread in a uniform fuel bed layer on a flat surface making an angle α with the horizontal datum $O_oX_oY_o$. Cartesian coordinate system $O_oX_oY_oZ_o$ is considered, in which O_oZ_o is perpendicular to the ground. Point ***A*** coincides initially with the origin of the reference cartesian frame with axis ***OX*** parallel to the slope gradient. The axis OX_1 represents the symmetry line of the fire configuration and can be defined by the angle δ that represents the angle between the bisector of the fire lines and the line with the highest slope. However, for each angle α and δ the maximum ROS happened according to axis OX_m and this axis is rotated some angle γ that represents the angle between the bisector of the fire lines and the maximum ROS. The fuel bed area is defined by ***ABC*** and is covered by a uniform layer of forest fuel able to support the spread of a surface fire. The merging of two linear fire fronts is illustrated schematically in Figure 1 a).

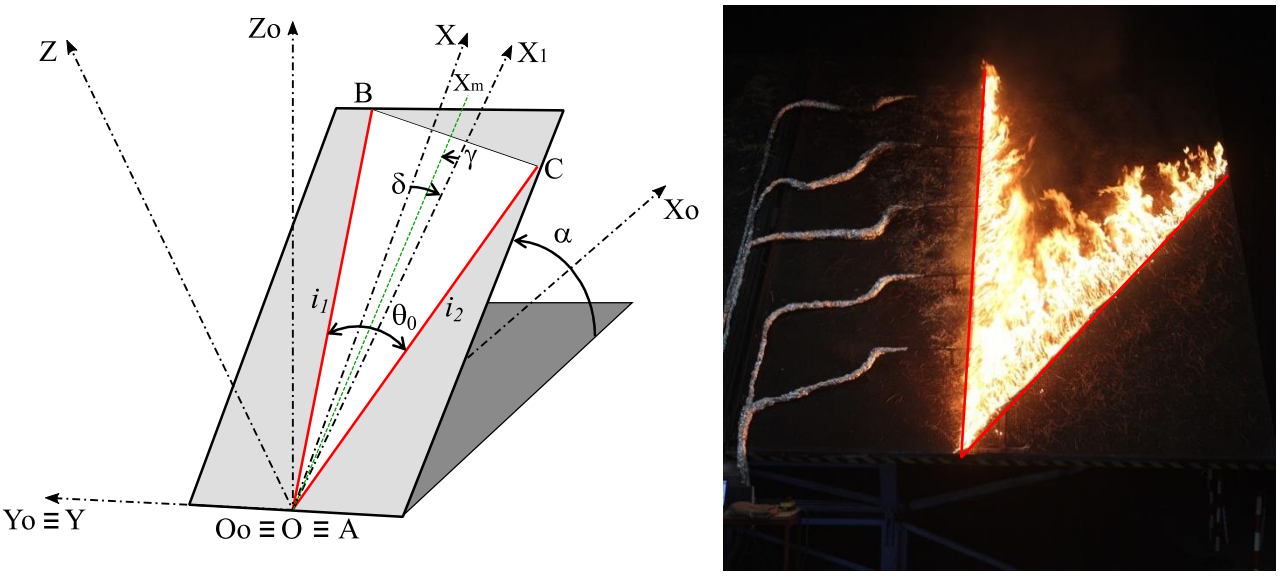

a) b)

Figure 1- a) Schematic layout of the merging of two non-symmetric straight fire lines making an initial angle 0 between them. The axis OX is parallel to the slope gradient, the axis OX1 represents the symmetry line of the fire configuration and the axis OXm, defined by the green dashed line, represents the maximum ROS happened. b) View of the Canyon Table DE4 of the Forest Fire Laboratory of the University of Coimbra.

We consider two linear fire fronts defined by two straight lines (***AB*** and ***AC***), non-symmetric in the OX axis, as shown in Figure 1 a). Henceforward, the linear fire lines ***AB*** and ***AC*** will be referred to as i_1 and i_2, respectively. In this study, it is assumed that the ambient air is still in accordance with the experimental conditions at the laboratory and at time $t_0=0s$, the fire lines are simultaneously and instantaneous ignited.

3. Material and Methods

3.1. Laboratory Experiments

Laboratory experiments were carried out at the Forest Fire Research Laboratory of the University of Coimbra using the Canyon Table DE4 and that has a useful area of $6.0x8.0m^2$ with a slope (α) that can be changed in the range of 0^o to 40^o. The initial angle θ_0 between the two fire lines was 30º. In Figure 1 b) typical performance conditions of these tests are shown.

During the preparation of each test, the conditions of the fuel load and bulk density were controlled, and the air temperature (^oC), relative humidity (%) and fuel moisture (m_f) were monitored. The fuel bed for the experiments was composed of dry particles of dead pine needles (*Pinus pinaster - PP*) with a constant load of 600g.m^{-2} (dry basis) (Viegas and Pita 2004; Xie et al. 2014; Raposo 2016; Raposo et al. 2018; Rodrigues et al. 2019; Viegas et al. 2021). The fuel bed height (h_f) was measured in five aleatory positions and on average it was 5.2cm. The basic rate of spread R_o (cm.s^{-1}) of a linear fire front in a fuel bed with the same properties was measured for

each series of tests using a 1x1m^2 horizontal fuel bed without slope and wind. The ignition of the two fire lines was made by two persons to assure that the lines started burning simultaneously and two wool threads soaked in a mixture of petrol and diesel fuel were used. A summary of the main test parameters is provided in Table 1.

Table 1 – Parameters of the tests.

Ref.	Test	α (º)	δ (º)	m_f (%)	R_o (cm.s^{-1})
1	JF003030_2	30	15	13.90	0.203
2	JF052530_2	30	10	14.29	0.218
3	JF102030_2	30	5	14.29	0.221
4	JF003030_1	30	15	12.49	0.245
5	JF052530_1	30	10	12.49	0.245
6	JF003040_1	40	15	11.88	0.197
7	JF052540_1	40	10	13.64	0.263
8	JF102030_1	30	5	14.03	0.247
9	JF151530_1	30	0	13.64	0.209
10	JF151540_1	40	0	11.86	0.255
11	JF003010_1	10	15	13.25	0.226
12	JF003020_1	20	15	13.25	0.289
13	JF052510_1	10	10	13.25	0.276
14	JF052520_1	20	10	13.25	0.221
15	JF102010_1	10	5	13.25	0.267
16	JF102020_1	20	5	13.89	0.228
17	JF102040_1	40	5	14.81	0.220

3.2. Evolution of the ROS

The instantaneous position x_A of the intersection point A along the axis OX_m was the main object of the present analysis and it is associated with the overall evolution of the fire fronts. The displacement velocity R_A is defined as:

$$R_A = \frac{\partial x_A}{\partial t} \tag{1}$$

In order to compare results performed with different fuels we use the non-dimensional displacement velocity R'_A defined by:

$$R'_A = \frac{R_A}{R_o} \tag{1}$$

where Ro is the basic ROS.

4. Results and discussion

4.1. Rate of Spread analysis

The evolution of the fire front during tests performed was recorded by IR camera and frames with pre-defined times were used to measure the ROS of point A. The area between two fire fronts is burned by the advance of the intersection point A.

Results of R'_A from a series of tests performed as a function of the time are shown in Figure 2. In general, the evolution of R'_A, for $\alpha=10^o$ and $\alpha=20^o$, happens with a market acceleration when the fire lines are ignited, but, during the time, a deceleration phase happens. Otherwise, for $\alpha=30^o$ and $\alpha=40^o$, the evolution of R'_A has a market non-monotonic behaviour, but after the R'_A reaches the maximum value the deceleration phase happens. For the angle δ and slope angle α performed, there is no marked difference between the R'_A for each combination. For $\alpha=30^o$ and $\alpha=40^o$, the R'_A for $\delta=0^o$ (JF151530_1 and JF151540_1, respectively) on average during the time is quite similar to the δ values performed.

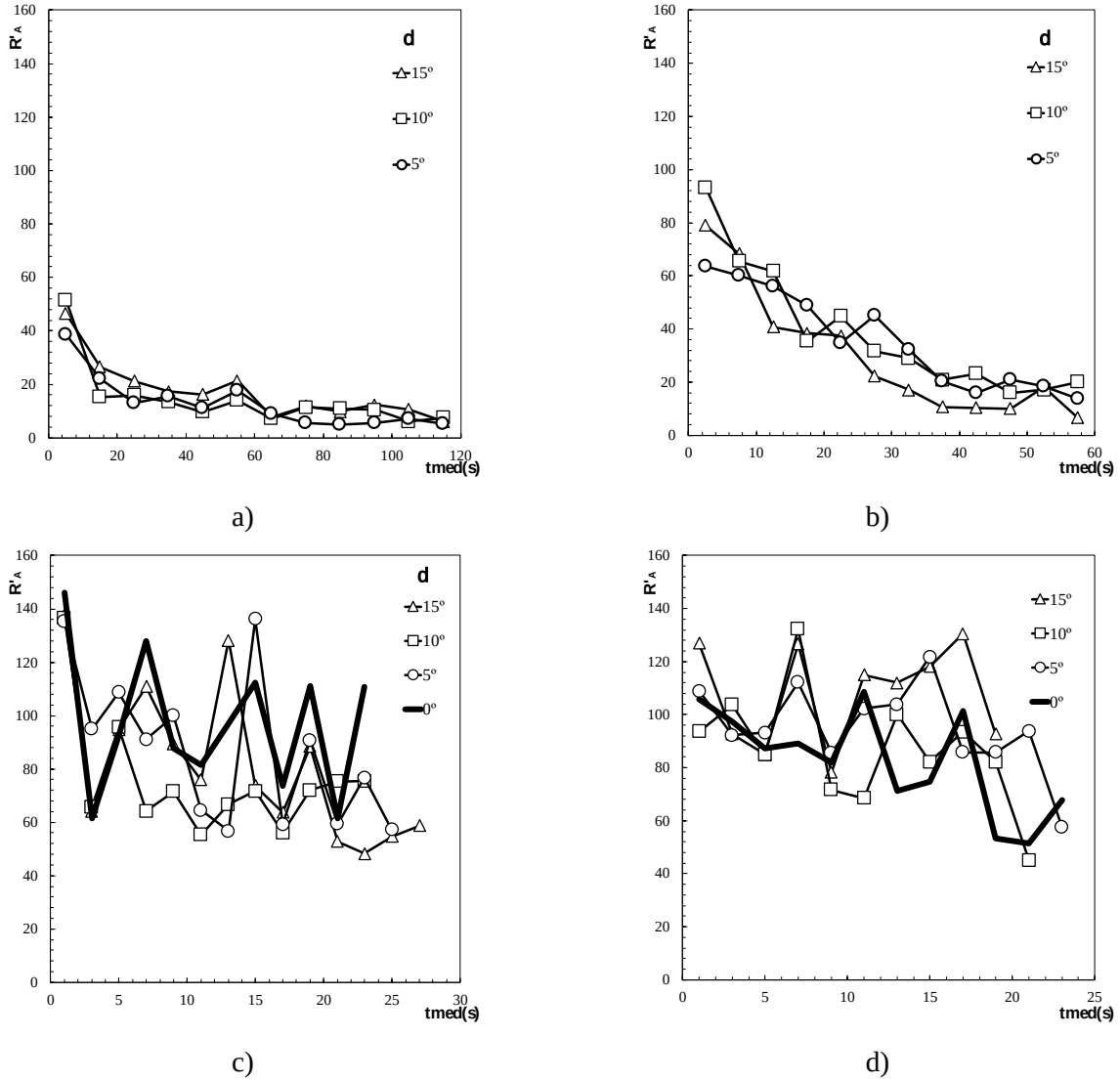

Figure 2 - Non-dimensional ROS R'_A of the intersection point A as a function of the time. The angle δ=5º, 10º and 15º were plotted in all analysis and, for α=30º and 40º, the angle δ=0º was added. a) α=10º; b) α=20º; c) α=30º and d) α=40º

4.2. Angle of the maximum ROS

In order to assess the overall role of the parameters α and δ, the angle γ for each set of parameters was measured. These values are plotted in Figure 3 as a function of the angle between the bisector of the fire lines and the line with the highest slope (δ), for all tests performed. As can be seen, for the highest value of the slope (α=30º and 40º) the angle γ has a similar trend and, in those cases, the axis, where happens the maximum ROS, is influenced more by the convection process. However, for the lower values of the slope the values (α=10º and 20º) the angle γ tends to decrease and the maximum ROS happens near the bisector of the fire lines. In that case, the radiation process in the vicinity of point ***A*** is dominant relative to the convection process.

The dashed lines, in Figure 3, represent the fitted linear regression of the data values for each slope angle (α) and the correlation coefficient R^2 for this fitting is for $a=10º$, $R^2=0.864$, and $a>10º$, $R^2=0.991$.

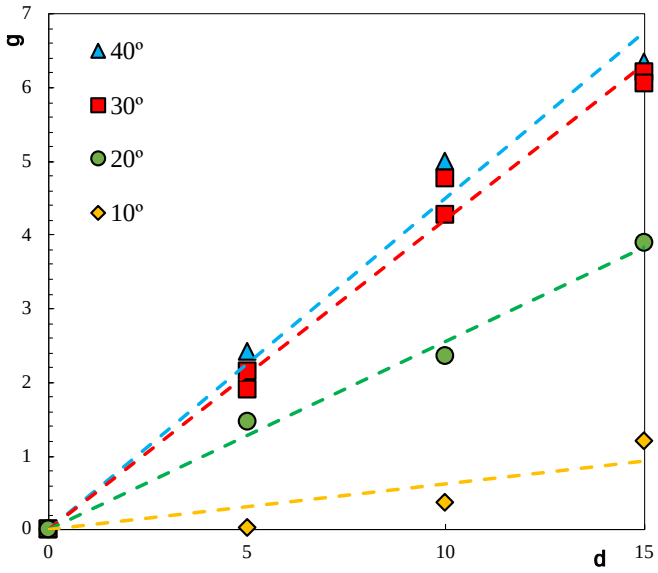

Figure 3- The angle between the bisector of the fire lines and the maximum ROS (γ) as a function of the angle between the bisector of the fire lines and the line with the highest slope (δ). The dashed lines represent the fitted linear regression of the data values for each slope angle (α).

5. Conclusion

Analysis of the Junction Fires with non-symmetric linear fire lines based on laboratory scale experiments was performed for different inclined terrain, ***α=10º, 20º, 30º*** and ***40º***. The evolution of the fire front consists mainly of the advance of the intersection point ***A***, with an initial angle θ_0***=30º*** between fire lines. For the δ angles performed, the non-ROS R'_A is quite similar for each slope angle and, for ***α=30º and 40º***, similar with symmetric condition ***δ=0º.*** With these preliminary laboratory tests, we conclude that the non-ROS of the intersection point ***A*** for small rotation angles depends on the slope angle and the initial angle of the fire fronts. However, for the highest slope angles, the convection process is dominant and changes the angle γ where the maximum ROS occurred but, for the lowest slope angles, the variation angle γ is lower and near to the bisector of the fire lines.

This study must be complemented by more tests to reduce experimental errors and to explore other conditions, different fuel bed types and scale effects.

6. References

Filkov A, Cirulis B, Penman T (2020) Quantifying merging fire behaviour phenomena using unmanned aerial vehicle technology. International Journal of Wildland Fire. doi:10.1071/WF20088.

Hilton JEA, Miller CA, Sharples JJB, Sullivan ALC (2016) Curvature effects in the dynamic propagation of wildfires. International Journal of Wildland Fire 2016, 25, 1238–1251. doi:10.1071/WF16070.

Raposo JR, Cabiddu S, Viegas DX, Salis M, Sharples J (2015) Experimental analysis of fire spread across a two-dimensional ridge under wind conditions. International Journal of Wildland Fire. doi:http://dx.doi.org/10.1071/WF14150.

Raposo JRN (2016) Extreme Fire Behaviour Associated to Merging of Two Linear Fire Fronts. Coimbra. http://hdl.handle.net/10316/31020.

Raposo JR, Viegas DX, Xie X, Almeida M, Figueiredo AR, Porto L, Sharples J (2018) Analysis of the physical processes associated with junction fires at laboratory and field scales. International Journal of Wildland Fire 27, 52–68. doi:10.1071/WF16173.

Rodrigues A, Ribeiro C, Raposo J, Viegas DX, André J (2019) Effect of canyons on a fire propagating laterally over slopes. Frontiers in Mechanical Engineering 5, 402–409. doi:10.14195/978-989-26-16-506_43.

Sharples JJ, Cary GJ, Fox-Hughes P, Mooney S, Evans JP, Fletcher MS, Fromm M, Grierson PF, McRae R, Baker P (2016) Natural hazards in Australia: extreme bushfire. Climatic Change 139, 85–99. doi:10.1007/s10584-016-1811-1.

Thomas CM, Sharples JJ, Evans JP (2017) Modelling the dynamic behaviour of junction fires with a coupled atmosphere-fire model. International Journal of Wildland Fire 26, 331–344. doi:10.1071/WF16079.

Viegas DX, Pita LP (2004) Fire spread in canyons. International Journal of Wildland Fire 13, 253. doi:10.1071/WF03050.

Viegas DX, Raposo JR, Davim D a., Rossa CG (2012) Study of the jump fire produced by the interaction of two oblique fire fronts. Part 1. Analytical model and validation with no-slope laboratory experiments. International Journal of Wildland Fire 21, 843–856. doi:http://dx.doi.org/10.1071/WF10155.

Viegas D, Raposo J, Figueiredo A (2013) Preliminary analysis of slope and fuel bed effect on jump behavior in forest fires. Procedia Engineering 62, 1032–1039. doi:10.1016/j.proeng.2013.08.158.

Viegas DX, Almeida M, Ribeiro L, Raposo J, Viegas MT, Oliveira R, Alves D, Pinto C, Humberto J, Rodrigues A, Lucas D, Lopes S, Silva L (2017) O COMPLEXO DE INCÊNDIOS DE PEDRÓGÃO GRANDE E CONCELHOS LIMÍTROFES, INICIADO A 17 DE JUNHO DE 2017. (Coimbra, Portugal)

Viegas D, Raposo J, Ribeiro C, Reis L, Abouali A, Viegas CX (2021) On the non-monotonic behaviour of fire spread. International Journal of Wildland Fire. doi:10.1071/WF21016.

Xie X, Liu N, Viegas DX, Raposo JR (2014) Experimental Research on Upslope Fire and Jump Fire. Fire Safety Science 11, 1430–1442. doi:10.3801/IAFSS.FSS.11-1430.

Spatiotemporal analysis of fire danger extremes in Europe between 1980 and 2019: Preliminary results

Theodore M. Giannaros*; Georgios Papavasileiou

[1]National Observatory of Athens, Institute for Environmental Research and Sustainable Development. Lofos Koufou, 15236 Penteli, Greece, {thgian, papavasileiou}@noa.gr

**Corresponding author*

Keywords

Extreme fire weather, Europe, ERA5, trends, change-points

Abstract

This work summarizes preliminary results of a spatiotemporal analysis focusing on changes in the occurrence of fire danger extremes in Europe between 1980 and 2019. Extreme danger days were defined based on the daily severity rating exceeding the locally defined 95th percentile. For the 2001 – 2019 period, we show that extreme fire danger days and total burnt area have a positive relationship across Europe, albeit stronger in the eastern half of it. Trend analysis results indicate that extreme fire danger days have overall increased in Europe, with the largest increases found in the north-eastern regions. Further, we illustrate that these increases may be related to abrupt shifts in the means, especially over the south-west Mediterranean, and central and north-eastern Europe. These shifts took place primarily during the 1990s, marking large increases in the mean annual number of extreme fire danger days before and after the years of change. It is hypothesized that these abrupt shifts in fire danger extreme means could be associated with changes in the large-scale circulation of the atmosphere. Overall, the approach followed in the present study is novel as it has not been implemented in previous studies focusing on fire weather extremes. In that view, it complements existing studies and provides new insights into the spatiotemporal variations and changes of fire danger extremes in Europe.

1. Introduction

According to the European Forest Fire Information System, the 2021 fire season in Europe was the second worst on record since 2000 (San-Miguel-Ayanz et al., 2021). Large and extreme wildfires burnt more than 500,000 ha across 22 EU27 Member States, with Mediterranean countries experiencing the most damages. These wildfires are the latest in a series of catastrophic events that affected Europe in recent years. Some of the worst cases include the wildfires that occurred in Portugal (2003, 2005, and 2017), Spain (2006 and 2017), Greece (2000, 2007, and 2018), and Sweden (2018). Researchers argue that the frequency and intensity of such events have been increasing due to the more frequent occurrence of extreme fire weather (e.g., Abatzoglou and Williams, 2016; Bowman et al., 2017; Jolly et al., 2015).

In this work, we present preliminary results of a spatiotemporal analysis focusing on the occurrence of fire danger extremes in Europe between 1980 and 2019. Our analysis is based on the daily severity rating (DSR), a sub-component of the Canadian Forest Fire Weather Index System (CFFWIS; Van Wagner, 1987) that indicates fire suppression difficulty. Trend analysis was conducted to quantify long-term changes in the occurrence of fire danger extremes in Europe. In addition, we applied statistical change-point detection methods to identify and quantify abrupt changes in the occurrence of extreme fire danger days.

2. Data and methods

Daily, gridded DSR data were retrieved from the 0.25^o x 0.25^o spatial resolution GEFF-ERA5 reanalysis dataset of the CFFWIS (Vitolo et al., 2020), developed by the European Centre for Medium-range Weather Forecasts (ECMWF). The data cover spatially the European region from 25^o W to 40^o E and from 34 ^{o}N to 72 ^{o}N (Figure 1) and extend temporally from 1 January 1980 to 31 December 2019 (40 years). Extreme fire danger days were defined based on DSR exceeding the locally (grid cell-specific) defined 95th percentiles (reference period 1981

– 2010). We opted for using percentile-based local thresholds since previous studies have shown that local extremes promote large fire growth (e.g., Abatzoglou et al., 2021).

The statistic used to quantify changes in extreme fire danger occurrence in Europe is the annual count of extreme DSR days. We applied the non-parametric Pettitt test (Pettitt, 1979) to detect abrupt changes in the time series of extreme DSR days, and the non-parametric Mann-Kendall (MK) test (Mann, 1945; Kendall, 1976) to quantify long-term trends. Finally, we supplemented our analysis with observed burnt area data for the 2001 – 2019 period, retrieved from the FireCCI v5.1 dataset (Lizundia-Loiola et al., 2020) of the European Space Agency (ESA) Climate Change Initiative.

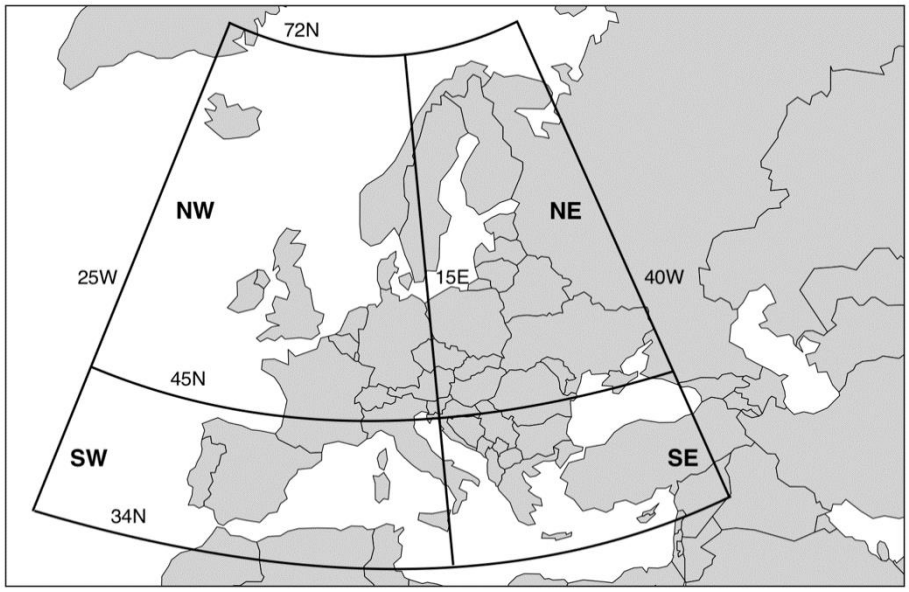

Figure 1 – Study area with identification of the different sub-regions used in the analysis.

3. Results

3.1. Relationship between fire danger and burnt area

Figure 2 summarizes a simple exploratory analysis between the annual count of extreme fire danger days and the annual total burnt area (in non-agricultural vegetation class categories) in the examined sub-regions of Europe (Figure 1). Results indicate a statistically significant ($p < 0.05$) positive relationship between the two variables (Figure 2a), which is stronger in the eastern part of the study area (SE, NE) than in the western part (SW, NW). Further, it can be seen that the most destructive years during the examined period (2001 – 2019) coincide well with peaks in the annual count of extreme fire danger days in all European sub-regions (Figure 2b).

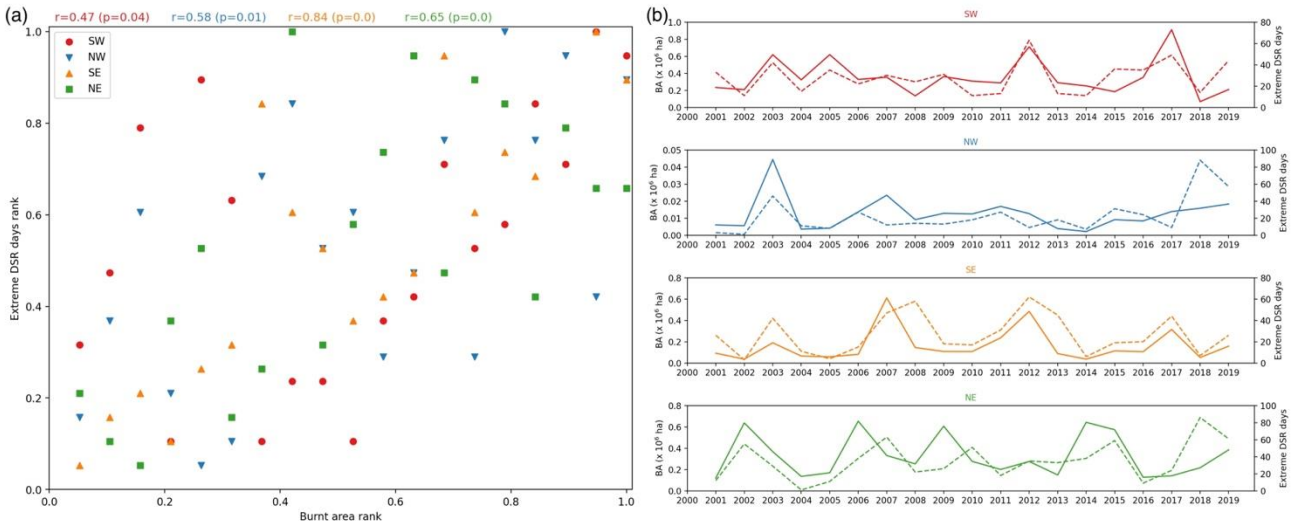

Figure 2 – (a) Scatter plot between the annual total burnt area in the different European sub-regions and the corresponding annual count of extreme DSR days. All data are plotted in their rank order, scaled between 0 and 1. Different colors and symbols are used for the data pooled from the different sub-regions. Spearman correlation coefficients (r) and their associated p-values are shown on top of the plot, with colors corresponding to the different European sub-regions. (b) Time series of the annual total burnt area (solid lines) and the corresponding annual count of extreme DSR days (dashed lines) in the different European sub-regions.

3.2. Seasonality and changes in extreme fire danger occurrence

Extreme fire danger days exhibit a clear seasonal cycle (Figure 3), occurring primarily during the warmest part of the year, from June to September in southern Europe (SW, SE) and from May to September in northern Europe (NW, NE). This suggests that the northern European countries are more prone to experiencing locally extreme fire danger days at the edge of the traditional fire season (May to October) compared to the southern Mediterranean countries, where occurrences of extreme fire danger days peak during the hottest months of July and August.

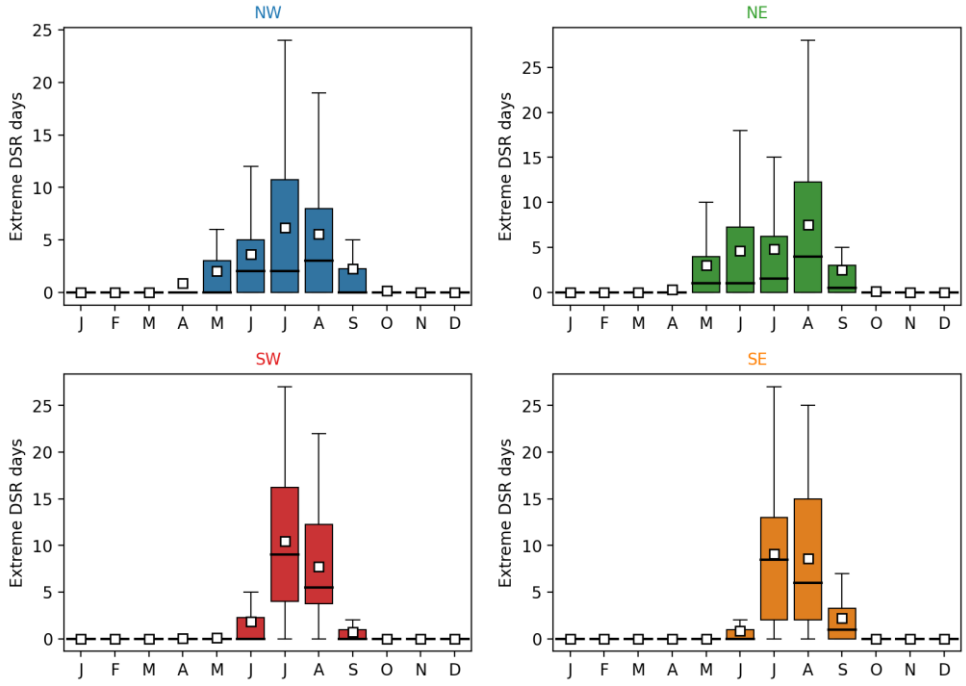

Figure 3 – Monthly distribution of extreme DSR days in the different European sub-regions for the period 1980 – 2019. Solid black lines and white boxes denote median and mean values, respectively. Error bars indicate the interquartile range of the data.

Extreme fire danger days have increased between 1980 and 2019 in all European sub-regions (Table 1). Statistically significant ($p < 0.05$) increases were computed for the SW, SE, and NE sub-regions, whereas a non-significant trend was found in the NW sub-region. The magnitude of the statistically significant increasing trends was found to range from an additional 4 days per decade in the SE sub-region to more than 10 days per decade in the NE sub-region.

Table 1 – Extreme DSR days trends in the different European sub-regions, computed for the 1980 – 2019 period. Show are the decadal trends computed using the MK test and the associated p values.

European sub-region	Trend (days decade^{-1})	p-value
SW	6.3	0.00
NW	3.0	0.23
SE	4.3	0.01
NE	10.9	0.00

Results of the Pettitt test indicate that the increasing occurrences of extreme fire danger days in the SW and NE European sub-regions may be linked to abrupt changes in the means. The change-points for the above two sub-regions occurred in the 1990s (1991 for the NE and 1997 for the SW), marking sharp increases in the mean annual number of extreme fire danger days (Figure 4).

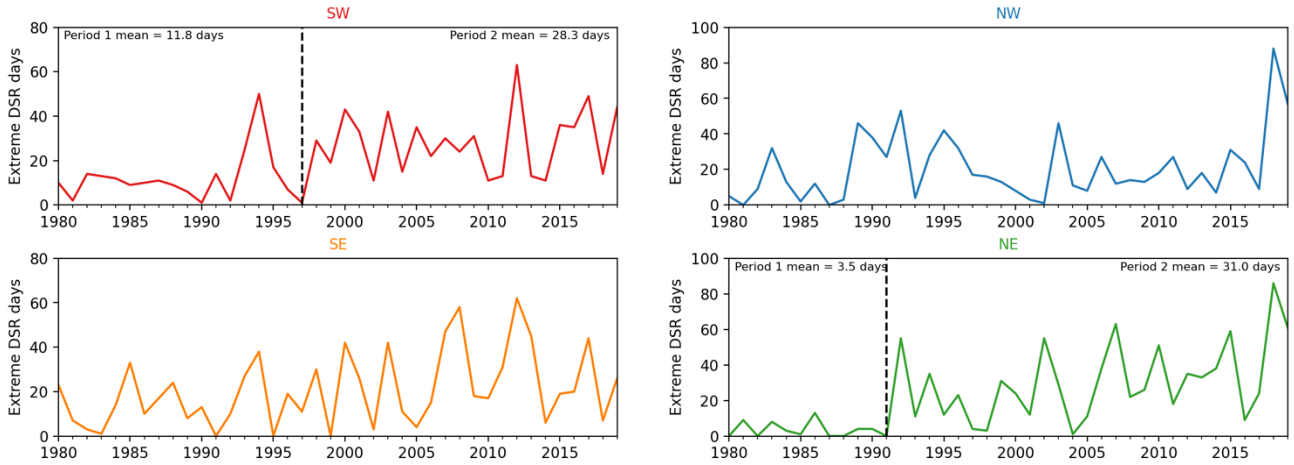

Figure 4 – Time series of the annual count of extreme DSR counts in the different European sub-regions. Vertical dashed lines denote statistically significant potential change-points.

Concerning the spatial variability of changes in extreme fire danger days, Figure 5 reveals widespread, statistically significant potential change-points over a large part of Europe. The largest changes were found in the eastern part of the study area, where many grid cells were found to experience up to more than 30 additional extreme fire danger days per year after the year of the potential change-point (Figure 5b). The related change-points were found to occur mostly in the early 1990s (Figure 5a, green-colored grid cells). Grid cells in south-eastern Spain were also found to experience large increases, up to more than 20 additional extreme fire danger days per year after potential change-points that occurred in the mid-1990s. Finally, grid cells in central Europe (eastern France, southern Germany) were found to exhibit 10 – 15 additional extreme fire danger days per year after potential change-points that occurred in the 2000s.

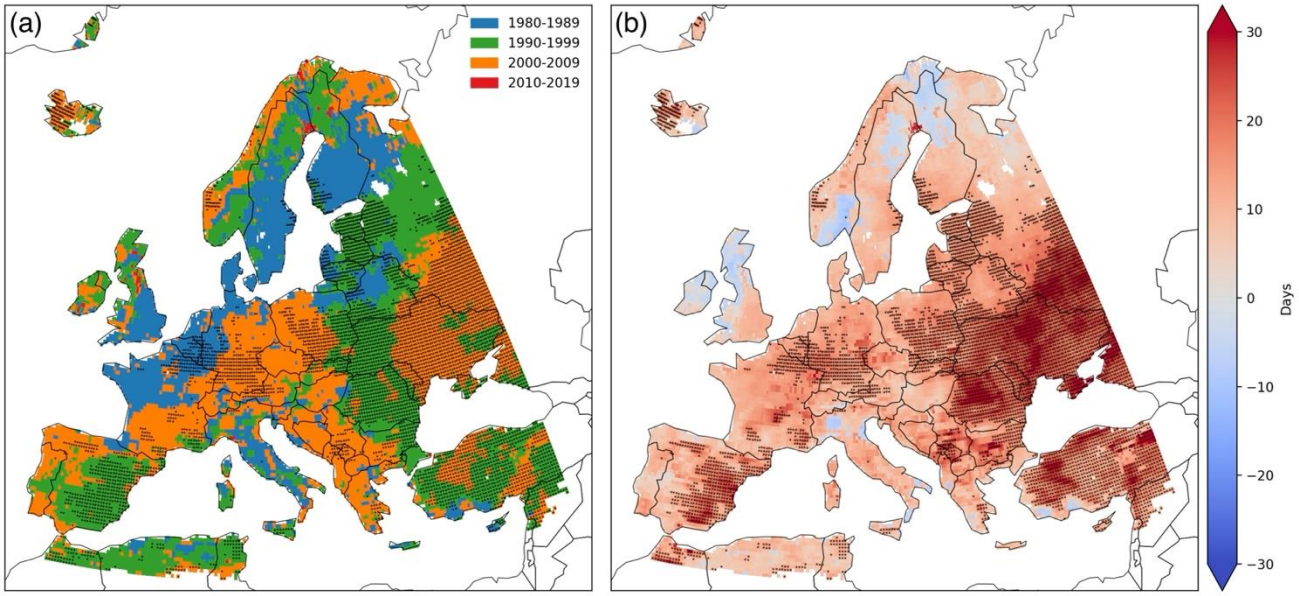

Figure 5 – (a) Years of potential change-points in the time series of the annual count of extreme DSR days. (b) Change in the mean annual count of extreme DSR days before and after the potential change-points. Stippling indicates statistical significance (at the 95 % confidence interval) of the potential change-points. Change points and the associated statistical significance were computed using the non-parametric Pettitt test.

4. Conclusions

The preliminary results of our spatiotemporal analysis indicate that extreme fire danger days have increased in Europe during the period from 1980 to 2019. Within large parts of the SW and NE European sub-regions, but also in central Europe, these increases seem to have taken place abruptly. This conclusion is supported by the statistically significant potential change-points that were identified in the time series of the extreme fire danger days. Abrupt changes appear to have occurred in the mid-1990s in the SW sub-region and over the largest part of the NE sub-region, marking very large changes in the mean annual occurrences of extreme fire danger days before and after the year of change. It can be speculated that these abrupt changes may be associated with changes in large-scale atmospheric circulation and atmospheric teleconnection patterns, which in turn gave rise to increases in temperature and decreases in humidity and precipitation. However, this is an hypothesis that needs to be statistically verified before reaching to robust conclusions.

5. Acknowledgments

This research was funded by the Hellenic Foundation for Research and Innovation (H.F.R.I.) under the "2nd Call for H.F.R.I. Research Projects to support Post-Doctoral Researchers" (Project Number: 00559).

6. References

Abatzoglou JT, Williams AP (2016) Impact of anthropogenic climate change on wildfire across western US forests. Proceedings of the National Academy of Sciences of the United States of America 113, 11770-11775.

Abatzoglou JT, Juang CS, Williams AP, Kolden CA, Westerling AL (2021) Increasing synchronous fire danger in forests of the Western United States. Geophysical Research Letters 48, e2020GL091377.

Bowman DMJS, Williamson GJ, Abatzoglou JT, Kolden CA, Cochrane MA, Smith AMS (2017) Human exposure and sensitivity to globally extreme wildfire events. Nature Ecology and Evolution 1, 1-6.

Jolly WM, Cochrane MA, Freeborn PH, Holden ZA, Brown T, Williamson GJ, Bowman DMJS (2015) Climate-induced variations in global wildfire danger from 1979 to 2013. Nature Communications 6, 7537.

Kendall MG (1976) Rank correlation methods. 4th Edition, London UK: Griffin.

Lizundia-Loiola J, Otón G, Ramo R, Chuvieco E (2020) A spatio-temporal active fire-clustering approach for global burned area mapping at 250 m from MODIS data. Remote Sensing of the Environment 236, 111493.
Mann HB (1945) Nonparametric tests against trend. Econometrica 13, 245-259.
Pettitt AN (1979) A non-parametric approach to the change-point problem. Journal of the Royal Statistical Society C: Applied Statistics 28, 126-135.
San-Miguel-Ayanz J, Durrant T, Boca R, Maianti P, Libertá G, Artés-Vivanco T, Oom D, Branco A, de Rigo D, Ferrari D, Pfeiffer H, Grecchi R, Nuijten D (2022) Advance Report on Forest Fires in Europe, Middle East and North Africa 2021. EUR 31028 EN, Publications Office of the European Union, Luxembourg, ISBN 978-92-76-49633-5.
Van Wagner CE (1987) Development and structure of the Canadian Forest Fire Weather Index System. Canadian Forestry Technical Report 35, Canadian Forestry Service, Ottawa, ON.
Vitolo C, Di Giuseppe F, Barnard C, Coughlan R, San-Miguel-Ayanz J, Libertá G, Krzeminski B (2020) ERA5-based global meteorological wildfire danger maps. Scientific Data 7, 216.

The economic benefits of planning before the fire

Jude Bayham*; Marissa Lee

Colorado State University, Fort Collins, CO 80523, USA, {jbayham, m.lee}@colostate.edu

**Corresponding author*

Keywords

Wildfire Management, Planning, Suppression Cost, Matching Methods

Abstract

Wildfire suppression expenditures in the United States regularly exceed a billion dollars and are expected to continue rising due to climate change, high fuel loads, and a growing wildland urban interface. Risk management research suggests that pre-fire planning reduces uncertainty and may lead to better wildfire management outcomes including lower suppression costs, less damage to values at risk and improve safety outcomes. One form of pre-fire planning in US National Forests is known as potential operating delineations (PODs) whereby stakeholders collaboratively identify area on the landscape where wildfire can be safely and effectively engaged. Moreover, the area defined by the PODs are classified based on the level of urgency to suppress fire.

The objective of this paper is to test whether fires that have occurred within areas that have undergone the POD process are systematically different from fires that have not undergone PODs. We evaluate the following wildfire outcomes: final fire cost, final fire size, cost per acre, and duration. We employ statistical matching methods to find comparable non-POD fires that serve as "control" units for our POD "treated" fires. Our results suggest that POD fires cost $373 per acre less than non-POD fires, and that the POD fires cost per acre is comparable to prescribed burning cost per acre in the Southwestern US. These results imply that pre-fire planning like the POD process may reduce suppression costs to a level comparable with prescribed burning facilitating the long-standing recommendation from fire ecologists to "restore fire to the landscape."

1. Introduction

Billions of dollars are spent on wildland fire management in the United States each year. These costs are a result of decisions to commit resources to manage and suppress fire. Climate change, a growing wildland urban interface, and the accumulation of fuels are expected to drive increased fire activity necessitating additional resources that will likely increase costs. For decades, the default response had been to suppress all fire as quickly as possible. This strategy has led to an accumulation of fuels that currently contribute to large costly incidents (Thompson et al., 2013). Risk management offers insights that when applied to wildfire management can improve effectiveness, reduce costs, and increase safety (Thompson et al., 2011, 2019). Risk management involves planning in advance of an incident to identify risks and make informed decisions.

The wildfire community has recognized the importance of planning in advance of incidents. The process to identify and characterize potential operational delineations (PODs) is an attempt to plan in advance of the incident (Dunn et al., 2020). PODS summarize wildfire risk before ignitions occur and may guide operations as fires progress. In cases where a fire is burning in a POD with a low risk rating, managers may employ less aggressive suppression strategies that may reduce cost. While less aggressive suppression may result in larger fires, they may provide ecological benefits and reduce the risk of firefighter injury.

Fuel treatments are another tool used to mitigate the impacts of fire. Fuel treatments are an important tool to reduce fuel loads thereby reducing the risk of uncontrollable wildfire. However, fuel treatments can be costly (US Forest Service, 2015). Mechanical treatments involve considerable machinery and labor. Prescribed burns carry political risk and generate smoke that impose additional costs on society (Navaro et al., 2018). Managing wildfire to achieve the benefits of fuel treatment may represent a less costly method for mitigating fuels and the potential for future fire damage.

We investigate the impact of the POD process on economic and operational aspects of fire management. Our approach is to compare fires that occur in forests that have developed PODs to statistically similar fires that

occur in forests that have not developed PODs. After controlling for numerous factors that may influence fire outcomes, we attribute differences in fire outcomes to the POD process. We find that POD fires have a lower cost per acre, which supports the idea that planning prior to the fire event can improve the efficient use of suppression resources. We then compare the average cost per acre of POD and non-POD fires to mechanical and prescribed treatments to see if cost savings are present.

2. Data and Methods

Our objective is to empirically analyze the impact of the POD process on suppression operations and to compare the cost of POD fires to alternative methods of fuel treatment. The POD process is relatively new and has only been administered on a few forests. In particular, the Tonto National Forest (Southwestern US) developed PODs in 2017. As of 2021, the Southwest Region has 40+ landscapes in national forests that have undergone the PODs process. We compare a set of fires that burned in the Southwest region in 2019 (POD fires) to statistically similar fires that were not in a forest with developed PODS (non-POD fires). We compare POD fires to non-POD fires across multiple outcome variables through regression analysis. We then compare the costs of wildfires managed under these strategies to fuel treatment costs in the same areas. Our methods are straightforward and contribute to the novel research around POD fires. Prior research on the benefits of PODs is qualitative in nature using mechanisms like interviews and surveys. Our econometric-driven approach is a useful lens to support other PODs research.

2.1. Data

We assemble a dataset from several disparate sources to investigate the impact of PODs on suppression operations. We begin with 20 fires from 2019 that occurred in US National Forests that underwent the POD planning process. We extract the ignition location point, start and end dates of suppression or management operations, and final fire size from USFS records. We cross-reference this list of fires with US Forest Service suppression billing records to estimate the cost of the fires. We also extract preparedness level from the National Interagency Fire Center to account for the level of strain on the wildfire response system during a fire.

In addition to location and dates, we use weather and topographical data to incorporate pre-fire conditions into our matching approach. Weather variables, including temperature, energy release component, precipitation, humidity, and wind speed were averaged for the 10 days leading up to the first reporting date from Gridmet data. Topographical features such as elevation, slope, aspect, and ruggedness are generated from a digital elevation model using the elevatr package in R.

2.2. Matching Methods

We employ several empirical strategies to analyze the impact of the POD process on suppression operations. Our primary empirical strategy is to match fires that ignite in forests that have undergone the PODs process, so called POD fires, with fires that ignite in forests that have not undergone the PODs process, non-POD fires. The intuition behind matching is that we are able to identify non-POD fires that are similar to POD fires along several observable dimensions to serve as the "control" group in our experimental design. Ideally, the occurrence of the fire in a POD forest is the only meaningful difference between the POD fire and its non-POD (control) counterparts.

To accurately investigate the cost savings and other benefits of POD fires, similar non-POD fires are needed for comparison. Using the data described above, we develop a propensity score matching model to find suitable non-POD matches for the set of POD fires. Specifically, fires are matched based on: region of the US (GACC), national preparedness level, fire cause, topographic and weather in the 10 days preceding ignition. Topographic data include elevation, slope, aspect, and ruggedness within 2km of the point of ignition. Weather data include energy release component, precipitation, minimum near-surface relative humidity, maximum near-surface air temperature, wind speed. We use the 10 days before fire ignition to avoid the effects of the fire progression and suppression operations that may confound our estimate of the effect of the POD process on wildfire outcomes.

POD fires were matched to non-POD fires at a ratio of 1 to 3. In total, we matched 17 POD fires to 51 non-POD fires. We requested management cost data for non-POD fires and received data for 24 fires where at least one of the 51 matched fires corresponded to a POD fire. Our end sample size included 16 POD fires and 24 non-POD fires. The locations of these fires are shown in Figure 1.

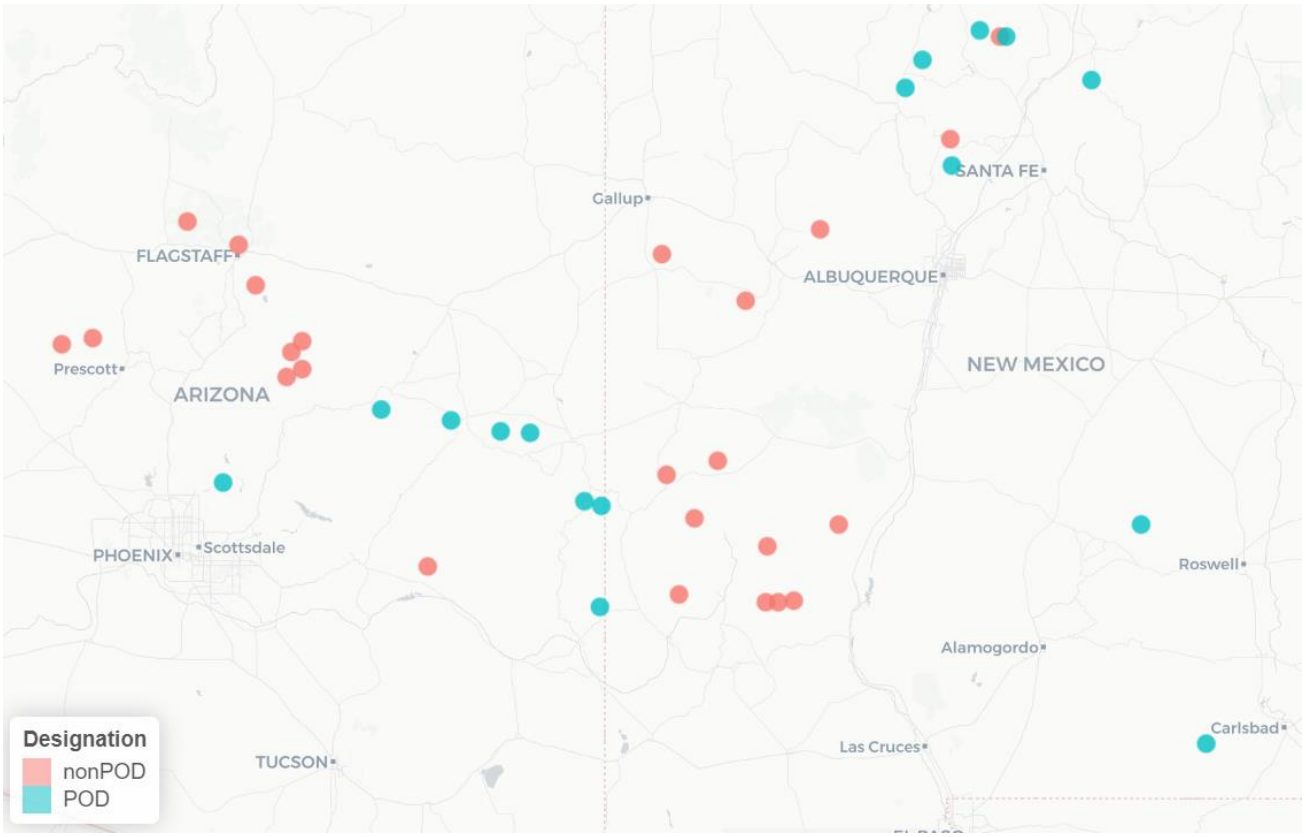

Figure 1: Map of Arizona and New Mexico (USA) showing location of POD and non-POD fires used in the sample.

Table 1 contains summary statistics for the set of POD and non-POD fires used in the matching analysis. Suppression costs are lower on POD fires than their non-POD counterparts both in total cost and cost per day. POD fires, on average, have a larger start size in acres than non-POD fire counterparts but also have a smaller ending size. This could indicate effective planning of POD fires before ignition. Interestingly, POD fires have shorter durations than non-POD fires, possibly suggesting a more efficient use of daily resources. POD fires are also shorter in duration and less expensive per acre when compared to fires managed under direct, modified, and limited suppression strategies from 2006-2008 (Gebert and Black, 2012).

Table 1. Summary statistics comparing POD and non-POD fires

Variable	N	Mean	SD
Fire Size first day (acres)			
POD	16	901	1,572
non-POD	24	265	243
Fire size last day (acres)			
POD	16	3,536	3,966
non-POD	24	4,041	5,466
Fire Cost			
POD	16	720,419	1,313,024
non-POD	24	1,011,137	1,783,758
Duration			
POD	16	13.69	8.52
non-POD	24	18.33	14.29
Fire Cost ($USD/Day)			
POD	16	57,287	84,080
non-POD	24	57,643	95,458
Fire Cost ($USD/Acre)			
POD	16	206	182
non-POD	24	591	971

3. Results and Discussion

Table 2 contains the results of the matching analysis. POD and non-POD fires are matched on characteristics and conditions that exist before ignition to mitigate the effect of matching on factors affected by management decisions over the course of the fire. We compare the POD and non-POD fires along four dimensions: Final Cost, Final Fire Size, Cost/Acre, Duration. We run regressions using only the POD indicator and then again with the variables the POD and non-POD fires are matched on.

Table 2. Regression results based on matched dataset

	Final Fire Cost	Final Fire Size	Cost/Acre	Duration
(Intercept)	30,577	308,778*	-33,864	419
	[-68,048, 129,202]	[-4,226, 621,782]	[-76,144, 8,414]	[-548, 1,388]
POD Fires	-222	603	-373*	-3.40
	[-1225, 779]	[-2,577, 3,784]	[-802, 56]	[-13.25, 6.44]
R2 Adj.	0.279	0.217	0.440	-0.158

Notes: N=40 in all regressions. All regressions include the following controls, but are omitted from the table for brevity: region of the US (GACC), national preparedness level, fire cause, topographic and weather

We find little statistical evidence that there are differences between POD and non-POD fires with the exception of Cost/Acre. Specifically, the cost per acre on POD fires is $373 less than comparable non-POD fires (statistically significant at 10% level. This result supports the hypothesis that less costly suppression effort is expended on POD fires. Suppression resources may be monitoring fire growth in areas with few values at risk or focusing containment effort on the operating delineations identified in the planning process rather than responding to fire growth as an emergency. The lack of statistical significance in the other regression models is likely the result of small sample sizes given the relatively recent implementation of the POD process.

3.1. Comparison to Mechanical and Prescribed Treatments

While we observe some evidence that POD fires are cost effective compared to non-POD fires, we also compare the average cost per acre to the costs of prescribed and mechanical treatments. We estimate per-acre prescribed burning and mechanical treatment costs in the Southwestern US (USFS Region 3) using data from the Hazardous Fuel Treatment Reduction dataset. We remove all prescribed and mechanical projects that fall outside of three standard deviations of the mean cost per acre. We find that POD fires average suppression expenditures of $206/ac and are less expensive per acre than mechanical treatments ($408) and non-POD fires ($591, Table 3). While not all POD fires are necessarily managed for resource benefits, our results suggest that the pre-fire planning during the POD process does curtail suppression expenditures making them comparable to prescribed burning treatments. This result suggests a potential role for managing POD fires for resource benefit.

Table 3: Cost per acre ($USD) of POD and non-POD fires and Southwestern US fuel treatments

Fire Treatment	**N**	**Mean**	**SD**
POD Fire	16	$206	$182
Non-POD Fire	24	$591	$971
Prescribed	982	$189	$1,268
Mechanical	3,356	$408	$612

4. References

Dunn, C.J., O'Connor, C.D., Abrams, J., Thompson, M.P., Calkin, D.E., Johnston, J.D., Stratton, R., Gilbertson-Day, J. 2020. Wildfire risk science facilitates adaptation of fire-prone social-ecological systems to the new fire reality. Environ. Res. Lett. 15, 1–13.

Gebert, K.M. and Black, A.E., 2012. Effect of suppression strategies on federal wildland fire expenditures. Journal of Forestry, 110(2), pp.65-73.

Navarro, K.M., Schweizer, D., Balmes, J.R. and Cisneros, R., 2018. A review of community smoke exposure from wildfire compared to prescribed fire in the United States. Atmosphere, 9(5), p.185.

National Interagency Coordination Center. (2020). Incident Management Situation Report (IMSR) Archives. Retrieved October 20, 2021, from https://www.predictiveservices.nifc.gov/intelligence/archive.htm

Thompson, M. P., Calkin, D. E., Finney, M. A., Ager, A. A., & Gilbertson-Day, J. W. 2011. Integrated national-scale assessment of wildfire risk to human and ecological values. Stochastic Environmental Research and Risk Assessment, 25(6), 761–780. https://doi.org/10.1007/s00477-011-0461-0

Thompson, M. P., Vaillant, N. M., Haas, J. R., Gebert, K. M., & Stockmann, K. D. 2013. Quantifying the Potential Impacts of Fuel Treatments on Wildfire Suppression Costs. Journal of Forestry, 111(1), 49–58. https://doi.org/10.5849/jof.12-027

Thompson, M.P., Wei, Y., Calkin, D.E., O'Connor, C.D., Dunn, C.J., Anderson, N.M. and Hogland, J.S., 2019. Risk management and analytics in wildfire response. Current Forestry Reports, 5(4), pp.226-239.

USDA Forest Service. 2015. The Rising Cost of Fire Operations: Effects on the Forest Service's Non-Fire Work. Available online:
https://www.fs.usda.gov/sites/default/files/2015-Fire-Budget-Report.pdf (accessed on 12 October 2021).

The geography of forest fires in Greece: fire resilience vis-à-vis management crises

Kostas Kalabokidis*[1]; Palaiologos Palaiologou[2]

[1]*Department of Geography, University of the Aegean, Mytilene 81100, Greece {kalabokidis@aegean.gr}*
[2]*Department of Forestry and Natural Environment Management, Agricultural University of Athens, Karpenisi 36100, Greece {palaiologou@aua.gr}*

**Corresponding author*

Keywords

Extreme wildfire events; fire regimes; fuels management; climate change; stochastic fire simulations; transboundary wildfire exposure

Abstract

Greece has an ever-increasing appeal for establishment of new and/or expansion of existing human settlements in the wildland-urban interface that in turn cause pressures on the natural environment, increasing the fire risk and decreasing resilience at a landscape level. A multitude of Mediterranean-type of ecosystems exist in the country, ranging from low shrubs and coniferous woodlands on coastal sites to high-elevation conifer and broadleaf forests. Fire plays a critical role on how these ecosystems were formed and function. Due to the topography, land uses, numerous islands, extensive coastlines and local microclimates, we find either broad zones with similar fire-related characteristics or enclaves where unique interactions with landscape fires prevail. We described the fuel and fire schemes in Greece as formed by different combinations of topography, weather, vegetation and human activity. A geographical context for this analysis was provided by examples of recent wildfires occurred in Greece during the 21st century, which re-shaped the landscape and affected in multiple ways the natural environment and human settlements from severe fire effects. In addition, we showed how these wildfires created crises that drove fire management policies; and we illustrated how fuels and wildfires should be managed based on their respective fire regimes and expected fire effects. Finally, we briefly reviewed future implications for wildfire management from the cumulative effects of climate change, urban sprawl and unmanaged forest growth.

1. Fire environment and regimes

The problem of forest fires in Greece is intensified when extreme events occur that cannot be suppressed immediately due to the inherent weaknesses of firefighting, the widespread wildland-urban interface (WUI) and the lack of forest management in the midst of climate change. Apart from the high and increasing risk of forest fires, a large number of deaths from wildfires in residential areas in Greece has shown that the problem cannot be solved by suppression alone. Extreme behavior of the recent catastrophic fires with human losses in Greece can be attributed to many explanatory factors, such as the ever-expanding urban footprint in forested areas, increasing human-caused fires, mountainous topography, fuel accumulations, intensifying drought and stronger winds from unexpected directions due to climate anomalies.

In Greece, the low elevation pine forests of the moderate-sized serotinous-cone species of Aleppo pine (*Pinus halepensis*) west of the 25th meridian, and Calabrian pine (*Pinus brutia*) at the east of the 25th meridian, have frequent crown fire regimes and transmit most of the catastrophic wildfires; trees can reach a height of up to 30 m, if left undisturbed, but usually they are between 10-20 m in frequently burned forests (Keeley *et al.* 2012). Other important conifers that burn less often and under surface fire regimes are the serotinous Mediterranean cypress (*Cupressus sempervirens*) and maritime pine (*Pinus pinaster*), and the non-serotinous stone pine (*Pinus pinea*), Scots pine (*Pinus sylvestris*) and black pine (*Pinus nigra*). Except Scots pine, all these pines have thick bark and large-sized buds to tolerate relatively high fire intensities and heating. The needle drape (suspended live and detached dead needles) of all these conifers is usually mixed with conifer saplings, broadleaf evergreen shrublands (referred as maquis or phrygana) and cured annual plants (Kalabokidis and Palaiologou 2019).

The shrub fuel types consist of non-tree, woody and foliage vegetation biomass (live with hard leaves or dead twigs) from the dominant shrub species. When assorted with conifers, the shrub fuelbed is mixed with conifer

needles and branches, and saplings in canopy openings. Maquis form high canopy density shrublands with heights between 2-8 m and foliar cover >30%, when they are dominant in open landscapes (scrub), forming woodlands with tree heights of more than 8 m if left undisturbed for several decades. When found on the understory of conifers, they can be either sparse and suppressed in closed canopy stands (low shrubs, 0-2 m tall) or dense and tall in open canopy or sparsely forested stands. These shrublands regenerate vigorously after fire through resprouting with high success rates or seedling recruitment, forming a densely covered post-fire fuelbed mixed with dead conifer biomass, fallen logs and annuals. The most typical maquis evergreen shrub is Kermes oak (*Quercus coccifera*), forming vast and severely burned shrublands (and sometimes low woodlands on moister sites), which has a strong post-fire resprouting capacity from rhizomes. In phrygana and/or garrigue shrublands, *Sarcopoterium spinosum* is a thorny dwarf shrub colonizer that accumulates high proportions of standing fine and dead fuel in over-burned and overgrazed areas with land degradation and desertification problems (Moreira *et al.* 2012). Oaks (*Quercus* spp.) have important contribution in the formation of fuelbeds forming woodlands on a transitional zone to temperate forests, including winter-deciduous species. Oaks epicormically resprout from dormant buds (buried in bark) after moderate-severity wildfires, but they may fail following high-intensity fires. Fuelbeds in oak-dominated landscapes consist of dead leaves and branches, mixed with annual vegetation (usually geophytes that resprout by means of underground buds) and short shrubs or maquis, and rarely support active crown fires. When mixed with conifers or tall maquis, oaks can be scorched or completely consumed by passive crown fires (Kalabokidis and Palaiologou 2019).

2. Fire activity during the 21st century

While the annually burned area in Greece has been around 40 thousand hectares on the average in the last 40 years from approximately 1,500 fires per year, certain years stand out as exceptionally catastrophic such as indicated from the European Union's wildfire history statistics (EFFIS 2020). These are the years of 2000 with 145,033 ha and 2007 with 225,734 ha burned in the 21st century. More than 2,500 ignitions occurred during the years 2000 and 2001. The largest fire events of history for the prefectures of Greece took place in the record year of 2007 in the region of Peloponnese, namely in Achaea (30,000 ha), Messenia (11,000 ha), Laconia (22,000 ha) and Ilia with four wildfires (40,000, 32,000, 30,000 and 12,000 ha). In 2000 the fire of Samos Island in the north-eastern Aegean burned 14,500 ha, summing up to a total of 18,000 ha burned during that year in the region. Evia also experienced a large-scale event during 2007 with 18,000 ha burned. During 2012, a large fire on Chios Island burned 15,000 ha including a significant area occupied by the precious and unique mastic producing tree (*Pistacia lentiscus* var. *chia*). Forest fires of 2021 in Greece amounted to 140,000 ha burned, from six large-scale events (more than 5,000 ha each) and one mega-fire in Evia (46,000 ha).

Attica experienced the largest fire event during 2009 with 20,500 ha burned and repeated catastrophic wildfire years in the vicinity of certain highly populated suburbs of Athens. On July 23, 2018, at the eastern foothills of Penteli Mountain in eastern Attica, a lethal forest fire burned through the urban settlements of Neos Voutzas and Mati where houses intermingled with pine stands, killing 102 people, destroying more than 1,500 homes and burning 1,450 ha. These wildfires caused a lot of pain, had a huge impact on society and demonstrated dramatically the urgent need for better fire prevention planning and coordination of fire control resources, including a major reform to obsolete wildfire management policies and tactics in Greece.

3. Fire management implications

Wildfire management of the various forest types needs to take into consideration the fire regime group to which they belong, that as a rule is linked to the adaptation of the particular species to fire effects (damage severity, capacity for post-fire regeneration), and the fuel hazard they represent (characteristics as fuel accumulation rate, fuel loading and arrangement, and ultimately fire behavior). Locally, of course, management needs to also consider non-forest values-at-risk, and the possibility for fire regime alterations due to the increased presence of humans as source of deliberate or accidental ignitions.

In response to the growing scale of fire risk in Greece, it is proposed to implement new forest management principles with landscape-scale fuel management activities and a more representative geography of risk in terms of setting goals and priorities. Effective fire risk management strategies and comprehensive preventive planning are required, rather than investing solely or mainly in forest firefighting and aerial firefighting. Without the

management of fuels and forests to mitigate the intensity and spread of fires before they occur, the effectiveness of firefighting is dramatically reduced. Preventing, suppressing and reducing the risk of wildfires follow interconnected paths, and require alternative practices of vegetation management, mitigation of accumulated fuel and clearing of forest areas with timely and valid scientific interventions to reduce fire risks (Palaiologou *et al.* 2020), in relation to the global climate change we are experiencing today.

The management of forest fuels has proven to be an effective method for stopping the continuity and reducing their quantity, reducing the rate of spread and the intensity of fires. Using stochastic forest fire simulations (Kalabokidis *et al.* 2014) and alternative scenario planning and evaluation tools, different fuel management priorities can be located in forest areas to: 1) block the main fire flows to protected areas; 2) decrease the possibility of high-intensity fires, 3) reduce the likelihood of fires spreading within residential areas, 4) protect areas of increased economic value, and 5) optimize the production of commercial forest products. Results show how investing and implementing one management priority can offer trade-offs to other priorities (Palaiologou *et al.* 2021), and where there are opportunities (spatial coincidence) for achieving multiple management objectives at the same time (e.g. Figure 1).

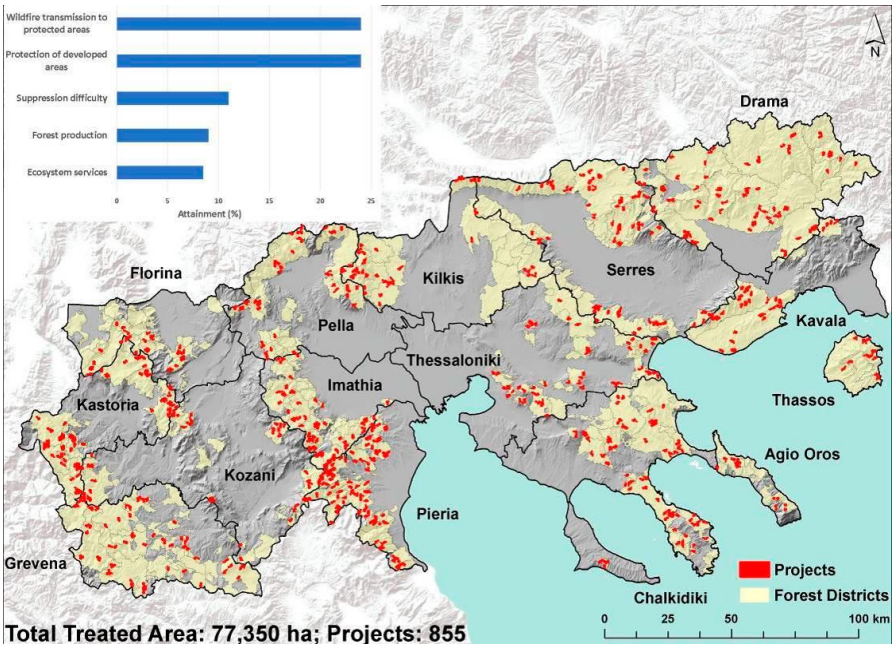

Figure 1: The best 100-ha projects in Macedonia, northern Greece, for each priority with a four-year fuel treatment plan. Attainment for each priority, if all stands that appear on the map are treated, is shown at the upper left corner (Palaiologou et al. 2021).

Post-management changes in forest structure and fuel loads can change the spread and intensity of wildfires and increase the resilience of forest ecosystems. Recent studies have examined the performance of appropriate spatial (composition and density) and temporal (seasonality, efficiency over time) strategies, as well as the effects of different institutional constraints (e.g. protected area management legislation, permitted land uses per property) in reducing the fire risk. In addition, the role and importance of forest management in the protection of settlements is highlighted, with emphasis on the strategic planning of projects and the consideration of the future fire occurrence and behavior (Palaiologou *et al.* 2018). Emphasis should be placed on a combination of thinning, mechanical treatments for managing or arranging the fuel and understory burning to reduce surface and canopy fuels (Omi 2015), while the appropriate planning of fire protection and other socio-economic values that are endangered will be needed, in combination with the fire size and fire regimes (Keane 2015).

4. Concluding remarks

Regions with Mediterranean-type of ecosystems have an ever-increasing appeal for establishment of new and/or expansion of existing human settlements in WUI, which in turn cause pressure on the natural environment (e.g. introduction of alien species, deforestation, human activities in formerly natural areas) that increase the fire risk. This complicated intermix of natural and human systems (Liu *et al.* 2007), aided by the catalyst role of wildfires,

leads to new risk governance systems and policies that aim to manage these ecosystems to reduce the loads, change the arrangement and alter the composition of forest fuels on the landscape. Communities can neither eliminate forest fuels (only manage them at a high economic cost on a limited extent), nor totally control the increasing frequency and intensity of wildfires that are influenced by the climate change (Kalabokidis *et al.* 2015), fire suppression policies, land abandonment and reforestation. Human adaptation requires a deep understanding of the role of forest fuels and their effective management, at scales that will prevent future wildfire loses and re-introduce the fire ecosystem resilience (Moritz *et al.* 2014).

5. References

EFFIS. 2020. European Forest Fire Information System, Joint Research Centre: Forest Fires in Europe, Middle East and North Africa. European Commission, Publications Office, Luxembourg. https://effis.jrc.ec.europa.eu/.

Kalabokidis K., Palaiologou P. 2019. Mediterranean forest fuels. *In:* Manzello S. (eds) Encyclopedia of Wildfires and Wildland-Urban Interface (WUI) Fires. Springer, Cham. https://doi.org/10.1007/978-3-319-51727-8_29-1. 13 p.

Kalabokidis K., Palaiologou P., Finney M. 2014. Fire behavior simulation in Mediterranean forests using the Minimum Travel Time algorithm. In Proceedings of 4th Fire Behavior and Fuels Conference, 18-22 Feb. 2013, Raleigh, NC, USA and 1-4 July 2013, St. Petersburg, Russia. Published by the International Association of Wildland Fire: Missoula, MT, USA. pp. 468-492.

Kalabokidis K., Palaiologou P., Gerasopoulos E., Giannakopoulos C., Kostopoulou E., Zerefos C. 2015. Effect of climate change projections on forest fire behavior and values-at-risk in southwestern Greece. *Forests* 6(6):2214-2240.

Keane R.E. 2015. Wildland fuel fundamentals and application. Springer International Publishing, Switzerland. doi:10.1007/978-3-319-09015-3.

Keeley J.E., Bond W.J., Bradstock R.A., Pausas J.G., Rundel P.W. 2012. Fire in Mediterranean ecosystems: ecology, evolution and management. Cambridge University Press, New York, USA.

Liu J., Dietz T., Carpenter S.R., Alberti M., Folke C., Moran E., Pell A.N., Deadman P., Kratz T., Lubchenco J., Ostrom E., Ouyang Z., Provencher W., Redman C.L., Schneider S.H., Taylor W. 2007. Complexity of coupled human and natural systems. *Science* 317 (5844):1513-1516. doi:10.1126/science.1144004.

Moreira F., Arianoutsou M., Corona P., De las Heras J. 2012. Post-fire management and restoration of southern European forests, vol 24. Springer Science & Business Media, Berlin, Germany.

Moritz M.A., Batllori E., Bradstock R.A., Gill A.M., Handmer J., Hessburg P., Leonard J., McCaffrey S., Odion D.C., Schoennagel T., Syphard A.D. 2014. Learning to coexist with wildfire. *Nature* 515 (7525):58-66. doi:10.1038/nature13946.

Omi P.N. 2015. Theory and practice of wildland fuels management. *Current Forestry Reports* 1 (2):100-117. doi:10.1007/s40725-015-0013-9.

Palaiologou P., Ager A.A., Nielsen-Pincus M., Evers C.R., Kalabokidis K. 2018. Using transboundary wildfire exposure assessments to improve fire management programs: a case study in Greece. *International Journal of Wildland Fire* 27(8):501-513.

Palaiologou P., Kalabokidis K., Ager A.A., Day M.A. 2020. Development of comprehensive fuel management strategies for reducing wildfire risk in Greece. *Forests* 11(8), 789.

Palaiologou P., Kalabokidis K., Ager A.A., Galatsidas S., Papalampros L., Day M.A. 2021. Spatial optimization and tradeoffs of alternative forest management scenarios in Macedonia, Greece. *Forests* 12(6), 697.

Two-dimensional model of heat transfer in a pine trunk under the influence of a forest fire environment

Eusébio Conceição*[1]; João Gomes[2]; Mª Manuela Lúcio[1]; Domingos Viegas[3]; Mª Teresa Viegas[3]

[1] FCT – Universidade do Algarve, Campus de Gambelas,
8005-139 Faro, Portugal, {econcei@ualg.pt, maria.manuela.lucio@gmail.com}
[2] CINTAL, Campus de Gambelas,
8005-139 Faro, Portugal, {jgomes@ualg.pt}
[3] FCT – Universidade de Coimbra - Pinhal de Marrocos - Pólo II,
3030 Coimbra, Portugal, {xavier.viegas, maria.viegas}@dem.uc.pt

**Corresponding author*

Keywords

Forest Fire, Numerical Simulation, Pine Trunk, Thermal Response, Wind Speed

Abstract

This article presents a numerical study on a two-dimensional model of heat transfers verified in a pine trunk under the effect of a forest fire. The thermal response model of the pine trunk was developed from a geometric model of complex topology of the trunk obtained using mesh generation. The thermal response model of the pine trunk is founded on energy energy balance integral and differential equations. Heat exchanges are considered by conduction inside the pine trunk, by convection between the outer surface of the pine trunk and the surrounding environment, and by radiation between the outer surface of the pine trunk and the and the surroundings, including the fire front. The radiative heat exchanges between the pine trunk and the fire front are calculated from the view factors obtained taking into account the meshing in the pine trunk and in the fire front. In this numerical study, it is considered that the fire front evolves with a spread rate with random and oscillatory characteristics, depending on wind speed, whose flame temperature has an average value of 500ºC. The evolution of the temperature distribution inside the pine trunk as well as in its outer surface was obtained for a variable and random wind speed. Temperature fluctuations on the outer surface of the trunk are affected by fluctuations in wind speed decreasing with time and with increasing distance from the fire front. Inside the trunk, temperature fluctuations occur mainly in the two outermost rings.

1. Introduction

The main influences on how fire spreads in forests are humidity, topography, wind and temperature (Tošić et al., 2019). The higher the temperature, the lower the humidity, and the lower the humidity, the drier the air, therefore dry fuel ignites and burns more easily. The slope of the landscape is also important: fires burn much faster uphill than downhill (Eftekharian et al., 2019). A fire creates radiation and convection phenomena that preheat the unburned fuel ahead of the fire front more effectively upslope than down. Fire spread is significantly affected by wind speed (Beer, 1991; Cruz and Alexander, 2019). Wind can bias fire behavior by moving moist air away from fuels, causing them to dry quickly. It transports burning embers that have been lifted aloft by convection air and starting spot fires ahead of the perimeter. It bends the convection column, which promotes preheating of unburned fuels in front of the fire. It brings a continuous supply of oxygen to the fire. Strong winds have a pressing dominant effect on the spread rate of wildfires when fuels are dry (Cruz et al., 2020). The environmental wind fluctuates in both direction and speed, with increased air instability implying greater fluctuations (Beer, 1991). Works on wildfire spread models (Nelson, 2002), simulations of spread and behavior of real fires (Jahdi et al., 2014), and fire spreads with variable wind strengths (Song and Li, 2017) present relevant aspects about the behavior of forest fires when under the effect of fluctuations in wind speed.

The numerical model used to simulate the pine trunk thermal response was founded on a numerical model used to simulate the human body thermal response (Conceição et al., 2010a; Conceição and Lúcio, 2016), because both models consider the use of energy equations in the boundary conditions in a similar way. These equations represent the following heat transfer processes: by conduction inside the pine trunk; by convection between the outer surface of the pine trunk and the surrounding environment; and by radiation between the outer surface of

the pine trunk and the surroundings (fire front included). In the assessment of the radiative exchanges between the outer surface of the pine trunk and the surroundings is utilized view factors. The sub-model used in the calculation of the view factors was established in the same way as the sub-models used in the calculation of the view factors in buildings (Conceição and Lúcio, 2010; Conceição et al., 2010b) and in passenger compartments (Conceição et al., 2000).

The purpose of this numerical study is to present a model that simulates the transient thermal response of a pine trunk under the influence of a forest fire, considering the variable wind speed. The forest fire is represented by a front fire with a variable spread rate. The transient thermal response will be assessed by the temperature distribution evolution inside and on the outer surface of the pine trunk.

2. Numerical Model

The differential energy equations and the generated mesh are utilized by the numerical model to evaluate the thermal response of the pine trunk, which consists of bark and cambium. This numerical model takes into account energy balance equations at the boundary between the pine trunk and the surrounds assuming the following thermal phenomena: heat conduction inside the pine trunk, heat convection (natural, forced and mixed) between the outer surface (bark) and the environment air and heat exchange by radiation between the outer surface (bark) and the surrounding body surfaces (fire front, fuel bed and sky).

These energy balance equations are established considering the following hypotheses:

- The heat flux is defined in two dimensions;
- The air temperature around the pine trunk, uniform and equal to the ambient temperature, will increase as the fire front approaches its vicinity;
- Use of heat transfer coefficients by convection developed for isothermal surfaces;
- The effects of fire around the pine trunk are neglected.

In the generation of the mesh of the pine trunk and fire front, the finite differences method is used. The numerical mesh generation considers a physical space and a computational space. The model transforms the physical domain into the computational plan, using two elliptic partial differential equations, of Poisson's type.

3. Methodology

The results of the numerical simulation will be the evolution of the temperature distribution inside and on the outer surface (bark) of the pine trunk obtained in a transient regime. In the numerical simulation carried out, it was considered that the wind speed is variable according to the profile represented in Figure 1, with an average value of 5.04 m/s.

The fire front progresses with a variable fire spread rate, according to the profile shown in Figure 2, with an average value of 0.0116 m/s, from a distance of 10 m upstream of the pine trunk. The pine trunk has a height of 2.0 m and an external diameter of 0.4 m. The fire front has a tilt angle of 70º relative to the ground plane, 2 m wide, 4 m high and an average flame temperature of 500ºC. The representation of fire propagation towards the pine trunk is shown in Figure 3. As environmental conditions, there is an air temperature of 20ºC and a relative humidity of 50% near the trunk. The temperature distribution was obtained at 33 points (P) equidistant distributed along the outer surface (bark) of the pine trunk in a plane located at a height of 2.0 m and at 20 points (Q) distributed along the radius of the pine trunk, as shown in Figure 4.

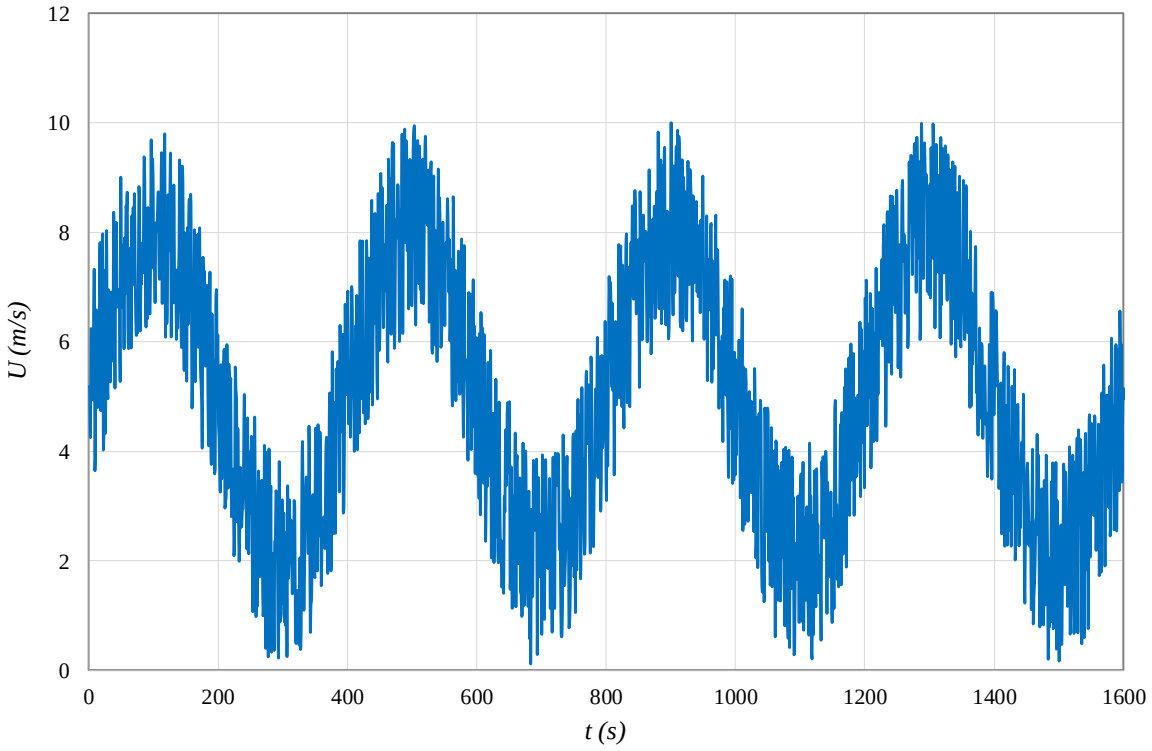

Figure 1 – Profile of wind speed.

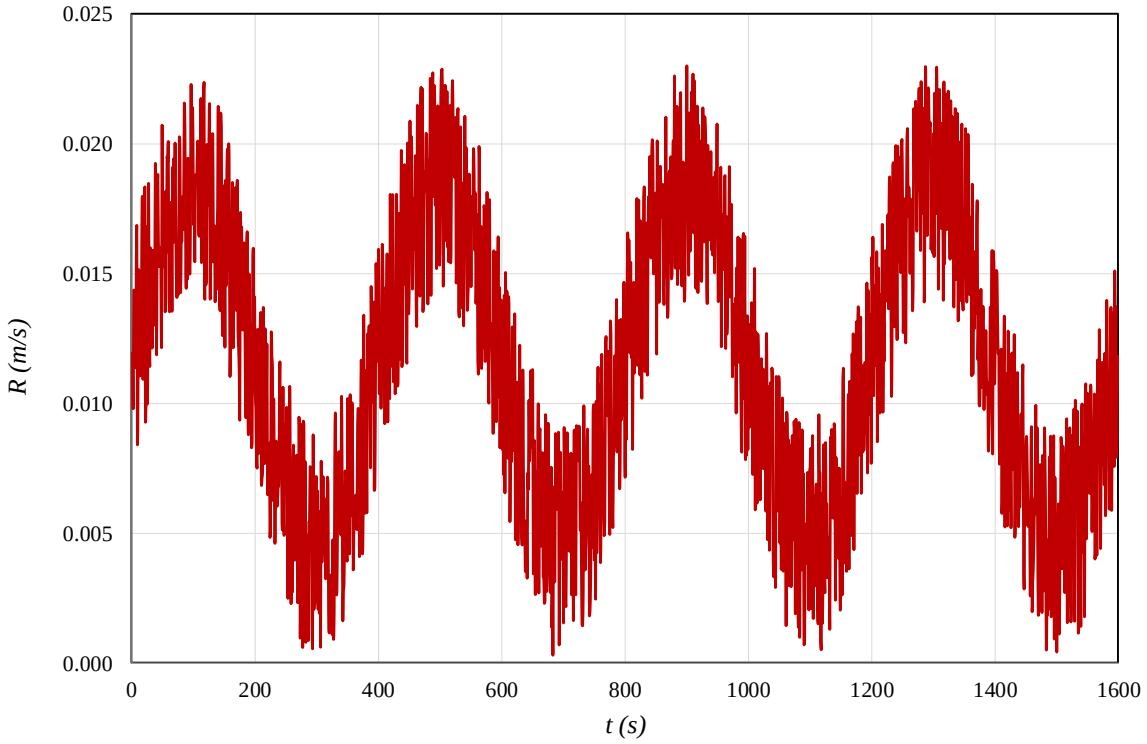

Figure 2 – Profile of fire spread rate.

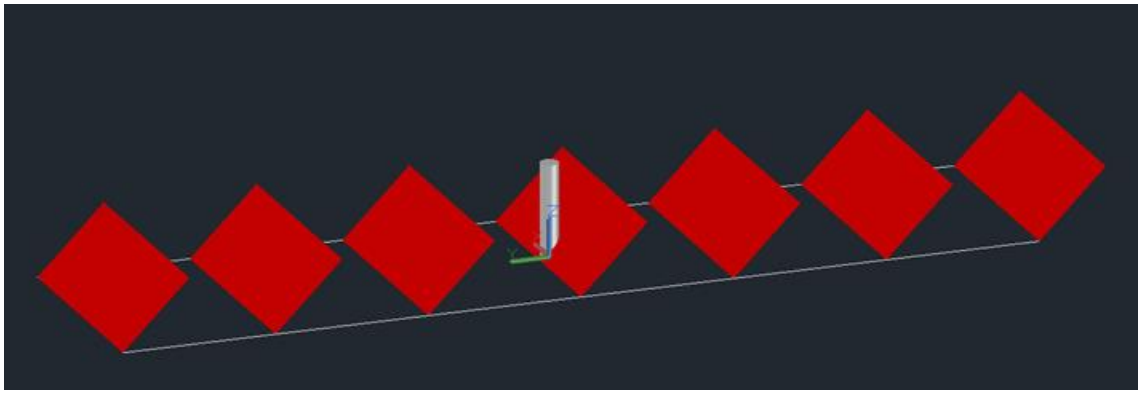

Figure 3 – Representation of the movement of the fire front towards the pine trunk.

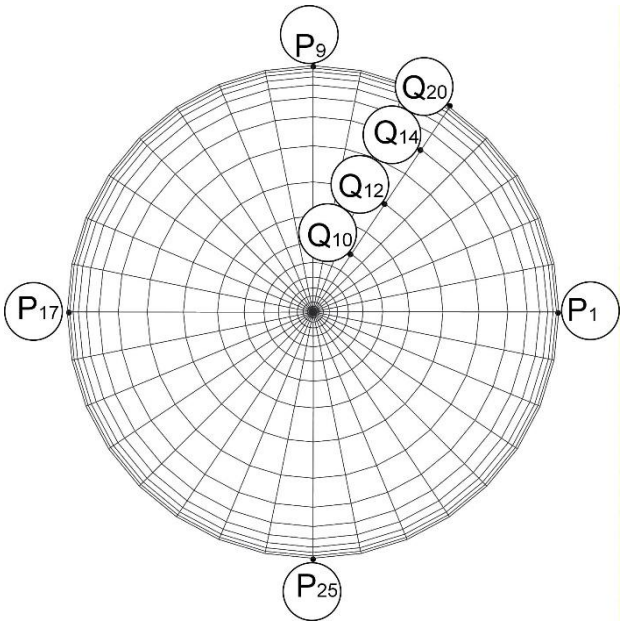

Figure 4 – Cross-section of the pine trunk with the location of the 33 P-points on its outer surface (bark) and the 20 Q-points on its interior.

4. Results and Discussion

The evolution of the temperature distribution on the outer surface (bark, points P1 to P33) of the pine trunk is shown in Figure 5. The results show that during the movement of the fire front, the upstream side of the pine trunk is the first to be affected by the increase in temperature on its outer surface. Fluctuations in wind speed and, consequently, in the fire spread rate, cause fluctuations in the temperature obtained at the marked points on the outer surface of the trunk. The maximum values of temperature fluctuations, as well as the amplitudes of these fluctuations, decrease with time and with the distance of the fire from the pine trunk. Temperatures are higher on the upstream side of the tree trunk than on the downstream side due to the slope of the flame caused by the spread of fire.

The evolution of the temperature distribution in the points Q1-Q20 located on the interior of the pine trunk, containing the point P1 on the side, on the upstream side, the point P9 on the upstream side and the point P25 on the downstream side (see Figure 4), is shown, respectively, in Figure 6, Figure 7 and Figure 8.

As can be seen from the temperature variation in relation to the ambient temperature of 20ºC, fire influences the four outermost rings, mainly the two rings represented by points Q18 and Q19. In these two rings, fluctuations in wind speed and fire spread rate have a noticeable impact on the fluctuations obtained in the evolution of temperature. Therefore, it can be seen that the passage of a forest fire with the characteristics presented here can cause the interior areas of the trunk to heat up to values around 60ºC on its upstream side.

Temperatures of 60ºC can cause the death of tree tissues (Kelsey and Westlind, 2017). Inside the trunk, temperatures are generally higher at points located on the upstream side of the trunk than on the downstream side. Again, this is due to the way the flame leans in the downstream direction of the fire's movement.

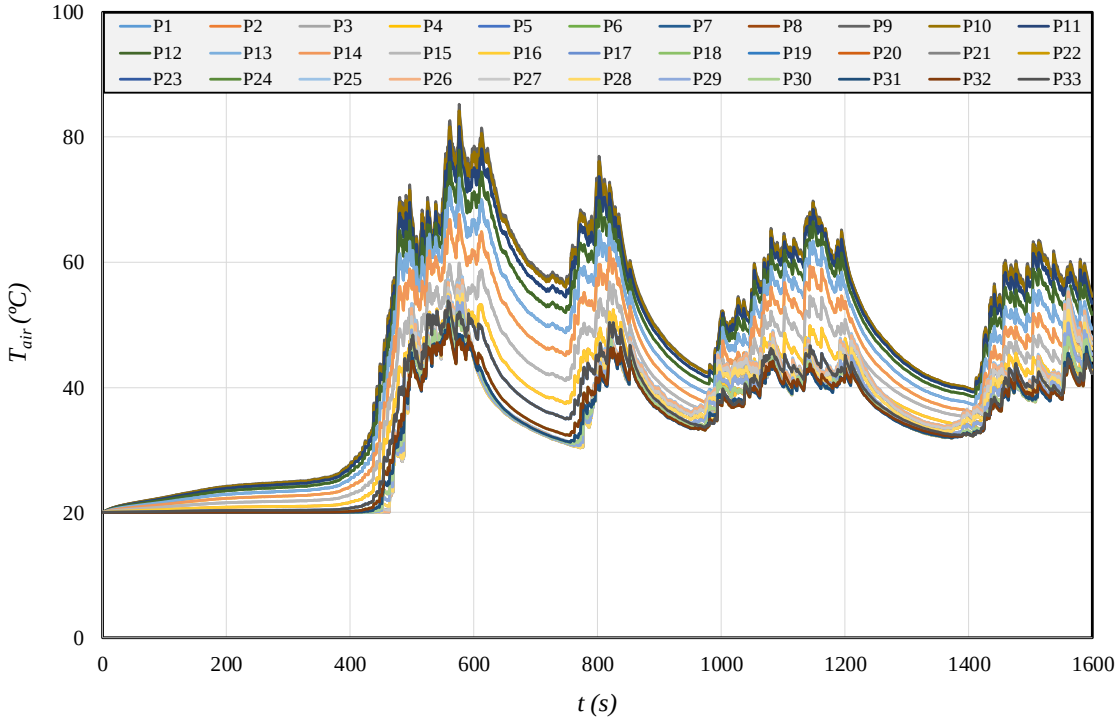

Figure 5 – Evolution of the temperature distribution on the outer surface (points P1 to P33) of the trunk according to the environmental conditions in which the fire propagates.

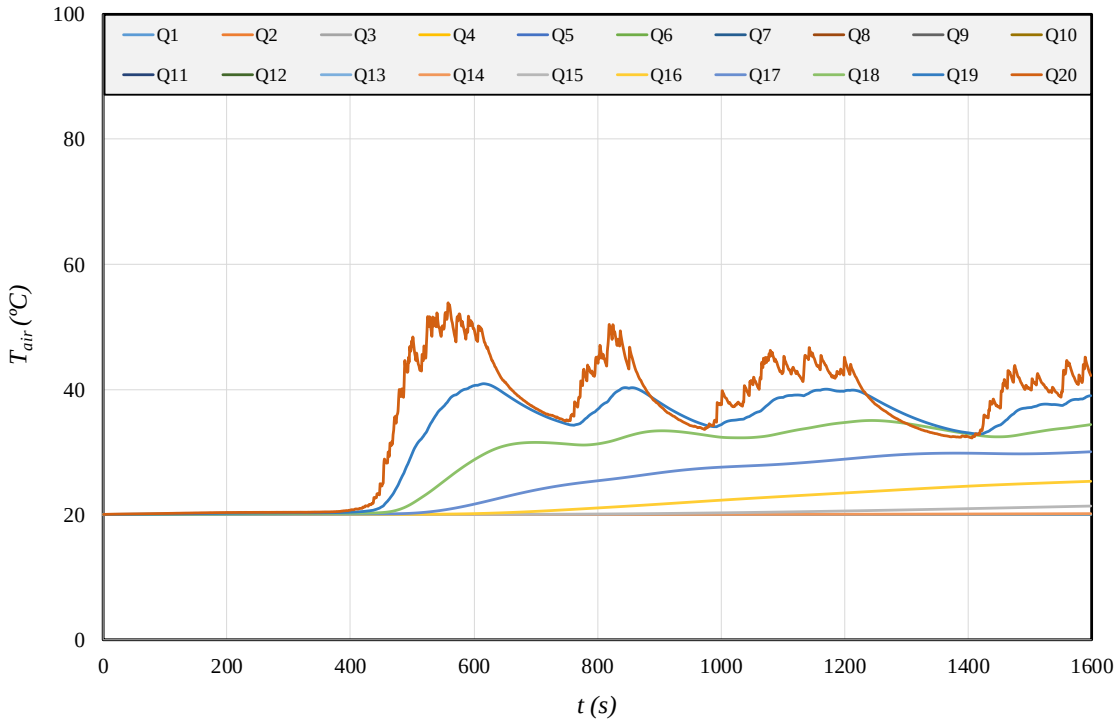

Figure 6 – Evolution of the temperature distribution in the points Q1-Q20 located inside the pine trunk containing the point P1 (coincident with point Q20) on the outer surface.

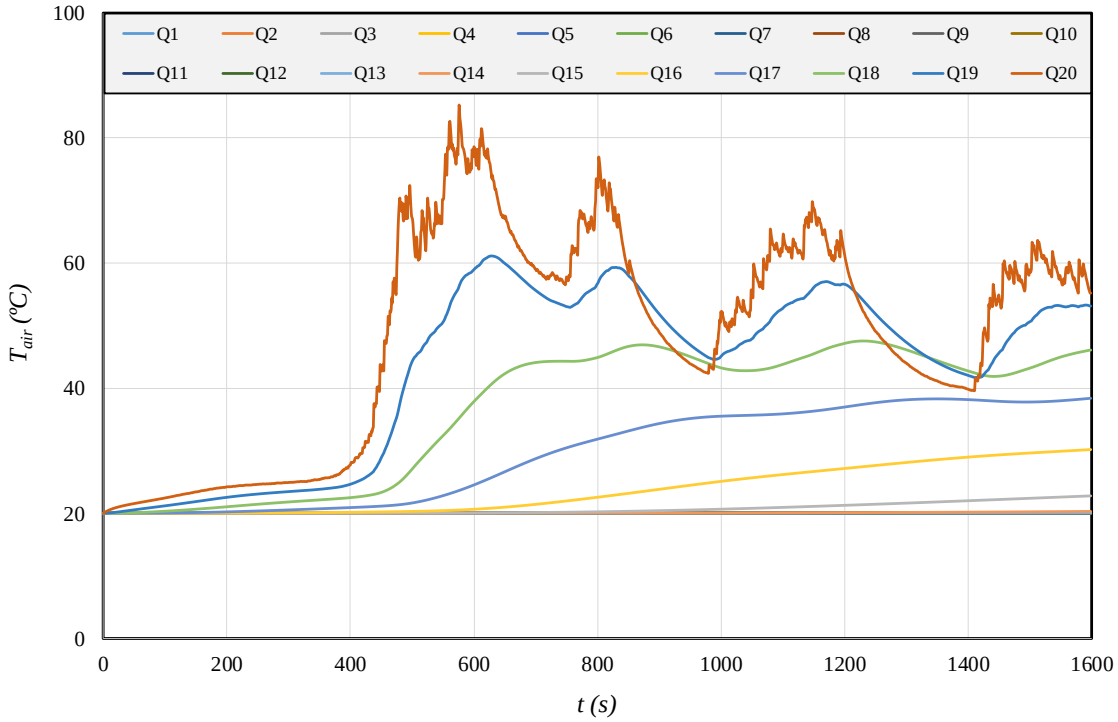

Figure 7 – Evolution of the temperature distribution in the points Q1-Q20 located inside the pine trunk containing the point P9 (coincident with point Q20) on the outer surface.

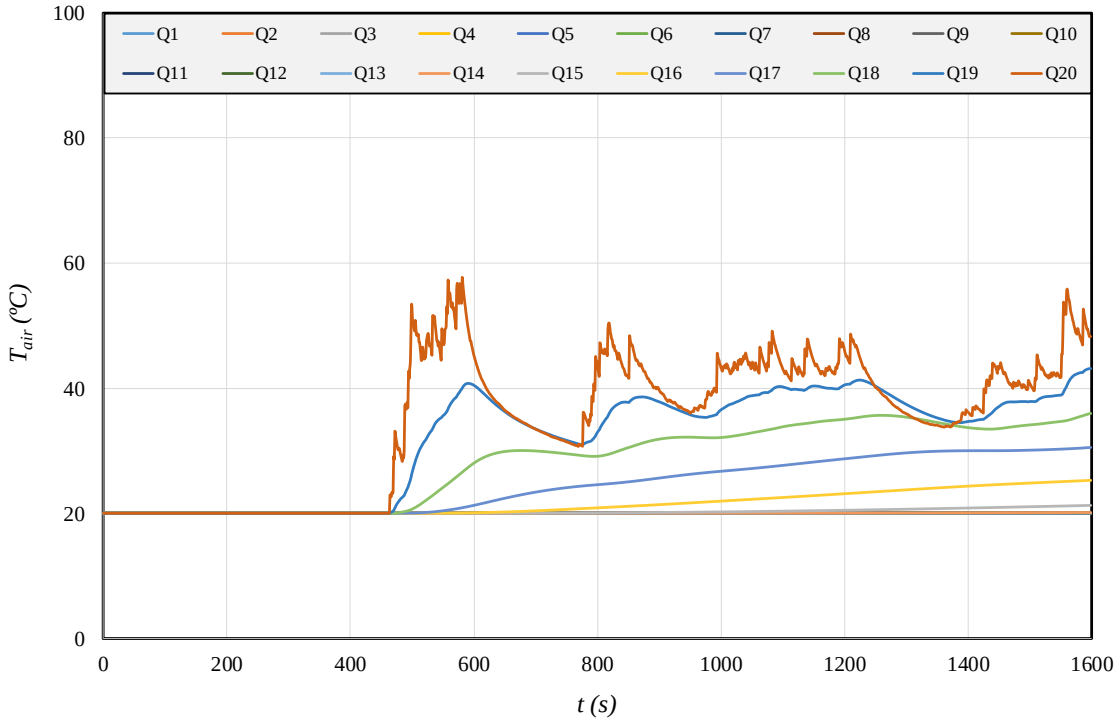

Figure 8 – Evolution of the temperature distribution in the points Q1-Q20 located inside the pine trunk containing the point P25 (coincident with point Q20) on the outer surface.

5. Conclusions

The thermal response of a pine trunk under the influence of a forest fire was numerically evaluated in this article. Forest fire is represented by a moving fire front. The temperature distributions inside and on the outer surface

of the pine trunk were obtained in a transitory regime. The numerical study was carried out assuming that the wind speed and the fire spread rate have a random evolution.

The results show that fluctuations in wind speed and fire spread rate also cause fluctuations in temperature calculated at points on the outer surface and in the four outermost rings of the pine trunk. At points on the outer surface, the maximum temperature values and the amplitudes of temperature variations decrease with time and with increasing distance from the fire to the pine trunk. Inside the trunk, on the upstream side, there are points on its outermost ring that reach 60ºC, which can cause tissue death there. Points on the upstream side of the pine trunk have higher temperatures than those on its downstream side due to the inclination of the flame in the direction of fire movement downstream of the pine trunk.

6. Acknowledgments

The authors would like to acknowledge the support of the project reference PCIF/MPG/0108/2017, funded by the Portuguese Foundation of Science and Technology (FCT).

7. References

Beer, T.: The interaction of wind and fire. Boundary-Layer Meteorology 54, 287-308 (1991).

Conceição, E., Silva, M., André, J., Viegas, D.: Thermal behaviour simulation of the passenger compartment of vehicles. International Journal of Vehicle Design 24(4), 372-387 (2000).

Conceição, E., Rosa, S., Custódio, A., Andrade, R., Meira, M., Lúcio, M.: Study of airflow around occupants seated in desks equipped with upper and lower air terminal devices for slightly warm environments. HVAC&R Research 16(4), 401-412 (2010a).

Conceição, E., Nunes, A., Gomes, J., Lúcio, M.: Application of a school building thermal response numerical model in the evolution of the adaptive thermal comfort level in the Mediterranean environment. International Journal of Ventilation 9(3), 287-304 (2010b).

Conceição, E., Lúcio, M.: Numerical study of the influence of opaque external trees with pyramidal shape in the thermal behaviour of a school building in summer conditions. Indoor and Built Environment 19, 657-667 (2010).

Conceição, E., Lúcio, M.: Numerical simulation of the application of solar radiant systems, internal airflow and occupants' presence in the improvement of comfort in winter conditions. Buildings 6(3), 38 (2016).

Cruz, M., Alexander, M.: The 10% wind speed rule of thumb for estimating a wildfire's forward rate of spread in forests and shrublands. Annals of Forest Science 76, 44 (2019).

Cruz, M., Alexander, M., Fernandes, P., Kilinc, M., Sil, A.: Evaluating the 10% wind speed rule of thumb for estimating a wildfire's forward rate of spread against an extensive independent set of observations. Environmental Modelling and Software 13, 104818 (2020).

Eftekharian, E. Ghodrat, M., He, Y., Ong, R., Kwok, K., Zhao, M., Samali, B.: Investigation of terrain slope effects on wind enhancement by a line source fire. Case Studies in Thermal Engineering 14, 100467 (2019).

Jahdi, R., Darvishsefat, A., Etemad, V., Mostafavi, M.: Wind effect on wildfire and simulation of its spread (Case study: Siahkal Forest in Northern Iran). Journal of Agricultural Science and Technology 16, 1109-1121 (2014).

Kelsey, R., Westlind, D.: Physiological stress and ethanol accumulation in tree stems and woody tissues at sublethal temperatures from fire. Bioscience 67, 443–451 (2017).

Nelson, R.: An effective wind speed for models of fire spread. International Journal of Wildland Fire 11, 153-161 (2002).

Song, H., Lee, S.: Effects of wind and tree density on forest fire patterns in a mixed-tree species forest. Forest Science and Technology 13(1), 9-16 (2017).

Tošić, I., Mladjan, D., Gavrilov, M., Živanović, S., Radaković, M., Putniković, S., Petrović, P., Mistridželović, I., Marković, S.: Potential influence of meteorological variables on forest fire risk in Serbia during the period 2000-2017. Open Geosciences 11, 414-425 (2019).

Uncovering the science-policy interface: applying bibliographic approaches to the wildfire risk management domain

Schlierkamp Juliane*; Berchtold Claudia; Neisser Florian; Linde-Frech Isabelle

[1]Fraunhofer INT. Appelsgarten 2, 53879 Euskirchen,
{juliane.schlierkamp, claudia.berchtold, florian.neisser, isabelle.linde-frech}@int.fraunhofer.de

**Corresponding author*

Keywords

Science-Policy Interfaces, Bibliometrie, Wildfire Risk Management, Altmetrics

Abstract

The impact of research is increasingly gaining importance as science is understood as a means to solve the challenges of humanity. Therefore, processes of interaction between science and policy makers are needed, these processes are named Science-Policy Interface (SPI). But who is actually participating in SPIs? This question is relevant since scientific findings can be subject to interpretation, might contradict each other or can be driven by normative frameworks. Additionally, complex challenges require the involvement of all relevant disciplines and if certain disciplines are not heard, policies might as well only address parts of the problem. To unpack respective processes, this paper explores the opportunities of bibliometrics to trace and track science-policy interactions applying it to the field of wildfire risk management (WFRM).

An analysis of bibliometric data provided by Dimensions (https://app.dimensions.ai) was carried out. Therefore, the development of the numbers of publications and policy documents over time as well as the numbers of publications and policy documents in different fields of research (FoR) are considered. Furthermore, the Altmetrics of publications which are cited in policy documents are compared to the total of publications with reference to WFRM.

It can be stated that the number of publications with reference to WFRM follows the general trend of an increasing publication rate. Individual deviations from the general trend can be attributed to extraordinary wildfire events. The number of policy documents with reference to WFRM seems to correlate more strongly with the number of scientific publications with reference to WFRM than to the general trend in the number of policy documents. In addition, indicators for delay of 6 to 7 years in knowledge uptake from science to policy were found. Regarding the FoRs, three clusters of were identified. While two of these clusters indicate a positive correlation between the number of publications in a FoR and the number of citations, one cluster of FoR has low numbers of citations in policy documents while the number of publications is high. That leads to the conclusion, that there are bias respective unknown impacting factors which affect whether or not a policy maker considers a particular FoR. One impacting factor seems to be the attention a publication receives in scientific but also non-scientific communities. The Altmetric Scores of publications with citations in policy documents are double as high as the Altmetric Scores of the total of publications with reference to WFRM. By analysing the composition of the Altmetric Scores of cited publications respective the Altmetric Donuts, it could be found that the vast majority of publications that are cited in policy documents did receive attention in social media, especially twitter.

Another result of the analysis is, that the data quality concerning the links between policy documents and publications is insufficient. However, the bias found in the SPI demonstrate the usefulness of this bibliometric approach. With increasing reliability of bibliometric databases, the methodology presented in this paper can be applied broadly as a tool to analyse SPIs and help to create transparency on the integration of scientific findings into policy processes.

1. Introduction: The Science-Policy Interface in WFRM

The impact of research is increasingly gaining importance as science is understood as a means to solve the challenges of humanity. Therefore, processes of interaction between science and policy makers are needed, these processes are named Science-Policy Interfaces (SPI). But who is actually participating in such SPIs? This question is relevant since scientific findings are often subject to interpretation, might contradict each other or can be based on normative frameworks. Additionally, complex challenges require the involvement and consideration of all relevant and related disciplines and if certain disciplines are not heard, policies only address parts of the problem.

However, SPI processes sometimes seem to be black-boxes that are hard to reconstruct or understand from an outside perspective. It is not necessarily clear who contributed to certain papers or who was involved in committees and fora. To unpack respective processes, the review of policy papers and their scientific input, this paper explores the opportunities of bibliometrics to trace and track science-policy interactions applying it to the field of wildfire risk management.

1.1. Research Questions

In many cases, it is not always comprehensible why scientific findings are considered in policies or why they have not been considered. This raises the question of potential biases that influence the transfer of knowledge. *In order to divide and specify this overarching question, the following subsequent research questions (RQs) have been devised:*

1. *Is there a time lag between the publication of scientific publications and the publication of the policy document? (RQ1)*
2. *Do more publications in a field of research lead to more citations in policy documents? (RQ2)*
3. *Are publications that are frequently mentioned online cited more often in policy documents? (RQ3)*
    a. Are there similarities or differences between the Altmetric Scores of the publications cited in policy documents and those of the publications as a whole?
    b. How are the Altmetric Scores of the publications cited in policy documents composed?

2. Methodology: bibliometric analysis

In this chapter Altmetrics are introduced, the development of the hypothesis and the used statistical tools are described.

2.1. Hypotheses and statistical tools

In order to answer the research questions by the use of statistical tool, hypothesis derived from the research questions are necessary.

To answer the RQ1 the hypothesis

"There is no time lag between the publication of scientific publications and the publication of the policy document."

is examined by comparing the timelines of publications with reference to WFRM and the timeline of all scientific publications. In addition to this descriptive approach, the hypothesis is also examined with multiple regression of the publication numbers.

The RQ2 is examined by testing the hypothesis

"The number of publications per field of research does not corelate with the number of citations in policy documents"

Therefore, histograms and scatter plots of the numbers of publications within the fields of research (FoR) are analysed and rank correlation test according to Spearman is applied (Handl und Kuhlenkasper 2018, pp. 169-173)

The hypothesis to answer the RQ3 is:

"The number of online citations does not correlate to the number of citations in policy documents."

This hypothesis is examined by analysing the key figures of the Altmetric Scores of the publications cited in policy documents compared to the total number of publications with reference to WFRM.

2.2. Altmetrics

Altmetrics were developed in response to the expansion of opportunities to publish and disseminate scientific results. They offer an insight into how often publications are used or discussed by others already after a short amount of time and are applicable on big numbers of publications. Furthermore, by including attention outside

of the scientific community can decrease the influence of bias which exist within the scientific community and affect scientific processes. (Priem et al. 2010; Howard 2012; Galligan und Dyas-Correia 2013, p. 56).

2.3. Data Collection

The Dimensions database is used to collect the bibliometric data. The database is characterised by the fact that different types of data are made available and shows linkages between different publications. (Dimensions n. a; Hook et al. 2018; Singh et al. 2021, p. 5).

3. Findings of the bibliometric analysis

The following chapter presents the results of the analysis of the bibliometric data of publications and policy documents with reference to WFRM. In addition, first findings with regard to data quality are presented.

3.1. Publications over time

The number of publications with refence to WFRM as well as the total of scientific publications has increased significantly over the 50 years (Figure 1, bottom graph). This trend, however, is not exclusive to WFRM publications, but number of publications in general (Figure 1, top graph).

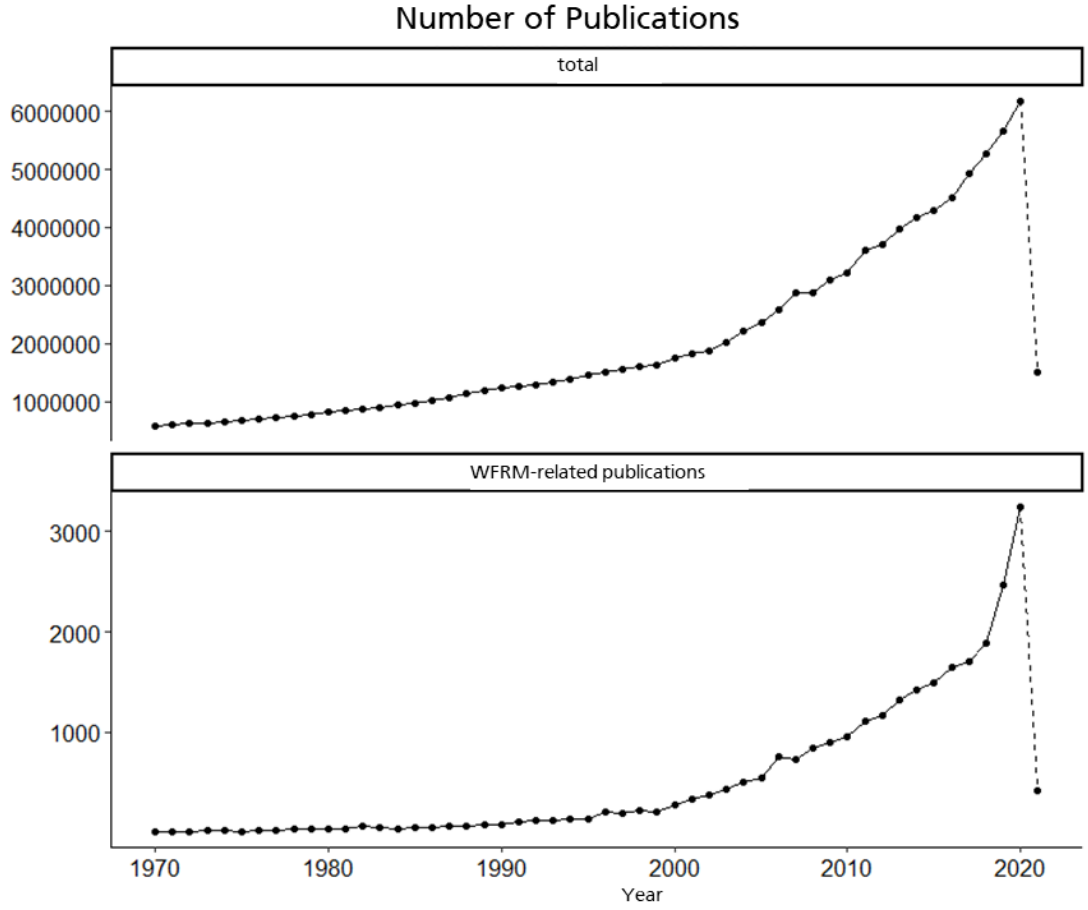

Figure 1 – Annual numbers of publication, total and with reference to WFRM

The numbers of publications with reference to wildfire follows the trend of exponentially increasing numbers of publications (Parthey und Biedermann 2002, p. 113) Exceptional effects can be attributed to outstanding wildfire events, e.g. wildfires as a consequence of a heatwave in Europe in 2003 can be associated with the exceptionally high number of publications in 2006 Spain (Lyamani et al. 2006, pp. 6456-6460). The average delay between these events and effects in the publication numbers is three years.

During the time period in question from 1970 to 2021, 476.548 policy documents were published. Out of those, 69 make reference to WFRM. Regarding the annual numbers of policy documents, a strong growth from 2010

to 2015 can be identified. From 2015 on, the numbers of policy documents declined (Figure 2). The numbers of publications with reference to WFRM fluctuate strongly during this time, still displaying a tendency of growing numbers of policy documents with reference to WFRM. That leads to the assumption that the number of policy documents with reference to WFRM possesses a stronger correlation to the number of publications with reference to WFRM than to the number of policy documents in general.

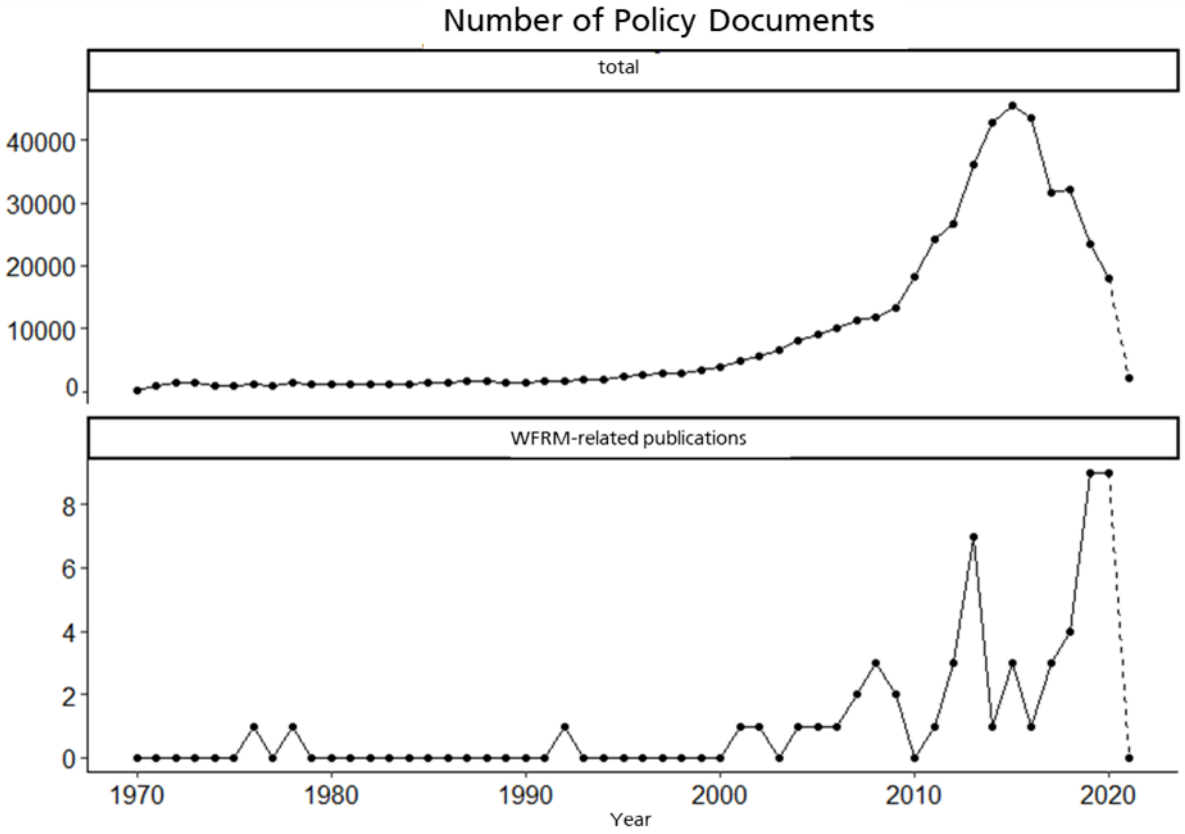

Figure 2- Annual numbers of policy documents, total and with reference to WFRM

To examine this assumption multiple regression analysis is carried out. The regression model considers the number of annual publications with reference to WFRM for the past 14 years as an impact number for the annual number of policy documents. Thus, a regression model was developed which contains the numbers of publication for the past 14 years as variables, 14 coefficients and one constant:

$$n_{PD}(t) = b_{t-1} * n_{pub}(t-1) + b_{t-2} * n_{pub}(t-2) + b_{t-3} * n_{pub}(t-3) + b_{t-4} * n_{pub}(t-4) + b_{t-5} * n_{pub}(t-5) + b_{t-6} * n_{pub}(t-6) + b_{t-7} * n_{pub}(t-7) + b_{t-8} * n_{pub}(t-8) + b_{t-9} * n_{pub}(t-9) + b_{t-10} * n_{pub}(t-10) + b_{t-11} * n_{pub}(t-11) + b_{t-12} * n_{pub}(t-12) + b_{t-13} * n_{pub}(t-13) + b_{t-14} * n_{pub}(t-14) + \epsilon$$

The result of the regression analysis is significant with values of $p=2{,}919*10^{-10}$ and $R^2=0{,}77$.

Table 1 – results of the multiple regression analysis

Ranking	*Coefficient*	*Value*	*Ranking*	*Coefficient*	*Value*
1.	b_{t-7}	0.0285282	8.	b_{t-12}	-0.0014705
2.	b_{t-13}	0.0197481	9.	b_{t-5}	-0.0036211
3.	b_{t-6}	0.0178220	10.	b_{t-1}	-0.0039888
4.	b_{t-14}	0.0068295	11.	b_{t-2}	-0.0057053
5.	b_{t-3}	0.0037625	12.	b_{t-10}	-0.0127954
6.	b_{t-11}	0.0026201	13.	b_{t-9}	-0.0142249
7.	b_{t-4}	0.0005291	14.	b_{t-8}	-0.0250294

Half of the coefficients is positive; the others are negative. While there is no factual explanation for the negative values of the coefficients, positive values might be an indicator for a certain delay of time. The coefficients b_{t-7}, b_{t-13} and b_{t-6} have the highest values, b_{t-10}, b_{t-9} and b_{t-8} have the lowest values (Table 1).

In the analysis of the publications over time it can be shown, that wildfire incidents lead to more publications with a delay of 3 years. Furthermore, a delay of 6 to 7 years from science to policies is indicated by the results of the multiple regression analysis.

3.2. Fields of Research

The scatter plot in Figure 3 shows a correlation between all publications with reference to WFRM and those which are cited in policy documents. Each dot represents a FoR. For the cited publications all values are increased by one (TC+1). Three cluster can be identified in the scatter plot.

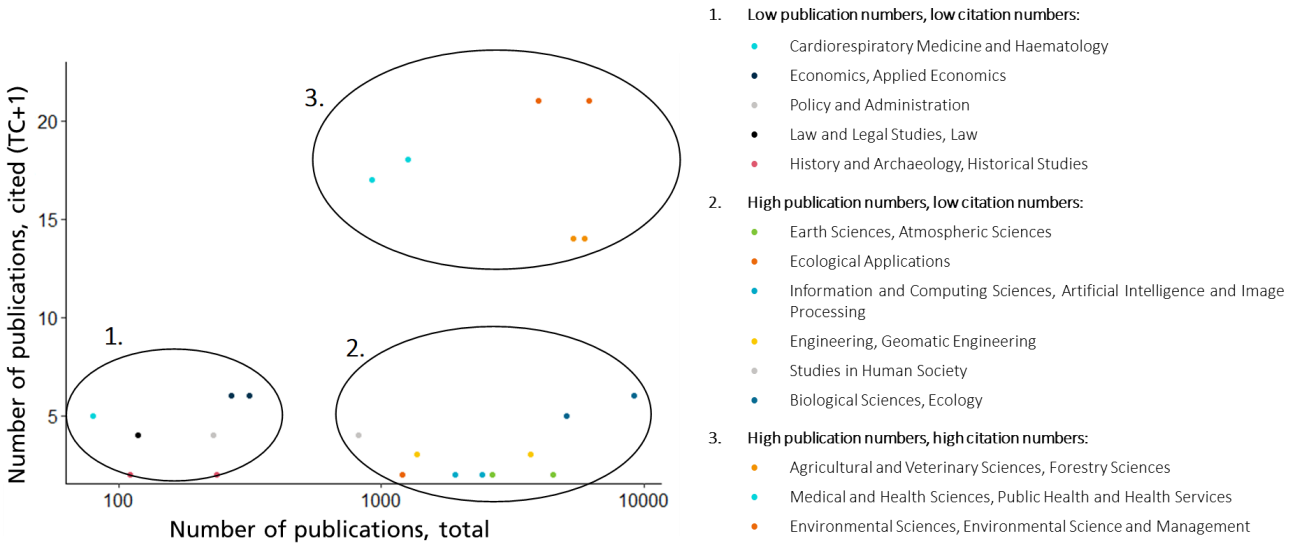

Figure 3-Number of publications per FoR, total and cited in policy documents

The rank correlation test by Spearman shows that the number of publications in the superordinate FoR corelates significantly (p=0,0022) with the number of publications cited in policy documents. With correlation coefficient ϱ= 0,62, which is a strong effect according to Cohen (1988). For the super- and subordinate FoR cumulated the correlation is also significant ($p=6{,}784*10^{-13}$) and with a strong effect (ϱ=0,52).

These results correspond with first and the third cluster which indicate that the numbers of publications in a FoR correlate to the number of citations in policy documents. The second cluster, where the number of publications is high and the number of citations is low contradicts this correlation which leads to the conclusion, that there are further impacting factors involved.

3.3. Altmetrics of the publications

For those publications which are cited in policy documents with reference to WFRM the Altmetric Scores and Donuts are analysed.

The arithmetic mean of Altmetric Scores of the cited publications is 50 and double the Altmetric Score of all publications, which is 25. The median is also double with a value of 6 for the cited publications and 3 for all publications. With a standard deviation of 124 the distribution of the Altmetric Scores of all publications is more homogeneous than the distribution of the Altmetric Scores of the cited publications with 213.

Table 2 – Comparison, key figures of the Altmetric Scores

Value	*Total of publication with reference to WFRM*	*Cited publication with reference to WFRM*
Arithmetic mean	25	50
Median	3	6
Standard deviation	124	213
Range	5289 (x_{min}=1; x_{max}=5290)	3089 (x_{min}= 3; x_{max}= 3092)

As the Altmetric Score is only an indicator for the amount of attention a publication receives, the Altmetric Donuts are analysed to get an insight of the platforms on which the publications are mentioned. All cited publications with a minimum score of 8 for the Altmetric Score are considered. These are 84 publications of which:

- 78 are cited on Twitter
- 41 are cited in Blogs
- 42 are cited on Facebook
- 15 are cited on Google+
- 5 are cited on Reddit
- 3 are cited on YouTube
- 1 is cited in the Stack Overflow Q&A

The Altmetric Scores of the cited publications have a higher arithmetic mean than the total of publications with reference to WFRM. Furthermore, it can be shown, that publications which were cited in policy documents were also often cited on Social Media as well.

3.4. Limitations of the results

The findings of this study of bibliometric data are limited by several factors. The results are only valid for the sector of WFRM. As the number of policy documents is generally low and most policy documents were published after the year 2000, which is a short observation timeframe when considering the observation that knowledge transfer from science to policies takes 6 to 7 years, this delay needs to be confirmed by further research.

Another limitation is given by the quality of data. To evaluate the quality of the data provided by Dimensions an exemplary manual analysis of citations in a policy document was carried out. The policy document "Advances in remote sensing and GIS applications in forest fire management - EU Law and Publications" includes 203 citations according to Dimensions. In a manual analysis, 445 citations were found. One reason for these 242 citations which are not regarded in Dimensions is that not all kinds of publications are considered by Dimensions, but 112 of the 242 missing citations are articles which should be included in Dimensions. Of these 112 articles only 18 are not listed in Dimensions. One reason might be inconsistencies in the references in the policy paper. At least in the exemplary policy paper, different styles of citation were used and several citations were incomplete. On the other hand it might be the case, that the AI which identifies the citations in Dimensions is not sufficientlytrained in analysing policy documents, because these are not the main focus of Dimensions. Another problem which was identified in the evaluation of the data is that Dimensions does not include all crucial policy documents, e.g. the policy document "Forest Fires: Sparking firesmart policies in the EU" which is a key publication of the EU is not listed in Dimensions.

4. Conclusion

The use of bibliometric data and analyses has great potential to understand and reconstruct SPIs on a larger scale. As a direct effect, this would allow to compare and complement the consideration of certain disciplines in policy processes. Particularly for complex settings such as WFRM, this could lead to an enhancement of a holistic perspective by integrating (potentially so far disregarded yet important inputs. From an indirect perspective, it would contribute to enhancing transparency and thus democratic principles. Specifically, in times of "fake news" and science scepticism, the suggested approach could provide important contributions to not only reconstructing science-policy relations but to enhance the overall credibility in science and policy making through transparency.

Nevertheless, the generated insights for the WFRM domain have to be assessed against the fact that the list of policy papers is incomplete, as do the listed citations. Assuming however that these systematic errors affect all fields of research evenly, we can for example assume that policy makers do not regard all FoR evenly. There are fields like Earth Sciences, Engineering or Ecology that publish articles with reference to WFRM and are not properly regarded by policy makers. This clustering can be used by policy makers to identify blind spots. At the same time, it might be the case, that scientists in these fields do not communicate and spread their findings as

efficient as scientists in other fields. For further research, it might be useful to analyse the communication and dissemination in Cluster 1 of the FoRs (Figure 3) to identify best practises.

Finally, this paper results in additional research questions and aspects that require for further analysis. First of all, the mentioned data base shortfalls have not yet been understood in their entirety and they seem to be related to systematic errors, most likely caused by artificial intelligence and the applied machine learning approaches. More detailed insights can only be provided by the operators and experts. Since the access to the policy paper database is a service that needs to be paid, it can be assumed that this challenge will be addressed in the near future.

In a second stage, the use of national (or even local) level language policy papers should be considered since the presented approach seems also useful for analysing SPIs at the national level. However, respective papers are currently not covered by any database and can hence not be subject to analysis.

5. References

Cohen, Jacob Willem (1988): Statistical power analysis for the behavioral sciences. 2. ed. Hillsdale, NJ: Erlbaum.

Dimensions (n. a.): Why did we build Dimensions? Online: https://www.dimensions.ai/why-dimensions/

Handl, Andreas; Kuhlenkasper, Torben (2018): Einführung in die Statistik. Theorie und Praxis mit R. Berlin, Germany: Springer Spektrum.

Hook, Daniel W.; Porter, Simon J.; Herzog, Christian (2018): Dimensions: Building Context for Search and Evaluation. In: Front. Res. Metr. Anal. 3. DOI: 10.3389/frma.2018.00023.

Lyamani, H.; Olmo, F. J.; Alcántara, A.; Alados-Arboledas, L. (2006): Atmospheric aerosols during the 2003 heat wave in southeastern Spain I: Spectral optical depth. In: Atmospheric Environment 40 (33), S. 6453–6464. DOI: 10.1016/j.atmosenv.2006.04.048.

Parthey, Heinrich; Biedermann, Wolfgang (Hg.) (2002): Wissenschaft und Innovation. Gesellschaft für Wissenschaftsforschung. 1. Ed. Berlin: GEWIF (Wissenschaftsforschung, 2001).

Singh, Vivek Kumar; Singh, Prashasti; Karmakar, Mousumi; Leta, Jacqueline; Mayr, Philipp (2021): The journal coverage of Web of Science, Scopus and Dimensions: A comparative analysis. In: Scientometrics. DOI: 10.1007/s11192-021-03948-5.

Turco, Marco; Jerez, Sonia; Augusto, Sofia; Tarín-Carrasco, Patricia; Ratola, Nuno; Jiménez-Guerrero, Pedro; Trigo, Ricardo M. (2019): Climate drivers of the 2017 devastating fires in Portugal. In: Scientific Reports 9 (1), S. 13886. DOI: 10.1038/s41598-019-50281-2.

Understanding Fire Response to Spatial Variations in Vegetation Distribution and Wind

Daniel Jimenez*[1]; Natalie Wagenbrenner[1]; Cyle Wold[1]; Paul Sopko[1]; Daniel Gorham[2]; Joe O'Brien[3]; Robert Spencer[4]; Matthew Nolasco[4]

[1]Fire Science Laboratory, Rocky Mountain Research Station, USDA Forest Service, Missoula Montana, USA, {dan.jimenez@usda.gov}
[2] Insurance Institute for Business & Home Safety, Rock Hill, South Carolina, USA, {dgorham@ibhs.org}
[3] Centre for Forest Disturbance Science, Southern Research Station, USDA Forest Service, Athens, Georgia, USA, {joseph.j.obrien@usda.gov}
[4]Tall Timbers Research Station & Land Conservancy, Tallahassee, Florida, USA, {mnolasco@talltimbers.org}

**Corresponding author*

Keywords

Radiant Heat Flux, Convective Heat Flux, Fuel Break Effectiveness, Windspeed, Fuel Moisture

Abstract

Fire spread can be characterized as a continuous sequence of ignitions. Ignition is a local phenomenon, governed by complex interactions between temporal and spatial variations in fuel and environment. Seemingly insignificant changes in vegetation orientation or spacing can significantly affect the ignition process and result in fire either bridging a gap in fuels or extinguishing at the gap boundary. This study seeks to improve understanding of ignition by exploring the physics underlying fire's response to gaps in vegetation under the influence of wind, fuel conditions and microtopography. A series of 70 experiments were conducted at the US Forest Service Missoula Fire Science Laboratory (MFSL) and the Insurance Institute of Business & Home Safety (IBHS) wind tunnel facilities to test fire's response to fuel discontinuities under varying wind conditions and fuel moistures. Winds speeds ranged between 0.5 to 9 m/s over 4 different levels. Fuel moistures varied between dry (2-6%) and wet (8-17%) by weight gravimetrically. Fuel discontinuity gap sizes varied from 10 to 160cm. Fuels consisted of long leaf (Pinus palustris) pine straw. Fuel loading was 0.56 kg/m^2 and packing ratio was 0.02. Six replicates were performed at each gap bridging threshold, three at the minimum gap and three at the minimum plus one for statistical significance and probability. Under all wind speeds and moisture conditions the gap threshold between fire bridging and fire extinction was 10cm.

1. Introduction

Fire professionals within land management agencies in the United States recognize that vegetation and environmental heterogeneity collectively drive fire behaviour and fire effects on soil and plants (SERDP, 2014). The interactions between energy transport in wildland fires and the spatial distribution of fuels and wind are complex. While intuition and anecdotal observations provide some guidance, the current state of wildland fire science lacks full understanding of the dependency between fire and the spatial distribution of wind and fuels (Arno, 1997). Improved understanding of how fire responds to changes in vegetation type and density combined with wind and topography would improve the ability of the fire science community to effectively model fire behaviour and the capability of operational fire managers to use fire as a land management tool (Finney, 2013).

Experienced fire practitioners recognize that seemingly insignificant changes in wind, topography (slope or aspect) or vegetation orientation can influence fire intensity and spread (Hessburg, 2005; Camp, 1995; Ottmar, 1996). The sensitivity of fire to variations in fuel element geometry, location, and orientation as well as local air flow complicates effective fire-based land management. The dependence of fire intensity on local winds is readily recognized, but we do not yet know which scales are most relevant. Knowledge gaps pertinent to this effort include: 1) dependence of ignition on wind; 2) relative contribution of radiant and convective heating across fuel gaps as a function of burning conditions; 3) probability of ignition success as a function of fuel moisture; 4) ignition critical scales for fuel composition, load, and distribution; 5) dependence of fuel

consumption as a function of arrangement of spatial discontinuities within the fuel matrix (Anderson, 1969; Anderson, 2010; Butler, 2004).

2. Methods

The underlying hypothesis for this work is that ignition is a dose verses response mechanism. The dose is total energy absorbed by fuel particles and the response is ignition or extinction. This study seeks to identify the minimum energy dose to affect ignition through study of fire's interaction to gaps in the fuel array. To address these knowledge gaps, a series of laboratory burn experiments were completed at two different wind tunnel facilities, the US Forest Service Missoula Fire Science Laboratory (MFSL) located in Missoula, MT and the Insurance Institute for Business & Home Safety (IBHS) located in Rock Hill, SC. The lower wind speed experiments were conducted at MFSL wind tunnel while the upper wind speed experiments were conducted at the IBHS test facility. Windspeed was digitally controlled at each test facility and ranged from 0.5 to 9 m/s at 4 different levels. Fuel beds of long leaf (Pinus palustris) pine straw (nominally 2.5-3.5 m wide by 5-12 m long) were constructed with artificially imposed gaps (10 to 160 cm wide) in the fuel bed (Figure 1). Pine straw fuels were conditioned in an environmental chamber to achieve desired dry (2-6%) and wet (8-17%) fuels moisture levels.

Figure 1 – Fuel bed with pine straw fuels and discontinuous fuel gap layout at IHBS wind tunnel

Fuels were evenly distributed on the burn bed once they were weighed and measured. Light detection and ranging (LiDAR) was used to characterize the 3-dimensional distribution of fuels for each test bed. Local microscale (<1 m) winds were measured at the fuel gap using mechanical 2-dimensional (horizontal and vertical) anemometers combined with fine scale wind simulations. Local energy transport within and above fuel gaps were characterized using established *in-situ* heat flux sensors and methods (Butler, 2004). Infrared and visible imagery of flames and fuels from both horizontal and nadir orientations characterized flame presence and geometry, and kinetic and radiometric fuel surface temperature at the fuel gap. For each wind speed and fuel moisture level, the fuel bed was burned with decreasing gap width until the fire bridged the gap. Once this gap width is identified four replicates, two at the threshold and two at the threshold plus one, were burned under the same environmental conditions to verify the results and aid in the statistical analysis. Measurements for each burn experiment included whether the fire successfully bridged the gap (Yes or No), fire front progression (rate of spread, ROS) using in-situ thermocouples and overhead infrared imagery, radiative and convective energy release from the flames, wind speed, fuel moisture, gap size, relative humidity, ambient air temperature. From these data a statistical dose verses response relation will be developed and analysed to identify critical spatial scales in fuels that affect ignition and subsequent fire spread. Lab and field-scale data will be used to evaluate a new heat transfer based coupled fire/atmosphere model.

3. Experimental Design

We hypothesize that fire can be characterized as a continuous sequence of ignitions and the physical processes governing fire are directly linked. We intend to differentiate ignitions across gaps based on incident energy transport and not from ember transport. This fundamental approach seeks to improve understanding of physical fire scales, identify critical fuel spatial and temporal scales in three dimensions and improve understanding of fuel consumption and fire effects. In order to differentiate ignitions across the gap a series and visual and infrared cameras were deployed from multiple positions.

A series of 70 experiments were conducted at the US Forest Service Missoula Fire Science Laboratory (MFSL) and the Insurance Institute of Business & Home Safety (IBHS) wind tunnel facilities to test fire's response to fuel discontinuities under varying wind conditions and fuel moistures. MFSL is a research facility owned and operated by a US Forest Service and is located in Missoula, MT. The facility encompasses several buildings, including the main test chamber that is equipped with a low-speed wind tunnel capable of generating wind speeds from 0.5-3.0 m/s. This low-speed wind tunnel has a 3x3m cross section and is 26.2m long. IHBS is a $40M research facility owned and operated by a consortium of insurance companies and is located in Richburg, SC. The facility encompasses several buildings, including the main test chamber that is equipped with a vertical wall comprised of 105 interlinked, process-controlled fans. The fan bank is capable of generating hurricane force winds in excess of 54 m/s.

Variables to be tested include wind speed (0.5-9 m/s), fuel moisture (dry and wet) and gap size (10 to 160 cm). Test order was chosen at random to eliminate bias. For each test, fuels were weighed and measured for moisture content to achieve a consistent fuel load (0.56 kg/m2) and a packing ratio (0.02). Fuels were conditioned in an environmental chamber to achieve dry (2-6%) and wet (8-17%) moisture levels. Fuels were evenly distributed on the burn bed once they were weighed and measured. The pre-determined gap size was left void of fuel. Fuel was place at the downwind edge of the gap at the same pre-determined loading and packing ratio.

Each fuel bed at the IHBS test facility was measured using light detection and ranging (LiDAR) prior to ignition. Four separate scans were performed on each burn bed in order the characterize the 3D nature of the fuels. The LiDAR unit used was a Leica BLK360. The laser scans at 830nm wavelength, has a range of 0.6 - 60m, scans up to 360,000 pts/sec and a 3D point accuracy of 6mm at 10m and 8mm at 10m. Most of the points within the fuel bed scans were within 20m. Fuel beds were not scanned at the MFSL due to the complexity and space limitations associated with the wind tunnel design.

Each burn was instrumented with a vast array of sensors. A fire behaviour sensor array was placed at the leading edge of the receiving bed to measure incident heat flux, 2-dimensional wind flow and air temperature. The sensor array contained a total of three Medtherm® heat flux sensors to measure total, radiant and convection incident energy on the receiving bed. The sensor array contained five 2-dimensional Keil static wind probes to measure horizontal and vertical wind velocity at the receiving bed. Finally, the sensor array contained five type K thermocouples to measure air temperature at the receiving bed. All sensors on the fire behaviour array scanned at 180 Hz. The sensor array was constructed of a 5.1 x 15.2 cm metal stud on wooden supports to provide a flush surface between the fuel bed and receiving bed. The gap was filled with 5.1 x 10.2 cm metal studs on wooden supports that were each instrumented with three type K thermocouples to measure air temperature in the gap. The list of imaging sensors used can be seen in Table 1.

Table 1: Visual and infrared sensors used during IBHS test burns.

Sensor	Resolution	Frame Rate	Orientation	Range	Field of View
GoPro	2.7k	24 fps	end, side, nadir	N/A	infinite
Sony	4k	30 fps	side	N/A	infinite
FLIR Duo IR	640 x 512	30 Hz	side	-300C - 1035C	45º
& Visible	4k	24 fpm	side	N/A	56º x 45º
FLIR A655sc	640 x 482	25 Hz	nadir	300C - 2000C	45º
Optris PI 400	382 x 288	27 Hz	nadir	-20C - 900C	13º

These imagers were deployed in several configurations to monitor fire rate of spread, flame geometry, flame impingement across the fuel gap, ember transport across the fuel gap, fuel particle temperature and radiant energy release. The GoPro cameras were placed in three separate configurations: end view, side view and nadir view (Figure 2). This imagery will be used to quantify flame geometry and fire rate of spread. The Sony camera was oriented side view at the gap to measure flame geometry as well as flame impingement on the receiving bed.

Figure 2: In order; GoPro screen capture of end view, side view at the gap and nadir view of burns.

Two infrared cameras were deployed during the MFSL experiments, and three infrared cameras were deployed during the IBHS experiments for each of the test burns. Ground control points were established for each infrared camera for image rectification. The Optris PI400 was oriented nadir to the fuel bed. The narrow field of view (FOV) on the Optris made it ideal for determining fuel particle temperature, whether fire crossed the gap and if ignition was derived from ember transport or flame impingement. The FLIR A655sc was oriented nadir to the fuel bed for the IBHS experiments. The wide angle on the A655sc allowed for full view of the fuel bed and was used primarily for fire rate of spread and radiate energy release. The FLIR Duo is a dual infrared and visible high-resolution imager. This camera was oriented to the side and above the gap and was primarily used to determine fuel particle temperature, whether fire crossed the gap and if ignition was derived from ember transport or flame impingement. (Figure 3).

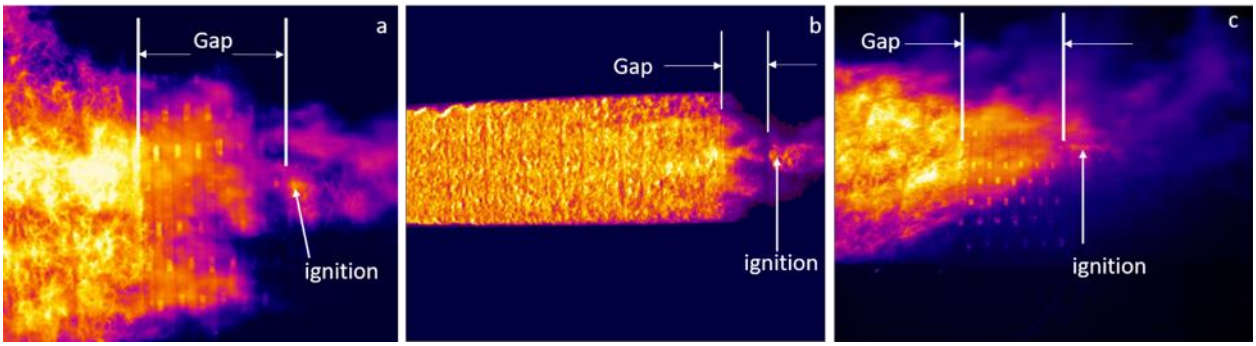

Figure 3: (a) imagine from the Optris PI400, (b) image from the FLIR A655sc, (c) image from the FLIR Duo.

4. Results

Four test scenarios were designed for the both the MFLS and IBHS test facilities. These include, 1) low wind speed/dry fuels, 2) low wind speed/wet fuels, 3) high wind speed/dry fuels and 4) high wind/speed wet fuels. The test scenarios were chosen at random to eliminate bias. All tests in a series were completed before changing to the next set of parameters to maintain consistent weather conditions. For each wind speed and fuel moisture level, the fuel beds were burned with decreasing gap width until the fire bridges the gap. Once the gap width was identified, four replicates were burned under the same environmental conditions to verify the results and aid in the statistical analysis. Two replicates were burned at the gap size where fire crossed the gap to identify probability of a false positive and two replicates were burned at the increased gap size where fire did not cross to identify probability of a false negative result. Table 2 outlines the results from the four test scenarios.

Table 2: Summary of test results showing wind speed, fuel moisture, gap size and whether the fire crossed the gap.

Test Series	Wind Speed (m/s)	Fuel Moisture	Gap Size (cm)	Crossed Gap (Y/N)	Replicate Crossed (Y/N)
MSFL					
Low Wind/Dry Fuel	0.5	Dry	10 17	Yes No	Yes/Yes No/No
Low Wind/Wet Fuel	0.5	Wet	15 23	Yes No	Yes No/No
High Wind/Dry Fuel	1.0	Dry	39 46	Yes No	Yes/Yes No/No
High Wind/Wet Fuel	1.0	Wet	23 39	Yes No	Yes/Yes No/No
IBHS					
Low Wind/Dry Fuel	6	Dry	100 110	Yes No/No	Yes/No No/No
Low Wind/Wet Fuel	6	Wet	90 100	Yes No	No/No No/No
High Wind/Dry Fuel	9	Dry	150 160	Yes No	Yes/Yes No/No
High Wind/Wet Fuel	9	Wet	120 130	Yes No	Yes/Yes No/No

The data suggests that the incident energy threshold required to cross the fuel gap is extremely narrow, in each case the separation distance was equal to or less than 10 cm. The low wind speed wet fuels scenario initially crossed a gap of 90 cm, but neither replicate crossed suggesting a false positive at this setting. This test scenario will be repeated at a future date. Comparing data between the two test facilities shows linear alignment, but mid-range wind speeds are lacking (Figure 4).

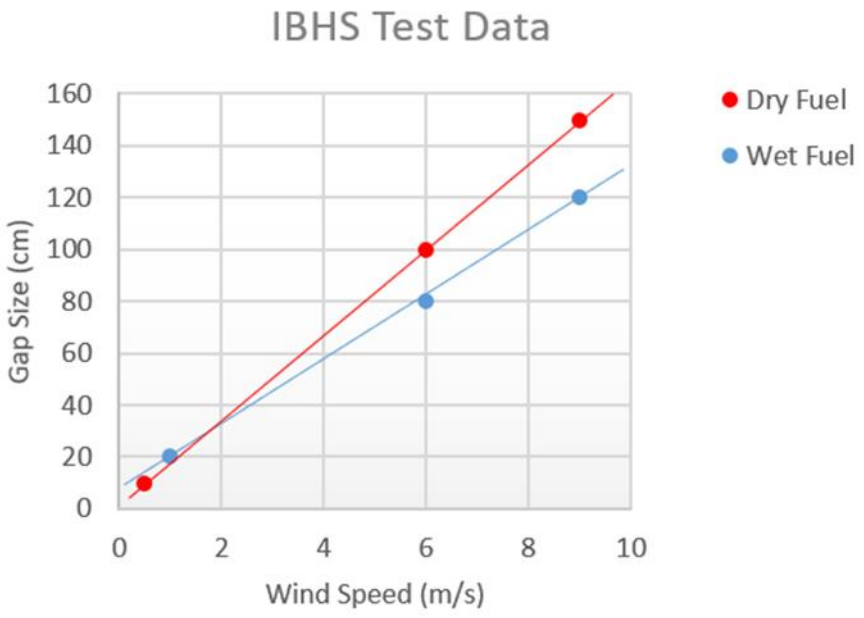

Figure 4: Test results comparing low wind speed data collect at FiSL and high wind speed data collected IBHS.

This poster will outline the methods, experimental design, and initial results from the data collected to date.

5. References

Anderson, H.E., Heat transfer and fire spread, 1969, USDA, Forest Service: Ogden, UT.

Anderson, W.R., E.A. Catchpole, and B.W. Butler, Convective heat transfer in fire spread through fine fuelbeds. International Journal of Wildland Fire, 2010. 19: p. 284-298.

Arno, S.F., H.Y. Smith, and M.A. Krebs, Old growth Ponderosa pine and Western larch stand structures: influences of pre-1900 fires and fire exclusion, 1997, Intermountain research station.

Butler, B.W., et al., Measurements of radiant emissive power and temperatures in crown fires. Canadian Journal of Forest Research, 2004. 34: p. 1577- 1587.

Camp, A., et al., Spatial changes in forest landscape patterns from altered disturbance regimes on the eastern slope of the Washington cascades. Proceedings: Symposium on Fire in Wilderness and Park Management, 1995. USDA Forest Service: Intermountain Research Station (General Technical Report INT-GTR-320): p. 169-172.

Finney, M.A., et al., On the need for a theory of wildland fire spread. International Journal of Wildland Fire, 2013. 22(1): p. 25-36.

Hessburg, P.F., J.K. Agee, and J.F. Franklin, Dry forests and wildland fires of the inland Northwest USA: Contrasting the landscape ecology of the pre-settlement and modern eras. FOREST ECOLOGY AND MANAGEMENT, 2005. 211(1): p. 117-139.

Ottmar, R.D., E. Alvarado, and P.F. Hessburg. Linking Recent Historical and Current Forest Vegetation Patterns to Smoke and Crown Fire in the Interior Columbia River Basin. in 13th Fire and Forest Meteorology Conference. 1996. Lorne, Australia: International Association of Wildland Fire.

SERDP. 2014; Available from: https://www.serdp-estcp.org/News-and-Events/Blog/SERDP-and-ESTCP-Release-a-Fire-Science-Strategy.

Usage of pouches with phase change materials (PCMs) to increase the thermal performance of a firefighter jacket - development and thermal behaviour evaluation of the multilayer system

Margarida Silva[1,2]; J. Ribeiro[3]; A. Moreira[3]; P. Fernandes[3]; Gilda Santos[4]; Rita Marques[4]; João B. L. M. Campos[1,2]; Soraia F. Neves[1,2*]

[1]CEFT - Transport Phenomena Research Centre, Faculty of Engineering, University of Porto, Rua Dr. Roberto Frias, 4200-465 Porto, Portugal, {up201909589@up.pt}, {jmc, sfneves}@fe.up.pt
[2]ALiCE - Associate Laboratory in Chemical Engineering, Faculty of Engineering, University of Porto, Rua Dr. Roberto Frias, 4200-465 Porto, Portugal
[3] CeNTI – Centre for Nanotechnology and Smart Materials, V. N. Famalicão, Portugal, {jpribeiro, amoreira, pfernandes}@centi.pt
[4] CITEVE – Technological Centre of the Textile and Clothing Industries of Portugal, V. N. Famalicão, Portugal {gsantos, rmarques}@citeve.pt

**Corresponding author*

Keywords

Multilayer system; Phase change materials; Transient behaviour; Thermal performance

Abstract

In recent years, the growth in size and duration of wildland fires and the increasing demand for high-performance protective clothing have led Thermal Protective Clothing (TPC) research and development to seek solutions to minimise firefighter thermal load and skin burns. In this context, the present work was developed under the framework of the DIF-Jacket project (https://difjacketproject.fe.up.pt), where the main goal is to develop a new multilayer system with phase change materials (PCMs) to be used in a jacket of wildland firefighters and the subsequent development of an experimental procedure to evaluate its transient behaviour. For that purpose, a small-scale multilayer system was developed, which consisted of three layers: an outer textile layer, a pouch with PCMs (intermediate layer) and an inner textile layer. The pouch with PCMs was incorporated into the multilayer system to absorb the incoming heat from the environment, increasing the time a firefighter can be exposed to it. Subsequently, an experimental set-up was developed to evaluate the transient behaviour of the solution with PCMs, simulating the different phases to which a firefighter is exposed to (i.e., direct exposure to a radiative heat flux followed by a post-fire period). Therefore, the effect of some pouch-related parameters on the multilayer system thermal behaviour was studied, namely different geometries of the pouches (square and rectangular) and two types of PCMs. As main conclusions, similar tendencies were obtained with the square and rectangular pouches. The best temperature homogeneity of the PCM pouches was obtained with the macro encapsulated PCM. The incorporation of PCMs in the multilayer system significantly delays its heating. Further research must be conducted to delay even more the increase of temperature during the exposure time. Nevertheless, the described set-up can be used to analyse several opposing requirements of a multilayer system with PCM pouches integrated, allowing the correlation of geometrical features and properties of the system components (either textiles or PCM pouches) with the system transient temperature behaviour.

1. Introduction

The intense demands of Thermal Protective Clothing (TPC) market and the technological development in the textile industry encourage the development of protective clothing with high thermal protection while maintaining high comfort performance (G. Song and F. Wang, 2019; R. Paul, 2019). Emerging technologies have come into sight to minimize the heat stress felt by users exposed to a hot environment, such as cooling vests either with water perfused tubes (L.P.J. Teunissen *et al*., 2014) or incorporating Phase Change Materials (PCMs) (C. Gao *et al*., 2012). Recently, A. Fonseca et al. (2020) obtained promising numerical results showing the potential of phase change materials (PCMs) to increase the thermal protection of firefighters' bodies.

Phase change materials (PCMs) are materials that can be used to absorb/release energy in the form of latent heat through a phase transition (L. F. Cabeza *et al*., 2015; A. Fonseca *et al*., 2018). The incorporation of PCMs into firefighter's protective clothing can target absorption of metabolic heat produced by the human body (enhancing comfort) or absorption of heat from the environment (enhancing protection). R. Paul, (2019) stated that when PCMs are incorporated into the firefighter's protective clothing, they can absorb the heat metabolically produced by the human body during its melting process, giving the wearer a cooling effect. However, A. Fonseca *et al*. (2018) found that the optimum position for the PCM layer is the closest to the external heat source, since it favours a higher use of the PCM storage capacity and takes advantage of its high thermal inertia in a more efficient way. As this work targets protection enhancement, PCMs were incorporated into the firefighter's protective jacket to absorb the heat from the fire, thus increasing the time that the firefighter can be safely exposed to it. However, it is also crucial to release the energy accumulated during fire exposure, as excessive heat accumulation promotes the occurrence of third-degree burns, limiting the time the firefighter has to remove the garment. For that reason, the next step is to develop an innovative solution following the multilayer system of a convectional jacket structure with the addition of PCMs incorporated through pouches. Additionally, it is necessary to consider the transient behaviour of PCMs and, consequently, a new methodology for evaluating the protective clothing under transient conditions was developed.

2. Materials and methods

2.1. PCMs and its incorporation in the multilayer system

To incorporate the multilayer system of the firefighter jacket, two different PCMs were studied and their main thermophysical properties are presented in Table 1.

Table 1 - PCMs and their thermophysical properties; T_m, ΔH_m, C_p, k, and T_{max} stand for melting temperature, latent heat of fusion, specific heat, thermal conductivity and maximum operation temperature, respectively.

PCM	Form (at 25 ºC)	T_m / ºC	ΔH_m / kJ·kg^{-1}	c_p / kJ·kg^{-1}·ºC^{-1}	k / W·m^{-1}·ºC^{-1}	T_{max} / ºC
A	Solid (pure state)	69-73	120	2	0.6	90
B	Solid (powder)	77-85	75	2	0.1	110

In the PCMs pouches construction, a low thickness polymeric film was chosen due to its high thermal resistance and ability to maintain its excellent mechanical properties under hot severe environmental conditions. Square 7 cm x 7 cm pouches and rectangular 7.0 cm x 3.5 cm pouches were constructed in order to evaluate the effect of the pouch geometry. PCM A was melted before being incorporated into the pouches to have a more homogeneous distribution across the pouch. It was not necessary to melt PCM B since it was already a uniform powder (macro encapsulated in silica).

2.2. Experimental set-up for the evaluation of transient behaviour

The experimental procedure developed to evaluate the transient behaviour consisted of two different phases:

1) Heating phase – the sample is placed between the installation table and the IR lamp and therefore exposed to a constant radiant heat flux;
2) Cooling phase – the sample is removed from the installation (i.e., not exposed to a heat flux) and is left to cool down to room temperature.

The installation shown in Figure 1 was used to evaluate the sample transient behaviour. It consisted of a table and an IR lamp at the height of 30 cm from the table top, corresponding to a heat flux of 3.07 kW·m^{-2}. Additionally, a thermal camera was used to monitor the surface temperature of the sample and three data loggers to monitor the temperature on the sample's inner layer. The samples were placed in the laboratory 24 hours before testing to ensure they were in equilibrium with ambient conditions at the start of the test. As test stopping criteria of the heating phase, the maximum operating temperature of the PCM was used, i.e., 90 °C and 110 °C, respectively, for the tests with PCM A and PCM B (maximum obtained in, at least, one of the data loggers).

Figure 1 – Installation for the evaluation of samples transient behavior.

The tests were performed with the PCMs pouches and the assembly (outer layer + PCM pouch + inner layer), both insulated with extruded polystyrene (XPS) to maximize a unidirectional heat transfer. Also, XPS surface reflectivity was increased by applying a white coating to reduce temperature increase and prevent it from melting. The PCM pouches' mass to surface area ratio was also considered since the mass influences the amount of energy that the PCM will accumulate. Thus, a mass to surface area ratio of 0.38 $g \cdot cm^{-2}$ (maximum achievable ratio) was used to make a comparative analysis of the efficiency of the PCMs. The experimental set-up for the transient behaviour evaluation tests is shown in Figure 2.

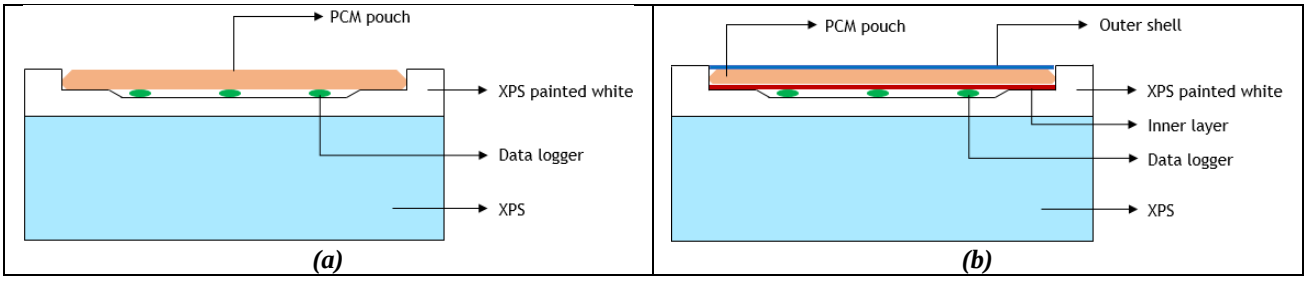

Figure 2 - Schematic representation of the experimental set-up for the transient behavior evaluation tests considering: (a) only the PCM pouch and (b) the assembly outer layer + PCM pouch + inner layer.

3. Results

This work focused mainly on evaluating the effects of the pouch geometry and the type of PCM introduced into it and, in addition, the influence of the incorporation of PCMs pouches into a firefighter jacket. Thus, the test described in section 2.2 was performed on square and rectangular pouches to study the transient behaviour of PCM pouches. Similar tendencies were obtained, so only the results obtained with the square pouches were included in this article. The comparison of the temperature profiles obtained during heating/cooling test of PCM pouches with PCM A or PCM B is shown in Figure 3. This figure contains the mean value (solid lines) of the temperatures of the three data loggers of three tests and the respective standard deviations (areas around the solid lines with the same colour).

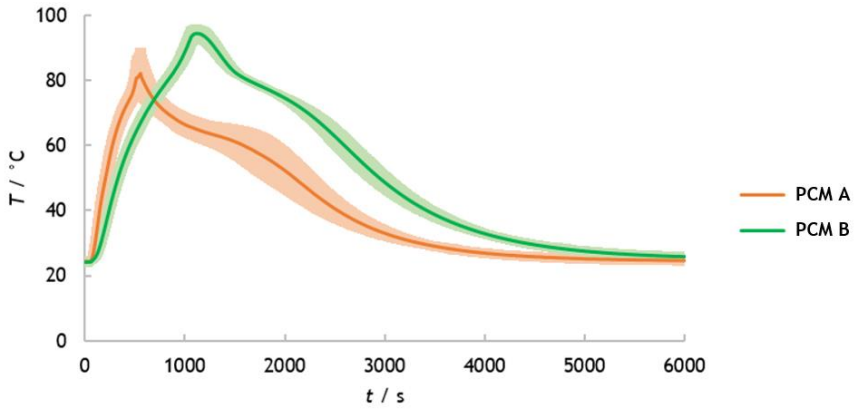

Figure 3 - Temperature profiles obtained in the PCM pouch during the heating/cooling test, considering PCM A and PCM B (three independent measurements per sample; standard deviation).

In Figure 3, it is shown that PCM B exhibits slower heating and cooling than PCM A, which can be explained by the fact that PCM B has a thermal conductivity six times lower than PCM A and equal specific heat (Table 1). The density of PCMs can also influence their heating and cooling rates. However, the supplier did not provide this information and, therefore, the density effect on the heating and cooling rates of the PCMs could not be analysed. In addition, PCM B is more homogeneous in the way it spreads across the pouch and it is easier to incorporate into pouches as it is already a uniform powder. As it is necessary to melt the PCM A before introducing it into the pouches, this PCM has the drawback of the appearance of air bubbles during the construction of the pouch. This air bubble is visible in the thermal camera image shown in Figure 4 and leads to a higher standard deviation in the results.

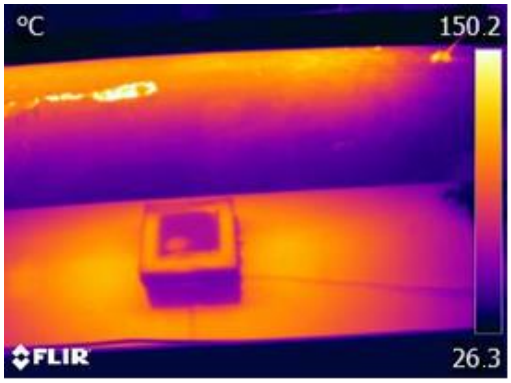

Figure 4 - Thermal camera image of the square pouch with PCM A after 4 min of exposure to IR radiation.

Lastly, the impact of the incorporation of PCM pouches on the thermal performance of the multilayer system was studied. PCM B was chosen for this study since it showed greater homogeneity (without bubbles) and was easier to incorporate into the pouches. The effect of the incorporation of PCM B on the sample's inner layer measured by the data loggers is presented in Figure 5, where the solid line is the mean value of the temperatures of the three data loggers of three tests and the area around the solid line with the same colour is the respective standard deviation.

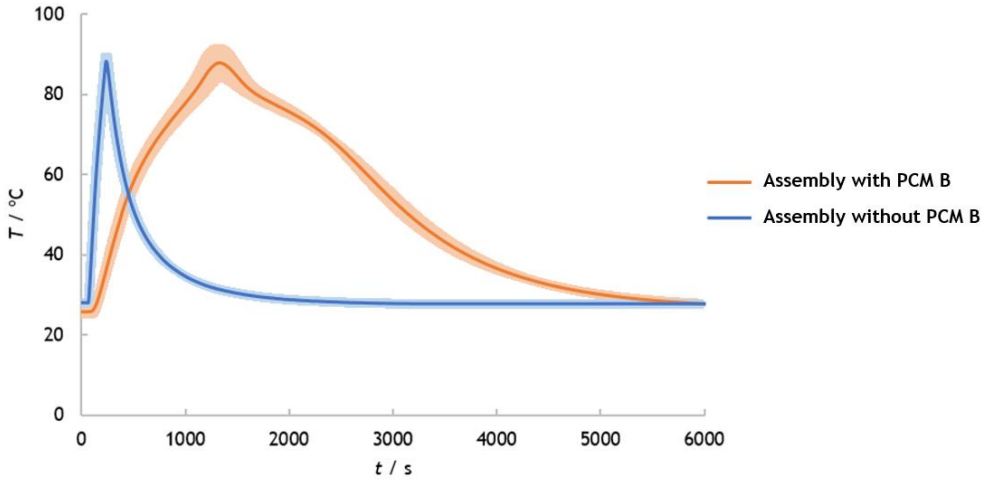

Figure 5 - Effect of the incorporation of PCM B on the multilayer system temperature (three independent measurements per sample; standard deviation).

Figure 5 shows that the assembly's behaviour without PCMs is different from the assembly with PCMs. During the exposure to the radiant heat flux, the assembly without PCM pouch (i.e., consists only of an outer shell and an inner layer) shows an increase in heating rate significantly sharper than the increase rate obtained for the assembly with PCM pouch, with an initial heating rate of 0.44 ± 0.01 ºC·s^{-1}. As the initial heating rate of the assembly with the incorporated PCMs is 0.09 ± 0.01 ºC·s^{-1}, it corresponds to a decrease of 79.5 %. This decrease is due to the fact that the assembly with PCM pouch has an additional layer, which provides higher thermal insulation (due to the addition of PCM and pouch material). Nevertheless, the effect of PCM latent heat on the pouch temperature is slightly evident at approximately 1600 s (beginning of the cooling phase); it is observed a slight change in the decline of the temperature profile. Further studies considering a large amount of PCM should be interesting to study. Although the incorporation of PCMs is beneficial since it decreases the heating rate of the assembly, it also dramatically delays its cooling by almost 4500 seconds.

As future considerations, to avoid the increase in the cooling time, further research must be conducted to delay even more the increase of temperature during the exposure time. Furthermore, it is important to study the impact of incorporating PCMs on the weight and on the evaporative resistance in the firefighter jacket. Also, since one of the most important considerations to be taken in the development of protective clothing is mass transfer, it is still necessary to optimise the performance of the developed multilayer system, considering relevant aspects related to mass transfer (e.g., the effect of the distribution/quantity of water inside the jacket on the occurrence of burns).

4. Conclusions

A multilayer system with integrated PCMs was studied at a small scale. The developed multilayer system consists of three layers: an outer shell, a PCM pouch, and an inner layer. An experimental procedure was also developed to evaluate the transient behaviour of PCMs pouches and the multilayer system, simulating different phases that a firefighter is exposed to in firefighting. As a result, the following conclusions were obtained:

- The pouch geometry does not significantly influence the thermal performance of the multilayer system;
- Powder rather than pure state PCMs must be selected to fill in the pouches to avoid operational problems. For instance, the macro encapsulated PCM showed the most promising results since it presented a greater homogeneity in its spread across the pouch and a more straightforward incorporation method into the pouches;
- The incorporation of PCMs is beneficial since it decreases the initial heating rate of the assembly, but it also dramatically delays its cooling.

Furthermore, the developed set-up can be used to analyse several opposing requirements of a multilayer system with PCM pouches integrated, allowing the correlation of geometrical features and properties of the system components (either textiles or PCM pouches) with the system transient temperature behaviour.

5. Acknowledgements

This work was financially supported by LA/P/0045/2020 (ALiCE), UIDB/00532/2020 and UIDP/00532/2020 (CEFT), and by PCIF/SSO/0106/2018 - Project for "Development of an innovative firefighter's jacket", funded by national funds through FCT/MCTES (PIDDAC).

6. References

G. Song and F. Wang, Firefighters' Clothing and Equipment, 1st Edition. New York, United States: CRC Press, 2019.

R. Paul, High Performance Technical Textiles, First Edit. Leeds, United Kingdom: John Wiley & Sons Ltd, 2019.

L.P.J. Teunissen, L.C. Wang, S.N. Chou, C. hsien Huang, G.T. Jou, H.A.M. Daanen, Evaluation of two cooling systems under a firefighter coverall, Appl. Ergon. 45 (2014) 1433–1438. https://doi.org/10.1016/j.apergo.2014.04.008.

C. Gao, K. Kuklane, F. Wang, I. Holmér, Personal cooling with phase change materials to improve thermal comfort from a heat wave perspective, Indoor Air. 22 (2012) 523–530. https://doi.org/10.1111/j.1600-0668.2012.00778.x.

A. Fonseca, S. F. Neves, and J. B. L. M. Campos, "Thermal performance of a PCM firefighting suit considering transient periods of fire exposure, post – fire exposure and resting phases," Appl. Therm. Eng., vol. 182, no. February 2020, p. 115769, 2021, doi: 10.1016/j.applthermaleng.2020.115769.

L. F. Cabeza, I. Martorell, L. Miró, A. I. Fernández, and C. Barreneche, Introduction to thermal energy storage (TES) systems. Woodhead Publishing Limited, 2015.

A. Fonseca, T. S. Mayor, and J. B. L. M. Campos, "Guidelines for the specification of a PCM layer in Firefighting Protective Clothing Ensembles," Appl. Therm. Eng., 2018, doi: 10.1016/j.applthermaleng.2018.01.028.

Validation of ERA5 fire weather conditions in Greece between 2007 and 2019: A preliminary analysis

Georgios Papavasileiou*; Theodore M. Giannaros

National Observatory of Athens (NOA), Institute for Environmental Research & Sustainable Development (IERSD), Greece, {papavasileiou, thgian}@noa.gr

**Corresponding author*

Keywords

Fire weather, extreme fire behavior, ERA5, validation, Greece

Abstract

Accurate simulations of fire weather conditions for both the past and future are of great importance for fire management and preparedness. With the advancement of numerical weather prediction models and data assimilation techniques, more accurate reanalysis products have been developed the recent years. Here we validate fire weather conditions in Greece which are computed based on ERA5 reanalysis data against surface observations from the automatic weather station network of the National Observatory of Athens (NOA). We assess the fire weather conditions in an application of the Canadian Forest Fire Weather Index (FWI) System in both datasets. Although, ERA5 FWI archive is available since 1979 here we limit our analysis during the period from 2007 to 2019, due to the limited data availability from the NOA network. The validation of FWI in ERA5 data shows good agreement with the NOA observations with a mean correlation of 0.87. Furthermore, FWI in ERA5 data is overall slightly underestimated compared to NOA observations, which is driven by an underestimation of the three moisture components of FWI, namely the Fine Fuel Moisture Code (FFMC), the Drought Code (DC) and the Duff Moisture Code (DMC). Preliminary results also indicate that the largest errors are found over the eastern and southern parts of Greece, which is the area that experiences the highest FWI values during the summer.

1. Introduction

The evaluation of the atmospheric conditions which are prone to extreme fire behavior is very critical for both the ecosystems and human life. Furthermore, accurate knowledge of fire weather conditions is also critical for civil protection preparedness and management. Fire weather conditions are determined by the meteorological conditions across weather and climate scales (Abatzoglou and Kolden, 2013; Flannigan and Wotton, 2001). Across longer time scales, such as sub-seasonal to seasonal and climate scales, changes in atmospheric state expressed via changes in basic meteorological variables (e.g. precipitation and temperature) influence the state of the fuels. On the other hand, across shorter time scales, changes in synoptic to mesoscale atmospheric conditions can modulate fire weather primarily via changes in temperature, wind speed and humidity.

These changes in fire weather conditions can be monitored by using fire weather indices. One of the mostly used fire weather indices is the Canadian Forest Fire Weather Index (FWI) System (Van Wagner, 1987). FWI is used by many agencies and national weather services to assess fire weather. Thus, its evaluation for both past conditions as well as for forecasting fire weather conditions is of great importance. Here we present preliminary results of an evaluation of ERA5 FWI and its components in Greece using observations from the network of automatic weather stations that is operated by the National Observatory of Athens (NOA).

2. Data and methods

For the purpose of this analysis we use the recently developed by the European Centre for Medium-range Weather Forecasts (ECMWF) daily gridded dataset of FWI based on ERA5 reanalysis. The ERA5 FWI dataset is based on an application of the Global ECMWF Fire Forecast (GEFF) model in ERA5 reanalysis data (Vitolo

et al., 2020). The ERA5-based FWI data extends from 1979 till present and has a spatial resolution of 0.25˚ x 0.25˚. However, for the validation analysis here we limit our analysis in the period of 2007—2019, when the NOA automatic weather station (AWS) observations are available. For the comparison we use the nearest land ERA5 grid point to the each AWS location. The locations of the 76 AWS that we use in this analysis are shown in Fig. 1. AWS-based FWI components are calculated in the same way as in Vitolo et al. (2020).

For the validation, following previous work of McElhinny et al. (2020), we consider four simple metrics: (1) mean bias error (MBE), (2) mean absolute error (MAE), (3) Spearman rank correlation and (4) root mean square error (RMSE) applied in the ERA5-based FWI and the AWS-based FWI time series.

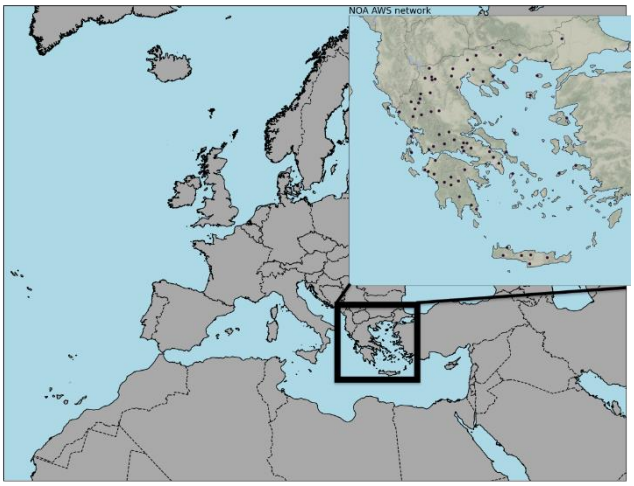

Figure 1- Study area (black box) and the locations (white dotes) of the automatic weather stations operated by the National Observatory of Athens (NOA) during the period of 2007—2019 that we use in this analysis.

3. Results

3.1. Climatology of fire weather in Greece

In Figure 2 we present the monthly climatological mean FWI values for four selected months based on ERA5 data during the period of 1981 to 2010 in Greece. This analysis illustrates, not surprisingly, the substantial spatiotemporal variability of FWI in Greece suggesting that a dense observational network is necessary for monitoring fire weather conditions. Results show that FWI is lower across the entire country during winter (Fig. 2a) and peaks during the summer particularly over the eastern and southern parts of the country (Fig. 2c). During spring and mostly during autumn FWI exhibits a NW-SE gradient with higher values over the southeastern parts and lower values over the northwestern parts of the country (Fig. 2b, d).

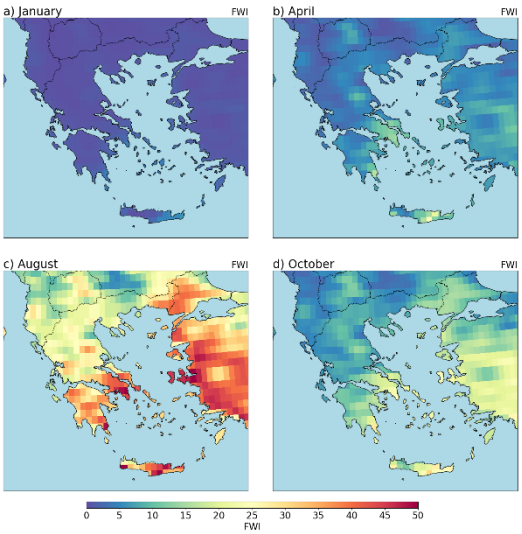

Figure 2- Monthly climatologies of mean FWI for (a) January, (b) April, (c) August and (d) October based on 1981-2010 ERA5 reanalysis data.

Similar spatiotemporal variability to the FWI exhibits the daily severity rating (DSR), which is a component of the FWI and it is a good indicator of fire suppression effort that is required (Fig. 3).

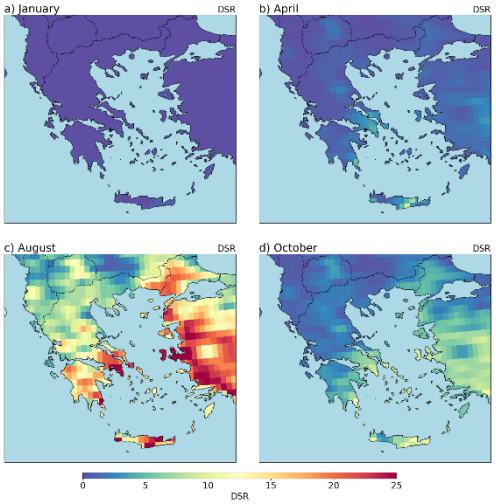

Figure 3- Monthly climatologies of mean DSR for (a) January, (b) April, (c) August and (d) October based on 1981-2010 ERA5 reanalysis data.

3.2. Validation of ERA5 fire weather

A validation analysis of ERA5-based FWI over the 76 NOA AWS locations in Figure 4 reveals that overall ERA5 is in good agreement with the AWS data exhibiting a mean Spearman rank correlation of 0.9, mean MAE of 5.19 and a slightly mean negative bias of -0.6 (Fig. 4). These findings are in line with previous analysis performed in Canada by McElhinny et al. (2020). The spatial distribution of MAE (Fig. 4b) and MBE (Fig. 4a) reveals that a negative bias is mainly evident in AWS near coastal areas and islands suggesting a model bias primarily in wind speed as it has also been discussed in previous studies (Betts et al., 2019; McElhinny et al., 2020). However, the source of this bias is beyond the scope of this study but users should be aware of these potential limitations (Vitolo et al., 2020).

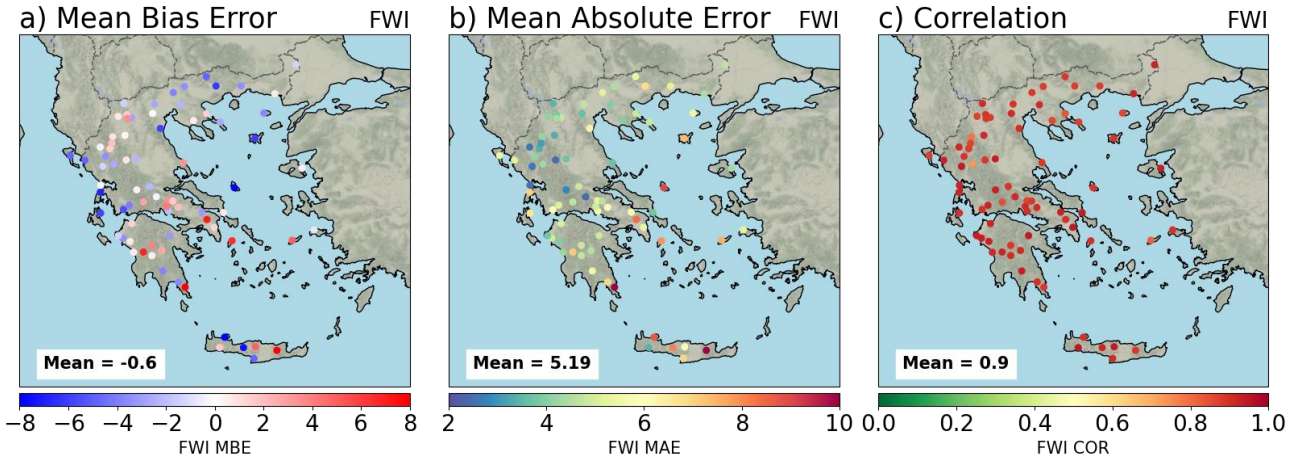

Figure 4- FWI (a) mean bias error, (b) mean absolute error and (c) Spearman rank correlation of ERA5 data against NOA AWS observations.

Validating ERA5 DSR data yields even greater agreement between ERA5 and NOA AWS with a mean Spearman correlation of 0.9, mean MAE of 2.54 and mean bias of -0.02. The mean biases in DSR are substantially smaller compared to FWI (near 50%) and are mainly identified in the southern parts of the country. These findings suggest that DSR might be a more useful indicator of fire behavior and fire weather conditions across broader regions in ERA5 data compared to FWI. Furthermore, DSR mean bias errors exhibit smaller variance suggesting an overall better agreement with the AWS data compared to FWI (Fig. 6).

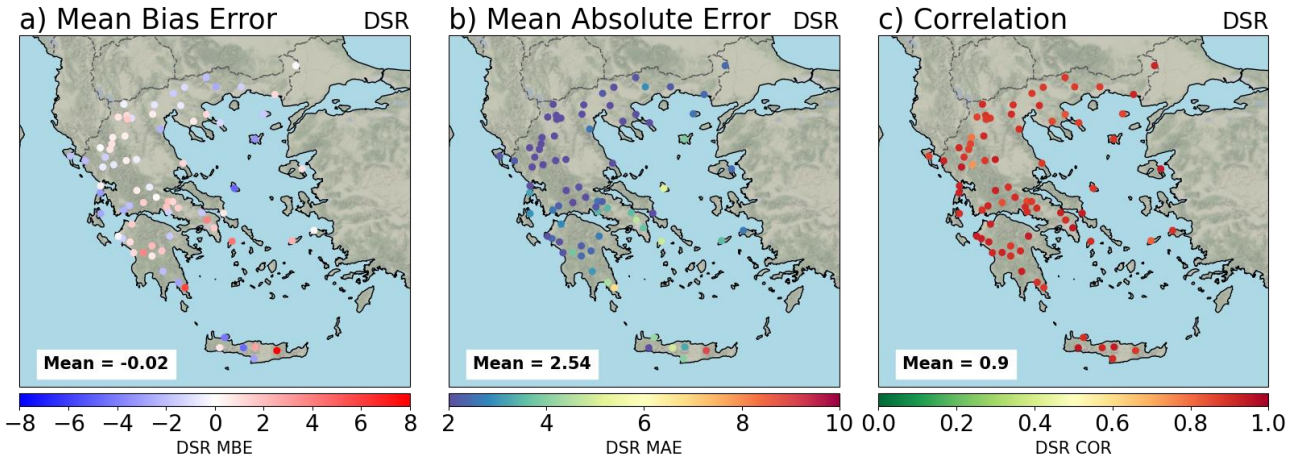

Figure 5- DSR (a) mean bias error, (b) mean absolute error and (c) Spearman rank correlation of ERA5 data against NOA AWS observations.

We further validate all the components of the CFFWIS and we provide a summary of the statistical metrics that use here in Table 1. Overall, we find that the largest biases are evident for the three moisture components of FWI, namely the Fine Fuel Moisture Code (FFMC), the Drought Code (DC) and the Duff Moisture Code (DMC) and therefore by construction the Build Up Index (BUI). The smallest mean biases are evident for DSR, Initial Spread Index (ISI) and FWI. Furthermore, the largest MAE are evident for DC, BUI, DMC, FFMC, while the smallest occur for ISI, DSR and FWI. It is notable that even though some moisture components exhibit high correlation, they are also accompanied by the largest MBE, MAE and RMSE.

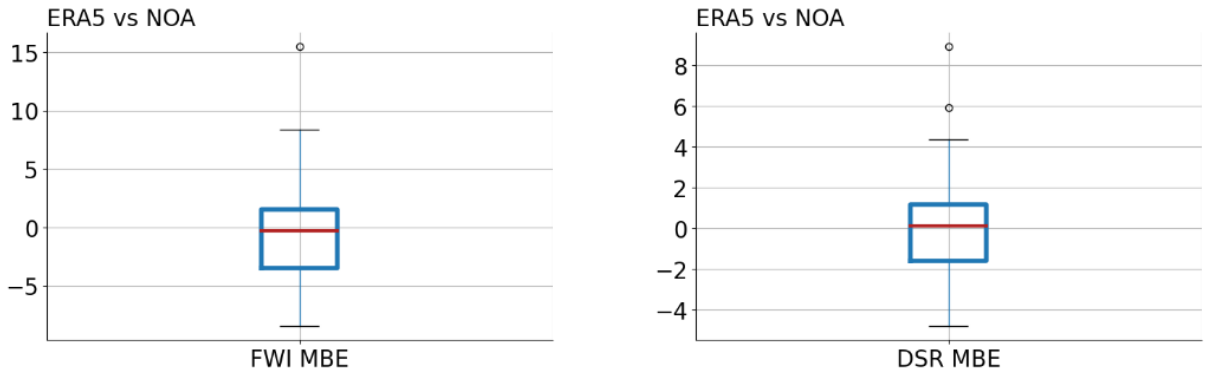

a) ***b)***

Figure 6- Distribution of ERA5 (a) FWI and (b) DSR mean bias errors across all 76 NOA AWS locations.

Our findings are in line with previous results from McElhinny et al. (2020), where similar magnitudes of MBE and MAE are shown, however here we find stronger Spearman rank correlation between ERA5-based and NOA AWS-based FWI suggesting an overall good performance of ERA5 despite the dataset limitations. As mentioned above, these limitations arise from ERA5 biases mainly in precipitation and wind, which then influences the computations of the CFFWIS components.

Table 1- Statistics of fire weather indices based on ERA5 data against NOA AWS observations.

	Mean Bias Error	Mean Absolute Error	Root Mean Square Error	Correlation
FWI	-0.6	5.19	8.05	0.9
ISI	0.24	1.2	3.03	0.81
FFMC	-4.43	7.42	11.5	0.86
DMC	-9.5	26.1	50.4	0.93
DC	-161.3	187.25	252.9	0.85
BUI	-18.7	31.23	54.9	0.93
DSR	-0.02	2.54	4.8	0.9

4. Conclusions

In this study we present preliminary results of the validation of ERA5 fire weather conditions in Greece using automatic weather station observations during the period from 2007 to 2019. Our results show that ERA5 overall perform well mostly in the continental parts of the country, while some biases are evident over the eastern and southern parts of the country. A detailed validation of each component of the Canadian Forest Fire Weather Index System suggests that the daily severity rating component performs better than any other component and could be a more reliable indicator of fire weather and fire behavior for future studies that focus over broader areas compared to other components.

5. Acknowledgments

This research was funded by the Hellenic Foundation for Research and Innovation (H.F.R.I.) under the "2nd Call for H.F.R.I. Research Projects to support Post-Doctoral Researchers" (Project Number: 00559).

6. References

Abatzoglou, J.T. and Kolden, C.A. (2013) Relationships between cli-mate and macroscale area burned in the western United States.International Journal of Wildland Fire, 22, 1003–1020.

Betts AK, Chan DZ and Desjardins RL (2019) Near-Surface Biases in ERA5 Over the Canadian Prairies. Front. Environ. Sci. 7:129. doi: 10.3389/fenvs.2019.0012

Flannigan, M.D. and Wotton, B.M. (2001) Climate, weather and area burned. In: Johnson, E.A. and Miyanishi, K. (Eds.)ForestFires: Behavior and Ecological Effects. New York, NY: AcademicPress, pp. 335–357.

McElhinny, M., Beckers, J. F., Hanes, C., Flannigan, M., and Jain, P.: A high-resolution reanalysis of global fire weather from 1979 to 2018 – overwintering the Drought Code, Earth Syst. Sci. Data, 12, 1823–1833, https://doi.org/10.5194/essd-12-1823-2020, 2020.

Van Wagner, C. E. Development and structure of the Canadian forest fire weather index system. Report No. 1992 (Canadian Forestry Service, Petawawa National Forestry Institute, Chalk River, ON, Canada, (1987).

Vitolo, C., Di Giuseppe, F., Barnard, C. et al. ERA5-based global meteorological wildfire danger maps. Sci Data 7, 216 (2020). https://doi.org/10.1038/s41597-020-0554-z

Validation of the Small World Network Model on a prescribed burning

Nadjet Hamamousse*[1]; Nouredine Zekri[1]; Ahmed Kaiss[2] ; Omar Mosbah[1]

[1] *Université des Sciences et de la Technologie d'Oran, LEPM, B.P.1505 El Mnaouer Oran, Algeria {nadjet.hamamousse@gmail.com, nzekri@yahoo.com}*
[2] *Aix Marseille Université. CNRS, IUSTI UMR 7343, 13453 Marseille, France {ahmed.kaiss@univ-amu.fr}*

**Corresponding author*

Keywords

Pinus Halepensis needles, prescribed burning, slope effect, Small World Model, vegetation fire.

Abstract

This work aims to validate the Small World Network Model by comparing the numerical predicted rate of spread results to those obtained from a prescribed burning in the city of Oran in Algeria using Pinus Halepensis needles. In the first part of the experimental tests pine needles partially dried using microwave oven and climatic chamber were used. Fire propagation tests were then realized at different fuel moisture contents. In the second part of the tests, dead Pinus Halepensis needles were used in order to evaluate the effect of the terrain slope on fire spread. This model may be used to simulate the fire patterns both in homogeneous and heterogeneous landscapes. This model takes into account both the deterministic effects induced by the flame, and the probabilistic long range effects due to the spotting process of firebrands. Therefore, it combines as well the advantages of network models and those of macroscopic semi-physical models.

1. Introduction

Forest fires are very complex to model because of the number of intricate factors that can influence their propagation, and their multi-scale nature. Indeed, the characterization of their behavior depends on several parameters such as the fuel moisture content and the inclination of the terrain.

The small world model was proposed for the first time in 1998 by Watts and Strogatz in order to describe social behavior (Watts D. J. and Strogatz S. H., 1998). It is characterized by a high clustering coefficient and its ability to include randomly generated long-range connections. It was applied to model various phenomena such as epidemics, propagation of rumors (Zanette., 2002), the synchronization networks of cortical neurons (Yu Shan et al., 2008) etc.

On 2005, this model was successfully applied for the first time to forest fires within a collaboration between the two laboratories IUSTI (Polytech Marseille, France) and LEPM (USTO, Oran, Algeria) (Zekri et al., 2005). This variant of the small world model is based on two important requirements : it takes into account the flame radiation and the convection induced by the flame. In fact, the flame is modeled as having a cylindrical shape that emits a thermal radiation from its surface. Indeed, from each m² of the flame surface, N quanta of energy q are randomly generated using the statistical Monte Carlo method. In the other side, it considers the physics of combustion and the ignition and combustion properties of fine fuel elements which lead to the energy balance. The Small World Model was previously validated for three cases studies: fire experiments conducted in South Africa in 1992 (Savanna fires), historical fires that occurred in Lançon (France) in 2005 (Adou et al., 2010), and the historical fire of Suartone in Corsica 2003 (Hamamousse et al., 2021). In this work, the most recent version of this model is used to compare the real and the numerical rate of spread at different fuel moisture contents (for partially dried samples) and different terrain slopes (for naturally fead fuel).

2. Small World Network Model overview

In this model, the fuel medium is preheated to ignition by wind-driven convective and radiative heat emitted by the fire front and loses, in turn, a fraction of this energy by radiation to its influence area.

Each fuel element has a cylindrical shape with a height *H* and a diameter *D*, and only a top layer of thickness δ corresponding to the mean free path of radiation through the considered combustible that can be related to its surface-to-volume ratio, $\boldsymbol{\sigma_k = \frac{S_k}{V_k}}$, and to the volume fraction of the solid phase, $\boldsymbol{\alpha_k = \frac{V_k}{V}}$, as $\boldsymbol{\delta = 4/\sigma_k \alpha_k}$ (De Mestre et al., 1989), and volume $\boldsymbol{V = \pi D^2 \delta}$ of this combustible is affected in the pre-heating process. Above this penetration length $\boldsymbol{\delta}$, it is supposed that the radiation do not interact with fuel elements. These latter are considered as having the same geometric and thermo-physical properties. We assume also that the wet and dry fine fuel elements absorptivities are equal ($\boldsymbol{a_{WFF} = a_{DFF}}$), and that their volume fraction $\boldsymbol{\alpha}$ and surface-to-volume ratio $\boldsymbol{\sigma}$ are not affected during the thermal degradation process, which implies that $\boldsymbol{\alpha_{WFF} = \alpha_{DFF}}$ and $\boldsymbol{\sigma_{WFF} = \sigma_{DFF}}$.

Following the Koo et al. model (Koo et al., 2005), the receptive vegetation cell is heated in three steps: First, its temperature is raised by the absorbed heat up to the boiling temperature of water, namely 373 K. Then, it stagnates until the moisture content of this combustible is evaporated. Hence, in this desiccation phase, the wet fine fuel (WFF) is dried by the evaporation process turning into a dried fine fuel (DFF). Finally, the temperature of the dried vegetation restarts to increase steadily until it attains the pyrolysis temperature. If the emitted quantity of VOC is sufficient, the ignition process occurs, marking the end of the endothermic phase of this cell. The energy conservation in a receptive cell $\boldsymbol{j}$ exposed to a fire ($\boldsymbol{N_{bc}}$ burning cells) yields to the following equations.

For a temperature below the boiling temperature of water ($\boldsymbol{T(j) < 373K}$), we have:

$$\sum_{i=1}^{N_{bc}}\left[q^{+}_{rad,fl}(i) + q^{+}_{rad,e}(i) + q^{+}_{conv}(i)\right] - q^{-}_{rad}(j) = \rho_{WFF}\, c_{p_{WFF}}\, \alpha_k \frac{dT(j)}{dt} \qquad (1)$$

$\boldsymbol{q^{+}_{rad,fl}}$, $\boldsymbol{q^{+}_{rad,e}}$, $\boldsymbol{q^{+}_{conv}}$ and $\boldsymbol{q^{-}_{rad}}$ correspond respectively to the radiation of the flame, the radiation of embers, the convective preheating of the site located in the influence zone of the burning cell by the emitted hot gases and the radiative losses due to the heat transfer from the cell *j* to the ambient. $\boldsymbol{\rho_{WFF}}$ is the volumetric mass density of the wet fine fuel element and $\boldsymbol{c_{p_{WFF}}}$is its heat capacity.

When the temperature of the receptive cell is equal to $\boldsymbol{373K}$, the equation becomes:

$$\sum_{i=1}^{N_{bc}}\left[q^{+}_{rad,fl}(i) + q^{+}_{rad,e}(i) + q^{+}_{conv}(i)\right] - q^{-}_{rad}(j) = -\rho_{DFF}\, L_{vap}\, \alpha_k \frac{dm_c(j)}{dt} \qquad (3)$$

The latent heat of water vaporization $\boldsymbol{L_{vap}}$ is equal to $\boldsymbol{.25 \times 10^6\ J/Kg}$.

Once the site temperature exceeds that of water evaporation ($\boldsymbol{373K < T(j) < T_{pyr}}$), we have:

$$\sum_{i=1}^{N_{bc}}\left[q^{+}_{rad,fl}(i) + q^{+}_{rad,e}(i) + q^{+}_{conv}(i)\right] - q^{-}_{rad}(j) = \rho_{DFF}\, \alpha_k \frac{dT(j)}{dt} \qquad (4)$$

When it attains the pyrolysis temperature $\boldsymbol{T(j) = T_{pyr}}$, the conservation of energy implies:

$$\sum_{i=1}^{N_{bc}}\left[q^{+}_{rad,fl}(i) + q^{+}_{rad,e}(i) + q^{+}_{conv}(i)\right] - q^{-}_{rad}(j) = -\rho_{DFF}\ L_{pyr}\, \alpha_k \frac{dFPC}{dt} \qquad (5)$$

FPC is the pyrolysis product content of the dry fuel and $\boldsymbol{L_{pyr}}$ is the latent heat of pyrolysis.

The figure bellow schematizes the flame spread, the energy transfer mechanisms and the control volume of the cell involved in preheating.

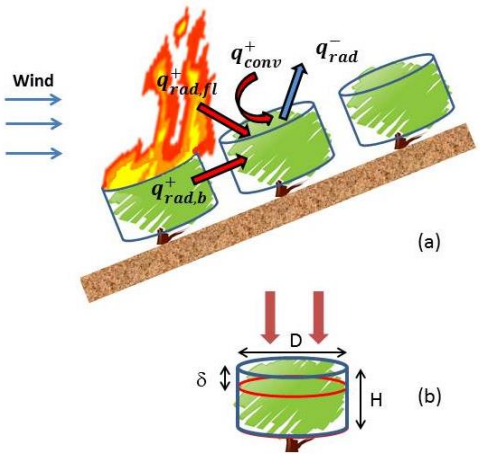

Figure 1: Flame spread schematic, with energy-transfer mechanisms indicated, and control volume of the cell involved in preheating.

We use a Monte Carlo method in order to estimate roughly the number of photons (quanta of energy) received by a healthy cell from the flame. This latter is modeled as a cylindrical solid body emitting radiation energy solely from its surface (solid flame model), this means that the properties of the flame such as its height, length, base diameter, angle and its emissive power are required. It is worth noting that the amount of energy received by a given cell depends on these flame properties, and may be affected by the air layer separating the flame and the cell, and the type of the vegetation cell. Moreover, some of these emitted quanta of energy may be absorbed by another burning cell situated between the emissive and the receptive sites. This screening effect that causes a loss of energy which does not contribute to the preheating of the healthy fuel is also taken into account by this MC method.

The radiated power is given by:

$$\boldsymbol{q^+_{rad,e}(i) = -a_{fm}\sigma\varepsilon_b T_b^4 \frac{d\tau}{dy} = a_{fm}\sigma\varepsilon_b T_b^4 \frac{1}{D_j}(exp(-d_1/\delta) - exp(-d_2/\delta))} \qquad (7)$$

Where $\boldsymbol{\sigma}$ is the Stefan-Boltzman constant (equal to $\boldsymbol{5.67 \times 10^{-8} Kg.s^{-3}.Kg^{-4}}$), $\boldsymbol{\varepsilon_b}$ is the embers emissivity (it is assumed to be equal to one) and $\boldsymbol{T_b}$ is the temperature of the radiating embers. $\boldsymbol{D_j}$ corresponds to the diameter of the preheating site whose center is located at a distance $\boldsymbol{d_{ij} = d_1 + \frac{D_i+D_j}{2} = d_2 - \frac{D_i+D_j}{2}}$ from the burning site.

The fuel cells situated in its influence area may be affected also by a wind-driven convective heat transfer mechanism which contributes to the heating of the receptive cell. If we suppose that the temperature difference decreases exponentially with the distance $\boldsymbol{y}$ as in (Pagni and Peterson., 1973). We can express this convective power as follows:

$$\boldsymbol{q^+_{conv}(i) = \frac{h}{\delta}(T_f - T_j)e^{-0.3d_{ij}/L_f}} \qquad (8)$$

We consider here that the length flame is approximately equal to one third of the characteristic length.
$\boldsymbol{L_f}$ is the flame length and $\boldsymbol{T_f}$ its temperature. $\boldsymbol{h}$ is an average heat transfer coefficient and is determined by the equation hereunder (Pagni and Peterson., 1973):

$$\boldsymbol{h = \frac{k_f}{d_{ij}} 0.037\, Re_{d_{ij}}^{0.8}\, Pr^{1/3}} \qquad (9)$$

$\boldsymbol{k_f}$ and $\boldsymbol{Pr}$ are the thermal conductivity and the dimensionless Prandtl number

Hence, the combustible cell exposed to the flame gains energy by radiative (flame and embers radiations) and convective (heat transported by hot gases) processes. However, it loses also a part of this stored heat by radiating it to the surrounding environment. These radiative losses can be expressed as:

$$q_{rad}^{-}(j) = \frac{1}{\delta}\varepsilon_{fm}\sigma\left(T_j{}^4 - T_\infty{}^4\right) \quad (10)$$

$\boldsymbol{\varepsilon_{fm}}$ is the fuel medium emissivity and $\boldsymbol{T_\infty}$ is the ambient temperature.

3. Validation of the Small world Network Model

In this work, the numerical rate of spread is compared to the experimental one :

- At different fuel moisture contents (for partially dried samples)
- At different terrain slopes (for naturally fead fuel).

The prescribed burning experiences were realized at the laboratory LEPM situated at the University of Sciences and Technology of Oran during spring 2021. 150 g masses of Pinus halepensis needles were homogeneously distributed on a metallic burning table of dimensions 88.5cm x 37.5cm. The fuel bed thickness and charge were about 1cm and 0.5kg/m², respectively. The fuel bed was divided into seven different positions (Figure 2); fire spread was then calculated by recording the time taken by the flame to pass between two successive positions.

Figure 2- Fire propagation table.

The first series of tests was realized on flat ground using pine needles dried partially using a microwave oven and a climatic chamber. The second series of tests was carried out according to different inclination angles (0, 5,9,13 and 17°) using naturally dried pine needles (dead needles) (figure 3).

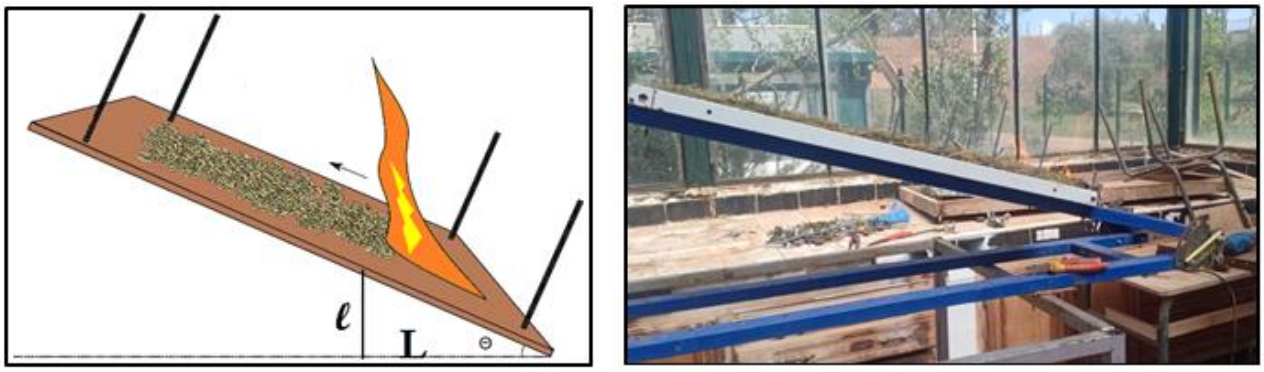

Figure 3- Inclined fire propagation table.

The study was divided into two main parts :

- Part 1 : The Network

2-dimentions network that contains homogeneous and uniform vegetation was constructed on a square based structure. The input data are occupancy, site radius, inclination, ignition type (punctual or linear).

- Part 2 : Fire propagation

The second part consists on the simulation of the fire propagation using the Small World Network Model. The network created in the previous section is integrated as an input of the Small World Network Model to simulate the fire propagation.

4. Results and discussions

In this section, we are going to present the experimental and the numerical results.

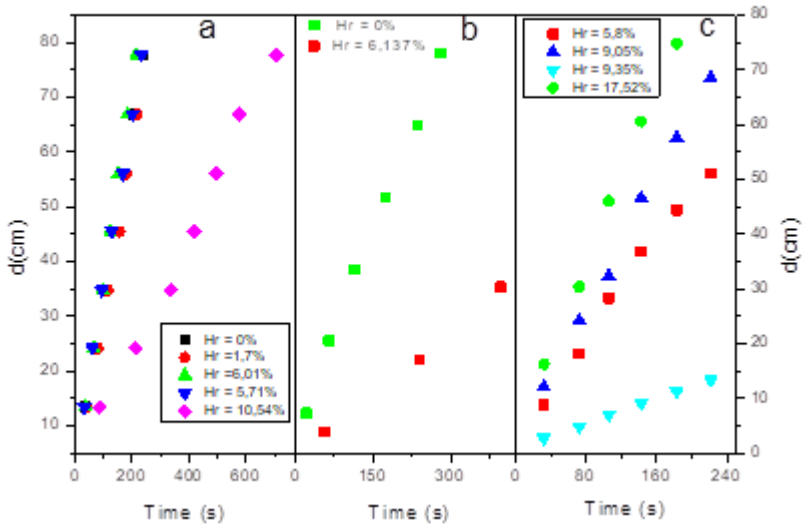

Figure 4- Fire spread evolution at different fuel moisture contents: Microwave oven , b) climatic chamber and c) naturally dead fuel.

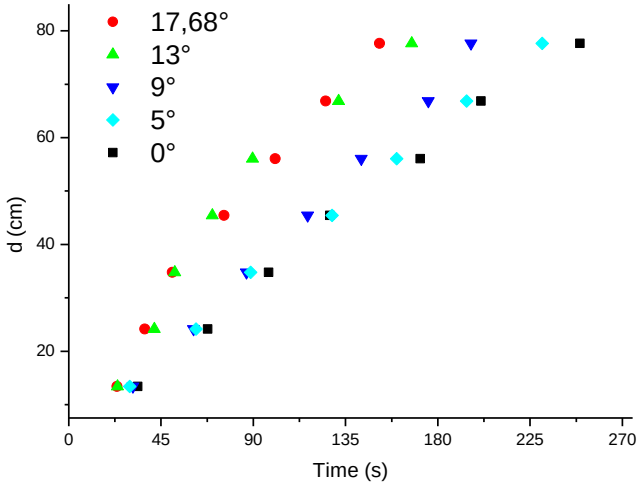

Figure 5- Fire spread at different table inclinations.

The comparison between the experimental and numerical results showed that the numerical simulations underestimate the fire rate of spread. This difference may be due to several reasons :

The intrinsic fuel parameters are not exactly estimated, some parameters differ from a region to another and from a season to another. Thus, it is important to characterize them experimentally.

The flame temperature captured by the thermocouples during the fire propagation indicates that the temperature decreases. This behavior is the same for low fuel moisture content.

5. Conclusion

The Small World Network model of fire propagation which combines the stochastic method of Monte Carlo and the semi-physicalapproach based on the resolution of the energy equation was validated on a prescribed burning realized at the laboratory LEPM situated at the University of Sciences and Technology of Oran during spring 2021. The comparison between the experimental and numerical results showed that the numerical simulations underestimate the fire rate of spread.

6. References

Adou, J. K., Y. Billaud, D. A. Brou, J. P. Clerc, J. L. Consalvi, A. Fuentes, A. Kaiss, F. Nmira, B. Porterie, L. Zekri, et al. 2010. Simulating wildfire patterns using a small-world network model. *Ecol Modell* 221 (11):1463–71. doi:10.1016/j.ecolmodel.2010.02.015.

De Mestre, N. J., E. A. Catchpole, D. H. Anderson, and R. C. Rothermel. 1989. Uniform propagation of a planar fire front without wind. *Combustion Science and Technology* 65 (4–6):231–44. doi:10.1080/00102208908924051.

Hamamousse,N., Kaiss,A., Giroud,F., Bozabalian,N., Clerc, J-P., & Zekri, N. (2021): Small World Network Model Validation. Case Study of Suartone Historical Fire in Corsica, Combustion Science and Technology, DOI: 10.1080/00102202.2021.1925890

Koo, E., P. J. Pagni, J. Woycheese, S. Stephens, D. R. Weise, and J. Huff (2005) A simple physical model for fire spread rate. In Fire Safety Science – Proc. of the 8th Int, 851–62.

Pagni, P. J., and T. P. Peterson (1973) Flame spread through porous fuels. In 14th Symposium (International) on Combustion, The Combustion Institute, 1099–107.

Watts, D. J., and S. H. Strogatz. 1998. Collective dynamics of 'small-world' networks. *Nature* 393 (6684):440–42. doi:10.1038/30918.

Zanette, D.H. 2002. Phys. Rev. E 65 041908.

Shan Yu; D. Huang; W. Singer; D. Nikolić. 2008. A Small World of Neuronal Synchrony. Cerebral Cortex. 18 (12): 2891–2901

Zekri, N., B. Porterie, J. P. Clerc, and J. C. Loraud. 2005. Propagation in a two-dimensional weighted local small-world network. *Physical Review E* 71 (4):046121. doi:10.1103/PhysRevE.71.046121.

OBRA PUBLICADA
COM A COORDENAÇÃO
CIENTÍFICA

1 2 9 0

IMPRENSA DA
UNIVERSIDADE
DE COIMBRA
COIMBRA UNIVERSITY PRESS